

# ORGANOMETALLICS

Volume 14, Number 1, January 1995

© Copyright 1995  
American Chemical Society

## Communications

### Mechanism of the Palladium-Catalyzed Elimination of Acetic Acid from Allylic Acetates

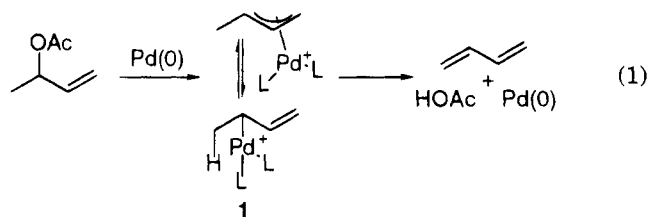
Pher G. Andersson\* and Szymon Schab

Department of Organic Chemistry, University of Uppsala, Box 531, S-751 21 Uppsala, Sweden

Received May 31, 1994<sup>⊗</sup>

**Summary:** The mechanism of the palladium-catalyzed elimination of acetic acid from allylic acetates has been studied. It was found that this process can take place not only via conventional *syn* elimination of palladium hydride but also via an *anti* elimination pathway.

**Introduction.** The palladium-catalyzed elimination of acetic acid from allylic acetates was first developed by Tsuji<sup>1</sup> and Trost<sup>2</sup> and has since then become a useful synthetic route to 1,3-dienes. This reaction (eq 1) has



been thought to proceed via a  $\beta$ -elimination from the intermediate ( $\sigma$ -allyl)palladium complex **1**, but the mechanism has never been subject to closer investigation. In this communication we present results which show that an *anti* elimination is an important pathway.

During our development of palladium-catalyzed an-

nulation chemistry<sup>3</sup> we prepared some of the requisite diene starting materials via the route outlined in Scheme 1. Palladium-catalyzed elimination of HOAc from the *cis*-acetate **3** under standard conditions<sup>4</sup> resulted in a 5:1 mixture of the two dienes **4** and **5**. During the optimization of the reaction conditions several bases were tried and it was found that sterically hindered amines favored the formation of **4**. Thus, triisobutylamine gave a 7:1 ratio between **4** and **5**.

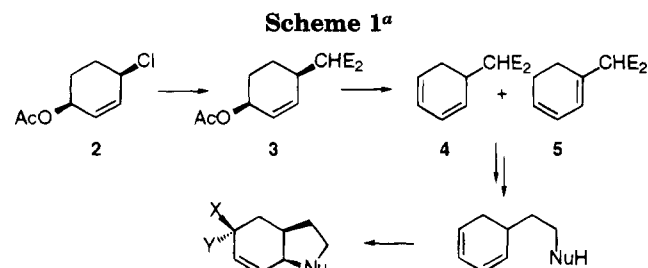
We have now undertaken further studies of this elimination and found that the ratio of **4** and **5** can be further shifted, depending on which base is used; for example, the use of DBU resulted in a very much faster reaction rate and the ratio of **4** and **5** in the isolated product was >25:1. These findings suggest that the base is at least in part responsible for the proton abstraction, a result which stands in sharp contrast to the commonly accepted *syn*  $\beta$ -elimination mechanism in which the base does not participate in the elimination step. In order to gain further insight into the mechanism, *trans*-acetate **6** was synthesized via an  $S_N2$  displacement of allylic chloride **2** with sodium mal-

(3) (a) Bäckvall, J. E.; Andersson, P. G.; Vågberg, J. O. *Tetrahedron Lett.* **1989**, *30*, 137. (b) Bäckvall, J. E.; Andersson, P. G. *J. Am. Chem. Soc.* **1990**, *112*, 3683. (c) Bäckvall, J. E.; Andersson, P. G.; Stone, G. B.; Gogoll, A. *J. Org. Chem.* **1991**, *56*, 2988. (d) Bäckvall, J. E.; Andersson, P. G. *J. Am. Chem. Soc.* **1993**, *114*, 6374. (e) Bäckvall, J. E.; Granberg, K. L.; Andersson, P. G.; Gatti, R.; Gogoll, A. *J. Org. Chem.* **1993**, *58*, 5445.

(4) The acetate (1 equiv) was dissolved in toluene under a nitrogen atmosphere. To this solution were added Pd(dba)<sub>2</sub> (0.02 equiv), dppe (0.04 equiv), and triethylamine (1.5 equiv). The resulting solution was heated to reflux until the reaction was complete.

<sup>⊗</sup> Abstract published in *Advance ACS Abstracts*, December 1, 1994.  
(1) Tsuji, J.; Yamakawa, T.; Kaito, M.; Mandai, T. *Tetrahedron Lett.* **1978**, 2075.

(2) Trost, B. M.; Verhoeven, T. R.; Fortunak, J. M. *Tetrahedron Lett.* **1979**, 2301.



<sup>a</sup> Legend: Nu = O, NR; E = CO<sub>2</sub>Me; X = Cl, RO, RCO<sub>2</sub>; Y = RCO<sub>2</sub>

**Table 1. Palladium-Catalyzed Elimination of Acetates 3 and 6<sup>a</sup>**

time (min)	acetates		dienes		acetates		dienes	
	3	6	4	5	3	6	4	5
0	95.8	4.2	0	0	5.7	94.3	0	0
5	87.4	4.1	7.6	0.9	5.5	93.9	0.4	0.2
10	74.2	3.8	19.6	2.4	5.4	93.8	0.5	0.3
15	63.7	3.2	29.3	3.8	5.3	93.1	1.0	0.6
30	31.6	2.1	58.3	8.0	5.0	91.5	1.9	1.6
45	0	0	88.2	11.8	4.6	88.2	4.8	2.4
60					4.3	83.5	7.9	4.3
90					3.8	76.4	12.9	6.9
120					2.8	59.3	23.1	14.8
240					0.5	26.7	46.6	26.2
480					0	0	62.1	37.9

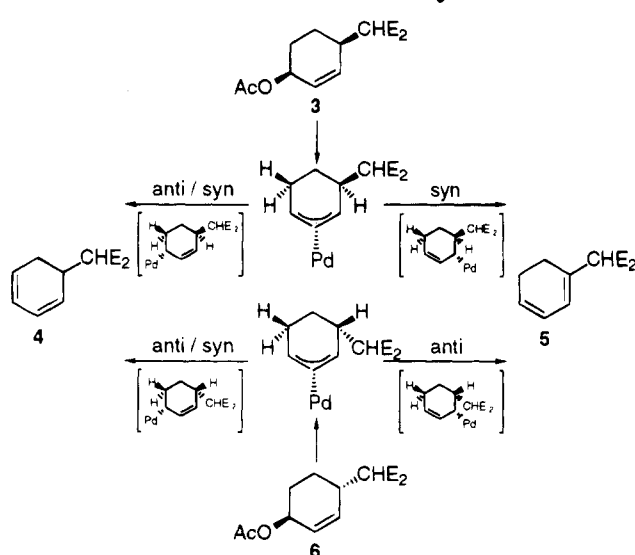
<sup>a</sup> The acetate **3** or **6** (1 equiv) was dissolved in toluene under a nitrogen atmosphere. To this solution were added Pd(dba)<sub>2</sub> (0.02 equiv), dppe (0.04 equiv) and triisobutylamine (1.5 equiv). The resulting yellow solution was heated to reflux and monitored by GC until the reaction was completed.

onate.<sup>5</sup> If the diene formation were to proceed via  $\beta$ -elimination of palladium hydride, this substrate would be expected to give rise to diene **4** exclusively, since only one hydrogen would be *syn* to palladium in the intermediate  $\sigma$ -allyl complexes. However, in contrast with such a prediction, a substantially greater amount of diene **5** was formed when **6** was reacted under the same conditions as **3**. As mentioned above, reaction of **3** in toluene at reflux in the presence of Pd(dba)<sub>2</sub>, 1,2-bis-(diphenylphosphino)ethane (dppe) and triisobutylamine gave a 7:1 mixture of **4** and **5** after 45 min (Table 1). When **6** was reacted under the same conditions, the corresponding value was 1.6:1.

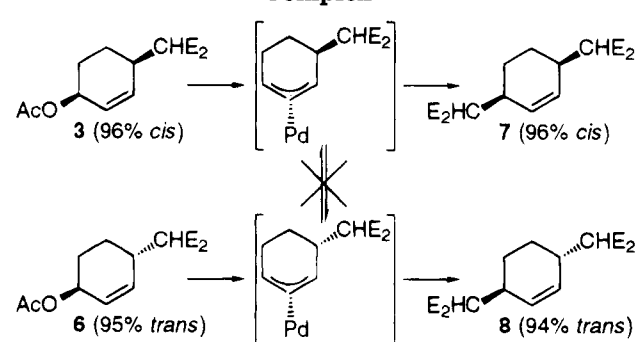
It is known that allylic acetates can isomerize in palladium(0)-catalyzed reactions.<sup>2</sup> This isomerization takes place via a *syn* migration of acetate from palladium to carbon in the allyl intermediate to give the stereoisomeric acetate. To ensure that this pathway was not operative here, the reactions were followed by GC, which showed that no isomerization of the starting material took place during the reaction (Table 1).

Another possible isomerization pathway involves S<sub>N</sub>2 attack by "free Pd(0)" on the ( $\pi$ -allyl)palladium complex and results in a new palladium species in which the configuration at the  $\pi$ -allyl is now inverted.<sup>6</sup> This isomerization is, however, known to be efficiently inhibited by the use of a bidentate phosphine ligand such as dppe.<sup>5a,c,d</sup> A control experiment was performed in

**Scheme 2. Elimination Pathways for 3 and 6**



**Scheme 3. Trapping of the Intermediate  $\pi$ -Allyl Complex<sup>a</sup>**



<sup>a</sup> To a THF solution of the acetate (**3** or **6**) was added Pd(OAc)<sub>2</sub> 0.05 equiv and dppe (0.10 equiv) under an atmosphere of nitrogen. The resulting solution was heated to reflux for 1 h after which a THF solution of sodium malonate was added. After the reaction was complete, the crude product was analyzed by NMR and GC.

which the intermediate  $\pi$ -allyl complex was trapped with sodium malonate after 1 h of reflux. Trapping the  $\pi$ -allyl complex derived from acetates **3** and **6**, respectively, produced the corresponding bis(malonates) **7** and **8** in a highly stereospecific manner, confirming that no isomerization of the ( $\pi$ -allyl)palladium complex had occurred.<sup>7</sup>

**Conclusion.** The above-mentioned findings strongly suggest that an *anti*-elimination pathway can operate in the palladium-catalyzed elimination of allylic acetates. A probable mechanism would be a base-assisted 1,2-diaxial elimination of the proton and Pd(0) from a ( $\sigma$ -allyl)palladium intermediate (cf. Scheme 2), which nicely explains the effect of the base on the regiochemical outcome of the reaction.

**Acknowledgment.** Financial support from the Swedish Natural Science Research Council is gratefully acknowledged. S.S. thanks the Swedish Institute for a fellowship. We are grateful to Prof. J. E. Bäckvall and Dr. D. Tanner for helpful discussions and to Johnson Matthey for a generous gift of palladium chloride.

OM9404083

(5) Bäckvall, J. E.; Vågberg, J. O. *Org. Synth.* **1990**, *69*, 38.

(6) (a) Moreno-Mañas, M.; Ribas, J.; Virgili, A. *J. Org. Chem.* **1988**, *22*, 5328. (b) Bäckvall, J. E.; Granberg, K. L.; Heumann, A. *Isr. J. Chem.* **1991**, *31*, 17. (c) Granberg, K. L.; Bäckvall, J. E. *J. Am. Chem. Soc.* **1992**, *114*, 6858. (d) Stary, I.; Zajicek, J.; Kocovsky, P. *Tetrahedron* **1992**, *48*, 7229.

(7) The spectral data of compounds **7** and **8** were identical with those reported in the literature: Bäckvall, J. E.; Juntunen, S. K. *J. Am. Chem. Soc.* **1987**, *109*, 6396.



# Organosamarium Tetrathiometalate Chemistry: Synthesis and Structure of the Mixed-Metal Complexes {[(C<sub>5</sub>Me<sub>5</sub>)<sub>2</sub>Sm]<sub>2</sub>Mo(μ-S)<sub>4</sub>}<sup>-</sup> and [(C<sub>5</sub>Me<sub>5</sub>)<sub>2</sub>Sm(μ-S)<sub>2</sub>WS<sub>2</sub>]<sup>-</sup>

William J. Evans,\* Mohammad A. Ansari, and Joseph W. Ziller

Department of Chemistry, University of California, Irvine, California 92717

Saeed I. Khan

Department of Chemistry and Biochemistry, University of California,  
Los Angeles, California 90024

Received August 1, 1994<sup>®</sup>

**Summary:** Mixed-metal Mo-Sm and W-Sm complexes can be readily made by reaction of (C<sub>5</sub>Me<sub>5</sub>)<sub>2</sub>Sm(THF)<sub>2</sub> with (PPh<sub>4</sub>)<sub>2</sub>MoS<sub>4</sub> and (PPh<sub>4</sub>)<sub>2</sub>WS<sub>4</sub>. In the molybdenum case, a trimetallic Mo(V) complex, {[(C<sub>5</sub>Me<sub>5</sub>)<sub>2</sub>Sm]<sub>2</sub>Mo(μ-S)<sub>4</sub>}<sup>-</sup>(PPh<sub>4</sub>)<sup>+</sup> (1), is obtained. With tungsten, a bimetallic W(VI) complex, [(C<sub>5</sub>Me<sub>5</sub>)<sub>2</sub>Sm(μ-S)<sub>2</sub>WS<sub>2</sub>](PPh<sub>4</sub>)<sup>-</sup> (2), is isolated. Both complexes contain tetrahedral MS<sub>4</sub> units which coordinate via bridging sulfur atoms to (C<sub>5</sub>Me<sub>5</sub>)<sub>2</sub>-Sm moieties.

Tetrathiometalates such as (MoS<sub>4</sub>)<sup>2-</sup>, (WS<sub>4</sub>)<sup>2-</sup>, and (ReS<sub>4</sub>)<sup>-</sup> have been found to coordinate to a wide variety of transition metals<sup>2-6</sup> with interesting ramifications in hydrodesulfurization catalysis<sup>7</sup> and molybdoenzyme chemistry,<sup>8</sup> but their utility as ligands for the lanthanide metals has not yet been explored. Although the electropositive lanthanide metals have a stronger preference for oxygen donor ligands than for sulfur, lanthanide complexes involving the lower congeners of main group 16 are known and recent work has shown that an extensive chemistry is available with these donor atoms.<sup>9-15</sup> Given the tendency of the tetrathiometalates to form chelating bidentate structures, they

seemed to be ideal ligands for formation of mixed-metal species with the (C<sub>5</sub>Me<sub>5</sub>)<sub>2</sub>Sm unit,<sup>16</sup> which prefers to coordinate to two additional ligands to form eight-coordinate structures.<sup>17</sup> We report here on the utility of (C<sub>5</sub>Me<sub>5</sub>)<sub>2</sub>Sm(THF)<sub>2</sub><sup>18</sup> in forming new heterometallic group 6 transition-metal lanthanide complexes using tetrathiometalate anions.

Purple (C<sub>5</sub>Me<sub>5</sub>)<sub>2</sub>Sm(THF)<sub>2</sub> reacts immediately with (PPh<sub>4</sub>)<sub>2</sub>MoS<sub>4</sub> to form a red product (1) and PPh<sub>3</sub>.<sup>19</sup> The IR spectrum of 1 contains an absorption at 431 cm<sup>-1</sup> in the Mo-S region which is shifted from the 458 cm<sup>-1</sup> absorption of (MoS<sub>4</sub>)<sup>2-</sup>. The <sup>1</sup>H and <sup>13</sup>C NMR spectra of 1 are consistent with the presence of Sm(III),<sup>20</sup> a single C<sub>5</sub>Me<sub>5</sub> ligand environment, and (PPh<sub>4</sub>)<sup>+</sup>. An X-ray diffraction study<sup>21</sup> revealed that the product contained one (PPh<sub>4</sub>)<sup>+</sup> per trimetallic Sm<sub>2</sub>Mo unit; i.e., 1 is the Mo(V) complex {[(C<sub>5</sub>Me<sub>5</sub>)<sub>2</sub>Sm]<sub>2</sub>MoS<sub>4</sub>}<sup>-</sup>(PPh<sub>4</sub>)<sup>+</sup> (Figure 1). Reduction of the metal center of a tetrathiometalate unit after complexation is rare and has been observed only in Fe/Mo cubanes.<sup>8b</sup>

(15) (a) Berardini, M.; Emge, T. J.; Brennan, J. G. *J. Am. Chem. Soc.* **1993**, *115*, 8501-8502. (b) Berardini, M.; Emge, T. J.; Brennan, J. G. *J. Chem. Soc., Chem. Commun.* **1993**, 1537-1538.

(16) Evans, W. J. *Polyhedron* **1987**, *6*, 803-835 and references therein.

(17) Evans, W. J.; Foster, S. E. *J. Organomet. Chem.* **1992**, *433*, 79-94.

(18) Evans, W. J.; Grate, J. W.; Choi, H. W.; Bloom, I.; Hunter, W. E.; Atwood, J. L. *J. Am. Chem. Soc.* **1985**, *107*, 941-946.

(19) In a glovebox, addition of (C<sub>5</sub>Me<sub>5</sub>)<sub>2</sub>Sm(THF)<sub>2</sub> (283 mg, 0.5 mmol) in 5 mL of THF to a suspension of (PPh<sub>4</sub>)<sub>2</sub>MoS<sub>4</sub> (226 mg, 0.25 mmol) in 10 mL of THF caused an immediate color change from purple to red. The reaction mixture was stirred for 20 min and centrifuged to remove solids, and the solvent was removed by rotary evaporation. The crude product was washed with hexanes to remove any soluble organic byproducts. The <sup>31</sup>P NMR spectrum of the hexane wash confirmed the presence of PPh<sub>3</sub>. No signals were observed in the EPR spectrum of 1, probably due to the presence of Sm(III). Recrystallization from toluene at -35 °C produced {[(C<sub>5</sub>Me<sub>5</sub>)<sub>2</sub>Sm]<sub>2</sub>Mo(μ-S)<sub>4</sub>}<sup>-</sup>(PPh<sub>4</sub>)<sup>+</sup> (1) as dark red crystals (316 mg, 90%). Anal. Calcd for C<sub>64</sub>H<sub>80</sub>PS<sub>4</sub>MoSm<sub>2</sub>: C, 54.65; H, 5.73; P, 2.20; S, 9.13; Mo, 6.82; Sm, 21.40. Found: C, 55.52; H, 5.81; P, 2.50; S, 8.44; Mo, 6.31; Sm, 21.55. <sup>1</sup>H NMR (C<sub>6</sub>D<sub>6</sub>): δ 7.39, 7.03, 6.85, 6.48 and 6.29 (PPh<sub>4</sub><sup>+</sup>), 1.76 (C<sub>5</sub>Me<sub>5</sub>). <sup>13</sup>C NMR (THF-*d*<sub>6</sub>): δ 137.3, 136.3, and 132.7 (PPh<sub>4</sub><sup>+</sup>), 119.9 (C<sub>5</sub>Me<sub>5</sub>), 34.0 (C<sub>5</sub>Me<sub>5</sub>). UV-vis (1.42 × 10<sup>-4</sup> M in THF; λ, nm (ε)): 470 (6320). IR (Nujol): 2980-2850 (s, br), 1460 (s), 1375 (s), 1186 (w), 1106 (m), 1066 (w), 996 (w), 742 (w), 722 (s), 689 (m), 526 (s), 431 (s, Mo-S), 301 (m, Sm-S) cm<sup>-1</sup>. Magnetic susceptibility (Evans method<sup>26</sup>): χ<sub>M</sub><sup>298 K</sup> = 290 × 10<sup>-6</sup> cgsu; μ<sub>eff</sub><sup>298 K</sup> = 1.2 μ<sub>B</sub>.

(20) Evans, W. J.; Ulibarri, T. A. *J. Am. Chem. Soc.* **1987**, *109*, 4292-4297.

(21) Crystal data for C<sub>64</sub>H<sub>80</sub>PS<sub>4</sub>MoSm<sub>2</sub>: monoclinic system with cell dimensions at 183 K of a = 17.212(3) Å, b = 13.754(2) Å, c = 26.378(4) Å, β = 103.63(1)°, and V = 6068(2) Å<sup>3</sup>. The space group is P<sub>2</sub><sub>1</sub>/c with Z = 4 and D<sub>calc</sub> = 1.538 Mg/m<sup>3</sup>. The structure was solved by direct methods and refined by full-matrix least-squares techniques using 6505 reflections with |F<sub>o</sub>| > 3.0σ(F<sub>o</sub>). At convergence, R<sub>F</sub> = 4.27%, R<sub>wF</sub> = 4.27%, and GOF = 1.37 for 649 variables. Recrystallization from THF/benzene at ambient glovebox temperature produces the same compound with one benzene solvent molecule per formula unit in the same space group with a = 18.139(7) Å, b = 14.208(5) Å, c = 27.3041(10) Å, β = 103.01(1)°, and V = 6858.4 (20) Å<sup>3</sup>.

<sup>®</sup> Abstract published in *Advance ACS Abstracts*, December 1, 1994.

(1) Reported in part at the 207th National Meeting of the American Chemical Society, San Diego, CA March 1994; INOR 73.

(2) Müller, A.; Diemann, E.; Jostes, R.; Bögge, H. *Angew. Chem., Int. Ed. Engl.* **1981**, *20*, 934-955.

(3) Müller, A.; Bögge, H.; Schimanski, U.; Penk, M.; Nieradzki, K.; Dartmann, M.; Krickemeyer, E.; Schimanski, J.; Römer, C.; Römer, M.; Dornfeld, H.; Wienböcker, U.; Hellmann, W.; Zimmerman, M. *Monatsh. Chem.* **1989**, *120*, 367-391.

(4) Howard, K. E.; Rauchfuss, T. B.; Wilson, J. R. *Inorg. Chem.* **1988**, *27*, 3561-3567.

(5) Secheresse, F.; Salis, M.; Potvin, C.; Manoli, J. M. *Inorg. Chim. Acta* **1986**, *114*, L19-L23.

(6) Manoli, J. M.; Potvin, C.; Secheresse, F.; Marzak, S. *Inorg. Chim. Acta* **1988**, *150*, 257-268.

(7) (a) Picoraro, T. A.; Chianelli, R. R. *Catalysis* **1981**, *67*, 430-435.

(b) Harris, S.; Chianelli, R. R. *Catalysis* **1984**, *86*, 400-412. (c) Chianelli, R. R.; Picoraro, T. A.; Halbert, T. R.; Pan, W.-H.; Steifel, E. I. *J. Catal.* **1984**, *86*, 226-230. (d) Müller, A. *Polyhedron* **1986**, *5*, 323-340.

(8) (a) Holm, R. H.; Berg, J. M. *Acc. Chem. Res.* **1986**, *19*, 363-370.

(b) Coucouvanis, D. *Acc. Chem. Res.* **1991**, *24*, 1-8.

(9) (a) Tilley, T. D.; Andersen, R. A.; Zalkin, A.; Templeton, D. H. *Inorg. Chem.* **1982**, *21*, 2644-2647. (b) Zalkin, A.; Henly, T. J.; Andersen, R. A. *Acta Crystallogr.* **1987**, *C43*, 233-236. (c) Berg, D. J.; Andersen, R. A.; Zalkin, A. *Organometallics* **1988**, *7*, 1858-1863. (d) Zalkin, A.; Berg, D. J. *Acta Crystallogr.* **1988**, *C44*, 1488-1489. (e) Berg, D. J.; Burns, C. J.; Andersen, R. A.; Zalkin, A. *Organometallics* **1989**, *8*, 1865-1870.

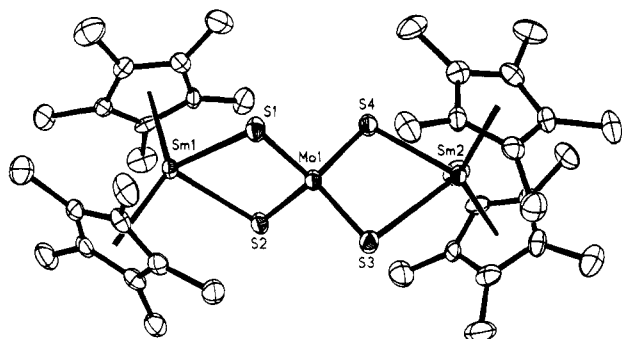
(10) Schumann, H.; Albrecht, I.; Hahn, E. *Angew. Chem., Int. Ed. Engl.* **1985**, *24*, 985-986.

(11) Recknagel, A.; Noltemeyer, M.; Stalke, D.; Pieper, U.; Schmidt, H.-G.; Edelman, F. T. *J. Organomet. Chem.* **1991**, *411*, 347-356.

(12) Evans, W. J.; Rabe, G. W.; Ziller, J. W.; Doedens, R. J. *Inorg. Chem.* **1994**, *33*, 2719-2726.

(13) Strzelecki, A. G.; Timinski, P. A.; Helsen, B. A.; Bianconi, P. A. *J. Am. Chem. Soc.* **1992**, *114*, 3159-3160.

(14) Cary, D. R.; Arnold, J. J. *J. Am. Chem. Soc.* **1993**, *115*, 2520-2521.

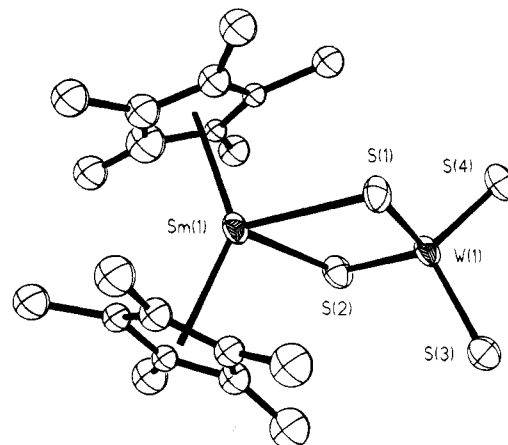


**Figure 1.** Thermal ellipsoid plot of  $[(C_5Me_5)_2Sm(\mu-S)_4]^-$  with ellipsoids drawn at the 50% probability level.

The solid-state structure of **1** contains essentially identical  $(C_5Me_5)_2Sm(\mu-S)_2$  units which have metrical parameters typical of eight-coordinate Sm(III).<sup>17</sup> The 2.791(2) and 2.796(2) Å Sm–S distances are longer than those in  $[(C_5Me_5)_2Sm(THF)]_2(\mu-S)$  (2.663(1) and 2.665(1) Å).<sup>12</sup>

Mo–S distances in tetrathiomolybdate complexes typically do not vary beyond a range of 2.2–2.4 Å,<sup>2</sup> and the 2.225(2)–2.241(2) Å Mo–S distances in **1** are no exception. For comparison, free  $MoS_4^{2-}$  has 2.178(5) Å distances<sup>22</sup> and the trimetallic  $MoS_4$ -bridged complexes  $(PPh_4)_2[(Cl_2Fe)_2MoS_4]^{23}$  and  $(NMe_4)_2[(NCCu)_2MoS_4]^{24}$  have distances of 2.204(5) and 2.209(3) Å, respectively. In mixed-valence  $[(MoS_4)_2Fe]^{3-}$ , the bridging Mo–S distances are 2.251(5) and 2.260(4) Å.<sup>23b</sup> The mixed-valence complex  $[(Mo^{VI}S_4)Mo^{IV}O(Mo^{VI}S_4)]^{2-}$  has an average Mo(IV)–S distance of 2.408(16) Å and an average Mo(VI)–S(bridging) distance of 2.245(14) Å.<sup>24</sup>

Interestingly, under similar conditions reactions of  $(PPh_4)_2WS_4$  with  $(C_5Me_5)_2Sm(THF)_2$  in THF did not produce a tungsten analog of **1** but instead yielded  $[(C_5Me_5)_2Sm(\mu-S)_2WS_2](PPh_4)$  (**2**).<sup>25</sup> Although the spectral characteristics of **2** were similar to those of **1**, they were not identical and X-ray crystallography was needed for definitive identification.<sup>26</sup> **2** crystallizes with two independent molecules in the unit cell, each containing a  $(PPh_4)^+$  group and a bimetallic monoanion having an eight-coordinate Sm center ligated to a  $(\mu-S)_2WS_2$  unit (Figure 2). Apparently, in this case reduction of the tetrathiometalate metal center did not occur. This is consistent with the difference in redox potentials of



**Figure 2.** Molecular structure of  $[(C_5Me_5)_2Sm(\mu-S)_2WS_2]^-$  with ellipsoids drawn at the 50% probability level.

$MoS_4^{2-}$  vs  $WS_4^{2-}$ . Similar differences have been noted in some monomeric Mo/W compounds.<sup>27</sup>

The structure of **2** is similar to that of **1** except that the  $WS_4^{2-}$  moiety in **2** is less symmetrical than the tetrathiometalate in **1** since only two of the sulfur atoms are bridging. As expected, the bridging W–S distances (2.209(7)–2.217(7) Å) are larger than the terminal W–S distances of 2.154(8)–2.164(9) Å. In comparison, uncoordinated  $WS_4^{2-}$  has an average W–S distance 2.177 Å.<sup>2</sup> W–S distances, like Mo–S distances, do not typically span a wide range, and the M–S distances in the two complexes are similar. The  $(C_5Me_5)$  ring centroid–Sm–(ring centroid) angles in **1** and **2** are similar (Mo, 136.8 and 136.2°; W, 135.1 and 138.5°), and the Sm–C and Sm–S distances are equivalent within statistical limits (Sm– $(C_5Me_5)$  ring centroid) distance: Mo, 2.439–2.462 Å; W, 2.400–2.419 Å and Sm–S: Mo, 2.784(2)–2.796(2) Å; W, 2.817(8)–2.841(7) Å). In both complexes, the cations are well separated from the anions and do not show any unusual features.

These results show that tetrathiometalates are viable ligands for the lanthanides and provide a facile way to make molecular mixed-metal species containing this combination of metals. In addition, by using  $(C_5Me_5)_2Sm(THF)_2$  with  $(MoS_4)^{2-}$  an unusual Mo(V) derivative can be obtained.

**Acknowledgment.** This research was supported by the National Science Foundation.

**Supplementary Material Available:** Tables of crystal data and refinement details, positional and thermal parameters, and bond distances and angles and fully labeled ORTEP drawings for compounds **1** and **2** (31 pages). Ordering information is given on any current masthead page.

OM940608E

(26) **2** crystallizes with two independent molecules in the asymmetric unit, and structure solution requires the determination of two cations, two anions and two noncoordinated THF molecules. Crystal data for  $C_{48}H_{58}OPS_4SmW$ : triclinic, space group  $P\bar{1}$ , with cell dimensions at 176 K  $a = 22.158(6)$  Å,  $b = 23.323(6)$  Å,  $c = 9.611(2)$  Å,  $\alpha = 98.28(1)^\circ$ ,  $\beta = 91.31(1)^\circ$ ,  $\gamma = 101.29(1)^\circ$ , and  $V = 4813(2)$  Å<sup>3</sup> with  $Z = 4$  and  $D_{\text{calcd}} = 1.561$  Mg/m<sup>3</sup>. The structure was solved by heavy-atom methods of SHELX 86 and refined by using SHELX 76. Due to a low data to parameter ratio all the phenyl carbon atoms of  $PPh_4^+$  were refined as rigid groups. All the  $C_5Me_5$  carbon atoms were treated isotropically. The final refinement using 4885 reflections with  $|F_o| > 6\sigma(|F_o|)$  converged to  $R_F = 6.20\%$  and  $R_{wF} = 6.0\%$ , for 476 variables.

(27) Pan, W.-H.; Halbert, T. R.; Hutching, L. L.; Stiefel, E. I. *J. Chem. Soc., Chem. Commun.* **1985**, 927–929.

(28) Evans, D. F. *J. Chem. Soc.* **1959**, 2003–2005. Becconsall, J. K. *Mol. Phys.* **1968**, 15, 129–139.

(22) Lapasset, P. J.; Chezeau, N.; Belougne, P. *Acta Crystallogr.* **1976**, B32, 3087–3088.

(23) (a) Coucouvanis, D.; Baenziger, N. C.; Simhon, E. D.; Stremple, P.; Swenson, D.; Simpoulos, A.; Kosticas, A.; Petrouleas, V.; Papaefthymiou, V. *J. Am. Chem. Soc.* **1980**, 102, 1732–1734. (b) Coucouvanis, D.; Simhon, E. D.; Baenziger, N. C. *J. Am. Chem. Soc.* **1980**, 102, 6644–6646.

(24) Müller, A.; Dartmann, M.; Römer, C.; Clegg, W.; Sheldrick, G. M. *Angew. Chem., Int. Ed. Engl.* **1981**, 20, 1060–1061.

(25) In a glovebox,  $(C_5Me_5)_2Sm(THF)_2$  (56 mg, 0.1 mmol) in 5 mL of THF was added to a suspension of  $(PPh_4)_2WS_4$  (99 mg, 0.1 mmol) in 5 mL of THF. The color of the solution changed immediately from purple to red. The reaction mixture was stirred for 30 min and centrifuged. Solvent was removed by rotary evaporation, and the resulting solid was washed with hexanes and toluene. Slow evaporation of a THF solution at ambient temperature produced  $[(C_5Me_5)_2Sm(\mu-S)_2WS_2](PPh_4) \cdot THF$  (**2**) as red crystals (67 mg, 60%).  $PPh_3$  was identified as a hexane-soluble byproduct. Anal. Calcd for  $C_{48}H_{58}OPS_4SmW$ : C, 50.37; H, 5.11; P, 2.71; S, 11.21. Found: C, 52.08; H, 5.19; P, 2.84; S, 9.28. <sup>1</sup>H NMR ( $THF-d_6$ ):  $\delta$  7.76, 7.72, and 7.31 ( $PPh_4^+$ ), 1.05 ( $C_5Me_5$ ). Bulk samples were observed to have an additional resonance in the  $C_5Me_5$  region at 1.13 ppm. <sup>13</sup>C NMR ( $THF-d_6$ ):  $\delta$  137.0, 136.1, and 132.4 ( $PPh_4^+$ ), 118.5 ( $C_5Me_5$ ), 44.7 ( $C_5Me_5$ ). UV–vis ( $7 \times 10^{-5}$  M in THF;  $\lambda$ , nm ( $\epsilon$ )) 397 (3735). IR (Nujol): 2980–2850 (s, br), 1460 (s), 1375 (s), 1185 (w), 1163 (w), 1106 (m), 1062 (w), 996 (w), 743 (w), 723 (s), 690 (m), 526 (s), 414, 426 (s,  $\nu(W-S)$ ), 300 (m, Sm–S)  $cm^{-1}$ . Magnetic susceptibility (Evans method<sup>28</sup>):  $\chi_M^{298 K} = 5138 \times 10^{-6}$  cgsu;  $\mu_{\text{eff}}^{298 K} = 1.1 \mu_B$ .

# Efficient Synthesis of *rac*-(Ethylenebis(indenyl))ZrX<sub>2</sub> Complexes via Amine Elimination

Gary M. Diamond, Stephan Rodewald, and Richard F. Jordan\*

Department of Chemistry, University of Iowa, Iowa City, Iowa 52242

Received September 2, 1994<sup>®</sup>

**Summary:** The amine elimination reaction of 1,2-bis(3-indenyl)ethane (**3**) and Zr(NMe<sub>2</sub>)<sub>4</sub> (**2**) affords pure *rac*-(EBI)Zr(NMe<sub>2</sub>)<sub>2</sub> (**4**; EBI = 1,2-ethylenebis(1-indenyl)) in 68% isolated yield. Treatment of **4** with 2 equiv of Me<sub>2</sub>NH·HCl affords *rac*-(EBI)ZrCl<sub>2</sub> (**1**) in 92% isolated yield. Compound **1** can also be prepared directly from **2** and **3** in a "one-pot" synthesis in 69% isolated yield.

Chiral group 4 *ansa*-metallocenes, originally developed by Brintzinger,<sup>1</sup> have been exploited as stereoselective catalysts or reagents for a wide variety of reactions.<sup>2</sup> Important examples include olefin polymerization,<sup>3,4</sup> hydrooligomerization,<sup>5a,b</sup> cyclopolymerization,<sup>5c,d</sup> hydrogenation,<sup>5e</sup> epoxidation<sup>5f,g</sup> and isomerization<sup>5h</sup> reactions, olefin-pyridine coupling,<sup>5i</sup> imine hydrogenation,<sup>5j</sup> Diels-Alder reactions,<sup>5k</sup> allylic amine synthesis,<sup>5l</sup> dehydrogenative phenylsilane oligomerization,<sup>5m</sup> and carbomagnesiation reactions.<sup>5n</sup>

Chiral *ansa*-metallocenes are normally prepared by chloride displacement reactions of MCl<sub>x</sub> compounds and bis(cyclopentadienyl) dianion reagents. However, these procedures are inefficient and are hampered by low yields and tedious separation and purification steps. For example, Brintzinger<sup>1c</sup> and Collins<sup>6</sup> prepared the important *ansa*-metallocene *rac*-(EBI)ZrCl<sub>2</sub> (**1**; EBI = 1,2-ethylenebis(1-indenyl)) by reaction of ZrCl<sub>4</sub>(THF)<sub>2</sub> and

(EBI)Li<sub>2</sub> and reported low, variable yields (30–50%). Buchwald employed (EBI)K<sub>2</sub> and obtained (EBI)ZrCl<sub>2</sub> in 70% yield with a *rac/meso* ratio of 2/1.<sup>7</sup> In general, current syntheses of chiral C<sub>2</sub> symmetric *ansa*-metallocenes produce the desired *rac* isomer in 10–40% yield, and separation of the chiral *rac* isomer from the undesired, achiral *meso* isomer is not always possible.<sup>4,8</sup> Here we report that chiral, racemic *ansa*-zirconocenes may be prepared in high yield via amine elimination reactions.

Group 4 organometallic complexes may be prepared by amine elimination reactions of metal dialkylamide compounds.<sup>9</sup> Lappert found that the reaction of Zr(NMe<sub>2</sub>)<sub>4</sub> (**2**) with excess cyclopentadiene affords Cp<sub>2</sub>Zr(NMe<sub>2</sub>)<sub>2</sub> and 2 equiv of Me<sub>2</sub>NH; in contrast, the reaction of **2** with excess indene affords the mono(indenyl) compound (η<sup>5</sup>-C<sub>9</sub>H<sub>7</sub>)Zr(NMe<sub>2</sub>)<sub>3</sub>.<sup>10</sup> Recently, Teuben showed that the reaction of the cyclopentadiene-amine species C<sub>5</sub>H<sub>5</sub>(CH<sub>2</sub>)<sub>3</sub>NHMe with M(NMe<sub>2</sub>)<sub>4</sub> (M = Zr, Hf) affords chelated {η<sup>5</sup>:η<sup>1</sup>-C<sub>5</sub>H<sub>4</sub>(CH<sub>2</sub>)<sub>3</sub>NMe}M(NMe<sub>2</sub>)<sub>2</sub> complexes in high yield.<sup>11</sup> We decided to study the reaction of *ansa*-bridged bis(indenes) and group 4 metal dialkylamides to test whether the chelate effect would favor the formation of bis(indenyl) *ansa*-metallocenes.

The reaction of Zr(NMe<sub>2</sub>)<sub>4</sub> (**2**)<sup>12,13</sup> with 1,2-bis(3-indenyl)ethane (**3**)<sup>6</sup> under N<sub>2</sub> in toluene at 100 °C for 17 h affords the *ansa*-zirconocene (EBI)Zr(NMe<sub>2</sub>)<sub>2</sub> (**4**) in 90% yield in a *rac/meso* ratio of 13/1. Crystallization from toluene affords pure *rac*-(EBI)Zr(NMe<sub>2</sub>)<sub>2</sub> (*rac*-**4**) as orange-red crystals in 68% yield (Figure 1). The evolved Me<sub>2</sub>NH was allowed to escape from the reaction vessel via an oil bubbler, but the vessel was not purged with N<sub>2</sub> during the reaction. The use of chlorobenzene or nonane as reaction solvent and recrystallization from hexane give similar results (90–95% crude **4** in a *rac/meso* ratio of >9/1; pure *rac*-**4** in 65–75% isolated yield after recrystallization). The exclusion of light from the reaction vessel has no effect upon the *rac/meso* ratio or yield. *rac*-**4** was characterized by <sup>1</sup>H and <sup>13</sup>C NMR,

(7) Grossman, R. B.; Doyle, R. A.; Buchwald, S. L. *Organometallics* 1991, 10, 1501.

(8) (a) Ellis, W. W.; Hollis, T. K.; Odenkirk, W.; Whelan, J.; Ostrander, R.; Rheingold, A. L.; Bosnich, B. *Organometallics* 1993, 12, 4391. (b) Wiesenfeldt, H.; Reinmuth, A.; Barsties, E.; Evertz, K.; Brintzinger, H. H. *J. Organomet. Chem.* 1989, 369, 359. (c) Erickson, M. S.; Fronczek, F. R.; McLaughlin, M. L. *J. Organomet. Chem.* 1991, 415, 75. (d) Collins, S.; Hong, Y.; Ramachandran, R.; Taylor, N. J. *Organometallics* 1991, 10, 2349.

(9) (a) Lappert, M. F.; Power, P. P.; Sanger, A. R.; Srivastava, R. C. *Metal and Metalloid Amides*; Ellis Horwood: Chichester, West Sussex, U.K., 1980. (b) Bradley, D. C. *Adv. Inorg. Chem. Radiochem.* 1972, 15, 259.

(10) Chandra, G.; Lappert, M. F. *J. Chem. Soc. A* 1968, 1940.

(11) Hughes, A. K.; Meetsma, A.; Teuben, J. H. *Organometallics* 1993, 12, 1936.

(12) Bradley, D. C.; Thomas, I. M. *Proc. Chem. Soc., London* 1959, 225; *J. Chem. Soc.* 1960, 3857.

(13) Chisholm, M. H.; Hammond, C. E.; Huffman, J. C. *Polyhedron* 1988, 7, 2515.

<sup>®</sup> Abstract published in *Advance ACS Abstracts*, November 15, 1994.

(1) (a) Schnutenhaus, H.; Brintzinger, H. H. *Angew. Chem.* 1979, 91, 837; *Angew. Chem., Int. Ed. Engl.* 1979, 18, 777. (b) Wild, F. R. W. P.; Zsolnai, L.; Huttner, G.; Brintzinger, H. H. *J. Organomet. Chem.* 1982, 232, 233. (c) Wild, F. R. W. P.; Wasjucioneck, M.; Huttner, G.; Brintzinger, H. H. *J. Organomet. Chem.* 1985, 288, 63.

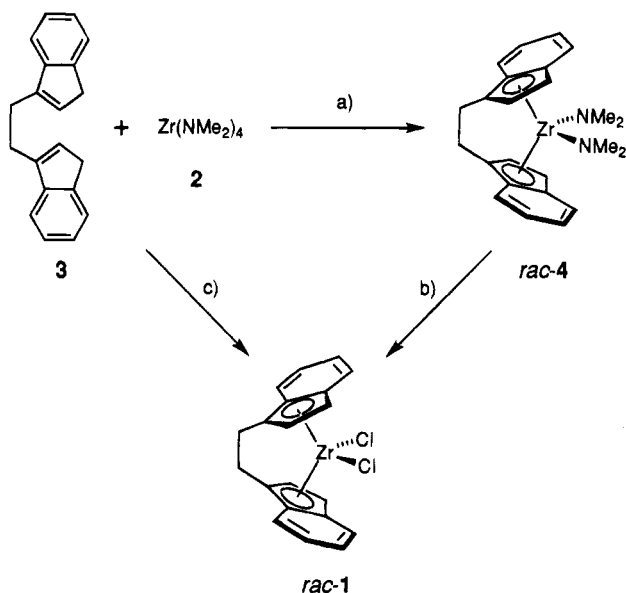
(2) Halterman, R. L. *Chem. Rev.* 1992, 92, 965.

(3) (a) Ewen, J. A. *J. Am. Chem. Soc.* 1984, 106, 6355. (b) Kaminsky, W.; Kulper, K.; Brintzinger, H. H.; Wild, F. R. W. P. *Angew. Chem.* 1985, 97, 507; *Angew. Chem., Int. Ed. Engl.* 1985, 24, 507. (c) Ewen, J. A.; Elder, M. J.; Jones, R. L.; Haspeslagh, L.; Atwood, J. L.; Bott, S. G.; Robinson, K. *Makromol. Chem. Makromol. Symp.* 1991, 48/49, 253. (d) Kaminsky, W.; Engehausen, R.; Zoumis, K.; Spaleck, W.; Rohrmann, J. *Makromol. Chem.* 1992, 193, 1643.

(4) (a) Spaleck, W.; Antberg, M.; Rohrmann, J.; Winter, A.; Bachmann, B.; Kiprof, P.; Behm, J.; Herrmann, W. A. *Angew. Chem.* 1992, 104, 1373; *Angew. Chem., Int. Ed. Engl.* 1992, 31, 1347. (b) Spaleck, W.; Kuber, F.; Winter, A.; Rohrmann, J.; Bachmann, B.; Antberg, M.; Dolle, V.; Paulus, E. F. *Organometallics* 1994, 13, 954. (c) Stehling, U.; Diebold, J.; Kirsten, R.; Roll, W.; Brintzinger, H. H.; Jungling, S.; Mulhaupt, R.; Langhauser, F. *Organometallics* 1994, 13, 964.

(5) (a) Pino, P.; Cioni, P.; Wei, J. *J. Am. Chem. Soc.* 1987, 109, 6189. (b) Pino, P.; Galimberti, M.; Prada, P.; Consiglio, G. *Makromol. Chem.* 1990, 191, 1677. (c) Coates, G. W.; Waymouth, R. M. *J. Am. Chem. Soc.* 1993, 115, 91. (d) Coates, G. W.; Waymouth, R. M. *J. Mol. Catal.* 1992, 76, 189. (e) Waymouth, R.; Pino, P. *J. Am. Chem. Soc.* 1990, 112, 4911. (f) Colletti, S. L.; Halterman, R. L. *J. Organomet. Chem.* 1993, 455, 99. (g) Halterman, R. L.; Ramsey, T. M. *Organometallics* 1993, 12, 2879. (h) Chen, Z.; Halterman, R. L. *J. Am. Chem. Soc.* 1992, 114, 2276. (i) Rodewald, S.; Jordan, R. F. *J. Am. Chem. Soc.* 1994, 116, 4491. (j) Willoughby, C. A.; Buchwald, S. L. *J. Am. Chem. Soc.* 1992, 114, 7562. (k) Hong, Y.; Kuntz, B. A.; Collins, S. *Organometallics* 1993, 12, 964. (l) Grossman, R. B.; Davis, W. M.; Buchwald, S. L. *J. Am. Chem. Soc.* 1991, 113, 2321. (m) Banovetz, J. P.; Stein, K. M.; Waymouth, R. M. *Organometallics* 1991, 10, 3430. (n) Morken, J. P.; Didiuk, M. T.; Hoveyda, A. H. *J. Am. Chem. Soc.* 1993, 115, 6997.

(6) (a) Collins, S.; Kuntz, B. A.; Taylor, N. J.; Ward, D. G. *J. Organomet. Chem.* 1988, 342, 21. (b) See footnote 7 in: Collins, S.; Kuntz, B. A.; Hong, Y. *J. Org. Chem.* 1989, 54, 4154.



**Figure 1.** Reagents and conditions: (a) toluene, 100 °C, 17 h, 68% isolated yield; (b) 2 Me<sub>2</sub>NH·HCl, CH<sub>2</sub>Cl<sub>2</sub>, -78 to +23 °C, 0.5 h, 92% isolated yield; (c) (i) chlorobenzene, 125 °C, 18 h and (ii) 2 Me<sub>2</sub>NH·HCl, CH<sub>2</sub>Cl<sub>2</sub>, 0 to 23 °C, 3 h, 69% isolated yield.

elemental analysis, and an X-ray crystal structure determination which confirmed the monomeric structure.<sup>14</sup>

Several observations provide insight to the mechanism and stereoselectivity of the reaction of **2** and **3**. (i) Monitoring the reaction at 100 °C in toluene, via <sup>1</sup>H NMR analysis of aliquots taken from the reaction solution, showed that the binuclear species ( $\mu$ - $\eta^5$ : $\eta^5$ -EBI){Zr(NMe<sub>2</sub>)<sub>3</sub>}<sub>2</sub> (**5**) was present initially (*ca.* 10 mol % after 2 h, *rac/meso* ratio approximately 1/1) but disappeared after several hours. Compound **5** was prepared independently by the reaction of 2 equiv of Zr(NMe<sub>2</sub>)<sub>4</sub> (**2**) with (EBI)H<sub>2</sub> (**3**) in toluene at room temperature. (ii) The NMR monitoring experiments also showed that the *rac/meso* ratio of product **4** was initially low (2/1 after 2 h) but increased with reaction time (>50/1 after 5 days). A reaction time of 15–20 h is optimum for the preparation of *rac*-4, since prolonged heating (>1 day) is accompanied by formation of insoluble products. (iii) When the reaction was performed in a closed vessel, from which the Me<sub>2</sub>NH could not escape, it did not go to completion (a mixture of **3**–**5** was obtained). (iv) When N<sub>2</sub> was bubbled through the reaction solution to sweep out the amine rapidly as it was formed, the reaction went to completion but the final *rac*-4/*meso*-4 ratio was low (1/1). These observations imply that (i) the amine elimination is reversible, (ii) *meso*-4 and *rac*-4 are formed at comparable rates but *rac*-4 is the thermodynamically preferred product, and (iii) the isomerization of *meso*-4 to *rac*-4 is catalyzed by Me<sub>2</sub>NH. These results may be rationalized by Scheme 1.

In Scheme 1, Zr(NMe<sub>2</sub>)<sub>4</sub> (**2**) reacts with (EBI)H<sub>2</sub> (**3**) to form the unobserved intermediate **6**. Mono(indenyl) species **6** may undergo reversible intermolecular amine elimination with a second equivalent of **2** to give binuclear species **5** or, alternatively, reversible intramolecular amine elimination to give either *meso*-4 or the

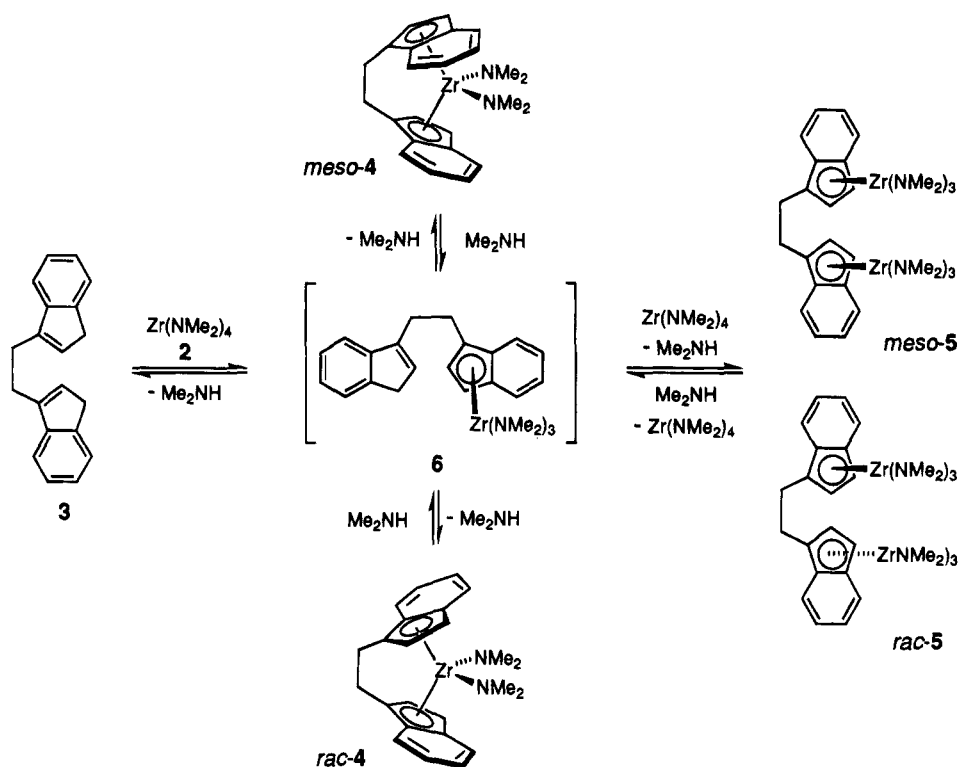
thermodynamically favored *rac*-4. A critical aspect of Scheme 1 is the amine-catalyzed *meso*-4/*rac*-4 interconversion; when Me<sub>2</sub>NH was swept from the reaction vessel, this epimerization was inhibited and a 1/1 *rac*-4/*meso*-4 product ratio was obtained.

It is likely that the bis(amide) complex *rac*-4 could be used directly as a catalyst or catalyst precursor in many applications. However, *rac*-4 may be converted to the commonly used dichloride derivative *rac*-(EBI)-ZrCl<sub>2</sub> (**1**) in high yield (92%) via reaction with 2 equiv of Me<sub>2</sub>NH·HCl in CH<sub>2</sub>Cl<sub>2</sub>.<sup>11</sup> Alternatively, *rac*-(EBI)-

(15) **Experimental Procedures.** All reactions were performed under an N<sub>2</sub> atmosphere using standard glovebox and Schlenk techniques. Zr(NMe<sub>2</sub>)<sub>4</sub> (**2**): Solid ZrCl<sub>4</sub> (12 g, 52 mmol) was added, in several portions over 2 h, to a suspension of LiNMe<sub>2</sub> (11 g, 220 mmol) in toluene (150 mL) at room temperature. The reaction mixture was stirred for an additional 18 h at room temperature. The solvent was removed under reduced pressure, leaving an off-white solid, from which pure Zr(NMe<sub>2</sub>)<sub>4</sub> (**2**) was obtained by sublimation at 80 °C/0.05 mmHg, in 83% yield (12 g). The use of toluene rather than THF as the solvent for this reaction avoids the formation of Li<sub>2</sub>(THF)<sub>2</sub>Zr(NMe<sub>2</sub>)<sub>6</sub> and results in an improved yield.<sup>12,13</sup> *rac*-(EBI)Zr(NMe<sub>2</sub>)<sub>2</sub> (*rac*-4): Zr(NMe<sub>2</sub>)<sub>4</sub> (**2**) (1.0 g, 3.7 mmol) and 1,2-bis(3-indenyl)ethane (**3**; 0.96 g, 3.7 mmol) were placed in a Schlenk vessel, and toluene (20 mL) was added. The reaction mixture was stirred and heated at 100 °C for 17 h. An aliquot was removed and analyzed by <sup>1</sup>H NMR. The <sup>1</sup>H NMR spectrum showed that (EBI)Zr(NMe<sub>2</sub>)<sub>2</sub> (**4**) was present in 90% yield in a *rac/meso* ratio of 13/1. The reaction mixture was filtered, concentrated under reduced pressure, and cooled to -20 °C. Filtration afforded pure *rac*-(EBI)Zr(NMe<sub>2</sub>)<sub>2</sub> (*rac*-4) as orange-red crystals in 68% yield (1.1 g). *rac*-4: Anal. Calcd for C<sub>24</sub>H<sub>28</sub>N<sub>2</sub>Zr: C, 66.16; H, 6.48; N, 6.43. Found: C, 66.42; H, 6.40; N, 6.24. <sup>1</sup>H NMR (360 MHz, C<sub>6</sub>D<sub>6</sub>, 298 K):  $\delta$  7.42 (d, *J* = 9 Hz, 2 H, indenyl), 7.40 (d, *J* = 9 Hz, 2 H, indenyl), 6.93 (dd, *J* = 7 Hz, *J* = 9 Hz, 2 H, indenyl), 6.71 (dd, *J* = 7 Hz, *J* = 9 Hz, 2 H, indenyl), 6.35 (d, *J* = 3 Hz, 2 H, C<sub>5</sub> indenyl), 5.88 (d, *J* = 3 Hz, 2 H, C<sub>5</sub> indenyl), 3.31 (m, 2 H, CH<sub>2</sub>), 3.10 (m, 2 H, CH<sub>2</sub>), 2.53 (s, 12 H, NMe<sub>2</sub>). <sup>13</sup>C{<sup>1</sup>H} NMR (90 MHz, C<sub>6</sub>D<sub>6</sub>, 298 K):  $\delta$  130.0 (C), 125.8 (CH), 123.3 (CH), 123.2 (CH), 121.3 (C), 120.7 (CH), 117.3 (C), 113.9 (CH), 100.6 (CH), 47.7 (NMe<sub>2</sub>), 28.9 (CH<sub>2</sub>CH<sub>2</sub>). *meso*-4: <sup>1</sup>H NMR (360 MHz, C<sub>6</sub>D<sub>6</sub>, 298 K):  $\delta$  7.56 (d, *J* = 8 Hz, 2 H, indenyl), 7.39 (d, *J* = 9 Hz, 2 H, indenyl), 6.88 (m, 2 H, indenyl), 6.70 (m, 2 H, indenyl), 6.41 (d, *J* = 3 Hz, 2 H, C<sub>5</sub> indenyl), 5.86 (d, *J* = 3 Hz, 2 H, C<sub>5</sub> indenyl), 3.50 (m, 2 H, CH<sub>2</sub>), 2.99 (s, 6 H, NMe<sub>2</sub>), 2.94 (m, 2 H, CH<sub>2</sub>), 1.82 (s, 6 H, NMe<sub>2</sub>). ( $\mu$ - $\eta^5$ : $\eta^5$ -EBI){Zr(NMe<sub>2</sub>)<sub>3</sub>}<sub>2</sub> (**5**): A solution of **3** (0.24 g, 0.93 mmol) in toluene (20 mL) was added dropwise at room temperature to a solution of **2** (0.50 g, 1.9 mmol) in toluene (20 mL). The reaction solution was stirred for 17 h at room temperature. The solvent was removed under reduced pressure, affording an orange oil. The <sup>1</sup>H NMR spectrum of the oil showed that ( $\mu$ - $\eta^5$ : $\eta^5$ -EBI){Zr(NMe<sub>2</sub>)<sub>3</sub>}<sub>2</sub> (**5**) was present in 75% yield in a *rac/meso* ratio of 1/1. Recrystallization from hexane afforded pure **5** in 19% yield (0.12 g) as a yellow crystalline solid in an isomeric ratio (**5a**/**5b**) of 2/1. Anal. Calcd for C<sub>33</sub>H<sub>52</sub>N<sub>6</sub>Zr<sub>2</sub>: C, 54.65; H, 7.45; N, 11.95. Found: C, 54.86; H, 7.26; N, 11.76. **5a**: <sup>1</sup>H NMR (360 MHz, C<sub>6</sub>D<sub>6</sub>, 298 K):  $\delta$  7.59–7.45 (m, 4 H, indenyl), 6.96–6.88 (m, 4 H, indenyl), 6.36 (d, *J* = 3 Hz, 2 H, C<sub>5</sub> indenyl), 6.20 (d, *J* = 3 Hz, 2 H, C<sub>5</sub> indenyl), 3.39–3.21 (m, 4 H, CH<sub>2</sub>CH<sub>2</sub>), 2.80 (s, 36 H, NMe<sub>2</sub>). <sup>13</sup>C{<sup>1</sup>H} NMR (90 MHz, C<sub>6</sub>D<sub>6</sub>, 298 K):  $\delta$  126.3 (C), 125.2 (C), 123.1 (CH), 122.6 (CH), 122.1 (CH), 121.7 (CH), 116.4 (CH), 114.3 (C), 96.0 (CH), 44.1 (NMe<sub>2</sub>), 29.4 (CH<sub>2</sub>CH<sub>2</sub>). **5b**: <sup>1</sup>H NMR (360 MHz, C<sub>6</sub>D<sub>6</sub>, 298 K):  $\delta$  7.59–7.45 (m, 4 H, indenyl), 6.96–6.88 (m, 4 H, indenyl), 6.26 (d, *J* = 3 Hz, 2 H, C<sub>5</sub> indenyl), 6.20 (d, *J* = 3 Hz, 2 H, C<sub>5</sub> indenyl), 3.43 (m, 2 H, CH<sub>2</sub>), 3.17 (m, 2 H, CH<sub>2</sub>), 2.79 (s, 36 H, NMe<sub>2</sub>). <sup>13</sup>C{<sup>1</sup>H} NMR (90 MHz, C<sub>6</sub>D<sub>6</sub>, 298 K):  $\delta$  126.5 (C), 125.0 (C), 123.1 (CH), 122.6 (CH), 122.2 (CH), 121.7 (CH), 116.9 (CH), 114.1 (C), 95.7 (CH), 44.1 (NMe<sub>2</sub>), 29.2 (CH<sub>2</sub>CH<sub>2</sub>). *rac*-(EBI)ZrCl<sub>2</sub> (**1**) from *rac*-(EBI)Zr(NMe<sub>2</sub>)<sub>2</sub>: A solution of Me<sub>2</sub>NH·HCl (0.093 g, 1.1 mmol) in CH<sub>2</sub>Cl<sub>2</sub> (20 mL) was added dropwise to a stirred solution of *rac*-4 (0.25 g, 0.57 mmol) in CH<sub>2</sub>Cl<sub>2</sub> (20 mL) at -78 °C. The resulting clear, yellow solution was stirred at room temperature for 30 min. Removal of solvent under reduced pressure followed by washing with hexane and extraction of the yellow product into toluene gave, upon removal of solvent, *rac*-(EBI)ZrCl<sub>2</sub> (**1**) in 92% yield (0.22 g). "One-pot" synthesis of *rac*-(EBI)ZrCl<sub>2</sub> (**1**) from Zr(NMe<sub>2</sub>)<sub>4</sub>: Zr(NMe<sub>2</sub>)<sub>4</sub> (**2**) (0.52 g, 1.9 mmol) and 1,2-bis(3-indenyl)ethane (**3**; 0.50 g, 1.9 mmol) were placed in a Schlenk vessel, and chlorobenzene (10 mL) was added. The reaction mixture was stirred and heated to 125 °C for 18 h. An aliquot was removed and analyzed by <sup>1</sup>H NMR. The <sup>1</sup>H NMR spectrum showed that **4** was present in 95% yield in a *rac/meso* ratio of 10/1. The reaction mixture was cooled to 0 °C, and a solution of Me<sub>2</sub>NH·HCl (0.30 g, 3.7 mmol) in CH<sub>2</sub>Cl<sub>2</sub> (65 mL) was added dropwise over 30 min, during which time the color changed from red-orange to yellow. The reaction mixture was stirred at room temperature for 3 h. The solvent was removed under reduced pressure to give a yellow powder. Recrystallization of the yellow powder from CH<sub>2</sub>Cl<sub>2</sub> gave pure *rac*-(EBI)ZrCl<sub>2</sub> (**1**) in 69% yield (0.54 g).

(14) Petersen, J. L. Unpublished results.

Scheme 1



ZrCl<sub>2</sub> may be prepared directly in 69% isolated yield in a "one-pot" synthesis via reaction of Zr(NMe<sub>2</sub>)<sub>4</sub> (2) and (EBI)<sub>2</sub> (3) in chlorobenzene (125 °C, 18 h), followed by addition of Me<sub>2</sub>NH·HCl (0 °C), solvent removal, and recrystallization from CH<sub>2</sub>Cl<sub>2</sub> (Figure 1).

We conclude that amine elimination offers a simple and efficient approach to the synthesis of *rac*-(EBI)ZrX<sub>2</sub> compounds.<sup>15</sup> We have successfully extended this approach to the synthesis of other *ansa*-metallocenes with Me<sub>2</sub>Si bridging groups and with different cyclopentadienyl substituents and will report on these later. We

anticipate that the use of homochiral metal amide starting materials will enable the efficient synthesis of enantiomerically pure *ansa*-metallocenes, which would greatly facilitate their use in asymmetric synthetic applications.<sup>5</sup>

**Acknowledgment.** This research was supported by the National Science Foundation and the Volkswagen Stiftung.

OM9406963

## Synthesis, X-ray Crystal Structure, and Thermal Stability of Y[DAC][CH<sub>2</sub>SiMe<sub>3</sub>] (DAC = Deprotonated 4,13-Diaza-18-crown-6)

Lawrence Lee, David J. Berg, and Gordon W. Bushnell

*Organometallics*, 1995, 14 (1), 8-10 • DOI: 10.1021/om00001a004 • Publication Date (Web): 01 May 2002

Downloaded from <http://pubs.acs.org> on March 9, 2009

### More About This Article

---

The permalink <http://dx.doi.org/10.1021/om00001a004> provides access to:

- Links to articles and content related to this article
- Copyright permission to reproduce figures and/or text from this article



ACS Publications  
High quality. High impact.

# Synthesis, X-ray Crystal Structure, and Thermal Stability of Y[DAC][CH<sub>2</sub>SiMe<sub>3</sub>] (DAC = Deprotonated 4,13-Diaza-18-crown-6)

Lawrence Lee, David J. Berg,\* and Gordon W. Bushnell

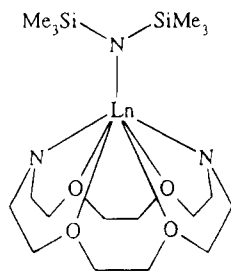
Department of Chemistry, University of Victoria, Victoria, British Columbia, Canada V8W 2Y2

Received September 20, 1994<sup>®</sup>

**Summary:** The deprotonated 4,13-diaza-18-crown-6 (DAC) ligand system allows isolation of the yttrium alkyl species Y(DAC)(CH<sub>2</sub>SiMe<sub>3</sub>). A crystallographic investigation reveals a monomeric complex containing a seven-coordinate yttrium center exhibiting no agostic interactions with the alkyl group. The complex is relatively stable in the solid state but decomposes by ligand metalation in solution.

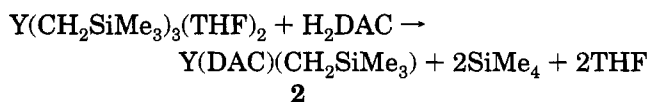
Despite the extensive coordination chemistry of the lanthanides with crown ethers and their N-substituted analogs (azacrowns),<sup>1</sup> no attempt has been made to utilize deprotonated azacrowns as ancillary ligands in organolanthanide chemistry. Indeed, the only examples of deprotonated azacrowns as ancillary ligands in organometallic chemistry are the aluminum alkyl complexes prepared by Robinson<sup>2</sup> and Gokel and Richey.<sup>3</sup>

Deprotonated azacrowns are intriguing as ancillary ligands because they provide a flexible donor array with the ability to fill one hemisphere of the lanthanide coordination sphere. We have previously shown that this coordination mode is realized with deprotonated 4,13-diaza-18-crown-6 (DAC)<sup>4</sup> in Ln(DAC)[N(SiMe<sub>3</sub>)<sub>2</sub>] (1).<sup>5,6</sup> In this contribution we report the successful extension of the DAC ligand system to the synthesis of a hydrocarbon-soluble monomeric alkyl: Y(DAC)(CH<sub>2</sub>SiMe<sub>3</sub>) (2).



1	Ln
a	Y
b	Ce
c	Sm

Complex **2** is conveniently prepared by the protonation reaction.<sup>7</sup>



Attempts to prepare **2** by metathetical routes have been

\* To whom correspondence should be addressed.

<sup>®</sup> Abstract published in *Advance ACS Abstracts*, November 15, 1994.

(1) For comprehensive reviews see: (a) Bünzli, J.-C. G.; Wessner, D. *Coord. Chem. Rev.* **1984**, *10*, 191. (b) Bünzli, J.-C. G. In *Handbook on the Physics and Chemistry of Rare Earths*; Gschneidner, K. A., Eyring, L., Eds.; Elsevier: Amsterdam, 1987; Vol. 9, p 321. (c) Hart, F. A. In *Comprehensive Coordination Chemistry*; Wilkinson, G., Ed.; Pergamon Press: Oxford, U.K., 1987; Vol. 3, p 1059. (d) Adachi, G.; Hirashima, Y. In *Cation Binding by Macrocycles; Complexation of Cationic Species by Crown Ethers*; Inoue, Y., Gokel, G. W., Eds.; Marcel Dekker: New York, 1990; p 701.

thwarted by difficulties in cleanly preparing suitable precursors such as Y(DAC)(Cl) or Y(DAC)(OC<sub>6</sub>H<sub>3</sub><sup>t</sup>Bu<sub>2</sub>-2,6). Colorless crystalline **2** is very air and moisture sensitive and undergoes slow thermal decomposition at room temperature (*vide infra*).

The NMR spectra of **2** are consistent with a monomeric alkyl complex. The DAC region of the <sup>1</sup>H NMR spectrum consists of six multiplets, while only three triplets are observed for the DAC carbons in the proton-coupled <sup>13</sup>C NMR spectrum, consistent with C<sub>2v</sub> molecular symmetry as found for **1a**. A doublet of triplets pattern is observed for the CH<sub>2</sub> carbon of the alkyl due to yttrium and proton coupling (<sup>1</sup>J<sub>YC</sub> = 39 Hz; <sup>1</sup>J<sub>CH</sub> = 102 Hz). In addition, the <sup>89</sup>Y NMR spectrum (Figure 1) shows a well-resolved triplet (δ +551.2 ppm, <sup>2</sup>J<sub>YH</sub> = 2.8 Hz), effectively ruling out a static bridging alkyl structure. The <sup>89</sup>Y chemical shift is far downfield of that in **1a** (+401 ppm), consistent with the strong deshielding effect of alkyls, as previously noted by Schaverien.<sup>9</sup>

The spectroscopic data for **2** do not provide compelling evidence for an agostic interaction between the α-CH<sub>2</sub> protons and Y. While the low value of <sup>1</sup>J<sub>CH</sub> is consistent with averaging of an agostic (typical range <sup>1</sup>J<sub>CH</sub> = 40–80 Hz) and a classical CH (<sup>1</sup>J<sub>CH</sub> in SiMe<sub>4</sub> = 117 Hz),

(2) (a) Robinson, G. H.; Rae, A. D.; Campana, C. F.; Byram, S. K. *Organometallics* **1987**, *6*, 1227. (b) Robinson, G. H.; Sangokoya, S. A. *Organometallics* **1988**, *7*, 1453. (c) Robinson, G. H.; Appel, E. S.; Sangokoya, S. A.; Zhang, H.; Atwood, J. L. *J. Coord. Chem.* **1988**, *17*, 373. (d) Sangokoya, S. A.; Moise, F.; Pennington, W. T.; Self, M. F.; Robinson, G. H. *Organometallics* **1989**, *8*, 2584. (e) Sangokoya, S. A.; Pennington, W. T. *J. Am. Chem. Soc.* **1989**, *111*, 1520. (f) Self, M. F.; Pennington, W. T.; Laske, J. A.; Robinson, G. H. *Organometallics* **1991**, *10*, 36.

(3) (a) Gokel, G. W.; Garcia, B. J. *Tetrahedron Lett.* **1977**, 317. (b) Pajerski, A. D.; Cleary, T. P.; Parvez, M.; Gokel, G. W.; Richey, H. G., Jr. *Organometallics* **1992**, *11*, 1400.

(4) Systematic name: 1,7,10,16-tetraoxa-4,13-diazacyclooctadecane.

(5) Ln refers to yttrium, lanthanum, and the lanthanides in general throughout this paper.

(6) Lee, L.; Berg, D. J.; Bushnell, G. W. *Inorg. Chem.*, in press.

(7) Synthesis of **2**: All operations were carried out in an argon-filled glovebox. A solution of H<sub>2</sub>DAC<sup>6</sup> (0.200 g, 0.762 mmol) in 20 mL of toluene was added dropwise over 10 min to a vigorously stirred solution of Y(CH<sub>2</sub>SiMe<sub>3</sub>)<sub>3</sub>(THF)<sub>2</sub><sup>8</sup> (0.377 g, 0.762 mmol) in 20 mL of toluene. The colorless solution was stirred for 30 min followed by removal of the solvent under reduced pressure. Recrystallization of the resulting white powder from a toluene-hexane mixture produced white crystals of **2** (0.310 g, 70%). Mp: 120 °C dec. <sup>1</sup>H NMR (250 MHz): δ 3.80 (m, 4 H, C<sub>6</sub>H), 3.38 (m, 8 H, overlapping C<sub>6</sub>H and C<sub>8</sub>H), 3.33 (m, 4 H, C<sub>8</sub>H), 3.14 (m, 4 H, C<sub>6</sub>H), 3.02 (m, 4 H, C<sub>6</sub>H), 0.42 (s, 9 H, SiMe<sub>3</sub>), -0.84 (d, 2 H, CH<sub>2</sub>Si, <sup>2</sup>J<sub>YH</sub> = 2.8 Hz). <sup>13</sup>C NMR (90.29 MHz): δ 74.2 (t, C<sub>6</sub>, <sup>1</sup>J<sub>CH</sub> = 143 Hz), 68.1 (t, C<sub>6</sub>, <sup>1</sup>J<sub>CH</sub> = 145 Hz), 55.2 (t, C<sub>8</sub>, <sup>1</sup>J<sub>CH</sub> = 128 Hz), 19.4 (dt, CH<sub>2</sub>Si, <sup>1</sup>J<sub>YC</sub> = 39 Hz, <sup>1</sup>J<sub>CH</sub> = 102 Hz), 4.9 (q, SiMe<sub>3</sub>, <sup>1</sup>J<sub>CH</sub> = 114 Hz). <sup>29</sup>Si NMR (49.69 MHz): δ -1.9 (s, SiMe<sub>3</sub>). NMR spectra were recorded in C<sub>6</sub>D<sub>6</sub> at room temperature; <sup>1</sup>H and <sup>13</sup>C spectra were referenced to residual solvent resonances, <sup>29</sup>Si to external TMS, and <sup>89</sup>Y to 3 M YCl<sub>3</sub> in D<sub>2</sub>O. <sup>1</sup>H and <sup>13</sup>C assignments refer to the unique portion of the DAC backbone NC<sub>6</sub>H<sub>2</sub>C<sub>6</sub>H<sub>2</sub>OC<sub>6</sub>H<sub>2</sub>; partial assignments were made by a <sup>1</sup>H-<sup>13</sup>C COSY experiment; endo and exo H assignments have not been made. Anal. Calcd for C<sub>16</sub>H<sub>35</sub>N<sub>2</sub>O<sub>4</sub>SiY: C, 44.03; H, 8.08; N, 6.42. Found: C, 43.00; H, 7.81; N, 6.35.

(8) Lappert, M. F.; Pearce, R. *J. Chem. Soc., Chem. Commun.* **1973**, 126.

(9) Schaverien, C. J. *Organometallics* **1994**, *13*, 69.



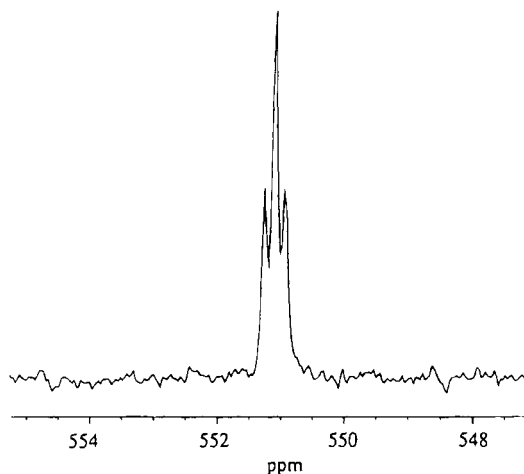


Figure 1.  $^{89}\text{Y}$  NMR spectrum of **2** (17.64 MHz,  $\text{C}_6\text{D}_6$ ).

comparable values have been found for  $(\text{OEP})\text{Lu}[\text{CH}(\text{SiMe}_3)_2]$  (95 Hz),<sup>10</sup>  $\{\text{LuCp}^*[\text{CH}(\text{SiMe}_3)_2]\text{Cl}_2\}\text{Li}(\text{TMEDA})$  (93 Hz),<sup>11</sup>  $\text{La}[\text{CH}(\text{SiMe}_3)_2]_3$  (95.2 Hz),<sup>12</sup> and  $\text{Mg}[\text{CH}(\text{SiMe}_3)_2]_2$  (100.8 Hz),<sup>13</sup> which have been shown crystallographically to contain no significant  $\alpha$ -CH agostic interactions. In fact, for these compounds, observation of a low  $^1J_{\text{CH}}$  value appears to be a rather unreliable criterion for establishing the presence of an agostic interaction since  $\text{Cp}^*\text{La}[\text{CH}(\text{SiMe}_3)_2]_2$  (100 Hz),<sup>14</sup>  $\text{Cp}^*\text{La}[\text{CH}(\text{SiMe}_3)_2]_2(\text{THF})$  (92 Hz),<sup>14</sup> and  $\text{Cp}^*_2\text{Y}[\text{CH}(\text{SiMe}_3)_2]$  (84.2 Hz),<sup>15</sup> which contain crystallographically verified  $\alpha$ -agostic interactions, span a comparable range of  $^1J_{\text{CH}}$  values.

The uncertainty regarding the presence of an  $\alpha$ -agostic CH interaction, as well as the possibility of agostic  $\beta$ -Si-Me to yttrium bonding,<sup>9</sup> prompted us to investigate the solid-state structure of **2** by X-ray crystallography (Figure 2).<sup>16</sup> The structure of **2** is monomeric, as suggested by NMR spectroscopy; the nearest intermolecular contacts are  $>3.5$  Å. The bonding geometry about Y, like that in **1a**,<sup>6</sup> can be viewed as consisting of primary trigonal-planar coordination of the anionic groups (alkyl C and amido N; sum of the angles about Y for the  $\text{YN}_2\text{C}$  unit is  $359.9^\circ$ ) with secondary coordina-

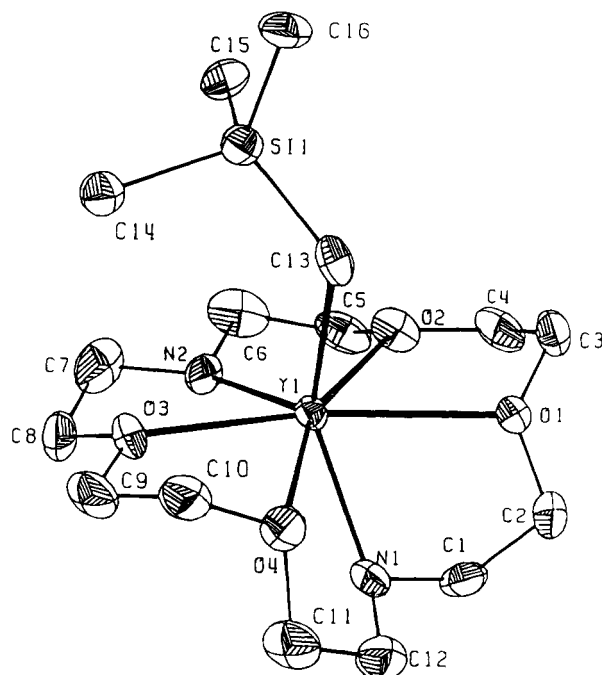


Figure 2. ORTEP drawing of **2**. Selected bond distances (Å) and angles (deg):  $\text{Y}(1)-\text{N}(1) = 2.27(2)$ ,  $\text{Y}(1)-\text{N}(2) = 2.26(2)$ ,  $\text{Y}(1)-\text{O}(1) = 2.622(11)$ ,  $\text{Y}(1)-\text{O}(2) = 2.442(13)$ ,  $\text{Y}(1)-\text{O}(3) = 2.431(12)$ ,  $\text{Y}(1)-\text{O}(4) = 2.534(11)$ ,  $\text{Y}(1)-\text{C}(13) = 2.45(2)$ ;  $\text{N}(1)-\text{Y}(1)-\text{N}(2) = 111.0(5)$ ,  $\text{N}(1)-\text{Y}(1)-\text{C}(13) = 137.4(6)$ ,  $\text{N}(2)-\text{Y}(1)-\text{C}(13) = 111.5(6)$ ,  $\text{Y}(1)-\text{C}(13)-\text{Si}(1) = 126.4(8)$ .

tion of the four ether oxygens above and below the  $\text{YN}_2\text{C}$  plane. The DAC N-Y and O-Y distances are very similar to those found in **1a**. The Y-C distance of 2.45(2) Å is comparable to that found in  $\text{Cp}^*_2\text{Y}[\text{CH}(\text{SiMe}_3)_2]$  (2.468(7) Å),<sup>15</sup> the only other structurally characterized neutral yttrium alkyl species containing a seven-coordinate yttrium center. Significantly, the long  $\text{Y}(1)\cdots\text{Si}(1)$  (3.84(2) Å) and  $\text{Y}(1)\cdots\text{C}(14)-\text{C}(16)$  (4.38(2), 4.38(2), and 5.49(2) Å) distances rule out any  $\beta$ - or  $\gamma$ -agostic interactions. Attempts to refine H(13a) and H(13b) isotropically resulted in an unreasonably short C(13)-H(13b) distance of 0.82(11) Å, but the  $\text{Y}(1)\cdots\text{H}(13a, 13b)$  nonbonding distance did not shorten significantly from the calculated (fixed) distance of 2.92 Å. This distance is far longer than that observed in compounds believed to contain an  $\alpha$ -CH agostic interaction and would appear to rule out this type of bonding.<sup>14,15</sup>

Complex **2** slowly decomposes (weeks) at room temperature but is stable indefinitely at  $-30^\circ\text{C}$  in the solid state. In  $d_6$ -benzene solution, **2** decomposes more rapidly to produce TMS. The ultimate fate of the Y(DAC) moiety is not known with certainty, although the presence of at least 15  $^{13}\text{C}$  resonances in the DAC region strongly suggests that decomposition involves metalation of the DAC ligand. No evidence for metalation of  $d_6$ -benzene (or  $d_8$ -toluene) or incorporation of deuterium into TMS was found. Fryzuk has reported a similar decomposition mode for  $\text{Ln}(\text{PNP}^{\text{Me}})_2\text{R}$  ( $\text{PNP}^{\text{Me}} = \text{N}(\text{SiMe}_2\text{CH}_2\text{PMe}_2)_2$ ; Ln = Y, R = Ph,  $\text{CH}_2\text{Ph}$ ; Ln = Lu, R = Ph).<sup>20</sup> Complex **2** is considerably more stable than  $\text{Y}(\text{PNP}^{\text{Me}})_2(\text{CH}_2\text{Ph})$ , which is somewhat surprising given the lower steric shielding anticipated for the DAC ligand. The higher stability of **2** may be explained by

(10) Schaverien, C. J.; Orpen, A. G. *Inorg. Chem.* **1991**, *30*, 4968.  
(11) van der Heijden, H.; Pasman, P.; de Boer, E. J. M.; Schaverien, C. J. *Organometallics* **1989**, *8*, 1459.

(12) Hitchcock, P. B.; Lappert, M. F.; Smith, R. G.; Bartlett, R. A.; Power, P. P. *J. Chem. Soc., Chem. Commun.* **1988**, 1007.

(13) Hitchcock, P. B.; Howard, J. A. K.; Lappert, M. F.; Leung, W.-P.; Mason, S. A. *J. Chem. Soc., Chem. Commun.* **1990**, 847.

(14) (a) van der Heijden, H.; Schaverien, C. J.; Orpen, A. G. *Organometallics* **1989**, *8*, 255. (b) Schaverien, C. J.; van der Heijden, H.; Orpen, A. G. *Polyhedron* **1989**, *8*, 1850.

(15) den Haan, K. H.; de Boer, J. L.; Teuben, J. H.; Spek, A. L.; Kojic-Prodic, B.; Hays, G. R.; Huis, R. *Organometallics* **1986**, *5*, 1726.

(16) Crystal data for **2**:  $\text{C}_{16}\text{H}_{35}\text{N}_2\text{O}_4\text{SiY}$ ,  $M_r = 436.46$ , monoclinic, space group  $P2_1/n$  (No. 14),  $a = 9.709(5)$  Å,  $b = 11.704(6)$  Å,  $c = 19.523(6)$  Å,  $\beta = 97.63(4)^\circ$ ,  $V = 2198.7$  Å<sup>3</sup>,  $Z = 4$ ,  $D_c = 1.319$  g cm<sup>-3</sup>,  $\mu(\text{Mo K}\alpha) = 27.40$  cm<sup>-1</sup> (graphite monochromated),  $\lambda = 0.70932$  Å,  $F(000) = 919.9$ . The data were collected on a Nonius CAD-4F diffractometer at ambient temperature (293 K) using the  $\omega$ - $\theta$  scan mode ( $2\theta = 2$ - $45^\circ$ ). The data were corrected for Lorentz and polarization effects, and an empirical absorption correction ( $\psi$  scan) was carried out. The structure was solved using direct methods (NRC Solver<sup>17</sup>). Of the 2851 unique reflections, 1402 with  $I > 4\sigma(I)$  were used in the refinement. A total of 219 parameters were refined using SHELX76,<sup>18</sup> and the structure converged satisfactorily (maximum shift/esd 0.018). The final residuals were  $R = 0.088$  and  $R_w = 0.118$ .

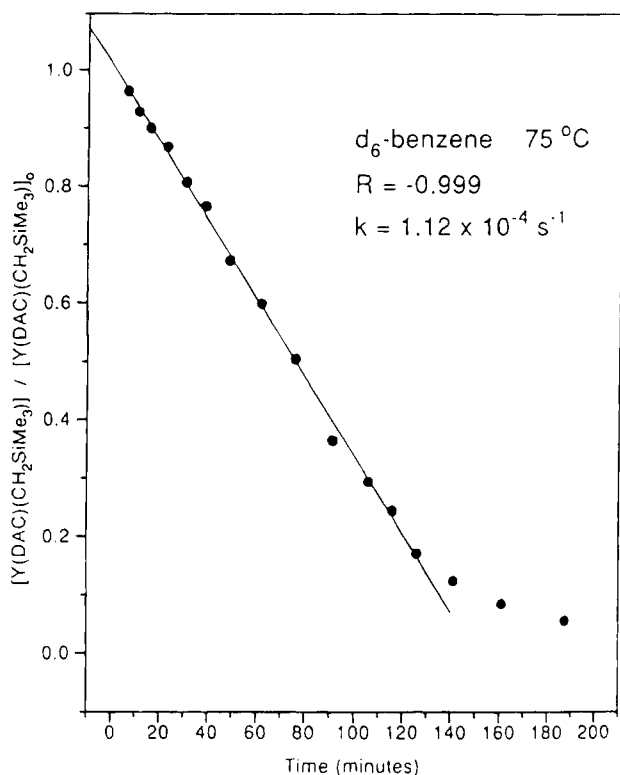
(17) Larson, A.; Lee, F.; Page, Y.; Webster, M.; Charland, J.; Gabe, E. NRC Vax Crystal Structure System; NRC: Ottawa, Canada, 1985.

(18) Sheldrick, G. M. SHELX76, Programs for Crystal Structure Determination; University of Cambridge: Cambridge, U.K., 1976.

(19) Johnson, C. K. ORTEPII; Oak Ridge National Laboratory: Oak Ridge, TN, 1976.

(20) Fryzuk, M. D.; Haddad, T. S.; Rettig, S. J. *Organometallics* **1991**, *10*, 2026.





**Figure 3.** Thermal decomposition of **2** at 75 °C ( $C_6D_6$ ).

electronic differences between PNP and DAC, since the soft P donors of the former ligand are expected to coordinate more weakly to a lanthanide center than the hard O donors of DAC. Lanthanide and group 3 alkyls containing dialkylamido ligation are rare, although the related  $Ln(OEP)R$  series ( $OEP = \text{octaethylporphyrin}$ ) have been investigated in some detail by Arnold<sup>21</sup> and Schaverien.<sup>10,22</sup> The greater thermal stability of the OEP system can probably be attributed to difficulties in achieving the necessary geometry to allow metalation of the rigid porphyrin backbone.

In contrast to the  $Ln(PNP^Me)_2R$  system, the thermal decomposition of **2** does not follow simple first-order kinetics. A plot of the relative amount of alkyl remaining versus time at 75 °C (Figure 3) shows essentially

(21) (a) Arnold, J.; Hoffman, C. G.; Dawson, D. W.; Hollander, F. J. *Organometallics* **1993**, *12*, 3645. (b) Brand, H.; Arnold, J. *Organometallics* **1993**, *12*, 3655. (c) Brand, H.; Arnold, J. *Angew. Chem., Int. Ed. Engl.* **1994**, *33*, 95.

(22) Schaverien, C. J. *J. Chem. Soc., Chem. Commun.* **1991**, 458.

zero-order kinetics until less than 15% of the alkyl remains. This behavior is typical of a heterogeneous reaction. Since the rate of decay is unaffected by variable treatment of the NMR tubes, including silicization, but is affected by *how recently* the sample of **2** used was isolated, we believe that the decomposition is autocatalytic and occurs at the surface of the insoluble Y(DAC) metalation product.<sup>23,24</sup> The same behavior is obtained throughout the 35–85 °C range, affording an  $E_a$  value of 79  $\text{kJ mol}^{-1}$  from the Arrhenius plot. It is clear from these results that the stability of **2** is critically dependent upon its purity.

Given the monomeric structure of **2**, it is clear that a single DAC ligand is capable of satisfying the steric requirements of the Y center in a manner similar to that for  $Cp^*$  ( $C_5Me_5^-$ ). The unique features of the DAC system, compared with  $Cp^*$ , are its flexible geometry and variable donor complement. These features may allow the remarkably simple DAC ligand to access areas of group 3 and lanthanide chemistry hitherto inaccessible with the less flexible  $Cp^*$  system.

**Acknowledgment.** We thank Mrs. C. Greenwood for assistance in recording the NMR spectra and Dr. Becky Chak for help with the X-ray structural study. L.L. thanks Mr. Gord Cross and Mrs. Alison Ingham for helpful discussions regarding preparation of the macrocycle. This research was supported by the NSERC (Canada) and a University of Victoria Internal Research Grant (to D.J.B.).

**Supplementary Material Available:** Tables of atomic positional and equivalent isotropic displacement parameters, bond distances and angles, anisotropic thermal parameters, and calculated hydrogen positions for **2** (9 pages). Ordering information is given on any current masthead page.

OM9407363

(23) Since decomposition of **2** at the glass surface of the NMR tube could also yield zero-order kinetics, we carried out the decomposition studies in tubes that had been cleaned with a variety of agents ( $HNO_3$ ,  $HCl$ , or  $H_2O_2$ /base prior to repeated water rinses) and dried for varying lengths of time (2–60 h) at different temperatures. Additionally, for some runs the tube was silicized with  $Me_2SiCl_2$ .<sup>24</sup> Regardless of the treatment used, plots very similar to Figure 3 were obtained in all cases.

(24) The procedure involved treatment of the tube with 10% HF followed by a deionized water rinse and oven drying (120 °C) for 1–2 h. After it was cooled, the tube was treated with 3%  $Me_2SiCl_2$  in toluene followed by oven drying (120 °C, 48 h). This procedure is a modification of that given in: *Model 303 Static Mercury Drop Electrode Operating and Service Manual*; EG+G Princeton Applied Research: Princeton, NJ, 1984.

# Synthesis and Characterization of the Encapsulated Stannocenes [(C<sub>3</sub>H<sub>7</sub>)<sub>3</sub>C<sub>5</sub>H<sub>2</sub>]<sub>2</sub>Sn and [(C<sub>3</sub>H<sub>7</sub>)<sub>4</sub>C<sub>5</sub>H]<sub>2</sub>Sn

David J. Burkey and Timothy P. Hanusa\*

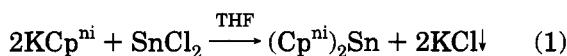
Department of Chemistry, Vanderbilt University, Nashville, Tennessee 37235

Received October 17, 1994<sup>®</sup>

**Summary:** The encapsulated stannocenes [(C<sub>3</sub>H<sub>7</sub>)<sub>4</sub>C<sub>5</sub>H]<sub>2</sub>Sn and [(C<sub>3</sub>H<sub>7</sub>)<sub>3</sub>C<sub>5</sub>H<sub>2</sub>]<sub>2</sub>Sn are isolated as an air-stable, high-melting solid and an air-sensitive oil, respectively; their physical properties mirror those of alkaline-earth metallocenes containing these ligands. The X-ray crystal structure of [(C<sub>3</sub>H<sub>7</sub>)<sub>4</sub>C<sub>5</sub>H]<sub>2</sub>Sn reveals a bent-metallocene geometry closely related to that of [(C<sub>3</sub>H<sub>7</sub>)<sub>4</sub>C<sub>5</sub>H]<sub>2</sub>Ca.

The wide use of the cyclopentadienyl ([C<sub>5</sub>H<sub>5</sub>]<sup>-</sup>) and pentamethylcyclopentadienyl ([C<sub>5</sub>Me<sub>5</sub>]<sup>-</sup>) ligands in organometallic chemistry often overshadows the unique properties possessed by compounds containing other substituted cyclopentadienyl rings.<sup>1</sup> For example, the difference of one isopropyl group between the 1,2,4-triisopropyl- and 1,2,3,4-tetraisopropylcyclopentadienyl ligands ([Cp<sup>3i</sup>]<sup>-</sup> and [Cp<sup>4i</sup>]<sup>-</sup>, respectively) induces dramatically different properties in their associated group 2 metallocenes.<sup>2–5</sup> In particular, the “encapsulated” (Cp<sup>4i</sup>)<sub>2</sub>Ae (Ae = Mg–Ba) metallocenes are high-melting (>150 °C) crystalline solids that do not react with nucleophiles such as ethers<sup>2</sup> or [N(SiMe<sub>3</sub>)<sub>2</sub>]<sup>-6</sup> and possess moderate air stability (up to 30 min). In contrast, the (Cp<sup>3i</sup>)<sub>2</sub>Ae metallocenes are lower melting (<92 °C) oils or waxes that readily form Lewis acid–base adducts with nucleophiles such as THF<sup>3</sup> and decompose in air within seconds. We were interested in determining whether the widely differing properties observed for the (Cp<sup>3i</sup>)<sub>2</sub>Ae and (Cp<sup>4i</sup>)<sub>2</sub>Ae compounds would be reproduced in other metallocenes containing these ligands,<sup>4</sup> and report here results for the corresponding tin compounds.

The stannocenes (Cp<sup>3i</sup>)<sub>2</sub>Sn and (Cp<sup>4i</sup>)<sub>2</sub>Sn are prepared by the metathetical reaction of KCp<sup>3i</sup> or KCp<sup>4i</sup> with SnCl<sub>2</sub> in THF (eq 1).<sup>7</sup> Hexane extraction of the reaction



mixtures gives both compounds in high (>80%) yield; (Cp<sup>4i</sup>)<sub>2</sub>Sn is isolated as a light yellow, crystalline solid, whereas (Cp<sup>3i</sup>)<sub>2</sub>Sn is a slightly viscous, deep yellow oil.<sup>8–11</sup> Any impurities in the compounds can be removed by high-vacuum sublimation (140 °C, 10<sup>-6</sup> Torr) for (Cp<sup>4i</sup>)<sub>2</sub>Sn or distillation (100 °C, 10<sup>-6</sup> Torr) for (Cp<sup>3i</sup>)<sub>2</sub>Sn.

Analytical and spectroscopic (<sup>1</sup>H, <sup>13</sup>C NMR, IR) data for the two metallocenes confirm the proposed formulations.<sup>7</sup>

An X-ray crystallographic study of (Cp<sup>4i</sup>)<sub>2</sub>Sn<sup>12</sup> reveals a bent-metallocene geometry (Figure 1). As observed in all other previously characterized bent stannocenes,<sup>13</sup> the Cp ligands are displaced from symmetrical η<sup>5</sup> coordination; this displacement renders the ring centroid–Sn–ring centroid angle for the complex (165.0°) substantially larger than the ring normal–Sn–ring normal angle (152.2°). Both angles are the largest so

(7) Synthesis of (Cp<sup>3i</sup>)<sub>2</sub>Sn. KCp<sup>3i</sup> (1.29 g, 5.58 mmol) and SnCl<sub>2</sub> (0.53 g, 2.79 mmol) were added to 45 mL of THF, and the yellowish suspension was stirred for 12 h. The THF was removed under vacuum, leaving a dark yellow residue, which was then extracted with 60 mL of hexane. Filtration of the extract removed a brown solid; vacuum evaporation of the hexane from the yellow filtrate gave 1.24 g (89% yield) of (Cp<sup>3i</sup>)<sub>2</sub>Sn as a yellow oil, mp ca. -18 °C. (Cp<sup>3i</sup>)<sub>2</sub>Sn can be distilled at 100 °C and 10<sup>-6</sup> Torr, but such distillations result in considerable high mechanical losses of product. Anal. Calcd for C<sub>28</sub>H<sub>46</sub>Sn: C, 67.08; H, 9.25. Found: C, 67.35; H, 9.17. <sup>1</sup>H NMR (C<sub>6</sub>D<sub>6</sub>): δ 5.68 (s, <sup>2</sup>J(Sn–H) = 22.9 Hz, 4 H, ring CH), 2.76–2.84 (two overlapping septets, 6 H, CHMe<sub>2</sub>), 1.22 (d, J = 6.7 Hz, 24 H, CH<sub>3</sub>), 1.20 (d, J = 6.6 Hz, 12 H, CH<sub>3</sub>). <sup>13</sup>C NMR (C<sub>6</sub>D<sub>6</sub>): δ 134.2 (1,2-ring CCHMe<sub>2</sub>), 131.1 (4-ring CCHMe<sub>2</sub>), 102.4 (<sup>1</sup>J(Sn–C) = 26.5 Hz, ring CH), 27.9 (4-CHMe<sub>2</sub>), 27.2 (CH<sub>3</sub>), 25.9 (1,2-CHMe<sub>2</sub>), 25.8 (CH<sub>3</sub>), 25.2 (CH<sub>3</sub>). Principal IR bands (neat, cm<sup>-1</sup>): 3072 (w), 2954 (vs, br), 1459 (m), 1412 (w), 1378 (m), 1360 (m), 1325 (w), 1268 (m), 1177 (m), 1151 (m), 1103 (m), 1051 (m), 1028 (m), 805 (s), 779 (m), 651 (w), 498 (w). Synthesis of (Cp<sup>4i</sup>)<sub>2</sub>Sn. By the procedure used for (Cp<sup>3i</sup>)<sub>2</sub>Sn, (Cp<sup>4i</sup>)<sub>2</sub>Sn was prepared from KCp<sup>4i</sup> (0.77 g, 2.83 mmol) and SnCl<sub>2</sub> (0.27 g, 1.41 mmol) in THF. Bright yellow (Cp<sup>4i</sup>)<sub>2</sub>Sn was isolated from a hexane extract of the reaction mixture. Purification of the product was achieved by sublimation at 140 °C and 10<sup>-6</sup> Torr, giving 0.685 g (83% yield) of (Cp<sup>4i</sup>)<sub>2</sub>Sn (mp 162–163 °C). Anal. Calcd for C<sub>34</sub>H<sub>58</sub>Sn: C, 69.74; H, 9.98. Found: C, 70.14; H, 10.09. <sup>1</sup>H NMR (C<sub>6</sub>D<sub>6</sub>): δ 5.31 (s, <sup>2</sup>J(Sn–H) = 29.6 Hz, 2 H, ring CH), 3.04 (septet, J = 7.2 Hz, 4 H, CHMe<sub>2</sub>), 2.93 (septet, J = 6.8 Hz, 4 H, CHMe<sub>2</sub>), 1.35 (d, J = 7.1 Hz, 12 H, CH<sub>3</sub>), 1.33 (d, J = 7.0 Hz, 12 H, CH<sub>3</sub>), 1.27 (d, J = 6.8 Hz, 12 H, CH<sub>3</sub>), 1.17 (d, J = 6.7 Hz, 12 H, CH<sub>3</sub>). <sup>13</sup>C NMR (C<sub>6</sub>D<sub>6</sub>): δ 132.1 (ring CCHMe<sub>2</sub>), 130.2 (<sup>1</sup>J(Sn–C) = 40.4 Hz, ring CCHMe<sub>2</sub>), 96.3 (ring CH), 27.3 (CH<sub>3</sub>), 26.45 (CHMe<sub>2</sub>), 26.35 (CHMe<sub>2</sub>), 26.0 (br, CH<sub>3</sub>), 25.7 (br, CH<sub>3</sub>), 25.3 (br, CH<sub>3</sub>). Principal IR bands (KBr, cm<sup>-1</sup>): 3074 (w), 2960 (s, br), 1454 (m), 1402 (w), 1375 (m), 1361 (m), 1341 (w), 1312 (m), 1264 (m), 1179 (m), 1143 (m), 1104 (m), 1055 (m), 984 (w), 886 (w), 780 (s), 668 (m), 619 (w), 491 (m), 373 (m), 344 (w).

(8) There are several previous examples in the literature of stannocenes that are oils or liquids at room temperature; e.g., (MeC<sub>5</sub>H<sub>4</sub>)<sub>2</sub>Sn,<sup>9</sup> [Me<sub>3</sub>Si]C<sub>5</sub>H<sub>4</sub>Sn,<sup>10</sup> (t-BuC<sub>5</sub>H<sub>4</sub>)<sub>2</sub>Sn,<sup>10</sup> and [(t-Bu)<sub>2</sub>C<sub>5</sub>H<sub>3</sub>]<sub>2</sub>Sn.<sup>11</sup>

(9) Dave, L. D.; Evans, D. F.; Wilkinson, G. *J. Chem. Soc.* **1959**, 3684–3688.

(10) Hani, R.; Geanangel, R. A. *J. Organomet. Chem.* **1985**, 293, 197–205.

(11) Jutzki, P.; Dickbreder, R.; Nöth, H. *Chem. Ber.* **1989**, 122, 865–870.

(12) Crystals of [(C<sub>3</sub>H<sub>7</sub>)<sub>4</sub>C<sub>5</sub>H]<sub>2</sub>Sn grown from hexane are monoclinic, space group C2/c, a = 34.05(1) Å, b = 12.40(1) Å, c = 16.604(6) Å, β = 111.52(4)°, V = 6522(13) Å<sup>3</sup>, and D<sub>calc</sub> = 1.192 g cm<sup>-3</sup> for Z = 8. Data were collected on a Rigaku AFC6S diffractometer at 293 K using graphite-monochromated Mo Kα radiation (λ = 0.710 73 Å). Continuous ω–2θ scans with fixed backgrounds were used to collect a total of 6174 reflections (6064 unique) in the range 6° ≤ 2θ ≤ 50°, of which 3036 had F > 2.00σ(F). Data were reduced to a unique set of intensities and associated σ values in the usual manner. No absorption correction was applied (μ = 8.03 cm<sup>-1</sup>). The structure was solved by direct methods (SHELXS-86 and DIRDIF) and Fourier techniques. Non-hydrogen atoms were refined anisotropically. All the hydrogen atoms were located on difference Fourier maps and were refined isotropically. The final difference maps were featureless. R = 0.032, R<sub>w</sub> = 0.036, and GOF = 1.21.

<sup>®</sup> Abstract published in *Advance ACS Abstracts*, December 1, 1994.

(1) Janiak, C.; Schumann, H. *Adv. Organomet. Chem.* **1991**, 33, 291–393.

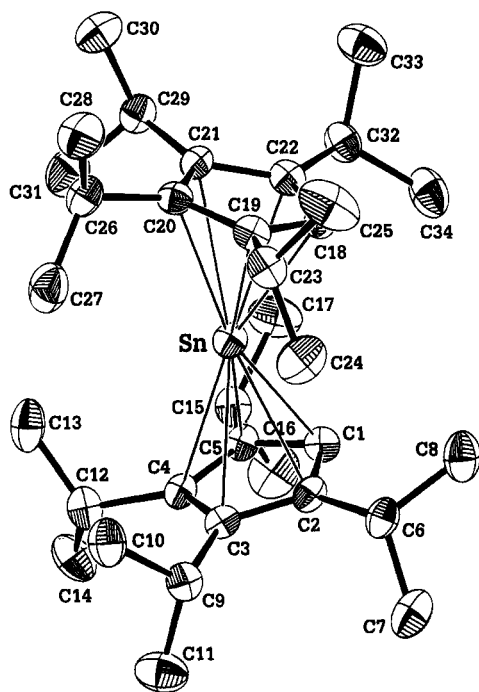
(2) Williams, R. A.; Tesh, K. F.; Hanusa, T. P. *J. Am. Chem. Soc.* **1991**, 113, 4843–4851.

(3) Burkey, D. J.; Williams, R. A.; Hanusa, T. P. *Organometallics* **1993**, 12, 1331–1337.

(4) Burkey, D. J.; Hanusa, T. P.; Huffman, J. C. *Adv. Mater. Opt. Electron.* **1994**, 4, 1–8.

(5) Burkey, D. J.; Hanusa, T. P., unpublished results for (Cp<sup>4i</sup>)<sub>2</sub>Mg and (Cp<sup>4i</sup>)<sub>2</sub>Sr.

(6) Burkey, D. J.; Alexander, E. K.; Hanusa, T. P. *Organometallics* **1994**, 13, 2773–2786.



**Figure 1.** ORTEP diagram of the non-H atoms of  $(\text{Cp}^{4i})_2\text{Sn}$ ; thermal ellipsoids are shown at the 35% level. Selected bond distances (Å) and angles (deg): Sn(1)–C(1), 2.575(6); Sn(1)–C(2), 2.641(5); Sn(1)–C(3), 2.772(6); Sn(1)–C(4), 2.821(5); Sn(1)–C(5), 2.706(5); Sn(1)–C(18), 2.596(6); Sn(1)–C(19), 2.721(5); Sn(1)–C(20), 2.812(5); Sn(1)–C(21), 2.769(6); Sn(1)–C(22), 2.627(6); Sn(1)–centroid(1), 2.423; Sn(1)–centroid(2), 2.424; ring normal–Sn–ring normal, 152.2; ring centroid–Sn(1)–ring centroid, 165.0.

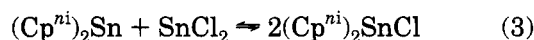
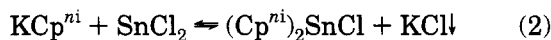
far observed for a *bent* stannocene<sup>13</sup> (the only larger value being 180° for both angles in the *linear* stannocene  $(\text{Ph}_5\text{C}_5)_2\text{Sn}^{14}$ ), underscoring the exceptional steric bulk of the  $[\text{Cp}^{4i}]^-$  ligand. However, the bulkiness of the ligand does not lengthen any of the Sn–C distances from their expected values; i.e., the Sn–ring centroid (2.423 and 2.424 Å) and Sn–C (range 2.575(6)–2.821(5) Å; average 2.703(9) and 2.705(9) Å) distances are similar to those in other previously characterized stannocenes.<sup>15</sup>

The isopropyl groups in  $(\text{Cp}^{4i})_2\text{Sn}$  orient themselves in a semi-g geared fashion so that they are rotated out of the plane of the cyclopentadienyl ring by 52.8–89.9° (average 77.8°) (Figure 1). The isopropyl group orientation leads to an almost complete encapsulation of the metal by the  $[\text{Cp}^{4i}]^-$  ligands. Interestingly, nearly the same orientation of the isopropyl groups is found in the solid state for  $(\text{Cp}^{4i})_2\text{Ca}$ ;<sup>2</sup> the similarities in isopropyl group orientation, combined with the resemblance in bending angles (ring centroid–Ca–ring centroid angle of 162.3°) and metal–carbon distances (Ca–C average of 2.64(1) Å), make the two complexes essentially isostructural. It is natural to view this similarity as a consequence of the extreme steric bulk of the  $[\text{Cp}^{4i}]^-$

ring, but detailed comparisons between the structural energetics of group 2 and group 14 metallocenes reveal that the two classes of compounds share quantitatively similar preferences for bent structures, in spite of differences in metal valence electron configuration.<sup>16</sup>

As observed previously for the corresponding alkaline-earth metallocenes, the properties of  $(\text{Cp}^{4i})_2\text{Sn}$  and  $(\text{Cp}^{3i})_2\text{Sn}$  are significantly different. The much lower melting point of  $(\text{Cp}^{3i})_2\text{Sn}$  (ca. –18 °C) relative to  $(\text{Cp}^{4i})_2\text{Sn}$  (mp 162–163 °C) parallels the behavior in the alkaline-earth metallocenes (e.g.,  $(\text{Cp}^{3i})_2\text{Ca}$  is isolated as a supercooled oil that eventually solidifies into a low-melting solid,<sup>4</sup> whereas  $(\text{Cp}^{4i})_2\text{Ca}$  melts at 196–200 °C). This trend is apparently linked to the increased freedom of movement of the isopropyl groups in the  $[\text{Cp}^{3i}]^-$  ligand relative to  $[\text{Cp}^{4i}]^-$ .<sup>4</sup> In addition, the relative air stability of the stannocenes is dramatically dissimilar. Solid  $(\text{Cp}^{4i})_2\text{Sn}$  can be stored for weeks in air without noticeable decomposition, and benzene solutions of the compound exposed to air do not begin to decompose for 2–4 h (as monitored by <sup>1</sup>H NMR). Even after 24 h exposure, over 90% of the metallocene can be recovered. In contrast,  $(\text{Cp}^{3i})_2\text{Sn}$  begins to decompose within minutes on exposure to air. Thus, the removal of an isopropyl group on each ring of  $(\text{Cp}^{4i})_2\text{Sn}$  allows greater access to the metal center (which leads to increased reactivity with oxygen) and increases the flexibility of the substituents on the Cp ligand (which leads to the reduction in melting point).

No difference between the  $[\text{Cp}^{3i}]^-$  and  $[\text{Cp}^{4i}]^-$  ligands was noted in attempts to prepare the corresponding (cyclopentadienyl)tin chlorides by either a 1:1 metathesis reaction (eq 2) or a comproportionation reaction (eq 3); both methods were unsuccessful.



Although NMR spectra ( $\text{C}_6\text{D}_6$  and  $\text{THF}-d_8$ ) of the product mixtures exhibit new resonances that could be attributed to the desired  $(\text{Cp}^{ni})\text{SnCl}$  compounds (especially a ring CH peak at  $\delta$  5.89 in  $\text{C}_6\text{D}_6$  for both), these were always accompanied by peaks for the corresponding metallocenes. Thus, the mono(ring) compounds appear to be susceptible to disproportionation in both polar and nonpolar solvents, frustrating attempts to isolate them in pure form. The disproportionational instability of  $(\text{Cp}^{3i})\text{SnCl}$  and  $(\text{Cp}^{4i})\text{SnCl}$  is in contrast with the stability of previously described mono(cyclopentadienyl)tin complexes of *unsubstituted* cyclopentadiene (i.e.,  $\text{CpSnCl}$ ,<sup>17</sup>  $\{\text{CpSn}[\mu\text{-N}=\text{C}(\text{NMe}_2)_2]_2\}$ ,<sup>18</sup>), but it is similar to the observed solution instability of the mono(pentamethylcyclopentadienyl)tin complexes  $\text{Cp}^*\text{SnCl}$ ,<sup>19</sup>  $\text{Cp}^*\text{Sn}(\text{O}_2\text{CCl}_3)$ , and  $\text{Cp}^*\text{Sn}(\text{O}_2\text{CCF}_3)$ .<sup>20,21</sup> Apparently, the enhanced electron-donating ability of highly alkylated Cp ligands renders the corresponding mono(ring)tin complexes more prone to disproportion-

(13)  $(\text{Me}_3\text{Si})_3\text{C}_5\text{H}_2\text{Sn}$  has been reported to have similarly large ring centroid–Sn–ring centroid and ring normal–Sn–ring normal angles of 162(2) and 164° in the solid state. However, the structural determination was of sufficiently poor quality ( $R = 0.13$ , ring C–C bonds as large as 1.57(4) Å) that the reliability of these values is in question. See: Cowley, A. H.; Jutzi, P.; Kohl, F. X.; Lasch, J. G.; Norman, N. C.; Schlüter, E. *Angew. Chem., Int. Ed. Engl.* **1984**, *23*, 616–617.

(14) Heeg, M. J.; Janiak, C.; Zuckerman, J. J. *J. Am. Chem. Soc.* **1984**, *106*, 4259–4261.

(15) Jutzi, P. *Adv. Organomet. Chem.* **1986**, *26*, 217–295.

(16) Burkey, D. J.; Hanusa, T. P. *Comments Inorg. Chem.*, in press.  
(17) Bos, K. D.; Bulten, E. J.; Noltes, J. G. *J. Organomet. Chem.* **1972**, *39*, C52–C54.

(18) Stalke, D.; Paver, M. A.; Wright, D. S. *Angew. Chem., Int. Ed. Engl.* **1993**, *32*, 428–429.

(19) Jutzi, P.; Kohl, F. *J. Organomet. Chem.* **1979**, *164*, 141–152.

(20) Jutzi, P.; Kohl, F. X. *Chem. Ber.* **1981**, *114*, 488–494.

ation, probably through increased stabilization of the  $[\text{Cp}^*\text{Sn}]^+$  fragment. It is worth noting that, unlike the case with tin, the  $[\text{Cp}^{4i}]^-$  ligand kinetically stabilizes mono(cyclopentadienyl)calcium complexes  $(\text{Cp}^{4i})\text{CaE}(\text{thf})_n$  against solution disproportionation.<sup>6</sup>

The different physical and chemical properties of  $(\text{Cp}^{3i})_2\text{Sn}$  and  $(\text{Cp}^{4i})_2\text{Sn}$  emphasize the dramatic effect that a single isopropyl group can have on metallocenes containing the  $[\text{Cp}^{3i}]^-$  and  $[\text{Cp}^{4i}]^-$  ligands. Further investigation of the reactivity of alkaline-earth and tin

---

(21) The synthesis of (pentamethylcyclopentadienyl)tin bromide by the *solid-state* reaction of  $(\eta^1\text{-Cp}^*)_2\text{SnBr}_2$  and  $\text{Cp}^*\text{Sn}$  at 90 °C has been reported. Apparently, the success of this reaction stems from the absence of a reaction solvent; no information on the solution stability of this complex was given (although it was purified by recrystallization from methylene chloride). See: Jutzi, P.; Hielscher, B. *Organometallics* **1986**, *5*, 1201–1204.

complexes of  $[\text{Cp}^{3i}]^-$  and  $[\text{Cp}^{4i}]^-$ , and the synthesis of other main-group complexes of these ligands, is in progress.

**Acknowledgment** is made to the Army Research Office and to the University Research Council of Vanderbilt University for support of this research. D.J.B. is the grateful recipient of an NSF Predoctoral Fellowship.

**Supplementary Material Available:** Tables of crystal data and data collection details, fractional coordinates, bond distances and angles, and anisotropic thermal parameters (6 pages). Ordering information is given on any current mast-head page.

OM940798T

# B–H Reactivity of a Dihydrobis(pyrazolyl)borate Ligand: Products of Intramolecular Acyl and Iminoacyl Hydroboration

Antonio Pizzano,<sup>†</sup> Luis Sánchez,<sup>†</sup> Enrique Gutiérrez,<sup>\*,‡</sup> Angeles Monge,<sup>‡</sup> and Ernesto Carmona<sup>\*,†</sup>

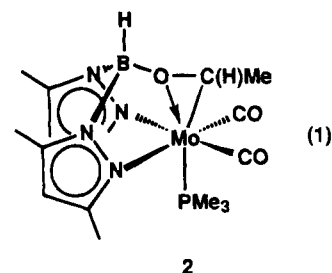
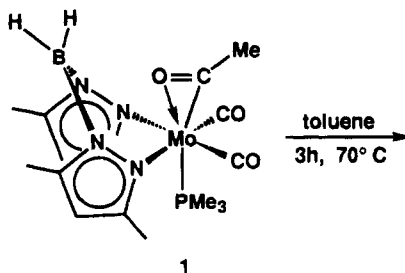
Departamento de Química Inorgánica-Instituto de Ciencia de Materiales, Universidad de Sevilla-Consejo Superior de Investigaciones Científicas, Apdo 553, 41071 Sevilla, Spain, Instituto de Ciencia de Materiales, Sede D, Consejo Superior de Investigaciones Científicas, Serrano 113, 28006 Madrid, Spain, and Facultad de Ciencias Químicas, Universidad Complutense, 28040 Madrid, Spain

Received October 26, 1994<sup>®</sup>

**Summary:** Upon heating at 70 °C, in toluene, the  $\eta^2$ -acyl  $H_2B(pz^*)_2Mo(\eta^2-C(O)Me)(CO)_2(PMe_3)$  (**1**;  $pz^* = 3,5$ -dimethylpyrazol-1-yl) rearranges to the complex  $HB(pz^*)_2Mo(HC(O)Me)(CO)_2(PMe_3)$  (**2**), which contains a functionalized acyl ligand resulting from the stereo- and regioselective intramolecular addition of one of the B–H bonds of the  $H_2B(pz^*)_2$  group across the C=O moiety of the  $\eta^2$ -acyl group. Other complexes of this type, e.g.  $H_2B(pz^*)_2Mo(\eta^2-C(O)CH_2CMe_3)(CO)(CN-t-Bu)(PMe_3)$  or the related  $\eta^2$ -iminoacyl  $H_2B(pz^*)_2Mo(\eta^2-C(N-t-Bu)Me)(CO)_2(PMe_3)$ , undergo a similar transformation, but the analogous derivatives containing the unsubstituted  $H_2B(pz)_2$  ligand are considerably less reactive toward hydroboration.

The reduction of a coordinated acyl ligand is a key step in some CO hydrogenation reactions, e.g. Fischer–Tropsch synthesis, hydroformylation, etc.<sup>1</sup> Recent reactivity studies of M–acyl complexes<sup>2</sup> have disclosed a number of interesting transformations.<sup>3</sup> Intermolecular hydrogen transfer from transition-metal hydrides to isolable acyl functionalities has been achieved,<sup>4</sup> and

similar acyl reductions by hydrogen, hydrosilanes, and other reductants have been investigated.<sup>5</sup> In this contribution we show that one the B–H bonds of a coordinated dihydrobis(pyrazolyl)borate ligand<sup>6</sup> can be smoothly and intramolecularly added across the C=O bond of a Mo-bound  $\eta^2$ -acyl moiety. A representative example of this (to our knowledge) unprecedented reaction,<sup>7</sup> which yields products formally derived from the hydroboration<sup>8</sup> of the acyl group, is shown in eq 1. Extension of this rearrangement to related  $\eta^2$ -iminoacyl systems has also been accomplished.



A toluene solution of complex **1**,<sup>9</sup> maintained at 70 °C for 3 h, results in the formation of the isomeric, red crystalline product **2**<sup>10</sup> in ca. 60% isolated yield. Evidence for the functionalization of the acyl moiety in the above transformation comes from NMR studies. Thus, the elaborated acyl ligand gives rise to two mutually

<sup>†</sup> Universidad de Sevilla-CSIC.

<sup>‡</sup> CSIC-Universidad Complutense.

<sup>®</sup> Abstract published in *Advance ACS Abstracts*, December 1, 1994.

(1) See for example: (a) *Homogeneous Catalysis*; Parshall, G. W., Ed.; Wiley New York, 1992; (b) Sneed, R. P. A. In *Comprehensive Organometallic Chemistry*; Wilkinson, G., Stone, F. G. A., Abel, E. W., Eds.; Pergamon Press: Oxford, U.K., 1982; Vol. VIII, Chapter 50.2.

(2) (a) Durfee, L. D.; Rothwell, I. P. *Chem. Rev.* **1988**, *88*, 1059. (b) Cutler, A. R.; Hanna, P. K.; Vites, J. C. *Chem. Rev.* **1988**, *88*, 1363.

(3) (a) Rusik, C. A.; Collins, M. A.; Gamble, A. S.; Tonker, T. L.; Templeton, J. L. *J. Am. Chem. Soc.* **1989**, *111*, 2550. (b) Campion, B. K.; Falk, J.; Tilley, T. D. *J. Am. Chem. Soc.* **1987**, *109*, 2049. (c) Elsner, F. H.; Woo, H.; Tilley, T. D. *J. Am. Chem. Soc.* **1988**, *110*, 313. (d) Arnold, J.; Tilley, T. D.; Rheingold, A. L.; Geib, S. J.; Arif, A. M. *J. Am. Chem. Soc.* **1989**, *111*, 149. (e) Zambrano, C. H.; McMullen, A. K.; Kobriger, L. M.; Fanwick, P. E.; Rothwell, I. P. *J. Am. Chem. Soc.* **1990**, *112*, 6565. (f) Villiers, C.; Adam, R.; Ephiritikhine, M. *J. Chem. Soc., Chem. Commun.* **1992**, 1555.

(4) (a) Erker, G.; Kropp, K.; Kruger, C.; Chiang, A.-P. *Chem. Ber.* **1982**, *115*, 2447. (b) Martin, B. D.; Matchett, S. A.; Norton, J. R.; Anderson, O. P. *J. Am. Chem. Soc.* **1985**, *107*, 7952. (c) Martin, B. D.; Warner, K. E.; Norton, J. R. *J. Am. Chem. Soc.* **1986**, *108*, 33. (d) Warner, K. E.; Norton, J. R. *Organometallics* **1985**, *4*, 2150. (e) Marsella, J. A.; Caulton, K. G. *J. Am. Chem. Soc.* **1980**, *102*, 1747. (f) Marsella, J. A.; Folting, K.; Huffman, J. C.; Caulton, K. G. *J. Am. Chem. Soc.* **1981**, *103*, 5596. (g) Maatta, E. A.; Marks, T. J. *J. Am. Chem. Soc.* **1981**, *103*, 3576. (h) Martin, J. T.; Baird, M. C. *Organometallics* **1983**, *2*, 1073.

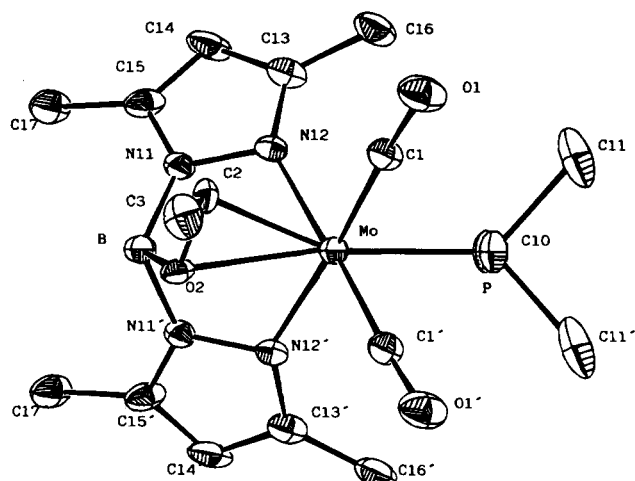
(5) (a) Gregg, B. T.; Cutler, A. R. *Organometallics* **1992**, *11*, 4276. (b) Gregg, B. T.; Hanna, P. K.; Crawford, E. J.; Cutler, A. R. *J. Am. Chem. Soc.* **1991**, *113*, 384. (c) Kovacs, I.; Sisak, A.; Ungvary, F.; Marko, L. *Organometallics* **1988**, *7*, 1025. (d) Wegman, R. W. *Organometallics* **1986**, *5*, 707. (e) Akita, M.; Mitani, O.; Sayama, M.; Morooka, Y. *Organometallics* **1991**, *10*, 1394. (f) Crawford, E. J.; Hanna, P. K.; Cutler, A. R. *J. Am. Chem. Soc.* **1989**, *111*, 6891. (g) Selover, J. C.; Vaughn, G. P.; Strouse, C. E.; Gladysz, J. A. *J. Am. Chem. Soc.* **1986**, *108*, 1455.

(6) Trofimenko, S. *Chem. Rev.* **1993**, *93*, 943.

(7) For a somewhat related transformation see: Gorrell, I. B.; Looney, A.; Parkin, G. *J. Am. Chem. Soc.* **1990**, *112*, 4068.

(8) (a) *Borane Reagents*; Pelter, A., Smith, K., Brown, H. C., Eds.; Academic Press: London, 1988. (b) Zaidlewicz, M. In *Comprehensive Organometallic Chemistry*; Wilkinson, G., Stone, F. G. A., Abel, E. W., Eds.; Pergamon Press: Oxford, U. K., 1982; Vol. VII, Chapter 45.2.

(9) **1**: A solution of  $MoCl(\eta^2-C(O)CH_2CO)(PMe_3)_3$ <sup>19</sup> (0.43 g, 1.0 mmol) in THF (40 mL) was treated with  $KBpz^*$  (0.29 g, 1.2 mmol). The suspension was stirred for 5 h, and then CO was bubbled through the mixture for about 15 min. The solvent was removed under reduced pressure and the residue extracted with a 1:1 petroleum ether–Et<sub>2</sub>O mixture. The insoluble components were filtered off and the solution cooled. **1** was obtained as yellow crystals (80% yield).



**Figure 1.** ORTEP diagram of  $\text{H}_2\text{B}(\text{pz}^*)_2\text{Mo}(\text{HC}(\text{O})\text{Me})(\text{CO})_2(\text{PMe}_3)$  (**2**) showing the atom-numbering scheme. Selected bond lengths (Å) and angles (deg): Mo–O2 = 2.16(1), Mo–C2 = 2.18(2), C2–O2 = 1.37(2), B–O2 = 1.48(2), O2–Mo–C2 = 36.8(5), Mo–O2–C2 = 72.5(9), C2–O2–B = 121(1).

coupled  $^1\text{H}$  NMR resonances at  $\delta$  2.18 and 4.00 (doublet, 3H, and quartet, 1H, respectively;  $^3J_{\text{HH}} = 5$  Hz), suggesting the formation of a  $\text{HC}(\text{O})\text{Me}$  group. This assumption is further supported by the observation of a  $^{13}\text{C}\{^1\text{H}\}$  NMR signal at  $\delta$  92.2 (d,  $^2J_{\text{CP}} = 10$  Hz), which experiences doublet splitting upon gate decoupling ( $^1J_{\text{CH}} = 170$  Hz) and longer range coupling to the methyl protons ( $^2J_{\text{CH}} = 6$  Hz). Moreover, a single, sharp absorption attributable to  $\nu(\text{B}-\text{H})$  is detected in the IR spectrum of **2** at ca.  $2475\text{ cm}^{-1}$ .

The molecular complexity and bonding mode of the functionalized ligand present in **2** has been ascertained by a single-crystal X-ray structural determination.<sup>11</sup> Figure 1 shows an ORTEP view, together with some important bond distances and angles. As can be seen, the fragment derived from the original acyl moiety is trans with respect to the phosphine ligand and is C- and O-bonded to the Mo atom, with relatively short Mo–C2 and Mo–O2 contacts.<sup>12</sup> Considering the small C2–Mo–O2 bite angle of  $36.8(5)^\circ$ , the C–O entity can be thought to occupy a single coordination position, and therefore, the structure of **2** is that of a distorted octahedron, with the two pyrazolyl nitrogens, N12 and N12', the two carbonyl carbons, C1 and C1', and the phosphine ligand occupying the remaining coordination sites. The B–O bond length of 1.48(2) Å is a normal value.<sup>13</sup>

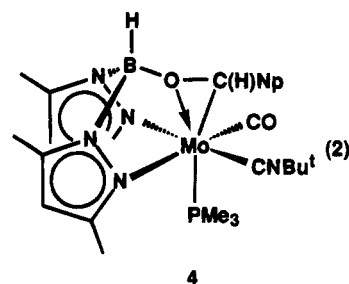
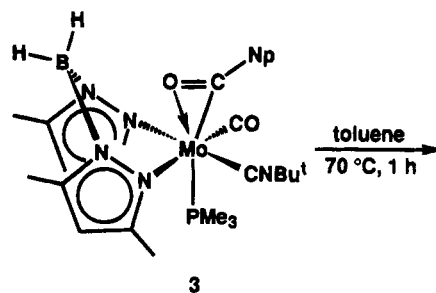
(10) **2**: After a solution of **1** (0.52 g, 1 mmol) was stirred in toluene (20 mL) at  $70^\circ\text{C}$  for 3 h, the solvent was stripped off and the residue extracted with  $\text{Et}_2\text{O}$  (15 mL), concentrated and cooled, to give dark pink crystals of **2** (60% yield). Anal. Calcd for  $\text{C}_{17}\text{H}_{23}\text{O}_3\text{N}_4\text{PBMo}$ : C, 43.0; H, 5.9; N, 11.8. Found: C, 42.2; H, 6.2; N, 11.4. Selected spectroscopic data are given in the text.

(11) Crystal data for **2**. This compound crystallizes in the monoclinic system, space group  $P2_1/m$ , with unit cell parameters  $a = 7.522(2)$  Å,  $b = 15.261(3)$  Å,  $c = 9.826(3)$  Å,  $\beta = 104.52(3)^\circ$ ,  $V = 1091.9(5)$  Å<sup>3</sup>, and  $\rho_{\text{calcd}} = 1.44\text{ g cm}^{-3}$  for  $Z = 2$ . Using MoK $\alpha$  radiation on a Kappa diffractometer, 3145 reflections were measured to  $2\theta_{\text{max}} = 60^\circ$ , 1339 of which were unique. Most of the calculations were carried out with the X-Ray 80 system. The structure was resolved by Patterson and Fourier methods, leading to final values of  $R(F) = 0.061$  and  $R_w(F) = 0.062$ .

(12) Atwood, J. L.; Hunter, W. E.; Rogers, R. D.; Carmona, E.; Wilkinson, G. J. *Chem. Soc., Dalton Trans.* **1979**, 1519.

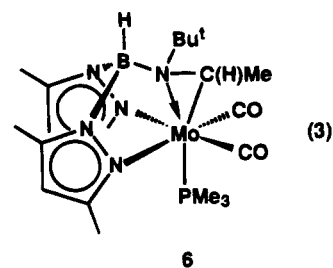
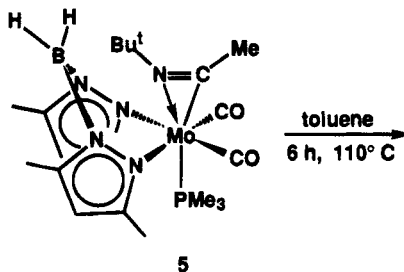
(13) Borodinski, L.; Sinn, E.; Grimes, R. N. *Inorg. Chem.* **1982**, *21*, 1928.

In order to gain a better understanding of this unusual reaction, other related systems have been investigated. The hydroboration reaction is more facile for complexes of the sterically demanding  $\text{H}_2\text{B}(\text{pz}^*)_2$  ligand, as compared to those of the less encumbered  $\text{H}_2\text{B}(\text{pz})_2$  group ( $\text{pz}^* = 3,5\text{-Me}_2\text{C}_3\text{N}_2\text{H}$ ;  $\text{pz} = \text{C}_3\text{N}_2\text{H}_3$ ). Thus, apart from **1**, other related  $\text{H}_2\text{B}(\text{pz}^*)_2$  complexes such as the neopentyl-derived species  $\text{H}_2\text{B}(\text{pz}^*)_2\text{Mo}(\eta^2\text{-C}(\text{O})\text{CH}_2\text{-}t\text{-Bu})(\text{CN-}t\text{-Bu})(\text{PMe}_3)$  (**3**) undergo readily the addition of B–H across the acyl C–O bond to yield the corresponding hydroborated product (e.g. **4**, eq 2).



However, the  $\text{H}_2\text{B}(\text{pz})_2$  analog of **1** requires considerably more forcing conditions: while the half-life of the **1**  $\rightarrow$  **2** conversion in toluene, at  $70^\circ\text{C}$ , is ca. 1 h, the equivalent transformation of the complex  $\text{H}_2\text{B}(\text{pz})_2\text{Mo}(\eta^2\text{-C}(\text{O})\text{Me})(\text{CO})_2(\text{PMe}_3)$ , under the same experimental requirements, is over 1 order of magnitude slower ( $t_{1/2} \approx 30$  h). As a result, in this  $\text{H}_2\text{B}(\text{pz})_2$  system observation of the hydroboration products is often hampered by other competitive reactions, leading to different products.<sup>14</sup>

Extension of this transformation to the analogous  $\eta^2$ -iminoacyl compounds proves attainable (eq 3). Some-



what more forcing conditions are nevertheless demanded and, for example, hydroboration of the C=N bond of  $\text{H}_2\text{B}(\text{pz}^*)_2\text{Mo}(\eta^2\text{-C}(\text{N-}t\text{-Bu})\text{Me})(\text{CO})_2(\text{PMe}_3)^{15,16}$  requires heating at 110 °C, in toluene for 6 h. Once again, the  $\text{H}_2\text{B}(\text{pz}_2)$  analogs are considerably less reactive, no conversion to the B-H addition product being detected after heating  $\text{H}_2\text{B}(\text{pz}_2)\text{Mo}(\eta^2\text{-C}(\text{N-}t\text{-Bu})\text{Me})(\text{CO})_2(\text{PMe}_3)$  in toluene, at 110 °C, for 6 h. The functionalized iminoacyls have also been characterized by spectroscopy.

Preliminary kinetic studies show the conversion of **3** into **4** is intramolecular and exhibits clean, first-order kinetics over at least 3-4 half-lives (toluene, 70 °C, as determined by  $^{31}\text{P}\{^1\text{H}\}$  NMR spectroscopy). A detailed kinetic and mechanistic investigation is presently under way. In the meantime, we note that a plausible reaction pathway could involve a concerted, stereospecific and regioselective addition<sup>17</sup> of one of the B-H bonds to the acyl or iminoacyl functionality.<sup>8</sup> Close proximity of the reacting B-H and C=X moieties may be facilitated by dissociation of one of the pyrazolyl rings of the  $\text{H}_2\text{B}(\text{pz}^*)_2$  ligands.<sup>18</sup> This hypothesis finds support in the aforementioned qualitative observations regarding the influence of the steric demands of the  $\text{H}_2\text{B}(\text{pz}^*)_2$  group

(14) For example,  $\text{H}_2\text{B}(\text{pz})_2\text{Mo}(\eta^2\text{-C}(\text{O})\text{CH}_2\text{-}t\text{-Bu})(\text{CN-}t\text{-Bu})(\text{CO})_2(\text{PMe}_3)$  yields mainly the  $\eta^2$ -iminoacyl  $\text{H}_2\text{B}(\text{pz})_2\text{Mo}(\eta^2\text{-C}(\text{N-}t\text{-Bu})\text{-neo-Pe})(\text{CO})_2(\text{PMe}_3)$ .

(15) **5**: To a stirred solution of **1** (0.52 g, 1 mmol) was added an equimolar amount of CN-*t*-Bu (1.0 mL, 1.0 M solution in THF). After 2 h complete reaction took place, and the mixture was evaporated to dryness. Redissolving the residue and cooling the resulting solution yielded **5** as a red crystalline product (80% yield).

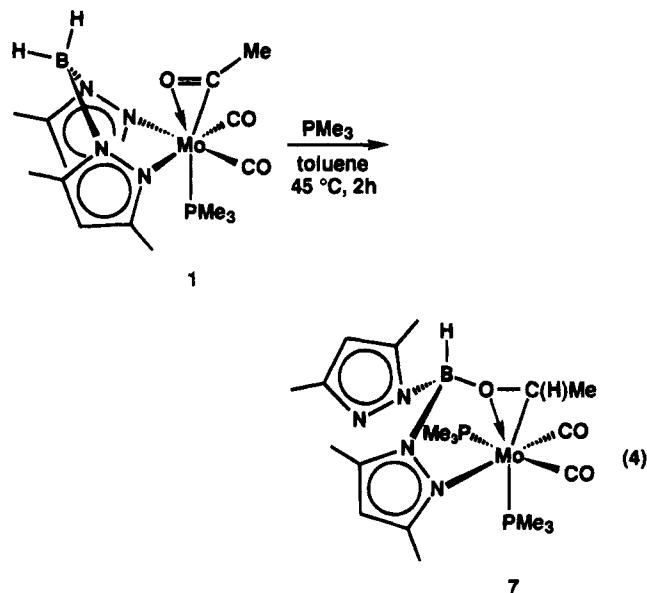
(16) **6**: A solution of **5** in toluene was stirred in toluene at 110 °C for 6 h. Removal of the solvent, extraction in hexanes (20 mL), and cooling of the resulting solution gave **6** as red crystals (60% yield). Anal. Calcd for  $\text{C}_{21}\text{H}_{37}\text{O}_2\text{N}_3\text{PBMo}$ : C, 47.6; H, 7.0; N, 13.3. Found: C, 47.4; H, 7.2; N, 12.8. Selected spectroscopic data: M-CO, IR bands (Nujol mull) at 1892 and 1774  $\text{cm}^{-1}$ ,  $^{13}\text{C}\{^1\text{H}\}$  NMR signals at  $\delta$  228.8 (d,  $^2J_{\text{CP}} = 9$  Hz) and 233.7 (d,  $^2J_{\text{CP}} = 18$  Hz). Hydroborated iminoacyl:  $^1\text{H}$  NMR (500 MHz,  $\text{C}_6\text{D}_6$ , 25 °C)  $\delta$  1.3 (s, 9 H, *CMe*), 2.1 (dd,  $^3J_{\text{HP}} = 5.0$  Hz,  $^3J_{\text{HH}} = 1.5$  Hz, 3 H, *HC(N-}t\text{-Bu)Me*), 2.8 (q,  $^3J_{\text{HH}} = 6.5$  Hz, 1 H, *HC(N-}t\text{-Bu)Me*).

(17) The reactions are highly stereospecific and furnish a single stereomer as the kinetic product of the hydroboration. Longer reaction times lead, however, to mixtures of two or three isomers whose nature is presently being investigated.

(18)  $\eta^1$  coordination of a poly(pyrazolyl)borate has been demonstrated recently. See: Gutiérrez, E.; Hudson, S. A.; Monge, A.; Nicasio, M. C.; Paneque, M.; Carmona, E. *J. Chem. Soc., Dalton Trans.* **1992**, 2651.

(19) Carmona, E.; Sanchez, L.; Marín, J. M.; Poveda, M. L.; Atwood, J. L.; Priester, R. D.; Rogers, R. D. *J. Am. Chem. Soc.* **1984**, *106*, 3214.

upon the course of this transformation. More compelling evidence is derived from the isolation, after the thermal activation of **1** in the presence of 3-5 equiv of  $\text{PMe}_3$ , of the complex  $\text{H}(\text{pz}^*)\text{B}(\text{pz}^*)\text{Mo}(\text{HC}(\text{O})\text{Me})(\text{CO})_2(\text{PMe}_3)_2$  **7** (eq 4), which has been shown by X-ray studies



(to be reported separately) to contain an  $\eta^1\text{-H}_2\text{B}(\text{pz}^*)_2$  fragment. Further studies directed toward clarifying some of the synthetic and mechanistic aspects of this unusual transformation that are, at present, incompletely understood are in progress.

**Acknowledgment.** We thank the Dirección General de Investigación Científica y Técnica (Grant No. PB 91-0612-C03-01) and Junta de Andalucía for the award of research fellowships. Thanks are also due to the University of Sevilla for free access to its analytical and NMR facilities.

**Supplementary Material Available:** Crystallographic tables for **2**, including crystal and refinement data, fractional coordinates, thermal parameters, and selected bond lengths and angles (7 pages). Ordering information is given on any current masthead page.

OM940820I

# Rhodium-Mediated Stoichiometric P=C Bond Cleavage and Catalytic Isomerization in Phosphacumulenes

Marie-Anne David, Sara N. Paisner, and David S. Glueck\*

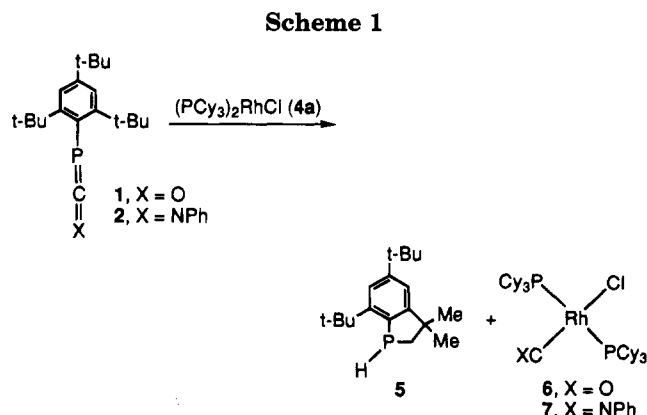
Department of Chemistry, Dartmouth College, 6128 Burke Laboratory,  
Hanover, New Hampshire 03755

Received November 17, 1994<sup>®</sup>

**Summary:** Reaction of  $Rh(PCy_3)_2Cl$  (**4a**,  $Cy = cyclo-C_6H_{11}$ ) with the phosphacumulenes  $Mes^*P=C=X$  ( $X = O$  (**1**),  $X = NPh$  (**2**);  $Mes^* = 2,4,6-(t-Bu)_3C_6H_2$ ) results in P=C bond cleavage to form  $[2,4-(t-Bu)_2C_6H_2(6-CMe_2CH_2PH)]$  (**5**) and *trans*- $Rh(PCy_3)_2Cl(CX)$  (**6**,  $X = O$ ; **7**,  $X = NPh$ ), respectively. In contrast, **4a** and related  $Rh(I)PPh_3$  complexes are catalyst precursors for the rearrangement of  $Mes^*P=C=CPh_2$  (**3**) to its isomer  $[2,4-(t-Bu)_2C_6H_2(6-CMe_2CH_2PCH=CPh_2)]$  (**8**); the intermediate  $[Rh(PCy_3)[\eta^2(P,C)-Mes^*P=C=CPh_2]Cl]_n$  (**9a**), which is itself an active catalyst for the isomerization, was isolated and characterized spectroscopically.

We report that the reactions of the phosphacumulenes<sup>1</sup>  $Mes^*P=C=X$  ( $X = O$  (**1**),  $X = NPh$  (**2**),  $X = CPh_2$  (**3**);  $Mes^* = 2,4,6-(t-Bu)_3C_6H_2$ ) with  $Rh(I)$  phosphine complexes result in stoichiometric P=C bond cleavage in **1** and **2** and catalytic isomerization of **3** with partial cleavage of the P=C double bond.

Reaction of **1** with  $Rh(PCy_3)_2Cl^2$  (**4a**;  $Cy = cyclo-C_6H_{11}$ ) in THF at ambient temperature rapidly gives the known compounds  $[2,4-(t-Bu)_2C_6H_2(6-CMe_2CH_2PH)]^3$  (**5**) and *trans*- $Rh(PCy_3)_2Cl(CO)^{2b}$  (**6**), while **2** and **4a** afford **5** and *trans*- $Rh(PCy_3)_2Cl(CNPh)$  (**7**) (Scheme 1).<sup>4</sup> The presence of an isocyanide ligand in **7** is consistent with the IR spectrum ( $\nu_{CN} = 1991\text{ cm}^{-1}$  with a shoulder at  $2050\text{ cm}^{-1}$ ) and the <sup>13</sup>C NMR spectrum ( $\delta$  166.5, dt, <sup>1</sup> $J_{RhC} = 72\text{ Hz}$ , <sup>2</sup> $J_{PC} = 17\text{ Hz}$ , CNPh); the latter confirms the *trans* geometry.<sup>5</sup> These results suggest that Rh-induced extrusion of CX ( $X = O, NPh$ ) from the phosphacumulenes generates the reactive intermediate



$Mes^*P$ , which is known to undergo intramolecular cyclization, forming **5**.<sup>6</sup> Related P=C bond cleavage has been observed in **1** on reaction with Fe and W complexes.<sup>7</sup>

In contrast, **4a** is a catalyst precursor for the isomerization of **3** to the phosphaindan derivative  $[2,4-(t-Bu)_2C_6H_2(6-CMe_2CH_2PCH=CPh_2)]$  (**8**), which is apparently produced by C-H activation of a *tert*-butyl methyl group with formation of a C-P bond and migration of the hydrogen to the central carbon of the phosphallene.<sup>8</sup> The complexes  $Rh(PPh_3)_3Cl$  and  $[(PPh_3)_2RhCl]_2$  (**4b,c**)<sup>9</sup> also act as catalyst precursors for this rearrangement, which proceeds in benzene or THF at ambient temperature and proceeds more quickly on heating (Scheme 2). Control experiments show that **3** is stable under the reaction conditions in the absence of the Rh complexes and that neither  $PPh_3$  nor  $PCy_3$  induces the isomerization.

Reaction of 500 mg of the phosphallene **3** with 5 mg of **4c** (146 equiv/Rh) in THF at 50 °C for 7 days affords the rearranged product **8** quantitatively, according to <sup>31</sup>P NMR. White crystals of **8** are obtained in 78% yield

(6) (a) Yoshifuji, M.; Sato, T.; Inamoto, N. *Chem. Lett.* **1988**, 1735-1738. (b) Cowley, A. H.; Gabbai, F.; Schluter, R.; Atwood, D. *J. Am. Chem. Soc.* **1992**, *114*, 3142-3144.

(7) (a) Cowley, A. H.; Pellerin, B.; Atwood, J. L.; Bott, S. G. *J. Am. Chem. Soc.* **1990**, *112*, 6734-6735. They also briefly describe a related CNPh extrusion from **2**. (b) Champion, D. H.; Cowley, A. H. *Polyhedron* **1985**, *4*, 1791-1792.

(8) Related ring closures in organic  $Mes^*$ -phosphorus compounds have been reported previously: (a) Bacereido, A.; Bertrand, G.; Mazerolles, P.; Majoral, J.-P. *J. Chem. Soc., Chem. Commun.* **1981**, 1197-1198. (b) Yoshifuji, M.; Shima, I.; Ando, K.; Inamoto, N. *Tetrahedron Lett.* **1983**, *24*, 933-936. Related metal-induced rearrangements have been observed by Nixon and co-workers in the diphosphaallene  $Mes^*P=C=PMes^*$  on heating with iron or tungsten carbonyls, but in these cases the phosphorus-containing product is formed stoichiometrically and remains complexed to the metal: (c) Akpan, C. A.; Hitchcock, P. B.; Nixon, J. F.; Yoshifuji, M.; Niitsu, T.; Inamoto, N. *J. Organomet. Chem.* **1988**, *338*, C35-C37. (d) Akpan, C. A. D. Phil. Thesis, University of Sussex, 1986.

(9) Osborn, J. A.; Jardine, F. H.; Young, J. F.; Wilkinson, G. *J. Chem. Soc.* **1966**, 1711-1732.

<sup>®</sup> Abstract published in *Advance ACS Abstracts*, December 15, 1994.

(1) For a review of phosphacumulene coordination chemistry, see: Nixon, J. F. *Chem. Rev.* **1988**, *88*, 1327-1362.

(2) (a) van Gaal, H. L. M.; Moers, F. G.; Steggerda, J. J. *J. Organomet. Chem.* **1974**, *65*, C43-C45. (b) van Gaal, H. L. M.; van den Bekerom, F. L. A. *J. Organomet. Chem.* **1977**, *134*, 237-248.

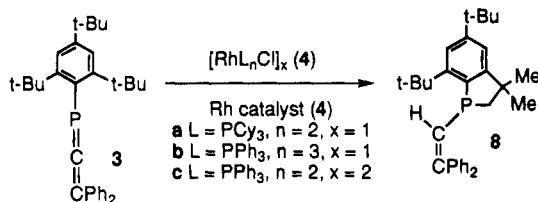
(3) Cowley, A. H.; Pakulski, M. *Tetrahedron Lett.* **1984**, *25*, 2125-2126.

(4) *trans*- $Rh(PCy_3)_2Cl(CNPh)$  (**7**). To a suspension of **4a** (184 mg, 0.26 mmol) in THF (1 mL) was added **2** (100 mg, 0.26 mmol) dissolved in THF (2 mL). The mixture was stirred at room temperature and became a clear orange solution after a few minutes. The solvent was then removed under reduced pressure. The residual yellow solid was washed with cold petroleum ether, filtered on a frit, and dried under vacuum to give 154 mg of **7** (73% yield). An analytical sample was recrystallized from petroleum ether at -25 °C. The petroleum ether filtrate contained phosphaindan **5**, identified by comparison of its NMR spectra to the literature values. In a separate experiment on a smaller scale (28 mg (0.04 mmol) of **4a**, concentration of the petroleum ether filtrate and cooling to -25 °C gave 7 mg of **5** (64% yield). For **7**: <sup>1</sup>H NMR ( $CD_2Cl_2$ )  $\delta$  7.33-7.28 (m, 2H), 7.24-7.19 (m, 1H), 7.12-7.09 (m, 2H), 2.37-2.29 (broad m, 6H), 2.05-2.01 (broad m, 12H), 1.79-1.65 (broad m, 30H), 1.30-1.11 (m, 18H); <sup>13</sup>C(<sup>1</sup>H) NMR ( $CD_2Cl_2$ )  $\delta$  166.5 (dt, <sup>1</sup> $J_{RhC} = 72$ , <sup>2</sup> $J_{PC} = 17\text{ Hz}$ , quat CN), 132.7 (quat Ph), 129.7 (Ph), 126.1 (Ph), 124.8 (Ph), 34.0 (dd, <sup>2</sup> $J_{RhC} = J_{PC} = 9\text{ Hz}$ , P-C-H), 30.6 ( $CH_2$ ), 28.3 (dd, <sup>3</sup> $J_{RhC} = J_{PC} = 5\text{ Hz}$ ,  $CH_2$ ), 27.2 ( $CH_2$ ); <sup>31</sup>P(<sup>1</sup>H) NMR ( $CD_2Cl_2$ )  $\delta$  38.5 (d, <sup>1</sup> $J_{RhP} = 125\text{ Hz}$ ); IR (KBr) 2915, 2847, 2652, 2050 (shoulder), 1991, 1590, 1490, 1445, 1264, 1173, 1004, 900, 847, 752, 736  $cm^{-1}$ . Anal. Calcd for  $C_{43}H_{71}ClNP_2Rh$ : C, 64.36; H, 8.94. Found: C, 64.36; H, 8.97.

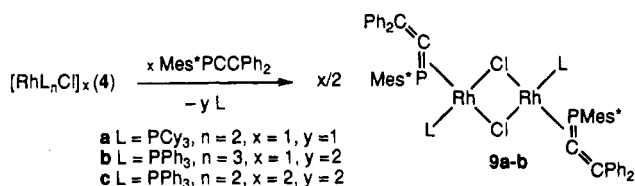
(5) Jones, W. D.; Hessel, E. T. *Organometallics* **1990**, *9*, 718-727.



Scheme 2



Scheme 3



after recrystallization from petroleum ether.<sup>10</sup> Elemental analysis and EI-MS show that **8** is an isomer of **3**, and its structure was determined spectroscopically. In the <sup>1</sup>H NMR spectrum (C<sub>6</sub>D<sub>6</sub>), for example, there are four sets of peaks due to methyl protons in a 9:9:3:3 ratio. The vinylic proton resonates at 6.86 ppm and does not show coupling to phosphorus, while signals for the methylene protons are a complex multiplet at 1.94–1.79 ppm (ABX spin system; <sup>2</sup>J<sub>HH</sub> = 14.4 Hz; <sup>2</sup>J<sub>HP</sub> = 1 Hz, <sup>2</sup>J<sub>HP</sub> = 21 Hz).<sup>11</sup> The CH<sub>2</sub> carbon signal appears at 42.0 ppm (d, <sup>1</sup>J<sub>PC</sub> = 8.3 Hz) and the vinylic carbon at 135.3 ppm (d, <sup>1</sup>J<sub>PC</sub> = 27.5 Hz).

When the reactions of **3** with PPh<sub>3</sub> complexes **4b,c** in THF are monitored by <sup>31</sup>P NMR spectroscopy, the intermediate **9b** (δ 52.4 (dd, <sup>2</sup>J<sub>PP</sub> = 10 Hz; <sup>1</sup>J<sub>RhP</sub> = 220 Hz, PPh<sub>3</sub>), -59.3 (broad dd, <sup>2</sup>J<sub>PP</sub> = 10 Hz; <sup>1</sup>J<sub>RhP</sub> = 37 Hz, Mes\*P=C=CPh<sub>2</sub>); Scheme 3) is observed, along with **3**, product **8**, both **4b** and **4c**, and PPh<sub>3</sub>. In both cases, once the supply of **3** is exhausted, the peaks due to the intermediate disappear. They reappear when more phosphorane is added. In an analogous experiment,

(10) [2,4-(*t*-Bu)<sub>2</sub>C<sub>6</sub>H<sub>2</sub>(6-CMe<sub>2</sub>CH<sub>2</sub>PCH=CPh<sub>2</sub>)] (**8**). An ampule was charged with **4c** (5 mg, 7.5 × 10<sup>-2</sup> mmol), **3** (500 mg, 1.1 mmol), and 10 mL of THF, sealed under nitrogen, and heated in an oil bath at 50 °C. The extent of reaction was monitored by <sup>31</sup>P NMR of aliquots of the orange solution; after 7 days the solvent was removed in vacuo and the residue was recrystallized at -25 °C from petroleum ether to give 392 mg (78%) of **8**, in three crops. An analytical sample was recrystallized from petroleum ether. For **8**: mp 155 °C; <sup>1</sup>H NMR (C<sub>6</sub>D<sub>6</sub>) δ 7.57–7.55 (m, 1H), 7.44–7.42 (m, 2H), 7.24–7.19 (m, 3H), 7.13–7.05 (m, 3H), 6.94–6.91 (m, 3H), 6.86 (1H, CH=CPh<sub>2</sub>), 1.94–1.79 (m, 2H, CH<sub>2</sub>, <sup>2</sup>J<sub>HH</sub> = 14.4, <sup>2</sup>J<sub>PH</sub> = 1, <sup>2</sup>J<sub>PH</sub> = 21 Hz), 1.60 (9H), 1.40 (3H), 1.31 (9H), 1.17 (3H); <sup>13</sup>C{<sup>1</sup>H} NMR (CD<sub>2</sub>Cl<sub>2</sub>) δ 159.5 (d, *J* = 2.3 Hz, quat), 153.1 (d, *J* = 14.3 Hz, quat), 152.8 (quat), 150.4 (d, *J* = 19.2 Hz, quat), 143.2 (d, *J* = 4.9 Hz, quat), 141.2, 141.1, 135.7 (d, *J* = 13.8 Hz, quat), 135.3 (d, *J* = 27.5 Hz, P-CH), 130.7 (d, *J* = 3.8 Hz), 128.8, 128.6, 128.1 (d, *J* = 2.7 Hz), 127.8, 122.4 (d, *J* = 4.9 Hz), 119.0 (d, *J* = 1.1 Hz), 47.3 (d, *J* = 6.0 Hz, quat), 42.0 (d, *J* = 8.3 Hz, P-CH<sub>2</sub>), 37.7 (d, *J* = 1.7 Hz, quat), 35.5 (quat), 32.8 (overlaps with next peak), 32.6 (d, *J* = 9.4 Hz), 32.3 (d, *J* = 5.0 Hz), 31.8; <sup>31</sup>P{<sup>1</sup>H} NMR (CD<sub>2</sub>Cl<sub>2</sub>) δ -22.2; <sup>31</sup>P NMR (C<sub>6</sub>D<sub>6</sub>) δ -20.5 (broad d, “*J*” = ca. 20 Hz); IR (KBr) 3052, 2956, 1591, 1554, 1540, 1491, 1442, 1394, 1380, 1360, 1331, 1244, 1225, 1203, 1164, 1144, 1129, 1072, 1030, 986, 952, 930, 902, 880, 852, 841, 810, 786, 770, 749, 713, 702, 656, 643, 621, 607, 559, 514, 483, 458, 428 cm<sup>-1</sup>; EI-MS *m/z* 454 (M<sup>+</sup>), 261 (MH - Me - C<sub>2</sub>Ph<sub>2</sub><sup>+</sup>), 57 (*t*-Bu). Anal. Calcd for C<sub>32</sub>H<sub>38</sub>P: C, 84.53; H, 8.66. Found: C, 84.57; H, 8.76. Catalysis by **4c** is unaffected by the presence of metallic Hg, suggesting that the reaction is homogeneous and is not catalyzed by Rh metal; see: Whitesides, G. M.; Hackett, M.; Brainard, R. L.; Lavalle, J.-P. P. M.; Sowinski, A. F.; Izumi, A. N.; Moore, S. S.; Brown, D. W.; Staudt, E. M. *Organometallics* **1985**, *4*, 1819–1830.

(11) The large difference in the two <sup>2</sup>J<sub>PH</sub> couplings has precedent in the results for **5**, for which we find <sup>2</sup>J<sub>PH</sub> = 15.3 and 1.8 Hz, respectively. See also: Benitude, W. G.; Setzer, W. N. In *Phosphorus-31 NMR Spectroscopy in Stereochemical Analysis*; Verkade, J. G., Quin, L. D., Eds.; VCH: Deerfield Beach, FL, 1987; pp 365–389.

**4a** is not seen, but PCy<sub>3</sub>, **3**, and **8** are observed, along with the similar, longer lived intermediate **9a**, which can be isolated directly from the reaction mixture. Alternatively, it can be prepared independently in 73% yield from the reaction of Rh(PCy<sub>3</sub>)<sub>2</sub>Cl (prepared *in situ* from [Rh(COE)<sub>2</sub>Cl]<sub>2</sub> in petroleum ether or ether) with **3**; this yields **9a** as an air-stable red-orange precipitate (Scheme 3).<sup>12</sup>

Elemental analysis and integration of the <sup>1</sup>H NMR spectrum show that **9a** has the formula Rh(PCy<sub>3</sub>)(Mes\*P=C=CPh<sub>2</sub>)Cl, while the <sup>1</sup>H and <sup>13</sup>C NMR spectra show that the Mes\* group remains intact. The <sup>31</sup>P{<sup>1</sup>H} NMR spectrum (THF-*d*<sub>8</sub>) is similar to that observed for **9b** (δ 62.1 (dd, <sup>2</sup>J<sub>PP</sub> = 2 Hz, <sup>1</sup>J<sub>RhP</sub> = 194 Hz, PCy<sub>3</sub>), -38.8 (dd, <sup>2</sup>J<sub>PP</sub> = 2 Hz, <sup>1</sup>J<sub>RhP</sub> = 37 Hz, Mes\*P=C=CPh<sub>2</sub>)).<sup>13</sup> The central carbon of the phosphorane ligand resonates at δ 179.6 (dd, <sup>1</sup>J<sub>RhC</sub> = 27 Hz, <sup>1</sup>J<sub>PC</sub> = 99 Hz).<sup>14</sup> An IR absorption at 1586 cm<sup>-1</sup> (KBr) may be assigned to an uncomplexed C=C bond.<sup>15</sup> These observations are consistent with π(P,C)-coordination of the phosphorane ligand in **9a,b**. Because of the low solubility of **9a** in most organic solvents, we assume it exists in the solid state as a chloride-bridged dimer (Scheme 3).<sup>16</sup> Com-

(12) COE = cyclooctene; van der Ent, A.; Onderdelinden, A. L. *Inorg. Synth.* **1973**, *14*, 92–95. To a slurry of [(COE)<sub>2</sub>RhCl]<sub>2</sub> (41 mg, 0.057 mmol) in ether (4 mL) was added a solution of PCy<sub>3</sub> (64 mg, 0.23 mmol) in 3 mL of ether. A red solution formed; it was filtered after ~3 min. A solution of **3** (52 mg, 0.11 mmol) in 2 mL of ether was added to the filtrate. After 3 h red crystals formed; the mixture was cooled overnight at -25 °C to induce further crystallization. The yellow-orange supernatant was decanted, and the red crystals were washed with 4 × 2 mL of cold ether to give, after drying in vacuo, 73 mg (73%) of red crystals. This synthetic method avoids the use of sparingly soluble isolated **4a** and allows precipitation of pure **9a** under mild conditions. For **9a**: <sup>1</sup>H NMR (CD<sub>2</sub>Cl<sub>2</sub>) δ 8.23 (d, *J* = 7.5 Hz, 2H), 7.40–7.26 (m, 3H), 7.00 (2H), 6.93–6.88 (m, 3H), 6.74–6.71 (m, 2H), 2.18–1.50 (broad m, 22H), 1.40 (broad, 18H), 1.25–1.10 (broad m, 11H), 1.14 (9H); <sup>13</sup>C{<sup>1</sup>H} NMR (CD<sub>2</sub>Cl<sub>2</sub>) δ 179.6 (dd, <sup>1</sup>J<sub>RhC</sub> = 27 Hz, <sup>1</sup>J<sub>PC</sub> = 99 Hz, quat, P=C), 155.4 (quat, broad), 149.9 (quat), 142.0 (quat), 141.7 (quat, broad), 141.4 (quat), 132.7 (d, *J* = 102 Hz, quat), 130.2, 128.2, 128.2 (d, *J* = 3.8 Hz), 127.7, 127.4, 126.4, 122.9, 37.5 (quat), 35.5 (dd, <sup>2</sup>J<sub>RhC</sub> = 5.5 Hz, <sup>1</sup>J<sub>PC</sub> = 25 Hz, P-C-H), 34.9 (quat), 32.1 (broad, CH<sub>3</sub>), 31.9 (broad, CH<sub>2</sub>), 31.4 (CH<sub>3</sub>), 29.9 (CH<sub>2</sub>), 28.4 (CH<sub>2</sub>), 28.2 (CH<sub>2</sub>), 26.9 (CH<sub>2</sub>); <sup>31</sup>P{<sup>1</sup>H} NMR (THF-*d*<sub>8</sub>) δ 62.1 (dd, <sup>1</sup>J<sub>RhP</sub> = 194 Hz, <sup>2</sup>J<sub>PP</sub> = 2 Hz), -38.8 (dd, <sup>1</sup>J<sub>RhP</sub> = 37 Hz, <sup>2</sup>J<sub>PP</sub> = 2 Hz); IR (KBr) 3054, 2924, 2849, 2644, 1586, 1490, 1441, 1389, 1361, 1249, 1198, 1175, 1122, 1074, 1030, 1004, 924, 899, 880, 851, 768, 748, 735, 700, 690, 648, 556, 518, 493, 451, 424 cm<sup>-1</sup>. The analytical sample cocrystallized with dichloromethane and ether, which was quantitatively confirmed by integration of the <sup>1</sup>H NMR spectrum. Anal. Calcd for C<sub>55</sub>H<sub>72</sub>Cl<sub>2</sub>PtRh<sub>2</sub>·0.35CH<sub>2</sub>Cl<sub>2</sub>·0.2C<sub>4</sub>H<sub>10</sub>O: C, 66.91; H, 8.22. Found: C, 66.53; H, 8.42.

(13) (a) For comparison, in L<sub>2</sub>Pt{η<sup>2</sup>(P,C)-Mes\*P=C=CPh<sub>2</sub>} (L<sub>2</sub> = (PPh<sub>3</sub>)<sub>2</sub>, Ph<sub>2</sub>PCH<sub>2</sub>CH<sub>2</sub>PPh<sub>2</sub>, (PEt<sub>3</sub>)<sub>2</sub>), the <sup>195</sup>Pt-<sup>31</sup>P coupling constants for the Mes\*(P) nucleus are 192, 234, and 268 Hz, respectively.<sup>8d</sup> (b) From the magnetogyric ratios of <sup>195</sup>Pt and <sup>103</sup>Rh, the magnitude of <sup>195</sup>Pt-X coupling is expected to be about 7 times that of <sup>103</sup>Rh-X (Kidd, R. G.; Goodfellow, R. J.; In *NMR and the Periodic Table*; Harris, R. K., Mann, B. E., Eds.; Academic: New York, 1978; p 249).

(14) For comparison, we prepared (Ph<sub>2</sub>PCH<sub>2</sub>CH<sub>2</sub>PPh<sub>2</sub>)Pt{η<sup>2</sup>(P,C)-Mes\*P=C=CPh<sub>2</sub>} as in ref 8d and obtained its <sup>13</sup>C NMR spectrum in CD<sub>2</sub>Cl<sub>2</sub>. The central P=C=C carbon signal appears at δ 171.6 (ddd, <sup>1</sup>J<sub>P-C</sub> = 118 Hz, <sup>2</sup>J<sub>PC</sub> = 70 Hz, <sup>2</sup>J<sub>PC</sub> = 6 Hz; Pt satellites were too low in intensity to be observed).

(15) Related absorptions at 1590, 1600, and 1590 cm<sup>-1</sup> are observed in the Pt-phosphorane complexes of ref 8d.

(16) Two spectroscopic observations suggest that **9a** contains an agostic interaction between Rh and C-H bonds of the PCy<sub>3</sub> ligand (for related complexes, see: Wasserman, H. J.; Kubas, G. J.; Ryan, R. R. *J. Am. Chem. Soc.* **1986**, *108*, 2294–2301). The IR spectrum includes an absorption at 2644 cm<sup>-1</sup>, and the <sup>13</sup>C NMR spectrum shows signals due to six different cyclohexyl carbons. In contrast, peaks due to four Cy carbons are observed for **6** and **7**. Interaction of Rh with a C-H bond on one PCy<sub>3</sub> cyclohexyl group in **9a** could make the six carbons inequivalent. Rapid exchange (on the NMR time scale) between such a bond and the other two cyclohexyl groups by a 3-fold rotation could make the three cyclohexyl groups equivalent. Unfortunately, we have not yet been able to obtain crystals suitable for X-ray analysis to check this assignment or to investigate related interactions in **6** and **7**, which show IR peaks at 2654 and 2652 cm<sup>-1</sup>, respectively.

plex **9a** is readily soluble in  $\text{CH}_2\text{Cl}_2$  but decomposes at ambient temperature in this solvent, preventing molecular weight measurements. Isolated **9a** is stable in solution in the presence of **3** and catalyzes its isomerization to **8**. This reaction also proceeds smoothly in the presence of 1 equiv of  $\text{PCy}_3$ .

The isolation of **9a** suggests that cumulenes **1** and **2** also initially bind to Rh with displacement of  $\text{PCy}_3$  to form the intermediates  $\text{Rh}(\text{PCy}_3)[\eta^2(\text{P},\text{C})\text{-Mes}^*\text{P}=\text{C}=\text{X}]\text{-Cl}$  ( $\text{X} = \text{O}, \text{NPh}$ ), which are not observed under the reaction conditions. Mechanistic investigations of the role of such species in the  $\text{P}=\text{C}$  cleavage and isomerization reactions are in progress as part of a broader study of phosphacumulene coordination chemistry.

**Acknowledgment.** We thank Dartmouth College and the donors of the Petroleum Research Fund, administered by the ACS, for partial support of this work. We also thank Johnson Matthey/Alfa/Aesar for a loan of Rh salts.

**Supplementary Material Available:** Text giving experimental details and spectroscopic data for complexes **5** and **6** and  $^{31}\text{P}$  NMR studies of catalysis by **4a-c** and **9a** (5 pages). This material is contained in many libraries on microfiche, immediately follows this article in the microfilm version of the journal, and can be ordered from the ACS; see any current masthead page for ordering information.

OM940876C

# Articles

## (Cyclopentadienylalkyl)phosphine Derivatives of Gallium(III) and Indium(III)

Alan H. Cowley,\* Christopher S. King, and Andreas Decken

Department of Chemistry and Biochemistry, The University of Texas at Austin,  
Austin, Texas 78712

Received May 6, 1994<sup>®</sup>

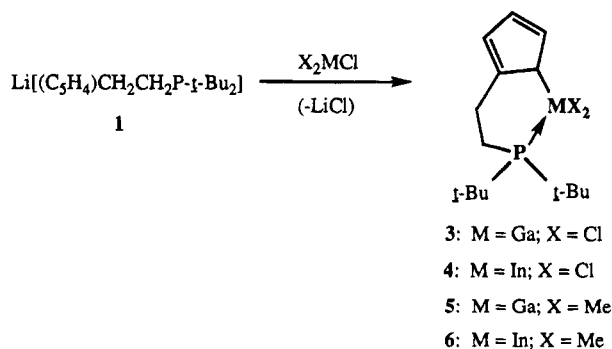
The bis(*tert*-butyl)phosphinoethylcyclopentadienide complexes [*t*-Bu<sub>2</sub>PCH<sub>2</sub>CH<sub>2</sub>C<sub>5</sub>H<sub>4</sub>]MX<sub>2</sub> with M = Ga, X = Cl (**3**); M = In, X = Cl (**4**); M = Ga, X = Me (**5**); and M = In, X = Me (**6**) have been prepared by the reaction of the phosphinoethylcyclopentadienide lithium salt with the appropriate group 13 chloride. Compounds **5** and **6** were also prepared by the methane elimination reactions of the phosphinoethylcyclopentadiene with MMe<sub>3</sub>. Each compound has been characterized by elemental analysis, <sup>1</sup>H, <sup>13</sup>C, and <sup>31</sup>P NMR, and mass spectroscopy. The structures of **4** and **5** were determined by X-ray crystallography. Crystal data for **4**: space group P2<sub>1</sub>2<sub>1</sub>2<sub>1</sub>, *a* = 8.782(2) Å, *b* = 14.039(1) Å, *c* = 15.116(2) Å, *V* = 1863.6(9) Å<sup>3</sup>, *Z* = 4, and *R* = 0.0352. Crystal data for **5**: space group P2<sub>1</sub>/c, *a* = 12.653(3) Å, *b* = 9.683(2) Å, *c* = 15.313(3) Å, β = 100.81(3)°, *V* = 1842.8(9) Å<sup>3</sup>, *Z* = 4, and *R* = 0.0562. The X-ray analyses reveal that for both compounds (i) the MX<sub>2</sub> fragment is η<sup>1</sup> attached to the cyclopentadienyl ring and (ii) the phosphorus atom is coordinated intramolecularly to the group 13 center.

### Introduction

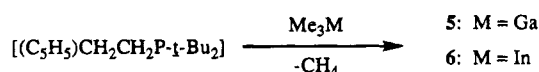
Cyclopentadienyl and phosphine ligands are ubiquitous in inorganic chemistry. Not surprisingly, therefore, the possibility of combining the special features of these ligands in a potentially chelating fashion has begun to attract attention. A few (cyclopentadienylalkyl)phosphines of the general type C<sub>5</sub>R<sub>4</sub>(CH<sub>2</sub>)<sub>*n*</sub>PR<sub>2</sub> (*n* = 1, 2) have now been prepared and employed as ligands.<sup>1</sup> However, with the exception of one trimethylstannyl derivative,<sup>1a</sup> these interesting heterodifunctional ligands have been used exclusively in the context of d-block chemistry. We have therefore become interested in exploring the utility of these ligand systems for the synthesis of main group compounds. Given the considerable current interest in a variety of 13/15 ring, cage, and acyclic compounds as single-source precursors to compound semiconductors,<sup>2</sup> we have chosen to initiate our studies by an investigation of the ligative behavior of some gallium(III) and indium(III) halides and alkyls.<sup>3</sup>

### Results and Discussion

The reagent lithium (2-{di-*tert*-butylphosphinoethyl}-cyclopentadienide) (**1**) was prepared via the reaction of LiP-*t*-Bu<sub>2</sub> with spiro[4.2]hepta-1,3-diene according to the method of Kauffman et al.<sup>1b</sup> The corresponding cyclopentadiene **2** was prepared by hydrolysis of **1**. The gallium(III) and indium(III) compounds **3-6** were prepared in excellent yields via the metathetical reactions of **1** with the appropriate metal chlorides in THF at low temperature.



A second synthetic strategy was employed for the synthesis of **5** and **6**,



namely, the methane elimination reactions between **2** and the relevant gallium or indium trialkyl.

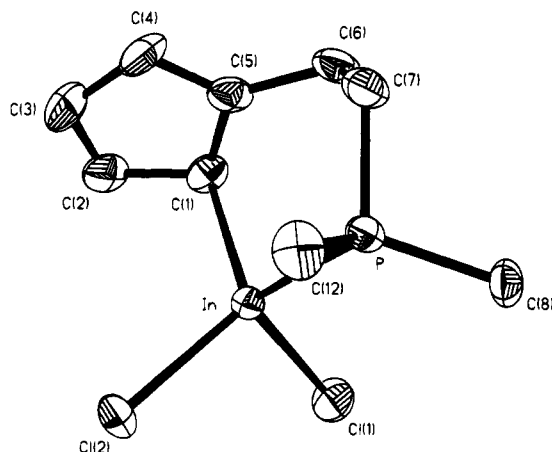
**3-5** were obtained as colorless crystals; **4** is a white powder. Each of the new compounds is slightly air

<sup>®</sup> Abstract published in *Advance ACS Abstracts*, November 1, 1994.

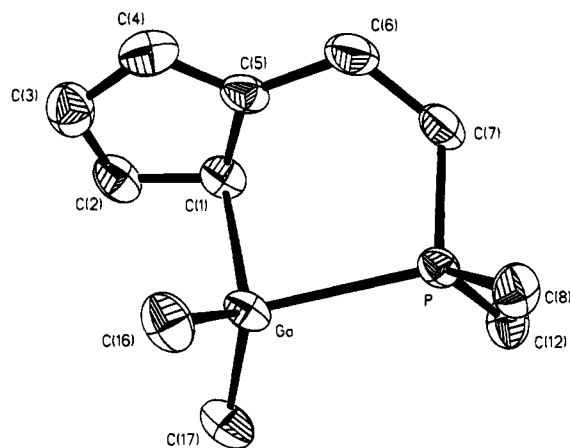
(1) (a) Charrier, C.; Mathey, F. *J. Organomet. Chem.* **1979**, *170*, C 41. (b) Kauffmann, T.; Ennen, J.; Lhotak, H.; Rensing, A.; Steinseifer, F.; Woltermann, A. *Angew. Chem., Int. Ed. Engl.* **1980**, *19*, 328. (c) Slawin, A. M. Z.; Williams, D. J.; Crosby, J.; Ramsden, J. A.; White, C. *J. Chem. Soc., Dalton Trans.* **1988**, 2491. (d) Szymoniak, J.; Besançon, J.; Dormond, A.; Moïse, C. *J. Org. Chem.* **1990**, *55*, 1429. (e) Kettenbach, R. T.; Butenschön, H. *New J. Chem.* **1990**, *14*, 599. (f) Miguel-Garcia, J. A.; Adams, H.; Bailey, N. A.; Maitlis, P. M. *J. Organomet. Chem.* **1991**, *413*, 427. (g) Butenschön, H.; Kettenbach, R. T.; Krüger, C. *Angew. Chem., Int. Ed. Engl.* **1992**, *31*, 1066.

(2) For reviews, see: Cowley, A. H.; Jones, R. A. *Angew. Chem., Int. Ed. Engl.* **1989**, *28*, 1208. Wells, R. L. *Coord. Chem. Rev.* **1992**, *112*, 273. Cowley, A. H.; Jones, R. A. *Polyhedron* **1994**, *13*, 1149.

(3) For interesting work on amine analogues, see: Jutzi, P.; Dahlhaus, J.; Bangel, M. *J. Organomet. Chem.* **1993**, *460*, C13.



**Figure 1.** View of  $[t\text{-Bu}_2\text{PCH}_2\text{CH}_2\text{C}_5\text{H}_4]\text{InCl}_2$  (**4**) showing the atom-labeling scheme. The  $\text{CH}_3$  groups are omitted for clarity.



**Figure 2.** View of  $[t\text{-Bu}_2\text{PCH}_2\text{CH}_2\text{C}_5\text{H}_4]\text{GaMe}_2$  (**5**) showing the atom-labeling scheme. The  $t\text{-Bu}$   $\text{CH}_3$  groups are omitted for clarity.

sensitive in the solid state. The methyl derivatives **5** and **6** are distinctly more volatile than the chloro analogues **3** and **4** and sublime readily at  $100^\circ\text{C}$  ( $10^{-5}$  Torr).

Satisfactory carbon and hydrogen analyses were obtained for the indium compounds **4** and **6**. However, despite several attempts, the carbon analyses for the analogous gallium compounds, **3** and **5**, were found to be 3–5% too low. This does not appear to be a consequence of the presence of impurities since both compounds have sharp melting points. Excellent HRMS data were obtained for **3–6** (Experimental Section).

The  $^{31}\text{P}$  NMR chemical shifts for **3–6** are less shielded than those of the free ligand **2** by between 5 and 24 ppm, thus suggesting that the pendent phosphine is coordinated to the group 13 center in each case. It was not clear from NMR data, however, how the  $\text{MX}_2$  moiety is attached to the cyclopentadienyl ring because only two types of ring proton and one type of ring carbon are detectable at ambient temperature. The question of the ground state geometries of **4** and **5** was resolved by X-ray analysis. The molecular structures of **4** and **5** are shown in Figures 1 and 2, respectively, along with the relevant atom-numbering schemes. In contrast to, for example,  $(\text{C}_5\text{H}_5)\text{GaMe}_2$ ,<sup>4</sup> crystals of **4** and **5** consist of

**Table 1.** Selected Bond Distances ( $\text{\AA}$ ) for  $(t\text{-Bu}_2\text{PCH}_2\text{CH}_2\text{C}_5\text{H}_4)\text{InCl}_2$  (**4**) and  $(t\text{-Bu}_2\text{PCH}_2\text{CH}_2\text{C}_5\text{H}_4)\text{GaMe}_2$  (**6**)

Compound 4			
In–P	2.595(2)	C(1)–C(2)	1.452(13)
P–C(7)	1.843(9)	C(2)–C(3)	1.318(17)
P–C(8)	1.860(9)	C(3)–C(4)	1.416(5)
P–C(12)	1.854(10)	C(4)–C(5)	1.339(15)
In–C(1)	2.202(9)	C(5)–C(6)	1.509(12)
In–Cl(1)	2.383(3)		
In–Cl(2)	2.364(3)		
Compound 5			
Ga–P	2.493(2)	C(1)–C(2)	1.437(9)
P–C(7)	1.839(5)	C(2)–C(3)	1.324(10)
P–C(8)	1.868(6)	C(3)–C(4)	1.407(10)
P–C(12)	1.863(7)	C(4)–C(5)	1.370(10)
Ga–C(1)	2.103(5)	C(1)–C(5)	1.433(8)
Ga–C(16)	1.964(6)		
Ga–C(17)	1.961(7)		

**Table 2.** Selected Bond Angles (deg) for  $(t\text{-Bu}_2\text{PCH}_2\text{CH}_2\text{C}_5\text{H}_4)\text{InCl}_2$  (**4**) and  $(t\text{-Bu}_2\text{PCH}_2\text{CH}_2\text{C}_5\text{H}_4)\text{GaMe}_2$  (**5**)

Compound 4			
In–P–C(7)	103.7(3)	Cl(1)–In–Cl(2)	101.9(1)
In–P–C(8)	112.3(3)	P–In–Cl(1)	113.0(1)
C(7)–P–C(8)	107.2(4)	P–In–Cl(2)	111.2(1)
In–P–C(12)	111.4(3)	P–In–C(1)	104.2(2)
C(7)–P–C(12)	104.8(5)	Cl(1)–In–C(1)	108.2(3)
C(8)–P–C(12)	116.2(4)	Cl(2)–In–C(1)	118.6(2)
Compound 5			
Ga–P–C(7)	104.5(2)	C(16)–Ga–C(17)	114.8(3)
Ga–P–C(8)	115.2(2)	P–Ga–C(16)	110.9(2)
C(7)–P–C(8)	106.5(3)	P–Ga–C(17)	112.7(2)
Ga–P–C(12)	113.8(2)	P–Ga–C(1)	91.3(2)
C(7)–P–C(12)	103.6(3)	C(16)–Ga–C(1)	115.0(3)
C(8)–P–C(12)	111.9(3)	C(17)–Ga–C(1)	109.9(2)

isolated molecules with no abnormally short intermolecular contacts. In both compounds, the group 13  $\text{MX}_2$  fragment is attached to the cyclopentadienyl ring in an  $\eta^1$  fashion in an  $\alpha$  position with respect to the phosphinoethane moiety. The patterns of bond distances (Table 1) and bond angles (Table 2) within the cyclopentadienyl ring are similar to those of other  $\eta^1$ -metalated systems, specifically, (i) the C(2)–C(3) and C(4)–C(5) bond distances are shorter than the others, and (ii) the smallest bond angle is C(2)–C(1)–C(5). The Ga–C(ring) bond distance in **5** (2.103(5)  $\text{\AA}$ ) is similar to that reported for  $(\eta^1\text{-C}_5\text{H}_5)_3\text{Ga}$  (average 2.05(2))  $\text{\AA}$ .<sup>5</sup> However, the In–C(ring) bond distance in **4** (2.202(9)  $\text{\AA}$ ) is slightly shorter than those reported for the  $\eta^1$ -attached cyclopentadienyl rings of  $(\text{C}_5\text{H}_5)_3\text{In}$  (average 2.240(9)  $\text{\AA}$ ).<sup>6</sup>

The X-ray crystallographic studies also reveal that the phosphine arm is coordinated to the  $\text{MX}_2$  center in **4** and **5**, thus confirming the  $^{31}\text{P}$  NMR spectroscopic indications discussed above. Both compounds therefore possess a bicyclic structure which is formed by fusion of a cyclopentadienyl and a six-membered  $\text{MC}_4\text{P}$  ring. The conformations of the  $\text{MC}_4\text{P}$  rings are twist-boat and boat in **4** and **5**, respectively. The P  $\rightarrow$  Ga dative bond distance in **5** (2.493(2)  $\text{\AA}$ ) is comparable to that in the Lewis acid–base complex  $\text{Me}_3\text{P} \rightarrow \text{GaMe}_3$  (2.52  $\text{\AA}$ ).<sup>7</sup> As expected, the geometries at phosphorus and the

(5) Beachley, O. T., Jr.; Getman, T. D.; Kirss, R. U.; Hallock, R. B.; Hunter, W. E.; Atwood, J. L. *Organometallics* **1985**, *4*, 751.

(6) Einstein, F. W. B.; Gilbert, M. M.; Tuck, D. G. *Inorg. Chem.* **1972**, *11*, 2832.

(7) Golubinskaya, L. M.; Golubinskii, A. V.; Mastryukov, V. S.; Vilkov, L. V.; Bregadze, V. I. *J. Organomet. Chem.* **1976**, *117*, C4.

(4) Mertz, K.; Zettler, F.; Hausen, H. D.; Weidlein, J. *J. Organomet. Chem.* **1976**, *122*, 159.

group 13 element are approximately tetrahedral. However, there are considerable departures from the ideal angle at both centers for both compounds.

Finally, we return to the question of the implied fluxionality of **3–6** in solution. Ligand **1** is not fluxional; hence it is evidently the  $\text{MX}_2$  moiety which shuttles back and forth between the C(1) and C(4) positions of the cyclopentadienyl ring in **3–6**. Presumably, the  $\text{P} \rightarrow \text{Ga}$  or  $\text{P} \rightarrow \text{In}$  dative bond is broken concomitantly in this process. Attempts to address this question were not successful; no spectral changes other than viscosity broadening were detected upon cooling toluene or THF solutions of **3–6** to  $-80^\circ\text{C}$ .

## Experimental Section

**General Considerations.** All reactions were performed under oxygen-free argon or under vacuum using standard Schlenk line or drybox techniques. All solvents were dried over sodium and distilled from sodium benzophenone under argon before use. The reagents  $\text{GaCl}_3$ ,  $\text{InCl}_3$ ,  $\text{Me}_3\text{Ga}$ ,  $\text{Me}_3\text{In}$ , and *n*-BuLi were procured commercially and used without further purification. The concentration of the *n*-BuLi was determined by titrimetric analysis prior to use. Spiro[4.2]hepta-1,3-diene<sup>8</sup> and *t*-Bu<sub>2</sub>PH<sup>9</sup> were prepared according to literature methods.

**Physical Measurements.** IR spectra were obtained as KBr pellets on a Bio-Rad FTS-40 spectrometer. Mass spectra, EI and CI, were run on a Bell and Howell 21-491 instrument, and NMR spectra were measured on a GE QE-300 spectrometer (<sup>1</sup>H, 300.17 MHz; <sup>13</sup>C, 75.48 MHz; <sup>31</sup>P, 121.5 MHz). NMR spectra are referenced to C<sub>6</sub>D<sub>6</sub> and THF-*d*<sub>8</sub>, both of which were dried over Na/K alloy and distilled prior to use. All chemical shifts are reported relative to TMS (0.00 ppm). Melting points (uncorrected) were obtained in sealed capillaries under argon (1 atm), and elemental analyses were performed by Atlantic Microlab, Norcross, GA.

**Synthesis of Lithium [2-(Di-*tert*-butylphosphinoethyl)cyclopentadienide] (1).** A hexane solution of 1.6 M *n*-BuLi (62.5 mL, 0.10 mol) was added to a stirred solution of *t*-Bu<sub>2</sub>PH (14.62 g, 0.10 mol) in 30 mL of THF at  $-78^\circ\text{C}$ . The stirred reaction mixture was allowed to warm slowly to  $0^\circ\text{C}$ . A THF solution of 1.13 M spiro[4.2]hepta-1,3-diene (88.5 mL, 0.10 mol) was then added and the solution heated to reflux for 13 h. The solution was cooled to room temperature and the solvent removed under reduced pressure. The residue was then washed with cold hexane (3 × 50 mL) and dried in vacuo to afford 20.7 g (84.7 mmol, 85% yield) of the light tan powder **1**, mp 235–237 °C.

**Synthesis of 2-(Di-*tert*-butylphosphinoethyl)cyclopentadiene (2).** A stirred solution of 0.33 g (1.0 mmol) of **1** in 10 mL of hexane was hydrolyzed by addition of 10 drops of water. The solution was dried over  $\text{MgSO}_4$  and filtered and the solvent removed under reduced pressure to yield 0.16 g of brown oil **2**, (0.5 mmol, 50% yield). <sup>1</sup>H NMR (C<sub>6</sub>D<sub>6</sub>): δ 1.06 (d, CH<sub>3</sub>, 18 H), 1.59 (m, CH<sub>2</sub>, 2 H), 2.63 (m, CH<sub>2</sub>, 2 H), 6.20 (m, ring H, 5 H); <sup>31</sup>P NMR (C<sub>6</sub>D<sub>6</sub>): δ 29.2 (s).

**Synthesis of Dichloro[1-η<sup>1</sup>-(2-di-*tert*-butylphosphino)ethylcyclopentadienyl]gallium (3).** A solution of 0.31 g (1.2 mmol) of **1** in 20 mL of THF was added at  $-78^\circ\text{C}$  to a stirred solution of  $\text{GaCl}_3$  (0.22 g, 1.2 mmol) in 30 mL of THF. After 3 h at  $-78^\circ\text{C}$ , the stirred reaction mixture was allowed to warm to room temperature. The solvent and volatiles were removed under reduced pressure. The residue was extracted with  $\text{CH}_2\text{Cl}_2$  (60 mL) and filtered, and the solvent removed under reduced pressure. The residue was then dissolved in a minimum amount of THF. A few drops of hexane were added to aid crystallization. Colorless crystals of **3** (mp 134–135 °C)

**Table 3. Crystal Data, Details of Intensity Measurement, and Structural Refinement for (*t*-Bu<sub>2</sub>PCH<sub>2</sub>CH<sub>2</sub>C<sub>5</sub>H<sub>4</sub>)InCl<sub>2</sub> (4) and (*t*-Bu<sub>2</sub>PCH<sub>2</sub>CH<sub>2</sub>C<sub>5</sub>H<sub>4</sub>)GaMe<sub>2</sub> (5)**

compd	4	5
formula	C <sub>15</sub> H <sub>26</sub> Cl <sub>2</sub> InP	C <sub>17</sub> H <sub>32</sub> GaP
fw	423.0	337.1
cryst dimen, mm	0.22 × 0.22 × 0.31	0.31 × 0.53 × 0.60
cryst syst	orthorhombic	monoclinic
space group	P2 <sub>1</sub> 2 <sub>1</sub> 2 <sub>1</sub>	P2 <sub>1</sub> /c
a, Å	8.782(2)	12.653(3)
b, Å	14.039(1)	9.683(2)
c, Å	15.116(2)	15.313(3)
α, deg	90.0	90.0
β, deg	90.0	100.81(3)
γ, deg	90.0	90.0
V, Å <sup>3</sup>	1863.6(9)	1842.8(9)
D <sub>calc</sub> , g cm <sup>-3</sup>	1.508	1.215
Z	4	4
radiation	Mo Kα	Mo Kα
no. of total reflns	2318	3234
no. of obsd reflns	1881	2116
sig test	$F > 4\sigma(F)$	$F > 4\sigma(F)$
no. of param	174	172
weighting scheme	0.0005	0.0005
g in $[(\sigma F)^2 + gF^2]^{-1}$		
final R	0.0352	0.0525
final R <sub>w</sub>	0.0395	0.0562

formed upon cooling this solution to  $-20^\circ\text{C}$  for 12 h. <sup>1</sup>H NMR (C<sub>6</sub>D<sub>6</sub>): δ 0.99 (d, CH<sub>3</sub>, 18 H), 1.46 (m, CH<sub>2</sub>, 2 H), 2.52 (m, CH<sub>2</sub>, 2 H), 5.14 (s, ring H, 2 H), 6.78 (s, ring H, 2 H); <sup>31</sup>P NMR (C<sub>6</sub>D<sub>6</sub>): δ 8.3 (s). MS(CI) 379 [M<sup>-</sup>]. HRMS calcd 377.048 326, found 377.047 549. Anal. Calcd for C<sub>15</sub>H<sub>26</sub>Cl<sub>2</sub>GaP: C, 47.66; H, 6.95. Found: C, 44.34; H, 6.61.

**Synthesis of Dichloro[1-η<sup>1</sup>-(2-di-*tert*-butylphosphino)ethylcyclopentadienyl]indium (4).** A solution of 1.32 g (5.4 mmol) of **1** in 20 mL of THF was added at  $-78^\circ\text{C}$  to a stirred solution of  $\text{InCl}_3$  (1.19 g, 5.4 mmol) in 30 mL of THF. After 3 h at  $-78^\circ\text{C}$ , the stirred reaction mixture was allowed to warm to room temperature. The solvent and volatiles were removed under reduced pressure, and the residue was extracted with toluene (3 × 60 mL). The mixture was filtered to separate the product **4** from  $\text{LiCl}$  and unreacted starting materials. The solvent was removed under reduced pressure. The resulting residue was dissolved in 5 mL of  $\text{CH}_2\text{Cl}_2$ . Several drops of hexane were added to aid crystallization. Colorless crystals of **4** (mp 194 °C) formed upon cooling this solution to  $-20^\circ\text{C}$  for 12 h (3.8 mmol, 70% yield). <sup>1</sup>H NMR (C<sub>6</sub>D<sub>6</sub>): δ 0.88 (d, CH<sub>3</sub>, 18 H), 1.34 (m, CH<sub>2</sub>, 2 H), 2.40 (m, CH<sub>2</sub>, 2 H), 5.40 (s, ring H, 2 H), 6.74 (s, ring H, 2 H). <sup>13</sup>C NMR (C<sub>6</sub>D<sub>6</sub>): δ 26.8 (d, CH<sub>2</sub>, <sup>2</sup>J(CP) 1.7 Hz), 28.5 (d, CH<sub>3</sub>, <sup>2</sup>J(CP) 3.2 Hz), 29.0 (d, CH<sub>2</sub>, <sup>1</sup>J(CP) 7.2 Hz), 34.1 (d, *t*-C, <sup>1</sup>J(CP) 12.2 Hz), 97.2 (s, ring C); <sup>31</sup>P NMR (C<sub>6</sub>D<sub>6</sub>) δ 24.0 (s). MS(CI) 457 [M + Cl<sup>-</sup>]. HRMS calcd 422.019 124, found 422.018 795. Anal. Calcd for C<sub>15</sub>H<sub>26</sub>Cl<sub>2</sub>InP: C, 42.97; H, 6.19. Found: C, 43.64; H, 6.60.

**Synthesis of Dimethyl[1-η<sup>1</sup>-(2-di-*tert*-butylphosphino)ethylcyclopentadienyl]gallium (5).** Method A. A solution of 0.24 g (1.0 mmol) of **1** in 20 mL of THF was added at  $-78^\circ\text{C}$  to a stirred solution of  $\text{Me}_2\text{GaCl}$  (0.13 g, 1.0 mmol) in 30 mL of THF. After 3 h at  $-78^\circ\text{C}$ , the stirred solution was allowed to warm to room temperature. The solvent and volatiles were removed under reduced pressure, and the resulting residue was extracted with hexane (60 mL), filtered, and concentrated. Colorless crystals of **5** (mp 98–99 °C) formed upon cooling this solution to  $-20^\circ\text{C}$  for 12 h. <sup>1</sup>H NMR (C<sub>6</sub>D<sub>6</sub>): δ -0.35 (d, GaCH<sub>3</sub>, 6 H), 0.94 (d, CH<sub>3</sub>, 18 H), 1.62 (m, CH<sub>2</sub>, 2 H), 2.81 (m, CH<sub>2</sub>, 2 H), 5.25 (s, ring H, 2 H), 6.55 (s, ring H, 2 H); <sup>13</sup>C{<sup>1</sup>H} NMR (C<sub>6</sub>D<sub>6</sub>): δ -5.5 (d, GaCH<sub>3</sub>, <sup>2</sup>J(CP) 16.7 Hz), 20.1 (d, CH<sub>2</sub>, <sup>2</sup>J(CP) 14.6 Hz), 29.2 (d, CH<sub>3</sub>, <sup>2</sup>J(CP) 4.7 Hz), 26.3 (d, CH<sub>2</sub>, <sup>1</sup>J(CP) 7.2 Hz), 32.7 (d, *t*-C, <sup>1</sup>J(CP) 7.4 Hz), 92.4 (s, ring C), 123.7 (s, ring C); <sup>31</sup>P NMR (C<sub>6</sub>D<sub>6</sub>): δ 5.5 (s). MS(CI) 339 [M<sup>+</sup>]. HRMS calcd 336.149 746, found 336.149 160. Anal. Calcd for C<sub>17</sub>H<sub>32</sub>GaP: C, 60.55; H, 9.59. Found: C, 55.52; H, 9.21.

(8) Wilcox, C. F.; Craig, R. R. *J. Am. Chem. Soc.* **1961**, *83*, 3866.

(9) Hoffmann, H.; Schellenbeck, P. *Chem. Ber.* **1966**, *99*, 1134.

**Table 4. Atomic Coordinates (10<sup>4</sup>) and Equivalent Isotropic Displacement Coefficients (Å<sup>2</sup> 10<sup>3</sup>) for 3 and 4**

atom	<i>x/a</i>	<i>y/b</i>	<i>z/c</i>	<i>U(eq)</i>
Compound 4				
In	8235(1)	9080(1)	2134(1)	38(1)
P	6821(3)	10379(1)	1231(1)	39(1)
Cl(1)	10256(3)	9704(2)	3012(2)	65(1)
Cl(2)	6628(4)	403(2)	3220(2)	69(1)
C(1)	9230(11)	8139(6)	1122(6)	52(3)
C(2)	8659(14)	7188(7)	1301(7)	68(4)
C(3)	7550(15)	6993(7)	741(8)	9(4)
C(4)	7347(13)	774(7)	160(7)	67(4)
C(5)	8353(14)	8461(6)	351(5)	56(3)
C(6)	8590(14)	9425(6)	-71(6)	64(4)
C(7)	7197(13)	10047(7)	72(5)	0(4)
C(8)	7644(11)	11586(6)	1407(7)	50(3)
C(9)	9344(11)	11516(7)	1163(7)	68(4)
C(10)	7566(11)	11861(6)	2389(6)	65(4)
C(11)	6908(12)	12357(6)	849(7)	69(4)
C(12)	4728(10)	10275(7)	1357(7)	60(4)
C(13)	3850(12)	10847(9)	669(8)	99(5)
C(14)	4317(11)	9225(7)	1266(7)	73(4)
C(15)	4245(10)	10616(7)	2283(6)	66(4)
Compound 5				
Ga	2290(1)	1284(1)	874(1)	51(1)
P	2538(1)	-471(2)	2086(1)	46(1)
C(1)	3710(4)	2310(5)	1465(4)	54(2)
C(2)	3817(5)	3283(6)	778(4)	67(2)
C(3)	4550(6)	2842(8)	30(4)	76(3)
C(4)	976(5)	1593(7)	714(5)	73(3)
C(5)	4512(4)	1277(6)	1428(4)	58(2)
C(6)	4763(5)	32(7)	2012(5)	76(3)
C(7)	3969(4)	-340(6)	603(4)	64(2)
C(8)	303(5)	-2299(6)	1710(4)	58(2)
C(9)	1237(5)	-2364(7)	1051(4)	79(3)
C(10)	2305(5)	-3360(6)	2455(4)	77(3)
C(11)	3201(5)	-2663(6)	1213(5)	79(3)
C(12)	1825(5)	-44(7)	3011(4)	68(3)
C(13)	2252(7)	-828(8)	3884(4)	106(4)
C(14)	1990(6)	1497(7)	3207(5)	97(3)
C(15)	632(5)	-313(8)	2722(5)	97(4)
C(16)	2335(5)	418(6)	-278(3)	68(2)
C(17)	1043(5)	2483(7)	884(4)	83(3)

**Method B.** A solution of 0.34 g (1.4 mmol) of **2** in 20 mL of toluene was added to a stirred solution of Me<sub>3</sub>Ga (0.23 g, 1.4 mmol) in 20 mL of toluene. The stirred solution was refluxed for 24 h. The solvent and volatiles were removed under reduced pressure to yield **5** as a white powder. The product was identified by <sup>31</sup>P NMR spectroscopy.

**Synthesis of Dimethyl[1-η<sup>1</sup>-(2-di-*tert*-butylphosphino)-ethylcyclopentadienyl]indium (**6**).** **Method A.** A solution

of 0.24 g (1.0 mmol) of **1** in 20 mL of THF was added at -78 °C to a stirred solution of Me<sub>2</sub>InCl (0.18 g, 1.0 mmol) in 30 mL of THF. After 3 h at -78 °C, the stirred solution was allowed to warm to room temperature. The solvent and volatiles were removed under reduced pressure, and the resulting residue was extracted with hexane (100 mL), filtered, and concentrated to 20 mL. Cooling the solution overnight at -20 °C resulted in a white, powdery **6** (mp 97–99 °C). <sup>1</sup>H NMR (C<sub>6</sub>D<sub>6</sub>): δ -0.11 (d, InCH<sub>3</sub>, 6 H), 0.81 (d, CH<sub>3</sub>, 18 H), 1.56 (m, CH<sub>2</sub>, 2 H), 2.82 (m, CH<sub>2</sub>, 2 H), 5.74 (s, ring H, 2 H), 6.79 (s, ring H, 2 H); <sup>13</sup>C{<sup>1</sup>H} NMR (C<sub>6</sub>D<sub>6</sub>): δ 1.4 (d, InCH<sub>3</sub>, <sup>2</sup>J(CP) 15.8 Hz), 21.5 (d, CH<sub>2</sub>, <sup>1</sup>J(CP) 15.2 Hz), 27.0 (d, CH<sub>2</sub>, <sup>2</sup>J(CP) 7.8 Hz), 29.2 (d, CH<sub>3</sub>, <sup>2</sup>J(CP) 4.6 Hz), 33.1 (d, *t*-C, <sup>1</sup>J(CP) 14.2 Hz), 96.1 (s, ring C), 118.4 (s, ring C). <sup>31</sup>P NMR (C<sub>6</sub>D<sub>6</sub>): δ 10.5 (s). MS (CI) 383 [M<sup>+</sup>]. HRMS calcd 383.135 865, found 383.134 827. Anal. Calcd for C<sub>17</sub>H<sub>32</sub>InP: C, 53.42; H, 8.44. Found: C, 52.68; H, 7.92.

**Method B.** A solution of 0.34 g (1.4 mmol) of **2** in 20 mL of toluene was added to a stirred solution of Me<sub>3</sub>In (0.23 g, 1.4 mmol) in 20 mL of toluene. The stirred solution was refluxed for 24 h. The solvent and volatiles were removed under reduced pressure to yield white powdery **6**. The product was identified by <sup>31</sup>P NMR spectroscopy.

**X-ray Crystallography.** Details of the crystal data and a summary of intensity data collection parameters for **4** and **5** are presented in Table 3. Atomic coordinates and equivalent isotropic thermal parameters for **4** and **5** are listed in Table 4. The crystals were mounted in thin-walled glass capillaries and sealed under argon. Both data sets were collected at 25 °C on an Enraf-Nonius CAD-4 diffractometer. The unit cell parameters were obtained by centering 25 reflections having 2θ values between 16 and 24°. For both structures, the data were corrected for Lorentz and polarization effects. The structures were solved by direct methods and successive cycles of difference maps followed by least-squares refinements. All calculations were performed using the Siemens SHELXTL PLUS (PC version) programs.

**Acknowledgment.** We thank the Robert A. Welch Foundation, the National Science Foundation, and the Science and Technology Center Program of the National Science Foundation (Grant CHE-8920120) for their generous support of this research.

**Supplementary Material Available:** Tables of atomic parameters, thermal parameters, bond distances and angles, and hydrogen atom coordinates for **4** and **5** (6 pages). Ordering information is given on any current masthead page.

OM9403535

# Phosphine Derivatives of ( $\mu$ - $\eta^2$ -Methylidyne)( $\mu$ -hydrido)dodecacarbonyltetrairon<sup>†,‡</sup>

Hubert Wadepohl\*

Anorganisch-chemisches Institut der Ruprecht-Karls-Universität, Im Neuenheimer Feld 270,  
D-69120 Heidelberg, Germany

Dario Braga\* and Fabrizia Grepioni

Dipartimento di Chimica "G. Ciamician", Università degli Studi di Bologna, Via Selmi, 2,  
I-40126 Bologna, Italy

Received March 2, 1994<sup>§</sup>

A number of phosphine monosubstitution products of the  $\mu$ - $\eta^2$ -methylidyne tetrairon cluster complex  $[\text{HFe}_4(\mu\text{-}\eta^2\text{-CH})(\text{CO})_{12}]$  (**1**) have been prepared from **1** and 1 equiv of tertiary phosphine  $\text{PR}_3$ . In the products  $[\text{HFe}_4(\mu\text{-}\eta^2\text{-CH})(\text{CO})_{11}\text{PR}_3]$  **2a** ( $\text{R} = \text{Ph}$ ), **2b** ( $\text{R}_3 = \text{Ph}_2\text{Me}$ ), **2c** ( $\text{R}_3 = \text{PhMe}_2$ ), and **2d** ( $\text{R} = \text{Me}$ ), the two hydrogen atoms assume C–H–Fe and Fe–H–Fe bridging positions, as in **1**. From **1** and  $\text{PCy}_3$  ( $\text{Cy} = \text{cyclo-C}_6\text{H}_{11}$ ) only the salt-like  $[\text{HPCy}_3][\text{HFe}_4\text{C}(\text{CO})_{12}]$  was obtained in quantitative yield. The molecular and crystal structure of the phosphine derivative **2a** has been determined by single-crystal X-ray diffraction: **2a** is monoclinic; space group  $P2_1/n$ ;  $a = 13.136(6)$ ,  $b = 15.084(7)$ , and  $c = 16.265(4)$  Å,  $\beta = 100.95(3)^\circ$ ;  $V = 3164(2)$  Å<sup>3</sup>,  $F(000) = 1616$ ;  $wR2 = 0.18$  [on  $F^2$ , all data, 5537 unique reflections];  $R_1 = 0.0546$  [on  $F$ , 2694 reflections with  $I < \sigma(I)$ ]. The molecular structure of **2a** is similar to that of the parent molecule **1** showing a  $\text{Fe}_4$  butterfly cluster core with a  $\eta^2$ -CH group between the wings and an equatorial  $\text{PPh}_3$  ligand bound to a wingtip iron atom. The H(hydride) ligand spans the  $\text{Fe}_4$  butterfly hinge. The intermolecular networks of hydrogen bonding interactions established by the  $\mu$ - $\eta^2$ -methylidyne hydrogen atom and by the bridging hydride with the CO ligands in **2a** and **1** have also been investigated. The variable temperature <sup>13</sup>C NMR spectra of isotopically enriched **2a** reveal several dynamic processes, which can be explained by intrametal site CO exchange. A slow dynamic process, detectable by <sup>1</sup>H NMR spectroscopy in the  $T_1$  regime, interconverts hydridic and agostic hydrogen sites in the cluster complexes **2**. Extended Hückel and Fenske–Hall MO calculations have been performed on **1** and the model complex  $[\text{HFe}_4(\mu\text{-}\eta^2\text{-CH})(\text{CO})_{11}\text{PH}_3]$  (**2e**) as well as on the corresponding deprotonated species  $[\text{1-H}]^-$  and  $[\text{2e-H}]^-$ . The structure of **2** can be rationalized using charge and frontier MO arguments. Fast intramolecular switches of the  $\mu$ -CH hydrogen between the two wing tips of the iron butterfly framework are predicted by the calculations.

## Introduction

Interactions of carbon–hydrogen groups with transition metal centers (some time ago named “agostic” hydrogens<sup>1</sup>) are of great scientific interest since they may resemble intermediate points in an important hydrocarbon reaction: carbon–hydrogen bond breaking on surfaces or in molecular organometallic compounds.<sup>2</sup> Agostic hydrogens have been observed in a variety of different mononuclear complexes as well as in molecular clusters.<sup>1</sup> Surface C–H–M multicenter bonded species have been proposed<sup>3</sup> as key intermediates in the dihy-

drogen reduction of carbide-like carbon atoms in heterogeneous Fischer–Tropsch reactions.

A reasonable model<sup>4</sup> of such an intermediate is the molecular  $\eta^2$ -methylidyne cluster complex  $[\text{HFe}_4(\mu\text{-}\eta^2\text{-CH})(\text{CO})_{12}]$  (**1**).<sup>5,6</sup> Within our efforts to seek comparisons of the hydrocarbon coordination chemistry on metal surfaces and molecular metal clusters,<sup>7,8</sup> we were interested in the effect of minor changes of the electronic and steric structure of the parent cluster backbone on the 3c-2e C–H–Fe bond present in **1**. Transition metal carbonyl cluster complexes are generally prone to CO substitution, and this behavior offered a convenient approach to our objective. Thus, we have prepared and

<sup>†</sup> This work was started in 1983 in the laboratory of Earl Muetterties at the University of California, Berkeley, CA. Prof. Muetterties's untimely death on January 12th, 1984, put a sudden end to his research projects. We have decided to take up these investigations again and are presenting them in commemoration of Prof. Muetterties's death ten years ago.

<sup>‡</sup> Dedicated to the memory of Earl L. Muetterties. Deceased January 12, 1984.

<sup>§</sup> Abstract published in *Advance ACS Abstracts*, November 1, 1994.

(1) Brookhart, M.; Green, M. L. H. *J. Organomet. Chem.* **1982**, *250*, 395.

(2) Muetterties, E. L. *Pure Appl. Chem.* **1982**, *54*, 3.

(3) Muetterties, E. L.; Stein, J. *Chem. Rev.* **1979**, *790*, 479.

(4) Gavin, R. M., Jr.; Reutt, J.; Muetterties, E. L. *Proc. Natl. Acad. Sci. U.S.A.* **1981**, *78*, 3981.

(5) (a) Tachikawa, M.; Muetterties, E. L. *J. Am. Chem. Soc.* **1980**, *102*, 4541. (b) Beno, M. A.; Williams, J. M.; Tachikawa, M.; Muetterties, E. L. *Ibid.* **1980**, *102*, 4542. (c) Beno, M. A.; Williams, J. M.; Tachikawa, M.; Muetterties, E. L. *Ibid.* **1981**, *103*, 1485.

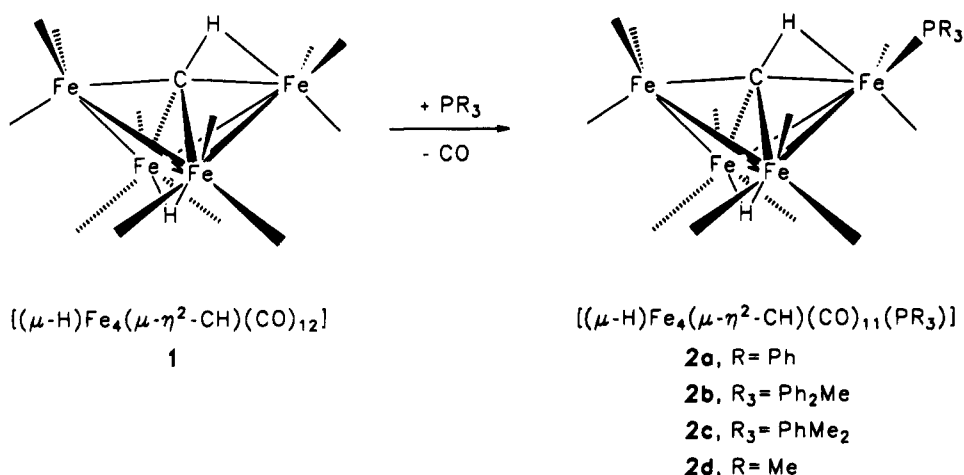
(6) (a) Holt, E. M.; Whitmire, K. H.; Shriver, D. F. *J. Organomet. Chem.* **1981**, *213*, 125. (b) Davis, J. H.; Beno, M. A.; Williams, J. M.; Zimmie, J.; Tachikawa, M. *Proc. Natl. Acad. Sci. U.S.A.* **1981**, *78*, 668.

(7) Muetterties, E. L.; Rhodin, T. N.; Band, E.; Brucker, C. F.; Pretzer, W. R. *Chem. Rev.* **1979**, *79*, 91.

(8) (a) Wadepohl, H. *Angew. Chem.* **1992**, *104*, 253. (b) Wadepohl, H. *Comments Inorg. Chem.* **1994**, *15*, 369.



Scheme 1



fully characterized a variety of phosphine monosubstituted derivatives of **1**.

We have also undertaken the single-crystal X-ray diffraction characterization of the triphenylphosphine derivative **2a**. Beside discussing in detail the structural features of this complex in comparison with that of the parent cluster **1**, we have carefully investigated the molecular organization in the solid state. This part of the study integrates with our more general interest in the intermolecular forces acting amongst molecules and in the relationship between molecular and crystal structure in organometallic materials.<sup>9</sup>

## Results and Discussion

**Substitution Reactions.** Compound **1** slowly underwent reaction with 1 equiv of tertiary phosphine at room temperature to form the monosubstituted derivatives **2a** (L = PPh<sub>3</sub>), **2b** (L = PPh<sub>2</sub>Me), **2c** (L = PPhMe<sub>2</sub>), and **2d** (L = PMe<sub>3</sub>) (Scheme 1). Compounds **2a–d** are dark brown or black crystalline solids which are only moderately air sensitive and can even be handled in air for short periods of time. When the reaction of **1** with trimethylphosphine in a mixture of pentane and tetrahydrofuran (THF) was carried out at  $-70^\circ\text{C}$ , the formation of a deep red solution was observed. On warming, its color changed to brown and the substituted cluster complex **2d** could be isolated. Since **1** is known<sup>5,10</sup> to be a strong acid, we suspected deprotonation by the basic phosphine. <sup>1</sup>H NMR analysis of such a red solution at low temperature indeed suggested the transient presence of the  $[\text{HPMe}_3]^+$  and  $[\text{HFe}_4\text{C}(\text{CO})_{12}]^-$  ions. Likewise the deep red salt  $[\text{HPCy}_3]^+[\text{HFe}_4\text{C}(\text{CO})_{12}]^-$  was isolated in quantitative yield when **1** was treated with the highly basic and bulky<sup>11</sup> tricyclohexylphosphine PCy<sub>3</sub>.  $[\text{HPCy}_3]^+[\text{HFe}_4\text{C}(\text{CO})_{12}]^-$  was stable as a solid and in solution up to ca.  $50^\circ\text{C}$ . Higher temperatures resulted in complete decomposition. No further reaction took place when  $[\text{HPCy}_3]^+[\text{HFe}_4\text{C}(\text{CO})_{12}]^-$  was treated with excess PCy<sub>3</sub>.

The phosphine substituted cluster complexes **2a–d** are strong acids. As judged from the infrared and <sup>1</sup>H

NMR spectra, the dominant species in ethanol or even THF solutions are the monoanions  $[\text{HFe}_4\text{C}(\text{CO})_{11}(\text{PR}_3)]^-$ . With stronger bases like triethylamine ( $\text{p}K_a = 18.5$ ), morpholine ( $\text{p}K_a = 16.6$ ), and pyridine ( $\text{p}K_a = 12.3$ )<sup>12</sup> in acetonitrile, complete deprotonation to give the dianions  $[\text{Fe}_4\text{C}(\text{CO})_{11}(\text{PR}_3)]^{2-}$  takes place. Reprotonation is effected with HCl etherate.

**Molecular Structure of  $[\text{HFe}_4(\mu\text{-}\eta^2\text{-CH})(\text{CO})_{11}(\text{PPh}_3)]$  (**2a**).** A ball-and-stick and space-filling representation of the molecular structure of **2a** is shown in Figure 1. Relevant structural parameters are reported in Table 1 and fractional atomic coordinates in Table 2. The essential structural features of **2a** correspond to those observed in the parent complex  $[\text{HFe}_4(\mu\text{-}\eta^2\text{-CH})(\text{CO})_{12}]$  (**1**). The comparison between **2a** and **1** is complicated by the presence of two independent molecules in the asymmetric unit of the latter crystal.<sup>5b,9</sup> Moreover, there are two different crystal structure determinations for complex **1**: an X-ray diffraction study at  $173\text{ K}$ <sup>5b</sup> and a neutron diffraction study at  $26\text{ K}$ .<sup>5c</sup> In the following we chose to compare our X-ray diffraction study with the corresponding study of **1** because, although the neutron study is certainly more accurate, the two X-ray experiments have comparable precision. The results of the neutron diffraction experiment will be reported in brackets as pairs of chemically corresponding values.

The most relevant structural features of **2a** can be summarized as follows: (i) The metal framework consists of a butterfly of iron atoms with Fe–Fe bonds ranging from 2.584(2) to 2.669(2) Å in compound **2a**. The shortest bond [Fe(2)–Fe(4)] corresponds to the butterfly hinge and is spanned by the H(hydride) bridge. The longest bond is between atoms Fe(1) and Fe(2). The lengthening of this bond with respect to the other wing bonds is attributable to the steric presence of the PPh<sub>3</sub> ligand, which cannot afford to approach the CO ligands bound to Fe(2) more closely. (ii) The PPh<sub>3</sub> ligand formally replaces one "equatorial" wing-tip CO in the structure of **1**; of the two "symmetry-distinguishable" equatorial coordination sites available on these atoms, the one *trans* to the agostic  $\eta$ -interaction with the C–H ligand is not preferred. (iii) As in **1**, the  $\mu\text{-}\eta^2$ -methylidyne ligand is roughly placed in the middle of the butterfly core, with the C atom simultaneously interact-

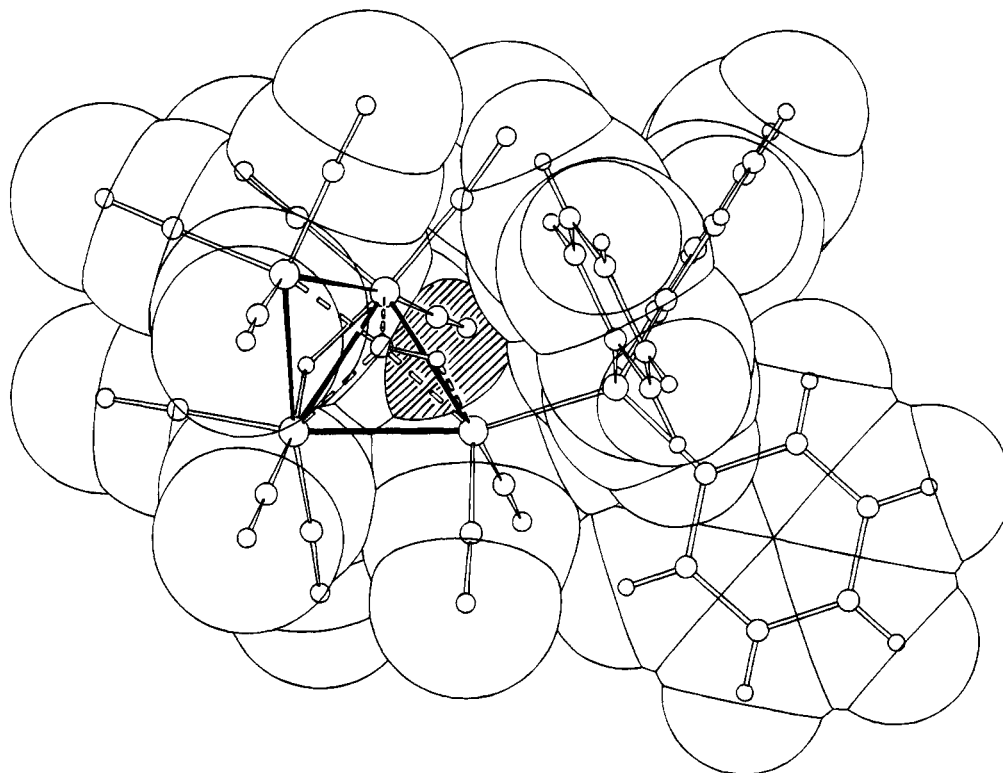
(9) Braga, D.; Grepioni, F. *Acc. Chem. Res.* **1994**, *27*, 51.

(10) Bradley, J. S. *Phil. Trans. R. Soc. London* **1982**, *A308*, 103.

(11)  $\text{p}K_a$  values for  $[\text{HPMe}_3]^+$  and  $[\text{HPCy}_3]^+$  are given as 8.65 and 9.7, respectively (Allman, T.; Goel, R. G. *Can. J. Chem.* **1982**, *60*, 716. Henderson, W. A., Jr.; Streuli, C. A. *J. Am. Chem. Soc.* **1960**, *82*, 5791). Cone angles are  $118^\circ$  for PMe<sub>3</sub> and  $170^\circ$  for PCy<sub>3</sub> (Tolman, C. A. *Chem. Rev.* **1977**, *77*, 313).

(12) Moore, E. J.; Sullivan, J. M.; Norton, J. R. *J. Am. Chem. Soc.* **1986**, *108*, 2257 and references cited therein.  $\text{p}K_a$  refers to  $[\text{HB}]^+$ .





**Figure 1.** Molecular structure of  $[\text{HFe}_4(\mu\text{-}\eta^2\text{-CH})(\text{CO})_{11}(\text{PPh}_3)]$  (**2a**). The space-filling outlines the ligand shell embedding the CH group.

**Table 1.** Selected Bond Lengths [Å] and Angles [deg] for **2a**

Fe(1)–Fe(2)	2.669(2)
Fe(1)–Fe(4)	2.613(2)
Fe(2)–Fe(3)	2.630(2)
Fe(2)–Fe(4)	2.584(2)
Fe(3)–Fe(4)	2.624(2)
Fe(1)–C(30)	1.908(7)
Fe(2)–C(30)	1.926(9)
Fe(3)–C(30)	1.803(7)
Fe(4)–C(30)	1.973(8)
Fe(1)–H(30)	1.69(1)
C(30)–H(30)	1.04(1)
Fe(2)–H(31)	1.57
Fe(4)–H(31)	1.44
Fe(1)–P(1)	2.238(2)
P(1)–C(12)	1.812(4)
P(1)–C(18)	1.830(5)
P(1)–C(24)	1.818(5)
mean Fe–C(CO)	1.78(1)
mean C–O	1.14(1)
mean Fe–C(CO)–O	177(1)
Fe(3)–C(30)–Fe(1)	172.4(5)
Fe(2)–C(30)–Fe(4)	83.0(3)
Fe(1)–C(30)–H(30)	85(1)
Fe(2)–H(31)–Fe(4)	119
C(12)–P(1)–C(18)	105.0(3)
C(12)–P(1)–C(24)	105.7(2)
C(24)–P(1)–C(18)	101.0(3)
C(12)–P(1)–Fe(1)	108.2(2)
C(18)–P(1)–Fe(1)	118.9(2)
C(24)–P(1)–Fe(1)	116.8(2)

ing (though in an asymmetric fashion) with all four metal centers. Fe–C(H) distances in **2a** range from 1.803(7) to 1.973(8) Å, again showing a wider spread with respect to **1**: 1.822(4)–1.958(4); 1.828(5)–1.946(5) Å [1.822(2)–1.952(2); 1.827(2)–1.949(2) Å]. (iv) The C–H distance is 1.04(1) Å, i.e. strictly comparable with the value observed for **1**, 1.00(4); 1.09(4),<sup>5b</sup> but appreciably shorter than that found in the neutron diffraction experiment [1.176(5), 1.191(4) Å].<sup>5c</sup> The reason

for this difference is inherent to the difference between the two types of experiments. The reader is referred to ref 5c for a thorough discussion of the relationship between X-ray and neutron diffraction results. The H(30)–Fe(1) separation of 1.69(1) Å in **2a** is somewhat midway between the two very different values obtained by X-ray diffraction in **1** [1.48(4) and 1.80(4) Å] and closer to those obtained by neutron diffraction [1.747(4) and 1.753(4) Å]. (v) The H(hydride) bridge in **2a** is in an asymmetric bridging position [1.57 and 1.45 Å] as found for **1** in the X-ray diffraction experiment [1.82(4), 1.58(4), 1.73(4), 1.63(4) Å]. The H(hydride) atom is, instead, symmetrically located in the neutron structure of **1** at 26 K [1.674(4), 1.670(4); 1.668(4), 1.670(4)].

**Intermolecular C–H–O(C) Hydrogen Bonds.** The existence of “weak” C–H–O(C) interactions in solid **1** was discussed by Muetterties *et al.*<sup>5b,c</sup> In the course of our study of the molecular organization in solid organometallic materials, we have illustrated several examples of these weak intermolecular interactions.<sup>9</sup> C–H–O(C) interactions have been detected in the crystals of both structural isomers of  $[\text{Ir}_4(\text{CO})_9(\mu_3\text{-trithiane})]$  (trithiane = 1,3,5-trithiacyclohexane),<sup>13a</sup> in various crystals of arene clusters,<sup>13b</sup> and in the binuclear carbene complex  $[\text{Cp}_2\text{Fe}_2(\text{CO})_3\{\mu\text{-C}(\text{H})\text{CN}\}]$ .<sup>13c</sup> In **1**, due to the presence of two independent molecular units (A, B) there are two types of C–H–O(C) interactions (see Figure 2). Molecules of type A present one single H-bond between the  $\mu\text{-}\eta^2\text{-methylidyne}$  ligand and a hinge CO ligand with a C–H–O(C) separation of 2.58 Å [O(32)–H(1)]. The second type of molecules (B) are,

(13) (a) Braga, D.; Grepioni, F. *J. Chem. Soc., Dalton Trans.* **1993**, 1223. (b) Braga, D.; Grepioni, F.; Parisini, E.; Johnson, B. F. G.; Martin, M. C.; Nairn, J. G. M.; Lewis, J.; Martinelli, M. *J. Chem. Soc., Dalton Trans.* **1993**, 1891. (c) Aime, S.; Cordero, L.; Gobetto, R.; Bordoni, S.; Busetto, L.; Zanotti, V.; Albano, V.; Braga, D.; Grepioni, F. *J. Chem. Soc., Dalton Trans.* **1992**, 2961.

Table 2. Atomic Coordinates ( $\times 10^4$ ) for 2a

	x	y	z		x	y	z
Fe(1)	467(1)	8843(1)	7503(1)	O(9)	-3213(6)	9719(6)	8430(5)
Fe(2)	-169(1)	8449(1)	8923(1)	C(10)	1167(6)	9791(5)	7910(5)
Fe(3)	-1777(1)	7633(1)	8030(1)	O(10)	1600(5)	10427(4)	8160(4)
Fe(4)	-1375(1)	9296(1)	7742(1)	C(11)	219(7)	9254(6)	6493(6)
C(30)	-645(5)	8150(5)	7762(6)	O(11)	17(6)	9560(5)	5826(4)
H(30)	-216(53)	7887(44)	7343(43)	P(1)	1882(2)	8045(1)	7424(1)
H(31)	-978	9200	8623	C(12)	1468(4)	7017(3)	6887(3)
C(1)	564(7)	7465(5)	9233(5)	C(13)	986(4)	6381(3)	7298(3)
O(1)	999(5)	6844(4)	9480(4)	C(14)	616(4)	5604(3)	6887(4)
C(2)	-1397(8)	6538(7)	8312(7)	C(15)	727(4)	5464(3)	6064(4)
O(2)	-1141(7)	5825(6)	8477(7)	C(16)	1209(4)	6100(4)	5653(3)
C(3)	-2471(7)	7328(7)	7019(7)	C(17)	1580(4)	6877(3)	6064(3)
O(3)	-2866(6)	7115(6)	6362(5)	C(18)	2844(4)	8509(4)	6864(4)
C(4)	771(7)	9164(6)	9507(6)	C(19)	2641(5)	9258(4)	6363(5)
O(4)	1344(5)	9615(5)	9940(4)	C(20)	3387(6)	9578(5)	5937(5)
C(5)	-953(8)	8303(6)	9698(7)	C(21)	4337(5)	9150(6)	6014(5)
O(5)	-1401(6)	8247(5)	10224(5)	C(22)	4541(4)	8400(6)	6515(5)
C(6)	-2881(8)	7660(8)	8556(8)	C(23)	3794(5)	8080(4)	6941(5)
O(6)	-3564(6)	7656(7)	8878(6)	C(24)	2701(4)	7725(4)	8409(3)
C(7)	-932(8)	10425(7)	7671(7)	C(25)	2937(4)	8383(3)	9013(3)
O(7)	-685(6)	11128(5)	7626(6)	C(26)	3577(5)	8193(4)	9777(3)
C(8)	-2028(8)	9234(7)	6702(8)	C(27)	3980(4)	7345(4)	9935(3)
O(8)	-2470(7)	9226(6)	6016(5)	C(28)	3743(5)	6687(3)	9331(4)
C(9)	-2517(7)	9524(7)	8144(7)	C(29)	3104(5)	6877(3)	8568(4)

instead, more efficiently "linked" by two identical interactions related to the crystallographic center of inversion. These interactions are much shorter, 2.48 Å, than those involving molecule A. In crystalline **2a**, on the contrary, no C-H-O(C) interaction is present, not it could be since the H-atom is completely embedded within the ligand shell and screened from the surroundings by one phenyl group. This can be appreciated from the space-filling diagram of **2a** shown in Figure 1.

A second aspect of interest concerns the intermolecular interactions between the H(hydride) atoms and the CO ligands. In **1**, two of these interactions join molecules of type A and B. They are, however, much longer

than those discussed above [2.66 and 2.70 Å, respectively] and are clearly detectable only in the structure determined at 26 K. If the observed H(hydride) atom in **2a** is shifted in the Fe-H-Fe plane to the symmetric bridging position observed for **1** in the neutron diffraction study (Fe-H 1.67 Å), a "dimer" similar to that present in **1** is recognizable around a crystallographic inversion center, as shown in Figure 3.

A systematic study of hydrogen bonding interactions in organometallic crystals is under way.<sup>14</sup>

**Spectroscopic Investigations.** (a) **The Salt**  $[HP-Cy_3]^+ [HFe_4C(CO)_{12}]^-$ . The formulation of the red product from the reaction of **1** with PCy<sub>3</sub> as a phospho-

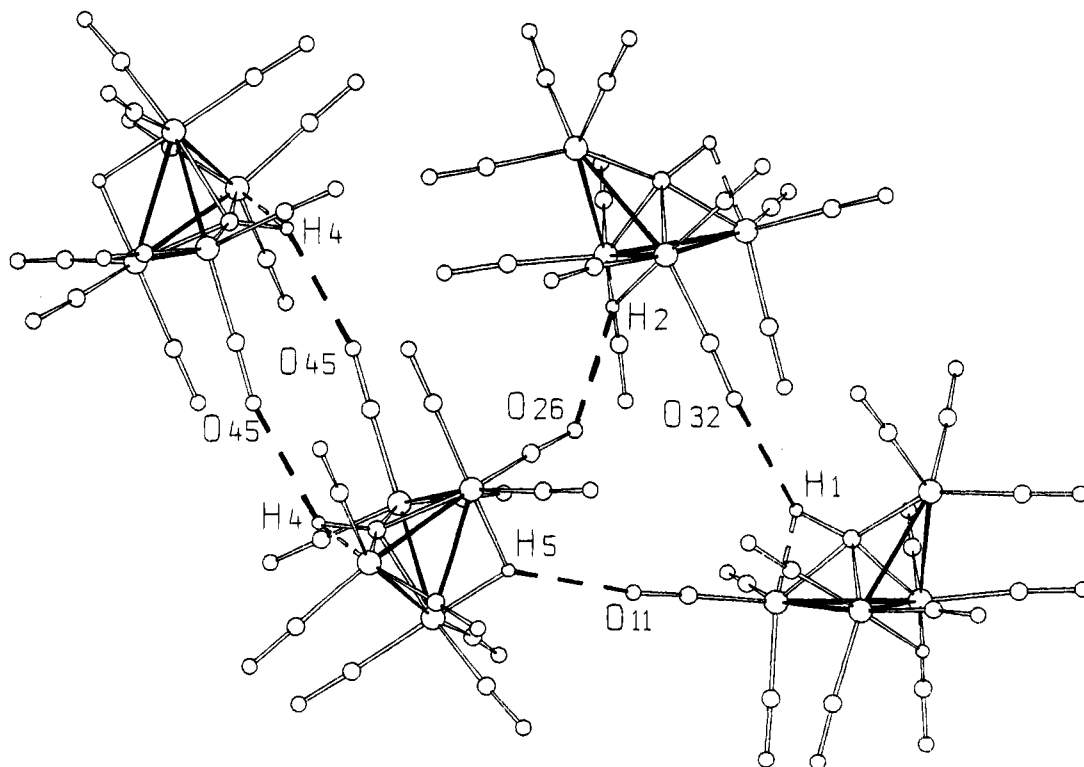
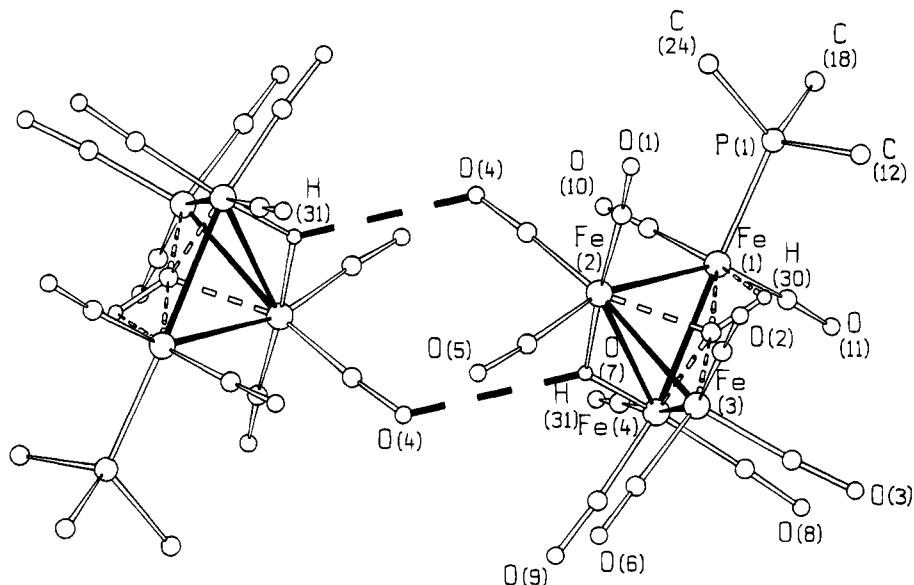


Figure 2. C-H...O and H(hydride)...O intermolecular interactions in  $[HFe_4(\mu-\eta^2-CH)(CO)_{12}]$  (**1**) between molecules of type A and B.



**Figure 3.** H(hydride)-O intermolecular interactions in **2a**. For sake of clarity only the phenyl *ipso* C atoms are drawn; the C(CO) atoms bear the same numbering as the corresponding O atoms.

**Table 3.** IR  $\nu_{\text{CO}}$  Data for compounds **2a-d**.

	$\nu_{\text{CO}}$ [ $\text{cm}^{-1}$ ]
<b>2a<sup>a</sup></b>	2075 (m), 2037 (vs), 2028 (vs), 2004 (s)
<b>2b<sup>b</sup></b>	2080 (m), 2040 (vs), 3032 (vs), 2018 (sh), 2008 (s)
<b>2c<sup>b</sup></b>	2080 (m), 2040 (vs), 2031 (vs), 2017 (sh), 2007 (s), 1994 (w)
<b>2d<sup>a</sup></b>	2077 (m), 2035 (vs), 2027 (vs), 2003 (s)

<sup>a</sup> In *n*-hexane. <sup>b</sup> In petroleum ether.

nium salt of the hydridocarbonyliron carbide cluster anion  $[\text{HFe}_4\text{C}(\text{CO})_{12}]^{-5,6}$  is mainly based on its NMR spectroscopic properties, namely a doublet in the  $^{31}\text{P}$  NMR spectrum at  $\delta = 34.4$  with  $J_{\text{PH}} = 442$  Hz, which is indicative of a phosphorus hydrogen bond, and the absence of  $^1\text{H}$  resonances in the region  $-3 \leq \delta(^1\text{H}) \leq 1$ . The hydride resonance ( $\delta = -26.6$ ) was somewhat broadened, but fast exchange with the phosphonium hydrogen can be ruled out since the latter showed coupling to both the phosphorus and alkyl hydrogens. The hydride resonance in  $[\text{PPN}]^+[\text{HFe}_4\text{C}(\text{CO})_{12}]^-$  (PPN =  $\text{N}[\text{P}\{\text{C}_6\text{H}_5\}_3]_2$ ) is also broad.<sup>5a,6a</sup> The infrared spectrum in the  $\nu_{\text{CO}}$  region closely resembles the spectrum of  $[\text{PPN}]^+[\text{HFe}_4\text{C}(\text{CO})_{12}]^-$ .<sup>5a</sup> In addition there is a band at  $2308$   $\text{cm}^{-1}$  which can be assigned to a P-H stretch.

**(b) Substitution Products 2a-d.** The infrared spectra (Table 3) indicate that the electronic structures of **2a-d**, as experienced by the CO ligands, are very similar. We attribute this observation to an extensive delocalization of the varying extra electron density which is introduced into the cluster by the phosphine ligands. Selected NMR spectroscopic data are presented in Tables 4 and 5. Our NMR spectroscopic results confirm that the  $\mu$ -hydrido( $\mu$ - $\eta^2$ -methylidyne) cluster structure, as determined for **2a** in the solid state by X-ray crystallography, is retained in solution. The high-field proton resonances around  $\delta -27$  (Table 2) are characteristic for metal bridging hydrides. The  $^1\text{H}(\text{CH})$  resonances between  $\delta -1.3$  and  $-2.3$ , and the low value for  $J(^{13}\text{CH})$  (102.7 Hz for **2a**) are indicative<sup>1</sup> of agostic hydrogens.

It is interesting to note that the chemical shift of the CH proton is nearly the same in **1** and **2a**, but this

**Table 4.** Selected  $^1\text{H}$  NMR Data<sup>a</sup> for Compounds **2a-d** and **1**

	CH			$\text{Fe}_2\text{H}$		
	$\delta$	$J_{\text{PH}}$	$J_{\text{HH}}$	$\delta$	$J_{\text{PH}}$	$J_{\text{HH}}$
<b>2a</b>	-1.29	6.5	0.8	-27.3	3	<i>b</i>
<b>2b</b>	-1.60	5.7	0.7	-27.4	<i>b</i>	<i>b</i>
<b>2c</b>	-2.00	6.0	1.0	-27.52	1	1
<b>2d</b>	-2.27	7.0	1.0	-27.41	1	1
<b>1</b>	-1.31		0.9	-27.95		0.9

<sup>a</sup> In *d*<sub>8</sub>-toluene at 20 °C. *J* in hertz. <sup>b</sup> Not resolved.

**Table 5.** Selected  $^{13}\text{C}$  and  $^{31}\text{P}$  NMR Data<sup>a</sup> for Compounds **2a-d** and **1**

	$\delta(^{13}\text{C})$	$J_{\text{CH}}$ [Hz]	$J_{\text{CP}}$ [Hz]	$\delta(^{31}\text{P})$
<b>2a<sup>b</sup></b>	333.5	102.7	9	61.1
<b>2b<sup>c</sup></b>	331.9	<i>d</i>	9	42.8
<b>2c<sup>c</sup></b>	328.5	<i>d</i>	9	19.3
<b>2d<sup>c</sup></b>	326.7	<i>d</i>	10	19.3
<b>1</b>	335	103.6		

<sup>a</sup> Methylidyne carbon resonance at 20 °C. <sup>b</sup> In  $\text{CD}_2\text{Cl}_2$ . <sup>c</sup> In *d*<sub>8</sub>-toluene. <sup>d</sup> Not determined.

resonance is markedly shifted upfield when the basicity of the phosphine ligand is increased. However, there is only a very small effect on the hydride resonance.  $^{31}\text{P}$ - $^1\text{H}$  spin-spin coupling was observed to both the  $\eta^2$ -CH and  $\text{Fe}_2\text{H}$  resonances. The coupling constants were not affected by cooling to  $-80$  °C. Very fast intramolecular switches of the  $\mu$ -CH hydrogen between the two wing tips of the iron butterfly framework were observed in solutions of **1**. The question of a possible CH hydrogen atom switch between the chemically different C-H-Fe(CO)<sub>2</sub>PR<sub>3</sub> and C-H-Fe(CO)<sub>3</sub> sites in **2** is difficult to answer on the basis of NMR studies. From the appearance of the spectra—sharp  $^1\text{H}$  resonances with well-resolved coupling to  $^{31}\text{P}$ —we conclude that such an exchange process in **2a-d** must either be very fast or very slow on the NMR time scale. In the first case, the observed value  $J'_{\text{PH}}$  of the coupling constant between the phosphorus and the methylidyne proton should be only about half of the real value  $J_{\text{PH}}$ , which would be observable in the second case. In hydrido cluster complexes, values of less than 3 Hz for  $J_{\text{HP}}$  are usually observed when the hydrido and the phosphine

(14) Braga, D.; Grepioni, F.; Sabatino, P.; Desiraju, G. R. *Organometallics*, in press.

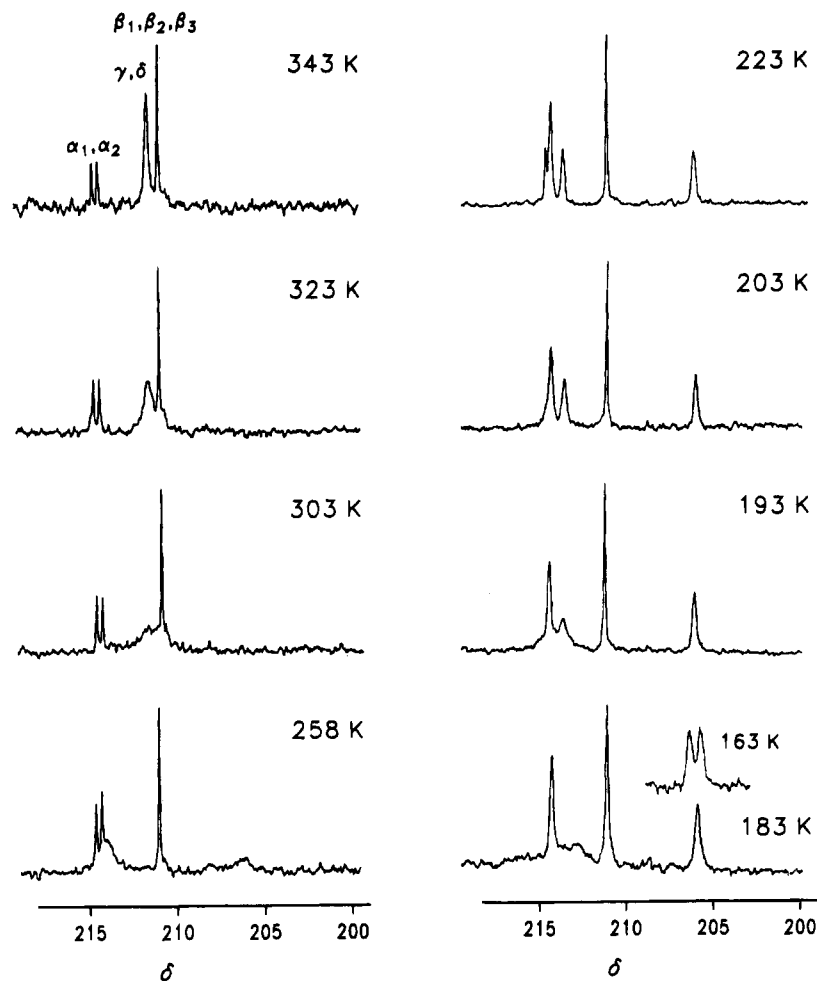


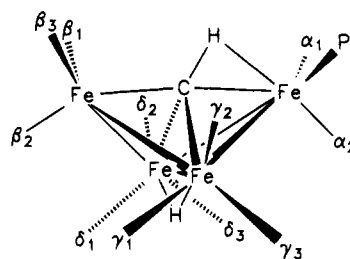
Figure 4. Dynamic  $^{13}\text{C}\{^1\text{H}\}$  spectra of **2a** (region of the carbonyl ligands only).

ligands are not bound to the same metal atom.<sup>15</sup> For bridging *hydrides* bound to a phosphine-substituted metal carbonyl moiety,  $J_{\text{HP}}$  typically is 9–18 Hz for the *cis* and 28–30 Hz for the *trans* arrangement.<sup>16</sup> In **2a–d** the phosphines are equatorial and therefore *cis* to the methylidyne H. The problem is the lack of a suitable reference for *agostic* CH–metal interactions in phosphine-substituted metal carbonyl cluster complexes. Therefore the observed small coupling constants of 5–6 Hz (Table 4) cannot be interpreted unambiguously. Our MO calculations (*vide infra*) however suggest that CHFe bridge switch does indeed take place rapidly in **2**.

Fast intramolecular CO exchange occurred in the clusters **2a–d** at 20 °C. In the  $^1\text{H}$  NMR spectrum of **2c**, there is only one doublet for the methyl groups, which broadens when the temperature is lowered to 190 K. In a rigid structure with the phosphine in one particular equatorial position on a wing-tip iron atom, these methyl groups would be diastereotopic, and two doublets should be observed. Therefore we can conclude that the phosphine ligand is participating in the intramolecular ligand exchange processes.

In Figure 4, the  $^{13}\text{C}$  dynamic NMR spectra in the metal carbonyl region of a  $^{13}\text{C}$ -enriched sample of **2a** are presented. At high temperature we observed only

Chart 1. Labeling Scheme Used for the Assignment of  $^{13}\text{C}$  Carbonyl Resonances in **2a**



three  $^{13}\text{C}$  carbonyl resonances of intensities ca. 2:6:3. Only the low-field resonance ( $\delta = 214.8$ ) was coupled to phosphorus ( $J_{\text{CP}} = 15$  Hz).<sup>17</sup> The signal at  $\delta = 211.8$  was further broadened, when the hydride resonance was not decoupled. This spectrum is consistent with fast intrametal site CO exchange (localized at a single metal atom), a process which is quite common in metal carbonyl cluster complexes.<sup>18</sup> It was also found to be operative in the parent compound **1**.<sup>5</sup> The assignment of the resonances at temperatures above room temperature in the direction of increasing field is apical (wing-tip)  $\text{Fe}(\text{CO})_2\text{PR}_3$  ( $\alpha$ , see Chart 1), basal (wing-base)  $\text{Fe}(\text{CO})_3$  ( $\gamma$ ,  $\delta$ ) and apical  $\text{Fe}(\text{CO})_3$  ( $\beta$ ). At lower temperatures, specific CO exchange processes become slow on the NMR time scale.

(15) Fox, J. R.; Gladfelter, W. L.; Wood, T. G.; Smegal, J. A.; Foreman, T. K.; Geoffroy, G. L.; Tavaniaepour, I.; Day, V. W.; Day, C. S. *Inorg. Chem.* **1981**, *20*, 3214.

(16) Shapley, J. R.; Richter, S. I.; Churchill, M. R.; Lashewycz, R. A. *J. Am. Chem. Soc.* **1977**, *99*, 7384.

(17) The two resonances centred at  $\delta = 214.7$  are indeed due to coupling  $^{13}\text{C}$ – $^{31}\text{P}$  as established by recording the spectra at several different magnetic fields.

(18) Band, E.; Muettterties, E. L. *Chem. Rev.* **1978**, *78*, 639.

Upon lowering of the temperature from 340 to 220 K, the resonance at  $\delta = 211.8$  collapsed and finally split into three distinct signals with an intensity ratio of ca. 2:2:2 ( $\delta = 214.3, 213.7,$  and  $206.4$ ). The signal at  $\delta = 213.7$  was a doublet when the hydride resonance was not decoupled. The resonances due to the CO ligands on apical iron sites were unchanged (one-half of the doublet due to the apical  $\text{Fe}(\text{CO})_2\text{P}$  carbonyl ligands accidentally coincided with the singlet at  $\delta 214.3$ ). Hence, at 220 K CO exchange in the basal  $\text{Fe}(\text{CO})_3$  sites is already slow, while CO exchange on the apical iron atoms is still fast on the NMR time scale. Tentatively, we assign the resonance at  $\delta = 213.7$ , which is coupled to the hydride, to the positions  $\gamma_2$  and  $\delta_2$ , *trans* to the bridging hydride ligand. Below 220 K the doublet at  $\delta = 214.7$  broadened and lost intensity. This was accompanied by a broadening of the resonances at  $\delta = 213.7$  and  $206.4$ . Spectra were also recorded below 180 K in toluene- $d_6$ /thf- $d_8$ . At 163 K, the signal at  $\delta = 211$  was still relatively sharp and the high-field signal had split into two lines. Unfortunately, a complete analysis of these data was prevented by minor impurities in that particular sample and severely limited spectral resolution. Clearly, at 160 K while CO exchange on the apical  $\text{Fe}(\text{CO})_3$  site (i.e.  $\beta_1, \beta_2,$  and  $\beta_3$ ) is still rapid, exchange of the apical  $\text{Fe}(\text{CO})_2\text{P}$  positions  $\alpha_1$  and  $\alpha_2$  occurs at a rate comparable to the NMR time scale.

**Comparison with the Ferraboranes**  $[\text{HFe}_4(\text{BH})(\text{CO})_{12-n}\text{L}_n]^-$  ( $\text{L} = \text{CO}, \text{PMe}_2\text{Ph}, n = 0, 1, 2$ ). The ferraborane cluster  $[\text{HFe}_4(\text{BH})(\text{CO})_{12}]^-$  (**3**)<sup>19,20</sup> is an interesting isoelectronic and isoprotonic analog to **1**. Unfortunately the crystal structure of this anion has not been reported. However, the structure of its formal protonation product  $[\text{HFe}_4(\mu\text{-BH}_2)(\text{CO})_{12}]$  [**3** + H] is known from an X-ray crystal structure determination.<sup>21b</sup> From spectroscopic evidence, there is no doubt that **3** has the same type of butterfly tetrairon cluster backbone with a hydride (bridging the hinge FeFe bond) and a  $\mu\text{-}\eta^2\text{-BH}$  bridge.<sup>19,20</sup> Two phosphine substitution products of **3**, namely  $[\text{HFe}_4(\text{BH})(\text{CO})_{11}(\text{PMe}_2\text{Ph})]^-$  (**4**) and  $[\text{Fe}_4(\text{BH}_2)(\text{CO})_{10}(\text{PMe}_2\text{Ph})_2]^-$  (**5**), were reported.<sup>20,22d</sup> The monosubstitution product **4** has the phosphine ligand in an equatorial position at a wing-tip iron atom. As in the parent **3**, of the two "endo" hydrogens one is in a hydridic FeHFe site and the other remains in the BHFe bridge. This is closely analogous to the behavior of the methylidyne cluster complex **1**. The disubstituted **5** has two BHFe interactions and no hydride ligand.<sup>20,22d</sup> Two transient intermediates with unknown structure but containing  $\text{PMe}_2\text{Ph}$  are involved in the substitution reactions. Thus no unambiguous conclusion could be reached about the primary site of nucleophilic attack by the phosphine.<sup>20</sup> Our system is even more complicated, since we know that **1** is involved in a deprotonation equilibrium with the more basic phosphines or even the solvent. At present we do not know whether **1** or the deprotonated  $[\text{1} - \text{H}]^-$  or both are attacked by the phosphines, nor do we know the primary product.

Addition of more than 1 molar equiv of phosphine to **1** or treatment of **2** with more phosphine does not lead to a single disubstituted product.<sup>23</sup> It is still not clear if the reported<sup>24a</sup> reductive elimination of dihydrogen to form highly substituted cluster complexes  $[\text{Fe}_4\text{C}(\text{CO})_{13-x}(\text{PR}_3)_x]$  represents a well-defined reaction pathway.

As for **1** and **2**, **3**–**5** are also dynamic. The most interesting exchange process is between the  $\text{Fe}_2\text{H}$  and the agostic  $\text{EIHFe}$  ( $\text{E} = \text{B}$  or  $\text{C}$ ) protons, because it involves the breaking and making of the EIH bond on the cluster "surface". This process is quite fast in **3**.<sup>21</sup> In the phosphine-substituted complex **4**, the barrier is considerably higher.<sup>20,22d</sup> In the methylidyne cluster complex **1**, exchange of the hydridic and agostic protons is slow on the conventional ( $T_2$ ) NMR time scale but can be observed in the  $T_1$  regime using magnetization transfer methods.<sup>25</sup> An Arrhenius activation energy of  $\sim 21$  kcal/mol was reported.<sup>24b</sup> It has been stated<sup>24a</sup> that phosphine substitution reduces this value.

We carried out further magnetization transfer experiments on **1** and **2a** to clarify this point.<sup>26</sup> The slow exchange between hydridic and agostic hydrogen sites in both molecules is confirmed by our experiments. However, there was considerable scatter of the experimental activation parameters obtained from different samples. Therefore no reasonable quantitative conclusion could be drawn. In view of the high acidity of the methylidyne H, we suspected that at least part of the observed exchange occurred via intermolecular pathways. Indeed when samples of **1** and  $[\text{DFe}_4(\mu\text{-}\eta^2\text{-CD})(\text{CO})_{12}]$  were mixed in  $\text{CD}_2\text{Cl}_2$ , complete scrambling of the D label was observed within a few hours at room temperature. Such reactions are likely catalyzed by the glass surface of the NMR tubes.

**Molecular Orbital Calculations.** The electronic structure of **1** and the closely related anions  $[\text{HFe}_4\text{C}(\text{CO})_{12}]^-$  ( $[\text{1} - \text{H}]^-$ ) and  $[\text{Fe}_4\text{C}(\text{CO})_{12}]^{2-}$  ( $[\text{1} - 2\text{H}]^{2-}$ ) were studied by several groups using the extended Hückel and the Fenske–Hall quantum chemical procedures.<sup>5c,22,27,28</sup> Experimentally,  $[\text{1} - 2\text{H}]^{2-}$  is monoprotonated at a hinge FeFe bond to give the monohydride anion  $[\text{1} - \text{H}]^-$ .<sup>5,6a</sup> The latter is attacked by a further proton at a  $\text{CFe}_{\text{apex}}$  bond to form the  $\text{CHFe } 3c\text{-}2e$  bond in **1**. Using a reactant-like geometry to model these reactions, the experimentally observed behavior was rationalized by Hoffmann *et al.*<sup>27</sup> in terms of a frontier orbital control of the protonation reactions. Housecroft and Fehlner<sup>22</sup> based their explanation on the interaction of the frontier orbitals of the fragments  $[\text{HFe}_4\text{C}(\text{CO})_{12}]^+$  and  $[\text{CH}]^-$  in the product of the second protonation step. The same arguments hold for the positions of the *endo* hydrogens in the ferraborane anion **3**.<sup>22</sup> From extended Hückel theory, the difference in energy between the tilted (EIHM bridge,  $|\varphi| > 0$  [Chart 2]) and upright (terminal EIH,  $\varphi = 0$ ) coordination geometries of the

(23) Hahn, S.; Wadepohl, H., unpublished results.

(24) (a) Muettterties, E. L.; Geerts, R. L.; Tachikawa, M.; Burch, R. R.; Sennett, M. S.; Williams, J.; Beno, M. *Abstracts of Papers*, 182nd National Meeting of the American Chemical Society, New York, NY, Fall 1981; American Chemical Society: Washington, DC, 1981; INOR 89. (b) Muettterties, E. L. *Chem. Soc. Rev.* **1982**, *11*, 283.

(25) (a) Forsén, S.; Hoffman, R. P. *J. Chem. Phys.* **1963**, *63*, 2892. (b) Campbell, I. D.; Dobson, C. M.; Ratcliffe, R. G.; Williams, J. P. *J. Magn. Reson.* **1978**, *29*, 397.

(26) The experiments were carried out in toluene- $d_6$  at 300–310 K. (27) Wijeyesekera, S. D.; Hoffmann, R.; Wilker, C. N. *Organometallics* **1984**, *3*, 962.

(28) Harris, S.; Bradley, J. S. *Organometallics* **1984**, *3*, 1086.

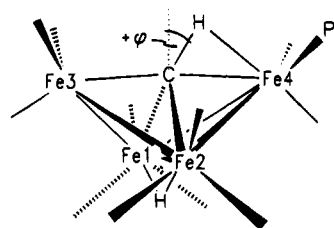
(19) Housecroft, C. E.; Fehlner, T. P. *Organometallics* **1986**, *5*, 379.

(20) Housecroft, C. E.; Buhl, M. L.; Long, G. J.; Fehlner, T. P. *J. Am. Chem. Soc.* **1987**, *109*, 3323.

(21) (a) Wong, K. S.; Scheidt, W. R.; Fehlner, T. P. *J. Am. Chem. Soc.* **1982**, *104*, 1111. Fehlner, T. P.; Housecroft, C. E.; Scheidt, W. R.; Wong, K. S. *Organometallics* **1983**, *2*, 825.

(22) (a) Housecroft, C. E.; Fehlner, T. P. *Organometallics* **1983**, *2*, 690. (b) Fehlner, T. P.; Housecroft, C. E. *Organometallics* **1984**, *3*, 764. (c) Housecroft, C. E. *J. Organomet. Chem.* **1984**, *276*, 297. (d) Housecroft, C. E.; Fehlner, T. P. *Organometallics* **1986**, *5*, 1279.

Chart 2

Table 6. Mulliken Atomic Charges<sup>a</sup> for **1** and **2e**

	<b>1</b>		<b>2e</b>	
	$C_{2v}$	$C_s$	$C_{2v}$	$C_s$
Fe1 <sup>b</sup>	0.131	0.137	0.133 <sup>c</sup>	0.138 <sup>c</sup>
Fe2 <sup>b</sup>	0.131	0.137	0.101 <sup>d</sup>	0.104 <sup>d</sup>
Fe3 <sup>e</sup>	0.059	0.044	0.046	0.033
Fe4 <sup>f</sup>	0.183	0.168	0.131	0.119
C(H)	-0.572	-0.544	-0.579	-0.550
(C)H	0.011	0.006	-0.009	-0.016
(Fe <sub>2</sub> )H	-0.233	-0.234	-0.231	-0.231

<sup>a</sup> Fenske–Hall calculations. <sup>b</sup> Wing base. <sup>c</sup> *Trans* to P. <sup>d</sup> *Cis* to P. <sup>e</sup> Wing tip. <sup>f</sup> Wing tip, CHFe.

$\mu$ -ElH moiety was calculated to be rather small, about 0.3 eV for **1** (El = C) and 0.8 eV for **3** (El = B).<sup>22d</sup>

Extended Hückel calculations on the model complex  $[HFe_4(BH)(CO)_{11}(PH_3)]^-$  gave a somewhat increased barrier for the BHFe bridge switch ( $\varphi < 0^\circ$  to  $\varphi > 0^\circ$ ) as compared to **3**; of the two possible BHFe sites the BH[Fe(CO)<sub>2</sub>PH<sub>3</sub>] bridge was favored by about 0.2 eV.<sup>20</sup> We performed extended Hückel (EH) and Fenske–Hall (FH) MO calculations on **1**, [**1** – H]<sup>-</sup>, [**1** – 2H]<sup>2-</sup>, and the PH<sub>3</sub> monosubstituted derivatives  $[HFe_4(CH)(CO)_{11}(PH_3)]^-$  (**2e**), [**2e** – H]<sup>-</sup>, and [**2e** – 2H]<sup>2-</sup>. The energies and composition of the frontier orbitals for the PH<sub>3</sub>-substituted species are quite similar to those of the parent carbonyl cluster complexes. Therefore, the same arguments as cited above can be put forward to explain the gross structure of **2e**. There are however some details which merit further attention. The atomic charges which are assigned to the atoms of the Fe<sub>4</sub>C core by a Mulliken population analysis do not change significantly on replacing a CO ligand by PH<sub>3</sub>. As has been remarked before,<sup>29</sup> the actual numbers are certainly not true in the absolute sense but they still allow us to make qualitative conclusions concerning changes in the electron distribution. As can be seen from Tables 6 and 7, the carbide carbons (in the monoanions) and methylidyne carbons (in the neutral cluster complexes) are the most negatively charged atoms. The HOMOs of [**1** – H]<sup>-</sup> and [**2e** – H]<sup>-</sup> are mainly centered on the wing-tip irons, with small contributions of the carbido carbon atoms. Therefore, both charge and frontier orbital control favor a CHFe bridge as the protonation product of [**1** – H]<sup>-</sup> and [**2e** – H]<sup>-</sup>. In addition, the values in Table 7 suggest protonation of [**2e** – H]<sup>-</sup> to occur preferentially at the C[Fe(CO)<sub>2</sub>P] bond. The differences in the charges of the Fe<sub>2</sub>H and CHFe hydrogens are in accord with the observed high acidity of the latter.

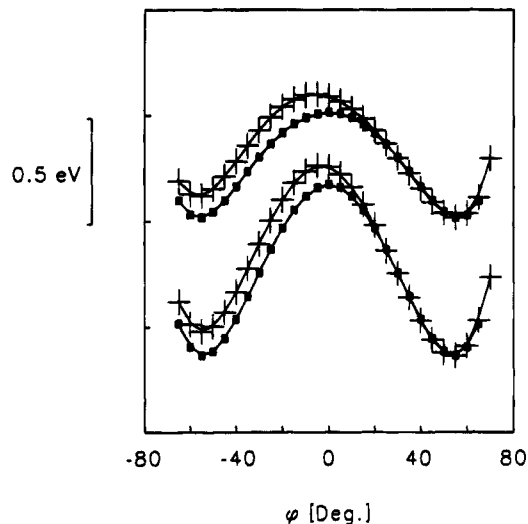
Although the symmetry of the cluster core is destroyed when a phosphine ligand is added to a wing-tip

(29) For more recent discussions of the drawbacks of Mulliken population analysis, see: (a) Schaefer, H. F., III. *The Electronic Structure of Atoms and Molecules*; Addison-Wesley: Reading, MA, 1972. (b) Streitwieser, A., Jr.; Berke, C. M.; Schriver, G. W.; Grier, D.; Collins, J. B. *Tetrahedron Suppl.* **1980**, *37*, 345. (c) Kostic, N. M.; Fenske, R. F. *J. Am. Chem. Soc.* **1981**, *103*, 4677.

Table 7. Mulliken Atomic Charges<sup>a</sup> and Compositions of the HOMO<sup>a</sup> for  $[HFe_4C(CO)_{12}]^-$  and  $[HFe_4C(CO)_{11}(PH_3)]^-$ 

	$[HFe_4C(CO)_{12}]^-$		$[HFe_4C(CO)_{11}(PH_3)]^-$	
	charge	HOMO [%]	charge	HOMO [%]
Fe1 <sup>b</sup>	0.154	8.9	0.162 <sup>c</sup>	6.0 <sup>c</sup>
Fe2 <sup>b</sup>	0.154	8.9	0.129 <sup>d</sup>	8.7 <sup>d</sup>
Fe3 <sup>e</sup>	0.052	23.7	0.050	19.8
Fe4 <sup>e</sup>	0.052	23.7	-0.008 <sup>f</sup>	34.1 <sup>f</sup>
C	-0.691	3.3	-0.731	5.6
(Fe <sub>2</sub> )H	-0.239	0	-0.237	0

<sup>a</sup> Fenske–Hall calculations. <sup>b</sup> Wing base. <sup>c</sup> *Trans* to P. <sup>d</sup> *Cis* to P. <sup>e</sup> Wing tip. <sup>f</sup> Wing tip, FeP.



**Figure 5.** Plot of the calculated one-electron total energies for **1** and **2e** versus bending angle  $\varphi$  of the methylidyne fragment. Points indicated with squares, **1**; with crosses, **2e**. Lower curves:  $d(CFe_{\text{apex}}) = 1.87, 1.92 \text{ \AA}$ . Upper curves:  $d(CFe_{\text{apex}}) = 1.96 \text{ \AA}$ .

iron, the hydrido ligand is still expected to bridge the hinge FeFe bond in a symmetrical manner. Mulliken overlap populations between the hydride and the two hinge iron atoms in **2e** are 0.303, 0.301 (EH) and 0.254, 0.252 (FH). This is because the FeHFe interaction is essentially localized in a single MO with negligible participation of the two wing-tip iron atoms.

In a series of EH calculations the angle  $\varphi$  in **1** and **2e** was varied from  $-70^\circ$  to  $70^\circ$  (cf. Chart 2) while all other distances and angles were kept constant. This is identical to the “test” process which was used by Housecroft *et al.*<sup>20</sup> to model the BHFe bridge switch in **1**, **3**, and **4**. These authors obtained a somewhat increased barrier for  $[HFe_4(BH)(CO)_{11}(PH_3)]^-$  as compared to **3**; of the two BHFe sites the BH[Fe(CO)<sub>2</sub>(PH<sub>3</sub>)] bridge was favored by about 0.2 eV.<sup>20</sup> Our results for the  $C_{2v}$  and  $C_s$  structures are depicted in Figure 5; they are again qualitatively similar to those obtained for the ferraboranes. The barrier for the “test” process is increased by phosphine substitution, and the CH[Fe(CO)<sub>2</sub>PH<sub>3</sub>] bridge is favored by about 0.1 eV relative to the CH[Fe(CO)<sub>3</sub>] site.<sup>30</sup>

## Experimental Section

**Reagents and Solvents.** All manipulations were carried out under an atmosphere of purified nitrogen using conven-

(30) It has to be noted here that the calculated energy minima are at larger angles  $\varphi$  ( $55^\circ$ ) than were found in the crystal structures ( $\varphi = 34^\circ$  for **1**,  $28^\circ$  for **2a**; the latter value is not reliable).

tional Schlenk techniques. Tetrahydrofuran (THF), pentane, hexanes, and petroleum ether (bp 40–60 °C) were distilled from sodium benzophenone ketyl prior to use. Toluene-*d*<sub>8</sub> and thf-*d*<sub>8</sub> were distilled from potassium mirrors. Dichloromethane-*d*<sub>2</sub> was distilled from calcium hydride powder and stored over sodium–lead alloy. The acetonitrile used for the deprotonation studies was refluxed over CaH<sub>2</sub> powder for several hours and carefully rectified over a Vigreux column (bp 81.5 °C). <sup>13</sup>C (90 atom % <sup>13</sup>C) was obtained from Bio-Rad and used without further purification.

**Spectroscopic and Analytical Methods.** NMR spectra were recorded at Berkeley on homebuilt instruments using Bruker or Cryomagnet Systems superconducting magnets (4.2, 4.7, 5.9, or 7.1 T) interfaced with Nicolet 1180 or 1280 computers and operating in the PFT mode. At Heidelberg, a Bruker AC 200 instrument with an Oxford 4.7 T magnet was used. Variable temperature <sup>13</sup>C NMR spectra were obtained from enriched samples at 45.3 MHz. <sup>13</sup>C NMR spectra of nonenriched samples were recorded at ambient temperature at 75.5 MHz. Chemical shifts are given relative to TMS (<sup>1</sup>H, <sup>13</sup>C) and external 85% H<sub>3</sub>PO<sub>4</sub> (<sup>31</sup>P). Infrared spectra were obtained on a Perkin-Elmer 283 grating spectrometer and on a Bruker IFS 28 Fourier instrument. Microanalyses were carried out at the U.C. Berkeley Microanalytical Laboratory and at the Mikroanalytisches Labor der chemischen Institute Heidelberg.

**Preparation of [(μ-H)Fe<sub>4</sub>(μ-η<sup>2</sup>-CH)(CO)<sub>11</sub>PPh<sub>3</sub>] (5 Fe–Fe) (2a).** To 200 mg (0.35 mmol) of [HFe<sub>4</sub>(CH)(CO)<sub>12</sub>] (1) dissolved in 25 mL of hexanes and 5 mL of THF was added a hexane solution (10 mL) of PPh<sub>3</sub> (91.5 mg, 0.35 mmol) over a period of several hours with vigorous stirring. The dark brown solution was allowed to stand at room temperature for ca. 20 h. Removal of solvent in vacuo resulted in a brown oily residue which was extracted twice with a total of 160 mL of hexanes. After filtration, the volume of the extracts was reduced in vacuo by approximately 50%, and the solution was cooled to –20 °C to afford small brown crystals (180 mg, 64%). Anal. Calcd for C<sub>30</sub>H<sub>17</sub>O<sub>11</sub>Fe<sub>4</sub>P (807.82): C, 44.60; H, 2.12; P, 3.83. Found: C, 44.47; H, 2.15; P, 4.0. <sup>1</sup>H NMR (CD<sub>2</sub>Cl<sub>2</sub>, 20 °C): δ 7.5–7.6 (m, Ph, 15H), –1.38 (dd, *J*<sub>PH</sub> = 6.5 Hz, *J*<sub>HH</sub> = 0.7 Hz, CH, 1H), –27.5 (br, Fe<sub>2</sub>H, 1H). <sup>31</sup>P{<sup>1</sup>H} NMR (CD<sub>2</sub>Cl<sub>2</sub>, 20 °C): δ 61.6.

<sup>13</sup>C-enriched 2a (60 atom % <sup>13</sup>C) was prepared from enriched 1 in the same way.

Enriched 1 was obtained starting from Fe(CO)<sub>5</sub> and <sup>13</sup>CO by published procedures.<sup>5,31</sup>

[HFe<sub>4</sub>(<sup>13</sup>CH)(<sup>13</sup>CO)<sub>11</sub>PPh<sub>3</sub>] (<sup>13</sup>C-2a): <sup>13</sup>C NMR (toluene-*d*<sub>8</sub>/thf-*d*<sub>8</sub>, 1:2, 45.3 MHz, –70 °C) δ 333.8 (dm, *J*<sub>CP</sub> = 10 Hz, *J*<sub>CH</sub> = 109 Hz, CH, 1C), 214.7 (d, *J*<sub>CP</sub> = 15 Hz, CO, 2C), 211.8 (br, CO, 6C), 211.3 (s, CO, 3C). 20 °C: δ 333.5 (ddd, *J*<sub>CP</sub> = 9 Hz, *J*<sub>CH</sub> = 102 Hz, 7 Hz, CH, 1C), 214.8 (d, *J*<sub>CP</sub> = 15 Hz, CO, 2C), 212 (br, CO), 211.4 (s, CO, 3C). The chemical shift of the center of the two lines at δ = 214.8 and their separation in hertz was unchanged when the spectrum was recorded at 75.5 MHz. The <sup>31</sup>P NMR spectrum of this sample (recorded at 72.9 MHz and 20 °C) was a symmetrical 15-line pattern due to the superimposed spectra of isotopomers containing one to three <sup>13</sup>C atoms coupled to phosphorus. It is consistent with *J*<sub>PC(H)}</sub> = 10 Hz and *J*<sub>PC(O)}</sub> = 15 Hz.

**Preparation of [(μ-H)Fe<sub>4</sub>(μ-η<sup>2</sup>-CH)(CO)<sub>11</sub>(PPh<sub>2</sub>Me)] (5 Fe–Fe) (2b).** As in the preparation of 2a, a hexane/THF solution of 1 (100 mg, 0.17 mmol) was treated with a hexane solution (10 mL) of PPh<sub>2</sub>Me (35 mg, 0.17 mmol). After standing at room temperature for 20 h, the solvent was removed in vacuo, hexanes (100 mL) were added, and the mixture was stirred vigorously for 24 h. The brown extract

was filtered from the residue, which was again extracted with hexanes (60 mL, 20 h). The combined extracts were concentrated in vacuo to ca. 50 mL and filtered. Cooling of the filtrate to –80 °C gave brown crystals of 2b (45 mg, 36%). Anal. Calcd for C<sub>25</sub>H<sub>15</sub>O<sub>11</sub>Fe<sub>4</sub>P (745.75): C, 40.26; H, 2.03; P, 4.15. Found: C, 39.00; H, 2.31; P, 4.01. <sup>1</sup>H NMR (toluene-*d*<sub>8</sub>, 20 °C): δ 6.9–7.3 (m, Ph, 10H, corrected for solvent contributions), 1.62 (d, *J*<sub>PH</sub> = 8.8 Hz, CH<sub>3</sub>, 3H), –1.60 (dd, *J*<sub>PH</sub> = 5.7 Hz, *J*<sub>HH</sub> = 0.7 Hz, CH, 1H), –27.4 (br, Fe<sub>2</sub>H, 1H). <sup>13</sup>C{<sup>1</sup>H} NMR (toluene-*d*<sub>8</sub>, 20 °C): δ 331.9 (d, *J*<sub>CP</sub> = 9 Hz, CH, 1C), 214.0 (d, *J*<sub>CP</sub> = 15 Hz, CO, 2C), 211.1 (s, CO, 3C). The <sup>13</sup>C resonances of the phosphine ligand coincide with solvent resonances. <sup>31</sup>P{<sup>1</sup>H} NMR (toluene-*d*<sub>8</sub>, 20 °C): δ 42.8.

**Preparation of [(μ-H)Fe<sub>4</sub>(μ-η<sup>2</sup>-CH)(CO)<sub>11</sub>(PPhMe<sub>2</sub>)] (5 Fe–Fe) (2c).** This was prepared in the same manner as 2a. From 100 mg (0.17 mmol) of 1 and 24 mg (0.17 mmol) of PPh<sub>2</sub>Me, brown crystals of 2c were obtained, yield 55 mg (48%). Anal. Calcd for C<sub>20</sub>H<sub>13</sub>O<sub>11</sub>Fe<sub>4</sub>P (638.68): C, 35.14; H, 1.92; P, 4.53. Found: C, 35.33; H, 1.99; P, 4.27. <sup>1</sup>H NMR (toluene-*d*<sub>8</sub>, 20 °C): δ 7.1–6.9 (m, Ph, 5H, corrected for solvent contributions), 1.20 (d, *J*<sub>PH</sub> = 9.0 Hz, CH<sub>3</sub>, 6H), –2.00 (dd, *J*<sub>PH</sub> = 6.0 Hz, *J*<sub>HH</sub> = 1.0 Hz, CH, 1H), –27.5 (br, Fe<sub>2</sub>H, 1H). <sup>13</sup>C{<sup>1</sup>H} NMR (toluene-*d*<sub>8</sub>, 20 °C): δ 328.5 (d, *J*<sub>CP</sub> = 10 Hz, CH, 1C), 213.6 (d, *J*<sub>CP</sub> = 16 Hz, CO, 2C), 211.3 (s, CO, 3C). The <sup>13</sup>C resonances of the phosphine ligand coincide with solvent resonances. <sup>31</sup>P{<sup>1</sup>H} NMR (toluene-*d*<sub>8</sub>, 20 °C): δ 27.3.

**Preparation of [(μ-H)Fe<sub>4</sub>(μ-η<sup>2</sup>-CH)(CO)<sub>11</sub>(PMe<sub>3</sub>)] (5 Fe–Fe) (2d).** A solution of 150 mg (0.26 mmol) of 1 in 30 mL of pentane and 5 mL of THF was treated with a pentane solution (10 mL) of PMe<sub>3</sub> (20 mg, 0.26 mmol) at –70 °C. Upon addition of the phosphine, the previously brown solution turned red. The mixture was allowed to warm up to room temperature where upon its color changed to deep brown. It was allowed to stand for 15 h; then the solvent was removed in vacuo. The residue was extracted with 20 mL portions of pentane. The combined extracts were filtered and cooled to –20 °C for 24 h to afford 2d as dark brown needles (60 mg, 37%). Anal. Calcd for C<sub>15</sub>H<sub>11</sub>O<sub>11</sub>Fe<sub>4</sub>P (621.61): C, 28.98; H, 1.78; P, 4.98. Found: C, 28.81; H, 1.94; P, 5.00. <sup>1</sup>H NMR (toluene-*d*<sub>8</sub>, 20 °C): δ 0.83 (d, *J*<sub>PH</sub> = 10.0 Hz, CH<sub>3</sub>, 3H), –2.27 (dd, *J*<sub>PH</sub> = 7.0 Hz, *J*<sub>HH</sub> = 1.0 Hz, CH, 1H), –27.4 (dd, *J*<sub>PH</sub> = 1.0 Hz, *J*<sub>HH</sub> = 1.0 Hz, Fe<sub>2</sub>H, 1H). <sup>13</sup>C{<sup>1</sup>H} NMR (toluene-*d*<sub>8</sub>, 20 °C): δ 326.7 (d, *J*<sub>CP</sub> = 10 Hz, CH, 1C), 213.4 (d, *J*<sub>CP</sub> = 17 Hz, CO, 2C), 211.5 (s, CO, 3C). The <sup>13</sup>C resonances of the phosphine ligand coincide with solvent resonances. <sup>31</sup>P{<sup>1</sup>H} NMR (toluene-*d*<sub>8</sub>): 40 °C, δ 19.3; –80 °C, δ 20.4.

**Reaction of 1 with PCy<sub>3</sub> (Cy = cyclo-C<sub>6</sub>H<sub>11</sub>).** PCy<sub>3</sub> (50 mg, 0.18 mmol) was added to a solution of 100 mg (0.17 mmol) of 1 in 20 mL of hexanes and 5 mL of THF. The solution turned immediately red and a red oil separated. The mixture was allowed to stand at room temperature for 20 h. Solvent was removed in vacuo, and the red powder of [(HPCy<sub>3</sub>)]-[HFe<sub>4</sub>C(CO)<sub>12</sub>] was washed with hexanes and dried in vacuo. The yield was quantitative. The same product was obtained using CH<sub>2</sub>Cl<sub>2</sub> as a solvent. Anal. Calcd for C<sub>31</sub>H<sub>35</sub>O<sub>12</sub>Fe<sub>4</sub>P (853.97): C, 43.60; H, 4.13; P, 3.63. Found: C, 43.73; H, 4.13; P, 3.76. <sup>1</sup>H NMR (CD<sub>2</sub>Cl<sub>2</sub>, 20 °C): δ 5.04 (dq, *J*<sub>PH</sub> = 441.3 Hz, *J*<sub>HH</sub> = 3.8 Hz, PH, 1H), 2.5–1.2 (m, Cy, 33H), –26.6 (br, *w*<sub>1/2</sub> = 44 Hz, Fe<sub>2</sub>H, 1H). <sup>31</sup>P NMR (CD<sub>2</sub>Cl<sub>2</sub>, 20 °C): δ 34.4 (d, *J*<sub>PH</sub> = 442 Hz). IR (CH<sub>2</sub>Cl<sub>2</sub>, ν<sub>CO</sub>, cm<sup>–1</sup>): 2017 (sh), 2010 (vs), 1991 (s), 1982 (sh), 1933 (br, w); (ν<sub>PH</sub>, cm<sup>–1</sup>) 2308.

**X-ray Crystal Structure Determination of 2a.** Crystals of 2a were obtained by slow evaporation of the solvent from a hexane solution. Diffraction data were collected on an Enraf-Nonius CAD-4 diffractometer equipped with a graphite monochromator (Mo Kα, λ = 0.71069 Å). The intensities were collected in the *w*/2θ scan mode at room temperature. Crystal data and details of measurements are summarized in Table 8. The structure was solved by direct methods, followed by difference Fourier syntheses and subsequent least-squares

(31) <sup>13</sup>C(carbide) chemical shifts for several carbido cluster complexes prepared en route to <sup>13</sup>C-enriched 2a were also recorded: [Fe<sub>3</sub>C(CO)<sub>15</sub>], δ 485.7 (in CD<sub>2</sub>Cl<sub>2</sub>, 20 °C); [NEt<sub>4</sub>]<sub>2</sub>[Fe<sub>5</sub>C(CO)<sub>14</sub>], δ 477.4 (in THF-*d*<sub>8</sub>, 20 °C); [PPN]<sub>2</sub>[Fe<sub>3</sub>C(CO)<sub>12</sub>], δ 477.2 (in CD<sub>2</sub>Cl<sub>2</sub>, 0 °C). Our values for [Fe<sub>3</sub>C(CO)<sub>15</sub>] and [PPN]<sub>2</sub>[Fe<sub>3</sub>C(CO)<sub>12</sub>] agree well with data reported by Bradley (ref 10).

**Table 8. Details of the Crystal Structure Determination of 2a**

formula	$C_{30}H_{17}Fe_4O_{11}P$
crystal system	monoclinic
space group	$P2_1/n$
$a$ [Å]	13.136(6)
$b$ [Å]	15.084(7)
$c$ [Å]	16.265(4)
$\beta$ [°]	100.95(3)
$V$ [Å <sup>3</sup> ]	3164(2)
$Z$	4
$M_r$	807.8
$d_c$ [g cm <sup>-3</sup> ]	1.70
$F_{000}$	1616
$\mu$ (Mo $K\alpha$ ) [mm <sup>-1</sup> ]	190.7
X-radiation, $\lambda$ [Å]	Mo- $K\alpha$ , graphite monochromated, 0.71069
data collect. temp	ambient
$2\theta$ range [deg]	6–50
$hkl$ range	–15/15, 0/17, 0/19
reflins measd	5742
unique	5537 [ $R(\text{int}) = 0.055$ ]
absorption correctn	empirical
param refined	398
GOF on $F^2$	1.003
$R$ values	
$R_1$ [on $F$ , 2694 reflns with $I \leq \sigma(I)$ ]	0.055
$wR_2$ (on $F^2$ , all reflexions)	0.180

refinement. For all calculations the SHELXS86<sup>32a</sup> and SHELXL93<sup>32b</sup> programs were used. Absorption correction was applied by azimuthal scan of four reflections with  $\chi > 80^\circ$  [transmission range 0.75–1.00]. All non-hydrogen atoms were refined anisotropically. H atoms of phenyl groups were added in calculated positions [ $d(C-H) = 0.93$  Å] and refined “riding” on their respective C atoms. The H atom of the system  $\eta^2-CH$  was located from the Fourier map, and its position and isotropic thermal parameter were refined. The H(hydride) position was also located from a difference Fourier map, but coordinates and thermal parameters were not refined. A rigid-body model (angle (CCC) =  $120^\circ$ ,  $d(C-C) = 1.395$  Å) was adopted to refine the phenyl groups.

**MO Calculations.** The gross geometry of the  $Fe_4C$  cluster core common to **1** and **2** was taken from the crystal structure of **1** and idealized to the point group  $C_{2v}$ . Fe–Fe distances

were set to 2.60 Å (base–base) and 2.62 Å (apex–apex). The carbide carbon atom was placed 1.94 Å from the wing-base and 1.96 Å from the wing-tip iron atoms.  $PH_3$  ( $d_{PH} = 1.42$  Å,  $d_{FeP} = 2.24$  Å) was taken to model the  $PR_3$  ligands.<sup>33</sup> Fe–C(O) bond lengths were set to 1.80 Å and C–O bonds to 1.15 Å.

Extended Hückel calculations were carried out with CAO<sup>34</sup> using the wave functions supplied with the package. The weighted Wolfsberg–Helmholtz formula<sup>35</sup> was employed. The iterative self-consistent field Fenske–Hall (FH) procedure<sup>36</sup> employs the atomic basis functions and the molecular geometry as the only adjustable parameters. The STO basis functions used in the FH calculations have been developed by the Fenske group using the numerical  $X\alpha$  atomic orbital program of Herman and Skillman<sup>37</sup> in conjunction with the X $\alpha$ -to-Slater basis program of Bursten and Fenske.<sup>38</sup> Exponents of 4s and 4p atomic orbitals for iron were set to 2.0. A value of 1.20 was used for the hydrogen exponent. The FH calculations were also carried out for structures with the methylidyne carbon shifted away from the wing-tip iron Fe4 which is involved in the CHFe interaction ( $d_{FeC} = 1.92, 1.87$  Å).

**Acknowledgment.** H.W. gratefully acknowledges the support of the NATO Office of Scientific Affairs and the Fonds der Chemischen Industrie. This collaborative research was also supported by the Deutscher Akademischer Austauschdienst, Bonn, and the Conferenza Permanente dei Rettori delle Università Italiane, Roma, with a Vigoni grant to H.W. and D.B.

**Supplementary Material Available:** Tables of anisotropic thermal parameters and fractional atomic coordinates and a complete list of bond lengths and angles (6 pages). Ordering information is given on any current masthead page.

OM940164M

(33) Kostic, N. M.; Fenske, R. F. *Organometallics* **1982**, *1*, 489.

(34) Mealli, C.; Proserpio, D. M. *J. Chem. Educ.* **1990**, *67*, 399.

(35) Ammeter, J. H.; Bürgi, H. B.; Thibeault, J. C.; Hoffmann, R. *J. Am. Chem. Soc.* **1978**, *101*, 3686.

(36) Hall, M. B.; Fenske, R. F. *Inorg. Chem.* **1972**, *11*, 768.

(37) Herman, F.; Skillman, S. *Atomic Structure Calculations*; Prentice-Hall: Englewood Cliffs, NJ, 1963.

(38) Bursten, B. E.; Fenske, R. F. *J. Chem. Phys.* **1977**, *67*, 3138. Bursten, B. E.; Jensen, R. J.; Fenske, R. F. *J. Chem. Phys.* **1978**, *68*, 3320.

(32) (a) Sheldrick, G. M. *Acta Crystallogr.* **1990**, *A46*, 467. (b) Sheldrick, G. M.: SHELXL93, University of Göttingen, 1993.



# Hydroformylation with a Rhodium/Bulky Phosphite Modified Catalyst. Catalyst Comparison for Oct-1-ene, Cyclohexene, and Styrene

Annemiek van Rooy, Edwin N. Orij, Paul C. J. Kamer, and  
Piet W. N. M. van Leeuwen\*

Van't Hoff Research Institute, Department of Inorganic Chemistry, University of Amsterdam,  
Nieuwe Achtergracht 166, 1018 WV Amsterdam, The Netherlands

Received March 17, 1994<sup>®</sup>

The rhodium-catalyzed hydroformylation of oct-1-ene, cyclohexene, and styrene has been studied using  $\text{Rh}(\text{CO})_2\text{Acac}$  as the catalyst precursor and tris(2-*tert*-butyl-4-methylphenyl) phosphite as the ligand ( $T = 40\text{--}100\text{ }^\circ\text{C}$ ,  $P_{\text{CO}} = 2.5\text{--}44\text{ bar}$ ,  $P_{\text{H}_2} = 2.5\text{--}50\text{ bar}$ , toluene as a solvent). For oct-1-ene, very high hydroformylation rates are obtained ( $39.8 \times 10^3\text{ mol} [\text{mol Rh}]^{-1}\text{ h}^{-1}$ ) under mild conditions ( $P_{\text{CO}} = 10\text{ bar}$ ,  $P_{\text{H}_2} = 10\text{ bar}$ ,  $T = 80\text{ }^\circ\text{C}$ ). The concentration dependencies of the reaction rate show that the rate-determining step is the reaction of  $\text{H}_2$  with the acylrhodium complex. A negative order in the CO concentration is observed. For cyclohexene, the reaction rate is lower under the same conditions ( $512\text{ mol} [\text{mol Rh}]^{-1}\text{ h}^{-1}$ ,  $[\text{cyclohexene}] = 0.91\text{ M}$ ), the addition of cyclohexene to the starting rhodium hydride complex now being rate-limiting. In the hydroformylation of styrene, the rate is 3 times lower than that of oct-1-ene. For the formation of the linear 3-phenylpropanal, the rate-determining step is the reaction of  $\text{H}_2$  with the rhodium acyl species. CO inhibits the reaction. In contrast with the formation of the secondary 2-octyl species from oct-1-ene, the formation of the secondary (1-phenylethyl)rhodium species is reversible. For the formation of the branched aldehyde, the kinetics depend strongly on the CO partial pressure. At low CO pressures, addition of CO to the proposed ( $\eta^3$ -1-phenylethyl)rhodium intermediate is slow. At higher CO pressures, hydrogenolysis of the rhodium acyl intermediate is the rate-determining step and the rate decreases with increasing CO.

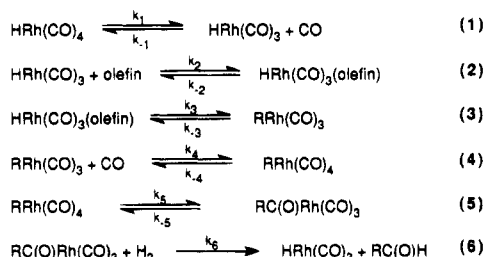
## Introduction

Much research has been conducted to elucidate the mechanism and the kinetics of the rhodium-catalyzed hydroformylation reaction.<sup>1</sup> It is commonly recognized that the reaction mechanism for the cobalt-catalyzed hydroformylation as pointed out by Heck and Breslow<sup>2</sup> is suitable for the rhodium analogue as well. Markó and co-workers<sup>3</sup> and more recently Garland<sup>4</sup> studied the unmodified rhodium carbonyl catalyst system very extensively. The active species is generally assumed to be  $\text{HRh}(\text{CO})_3$ , which is formed by dissociation of a CO ligand from the  $\text{HRh}(\text{CO})_4$  complex as Vidal and Walker<sup>5</sup> have evidenced. Very recently Garland<sup>6</sup> identified  $\text{RC}(\text{O})\text{Rh}(\text{CO})_4$  as the only observable reaction intermediate, using high-pressure infrared spectroscopy during the rhodium-catalyzed hydroformylation of 3,3-dimethylbut-1-ene starting with  $\text{Rh}_4(\text{CO})_{12}$ .

Markó found different kinetic equations for different types of alkenes.<sup>3</sup> Using hept-1-ene, under the typical reaction conditions of  $P_{\text{H}_2} = 33\text{--}126\text{ bar}$ ,  $P_{\text{CO}} = 40\text{--}170\text{ bar}$ ,  $T = 75\text{ }^\circ\text{C}$ , the kinetic expression is the following:

$$\frac{d[\text{aldehyde}]}{dt} = \frac{k[\text{Rh}][\text{H}_2]}{[\text{CO}]} \quad (1)$$

## Scheme 1. Generally Accepted Mechanism for the Hydroformylation Reaction Catalyzed by the Unmodified Rhodium Carbonyl Complex



This corresponds with the reaction of  $\text{H}_2$  and the rhodium acyl intermediate (Scheme 1, step 6) as rate-determining. Thus as these high pressures, the reaction is inhibited by CO. At lower CO pressures ( $P_{\text{CO}} \leq 20\text{ bar}$ ), the reaction is first order in  $[\text{CO}]$ , the coordination of CO to the rhodium-alkyl complex (Scheme 1, step 4) now appearing as rate-limiting. This proposal is contradicted<sup>6</sup> by the observation of  $\text{RC}(\text{O})\text{Rh}(\text{CO})_4$  as the only species present in the reaction mixture at 20 bars of pressure. However, the substrate used, 3,3-dimethylbut-1-ene, is a highly substituted alkene and the conditions are not quite the same. This can influence the reaction kinetics rigorously as has been shown recently.<sup>7</sup> For an internal olefin like cyclohexene and  $\text{Rh}_4(\text{CO})_{12}$  as the catalyst precursor, the rate expression

<sup>®</sup> Abstract published in *Advance ACS Abstracts*, November 1, 1994.

(1) Heil, B.; Markó, L. *Chem. Ber.* **1968**, *101*, 2209.

(2) Heck, R. F.; Breslow, D. S. *J. Am. Chem. Soc.* **1961**, *83*, 4023.

(3) (a) Csontos, G.; Heil, B.; Markó, L. *Ann. N.Y. Acad. Sci.* **1974**, *239*, 47. (b) Heil, B.; Markó, L.; Bor, G. *Chem. Ber.* **1971**, *104*, 3418.

(4) Garland, M.; Pino, P. *Organometallics* **1991**, *10*, 1693.

(5) Vidal, J. L.; Walker, W. E. *Inorg. Chem.* **1981**, *20*, 249.

(6) (a) Garland, M.; Bor, G. *Inorg. Chem.* **1989**, *28*, 410. (b) Garland, M.; Pino, P. *Inorg. Chem.* **1989**, *28*, L411.

reported by Markó<sup>3</sup> is

$$\frac{d[\text{aldehyde}]}{d[t]} = k[\text{cyclohexene}][\text{Rh}]^{0.25}[\text{H}_2]^{0.5} \quad (2)$$

From the kinetic equation and infrared data,<sup>3</sup> it was concluded that the addition of cyclohexene to the hydrido rhodium carbonyl complex is rate-determining with rhodium predominantly in the tetranuclear cluster.

The phosphine- or phosphite-modified catalyst system behaves differently. Several active species may be present in this catalytic system, and the complex that shows the highest linearity is generally accepted to be  $\text{HRh}(\text{CO})_2\text{L}_2$ , in which L represents an arylphosphine or a small phosphite.<sup>8</sup> Much research on the kinetics has been conducted, but only Cavalieri d'Oro and his co-workers have studied the catalysis under actual process conditions ( $P = 10\text{--}50$  bar,  $T = 80\text{--}120$  °C).<sup>9</sup> Their results (using propene as substrate and triphenylphosphine as ligand) showed that the reaction was zeroth order in both CO and  $\text{H}_2$  concentrations, which excludes the hydrogenolysis (Scheme 1, step 6) as being rate-determining. Despite these data, many authors still consider the hydrogenolysis as the turnover-limiting step.

Several reports<sup>10–12</sup> have appeared using phosphites as auxiliary ligands. These ligands are considered too sensitive to hydrolysis and alcoholysis.<sup>13</sup> However, phosphites are less sensitive toward oxidation than phosphines and they show, besides lower  $\sigma$ -donor capacities, better  $\pi$ -acceptor properties. The latter feature should make them interesting as modifying ligands covering a wide range of electronic variation. Since the early 1980s, the use of bulky phosphites in the rhodium-catalyzed hydroformylation has been a field of interest.<sup>11d,f,12a</sup> These ligands show a high reactivity in the hydroformylation of otherwise unreactive olefins<sup>12</sup> and are commercially applied for the formation of 3-methylpentane-1,5-diol.<sup>12c</sup> In contrast to the assertion that bulky phosphite containing catalysts are not applicable in the hydroformylation of alk-1-enes, we showed earlier a very high reaction rate of the hydroformylation of oct-1-ene using tris(2-*tert*-butyl-4-methyl-

**Table 1.** Influence of the Phosphite/Rhodium Ratio on the Different Reaction Parameters (Conditions:  $T = 80$  °C,  $P_{\text{CO}} = P_{\text{H}_2} = 10$  bar,  $[\text{Rh}(\text{CO})_2\text{Acac}] = 0.1$  mmol  $\text{dm}^{-3}$ ,  $[\text{oct-1-ene}] = 0.86$  mol  $\text{dm}^{-3}$  in 20 mL of toluene)

run	P/Rh	convn (%)	$k_{\text{ald}} (\times 10^3 \text{ mol mol}^{-1} \text{ h}^{-1})$	$n/\text{iso}$	isom (%)
1	10	31	39.7	2.0	16
2	50	23	38.4	1.9	12
3	50	32	42.5	1.9	12
4	50	30	38.5	1.9	14
5	250	29	43.2	1.9	12

phenyl) phosphite,<sup>14</sup> combined with an average regioselectivity (linear aldehyde:branched aldehyde = 2:1) and a low isomerization rate. A preliminary mechanistic study of this catalytic system was carried out by Jongmsma<sup>15</sup> using less reactive cycloalkenes as the substrates. Under 20 bar  $\text{H}_2/\text{CO}$ , the main rhodium species is  $\text{HRh}(\text{CO})_3\text{P}$  ( $\text{P} = \text{tris}(2\text{-}i\text{-tert-butylphenyl})$  phosphite) as was evidenced by NMR and IR spectroscopy, meaning that only one CO ligand is replaced by the bulky phosphite instead of two, which is the case with triphenylphosphine. Under hydroformylation conditions (after adding alkene), *in situ* IR showed that the same species was most abundant. Thus, his results indicate that the bulky phosphite modified system behaves differently from the triphenylphosphine-modified system.

In this article, we report on the kinetics of the bulky phosphite, tris(2-*tert*-butyl-4-methylphenyl) phosphite, modified system and the mechanism of the hydroformylation reaction is discussed. We studied the effects of  $\text{H}_2$  and CO pressures in the hydroformylation of oct-1-ene, cyclohexene, and styrene as well as the influence of the rhodium, ligand, and substrate concentrations.

## Results

For all substrates a 100% conversion could eventually be reached. To compare the results properly, we decided to present in the tables data obtained at similar substrate conversions.

**Oct-1-ene.** First, it was determined which tris(2-*tert*-butyl-4-methylphenyl) phosphite/rhodium ratio was sufficient to be certain that all rhodium particles are converted *in situ* into the active complexes and all the effects measured could be ascribed to the other varied conditions.<sup>5</sup> Jongmsma<sup>15</sup> found an enhancement in reaction rate at increasing phosphite/rhodium ratio and proved that at low phosphite concentrations  $\text{Rh}(\text{CO})_2\text{Acac}$  is not converted completely to a hydride. Table 1 summarizes the results of varying the P/Rh ratio. All results remained equal as the P/Rh ratio increased, and it was decided to use a minimum ratio of 50 in the kinetic experiments at a total rhodium concentration of 0.1 mmol  $\text{dm}^{-3}$ .

An increase of the reaction temperature causes an enhancement of both the rate of hydroformylation and that of isomerization, as can be seen in Table 2. Also a slight increase of the  $n/\text{iso}$  ( $n/i$ ) ratio is observable. The zeroth-order reaction rate constant for the formation of aldehyde changes from  $1.7 \times 10^3$  [mol] [mol Rh]<sup>-1</sup> h<sup>-1</sup> at 50 °C to  $87.3 \times 10^3$  [mol] [mol Rh]<sup>-1</sup> h<sup>-1</sup> at 90 °C,

(7) Van Rooy, A.; De Bruijn, J. N. H.; Van Leeuwen, P. W. N. M.; Roobeek, C. F. To be published.

(8) Brown, J. M.; Kent, A. G. *J. Chem. Soc., Perkin Trans. 2*, **1987**, 1, 597.

(9) (a) Cavalieri d'Oro, P.; Raimonde, L.; Pagani, G.; Montrasi, G.; Gresorio, G.; Andreetta, A. *Chim. Ind.* **1980**, 62(7-8), 572. (b) Cavalieri d'Oro, P.; Raimondt, L.; Pagani, G.; Montrasi, G.; Gregorio, G.; Oliveri del Castillo, G. F.; Andreetta, A. *Symposium on rhodium in homogeneous catalysis*; Veszprem, **1978**; pp 76–83.

(10) (a) Trzeciak, A. M.; Ziolkowski, J. J.; Aygen, S.; Van Eldik, R. *J. Mol. Catal.* **1986**, 34, 337. (b) Trzeciak, A. M.; Ziolkowski, J. J. *Trans. Met. Chem.* **1987**, 12, 408. (c) Trzeciak, A. M.; Ziolkowski, J. J. *Inorg. Chim. Acta Lett.* **1982**, 64, L267. (d) Trzeciak, A. M.; Ziolkowski, J. J. *J. Mol. Catal.* **1986**, 34, 213. (e) Janecko, H.; Trzeciak, A. M.; Ziolkowski, J. J. *J. Mol. Catal.* **1984**, 26, 355. (f) Trzeciak, A. M.; Ziolkowski, J. J. *J. Mol. Catal.* **1987**, 43, 13.

(11) (a) Pruett, R. L.; Smith, J. A. *J. Org. Chem.* **1969**, 34, 327. (b) Keblys, K. A. U.S. Patent 3 907 847, 1975, to Ethyl Corporation. (c) Van Leeuwen, P. W. N. M.; Roobeek, F. Brit. Pat. 2 068 377 A, 1981, to Shell. (d) Billig, E.; Abatjoglou, A. G.; Bryant, D. R. Eur. Pat. 861 122-562, 1986, to Union Carbide Corporation. (e) Bahrman, H.; Fell, B.; Papadogianakis, G. DE 3 942 954 A1, 1991, to Hoechst. (f) Bryant, D. R. 203rd National Meeting of the American Chemical Society, San Francisco, CA, 1992.

(12) (a) Van Leeuwen, P. W. N. M.; Roobeek, C. F. *J. Organomet. Chem.* **1983**, 258, 343. (b) Polo, A.; Real, J.; Claver, C.; Castillón, S.; Bayón, J. C. *J. Chem. Soc., Chem. Commun.* **1990**, 600. (c) Yoshinura, N. and Tokito, Y. Eur. Pat. 223 103, 1987, to Kuraray.

(13) Morrison, J. D. *Asym. Synth.* **1983**, 5.

(14) Van Rooy, A.; Orij, E. N.; Kamer, P. C. J.; Van den Aardweg, F.; Van Leeuwen, P. W. N. M. *J. Chem. Soc., Chem. Commun.* **1991**, 1096.

(15) Jongmsma, T.; Challa, G.; Van Leeuwen, P. W. N. M. *J. Organomet. Chem.* **1991**, 421, 121.

**Table 2. Temperature Effect on the Hydroformylation Results (Conditions:  $p_{\text{CO}} = p_{\text{H}_2} = 10$  bar,  $[\text{Rh}(\text{CO})_2\text{Acac}] = 0.1$  mmol dm<sup>-3</sup>,  $P/\text{Rh} = 50$ ,  $[\text{oct-1-ene}] = 0.86$  mol dm<sup>-3</sup> in 20 mL of Toluene)**

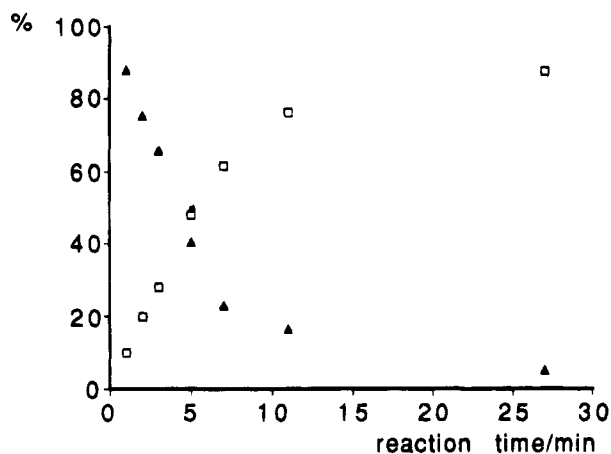
run	$T$ (°C)	convn (%)	$k_{\text{ald}} (\times 10^3 \text{ mol mol}^{-1} \text{ h}^{-1})$	$n/\text{iso}$	isom (%)
6	50	18	1.7	1.5	3
7	60	23	5.3	1.6	4
8	70	38	16.9	1.7	7
2-4 <sup>a</sup>	80	28	39.8	1.9	13
9	90	38	87.3	2.1	24

<sup>a</sup> The average values of runs 2, 3, and 4 are given,  $\sigma(n-1)(\text{TOF}) = 2.54 \times 10^3$ .

**Table 3. Substrate Dependency of the Hydroformylation Reaction Rate and Reaction Products (Conditions:  $T = 80$  °C,  $p_{\text{CO}} = p_{\text{H}_2} = 10$  bar,  $P/\text{Rh} = 50$ ,  $[\text{Rh}(\text{CO})_2\text{Acac}] = 0.1$  mmol dm<sup>-3</sup>,  $P/\text{Rh} = 50$ ,  $[\text{oct-1-ene}] = 0.86$  mol dm<sup>-3</sup> in 20 mL of Toluene)**

run	[oct-1-ene] (M)	convn (%)	$k_{\text{ald}} (\times 10^3 \text{ mol mol}^{-1} \text{ h}^{-1})$	$n/\text{iso}$	isom (%)
10	0.46	44	28.5	1.9	14
11	1.21	24	29.6	1.8	14
12	0.86	43	32.1	1.9	13
13 <sup>a</sup>	1.73	13	46.2	1.7	1.1
14 <sup>a</sup>	0.86	23	43.1	1.7	2.1
15 <sup>a</sup>	0.43	11	30.3	1.7	0.6
15 <sup>a</sup>	0.43	17	24.6	1.7	0.4
15 <sup>a</sup>	0.43	41	23.0	1.7	1.2

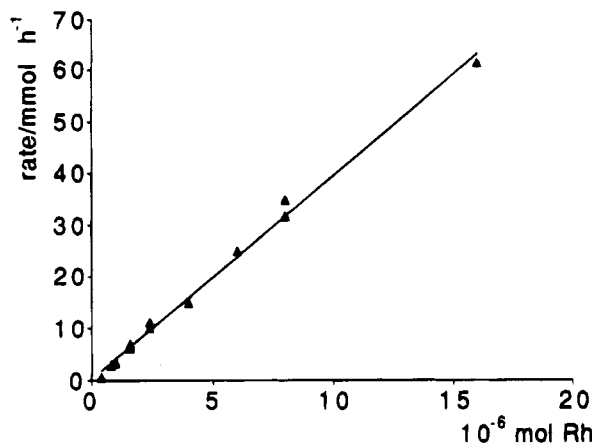
<sup>a</sup>  $p_{\text{CO}} = p_{\text{H}_2} = 40$  bar.



**Figure 1.** Course of a typical hydroformylation experiment: ( $\blacktriangle$ ) percentage of oct-1-ene in the reaction mixture, ( $\square$ ) percentage of formed aldehydes. Conditions:  $T = 80$  °C,  $p_{\text{CO}} = p_{\text{H}_2} = 10$  bar,  $[\text{Rh}(\text{CO})_2\text{Acac}] = 0.5$  mmol dm<sup>-3</sup>,  $[(2-t\text{-Bu-4-MeC}_6\text{H}_4\text{O})_3\text{P}] = 5$  mmol dm<sup>-3</sup>,  $[\text{oct-1-ene}] = 0.86$  mol dm<sup>-3</sup> in 20 mL of toluene.

and the amount of isomerization products is enlarged from 3% to 24%.

As can be concluded from Table 3 and Figure 1, in our dilute solution, the reaction rate is independent of the octene concentration up to at least 30% conversion. This concentration corresponds to a conversion of 95% if the reaction were carried out in pure octene. In Figure 1, the course of a typical reaction, performed at standard conditions, is drawn and it shows that the octene concentration decreases linearly with the reaction time up to even 60% conversion in this dilute solution. The ratio of the products that are formed (both of the aldehydes and internal octenes) is constant during that time. When the reaction of oct-1-ene begins to slow down, the internal octenes, formed via isomerization of oct-1-ene, are hydroformylated as well, resulting in



**Figure 2.** Dependency of the reaction rate on the concentration of the catalyst precursor (runs 16-29).  $\blacktriangle$  = turnover number. Conditions:  $T = 60$  °C,  $p_{\text{H}_2} = p_{\text{CO}} = 10$  bar,  $[(2-t\text{-Bu-4-MeC}_6\text{H}_4\text{O})_3\text{P}] = 5$  mmol dm<sup>-3</sup>,  $[\text{oct-1-ene}] = 0.86$  mol dm<sup>-3</sup> in 20 mL of toluene.

several branched aldehydes and hence causing a disturbance in the initial normal to branched ratios.

We repeated these reactions under pseudo-zeroth-order conditions in CO and H<sub>2</sub>, *i.e.* 80 bar CO/H<sub>2</sub> (runs 13-15), and these results confirmed what we stated before: in the higher concentration region, no substrate dependency was observed. From  $\approx 50\%$  conversion of our standard oct-1-ene concentration ( $=0.86$  M), the octene appears in the reaction equation as we found indeed for the low concentration experiment a lower initial rate in agreement with Figure 1. The order we determined for that region was around 0.3.

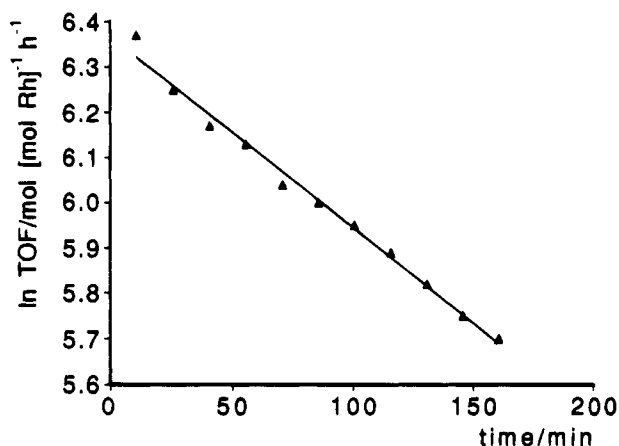
We also studied the effects of the rhodium precursor concentration on the rate of the hydroformylation reaction. To avoid exothermic temperature effects at high catalyst concentrations and 80 °C, we did the measurements at 60 °C and we varied the rhodium concentration from 0.2 to 8 times our standard concentration. From Figure 2 it is clear that the rate of formation of the product aldehydes is linearly proportional to the rhodium precursor concentration. So it can be concluded that the reaction rate has in this low concentration region a first-order dependency on the rhodium concentration. From this figure, it can also be concluded that diffusion of the gases into the solution is not rate-limiting. Otherwise, at enhanced rhodium concentrations, *i.e.* at higher overall gas consumptions, this diffusion limitation would have shown up in decreased reaction rates, higher amounts of isomerized alkene, and a higher normal ( $n$ ) to iso ratio. None of these phenomena were observed (see also Experimental Section).

Variation of the total pressure ( $p_{\text{CO}}/p_{\text{H}_2} = 1$ ) causes a slight increase in the hydroformylation reaction rate, and the normal to iso ratio decreases from 2.1 to 1.8 (Table 4). However, the formation of internal octenes, caused by isomerization of oct-1-ene, decreases significantly at higher overall pressures. The table shows that the rate of formation of both the normal and the branched aldehydes as well as the rate of the isomerization reaction is first order in H<sub>2</sub> concentration. No significant change in the  $n/\text{iso}$  ratio is observable. The hydroformylation reaction rate, however, shows an inverse dependency on the CO partial pressure. At very low CO pressures, the reaction even has a runaway

**Table 4. Effect of Variation of Pressures on the Hydroformylation of Oct-1-ene (Conditions:  $P_{\text{Rh}} = 50$ ,  $T = 80$  °C,  $[\text{Rh}(\text{CO})_2\text{Acac}] = 0.1 \text{ mol dm}^{-3}$ ,  $[\text{oct-1-ene}] = 0.86 \text{ mol dm}^{-3}$  in 20 mL of toluene)**

run	$P_{\text{H}_2}$ (bar)	$P_{\text{CO}}$ (bar)	convn (%)	$k_{\text{ald}} (\times 10^3 \text{ mol mol}^{-1} \text{ h}^{-1})$	$n/\text{iso}$	isom (%)
30	2.5	2.5	28	30.5	2.1	28
4	10	10	30	38.5	1.9	14
31	15	15	28	43.7	1.8	9
32	20	20	32	45.4	1.8	6
4	10	10	30	38.5	1.9	12
33	10	21	28	25.6	1.7	8
34	10	32	30	14.3	1.7	6
35	10	40	17	7.6	1.7	3
8	10 <sup>a</sup>	10	38	16.9	1.7	7
36	20 <sup>a</sup>	10	28	34.9	1.7	6
37	30 <sup>a</sup>	10	28	39.4	1.7	5
38	30 <sup>a</sup>	10	28	42.3	1.7	5
39	40 <sup>a</sup>	10	32	72.4	1.7	5
40	50 <sup>a</sup>	10	28	85.2	1.7	5

<sup>a</sup>  $T = 70$  °C.



**Figure 3.** In plot of the average turnover frequency of the hydroformylation of cyclohexene (calculated by means of the pressure drop) against the reaction time.  $\blacktriangle$  = turnover number. Conditions:  $T = 80$  °C,  $P_{\text{CO}} = P_{\text{H}_2} = 10$  bar  $P/\text{Rh} = 10$ ,  $[\text{Rh}(\text{CO})_2\text{Acac}] = 1 \text{ mmol dm}^{-3}$  [cyclohexene] =  $0.91 \text{ mol dm}^{-3}$  in 20 mL of toluene.

character. The CO present in the reaction mixture is consumed so fast that diffusion of CO from the vapor into the solution becomes rate-determining. At increasing CO pressure, the isomerization reaction is suppressed.

**Cyclohexene.** The hydroformylation of substituted alkenes is, as known, much slower than the hydroformylation of 1-alkenes. For cyclohexene, the ln plot (Figure 3) of conversion *vs* time shows clearly that the reaction rate is first order in cyclohexene concentration. The rate constant determined from the ln plot is  $512 \text{ [mol] [mol Rh]}^{-1} \text{ h}^{-1}$  ( $T = 80$  °C,  $P_{\text{CO}} = P_{\text{H}_2} = 10$  bar, initial cyclohexene concentration =  $0.91 \text{ M}$ ), being 80 times lower than for oct-1-ene (note: this comparison is of limited value because the hydroformylation of oct-1-ene shows a zeroth-order dependency in substrate concentration).

In Table 5, the influence of the reaction temperature on the reaction rate is presented. Raising the initial temperature results in an increase of the rate constant. Going from 70 to 100 °C, the reaction proceeds faster by a factor of approximately 10. The determined initial turnover frequencies are respectively 176 and 1636  $[\text{mol}][\text{mol Rh}]^{-1} \text{ h}^{-1}$  ( $P_{\text{CO}} = P_{\text{H}_2} = 10$  bar, initial cyclohexene concentration =  $0.91 \text{ M}$ ).

**Table 5. Influence of the Temperature on the Rate of Hydroformylation of Cyclohexene (Conditions:  $P_{\text{CO}} = P_{\text{H}_2} = 10$  bar,  $P/\text{Rh} = 10$ ,  $[\text{Rh}(\text{CO})_2\text{Acac}] = 1 \text{ mmol dm}^{-3}$ , [cyclohexene] =  $0.91 \text{ mol dm}^{-3}$  in 20 mL of Toluene)**

run	$T$ (°C)	convn (%)	$k_{\text{ald}} (\text{mol mol}^{-1} \text{ h}^{-1})$
41	70	27	176
42	80	34	512
43	90	37	788
44	100	41	1636

**Table 6. CO- and H<sub>2</sub>-Pressure Influence on the Rate of Hydroformylation of Cyclohexene (Conditions:  $T = 80$  °C,  $P/\text{Rh} = 10$ ,  $[\text{Rh}(\text{CO})_2\text{Acac}] = 1 \text{ mmol dm}^{-3}$ , [cyclohexene] =  $0.91 \text{ mol dm}^{-3}$  in 20 mL of Toluene)**

run	$P_{\text{H}_2}$ (bar)	$P_{\text{CO}}$ (bar)	$k_{\text{ald}} (\text{mol mol}^{-1} \text{ h}^{-1})$
45	10	10	512
46	15	10	555
47	20	10	573
48	30	10	652
49	10	5	607
50	10	20	324
51	10	30	244
52	10	40	219

**Table 7. P/Rh Dependency of Hydroformylation of Styrene (Conditions:  $T = 80$  °C,  $P_{\text{CO}} = P_{\text{H}_2} = 11$  bar,  $[\text{Rh}(\text{CO})_2\text{Acac}] = 0.25 \text{ mmol dm}^{-3}$ , [styrene] =  $0.89 \text{ mol dm}^{-3}$  in 20 mL of Toluene)**

run	P/Rh	convn (%)	$k_{\text{ald}} (\times 10^3 \text{ mol mol}^{-1} \text{ h}^{-1})$	iso/n
53	5	21	4.1	3.3
54	20	25	19.8	3.0
55	20	21	14.6	3.4
56	20	19	15.0	3.4
57 <sup>a</sup>	50	19	16.0	3.7
58	200	25	19.6	3.1

<sup>a</sup>  $[\text{Rh}(\text{CO})_2\text{Acac}] = 0.002 \text{ mmol}$  in 20 mL.

**Table 8. Influence of the Initial Styrene Concentration on the Reaction Rate and Selectivity (Conditions:  $T = 70$  °C,  $P_{\text{CO}} = P_{\text{H}_2} = 11$  bar,  $[\text{Rh}(\text{CO})_2\text{Acac}] = 0.25 \text{ mmol dm}^{-3}$ ,  $P/\text{Rh} = 20$  in 20 mL of Toluene)**

run	[styrene] (M)	convn (%)	iso/n	$k_{\text{ald}} (\times 10^3 \text{ mol mol}^{-1} \text{ h}^{-1})$
59	0.47	38	5.1	11.3
60	0.89	23	5.9	12.0
61	1.27	24	5.5	10.9

The pressure dependencies are clear; the H<sub>2</sub> concentration has a slightly positive effect on the reaction rate (see Table 6), the order in  $p_{\text{H}_2}$  being approximately 0.2. The CO pressure affects the reaction rate very significantly. The  $k_0$  is decreased by a factor of 3, going from 5 to 40 bar of CO, which corresponds with a negative order in CO ( $\approx -0.65$ ).

**Styrene.** From Table 7 it is clear that a P/Rh ratio of 5 is too small to transform all rhodium into an active catalyst but that a ratio of 20 is sufficient.

Variation of the initial styrene concentration hardly influenced the reaction rate and the normal to branched ratio (Table 8). We found an average overall reaction rate of  $10.2 \times 10^3 \text{ [mol] [mol Rh]}^{-1} \text{ h}^{-1}$  ( $T = 70$  °C, [styrene] =  $0.89 \text{ M}$ , rate averaged over about 30% conversion of styrene) which is a factor of 3 lower than the rate found for oct-1-ene.

As in the hydroformylation of other substrates, an increase in temperature leads to an enlarged overall reaction rate but, more noteworthy, to a considerable decrease of the selectivity toward the branched aldehyde

**Table 9. Influence of the Reaction Temperature on the Rate and Selectivity of the Hydroformylation of Styrene (Conditions:  $P_{\text{CO}} = P_{\text{H}_2} = 11$  bar,  $[\text{Rh}(\text{CO})_2\text{Acac}] = 0.25$  mmol dm<sup>-3</sup>,  $[\text{styrene}] = 0.89$  mol dm<sup>-3</sup>,  $P/\text{Rh} = 20$  in 20 mL of Toluene)**

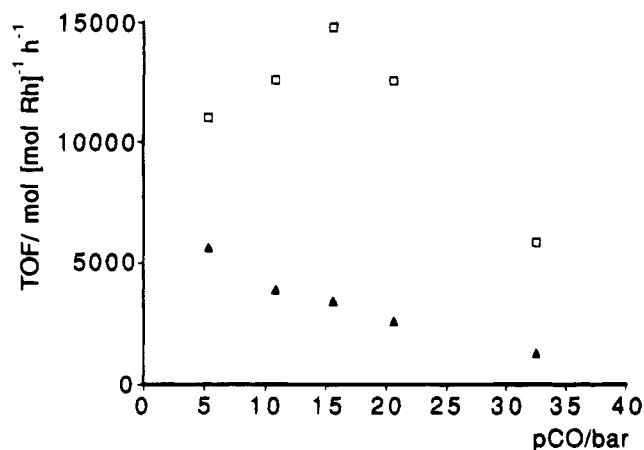
run	$T$ (°C)	convn (%)	iso/n	$k_{n\text{-ald}}$ ( $\times 10^3$ mol mol <sup>-1</sup> h <sup>-1</sup> )	$k_{\text{isoald}}$ ( $\times 10^3$ mol mol <sup>-1</sup> h <sup>-1</sup> )
62	51	23	10.6	0.2	2.1
63	60	22	7.6	0.8	5.8
64	70	23	5.9	1.8	10.2
54–56 <sup>a</sup>	80	22	3.3	3.9	12.6
65	90	27	2.1	6.2	12.6

<sup>a</sup> Average of runs 54, 55, 56 is given,  $\sigma(n-1)(\text{TOF}) = 2.00 \times 10^3$ .

**Table 10.  $P_{\text{H}_2}$  and  $P_{\text{CO}}$  Influence on the Rate and Selectivity of the Hydroformylation of Styrene (Conditions:  $T = 80$  °C,  $[\text{Rh}(\text{CO})_2\text{Acac}] = 0.25$  mmol dm<sup>-3</sup>,  $P/\text{Rh} = 20$ ,  $[\text{styrene}] = 0.89$  mol dm<sup>-3</sup> in 20 mL of Toluene)**

run	$P_{\text{H}_2}$ (bar)	$P_{\text{CO}}$ (bar)	convn (%)	iso/n	$k_{n\text{-ald}}$ ( $\times 10^3$ mol mol <sup>-1</sup> h <sup>-1</sup> )	$k_{\text{isoald}}$ ( $\times 10^3$ mol mol <sup>-1</sup> h <sup>-1</sup> )
66	5	11	11	2.3	2.7	6.3
54–56 <sup>a</sup>	11	11	22	3.3	3.9	12.6
67	17	11	20	4.4	5.5	24.4
68	24	11	21	4.7	8.0	37.8
69	11	5	21	2.0	5.6	11.0
54–56 <sup>a</sup>	11	11	22	3.3	3.9	12.6
70	10	16	23	4.3	3.4	14.8
71	10	21	23	5.0	2.3	11.4
72	10	33	18	4.5	1.3	5.9

<sup>a</sup> Average of runs 54, 55, 56 is given,  $\sigma(n-1)(\text{TOF}) = 2.00 \times 10^3$ .



**Figure 4.** Dependency of the rate of formation of aldehydes on CO pressure. TOF = turnover frequency,  $\square$  = turnover frequency for the branched aldehydes,  $\blacktriangle$  = turnover frequency for the normal aldehydes. Conditions:  $T = 80$  °C,  $P_{\text{H}_2} = 11$  bar,  $[\text{Rh}(\text{CO})_2\text{Acac}] = 0.25$  mmol dm<sup>-3</sup>,  $[(2\text{-tBu-4-MeC}_6\text{H}_4\text{O})_3\text{P}] = 5$  mmol dm<sup>-3</sup>,  $[\text{styrene}] = 0.89$  mol dm<sup>-3</sup> in 20 mL of toluene.

(Table 9). At temperatures above 80 °C, the observed rate for isoaldehydes remains equal. Remarkably (Table 10), the order in  $\text{H}_2$  for the formation of linear aldehydes is lower than 1 and the order in  $\text{H}_2$  for the formation of isoaldehydes is larger than 1. This means that the regioselectivity is also dependent on the  $\text{H}_2$  pressure; at increasing  $\text{H}_2$  pressure the formation of branched aldehyde is more favored. At an increasing  $\text{CO}/\text{H}_2$  ratio, the hydroformylation reaction is suppressed, the formation of the isoaldehyde being slightly less affected (Table 10). As a result the plot of the rate of formation of branched aldehydes vs CO pressure shows a maximum (Figure 4).

## Discussion

**Oct-1-ene.** The high hydroformylation rates are remarkable. As reported by Jongsmas,<sup>15</sup> in competition with CO, only one phosphite coordinates to the Rh center due to its large cone angle ( $180^\circ$ , cf.  $\text{PPh}_3$   $145^\circ$ ).<sup>16</sup> This complex has, similar to the  $\text{HRh}(\text{CO})_4$  catalyst, a strong aptitude for CO dissociation compared with the triphenylphosphine-modified catalyst. With only one phosphite bonded to the rhodium, the 16-electron complex easily binds to the olefin, thus initiating a very fast reaction cycle. Due to the large space available in comparison with the  $\text{HRh}(\text{CO})_2(\text{PPh}_3)_2$  system, the reaction to the branched aldehyde proceeds with relative ease as well, resulting in a moderate overall linearity.

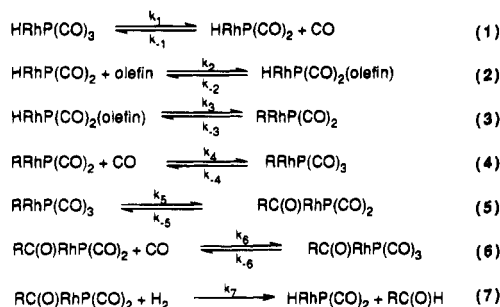
Another remarkable result is the runaway character of the reaction. This is probably the reason that some other authors<sup>6,11</sup> postulated that bulky phosphite ligands induce a high isomerization rate and hence are not applicable as modifying ligands in the hydroformylation of terminal alkenes. The hydroformylation reaction proceeds so fast that all CO present in solution is consumed. At very low concentrations of CO, the mass transport is now rate-determining and the system catalyzes isomerization (see also Experimental Section). When all terminal alkenes are converted into aldehydes, the internal alkenes start to participate in the hydroformylation as well. As a result, the high isomerization rates give low  $n/\text{iso}$  ratios. To circumvent this problem, the reaction rate has to be low or the stirring of the reaction mixture has to be efficient. In our apparatus with magnetic stirring bars, no kinetic measurements could be done at CO pressures below 5 bar and a rhodium concentration above 0.8 mmol dm<sup>-3</sup>, but otherwise stirring was effective.

A first-order dependency in  $\text{H}_2$  concentration indicates that the  $\text{H}_2$  reaction with the rhodiumacyl intermediate is the rate-determining step. Cavalieri d'Oro and co-workers<sup>9</sup> found that when propene was hydroformylated with the  $\text{PPh}_3$ -modified rhodium carbonyl complex, higher  $\text{H}_2$  pressures affect the reaction rate only slightly and the value found for the order in  $\text{H}_2$  was between 0.0 and 0.05. Thus, the bulky phosphite system does not resemble the triphenylphosphine-modified catalyst but our reaction appears to fit the kinetics found for the unmodified rhodium carbonyl catalyst by Markó *et al.*<sup>3</sup> (eq 1) who used 1-heptene as a substrate and performed the reaction at pressures above 75 bar. We found approximately the same dependency on  $\text{H}_2/\text{CO}$  and Rh, and our initial reaction rate was also independent of the olefin concentration when oct-1-ene was used as a substrate (even at these low concentrations). After 50% conversion or at the corresponding initial oct-1-ene concentrations, the reaction rate becomes dependent on the alkene concentration, but for further considerations we choose to focus on the catalyst behavior at the initial conditions. The only step of the reaction mechanism featuring a reaction with  $\text{H}_2$  is the hydrogenolysis of  $\text{RC}(\text{O})\text{Rh}(\text{CO})_{4-n}\text{P}_n$  forming the aldehyde and regenerating the starting catalytic active rhodium complex (step 7 in Scheme 2).

The negative order in CO can be due to two steps in the reaction cycle where CO can play an inhibiting role (steps 1 and 6 of Scheme 2). Step 1 can be ruled out

(16) Tolman, C. A. *Chem. Rev.* **1977**, 313.

**Scheme 2. Proposed Mechanism of the Tris(2-*tert*-butyl-4-methylphenyl) Phosphite Modified Rhodium-Catalyzed Hydroformylation**



from any significant importance because the reaction rate is found to be independent of the oct-1-ene concentration (provided that  $k_{-1}[\text{CO}] \gg k_2[\text{oct-1-ene}]$ ).<sup>17</sup> The second step where the presence of a CO molecule can inhibit the reaction is in step 6, after the rhodium acyl complex has been formed. After step 5, two onward reactions are possible. First, reaction with H<sub>2</sub> can take place, which finally results in the starting catalyst complex and product aldehyde. Second, a molecule of CO can occupy the vacant site and a saturated inactive complex is formed, thus inhibiting the completion of the cycle. The order in CO is explained by the equilibrium represented by step 6 in Scheme 2. The resulting negative order in CO suggests that the acyl species rather than the alkyl species is the most abundant species under the reaction conditions; Garland<sup>6</sup> observed  $\text{RC(O)Rh}(\text{CO})_4$  in the system without modifying ligands, and although he used a different substrate, neohexene, he found approximately the same rate equation (zeroth order in substrate concentration). The fact that we found an order in CO that is somewhat larger than -1 (about -0.5 to -1) suggests that certain reaction steps have rates of similar magnitude, which results in a less clear-cut rate equation. It was nearly impossible to derive a useful rate equation comprising all seven steps which can be applied for all substrates,<sup>18</sup> and we are forced to treat the different substrates separately. We start from the experimentally determined concentration dependencies and choose only that part of the scheme that is likely to fit the data (see also cyclohexene discussion).

For oct-1-ene, the hydrogenolysis is rate-determining (step 7, Scheme 2):

$$r = k_7[\text{RhP}(\text{CO})_2\text{C(O)R}][\text{H}_2] \quad (3)$$

It is assumed that all forward steps are faster and that step 6 is in equilibrium. Furthermore we prefer a preequilibrium treatment rather than a steady state approach since after some time the equilibrium of step 6 will be established. With  $[\text{Rh}_t] \approx [\text{RhP}(\text{CO})_2\text{C(O)R}] + [\text{RhP}(\text{CO})_3\text{C(O)R}]$ , the next equation is obtained:

$$r = \frac{k_7[\text{H}_2][\text{Rh}_t]}{K_6[\text{CO}] + 1} \quad (4)$$

When  $K_6[\text{CO}] \gg 1$ , (4) is reduced to

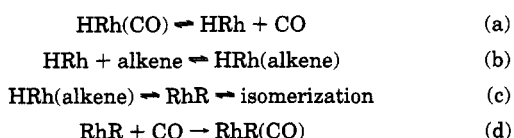
$$r = \frac{k_7[\text{H}_2][\text{Rh}_t]}{K_6[\text{CO}]} \quad (5)$$

This equation describes the observed first order in H<sub>2</sub> and inverse first order in CO and is indeed similar to that of the unmodified system, eq 1, described by Markó.<sup>3</sup>

A regularly recurring subject is the selectivity to hydroformylation *vs* isomerization and the normal to branched ratio. The relation between the observed isomerization and the normal to branched ratio has been clearly explained by Lazzaroni.<sup>19,20</sup> Isomerization is a result of  $\beta$ -hydride elimination of the isoalkyl bonded to the rhodium. The elimination can occur from two different sides of the secondary bonded alkyl forming either 1-alkene or 2-alkene. Because this reaction has a higher free energy of activation than the hydroformylation reaction and because  $\beta$ -hydride elimination requires a vacant site, the proportion of isomerization is expected to increase with higher temperatures and lower pressures. Lazzaroni showed by means of deuterioformylation of hex-1-ene that indeed the degree of isomerization depended on the reaction conditions. No isomerization occurred at low temperatures, and the amount of deuterated rearrangement products was higher for the branched than for the linear metal-alkyl. At a reaction temperature of 100 °C, for linear alkyls, the hydroformylation predominates  $\beta$ -hydride elimination, but for the branched alkyl, elimination predominates hydroformylation. This was also observed for the bulky phosphite system (see Table 2). In the present system the degree of isomerization increases with temperature. Although isomerization of the linear alkyl is not productive, we exclude  $\beta$ -hydride elimination. Otherwise, our kinetic data would be distributed and not give such a clear picture as is shown here;  $\beta$ -hydride elimination of the linear alkyl species would cause a decrease in the overall rate of formation of aldehydes.

(17) The *in situ* infrared spectrum during the hydroformylation of oct-1-ene showed a species clearly different from the  $\text{HRhP}(\text{CO})_3$  (P = tris(2-*tert*-butyl-4-methylphenyl) phosphite) complex (2093 (w), 2045 (s), and 2016  $\text{cm}^{-1}$  (s)), the predominant species expected if the rate-limiting step is the addition of the substrate as indeed occurred when cyclohexene was hydroformylated. The observed carbonyl frequencies during the hydroformylation of oct-1-ene were 1955 (w), 2027 (s), and 2043 (s), and no change occurred when H<sub>2</sub> was replaced by D<sub>2</sub> (conditions:  $T = 65$  °C,  $P_{\text{H}_2} = 5$  bar,  $P_{\text{CO}} = 15$  bar,  $[\text{Rh}(\text{CO})_2\text{Acac}] = 3.24$  mmol  $\text{dm}^{-3}$ ,  $[\text{tris}(2\text{-}i\text{-tert-butyl-4-methylphenyl) phosphite}] = 52.83$  mmol  $\text{dm}^{-3}$ , and  $[\text{oct-1-ene}] = 1.04$  mol  $\text{dm}^{-3}$  in 12 mL of cyclohexane). No acyl CO frequency could be observed probably because (if present) it would absorb in the same region as the aldehyde carbonyl group.

(18) We made an attempt to describe the kinetic behavior with four steps involved. The mechanism was reduced to the following sequence:



With eq a in preequilibrium, employing a steady state approach for  $[\text{HRh}(\text{alkene})]$  and  $[\text{RhR}]$  and making the assumption that  $[\text{Rh}_t] = [\text{HRh}(\text{CO})] + [\text{HRh}] + [\text{HRh}(\text{alkene})] + [\text{RhR}]$  we obtained the following

equation:

$$r = \frac{K_1 k_2 k_3 k_4 [\text{Rh}_t] [\text{alkene}] [\text{CO}]}{A + B[\text{alkene}] + C[\text{alkene}][\text{CO}] + D[\text{CO}] + E[\text{CO}]^2}$$

with  $A = K_1 k_2 k_3$ ,  $B = K_1 k_2 k_3 + K_1 k_2 k_{-3}$ ,  $C = K_1 k_2 k_4$ ,  $D = K_1 k_{-2} k_4 + K_1 k_3 k_4 + k_{-2} k_{-3}$ , and  $E = k_{-2} k_4 + k_3 k_4$ , which reduces under suitable conditions to (a). The total derivation as well as those of the used rate equations are available as supplementary material.

(19) Lazzaroni, R.; Ucello-Barretta, G.; Benetti, M. *Organometallics* **1989**, *8*, 2323.

(20) Lazzaroni, R.; Raffaelli, A.; Settambolo, R.; Bertozzi, S.; Vitulli, G. *J. Mol. Catal.* **1989**, *50*, 1.

As only the isoalkylrhodium will form internal alkenes (Scheme 3), the relative amount of branched aldehyde diminishes and the apparent initial normal to branched ratio will be higher, and is indeed the case (see tables). Since 1-alkenes are much more reactive than internal alkenes, significant hydroformylation of the latter will take place only after most of the alk-1-ene has been consumed.

When no  $\beta$ -hydride elimination takes place ( $k_3 \gg k_{-3}$ ), the irreversible step 3 (Scheme 2) determines the regioselectivity and yet the hydrogenolysis step 7 (Scheme 2) is rate-determining. When the substrate conversion is high and the conditions are chosen such that step 3 (Scheme 2) is only reversible for 2-alkyl intermediates, the isomerization products are hydroformylated and the regioselectivity depends on the degree of conversion. The kinetics of the internal alkenes are different, as now coordination of alkene to rhodium (step 2) is rate-determining.

**Cyclohexene.** A first-order dependency in cyclohexene concentration, a negative order in CO, and a very slightly positive order in  $H_2$  leads to the conclusion that the rate-determining step is no longer the hydrogenolysis reaction (Scheme 2, step 7) as was found for oct-1-ene. The data clearly indicate that one of the steps preceding step 7 is now rate-determining. Most likely, the exchange of one CO ligand for cyclohexene (Scheme 2, step 2) is the slowest step. Due to its internal double bond cyclohexene approaches the rhodium center less easily, *i.e.*

$$r = k_2[\text{RhH}][\text{cyclohexene}] \quad (6)$$

From the assumption that  $\text{RhP}(\text{CO})_3\text{H}$  and  $\text{RhP}(\text{CO})_2\text{H} + \text{CO}$  occur in preequilibrium and  $[\text{Rh}_t] = [\text{RhP}(\text{CO})_2\text{H}] + [\text{RhP}(\text{CO})_3\text{H}]$ , it follows that

$$r = \frac{K_1 k_2 [\text{Rh}_t] [\text{cyclohexene}]}{K_1 + [\text{CO}]} \quad (7)$$

This relation describes both the observed orders in the rhodium precursor and cyclohexene and the negative order in CO. The kinetic expression would also be in accordance with step 3 being the rate-determining step following a fast preequilibrium of steps 1 and 2. However, this seems unlikely since upon migration (Scheme 2, step 3) the steric repulsion is released.

Our results are not completely in agreement with the kinetic results that Markó obtained with the rhodium carbonyl system. He observed an equal dependence in the cyclohexene concentration but he did not notice any influence of the CO partial pressure, for which we found an order between  $-0.6$  and  $-0.7$ . This can be due to the different nature of the active complexes  $\text{HRh}(\text{CO})_4$  and  $\text{HRhP}(\text{CO})_3$  ( $P = \text{tris}(2\text{-tert-butyl-4-methylphenyl})\text{phosphite}$ ). Furthermore,  $\text{HRh}(\text{CO})_4$  is in equilibrium with a tetrameric rhodium cluster. The complexes may have a different aptitude for CO dissociation resulting in a different overall kinetic equation. Little mechanistic research has been done on the triphenylphosphine-modified rhodium-catalyzed hydroformylation of cyclic alkenes because of their poor reactivity,<sup>21</sup> but it

would seem that also for these catalysts the association of metal and alkene is rate-determining.

**Styrene.** The hydroformylation of styrene with the bulky phosphite modified catalyst is somewhat slower than that of oct-1-ene. This is in contrast with results obtained with  $\text{Rh}_4(\text{CO})_{12}$  and  $\text{RhH}(\text{CO})(\text{PPh}_3)_3$  as catalyst. With  $\text{Rh}_4(\text{CO})_{12}$  as the catalyst, styrene reacted more than twice as fast ( $124 \times 10^3$  [mol] [min]<sup>-1</sup> for styrene vs  $50.1 \times 10^3$  [mol] [min]<sup>-1</sup> for oct-1-ene,  $5.3 \times 10^{-2}$  mM  $\text{Rh}_4(\text{CO})_{12}$ ,  $75^\circ\text{C}$ ,  $P = 130$  bar).<sup>22</sup> With the triphenylphosphine-modified catalyst, styrene reacted somewhat faster than the unsubstituted 1-alkenes as hex-1-ene, hept-1-ene, and dodec-1-ene<sup>21</sup> (styrene: 2.8 cycles/h vs hex-1-ene and hept-1-ene 2.3 and dodec-1-ene 2.0 cycles/h, 2.5 mM catalyst concentration, 1.0 M substrate in benzene,  $25^\circ\text{C}$ , 0.7 bar,  $\text{CO}/\text{H}_2 = 1$ ) although comparison were is difficult because of the different kinetic expression found for this catalyst system. The lower rate of the bulky phosphite catalyst for styrene vs 1-octene cannot be assigned to the larger phenyl substituent at the alkene, since the addition of alkene to rhodium does not show up in the rate equation; also in the report of Lazzaroni<sup>23</sup> the rate of styrene conversion is independent of the styrene concentration in the range of 0.4 to 2.4 mol dm<sup>-3</sup> (180 bar,  $90^\circ\text{C}$ ,  $\text{Rh}_4(\text{CO})_{12}$  catalyst). It is also unlikely that the hydrogenolysis reaction would strongly depend on the nature of the organic fragment of the rhodium acyl group (respectively 1-nonanoyl, 2-methyloctanoyl, 2-phenylpropanoyl, 3-phenylpropanoyl), although a slightly different rate ( $k_7$  and  $K_6$ ) for the 2-phenylpropanoyl might be expected. In the extreme situation, the iso/normal product distribution reflects the concentrations of the iso and normal acyl species, which on their turn are determined by the rates of the insertion reactions (step 3, Scheme 2) leading to the iso and normal alkyl species, provided that these reactions are irreversible. Since the overall reaction rate is independent of styrene concentration but lower than that of oct-1-ene, and since the hydrogenolysis rate and  $K_6$  are expected to be of similar magnitude, we conclude that the concentrations of the acylrhodium species with styrene are lower than those with oct-1-ene in the concentration regime studied here. In other words, rhodium does not reside completely in the acyl stage (as it does with oct-1-ene), but it does not reside in the hydride stage either (as it does with cyclohexene or cyclooctene).<sup>15</sup> The product distribution and its dependency on the CO pressure hint as to the explanation of these phenomena.

Deuterioformylation of styrene at  $60^\circ\text{C}$ <sup>24</sup> has been shown to involve an irreversible alkene insertion step. The iso to normal ratio reported was 15 (180 bar). At higher temperatures the iso/n ratio decreases (*i/n* = 5 at  $90^\circ\text{C}$ , total pressure = 180 bar). The present rhodium catalyst modified with a bulky phosphite gives a lower iso/n ratio (10.6 at  $51^\circ\text{C}$ , 2.1 at  $90^\circ\text{C}$ , total pressure = 22 bar). We presume that also in this instance the styrene insertion is irreversible. The isomer ratio reflects the preference of the styrene insertion reaction, modified by small differences in the

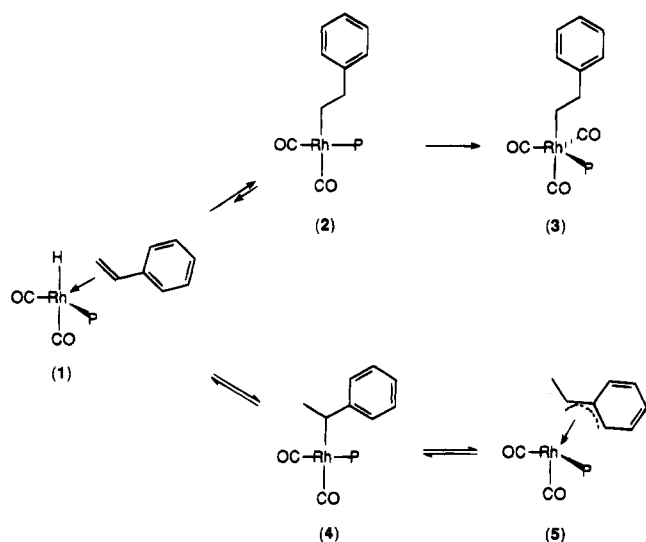
(22) Heil, B.; Markó, M. *Chem. Ber.* **1969**, *102*, 2238.

(23) Lazzaroni, R.; Pertici, P.; Bertozzi, S.; Fabrizi, G. *J. Mol. Catal.* **1990**, *58*, 75.

(24) Ucello-Baretta, G.; Lazzaroni, R.; Settambolo, R.; Salvadori, P. *J. J. Organomet. Chem.* **1991**, *417*, 111.

(21) (a) Brown, C. K.; Wilkinson, G. *J. Chem. Soc. A* **1970**, *5*, 2753.  
(b) Brown, C. K.; Wilkinson, G. *Tetrahedron Lett.* **1969**, *22*, 1725.



**Scheme 3. Possible Reactions for the Styrene-Coordinated Rhodium Complex**


rate constants that may follow this step. For oct-1-ene the ratio *iso/n* is 0.7, *i.e.* considerably lower than for styrene. The strong preference of styrene to form the branched alkyl species (1-phenylethyl, Scheme 3, 4) must be related to the resonance-stabilized species (Scheme 3, 5) suggested before in 1974 by Tanaka *et al.*<sup>25</sup> and in 1983 by Tolman and Faller.<sup>26</sup> These kinds of benzyl complexes are known for rhodium<sup>27</sup> and platinum.<sup>28</sup> After the migratory insertion, a coordinatively and electronically unsaturated metal complex is formed. For 1-phenylethyl, however, this unsaturation is released by coordination in an  $\eta^3$ -fashion (5). The relative stability of this species is crucial in styrene carbonylation and hydroformylation, *e.g.* insertion of styrene into a palladium acetyl bond gives an  $\eta^3$ -bonded 1-phenylethyl group.<sup>29</sup> Depending upon the conditions of the rhodium-catalyzed hydroformylation of styrene, a substantial amount of the rhodium complex may reside in this  $\eta^3$ -1-phenylethyl state. When migratory insertion of the alkene into rhodium hydride leads to an  $\eta^2$ -alkylrhodium species (1-octyl, 2-methylheptyl, 2-phenylethyl, Scheme 3, 2), the vacant site will be occupied by carbon monoxide or phosphine ligand with a high rate; under these reaction conditions the insertion is now irreversible and the regioselectivity of the reaction has been determined. The  $\eta^3$ -1-phenylethyl species (Scheme 3, 5) remains in a state that may easily undergo deinsertion.

Ojima<sup>30</sup> presented a different explanation for the higher selectivity toward the branched aldehyde. When electron-withdrawing substituents are involved, the  $C_\alpha$ -metal bond of a  $\pi$ -olefin complex should be stronger than

the  $C_\beta$ -metal bond, resulting in a preferred migration of the hydride to the  $C_\beta$  forming an isoalkyl metal species. According to the author, the normal to branched aldehyde ratio reflects the ratio of the isoacyl and *n*-acyl metal species provided that the hydrogenolysis is not rate-determining. If hydrogenolysis is the rate-determining step, isomerization of the acyl metal complexes can occur, giving rise to an increased *iso/n* aldehyde ratio.<sup>30</sup> Although an ( $\eta^3$ -1-phenylethyl)rhodium species was never observed during a catalytic reaction, the recent results of Lazzaroni about the extreme susceptibility of the 1-phenylethyl intermediate toward  $\beta$ -hydride elimination support the occurrence of the  $\eta^3$ -1-phenylethyl compound.

From the reaction data it becomes immediately clear that more so than for oct-1-ene, the  $\beta$ -hydride elimination is a crucial step in determining the product distribution. For styrene, however, the progress of this reaction cannot be established by the presence of isomerization products. As for oct-1-ene,  $\beta$ -hydride elimination has a higher free energy of activation than the hydrogenolysis reaction at the end of the hydroformylation cycle. As a result, the proportion of  $\beta$ -hydride elimination increases with temperature. The branched alkyl species, in this instance 1-phenylethyl, is more sensitive to elimination than the linear alkyl species and hence the observed linearity of the product increases, as was clearly pointed out by Lazzaroni.<sup>19,20</sup> The results with bulky phosphite rhodium catalysts fit perfectly well with those obtained with rhodium carbonyl catalysts, although the latter are slower.

the importance of intermediate 5 is also expressed in the ratio of the formation of branched and linear products as a function of  $H_2$  and CO pressures (Figure 4, Table 10). The first-order dependency of the rate of formation of linear aldehyde (3-phenylpropanal) on  $H_2$  pressure indicates that the hydrogenolysis of the acyl complex (Scheme 2, step 7) is rate-determining. The turnover frequency (TOF) to the branched aldehyde (2-phenylpropanal) shows an observed reaction order in  $H_2$  slightly higher than 1. The reaction rates do not exceed those of oct-1-ene. We explain this as follows. The rate-determining step is again the hydrogenolysis reaction (Scheme 2, step 7) but upon depletion of the acyl species the branched one can be replenished at a higher rate because of the reservoir of 5 and the fast reaction 3 (Scheme 2) leading to 5. In other words the ratio of the concentrations of the rhodium acyl and  $\eta^3$ -1-phenylethyl species changes with the syngas pressure, and a rigid treatment with reaction 7 (Scheme 2) as being rate-determining is no longer valid. The dependency on CO pressure is more instructive. The rate of formation of 3-phenylpropanal decreases proportionally with the inverse of the CO pressure. Again this is the same as found for the kinetics of the reaction of oct-1-ene to nonanal. Interestingly, the rate of formation of 2-phenylpropanal increases when the CO pressure is raised from 5 to 16 bar ( $p_{H_2} = 11$  bar, 80 °C) and decreases again when the pressure is raised from 16 to 33 bar (Figure 4). The initial increase is caused by the conversion of 5 to the corresponding acyl species; a higher concentration of the acyl species gives a higher overall rate of reaction. When most of the rhodium rests in the acyl state, a further increase of the CO pressure

(25) Tanaka, M.; Watanabe, Y.; Mitsudo, T.; Takegami, Y. *Bull. Chem. Soc. Jpn.* **1974**, 47(7), 1698.

(26) Tolman, C. A.; Faller, J. W. *Homogeneous Catalysis with Metal Phosphine Complexes*; Pignolet, L. H., Ed.; Plenum Press: New York and London, 1983; Chapter 2, pp 88–89.

(27) (a) Stühler, H.-O.; Pickardt, J. *Z. Naturforsch., B* **1981**, 36, 315. (b) Werner, H.; Feser, R. *J. Organomet. Chem.* **1982**, 232, 351.

(28) Craswell, L. E.; Litster, S. A.; Redhouse, A. D.; Spencer, J. L. *J. Organomet. Chem.* **1990**, 394, C35.

(29) (a) Dekker, G. P. C. M.; Elsevier, C. J.; Vrieze, K.; Van Leeuwen, P. W. N. M.; Roobeek, C. F. *J. Organomet. Chem.* **1992**, 430, 357. (b) Granberg, K. L.; Bäckvall, J.-E. *J. Am. Chem. Soc.* **1992**, 114, 6858. (c) Brookhart, M.; Rix, F. C.; De Simone, J. M.; Barborak, J. C. *J. Am. Chem. Soc.* **1992**, 114, 5894.

(30) Ojima, I. *Chem. Rev.* **1988**, 88, 1011.



cannot lead to further acceleration, instead the "normal" inhibition via equilibrium 6 becomes dominating.

The influence of the CO pressure on the rate of the formation of the branched product clearly explains why the product ratios in literature data of styrene hydroformylation depend so strongly on the pressure. If both modes of styrene insertion are irreversible (low temperature, high CO pressure, high ligand concentration), the *iso/n* ratio is very high (10–25) (case 1). Conditions can be set such that only the formation of the linear (2-phenylethyl)rhodium complex is irreversible. Now, kinetically, a highly linear product can be produced (case 2). A third possibility arises when all reactions 1–6 are reversible and yet reaction 7 (Scheme 2) is rate-determination. In this instance (case 3) the normal to branched ratio is determined by the ratio of the concentrations of the equilibrated acyl species.

Looking at these mechanistic considerations, it is clear that neither the kinetic expression for oct-1-ene nor the expression for cyclohexene is suitable for the styrene substrate. An analytic expression taking into account all reactions describing these features would be rather complicated.<sup>18</sup>

### Conclusions

In general, the tris(2-*tert*-butyl-4-methylphenyl) phosphite modified rhodium hydroformylation catalyst is an excellent catalyst, particularly for unsubstituted alk-1-enes, yielding high rates under mild conditions.

The catalyst system exhibits simple kinetics for oct-1-ene and cyclohexene while those for styrene are more complicated. The kinetics of oct-1-ene and cyclohexene resemble those of the  $\text{Rh}_4(\text{CO})_{12}$  system as studied by Markó and are clearly different from the triphenylphosphine-modified rhodium catalyst. The kinetics of oct-1-ene are reduced to a simple equation by virtue of the relative inertness of the isomerization product. Reaction 3 of Scheme 2 is irreversible under the conditions studied, while reaction 7 is rate-determining. As a result the regioselectivity is determined in step 3, and beyond this step no normal to iso equilibration takes place.

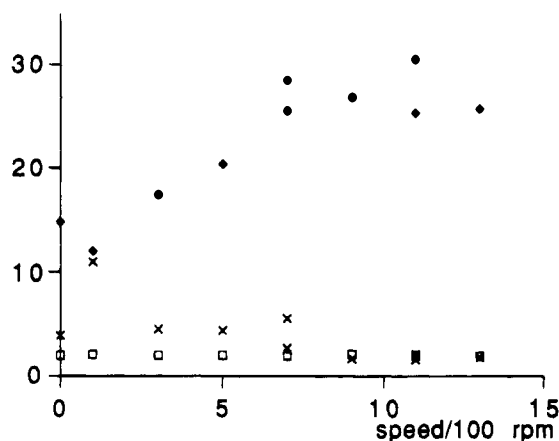
For cyclohexene, the rate-limiting step lies at the beginning of the cycle; the initial reaction of the alkene with the rhodium hydride species is the slowest step.

For styrene, in contrast to oct-1-ene,  $\beta$ -hydride elimination has an important influence on the regioselectivity; the selectivity for the branched product increases at lower temperatures and higher pressures.

### Experimental Section

**General Information.** All preparations were carried out under an atmosphere of nitrogen or argon by using standard Schlenk techniques. Solvents were distilled from sodium/benzophenone prior to use. Oct-1-ene was distilled from sodium; cyclohexene and styrene were percolated over neutral alumina.  $\text{Rh}(\text{CO})_2\text{Acac}$  was purchased from Johnson Matthey and trimethyl phosphite from Aldrich and both were used as received. Gas-liquid chromatography analyses were done using a DB 5 column and a Carlo Erba GC 6000Vega series 2 chromatograph. NMR measurements were performed on a Bruker AC 100 or AMX 300 spectrometer. Chemical shifts are given in ppm using TMS or  $\text{H}_3\text{PO}_4$  as standard.

Hydroformylation studies were performed in a stainless steel autoclave (181 mL) containing a glass beaker. The



**Figure 5.** Dependency of the turnover frequency (TOF) isomerization and regioselectivity on the stirring rate. ◆ = TOF/1000 mol [mol Rh]<sup>-1</sup> h<sup>-1</sup>, × = % isomerization products, □ = *n/i* ratio. Conditions:  $T = 80^\circ\text{C}$ ,  $P_{\text{H}_2} = P_{\text{CO}} = 10$  bar,  $[\text{Rh}(\text{CO})_2\text{Acac}] = 0.1$  mmol dm<sup>-3</sup>,  $[(2\text{-tBu-4-MeC}_6\text{H}_4\text{O})_3\text{P}] = 5$  mmol dm<sup>-3</sup>,  $P/\text{Rh} = 50$ ,  $[\text{oct-1-ene}] = 0.86$  mol dm<sup>-3</sup> in 20 mL of toluene.

autoclave is magnetically stirred and equipped with a reservoir, a pressure transducer, a thermocouple, and a sampling device. The beaker was charged with the rhodium precursor ( $\text{Rh}(\text{CO})_2\text{Acac}$ ), the tris(2-*tert*-butyl-4-methylphenyl) phosphite, and an internal standard (decane) and filled with toluene up to 20 mL. The autoclave with the beaker was closed and flushed several times with  $\text{CO}/\text{H}_2$  and was brought under pressure. After the catalyst solution was heated, the substrate was charged to the reservoir and added to the reaction mixture by overpressure. Upon this addition, the reaction started immediately as was evidenced by a pressure drop and an increase of the temperature. Attention was paid to the gas consumption at 30% conversion; at the given alkene concentration and gas volume, less than 10% of the gases was consumed. During the reaction, a number of samples were taken and immediately quenched (by  $\text{P}(\text{OMe})_3$ ) so that a catalytically inactive rhodium complex was formed. These samples were analyzed by GC. The reaction rates for oct-1-ene and styrene are represented by the turnover frequencies (TOF), *i.e.* the total amount of formed aldehydes recalculated to moles of aldehydes per mole of rhodium per hour. The zeroth-order dependence of the reaction rate of the substrate concentration allowed us to average the TOFs over the reaction time. The tables were composed using samples with similar conversions. For cyclohexene, a different order in the substrate concentration was observed and the  $k_0$  of the reaction could be determined. During the reaction, several averaged turnover frequencies were calculated from the observed decrease in  $\text{CO}/\text{H}_2$  pressure. These data were used to obtain a plot of the  $\ln(\text{TOF})$  vs reaction time. Extrapolation of the calculated line produced the  $k_0$  of the reaction.

To exclude a diffusion-limited reaction, we carried out experiments in which we varied the stirring velocity. Figure 5 shows that at very low stirring speeds or with no stirring at all, the reaction is diffusion-limited and at increasing velocity the reaction rate eventually remains constant. Up to 100 rpm, the turnover frequency deviates during the reaction, so average values are presented here. Furthermore at low stirring rates the isomerization rate is somewhat higher; at 100 rpm 10.8% isomerized oct-1-ene is formed and from 900 rpm the amount of isomerized oct-1-ene stays around 2%. Consequently the percentage of linear aldehydes is somewhat lower at high stirring rates (a very slight change was obtained; the *n/i* decreased from 2.10 to 1.91). We worked at a stirring rate of 1100 rpm, situated in the adequate region. At the extremely low rhodium concentrations applied and our standard reaction conditions it is not likely that the reaction rate is limited by

mass transfer. As we work with 2  $\mu$ mol of rhodium precursor, the overall gas consumption will be low in spite of the high TOF's.

**Preparation of Tris(2-*tert*-butyl-4-methylphenyl) Phosphite.** PCl<sub>3</sub> (10.1 g, 73.3 mmol) was added dropwise under stirring at 70 °C to 48.15 g (293.1 mmol) of 2-*tert*-butyl-4-methylphenol in 30 mL of toluene. When all PCl<sub>3</sub> was added, the mixture was heated slowly (in 30 min) to 150 °C and stirred at this temperature for 3 h. Meanwhile, the formed HCl was removed several times by evacuating the mixture. After being cooled to 70 °C, the mixture was again evacuated for 15 min. The product was precipitated by addition of 100 mL of CH<sub>3</sub>-

CN. The precipitate was filtered off and washed with 100 mL of CH<sub>3</sub>CN. The product was purified by recrystallization from toluene/CH<sub>3</sub>CN. Yield: 23.26 g (61%) of white crystals. <sup>31</sup>P NMR (CDCl<sub>3</sub>):  $\delta$  131 ppm. <sup>1</sup>H NMR (CDCl<sub>3</sub>):  $\delta$  1.4 ppm (s, 9H, tBu), 2.3 (s, 3H, Me), 7.1. (m, 3 H, aromatic). Mp: 111 °C.

**Supplementary Material Available:** Total derivation of equations in ref 18 and the rate equations used (4 pages). Ordering information is given on any current masthead page.

OM940207Z

# ( $\eta^5$ -Cyclopentadienyl)( $\eta^5$ -cyclooctatrienyl)iron Complexes: Demonstration of Two Different Intramolecular Rearrangements<sup>†</sup>

Erhard T. K. Haupt, Jürgen Heck,\* Michiel Maters, and Bea Voss

Institut für Anorganische und Angewandte Chemie, Universität Hamburg,  
Martin-Luther-King-Platz 6, D-20146 Hamburg, Germany

Mark Damen

Vakgroep Anorganische en Algemene Chemie, Universiteit Nijmegen, Toernooiveld,  
NL-6525 ED Nijmegen, The Netherlands

Received April 25, 1994<sup>⊗</sup>

Nucleophilic additions of methanolate and the acetylides  $\text{PhC}\equiv\text{C}^-$  and  $t\text{-BuC}\equiv\text{C}^-$  to the cationic complex  $[\text{CpFe}(\eta^6\text{-Cot})]^+(1^+)$  (Cot = cyclooctatetraene) exclusively occur on the Cot ring in high yield. However, the new products are not stable with respect to molecular fluxionalities. To establish the mechanism of the fluxional processes, different NMR techniques were applied on  $\text{CpFe}(\eta^5\text{-C}_8\text{H}_9)$  (**3**) and  $\text{CpFe}(\eta^5\text{-C}_8\text{H}_8\text{D})$  (**3-d**<sub>1</sub>). The monodeuterated complex **3-d**<sub>1</sub> has been obtained in two ways: (i) by nucleophilic addition of  $\text{D}^-$  from  $\text{Li}[\text{BEt}_3\text{D}]$  to  $1^+$  and (ii) by deprotonation of **3** with  $\text{Lin-Bu}$  at  $-30^\circ\text{C}$ , forming the anionic complex  $[\text{CpFeCot}]^-$  (**4**), and successive deuterolysis with  $\text{MeOD}$ . The addition of  $\text{D}^+$  to **4**, as well as the addition of  $\text{D}^-$  to  $1^+$ , initially yielded  $\text{CpFe}(\eta^5\text{-C}_8\text{H}_8\text{-1-}exo\text{-D})$ , although the deuterium is later distributed over all positions of the *cyclo*-C<sub>8</sub> ligand with the exception of the *endo*-position. Various NMR studies demonstrate two different exchange processes: a slow 1,3-metal shift, as shown by spin saturation transfer (SST) experiments, which leads to an enantiotopomerization of **3**, and a 1,4-hydrogen shift as an even slower process.

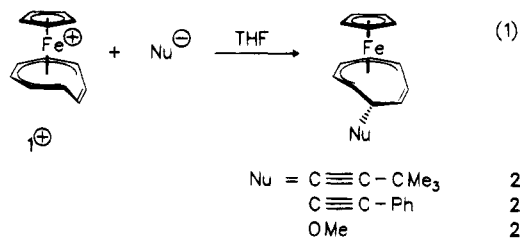
## Introduction

The C-C bond formation reactions of coordinated cyclooctatetraene (Cot) have become the focus of some attention.<sup>1</sup> Recently, we were able to show that nucleophilic addition to coordinated Cot in the cationic complex  $[\text{CpFe}(\eta^6\text{-Cot})]^+(1^+)$ <sup>1d</sup> is a new complementary way<sup>2</sup> in which to introduce special functionalities to Cot in a highly stereo- and regioselective manner. The nucleophilic addition products from malonate nucleophiles seem to be inert with respect to intramolecular fluxional processes, e.g., ring contractions or H-migrations.<sup>3,5</sup> Further to our previous findings, we report herein new results indicating two different intramolecular fluxional

processes with activation barriers dependent on the substituent of the *cyclo*-C<sub>8</sub> ligand.

## Results and Discussion

Since we were interested in acetylenic and methoxy substitution of the Cot ligand, we have chosen two representative acetylides and methanolate as nucleophiles in reactions with  $1^+$ . As mentioned earlier,<sup>1d</sup> the reactions (eq 1) occur almost quantitatively.



If the reaction products are isolated within 1 h, it is possible to obtain the <sup>1</sup>H-NMR spectra of **2a** and **2c**, which show the formation of only one product.

The <sup>1</sup>H-NMR spectra are in very good agreement with those described recently for Nu =  $\text{CH}(\text{CO}_2\text{R})_2$  (R = Me, Et) and  $\text{NMe}_2$ .<sup>1d</sup> The two proton resonance signals between 5.1 and 5.6 ppm correspond to the olefinic protons belonging to the uncoordinated double bond of the *cyclo*-C<sub>8</sub> ligand. After three days, however, the <sup>1</sup>H-NMR spectrum of **2a** changes dramatically, showing at least four different products, which can be identified by four Cp and *t*-Bu signals at ca. 4 and 1.2 ppm, respectively. Warming up the NMR tube to  $60^\circ\text{C}$  for 16 h

<sup>†</sup> Dedicated to Prof. Dr. Dr. E. h. H. Sinn on the occasion of his 65th birthday.

<sup>⊗</sup> Abstract published in *Advance ACS Abstracts*, November 1, 1994.  
(1) (a) Connelly, N. G.; Hopkins, P. M.; Orpen, A. G.; Slater, J. J. *Chem. Soc., Dalton Trans.* **1992**, 3302. (b) Chen, J.; Li, D.; Yu, Y.; Jin, Z.; Zhou, Q.; Wei, G. *Organometallics* **1993**, *12*, 3885. (c) Wieser, M.; Sünkel, K.; Beck, W. *Chem. Ber.* **1992**, *125*, 1369. (d) Beurskens, P. T.; Bosman, W. P.; Brussaard, H. C.; Heck, J.; Klein Gebbink, R. J. M.; Maters, M.; Smits, J. M. M. *J. Organomet. Chem.* **1994**, *469*, 197.

(2) Concerning the use of Cot for synthetic purposes, see: Paquette, L. A.; Henzel, K. A. *J. Am. Chem. Soc.* **1975**, *97*, 4649 and literature cited therein. See also: Johnson, B. F. G.; Lewis, J.; Randall, G. L. P. *J. Chem. Soc. A* **1971**, 422. Connelly, N. G.; Gilbert, M.; Orpen, A. G.; Sheridan, J. B. *J. Chem. Soc., Dalton Trans.* **1990**, 1291. Aggerwal, R. P.; Connelly, N. G.; Dunne, B. J.; Gilbert, M.; Orpen, A. G. *J. Chem. Soc., Dalton Trans.* **1991**, 1. Mann, B. E. *Comprehensive Organometallic Chemistry*; Wilkinson, G.; Stone, F. G. A., Eds.; Abel, E. W., Eds.; Pergamon Press: New York, 1982; Vol. 3, p 134.

(3) Brookhart, M.; Noh, S. K.; Timmers, F. J.; Hong, Y. H. *Organometallics* **1988**, *7*, 2458.

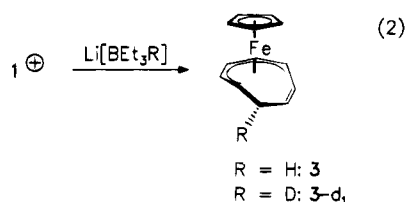
(4) Davison, A.; McFarlane, W.; Pratt, L.; Wilkinson, G. *J. Chem. Soc.* **1962**, 4821. McFarlane, W.; Pratt, L.; Wilkinson, G. *Ibid.* **1963**, 2162.

(5) Aumann, R.; Knecht, J. *Chem. Ber.* **1976**, *109*, 174.

(6) Greco, A.; Carbonaro, A.; Cambisi, F.; Dall'Asta, G. *Chim. Ind. (Italy)* **1970**, *52*, 877.

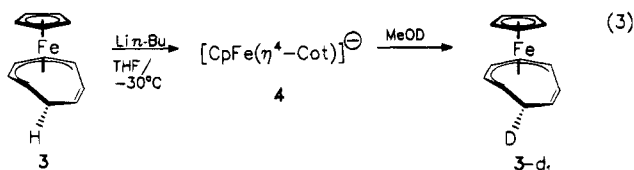
simplifies the  $^1\text{H-NMR}$  spectrum to a set of signals indicating two different products with the ratio 2:1. However, these products could not be isolated separately by either fractional crystallization or column chromatography. A similar fluxional behavior, within a shorter period of time, is observed for **2c** ( $\text{Nu} = \text{OMe}$ ). The phenylethynyl derivative **2b** is even more labile, and in contrast to **2a**, the number of different products caused by the fluxionality is even larger for **2b** and **2c**.

The molecular transformation in **2a–2c** is at variance with our former results,<sup>1d</sup> and we have thus been forced to investigate this behavior more thoroughly. We decided therefore to study the stereochemistry in the monodeuterated cyclooctatrienyl complex  $\text{CpFe}(\eta^5\text{-C}_8\text{H}_7\text{D})$  (**3-d<sub>1</sub>**), which can be obtained from deuteride addition to **1**<sup>+</sup> similar to the synthesis of  $\text{CpFe}(\eta^5\text{-C}_8\text{H}_9)$  (**3**)<sup>1d</sup> (eq 2).



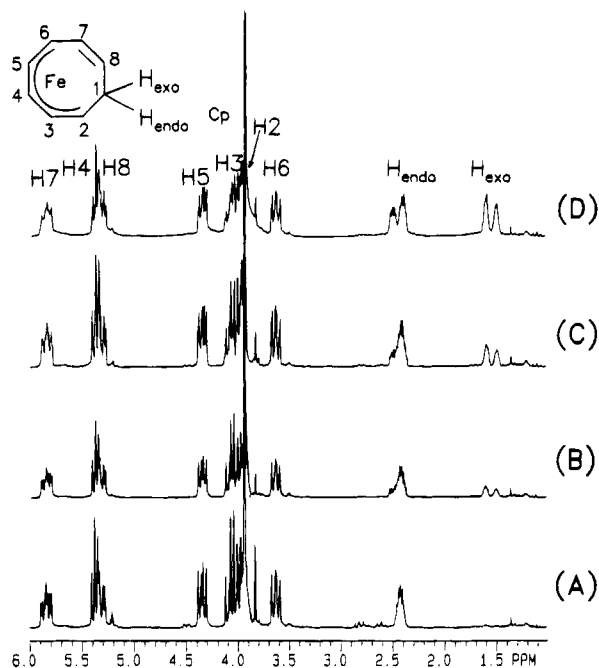
Providing that the addition of  $\text{D}^-$  to the cyclooctatetraene ligand in **1**<sup>+</sup> occurs stereo- and regioselectively, as with normal nucleophilic additions to coordinated olefinic ligands, only one signal should be observed in a  $^2\text{H-NMR}$  spectrum. In the case of molecular transformations in **3-d<sub>1</sub>**, for each isomer, one singlet is to be expected.

A monodeuterated derivative of **3** can also be prepared by the deprotonation of **3** with  $\text{Li}n\text{-Bu}$  and subsequent protolysis with  $\text{MeOD}$  (eq 3).



When the first  $^1\text{H-NMR}$  spectra of **3-d<sub>1</sub>** were obtained from both synthetic routes (recorded within a few hours after the reaction had been performed), a doublet of multiplets of very low intensity at  $\delta = 1.78$  ppm was observed. This corresponds to a negligible number of *exo*-protons of the  $\text{C}_8$ -ring ligand, as it is this position that is occupied by the deuterium (Figure 1A). The *endo*-proton only shows a broad multiplet, which gradually sharpens to reveal a doublet of multiplets. Meanwhile, the intensity of the signal belonging to the *exo*-proton increases until it is eventually equal to that of the *endo*-proton (Figure 1B–D).

Since no significant alteration of the other *cyclo-C<sub>8</sub>* proton signals could be observed, with the exception of some changes in the splitting pattern, time-dependent  $^2\text{H-NMR}$  experiments were used to obtain a deeper understanding of the mechanism of this molecular rearrangement (Figure 2). As expected from  $^1\text{H-NMR}$  spectra, the signal of the *exo*-position can be recognized immediately (Figure 2A), confirming the regioselective addition of the proton (or deuteron) to the metallated complex **4**. After 24 h two peaks corresponding to

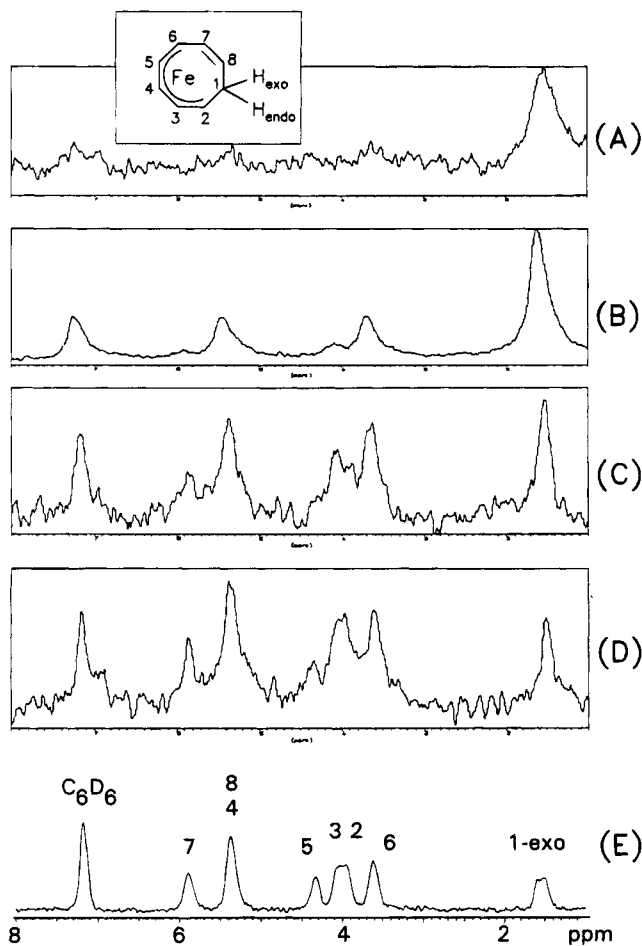


**Figure 1.** Time-dependent  $^1\text{H-NMR}$  spectra of  $\text{CpFe}(\eta^5\text{-C}_8\text{H}_7\text{D})$  (**3-d<sub>1</sub>**). (A) Recorded within 2 h after preparation. (B) Recorded after 17 h. (C) Recorded after 23 h. (D) Recorded after 1 week (200 MHz,  $\text{C}_6\text{D}_6$ ).

positions 4 and 6 appear with similar intensities (Figure 2B). Furthermore, weak signals originating from positions 3 and 7 can be observed, which become stronger after another day (Figure 2C). In spectrum D of Figure 2, the signals of positions 2 and 8 can be distinguished and the intensity of the signal of position 5 at last increases. Finally, the  $^2\text{H-NMR}$  spectrum of **3-d<sub>1</sub>** shows signals for all of the *cyclo-C<sub>8</sub>* positions, though not for the *endo*-position, which indicates an even distribution of the deuterium atom over all cyclooctatrienyl positions with the exception of the *endo*-position (Figure 2E). The lack of any Cp signal in spectrum E proves that the rearrangement strictly occurs within the  $\text{C}_8$  ligand.

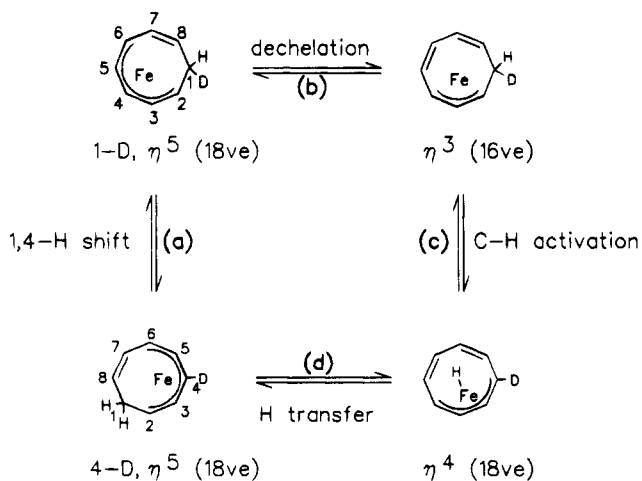
The most surprising result that emerges from the  $^2\text{H-NMR}$  spectra is the successive population in pairs of the positions 4 and 6, 3 and 7, and 2 and 8, respectively, by deuterium; this can best be explained by two different molecular transformations occurring at different rates. One dynamic process is an energetically degenerate 1,3-metal shift (Scheme 1a) as indicated by spin saturation transfer (SST) experiments. In an SST experiment, a proton **a** is irradiated, and as a result, this proton will transfer its spin information to the interchanging position **b**. Consequently, the population difference between the ground state and the excited state will be diminished for **b**, revealing a reduced intensity of the resonance signal of proton **b**, too. Hence, after subtracting a normal  $^1\text{H-NMR}$  spectrum, used as a reference (Figure 3A), from the SST spectrum, a difference  $^1\text{H-NMR}$  spectrum is thus obtained. This shows a strong negative signal for the irradiated proton **a** and a smaller negative one for proton **b**, whereas all other signal intensities have to be zero. Compared to the SST spectra of **3**, however, some signals are left with positive intensities as in Figure 3.

These are caused by nuclear Overhauser effects (NOEs) which stem from dipolar interactions between

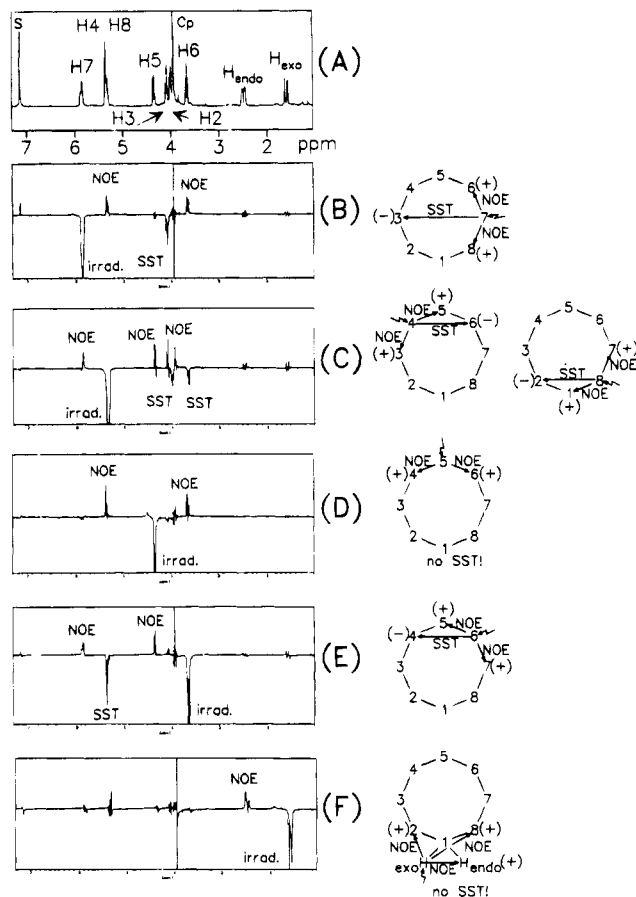


**Figure 2.** Time-dependent <sup>2</sup>H-NMR spectra of CpFe(η<sup>5</sup>-C<sub>8</sub>H<sub>8</sub>D) (3-d<sub>1</sub>). (A) Recorded within 3 h after preparation. (B) Recorded after 1 day. (C) Recorded after 2 days. (D) Recorded after 4 days (360 MHz, proton decoupled, C<sub>6</sub>D<sub>6</sub>). (E) Recorded after 1 week (200 MHz, not proton decoupled; note line width of signal δ < 2 ppm, C<sub>6</sub>D<sub>6</sub>).

### Scheme 1



vicinal protons, thereby giving rise to positive resonance signals. Hence, the irradiation of proton 7, for example, reveals a negative signal for the interchanging proton 3 in the difference spectrum caused by SST (Figure 3, spectrum B), whereas protons 6 and 8 show positive signals caused by NOEs. The chosen timing of the experiment does not allow one to observe the NOE effects on the "new" position, however, because it has

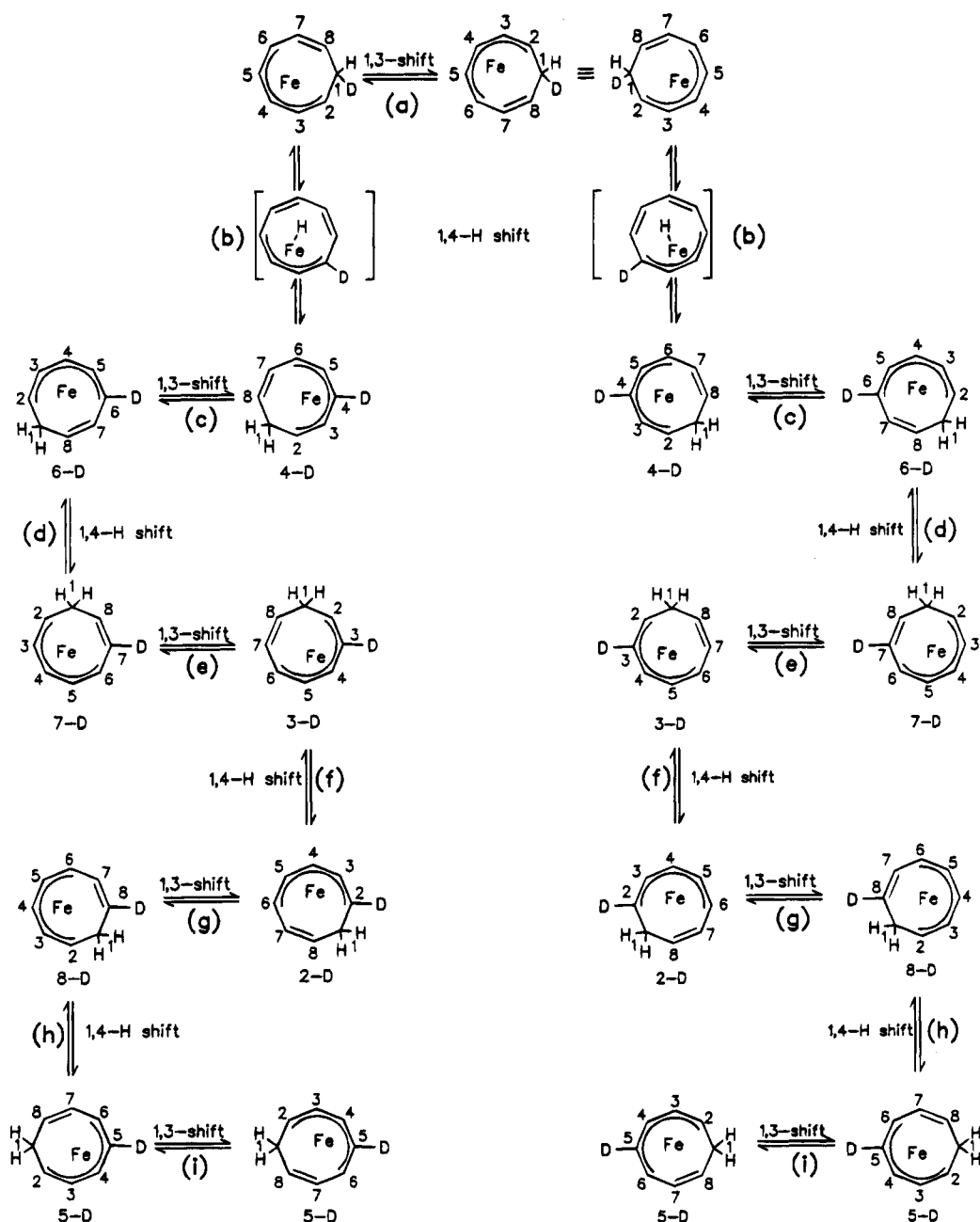


**Figure 3.** <sup>1</sup>H-NMR spectra of CpFe(η<sup>5</sup>-C<sub>8</sub>H<sub>9</sub>) (3). (A) Normal <sup>1</sup>H-NMR spectrum of 3 as reference (S = C<sub>6</sub>D<sub>5</sub>H). (B–F) Spectra obtained by means of spin saturation transfer experiments. Irradiated protons are marked Irrad. NOE denotes the nuclear Overhauser enhancement. SST denotes the signals of the protons suffering spin saturation transfer. The ideograms elucidate the interaction pattern.

still not built up in any reasonable amount. Comparable intensity alterations can be seen for the other irradiation experiments depicted in Figure 3. For every difference spectrum, the SST and NOE interactions are depicted in the ideograms of Figure 3 as well as the signs (±) of the signals. From these spectra the interconversion of protons 2 and 8, 3 and 7, and 4 and 6, respectively, can be clearly deduced, yielding the enantiomer of 3 by means of a 1,3-metal shift. Since this enantiotopomerization is slow, with respect to the NMR time scale, it becomes obvious that no indication of this process has been observed before. However, a 1,3-metal shift is not uncommon for η<sup>5</sup>-cyclooctatrienyl<sup>3</sup> and η<sup>5</sup>-cycloheptatrienyl complexes,<sup>7</sup> although for 3 a complete circulation of the metal center is hindered by the interruption of the conjugation of the cyclo-C<sub>8</sub> ligand in position 1. Hence, a "twitching" motion will only occur in 3, the activation barrier of which has to be considerably higher (ΔG<sup>‡</sup> > 71 kJ/mol) than that for the valence isoelectronic complex Mn(CO)<sub>3</sub>(η<sup>5</sup>-C<sub>8</sub>H<sub>9</sub>) (5) (ΔG<sup>‡</sup> = 52.7 kJ/mol).<sup>3</sup> The higher activation barrier of metallotropic shifts in the cyclopentadienyl complex 3, compared to the tricarbonyl complex 5, parallels the results obtained

(7) Alibrandi, G.; Mann, B. E. *J. Chem. Soc., Dalton Trans.* **1992**, 1439. Hails, M. J.; Mann, B. E.; Spencer, C. M. *J. Chem. Soc., Dalton Trans.* **1985**, 693.

Scheme 2



for the cyclooctatetraene compounds  $\text{Cr}(\text{CO})_3(\eta^6\text{-Cot})$ ,<sup>8</sup>  $\text{CrCp}(\eta^6\text{-Cot})$ ,<sup>9</sup> and  $[\text{FeCp}(\eta^6\text{-Cot})]^+$ .<sup>10</sup>

The second dynamic process in **3** has to be distinctly slower than the 1,3-metal shift; otherwise additional SST and NOE signals would have to have been recorded. The slower dynamic process is assumed to be a metal-mediated 1,4-shift of the *endo*-proton (Scheme 1) similar to the 1,5-shift discussed for  $(\eta^6\text{-cycloheptatriene})\text{-}(\text{tricarbonyl})\text{chromium}$ .<sup>11</sup> In analogy to other hydrogen shifts in organometallic complexes,<sup>12</sup> the 1,4-hydrogen migration may be initiated by the dechelation of the

terminal double bond, which is in conjugation with the free double bond of the  $\eta^5$ -cyclooctatrienyl unit, to generate an unsaturated 16 valence electron (ve)  $\eta^3$ -cyclooctatrienyl complex (Scheme 1b). Then C-H activation takes place on C1 to form the 18 ve hydride intermediate (Scheme 1c), which is able to transfer the hydride either to position 1 to reveal the starting complex or to position 4 to create the 4-D derivative (Scheme 1d). A subsequent 1,3-shift places the deuterium atom in position 6 (Scheme 2, equilibrium c). From the 6-D derivative, the 7-D compound is formed by the metal-mediated 1,4-shift of the *endo*-proton (Scheme 2, equilibrium d), with the ensuing degenerate 1,3-shift revealing the 3-D product (Scheme 2, equilibrium e). After this procedure, all of the positions of the cyclooctatrienyl ligand are deuterated in the sequence which was elucidated from the <sup>2</sup>H-NMR spectra (see Scheme 2, equilibria f-i).

From these intramolecular rearrangements it is clear

(8) Lawless, M. S.; Marynick, D. S. *J. Am. Chem. Soc.* **1991**, *113*, 7513 and references cited therein.

(9) Heck, J.; Rist, G. *J. Organomet. Chem.* **1988**, *342*, 45.

(10) Reger, D. L.; Colemann, C. *J. Organomet. Chem.* **1977**, *131*, 153.

(11) Foreman, M. I.; Knox, G. R.; Pauson, P. L.; Todd, K. H.; Watts, W. E. *J. Chem. Soc., Perkin Trans. 2* **1972**, 1141. Roth, W. R.; Grimme, W. *Tetrahedron Lett.* **1966**, 2347.

(12) Karel, K. J.; Brookhart, M.; Aumann, R. *J. Am. Chem. Soc.* **1981**, *103*, 2695.

that, in principle, eight different isomers can be formed upon nucleophilic addition to  $1^+$ . The absence<sup>1d</sup> or formation of different isomers is apparently controlled by the electronic behavior of the added nucleophiles and seems to be restricted only to iron compounds. The corresponding Ru complexes give no indications for comparable fluxional processes under the described conditions.<sup>13</sup> Some efforts are still necessary to isolate different isomers of cyclooctatrienyl complexes, e.g., of **2a**, in order to confirm that the rearrangements discussed above are the reason for their formation.

The strict intramolecular 1,4-hydrogen shift in **3** is in accordance with the proposed hydrogen shift in  $\text{CpV}(\eta^7\text{-C}_8\text{H}_9)$ ,<sup>14</sup> however, it disagrees with  $\text{Cp}^*\text{ZrC}_8\text{H}_9\text{-}d_1$  wherein a *complete* (statistical) distribution of the deuterium atom is found over all *cyclo-C*<sub>8</sub> positions including the *endo*- and *exo*-positions.<sup>15</sup>

### Experimental Section

All manipulations were performed under nitrogen with thoroughly dried solvents. Standard <sup>1</sup>H-NMR spectra were recorded on a VARIAN Gemini 200 BB spectrometer, while the <sup>2</sup>H-NMR spectra were recorded in 10-mm tubes with the broad-band equipment of a BRUKER-AM-360 spectrometer. The initial assignment of the <sup>1</sup>H-NMR signals has been performed by means of chemical arguments: the addition of nucleophiles to coordinated -ene and -enyl ligands (e.g., D<sup>-</sup> from Li[BEt<sub>3</sub>D]; see eq 1) exclusively occurs in *exo*-position with respect to the metal center. Therefore, the signal of the *exo*-proton is easily found by comparison of the spectra of **3** and **3-d**<sub>1</sub>, when the NMR sample of **3-d**<sub>1</sub> has freshly been prepared. The assignment of the remaining <sup>1</sup>H-resonance signals *via* standard <sup>1</sup>H-COSY is straightforward. The SST experiments are performed on the AM-360 using the standard NOE-difference procedure with relaxation delay and mixing times of 0.5 s. Differences were calculated to reference spectra with an irradiation frequency close to the on-resonance frequencies. All spectra were recorded at room temperature.  $[\text{CpFe}(\eta^6\text{-Cot})\text{PF}_6$  (**1**) has been prepared according to reference 16. The Li salts Li[C≡Ct-Bu] and Li[C≡CPh] were obtained as solids from reactions of the corresponding acetylenes with *Lin*-Bu in hexane.

**Preparation of CpFe( $\eta^5\text{-C}_8\text{H}_9\text{-1-}exo\text{-C}\equiv\text{Ct-Bu}$ ) (**2a**).** Twenty-five milliliters of a THF solution containing 3.07 mmol of LiC≡Ct-Bu are added dropwise to a cooled, stirred suspension ( $T = -78^\circ\text{C}$ ) of 1.07 g (2.8 mmol) of **1** in 40 mL of THF. The orange-colored suspension immediately changes to a clear solution, which is allowed to warm up to room temperature. The solvent is removed *in vacuo*, and the oily residue is extracted with hexane. Crystalline product can be obtained from pentane solution at  $-78^\circ\text{C}$ . Yield: 0.85 g (98% based on **1**). EI-MS:  $m/e$  306 (18) [ $M^+$ ], 291 (9) [ $M^+ - \text{Me}$ ], 249 (100) [ $M^+ - t\text{-Bu}$ ], 240 (44) [ $M^+ - \text{C}_5\text{H}_8$ ], 199 (23) [ $\text{CpFeC}_6\text{H}_6$ ]<sup>+</sup>, 184 (16), 162 (14), 128 (12), 121 (80), 56 (48). IR (KBr, hexane),  $\text{cm}^{-1}$ : 1648 m (uncoordinated C=C of the C<sub>8</sub>-ring). <sup>1</sup>H-NMR (obtained within 30 min after isolation, C<sub>6</sub>D<sub>6</sub>, TMS, 200 MHz):  $\delta$  5.55 (dd, 1H, uncoordinated C=C of the C<sub>8</sub>-ring), 5.25 (dd, 1H, uncoordinated C=C of the C<sub>8</sub>-ring bond), 4.65 (dd,

1H, C<sub>8</sub>-ring), 3.90 (m, 2H, C<sub>8</sub>-ring), 3.75 (s, 5H, Cp), 2.90 (t, 1H, C<sub>8</sub>-ring), 2.75 (t, 1H, C<sub>8</sub>-ring), 1.05 (s, 9H, *t*-Bu). Anal. Calcd for C<sub>19</sub>H<sub>22</sub>Fe (M = 306.21): C, 74.52; H, 7.24. Found: C, 73.83; H, 7.24.

**Preparation of CpFeC( $\eta^5\text{-C}_8\text{H}_9\text{C}\equiv\text{CPh}$ ) (**2b**).** The reaction is performed identically to the synthesis of **2a** with 1.3 g (3.5 mmol) of **1** in 40 mL of THF and with 3.7 mmol of LiC≡CPh dissolved in 20 mL of THF. Extraction of the dry reaction residue in hexane yields 1.09 g (96%) of **2b**. The <sup>1</sup>H-NMR spectrum obtained within 30 min after isolation already reveals signals of different compounds (C<sub>6</sub>D<sub>6</sub>, TMS, 200 MHz): 6.9, 7.3, 7.5 (m, 5H, phenyl group), 5.3–5.6 (m, 2H, uncoordinated C=C bond of the C<sub>8</sub>-ring), 3.9–4.7 (m, 5H, C<sub>8</sub>-ring), 3.78 and 3.9 (s, 5H, Cp ligand), 2.7–2.9 (m, 1H, C<sub>8</sub>-ring).

**Preparation of CpFe( $\eta^5\text{-C}_8\text{H}_9\text{-1-}exo\text{-OMe}$ ) (**2c**).** A THF solution (0.63 mL) containing 0.87 mmol of NaOMe is added dropwise to a stirred suspension of 0.31 g (0.83 mmol) of **1**. After 5 min, a clear red solution is obtained, which is dried *in vacuo*. The residue is extracted with 15 mL of hexane. The hexane is removed, and the dark red oily residue is thoroughly dried *in vacuo*, during which it becomes crystalline. Yield: 186 mg (88%). EI-MS:  $m/e$  256 (18) [ $M^+$ ], 241 (5) [ $M^+ - \text{Me}$ ], 225 (20) [ $M^+ - \text{OMe}$ ], 199 (7), 186 (25) [ $\text{FeCp}_2^+$ ], 160 (12), 152 (30), 134 (17), 121 (75) [ $\text{FeCp}^+$ ], 104 (52), 91 (100), 78 (68), 65 (79), 56 (86). IR (KBr, *nujol*),  $\text{cm}^{-1}$ : 1656 w (uncoordinated C=C of the C<sub>8</sub>-ring), 1151 m (C–O–Me). <sup>1</sup>H-NMR (C<sub>6</sub>D<sub>6</sub>, TMS, 200 MHz):  $\delta$  5.4 (dd, 1H, uncoordinated C=C of the C<sub>8</sub>-ring) 5.1 (dd, 1H, uncoordinated C=C of the C<sub>8</sub>-ring), 3.9 (m, 2H, C<sub>8</sub>-ring), 3.78 (s, 5H, Cp), 3.3 (m, 1H, C<sub>8</sub>-ring). Anal. Calcd for C<sub>14</sub>H<sub>16</sub>FeO (M = 256.11): C, 65.65; H, 6.25. Found: C, 65.0; H, 6.3.

**Preparation of CpFe( $\eta^5\text{-C}_8\text{H}_9\text{D}$ ) (**3-d**<sub>1</sub>).** (a) **Via Nucleophilic Addition.** The reaction is performed in strict analogy to the synthesis of **3**.<sup>1d</sup> Li[BEt<sub>3</sub>D] (1.5 mL; 1.0 M in THF) is added to a cooled, stirred suspension ( $-78^\circ\text{C}$ ) of 0.52 g (1.4 mmol) of **1** in 10 mL of THF. The mixture is allowed to warm to room temperature. After 45 min of stirring, the reaction mixture is evaporated to dryness and the residue is extracted with pentane. The pentane extract is reduced in volume until precipitation occurs. Storage at  $-30^\circ\text{C}$  for 3 days yields 0.23 g (71%) **3-d**<sub>1</sub> as orange-red crystals.

(b) **Via Deprotonation and Addition of D<sup>+</sup>.** *Lin*-Bu (0.4 mL; 1.6 in hexane) is added to a cooled solution ( $-30^\circ\text{C}$ ) of 0.14 g (0.6 mmol) of CpFe( $\eta^5\text{-C}_8\text{H}_9$ ) (**3**) in 10 mL of THF. The color of the solution immediately changes from orange-red to deep green. After 15 min of stirring, 25  $\mu\text{L}$  of the MeOD is added, yielding an orange-red solution. The reaction mixture is then evaporated to dryness, and the residue is extracted with hexane. The hexane is removed to yield 0.13 g (93%) of **3-d**<sub>1</sub>. <sup>1</sup>H-NMR: see Figure 1 and reference 1d. EI-MS:  $m/e$  (% of **3-d**<sub>1</sub>) [% of **3**] 228 (15) [–], 227 (90) [5], 226 (80) [100], 225 (42) [71], 224 (14) [27], 223 (4) [3], 200 (15) [2], 199 (28) [15], 198 (10) [11], 197 (2) [1], 162 (50) [5], 160 (32) [62], 159 (15) [2], 158 (13) [19], 135 (26) [5], 134 (30) [35], 133 (4) [2], 122 (42) [25], 121 (70) [48], 56 (100) [76].

**Acknowledgment.** We thank Professor M. Brookhart for the fruitful discussion concerning the 1,4-hydrogen shift. This work was supported by the European Commission, Science Project CT 910 740, and by the Fonds der Chemischen Industrie (Germany). We also acknowledge the generous donation of Cot by the BASF.

OM9403028

(13) Lange, G. Diplomarbeit, Universität Hamburg, 1993. Heck, J.; Lange, G. Manuscript in preparation.

(14) Bachmann, B.; Heck, J. *Organometallics* **1991**, *5*, 1373.

(15) Teuben, J. H.; Sinnema, P.-J. Personal communication.

(16) Heck, J.; Massa, W. J. *Organomet. Chem.* **1989**, *376*, C15.

# Characterization of *mer,mer*-{Cr(CO)<sub>3</sub>(η<sup>2</sup>-dpe)}<sub>2</sub>(μ-dpe) (dpe = Ph<sub>2</sub>PCH<sub>2</sub>CH<sub>2</sub>PPh<sub>2</sub>) and an Investigation of Its Chemical, Redox, and Photochemical Reactivity

Alan M. Bond,\* Ray Colton,\* John B. Cooper,<sup>1</sup> Katherine McGregor,<sup>2</sup> Jacky N. Walter, and David M. Way

School of Chemistry, La Trobe University, Bundoora, Victoria 3083, Australia

Received May 25, 1994<sup>⊗</sup>

Reaction of (C<sub>7</sub>H<sub>8</sub>)Cr(CO)<sub>3</sub> with dpe (dpe = Ph<sub>2</sub>PCH<sub>2</sub>CH<sub>2</sub>PPh<sub>2</sub>) in refluxing hexane gives *mer,mer*-{Cr(CO)<sub>3</sub>(η<sup>2</sup>-dpe)}<sub>2</sub>(μ-dpe) instead of the expected *mer*-Cr(CO)<sub>3</sub>(η<sup>1</sup>-dpe)(η<sup>2</sup>-dpe). The dinuclear species has been characterized by <sup>31</sup>P NMR and IR spectroscopies, elemental analysis, and voltammetry which shows two closely spaced reversible one-electron oxidation processes at about 75 and 225 mV vs Ag/AgCl due to the reactions {Cr(CO)<sub>3</sub>(η<sup>2</sup>-dpe)}<sub>2</sub>(μ-dpe) ⇌ [{Cr(CO)<sub>3</sub>(η<sup>2</sup>-dpe)}<sub>2</sub>(μ-dpe)]<sup>+</sup> + e<sup>-</sup> and [{Cr(CO)<sub>3</sub>(η<sup>2</sup>-dpe)}<sub>2</sub>(μ-dpe)]<sup>+</sup> ⇌ [{Cr(CO)<sub>3</sub>(η<sup>2</sup>-dpe)}<sub>2</sub>(μ-dpe)]<sup>2+</sup> + e<sup>-</sup>. On the synthetic time scale at -78 °C the *mer,mer*-[{Cr(CO)<sub>3</sub>(η<sup>2</sup>-dpe)}<sub>2</sub>(μ-dpe)]<sup>+</sup> cation is moderately stable whereas the *mer,mer*-[{Cr(CO)<sub>3</sub>(η<sup>2</sup>-dpe)}<sub>2</sub>(μ-dpe)]<sup>2+</sup> cation is completely unstable. The decomposition reactions of *mer,mer*-{Cr(CO)<sub>3</sub>(η<sup>2</sup>-dpe)}<sub>2</sub>(μ-dpe) have been studied in the dark and in the presence of light to give novel and distinctively different decomposition pathways. In the light, photochemical oxidation of *mer,mer*-{Cr(CO)<sub>3</sub>(η<sup>2</sup>-dpe)}<sub>2</sub>(μ-dpe) occurs to generate *mer,mer*-[{Cr(CO)<sub>3</sub>(η<sup>2</sup>-dpe)}<sub>2</sub>(μ-dpe)]<sup>+</sup>, which then decomposes to give several products, among which *mer*-[Cr(CO)<sub>3</sub>(η<sup>1</sup>-dpe)(η<sup>2</sup>-dpe)]<sup>+</sup>, *trans*-[Cr(CO)<sub>2</sub>(dpe)<sub>2</sub>]<sup>+</sup>, and Cr(CO)<sub>4</sub>(dpe) have been identified. In the dark, *mer*-Cr(CO)<sub>3</sub>(η<sup>1</sup>-dpe)(η<sup>2</sup>-dpe) is a decomposition product. In the presence of an external oxidant such as NO<sup>+</sup> or an electrode, *mer*-[Cr(CO)<sub>3</sub>(η<sup>1</sup>-dpe)(η<sup>2</sup>-dpe)]<sup>+</sup> is a product. Evidence for these products is gained by voltammetric and spectroscopic studies.

## Introduction

Photochemical and electrochemical studies of monomeric 18-electron metal carbonyl species are extensive.<sup>3–5</sup> In general, oxidation or reduction by one electron leads to reactive species which undergo a wide range of subsequent reactions.<sup>4,5</sup>

Recently, there has been considerable interest in the redox and photochemistry of dinuclear species, particularly because of the possibilities of electronic communication between the metal centers. In the specific case of dinuclear chromium carbonyl derivatives linked by diphosphine or other ligands, Geiger<sup>6</sup> and Shaw<sup>7</sup> and their co-workers have investigated electrochemical oxidations and observed two distinct one-electron steps, which suggests some electronic interaction between the metal centers. Photochemical studies on this class of chromium compound do not appear to have been investigated, although photochemical and optical studies

have been reported, for example, on some diphosphine-bridged dinuclear ruthenium and osmium compounds.<sup>8,9</sup>

Typically, interaction of M(CO)<sub>3</sub>(C<sub>7</sub>H<sub>8</sub>) (M = Cr, Mo, W) with 2 molar equiv of L-L (L-L = potentially bidentate group 15 ligand) leads to the formation of compounds of the type M(CO)<sub>3</sub>(η<sup>1</sup>-L-L)(η<sup>2</sup>-L-L).<sup>10,11</sup> When the reaction is carried out at room temperature, the facial isomer of M(CO)<sub>3</sub>(η<sup>1</sup>-L-L)(η<sup>2</sup>-L-L) is usually obtained, and at ~80 °C the meridional isomer is often formed. These geometries can be readily distinguished by infrared (IR) and <sup>31</sup>P nuclear magnetic resonance (NMR) spectroscopies. However, in the specific case of M = Cr and L-L = dpe (dpe = Ph<sub>2</sub>PCH<sub>2</sub>CH<sub>2</sub>PPh<sub>2</sub>), the system is unusual in that attempts to prepare the *mer* isomer as described above yielded instead a species which is shown in this paper to be the dinuclear complex *mer,mer*-{Cr(CO)<sub>3</sub>(η<sup>2</sup>-dpe)}<sub>2</sub>(μ-dpe). *Mer*-Cr(CO)<sub>3</sub>(η<sup>1</sup>-dpe)(η<sup>2</sup>-dpe) may be prepared in solution<sup>11</sup> by an electrochemical oxidation-reduction sequence involving oxidation of *fac*-Cr(CO)<sub>3</sub>(η<sup>1</sup>-dpe)(η<sup>2</sup>-dpe) to give *fac*-[Cr(CO)<sub>3</sub>(η<sup>1</sup>-dpe)(η<sup>2</sup>-dpe)]<sup>+</sup> which rapidly isomerizes to *mer*-[Cr(CO)<sub>3</sub>(η<sup>1</sup>-dpe)(η<sup>2</sup>-dpe)]<sup>+</sup>, followed by subsequent electrochemical reduction to give the required *mer*-Cr(CO)<sub>3</sub>(η<sup>1</sup>-dpe)(η<sup>2</sup>-dpe). A more elegant solution synthesis<sup>11</sup> utilizes a catalytic cycle involving the same redox reactions, but which is initiated by addition of a small amount of oxidant such as NOBF<sub>4</sub> to *fac*-Cr(CO)<sub>3</sub>(η<sup>1</sup>-dpe)(η<sup>2</sup>-dpe).

\* Abstract published in *Advance ACS Abstracts*, October 1, 1994.

(1) Present address: Department of Chemistry and Biochemistry, Old Dominion University, Norfolk, VA 23529-0126.

(2) Present address: CSIRO, Division of Mineral Products, Port Melbourne 3207, Australia.

(3) *Comprehensive Organometallic Chemistry*; Wilkinson, G., Stone, F. G. A., Abel, E. W., Eds.; Pergamon Press: Oxford, 1982.

(4) Geiger, W. E. *Prog. Inorg. Chem.*, **1985**, *33*, 275.

(5) Vlcek, A., Jr. *Chemtracts—Inorg. Chem.* **1993**, *5*, 1.

(6) (a) Van Order, N.; Geiger, W. E.; Bitterwolf, T. E.; Rheingold, A. L. *J. Am. Chem. Soc.* **1987**, *109*, 5680. (b) Merkert, J. W.; Geiger, W. E.; Paddon-Row, M. N.; Oliver, A. M.; Rheingold, A. L. *Organometallics* **1992**, *11*, 4109.

(7) Taylor, N.; Boddington, T.; Dobson, I.; Gill, B.; Luo, R.; Shaw, B. L. *NATO ASI Series, Series C: Mathematical and Physical Sciences*; Kluwer Academic Publishers: Dordrecht, The Netherlands, 1993; Vol 385, pp 467–475.

(8) Sullivan, B. T.; Meyer, T. J. *Inorg. Chem.* **1980**, *19*, 752.

(9) Kober, E. M.; Goldsby, K. A.; Narayana, D. N. S.; Meyer, T. J. *J. Am. Chem. Soc.* **1983**, *105*, 4303.

(10) Isaacs, E. E.; Graham, W. A. G. *Inorg. Chem.* **1975**, *14*, 2560.

(11) Bond, A. M.; Colton, R.; McGregor, K. *Inorg. Chem.* **1986**, *25*, 2378.



During the course of the present studies which led to the characterization of the structure of *mer,mer*-{Cr(CO)<sub>3</sub>(η<sup>2</sup>-dpe)}<sub>2</sub>(μ-dpe), photoactivity in sunlight, as well as a much higher degree of chemical reactivity than found with the stable, well characterized monomeric *fac*-Cr(CO)<sub>3</sub>(η<sup>1</sup>-dpe)(η<sup>2</sup>-dpe) complex, was noted. Consequently, detailed studies of the products formed in dichloromethane solutions of *mer,mer*-{Cr(CO)<sub>3</sub>(η<sup>2</sup>-dpe)}<sub>2</sub>(μ-dpe) both in the dark and after exposure to light were undertaken. The products of electrochemical and chemical oxidation of *mer,mer*-{Cr(CO)<sub>3</sub>(η<sup>2</sup>-dpe)}<sub>2</sub>(μ-dpe) in dichloromethane solution also were studied. The present paper, therefore, in addition to describing the synthesis and structural characterization of a new form of a chromium carbonyl-dpe complex, contains a report of the unusual reactivity which is introduced by structural factors related to having an uncommon dinuclear rather than the usual monomeric structure.

### Experimental Section

**Materials.** All solvents used were of AR-grade purity. Tetrabutylammonium hexafluorophosphate used as one of the supporting electrolytes in the voltammetric studies was prepared by the method of Swain et al.<sup>12</sup> Other electrolytes, tetrabutylammonium tetrafluoroborate and tetrabutylammonium perchlorate (GFS Chemicals) and NOPF<sub>6</sub> (Aldrich), used in chemical oxidation studies were used as supplied by the manufacturers. Cr(CO)<sub>6</sub> and dpe (Strem) also were used as purchased.

**Preparations.** The dinuclear species *mer,mer*-{Cr(CO)<sub>3</sub>(η<sup>2</sup>-dpe)}<sub>2</sub>(μ-dpe) was prepared by the interaction of Cr(CO)<sub>3</sub>(C<sub>7</sub>H<sub>8</sub>) and dpe (1:2) in refluxing hexane for 4.5 h. Anal. Found (CMAS, Geelong, Australia): C, 68.71; H, 5.13. Req'd for *mer,mer*-{Cr(CO)<sub>3</sub>(η<sup>2</sup>-dpe)}<sub>2</sub>(μ-dpe): C, 68.8; H, 4.9. IR absorptions (carbonyl region): 1950, 1850, and 1834 cm<sup>-1</sup>. <sup>31</sup>P NMR: δ 92.7, 74.8, 67.0. *cis*-<sup>13</sup>C and *trans*-Cr(CO)<sub>2</sub>(dpe)<sub>2</sub>,<sup>13b</sup> *mer*-Cr(CO)<sub>3</sub>(η<sup>1</sup>-dpe)(η<sup>2</sup>-dpe),<sup>11</sup> and *trans*-[Cr(CO)<sub>2</sub>(dpe)<sub>2</sub>]<sup>14</sup> used in studies to characterize the reactions of the dinuclear complex were prepared by literature methods.

**Instrumentation.** <sup>31</sup>P NMR spectra were recorded on either a JEOL FX 100 (CH<sub>2</sub>Cl<sub>2</sub>, external <sup>7</sup>Li lock) or a Bruker AM 300 (CDCl<sub>3</sub>, internal <sup>2</sup>D lock) spectrometer at 40.32 or 121.5 MHz, respectively. Chemical shifts were referenced against external 85% H<sub>3</sub>PO<sub>4</sub> and the high frequency positive sign convention is used in reporting the data. ESR spectra were recorded using a Varian E-9 spectrometer at room temperature in either the solid state or in dichloromethane solution. IR spectra in the carbonyl region were recorded in dichloromethane solution on either a Perkin-Elmer FT-IR 1720 X or a JASCO A-302 spectrophotometer, with spectra on the latter instrument being calibrated against polystyrene (1601 cm<sup>-1</sup>).

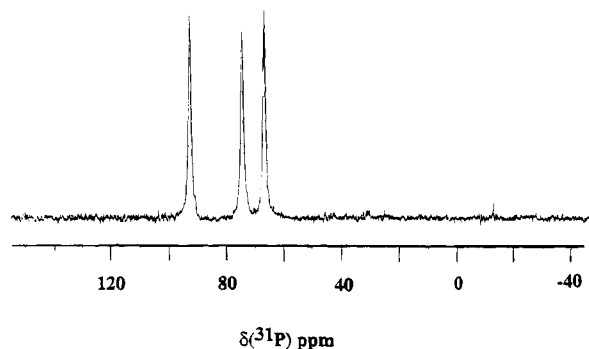
All UV irradiation experiments were conducted in a 1.5 cm radius Pyrex test tube in dichloromethane solution at room temperature using a 125 W Hg lamp.

Cyclic voltammograms in dichloromethane were obtained with a Cypress System Model CYSY-1 computer-controlled electrochemical system. For studies with electrolyte, a conventional 0.5 mm radius platinum disk working electrode, a platinum wire auxiliary electrode, and a Ag/AgCl (satd. LiCl in CH<sub>2</sub>Cl<sub>2</sub>) reference electrode were used. Voltammetric data without electrolyte were obtained with a 5 μm radius platinum disk microelectrode. The same auxiliary and reference electrodes were used as in conventional studies with electrolyte.

(12) Swain, C. G.; Ohno, A.; Roe, D. K.; Brown, R.; Maugh, T. II. *J. Am. Chem. Soc.* **1967**, *89*, 2648.

(13) (a) Chatt, J.; Watson, H. R. *J. Chem. Soc.* **1961**, 4980. (b) Bond, A. M.; Colton, R.; Jackowski, J. *J. Inorg. Chem.* **1975**, *14*, 274.

(14) Crossing, P. F.; Snow, M. R. *J. Chem. Soc. A* **1971**, 610.

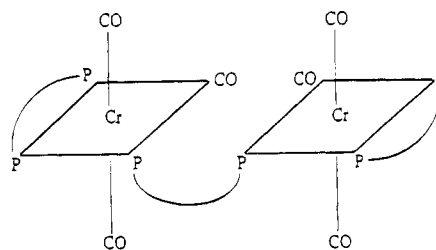


**Figure 1.** <sup>31</sup>P NMR spectra at room temperature of a dichloromethane solution of *mer,mer*-{Cr(CO)<sub>3</sub>(η<sup>2</sup>-dpe)}<sub>2</sub>(μ-dpe).

Bulk electrolysis experiments were undertaken with either a PAR Model 273 potentiostat or a BAS 100A electrochemical analyzer using a large platinum basket working electrode and a platinum gauze auxiliary electrode separated from the test solution by a salt bridge and the same reference electrode as used in voltammetric studies.

### Results and Discussion

**Characterization of *mer,mer*-{Cr(CO)<sub>3</sub>(η<sup>2</sup>-dpe)}<sub>2</sub>(μ-dpe).** When Cr(CO)<sub>3</sub>(C<sub>7</sub>H<sub>8</sub>) and dpe (1:2) are reacted in refluxing hexane for 4.5 h a yellow precipitate is formed. When dissolved in dichloromethane, the IR spectrum in the carbonyl region contains bands at 1950, 1850, and 1834 cm<sup>-1</sup> which are very similar to those found for *mer*-Cr(CO)<sub>3</sub>(η<sup>1</sup>-dpe)(η<sup>2</sup>-dpe)<sup>11</sup> and are typical of a meridional isomer. The <sup>31</sup>P NMR spectrum<sup>11</sup> of *mer*-Cr(CO)<sub>3</sub>(η<sup>1</sup>-dpe)(η<sup>2</sup>-dpe), prepared in dichloromethane by the electrochemical sequence described in the Introduction, displays four <sup>31</sup>P resonances of equal intensities at δ 92.6, 74.4, 66.8, and -13.2 with the appropriate coupling constants expected for the *mer* isomer,<sup>11</sup> with the signal at lowest frequency being due to the pendant phosphorus whose chemical shift is the same as for free dpe, but it appears as a doublet due to phosphorus-phosphorus coupling.<sup>11</sup> The <sup>31</sup>P NMR spectrum (Figure 1) of the new chromium carbonyl compound gives resonances at δ 92.7, 74.8, and 67.0, almost identical chemical shifts to those for *mer*-Cr(CO)<sub>3</sub>(η<sup>1</sup>-dpe)(η<sup>2</sup>-dpe), but phosphorus-phosphorus coupling is not resolved. The resonance at δ -13.2 due to the pendant phosphorus in *mer*-Cr(CO)<sub>3</sub>(η<sup>1</sup>-dpe)(η<sup>2</sup>-dpe) is absent in the spectrum for the new compound. Thus the IR and NMR spectra both indicate that the environments of all the donor atoms bonded to chromium are essentially the same in both compounds. <sup>31</sup>P NMR and IR spectral data are summarized in Table 1. The only stereochemistry consistent with all the data is *mer,mer*-{Cr(CO)<sub>3</sub>(η<sup>2</sup>-dpe)}<sub>2</sub>(μ-dpe) as represented in structure I. Analytical

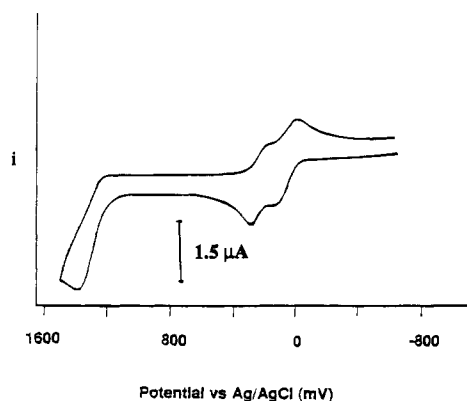


I (P-P = dpe)

**Table 1.** IR (Carbonyl Region) and <sup>31</sup>P NMR Data for mer,mer-{Cr(CO)<sub>3</sub>(η<sup>2</sup>-dpe)}<sub>2</sub>(μ-dpe) and Its Possible Decomposition Products

	dinucl <sup>a</sup>	dinucl <sup>a</sup> (after irrad)	Cr(CO) <sub>3</sub> (dpe) <sub>2</sub> <sup>b</sup>	Cr(CO) <sub>4</sub> (dpe)	[Cr(CO) <sub>2</sub> (dpe) <sub>2</sub> ] <sup>+</sup>	dpe	dpeO <sub>2</sub>
IR <sup>c</sup>		2009		2009			
	1950	1950	1955				
		1912		1914			
		1900		1899			
		1877		1877			
	1850	1850	1850		1850		
	1834	1834	1830				
<sup>31</sup> P <sup>d</sup>	92.7	92.9	92.6				
		78.6		79.4			
	74.8	74.8	74.4				
	67.0	66.9	66.8				
		31.1					31.1
		-13.0	-13.2			-13.3	

<sup>a</sup> Dinucl = mer,mer-{Cr(CO)<sub>3</sub>(η<sup>2</sup>-dpe)}<sub>2</sub>(μ-dpe). <sup>b</sup> Cr(CO)<sub>3</sub>(dpe)<sub>2</sub> = mer-Cr(CO)<sub>3</sub>(η<sup>1</sup>-dpe)(η<sup>2</sup>-dpe). <sup>c</sup> cm<sup>-1</sup>. <sup>d</sup> δ.

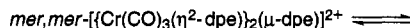
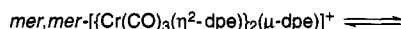
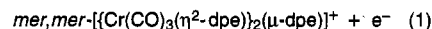
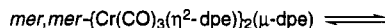


**Figure 2.** Cyclic voltammograms at 22 °C for the oxidation of  $5 \times 10^{-4}$  M mer,mer-{Cr(CO)<sub>3</sub>(η<sup>2</sup>-dpe)}<sub>2</sub>(μ-dpe) in dichloromethane (0.1 M Bu<sub>4</sub>NPF<sub>6</sub>) at a 0.5 mm radius Pt disk electrode at a scan rate of 100 mV s<sup>-1</sup>.

data are also consistent with this formulation. We have recently characterized<sup>15</sup> by X-ray crystallography a related dinuclear molybdenum complex, fac, fac-{Mo(CO)(η<sup>2</sup>-ape)}<sub>2</sub>(μ-ape) (ape = Ph<sub>2</sub>AsCH<sub>2</sub>CH<sub>2</sub>PPh<sub>2</sub>), which was also prepared by the M(CO)<sub>3</sub>(C<sub>7</sub>H<sub>8</sub>) method.

**Voltammetric Studies in Dichloromethane.** In keeping with the proposed dinuclear structure, the cyclic voltammogram of the yellow product dissolved in dichloromethane (0.1 M Bu<sub>4</sub>NPF<sub>6</sub>) shows two closely spaced chemically reversible one-electron redox couples (Figure 2) with  $E_{1/2}^r$  values (reversible halfwave potentials) at 75 and 225 mV vs Ag/AgCl, which formally corresponds to the consecutive oxidation of the two zero valent chromium centers to the chromium(I) oxidation state. This is in contrast to the monomeric mer-Cr(CO)<sub>3</sub>(η<sup>1</sup>-dpe)(η<sup>2</sup>-dpe) which shows a single oxidation response with an  $E_{1/2}^r$  value of 155 mV vs Ag/AgCl. The reversible potentials were calculated from the average of the oxidation and reduction potentials from the cyclic voltammograms. The 150 mV separation between the two redox couples for the dimer suggests some degree of interaction between the two metal centers. Similar separations have been observed previously<sup>6a,8,9</sup> for dpm-bridged dimers (dpm = Ph<sub>2</sub>PCH<sub>2</sub>PPh<sub>2</sub>). Shaw and co-workers<sup>7</sup> also have reported analogous data for bimetallic compounds of the type cis,cis-{M'(CO)<sub>4</sub>(μ-dpe)<sub>2</sub>-M''(CO)<sub>4</sub>} (M', M'' = Cr, Mo, W) and for the corresponding monomeric species M(CO)<sub>4</sub>(dpe). At more positive potentials, an irreversible two-electron oxidation process

is observed for mer,mer-{Cr(CO)<sub>3</sub>(η<sup>2</sup>-dpe)}<sub>2</sub>(μ-dpe) (peak potential at 1390 mV vs Ag/AgCl for a scan rate of 100 mV s<sup>-1</sup>) which corresponds to a second oxidation of the chromium centers. This potential may be compared to that of the second oxidation of the meridional monomer mer-Cr(CO)<sub>3</sub>(η<sup>1</sup>-dpe)(η<sup>2</sup>-dpe) (1240 mV vs Ag/AgCl). Data in dichloromethane with 0.1 M Bu<sub>4</sub>NBF<sub>4</sub> and Bu<sub>4</sub>NCIO<sub>4</sub> as the electrolyte are very similar to that found with 0.1 M Bu<sub>4</sub>NPF<sub>6</sub>. The voltammetry in dichloromethane in the dark is therefore summarized by eqs 1–3

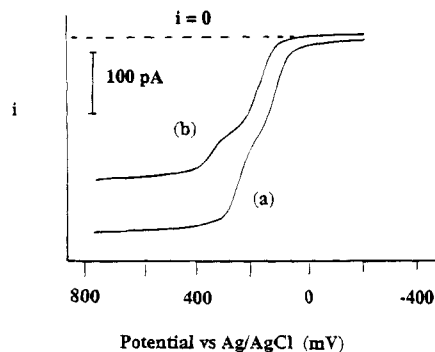


where mer,mer-[\{Cr(CO)<sub>3</sub>(η<sup>2</sup>-dpe)}<sub>2</sub>(μ-dpe)]<sup>3+</sup> is probably an intermediate in eq 3, but mechanistic details of this irreversible overall two-electron step are unknown.

Steady-state voltammograms obtained at a 5 μm radius Pt disk microelectrode over the restricted range -200 mV to +800 mV, to cover the initial two one-electron oxidations, are shown in Figure 3. The process described for the cyclic voltammograms at higher positive potential is also observed with the microdisk electrode, but this process is not relevant to this discussion. In the presence of electrolyte (Figure 3a), two processes of equal limiting currents are observed with  $E_{1/2}^r$  values of 75 and 225 mV vs Ag/AgCl. These values and their separation are the same as those observed in cyclic voltammetry using a conventional electrode. Interestingly, in the absence of electrolyte (Figure 3b) the ratio of the currents for the two processes alters dramatically. Presumably, the charged one-electron-oxidized species mer,mer-[\{Cr(CO)<sub>3</sub>(η<sup>2</sup>-dpe)}<sub>2</sub>(μ-dpe)]<sup>+</sup> migrates from the positively charged electrode which causes the current response for the second process to decrease in height (see for example refs 16–19). Oxidation of the neutral dinuclear species

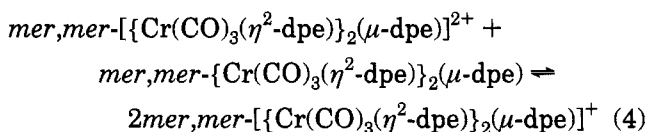
(15) Abrahams, B. F.; Colton, R.; Hoskins, B. F.; McGregor, K. *Aust. J. Chem.* **1992**, *45*, 941.

(16) Cooper, J. B.; Bond, A. M. *J. Electroanal. Chem. Interfacial Electrochem.* **1992**, *315*, 143.



**Figure 3.** Steady-state microdisk electrode voltammograms at 22 °C for the oxidation of  $5 \times 10^{-4}$  M *mer,mer*- $\{Cr(CO)_3(\eta^2-dpe)\}_2(\mu-dpe)$  in dichloromethane (a) with 0.1 M  $Bu_4NPF_6$  as supporting electrolyte and (b) without deliberately added electrolyte. Voltammograms recorded at a 5  $\mu$ m radius Pt microdisk electrode, scan rate 30  $mV s^{-1}$ .

to the corresponding monocation should of course not be altered by migration under steady state conditions, and this is observed (Figure 3). The reaction in eq 4 also may be important<sup>20</sup> in the absence of electrolyte.



The more positive half wave potentials observed in the absence of any electrolyte is attributed predominantly to Ohmic ( $iR$ ) drop.

Controlled potential oxidative electrolysis of *mer,mer*- $\{Cr(CO)_3(\eta^2-dpe)\}_2(\mu-dpe)$  was performed at a large platinum gauze basket electrode with the potential held between the first and second oxidation processes, or at a potential more positive than the second process. The progress of the experiment was monitored by steady-state microelectrode voltammetry and the data indicated that neither the dinuclear monocation nor dication are stable on the bulk electrolysis (synthetic) time scale at room temperature. If the dinuclear monocation had been stable, then after completion of a one-electron reversible oxidation the zero of current would lie between the two original processes. In fact, both one-electron processes disappear and are replaced by a number of other processes which included reversible reduction and oxidation processes assigned to formation of *trans*- $[Cr(CO)_2(dpe)_2]^+$  (see later). The presence of paramagnetic *trans*- $[Cr(CO)_2(dpe)_2]^+$  was confirmed by subsequent observation of its characteristic 1:4:6:4:1 ESR signal<sup>21</sup> (also see later).

Microelectrode steady-state voltammetric monitoring of the oxidation of *mer,mer*- $\{Cr(CO)_3(\eta^2-dpe)\}_2(\mu-dpe)$  in dichloromethane with  $NOPF_6$  at 0 °C in the dark was consistent with the bulk electrolysis data in that no

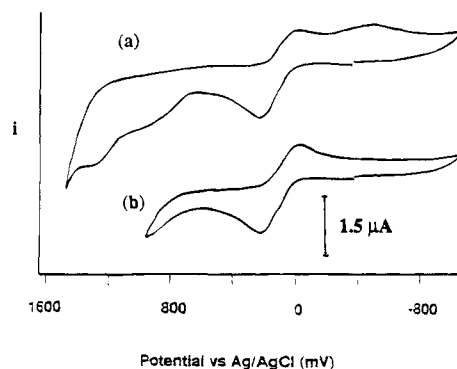
(17) Cooper, J. B.; Bond, A. M.; Oldham, K. B. *J. Electroanal. Chem. Interfacial Electrochem.* **1992**, *331*, 877.

(18) Oldham, K. B., *J. Electroanal. Chem. Interfacial Electrochem.* **1992**, *337*, 91.

(19) Heinze, J. *Angew. Chem., Int. Ed. Engl.* **1993**, *32*, 1268 and references cited therein.

(20) Norton, J. D.; Benson, W. E.; White, H. S.; Pendley, B. D.; Abruna, H. D. *Anal. Chem.* **1991**, *63*, 1909.

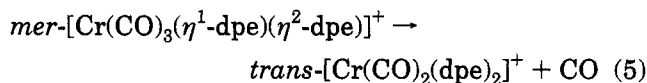
(21) (a) Bagchi, R. N.; Bond, A. M.; Colton, R.; Creece, I.; McGregor, K.; Whyte, T. *Organometallics* **1991**, *10*, 2611. (b) Bond, A. M.; Colton, R.; Cooper, J. B.; Traeger, J. C.; Walter, J. N.; Way, D. M. *Organometallics* **1994**, *13*, 3434.



**Figure 4.** Cyclic voltammograms at 26 °C for a solution initially containing  $5 \times 10^{-4}$  M *mer,mer*- $\{Cr(CO)_3(\eta^2-dpe)\}_2(\mu-dpe)$  in dichloromethane (0.1 M  $Bu_4NPF_6$ ) kept in the dark for 10 h at 26 °C. (a) Full potential range. (b) Restricted potential range. The voltammograms were recorded at a 0.5 mm radius Pt disk electrode, scan rate 100  $mV s^{-1}$ .

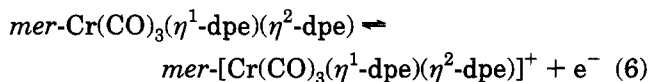
evidence for formation of *mer,mer*- $\{Cr(CO)_3(\eta^2-dpe)\}_2(\mu-dpe)^+$  was found on the synthetic time scale. However, at  $-78$  °C, maintained by a dry ice/acetone slush bath, after oxidation with  $NOPF_6$  the zero of current could be observed to lie between the two original one-electron processes for a short period of time. That is, there is now one reversible oxidation and one reversible reduction process. This result is consistent with *mer,mer*- $\{Cr(CO)_3(\eta^2-dpe)\}_2(\mu-dpe)^+$  exhibiting transient stability at this temperature.

The monocation voltammetric response observed after  $NOPF_6$  oxidation of *mer,mer*- $\{Cr(CO)_3(\eta^2-dpe)\}_2(\mu-dpe)$  gradually disappeared even at  $-78$  °C and was replaced by a process assigned to the *mer*- $[Cr(CO)_3(\eta^1-dpe)(\eta^2-dpe)]^{+/0}$  redox couple (see later). The presence of the *mer*<sup>+</sup> species also was confirmed by observing its characteristic ESR spectrum.<sup>21</sup> On warming the solution, the ESR spectrum of *mer*<sup>+</sup> was replaced by that of *trans*<sup>+</sup> in accordance with the known<sup>21</sup> reaction

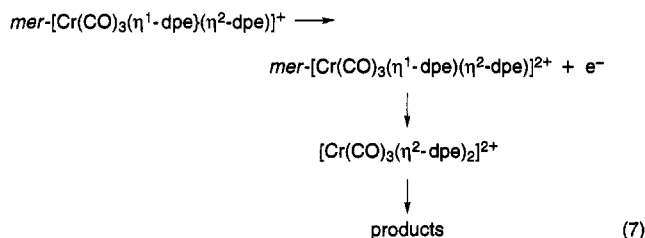


**Decomposition Reactions of *mer,mer*- $\{Cr(CO)_3(\eta^2-dpe)\}_2(\mu-dpe)$  in the Dark. Voltammetric Studies.** When the solution of *mer,mer*- $\{Cr(CO)_3(\eta^2-dpe)\}_2(\mu-dpe)$  in dichloromethane (0.1 M  $Bu_4NPF_6$ ) was kept in the dark at 0 °C, no voltammetric evidence of decomposition was found even after 10 h; that is, the response remains as in Figure 2. However, when the solution was left standing at 26 °C in the dark for the same period of time, the voltammetric responses for *mer,mer*- $\{Cr(CO)_3(\eta^2-dpe)\}_2(\mu-dpe)$  had disappeared. Instead, a chemically reversible couple with an  $E^{r_{1/2}}$  value of 155 mV vs Ag/AgCl is observed, as well as irreversible oxidation processes with oxidation peak potentials at about 1000 and 1365 mV vs Ag/AgCl. On the reverse scan an irreversible reduction process occurs at  $-350$  mV vs Ag/AgCl (Figure 4a). If the potential is scanned over a restricted range to include only the first two oxidation responses, then the reduction process at  $-350$  mV vs Ag/AgCl is absent (Figure 4b). This demonstrates that the reduction response is due to products generated at very positive potentials. The new reversible redox couple with an  $E^{r_{1/2}}$  value of 155 mV is

tentatively assigned (definite evidence is presented below) to the first oxidation process for *mer*-Cr(CO)<sub>3</sub>(η<sup>1</sup>-dpe)(η<sup>2</sup>-dpe)<sup>11</sup> and is therefore attributed to the presence and subsequent electrochemical oxidation of this compound according to eq 6



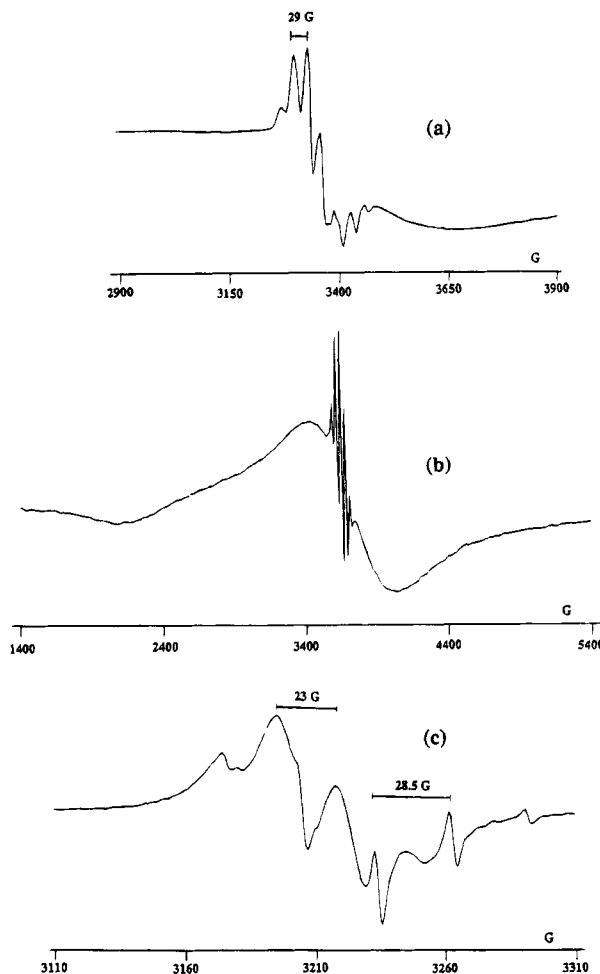
The most positive response in Figure 4a at 1350 mV vs Ag/AgCl is assigned to oxidation of *mer*-[Cr(CO)<sub>3</sub>(η<sup>1</sup>-dpe)(η<sup>2</sup>-dpe)]<sup>+</sup> as in eq 7



and the process on the reverse scan is a result of reduction of [Cr(CO)<sub>3</sub>(η<sup>2</sup>-dpe)<sub>2</sub>]<sup>2+</sup> and/or products of its decomposition.

Cyclic voltammetry, being a transient technique, cannot unambiguously be used to distinguish whether the process at 155 mV vs Ag/AgCl generated in the dark at 26 °C for a solution of *mer,mer*-{Cr(CO)<sub>3</sub>(η<sup>2</sup>-dpe)}<sub>2</sub>(μ-dpe) in dichloromethane is in fact due to *mer*-Cr(CO)<sub>3</sub>(η<sup>1</sup>-dpe)(η<sup>2</sup>-dpe) or *mer*-[Cr(CO)<sub>3</sub>(η<sup>1</sup>-dpe)(η<sup>2</sup>-dpe)]<sup>+</sup>. However, voltammetry at a microelectrode under steady-state conditions can make the distinction by observation of the sign of the current. At a scan rate of 25 mV s<sup>-1</sup> and with a 5 μm radius platinum microdisk working electrode, near steady-state voltammetric conditions prevail. A steady-state voltammogram at a microelectrode of the dichloromethane solution of *mer,mer*-{Cr(CO)<sub>3</sub>(η<sup>2</sup>-dpe)}<sub>2</sub>(μ-dpe) which was stored in the dark at 26 °C for 10 h showed that zero current was achieved only at potentials more negative than the process at 155 mV vs Ag/AgCl. This result shows that the process at 155 mV vs Ag/AgCl is an oxidative process and confirms that the species in solution is *mer*-Cr(CO)<sub>3</sub>(η<sup>1</sup>-dpe)(η<sup>2</sup>-dpe) rather than *mer*-[Cr(CO)<sub>3</sub>(η<sup>1</sup>-dpe)(η<sup>2</sup>-dpe)]<sup>+</sup>.

**Electron Spin Resonance and Infrared Spectroscopies.** Although the uncharged dinuclear compound *mer,mer*-{Cr(CO)<sub>3</sub>(η<sup>2</sup>-dpe)}<sub>2</sub>(μ-dpe) is expected to be diamagnetic, the ESR spectrum of a solid powder sample showed a weak S = 1/2 signal (Figure 5a). The low-field tensor shows resolved hyperfine structure, and the spectrum contains an anisotropic seven-line pattern. The splitting is most reasonably assigned to three non-equivalent phosphorus nuclei with I = 1/2 and hyperfine coupling constants in the approximate ratios of 1:2:3 where the smallest constant is 29 G. The ESR spectrum of *mer*-[Cr(CO)<sub>3</sub>(η<sup>1</sup>-dpe)(η<sup>2</sup>-dpe)]<sup>+</sup> consists of an S = 1/2 signal with a four-line splitting pattern, indicating three near-equivalent phosphorus nuclei.<sup>11,21</sup> In the case of the singly oxidized *mer,mer*-[Cr(CO)<sub>3</sub>(η<sup>2</sup>-dpe)]<sub>2</sub>(μ-dpe)<sup>+</sup>, this near-degeneracy of the hyperfine coupling constants to the Cr(I) center could be removed when the pendant phosphine in *mer*-[Cr(CO)<sub>3</sub>(η<sup>1</sup>-dpe)(η<sup>2</sup>-dpe)]<sup>+</sup> is coordinated to another chromium center in *mer,mer*-[Cr(CO)<sub>3</sub>(η<sup>2</sup>-dpe)]<sub>2</sub>(μ-dpe)<sup>+</sup>. Indeed, such a perturbation



**Figure 5.** ESR spectra of (a) solid powder *mer,mer*-{Cr(CO)<sub>3</sub>(η<sup>2</sup>-dpe)}<sub>2</sub>(μ-dpe), (b) a solution of *mer,mer*-{Cr(CO)<sub>3</sub>(η<sup>2</sup>-dpe)}<sub>2</sub>(μ-dpe) in dichloromethane kept in the dark for 3 days at 26 °C, and (c) a solution of *mer,mer*-{Cr(CO)<sub>3</sub>(η<sup>2</sup>-dpe)}<sub>2</sub>(μ-dpe) in dichloromethane at -77 °C to which has been added NOPF<sub>6</sub>.

is very likely since the separation of the two oxidation potentials of *mer,mer*-{Cr(CO)<sub>3</sub>(η<sup>2</sup>-dpe)}<sub>2</sub>(μ-dpe) in the voltammetry does indicate some interaction between the two metal centers (an interaction which is mediated by the dpe bridge). Accordingly, the ESR spectrum in Figure 5a is assigned to the singly oxidized species *mer,mer*-[Cr(CO)<sub>3</sub>(η<sup>2</sup>-dpe)]<sub>2</sub>(μ-dpe)<sup>+</sup>. Presumably, a small amount of surface oxidation occurs when *mer,mer*-{Cr(CO)<sub>3</sub>(η<sup>2</sup>-dpe)}<sub>2</sub>(μ-dpe) is exposed to light and/or air (see later).

The ESR spectrum of a dichloromethane solution of *mer,mer*-{Cr(CO)<sub>3</sub>(η<sup>2</sup>-dpe)}<sub>2</sub>(μ-dpe) which was kept in the dark for 3 days at 26 °C was also investigated. The spectrum (Figure 5b) indicates the presence of two paramagnetic species. One S = 1/2 signal gives a sharp symmetric five-line pattern which can be assigned to a very small concentration of *trans*-[Cr(dpe)<sub>2</sub>(CO)<sub>2</sub>]<sup>+</sup> on the basis of its g value of 2.012 and hyperfine coupling constant<sup>21</sup> (see later for confirmation of the assignment). The other S = 1/2 signal is very broad, shows no resolved hyperfine splitting, and cannot be assigned.

The infrared spectrum in the carbonyl region of the same solution shows peaks due to the presence of *mer*-Cr(CO)<sub>3</sub>(η<sup>1</sup>-dpe)(η<sup>2</sup>-dpe) and/or *mer,mer*-{Cr(CO)<sub>3</sub>(η<sup>2</sup>-dpe)}<sub>2</sub>(μ-dpe) (these cannot be distinguished by IR, see earlier) together with a small unidentified peak just

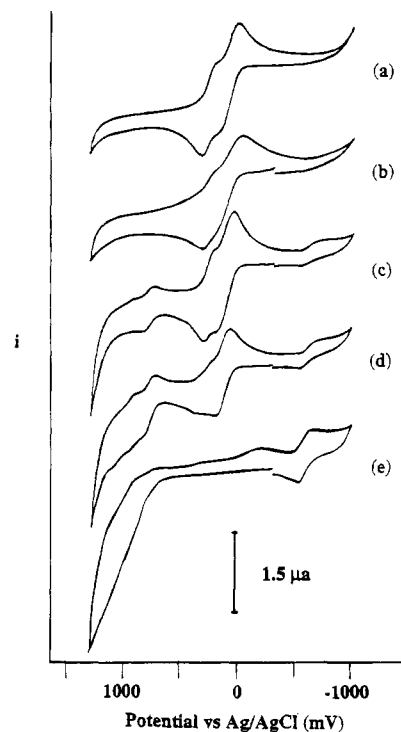
above 1600  $\text{cm}^{-1}$ . The small concentration of *trans*-[Cr(dpe)<sub>2</sub>(CO)<sub>2</sub>]<sup>+</sup> detected by ESR spectroscopy would be expected to give rise to an absorption at 1850  $\text{cm}^{-1}$ , but unfortunately the spectra of the other carbonyl compounds present at high concentration dominate this region of the spectrum.

### <sup>31</sup>P Nuclear Magnetic Resonance Spectroscopy.

The <sup>31</sup>P NMR spectrum of a freshly prepared dichloromethane solution of *mer,mer*-{Cr(CO)<sub>3</sub>( $\eta^2$ -dpe)}<sub>2</sub>( $\mu$ -dpe) gives the spectrum shown in Figure 1, with resonances at  $\delta$  92.7, 74.8, and 67 ppm. The spectrum of the same solution after standing 2 days in the dark at room temperature resembles that of *mer*-Cr(CO)<sub>3</sub>( $\eta^1$ -dpe)( $\eta^2$ -dpe). That is, the three resonances close to  $\delta$  92.7, 74.8, and 67 are still present, but a new doublet has appeared at  $\delta$  -13.3 ppm. This resonance cannot be assigned to free dpe, which gives a singlet, and therefore must be assigned to the pendant phosphorus of *mer*-Cr(CO)<sub>3</sub>( $\eta^1$ -dpe)( $\eta^2$ -dpe),<sup>11</sup> thus confirming the formation of this compound in the dark. Based on the intensity of the peak at  $\delta$  -13.3 compared with the other peaks, it is likely that this solution contains a mixture of *mer,mer*-{Cr(CO)<sub>3</sub>( $\eta^2$ -dpe)}<sub>2</sub>( $\mu$ -dpe) and *mer*-Cr(CO)<sub>3</sub>( $\eta^1$ -dpe)( $\eta^2$ -dpe).

### Decomposition Reactions of *mer,mer*-{Cr(CO)<sub>3</sub>( $\eta^2$ -dpe)}<sub>2</sub>( $\mu$ -dpe) in the Presence of Light. Voltammetric Studies.

Recently we have reported data on systematic photoelectrochemical studies on carbonyl complexes,<sup>22,23</sup> and it appears that photochemistry in the 17 electron, as well as in the 18 electron state is important. In order to ascertain whether the very slow decomposition reactions described are light catalyzed or modified in the presence of light, three identical dichloromethane solutions of *mer,mer*-{Cr(CO)<sub>3</sub>( $\eta^2$ -dpe)}<sub>2</sub>( $\mu$ -dpe) ( $5 \times 10^{-4}$  M) in CH<sub>2</sub>Cl<sub>2</sub> (0.1 M Bu<sub>4</sub>NPF<sub>6</sub>) were prepared and kept at 0 °C. One, the control, was left standing in the laboratory on the bench top in the presence of air and a moderate amount of light, another was stored in the dark, and the remaining sample was purged with N<sub>2</sub> while left standing on the bench top, again in the presence of a moderate amount of light. Cyclic voltammograms were then recorded on each solution at approximately 2 h intervals. After 4 h, the two samples which were exposed to normal laboratory light began to show evidence of decomposition, whereas the solution maintained in the dark remained unchanged. A new sample of the dinuclear complex was therefore prepared and exposed to a mercury light source and voltammograms recorded every 10 min while keeping the solution at 0 °C. Some of the resulting voltammograms are shown in Figure 6. Figure 6a shows the cyclic voltammogram of the freshly prepared solution of *mer,mer*-{Cr(CO)<sub>3</sub>( $\eta^2$ -dpe)}<sub>2</sub>( $\mu$ -dpe). The initial evidence for decomposition is detected in Figure 6b (10 mins) by noting that the resolution between the two chromium oxidation responses apparently decreases. Upon further irradiation (Figure 6c, 20 min), oxidation processes for *mer,mer*-{Cr(CO)<sub>3</sub>( $\eta^2$ -dpe)}<sub>2</sub>( $\mu$ -dpe) have almost disappeared. In fact, the two one-electron oxidation processes associated with *mer,mer*-{Cr(CO)<sub>3</sub>( $\eta^2$ -dpe)}<sub>2</sub>( $\mu$ -dpe) are being replaced by a new reversible one-



**Figure 6.** Cyclic voltammograms at 26 °C for a solution initially containing  $5 \times 10^{-4}$  M *mer,mer*-{Cr(CO)<sub>3</sub>( $\eta^2$ -dpe)}<sub>2</sub>( $\mu$ -dpe) in dichloromethane (0.1 M Bu<sub>4</sub>NPF<sub>6</sub>) after UV irradiation for various times: (a) freshly prepared solution, (b) 10 min irradiation, (c) 20 min, (d) 30 min, (e) 60 min. The voltammograms were recorded at a 0.5 mm radius Pt disk electrode, scan rate 100  $\text{mV s}^{-1}$ .

electron oxidation process at 155 mV vs Ag/AgCl. Additionally, two new reversible redox couples are seen at -575 and 935 mV vs Ag/AgCl. With time, the positive potential region becomes very complex and consistent with the presence of many unresolved processes (Figure 6d, 30 min). The reversible process at -575 mV vs Ag/AgCl increases in magnitude with further irradiation. The new couple at 155 mV vs Ag/AgCl then begins to decrease in magnitude until eventually the response disappears (Figure 6e, 60 min). Periodic examination of a solution of the dinuclear complex placed in bright sunlight also exhibited the same characteristics as the solution exposed to UV irradiation.

The initial distortion of the cyclic voltammogram is due to a decrease in the two reversible oxidation processes of *mer,mer*-{Cr(CO)<sub>3</sub>( $\eta^2$ -dpe)}<sub>2</sub>( $\mu$ -dpe) and the concomitant growth of the new oxidation process at 155 mV vs Ag/AgCl which is assigned to the formation and then voltammetric oxidation of *mer*-Cr(CO)<sub>3</sub>( $\eta^1$ -dpe)( $\eta^2$ -dpe) (see later). The reversible oxidation at 935 mV and the reversible reduction process at -575 mV vs Ag/AgCl correspond respectively to the formation and then electrochemical oxidation and reduction of *trans*-[Cr(CO)<sub>2</sub>(dpe)<sub>2</sub>]<sup>+</sup> (also see later). The irreversible oxidation processes at positive potentials are also consistent with formation and oxidation of Cr(CO)<sub>4</sub>(dpe)<sup>24</sup> (see spectroscopic data below) although the lack of resolution does not allow definitive conclusions to be made on this assignment.

(22) Compton, R. G.; Barghout, R.; Eklund, J. C.; Fisher, A. C.; Bond, A. M.; Colton, R. *J. Phys. Chem.* **1993**, *97*, 1661.

(23) Compton, R. G.; Barghout, R.; Eklund, J. C.; Fisher, A. C.; Davies, S. G.; Metzler, M. R.; Bond, A. M.; Colton, R.; Walter, J. N. *J. Chem. Soc., Dalton Trans.* **1993**, 3641.

(24) Bond, A. M.; Colton, R.; Kevekordes, J. E.; Panagiotidou, P. *Inorg. Chem.* **1987**, *26*, 1430.

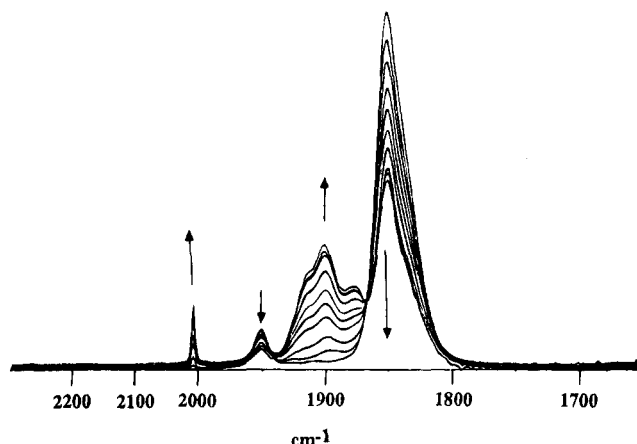
The position of zero current (and hence the unambiguous identification of the complex formed in the presence of light) for each process in Figure 6 was ascertained by obtaining steady-state voltammograms at the 5 μm radius platinum microdisk electrode. In all cases, the zero of current was observed to lie at potentials between the *trans*-[Cr(CO)<sub>2</sub>(dpe)<sub>2</sub>]<sup>+0</sup> (reduction) process and the *mer*-[Cr(CO)<sub>3</sub>(η<sup>1</sup>-dpe)(η<sup>2</sup>-dpe)]<sup>0/+</sup> (oxidation) process as required when *trans*-[Cr(CO)<sub>2</sub>(dpe)<sub>2</sub>]<sup>+</sup> is present in the +1 oxidation state and *mer*-Cr(CO)<sub>3</sub>(η<sup>1</sup>-dpe)(η<sup>2</sup>-dpe) is present in the zerovalent state.

**Electron Spin Resonance Spectroscopy.** The decomposition of a dichloromethane solution of *mer,mer*-[Cr(CO)<sub>3</sub>(η<sup>2</sup>-dpe)]<sub>2</sub>(μ-dpe) in the presence of light also was monitored by ESR spectroscopy. A sample exposed to either sunlight or the mercury light source at 26 °C gives a symmetric five-line pattern (with chromium isotopic satellites) due to *trans*-[Cr(CO)<sub>2</sub>(dpe)<sub>2</sub>]<sup>+</sup>.<sup>21</sup> The same ESR spectrum also was generated when a bulk oxidative electrolysis experiment was undertaken at the potential corresponding to either the first or second oxidation processes of the neutral dinuclear complex (see above).

To show the similarity between photochemical and chemical oxidation of *mer,mer*-[Cr(CO)<sub>3</sub>(η<sup>2</sup>-dpe)]<sub>2</sub>(μ-dpe) the ESR spectrum of a solution of the dinuclear compound also was monitored as the chemical oxidant NOPF<sub>6</sub> was added to a solution of the compound in dichloromethane. At room temperature, the characteristic five-line signal for *trans*-[Cr(CO)<sub>2</sub>(dpe)<sub>2</sub>]<sup>+</sup> was once again seen. However, when the experiment was conducted at -77 °C, a new ESR signal was seen superimposed on the familiar five line pattern (Figure 5c). It consisted of four lines with a *g* value and hyperfine splitting constants the same as reported<sup>21</sup> for *mer*-[Cr(CO)<sub>3</sub>(η<sup>1</sup>-dpe)(η<sup>2</sup>-dpe)]<sup>+</sup>. The conversion of *mer*-[Cr(CO)<sub>3</sub>(η<sup>1</sup>-dpe)(η<sup>2</sup>-dpe)]<sup>+</sup> to *trans*-[Cr(CO)<sub>2</sub>(dpe)<sub>2</sub>]<sup>+</sup> has been reported previously,<sup>21a</sup> and the observation of this complex suggests it is a precursor of *trans*-[Cr(CO)<sub>2</sub>(dpe)<sub>2</sub>]<sup>+</sup> in the decomposition pathway. Clearly, there is a close relationship between the reactions of *mer,mer*-[Cr(CO)<sub>3</sub>(η<sup>2</sup>-dpe)]<sub>2</sub>(μ-dpe) in the presence of light or following bulk electrolysis or chemical oxidation. The reaction in the light is therefore consistent with photochemical oxidation.

**Infrared Spectroscopy.** Time-dependent FTIR spectra of the carbonyl stretching region are shown in Figure 7 for a dichloromethane solution of *mer,mer*-[Cr(CO)<sub>3</sub>(η<sup>2</sup>-dpe)]<sub>2</sub>(μ-dpe) as it was exposed to UV light. Prior to exposure to light, the IR spectrum of *mer,mer*-[Cr(CO)<sub>3</sub>(η<sup>2</sup>-dpe)]<sub>2</sub>(μ-dpe) consists of three peaks at 1950, 1850, and 1834 (sh) cm<sup>-1</sup>. Upon exposure to UV radiation, new peaks grew at 2009, 1912, 1900, and 1877 cm<sup>-1</sup> concomitant with a decrease in the three original peak intensities. All four of these new carbonyl stretching frequencies can be assigned to Cr(CO)<sub>4</sub>(dpe) (see Table 1).<sup>13</sup> The IR bands due to *mer*-Cr(CO)<sub>3</sub>(η<sup>1</sup>-dpe)(η<sup>2</sup>-dpe) and *trans*-[Cr(CO)<sub>2</sub>(dpe)<sub>2</sub>]<sup>+</sup> (detected voltammetrically and by other spectroscopic procedures) are unresolved from those of the starting material, *mer,mer*-[Cr(CO)<sub>3</sub>(η<sup>2</sup>-dpe)]<sub>2</sub>(μ-dpe). Thus the IR experiments unambiguously only show the formation of Cr(CO)<sub>4</sub>(dpe).

Prolonged exposure to UV radiation at room tempera-



**Figure 7.** Time-dependent FTIR spectra for a dichloromethane solution of *mer,mer*-[Cr(CO)<sub>3</sub>(η<sup>2</sup>-dpe)]<sub>2</sub>(μ-dpe) during UV irradiation.

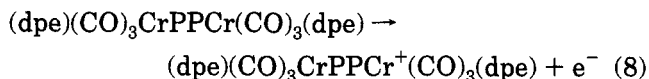
ture in the IR cell results in a gradual decrease in all carbonyl peaks until eventually no evidence for any carbonyl bands is seen.

**<sup>31</sup>P Nuclear Magnetic Resonance Spectroscopy.** The decomposition of *mer,mer*-[Cr(CO)<sub>3</sub>(η<sup>2</sup>-dpe)]<sub>2</sub>(μ-dpe) in dichloromethane under UV irradiation also was followed by <sup>31</sup>P NMR spectroscopy, and relevant data are given in Table 1. As mentioned earlier the dinuclear complex gives three resonances at δ 92.7, 74.8, and 67.0. Upon irradiation with a mercury light source, the three peaks remain in the same positions but new singlets soon appear at δ 78.6, 31.1 together with a doublet at δ -13. The relative intensities of these peaks vary between samples suggesting that they are due to separate compounds. These peaks are assigned to Cr(CO)<sub>4</sub>(dpe), dpeO<sub>2</sub> and *mer*-Cr(CO)<sub>3</sub>(η<sup>1</sup>-dpe)(η<sup>2</sup>-dpe) respectively (Table 1) but for the last compound its other resonances are obscured by those of remaining *mer,mer*-[Cr(CO)<sub>3</sub>(η<sup>2</sup>-dpe)]<sub>2</sub>(μ-dpe). If the sample is left standing on the bench in the laboratory light for several days, the spectrum shows only the peaks at δ 78.6, 31.1 and now a singlet at δ -13, which are assigned to Cr(CO)<sub>4</sub>(dpe), dpeO<sub>2</sub> and free dpe, respectively (Table 1).

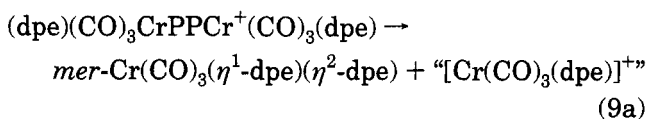
**Discussion of the Mechanism of Electrochemical and Chemical Oxidation and Photochemistry of *mer,mer*-[Cr(CO)<sub>3</sub>(η<sup>2</sup>-dpe)]<sub>2</sub>(μ-dpe).** The electrochemical and chemical oxidation studies and the photochemistry are all consistent with the initial generation of a *mer,mer*-[Cr(CO)<sub>3</sub>(η<sup>2</sup>-dpe)]<sub>2</sub>(μ-dpe)<sup>+</sup> species which then undergoes a series of additional reactions which are determined by the conditions of the experiment, but not all the products or intermediates have been identified.

An important piece of evidence for the first step in the mechanism(s) of the light-catalyzed decomposition of *mer,mer*-[Cr(CO)<sub>3</sub>(η<sup>2</sup>-dpe)]<sub>2</sub>(μ-dpe) is the weak ESR signal obtained from the solid sample which is assigned to the singly oxidized *mer,mer*-[Cr(CO)<sub>3</sub>(η<sup>2</sup>-dpe)]<sub>2</sub>(μ-dpe)<sup>+</sup> and presumably this cation is stabilized in the solid state. The solid-state oxidation of *mer,mer*-[Cr(CO)<sub>3</sub>(η<sup>2</sup>-dpe)]<sub>2</sub>(μ-dpe) (presumably by light and/or oxygen to form a peroxide salt) is not unexpected since the potential at which it is produced is less than 100 mV positive of Ag/AgCl. The compounds *trans*-Cr(CO)<sub>2</sub>(dpe)<sub>2</sub> and *mer*-Cr(CO)<sub>3</sub>(η<sup>1</sup>-dpe)(η<sup>2</sup>-dpe) are also photochemically oxidized under similar conditions (ESR evidence). However, the quantity of singly oxidized

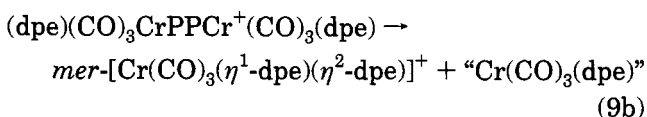
dinuclear cation in the solid is very small and is possibly only detectable via the (typically) nanomolar sensitivity of the ESR method. Thus, on the basis of voltammetric and solid-state ESR evidence, the first step of the mechanism for electrochemical, chemical, or photochemical oxidation can be written



where the new notation for the dinuclear compound is introduced for convenience to distinguish the two chromium centers. The next step in the reaction then appears to involve cleavage of the dpe bridge ( $-\text{PP}-$ ). The two possibilities are either cleavage at the oxidized 17 electron center



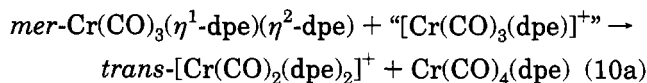
or cleavage at the 18-electron center



but only one of the products of each reaction can be identified in the solution and the other "product" is included merely to balance the equations.

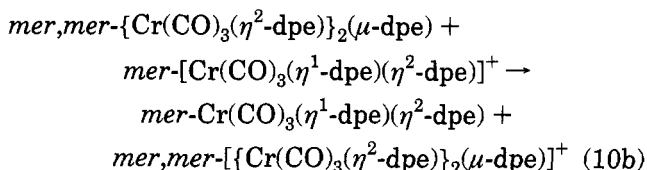
Step 9a results in the formation of  $\text{mer-Cr}(\text{CO})_3(\eta^1\text{-dpe})(\eta^2\text{-dpe})$  which is consistent with voltammetric,  $^{31}\text{P}$  NMR and IR evidence. The detection of  $\text{mer-}[\text{Cr}(\text{CO})_3(\eta^1\text{-dpe})(\eta^2\text{-dpe})]^{+\bullet}$  (four-line ESR spectrum at  $-77^\circ\text{C}$ ) only in the presence of the strong oxidant  $\text{NOPF}_6$ , or in bulk electrolysis experiments, suggests the initial formation of  $\text{mer-Cr}(\text{CO})_3(\eta^1\text{-dpe})(\eta^2\text{-dpe})$  occurs in the oxidation state of zero (eq 6a). However,  $\text{NO}^+$  oxidizes  $\text{mer-Cr}(\text{CO})_3(\eta^1\text{-dpe})(\eta^2\text{-dpe})$  to  $\text{mer-}[\text{Cr}(\text{CO})_3(\eta^1\text{-dpe})(\eta^2\text{-dpe})]^{+\bullet}$ , and the potential applied to oxidize  $\text{mer,mer-}[\text{Cr}(\text{CO})_3(\eta^2\text{-dpe})]_2(\mu\text{-dpe})$  in a bulk electrolysis experiment also is sufficient to oxidize any  $\text{mer-Cr}(\text{CO})_3(\eta^1\text{-dpe})(\eta^2\text{-dpe})$  formed to  $\text{mer-}[\text{Cr}(\text{CO})_3(\eta^1\text{-dpe})(\eta^2\text{-dpe})]^{+\bullet}$ .

The unidentified product(s) of step 6a would be coordinatively unsaturated and expected to be very reactive. A reaction such as



may occur which would result in the formation of the paramagnetic trans dicarbonyl complex as well as the diamagnetic tetracarbonyl complex, both of which have been identified in the presence of light. The solubility of carbon monoxide in the solvents used would aid the transfer of this ligand between species.

The alternative route to decomposition of the monocation (eq 9b) would give rise to the formation of  $\text{mer-}[\text{Cr}(\text{CO})_3(\eta^1\text{-dpe})(\eta^2\text{-dpe})]^{+\bullet}$  and  $[\text{Cr}(\text{CO})_3(\text{dpe})]^{+\bullet}$ . Although no evidence has been obtained for the formation of  $\text{mer-}[\text{Cr}(\text{CO})_3(\eta^1\text{-dpe})(\eta^2\text{-dpe})]^{+\bullet}$  in the absence of a chemical oxidant such as  $\text{NO}^+$ , it is possible that such a decomposition pathway exists which is followed by rapid intermolecular electron transfer. Voltammetric data shows that potentials for oxidation of  $\text{mer,mer-}[\text{Cr}(\text{CO})_3(\eta^2\text{-dpe})]_2(\mu\text{-dpe})$  and  $\text{mer-Cr}(\text{CO})_3(\eta^1\text{-dpe})(\eta^2\text{-dpe})$  complexes are similar so that the redox reaction



is a reasonably favorable process. If this reaction occurs, then  $\text{mer-Cr}(\text{CO})_3(\eta^1\text{-dpe})(\eta^2\text{-dpe})$  (which is the product of eq 9a) is formed together with more of the singly charged dinuclear cation, which can participate in step 9 again. The net result of this pathway is predicted to be the formation of  $\text{mer-Cr}(\text{CO})_3(\eta^1\text{-dpe})(\eta^2\text{-dpe})$  and  $[\text{Cr}(\text{CO})_3(\text{dpe})]^{+\bullet}$  complexes.

**Acknowledgment.** K.M. and J.N.W. thank the Commonwealth Government for Australian Postgraduate Research Awards. Financial support from the Australian Research Council is gratefully acknowledged.

OM9404036



**Electrophilic Attack of Group 11 and 12 Metal  
Fragments on the Dinuclear Anions  
[M<sub>2</sub>(μ-σ:C<sub>2</sub>Ph)(CO)<sub>4</sub>(η-C<sub>5</sub>H<sub>5</sub>)<sub>2</sub>]<sup>-</sup> (M = Mo, W). Crystal  
Structure of the Transversally Bridged Alkyne Complex  
[W<sub>2</sub>(μ-PhC<sub>2</sub>AuPPh<sub>3</sub>)(CO)<sub>4</sub>(η-C<sub>5</sub>H<sub>5</sub>)<sub>2</sub>]**

Montserrat Ferrer, Oriol Rossell, and Miquel Seco

*Departament de Química Inorgànica, Universitat de Barcelona, Diagonal 647,  
E-08028 Barcelona, Spain*

Maria Angela Pellinghelli and Antonio Tiripicchio\*

*Dipartimento di Chimica Generale ed Inorganica, Chimica Analitica, Chimica Fisica,  
Università di Parma, Centro di Studio per la Strutturistica Diffraattometrica del C.N.R., Viale  
delle Scienze 78, I-43100 Parma, Italy*

Received May 31, 1994<sup>®</sup>

The dinuclear anions [M<sub>2</sub>(μ-σ:C<sub>2</sub>Ph)(CO)<sub>4</sub>(η-C<sub>5</sub>H<sub>5</sub>)<sub>2</sub>]<sup>-</sup> (M = Mo, W) react with gold halides ClAuPR<sub>3</sub> (R = Ph, Me) in tetrahydrofuran to yield the μ-alkyne bonded complexes [M<sub>2</sub>(μ-PhC<sub>2</sub>AuPR<sub>3</sub>)(CO)<sub>4</sub>(η-C<sub>5</sub>H<sub>5</sub>)<sub>2</sub>] [M = Mo, R = Ph (**1a**), R = Me (**2a**); M = W, R = Ph (**1b**), R = Me (**2b**)] in good yield. The structure of **1b** has been determined by X-ray diffraction methods. The crystals are monoclinic, space group *P2<sub>1</sub>/c* with *Z* = 4 in a unit cell of dimensions *a* = 8.417(4) Å, *b* = 16.386(6) Å, *c* = 25.352(9) Å, β = 90.55(2)°. The structure has been solved from diffractometer data by direct and Fourier methods and refined by full-matrix least-squares on the basis of 3865 observed reflections to *R* and *R<sub>w</sub>* values of 0.0314 and 0.0362, respectively. The complex displays a W<sub>2</sub>C<sub>2</sub> tetrahedral core with W–W and the C–C bond distances of 2.958(1) and 1.387(15) Å, respectively. The reaction between the dinuclear anions and HgCl<sub>2</sub> leads to a new class of pentametallic symmetric mercury derivatives where the mercury atom forms two Hg–C(μ-alkyne) bonds bridging two cluster units.

### Introduction

In the course of the last years, we have been investigating the incorporation of group 11 or 12 metal fragments, such as AuPR<sub>3</sub><sup>+</sup> or Hg{Mo(CO)<sub>3</sub>(η-C<sub>5</sub>H<sub>5</sub>)<sub>2</sub>}<sup>+</sup>, in preformed polymetallic anions to give mixed transition-metal clusters.<sup>1</sup> Results concerning group 6 metals involve the unsuccessful synthesis of the molybdenum (or tungsten)–mercury derivatives, M<sub>2</sub>Hg, from the dinuclear [M<sub>2</sub>(CO)<sub>10</sub>]<sup>2-</sup> (M = Cr, Mo, W) anion and ClHg{Mo(CO)<sub>3</sub>(η-C<sub>5</sub>H<sub>5</sub>)<sub>2</sub>} because of the cleavage of the M–M bond.<sup>2</sup> On the other hand, the reaction between the hydrido anion [Mo<sub>2</sub>(μ-H)(μ-dppm)(CO)<sub>8</sub>]<sup>-</sup> and ClAuPPh<sub>3</sub> resulted in the formation of [Mo<sub>2</sub>(CO)<sub>8</sub>(μ-dppm)(μ<sub>3</sub>-H)(μ-AuPPh<sub>3</sub>)]<sup>3</sup> with an in-plane μ<sub>3</sub>-hydride ligand which holds three metal atoms together by means of a four-center–two-electron bond. As a consequence, the Mo–Au separations are only consistent with the existence of weak Mo–Au interactions. Other potentially interesting group 6 precursors for the synthesis of mixed M<sub>2</sub>Au or M<sub>2</sub>Hg clusters are the anionic complexes [M<sub>2</sub>(μ-

σ:C<sub>2</sub>Ph)(CO)<sub>4</sub>(μ-C<sub>5</sub>H<sub>5</sub>)<sub>2</sub>]<sup>-</sup> (M = Mo, W).<sup>4,5</sup> These species are of particular interest because it has been suggested that the negative charge is delocalized between the metal atoms and the β-carbon atom of the acetylenic ligand. Green et al.<sup>5</sup> proposed the contribution of two canonical forms to the electronic structure of the anionic compound (Scheme 1).

Consequently, electrophilic agents can add to the anionic species by interaction either with the β-carbon atom or with the metal atoms. In fact, the reaction of the bimetallic anions with different electrophilic species (H<sup>+</sup>, Me<sup>+</sup>, Et<sup>+</sup>) was reported<sup>5</sup> to yield, without exception, the side-on bonded μ-σ:η<sup>2</sup>-vinylidenes by nucleophilic attack on the β-carbon atom. Interestingly, however, electrophilic attack on the metal centers has never been observed. All these facts prompted us to explore the reactivity of the proton isolobal agents AuL<sup>+</sup> (L = PR<sub>3</sub>, R = Me, Ph) or HgR<sup>+</sup> [R = Mo(CO)<sub>3</sub>(η-C<sub>5</sub>H<sub>5</sub>), Ph] with these [M<sub>2</sub>(μ-σ:C<sub>2</sub>Ph)(CO)<sub>4</sub>(η-C<sub>5</sub>H<sub>5</sub>)<sub>2</sub>]<sup>-</sup> (M = Mo, W) anions in order to ascertain the nature of the resulting products as well as some aspects of the mechanism involved in this type of process.

### Results and Discussion

Treatment of the "in situ" generated anionic compounds Li[M<sub>2</sub>(μ-σ:C<sub>2</sub>Ph)(CO)<sub>4</sub>(η-C<sub>5</sub>H<sub>5</sub>)<sub>2</sub>] (M = Mo, W)

<sup>®</sup> Abstract published in *Advance ACS Abstracts*, November 1, 1994.

(1) (a) Reina, R.; Rossell, O.; Seco, M. *J. Organomet. Chem.* **1990**, *398*, 285. (b) Rossell, O.; Seco, M.; Jones, P. G. *Inorg. Chem.* **1990**, *29*, 348. (c) Ferrer, M.; Reina, R.; Rossell, O.; Seco, M.; Solans, X. *J. Chem. Soc., Dalton Trans.* **1991**, 347. (d) Reina, R.; Rossell, O.; Seco, M.; Ros, J.; Yañez, R.; Perales, A. *Inorg. Chem.* **1991**, *30*, 3973.

(2) Reina, R.; Rossell, O.; Seco, M.; Perales, A. *J. Organomet. Chem.* **1991**, *415*, 101.

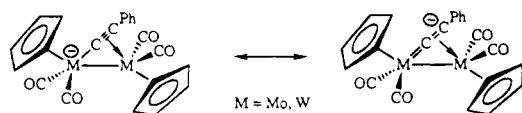
(3) Ferrer, M.; Reina, R.; Rossell, O.; Seco, M.; Alvarez, S.; Ruiz, E.; Pellinghelli, M. A.; Tiripicchio, A. *Organometallics* **1992**, *11*, 3753.

(4) Green, M.; Mercer, A. G.; Orpen, A. G. *J. Chem. Soc., Chem. Commun.* **1986**, 567.

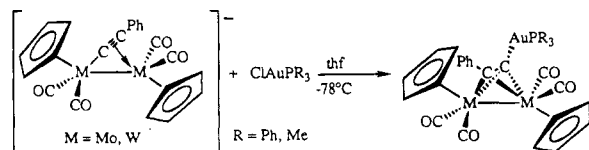
(5) Froom, S. F. T.; Green, M.; Mercer, R. J.; Nagle, K. R.; Orpen, A. G.; Rodrigues, R. A. *J. Chem. Soc., Dalton Trans.* **1991**, 3171.



Scheme 1



with  $\text{ClAuPR}_3$  ( $R = \text{Me, Ph}$ ) in THF solution at  $-78^\circ\text{C}$  afforded the  $\mu$ -alkyne neutral compounds  $[\text{M}_2(\mu\text{-PhC}_2\text{-AuPR}_3)(\text{CO})_4(\eta\text{-C}_5\text{H}_5)_2]$  [ $\text{M} = \text{Mo}$ ,  $R = \text{Ph}$  (**1a**),  $R = \text{Me}$  (**2a**);  $\text{M} = \text{W}$ ,  $R = \text{Ph}$  (**1b**),  $R = \text{Me}$  (**2b**)] in good yield according to eq 1.



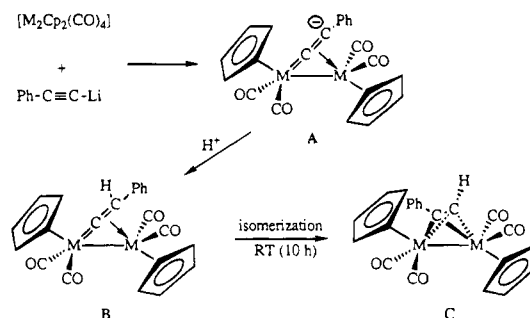
Equation 1

The reaction was monitored by IR spectroscopy and no changes were observed after the quick formation of the  $\mu$ -alkyne compounds. No intermediate products were detected.

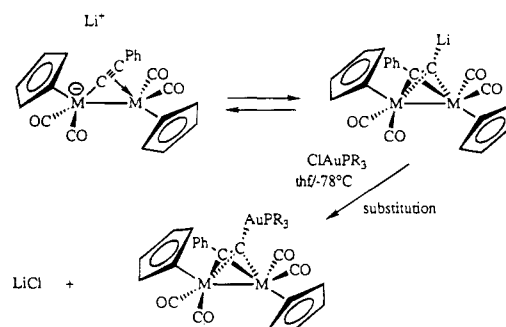
Compounds **1a,b** and **2a,b** were characterized by elemental analyses and spectroscopic methods. The IR spectra of either THF or toluene solutions showed an identical pattern in the  $\nu(\text{CO})$  region for the four compounds, in agreement with previous data on molecules of this type.<sup>6</sup> In all, low-frequency absorptions indicated for the presence of a semibridging CO ligand. However,  $^1\text{H}$  NMR spectra recorded at  $25^\circ\text{C}$  only showed one signal attributable to Cp rings that splits in two different signals on cooling of the solutions to  $-80^\circ\text{C}$ , indicating that these complexes undergo a fluxionality process. Accordingly,  $^{13}\text{C}$  NMR spectra at room temperature showed only two peaks corresponding to the four inequivalent CO ligands. This fluxionality process prevented the observation of the quaternary carbons of the acetylenic ligands.<sup>7</sup> The FAB mass spectra were recorded using nitrobenzyl alcohol (NBA) as the matrix and the patterns in all these spectra are very similar. They showed the parent molecular ion and several fragments that correspond to subsequent losses of carbonyl ligands. In the case of  $\text{PMe}_3$  derivatives (**2a,b**),  $\text{Au}(\text{PMe}_3)^+$  and  $\text{Au}(\text{PMe}_3)_2^+$  fragments are the most abundant.

The formation of the  $\mu$ -alkyne neutral compounds **1a,b** and **2a,b** from the lithium salt of  $[\text{M}_2(\mu\text{-}\sigma\text{-C}_2\text{Ph})(\text{CO})_4(\eta\text{-C}_5\text{H}_5)_2]^-$  and the corresponding gold derivative is not yet clearly understood. According to the literature<sup>5</sup> (Scheme 2), the  $\text{Mo}_2$   $\mu$ -acetylide anionic species  $[\text{Mo}_2(\mu\text{-}\sigma\text{-C}_2\text{Ph})(\text{CO})_4(\eta\text{-C}_5\text{H}_5)_2]^-$  (**A**) reacts with proton sources to give a dark blue solution, which on low-temperature crystallization affords a high yield of the relatively unstable "side-on" bonded vinylidene complex  $[\text{Mo}_2\{\mu\text{-}\sigma\text{-C}=\text{CH}(\text{Ph})\}(\text{CO})_4(\eta\text{-C}_5\text{H}_5)_2]$  (**B**). This dark blue complex is thermally unstable, rearranging in solution at room temperature (10 h) to the red  $\mu$ -alkyne complex  $[\text{Mo}_2(\mu\text{-PhC}_2\text{H})(\text{CO})_4(\eta\text{-C}_5\text{H}_5)_2]$  (**C**). This unusual rearrangement reaction of a "side-on" bonded

Scheme 2



Scheme 3



vinylidene into a  $\mu$ -alkyne involves an apparent 1,2-hydrogen shift from the  $\beta$ - to the  $\alpha$ -carbon.

In our case, the reaction of the electrophilic agent  $\text{AuPR}_3^+$  instead of the isolobal  $\text{H}^+$  with the same  $\text{Mo}_2$  (or  $\text{W}_2$ )  $\mu$ -acetylide anions seems to proceed through a mechanism involving the previous rearrangement of the  $\mu$ -acetylide into the  $\mu$ -alkyne lithium complexes  $[\text{M}_2(\mu\text{-PhC}_2\text{Li})(\text{CO})_4(\eta\text{-C}_5\text{H}_5)_2]$  and subsequent substitution of the lithium by the  $\text{AuPR}_3^+$  fragment. The presence of these species in solution has been already postulated<sup>5</sup> to explain the mechanism of the deprotonation process of the corresponding  $\mu$ -alkyne complexes which yields, through the less thermodynamically stable transversally bridged lithium intermediate, the anionic  $\mu$ -acetylide compounds (Scheme 3). Otherwise, the initial attack at the  $\beta$ -carbon by the gold reagent would be followed by an improbable 1,2-diphenyl or  $\text{AuPR}_3^+$  shift from the  $\beta$ - to the  $\alpha$ -carbon atom. Moreover, no observation of a dark blue intermediate in the course of any of the reactions carried out may confirm the suggested mechanism which, on other hand, has been also considered in the protonation of the closely related adducts obtained from  $\text{CH}_2=\text{C}(\text{Me})\text{C}\equiv\text{CLi}$  and  $[\text{M}_2(\text{CO})_4(\eta\text{-C}_5\text{H}_5)_2]$ .<sup>8</sup>

The molecular structure of **1b**, confirmed by an X-ray crystal study, is shown in Figure 1 together with the atomic numbering scheme. Selected bond distances and angles are given in Table 1. The acetylenic part of **1b** coordinates perpendicularly to the ditungsten center to form the dimetallatetrahedral core. The C-C, 1.387-(15) Å distance is lengthened by ca. 0.22 compared to that in  $\text{PhC}\equiv\text{CAuPPh}_3$ .<sup>9</sup> At the same time, this distance is a bit longer than the ones found in analogous compounds with a tetrahedral  $\text{C}_2\text{M}_2$  core, such as  $[\text{Co}_2(\text{CO})_6(\mu\text{-FpC}\equiv\text{CH})]$ ,<sup>10</sup>  $[\text{Ni}_2(\mu\text{-FpC}\equiv\text{CH})(\eta\text{-C}_5\text{H}_5)_2]$ ,<sup>11</sup> or  $[\text{Mo}_2(\text{CO})_4(\eta\text{-C}_5\text{H}_5)_2(\mu\text{-FpC}\equiv\text{CH})]$ <sup>7</sup> [ $\text{Fp} = \text{Fe}(\text{CO})_2(\text{C}_5\text{H}_5)$ ],

(8) Froom, S. F. T.; Green, M.; Mercer, R. J.; Nagle, K. R.; Orpen, A. G.; Schwiegk, S. *J. Chem. Soc., Chem. Commun.* **1986**, 1666.

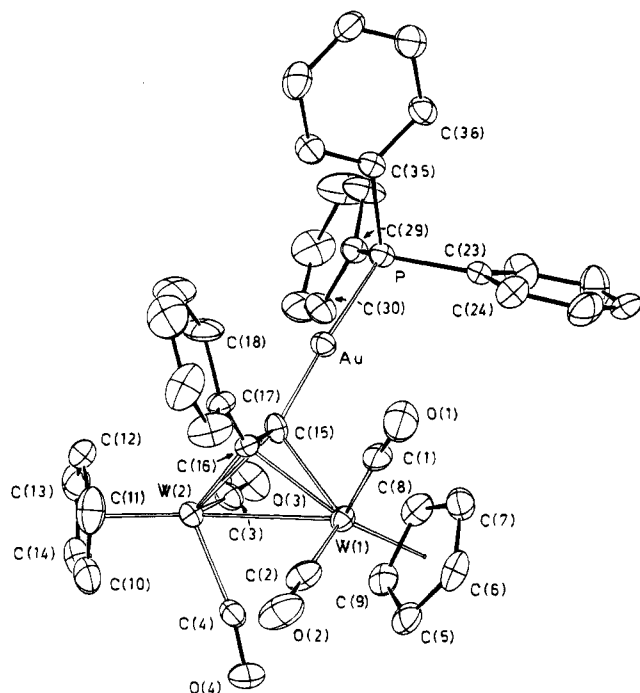
(9) Bruce, M. I.; Duffy, D. N. *Aust. J. Chem.* **1986**, *39*, 1697.

(10) Akita, M.; Terada, M.; Moro-oka, Y. *Organometallics* **1992**, *11*, 1825.

(11) Akita, M.; Terada, M.; Moro-oka, Y. *Organometallics* **1992**, *11*, 3468.

(6) Winter, M. J. *Adv. Organomet. Chem.* **1989**, *29*, 101 and references therein.

(7) Akita, M.; Sugimoto, S.; Takabuchi, A.; Tanaka, M.; Moro-oka, Y. *Organometallics* **1993**, *12*, 2925.



**Figure 1.** ORTEP view of the molecular structure of the complex  $[W_2(\mu\text{-PhC}_2\text{AuPPh}_3)(CO)_4(\eta\text{-C}_5\text{H}_5)_2]$  (**1b**) together with the atomic numbering scheme. The thermal ellipsoids are drawn at the 30% probability level.

**Table 1.** Selected Bond Distances (Å) and Angles (deg) for Compound **1b**<sup>a</sup>

Au-P	2.273(3)	W(2)-C(4)	1.960(12)
Au-C(15)	1.998(10)	W(2)-C(15)	2.226(10)
W(1)-W(2)	2.958(1)	W(2)-C(16)	2.148(11)
W(1)-CE(1)	2.011(13)	C(1)-O(1)	1.167(16)
W(1)-C(1)	1.935(13)	C(2)-O(2)	1.155(17)
W(1)-C(2)	1.955(13)	C(3)-O(3)	1.202(14)
W(1)-C(15)	2.231(11)	C(4)-O(4)	1.155(15)
W(1)-C(16)	2.237(11)	C(15)-C(16)	1.387(15)
W(2)-CE(2)	2.010(15)	C(16)-C(17)	1.459(16)
W(2)-C(3)	1.913(11)		
P-Au-C(15)	175.6(3)	CE(2)-W(2)-C(4)	111.1(6)
CE(1)-W(1)-W(2)	121.4(4)	W(1)-W(2)-C(3)	88.6(3)
CE(1)-W(1)-C(1)	111.4(5)	W(1)-W(2)-C(4)	66.2(4)
CE(1)-W(1)-C(2)	122.0(5)	C(3)-W(2)-C(4)	93.7(5)
W(2)-W(1)-C(1)	123.6(4)	W(1)-C(1)-O(1)	178.1(11)
W(2)-W(1)-C(2)	85.9(4)	W(1)-C(2)-O(2)	177.2(12)
C(1)-W(1)-C(2)	82.4(5)	W(2)-C(3)-O(3)	175.9(9)
CE(2)-W(2)-W(1)	152.0(4)	W(2)-C(4)-O(4)	169.6(11)
CE(2)-W(2)-C(3)	119.2(5)		

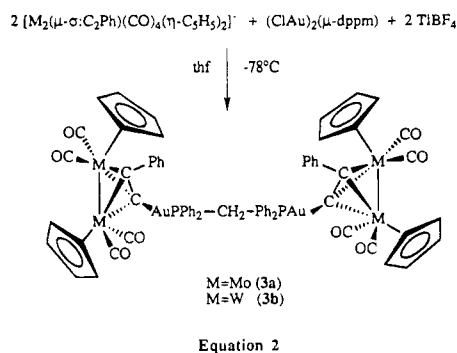
<sup>a</sup> CE(1) and CE(2) are the centroids of the C(5)-C(9) and C(10)-C(14) cyclopentadienyl rings, respectively.

that have been prepared very recently by direct interaction of the substituted iron acetylene with the corresponding metal dimer. The distances Au-C, 1.998(10) Å, and Au-P, 2.273(3) Å, are within the range of similar compounds. The semibridging carbonyl group is found in the W(2)-C(4)-O(4) unit. The nonlinearity of the unit 169.6(11)° and the closeness of the W(1)-C(4) contact distance 2.814(11) Å are both consistent with an incipient bond formation taking place between W(1) and C(4). The structure of **1b** is comparable to that of the complex  $[W_2(\mu\text{-C}_2\text{H}_2)(CO)_4(\eta\text{-C}_5\text{H}_5)_2]$ , the unique tungsten compound of this type the X-ray structure<sup>12</sup> of which showed  $d(W-W) = 2.958(1)$  Å,

$d(C-C) = 1.33(3)$  Å, and also a semibridging carbonyl [W(1)-C = 1.91(3) and W(2)-C = 2.97(3) Å, W(1)-C-O = 173(2)°].

Since  $ClAuPR_3$  species reacted cleanly with the anionic dimers, the reaction with digold derivatives  $(ClAu)_2(\mu\text{-PP})$  (PP = dpmm, dppe) was next investigated. This type of compounds allows the syntheses of compounds in which two clusters units are linked by the chelating ligand.<sup>13</sup> Moreover, condensation processes are likely to occur, leading to the formation of new polymetallic clusters of higher nuclearity than their precursors.

When  $(ClAu)_2dpmm$  was added to an "in situ" generated THF solution of  $Li[M_2(\mu\text{-}\sigma\text{-C}_2\text{Ph})(CO)_4(\eta\text{-C}_5\text{H}_5)_2]$  (M = Mo, W) in a 1:2 ratio at -78 °C in the presence of TIBF<sub>4</sub>, the compounds  $[(\mu\text{-dpmm})\{M_2(\mu\text{-AuC}_2\text{Ph})(CO)_4(\eta\text{-C}_5\text{H}_5)_2\}_2]$  [M = Mo (**3a**), M = W (**3b**)] were isolated along with other products that did not contain phosphorus that were not fully characterized (eq 2).



Compounds **3a** and **3b** were isolated as red solids and characterized by elemental analyses and spectroscopic methods. The IR spectra are consistent with the proposed structure since the  $\nu(CO)$  pattern is very similar to that previously observed for compounds **1** and **2**. Their <sup>1</sup>H NMR spectra showed the signals assignable to CH<sub>2</sub> protons in the dpmm ligand. The <sup>13</sup>C NMR spectrum of **3a** was not recorded due to the low solubility of the compound in common deuterated solvents. Surprisingly, the use of  $(ClAu)_2dppe$  did not yield any characterizable product even when the workup of the reaction mixture was performed at temperatures below 0 °C. As could be inferred from <sup>31</sup>P NMR VT studies, complicated reactions took place that are now under investigation.

**Reactivity Studies of  $[M_2(\mu\text{-PhC}_2\text{AuPPh}_3)(CO)_4(\eta\text{-C}_5\text{H}_5)_2]$  (M = Mo, W)** Since complexes of the type  $[M_2(\mu\text{-RC}_2\text{R}')(CO)_4(\eta\text{-C}_5\text{H}_5)_2]$  (R, R' = organic fragments) have been proved to be very reactive toward a great variety of substrates, it was of interest to investigate the variations of this reactivity produced by the substitution of an organic fragment by a transition-metal fragment.

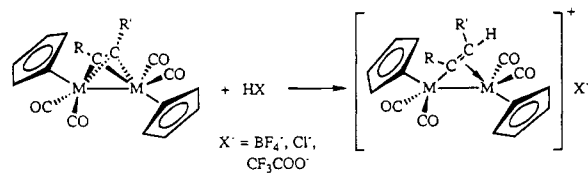
Thus, reactions of sequential linking of alkynes were tested, by treating toluene solutions of  $[M_2(\mu\text{-PhC}_2\text{AuPPh}_3)(CO)_4(\eta\text{-C}_5\text{H}_5)_2]$  (M = Mo, W) with an excess of PhC≡CPh at 60 °C for several hours. The reactions were monitored by IR spectroscopy and no changes were observed after a reaction time of 24 h. In a different experiment, **1a,b** were treated with an excess of the activated acetylene MeO<sub>2</sub>CC≡CCO<sub>2</sub>Me under the same

(12) Ginley, D. S.; Bock, C. R.; Wrighton, M. S.; Fischer, B.; Tipton, D. L.; Bau, R. J. *Organomet. Chem.* **1978**, *157*, 41.

(13) Salter, I. D. *Adv. Organomet. Chem.* **1989**, *29*, 249.

conditions. Neither insertion nor substitution of the acetylene were detected.

Since strong acids (HCl, HBF<sub>4</sub>, CF<sub>3</sub>COOH) react with [M<sub>2</sub>(μ-RCCR')(CO)<sub>4</sub>(η-C<sub>5</sub>H<sub>5</sub>)<sub>2</sub>] adducts to yield the corresponding addition products (eq 3),<sup>14</sup> a toluene solution



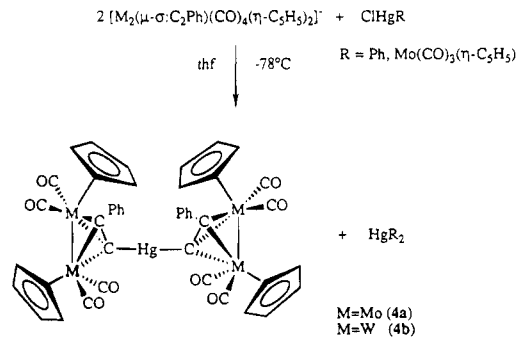
Equation 3

of CF<sub>3</sub>COOH was added dropwise to an equimolar amount of [M<sub>2</sub>(μ-PhC<sub>2</sub>AuPPh<sub>3</sub>)(CO)<sub>4</sub>(η-C<sub>5</sub>H<sub>5</sub>)<sub>2</sub>] dissolved in the same solvent. An immediate change of color was observed. The IR spectrum of the toluene solution revealed the formation of [M<sub>2</sub>(μ-PhCCH)(CO)<sub>4</sub>(η-C<sub>5</sub>H<sub>5</sub>)<sub>2</sub>]. This process can be understood in terms of the cleavage of the Au–C bond and subsequent formation of the C–H bond. These observations are in agreement with previous results reported by Stone<sup>15</sup> and Curtis<sup>14</sup> for compounds containing C–Si and C–Sn bonds, respectively.

In another experiment, the reaction was repeated with a weaker acid. Solid NH<sub>4</sub>PF<sub>6</sub> was added to a toluene solution of **1b**. The reaction was monitored by IR. A reaction time of 3 h was necessary for total conversion of [W<sub>2</sub>(μ-PhC<sub>2</sub>AuPPh<sub>3</sub>)(CO)<sub>4</sub>(η-C<sub>5</sub>H<sub>5</sub>)<sub>2</sub>] to [W<sub>2</sub>(μ-PhCCH)(CO)<sub>4</sub>(η-C<sub>5</sub>H<sub>5</sub>)<sub>2</sub>]. In spite of the weaker acid used, the cleavage of the C–Au bond took place and no addition products were obtained.

In a further experiment, a toluene solution of **1a** was irradiated with a medium-pressure mercury lamp with the object of promoting decarbonylation processes that could provoke the formation of new metal–metal bonds. The results, however, were quite different from that expected. After 2 h of irradiation, decomposition products that did not contain carbonyl ligands were isolated. The observed behavior of the alkyne dimers toward irradiation is in agreement with the recently reported photochemical decarbonylation of the adducts [Mo<sub>2</sub>(μ-FpCCH)(CO)<sub>4</sub>(η-C<sub>5</sub>H<sub>5</sub>)<sub>2</sub>] that leads to the formation of μ<sub>3</sub>-vinylidene derivatives through the generation of an unsaturation on the iron center due to the photoinduced loss of a carbonyl ligand.<sup>7</sup>

In order to extend the synthetic method to other transition-metal fragments, the reactions of the bimetallic anions with RHgCl compounds [R = Mo(CO)<sub>3</sub>(η-C<sub>5</sub>H<sub>5</sub>) and Ph] were examined. When the molar ratio between both reagents was 1:1, two different symmetrical mercury species were identified, HgR<sub>2</sub> and [Hg{M<sub>2</sub>(μ-CCPh)(CO)<sub>4</sub>(η-C<sub>5</sub>H<sub>5</sub>)<sub>2</sub>}<sub>2</sub>], as a result of a ligand redistribution process (eq 4) that took place even when the reaction mixture was kept at –78 °C. This behavior is quite unusual due to the well-documented<sup>16</sup> stability of unsymmetrical mercury derivatives of the type R<sub>2</sub>HgR' (R, R' = organic fragments). However, compounds **4a,b** are the first reported examples of Hg–C(μ-alkyne) bonds.



Equation 4

In the case of R = Mo(CO)<sub>3</sub>(η-C<sub>5</sub>H<sub>5</sub>), the instability of the asymmetric derivatives is in agreement with our previous observations on analogous compounds of the type [(η-C<sub>5</sub>H<sub>5</sub>)(OC)<sub>3</sub>M–HgR] (R = alkyl or aryl groups, M = Mo, W).<sup>17</sup>

The reaction of HgCl<sub>2</sub> with the bimetallic anion in a 1:2 ratio, in THF solution at –78 °C, yielded [Hg{M<sub>2</sub>(μ-CCPh)(CO)<sub>4</sub>(η-C<sub>5</sub>H<sub>5</sub>)<sub>2</sub>}<sub>2</sub>] [M = Mo (**4a**), M = W (**4b**)] in nearly quantitative yield. The reaction was monitored by IR and no further changes were observed after the formation of the μ-alkyne products at –78 °C.

Compounds **4a,b** were characterized by elemental analyses and spectroscopically. Their IR and NMR spectra are consistent with the proposed formulation. Elemental analysis and the observation of the M<sup>+</sup> in the FAB mass spectra confirmed unequivocally the nature of the products. All attempts to synthesize asymmetric species from **4a,b** by adding HgCl<sub>2</sub> in a 1:1 molar ratio were unsuccessful.

It is well-known that the Pt(PPh<sub>3</sub>)<sub>2</sub> fragment inserts into Hg–C bonds, leading to the formation of Hg–Pt bonds.<sup>18</sup> The presence of two Hg–C(μ-alkyne) bonds prompted us to investigate the possibility of insertion of platinum fragments in the new Hg–C bonds with the aim of increasing the metallic nuclearity. The reaction between **4a,b** and [Pt(PPh<sub>3</sub>)<sub>2</sub>(C<sub>2</sub>H<sub>4</sub>)] was carried out in toluene at 60 °C and monitored by IR and <sup>31</sup>P NMR spectroscopy. After several hours, IR ν(CO) bands characteristic of **4a,b** as well as the phosphorus signal corresponding to the platinum derivative remained unaltered.

## Experimental Section

All manipulations were performed under an atmosphere of prepurified N<sub>2</sub> using standard Schlenk techniques. All solvents were distilled from appropriate drying agents. Elemental analyses of C and H were carried out at the Institut de Bioorgànica de Barcelona.

Infrared spectra were measured using a FTIR 520 Nicolet spectrometer. <sup>31</sup>P{<sup>1</sup>H} NMR spectra were recorded on a Bruker WP 80SY instrument (δ(85% H<sub>3</sub>PO<sub>4</sub>) = 0.0 ppm). <sup>1</sup>H and <sup>13</sup>C NMR were recorded on a Varian XL-200 instrument operating at 200 and 50 MHz, respectively, for <sup>1</sup>H and <sup>13</sup>C (δ-(TMS) = 0.00 ppm). Fast atom bombardment (FAB) mass spectra were recorded on an Auto SPEC U, Cs<sup>+</sup>, 30 kV mass spectrometer employing a 3-nitrobenzyl alcohol matrix (NBA).

(14) Gerlach, R. F.; Duffy, D. N.; Curtis, M. D. *Organometallics* **1983**, *2*, 1172.

(15) Beck, J. A.; Knox, S. A. R.; Stansfield, R. F. D.; Stone, F. G. A.; Winter, M. J.; Woodward, P. *J. Chem. Soc., Dalton. Trans.* **1982**, 195.

(16) Roberts, D. A.; Geoffroy, G. L. In *Comprehensive Organometallic Chemistry*; Wilkinson, G.; Stone, F. G. A.; Abel, E. W., Eds.; Pergamon: Oxford, 1982.

(17) Rossell, O.; Seco, M.; Braunstein, P. *J. Organomet. Chem.* **1984**, *273*, 233.

(18) (a) Sokolov, V. I.; Reutov, O. A. *Coordination Chem. Rev.* **1978**, *27*, 89 and references therein. (b) Braunstein, P.; Rossell, O.; Seco, M.; Torra, I.; Solans, X.; Miravittles, C. *Organometallics* **1986**, *5*, 1113.

**Table 2. Summary of Crystallographic Data for Complex 1b**

mol formula	$\text{C}_{40}\text{H}_{30}\text{AuO}_4\text{PW}_2$	$V, \text{\AA}^3$	3496(2)
mol wt	1170.32	$Z$	4
cryst syst	monoclinic	$D_{\text{calcd}}, \text{g cm}^{-3}$	2.223
space group	$P2_1/c$	$F(000)$	2176
$a, \text{\AA}$	8.417(4)	$\mu(\text{Mo K}\alpha), \text{cm}^{-1}$	108.36
$b, \text{\AA}$	16.386(6)	$R$	0.0314
$c, \text{\AA}$	25.352(9)	$R_w$	0.0362
$\beta, \text{deg}$	90.55(2)		

$[\text{M}_2(\text{CO})_6(\eta\text{-C}_5\text{H}_5)_2]$  ( $\text{M} = \text{Mo}, \text{W}$ ),<sup>19</sup>  $[\text{M}_2(\text{CO})_4(\eta\text{-C}_5\text{H}_5)_2]$  ( $\text{M} = \text{Mo}, \text{W}$ ),<sup>20</sup> and  $\text{ClAuPPh}_3$ <sup>21</sup> were prepared as described previously. The complexes  $\text{ClAuPMe}_3$ ,  $(\text{ClAu})_2(\mu\text{-dppm})$ , and  $(\text{ClAu})_2(\mu\text{-dppe})$  were synthesized and isolated as solids from  $\text{ClAu}(\text{tht})$ <sup>22</sup> by adding the appropriate amount of the corresponding mono- or diphosphine.

**Preparation of  $[\text{M}_2(\mu\text{-PhC}_2\text{AuPPh}_3)(\text{CO})_4(\eta\text{-C}_5\text{H}_5)_2]$  [ $\text{M} = \text{Mo}$  (**1a**),  $\text{W}$  (**1b**)].** A solution of  $\text{Li}[\text{Mo}_2(\mu\text{-}\sigma\text{-C}_2\text{Ph})(\text{CO})_4(\eta\text{-C}_5\text{H}_5)_2]^4$  in THF was generated "in situ" by adding dropwise a solution of  $\text{PhC}_2\text{Li}$  (1.0 mmol) in THF (15 mL,  $-78^\circ\text{C}$ ) to a precooled ( $-78^\circ\text{C}$ ) solution of  $[\text{Mo}_2(\text{CO})_4(\eta\text{-C}_5\text{H}_5)_2]$  (450 mg, 1.0 mmol) in the same solvent. Once the anion was formed, solid  $\text{ClAuPPh}_3$  (490 mg, 1.0 mmol) was added and the mixture was stirred and allowed to warm slowly to room temperature. The resulting red solution was evaporated to dryness and the solid residue was extracted twice ( $2 \times 10$  mL) with toluene. Subsequent addition of hexane and cooling overnight ( $-30^\circ\text{C}$ ) afforded purple microcrystals of compound **1a**: yield 75%. IR (toluene,  $\text{cm}^{-1}$ ):  $\nu(\text{CO})$  1959 s, 1898 vs, 1823 s.  $^{31}\text{P}\{^1\text{H}\}$  NMR ( $-40^\circ\text{C}$ , toluene):  $\delta$  39.4.  $^1\text{H}$  NMR (25  $^\circ\text{C}$ ,  $\text{C}_6\text{D}_6$ ):  $\delta$  8.0–6.9 (m, 20H, Ph), 5.18 (s, 10H, Cp).  $^{13}\text{C}$  NMR (25  $^\circ\text{C}$ ,  $\text{C}_6\text{D}_6$ ):  $\delta$  236.2, 234.1 (CO), 134.6–125.6 (Ph), 94.4 (Cp). FAB mass spectrum:  $m/z$  995  $[\text{M}]^+$ , 967  $[\text{M} - \text{CO}]^+$ , 940  $[\text{M} - 2\text{CO}]^+$ , 883  $[\text{M} - 4\text{CO}]^+$ . Anal. Calcd for  $\text{C}_{40}\text{H}_{30}\text{AuMo}_2\text{O}_4\text{P}$ : C, 48.31; H, 3.04. Found: C, 47.98; H, 2.97.

A similar procedure was used to prepare the tungsten derivative **1b**: yield 80%. IR (toluene,  $\text{cm}^{-1}$ ):  $\nu(\text{CO})$  1957 s, 1894 vs, 1811 s.  $^{31}\text{P}\{^1\text{H}\}$  NMR ( $-40^\circ\text{C}$ , toluene):  $\delta$  39.1.  $^1\text{H}$  NMR (25  $^\circ\text{C}$ ,  $\text{C}_6\text{D}_6$ ):  $\delta$  8.0–6.9 (m, 20H, Ph), 5.17 (s, 10H, Cp).  $^{13}\text{C}$  NMR (25  $^\circ\text{C}$ ,  $\text{C}_6\text{D}_6$ ):  $\delta$  222.7, 222.0 (CO), 134.6–125.2 (Ph), 90.3 (Cp). FAB mass spectrum:  $m/z$  1171  $[\text{M}]^+$ , 1115  $[\text{M} - 2\text{CO}]^+$ , 1087  $[\text{M} - 3\text{CO}]^+$ , 1060  $[\text{M} - 4\text{CO}]^+$ . Anal. Calcd for  $\text{C}_{40}\text{H}_{30}\text{AuO}_4\text{PW}_2$ : C, 41.05; H, 2.58. Found: C, 41.23; H, 2.69.

**Preparation of  $[\text{M}_2(\mu\text{-PhC}_2\text{AuPMe}_3)(\text{CO})_4(\eta\text{-C}_5\text{H}_5)_2]$  [ $\text{M} = \text{Mo}$  (**2a**),  $\text{W}$  (**2b**)].** A solution of  $\text{Li}[\text{Mo}_2(\mu\text{-}\sigma\text{-C}_2\text{Ph})(\text{CO})_4(\eta\text{-C}_5\text{H}_5)_2]$  in THF was generated "in situ" by adding dropwise a solution of  $\text{PhC}_2\text{Li}$  (1.0 mmol) in THF (15 mL,  $-78^\circ\text{C}$ ) to a precooled ( $-78^\circ\text{C}$ ) solution of  $[\text{Mo}_2(\text{CO})_4(\eta\text{-C}_5\text{H}_5)_2]$  (450 mg, 1.0 mmol) in the same solvent. Once the anion was formed, solid  $\text{ClAuPMe}_3$  (305 mg, 1.0 mmol) was added and the mixture was stirred and allowed to warm slowly to room temperature. The resulting red solution was evaporated to dryness and the solid residue was extracted twice ( $2 \times 10$  mL) with toluene. Subsequent addition of hexane and cooling overnight ( $-30^\circ\text{C}$ ) afforded purple-red microcrystals of compound **2a**: yield 70%. IR (toluene,  $\text{cm}^{-1}$ ):  $\nu(\text{CO})$  1958 s, 1898 vs, 1823 s.  $^{31}\text{P}\{^1\text{H}\}$  NMR ( $-40^\circ\text{C}$ , toluene):  $\delta$  2.2.  $^1\text{H}$  NMR (25  $^\circ\text{C}$ ,  $\text{C}_6\text{D}_6$ ):  $\delta$  7.9–7.0 (m, 5H, Ph), 5.24 (s, 10H, Cp), 0.50 (d, 9H,  $\text{P}(\text{CH}_3)_3$ ,  $^2J(\text{P}-\text{H}) = 9.72$  Hz).  $^{13}\text{C}$  NMR (25  $^\circ\text{C}$ ,  $\text{C}_6\text{D}_6$ ):  $\delta$  237.2, 234.5 (CO), 130.8–125.4 (Ph), 92.25 (Cp), 14.4 (d,  $\text{P}(\text{CH}_3)_3$ ,  $J(\text{C}-\text{P}) = 33.5$  Hz). FAB mass spectrum:  $m/z$  808  $[\text{M}]^+$ , 752  $[\text{M} - 2\text{CO}]^+$ , 349  $\text{Au}(\text{PMe}_3)_2^+$ , 273  $\text{AuPMe}_3^+$ . Anal. Calcd for  $\text{C}_{25}\text{H}_{24}\text{-AuMo}_2\text{O}_4\text{P}$ : C, 37.15; H, 2.99. Found: C, 37.42; H, 2.97.

A similar procedure was used to prepare the tungsten derivative **2b**: yield 75%. IR (toluene,  $\text{cm}^{-1}$ ):  $\nu(\text{CO})$  1954 s, 1894 vs, 1811 s.  $^{31}\text{P}\{^1\text{H}\}$  NMR ( $-40^\circ\text{C}$ , toluene):  $\delta$  2.6.  $^1\text{H}$

**Table 3. Atomic Coordinates ( $\times 10^4$ ) and Isotropic Thermal Parameters ( $\text{\AA}^2 \times 10^4$ ) with esd's in Parentheses for the Non-Hydrogen Atoms of Compound 1b**

atom	$x/a$	$y/b$	$z/c$	$U^a$
Au	3514.3(5)	1921.7(3)	1697.8(2)	390(1)
W(1)	-141.5(5)	2031.9(3)	894.1(2)	369(2)
W(2)	2444.8(6)	1645.2(3)	153.0(2)	357(1)
P	4554(3)	1676(2)	2513(1)	387(9)
O(1)	-533(13)	3699(6)	1457(4)	906(46)
O(2)	-1734(12)	2946(6)	-47(4)	926(47)
O(3)	3426(12)	175(5)	863(3)	726(38)
O(4)	-724(11)	891(5)	-249(4)	671(36)
C(1)	-360(15)	3076(7)	1242(5)	565(46)
C(2)	-1120(14)	2624(8)	306(5)	557(47)
C(3)	2990(14)	731(7)	588(4)	439(40)
C(4)	379(15)	1189(7)	-56(4)	443(41)
C(5)	-2108(16)	1039(8)	890(5)	609(51)
C(6)	-2386(16)	1609(9)	1305(6)	668(54)
C(7)	-1165(16)	1539(8)	1686(5)	599(50)
C(8)	-136(15)	926(8)	1515(5)	577(48)
C(9)	-702(15)	625(7)	1021(5)	535(47)
C(10)	2616(20)	1881(12)	-758(5)	836(72)
C(11)	3218(21)	2561(10)	-511(6)	812(69)
C(12)	4588(18)	2323(11)	-234(5)	740(62)
C(13)	4828(18)	1493(11)	-288(5)	735(64)
C(14)	3610(20)	1218(9)	-618(5)	683(57)
C(15)	2495(13)	2063(7)	989(4)	417(37)
C(16)	2061(12)	2688(7)	648(4)	395(36)
C(17)	2540(14)	3540(7)	599(4)	467(41)
C(18)	3968(18)	3796(8)	839(5)	773(59)
C(19)	4451(24)	4599(11)	762(6)	1093(87)
C(20)	3607(27)	5155(10)	510(7)	1023(92)
C(21)	2219(21)	4925(9)	277(7)	889(76)
C(22)	1714(17)	4118(8)	316(6)	768(61)
C(23)	2959(13)	1493(7)	2978(4)	403(37)
C(24)	1689(15)	2021(8)	2981(5)	583(48)
C(25)	420(16)	1888(10)	3309(6)	758(62)
C(26)	423(16)	1225(10)	3648(6)	683(57)
C(27)	1662(19)	720(9)	3654(5)	774(62)
C(28)	2907(17)	838(8)	3309(5)	656(53)
C(29)	5801(13)	772(7)	2523(4)	420(38)
C(30)	5651(16)	210(7)	2124(5)	520(46)
C(31)	6536(18)	-483(8)	2129(6)	701(59)
C(32)	7595(19)	-641(8)	2522(7)	812(68)
C(33)	7797(19)	-86(9)	2922(7)	993(74)
C(34)	6910(16)	622(8)	2909(5)	707(54)
C(35)	5738(12)	2502(6)	2801(4)	379(36)
C(36)	5944(14)	2598(8)	3343(4)	491(42)
C(37)	6909(15)	3203(8)	3534(5)	645(51)
C(38)	7654(15)	3715(9)	3195(6)	652(54)
C(39)	7459(17)	3644(8)	2652(6)	658(54)
C(40)	6501(15)	3021(7)	2469(5)	518(44)

<sup>a</sup> Equivalent isotropic  $U$  defined as one-third of the trace of the orthogonalized  $U_{ij}$  tensor.

NMR (25  $^\circ\text{C}$ ,  $\text{C}_6\text{D}_6$ ):  $\delta$  7.9–7.0 (m, 5H, Ph), 5.23 (s, 10H, Cp), 0.52 (d, 9H,  $\text{P}(\text{CH}_3)_3$ ,  $^2J(\text{P}-\text{H}) = 9.52$  Hz).  $^{13}\text{C}$  NMR (25  $^\circ\text{C}$ ,  $\text{C}_6\text{D}_6$ ):  $\delta$  222.9, 222.2 (CO), 131.6–124.9 (Ph), 90.1 (Cp), 14.45 (d,  $\text{P}(\text{CH}_3)_3$ ,  $J(\text{C}-\text{P}) = 33.0$  Hz). FAB mass spectrum:  $m/z$  984  $[\text{M}]^+$ , 928  $[\text{M} - 2\text{CO}]^+$ , 900  $[\text{M} - 3\text{CO}]^+$ , 872  $[\text{M} - 4\text{CO}]^+$ , 349  $\text{Au}(\text{PMe}_3)_2^+$ , 273  $\text{AuPMe}_3^+$ . Anal. Calcd for  $\text{C}_{25}\text{H}_{24}\text{-AuO}_4\text{PW}_2$ : C, 30.51; H, 2.46. Found: C, 30.83; H, 2.59.

**Preparation of  $[(\mu\text{-dppm})\{\text{M}_2(\mu\text{-AuC}_2\text{Ph})(\text{CO})_4(\eta\text{-C}_5\text{H}_5)_2\}]$  [ $\text{M} = \text{Mo}$  (**3a**),  $\text{W}$  (**3b**)].** To a cooled THF (30 mL) solution of  $\text{Li}[\text{Mo}_2(\mu\text{-}\sigma\text{-C}_2\text{Ph})(\text{CO})_4(\eta\text{-C}_5\text{H}_5)_2]$  (0.8 mmol), prepared as described above, was added  $(\text{ClAu})_2(\mu\text{-dppm})$  (340 mg, 0.4 mmol) and  $\text{TlBF}_4$  (233 mg, 0.8 mmol). The mixture was allowed to warm up to  $-20^\circ\text{C}$ , and  $\text{TlCl}$  and  $\text{LiBF}_4$  salts were removed by filtration. The resulting solution was evaporated to dryness and the solid residue extracted twice ( $2 \times 15$  mL) with precooled toluene. Subsequent addition of hexane and cooling overnight ( $-30^\circ\text{C}$ ) afforded red microcrystals of the compound **3a**: yield 30%. IR (toluene,  $\text{cm}^{-1}$ ):  $\nu(\text{CO})$  1957 s, 1901 vs, 1825 s.  $^{31}\text{P}\{^1\text{H}\}$  NMR ( $-40^\circ\text{C}$ , toluene):  $\delta$  25.1.  $^1\text{H}$  NMR (25  $^\circ\text{C}$ ,  $\text{C}_6\text{D}_6$ ):  $\delta$  7.8–6.9 (m, 30H, Ph), 5.08 (s, 20H, Cp), 3.12 (t,  $\text{PCH}_2\text{P}$ ,  $^2J(\text{P}-\text{H}) = 8.9$  Hz).

(19) Birdwhistell, R.; Hackett, P.; Manning, A. R. *J. Organomet. Chem.* **1978**, *157*, 239.

(20) Curtis, M. D.; Fotinos, N. A.; Messerle, L.; Sattelberger, A. P. *Inorg. Chem.* **1983**, *22*, 1559.

(21) Kowala, C.; Swan, J. M. *Aust. J. Chem.* **1966**, *19*, 547.

(22) Usón, R.; Laguna, A. *Organomet. Synth.* **1986**, *3*, 324.

A similar procedure was used to prepare the tungsten derivative **3b**: yield 40%. IR (toluene,  $\text{cm}^{-1}$ ):  $\nu(\text{CO})$  1954 s, 1897 vs, 1815 s.  $^{31}\text{P}\{^1\text{H}\}$  NMR ( $-40^\circ\text{C}$ , toluene):  $\delta$  25.1.  $^1\text{H}$  NMR (25  $^\circ\text{C}$ ,  $\text{C}_6\text{D}_6$ ):  $\delta$  7.8–6.9 (m, 30H, Ph), 5.06 (s, 20H, Cp), 3.13 (t,  $\text{PCH}_2\text{P}$ ,  $^2J(\text{P}-\text{H}) = 8.9$  Hz).  $^{13}\text{C}$  NMR (25  $^\circ\text{C}$ ,  $\text{C}_6\text{D}_6$ ):  $\delta$  133.9–125.1 (Ph), 90.2 (Cp), 30.0 ( $\text{PCH}_2\text{P}$ ).

**Preparation of  $[\text{Hg}\{\text{M}_2(\mu\text{-CCPh})(\text{CO})_4(\eta\text{-C}_5\text{H}_5)_2\}_2]$  [**M** = Mo (**4a**), W (**4b**)].** A solution of  $\text{Li}[\text{Mo}_2(\mu\text{-}\sigma\text{-C}_2\text{Ph})(\text{CO})_4(\eta\text{-C}_5\text{H}_5)_2]$  in THF was generated "in situ" by adding dropwise a solution of  $\text{PhC}_2\text{Li}$  (1.0 mmol) in THF (15 mL,  $-78^\circ\text{C}$ ) to a precooled ( $-78^\circ\text{C}$ ) solution of  $[\text{Mo}_2(\text{CO})_4(\eta\text{-C}_5\text{H}_5)_2]$  (675 mg, 1.5 mmol) in the same solvent. Once the anion was formed, solid  $\text{HgCl}_2$  (200 mg, 0.75 mmol) was added and the mixture was stirred and allowed to warm slowly to room temperature. The resulting deep red solution was evaporated to dryness and the solid residue was extracted twice ( $2 \times 10$  mL) with toluene. Subsequent addition of hexane and cooling overnight ( $-30^\circ\text{C}$ ) afforded purple-red microcrystals of compound **4a**: yield 80%; IR (toluene,  $\text{cm}^{-1}$ ):  $\nu(\text{CO})$  1976 s, 1916 vs, 1837 s.  $^1\text{H}$  NMR (25  $^\circ\text{C}$ ,  $\text{C}_6\text{D}_6$ ):  $\delta$  7.7–6.9 (m, 10H, Ph), 4.98 (s, 20H, Cp).  $^{13}\text{C}$  NMR (25  $^\circ\text{C}$ ,  $\text{C}_6\text{D}_6$ ):  $\delta$  231.7, 230.2 (CO), 130.0–125.9 (Ph), 91.8 (Cp). FAB mass spectrum:  $m/z$  1271 [**M**] $^+$ . Anal. Calcd for  $\text{C}_{44}\text{H}_{30}\text{HgMo}_4\text{O}_8$ : C, 41.58; H, 2.38. Found: C, 41.43; H, 2.37.

A similar procedure was used to prepare the tungsten derivative **4b**: yield 85%. IR (toluene,  $\text{cm}^{-1}$ ):  $\nu(\text{CO})$  1971 s, 1907 vs, 1825 s.  $^1\text{H}$  NMR (25  $^\circ\text{C}$ ,  $\text{C}_6\text{D}_6$ ):  $\delta$  7.7–6.9 (m, 10H, Ph), 4.97 (s, 20H, Cp).  $^{13}\text{C}$  NMR (25  $^\circ\text{C}$ ,  $\text{C}_6\text{D}_6$ ):  $\delta$  220.7, 217.1 (CO), 130.8–125.6 (Ph), 90.0 (Cp). FAB mass spectrum:  $m/z$  1623 [**M**] $^+$ . Anal. Calcd for  $\text{C}_{44}\text{H}_{30}\text{HgW}_4\text{O}_8$ : C, 32.57; H, 1.86. Found: C, 32.56; H, 1.90.

**X-ray Data Collection, Structure Determination, and Refinement for  $[\text{W}_2(\mu\text{-PhC}_2\text{AuPPh}_3)(\text{CO})_4(\eta\text{-C}_5\text{H}_5)_2]$  (**1b**).** A single crystal of ca.  $0.20 \times 0.24 \times 0.32$  mm was selected and used for data collection. The crystallographic data are summarized in Table 2. Data were collected at room temperature on a Philips PW 1100 diffractometer, using the graphite-monochromated Mo K $\alpha$  radiation ( $\lambda = 0.71073$  Å) and the  $\theta/2\theta$  scan type. The reflections were collected with a variable scan speed of  $3\text{--}12^\circ \text{min}^{-1}$  and a scan width from ( $\theta - 0.60$ ) $^\circ$  to ( $\theta + 0.60 + 0.346 \tan \theta$ ) $^\circ$ . Of 7638 unique reflections, with  $\theta$  in the range  $3\text{--}27^\circ$ , 3865 with  $I \geq 2\sigma(I)$  were used for the analysis. One standard reflection was monitored every 50 measurements; no significant decay was noticed over the time of data collection. The individual profiles have been analyzed following the method of Lehmann and Larsen.<sup>23</sup> Intensities were corrected for Lorentz and polarization effects.

(23) Lehmann, M. S.; Larsen, F. K. *Acta Crystallogr., Sect. A* **1974**, *30*, 580.

A correction for absorption was applied (maximum and minimum values for the transmission factors were 1.217 and 0.809).<sup>24</sup>

The structure was solved by direct and Fourier methods and refined first by full-matrix least-squares with isotropic thermal parameters and then by full-matrix least-squares with anisotropic thermal parameters for all non-hydrogen atoms. All hydrogen atoms were placed at their geometrically calculated positions ( $\text{C}-\text{H} = 0.96$  Å) and refined "riding" on the corresponding carbon atoms. The final cycles of refinement were carried out on the basis of 437 variables; after the last cycles, no parameters shifted by more than 0.61 esd. The biggest remaining peak (close to a W atom) in the final difference map was equivalent to about  $1.16 \text{ e}/\text{Å}^3$ . In the final cycles of refinement a weighting scheme,  $w = K[\sigma^2(F_o) + gF_o^2]^{-1}$  was used; at convergence, the  $K$  and  $g$  values were 0.626 and 0.0018, respectively. The analytical scattering factors, corrected for the real and imaginary parts of anomalous dispersions, were taken from ref 25. All calculations were carried out on the GOULD POWERNODE 6040 and ENCORE 91 computers of the "Centro di Studio per la Strutturistica Diffattometrica" del C.N.R., Parma, Italy, using the SHELX-76 and SHELXS-86 systems of crystallographic computer programs.<sup>26</sup> The final atomic coordinates for the non-hydrogen atoms are given in Table 3. The atomic coordinates of the hydrogen atoms are given in Table SI and the thermal parameters in Table SII of the supplementary material.

**Acknowledgment.** Financial support for this work was given by the DGICYT (Spain), through Grant PB90-0055-C02-01, and by MURST (Italy). We thank X. Huguet and J. Caixac for use of their facilities in recording the FAB spectra.

**Supplementary Material Available:** Tables of hydrogen atom coordinates (Table SI), anisotropic thermal parameters for the non-hydrogen atoms (Table SII), and complete bond distances and angles (Table SIII) for **1b** (4 pages). Ordering information is given on any current masthead page.

OM940414Z

(24) Walker, N.; Stuart, D. *Acta Crystallogr., Sect. A* **1983**, *39*, 158. Ugozzoli, F. *Comput. Chem.* **1987**, *11*, 109.

(25) *International Tables for X-Ray Crystallography*; Kynoch Press: Birmingham, England, 1974; Vol. IV.

(26) Sheldrick, G. M. SHELX-76 Program for crystal structure determination. University of Cambridge, England, 1976. SHELXS-86 Program for the solution of crystal structures. University of Göttingen, 1986.

# A Theoretical Study of the (Cyclobutane)diazadivanadium Complex

Nazzareno Re and Antonio Sgamellotti

*Dipartimento di Chimica, Università di Perugia, Via Elce di Sotto 8, I-06100 Perugia, Italy*

B. Joakim Persson and Björn O. Roos\*

*Department of Theoretical Chemistry, Chemical Centre, P.O. Box 124, S-221 00 Lund, Sweden*

Carlo Floriani

*Section de Chimie, Université de Lausanne, Place du Château 3,  
CH-1005, Lausanne, Switzerland*

Received May 10, 1994<sup>®</sup>

*Ab initio* CASSCF/CASPT2 calculations have been carried out on the  $V_2N_2H_6$  complex, as a model of a series of (cyclobutane)diazadivanadium complexes, in order to study the electronic structure and bonding in these complexes. Analogous calculations were performed also on the cationic and anionic species in order to study the behavior of the complexes toward oxidation and reduction. Geometry optimizations have been performed on the lowest singlet and triplet states and on the ground states of the ions, using wave functions of the restricted active space (RAS) SCF type. Dynamic correlation effects are included by means of second-order perturbation theory (CASPT2) with a CASSCF reference function based on an active space comprising the V–V bonding and antibonding orbitals. The results indicate the presence of a weak  $\sigma$  metal–metal bond and a relatively large singlet–triplet splitting ( $8400\text{ cm}^{-1}$ ), with the singlet as the ground state. The computed structure for the singlet state is in agreement with experiment.

## 1. Introduction

The synthesis of a series of novel binuclear complexes of V(IV) with two bridging arylimido ligands has recently been reported.<sup>1</sup> Complexes, of the type  $\{L_2V[\mu\text{-N}(p\text{-MeC}_6\text{H}_4)]\}_2$  with  $L = \text{CH}_2\text{Ph}$ ,  $\text{Mes} = 2,4,6\text{-Me}_3\text{C}_6\text{H}_2$ , hereafter called complex **1** and **2**, respectively, show a short V–V distance in the range 2.45–2.50 Å. Although rare, analogous compounds with heteroatom ligands on vanadium atoms have also been synthesized with similar V–V distances.<sup>2–4</sup> Such bond lengths fall in the typical range for single vanadium–vanadium bonds.<sup>5</sup> Magnetic susceptibility measurements<sup>1</sup> indicate diamagnetic character and therefore spin pairing of all the electrons. Both features suggest a single bond between the two V(IV)  $d^1$  species. However there are only few examples of metal–metal bonded divanadium complexes<sup>6</sup> and they must be considered labile entities. Moreover, recent *ab initio* calculations on bridged dinuclear complexes of early-transition metals<sup>6–15</sup> have shown an interesting interplay between the metal–

metal and the metal–ligand interactions. It is therefore of interest to study theoretically the electronic structure and the chemical bonding in such complexes. The real systems have two transition metals and large ligands, which would be prohibitively expensive for accurate *ab initio* calculations, especially when correlation energy is to be included and geometry optimization is to be performed. Two strategies are usually employed in such cases: either to deal with real systems performing low accuracy calculations or even using model hamiltonians (e.g. extended Huckel) or to perform highly accurate calculations on appropriate model systems. We have chosen the latter approach, taking the  $\{H_2V(\mu\text{-NH})\}_2$  species, **3**, as a model system of these complexes and performing accurate *ab initio* calculations. The chosen system is in our opinion a chemically significant model and represents well the  $V_2N_2$  unit of the real complexes **1** and **2**. The *ab initio* complete active space (CAS) SCF method and second-order perturbation theory correction (CASPT2) to the CASSCF wave function have been used with the molecular orbitals expanded in atomic contracted Gaussian-type functions. The CASSCF method is used to obtain a zeroth-order wave function where

<sup>®</sup> Abstract published in *Advance ACS Abstracts*, November 1, 1994.

(1) Solan, G.; Cozzi, P. G.; Floriani, C.; Chiesi-Villa, A.; Rizzoli, C. *Organometallics* **1994**, *13*, 2572.

(2) Ruiz, J.; Vivanco, M.; Floriani, C.; Chiesi-Villa, A.; Rizzoli, C. *J. Chem. Soc., Chem. Commun.* **1991**, 214.

(3) Ruiz, J.; Vivanco, M.; Floriani, C.; Chiesi-Villa, A.; Rizzoli, C. *Organometallics* **1993**, *12*, 1811.

(4) Preuss, F.; Overhoff, G.; Becker, H.; Häusler, H. J.; Frank, W.; Reiss, G. *Z. Anorg. Allg. Chem.* **1993**, *619*, 1827.

(5) Messerle, L. *Chem. Rev.* **1988**, *88*, 1229.

(6) Cotton, F. A.; Diebold, M. P.; Shim, I. *Inorg. Chem.* **1985**, *24*, 1510.

(7) Arif, A. M.; Cowley, A. H.; Pakulski, M.; Norman, N. C.; Orpen, A. G. *Organometallics* **1987**, *6*, 189.

(8) Luthi, H. P.; Bauschlicher, C. W., Jr. *J. Am. Chem. Soc.* **1987**, *109*, 2046.

(9) Mougnot, P.; Demuynck, J.; Benard, M.; Bauschlicher, C. W., Jr. *J. Am. Chem. Soc.* **1988**, *110*, 4503.

(10) Weber, J.; Chermette, H. *Organometallics* **1989**, *8*, 2544.

(11) Poumbga, C.; Daniel, C.; Benard, M. *Inorg. Chem.* **1990**, *29*, 2337.

(12) Poumbga, C.; Daniel, C.; Benard, M. *J. Am. Chem. Soc.* **1991**, *113*, 1090.

(13) Rohmer, M.-M.; Benard, M. *Organometallics* **1991**, *10*, 157.

(14) Cotton, F. A.; Daniels, L. M.; Murillo, C. A. *Inorg. Chem.* **1993**, *32*, 2881.

(15) Rohmer, M.-M.; Benard, M. *J. Am. Chem. Soc.* **1992**, *114*, 4785.

all spin couplings in the vanadium atoms 3d shell are properly treated and near degeneracy effects are taken into account. The CASPT2 correction to this CASSCF wave function is used to account for the dynamic correlation effects which are necessary in order to make reasonable quantitative predictions of the singlet-triplet splitting energy. The CASPT2 method has recently been shown to yield accurate binding energies for the transition metal diatomics Ni<sub>2</sub> and Cu<sub>2</sub>.<sup>16</sup> As the complexes discussed here are reported to show an interesting redox reactivity,<sup>1</sup> analogous calculations have been performed also on the cationic and anionic species in order to study their behavior toward oxidation and reduction.

## 2. Computational Details

Generally contracted basis sets of the averaged atomic natural orbital (ANO) type have been used throughout this study. They have been obtained from (17s12p5d4f), (14s9p4d3f), and (8s4p3d) primitive sets for the vanadium, nitrogen, and hydrogen atoms, respectively. The ANO's were constructed by averaging over several atomic states and positive and negative ions.<sup>17</sup> They were contracted to [V,6s4p3d1f], [N,4s3p2d1f], and [H,-3s1p].

The lowest states of singlet and triplet character were studied at essentially two levels of accuracy. The purpose was to compute the relative energies of the different spin states using multiconfigurational second-order perturbation theory (CASPT2).<sup>18–20</sup> The CASPT2 calculation is based on a reference function of the complete active space (CAS) SCF type.<sup>21,22</sup> Thus a CASSCF calculation has first to be carried out. The choice of the active orbital space is crucial, since it is important that all near-degeneracy effects are included at the CASSCF level. If not, CASPT2 will not be a valid approach for treating remaining correlation effects. In a weakly bonded system like V<sub>2</sub>N<sub>2</sub>H<sub>6</sub>, it is not obvious which orbitals have to be included in the active space. Therefore the restricted active space (RAS) SCF method<sup>23</sup> was used in the preliminary studies. This approach was also used for the geometry optimizations.

In the CASSCF method,<sup>21,22</sup> the wave function is defined through the choice of the active orbital subspace and the number of active electrons. The wave function includes all the configuration state functions which can be generated by distributing the active electrons among the active orbitals in all possible ways. In the {H<sub>2</sub>V-(μ-NH)}<sub>2</sub> molecule there are 26 valence electrons and 26 valence orbital which would lead, of course, to an active space much too big for a feasible CASSCF calculation. After some trial studies, we realized that,

for a balanced description of the electronic structure in the metallacycle unit, the wave function should include terms necessary to describe at least the vanadium–vanadium, the vanadium–nitrogen, and the vanadium–hydrogen bonds. However, this leads to an active space of 22 orbitals with 22 electrons, which is still prohibitively big for a conventional CASSCF calculation. We therefore used a restricted active space (RAS) SCF scheme. This is a generalization of the CASSCF method in which, instead of a single active space, three active spaces are distinguished and called RAS-1, RAS-2 and RAS-3, respectively. Again, a certain number of electrons are distributed among the three orbital spaces, but now with the added restriction that at most a specified number of holes are allowed in the RAS-1 space and at most a specified number of electrons are allowed in RAS-3. The present RASSCF wave function used 22 active orbitals corresponding to the V 3d, N 2p, and H(V) 1s orbitals. Two of these orbitals (the HOMO and the LUMO) were placed in the RAS-2 space; at most two holes were allowed in the RAS-1 space and a maximum of two electrons in RAS-3. This is equivalent to performing an MR-SDCI calculation with one (or two) reference configurations, in a small but optimized orbital space. The two reference configurations (one for the triplet state) are necessary to take into account the near degeneracy of the HOMO and LUMO orbitals, which leads to a high weight of the biexcited configuration. The RASSCF calculations showed that apart from the HOMO–LUMO pair, no severe near degeneracies occurred in the wave function. It was therefore decided that a CASSCF wave function with two active orbitals should be used as the reference function for the CASPT2 treatment.

In the CASPT2 method, a Möller–Plesset-like second-order perturbation theory is used, with the CASSCF wave function as the unperturbed wave function. The zero-order hamiltonian is built from a Fock-type one-electron operator that reduces to the Möller–Plesset operator for a closed-shell case. The CASPT2 method computes the first-order wave function and the second order energy in the full space of configurations generated by the basis set. All calculations were performed in the “nondiagonal” approach, i.e. the full Fock matrix (including the nondiagonal elements) were used in the construction of the zero-order hamiltonian. For both the singlet and the triplet states the CASSCF calculation with two electrons in two active orbitals (the HOMO and LUMO) was followed by CASPT2 calculations differing only in the number of correlated electrons. In a first calculation all valence electrons, originating from the vanadium 3d, the nitrogen 2s, and 2p, and the hydrogen 1s orbitals, were correlated; in the second calculation also the vanadium core 3s and 3p orbitals were included. Recent studies of the electronic spectra of transition metal ions have shown that 3s,3p correlation effects can have a sizable effect on relative energies<sup>24</sup> which is to a large extent determined by (3p)<sup>2</sup> → (3d)<sup>2</sup> type excitations. Studies of hexacyanometalate complexes<sup>25</sup> showed that these core correlation effects are not specific to the free atoms, but also occur in

(16) Pou-Amérigo, R.; Merchán, M.; Nebot-Gil, I.; Roos, B. O. *J. Chem. Phys.*, submitted.

(17) Pierlott, K.; Dumez, B.; Widmark, P.-O.; Roos, B. O. Medium size ano basis sets for the atoms H-Kr. To be published.

(18) Andersson, K.; Malmqvist, P.-Å.; Roos, B. O.; Sadlej, A. J.; Wolinski, K. *J. Phys. Chem.* **1990**, *94*, 5483.

(19) Andersson, K.; Malmqvist, P.-Å.; Roos, B. O. *J. Chem. Phys.* **1992**, *96*, 1218.

(20) Andersson, K. *Multiconfigurational Perturbation Theory*. Ph.D. thesis, University of Lund, Theor. Chemistry, Chem. Center, Lund, Sweden, 1992.

(21) Roos, B. O.; Taylor, P. R.; Siegbahn, P. E. M. *Chem. Phys.* **1980**, *48*, 157.

(22) Roos, B. O. *Int. J. Quant. Chem.* **1980**, *S14*, 175.

(23) Malmqvist, P.-Å.; Rendell, A.; Roos, B. O. *J. Phys. Chem.* **1990**, *94*, 5477.

(24) Pierlott, K.; Tsokos, E.; Roos, B. O. *Chem. Phys. Lett.* **1993**, *214*, 583.

(25) Pierlott, K.; Van Praet, E.; Vanquickenborne, L. G.; Roos, B. O. *J. Phys. Chem.* **1993**, *97*, 12220.



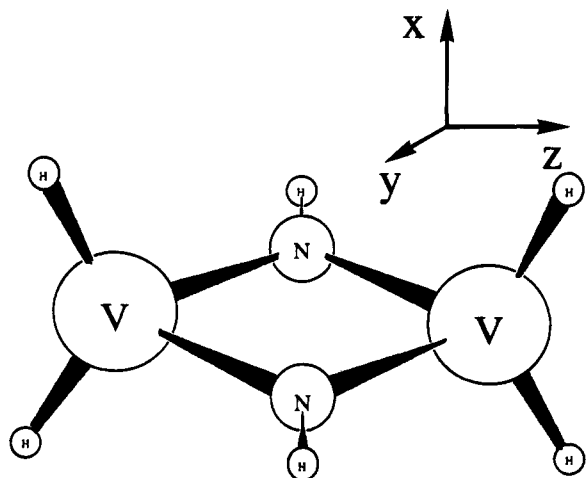


Figure 1. The model system  $\{H_2V(\mu-NH)\}_2$  studied.

Table 1. Optimized (RASSCF) Geometries for the  $[V_2N_2H_6]$  Complex in the Lowest Singlet and Triplet States (units, angstroms and degrees)

	V-V	V-N	V-H	N-H	$\angle HVH$
$^1A_g$	2.438	1.836	1.668	0.997	123.5
$^3B_{1u}$	2.691	1.860	1.667	0.996	121.2
expl <sup>a</sup>	2.487	1.853			

<sup>a</sup> For the  $\{(Mes)_2V[\mu-(p-MeC_6H_4)]\}_2$  complex.

Table 2. Calculated Triplet-Singlet Splittings,  $cm^{-1}$ , at Different Levels of Theory

	RASSCF	CASPT2	CASPT2 (3s,3p)
$\Delta E_{ST}$ (vertical)	6500	9550	9860
$\Delta E_{ST}$ (adiabatic)	4060	7450	8400

complexes. Their importance for the singlet-triplet splitting in the present system therefore cannot be neglected.

Geometries have been optimized at RASSCF level for both the lowest singlet and triplet states under a  $D_{2h}$  symmetry constraint. The coordinate system has been chosen such that the  $z$  axis is in the V-V direction and the planar  $V_2N_2$  unit lies in the  $yz$  plane (cf. Figure 1). All computations were performed with the MOLCAS-2 quantum chemistry package,<sup>26</sup> implemented on IBM RS6000 workstations.

### 3. Results and Discussion

The RASSCF geometry optimization of the complex **3** in the lowest singlet and triplet states leads to the optimized geometries reported in Table 1. The relative energies of the two electronic states are presented in Table 2. At all levels of theory, the ground state is a closed shell  $^1A_g$  state with the lowest triplet state,  $^3B_{1u}$ , about 1 eV above. The dynamic correlation effects treated with the CASPT2 method leads to an increase in the energy separation. A slight further increase is obtained by including also the 3s,3p correlation effects. The optimized geometry for the singlet state of the model molecule is close to the experimental geometry for complex **2**. This confirms the close analogy of the chosen model to the real molecule. The optimized

Table 3. Natural Orbital Occupation Numbers for the Lowest Singlet and Triplet States of  $[V_2N_2H_6]$ , Metal Character, and Metal Bonding Character of These Orbitals

NO	singlet		triplet		character
	occ no.	metal %	occ no.	metal %	
$9a_g$	1.97	8	1.98	9	$\delta$
$4b_{3u}$	1.96	22	1.97	25	$\pi$
$5b_{2u}$	1.98	18	1.97	19	$\pi$
$1b_{1g}$	1.95	19	1.96	20	$\delta$
$7b_{1u}$	1.97	27	1.97	28	$\delta^*$
$3b_{3g}$	1.97	19	1.98	21	$\pi^*$
$10a_g$	1.69	99	1.00	98	$\sigma$
$8b_{1u}$	0.31	91	0.99	98	$\sigma^*$

geometry for the triplet state is, instead, very different, with a much longer V-V distance.

An analysis of the electronic structure of the singlet ground state may be obtained from the RASSCF calculations. The leading configuration in the final RASSCF expansion corresponds to  $(3d\sigma)^2$ , which has a weight of 73%. The second most important configuration corresponds to a  $(3d\sigma)^2 \rightarrow (3d\sigma^*)^2$  electron excitation with a weight of 12%, while all other configurations account for less than 0.5% each. The results of the RASSCF calculation can also be interpreted in terms of population of bonding/antibonding pairs of natural orbitals (NOs) with some metal character. Table 3 gives the natural orbital occupations of these NOs for both the singlet and the triplet states. It is clear from these results that there is only one pair of orbitals with the dominating metal character, ( $10a_g/8b_{1u}$ ), corresponding to the vanadium  $\sigma$  and  $\sigma^*$  orbitals. A more detailed analysis of these two natural orbitals reveals that  $10a_g$  has a metal-metal bonding character and is essentially built from overlapping hybrid 3d orbitals (about 89%  $d_{z^2}$  and 11%  $d_{x^2-y^2}$ ), while  $8b_{1u}$  is the corresponding antibonding orbital.

Moreover the occupation analysis gives for the singlet state a  $\sigma^{1.69}\sigma^{*0.31}$  configuration, which is characteristic of a relatively strong metal-metal bond. We recall<sup>12</sup> that the relative distribution of the population between the bonding/antibonding pair of NOs determines the degree of delocalization of the corresponding electron pair. That is, an almost zero population of the antibonding NO indicates an almost complete delocalization of the electron pair and therefore a strong metal-metal bond, while nearly equal populations for the two NO indicates an almost complete localization of the two electrons, one on each metal atom, and antiferromagnetic coupling between them. This metal-metal bonding picture is consistent with the computed relatively large singlet-triplet energy splitting, which at the most accurate CASPT2 level is  $9860\text{ cm}^{-1}$ , in agreement with the diamagnetic character observed for such complexes. Although the formal V-V bond order in this V(IV)-V(IV) complex is 1, the partial occupation of the  $\sigma^*$  NO leads to an actual lower bond order. Indeed, the bond order computed from the RASSCF wave function as

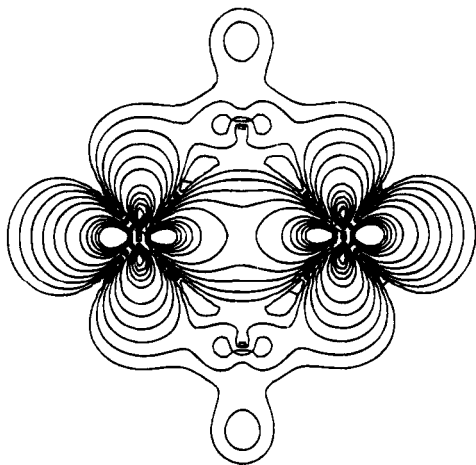
$$1/2 \sum_{NO} [\rho(V_2^{\text{bond}}) - \rho(V_2^{\text{antibond}})]$$

where  $\rho(V_2i)$  represents the contribution of the occupation of orbital  $i$ , which can be assigned to the dimetallic unit on the basis of the metal character of that orbital, is 0.7 and clearly shows the partial localization effects.

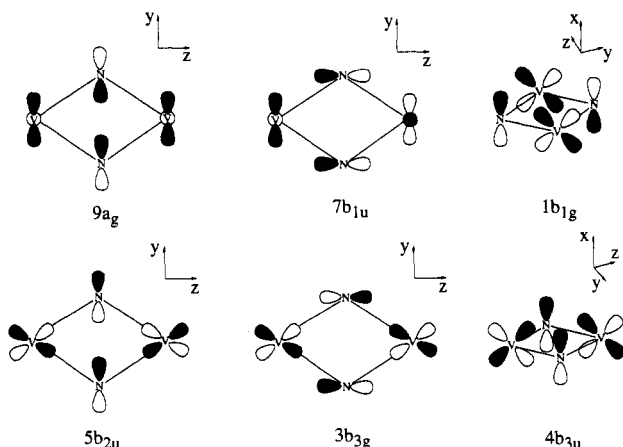
The electron density generated by this  $\sigma/\sigma^*$  NO pair is represented in Figure 2. It shows the mainly  $d_{z^2}$

(26) Andersson, K.; Blomberg, M. R. A.; Fülcher, M. P.; Kellö, V.; Lindh, R.; Malmqvist, P.-Å.; Noga, J.; Olsen, J.; Roos, B. O.; Sadlej, A. J.; Siegbahn, P. E. M.; Urban, M.; Widmark, P.-O. *MOLCAS Version 2 User's Guide*. Dept. of Theor. Chem., Chem. Center, Univ. of Lund, Lund, 1992.





**Figure 2.** Plot of the summed electron density from the V–V bonding and antibonding orbital pair. The values of the density contours are  $\pm 0.30$ ,  $\pm 0.25$ ,  $\pm 0.20$ ,  $\pm 0.15$ ,  $\pm 0.10$ ,  $\pm 0.04$ ,  $\pm 0.02$ ,  $\pm 0.01$ ,  $\pm 0.005$ ,  $\pm 0.0025$ , and  $\pm 0.00125$  e/au<sup>3</sup>.



**Figure 3.** The six molecular orbitals involved in the bonding of the vanadium atoms to the ligands.

character of the d hybrids, which constitute such bonding/antibonding pair, with a minor  $3d_{x^2-y^2}$  component. As Table 3 illustrates there are also six lower lying frontier orbitals with a relevant metal character, namely  $9a_g$ ,  $4b_{3u}$ ,  $5b_{2u}$ ,  $1b_{1g}$ ,  $7b_{1u}$ , and  $3b_{3g}$ , showing an almost negligible degree of localization (with occupations in the range 1.96–1.98). These six bonding orbitals represent essentially the four combinations of the  $2p_y$  and  $2p_z$  orbitals of the bridging nitrogen atoms with the unoccupied metal–metal orbitals of appropriate symmetry in the metallacycle plane ( $yz$ ), and the analogous two combinations of the  $2p_x$  nitrogen orbitals with corresponding  $3d$  metal orbitals (cf. Figure 3). The corresponding electron pairs take part in delocalized metal–bridging ligand interactions giving rise to the four vanadium–nitrogen  $\sigma$  bonds and two delocalized  $\pi$  bonds of the metallacycle moiety. The  $\pi$  or  $\delta$  metal–metal bonding character of four of these orbitals overcomes the antibonding character of the remaining two (see Table 3) and indicates an appreciable net contribution to the V–V bond order (about 0.2 of mainly  $\pi$  character). Thus, the overall metal–metal interaction results from the interplay of the direct vanadium–vanadium bond and through the vanadium–ligand bonds. This bonding picture for the metallacycle moiety is in agreement with intuitive considerations based on the ionic and covalent models that are commonly used

**Table 4.** Atomic Charges and Partial Mulliken Gross Atomic Populations for the Lowest Singlet and Triplet States of  $[V_2N_2H_6]$  Complex and for the  $H_2V^{2+}$  Fragment in Its  $^2A_1$  Ground State

	singlet	triplet	fragment
V charge	1.05	1.10	1.84
4s	0.50	0.51	0.35
4p	0.32	0.33	0.18
$3d_{z^2}$	0.93	0.99	0.96
$3d_{x^2-y^2}$	0.73	0.64	0.50
$3d_{xy}$	0.25	0.22	0.00
$3d_{xz}$	0.78	0.72	1.17
$3d_{yz}$	0.38	0.42	0.00
3d	3.07	3.00	2.63
H(V) charge	−0.20	−0.20	+0.08
NH charge	−0.66	−0.69	

in connection with electron counting. Indeed, the imino ligands must be formally considered as  $(HN)^{2-}$  while the metal is V(IV). Each vanadium ion (with a  $d^1$  configuration) accepts one electron pair from each of the NH ligands, forming two V–N  $\sigma$  bonds, and one  $\pi$  electron pair from one of the NH ligands, forming a delocalized V–N  $\pi$  bond of order 0.5 with the two imino ligands. The d electrons on the two vanadium atoms couple together to form a  $\sigma$  metal–metal bond. This picture is confirmed by the Mulliken population analysis of the RASSCF wave function reported in Table 4.

The Mulliken gross atomic charge on each metal atom is 1.05, which is of course much lower than the formal 4 value because of the covalent bonding with the bridging NH and the hydrogen ligands. An analysis of the interactions within the metallacycle moiety can be performed by comparing the Mulliken analysis population of our complex with that of the monomeric  $H_2V^{2+}$  fragment, also reported in Table 4. For these fragments, still of V(IV) character, the positive net charge is 1.84. The metallacycle formation thus leads to a reduction of the vanadium charge by 0.79 units. Most of this extra electronic charge is distributed on the metal  $3d_{x^2-y^2}$ ,  $3d_{xy}$ ,  $3d_{xz}$ , and  $3d_{yz}$  orbitals and is due to the bonding interactions of these formally unoccupied 3d orbitals with the NH bridging ligands within the metallacycle unit as described above. Among the results of our calculations, we see from Table 4 that the  $10a_g$  NO representing the V–V  $\sigma$  interaction is an almost pure (99%) metallic orbital. Although unusual in SCF or semiempirical calculations, in which a relevant contribution from the NH  $\sigma$  lone pair is expected (see, for example, ref 27), a HOMO of almost pure metallic character describing a metal–metal bond may be quite common in accurate calculations including electron correlation.<sup>11–13</sup>

The electronic structure of the triplet state,  $^3B_{1u}$ , is described by a  $\sigma^1\sigma^{*1}$  configuration (cf. Table 3) corresponding to a nonbonding character of the metal–metal interaction. However, the nature of the metal–bridging ligand interactions in this triplet state is essentially identical to that found for the singlet state and described above. This is further illustrated by the NO occupation numbers and the Mulliken analysis presented in Tables 3 and 4. The character of the bond is reflected in the optimized geometry found for the triplet state where the metal–metal distance is elongated to 2.69 Å (typical of nonbonded V–V interactions).

(27) Shaik, S.; Hoffmann, R.; Fisel, C. R.; Summerville, R. H. *J. Am. Chem. Soc.* **1980**, *102*, 4555.

**Table 5. Optimized Geometries for the Dication, Monocation, Monoanion, and Dianion Species in Their  $^1A_g$ ,  $^2A_g$ ,  $^2B_{1u}$ , and  $^1A_g$  Ground States (units, angstroms and degrees)**

	V-V	V-N	V-H	N-H	$\angle$ HVH
dication	2.688	1.811	1.585	1.015	123.9
monocation	2.549	1.816	1.626	1.003	125.0
monoanion	2.537	1.870	1.759	1.007	116.5
dianion	2.625	1.922	1.836	1.000	104.4

**Table 6. Relative RASSCF and CASPT2 (both with and without 3s,3p correlation) Energies (in kcal/mol) for the Dication, Monocation, Monoanion and Dianion Species in Their  $^1A_g$ ,  $^2A_g$ ,  $^2B_{1u}$ , and  $^1A_g$  Ground States, with Respect to the Ground State of the Neutral Compound**

	RASSCF	CASPT2	CASPT2 (3s3p)
dication	488	512	502
monocation	184	150	142
monoanion	-28	-30	-29
dianion	63	122	120

**Table 7. Natural Orbital Occupation Numbers for the Dication, Monocation, Monoanion, and Dianion Species in Their  $^1A_g$ ,  $^2A_g$ ,  $^2B_{1u}$ , and  $^1A_g$  Ground States**

NO	dicat	monocat	monoan	dian
9a <sub>g</sub>	1.98	1.95	1.96	1.96
4b <sub>3u</sub>	1.96	1.97	1.98	1.98
5b <sub>2u</sub>	1.98	1.96	1.97	1.97
1b <sub>1g</sub>	1.95	1.98	1.98	1.98
7b <sub>1u</sub>	1.97	1.97	1.97	1.98
3b <sub>2g</sub>	1.97	1.98	1.96	1.96
10a <sub>g</sub>	0.02	0.96	1.91	1.98
8b <sub>1u</sub>	0.01	0.09	1.03	1.97

The structure is, however, still kept together by the strong metal-bridging ligand interaction. The vertical singlet-triplet energy separation computed at the most accurate CASPT2 level is 9860 cm<sup>-1</sup> (cf. Table 2). The large values found for this splitting rules out any possible thermal contamination of the singlet ground state and is therefore in agreement with the diamagnetic character found experimentally for the complexes **1** and **2**. From Table 2 we see also that geometry relaxation leads to a slightly lower value of the adiabatic singlet-triplet splitting, 8400 cm<sup>-1</sup>. It is moreover worth noting that the energy splitting depends on the inclusion of dynamic correlation. The RASSCF calculation underestimates the splitting, which is probably due to the inadequate accounting for the differential Pauli correlation effects in the RASSCF wave function.

We have performed RASSCF and CASSCF/CASPT2 calculations also on the mono- and dianion and on the mono- and dication species, {H<sub>2</sub>V[μ-NH]}<sub>2</sub><sup>2+</sup>, **4**, {H<sub>2</sub>V[μ-NH]}<sub>2</sub><sup>+</sup>, **5**, {H<sub>2</sub>V[μ-NH]}<sub>2</sub><sup>-</sup>, **6**, and {H<sub>2</sub>V[μ-NH]}<sub>2</sub><sup>2-</sup>, **7**, in order to study the behavior of complex **3** toward reduction and oxidation. The corresponding optimized geometries and relative energies are reported in Tables 5 and 6. In Table 7 we report the natural orbital occupation numbers of the NOs with some metal character for all four charged species. A detailed analysis of the orbitals shows that they are qualitatively similar to those of the neutral species **3**, describing the σ and π vanadium bridging ligands interactions and discussed above. However, all these orbitals have a higher metallic character in the cationic species and a lower metallic character in the anionic species. Moreover, from Table 7 we note that the configurations for these four charged species are approximately (3dσ)<sup>0</sup>-(3dσ\*)<sup>0</sup>, (3dσ)<sup>1</sup>(3dσ\*)<sup>0</sup>, (3dσ)<sup>2</sup>(3dσ\*)<sup>1</sup>, and (3dσ)<sup>2</sup>(3dσ\*)<sup>2</sup>,

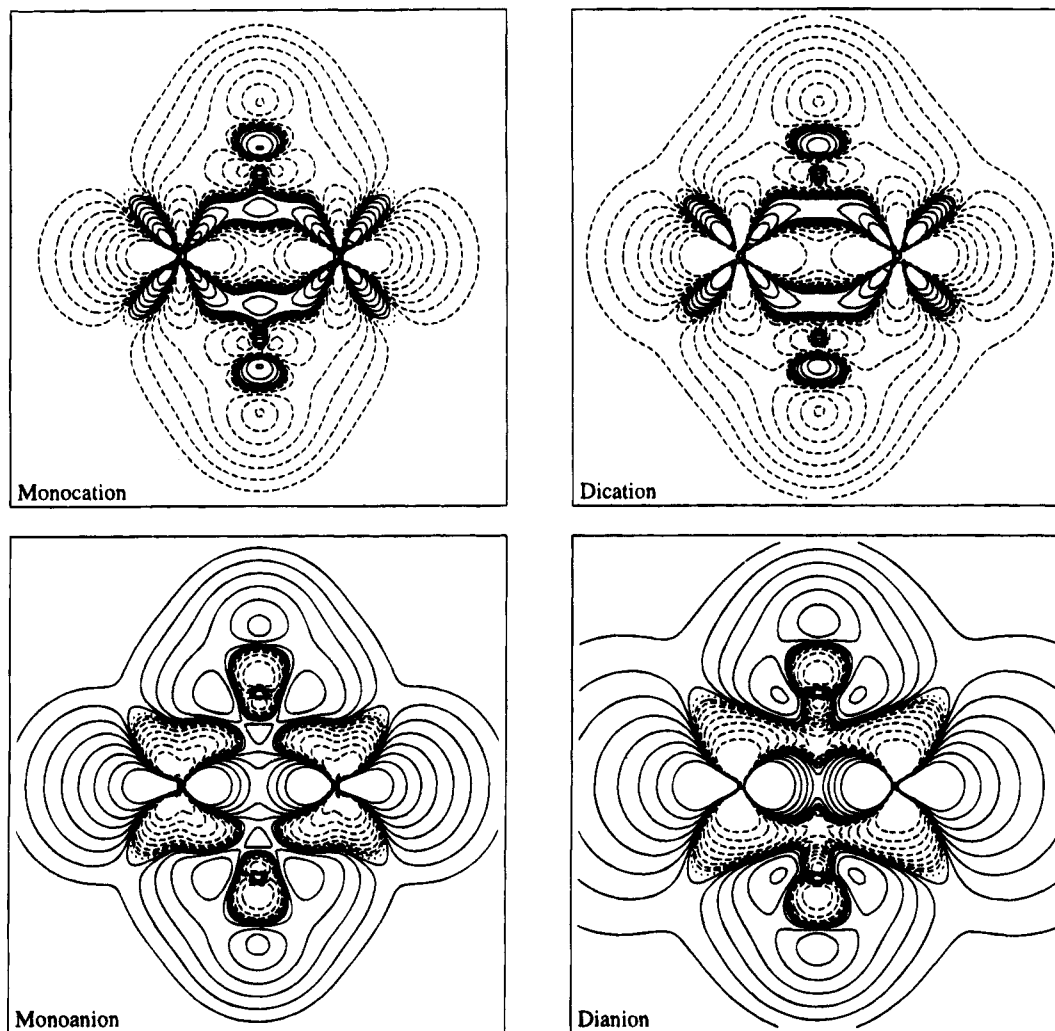
**Table 8. Atomic Charges and Partial Mulliken Population Analysis for the Dication, Monocation, Monoanion, and Dianion Species in Their  $^1A_g$ ,  $^2A_g$ ,  $^2B_{1u}$ , and  $^1A_g$  Ground States**

	dicat	monocat	monoan	dian
V charge	1.32	1.14	1.11	1.18
4s	0.43	0.51	0.48	0.40
4p	0.28	0.31	0.31	0.28
3d <sub>z<sup>2</sup></sub>	0.11	0.45	1.40	1.86
3d <sub>x<sup>2</sup>-y<sup>2</sup></sub>	0.86	0.86	0.57	0.41
3d <sub>xy</sub>	0.25	0.25	0.23	0.17
3d <sub>xz</sub>	1.07	0.93	0.58	0.42
3d <sub>yz</sub>	0.72	0.50	0.26	0.23
3d	3.01	3.00	3.04	3.09
H(V) charge	0.09	-0.04	-0.39	-0.58
NH charge	-0.50	-0.55	-0.82	-1.02

respectively, going from the dication to the dianion, which formally corresponds to no metal-metal bond for the dication and the dianion species ... to a weak metal-metal bond (with a bond order of about 0.5) for the monocation and the monoanion. The different V-V bond strengths resulting from these electronic structures are reflected by the optimized geometries (cf. Table 5), with a metal-metal distance of 2.60–2.70 Å for the dication and dianion species, similar to that found for the triplet state of the neutral species and typical of nonbonded V-V interactions, and of 2.50–2.55 Å for the monocation and monoanion species, intermediate between those of the singlet and triplet states of the neutral molecule.

The Mulliken analysis population for all these four charged species is given in Table 8. The main interesting feature in these results is the small change of the charge on the vanadium atom in going from the dication to the dianion. This redistribution of the electron charge removed from or put into metallic 3dσ or 3dσ\* orbitals can be ascribed to the change in the metallic character of all the low lying frontier orbitals going from the neutral species to the cationic and anionic species, as reported above. A large fraction of the extra charge is located at the four hydrogens directly bound to the metal. Although this effect could be partly due to the extended basis set with many polarization functions, it is significant and should be even larger in the real system where hydrogens are substituted by the more polarizable mesityl groups. The hydrogen atoms (mesityl groups in the real system) act as effective reservoirs for the electrons put on the HOMO and LUMO orbitals.

The analysis of the six low lying frontier orbitals representing the σ and π vanadium-bridging ligand interactions for ionic species **4**–**7** shows that metal-bridging ligand bonding is not overly weakened by oxidation or reduction. Moreover, the obtained V-N bond distances, although slightly elongated with respect to the neutral molecule in the anionic species, still fall in the range of typical vanadium-nitrogen bonds for all the four ionic species. This suggests that, in spite of the two lost or gained electrons, the metallacycle V<sub>2</sub>N<sub>2</sub> unit is still a fairly strongly bound moiety so that complex **3** should survive both one or two electron oxidation or reduction steps. Considering the energy needed to form the four ionic species from complex **3** (cf. Table 6), it is found that mono- and dioxidation requires much energy (142 and 501 kcal/mol, respectively) while mono and direduction are much easier with the first electron affinity positive; that is, the monoanion



**Figure 4.** Plots of the total density difference between the ionic species and the singlet ground state of the molecule. The figures show the density shifts in the VNVN plane with the vanadium atoms along a horizontal axis. Full contours correspond to an increased density and dashed contours to a decreased. The values of the density contours are  $\pm 0.032$ ,  $\pm 0.016$ ,  $\pm 0.008$ ,  $\pm 0.004$ ,  $\pm 0.002$ ,  $\pm 0.001$ ,  $\pm 0.0005$ , and  $\pm 0.00025$  e/au<sup>3</sup>.

is lower in energy than the neutral complex (by 29 kcal/mol). Also the computed energy required for the double reduction of the model  $\{\text{H}_2\text{V}[\mu\text{-NH}]\}_2$  complex is only 120 kcal/mol and will be even lower considering that the real system has six mesityl groups instead of hydrogens which, because of their electron withdrawing properties, should further stabilize the dianion species. Moreover, taking into account solvation effects in the real liquid phase reactions, the results above suggest that monoreduction of complex **3** in solution should be easy and that also its direduction could be possible. The value for the second electron affinity is in a way artificial, since it has been computed to be negative. However, the extra electron naturally goes into a 3d antibonding orbital, which then becomes a closed shell. The calculation therefore describes the situation which would occur in solution, where the dianion is stable and the computed energy is more a measure of the solvation energy needed to make the ion stable. There is a strong negative correlation contribution to the relative energy of the dianion. The CASSCF value is only 63 kcal/mol, which is almost doubled at the CASPT2 level of theory. This is somewhat surprising, since dynamic correlation is normally more important in the negative ions than in the corresponding neutral species.

The electron density difference for the four ionic species is shown in Figure 4. It is clear that ionization leads to a decreased density in the V–V bonding region, which is to some extent compensated by an increased density in the V–N and V–H regions. As a result, the corresponding bond distances decrease (cf. Tables 1 and 5). In the anions the extra electron goes into the antibonding V–V orbital, so even if the figure shows an increased density in this region the bond distance will increase. The decreased density in the V–N and V–H regions leads to elongated bonds.

The results obtained for the mono- and dianionic species indicate that the  $8b_{1u}$  LUMO can be seen as a low-energy orbital available for the molecule to easily accept one or two electrons without undergoing drastic structure *i* alterations, the extra charge being buffered into the hydrogen atoms (mesityl groups).

#### 4. Conclusions

The electronic structure and geometry of the model compound  $\{\text{H}_2\text{V}[\mu\text{-NH}]\}_2$  in its lowest singlet and triplet state has been determined using multiconfigurational SCF methods with dynamic correlation effects on the total energy obtained using second-order perturbation

theory. The molecule has been found to have a singlet ground state with the lowest triplet state about 1 eV higher in energy. The computed equilibrium geometry is in agreement with measured data for related compounds. Analysis of the wave function shows that the two vanadium atoms are bound together with a single bond in the singlet state, while no such bond exists in the triplet state. Corresponding calculations on the positive and negative ions yields structures with half a bond for the singly ionized systems and no V-V bond

for the doubly ionized systems. The first electron affinity is found to be positive.

**Acknowledgment.** The present work has been carried out within the program "Progetto finalizzato CNR Materiali Speciali per Tecnologie Avanzate". Support by the Fond Nationale Suisse de la Recherche Scientifique and the Swedish Natural Science Research Council (NFR) is gratefully acknowledged.

OM9403582

# Regiocontrolled Hydrosilation of $\alpha,\beta$ -Unsaturated Carbonyl Compounds Catalyzed by Hydridotetrakis(triphenylphosphine)rhodium(I)

G. Z. Zheng and T. H. Chan\*

Department of Chemistry, McGill University, Montreal, Quebec, Canada H3A 2K6

Received June 3, 1994<sup>⊗</sup>

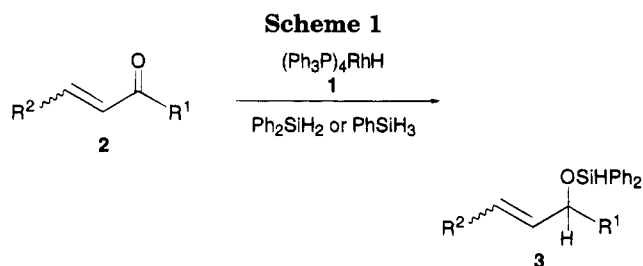
Hydrosilation of  $\alpha,\beta$ -unsaturated carbonyl compounds catalyzed by hydridotetrakis(triphenylphosphine)rhodium(I) (**1**) was found to be highly regioselective, depending on the silanes used. Diphenylsilane was found to give 1,2-hydrosilation, whereas dimethylphenylsilane and other monohydrosilanes gave 1,4-addition. The kinetic isotope effect of the hydrosilation reaction was examined, and a mechanism was proposed to account for the regioselection and the kinetic isotope effect.

## Introduction

Reactions which selectively reduce  $\alpha,\beta$ -unsaturated carbonyl compounds are of considerable interest for organic synthesis. Among the many procedures available, metal complex catalyzed homogeneous hydrosilation<sup>1</sup> offers some interesting advantages. For example, regioselective 1,4-reductions of  $\alpha,\beta$ -unsaturated carbonyl compounds with hydrosilanes give the corresponding enol silyl ethers, which are themselves useful synthons.<sup>2</sup> A number of metal complexes can be used as catalysts for the hydrosilation reaction.<sup>1,3</sup> Of particular significance is the report by Ojima that tris(triphenylphosphine)chlororhodium (**2**) catalyzed by the reduction of  $\alpha,\beta$ -unsaturated carbonyl compounds regioselectively.<sup>4</sup> Recently, we found that hydridotetrakis(triphenylphosphine)rhodium (**1**) is an efficient catalyst for the 1,4-reduction of  $\alpha,\beta$ -unsaturated carbonyl compounds to give the corresponding enol silyl ethers.<sup>5</sup> We have since found that the same catalyst **1** can also be an efficient catalyst for the 1,2-reduction reactions when di- or trihydrosilanes are used in the hydrosilation reactions. Compared to **2**, catalyst **1** appears to offer milder reaction conditions and higher regioselectivity. We describe here an account of our research on this subject.

## Results and Discussion

**1,2-Hydrosilations.** A number of carbonyl compounds were reduced to the corresponding alcohols (after hydrolysis of the silyl ether products) with diphenylsilane or phenylsilane using **1** as the catalyst (Scheme 1). The results are summarized in Table 1. Of the  $\alpha,\beta$ -unsaturated ketones examined (entries 1-4, Table 1),



only 1,2-reduction products were obtained. No detectable 1,4-reduction products were observed in the <sup>1</sup>H NMR of the crude product mixtures prior to hydrolysis, and GC analyses of the allylic alcohols **3a-c** showed the absence of the corresponding saturated ketones. In the case of carvone (**2c**), the product was a mixture of *cis*- and *trans*-carveol in a ratio of 65:35. Such stereoselectivity is similar to the results reported in the literature for the hydrosilation of **2c** using ((+)-DIOP)-Rh as catalyst.<sup>6</sup> In the reduction of cholestenone **2d** (entry 4, Table 1), cholestadiene **3d** was obtained as the sole product in good yield, presumably due to the acid-catalyzed elimination of the allylic alcohol in the hydrolysis step. The 1,4-reduction product, cholestanone, was not observed.

Simple ketones can be reduced effectively as well. The reduction of 4-*tert*-butylcyclohexanone (**5b**) led to two diastereomers, **7a** and **7b**, in a ratio of 84:16 (*trans*:*cis*). This stereoselectivity appeared to be superior to that reported previously for similar hydrosilation,<sup>7</sup> indicating a preference for axial attack during the course of hydrosilation. Such stereoselectivity is also evident in the reduction of **2e**. The only product obtained was the alcohol **3e**. On the other hand, reduction of camphor (**5c**) gave a mixture of two diastereomers (**7c** and **7d**) in a ratio of 64:36, a stereoselectivity which is somewhat lower than expected from similar hydrosilations reported previously.<sup>8</sup> Interestingly, the catalyst **1** tolerated the presence of the hydroxy group in the substrate (**5e**), an observation

\* Abstract published in *Advance ACS Abstracts*, November 1, 1994.

(1) (a) Ojima, I.; Kogure, T. *Rev. Silicon, Germanium, Tin, Lead Compd.* **1981**, 5, 7. (b) Ojima, I.; Kogure, T. *Organometallics* **1982**, 1, 1390.

(2) (a) Mukaiyama, T. *Angew. Chem., Int. Ed. Engl.* **1977**, 16, 817. (b) Brownbridge, P. *Synthesis* **1983**, 1, 83. (c) Chan, T. H. In *Comprehensive Organic Synthesis*; Trost, B. M., Fleming, I., Heathcock, C. H., Eds.; Pergamon Press: Oxford, U.K., 1991; Vol. 2, Part 2, pp 595-628.

(3) (a) Speier, J. L.; Webster, J. A.; Barnes, G. H. *J. Am. Chem. Soc.* **1957**, 79, 974. (b) Revis, A.; Hilty, K. T. *J. Org. Chem.* **1990**, 55, 2972.

(4) Ojima, I.; Kogure, T.; Nagai, Y. *Tetrahedron Lett.* **1972**, 5035.

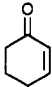
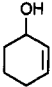
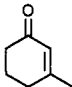
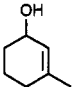
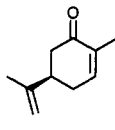
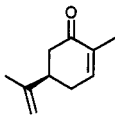
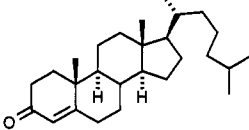
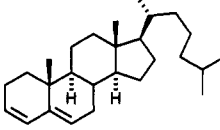
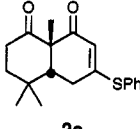
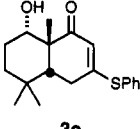
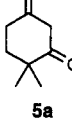
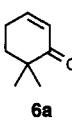

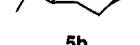
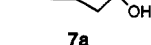
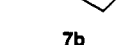
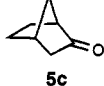
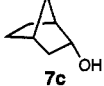
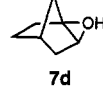
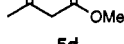
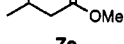
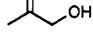
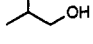
(5) Chan, T. H.; Zheng, G. Z. *Tetrahedron Lett.* **1993**, 34, 3095.

(6) Kogure, T.; Ojima, I. *J. Organomet. Chem.* **1982**, 234, 249.

(7) Nishiyama, H.; Park, S. B.; Itoh, K. *Tetrahedron: Asymmetry* **1992**, 3, 1029.

(8) French Patent 2,187,798, 1974; *Chem. Abstr.* **1974**, 81, 25799c.

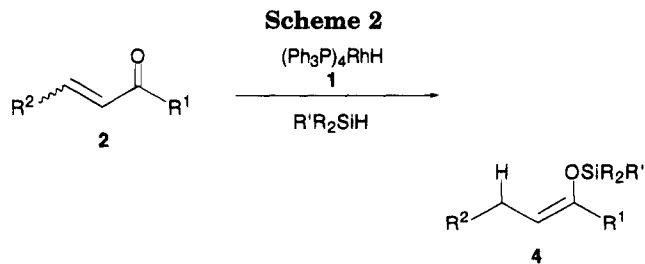
Table 1. 1,2-Hydrosilation of Carbonyl Compounds with  $\text{Ph}_2\text{SiH}_2$ 

entry no.	substrate	amt of Rh(I), % mol/mol; time, h <sup>a</sup>	product <sup>b</sup>	yield, % <sup>c</sup>
1		0.4; 4		83
2		0.3; 4		86
3		0.4; 12		84 (cis:trans = 65:35)
4		0.4; 12		76
5		0.5; 12		56
6		0.5; 12	 	49 (19:1)
7		0.3; 5	 	81 (trans:cis = 84:16)
8		0.4; 7	 	85 (endo:exo = 36:64)
9		0.3; 4		86
10		0.4; 12		80

<sup>a</sup> Reaction time;  $\text{CH}_2\text{Cl}_2$  is the solvent used in all cases. <sup>b</sup> The products are hydrolyzed products from hydrosilations. <sup>c</sup> Purified yields.

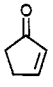
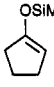
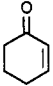
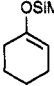
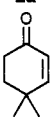
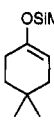
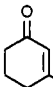
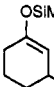
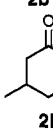
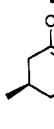
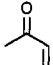
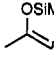
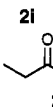
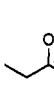
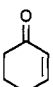
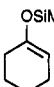
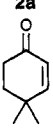
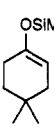
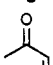
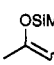
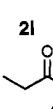
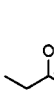
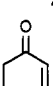
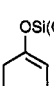

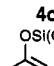
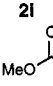
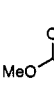
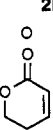
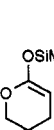
which may well be useful in the synthesis of compounds of biological interest. The presence of the thioether function in the substrate (**2e**) presented no problem as well. 1,3-Dicarbonyl compounds were also reduced in a 1,2-reduction fashion. In the case of **5d**, the chemoselective reduction of the ketone function over the ester function is to be expected. Steric factors are likely to play a role in the selective reduction of **5a** in giving **6a** as the major product.

**1,4-Hydrosilations.** A number of  $\alpha,\beta$ -unsaturated carbonyl compounds were reduced by various monohydrosilanes with **1** as the catalyst to give the corresponding enol silyl ethers (Scheme 2). The results are summarised in Table 2. In all cases, only 1,4-reduction was observed. By comparing the hydrosilation of **2a** with that of **2b**, it is evident that substitution at the  $\beta$ -position reduces the rate of reaction but did not change the regioselection. In the case of 3,5-dimethyl-



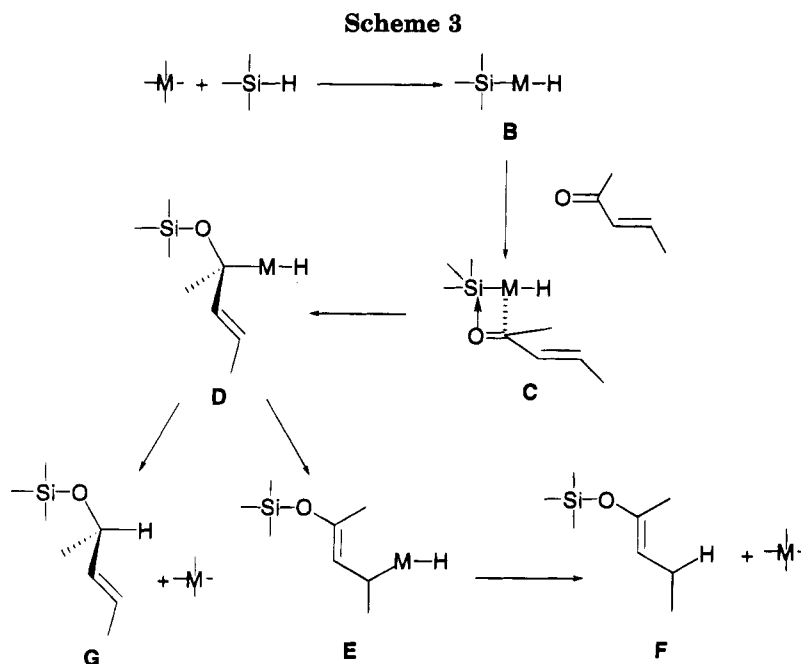
2-cyclohexen-1-one (**2h**), the result was quite interesting. Previously, it was reported that this substrate underwent only isomerization of the  $\text{C}=\text{C}$  bond to form 3,5-dimethyl-3-cyclohexen-1-one, irrespective of the catalyst or silanes used.<sup>9</sup> We found that **2h** was reduced in a 1,4-fashion to give **4h** in good yield and with high stereoselectivity (cis:trans = 92:8). Catalyst **1** is also capable of mediating the hydrosilation of  $\alpha,\beta$ -unsatur-

Table 2. 1,4-Hydrosilation of  $\alpha,\beta$ -Unsaturated Carbonyl Compounds

entry no.	substrate	amt of Rh(I), % mol/mol; conditions	silane <sup>a</sup>	product <sup>b</sup>	yield, %
1	 <b>2f</b>	0.3; room temp. 12 h	<b>8a</b>	 <b>4f</b>	83
2	 <b>2a</b>	0.3; room temp, 12 h	<b>8a</b>	 <b>4a</b>	84
3	 <b>2g</b>	0.4; room temp, 12 h	<b>8a</b>	 <b>4g</b>	96
4	 <b>2b</b>	0.5; 50 °C, 24 h	<b>8a</b>	 <b>4b</b>	89
5	 <b>2h</b>	0.5; 50 °C, 24 h	<b>8a</b>	 <b>4h</b>	87 (cis:trans = 92:8)
6	 <b>2i</b>	0.2; room temp, 6 h	<b>8a</b>	 <b>4i</b>	73 ( <i>E</i> : <i>Z</i> = 33:67)
7	 <b>2j</b>	0.2; room temp, 6 h	<b>8a</b>	 <b>4j</b>	82 ( <i>E</i> : <i>Z</i> = 77:23)
8	 <b>2a</b>	0.1; room temp, 0.5 h	<b>8b</b>	 <b>4k</b>	83
9	 <b>2g</b>	0.3; room temp, 4 h	<b>8b</b>	 <b>4l</b>	80
10	 <b>2i</b>	0.2; room temp, 1.5 h	<b>8b</b>	 <b>4m</b>	85 ( <i>E</i> : <i>Z</i> = 1:2)
11	 <b>2j</b>	0.3; room temp, 10 h	<b>8b</b>	 <b>4n</b>	83 ( <i>E</i> : <i>Z</i> = 4:1)
12	 <b>2a</b>	0.3; room temp, 12 h	<b>8c</b>	 <b>4o</b>	93
13	 <b>2i</b>	0.3; room temp, 20 h	<b>8c</b>	 <b>4p</b>	75 ( <i>E</i> : <i>Z</i> = 56:44)
14	 <b>2k</b>	0.3; room temp, 1.5 h	<b>8a</b>	 <b>4q</b>	91
15	 <b>2l</b>	0.3; room temp, 12 h	<b>8a</b>	 <b>4r</b>	85

<sup>a</sup> **8a**, PhMe<sub>2</sub>SiH; **8b**, (ClCH<sub>2</sub>)Me<sub>2</sub>SiH; **8c**, (EtO)<sub>3</sub>SiH. <sup>b</sup> The products were distilled via Kugelrohr apparatus.





ated esters to give the corresponding silyl ketene acetals (entries 14 and 15). Transition metal catalyzed hydrosilation of  $\alpha,\beta$ -unsaturated esters have previously been reported.<sup>10</sup> Since silyl ketene acetals are useful synthons as well as in group transfer polymerization,<sup>11</sup> the present catalytic process may find considerable applications. Finally, functionalized silanes are compatible with catalyst **1** and can be used in the hydrosilation reaction. Thus, triethoxysilane (**8c**) and (chloromethyl)dimethylsilane (**8b**) gave the corresponding 1,4-addition products.

**Mechanism of Hydrosilation of Carbonyl Compounds.** The general features of the mechanism of homogeneous hydrosilation reactions were first outlined by Chalk and Harrod<sup>12</sup> and subsequently elaborated by numerous studies.<sup>13</sup> In adapting the hydrosilation mechanism to the reduction of carbonyl compounds, and to account for the regioselection, Ojima proposed a general mechanism for the hydrosilation of carbonyl compounds as depicted in Scheme 3. The metal complex undergoes insertion into the silicon hydrogen bond to give the silyl metal hydride complex **B**. Coordination of **B** with the carbonyl substrate gives **C**, in which there is a four-membered ring. In the next step, the four-membered ring is transformed into the  $\alpha$ -metalated silyl ether intermediate **D**. Reductive elimination of **D** gives the 1,2-addition product **G** with the regeneration of the metal **M** to start another catalytic cycle. Alternatively, **D** can undergo an allylic rearrangement to give the intermediate **E**, which on reductive elimination gives the 1,4-addition product **F**. Spin trapping experiments were used by Ojima to provide supporting evidence for the intermediacy of **D** and **E**.

In trying to adapt the Ojima mechanism to the observed regioselection in our experiments, we were puzzled by several points. The most glaring one is the fact that monohydrosilanes gave exclusively 1,4-addition and di- or trihydrosilanes gave 1,2-addition. It is difficult to understand why the isomerization of **D** to **E** or their subsequent eliminations should be drastically altered by the presence (or absence) of a hydrogen on silicon in the Ojima mechanism. The second point is that in a substrate where only 1,2-addition is possible, for example, in the hydrosilation of acetophenone, diphenylsilane was found to react much faster than dimethylphenylsilane using the same catalyst **1**. Again, this is difficult to reconcile on the basis of the proposed mechanism. The third point is that when there is an additional substituent in the  $\beta$ -position of the C=C bond, one would expect the isomerization of **D** to **E** to be diminished on both kinetic and thermodynamic grounds, thus reducing the regioselectivity. Our observation is that regioselection was not affected (*vide supra*). We seek, therefore, an alternative explanation to accommodate these observations, at least for **1** as the catalyst.

For the 1,2-hydrosilation of carbonyl compounds with di- and trihydrosilanes, a possible mechanism is outlined in Scheme 4. The critical feature in this mechanism is that, in the step from the complex **J** to the intermediate **K**, it is the hydrogen on silicon that is transferred. When the silane used is a monohydrosilane, this pathway is not available. Complex **J** then rearranges to the intermediate **L**, which reductively eliminates to the silyl ether product. The mechanism accounts for the substantial difference in rates in the 1,2-reduction of carbonyl compounds with diphenylsilane versus dimethylphenylsilane.

We have examined the kinetic isotope effect in the hydrosilation of acetophenone, and the results appear to be more compatible with the mechanism in Scheme 4 than with the Ojima mechanism. When dideuterio-diphenylsilane (1 mmol) and diphenylsilane (1 mmol) were reacted with acetophenone (1 mmol) using **1** as the catalyst, the product *sec*-phenethyl alcohol had a ratio of 2:1 for proton and deuterium incorporation in

(9) Marciniak, B.; Gulinski, J.; Urbaniak, W.; Kornetka, Z. W. In *Comprehensive Handbook on Hydrosilylation*; Marciniak, B. Ed.; Pergamon Press: Oxford, U.K., 1992; p 148.

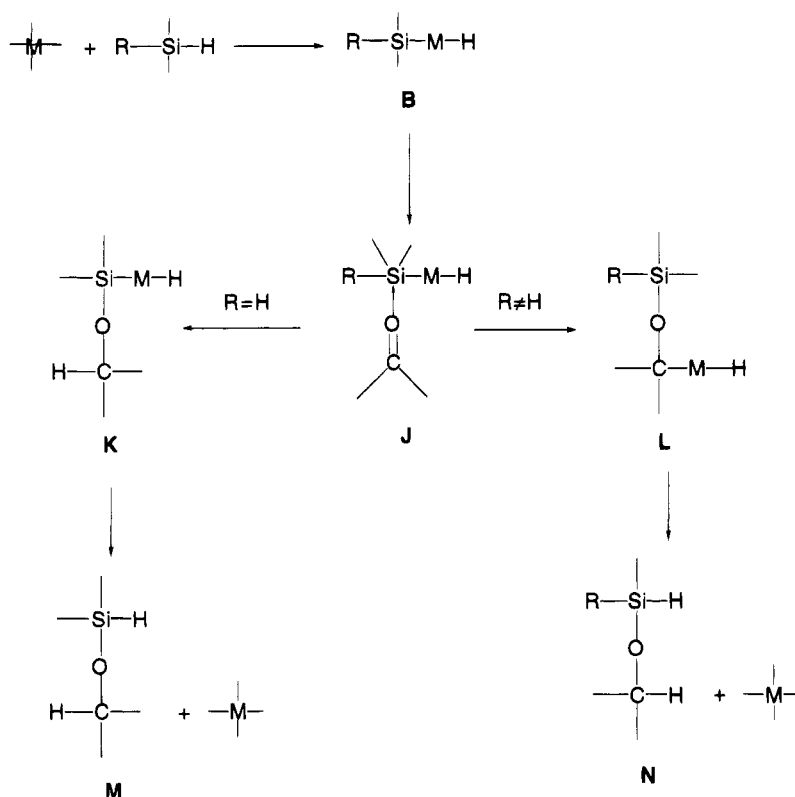
(10) Revis, A.; Hilty, T. K. *J. Org. Chem.* **1990**, *55*, 2972 and references therein.

(11) Sogah, D. Y.; Hertler, W. R.; Webster, O. W.; Cohen, G. M. *Macromolecules* **1987**, *20*, 1473 and references cited therein.

(12) Chalk, A. J.; Harrod, J. F. *J. Am. Chem. Soc.* **1965**, *87*, 16.

(13) (a) Kolb, I.; Hetflejš, J. *Collect. Czech. Chem. Commun.* **1980**, *45*, 2224. (b) Corriu, R. J. P.; Moreau, J. J. E. *J. Organomet. Chem.* **1975**, *85*, 19. (c) Bergens, S. H.; Noheda, P.; Whelan, J.; Bosnich, B. *J. Am. Chem. Soc.* **1992**, *114*, 2128. (d) Marciniak, B.; Duczmal, W.; Urbaniak, W.; Silwinska, E. *J. Organomet. Chem.* **1990**, *385*, 319.

Scheme 4



the methine carbon. This gives an isotope effect of  $k_{\text{H}}/k_{\text{D}} = 2$ . In contrast, when deuteriodimethylphenylsilane (1 mmol) and dimethylphenylsilane (1 mmol) were reacted with acetophenone (1 mmol) using catalyst **1** under identical conditions, the product ratio was 1:1 for hydrogen and deuterium incorporation, giving a kinetic isotope effect of  $k_{\text{H}}/k_{\text{D}} = 1$ . It can be estimated from stretching vibrational frequencies of silanes and rhodium hydrides<sup>14</sup> that in a rate-determining step where a Si-H or Rh-H bond is broken, the primary kinetic isotope effect would be  $k_{\text{H}}/k_{\text{D}} = 3-4$ . The absence of any significant kinetic isotope effect in the reaction of dimethylphenylsilane with acetophenone suggests that neither the formation of the silylhydridorhodium complex **B** nor the elimination of **L** to **N** can be the rate-determining step. On the other hand, the observation of a significant primary kinetic isotope effect in the reduction of acetophenone by diphenylsilane is consistent with the possibility that the rate-determining step is the formation of the intermediate **K** from the complex **J**. The observed  $k_{\text{H}}/k_{\text{D}} = 2$  is similar to the primary kinetic isotope effect observed in the reduction of sulfoxide by silane, where cleavage of a Si-H bond in a four-membered-ring transition state is believed to be the rate-determining step.<sup>15</sup>

A possible mechanism for 1,4-hydrosilylation reaction is outlined in Scheme 5. When the substrate is an  $\alpha,\beta$ -unsaturated carbonyl compound, it complexes with **B** to form **O**, where there is  $\sigma$ -coordination between oxygen and silicon and  $\pi$ -coordination between the metal and the double bond. When the silane used is a di- or trihydrosilane, the hydrogen on silicon migrates as in Scheme 4 to give **P** and then the 1,2-reduction product

**Q**. On the other hand, when the silane used is a monohydrosilane, complex **O** rearranges with Si-M cleavage to give the intermediate **R**, which then reductively eliminates to give the enol silyl ether **S**. In such a mechanism, one can rationalize the divergent regioselection of di- versus monohydrosilane readily.

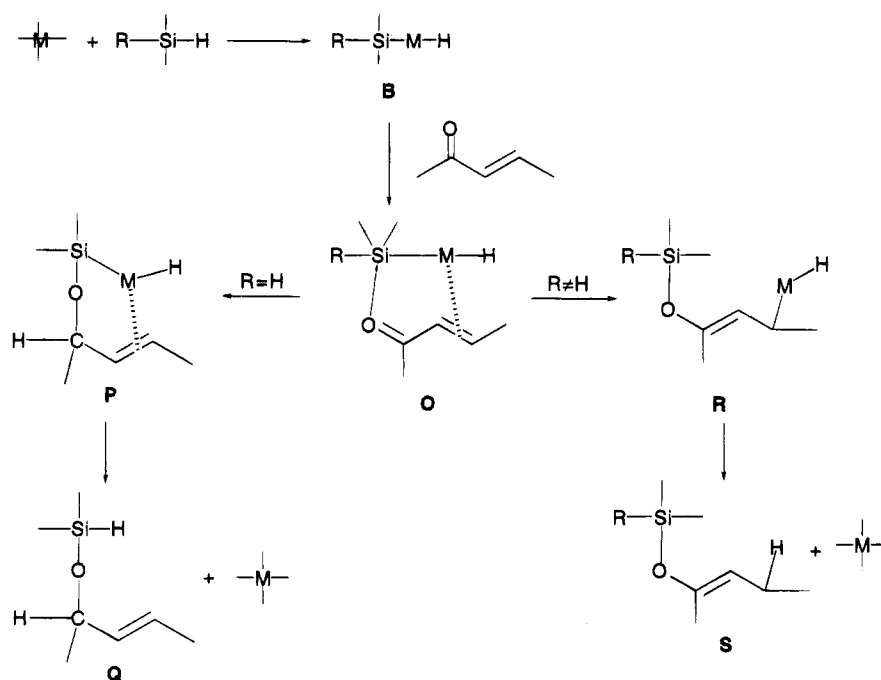
We have also examined the isotope effect of the 1,4-hydrosilylation reaction. When deuteriodimethylphenylsilane (1 mmol) and dimethylphenylsilane (1 mmol) were reacted with 4,4-dimethyl-2-cyclohexen-1-one (**2g**; 1 mmol) with **1** as the catalyst, the product enol silyl ether **4g** was found to be a 1:1 mixture of the mono-deuterated and non-deuterated compounds. The absence of a significant primary kinetic isotope effect suggests that the rate-determining step is either the formation of the complex **O** or the formation of the intermediate **R**. In a kinetic study of the hydrosilylation of *tert*-butyl phenyl ketone using a  $[\text{Rh}(1,5\text{-COD})(\text{-DIOP})]^+\text{ClO}_4^-$  catalyst, Kolb and Heflejs were able to show that the coordination of the ketone with the silylhydridorhodium species was the rate-determining step in that reaction. It is possible that in the present case the coordination of the  $\alpha,\beta$ -unsaturated ketone with the silylhydridorhodium species **B** to form **O** is the rate-determining step. This is also consistent with the absence of a primary kinetic isotope effect in the 1,2-hydrosilylation of 4,4-dimethyl-2-cyclohexen-1-one with an equal mixture of dideuteriodiphenylsilane and diphenylsilane using **1** as the catalyst. A 1:1 mixture of 1-deuterio-4,4-dimethyl-2-cyclohexen-1-ol (**3g**) and 4,4-dimethyl-2-cyclohexen-1-ol (**3f**) was obtained.

The presence of  $\pi$ -coordination between rhodium and the double bond can also account for the stereoselection observed in the 1,4-reduction of **2h**. In this particular case, the intermediate **T** would be favored over the intermediate **U**, where there is more serious steric interaction between the axial methyl group and the

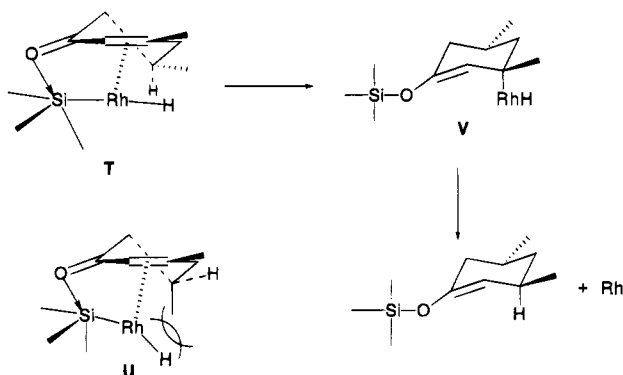
(14) (a) Ito, T.; Kitazume, S.; Yamamoto, A.; Ikeda, S. *J. Am. Chem. Soc.* **1974**, *92*, 3012. (b) Kono, H.; Wakao, N.; Ojima, I.; Nagai, Y. *Chem. Lett.*, **1975**, 189.

(15) Chan, T. H.; Melnyk, A. *J. Am. Chem. Soc.* **1970**, *92*, 3718.

Scheme 5



rhodium moiety. Subsequent transformation of **T** to the intermediate **V** would then give the *cis* product selectively.



### Conclusion

Hydridotetrakis(triphenylphosphine)rhodium (**1**) was found to be a very efficient catalyst for the regioselective hydrosilation of  $\alpha,\beta$ -unsaturated carbonyl compounds. A new mechanism for the hydrosilation of carbonyl compounds is proposed to account for the observed regioselectivity and kinetic isotope effect.

### Experimental Section

**General Considerations.** Most of the chemicals used were purchased from Aldrich. Hydridotetrakis(triphenylphosphine)rhodium(I) was purchased from Johnson Matthey. Diphenylchlorosilane was purchased from Hüls America. THF was distilled over sodium/benzophenone ketyl radical before use. Hexanes, ethyl acetate, and dichloromethane were distilled over calcium hydride. Nuclear magnetic resonance spectra were recorded on Varian Gemini 200 ( $^1\text{H}$ , 200 MHz;  $^{13}\text{C}$ , 50 MHz), XL-200 ( $^1\text{H}$ , 200 MHz;  $^{13}\text{C}$ , 50 MHz), XL-300 ( $^1\text{H}$ , 300 MHz;  $^{13}\text{C}$ , 75 MHz), and Unity 500 ( $^1\text{H}$ , 500 MHz;  $^{13}\text{C}$ , 125 MHz) spectrometers. Chemical shifts are expressed in parts per million (ppm) and the reference is a trace of chloroform in  $\text{CDCl}_3$  giving a signal at 7.24 ppm for  $^1\text{H}$  and at 77.00 ppm ( $\text{CDCl}_3$ ) for  $^{13}\text{C}$ . IR spectra were recorded on an Analet FT A25-18 spectrometer between NaCl plates (neat liquids) or as

KBr disks. Mass spectra were recorded on a Kratos MS25RFA mass spectrometer and are reported in  $m/z$  units. Melting points were determined on a Gallenkamp block and are uncorrected. Elemental analyses were obtained on a CEC 240XA elemental analyzer in the Department of Chemical Engineering, McGill University. Analytical samples for elemental analysis were obtained via column chromatography (silica gel, deactivated with 2% triethylamine in hexanes) using hexanes as eluent.

**Deuteriodimethylphenylsilane (8d).** Chlorodimethylphenylsilane (99%, 10 mmol, 1.72 g) was placed in a 150-mL flask with 40 mL of diethyl ether.  $\text{LiAlD}_4$  (96% D, 5 mmol, 0.210 g) was added at room temperature. The reaction mixture was stirred for 3 h at room temperature and then quenched with saturated aqueous  $\text{NH}_4\text{Cl}$  solution. The organic layer was separated, and the aqueous layer was extracted by diethyl ether ( $2 \times 10$  mL). The combined organic layers were dried over  $\text{Na}_2\text{SO}_4$  and filtered. Removal of ether gave a colorless liquid, which was purified via Kugelrohr distillation (55  $^\circ\text{C}/5$  mmHg) to give 1.10 g of **8d** (80% yield) which contained about 95% deuterated product.  $^1\text{H}$  NMR (200 MHz,  $\text{CDCl}_3$ ): 7.53 (m, 2H), 7.36 (m, 3H), 0.33 (s, 6H).  $^{13}\text{C}$  NMR (50 MHz,  $\text{CDCl}_3$ ): 142.2, 133.3, 128.5, 127.2, -2.9. IR (neat): 699.5, 732.3, 794.1, 836.3, 1116.1, 1252.6, 1541.1, 1589.4, 2119.7, 2960.6, 3016.0, 3052.1, 3068.7  $\text{cm}^{-1}$ . HRMS: calcd for  $\text{C}_8\text{D}_{11}\text{DSi}$  137.0771, found 137.0774.

**Dedeuteriodiphenylsilane<sup>13a</sup> (8f).** Dichlorodiphenylsilane (97%, 4.9 mmol, 1.27 g) was placed in a 150 mL flask with 40 mL of diethyl ether.  $\text{LiAlD}_4$  (96% D, 5 mmol, 0.210 g) was added at room temperature. The reaction mixture was stirred for 3 h at room temperature and then quenched with saturated aqueous  $\text{NH}_4\text{Cl}$  solution. The reaction mixture was worked up as in **8d**. This gave a colorless liquid which was purified via Kugelrohr distillation (100  $^\circ\text{C}/5$  mmHg) to give 0.84 g of **8f** (90% yield) which contained about 93% dideuterated product.  $^1\text{H}$  NMR (200 MHz,  $\text{CDCl}_3$ ): 7.61 (m, 4H), 7.41 (m, 6H).  $^{13}\text{C}$  NMR (50 MHz,  $\text{CDCl}_3$ ): 134.9, 130.7, 129.2, 127.4. IR (neat) 1121.4, 1428.3, 1548.3, 1655.5, 1819.6, 1884.8, 1956.8, 2140.7, 3016.3, 3050.0, 3066.9  $\text{cm}^{-1}$ . HRMS: calcd for  $\text{C}_{12}\text{H}_{10}\text{D}_2\text{Si}$  186.0834, found 186.0832.

**General Procedure for the 1,2-Reduction of  $\alpha,\beta$ -Unsaturated Ketones.** Hydridotetrakis(triphenylphosphine)rhodium(I) (ca. 5 mg) was placed in a 10 mL flask furnished with a magnetic stirring bar and sealed with a rubber septum under argon. Dried  $\text{CH}_2\text{Cl}_2$  (1 mL) was added via a syringe

followed by the  $\alpha,\beta$ -unsaturated ketone (1 mmol). After 10 min, diphenylsilane (1.3 mmol) was added dropwise. The reaction mixture was stirred at room temperature for 4 h and then transferred to a 25 mL flask with a solution of HCl (2 N, 3 mL)-acetone (3 mL). The mixture was stirred at room temperature for 2 h. Acetone was removed via rotary evaporation. The aqueous residue was then extracted with dichloromethane (4  $\times$  3 mL). The combined organic layers were dried over  $\text{Na}_2\text{SO}_4$ . Removal of solvent gave the crude product, which was purified by flash column chromatography separation or Kugelrohr distillation.

**2-Cyclohexen-1-ol (3a).**<sup>16</sup> Compound **3a** was obtained from 2-cyclohexen-1-one (97%; 1 mmol, 0.099 g, 100  $\mu\text{L}$ ) as a yellowish liquid, which was subjected to flash column chromatography separation (hexanes:ethyl acetate = 6:1) to give product **3a** (81 mg, 83% yield).  $^1\text{H}$  NMR (200 MHz,  $\text{CDCl}_3$ ): 5.82 (dt,  $J = 3.0, 10.1$  Hz, 1H), 5.72 (m, 1H), 4.17 (m, 1H), 1.97 (m, 2H), 1.45–1.92 (m, 4H).  $^{13}\text{C}$  NMR (50 MHz,  $\text{CDCl}_3$ ): 130.0, 129.2, 65.6, 32.5, 25.7, 19.6. IR (neat) 1054.2, 1435.6, 1451.9, 1651.4, 1706.3, 2864.4, 2935.7, 3024.6, 3363.5  $\text{cm}^{-1}$ . MS (EI): 99 (4), 98 (54, M), 97 (41), 83 (35), 70 (100), 55 (22).

**3-Methyl-2-cyclohexen-1-ol**<sup>17</sup> (**3b**). Compound **3b** was obtained from 3-methyl-2-cyclohexen-1-one (98%, 1 mmol, 0.112 g, 116  $\mu\text{L}$ ) as a yellowish liquid, which was subjected to flash column chromatography separation (hexanes:ethyl acetate = 6:1). Compound **3b** was obtained as a colorless liquid (96 mg, 86% yield).  $^1\text{H}$  NMR (200 MHz,  $\text{CDCl}_3$ ): 5.47 (m, 1H), 4.12 (m, 1H), 1.89 (m, 2H), 1.75 (m, 2H), 1.67 (s, 3H), 1.56 (m, 2H), 1.55 (s, 1H).  $^{13}\text{C}$  NMR (50 MHz,  $\text{CDCl}_3$ ): 137.7, 123.7, 65.7, 32.1, 30.5, 24.2, 19.7. IR (neat) 957.9, 993.1, 1034.6, 1436.5, 1448.3, 1671.6, 2867.1, 2875.6, 2895.5, 2925.5  $\text{cm}^{-1}$ . MS (EI): 112 (17, M), 97 (100), 84 (30), 79 (22), 69 (18).

**(1R,5R)-5-Isopropenyl-2-cyclohexen-1-ol**<sup>18</sup> (**Carveol**, **3c**). Compound **3c** was obtained from (*R*)-(-)-carvone (127 mg, 84% yield) as a colorless liquid with a ratio for cis:trans isomers of 65:35.  $^1\text{H}$  NMR (200 MHz,  $\text{CDCl}_3$ ): 5.58 (m, 35% of 1H), 5.48 (m, 65% of 1H), 4.71 (s, 4H), 4.18 (m, 65% of 1H), 4.01 (m, 35% of 1H), 1.87–2.40 (m, 6H), 1.68–1.84 (m, 12H), 1.40–1.65 (m, 4H).  $^{13}\text{C}$  NMR (50 MHz,  $\text{CDCl}_3$ ): 148.3, 148.1, 135.4, 133.6, 124.8, 123.3, 108.7, 108.6, 71.0, 68.6, 40.8, 38.4, 37.2, 35.7, 31.5, 21.6, 21.5, 21.3, 19.7. IR (neat) 1035.0, 1439.1, 1645.3, 2858.3, 2884.2, 2915.8, 2940.1, 2967.7, 3319.5  $\text{cm}^{-1}$ . MS (EI): 152 (23, M), 137 (16), 134 (58), 109 (100), 93 (28), 84 (99).

**3,5-Cholestadiene**<sup>19</sup> (**3d**). Compound **3d** was obtained from (+)-4-cholesten-3-one (1 mmol, 0.385 g) as a solid, which was recrystallized from  $\text{CH}_2\text{Cl}_2$ -MeOH (281 mg, 76% yield). Mp: 76.5–77.5  $^\circ\text{C}$ .  $^1\text{H}$  NMR (200 MHz,  $\text{CDCl}_3$ ): 5.91 (d,  $J = 10.0$  Hz, 1H), 5.58 (m, 1H), 5.38 (m, 1H), 2.14 (m, 2H), 2.00 (dt,  $J = 3.4, 12.3$  Hz, 1H), 0.96–1.88 (m, 23H), 0.94 (s, 3H), 0.90 (d,  $J = 6.6$  Hz, 3H), 0.85 (d,  $J = 6.6$  Hz, 6H), 0.67 (s, 3H).  $^{13}\text{C}$  NMR (50 MHz,  $\text{CDCl}_3$ ): 140.7, 128.4, 124.4, 122.6, 57.2, 56.4, 48.7, 42.9, 40.3, 40.0, 36.7, 36.3, 35.7, 34.3, 32.3, 28.8, 28.6, 24.8, 24.6, 24.0, 23.5, 23.2, 21.6, 19.5, 19.4, 12.8. IR (KBr): 1333.5, 1374.6, 1463.9, 1650.6, 2857.5, 2908.8, 2962.3, 3017.7  $\text{cm}^{-1}$ . MS (EI): 370 (16), 369 (30), 368 (100, M), 353 (20), 260 (19), 255 (16), 147 (43), 107 (27), 105 (30).

**cis-3-(Phenylthio)-1,4,4a,5,6,7,8,8a-octahydro-8 $\alpha$ -hydroxy-5,5,8a-trimethylnaphthalen-1-one**<sup>20</sup> (**3e**). Compound **3e** was obtained from *cis*-3-(phenylthio)-1,4,4a,5,6,7,8,8a-octahydro-5,5,8a-trimethylnaphthalen-1,8-dione<sup>18</sup> (0.06 mmol, 0.018 g) as a yellowish solid, which was subjected to flash column chromatography purification (hexanes:ethyl acetate = 6:1) to give the white solid  $\alpha$ -isomer (10.5 mg, 56% yield). Mp: 183.0–184.0  $^\circ\text{C}$ .  $^1\text{H}$  NMR (200 MHz,  $\text{CDCl}_3$ ): 7.44 (m, 5H), 5.32 (d,  $J = 2.4$  Hz, 1H), 4.77 (d,  $J = 11.0$  Hz, 1H), 3.13 (td,  $J = 11.3, 4.6$  Hz, 1H), 2.87 (ddd,  $J = 19.0, 6.4, 2.4$  Hz, 1H), 2.48 (dd,  $J = 19.0, 1.1$  Hz, 1H), 1.24–1.86 (m, 5H), 1.44 (s, 3H), 0.92 (s, 3H), 0.75 (s, 3H).  $^{13}\text{C}$  NMR (50 MHz,  $\text{CDCl}_3$ ): 202.2, 163.2, 134.9, 129.6, 129.3, 127.2, 119.9, 78.6, 52.8, 47.7, 40.7, 35.2, 31.7, 29.6, 29.4, 25.0, 24.0. IR (film): 1030.7, 1222.4, 1341.9, 1378.3, 1433.8, 1580.3, 1618.8, 1713.6, 2863.9, 2930.2, 2955.8, 3449.1  $\text{cm}^{-1}$ . MS (EI): 316 (7, M), 219 (6), 218 (16), 217 (100), 176 (24), 139 (19), 108 (11).

**6,6-Dimethyl-2-cyclohexen-1-one**<sup>21</sup> (**6a**) and **4,4-Dimethyl-2-cyclohexen-1-one**<sup>22</sup> (**6b**). Compounds **6a** and **6b** were obtained from 4,4-dimethylcyclohexane-1,3-dione (98%, 1 mmol, 143.0 mg) as a yellowish liquid which was subjected to Kugelrohr distillation (90  $^\circ\text{C}/20$  mmHg) to give a mixture of **6a** and **6b** (95:5; 61 mg, 49% yield) [or flash column chromatography separation (hexanes:ethyl acetate = 10:1)].

**6,6-Dimethyl-2-cyclohexen-1-one (6a):**  $^1\text{H}$  NMR (200 MHz,  $\text{CDCl}_3$ ) 6.84 (dt,  $J = 10.0, 4.0$  Hz, 1H), 5.89 (dt,  $J = 10.0, 2.0$  Hz, 1H), 2.35 (m, 2H), 1.81 (t,  $J = 6.0$  Hz, 2H), 1.09 (s, 6H);  $^{13}\text{C}$  NMR (50 MHz,  $\text{CDCl}_3$ ) 203.1, 147.7, 127.7, 41.8, 36.7, 24.7, 24.0; IR (neat): 1125.9, 1301.9, 1385.5, 1427.4, 1453.9, 1679.1, 1708.5, 2867.3, 2930.5, 2963.4, 3033.7  $\text{cm}^{-1}$ ; MS (EI) 126 (5), 124 (41, M), 109 (11), 96 (18), 69 (11), 68 (100).

**4,4-Dimethyl-2-cyclohexen-1-one (6b):**  $^1\text{H}$  NMR (200 MHz,  $\text{CDCl}_3$ ) 6.62 (d,  $J = 10.0$  Hz, 1H), 5.80 (d,  $J = 10.0$  Hz, 1H), 2.42 (t,  $J = 6.5$  Hz, 2H), 1.83 (t,  $J = 6.7$  Hz, 2H), 1.13 (s, 6H);  $^{13}\text{C}$  NMR (50 MHz,  $\text{CDCl}_3$ ) 198.1, 158.8, 126.2, 36.5, 34.9, 33.3, 28.3; IR (neat) 803.6, 1122.0, 1236.5, 1418.9, 1467.0, 1618.4, 1687.9, 2930.1, 2962.7  $\text{cm}^{-1}$ ; MS (EI) 125 (7), 124 (72, M), 109 (13), 96 (67), 82 (100), 81 (48).

**cis-4-tert-Butyl-1-cyclohexanol**<sup>23</sup> (**7b**) and **trans-4-tert-Butyl-1-cyclohexanol**<sup>24</sup> (**7a**). Compounds **7a** and **7b** were obtained from 4-*tert*-butylcyclohexan-1-one (99%; 1 mmol, 156 mg) as a solid (*cis:trans* = 16:84), which was subjected to flash column chromatography separation (hexanes:ethyl acetate = 6:1). White solids were obtained (*cis*, 27 mg; *trans*, 100 mg; 81% yield).

**trans-4-tert-Butyl-1-cyclohexanol (7a):** mp 80.5–81.5  $^\circ\text{C}$ ;  $^1\text{H}$  NMR (200 MHz,  $\text{CDCl}_3$ ) 3.43 (m, 1H), 2.47 (br, 1H), 1.93 (m, 2H), 1.71 (m, 2H), 0.87–1.27 (m, 5H), 0.78 (s, 9H);  $^{13}\text{C}$  NMR (50 MHz,  $\text{CDCl}_3$ ) 71.0, 47.4, 36.3, 32.7, 28.1, 26.1; IR (KBr) 1068.5, 1367.6, 1450.7, 1473.3, 2862.8, 2917.8, 2964.4, 3215.0  $\text{cm}^{-1}$ ; MS (CI) 174 (33, M + 18), 156 (2, M), 155 (5), 139 (35), 138 (100), 123 (83).

**cis-4-tert-Butyl-1-cyclohexanol (7b):** mp 82.0–83.0  $^\circ\text{C}$ ;  $^1\text{H}$  NMR (200 MHz,  $\text{CDCl}_3$ ) 4.00 (br, 1H), 1.80 (m, 2H), 1.50 (m, 2H), 1.29–1.54 (m, 5H), 0.96 (tt,  $J = 11.4, 2.9$  Hz, 1H), 0.83 (s, 9H);  $^{13}\text{C}$  NMR (50 MHz,  $\text{CDCl}_3$ ) 66.0, 48.3, 33.9, 33.1, 28.0, 21.5; IR (KBr) 960.5, 1007.3, 1032.5, 1114.3, 1147.4, 1180.5, 1232.1, 1275.0, 1337.3, 1365.9, 1439.9, 1476.3, 2839.6, 2866.8, 2952.5, 3287.4  $\text{cm}^{-1}$ ; MS (CI) 174 (8, M + 18), 155 (3), 139 (15), 123 (21).

**(1S,2R,4S)-1,7,7-Trimethylbicyclo[2.2.1]hepten-2-ol**<sup>24</sup> (**Isoborneol**, **7d**) and **(1S,2S,4S)-1,7,7-trimethylbicyclo[2.2.1]hepten-2-ol**<sup>24</sup> (**Borneol**, **7c**). Compounds **7c** and **7d** were obtained from (-)-camphor (99%; 1 mmol, 153.8 mg) as a yellowish solid, which was subjected to flash column chromatography separation (hexanes:ethyl acetate = 6:1). White solid products were obtained (83.8 mg of *exo* isomer **7d**, 4.2 mg of *endo* isomer **7c**, 85% yield).

**Isoborneol (7d):** mp 218.0–219.0  $^\circ\text{C}$ ;  $^1\text{H}$  NMR (200 MHz,  $\text{CDCl}_3$ ) 3.61 (m, 1H), 1.40–1.74 (m, 8H), 1.00 (s, 3H), 0.86 (s, 3H), 0.80 (s, 3H);  $^{13}\text{C}$  NMR (50 MHz,  $\text{CDCl}_3$ ) 79.7, 49.2, 46.6, 45.3, 40.8, 34.4, 27.8, 21.1, 20.7, 12.1; IR (KBr) 1005.1, 1070.3, 1455.9, 1477.7, 2875.0, 2955.0, 3434.3  $\text{cm}^{-1}$ ; MS (EI) 154 (3, M), 139 (16), 136 (27), 121 (21), 110 (32), 96 (10), 95 (100), 93 (22).

(16) Mincione, E. *J. Org. Chem.* **1978**, *43*, 1829.

(17) Mori, K.; Tamada, S.; Uchida, M.; Mizumachi, N.; Tachibana, Y.; Matsui, M. *Tetrahedron* **1978**, *34*, 1901.

(18) Gradi, R.; Pagnoni, U. M.; Trave, R. *Tetrahedron* **1974**, *30*, 4037.

(19) Achmatowicz, S.; Barton, D. H. R.; Magnus, P. D.; Poulton, G. A.; West, P. J. *J. Chem. Soc., Perkin Trans. 1* **1973**, *15*, 1567.

(20) Chan, T. H.; Guertin, K. R.; Prasad, C. V. C.; Thomas, A. W.; Strunz, G. M.; Saloni, A. *Can. J. Chem.* **1990**, *68*, 1170.

(21) Oppolzer, W.; Sarkar, T.; Mahalanabis, K. K. *Helv. Chim. Acta* **1976**, *59*, 2012.

(22) Chan, Y. L.; Epstein, W. W. *Org. Synth.* **1973**, *53*, 48.

(23) Winstein, S.; Holness, N. J. *J. Am. Chem. Soc.* **1955**, *77*, 5562.

(24) Gream, G. E.; Wege, D.; Mular, M. *Aust. J. Chem.* **1974**, *27*, 567.

Borneol (**7c**): mp 206.0–208.0 °C;  $^1\text{H}$  NMR (200 MHz,  $\text{CDCl}_3$ ) 4.01 (m, 1H), 2.26 (m, 1H), 1.56–1.94 (m, 3H), 1.14–1.38 (m, 3H), 0.92 (dd,  $J = 13.5, 3.6$  Hz, 1H), 0.85 (s, 3H), 0.84 (s, 3H), 0.83 (s, 3H);  $^{13}\text{C}$  NMR (50 MHz,  $\text{CDCl}_3$ ) 77.4, 49.8, 48.4, 45.5, 39.5, 28.9, 26.5, 20.9, 19.4, 14.1; IR (KBr) 1024.5, 1056.8, 1109.7, 1455.6, 2874.0, 2952.0, 3305.6  $\text{cm}^{-1}$ ; MS (EI) 154 (2, M), 139 (15), 136 (11), 110 (32), 95 (100), 93 (8).

**Methyl 3-Hydroxybutyrate**<sup>25</sup> (**7e**). Compound **7e** was obtained from methyl acetoacetate (1 mmol, 0.117 g, 109  $\mu\text{L}$ ) as a yellowish liquid, which was subjected to Kugelrohr distillation (50 °C/10 mmHg, 101 mg, 86% yield).  $^1\text{H}$  NMR (200 MHz,  $\text{CDCl}_3$ ): 4.18 (m, 1H), 3.69 (s, 3H), 2.95 (m, 1H), 2.49 (dd,  $J = 16.5, 4.3$  Hz, 1H), 2.37 (dd,  $J = 16.5, 8.0$  Hz, 1H), 1.21 (d,  $J = 6.4$  Hz, 3H).  $^{13}\text{C}$  NMR (50 MHz,  $\text{CDCl}_3$ ): 172.0, 64.3, 51.9, 43.0, 23.0. IR (neat): 1007.2, 1072.3, 1087.9, 1174.0, 1197.4, 1296.9, 1440.0, 1742.7, 2973.7, 3459.0  $\text{cm}^{-1}$ . MS (CI): 136 (5, M + 18), 120 (5), 119 (100, M + 1), 101 (15), 74 (12).

**1,2-Propanediol**<sup>26</sup> (**7f**). Compound **7f** was obtained (at –78 °C, and then room temperature) from acetol (90%, 1 mmol, 0.082 g, 76  $\mu\text{L}$ ) as a yellowish liquid, which was subjected to Kugelrohr distillation (80 °C/20 mmHg, 61 mg, 80% yield).  $^1\text{H}$  NMR (200 MHz,  $\text{CDCl}_3$ ): 3.86 (m, 1H), 3.58 (d,  $J = 10.9$  Hz, 1H), 3.38 (d,  $J = 8.1$  Hz, 1H), 3.25 (s (br), 2H), 1.12 (d,  $J = 6.2$  Hz, 3H).  $^{13}\text{C}$  NMR (50 MHz,  $\text{CDCl}_3$ ): 68.4, 68.1, 19.4. IR (neat): 1037.6, 1052.6, 1079.5, 1139.0, 1414.9, 1458.9, 2879.8, 2929.0, 2974.4, 3313.6  $\text{cm}^{-1}$ . MS (EI): 76 (1, M), 61 (6), 45 (100), 44 (9), 43 (14), 40 (10).

**General Procedure for 1,4-Reduction of  $\alpha,\beta$ -Unsaturated Carbonyl Compounds.** In a 5 mL flask furnished with a magnetic stirring bar and sealed with a rubber septum, hydridotetrakis(triphenylphosphine)rhodium(I) (**1**; ca. 5 mg) was placed under argon. The  $\alpha,\beta$ -unsaturated ketone (1 mmol) was introduced to the flask via a syringe followed by the silane (1.1 mmol). The reaction mixture was stirred at room temperature for 12 h, and then hexanes (1 mL) were added. The mixture was filtered and the solvent was removed to get the crude product, which was purified by Kugelrohr distillation.

**1-Cyclopenten-1-yl Dimethylphenylsilyl Ether (4f).** Catalyst **1** (0.0035 mmol, 4 mg) and 2-cyclopenten-1-one (1.0 mmol, 0.082 g, 85  $\mu\text{L}$ ) were treated with dimethylphenylsilyl ether (1.1 mmol, 0.150 g, 169  $\mu\text{L}$ ) at room temperature for 12 h. After standard workup, the crude mixture was distilled at 95 °C/5 mmHg (Kugelrohr) to give **4f** as a colorless liquid (182 mg, 83% yield).  $^1\text{H}$  NMR (200 MHz,  $\text{CDCl}_3$ ): 7.68 (m, 2H), 7.46 (m, 3H), 4.66 (m, 1H), 2.33 (m, 4H), 1.89 (q,  $J = 7.0$  Hz, 2H), 0.55 (s, 6H).  $^{13}\text{C}$  NMR (50 MHz,  $\text{CDCl}_3$ ): 154.8, 137.4, 133.3, 129.7, 127.8, 102.7, 33.4, 28.7, 21.2, –1.3. IR (neat): 2958.0, 2850.5, 1645.9, 1428.4, 1344.9, 1253.0, 1119.3, 831.4, 699.2  $\text{cm}^{-1}$ . MS (EI): calcd for  $\text{C}_{13}\text{H}_{18}\text{OSi}$  218.1127, found 218.1139. Anal. Calcd for  $\text{C}_{13}\text{H}_{18}\text{OSi}$ : C, 71.52; H, 8.32. Found: C, 71.48; H, 8.37.

**1-Cyclohexen-1-yl Dimethylphenylsilyl Ether (4a).** Catalyst **1** (0.0035 mmol, 4 mg) and 2-cyclohexen-1-one (1.0 mmol, 0.096 g, 97  $\mu\text{L}$ ) were treated with dimethylphenylsilyl ether (1.1 mmol, 0.150 g, 169  $\mu\text{L}$ ) at room temperature for 12 h. After standard workup, the crude mixture was distilled at 90 °C/5 mmHg (Kugelrohr) to give **4a** as a colorless liquid (195 mg, 84% yield).  $^1\text{H}$  NMR (200 MHz,  $\text{CDCl}_3$ ): 7.66 (m, 2H), 7.42 (m, 3H), 4.91 (m, 1H), 2.03 (m, 4H), 1.68 (m, 2H), 1.55 (m, 2H), 0.49 (s, 6H).  $^{13}\text{C}$  NMR (50 MHz,  $\text{CDCl}_3$ ): 170.9, 158.8, 154.0, 150.2, 148.5, 125.4, 50.5, 44.5, 43.8, 43.0, 19.7. IR (neat): 2930.5, 1669.4, 1252.6, 1186.8, 1169.9, 893.6  $\text{cm}^{-1}$ . MS (EI): calcd for  $\text{C}_{14}\text{H}_{20}\text{OSi}$  232.1283, found 232.1288. Anal. Calcd for  $\text{C}_{14}\text{H}_{20}\text{OSi}$ : C, 72.37; H, 8.68. Found: C, 71.97; H, 8.70.

**4,4-Dimethyl-1-cyclohexen-1-yl Dimethylphenylsilyl Ether (4g).** Catalyst **1** (0.0043 mmol, 5 mg) and 4,4-dimethyl-2-cyclohexen-1-one (1.0 mmol, 0.124 g, 132  $\mu\text{L}$ ) were treated with dimethylphenylsilyl ether (1.1 mmol, 0.150 g, 169  $\mu\text{L}$ ) at room

temperature for 12 h. After standard workup, the crude mixture was distilled at 100 °C/5 mmHg (Kugelrohr) to give **4g** as a colorless liquid (250 mg, 96% yield).  $^1\text{H}$  NMR (200 MHz,  $\text{CDCl}_3$ ): 7.66 (m, 2H), 7.41 (m, 3H), 4.82 (m, 1H), 2.03 (m, 2H), 1.82 (m, 2H), 1.42 (t,  $J = 6.5$  Hz, 2H), 0.93 (s, 6H), 0.50 (s, 6H).  $^{13}\text{C}$  NMR (50 MHz,  $\text{CDCl}_3$ ): 149.2, 138.0, 133.3, 129.6, 127.7, 103.6, 37.8, 35.8, 28.5, 27.9, 27.5, –1.0. IR (neat): 2952.0, 2919.9, 1669.6, 1366.3, 1197.3, 1167.7, 1119.1, 889.2, 873.3, 834.2, 784.8  $\text{cm}^{-1}$ . MS (EI): calcd for  $\text{C}_{16}\text{H}_{24}\text{OSi}$  260.1596, found 260.1595. Anal. Calcd for  $\text{C}_{16}\text{H}_{24}\text{OSi}$ : C, 73.80; H, 9.30. Found: C, 73.82; H, 9.34.

**Deuterium Isotope Effect for the 1,4-Reduction of 4,4-Dimethyl-2-cyclohexen-1-one.** Catalyst **1** (0.0043 mmol, 5 mg) and 4,4-dimethyl-2-cyclohexen-1-one (1.0 mmol, 0.124 g, 132  $\mu\text{L}$ ) were treated with dimethylphenylsilyl ether (98%, 1 mmol, 0.140 g) and deuteriodimethylphenylsilyl ether (96% D; 1 mmol, 0.140 g) at room temperature for 12 h. After standard workup, the crude product was distilled at 100 °C/5 mmHg (Kugelrohr) to give a colorless liquid (237 mg, ca. 91% yield) as a mixture of **4g** and its 3-deuterated compound. The amount of deuterium incorporation was determined by comparing the signal at 1.82 ppm (m, 1.52H) and that at 2.03 ppm (m, 2.00H). The ratio of nondeuterated to deuterated products was 50.6:47.3 (1.1:1).

**3-Methyl-1-cyclohexen-1-yl Dimethylphenylsilyl Ether (4b).** Catalyst **1** (0.0052 mmol, 6 mg) and 3-methyl-2-cyclohexen-1-one (1.0 mmol, 0.110 g, 114  $\mu\text{L}$ ) were treated with dimethylphenylsilyl ether (1.3 mmol, 0.177 g, 199  $\mu\text{L}$ ) at 50 °C for 24 h. After standard workup, the crude mixture was distilled at 110 °C/5 mmHg (Kugelrohr) to give **4b** as a colorless liquid (220 mg, 89% yield).  $^1\text{H}$  NMR (300 MHz,  $\text{CDCl}_3$ ): 7.70 (m, 2H), 7.45 (m, 3H), 4.83 (d,  $J = 1.4$  Hz, 1H), 2.28 (m, 1H), 2.04 (m, 2H), 1.70–1.86 (m, 2H), 1.59 (m, 1H), 1.11 (m, 1H), 0.99 (d,  $J = 7.0$  Hz, 3H), 0.53 (s, 6H).  $^{13}\text{C}$  NMR (75 MHz,  $\text{CDCl}_3$ ): 149.9, 137.9, 133.3, 129.5, 127.7, 111.5, 31.0, 29.7, 29.4, 22.4, 21.7, –1.0, –1.1. IR (neat): 2952.0, 2930.3, 2864.5, 2853.0, 1664.5, 1455.8, 1428.5, 1252.9, 1185.0, 1119.4, 1063.9, 1047.9, 886.4, 831.4, 786.8, 699.4  $\text{cm}^{-1}$ . MS (EI): calcd for  $\text{C}_{15}\text{H}_{22}\text{OSi}$  246.1440, found 246.1443. Anal. Calcd for  $\text{C}_{15}\text{H}_{22}\text{OSi}$ : C, 73.13; H, 9.01. Found: C, 73.22; H, 9.28.

**3,5-Dimethyl-1-cyclohexen-1-yl Dimethylphenylsilyl Ether (4h).** Catalyst **1** (0.0052 mmol, 6 mg) and 3,5-dimethyl-2-cyclohexen-1-one (1.0 mmol, 0.124 g, 141  $\mu\text{L}$ ) were treated with dimethylphenylsilyl ether (1.3 mmol, 0.177 g, 199  $\mu\text{L}$ ) at 50 °C for 48 h. After standard workup, the crude mixture was distilled at 90 °C/1 mmHg (Kugelrohr) to give **4h** as a colorless liquid (225 mg, 87% yield).  $^1\text{H}$  NMR (200 MHz,  $\text{CDCl}_3$ ): 7.58 (m, 2H), 7.37 (m, 3H), 4.66 (s, 1H), 2.21 (br, 1H), 1.93 (m, 1H), 1.63 (m, 4H), 0.90 (d,  $J = 7.9$  Hz, 3H), 0.86 (d,  $J = 7.0$  Hz, 3H), 0.43 (s, 6H).  $^{13}\text{C}$  NMR (50 MHz,  $\text{CDCl}_3$ ): 149.7, 138.0, 133.4, 129.5, 127.7, 111.3, 40.8, 38.4, 30.3, 29.6, 22.6, 22.0, –0.9, –1.0. IR (neat): 2952.0, 2917.6, 2912.9, 2901.5, 2870.0, 1666.1, 1428.4, 1368.9, 1252.9, 1196.8, 1182.4, 1120.8, 1079.3, 826.2, 786.5, 699.3  $\text{cm}^{-1}$ . MS (EI): calcd for  $\text{C}_{16}\text{H}_{24}\text{OSi}$  260.1596, found 260.1584. Anal. Calcd for  $\text{C}_{16}\text{H}_{24}\text{OSi}$ : C, 73.80; H, 9.30. Found: C, 73.78; H, 9.25.

**2-Buten-2-yl Dimethylphenylsilyl Ether (4i).** Catalyst **1** (0.0017 mmol, 2 mg) and 3-buten-2-one (1.0 mmol, 0.070 g, 83  $\mu\text{L}$ ) were treated with dimethylphenylsilyl ether (1.1 mmol, 0.150 g, 169  $\mu\text{L}$ ) at room temperature for 6 h. After standard workup, the crude mixture (205 mg,  $E:Z = 33:67$ ) was distilled at 60 °C/5 mmHg (Kugelrohr) to give a colorless liquid (151 mg, 73% yield).  $^1\text{H}$  NMR (200 MHz,  $\text{CDCl}_3$ ): 7.66 (m, 2H), 7.42 (m, 3H), 4.70 (dq,  $J = 6.9, 1.0$  Hz, 0.33H), 4.52 (dq,  $J = 6.6, 1.0$  Hz, 0.67H), 1.74 (m, 3H), 1.53 (m, 3H), 0.49 (s, 4.02H), 0.46 (s, 1.98H).  $^{13}\text{C}$  NMR (50 MHz,  $\text{CDCl}_3$ ): 147.9, 147.2, 138.1, 138.0, 133.3, 129.6, 127.8, 103.0, 102.3, 22.6, 17.3, 12.1, 10.7, –0.7, –1.1. IR (neat): 2960.8, 2944.1, 1682.4, 1428.4, 1383.8, 1316.0, 1252.9, 1119.2, 1100.5, 1048.0, 834.2, 784.9, 699.2  $\text{cm}^{-1}$ . MS (EI): calcd for  $\text{C}_{12}\text{H}_{18}\text{OSi}$  206.1127, found 206.1117.

**3-Hexen-3-yl Dimethylphenylsilyl Ether (4j).** Catalyst **1** (0.0017 mmol, 2 mg) and 4-hexen-3-one (1.0 mmol, 0.098 g,

(25) Meyers, A. I.; Knaus, G. *Tetrahedron Lett.* **1974**, 1333.

(26) Levene, P. A.; Walti, A. *Organic Syntheses*; Wiley: New York, 1943, Collect. Vol. 2, p 545.

114  $\mu\text{L}$ ) were treated with dimethylphenylsilane (1.1 mmol, 0.150 g, 169  $\mu\text{L}$ ) at room temperature for 6 h. After standard workup, the crude mixture (*E:Z* = 77:23) was distilled at 70 °C/5 mmHg (Kugelrohr) to give a colorless liquid (192 mg, 82% yield).  $^1\text{H NMR}$  (200 MHz,  $\text{CDCl}_3$ ): 7.70 (m, 2H), 7.46 (m, 3H), 4.68 (t,  $J$  = 7.6 Hz, 0.77H), 4.54 (t,  $J$  = 7.0 Hz, 0.23H), 2.17 (m, 2H), 2.00 (m, 2H), 1.12 (m, 3H), 0.99 (m, 3H), 0.54 (s, 6H).  $^{13}\text{C NMR}$  (50 MHz,  $\text{CDCl}_3$ ): 152.3, 151.1, 138.2, 138.1, 133.4, 133.3, 129.6, 129.5, 127.7, 109.2, 109.1, 29.3, 24.3, 20.1, 18.7, 15.4, 14.4, 12.0, 11.7, -0.8, -1.0. IR (neat): 2963.3, 1662.1, 1654.0, 1458.3, 1428.5, 1252.6, 1199.3, 1119.2, 1084.5, 831.4, 786.5  $\text{cm}^{-1}$ . MS (EI): calcd for  $\text{C}_{14}\text{H}_{22}\text{OSi}$  234.1440, found 234.1437.

**1-Cyclohexen-1-yl (Chloromethyl)dimethylsilyl Ether (4k).** Catalyst 1 (0.010 mmol, 12 mg) and 2-cyclohexen-1-one (10.0 mmol, 0.096 g, 968  $\mu\text{L}$ ) were treated with (chloromethyl)dimethylsilane (11.0 mmol, 1.196 g, 1.34 mL) at 0 °C. The mixture was then warmed up to room temperature and stirred for 30 min. After standard workup, the crude mixture (2.3681 g) was distilled at 70 °C/5 mmHg (Kugelrohr) to give **4k** as a colorless liquid (1.6852 g, 83%).  $^1\text{H NMR}$  (200 MHz,  $\text{CDCl}_3$ ): 4.87 (m, 1H), 2.82 (s, 2H), 1.98 (m, 4H), 1.62 (m, 2H), 1.51 (m, 2H), 0.28 (m, 6H).  $^{13}\text{C NMR}$  (50 MHz,  $\text{CDCl}_3$ ): 149.8, 104.9, 29.6, 29.5, 23.7, 23.0, 22.1, -2.9. IR (neat): 2931.1, 1669.8, 1265.1, 1255.1, 1190.0, 1169.8, 987.8, 898.4  $\text{cm}^{-1}$ . MS (EI): calcd for  $\text{C}_9\text{H}_{17}\text{OSiCl}$  204.0737, found 204.0742.

**4,4-Dimethyl-1-cyclohexen-1-yl (Chloromethyl)dime-thylsilyl Ether (4l).** Catalyst 1 (0.0061 mmol, 7 mg) and 4,4-dimethyl-2-cyclohexen-1-one (2.0 mmol, 0.248 g, 264  $\mu\text{L}$ ) were treated with (chloromethyl)dimethylsilane (2.4 mmol, 0.261 g, 292  $\mu\text{L}$ ) at room temperature for 4 h. After standard workup, the crude mixture (488 mg) was distilled at 70 °C/5 mmHg (Kugelrohr) to give **4l** as a colorless liquid (371 mg, 80% yield).  $^1\text{H NMR}$  (300 MHz,  $\text{CDCl}_3$ ): 4.75 (m, 1H), 2.79 (s, 2H), 1.96 (m, 2H), 1.76 (m, 2H), 1.37 (t,  $J$  = 6.5 Hz, 2H), 0.88 (s, 6H), 0.26 (s, 6H).  $^{13}\text{C NMR}$  (75 MHz,  $\text{CDCl}_3$ ): 148.7, 103.7, 37.7, 35.7, 29.4, 28.5, 27.8, 27.3, -3.0. IR (neat): 2952.0, 2923.6, 1673.8, 1366.4, 1255.2, 1196.8, 1167.5, 898.3, 876.3, 847.4, 825.1  $\text{cm}^{-1}$ . MS (EI): calcd for  $\text{C}_{11}\text{H}_{21}\text{OCiSi}$  232.1050, found 232.1051.

**2-Buten-2-yl (Chloromethyl)dimethylsilyl Ether (4m).** Catalyst 1 (0.0043 mmol, 5 mg) and 3-buten-2-one (2.0 mmol, 0.140 g, 167  $\mu\text{L}$ ) were treated with (chloromethyl)dimethylsilane (2.2 mmol, 0.239 g, 268  $\mu\text{L}$ ) at room temperature for 1.5 h. After standard workup, the crude mixture (350 mg, *E:Z* = 1:2) was distilled at 60 °C/15 mmHg (Kugelrohr) to give **4m** as a colorless liquid (305 mg, 85%).  $^1\text{H NMR}$  (300 MHz,  $\text{CDCl}_3$ ): *E* isomer (33%), 4.65 (g,  $J$  = 6.7 Hz, 1H), 2.79 (s, 2H), 1.69 (d,  $J$  = 1.0 Hz, 3H), 1.48 (d,  $J$  = 6.8 Hz, 3H), 0.25 (s, 6H); *Z* isomer (67%), 4.48 (q,  $J$  = 6.6 Hz, 1H), 2.80 (s, 2H), 1.73 (d,  $J$  = 1.0 Hz, 3H), 1.45 (dd,  $J$  = 6.7, 1.4 Hz, 3H), 0.28 (s, 6H).  $^{13}\text{C NMR}$  (75 MHz,  $\text{CDCl}_3$ ): *E* isomer, 147.5, 102.6, 29.4, 17.1, 11.9, -3.1; *Z* isomer, 146.5, 103.3, 29.6, 22.4, 10.5, -2.8. IR (neat): 2963.3, 2922.5, 1685.8, 1384.2, 1315.5, 1255.6, 1202.0, 1107.0, 1100.0, 1048.3, 1003.0, 888.9, 847.5, 823.1, 799.7  $\text{cm}^{-1}$ . MS (EI): calcd for  $\text{C}_7\text{H}_{16}\text{OSiCl}$  178.0581, found 178.0571.

**3-Hexen-3-yl (Chloromethyl)dimethylsilyl Ether (4n).** Catalyst 1 (0.005 mmol, 6 mg) and 4-hexen-3-one (2.0 mmol, 0.196 g, 229  $\mu\text{L}$ ) were treated with (chloromethyl)dimethylsilane (2.4 mmol, 0.261 g, 293  $\mu\text{L}$ ) at room temperature for 10 h. After standard workup, the crude product mixture (400 mg, *E:Z* = 4:1) was distilled at 40 °C/5 mmHg (Kugelrohr) to give **4n** as a colorless liquid (342 mg, 83% yield).  $^1\text{H NMR}$  (300 MHz,  $\text{CDCl}_3$ ): 4.55 (t,  $J$  = 7.6 Hz, 0.75H), 4.42 (t,  $J$  = 6.7 Hz, 0.25H), 2.79 (s, 1.50H), 2.78 (s, 0.50H), 2.03 (q,  $J$  = 7.6 Hz, 2H), 1.89 (p,  $J$  = 7.6 Hz, 2H), 0.84-1.00 (m, 6H), 0.26 (s, 6H).  $^{13}\text{C NMR}$  (75 MHz,  $\text{CDCl}_3$ ): *E* isomer, 151.9, 109.2, 29.4, 24.1, 20.0, 15.2, 11.8, -3.1; *Z* isomer, 150.5, 109.4, 29.6, 24.1, 18.5, 14.2, 11.6, -2.9. IR (neat): 2965.6, 2935.4, 1668.7, 1654.0, 1465.6, 1458.4, 1255.5, 1196.8, 1086.2, 1064.0, 1044.9, 876.3, 847.2, 821.1  $\text{cm}^{-1}$ . MS (EI): calcd for  $\text{C}_9\text{H}_{16}\text{OCiSi}$  206.0894, found 206.0894.

**1-Cyclohexen-1-yl Triethoxysilyl Ether (4o).** Catalyst

1 (0.0026 mmol, 3 mg) and 2-cyclohexen-1-one (1 mmol, 0.096 g, 97  $\mu\text{L}$ ) were treated with triethoxysilane (1.1 mmol, 0.181 g, 207  $\mu\text{L}$ ) at room temperature for 12 h. After standard workup, the crude product (242 mg, 93%) was distilled at 70 °C/5 mmHg (Kugelrohr) to give **4o** as a colorless liquid (202 mg, 78%).  $^1\text{H NMR}$  (200 MHz,  $\text{CDCl}_3$ ): 5.05 (m, 1H), 3.84 (q,  $J$  = 7.0 Hz, 6H), 2.04 (m, 4H), 1.64 (m, 2H), 1.48 (m, 2H), 1.21 (t,  $J$  = 7.0 Hz, 9H).  $^{13}\text{C NMR}$  (50 MHz,  $\text{CDCl}_3$ ): 148.8, 104.5, 59.4, 28.9, 23.6, 23.0, 22.1, 18.0. IR (neat): 2978.0, 2930.2, 2859.7, 1674.7, 1368.5, 1199.4, 1167.9, 1105.0, 1083.7, 524.6  $\text{cm}^{-1}$ . MS (EI): calcd for  $\text{C}_{12}\text{H}_{24}\text{O}_4\text{Si}$  260.1444, found 260.1453. Anal. Calcd for  $\text{C}_{12}\text{H}_{24}\text{O}_4\text{Si}$ : C, 55.35; H, 9.30. Found: C, 55.33; H, 9.35.

**2-Buten-2-yl Triethoxysilyl Ether (4p).** Catalyst 1 (0.0026 mmol, 3 mg) and 3-buten-2-one (1 mmol, 0.070 g, 83  $\mu\text{L}$ ) were treated with triethoxysilane (1.1 mmol, 0.181 g, 207  $\mu\text{L}$ ) at room temperature for 20 h. After standard workup, the crude product (*E:Z* = 56:44) was distilled at 60 °C/5 mmHg (Kugelrohr) to give **4p** as a colorless liquid (176 mg, 75%).  $^1\text{H NMR}$  (200 MHz,  $\text{CDCl}_3$ ): 4.82 (q,  $J$  = 6.9 Hz, 0.56H), 4.40 (q,  $J$  = 6.6 Hz, 0.44H), 3.81 (m, 6H), 1.78 (s, 1.32H), 1.72 (s, 1.68H), 1.47 (m, 3H), 1.16 (m, 9H).  $^{13}\text{C NMR}$  (50 MHz,  $\text{CDCl}_3$ ): 146.4, 145.8, 102.6, 102.1, 59.2, 21.5, 18.1, 17.9, 16.4, 11.8. IR (neat): 2978.1, 2926.1, 2895.9, 1722.1, 1682.7, 1388.6, 1106.8, 1083.6, 792.0  $\text{cm}^{-1}$ . MS (EI): calcd for  $\text{C}_{10}\text{H}_{22}\text{O}_4\text{Si}$  234.1287, found 234.1295.

**1-Methoxy-1-(dimethylphenylsiloxy)-2-methyl-1-pro-pene (4q).** Catalyst 1 (0.0069 mmol, 8 mg) and methyl methacrylate (2.0 mmol, 0.200 g, 214  $\mu\text{L}$ ) were treated with dimethylphenylsilane (2.2 mmol, 0.300 g, 337  $\mu\text{L}$ ) at room temperature for 1.5 h. After standard workup, the crude mixture was distilled at 85 °C/5 mmHg (Kugelrohr) to give a colorless liquid (430 mg, 91% yield).  $^1\text{H NMR}$  (200 MHz,  $\text{CDCl}_3$ ): 7.63 (m, 2H), 7.39 (m, 3H), 3.41 (s, 3H), 1.55 (s, 3H), 1.50 (s, 3H), 0.47 (s, 6H).  $^{13}\text{C NMR}$  (50 MHz,  $\text{CDCl}_3$ ): 149.4, 137.2, 133.4, 129.8, 127.8, 91.4, 56.9, 16.9, 16.1, -1.5. IR (neat): 2962.4, 2933.2, 2917.6, 2858.4, 1706.5, 1428.6, 1253.1, 1204.6, 1173.8, 1147.3, 1121.1, 1026.1, 943.0, 859.8, 834.2, 789.7  $\text{cm}^{-1}$ . MS (EI): calcd for  $\text{C}_{13}\text{H}_{20}\text{O}_2\text{Si}$  236.1233, found 236.1229.

**5,6-Dihydro-4H-pyran-2-yl Dimethylphenylsilyl Ether (4r).** Catalyst 1 (0.0069 mmol, 8 mg) and 5,6-dihydro-2H-pyran-2-one (2.0 mmol, 0.196 g, 172  $\mu\text{L}$ ) were treated with dimethylphenylsilane (2.2 mmol, 0.300 g, 337  $\mu\text{L}$ ) at room temperature for 12 h. After standard workup, the crude mixture was distilled at 110 °C/5 mmHg (Kugelrohr) to give **4r** as a colorless liquid (398 mg, 85% yield).  $^1\text{H NMR}$  (200 MHz,  $\text{CDCl}_3$ ): 7.67 (m, 2H), 7.44 (m, 3H), 4.04 (dd,  $J$  = 5.1, 5.1 Hz, 2H), 3.88 (t,  $J$  = 3.7 Hz, 1H), 2.04 (dt,  $J$  = 6.3, 3.9 Hz, 2H), 1.76 (m, 2H), 0.53 (s, 6H).  $^{13}\text{C NMR}$  (50 MHz,  $\text{CDCl}_3$ ): 154.2, 137.0, 133.2, 129.6, 127.6, 74.3, 67.1, 22.2, 19.7, -1.3. IR (neat): 2955.1, 2932.9, 2850.5, 1736.0, 1688.6, 1428.5, 1386.3, 1278.5, 1250.1, 1209.8, 1121.1, 1063.2, 911.9, 844.6, 821.1, 792.4  $\text{cm}^{-1}$ . MS (EI): calcd for  $\text{C}_{13}\text{H}_{18}\text{O}_2\text{Si}$  234.1076, found 234.1078.

**1-Phenylethanol<sup>27</sup> (7h).** Catalyst 1 (0.0043 mmol, 5 mg) and acetophenone (1 mmol, 0.121 g, 118  $\mu\text{L}$ ) were treated with diphenylsilane (1.3 mmol, 0.245 g, 250  $\mu\text{L}$ ) at room temperature for 4 h. After standard workup, the crude product was distilled at 75 °C/5 mmHg (Kugelrohr) to give **7h** as a colorless liquid (100 mg, 82% yield).  $^1\text{H NMR}$  (200 MHz,  $\text{CDCl}_3$ ): 7.22-7.38 (m, 5H), 4.88 (q,  $J$  = 6.5 Hz, 1H), 1.87 (s, 1H), 1.45 (d,  $J$  = 8.2 Hz, 3H).  $^{13}\text{C NMR}$  (50 MHz,  $\text{CDCl}_3$ ): 145.0, 127.9, 126.9, 124.8, 70.5, 25.8. IR (neat): 699.4, 1077.1, 1452.1, 1493.3, 1603.6, 2875.1, 2927.5, 2974.4, 3366.4  $\text{cm}^{-1}$ . MS (EI): 122 (39, M), 107 (100), 79 (67), 77 (36), 51 (14).

**Deuterium Isotope Effects for the Reduction of Acetophenone. (a) With Dideuteriodiphenylsilane-Diphenylsilane (7h/7g).** Catalyst 1 (0.0026 mmol, 3 mg) and acetophenone (1 mmol, 0.121 g, 118  $\mu\text{L}$ ) were treated with diphenylsilane (1.3 mmol, 0.245 g) and dideuteriodiphenylsi-



lane (1.3 mmol, 96% D, 0.245 g) at room temperature for 12 h. The crude mixture was used to measure the product ratio by 500 MHz NMR:  $\delta$  1.46, s, 33.6%;  $\delta$  1.47, d, 7.0 Hz, 67.7%. The ratio of nondeuterated to deuterated 1-phenylethyl diphenylsilyl ether was 65.1:33.6 (1.9:1). Hydrolysis of the product with HCl (2 N) and distilled (Kugelrohr) at 75 °C/5 mmHg gave 1-phenylethanol and its 1-deuterated compound (103 mg, ca. 84% yield).

**(b) With Deuteriodimethylphenylsilane–Dimethylphenylsilane (7h/7g).** Catalyst **1** (0.0095 mmol, 11 mg) in CH<sub>2</sub>Cl<sub>2</sub> (0.5 mL) and acetophenone (1 mmol, 0.121 g, 118  $\mu$ L) were treated with deuteriodimethylphenylsilane (1 mmol, 96% D; 0.140 g) and dimethylphenylsilane (1 mmol, 0.140 g) at room temperature for 4 days. The crude mixture was used for measuring the product ratio by 500 MHz NMR:  $\delta$  1.40, s, 49%;  $\delta$  1.47, d, 6.5 Hz, 51%. The ratio of nondeuterated to deuterated 1-phenylethyl dimethylphenylsilyl ether was 49:41 (1:1). Distillation (Kugelrohr) at 105 °C/5 mmHg gave the product (112 mg, ca. 91% yield), which was contaminated with some disiloxane.

**4,4-Dimethyl-2-cyclohexen-1-ol (3f).** Catalyst **1** (0.0034 mmol, 4 mg) and 4,4-dimethyl-2-cyclohexen-1-one (1 mmol, 0.128 g, 136  $\mu$ L) were treated with diphenylsilane (1.3 mmol, 0.245 g, 250 mL) at room temperature for 12 h. After standard workup, the crude product was distilled at 80 °C/5 mmHg (Kugelrohr) to give **3r** (109 mg, 87% yield). <sup>1</sup>H NMR (200

MHz, CDCl<sub>3</sub>): 5.56 (dd,  $J$  = 10.1, 2.6 Hz, 1H), 5.47 (d,  $J$  = 10.3 Hz, 1H), 4.11 (m, 1H), 1.85 (m, 1H), 1.28–1.70 (m, 4H), 0.98 (s, 3H), 0.93 (s, 3H). <sup>13</sup>C NMR (50 MHz, CDCl<sub>3</sub>): 139.8, 126.7, 66.0, 34.1, 32.3, 29.7, 29.6. IR (neat): 1055.6, 1366.4, 1458.1, 1650.9, 2864.7, 2955.6, 3317.1 cm<sup>-1</sup>. MS (EI): 126 (18, M), 111 (30), 92 (18), 84 (11), 70 (100).

**Deuterium Isotope Effect for the 1,2-Reduction of 4,4-Dimethyl-2-cyclohexen-1-one (3f/3g).** Catalyst **1** (0.0043 mmol, 5 mg) in CH<sub>2</sub>Cl<sub>2</sub> (2 mL) and 4,4-dimethyl-2-cyclohexen-1-one (1 mmol, 0.128 g, 136  $\mu$ L) were treated with diphenylsilane (1.3 mmol, 0.250 g) and dideuteriodiphenylsilane (1.3 mmol, 96% D, 0.250 g) at room temperature for 12 h. After standard workup, the crude mixture was distilled (Kugelrohr; 80 °C/5 mmHg) to give **3f** and **3g** (107 mg, ca. 85% yield). The <sup>1</sup>H NMR signal of HOCH at 4.11 had 54% of the intensity of the signal (100%) at 5.47 ppm. The ratio of nondeuterated to deuterated products was therefore 52:48 (1.1:1).

**Acknowledgment.** We thank the NSERC and FCAR for financial support of this research.

**Supplementary Material Available:** Figures giving NMR spectra for the compounds reported (64 pages). Ordering information is given on any current masthead page.

OM940425S



# Oxidative Carbonylation of Aliphatic Mono-, Di-, and Triamines Catalyzed by Montmorillonite–Bipyridinylpalladium(II) Acetate

V. L. K. Valli and Howard Alper\*

Ottawa-Carleton Chemistry Institute, Department of Chemistry, University of Ottawa,  
10 Marie Curie, Ottawa, Ontario, Canada K1N 6N5

Received June 24, 1994<sup>®</sup>

A simple, efficient, and highly selective non-phosgene route has been developed for the preparation of aliphatic, alicyclic, and/or aromatic mono-, di-, and triurethanes from the corresponding amines using montmorillonite–bipyridinylpalladium(II) acetate (Pd–Clay) in the presence of NaI as a promoter. The catalytic activity of other palladium catalysts was studied and compared with Pd–Clay. The difference in reactivity, as well as the selectivity between the immobilized palladium catalyst, i.e., Pd–Clay, and the homogeneous catalyst systems is accounted for in terms of the position and the electronic environment of the metal in the interlayers of the clay system surrounded by the surface Brønsted acidic sites. The versatility of the present catalytic system was demonstrated by the synthesis of commercially important isocyanate precursors, including those of Dytek-A-diurethane and isophorone diurethane.

## Introduction

Alkyl isocyanates such as methyl *N*-methyl isocyanate have industrial applications in the preparation of various insecticides and pesticides.<sup>1</sup> Also, the major demand for aliphatic and/or alicyclic diisocyanates is for the production of polyurethane elastomers. Polyurethanes based on aromatic diisocyanates turn yellow upon exposure to extended sunlight. As a result, alkyl diisocyanates are used almost exclusively in the synthesis of high-performance polyurethane elastomers which require light stability and weatherability. Phosgene has been used to prepare isocyanates on a commercial basis, and less hazardous non-phosgene routes have attracted considerable attention in the last two decades.<sup>2,3</sup> One of the approaches being advanced is to first synthesize the urethane, either by oxidative carbonylation of amines<sup>3–6</sup> or by reductive carbonylation of nitro compounds in the presence of an alcohol,<sup>9–15</sup> followed by the thermal elimination of alcohol to form isocyanates.

The oxidative carbonylation of aromatic amines to form arylurethanes can be realized quite easily using various transition-metal catalysts.<sup>3–6</sup> However, the synthesis of aliphatic urethanes and, in particular, aliphatic diurethanes by a non-phosgene route is not as facile due to the reduced reactivity of the aliphatic reactants. As a result, there are few publications in the literature on the oxidative carbonylation of aliphatic

amines.<sup>1,7,8</sup> A report by Chaudhari and co-workers showed that palladium on carbon in the presence of NaI as a promoter can catalyze the conversion of aliphatic amines to urethanes. The reaction proceeds well for methylamine, but higher amines gave low conversion to products. Recently, we described the use of a transition-metal complex immobilized on a smectite clay, i.e., montmorillonite–bipyridinylpalladium(II) acetate (Pd–Clay), for the reductive carbonylation of aromatic mono- and dinitro arenes to the corresponding mono- and diurethanes in good to excellent yields.<sup>9</sup> We now wish to report the highly selective oxidative carbonylation of aliphatic and alicyclic mono-, di-, and triamines to their corresponding mono-, di-, and triurethanes using catalytic amounts of Pd–Clay, a nitrogen-containing donor ligand, and NaI added as a promoter. Pd–Clay is prepared by anchoring 2,2'-bipyridine in the interlayers of montmorillonite and subsequent complexation with Pd(OAc)<sub>2</sub>.<sup>16</sup>

## Results and Discussion

Treatment of aliphatic and/or alicyclic monoamines with carbon monoxide (70 atm) and oxygen (11 atm) in methanol in the presence of catalytic amounts of Pd–

<sup>®</sup> Abstract published in *Advance ACS Abstracts*, October 15, 1994.

(1) Kelkar, A. A.; Kohle, D. S.; Kanagasabhapathy, S.; Chaudhari, R. V. *Ind. Eng. Chem. Res.* **1992**, *31*, 172.

(2) Senekar, S. D.; Rosthauser, J. W.; Markus, P. H. *34th Annual Polyurethane Technical/Marketing Conference*; Oct 21–24, 1992; p 588.

(3) Cenini, S.; Pizzotti, M.; Crotti, C.; In *Aspects of Homogeneous Catalysis*; Ugo, R., Ed.; Reidel: Dordrecht, The Netherlands, 1988; Vol. 6, p 97.

(4) Fukuoka, S.; Chono, M.; Khono, M. *CHEMTECH* **1984**, 670.

(5) Alper, H.; Hartstock, F. W. *J. Chem. Soc., Chem. Commun.* **1985**, 1141.

(6) Benedini, F.; Nali, M.; Rindone, B.; Tollari, S.; Cenini, S.; La, G. M.; Porta, F. *J. Mol. Catal.* **1986**, *34*, 155.

(7) Leung, T. W.; Dombek, B. D. *J. Chem. Soc., Chem. Commun.* **1992**, 205 and references therein.

(8) Giannoccaro, P.; Nobile, C. F.; Mastroilli, P.; Ravasio, N. *J. Organomet. Chem.* **1991**, *419*, 251.

(9) Valli, V. L. K.; Alper, H. *J. Am. Chem. Soc.* **1993**, *115*, 3778.

(10) Gargulak, J. D.; Berry, A. J.; Noirot, M. D.; Gladfelter, W. L. *J. Am. Chem. Soc.* **1992**, *114*, 8933.

(11) Gargulak, J. D.; Noirot, M. D.; Gladfelter, W. L.; *J. Am. Chem. Soc.* **1991**, *113*, 1054.

(12) Cenini, S.; Ragaini, F.; Pizzotti, M.; Porta, F.; Mestroni, G.; Alessio, E. *J. Mol. Catal.* **1991**, *64*, 179.

(13) Bhaduri, S.; U. S. Patent 4,491,670, 1985.

(14) Cenini, S.; Pizzotti, M.; Crotti, C.; Porta, F. *J. Org. Chem.* **1988**, *53*, 1243.

(15) Balabanov, G. P.; Dergunov, Y. I.; Khoshdurdyev, K. O.; Manov-Yunskii, V. I.; Neredov, B. K.; Rysikhin, A. I. U.S. Patent 4,207,212, 1980.

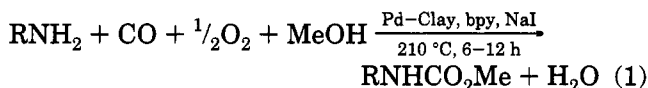
(16) Choudary, B. M.; Bharati, P. *J. Chem. Soc., Chem. Commun.* **1987**, 1505.

**Table 1. Effect of NaI on the Carbonylation of *n*-Hexylamine Catalyzed by Pd-Clay with 2,2'-bpy<sup>a</sup>**

expt no.	substrate:NaI	conversion (%)	yield (%) by NMR	
			urethane	urea
1	no NaI <sup>b</sup>	100	80	20
2	1:1	72	68	4
3	3:1	100	91	9
4	5:1	100	99 <sup>c</sup>	traces
5	10:1	100	75	25
6	5:1 <sup>d</sup>	100	50	50

<sup>a</sup> Reaction conditions for expt 4: substrate (2 mmol), Pd-Clay (20 mg, 0.004 mmol), 2,2'-bpy (16 mg, 0.1 mmol), NaI (60 mg, 0.4 mmol), methanol (6 mL), CO/O<sub>2</sub> (70/11 atm), 210 °C, 8 h. Ratio of substrate to NaI changes as indicated above. <sup>b</sup> Carried out for 36 h. <sup>c</sup> Isolated yield. <sup>d</sup> Carried out without 2,2'-bpy.

Clay, NaI as promoter, and a nitrogen donor ligand, 2,2'-bipyridine, at 210 °C for 6–12 h afforded the corresponding urethanes in 62–91% isolated yield (eq 1).



The reaction is highly selective, and only trace amounts of ureas were obtained as byproducts. However, the formation of urea is dependent on the amount of NaI used as a promoter. The best ratio of substrate to NaI is 5:1. In the presence of more NaI, i.e., using a substrate to NaI ratio of 3:1, the results were comparable to the 5:1 ratio of substrate to NaI. However, when the ratio of the substrate to NaI was 10:1, the selectivity toward urethanes was inferior, affording 75% urethane and 25% urea when *n*-hexylamine was used as the substrate. This result can be compared with the control experiment performed in the absence of NaI. Using *n*-hexylamine as a model reactant, a control experimental run without NaI afforded complete conversion to give 80% urethane and 20% urea. Although the conversion of *n*-hexylamine was 100% in the absence of 2,2'-bipyridine, virtually no selectivity was observed with urethane to urea formed in a 1:1 ratio (Table 1). Thus, the nitrogen donor, i.e., 2,2'-bipyridine, and the amount of NaI play important roles in the selectivity of the reaction. Use of a monodentate nitrogen donor requires longer reaction time for complete conversion and gave poor selectivities. Thus, using *N*-methylpyrrolidine as a donor, carbonylation of *n*-hexylamine required 18 h, affording 69% of the corresponding urethane and 31% urea, while 1,10-phenanthroline can be used instead of 2,2'-bipyridine, affording 82% urethane and 18% urea when *n*-hexylamine is the model substrate.

The use of Pd(PPh)<sub>4</sub> in place of Pd-Clay afforded complete conversion with slightly inferior selectivities (78% urethane, 22% urea) compared with the clay system. In the absence of NaI, Pd(PPh)<sub>4</sub> gave poor selectivity toward urethane (12%) formation, with ureas obtained as the major compounds. Other palladium catalysts, for example Pd/C, gave a result comparable to that for Pd(PPh)<sub>4</sub>. However, when homogeneous Pd(OAc)<sub>2</sub> was used instead of Pd-Clay, decomposition of Pd(OAc)<sub>2</sub> was observed, resulting in poor yields (12%) of ureas, and no urethane was obtained in the case of *n*-hexylamine as the starting amine (Table 2).

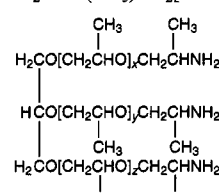
The method reported herein shows excellent selectivity for the formation of aliphatic and alicyclic diure-

**Table 2. Comparison of Various Palladium Catalysts for the Carbonylation of *n*-Hexylamine<sup>a</sup>**

expt no.	catalyst	conversion	yield (%) by NMR	
			urethane	urea
1	Pd(PPh <sub>3</sub> ) <sub>4</sub>	100	78	22
2	Pd(PPh <sub>3</sub> ) <sub>4</sub> <sup>b</sup>	89	12	77
3	Pd(OAc) <sub>2</sub> <sup>c</sup>	52	0	12
4	Pd/C	94	73	11
5	Pd-Clay	100	85	traces
6	Pd-Clay <sup>d</sup>	100	50	50
7	Pd-Clay <sup>b</sup>	100	80	20

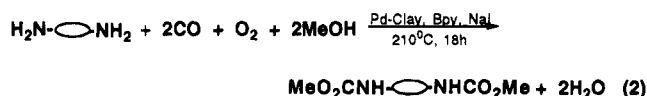
<sup>a</sup> For reaction conditions, see footnote a of Table 1, the amount of Pd catalyst being 0.004 mmol. <sup>b</sup> Without NaI. <sup>c</sup> Catalyst decomposed. <sup>d</sup> Without 2,2'-bpy.

**Table 3. Oxidative Carbonylation of Mono-, Di-, and Triamines Catalyzed by Pd-Clay, 2,2'-bpy, and NaI<sup>a</sup>**

expt	amine	yield (%) by NMR (isolated)	
		urethane	urea
1	<i>n</i> -C <sub>6</sub> H <sub>13</sub> NH <sub>2</sub>	85 (83)	2–3 (traces)
2	<i>n</i> -C <sub>12</sub> H <sub>25</sub> NH <sub>2</sub>	91 (81)	6 (traces)
3	<i>i</i> -C <sub>3</sub> H <sub>7</sub> NH <sub>2</sub>	79 (62)	20 (18)
4	cyclo-C <sub>6</sub> H <sub>11</sub> NH <sub>2</sub>	99 (91)	
5	H <sub>2</sub> N(CH <sub>2</sub> ) <sub>8</sub> NH <sub>2</sub>	89 (72)	
6	H <sub>2</sub> NCH <sub>2</sub> (CH <sub>3</sub> )CH(CH <sub>2</sub> ) <sub>3</sub> NH <sub>2</sub> <sup>b</sup>	100 (88)	
7	H <sub>2</sub> NCH <sub>2</sub> (CH <sub>3</sub> )CH(CH <sub>2</sub> ) <sub>3</sub> NH <sub>2</sub> <sup>c</sup>	100 (94)	
8	H <sub>2</sub> NCH <sub>2</sub> (CH <sub>3</sub> )CH(CH <sub>2</sub> ) <sub>3</sub> NH <sub>2</sub> <sup>d</sup>	91	
9	1,4-(NH <sub>2</sub> ) <sub>2</sub> -cyclo-C <sub>6</sub> H <sub>10</sub>	32	
10	1-NH <sub>2</sub> -3-CH <sub>2</sub> NH <sub>2</sub> -3,5,5-(CH <sub>3</sub> )-cyclo-C <sub>6</sub> H <sub>7</sub>	100 (96)	
11	1,3-(NH <sub>2</sub> ) <sub>2</sub> -4-CH <sub>3</sub> -C <sub>6</sub> H <sub>3</sub>	98 (69)	
12	H <sub>2</sub> NCH(CH <sub>3</sub> )CH <sub>2</sub> [OCH <sub>2</sub> CH(CH <sub>3</sub> )] <sub>x</sub> NH <sub>2</sub> <sup>e</sup>	quantitative	
13	H <sub>2</sub> NCH(CH <sub>3</sub> )CH <sub>2</sub> [OCH <sub>2</sub> CH(CH <sub>3</sub> )] <sub>y</sub> NH <sub>2</sub> <sup>f</sup>	quantitative	
14		quantitative	

<sup>a</sup> For reaction conditions, see footnote a of Table 1. The amounts of catalyst, promoter, donor, and solvent are double and triple in case of di- and triamines, respectively. Reaction time for di- and triamines is 18 h. <sup>b</sup> Dytek-A. <sup>c</sup> Pd-Clay, 2,2'-bpy, NaI, EtOH. <sup>d</sup> Pd(PPh<sub>3</sub>)<sub>4</sub>, 2,2'-bpy, NaI. <sup>e</sup> Jeffamine-D-400, *x* = 5–6. <sup>f</sup> Jeffamine-D-2000, *y* = 33 (av). <sup>g</sup> Jeffamine-T-5000, *x* + *y* + *z* = 83.

thanes directly by the carbonylation of the corresponding diamines (eq 2).



To our knowledge, there are no efficient catalysts described in the literature for the preparation of diurethane precursors of isophorone diisocyanate (IPDI) and Dytek-A-diisocyanate (DDI) by direct oxidative carbonylation methods. A method reported by Leung and Dombek claimed 73% selectivity toward the IPDI precursor using complex metallamacrocyclic compounds as catalysts.<sup>7</sup>

A series of diamines was subjected to carbonylation in the same manner as for *n*-hexylamine to give diurethanes in good to excellent yields (Table 3). Of particular note are the preparation of the diurethane precursors to isophorone diisocyanate (IPDI), Dytek-A-diisocyanate (DDI), and 2,4-toluene diisocyanate (TDI). Di- and triamines of Jeffamine 400, 2000, and T-5000 (Jeffamines are poly(propyleneoxy) amines) were also

carbonylated efficiently, affording the corresponding di- and triurethanes in quantitative yields. Attempts to prepare *trans,trans*-(1,4-cyclohexanediyl)diurethane (convertible to *trans,trans*-CDI) resulted in complete conversion of the starting material, but the yield of the diurethane was moderate, with the balance of the product being an uncharacterized polymer.

The recycling capacity of Pd-Clay was examined for the carbonylation of *n*-hexylamine. It was found that Pd-Clay is active for up to three cycles, affording 68% conversion in the third run. Addition of 2,2'-bipyridine and NaI is necessary in each run. However, the selectivity toward the formation of urethane was unchanged, affording 55% urethane (81% selectivity). After the third cycle, no considerable amount of conversion was noticed, indicating the loss of activity. Use of a high reaction temperature and pressure might have caused the gradual leaching of the palladium metal from the interlayers of the clay.

It is conceivable that, in these reactions, the surface Brønsted and Lewis acidities of the smectite clay can promote carbon monoxide insertion to generate the intermediate species  $\text{RNH}_2^+(\text{CO})\text{MHLn}$ , bound to the silicate sheets of montmorillonite, which in turn can react with alcohol to give urethanes. The superior selectivity of Pd-Clay over other palladium catalysts could be due to the change in electronic environment around the palladium in the clay interlayers. ESCA studies reported on Pd-Clay indicated that palladium is present as a divalent palladium species in the interlayers of clay.<sup>16</sup> However, the corresponding homogeneous  $\text{Pd}(\text{OAc})_2$  afforded only ureas as the major products under the same experimental conditions. This confirms the difference in electronic environment around palladium in Pd-Clay. Also, the presence of surface Brønsted and Lewis acidic centers in the smectite clay can enhance the polarization of carbon monoxide and result in a more selective reaction.<sup>17</sup>

## Conclusion

A simple, efficient, and highly selective non-phosgene route was developed for the preparation of aliphatic and/or alicyclic mono-, di-, and triurethanes from the corresponding amines in good to excellent yields. This methodology, coupled with the recently developed conversion of urethanes to isocyanates by using chlorocatecholborane<sup>18</sup> constitutes an attractive route for the preparation of commercially important isocyanates from amines by carbonylation.

## Experimental Section

**General Considerations.** The following spectrometers were used to obtain spectral data: Bomem MB100-C15 (FT-IR), Varian XL-300 and/or Gemini 200 (NMR), and VG 7070E (MS). X-ray basal spacings of Pd-Clay were determined with a Philips PW 3710 based analytical diffractometer using Ni-filtered  $\text{Cu K}\alpha$  radiation. Pd-Clay was synthesized by a known method,<sup>16</sup> and the  $d_{(001)}$  expansion of Pd-Clay was determined to be 5.3 Å. Organic solvents were dried and distilled prior to use.

**General Procedure for the Pd-Clay-Catalyzed Oxidative Carbonylation of Amines.** A mixture of the substrate (2 mmol), Pd-Clay (20 mg, contains 0.004 mmol of Pd), 2,2'-

bipyridine (16 mg, 0.1 mmol), NaI (60 mg, 0.4 mmol), and dry methanol (6 mL) was charged in a 30 mL autoclave. The autoclave was flushed with carbon monoxide, pressurized to 70 atm, and then carefully pressurized with 11 atm of oxygen. (*Caution!* Reverse addition, i.e.,  $\text{O}_2$  before CO, is dangerous.) The autoclave was transferred to a preheated oil bath at 210 °C and stirred for 6–18 h. The reaction mixture was cooled to room temperature, filtered through neutral alumina, and then concentrated by rotary evaporation. The crude material was washed with pentane and further purified by column chromatography (neutral alumina, eluant 9:1 pentane/chloroform). Di- and triamines were also reacted in a similar procedure using amounts of catalyst and NaI proportional to the number of amine groups (e.g., in the case of Dytek-A, double the amount of catalyst, promoter and solvents were used compared to the case for *n*-hexylamine).

**Preparation of *n*-Hexylmethylurethane Using Pd-(PPh)<sub>4</sub>, 2,2'-Bipyridine, and NaI.** A mixture of *n*-hexylamine (2 mmol), Pd(PPh)<sub>4</sub> (4.6 mg, 0.004 mmol), 2,2'-bipyridine (16 mg, 0.1 mmol), and dry methanol (6 mL) was charged in a 30 mL autoclave. The autoclave was flushed with carbon monoxide, pressurized to 70 atm, and then pressurized with 11 atm of oxygen. The autoclave was transferred to a preheated oil bath at 210 °C and stirred for 6 h. The reaction mixture was cooled to room temperature, filtered through neutral alumina, and then concentrated by rotary evaporation. Urea was separated as a solid material from the reaction mixture and was isolated by filtration. The crude *n*-hexylmethylurethane was purified by column chromatography (neutral alumina, with 9:1 pentane/chloroform as the eluant). The isolated yield of urethane was 78%. IR  $\nu(\text{CO})$  1718  $\text{cm}^{-1}$ . <sup>1</sup>H NMR ( $\text{CDCl}_3$ ):  $\delta$  0.80 (t, 3H,  $\text{CH}_3$ ), 1.25 (m, 6H,  $\text{CH}_2$ ), 1.48 (m, 2H,  $\text{CH}_2$ ), 3.11 (q, 2H,  $\text{CH}_2$ ), 3.60 (s, 3H,  $\text{OCH}_3$ ), 4.72 (br, 1H, NH). <sup>13</sup>C NMR ( $\text{CDCl}_3$ ):  $\delta$  12.9, 21.5, 25.3, 28.9, 30.4, 40.1, 51.3, 156.8; MS (*m/e*): 159 ( $\text{M}^+$ ).

The same procedure was followed for other palladium-catalyzed carbonylation reactions using 0.004 mmol of the respective palladium catalyst. The urethanes 1–11 (Table 3) were characterized by comparison with literature data.<sup>4–12,19–26</sup> The following urethanes are new.

**12, Jeffamine-D-400 methyl diurethane:** IR  $\nu(\text{CO})$  1712  $\text{cm}^{-1}$ ; <sup>1</sup>H NMR ( $\text{CDCl}_3$ )  $\delta$  1.12 (d,  $\text{CH}_3$ ), 2.31 (m, CH), 3.48 (m, OCH), 3.75 (s,  $\text{OCH}_3$ ), 5.18 (br, NH), 5.52 (br, NH); <sup>13</sup>C NMR ( $\text{CDCl}_3$ )  $\delta$  51.68 ( $\text{OCH}_3$ ), 156.52 (carbonyl).

**13, Jeffamine-D-2000 methyl diurethane:** IR  $\nu(\text{CO})$  1714  $\text{cm}^{-1}$ ; <sup>1</sup>H NMR ( $\text{CDCl}_3$ )  $\delta$  1.12 (d,  $\text{CH}_3$ ), 2.32 (m, CH), 3.48 (m, OCH), 3.78 (s,  $\text{OCH}_3$ ), 5.20 (br, NH), 5.49 (br, NH); <sup>13</sup>C NMR ( $\text{CDCl}_3$ )  $\delta$  51.64 ( $\text{OCH}_3$ ), 156.60 (carbonyl).

**14, Jeffamine-T-5000 methyl triurethane:** IR  $\nu(\text{CO})$  1720  $\text{cm}^{-1}$ ; <sup>1</sup>H NMR ( $\text{CDCl}_3$ )  $\delta$  1.19 ( $\delta$ ,  $\text{CH}_3$ ), 2.34 (m, CH), 3.49 (m, OCH), 3.62 (m,  $\text{OCH}_3$ ), 5.32 (br, NH), 5.50 (br, NH); <sup>13</sup>C NMR ( $\text{CDCl}_3$ )  $\delta$  51.70 ( $\text{OCH}_3$ ), 55.07 ( $\text{OCH}_3$ ), 155.20 (carbonyl), 156.48 (carbonyl).

**Acknowledgment.** We are indebted to the Institute for Chemical Science and Technology and the University Research Incentive Fund for financial support of this research. We are grateful to DuPont, Dow Chemical Canada Inc., and Texaco for providing samples of Dytek A and Jeffamines.

OM9404947

(19) Merger, F.; Nestler, G.; Towae, F.; Hellbach, H.; Eur. Pat. Appl. EP 100 047; *Chem. Abstr.* **1984**, *100*, 157138g.

(20) Disteldorf, J.; Huebel, W.; Reiffer, J. Eur. Pat. Appl. EP 106 138; *Chem. Abstr.* **1984**, *101*, 170702b.

(21) Disteldorf, J.; Huebel, W.; Wolf, E. Ger. Offen. DE 3 151 855; *Chem. Abstr.* **1983**, *99*, 176959c.

(22) Burgess, E. M.; Penton, H. R., Jr.; Taylor, E. A.; Williams, W. M. *Org. Synth.* **1973**, *53*, 1857.

(23) Zhou, X.; Huang, Z. *Synth. Commun.* **1989**, *19*, 1347.

(24) Alper, H.; Vasapollo, G.; Hartstock, F. W.; Mlekuz, M.; Smith, D. J. H.; Morris, G. E.; *Organometallics* **1987**, *6*, 2391.

(25) Wallace, G. C.; Zerba, E. N. *Pestic. Sci.* **1989**, *26*, 215.

(26) Crosby, J.; Paton, R. M.; Rennie, R. A. C. Ger. Offen. DE 2 336 403; *Chem. Abstr.* **1974**, *81*, 49257a.

(17) Pinnavaia, T. J.; Raythatha, R.; Lee, J. G. S.; Hollaran, L. J.; Hoffman, J. F. *J. Am. Chem. Soc.* **1979**, *101*, 6891.

(18) Valli, V. L. K.; Alper, H. *J. Org. Chem.*, in press.

# Metal-Assisted Formation of Phosphorus–Oxygen Heterocyclic Complexes

Xiaoyong Sun,<sup>†</sup> Edward H. Wong,<sup>\*,†</sup> Mark M. Turnbull,<sup>\*,‡</sup> Arnold L. Rheingold,<sup>\*,§</sup>  
Beth E. Waltermire,<sup>§</sup> and Robert L. Ostrander<sup>§</sup>

Department of Chemistry, University of New Hampshire, Durham, New Hampshire 03824,  
Department of Chemistry, Clark University, Worcester, Massachusetts 01610, and  
Department of Chemistry, University of Delaware, Newark, Delaware 19716

Received June 9, 1994<sup>⊙</sup>

Starting with bis(dialkylamino)phosphine oxides or triphosphoxane [R<sub>2</sub>NPO]<sub>3</sub> rings, transition metal complexes containing P<sub>4</sub>O<sub>4</sub>, P<sub>5</sub>O<sub>5</sub>, and P<sub>6</sub>O<sub>6</sub> heterocycles have been assembled. Specific products isolated were found to depend critically on reaction conditions, the metal, and its ancillary ligands, as well as the phosphorus substituent. While only monometallic products were obtained from divalent precursors of the nickel triad, bimetallic complexes were also produced from the group 6 metal carbonyls. In general, larger rings were obtained at higher temperatures. Only P<sub>3</sub>O<sub>3</sub> and P<sub>4</sub>O<sub>4</sub> products were formed around molybdenum, while P<sub>5</sub>O<sub>5</sub> structures could also be assembled about chromium, nickel, palladium, and platinum centers. One of the iron carbonyl complexes was found to feature an unusual η<sup>1</sup>-P[OP(O)]<sub>2</sub>P ring, the product of a double POP to PP(=O) rearrangement. In addition, a dichromium P<sub>6</sub>O<sub>6</sub> cluster complex featuring the novel hexaphosphoxane ring was synthesized from bis(*cis*-2,6-dimethylpiperidino)phosphine oxide. Use of isolated monometallic P<sub>n</sub>O<sub>n</sub> complexes as ligands yielded heterobimetallic products as well as phosphoxane ring transfer reactions. The X-ray crystal structures of five representative complexes containing FeP<sub>4</sub>O<sub>4</sub> (**14**), Cr<sub>2</sub>P<sub>4</sub>O<sub>4</sub> (**19a**, **19b**), Cr<sub>2</sub>P<sub>6</sub>O<sub>6</sub> (**21**), and MoFeP<sub>4</sub>O<sub>4</sub> (**25**) cores, respectively, are reported.

## Introduction

Inorganic rings, cages, and clusters have relevance in many areas of chemical research including coordination, catalytic, polymer, and materials chemistry.<sup>1</sup> Trivalent phosphorus–oxygen heterocycles or cyclic phosphoxanes are potentially useful multidentate ligands that can lead to polycyclic, cage, or cluster complexes with M<sub>n</sub>P<sub>n</sub>O<sub>n</sub> cores (Figure 1). We have previously shown that bis(dialkylamino)phosphine oxides and related triphosphoxane ([R<sub>2</sub>NPO]<sub>3</sub>) rings are suitable precursors to MP<sub>n</sub>O<sub>n</sub> and MP<sub>n</sub>O<sub>n</sub>M complexes (M = Cr, n = 4, 5; M = Mo, n = 3, 4; M = W, Ni, Pd, n = 4) with bicyclic and cage structures (Figure 2A–F).<sup>2</sup> These syntheses depend critically on the presence of metal centers to provide templating sites for the linking up of R<sub>2</sub>NP=O phosphinidene units. In this article, we will further expand the scope of these reactions and demonstrate the variety of products and structural types now accessible, including a novel hexaphosphoxane Cr<sub>2</sub>P<sub>6</sub>O<sub>6</sub> cluster. Interesting ring transfer and metallaligand chemistry of several of these products will also be presented.

## Results

**Syntheses from Triphosphoxane ([R<sub>2</sub>NPO]<sub>3</sub>) Rings. (1) The Nickel Triad.** In hexane, tris(diisopropylaminophosphoxane) ([<sup>i</sup>Pr<sub>2</sub>NPO]<sub>3</sub>) and various metal dihalide MX<sub>2</sub> complexes (MX<sub>2</sub> = NiCl<sub>2</sub>DME, NiBr<sub>2</sub>DME, PdCl<sub>2</sub>2PhCN, PdBr<sub>2</sub>2PhCN, PtCl<sub>2</sub>NBD) all yielded tetraphosphoxane MX<sub>2</sub>[<sup>i</sup>Pr<sub>2</sub>NPO]<sub>4</sub> complexes (**1A**, **B**, **2A**, **B**, **3**). These light-yellow to orange-red solids have been characterized by IR, <sup>31</sup>P (Table 1), and, in some cases, <sup>1</sup>H and <sup>13</sup>C (Tables 2 and 3) NMR spectroscopy. The NiBr<sub>2</sub> (**1B**), PdCl<sub>2</sub> (**2A**), and PdBr<sub>2</sub> (**2B**) products were also sufficiently stable for satisfactory elemental analyses to be obtained. The X-ray crystal structure of complex **2A** has been reported.<sup>2</sup> By <sup>31</sup>P NMR spectroscopy, the other palladium (**2B**) and platinum (**3**) products can also be assigned the same structure with a 1,5-chelating P<sub>4</sub>O<sub>4</sub> ring in a chair–chair conformation (Figure 2A), accounting for their A<sub>2</sub>X<sub>2</sub> spectra. The unique 1,3-ring coordination mode (Figure 2B) of the two nickel complexes (**1A**, **B**) can be deduced from their distinctive AA'XX' <sup>31</sup>P NMR (Table 1) spectra.<sup>2</sup>

Reactions using the tris(dicyclohexylaminophosphoxane) ([Cy<sub>2</sub>NPO]<sub>3</sub>) precursor gave analogous MX<sub>2</sub>P<sub>4</sub>O<sub>4</sub> products (MX<sub>2</sub> = NiCl<sub>2</sub>, **4A**; NiBr<sub>2</sub>, **4B**; NiI<sub>2</sub>, **4C**; PdCl<sub>2</sub>, **5A**; PdBr<sub>2</sub>, **5B**; PtCl<sub>2</sub>, **6**, but in addition, MX<sub>2</sub>P<sub>5</sub>O<sub>5</sub> (MX<sub>2</sub> = NiCl<sub>2</sub>, **7**; PdCl<sub>2</sub>, **8A**; PdBr<sub>2</sub>, **8B**; and PtCl<sub>2</sub>, **9**) were also isolable under different reaction conditions. Specifically, reaction in hot-toluene (90 °C) afforded unstable NiCl<sub>2</sub>[Cy<sub>2</sub>NPO]<sub>4</sub> (**4A**; <sup>31</sup>P NMR, AA'XX' pattern) while room-temperature reaction in hexane yielded NiCl<sub>2</sub>[Cy<sub>2</sub>NPO]<sub>5</sub> (**7**). A mixture of both (**4A**, **7**) was obtained by reaction at room temperature in toluene. In contrast, the palladium and platinum P<sub>5</sub>O<sub>5</sub> complexes (**8A**, **B**, **9**) were obtained from reactions in refluxing hexane while

<sup>†</sup> University of New Hampshire.

<sup>‡</sup> Clark University.

<sup>§</sup> University of Delaware.

<sup>⊙</sup> Abstract published in *Advance ACS Abstracts*, November 1, 1994.

(1) Armitage, D. A. *Inorganic Rings and Cages*; E. Arnold: London, 1972. Heal, H. G. *The Inorganic Heterocyclic Chemistry of Sulfur, Nitrogen, and Phosphorus*; Academic Press: London, 1980. Haiduc, I., Sowerby, D. B., Eds. *The Chemistry of Inorganic Homo- and Heterocycles*; Academic Press: London, 1987. Wollins, J. D. *Non-Metal Rings, Cages, and Clusters*; Wiley and Sons: New York, 1988. Mark, J. E.; Allcock, H. R.; West, R. *Inorganic Polymers*; Prentice Hall: New York, 1992.

(2) Wong, E. H.; Sun, X.; Gabe, E. J.; Lee, F. L.; Charland, J.-P. *Organometallics* 1991, 10, 3010.

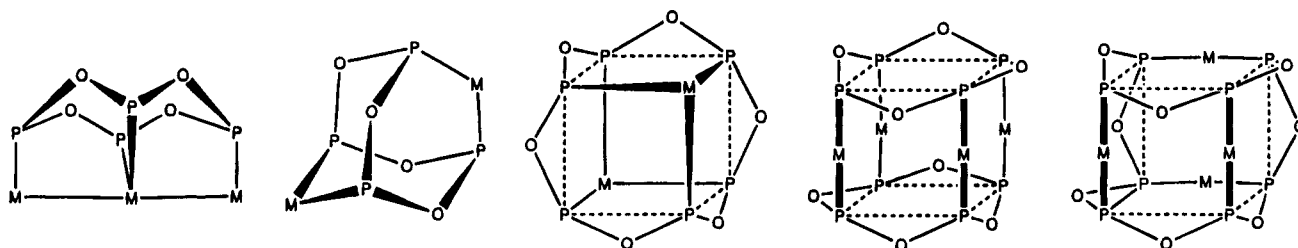


Figure 1. Possible structures based on  $M_m P_n O_n$  cyclic polyphosphoxane metal complexes ( $P = RP$ ).

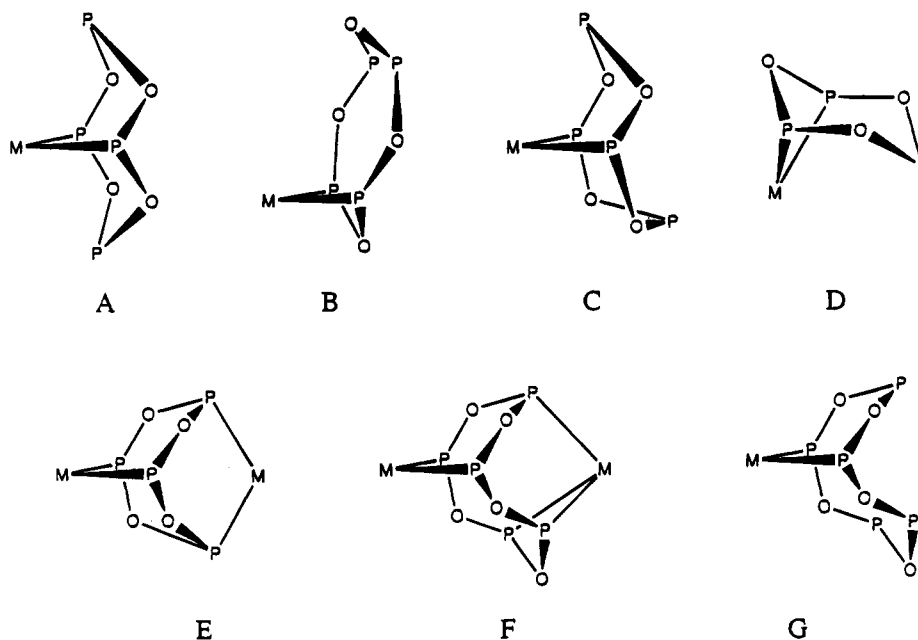


Figure 2. Bicyclic and cage structures of  $M P_n O_n$  and  $M_2 P_n O_n$  complexes ( $P = R_2 NP$ ).

the  $MP_4O_4$  products (**5A,B, 6**) only formed in cold hexane at 4 °C.  $^{31}P$  NMR spectroscopy ( $A_2X_2$  patterns) supported similar structural assignments for the various  $MX_2P_4O_4$  complexes as made above for their diisopropylamino analogues. It also revealed the presence of two isomers of the  $PtCl_2[Cy_2NPO]_4$  complex, one with the familiar  $A_2X_2$  pattern (**6A**) and the second with an  $AMX_2$  pattern (**6B**). These can be assigned to the 1,5-chelated  $P_4O_4$  ring in chair–chair (Figure 2A) and boat–chair (Figure 2C) conformations, respectively. All the  $MX_2P_5O_5$  complexes exhibited  $AA'MXX'$  patterns consistent only with the novel 1,5-chelating  $\eta^2-P_5O_5$  coordination mode (Figure 2G).

**(2) Metal Carbonyls.** Room-temperature reaction of  $Mo(CO)_4(NBD)$  with  $[^iPr_2NPO]_3$  or  $[Cy_2NPO]_3$  in hexanes afforded the simple substitution products  $cis-Mo(CO)_4[R_2NPO]_3$  ( $R = ^iPr, Cy$ ; **10A,B**, Figure 2D). These unstable white compounds slowly transformed to the known  $Mo(CO)_4[R_2NPO]_4Mo(CO)_4$  cage complexes (Figure 2E) in solution or in the solid state.<sup>2</sup> Similar reaction using  $Cr(CO)_4(NBD)$  required prolonged reaction times or refluxing to give  $cis-Cr(CO)_4[R_2NPO]_4$  (**11a**) instead as a white solid. Its  $^{31}P$  NMR spectrum with an  $A_2XY$  pattern is consistent with a boat–chair 1,5-chelating mode for the tetraphosphoxane heterocycle (Figure 2C).

In refluxing toluene, diiron nonacarbonyl gave different products with the two triphosphoxanes. Specifically,  $[Cy_2NPO]_3$  yielded complex **12**,  $Fe(CO)_3[Cy_2NPO]_4$ , also with an  $A_2XY$   $^{31}P$  NMR spectrum (Table 1) as observed for the chromium complex **11** (Figure 2C). By contrast,

$[^iPr_2NPO]_3$  gave two isolable products in a 60:40 ratio; the first analyzed as  $Fe(CO)_3[^iPr_2NPO]_4$  (**13**) and the second as  $Fe(CO)_4[^iPr_2NPO]_4$  (**14**). Complex **13** can be assigned the chair–chair ligand ring conformation based on its  $A_2X_2$   $^{31}P$  NMR spectrum (Table 1, Figure 2A). Complex **14**, however, has a spectrum that indicated presence of high-field ( $\delta +24.5$ ) phosphoryl resonances in a distinctive  $AX_2Y$  pattern (Table 1). Its novel structure as revealed by an X-ray study (Figure 3) actually features a  $P[OP(=O)]_2P$  heterocycle as a monodentate ligand toward the tetracarbonyl iron.

**Syntheses from Bis(dialkylamino)phosphine Oxide Precursors.** We have previously reported the formation of complexes with  $MoP_3O_3$ ,  $MoP_4O_4$ ,  $Mo_2P_4O_4$ ,  $CrP_4O_4$ ,  $Cr_2P_4O_4$ ,  $Cr_2P_5O_5$ , and  $WP_4O_4$  (Figure 2A–F) cores from reactions of the respective metal hexacarbonyl and  $(^iPr_2N)_2P(O)H$ .<sup>2</sup> Similarly,  $(Cy_2N)_2P(O)H$  and  $Cr(CO)_6$  also produced two isomers of  $Cr(CO)_4[Cy_2NPO]_4$  with chair–chair (**11b**) and boat–chair (**11a**)  $P_4O_4$  conformations,  $Cr_2(CO)_3[Cy_2NPO]_4$  (**15**), and  $Cr_2(CO)_7[Cy_2NPO]_5$  (**16**), with higher reaction temperatures favoring formation of the pentaphosphoxane complex **16** (Figure 2F). Traces of an unstable white solid characterized as the O-bonded  $Cr(CO)_5O=P(Cy_2N)_2H$  were also isolated ( $^{31}P$  NMR: singlet at  $\delta 94.1$ ,  $^1J_{PH} = 366$  Hz). Tungsten hexacarbonyl yielded  $W_2(CO)_7[Cy_2NPO]_5$  (**17**), a product analogous to **16**, although it was found to be quite unstable. In addition, prolonged reaction times led to isolation of small amounts of a red solid characterized as  $W_2(CO)_6[Cy_2NPO]_4$  (**18**), the  $^{31}P$  NMR spectrum of which contained a very low-field

Table 1.  $^{31}\text{P}\{^1\text{H}\}$  NMR Spectra of the Cyclic Phosphoxane Complexes<sup>a</sup>

complex		splitting pattern [chemical shift, ppm] ( <i>J</i> , Hz)
NiCl <sub>2</sub> [ <sup>1</sup> Pr <sub>2</sub> NPO] <sub>4</sub> ( <b>1A</b> )	AA'XX'	[ $\delta_A = \delta_{A'} = 144.2, \delta_X = \delta_{X'} = 55.7$ ] ( $J_{AA'} = J_{XX'} = 50, J_{AX} = J_{A'X'} = 20, J_{AX'} = J_{A'X} = 1$ )
NiBr <sub>2</sub> [ <sup>1</sup> Pr <sub>2</sub> NPO] <sub>4</sub> ( <b>1B</b> )	AA'XX'	[ $\delta_A = \delta_{A'} = 144.4, \delta_X = \delta_{X'} = 63.4$ ] ( $J_{AA'} = J_{XX'} = 50, J_{AX} = J_{A'X'} = 20, J_{AX'} = J_{A'X} = 1$ )
PdCl <sub>2</sub> [ <sup>1</sup> Pr <sub>2</sub> NPO] <sub>4</sub> ( <b>2A</b> )	A <sub>2</sub> X <sub>2</sub>	[ $\delta_A = 147.8, \delta_X = 88.3$ ] ( $J_{AX} = 44$ )
PdBr <sub>2</sub> [ <sup>1</sup> Pr <sub>2</sub> NPO] <sub>4</sub> ( <b>2B</b> )	A <sub>2</sub> X <sub>2</sub>	[ $\delta_A = 146.1, \delta_X = 88.3$ ] ( $J_{AX} = 49$ )
PtCl <sub>2</sub> [ <sup>1</sup> Pr <sub>2</sub> NPO] <sub>4</sub> ( <b>3</b> )	A <sub>2</sub> X <sub>2</sub>	[ $\delta_A = 142.8, \delta_X = 59.0$ ] ( $J_{AX} = 34$ )
NiCl <sub>2</sub> [Cy <sub>2</sub> NPO] <sub>4</sub> ( <b>4A</b> )	AA'XX'	[ $\delta_A = \delta_{A'} = 142.3, \delta_X = \delta_{X'} = 54.0$ ] ( $J_{AA'} = J_{XX'} = 50, J_{AX} = J_{A'X'} = 20, J_{AX'} = J_{A'X} = 1$ )
NiBr <sub>2</sub> [Cy <sub>2</sub> NPO] <sub>4</sub> ( <b>4B</b> )	AA'XX'	[ $\delta_A = \delta_{A'} = 142.4, \delta_X = \delta_{X'} = 62.3$ ] ( $J_{AA'} = J_{XX'} = 50, J_{AX} = J_{A'X'} = 20, J_{AX'} = J_{A'X} = 1$ )
NiI <sub>2</sub> [Cy <sub>2</sub> NPO] <sub>4</sub> ( <b>4C</b> )	AA'XX'	[ $\delta_A = \delta_{A'} = 142.4, \delta_X = \delta_{X'} = 75.4$ ] ( $J_{AA'} = J_{XX'} = 50, J_{AX} = J_{A'X'} = 20, J_{AX'} = J_{A'X} = 1$ )
PdCl <sub>2</sub> [Cy <sub>2</sub> NPO] <sub>4</sub> ( <b>5A</b> )	A <sub>2</sub> X <sub>2</sub>	[ $\delta_A = 143.9, \delta_X = 88.9$ ] ( $J_{AX} = 83$ )
PdBr <sub>2</sub> [Cy <sub>2</sub> NPO] <sub>4</sub> ( <b>5B</b> )	A <sub>2</sub> X <sub>2</sub>	[ $\delta_A = 141.9, \delta_X = 88.8$ ] ( $J_{AX} = 88$ )
PtCl <sub>2</sub> [Cy <sub>2</sub> NPO] <sub>4</sub> ( <b>6A</b> )	A <sub>2</sub> X <sub>2</sub>	[ $\delta_A = 146.8, \delta_X = 59.3$ ] ( $J_{AX} = 64, J_{\text{Pr-P}} = 4826$ )
PtCl <sub>2</sub> [Cy <sub>2</sub> NPO] <sub>4</sub> ( <b>6B</b> )	AMX <sub>2</sub>	[ $\delta_A = 140.1, \delta_M = 134.4, \delta_X = 58.1$ ] ( $J_{AM} \sim 0, J_{AX} = 44, J_{MX} = 13$ )
NiCl <sub>2</sub> [Cy <sub>2</sub> NPO] <sub>5</sub> ( <b>7</b> )	AA'MXX'	[ $\delta_A = \delta_{A'} = 143.9, \delta_M = 124.6, \delta_X = \delta_{X'} = 91.7$ ] ( $J_s < 15$ , poorly resolved)
PdCl <sub>2</sub> [Cy <sub>2</sub> NPO] <sub>5</sub> ( <b>8A</b> )	AA'MXX'	[ $\delta_A = \delta_{A'} = 143.4, \delta_M = 127.5, \delta_X = \delta_{X'} = 87.9$ ] ( $J_{AA'} = J_{XX'} = 50, J_{AX} = J_{A'X'} = 15, J_{AM} = J_{A'M} = 3, J_{MX} = J_{M'X'} = 12$ )
PdBr <sub>2</sub> [Cy <sub>2</sub> NPO] <sub>5</sub> ( <b>8B</b> )	AA'MXX'	[ $\delta_A = \delta_{A'} = 142.7, \delta_M = 127.3, \delta_X = \delta_{X'} = 87.4$ ] ( $J_{AA'} = J_{XX'} = 50, J_{AX} = J_{A'X'} = 19, J_{AM} = J_{A'M} = 3, J_{MX} = J_{M'X'} = 19$ )
PtCl <sub>2</sub> [Cy <sub>2</sub> NPO] <sub>5</sub> ( <b>9</b> )	AA'MXX'	[ $\delta_A = \delta_{A'} = 141.8, \delta_M = 127.5, \delta_X = \delta_{X'} = 60.1$ ] ( $J_{AA'} = J_{XX'} = 50, J_{AM} = J_{A'M} = 3, J_{AX} = J_{A'X'} = 14, J_{MX} = J_{M'X'} = 11, J_{\text{Pr-P}} = 5206$ )
Mo(CO) <sub>4</sub> [ <sup>1</sup> Pr <sub>2</sub> NPO] <sub>3</sub> ( <b>10A</b> )	A <sub>2</sub> X	[ $\delta_A = 138.5, \delta_X = 130.1$ ] ( $J_{AX} = 2$ )
Mo(CO) <sub>4</sub> [Cy <sub>2</sub> NPO] <sub>3</sub> ( <b>10B</b> )	A <sub>2</sub> X	[ $\delta_A = 136.8, \delta_X = 128.2$ ] ( $J_{AX} = 15$ )
Cr(CO) <sub>4</sub> [Cy <sub>2</sub> NPO] <sub>4</sub> ( <b>11A</b> )	A <sub>2</sub> XY	[ $\delta_A = 177.1, \delta_X = 129.4, \delta_Y = 123.4$ ] ( $J_{AX} = 37, J_{AY} = 10, J_{XY} = 3$ )
Cr(CO) <sub>4</sub> [Cy <sub>2</sub> NPO] <sub>4</sub> ( <b>11b</b> )	A <sub>2</sub> X <sub>2</sub>	[ $\delta_A = 174.0, \delta_X = 138.7$ ] ( $J_{AX} = 63$ )
Fe(CO) <sub>3</sub> [Cy <sub>2</sub> NPO] <sub>4</sub> ( <b>12</b> )	A <sub>2</sub> XY	[ $\delta_A = 163.8, \delta_X = 131.6, \delta_Y = 125.6$ ] ( $J_{AX} = 54, J_{AY} = 0.2, J_{XY} \approx 0$ )
Fe(CO) <sub>3</sub> [ <sup>1</sup> Pr <sub>2</sub> NPO] <sub>4</sub> ( <b>13</b> )	A <sub>2</sub> X <sub>2</sub>	[ $\delta_A = 160.6, \delta_X = 145.0$ ] ( $J_{AX} = 39$ )
Fe(CO) <sub>4</sub> [ <sup>1</sup> Pr <sub>2</sub> NPO] <sub>4</sub> ( <b>14</b> )	AX <sub>2</sub> Y	[ $\delta_A = 152.5, \delta_X = 24.5, \delta = 6.6$ ] ( $J_{AX} = 15, J_{AY} \approx 0, J_{XY} = 187$ )
Cr <sub>2</sub> (CO) <sub>8</sub> [Cy <sub>2</sub> NPO] <sub>4</sub> ( <b>15</b> )	singlet	[ $\delta = 157.8$ ] ( $J_{AB} = 6, J_{BX} = 34, J_{AX} \approx 0$ )
Cr <sub>2</sub> (CO) <sub>7</sub> [Cy <sub>2</sub> NPO] <sub>5</sub> ( <b>16</b> )	A <sub>2</sub> BX <sub>2</sub>	[ $\delta_A = 176.1, \delta_B = 175.1, \delta_X = 155.4$ ] ( $J_{AB} = 2, J_{AX} = 1, J_{BX} = 17, J_{\text{WP}} = 186$ )
W <sub>2</sub> (CO) <sub>7</sub> [Cy <sub>2</sub> NPO] <sub>5</sub> ( <b>17</b> )	A <sub>2</sub> BX <sub>2</sub>	[ $\delta_A = 267.7, \delta_X = 133.2, \delta_Y = 100.1, \delta_Z = 84.2$ ] ( $J_{AX} = J_{AY} = 13, J_{AZ} = 20, J_{XY} = 101, J_{XZ} = 140, J_{YZ} = 33$ )
W <sub>2</sub> (CO) <sub>6</sub> [Cy <sub>2</sub> NPO] <sub>4</sub> ( <b>18</b> )	AXYZ	[ $\delta = 171.1$ ] ( $\delta = 155.4$ )
Cr <sub>2</sub> (CO) <sub>8</sub> [DMP-PO] <sub>4</sub> ( <b>19a</b> )	singlet	[ $\delta = 171.1$ ] ( $\delta = 155.4$ )
Cr <sub>2</sub> (CO) <sub>8</sub> [DMP-PO] <sub>4</sub> ( <b>19b</b> )	singlet	[ $\delta = 155.4$ ] ( $\delta = 171.1$ )
Cr <sub>2</sub> (CO) <sub>7</sub> [DMP-PO] <sub>5</sub> ( <b>20</b> )	A <sub>2</sub> BX <sub>2</sub>	[ $\delta_A = 176.1, \delta_B = 175.1, \delta_X = 155.4$ ] ( $J_{AB} = 6, J_{AX} \approx 0, J_{BX} = 42$ )
Cr <sub>2</sub> (CO) <sub>6</sub> [DMP-PO] <sub>6</sub> ( <b>21</b> )	singlet	[ $\delta = 175.5$ ] ( $\delta = 149.6$ )
Mo <sub>2</sub> (CO) <sub>8</sub> [DMP-PO] <sub>4</sub> ( <b>22</b> )	singlet	[ $\delta = 149.6$ ] ( $\delta_A = \delta_{A'} = 137.9, \delta_X = \delta_{X'} = 60.7$ ] ( $J_{AX} = J_{A'X'} = 15, J_{AX'} = J_{A'X} = 12$ )
NiBr <sub>2</sub> [Cy <sub>2</sub> NPO] <sub>4</sub> Mo(CO) <sub>4</sub> ( <b>23</b> )	AA'XX'	[ $\delta_A = 157.1, \delta_M = 137.5, \delta_X = 88.9$ ] ( $J_{AM} = J_{A'M} = 28.9, J_{AX} = J_{A'X'} = 9.5, J_{MX} = J_{M'X'} = J_{M'X} = J_{MX'} \approx 0$ )
PtCl <sub>2</sub> [Cy <sub>2</sub> NPO] <sub>5</sub> Mo(CO) <sub>3</sub> ( <b>24</b> )	AMM'XX'	[ $\delta_A = 157.1, \delta_M = 137.5, \delta_X = 88.9$ ] ( $J_{AM} = J_{A'M} = 28.9, J_{AX} = J_{A'X'} = 9.5, J_{MX} = J_{M'X'} = J_{M'X} = J_{MX'} \approx 0$ )
Fe(CO) <sub>3</sub> [ <sup>1</sup> Pr <sub>2</sub> NPO] <sub>4</sub> Mo(CO) <sub>4</sub> ( <b>25</b> )	AB <sub>2</sub> X	[ $\delta_A = 163.5, \delta_B = 160.5, \delta_X = 137.4$ ] ( $J_{AB} = 85, J_{AX} \approx 0, J_{BX} = 5$ )
Ni <sub>2</sub> (CO) <sub>4</sub> [Cy <sub>2</sub> NPO] <sub>4</sub> ( <b>26</b> )	singlet	[ $\delta = 133.8$ ] ( $\delta = 133.8$ )

<sup>a</sup> All spectra were run in CDCl<sub>3</sub>.

phosphido resonance ( $\delta +267.8$ ). An analogous Mo<sub>2</sub>(CO)<sub>6</sub>-[<sup>1</sup>Pr<sub>2</sub>NPO]<sub>4</sub> complex containing a phosphido-bridged metal–metal bond and a cleaved P–O linkage has been reported (Figure 4).<sup>3</sup> Diiron nonacarbonyl gave the same Fe(CO)<sub>3</sub>[Cy<sub>2</sub>NPO]<sub>4</sub> (**13**) product as described above from its reaction with [Cy<sub>2</sub>NPO]<sub>3</sub>.

From bis(2,6-dimethylpiperidino)phosphine oxide ((DMP)<sub>2</sub>P(O)H) and Cr(CO)<sub>6</sub> in refluxing toluene we obtained both isomers of Cr<sub>2</sub>(CO)<sub>8</sub>[DMP-PO]<sub>4</sub> (**19a,b**), Cr<sub>2</sub>(CO)<sub>7</sub>[DMP-PO]<sub>5</sub> (**20**) and traces of a white solid with high spectral (Table 1) symmetry that analyzed as Cr(CO)<sub>3</sub>[DMP-PO]<sub>3</sub> (**21**). The X-ray crystal structures of **19a** and **19b** confirmed their being configurational isomers of the Cr<sub>2</sub>P<sub>4</sub>O<sub>4</sub> core. Complex **19a** adopts the familiar adamantanoid cage structure featuring a tetradentate P<sub>4</sub>O<sub>4</sub> ring in a boat–boat form (Figures 5 and 2E). Complex **19b** has the heterocycle in the long chair form serving to link two four-membered CrPOP chelate rings (Figure 6). X-ray crystallography also revealed the symmetrical **21** to be the novel Cr<sub>2</sub>(CO)<sub>6</sub>[DMP-PO]<sub>6</sub> (Figure 7), a cluster structure featuring the heretofore unknown hexaphosphoxane ring. Significantly, quantitative yields of this same product can be obtained from the cage expansion reaction of Cr<sub>2</sub>(CO)<sub>7</sub>[DMP-PO]<sub>5</sub> (**20**) with (DMP)<sub>2</sub>P(O)H in refluxing xylene. By contrast,

molybdenum hexacarbonyl gave the Mo<sub>2</sub>P<sub>4</sub>O<sub>4</sub> cage complex **22** as the only product regardless of reaction conditions.

No tractable products were obtained from Fe<sub>2</sub>(CO)<sub>9</sub> or dihalide precursors of the nickel triad in this type of thermal reaction. Substitution of the bis(amino)phosphine oxides with various phosphoramidites like (R<sub>2</sub>N)-(R'O)P(O)H also failed to produce any alkoxy- or aryloxy-substituted phosphoxane complexes.

**Reactions of Monometallic Phosphoxane Complexes.** The monometallic phosphoxane complexes synthesized above contain additional available phosphorus donor sites. Several heterobimetallic complexes have been prepared using them as metalla-ligands. These include the Mo(CO)<sub>4</sub>[Cy<sub>2</sub>NPO]<sub>4</sub>NiBr<sub>2</sub> complex (**23**), the Mo(CO)<sub>3</sub>[Cy<sub>2</sub>NPO]<sub>5</sub>PdCl<sub>2</sub> complex **24**, and the Mo(CO)<sub>4</sub>[<sup>1</sup>Pr<sub>2</sub>NPO]<sub>4</sub>Fe(CO)<sub>3</sub> complex **25** (Scheme 1). All have been characterized spectrally and by elemental analyses. The Ni/Mo complex **23** can be assigned a basic structure similar to that of complex **19b** (Figure 6) with the P<sub>4</sub>O<sub>4</sub> ring in the long chair conformation and metals coordinating at opposite ends of the heterocycle. Complex **24** should be a Mo/Pd mixed-metal analogue of the Cr<sub>2</sub>P<sub>5</sub>O<sub>5</sub> cage (complex **16**, Figure 2F) structure. Complex **25** exhibited an AB<sub>2</sub>X pattern in its solution <sup>31</sup>P NMR spectrum (Table 1) and numerous bands in its IR carbonyl spectrum (see Experimental Section). A single-

(3) Yang, H. Y.; Wong, E. H.; Jasinski, J. P.; Pozdniakov, R. Y.; Woudenberg, R. *Organometallics* **1992**, *11*, 1579.

**Table 2.**  $^{13}\text{C}$  NMR Data for the Cyclic Phosphoxane Complexes<sup>a</sup>

compd	assgnt [ $\delta$ , ppm ( <i>J</i> , Hz)]
<b>1B</b>	CH [48.6, 45.1], CH <sub>3</sub> [24.5, 22.9]
<b>2A</b>	CH [47.7, 47.2], CH <sub>3</sub> [23.2, 19.2]
<b>4B</b>	CH [58.1, 53.5], CH <sub>2</sub> [33.3, 33.1, 26.7, 26.4, 26.1, 25.5, 24.8]
<b>7</b>	CH [58.1, 53.8, 52.7], CH <sub>2</sub> [33.4, 32.4, 29.3, 27.1, 26.5, 25.6, 25.4, 24.9, 21.5]
<b>8A</b>	CH [58.5, 53.7, 52.7], CH <sub>2</sub> [37.7, 35.7, 35.2, 33.2, 32.5, 31.5, 29.2, 26.9, 26.3, 25.3, 24.7]
<b>8B</b>	CH [58.5, 54.1, 53.0], CH <sub>2</sub> [37.6, 37.3, 33.4, 33.1, 32.7, 32.4, 29.1, 27.1, 26.4, 25.8, 25.4, 24.8]
<b>9</b>	CH [58.0, 53.6, 52.9], CH <sub>2</sub> [37.8, 37.2, 33.1, 32.5, 29.3, 27.1, 26.4, 25.8, 25.6, 25.4, 24.8]
<b>10A</b>	CH [47.8, 44.5], CH <sub>3</sub> [24.4, 23.6, 23.2]
<b>10B</b>	CH [57.4, 53.7], CH <sub>2</sub> [34.9, 33.7, 34.2, 26.9, 26.6, 26.5, 25.4, 25.1]
<b>11a</b>	CO [226.0, triplet (10)], 219.4, triplet (20)], CH [57.4, 53.2, 52.5], CH <sub>2</sub> [33.7, 33.1, 26.8, 25.6]
<b>12</b>	CO [218.1, multiplet], CH [57.8, 53.5 doublet (9); 52.5, doublet (12)] CH <sub>2</sub> [33.5, 33.0, 26.9, 26.8, 26.3, 25.8, 25.7]
<b>13</b>	CO [218.0, multiplet], CH [47.5; 44.4, doublet (15)], CH <sub>3</sub> [24.1, 22.8]
<b>14</b> ( $-10^\circ$ )	CO [215.8, doublet (15); 215.0, doublet (15)] CH [56.9, doublet (11); 48.0, doublet (12); 46.9, doublet (7); 44.6, doublet (27)] CH <sub>3</sub> [26.4, doublet (11); 23.9, 23.5, 23.2, 22.9]
<b>16</b>	CO [229.9, multiplet; 229.1, triplet (14); 224.4, triplet (9); 219.7, triplet (20); 216.7, triplet (20)] CH [58.5, 58.3, 57.5, doublet (10)], CH <sub>2</sub> [36.2, 35.9, 35.3, 34.8, 34.3, 27.3, 27.1, 26.9, 26.7, 25.8, 25.6, 25.2]
<b>17</b>	CO [213.5, 209.8, 203.6, multiplets]; CH [59.0, 58.7, 58.0, doublet (14)], CH <sub>2</sub> [36.0, 35.4, 35.2, 34.8, 34.3, 27.1, 27.0, 26.9, 26.6, 25.7, 25.5, 25.2, 24.8]
<b>18</b>	CO [212.9, 217.6, 210.8, 210.3, 209.8, 206.9, multiplets], CH [57.8, doublet (10); 57.2, doublet (9); 57.5, doublet (8)], CH <sub>2</sub> [34.0, 33.9, 33.7, 33.6, 33.4, 31.5, 26.9, 26.6, 26.5, 25.4, 25.3, 24.9, 22.6]
<b>19a</b>	CO [224.1, triplet (9); 217.1, triplet (19)], CH [45.6], CH <sub>2</sub> [30.9, 14.2], CH <sub>3</sub> [23.2]
<b>19b</b>	CO [213.5, 209.8, 203.6, multiplets], CH [47.3, triplet (4); 46.1], CH <sub>2</sub> [31.0, 30.1, 13.6], CH <sub>3</sub> [23.3, 21.7]
<b>20</b>	CO [229.5, multiplet; 228.3, multiplet; 226.4, triplet (11); 219.3, triplet (21); 216.2, triplet (20)]; CH [47.6, triplet (7); 45.8, 45.6, multiplets], CH <sub>2</sub> [31.4, 31.9, 31.1, 30.9, 30.6, 30.5, 14.2, 14.1, 13.9], CH <sub>3</sub> [23.4, 23.0, 22.9, 22.8, 22.5, 22.4]
<b>21</b>	CO [213.5, triplet (15); 206.9, triplet (12)], CH [45.6, triplet (7)], CH <sub>2</sub> [31.0, 14.1], CH <sub>3</sub> [23.0]
<b>22</b>	CO [213.5, triplet (15); 206.9, triplet (12)] CH [45.6, triplet (7)], CH <sub>2</sub> [31.0, 14.1], CH <sub>3</sub> [23.0]
<b>23</b>	CO [215.9, doublet (12); 215.4, doublet (12); 208.7, triplet (8); 207.7, triplet (10)], CH [58.4, 58.2], CH <sub>2</sub> [36.4, 34.2, 33.5, 32.9, 26.4, 25.9, 25.3, 25.1]
<b>24</b>	CO [218.9, doublet of triplets (39, 13); 216.4, doublet of triplets (39, 13)], CH [59.3, 58.2, 57.7], CH <sub>2</sub> [35.8, 35.4, 34.7, 33.3, 27.0, 26.7, 26.1, 25.4, 25.2, 24.9]
<b>25</b>	CO [219.2, triplet (6); 218.8, doublet (9); 216.7, doublet (54); 211.0, doublet of doublets (9, 3); 207.5, quartet (9)], CH [49.2; 47.6, doublet (9); 44.3, doublet (14)], CH <sub>3</sub> [23.4, 23.0, 22.4]
<b>26</b>	CO [198.0, triplet (2)], CH [55.4, triplet (6)], CH <sub>2</sub> [34.2, 26.6, 25.5]

<sup>a</sup> All spectra were run in CDCl<sub>3</sub> at ambient temperature unless otherwise noted.

**Table 3.** Proton NMR Data for the Cyclic Phosphoxane Complexes<sup>a</sup>

compd	assgnt [ $\delta$ , ppm ( <i>J</i> , Hz)]
<b>1B</b>	CH [4.20, multiplets], CH <sub>3</sub> [1.36, 1.32, 1.31, doublets (6.8 Hz)]
<b>2A</b>	CH [3.74, multiplets], CH <sub>3</sub> [1.36, 1.28, doublet (6.7)]
<b>4B</b>	CH [3.8, broad], CH <sub>2</sub> [1.99–0.84, multiplets]
<b>7</b>	CH [3.6, 3.1, 2.9, broad], CH <sub>2</sub> [2.14–1.07, multiplets]
<b>8A</b>	CH [3.52, 3.04, 2.82, broad], CH <sub>2</sub> [2.25–0.88, multiplets]
<b>8B</b>	CH [3.51, 3.17, 2.80, broad], CH <sub>2</sub> [2.26–0.85, multiplets]
<b>9</b>	CH [3.56, 3.06, 2.79, broad], CH <sub>2</sub> [2.19–0.82, multiplets]
<b>10A</b>	CH [3.86, septet (6.9); 3.7, broad], CH <sub>3</sub> [1.32, 1.31, 1.26, doublets (6.9)]
<b>10B</b>	CH [3.25, broad], CH <sub>2</sub> [1.70–1.18, multiplets]
<b>11a</b>	CH [3.48, broad], CH <sub>2</sub> [1.76–0.84, multiplets]
<b>12</b>	CH [3.52, broad], CH <sub>2</sub> [1.82–0.84, multiplets]
<b>13</b>	CH [3.92, 3.79, broad], CH <sub>3</sub> [1.26, doublet (23)]
<b>14</b> ( $-10^\circ$ )	CH [4.58, 4.15, 3.50, 3.33], CH <sub>3</sub> [1.35, 1.31, 1.24, 1.19, doublets (6)]
<b>16</b>	CH [4.19, 3.76, 3.51, multiplets], CH <sub>2</sub> [1.98–0.84, multiplets]
<b>17</b>	CH [4.21, 3.73, 3.10, multiplets], CH <sub>2</sub> [1.92–0.84, multiplets]
<b>18</b>	CH [3.41, 3.30, 3.20, multiplets], CH <sub>2</sub> [2.03–0.84, multiplets]
<b>19a</b>	CH [4.46], CH <sub>2</sub> [1.15–1.18, multiplets], CH <sub>3</sub> [1.35, doublet (7)]
<b>19b</b>	CH [4.46, 4.22, multiplets], CH <sub>2</sub> [1.87–1.55, multiplets], CH <sub>3</sub> [1.35, 1.40, doublets (7)]
<b>20</b>	CH [4.55, 4.46, 4.37, 4.25, 4.13, multiplets], CH <sub>2</sub> [1.87–1.55, multiplets], CH <sub>3</sub> [1.41, 1.37, 1.32, doublets (7)]
<b>21</b>	CH [4.47, multiplet], CH <sub>2</sub> [1.51–1.19, multiplets], CH <sub>3</sub> [1.37, doublet (7)]
<b>22</b>	CH [4.40, multiplet], CH <sub>2</sub> [1.92–1.50, multiplets], CH <sub>3</sub> [1.31, doublet (7)]
<b>23</b>	CH [3.98, multiplet; 3.8, broad], CH <sub>3</sub> [1.95–0.84, multiplets]
<b>24</b>	CH [4.11, 3.66, multiplets; 3.0, broad], CH <sub>3</sub> [2.06–1.00, multiplets]
<b>25</b>	CH [4.03, 3.87, septets (7); 3.63, broad], CH <sub>3</sub> [1.44, 1.38, 1.33, 1.19, doublets (7)]
<b>26</b>	CH [3.38, broad], CH <sub>2</sub> [2.18–0.72, multiplets]

<sup>a</sup> All spectra were run at ambient temperature in CDCl<sub>3</sub> unless noted otherwise.

crystal X-ray analysis revealed an  $\eta^3\text{-P}_4\text{O}_4$  ring bridging the two metals with an iron–molybdenum bond completing pseudooctahedral coordination spheres at both metals (Figure 8).

In attempts to prepare heterobimetallic complexes of the nickel triad, phosphoxane ring transfer reactions were observed instead. For example, PdBr<sub>2</sub> and PtCl<sub>2</sub> were found to displace the 1,3-chelated NiBr<sub>2</sub> from



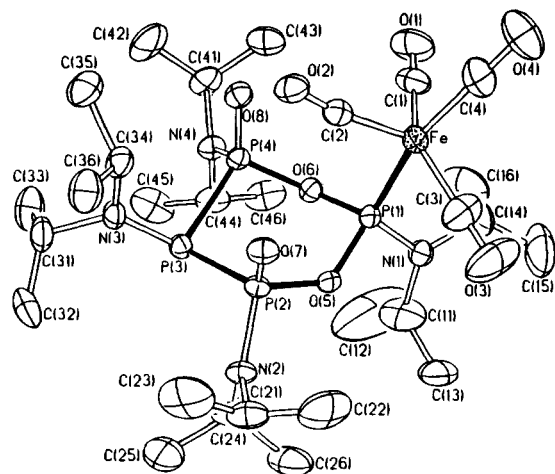


Figure 3. Molecular structure of  $\text{Fe}(\text{CO})_4[{}^1\text{Pr}_2\text{NPO}]_4$  (14).

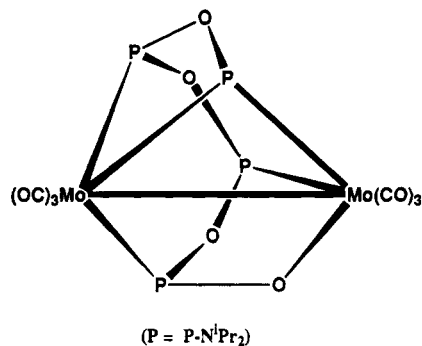


Figure 4. Molecular structure of  $\text{Mo}_2(\text{CO})_6[{}^1\text{Pr}_2\text{NPO}]_4$ .<sup>3</sup>

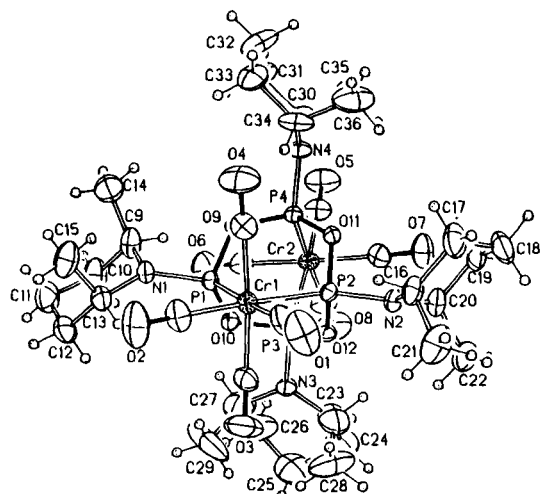


Figure 5. Molecular structure of  $\text{Cr}_2(\text{CO})_8[\text{DMP-PO}]_4$  (19a).

complex **4B** to give the respective 1,5- $\text{P}_4\text{O}_4$  complexes (**5B**, **6**) at room temperature (Scheme 2). At lower temperature, an intermediate 1,3-chelated  $\text{PtCl}_2$  complex (Figure 2B) can be identified by  $^{31}\text{P}$  NMR spectroscopy (AA'XX' pattern).

A reductive decarbonylation occurred in the thermal reactions of either  $\text{Fe}(\text{CO})_5$  or  $\text{Fe}_2(\text{CO})_9$  with  $\text{NiBr}_2[\text{Cy}_2\text{N-PO}]_4$  (**4B**) in attempts to prepare a Ni/Fe complex. The only isolated phosphoxane product was identified as  $\text{Ni}_2(\text{CO})_4[\text{Cy}_2\text{NPO}]_4$  complex **26**, a nickel analogue of adamantanoid cages like **19a** (see Figures 2E and 5).

**X-Ray Structural Studies.** (1) **Molecular Structure of  $\text{Fe}(\text{CO})_4[{}^1\text{Pr}_2\text{NPO}]_4$  (14).** The coordination geometry around iron is essentially trigonal bipyramidal

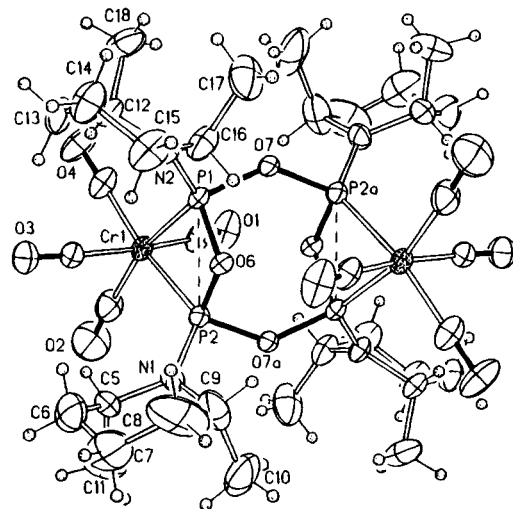


Figure 6. Molecular structure of  $\text{Cr}_2(\text{CO})_8[\text{DMP-PO}]_4$  (19b).

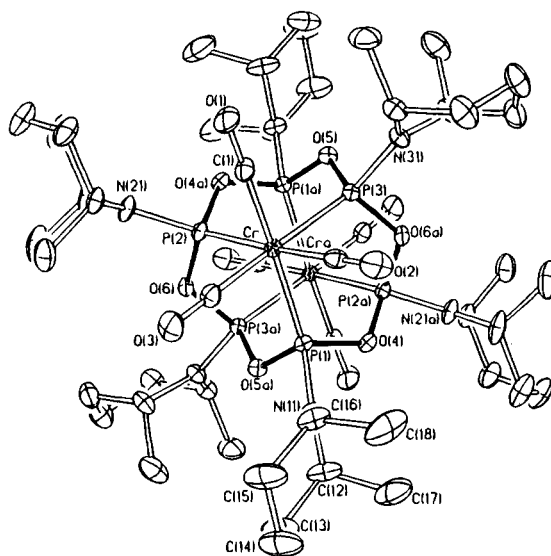
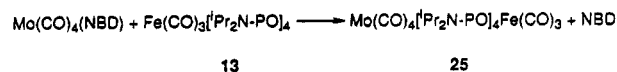
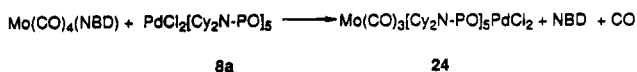
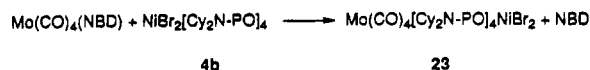


Figure 7. Molecular structure of  $\text{Cr}_2(\text{CO})_6[\text{DMP-PO}]_6$  (21).

### Scheme 1



with the lone phosphorus donor in one axial site (Figure 3). An Fe–P bond length of 2.189(2) Å is toward the short side of typical values for phosphine– $\text{Fe}(\text{CO})_4$  structures (2.22–2.37 Å).<sup>4</sup> The axial Fe–C(4) bond is at 1.763(10) Å. The diaxial P(1)–Fe–C(4) angle is considerably bent from linearity at 161.3(2)°. While the equatorial coordination plane is well defined by Fe, C(1), C(2), and C(3), the C(1)–Fe–C(3) angle has opened up

(4) Riley, P. E.; Davis, R. E. *Inorg. Chem.* **1980**, *19*, 159. Massimbeni, L. R. *Inorg. Nucl. Chem. Lett.* **1971**, *7*, 187. Wong, E. H.; Bradley, F. C.; Prasad, L.; Gabe, E. J. *J. Organomet. Chem.* **1984**, *263*, 167. Pickardt, J.; Rosch, L.; Schumann, H. *J. Organomet. Chem.* **1976**, *107*, 241. Kilbourn, B. T.; Raeburn, U. A.; Thompson, D. T. *J. Chem. Soc. A* **1969**, 1906. Einstein, F. W. B.; Jones, R. D. G. *J. Chem. Soc., Dalton Trans.* **1972**, 442.





**Table 6. Selected Bond Distances and Angles for Complex 19b**

Bond Distances (Å)			
Cr(1)–P(1)	2.337(1)	Cr(1)–P(2)	2.333(1)
Cr(1)–C(1)	1.884(4)	Cr(1)–C(2)	1.862(6)
Cr(1)–C(3)	1.875(4)	Cr(1)–C(4)	1.872(5)
P(1)–P(2)	2.560(1)	P(1)–N(2)	1.633(3)
P(1)–O(1)	1.657(3)	P(1)–O(7)	1.635(3)
P(2)–N(1)	1.627(4)	P(2)–O(6)	1.664(3)
P(2)–O(7A)	1.630(2)	O(1)–C(1)	1.152(5)
O(2)–C(2)	1.144(8)	O(3)–C(3)	1.141(5)
O(4)–C(4)	1.141(6)	O(7)–P(2A)	1.630(2)

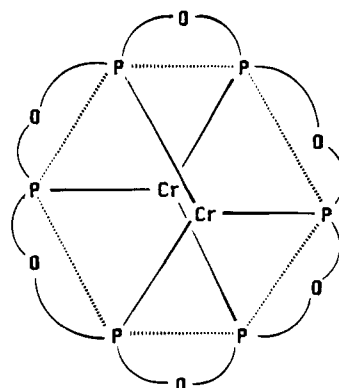
  

Bond Angles (deg)			
P(1)–Cr(1)–P(2)	66.5(1)	P(1)–Cr(1)–C(1)	97.9(2)
P(2)–Cr(1)–C(1)	98.7(2)	P(1)–Cr(1)–C(2)	162.7(2)
P(2)–Cr(1)–C(2)	96.3(2)	C(1)–Cr(1)–C(2)	85.5(2)
P(1)–Cr(1)–C(3)	89.9(2)	P(2)–Cr(1)–C(3)	91.3(2)
C(1)–Cr(1)–C(3)	169.2(2)	C(2)–Cr(1)–C(3)	89.3(2)
P(1)–Cr(1)–C(4)	100.2(2)	P(2)–Cr(1)–C(4)	166.4(2)
C(1)–Cr(1)–C(4)	85.6(4)	C(2)–Cr(1)–C(4)	96.9(2)
C(3)–Cr(1)–C(4)	85.6(2)	O(6)–P(2)–O(7A)	98.8(1)
P(1)–O(6)–P(2)	100.9(2)	P(1)–O(7)–P(2A)	134.5(2)

and leg and P(1), P(2), O(7a), P(1a), P(2a), and O(7) the planar seat (Figure 6). Significantly longer P–O bonds of 1.660(4) Å are observed in the strained chelate rings compared to those in the rest of the ring (1.632(4) Å). Also, the compressed P(1)–O(6)–P(2) angle of 100.9(2)° in the four-membered chelate rings can be contrasted with the much larger 134.5(2)° found for the remaining P–O–P angles. Transannular P(1)–P(2) separations are at only 2.560(1) Å. Two Cr(CO)<sub>4</sub> groups are coordinated to opposite sides of this heterocycle by four-membered chelate rings to give approximately octahedral environments at the metals. Bending of the axial carbonyls away from the phosphoxane ring is observed with a C(1)–Cr(1)–C(3) angle of 169.2(2)°. The cramped P(1)–Cr(1)–P(2) and P(1)–O(6)–P(2) angles of 66.5(1)° and 100.9(2)°, respectively have precedence in related chromium phosphoxane chelate rings.<sup>2,6</sup> Metal–phosphorus distances at 2.333(1) and 2.337(1) Å are unexceptional. Selected bond distances and angles are listed in Table 6. Interestingly, the two methyl substituents in each of the dimethylpiperidino groups adopt diaxial positions with the piperidino nitrogens effectively planar.

**(4) Molecular Structure of Cr<sub>2</sub>(CO)<sub>6</sub>[DMP-PO]<sub>6</sub> (21).** The centrosymmetric core structure of the hexaphosphoxane complex 21 (Figure 7) features two *fac*-Cr(CO)<sub>3</sub>, six phosphorus, and six oxygen vertices. A novel P<sub>6</sub>O<sub>6</sub> macrocycle serves as a hexadentate donor toward two metal centers, one above and one below. This can also be viewed as a Cr<sub>2</sub>P<sub>6</sub> cube with oxygens bridging only the P–P edges (Figure 9). Cage phosphoxane P–O–P angles range from 123.3(3)° to 124.8(2)°. Bond angles around the metals are reasonably close to orthogonal values with P–Cr–P angles ranging from 92.7(1)° to 93.0(1)° and C–Cr–C angles from 88.0(3)° to 90.2(3)°. Average Cr–P bond lengths of 2.335(2) Å and Cr–C distances of 1.857(6) Å are found. The intracage Cr–Cr separation is down to 4.700(1) Å. Other selected bond distances and angles are listed in Table 7.

**(5) Molecular Structure of Fe(CO)<sub>3</sub>[Pr<sub>2</sub>NPO]<sub>4</sub>Mo(CO)<sub>4</sub> (25).** This heterobimetallic complex contains a

**Figure 9.** Schematic view of the Cr<sub>2</sub>P<sub>6</sub>O<sub>6</sub> core in complex 21.**Table 7. Selected Bond Distances and Angles for Complex 21**

Bond Distances (Å)			
Cr–P(1)	2.325(1)	Cr–P(2)	2.325(1)
Cr–P(3)	2.321(1)	Cr–C(1)	1.866(5)
Cr–C(2)	1.857(5)	Cr–C(3)	1.860(4)
P(1)–O(4)	1.647(2)	P(1)–N(11)	1.649(4)
P(1)–O(5A)	1.638(3)	P(2)–O(6)	1.648(3)
P(2)–N(21)	1.645(4)	P(2)–O(4A)	1.639(3)
P(3)–O(6A)	1.641(3)	O(1)–C(1)	1.145(6)
O(2)–C(2)	1.152(6)	O(3)–C(3)	1.145(5)
O(4)–P(2A)	1.639(3)	O(5)–P(1A)	1.638(3)
O(6)–P(3A)	1.641(3)		

Bond Angles (deg)			
P(1)–Cr–P(2)	92.8(1)	P(1)–Cr–P(3)	93.1(1)
P(2)–Cr–P(3)	93.0(1)	P(1)–Cr–C(1)	177.1(1)
P(2)–Cr–C(1)	87.0(1)	P(3)–Cr–C(1)	89.8(1)
P(1)–Cr–C(2)	90.0(1)	P(2)–Cr–C(2)	177.2(1)
P(3)–Cr–C(2)	87.0(1)	C(1)–Cr–C(2)	90.2(2)
P(1)–Cr–C(3)	87.0(1)	P(2)–Cr–C(3)	89.7(1)
P(3)–Cr–C(3)	177.3(1)	C(1)–Cr–C(3)	90.1(2)
C(2)–Cr–C(3)	90.3(2)	O(4)–P(1)–O(5A)	97.0(1)
O(6)–P(2)–O(4A)	96.8(1)	O(5)–P(3)–O(6A)	96.8(1)
P(1)–O(4)–P(2A)	123.7(2)	P(3)–O(5)–P(1A)	123.7(2)
P(2)–O(6)–P(3A)	123.7(1)		

metal-bridging tridentate P<sub>4</sub>O<sub>4</sub> ring in a chair–chair conformation (Figure 8). In addition to the often observed 1,5-chelating coordination mode toward Fe (Figure 2A), a third phosphorus is also ligating to the Mo(CO)<sub>4</sub> fragment. A long Fe–Mo bond of 3.034(2) Å completes the pseudooctahedral coordination sphere at each metal. At Mo, an acute Fe–Mo–P(1) angle of 72.9(1)° is found while all four carbonyls are pushed away from the FeP<sub>4</sub>O<sub>4</sub> unit with Fe–Mo–C and P(1)–Mo–C angles ranging from 93.7(2)° to as much as 102.1(2)° (P(1)–Mo–C(3)). The Mo–C(3) bond *trans* to the Fe is the shortest at 1.946(8) Å while those *cis* to both the Fe and P(1) are longest at 2.036(8)–2.057(8) Å. A Mo–P(1) bond of 2.473(2) Å can also be noted. At the Fe center, the two carbonyls *trans* to the phosphorus atoms are bent toward the Mo(CO)<sub>4</sub> moiety with Mo–Fe–C(5) and Mo–Fe–C(6) angles of only 71.8(3)° and 73.7(2)°, respectively, while that *trans* to the Mo is bent away from the P<sub>4</sub>O<sub>4</sub> ring with the P–Fe–C(7) angle at about 100°. The two Fe–P distances are at 2.218(2) and 2.225(2) Å. Other selected bond distances and angles are listed in Table 8.

The tetraphosphoxane ring itself retains the approximate chair–chair conformation as was found for complex 2A.<sup>2</sup> Interestingly, two ranges of P–O bond lengths are observed. Those at the chelating P(2) and

Table 8. Selected Distances and Angles for Complex 25

Bond Distances (Å)			
Mo-Fe	3.034(2)	Mo-P(1)	2.473(2)
Mo-C(1)	1.984(6)	Mo-C(2)	2.057(8)
Mo-C(3)	1.946(8)	Mo-C(4)	2.036(8)
Fe-P(2)	2.225(2)	Fe-P(4)	2.218(2)
Fe-C(5)	1.796(7)	Fe-C(6)	1.798(7)
Fe-C(7)	1.792(7)	P(1)-O(8)	1.663(4)
P(1)-O(11)	1.669(5)	P(2)-O(8)	1.621(4)
P(2)-O(9)	1.621(5)	P(3)-O(9)	1.675(6)
P(3)-O(10)	1.658(4)	P(4)-O(10)	1.621(5)
P(4)-O(11)	1.622(4)	O(1)-C(1)	1.152(8)
O(2)-C(2)	1.124(9)	O(3)-C(3)	1.152(10)
O(4)-C(4)	1.139(11)	O(5)-C(5)	1.142(8)
O(6)-C(6)	1.143(8)	O(7)-C(7)	1.138(9)
Bond Angles (deg)			
Fe-Mo-P(1)	72.9(1)	Fe-Mo-C(1)	94.8(2)
P(1)-Mo-C(1)	167.6(2)	Fe-Mo-C(2)	97.5(3)
P(1)-Mo-C(2)	96.0(2)	C(1)-Mo-C(2)	86.8(3)
Fe-Mo-C(3)	174.7(2)	P(1)-Mo-C(3)	102.1(2)
C(1)-Mo-C(3)	90.1(3)	C(2)-Mo-C(3)	84.5(3)
Fe-Mo-C(4)	95.0(3)	P(1)-Mo-C(4)	93.7(2)
C(1)-Mo-C(4)	85.9(3)	C(2)-Mo-C(4)	166.0(4)
C(3)-Mo-C(4)	83.6(3)	Mo-Fe-P(2)	89.8(1)
Mo-Fe-P(4)	90.4(1)	P(2)-Fe-P(4)	83.0(1)
Mo-Fe-C(5)	73.7(2)	P(2)-Fe-C(5)	91.9(2)
P(4)-Fe-C(5)	163.4(2)	Mo-Fe-C(6)	71.8(3)
P(2)-Fe-C(6)	160.5(2)	P(4)-Fe-C(6)	90.6(2)
C(5)-Fe-C(6)	89.0(3)	Mo-Fe-C(7)	166.2(2)
P(2)-Fe-C(7)	100.1(2)	P(4)-Fe-C(7)	100.2(2)
C(5)-Fe-C(7)	96.3(2)	C(6)-Fe-C(7)	99.2(3)
Mo-P(1)-O(8)	109.5(1)	Mo-P(1)-O(11)	112.3(1)
O(8)-P(1)-O(11)	97.9(2)	Fe-P(2)-O(8)	112.4(2)
Fe-P(2)-O(9)	113.5(2)	O(8)-P(2)-O(9)	97.7(2)
O(9)-P(3)-O(10)	96.1(2)	Fe-P(4)-O(10)	113.0(1)
Fe-P(4)-O(11)	111.1(2)	O(10)-P(4)-O(11)	99.9(2)
P(1)-O(8)-P(2)	117.7(2)	P(2)-O(9)-P(3)	127.0(2)
P(3)-O(10)-P(4)	127.4(2)	P(1)-O(11)-P(4)	119.5(2)
Mo-C(1)-O(1)	178.4(7)	Mo-C(2)-O(2)	171.4(8)
Mo-C(3)-O(3)	178.2(5)	Mo-C(4)-O(4)	170.2(8)
Fe-C(5)-O(5)	172.9(6)	Fe-C(6)-O(6)	171.6(6)
Fe-C(7)-O(7)	174.8(5)		

P(4) are all around 1.621(5) Å while the remainders are significantly longer, varying from 1.658(4) to 1.675(6) Å.

## Discussion

**Formation of the Cyclic Phosphoxane Complexes.** The variety of products obtained from preformed triphosphoxane rings  $[R_2NPO]_3$  ( $R = {}^iPr, Cy$ ) with nickel, palladium, or platinum dihalides illustrates some of the subtle and still not well-understood factors that influenced the reaction course. Though diisopropylamino and dicyclohexylamino substituents would not be expected to differ dramatically in their stereoelectronic influences,<sup>7</sup>  $[{}^iPr_2NPO]_3$  yielded only  $P_4O_4$  complexes while  $[Cy_2NPO]_3$  led to both  $P_4O_4$  and  $P_5O_5$  products. There is a general pattern in higher reaction temperatures favoring formation of the larger  $P_5O_5$  rings except in the nickel dichloride case. The nature of the ancillary halides in  $NiX_2$  ( $X = Cl, Br, I$ ) also made a difference. Of the three, only  $NiCl_2$  yielded a  $P_5O_5$  complex.

The 1,3-coordination mode (Figure 2B) in the  $NiP_4O_4$  (Figures 4A-C and 7) products as revealed by a characteristic  $AA'XX'$   ${}^{31}P$  NMR spectrum was unique to the nickel dihalides, presumably due to a superior fit in the resulting four-membered  $NiPOP$  chelate ring. Although the actual conformation of the tetraphosphox-

ane ring itself has not been determined, its ability to further coordinate a second metal to give  $Mo(CO)_4[Cy_2NPO]_4NiBr_2$  (**23**) suggests the long chair form with the opposite side of the ring available for coordination of a second metal (Figures 2B and 6). The X-ray structure of  $Cr(CO)_4[DMP-PO]_4Cr(CO)_4$  (**19b**, Figure 6) lends credence to this premise. Observation of well-resolved NMR resonances for all the isolated  $NiX_2$  phosphoxane complexes (**1A,B**, **4A-C**, **7**, **23**) is consistent with near-square-planar nickel coordination geometries and diamagnetism in all these cases.

The assembly of  $P_4O_4$  and  $P_5O_5$  complexes from cyclic triphosphoxane under reaction conditions as mild as 4° requires exclusive head-to-tail grafting in of extra  $R_2NP=O$  phosphinidene units. Existence of such intermediates has been substantiated by several previous reports.<sup>8</sup> It is very likely that prior metal coordination represents an essential prerequisite to these ring expansions. It is also noteworthy that we failed to isolate any products incorporating more than one divalent metal center regardless of the reaction stoichiometry. Subsequent studies indeed revealed the reluctance of divalent metal  $MP_nO_n$  complexes to coordinate a second divalent metal center even though zero-valent metals were readily bound. Electronic effects transmitted through the P-O-P linkages may be responsible for this selectivity. We have recently reported on such intramolecular influences in a series of heterobimetallic  $P_4O_4$  cage complexes.<sup>9,10</sup> Cage complexes containing two  $Mo^{II}$  vertices can be synthesized indirectly from halogenation reactions of  $Mo^0P_4O_4Mo^0$  precursors.<sup>14</sup>

Under similar reaction conditions,  $Fe_2(CO)_9$  gave significantly different products, depending on the cyclic triphosphoxane used. While  $[Cy_2NPO]_3$  yielded  $Fe(CO)_3[Cy_2NPO]_4$  (**12**) with an 1,5- $\eta^2$ - $P_4O_4$  ring in a boat-chair configuration (Figure 2C),  $[{}^iPr_2NPO]_3$  produced instead  $Fe(CO)_3[{}^iPr_2NPO]_4$  (**13**), the chair-chair (Figure 2A) isomer, and a novel  $Fe(CO)_4-\eta^1-({}^iPr_2NPO)_4$  complex (**14**). The X-ray structure of the latter (Figure 3) revealed coordination of a  $Fe(CO)_4$  fragment to a  $P[OP(=O)]_2P$  ring. This unusual six-membered ring can be viewed as the product of a double P-O-P to P-P(=O) rearrangement, converting a tetraphosphoxane  $\eta^1$ - $P_4O_4$  ring into a mondentate  $P[OP(=O)]_2P$  heterocycle. It is conceivable that the eight-membered  $P_4O_4$  ring was initially formed but was unstable toward such a rearrangement to a six-membered ring with two strong phosphoryl P=O bonds. We have previously reported a single P-O-P to P-P(=O) rearrangement in the metallocycle  $cis-M(CO)_4(PPh_2O)_2PPh$  to form  $cis-M(CO)_4[PPh_2P(O)PhOPPh_2]$  ( $M = Cr, Mo, W$ ).<sup>11a</sup>

Three diaminophosphine oxides,  $(R_2N)_2P(O)H$  ( $R_2N = {}^iPr_2N, Cy_2N, DMP$ ), were used as sources of  $R_2NP=O$  phosphinidene oxide units in thermal reactions with group 6 metal carbonyls. All three have in common

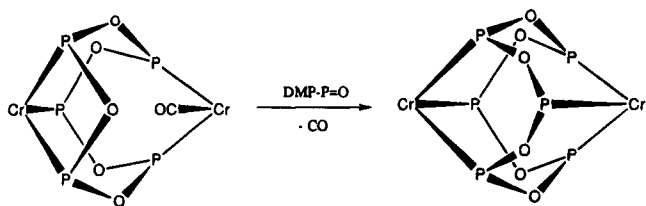
(8) Niecke, E.; Engelmann, M.; Zorn, H.; Krebs, B.; Henkel, G. *Angew. Chem., Int. Ed. Engl.* **1980**, *19*, 710. Chasar, D. W.; Fackler, J. P.; Mazany, A. M.; Komoroski, R. A.; Kroenke, W. J. *J. Am. Chem. Soc.* **1986**, *108*, 5956. Quast, H.; Heuschmann, M. *Angew. Chem., Int. Ed. Engl.* **1978**, *17*, 867.

(9) Yang, H. Y.; Wong, E. H.; Rheingold, A. L.; Owens-Waltermire, B. E. *J. Chem. Soc., Chem. Commun.* **1993**, 35.

(10) Yang, H. Y.; Wong, E. H.; Rheingold, A. L.; Waltermire, B. E. *Organometallics*, in press.

(11) (a) Wong, E. H.; Bradley, F. C.; Gabe, E. J. *J. Organomet. Chem.* **1983**, *244*, 235. (b) Bader, D. S.; Turnbull, M. M. *Polyhedron* **1990**, *9*, 2619.

Scheme 3



amino substituents with secondary  $\alpha$ -carbons. We have previously found that less bulky dialkylamino groups like Et<sub>2</sub>N failed to lead to P<sub>*n*</sub>O<sub>*n*</sub> products under these conditions.<sup>2</sup> Presumably the dialkylamine elimination critical to the generation of R<sub>2</sub>NP=O units from (R<sub>2</sub>N)<sub>2</sub>P(O)H is only viable with the bulkier R groups. A correlation between the steric bulk of the dialkylamino substituents and success of cage formation from dialkylamino phosphine oxides has been made.<sup>11b</sup>

Again, the size and coordination mode of the P<sub>*n*</sub>O<sub>*n*</sub> rings formed in the complexes isolated were sensitive to the nature of both precursors and the reaction conditions. In general, only P<sub>3</sub>O<sub>3</sub> and P<sub>4</sub>O<sub>4</sub> complexes were formed around the Mo(CO)<sub>4</sub> moiety. Although a lone Mo<sub>2</sub>(CO)<sub>6</sub>[Me-AsO]<sub>6</sub> structure has been reported previously,<sup>12</sup> no Mo<sub>2</sub>P<sub>6</sub>O<sub>6</sub> species was isolated here in our studies. It may be that the smaller P<sub>6</sub>O<sub>6</sub> core cannot accommodate two *fac*-Mo(CO)<sub>3</sub> vertices. By contrast, in addition to two isomers of the Cr<sub>2</sub>P<sub>4</sub>O<sub>4</sub> cores (19a,b), larger ring P<sub>5</sub>O<sub>5</sub> and P<sub>6</sub>O<sub>6</sub> products were also isolated around Cr(CO)<sub>*n*</sub> (*n* = 3, 4) fragments. Further, among the products isolated, only chromium formed stable four-membered MPOP chelate rings (complexes 16 and 19b), the shorter Cr–P bond apparently resulting in less strained ring geometries. Larger cages incorporating Cr(CO)<sub>3</sub> vertices are increasingly favored with higher reaction temperatures. Conceivably, progressive assembly of P<sub>3</sub>O<sub>3</sub> to P<sub>4</sub>O<sub>4</sub> to P<sub>5</sub>O<sub>5</sub> to P<sub>6</sub>O<sub>6</sub> rings about the metal carbonyl centers as more CO's are lost underlie the syntheses of these products. This is not unexpected since the loss of a third carbonyl from the Cr(CO)<sub>4</sub> center should be possible only under more forcing conditions.<sup>13</sup> Indeed, it is tempting upon examining the related structures of the Cr<sub>2</sub>P<sub>5</sub>O<sub>5</sub> (20) and Cr<sub>2</sub>P<sub>6</sub>O<sub>6</sub> (21) cores to speculate on the loss of a third CO from the *cis*-Cr(CO)<sub>4</sub> vertex in 20 with incorporation of an extra phosphinidene oxide unit (Scheme 3) to build up to the hexaphosphoxane complex 21. This speculation was amply supported by the quantitative conversion of 20 to 21 upon refluxing in xylene in the presence of extra (DMP)<sub>2</sub>P(O)H as the phosphinidene oxide source.

**Metal Coordination Reactions of Monometallic Cyclic Phosphoxane Complexes.** Heterobimetallic complexes were accessible from the monometallic polyphosphoxane complexes since they have phosphorus lone pairs available. Isolated complexes include Mo(CO)<sub>4</sub>[Cy<sub>2</sub>NPO]<sub>4</sub>NiBr<sub>2</sub> (23), Mo(CO)<sub>3</sub>[Cy<sub>2</sub>NPO]<sub>5</sub>PdCl<sub>2</sub> (24), and Mo(CO)<sub>4</sub>[<sup>1</sup>Pr<sub>2</sub>NPO]<sub>4</sub>Fe(CO)<sub>3</sub> (25) (Scheme 1). The first two have parallels in known M<sub>2</sub>P<sub>*n*</sub>O<sub>*n*</sub> structures. Complex 23 can be assigned a long chair ring conformation based on its <sup>31</sup>P NMR spectrum (Table 1), at its core a configurational isomer of the previously

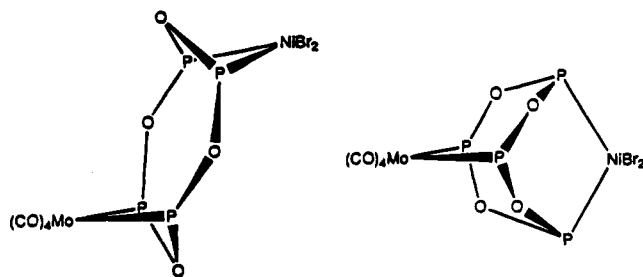


Figure 10. Two core geometries of Mo(CO)<sub>4</sub>[R<sub>2</sub>NPO]<sub>4</sub>NiBr<sub>2</sub> (P = R<sub>2</sub>NP).

reported Mo(CO)<sub>4</sub>[<sup>1</sup>Pr<sub>2</sub>NPO]<sub>4</sub>NiBr<sub>2</sub> cage complex (Figure 10).<sup>9,10</sup> Interestingly, the latter is paramagnetic and has been found to have a pseudotetrahedral geometry at the Ni center.<sup>9</sup> We ascribe these different nickel coordination geometries to steric factors engendered by the positioning of the cage dialkylamino groups, which disfavors a square-planar Ni coordination geometry. Complex 24 is a Pd/Mo analogue of the Cr<sub>2</sub>P<sub>5</sub>O<sub>5</sub> cage core (complexes 16 and 20, Figure 2F). Its ready formation from PdCl<sub>2</sub>[Cy<sub>2</sub>NPO]<sub>5</sub> (8A) supports the <sup>31</sup>P NMR-based geometry of the precursor (Figure 2G). The unique complex 25 was found to have an η<sup>3</sup>-P<sub>4</sub>O<sub>4</sub> ring bridging the two metal centers. Furthermore, EAN electron counting would be consistent with a dative iron to molybdenum bond, completing pseudooctahedral environments at both sites.

Again, no bimetallic products containing two divalent metal vertices were isolated. This confirms the reluctance of such P<sub>*n*</sub>O<sub>*n*</sub> rings to incorporate two relatively electron-demanding centers. The only such complexes we know of are the tetrahalogenated molybdenum cage species Mo(CO)<sub>2</sub>X<sub>2</sub>[RPO]<sub>4</sub>Mo(CO)<sub>2</sub>X<sub>2</sub> (X = Cl, Br, I; R = <sup>1</sup>Pr<sub>2</sub>N, Ph) prepared from direct halogenations of the parent cages. Even these rare exceptions were found to be relatively less tractable species.<sup>14</sup>

Attempts at synthesizing Ni/Pd and Ni/Pt complexes revealed instead phosphoxane ring transfer reactions whereby the P<sub>*n*</sub>O<sub>*n*</sub> heterocycle was displaced from NiBr<sub>2</sub>[Cy<sub>2</sub>NPO]<sub>4</sub> (4B) by the heavier metals to form the more stable 1,5-chelates (5B, 6). Previously, we reported a pyridine displacement of the [<sup>1</sup>Pr<sub>2</sub>NPO]<sub>4</sub> tetraphosphoxane free ligand from its NiBr<sub>2</sub> complex at –30 °C.<sup>2</sup> Similar displacements failed with the palladium complexes. Observation of the PtCl<sub>2</sub>-1,3-[Cy<sub>2</sub>NPO]<sub>4</sub> intermediate at low temperature (<sup>31</sup>P NMR, AA'XX' pattern) suggested that the transfer reaction may proceed via a bimetallic intermediate followed by loss of nickel and a subsequent 1,3- to 1,5-rearrangement of the chelation mode (Scheme 4).

Reductive carbonylation of the NiBr<sub>2</sub> vertex in the reactions of complex 4B with Fe(CO)<sub>5</sub> and Fe<sub>2</sub>(CO)<sub>9</sub> to give Ni<sub>2</sub>(CO)<sub>4</sub>[Cy<sub>2</sub>NPO]<sub>4</sub> (26) has precedence in the reported use of iron carbonyls as both reducing and carbonylating agents toward metal dihalides.<sup>15</sup> The initially formed Ni(CO)<sub>2</sub>[Cy<sub>2</sub>NPO]<sub>4</sub> then can dimerize with loss of four phosphinidene oxide units to form the cage complex 26.

**<sup>31</sup>P NMR Spectroscopy of the Cyclic Phosphoxane Complexes.** <sup>31</sup>P NMR spectroscopy remains the

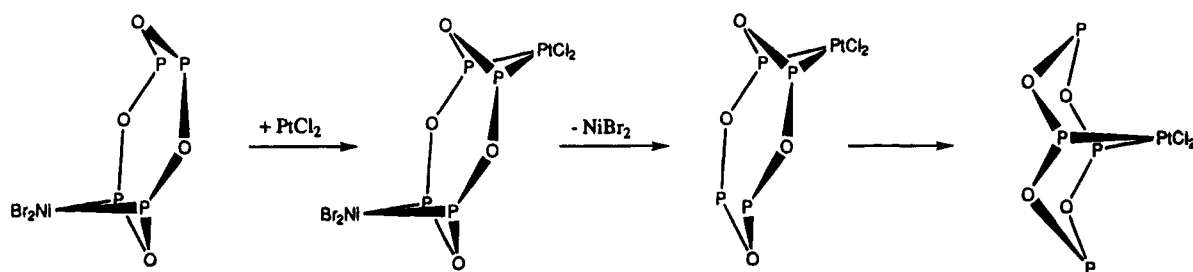
(12) Rheingold, A. L. *Organometallics* 1986, 5, 393.

(13) Kirtly, S. W. *Comprehensive Organometallic Chemistry*; Wilkinson, G., Stone, F. G. A., Abel, E. W., Eds.; Pergamon Press: New York, 1982; Vol. 3.

(14) Turnbull, M. M.; Valdez, C.; Wong, E. H.; Gabe, E. J.; Lee, F. L. *Inorg. Chem.* 1992, 31, 208.

(15) Booth, B. L.; Else, M. J.; Fields, R.; Goldwhile, H.; Hazeldine, R. N. J. *Organomet. Chem.* 1968, 14, 417. Nesmeynov, A. N.; Isaeva, L. S.; Morozova, L. N. *Inorg. Chim. Acta* 1978, 29, L210.

Scheme 4



single most powerful tool for structural determination of the described cyclic phosphoxane complexes in solution. The well-known dependence of  $^2J_{PP}$  on lone pair orientation has proven to be useful for structural assignments in a variety of polyphosphorus compounds.<sup>16</sup> In the known cyclic phosphoxane complexes, magnitudes of observed  $^2J_{POP}$  range from less than 1 to over 60 Hz, with lone pairs *syn* to the coordinated metals accounting for most of the larger values. For example, in the chair–chair form (Figure 11A) of  $MP_4O_4$  ( $M = Cr, Mo, W, Fe, Pd, Pt$ ) possessing *syn* lone pairs,  $^2J_{POP}$  were observed at 28–88 Hz. For the chair–boat form (Figure 11B) ( $M = Cr, Mo, W, Fe, Pt$ ), the *syn* values range from 38 to 59 Hz while the *anti* couplings are significantly smaller at 1–13 Hz. In the lone boat–boat complex  $Mo(CO)_4[Pr_2NPO]_4$  (Figure 11C) with both lone pairs *anti* to the coordinated metal,  $^2J_{POP}$  is 2 Hz only.<sup>9,10</sup> We also noted that high-temperature (to 100 °C) spectral studies failed to reveal any interconversions between these isomeric structures (Figure 11A–C), thus confirming typically high phosphorus inversion barriers. These coupling data also allowed us to propose solution structures of several  $MP_5O_5$  complexes with some confidence. For example,  $PdX_2P_5O_5$  (**8A**, **8B**) and  $PtCl_2P_5O_5$  (**9**) are assigned structures (Figure 11D) on the basis of their  $AA'MXX'$  spectral patterns, their small  $^2J_{AX}$  and  $^2J_{MX}$  of 11–19 Hz, and the actual observation of  $^4J_{AM}$ 's of about 3 Hz in each case. The ready formation of the  $MoP_5O_5Pd$  (**24**, Figure 2F) cage complex from **8A** lends further support for these structural designations.

The well-known “ring effect” or ring contribution ( $\Delta_R$ ) to the  $^{31}P$  chemical shifts of four- to six-membered phosphine chelates has been recently ascribed by Lindner to originate from the component of the shift tensor perpendicular to the ring plane.<sup>17–19</sup> For our complexes, it proved very helpful in identifying the existence of four-membered chelate rings. For example, the four-membered CrPOP chelate rings in complex **19b** ( $\delta$  155.4) can be distinguished from the six-membered rings in the adamantanoid cage structure of **19a** ( $\delta$  171.1) by their upfield shift. This effect also manifested itself in the mixed-metal complex **23**, where the relatively upfield shift ( $\delta$  137.9) of the Mo-bounded P's compared to typical larger chelate ring values ( $\delta \sim 150$ ) is fully consistent with formation of four-membered chelate rings using the long chair form of  $P_4O_4$  (Figure

2B). Similarly, the 1,3-coordination mode of the  $NiX_2P_4O_4$  complexes can be gauged from their upfield  $\delta$ 's of 54–63. Nickel analogues of the 1,5-chelated  $PdX_2P_4O_4$  structure would be expected to have chemical shifts downfield from the 88 ppm region.<sup>17</sup> Thus, the  $NiP_5O_5$  complex was assigned its structure (Figures 2G and 11D) partly on the basis of this downfield  $\delta$  value of 91.7 observed for its coordinated P's, invalidating the presence of any four-membered chelate rings.

Bridging phosphido and phosphoryl units in these complexes are readily identified by their unique chemical shifts at very low and high fields, respectively, compared to typical  $P(NR_2)(OR')_2$  centers whose shifts range from  $\delta +60$  to  $+180$ .<sup>16,20</sup> Finally, complexes **10A** and **10B** both contain a  $P_3O_3$  ring which can be either in a boat or in a chair form. We favor the chair form (Figure 2D) in both cases since the upfield shift of the lone uncoordinated  $P_x$  from  $\delta$  140.3 to 130.1 and 128.2, respectively, upon complex formation should be a result of the parent triphosphoxane flipping into a chair form. This will remove the transannular P–O interaction present in the parent boat-form heterocycle and lead to the observed upfield shift.

Room-temperature  $^{13}C$  NMR studies of the iron  $FeP_4O_4$  complex **14** in  $CDCl_3$  revealed fluxional carbonyls resulting in observation of a single doublet resonance at  $\delta +215.8$  ( $^2J_{CP} = 15$  Hz). Interestingly, in addition to the usual sharp signals, both the methyl ( $\delta$ 's 26.4 and 23.1) and methine ( $\delta$ 's 56.9, 44.9) regions exhibited two broad resonances at room temperature which sharpened into doublets at  $-10$  °C. In toluene- $d_8$  at about 100 °C, these coalesced to broad singlets at around  $\delta$  25 and  $\delta$  51. Decomposition precluded observation of spectra at the fast-exchange regime. We ascribe these changes to a hindered rotation around the P–N $^i$ Pr $_2$  bond at the iron-coordinating phosphorus center since the solid-state structure (Figure 3) showed a significant bending back of the  $Fe(CO)_4$  unit away from the two axial phosphoryl oxygens and toward this particular diisopropylamino group.

**X-Ray Structures of Cyclic Phosphoxane Complexes.** The highly distorted equatorial C(1)–Fe–C(3) angle of  $144.5(3)^\circ$  in the structure of complex **14** may be traced to two origins. One of the P(1)–N(1)–diisopropyl groups is oriented so that a methine C(14)–H is pointed directly into the region between C(1) and C(3) (Figure 3). Concurrently, a tilting away of the equatorial iron coordination plane at C(2) (C(2)–Fe–P(1) angle of  $101.6(2)^\circ$ ) from the two axial ring phosphoryl oxygens toward this methine group may also contribute to the opening up of this angle. As a consequence of this, an elongated Fe–C(2) bond ( $1.821(5)$  Å) also results while

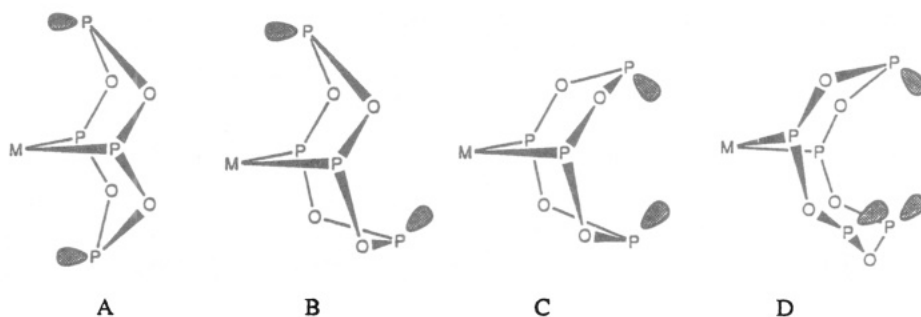
(16) Verkade, J. G.; Quin, L. D., Eds. *Phosphorus-31 NMR Spectroscopy in Stereochemical Analysis: Organic Compounds and Metal Complexes*; VCH Publishers: Deerfield Beach, FL, 1987.

(17) Garrou, P. E. *Chem. Rev.* **1981**, *81*, 229.

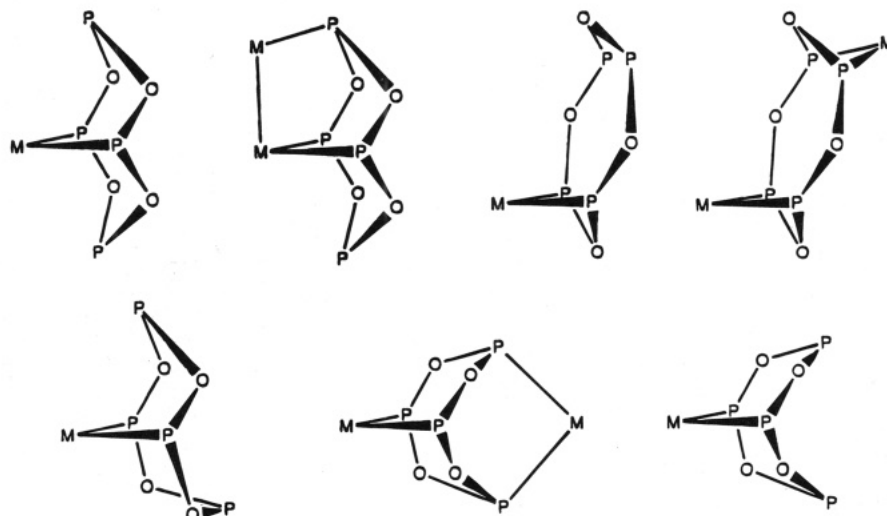
(18) Lindner, E.; Fawzi, R.; Mayer, H. A.; Eichele, K.; Hiller, W. *Organometallics* **1992**, *11*, 1033.

(19) Pregosin, P. S.; Kunz, R. W.  *$^{31}P$  and  $^{13}C$  NMR of Transition Metal Phosphine Complexes*; Springer-Verlag: New York, 1979.

(20) Gorenstein, D. G.  *$^{31}P$  NMR*; Academic Press: New York, 1984.



**Figure 11.** *Syn* and *anti* phosphorus lone pairs in  $MP_4O_4$  and  $MP_5O_5$  ( $P = R_2NP$ ).



**Figure 12.** Known coordination modes of the  $P_4O_4$  tetraphosphoxane heterocycle ( $P = R_2NP$ ).

the remaining Fe–C distances are quite similar to each other (1.76–1.78 Å).

Comparison to the original  $Mo_2P_4O_4$  geometry reveals the slightly more compact  $Cr_2P_4O_4$  core in complex **19a** with shorter average Cr–P distances of 2.332(3) Å compared to 2.501(2) Å in the former.<sup>21</sup> Average cage P–O–P angles are also less in **19a** (128.0(3)°) than in the molybdenum cage (131.0(2)°). Further, the intracage Cr–Cr separation is down to 5.656(1) Å from the Mo–Mo value of 6.001(1) Å. The deviations from idealized octahedral geometry about the metal center are also less in the dichromium cage structure. For example, the axial carbonyls subtend an angle of 172° at Cr and 167° at Mo while the P–M–P angles are 79.7(2)° and 75.96(5)°, respectively, indicative of the better fit of the more compact chromium vertices.

Aside from the distinct coordination modes and conformations of the  $\eta^4$ - $P_4O_4$  ring, comparison of structural details between the **19a** cage and its long chair configurational isomer **19b** revealed only a few dramatic differences. The presence of two strained four-membered CrPOP chelate rings in the latter resulted in two types of wildly differing P–O–P angles of 100.9(2)° and 134.5(2)°. These smaller chelate rings enforced a P–Cr–P angle of 66.5(1)° and a wider C(eq)–Cr–C(eq) angle of 96.9(2)° than similar values in the cage structure of 80° and around 86°, respectively. In spite of these, no significant variations in Cr–P, Cr–C, or P–O distances were found.

The lone precedent for the  $M_2P_6O_6$  core geometry of complex **21** (Figures 7 and 9) is the  $Mo_2(CO)_6[Me-AsO]_6$  complex formed in the reaction of  $Mo(CO)_6$  with  $[Me-AsO]_5$  in the presence of air.<sup>12</sup> A description of the latter

structure as a flattened  $As_6O_6$  cubooctahedron *trans*-capped by  $Mo(CO)_3$  units can also describe the geometry of **21**. The longer As–O distances apparently allowed accommodation of two *fac*- $Mo(CO)_3$  vertices while only smaller  $Cr(CO)_3$  units are incorporated into the hexaphosphoxane core. This superior fit can be seen in the nearly ideal octahedral angles observed at the chromium centers with all their structural details closely mirroring those reported for the acyclic *fac*- $Cr(CO)_3$ -( $PH_3$ )<sub>3</sub>.<sup>22</sup> The considerable decrease of intracage Cr–Cr distance from the  $Cr_2P_4O_4$  cage value of 5.656(1) to 4.700(1) Å in the  $Cr_2P_6O_6$  cage reflects a flattening of the  $P_6O_6$  core. Consistent with this observation, slightly smaller phosphoxane P–O–P angles of around 124° are observed compared to that of 128° in the  $Cr_2P_4O_4$  cage.

All three structures featuring the dimethylpiperidino substituent (**19a**, **19b**, **21**) revealed diaxial positioning of their 2,6-dimethyls. Adoption of this normally unfavored conformation is presumably due to the near-planarity at their ring nitrogens and a similar preference for axial methyls in substituted piperidines containing *N*-nitroso, *N*-acetyl, and *N*-nitro groups.<sup>23</sup>

The novel tridentate coordination geometry of the  $P_4O_4$  ring in the iron–molybdenum complex **25** extends to seven the known ligating modes of the versatile tetraphosphoxane ligand (Figure 12). The long Fe–Mo bond of 3.034(2) Å has ample precedence in known Fe/

(21) Wong, E. H.; Turnbull, M. M.; Hutchinson, K. D.; Valdez, C.; Gabe, E. J.; Lee, F. L.; LePage, Y. *J. Am. Chem. Soc.* **1988**, *110*, 8422.

(22) Huttner, G.; Schelle, S. *J. Organomet. Chem.* **1973**, *47*, 383.

(23) Fraser, R. R.; Grindley, C. *J. Chem. Soc.* **1975**, *53*, 2465. Ripperger, H. *Z. Chem.* **1977**, *17*, 177.



Mo cluster compounds, and its presence ensures the electron-precise nature of the complex.<sup>24</sup> In accord with this dative Fe → Mo bonding, a distinctly strengthened and shorter Mo–C(3) bond *trans* to this interaction of 1.946(8) Å is observed compared to the other Mo–C bonds which range from 1.98 to 2.06 Å.

### Experimental Section

All manipulations were carried out using standard Schlenk techniques under an atmosphere of prepurified nitrogen. Hexane was distilled from CaH<sub>2</sub> and toluene from sodium, while THF was distilled from sodium benzophenone ketyl. Triethylamine was distilled from KOH before use. Phosphorus trichloride, diisopropylamine, dicyclohexylamine, dimethylpiperidine, and xylene were reagent grade chemicals obtained from Aldrich Chemicals. Group 6 metal hexacarbonyls and iron carbonyls were purchased from Pressure Chemicals, Inc. Norbornadiene chromium tetracarbonyl,<sup>25</sup> (NBD)Mo(CO)<sub>4</sub>,<sup>26</sup> (NBD)W(CO)<sub>4</sub>,<sup>27</sup> (cycloheptatriene)Mo(CO)<sub>3</sub>,<sup>28</sup> NiCl<sub>2</sub>·DME, NiBr<sub>2</sub>·DME,<sup>29</sup> NiI<sub>2</sub>·2THF,<sup>30</sup> PdCl<sub>2</sub>(PhCN)<sub>2</sub>,<sup>31</sup> PdBr<sub>2</sub>(PhCN)<sub>2</sub>,<sup>32</sup> and (NBD)PtCl<sub>2</sub><sup>33</sup> were all prepared according to literature methods. The phosphine oxides (iPr<sub>2</sub>N)<sub>2</sub>P(O)H and (Cy<sub>2</sub>N)<sub>2</sub>P(O)H and the triphosphoxane [iPr<sub>2</sub>NPO]<sub>3</sub> were prepared as described previously.<sup>2</sup>

Proton, <sup>13</sup>C{<sup>1</sup>H}, <sup>31</sup>P{<sup>1</sup>H} NMR spectra were recorded on JEOL FX90Q and Bruker AM 360 spectrometers using internal deuterium lock. Proton and <sup>13</sup>C chemical shifts were referenced to internal TMS while <sup>31</sup>P shifts were referenced to external 85% phosphoric acid. Infrared spectra were recorded on a Perkin-Elmer 283B instrument using KBr pellets. Elemental analyses were performed at the University of New Hampshire Instrumentation Center with a Perkin-Elmer 2400 elemental analyzer.

**NiCl<sub>2</sub>[iPr<sub>2</sub>NPO]<sub>4</sub> (1A) and NiBr<sub>2</sub>[iPr<sub>2</sub>NPO]<sub>4</sub> (1B).** The synthesis and elemental analyses of complex **1B** have been described in ref 2. A similar procedure was used to prepare **1A**: A 2.0 g (4.5 mmol) amount of [iPr<sub>2</sub>NPO]<sub>3</sub> and 0.60 g (2.7 mmol) of NiCl<sub>2</sub>·DME were stirred in 30 mL of hexane for 24 h. The yellow suspension turned brown and was filtered, and the residue was washed with hexane. After dissolution of the brown solid in CH<sub>2</sub>Cl<sub>2</sub> and filtration through Celite to remove residual NiCl<sub>2</sub>·DME, the filtrate was evaporated to dryness to give crude **1A** as a brown powder (0.80 g, 44% based on Ni). Although a satisfactory <sup>31</sup>P NMR spectrum was obtained (Table 1), acceptable elemental analyses were not available due to its low stability. IR, ν<sub>POP</sub> 939 cm<sup>-1</sup>.

**PdCl<sub>2</sub>[iPr<sub>2</sub>NPO]<sub>4</sub> (2A) and PdBr<sub>2</sub>[iPr<sub>2</sub>NPO]<sub>4</sub> (2B).** The synthesis and spectral and structural characterization of **2A** were described in ref 2. A similar procedure was used to prepare **2B**: Triphosphoxane [iPr<sub>2</sub>NPO]<sub>3</sub> (0.30 g, 0.68 mmol) and 0.20 g (0.42 mmol) of PdBr<sub>2</sub>·2PhCN were refluxed in 30 mL of hexane for 6 h. The orange suspension turned yellow and after cooling to room temperature was filtered to give a light yellow residue. This was washed with hexane and dried

under reduced pressure to give 0.41 g (40% based on Pd) of **2B**: IR, ν<sub>POP</sub> 896 cm<sup>-1</sup>. Anal. Calcd for C<sub>24</sub>H<sub>56</sub>Br<sub>2</sub>N<sub>4</sub>O<sub>4</sub>P<sub>4</sub>Pd: N, 6.60; C, 33.71; H, 6.60. Found: N, 6.46; C, 34.12; H, 6.77.

**PtCl<sub>2</sub>[iPr<sub>2</sub>NPO]<sub>4</sub> (3).** The triphosphoxane (0.30 g, 0.68 mmol) and 0.15 g (0.42 mmol) of (NBD)PtCl<sub>2</sub> were refluxed in 20 mL of hexane for 6 h. After cooling to room temperature, the white residue was filtered off, washed with hexane, and dried to give 0.27 g (75% based on Pt) of crude **3**. Attempts to further purify this white powder were not successful.

**[Cy<sub>2</sub>NPO]<sub>3</sub>.** The triphosphoxane was prepared from Cy<sub>2</sub>-NPCl<sub>2</sub> as follows: An amount of 27.5 g (87.0 mmol) of Cy<sub>2</sub>-NPCl<sub>2</sub> and 27.0 mL (194 mmol) of triethylamine in 100 mL of THF were chilled in an ice bath. From a dropping funnel, 30 mL of the THF containing 1.70 mL (94.0 mmol) of water was added dropwise over 2 h with rigorous stirring of the reaction mixture. After complete addition, the mixture was allowed to warm to room temperature and then heated to reflux for about 1 h. The thick white precipitate of amine hydrochloride was filtered off and the filtrate evaporated to dryness under reduced pressure. The white residue resulting was then extracted with hot hexane and filtered. Upon cooling, a white solid precipitated which was filtered and dried to give 33 g (56%) of the pure triphosphoxane: IR, ν<sub>POP</sub> 820, 846 cm<sup>-1</sup>. Anal. Calcd for C<sub>36</sub>H<sub>66</sub>N<sub>3</sub>O<sub>3</sub>P<sub>3</sub>: N, 6.16; C, 63.43; H, 9.69. Found: N, 6.29; C, 63.23; H, 9.75.

**NiCl<sub>2</sub>[Cy<sub>2</sub>NPO]<sub>4</sub> (4B).** A 6.2 g (9.1 mmol) amount of triphosphoxane and 1.0 g (4.6 mmol) of NiCl<sub>2</sub>·DME were stirred in 30 mL of hot toluene at 90 °C. After 5 h, the initially yellow suspension became red. Cooling, filtration, and evaporation of the filtrate gave 2.4 g (50% based on Ni) of crude **4A**. This unstable red powder gave satisfactory NMR data but could not be further purified due to ready decomposition.

**NiBr<sub>2</sub>[Cy<sub>2</sub>NPO]<sub>4</sub> (4B).** Triphosphoxane (1.7 g, 2.5 mmol) and NiBr<sub>2</sub>·DME (0.56 g, 1.8 mmol) were stirred in 30 mL of hexane for 24 h. The orange-red suspension turned brown. After filtration and washing with hexane, the residue was dissolved in CH<sub>2</sub>Cl<sub>2</sub> and filtered through Celite to give 1.2 g (60% based on Ni) of orange **4B**: IR, ν<sub>POP</sub> 932 cm<sup>-1</sup>. Anal. Calcd for C<sub>48</sub>H<sub>88</sub>Br<sub>2</sub>N<sub>4</sub>NiO<sub>4</sub>P<sub>4</sub>: N, 4.96; C, 51.12; H, 7.86. Found: N, 4.75; C, 50.93; H, 8.18.

**NiI<sub>2</sub>[Cy<sub>2</sub>NPO]<sub>4</sub> (4C).** A 0.60 g (0.90 mmol) amount of the triphosphoxane and 0.18 g (0.39 mmol) of NiI<sub>2</sub>·2THF were stirred in 30 mL of THF. After 3 h, the purple suspension turned red-purple and was filtered through Celite. The filtrate was evaporated to dryness, washed by hexane, and dried under reduced pressure to give unstable **4C** as a red-purple powder.

**PdCl<sub>2</sub>[Cy<sub>2</sub>NPO]<sub>4</sub> (5A).** Triphosphoxane (1.1 g, 1.6 mmol) and PdCl<sub>2</sub>·2PhCN (0.46 g, 1.2 mmol) were stirred in 30 mL of hexane at 4 °C in the cold room. After 72 h, the orange suspension turned yellow. Filtration, washing with hexane, and drying gave a yellow powder (1.0 g, 77% based on Pd) of crude **5A** which was not further purified: IR, ν<sub>POP</sub> 880 cm<sup>-1</sup>.

**PdBr<sub>2</sub>[Cy<sub>2</sub>NPO]<sub>4</sub> (5B).** Triphosphoxane (1.1 g, 1.6 mmol) and PdBr<sub>2</sub>·2PhCN (0.50 g, 1.1 mmol) were stirred at 4 °C in 30 mL of hexane. After 72 h, the yellow suspension was filtered, and the residue was washed with hexane and dried under reduced pressure to give 0.91 g (70% based on Pd) of complex **5B**: IR, ν<sub>POP</sub> 878 cm<sup>-1</sup>. Anal. Calcd for C<sub>48</sub>H<sub>88</sub>Br<sub>2</sub>N<sub>4</sub>O<sub>4</sub>P<sub>4</sub>Pd: N, 4.77; C, 49.05; H, 7.55. Found: N, 4.61; C, 49.34; H, 7.70.

**PtCl<sub>2</sub>[Cy<sub>2</sub>NPO]<sub>4</sub> (6).** Triphosphoxane (0.44 g, 0.64 mmol) and 0.15 g (0.40 mmol) of PtCl<sub>2</sub>(NBD) were stirred at 4 °C in 20 mL of hexane for 72 h. The white suspension was filtered and dried to give a white solid. Solution <sup>31</sup>P NMR indicated the **6a** isomer to be the major component. Similar reaction at room temperature gave both isomers with **6b** being the major product. Both **6a** and **6b** were too unstable for further purifications.

**NiCl<sub>2</sub>[Cy<sub>2</sub>NPO]<sub>5</sub> (7).** A 2.6 g (3.8 mmol) amount of triphosphoxane and 0.60 g (2.7 mmol) of NiCl<sub>2</sub>·DME were stirred in 40 mL of hexane at room temperature. After 24 h, the dark-yellow suspension was filtered and the residue washed with

(24) Coucouvanis, D.; Salifoglou, A.; Kantzidis, M. G.; Dunham, W. R.; Simopoulos, A.; Kostikas, A. *Inorg. Chem.* **1988**, *27*, 4071. Gorzelli, M.; Nuber, B.; Ziegler, M. L. *J. Organomet. Chem.* **1992**, *436*, 207.

(25) Bennett, M. A.; Pratt, L.; Wilkinson, G. *J. Chem. Soc.* **1961**, 2037.

(26) King, R. B., Ed. *Organometallic Synthesis*; Academic Press: New York, 1965; p 124.

(27) King, R. B.; Fronzaglia, A. *Inorg. Chem.* **1966**, *5*, 1837.

(28) Abel, E. W.; Bennett, M. A.; Burton, R.; Wilkinson, G. *J. Chem. Soc.* **1958**, 4559.

(29) Ward, L. G. L. *Inorg. Synth.* **1972**, *13*, 154.

(30) McMullen, A. K.; Tilley, T. D.; Rheingold, A. L.; Geib, S. J. *Inorg. Chem.* **1990**, *27*, 2228. Brauer, G., Ed. *Handbook of Preparatory Inorganic Chemistry*; Academic Press: New York, 1965; Vol. 2, p 1547.

(31) Doyle, J. R.; Slade, P. E.; Jonassen, H. B. *Inorg. Synth.* **1960**, *6*, 218.

(32) McCrindle, R.; Alyea, E. C.; Ferguson, G.; Dias, S. A.; McAlees, A. J.; Parvez, M. J. *Chem. Soc., Dalton Trans.* **1980**, 137.

(33) Drew, D.; Doyle, J. R. *Inorg. Synth.* **1990**, *28*, 346.



hexane and then dissolved in  $\text{CH}_2\text{Cl}_2$ . This was filtered through Celite and the filtrate evaporated to give 1.65 g (48% based on Ni) of the yellow complex **7**. An analytical sample was prepared by recrystallization from toluene: IR,  $\nu_{\text{POP}}$  863  $\text{cm}^{-1}$ . Anal. Calcd for  $\text{C}_{60}\text{H}_{110}\text{Cl}_2\text{N}_5\text{NiO}_5\text{P}_5$ : N, 5.15; C, 59.24; H, 8.75. Found: N, 5.13; C, 59.26; H, 8.96.

**PdCl<sub>2</sub>[Cy<sub>2</sub>NPO]<sub>5</sub> (8A)**. Triphosphoxane (2.0 g, 2.9 mmol) and 0.60 g (1.5 mmol) of  $\text{PdCl}_2\cdot 2\text{PhCN}$  were refluxed in 40 mL of hexane for 12 h. The orange suspension turned yellow and was cooled and filtered. The yellow residue was washed with hexane and dried under reduced pressure to give 1.6 g (81% based on Pd) of **8A**: IR,  $\nu_{\text{POP}}$  868  $\text{cm}^{-1}$ . Anal. Calcd for  $\text{C}_{60}\text{H}_{110}\text{Cl}_2\text{N}_5\text{O}_5\text{P}_5\text{Pd}$ : N, 5.33; C, 54.85; H, 8.44. Found: N, 5.29; C, 54.49; H, 8.69.

**PdBr<sub>2</sub>[Cy<sub>2</sub>NPO]<sub>5</sub> (8B)**. A 0.90 g (1.3 mmol) amount of triphosphoxane and 0.30 g (0.60 mmol) of  $\text{PdBr}_2\cdot 2\text{PhCN}$  were refluxed in 40 mL of hexane for 12 h. Cooling of the yellow suspension, filtration, hexane washing, and drying of the residue gave the light-yellow solid **8B** (0.60 g, 71% based on Pd): IR,  $\nu_{\text{POP}}$  869  $\text{cm}^{-1}$ . Anal. Calcd for  $\text{C}_{60}\text{H}_{110}\text{Br}_2\text{N}_5\text{O}_5\text{P}_5\text{Pd}$ : N, 4.99; C, 51.38; H, 7.85. Found: N, 4.83; C, 51.45; H, 8.18.

**PtCl<sub>2</sub>[Cy<sub>2</sub>NPO]<sub>5</sub> (9)**. Triphosphoxane (0.44 g, 0.64 mmol) and 0.15 g (0.42 mmol) of  $\text{PtCl}_2(\text{NBD})$  were refluxed in 20 mL of hexane for 16 h. After cooling to room temperature and filtering, the white residue was washed with hexane and dried under reduced pressure to give about 0.47 g (80% based on Pt) of complex **9**. An analytical sample was obtained by recrystallization from toluene: IR,  $\nu_{\text{POP}}$  870  $\text{cm}^{-1}$ . Anal. Calcd for  $\text{C}_{60}\text{H}_{110}\text{Cl}_2\text{N}_5\text{O}_5\text{P}_5\text{Pt}$ : N, 4.69; C, 53.84; H, 7.96. Found: N, 4.67; C, 53.51; H, 8.42.

**Mo(CO)<sub>4</sub>[<sup>18</sup>Pr<sub>2</sub>NPO]<sub>3</sub> (10A) and Mo(CO)<sub>4</sub>[Cy<sub>2</sub>NPO]<sub>3</sub> (10B)**. The synthesis and analyses of complex **10A** were described in ref 2. Complex **10B** was similarly prepared: The triphosphoxane [ $\text{Cy}_2\text{NPO}$ ]<sub>3</sub> (1.0 g, 1.5 mmol) and 0.40 g (1.3 mmol) of  $\text{Mo(CO)}_4(\text{NBD})$  were dissolved in 30 mL of hexane to give a yellow solution. After stirring for 2 h, a pale yellow suspension formed. The solid was filtered off, washed with cold hexane, and dried under reduced pressure to give 1.1 g (91% based on Mo) of white complex **10B**: IR,  $\nu_{\text{CO}}$  2000, 1918, 1889, 1885;  $\nu_{\text{POP}}$  826  $\text{cm}^{-1}$ . Anal. Calcd for  $\text{C}_{40}\text{H}_{66}\text{MoN}_3\text{O}_7\text{P}_3$ : N, 4.72; C, 53.99; H, 7.48. Found: N, 4.78; C, 53.66; H, 7.57.

**Cr(CO)<sub>4</sub>[Cy<sub>2</sub>NPO]<sub>4</sub> (11a)**. Triphosphoxane (1.6 g, 2.3 mmol) and  $\text{Cr(CO)}_4(\text{NBD})$  (0.20 g, 0.78 mmol) were refluxed in 50 mL of hexane for 40 h. Upon cooling to room temperature and standing overnight,  $\text{Cr(CO)}_6$  crystallized out and was filtered off. The solution was decolorized by stirring with alumina and filtering through Celite. The filtrate was then evaporated and the residue recrystallized from hot hexane to give 0.25 g (30% based on Cr) of complex **11a**: IR,  $\nu_{\text{CO}}$ , 2000, 1912, 1896, 1886  $\text{cm}^{-1}$ ;  $\nu_{\text{POP}}$  829  $\text{cm}^{-1}$ . Anal. Calcd for  $\text{C}_{52}\text{H}_{88}\text{CrN}_4\text{O}_8\text{P}_4$ : N, 5.22; C, 58.24; H, 8.21. Found: N, 5.12; C, 58.21; H, 8.35.

**Fe(CO)<sub>3</sub>[Cy<sub>2</sub>NPO]<sub>4</sub> (12)**. Triphosphoxane (0.60 g, 0.88 mmol) and  $\text{Fe}_2(\text{CO})_9$  (0.29 g, 0.80 mmol) were refluxed in 20 mL of hexane for 10 h. After cooling to room temperature and filtering through Celite, the filtrate was evaporated to dryness and the residue chromatographed on an alumina column using 2.5% ethyl acetate/hexane as the eluant. Complex **12** was isolated as a yellow solid and recrystallized from hot hexane to give 0.21 g (25% based on Fe) of **12**: IR,  $\nu_{\text{CO}}$  1995, 1926, 1899  $\text{cm}^{-1}$ ;  $\nu_{\text{POP}}$  832  $\text{cm}^{-1}$ . Anal. Calcd for  $\text{C}_{51}\text{H}_{88}\text{FeN}_4\text{O}_7\text{P}_4$ : N, 5.34; C, 58.43; H, 8.39. Found: N, 5.11; C, 58.77; H, 8.82.

**Fe(CO)<sub>5</sub>[<sup>18</sup>Pr<sub>2</sub>NPO]<sub>4</sub> (13) and "Fe(CO)<sub>4</sub>[<sup>18</sup>Pr<sub>2</sub>NPO]<sub>4</sub>" (14)**. Triphosphoxane (3.4 g, 7.7 mmol) and 2.0 g (5.5 mmol) of  $\text{Fe}_2(\text{CO})_9$  were refluxed in 60 mL of toluene for 18 h. After cooling and filtration through Celite, the filtrate was evaporated to dryness and the residue chromatographed on an alumina column using 2.5% ethyl acetate/hexane as the eluant. The yellow fraction was evaporated to dryness and recrystallized from hot hexane to give a mixture of large yellow cubic crystals of **13** and small light-yellow prisms of **14** suitable for X-ray

studies which were manually separated. Total yield of **13** and **14** was around 20% based on Fe. Anal. Calcd for **13**,  $\text{C}_{27}\text{H}_{56}\text{FeN}_4\text{O}_7\text{P}_4$ : N, 7.69; C, 44.54; H, 7.69. Found: N, 7.57; C, 44.32; H, 7.91. IR,  $\nu_{\text{CO}}$  1999, 1936, 1908  $\text{cm}^{-1}$ ;  $\nu_{\text{POP}}$  829  $\text{cm}^{-1}$ . Anal. Calcd for **14**,  $\text{C}_{28}\text{H}_{56}\text{FeN}_4\text{O}_8\text{P}_4$ : N, 7.41; C, 44.48; H, 7.41. Found: N, 7.38; C, 44.81; H, 7.57. IR,  $\nu_{\text{CO}}$  2047, 1987, 1947, 1933  $\text{cm}^{-1}$ ;  $\nu_{\text{POP}}$  875  $\text{cm}^{-1}$ .

**Cr(CO)<sub>4</sub>[Cy<sub>2</sub>NPO]<sub>4</sub> (11b), Cr<sub>2</sub>(CO)<sub>8</sub>[Cy<sub>2</sub>NPO]<sub>4</sub> (15), and Cr<sub>2</sub>(CO)<sub>7</sub>[Cy<sub>2</sub>NPO]<sub>5</sub> (16)**. The phosphine oxide ( $\text{Cy}_2\text{N})_2\text{P(O)H}$  (4.5 g, 11 mmol) and  $\text{Cr(CO)}_6$  (0.80 g, 3.6 mmol) were refluxed in 20 mL of toluene for 36 h. The dark-brown suspension was allowed to cool and then filtered through Celite. After evaporation of the filtrate, the residue was washed with about 20 mL of acetone and then extracted with 30 mL of hot hexane. The hexane extract was concentrated and chilled to precipitate about 0.61 g (32% based on Cr) of complex **11a**. The filtrate from this contained **11b** and **15** in about a 1:4 ratio according to its <sup>31</sup>P NMR spectrum. Further purification was not attempted. The acetone wash was evaporated to dryness and chromatographed on an alumina column using 0.5% ethyl acetate/hexane as the eluant. A first fraction contained a small amount of unstable  $\text{Cr(CO)}_5\text{OP(H)(NCy}_2)_2$  (IR,  $\nu_{\text{CO}}$  2047, 1975, 1927  $\text{cm}^{-1}$ ;  $\nu_{\text{P=O}}$  968  $\text{cm}^{-1}$ ) and the second gave 0.52 g (20% based on Cr) of **16** upon evaporation: IR,  $\nu_{\text{CO}}$  2005, 1961, 1930, 1905, 1892, 1875  $\text{cm}^{-1}$ ;  $\nu_{\text{POP}}$  900  $\text{cm}^{-1}$ . Anal. Calcd for  $\text{C}_{67}\text{H}_{110}\text{Cr}_2\text{N}_5\text{O}_{12}\text{P}_5$  (**16**): N, 4.88; C, 56.05; H, 7.72. Found: N, 4.43; C, 56.14; H, 8.22.

Complex **16** was also prepared by refluxing 4.5 g (11 mmol) of the phosphine oxide with  $\text{Cr(CO)}_6$  (0.80 g, 3.6 mmol) in 25 mL of xylene for 36 h. The dark brown suspension was cooled and filtered through Celite. The filtrate was evaporated to dryness and extracted with 30 mL of acetone. The acetone extract was dried under reduced pressure and chromatographed on an alumina column using 0.5% ethyl acetate/hexane eluant. A total of 1.7 g (65% based on Cr) of **16** was isolated.

**W<sub>2</sub>(CO)<sub>7</sub>[Cy<sub>2</sub>NPO]<sub>5</sub> (17) and W<sub>2</sub>(CO)<sub>6</sub>[Cy<sub>2</sub>NPO]<sub>4</sub> (18)**. An amount of the phosphine oxide (3.5 g, 8.6 mmol) and  $\text{W(CO)}_6$  (1.0 g, 2.8 mmol) was refluxed in 20 mL of toluene for 48 h. The dark-brown suspension was allowed to cool and filtered through Celite, and the filtrate was evaporated to dryness. The residue was chromatographed on an alumina column with hexane as the eluant. The first fraction to elute was the unstable yellow complex **17**, which was only characterized spectroscopically (Table 1). The second fraction yielded red crystalline complex **18** upon prolonged standing: IR,  $\nu_{\text{CO}}$  2000, 1973, 1930, 1908, 1904, 1876  $\text{cm}^{-1}$ ;  $\nu_{\text{POP}}$  885  $\text{cm}^{-1}$ . Anal. Calcd for  $\text{C}_{54}\text{H}_{88}\text{N}_4\text{O}_{10}\text{P}_4\text{W}_2\cdot 1.5\text{hexane}$ : N, 3.56; C, 48.09; H, 6.93. Found: N, 3.59; C, 47.94; H, 7.20.

**Cr<sub>2</sub>(CO)<sub>8</sub>[DMP-PO]<sub>4</sub> (19a), Cr<sub>2</sub>(CO)<sub>8</sub>[DMP-PO]<sub>4</sub> (19b), and Cr<sub>2</sub>(CO)<sub>7</sub>[DMP-PO]<sub>5</sub> (20)**. The phosphine oxide ( $\text{DMP})_2\text{P(O)H}$  (3.0 g, 11 mmol; synthesized from  $\text{DMP}_2\text{-PCL}$  in the same way as the dialkylaminophosphine oxides described in ref 2) and  $\text{Cr(CO)}_6$  (0.90 g, 4.1 mmol) were refluxed in 20 mL of toluene for 48 h. The dark-brown suspension was allowed to cool and filtered through Celite. The filtrate was evaporated to dryness and chromatographed on an alumina column using hexane eluant. The fraction collected was recrystallized from hexane to give complex **20** (0.28 g, 18% based on Cr): IR,  $\nu_{\text{CO}}$  2011, 1963, 1933, 1912, 1898, 1869  $\text{cm}^{-1}$ ;  $\nu_{\text{POP}}$  898  $\text{cm}^{-1}$ . The mother liquor was concentrated and a small amount of **19a** (0.10 g, 5%) crystallized out: IR,  $\nu_{\text{CO}}$  2006, 1942, 1892  $\text{cm}^{-1}$ ;  $\nu_{\text{POP}}$  819  $\text{cm}^{-1}$ . Prolonged standing gave 40 mg (2%) of large crystals of complex **19b**: IR,  $\nu_{\text{CO}}$  2004, 1927, 1908, 1897  $\text{cm}^{-1}$ ;  $\nu_{\text{POP}}$  881  $\text{cm}^{-1}$ . Anal. Calcd for  $\text{C}_{36}\text{H}_{56}\text{Cr}_2\text{N}_4\text{O}_{12}\text{P}_4$  (**19a**): N, 5.80; C, 44.80; H, 5.80. Found: N, 5.78; C, 45.11; H, 5.93. Calcd for  $\text{C}_{36}\text{H}_{56}\text{Cr}_2\text{N}_4\text{O}_{12}\text{P}_4$  (**19b**): N, 5.80; C, 44.80; H, 5.80. Found: N, 5.77; C, 45.07; H, 6.04. Calcd for  $\text{C}_{42}\text{Cr}_2\text{H}_{70}\text{N}_5\text{O}_{12}\text{P}_5\cdot 1.3\text{hexane}$  (**20**): N, 5.78; C, 49.61; 7.33. Found: N, 5.96; C, 49.35; H, 6.95.

**Cr<sub>2</sub>(CO)<sub>6</sub>[DMP-PO]<sub>6</sub> (21)**. Phosphine oxide (0.10 g, 0.37 mmol) and  $\text{Cr}_2(\text{CO})_7[\text{DMP-PO}]_5$  (complex **20**; 0.10 g, 0.090

Table 9. Crystallographic Data for Complexes 14, 19a, 19b, 21, and 25

	14	19a	19b	25	21
(a) Crystal Parameters					
formula	C <sub>28</sub> H <sub>56</sub> FeN <sub>4</sub> O <sub>8</sub> P <sub>4</sub>	C <sub>36</sub> H <sub>56</sub> Cr <sub>2</sub> N <sub>4</sub> O <sub>12</sub> P <sub>4</sub>	C <sub>36</sub> H <sub>56</sub> Cr <sub>2</sub> N <sub>4</sub> O <sub>12</sub> P <sub>4</sub>	C <sub>34</sub> H <sub>62</sub> FeMoN <sub>4</sub> O <sub>11</sub> P <sub>4</sub>	C <sub>56</sub> H <sub>94</sub> Cr <sub>2</sub> N <sub>6</sub> O <sub>12</sub> P <sub>6</sub>
formula weight	756.5	964.7	964.7	978.5	1333.2
crystal system	monoclinic	monoclinic	triclinic	monoclinic	triclinic
space group	<i>C2/c</i>	<i>I2/a</i>	<i>P1̄</i>	<i>P2<sub>1</sub>/c</i>	<i>P1̄</i>
<i>a</i> , Å	42.583(14)	27.593(8)	9.905(3)	20.200(13)	10.650(2)
<i>b</i> , Å	13.298(4)	18.105(7)	11.668(4)	12.003(4)	12.407(3)
<i>c</i> , Å	14.828(4)	18.648(5)	12.189(3)	21.881(12)	13.064(3)
$\alpha$ , deg			96.62(2)		106.64(2)
$\beta$ , deg	109.48(3)	91.45(2)	110.81(2)	117.45(2)	93.60(2)
$\gamma$ , deg			112.59(2)		95.92(2)
<i>V</i> , Å <sup>3</sup>	7916.3(4)	9313	1162.9(5)	4708(4)	1637.3(6)
<i>Z</i>	8	8	1	4	1
cryst dimens, mm	0.25 × 0.28 × 0.44	0.40 × 0.40 × 0.45	0.40 × 0.40 × 0.45	0.25 × 0.30 × 0.30	0.18 × 0.30 × 0.60
cryst color	yellow	colorless	yellow	colorless	colorless
<i>D</i> <sub>calc</sub> , g cm <sup>-3</sup>	1.270	1.376	1.378	1.381	1.352
$\mu$ (Mo K $\alpha$ ), cm <sup>-1</sup>	5.89	6.47	6.47	7.64	5.39
temp, K	244	296	296	233	237
(b) Data Collection					
diffractometer			Siemens P4		
monochromator			graphite		
radiation			Mo K $\alpha$ ( $\lambda$ = 0.710 73 Å)		
2 $\theta$ scan range, deg	4.0–52.0	4.0–52.0	4.0–52.0	4.0–54.0	4.0–50.0
data collected ( <i>h, k, l</i> )	±49, ±16, ±18	±34, ±22, ±22	±12, ±14, ±15	±22, ±15, ±27	±12, ±14, ±15
no. of colld rflns	8467	9465	4799	11220	6055
no. of ind rflns	7747	9164	4571	11043	5778
no. of ind obsd rflns	4391	5611	3489	5730	4515
$F_o \geq n\sigma(F_o)$ ( $n = 4$ )					
std rflns	3 std/197 rflns	3 std/197 rflns	3 std/197 rflns	3 std/197 rflns	3 std/197 rflns
var in std, %	2	<1	2	1	2
(c) Refinement					
<i>R</i> ( <i>F</i> ), %	6.08	5.89	4.81	5.49	4.66
<i>R</i> ( <i>wF</i> ), %	6.97	6.95	6.99	5.72	5.19
$\Delta/\sigma$ (max)	0.031	0.598	0.108	0.549	0.054
$\Delta(\rho)$ , eÅ <sup>-3</sup>	0.67	1.10	1.02	0.65	0.94
<i>N</i> <sub>o</sub> / <i>N</i> <sub>v</sub>	10.8	10.7	13.3	11.3	12.9
GOF	1.28	1.35	1.20	1.10	1.44

mmol) were refluxed in 20 mL of xylene for 6 h. After cooling to room temperature and filtration, the solid residue was recrystallized from toluene to give 0.10 g (90% based on **20**) of complex **21**: IR,  $\nu_{CO}$  1949, 1893, 1876 cm<sup>-1</sup>;  $\nu_{POP}$  912 cm<sup>-1</sup>. Slow cooling of a hot xylene solution of **21** gave X-ray quality crystals. Anal. Calcd for C<sub>48</sub>H<sub>84</sub>Cr<sub>2</sub>N<sub>4</sub>O<sub>12</sub>P<sub>4</sub>·2toluene: N, 5.96; C, 52.79; H, 7.09. Found: N, 5.82; C, 52.21; H, 7.14.

**Mo<sub>2</sub>(CO)<sub>8</sub>[DMP-PO]<sub>4</sub> (22).** The phosphine oxide (DMP)<sub>2</sub>P-(O)H (1.0 g, 3.6 mmol) and 0.50 g Mo(CO)<sub>6</sub> (1.8 mmol) were refluxed in 20 mL of toluene for 48 h. The dark-brown suspension was cooled, filtered through Celite, and the filtrate was evaporated to dryness. Chromatography of the residue on an alumina column using hexane yielded a white solid. It was recrystallized from hexane to give 0.31 g (32% based on Mo) of **22**: IR,  $\nu_{CO}$  2012, 1928, 1914, 1898 cm<sup>-1</sup>;  $\nu_{POP}$  885 cm<sup>-1</sup>. Anal. Calcd for C<sub>36</sub>H<sub>56</sub>Mo<sub>2</sub>N<sub>4</sub>O<sub>12</sub>P<sub>4</sub>: N, 5.32; C, 41.09; H, 5.32. Found: N, 5.28; C, 41.19; H, 5.50.

**Mo(CO)<sub>4</sub>[Cy<sub>2</sub>NPO]<sub>4</sub>NiBr<sub>2</sub> (23).** The complex NiBr<sub>2</sub>[Cy<sub>2</sub>NPO]<sub>4</sub> (0.45 g, 0.40 mmol of **4B**) and Mo(CO)<sub>4</sub>(NBD) (0.12 g, 0.40 mmol) were stirred in 25 mL of toluene at 90 °C for 3 h. The clear red solution turned pale brown as the reaction progressed. After cooling and filtration through Celite, the filtrate was evaporated and the residue chromatographed on an alumina column using 2.5% ethyl acetate/hexane as the eluant. The red-brown solid isolated was 0.25 g (47% based on Mo) of complex **23**: IR,  $\nu_{CO}$  2022, 1945, 1928, 1909 cm<sup>-1</sup>;  $\nu_{POP}$  904 cm<sup>-1</sup>. Anal. Calcd for C<sub>52</sub>H<sub>88</sub>Br<sub>2</sub>MoN<sub>4</sub>NiO<sub>8</sub>P<sub>4</sub>: N, 4.19; C, 46.79; H, 6.59. Found: N, 4.10; C, 46.76; H, 6.87.

**Mo(CO)<sub>3</sub>[Cy<sub>2</sub>NPO]<sub>5</sub>PdCl<sub>2</sub> (24).** The complex PdCl<sub>2</sub>[Cy<sub>2</sub>NPO]<sub>5</sub> (0.26 g, 0.20 mmol of **4A**) and Mo(CO)<sub>4</sub>(NBD) (60 mg, 0.20 mmol) were stirred in 30 mL of toluene at 90 °C for 5 h. After cooling to room temperature and filtration through Celite, the filtrate was evaporated to dryness. The residue was then chromatographed on an alumina column using 5%

ethyl acetate/hexane eluant. The pale-yellow solid complex **24** was isolated (0.12 g, 40% based on Mo): IR,  $\nu_{CO}$  1979, 1912, 1902, 1890 cm<sup>-1</sup>;  $\nu_{POP}$  919 cm<sup>-1</sup>. Anal. Calcd for C<sub>63</sub>H<sub>110</sub>Cl<sub>2</sub>MoN<sub>5</sub>O<sub>8</sub>P<sub>5</sub>Pd: N, 4.69; C, 50.69; H, 7.37. Found: N, 4.36; C, 50.41; H, 7.78.

**Mo(CO)<sub>4</sub>[Pr<sub>2</sub>NPO]<sub>4</sub>Fe(CO)<sub>3</sub> (25).** The complex Fe(CO)<sub>3</sub>-[Pr<sub>2</sub>NPO]<sub>4</sub> (0.20 g, 0.27 mmol of **13**) and Mo(CO)<sub>4</sub>(NBD) (0.10 g, 0.33 mmol) were refluxed in 20 mL of hexane for 5 h. After cooling, the solution was evaporated to dryness and chromatographed on an alumina column using 0.5% ethyl acetate/hexane as the eluant. The isolated product was recrystallized from benzene/hexane to give 0.19 g (75% based on Fe) of **25** as pale yellow crystals suitable for X-ray analysis: IR,  $\nu_{CO}$  2021, 1999, 1962, 1944, 1922, 1912, 1899, 1877, 1869 cm<sup>-1</sup>;  $\nu_{POP}$  873 cm<sup>-1</sup>. Anal. Calcd for C<sub>31</sub>H<sub>56</sub>FeMoN<sub>4</sub>O<sub>11</sub>P<sub>4</sub>: N, 5.98; C, 39.78; H, 5.98. Found: N, 6.03; C, 39.83; H, 5.98.

**Ni(CO)<sub>2</sub>[Cy<sub>2</sub>NPO]<sub>4</sub>Ni(CO)<sub>2</sub> (26).** NiBr<sub>2</sub>[Cy<sub>2</sub>NPO]<sub>4</sub> (1.50 g, 1.3 mmol) and Fe<sub>2</sub>(CO)<sub>9</sub> (0.48 g, 1.3 mmol) were stirred in 40 mL of toluene at 90 °C. After 2 h, the suspension was cooled to room temperature and filtered through Celite. The filtrate was evaporated to dryness and the residue chromatographed on an alumina column using 2.5% ethyl acetate/hexane eluant. A yield of 0.27 g (18% based on Ni) of white complex **26** was isolated: IR,  $\nu_{CO}$  2000, 1947 cm<sup>-1</sup>;  $\nu_{POP}$  870 cm<sup>-1</sup>. Anal. Calcd for C<sub>52</sub>H<sub>88</sub>N<sub>4</sub>Ni<sub>2</sub>O<sub>8</sub>P<sub>4</sub>: N, 4.92; C, 54.89; H, 7.73. Found: N, 4.71; C, 54.87; H, 8.11.

**Crystallographic Studies.** Crystal, data collection, and refinement parameters are listed in Table 9. Single crystals of complexes **14**, **19a**, and **19b** were grown from saturated hexane solutions. Crystals of **21** and **25** were from xylene and benzene, respectively. Suitable crystals were selected and mounted on glass fibers with epoxy cement. The unit cell parameters were obtained by least-squares refinement of the

angular settings of 25 reflections ( $20^\circ \leq 2\theta \leq 25^\circ$ ). The XABS program was used to correct the data for absorption for **25**.<sup>34</sup>

The systematic absences in the diffraction data for **14** are consistent for space groups  $C2/c$  and  $Cc$ ; for **19a**,  $I2/a$  and  $Ia$ ; for **19b** and **21**,  $P1$  and  $P1$ ; and uniquely for **25**,  $P2_1/c$ . The  $E$ -statistics suggested the centrosymmetric alternatives for **14**, **19a**, **19b**, and **21** and were verified by subsequent refinements.

The centers of the molecules of **19b** and **25** are located on inversion centers. In **21** and **25**, several peaks on the Fourier difference maps, not connected with the compound molecules, were observed and modeled as *p*-xylene and benzene, respectively. These solvent molecules were isotropically refined.

All structures were solved by direct methods, completed by subsequent difference Fourier syntheses, and refined by full-matrix least-squares procedures. All non-hydrogen, nonsol-

vent atoms were refined with anisotropic displacement coefficients. Hydrogen atoms were treated as idealized contributions.

All software and sources of the scattering factors are contained in either in SHELXTL (5.1) or the SHELXTL PLUS (4.2) program libraries (G. Sheldrick, Siemens XRD, Madison, WI).

**Acknowledgment.** We acknowledge financial support from the Petroleum Research Fund, administered by the American Chemical Society.

**Supplementary Material Available:** Listings of atomic coordinates, anisotropic thermal factors, and complete bond distances and angles (35 pages). Ordering information is given on any current masthead page.

---

(34) Hope, H.; Moezzi, B., University of California, Davis, CA.

OM940442H

**Synthesis, Characterization, and Reactions of the  
Cluster Complexes Containing the Tetrahedral Cluster  
Core MFeCoS (M = Mo, W) and a Functionally  
Substituted Cyclopentadienyl Ligand. The Single  
Crystal X-ray Structures of Two Double Clusters,  
[ $\eta^5\text{-C}_5\text{H}_4\text{C}(\text{O})\text{CH}_2\text{CH}_2\text{C}(\text{O})\text{C}_5\text{H}_4\text{-}\eta^5$ ]-  
[M(CO)<sub>2</sub>Fe(CO)<sub>3</sub>Co(CO)<sub>3</sub>( $\mu_3\text{-S}$ )]<sub>2</sub> (M = Mo, W)<sup>†</sup>**

Li-Cheng Song,\* Jin-Yu Shen, and Qing-Mei Hu

*Department of Chemistry, Nankai University, Tianjin 300071, People's Republic of China*

Xiao-Ying Huang

*State Key Laboratory of Structural Chemistry,  
Fuzhou, Fujian 350002, People's Republic of China*

Received June 6, 1994<sup>⊗</sup>

Reactions of monoanions  $\eta^5\text{-RC}_5\text{H}_4(\text{CO})_3\text{M}^-$  with  $\text{FeCo}_2(\text{CO})_9(\mu_3\text{-S})$  gave the functional cluster complexes  $\eta^5\text{-RC}_5\text{H}_4(\text{CO})_2\text{MFeCo}(\text{CO})_6(\mu_3\text{-S})$  (**1a-e**, M = Mo, R = CO<sub>2</sub>Me, CO<sub>2</sub>Et; M = W, R = CO<sub>2</sub>Me, CO<sub>2</sub>Et, C(O)Me). **1e** reacted with MeMgI, followed by hydrolysis, giving tertiary alcohol cluster  $\eta^5\text{-Me}_2\text{C}(\text{OH})\text{C}_5\text{H}_4(\text{CO})_2\text{WFeCo}(\text{CO})_6(\mu_3\text{-S})$  (**2**), while it reacted with NaBH<sub>4</sub> to give the secondary alcohol cluster  $\eta^5\text{-MeCH}(\text{OH})\text{C}_5\text{H}_4(\text{CO})_2\text{WFeCo}(\text{CO})_6(\mu_3\text{-S})$  (**3**). Treatment of **3** with Et<sub>3</sub>OBf<sub>4</sub> afforded both a single cluster ether complex,  $\eta^5\text{-MeCH}(\text{OEt})\text{C}_5\text{H}_4(\text{CO})_2\text{WFeCo}(\text{CO})_6(\mu_3\text{-S})$  (**4**), and a double cluster ether complex,  $(\eta^5\text{-C}_5\text{H}_4\text{MeCHO-CHMeC}_5\text{H}_4\text{-}\eta^5)[(\text{CO})_2\text{WFeCo}(\text{CO})_6(\mu_3\text{-S})]_2$  (**5**). Similarly, reactions of dianions  $^-\text{M}(\text{CO})_3[\eta^5\text{-C}_5\text{H}_4\text{C}(\text{O})\text{CH}_2\text{CH}_2\text{C}(\text{O})\text{C}_5\text{H}_4\text{-}\eta^5](\text{CO})_3\text{M}^-$  with two molecules of  $\text{FeCo}_2(\text{CO})_9(\mu_3\text{-S})$  gave 1,4-succinoyl(biscyclopentadienyl)-bridged double cluster complex  $[\eta^5\text{-C}_5\text{H}_4\text{C}(\text{O})\text{CH}_2\text{CH}_2\text{C}(\text{O})\text{C}_5\text{H}_4\text{-}\eta^5][(\text{CO})_2\text{MFeCo}(\text{CO})_6(\mu_3\text{-S})]_2$  (**6a**, M = Mo, **6b**, M = W). These complexes could be further reduced by NaBH<sub>4</sub> to give dihydroxyl derivatives  $[\eta^5\text{-C}_5\text{H}_4\text{CH}(\text{OH})\text{CH}_2\text{CH}_2\text{CH}(\text{OH})\text{C}_5\text{H}_4\text{-}\eta^5][(\text{CO})_2\text{MFeCo}(\text{CO})_6(\mu_3\text{-S})]_2$  (**7a**, M = Mo; **7b**, M = W). Treatment of **7a** and **7b** with Et<sub>3</sub>OBf<sub>4</sub> afforded two unexpected double clusters containing a biscyclopentadienyl-substituted tetrahydrofuran bridge  $(\alpha\text{-}\eta^5\text{-C}_5\text{H}_4\text{-C}_4\text{H}_6\text{O-C}_5\text{H}_4\text{-}\eta^5\text{-}\alpha)[(\text{CO})_2\text{MFeCo}(\text{CO})_6(\mu_3\text{-S})]_2$  (**8a**, M = Mo, **8b**, M = W). X-ray structures of **6a** and **6b** have been determined. Crystal data for **6a**: triclinic, space group *P*-1 (No. 2), *a* = 7.602(3) Å, *b* = 8.112(4) Å, *c* = 16.208(3) Å,  $\alpha$  = 97.58(3)°,  $\beta$  = 94.05(2)°,  $\gamma$  = 109.50(3)°, *V* = 927(1) Å<sup>3</sup>, *Z* = 1. Crystal data for **6b**: monoclinic, space group *C*2/*c* (No. 15), *a* = 26.448(7) Å, *b* = 9.660(4) Å, *c* = 14.687(5) Å,  $\beta$  = 100.72(2)°, *V* = 3687(4) Å<sup>3</sup>, *Z* = 4.

### Introduction

In recent years transition metal cluster complexes have been receiving considerable attention, largely because of their potential applications in catalysis and because of the novelty and versatility of their reactions and structures.<sup>1-13</sup> Among these, however, there are very few cluster complexes containing a functionally

substituted cyclopentadienyl ligand attached to group 6 metals,<sup>14</sup> although the corresponding mono-,<sup>15,16</sup> di-

<sup>†</sup> Dedicated to Professor Dietmar Seyferth, on the occasion of his 65th birthday and in recognition of his outstanding contributions to organometallic chemistry.

<sup>⊗</sup> Abstract published in *Advance ACS Abstracts*, November 1, 1994.

(1) Vahrenkamp, H. In *Transition Metal Chemistry-Current Problems of General, Biological and Catalytic Relevance*; Müller, A., Diemann, E., Eds.; Verlag Chemie, 1981; p 35.

(2) Cotton, F. A.; Chisholm, M. H. *Chem. Eng. News* **1982**, *60*, 40.

(3) Roberts, D. A.; Geoffroy, G. L. In *Comprehensive Organometallic Chemistry*; Wilkinson, G., Stone, F. G. A., Abel, E. W., Eds.; Pergamon Press: Oxford, England, 1982; Vol. 6, pp 763-877.

(4) Muettterties, E. L.; Krause, M. J. *Angew. Chem., Int. Ed. Engl.* **1983**, *22*, 135.

(5) Stone, F. G. A. *Angew. Chem., Int. Ed. Engl.* **1984**, *23*, 89.

(6) Fischer, K.; Müller, M.; Vahrenkamp, H. *Angew. Chem., Int. Ed. Engl.* **1984**, *23*, 140.

(7) Mlekuz, M.; Bougeard, P.; Sayer, B. G.; Faggiani, R.; Lock, C. J. L.; McGlinchey, M. J.; Jaouen, G. *Organometallics* **1985**, *4*, 2046.

(8) Chen, W.; Goh, L. Y.; Mak, T. C. W. *Organometallics* **1986**, *5*, 1997.

(9) Li, P.; Curtis, M. D. *Inorg. Chem.* **1990**, *29*, 1242.

(10) Chetcuti, M. J.; Gordon, J. C.; Fanwick, P. E. *Inorg. Chem.* **1990**, *29*, 3781.

(11) (a) Adams, R. D.; Pompeo, M. P. *Organometallics* **1992**, *11*, 1460. (b) Adams, R. D.; Belinski, J. A. *Organometallics* **1992**, *11*, 2488.

(c) Adams, R. D.; Cortopass, J. E.; Falloon, S. B. *Organometallics* **1992**, *11*, 3794.

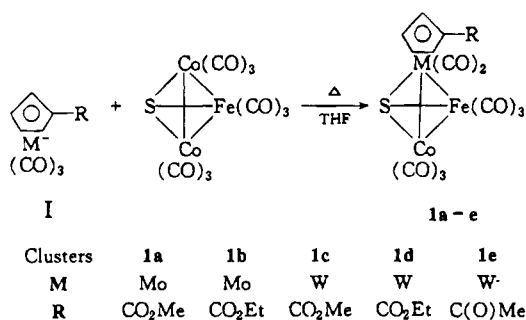
(12) (a) Seyferth, D.; Song, L.-C.; Henderson, R. S. *J. Am. Chem. Soc.* **1981**, *103*, 5103. (b) Seyferth, D.; Henderson, R. S.; Song, L.-C. *Organometallics* **1982**, *1*, 125. (c) Cowie, M.; DeKock, R. L.; Wagenmaker, T. R.; Seyferth, D.; Henderson, R. S.; Gallagher, M. K. *Organometallics* **1989**, *8*, 119. (d) Seyferth, D.; Womack, G. B.; Archer, C. M.; Dewan, J. C. *Organometallics* **1989**, *8*, 430. (e) Seyferth, D.; Womack, G. B.; Archer, C. M.; Fackler, J. P., Jr.; Marler, D. O. *Organometallics* **1989**, *8*, 443.

(13) (a) Song, L.-C.; Kadiata, M.; Wang, J.-T.; Wang, R.-J.; Wang, H.-G. *J. Organomet. Chem.* **1988**, *340*, 239. (b) Song, L.-C.; Kadiata, M.; Wang, J.-T.; Wang, R.-J.; Wang, H.-G. *J. Organomet. Chem.* **1990**, *391*, 387. (c) Song, L.-C.; Hu, Q.-M. *J. Organomet. Chem.* **1991**, *414*, 219. (d) Song, L.-C.; Hu, Q.-M.; Zhang, L.-Y.; Wang, H.; Zhou, Z.-Y.; Liu, L. *J. Organomet. Chem.* **1991**, *412*, C19.

(14) Song, L.-C.; Shen, J.-Y.; Hu, Q.-M.; Wang, R.-J.; Wang, H.-G. *Organometallics* **1993**, *12*, 408.

(15) Macomber, D. W.; Hart, W. P.; Rausch, M. D. *Advances in Organometallic Chemistry*, Academic Press, Inc.: New York, 1982; Vol. 21, p 1.

Scheme 1



15-17 and linear trinuclear<sup>18</sup> complexes have been well-studied. In this article, we wish to report the synthesis, characterization, and some of the interesting reactions of this novel type of cluster complex, as well as the X-ray structure analyses for two such compounds.

## Results and Discussion

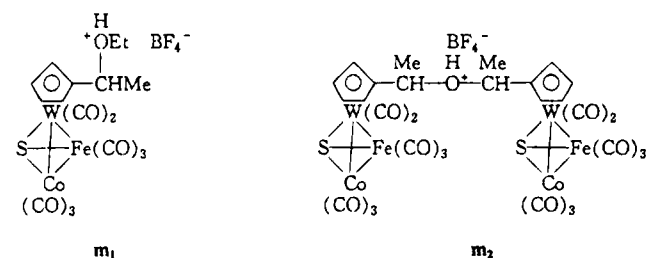
**Part 1. The Chemistry Starting from the Monoanions  $\eta^5\text{-RC}_5\text{H}_4(\text{CO})_3\text{M}^-$  (I). Preparations of 1a-e.** Functionally substituted cyclopentadienyl tricarbonyl group 6 metal anions  $\eta^5\text{-RC}_5\text{H}_4(\text{CO})_3\text{M}^-$  (R = MeCO, MeO<sub>2</sub>C, etc.) (I) have proved to be important in the synthesis of organometallic and metal cluster complexes containing the structural unit  $\eta^5\text{-RC}_5\text{H}_4(\text{CO})_2\text{M}$ .<sup>14-18</sup> This is because the commonly used electrophilic substitution of the cyclopentadienyl ring of their parent compounds could not be applied to prepare this type of complex, due to their inherent lack of aromatic character and/or their decomposition under substitution conditions involved.<sup>14,15</sup> Now we have found an additional use of the monoanions I in the synthesis of the tetrahedral MFeCoS (M = Mo, W) cluster complexes. For instance, complexes 1a-e can be prepared by their reaction with the cluster complex  $\text{FeCo}_2(\text{CO})_9(\mu_3\text{-S})$  in THF at reflux in 41-69% yield, as shown in Scheme 1. Actually, this is an isolobal displacement<sup>19</sup> of  $\text{Co}(\text{CO})_3(\text{d}^9\text{ML}_3)$  in  $\text{FeCo}_2(\text{CO})_9(\mu_3\text{-S})$  by  $\eta^5\text{-RC}_5\text{H}_4(\text{CO})_2\text{M}(\text{d}^5\text{ML}_5)$  generated in situ from the anions I.

However, it is worth noting that our initial attempts to obtain cluster 1e failed when an electrophilic aromatic substitution reaction of the parent compound  $\text{CpWFeCo}(\text{CO})_8(\mu_3\text{-S})$  with acetyl chloride in the presence of  $\text{AlCl}_3$  in  $\text{CH}_2\text{Cl}_2$  at room temperature was tried. From the reaction mixture only 48% of the parent cluster was recovered, showing the inherent lack of aromaticity and the severe decomposition of the parent cluster under the Friedel-Crafts conditions.

**Reactions of 1 and Formation of 2-5.** Although reactions of the functional group of a cyclopentadienyl

ring in mononuclear transition metal complexes, such as ferrocene derivatives<sup>20</sup> and group 6 monometallic compounds,<sup>21</sup> have been extensively studied, the investigations of this kind of reaction involved in dinuclear compounds and especially in cluster systems are relatively few.<sup>15,16c</sup> In principle, the cluster core in cluster complexes may influence the reactivity of the functional group on the cyclopentadienyl ring and also could be destroyed under the reaction conditions used. Rausch reported that  $(\eta^5\text{-carbomethoxycyclopentadienyl})\text{tricarboxylmethyl tungsten}$  was saponified with potassium hydroxide in aqueous methanol at 25 °C to give, after acidification, the corresponding carboxylic acid in 82% yield.<sup>21a</sup> However, treatment of cluster 1c in methanol with aqueous potassium hydroxide, followed by acidification, did not give the expected carboxylic acid. In fact, when potassium hydroxide was added to the solution of 1c, a color change from brown-red to brown-black occurred immediately, presumably due to the decomposition of cluster 1c under the basic conditions of saponification. In contrast to the different hydrolysis behavior of the carbomethoxy group as mentioned above, the acetyl group in cluster 1e showed chemical behavior similar to that of some mononuclear compounds<sup>21b,c</sup> toward Grignard reagents and  $\text{NaBH}_4$ . For instance, 1e reacted with  $\text{MeMgI}$  in ether at room temperature, after hydrolysis of the addition intermediate, to give tertiary alcohol 2 in 39% yield as shown in Scheme 2. Also as shown in Scheme 2, 1e could be reduced by  $\text{NaBH}_4$  in MeOH at room temperature to give secondary alcohol 3 in 55% yield. It is interesting that 3 could further react with triethyloxonium tetrafluoroborate salt  $\text{Et}_3\text{O}^+\text{BF}_4^-$ , as in the case of an organic alcohol,<sup>22</sup> in  $\text{CH}_2\text{Cl}_2$  at room temperature to give the expected alkylation product 4 in 29% yield. However, the reaction also gave an unexpected product, 5, formally viewed as derived by loss of one molecule of water from two molecules of 3, in 31% yield, as shown in Scheme 2.

The mechanisms for ether formation from alcohols under acidic conditions are well-known in organic and organometallic chemistry. So, as in the case of organic alcohols,<sup>22</sup> the alkylation product 4 would be produced through a pathway which involves the attack of the  $\text{Et}^+$  cation generated from dissociation of the oxonium salt at the oxygen atom of hydroxy group of the cluster 3 to form the intermediate  $\mathbf{m}_1$ , followed by loss of  $\text{HBF}_4$ .



However, the carbon atom attached to the Cp ring of the intermediate  $\mathbf{m}_1$  might be possibly further attacked

(20) Bublitz, D. E.; Rinehart, K. L., Jr. In *Organic Reactions*; Dauben, W. G., Ed.; John Wiley & Sons, Inc.: New York, 1969; Vol. 17, pp 1-154.

(21) (a) Macomber, D. W.; Rausch, M. D. *J. Organomet. Chem.* 1983, 258, 331. (b) Rausch, M. D.; Mintz, E. A.; Macomber, D. W. *J. Org. Chem.* 1980, 45, 689. (c) Hart, W. P.; Rausch, M. D. *J. Organomet. Chem.* 1988, 355, 455.

(22) Diem, M. J.; Burow, D. F.; Fry, J. L. *J. Org. Chem.* 1977, 42, 1801.

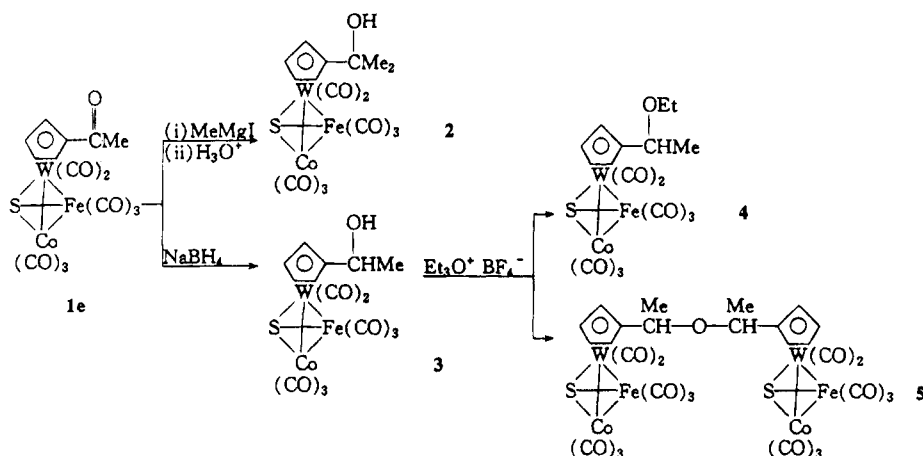
(16) (a) Song, L.-C.; Dong, Q.; Hu, Q.-M. *Acta. Chim. Sin.* 1991, 49, 1129. (b) Song, L.-C.; Dong, Q.; Hu, Q.-M. *Youji Huaxue* 1992, 12, 35. (c) Song, L.-C.; Shen, J.-Y.; Hu, Q.-M. *Sci. China* (series B) 1993, 36, 1281.

(17) (a) Song, L.-C.; Shen, J.-Y. *Chem. J. Chin. Univ.* 1992, 13, 1227. (b) Edelmann, F.; Töfke, S.; Behrens, U. *J. Organomet. Chem.* 1986, 309, 87. (c) Avey, A.; Tenhaeff, S. C.; Weakley, T. J. R.; Tyler, D. R. *Organometallics* 1991, 10, 3607.

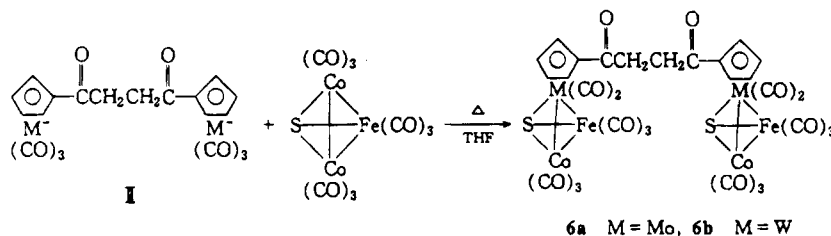
(18) (a) Song, L.-C.; Dong, Q.; Hu, Q.-M. *Acta Chim. Sin.* 1992, 50, 193. (b) Song, L.-C.; Yang, H.; Dong, Q.; Hu, Q.-M. *J. Organomet. Chem.* 1991, 414, 137. (c) Medina, R. M.; Masaguer, J. R.; Moran, M.; Losada, J. *Inorg. Chim. Acta* 1988, 146, 115.

(19) (a) Hoffmann, R. *Angew. Chem., Int. Ed. Engl.* 1982, 21, 711. (b) Vahrenkamp, H. *Comments Inorg. Chem.* 1985, 4, 253. (c) Kaganovich, V. S.; Slovokhotov, Yu. L.; Mironov, A. V.; Struchkov, Yu. T.; Rybinskaya, M. I. *J. Organomet. Chem.* 1989, 372, 339.

Scheme 2



Scheme 3



6a M = Mo, 6b M = W

by the nucleophilic oxygen atom of the hydroxyl group of **3** with loss of one molecule of EtOH to generate another intermediate, **m<sub>2</sub>**. Then, **5** would be finally afforded from **m<sub>2</sub>** by loss of HBF<sub>4</sub>. Interestingly, to our knowledge, this reaction is the first example so far for producing a symmetrical double cluster ether such as **5** by the action of a trialkyloxonium salt upon the corresponding alcohol. However, the detailed mechanism for this reaction still needs further study.

**Characterization of 1a-e and 2-5.** Compounds **1a-e** are solid colored from brown-red to black, while **2-5** are red viscous oils. They were all fully characterized by elemental analysis and IR, <sup>1</sup>H NMR and MS spectroscopies. In their IR spectra all showed terminal carbonyl absorption bands<sup>23</sup> in the range of 2082–1901 cm<sup>-1</sup>, and bridging carbonyls<sup>23</sup> might exist for **1a,c,e** and **3-5**, evidenced by one absorption band present between 1860 and 1890 cm<sup>-1</sup>. The IR spectra of **1a-e** also showed corresponding carbonyl absorption bands of ester at around 1720 cm<sup>-1</sup> and acetyl at 1685 cm<sup>-1</sup>, while the IR spectra of **2** and **3** showed the hydroxyl group at around 3427 cm<sup>-1</sup>. As we know, <sup>1</sup>H NMR spectra of a monosubstituted cyclopentadienyl ring in transition metal compounds vary greatly in complexity, such as a single resonance, an A<sub>2</sub>B<sub>2</sub> or A<sub>2</sub>BB' pattern or a multiplet pattern, all depending on the nature of the substituent.<sup>21</sup> For the <sup>1</sup>H NMR spectra of **1a-e**, the four protons on the cyclopentadienyl ring exhibited an A<sub>2</sub>BB' pattern. The A<sub>2</sub>BB' pattern consisted of two closely spaced quartets of relative intensity 1H upfield from 5.40 ppm and a triplet (or a quartet for **1e**) of relative intensity 2H downfield from 6.04 ppm. The two upfield quartets had been assigned to the H<sup>3</sup> and H<sup>4</sup> protons remote from the electron-withdrawing substituent,

since they were deshielded to a less extent than H<sup>2</sup> and H<sup>5</sup> close to the substituent. We believe that the A<sub>2</sub>BB' pattern was caused by the chirality of the tetrahedral cluster core MFeCoS. It is the chiral core that makes H<sup>3</sup> and H<sup>4</sup> protons diastereotopic. However, at present, we do not fully understand why H<sup>3</sup> and H<sup>4</sup> are diastereotopic whereas H<sup>2</sup> and H<sup>5</sup> are not. Perhaps, this is due to H<sup>3</sup> and H<sup>4</sup> being closer than H<sup>2</sup> and H<sup>5</sup> to the chiral cluster core. In contrast to the <sup>1</sup>H NMR spectra of **1a-e**, the <sup>1</sup>H NMR spectra of the cyclopentadienyl protons of **2-5** showed more complicated patterns. Obviously, this can be attributed (except for cluster **2**) to the influences from both the chiral cluster core and the chiral α-carbon atom attached to cyclopentadienyl ring.

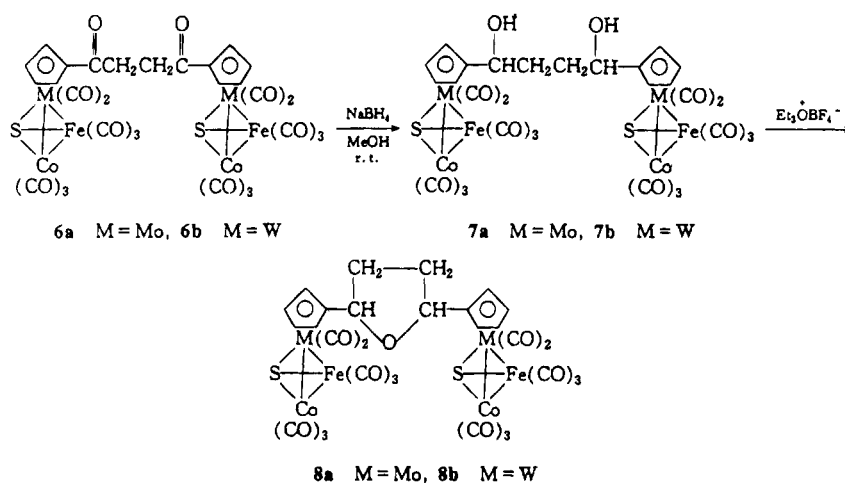
The mass spectra of **1a,b,d,e** and **4** showed their parent ion peaks, the fragment ion peaks of successive loss of a given number of CO from parent ion, the respective cluster core peaks, and so on. Although no parent ion peaks appeared in the mass spectra of **1c**, **2**, and **3**, the peaks of corresponding fragment ions similar to those mentioned above existed.

**Part 2. The Chemistry Generated from the Bridging Dianions (η<sup>5</sup>-C<sub>5</sub>H<sub>4</sub>C(O)CH<sub>2</sub>CH<sub>2</sub>C(O)C<sub>5</sub>H<sub>4</sub>-η<sup>5</sup>)(CO)<sub>6</sub>M<sub>2</sub><sup>2-</sup> (II). Preparations of **6a,b**.** Reactions of 1,4-succinoylbis(cyclopentadienyl)sodium with Mo(CO)<sub>6</sub> in THF or with W(CO)<sub>6</sub> in diglyme at reflux for several hours gave dianions II, which could react in situ with two molecules of FeCo<sub>2</sub>(CO)<sub>9</sub>(μ<sub>3</sub>-S), through d<sup>5</sup>ML<sub>5</sub>/d<sup>9</sup>ML<sub>3</sub> double isolobal displacement, to afford **6a** and **6b** in 31% and 43% yields, respectively, as shown in Scheme 3. This type of double isolobal displacement, to our knowledge, is unprecedented.

**Reactions of **6a,b** and Formation of **7a,b** and **8a,b**.** The functionality in double cluster complexes **6a** and **6b**, just like those in the above single cluster complexes, could be transformed into other functional-

(23) Collman, J. P.; Hegedus, L. S.; Norton, J. R.; Finke, R. G. *Principles and Applications of Organotransition Metal Chemistry*; 2nd ed.; California University Science Books: Mill Valley, 1987.

Scheme 4

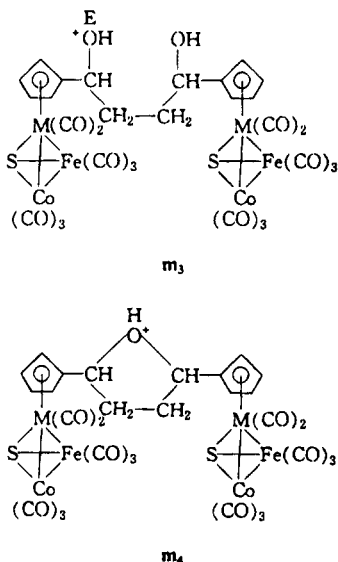


ities. Thus, **6a** and **6b** reacted with  $\text{NaBH}_4$  in  $\text{CH}_3\text{OH}$  at room temperature, giving dihydroxy derivatives **7a** and **7b** in 31% and 23% yields, as shown in Scheme 4.

Interestingly, the 1,4-dihydroxybutylene group in **7a** and **7b**, under the action of  $\text{Et}_3\text{OBF}_4$  in  $\text{CH}_2\text{Cl}_2$  at reflux, was converted into an  $\alpha, \alpha'$ -disubstituted tetrahydrofuran ring affording **8a** and **8b** in 90% and 89% yields, as shown in Scheme 4.

TLC showed no formation of **8a** and **8b** below  $0^\circ\text{C}$  after 2 h, while **8a** and **8b** were produced at  $18^\circ\text{C}$  after 2 h in 86% and 39% yields, respectively. **8a** and **8b** might also be produced by use of  $\text{HBF}_4$  or  $\text{HCl}$  instead of  $\text{Et}_3\text{OBF}_4$ , in spite of the lower yields. For example, in the case of using  $\text{HBF}_4$  the reaction at reflux for 2 h gave **8a** in 58% yield whereas the reaction, when  $\text{HCl}$  was used, at reflux for 9 h gave **8b** only in 12% yield. The mechanism for producing complexes **8a** and **8b** under these conditions is similar to that for formation of **4** and **5** described above.

The reaction may involve initial attack of electrophilic E (representing  $\text{H}^+$  or  $\text{Et}^+$  generated by dissociation from  $\text{HCl}$ ,  $\text{HBF}_4$  and  $\text{Et}_3\text{OBF}_4$ ) at the oxygen atom of one hydroxy group of **7a** or **7b** to form the intermediate **m<sub>3</sub>**, which in turn loses one molecule of water or ethanol



by the intramolecular attack of the oxygen atom of another hydroxyl group at the carbon atom attached to

EOH moiety to give the protonated species **m<sub>4</sub>**. Finally the **m<sub>4</sub>** loses one proton to give **8a** or **8b**. Although the dehydration from diols leading to a substituted tetrahydrofuran derivatives by the action of proton acid or the others is a known process,<sup>24</sup> the process occurred by the action of  $\text{Et}_3\text{OBF}_4$  to form  $\alpha, \alpha'$ -bis(cyclopentadienyl)-tetrahydrofuran bridged double cluster complexes **8a** and **8b** is unprecedented in literature.

**Characterization of 6a,b, 7a,b, and 8a,b.** Except for **8a**, which is a brown viscous oil, **6a,b**, **7a,b**, and **8b** are brown solids and have been characterized by C/H analysis and IR and  $^1\text{H}$  NMR spectroscopies. In their IR spectra, there exist four absorption bands, in which three bands in the range of  $2077\text{--}1967\text{ cm}^{-1}$  are assigned to terminal carbonyls and one band around  $1885\text{ cm}^{-1}$  is assigned to a bridging carbonyl.<sup>23</sup> Besides these absorptions for carbonyls attached to metals, there is a moderately strong absorption band around  $1682\text{ cm}^{-1}$  for the ketonic carbonyl of **6a,b**, while there is a broad absorption band around  $3400\text{ cm}^{-1}$  for the hydroxyl group of **7a,b**. The  $^1\text{H}$  NMR spectra of cyclopentadienyl protons for double clusters **6a,b**, **7a,b**, and **8a,b** are also as complicated as those for clusters **1–5** mentioned above. This is reasonable because these double clusters all contain the chiral tetrahedral cluster core MFeCoS and **7a,b** and **8a,b** contain the chiral  $\alpha$ -carbon atom attached to the cyclopentadienyl ring as well. For **6a,b** the  $^1\text{H}$  NMR spectra of each cyclopentadienyl protons show an  $\text{A}_2\text{BB}'$  pattern, of which the two upfield sets of quartets are assigned to  $\text{H}^3$  and  $\text{H}^4$  remote from succinyl bridge and the downfield triplet or multiplet is assigned to  $\text{H}^2$  and  $\text{H}^5$  close to the bridge, due to the electron-withdrawing effect of the succinyl group. However, for **7a,b** the  $^1\text{H}$  NMR spectra show two multiplets, while for **8a,b** there is one multiplet. Based on the same reason, for **7a,b** the upfield multiplet should be assigned to  $\text{H}^3$  and  $\text{H}^4$ , while the downfield multiplet is assigned to  $\text{H}^2$  and  $\text{H}^5$ . The chemical shifts of the hydroxyl group for **7a,b** were established by the D/H exchange method, which included adding  $\text{D}_2\text{O}$  to the  $^1\text{H}$  NMR tube and redetermination of the  $^1\text{H}$  NMR of **7a,b**, showing complete disappearance of the peak for the hydroxyl group.

**X-ray Structure Analysis.** In order to confirm the structures of **6a** and **6b**, a study of their X-ray diffrac-

(24) Jacobus, J. J. *Org. Chem.* **1973**, *38*, 403.

**Table 1. Fractional Coordinates and Equivalent Isotropic Thermal Parameters for 6a**

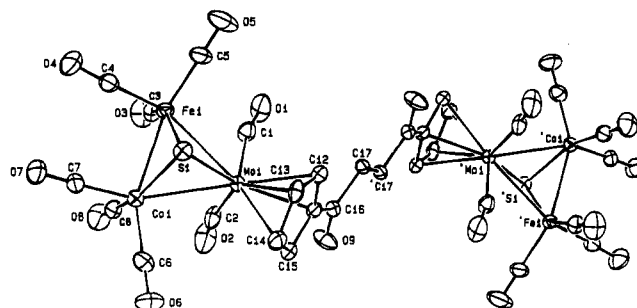
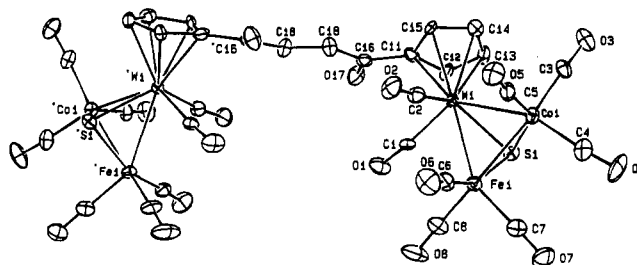
atom	x	y	z	B(eq), Å <sup>2</sup>
Mo(1)	0.4244(1)	0.19938(9)	0.79774(4)	2.39(2)
Co(1)	0.5758(1)	0.4178(1)	0.68230(7)	3.05(4)
Fe(1)	0.2791(1)	0.1434(1)	0.62866(7)	2.81(4)
S(1)	0.5520(3)	0.1417(3)	0.6749(1)	3.05(7)
O(1)	-0.0089(9)	0.026(1)	0.7703(5)	6.6(3)
C(1)	0.155(1)	0.091(1)	0.7688(6)	4.0(4)
O(2)	0.332(1)	0.540(1)	0.8523(5)	7.7(4)
C(2)	0.370(1)	0.419(1)	0.8252(6)	4.3(4)
O(3)	0.004(1)	0.324(1)	0.6297(5)	6.7(4)
C(3)	0.109(1)	0.251(1)	0.6302(5)	3.5(3)
O(4)	0.328(1)	0.152(1)	0.4535(4)	6.2(3)
C(4)	0.313(1)	0.150(1)	0.5230(6)	3.9(3)
O(5)	0.049(1)	-0.233(1)	0.5975(6)	8.0(4)
C(5)	0.135(1)	-0.088(1)	0.6092(6)	4.5(4)
O(6)	0.923(1)	0.611(1)	0.7955(5)	6.7(3)
C(6)	0.789(1)	0.538(1)	0.7518(7)	4.7(4)
O(7)	0.721(1)	0.456(1)	0.5205(4)	5.6(3)
C(7)	0.668(1)	0.443(1)	0.5832(6)	3.6(3)
O(8)	0.387(1)	0.679(1)	0.6852(5)	6.3(3)
C(8)	0.458(1)	0.573(1)	0.6843(5)	3.8(3)
C(11)	0.398(1)	0.135(1)	0.9306(5)	2.8(3)
C(12)	0.409(1)	-0.018(1)	0.8810(5)	3.4(3)
C(13)	0.585(1)	0.026(1)	0.8528(6)	3.5(3)
C(14)	0.686(1)	0.206(1)	0.8858(6)	4.0(4)
C(15)	0.575(1)	0.275(1)	0.9344(5)	3.2(3)
C(16)	0.243(1)	0.151(1)	0.9765(5)	3.1(3)
O(9)	0.251(1)	0.2917(8)	1.0156(4)	5.3(3)
C(17)	0.071(1)	-0.016(1)	0.9732(5)	3.0(3)

**Table 2. Fractional Coordinates and Equivalent Isotropic Thermal Parameters for 6b**

atom	x	y	z	B(eq), Å <sup>2</sup>
W(1)	0.62278(2)	0.27121(5)	0.01240(4)	1.88(2)
Co(1)	0.65727(7)	0.2129(2)	0.1975(1)	2.41(8)
Fe(1)	0.62502(8)	0.0078(2)	0.0925(1)	2.56(9)
S(1)	0.6928(1)	0.1352(3)	0.0845(3)	2.4(1)
O(1)	0.5946(5)	0.080(1)	-0.1606(8)	4.5(6)
C(1)	0.6060(5)	0.145(1)	-0.093(1)	2.3(6)
O(2)	0.5087(4)	0.242(1)	0.034(1)	5.2(6)
C(2)	0.5520(6)	0.245(1)	0.030(1)	3.1(7)
O(3)	0.7125(4)	0.470(1)	0.2517(8)	4.7(6)
C(3)	0.6904(6)	0.370(2)	0.228(1)	3.3(7)
O(4)	0.7070(6)	0.060(1)	0.3629(9)	6.6(8)
C(4)	0.6881(6)	0.113(2)	0.297(1)	3.6(8)
O(5)	0.5579(5)	0.270(1)	0.2466(9)	5.0(6)
C(5)	0.5958(6)	0.244(2)	0.226(1)	3.4(7)
O(6)	0.5234(5)	-0.040(1)	0.139(1)	5.8(7)
C(6)	0.5625(7)	-0.019(2)	0.119(1)	3.5(7)
O(7)	0.6802(5)	-0.198(1)	0.217(1)	6.1(7)
C(7)	0.6579(7)	-0.116(2)	0.171(1)	3.5(8)
O(8)	0.6138(6)	-0.193(1)	-0.058(1)	6.8(8)
C(8)	0.6177(7)	-0.112(2)	0.002(1)	3.5(7)
C(11)	0.6064(6)	0.434(1)	-0.102(1)	3.1(7)
C(12)	0.6600(6)	0.407(2)	-0.084(1)	4.0(8)
C(13)	0.6785(6)	0.457(2)	0.003(1)	3.2(7)
C(14)	0.6384(6)	0.509(2)	0.043(1)	3.1(7)
C(15)	0.5949(6)	0.498(1)	-0.022(1)	3.1(6)
C(16)	0.5712(6)	0.414(1)	-0.196(1)	2.9(7)
O(17)	0.5914(5)	0.391(1)	-0.2643(8)	4.5(6)
C(18)	0.5147(5)	0.425(2)	-0.201(1)	2.9(7)

tion was undertaken. The final fractional coordinates with equivalent isotropic thermal parameters are listed in Tables 1 and 2. Tables 3 and 4 list the selected bond lengths and bond angles. The perspective views of **6a** and **6b** are presented in Figures 1 and 2, respectively.

As seen from Figure 1, the molecule **6a** consists of two identical tetrahedral subclusters, FeMoCoS, carrying eight carbonyls and one 1,4-succinoyl-bridged bis-cyclopentadienyl ligand. The two subclusters are connected through Mo atoms to two  $\eta^5$ -cyclopentadienyl rings in a trans fashion. Among the eight carbonyls attached to the metals, two carbonyls attached to the

**Figure 1.** ORTEP diagram of **6a** showing 30% probability thermal ellipsoids.**Figure 2.** ORTEP diagram of **6b** showing 30% probability thermal ellipsoids.**Table 3. Selected Bond Lengths (Å) and Angles (deg) for 6a**

atoms	distance	atoms	distance
Mo(1)-C(1)	1.937(9)	Fe(1)-S(1)	2.161(2)
Mo(1)-C(2)	1.96(1)	O(1)-C(1)	1.18(1)
Mo(1)-C(11)	2.288(8)	Co(1)-S(1)	2.172(3)
Mo(1)-S(1)	2.335(2)	Co(1)-Fe(1)	2.580(2)
Mo(1)-Co(1)	2.790(2)	C(11)-C(16)	1.47(1)
Mo(1)-Fe(1)	2.801(1)	C(16)-O(9)	1.21(1)
atoms	angle	atoms	angle
C(1)-Mo(1)-C(2)	84.1(4)	S(1)-Fe(1)-Mo(1)	54.31(6)
C(1)-Mo(1)-Fe(1)	62.1(3)	Co(1)-Fe(1)-Mo(1)	62.29(5)
C(2)-Mo(1)-Co(1)	72.5(3)	Fe(1)-S(1)-Co(1)	73.09(8)
S(1)-Co(1)-Fe(1)	53.25(7)	Fe(1)-S(1)-Mo(1)	76.96(7)
S(1)-Co(1)-Mo(1)	54.45(7)	Co(1)-S(1)-Mo(1)	76.38(8)
Fe(1)-Co(1)-Mo(1)	62.74(5)	S(1)-Mo(1)-Co(1)	49.18(6)
S(1)-Fe(1)-Co(1)	53.66(7)	S(1)-Mo(1)-Fe(1)	48.72(6)

**Table 4. Selected Bond Lengths (Å) and Angles (deg) for 6b**

atoms	distance	atoms	distance
W(1)-C(2)	1.95(1)	Fe(1)-S(1)	2.194(4)
W(1)-C(1)	1.96(1)	O(1)-C(1)	1.16(2)
W(1)-C(11)	2.28(1)	Co(1)-S(1)	2.187(4)
W(1)-S(1)	2.355(4)	Co(1)-Fe(1)	2.558(3)
W(1)-Co(1)	2.761(2)	C(11)-C(16)	1.54(2)
W(1)-Fe(1)	2.799(2)	C(16)-O(17)	1.24(2)
atoms	angle	atoms	angle
C(2)-W(1)-C(1)	86.8(6)	S(1)-Fe(1)-W(1)	54.7(1)
C(2)-W(1)-Fe(1)	76.8(4)	Co(1)-Fe(1)-W(1)	61.85(7)
C(1)-W(1)-Fe(1)	75.6(4)	Co(1)-S(1)-Fe(1)	71.4(1)
C(4)-Co(1)-W(1)	156.9(5)	Co(1)-S(1)-W(1)	74.8(1)
S(1)-Co(1)-Fe(1)	54.4(1)	Fe(1)-S(1)-W(1)	75.9(1)
S(1)-Co(1)-W(1)	55.4(1)	S(1)-W(1)-Co(1)	49.8(1)
S(1)-Fe(1)-Co(1)	54.1(1)	S(1)-W(1)-Fe(1)	49.5(1)

Mo atom are semibridging and the other terminal. The existence of both terminal and semibridging CO's confirmed by X-ray diffraction is consistent with the IR spectrum of **6a** described above. For semibridging carbonyls Curtis's definition<sup>25</sup> is  $0.1 \leq \alpha = (d_2 - d_1)/d_2 \leq 0.6$ . Since  $d_2 = \text{Fe(1)-C(1)} = 2.554 \text{ \AA}$  and  $d_1 = \text{Mo(1)-C(1)} = 1.937 \text{ \AA}$ ,  $\alpha$  for C(1)O(1) = 0.32; since  $d_2 =$



Table 5. Comparison of the Bond Lengths (Å) of the Cluster Core in **6a** and **6b** with Those of Two Single Clusters

clusters <sup>a</sup>	Mo-Fe	Mo-Co	Fe-Co	Mo-S	Fe-S	Co-S
CpMoFeCo(CO) <sub>7</sub> L(μ <sub>3</sub> -S)	2.793(2)	2.750(2)	2.568(2)	2.363(3)	2.182(3)	2.170(3)
<b>6a</b>	2.801(1)	2.790(2)	2.580(2)	2.335(2)	2.161(2)	2.172(3)
clusters	W-Fe	W-Co	Fe-Co	W-S	Fe-S	Co-S
CpWFeCo(CO) <sub>7</sub> L(μ <sub>3</sub> -S)	2.792(2)	2.730(2)	2.574(2)	2.348(3)	2.187(3)	2.179(4)
<b>6b</b>	2.799(2)	2.761(2)	2.558(3)	2.355(4)	2.194(4)	2.187(4)

<sup>a</sup> L = MePrPhP.

Co(1)-C(2) = 2.89 Å and  $d_1 = \text{Mo}(1)-\text{C}(2) = 1.96 \text{ \AA}$ ,  $\alpha$  for C(2)O(2) = 0.47. So, they all fall into the  $\alpha$  value range for semibridging carbonyls. Since the angle of Fe(1)Mo(1)C(1) is 62.1°, the C(1)O(1) is bridged across the Mo(1)Fe(1) bond while C(2)O(2) is bridged across the Co(1)Mo(1) bond due to the angle (72.5°) Co(1)Mo(1)C(2). The cyclopentadienyl ring is tilted to the triangular plane Fe(1)-Co(1)-S(1) and gives a dihedral angle of 48.12°. The Mo atom-Cp ring centroid distance is 2.001 Å. Since the dihedral angle between the cyclopentadienyl ring and the plane C(16)-O(9)-C(17) is rather small (4.76°), the  $\pi$ -system of half of the succinoyl bridge C(16)O(9)C(17) would be quite well conjugated with the Cp ring  $\pi$ -system and thus the bond length of C(11)-C(16) (1.47 Å) becomes much shorter than a normal C-C single bond.

Also, **6b** as seen from Figure 2, consists of two identical tetrahedral subclusters, FeCoWS, carrying eight carbonyls and one 1,4-succinoyl-bridged bicyclopentadienyl ligand. Just like **6a**, two carbonyls, i.e., C(1)O(1) and C(2)O(2) attached to the W atom, are semibridging and the other six terminal. This is in good agreement with the IR spectrum of **6b**. However, since the angles Fe(1)W(1)C(1) and Fe(1)W(1)C(2) are 75.6-(4)° and 76.8 (4)°, respectively, these two carbonyls appear to be both bridged across the Fe(1)-W(1) bond. For C(1)O(1),  $\alpha = 0.53$  [since W(1)-C(1) = 1.96(1) Å, Fe(1)-C(1) = 2.99 (1) Å]. For C(2)O(2),  $\alpha = 0.55$  [since W(1)-C(2) = 1.95(1) Å, Fe(1)-C(2) = 3.03(1) Å].<sup>25</sup> The cyclopentadienyl ring of **6b** is tilted to the triangular plane Fe(1)-Co(1)-S(1) and gives a dihedral angle of 46.87°, a value slightly less than that in the case of **6a**. The distance W atom-Cp-ring centroid (1.998 Å) is almost the same as the corresponding one in **6a**. However, the  $\pi$ -system of half of the succinoyl bridge, C(16)-O(17)-C(18), is not well conjugated with the cyclopentadienyl ring  $\pi$ -system, since the dihedral angle between the cyclopentadienyl plane and the plane C(16)-O(17)-C(18) is quite larger (15.32°). This can be reflected by the fact that the bond length of C(11)-C(16) (1.54 Å) is actually the same as the value of a normal C-C single bond.

So far, no double cluster complexes containing tetrahedral subcluster core MFeCoS are reported, although a few such single cluster complexes have appeared in the literature.<sup>26</sup> The related bond lengths for the cluster core of **6a** and **6b** are compared with those of two known single clusters<sup>26d</sup>(+)-CpMoFeCo(CO)<sub>7</sub>(MePrPhP)(μ<sub>3</sub>-S)

and (-)-CpWFeCo(CO)<sub>7</sub>(MePrPhP)(μ<sub>3</sub>-S), as shown in Table 5.

From Table 5 it can be seen that all the corresponding bond lengths are basically the same, except that the Mo-Co bond of **6a** and the W-Co bond of **6b** are slightly longer than those of corresponding bond in (+)-CpMoFeCo(CO)<sub>7</sub>(MePrPhP)(μ<sub>3</sub>-S) and (-)-CpWFeCo(CO)<sub>7</sub>(MePrPhP)(μ<sub>3</sub>-S), respectively.

It should be mentioned that the crystal molecule of **6a** is that of an achiral molecule containing a symmetric center, which is actually one of three possible optical isomers, namely the meso form; the crystal molecule of **6b** is that of a chiral molecule containing a 2-fold symmetric axis, which is the R form of three possible optical isomers. However, no matter what they are, the <sup>1</sup>H NMR spectra of the cyclopentadienyl protons of **6a** and **6b** should show an A<sub>2</sub>BB' pattern as mentioned above. This is because they all contain a chiral tetrahedral subcluster, MFeCoS, which would make the two protons H<sup>3</sup> and H<sup>4</sup> of the cyclopentadienyl diastereotopic.

## Experimental Section

All reactions were carried out under prepurified nitrogen atmosphere using standard Schlenk or vacuum line techniques. THF and diglyme were distilled from sodium-benzophenone ketyl under nitrogen. Column chromatography and TLC were carried out by using silica gel of 300-400 mesh and silica gel G (10-40 μm), respectively. Mo(CO)<sub>6</sub>, W(CO)<sub>6</sub>, and Co<sub>2</sub>(CO)<sub>8</sub> were purchased from Strem Chemicals Inc. Et<sub>3</sub>OBF<sub>4</sub>,<sup>27</sup> FeCo<sub>2</sub>(CO)<sub>9</sub>S,<sup>12c</sup> RC<sub>5</sub>H<sub>4</sub>Na (R = MeCO, MeO<sub>2</sub>C, EtO<sub>2</sub>C),<sup>28,29</sup> and [NaC<sub>5</sub>H<sub>4</sub>C(O)CH<sub>2</sub>]<sub>2</sub><sup>30</sup> were prepared according to literature methods. IR spectra were recorded on a NICOLET FT-IR 5DX infrared spectrophotometer; <sup>1</sup>H NMR spectra were recorded on a JEOL FX 90Q NMR spectrometer. C/H analyses and MS determinations were performed by a 240 C analyzer and HP 5988 A spectrometer, respectively. Melting points were determined on a Yanaco micromelting point apparatus MP-500.

**Preparations of 1a-e.** A 100 mL two-necked flask fitted with a magnetic bar, a rubber septum, and reflux condenser topped with a nitrogen inlet tube was charged with 528 mg (2.0 mmol) of Mo(CO)<sub>6</sub>, 292 mg (2.0 mmol) of MeO<sub>2</sub>CC<sub>5</sub>H<sub>4</sub>Na, and 20 mL of THF. The mixture was refluxed for 15 h. Upon cooling to room temperature, 458 mg (1.0 mmol) of FeCo<sub>2</sub>(CO)<sub>9</sub>(μ<sub>3</sub>-S) was added and the mixture stirred at reflux for an additional 1 h. Solvent was removed under reduced pressure and the residue extracted with CH<sub>2</sub>Cl<sub>2</sub>. The extracts were subjected to chromatographic separation on a silica gel column. After elution with 1:1 petroleum ether/CH<sub>2</sub>Cl<sub>2</sub>, followed by evaporation of solvents, 240 mg (41%) of **1a** as a black solid was obtained. The sample for analysis was further purified

(25) Curtis, M. D.; Han, K. R.; Butler, W. M. *Inorg. Chem.* **1980**, *19*, 2096.

(26) (a) Richter, F.; Vahrenkamp, H. *Angew. Chem. Int. Ed. Engl.* **1978**, *17*, 863. (b) Richter, F.; Vahrenkamp, H. *Angew. Chem. Int. Ed. Engl.* **1978**, *17*, 864. (c) Richter, F.; Vahrenkamp, H. *Organometallics* **1982**, *1*, 756. (d) Richter, F.; Vahrenkamp, H. *Chem. Ber.* **1982**, *115*, 3243. (e) Yang, H.; Zhao, Z.-Y.; Yin, Y.-Q.; Huang, L.-R. *Chinese Sci. Bull.* **1992**, *37*, 1804. (f) Sun, W.-H.; Yang, S.-Y.; Wang, H.-Q.; Zhou, Q.-F.; Yu, K.-B. *J. Organomet. Chem.* **1994**, *465*, 263.

(27) Meerwein, H. *Org. Synth.* **1966**, *46*, 113.

(28) Rogers, R. D.; Atwood, J. L.; Rausch, M. D.; Macomber, D. W.; Hart, W. P. *J. Organomet. Chem.* **1982**, *238*, 79.

(29) Hart, W. P.; Dong, S.; Rausch, M. D. *J. Organomet. Chem.* **1985**, *282*, 111.

(30) Bitterwolf, T. E. *J. Organomet. Chem.* **1990**, *386*, 9.

by recrystallization from 1:1 petroleum ether/ $\text{CH}_2\text{Cl}_2$ . **1a**: mp 73–75 °C. Anal. Calcd for  $\text{C}_{15}\text{H}_7\text{CoFeMoO}_{10}\text{S}$ : C, 30.54; H, 1.20. Found: C, 30.55; H, 1.14. IR (KBr disk):  $\nu_{(\text{C}=\text{O})}$  1713(s)  $\text{cm}^{-1}$ ;  $\nu_{(\text{C}=\text{O})}$  2082 (s), 2032(s), 2000(s), 1983(s), 1942(s), 1860(s)  $\text{cm}^{-1}$ .  $^1\text{H NMR}$  ( $\text{CDCl}_3$ ):  $\delta$  3.92 (s, 3H,  $\text{CH}_3$ ), 5.48, 5.66 (q, 2H,  $\text{H}^3$ ,  $\text{H}^4$ ), 6.02 (t, 2H,  $\text{H}^2$ ,  $\text{H}^5$ ) ppm. MS (EI,  $\text{Mo}^{98}$ ),  $m/z$  (relative intensity): 592 [ $\text{M}^+$ , 1.4], 564 [( $\text{M} - \text{CO}$ ) $^+$ , 1.3], 536 [( $\text{M} - 2\text{CO}$ ) $^+$ , 2.4], 508 [( $\text{M} - 3\text{CO}$ ) $^+$ , 1.3], 480 [( $\text{M} - 4\text{CO}$ ) $^+$ , 3.4], 452 [( $\text{M} - 5\text{CO}$ ) $^+$ , 6.7], 424 [( $\text{M} - 6\text{CO}$ ) $^+$ , 12.8], 396 [( $\text{M} - 7\text{CO}$ ) $^+$ , 7.7], 368 [( $\text{M} - 8\text{CO}$ ) $^+$ , 7.3], 533 [ $\text{SFeCoMoC}_5\text{H}_4(\text{CO})_8$ ] $^+$ , 1.4], 505 [ $\text{SFeCoMoC}_5\text{H}_4(\text{CO})_7$ ] $^+$ , 1.2], 477 [ $\text{SFeCoMoC}_5\text{H}_4(\text{CO})_6$ ] $^+$ , 2.8], 449 [ $\text{SFeCoMoC}_5\text{H}_4(\text{CO})_5$ ] $^+$ , 4.4], 421 [ $\text{SFeCoMoC}_5\text{H}_4(\text{CO})_4$ ] $^+$ , 7.4], 393 [ $\text{SFeCoMoC}_5\text{H}_4(\text{CO})_3$ ] $^+$ , 4.5], 365 [ $\text{SFeCoMoC}_5\text{H}_4(\text{CO})_2$ ] $^+$ , 4.4], 337 [ $\text{SFeCoMoC}_5\text{H}_4(\text{CO})$ ] $^+$ , 1.5], 309 [ $\text{SFeCoMoC}_5\text{H}_4$ ] $^+$ , 6.2], 301 [ $\text{SFeCoMo}(\text{CO})_2$ ] $^+$ , 1.4], 273 [ $\text{SFeCoMo}(\text{CO})$ ] $^+$ , 1.1], 245 [ $\text{SFeCoMo}^+$ ], 1.5].

**Compound 1b**. The workup for **1b–e** was similar to that of the preparation of **1a**. To the flask described above were added 528 mg (2.0 mmol) of  $\text{Mo}(\text{CO})_6$ , 320 mg (2.0 mmol) of  $\text{EtO}_2\text{CC}_5\text{H}_4\text{Na}$ , and 20 mL of THF. The solution was refluxed for 15 h. After the reaction of the resulting  $\eta^5\text{-EtO}_2\text{CC}_5\text{H}_4\text{Mo}(\text{CO})_3\text{Na}$  with 458 mg (1.0 mmol) of  $\text{FeCo}_2(\text{CO})_9(\mu_3\text{-S})$ , 305 mg (50%) of **1b** as a black solid was obtained. **1b**: mp 74–75 °C. Anal. Calcd for  $\text{C}_{16}\text{H}_9\text{CoFeMoO}_{10}\text{S}$ : C, 31.82; H, 1.50. Found: C, 31.67; H, 1.44. IR (KBr disk):  $\nu_{(\text{C}=\text{O})}$  1719(s)  $\text{cm}^{-1}$ ;  $\nu_{(\text{C}=\text{O})}$  2077 (s), 2018(s), 1991(s), 1963(s), 1900(s)  $\text{cm}^{-1}$ .  $^1\text{H NMR}$  ( $\text{CDCl}_3$ ):  $\delta$  1.32 (t, 3H,  $J = 7.2$  Hz,  $\text{CH}_3$ ), 4.30 (q, 2H,  $J = 7.2$  Hz,  $\text{CH}_2$ ), 5.40, 5.58 (q, q, 2H,  $\text{H}^3$ ,  $\text{H}^4$ ), 5.96 (t, 2H,  $\text{H}^2$ ,  $\text{H}^5$ ) ppm. MS (EI,  $\text{Mo}^{98}$ ),  $m/z$  (relative intensity): 606 [ $\text{M}^+$ , 0.7], 550 [( $\text{M} - 2\text{CO}$ ) $^+$ , 2.4], 522 [( $\text{M} - 3\text{CO}$ ) $^+$ , 1.6], 494 [( $\text{M} - 4\text{CO}$ ) $^+$ , 4.0], 466 [( $\text{M} - 5\text{CO}$ ) $^+$ , 8.4], 438 [( $\text{M} - 6\text{CO}$ ) $^+$ , 10.8], 410 [( $\text{M} - 7\text{CO}$ ) $^+$ , 5.8], 382 [( $\text{M} - 8\text{CO}$ ) $^+$ , 4.6], 309 [ $\text{SFeCoMoC}_5\text{H}_4$ ] $^+$ , 4.6], 469 [ $\text{SFeCoMo}(\text{CO})_8$ ] $^+$ , 0.6], 441 [ $\text{SFeCoMo}(\text{CO})_7$ ] $^+$ , 0.7], 301 [ $\text{SFeCoMo}(\text{CO})_2$ ] $^+$ , 1.5], 245 [ $\text{SFeCoMo}^+$ ], 1.9].

**Compound 1c**. To the flask described above were added 704 mg (2.0 mmol) of  $\text{W}(\text{CO})_6$ , 292 mg (2.0 mmol) of  $\text{MeO}_2\text{-CC}_5\text{H}_4\text{Na}$ , and 20 mL of diglyme. The solution was refluxed for 6 h. After the solvent was stripped at reduced pressure, 20 mL of THF and 458 mg (1.0 mmol) of  $\text{FeCo}_2(\text{CO})_9(\mu_3\text{-S})$  were added. After stirring of the mixture at reflux for an additional 1 h, 465 mg (68%) of **1c** as a brown-red solid was obtained. **1c**: mp 62–64 °C. Anal. Calcd for  $\text{C}_{15}\text{H}_7\text{CoFeO}_{10}\text{SW}$ : C, 26.58; H, 1.04. Found: C, 26.64; H, 1.02. IR (KBr, disk):  $\nu_{(\text{C}=\text{O})}$  1719(s)  $\text{cm}^{-1}$ ;  $\nu_{(\text{C}=\text{O})}$  2075(s), 2028(s), 1985(s), 1946(s), 1887(s)  $\text{cm}^{-1}$ .  $^1\text{H NMR}$  ( $\text{CDCl}_3$ ):  $\delta$  3.88 (s, 3H,  $\text{CH}_3$ ), 5.50, 5.70 (q, q, 2H,  $\text{H}^3$ ,  $\text{H}^4$ ), 6.00 (t, 2H,  $\text{H}^2$ ,  $\text{H}^5$ ) ppm. MS (EI,  $\text{W}^{184}$ ),  $m/z$  (relative intensity): 622 [( $\text{M} - 2\text{CO}$ ) $^+$ , 3.0], 594 [( $\text{M} - 3\text{CO}$ ) $^+$ , 2.0], 566 [( $\text{M} - 4\text{CO}$ ) $^+$ , 4.4], 538 [( $\text{M} - 5\text{CO}$ ) $^+$ , 9.0], 510 [( $\text{M} - 6\text{CO}$ ) $^+$ , 12.1], 482 [( $\text{M} - 7\text{CO}$ ) $^+$ , 9.0], 454 [( $\text{M} - 8\text{CO}$ ) $^+$ , 8.6], 535 [ $\text{SFeCoWC}_5\text{H}_4(\text{CO})_6$ ] $^+$ , 0.8], 423 [ $\text{SFeCoWC}_5\text{H}_4(\text{CO})$ ] $^+$ , 3.6], 395 [ $\text{SFeCoWC}_5\text{H}_4$ ] $^+$ , 4.8], 387 [ $\text{SFeCoW}(\text{CO})_2$ ] $^+$ , 1.9], 359 [ $\text{SFeCoW}(\text{CO})$ ] $^+$ , 1.4], 331 [ $\text{SFeCoW}^+$ ], 1.4].

**Compound 1d**. To the flask described above were added 704 mg (2.0 mmol) of  $\text{W}(\text{CO})_6$ , 320 mg (2.0 mmol) of  $\text{EtO}_2\text{-CC}_5\text{H}_4\text{Na}$ , and 20 mL of diglyme. The solution was refluxed for 6 h. After the reaction of the resulting  $\eta^5\text{-EtO}_2\text{CC}_5\text{H}_4\text{W}(\text{CO})_3\text{Na}$  with 458 mg (1.0 mmol) of  $\text{FeCo}_2(\text{CO})_9(\mu_3\text{-S})$ , 450 mg (65%) of **1d** as a brown-red solid was obtained. **1d**: mp 83–84 °C. Anal. Calcd for  $\text{C}_{16}\text{H}_9\text{CoFeO}_{10}\text{SW}$ : C, 27.77; H, 1.31. Found: C, 27.88; H, 1.30. IR (KBr, disk):  $\nu_{(\text{C}=\text{O})}$  1721(s)  $\text{cm}^{-1}$ ;  $\nu_{(\text{C}=\text{O})}$  2076(s), 2022(s), 1988(s), 1957(s), 1901 (s)  $\text{cm}^{-1}$ .  $^1\text{H NMR}$  ( $\text{CDCl}_3$ ):  $\delta$  1.34 (t, 3H,  $J = 7.2$  Hz,  $\text{CH}_3$ ), 4.34 (q, 2H,  $J = 7.2$  Hz,  $\text{CH}_2$ ), 5.50, 5.68 (q, q, 2H,  $\text{H}^3$ ,  $\text{H}^4$ ), 5.98 (t, 2H,  $\text{H}^2$ ,  $\text{H}^5$ ) ppm. MS (EI,  $\text{W}^{184}$ ),  $m/z$  (relative intensity): 692 [ $\text{M}^+$ , 5.7], 664 [( $\text{M} - \text{CO}$ ) $^+$ , 4.9], 636 [( $\text{M} - 2\text{CO}$ ) $^+$ , 11.4], 608 [( $\text{M} - 3\text{CO}$ ) $^+$ , 9.3], 580 [( $\text{M} - 4\text{CO}$ ) $^+$ , 25.6], 552 [( $\text{M} - 5\text{CO}$ ) $^+$ , 60.7], 524 [( $\text{M} - 6\text{CO}$ ) $^+$ , 80.9], 496 [( $\text{M} - 7\text{CO}$ ) $^+$ , 48.0], 468 [( $\text{M} - 8\text{CO}$ ) $^+$ , 47.5], 479 [ $\text{SFeCoWC}_5\text{H}_4(\text{CO})_3$ ] $^+$ , 3.3], 451 [ $\text{SFeCoWC}_5\text{H}_4(\text{CO})_2$ ] $^+$ , 5.5], 423 [ $\text{SFeCoWC}_5\text{H}_4(\text{CO})$ ] $^+$ , 5.0], 395 [ $\text{SFeCoWC}_5\text{H}_4$ ] $^+$ , 33.6], 555 [ $\text{SFeCoW}(\text{CO})_8$ ] $^+$ , 13.9], 527 [ $\text{SFeCoW}(\text{CO})_7$ ] $^+$ , 9.1], 499 [ $\text{SFeCoW}(\text{CO})_6$ ] $^+$ , 8.3], 471 [ $\text{SFeCoW}(\text{CO})_5$ ] $^+$ , 3.2], 415 [ $\text{SFeCoW}$ ]

( $\text{CO})_3$ ] $^+$ , 7.2], 387 [ $\text{SFeCoW}(\text{CO})_2$ ] $^+$ , 16.6], 359 [ $\text{SFeCoW}(\text{CO})$ ] $^+$ , 10.1], 331 [ $\text{SFeCoW}^+$ ], 22.4].

**Compound 1e**. To the flask described above were added 704 mg (2.0 mmol) of  $\text{W}(\text{CO})_6$ , 260 mg of  $\text{MeC}(\text{O})\text{C}_5\text{H}_4\text{Na}$ , and 20 mL of diglyme. The solution was refluxed for 6 h. After the reaction of the resulting  $\eta^5\text{-MeC}(\text{O})\text{C}_5\text{H}_4\text{W}(\text{CO})_3\text{Na}$  with 458 mg (1.0 mmol) of  $\text{FeCo}_2(\text{CO})_9(\mu_3\text{-S})$ , 458 mg (69%) of **1e** as a brown-red solid was obtained. **1e**: mp 102–104 °C. Anal. Calcd for  $\text{C}_{15}\text{H}_7\text{CoFeO}_9\text{SW}$ : C, 27.22; H, 1.07. Found: C, 27.27; H, 0.97. IR (KBr, disk):  $\nu_{(\text{C}=\text{O})}$  1685(s)  $\text{cm}^{-1}$ ;  $\nu_{(\text{C}=\text{O})}$  2075(s), 2034(s), 2016(s), 1998(s), 1969(s), 1907(m), 1874(m)  $\text{cm}^{-1}$ .  $^1\text{H NMR}$  ( $\text{CDCl}_3$ ):  $\delta$ : 2.48 (s, 3H,  $\text{CH}_3$ ), 5.64, 5.82 (q, q, 2H,  $\text{H}^3$ ,  $\text{H}^4$ ), 6.04 (q, 2H,  $\text{H}^2$ ,  $\text{H}^5$ ) ppm. MS (EI,  $\text{W}^{184}$ ),  $m/z$  (relative intensity): 662 [ $\text{M}^+$ , 1.2], 634 [( $\text{M} - \text{CO}$ ) $^+$ , 1.9], 606 [( $\text{M} - 2\text{CO}$ ) $^+$ , 3.1], 578 [( $\text{M} - 3\text{CO}$ ) $^+$ , 2.3], 550 [( $\text{M} - 4\text{CO}$ ) $^+$ , 4.3], 522 [( $\text{M} - 5\text{CO}$ ) $^+$ , 13.4], 494 [( $\text{M} - 6\text{CO}$ ) $^+$ , 18.3], 466 [( $\text{M} - 7\text{CO}$ ) $^+$ , 10.7], 438 [( $\text{M} - 8\text{CO}$ ) $^+$ , 26.5], 395 [ $\text{SFeCoWC}_5\text{H}_4$ ] $^+$ , 2.5], 387 [ $\text{SFeCoW}(\text{CO})_2$ ] $^+$ , 1.43], 359 [ $\text{SFeCoW}(\text{CO})$ ] $^+$ , 1.3], 331 [ $\text{SFeCoW}^+$ ], 1.5].

**Reaction of 1e with MeMgI**. The three-necked flask described above was charged with 200 mg (0.30 mmol) of **1e** and 15 mL of ethyl ether and then 2 mL (0.59 M, 1.18 mmol) of  $\text{MeMgI}$ /ether solution was added slowly during stirring. After stirring at room temperature for 3 h, 50 mL of distilled water and 10 mL of (0.167M) of dilute HCl acid were added. The ether phase was separated from the mixture and the aqueous phase was extracted twice with 10 mL of ethyl ether. The ethyl ether layers were combined and dried with anhydrous  $\text{MgSO}_4$ . Solvent was removed under reduced pressure and the residue was subjected to TLC separation using 2:1  $\text{CH}_2\text{Cl}_2$ /petroleum ether as eluant. Four orange bands were developed. The third band, as the main band gave 80 mg (39%) of **2** as a brown-red viscous oil. **2**: Anal. Calcd for  $\text{C}_{16}\text{-H}_{11}\text{CoFeO}_9\text{SW}$ : C, 28.35; H, 1.64. Found: C, 28.40; H, 1.55. IR (KBr, disk):  $\nu_{(\text{OH})}$  3480 (br, m)  $\text{cm}^{-1}$ ;  $\nu_{(\text{C}=\text{O})}$  2073(s), 2016(s), 1984(s), 1893(m)  $\text{cm}^{-1}$ .  $^1\text{H NMR}$  ( $\text{CDCl}_3$ ):  $\delta$  1.64 (s, 6H, 2 $\text{CH}_3$ ), 2.28 (s, 1H, OH), 5.28–5.64 (m, 4H,  $\text{C}_5\text{H}_4$ ) ppm. MS (EI,  $\text{W}^{184}$ ),  $m/z$  (relative intensity): 622 [( $\text{M} - 2\text{CO}$ ) $^+$ , 0.08], 538 [( $\text{M} - 5\text{CO}$ ) $^+$ , 0.12], 510 [( $\text{M} - 6\text{CO}$ ) $^+$ , 0.18], 482 [( $\text{M} - 7\text{CO}$ ) $^+$ , 0.42], 454 [( $\text{M} - 8\text{CO}$ ) $^+$ , 0.54], 451 [ $\text{SFeCoWC}_5\text{H}_4(\text{CO})_2$ ] $^+$ , 0.18], 395 [ $\text{SFeCoWC}_5\text{H}_4$ ] $^+$ , 0.10].

**Reaction of 1e with NaBH<sub>4</sub>**. To the flask described above were added 199 mg (0.3 mmol) of **1e**, 11.4 mg (0.3 mmol) of  $\text{NaBH}_4$ , and 10 mL of MeOH. The mixture was stirred at room temperature for 7 h. Solvent was removed under reduced pressure and the residue extracted with  $\text{CH}_2\text{Cl}_2$ . The extracts were concentrated and subjected to chromatographic separation on silica gel plates. Two bands were developed when 2:1  $\text{CH}_2\text{Cl}_2$ /petroleum ether was used as eluant. From the second orange band, 110 mg (55%) of **3** as a red oil was obtained. **3**: Anal. Calcd for  $\text{C}_{15}\text{H}_9\text{CoFeO}_9\text{SW}$ : C, 27.14; H, 1.37. Found: C, 27.43; H, 1.48. IR (KBr, disk):  $\nu_{(\text{C}=\text{O})}$  2071(s), 2022(s), 1980(s), 1890(s)  $\text{cm}^{-1}$ ;  $\nu_{(\text{OH})}$  3427 (br, s)  $\text{cm}^{-1}$ .  $^1\text{H NMR}$  ( $\text{CDCl}_3$ ):  $\delta$  1.56 (d, 3H,  $J = 5.4$  Hz,  $\text{CH}_3$ ), 2.00–2.32 (m, 1H, OH), 4.56–4.96 (m, 1H, CH), 5.16–5.76 (m, 4H,  $\text{C}_5\text{H}_4$ ) ppm. MS (EI,  $\text{W}^{184}$ ),  $m/z$  (relative intensity): 608 [( $\text{M} - 2\text{CO}$ ) $^+$ , 1.1], 580 [( $\text{M} - 3\text{CO}$ ) $^+$ , 0.17], 552 [( $\text{M} - 4\text{CO}$ ) $^+$ , 1.4], 524 [( $\text{M} - 5\text{CO}$ ) $^+$ , 1.6], 496 [( $\text{M} - 6\text{CO}$ ) $^+$ , 3.0], 468 [( $\text{M} - 7\text{CO}$ ) $^+$ , 9.3], 440 [( $\text{M} - 8\text{CO}$ ) $^+$ , 10.8], 395 [ $\text{SFeCoWC}_5\text{H}_4$ ] $^+$ , 0.8], 471 [ $\text{SFeCoW}(\text{CO})_5$ ] $^+$ , 0.9], 443 [ $\text{SFeCoW}(\text{CO})_4$ ] $^+$ , 0.6], 387 [ $\text{SFeCoW}(\text{CO})_2$ ] $^+$ , 0.6], 359 [ $\text{SFeCoW}(\text{CO})$ ] $^+$ , 3.2], 331 [ $\text{SFeCoW}^+$ ], 2.2].

**Reaction of 3 with Et<sub>3</sub>OBf<sub>4</sub>**. To a 50 mL flask described above were added 166 mg (0.25 mmol) of **3** and 5 mL of  $\text{CH}_2\text{-Cl}_2$  to form a brown-red solution, and then 143 mg (0.75 mmol) of  $\text{Et}_3\text{OBf}_4$  was added. After the mixture had been stirred for 16 h, solvent was removed under reduced pressure to leave a residue. The residue was subjected to TLC separation using 2:1  $\text{CH}_2\text{Cl}_2$ /petroleum ether as eluant. Seven orange-red bands were developed. From the third band was obtained 51 mg (29%) of **4** as a red viscous oil. **4**: Anal. Calcd for  $\text{C}_{17}\text{-H}_{13}\text{CoFeO}_9\text{SW}$ : C, 29.51; H, 1.89. Found: C, 29.69; H, 1.70. IR (KBr, disk):  $\nu_{(\text{C}=\text{O})}$  2073(s), 2024(s), 1959(s), 1885(m)  $\text{cm}^{-1}$ .

**Table 6. Crystal Data, Data Collection, and Refinement of Compounds 6a and 6b**

	6a	6b
empirical formula	C <sub>30</sub> H <sub>12</sub> Co <sub>2</sub> Fe <sub>2</sub> Mo <sub>2</sub> O <sub>18</sub> S <sub>2</sub>	C <sub>30</sub> H <sub>12</sub> Co <sub>2</sub> Fe <sub>2</sub> O <sub>18</sub> S <sub>2</sub> W <sub>2</sub>
fw	1145.97	1321.79
cryst syst	triclinic	monoclinic
space group	<i>P</i> - 1 (No. 2)	<i>C</i> 2/c (No. 15)
<i>a</i> /Å	7.602(3)	26.448(7)
<i>b</i> /Å	8.112(4)	9.660(4)
<i>c</i> /Å	16.208(3)	14.687(5)
$\alpha$ /deg	97.58(3)	
$\beta$ /deg	94.05(2)	100.72(2)
$\gamma$ /deg	109.50(3)	
<i>V</i> /Å <sup>3</sup>	927(1)	3687(4)
<i>Z</i>	1	4
<i>D</i> <sub>c</sub> /g cm <sup>-3</sup>	2.05	2.38
cryst size/mm	0.4 × 0.45 × 0.25	0.28 × 0.05 × 0.75
<i>F</i> (000)	558	2488
$\mu$ (Mo K $\alpha$ )/cm <sup>-1</sup>	24.60	81.80
radiation	Mo K $\alpha$ ( $\lambda$ = 0.71069 Å)	Mo K $\alpha$ ( $\lambda$ = 0.71069 Å)
temp/k	296	296
scan type	$\omega$ - 2 $\theta$	$\omega$ - 2 $\theta$
2 $\theta$ /deg (max)	49.9	49.9
data limits/deg	1° < $\theta$ < 25°	1° < $\theta$ < 25°
no. of observations ( <i>I</i> > 3.00 $\sigma$ ( <i>I</i> ))	2197	2192
no. of variables	277	253
<i>R</i> ; <i>R</i> <sub>w</sub>	0.044; 0.048	0.046; 0.051
goodness of fit	1.05	1.08
indicator		
maximum shift in final cycle	0.05	0.04
largest peak in final diff map/e Å <sup>-3</sup>	0.76	1.04

<sup>1</sup>H NMR (CDCl<sub>3</sub>):  $\delta$  1.22 (t, *J* = 7.2 Hz, 3H, CH<sub>2</sub>CH<sub>3</sub>), 1.50 (d, *J* = 7.2 Hz, 3H, CHCH<sub>3</sub>), 3.40–3.76 (m, 2H, CH<sub>2</sub>), 4.36 (q, *J* = 7.2 Hz, H, CH), 5.28–5.68 (m, 4H, C<sub>5</sub>H<sub>4</sub>) ppm. MS (EI, W<sup>184</sup>), *m/z* (relative intensity): 692 [M<sup>+</sup>, 0.9], 636 [(M - 2CO)<sup>+</sup>, 2.7], 608 [(M - 3CO)<sup>+</sup>, 1.9], 580 [(M - 4CO)<sup>+</sup>, 4.4], 552 [(M - 5CO)<sup>+</sup>, 5.7], 524 [(M - 6CO)<sup>+</sup>, 4.2], 496 [(M - 7CO)<sup>+</sup>, 19.0], 468 [(M - 8CO)<sup>+</sup>, 9.1], 423 [SFeCoWC<sub>5</sub>H<sub>4</sub>(CO)<sup>+</sup>, 4.5], 395 [SFeCoWC<sub>5</sub>H<sub>4</sub><sup>+</sup>, 2.7], 555 [SFeCoW(CO)<sub>8</sub><sup>+</sup>, 0.9], 499 [SFeCoW(CO)<sub>6</sub><sup>+</sup>, 2.5], 471 [SFeCoW(CO)<sub>5</sub><sup>+</sup>, 1.1], 387 [SFeCoW(CO)<sub>2</sub><sup>+</sup>, 1.3], 359 [SFeCoW(CO)<sup>+</sup>, 4.1], 331 [SFeCoW<sup>+</sup>, 2.2]. From the second band was obtained 50 mg (31%) of **5** as a brown-red viscous oil. **5**: Anal. Calcd for C<sub>30</sub>H<sub>16</sub>Co<sub>2</sub>Fe<sub>2</sub>O<sub>17</sub>S<sub>2</sub>W<sub>2</sub>: C, 27.51; H, 1.23. Found: C, 27.79; H, 1.23. IR (KBr, disk):  $\nu$ (C=O) 2073(s), 2016(s), 1975(s), 1868(m) cm<sup>-1</sup>. <sup>1</sup>H NMR (CDCl<sub>3</sub>):  $\delta$  1.50 (d, *J* = 7.2 Hz, 6H, 2CH<sub>3</sub>), 4.40–4.80 (m, 2H, 2CH), 5.16–5.80 (m, 8H, 2C<sub>5</sub>H<sub>4</sub>) ppm.

**Preparations of 6a,b.** To the flask described above were added 258 mg (1.0 mmol) of [NaC<sub>5</sub>H<sub>4</sub>C(O)CH<sub>2</sub>]<sub>2</sub>, 528 mg (2.0 mmol) of Mo(CO)<sub>6</sub>, and 20 mL of THF. The mixture was refluxed for 12 h. Upon cooling of the mixture to room temperature, 916 mg (2.0 mmol) of FeCo<sub>2</sub>(CO)<sub>9</sub>( $\mu_3$ -S) was added and the mixture refluxed for an additional 1 h. Solvent was removed under reduced pressure to give a residue. The residue was extracted with CH<sub>2</sub>Cl<sub>2</sub>, and then the extracts were subjected to column chromatography. The 2:1 CH<sub>2</sub>Cl<sub>2</sub>/petroleum ether eluted the unreacted FeCo<sub>2</sub>(CO)<sub>9</sub>( $\mu_3$ -S) and then a brown-red band. After evaporation of the solvent from the brown-red band solution and drying under vacuum, 360 mg (31%) of **6a** as a brown solid was obtained. Analytical sample was obtained by recrystallization from 1:2 CH<sub>2</sub>Cl<sub>2</sub>/petroleum ether. **6a**: mp 134–136 °C. Anal. Calcd for C<sub>30</sub>H<sub>12</sub>Co<sub>2</sub>Fe<sub>2</sub>Mo<sub>2</sub>O<sub>18</sub>S<sub>2</sub>: C, 31.44; H, 1.06. Found: C, 31.57; H, 1.15. IR (KBr, disk):  $\nu$ (C=O) 2077(s), 2028(vs), 1977 (s), 1884 (m) cm<sup>-1</sup>;  $\nu$ (C-O) 1681 (m) cm<sup>-1</sup>. <sup>1</sup>H NMR (CDCl<sub>3</sub>):  $\delta$  3.16 (s, 4H, CH<sub>2</sub>CH<sub>2</sub>), 5.60, 5.72 [q, q, 4H, 2(H<sup>3</sup>, H<sup>4</sup>)], 6.08 [t, 4H, 2(H<sup>2</sup>, H<sup>5</sup>)] ppm.

**Compound 6b.** To the flask described above were added 258 mg (1.0 mmol) of [NaC<sub>5</sub>H<sub>4</sub>C(O)CH<sub>2</sub>]<sub>2</sub>, 704 mg (2.0 mmol) of W(CO)<sub>6</sub>, and 20 mL of diglyme. The mixture was refluxed for 6 h. After the solvent was removed under reduced

pressure, 916 mg (2.0 mmol) of FeCo<sub>2</sub>(CO)<sub>9</sub>( $\mu_3$ -S) and 20 mL of THF were added. The mixture was refluxed for an additional 1 h. After a workup similar to that of **6a**, 570 mg (43%) of **6b** was obtained as a brown solid. **6b**: mp 139–141 °C dec. Anal. Calcd for C<sub>30</sub>H<sub>12</sub>Co<sub>2</sub>Fe<sub>2</sub>O<sub>18</sub>S<sub>2</sub>W<sub>2</sub>: C, 27.26; H, 0.92. Found: C, 27.22, H, 0.82. IR (KBr, disk):  $\nu$ (C=O) 2075-(s), 2026(vs), 1978(s) 1886(m) cm<sup>-1</sup>.  $\nu$ (C-O) 1683(m) cm<sup>-1</sup>. <sup>1</sup>H NMR (CDCl<sub>3</sub>): 3.18 (s, 4H, CH<sub>2</sub>CH<sub>2</sub>), 5.66, 5.80 [q, q, 4H, 2(H<sup>3</sup>, H<sup>4</sup>)], 5.98–6.18 [m, 4H, 2(H<sup>2</sup>, H<sup>5</sup>)] ppm.

**Reaction of 6a with NaBH<sub>4</sub>.** To the three-necked flask described above were added 115 mg (0.1 mmol) of **6a**, 7.6 mg (0.2 mmol) of NaBH<sub>4</sub>, and 6 mL of methanol. The mixture was stirred for 7 h at room temperature. Solvent was removed under reduced pressure and then the residue was extracted with CH<sub>2</sub>Cl<sub>2</sub>. The extracts were subjected to TLC using CH<sub>2</sub>-Cl<sub>2</sub> as eluant. There are three bands on the TLC plates. From the third band was obtained 36 mg (31%) of **7a** as a brown solid. **7a**: mp 42–44 °C. Anal. Calcd for C<sub>30</sub>H<sub>16</sub>Co<sub>2</sub>Fe<sub>2</sub>Mo<sub>2</sub>O<sub>18</sub>S<sub>2</sub>: C, 31.33; H, 1.40. Found: C, 31.81; H, 1.49. IR (KBr, disk):  $\nu$ (OH) 3435 (br, m) cm<sup>-1</sup>;  $\nu$ (C=O) 2073 (s), 2016 (vs), 1975(vs), 1885(m) cm<sup>-1</sup>. <sup>1</sup>H NMR (CDCl<sub>3</sub>):  $\delta$  1.96–2.14 (m, 4H, CH<sub>2</sub>CH<sub>2</sub>), 2.14–2.34 (m, 2H, 2OH), 4.58–4.82 (m, 2H, 2CH), 5.34–5.52 [m, 4H, 2(H<sup>3</sup>, H<sup>4</sup>)], 5.52–5.78 [m, 4H, 2(H<sup>2</sup>, H<sup>5</sup>)] ppm.

**Reaction of 6b with NaBH<sub>4</sub>.** To the three-necked flask described above were added 138 mg (0.1 mmol) of **6b**, 7.6 mg (0.2 mmol) of NaBH<sub>4</sub>, and 6 mL of methanol. The mixture was stirred for 7 h at room temperature. Solvent was removed under reduced pressure and then the residue was extracted with CH<sub>2</sub>Cl<sub>2</sub>. The extracts were subjected to TLC using CH<sub>2</sub>-Cl<sub>2</sub> as eluant to give three brown-red bands on the plates. From the third band was obtained 30 mg (23%) of **7b** as a brown solid. **7b**: mp 49–51 °C. Anal. Calcd for C<sub>30</sub>H<sub>16</sub>Co<sub>2</sub>Fe<sub>2</sub>O<sub>18</sub>S<sub>2</sub>W<sub>2</sub>: C, 27.18; H, 1.22. Found: C, 27.27; H, 1.28. IR (KBr, disk):  $\nu$ (OH) 3443 (br, m) cm<sup>-1</sup>;  $\nu$ (C=O) 2071(s), 2020(vs), 1974(vs), 1877 (m) cm<sup>-1</sup>. <sup>1</sup>H NMR (CDCl<sub>3</sub>):  $\delta$  1.74–2.10 (m, 4H, CH<sub>2</sub>CH<sub>2</sub>), 2.50–2.82 (m, 2H, 2OH), 4.58–4.86 (m, 2H, 2CH), 5.22–5.50 [m, 4H, 2(H<sup>3</sup>, H<sup>4</sup>)], 5.50–5.78 [m, 4H, 2(H<sup>2</sup>, H<sup>5</sup>)] ppm.

**Reaction of 7a with Et<sub>3</sub>OBF<sub>4</sub>. Method 1.** To the 50 mL flask described above were added 50 mg (0.043 mmol) of **7a** and 6 mL of CH<sub>2</sub>Cl<sub>2</sub>, after stirring for a while, to give a brown-red solution, and then 50 mg (0.26 mmol) of Et<sub>3</sub>OBF<sub>4</sub> was added. The mixture was refluxed for 0.5 h. Solvent was removed under reduced pressure and then the residue was subjected to TLC using 1:1 CH<sub>2</sub>Cl<sub>2</sub>/petroleum ether as eluant to give a pink band, from which 44 mg (90%) of **8a** was obtained as a brown-red viscous oil. **8a**: Anal. Calcd for C<sub>30</sub>H<sub>14</sub>Co<sub>2</sub>Fe<sub>2</sub>Mo<sub>2</sub>O<sub>17</sub>S<sub>2</sub>: C, 31.83; H, 1.25. Found: C, 31.83; H, 1.45. IR (KBr, disk):  $\nu$ (C=O) 2073(s), 2024(vs), 1967 (vs), 1877 (m) cm<sup>-1</sup>. <sup>1</sup>H NMR (CDCl<sub>3</sub>):  $\delta$  1.80–2.20 (m, 2H, CH<sub>2</sub>), 2.20–2.60 (m, 2H, CH<sub>2</sub>), 4.68–5.08 (m, 2H, 2CH), 5.28–5.68 (m, 8H, 2C<sub>5</sub>H<sub>4</sub>) ppm.

**Method 2.** To the flask described above were added 50 mg (0.043 mmol) of **7a** and 6 mL of CH<sub>2</sub>Cl<sub>2</sub>. Upon cooling to 0 °C, 50 mg (0.26 mmol) of Et<sub>3</sub>OBF<sub>4</sub> was added. After stirring for 2 h at this temperature, TLC showed that no **8a** was formed. The reaction mixture continued to be stirred for 2 h at room temperature, and TLC showed that no starting material **7a** was left. After the same workup as before, 42 mg (86%) of **8a** was obtained.

**Method 3.** To the flask described above were added 50 mg (0.043 mmol) of **7a** and 6 mL of CH<sub>2</sub>Cl<sub>2</sub>. Upon cooling to 0 °C, 0.05 mL (6.4 M, 0.32 mmol) of aqueous solution of HBF<sub>4</sub> was added. After stirring for 2 h at this temperature, TLC showed that no **8a** was produced. The mixture was then refluxed for an additional 2 h. After the same workup as before, 28 mg (58%) of **8a** was obtained.

**Reaction of 7b with Et<sub>3</sub>OBF<sub>4</sub>. Method 1.** To the flask described above were added 57 mg (0.043 mmol) of **7b**, 6 mL of CH<sub>2</sub>Cl<sub>2</sub>, and 50 mg (0.26 mmol) of Et<sub>3</sub>OBF<sub>4</sub>. The mixture was refluxed for 0.5 h. After the same workup as above, 50

mg (89%) of **8b** as a brown solid was obtained. **8b**: mp 35–36 °C. Anal. Calcd for  $C_{30}H_{14}Co_2Fe_2O_{17}S_2W_2$ : C, 27.55; H, 1.08. Found: C, 27.68; H, 1.07. IR (KBr, disk):  $\nu_{(C=O)}$  2073-(s), 2024(s), 1967(vs), 1877(m)  $cm^{-1}$ .  $^1H$  NMR ( $CDCl_3$ ):  $\delta$  1.80–2.20 (m, 2H,  $CH_2$ ), 2.20–2.60 (m, 2H,  $CH_2$ ), 4.68–5.20 (m, 2H, 2CH), 5.28–5.64 (m, 8H,  $2C_5H_4$ ) ppm.

**Method 2.** To the flask described above were added 57 mg (0.043 mmol) of **7b**, 6 mL of  $CH_2Cl_2$ , and 50 mg (0.26 mmol) of  $Et_3OBF_4$ . Then the mixture was stirred for 2h at room temperature. After the same workup as above, 22 mg (39%) of **8b** was obtained.

**Method 3.** To the flask described above were added 57 mg (0.043 mmol) of **7b**, 6 mL of  $CH_2Cl_2$ , and 0.05 mL (12.4 M, 0.62 mmol) of aqueous solution of HCl. The mixture was refluxed for 9 h. After the same workup as above, 7 mg (12%) of **8b** was obtained.

**X-ray Structure Determination of 6a and 6b.** Samples of **6a** and **6b** were prepared as detailed above. X-ray quality crystals were grown for **6a** and **6b** by slow evaporation of their solutions in 2:1  $CH_2Cl_2$ /hexane. Both crystalline samples were in the form of brown plates. The crystal of **6a** or **6b** was mounted on a glass fiber in an arbitrary orientation and

determined on an Enraf-Nonius CAD4 diffractometer equipped with a graphite monochromator. Details of the crystals, data collections, and structure refinements are summarized in Table 6. The structures were solved by a direct phase determination method (MULTAN82). The final refinement was accomplished by the full-matrix least-squares method with anisotropic thermal parameters for non-hydrogen atoms. All calculations were performed on a MICRO-VAX II computer using the TAXSAN program system.

**Acknowledgment.** We are grateful to the National Science Foundation of China and State Key Laboratory of Structural Chemistry for financial support of this work.

**Supplementary Material Available:** Full tables of crystal data, atomic coordinates and thermal parameters, and bond lengths and angles for **6a** and **6b** (10 pages). Order information is given on any current masthead page.

OM940431O

# Time-Resolved Raman Spectroscopy and Matrix Isolation Studies of *Anti*–*Syn* Photoisomerization in Metal Carbonyl Carbenes

A. Denise Rooney,<sup>\*,†</sup> John J. McGarvey,<sup>\*</sup> and Keith C. Gordon<sup>‡</sup>

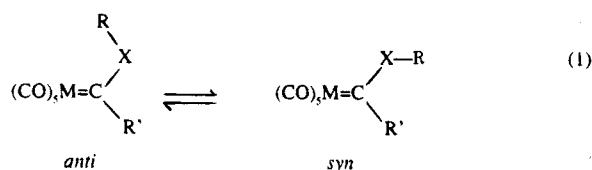
School of Chemistry, The Queen's University of Belfast, Belfast BT9 5AG, Northern Ireland

Received June 13, 1994<sup>⊗</sup>

Photoinduced *anti*–*syn* isomerization in tungsten carbonyl carbenes,  $(\text{CO})_5\text{W}=\text{C}(\text{OR})\text{R}'$ , [1 with R = Me, R' = Me; 2 with R = Me, R' = *p*-Tolyl; 3 with R = Et, R' = Ph] brought about by irradiation in the MLCT absorption region has been investigated by laser flash photolysis coupled with transient absorbance and time-resolved resonance Raman spectroscopy (TR<sup>3</sup>S). The studies, carried out in solution in solvents of varying polarity, have been supplemented by matrix isolation studies using UV-vis and IR detection. Pulsed irradiation in the MLCT absorption region of 1–3 results in the formation within the pulse risetime of the *syn* isomer from the ground state (*anti*) form, followed by thermal relaxation/isomerization back to the ground state. In all three complexes the transient lifetimes increase with increasing solvent polarity falling in the range 120 μs–3 ms for 1 and 1–2 orders of magnitude shorter for 2 and 3. Growth and decay of the *syn* isomer were also monitored by TR<sup>3</sup>S. For 1, bands in the Raman attributable to modes of the carbene group showed little change in frequency between the *anti* and *syn* isomers. In the case of the *anti* forms of 2 and 3, a band near 1235 cm<sup>-1</sup> attributable to  $\nu(\text{C}_{\text{carbene}}-\text{OR})$  shifts to ca. 1270 cm<sup>-1</sup> in the spectra of the *syn* isomer. The differences between 1, 2 and 3 in respect of both vibrational spectra and rates of isomerization are discussed in relation to the possible influence on electronic stabilization of reorientation of the R' group which accompanies *anti*–*syn* transformation. Comparison of the *anti*–*syn* photoisomerization of 1 in an argon matrix with that of 4 (R = Me, R' = Ph) shows that the process is photoreversible only in the case of 1.

## Introduction

The existence of *anti* and *syn* isomers (eq 1) in solution for metal carbenes of the type  $[\text{M}]-\text{C}(\text{XR})(\text{R}')$ , X=O, N,



S, has been established since the NMR studies carried out on chromium pentacarbonyl carbenes.<sup>1</sup> The isomers arise as a result of inhibited rotation about the C–X bond in which the partial double bond character is due to the  $\pi$  interaction between the lone pair of electrons on the heteroatom and the carbene carbon  $2p_z$  orbital. The energy difference  $E_{\text{syn}} - E_{\text{anti}}$  between the two isomers is very dependent on the heteroatom (N > O > S), the  $\pi$  donating ability of R', steric interactions and the solvent environment. Which isomer is energetically the more favored will depend on the steric demands of the complex. However, in complexes of the type  $(\text{CO})_5\text{WC}(\text{OR})(\text{R}')$ , which are studied here, the *anti* isomer predominates.<sup>2</sup>

The electronic absorption spectra of  $(\text{CO})_5\text{WC}(\text{OR})-\text{R}'$  generally exhibit two bands, a higher energy LF transition, assigned in one-electron terms as  $(b_2^2) \rightarrow (2a_1^1, b_2^1)$  in the assumed<sup>3</sup> local  $C_{2v}$  symmetry of the carbene group, and a lower energy MLCT transition, assigned as  $(b_2^2) \rightarrow (3a_1^1, b_2^1)$ . The latter transition formally promotes electron density into the carbene carbon  $2p_z$  orbital. The photochemistry associated with the LF transition involves CO dissociation.<sup>3</sup> Until recently photoexcitation within the MLCT region has been less extensively investigated.<sup>4</sup>

Previous work from this laboratory on the photochemistry of  $(\text{CO})_5\text{WC}(\text{OMe})(\text{Ph})$ , the first time-resolved resonance Raman (TR<sub>3</sub>) study on an organometallic complex,<sup>5</sup> noted that LF excitation resulted in the formation of a transient with a lifetime in the μs range. Originally it was believed that this was a 16-electron species arising from CO loss. Subsequent work on this same complex in a matrix by Stufkens et al. demonstrated that irradiation into the MLCT band of the complex resulted in *anti* to *syn* photoisomerization,<sup>2</sup> according to eq 1. Furthermore, these workers showed that irradiation into the higher energy LF band also resulted in the same photoisomerization, apparently

(2) Servaas, P. C.; Stufkens, D. J.; Oskam, A. *J. Organomet. Chem.* **1990**, *390*, 61.

(3) Foley, H. C.; Strubinger, L. M.; Targos, T. S.; Geoffroy, G. L. *J. Am. Chem. Soc.* **1983**, *105*, 3064; Fong, L. K.; Cooper, N. J. *Ibid.* **1984**, *106*, 2595.

(4) Poirreau, D.; Geoffroy, G. L. *Adv. Organomet. Chem.* **1985**, *24*, 249.

(5) Bell, S. E. J.; Gordon, K. C.; McGarvey, J. J. *J. Am. Chem. Soc.* **1988**, *110*, 3107.

<sup>†</sup> Present address: Department of Chemistry, St. Patrick's College, National University, Maynooth, Ireland.

<sup>‡</sup> Present address: Chemistry Department, University of Otago, Dunedin, N. Zealand.

<sup>⊗</sup> Abstract published in *Advance ACS Abstracts*, November 1, 1994.

(1) Kreiter, C. G.; Fischer, E. O. *Angew. Chem. Int. Ed. Engl.* **1969**, *8*, 761.

arising as a result of efficient radiationless decay from the initially populated LF state into the lower lying MLCT state. The transient species originally reported<sup>5</sup> in the TR<sub>3</sub> studies in solution was identified<sup>2</sup> as the *syn* isomer of (CO)<sub>5</sub>WC(OMe)(Ph) as observed in the matrix experiments. More recently we have reported the observation of a photogenerated transient *syn* isomer in the related carbene complex (CO)<sub>5</sub>WC(OEt)(SiPh<sub>3</sub>).<sup>6</sup>

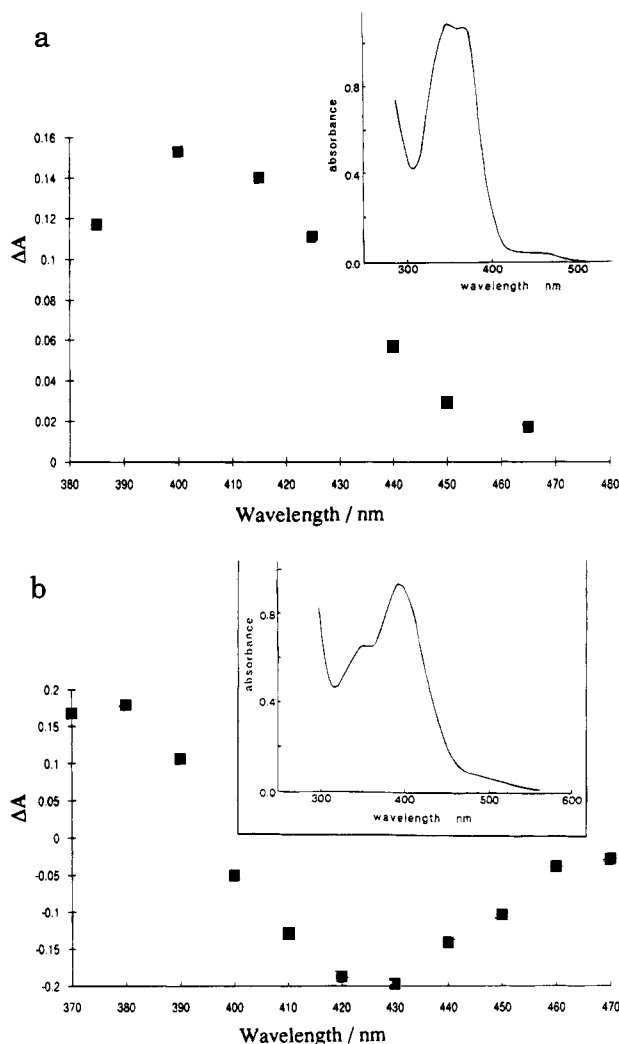
The primary aim of the present work has been to carry out a comparative study of the photoisomerization of (CO)<sub>5</sub>WC(OR)(R') complexes in solution, using the methods of flash photolysis and TR<sub>3</sub> spectroscopy, and in an argon matrix, using IR and UV/vis spectroscopic detection. The following complexes, containing both aryl and alkyl substituents have been investigated: (CO)<sub>5</sub>WC(OMe)(Me), **1**, (CO)<sub>5</sub>WC(OMe)(*p*-C<sub>6</sub>H<sub>4</sub>CH<sub>3</sub>), **2**, and (CO)<sub>5</sub>WC(OEt)(Ph), **3**. The results are considered in relation to the earlier studies<sup>5</sup> of the Fischer carbene, (CO)<sub>5</sub>WC(OMe)(Ph), **4**.

### Experimental Section

Flash photolysis experiments were carried out using either a Nd/YAG laser (355 nm, 10 ns pulse width, *ca.* 10–30 mJ pulse<sup>-1</sup>) or a XeCl excimer laser (308 nm, 30 ns pulse width, up to 40 mJ pulse<sup>-1</sup>). Both systems have previously been described in detail.<sup>7,8</sup> For resonance Raman studies the Nd/YAG laser coupled with a Raman shifter was used for recording the transient spectra and an argon ion laser for the ground state spectra.<sup>5,9</sup> Two-color TR<sub>3</sub> experiments were carried out at the Central Laser Facility, Rutherford Appleton Laboratory (RAL), using excimer and excimer-pumped dye lasers as pump and probe sources respectively. The matrix isolation experiments were carried out at the University of York and the apparatus has been described in detail elsewhere.<sup>10</sup> The samples were deposited on a BaF<sub>2</sub> window which was cooled to 12–20 K by an Air Products CS202 closed-cycle Displex refrigerator. The complexes were sublimed onto the window from a tube, concurrent with the gas stream that entered the vacuum shroud from a separate inlet.

Matrices were photolysed using a 300W Xe arc (ILC, model 302UV) with appropriate filters. The IR spectra were recorded on either a Mattson Sirius FTIR or Mattson Research Series FTIR spectrometer with a PbS detector and a KBr beam splitter (4000–450 cm<sup>-1</sup>) or a CsI beam splitter (4000–200 cm<sup>-1</sup>). The spectrometer was continuously purged with CO<sub>2</sub>-free dry air. The spectra were recorded as the average of 128 scans with 1 cm<sup>-1</sup> resolution (25K data points). The UV/vis spectra were recorded on a Perkin-Elmer Lambda 1G spectrometer. The complexes and their deuteriated analogs were synthesized by standard literature procedures.<sup>11</sup>

For the flash photolysis experiments the samples were dissolved in the appropriate solvent in a 1 cm path length quartz cuvette. The absorbances of the solutions were in the range 0.5–1.0 at the excitation wavelength. The solutions were either purged with argon or degassed by several freeze-pump thaw cycles to 10<sup>-4</sup> mbar before back filling to 1 atm of argon. For the transient resonance Raman spectra the argon-purged samples were circulated through a quartz capillary (*ca.*



**Figure 1.** Transient absorbance difference ( $\Delta A$ ) spectra recorded following flash photolysis at 354.7 nm of (a) (CO)<sub>5</sub>W=C(OCH<sub>3</sub>)CH<sub>3</sub> and (b) (CO)<sub>5</sub>W=C(OCH<sub>2</sub>CH<sub>3</sub>)C<sub>6</sub>H<sub>5</sub>. Solution concentrations were *ca.* 10<sup>-3</sup> mol dm<sup>-3</sup> in CH<sub>2</sub>Cl<sub>2</sub> in both cases. Insets: corresponding ground electronic absorption spectra.

1 mm i.d.) at a rate which ensured that each laser pulse irradiated a fresh volume of solution, thus minimizing sample decomposition in the laser beam.

### Results

**(a) Flash Photolysis.** Complex **1** exhibits two absorption bands at 350 nm (LF) and 370 nm (MLCT) in cyclohexane solution. Irradiation of a solution of **1** in dichloromethane at 355 nm resulted in a rise in absorption in the range 390–460 nm occurring within the time resolution of the apparatus (*ca.* 10 ns) and followed by an exponential decay to the preflash absorbance level. The maximum in the  $\Delta A$  spectrum measured in CH<sub>2</sub>Cl<sub>2</sub> (Figure 1a) exhibited a red shift of *ca.* 15 nm from the ground state absorption maximum (365 nm). Little change was observed in the  $\Delta A$  maximum with solvent. The transient lifetime however was markedly solvent-dependent (Table 1) and varied with temperature, yielding an activation enthalpy of 51 ± 2 kJ mol<sup>-1</sup> in cyclohexane from an Eyring plot over the range (283–328) K.

Complex **2**, with absorption bands at 354 nm (LF) and 410 nm (MLCT) in cyclohexane displayed similar tran-

(6) Rooney, A. D.; McGarvey, J. J.; Gordon, K. C.; McNicholl, R.-A.; Schubert, U.; Hepp, W.; *Organometallics* **1993**, *12*, 1277.

(7) Bell, S. E. J.; Gordon, K. C.; McGarvey, J. J. *Inorg. Chem.* **1988**, *27*, 4003.

(8) Belt, S. T.; Grevels, F.-W.; Klotzbucher, W.; McCamley, A.; Perutz, R. N. *J. Am. Chem. Soc.* **1989**, *111*, 8373.

(9) Bell, S. E. J.; Gordon, K. C.; McGarvey, J. J. *J. Raman Spectrosc.* **1989**, *20*, 105.

(10) Haddleton, D. M.; McCamley, A.; Perutz, R. N. *J. Am. Chem. Soc.* **1988**, *110*, 1810.

(11) (a) Villemin, D. *J. Chem. Ed.* **1987**, *64*, 183. (b) Schubert, U.; Fischer, E. O. *Liebigs Ann. Chem.* **1975**, 393.



**Table 1. Lifetimes ( $\mu\text{s}$ ) of *Syn* Isomers of Tungsten Carbenes in Solution<sup>a</sup>**

solvent	(CO) <sub>5</sub> WC-(OMe)Me	(CO) <sub>5</sub> WC-(OEt)Ph	(CO) <sub>5</sub> WC-(OMe)p-tol
hexane	126 ± 4	4.65 ± 0.10	1.1 ± 0.05
cyclohexane	294 ± 15	5.0 ± 0.2	1.62 ± 0.05
dichloromethane	1200 ± 100	14.3 ± 0.3	3.70 ± 0.15
methanol	2642 ± 211	20.7 ± 0.4	6.6 ± 0.3
acetonitrile	3356 ± 300	23 ± 2	7.1 ± 0.3

<sup>a</sup> Measurements at 20 °C, *ca.* 10<sup>-3</sup> mol dm<sup>-3</sup>.

**Table 2. Principal Bands (cm<sup>-1</sup>) in CW and Pulsed (Single Color) RR Spectra of Carbene Complexes**

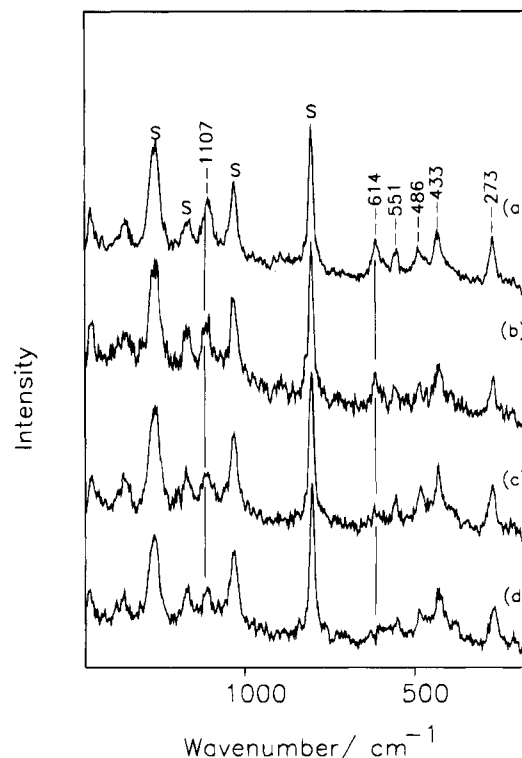
complex	$\lambda_{\text{exc}}/\text{nm}$	Raman bands/cm <sup>-1</sup>					
		273	430	486	557	1107	1264
(CO) <sub>5</sub> WC(OMe)Me	363.8 (CW)	273	433	486	557	1107	1170 1264
	354.7 (pulsed)					<i>a</i>	1107 1170 1264
	396 (pulsed)	273	430	486	557	614	<i>b</i>
(CO) <sub>5</sub> WC(OMe)p-tol	363.8 (CW)			878	990	1181	1210 1235
	354.7 (pulsed)			878	920	1181	1235 1270
(CO) <sub>5</sub> WC(OEt)Ph	363.8 (CW)			903		1181	1233
	354.7 (pulsed)			903	935	1181	1266

<sup>a</sup> Frequency range <1000 cm<sup>-1</sup> not probed. <sup>b</sup> Frequency range >1000 cm<sup>-1</sup> not probed.

sient behavior, again showing a rise in <10 ns (the response time of the experiment) in the absorbance between 370 and 390 nm and in this case a ground state depletion in the range 400–450 nm. The first order transient decay was temperature- and solvent-dependent as for **1** but the lifetime was some two orders of magnitude shorter.

Irradiation at 355 nm of the EtO-substituted analogue, **3**, which has absorption bands at 356 nm (LF) and 403 nm (MLCT) also resulted in formation of a transient within the laser pulse risetime and with a very similar  $\Delta A$  spectrum to that observed for **2**, positive over the range 370–390 nm and showing depletion between 400 and 460 nm (Figure 1b). The transient decayed exponentially as a function of temperature and solvent with a lifetime slightly longer than that of the phenyl analogue, **2**. In general, the behavior of **3** was very similar to the Fischer carbene, (CO)<sub>5</sub>WC(OMe)(Ph) **4**, reported in an earlier paper.<sup>5</sup> The latter investigation has been extended in the present work by investigating the temperature dependence of the thermal isomerization of the *syn* back to the *anti* form following photogeneration by flash photolysis at 308 nm. Measurements over the temperature range (283–328) K in cyclohexane solution, yielded an activation enthalpy from the Eyring plot of 37 ± 3 kJ mol<sup>-1</sup> for the thermal relaxation to the *anti* ground state.

**(b) Resonance Raman spectroscopy.** Principal features in the resonance Raman (RR) spectra recorded under CW- and pulsed-excitation for complexes **1**–**3** are summarized in Table 2. For complex **1**, spectra generated at either  $\lambda_{\text{exc}} = 363.8$  nm (CW) or 355 nm (pulsed) in CH<sub>2</sub>Cl<sub>2</sub> solution showed features at 1107, 1170 and 1264 cm<sup>-1</sup>. In the lower frequency region of the RR spectrum, generated at 363.8 nm in cyclohexane as solvent, bands appeared at 277, 430, 486, 557 and 594 cm<sup>-1</sup>. With pulsed excitation at 396 nm a new band grew in at 614 cm<sup>-1</sup>. The results of a two-color time-resolved experiment carried out on the same sample are shown in Figure 2. The spectra were recorded using a pump wavelength of 351 nm and a probe wavelength of 406 nm at a series of pump-probe delays over the time range 120 ns–600  $\mu\text{s}$ . The rate of decay which can be

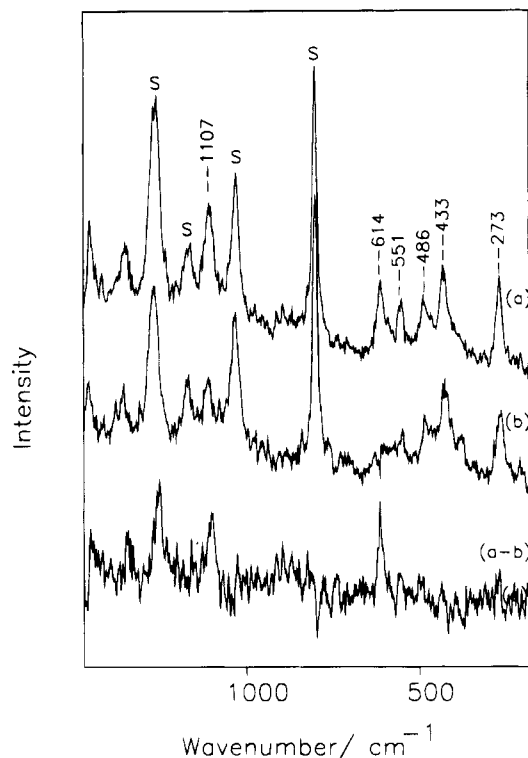


**Figure 2.** Two-color time-resolved resonance Raman study of (CO)<sub>5</sub>W=C(OCH<sub>3</sub>)CH<sub>3</sub> in C<sub>6</sub>H<sub>12</sub> (*ca.* 10<sup>-3</sup> mol dm<sup>-3</sup>); Pump  $\lambda$  351 nm; probe  $\lambda$  406 nm. Pump-probe time delays: (a) 120 ns; (b) 100  $\mu\text{s}$ ; (c) 300  $\mu\text{s}$ ; (d) 600  $\mu\text{s}$ .

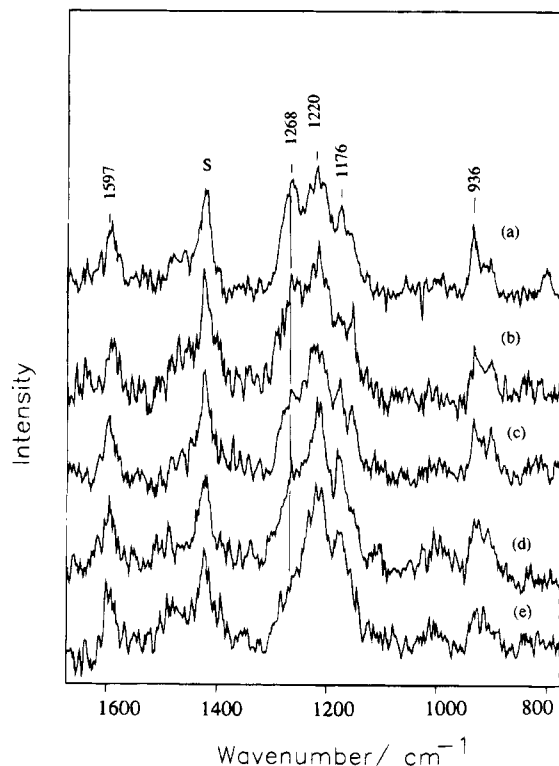
estimated from the gradual disappearance with increasing pump-probe delay of the 614 cm<sup>-1</sup> feature in Figure 2 is consistent with the 300  $\mu\text{s}$  lifetime recorded in the flash photolysis experiments in the same solvent (Table 1). CO saturation of the solution had no measurable effect on the rate of transient decay.

The intensity of the 1107 cm<sup>-1</sup> band relative to the solvent peak at 1028 cm<sup>-1</sup> also changes with pump-probe delay confirming it as a transient feature, unshifted from the ground state position. This is also the case for the band near 1264 cm<sup>-1</sup> although the variation of band intensity is not immediately evident from Figure 2 because of an overlapping solvent feature at 1266 cm<sup>-1</sup>. However a careful comparison of the spectra from Figure 2, recorded at the shortest and longest pump-probe delays brings out the point. The two spectra are replotted in Figure 3, along with the corresponding difference spectrum, from which the enhanced intensity of the 1264 cm<sup>-1</sup> band at the shortest delay is evident. The decrease in intensity of both this band and that at 1107 cm<sup>-1</sup> for the transient compared to the ground state is what would be expected from resonance enhancement considerations. The monitoring beam at 406 nm is more in resonance with the MLCT absorption of the transient (Figure 1a) than that of the ground state ( $\lambda_{\text{max}}$  370 nm). The observed changes in intensity confirm that the bands observed at the short time delays are transient features, unshifted in frequency from the ground state.

In the case of complex **2** several bands also appear at the same frequencies in CW- (363.8 nm) and pulse- (355 nm) generated spectra but additional, transient bands were observed at 920 cm<sup>-1</sup> and 1270 cm<sup>-1</sup> in the pulse-generated spectra. The pattern for complex **3** was very similar, with several features common to the CW-

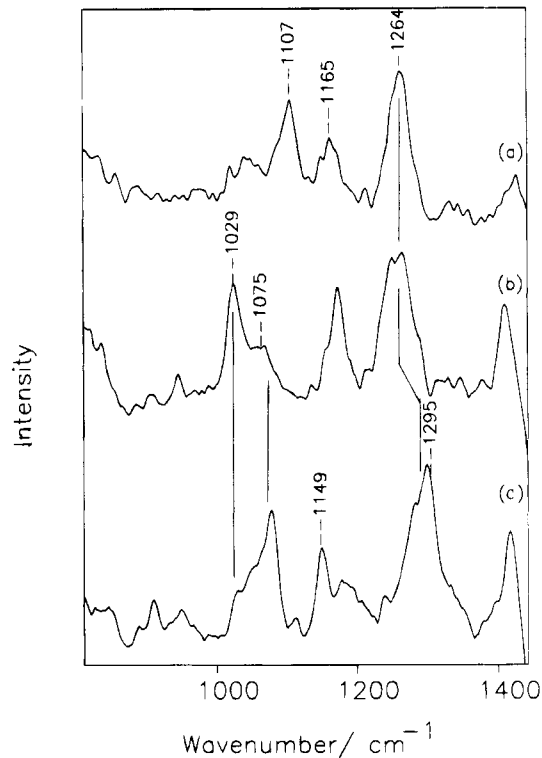


**Figure 3.** Two-color RR spectra from Figure 2 at shortest (120 ns, trace a) and longest (600  $\mu$ s, trace b) pump-probe delays, showing the increased intensity of the 1264  $\text{cm}^{-1}$  band at the shortest delay.



**Figure 4.** Two-color time-resolved resonance Raman study of  $(\text{CO})_5\text{W}=\text{C}(\text{OCH}_2\text{CH}_3)\text{C}_6\text{H}_5$  in  $\text{CH}_2\text{Cl}_2$  ( $\text{ca. } 10^{-3}$  mol  $\text{dm}^{-3}$ ): Pump  $\lambda$  351 nm; probe  $\lambda$  420 nm. Pump-probe time delays: (a) 100 ns; (b) 500 ns; (c) 1  $\mu$ s; (d) 10  $\mu$ s; (e) 50  $\mu$ s.

and pulse-excited spectra as well as additional bands at 935  $\text{cm}^{-1}$  and 1266  $\text{cm}^{-1}$  in the spectra recorded under pulsed excitation at 355 nm. Figure 4 shows two color TR<sub>3</sub> spectra recorded for complex **3** in  $\text{CH}_2\text{Cl}_2$  using



**Figure 5.** Influence of deuteration on resonance Raman spectra of  $(\text{CO})_5\text{W}=\text{C}(\text{OCH}_3)\text{CH}_3$ , recorded at an excitation wavelength of 363.8 nm in  $\text{CH}_2\text{Cl}_2$  ( $\text{ca. } 10^{-3}$  mol  $\text{dm}^{-3}$ ): (a) Undeuterated species; (b)  $(\text{CO})_5\text{W}=\text{C}(\text{OCH}_3)(\text{CD}_3)$ ; (c)  $(\text{CO})_5\text{W}=\text{C}(\text{OCD}_3)(\text{CD}_3)$ .

a pump wavelength of 351 nm and a probe of 420 nm. The transient nature of the 1266 and 935  $\text{cm}^{-1}$  features is clear and the observed decay on a time scale of  $\text{ca. } 20$   $\mu$ s is consistent with flash photolysis measurements (Table 1).

For purposes of comparison RR spectra were also recorded for the Cr- analogue of **4**,  $(\text{CO})_5\text{Cr}(\text{OMe})(\text{Ph})$ . The spectra were generated using CW and pulsed excitation at 363.8 nm and 355 nm respectively. In the CW-excited spectrum the primary features appear at 935  $\text{cm}^{-1}$ , 997  $\text{cm}^{-1}$ , 1235  $\text{cm}^{-1}$  and 1270  $\text{cm}^{-1}$ , suggesting the presence of both *anti* and *syn* isomers. To establish that this was not simply due to the creation of a photostationary state, RR spectra were also recorded at an excitation wavelength of 457.9 nm. At this wavelength negligible photochemical transformation to *syn* isomer would be expected yet the spectrum (not shown here) clearly displayed features characteristic of both species. NMR studies<sup>1</sup> of  $(\text{CO})_5\text{Cr}(\text{OMe})\text{Ph}$  do in fact confirm the existence of both isomers in solution under ambient conditions.

Resonance Raman studies were also carried out on samples of **1** with deuterated methyl and methoxy groups. The spectra recorded using CW excitation at 363.8 nm are displayed in Figure 5. When the  $\text{CH}_3$  group alone is deuterated the band at 1264  $\text{cm}^{-1}$  remains unshifted but additional features appear at 1029  $\text{cm}^{-1}$  and 1075  $\text{cm}^{-1}$ . The spectrum recorded when the  $\text{OCH}_3$  and  $\text{CH}_3$  groups are both deuterated shows bands near 1149  $\text{cm}^{-1}$  and 1295  $\text{cm}^{-1}$  as the primary features.

**(c) Low Temperature Matrix Isolation Studies.** When  $(\text{CO})_5\text{WC}(\text{OMe})(\text{Ph})$  was deposited in an argon matrix at 20 K the IR spectrum exhibited CO stretching



**Table 3.** IR Bands ( $\text{cm}^{-1}$ ) for Carbene Complexes in Ar Matrix at 20 K

complex	bands
<i>anti</i> -(CO) <sub>5</sub> WC(OMe)Ph	2074, 1985, 1950, 1223, 1212, 1181, 1149, 993, 876
<i>syn</i> -(CO) <sub>5</sub> WC(OMe)Ph <sup>a</sup>	2074, 1985, 950, 1260, 1191, 1171, 1128, 936, 917, 878
<i>anti</i> -(CO) <sub>5</sub> WC(OMe)Me	2075, 1985, 1950, 1456, 1348, 1255, 1174, 910, 898
<i>syn</i> -(CO) <sub>5</sub> WC(OMe)Me <sup>a</sup>	2075, 1985, 1950, 1340, 1250, 1175, 1099, 1081, 998

<sup>a</sup> Bands observed after matrix irradiation (see text for details); features attributable to CO stretching modes are unshifted between *anti* and *syn* isomers.

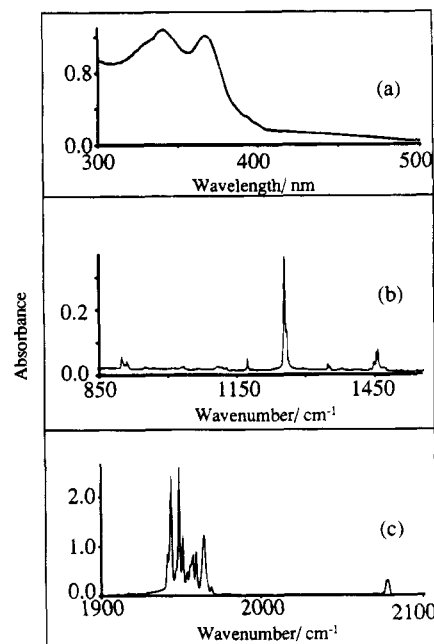
modes at 2074  $\text{cm}^{-1}$ , 1985  $\text{cm}^{-1}$  and at 1950  $\text{cm}^{-1}$  though with extensive matrix splitting. Several IR bands associated with the carbene moiety were also observed and are summarized in Table 3. Irradiation of the matrix-isolated sample at 434 nm, within the MLCT band ( $\lambda_{\text{max}} = 404$  nm) resulted in some intensity decrease and frequency shifts in the carbene IR bands as listed in Table 3. Irradiation at 434 nm for 3 h resulted in *ca.* 70% conversion of the *anti* isomer as estimated from the observed decrease in intensity of the carbene band at 1223  $\text{cm}^{-1}$ . There were no apparent changes in the positions of the CO stretching modes though minor alterations could have been masked by the matrix splitting. As well as the changes in the carbene IR bands upon irradiation a blue shift in the MLCT band from 404 nm to 394 nm was observed. The results are consistent with earlier observations by Stufkens and co-workers on this complex in low temperature matrices<sup>2</sup> and have been attributed to photoconversion of the *anti* to the *syn* isomer of (CO)<sub>5</sub>WC(OMe)(Ph). Irradiation of the sample in the matrix for 3 h within the MLCT band (394 nm) of the *syn* isomer failed to bring about any conversion back to the *anti* form, again consistent with previous work<sup>2</sup>.

The UV and IR spectra for the (CO)<sub>5</sub>WC(OMe)(Me) complex deposited in an argon matrix at 20 K are shown in Figure 6. Irradiation within the MLCT band of the *anti* isomer ( $\lambda_{\text{max}} 368$  nm) resulted in frequency shifts in several of the carbene IR bands, as shown in Table 3 and also a red shift in the UV spectrum from 368 nm to 375 nm. There was no evidence for CO loss upon irradiation and no apparent changes in the CO stretching region, apart from matrix site splitting as in the case of (CO)<sub>5</sub>WC(OMe)(Ph). The observations are consistent with formation of the *syn* isomer. Irradiation for *ca.* 1.5 h within the MLCT band of the *anti* isomer resulted in about 50% photoconversion as estimated from the decrease in the intensity of the carbene IR bands of the starting material. Interestingly in this case and in contrast to the situation with complex 4, matrix irradiation into the MLCT band of the *syn* isomer (*ca.* 1.5 h at 397 nm) did result in regeneration of the *anti* isomer as judged by the grow-in of features in both the IR and UV/vis spectra (Table 3).

For both complexes the changes in the IR and UV spectra in the matrix experiments are consistent with the data recorded in the solution studies, indicating that the same process is being observed in both media.

## Discussion

**(1) Identification of the Transient.** The time-resolved spectroscopic studies on the three carbene



**Figure 6.** UV and IR spectra recorded for (CO)<sub>5</sub>WC(OMe)(Me) upon deposition in an argon matrix at 20 K: (a) UV spectrum; (b, c)  $\nu(\text{carbene})$  and  $\nu(\text{CO})$  regions respectively. Arbitrary absorbance scales for (b) and (c) indicate relative band intensities.

complexes 1–3 in solution show that excitation into either LF or MLCT bands results in formation of the same single transient in <10 ns. The transient UV/vis and vibrational spectra for both the alkyl- and aryl-substituted carbenes closely resemble the corresponding spectra of the low temperature matrix photoproducts. The rate of decay of the transient is also independent of added CO. The evidence supports the identification of the major photoreaction in these metal carbonyl carbene complexes in solution as an *anti* to *syn* isomerization (eq 1) about the C–OR (R = Me, Et) carbene bond, as established by the matrix studies of Stufkens et al. for the Fischer carbene 4 and its Cr analogue.<sup>2</sup> Free rotation about the C–OR bond is inhibited by the partial double bond character, due to  $\pi$  interaction between the oxygen lone pair and the carbene carbon 2p<sub>z</sub> orbital.

## (2) Comparative Kinetics and Spectroscopy of Aryl- and Alkyl-Substituted Carbenes in Solution.

The flash photolysis studies show that the transient lifetimes (Table 1) for the alkyl-substituted carbenes are 1–2 orders of magnitude longer than for the aryl-substituted species. These differences are reflected in the activation enthalpies 51  $\text{kJ mol}^{-1}$  and 37  $\text{kJ mol}^{-1}$  for the *syn* to *anti* thermal isomerization measured in cyclohexane solution for (CO)<sub>5</sub>WC(OMe)Me and (CO)<sub>5</sub>WC(OMe)Ph, respectively. Steric interactions by the more bulky aryl group may be one factor influencing the thermal relaxation of the *syn* isomer. However this cannot be the only factor since previous flash photolysis studies<sup>6</sup> on the silyl-substituted carbene, (CO)<sub>5</sub>WC(OEt)(SiPh<sub>3</sub>), show the lifetime of the *syn* isomer to be similar to those determined for the sterically less crowded aryl-substituted carbenes. It appears that the aryl ring must also be exerting an electronic effect, possibly via an alteration during the isomerization of the extent of  $\pi$  delocalization over the carbene ligand. This point is expanded upon below. The kinetic data

in Table 1 also show that the rate of decay of the *syn* isomer is influenced by the solvent, being slower in more polar solvents for both alkyl- and aryl-substituted carbenes. This could be due to an increased stabilization of the *syn* isomer or a decrease in that of the transition state or more likely the result of some contribution from both.

The transient UV/vis spectra are significantly different for the alkyl- and aryl-substituted carbenes. The  $\lambda_{\text{max}}$  of the MLCT absorption for the *syn* isomer of the aryl-substituted complexes shifts to shorter wavelengths compared to the ground state spectrum while for the alkyl-substituted complex the corresponding spectra shift to longer wavelength. The spectral results in the latter case are consistent with those previously reported<sup>6</sup> for the silyl-substituted carbenes and a similar change in the relative stabilities of the HOMO and LUMO might have been expected upon photoisomerization of the closely related aryl-substituted carbenes. The shift to higher energy which is actually observed in the latter therefore suggests the operation of an additional factor in this case. As alluded to earlier, this might arise from a reduction in the degree of  $\pi$  delocalization over the carbene moiety between the *anti* and *syn* isomers. The isomerization of  $(\text{CO})_5\text{WC}(\text{OR})(\text{R}')$  according to eq 1 can involve not only rotation of the alkoxy group but an associated reorientation of  $\text{R}'$ . When an aryl group rotates away from the plane of the carbene in order to minimize its steric interaction with the alkoxy group in the *syn* isomer there will be a reduction in the degree of  $\pi$  interaction of the aryl ring with the carbene carbon  $2p_z$  orbital in the *syn* isomer.<sup>12</sup> This situation does not arise when  $\text{R}'$  is alkyl. Any effect of reorientation of the aryl group might be reflected in frequency changes in vibrational modes of the carbene.

Before discussing the resonance Raman spectra of 1–3 reference is made to the results obtained from studying the spectra of the deuterated analogs of 1. The *anti* isomer of complex 1 exhibits significant shifts in the three bands in its RR spectrum at 1107, 1165 and  $1264\text{ cm}^{-1}$  (Figure 5a) upon successive deuteration of the  $(\text{CH}_3)$  and  $(\text{OCH}_3)$  groups (Figure 5b,c, respectively). However attempts to assign the bands to specific vibrational modes by comparison of the frequency shifts observed upon deuteration with those calculated on the basis of reduced mass considerations were inconclusive. It appears that mode coupling within the carbene moiety is involved but further speculation is unwarranted without additional data. Studies with isotopically labeled species in low temperature matrices are planned to aid band assignment.

The most significant feature of the resonance Raman data for these carbenes is the general similarity in the frequencies of modes assignable to the *anti* and *syn* isomers. This is illustrated for instance by the CW- and pulse-excited spectra for 1 (Table 1 and Figure 2). The notable lack of frequency shifts suggests that the change in position of the alkoxy group which characterises the isomerization between the *anti* and *syn* forms does not significantly perturb the vibrational modes of the com-

plex. Available X-ray data,<sup>13</sup> although for somewhat different systems, appear to be consistent with this conclusion.

The significant shift in the position of a mode between the two isomers which is observed occurs only for the aryl-substituted carbenes. The feature near  $1235\text{ cm}^{-1}$  in the RR spectra of the *anti* forms of 2 and 3 shifts to  $1266\text{--}1270\text{ cm}^{-1}$  in the respective *syn* isomer spectra. The analogous band ( $1264\text{ cm}^{-1}$ ) in the RR spectra of the alkyl-substituted complex 1 (Table 1 and Figure 2) shows no shift in frequency between the spectra of the two isomers. This band is associated<sup>2,15</sup> with modes involving a substantial contribution from a  $(\text{C}_{\text{carbene}}-\text{OMe})$  stretching motion, consistent with its significant intensity in both the RR and IR spectra of these complexes. As proposed above, the flash photolysis experiments suggest that the formation of the *syn* isomer of 2 and 3 requires a further rotation of the aryl group away from the plane of the carbene to minimize the steric interaction between the alkoxy group and the aryl ring. Stabilization of the *syn* isomer would then arise largely<sup>16</sup> from oxygen lone pair donation into the carbon  $2p_z$  orbital with a consequent increase in the C–OMe bond order. Our spectral data are consistent with this although as stated earlier in relation to the results of the isotopic substitution studies, the vibrational spectra of the carbenes are complicated. That a shift in position of this band is only observed for the aryl-substituted carbenes ties in with the proposal that in this case an additional perturbation associated with phenyl ring reorientation is occurring in the course of the *anti* to *syn* isomerization.

**(3) Comparative Spectroscopy of Aryl- and Alkyl-Substituted Carbenes in Cryogenic Argon Matrices.** Stufkens and co-workers reported that isomerization of  $(\text{CO})_5\text{WC}(\text{OMe})(\text{Ph})$ , 4, could be photochemically induced in one direction only, *anti* to *syn*, and we have confirmed this here. The reverse *syn* to *anti* isomerization was not observed, even following direct irradiation into the MLCT band of the *syn* isomer. The only photoreaction observed<sup>2</sup> for the *syn* isomer of 4 in the matrix was CO dissociation via the LF state and it was suggested<sup>2</sup> that the MLCT and LF states of 4 were so close in energy that reaction occurred preferentially from the more reactive LF state irrespective of the state initially populated. However, the matrix isolation studies reported in the present work show that for 1 the isomerization is photochemically reversible. In reported cases of "one-way" photoisomerization in stilbene-type molecules such as that observed in 1-(2-anthryl)-3,3-dimethyl-1-butene the suggested explanation was that a local minimum exists on the excited state potential energy surface close to the geometry of the photochemically inert isomer.<sup>17</sup> We propose here that in the aryl-substituted carbenes the first distortion in the MLCT state upon excitation of the *syn* isomer is a rotation of the aryl ring to a more conjugating position, the driving force being the resulting resonance stabilization. The relative rates of conversion of this localized thermally

(13) Schubert, U.; Ackeremann, K.; Rustenmeyer, P. *J. Organomet. Chem.* **1982**, *231*, 323.

(14) Mills, O. S.; Redhouse, A. D. *J. Chem. Soc. A* **1968**, 642.

(15) Fischer, E. O.; Massbol, A. *Chem. Berichte* **1967**, *100*, 2445.

(16) Casey, C. P.; Burkhardt, T. J.; Bunnett, C. A.; Calabrese, J. C. *J. Am. Chem. Soc.* **1977**, *99*, 2127.

(17) Arai, T.; Karatsu, T.; Sakuragi, H.; Tokumaru, K. *Tetrahedron Lett.* **1983**, *24*, 2873.

(12) X-ray crystallographic studies<sup>14</sup> on  $(\text{CO})_5\text{CrC}(\text{OMe})(\text{Ph})$  show that in the solid state this complex exists as the *anti* isomer, with the phenyl ring lying at  $90^\circ$  to the carbene plane so that there is no  $\pi$  interaction between the phenyl ring and the carbene carbon  $2p_z$  orbital. However this situation may be different in solution where for instance crystal packing effects will not operate.

equilibrated excited state to either the *anti* or the *syn* forms will depend upon the relative dispositions of the three potential energy surfaces. The data suggest that in the present case decay occurs preferentially back into the potential energy well of the *syn* isomer; the MLCT state of the *syn* isomer is photochemically inert. For the *anti* isomer the solution studies suggest that some degree of conjugation extends over the carbene moiety in the ground state. Therefore, no significant rotation of the aryl ring need occur upon MLCT excitation. The initial excited state rapidly decays via rotation of the C-OMe bond into a lower energy "twisted excited" state in which the original geometry of the complex is lost. From this state decay to either ground state isomer is possible. Hence in the aryl-substituted carbenes the MLCT excited state of the *anti* isomer is photochemically active to isomerization. Support for this explanation of "one way" photoisomerization for  $(\text{CO})_5\text{WC}(\text{OMe})(\text{Ph})$  comes from the matrix experiments on the alkyl-substituted carbene **1**. The MLCT excited states of the *anti* and *syn* isomers of complex **1** are both active to isomerization. This is consistent with the above proposed explanation for "one way" photoisomerization in the aryl-substituted case since "localized" stabilization of the MLCT excited state by increased conjugation cannot operate in complex **1** and both the *syn* and *anti* isomers would be expected to behave like the *anti* isomer of  $(\text{CO})_5\text{WC}(\text{OMe})(\text{Ph})$ .

### Summary and Conclusions

1. The transient observed upon pulsed irradiation in solution into both the LF and MLCT band of these carbenes is assigned as the *syn* isomer. This assignment is supported by comparison with results from experiments carried out in cryogenic matrices. LF excitation provides no evidence in support of a transient arising from CO dissociation, although continuous irradiation experiments<sup>3,5,6</sup> show that the reaction should occur. Presumably the quantum yield for the process is so low that the transient is not detectable.

2. The lifetime of the *syn* isomer is dependent on the polarity of the solvent and on the nature of the ancillary (*R'*) group on the carbene carbon.

3. Distinctive photochemical behaviour is exhibited by the *syn* isomer of alkyl- and aryl-substituted carbenes. The most notable difference is that the MLCT excited state of the *syn* isomer of aryl-substituted carbenes is photoinert, while that of the alkyl-substituted complex leads to photoisomerization. These differences are consistent with the proposal that the isomerization of the aryl-substituted carbenes also involves a reorientation of the aryl ring to a less  $\pi$ -interacting position in the *syn* isomer.

4. There are clear parallels between *anti-syn* photoisomerization of metal carbenes<sup>18,19</sup> as investigated in the present work and the extensively studied *cis-trans* photoisomerization of organic alkenes.<sup>20</sup> However the novel feature which appears in the metal carbene complexes is that although the geometric change is centered on the carbene ligand it is not the direct result of an *intraligand* excitation process. The metal center is in effect acting as an intramolecular photosensitizer resulting in light absorption and the transfer of electron density onto the carbene ligand, thereby facilitating the isomerization.

**Acknowledgment.** We thank the U.K. Science & Engineering Research Council for support (Grant GR/F42980), Dr. A. W. Parker and Sue Tavender at the Central Laser Facility, Rutherford Appleton Laboratory, for assistance with two-laser TR<sub>3</sub> experiments, and Professor R. N. Perutz for providing access to the matrix isolation apparatus in York. We also gratefully acknowledge several useful discussions with Dr. S. E. J. Bell and for some preliminary flash photolysis data on **1**. We also thank Dr. Ala H. R. Al-Obaidi for assistance with processing of Raman spectra and for useful discussions.

OM940449Z

(18) (a) Kiel, W. A.; Lin, G.-Y.; Constable, A. G.; McCormick, F. B.; Strouse, C. E.; Eisenstein, O.; Gladysz, J. A. *J. Am. Chem. Soc.* **1982**, *104*, 4865. (b) McCormick, F. B.; Kiel, W. A.; Gladysz, J. A. *Organometallics* **1982**, *1*, 405.

(19) Voran, S.; Blau, H.; Wolfgang, M.; Schubert, U. *J. Organomet. Chem.* **1982**, *232(C)*, 33.

(20) Allen, M. T.; Whitten, D. G. *Chem. Rev.* **1989**, *89*, 1691.

# Silicon-Carbon Unsaturated Compounds. 51. Nickel-Catalyzed Reactions of 3,4-Benzo-1,1,2,2-tetraethyl-1,2-disilacyclobut-3-ene with Alkenes and Dienes

Mitsuo Ishikawa,\* Shougo Okazaki, and Akinobu Naka

Department of Applied Chemistry, Faculty of Engineering, Hiroshima University,  
Higashi-Hiroshima 724, Japan

Akitomo Tachibana,\* Susumu Kawauchi,† and Tokio Yamabe

Division of Molecular Engineering, Faculty of Engineering, Kyoto University,  
Sakyo-ku, Kyoto 60601, Japan

Received June 8, 1994<sup>®</sup>

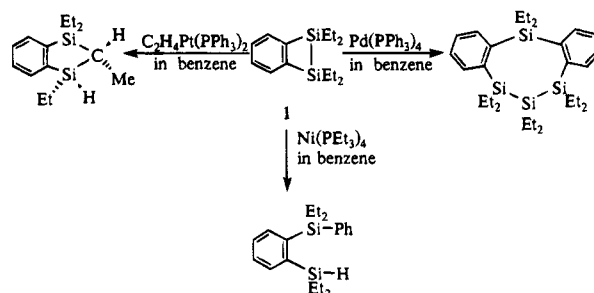
The reactions of 3,4-benzo-1,1,2,2-tetraethyl-1,2-disilacyclobut-3-ene (**1**) with alkenes in the presence of a catalytic amount of tetrakis(triethylphosphine)nickel(0) at 150 °C have been investigated. With 1,1-diphenylethylene, **1** afforded 1,2-bis(diethylsilyl)benzene (**2**), 4,5-benzo-1,1,3,3-tetraethyl-2-diphenylmethylene-1,3-disilacyclopent-4-ene, and 1-[diethyl-(2,2-diphenylethenyl)silyl]-2-diethylsilylbenzene in 4%, 55%, and 7% yields. The reaction of **1** with styrene gave 4,5-benzo-1,1,3,3-tetraethyl-2-phenylmethylene-1,3-disilacyclopent-4-ene and (*E*)-1-tetraethyl(2-phenyl)disilanyl-2-phenylethene in 12% and 47% yields, while with 1- and 2-hexene, **1** produced 4,5-benzo-1,1,3,3-tetraethyl-2-(*n*-pentylidene)-1,3-disilacyclopent-4-ene, together with a product arising from hydrosilation of **2** and 1-hexene. Similar treatment of **1** with ethylene in an autoclave afforded 4,5-benzo-1,1,3,3-tetraethyl-2-methylene-1,3-disilacyclopent-4-ene, tetraethyl-1-phenyl-2-vinyl-disilane, and 2,3-benzo-1,1,4,4-tetraethyl-1,4-disilacyclohex-2-ene in 7%, 34%, and 10% yields. Similarly, the nickel-catalyzed reaction of **1** with 2,3-dimethylbutadiene yielded 4,5-benzo-1,1,3,3-tetraethyl-2-(1,2,2-trimethylethenyl)-1,3-disilacyclopent-4-ene and 2,3-benzo-1,1,4,4-tetraethyl-6,7-dimethyl-1,4-disilacycloocta-2,6-diene in 33% and 30% yields, while with 1,3- and 1,4-cyclohexadiene, **1** afforded 5,5,10,10-tetraethyl-8,9,13,14-tetrahydrosilanthrene, as the sole product. The results of MO calculations for 1-nickela-2,5-disilacyclopent-3-ene are also reported.

## Introduction

3,4-Benzo-1,1,2,2-tetraethyl-1,2-disilacyclobut-3-ene (**1**) shows unique chemical behavior. The thermolysis of **1** produces an *o*-quinodisilane as a reactive species,<sup>1</sup> while its photolysis gives 1-ethyl-1-(*o*-diethylsilylphenyl)-2-methylsilene.<sup>2</sup> These intermediates can be readily trapped by various trapping agents such as alcohols, carbonyl compounds, and alkynes. On the other hand, the reaction of **1** with transition-metal complexes gives reactive species containing the transition-metal, and their reactivities highly depend on the nature of the metal in these complexes.<sup>3-6</sup> For examples, the reaction of **1** with a catalytic amount of ( $\eta^2$ -ethylene)bis(triphenylphosphine)platinum(0) in refluxing benzene affords an isomerization product, *cis*-4,5-benzo-1,1,3-tri-

ethyl-2-methyl-1,3-disilacyclopent-4-ene, along with a small amount of 1-(diethylphenylsilyl)-2-diethylsilylbenzene,<sup>5</sup> while with a tetrakis(triphenylphosphine)-palladium(0) catalyst in benzene at 150 °C, **1** produces a dimerization product, 4,5,7,8-dibenzo-1,1,2,2,3,3,6,6-octaethyl-1,2,3,6-tetrasilacycloocta-4,7-diene as the sole product.<sup>6</sup>

The reaction of **1** with a catalytic amount of tetrakis(triethylphosphine)nickel(0) in refluxing benzene gives neither isomerization product nor dimerization product, but affords 1-(diethylphenylsilyl)-2-diethylsilylbenzene arising from C-H bond activation of the phenyl ring.<sup>3</sup>



Recently, we have found that the similar nickel-catalyzed reaction of **1** with enolizable ketones such as

\* Information and Systems Department, Showa Denko K. K., 1-13-9 Shiba Daimon, Minato-ku, Tokyo 105, Japan.

<sup>®</sup> Abstract published in *Advance ACS Abstracts*, November 1, 1994.

(1) Ishikawa, M.; Sakamoto, H.; Tabuchi, T. *Organometallics* **1991**, *10*, 3173.

(2) Sakamoto, H.; Ishikawa, M. *Organometallics* **1992**, *11*, 2580.

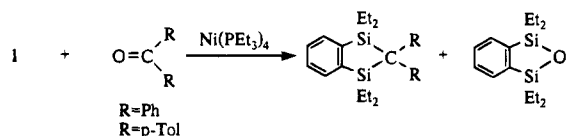
(3) Ishikawa, M.; Okazaki, S.; Naka, A.; Sakamoto, H. *Organometallics* **1992**, *11*, 4135.

(4) Ishikawa, M.; Naka, A.; Okazaki, S.; Sakamoto, H. *Organometallics* **1993**, *12*, 87.

(5) Ishikawa, M.; Naka, A.; Ohshita, J. *Organometallics* **1993**, *12*, 4987.

(6) Naka, A.; Hayashi, M.; Okazaki, S.; Ishikawa, M. submitted to *Organometallics*, in press.

acetone and acetophenone affords 1-[diethyl(isopropoxy)silyl]-2-(diethylsilyl)benzene and 1-[diethyl[(1-phenylvinyl)-oxy]silyl]-2-(diethylsilyl)benzene, in addition to 4,5-benzo-1,1,3,3-tetraethyl-1,3-disila-2-oxacyclopent-4-ene. The reaction of **1** with benzophenone and 4,4'-dimethylbenzophenone, however, gives products arising from insertion of diphenylcarbene and di(*p*-tolyl)carbene into a silicon-silicon bond of **1** and 4,5-benzo-1,1,3,3-tetraethyl-1,3-disila-2-oxacyclopent-4-ene, respectively.<sup>4</sup>

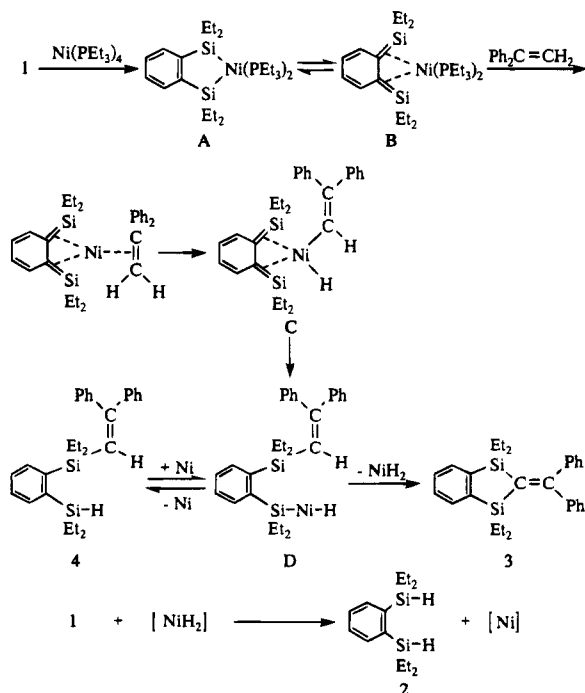


In order to obtain more information about the reactive species in the nickel-catalyzed reaction, we investigated the reaction of **1** with alkenes and dienes in the presence of a catalytic amount of tetrakis(triethylphosphine)nickel(0). We also carried out MO calculations for 1-nickela-2,5-disilacyclopent-3-ene as a model of 3,4-benzo-2,2,5,5-tetraethyl-1-nickela-2,5-disilacyclopent-3-ene.

## Results and Discussion

When a mixture of 3,4-benzo-1,1,2,2-tetraethyl-1,2-disilacyclobut-3-ene (**1**) and 1.5 equiv of 1,1-diphenylethylene in the presence of a catalytic amount of tetrakis(triethylphosphine)nickel(0) in a sealed degassed tube was heated at 150 °C for 24 h, three products, 1,2-bis(diethylsilyl)benzene (**2**) and 4,5-benzo-1,1,3,3-tetraethyl-2-(diphenylmethylene)-1,3-disilacyclopent-4-ene (**3**), and 1-[diethyl(2,2-diphenylethenyl)silyl]-2-diethylsilylbenzene (**4**) were obtained in 4%, 55%, and 7% yields, respectively (Scheme 1). In this reaction, a trace amount of an isomer of **4** was also detected by mass spectrometric analysis. GC-Mass spectrometric analysis of the recovered 1,1-diphenylethylene fraction showed

Scheme 1



that the hydrogenated product of the starting olefin, 1,1-diphenylethane was produced in 28% yield. The formation of compound **2** and 1,1-diphenylethane shows that nickel dihydride species is formed in this reaction (see below).

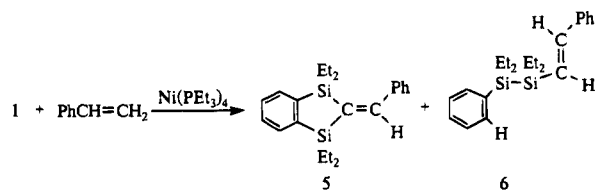
The structures of **3** and **4** were verified by spectroscopic analysis, as well as by elemental analysis. The mass spectrum for **3** shows a parent ion at  $m/z$  426, corresponding to the calculated molecular weight for  $C_{28}H_{34}Si_2$  (adduct - 2H). Its  $^{13}C$  NMR spectrum shows two resonances at 137.4 and 170.1 ppm, attributed to olefinic carbons, as well as seven resonances due to phenylene and phenyl carbons. The  $^{29}Si$  NMR spectrum for **3** reveals a single resonance at -2.82 ppm, showing the presence of two equivalent silicon atoms. These results clearly indicate that **3** has a 4,5-benzo-2-(diphenylmethylene)-1,3-disilacyclopent-3-ene structure. The mass spectrum for **4** shows a fragment ion at  $m/z$  428, corresponding to the calculated value for  $C_{28}H_{36}Si_2$ . Its  $^1H$  NMR spectrum shows a quintet resonance at  $\delta$  4.57 ppm and a singlet at 6.45 ppm, due to an Si-H proton and a vinylic proton, respectively. The IR spectrum for **4** shows Si-H stretching frequencies at  $2147\text{ cm}^{-1}$ . These results are wholly consistent with the structure proposed for **4**. All spectral data obtained for **2** were identical with those of an authentic sample reported previously.<sup>1</sup>

In the nickel-catalyzed reactions of **1** with arenes and carbonyl compounds<sup>4</sup> and also in the platinum-catalyzed reactions<sup>5</sup> with alkenes and alkynes, we suggested the formation of 3,4-benzo-1-metala-2,5-disilacyclopent-3-enes (**A**) and *o*-quinodisilane-transition metal complexes (**B**) as key reactive species. The production of **3** and **4** in the present reaction may be best explained in terms of the reaction of *o*-quinodisilane-nickel complex **B**, which would be formed from isomerization of 3,4-benzo-1-nickela-2,5-disilacyclopent-3-ene **A** arising from insertion of a nickel species into an Si-Si bond of **1**, with 1,1-diphenylethylene. Oxidative addition of an olefinic C-H bond of 1,1-diphenylethylene to the nickel atom in complex **B** would produce nickel complex **C**. The shift of a diphenylethenyl group from the nickel atom to one of two silicon atoms in the complex **C** would yield nickel complex **D**. Reductive elimination of nickel dihydride from **D** leads to the formation of **3**, while elimination of nickel species from **D** results in the production of **4** (Scheme 1).

Interestingly, addition of a hydrosilane to the nickel-catalyzed reaction of **1** with 1,1-diphenylethylene results in acceleration of the reaction rate, and also affects the product distribution. Thus, the reaction of **1** with 1,1-diphenylethylene in the presence of 5 mol% of the nickel(0) catalyst and 89 mol% of dimethylphenylsilane in refluxing hexane for 20 h gave compound **4** in 70% yield, in addition to a trace amount of **3**. The selective formation of **4** is probably due to rapid nickel transfer from complex **D** to dimethylphenylsilane. The reaction of **4** isolated in a pure form with a catalytic amount of tetrakis(triethylphosphine)nickel(0) in a sealed tube at 150 °C for 24 h gave **3** in 76% yield. These results strongly suggest that the initial step of the reaction involves oxidative addition of an  $sp^2$  C-H bond of 1,1-diphenylethylene to *o*-quinodisilane-nickel complex **B** giving complex **C**,<sup>7</sup> which undergoes further reaction to form complex **D**, as shown in Scheme 1. That the

product **2** was produced by the reaction of **1** with nickel dihydride which would be eliminated from **D** was confirmed by the fact that the reaction of **1** with hydrogen in the presence of a catalytic amount of tetrakis(triethylphosphine)nickel(0) in an autoclave at 150 °C for 24 h produced **2** in quantitative yield. Furthermore, treatment of **4** with the nickel(0) catalyst in the presence of 1 equiv of **1** at 150 °C for 24 h produced **2** and **3** in 47% and 84% yields, together with 15% of the unchanged compound **1**. Similar treatment of **4** in the presence of 3.4 equiv of 1,1-diphenylethylene at 150 °C for 24 h gave **3** and 1,1-diphenylethane in 70% and 43% yields. These results can best be understood by elimination of nickel dihydride species from nickel complex **D** arising from insertion of a nickel catalyst into an Si-H bond in compound **4**. The resulting nickel dihydride reacts with **1** or 1,1-diphenylethylene to give the observed products.

The nickel-catalyzed reaction of **1** with styrene under the same conditions afforded two products, which were identified as 4,5-benzo-1,1,3,3-tetraethyl-2-phenylmethylene-1,3-disilacyclopent-4-ene (**5**) and (*E*)-1-tetraethyl-(2-phenyl)disilanyl-2-phenylethene (**6**) in 12% and 47% yields, in addition to a trace amount of compound **2**. In

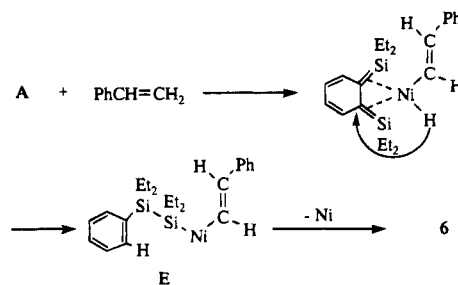


this reaction, no 1-[diethyl(2-phenylethenyl)silyl]-2-diethylsilylbenzene, analogous to **4** was detected in the reaction mixture by spectrometric analysis. Pure **5** and **6** could readily be isolated by preparative HPLC.

The mass spectrum of **5** reveals a molecular ion at  $m/z$  350, corresponding to the calculated value for  $\text{C}_{22}\text{H}_{30}\text{Si}_2$  (adduct - 2H). The  $^1\text{H}$  NMR spectrum of **5** shows a singlet resonance at  $\delta$  7.89 ppm, attributed to an olefinic proton, along with resonances at 0.71–0.99 and 7.30–7.63 ppm, due to ethyl protons, and phenyl and phenylene protons, respectively. The  $^{13}\text{C}$  NMR spectrum indicates two resonances at  $\delta$  139.0 and 155.5 ppm attributable to olefinic carbons, while its  $^{29}\text{Si}$  NMR spectrum reveals two resonances at 6.46 and 0.50 ppm due to two nonequivalent silicon atoms. These results are wholly consistent with the structure proposed for **5**. The mass spectrum of **6**, however, shows a parent peak at  $m/z$  352, and its  $^1\text{H}$  NMR spectrum reveals two doublets at 6.44 and 6.79 ppm due to two olefinic protons. The  $^{13}\text{C}$  NMR spectrum also reveals two olefinic carbons at 126.3 and 144.5 ppm, together with eight resonances for phenyl carbons, while the  $^{29}\text{Si}$  NMR spectrum reveals two resonances at -14.81 and -17.90 ppm. On the basis of the coupling constant ( $J = 19.1$  Hz) of the olefinic protons, compound **6** must have the trans configuration.

The formation of compound **5** may be explained by a series of the reaction involving activation of a terminal  $\text{sp}^2$  C-H bond,<sup>7</sup> which is similar to the mechanism proposed for the formation of compound **3**. The produc-

## Scheme 2

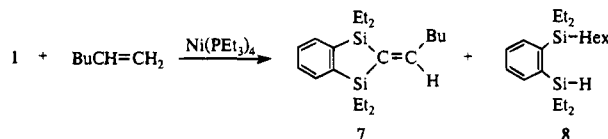


tion of **6** is of considerable interest, because scission of a silicon-phenylene bond is involved. In the nickel-catalyzed reactions of **1** with aromatic compounds and carbonyl compounds reported previously,<sup>3,4</sup> no compounds derived from scission of the silicon-phenylene bond were detected at all.

Two possible mechanism may be considered for the formation of **6**. One involves isomerization of a nickel complex, analogous to **C**, which would be formed from oxidative addition of an  $\text{sp}^2$  C-H bond of styrene to *o*-quinodisilane **B**. Hydrogen on the nickel atom in this complex migrates to the silene carbon and produces a silicon-silicon bond to give nickel complex **E**. Finally reductive elimination of a nickel species from **E** produces compound **6** (Scheme 2). The other comprises direct insertion of a nickel species into a silicon-phenylene bond to give 4,5-benzo-2,2,3,3-tetraethyl-1-nickela-2,3-disilacyclopent-4-ene, followed by the reaction of this nickel complex with styrene leading to nickel complex **E**.

Although, at present, evidence to support the former mechanism has not yet been obtained, it seems likely that direct insertion of the nickel species into a silicon-phenylene bond is highly unfavorable because of the steric reasons.

Similarly, 1-hexene reacted with **1** under the same conditions to give 4,5-benzo-1,1,3,3-tetraethyl-2-(*n*-pentylidene)-1,3-disilacyclopent-4-ene (**7**) and 1-[diethyl(*n*-hexyl)silyl]-2-(diethylsilyl)benzene (**8**) in 52% and 44% yields. Compound **7** is probably produced from the



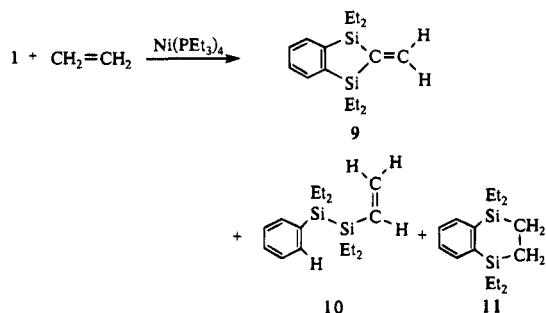
reaction which is similar to that of **3** and **5**. Compound **8**, however, would be produced from hydrosilation of **2** to 1-hexene. Indeed, the reaction of **2** with 1-hexene in the presence of a catalytic amount of tetrakis(triethylphosphine)nickel(0) under the same conditions afforded **8** in 58% yield, in addition to 28% of the unchanged starting compound **1**. No other products were detected in the reaction mixture by either GLC analysis or spectrometric analysis. Products **7** and **8** could be readily isolated by preparative HPLC.

2-Hexene also reacted with *o*-quinodisilane-nickel complex **B** to give **7** in 56% yield, indicating that isomerization of an internal double bond to the terminal one takes place. Isomerization of internal olefins to terminal ones in the presence of a transition metal catalyst is well known. In this reaction, **2** and a hydrosilation product were also obtained in 11% and

(7) For C-H bond activation by transition metal catalysts, see Jones, W. D.; Feher, F. J. *Acc. Chem. Res.* **1989**, *22*, 91 and also Tanaka, M.; Sakakura, T. *Pure Appl. Chem.* **1990**, *62*, 1147.

20% yields.  $^1\text{H}$  and  $^{13}\text{C}$  NMR spectra for the hydrosilation product show the presence of compound **8** as a major product (16% yield), but the other two hydrosilation products (4% combined yield), which are probably formed by hydrosilation of **2** to an internal double bond were detected. Unfortunately, all attempts to separate these two isomers from the mixture were unsuccessful. The structures of **7** and **8** were verified by spectrometric analysis (see Experimental Section).

Interestingly, the nickel-catalyzed reaction of **1** with ethylene in an autoclave at 150 °C gave three products, 4,5-benzo-1,1,3,3-tetraethyl-2-methylene-1,3-disilacyclopent-3-ene (**9**), tetraethyl-1-phenyl-2-vinyldisilane (**10**), and 2,3-benzo-1,1,4,4-tetraethyl-1,4-disilacyclohex-2-ene (**11**) in 7%, 34%, and 10% yields, respectively. Products

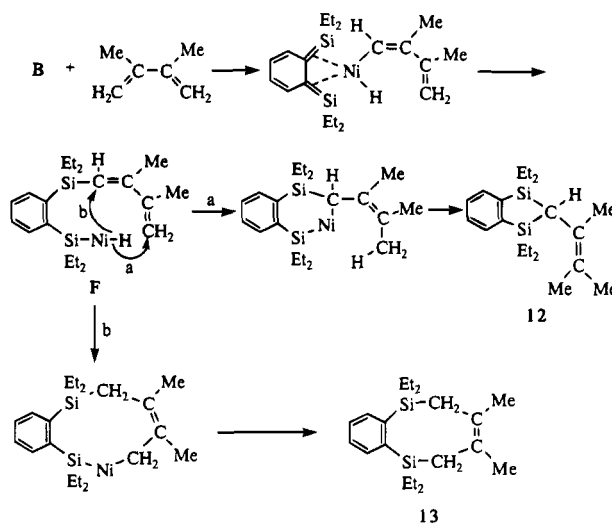


**9**, **10**, and **11** were isolated by preparative HPLC, and the structures of **9** and **10** were confirmed by spectroscopic analysis. All spectral data for **11** were identical with those of an authentic sample.<sup>5</sup> As reported recently, the platinum-catalyzed reaction of **1** with ethylene under the same conditions proceeds [4 + 2] cycloaddition to give **11** as the sole product. The present reaction, however, seems to proceed with two different pathways,  $\text{sp}^2$  C-H bond activation of ethylene leading to the formation of **9** and **10**, and [4 + 2] cycloaddition which was observed in the platinum-catalyzed reactions.<sup>5</sup>

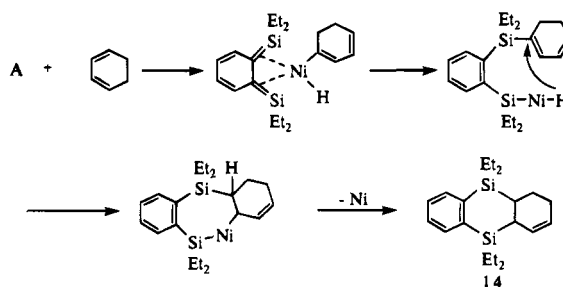
The nickel-catalyzed reaction of **1** with dienes gives the products whose formation can be explained in terms of activation of an  $\text{sp}^2$  C-H bond of dienes. Thus, the reaction of **1** with 2,3-dimethylbutadiene in the presence of a catalytic amount of tetrakis(triethylphosphine)nickel(0) at 150 °C for 20 h produced two products, 4,5-benzo-1,1,3,3-tetraethyl-2-(1,2,2-trimethylethenyl)-1,3-disilacyclopent-4-ene (**12**) and 2,3-benzo-1,1,4,4-tetraethyl-6,7-dimethyl-1,4-disilacycloocta-2,6-diene (**13**) in 33% and 30% yields, respectively. The migration of a diene group in the nickel complex formed from oxidative addition of an  $\text{sp}^2$  C-H bond of 2,3-dimethylbutadiene to a nickel atom of *o*-quinodisilane-nickel complex **B** to one of two silicon atoms gives complex **F**. Intramolecular addition of the Ni-H bond across the terminal carbon-carbon double bond affords **12**, while addition of this Ni-H bond to an internal carbon-carbon double bond produces **13** (Scheme 3).

Similar nickel-catalyzed reaction of **1** with 1,3-cyclohexadiene gave 5,5,10,10-tetraethyl-8,9,13,14-tetrahydro-silanthrene (**14**) in 80% yield. With 1,4-cyclohexadiene, **1** also afforded **14** in 80% yield as the sole product, indicating that rapid isomerization of a double bond to the conjugated system takes place during the reaction. The formation of **14** may also be understood in terms of  $\text{sp}^2$  C-H bond activation of cyclohexadiene,

## Scheme 3



## Scheme 4

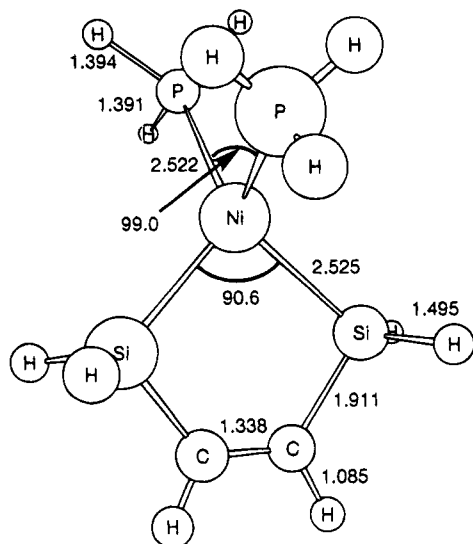


followed by intramolecular addition of a Ni-H bond to a diene moiety (Scheme 4). Since the reaction of **1** with cyclohexene under the same conditions gave no volatile products, formal [4 + 2] cycloaddition would not be involved for the production of **14**.

In an effort to learn more about the reactive species in the present reaction, we carried out the stoichiometric reaction of **1** with tetrakis(triethylphosphine)nickel(0) in benzene- $d_6$ . The reactions of **1** with a stoichiometric amount of ( $\eta^2$ -ethylene)bis(triphenylphosphine)platinum(0)<sup>8</sup> in toluene- $d_8$  and tetrakis(triphenylphosphine)palladium(0)<sup>6</sup> in benzene- $d_6$  at room temperature proceed cleanly to give the reactive 3,4-benzo-2,2,5,5-tetraethyl-1-metala-2,5-disilacyclopent-3-enes in almost quantitative yields. However, similar reaction of **1** with tetrakis(triethylphosphine)nickel(0) produces no 3,4-benzo-1-nickela-2,5-disilacyclopent-3-ene **A**. Thus, when compound **1** was added to a benzene- $d_6$  solution containing 1 equiv of tetrakis(triethylphosphine)nickel(0) at room temperature, the light yellow solution changed to a dark red color. However, the  $^1\text{H}$  NMR spectrum of this solution showed only resonances attributed to **1** and tetrakis(triethylphosphine)nickel(0). Furthermore, the  $^{29}\text{Si}$  NMR spectrum of the solution reveals a single resonance whose chemical shift is identical with that of **1**. When the solution was stirred for 36 h at room temperature, no change was observed in its  $^1\text{H}$  and  $^{29}\text{Si}$  NMR spectra. Heating the solution at 80 °C for 12 h

(8) 3,4-Benzo-2,2,5,5-tetraethyl-1,1-bis(triphenylphosphine)-1-platina-2,5-disilacyclopent-3-ene: mp 119–121 °C (dec.);  $^1\text{H}$  NMR  $\delta$  ( $\text{C}_6\text{D}_6\text{CD}_3$ ) 0.53–1.19 (m, 20H, EtSi), 6.88–7.72 (m, 34H, phenyl and phenylene ring protons);  $^{29}\text{Si}$  NMR  $\delta$  ( $\text{C}_6\text{D}_6\text{CD}_3$ ) 36.43;  $^{31}\text{P}$  NMR  $\delta$  ( $\text{C}_6\text{D}_6\text{CD}_3$ ) 24.95 ( $J_{\text{Pt-P}} = 1540.6$  Hz). Anal. Calcd for  $\text{C}_{60}\text{H}_{84}\text{P}_2\text{Pt}_1\text{Si}_2$ : C, 62.03; H, 5.62. Found: C, 61.89; H, 5.53.





**Figure 1.** HF/HUZSP\* optimized structure for 1-nickela-2,5-disilacyclopent-3-ene (**G**). Bond lengths are in angstroms and bond angles in degrees.

gave an oligomer whose  $^1\text{H}$  NMR spectrum showed broad signals in the region of ethyl protons and also phenylene protons. The molecular weight of the oligomer was determined to be 700, relative to polystyrene standards. Unfortunately, all attempts to detect 3,4-benzo-1-nickela-2,5-disilacyclopent-3-ene **A** in the present system were unsuccessful.

**Quantum Chemical Study of 1-Nickela-2,5-disilacyclopent-3-ene.** We carried out molecular orbital calculations for 1-nickela-2,5-disilacyclopent-3-ene (**G**), as a model of complex **A**. The MO calculations were performed with the GAUSSIAN 92 program.<sup>9</sup> The geometry was optimized under constraint of  $C_{2v}$  symmetry by using the Hartree-Fock (HF) theory.<sup>10</sup> The Huzinaga basis set, (43321/4211\*/31), was used for Ni which includes a split valence shell and a p-type polarization function.<sup>11a</sup> The basis sets for H, C, Si, and P were taken from the standard 6-31G\* basis sets, respectively.<sup>11b</sup> These basis sets will be referred to as HUZSP\*. Theoretical harmonic vibrational frequencies were obtained from analytical second derivatives.<sup>10</sup> The optimized geometry has all positive frequencies to be verified as a true energy minimum.

The HF/HUZSP\* geometry of complex **G** is displayed in Figure 1. The Ni-P bond length of 2.522 Å, which is comparable with the Ni-Si bond length of 2.525 Å, is somewhat larger than the experimental value of 2.15 Å in  $\text{Ni}(\text{PPh}_3)_2(\text{C}_2\text{H}_4)$  and  $\text{Ni}(\text{PCy}_3)_2(\eta\text{-CO}_2)$ .<sup>12,13</sup> This

may indicate that the Ni-Si and Ni-P bond in **1** are relatively weak, because the HOMO is the  $\sigma$ -orbital of Ni-Si, while the LUMO the  $\sigma^*$  of Ni-Si and Ni-P. The Si-C bond of 1.911 Å may be compared to the single bond in methylsilane of 1.888 Å,<sup>11</sup> while the C-C bond of 1.338 Å may be compared to the double bond in cyclobutene of 1.322 Å.<sup>11</sup> In addition, HOMO-1 is mainly composed of p orbitals on C atoms, which correspond to the  $\pi$ -orbital. Therefore, it is concluded that the Si-C and C-C bonds in complex **G** have the single and double bond character, respectively.

In order to clarify the role of 3,4-benzo-1-nickela-2,5-disilacyclopent-3-ene **A** and its another isomer, *o*-quinodisilane-nickel complex **B** in catalytic reactions, further study by using higher level of theory including electron correlation effect is now in progress.

## Experimental Section

**General Procedure.** All nickel-catalyzed reactions of compound **1** with olefinic compounds were carried out in a degassed sealed glass tube (1.0 cm x 10 cm) with one exception of a experiment to reflux hexane. Yields of the products were determined by analytical GLC with the use of tridecane as an internal standard. NMR spectra were recorded on a JEOL Model EX-270 spectrometer. Infrared spectra were recorded on a Perkin-Elmer 1600 FT infrared spectrometer. Mass spectra were measured on a Shimadzu Model GCMS-QP 1000 instrument. Gas chromatographic separations were carried out using a column (3 x 10 mm) packed with 30% SE-30 silicone on Chromosorb P. Gel permeation chromatographic separation was performed with a Model LC-908 Recycling Preparative HPLC (Japan Analytical Industry Co., Ltd.). Tetrakis(triethylphosphine)nickel(0) was prepared by the method reported in the literature.

**Materials.** 3,4-Benzo-1,1,2,2-tetraethyl-1,2-disilacyclobutene **1** was prepared as reported previously.<sup>1</sup> Hexane was dried over lithium aluminum hydride and distilled before use.

**Reaction of 1 with 1,1-Diphenylethylene.** A mixture of 0.110 g (0.443 mmol) of **1**, 0.118 g (0.655 mmol) of 1,1-diphenylethylene, and 0.009 g (0.017 mmol) of tetrakis(triethylphosphine)nickel(0) was heated at 150 °C for 24 h. The mixture was analyzed by GLC as being **2** (4% yield), **3** (55% yield), and **4** (7% yield). The mixture was treated with a short silica gel column to remove nickel species from the reaction mixture. Compound **2** was isolated by preparative GLC. The product **3** was obtained from recrystallization of the mixture from ethanol. Compound **4** was isolated by preparative HPLC. For **3**: mp 102 °C–103 °C; MS  $m/z$  426 ( $M^+$ ); IR 2961, 2862, 1563, 1456, 1120, 966, 818, 748, 701, 668  $\text{cm}^{-1}$ ;  $^1\text{H}$  NMR  $\delta$ ( $\text{CDCl}_3$ ) 0.28–0.39 (m, 2H,  $\text{CH}_2$ ), 0.56–0.67 (m, 2H,  $\text{CH}_2$ ), 0.76–0.82 (m, 6H,  $\text{CH}_3$ ), 7.23–7.52 (m, 14H, phenyl and phenylene ring protons);  $^{13}\text{C}$  NMR  $\delta$ ( $\text{CDCl}_3$ ) 7.51, 7.91 (EtSi), 126.9, 127.0, 127.9, 128.2, 132.5, 146.7, 148.2 (phenyl and phenylene ring carbons), 137.4, 170.1 (olefinic carbons);  $^{29}\text{Si}$  NMR  $\delta$ ( $\text{CDCl}_3$ ) –2.82. Anal. Calcd for  $\text{C}_{28}\text{H}_{34}\text{Si}_2$ : C, 78.81; H, 8.03. Found: C, 78.62; H, 8.02. For **4**: MS  $m/z$  428 ( $M^+$ ); IR 3059, 2954, 2873, 2147, 1564, 1489, 1416, 1232, 1116, 1009, 972, 896, 793, 692, 604  $\text{cm}^{-1}$ ;  $^1\text{H}$  NMR  $\delta$ ( $\text{CDCl}_3$ ) 0.51–0.94 (m, 20H, EtSi), 4.57 (quint, 1H, HSi,  $J = 3.3$  Hz), 6.45 (s, 1H,  $\text{HC}=\text{C}$ ), 6.91–7.52 (m, 14H, phenyl and phenylene ring protons);  $^{13}\text{C}$  NMR  $\delta$ ( $\text{CDCl}_3$ ) 4.56, 5.28, 7.60, 8.34 (EtSi), 127.2, 127.3, 127.5, 127.8 (two carbons), 127.9 (two carbons), 128.1, 129.5, 134.7, 135.0, 142.2, 142.5, 143.8, 146.1, 157.4 (phenyl and phenylene ring and olefinic carbons);  $^{29}\text{Si}$  NMR  $\delta$ ( $\text{CDCl}_3$ ) –8.44 (two silicons). Anal. Calcd for  $\text{C}_{28}\text{H}_{36}\text{Si}_2$ : C, 78.44; H, 8.46. Found: C, 78.44; H, 8.49. All spectral data for **2** were identical with those of authentic samples.<sup>1</sup>

**Reaction of 1 with 1,1-Diphenylethylene in the Presence of Hydrosilane in Hexane.** A mixture of 0.309 g (1.24

(9) Frisch, M. J.; Trucks, G. W.; Head-Gordon, M.; Gill, P. M. W.; Wong, M. W.; Foresman, J. B.; Jonson, B. G.; Schlegel, H. B.; Robb, M. A.; Replogle, E. S.; Gomperts, R.; Andres, J. L.; Raghavachari, K.; Binkley, J. S.; Gonzales, C.; Martin, R. L.; DeFrees, D. J.; Baker, J.; Stewart, J. J. P.; Pople, J. A. GAUSSIAN 92, Revision A, Gaussian Inc., Pittsburgh, PA, 1992.

(10) Hehre, W. J.; Radom, L.; Schleyer, P. v. R.; Pople, J. A. *Ab Initio Molecular Orbital Theory*, Wiley, New York, 1986.

(11) (a) Huzinaga basis set; Huzinaga, S.; Andzelm, J.; Klobukowski, M.; Radzio-Andzelm, E.; Sasaki, Y.; Tatewaki, H.; *Gaussian Basis Sets for Molecular Calculations*, Elsevier, New York, 1984. (b) 6-31G\* basis sets; Hariharan, P. C.; Pople, J. A. *Theor. Chim. Acta* 1973, 28, 213; Francl, M. M.; Pietro, W. J.; Hehre, W. J.; Binkley, J. S.; Gordon, M. S.; DeFrees, D. J.; DeFrees; Pople, J. A. *J. Chem. Phys.* 1982, 77, 3654.

(12) Jolly, P. W.; Wilke, G. *The Organic Chemistry of Nickel*, Academic Press, New York and London, 1974, Vol. I, Chapter V.

(13) Aresta, M.; Nobile, C. F.; Albano, V. G.; Forni, E.; Manassero, M. *J. Chem. Soc. Chem. Commun.* 1975, 636.



mmol) of **1**, 0.396 g (2.20 mmol) of 1,1-diphenylethylene, 0.149 g (1.10 mmol) of dimethylphenylsilane, and 0.033 g (0.062 mmol) of tetrakis(triethylphosphine)nickel(0) in 10 mL of hexane was heated to reflux for 20 h. The mixture was analyzed by GLC as being **4** (70% yield) and 4% of the starting compound **1**. The mixture was treated with a short silica gel column to remove nickel species from the reaction mixture. Compound **4** was isolated by preparative HPLC. All spectral data for **4** were identical with those of authentic samples.

**Reaction of **4** in the Presence of Nickel Catalyst.** A mixture of 0.100 g (0.233 mmol) of **4**, and 0.017 g (0.032 mmol) of tetrakis(triethylphosphine)nickel(0) in 1 mL of hexane was heated at 150 °C for 24 h. The mixture was analyzed by GLC as being **3** (76% yield). The mixture was treated with a short silica gel column to remove nickel species from the reaction mixture. Compound **3** was isolated by preparative HPLC. All spectral data for **3** were identical with those of authentic samples.

**Reaction of **1** with Hydrogen.** Into a 50-mL autoclave was placed 0.300 g (1.21 mmol) of **1** and 0.031 g (0.058 mmol) of tetrakis(triethylphosphine)nickel(0), and then hydrogen gas (60 kg/cm<sup>2</sup>) was compressed into autoclave. The autoclave was heated at 150 °C for 24 h. The mixture was analyzed by GLC as being **2** (98% yield). The mixture was treated with a short silica gel column to remove nickel species from the reaction mixture. Compound **2** was isolated by preparative GLC. All spectral data for **2** were identical with those of authentic samples.<sup>1</sup>

**Reaction of **1** and **4** in the Presence of Nickel Catalyst.** A mixture of 0.335 g (1.35 mmol) of **1**, 0.557 g (1.23 mmol) of **4** and 0.053 g (0.100 mmol) of tetrakis(triethylphosphine)nickel(0) was heated at 150 °C for 24 h. The mixture was analyzed by GLC as being **2** (47% yield), **3** (84% yield) and 15% of the compound **1**. The mixture was treated with a short silica gel column to remove nickel species from the reaction mixture. Compound **2** was isolated by preparative GLC. Compound **3** was isolated by preparative HPLC. All spectral data for **2** and **3** were identical with those of authentic samples.

**Reaction of **4** and 1,1-Diphenylethylene in the Presence of Nickel Catalyst.** A mixture of 0.063 g (0.147 mmol) of **4**, 0.089 g (0.494 mmol) of 1,1-diphenylethylene and 0.007 g (0.013 mmol) of tetrakis(triethylphosphine)nickel(0) was heated at 150 °C for 24 h. The mixture was analyzed by GLC as being **3** (70% yield) and 1,1-diphenylethane (43% yield). The mixture was treated with a short silica gel column to remove nickel species from the reaction mixture. Compound **3** and 1,1-diphenylethane was isolated by preparative HPLC. All spectral data for **3** and 1,1-diphenylethane were identical with those of authentic samples.

**Reaction of **1** with Styrene.** A mixture of 0.374 g (1.51 mmol) of **1**, 0.255 g (2.45 mmol) of styrene, and 0.040 g (0.075 mmol) of tetrakis(triethylphosphine)nickel(0) was heated at 150 °C for 24 h. The mixture was analyzed by GLC as being **5** (12% yield) and **6** (47% yield). The mixture was treated with a short silica gel column to remove nickel species from the reaction mixture. Compounds **5** and **6** were isolated by preparative HPLC. For **5**: MS *m/z* 350 (M<sup>+</sup>); IR 3045, 2954, 2908, 2872, 1585, 1490, 1458, 1412, 1376, 1257, 1231, 1119, 1053, 1003, 960, 886, 752, 695 cm<sup>-1</sup>; <sup>1</sup>H NMR δ(CDCl<sub>3</sub>) 0.71–0.99 (m, 20H, EtSi), 7.30–7.63 (m, 9H, phenyl and phenylene ring protons), 7.89 (s, 1H, olefinic carbons); <sup>13</sup>C NMR δ(CDCl<sub>3</sub>) 6.31, 7.35, 7.67, 7.82 (EtSi), 127.7, 128.0, 128.2, 128.3, 128.6, 132.5, 132.8, 141.5, 147.4, 149.0 (phenyl and phenylene ring carbons), 139.0, 155.5 (olefinic carbons); <sup>29</sup>Si NMR δ(CDCl<sub>3</sub>) 0.50, 6.46. Anal. Calcd for C<sub>22</sub>H<sub>30</sub>Si<sub>2</sub>: C, 75.36; H, 8.62. Found: C, 75.38; H, 8.63. For **6**: MS *m/z* 352 (M<sup>+</sup>); IR 3065, 2953, 2906, 2872, 1596, 1493, 1458, 1460, 1376, 1330, 1231, 1196, 1069, 1006, 987, 910, 826, 775, 699 cm<sup>-1</sup>; <sup>1</sup>H NMR δ(CDCl<sub>3</sub>) 0.75–1.07 (m, 20H, EtSi), 6.44 (d, 1H, HC=CHPh, *J* = 19.1 Hz), 6.79 (d, 1H, HPhC=CH, *J* = 19.1 Hz), 7.22–7.47 (m, 10H, phenyl and phenylene ring protons); <sup>13</sup>C NMR δ(CDCl<sub>3</sub>) 3.92, 3.99, 8.25, 8.30 (EtSi), 127.7, 127.8, 128.3, 128.5,

134.5, 137.6, 138.7 (two carbons) (phenyl and phenylene ring carbons), 126.3, 144.5 (olefinic carbons); <sup>29</sup>Si NMR δ(CDCl<sub>3</sub>) -17.90, -14.81. Anal. Calcd for C<sub>22</sub>H<sub>32</sub>Si<sub>2</sub>: C, 74.93; H, 9.15. Found: C, 74.85; H, 9.12.

**Reaction of **1** with 1-Hexene.** A mixture of 0.449 g (1.81 mmol) of **1**, 0.272 g (3.23 mmol) of 1-hexene, and 0.048 g (0.090 mmol) of tetrakis(triethylphosphine)nickel(0) was heated at 150 °C for 24 h. The mixture was analyzed by GLC as being **7** (52% yield) and **8** (44% yield). The mixture was treated with a short silica gel column to remove nickel species from the reaction mixture. Compounds **7** and **8** were isolated by preparative HPLC. For **7**: MS *m/z* 330 (M<sup>+</sup>); IR 3045, 2955, 2873, 1595, 1462, 1413, 1376, 1254, 1231, 1118, 1052, 1017, 960, 860, 788, 712, 618 cm<sup>-1</sup>; <sup>1</sup>H NMR δ(CDCl<sub>3</sub>) 0.71–0.99 (m, 23H, EtSi, CH<sub>3</sub>), 1.33–1.50 (m, 4H, CH<sub>2</sub>), 2.30 (q, 2H, CH<sub>2</sub>, *J* = 7.3 Hz), 6.91 (t, 1H, HC=C, *J* = 6.9 Hz), 7.34–7.59 (m, 4H, phenylene ring protons); <sup>13</sup>C NMR δ(CDCl<sub>3</sub>) 6.40, 7.08, 7.68, 7.93 (EtSi), 14.11 (Me), 22.57 (CH<sub>2</sub>), 31.57 (CH<sub>2</sub>), 38.92 (CH<sub>2</sub>), 128.2, 128.3, 132.6, 132.7, 148.5, 148.7 (phenylene ring carbons), 133.8, 159.6 (olefinic carbons); <sup>29</sup>Si NMR δ(CDCl<sub>3</sub>) 0.36, 1.66. Anal. Calcd for C<sub>20</sub>H<sub>34</sub>Si<sub>2</sub>: C, 72.65; H, 10.36. Found: C, 72.57; H, 10.34. For **8**: MS *m/z* 334 (M<sup>+</sup>); IR 2955, 2918, 2873, 2148, 1260, 1235, 1168, 1117, 1015, 972, 811, 743, 715, 698 cm<sup>-1</sup>; <sup>1</sup>H NMR δ(CDCl<sub>3</sub>) 0.78–1.26 (m, 33H, EtSi, n-Hex), 4.53 (quint, 1H, HSi, *J* = 3.3 Hz), 7.29–7.55 (m, 4H, phenylene ring protons); <sup>13</sup>C NMR δ(CDCl<sub>3</sub>) 4.69, 5.25, 7.66, 8.37 (EtSi), 13.99, 14.12, 22.64, 23.94, 31.54, 33.57 (n-Hex), 127.5, 127.8, 134.8, 135.4, 142.8, 144.6 (phenylene ring carbons), 133.8, 159.6 (olefinic carbons); <sup>29</sup>Si NMR δ(CDCl<sub>3</sub>) -9.69, 2.00. Anal. Calcd for C<sub>20</sub>H<sub>38</sub>Si<sub>2</sub>: C, 71.77; H, 11.44. Found: C, 71.59; H, 11.52.

**Reaction of **1** with 2-Hexene.** A mixture of 0.389 g (1.57 mmol) of **1**, 0.249 g (2.96 mmol) of 2-hexene, and 0.040 g (0.075 mmol) of tetrakis(triethylphosphine)nickel(0) was heated at 150 °C for 24 h. The mixture was analyzed by GLC as being **2** (11% yield), **7** (56% yield) and **8** (20% yield). The mixture was treated with a short silica gel column to remove nickel species from the reaction mixture. Compound **2** was isolated by preparative GLC. Compounds **7** and **8** were isolated by preparative HPLC. All spectral data for **2**, **7** and **8** were identical with those of authentic samples.

**Reaction of **1** with Ethylene.** Into a 50-mL autoclave was placed 0.195 g (0.785 mmol) of **1** and 0.022 g (0.041 mmol) of tetrakis(triethylphosphine)nickel(0), and then ethylene gas (60 kg/cm<sup>2</sup>) was compressed into autoclave. The autoclave was heated at 150 °C for 24 h. The mixture was analyzed by GLC as being **9** (7% yield), **10** (34% yield) and **11** (10% yield). The mixture was treated with a short silica gel column to remove nickel species from the reaction mixture. Compounds **9**, **10** and **11** were isolated by preparative HPLC. For **9**: MS *m/z* 274 (M<sup>+</sup>); IR 2954, 2872, 1508, 1458, 1120, 1032, 697 cm<sup>-1</sup>; <sup>1</sup>H NMR δ(CDCl<sub>3</sub>) 0.72–1.26 (m, 20H, EtSi), 6.62 (s, 2H, H<sub>2</sub>C=C), 7.28–7.59 (m, 4H, phenylene ring protons); <sup>13</sup>C NMR δ(CDCl<sub>3</sub>) 5.88, 7.55 (EtSi), 128.4, 133.0, 141.4, 148.3, 148.6 (phenylene ring and olefinic carbons); <sup>29</sup>Si NMR δ(CDCl<sub>3</sub>) 0.89. Anal. Calcd for C<sub>16</sub>H<sub>26</sub>Si<sub>2</sub>: C, 70.00; H, 9.55. Found: C, 69.74; H, 9.47. For **10**: MS *m/z* 276 (M<sup>+</sup>); IR 3047, 2954, 2873, 1462, 1008, 699 cm<sup>-1</sup>; <sup>1</sup>H NMR δ(CDCl<sub>3</sub>) 0.65–1.02 (m, 20H, EtSi), 5.61 (dd, 1H, olefinic proton, *J*<sub>trans</sub> = 19.8 Hz, *J*<sub>gem</sub> = 4.3 Hz), 5.97 (dd, 1H, olefinic proton, *J*<sub>cis</sub> = 14.5 Hz, *J*<sub>gem</sub> = 4.3 Hz), 6.13 (dd, 1H, olefinic proton, *J*<sub>trans</sub> = 19.8 Hz, *J*<sub>cis</sub> = 14.5 Hz), 7.28–7.53 (m, 5H, phenyl ring protons); <sup>13</sup>C NMR δ(CDCl<sub>3</sub>) 3.65, 3.92, 8.12, 8.27 (EtSi), 127.7, 128.3, 132.7, 134.5, 136.6, 136.8 (phenyl ring and olefinic carbons); <sup>29</sup>Si NMR δ(CDCl<sub>3</sub>) -18.58, -15.24. Anal. Calcd for C<sub>16</sub>H<sub>28</sub>Si<sub>2</sub>: C, 69.49; H, 10.20. Found: C, 69.43; H, 10.20. All spectral data for **11** were identical with those of authentic samples.<sup>5</sup>

**Reaction of **1** with 2,3-Dimethyl-1,3-butadiene.** A mixture of 0.134 g (0.541 mmol) of **1**, 0.081 g (0.981 mmol) of 2,3-dimethyl-1,3-butadiene, and 0.013 g (0.025 mmol) of tetrakis(triethylphosphine)nickel(0) was heated at 150 °C for 24 h. The mixture was analyzed by GLC as being **12** (33% yield),

**13** (29% yield). The mixture was treated with a short silica gel column to remove nickel species from the reaction mixture. Compound **12** and **13** were isolated by preparative HPLC. For **12**: MS  $m/z$  330 ( $M^+$ ); IR 3044, 2954, 2874, 1458, 1414, 1375, 1230, 1156, 1113, 1008, 766, 731, 608  $\text{cm}^{-1}$ ;  $^1\text{H}$  NMR  $\delta(\text{CDCl}_3)$  0.71–1.10 (m, 20H, EtSi), 1.59–1.69 (three broad peaks, 9H, Me), 2.00–2.01 (br s, 1H, CH), 7.24–7.58 (m, 4H, phenylene ring protons);  $^{13}\text{C}$  NMR  $\delta(\text{CDCl}_3)$  5.82, 6.52, 7.46, 7.64 (EtSi), 19.01 (CH), 20.77, 21.06, 21.24 (Me), 128.2, 132.8, 149.0 (phenylene ring carbons), 119.2, 125.6 (olefinic carbons);  $^{29}\text{Si}$  NMR  $\delta(\text{CDCl}_3)$  10.89. Anal. Calcd for  $\text{C}_{20}\text{H}_{34}\text{Si}_2$ : C, 72.65; H, 10.36. Found: C, 72.65; H, 10.36. For **13**: MS  $m/z$  330 ( $M^+$ ); IR 3045, 2954, 2872, 1457, 1417, 1379, 1273, 1233, 1182, 1116, 1007, 773, 716  $\text{cm}^{-1}$ ;  $^1\text{H}$  NMR  $\delta(\text{CDCl}_3)$  0.80–1.04 (m, 20H, EtSi), 1.68 (s, 6H, Me), 1.78 (s, 4H,  $\text{CH}_2$ ), 7.24–7.60 (m, 4H, phenylene ring protons);  $^{13}\text{C}$  NMR  $\delta(\text{CDCl}_3)$  6.24, 7.51 (EtSi), 21.10 (Me), 21.76 ( $\text{CH}_2$ ), 127.4, 135.9, 143.6 (phenylene ring carbons), 122.7 (olefinic carbon);  $^{29}\text{Si}$  NMR  $\delta(\text{CDCl}_3)$  5.53. Anal. Calcd for  $\text{C}_{20}\text{H}_{34}\text{Si}_2$ : C, 72.65; H, 10.36. Found: C, 72.64; H, 10.31.

**Reaction of 1 with 1,3-Cyclohexadiene.** A mixture of 0.238 g (0.958 mmol) of **1**, 0.139 g (1.67 mmol) of 1,3-cyclohexadiene, and 0.024 g (0.045 mmol) of tetrakis(triethylphosphine)nickel(0) was heated at 150 °C for 24 h. The mixture was analyzed by GLC as being **14** (80% yield). The mixture was treated with a short silica gel column to remove nickel species from the reaction mixture. Compound **14** were isolated by preparative GLC: MS  $m/z$  328 ( $M^+$ ); IR 3011, 2952, 2873, 1462, 1414, 1234, 1146, 1117, 1008, 794, 742, 708  $\text{cm}^{-1}$ ;  $^1\text{H}$  NMR  $\delta(\text{CDCl}_3)$  0.63–1.09 (m, 20H, EtSi), 1.50–1.58 (m, 2H, CH,  $\text{CH}_2$  (axial)), 1.79–1.84 (m, 1H,  $\text{CH}_2$  (equatorial)), 1.98–2.14 (m, 3H, CH,  $\text{CH}_2$ ), 5.60–5.66 (m, 1H,  $\text{CH}=\text{CH}$ ), 5.92–5.98 (m, 1H,  $\text{CH}=\text{CH}$ ), 7.21–7.52 (m, 4H, phenylene ring

protons);  $^{13}\text{C}$  NMR  $\delta(\text{CDCl}_3)$  2.28, 5.45, 6.24, 6.61, 7.57, 7.62, 7.73, 7.89 (EtSi), 19.12 (CH), 22.98 ( $\text{CH}_2$ ), 24.47 (CH), 25.82 ( $\text{CH}_2$ ), 127.8 (two carbons), 134.2, 134.3, 143.3, 143.4 (phenylene ring carbons), 124.1, 130.5 (olefinic carbons);  $^{29}\text{Si}$  NMR  $\delta(\text{CDCl}_3)$  -4.28, -6.66. Anal. Calcd for  $\text{C}_{20}\text{H}_{32}\text{Si}_2$ : C, 73.09; H, 9.81. Found: C, 73.19; H, 9.68.

**Reaction of 1 with 1,4-Cyclohexadiene.** A mixture of 0.212 g (0.854 mmol) of **1**, 0.134 g (1.67 mmol) of 1,4-cyclohexadiene, and 0.015 g (0.028 mmol) of tetrakis(triethylphosphine)nickel(0) was heated at 150 °C for 24 h. The mixture was analyzed by GLC as being **14** (80% yield). The mixture was treated with a short silica gel column to remove nickel species from the reaction mixture. Compound **14** were isolated by preparative GLC. All spectral data for **14** were identical with those of the authentic sample.

**Acknowledgment.** This work was supported by a Grant-in-Aid for Scientific Research from the Ministry of Education, Science and Culture of Japan, for which the authors express their gratitude. We wish to thank the Computer Center of the Institute for Molecular Science and the Data Processing Center of Kyoto University, for their generous permission to use HITAC M-680 and S-820, and FACOM M-780/30, VP-400E, and VP-200 computers, respectively. We also express our appreciation to Shin-Etsu Chemical Co. Ltd., Nitto Electric Industrial Co. Ltd., Kaneka Corp., and Sumitomo Electric Industry Ltd. for financial support. SK thanks Masahito Mori and Yoshihiro Shibusa for their support and assistance.

OM9404386

# Molecular Structure, Dynamics, and Crystal Organization of $[(\mu\text{-Cl})_3\{\eta^6\text{-arene}\}\text{Ru}]_2[\text{BF}_4]$ (Arene = $\text{C}_6\text{H}_6$ and $\text{C}_6\text{H}_5\text{Me}$ ) and a Bonding Study by Extended Hückel Calculations

Fabrizia Grepioni\* and Dario Braga

*Dipartimento di Chimica G. Ciamician, Università di Bologna, Via Selmi 2, 40126 Bologna, Italy*

Paul J. Dyson, Brian F. G. Johnson,\* and Fiona M. Sanderson

*Department of Chemistry, The University of Edinburgh, West Mains Road, Edinburgh EH9 3JJ, U.K.*

Maria José Calhorda\* and Luis F. Veiros

*Centro de Tecnologia Química e Biológica, R. da Quinta Grande 6, 2780 Oeiras, Portugal, and Instituto Superior Técnico, Lisboa, Portugal*

Received June 8, 1994<sup>®</sup>

The complexes  $[(\mu\text{-Cl})_3\{\eta^6\text{-arene}\}\text{Ru}]_2^+$  (arene =  $\text{C}_6\text{H}_6$ , **1**, and  $\text{C}_6\text{H}_5\text{Me}$ , **2**) have been synthesized by reaction of the appropriate dihydroarene and ruthenium(III) chloride in ethanol, yielding  $\{(\mu\text{-Cl})_2[\eta^6\text{-arene}\}\text{RuCl}_2\}$ , which then affords the desired product on treatment with aqueous  $\text{HBF}_4$  in trifluoroacetic acid. Single crystal X-ray diffraction data have been collected at 296 and 150 K for **1** (**1a**, and **1b**, respectively) and at 150 K for **2**. Compound **1a** is monoclinic, space group  $P2_1/a$ ,  $a = 8.4449(6)$ ,  $b = 18.9448(12)$ ,  $c = 10.3154(7)$  Å,  $\beta = 103.416(4)^\circ$ ,  $V = 1605.3$  Å<sup>3</sup>,  $Z = 4$ ; **1b** is monoclinic, space group  $P2_1/a$ ,  $a = 8.43(2)$ ,  $b = 18.68(14)$ ,  $c = 10.25(2)$  Å,  $\beta = 104.8(1)^\circ$ ,  $V = 1560.5$  Å<sup>3</sup>,  $Z = 1$ ; **2** is triclinic, space group  $P\bar{1}$ ,  $a = 9.355(5)$ ,  $b = 9.668(4)$ ,  $c = 10.190(4)$  Å,  $\alpha = 92.12(3)$ ,  $\beta = 104.71(4)$ ,  $\gamma = 93.07(3)^\circ$ ,  $V = 888.9$  Å<sup>3</sup>,  $Z = 2$ . The hydrogen atoms in **1**, as well as the methyl groups in **2**, have been found to bend significantly towards the metal atoms. The bonding interactions between the arene fragments and the metals have been studied by means of extended Hückel calculations showing that a 6° bending is required in order to optimize the overlap between the  $(\mu\text{-Cl})_3\text{Ru}_2$  fragment and the arenes. The molecular structures of both complexes have been investigated in relation with the respective crystal structures. The ion organization in crystalline **1** and **2** has been compared with that in analogous *bis*(arene) derivatives. The dynamics about equilibrium positions as well as the reorientational motion of the benzene ligands in **1** at the two temperatures have been investigated by means of thermal motion analysis and packing potential energy calculations.

## Introduction

Chloro-bridged arene diruthenium complexes date back many years. The primary complex,  $[(\text{arene})\text{-RuCl}_2]_2$ , from which all subsequent products are derived, was first reported in 1967 for benzene. The complex was obtained from the reaction between cyclohexa-1,3-diene and ruthenium(III) chloride in ethanol.<sup>1</sup> It was later found that virtually any dihydroarene would react under similar conditions to afford the appropriate arene derivatives.<sup>2</sup> It is from these species that the complexes described herein, namely  $[(\mu\text{-Cl})_3\{\eta^6\text{-arene}\}\text{Ru}]_2^+$  (arene = benzene, **1**, and toluene, **2**) are produced by merely heating with aqueous tetrafluoroboric acid in trifluoroacetic acid. Both types of complexes described above have been the subject of extensive reactivity studies, usually concerning halide ion substitution.

Many of these reactions have been well documented quite recently.<sup>3</sup>

In this paper, beside reporting the synthesis and spectroscopic characterization of the two title complexes, we investigate in detail the structures of the two cationic complexes in the solid state as well as the structure of the respective crystals. Attention is focused on the *relationship* between molecular and crystal structures and on the intermolecular organization of the component ions in the crystalline material. The structural features observed in the solid state are examined in the light of the results of extended Hückel calculations whereas the crystal structures are investigated in terms of intermolecular interactions and anion-cation organization. A similar approach has been used to study the relationship between face-capping and terminal bonding modes of benzene in neutral ruthenium clusters.<sup>4</sup>

<sup>®</sup> Abstract published in *Advance ACS Abstracts*, November 1, 1994.

(1) Winkhans, G.; Singer, H. *J. Organomet. Chem.* **1967**, *7*, 487.

(2) Bennet, M. A.; Smith, A. K. *J. Chem. Soc., Dalton Trans.* **1974**, 233.

(3) Le Bozec, H.; Touchard, D.; Dixneuf, P. H. *Adv. Organomet. Chem.* **1989**, *29*, 163.

(4) Braga, D.; Dyson, P. J.; Grepioni, F.; Johnson, B. F. G.; Calhorda, M. J. *Inorg. Chem.* **1994**, *33*, 3218.

**Table 1. Selected Bond Lengths (Å) and Angles (deg) for 1**

	1a	1b
Ru(1)–Cl(1)	2.451(2)	2.454(1)
Ru(1)–Cl(2)	2.422(2)	2.425(1)
Ru(1)–Cl(3)	2.425(2)	2.434(1)
Ru(2)–Cl(1)	2.455(2)	2.458(1)
Ru(2)–Cl(2)	2.423(1)	2.428(1)
Ru(2)–Cl(3)	2.415(2)	2.421(1)
Ru(1)–C(1)	2.173(6)	2.167(5)
Ru(1)–C(2)	2.169(6)	2.171(5)
Ru(1)–C(3)	2.167(6)	2.168(5)
Ru(1)–C(4)	2.156(6)	2.167(5)
Ru(1)–C(5)	2.165(6)	2.171(5)
Ru(1)–C(6)	2.171(6)	2.163(5)
Ru(2)–C(7)	2.140(6)	2.155(5)
Ru(2)–C(8)	2.172(6)	2.163(5)
Ru(2)–C(9)	2.166(6)	2.178(5)
Ru(2)–C(10)	2.158(7)	2.178(5)
Ru(2)–C(11)	2.164(6)	2.177(5)
Ru(2)–C(12)	2.151(7)	2.161(5)
C(1)–C(2)	1.41(1)	1.392(7)
C(1)–C(6)	1.42(1)	1.431(7)
C(2)–C(3)	1.40(1)	1.415(8)
C(3)–C(4)	1.41(1)	1.418(8)
C(4)–C(5)	1.40(1)	1.419(8)
C(5)–C(6)	1.39(1)	1.402(8)
C(7)–C(8)	1.39(1)	1.418(8)
C(7)–C(12)	1.38(1)	1.404(7)
C(8)–C(9)	1.41(1)	1.394(8)
C(9)–C(10)	1.42(2)	1.424(10)
C(10)–C(11)	1.38(1)	1.409(8)
C(11)–C(12)	1.41(1)	1.427(8)
B–F(1)	1.38(2)	1.383(8)
B–F(2)	1.37(2)	1.390(7)
B–F(3)	1.39(2)	1.410(7)
B–F(4)	1.38(2)	1.375(7)
Ru(1)–Cl(1)–Ru(2)	84.10(5)	84.01(4)
Ru(1)–Cl(2)–Ru(2)	85.39(5)	85.27(4)
Ru(2)–Cl(3)–Ru(1)	85.49(5)	85.22(4)

Anion–cation interactions,<sup>5</sup> hydrogen bonding,<sup>6</sup> and van der Waals interactions have been studied in detail.<sup>7</sup> These aspects are related to our studies of the factors controlling the *crystal engineering* of organometallic materials.<sup>8</sup> Another aspect of relevance is concerned with the dynamic behavior about equilibrium positions and far from equilibrium of the atoms or atomic groupings in the solid state. Investigatory “tools” such as thermal motion analysis and atom-atom potential energy barrier calculations have been used to estimate the extent of such dynamics.<sup>9</sup>

## Results and Discussion

**Molecular Structure of 1 and 2 in the Solid State.** The molecular structures of **1** and **2** have been determined by single-crystal X-ray diffraction measurements at 296 and 150 K for **1** (**1a** and **1b**, respectively) and at 150 K for **2**. The two molecules are closely related and will be discussed together. Relevant structural parameters are reported in Tables 1 and 2 for **1**

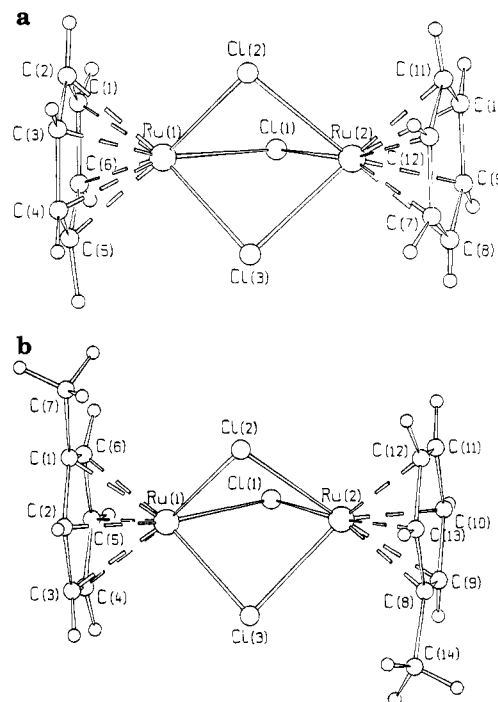
(5) (a) Braga, D.; Grepioni, F.; Milne, P.; Parisini, E. *J. Am. Chem. Soc.* **1993**, *115*, 5115. (b) Braga, D.; Grepioni, F. *Organometallics* **1992**, *11*, 1256.

(6) (a) Braga, D.; Grepioni, F.; Sabatino, P.; Desiraju, G. R. *Organometallics* **1994**, *13*, 3532. (b) Biradha, K.; Peddireddi, V. R.; Braga, D.; Grepioni, F.; Desiraju, G. R. Submitted for publication.

(7) (a) Braga, D.; Grepioni, F. *Organometallics* **1991**, *10*, 1255. (b) Braga, D.; Grepioni, F.; Sabatino, P. *J. Chem. Soc. Dalton Trans.* **1990**, 3137. (c) Braga, D.; Grepioni, F.; Sabatino, P.; Gavezzotti, A. *J. Chem. Soc. Dalton Trans.* **1992**, 1185. (d) Braga, D.; Grepioni, F. *Acta Crystallogr. Sect. B* **1989**, *B45*, 378. (e) Braga, D.; Grepioni, F. *Organometallics* **1991**, *10*, 2563.

(8) Braga, D.; Grepioni, F. *Acc. Chem. Res.* **1994**, *27*, 51.

(9) Braga, D. *Chem. Rev.* **1992**, *92*, 633.

**Figure 1.** Structures of **1** (a) and **2** (b) in the solid state showing the atomic labeling schemes.**Table 2. Selected Bond Lengths (Å) and Angles (deg) for 2**

Ru(1)–Cl(1)	2.438(1)	C(1)–C(2)	1.426(5)
Ru(1)–Cl(2)	2.419(1)	C(1)–C(6)	1.401(5)
Ru(1)–Cl(3)	2.434(1)	C(2)–C(3)	1.403(5)
Ru(2)–Cl(1)	2.438(1)	C(3)–C(4)	1.418(6)
Ru(2)–Cl(2)	2.420(1)	C(4)–C(5)	1.394(5)
Ru(2)–Cl(3)	2.441(1)	C(5)–C(6)	1.421(5)
Ru(1)–C(1)	2.188(3)	C(1)–C(7)	1.493(5)
Ru(1)–C(2)	2.167(3)	C(8)–C(9)	1.418(5)
Ru(1)–C(3)	2.157(3)	C(8)–C(13)	1.415(5)
Ru(1)–C(4)	2.175(3)	C(9)–C(10)	1.413(5)
Ru(1)–C(5)	2.154(3)	C(10)–C(11)	1.416(5)
Ru(1)–C(6)	2.161(3)	C(11)–C(12)	1.411(6)
Ru(2)–C(8)	2.190(3)	C(12)–C(13)	1.415(6)
Ru(2)–C(9)	2.163(3)	C(8)–C(14)	1.488(5)
Ru(2)–C(10)	2.156(3)	B(1)–F(1)	1.378(5)
Ru(2)–C(11)	2.175(3)	B(1)–F(3)	1.386(5)
Ru(2)–C(12)	2.160(3)	B(1)–F(4)	1.385(5)
Ru(2)–C(13)	2.170(3)	B(1)–F(2)	1.385(5)
Ru(1)–Cl(1)–Ru(2)	84.38(2)	Ru(1)–Cl(3)–Ru(2)	84.42(3)
Ru(1)–Cl(2)–Ru(2)	85.19(3)		

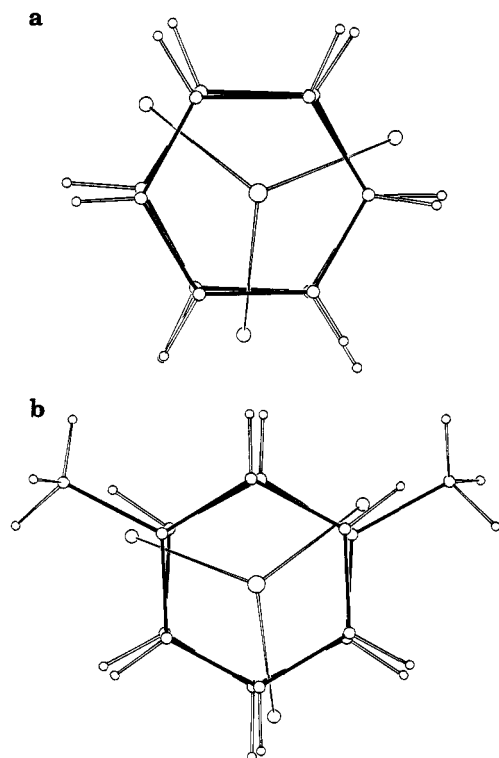
and **2**, respectively. Sketches of the two molecules are shown in Figure 1a,b for **1** and **2**, respectively.

The relevant structural features of the two complexes can be summarized as follows:

(i) Both complexes are constituted of two Ru(II) atoms closely joined by three bridging chlorine ligands, each Ru-atom also carries an  $\eta^6$ -coordinated arene ligand (benzene in **1**, toluene in **2**).

(ii) The Ru··Ru separation is slightly shorter in the toluene complex than in the benzene derivative [3.275(1) in **2** vs. 3.285(1) at 296 and 3.287(1) Å at 150 K in **1**].

(iii) The Ru-atoms are almost equidistant from the plane formed by the bridging Cl-atoms; Ru–Cl distances range between 2.415(2) and 2.455(2) Å in **1a**, between 2.421(1) and 2.458(1) Å in **1b**, and between 2.419(1) and 2.441(1) Å in **2**. The Ru–Cl–Ru angles vary accordingly [84.10(5)–85.49(5)° in **1a**; 84.01(4)–85.27(4) in **1b**; 84.38(2)–85.19(3)° in **2**].



**Figure 2.** Different conformations of the arene rings in **1** (a) and **2** (b) with respect to the chlorine bridges. In **1** the two benzene rings are almost exactly eclipsed but staggered with respect to the Cl-atoms. In **2**, the ring carbons and the Cl-atoms are eclipsed, while the methyl groups are 120° apart in projection and adopt a *pseudo* 1,3-arrangement overlapping two Cl-atoms.

(iv) Ru–C distances are fairly constant and comparable in the two complexes [ranges: 2.14(1)–2.17(1) **1a**; 2.155(5)–2.178(5) **1b**; 2.154(3)–2.190(3) Å in **2**]; the longest distances in **2** are associated with the ring atoms carrying the methyl groups [Ru(1)–C(1) 2.188(3), Ru(2)–C(8) 2.190(3) Å].

(v) The arene rings in **1** and **2** have different conformations with respect to the chlorine bridges. In **1** the two benzene rings are almost exactly eclipsed, but are staggered with respect to the Cl-atoms (see Figure 2a). In **2**, on the other hand, the ring carbons and the Cl-atoms are eclipsed, while the methyl groups are 120° apart in projection and adopt a *pseudo* 1,3-arrangement overlapping (see Figure 2b) two Cl-atoms. The conformational aspect of these molecules will be discussed in more detail in the crystal structure section.

(vi) Although only a neutron diffraction study can afford an unequivocal location of H-atoms, an interesting feature shared by **1** and **2** is revealed by the X-ray diffraction data. Both the C–H and the C–Me bonds bend *towards* the metal atoms from the planes defined by the C<sub>6</sub> rings. The high quality of the diffraction data allowed direct location of all the H-atoms including those of the methyl groups. The H-atom location is more precise in the 150 K data sets. The average deviation of the H-atoms from the mean least-square plane of the rings towards the metal atom is 0.07, and 0.04 Å in **1a**; 0.08, 0.09 Å in **1b**; C(7) 0.09, H-atoms 0.10; C(14) 0.09; H-atoms 0.9 Å in **2**. The mean Ru–C(arene) are in **1a**, Ru(1)–C 2.17(1), Ru(2)–C 2.16(1) Å; in **1b**, Ru(1)–C 2.168(5), Ru(2)–C 2.169(5) Å; and in **2**, 2.167(3), Ru(2)–C 2.169(3) Å.

**Table 3.** Results of Rigid-Body-Motion Analysis for **1a**, **1b**, and **2**

	<b>1a</b> (296 K)	<b>1b</b> (150 K)	<b>2</b> (150 K)
Model 1 (Whole Molecule)			
L <sub>1</sub> (deg <sup>2</sup> )	60.4	21.1	29.1
L <sub>2</sub> (deg <sup>2</sup> )	7.3	3.3	3.0
L <sub>3</sub> (deg <sup>2</sup> )	4.7	2.2	2.1
Model 2.1 (Ru and First Ring C Atoms)			
L <sub>1</sub> (deg <sup>2</sup> )	52.1	21.3	20.6
L <sub>2</sub> (deg <sup>2</sup> )	6.1	2.8	3.5
L <sub>3</sub> (deg <sup>2</sup> )	4.5	1.3	2.4
Model 2.2 (Ru and Second Ring C Atoms)			
L <sub>1</sub> (deg <sup>2</sup> )	77.5	36.0	31.4
L <sub>2</sub> (deg <sup>2</sup> )	7.4	2.6	3.7
L <sub>3</sub> (deg <sup>2</sup> )	5.5	1.0	3.0
Model 2.3 (Ru and Cl Atoms)			
L <sub>1</sub> (deg <sup>2</sup> )	61.7	21.4	30.8
L <sub>2</sub> (deg <sup>2</sup> )	7.8	3.9	3.6
L <sub>3</sub> (deg <sup>2</sup> )	5.4	2.5	2.9

(vii) The ring planes are nearly parallel in **2**, whereas they form an angle of 3.9° in **1a** which increases to 4.3° on passing from room temperature to 150 K.

(viii) A slight, but significant C–C bond length alternation is observed in complex **1** (see Table 1), the “short” bonds being those *trans* to the Cl-bridges, whereas in **2** there is no systematic alternation nor there is any symmetry pattern conforming to the mirror symmetry of the toluene ligands.

The molecular structures of **1** and **2** are related to that of the *bis*(cymene) complex [( $\mu$ -Cl)<sub>3</sub>{(*p*-CH<sub>3</sub>-C<sub>6</sub>H<sub>4</sub>-CH(CH<sub>3</sub>)<sub>2</sub>)Ru}<sub>2</sub>][BPh<sub>4</sub>], which also contains three Cl-bridges and two  $\eta^6$ -arene fragments bound to the Ru(II) atoms,<sup>10</sup> and to the neutral complex ( $\mu$ -Cl)<sub>2</sub>{RuCl( $\eta^6$ -C<sub>6</sub>Me<sub>6</sub>)<sub>2</sub>} which presents only two Cl-atoms in bridging position while the other two are terminally bound.<sup>11</sup>

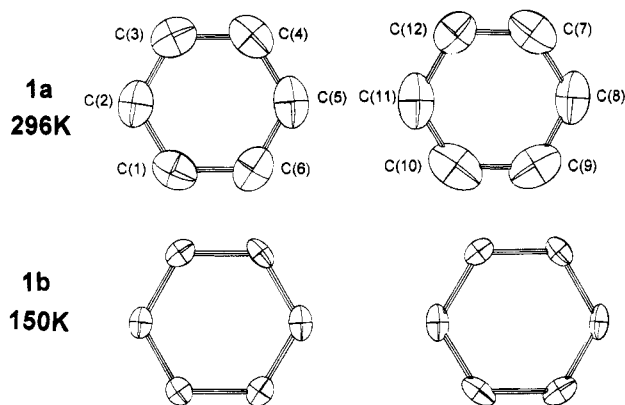
**Thermal Motion Analysis.** The dynamic behavior of the arene rings about equilibrium positions will now be discussed. The available anisotropic displacement parameters (the anisotropic U<sub>s</sub>) were used to carry out a rigid-body motion analysis based on the libration (L), translation (T) and correlation, or roto-translation (S) tensors (TLS approach<sup>12 a,b</sup>). In order to evaluate the mean-square amplitudes for the arenes motion around equilibrium, thermal motion analysis was performed with the program THMA11<sup>12c</sup> and the results are summarized in Table 3.

A rigid body motion was first assumed to describe the motion about equilibrium of the whole molecules **1a**, **1b** and **2** (model 1 in Table 3). In all cases the overall librational motion is strongly anisotropic, the value of the L<sub>1</sub> component being one order of magnitude larger than those of L<sub>2</sub> and L<sub>3</sub>. In the case of molecule **1** the librational motion decreases appreciably with temperature on passing from 60.4 to 21.1 deg<sup>2</sup>. The maximum libration axis L<sub>1</sub> is almost coincident with the molecular axis, i.e. the axis passing through the two ruthenium atoms. The translational motion, on the contrary, is fairly isotropic, therefore the eigenvalues of the three

(10) Tocher, D. A.; Walkinshaw, M. D. *Acta Crystallogr., Sect. B* **1982**, *B38*, 3083

(11) McCormick, F. B.; Cleason, W. N. *Acta Crystallogr., Sect. C* **1988**, *C44*, 603.

(12) (a) Dunitz, J. D.; Schomaker, V.; Trueblood, K. N. *J. Phys. Chem.* **1988**, *92*, 856. (b) Dunitz, J. D.; Maverick, E. F.; Trueblood, K. N. *Angew. Chem. Int. Ed. Engl.* **1988**, *27*, 880. (c) Trueblood, K. N. **THMA11**. *Thermal Motion Analysis*. University of California, Los Angeles, CA, 1987.



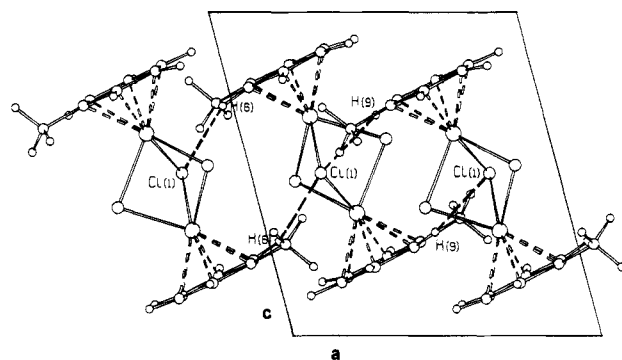
**Figure 3.** Comparison of the ADP of the two independent benzene rings in **1** at 296 and 150 K.

translational components are not reported in Table 3.

Because of the delocalized nature of the arene-metal bonding interactions, however, the motion of these molecules as rigid bodies represents an obvious approximation.<sup>9</sup> A more realistic model for the dynamics about equilibrium positions can be attained if the arene fragments are allowed independent motion. Three alternative models were then tested to analyze the motion of the three separate fragments formed by the two Ru atoms and the first arene (model 2.1), the second arene (model 2.2), and the three Cl atoms (model 2.3). As in the case of model 1, attention is focused on the extent of librational motion about the three librational axes. The results are summarized in Table 3. It can be appreciated that, while model 1 describes fairly accurately the motion around equilibrium of the fragment  $\text{Ru}_2\text{Cl}_3$  in all molecules (compare with model 2.3), the librational motion of the benzene and toluene rings around the Ru–Ru axis is better described if the two rings are treated separately (model 2.1 and 2.2) in each molecule. In summary, the results collected in Table 3 show that in both **1** and **2** the first arene ligand moves more than the second, while when model 1 is used this difference is “averaged” in the librational motion of the whole molecule. Potential energy barrier calculations (see section below) also indicate that the two rings differ in their reorientational motion.

The anisotropic displacement parameters (ADP) of the two independent benzene rings in **1** and their variation with temperature are shown in Figure 3. The reduction of the ADP on passing from 296 K to 150 K is indicative of a true librational motion, and excludes the presence of some kind of static disorder. Similar behavior has been observed in many other instances. It is worth recalling here, as an example, the variable temperature structural analysis of the benzene complexes  $(\text{C}_6\text{H}_6)\text{-Cr}(\text{CO})_3$ <sup>13a</sup> and of  $(\text{C}_6\text{H}_6)\text{Mo}(\text{CO})_3$ .<sup>13b</sup>

**Discussion of the Crystal Structures of 1 and 2 and Related Materials.** The organization of anions and cations in the crystal structure is now described. Emphasis will be given to the patterns of intermolecular interactions observed in crystalline **1** and **2** and on the relationship between these crystal structures and those of related complexes.



**Figure 4.** Intermolecular Cl–H–C interactions (filled broken lines) in crystalline **2**.

**Table 4.** Intermolecular Contacts in **1a**, **1b** and **2**<sup>a</sup>

inter-molecular contact	Cl···H (Å) (<3.00 Å)	C–H···Cl angle (deg)	F···H (Å) (<3.00 Å)	C–H···F angle (deg)	
<b>1b</b> Cl1···H2	2.69	134	F1···H11	2.47	155
Cl2···H1	2.74	168	F2···H4	2.38	129
Cl2···H12	2.81	125	F2···H9	2.26	147
Cl3···H6	2.71	121	F3···H10	2.48	132
Cl3···H7	2.88	169	(F4···H) <sub>min</sub>	2.65	
Cl1···H7	2.98	126			
Cl2···H11	2.99	119			
Cl3···H5	2.84	119			
<b>1a</b> Cl1···H2	2.74	141	F2···H4	2.36	142
Cl2···H1	2.86	153	F2···H9	2.35	147
Cl2···H12	2.82	129	F3···H10	2.45	145
Cl3···H6	2.70	124	(F1···H) <sub>min</sub>	2.56	
Cl3···H7	2.94	167			
<b>2</b> Cl1···H6	2.55	157	F1···H10	2.32	129
Cl1···H9	2.63	157	F2···H2	2.39	151
Cl2···H73	2.73	144	F3···H71	2.38	177
Cl3···H13	2.93	155	F4···H5	2.45	116
Cl3···H141	2.98	157	F1···H71	2.52	125
			F2···H12	2.51	127
			F4···H3	2.52	115

<sup>a</sup> Intermolecular contacts are based on a normalized C–H distance of 1.08 Å.

Short intermolecular contacts are observed between the F-atoms of the  $\text{BF}_4^-$  anions as well as between the Cl-atoms and the arene H-atoms. In order to compare these interactions the C–H distances were first normalized to 1.08 Å. C–H···Cl and C–H···F intermolecular interactions lower than 3.00 and 2.55 Å (i.e. lower than the sum of van der Waals radii) were calculated.

A short Cl–H–C(<sub>sp</sub><sup>2</sup>) contact of 2.55 Å is found between two molecules of compound **2** which are related by an inversion center; because of this symmetry element the interaction is acting twice between the two molecules which constitute a sort of dimer (see Figure 4). The same chlorine atom is also involved in a second, slightly longer contact of 2.63 Å with another H(C<sub>sp</sub><sup>2</sup>–H) atom of a second molecule, also related by an inversion center (second “dimer”, see Figure 4). Atoms Cl(2) and Cl(3), which are eclipsed each with one methyl group, form longer Cl···H contacts (see Table 4).

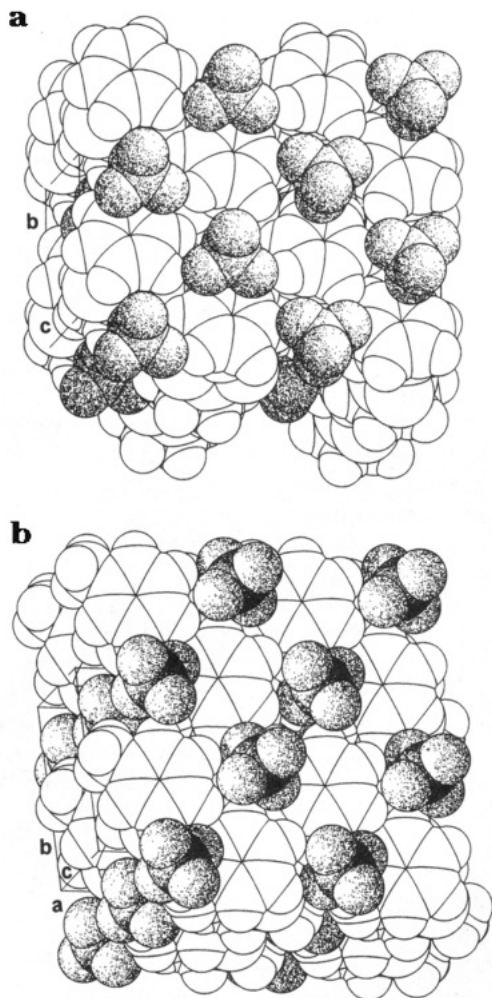
Short intermolecular contacts between H- and F-atoms are present also in **2**; each fluorine atom participates in one short interaction (C–H···F distances fall in the range 2.32–2.45 Å).

The pattern of F···H interactions offers an interesting explanation for the anomalously high ADP of F(4) in

(13) (a) Wang, Y.; Angermund, K.; Goddard, R.; Krüger, C. *J. Am. Chem. Soc.* **1987**, *109*, 587. (b) Bürgi, H.-B.; Raselli, A.; Braga, D.; Grepioni, F. *Acta Crystallogr., Sect. B* **1992**, *B48*, 428.

(14) (a) Desiraju, G. R. *Acc. Chem. Res.* **1991**, *24*, 290.





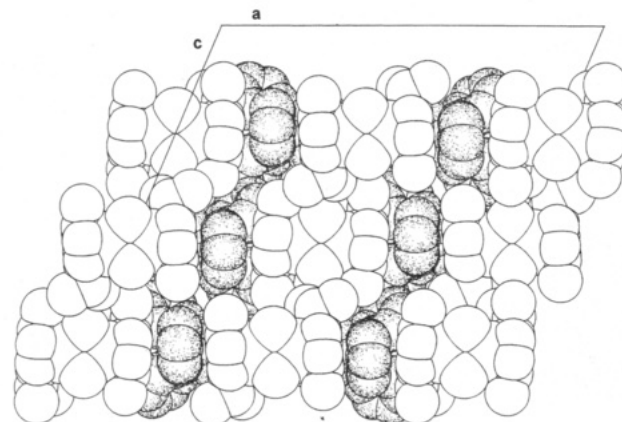
**Figure 5.** Cations pile in crystalline **1** (a) and in crystalline **2** (b).

both **1a** and **1b** structures (see Experimental Section). It appears that, while F(2) and F(3) are at short intermolecular distance from three H-atoms (C–H···F distances in the range 2.36–2.45 Å), and F(1) is at “normal” distance from an H-atom (2.56 Å), the minimum intermolecular separation between F(4) and an H-atom of the surroundings is 2.75 Å, whereas the minimum F(4)···C contact is 2.89 Å. The F–H separation becomes slightly shorter (2.65 Å) in **1b**. Although the F(4) atom could be refined anisotropically at low temperature (see Experimental Section) it still shows the highest ADP values.

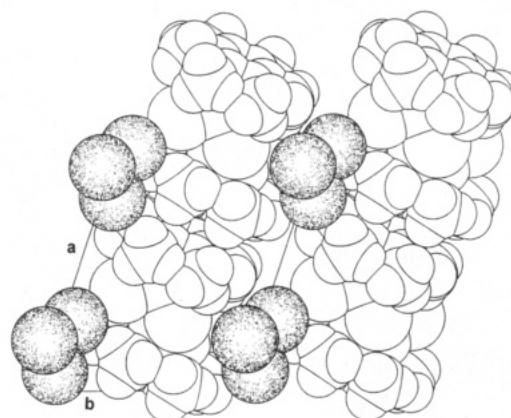
The  $[(\mu\text{-Cl})_3\{\eta^6\text{-C}_6\text{H}_6\}\text{Ru}]_2^+$  cations in crystalline **1** organize themselves in piles extending along the (001) direction, as it can be seen from Figure 5a. The distance between arene planes belonging to two adjacent molecules in the same pile is ca. 3.4 Å in both **1a** and **1b**. Small cavities left in the packing along the same direction are filled by the  $[\text{BF}_4]^-$  anions.

Neat cationic piles also constitute the fundamental packing motif in crystalline **2**. As shown in Figure 5b the cations pile along the *c*-axis, whereas the small  $[\text{BF}_4]^-$  anions occupy the interstices in the vicinity of the ligand methyl groups. The toluene–toluene distance is 3.43 Å.

The crystal of the bis(cymene) complex<sup>10</sup> can be described as formed by ionic piles. Each pile results from the stacking of cations intermixed with phenyl



**Figure 6.** (a) Projection in the *bc*-plane of the ion organization in the crystal of the bis(cymene) complex. (b) An ionic pile along the *c*-axis, note how one phenyl group of the  $[\text{BPh}_4]^-$  anions is “sandwiched” between the cymene ligands of two consecutive cations along the pile.



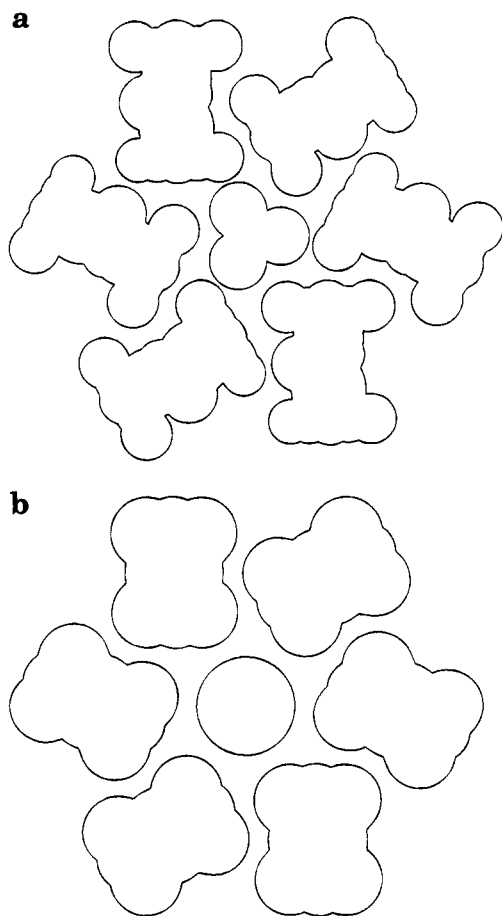
**Figure 7.** (a) Arene–arene interactions (arene–arene distance 3.64 Å) in crystalline  $(\mu\text{-Cl})_2\{\eta^6\text{-C}_6\text{Me}_6\}\text{RuCl}_2$ . Note how the chloroform molecules formally replace the  $[\text{BF}_4]^-$  anions present in the packing of **2**.

groups of the  $[\text{BPh}_4]^-$  counterion. This is shown in Figure 6. The crystal structure also contains some disordered  $\text{CH}_3\text{OH}$ , which could not be properly located. It is interesting that one anion phenyl group is sandwiched between two consecutive cymene ligands along the pile at graphitic-like separation (cymene1–phenyl 3.65, phenyl–cymene2 3.46 Å).

The crystal structure of the neutral complex  $(\mu\text{-Cl})_2\{\eta^6\text{-C}_6\text{Me}_6\}\text{RuCl}_2$  is also noteworthy because the arene–arene interactions present in the other crystalline materials thus far discussed persist in this neutral crystal as shown in Figure 7. Interestingly, the crystal structure interstices are “filled” by chloroform molecules which formally replace the  $[\text{BF}_4]^-$  anions present in the packing of **2**. The shortest Cl–H intermolecular contact [Cl(2)–H(19) 2.738 Å] is between the terminally bound Cl atom and one of chloroform H-atoms.

The packing pattern in crystalline  $[(\mu\text{-Cl})_3\{\eta^6\text{-C}_6\text{H}_3\text{Me}_3\text{-1,3,5}\}\text{Ru}]_2[\text{BF}_4]$  presents a complex intercation interlocking along the three-fold axis of symmetry in the space group  $P2_13$ . The cation helix is wrapped around the molecule located on the axis. This arrangement is not unique, a similar packing having been previously observed in the crystal of dibenzenechromium. The packing arrangement is shown in Figure 8a, and compared with the arrangement observed in crystalline  $(\text{C}_6\text{H}_6)_2\text{Cr}$  (see Figure 8b).<sup>7e</sup>





**Figure 8.** Packing arrangement in  $[(\mu\text{-Cl})_3\{(\eta^6\text{-C}_6\text{H}_5\text{Me}_{3-1,2,3})\text{Ru}\}_2]$  section through the  $\text{Cl}_3$  plane of a reference (central) molecule (a) and comparison with a section perpendicular to the molecular axis of the central molecule in (dibenzene)chromium (b).

**Potential Energy Barrier Calculations.** Having examined the solid state molecular structure as well as the crystal structures of complexes **1** and **2**, we can now attempt to evaluate the ease of reorientational motion of the  $\pi$ -bound arene fragments in the crystals. Benzene reorientation in solid **1a** and **1b** can be evaluated by means of the pairwise potential energy method<sup>15</sup> (see Experimental Section). The intermolecular potential energy profiles  $\Delta E$  were calculated for a complete reorientation of the two benzene fragments, at  $10^\circ$  rotational steps and at the two temperatures, around the axes passing through the Ru-atoms and the midpoint of the coordinated  $\text{C}_6$ -rings. The  $\Delta E$  profiles show minima of almost equal energy every  $60^\circ$ , corresponding to the idealized symmetry of the fragment. The  $\Delta E$  barrier values are different for the two benzene ligands and increase, as expected, on passing from 296 K to 150 K ( $\Delta E$  3.9 and 2.6 kcal·mol<sup>-1</sup> for first and second ring, respectively, at 296 K;  $\Delta E$  6.5 and 5.0 kcal·mol<sup>-1</sup> for first and second ring, respectively, at 150 K). The intramolecular contribution to the barrier is almost negligible ( $\Delta E_{\text{intra}} = 0.1$  kcal·mol<sup>-1</sup>). Interestingly, the motion far from equilibrium of the two benzene rings parallels the

behavior about equilibrium, i.e. the first ring, which shows the lower librational motion (see Table 3, models 2.1 and 2.2), is also the one which is more hindered in its reorientational motion around the molecular axis at both temperatures. Similar relationship between motion about equilibrium and ease of reorientation has been observed, for instance, in the case of the *cis*-isomer of  $(\eta^5\text{-C}_5\text{H}_5)_2\text{Fe}_2(\text{CO})_4$ .<sup>16</sup>

As previously observed in crystalline  $(\text{C}_6\text{H}_5\text{Me})\text{M}(\text{CO})_3$  [ $\text{M} = \text{Cr}$ ,<sup>17a</sup>  $\text{Mo}$ <sup>17b</sup>], a complete reorientation of the toluene fragment around the axis passing through the  $\text{C}_6$ -ring center and the metal atom to which the ring is bonded, is not allowed. Nonetheless, the intermolecular potential energy profile  $\Delta E$  in **2** is almost flat in the range  $\pm 15^\circ$  around the equilibrium position (maximum  $\Delta E$  value 4.3 and 4.6 kcal·mol<sup>-1</sup> for the first and second toluene rings, respectively). This indicates that, even though full scale reorientation of the ligand is forbidden by the intermolecular interlocking, large amplitude swinging motion is permitted.<sup>16b</sup>

**Molecular Orbital Calculations.** The  $[(\mu\text{-Cl})_3\{(\eta^6\text{-arene})\text{Ru}\}_2]^+$  complexes exhibit a bending of the arene substituents (H or methyl groups) toward the metal. This behavior has been observed before and is the opposite of that found when benzene binds at a surface,<sup>18</sup> a triangular face on a cluster, or even one single atom of a cluster.<sup>19</sup> Less striking, although also showing variation, is the relative position of the arene rings relative both to each other and to the  $(\mu\text{-Cl})_3$  frame.

Bending of benzene substituents toward the metal atom has been referred in the literature,<sup>18</sup> following theoretical predictions,<sup>20,21</sup> though the real examples are more recent.

Hoffmann and co-workers<sup>20</sup> discussed the possibility of bending in both directions the substituents in the series of  $\text{C}_n\text{H}_n$  polyenes, using the simplified model  $\text{M}(\text{CH})_n$ . The values they obtained for bending in the chromiumbenzene derivative were much smaller ( $3^\circ$ ) than those later experimentally found in ruthenium complexes such as those described in this work (around  $6^\circ$ ). The same result had been anticipated, on symmetry arguments, by Kettle.<sup>21</sup> As the plane of benzene is no longer a symmetry plane of the complex, the  $\sigma$  and  $\pi$  orbitals of benzene will tend to mix to maximize overlap. The behavior of benzene and other large polyenes is opposite to those of the small ones. In the limit, the

(16) (a) Braga, D.; Grepioni, F.; Gradella, C. *J. Chem. Soc. Dalton Trans.* **1989**, 1721. (b) Braga, D. *Chem. Rev.* **1992**, *93*, 636.

(17) (a) Braga, D.; Grepioni, F. *J. Chem. Soc. Dalton Trans.* **1990**, 3143. (b) van Meurs, F.; van Koningsveld, H. J. *J. Organomet. Chem.* **1977**, *131*, 423.

(18) (a) Garfunkel, E. L.; Minot, C.; Gavezzotti, A.; Simonetta, M. *Surf. Sci.* **1986**, *167*, 177. (b) Friend, C. M.; Muettterties, E. L. *J. Am. Chem. Soc.* **1981**, *103*, 773. (c) Somorjai, G. A. *The Building of Catalysts: A Molecular Surface Science Approach in Catalyst Design-Progress and Perspectives*, Hegedus, L. L., Ed.; John Wiley & Sons: NY, 1987. (d) Somorjai, G. A. *Chemistry in Two Dimensions: Surfaces*; Cornell University Press: Ithaca, NY, 1981.

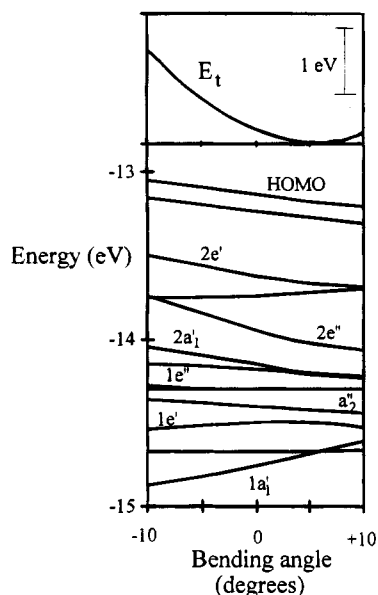
(19) (a) Braga, D.; Grepioni, F.; Johnson, B. F. G.; Chen, H.; Lewis, J. *J. Chem. Soc. Dalton Trans.* **1991**, 2559. (b) Braga, D.; Grepioni, F.; Righi, S.; Dyson, P. J.; Johnson, B. F. G.; Bailey, P. J.; Lewis, J. *Organometallics* **1992**, *11*, 4042. (c) Braga, D.; Grepioni, F.; Righi, S.; Johnson, B. F. G.; Bailey, P. J.; Dyson, P. J.; Lewis, J.; Martinelli M. *J. Chem. Soc. Dalton Trans.* **1992**, 2121.

(20) Elian, M.; Chen, M. M. L.; Mingos, D. M. P.; Hoffmann, R. *Inorg. Chem.* **1976**, *15*, 1148.

(21) Kettle, S. F. A. *Inorg. Chim. Acta* **1967**, *1*, 303.

(22) Mingos, D. M. P. *Bonding of Unsaturated Organic Molecules to Transition Metals*; in *Comprehensive Organometallic Chemistry*, Wilkinson, G., Stone, F. G. A., Abel, W., Eds.; Pergamon Press: Oxford, U.K., 1987; Vol. 3.

(15) (a) Gavezzotti, A.; Simonetta, M. *Chem. Rev.* **1981**, *82*, 1. (b) *Organic Solid State Chemistry*; Desiraju, G. R., Ed.; Elsevier: Amsterdam, 1987. (c) Kitaigorodsky, A. I. *Molecular Crystals and Molecules*; Academic Press: New York, 1973. (d) Gavezzotti, A. *J. Am. Chem. Soc.* **1989**, *111*, 1835. (e) Desiraju, G. R. *Crystal Engineering. The Design of Organic Solids*; Elsevier: Amsterdam, 1989.



**Figure 9.** Change in total energy and Walsh diagram for bending the benzene hydrogen atoms away (negative values) and toward (positive values) the ruthenium atoms in  $[(\mu\text{-Cl})_3\{\eta^6\text{-C}_6\text{H}_6\}\text{Ru}]_2^+$ .

binding of an ethylene molecule to a metal is accompanied by the bending away from the metal, by ca. 20°, of the hydrogen atoms or any other substituents.<sup>22</sup>

In order to explain in more detail these structural characteristics, extended Hückel molecular orbital calculations<sup>23</sup> were performed on a  $[(\mu\text{-Cl})_3\{\eta^6\text{-arene}\}\text{Ru}]_2^+$  model. The change in total energy accompanying the bending of the hydrogen atoms either away or toward the metal atom is shown in the top of Figure 9. The bottom of the figure is the Walsh diagram for the same distortion. For the sake of simplicity only part of the levels are labeled, namely, those involved in the metal–benzene bonding (the ruthenium d-orbitals and the benzene  $\pi$ -orbitals). The energy of the other levels, such as benzene  $\sigma$ -orbitals, does not change significantly with the bending distortion.

Though the potential energy surface is very soft in the neighborhood of a 0° angle (planar arene ligand), there is a distinct minimum (0.23 eV) at ca. 6°. The general explanation is the increased overlap between certain benzene and metal orbitals which, by making the resulting mo's more bonding, lowers their energy.<sup>20</sup> This is not the whole story, because, as stems from the Walsh diagram, there is at least one level which is strongly destabilized. Indeed, the Walsh diagram reveals that the minimum results from the balance of the energy of two groups of orbitals. For the first group, exemplified by  $2e'$ , the energy always drops in the region shown, when the hydrogens approach the metal, while for the second ( $1a'_1$ ) the opposite is found.

The Ru–benzene interaction in this binuclear species is similar to that described previously,<sup>24</sup> namely five of the  $\pi$  molecular orbitals, the  $a_{2u}$ , the  $e_{1g}$  and the  $e_{2u}$  sets (now in their symmetric and antisymmetric combinations) interact with essentially the Ru d and s orbitals of appropriate symmetry. For a better understanding,

however, we should start with the levels of the fragment  $[(\mu\text{-Cl})_3\text{Ru}_2]^+$ , which in turn is derived from the well known conical  $\text{ML}_3$  fragment with the three L ligands fused.

The orbitals of this fragment, a half octahedron, have been described in detail when  $L = \text{CO}$ .<sup>24,25</sup> Their difference relative to the traditional octahedron comes from another choice of coordinate system, more suitable in this case, which defines the  $z$  axis as the 3-fold axis. Consequently,  $xz$ ,  $yz$  mix with  $xy$ ,  $x^2 - y^2$  to give two equivalent sets of fragment orbitals, a lower energy one, with the orbitals between the direction of the ligands ( $t_{2g}$  like orbitals) and a higher energy one, where they are in the direction of the ligands (the  $e_g$  like set), suitable for making  $\sigma$  bonds. The first set of orbitals along with the third " $t_{2g}$ " orbital will be used to make  $\pi$  bonds. They are represented on the left side of Figure 10.

Fusing together the two RuCl groups will result in the in-phase and out-of-phase combinations of the described orbitals (second column from left in Figure 10). These will in turn interact with the  $\pi$  orbitals of the two benzenes,<sup>4</sup> which come also in pairs. As expected, there are three pairs of major interactions, corresponding to donation from filled benzene orbitals ( $1e'$ ,  $1e''$ ,  $a'_1$ ,  $a''_2$ ) to empty  $\sigma$ -type ruthenium orbitals ( $2e'$ ,  $2e''$ ,  $2a'_1$ ,  $2a''_2$ ) of  $\text{Ru}_2\text{Cl}_3$ . The  $\pi$ -type filled metal orbitals ( $1e'$ ,  $1e''$ ) enter weaker interactions with the empty pairs of  $e_{2u}$  benzene orbital ( $2e'$ ,  $2e''$ ). There are no orbitals of appropriate symmetry to back donate to the highest  $\pi$  orbital ( $b_{2g}$ ) of the benzenes, which is not shown. The HOMO of the complex is a mostly  $\sigma$  orbital of benzene, made slightly antibonding by a weak interaction with the metal.

There is one interaction which deserves to be described in more detail as it gives rise to the molecular orbital which is destabilized upon bending of the hydrogen atoms toward the metal and therefore prevents a larger distortion: it is a three orbital interaction between  $a'_1$  orbitals, the high energy sp hybrid  $2a'_1$ , the  $z^2$  and the out of phase combination of benzene  $a_{2u}$ . Though the overall stabilizing interaction is between benzene  $a_{2u}$  and  $\text{Ru}_2\text{Cl}_3$   $2a'_1$ , there is mixing of  $1a'_1$ , which is essentially  $z^2$ . The bonding molecular orbital of  $[(\mu\text{-Cl})_3\{\eta^6\text{-arene}\}\text{Ru}]_2^+$  is  $1a'_1$ , followed by almost nonbonding  $2a'_1$ , while the high energy antibonding counterpart is not represented. The energy of this orbital increases along the distortion (Figure 9) because the amount of mixing of  $z^2$  varies and bonding character is lost, as the p orbital in each carbon overlaps nearer to the nodal plane (see Figure 11a).

For most of the other molecular orbitals, the energy decreases when the hydrogen atoms bend toward the metal. This is caused by the increased overlap between the orbitals in each fragment after the redirection of the benzene  $\pi$  orbitals, as shown schematically in Figure 11b.

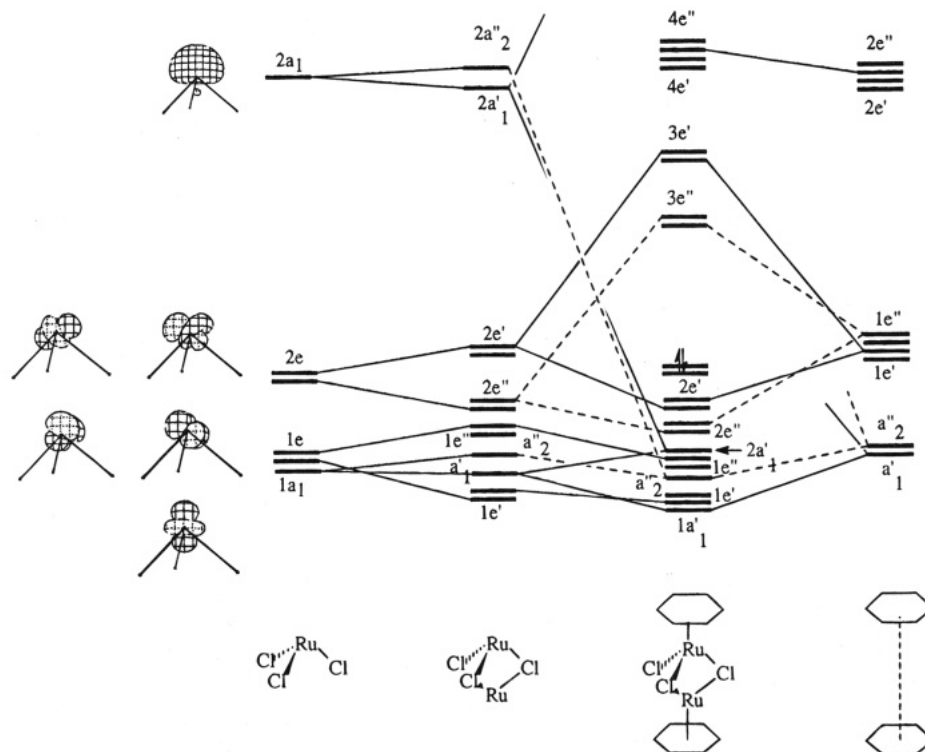
Having found out that a benzene ring coordinated to a single metal atom favors the bending of its hydrogen

(25) Albright, T. A.; Hoffmann, P.; Hoffmann, R. *J. Am. Chem. Soc.* **1977**, *99*, 7546.

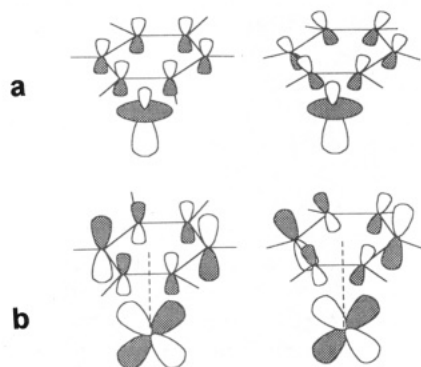
(26) (a) Beck, U.; Hummel, W.; Bürgi, H.-B.; Ludi, H. *Organometallics* **1987**, *6*, 20. (b) Stebler-Röthlisberger, M.; Hummel, W.; Pittet, P. A.; Bürgi, H.-B.; Ludi, H.; Merbach, A. E. *Inorg. Chem.* **1988**, *27*, 1358. (c) Luginbühl, W.; Zbinden, P.; Pittet, P. A.; Armbruster, T.; Bürgi, H.-B.; Ludi, H. *Inorg. Chem.* **1991**, *30*, 2350.

(23) (a) Hoffmann, R. *J. Chem. Phys.* **1963**, *39*, 1397. (b) Hoffmann, R.; Lipscomb, W. N. *J. Chem. Phys.* **1962**, *37*, 2179.

(24) Albright, T. A.; Burdett, J. K.; Whangbo, M.-H. *Orbital Interactions in Chemistry*; John Wiley & Sons: New York, 1985.



**Figure 10.** Building the molecular orbitals of  $[(\mu\text{-Cl})_3\{\eta^6\text{-C}_6\text{H}_6\}\text{Ru}_2]^+$  from those of  $\text{RuCl}_3$  and benzene.



**Figure 11.** Interaction of benzene  $\pi$  orbitals with the  $1a'_1$ -( $z^2$ ) (a) and the  $xz(2e'')$  (b) orbital of one ruthenium atom for planar benzene (left) and bent benzene (right).

atoms toward the metal, one can question why this behavior is not always found. The first reason may be the difficulty of adequately locating hydrogen atoms in X-ray diffraction experiments. Rings assigned as planar may actually be bent. The examples of bent coordinated arenes are still quite rare.<sup>9</sup> We have performed calculations for a few of these systems and observed a good agreement between our findings and experimental results. For instance, the toluene derivative described in this work has an energy minimum for a bending of  $6^\circ$  toward the ruthenium atom.

The exceptions are, to our knowledge, found for hexamethylbenzene complexes<sup>27</sup> and in these the ring substituents are bent away from the metal. Calculations on benzene and hexamethylbenzene confirmed the data and indicated that steric repulsions between adjacent methyl groups play an important role. On the other hand, if the substituents move away from the metal, to the other side of the ring, the steric constraints

will be minimized. This behavior becomes important as the number of methyl substituents on the ring increases, therefore it is not seen in the toluene complex.

The last question to address refers to the rotation of benzene or toluene around the  $\text{Ru}_2$ -axis. The potential energy surface is very soft,<sup>24</sup> though a small minimum was found for the conformations actually observed in **1** and **2**.

## Experimental Section

**Synthesis of  $[(\mu\text{-Cl})_3\{\eta^6\text{-arene}\}\text{Ru}_2][\text{BF}_4]$  (Arene =  $\text{C}_6\text{H}_6$ , **1**, and  $\text{C}_6\text{H}_5\text{Me}_2$ , **2**).** The synthesis of **1** and **2** follows a method reported earlier.<sup>28</sup> In a typical reaction,  $[\text{Ru}_2\text{Cl}_3(\eta^6\text{-arene})_2]$  ( $\sim 0.15$  g) was dissolved in  $\text{CH}_3\text{COOF}$  ( $\sim 3$  mL) and to this solution aqueous  $\text{HBF}_4$  (48% v/v, 0.4 mL) was added. The mixture was heated to reflux for 3 h during which time the solution changed colour from brown to dark orange. The solvents were removed under a reduced pressure, yielding an orange residue of  $[(\mu\text{-Cl})_3\{\eta^6\text{-arene}\}\text{Ru}_2][\text{BF}_4]$  (90%).

Crystals of **1** and **2** were grown by slow evaporation from  $\text{MeNO}_2$  at room temperature over a period of approximately 1 week. Both sets of crystals appeared to be stable out of the mother liquor in air. Crystals of **1** were orange-red tablets, the one used for the two data collections had dimensions of  $0.40 \times 0.25 \times 0.12$  mm. Anal. Found: C, 25.62; H, 2.25. Calcd: C, 26.13; H, 2.19. Positive fast atom bombardment mass spectrum  $M^+$  465 (calculated 465, corresponding to  $[(\mu\text{-Cl})_3\{\eta^6\text{-arene}\}\text{Ru}_2]^+$ ).

Crystals of **2** were red columns, the dimensions of the one used in the data collection being  $0.44 \times 0.24 \times 0.22$  mm. Anal. Found: C, 28.35; H, 2.80. Calcd: C, 29.01; H, 2.78. Positive fast atom bombardment mass spectrum  $M^+$  493 (calculated 493, corresponding to  $[(\mu\text{-Cl})_3\{\eta^6\text{-arene}\}\text{Ru}_2]^+$ ).

**Crystal Structure Determination.** X-ray measurements were made on a Stöe Stadi-4 four-cycle diffractometer. Data were collected at 295 and 150 K for compound **1**, and at 150 K

(27) Muetterties, E. L.; Bleeke, J. R.; Wucherer, E. J.; Albright, T. A. *Chem. Rev.* **1982**, *82*, 499.

(28) Rybinskaya, M. I.; Kudinov, A. R.; Kaganovich, V. S. *J. Organomet. Chem.* **1983**, *246*, 279.

Table 5. Crystal Data and Details of Measurements for 1 and 2

	1a	1b	2
formula	C <sub>12</sub> H <sub>12</sub> BCl <sub>3</sub> F <sub>4</sub> Ru <sub>2</sub>	C <sub>12</sub> H <sub>12</sub> BCl <sub>3</sub> F <sub>4</sub> Ru <sub>2</sub>	C <sub>14</sub> H <sub>16</sub> BCl <sub>3</sub> F <sub>4</sub> Ru <sub>2</sub>
M <sub>r</sub>	551.52	551.52	579.57
temp (K)	296	150	150
system	monoclinic	monoclinic	triclinic
space group	P2 <sub>1</sub> /a	P2 <sub>1</sub> /a	P1
a (Å)	8.4449(6)	8.43(2)	9.355(5)
b (Å)	18.9448(12)	18.68(4)	9.668(4)
c (Å)	10.3154(7)	10.25(2)	10.190(4)
α (deg)			92.12(3)
β (deg)	103.416(4)	104.8(1)	104.71(4)
γ (deg)			93.07(3)
V (Å <sup>3</sup> )	1605.3	1560.5	888.9
Z	4	4	2
F(000)	1056	1056	560
D <sub>calcd</sub> (g cm <sup>-3</sup> )	2.28	2.35	2.17
λ(Mo Kα) (Å)	0.71069	0.71069	0.71069
μ(Mo Kα) (mm <sup>-1</sup> )	2.260	2.325	2.047
θ-range (deg)	2.5–25	2.5–25	2.5–25
octants explored (h <sub>min</sub> , h <sub>max</sub> ; k <sub>min</sub> , k <sub>max</sub> ; l <sub>min</sub> , l <sub>max</sub> )	–10, 9; 0, 22; 0, 12	–10, 9; 0, 22; 0, 12	–11, 10; –11, 11; 0, 12
no. of measd rflns	2924	2811	3278
no. of unique rflns used in the refinement	2812	2708	3143
no. of refined params	239	248	281
GOF on F <sup>2</sup>	1.05	1.06	1.15
R <sub>1</sub> (on F, I > 2σ(I))	0.0392	0.0378	0.0220
wR <sub>2</sub> (on F <sup>2</sup> , all data)	0.1279	0.1117	0.0596

Table 6. Atomic Coordinates (×10<sup>4</sup>) for 1a

	x	y	z
Ru(1)	1608(1)	3811(1)	1378(1)
Ru(2)	2799(1)	3684(1)	–1427(1)
Cl(1)	89(2)	3775(1)	–955(1)
Cl(2)	3310(2)	4551(1)	348(2)
Cl(3)	3081(2)	2909(1)	473(2)
C(1)	–227(9)	4340(4)	2195(6)
C(2)	1314(9)	4618(4)	2795(6)
C(3)	2580(9)	4164(4)	3405(6)
C(4)	2313(10)	3431(4)	3401(6)
C(5)	780(10)	3151(4)	2802(6)
C(6)	–488(9)	3598(4)	2200(7)
C(7)	4692(9)	3167(4)	–2132(7)
C(8)	3224(10)	2884(4)	–2817(7)
C(9)	1964(10)	3333(5)	–3471(6)
C(10)	2260(12)	4070(6)	–3450(7)
C(11)	3735(11)	4343(4)	–2792(7)
C(12)	4969(9)	3883(4)	–2125(8)
H(1)	–1134(87)	4567(38)	1809(65)
H(2)	1451(78)	5153(36)	2577(60)
H(3)	3724(76)	4436(33)	3748(55)
H(4)	3050(100)	3034(48)	3720(73)
H(5)	751(95)	2654(42)	2782(73)
H(6)	–1485(74)	3369(32)	1842(54)
H(7)	5481(83)	2828(36)	–1598(63)
H(8)	2855(108)	2334(48)	–2975(85)
H(9)	877(116)	3069(49)	–3856(84)
H(10)	1738(196)	4375(92)	–3822(141)
H(11)	3858(93)	4735(43)	–2717(73)
H(12)	5809(94)	4050(41)	–1697(68)
B	2325(6)	1256(2)	4679(4)
F(1)	1402(7)	1204(3)	3393(5)
F(2)	3178(7)	1877(2)	4766(6)
F(3)	3390(8)	687(3)	4876(7)
F(4)	1253(10)	1233(4)	5505(6)

Table 7. Atomic Coordinates (×10<sup>4</sup>) for 1b

	x	y	z
Ru(1)	1644(1)	3827(1)	1413(1)
Ru(2)	2776(1)	3678(1)	–1415(1)
Cl(1)	62(1)	3770(1)	–954(1)
Cl(2)	3321(2)	4572(1)	362(1)
Cl(3)	3126(2)	2904(1)	532(1)
C(1)	–162(6)	4369(3)	2229(5)
C(2)	1378(7)	4654(3)	2828(5)
C(3)	2697(6)	4200(3)	3453(5)
C(4)	2443(7)	3450(3)	3476(5)
C(5)	876(7)	3157(3)	2871(5)
C(6)	–418(7)	3613(3)	2251(5)
C(7)	4645(6)	3123(3)	–2112(5)
C(8)	3085(7)	2864(3)	–2830(5)
C(9)	1860(7)	3332(3)	–3501(5)
C(10)	2183(7)	4081(3)	–3477(5)
C(11)	3727(7)	4350(3)	–2776(5)
C(12)	4965(7)	3861(3)	–2096(5)
H(1)	–991(68)	4648(30)	1711(53)
H(2)	1454(60)	5144(28)	2735(46)
H(3)	3705(71)	4410(31)	3812(53)
H(4)	3283(76)	3093(35)	3801(59)
H(5)	643(80)	2568(36)	2747(64)
H(6)	–1411(76)	3437(34)	1807(57)
H(7)	5352(71)	2837(32)	–1498(57)
H(8)	2909(75)	2487(35)	–2830(59)
H(9)	988(74)	3101(31)	–3879(56)
H(10)	1416(73)	4423(34)	–3821(56)
H(11)	3908(63)	4825(31)	–2661(50)
H(12)	5824(65)	3998(27)	–1609(49)
B	2311(8)	1249(3)	4618(7)
F(1)	1329(4)	1188(2)	3317(3)
F(2)	3136(4)	1900(2)	4756(3)
F(3)	3477(5)	692(2)	4825(4)
F(4)	1395(6)	1190(3)	5547(5)

only for compound 2. An Oxford Cryosystems low-temperature device was used for the low temperature determinations.<sup>29</sup>

Diffraction data were corrected for absorption by azimuthal scanning of high-γ reflections. All non-H atoms were allowed

to vibrate anisotropically. SHELX93<sup>30</sup> was used for data treatment and refinement based on F<sup>2</sup>. The position of F(4) in 1a had to be refined with constraints on B–F and F··F distances, and the atom could only be treated isotropically. Crystal data and details of measurement are reported in Table 5. Fractional atomic coordinates are reported in Tables 6–8. Anisotropic displacement parameters are deposited as Supplementary Material. SCHAKAL93 was used for the graphical representation of the results.<sup>31a</sup>

**Packing Potential Energy Barrier Calculations.** The packing potential energy of an organometallic molecule (p.p.e.) can be estimated by applying empirical methods similar to

(29) Cosier, J.; Glaser, A. M. *J. Appl. Cryst.* **1986**, *19*, 105.

(30) (a) Sheldrick, G. M. *Acta Crystallogr.* **1990**, *A46*, 467. (b) Sheldrick, G. M.: **SHELXL93**, University of Gottingen, Germany, 1993.

(31) Keller, E.: **SCHAKAL93**, University of Freiburg, Germany, 1993. (b) Gavezzotti, A. **OPEC, Organic Packing Potential Energy Calculations**, University of Milano, Italy. See also: Gavezzotti, A. *J. Am. Chem. Soc.* **1983**, *195*, 5220.

Table 8. Atomic Coordinates ( $\times 10^4$ ) for 2

	x	y	z
Ru(1)	2408(1)	2057(1)	6767(1)
Ru(2)	3089(1)	2115(1)	3770(1)
Cl(1)	2263(1)	245(1)	5001(1)
Cl(2)	1358(1)	3287(1)	4758(1)
Cl(3)	4651(1)	2660(1)	6061(1)
C(1)	772(4)	2801(4)	7779(3)
C(2)	2184(4)	3501(4)	8370(3)
C(3)	3429(4)	2738(4)	8850(3)
C(4)	3305(4)	1267(4)	8760(3)
C(5)	1932(4)	582(4)	8156(3)
C(6)	666(4)	1348(4)	7671(3)
C(7)	-530(6)	3610(6)	7182(5)
C(8)	4901(4)	2782(4)	2889(3)
C(9)	4644(4)	1319(4)	2729(3)
C(10)	3214(4)	702(4)	2121(3)
C(11)	2009(4)	1537(4)	1652(3)
C(12)	2261(4)	2992(4)	1824(3)
C(13)	3691(4)	3613(4)	2437(3)
C(14)	6394(5)	3405(5)	3619(4)
B(1)	2208(4)	-2694(4)	9788(4)
F(1)	1406(3)	-1861(2)	10422(2)
F(2)	1310(3)	-3166(3)	8534(2)
F(3)	2710(3)	-3809(2)	10552(3)
F(4)	3418(2)	-1927(3)	9583(3)
H(2)	2271(44)	4399(45)	8396(40)
H(3)	4347(47)	3229(42)	9125(40)
H(4)	4146(45)	757(41)	8998(39)
H(5)	1851(46)	-388(46)	7946(43)
H(6)	-196(42)	871(38)	7181(37)
H(71)	-1161(57)	3636(52)	7794(54)
H(72)	-1194(61)	3032(57)	6478(59)
H(73)	-276(58)	4485(60)	6855(57)
H(9)	5307(41)	752(38)	3101(37)
H(10)	3061(49)	-186(50)	2089(46)
H(11)	1068(49)	1132(43)	1296(43)
H(12)	1501(52)	3620(48)	1684(46)
H(13)	3819(41)	4515(42)	2575(38)
H(141)	6302(47)	4283(49)	3956(44)
H(142)	6995(56)	3441(51)	3077(52)
H(143)	6906(54)	2760(50)	4291(52)

those usually employed in the neighboring field of solid state organic chemistry.<sup>15</sup> Use is made of the expression p.p.e. =  $\sum_i \sum_j [A \exp(-Br_{ij}) - Cr_{ij}^{-6}]$ , where p.p.e. represents the packing potential energy and  $r_{ij}$  the non-bonded atom-atom intermolecular distance. Index ( $i$ ) in the summation runs over all atoms of the reference molecule and index ( $j$ ) over the atoms

of the surrounding molecules within a preset cutoff distance (10 Å in the present work). The ruthenium atoms were attributed the potential coefficients available for argon. The PPE can be recalculated at given rotational steps for fragments undergoing reorientation in the solid state thus yielding the atom-atom potential energy barrier [ $\Delta E$ ]. This procedure has been successfully applied in a number of cases to estimate the reorientational barriers opposing motion of various types of discoidal ligands in the solid state. The reader is addressed to ref 9 for references. The calculations have been performed with the computer program OPEC.<sup>31b</sup>

**Molecular Orbital Calculations.** All the calculations were carried out using the extended Hückel method<sup>23</sup> with modified  $H_{ij}$ 's.<sup>32</sup> The basis set for the metal atom consisted of  $ns$ ,  $np$ , and  $(n-1)d$  orbitals. The  $s$  and  $p$  orbitals were described by single Slater-type wave functions, and the  $d$  orbitals were taken as contracted linear combinations of two Slater-type wave functions. Standard parameters were used for C and H, while those for Ru were as follows ( $H_{ij}/eV$ ,  $\zeta$ ): 5s -10.40, 2.078; 5p -6.89, 2.043; 4d -14.90, 5.378, 2.303 ( $\zeta_2$ ), 0.5340 ( $c_1$ ), 0.6365 ( $c_2$ ). Three-dimensional representations of orbitals were drawn using the program CACAO.<sup>33</sup>

In all calculations idealized models were used, based on the experimentally observed structures. The RuCl<sub>3</sub> fragment was taken as a half octahedron. The following distances were used: Ru-Ru 3.14, Ru-Cl 2.44, Ru-C(benzene) 2.22, C-C 1.40, C-H 1.08 Å.

**Acknowledgment.** D.B., F.G., M.J.C., and L.F.V. acknowledge CNR (Italy) and JNICT (Portugal) for joint financial support. D.B., F.G., and B.F.G.J. thank NATO for a travel grant. P.J.D. thanks the SERC and British Petroleum for financial support.

**Supplementary Material Available:** ORTEP figures and tables of anisotropic thermal parameters, hydrogen fractional coordinates and  $u$  values, and complete bond lengths and angles (19 pages). Ordering information is given on any current masthead page.

OM940437D

(32) Ammeter, J. H.; Bürgi, H.-B.; Thibault, J. C.; Hoffmann, R. *J. Am. Chem. Soc.* **1978**, *100*, 3686.

(33) Mealli, C.; Proserpio, D. M. *J. Chem. Ed.* **1990**, *67*, 39.

# Carbonyl Insertions into Metal–Nitrogen Bonds of Group 4 Dialkylamido Complexes. X-ray Structure of $\text{Cp}^*(\text{Me}_2\text{N})_2\text{Ti}[\text{O}(\text{Me}_2\text{N})\text{C}]\text{W}(\text{CO})_5$

Mikhail Galakhov, Avelino Martín, Miguel Mena,<sup>\*,†</sup> Federico Palacios, and Carlos Yélamos

Departamento de Química Inorgánica, Universidad de Alcalá de Henares, Campus Universitario, 28871 Alcalá de Henares, Spain

Paul R. Raithby

University Chemical Laboratory, University of Cambridge, Cambridge CB2 1EW, England

Received June 15, 1994<sup>®</sup>

$[\text{Cp}^*\text{M}(\text{NMe}_2)_3]$  [ $\text{Cp}^* = \eta^5\text{-C}_5\text{Me}_5$ ; **1**,  $\text{M} = \text{Ti}$ ; **2**,  $\text{M} = \text{Zr}$ ] reacts with metal carbonyls,  $\text{M}'(\text{CO})_n$  ( $n = 6$ ,  $\text{M}' = \text{Cr}, \text{Mo}, \text{W}$ ;  $n = 5$ ,  $\text{M}' = \text{Fe}$ ), to give the corresponding insertion products,  $\text{Cp}^*(\text{Me}_2\text{N})_2\text{M}[\text{O}(\text{Me}_2\text{N})\text{C}]\text{M}'(\text{CO})_{n-1}$  ( $\text{M} = \text{Ti}$ ; **3**,  $\text{M}' = \text{W}$ ; **4**,  $\text{M}' = \text{Mo}$ ; **5**,  $\text{M}' = \text{Cr}$ ; **6**,  $\text{M}' = \text{Fe}$ ;  $\text{M} = \text{Zr}$ ; **7**,  $\text{M}' = \text{W}$ ; **8**,  $\text{M}' = \text{Mo}$ ; **9**,  $\text{M}' = \text{Cr}$ ; **10**,  $\text{M}' = \text{Fe}$ ), in good yield. When complexes **3–5** were heated at 80 °C in toluene for several days,  $\text{Cp}^*\text{Ti}(\mu\text{-NMe}_2)_2[\text{O}(\text{NMe}_2)\text{C}]\text{M}'(\text{CO})_3$  (**11**,  $\text{M}' = \text{W}$ ; **12**,  $\text{M}' = \text{Mo}$ ; **13**,  $\text{M}' = \text{Cr}$ ) were obtained. However, heating **6** under the same conditions gave  $\text{Cp}^*(\text{Me}_2\text{N})\text{Ti}[\text{O}(\text{Me}_2\text{N})\text{C}]_2\text{Fe}(\text{CO})_3$  (**14**). Reactions of **12** with CO and Bu<sup>t</sup>NC have been carried out, giving compound **4** in the first case and  $\text{Cp}^*(\text{Me}_2\text{N})_2\text{Ti}[\text{O}(\text{Me}_2\text{N})\text{C}]\text{Mo}(\text{CO})_3(\text{CNBu}^t)_2$  (**15**) in the second. The structure of **3** has been proved unequivocally by a X-ray diffraction study (space group  $P2_1$ ,  $a = 8.828(2)$  Å,  $b = 13.001(4)$  Å,  $c = 12.045(2)$  Å,  $\beta = 98.22(2)^\circ$ ,  $Z = 2$ ,  $R_1 = 0.044$  and  $wR_2 = 0.109$ ). **3** consists of two moieties,  $\text{Cp}^*\text{Ti}(\text{NMe}_2)_2$  and  $\text{W}(\text{CO})_5$ , bridged by a  $[\text{O}(\text{Me}_2\text{N})\text{C}]$  unit where the oxygen atom is bound to the oxophilic titanium atom, while the carbon is forming a Fischer carbene-like complex with tungsten.

## Introduction

A wide variety of early–late heterobimetallic transition metal complexes have been studied. Two of the reasons for interest in such species arise from their potential applications in homogeneous catalytic processes with the cooperative activation of small molecular substrates such as carbon monoxide<sup>1</sup> and their relation to strong metal–support interaction (SMSI) seen in some heterogeneous catalytic systems.<sup>2</sup>

In 1968, Bradley suggested that reactions between  $\text{CpTi}(\text{NMe}_2)_3$  and  $\text{M}'(\text{CO})_6$  ( $\text{M}' = \text{Cr}, \text{Mo}, \text{W}$ ) gave simple acid–base compounds of the general formula  $\text{CpTi}(\text{NMe}_2)_3\text{M}'(\text{CO})_3$  with three bridging dimethylamido groups joining the titanium and the group 6 metals, which were terminally bonded to the  $\pi$ -cyclopentadienyl group and the three carbonyls, respectively.<sup>3</sup> More recently, Petz has reported that complexes similar to Fischer carbenes can be obtained in a single step by insertion of carbon monoxide ligands from  $\text{M}'(\text{CO})_n$  compounds into E–N bonds of dialkylamides, where E

belongs to the groups 4, 13, and 14.<sup>4,1f</sup> The formulation of these complexes have been confirmed crystallographically only for the aluminometallobenzenes  $\text{Fe}_2(\text{CO})_8\text{-}[\text{C}(\text{NMe}_2)\text{OAl}(\text{NMe}_2)_2]_2$  and  $\text{Mn}_2(\text{CO})_9[\text{C}(\text{NMe}_2)\text{OAl}_2(\text{NMe}_2)_5]$ .<sup>5</sup>

We have recently reported a series of mono(pentamethylcyclopentadienyl)titanium(IV) amides and are interested in the study of their chemical reactivity.<sup>6</sup> In this paper, we describe the reactions of  $\text{Cp}^*\text{M}(\text{NMe}_2)_3$  ( $\text{M} = \text{Ti}, \text{Zr}$ ) with several group 6 and 8 metal carbonyls. Also, we report the first X-ray structure of a heterobimetallic titanium–tungsten complex, with formation of carbene-bridged species via insertion of a metal carbonyl moiety into a Ti–N bond. Thermal behavior of the titanium insertion products and reactions with carbon monoxide or isocyanides are also presented.

## Results and Discussion

$\text{Cp}^*(\text{Me}_2\text{N})_2\text{M}[\text{O}(\text{Me}_2\text{N})\text{C}]\text{M}'(\text{CO})_{n-1}$  compounds, where the M metal atom belongs to group 4 and the M' metal atom to the groups 6–8, can be easily obtained from the known  $[\text{Cp}^*\text{M}(\text{NMe}_2)_3]$  complexes by addition of the corresponding metal carbonyls of groups 6–8,  $\text{M}'(\text{CO})_n$ , in a toluene solution (see Scheme 1) and heating at different temperatures (Experimental Section).

<sup>†</sup> E-mail: MMENA@INORG.ALCALA.ES.

<sup>®</sup> Abstract published in *Advance ACS Abstracts*, November 1, 1994.

(1) (a) For a comprehensive review see: Stephan, D. W. *Coord. Chem. Rev.* **1989**, *95*, 41. (b) Ferguson, G. S.; Wolczanski, P. T.; Parkanyi, L.; Zonneville, M. C. *Organometallics* **1988**, *7*, 1967. (c) Anslyn, E. V.; Santarsiero, B. D.; Grubbs, R. H. *Organometallics* **1988**, *7*, 2137. (d) Erker, G.; Mena, M.; Hoffmann, U.; Menjón, B. *Organometallics* **1991**, *10*, 291, and references cited therein. (e) Beckhaus, R.; Strauss, I.; Wagner, T.; Kiprof, P. *Angew. Chem., Int. Ed. Engl.* **1993**, *32*, 264. (f) Petz, W. *J. Organomet. Chem.* **1993**, *456*, 85.

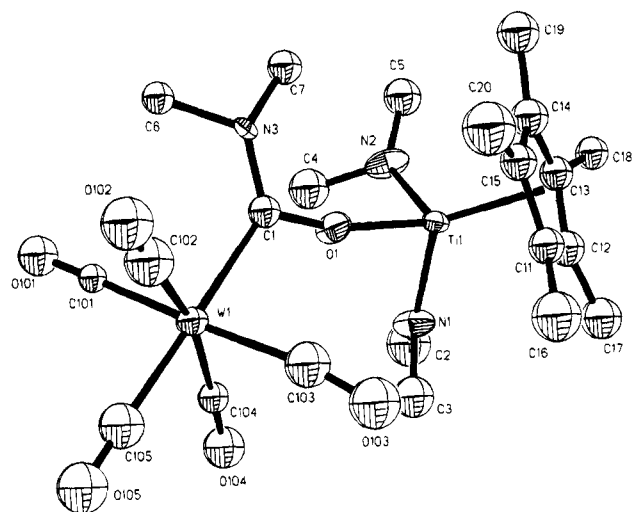
(2) (a) *Metal-Support Interactions in Catalysis, Sintering and Redispersion*; Stevenson, S. A., Dumesic, J. A., Baker, R. T., Ruckenstein, E., Eds.; Van Nostrand-Reinhold: New York, 1987. (b) *Strong Metal-Support Interactions*; Backer, R. T. K., Tauster, S. J., Dumesic, J. A., Eds.; American Chemical Society: Washington, DC, 1986.

(3) Bradley, D. C.; Kasenally, A. S. *J. Chem. Soc., Chem. Comm.* **1968**, 1430.

(4) (a) Petz, W.; Schmid, G. *J. Organomet. Chem.* **1972**, *35*, 321. (b) Petz, W.; Schmid, G. *Angew. Chem., Int. Ed. Engl.* **1972**, *11*, 934. (c) Petz, W. *J. Organomet. Chem.* **1973**, *55*, C42. (d) Petz, W. *J. Organomet. Chem.* **1974**, *72*, 369. (e) Petz, W.; Jonas, A. *J. Organomet. Chem.* **1976**, *120*, 423. (f) Petz, W. *J. Organomet. Chem.* **1979**, *165*, 199.

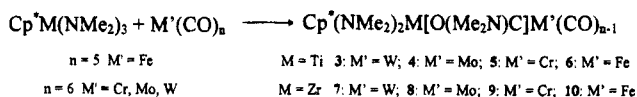
(5) Janik, J. Fr.; Duesler, E. N.; Paine, R. T. *J. Organomet. Chem.* **1987**, *323*, 149.

(6) (a) Martín, A.; Mena, M.; Raithby, P. R.; Serrano, R.; Yélamos, C. *J. Organomet. Chem.* **1994**, *467*, 79. (b) Galakhov, M.; Irigoyen, A. M.; Martín, A.; Mena, M.; Monge, M.; Palacios, F.; Yélamos, C., manuscripts in preparation.



**Figure 1.** ORTEP drawing of  $\text{Cp}^*(\text{Me}_2\text{N})_2\text{Ti}[\text{O}(\text{Me}_2\text{N})\text{C}]\text{W}(\text{CO})_5$  (**3**). Thermal ellipsoids at the 30% level are shown.

### Scheme 1



IR spectra of complexes **3–10** show the characteristic frequencies of the  $\text{MCp}^*$ ,  $\text{MNMe}_2$ , and  $\text{M}'(\text{CO})_{n-1}$  fragments and are consistent with reported values for compounds with such groups.<sup>1f,4,6,7</sup> Complexes **3–6** are monomeric in the gas phase according to mass spectrometry data (see Experimental Section) and in the solid state as shown by the X-ray crystal structure for **3**.

**X-ray Structure of  $\text{Cp}^*(\text{Me}_2\text{N})_2\text{Ti}[\text{O}(\text{Me}_2\text{N})\text{C}]\text{W}(\text{CO})_5$  (**3**).** The molecular structure of  $\text{Cp}^*(\text{Me}_2\text{N})_2\text{Ti}[\text{O}(\text{Me}_2\text{N})\text{C}]\text{W}(\text{CO})_5$  is shown in Figure 1, the final atomic coordinates for the non-hydrogen atoms are presented in Table 1, and selected bond distances and angles in Table 2. Compound **3** is a monomer, and the titanium atom has a classical three-legged piano stool arrangement. The  $\text{Cp}^*(\text{centroid})\text{--Ti}$ –substituent angles are  $134.9^\circ$  for  $\text{Cp}^*\text{--Ti}(1)\text{--O}(1)$ ,  $121.8^\circ$  for  $\text{Cp}^*\text{--Ti}(1)\text{--N}(1)$ , and  $117.6^\circ$  for  $\text{Cp}^*\text{--Ti}(1)\text{--N}(2)$ ; the angles formed by the legs are  $91.5(6)^\circ$  for  $\text{O}(1)\text{--Ti}(1)\text{--N}(1)$ ,  $90.4(7)^\circ$  for  $\text{O}(1)\text{--Ti}(1)\text{--N}(2)$ , and  $88.6(6)^\circ$  for  $\text{N}(1)\text{--Ti}(1)\text{--N}(2)$ .

It is interesting to compare the bonding parameters around the titanium atom. The distances from titanium to cyclopentadienyl ring carbons are in the normal range, but the presence of a large  $\text{Ti}(1)\text{--O}(1)\text{--C}(1)$  bond angle [ $164.5(12)^\circ$ ] and a short  $\text{Ti}(1)\text{--O}(1)$  bond distance [ $1.895(8)$  Å], similar to those reported for  $\text{Cp}^*_2\text{Ti}(\text{CH}=\text{CH}_2)[\text{OC}(=\text{CH}_2)\text{C}_6\text{H}_{11}]$  [ $165.9(2)^\circ$  and  $1.859(2)$  Å, respectively],<sup>8</sup> indicates a considerable oxygen to metal  $p_\pi \rightarrow d_\pi$  interaction, as we have proposed for other oxotitanium compounds containing the “ $\text{Cp}^*\text{TiO}$ ” unit.<sup>9</sup> This interaction weakens the donation of the nitrogen lone pair to titanium ( $p_\pi \rightarrow d_\pi$ ) and as a result the  $\text{Ti}(1)\text{--N}(1)$  [ $2.048(13)$  Å] and  $\text{Ti}(1)\text{--N}(2)$  [ $2.067(12)$  Å] distances are longer than those observed for  $\text{Cp}^*\text{Ti}$ –

**Table 1.** Atomic Coordinates ( $\times 10^4$ ) and Equivalent Isotropic Displacement Parameters ( $\text{\AA}^2 \times 10^3$ ) for Compound  $\text{Cp}^*(\text{Me}_2\text{N})_2\text{Ti}[\text{O}(\text{Me}_2\text{N})\text{C}]\text{W}(\text{CO})_5$  (**3**)

	x	y	z	U(eq)
W(1)	983(1)	0	9179(1)	43(1)
Ti(1)	2898(2)	39(5)	13162(1)	45(1)
N(1)	1094(13)	−940(10)	13217(10)	61(3)
N(2)	4351(15)	−1213(11)	13407(12)	66(4)
N(3)	4517(10)	−13(21)	10450(8)	76(4)
O(1)	2760(9)	−120(18)	11587(6)	60(3)
O(101)	2497(13)	−1909(7)	8074(11)	72(3)
O(102)	2262(16)	1697(9)	7636(12)	94(5)
O(103)	−657(16)	1648(10)	10570(12)	100(5)
O(104)	−1174(13)	−1606(9)	10204(12)	84(4)
O(105)	−1822(10)	228(11)	7208(7)	95(4)
C(101)	1946(15)	−1172(8)	8457(12)	36(4)
C(102)	1815(27)	1023(14)	8184(18)	87(8)
C(103)	89(23)	1076(14)	10083(18)	85(8)
C(104)	−263(15)	−1039(9)	9874(12)	42(4)
C(105)	−807(11)	18(23)	7955(9)	80(4)
C(1)	3013(11)	−98(18)	10564(8)	45(3)
C(2)	795(29)	−1842(19)	13700(23)	111(8)
C(3)	−385(20)	−491(14)	12660(15)	82(5)
C(4)	4041(29)	−2097(19)	12601(20)	88(7)
C(5)	5881(21)	−1456(16)	14100(16)	76(5)
C(6)	5034(13)	−204(10)	9333(9)	45(3)
C(7)	5836(15)	−283(10)	11373(11)	55(4)
C(11)	2127(9)	1561(8)	13712(8)	58(4)
C(12)	2239(9)	884(8)	14646(8)	62(4)
C(13)	3799(1)	602(8)	14934(7)	56(4)
C(14)	4652(8)	1104(9)	14179(10)	64(4)
C(15)	3618(12)	1697(8)	13424(8)	65(5)
C(16)	765(19)	2160(16)	13170(20)	103(7)
C(17)	987(16)	577(14)	15303(14)	85(5)
C(18)	4406(15)	179(14)	16059(8)	64(4)
C(19)	6362(10)	1132(18)	14276(17)	87(6)
C(20)	3984(34)	2353(20)	12473(18)	116(11)

**Table 2.** Selected Bond Lengths (Å) and Angles (deg) for Compound  $\text{Cp}^*(\text{Me}_2\text{N})_2\text{Ti}[\text{O}(\text{Me}_2\text{N})\text{C}]\text{W}(\text{CO})_5$  (**3**)<sup>a</sup>

W(1)–C(1)	2.271(10)	Ti(1)–O(1)	1.895(8)
Ti(1)–N(1)	2.048(13)	Ti(1)–N(2)	2.067(12)
N(1)–C(2)	1.35(3)	N(1)–C(3)	1.50(2)
N(2)–C(4)	1.50(3)	N(2)–C(5)	1.52(2)
N(3)–C(1)	1.359(13)	N(3)–C(6)	1.502(14)
N(3)–C(7)	1.53(2)	O(1)–C(1)	1.284(12)
Ti(1)–Cp*	1.912		
O(1)–Ti(1)–N(1)	91.5(6)	O(1)–Ti(1)–N(2)	90.4(7)
N(1)–Ti(1)–N(2)	88.6(6)	C(1)–N(3)–C(6)	120.3(9)
C(1)–N(3)–C(7)	124.1(12)	C(6)–N(3)–C(7)	108.4(11)
C(1)–O(1)–Ti(1)	164.5(12)	O(1)–C(1)–N(3)	113.9(9)
O(1)–C(1)–W(1)	118.6(7)	N(3)–C(1)–W(1)	126.9(8)
Cp*–Ti(1)–O(1)	134.9	Cp*–Ti(1)–N(1)	121.8
Cp*–Ti(1)–N(2)	117.6	C(2)–N(1)–C(3)	109(2)
C(2)–N(1)–Ti(1)	139.0(13)	C(3)–N(1)–Ti(1)	112.0(10)
C(4)–N(2)–C(5)	105.1(14)	C(4)–N(2)–Ti(1)	117.2(12)
C(5)–N(2)–Ti(1)	136.8(12)		

<sup>a</sup> Cp\* is the centroid of the  $\text{C}_5\text{Me}_5$  ring.

$(\text{NMe}_2)_3$  [ $1.918(12)$  Å (average)]<sup>6a</sup> and very similar, within experimental error, to those found for  $\text{Cp}^*_2\text{Ti}(\text{III})\text{--}(\text{NMePh})$  [ $2.054(2)$  Å]<sup>10</sup> where it is suggested that the  $\text{Ti}\text{--N}$  is a single bond and there is absence of multiple bonding.

The  $\text{W}\text{--C}(\text{carbene})$  bond length,  $2.271(10)$  Å, is slightly longer than those generally found for  $\text{W}\text{--C}(\text{carbene})$  bonds in other complexes ( $1.81\text{--}2.23$  Å).<sup>11</sup> The  $\text{O}(1)\text{--}$

(7) (a) Nakamoto, K. *Infrared and Raman Spectra of Inorganic and Coordination Complexes*, 4th ed., Wiley: New York, 1986. (b) King, R. B.; Bisnette, M. B. *J. Organomet. Chem.* **1967**, *8*, 287. (c) Bradley, D. C.; Gitlitz, M. H. *J. Chem. Soc. A*, **1969**, 980. (d) Bürger, H.; Dämmgen, U. *J. Organomet. Chem.* **1975**, *101*, 295.

(8) Beckhaus, R.; Strauss, I.; Wagner, T., *J. Organomet. Chem.* **1994**, *464*, 155.

(9) (a) Gómez Sal, M. P.; Martín, A.; Mena, M.; Royo, P.; Serrano, R. *J. Organomet. Chem.* **1991**, *419*, 77. (b) Gómez-Sal, M. P.; Mena, M.; Royo, P.; Serrano, R. *J. Organomet. Chem.* **1988**, *358*, 147. (c) Mena, M.; Royo, P.; Serrano, R.; Pellinghelli, M. A.; Tiripicchio, A. *Organometallics* **1989**, *8*, 476. (d) Gómez-Sal, M. P.; Mena, M.; Palacios, F.; Royo, P.; Serrano, R.; Martínez-Carreras, S. *J. Organomet. Chem.* **1989**, *375*, 59.

(10) Feldman, J.; Calabrese, J. C. *J. Chem. Soc., Chem. Commun.* **1991**, 1042.



Table 3.  $^1\text{H}$  and  $^{13}\text{C}\{^1\text{H}\}$  Chemical Shifts of **1**, **2**, and  $\text{Cp}^*(\text{Me}_2\text{N})_2\text{M}[\text{O}(\text{Me}_2\text{N})\text{C}]\text{X}$  (**3–10**, **14**) in  $\text{C}_6\text{D}_6$  at 293 K

Compounds	$\delta(^1\text{H})$			$\delta(^{13}\text{C})$					
	$\text{C}_5\text{Me}_5$	$\text{OCNMeMe}$	$\text{NMe}_2$	$\text{C}_5\text{Me}_5$	$\text{C}_5\text{Me}_5$	$\text{NMe}_2$	$\text{OCNMeMe} (\Delta\delta)$	$\text{OCNMeMe}$	CO
$\text{Cp}^*\text{Ti}(\text{NMe}_2)_3$ , <b>1</b>	1.95		3.09	11.9	118.4	48.5			
$\text{Cp}^*\text{Zr}(\text{NMe}_2)_3$ , <b>2</b>	1.97		2.92	10.9	117.6	43.6			
$\text{M} = \text{Ti}; \text{X} = \text{W}(\text{CO})_5$ , <b>3</b>	1.73	2.07, 3.06	2.92	10.8	121.6	47.0	30.8; 45.6 (14.7)	229.6	200.4 <sup>a</sup> 202.5 <sup>b</sup>
$\text{M} = \text{Ti}; \text{X} = \text{Mo}(\text{CO})_5$ , <b>4</b>	1.74	2.01; 3.07	2.93	11.5 <sup>c</sup> 11.1	122.3 <sup>c</sup> 121.9	46.0 <sup>c</sup> 47.4	31.4; <sup>c</sup> 46.0 <sup>c</sup> (14.6) 31.2; 44.7 (13.5)	227.5 <sup>c</sup> 239.3	200.0 <sup>c</sup> 208.6 <sup>a</sup> 213.7 <sup>b</sup>
$\text{M} = \text{Ti}; \text{X} = \text{Cr}(\text{CO})_5$ , <b>5</b>	1.72	1.98; 3.08	2.92	11.1	121.9	47.4	32.2; 44.0 (11.8)	244.3	219.8 <sup>a</sup> 223.1 <sup>b</sup>
$\text{M} = \text{Ti}; \text{X} = \text{Fe}(\text{CO})_4$ , <b>6</b>	1.80	2.21; 3.21	2.94	11.3	122.3	47.6	35.6; 44.8 (9.2)	232.0	218.3
$\text{M} = \text{Zr}; \text{X} = \text{W}(\text{CO})_5$ , <b>7</b>	1.80	2.09; 2.99	2.74	10.8	120.0	42.6	32.1; 46.0 (13.9)	229.6	200.3 <sup>a</sup> 202.6 <sup>b</sup>
$\text{M} = \text{Zr}; \text{X} = \text{Mo}(\text{CO})_5$ , <b>8</b>	1.80	2.07; 2.99	2.74	10.7	120.0	42.7	31.9; 44.7 (12.8)	239.1	208.3 <sup>a</sup> 213.0 <sup>b</sup>
$\text{M} = \text{Zr}; \text{X} = \text{Cr}(\text{CO})_5$ , <b>9</b>	1.79	2.08; 3.02	2.74	10.7	120.2	42.7	33.2; 44.0 (10.8)	245.1	219.5 <sup>a</sup> 222.8 <sup>b</sup>
$\text{M} = \text{Zr}; \text{X} = \text{Fe}(\text{CO})_4$ , <b>10</b>	1.88	2.33; 3.19	2.75	10.8	120.3	42.9	36.2; 44.9 (8.7)	231.9	217.6
$\text{M} = \text{Ti}; \text{X} = \text{Mo}(\text{CO})_5(\text{CNBu}^t)_2$ , <b>15</b>	1.91	2.29; 3.58	3.16	11.3	121.1	47.8	30.1; 45.0 (14.9)	248.7	218.0 <sup>a</sup> 221.0 <sup>b</sup>

<sup>a</sup> Four CO cis with respect to carbene carbon. <sup>b</sup> One CO trans with respect to carbene carbon. <sup>c</sup>  $^{13}\text{C}$  CP MAS spectrum.

$\text{C}(1)(\text{carbene})$  [1.284(12) Å] and  $\text{N}(3)–\text{C}(1)$  [1.359(13) Å] bond lengths are indeed shorter than the theoretical single bond distances [ $\text{C}(\text{sp}^3)–\text{O}$ , 1.41 Å;  $\text{C}(\text{sp}^3)–\text{N}$ , 1.45 Å] and similar to those found for organic amides.<sup>12</sup> These structural features are consistent with the presence of a considerable multiple bond character for  $\text{O}(1)–\text{C}(1)(\text{carbene})$ , the trigonal planar geometry around  $\text{C}(1)$  (the sum of bond angles is 359°), and a degree of double bond in  $\text{N}(3)–\text{C}(1)(\text{carbene})$ , where the  $\text{N}(3)$ , located  $\approx 0.2$  Å out of the plane of the three adjacent C-atoms, adopts a very slight pyramidal (nearly planar, sum of angles 353°) environment. The dihedral angle formed by the  $\text{O}(1)–\text{C}(1)–\text{N}(3)–\text{C}(7)$  and the  $\text{W}(1)–\text{C}(1)–\text{N}(3)–\text{C}(6)$  planes is 10.6°.

**NMR Spectra.**  $^1\text{H}$ - and  $^{13}\text{C}\{^1\text{H}\}$ -NMR spectra data for complexes **3–10** are shown in Table 3 and confirm the insertion of only one molecule of  $\text{M}'(\text{CO})_n$  ( $\text{M}' = \text{Cr}, \text{Mo}, \text{W}, \text{Fe}$ ) in complexes **1** and **2**.  $^1\text{H}$ -NMR data establish the presence of only one signal for the  $\text{Cp}^*$  groups, shifted 0.2 ppm upfield with respect to the starting materials **1** and **2**, respectively. The signals of the  $\text{O}^{13}\text{CNMe}_2$  are in the range 225–245 ppm and, as can be seen in Table 3, their chemical shifts depend on the nature of  $\text{M}'$ , increasing in the order  $\text{Cr} > \text{Mo} > \text{Fe} > \text{W}$ , but are independent of the nature of  $\text{M}$  ( $\text{Ti}, \text{Zr}$ ). Other signals assignable to two equivalent  $\text{M}-\text{NMe}_2$  fragments and two inequivalent methyl groups of the  $\text{OCNMe}_2$  moiety are observed in the  $^1\text{H}$ - and  $^{13}\text{C}\{^1\text{H}\}$ -NMR for complexes **3–10**.

Similar  $^{13}\text{C}$  chemical shifts (see Table 3) have been recorded for complex **3** both in solution and in the solid state (CP MAS spectrum), which allow us to assume that the structure of this compound in solution is the same as the structure in the solid state, as determined by X-ray crystallography, and that the nonequivalence of the  $\text{OCNMe}_2$  methyl groups observed at room tem-

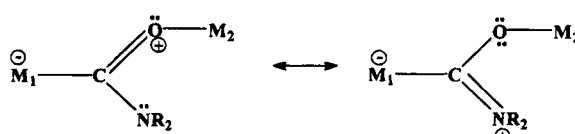
perature by NMR is consistent with a high rotational barrier around the  $\text{C}(\text{carbene})–\text{N}$  axis arising from a significant CN double bond character, typical for aminocarbenes.

We have attempted to determine the activations parameters of this rotation for complex **3**, but only small broadening of the two signals of the dimethylaminocarbenes protons have been observed in the  $^1\text{H}$  NMR (300 MHz) spectrum at 323 K ( $\Delta G^\ddagger > 18$  kcal/mol). This value is similar to those reported for the same process in other complexes.<sup>4e,11a</sup> The linear correlation between  $\Delta G^\ddagger$  of the rotation around the  $\text{C}–\text{N}$  bond and the  $\delta^{13}\text{C}$  of this carbon in the ground state<sup>13</sup> is well-known; consequently, in our case for the complexes **3–5** and **7–9** the  $\Delta G^\ddagger$  increases in the order  $\text{Cr} > \text{Mo} > \text{W}$ .

According to dynamic NMR theory,<sup>14</sup> the position of the average resonance ( $\delta_{\text{av}}$ ) of two equally populated sites at high-temperature (in the transition state) is simply the weighted average of the resonance positions ( $\delta_1$  and  $\delta_2$ ) at low temperature (in the ground state). For complexes **3–10**, the  $\delta_{\text{av}}(^{13}\text{C})$  values of the methyl carbon signals ( $\delta_1$  and  $\delta_2$ ) in the aminocarbenes groups are very similar (between 38.0 and 40.6 ppm), suggesting that the transition state when the carbene carbon has no  $\pi$  interaction with the dimethylamide group is not affected considerably by the  $\text{M}'(\text{CO})_5$  moiety. However the values of the differences between chemical shifts  $\Delta\delta(^{13}\text{C})$  in the ground state for complexes **3–10** depend on the nature of  $\text{M}'$  ( $\text{W}, \text{Mo},$  and  $\text{Cr}$ ) (see Table 3), while the fragments  $\text{Cp}^*\text{M}(\text{NMe}_2)_2$  ( $\text{M} = \text{Ti}, \text{Zr}$ ) do not affect them significantly.

So, most of these results (X-ray and NMR data principally) are reasonably consistent with a description of the bonding system between two canonical forms (Scheme 2) in valence bond theory terms.

Scheme 2



**Thermal Stability of  $\text{Cp}^*(\text{Me}_2\text{N})_2\text{Ti}[\text{O}(\text{Me}_2\text{N})\text{C}]\text{W}(\text{CO})_5$  ( $\text{M}' = \text{W}$ , **3**;  $\text{Mo}$ , **4**;  $\text{Cr}$ , **5**).** When complexes **3–5**

(11) (a) Orpen, A. G.; Brammer, L.; Allen, F. H.; Kennard, O.; Watson, D. G.; Taylor, R. *J. Chem. Soc. Dalton Trans.* **1989**, S1. (b) Dötz, K. H.; Fischer, H.; Hofmann, P.; Kreissl, F. R.; Schubert, U.; Weiss, K. *Transition Metal Carbene Complexes*; Verlag Chemie: Weinheim, 1983; p 103. (c) Erker, G.; Dorf, U.; Benn, R.; Reinhardt, R. D.; Petersen, J. L. *J. Am. Chem. Soc.* **1984**, *106*, 7649. (d) Erker, G.; Dorf, U.; Lecht, R.; Ashby, M. T.; Aulbach, M.; Schlund, R.; Krüger, C.; Mynott, R. *Organometallics* **1989**, *8*, 2037.

(12) March, J. *Advanced Organic Chemistry: Reactions, Mechanisms and Structure*, 3rd ed.; John Wiley & Sons: New York, 1985; p 19 and references therein.

Scheme 3

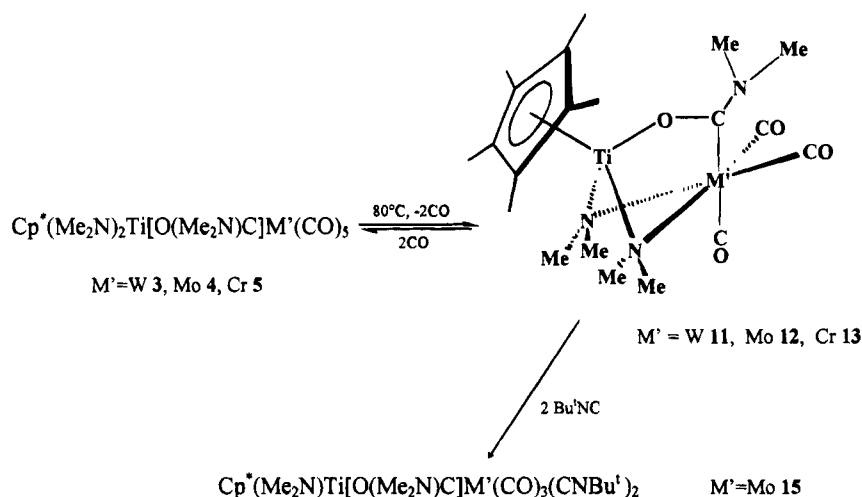


Table 4.  $^1\text{H}$  and  $^{13}\text{C}$  Chemical Shifts of  $\text{Cp}^*\text{Ti}(\mu\text{-NMe}_2)_2[\text{O}(\text{Me}_2\text{N})\text{C}]\text{X}$  (11–13) and  $\text{Cp}^*(\text{Me}_2\text{N})\text{Ti}[\text{O}(\text{Me}_2\text{N})\text{C}]_2\text{Fe}(\text{CO})_3$  (14) in  $\text{C}_6\text{D}_6$  at 293 K

Compounds	$\delta(^1\text{H})$			$\delta(^{13}\text{C})$					
	$\text{C}_5\text{Me}_5$	$\text{OCNMeMe}$	$\mu\text{-NMeMe}$	$\text{C}_5\text{Me}_5$	$\text{C}_5\text{Me}_5$	$\mu\text{-NMeMe}$	$\text{OCNMeMe} (\Delta\delta)$	$\text{OCNMeMe}$	CO
X = W(CO) <sub>3</sub> , <b>11</b>	1.62	2.26; 3.07	2.97; 3.18	10.5	123.2	56.2; 56.9	33.8; 42.7 (8.9)	225.3	224.7 <sup>a</sup> 230.7 <sup>b</sup>
X = Mo(CO) <sub>3</sub> , <b>12</b>	1.62	2.32; 3.20	2.81; 3.03	10.5	122.9	55.3; 56.0	33.7; 41.9 (8.2)	228.5	225.7 <sup>a</sup> 234.5 <sup>b</sup>
X = Cr(CO) <sub>3</sub> , <b>13</b>	1.63	2.34; 3.15	2.74; 2.96	10.4	121.7	55.0; 55.7	34.9; 41.1 (6.2)	233.9	233.2 <sup>a</sup> 244.6 <sup>b</sup>
<b>14</b>	1.97	2.76; 2.96		10.8	121.3		34.4; 40.1 (5.7)	225.9	220.4

<sup>a</sup> Two CO cis respect to carbene carbon. <sup>b</sup> One CO trans respect to carbene carbon.

are heated at 80 °C for several days, CO evolution is detected and the complexes 11–13 are formed (see Scheme 3).

These complexes can also be obtained if the conditions to prepare 3–5 are changed to 80 °C and the reaction mixtures stirred for longer periods of time. It is noticeable that no evolution of CO was observed if the temperature was not increased or only UV was used, different from what was reported by Bradley et al.<sup>3</sup>

In the IR spectra of complexes 11–13, one of the three frequencies corresponding to the carbonyl groups bonded to M' (W, Mo, and Cr) has disappeared, leaving the other two in the range 1820–1920  $\text{cm}^{-1}$ . This situation is similar to that found for *fac*-M(CO)<sub>3</sub>X<sub>3</sub> complexes, with a  $\text{C}_{3v}$  symmetry,<sup>15</sup> indicating a similar donor character of the carbene and the two bridging amido groups.

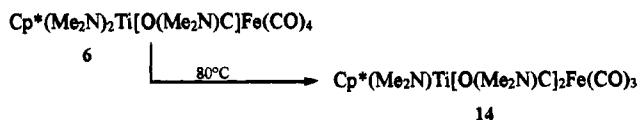
Similarly to complexes 3–5, the  $^1\text{H}$  and  $^{13}\text{C}\{^1\text{H}\}$  NMR spectra of 11–13 show only one type of Cp\* ring (see Table 4). Comparing the  $^{13}\text{C}\{^1\text{H}\}$  NMR data for complexes 11–13 with those for 3–5 shows that the signal assignable to OCNMe<sub>2</sub> has shifted upfield whereas the two CO resonances (now in 2:1 ratio) shifted downfield. The signals corresponding to the methyl groups of the OCNMe<sub>2</sub> fragments still appear different and keep the same average resonances [ $\delta_{\text{av}}(^{13}\text{C})$ : 37.8–38.3 ppm], but the  $\Delta\delta(^{13}\text{C})$  for these compounds are smaller than those found for the complexes 3–5 (see Table 4).

The  $^1\text{H}$  and  $^{13}\text{C}\{^1\text{H}\}$  NMR spectra also show two signals assignable to the inequivalent methyl groups of the  $\mu\text{-NMe}_2$  fragments,<sup>16</sup> with a very small difference

for chemical shifts in either  $^1\text{H}$  ( $\Delta\delta = 0.2$  ppm) and  $^{13}\text{C}\{^1\text{H}\}$  NMR ( $\Delta\delta = 0.7$  ppm) spectra (see Table 4). This difference could be caused by the different spacial distribution of the methyl groups (inside and outside, see Scheme 3) in each  $\mu\text{-NMe}_2$  fragment.

The same reaction conditions were used with the complex  $\text{Cp}^*(\text{Me}_2\text{N})_2\text{Ti}[\text{O}(\text{Me}_2\text{N})\text{C}]\text{Fe}(\text{CO})_4$  (6), but instead of CO evolution, a double insertion and hence formation of two carbene groups was observed (see Scheme 4). The metallocyclic carbene complex 14 obtained is similar to those reported by Petz et al.:  $(\text{CO})_4\text{FeC}(\text{NMe}_2)\text{OTi}(\text{NMe}_2)[\text{O}(\text{NMe}_2)\text{C}]_2\text{Fe}(\text{CO})_3$ ,<sup>1f</sup>  $(\text{CO})_3\text{Fe}[\text{C}(\text{NMe}_2)\text{O}]_2\text{SnMe}_2$ ,<sup>4e</sup> and  $(\text{CO})_3\text{Fe}[\text{C}(\text{NMe}_2)\text{O}]_2\text{SnM}(\text{CO})_5$  (M = Cr, Mo, W).<sup>4f</sup>

Scheme 4



The  $^1\text{H}$  and  $^{13}\text{C}$  NMR spectra of 14 show only one type of Cp\* ring, one signal due to the NMe<sub>2</sub> terminal group and other two attributable to the inequivalent methyl groups of the OCNMe<sub>2</sub> fragments. Comparing with the spectra for complex 6 shows that the signal corresponding to the OCNMe<sub>2</sub> carbon atom has been shifted 6.1 ppm upfield, the Fe(CO)<sub>3</sub> signal 2.1 ppm downfield, and the average resonance of the OCNMe<sub>2</sub> signals [ $\delta_{\text{av}}(^{13}\text{C}) = 37.5$  ppm,  $\Delta\delta(^{13}\text{C}) = 5.7$  ppm] 3 ppm upfield. Hence, the spectra imply the presence of a symmetry plane formed by the atoms Ti, Fe, and the N linked to

(13) Martin, G. J.; Gouesnard, J. P.; Dorie, J.; et al., *J. Am. Chem. Soc.* **1977**, *99*, 1381.

(14) Binsch, G. *Top. Stereochem.* **1968**, *3*, 97.

(15) Nakamoto, K.; McCarthy, P. J. *Spectroscopy and Structure of Metal Chelate Compounds*; Wiley: New York, 1968.

(16) A similar situation has been found for methyl groups of the  $\mu\text{-AsMe}_2$  fragment in  $\text{Fe}_2(\text{CO})_6(\mu\text{-AsMe}_2)(\mu\text{-OCNMe}_2)$ : Keller, E.; Trenkle, A.; Vahrenkam, H. *Chem. Ber.* **1977**, *110*, 441.

the titanium atom and are in agreement with the participation of the two OCNMe<sub>2</sub> fragments in the electronic delocalization. <sup>13</sup>C NMR spectrum of the compound **14** shows also only one signal for the Fe(CO)<sub>3</sub> fragment at 220.4 ppm, similar to that found for the complex (CO)<sub>4</sub>FeC(NMe<sub>2</sub>)OTi(NMe<sub>2</sub>)[O(NMe<sub>2</sub>)C]<sub>2</sub>Fe(CO)<sub>3</sub>.<sup>1f</sup>

In the IR spectrum of **14** three vibrations in the range 1968–2044 cm<sup>-1</sup> are observed, making clear again the difference with respect to the complexes **11–13**, with only two bands at smaller frequencies (1820–1920 cm<sup>-1</sup>).

Further studies were carried out to check the reversibility of the reactions used to get the complexes **11–13**. Thus, two experiments were performed in sealed NMR tubes, utilizing the complex **12** as starting material. In the first one, **12** was exposed to a carbon monoxide atmosphere (1 atm) and, after 15 h, the resulting product was pure complex **4** (see Scheme 3), confirming the reversibility of this kind of reactions. The second experiment consisted of adding the stoichiometric amount of Bu<sup>t</sup>NC over a hexadeuteriobenzene solution of **12**; after 2 h the solution quantitatively afforded orange **15** (see Scheme 3). The <sup>1</sup>H and <sup>13</sup>C{<sup>1</sup>H}-NMR spectra of **15** (see Table 3 and Experimental Section) confirm the existence of only one bridging OCNMe<sub>2</sub> fragment and two terminal NMe<sub>2</sub> groups joined to the titanium atom, the signals corresponding to the two terminal Bu<sup>t</sup>NC groups bonded to the molybdenum atom are present as well. Complex **15** is unstable in solution and decomposes slowly to give Cp\*Ti(NMe<sub>2</sub>)<sub>3</sub> and another residue with signals in the <sup>1</sup>H NMR that could be assigned to Mo(CO)<sub>4</sub>(Bu<sup>t</sup>NC)<sub>2</sub>.

### Experimental Section

All reactions were carried out under argon by Schlenk techniques or in a MBraun glovebox. Heptane, hexane, and pentane were refluxed over Na/K amalgam, toluene was refluxed over sodium, and all solvents were distilled under argon. Cr(CO)<sub>6</sub>, Mo(CO)<sub>6</sub>, W(CO)<sub>6</sub>, and C≡NCMe<sub>3</sub> were purchased from FLUKA and used without further purification. Fe(CO)<sub>5</sub> purchased from FLUKA was used freshly distilled. Cp\*Ti(NMe<sub>2</sub>)<sub>3</sub> and Cp\*Zr(NMe<sub>2</sub>)<sub>3</sub> were prepared by known procedures.<sup>6</sup> IR spectra were measured on a Perkin-Elmer 883 spectrophotometer. <sup>1</sup>H and <sup>13</sup>C NMR spectra were recorded on a Varian Unity 300 MHz spectrometer. Electron impact mass spectra were obtained at 70 eV with a Hewlett-Packard 5890 spectrometer. C, H, and N analysis were carried out with a Perkin-Elmer 240B microanalyzer.

**Synthesis of Cp\*(Me<sub>2</sub>N)<sub>2</sub>Ti[O(Me<sub>2</sub>N)C]W(CO)<sub>5</sub> (3).** A solution of 2.18 g (6.91 mmol) of Cp\*Ti(NMe<sub>2</sub>)<sub>3</sub> in toluene (100 mL) was added to 2.43 g (6.91 mmol) of W(CO)<sub>6</sub> and the mixture stirred at 50 °C for 24 h. The resulting reddish-brown solution was concentrated to a volume of ca. 15 mL and allowed to stay at room temperature. A first portion of red crystals of **3** was collected by filtration. From the filtrate, a second portion of red crystals was obtained after cooling to -30 °C. The combined yield of the titanaoxycarbene **3** was 4.38 g (95%). IR (KBr, cm<sup>-1</sup>): 2057s, 1897 vs, 1491m, 1441m, 1366m, 1295s, 1240m, 1222m, 1090m, 1043m, 949s, 918s, 698s, 605s, 583s, 484m, 432m, 381s; ν(CO) (in heptane): 2058w, 1984s, 1918s. Anal. Calcd for C<sub>22</sub>H<sub>33</sub>N<sub>3</sub>O<sub>6</sub>TiW: C, 39.60; H, 4.98; N, 6.30. Found: C, 40.05; H, 4.73; N, 6.03. MS: *m/e* [assignment, rel int (%)] 611 [(M - 2CO)<sup>+</sup>, 7], 510 [(M - 4CO - NHMe<sub>2</sub>)<sup>+</sup>, 10], 482 [(M - 5CO - NHMe<sub>2</sub>)<sup>+</sup>, 19].

**X-ray Structure Determination of Cp\*(Me<sub>2</sub>N)<sub>2</sub>Ti[O(Me<sub>2</sub>N)C]W(CO)<sub>5</sub> (3).** A red, block crystal of compound **3** crystallized from toluene (-40 °C) was mounted in a glass capillary in a random orientation. A summary of the crystal and X-ray structural analysis data for compound **3** is presented

**Table 5. Crystal and X-ray Structural Analysis Data for Compound Cp\*(Me<sub>2</sub>N)<sub>2</sub>Ti[O(Me<sub>2</sub>N)C]W(CO)<sub>5</sub> (3)**

empirical formula	C <sub>22</sub> H <sub>33</sub> N <sub>3</sub> O <sub>6</sub> TiW
molecular weight	667.26
crystal color/habit	red/prismatic
crystal system; space group	monoclinic; P2 <sub>1</sub>
<i>a</i> /Å	8.828(2)
<i>b</i> /Å	13.001(4)
<i>c</i> /Å	12.045(2)
β/(deg)	98.22(2)
<i>U</i> /Å <sup>3</sup>	1368.2(6)
<i>D</i> <sub>c</sub> /gcm <sup>-3</sup>	1.620
μ(Mo Kα)/cm <sup>-1</sup>	45.3
<i>F</i> (000)	660
<i>Z</i>	2
reflections measured	4162
unique reflections	3573
observed reflections [ <i>F</i> <sub>o</sub> > 4σ( <i>F</i> <sub>o</sub> )]	3238
number of parameters refined	154
Goodness of fit	1.281
<i>R</i> <sub>1</sub>	0.0436, <i>R</i> <sub>1</sub> = Σ   <i>F</i> <sub>o</sub> -   <i>F</i> <sub>c</sub>   /Σ  <i>F</i> <sub>o</sub>
<i>wR</i> <sub>2</sub>	0.1091, <i>wR</i> <sub>2</sub> = {Σ[w( <i>F</i> <sub>o</sub> <sup>2</sup> - <i>F</i> <sub>c</sub> <sup>2</sup> ) <sup>2</sup> ]/Σ[w( <i>F</i> <sub>o</sub> <sup>2</sup> ) <sup>2</sup> ]} <sup>1/2</sup>
weighting scheme	<i>w</i> = [σ <sup>2</sup> ( <i>F</i> <sup>2</sup> ) + (0.0479 <i>P</i> ) <sup>2</sup> + 9.5800 <i>P</i> ] <sup>-1</sup> <i>P</i> = ( <i>F</i> <sub>o</sub> <sup>2</sup> + 2 <i>F</i> <sub>c</sub> <sup>2</sup> )/3

in Table 5.<sup>19</sup> Preliminary examinations and data collection were performed at 20 °C using Mo Kα radiation (λ = 0.71073 Å) and a graphite-oriented monochromator on a Nicolet 3Rm/V diffractometer. From the systematic absences of 0*k*0 (*k* = 2*n* + 1), the space group could be determined to be monoclinic P2<sub>1</sub> (No. 4) or P2<sub>1</sub>/m (No. 11). Structure solution and refinement were carried out in either space groups but only P2<sub>1</sub> led to a sensible chemical model. A total of 4162 reflections were collected in the range 7° ≤ 2θ ≤ 45°, of which 3573 were independent with 3238 reflections having *F* ≥ 4σ(*F*). Three check reflections were monitored periodically throughout data collection and showed no significant variations. All intensity data were corrected for Lorentz-polarization effects and absorption corrections by the Ψ-scan method. No extinction correction was made. Calculations were carried out on a PC486 computer using the SHELXTL PLUS (PC version)<sup>17</sup> and SHELX-93.<sup>18</sup>

The structure was solved by a combination of Patterson synthesis and Fourier difference techniques and refined by full-matrix least-squares with W(1), Ti(1), N(1), N(2), N(3), and O(1) atoms assigned anisotropy displacement parameters. Methyl hydrogens were placed in idealized positions, C-H = 0.96 Å and H-C-H = 109.5°, and the methyl group was allowed to refine as a rigid group. The cyclopentadienyl ring was treated like a rigid group with C-C bonds of 1.420 Å and C-C-C angles of 108.0°. A weighting scheme, which gave satisfactory agreement analyses, was introduced in the final cycles of refinement. The final converged agreement factors were *R*<sub>1</sub> = 0.044, *wR*<sub>2</sub> = 0.109, and GOF = 1.28.

**Synthesis of Cp\*(Me<sub>2</sub>N)<sub>2</sub>Ti[O(Me<sub>2</sub>N)C]Mo(CO)<sub>5</sub> (4).** A toluene solution (50 mL) of 0.54 g (1.72 mmol) of Cp\*Ti(NMe<sub>2</sub>)<sub>3</sub> was added to 0.46 g (1.72 mmol) of Mo(CO)<sub>6</sub>. After stirring at 45 °C for 30 h, volatiles were removed in vacuo. The red solid was washed with cold pentane and dried under vacuum to yield 0.93 g (93%) of **4**. IR (KBr, cm<sup>-1</sup>): 2058s, 1906 vs, 1491m, 1440m, 1366m, 1290s, 1222m, 1087m, 1043m, 949s, 919s, 698m, 611s, 480m, 379s; ν(CO) (in heptane): 2060w, 1990m, 1922s. Anal. Calcd for C<sub>22</sub>H<sub>33</sub>N<sub>3</sub>O<sub>6</sub>TiMo: C, 45.61; H, 5.74; N, 7.25. Found: C, 46.03; H, 5.70; N, 7.03. MS: *m/e* [assignment, rel int (%)] 523 [(M - 2CO)<sup>+</sup>, 13], 495 [(M - 3CO)<sup>+</sup>, 35], 467 [(M - 4CO)<sup>+</sup>, 31], 439 [(M - 5CO)<sup>+</sup>, 44], 394 [(M - 5CO - NHMe<sub>2</sub>)<sup>+</sup>, 74].

(17) SHELXTL PLUS, version 4.0; Siemens Analytical Instruments, Madison, WI, 1990.

(18) Sheldrick, G. M. *J. Appl. Cryst.*, manuscript in preparation.

(19) The author has deposited atomic coordinates for structure with the Cambridge Crystallographic Data Centre. The coordinates can be obtained, on request, from the Director, Cambridge Crystallographic Data Centre, 12 Union Road, Cambridge, CB2 1EZ, UK.

**Synthesis of Cp\*(Me<sub>2</sub>N)<sub>2</sub>Ti[O(Me<sub>2</sub>N)C]Cr(CO)<sub>5</sub> (5).** The same method used to prepare **3** and **4** was followed using 0.54 g (1.72 mmol) of Cp\*Ti(NMe<sub>2</sub>)<sub>3</sub> and 0.38 g (1.72 mmol) of Cr(CO)<sub>5</sub> in toluene (40 mL) at 45 °C for 5 days. Volatiles were removed in vacuo, the dark red solid was extracted with several portions of pentane, and the combined extracts were filtered, concentrated, and kept at ca. -40 °C overnight. Red crystals of **5** were isolated in 78% yield (0.72 g). IR (KBr, cm<sup>-1</sup>): 2047s, 1900vs, 1490m, 1445m, 1369m, 1289s, 1220m, 1089m, 1043m, 949s, 920s, 670s, 567m, 464m, 390m; ν(CO) (in heptane): 2051w, 1987w, 1917vs. Anal. Calcd for C<sub>22</sub>H<sub>33</sub>N<sub>3</sub>O<sub>6</sub>TiCr: C, 49.35; H, 6.21; N, 7.85. Found: C, 49.87; H, 6.21; N, 7.70. MS: *m/e* [assignment, rel. int. (%)], 479 [(M-2CO)<sup>+</sup>, 4], 451 [(M-3CO)<sup>+</sup>, 9], 423 [(M-4CO)<sup>+</sup>, 3], 395 [(M-5CO)<sup>+</sup>, 54], 350 [(M-5CO-NHMe<sub>2</sub>)<sup>+</sup>, 29].

**Synthesis of Cp\*(Me<sub>2</sub>N)<sub>2</sub>Ti[O(Me<sub>2</sub>N)C]Fe(CO)<sub>4</sub> (6).** Fe(CO)<sub>5</sub> (0.26 mL, 1.90 mmol) was added over a solution of 0.54 g (1.72 mmol) of Cp\*Ti(NMe<sub>2</sub>)<sub>3</sub> in toluene (70 mL). After stirring for 40 h at room temperature, the orange solution was concentrated to ca. 10 mL and cooled to -40 °C overnight; 0.79 g (90%) of orange crystals of **6** were obtained. IR (KBr, cm<sup>-1</sup>): 2030s, 1996s, 1921 vs, 1496m, 1445m, 1373m, 1310m, 1280m, 1132m, 1097m, 1045m, 946s, 924s, 700m, 628s, 468m, 398s; ν(CO) (heptane): 2037m, 1955m, 1916vs. Anal. Calcd for C<sub>21</sub>H<sub>33</sub>N<sub>3</sub>O<sub>5</sub>TiFe: C, 49.34; H, 6.51; N, 8.22. Found: C, 49.62; H, 6.73; N, 8.01. MS: *m/e* [assignment, rel. int. (%)] 455 [(M-2CO)<sup>+</sup>, 26], 427 [(M-3CO)<sup>+</sup>, 47], 399 [(M-4CO)<sup>+</sup>, 58], 354 [(M-4CO-NHMe<sub>2</sub>)<sup>+</sup>, 100].

**Synthesis of Cp\*(Me<sub>2</sub>N)<sub>2</sub>Zr[O(Me<sub>2</sub>N)C]W(CO)<sub>5</sub> (7).** A toluene solution (50 mL) of 0.50 g (1.39 mmol) of Cp\*Zr(NMe<sub>2</sub>)<sub>3</sub> was added to 0.49 g (1.39 mmol) of W(CO)<sub>6</sub>. After stirring at 40 °C for 2 days, volatiles were removed in vacuo. The orange solid was washed with cold pentane and dried under vacuum to yield 0.88 g (89%) of **7**. IR (Nujol, cm<sup>-1</sup>): 2058m, 1982s, 1916s, 1462s, 1376s, 1288s, 1094m, 942m, 912m, 802w, 604m, 584m, 542w, 380s. Anal. Calcd for C<sub>22</sub>H<sub>33</sub>N<sub>3</sub>O<sub>6</sub>ZrW: C, 37.19; H, 4.68; N, 5.91. Found: C, 36.85; H, 4.50; N, 5.63.

**Synthesis of Cp\*(Me<sub>2</sub>N)<sub>2</sub>Zr[O(Me<sub>2</sub>N)C]Mo(CO)<sub>5</sub> (8).** A toluene solution (50 mL) of 0.50 g (1.39 mmol) of Cp\*Zr(NMe<sub>2</sub>)<sub>3</sub> was added to 0.36 g (1.39 mmol) of Mo(CO)<sub>6</sub>. After stirring at room temperature for 3 days, volatiles were removed in vacuo. The yellow solid was washed with cold pentane and dried under vacuum to yield 0.77 g (89%) of **8**. IR (Nujol, cm<sup>-1</sup>): 2060s, 1988s, 1966m, 1924s, 1462s, 1376s, 1284s, 1230m, 1140w, 1094w, 1058w, 942m, 912m, 612s, 594m, 540w, 376s. Anal. Calcd for C<sub>22</sub>H<sub>33</sub>N<sub>3</sub>O<sub>6</sub>ZrMo: C, 42.44; H, 5.34; N, 6.75. Found: C, 42.03; H, 5.07; N, 6.66.

**Synthesis of Cp\*(Me<sub>2</sub>N)<sub>2</sub>Zr[O(Me<sub>2</sub>N)C]Cr(CO)<sub>5</sub> (9).** A toluene solution (50 mL) of 0.50 g (1.39 mmol) of Cp\*Zr(NMe<sub>2</sub>)<sub>3</sub> was added to 0.30 g (1.39 mmol) of Cr(CO)<sub>6</sub>. After stirring at 60 °C for 2 days, volatiles were removed in vacuo. The greenish-yellow solid was washed with cold pentane and dried under vacuum to yield 0.74 g (92%) of **9**. IR (Nujol, cm<sup>-1</sup>): 2048m, 1986s, 1960m, 1918s, 1462s, 1376s, 1282s, 1248m, 1228m, 1140w, 1092w, 1056w, 942m, 910m, 674s, 540w, 464w, 406w, 362w. Anal. Calcd for C<sub>22</sub>H<sub>33</sub>N<sub>3</sub>O<sub>6</sub>ZrCr: C, 45.66; H, 5.75; N, 7.26. Found: C, 45.03; H, 5.70; N, 7.03.

**Synthesis of Cp\*(Me<sub>2</sub>N)<sub>2</sub>Zr[O(Me<sub>2</sub>N)C]Fe(CO)<sub>4</sub> (10).** A toluene solution (50 mL) of 0.50 g (1.39 mmol) of Cp\*Zr(NMe<sub>2</sub>)<sub>3</sub> was added to 0.27 g (1.39 mmol) of Fe(CO)<sub>5</sub>. After stirring at room temperature for 2 days, volatiles were removed in vacuo. The yellowish-green solid was washed with cold pentane and dried under vacuum to yield 0.69 g (89%) of **10**. IR (Nujol, cm<sup>-1</sup>): 2032s, 1960s, 1918s, 1462s, 1340m, 1300s, 1238m, 1144w, 1110w, 1052w, 944m, 912m, 886w, 666m, 630s, 538w, 488w, 466w, 368m. Anal. Calcd for C<sub>21</sub>H<sub>33</sub>N<sub>3</sub>O<sub>5</sub>ZrFe: C, 45.48; H, 6.00; N, 7.58. Found: C, 45.38; H, 5.86; N, 7.38.

**Synthesis of Cp\*Ti(μ-NMe<sub>2</sub>)<sub>2</sub>[O(Me<sub>2</sub>N)C]W(CO)<sub>3</sub> (11).** Following the method to prepare **3**; the dark red solution of **3** was heated at 80 °C for 6 days and then concentrated to ca. 25 mL and kept -40 °C for 2 days. Red crystals of **11** were isolated in 57% yield. IR (KBr, cm<sup>-1</sup>): 1898vs, 1797vs, 1500m, 1459m, 1382m, 1255m, 1168s, 1090m, 1024m, 922s, 715s,

602m, 534m, 491m, 447m, 384s; ν(CO) (in toluene): 1914s, 1824s. Anal. Calcd for C<sub>20</sub>H<sub>33</sub>N<sub>3</sub>O<sub>4</sub>TiW: C, 39.30; H, 5.44; N, 6.87. Found: C, 39.76; H, 5.47; N, 6.71.

**Synthesis of Cp\*Ti(μ-NMe<sub>2</sub>)<sub>2</sub>[O(Me<sub>2</sub>N)C]Mo(CO)<sub>3</sub> (12).** Following the method to prepare **11**, from 1.00 g (1.72 mmol) of **4** in toluene (50 mL), red crystals (0.70 g, 78%) of **12** were obtained. IR (KBr, cm<sup>-1</sup>): 1904vs, 1805vs, 1502s, 1450m, 1383s, 1254m, 1170s, 1100m, 1026m, 923s, 717s, 618s, 533m, 475m, 444m, 382s; ν(CO) (in toluene): 1920s, 1828s. Anal. Calcd for C<sub>20</sub>H<sub>33</sub>N<sub>3</sub>O<sub>4</sub>TiMo: C, 45.90; H, 6.36; N, 8.03. Found: C, 45.60; H, 6.22; N, 7.86. MS: *m/e* [assignment, rel. int. (%)] 523 [M<sup>+</sup>, 33], 495 [(M-CO)<sup>+</sup>, 61], 467 [(M-2CO)<sup>+</sup>, 39], 439 [(M-3CO)<sup>+</sup>, 51], 394 [(M-3CO-NHMe<sub>2</sub>)<sup>+</sup>, 78].

**Synthesis of Cp\*Ti(μ-NMe<sub>2</sub>)<sub>2</sub>[O(Me<sub>2</sub>N)C]Cr(CO)<sub>3</sub> (13).** This was prepared in the same way as **5** from 0.54 g (1.72 mmol) of Cp\*Ti(NMe<sub>2</sub>)<sub>3</sub> and 0.38 g (1.72 mmol) of Cr(CO)<sub>6</sub> in toluene (50 mL) with heating at 80 °C for 8 days. After crystallization, the red solid **13** was washed with several portions of pentane and dried. Yield: 64%. IR (KBr, cm<sup>-1</sup>): 1892vs, 1798vs, 1499s, 1452m, 1379s, 1252m, 1169s, 1094m, 1026m, 925s, 718s, 642m, 549m, 482m, 422m, 394s; ν(CO) (in toluene): 1908s, 1823s. Anal. Calcd for C<sub>20</sub>H<sub>33</sub>N<sub>3</sub>O<sub>4</sub>TiCr: C, 50.11; H, 6.94; N, 8.77. Found: C, 50.62; H, 7.11; N, 8.53.

**Synthesis of Cp\*(Me<sub>2</sub>N)Ti[O(Me<sub>2</sub>N)C]<sub>2</sub>Fe(CO)<sub>3</sub> (14).** A 0.33 mL portion of Fe(CO)<sub>5</sub> (2.43 mmol) was added to 0.73 g (2.31 mmol) of Cp\*Ti(NMe<sub>2</sub>)<sub>3</sub> in 80 mL of toluene. After 2 days at room temperature an orange solution of **6** was obtained. Heating to 80 °C for a week gave a dark red solution of **14**. The solution was concentrated to ca. 15 mL and cooled to -40 °C for 6 h; 0.96 g (81%) of reddish brown crystals of **14** were obtained. IR (KBr, cm<sup>-1</sup>): 1968vs, 1496m, 1446m, 1376s, 1305m, 1270m, 1240m, 1097s, 1023m, 953m, 606s, 399s; ν(CO) (in toluene): 2044w, 2002m, 1968vs(br). <sup>1</sup>H NMR (C<sub>6</sub>D<sub>6</sub>, 20 °C, δ): 1.97 (s, 15H, C<sub>5</sub>Me<sub>5</sub>), 2.76, 2.96 (s, 6H, OCNMe<sub>2</sub>), 2.83 (s, 6H, TiNMe<sub>2</sub>); <sup>13</sup>C NMR (C<sub>6</sub>D<sub>6</sub>, 20 °C, δ): 10.8 (q, <sup>1</sup>J<sub>CH</sub> = 125, C<sub>5</sub>Me<sub>5</sub>), 34.4, 40.1 (qq, <sup>1</sup>J<sub>CH</sub> = 137, <sup>3</sup>J<sub>CH</sub> = 3, OCNMe<sub>2</sub>), 46.8 (qq, <sup>1</sup>J<sub>CH</sub> = 133, <sup>3</sup>J<sub>CH</sub> = 6, TiNMe<sub>2</sub>), 121.3 (s, C<sub>5</sub>Me<sub>5</sub>), 220.4 (s, Fe(CO)<sub>3</sub>), 225.9 (m, OCNMe<sub>2</sub>). Anal. Calcd for C<sub>21</sub>H<sub>33</sub>N<sub>3</sub>O<sub>5</sub>TiFe: C, 49.34; H, 6.51; N, 8.22. Found: C, 49.52; H, 6.35; N, 7.91. MS: *m/e* [assignment, rel. int. (%)] 511 [M<sup>+</sup>, 2], 483 [(M-CO)<sup>+</sup>, 32], 455 [(M-2CO)<sup>+</sup>, 20], 427 [(M-3CO)<sup>+</sup>, 86], 382 [(M-3CO-NHMe<sub>2</sub>)<sup>+</sup>, 75], 354 [(M-4CO-NHMe<sub>2</sub>)<sup>+</sup>, 100].

**Reaction of 12 with CO.** Hexadeuteriobenzene (0.50 mL) was added to a 5 mm NMR tube containing compound **12** (0.01g, 0.02 mmol). The red solution was placed under 1 atm CO at -78 °C and the tube sealed and warmed at room temperature. After 15 h the product was identified as pure Cp\*(Me<sub>2</sub>N)<sub>2</sub>Ti[O(Me<sub>2</sub>N)C]Mo(CO)<sub>5</sub> (**4**) by <sup>1</sup>H NMR spectroscopy.

**Reaction of 12 with Bu<sup>1</sup>NC.** A 4.3 μL (0.04 mmol) portion of Bu<sup>1</sup>NC was added to a solution of **12** (0.01 g, 0.02 mmol) in hexadeuteriobenzene (0.50 mL) in a 5 mm NMR tube. The tube was sealed and within 2 h the solution afforded orange Cp\*(Me<sub>2</sub>N)<sub>2</sub>Ti[O(Me<sub>2</sub>N)C]Mo(CO)<sub>3</sub>(CNBu<sup>1</sup>)<sub>2</sub> (**15**) quantitatively according to <sup>1</sup>H and <sup>13</sup>C{<sup>1</sup>H} NMR spectroscopy. <sup>1</sup>H NMR (C<sub>6</sub>D<sub>6</sub>, 20 °C, δ): 1.07 (s, 18H, CNCMe<sub>3</sub>), 1.91 (s, 15H, C<sub>5</sub>Me<sub>5</sub>), 2.29, 3.58 (s, 3H, OCNMe<sub>2</sub>), 3.16 (s, 12H, TiNMe<sub>2</sub>); <sup>13</sup>C{<sup>1</sup>H} NMR (C<sub>6</sub>D<sub>6</sub>, 20 °C, δ): 11.3 (C<sub>5</sub>Me<sub>5</sub>), 30.1, 45.0 (OCNMe<sub>2</sub>), 30.8 (CNCMe<sub>3</sub>), 47.8 (TiNMe<sub>2</sub>), 55.6 (CNCMe<sub>3</sub>), 121.1 (C<sub>5</sub>Me<sub>5</sub>), 168.9 (CNCMe<sub>3</sub>), 218.0, 221.0 [Mo(CO)<sub>3</sub>], 248.7 (OCNMe<sub>2</sub>).

**Acknowledgment.** Financial support from the DGI-CYT (PB90-0294), the Comunidad Autónoma de Madrid (CAM C198/91), and the Universidad de Alcalá de Henares is gratefully acknowledged.

**Supplementary Material Available:** Tables of crystal data, atomic coordinates, equivalent displacement parameters, and bond lengths and angles for **3** (7 pages). Ordering information is given on any current masthead page.

OM9404588

# Reactions of $(\text{PMe}_3)_4\text{Ru}(\text{C}_2\text{H}_4)$ and $(\text{DMPE})_2\text{Ru}(\text{C}_2\text{H}_4)$ with Weak Proton-Donating Electrophiles $\text{HX}$ ( $\text{X} = \text{OAr}, \text{SAr}, \text{NHPH}, \text{PPh}$ ). Synthesis of Complexes with Metal-Heteroatom Single Bonds

Melinda J. Burn,<sup>†</sup> Michael G. Fickes,<sup>‡</sup> Frederick J. Hollander, and Robert G. Bergman\*

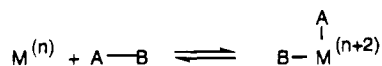
Department of Chemistry, University of California, Berkeley, California 94720

Received June 21, 1994<sup>Ⓞ</sup>

Reactions of the ruthenium ethylene complexes  $(\text{PMe}_3)_4\text{Ru}(\text{C}_2\text{H}_4)$  and  $(\text{DMPE})_2\text{Ru}(\text{C}_2\text{H}_4)$  with a variety of  $\text{HX}$  compounds ( $\text{X} = \text{SAr}, \text{OAr}, \text{PPhH}, \text{NHPH}$  and  $\text{Ph}$ ) have been explored. In all cases, the tetrakis(trimethylphosphine) complex reacted to form ethylene and the hydrido species,  $(\text{PMe}_3)_4\text{Ru}(\text{H})(\text{X})$ . However, parallel studies with the related material  $(\text{DMPE})_2\text{Ru}(\text{C}_2\text{H}_4)$  suggest that these complexes react as strained metallacycles toward  $\text{HX}$ . Thus, the bis(DMPE) analog gave the ethyl species  $(\text{DMPE})_2\text{Ru}(\text{X})(\text{CH}_2\text{CH}_3)$  in its reactions with  $\text{HSAr}$  and  $\text{PH}_2\text{Ph}$ , and thermolysis of these ethyl complexes led to the formation of the hydrides and free ethylene. The reaction of the DMPE ethylene complex with *p*-cresol allowed isolation of an intermediate cationic ethylene hydride species, but this was converted rapidly to the corresponding aryloxy hydride complex, even at room temperature. With  $\text{NH}_2\text{Ph}$  the bis(DMPE) complex formed only the corresponding hydride species. In an attempt to generate an acetylene complex that similarly might react as a strained metallacyclopropene,  $(\text{PMe}_3)_4\text{Ru}(\text{CH}=\text{CH}_2)_2$  was generated from the reaction of  $\text{CH}=\text{CH}_2\text{MgBr}$  with  $(\text{PMe}_3)_4\text{RuCl}_2$ . However, thermolysis of the divinyl species led only to the formation of the butadiene complex,  $(\text{PMe}_3)_3\text{Ru}(\text{C}_4\text{H}_6)$ .

## Introduction

Oxidative addition and reductive elimination reactions are critical processes in the catalytic and stoichiometric applications of transition-metal reagents in organic synthesis.<sup>1</sup> Two-electron oxidative addition reactions can be described as shown:



The addition of C-H bonds across a metal center has been well studied, but much less is known about the addition of X-H bonds, where X is a heteroatom (O, S, N, P). Recent syntheses of late transition metal-heteroatom compounds have resulted in the formation of new metal alkoxides, arylamides, thiolates and phosphides, formed primarily by the metathesis reaction of a metal halide and an alkali alkoxide, amide, thiolate or phosphide, rather than by an oxidative addition reaction. Recent examples include  $\text{Cp}^*\text{Ir}(\text{PPh}_3)(\text{Y})(\text{H})$  where  $\text{Y} = \text{OEt}^2$  and  $\text{NHPH}$ ,<sup>3</sup> *trans*- $(\text{PR}_3)_2\text{Pt}(\text{H})(\text{YAr})$

where  $\text{Y} = \text{O}$  and  $\text{NH}$ ,<sup>4,5</sup>  $[(\text{PMe}_3)_4\text{Ir}(\text{H})(\text{Y})]\text{PF}_6$  where  $\text{Y} = \text{OMe}$  and  $\text{SH}$ ,<sup>6</sup>  $(\text{PMe}_3)_4\text{Ru}(\text{YPh})(\text{H})$  where  $\text{Y} = \text{O}$  and  $\text{NH}$ ,<sup>7</sup> and  $\text{Os}(\text{PPhCl})(\text{CO})_2(\text{PPh}_3)_2$ .<sup>8</sup>

We have discovered a versatile route into metal-heteroatom compounds using ruthenium ethylene complexes. In this study, we have found that  $(\text{PMe}_3)_4\text{Ru}(\text{C}_2\text{H}_4)$  (**1**) is a useful precursor to a variety of complexes containing metal-heteroatom bonds. Complex **1** is conveniently prepared by treatment of  $(\text{PMe}_3)_4\text{RuCl}_2$  (**2**) with two equivalents of  $\text{EtMgCl}$ .<sup>9</sup> As shown previously,  $(\text{PMe}_3)_4\text{Ru}(\text{C}_2\text{H}_4)$  (**1**) reacts with *p*-cresol and aniline.<sup>7</sup> The reaction of **1** and *p*-cresol occurred at room temperature to form the cresolate hydride,  $(\text{PMe}_3)_4\text{Ru}(\text{H})(\text{OC}_6\text{H}_4\text{-}p\text{-CH}_3)$  (**3**, Scheme 1). Neither phosphine dissociation nor ethylene dissociation occurs in **1** at an appreciable rate at room temperature.<sup>10</sup> Although with late transition metals like Ru such species are often regarded as alkene complexes, the Ru-ethylene moiety reacts (at least in an overall sense) as a strained metallacyclopropane. It was proposed that the *p*-cresol reaction proceeded by initial protonation of the electron-rich ruthenium center, followed by olefin insertion into the metal-hydride bond and reaction with aryloxy to form the unobserved ruthenium ethyl cresolate,  $(\text{PMe}_3)_4\text{Ru}(\text{Et})(\text{OC}_6\text{H}_4\text{-}p\text{-CH}_3)$ .<sup>7</sup> Ionization of the aryloxy to

<sup>†</sup> Present address: Central Research and Development Dept., Experimental Station, E. I. duPont de Nemours and Co., Wilmington, DE 19880-0328.

<sup>‡</sup> Present address: Department of Chemistry, Massachusetts Institute of Technology, Cambridge, MA 02139.

<sup>Ⓞ</sup> Abstract published in *Advance ACS Abstracts*, November 1, 1994.

(1) Collman, J. P.; Hegedus, L. S.; Norton, J. R.; Finke, R. G. *Principles and Applications of Organotransition Metal Chemistry*; University Science Books: Mill Valley, CA, 1987.

(2) Newman, L. J.; Bergman, R. G. *J. Am. Chem. Soc.* **1985**, *107*, 5314.

(3) Glueck, D. S.; Winslow, L. N.; Bergman, R. G. *Organometallics* **1991**, *10*, 1462.

(4) Fornies, T.; Green, M.; Spencer, J. L.; Stone, F. G. A. *J. Chem. Soc., Dalton Trans.* **1977**, 1006.

(5) Cowan, R. L.; Trogler, W. C. *J. Am. Chem. Soc.* **1989**, *111*, 475.

(6) Milstein, D.; Calabrese, J. C.; Williams, I. D. *J. Am. Chem. Soc.* **1986**, *108*(20), 6387.

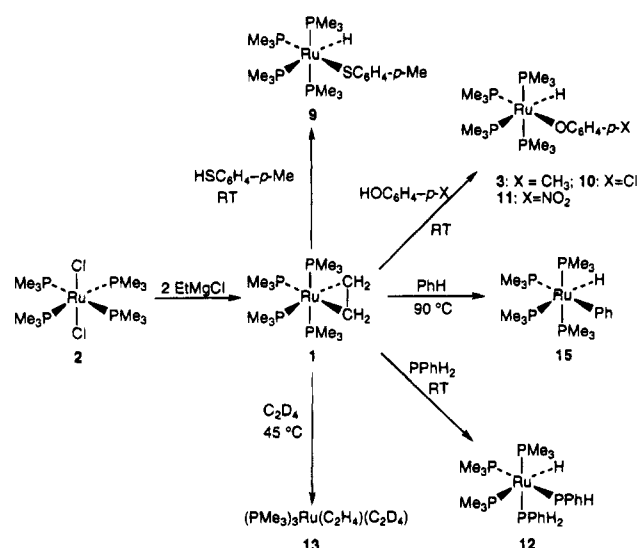
(7) Hartwig, J. F.; Andersen, R. A.; Bergman, R. G. *Organometallics* **1991**, *10*, 1875.

(8) Bohle, D. S.; Jones, T. C.; Rickard, C. E. F.; Roper, W. R. *J. Chem. Soc., Chem. Commun.* **1984**, 865.

(9) Wong, W.-K.; Chiu, K. W.; Statler, J. A.; Wilkinson, G.; Motavelli, M.; Hursthouse, M. B. *Polyhedron* **1984**, *3*, 1255.

(10) Hartwig, J. F. *Ph. D. Thesis* **1991**, University of California, Berkeley.

Scheme 1



form an ion pair,  $[(\text{PMe}_3)_4\text{Ru}(\text{Et})]^+[\text{OAr}]^-$ , to facilitate  $\beta$ -hydride elimination, followed by loss of ethylene and ion pair collapse would form the observed product **3**. The reaction of the complex **1** with aniline required heating to form the analogous product,  $(\text{PMe}_3)_4\text{Ru}(\text{NPh})(\text{H})$  (**4**).<sup>7</sup>

Studies of the reactivity of the related  $(\text{DMPE})_2\text{Ru}$  system began in 1965<sup>11</sup> when the dihydride complex,  $(\text{DMPE})_2\text{RuH}_2$  (**5**), was first reported.<sup>12</sup>  $(\text{DMPE})_2\text{RuH}_2$  has received recent attention as a source of the coordinately unsaturated species,  $(\text{DMPE})_2\text{Ru}$ .<sup>13,14</sup> The 16-electron species has been generated by photo-induced loss of  $\text{H}_2$  from  $(\text{DMPE})_2\text{RuH}_2$ .<sup>13,15</sup> The ethylene complex,  $(\text{DMPE})_2\text{Ru}(\text{C}_2\text{H}_4)$  (**6**), was briefly mentioned in the literature but no preparative details were given.<sup>13,16</sup> Complex **6** offers a potential route to ruthenium-heteroatom complexes with a bidentate ligand system.

In this paper we report further investigations of the reactions of ruthenium ethylene complexes,  $(\text{PMe}_3)_4\text{Ru}(\text{C}_2\text{H}_4)$  (**1**) and  $(\text{DMPE})_2\text{Ru}(\text{C}_2\text{H}_4)$  (**6**), with a variety of  $\text{HX}$  compounds, where  $\text{X} = \text{SAr}$ ,  $\text{OAr}$ ,  $\text{NHAr}$ , and  $\text{PPhH}$ . We have observed that, in the tetrakis(trimethylphosphine) system, the hydrido products  $(\text{PMe}_3)_4\text{Ru}(\text{H})(\text{X})$  are formed. In contrast, in the bis(DMPE) system the ethyl products  $(\text{DMPE})_2\text{Ru}(\text{Et})(\text{X})$  and an ethylene hydride cationic intermediate  $(\text{DMPE})_2\text{Ru}(\text{C}_2\text{H}_4)\text{H}^+\text{X}^-$  were isolated. Thermolysis of the ethyl and ethylene hydride complexes led to the formation of the hydrido analogues,  $(\text{DMPE})_2\text{Ru}(\text{H})(\text{X})$ .

In an attempt to generate a strained metallacyclopentene, dichloride **2** was treated with vinyl Grignard reagent to form the divinyl species,  $(\text{PMe}_3)_4\text{Ru}(\text{CH}=\text{CH}_2)_2$  (**7**). However,  $\beta$ -hydrogen elimination to form a metallacycle did not occur. Thermolysis of complex **7** led to the formation of a butadiene complex,  $(\text{PMe}_3)_3\text{Ru}(\eta^4\text{-C}_4\text{H}_6)$  (**8**).

## Results

### Synthesis of Trimethylphosphine Complexes.

The electron donating, monodentate trimethylphosphine ligand facilitated the addition of a variety of  $\text{HX}$  complexes to  $(\text{PMe}_3)_4\text{Ru}(\text{C}_2\text{H}_4)$  (**1**) to form  $(\text{PMe}_3)_4\text{Ru}(\text{H})(\text{X})$  complexes. Reaction of  $(\text{PMe}_3)_4\text{Ru}(\text{C}_2\text{H}_4)$  (**1**)<sup>9</sup> with one equivalent of *p*-thiocresol in a pentane solution at ambient temperature resulted in the formation of the *p*-thiocresolate hydride complex, *cis*- $(\text{PMe}_3)_4\text{Ru}(\text{H})(\text{SC}_6\text{H}_4\text{CH}_3)$  (**9**) in 49% yield as shown in Scheme 1. The reaction occurred rapidly and the yellow product immediately precipitated out of the pentane solution. The presence of the hydride ligand is confirmed by a doublet of doublets of triplets in the  $^1\text{H}$  NMR spectrum at  $\delta -8.95$  ( $J(\text{triplet}) = 28.1$  Hz,  $J(\text{doublet}) = 28.1$  Hz and 85.1 Hz), the result of coupling to the three types of phosphine ligands. The  $\text{A}_2\text{MX}$  pattern in the  $^{31}\text{P}\{^1\text{H}\}$  NMR spectrum confirms the *cis* geometry of complex **9**. The phosphine,  $\text{P}_\text{X}$ , trans to the strongest trans-influence ligand, the hydride, resonates furthest upfield.

In an analogous manner aryloxy complexes *cis*- $(\text{PMe}_3)_4\text{Ru}(\text{H})(\text{OC}_6\text{H}_4\text{-}p\text{-Y})$  ( $\text{Y} = \text{Cl}$  (**10**),  $\text{NO}_2$  (**11**)) were prepared by treatment of  $(\text{PMe}_3)_4\text{Ru}(\text{C}_2\text{H}_4)$  (**1**) with the corresponding para-substituted phenol at room temperature in pentane in 45% and 78% isolated yield, respectively. Both complexes display an  $\text{A}_2\text{MX}$ -type splitting pattern in the  $^{31}\text{P}\{^1\text{H}\}$  NMR spectrum and diagnostic hydride resonances in the  $^1\text{H}$  NMR spectrum at  $\delta -7.8$  for **10** and  $\delta -8.1$  for **11**.

Unlike the weakly acidic  $\text{HXAr}$  complexes, phenyl phosphine reacted with ethylene complex **1** to form *fac*- $(\text{PMe}_3)_3(\text{PPhH}_2)\text{Ru}(\text{H})(\text{PPhH})$  (**12**) (50% yield), the result of the addition of the P-H bond to the ruthenium center and the exchange of one  $\sigma$ -bound trimethylphosphine for a  $\sigma$ -bound phenylphosphine. The reaction was accompanied by a color change from pale yellow to deep yellow. The  $^{31}\text{P}\{^1\text{H}\}$  NMR spectrum shows a pattern indicating that all of the phosphine groups are magnetically and chemically inequivalent. The phosphide ligand appears furthest upfield as a broad multiplet at  $\delta -47.3$ . The presence of a hydride is confirmed in the  $^1\text{H}$  NMR spectrum by a multiplet at  $\delta -9.42$ .

In an attempt to investigate ligand lability in ethylene complex **1**, a benzene solution of  $(\text{PMe}_3)_4\text{Ru}(\text{C}_2\text{H}_4)$  (**1**) was heated in the presence of 1 equivalent of  $\text{C}_2\text{D}_4$  at 45 °C. After 6 h  $(\text{PMe}_3)_3\text{Ru}(\text{C}_2\text{H}_4)(\text{C}_2\text{D}_4)$  (**13**) and free  $\text{PMe}_3$  were formed. Identification of **13** is based on comparison to the known complex  $(\text{PMe}_3)_3\text{Ru}(\text{C}_2\text{H}_4)_2$  (**14**).<sup>17</sup> An  $\text{A}_2\text{B}$  pattern in the  $^{31}\text{P}\{^1\text{H}\}$  NMR spectrum indicates three  $\sigma$ -bound phosphine groups on the ruthenium center and the  $^1\text{H}$  NMR spectrum confirms the presence of bound ethylene groups. Free ethylene was not observed. As alluded to previously, thermolysis of a benzene solution of ethylene complex **1** at 90 °C resulted in the initial formation of a mixture of *cis*- $(\text{PMe}_3)_4\text{Ru}(\text{Ph})(\text{H})$  (**15**) and  $(\text{PMe}_3)_3\text{Ru}(\text{C}_2\text{H}_4)_2$  (**14**), which was transformed to pure **15** after 12 h.<sup>7</sup> Identification of phenyl hydride **15** was based on a comparison of its

(11) Chatt, J.; Davidson, J. M. *J. Chem. Soc.* **1965**, 843.

(12) The dihydride was more thoroughly characterized in: Ittel, S. D.; Tolman, C. A.; English, A. D.; Jesson, J. P. *J. Am. Chem. Soc.* **1976**, *98*, 6073.

(13) Bergamini, P.; Sostero, S.; Traverso, O. *J. Organomet. Chem.* **1986**, *299*, C11.

(14) Jones, W. D.; Kosar, W. P. *J. Am. Chem. Soc.* **1986**, *108*, 5640.

(15) Hall, C.; Jones, W. D.; Mawby, R. J.; Osman, R.; Perutz, R. N.; Whittlesey, M. K. *J. Am. Chem. Soc.* **1992**, *114*, 7425.

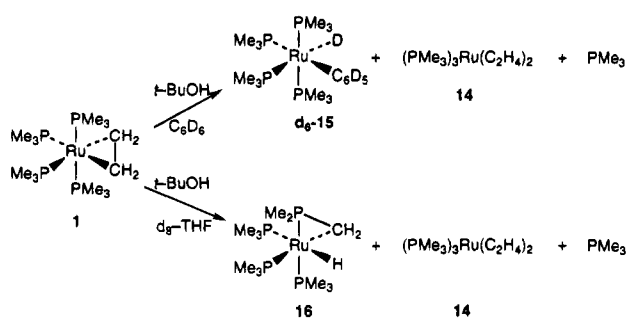
(16) Tolman, C. A.; Ittel, S. D.; English, A. D.; Jesson, J. P. *J. Am. Chem. Soc.* **1978**, *100*, 4080.

(17) Hartwig, J. F.; Bergman, R. G.; Andersen, R. A. *J. Am. Chem. Soc.* **1991**, *113*, 3404. We did not determine whether the compound isolated in this reaction is one pure isotopomer or whether it is a statistical mixture of 50% **13** and 25% each of the corresponding bis-ethylene and bis-tetra-deuterioethylene complexes.

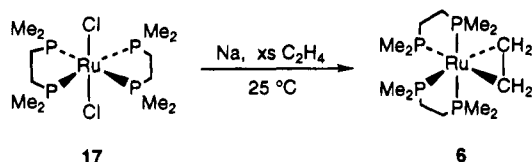
(18) Werner, H.; Werner, R. *J. Organomet. Chem.* **1981**, *209*, C60.

(19) Chatt, J.; Hayter, R. G. *J. Chem. Soc.* **1961**, 896.

Scheme 2



Scheme 3



NMR spectral data to literature data for *cis*-(PMe<sub>3</sub>)<sub>4</sub>-Ru(Ph)(H).<sup>17</sup>

Attempts to obtain a simple addition product of *t*-butyl alcohol to **1** were not successful. Instead, formation of *cis*-(PMe<sub>3</sub>)<sub>4</sub>Ru(C<sub>6</sub>D<sub>5</sub>)(D) (**d<sub>6</sub>-15**), (PMe<sub>3</sub>)<sub>3</sub>Ru(C<sub>2</sub>H<sub>4</sub>)<sub>2</sub> (**14**)<sup>17</sup> and free PMe<sub>3</sub> was observed when a  $d_6$ -benzene solution of ethylene complex **1** and *t*-BuOH was heated to 80 °C led to (Scheme 2). No reaction occurred at room temperature. When the same reactants were heated in  $d_8$ -THF, the products formed were the cyclometalated hydride (PMe<sub>3</sub>)<sub>3</sub>Ru(H)(Me<sub>2</sub>PCH<sub>2</sub>) (**16**),<sup>18</sup> the bis-ethylene complex **14**, and free PMe<sub>3</sub>.

**Synthesis of DMPE Complexes.** In order to study the effect of the phosphine ligands on the reactivity of ruthenium ethylene complexes, a room temperature synthesis of (DMPE)<sub>2</sub>Ru(C<sub>2</sub>H<sub>4</sub>) (**6**) was developed. The reaction of *trans*-(DMPE)<sub>2</sub>RuCl<sub>2</sub> (**17**),<sup>19</sup> excess ethylene and sodium in THF afforded complex **6** in 90% isolated yield (Scheme 3). Complex **6** has been reported previously<sup>13,16</sup> although no preparative data were given. Ethylene complex **6** exhibits an AA'XX' splitting pattern in the <sup>31</sup>P{<sup>1</sup>H} NMR spectrum but due to similar coupling constants, two pseudo triplets are observed at  $\delta$  43.9 and 37.2.

In contrast to the tetrakis(trimethylphosphine) ruthenium ethylene complex **1**, bis(DMPE)ethylene com-

Table 2. Selected Intramolecular Distances (Å) for *cis*-(DMPE)<sub>2</sub>Ru(CH<sub>2</sub>CH<sub>3</sub>)(SC<sub>6</sub>H<sub>4</sub>-*p*-CH<sub>3</sub>) (**18**)

Ru–S	2.522(3)	P <sub>1</sub> –C <sub>10</sub>	1.869(13)
Ru–P <sub>1</sub>	2.346(3)	P <sub>1</sub> –C <sub>11</sub>	1.847(13)
Ru–P <sub>2</sub>	2.342(3)	P <sub>1</sub> –C <sub>12</sub>	1.874(13)
Ru–P <sub>3</sub>	2.270(3)	P <sub>2</sub> –C <sub>13</sub>	1.848(14)
Ru–P <sub>4</sub>	2.302(3)	P <sub>2</sub> –C <sub>14</sub>	1.829(12)
Ru–C <sub>1</sub>	2.230(10)	P <sub>2</sub> –C <sub>15</sub>	1.820(13)
C <sub>1</sub> –C <sub>2</sub>	1.548(16)	C <sub>12</sub> –C <sub>13</sub>	1.561(17)
S–C <sub>3</sub>	1.791(11)	P <sub>3</sub> –C <sub>16</sub>	1.834(12)
C <sub>3</sub> –C <sub>4</sub>	1.398(15)	P <sub>3</sub> –C <sub>17</sub>	1.852(13)
C <sub>3</sub> –C <sub>8</sub>	1.402(15)	P <sub>3</sub> –C <sub>18</sub>	1.859(11)
C <sub>4</sub> –C <sub>5</sub>	1.435(15)	P <sub>4</sub> –C <sub>19</sub>	1.843(12)
C <sub>5</sub> –C <sub>6</sub>	1.404(15)	P <sub>4</sub> –C <sub>20</sub>	1.838(13)
C <sub>6</sub> –C <sub>7</sub>	1.410(15)	P <sub>4</sub> –C <sub>21</sub>	1.821(12)
C <sub>7</sub> –C <sub>8</sub>	1.395(15)	C <sub>18</sub> –C <sub>19</sub>	1.561(16)
C <sub>6</sub> –C <sub>9</sub>	1.523(16)		

plex **6** reacted with HSC<sub>6</sub>H<sub>4</sub>-*p*-Me in benzene at room temperature (Scheme 4) to afford *cis*-(DMPE)<sub>2</sub>Ru(SC<sub>6</sub>H<sub>4</sub>-*p*-Me)(CH<sub>2</sub>CH<sub>3</sub>) (**18**) in 75% yield. The <sup>31</sup>P{<sup>1</sup>H} NMR spectrum of **18** exhibits a six line pattern of multiplets due to the unsymmetrical *cis* orientation of the phosphorus ligands. Thermolysis of a benzene solution of ethyl thiocresolate **18** at 85 °C for 14 h resulted in the formation of *trans*-(DMPE)<sub>2</sub>Ru(SC<sub>6</sub>H<sub>4</sub>Me)(H) (**19**) (48% yield). The <sup>31</sup>P{<sup>1</sup>H} NMR spectrum shows the characteristic singlet for a *trans* complex, and the ruthenium hydride signal appears at  $\delta$  –18.01 in the <sup>1</sup>H NMR spectrum.

A suitable crystal of the DMPE ethyl thiolate complex **18** was obtained by crystallization from a benzene/pentane (1:10) solution at –30 °C, and an X-ray diffraction study of its structure was carried out. Crystal and data collection parameters are provided in Table 1, intramolecular bond distances are tabulated in Table 2, and intramolecular angles are provided in Table 3. An ORTEP drawing of complex **18** is shown in Figure 1. The structure of **18** is approximately octahedral with a Ru–S bond length of 2.552(3) Å and a ruthenium ethyl (Ru–C<sub>1</sub>) bond length of 2.230(10) Å. The C–C bond length in the ethyl fragment is 1.548(16) Å. The aryl ring is twisted out of the Ru–C<sub>1</sub>–X plane with a torsion angle between S–Ru–C<sub>1</sub>–C<sub>2</sub> of 106.85(0.77)°.

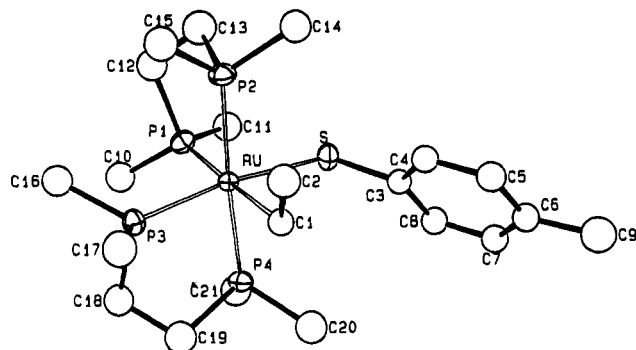
Addition of one equivalent of aniline to (DMPE)<sub>2</sub>Ru(C<sub>2</sub>H<sub>4</sub>) (**6**) followed by heating to 120 °C for eight days afforded *cis*-(DMPE)<sub>2</sub>Ru(NHPh)(H) (**20a**), small amounts of the *trans* isomer **20b** and *cis*-(DMPE)<sub>2</sub>RuH<sub>2</sub>. Complex **20a** was isolated in 45% yield by recrystallization

Table 1. Crystal Parameters<sup>a,b</sup> for Compounds **18**, **20a**, **21**, **23** and **24**

	C <sub>21</sub> H <sub>44</sub> P <sub>4</sub> RuS ( <b>18</b> )	C <sub>18</sub> H <sub>39</sub> NP <sub>4</sub> Ru ( <b>20a</b> )	C <sub>20</sub> H <sub>43</sub> P <sub>5</sub> Ru ( <b>21</b> )	C <sub>19</sub> H <sub>40</sub> OP <sub>4</sub> Ru ( <b>23</b> )	C <sub>35</sub> H <sub>60</sub> O <sub>3</sub> P <sub>4</sub> Ru <sup>c</sup> ( <b>24</b> )
FW	553.6	494.5	539.5	509.5	753.8
cryst system	orthorhombic	monoclinic	monoclinic	monoclinic	monoclinic
space group	P2 <sub>1</sub> 2 <sub>1</sub> 2 <sub>1</sub>	P2 <sub>1</sub> /n	C2/c	P2 <sub>1</sub> /n	P2 <sub>1</sub> /n
a, Å	9.3977(9)	9.496(2)	33.628(7)	12.6944(19)	12.528(8)
b, Å	15.2531(20)	16.714(3)	9.1956(13)	10.5119(16)	18.202(5)
c, Å	18.6320(20)	15.191(5)	18.440(3)	19.456(3)	16.592(5)
α, deg	90.0	90.0	90.0	90.0	90.0
β, deg	90.0	99.07(2)	114.910(16)	107.377(13)	98.27(4)
γ, deg	90.0	90.0	90.0	90.0	90.0
V, Å <sup>3</sup>	2670.8(8)	2380.9(18)	5172.3(33)	2477.6(14)	3744.4(49)
Z	4	4	8	4	4
size, mm	0.28 × 0.28 × 0.33	0.12 × 0.28 × 0.35	0.25 × 0.50 × 0.50	0.20 × 0.27 × 0.32	0.22 × 0.26 × 0.38
color	yellow	brown	yellow	pale yellow	colorless
d(calc), g cm <sup>–3</sup>	1.38	1.38	1.39	1.37	1.34
μ(calc), cm <sup>–1</sup>	8.9	9.1	9.0	8.8	5.8
2θ between	24° and 28°	24° and 26°	24° and 32°	24° and 34°	26° and 32°

<sup>a</sup> Unit cell parameters and their esd's were derived by a least-squares fit to the setting angles of the unresolved Mo Kα components of 24 reflections with 2θ between the angles listed in the last row of the Table. <sup>b</sup> In this and all subsequent tables the esd's of all parameters are given in parentheses, right-justified to the least significant digit(s) of the reported value. <sup>c</sup> Formula, density and absorption coefficient are all calculated for the pure compound as hydride. The particular crystal studied apparently had 15% chloride impurity.





**Figure 1.** ORTEP diagram of *cis*-(DMPE)<sub>2</sub>Ru(CH<sub>2</sub>CH<sub>3</sub>)-(SC<sub>6</sub>H<sub>4</sub>-*p*-Me) (**18**).

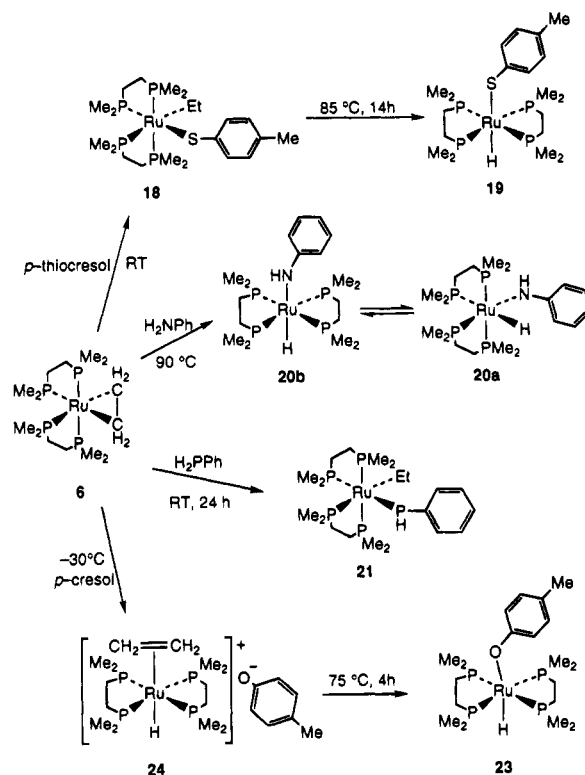
**Table 3.** Selected Intramolecular Angles (deg) for *cis*-(DMPE)<sub>2</sub>Ru(CH<sub>2</sub>CH<sub>3</sub>)(SC<sub>6</sub>H<sub>4</sub>-*p*-CH<sub>3</sub>) (**18**)

S-Ru-P <sub>1</sub>	85.68(10)	Ru-P <sub>1</sub> -C <sub>11</sub>	120.9(4)
S-Ru-P <sub>2</sub>	89.90(10)	Ru-P <sub>1</sub> -C <sub>12</sub>	108.3(4)
S-Ru-P <sub>3</sub>	170.16(10)	C <sub>10</sub> -P <sub>1</sub> -C <sub>11</sub>	98.9(6)
S-Ru-P <sub>4</sub>	86.17(9)	C <sub>10</sub> -P <sub>1</sub> -C <sub>12</sub>	100.7(6)
S-Ru-C <sub>1</sub>	92.3(3)	C <sub>11</sub> -P <sub>1</sub> -C <sub>12</sub>	100.9(6)
P <sub>1</sub> -Ru-P <sub>2</sub>	83.51(11)	Ru-P <sub>2</sub> -C <sub>13</sub>	109.2(5)
P <sub>1</sub> -Ru-P <sub>3</sub>	93.47(11)	Ru-P <sub>2</sub> -C <sub>14</sub>	121.9(4)
P <sub>1</sub> -Ru-P <sub>4</sub>	96.23(10)	Ru-P <sub>2</sub> -C <sub>15</sub>	122.3(4)
P <sub>1</sub> -Ru-C <sub>1</sub>	177.8(3)	C <sub>13</sub> -P <sub>2</sub> -C <sub>14</sub>	98.2(6)
P <sub>2</sub> -Ru-P <sub>3</sub>	99.75(10)	C <sub>13</sub> -P <sub>2</sub> -C <sub>15</sub>	100.8(6)
P <sub>2</sub> -Ru-P <sub>4</sub>	176.08(11)	C <sub>14</sub> -P <sub>2</sub> -C <sub>15</sub>	100.2(6)
P <sub>2</sub> -Ru-C <sub>1</sub>	95.8(3)	P <sub>1</sub> -C <sub>12</sub> -C <sub>13</sub>	107.2(9)
P <sub>3</sub> -Ru-P <sub>4</sub>	84.18(10)	P <sub>2</sub> -C <sub>13</sub> -C <sub>12</sub>	108.8(9)
P <sub>3</sub> -Ru-C <sub>1</sub>	88.7(3)	Ru-P <sub>3</sub> -C <sub>16</sub>	123.7(4)
P <sub>4</sub> -Ru-C <sub>1</sub>	84.3(3)	Ru-P <sub>3</sub> -C <sub>17</sub>	121.1(4)
Ru-C <sub>1</sub> -C <sub>2</sub>	120.1(7)	Ru-P <sub>3</sub> -C <sub>18</sub>	109.7(4)
Ru-S-C <sub>3</sub>	116.6(4)	C <sub>16</sub> -P <sub>3</sub> -C <sub>17</sub>	97.1(6)
S-C <sub>3</sub> -C <sub>4</sub>	122.4(8)	C <sub>16</sub> -P <sub>3</sub> -C <sub>18</sub>	101.2(5)
S-C <sub>3</sub> -C <sub>8</sub>	117.8(8)	C <sub>17</sub> -P <sub>3</sub> -C <sub>18</sub>	100.1(5)
C <sub>4</sub> -C <sub>3</sub> -C <sub>8</sub>	119.7(10)	Ru-P <sub>4</sub> -C <sub>19</sub>	110.4(4)
C <sub>3</sub> -C <sub>4</sub> -C <sub>5</sub>	119.4(10)	Ru-P <sub>4</sub> -C <sub>20</sub>	118.5(4)
C <sub>4</sub> -C <sub>5</sub> -C <sub>6</sub>	120.7(10)	Ru-P <sub>4</sub> -C <sub>21</sub>	121.0(4)
C <sub>5</sub> -C <sub>6</sub> -C <sub>7</sub>	118.4(10)	C <sub>19</sub> -P <sub>4</sub> -C <sub>20</sub>	98.9(6)
C <sub>5</sub> -C <sub>6</sub> -C <sub>9</sub>	120.2(11)	C <sub>19</sub> -P <sub>4</sub> -C <sub>21</sub>	103.1(6)
C <sub>7</sub> -C <sub>6</sub> -C <sub>9</sub>	121.3(10)	C <sub>20</sub> -P <sub>4</sub> -C <sub>21</sub>	101.7(6)
C <sub>6</sub> -C <sub>7</sub> -C <sub>8</sub>	121.0(11)	P <sub>3</sub> -C <sub>18</sub> -C <sub>19</sub>	108.9(8)
C <sub>3</sub> -C <sub>8</sub> -C <sub>7</sub>	120.8(11)	P <sub>4</sub> -C <sub>19</sub> -C <sub>18</sub>	108.0(8)
Ru-P <sub>1</sub> -C <sub>10</sub>	123.3(4)		

from a benzene/pentane (1/10) mixture. The *cis* configuration was determined by the ABMX pattern in the <sup>31</sup>P{<sup>1</sup>H} NMR spectrum. The hydride appears as a pseudo doublet of quartets at δ -7.26 in the <sup>1</sup>H NMR spectrum. Heating a solution of (DMPE)<sub>2</sub>Ru(C<sub>2</sub>H<sub>4</sub>) and one equivalent of aniline at lower temperature (90 °C) for 5.5 days allowed selective formation of *trans*-(DMPE)<sub>2</sub>Ru(NPhH)(H) (**20b**) in 15% yield (Scheme 4). Under these milder conditions complex **6** was not fully converted to **20b** but the 2:1 mixture of ethylene complex **6** and **20b** was easily separated by recrystallization. Complex **20b** exhibits a singlet in the <sup>31</sup>P{<sup>1</sup>H} NMR spectrum at δ 44.5. The hydride appears as a quintet at δ -19.13 in the <sup>1</sup>H NMR spectrum.

An X-ray quality crystal of the DMPE anilido hydride **20a** was obtained from a concentrated toluene solution, and its structure was solved by Patterson methods. Crystal and data parameters are provided in Table 1, intramolecular bond distances are tabulated in Table 4 and intramolecular angles are provided in Table 5. An ORTEP drawing of complex **20a** is shown in Figure 2. The structure is approximately octahedral, with a Ru-N bond length of 2.168(9) Å and a Ru-N-C13 bond angle of 132.8(7)°. The hydride was not located.

**Scheme 4**



**Table 4.** Selected Intramolecular Distances (Å) for *cis*-(DMPE)<sub>2</sub>Ru(H)(NPh) (**20a**)

Ru-P <sub>1</sub>	2.298(3)	P <sub>3</sub> -P <sub>8</sub>	1.860(13)
Ru-P <sub>2</sub>	2.335(3)	P <sub>3</sub> -P <sub>9</sub>	1.868(13)
Ru-P <sub>3</sub>	2.244(3)	P <sub>4</sub> -P <sub>10</sub>	1.840(13)
Ru-P <sub>4</sub>	2.274(3)	P <sub>4</sub> -C <sub>11</sub>	1.850(14)
Ru-N	2.168(9)	P <sub>4</sub> -C <sub>12</sub>	1.831(13)
P <sub>1</sub> -C <sub>1</sub>	1.861(13)	C <sub>9</sub> -C <sub>10</sub>	1.537(16)
P <sub>1</sub> -C <sub>2</sub>	1.827(15)	N-C <sub>13</sub>	1.345(13)
P <sub>1</sub> -C <sub>3</sub>	1.848(13)	C <sub>13</sub> -C <sub>14</sub>	1.419(15)
P <sub>2</sub> -C <sub>4</sub>	1.872(13)	C <sub>13</sub> -C <sub>18</sub>	1.429(15)
P <sub>2</sub> -C <sub>5</sub>	1.833(13)	C <sub>14</sub> -C <sub>15</sub>	1.394(16)
P <sub>2</sub> -C <sub>6</sub>	1.835(13)	C <sub>15</sub> -C <sub>16</sub>	1.400(16)
C <sub>3</sub> -C <sub>4</sub>	1.542(18)	C <sub>16</sub> -C <sub>17</sub>	1.418(15)
P <sub>3</sub> -C <sub>7</sub>	1.844(12)	C <sub>17</sub> -C <sub>18</sub>	1.393(15)

In a manner similar to that used in the reaction with *p*-thiocresol, treatment of (DMPE)<sub>2</sub>Ru(C<sub>2</sub>H<sub>4</sub>) (**6**) with PPhH<sub>2</sub> at room temperature led to the formation of (DMPE)<sub>2</sub>Ru(PPhH)(CH<sub>2</sub>CH<sub>3</sub>) (**21**) after 30 h. The <sup>31</sup>P{<sup>1</sup>H} NMR spectrum of this material shows eight complicated multiplets due to the unsymmetrical *cis* orientation of the phosphorus ligands. The phosphide phosphorus atom resonates far upfield (δ -62.5) as a very broad multiplet. The signal due to the hydrogen atom attached to the phosphide ligand appears as a doublet at δ 2.82 (*J* = 198 Hz).

A crystal suitable for X-ray determination of the DMPE ethyl phosphide **21** was obtained at -30 °C. Complex **21** crystallized in space group C2/c. An ORTEP drawing of compound **21** is shown in Figure 3. Crystal and data parameters are tabulated in Table 1; intramolecular bond distances and angles are shown in Tables 6 and 7, respectively. As in the case of the ethyl thiocresolate **18**, complex **21** is approximately octahedral. The metal phosphide (Ru-P5) bond length in **21** is 2.453(2) Å and the ruthenium ethyl (Ru-C1) distance is 2.225(7) Å. The C-C bond length in the ethyl fragment is 1.556(9) Å. Thermolysis of a THF solution of the ethyl phosphido complex **21** at 90 °C for six days

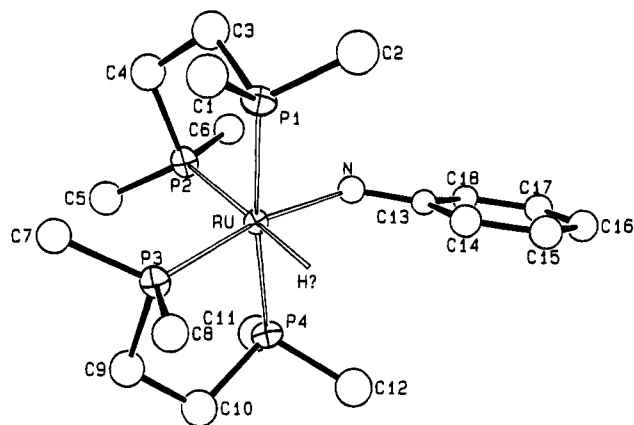


Figure 2. ORTEP diagram of *cis*-(DMPE)<sub>2</sub>Ru(H)(NHPh) (**20a**).

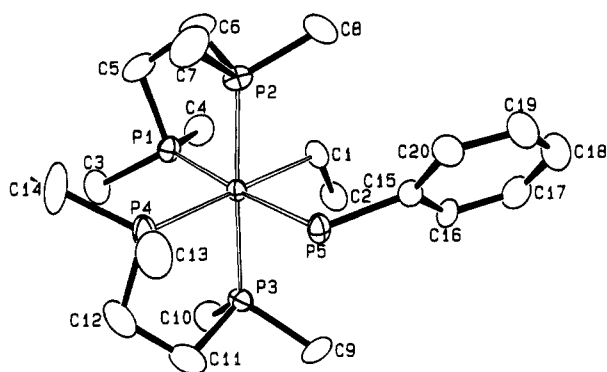


Figure 3. ORTEP diagram of *cis*-(DMPE)<sub>2</sub>Ru(CH<sub>2</sub>CH<sub>3</sub>)(PPhH) (**21**).

Table 5. Selected Intramolecular Angles (deg) for *cis*-(DMPE)<sub>2</sub>Ru(H)(NHPh) (**20a**)

P <sub>1</sub> -Ru-P <sub>2</sub>	84.56(11)	Ru-P <sub>3</sub> -C <sub>7</sub>	125.9(4)
P <sub>1</sub> -Ru-P <sub>3</sub>	99.45(12)	Ru-P <sub>3</sub> -C <sub>8</sub>	117.9(4)
P <sub>1</sub> -Ru-P <sub>4</sub>	173.76(12)	Ru-P <sub>3</sub> -C <sub>9</sub>	109.4(4)
P <sub>1</sub> -Ru-N	89.7(2)	C <sub>7</sub> -P <sub>3</sub> -C <sub>8</sub>	98.6(5)
P <sub>2</sub> -Ru-P <sub>3</sub>	96.35(11)	C <sub>7</sub> -P <sub>3</sub> -C <sub>9</sub>	99.9(6)
P <sub>2</sub> -Ru-P <sub>4</sub>	100.13(11)	C <sub>8</sub> -P <sub>3</sub> -C <sub>9</sub>	101.4(6)
P <sub>2</sub> -Ru-N	89.0(3)	Ru-P <sub>4</sub> -C <sub>10</sub>	111.6(4)
P <sub>3</sub> -Ru-P <sub>4</sub>	84.20(12)	Ru-P <sub>4</sub> -C <sub>11</sub>	119.4(4)
P <sub>3</sub> -Ru-N	169.8(2)	Ru-P <sub>4</sub> -C <sub>12</sub>	118.7(5)
P <sub>4</sub> -Ru-N	86.3(2)	C <sub>10</sub> -P <sub>4</sub> -C <sub>11</sub>	104.2(6)
Ru-P <sub>1</sub> -C <sub>1</sub>	121.7(4)	C <sub>10</sub> -P <sub>4</sub> -C <sub>12</sub>	101.4(6)
Ru-P <sub>1</sub> -C <sub>2</sub>	117.2(5)	C <sub>11</sub> -P <sub>4</sub> -C <sub>12</sub>	99.1(6)
Ru-P <sub>1</sub> -C <sub>3</sub>	109.9(4)	P <sub>3</sub> -C <sub>9</sub> -C <sub>10</sub>	108.8(9)
C <sub>1</sub> -P <sub>1</sub> -C <sub>2</sub>	100.4(6)	P <sub>4</sub> -C <sub>10</sub> -C <sub>9</sub>	109.4(9)
C <sub>1</sub> -P <sub>1</sub> -C <sub>3</sub>	102.4(6)	Ru-N-C <sub>13</sub>	132.8(7)
C <sub>2</sub> -P <sub>1</sub> -C <sub>3</sub>	102.8(7)	N-C <sub>13</sub> -C <sub>14</sub>	122.9(10)
Ru-P <sub>2</sub> -C <sub>4</sub>	107.5(4)	N-C <sub>13</sub> -C <sub>18</sub>	121.5(10)
Ru-P <sub>2</sub> -C <sub>5</sub>	125.0(4)	C <sub>14</sub> -C <sub>13</sub> -C <sub>18</sub>	115.6(10)
Ru-P <sub>2</sub> -C <sub>6</sub>	118.9(4)	C <sub>13</sub> -C <sub>14</sub> -C <sub>15</sub>	122.2(11)
C <sub>4</sub> -P <sub>2</sub> -C <sub>5</sub>	101.1(6)	C <sub>14</sub> -C <sub>15</sub> -C <sub>16</sub>	121.6(11)
C <sub>4</sub> -P <sub>2</sub> -C <sub>6</sub>	100.0(6)	C <sub>15</sub> -C <sub>16</sub> -C <sub>17</sub>	117.5(11)
C <sub>5</sub> -P <sub>2</sub> -C <sub>6</sub>	100.4(6)	C <sub>16</sub> -C <sub>17</sub> -C <sub>18</sub>	121.0(10)
P <sub>1</sub> -C <sub>3</sub> -C <sub>4</sub>	110.6(9)	C <sub>13</sub> -C <sub>18</sub> -C <sub>17</sub>	122.1(10)
P <sub>2</sub> -C <sub>4</sub> -C <sub>5</sub>	108.5(9)		

afforded an equilibrium mixture of two products, **22a** and **22b**, in a 2:1 ratio. Although we were not able to separate and fully characterize these materials, the NMR and IR data for this mixture are consistent with the formation of the *cis* and *trans* isomers of the corresponding hydrido phosphido complexes (DMPE)<sub>2</sub>Ru(PPhH)(H), respectively.

Unlike the reactions of HSAr, H<sub>2</sub>NPh, and H<sub>2</sub>PPh, *p*-cresol reacted with (DMPE)<sub>2</sub>Ru(C<sub>2</sub>H<sub>4</sub>) to form *trans*-(DMPE)<sub>2</sub>Ru(OC<sub>6</sub>H<sub>4</sub>-*p*-CH<sub>3</sub>)(H) (**23**) directly. Heating **6**

Table 6. Selected Intramolecular Distances (Å) for *cis*-(DMPE)<sub>2</sub>Ru(CH<sub>2</sub>CH<sub>3</sub>)(PPh) (**21**)

Ru-P <sub>1</sub>	2.312(2)	P <sub>3</sub> -C <sub>9</sub>	1.858(7)
Ru-P <sub>2</sub>	2.289(2)	P <sub>3</sub> -C <sub>10</sub>	1.839(8)
Ru-P <sub>3</sub>	2.337(2)	P <sub>3</sub> -C <sub>11</sub>	1.845(8)
Ru-P <sub>4</sub>	2.334(2)	C <sub>11</sub> -C <sub>12</sub>	1.584(12)
Ru-P <sub>5</sub>	2.453(2)	P <sub>4</sub> -C <sub>12</sub>	1.843(9)
Ru-C <sub>1</sub>	2.225(7)	P <sub>4</sub> -C <sub>13</sub>	1.869(8)
C <sub>1</sub> -C <sub>2</sub>	1.556(9)	P <sub>4</sub> -C <sub>14</sub>	1.864(8)
P <sub>1</sub> -C <sub>3</sub>	1.834(8)	P <sub>5</sub> -C <sub>15</sub>	1.835(7)
P <sub>1</sub> -C <sub>4</sub>	1.847(7)	C <sub>15</sub> -C <sub>16</sub>	1.402(9)
P <sub>1</sub> -C <sub>5</sub>	1.866(7)	C <sub>15</sub> -C <sub>20</sub>	1.399(9)
C <sub>5</sub> -C <sub>6</sub>	1.555(11)	C <sub>16</sub> -C <sub>17</sub>	1.408(10)
P <sub>2</sub> -C <sub>6</sub>	1.849(7)	C <sub>17</sub> -C <sub>18</sub>	1.378(11)
P <sub>2</sub> -C <sub>7</sub>	1.840(7)	C <sub>18</sub> -C <sub>19</sub>	1.416(12)
P <sub>2</sub> -C <sub>8</sub>	1.836(8)	C <sub>19</sub> -C <sub>20</sub>	1.399(11)

Table 7. Selected Intramolecular Angles (deg) for *cis*-(DMPE)<sub>2</sub>Ru(CH<sub>2</sub>CH<sub>3</sub>)(PPh) (**21**)

P <sub>5</sub> -Ru-P <sub>4</sub>	87.25(7)	Ru-P <sub>4</sub> -C <sub>13</sub>	120.2(3)
P <sub>5</sub> -Ru-P <sub>3</sub>	86.27(7)	Ru-P <sub>4</sub> -C <sub>12</sub>	109.0(3)
P <sub>5</sub> -Ru-P <sub>1</sub>	174.82(7)	C <sub>13</sub> -P <sub>4</sub> -C <sub>14</sub>	97.9(4)
P <sub>5</sub> -Ru-P <sub>2</sub>	90.28(6)	C <sub>14</sub> -P <sub>4</sub> -C <sub>12</sub>	100.3(4)
P <sub>5</sub> -Ru-C <sub>1</sub>	92.12(19)	C <sub>13</sub> -P <sub>4</sub> -C <sub>12</sub>	101.2(4)
P <sub>3</sub> -Ru-P <sub>4</sub>	83.71(7)	Ru-P <sub>3</sub> -C <sub>11</sub>	109.2(3)
P <sub>1</sub> -Ru-P <sub>4</sub>	93.64(7)	Ru-P <sub>3</sub> -C <sub>9</sub>	122.5(3)
P <sub>2</sub> -Ru-P <sub>4</sub>	96.51(7)	Ru-P <sub>3</sub> -C <sub>10</sub>	121.3(3)
P <sub>4</sub> -Ru-C <sub>1</sub>	179.36(19)	C <sub>9</sub> -P <sub>3</sub> -C <sub>11</sub>	99.0(4)
P <sub>1</sub> -Ru-P <sub>2</sub>	84.55(7)	C <sub>10</sub> -P <sub>3</sub> -C <sub>11</sub>	101.2(4)
P <sub>1</sub> -Ru-C <sub>1</sub>	86.99(19)	C <sub>9</sub> -P <sub>3</sub> -C <sub>10</sub>	99.8(4)
P <sub>1</sub> -Ru-P <sub>3</sub>	98.90(7)	P <sub>2</sub> -C <sub>12</sub> -C <sub>11</sub>	108.1(6)
P <sub>2</sub> -Ru-P <sub>3</sub>	176.53(7)	P <sub>3</sub> -C <sub>11</sub> -C <sub>12</sub>	108.1(5)
P <sub>3</sub> -Ru-C <sub>1</sub>	96.12(18)	Ru-P <sub>1</sub> -C <sub>3</sub>	125.2(3)
P <sub>2</sub> -Ru-C <sub>1</sub>	83.63(18)	Ru-P <sub>1</sub> -C <sub>4</sub>	122.0(3)
Ru-C <sub>1</sub> -C <sub>2</sub>	118.7(5)	Ru-P <sub>1</sub> -C <sub>5</sub>	107.8(2)
Ru-P <sub>5</sub> -C <sub>15</sub>	117.7(2)	C <sub>3</sub> -P <sub>1</sub> -C <sub>4</sub>	96.9(4)
P <sub>5</sub> -C <sub>15</sub> -C <sub>16</sub>	120.2(5)	C <sub>3</sub> -P <sub>1</sub> -C <sub>5</sub>	101.0(4)
P <sub>5</sub> -C <sub>15</sub> -C <sub>20</sub>	121.4(5)	C <sub>4</sub> -P <sub>1</sub> -C <sub>5</sub>	99.6(4)
C <sub>16</sub> -C <sub>15</sub> -C <sub>20</sub>	118.1(6)	Ru-P <sub>2</sub> -C <sub>6</sub>	109.1(2)
C <sub>15</sub> -C <sub>16</sub> -C <sub>17</sub>	120.5(7)	Ru-P <sub>2</sub> -C <sub>8</sub>	121.2(3)
C <sub>16</sub> -C <sub>17</sub> -C <sub>18</sub>	121.6(7)	Ru-P <sub>2</sub> -C <sub>7</sub>	121.3(3)
C <sub>17</sub> -C <sub>18</sub> -C <sub>19</sub>	118.2(7)	C <sub>6</sub> -P <sub>2</sub> -C <sub>8</sub>	101.0(4)
C <sub>18</sub> -C <sub>19</sub> -C <sub>20</sub>	120.3(7)	C <sub>6</sub> -P <sub>2</sub> -C <sub>7</sub>	101.8(4)
C <sub>15</sub> -C <sub>20</sub> -C <sub>19</sub>	121.3(7)	C <sub>7</sub> -P <sub>2</sub> -C <sub>8</sub>	99.1(4)
Ru-P <sub>4</sub> -C <sub>14</sub>	124.5(3)	P <sub>1</sub> -C <sub>5</sub> -C <sub>6</sub>	107.0(5)
		P <sub>2</sub> -C <sub>6</sub> -C <sub>5</sub>	108.2(5)

with 1 equivalent of *p*-cresol at 75 °C for 3 h led to the formation of **23** in 71% yield (Scheme 4). An X-ray diffraction study was carried out on a crystal of the hydrido *p*-cresolato complex **23** obtained from a toluene/pentane (1:10) solution at -30 °C. An ORTEP drawing of **23** is shown in Figure 4, crystal and data parameters are listed in Table 1, and intramolecular bond distances and angles are tabulated in Tables 8 and 9, respectively. The Ru-O bond length is 2.239(2) Å and the Ru-H bond length is 1.63(3) Å. The hydride was located; it lies below the DMPE phosphorus plane and the cresolate oxygen is located above the plane, tilted out of the normal by approximately 15°.

When (DMPE)<sub>2</sub>Ru(C<sub>2</sub>H<sub>4</sub>) was treated with excess *p*-cresol at -30 °C rapid precipitation of the salt [*trans*-(DMPE)<sub>2</sub>Ru(C<sub>2</sub>H<sub>4</sub>)(H)]<sup>+</sup>[OC<sub>6</sub>H<sub>4</sub>-*p*-CH<sub>3</sub>-2HOOC<sub>6</sub>H<sub>4</sub>-*p*-CH<sub>3</sub>]<sup>-</sup> (**24**) (Scheme 4) was observed. Two equivalents of unreacted *p*-cresol remain hydrogen-bonded to the cresolate counterion of **24** even after recrystallization. The <sup>31</sup>P{<sup>1</sup>H} NMR spectrum of **24** at 25 °C shows a broad singlet at δ 41.5; the <sup>1</sup>H NMR spectrum displays a singlet at δ 14.32 for the hydrogen-bonded protons, one broadened multiplet for the ethylene protons at δ 1.92 and the hydride multiplet at δ -9.88.

An X-ray crystal structure study was carried out on the ethylene hydrido complex **24**. Approximately 15%

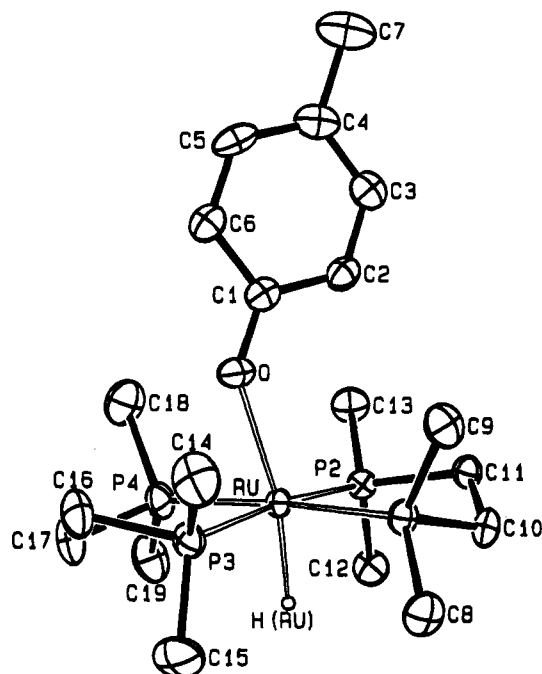


Figure 4. ORTEP diagram of *trans*-(DMPE)<sub>2</sub>Ru(H)(OC<sub>6</sub>H<sub>4</sub>-*p*-Me) (**23**).

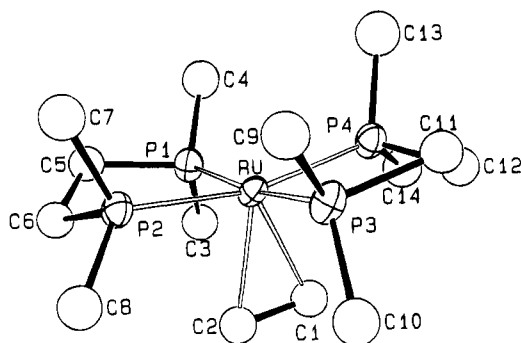


Figure 5. ORTEP diagram of the cation in [*trans*-(DMPE)<sub>2</sub>Ru(C<sub>2</sub>H<sub>4</sub>)(H)]<sup>+</sup>[OC<sub>6</sub>H<sub>4</sub>-*p*Me-2HOC<sub>6</sub>H<sub>4</sub>-*p*Me] (**24**).

Table 8. Selected Intramolecular Distances (Å) for *trans*-(DMPE)<sub>2</sub>Ru(H)(OC<sub>6</sub>H<sub>4</sub>-*p*-CH<sub>3</sub>) (**23**)

Ru-P <sub>1</sub>	2.289(1)	P <sub>1</sub> -C <sub>8</sub>	1.832(3)
Ru-P <sub>2</sub>	2.296(1)	P <sub>1</sub> -C <sub>9</sub>	1.822(3)
Ru-P <sub>3</sub>	2.299(1)	P <sub>1</sub> -C <sub>10</sub>	1.840(3)
Ru-P <sub>4</sub>	2.295(1)	P <sub>2</sub> -C <sub>11</sub>	1.844(3)
Ru-O	2.239(2)	P <sub>2</sub> -C <sub>12</sub>	1.830(3)
Ru-H(Ru)	1.63(3)	P <sub>2</sub> -C <sub>13</sub>	1.829(3)
O-C <sub>1</sub>	1.302(3)	C <sub>10</sub> -C <sub>11</sub>	1.518(4)
C <sub>1</sub> -C <sub>2</sub>	1.404(4)	P <sub>3</sub> -P <sub>14</sub>	1.822(3)
C <sub>1</sub> -C <sub>6</sub>	1.414(3)	P <sub>3</sub> -C <sub>15</sub>	1.819(3)
C <sub>2</sub> -C <sub>3</sub>	1.386(4)	P <sub>3</sub> -P <sub>16</sub>	1.846(3)
C <sub>3</sub> -C <sub>4</sub>	1.381(4)	P <sub>4</sub> -C <sub>17</sub>	1.848(3)
C <sub>4</sub> -C <sub>5</sub>	1.389(4)	P <sub>4</sub> -C <sub>18</sub>	1.822(3)
C <sub>4</sub> -C <sub>7</sub>	1.508(4)	P <sub>4</sub> -C <sub>19</sub>	1.821(3)
C <sub>5</sub> -C <sub>6</sub>	1.373(4)	C <sub>16</sub> -C <sub>17</sub>	1.514(4)

of the hydride sites in the crystal examined contained chloride presumably derived from the CH<sub>2</sub>Cl<sub>2</sub> used in crystallization. Although we were not able to obtain NMR evidence for the chloride contaminant, mass spectral analysis registered the chloride impurity. An ORTEP drawing of the organometallic portion of **24** is shown in Figure 5, and an ORTEP diagram of the hydrogen-bonded *p*-cresolate anion is provided in Figure 6. The crystal and data collection parameters are given in Table 1; the intramolecular bond distances are tabulated in Tables 10 and 12 and the intramolecular

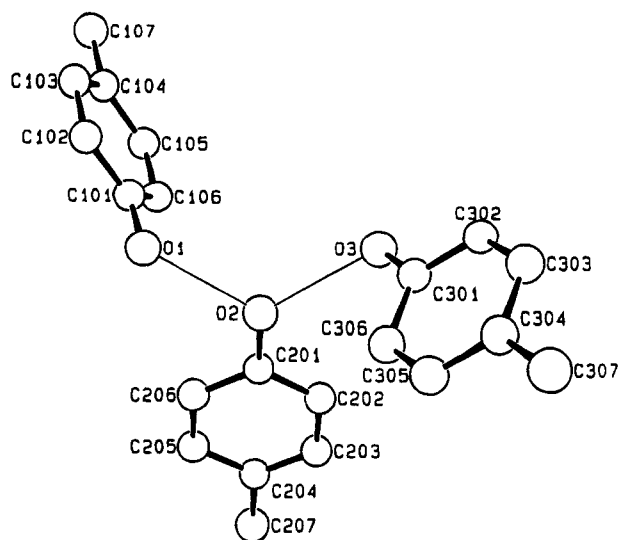


Figure 6. ORTEP diagram of the anion [*p*-Me-C<sub>6</sub>H<sub>4</sub>O-2HOC<sub>6</sub>H<sub>4</sub>-*p*-Me]<sup>-</sup> in **24**.

Table 9. Selected Intramolecular Angles (deg) for *trans*-(DMPE)<sub>2</sub>Ru(H)(OC<sub>6</sub>H<sub>4</sub>-*p*-CH<sub>3</sub>) (**23**)

P <sub>1</sub> -Ru-P <sub>2</sub>	84.16(2)	Ru-P <sub>1</sub> -C <sub>9</sub>	119.85(11)
P <sub>1</sub> -Ru-P <sub>3</sub>	94.45(2)	Ru-P <sub>1</sub> -C <sub>10</sub>	108.84(9)
P <sub>1</sub> -Ru-P <sub>4</sub>	175.68(2)	C <sub>8</sub> -P <sub>1</sub> -C <sub>9</sub>	100.64(15)
P <sub>1</sub> -Ru-O	100.80(5)	C <sub>8</sub> -P <sub>1</sub> -C <sub>10</sub>	102.07(14)
P <sub>1</sub> -Ru-H	85.7(10)	C <sub>9</sub> -P <sub>1</sub> -C <sub>10</sub>	102.38(14)
P <sub>2</sub> -Ru-P <sub>3</sub>	173.78(2)	Ru-P <sub>2</sub> -C <sub>11</sub>	109.69(8)
P <sub>2</sub> -Ru-P <sub>4</sub>	96.28(2)	Ru-P <sub>2</sub> -C <sub>12</sub>	116.69(10)
P <sub>2</sub> -Ru-O	106.43(5)	Ru-P <sub>2</sub> -C <sub>13</sub>	123.94(11)
P <sub>2</sub> -Ru-H	85.6(10)	C <sub>11</sub> -P <sub>2</sub> -C <sub>12</sub>	100.56(14)
P <sub>3</sub> -Ru-P <sub>4</sub>	84.66(2)	C <sub>11</sub> -P <sub>2</sub> -C <sub>13</sub>	102.39(13)
P <sub>3</sub> -Ru-O	79.79(5)	C <sub>12</sub> -P <sub>2</sub> -C <sub>13</sub>	100.38(14)
P <sub>3</sub> -Ru-H	88.2(10)	P <sub>1</sub> -C <sub>10</sub> -C <sub>11</sub>	110.16(18)
P <sub>4</sub> -Ru-O	83.21(5)	C <sub>10</sub> -C <sub>11</sub> -P <sub>2</sub>	108.82(18)
P <sub>4</sub> -Ru-H	90.0(10)	Ru-P <sub>3</sub> -C <sub>14</sub>	119.64(13)
O-Ru-H	166.7(10)	Ru-P <sub>3</sub> -C <sub>15</sub>	120.41(12)
Ru-O-C <sub>1</sub>	137.58(16)	Ru-P <sub>3</sub> -C <sub>16</sub>	107.83(11)
O-C <sub>1</sub> -C <sub>2</sub>	124.5(2)	C <sub>14</sub> -P <sub>3</sub> -C <sub>15</sub>	102.24(19)
O-C <sub>1</sub> -C <sub>6</sub>	120.4(2)	C <sub>14</sub> -P <sub>3</sub> -C <sub>16</sub>	101.69(16)
C <sub>2</sub> -C <sub>1</sub> -C <sub>6</sub>	115.1(2)	C <sub>15</sub> -P <sub>3</sub> -C <sub>16</sub>	102.26(18)
C <sub>1</sub> -C <sub>2</sub> -C <sub>3</sub>	121.8(2)	Ru-P <sub>4</sub> -C <sub>17</sub>	108.87(10)
C <sub>2</sub> -C <sub>3</sub> -C <sub>4</sub>	122.3(3)	Ru-P <sub>4</sub> -C <sub>18</sub>	117.14(13)
C <sub>3</sub> -C <sub>4</sub> -C <sub>5</sub>	116.6(2)	Ru-P <sub>4</sub> -C <sub>19</sub>	122.77(12)
C <sub>3</sub> -C <sub>4</sub> -C <sub>7</sub>	121.7(3)	C <sub>17</sub> -P <sub>4</sub> -C <sub>18</sub>	102.52(19)
C <sub>5</sub> -C <sub>4</sub> -C <sub>7</sub>	121.7(3)	C <sub>17</sub> -P <sub>4</sub> -C <sub>19</sub>	101.33(16)
C <sub>4</sub> -C <sub>5</sub> -C <sub>6</sub>	122.0(3)	C <sub>18</sub> -P <sub>4</sub> -C <sub>19</sub>	101.44(19)
C <sub>1</sub> -C <sub>6</sub> -C <sub>5</sub>	122.2(3)	P <sub>3</sub> -C <sub>16</sub> -C <sub>17</sub>	109.16(21)
Ru-P <sub>1</sub> -C <sub>8</sub>	120.37(11)	C <sub>16</sub> -C <sub>17</sub> -P <sub>4</sub>	109.80(20)

Table 10. Selected Intramolecular Distances (Å) for [*trans*-(DMPE)<sub>2</sub>Ru(C<sub>2</sub>H<sub>4</sub>)(H)]<sup>+</sup> (**24**)

Ru-P <sub>1</sub>	2.328(3)	P <sub>2</sub> -C <sub>6</sub>	1.834(9)
Ru-P <sub>2</sub>	2.324(2)	P <sub>2</sub> -C <sub>7</sub>	1.827(10)
Ru-P <sub>3</sub>	2.314(3)	P <sub>2</sub> -C <sub>8</sub>	1.842(10)
Ru-P <sub>4</sub>	2.317(2)	C <sub>5</sub> -C <sub>6</sub>	1.550(12)
Ru-C <sub>1</sub>	2.265(10)	P <sub>3</sub> -C <sub>9</sub>	1.844(10)
Ru-C <sub>2</sub>	2.269(10)	P <sub>3</sub> -C <sub>10</sub>	1.843(10)
Ru-Cl**	2.425(15)	P <sub>3</sub> -C <sub>11</sub>	1.862(10)
C <sub>1</sub> -C <sub>2</sub>	1.430(12)	P <sub>4</sub> -C <sub>12</sub>	1.847(10)
P <sub>1</sub> -C <sub>3</sub>	1.826(11)	P <sub>4</sub> -C <sub>13</sub>	1.842(12)
P <sub>1</sub> -C <sub>4</sub>	1.840(10)	P <sub>4</sub> -C <sub>14</sub>	1.852(11)
P <sub>1</sub> -C <sub>5</sub>	1.847(9)	C <sub>11</sub> -C <sub>12</sub>	1.540(13)

angles in Tables 11 and 13. The structure of **24** is pseudo-octahedral, with the ethylene ligand occupying an axial position and exhibiting nearly identical Ru-C distances of 2.26 and 2.27 Å. The ethylene C-C bond distance is 1.43 Å. These values should be interpreted with caution because of the 15% chloride impurity in the crystal.

**Table 11.** Selected Intramolecular Angles (deg) for  $[(trans-(DMPE)_2Ru(C_2H_4)(H))^+ (24)]$ 

P <sub>1</sub> -Ru-P <sub>2</sub>	83.69(8)	C <sub>4</sub> -P <sub>1</sub> -C <sub>5</sub>	100.1(4)
P <sub>1</sub> -Ru-P <sub>3</sub>	171.28(10)	Ru-P <sub>2</sub> -C <sub>6</sub>	109.3(3)
P <sub>1</sub> -Ru-P <sub>4</sub>	95.90(9)	Ru-P <sub>2</sub> -C <sub>7</sub>	116.9(3)
P <sub>1</sub> -Ru-C <sub>1</sub>	93.7(3)	Ru-P <sub>2</sub> -C <sub>8</sub>	122.4(3)
P <sub>1</sub> -Ru-C <sub>2</sub>	93.3(3)	C <sub>6</sub> -P <sub>2</sub> -C <sub>7</sub>	102.0(4)
P <sub>2</sub> -Ru-P <sub>3</sub>	94.73(9)	C <sub>6</sub> -P <sub>2</sub> -C <sub>8</sub>	102.4(4)
P <sub>2</sub> -Ru-P <sub>4</sub>	164.35(9)	C <sub>7</sub> -P <sub>2</sub> -C <sub>8</sub>	101.2(4)
P <sub>2</sub> -Ru-C <sub>1</sub>	116.16(24)	P <sub>1</sub> -C <sub>5</sub> -C <sub>6</sub>	111.0(6)
P <sub>2</sub> -Ru-C <sub>2</sub>	79.54(24)	P <sub>2</sub> -C <sub>6</sub> -C <sub>5</sub>	108.7(6)
P <sub>3</sub> -Ru-P <sub>4</sub>	83.30(9)	Ru-P <sub>3</sub> -C <sub>9</sub>	119.1(3)
P <sub>3</sub> -Ru-C <sub>1</sub>	94.64(25)	Ru-P <sub>3</sub> -C <sub>10</sub>	120.0(3)
P <sub>3</sub> -Ru-C <sub>2</sub>	94.85(25)	Ru-P <sub>3</sub> -C <sub>11</sub>	110.4(3)
P <sub>4</sub> -Ru-C <sub>1</sub>	79.49(24)	C <sub>9</sub> -P <sub>3</sub> -C <sub>10</sub>	101.6(4)
P <sub>4</sub> -Ru-C <sub>2</sub>	116.07(24)	C <sub>9</sub> -P <sub>3</sub> -C <sub>11</sub>	100.2(4)
C <sub>1</sub> -Ru-C <sub>2</sub>	36.8(3)	C <sub>10</sub> -P <sub>3</sub> -C <sub>11</sub>	102.6(4)
**Cl-Ru-P <sub>1</sub>	81.8(4)	Ru-P <sub>4</sub> -C <sub>12</sub>	109.0(3)
**Cl-Ru-P <sub>2</sub>	85.2(3)	Ru-P <sub>4</sub> -C <sub>13</sub>	115.8(4)
**Cl-Ru-P <sub>3</sub>	89.5(4)	Ru-P <sub>4</sub> -C <sub>14</sub>	123.0(4)
**Cl-Ru-P <sub>4</sub>	79.3(3)	C <sub>12</sub> -P <sub>4</sub> -C <sub>13</sub>	101.5(5)
Ru-P <sub>1</sub> -C <sub>3</sub>	120.0(3)	C <sub>12</sub> -P <sub>4</sub> -C <sub>14</sub>	102.1(5)
Ru-P <sub>1</sub> -C <sub>4</sub>	119.5(3)	C <sub>13</sub> -P <sub>4</sub> -C <sub>14</sub>	102.7(5)
Ru-P <sub>1</sub> -C <sub>5</sub>	109.5(3)	P <sub>3</sub> -C <sub>11</sub> -C <sub>12</sub>	109.4(7)
C <sub>3</sub> -P <sub>1</sub> -C <sub>4</sub>	101.6(5)	P <sub>4</sub> -C <sub>12</sub> -C <sub>11</sub>	108.5(6)
C <sub>3</sub> -P <sub>1</sub> -C <sub>5</sub>	103.4(5)		

**Table 12.** Selected Intramolecular Distances (Å) for  $[(p-CH_3-C_6H_4O)2HOC_6H_4-p-CH_3]^- (24)$ 

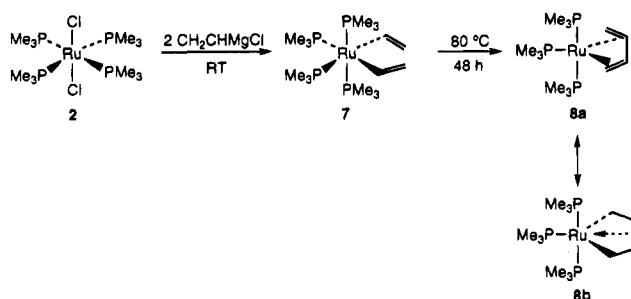
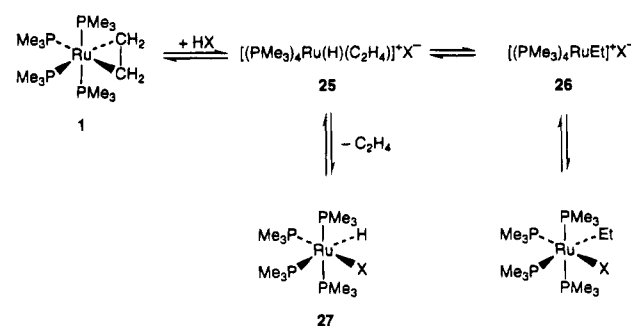
C <sub>101</sub> -O <sub>1</sub>	1.365(10)	C <sub>203</sub> -C <sub>204</sub>	1.411(12)
C <sub>101</sub> -C <sub>102</sub>	1.413(12)	C <sub>204</sub> -C <sub>205</sub>	1.393(12)
C <sub>101</sub> -C <sub>106</sub>	1.385(12)	C <sub>204</sub> -C <sub>207</sub>	1.554(13)
C <sub>102</sub> -C <sub>103</sub>	1.411(12)	C <sub>205</sub> -C <sub>206</sub>	1.403(12)
C <sub>103</sub> -C <sub>104</sub>	1.379(12)	C <sub>301</sub> -O <sub>3</sub>	1.360(10)
C <sub>104</sub> -C <sub>105</sub>	1.406(12)	C <sub>301</sub> -C <sub>302</sub>	1.386(12)
C <sub>104</sub> -C <sub>107</sub>	1.533(12)	C <sub>301</sub> -C <sub>306</sub>	1.406(12)
C <sub>105</sub> -C <sub>106</sub>	1.401(12)	C <sub>302</sub> -C <sub>303</sub>	1.419(12)
C <sub>201</sub> -O <sub>2</sub>	1.342(10)	C <sub>303</sub> -C <sub>304</sub>	1.393(13)
C <sub>201</sub> -C <sub>202</sub>	1.396(12)	C <sub>304</sub> -C <sub>305</sub>	1.391(12)
C <sub>201</sub> -C <sub>206</sub>	1.406(12)	C <sub>304</sub> -C <sub>307</sub>	1.519(13)
C <sub>202</sub> -C <sub>203</sub>	1.422(12)	C <sub>305</sub> -C <sub>306</sub>	1.420(12)
		O <sub>1</sub> ···O <sub>2</sub>	2.479(8)
		O <sub>2</sub> ···O <sub>3</sub>	2.543(9)

**Table 13.** Selected Intramolecular Angles (deg) for  $[(p-CH_3-C_6H_4O)2HOC_6H_4-p-CH_3]^- (24)$ 

C <sub>101</sub> -O <sub>1</sub> -O <sub>2</sub>	113.1(5)	C <sub>201</sub> -C <sub>202</sub> -C <sub>203</sub>	119.8(8)
C <sub>201</sub> -O <sub>2</sub> -O <sub>1</sub>	121.1(5)	C <sub>202</sub> -C <sub>203</sub> -C <sub>204</sub>	120.7(8)
C <sub>201</sub> -O <sub>2</sub> -O <sub>3</sub>	122.2(5)	C <sub>203</sub> -C <sub>204</sub> -C <sub>205</sub>	118.6(8)
C <sub>301</sub> -O <sub>3</sub> -O <sub>2</sub>	113.1(5)	C <sub>203</sub> -C <sub>204</sub> -C <sub>207</sub>	120.8(8)
O <sub>1</sub> -C <sub>101</sub> -C <sub>102</sub>	118.3(8)	C <sub>205</sub> -C <sub>204</sub> -C <sub>207</sub>	120.5(8)
O <sub>1</sub> -C <sub>101</sub> -C <sub>106</sub>	121.6(8)	C <sub>204</sub> -C <sub>205</sub> -C <sub>206</sub>	121.1(8)
C <sub>102</sub> -C <sub>101</sub> -C <sub>106</sub>	120.1(8)	C <sub>201</sub> -C <sub>206</sub> -C <sub>205</sub>	120.5(8)
C <sub>101</sub> -C <sub>102</sub> -C <sub>103</sub>	118.7(8)	O <sub>3</sub> -C <sub>301</sub> -C <sub>302</sub>	118.5(8)
C <sub>102</sub> -C <sub>103</sub> -C <sub>104</sub>	122.0(8)	O <sub>3</sub> -C <sub>301</sub> -C <sub>306</sub>	120.9(8)
C <sub>103</sub> -C <sub>104</sub> -C <sub>105</sub>	118.0(8)	C <sub>302</sub> -C <sub>301</sub> -C <sub>306</sub>	120.5(8)
C <sub>103</sub> -C <sub>104</sub> -C <sub>107</sub>	121.5(8)	C <sub>301</sub> -C <sub>302</sub> -C <sub>303</sub>	119.9(8)
C <sub>105</sub> -C <sub>104</sub> -C <sub>107</sub>	120.5(8)	C <sub>302</sub> -C <sub>303</sub> -C <sub>304</sub>	120.8(9)
C <sub>104</sub> -C <sub>105</sub> -C <sub>106</sub>	121.4(9)	C <sub>303</sub> -C <sub>304</sub> -C <sub>305</sub>	118.5(9)
C <sub>101</sub> -C <sub>106</sub> -C <sub>105</sub>	119.7(8)	C <sub>303</sub> -C <sub>304</sub> -C <sub>307</sub>	120.7(8)
O <sub>2</sub> -C <sub>201</sub> -C <sub>202</sub>	120.1(8)	C <sub>305</sub> -C <sub>304</sub> -C <sub>307</sub>	120.7(9)
O <sub>2</sub> -C <sub>201</sub> -C <sub>206</sub>	120.5(8)	C <sub>304</sub> -C <sub>305</sub> -C <sub>306</sub>	121.9(9)
C <sub>202</sub> -C <sub>201</sub> -C <sub>206</sub>	119.4(8)	C <sub>301</sub> -C <sub>306</sub> -C <sub>305</sub>	118.3(8)

**Synthesis of Divinyl Complex  $(PMe_3)_4Ru(CH=CH_2)_2$  (7) and Its Conversion to Butadiene Complex  $(PMe_3)_3Ru(\eta^4-C_4H_6)$  (8).** Treatment of  $(PMe_3)_4RuCl_2$  (2) with two equivalents of  $CH_2CHMgCl$  at room temperature afforded *cis*- $(PMe_3)_4Ru(CH=CH_2)_2$  in 50% yield (Scheme 5). The *cis* orientation of 7 was confirmed by the  $A_2X_2$  splitting pattern in the  $^{31}P\{^1H\}$  NMR spectrum.

Thermolysis of a benzene solution of divinyl complex 7 for two days at 80 °C yielded an orange solution that exhibited an  $A_2B$  pattern in the  $^{31}P\{^1H\}$  NMR spectrum. The presence of free  $PMe_3$  in both the  $^{31}P\{^1H\}$  and  $^1H$

**Scheme 5****Scheme 6**

NMR spectra indicated the dissociation of a phosphine group. Cooling a hexane solution of the product of this reaction afforded pure butadiene complex 8a in 48% isolated yield. The  $^1H$  NMR spectrum shows a doublet at  $\delta$  1.37, corresponding to the unique  $PMe_3$  group *trans* to the butadiene ligand, and a virtual triplet at  $\delta$  1.01 for the methyl groups on the mutually *trans* phosphine ligands. The  $^1H$  and  $^{13}C\{^1H\}$  NMR spectra are consistent with the formation of a butadiene complex (8a, Scheme 5). The assignment of peaks in the  $^1H$  NMR spectrum was made in analogy to the known  $Ru(CO)_3$ -(butadiene) $_2$  formed from the reaction of  $Ru_3(CO)_{12}$  and 1,3-butadiene.<sup>20</sup> The difference in the  $^{13}C\{^1H\}$  NMR chemical shifts of the butadiene carbons ( $\delta$  79.1 (CH) and  $\delta$  28.9 (CH<sub>2</sub>)) and the lack of coupling in the  $^1H$  NMR spectrum suggest that the structure is that of a chelating butadiene with substantial metallacyclopentene character (8a and 8b, Scheme 5).

## Discussion

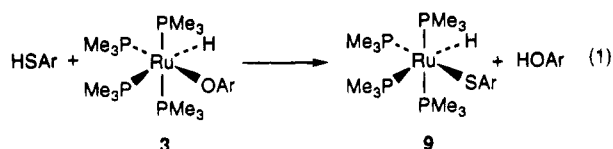
**Trimethylphosphine Complexes.** The reactions of  $(PMe_3)_4Ru(C_2H_4)$  (1) can be divided into two groups: those that occur at 25 °C and those that occur at higher temperatures. We consider the room temperature reactions first.

Previous studies on the reactivity of  $(PMe_3)_4Ru(C_2H_4)$  (1) showed that the ethylene complex readily reacts with *p*-cresol at room temperature to form the cresolate hydride by a protonation mechanism.<sup>7</sup> We find that treatment of ethylene complex 1 with *p*-thiocresol, *p*-chlorophenol, or *p*-nitrophenol at room temperature resulted in the immediate conversion of 1 to the hydrides  $(PMe_3)_4Ru(H)(ZC_6H_4-p-Y)$  (9, Z = S, Y = CH<sub>3</sub>; 10, Z = O, Y = Cl; 11, Z = O, Y = NO<sub>2</sub>). Similarities between the reaction conditions and the presence of an acidic hydrogen in the organic reagent support a mechanism analogous to that in the *p*-cresol reaction<sup>7</sup> despite

(20) Zobl-Ruh, S.; vonPhilipsborn, W. *Helv. Chim. Acta* 1980, 63, 773.

the large differences in  $pK_a$ 's of the acidic hydrogens. The mechanism proposed for the reaction of *p*-cresol involves initial protonation of the electron-rich ruthenium center by  $HXAr$ , followed by ethylene insertion to form a possible ruthenium ethyl cresolate intermediate, *cis*-( $PMe_3$ )<sub>4</sub>Ru(Et)(OC<sub>6</sub>H<sub>4</sub>-*p*-CH<sub>3</sub>). This is supported by the studies done on the bis(DMPE) complexes discussed in the next section. Ionization of the aryloxide to form an ion pair [( $PMe_3$ )<sub>4</sub>Ru(Et)]<sup>+</sup>[OAr]<sup>-</sup> would facilitate  $\beta$ -hydride elimination to form the observed product **3** (Scheme 6).

Addition of *p*-thiocresol to the *p*-cresolate complex **3** resulted in the complete conversion to the *p*-thiolato complex **9** and *p*-cresol (eq 1) at room temperature. The facility of this process is a consequence of the formation of (a) a stronger O-H bond relative to an S-H bond and (b) a stronger Ru-S bond compared to a Ru-O bond.<sup>21</sup>

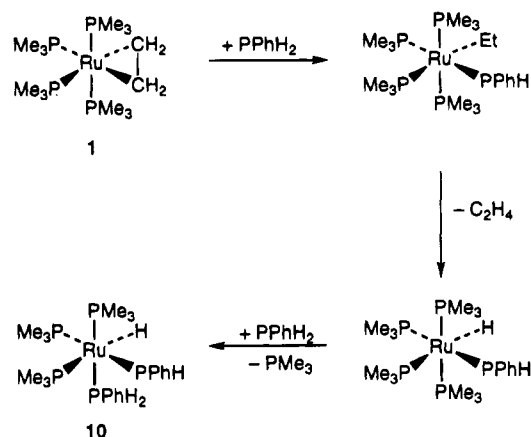


Studies performed on the related metal-hydroxy and metal-thiol systems suggest that the stronger interaction between the soft sulfur atom and the soft metal center is a result of more covalent character in the metal sulfur bond.<sup>6,22-24</sup>

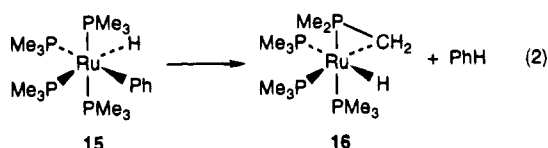
The reaction of ethylene complex **1** with one equivalent of phenylphosphine also occurs readily at room temperature. Neither dissociation of trimethylphosphine nor dissociation of ethylene from **1** occurs at this temperature. However, the fact that the phosphine-substituted complex ( $PMe_3$ )<sub>3</sub>(PPhH<sub>2</sub>)Ru(H)(PPhH) (**12**) is the final product suggests that the mechanism is more complicated than a simple protonation reaction. No mechanistic studies were performed as hydrido phosphido **12** is relatively unstable at room temperature and decomposes in solution to a complex mixture of products after 15 min. Support for the formation of an intermediate ethyl phosphide species was obtained, however, by reactivity studies in the bis(DMPE) system discussed in the next section.  $\beta$ -Hydride elimination to form the phosphido hydride followed by phosphine exchange of one  $PMe_3$  by  $PhPH_2$  is one possible pathway to the final product **12** (Scheme 7). Electron donation from the phosphido phosphorus atom may make the ruthenium center in ( $PMe_3$ )<sub>4</sub>Ru(H)(PPhH) more substitutionally labile than that in **1**.

At temperatures above 25 °C, the ethylene complex **1** can react by a number of pathways as seen from the product distributions in the following reactions. Deuterated ethylene displaces one phosphine ligand to form the bis(ethylene) complex **13** (Scheme 1) at 45 °C. At temperatures above 90 °C in benzene, ethylene complex **1** leads to phenyl hydride **15**.<sup>7</sup> Complex **15** has been previously prepared from the reaction of the tetrakis(trimethylphosphine) ruthenium benzyne complex with *n*-propanol.<sup>17</sup> Detailed studies of the reductive elimina-

Scheme 7



tion reaction of the phenyl hydride **15** to form benzene and the cyclometalated hydride **16** (eq 2) were reported



previously.<sup>25</sup> We propose that at 90 °C, dissociation of free ethylene forms an L<sub>4</sub>Ru intermediate that can activate the benzene solvent to form the phenyl hydride. The free ethylene liberated reacts with ( $PMe_3$ )<sub>4</sub>Ru(C<sub>2</sub>H<sub>4</sub>) to form the bis(ethylene) complex, ( $PMe_3$ )<sub>3</sub>Ru(C<sub>2</sub>H<sub>4</sub>)<sub>2</sub>, and free  $PMe_3$ .

**DMPE Complexes.** The behavior of bis(DMPE) system provides a useful comparison with that of the tetrakis(trimethylphosphine) system. The enhanced stability of the DMPE complexes, attributed to the chelate effect of the bidentate ligand, makes phosphine dissociation pathways less feasible and facilitates the isolation of intermediates, such as the cationic ethylene hydrido and ethyl complexes, not observed in the trimethylphosphine system.

Although (DMPE)<sub>2</sub>Ru(C<sub>2</sub>H<sub>4</sub>) (**6**) has been mentioned previously in the literature,<sup>13,16</sup> we have found a new route to complex **6** (Scheme 3) and have explored its reactivity with various HX complexes (Scheme 4). Complex **6** readily reacts with *p*-thiocresol at room temperature to form (DMPE)<sub>2</sub>Ru(SC<sub>6</sub>H<sub>4</sub>-*p*-CH<sub>3</sub>)(Et) (**18**). Thermolysis of complex **18** at 85 °C for 14 h results in the loss of ethylene and the formation of *trans*-(DMPE)<sub>2</sub>RuH(SAr) (**19**) (Ar = C<sub>6</sub>H<sub>4</sub>-*p*-CH<sub>3</sub>, Scheme 4). By contrast, we have not observed the ethyl species in the reaction of the tetrakis(trimethylphosphine) ethylene complex **1** and HSC<sub>6</sub>H<sub>4</sub>-*p*-CH<sub>3</sub>, where the reaction occurred rapidly at room temperature to form only the corresponding hydride complex (Scheme 1).

PPhH<sub>2</sub> reacted with bis(DMPE) ethylene complex **6** in a manner analogous to *p*-thiocresol, leading at room temperature to the ethyl phosphido complex **21**. Complex **21** is stable at room temperature and only undergoes  $\beta$ -hydride elimination at temperatures above 60 °C to form a mixture of *trans* and *cis*-(DMPE)<sub>2</sub>Ru(H)-(PPh) (**22a** and **22b**). Unlike the trimethylphosphine

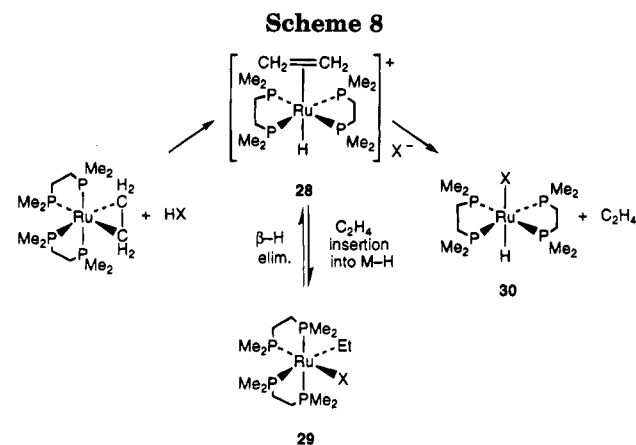
(21) Huheey, J. E.; Keiter, E. A.; Keiter, R. L. *Inorganic Chemistry: Principles of Structure and Reactivity*; 4th ed.; Harper and Row: New York, 1993, Ch. 9.

(22) Pearson, R. G. *J. Chem. Ed.* **1968**, *45*, 581.

(23) Pearson, R. G. *J. Chem. Ed.* **1968**, *45*, 643.

(24) Burn, M. J.; Fickes, M. G.; Hartwig, J. F.; Hollander, F. J.; Bergman, R. G. *J. Am. Chem. Soc.* **1993**, *115*, 5875.

(25) Hartwig, J. F.; Andersen, R. A.; Bergman, R. G. *J. Am. Chem. Soc.* **1991**, *113*, 6492.



system, phosphine substitution of the DMPE ligands by PPhH<sub>2</sub> was not observed.

In contrast to the reactions of *p*-thiocresol and PPhH<sub>2</sub>, aniline does not react with ethylene complex **6** at room temperature. However, at 90 °C formation of the anilido hydride (DMPE)<sub>2</sub>Ru(NPhH)(H) (**20b**) is observed. Monitoring the reaction by <sup>1</sup>H NMR spectrometry showed that the trans isomer **20b** is formed initially and subsequently rearranges to the cis form **20a**, suggesting that trans **20b** is the kinetic product of the reaction of **6** and aniline. This indicates that the reaction does not proceed by direct oxidative addition as is presumed in the case of the (PMe<sub>3</sub>)<sub>4</sub> analogue.<sup>7</sup>

The reaction of HOC<sub>6</sub>H<sub>4</sub>-*p*-CH<sub>3</sub> with bis(DMPE) ethylene complex **6** at room temperature slowly forms the *p*-cresolate hydride **23** with no observable ruthenium-ethyl species. However, at low temperature only the protonated ethylene hydride cation **24** is formed, presumably due to stabilization of the cresolate counterion by unreacted *p*-cresol. At room temperature, the reaction proceeded slowly to afford the *p*-cresolate hydride **23** with no observable ruthenium ethyl species as a second intermediate.

The isolation of the ethyl thiocresolate **18**, ethyl phosphide **21**, and ethylene hydride cation **24** provides some insight regarding the mechanism of reactions of weakly acidic reagents with **6** (Scheme 8). As previously mentioned, we propose that (PMe<sub>3</sub>)<sub>4</sub>Ru(C<sub>2</sub>H<sub>4</sub>) (**1**) reacts by initial protonation of the metal center to form an ethylene-hydrido cationic complex (**25**, Scheme 6), which may undergo reversible ethylene insertion to form the corresponding ruthenium ethyl species. Loss of ethylene from the ethylene-hydride cation leads to the neutral hydride product **27**. However, these proposed intermediates were not observed in the tetrakis(trimethylphosphine) system. The increased stability of the bis(DMPE) complexes allows for the isolation of the intermediate ethyl species, (DMPE)<sub>2</sub>Ru(Et)(X), and ethylene species [(DMPE)<sub>2</sub>Ru(H)(C<sub>2</sub>H<sub>4</sub>)]<sup>+</sup>[OC<sub>6</sub>H<sub>4</sub>-*p*-CH<sub>3</sub>-2HOC<sub>6</sub>H<sub>4</sub>-*p*-CH<sub>3</sub>]<sup>-</sup> and provides support for the mechanistic hypothesis.

A number of complexes similar to the protonated ethylene species **24** are known, and the reversible migratory insertion process of metal-complexed alkene into an M-H bond has been studied extensively.<sup>26-32</sup> Whether the Ru ethyl or the Ru ethylene hydride

cationic complex is isolated must in part be controlled by the ability of the counteranion to coordinate to the protonated metal center. Soft-soft interactions, such as Ru-S and Ru-P, favor the ethyl species. By comparison, the soft-hard Ru-O interaction that would be present with *p*-cresolate as the counterion provides less driving force for insertion, and the ionic intermediate is isolated.

**X-ray Structures of 18, 21, 20a, 23, and 24.** X-ray structural analyses of the ethyl thiolate **18** and the ethyl phosphide **21** reveal that these complexes are very similar. Although a slightly shorter Ru-S distance might be expected, based on the smaller atomic radius of sulfur compared to phosphorus,<sup>21</sup> the Ru-P bond is significantly shorter than the Ru-S bond (Ru-P = 2.453(2) compared to Ru-S = 2.522(3) Å) suggesting the presence of some multiple bond character in the Ru-P bond (see discussion below). The Ru-ethyl bond lengths in complexes **18** (2.230(10) Å) and **21** (2.225(7) Å) are not statistically different despite the change in environment at the metal center. These bond lengths are slightly longer than the metal-ethyl bond distances in other ruthenium-ethyl compounds such as Ru(Et)<sub>2</sub>(*t*-Bu<sub>2</sub>bipy)<sub>2</sub> where the Ru-Et distances are 2.138(7) and 2.142(8) Å.<sup>33</sup>

The Ru-P distances in the structures of both **18** and **21** reflect the relative trans influence properties of the various ligands. Comparison of the tabulated data of the Ru-P bond distances trans to the ethyl groups, or to another phosphine ligand, reveal the increasing trans influence trend SAR < phosphine ≈ phosphide ≈ ethyl.<sup>1</sup> The Ru-S-C angle in **18** is 116.6 (4)° and the Ru-P-C angle in **21** is 117.7 (2)°, indicating that this angle is not particularly sensitive to the difference in π-donating abilities of the thiolate and phosphide ligands.

There are only a few examples in the literature of structurally characterized terminal phosphidometal complexes.<sup>8,34-37</sup> A terminal phosphido-ligand in an L<sub>n</sub>M-PR<sub>2</sub> complex can be either planar or pyramidal at phosphorus. A planar phosphorus center (A) should



have a short M-P bond length and a large (approx. 130°) M-P-R bond angle. In contrast, a longer M-P bond length and a smaller (<114°) M-P-R angle would be consistent with a pyramidal phosphorus center (B). The Ru-P5 (phosphide) bond length in **21** is 2.453(2) Å, longer than the Ru-P (phosphine) distances in the literature that range from 2.289–2.337 Å, and the Ru-P5-Ar(C15) angle is 117.7(2)°. Although the phosphorus-bound hydrogen was not located, the structure appears

(28) Benfield, R. E.; Cragg, H. R.; Jones, R. G.; Swain, A. C. *Nature* **1991**, *353*, 340.

(29) Werner, H.; Feser, R. *Angew. Chem. Int. Ed. (Engl.)* **1979**, *18*, 157.

(30) Werner, H.; Werner, R. *J. Organomet. Chem.* **1979**, *174*, C63.

(31) Werner, H.; Feser, R. *J. Organomet. Chem.* **1982**, *232*, 351.

(32) Doherty, N. M.; Bercaw, J. E. *J. Am. Chem. Soc.* **1985**, *107*, 2670.

(33) Black, S. I.; Skapski, A. C.; Young, G. B. *J. Chem. Soc., Chem. Commun.* **1989**, 911.

(34) Roddick, D. M.; Santarsiero, B. D.; Bercaw, J. E. *J. Am. Chem. Soc.* **1985**, *107*, 4670.

(35) Stephen, D. W.; Ho, J. *Organometallics* **1992**, *11*, 1014.

(36) Weber, L.; Meine, G.; Boese, R.; Augart, N. *Organometallics* **1987**, *6*(12), 2484.

(37) Vaughan, G. A.; Hillhouse, G. L.; Rheingold, A. L. *Organomet.* **1989**, *8*, 1760.

(26) Byrne, J. W.; Kress, J. R. M.; Osborn, J. A.; Ricard, L.; Weiss, R. E. *J. Chem. Soc., Chem. Comm.* **1977**, 662.

(27) Brookhart, M.; Lincoln, M. *J. Am. Chem. Soc.* **1988**, *110*, 8719.

to be consistent with a phosphorus center that has a pyramidal geometry (B). However, the short Ru-P (phosphide) bond length suggests some double bond character may be present in the metal-phosphide bond.

In contrast the metal-nitrogen bond distance in **20a** is very similar to that of the previously reported tetrakis(trimethylphosphine) analogue (Ru-N 2.160(6) Å).<sup>7</sup> The Ru-P3 (trans to the amido ligand) distance of 2.244(3) Å in **20a** is similar to Ru-P3 (trans to the thiocresolate group) in **18** (2.270(3) Å) and consistent with a comparable trans influence. A Ru-P2 distance of 2.335(3) Å (trans to the hydride ligand, which was not located in the structural study) is slightly longer than the Ru-P distances in **18** and **21** trans to the ethyl ligand, also in accord with the expected stronger trans influence of H relative to C.<sup>1</sup>

In comparison to (PMe<sub>3</sub>)<sub>4</sub>Ru(H)(OC<sub>6</sub>H<sub>4</sub>-*p*-CH<sub>3</sub>)<sup>7</sup>, the structure of *trans*-(DMPE)<sub>2</sub>Ru(H)(OC<sub>6</sub>H<sub>4</sub>-*p*-CH<sub>3</sub>) (**23**) shows the Ru-O bond length of 2.239(2) Å to be slightly longer and the Ru-O-C<sub>ipso</sub> bond angle of 137.9(4)° slightly larger than that in the *cis* tetrakis(trimethylphosphine) analog. The increased bond length could be attributed to the trans influence of the hydride ligand. One unusual feature of the structure is the 15.4° tilt of the Ru-O vector from the normal to the phosphorus plane in the direction between P3 and P4. This detail is ascribed in part to steric interaction between the *p*-cresolate phenyl ring and the DMPE methyl groups. The Ru-H distance of 1.63(3) Å is slightly smaller than that for the related PMe<sub>3</sub> complex.<sup>7</sup>

The most unique structure described in this paper<sup>38</sup> is the cationic complex, [*trans*-(DMPE)<sub>2</sub>Ru(C<sub>2</sub>H<sub>4</sub>)(H)]<sup>+</sup>[OC<sub>6</sub>H<sub>4</sub>-*p*-CH<sub>3</sub>·2HOC<sub>6</sub>H<sub>4</sub>-*p*-CH<sub>3</sub>]<sup>-</sup> (**24**). Analysis of the X-ray data for this structure detected approximately 15% chloride presence in the hydride position. The source of chloride is undoubtedly the CH<sub>2</sub>Cl<sub>2</sub> used as a recrystallization solvent as no halogenated solvents were used in the synthesis of the complex. The hydride-chloride exchange suggests a fairly reactive hydride. The Ru-C1 and Ru-C2 bond lengths are 2.265(10) Å and 2.269(10) Å, respectively, and the ethylene C1-C2 bond distance is 1.430(12) Å. The [OC<sub>6</sub>H<sub>4</sub>-*p*-CH<sub>3</sub>·2HOC<sub>6</sub>H<sub>4</sub>-*p*-CH<sub>3</sub>]<sup>-</sup> counter-ion is propeller shaped; the O1-O2 and O2-O3 distances of 2.479(8) Å and 2.543(9) Å, respectively, constitute examples of very strong hydrogen bonding.<sup>39</sup>

**Behavior of Divinyl Complex 7.** It was initially hoped that, in a manner similar to the reaction with EtMgCl, reaction of dichloride **2** with vinylmagnesium bromide would yield a metallacyclopentene. However, the product isolated was the divinyl species, (PMe<sub>3</sub>)<sub>4</sub>-Ru(CH=CH<sub>2</sub>)<sub>2</sub> (**7**). Thermolysis of **7** could result in either coupling of the vinylic groups to give a butadiene ligand or loss of one of the vinyl groups as ethylene to give a metallacyclopentene, analogous to preparation of the benzyne complex (**23**) from (PMe<sub>3</sub>)<sub>4</sub>Ru(Ph)<sub>2</sub> (**24**).<sup>17</sup> In the event, thermolysis of **7** in benzene led to the formation of butadiene complex **8**. Spectroscopic details indicate that the chelating butadiene ligand has substantial metallacyclopentene character.<sup>20</sup>

The most plausible mechanism for the formation of butadiene **8** would be a direct concerted C-C reductive

elimination of the two vinyl ligands to form the butadiene species. Although C-C reductive elimination is not as well known as C-H reductive elimination for ruthenium complexes it has been invoked in a number of other systems such as the thermolysis of (alkyl)(acyl)ruthenium complexes to form ketones.<sup>40</sup> Butadiene complexes of transition metals are well known and are typically prepared by the reaction of butadiene with a coordinatively unsaturated metal species.<sup>20,41-44</sup> However, there is literature precedent for butadiene species formed from C-C coupling reactions. For example, addition of diphenylacetylene to Cp(PPh<sub>3</sub>)Co(Me)<sub>2</sub> forms Cp(PPh<sub>3</sub>)Co(C<sub>4</sub>Ph<sub>4</sub>)<sup>45,46</sup> and Cp<sub>2</sub>MCl<sub>2</sub> (M = Zr or Hf) reacts with CH<sub>2</sub>CHLi to form Cp<sub>2</sub>M(C<sub>4</sub>H<sub>6</sub>).<sup>47</sup> Interestingly, in direct contrast to the formation and relative stability of divinyl complex **7**, intermediate divinyl species are not observed in the Co, Zr or Hf cases.

## Summary

The reactivity of two strained phosphine-substituted ruthenium metallacyclopentanes (or ruthenium ethylene species) has been explored. The reactivity depends dramatically upon whether four PMe<sub>3</sub> ligands or two bis-dimethylphosphinoethane (DMPE) ligands are bound to ruthenium. For example, stable intermediate ethyl complexes could be isolated from the reaction of a variety of HX compounds (X = SAr, OAr, PPhH) with (DMPE)<sub>2</sub>Ru(C<sub>2</sub>H<sub>4</sub>) (**6**). Thermolysis of (DMPE)<sub>2</sub>Ru(Et)(SC<sub>6</sub>H<sub>4</sub>-*p*-Me) resulted in the formation of the hydride, *trans*-(DMPE)<sub>2</sub>Ru(H)(SC<sub>6</sub>H<sub>4</sub>-*p*-Me). In contrast, reactions of (PMe<sub>3</sub>)<sub>4</sub>Ru(C<sub>2</sub>H<sub>4</sub>) (**1**) with HX immediately resulted in the formation of the hydride species, and no ethyl intermediates could be observed.

A possible mechanism for these reactions involves initial protonation of the metal center by HX. This was initially proposed by Hartwig *et al.* for the reaction of (PMe<sub>3</sub>)<sub>4</sub>Ru(C<sub>2</sub>H<sub>4</sub>) with cresol.<sup>7</sup> Due to the reactivity of the PMe<sub>3</sub> complexes no intermediates were observed. We have observed similar behavior in the reactions of (PMe<sub>3</sub>)<sub>4</sub>Ru(C<sub>2</sub>H<sub>4</sub>) with HX (X = SC<sub>6</sub>H<sub>4</sub>-*p*-Me, OC<sub>6</sub>H<sub>4</sub>-*p*-Me, PPhH). Once again the presence of bidentate phosphine ligands provided additional stability to the intermediate ethyl species. The ethyl species have been isolated and shown to undergo conversion to the hydride products, and a unique ethylene hydride species, [(DMPE)<sub>2</sub>Ru(C<sub>2</sub>H<sub>4</sub>)(H)]<sup>+</sup>[OAr·2HOAr]<sup>-</sup> has been isolated and characterized by X-ray crystallography. This species rapidly rearranges to form (DMPE)<sub>2</sub>Ru(H)(OAr) in solution at room temperature.

Attempts to extend the metallacyclopentane-like behavior of ethylene complex **6** to the corresponding metallacyclopentene analog were not successful. Treatment of dichloride **2** with vinyl Grignard reagent resulted in the formation of a divinyl species, (PMe<sub>3</sub>)<sub>4</sub>-

(40) Goldberg, K. I.; Bergman, R. G. *J. Am. Chem. Soc.* **1989**, *111*, 1285.

(41) Ruh, S.; vonPhilipsborn, W. *J. Organomet. Chem.* **1977**, *127*, C59.

(42) Chang, J.; Bergman, R. G. *J. Am. Chem. Soc.* **1987**, *109*, 4298.

(43) Wreford, S. S.; Whitney, J. F. *Inorg. Chem.* **1981**, *20*, 3918.

(44) Yamamoto, H.; Yasuda, H.; Tatsumi, K.; Lee, K.; Nakamura, A.; Chen, J.; Kai, Y.; Kasai, N. *Organometallics* **1989**, *8*, 105.

(45) Evitt, E. R.; Bergman, R. G. *J. Am. Chem. Soc.* **1978**, *100*, 3237.

(46) Yamazaki, H.; Hagihara, N. *J. Organomet. Chem.* **1970**, *21*, 431.

(47) Beckhaus, R.; Thiele, K.-H. *J. Organomet. Chem.* **1986**, *317*, 23.

(38) Benfield, F. W. S.; Green, M. L. H. *J. Chem. Soc. Dalton Trans.* **1974**, 1324.

(39) Emsley, J. *Chem. Soc. Rev.* **1980**, 91.



$\text{Ru}(\text{CH}=\text{CH}_2)_2$  which led upon thermolysis to the butadiene complex **8**.

## Experimental Section

**General Considerations.** Unless otherwise noted, all reactions and manipulations were carried out under a nitrogen atmosphere in a Vacuum Atmospheres 553-2 Dri-Lab inert atmosphere box with attached M6-40-1H Dri-Train or under argon using standard Schlenk and vacuum techniques. Glassware was dried in an oven at 150 °C.

Reactions involving gaseous reagents were handled on a vacuum line equipped with a MKS Baratron gauge. A known pressure of volatile gaseous reagents, calculated from the ideal gas law, was expanded into a bulb of known volume and then condensed at -196 °C into a high pressure vessel consisting of a thick-walled glass bomb attached to a Kontes vacuum stopcock.

Infrared spectra were taken on a Mattson Galaxy 3000 - Fourier Transform Infrared spectrometer (FTIR). All  $^1\text{H}$ ,  $^{31}\text{P}$ - $\{^1\text{H}\}$  and  $^{13}\text{C}\{^1\text{H}\}$  NMR spectra were obtained at room temperature on a superconducting FT spectrometer incorporating Nicolet computers and cryomagnets assembled in the UC Berkeley NMR laboratory by Mr. Rudi Nunlist. The  $^1\text{H}$ ,  $^{31}\text{P}\{^1\text{H}\}$  and  $^{13}\text{C}\{^1\text{H}\}$  spectra were determined at 300 MHz, 121 MHz and 75 MHz, respectively. Elemental analyses were conducted by the U.C. Berkeley Microanalysis Facility. FAB-MS was carried out on a VG-70SE instrument in the U.C. Berkeley Mass Spectrometry Facility.

To prepare sealed NMR tubes, the sample tube was attached by Cajon adapters directly to Kontes vacuum stopcocks. Known volume bulb vacuum transfers were accomplished with an MKS Baratron gauge attached to a high vacuum line.

Unless otherwise specified, all reagents were purchased from commercial suppliers and used without further purification. Trimethylphosphine (Aldrich) was dried over Na and vacuum transferred prior to use. *p*-Thiocresol was recrystallized from pentane and *p*-nitrophenol and *p*-chlorophenol were purified by sublimation. Aniline was heated to reflux in benzene using a Dean-Stark trap and then vacuum distilled.  $(\text{PMe}_3)_4\text{Ru}(\text{C}_2\text{H}_4)$  (**1**),<sup>9</sup>  $(\text{PMe}_3)_4\text{RuCl}_2$  (**2**),<sup>48</sup>  $(\text{PMe}_3)_3\text{Ru}(\text{C}_2\text{H}_4)_2$  (**14**)<sup>17</sup> and *trans*-(DMPE)<sub>2</sub>RuCl<sub>2</sub><sup>19</sup> were prepared by literature methods.

Pentane and hexane (UV grade) were distilled from LiAlH<sub>4</sub> under nitrogen. Benzene and toluene were distilled from sodium benzophenone ketyl under nitrogen. Ether and tetrahydrofuran were distilled from sodium/benzophenone ketyl. Deuterated solvents for use in NMR experiments were dried as their protiated analogues and vacuum transferred from the drying agent.

**$(\text{PMe}_3)_4\text{Ru}(\text{H})(\text{SC}_6\text{H}_4\text{CH}_3)$  (**9**).** One equivalent of *p*-thiocresol (15.9 mg, 0.128 mmol) dissolved in 5 mL of pentane was slowly added to a pentane solution of  $(\text{PMe}_3)_4\text{Ru}(\text{C}_2\text{H}_4)$  (**1**) (53.6 mg, 0.124 mmol) at room temperature. A yellow precipitate formed immediately. The mixture was stirred at room temperature for 3 h to insure complete reaction. The solution was filtered and the remaining solvent was removed from the yellow precipitate *in vacuo*. The product was recrystallized at -30 °C from a CH<sub>2</sub>Cl<sub>2</sub>/ether mixture obtained by room temperature diffusion of ether into CH<sub>2</sub>Cl<sub>2</sub> solution of **9** (32.1 mg, 49% yield).  $^1\text{H}$  NMR (CD<sub>2</sub>Cl<sub>2</sub>)  $\delta$  7.58 (d, *J* = 7.9 Hz), 6.74 (d, *J* = 7.9 Hz), 2.16 (s), 1.42 (d, *J* = 7.1 Hz), 1.34 (t, *J* = 2.6 Hz), 1.32 (d, *J* = 5.5 Hz), -8.95 (dq, *J* = 28.1 Hz, *J* = 85.1 Hz);  $^{31}\text{P}\{^1\text{H}\}$  NMR (CD<sub>2</sub>Cl<sub>2</sub>)  $\delta$  20.6 (m, *J* = 17.9 Hz, *J* = 31.0 Hz), 9.8 (dd, *J* = 31.0 Hz, *J* = 26.7 Hz), -0.74 (m);  $^{13}\text{C}\{^1\text{H}\}$  NMR (CD<sub>2</sub>Cl<sub>2</sub>)  $\delta$  131.84 (s), 131.43 (d, *J* = 2.7 Hz), 130.28 (s), 127.83 (t, *J* = 12.8 Hz), 27.95 (d, *J* = 23.6 Hz), 23.76 (dt, *J* = 3.7 Hz, *J* = 13.0 Hz), 22.64 (d, *J* = 17.5 Hz), 20.60 (s). IR (CD<sub>2</sub>Cl<sub>2</sub>)  $\nu_{\text{Ru-H}}$  1860 cm<sup>-1</sup>. Anal. Calcd for C<sub>19</sub>H<sub>44</sub>P<sub>4</sub>RuS: C, 43.09; H, 8.37. Found: C, 42.91; H, 8.27.

**$(\text{PMe}_3)_4\text{Ru}(\text{H})(\text{OC}_6\text{H}_4\text{-}p\text{-Cl})$  (**10**).** Treatment of  $(\text{PMe}_3)_4\text{Ru}(\text{C}_2\text{H}_4)$  (**1**) (74.2 mg, 0.171 mmol) dissolved in 5 mL of pentane with HOC<sub>6</sub>H<sub>4</sub>-*p*-Cl (25.5 mg, 0.199 mmol) resulted in a change in color of the solution from yellow to white and the formation of a white precipitate over 15 min at room temperature. The mixture was allowed to stir an additional 15 min to ensure complete reaction before the pentane solvent was removed *in vacuo*. The white residue was dissolved in a minimum amount of ether (0.5 mL) and 5 mL of pentane was diffused into the solution at room temperature. The ether/pentane mixture was cooled to -30 °C. After 2 days, 40.8 mg (48%) of pure white solid **10** was collected by filtration.  $^1\text{H}$  NMR (d<sub>8</sub>-THF)  $\delta$  6.70 (d, *J* = 8.9 Hz), 6.60 (d, *J* = 8.9 Hz), 1.38 (d, *J* = 5.71 Hz), 1.33 (d, *J* = 7.8 Hz), 1.30 (t, *J* = 2.8 Hz), -7.93 (ddt, *J* = 26.5 Hz (triplet), *J* = 26.5 Hz, *J* = 101.2 Hz, 1H);  $^{31}\text{P}$  NMR (C<sub>6</sub>D<sub>6</sub>)  $\delta$  A<sub>2</sub>MX 16.2 (dt, P<sub>M</sub>), 1.76 (dd, P<sub>A</sub>), -12.50 (dt, P<sub>X</sub>) *J*<sub>AM</sub> = 33.0 Hz, *J*<sub>AX</sub> = 26.7 Hz, *J*<sub>MX</sub> = 16.5 Hz;  $^{13}\text{C}\{^1\text{H}\}$  NMR (d<sub>8</sub>-THF)  $\delta$  170.7 (d, *J* = 4.4 Hz), 128.4 (s), 121.6 (s), 113.8 (s), 27.4 (dm, *J* = 26.5 Hz), 23.2 (dt, *J* (triplet) = 12.9 Hz, *J* (doublet) = 3.8 Hz), 20.8 (dm, *J* = 15.9 Hz); IR (d<sub>8</sub>-THF) 2814 (w), 2908 (m), 2978 (m), 2225 (w), 1873 (m), 1483 (s), 1319 (s), 1423 (m). Anal. Calcd for C<sub>18</sub>H<sub>41</sub>ClO<sub>4</sub>Ru: C, 40.49; H, 7.74. Found: C, 40.04; H, 7.52.

**$(\text{PMe}_3)_4\text{Ru}(\text{H})(\text{OC}_6\text{H}_4\text{-}p\text{-NO}_2)$  (**11**).** A benzene solution of *p*-nitrophenol (37.9 mg, 0.272 mmol) was added dropwise to a solution of  $(\text{PMe}_3)_4\text{Ru}(\text{C}_2\text{H}_4)$  (**1**) (95.4 mg, 0.220 mmol) over 15 min at room temperature. The solution color turned from yellow to orange immediately upon addition of *p*-nitrophenol. The solution was stirred at room temperature for an additional 8 h to insure complete reaction. The solution was filtered through Celite and the solvent was removed under vacuum. Recrystallization from a 10:1 mixture of pentane:benzene at -30 °C gave 89.4 mg (78%) of orange solid **11**.  $^1\text{H}$  NMR (d<sub>8</sub>-THF)  $\delta$  7.82 (d, *J* = 9.4 Hz, 2H), 6.63 (d, *J* = 9.0 Hz, 2H), 1.41 (d, *J* = 5.7 Hz), 1.36 (d, *J* = 8.0 Hz), 1.30 (t, *J* = 2.7 Hz), -8.03 (ddt, *J* = 25.7 Hz, *J* = 101.2 Hz, 1H);  $^{31}\text{P}$  NMR (CD<sub>2</sub>Cl<sub>2</sub>)  $\delta$  A<sub>2</sub>MX 19.4 (dt, P<sub>M</sub>), 2.48 (dd, P<sub>A</sub>), -0.74 (dt, P<sub>X</sub>) *J*<sub>AM</sub> = 33.8 Hz, *J*<sub>AX</sub> = 25.9 Hz, *J*<sub>MX</sub> = 16.9 Hz;  $^{31}\text{P}\{^1\text{H}\}$  NMR (d<sub>8</sub>-THF)  $\delta$  A<sub>2</sub>MX 17.8 (dt, P<sub>M</sub>), 17.1 (dd, P<sub>A</sub>), -12.9 (dt, P<sub>X</sub>) *J*<sub>AM</sub> = 34.2 Hz, *J*<sub>AX</sub> = 25.9 Hz, *J*<sub>MX</sub> = 17.1 Hz.  $^{13}\text{C}\{^1\text{H}\}$  NMR (d<sub>8</sub>-THF)  $\delta$  179.8 (d, *J* = 3.9 Hz), 133.7 (s), 126.6 (s), 120.0 (s), 27.1 (dd, *J* = 1.5 Hz, *J* = 31.9 Hz), 23.2 (dt, *J* = 3.5 Hz, *J* = 13.1 Hz), 20.8 (d, *J* = 16.8 Hz); IR (C<sub>6</sub>H<sub>6</sub>)  $\nu_{\text{Ru-H}}$  2003 cm<sup>-1</sup>. Anal. Calcd for C<sub>18</sub>H<sub>41</sub>P<sub>4</sub>NO<sub>3</sub>Ru: C, 39.71; H, 7.59. Found: C, 39.53; H, 7.36.

**$(\text{PMe}_3)_3(\text{PPhH}_2)\text{Ru}(\text{H})(\text{PPh})$  (**12**).** To a benzene solution (10 mL) of  $(\text{PMe}_3)_4\text{Ru}(\text{C}_2\text{H}_4)$  (**1**) (56.7 mg, 0.131 mmol) was added one equivalent of phenylphosphine (15.0 mg, 0.136 mmol) dissolved in 1 mL of benzene. The solution became vivid yellow immediately. The solution was allowed to stir at room temperature for 5 min before the solvent was removed *in vacuo*. The yellow residue was dissolved in 1 mL of pentane and cooled to -30 °C. After 24 h, 36.8 mg (51%) of yellow crystalline product was isolated.  $^1\text{H}$  NMR (C<sub>6</sub>D<sub>6</sub>)  $\delta$  6.47 (m), 6.05 (m), 6.26 (d, *J* = 125.3 Hz), 5.32 (d, *J* = 75.5 Hz), 5.11 (m), 3.02 (m), 2.72 (d, *J* = 180.7 Hz), 1.42 (d, *J* = 5.97 Hz), 1.32 (m), 1.03 (d, *J* = 5.7 Hz), 0.99 (d, *J* = 6.4 Hz), -9.42 (m).  $^{31}\text{P}\{^1\text{H}\}$  NMR (C<sub>6</sub>D<sub>6</sub>)  $\delta$  -6.0 (m), -7.8 (M), -10.1 (m), -12.9 (m), -14.8 (m), -19.8 (m), -47.3 (m).  $^{13}\text{C}\{^1\text{H}\}$  NMR (C<sub>6</sub>D<sub>6</sub>)  $\delta$  134.2 (d, *J* = 10.4 Hz), 132.8 (d, *J* = 12.9 Hz), 128.7 (s), 126.9 (s), 122.5 (s), 65.4 (s), 63.5 (s), 25.3 (d, *J* = 19.0 Hz), 21.3 (d, *J* = 19.5 Hz), 23.8 (dd, *J* = 11.3 Hz, *J* = 19.2 Hz). Anal. Calcd for C<sub>21</sub>H<sub>4</sub>P<sub>5</sub>Ru: C, 45.90; H, 7.52. Found C, 45.65; H, 7.84.

**$(\text{PMe}_3)_3\text{Ru}(\text{C}_2\text{H}_4)(\text{C}_2\text{D}_4)$  (**13**).** A degassed benzene solution (0.7 mL) of  $(\text{PMe}_3)_4\text{Ru}(\text{C}_2\text{H}_4)$  (8.3 mg, 0.019 mmol) in an NMR tube was pressurized with C<sub>2</sub>D<sub>4</sub> (0.019 mmol) and the tube was sealed under vacuum. The tube was placed in a 45 °C oil bath and heated at 45 °C for 6 h. Comparison of the NMR spectra of the single product formed to literature data for  $(\text{PMe}_3)_3\text{Ru}(\text{C}_2\text{H}_4)_2$ <sup>17</sup> confirmed its assignment as complex **13**.

**$(\text{DMPE})_2\text{Ru}(\text{C}_2\text{H}_4)$  (**6**).** *trans*-(DMPE)<sub>2</sub>RuCl<sub>2</sub> (**17**) (3.619 g, 7.68 mmol) was dissolved in 60 mL of THF in a glass vessel

Table 14. Data Collection Parameters<sup>a</sup>

	18	20a	21	23	24
temp, K	-89 °C	-114 °C	-100 °C	-95 °C	-112 °C
2 $\theta$ range	3-50°	3-45°	3-45°	3-50°	3-45°
scan width ( $\Delta\theta$ )	0.70 + 0.35 tan $\theta$	0.90 + 0.35 tan $\theta$	0.85 + 0.35 tan $\theta$	0.80 + 0.35 tan $\theta$	1.00 + 0.35 tan $\theta$
scan type	$\theta-2\theta$	$\theta-2\theta$	$\theta-2\theta$	$\theta-2\theta$	$\omega$
scan speed ( $\theta$ , deg/min)	5.49	8.24	5.49	5.49	8.24
vert aperture (mm)	4.0	4.0	4.0	6.0	6.0
horiz aperture (mm)	2.0 + 1.0 tan $\theta$	2.2 + 1.0 tan $\theta$	2.0 + 1.0 tan $\theta$	2.0 + 1.0 tan $\theta$	2.3 + 1.0 tan $\theta$
reflections measured	+h,+k,+l	+h,+k, $\pm$ l	+h,+k, $\pm$ l	+h,+k, $\pm$ l	+h,+k, $\pm$ l
no. rflns collected	2687	3243	3671	4694	5080
no. unique rflns	2663	3107	3359	4244	4885
min/max transmission	0.931/0.984	0.810/0.999	0.833/0.998	0.94	0.925/1.000
no. params refined	139	122	235	387	203
R(F), %	4.6	6.4	4.6	2.20	6.1
R <sub>w</sub> (F), %	6.0	7.8	7.2	2.77	7.7
R <sub>all</sub> , %	7.1	8.4	5.2	2.93	8.3
goodness of fit	2.30	2.95	3.44	1.319	2.99
p factor	0.03	0.03	0.03	0.03	0.03

<sup>a</sup> General information: Diffractometer: ENRAF-Nonius CAD-4. Background: measured over 0.25( $\Delta\theta$ ) (in the case of **24**, measured over 0.25( $\Delta\omega$ )) added to each of the scan. Monochromator: highly oriented graphite, (2 $\theta$  = 12.2°). Radiation: Mo K $\alpha$  ( $\lambda$  = 0.71073 Å). Absorption correction: empirical.

containing finely cut Na (1.60 g, 69.6 mmol). The vessel was degassed with three freeze-pump-thaw cycles on a vacuum line and excess ethylene (54.1 mmol, 1.7 atm) was transferred from a known-volume bulb. The reaction mixture was stirred vigorously at room temperature for 8 d, during which time purple (presumably NaCl and colloidal Na<sup>28</sup>) solid was formed. The excess ethylene and the THF solvent were removed under vacuum, and product **6** was extracted with pentane (6  $\times$  8 mL) to yield 2.97 g (90%) pure product. <sup>1</sup>H NMR (C<sub>6</sub>D<sub>6</sub>)  $\delta$  1.48 (d,  $J$  = 4.2 Hz), 1.35 (m), 1.22 (m), 1.17 (vt,  $J$  = 42.2 Hz), 1.06 (s), 1.02 (m), 0.85 (m), 0.79 (t,  $J$  = 2.3 Hz); <sup>31</sup>P NMR (C<sub>6</sub>D<sub>6</sub>)  $\delta$  A<sub>2</sub>B<sub>2</sub> 43.9 (t,  $J$  = 28.6 Hz), 37.2 (t,  $J$  = 28.5 Hz), <sup>13</sup>C{<sup>1</sup>H} NMR (C<sub>6</sub>D<sub>6</sub>)  $\delta$  33.0 (m), 25.8 (t,  $J$  = 11.5 Hz), 21.0 (m), 8.5 (m), 7.9 (m); IR 2967 (s), 2898 (vs), 2803 (w), 1427 (m), 1270 (w), 1100 (m), 923 (vs), 880 (m), 684 (m), 630 (m) cm<sup>-1</sup>. Anal. Calcd for C<sub>14</sub>H<sub>36</sub>P<sub>4</sub>Ru: C, 39.16; H, 8.45. Found C, 39.34; H, 8.41.

**cis-(DMPE)<sub>2</sub>Ru(SC<sub>6</sub>H<sub>4</sub>Me)(CH<sub>2</sub>CH<sub>3</sub>) (18).** A solution of *p*-thiocresol (29.2 mg, 0.235 mmol) in 3.0 mL of benzene was added slowly to a benzene solution of (DMPE)<sub>2</sub>Ru(C<sub>2</sub>H<sub>4</sub>) (**6**) (100 mg, 0.234 mmol) dissolved in 10 mL of benzene. After two hours, the solvent was removed under vacuum and the product was recrystallized from a pentane/benzene solution (10/1) at -30 °C to yield 99.5 mg (75%) of yellow crystals. <sup>1</sup>H NMR (C<sub>6</sub>D<sub>6</sub>)  $\delta$  7.86 (d,  $J$  = 7.9 Hz, 2H), 6.99 (d,  $J$  = 7.8 Hz, 2H), 2.18 (s), 1.82 (dq,  $J$  = 2.7 Hz, 7.1 Hz), 1.74 (dd,  $J$  = 1.4 Hz,  $J$  = 7.4 Hz), 1.44 (d,  $J$  = 6.6 Hz), 1.30 (d,  $J$  = 7.2 Hz), 1.09 (d,  $J$  = 7.6 Hz), 1.02 (d,  $J$  = 5.7 Hz), 0.92 (dd,  $J$  = 1.3 Hz, 8.1 Hz), 0.82 (d,  $J$  = 5.0 Hz), 0.74 (d,  $J$  = 6.6 Hz), 0.46 (br s); <sup>31</sup>P NMR (C<sub>6</sub>D<sub>6</sub>)  $\delta$  48.3 (ddd,  $J$  = 11.6 Hz,  $J$  = 20.0 Hz,  $J$  = 28.7 Hz), 43.8 (t,  $J$  = 21.8 Hz,  $J$  = 20.8 Hz), 41.0 (t,  $J$  = 21.6 Hz,  $J$  = 21.0 Hz), 29.9 (dd,  $J$  = 7.7 Hz,  $J$  = 28.6 Hz), 27.1 (dd,  $J$  = 7.7 Hz,  $J$  = 28.6 Hz), 21.3 (seven line multiplet,  $J$  = 8.1 Hz,  $J$  = 11.6 Hz,  $J$  = 22.2 Hz); <sup>13</sup>C{<sup>1</sup>H} NMR (C<sub>6</sub>D<sub>6</sub>)  $\delta$  45.6 (d,  $J$  = 8.2 Hz), 137.2 (s), 130.8 (s), 32.8 (m), 32.1 (m), 31.1 (dd,  $J$  = 21.9 Hz,  $J$  = 27.2 Hz), 29.4 (dd,  $J$  = 16.7 Hz,  $J$  = 25.1 Hz), 24.4 (dd,  $J$  = 6.6 Hz,  $J$  = 12.1 Hz), 22.1 (dd,  $J$  = 3.0 Hz,  $J$  = 19.3 Hz), 21.3 (s), 20.5 (d,  $J$  = 14.1 Hz), 18.5 (m), 15.7 (dd,  $J$  = 2.5 Hz,  $J$  = 23.1 Hz), 15.2 (d,  $J$  = 17.2 Hz), 14.3 (dd,  $J$  = 3.1 Hz,  $J$  = 20.3 Hz), 9.2 (d,  $J$  = 20.9 Hz), 5.1 (d,  $J$  = 60.0 Hz); IR 2966 (m), 2906 (s), 2013 (m), 1953 (m), 1481 (m), 1402 (m), 1257 (m), 1085 (w), 966 (s), 890 (m) cm<sup>-1</sup>. Anal. Calcd for C<sub>21</sub>H<sub>44</sub>P<sub>4</sub>RuS: C, 45.56; H, 8.01. Found C, 45.37; H, 7.90.

**X-ray Crystal Structure Determination of 18.** Yellow crystals of **18** were obtained by vapor diffusion of pentane into a benzene solution of **18** followed by cooling to -30 °C for 2 days. A single crystal was mounted on a glass fiber using Paratone N hydrocarbon oil. The crystal used for data collection was then transferred to an Enraf-Nonius CAD-4 diffractometer, centered in the beam, and cooled to -89 °C by a nitrogen flow low-temperature apparatus which had been previously calibrated by a thermocouple placed at the sample

position. Automatic peak search and indexing procedures yielded an orthorhombic reduced primitive cell for **18**. Inspection of the Niggli values revealed no conventional cell of higher symmetry.

The 2687 raw intensity data were converted to structure factor amplitudes and their esd's by correction for scan speed, background and Lorentz and polarization effects. No correction for crystal decomposition was necessary. Inspection of the azimuthal scan data showed a variation I<sub>min</sub>/I<sub>max</sub> = 0.95 for the average curve. An empirical correction based on the observed variation was applied to the data. Inspection of the systematic absences indicated uniquely space group P2<sub>1</sub>2<sub>1</sub>2<sub>1</sub>. Removal of systematically absent and redundant data left 2663 unique data in the final data set.

The structure was solved by Patterson methods and refined by standard least-squares and Fourier techniques, and all non-hydrogen atoms were refined with anisotropic thermal parameters.

The final residuals for 139 variables refined against the 2239 accepted data for which  $F^2 > 3\sigma(F^2)$  were  $R$  = 4.6%,  $R_w$  = 6.0% and G.O.F. = 2.30. The  $R$  value for all 2663 data was 7.1%.

The quantity minimized by the least-squares program was  $\sum w(|F_o| - |F_c|)^2$ , where  $w$  is the weight of a given observation. The  $p$ -factor, used to reduce the weight of the intense reflections, was set to 0.03 throughout the refinement. The analytical forms of the scattering factor tables for the neutral atoms were used, and all scattering factors were corrected for both the real and imaginary components of anomalous dispersion.

Inspection of the residuals ordered in ranges of  $\sin\theta/\lambda$ ,  $|F_o|$ , and parity and value of the individual indexes showed no unusual features or trends. The largest peak in the final difference Fourier map had an electron density of 0.87 e<sup>-</sup>/Å<sup>3</sup>, and the lowest excursion -0.22 e<sup>-</sup>/Å<sup>3</sup>.

Crystal parameters for **18** are listed in Table 1. The bond distances and bond angles are given in Tables 2 and 3, and the data collection parameters are listed in Table 14. The positional, thermal and anisotropic parameters of the non-hydrogen atoms and their estimated standard deviations are available as supplementary material.

**trans-(DMPE)<sub>2</sub>Ru(SC<sub>6</sub>H<sub>4</sub>Me)(H) (19).** In an NMR tube *cis*-(DMPE)<sub>2</sub>Ru(Et)(*p*-thiocresolate) (46.5 mg, 0.084 mmol) was dissolved in 0.7 mL of benzene. The solution was degassed with one freeze-pump-thaw cycle and the NMR tube was sealed under vacuum. The solution was heated to 85 °C for 24 h. The tube was cracked open under an N<sub>2</sub> atmosphere and the solvent removed by lyophilization. Complex **19** was recrystallized at -30 °C from a benzene/pentane solution obtained by room temperature vapor diffusion of pentane into a concentrated benzene solution of **19**. Pale yellow crystals of **19** were obtained (21.3 mg, 48% yield). <sup>1</sup>H NMR (C<sub>6</sub>D<sub>6</sub>)  $\delta$

7.65 (d,  $J = 7.9$  Hz), 6.88 (d,  $J = 7.7$  Hz), 2.19 (s), 1.67 (m), 1.44 (s), 1.23 (m), 1.12 (s), -18.01 (quintet,  $J = 22.0$  Hz);  $^{31}\text{P}\{^1\text{H}\}$  NMR ( $\text{C}_6\text{D}_6$ )  $\delta$  43.2 (s);  $^{13}\text{C}\{^1\text{H}\}$  NMR ( $\text{CD}_3\text{CN}$ )  $\delta$  149.5 (s), 136.0 (s), 130.1 (s), 128.4 (s), 31.6 (quintet,  $J = 13.5$  Hz), 24.6 (quintet,  $J = 6.5$  Hz), 20.8 (s), 15.3 (quintet,  $J = 5.6$  Hz); IR 2962 (m), 2910 (m), 2896 (s), 1856 (m,  $\nu_{\text{Ru-H}}$ ), 1478 (m), 1425 (m), 1296 and 1276 (w), 1074 (m), 935 (s), 890 (m), 725 and 705 (m), 637 (w)  $\text{cm}^{-1}$ . Anal. Calcd for  $\text{C}_{19}\text{H}_{40}\text{P}_4\text{RuS}$ : C, 43.42; H, 7.67. Found C, 43.65; H, 7.52.

**cis-(DMPE) $_2$ Ru(NHPh)(H) (20a).** (DMPE) $_2$ Ru( $\text{C}_2\text{H}_4$ ) (6) (0.208 g, 0.485 mmol) was dissolved in 20 mL of THF in a high pressure vessel. Aniline (45  $\mu\text{L}$ , 0.48 mmol) was syringed directly into the solution in one portion and the resulting mixture was degassed once by a freeze-pump-thaw cycle. The solution was heated at 120  $^\circ\text{C}$  for eight days, interrupted once to be degassed a by freeze-pump-thaw cycle to remove free ethylene. The solvent was removed *in vacuo* and the product recrystallized by vapor diffusion of pentane into a concentrated benzene solution at room temperature and cooling the resulting pentane/benzene solution to -30  $^\circ\text{C}$  to induce crystallization. This single crystallization gave clean product as golden crystalline clusters (107.3 mg, 45% yield).  $^1\text{H}$  NMR ( $d_8$ -THF)  $\delta$  6.47 (br, 4H), 5.57 (t,  $J = 7.1$  Hz, 1H), 1.65 (m), 1.42 (d,  $J = 6.1$  Hz), 1.39 (d,  $J = 5.3$  Hz), 1.34 (d,  $J = 8.2$  Hz), 1.30 (d,  $J = 6.3$  Hz), 1.25 (s), 1.23 (m), 1.19 (s), 1.16 (d,  $J = 6.8$  Hz), -7.53 (dq,  $J = 28.1$  Hz, 96.0 Hz);  $^{31}\text{P}\{^1\text{H}\}$  NMR ( $d_8$ -THF)  $\delta$  49.4 (t,  $J = 21.8$  Hz), 47.5 (br. m), 46.6 (t,  $J = 21.8$  Hz), 44.3 (dd,  $J = 17.0$ , 26.1 Hz), 41.6 (dd,  $J = 16.2$ , 26.6 Hz), 31.6 (br. m);  $^{13}\text{C}\{^1\text{H}\}$  NMR ( $d_8$ -THF)  $\delta$  163.8 (s), 128.0 (br), 117.1 (br), 105.9 (s), 36.1 (m), 33.4 (m), 31.0 (t,  $J = 21.8$  Hz), 30.2 (dd,  $J = 16.1$ , 25.6 Hz), 28.0 (dd,  $J = 7.1$ , 28.4 Hz), 21.6 (d,  $J = 16.6$  Hz), 20.9 (d,  $J = 15.7$  Hz), 20.5 (m), 19.0 (m), 16.0 (d,  $J = 20.4$  Hz), 12.8 (d,  $J = 9.6$  Hz); IR 3353 (vw), 2962 (m), 2896 (s), 2803 (w), 1829 (m,  $\nu_{\text{Ru-H}}$ ), 1591 (s), 1492 (vs), 1419 (m), 1313 (m), 922 (s), 889 (m), 696 (m)  $\text{cm}^{-1}$ . Anal. Calcd for  $\text{C}_{18}\text{H}_{39}\text{NP}_4\text{Ru}$ : C, 43.72; H, 7.95; N, 2.83. Found C, 43.50; H, 8.03; N, 2.87.

**X-ray Crystal Structure Determination of 20a.** Brownish-red crystals of **20a** were obtained from a concentrated toluene solution cooled to -30  $^\circ\text{C}$ . A single crystal was mounted on a glass fiber using Paratone N hydrocarbon oil. Data were collected and refined as described for **18**. Crystal parameters for **20a** are listed in Table 1. The bond distances and bond angles are given in Tables 4 and 5, and the data collection parameters are listed in Table 14. The positional, thermal and anisotropic parameters of the non-hydrogen atoms and their estimated standard deviations are available as supplementary material.

**trans-(DMPE) $_2$ Ru(NHPh)(H) (20b).** (DMPE) $_2$ Ru( $\text{C}_2\text{H}_4$ ) (99.5 mg, 0.23 mmol) was dissolved in 20 mL of THF and aniline (22.0  $\mu\text{L}$ , 0.24 mmol) was syringed into the solution. The bomb was degassed once by a freeze-pump-thaw cycle and the mixture heated at 90  $^\circ\text{C}$  for 5.5 days. The solvent was removed *in vacuo*, and the product was isolated from the remaining starting material by recrystallization under  $\text{N}_2$ . The solid was dissolved in a minimum amount of benzene and pentane vapor was slowly diffused into the benzene solution at room temperature. The resulting benzene/pentane solution was cooled to -30  $^\circ\text{C}$  to induce crystallization. Reddish crystals were obtained (17.6 mg, 15% yield).  $^1\text{H}$  ( $\text{C}_6\text{D}_6$ )  $\delta$  7.22 (t,  $J = 7.4$ ), 6.38 (m), 6.24 (d,  $J = 7.8$  Hz), 1.42 (m), 1.27 (s), 1.16 (m), 1.10 (s), -19.13 (quin,  $J = 22.9$  Hz);  $^{31}\text{P}\{^1\text{H}\}$  NMR ( $\text{C}_6\text{D}_6$ )  $\delta$  44.5 (s);  $^{13}\text{C}\{^1\text{H}\}$  NMR ( $d_8$ -THF)  $\delta$  128.2 (s), 115.8 (s), 104.7 (s), 32.3 (quintet,  $J = 13.6$  Hz), 24.7 (m), 16.3 (br s). Anal. Calcd for  $\text{C}_{18}\text{H}_{39}\text{NP}_4\text{Ru}$ : C, 43.72; H, 7.95; N, 2.83. Found C, 43.92; H, 7.74; N, 2.68.

**cis-(DMPE) $_2$ Ru(PPh)(CH $_2$ CH $_3$ ) (21).** Phenylphosphine (66.5  $\mu\text{L}$ , 0.605 mmol) was syringed into a THF solution of (DMPE) $_2$ Ru( $\text{C}_2\text{H}_4$ ) (**6**, 252.8 mg, 0.589 mmol, dissolved in 10 mL THF). After stirring for 29 h at room temperature, the solvent was removed *in vacuo* and the product was recrystallized from a pentane/benzene (10:1) solution at -30  $^\circ\text{C}$ . The

recrystallization procedure was repeated once to yield 269 mg (89.4%) of yellow crystals.  $^1\text{H}$  ( $\text{C}_6\text{D}_6$ )  $\delta$  7.84 (dd,  $J = 5.2$ , 6.7), 7.17 (t,  $J = 7.7$  Hz), 7.06 (t,  $J = 6.8$  Hz), 2.82 (d,  $J = 198.2$  Hz), 1.76 (dq,  $J = 2.5$ , 6.7 Hz), 1.62 (d,  $J = 6.0$  Hz), 1.40 (m), 1.30 (d,  $J = 3.0$  Hz), 1.10 (m), 1.01 (d,  $J = 5.7$  Hz), 0.86 (m), 0.80 (m), 0.69 (d,  $J = 7.7$  Hz), 0.14 (m);  $^{31}\text{P}\{^1\text{H}\}$  NMR ( $\text{C}_6\text{D}_6$ )  $\delta$  43.0 (m), 40.4 (m), 40.0 (m), 39.0 (m), 30.1 (7 line m), 27.5 (m), 22.0 (broad s), -62.5 (very broad m, 1820 Hz);  $^1\text{H}$  ( $d_8$ -THF)  $\delta$  7.33 (m), 6.81 (t,  $J = 7.3$  Hz), 6.74 (t,  $J = 6.9$  Hz), 2.36 (d,  $J = 189.1$  Hz), 1.60 (m), 1.55 (d,  $J = 6.8$  Hz), 1.47 (m), 1.33-1.31 (complicated m), 1.25 (d,  $J = 5.1$  Hz), 0.58 (d,  $J = 7.4$  Hz), 0.15 (d,  $J = 131.8$  Hz);  $^{13}\text{C}\{^1\text{H}\}$  NMR ( $d_8$ -THF)  $\delta$  154.5 (d,  $J = 34.3$  Hz), 134.0 (d,  $J = 12.9$  Hz), 126.9 (d,  $J = 3.3$  Hz), 122.5 (s), 33.1 (m), 32.1 (m), 23.9 (t,  $J = 10.8$  Hz), 22.5 (d,  $J = 15.5$  Hz), 21.8 (d,  $J = 14.2$  Hz), 20.4 (m), 19.2 (dd,  $J = 7.6$ , 22.8 Hz), 16.7 (t,  $J = 17.8$  Hz), 15.2 (dd,  $J = 3.5$ , 19.1 Hz), 12.7 (m), 9.0 (d,  $J = 21.9$  Hz), 2.5 (dq,  $J = 9.7$ , 56.6 Hz); IR 3055 (w), 2967 (m), 2905 (s), 2830 (m), 1576 (w), 1465 (w) 1427 (w), 1290 (w), 1257 (w), 1205 and 1188 (w), 1099 and 1070 (m), 1018 (m), 930 (s), 896 (m), 691 (m)  $\text{cm}^{-1}$ . Anal. Calcd for  $\text{C}_{20}\text{H}_{43}\text{P}_5\text{Ru}$ : C, 44.53; H, 8.03. Found C, 44.60; H, 7.99.

**X-ray Crystal Structure Determination of 21.** Bright yellow crystals of air-sensitive **21** were obtained from a benzene/pentane solution at -30  $^\circ\text{C}$ . A single crystal was mounted on a glass fiber using Paratone N hydrocarbon oil. Data were collected and refined as described for **18**. Crystal parameters for **21** are listed in Table 1. The bond distances and bond angles are given in Tables 6 and 7, and the data collection parameters are listed in Table 14. The positional, thermal and anisotropic parameters of the non-hydrogen atoms and their estimated standard deviations are available as supplementary material.

**Thermolysis of cis-(DMPE) $_2$ Ru(Et)(PPh) (21).** A THF solution (6 mL) of cis-Ru(Et)(PPh)(DMPE) $_2$  (**21**) (0.284 g, 0.526 mmol) was transferred to a 100 mL high pressure vessel and heated at 90  $^\circ\text{C}$  for 6 d. The solvent was removed *in vacuo*, and the yellow solid was triturated with 2  $\times$  3 mL of pentane and dried *in vacuo* to yield 0.2667 g (99%) of crude product. NMR analysis of this material indicated it to be a 2:1 mixture of (hydrido)(phosphido)ruthenium complexes **22a** and **22b** (see text).  $^1\text{H}$  ( $\text{C}_6\text{D}_6$ )  $\delta$  8.26 (m, *cis*), 7.64 (m, *trans*), 7.18 (t,  $J = 7.3$  Hz, *cis*), 7.04 (m, *trans*), 6.99 (m, *cis*), 3.00 (br, *cis* P-H), 2.8 (br, *trans* P-H), 2.40 (br, *cis* P-H), 2.2 (br, *trans* P-H) 1.62 (m), 1.58 (d,  $J = 6.9$  Hz, *cis*), 1.32 (s, *trans* DMPE Me), 1.27 (d,  $J = 8.0$  Hz, *cis*), 1.22 (d,  $J = 5.9$  Hz, *cis*), 1.13 (s, *trans* DMPE Me), 1.10 (m, *cis*), 1.05 (m, *cis*), 0.85 (d,  $J = 5.6$  Hz, *cis*), 0.82 (m), -9.33 (m, *cis* Ru-H), -13.55 (m, *trans* Ru-H);  $^{31}\text{P}\{^1\text{H}\}$  NMR ( $\text{C}_6\text{D}_6$ )  $\delta$  47.3 (br, *cis*), 44.8 (br, *cis*), 43.6 (s, *trans*), 40.9 (br, *cis*), 40.3 (br, *cis*), 28.5 (br, *cis*), -63.0 (dd,  $J = 13.0$ , 87.2 Hz, *cis* Ru-PPh), -78.0 (s, *trans* Ru-PPh);  $^{13}\text{C}\{^1\text{H}\}$  NMR ( $\text{C}_6\text{D}_6$ )  $\delta$  133.1 ((d,  $J = 14.3$  Hz, *trans* C<sub>ortho</sub>), 132.9 (d,  $J = 11.4$  Hz, *cis* C<sub>ortho</sub>), 127.3 (d,  $J = 4.2$  Hz, *trans* C<sub>meta</sub>), 126.9 (d,  $J = 1.8$  Hz, *cis* C<sub>meta</sub>), 122.0 (s, *cis*), 121.7 (s, *trans*), 33.9 (m), 33.0 (m), 31.5 (m), 31.2 (m), 30.2 (m), 28.0 (m), 26.6 (m), 21.8 (m), 18.4 (m), 16.4 (m), 15.9 (m), 15.1 (m); IR ( $\text{C}_6\text{H}_6$ ) 3055 (w), 2962 (s), 2896 (s), 1829 (m,  $\nu_{\text{Ru-H}}$ ), 1776 (m,  $\nu_{\text{Ru-H}}$ ), 1571 (m), 1419 (m), 1260 (s), 1087 (vs), 1021 (s), 928 (s), 703 (s)  $\text{cm}^{-1}$ .

**trans-(DMPE) $_2$ Ru(H)(OC $_6$ H $_4$ -*p*-CH $_3$ ) (23).** A benzene solution (6 mL) of *p*-cresol (61.3 mg, 0.567 mmol) was added slowly to a stirred benzene solution of (DMPE) $_2$ Ru( $\text{C}_2\text{H}_4$ ) (221.0 mg, 0.515 mmol, dissolved in 2 mL of  $\text{C}_6\text{H}_6$ ) in a 100 mL high pressure vessel. The mixture was heated for 4 h at 75  $^\circ\text{C}$  and then the warm solution was degassed *in vacuo*. The reaction mixture was lyophilized, and the product was extracted with 3 mL toluene leaving behind a white insoluble solid. After removing the toluene *in vacuo*, the product was recrystallized from a pentane/toluene (10:1) solution at -30  $^\circ\text{C}$  to yield 187 mg (71%) of light yellow crystals.  $^1\text{H}$  ( $\text{C}_6\text{D}_6$ )  $\delta$  7.11 (d,  $J = 8.1$ ), 6.38 (d,  $J = 7.7$  Hz), 2.40 (s), 1.66 (m), 1.32 (s), 1.26 (m), 1.00 (s), -23.20 (quintet,  $J = 21.8$  Hz);  $^{31}\text{P}\{^1\text{H}\}$  NMR ( $\text{C}_6\text{D}_6$ )  $\delta$  45.5 (s);  $^{13}\text{C}\{^1\text{H}\}$  NMR ( $\text{C}_6\text{D}_6$ )  $\delta$  171.4 (s), 129.5 (s), 119.9 (s),

116.8 (s), 31.1 (quintet,  $J = 13.4$  Hz), 22.8 (quintet,  $J = 7.5$  Hz), 21.1 (s), 15.4 (quintet,  $J = 5.3$  Hz); IR ( $C_6H_6$ ) 2969 (w), 2903 (m), 1929 (m,  $\nu_{Ru-H}$ ), 1604 (m), 1489 (vs), 1419 (w), 1313 (m), 928 (s), 889 (m), 730 (w), 710 (w)  $cm^{-1}$ . Anal. Calcd for  $C_{19}H_{40}OP_4Ru$ : C, 44.79; H, 7.91. Found C, 44.60; H, 7.99.

**X-ray Crystal Structure Determination of 23.** Large, pale yellow crystals of **23** were collected by vapor diffusing pentane (10 mL) into a toluene solution of **23** (1 mL) and cooling the resulting pentane/toluene solution to  $-30$  °C for 24 h. A single crystal was mounted on a glass fiber using Paratone N hydrocarbon oil and data taken and analyzed as described for complex **18** (see Table 1).

In a difference Fourier map calculated following the refinement of all non-hydrogen atoms with anisotropic thermal parameters, peaks were found corresponding to the positions of all the hydrogen atoms. Hydrogen atoms were included in structure factor calculations and refined with isotropic thermal parameters. In the final cycles of least-squares, 51 data in two regions of the  $h_0/$  plane were given zero weight because they had abnormally large weighted difference values.

The final residuals for 387 variables refined against the 3563 accepted data for which  $F^2 > 3\sigma(F^2)$  were  $R = 2.20\%$ ,  $R_w = 2.77\%$  and  $GOF = 1.319$ . The  $R$  value for all 4244 data was 2.93%. In the final cycles of refinement a secondary extinction parameter was included (maximum correction: 11% on  $F$ ).

Inspection of the residuals ordered in ranges of  $\sin\theta/\lambda$ ,  $|F_o|$ , and parity and value of the individual indexes showed no unusual features or trends. The largest peak in the final difference Fourier map had an electron density of  $0.43 e^{-}/\text{\AA}$ , and the lowest excursion  $-0.10 e^{-}/\text{\AA}$ .

Crystal data parameters for **23** are listed in Table 1. The bond distances and bond angles are given in Tables 8 and 9, and the data collection parameters are listed in Table 14. The positional, thermal and anisotropic parameters of the non-hydrogen atoms and their estimated standard deviations are available as supplementary material.

**[trans-(DMPE)<sub>2</sub>Ru(C<sub>2</sub>H<sub>4</sub>)(H)]<sup>+</sup>[OC<sub>6</sub>H<sub>4</sub>-*p*-CH<sub>3</sub>2HOC<sub>6</sub>H<sub>4</sub>-*p*-CH<sub>3</sub>]<sup>-</sup> (**24**).** A toluene solution (3.0 mL) of *p*-cresol (30 mg, 0.276 mmol) was cooled to  $-30$  °C and added rapidly to a cold ( $-30$  °C) toluene solution of (DMPE)<sub>2</sub>Ru(C<sub>2</sub>H<sub>4</sub>) (55 mg, 0.139 mmol dissolved in 0.5 mL of toluene), instantly generating a white precipitate. The temperature of the reaction solution was maintained at  $-30$  °C for 10 min, at which point the supernatant was decanted off and the white solid washed with  $2 \times 1$  mL cold ( $-30$  °C) pentane. The solid was dried *in vacuo* to yield 63.2 mg (91.1%) of the crude product. The crude product (50.0 mg) was dissolved in  $CH_2Cl_2$ , and pentane (10:1 pentane to  $CH_2Cl_2$ ) was slowly diffused into the solution at  $-30$  °C. Clear, colorless crystals of the pure product were obtained (30.3 mg, 55%). <sup>1</sup>H NMR ( $CD_2Cl_2$ )  $\delta$  14.32 (s, 2H), 6.84 (d,  $J = 8.1$  Hz, 6H), 6.71 (d,  $J = 8.1$  Hz, 6H), 2.18 (s, 9H), 1.89 (m, 4H), 1.64 (m, 8H), 1.43 (s, 12H), 1.20 (s, 12H),  $-9.91$  (quintet,  $J = 22.6$  Hz, 1H); <sup>31</sup>P{<sup>1</sup>H} NMR ( $CD_2Cl_2$ )  $\delta$  41.5 (s); <sup>13</sup>C{<sup>1</sup>H} NMR ( $CH_2Cl_2$ )  $\delta$  160.3 (s), 129.7 (s), 124.2 (s), 117.0 (s), 46.3 (s), 30.5 (quintet,  $J = 13.2$  Hz), 22.8 (quintet,  $J = 8.8$  Hz), 20.5 (s), 13.0 (quintet,  $J = 6.7$  Hz); MS-FAB [sulfolane]  $m/z = 431.089 [M^+]$ . The spectrum also contained a small pattern centered around  $m/z = 465$  with relative intensities

that match exactly those predicted for the corresponding chloride; a 15% contamination by this material was noted in the X-ray study summarized below.

**X-ray Crystal Structure Determination of 24.** Clear, colorless crystals of **24** formed from vapor diffusion of pentane into  $CH_2Cl_2$  carried out at  $-30$  °C. A single crystal was mounted on a glass fiber using Paratone N hydrocarbon oil. Data were collected and refined as described for **18**. The specific crystal parameters for **24** are listed in Table 1. The positional, thermal and anisotropic parameters of the non-hydrogen atoms and their estimated standard deviations are available as supplementary material. The bond distances and bond angles are given in Tables 10 and 12 and Tables 11 and 13, respectively, and the data collection parameters are listed in Table 14.

**Ru(CH=CH<sub>2</sub>)<sub>2</sub>(PMe<sub>3</sub>)<sub>4</sub> (**7**).** Vinylmagnesium bromide (5.0 mL of a 1.0 M ether solution, 0.50 mmol) was added by syringe to an ether (10 mL) slurry of Ru(PMe<sub>3</sub>)<sub>4</sub>(Cl)<sub>2</sub> (**2**) (111 mg, 0.234 mmol) at room temperature. After stirring for 6 h the orange solution turned white. The ether was removed *in vacuo* and the product was extracted with pentane ( $8 \times 10$  mL). The pentane was removed *in vacuo* and **7** was crystallized from hexane at  $-30$  °C. After 2 d, 55.0 mg of white product **7** (50%) was obtained. <sup>1</sup>H NMR ( $C_6D_6$ )  $\delta$  8.2 (m, 2H), 6.6 (m, 2H), 5.7 (m, 2H), 1.18 (t,  $J = 27$  Hz, 18H), 1.13 (d,  $J = 4.7$  Hz, 18H); <sup>13</sup>C{<sup>1</sup>H} NMR ( $C_6D_6$ )  $\delta$  121.6 (t,  $J = 4.7$  Hz), 69.52 (s), 24.03 (m), 20.19 (t,  $J = 13.2$ ); <sup>31</sup>P{<sup>1</sup>H} NMR ( $C_6D_6$ )  $\delta$   $-6.44$  (t,  $J = 25.8$  Hz),  $-12.43$  (t,  $J = 25.8$  Hz). Anal. Calcd for  $C_{16}H_{42}P_4Ru$ : C, 41.83; H, 9.21. Found: C, 41.78; H, 9.01.

**Ru( $\eta^4$ -C<sub>4</sub>H<sub>6</sub>)(PMe<sub>3</sub>)<sub>3</sub> (**8**).** A degassed benzene (10 mL) solution of **7** (72.5 mg, 0.158 mmol) was heated to 55 °C for 48 h during which time the colorless starting solution turned orange. The solvent was removed *in vacuo* and the product was crystallized from hexanes at  $-30$  °C yielding 29.0 mg (48%) of orange crystals: mp 165–170 °C; <sup>1</sup>H NMR ( $C_6D_6$ )  $\delta$  4.3 (br. s, 2H), 1.33 (d,  $J = 6.8$  Hz), 1.01 (t,  $J = 5.5$  Hz),  $-0.42$  (m); <sup>31</sup>P{<sup>1</sup>H} NMR ( $C_6D_6$ )  $\delta$  2.81 (t,  $J = 6.8$  Hz),  $-1.79$  (d,  $J = 6.7$  Hz); <sup>13</sup>C{<sup>1</sup>H} NMR ( $C_6D_6$ )  $\delta$  79.1 (m), 28.9(m), 25.8(m), 24.1 (m); MS-FAB [sulfolane]  $m/z = 384 [M^+]$ .

**Acknowledgment.** We are grateful for financial support of this work from the National Institutes of Health (Grant no. R37 GM25459). The authors would like to express their gratitude to Dr. Robert D. Simpson for his suggestion of the synthesis of (DMPE)<sub>2</sub>Ru(C<sub>2</sub>H<sub>4</sub>)-(6).

**Supplementary Material Available:** Tables of crystal and data collection parameters, positional and thermal parameters, bond distances and angles, and torsion angles for **18**, **20a**, **21**, **23**, and **24** (34 pages). This material is contained in many libraries on microfiche, immediately follows this article in the microfilm version of the journal, and can be ordered from the ACS; ordering information is given on any current masthead page.

OM940486Q

# Ab Initio Molecular Orbital and Experimental Studies of Hydride Addition to Phosphine-Substituted Manganese Carbonyl Complexes

Dermot F. Brougham, David A. Brown,\* Noel J. Fitzpatrick, and William K. Glass

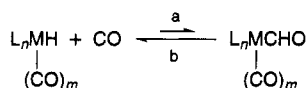
Department of Chemistry, University College Dublin, Belfield, Dublin 4, Ireland

Received June 29, 1994<sup>®</sup>

Ab initio molecular orbital calculations on  $[\text{Mn}(\text{CO})_6]^+$ ,  $[\text{Mn}(\text{CO})_5(\text{PH}_3)]^+$ , and the formyl and hydride complexes derived from these show that the increased stability of *cis*- $\text{Mn}(\text{CO})_4(\text{PR}_3)(\text{CHO})$  and similar formyl complexes is largely kinetic in origin. The transition state for the unsubstituted formyl complex, which forms the corresponding hydride by a simple dissociative mechanism, differs from the transition states for the substituted formyl complexes, which form the corresponding hydrides by concerted mechanisms. Experimental studies of hydride addition to diphenylphosphinoalkane-substituted hexacarbonylmanganese cations are in accord with the theoretical conclusions.

## Introduction

For nearly two decades, there has been continued interest in the hydride reduction of metal carbonyl complexes, motivated at least in part by interest in the Fischer–Tropsch reaction involving hydrogenation of carbon monoxide catalyzed by transition metal compounds.<sup>1</sup> In a number of cases, e.g., hydride addition to  $[\text{CpFe}(\text{CO})_3]^+$ , low-temperature spectroscopy has provided clear evidence for the intermediacy of metal formyl complexes such as  $\text{CpFe}(\text{CO})_2(\text{CHO})$ .<sup>2</sup> In the case of the prototype manganese formyl,  $\text{Mn}(\text{CO})_5(\text{CHO})$ , no spectroscopic evidence has yet been obtained for its existence although it is strongly implicated as an intermediate in both the reaction of  $\text{NaMn}(\text{CO})_5$  with acetic  $^{13}\text{C}$ formic anhydride<sup>3</sup> and the substitution reactions of  $\text{Mn}(\text{CO})_5\text{H}$  with labeled CO.<sup>4</sup> In general, attempts to prepare stable metal formyls by CO insertion into metal hydrogen bonds (pathway a) have been



unsuccessful in contrast to the well-documented CO insertion into metal–alkyl bonds; this failure is attributed to the greater M–H bond strength compared to the homologous M–C bonds.<sup>5,6</sup> It is still not clear whether the reverse reaction (pathway b) of a metal formyl to form the corresponding metal hydride with loss of CO is determined by thermodynamic factors or is kinetic in origin. The balance between these will depend on the mechanism of CO loss. For example, third-row metals (e.g., Re) form stronger metal ligand bonds than first row (e.g., Mn), so if the loss of CO from

the formyl proceeds by a dissociative mechanism, then third-row metal formyls should have greater kinetic stability as discussed by Gladysz.<sup>7</sup>

The nature of the  $\text{L}_n$  ligands is also very important, and as noted above, if the ligands  $\text{L}_n$  are replaced by a  $\pi$ -acid such as a Cp ring, the formyls can be observed spectroscopically and only lose CO to form the corresponding metal hydrides on raising the temperature. In the case of  $\text{Mn}(\text{CO})_5(\text{CHO})$ , replacement of some of the carbonyl groups by phosphines and phosphites leads to the formation of stable metal formyls. For example, the crystal structure of  $[\text{Mn}(\text{CO})_2(\text{P}(\text{O}(\text{Ph})_2)_3)_3(\text{CHO})]$  has been reported<sup>8</sup> and a range of the *trans* complexes,  $[\text{Mn}(\text{CO})_{5-n}(\text{PPh}_3)_n(\text{CHO})]$ ,  $n = 1, 2$ , prepared.<sup>9</sup> Clearly, replacement of CO by weaker  $\pi$ -acceptors such as phosphites and phosphines, which should lead to increased electron density on the metal, also leads to enhanced stability of the corresponding metal formyls.

The object of the theoretical part of this paper is to examine in detail the various factors influencing the relative stabilities of a series of manganese formyls and hydrides of the above types and, in particular, to assess the relative importance of thermodynamic and kinetic factors. Ab initio calculations were completed on the cationic parent complexes,  $[\text{Mn}(\text{CO})_6]^+$  and  $[\text{Mn}(\text{CO})_5(\text{PH}_3)]^+$ , on the three daughter formyl complexes,  $\text{Mn}(\text{CO})_5(\text{CHO})$ , *cis*- $\text{Mn}(\text{CO})_4(\text{PH}_3)(\text{CHO})$ , and *trans*- $\text{Mn}(\text{CO})_4(\text{PH}_3)(\text{CHO})$ , and also on the corresponding hydride complexes,  $\text{Mn}(\text{CO})_5\text{H}$ , *cis*- $\text{Mn}(\text{CO})_4(\text{PH}_3)\text{H}$ , and *trans*- $\text{Mn}(\text{CO})_4(\text{PH}_3)\text{H}$ . In addition, stationary points for the decomposition of each of the three formyl complexes to the corresponding hydride complexes were located.

## Computational Details

Ab initio molecular orbital calculations on the species I–XI were carried out using the Gaussian 92 program.<sup>10</sup>

The stationary points were initially located at the Hartree–Fock level using the 3-21G\*\* basis set.<sup>11</sup>

(7) Gladysz, J. A. *Adv. Organomet. Chem.* 1982, 20, 1.

(8) Berke, H.; Huttner, G.; Scheidsteger, O.; Weiler, G. *Angew. Chem., Int. Ed. Engl.* 1984, 23, 737.

(9) Gibson, D. H.; Owens, K.; Mandal, S. K.; Sattich, W. E.; Franco, J. O. *Organometallics* 1989, 8, 498.

<sup>®</sup> Abstract published in *Advance ACS Abstracts*, November 1, 1994.

(1) Pichler, H.; Schulz, H. *Chem.-Ing.-Tech.* 1970, 42, 1162.

(2) Brown, D. A.; Glass, W. K.; Ubeid, M. T. *Inorg. Chim. Acta* 1984, 89, L45.

(3) Fiato, R. A.; Vidal, J. L.; Pruet, R. L. *J. Organomet. Chem.* 1979, 172, C4.

(4) Byers, B. H.; Brown, T. L. *J. Organomet. Chem.* 1977, 127, 181.

(5) Berke, H.; Hoffmann, R. *J. Am. Chem. Soc.* 1978, 100, 7224.

(6) Ziegler, T.; Versluis, L.; Tschinke, V. *J. Am. Chem. Soc.* 1986, 108, 612.



$[\text{Mn}(\text{CO})_6]^+$	$[\text{Mn}(\text{CO})_5(\text{PH}_3)]^+$	
I	II	
$\text{Mn}(\text{CO})_5(\text{CHO})$	<i>cis</i> - $\text{Mn}(\text{CO})_4(\text{PH}_3)(\text{CHO})$	<i>trans</i> - $\text{Mn}(\text{CO})_4(\text{PH}_3)(\text{CHO})$
III	IV	V
$\text{Mn}(\text{CO})_5\text{H}$	<i>cis</i> - $\text{Mn}(\text{CO})_4(\text{PH}_3)\text{H}$	<i>trans</i> - $\text{Mn}(\text{CO})_4(\text{PH}_3)\text{H}$
VI	VII	VIII
T.S.	T.S.	T.S.
IX	X	XI

These points were characterized by harmonic vibrational analyses at the HF/3-21G\*\* level (designated by HF). The geometrical parameters were then refined using second-order Møller–Plesset perturbation calculations for all the species considered, except the transition states (IX–XI), using the 3-21G basis set with d polarization function on phosphorus only, MP2/3-21G (d p) (designated by MP2). The zero-point corrections were estimated from HF harmonic vibrational wave-number calculations.

All the bond angles at Mn were assumed to be 90° throughout. The formyl groups were kept planar. This assumption is justified by published X-ray data.<sup>8</sup> All the carbonyl groups were assumed to be linear. C–O and M–C bond lengths of the carbonyl groups were considered equal if they possessed the same *trans* group, and the geometry of the PH<sub>3</sub> group was frozen throughout at the standard value.<sup>12</sup> The other geometrical parameters were allowed to optimize freely.

These choices were dictated by computational limitations. Similar choices have been adequate in discussing hydride attack on  $[\text{CpFe}(\text{CO})_3]^+$ .<sup>13</sup>

Initial calculations indicated that the energy surface for rotation of the formyl group is almost flat in agreement with the conclusions for the  $\text{CpFe}(\text{CO})_2(\text{CHO})$  system.<sup>13</sup> At the HF level optimization of  $\text{Mn}(\text{CO})_5(\text{CHO})$  (III) gave the eclipsed form, which is less than 1 kcal mol<sup>-1</sup> lower in energy than the staggered form. The *cis*- $\text{Mn}(\text{CO})_4(\text{PH}_3)(\text{CHO})$  complex (IV) optimized to the eclipsed form, with the formyl hydrogen syn to the PH<sub>3</sub> group. The *trans*- $\text{Mn}(\text{CO})_4(\text{PH}_3)(\text{CHO})$  complex optimized to the eclipsed form. Preliminary calculations, at the HF level, showed that rotation of the phosphine group is a very low energy process (<0.01 kcal mol<sup>-1</sup>) in these systems. Thus, the phosphine group was rotationally frozen during the geometry optimizations at values which maximize the distances from the phosphine hydrogens to the atoms of the other ligands.

## Results and Discussion

**Energies.** At the HF level both the parent cations I and II are minima, having all real frequencies.  $\text{Mn}(\text{CO})_5(\text{CHO})$  (III) has one imaginary frequency corresponding to a rotation of the formyl group. As mentioned above, rotation of the formyl group is a low-

energy process; thus, the stationary state is considered a minimum. A similar result was obtained for  $\text{CpFe}(\text{CO})_2(\text{CHO})$ .<sup>13</sup>

The complex *cis*- $\text{Mn}(\text{CO})_4(\text{PH}_3)(\text{CHO})$  (IV) has all frequencies real and thus is a minimum. However *trans*- $\text{Mn}(\text{CO})_4(\text{PH}_3)(\text{CHO})$  (V) has one imaginary frequency, corresponding to a movement of two mutually *trans* carbonyls towards the phosphine and the other carbonyls away from it. Thus the minimum of this species has a slightly distorted octahedral structure.

The three hydride structures (VI–VIII) have imaginary frequencies. However,  $\text{Mn}(\text{CO})_5\text{H}$  is a stable molecule with geometry<sup>14</sup> quite close to the calculated HF geometry. Calculations of the frequencies at the MP2 level were computationally too expensive.

Stationary points along the decomposition pathway of  $\text{Mn}(\text{CO})_5(\text{CHO})$  (III) to  $\text{Mn}(\text{CO})_5\text{H}$  (VI) and CO and for *cis*- and *trans*- $\text{Mn}(\text{CO})_4(\text{PH}_3)(\text{CHO})$  (IV and V) to the corresponding hydrides VII and VIII and CO were located at the HF level, using the constraint, as noted above, of keeping the 90° angles at Mn. Due to this constraint the “transition states” exhibited three imaginary frequencies. In the *cis* transition state X these were at -934, -392, and -156 cm<sup>-1</sup>, essentially corresponding to in-plane H migration, out-of-plane H migration, and formyl group rearrangement. In the *trans* transition state XI, the corresponding frequencies were at -914, -335, and -242 cm<sup>-1</sup>, with assignments as in the *cis* case.

Table 1 gives the total and relative energies for various species, at both HF and MP2 levels, with and without ZPE corrections. From these values it is noted that, at both the HF and the MP2 levels, the *cis* isomers have lower energies than the *trans* isomers for the formyl and hydride complexes. The extra stability is possibly due to weaker  $\pi$  accepting ligands *trans* to CO enhancing the  $\pi$ -back-bonding to the carbonyls. This mechanism to increase the thermodynamic stability of the *cis* isomers is vindicated by the details of this study discussed below.

Table 1 also gives the enthalpies for the formation reaction ( $\Delta H_f$ )  $[\text{Mn}(\text{CO})_5(\text{L})]^+ + \text{H}^- \rightarrow \text{Mn}(\text{CO})_4(\text{L})(\text{CHO})$  and for the dissociation reaction ( $\Delta H_d$ )  $\text{Mn}(\text{CO})_4(\text{L})(\text{CHO}) \rightarrow \text{Mn}(\text{CO})_4(\text{L})\text{H} + \text{CO}$ , where L = CO, PH<sub>3</sub>.  $\Delta H_f$  and  $\Delta H_d$  were calculated from the MP2 results, and a zero-point correction calculated at the HF level, due to computational limitations, was included. The results in Table 1 show that the formation of the formyl is exothermic in all three cases, and the results in the three series differ little. The evidence for the existence of  $\text{Mn}(\text{CO})_5(\text{CHO})$  is indirect, yet phosphine-substituted formyls exist. Thus  $\Delta H_f$ , whose absolute value is greater in the unsubstituted case, does not reflect the instability of  $\text{Mn}(\text{CO})_5(\text{CHO})$ . The theoretical enthalpies of formation presented here compare favorably with values in other studies. In  $\text{CpFe}(\text{CO})_2(\text{CHO})$ , a corresponding value of -202 kcal mol<sup>-1</sup> was calculated.<sup>13</sup> Lane and Squires<sup>15</sup> obtained a value of -194 kcal mol<sup>-1</sup> for the gas phase enthalpy of formation of  $[\text{Fe}(\text{CO})_4(\text{CHO})]^-$  from the corresponding carbonyl complex and H<sup>-</sup>. Similarly, the  $\Delta H_d$  values do not explain the increased stability of the formyls with monosubstitution

(10) Frisch, J. M.; Head-Gordon, M.; Schlegel, H. B.; Raghavachari, K.; Binkley, J. S.; Gonzalez, C.; De Frees, D. J.; Fox, D. J.; Whiteside, R. A.; Seeger, R.; Melius, C. F.; Baker, J.; Kahn, L. R.; Stewart, J. J. P.; Fluder, E. M.; Topiol, S.; Pople, J. A. *GAUSSIAN 92*; Gaussian Inc.: Pittsburgh, PA, 1992.

(11) Binkley, J. S.; Pople, J. A.; Hehre, W. J. *J. Am. Chem. Soc.* **1980**, *102*, 939.

(12) Hehre, W. J.; Ditchfield, R.; Stewart, R. F.; Pople, J. A. *J. Chem. Phys.* **1970**, *52*, 2769.

(13) Brown, D. A.; Fitzpatrick, N. J.; Groarke, P. J.; Koga, N.; Morokuma, K. *Organometallics* **1993**, *12*, 2521.

(14) La Placa, S. L.; Hamilton, W. C.; Ibers, J. A.; Davidson, A. *Inorg. Chem.* **1969**, *9*, 1928.

(15) Lane, K. R.; Squires, R. L. *Polyhedron* **1988**, *7*, 1609.

Table 1. Energetics

	HF	MP2
Total Energies (au)		
[Mn(CO) <sub>6</sub> ] <sup>+</sup> (I)	-1816.91034	-1818.09157
[Mn(CO) <sub>5</sub> (PH <sub>3</sub> ) <sup>+</sup> (II)	-2045.49798	-2046.64128
H <sup>-</sup>	-0.40042	-0.40638
CO	-112.09330	-112.30484
Relative Energies (kcal mol <sup>-1</sup> ) <sup>a</sup>		
[Mn(CO) <sub>6</sub> ] <sup>+</sup> (I) + H <sup>-</sup>	0.0 (0.0)	0.0 (0.0)
Mn(CO) <sub>5</sub> (CHO) (III)	-181.5 (-175.1)	-228.1 (-221.7)
Mn(CO) <sub>5</sub> H (VI) + CO	-141.2 (-139.5)	-233.2 (-231.5)
Mn(CO) <sub>5</sub> (CHO) (IX, TS)	-154.7	
[Mn(CO) <sub>5</sub> (PH <sub>3</sub> ) <sup>+</sup> (II) + H <sup>-</sup>	0.0 (0.0)	0.0 (0.0)
<i>cis</i> -Mn(CO) <sub>4</sub> (PH <sub>3</sub> )(CHO) (IV)	-176.1 (-169.6)	-217.2 (-210.7)
<i>trans</i> -Mn(CO) <sub>4</sub> (PH <sub>3</sub> )(CHO) (V)	-175.0 (-168.4)	-202.2 (-195.6)
<i>cis</i> -Mn(CO) <sub>4</sub> (PH <sub>3</sub> )H (VII) + CO	-134.7 (-133.2)	-221.7 (-220.2)
<i>trans</i> -Mn(CO) <sub>4</sub> (PH <sub>3</sub> )H (VIII) + CO	-130.7 (-129.6)	-201.0 (-199.9)
<i>cis</i> -Mn(CO) <sub>4</sub> (PH <sub>3</sub> )(CHO) (X, TS)	-136.4	
<i>trans</i> -Mn(CO) <sub>4</sub> (PH <sub>3</sub> )(CHO) (XI, TS)	-138.8	
Thermochemical Data <sup>b</sup> (kcal mol <sup>-1</sup> )		
	$\Delta H_f$	$\Delta H_d$
unsubstituted complexes	-221.7	-9.8
<i>cis</i> -substituted complexes	-210.7	-9.5
<i>trans</i> -substituted complexes	-195.5	-4.3

<sup>a</sup> Values with HF ZPE corrections in parentheses. <sup>b</sup> Values at the MP2 level with ZPE corrections.

by phosphines, since  $\Delta H_d$  for the unsubstituted and *cis*-substituted complexes differ by an insignificant amount, -9.8 and -9.5 kcal mol<sup>-1</sup>, respectively. It is noted that it is the *cis*-monosubstituted form that is found experimentally.<sup>9</sup> Lane and Squires<sup>15</sup> recently estimated from published thermochemical data that the decomposition of [Fe(CO)<sub>4</sub>(CHO)]<sup>-</sup> to [Fe(CO)<sub>4</sub>H]<sup>-</sup> and CO was moderately exothermic, -21 kcal mol<sup>-1</sup>. This compares favorably with the values of  $\Delta H_d$  in this study. These small exothermic values for  $\Delta H_d$  suggest that the view<sup>5,6</sup> that large metal hydrogen bond strengths render CO insertion into neutral metal hydride complexes difficult and that neutral formyl complexes are thermodynamically unstable is suspect.

On the other hand, the values for the *trans*-monosubstituted complexes do differ substantially from both the *cis*-monosubstituted and unsubstituted forms.  $\Delta H_d$  for the *trans*-substituted complexes is -4.3 kcal mol<sup>-1</sup>, which is significantly less exothermic than the previous values of -9.8 and -9.5 kcal mol<sup>-1</sup>. This thermodynamic difference is due to the *trans* geometry being less favorable in the hydride complex than in the formyl complex because of the presence of two strong donor ligands along one coordinate axis in the *trans* hydride, an arrangement which leads to electron density being forced back into the phosphine ligand.

The optimized geometries at the MP2 level for species I–VIII and at the HF level for the transition states IX–XI are given in Figure 1. The effects of substituting CO with PH<sub>3</sub> are clearly evident. For example, the Mn–C(O) bonds *trans* to PH<sub>3</sub> in [Mn(CO)<sub>5</sub>(PH<sub>3</sub>)<sup>+</sup> are shorter than in [Mn(CO)<sub>6</sub>]<sup>+</sup>, and correspondingly, the C–O bonds in the phosphine-substituted species are longer, in accord with the presence of the phosphine increasing back-bonding to the other carbonyls, particularly in the *trans* position.

A similar effect is observed on those bond lengths in Mn(CO)<sub>5</sub>H compared to [Mn(CO)<sub>6</sub>]<sup>+</sup> (Figure 1). Again comparing the *cis* and *trans* hydrides VII and VIII, the Mn–C(O) bonds *trans* to PH<sub>3</sub> and H are shorter than

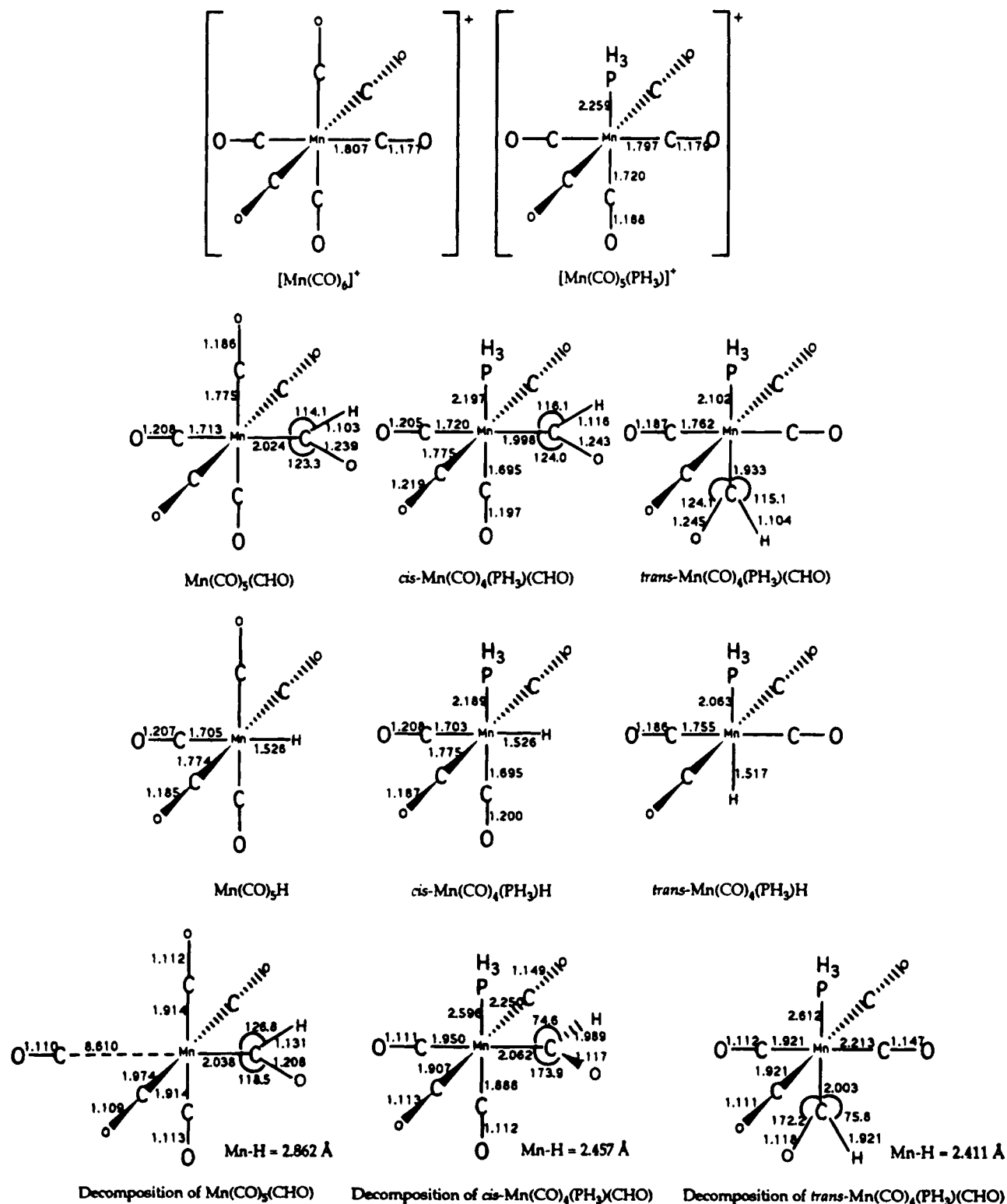
those which are *cis*, and the corresponding C–O bonds are longer, suggesting that the relative thermodynamic stability of VII is due to enhanced back-bonding to the carbonyls *trans* to substituents of less back-bonding ability. In the case of the formyls III–V, the calculated Mn–C(O) and C–O bond lengths are shorter and longer, respectively, than those in [Mn(CO)<sub>6</sub>]<sup>+</sup>, and moreover, the Mn–C(O) bond lengths in III are shorter than those in [Mn(CO)<sub>5</sub>(PH<sub>3</sub>)<sup>+</sup> (II), indicating greater back-bonding to carbonyls in the neutral formyl species III than in the cationic phosphine complex II. A comparison of the *cis* and *trans* species IV and V is also of interest (see Figure 1). In *trans*-Mn(CO)<sub>4</sub>(PH<sub>3</sub>)(CHO) (V), the Mn–C(O) and C–O bond lengths *trans* to CO are 1.762 and 1.187 Å, respectively, whereas in the *cis* complex IV the Mn–C(O) *trans* to PH<sub>3</sub> is 1.695 Å and to CHO is 1.720 Å. Thus, carbonyls *trans* to PH<sub>3</sub> and CHO show enhanced back-bonding leading to a slightly greater thermodynamic stability for *cis*-Mn(CO)<sub>4</sub>(PH<sub>3</sub>)(CHO) (IV) than the *trans* isomer V. The calculated Mn–CHO bond lengths may be discussed in terms of the relative contribution of the carbenoid resonance form B (Figure 2). In general, unsubstituted anionic formyls such as [Cr(CO)<sub>5</sub>(CHO)]<sup>-</sup><sup>16</sup> and [Fe(CO)<sub>4</sub>(CHO)]<sup>-</sup><sup>17</sup> are stabilized by significant contributions from the carbenoid resonance form D,<sup>7</sup> as indicated by their unusually low formyl CO stretching frequencies, ~1570 cm<sup>-1</sup> as opposed to the value of ~1600 cm<sup>-1</sup> for neutral formyls, which thus involve a smaller contribution from the carbenoid form B. Comparing Mn(CO)<sub>5</sub>(CHO) (III) with the corresponding *cis* and *trans* PH<sub>3</sub>-substituted formyls IV and V, it is immediately obvious that phosphine substitution leads to an increase in electron density on the metal and hence increased importance from (B). Thus, in Mn(CO)<sub>5</sub>(CHO),  $r(\text{Mn}-\text{CHO}) = 2.024$  Å, while in *cis*- and *trans*-Mn(CO)<sub>4</sub>(PH<sub>3</sub>)(CHO) the values of  $r(\text{Mn}-\text{CHO})$  are 1.998 and 1.933 Å, respectively. Similarly, without phosphine substitution,  $r(\text{C}(\text{H})-\text{O}) = 1.239$  Å, while in the *cis*- and *trans*-Mn(CO)<sub>4</sub>(PH<sub>3</sub>)(CHO),  $r(\text{C}(\text{H})-\text{O}) = 1.243$  (IV) and 1.245 Å (V).

**Kinetic Factors.** The similarity of the above calculated enthalpies ( $\Delta H_d$ ) suggests that the difference in stabilities of the unsubstituted formyl Mn(CO)<sub>5</sub>(CHO) and the corresponding *cis* and *trans* monophosphine-substituted formyls is not thermodynamic in origin and may be kinetic. Accordingly we searched for transition states for decomposition of the formyl species III–V to their corresponding hydrides VI–VIII. The respective transition states which we located using the basis sets discussed above are shown in IX–XI. The transition states X and XI are similar, and in both cases, the geometry of the formyl group has changed from that of the parent formyl, with the formyl hydrogen now being less associated with the carbon and more with the metal and with the C–H bond length being significantly longer and the Mn–H bond significantly shorter while the MnCH bond angle is very small and the formyl MnCO bond angle approaches 180°. These transition states correspond to a concerted mechanism for hydride formation and are in accord with experimental evidence for the decomposition of both monophosphine- and diphosphine-substituted metal formyls to their corresponding hydrides. For example, the decomposition

(16) Casey, C. P.; Neumann, S. M. *J. Am. Chem. Soc.* **1976**, *98*, 5395.

(17) Collman, J. P.; Winter, S. R. *J. Am. Chem. Soc.* **1973**, *95*, 4089.





**Figure 1.** Optimized geometries at the MP2 level of the complexes of this study. Bond lengths are in angstroms and bond angles in degrees. Decomposition transition states are at the HF level.

of the neutral stable formyl  $Mn(CO)_2(P(OPh)_3)_3(CHO)$  to the corresponding hydride shows a clear kinetic isotope effect,  $k_H/k_D = 3.24$  consistent with considerable C-H bond breaking in the transition state.<sup>8</sup> In the case of the formation of  $trans-[RuH(CO)(dppb)_2]$  ( $dppb = 1,4$ -bis(diphenylphosphino)butane,  $PPh_2(CH_2)_4PPh_2$ ) from  $trans-[Ru(CHO)(CO)(dppb)_2]$ , Barratt and Cole-Hamilton<sup>18</sup> invoked a three-centered transition state to explain an isotope effect of  $k_H/k_D = 2.3$ . Their transition state is very similar to that calculated above. In

addition, our own experimental studies described below also indicate a different mechanism for hydride formation as between unsubstituted and phosphine-substituted formyl complexes.

In the case of the unsubstituted formyl,  $Mn(CO)_5(CHO)$ , we were not able to locate a transition state of the above type. Instead, a transition state was located

(18) Barratt, D. S.; Cole-Hamilton, D. J. *J. Chem. Soc., Dalton Trans.* 1987, 2683.

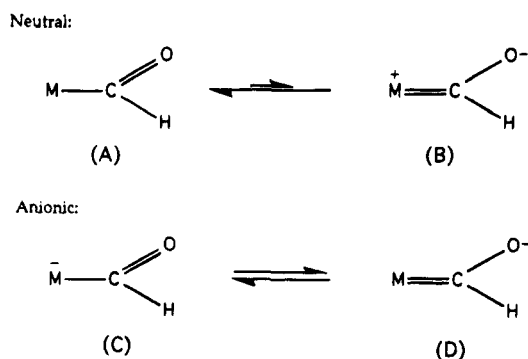


Figure 2. Significant resonance forms.

as shown in IX in which one carbonyl group has almost fully dissociated from the metal,  $r(\text{Mn}(\text{C}(\text{O})) = 8.610 \text{ \AA}$ , while the geometry of the formyl group remains close to that of the parent formyl complex at the HF level. This result suggests that the unsubstituted formyl decomposes to the corresponding hydride by a mechanism different from that of the phosphine-substituted formyls. It appears that initial carbonyl dissociation occurs, possibly with subsequent migration of the CO of the formyl group and formation of the corresponding hydride. Unfortunately we were not able to locate any other transition states to support this argument, so it must remain speculative. Nevertheless, the phosphine-substituted complexes, IV and V, clearly have different transition states from III involving a concerted mechanism and so we conclude that the difference in stability between the unsubstituted and phosphine-substituted metal formyls is kinetic in origin with thermodynamic factors only playing a small part.

**Comparison with Experiment. Hydride Addition to  $[\text{Mn}(\text{CO})_4(\text{PPh}_2(\text{CH}_2)_n\text{PPh}_2)]\text{ClO}_4$  ( $n = 1$ , dppm;  $n = 2$ , dppe;  $n = 3$ , dppp).** In view of the above theoretical results, it was of interest to compare them with detailed studies of the reaction of a hydride donor such as borohydride with the related series of diphosphine-substituted manganese carbonyl complexes,  $[\text{Mn}(\text{CO})_4(\text{PPh}_2(\text{CH}_2)_n\text{PPh}_2)]\text{ClO}_4$ ,  $n = 1, 2$ , and 3, using low-temperature  $^1\text{H}$  NMR spectroscopy to identify intermediates as in analogous studies of hydride addition to  $[(\eta^5\text{-C}_5\text{H}_5)\text{Fe}(\text{CO})_3]^+$ <sup>2</sup> and  $[(\eta^5\text{-C}_9\text{H}_7)\text{Fe}(\text{CO})_3]^+$ .<sup>19</sup>

**Room-Temperature Studies.** Addition of  $\text{NaBH}_4$  to a solution of  $[\text{Mn}(\text{CO})_4(\text{dppe})]\text{ClO}_4$  in THF or acetone gave an immediate color change from yellow to a red/brown suspension and formation of *fac*- $[\text{Mn}(\text{CO})_3(\text{dppe})\text{H}]$  as indicated by replacement of the starter  $\nu(\text{CO})$  infrared peaks with bands at 2003, 1928, and  $1915 \text{ cm}^{-1}$  in agreement with published values.<sup>20</sup> Attempts to isolate and purify  $[\text{Mn}(\text{CO})_3(\text{dppe})\text{H}]$  were unsuccessful but the  $^1\text{H}$  NMR spectrum of the product contained a metal-hydride peak at  $\delta -8.0$  ppm (t,  $J$  46.5 Hz) identical with the published value.<sup>21</sup> Similar results were obtained with  $[\text{Mn}(\text{CO})_4(\text{PPh}_2(\text{CH}_2)_n\text{PPh}_2)]\text{ClO}_4$ ,  $n = 2$  and 3, but again attempts to isolate the hydrides were unsuccessful.

**Low-Temperature Studies.** The reaction of  $[\text{Mn}(\text{CO})_4(\text{dppe})]\text{ClO}_4$  and  $\text{NaBH}_4$  in a 2:1 molar ratio in acetone- $d_6$  was carried out at  $-80$  °C by use of tech-

Table 2. Low-Temperature ( $-65$  °C)  $^1\text{H}$  NMR Data (in ppm) from the Reactions of  $[\text{Mn}(\text{CO})_4(\text{dppx})]\text{ClO}_4$  (dppx = Bis(diphenylphosphinoalkane) with  $\text{NaBH}_4$  in Acetone- $d_6$

	dppx		
	dppm	dppe	dppp
$\delta(^1\text{H})$	14.6(s)	13.4(t), 4 H 15.2(d), 1 H	14.5(s), 12 H 13.7(d), 1 H
$J(\text{PH})$ (Hz)		(t) 10.3 (d) 12.5	(d) 8.9
thermal stability (min)	15, RT <sup>a</sup>	(t) 15, RT (d) 5, RT	(s) 15, RT (d) <1, $-20$ °C

<sup>a</sup> RT, room temperature.

niques previously published.<sup>19</sup> At  $-65$  °C, clear evidence for the initial formation of metal formyls was obtained with characteristic peaks at  $\delta 15.2$  (d, 12.5 Hz) and 13.4 ppm (t, 10.3 Hz), the upfield resonance being about 4 times more intense than the other formyl resonance. No signal corresponding to a metal-hydride ( $\delta -5$  to  $-20$  ppm) was present at this temperature nor did it appear on raising the temperature to  $0$  °C in marked contrast to the behavior of  $[\text{CpFe}(\text{CO})_3]^+$  and  $[\text{IndFe}(\text{CO})_3]^+$ , where on raising the temperature to  $0$  °C the characteristic metal-formyl peaks disappear with concomitant development of metal hydride peaks.<sup>2,19</sup> In the present system, the metal formyl peaks were stable even at room temperature for several minutes with the peak at  $\delta 15.2$  ppm decomposing more rapidly ( $\sim 5$  min) than that at  $\delta 13.4$  ppm ( $\sim 15$  min) (Table 2). At the same time, the region  $\delta 0$ – $10$  ppm became complex, suggesting formation of a number of products, e.g., hydroxymethyl and methyl derivatives formed by further reactions of the metal formyls similar to those occurring with  $[\text{CpFe}(\text{CO})_2(\text{PR}_3)]^+$ .<sup>21</sup> However, on repeating the reaction at low temperatures with an increased molar ratio of  $\text{NaBH}_4$  to substrate (e.g., 1:1), initial formation of the metal formyls was still observed, but on increasing the temperature to  $0$  °C, when there was still some  $\text{NaBH}_4$  present, the metal-hydride peak at  $\delta -8.0$  ppm due to *fac*- $[\text{Mn}(\text{CO})_3(\text{dppe})\text{H}]$  now appeared. The presence of two metal formyl peaks in the region  $\delta 12$ – $15$  ppm often arises because of the formation of a simple metal formyl, e.g.,  $\text{CpFe}(\text{CO})_2(\text{CHO})$  and an adduct, e.g.,  $\text{CpFe}(\text{CO})_2(\text{CHO})\text{BH}_2\text{CN}$ .<sup>2</sup> In the present case, adduct formation may be discounted because on addition of a small quantity of pyridine to the reaction mixture at  $-20$  °C both metal formyl peaks were unaffected. On the basis of the observed coupling constants, we assign the  $\delta 15.2$  ppm peak to *mer*- $\text{Mn}(\text{CO})_3(\text{dppe})(\text{CHO})$  and that at  $\delta 13.4$  to *fac*- $\text{Mn}(\text{CO})_3(\text{dppe})(\text{CHO})$ .

These results show that, in the absence of excess  $\text{NaBH}_4$ , the above formyls do not decompose dissociatively by loss of CO and formation of the corresponding metal-hydride as in our previous studies of  $[\text{CpFe}(\text{CO})_3]^+$  and  $[\text{IndFe}(\text{CO})_3]^+$ .<sup>19</sup> It follows that the diphosphine ligands stabilize the formyl complexes relative to the parent neutral  $\text{Mn}(\text{CO})_5(\text{CHO})$ , which has not been observed spectroscopically. Similar low-temperature results were obtained with  $[\text{Mn}(\text{CO})_4(\text{PPh}_2(\text{CH}_2)_n\text{PPh}_2)]\text{ClO}_4$ ,  $n = 1$  and 3, using  $^1\text{H}$  NMR spectroscopy to monitor the course of reaction, except that for  $[\text{Mn}(\text{CO})_4(\text{PPh}_2\text{CH}_2\text{PPh}_2)]^+$  only one metal formyl at  $\delta 14.6$  ppm was observed (see Table 2).

During the preparation of this paper, a paper by Orchin and co-workers<sup>22</sup> was published reporting a

(19) Ahmed, H. A.; Brown, D. A.; Fitzpatrick, N. J.; Glass W. K. *Inorg. Chim. Acta* **1989**, *164*, 5.

(20) Booth, R. L.; Hazeldine, R. N. *J. Chem. Soc. A* **1966**, 157.

(21) Lapinte, C.; Cathelin, D.; Astruc, D. *Organometallics* **1988**, *7*, 1683.

room-temperature study of the same systems as above but in a different solvent mixture ( $\text{CH}_3\text{CN}/\text{CH}_3\text{OH}/\text{H}_2\text{O}$ ). This enabled them to isolate both the *mer*- and *fac*-metal formyls and record spectroscopic data before decomposition occurred together with an X-ray structure of the methoxymethyl derivative *fac*-(dppb) $\text{Mn}(\text{CO})_3\text{CH}_2\text{OCH}_3$ . Low-temperature  $^1\text{H}$  NMR studies were not reported.

Unlike the acetone system of our study, they found the formyl complexes decomposed directly to the hydride complexes. The  $^1\text{H}$  data for the complexes of their study are similar to ours, given that a different solvent was used. It appears therefore that the reaction is solvent dependent, indicating that the decomposition of both diphosphine and monophosphine formyls is under kinetic control.

### Experimental Section

Solvents were freshly dried by standard methods. All reactions and workup were carried out under high-purity nitrogen. Tertiary diphosphines (dppm, dppe, and dppp) were

---

(22) Mandal, S. K.; Krause, J. A.; Orchin, M. *J. Organomet. Chem.* **1994**, *467*, 113.

obtained commercially and used without further purification. Infrared spectra were measured using a 0.1 mm  $\text{CaF}_2$  cell on a Perkin-Elmer 1720FT spectrometer linked to a 3700 data station.  $^1\text{H}$ ,  $^{13}\text{C}$ , and  $^{31}\text{P}$  NMR spectra were recorded on a JEOL GX270 spectrometer. The complexes  $[\text{Mn}(\text{CO})_4(\text{dppx})]\text{ClO}_4$ ,  $x = m, e, \text{ and } p$ , were prepared by published methods.<sup>23</sup>

### Conclusion

The increased stability of monosubstituted phosphine carbonyl formyl complexes is shown theoretically to be largely kinetic in origin and to arise from quite different transition states between the unsubstituted formyl which forms the corresponding hydride by a simple carbonyl dissociative mechanism and the monophosphine-substituted formyls which form the corresponding hydrides by a concerted mechanism. Experimental studies are in accord with the theoretical conclusions.

**Acknowledgment.** We thank Ms. Geraldine Fitzpatrick for her expert help with the NMR studies and also the reviewers for helpful comments.

OM940511S

---

(23) Carriedo, G. A.; Riera, V.; Santamaria, J. *J. Organomet. Chem.* **1982**, *234*, 17.

**Photochemical Reimer–Tiemann Reactions of  
( $\eta^5\text{-C}_5\text{H}_5$ )<sub>2</sub>Fe<sub>2</sub>( $\mu\text{-CO}$ )<sub>2</sub>( $\mu\text{-Ph}_2\text{PCH}_2\text{PPh}_2$ ) and  
( $\eta^5\text{-C}_5\text{H}_5$ )<sub>2</sub>Fe<sub>2</sub>( $\mu\text{-CO}$ )<sub>2</sub>( $\mu\text{-Ph}_2\text{PCH}_2\text{CH}_2\text{PPh}_2$ ). Molecular  
Structures of ( $\eta^5\text{-C}_5\text{H}_5$ )<sub>2</sub>Fe<sub>2</sub>( $\mu\text{-CO}$ )<sub>2</sub>( $\mu\text{-Ph}_2\text{PCH}_2\text{CH}_2\text{PPh}_2$ )  
and  
( $\eta^5\text{-CHOC}_5\text{H}_4$ )( $\eta^5\text{-C}_5\text{H}_5$ )Fe<sub>2</sub>( $\mu\text{-CO}$ )<sub>2</sub>( $\mu\text{-Ph}_2\text{PCH}_2\text{CH}_2\text{PPh}_2$ )**

Joyce E. Shade,\* Wayne H. Pearson,\* and James E. Brown

*Department of Chemistry, U. S. Naval Academy, Annapolis, Maryland 21402-5026*

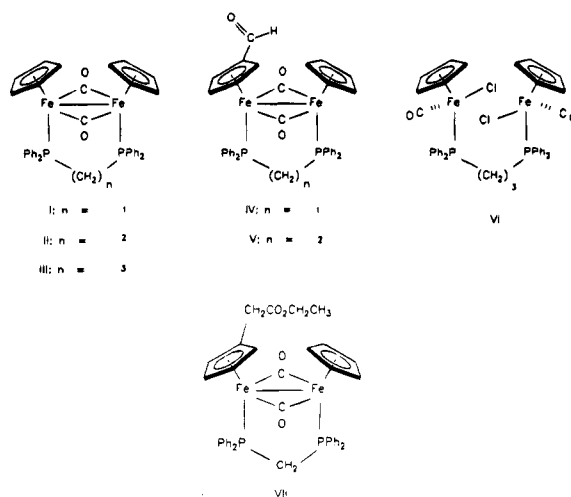
Thomas E. Bitterwolf\*

*Department of Chemistry, University of Idaho, Moscow, Idaho 83844-2343*

Received July 28, 1994<sup>⊗</sup>

Photolysis of either ( $\eta^5\text{-C}_5\text{H}_5$ )<sub>2</sub>Fe<sub>2</sub>( $\mu\text{-CO}$ )<sub>2</sub>( $\mu\text{-DPPM}$ ) (DPPM = Ph<sub>2</sub>PCH<sub>2</sub>PPh<sub>2</sub>), **I**, or ( $\eta^5\text{-C}_5\text{H}_5$ )<sub>2</sub>Fe<sub>2</sub>( $\mu\text{-CO}$ )<sub>2</sub>( $\mu\text{-DPPE}$ ) (DPPE = Ph<sub>2</sub>PCH<sub>2</sub>CH<sub>2</sub>PPh<sub>2</sub>), **II**, in CHCl<sub>3</sub> followed by chromatography on wet alumina results in the formation of products in which one cyclopentadienyl ring has been formylated. In contrast, photolysis of ( $\eta^5\text{-C}_5\text{H}_5$ )<sub>2</sub>Fe<sub>2</sub>( $\mu\text{-CO}$ )<sub>2</sub>( $\mu\text{-DPPP}$ ), **III**, under analogous conditions gives the chloride derivative expected from Fe–Fe bond homolysis. Available evidence suggests that the reactions of **I** and **II** proceed via a photochemical Reimer–Tiemann reaction involving an irreversible charge transfer to yield the respective radical cation and a dichloromethyl radical. Subsequent coupling of these radicals forms a ring-substituted dichloromethyl intermediate which is in turn hydrolyzed to the aldehyde upon workup. Formyl derivatives have been fully characterized by IR, <sup>1</sup>H, <sup>13</sup>C, and <sup>31</sup>P NMR, mass spectrometry, and elemental analysis. Reaction of [( $\eta^5\text{-C}_5\text{H}_5$ )<sub>2</sub>Fe<sub>2</sub>( $\mu\text{-CO}$ )<sub>2</sub>( $\mu\text{-DPPM}$ )]PF<sub>6</sub>, I<sup>+</sup>PF<sub>6</sub><sup>-</sup>, with ICH<sub>2</sub>CO<sub>2</sub>C<sub>2</sub>H<sub>5</sub>, under conditions known to generate the alkyl radical, yielded the ring substituted compound ( $\eta^5\text{-C}_5\text{H}_4\text{CH}_2\text{CO}_2\text{C}_2\text{H}_5$ )(C<sub>5</sub>H<sub>5</sub>)Fe<sub>2</sub>( $\mu\text{-CO}$ )<sub>2</sub>( $\mu\text{-DPPM}$ ), providing additional support for a radical pathway to ring substitution in these compounds. The molecular structures of ( $\eta^5\text{-C}_5\text{H}_5$ )<sub>2</sub>Fe<sub>2</sub>( $\mu\text{-CO}$ )<sub>2</sub>( $\mu\text{-DPPE}$ ), **II**, and ( $\eta^5\text{-CHOC}_5\text{H}_4$ )( $\eta^5\text{-C}_5\text{H}_5$ )Fe<sub>2</sub>( $\mu\text{-CO}$ )<sub>2</sub>( $\mu\text{-DPPE}$ ), **V**, have been characterized by X-ray crystallography: **II**, rhombohedral, *R* $\bar{3}$ , *a* = *b* = *c* = 27.749(2) Å,  $\alpha$  =  $\beta$  =  $\gamma$  = 116.52(9)°, *V* = 10104(15) Å<sup>3</sup>, *Z* = 12, *R*(*F*) = 4.1%; **V**, orthorhombic, *Pna*2<sub>1</sub>, *a* = 13.988(10) Å, *b* = 13.371(3) Å, *c* = 17.358(6) Å, *V* = 3246.5(41) Å<sup>3</sup>, *Z* = 4, *R*(*F*) = 6.9%.

The photochemical behavior of metal–metal bonded, metal–carbonyl complexes has been the subject of substantial investigation.<sup>1</sup> It is now well-established that two principle reaction modes are possible: metal–metal bond homolysis and carbonyl loss. We have been interested for some time in the behavior of bimetallic compounds in which the metal atoms are linked by either a bridging ligand such as a diphosphine, coupled cyclopentadienyl rings, or both. We hypothesized that these additional linkages between the metals would reduce the importance of the radical pathway by either eliminating homolysis or facilitating facile recombination of metal radicals. To test this hypothesis we examined the photolysis of ( $\eta^5\text{-C}_5\text{H}_5$ )<sub>2</sub>Fe<sub>2</sub>( $\mu\text{-CO}$ )<sub>2</sub>( $\mu\text{-DPPM}$ ), **I**, ( $\eta^5\text{-C}_5\text{H}_5$ )<sub>2</sub>Fe<sub>2</sub>( $\mu\text{-CO}$ )<sub>2</sub>( $\mu\text{-DPPE}$ ), **II**, and ( $\eta^5\text{-C}_5\text{H}_5$ )<sub>2</sub>Fe<sub>2</sub>( $\mu\text{-CO}$ )<sub>2</sub>( $\mu\text{-DPPP}$ ), **III**, in CHCl<sub>3</sub>, anticipating that CHCl<sub>3</sub> would serve as an efficient radical scavenger for any long-lived iron–iron bond homolysis products.



As will be discussed in this paper, photolysis of **III** proceeds by the expected homolysis pathway while photolysis of **I** and **II** revealed a wholly unexpected, and previously unobserved, charge transfer pathway for the photolysis of metal–metal bonded complexes. Further evidence for a radical pathway to ring substitution of these compounds is presented.

<sup>⊗</sup> Abstract published in *Advance ACS Abstracts*, November 1, 1994.  
(1) For major references, please see: (a) Zhang, S.; Brown, T. L. *Organometallics* **1992**, *11*, 4166. (b) Dixon, A. J.; George, M. W.; Hughes, C.; Poliakov, M.; Turner, J. J. *J. Am. Chem. Soc.* **1992**, *114*, 1719. (c) Bloyce, P. E.; Campen, A. K.; Hooker, R. H.; Rest, A. J.; Thomas, N. R.; Bitterwolf, T. E.; Shade, J. E. *J. Chem. Soc., Dalton Trans.* **1990**, 2833.

Table 1. UV/Visible Data for  $(C_5H_5)_2Fe_2(\mu-CO)_2L_2$  and Related Complexes

$L_2$	$\lambda_{max}$ , nm ( $\epsilon$ , L/mol cm)			
	$(C_5H_5)_2Fe_2(\mu-CO)_2L_2^a$	$Me_2Si(C_5H_4)_2Fe_2(\mu-CO)_2L_2^b$	$CH_2(C_5H_4)_2Fe_2(\mu-CO)_2L_2^{a,c}$	$(C_5H_4CHO)(C_5H_5)Fe_2(\mu-CO)_2L_2^d$
DPPM	634 ( $5.8 \times 10^2$ )	616 ( $4.4 \times 10^2$ )	580 ( $3.6 \times 10^2$ )	660 ( $3.7 \times 10^2$ )
	342 ( $7.4 \times 10^3$ )	385 ( $3.9 \times 10^3$ )	332 ( $5.3 \times 10^3$ )	390 ( $3.7 \times 10^3$ )
DPPE	655 ( $5.7 \times 10^2$ )	648 ( $4.0 \times 10^2$ )	604 ( $2.5 \times 10^2$ )	330 ( $5.0 \times 10^3$ )
	376 ( $4.7 \times 10^3$ )	385 ( $3.8 \times 10^3$ )	360 ( $3.7 \times 10^3$ )	670 ( $5.5 \times 10^2$ )
DPPP	681 ( $5.5 \times 10^2$ )	682 ( $4.3 \times 10^2$ )		400 ( $4.7 \times 10^3$ )
	376 ( $5.5 \times 10^3$ )	389 ( $4.2 \times 10^3$ )		

<sup>a</sup> Spectra were recorded in benzene. <sup>b</sup> Spectra were recorded in  $CH_2Cl_2$ . <sup>c</sup> Reference 9.

## Results and Discussion

$(\eta^5-C_5H_5)_2Fe_2(\mu-CO)_2(\mu-L_2)$ , where  $L_2 =$  DPPM (I), DPPE (II), and DPPP (III), were prepared as described by Haines.<sup>2</sup> Photolysis of I or II in  $CHCl_3$  resulted in a change in color of the reaction mixture from green to brown. After solvent removal, the resulting oil was chromatographed on wet (6% water) alumina, grade III, using petroleum ether: $CHCl_3$ . In each case, a single golden brown band was eluted from the column, yielding a brown solid after removal of solvent.

Analysis of  $^1H$  and  $^{13}C$  NMR spectra of the product compounds, IV and V, where  $L_2 =$  DPPM and DPPE, respectively, revealed that one cyclopentadienyl ring had been substituted during the course of the reaction. Characteristic resonances in both the proton and carbon spectra and the appearance of new IR bands at 1658 and  $1655\text{ cm}^{-1}$ , respectively, strongly suggested the presence of a formyl group in the molecule. The IR spectra also contained bands which were almost identical in position in the  $\mu-CO$  stretching bands of the starting materials. We have been unable to locate the  $^{13}C$  bridging carbonyl resonances of these compounds. The  $^{31}P$  NMR spectrum of IV consisted of a clean AB pattern centering on 84.48 and 81.47 ppm which is upfield of the singlet resonance observed at 86.56 ppm for I. V was found to have two singlets at 68.52 and 64.11 ppm which are slightly upfield from the singlet resonance of II which is found at 69.82 ppm. Mass spectrometry of IV (EI/CI) and V (FAB) revealed a parent mass and fragmentation pattern consistent with formyl derivatives of I and II. Final confirmation of the structure of V, and by inference IV, was provided by a molecular structure of V (vide infra).

The color change from the green starting materials to the golden brown formyl products can be understood by examination of the UV/visible spectra. The band positions of compounds I–V and representative, similar compounds are presented in Table 1. Compounds I and II have two bands in their electronic spectra. The lower energy bands are assigned to the Fe–Fe ( $\sigma \rightarrow \sigma^*$ ) and the higher energy band to the Fe  $\rightarrow$  ring (MLCT) transitions. Introduction of a formyl group onto one ring causes the  $\sigma \rightarrow \sigma^*$  bands to shift to longer wavelength and splits the Fe  $\rightarrow$  ring charge transfer bands. In the case of IV, two charge transfer bands are clearly observed, while for V a broad plateau is observed that, presumably, contains the two overlapping bands. We suggest that the two bands correspond to Fe  $\rightarrow C_5H_5$  and Fe  $\rightarrow C_5H_4CHO$  charge transfer bands, respectively. In both IV and V, the net effect of formylation is to shift the strongly absorbing charge transfer bands toward the

blue end of the visible range, resulting in a color change from green to golden-brown.

IR spectra of the reaction mixture of I prior to chromatographic purification contains bands which are similar in position to those of the product although the shoulder assigned to the formyl group was not observed. No bands were observed that might be attributable to a CpFe(CO)Cl product. Several attempts to obtain NMR spectra of these reaction mixtures were unsuccessful, due, apparently, to the presence of paramagnetic decomposition products. Ultraviolet photolysis of I in Nujol at 77 K yielded no change in the IR spectrum after 1 h, ruling out the possibility of photochemical carbonyl bridge opening. Similarly, photolysis of I in benzene resulted in some decomposition with no isolable product.

Photolysis of III proceeds similarly to that of I and II with a color change from green to brown although chromatography of the resulting product required a more polar solvent mixture (20:1 dichloromethane:methanol) for elution of the brown product, VI, which is unstable in solution and upon storage. It was not possible to record an NMR spectrum of VI. VI has a single carbonyl stretching band at  $1967\text{ cm}^{-1}$ . No bands which might be associated with either bridging carbonyl or formyl groups were observed. The observed IR band is similar in position to that of an authentic sample of  $(\eta^5-C_5H_5)Fe(CO)(PPh_3)Cl$  which has a terminal carbonyl stretching band at  $1963\text{ cm}^{-1}$ . These observations suggest that photolysis of III proceeds by homolysis of the Fe–Fe bond followed by reaction of the iron radicals with the chlorinated solvent.

The reactions of I and II are reminiscent of those reported by Sugimori and co-workers<sup>3</sup> involving the photochemistry of ferrocene in halocarbon solvents in which formyl, carboxylic acid, and ester (alcohol solvolysis) derivatives were isolated. Similar studies involving electron rich arene compounds have been reported.<sup>4</sup> These authors suggested that the observed products could be explained by a photochemical Reimer–Tiemann reaction whose initiating step is the photoinduced transfer of an electron from the ferrocene to  $CHCl_3$ , yielding a ferrocenium ion, a chloride ion, and the  $CHCl_2$  radical. Exo attack of the  $CHCl_2$  radical on a cyclopentadienyl ring of the  $17-e^-$  ferrocenium ion gives a protonated ferrocene intermediate. Deprotonation and hydrolysis of this species upon workup yields the formyl derivative. The literature on photooxidation of metal complexes has been reviewed.<sup>5</sup>

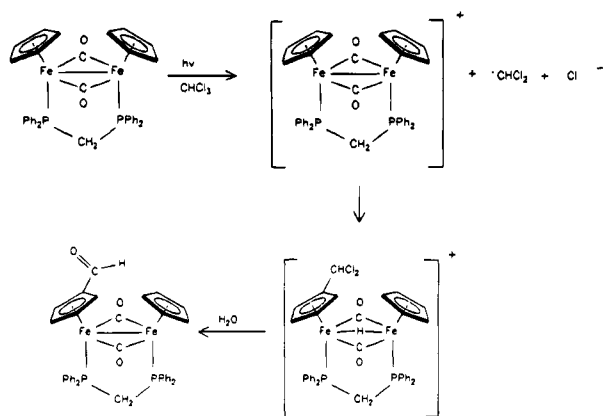
We propose that photolysis of I and II proceeds by a

(3) Hoshi, Y.; Akiyama, T.; Sugimori, A. *Tetrahedron Lett.* **1970**, 1485.

(4) (a) Hirao, K.; Ikegame, M.; Yonemitsu, O. *Tetrahedron* **1974**, *30*, 2301. (b) Kurz, M. E.; Lapin, S. C.; Mariam, K.; Hagen, T. J.; Qian, X. Q. *J. Org. Chem.* **1984**, *49*, 2728.

(2) (a) Haines, R. J.; DuPreez, A. L. *J. Organometal. Chem.* **1970**, *21*, 181. (b) Haines, R. J.; DuPreez, A. L. *Inorg. Chem.* **1970**, *11*, 330.

**Scheme 1. Postulated Mechanism for Formylation of I**



similar mechanism (Scheme 1) involving photoinduced electron transfer from the bimetallic compound to the solvent, followed by radical attack to form a protonated intermediate containing a  $\mu$ -H. Hydrolysis upon workup yields the isolated formyl derivative. The good yields of formyl products suggest that the bimetallic radical cation and the dichloromethyl radical are formed within a solvent cage, enhancing the likelihood of a favorable attack of the dichloromethyl radical onto one of the cyclopentadienyl rings. Since formylcyclopentadienyl iron compounds have proven to be particularly difficult to prepare by other strategies, this reaction provides an attractive synthetic entry to this class of compounds. We are presently exploring the organic reaction chemistry of these compounds.

Previous studies have shown that **I** and **II** can be oxidized to the corresponding stable radical cations both chemically and electrochemically.<sup>2b,6</sup> Additionally,  $(\eta^5\text{-C}_5\text{H}_5)_2\text{Fe}_2(\mu\text{-CO})_2(\mu\text{-Ph}_2\text{PN}(\text{Et})\text{PPh}_2)$  undergoes one-electron charge transfer oxidation with 7,7,8,8-tetracyano-*p*-quinodimethane to yield a product which has been crystallographically characterized.<sup>7</sup> Generating the monocations of **I** and **II** by photochemical charge transfer is entirely reasonable under the conditions of our reactions.

In order to provide further support for the proposal that these reactions proceed via radical attack on the ring of a bimetallic radical cation, we have carried out the reaction of  $\text{I}^+\text{PF}_6^-$  under conditions that are reported to involve alkyl radicals. Floris and co-workers<sup>8</sup> have described the reactions of ferrocene and ferrocenium ions with alkyl radicals generated by reaction of alkyl iodides with  $\text{Fe}^{+2}$ ,  $\text{H}_2\text{O}_2$ , and DMSO. Directly adopting the reported protocol,  $\text{I}^+\text{PF}_6^-$  was reacted with  $\text{ICH}_2\text{CO}_2\text{C}_2\text{H}_5$ . Upon workup and careful chromatography, a small quantity of green product was obtained that was shown to be free of **I** by HPLC. IR confirmed the presence of both ester and  $\mu$ -CO bands, and  $^1\text{H}$ ,  $^{13}\text{C}$ , and  $^{31}\text{P}$  NMR spectra were consistent with the expected ring substituted

product, **VII**. Mass spectrometry (EI/CI) yielded the required parent mass and a fragmentation pattern diagnostic of an ethyl ester. As found in the mass spectrum of **IV** and **V**, fragmentation of these asymmetrically substituted compounds gives rise to  $(\text{C}_5\text{H}_5)\text{-FeL}_2^+$  and  $(\text{C}_5\text{H}_4\text{R})\text{FeL}_2^+$  species that provide further confirmatory evidence for the identity of the compounds. The ultimate yield of **VII** was insufficient to permit elemental analysis.

The differences in behavior among compounds **I**, **II**, and **III** are probably attributable to the effect of the increasing length of the phosphine bridge upon the stability of the  $\text{Fe}_2(\mu\text{-CO})_2$  core of the molecule. Several physical properties of these and related compounds support this argument. Iron-Iron bond lengths are found to increase with increasing bridge length. The Fe-Fe bond length in **I** has been found to be 2.516 Å,<sup>9</sup> while the same bond length in **II** is 2.527 Å. Wright and co-workers<sup>10</sup> have found the Fe-Fe bond lengths in the compounds  $(\text{CH}_3)_2\text{Si}(\text{C}_5\text{H}_4)_2\text{Fe}_2(\mu\text{-CO})(\mu\text{-X})$ , where X = DPPM and DPPP, to be 2.497 and 2.521 Å, respectively. It should be noted that introduction of the  $(\text{CH}_3)_2\text{Si}$  bridge between the rings in the DPPM derivative compresses the Fe-Fe bond relative to **I**. These changes in bond length are reflected in changes in the Fe-Fe ( $\sigma \rightarrow \sigma^*$ ) band positions as presented in Table 1 for compounds **I-III** and analogous ring-coupled derivatives. As the diphosphine ligand bridge grows, this band moves to lower energy, reflecting the increasing strain on the Fe-Fe bond. Similarly, Wright has found that the first oxidation potentials for the series  $(\text{CH}_3)_2\text{-Si}(\text{C}_5\text{H}_4)_2\text{Fe}_2(\mu\text{-CO})(\mu\text{-X})$ , where X = DPPM, DPPE, and DPPP, undergo a negative shift with increasing bridge length.<sup>10</sup> These various trends are consistent with a gradual weakening of the Fe-Fe bond with increasing bridge length, but do not explain why only ring substitution is observed for compounds **I** and **II** and only bond homolysis is observed for **III**.

The X-ray crystallographic results for both **II** and **V** were obtained. Crystallographic data for **II** and **V** appear in Table 2 and selected bond lengths and angles appear in Tables 3 and 4, respectively. The solid state structure of **II** contains a racemic mixture resulting from the  $\text{C}_2$  symmetry of the compound. The two independent molecules in the unit cell are chemically indistinguishable. The structures of compounds **II** (Figure 1) and **V** (Figure 2) are also effectively superimposable with no chemically significant differences in bond lengths or angles arising from the presence of the formyl group. The Fe-Fe bond length of 2.527(1) Å for **V** and 2.516(1) and 2.512(1) Å for the two independent molecules of **II** indicate a slight weakening of the Fe-Fe bond, as reflected in the electronic spectra.

The observation of photochemical charge transfer for one class of bimetallic complexes raises the possibility that similar reactions might be possible for other complexes such as  $(\eta^5\text{-C}_5\text{H}_5)_2\text{Fe}_2(\text{CO})_4$  and  $(\eta^5\text{-C}_5\text{H}_5)_2\text{-Mo}_2(\text{CO})_6$ . Recent elegant work by Bullock et al.<sup>11</sup> examined the electrochemical formation of the  $[(\eta^5\text{-C}_5\text{H}_5)_2\text{Fe}_2(\text{CO})_4]^{1+}$  radical cation and provided detailed

(5) Giannotti, C.; Gaspard, S.; Kramer, P. In *Photoinduced Electron Transfer. Part D. Photoinduced Electron Transfer Reactions: Inorganic Substrates and Applications*; Fox, M. A.; Chanon, M., Eds.; Elsevier: Amsterdam, 1988; p 200-240.

(6) (a) Furguson, J. A.; Meyer, T. J. *Inorg. Chem.* **1971**, *10*, 1025.  
(b) Furguson, J. A.; Meyer, T. J. *Inorg. Chem.* **1971**, *11*, 631.

(7) Bell, S. E.; Field, J. S.; Haines, R. J. *J. Chem. Soc., Chem. Commun.* **1991**, 489.

(8) Baciocchi, E.; Floris, B.; Muragila, E. *J. Org. Chem.* **1993**, *58*, 2013. See also, Minisci, F.; Vismara, E.; Fontana, F. *J. Org. Chem.* **1989**, *54*, 5224.

(9) Bitterwolf, T. E.; Shade, J. E.; Pearson, W. H.; Brown, J. E., Unpublished results, **1994**.

(10) Wright, M. E.; Mezza, T. M.; Nelson, G. O.; Armstrong, N. R.; Day, V. W.; Thompson, M. R. *Organometallics* **1983**, *2*, 1711.

(11) Bullock, J. P.; Palazzotto, M. C.; Mann, K. R. *Inorg. Chem.* **1991**, *30*, 1284.

**Table 2. Crystal Data for**  
 $(\eta^5\text{-C}_5\text{H}_5)_2\text{Fe}_2(\text{CO})_2[(\text{C}_6\text{H}_5)_2\text{PC}_2\text{H}_4\text{P}(\text{C}_6\text{H}_5)_2]$  (II) and  
 $(\eta^5\text{-C}_5\text{H}_5)(\eta^5\text{-C}_5\text{H}_4\text{CHO})\text{Fe}_2[(\text{C}_6\text{H}_5)_2\text{PC}_2\text{H}_4\text{P}(\text{C}_6\text{H}_5)_2]$  (V)<sup>a</sup>

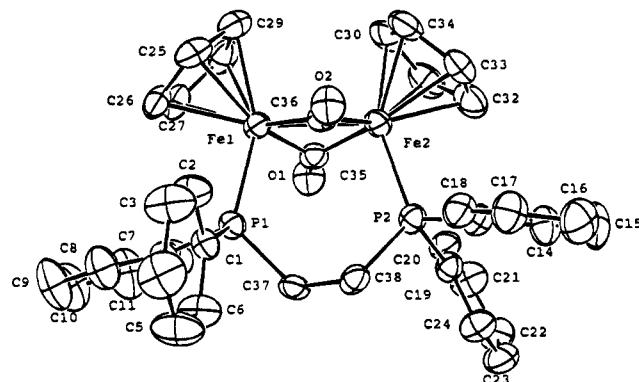
(i) Crystal Data		
formula	$\text{C}_{38}\text{H}_{34}\text{O}_2\text{P}_2\text{Fe}_2$	$\text{C}_{39}\text{H}_{34}\text{O}_3\text{P}_2\text{Fe}_2$
crystal system	trigonal	orthorhombic
space group	$R\bar{3}$ (No. 148)	$Pna2_1$ (No. 33)
<i>a</i>	27.749 (2)	13.988 (10)
<i>b</i>	27.749(2)	13.371(3)
<i>c</i>	27.749(2)	17.358(6)
$\alpha$	116.52(9)	90
$\beta$	116.52(9)	90
$\gamma$	116.52(9)	90
volume, Å <sup>3</sup>	10109(15)	3246.5(41)
<i>z</i>	12 <sup>b</sup>	4
<i>D</i> (calc), g/cm <sup>3</sup>	1.373	1.481
<i>D</i> (obs), g/cm <sup>3</sup>	1.410	1.463
$\mu$ (Mo K $\alpha$ ), cm <sup>-1</sup>	10.5	10.5
temp, K	296	296
crystal size, mm	0.30 × 0.20 × 0.25	0.25 × 0.25 × 0.20
crystal color	dark green	dark brown
(ii) Data Collection		
diffractometer	Enraf-Nonius CAD4	Enraf-Nonius CAD4
monochromator	oriented graphite	oriented graphite
radiation	Mo K $\alpha$	Mo K $\alpha$
wavelength	0.71073	0.71073
2 $\theta$ limits, deg	2–50	2–50
scan technique	$\omega$	$\theta$ –2 $\theta$
standards	3 std/100 rfls	3 std/100 rfls
decay (max), %	4.2	1.6
octants colld	$\pm h, k, \pm l$ (1–30° 2 $\theta$ ) <sup>d</sup>	$\pm h, \pm k \pm l$ (0–24° 2 $\theta$ )
	$h, k, \pm l$ (30–50° 2 $\theta$ )	$h, k, \pm l$ (24–50° 2 $\theta$ )
no. of rfls colld	17970	5360
no. of independt rfls	11832	4704
no. of independt rfls		
$I \geq 3\sigma(I)$	5413	3368
<i>R</i> ( <i>I</i> ) on averaging, %	3.8	1.7
<i>T</i> (max)/ <i>T</i> (min)	1.02	1.35
(iii) Refinement		
<i>R</i> ( <i>F</i> ), %	4.1	5.4
<i>R</i> <sub>w</sub> ( <i>F</i> ), %	5.9	6.3
GOF	1.936	1.667
$\Delta/\sigma$	0.01	0.01
$\Delta(\rho)$ , e Å <sup>-3</sup>	1.03	2.75
<i>N</i> <sub>o</sub> / <i>N</i> <sub>v</sub>	6.83	8.13

<sup>a</sup> Cell parameters for the idealized cells were determined from 25 reflections in the range 20° < 2 $\theta$  < 35° followed by least-squares refinement. Setting angles for the 25 reflections were based upon 100 reflections (four settings of each reflection including  $\pm 2\theta$  values). <sup>b</sup> This is the number of molecules in the unit cell. The number of asymmetric units per unit cell is six, with two molecules per asymmetric unit. <sup>c</sup> Same as II. <sup>d</sup> Data were collected with hexagonal setting and converted to rhombohedral for structure solution and refinement.

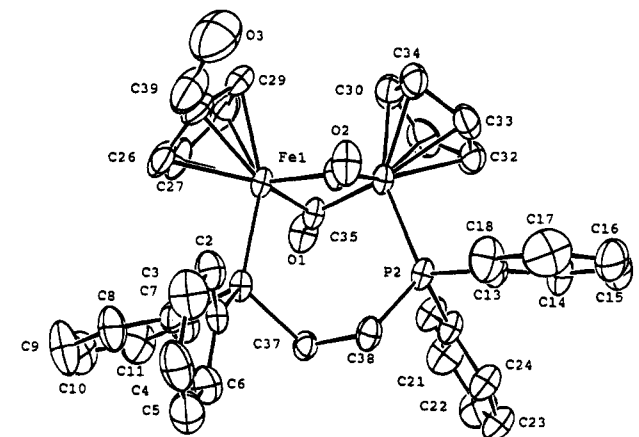
**Table 3. Selected Bond Distances (Å) for II and V**

atoms	II	V	atoms	II	V
Fe1–Fe2	2.516(1)	2.527(1)	C36–O2	1.202(8)	1.187(8)
Fe1–P1	2.172(2)	2.198(2)	C35–O1	1.181(8)	1.171(8)
Fe2–P2	2.180(2)	2.186(2)	P1–C37	1.825(4)	1.817(7)
Fe1–C36	1.884(8)	1.917(7)	P2–C38	1.838(8)	1.833(8)
Fe1–C35	1.922(4)	1.925(6)	C37–C38	1.51(1)	1.55(1)
Fe2–C36	1.902(6)	1.919(7)	C25–C39	1.41(1)	1.41(1)
Fe2–C35	1.908(8)	1.903(7)	O3–C39		1.25(2)

information on its reactions with nucleophiles. Earlier work by Kadish<sup>12</sup> demonstrated that the  $[(\eta^5\text{-C}_5\text{H}_5)_2\text{Mo}_2(\text{CO})_6]^{1+}$  cation radical is an intermediate in the oxidation of the bimetallic molybdenum compound. Bullock and co-workers have demonstrated that reactions of the cation radicals with nucleophiles yield products which are similar to those observed by Tyler and attributed to an intermediate 19-electron species.<sup>13</sup> Additional



**Figure 1.**



**Figure 2.**

**Table 4. Selected Bond Angles (deg) for II and V**

atoms	II	V
Fe2–Fe1–P1	105.64(6)	104.83(6)
Fe1–Fe2–P2	105.65(7)	106.24(7)
Fe1–P1–C37	117.6(3)	117.7(2)
Fe2–P2–C38	119.5(2)	118.0(2)
Fe1–C36–Fe2	83.3(3)	82.4(3)
Fe1–C35–Fe2	82.1(2)	82.6(3)
O3–C39–C25		124.(1)

work will be necessary to establish whether photochemical charge transfer reactions compete with the more familiar radical formation processes and contribute to the photochemistry of these bimetallic complexes.

## Experimental Section

Compounds I,<sup>2</sup> II,<sup>2</sup> III,<sup>2</sup> and I<sup>+</sup>PF<sub>6</sub><sup>2b,5</sup> were prepared by literature procedures. Crystals of II and V for X-ray crystallography were grown from CHCl<sub>3</sub>:pentane mixtures. IR spectra were recorded on a Perkin-Elmer 1750 FT-IR spectrometer. NMR spectra were recorded on a GE-QE300 NMR spectrometer and referenced to solvent resonances. Mass spectra of IV were recorded by Dr. Mark Ross of the Naval Research Laboratory and Dr. Gary Knerr of the University of Idaho. Elemental analyses were performed by Desert Analytics, Inc. Tucson, AZ.

**Synthesis of  $(\eta^5\text{-C}_5\text{H}_4\text{CHO})(\eta^5\text{-C}_5\text{H}_5)\text{Fe}_2(\mu\text{-CO})_2(\mu\text{-DPPM})$ , IV.** I (0.50 g, 0.73 mmol) is taken up in 125 mL of CHCl<sub>3</sub> in a Pyrex water-jacketed reaction vessel and photolyzed using a 250 W General Electric sun lamp for 4 h. During this time the solution changes color from olive green to brown. After the reaction is complete, the solvent is removed and the oily residue is chromatographed on a grade III alumina column

(12) Kadish, K. M.; Lacombe, D. A.; Anderson, J. E. *Inorg. Chem.* **1986**, *25*, 2246.

(13) Avey, A.; Tyler, D. R. *Organometallics* **1992**, *11*, 3856, and references therein.



using 6:1 petroleum ether:CHCl<sub>3</sub> as an eluant. A green band of **I** is eluted first from the column followed by a golden band. Removal of solvent from the golden band and recrystallization from dichloromethane:pentane yields 0.19 g of **IV** as a brown solid. Mp: 224–225 °C. Yield 37%. IR: (CHCl<sub>3</sub>): 1690 (m), 1682 (sh), 1658 (sh). <sup>1</sup>H NMR: (CDCl<sub>3</sub>) 9.15 (s, 1 H, CHO), 7.44–7.22 (m, 20 H, Ph), 4.70 and 4.66 (AA'BB', 4 H, C<sub>5</sub>H<sub>4</sub>-CHO), 4.37 (s, 5 H, C<sub>5</sub>H<sub>5</sub>), 1.89 (t, 2 H, <sup>2</sup>J<sub>P-H</sub> = 10.06 Hz, PCH<sub>2</sub>P). <sup>13</sup>C NMR: (CDCl<sub>3</sub>) 191.2 (CHO), 136.28 (dd, *ipso*-Ph, <sup>1</sup>J<sub>P-C</sub> = 32.6 Hz, <sup>3</sup>J<sub>P-C</sub> = 4.8 Hz), 135.75 (dd, *ipso*-Ph', <sup>1</sup>J<sub>P-C</sub> = 33.6 Hz, <sup>3</sup>J<sub>P-C</sub> = 6.3 Hz), 132.35 (d, *o*-Ph, <sup>2</sup>J<sub>P-C</sub> = 9.6 Hz), 132.22 (d, *o*-Ph', <sup>2</sup>J<sub>P-C</sub> = 9.1 Hz), 129.96 (d, *p*-Ph and -Ph', <sup>4</sup>J<sub>P-C</sub> = 8.0 Hz), 128.26 (d, *m*-Ph, <sup>3</sup>J<sub>P-C</sub> = 9.4 Hz), 128.22 (d, *m*-Ph', <sup>3</sup>J<sub>P-C</sub> = 9.0 Hz), 94.28 (*ipso*-Cp), 90.37 (CHOCp), 86.91 (Cp), 85.31 (CHOCp), 28.29 (t, <sup>1</sup>J<sub>P-C</sub> = 22.8 Hz). <sup>31</sup>P NMR: (CDCl<sub>3</sub>) 84.48 and 81.47 (AB, <sup>2</sup>J<sub>P-P</sub> = 92.38 Hz). Mass Spectrometry: 710 (M<sup>+</sup>), 682 (M<sup>+</sup> - CO), 658 (M<sup>+</sup> - 2CO), 589 (CHOC<sub>5</sub>H<sub>4</sub>-Fe<sub>2</sub>DPPM), 561 (C<sub>5</sub>H<sub>5</sub>Fe<sub>2</sub>DPPM), 533 (CHOC<sub>5</sub>H<sub>4</sub>FeDPPM), 505 (C<sub>5</sub>H<sub>5</sub>FeDPPM), 440 (FeDPPM). Calcd for C<sub>38</sub>H<sub>32</sub>Fe<sub>2</sub>O<sub>3</sub>P<sub>2</sub>: C, 64.25; H, 4.55; P, 8.72. Found: C, 64.36; H, 4.55; P, 8.63.

**Synthesis of (η<sup>5</sup>-C<sub>5</sub>H<sub>5</sub>CHO)(C<sub>5</sub>H<sub>5</sub>)Fe<sub>2</sub>(μ-CO)<sub>2</sub>(μ-DPPE), **V**.** **II** (0.50 g, 0.72 mmol) was photolyzed and purified as described above. **V** was recovered as a brown solid. Mp: 243–244 °C dec. Yield: 40%. IR: (CHCl<sub>3</sub>) 1687 (m), 1655 (sh). <sup>1</sup>H NMR: (CDCl<sub>3</sub>) 8.90 (s, 1 H, CHO), 7.89 (m, 8 H, Ph), 7.45 (m, 12 H, Ph), 4.57 and 4.53 (AA'BB', 4 H, CHOC<sub>5</sub>H<sub>4</sub>), 4.72 (s, 5 H, C<sub>5</sub>H<sub>5</sub>), 1.35 (m, 4 H, P-C<sub>2</sub>H<sub>4</sub>-P). <sup>13</sup>C: (CDCl<sub>3</sub>) 191.23 (CHO), 136.67 (br, *ipso*-Ph), 132.87 (br s, *o*-Ph), 130.04 (d, <sup>4</sup>J<sub>P-C</sub> = 12.8 Hz, *p*-Ph), 128.37 (pseudo t, <sup>3</sup>J<sub>P-C</sub> = 8.3 Hz, *m*-Ph), 95.26 (*ipso*-CHOCp), 90.37 (CHOCp), 86.88 (Cp), 84.55 (CHOCp), 22.54 (d, <sup>1</sup>J<sub>P-C</sub> = 25.23 Hz, PC<sub>2</sub>H<sub>4</sub>P), 22.30 (d, <sup>1</sup>J<sub>P-C</sub> = 25.72 Hz, PC<sub>2</sub>H<sub>4</sub>P). <sup>31</sup>P NMR: (CDCl<sub>3</sub>) 68.52 and 64.11. MS: (FAB) 724 (M<sup>+</sup>), 696 (M<sup>+</sup> - CO), 668 (M<sup>+</sup> - 2 CO), 640 (M<sup>+</sup> - 3 CO), 575 [CHOC<sub>5</sub>H<sub>4</sub>Fe(DPPE)(CO)], 547 [CHOC<sub>5</sub>H<sub>4</sub>Fe(DPPE)] or [C<sub>5</sub>H<sub>5</sub>Fe(DPPE)(CO)], 519 [C<sub>5</sub>H<sub>5</sub>Fe(DPPE)], 454 [Fe(DPPE)].

**Synthesis of (η<sup>5</sup>-C<sub>5</sub>H<sub>5</sub>CH<sub>2</sub>CO<sub>4</sub>C<sub>2</sub>H<sub>5</sub>)(C<sub>5</sub>H<sub>5</sub>)Fe<sub>2</sub>(μ-CO)<sub>2</sub>(μ-DPPM), **VIII**.** I<sup>+</sup>PF<sub>6</sub><sup>-</sup> (0.51 g, 0.61 mmol) and FeSO<sub>4</sub>·7H<sub>2</sub>O (0.28 g, 1.0 mmol) were taken up in DMSO, 35 mL of ICH<sub>2</sub>-CO<sub>2</sub>C<sub>2</sub>H<sub>5</sub>, and 5.0 mL of a 0.20 M solution in DMSO (1.0 mmol), and the solution stirred for 15 min, at which time the solution was green. Freshly prepared H<sub>2</sub>O<sub>2</sub> in DMSO (0.140 mL of 30% solution in 10 mL of DMSO, 1.0 mmol) was added dropwise to the solution during which the solution changes to reddish brown. Note: addition of excess H<sub>2</sub>O<sub>2</sub> results in complete decomposition of the metal compounds. After stirring for 15 min, the solution was diluted with brine and an excess of ascorbic acid was added. The solution immediately produces a green suspension that was stirred for at least 30 min. Extraction with benzene (30 mL) gave a green solution that was washed with brine and dried with MgSO<sub>4</sub>. Removal of solvent gave a green solid that was taken up in minimal benzene and chromatographed on a 40 × 2 cm alumina (grade III) column using benzene as the eluant. Slow elution resulted in the partial separation of two green bands. The first band was shown by IR and HPLC to be **I**. The second band recovered in this way was consistently contaminated with **I** and had to be rechromatographed to obtain a small amount of **VII** as a dark green solid. **VII** appears to decompose slowly on the column to a purple product resulting in a reduction of the total yield. IR: (CH<sub>2</sub>Cl<sub>2</sub>) 1728 (m), 1676 (s), 1095 (m) cm<sup>-1</sup> (m). <sup>1</sup>H NMR: (C<sub>6</sub>D<sub>6</sub>) 7.50 (8H, Ph), 7.00 (12 H, Ph), 4.59 (t, 2H, CpR), 4.39 (s, 5H, Cp), 4.09 (m, 2H, CpR), 3.92 (q, 2H, J = 7.1 Hz, CH<sub>2</sub>CH<sub>3</sub>), 3.59 (s, 2H, CpCH<sub>2</sub>CO<sub>2</sub>), 1.76 (t, 2H, J<sub>P-H</sub> = 10 Hz, PCH<sub>2</sub>P), 0.93 (t, 3H, J = 7.1, CH<sub>2</sub>CH<sub>3</sub>). <sup>13</sup>C NMR: (C<sub>6</sub>D<sub>6</sub>) 295.1 (t, J<sub>P-C</sub> = 14.6 Hz, μ-CO), 170.6 (CO<sub>2</sub>C<sub>2</sub>H<sub>5</sub>), 136.3

(m, *ipso*-Ph), 131.7 (m, *o*-Ph), 128.4 (s, *m*-Ph), 127.0 (*p*-Ph), 95.7 (*ipso*-Cp), 86.2 (CpR), 85.8 (Cp), 83.7 (CpR), 59.3 (CpCH<sub>2</sub>-CO<sub>2</sub>), 32.4 (CH<sub>2</sub>CH<sub>3</sub>), 27.5 (t, J<sub>P-C</sub> = 21.7 Hz), 13.2 (CH<sub>2</sub>CH<sub>3</sub>). <sup>31</sup>P NMR: (C<sub>6</sub>D<sub>6</sub>) 83.8 and 81.1 (AB q, J<sub>Pa-Pb</sub> = 91.9 Hz). Mass spectrometry: (EI/CI) 768 (M<sup>+</sup>), 740 (M<sup>+</sup> - C<sub>2</sub>H<sub>4</sub> or CO), 712 (M<sup>+</sup> - 2CO or CO and C<sub>2</sub>H<sub>4</sub>), 696 (M<sup>+</sup> - C<sub>2</sub>H<sub>4</sub> and CO<sub>2</sub>), 682 (M<sup>+</sup> - C<sub>4</sub>H<sub>7</sub>O<sub>2</sub>), 654 (M<sup>+</sup> - C<sub>4</sub>H<sub>7</sub>O<sub>2</sub> and CO), 591 ((η<sup>5</sup>-C<sub>5</sub>H<sub>4</sub>C<sub>3</sub>H<sub>7</sub>O<sub>2</sub>)<sub>2</sub>FeDPPE<sup>+</sup>), 505 ((C<sub>5</sub>H<sub>5</sub>)<sub>2</sub>FeDPPE<sup>+</sup>), 440 (FeDPPM<sup>+</sup>).

**X-ray Structure Determination.** Crystal data are presented in Table 1. Crystals of both **II** and **V** were grown by evaporation of chloroform:pentane solutions. Suitable crystals were chosen from each compound and mounted in random orientations on glass fibers. Rotation photographs were used to locate reflections which were then indexed to obtain the unit cells for both crystals. Axial photographs confirmed axial lengths for both unit cells and *mmm* Laue diffraction symmetry for **V**. Compound **II** was originally indexed in the nonprimitive hexagonal cell for which *a* = 47.2 Å and *c* = 15.7 Å. Data were collected in the hexagonal cell but were later transformed to the primitive rhombohedral cell for structure solution and refinement. Conditions of reflection of *h* + *k* + *l* = 3*n* confirmed space group *R*3̄ for **II**. Conditions of reflection 0*kl* (*k* + *l* = 2*n*) and *h*0*l* (*h* = 2*n*) for **V** were not sufficient to choose between the centrosymmetric *Pnam* and the noncentrosymmetric *Pna*2<sub>1</sub>. Intensity statistics indicated a noncentrosymmetric structure. A linear decay correction was applied to both data sets. Empirical absorption corrections for both crystals were based on  $\psi$  scans of three reflections at 10°  $\psi$  intervals.

Both structures were solved via direct methods and completed with difference Fourier synthesis. Structure solutions for **V** were attempted in both *Pnam* and *Pna*2<sub>1</sub>, but could only be obtained in *Pna*2<sub>1</sub>. The absolute configuration of the space group was assigned on the basis of the difference in *R*(*F*) between refinements of both hands without hydrogen atoms. The two forms refined to *R*(*F*) of 0.066 for the correct structure and *R*(*F*) of 0.072 for the incorrect structure. All non-hydrogen atoms were refined with anisotropic temperature factors in both structures. Hydrogen atoms were located in the difference Fourier maps but were calculated at idealized positions and assigned a temperature factor 30% larger than the corresponding carbon isotropic temperature factor. Hydrogen atom positions were updated throughout the final cycles of refinement. Examination of strong, low-angle reflections revealed no extinction effects.

An interesting feature of **II** is the existence of both enantiomers of the compound in the asymmetric unit. Cocrystallization of both enantiomers accounts for the usually large unit cell with six asymmetric units per cell.

**Acknowledgment.** We thank Prof. Barbara Floris for providing us with preprints of her manuscript describing alkyl radical reactions with ferrocene and ferrocenium. J.E.S. thanks the United States Naval Academy Research Council for generous support. J.E.B. thanks the Naval Academy for a Trident Scholarship.

**Supplementary Material Available:** Tables of bond distances and angles, positional parameters, and general displacement parameters for **II** and **V** (36 pages). Ordering information is given on any current masthead page.

OM9406660

# Unexpected Synthesis of Ortho-Substituted Diselenophenylenezirconocenes from the Para-Substituted Diphenylzirconocenes. Chemical and Structural Evidence of the Participation of a Cyclometalated Intermediate That Behaves as a Benzyne Zirconocene Equivalent

Corinne Legrand,<sup>†</sup> Philippe Meunier,<sup>\*,†</sup> Jeffrey L. Petersen,<sup>\*,‡</sup> Pascale Tavares,<sup>†</sup> Jacques Bodiguel,<sup>†</sup> Bernard Gautheron,<sup>†</sup> and Gabriel Dousse<sup>§</sup>

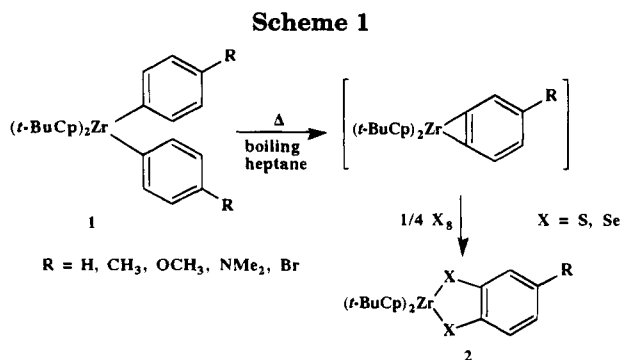
Laboratoire de Synthèse et d'Electrosynthèse Organométalliques (URA CNRS 1685), Université de Bourgogne, 6 boulevard Gabriel, BP 138, 21004 Dijon Cedex, France, Department of Chemistry, West Virginia University, Morgantown, West Virginia, 26506-6045, and Laboratoire de Chimie des Organominéraux (URA CNRS 477), Université Paul Sabatier, 118, route de Narbonne, 31062 Toulouse Cedex, France

Received July 12, 1994<sup>®</sup>

Heating grey selenium with  $[\eta^5\text{-C}_5\text{H}_4(t\text{-Bu})_2\text{Zr}(\text{C}_6\text{H}_4(p\text{-OCH}_3))_2]$  in boiling octane affords the diselenophenylenezirconocene complex containing a methoxy group in the ortho position. A similar reaction, although less selective, occurs when starting from  $[\eta^5\text{-C}_5\text{H}_4(t\text{-Bu})_2\text{Zr}(\text{C}_6\text{H}_4(p\text{-CH}_3))_2]$ . The structures of the diselenophenylenezirconocenes obtained were confirmed by NMR spectroscopy and definitively proved by comparison with the authentic ortho-substituted derivatives prepared from the corresponding methyl-*o*-anisyl- and methyl-*o*-tolylzirconocene. The mechanism proposed to explain this transformation involves the activation of a *tert*-butyl C-H bond by a transient benzynezirconocene species. The cyclometalation product, which is obtained by heating the diphenylzirconocene, reacts toward selenium and unsaturated organic compounds like the benzynezirconocene but the reaction takes place at room temperature. The cyclometalation pathway allows a more sterically hindered selenium-containing derivative  $[\eta^5\text{-C}_5\text{H}_4(t\text{-Bu})_2\text{ZrSe}_2\text{C}_6\text{H}_3(o,o'\text{-}(\text{CH}_3)_2)]$  to be prepared. The new diselenophenylenezirconocenes described are good precursors to generate benzodiselenagermoles and related spiro compounds by a zirconium-germanium transmetalation reaction. All the new products synthesized, zirconocene complexes and cyclometalated derivatives, benzodiselenagermoles, and spirobisbenzodiselenagermoles, were identified by the multinuclear NMR methods and mass spectrometry. The structure of the cyclometalated product  $[\eta^5\text{-C}_5\text{H}_4(t\text{-Bu})\text{Zr}[(2,5\text{-}(\text{CH}_3)_2\text{C}_6\text{H}_3)(\eta^1\text{-}\eta^5\text{-CH}_2\text{C}(\text{CH}_3)_2\text{C}_5\text{H}_4)]]$  was determined by X-ray diffraction analysis. This compound crystallizes in the monoclinic space group  $P2_1/c$  with two molecules per asymmetric unit with cell dimensions  $a = 8.278(3)$  Å,  $b = 20.113(9)$  Å,  $c = 27.661(9)$  Å, and  $\beta = 93.13(2)^\circ$  at 295 K. Least-squares refinement led to a value for the final  $R$  index of 0.0642 for 2701 reflections with  $I > 2\sigma(I)$ .

## Introduction

We have previously shown that chalcogens readily insert in the zirconium-carbon bonds of arynezirconocene complexes.<sup>1-3</sup> In this way, dichalcogenatozirconocyclic complexes are obtained in good yield by refluxing various diphenylzirconocenes with chalcogens in heptane (Scheme 1). In the case of para-substituted diphenylzirconocenes, complexes **2** (in which the substituent is positioned meta and para relative to the two carbon atoms bonded to the chalcogens) are selectively obtained.



Such compounds represent very useful reagents for the generation of various organic or organometallic species.<sup>4-9</sup> For example, they are used as a source of the *o*-diselenophenyl moiety through reactions with

(4) Meunier, P.; Gautheron, B.; Mazouz, A. *J. Chem. Soc., Chem. Comm.* **1986**, 424.

<sup>†</sup> Université de Bourgogne.

<sup>‡</sup> West Virginia University.

<sup>§</sup> Université Paul Sabatier.

<sup>®</sup> Abstract published in *Advance ACS Abstracts*, November 1, 1994.

(1) Gautheron, B.; Tainturier, G.; Pouly, S.; Théobald, F.; Vivier, H.; Laarif, A. *Organometallics* **1984**, *3*, 1495.

(2) Meunier, P.; Gautheron, B.; Mazouz, A. *J. Organomet. Chem.* **1987**, *320*, C39.

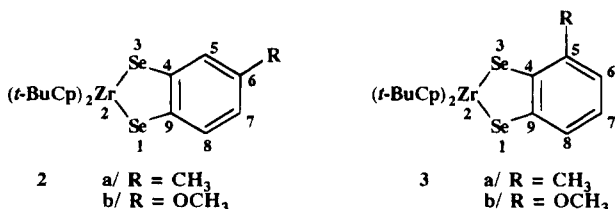
(3) Bodiguel, J.; Meunier, P.; Gautheron, B. *Appl. Organomet. Chem.* **1991**, *5*, 479.

monofunctional (acid and benzyl halides), bi- and tetrafunctional (metal halides) electrophiles, affording *o*-diselenium-containing benzenic compounds,<sup>4</sup> bicyclic<sup>5</sup> and spiro<sup>6,7</sup> derivatives. Some selenium-containing crown ethers have also been prepared by this way.<sup>9</sup>

When the reaction of elemental selenium with para-substituted diphenylzirconocenes is performed in boiling octane, the reaction proceeds with the formation of the ortho-substituted diselenophenylenezirconocene in some cases. The mechanism of the thermal isomerization involves a cyclometalated derivative resulting from the C–H bond activation of a *tert*-butyl group. We have isolated one representative of such intermediates for which the X-ray structure has been established. From the reactivity point of view, these cyclometalated complexes behave as arynezirconocene species, as evidenced by their analogous insertion chemistry with nitriles, alkynes, and ketones.

## Results and Discussion

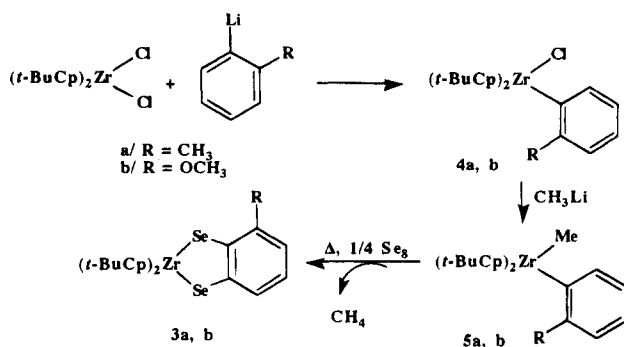
The products obtained by heating para-substituted diphenylzirconocenes **1** with grey selenium powder in refluxing octane are dependent on the substituents of the phenyl ring. When the substituent is a bromine atom or a dimethylamino group, decomposition is observed. When R is methyl, the reaction results in the formation of a mixture of complexes **2** and **3** (60/40). In the case where R is methoxy, complex **3** is the only observed product and the reaction proceeds with a satisfactory yield (60–65%).



As already observed for the meta-substituted derivatives,<sup>1,2</sup> the mass spectra of compounds **3** show the molecular isotopic pattern in perfect accordance with theoretical prediction. The fragmentation initially involves the breaking of the zirconium–carbon bonds and is followed by loss of the metal atom and the subsequent fragmentation of the selenium-containing ring.

The ortho- and meta-substituted complexes, **3** and **2**, can be differentiated by <sup>1</sup>H and <sup>77</sup>Se NMR.<sup>10</sup> As expected, the position of the R group on the phenyl ring does not influence the chemical shifts of the cyclopentadienyl protons. The methyl protons of the R group in the ortho isomer, being closer to a selenium atom, are more deshielded than those of the corresponding meta isomer. The increment is about 0.13 ppm for the methoxy series and lies close to 0.60 ppm for the methyl one. The phenyl protons are more sensitive to the sub-

## Scheme 2



stitution: H<sup>8</sup> appears as a doublet (*J*<sub>ortho</sub> = 8 Hz) with approximately the same chemical shift for both the ortho- and meta-substituted compounds. On the contrary, in the methoxy series, the proton H<sup>8</sup> is more shielded for the ortho isomer than for the meta one ( $\Delta\delta = 0.1$  ppm). Proton H<sup>7</sup>, which appears as a doublet of doublets (<sup>3</sup>*J* = 8 Hz, <sup>4</sup>*J* = 2 Hz) for the meta complex, is a triplet (<sup>3</sup>*J* = 7.8 Hz) in the ortho series.

The <sup>77</sup>Se NMR signals were assigned by comparing the proton-decoupled and normal spectra and considering the coupling constants between the aromatic protons and the selenium atoms. A selenium atom in a position meta to a methoxy group is slightly more deshielded than when located in the ortho position and is significantly more deshielded when located in the para position.

The structures of the ortho-substituted complexes **3** were also confirmed by comparison of their NMR spectra with those of authentic samples prepared according to Scheme 2. Complexes **4** and **5** are prepared in good yield starting from the [ $\eta^5$ -C<sub>5</sub>H<sub>4</sub>(*t*-Bu)]<sub>2</sub>ZrCl<sub>2</sub>. The mono-substituted derivative **4** is exclusively formed due to the steric hindrance of the ortho substituent. The action of methyl lithium on **4** leads to complex **5** which, when heated, loses a molecule of methane and affords the transient arynezirconocene able to insert two chalcogen atoms. Both methods afford the same compounds, but the latter is less efficient with the observed yields being 8% (R = CH<sub>3</sub>) and 24% (R = OCH<sub>3</sub>).

**1. Mechanism of the Thermal Transformation of **1** into **3**.** In view of the results previously published on the thermolysis of diphenylzirconocenes,<sup>11–13</sup> it is well established that the reactive species is the benzynezirconocene. Such species has been isolated and characterized by Buchwald<sup>14</sup> as a complex with trimethylphosphine. For the related *tert*-butyl-substituted cyclopentadienyl analog, the transient benzynezirconocene intermediate promotes a C–H bond activation of a methyl substituent of a *tert*-butyl group<sup>15</sup> leading to the metallacyclic complex **I** (Scheme 3). Alternatively, the thermolysis of [C<sub>5</sub>H<sub>4</sub>CMe<sub>2</sub>Ph]<sub>2</sub>ZrPh<sub>2</sub> gives a mixture of two compounds resulting from the C–H bond activation and cyclometalation, in a highly tempera-

(5) Meunier, P.; Gautheron, B.; Mazouz, A. *Phosphorus Sulfur Relat. Elem.* **1987**, *33*, 33.

(6) Tavares, P.; Meunier, P.; Gautheron, B.; Dousse, G.; Lavayssière, H. *Phosphorus, Sulfur Silicon Relat. Elem.* **1991**, *55*, 249.

(7) Tavares, P.; Meunier, P.; Kubicki, M. M.; Gautheron, B.; Dousse, G.; Lavayssière, H.; Satgé, J. *Heteroatom Chem.* **1993**, *4*, 383.

(8) Fagan, P. J.; Nugent, W. A.; Calabrese, J. C. *J. Am. Chem. Soc.* **1994**, *116*, 1880.

(9) Mazouz, A.; Bodiguel, J.; Meunier, P.; Gautheron, B. *Phosphorus, Sulfur Silicon Relat. Elem.* **1991**, *61*, 247.

(10) Granger, P.; Gautheron, B.; Tainturier, G.; Pouly, S. *Org. Magn. Reson.* **1984**, *22*, 701.

(11) Kolomnikov, I. S.; Lobeveva, T. S.; Gorbachevskaya, V. V.; Aleksandrov, G. G.; Struckhov, Y. T.; Vol'pin, M. E. *J. Chem. Soc., Chem. Commun.* **1971**, 972.

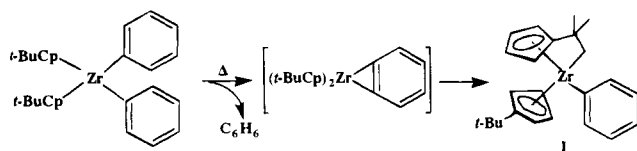
(12) Erker, G. *J. Organomet. Chem.* **1977**, *134*, 189.

(13) Buchwald, S. L.; Nielsen, R. B. *Chem. Rev.* **1988**, *88*, 1047.

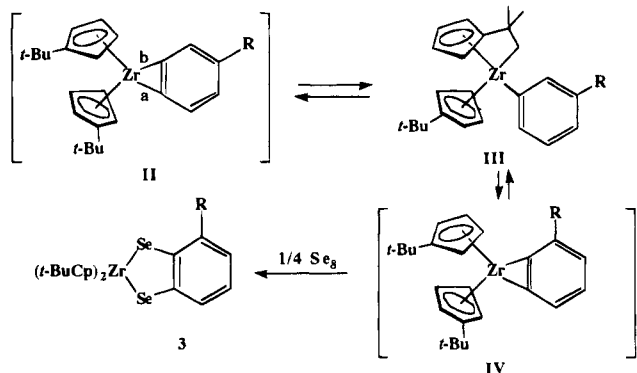
(14) Buchwald, S. L.; Watson, B. T.; Huffman, J. C. *J. Am. Chem. Soc.* **1986**, *108*, 7411.

(15) Erker, G.; Mühlenbernd, T. *J. Organomet. Chem.* **1987**, *319*, 201.

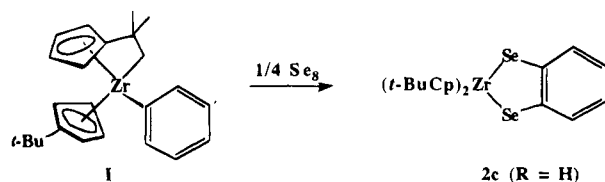
Scheme 3



Scheme 4



Scheme 5



ture dependent equilibrium.<sup>16</sup> Similar behavior has been observed in the pentamethylcyclopentadienyl series.<sup>17,18</sup>

From our experimental results, cyclometalation products similar to **I** are assumed to be the transient species involved in the reaction of diarylzirconocenes with chalcogens. Isomerization of the arynezirconocene intermediate via the cyclometalation product provides a reasonable explanation of the origin of the ortho isomer in the substituted phenyl ring (Scheme 4). Near 80 °C, the arynezirconocene **II** is transformed into the cyclometalation product **III**, able to afford intermediate **IV** (isomer of **II**). By varying the temperature and the electronic nature of R, the equilibrium **III** ⇌ **IV** can be shifted to favor the formation of **IV**. The subsequent reaction of selenium with **IV** produces selectively the ortho-substituted compound **3**.

We have tried to investigate this mechanism further by isolating the intermediates **III**. Unfortunately, for the experimental conditions used, only a mixture of isomers is obtained arising from the two ways of opening the three-membered zirconacyclic ring of **II**. As an alternative strategy, we reacted grey selenium with the complex **I** (Scheme 5). At 80 °C this reaction affords, in satisfactory yield, the diselenophenylenezirconocene **2c**.<sup>1</sup> This result provides good evidence of complex **I** as the intermediate in the transformation of  $(\eta^5\text{-C}_5\text{H}_4(t\text{-Bu}))_2\text{Zr}(\text{C}_6\text{H}_5)_2$  into **2c**. From these results, it is apparent that **I** and **III** provide a source of the corresponding arynezirconocene.

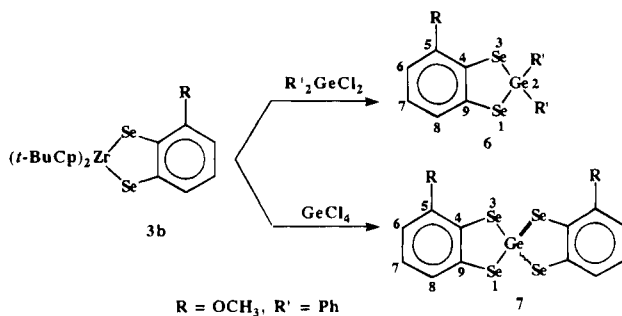
## 2. Reactivity of the Ortho-Substituted Diselenophenylenezirconocenes (**3**). Like complexes **2**,

(16) Erker, G.; Korek, U.; Petrenz, R.; Rheingold, A. L. *J. Organomet. Chem.* **1991**, *421*, 215.

(17) Schock, L. E.; Brock, C. P.; Marks, T. J. *Organometallics* **1987**, *6*, 232, and references therein.

(18) Schock, L. E.; Marks, T. J. *J. Am. Chem. Soc.* **1988**, *110*, 7701.

Scheme 6

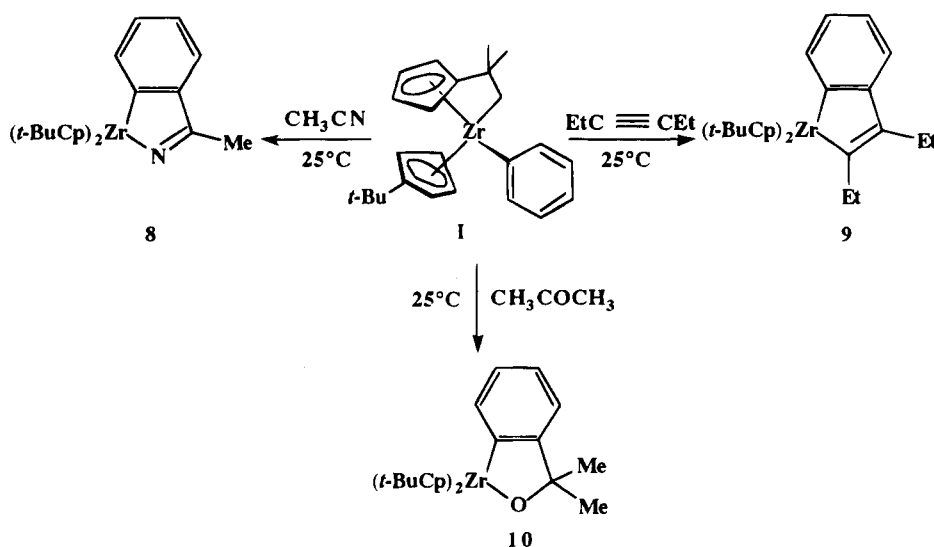


complexes **3** are good precursors for the substituted *o*-diselenophenylene unit. For instance, a zirconium–germanium transmetalation (Scheme 6)<sup>6–8</sup> provides a synthesis of several benzodiselenagermole and spiro-benzodiselenagermole. Particularly a selenium insertion followed by the exchange with reagents containing a main group element represents a new way of access to selenium-containing heterocyclic molecules. The exchange reactions were usually carried out at room temperature in tetrahydrofuran solutions. The reaction was complete when the deep red color of the starting solutions turned to yellow. Sometimes (in particular with germanium tetrachloride), the reaction took only a few seconds but generally it needed several minutes. Diselenagermoles **6** and **7**, which are noticeably more soluble than the side product zirconocene dichloride, were dissolved in pentane or in a pentane/ether mixture and chromatographed after the solvent was removed. Compounds **6** and **7** were obtained in a 60–70% yield of isolated product. They were characterized by microanalysis, mass spectrometry, and multinuclear NMR.

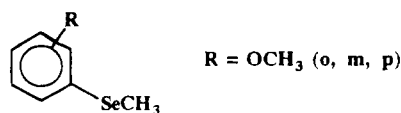
The influence of the position of the substituent in the phenyl ring on the chemical shifts of the <sup>1</sup>H and <sup>77</sup>Se atoms has been pointed out in **6** and **7** synthesized from complexes **3b** and in their isomers previously synthesized<sup>7</sup> from diselenophenylenezirconocene **2b**. The protons H<sup>7</sup> and H<sup>8</sup> are the most sensitive to the position of the methoxy substituent. A shielding (0.2–0.25 ppm) of the signal of H<sup>8</sup>, associated with a deshielding (0.5 ppm) of the resonance of H<sup>7</sup>, is observed when the substituent is moved from C<sup>6</sup> to C<sup>5</sup>. The resonances of the <sup>77</sup>Se are also dependent on the position of the substituent in the phenyl ring. The assignment of the <sup>77</sup>Se signals to the ortho and para isomers, respectively, is the result of the comparison between the proton-decoupled and nondecoupled <sup>77</sup>Se NMR spectra. The Se–H coupling constant observed (about 9 Hz) is assigned to the Se<sup>1</sup>–H<sup>8</sup> set ( $\delta = 185.9$  ppm) in **6** (R = OCH<sub>3</sub>). The other selenium atom (Se<sup>3</sup>) leads to a slightly more shielded singlet (140.4 ppm). The comparison between the values collected for the Se resonance versus the position of the methoxy group leads to the following sequence: ortho (about 140 ppm); para (about 156 ppm);<sup>7</sup> meta (about 190 ppm).

The <sup>77</sup>Se NMR results related to the spiran derivatives **7** and their isomers previously described<sup>7</sup> follow the same sequence with values largely shifted to low field (ortho position about 300 ppm; para about 320 ppm;<sup>7</sup> meta about 350 ppm). The same order (ortho position at 150.0 ppm; para at 189.5 ppm; and meta at

Scheme 7



207.0 ppm) has already been assigned to similar selenide compounds<sup>19</sup> of general formula



### 3. Reactivity of the Cyclometalated Products.

Complex **I** also behaves as a source of benzynezirconocene, and its reactivity is comparable to that of the benzynezirconocene trimethylphosphine adduct.<sup>14</sup> For example, in the presence of elemental selenium, complex **I** affords the diselenolato-zirconocyclic complex **2c** ( $\text{R} = \text{H}$ ), whereas the benzynezirconocene trimethylphosphine adduct leads to the corresponding diselenophenylenezirconocene. In addition, the insertion reactions of **I** with unsaturated organic molecules (nitrile, alkyne, ketone) have been performed (Scheme 7). The yields obtained by this route are slightly lower than when starting from the trimethylphosphinebenzynezirconocene complex<sup>14</sup> or from the corresponding diphenylzirconocene precursor. However, because these insertion reactions with **I** take place at room temperature, they allow thermally unstable species to be studied without use of trimethylphosphine.<sup>20</sup>

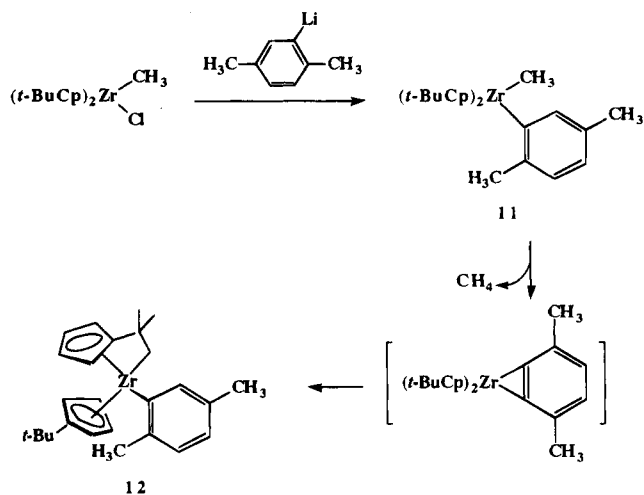
We have also been interested in the synthesis of sterically hindered compounds with a substituent in the position ortho to the zirconium-phenyl bond. We have prepared complex **12** following the reaction sequence shown in Scheme 8. The precursor compound **11** readily eliminates methane at room temperature leading easily to **12**.

Spectroscopic data for **12** are consistent with the proposed structure. The two diastereotopic methylene protons display two doublets at 0.30 and  $-1.22$  ppm in the  $^1\text{H}$  NMR spectrum. The cyclopentadienyl protons are also diastereotopic and appear as eight pseudoquartets. Seven signals in the range 99.3–117.5 ppm (one is of double intensity) are detected by  $^{13}\text{C}$  NMR for the eight unsubstituted carbons of the cyclopentadienyl rings.

(19) Llabrès, G.; Baiwir, M.; Piette, J. L.; Christiaens, L. *Org. Magn. Reson.* **1981**, *2*, 152.

(20) Meunier, P.; et al. Unpublished results.

Scheme 8



The molecular structure of complex **12** was confirmed by X-ray diffraction methods. The final atomic coordinates and selected interatomic distances and bond angles are given in Tables 1 and 2, respectively. This compound crystallizes in a monoclinic crystal lattice with two independent molecules per asymmetric unit. The structures of these two molecules differ only in terms of the spatial orientation of the *tert*-butyl-substituted cyclopentadienyl ring. As illustrated by the perspective view of **12** (Figure 1), the coordination environment about Zr is compatible with that of a bent pseudotetrahedral zirconocene complex with a  $\text{Cp}(c)\text{-Zr-Cp}(c)$  angle of *ca.*  $134^\circ$ . One of the *tert*-butyl-substituted cyclopentadienyl rings remains coordinated in a typical  $\eta^5$  fashion. The other has been transformed as a consequence of intramolecular C–H activation into a dianionic bifunctional cyclopentadienyl ligand which is further linked to the same Zr center through an  $\eta^1$ -1,1-dimethylethano bridge. Although the Zr–Cp(*c*) distance for the bifunctional cyclometalated cyclopentadienyl ligand is *ca.*  $0.05 \text{ \AA}$  shorter than that for a normal cyclopentadienyl ring, the Zr–C(ring) distances similarly vary by *ca.*  $0.1 \text{ \AA}$  within each ring. The Zr–C(methylene) bond of *ca.*  $2.34 \text{ \AA}$  (av) is noticeably longer than the Zr–C(aryl) bond of  $2.30 \text{ \AA}$  (av).

This type of "tucked-in" or cyclometalated structure has been reported by Marks and co-workers for ( $\eta^5\text{-C}_5$ -

**Table 1. Positional Parameters ( $\times 10^4$ ) and Equivalent Isotropic Displacement Coefficients ( $\text{\AA}^2 \times 10^3$ ) for Complex 12**

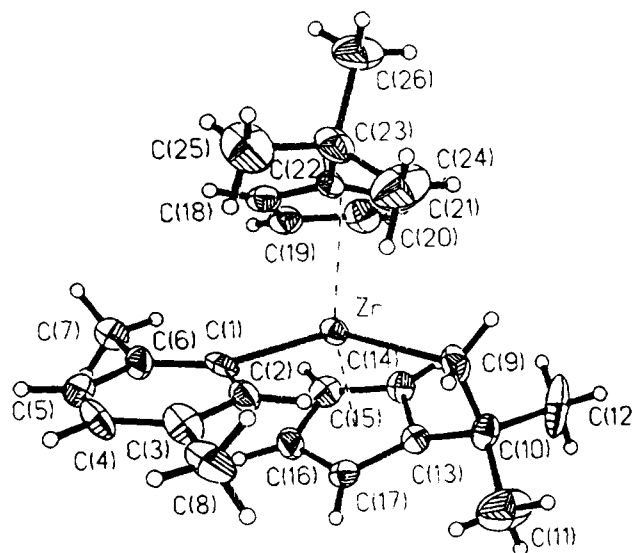
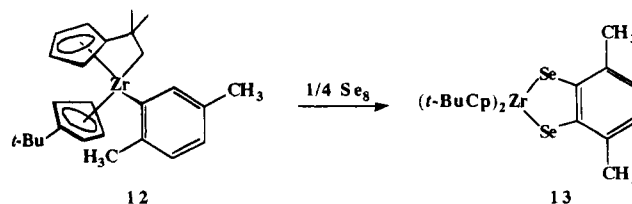
atom	x	y	z	$U(\text{eq})^a$
Zr(1)	1544(2)	2207(1)	803(1)	39(1)
C(1)	803(21)	1960(6)	15(4)	45(6)
C(2)	2195(18)	1946(6)	-250(5)	47(6)
C(3)	2194(20)	1794(7)	-742(5)	54(7)
C(4)	713(22)	1670(7)	-971(5)	58(7)
C(5)	-669(21)	1696(7)	-728(5)	55(7)
C(6)	-652(21)	1829(7)	-237(5)	52(6)
C(7)	-2246(18)	1832(7)	5(5)	69(7)
C(8)	3711(19)	1782(7)	-1014(5)	80(7)
C(9)	4304(16)	2451(7)	918(5)	59(6)
C(10)	4300(17)	3203(7)	1032(5)	49(6)
C(11)	5263(19)	3600(8)	693(7)	119(10)
C(12)	4928(18)	3344(8)	1554(5)	101(8)
C(13)	2502(18)	3349(6)	958(5)	40(5)
C(14)	1362(18)	3184(6)	1310(5)	46(6)
C(15)	-178(18)	3140(6)	1066(6)	52(6)
C(16)	12(20)	3257(7)	576(6)	57(7)
C(17)	1646(19)	3379(6)	503(5)	43(6)
C(18)	274(19)	1063(7)	897(5)	51(6)
C(19)	-404(19)	1515(7)	1221(6)	58(7)
C(20)	817(22)	1666(8)	1567(5)	64(7)
C(21)	2244(21)	1350(7)	1451(5)	59(7)
C(22)	1884(18)	958(6)	1026(5)	42(6)
C(23)	2983(21)	439(8)	815(6)	66(7)
C(24)	4650(20)	697(7)	732(6)	108(9)
C(25)	2245(21)	165(8)	329(6)	105(9)
C(26)	3124(20)	-140(7)	1174(6)	97(9)

<sup>a</sup> Equivalent isotropic  $U$  is defined as one-third of the trace of the orthogonalized  $U_{ij}$  tensor.

**Table 2. Selected Bond Lengths ( $\text{\AA}$ ) and Angles (deg) for Complex 12**

Bond Lengths			
Zr-C(1)	2.285(13)	C(10)-C(13)	1.520(20)
Zr-Cp(1)	2.172	C(13)-C(14)	1.430(20)
Zr-Cp(2)	2.227	C(13)-C(17)	1.411(19)
Zr-C(9)	2.342(13)	C(14)-C(15)	1.412(20)
Zr-C(13)	2.460(13)	C(15)-C(16)	1.392(23)
Zr-C(22)	2.599(13)	C(16)-C(17)	1.400(23)
C(1)-C(2)	1.399(22)	C(22)-C(23)	1.522(22)
C(9)-C(10)	1.545(20)	C(23)-C(24)	1.504(24)
C(10)-C(11)	1.495(23)	C(23)-C(25)	1.547(22)
C(10)-C(12)	1.533(20)	C(23)-C(26)	1.529(22)
Bond Angles			
C(1)-Zr-C(9)	112.6(6)	C(10)-C(13)-C(14)	122.7(12)
Cp(1)-Zr-Cp(2)	133.7	C(10)-C(13)-C(17)	124.7(13)
Zr-C(1)-C(2)	108.5(10)	C(14)-C(13)-C(17)	107.3(12)
Zr-C(1)-C(6)	134.7(12)	C(13)-C(14)-C(15)	107.6(12)
C(1)-C(6)-C(7)	122.2(13)	C(14)-C(15)-C(16)	107.9(13)
Zr-C(9)-C(10)	102.7(8)	C(15)-C(16)-C(17)	109.4(13)
C(9)-C(10)-C(11)	112.7(12)	C(13)-C(17)-C(16)	107.8(13)
C(9)-C(10)-C(12)	111.7(12)	C(18)-C(22)-C(23)	126.7(13)
C(11)-C(10)-C(12)	109.1(12)	C(21)-C(22)-C(23)	126.1(13)
C(9)-C(10)-C(13)	100.1(11)	C(22)-C(23)-C(24)	113.2(13)
C(11)-C(10)-C(13)	111.3(12)	C(22)-C(23)-C(25)	111.2(13)
C(12)-C(10)-C(13)	111.8(12)	C(22)-C(23)-C(26)	107.4(13)

$\text{Me}_5\text{Zr}(\eta^6\text{-C}_5\text{Me}_4\text{CH}_2)(\text{C}_6\text{H}_5)$ ,<sup>17</sup> obtained by the thermolysis of  $(\eta^5\text{-C}_5\text{Me}_5)_2\text{Zr}(\text{C}_6\text{H}_5)_2$ . In this case the bifunctional  $(\eta^6\text{-C}_5\text{Me}_4\text{CH}_2)$  ligand is linked by a single C atom to the metal rather than by a two-carbon-atom bridge as observed in **12**. As one might expect, the length of the hydrocarbon chain significantly affects the extent to which the methylene group of the metalated cyclopentadienyl ring is displaced from the mean plane defined by the internal carbons of the ring and the degree of canting of the cyclopentadienyl rings. The methylene group of  $(\eta^5\text{-C}_5\text{Me}_5)\text{Zr}(\eta^6\text{-C}_5\text{Me}_4\text{CH}_2)(\text{C}_6\text{H}_5)$  is displaced by 0.89  $\text{\AA}$  whereas the substituted methylene group of **12** is displaced by only 0.48  $\text{\AA}$  from the corresponding ring plane toward the Zr. The Cp(c)-

**Figure 1. ORTEP view of compound 12.****Scheme 9**

Zr-Cp(c) angle falls within the normal range of 125–135° observed for  $\text{Cp}_2\text{Zr}(\text{IV})\text{L}_2$ -type complexes;<sup>21,22</sup> the corresponding angle of 143.6° in  $(\eta^5\text{-C}_5\text{Me}_5)\text{Zr}(\eta^6\text{-C}_5\text{Me}_4\text{CH}_2)(\text{C}_6\text{H}_5)$  reflects significantly less canting of the cyclopentadienyl rings in this case. The additional carbon atom in the hydrocarbon linkage, however, does not notably affect the C(methylene)-Zr-C(phenyl) bond angle in **12** of 111.7° (av), which is comparable to the value of 110.5(2)° observed in  $(\eta^5\text{-C}_5\text{Me}_5)\text{Zr}(\eta^6\text{-C}_5\text{Me}_4\text{CH}_2)(\text{C}_6\text{H}_5)$ .<sup>17</sup> Finally, within the bridging ethano group of **12** the C(ring)-C-C and C-C-Zr bond angles of 102.7(8) and 100.1(11)° deviate significantly from that normally expected for a  $\text{sp}^3$  carbon.

The cyclometalation product **12** represents a useful precursor for the synthesis of crowded complexes containing two selenium atoms for which the corresponding diarylzirconocenes are not accessible for steric reasons (Scheme 9). The reaction of **12** with selenium proceeds in a good yield (83%), but the corresponding reaction for complex **11** affords a complex mixture. Moreover, the chemical intermediacy of **12** avoids the need to stabilize a benzynezirconocene with  $\text{PMe}_3$ .<sup>14</sup> Spectroscopic data for **13** are in agreement with its high symmetry. The  $^1\text{H}$  NMR displays the signal of the two homotopic phenyl protons near 7 ppm. In  $\text{C}_6\text{D}_6$ , the cyclopentadienyl protons appear as a singlet but this fortuitous equivalence is not observed in  $\text{CDCl}_3$ . As expected the *tert*-butyl and methyl groups resonate as two singlets at 1.11 and 2.73 ppm, respectively. The  $^{13}\text{C}$  NMR spectrum of **13** is very comparable to that of **2** and fits well with the proposed structure. In addition, only one signal is viewed in  $^{77}\text{Se}$  NMR, the chemical shift of which (559.3 ppm) is close to that of the

(21) Hunter, W. E.; Hrcir, D. C.; Vann Bynum, R.; Penttila, R. A.; Atwood, J. L. *Organometallics* **1983**, *2*, 750.

(22) Atwood, J. L.; Barker, G. K.; Holton, J.; Hunter, W. E.; Lappert, M. F.; Pearce, R. *J. Am. Chem. Soc.* **1977**, *99*, 6645.

unsubstituted congener **2c** (562.9 ppm)<sup>1</sup> and those related to **3a** (583.6 and 546.0 ppm).

### Conclusion

We have proposed a mechanism for the thermal isomerization of a  $\eta^2$ -arynezirconocene species based on the formation of a cyclometalation product resulting from the activation of a C–H bond of a *tert*-butyl group by the transient benzynezirconocene precursor. A crystallized representative has been isolated for the first time starting from the methyl(2,5-dimethylphenyl)di-*tert*-butylzirconocene, and its molecular structure has been determined by X-ray diffraction. Like **I**, this cyclometalated product is very reactive at room temperature toward grey selenium powder. Some complementary results concerning this reactivity will be reported in due time.

### Experimental Section

**General Procedures.** Reactions were carried out under an atmosphere of argon by means of conventional Schlenk techniques. Solvents (except benzene) were dried and deoxygenated before distillation from sodium benzophenone ketyl. Benzene and hexadeuteriobenzene were distilled from Na/K alloy. Acetonitrile was dried over anhydrous CaCl<sub>2</sub> and distilled from P<sub>2</sub>O<sub>5</sub>. Acetone was dried over anhydrous CaCl<sub>2</sub> and distilled from K<sub>2</sub>CO<sub>3</sub>. Di-*tert*-butylzirconocene dichloride was prepared according to literature.<sup>23</sup> Chloromethyl-di-*tert*-butylzirconocene was prepared with the method Wailes used for the chloromethylzirconocene.<sup>24</sup> Flash chromatography<sup>25</sup> was performed using silica gel Merck 9385.

Melting points were measured on a Kofler beam without any correction. Elemental analysis were performed by the Service Central d'Analyses du CNRS. Mass spectra (electronic ionization 70 eV) were recorded on a Kratos concept IS.

<sup>1</sup>H and <sup>13</sup>C NMR spectra were recorded on a Bruker AC 200 (<sup>1</sup>H, 200 MHz; <sup>13</sup>C, 50.3 MHz) or a Bruker WM 400 apparatus (<sup>13</sup>C, 100.4 MHz). The spectra were referenced to TMS (external), <sup>13</sup>C spectra being recorded using the JMOD technique. <sup>77</sup>Se NMR drawings were obtained on a Bruker WM 400 (76.31 MHz) or Bruker WR 300 (57.24 MHz) spectrometer and referenced to dimethylselenide (external).

The following abbreviations were used: C<sub>prim</sub>, C<sub>sec</sub>, C<sub>tert</sub>, and C<sub>quat</sub> for the primary, secondary, tertiary, and quaternary carbon atoms, respectively.

**Preparation of 3a.** A mixture of di(*p*-tolyl)zirconocene<sup>1</sup> (0.59 g, 1.14 mmol) and grey selenium powder (0.19 g, 2.40 mmol) was heated with reflux for 17 h in octane (14 mL). The resulting brown mixture was then hot filtered. When cooled, the solution gave 0.29 g of brown crystals containing a mixture of the two isomers **3a** and **2a** (60/40) from which **3a** has never been obtained in a pure state.

The <sup>1</sup>H NMR of the meta isomer **2a** had been previously published<sup>1</sup> at 100 MHz. More precise values (at 200 MHz) and <sup>13</sup>C NMR data are reported here. <sup>1</sup>H NMR, C<sub>6</sub>D<sub>6</sub>: 7.86 (d, H8, *J* = 7.81 Hz), 7.83 (s, H5), 6.81 (dd, H7, *J* = 7.81, 1.95 Hz), 5.85 (pt, 4H, Cp), 5.73 (m, 4H, Cp), 2.07 (s, 3H, CH<sub>3</sub>), 1.13 (s, 18H, *t*-Bu). <sup>13</sup>C NMR, CDCl<sub>3</sub>: 145.9 (C<sub>quat</sub>), 142.6 (C<sub>quat</sub>), 141.3 (C<sub>quat</sub>, 2C), 135.4 (C<sub>tert</sub>, C<sub>6</sub>H<sub>3</sub>), 134.5 (C<sub>tert</sub>, C<sub>6</sub>H<sub>3</sub>), 126.9 (C<sub>tert</sub>, C<sub>6</sub>H<sub>3</sub>), 111.2 (C<sub>tert</sub>, 4C, Cp), 108.1 (C<sub>tert</sub>, 4C, Cp), 33.2 (C<sub>quat</sub>; *t*-Bu), 31.8 (C<sub>prim</sub>, *t*-Bu), 21.0 (C<sub>prim</sub>, CH<sub>3</sub>). <sup>77</sup>Se NMR, CDCl<sub>3</sub>: 567.9 (Se-1), 561.6 (Se-3).

Spectroscopic data for **3a**. Anal. Calcd for C<sub>25</sub>H<sub>32</sub>Se<sub>2</sub>Zr: C, 51.62; H, 5.54. Found: C, 51.43; H, 5.49. <sup>1</sup>H NMR, C<sub>6</sub>D<sub>6</sub>: 7.88 (d, H8, *J* = 7.81 Hz), 7.02 (d, H6, *J* = 7.81 Hz), 6.97 (t, H7, *J*

= 7.81 Hz), 5.79 (pt, 4H, Cp), 5.66 (m, 4H, Cp), 2.67 (s, 3H, CH<sub>3</sub>), 1.12 (s, 18H, *t*-Bu). <sup>13</sup>C NMR, CDCl<sub>3</sub>: 148.4 (C<sub>quat</sub>), 147.4 (C<sub>quat</sub>), 140.7 (C<sub>quat</sub>, 2C), 132.5 (C<sub>tert</sub>, C<sub>6</sub>H<sub>3</sub>), 126.1 (C<sub>tert</sub>, C<sub>6</sub>H<sub>3</sub>), 125.7 (C<sub>tert</sub>, C<sub>6</sub>H<sub>3</sub>), 111.3 (C<sub>tert</sub>, 4C, Cp), 108.3 (C<sub>tert</sub>, 4C, Cp), 33.1 (C<sub>quat</sub>; *t*-Bu), 31.9 (C<sub>prim</sub>, *t*-Bu), 26.6 (C<sub>prim</sub>, CH<sub>3</sub>). <sup>77</sup>Se NMR, CDCl<sub>3</sub>: 583.6 (Se-1), 546.0 (Se-3).

**Preparation of 3b.** A mixture of di(*p*-anisyl)zirconocene (0.75 g, 1.37 mmol) and grey selenium powder (0.22 g, 2.79 mmol) in 16 mL of octane was heated with reflux for 17 h. The obtained dark-red solution was hot filtered and gave after cooling 0.42 g (0.70 mmol, 51% yield) of brown crystals. mp: 160 °C. Anal. Calcd for C<sub>25</sub>H<sub>32</sub>OSe<sub>2</sub>Zr: C, 50.24; H, 5.40. Found: C, 49.99; H, 5.24. <sup>1</sup>H NMR, C<sub>6</sub>D<sub>6</sub>: 7.68 (d, H8, *J* = 7.81 Hz), 7.01 (t, H7, *J* = 7.81 Hz), 6.44 (d, H6, *J* = 7.81 Hz), 5.86 (pt, 4H, Cp), 5.76 (m, 4H, Cp), 3.41 (s, 3H, OCH<sub>3</sub>), 1.14 (s, 18H, *t*-Bu). <sup>13</sup>C NMR, CDCl<sub>3</sub>: 158.6 (C<sub>quat</sub>, C<sub>6</sub>H<sub>3</sub>), 147.8 (C<sub>quat</sub>, C<sub>6</sub>H<sub>3</sub>), 141.4 (C<sub>quat</sub>, 2C, Cp), 135.8 (C<sub>quat</sub>, C<sub>6</sub>H<sub>3</sub>), 127.6 (C<sub>tert</sub>, C<sub>6</sub>H<sub>3</sub>), 126.6 (C<sub>tert</sub>, C<sub>6</sub>H<sub>3</sub>), 111.5 (C<sub>tert</sub>, 2C, Cp), 111.0 (C<sub>tert</sub>, 2C, Cp), 108.2 (C<sub>tert</sub>, 2C, Cp), 107.9 (C<sub>tert</sub>, 2C, Cp), 106.4 (C<sub>tert</sub>, C<sub>6</sub>H<sub>3</sub>), 56.3 (C<sub>prim</sub>, OCH<sub>3</sub>), 33.1 (C<sub>quat</sub>; *t*-Bu), 31.8 (C<sub>prim</sub>; *t*-Bu). <sup>77</sup>Se NMR, C<sub>6</sub>D<sub>6</sub>: 576.1 (Se-1), 574.6 (Se-3).

**Preparation of 4a.** *o*-Tolylolithium was prepared by action of lithium metal on *o*-tolyl bromide in ether. The aryllithium (65 mL, 20 mmol) was added dropwise at 0 °C to a solution of 4.04 g (10 mmol) of di-*tert*-butylzirconocene dichloride in 100 mL of diethyl ether. The stirring was maintained for 1 h at 0 °C and for 2 h more at room temperature. The solvent was then removed. The solid residue was extracted by 60 mL of hot octane, and the mixture was hot filtered. After cooling, 2.3 g of colorless crystals (5 mmol, 50% yield) were isolated. mp: 151 °C. Anal. Calcd for C<sub>25</sub>H<sub>33</sub>ClZr: C, 65.25; H, 7.23. Found: C, 65.01; H, 7.18. <sup>1</sup>H NMR, C<sub>6</sub>D<sub>6</sub>: 7.98 (m, 1H, C<sub>6</sub>H<sub>4</sub>), 7.02 (m, 3H, C<sub>6</sub>H<sub>4</sub>), 6.31 (q, 2H, Cp), 5.90 (q, 2H, Cp), 5.76 (q, 2H, Cp), 5.44 (q, 2H, Cp), 2.00 (s, 3H, CH<sub>3</sub>), 1.19 (s, 18H, *t*-Bu).

**Preparation of 4b.** **4b** was prepared according to the same method used for **4a** (77% yield). Anal. Calcd for C<sub>25</sub>H<sub>33</sub>-ClOZr: C, 63.06; H, 6.98. Found: C, 62.84; H, 6.87. <sup>1</sup>H NMR, C<sub>6</sub>D<sub>6</sub>: 7.81 (m, 2H, C<sub>6</sub>H<sub>4</sub>), 7.00 (dd, 1H, C<sub>6</sub>H<sub>4</sub>), 6.85 (dd, 1H, C<sub>6</sub>H<sub>4</sub>), 6.40 (pq, 2H, Cp), 5.94 (pt, 4H, Cp), 5.64 (pq, 2H, Cp), 3.29 (s, 3H, OCH<sub>3</sub>), 1.24 (s, 18H, *t*-Bu).

**Preparation of 5a.** To 3.53 g (7.68 mmol) of (*t*-BuCp)<sub>2</sub>Zr-(Cl)(*o*-C<sub>6</sub>H<sub>4</sub>CH<sub>3</sub>) in ether at 0 °C were added dropwise 3.3 mL (7.99 mmol) of an ethereal solution of CH<sub>3</sub>Li. The stirring was maintained for 1 h at 0 °C and for 2 h more at room temperature. The solvent was then removed and the residual solid extracted by 60 mL of hot hexane. After filtration and cooling, 2.18 g (4.96 mmol, 64% yield) of white crystals was obtained. Anal. Calcd for C<sub>36</sub>H<sub>36</sub>Zr: C, 71.01; H, 8.25. Found: C, 71.21; H, 8.27. <sup>1</sup>H NMR, C<sub>6</sub>D<sub>6</sub>: 7.02 (m, 4H, C<sub>6</sub>H<sub>4</sub>), 6.20 (pq, 2H, Cp), 5.84 (pq, 2H, Cp), 5.57 (pq, 2H, Cp), 5.35 (pq, 2H, Cp), 2.10 (s, 3H, CH<sub>3</sub>), 1.06 (s, 18H, *t*-Bu), 0.47 (s, 3H, CH<sub>3</sub>).

**Preparation of 5b.** **5b** was isolated as white crystals according to the same method used for **5a** (62% yield). mp: 69–70 °C. Anal. Calcd for C<sub>26</sub>H<sub>36</sub>OZr: C, 68.52; H, 7.96. Found: C, 68.42; H, 7.90. <sup>1</sup>H NMR, C<sub>6</sub>D<sub>6</sub>: 7.06 (m, 2H, C<sub>6</sub>H<sub>4</sub>), 6.91 (dd, 1H, C<sub>6</sub>H<sub>4</sub>), 6.41 (dd, 1H, C<sub>6</sub>H<sub>4</sub>), 6.27 (pq, 2H, Cp), 5.87 (pq, 2H, Cp), 5.75 (pq, 2H, Cp), 5.52 (pq, 2H, Cp), 3.26 (s, 3H, OCH<sub>3</sub>), 1.12 (s, 18H, *t*-Bu).

**Preparation of 3a from 5a.** A mixture of 0.68 g (1.55 mmol) of (*t*-BuCp)<sub>2</sub>Zr(CH<sub>3</sub>)(*o*-C<sub>6</sub>H<sub>4</sub>CH<sub>3</sub>) and 0.25 g (3.16 mmol) of grey selenium in 40 mL of hexane was heated with reflux for 4 h. The hot filtered mixture led after cooling to 0.07 g (0.12 mmol, 8% yield) of red crystals identified to **3a** by the usual spectroscopic methods.

**Preparation of 2 (R = H, X = Se) from I.** A 0.27 g (0.66 mmol) sample of **I** was heated for 2 h with grey selenium powder (0.112 g, 1.42 mmol) in refluxing benzene (8 mL). The red reaction mixture was then filtered and the solvent was removed, leading to a red-brown solid (quantitative yield) identified as **2** by the usual spectroscopic methods.<sup>2</sup>

**Preparation of 6 from 3 (R = OCH<sub>3</sub>, R' = C<sub>6</sub>H<sub>5</sub>).** A red solution of 0.44 g (0.74 mmol) of (*t*-BuCp)<sub>2</sub>ZrSe<sub>2</sub>(*o*-C<sub>6</sub>H<sub>5</sub>OCH<sub>3</sub>)

(23) Howie, R. A.; McQuillan, G. P.; Thompson, D. W.; Lock, G. A. *J. Organomet. Chem.* **1986**, *303*, 213.

(24) Wailes, P. C.; Weigold, H.; Bell, A. P. *J. Organomet. Chem.* **1972**, *34*, 155.

(25) Still, W. C.; Kahn, M.; Mitra, A. *J. Org. Chem.* **1978**, *43*, 2923.



in 14 mL of THF was added dropwise at room temperature to a colorless solution of dichlorodiphenylgermane (0.22 g, 0.74 mmol) in THF (9 mL). After 15 h under stirring, the mixture had become yellow. The solvent was removed and the product extracted with a mixture of pentane and diethyl ether (1/1). After evaporation of the solvents, the residue was chromatographed on silica gel with pentane/ether (8/2). The solvents were then removed, and the product was obtained as a pale yellow crystalline solid (0.23 g, 0.47 mmol, 64% yield). mp: 148 °C. Anal. Calcd for  $C_{19}H_{16}OSe_2Ge$ : C, 46.49; H, 3.28. Found: C, 46.69; H, 3.56.  $^1H$  NMR,  $C_6D_6$ : 7.78 (m, 4H,  $C_6H_5$ ), 7.44 (m, 6H,  $C_6H_5$ ), 7.16 (dd, H8,  $J = 7.86$  and 1.22 Hz), 7.07 (t, H7,  $J = 7.86$  Hz), 6.60 (dd, H6,  $J = 7.86$ , 1.22 Hz), 3.87 (s, 3H, OCH<sub>3</sub>).  $^{77}Se$  NMR,  $C_6D_6$ : 185.9 (Se-1), 140.4 (Se-3).

**Preparation of 7.** To a solution of (*t*-BuCp)<sub>2</sub>ZrSe<sub>2</sub>(*o*-C<sub>6</sub>H<sub>3</sub>-OCH<sub>3</sub>) (0.93 g, 1.56 mmol) in THF (43 mL) was added a solution of germanium tetrachloride (0.17 g, 0.78 mmol) in THF (17 mL). The mixture progressively discolored. After 3 h under stirring at room temperature, the solvent was removed under vacuum. The residual product was extracted by a mixture of pentane and diethyl ether (3/2). After evaporation of the solvents, the residue was chromatographed on silica gel with pentane/ether (3/2). The yellow fraction was collected, and the solvents were evaporated. The resulting solid was recrystallized from a mixture of methylene dichloride/hexane (1/1). After cooling, 0.26 g (0.43 mmol, 56% yield) of yellow crystals was isolated. mp: 197 °C. Anal. Calcd for  $C_{14}H_{12}GeO_2Se_4$ : C, 27.99; H, 2.01. Found: C, 27.75; H, 1.89.  $^1H$  NMR, CDCl<sub>3</sub>: 7.14 (dd, H8,  $J = 7.8$ , 1.3 Hz), 7.11 (t, H7,  $J = 7.8$  Hz), 6.60 (dd, H6,  $J = 7.8$ , 1.3 Hz), 3.88 (s, 6H, OCH<sub>3</sub>).  $^{13}C$  NMR, CDCl<sub>3</sub>: 157.9 (C<sub>quat</sub>), 156.2 (C<sub>quat</sub>), 139.4 (C<sub>quat</sub>), 126.9 (C<sub>tert</sub>, C<sub>6</sub>H<sub>3</sub>), 121.0 (C<sub>tert</sub>, C<sub>6</sub>H<sub>3</sub>), 107.4 (C<sub>tert</sub>, C<sub>6</sub>H<sub>3</sub>), 56.5 (C<sub>prim</sub>, OCH<sub>3</sub>).  $^{77}Se$  NMR,  $C_6D_6$ : 346.5 (Se-1), 296.6 (Se-3).

**Preparation of 8. (a) From I.** To a yellow solution of 0.30 g (0.73 mmol) of I in benzene (12 mL) was added dropwise a solution of CH<sub>3</sub>CN (0.04 mL, 0.76 mmol) in benzene (4 mL). The stirring was maintained for 24 h at room temperature after what the solution had become orange. The solvent was then removed, leading to an orange solid containing a little amount of nonreacted II (quantitative yield from I).

**(b) Direct Synthesis.** Compound 8 can also be synthesized directly from the diphenyldi-*tert*-butylzirconocene<sup>1</sup> via the following way: a mixture of 0.60 g (1.23 mmol) of diphenyldi-*tert*-butylzirconocene and 0.07 mL of CH<sub>3</sub>CN (1.33 mmol) in heptane (20 mL) was heated with reflux for 17 h. After this, the solution had turned from yellow to dark orange. The solvent was then removed, and the residue was recrystallized from heptane (15 mL), leading, after cooling, to 0.42 g (0.93 mmol, 76% yield) of orange crystals. mp: 136–7 °C. Anal. Calcd for  $C_{26}H_{33}NZr$ : C, 69.27; H, 7.37. Found: C, 69.42; H, 7.37.  $^1H$  NMR,  $C_6D_6$ : 7.74 (dd,  $J = 6$ , 2.2 Hz, 1H, C<sub>6</sub>H<sub>4</sub>), 7.40 (dd,  $J = 6.8$ , 1.7 Hz, 1H, C<sub>6</sub>H<sub>4</sub>), 7.22 (m, 2H, C<sub>6</sub>H<sub>4</sub>), 5.93 (q, 2H, Cp), 5.62 (q, 2H, Cp), 5.55 (q, 2H, Cp), 5.41 (q, 2H, Cp), 1.61 (s, 3H, CH<sub>3</sub>), 0.97 (s, 18H, *t*-Bu).  $^{13}C$  NMR,  $C_6D_6$ : 186.3 (C<sub>quat</sub>), 172.4 (C<sub>quat</sub>), 156.3 (C<sub>quat</sub>), 148.8 (C<sub>quat</sub>), 140.8 (C<sub>tert</sub>, C<sub>6</sub>H<sub>4</sub>), 125.5 (C<sub>tert</sub>, C<sub>6</sub>H<sub>4</sub>), 123.9 (C<sub>tert</sub>, C<sub>6</sub>H<sub>4</sub>), 123.1 (C<sub>tert</sub>, C<sub>6</sub>H<sub>4</sub>), 113.8 (C<sub>tert</sub>, 2C, Cp), 109.8 (C<sub>tert</sub>, 2C, Cp), 105.8 (C<sub>tert</sub>, 2C, Cp), 101.1 (C<sub>tert</sub>, 2C, Cp), 32.7 (C<sub>quat</sub>, *t*-Bu), 31.2 (C<sub>prim</sub>, *t*-Bu), 24.1 (C<sub>prim</sub>, CH<sub>3</sub>).

**Preparation of 9. (a) From I.** To a yellow solution of 0.30 g (0.73 mmol) of I in benzene (12 mL) was added dropwise a solution of hex-3-yne (0.08 mL, 0.76 mmol) in benzene (4 mL). The stirring was maintained for 24 h at room temperature. The solution had then become orange. The solvent was removed and the residue was washed several times with pentane. The product was obtained as an orange solid (0.25 g, 0.51 mmol, 70% yield).

**(b) Direct Synthesis.** A mixture of 0.35 g (0.72 mmol) of diphenyldi-*tert*-butylzirconocene<sup>1</sup> and 0.09 mL of hex-3-yne (0.79 mmol) in heptane (12 mL) was heated with reflux for 20 h. After this period, the solution had turned from yellow to dark orange. The solvent was then evaporated, leading to 0.36 g (0.72 mmol, 100% yield in crude product) of an orange solid.

mp: 85–6 °C.  $^1H$  NMR,  $C_6D_6$ : 7.28 (dd, 1H, C<sub>6</sub>H<sub>4</sub>,  $J = 8$ , 1.16 Hz), 7.15 (td, 1H, C<sub>6</sub>H<sub>4</sub>,  $J = 7$ , 1.66 Hz), 6.96 (td, 1H, C<sub>6</sub>H<sub>4</sub>,  $J = 7$ , 1.16 Hz), 6.85 (dd, 1H, C<sub>6</sub>H<sub>4</sub>,  $J = 7$ , 1.66 Hz), 6.39 (pq, 1H, Cp), 6.11 (pq, 1H, Cp), 5.87 (pq, 1H, Cp), 5.70 (pq, 1H, Cp), 2.46 (q, 2H, CH<sub>2</sub>,  $J = 7.5$  Hz), 2.06 (q, 2H, CH<sub>2</sub>,  $J = 7.5$  Hz), 1.23 (t, 3H, CH<sub>3</sub>,  $J = 7.5$  Hz), 1.03 (s, 18H, *t*-Bu), 1.02 (t, 3H, CH<sub>3</sub>,  $J = 7.4$  Hz).  $^{13}C$  NMR,  $C_6D_6$ : 196.5 (C<sub>quat</sub>), 185.1 (C<sub>quat</sub>), 146.6 (C<sub>quat</sub>), 144.1 (C<sub>quat</sub>), 141.3 (C<sub>quat</sub>), 137.7 (C<sub>tert</sub>, C<sub>6</sub>H<sub>4</sub>), 126.3 (C<sub>tert</sub>, C<sub>6</sub>H<sub>4</sub>), 122.6 (C<sub>tert</sub>, C<sub>6</sub>H<sub>4</sub>), 121.8 (C<sub>tert</sub>, C<sub>6</sub>H<sub>4</sub>), 111.5 (C<sub>tert</sub>, 2C, Cp), 111.3 (C<sub>tert</sub>, 2C, Cp), 108.3 (C<sub>tert</sub>, 4C, Cp), 33.0 (C<sub>quat</sub>, *t*-Bu), 31.5 (C<sub>prim</sub>, *t*-Bu), 28.1 (C<sub>sec</sub>, CH<sub>2</sub>), 21.8 (C<sub>sec</sub>, CH<sub>2</sub>), 15.3 (C<sub>prim</sub>, CH<sub>3</sub>), 13.9 (C<sub>prim</sub>, CH<sub>3</sub>).

**Preparation of 10. (a) From I.** To a yellow solution of 0.29 g (0.71 mmol) of I in benzene (15 mL) was added dropwise 0.08 mL (0.82 mmol) of CH<sub>3</sub>COCH<sub>3</sub>. After 5 h stirring at room temperature, the solution had discolored. The solvent was removed, and the residue was recrystallized from pentane. After cooling, 0.16 g (0.34 mmol, 48% yield) of pale yellow crystals was isolated (the yield was limited by the presence of diphenyldi-*tert*-butylzirconocene<sup>1</sup> which was not totally transformed into I).

**(b) Direct Synthesis.** A mixture of 0.74 g (1.52 mmol) of diphenyldi-*tert*-butylzirconocene and 0.12 mL of CH<sub>3</sub>COCH<sub>3</sub> (1.63 mmol) in heptane (30 mL) was heated with reflux for 16 h. The solvent was then removed, and the residue was recrystallized from heptane. After cooling, 0.57 g (1.22 mmol, 80% yield) of pale yellow crystals was isolated. mp: 152–3 °C. Anal. Calcd for  $C_{27}H_{36}ZrO$ : C, 69.32; H, 7.75. Found: C, 69.49; H, 7.70. Mass spectrum (main fragments): 451 (M<sup>+</sup> – CH<sub>3</sub>, 39), 409 (M<sup>+</sup> – *t*-Bu, 100), 351 (M<sup>+</sup> – *t*-Bu-CH<sub>3</sub>COCH<sub>3</sub>, 20), 211 (*t*-BuCpZr<sup>+</sup>, 38).  $^1H$  NMR,  $C_6D_6$ : 7.20 (m, 3H, C<sub>6</sub>H<sub>4</sub>), 6.85 (dd, 1H, C<sub>6</sub>H<sub>4</sub>,  $J = 4.7$ , 2.2 Hz), 6.36 (pq, 2H, Cp), 6.08 (pq, 2H, Cp), 5.93 (pq, 2H, Cp), 5.35 (pq, 2H, Cp), 1.55 (s, 6H, CH<sub>3</sub>), 1.17 (s, 18H, *t*-Bu).  $^{13}C$  NMR,  $C_6D_6$ : 180.2 (C<sub>quat</sub>), 170.3 (C<sub>quat</sub>), 142.7 (C<sub>quat</sub>), 139.2 (C<sub>tert</sub>, C<sub>6</sub>H<sub>4</sub>), 124.8 (C<sub>tert</sub>, C<sub>6</sub>H<sub>4</sub>), 124.7 (C<sub>tert</sub>, C<sub>6</sub>H<sub>4</sub>), 124.5 (C<sub>tert</sub>, C<sub>6</sub>H<sub>4</sub>), 117.9 (C<sub>tert</sub>, 2C, Cp), 110.4 (C<sub>tert</sub>, 2C, Cp), 110.0 (C<sub>tert</sub>, 2C, Cp), 103.8 (C<sub>tert</sub>, 2C, Cp), 87.5 (C<sub>quat</sub>), 32.6 (C<sub>quat</sub>, *t*-Bu), 32.1 (C<sub>prim</sub>, CH<sub>3</sub>), 31.8 (C<sub>prim</sub>, *t*-Bu).

**Preparation of 11. (a) (C<sub>6</sub>H<sub>3</sub>)(CH<sub>3</sub>)<sub>2</sub>Li.** The aryllithium was prepared by action of 2-bromo-*p*-xylo (2.76 g, 14.91 mmol) in ether (15 mL) on lithium metal (0.23 g, 32.81 mmol) in ether (30 mL). The stirring was maintained for a night and the mixture was then filtered leading to a yellow solution (which concentration was found to be 0.255 mol·L<sup>-1</sup>, 77% yield).

**(b) (*t*-BuCp)<sub>2</sub>Zr(CH<sub>3</sub>)[C<sub>6</sub>H<sub>3</sub>(CH<sub>3</sub>)<sub>2</sub>].** To a 0 °C cooled solution of chloromethyl-di-*tert*-butylzirconocene (0.90 g, 2.35 mmol) in ether (20 mL) was added dropwise 10 mL of the above aryllithium solution (2.55 mmol). The stirring was maintained for 2 h at 0 °C and for 30 min at room temperature. The solvent was then removed. The residue was extracted with 20 mL of hexane, and the mixture was filtered. After cooling, 0.30 g (0.66 mmol) of yellow crystals was isolated (28% yield). mp: 90 °C.  $^1H$  NMR,  $C_6D_6$ : 6.99 (d, 1H, C<sub>6</sub>H<sub>3</sub>,  $J = 6.6$  Hz), 6.86 (d, 1H, C<sub>6</sub>H<sub>3</sub>,  $J = 6.6$  Hz), 6.78 (s, 1H, C<sub>6</sub>H<sub>3</sub>), 6.19 (pq, 2H, Cp), 5.88 (pq, 2H, Cp), 5.55 (pq, 2H, Cp), 5.34 (pq, 2H, Cp), 2.18 (s, 3H, CH<sub>3</sub>), 2.12 (s, 3H, CH<sub>3</sub>), 1.05 (s, 18H, *t*-Bu), 0.51 (s, 3H, CH<sub>3</sub>).  $^{13}C$  NMR,  $C_6D_6$ : 142.3 (C<sub>quat</sub>), 140.0 (C<sub>quat</sub>), 133.0 (C<sub>quat</sub>), 132.9 (C<sub>quat</sub>), 128.5 (C<sub>tert</sub>, C<sub>6</sub>H<sub>3</sub>), 127.0 (C<sub>tert</sub>, C<sub>6</sub>H<sub>3</sub>), 124.9 (C<sub>tert</sub>, C<sub>6</sub>H<sub>3</sub>), 111.3 (C<sub>tert</sub>, 2C, Cp), 110.9 (C<sub>tert</sub>, 2C, Cp), 106.3 (C<sub>tert</sub>, 2C, Cp), 103.2 (C<sub>tert</sub>, 2C, Cp), 33.2 (C<sub>quat</sub>, *t*-Bu), 31.3 (C<sub>prim</sub>, *t*-Bu), 28.7 (C<sub>prim</sub>, CH<sub>3</sub>), 25.2 (C<sub>prim</sub>, CH<sub>3</sub>), 21.8 (C<sub>prim</sub>, CH<sub>3</sub>).

**Preparation of 12.** A solution of (*t*-BuCp)<sub>2</sub>Zr(CH<sub>3</sub>)[C<sub>6</sub>H<sub>3</sub>(CH<sub>3</sub>)<sub>2</sub>] (1.58 g, 3.49 mmol) in benzene (25 mL) was heated with reflux for 2.5 h. After removal of the solvent, the residual solid was recrystallized from pentane, leading to pale yellow crystals suitable for X-ray analysis. mp: 94–5 °C. Anal. Calcd for  $C_{26}H_{34}Zr$ : C, 71.33; H, 7.83. Found: C, 71.22; H, 7.89.  $^1H$  NMR,  $C_6D_6$ : 7.01 (d, 1H, C<sub>6</sub>H<sub>3</sub>,  $J = 7.5$  Hz), 6.85 (d, 1H, C<sub>6</sub>H<sub>3</sub>,  $J = 7.5$  Hz), 6.42 (s, 1H, C<sub>6</sub>H<sub>3</sub>), 6.29 (q, 2H, Cp), 6.16 (q, 1H, Cp), 5.64 (q, 1H, Cp), 5.27 (q, 1H, Cp), 5.15 (q, 1H, Cp), 5.08 (q, 1H, Cp), 5.03 (q, 1H, Cp), 2.16 (s, 3H, CH<sub>3</sub>), 2.14 (s, 3H, CH<sub>3</sub>), 1.49 (s, 3H, CH<sub>3</sub>), 1.23 (s, 3H, CH<sub>3</sub>), 0.99 (s, 9H,

Table 3. Structure Determination Summary

Crystal Data	
empirical formula	C <sub>26</sub> H <sub>34</sub> Zr
color, habit	pale yellow, rectangular
crystal size (mm)	0.080 × 0.120 × 0.230
crystal system	monoclinic
space group	P2 <sub>1</sub> /c
unit cell dimens	a = 8.278(3) Å, b = 20.113(9) Å, c = 27.661(9) Å, β = 93.13 (2)°
volume	4599(2) Å <sup>3</sup>
Z	8
formula wt	437.8
density (calc)	1.264 g/cm <sup>3</sup>
absorption coeff	4.85 cm <sup>-1</sup>
F(000)	1840
Data Collection	
diffractometer used	Siemens P4
radiation	Mo Kα (λ = 0.710 73 Å)
temp (K)	295
monochromator	highly oriented graphite crystal
2θ range	3.0–45.0°
scan type	ω
scan speed	fixed, 5.00°/min in ω
scan range (ω)	±0.55°
background measurement	stationary crystal and stationary counter at beginning and end of scan, each for 0.5% of total scan time
std reflns	3 measured every 200 reflections
index ranges	0 ≤ h ≤ 8, 0 ≤ k ≤ 21, -29 ≤ l ≤ 29
reflcs collected	6470
independent reflns	5989 (R <sub>int</sub> = 1.64%)
observed reflns	2701 (F > 4.0σ(F))
absorptn correction	face-indexed numerical
min/max transmission	0.9450/0.9673
Solution and Refinement	
system used	Siemens SHELXTL PLUS (PC Version)
solution	direct methods
refinement method	full-matrix least squares
quantity minimized	Σw(F <sub>o</sub> - F <sub>c</sub> ) <sup>2</sup>
hydrogen atoms	riding model, fixed isotropic U
weighting scheme	w <sup>-1</sup> = σ <sup>2</sup> (F) + 0.0008F <sup>2</sup>
no. of params refined	487
final R indices (obs data)	R = 6.42%, R <sub>w</sub> = 5.90%
R indices (all data)	R = 15.92%, R <sub>w</sub> = 8.12%
goodness of fit	1.10
largest and mean Δ/σ	0.002, 0.000
data-to-parameter ratio	5.5:1
largest difference peak	0.52 eÅ <sup>-3</sup>
largest difference hole	-0.46 eÅ <sup>-3</sup>

*t*-Bu), 0.30 (d, 1H, CH<sub>2</sub>, *J* = 11.3 Hz), -1.22 (d, 1H, CH<sub>2</sub>, *J* = 11.3 Hz). <sup>13</sup>C NMR, C<sub>6</sub>D<sub>6</sub>: 187.1 (C<sub>quat</sub>, C<sub>6</sub>H<sub>3</sub>), 142.4 (C<sub>quat</sub>), 140.0 (C<sub>quat</sub>), 132.9 (C<sub>quat</sub>), a C<sub>quat</sub> was not observed, 127.1 (C<sub>tert</sub>, 2C, C<sub>6</sub>H<sub>3</sub>), 121.0 (C<sub>tert</sub>, C<sub>6</sub>H<sub>3</sub>), 113.5 (C<sub>tert</sub>, Cp), 111.9 (C<sub>tert</sub>, Cp), 111.1 (C<sub>tert</sub>, 2C, Cp), 104.0 (C<sub>tert</sub>, Cp), 103.6 (C<sub>tert</sub>, Cp), 100.9 (C<sub>tert</sub>, Cp), 99.3 (C<sub>tert</sub>, Cp), 34.3 (C<sub>quat</sub> or C<sub>sec</sub>), 33.6 (C<sub>quat</sub> or C<sub>sec</sub>), 32.9 (C<sub>quat</sub> or C<sub>sec</sub>), 31.2 (C<sub>prim</sub>, *t*-Bu), 30.4 (C<sub>prim</sub>, CH<sub>3</sub>), 25.2 (C<sub>prim</sub>, CH<sub>3</sub>), 21.6 (C<sub>prim</sub>, CH<sub>3</sub>).

**Preparation of 13.** A mixture of **12** (57.6 mg, 0.132 mmol) and grey selenium powder (21.1 mg, 0.264 mmol) in benzene (6 mL) was heated with reflux for 15 h. The mixture was then filtered, and the benzene was removed. The product extracted with pentane was obtained as a red product (65.5 mg, 83% yield). Anal. Calcd for C<sub>26</sub>H<sub>34</sub>Se<sub>2</sub>Zr: C, 52.42; H, 5.75. Found: C, 52.31; H, 5.78. Mass spectrum (main fragments): 596 (M<sup>+</sup>, 23), 475 (M<sup>+</sup> - *t*-Bu, 18), 335 ([*t*-BuCp]<sub>2</sub>Zr<sup>+</sup>, 68), 264 (C<sub>6</sub>H<sub>2</sub>(CH<sub>3</sub>)<sub>2</sub>Se<sub>2</sub>, 20), 170 (C<sub>6</sub>H<sub>3</sub>SeCH<sub>3</sub>, 43). <sup>1</sup>H NMR, C<sub>6</sub>D<sub>6</sub>: 7.08 (s, 2H, C<sub>6</sub>H<sub>2</sub>), 5.81 (t, 8H, Cp), 2.73 (s, 6H, CH<sub>3</sub>), 1.11 (s, 18H, *t*-Bu). <sup>13</sup>C NMR, C<sub>6</sub>D<sub>6</sub>: 150.3 (C<sub>quat</sub>, C<sub>6</sub>H<sub>2</sub>), 140.6 (C<sub>quat</sub>, C<sub>6</sub>H<sub>2</sub>), 138.2 (C<sub>quat</sub>, Cp), 126.9 (C<sub>tert</sub>, C<sub>6</sub>H<sub>2</sub>), 110.8 (C<sub>tert</sub>, Cp), 108.3 (C<sub>tert</sub>, Cp), 32.8 (C<sub>quat</sub>, *t*-Bu), 31.8 (C<sub>prim</sub>, *t*-Bu), 26.9 (C<sub>prim</sub>, CH<sub>3</sub>). <sup>77</sup>Se NMR, CDCl<sub>3</sub>: 559.5.

**Action of the Selenium Powder on the Benzyneszirconocene Trimethylphosphine Adduct.** A mixture of Cp<sub>2</sub>Zr(PMe<sub>3</sub>)(C<sub>6</sub>H<sub>4</sub>)<sup>14</sup> (0.10 g, 0.27 mmol) and grey selenium powder (0.05 g, 0.63 mmol) in benzene (20 mL) was heated

with reflux for 18 h. The red mixture was then filtered, the benzene was removed, and the residual solid was washed with pentane (20 mL). The product was obtained as a red solid (0.07 g, 55% yield) and identified by the usual spectroscopic method.<sup>2</sup>

**X-ray Structural Analysis of 12.** Suitable crystals of **12** were obtained by slow crystallization from a pentane solution. A single crystal of C<sub>26</sub>H<sub>34</sub>Zr was sealed under nitrogen in a capillary tube and then optically aligned on the goniostat of a Siemens P4 automated X-ray diffractometer. The corresponding lattice parameters and orientation matrix for the sample were determined from a least-squares fit of the orientation angles for 25 reflections at 22 °C. The systematic absences are consistent with the centrosymmetric monoclinic space group, P2<sub>1</sub>/c. The refined lattice parameters and other pertinent crystallographic information are provided in the structure determination summary.

Intensity data were measured with graphite-monochromated Mo Kα radiation (λ = 0.710 73 Å) and variable ω scans. Background counts were measured at the beginning and at the end of each scan with the crystal and counter kept stationary. The intensities of three standard reflections were measured periodically during data collection and decreased by ca. 21% during data collection. The data were corrected for Lorentz-polarization effects, crystal decomposition, and absorption; the symmetry-equivalent reflections were averaged.

Approximate positions for the two independent Zr atoms were located by using direct methods (SHELXTL PLUS operating on a Professional Computing Systems 486 66 MHz computer), and all non-hydrogen atoms were revealed by successive difference Fourier syntheses. Following anisotropic refinement of the non-hydrogen atoms, idealized positions for the hydrogen atoms were included as fixed contributions by using a riding model. Full-matrix least-squares refinement, based upon the minimization of Σw<sub>i</sub>|F<sub>o</sub> - F<sub>c</sub>|<sup>2</sup>, with w<sub>i</sub><sup>-1</sup> = σ<sup>2</sup>(F<sub>o</sub>) + 0.0008F<sub>o</sub><sup>2</sup>, converged to give final discrepancy indices<sup>26</sup> of R(F<sub>o</sub>) = 0.0642, R<sub>w</sub>(F<sub>o</sub>) = 0.0590, and σ<sub>1</sub> = 1.10 for 2701 reflections with F<sub>o</sub> > 4.0σ(F<sub>o</sub>). The refined positional parameters are provided in Table 1, and selected interatomic distances and bond angles for the C<sub>26</sub>H<sub>34</sub>Zr are given in Tables 2.

A summary of crystallographic data for the structural analysis of **12** is provided in Table 3.

**Acknowledgment.** J.L.P. acknowledges the financial support provided by the Chemical Instrumentation Program of the National Science Foundation (Grant CHE-9120098) for the acquisition of a Siemens P4 X-ray diffractometer by Department of Chemistry at West Virginia University. Authors from the University of Bourgogne thank Mrs. S. Gourier for her technical assistance.

**Supplementary Material Available:** The positional parameters and equivalent isotropic displacement coefficients for C<sub>26</sub>H<sub>34</sub>Zr are given in Table I. The whole of interatomic distances and angles for the two independent molecules of C<sub>26</sub>H<sub>34</sub>Zr are given in Tables II and III, respectively. The anisotropic thermal parameters for the 54 non-hydrogen atoms and the idealized coordinates for the 68 hydrogen atoms are given in Tables IV and V, respectively (6 pages). Ordering information is given on any current masthead page.

OM9405495

(26) The discrepancy indices were calculated from the expressions R(F<sub>o</sub>) = Σ|F<sub>o</sub> - F<sub>c</sub>|/ΣF<sub>o</sub> and R<sub>w</sub>(F<sub>o</sub>) = Σ(w<sub>i</sub><sup>1/2</sup>|F<sub>o</sub> - F<sub>c</sub>|)/Σ(w<sub>i</sub><sup>1/2</sup>F<sub>o</sub>), and the standard deviation of an observation of unit weight σ<sub>1</sub> is equal to [(Σw<sub>i</sub>(F<sub>o</sub> - F<sub>c</sub>)<sup>2</sup>/(n - p)]<sup>1/2</sup>, where n is the number of observations and p is the number of parameters varied during the last refinement cycle.

# The Gas-Phase Chemistry of Silamide Ions

Michèle Krempf<sup>†</sup> and Robert Damrauer<sup>\*,‡</sup>

Departments of Chemistry, University of Colorado at Denver, Denver, Colorado 80217-3364,  
and University of Colorado at Boulder, Boulder, Colorado 80309

Received July 20, 1994<sup>⊙</sup>

A series of silamide (silanamide) anions,  $\text{SiH}_3\text{NH}^-$  (1),  $\text{C}_6\text{H}_5\text{SiH}_2\text{NH}^-$  (2),  $\text{CH}_3\text{OSiH}_2\text{NH}^-$  (3), and  $\text{CH}_3\text{SiF}_2\text{NH}^-$  (4), has been studied in detail in a tandem flowing afterglow selected-ion flow tube. Their reaction chemistry has been probed with  $\text{CO}_2$ ,  $\text{CS}_2$ ,  $\text{COS}$ ,  $\text{SO}_2$ , and  $\text{N}_2\text{O}$  as well as a number of alcohols and other reagents and shows not only features expected from amides but also ones that result from silyl substitution. Collision-induced dissociations (CID) were carried out to expand our knowledge of the effect of silyl substitution on amide behavior. A prevalent pattern for the CID behavior of anions 1-4 reveals that a substituent borne by silicon cleaves as an anion. The resulting fragments either separate immediately or the anion abstracts a proton before separation. The gas-phase acidities of  $\text{SiH}_3\text{NH}_2$ ,  $\text{FSiH}_2\text{NH}_2$ ,  $\text{C}_6\text{H}_5\text{SiH}_2\text{NH}_2$ ,  $\text{CH}_3\text{OSiH}_2\text{NH}_2$ , and  $\text{CH}_3\text{SiF}_2\text{NH}_2$  have been measured using bracketing techniques. The acidity values fall in a small range, indicating that  $\beta$ -substitution effects on silicon are small. G2 computational studies have been used to probe the Si-H and N-H acidity of  $\text{SiH}_3\text{NH}_2$ , showing that the N-H position is the more strongly acidic one.

## Introduction

Amide ions ( $\text{RNH}^-$ ) are the strongest bases routinely used in the gas phase. They are generally prepared by electron impact of amines and are used to prepare conjugate bases of acids that are more acidic than the amines.<sup>1-5</sup> A great deal of work has focused on determining the acidities of amines, particularly as they relate to the effects of substitution on nitrogen.<sup>1,4,6</sup>

Although the reactivity of  $\text{H}_2\text{N}^-$  has been studied in detail,<sup>2</sup> only a few studies have concentrated on the reactivity of other amide ions, despite the ease with which they can be prepared.<sup>1,3,5</sup> *tert*-Butylamide, di-*sec*-butylamide, and 2,2,6,6-tetramethylpiperidine have recently been prepared to study both their reactivity and the acidity of their corresponding amines.<sup>5</sup> Each was found to have a rich reaction chemistry with a variety of neutral reagents. There has also been recent interest in amines and amide ions substituted by silicon substituents<sup>3,7</sup> because of the importance of some  $\alpha$ -silyl amines as precursors to synthetically important bases.<sup>3</sup> Such silamines (silanamines) are considerably more acidic than carbon-substituted amines in both the gas and condensed phases.<sup>1,3</sup> Indeed, Grimm and Bartmess have recently shown that the disilamine hexamethyl-

disilazane is more acidic in the gas phase than expected on the basis of its solution behavior. They have suggested that such anomalous behavior results from counterion effects in solution.<sup>3</sup> Several years ago, we reported an experimental and computational study of the reactions of two silamides (silanamides),  $[(\text{CH}_3)_3\text{Si}]_2\text{N}^-$  and  $[(\text{CH}_3)_3\text{SiNCH}_3]^-$ , with  $\text{CO}_2$ ,  $\text{COS}$ , and  $\text{CS}_2$ .<sup>7</sup> More recently, we have prepared several silamides as possible precursors to low-valent silicon-containing species<sup>8</sup> such as  $\text{HSiNH}^-$ . We have studied the properties of four silamides in some detail and report on them here.

## Experimental Section

All experiments are carried out at room temperature in a tandem flowing afterglow-selected ion flow tube (FA-SIFT) which has been described in detail previously.<sup>9</sup> The FA-SIFT consists of four sections: a source (first) flow tube for ion preparation, an ion selection region, a second flow tube for studying the chemical reactions of the selected ions, and an ion detection region. In the typical experiment whose results are reported in this paper, silamide ions are prepared in the first flow tube by reaction of  $\text{H}_2\text{N}^-$  and the appropriate silane ( $\text{C}_6\text{H}_5\text{SiH}_3$  for  $\text{SiH}_3\text{NH}^-$  (1),  $\text{C}_6\text{H}_5\text{SiH}_2\text{NH}^-$  (2),  $\text{CH}_3\text{OSiH}_2\text{NH}^-$  (3) (with added  $\text{CH}_3\text{OH}$  for the latter), and  $\text{CH}_3\text{SiF}_3$  for  $\text{CH}_3\text{SiF}_2\text{NH}^-$  (4)).  $\text{FSiH}_2\text{NH}^-$  was prepared in the source from a mixture of  $\text{H}_2\text{N}^-$ ,  $\text{C}_6\text{H}_5\text{SiH}_3$ , and  $\text{NF}_3$ . The desired anions were readily mass selected as described below. The silamides formed in the source are entrained in a rapidly flowing helium stream (0.3 Torr) and sampled at the end of the first flow through a nose cone orifice into an ion separation region. The helium and other neutrals are removed by pumping while the silamides are focused into a quadrupole mass filter by a series of electrostatic lenses. This SIFT quadrupole can be tuned to an appropriate  $m/z$  and the desired anions are injected into the second flow tube, where they are entrained in helium (0.5 Torr). The reactions of the injected silamides can then be studied by the addition of a variety of neutral reactants in the

<sup>†</sup> University of Colorado at Boulder.

<sup>‡</sup> University of Colorado at Denver.

<sup>⊙</sup> Abstract published in *Advance ACS Abstracts*, November 1, 1994.

(1) Mackay, G. I.; Hemsforth, R. S.; Bohme, D. K. *Can. J. Chem.* **1976**, *54*, 1624-42.

(2) Bierbaum, V. M.; Grabowski, J. J.; DePuy, C. H. *J. Phys. Chem.* **1984**, *88*, 1389-93.

(3) Grimm, D. T.; Bartmess, J. E. *J. Am. Chem. Soc.* **1992**, *114*, 1227-31.

(4) Lias, S. G.; Bartmess, J. E.; Liebman, J. F.; Holmes, J. L.; Levin, R. D.; Mallard, W. G. *J. Phys. Chem. Ref. Data* **1988**, *17* (Suppl 1). This is the primary source for gas-phase acidity data. Unless otherwise specified, all gas-phase acidities used in this paper come from this source.

(5) Damrauer, R.; Krempf, M.; O'Hair, R. A. J.; Simon, R. A. *Int. J. Mass Spectrom. Ion Process* **1992**, *117*, 199-211.

(6) Brauman, J. I.; Blair, L. K. *J. Am. Chem. Soc.* **1971**, *93*, 3911-14.

(7) O'Hair, R. A. J.; Sheldon, J. C.; Bowie, J. H.; Damrauer, R.; Depuy, C. H. *Aust. J. Chem.* **1989**, *42*, 489-96.

(8) Damrauer, R.; Krempf, M.; O'Hair, R. A. J. *J. Am. Chem. Soc.* **1993**, *115*, 1998-2005.

(9) Van Doren, J. M.; Barlow, S. E.; DePuy, C. H.; Bierbaum, V. M. *Int. J. Mass Spectrom. Ion Processes* **1987**, *81*, 85-100.

second flow tube. At the end of the second flow tube, the ionic products are sampled through a nose cone orifice, mass analyzed, and detected by an electron multiplier. The structures of the product ions discussed in this paper are based on a recording of their  $m/z$ . Since neutral products are not detected, their identity is assumed on the basis of mechanistic rationale.

Branching ratios for the reactions of  $\text{SiH}_3\text{NH}^-$  (1) and  $\text{C}_6\text{H}_5\text{SiH}_2\text{NH}^-$  (2) were determined by injecting the silamides into the second flow tube and adding a particular neutral reactant at various points along the second tube. These ratios were determined as a function of reaction distance and are reported as extrapolations to zero reaction distance to eliminate any effects of secondary reactions or differential diffusion among the ions. Mass discrimination corrections were made for all the reactions. Rate coefficients were determined under pseudo-first-order conditions by monitoring the silamide ion density as a function of reaction distance (which is proportional to time) for a measured flow of neutral acid reagent. Reported values are the average of at least three measurements with different flows and are reproducible to 10%. Reaction efficiencies have been calculated from ion-neutral collision rates using the variational transition state theory model of Bowers and co-workers.<sup>10</sup> Two small impurities in  $\text{CH}_3\text{OSiH}_2\text{NH}^-$  (3) (not present in the few reactions of  $\text{CD}_3\text{OSiH}_2\text{NH}^-$  we studied) limited its quantitative study.

To inject ions from the low pressure ( $10^{-6}$  Torr) region of the SIFT quadrupole into the higher pressure region of the second flow tube, they must be extracted by an electrical potential which imparts kinetic energy to them. Multiple collisions with the helium buffer gas generally cool such ions; however, if the potential is made sufficiently high, ions can often undergo collision-induced dissociation (CID), forming new ions.<sup>11</sup> In a field-free region, the resulting ions can subsequently undergo multiple collisions with helium where they are usually cooled to room temperature. The injection potential leading to decomposition of ions is the potential difference between the ion source and the injector plate. The resulting kinetic energy of the ions is a sensitive function of a variety of factors and is not well characterized.

All reactions were studied at a He flow of  $\sim 225$  STP  $\text{cm}^3 \text{ s}^{-1}$ . Gases were obtained from commercial sources and were of the following purities: He (99.995%),  $\text{NH}_3$  (99.99%),  $\text{CO}_2$  (99.5%), COS (97.7%),  $\text{SO}_2$  (99.9%), and  $\text{N}_2\text{O}$  (99.99%). Other reagents were obtained from commercial sources. The helium buffer gas was passed through a liquid nitrogen cooled molecular sieve trap before entering the flow tubes.

## Results and Discussion

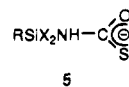
We report here on the reaction chemistry of silamide ions  $\text{SiH}_3\text{NH}^-$  (1),  $\text{C}_6\text{H}_5\text{SiH}_2\text{NH}^-$  (2),  $\text{CH}_3\text{OSiH}_2\text{NH}^-$  (3), and  $\text{CH}_3\text{SiF}_2\text{NH}^-$  (4), their collision-induced dissociation behavior, and the N-H acidities of  $\text{SiH}_3\text{NH}_2$ ,  $\text{FSiH}_2\text{NH}_2$ ,  $\text{C}_6\text{H}_5\text{SiH}_2\text{NH}_2$ ,  $\text{CH}_3\text{OSiH}_2\text{NH}_2$ , and  $\text{CH}_3\text{SiF}_2\text{NH}_2$ . Silamides with such different substitution patterns are well suited for exploring reactivity differences. These silamides will be compared with those previously studied,<sup>7</sup>  $[(\text{CH}_3)_3\text{Si}]_2\text{N}^-$  and  $[(\text{CH}_3)_3\text{SiNCH}_3]^-$ , and with the simple amides<sup>2,5</sup>  $\text{H}_2\text{N}^-$  and  $\text{t-BuNH}^-$ . Although the previous studies of  $[(\text{CH}_3)_3\text{Si}]_2\text{N}^-$  and  $[(\text{CH}_3)_3\text{SiNCH}_3]^-$  have not been exhaustive, their reactions with  $\text{CO}_2$ , COS, and  $\text{CS}_2$  have been explored. The two amides, on the other hand, have been studied in more detail.<sup>2,5</sup> The major objectives in our work have been (1) to identify

any unusual reactivity in amides caused by substitution of silicon on nitrogen, (2) to identify any unusual reactivity in silamides caused by substitution of different groups on silicon, and (3) to determine the effect of  $\beta$ -substitution on silamine acidity.

**Reactivity Studies with  $\text{CO}_2$ ,  $\text{CS}_2$ , COS,  $\text{SO}_2$ , and  $\text{N}_2\text{O}$ .** It is important to validate the structures of anions 1–3 since their preparation (see Experimental Section) might lead to either the amide anions proposed or corresponding silyl anions. In earlier work, we determined that  $\text{SiH}_3\text{CH}_3$  gave predominantly  $\text{SiH}_3\text{CH}_2^-$  on reaction with amide even though its Si–H is more strongly acidic than its C–H.<sup>12a</sup> This not only suggested that the C–H abstraction pathway was kinetically more accessible but raised the question of whether similar behavior would be observed in other systems. We believe that silyl amines as demonstrated in the structures of ions 1–3 undergo predominant N–H over Si–H deprotonation (see G2 calculations). The validity of these structures was determined by reactivity studies with simple neutral characterization reagents that have been used previously to characterize gas-phase anions.<sup>5,7,8,12b</sup>

Table 1 summarizes the reactivity of the two previously studied silamides with  $\text{CO}_2$ ,  $\text{CS}_2$ , and COS. In addition, the reactions of 1–4 with  $\text{CO}_2$ ,  $\text{CS}_2$ , COS,  $\text{SO}_2$ , and  $\text{N}_2\text{O}$  are presented. We have also determined the rate coefficients and efficiencies<sup>10</sup> of 1 and 2 with  $\text{CO}_2$ ,  $\text{CS}_2$ , COS, and  $\text{SO}_2$ .

Anions 1–4 react with these reagents in a very similar way to the amides and silamides previously studied, indicating the validity of their proposed structures. The mechanistic picture developed by DePuy and co-workers for amide ions thus serves well to explain most of the products of the newly studied silamides reactions.<sup>2</sup> In its reaction with COS, which is the reagent that often best reveals the mechanistic pathways of importance, amide either adds to the central carbon (ultimately giving  $\text{NCO}^-$  and  $\text{HS}^-$ ) or undergoes sulfur transfer by reaction at sulfur (ultimately giving  $\text{H}_2\text{NS}^-$ ). In the silamides studied here and previously, another mechanistic channel occurs as well when the DePuy intermediate **5** formed by reaction at the central



carbon is diverted by a further interaction at silicon. Although either sulfur or oxygen attachment at silicon is possible for this ambident intermediate, there is a strong tendency for S–Si over Si–O bond formation. Thus, for 1–4 and  $(\text{CH}_3)_3\text{SiNCH}_3^-$ , no Si–O bond formation is observed,<sup>7</sup> while the structurally more complex disilamide<sup>7</sup>  $[(\text{CH}_3)_3\text{Si}]_2\text{N}^-$  gives both  $\text{NCO}^-$  and  $\text{NCS}^-$ . The products in this last case are most easily rationalized by formation of complexes  $[(\text{CH}_3)_3\text{SiS}\cdots(\text{CH}_3)_3\text{SiNCO}]$  and  $[(\text{CH}_3)_3\text{SiO}\cdots(\text{CH}_3)_3\text{SiNCS}]$ . The first complex can either separate giving  $(\text{CH}_3)_3\text{SiS}^-$  and  $(\text{CH}_3)_3\text{SiNCO}$ , or react further at the neutral silicon component, giving  $\text{NCO}^-$  and  $(\text{Me}_3\text{Si})_2\text{S}$ . An analogous pathway for the other complex would give  $(\text{CH}_3)_3\text{SiO}^-$  and  $(\text{CH}_3)_3\text{SiNCS}$ , and  $\text{NCS}^-$  and  $(\text{Me}_3\text{Si})_2\text{O}$ , respectively. The minor yield of the reaction channel leading

(10) Chesnavich, W. J.; Su, T.; Bowers, M. T. *J. Chem. Phys.* **1980**, *72*, 2641–55.

(11) Gronert, S.; O'Hair, R. A. J.; Prodnuk, S.; Sülzle, D.; Damrauer, R.; DePuy, C. H. *J. Am. Chem. Soc.* **1990**, *112*, 997–1003.

(12) (a) Damrauer, R.; Kass, S. R.; DePuy, C. H. *Organometallics* **1988**, *7*, 637–40. (b) DePuy, C. H.; Damrauer, R. *Organometallics* **1984**, *3*, 362–5.

**Table 1. Products, Branching Ratios,<sup>a</sup> Rate Coefficients,<sup>b</sup> and Efficiencies<sup>c</sup> of Two Previously Studied Silamides and 1–4 with CO<sub>2</sub>, CS<sub>2</sub>, COS, N<sub>2</sub>O, and SO<sub>2</sub>**

amide ion	reactant = CO <sub>2</sub>	reactant = CS <sub>2</sub>	reactant = COS	reactant = N <sub>2</sub> O	reactant = SO <sub>2</sub>
Me <sub>3</sub> SiNMe <sup>-</sup>	NCO <sup>-</sup> + Me <sub>3</sub> SiOMe (51) Me <sub>3</sub> SiO <sup>-</sup> + MeNCO (21) adduct (28)	Me <sub>3</sub> SiS <sup>-</sup> + MeNCS (53) CS <sub>2</sub> <sup>-</sup> + Me <sub>3</sub> SiNMe (47)	Me <sub>3</sub> SiS <sup>-</sup> + MeNCO (76) NCO <sup>-</sup> + Me <sub>3</sub> SiSMe (10) HS <sup>-</sup> + C <sub>5</sub> H <sub>11</sub> NOSi (14) (the HS <sup>-</sup> likely forms from H <sub>2</sub> S impurities in COS)		
(Me <sub>3</sub> Si) <sub>2</sub> N <sup>-</sup>	NCO <sup>-</sup> + (Me <sub>3</sub> Si) <sub>2</sub> O (59) adduct (41)	NCS <sup>-</sup> + (Me <sub>3</sub> Si) <sub>2</sub> S (84) Me <sub>3</sub> SiS <sup>-</sup> + Me <sub>3</sub> SiNCS (16)	Me <sub>3</sub> SiS <sup>-</sup> + Me <sub>3</sub> SiNCO (53) NCO <sup>-</sup> + (Me <sub>3</sub> Si) <sub>2</sub> S (38) NCS <sup>-</sup> + (Me <sub>3</sub> Si) <sub>2</sub> O (9)		
SiH <sub>3</sub> NH <sup>-</sup> (1)	NCO <sup>-</sup> + SiH <sub>3</sub> OH (92) SiH <sub>3</sub> O <sup>-</sup> + HNCO (8) <b>7.24 (0.86)</b>	SiH <sub>3</sub> S <sup>-</sup> + HNCS (50) NCS <sup>-</sup> + SiH <sub>3</sub> SH (50) <b>2.28 (0.18)</b>	SiH <sub>3</sub> S <sup>-</sup> + HNCO (79) NCO <sup>-</sup> + SiH <sub>3</sub> SH (21) <b>6.17 (0.42)</b>	N <sub>3</sub> <sup>-</sup> + SiH <sub>3</sub> OH <b>very slow</b>	NSO <sup>-</sup> + SiH <sub>3</sub> OH (61) SiH <sub>3</sub> O <sup>-</sup> + HNSO (39) <b>16.6 (0.86)</b>
C <sub>6</sub> H <sub>5</sub> SiH <sub>2</sub> NH <sup>-</sup> (2)	NCO <sup>-</sup> + C <sub>6</sub> H <sub>5</sub> SiH <sub>2</sub> OH <b>6.02 (0.88)</b>	C <sub>6</sub> H <sub>5</sub> SiH <sub>2</sub> S <sup>-</sup> + HNCS (69) NCS <sup>-</sup> + C <sub>6</sub> H <sub>5</sub> SiH <sub>2</sub> SH (31) <b>0.84 (0.08)</b>	C <sub>6</sub> H <sub>5</sub> SiH <sub>2</sub> S <sup>-</sup> + HNCO (13) NCO <sup>-</sup> + C <sub>6</sub> H <sub>5</sub> SiH <sub>2</sub> SH (87) <b>6.05 (0.51)</b>	N <sub>3</sub> <sup>-</sup> + C <sub>6</sub> H <sub>5</sub> SiH <sub>2</sub> OH <b>very slow</b>	NSO <sup>-</sup> + C <sub>6</sub> H <sub>5</sub> SiH <sub>2</sub> OH (95) C <sub>6</sub> H <sub>5</sub> SiH <sub>2</sub> O <sup>-</sup> + HNSO (5) <b>14.5 (0.93)</b>
CH <sub>3</sub> OSiH <sub>2</sub> NH <sup>-</sup> (3)	NCO <sup>-</sup> + CH <sub>3</sub> OSiH <sub>2</sub> OH	NCS <sup>-</sup> + CH <sub>3</sub> OSiH <sub>2</sub> SH CH <sub>3</sub> OSiH <sub>2</sub> S <sup>-</sup> + HNCS	CH <sub>3</sub> OSiH <sub>2</sub> S <sup>-</sup> + HNCO (major) NCO <sup>-</sup> + CH <sub>3</sub> OSiH <sub>2</sub> SH (minor)	N <sub>3</sub> <sup>-</sup> + CH <sub>3</sub> OSiH <sub>2</sub> OH <b>very slow</b>	NSO <sup>-</sup> + CH <sub>3</sub> OSiH <sub>2</sub> OH
CH <sub>3</sub> SiF <sub>2</sub> NH <sup>-</sup> (4)	NCO <sup>-</sup> + CH <sub>3</sub> SiF <sub>2</sub> OH	NCS <sup>-</sup> + CH <sub>3</sub> SiF <sub>2</sub> SH CH <sub>3</sub> SiF <sub>2</sub> S <sup>-</sup> + HNCS	CH <sub>3</sub> SiF <sub>2</sub> S <sup>-</sup> + HNCO NCO <sup>-</sup> + CH <sub>3</sub> SiF <sub>2</sub> SH	N <sub>3</sub> <sup>-</sup> + CH <sub>3</sub> SiF <sub>2</sub> OH	NSO <sup>-</sup> + CH <sub>3</sub> SiF <sub>2</sub> OH CH <sub>3</sub> SiF <sub>2</sub> O <sup>-</sup> + HNSO

<sup>a</sup> The branching ratios are given in parentheses. <sup>b</sup> Experimental rate coefficients are given in bold type. Their units are cm<sup>3</sup> s<sup>-1</sup> molecule<sup>-1</sup> × 10<sup>-10</sup>. <sup>c</sup> The efficiencies (given in bold type) are the ratio of the experimental to the computed rate coefficients. The latter are obtained as *k<sub>L</sub>* (Langevin) or *k<sub>var</sub>* (variational) depending on the whether the reactant has a permanent dipole moment. References to their calculation are given in ref 10.

**Table 2. Products, Branching Ratios,<sup>a</sup> Rate Coefficient,<sup>b</sup> and Efficiencies<sup>c</sup> of 1–4 with Deuterated Neutrals**

amide ion	reactant = D <sub>2</sub> O	reactant = CH <sub>3</sub> OD	reactant = CD <sub>3</sub> CN
SiH <sub>3</sub> NH <sup>-</sup> (1)	SiH <sub>2</sub> (NHD)O <sup>-</sup> + HD (92) H <sub>3</sub> SiO <sup>-</sup> + NHD <sub>2</sub> (5)  H <sub>2</sub> Si(OD)O <sup>-</sup> + HD (3) <b>5.50 (0.20)</b>	SiH <sub>2</sub> (OCH <sub>3</sub> )NH <sup>-</sup> + HD (44)  SiH <sub>2</sub> (OCH <sub>3</sub> )ND <sup>-</sup> + H <sub>2</sub> (39)  H <sub>3</sub> SiND <sup>-</sup> + CH <sub>3</sub> OH (17) <b>13.31 (0.57)</b>	NCCD <sub>2</sub> <sup>-</sup> + SiH <sub>3</sub> NHD
C <sub>6</sub> H <sub>5</sub> SiH <sub>2</sub> NH <sup>-</sup> (2)	SiH <sub>2</sub> (NHD)O <sup>-</sup> + C <sub>6</sub> H <sub>5</sub> D (40) C <sub>6</sub> H <sub>5</sub> SiH(NHD)O <sup>-</sup> + HD (60)  <b>10.57 (0.43)</b>	SiH <sub>2</sub> (OCH <sub>3</sub> )NH <sup>-</sup> + C <sub>6</sub> H <sub>5</sub> D (32) SiH <sub>2</sub> (OCH <sub>3</sub> )ND <sup>-</sup> + C <sub>6</sub> H <sub>6</sub> (30) C <sub>6</sub> H <sub>5</sub> SiH(OCH <sub>3</sub> )NH <sup>-</sup> + HD (13) C <sub>6</sub> H <sub>5</sub> SiH(OCH <sub>3</sub> )ND <sup>-</sup> + H <sub>2</sub> (11) adduct (14) <b>13.11 (0.65)</b>	C <sub>6</sub> H <sub>5</sub> SiH <sub>2</sub> ND <sup>-</sup> + CHD <sub>2</sub> CN NCCD <sub>2</sub> <sup>-</sup> + C <sub>6</sub> H <sub>5</sub> SiH <sub>2</sub> NHD
CH <sub>3</sub> OSiH <sub>2</sub> NH <sup>-</sup> (3)	SiH <sub>2</sub> (NHD)O <sup>-</sup> + CH <sub>3</sub> OD CH <sub>3</sub> OSiH(NHD)O <sup>-</sup> + HD	SiH(OCH <sub>3</sub> ) <sub>2</sub> NH <sup>-</sup> + HD SiH(OCH <sub>3</sub> ) <sub>2</sub> ND <sup>-</sup> + H <sub>2</sub> adduct	CH <sub>3</sub> OSiH <sub>2</sub> ND <sup>-</sup> + CHD <sub>2</sub> CN NCCD <sub>2</sub> <sup>-</sup> + CH <sub>3</sub> OSiH <sub>2</sub> NHD
CH <sub>3</sub> SiF <sub>2</sub> NH <sup>-</sup> (4)	CH <sub>3</sub> SiF <sub>2</sub> ND <sup>-</sup> + HOD SiF <sub>2</sub> (NHD)O <sup>-</sup> + CH <sub>3</sub> D CH <sub>3</sub> SiF(NHD)O <sup>-</sup> + DF adduct	adduct (major) CH <sub>3</sub> SiF <sub>2</sub> ND <sup>-</sup> + CH <sub>3</sub> OH	adduct

<sup>a</sup> The branching ratios are given in parentheses. <sup>b</sup> Experimental rate coefficients are given in bold type. Their units are cm<sup>3</sup> s<sup>-1</sup> molecule<sup>-1</sup> × 10<sup>-10</sup>. <sup>c</sup> The efficiencies (given in bold type) are the ratio of the experimental to the computed rate coefficients. The latter are obtained as *k<sub>L</sub>* (Langevin) or *k<sub>var</sub>* (variational) depending on the whether the reactant has a permanent dipole moment. References to their calculation are given in ref 10.

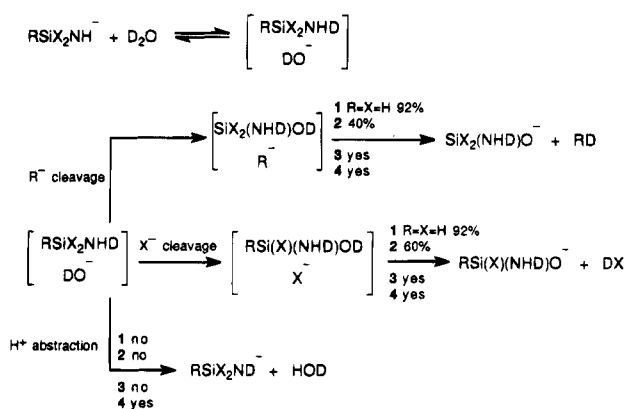
to NCS<sup>-</sup> (9%) as well as the absence of any such products for the other silamides indicates the strength of the tendency to form a Si–S rather than a Si–O bond in silamide reactions with COS. Previous studies of the reaction of the low-valent HSiNH<sup>-</sup> with COS demonstrated exclusive formation of Si–S bonds as well.<sup>8</sup> These results clearly demonstrate that the anions 1–4 display both the predominant characteristics of amide ions and those of their silicon substitution.

The rate coefficients of 1 and 2 with CO<sub>2</sub>, CS<sub>2</sub>, COS, and SO<sub>2</sub> parallel each other closely (Table 1). Both anions react at nearly the collision rate with CO<sub>2</sub> and SO<sub>2</sub>, at about half that rate with COS, and even more slowly with CS<sub>2</sub>. Both anions react very slowly with N<sub>2</sub>O. Previous rate coefficient measurements on (CH<sub>3</sub>)<sub>3</sub>SiNCH<sub>3</sub><sup>-</sup> give very similar results for reaction with CS<sub>2</sub> and COS, but reaction with CO<sub>2</sub> was about

10-fold slower.<sup>7</sup> The more weakly basic anion [(CH<sub>3</sub>)<sub>3</sub>Si]<sub>2</sub>N<sup>-</sup> reacted at about a quarter the rate of 1 and 2 with CO<sub>2</sub> but at a greatly reduced rate with CS<sub>2</sub> and COS.<sup>7</sup> The simple amide H<sub>2</sub>N<sup>-</sup> reacts at or near the collision rate with CO<sub>2</sub>, CS<sub>2</sub>, COS, and SO<sub>2</sub> (efficiencies are 0.84, 0.95, 1.0, and 1.4) and at about a quarter of that rate with N<sub>2</sub>O.<sup>2</sup> Low-valent HSiNH<sup>-</sup> reacts with CO<sub>2</sub>, CS<sub>2</sub>, COS, and SO<sub>2</sub> with efficiencies of 0.41, 0.35, 0.24, and 0.87.<sup>10</sup> Thus, while SO<sub>2</sub> always seems to react near the collision rate with the amine nucleophiles that have been studied, there is a large variation in efficiencies between H<sub>2</sub>N<sup>-</sup> and silicon-substituted amines and between the silicon substituted amines themselves in other reactions with neutrals.

**Reactions with Deuterated Neutrals.** Strongly basic amides react with water and alcohols by proton abstraction while silamides have a quite different fate

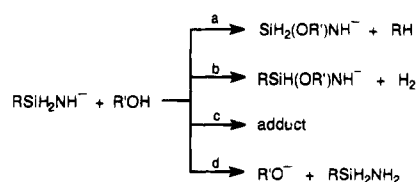
Scheme 1



in their corresponding reactions as shown in Table 2. Reaction of  $\text{D}_2\text{O}$  with 1–4 occurs by the general reaction Scheme 1. Since the silamides are less basic than  $\text{DO}^-$  (see following section on acidity), the endergonic proton abstraction reactions are driven by an ion–dipole attraction (ion–dipole attractions of 15–20 kcal/mol are common<sup>13</sup>). Subsequent attack of the  $\text{DO}^-$  at silicon cleaves a basic group (either  $\text{X}^-$  or  $\text{R}^-$ ) from silicon. The bases so cleaved abstract a proton before departing the reaction complex and, as a result, give  $\text{RSi(X)(NHD)O}^-$  plus  $\text{DX}$  and  $\text{SiX}_2(\text{NHD})\text{O}^-$  plus  $\text{RD}$  products. Such cleavage pathways account for more than 90% of the products of 1 and 2, the two reactants that have been studied quantitatively. We account for the 5 and 3% channels in the reaction of 1 with  $\text{D}_2\text{O}$  by formation of  $\text{H}_3\text{SiO}^-$  and the reaction product  $\text{H}_2\text{Si(OD)O}^-$ , respectively. These form by initial formation of  $\text{H}_3\text{SiNH}$  and  $\text{DO}^-$  followed by addition of  $\text{DO}^-$  with cleavage of  $\text{NHD}^-$ . The other product somehow must form from  $\text{H}_3\text{SiO}^-$  by a similar mechanism. We have obtained no evidence for H–D exchange of 1 with  $\text{D}_2\text{O}$  or with the more acidic  $\text{CD}_3\text{CN}$ , but 1 does exchange with  $\text{CH}_3\text{OD}$ . This result is perplexing, given that exchange is endergonic by 18 and 6 kcal/mol with  $\text{D}_2\text{O}$  and  $\text{CH}_3\text{OD}$  but exergonic by 3 kcal/mol with  $\text{CD}_3\text{CN}$ . It might be argued that the C–D exchange has a kinetic barrier; however 2 undergoes no exchange with  $\text{D}_2\text{O}$  or  $\text{CH}_3\text{OD}$  but exchanges with  $\text{CD}_3\text{CN}$ . These three cases are endergonic by 20 and 8 kcal/mol and exergonic by 1 kcal/mol, respectively. In contrast, anion 4 undergoes exchange with both  $\text{D}_2\text{O}$  and  $\text{CH}_3\text{OD}$ .

The major reaction chemistry of anions 1–4 with  $\text{CH}_3\text{OD}$  is detailed in Table 2 and readily explained with reference to Scheme 1. For  $\text{H}_3\text{SiNH}^-$  (1), 83% of the products result from  $\text{H}^-$  cleavage with a slight preference for HD (44%) over  $\text{H}_2$  (39%). The exchange product mentioned above is formed in fairly large amounts (17%). Similar results are obtained in the reaction of 1 and  $\text{CH}_3\text{CH}_2\text{OD}$ . The reaction of  $\text{C}_6\text{H}_5\text{SiH}_2\text{NH}^-$  (2) and  $\text{CH}_3\text{OD}$  gives all of the expected cleavage products, with  $\text{C}_6\text{H}_5\text{D}$  (32%) being formed in slightly greater amounts than  $\text{C}_6\text{H}_5\text{H}$  (30%) and HD (13%) in greater yield than  $\text{H}_2$  (11%). There is no evidence here of exchange, but an adduct is observed (14%), suggesting again that structurally more complex features in silamides larger

Scheme 2



than  $\text{H}_3\text{SiNH}^-$  provide lifetimes sufficient for adduct stabilization.<sup>14</sup> The rate coefficients for the reactions of 1 and 2 with both  $\text{D}_2\text{O}$  and  $\text{CH}_3\text{OD}$  have been measured (Table 2). These are relatively slow reactions that occur with efficiencies between 0.20 and 0.65 of the collision rate. Although no exchange reaction of 1 with  $\text{CD}_3\text{CN}$  occurs, anion 2 does give observable H–D exchange. Both anions abstract  $\text{D}^+$  from  $\text{CD}_3\text{CN}$ , giving  $\text{NCCD}_2^-$  as would be expected from their basicities compared to that of  $\text{NCCD}_2^-$  ( $\Delta G_{\text{acid}}^\circ$  of  $\text{CH}_3\text{CN} = 365$  kcal/mol)<sup>4</sup> (3 kcal/mol exergonic for 1 and 1 kcal/mol exergonic for 2).

The general features of the reactions just described have been observed with a number of other alcohols, although the proton abstraction channel described in Scheme 1 is invisible for reactions of undeuterated alcohols. A qualitative picture of the reactivity of anions 1, 2, and 3 (each a  $\text{RSiH}_2\text{NH}^-$  species) with a number of alcohols ( $\text{R}'\text{OH}$ ) is given in Scheme 2 and in Table 3. Products of pathways a and b,  $\text{SiH}_2(\text{OR}')\text{NH}^-$  plus  $\text{RH}$  and  $\text{RSiH}(\text{OR}')\text{NH}^-$  plus  $\text{H}_2$ , respectively, correspond to the cleavage reactions of  $\text{R}^-$  and  $\text{H}^-$ , while c corresponds to adduct formation and d to a simple acid–base reaction to give  $\text{R}'\text{O}^-$ . Anion 1 reacts with the aliphatic alcohols to give cleavage products almost exclusively, the only exceptions being its reaction with *tert*-butyl alcohol, where some d is observed, and hexanol, where adduct forms. The slightly greater acidity of *tert*-butyl alcohol<sup>4</sup> may explain the occurrence of pathway d while adduct formation in hexanol case is likely a reflection of the greater molecular complexity of hexanol. The more acidic fluoro alcohols<sup>4</sup> give greater amounts of the proton abstraction product d and less of the corresponding cleavage product a = b. Anion 2 exhibits a more complicated reactivity pattern, since two cleavage products are possible. Its reaction with small aliphatic alcohols generally gives phenide and hydride cleavage products a and b as well as adduct formation. Phenide cleavage is slightly favored in these qualitative studies. As the aliphatic group of the alcohol becomes larger, the amount of adduct increases to the point where it is nearly the exclusive product for hexanol. The fluoro alcohols are observed to form cleavage products a and b as well as adduct c, but only trifluoroethanol consistently gives  $\text{R}'\text{O}^-$  (d). The methoxy-substituted anion  $\text{H}_2\text{Si}(\text{OCH}_3)\text{NH}^-$  (3) has a similar pattern of reactivity, with hydride over methoxide cleavage generally predominating.

The reactivity pattern of these anions with alcohols is reasonably explained in terms of an initial acid–base reaction giving  $[\text{RSiH}_2\text{NH}_2 \cdots \text{R}'\text{O}^-]$ . This intermediate complex can (1) undergo cleavage reactions initiated by nucleophilic attack of the alkoxide at silicon (pathways

(13) Bartmess, J. E. *Mass Spectrom. Rev.* **1989**, *8*, 297–343. The 15–20 kcal/mol generally cited as the ion–dipole attraction is typical of the attraction of anions with water, alcohols, and simple organic molecules that do not form covalent products. The source cited here reviews a number of anion affinity relationships as well.

(14) Berry, R. S.; Rice, S. A.; Ross, J. *Physical Chemistry*; John Wiley and Sons: New York, 1980; pp 1204–1209. RRMK and similar kinetic treatments account for the distribution of energy in ion–dipole complexes.



Table 3. Reactions with 1–3 with Various Alcohols (R'OH)

Reactions of 1 <sup>a</sup>										
products	R'									
	Me	Et	n-Pr	i-Pr	n-Bu	t-Bu	n-hexyl	CH <sub>2</sub> FCH <sub>2</sub>	CHF <sub>2</sub> CH <sub>2</sub>	CF <sub>3</sub> CH <sub>2</sub>
a = b <sup>b</sup>	+	+	+	+	+	+++	++	++	+	–
c <sup>c</sup>	–	–	–	–	–	–	+	–	–	trace
d <sup>d</sup>	–	–	–	–	–	+	–	+	++	+
Reactions of 2 <sup>a</sup>										
products	R'									
	Me	Et	n-Pr	i-Pr	n-Bu	t-Bu	n-hexyl	CH <sub>2</sub> FCH <sub>2</sub>	CHF <sub>2</sub> CH <sub>2</sub>	CF <sub>3</sub> CH <sub>2</sub>
a <sup>b</sup>	++	+++	++	++	+	+	trace	+	++	++
b <sup>c</sup>	+	+	–	+	+	+	–	+	+	+
c <sup>d</sup>	+	++	+	+++	+++	+++	+++	++	++	++
d <sup>e</sup>	–	–	–	–	–	–	–	–	+ <sup>f</sup>	+++
Reactions of 3 <sup>a</sup>										
products	R'									
	Me	Et	i-Pr	n-Bu	t-Bu	n-hexyl	CH <sub>2</sub> FCH <sub>2</sub>	CHF <sub>2</sub> CH <sub>2</sub>	CF <sub>3</sub> CH <sub>2</sub>	
a <sup>b</sup>	+	+	trace	++	+	–	++	+	–	
b <sup>c</sup>	+++	+++	++	–	+	+	+++	++	–	
c <sup>d</sup>	++	++	+	+	trace	++	trace	–	–	
d <sup>e</sup>	–	trace	trace	–	–	–	+ <sup>f</sup>	+++	+	

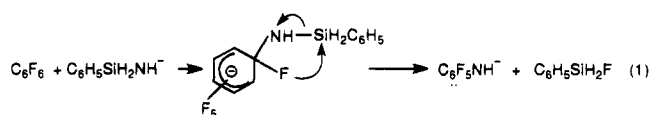
<sup>a</sup> These reactions have been carried out to determine the relative reactivities of 1–3 with alcohols of widely varying structure. When only one product is observed in such a reaction, it is designated by +. If no reaction occurs, a – designation signifies this. In those cases where more than one product is observed, we have tried to give a sense of the relative amounts of these by using multiple plus signs. Without careful branching ratio measurements these data can only be considered qualitatively as pointed out in the text. <sup>b–e</sup> The designations a, b, c, and d correspond to the reaction channels given in Scheme 2 in the text. <sup>f</sup> These products have not been consistently observed.

Table 4. Reactions of 1 and 2 with C<sub>6</sub>F<sub>6</sub>, HCO<sub>2</sub>CH<sub>3</sub>, and CH<sub>3</sub>CO<sub>2</sub>CH<sub>3</sub>

amide ion	reactant = C <sub>6</sub> F <sub>6</sub>	reactant = HCO <sub>2</sub> CH <sub>3</sub>	reactant = CH <sub>3</sub> CO <sub>2</sub> CH <sub>3</sub>
SiH <sub>3</sub> NH <sup>–</sup> (1)	C <sub>6</sub> F <sub>5</sub> NH <sup>–</sup> + SiH <sub>3</sub> F	HCONH <sup>–</sup> + SiH <sub>3</sub> OCH <sub>3</sub>	CH <sub>3</sub> O <sub>2</sub> CCH <sub>2</sub> <sup>–</sup> + SiH <sub>3</sub> NH <sub>2</sub>
C <sub>6</sub> H <sub>5</sub> SiH <sub>2</sub> NH <sup>–</sup> (2)	C <sub>6</sub> F <sub>5</sub> NH <sup>–</sup> + C <sub>6</sub> H <sub>5</sub> SiH <sub>2</sub> F	HCONH <sup>–</sup> + C <sub>6</sub> H <sub>5</sub> SiH <sub>2</sub> OCH <sub>3</sub> (major) [C <sub>6</sub> H <sub>5</sub> SiH <sub>2</sub> (OCH <sub>3</sub> )NH <sub>2</sub> ] <sup>–</sup> + CO [C <sub>6</sub> H <sub>5</sub> SiH <sub>2</sub> (NCHO)] <sup>–</sup> + CH <sub>3</sub> OH SiH <sub>2</sub> (OCH <sub>3</sub> )NH <sup>–</sup> + C <sub>6</sub> H <sub>6</sub> + CO	CH <sub>3</sub> O <sub>2</sub> CCH <sub>2</sub> <sup>–</sup> + C <sub>6</sub> H <sub>5</sub> SiH <sub>2</sub> NH <sub>2</sub> CH <sub>3</sub> CONH <sup>–</sup> + C <sub>6</sub> H <sub>5</sub> SiH <sub>2</sub> OCH <sub>3</sub>

a and b), (2) be stabilized by collision after the penta-coordinate silicon intermediate forms (pathway c), and/or (3) dissociate to alkoxide and RSiH<sub>2</sub>NH<sub>2</sub> (pathway d). The observed trends are consistent with expectations, since increased molecular complexity tends to increase the amount of pathway c and increased acidity of R'OH tends to increase the amount of d.

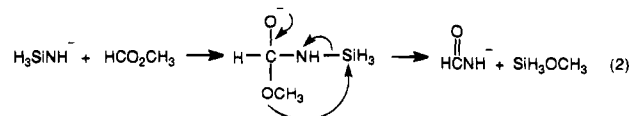
**Other Reactions.** Hexafluorobenzene has been shown<sup>11,15</sup> to give a number of unusual reactions with a wide variety of anions (Table 4). Its reaction with C<sub>6</sub>H<sub>5</sub>SiH<sub>2</sub>NH<sup>–</sup> giving C<sub>6</sub>F<sub>5</sub>NH<sup>–</sup> is reminiscent<sup>15</sup> of O<sup>–</sup> transfer from (CH<sub>3</sub>)<sub>2</sub>AlO<sup>–</sup>. In reactions of this type, we believe the anion adds to hexafluorobenzene, giving an adduct that loses F<sup>–</sup> while transferring it to the electropositive element (silicon here and aluminum in the previous case studied) as shown in eq 1. Another silicon



anion, HSiO<sup>–</sup>, has been shown to behave in a similar manner, although, in this example, the F<sup>–</sup> transfer to silicon results in the loss of HFSiO, giving C<sub>6</sub>F<sub>5</sub><sup>–</sup> as one of several products.<sup>11</sup>

The reactions of methyl formate and methyl acetate have also been studied briefly to chart the range of

reactivity of silylamines (Table 4). These neutrals react with anionic bases to give a variety of products that depend on the substitution pattern of the ester and the nature of the base.<sup>16–18</sup> Typical products that have been observed arise from processes including S<sub>N</sub>2 displacement at the methyl ester, proton abstraction of an aldehydic hydrogen followed by methoxide loss (the Riveros reaction of methylformate), and carbonyl addition through a tetracoordinate intermediate (B<sub>AC</sub>2). Anion 1 reacts with methyl formate in a simple fashion by a process that we believe begins as a carbonyl addition. Product HC(=O)NH<sup>–</sup> then forms as shown in eq 2 with the tetracoordinate adduct losing methox-



ide, which is transferred to silicon without escaping the reaction complex. The major product of the reaction of 2 follows this same pathway, although smaller amounts of other products suggest that some variations of the familiar pathways discussed above for other anions with ester are active. In the reaction of 2 with methyl

(16) DePuy, C. H.; Grabowski, J. J.; Bierbaum, V. M.; Ingemann, S.; Nibbering, N. M. M. *J. Am. Chem. Soc.* **1985**, *107*, 1093–8.

(17) Faigle, J. F. G.; Isolani, P. C.; Riveros, J. M. *J. Am. Chem. Soc.* **1976**, *98*, 2049–52.

(18) Takashima, K.; Riveros, J. M. *J. Am. Chem. Soc.* **1978**, *100*, 6128–32.

(15) Damrauer, R.; Krempp, M.; Schmidt, M. W.; Gordon, M. S. *J. Am. Chem. Soc.* **1991**, *113*, 2393–2400.



Table 5. Collision-Induced Dissociation of Silamides 1–4

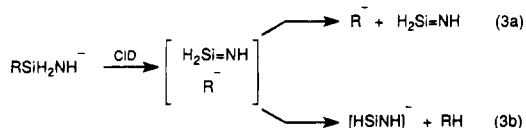
amide ion	collision-induced dissociation (CID)
SiH <sub>3</sub> NH <sup>-</sup> (1)	HSiNH <sup>-</sup> + H <sub>2</sub> (major) SiH <sub>2</sub> <sup>-</sup> + H <sub>2</sub> N (minor)
SiD <sub>3</sub> NH <sup>-</sup>	DSiNH <sup>-</sup> + D <sub>2</sub> (major) SiD <sub>2</sub> <sup>-</sup> + HDN (minor) D <sup>-</sup> + D <sub>2</sub> SiNH (minor)
C <sub>6</sub> H <sub>5</sub> SiH <sub>2</sub> NH <sup>-</sup> (2)	HSiNH <sup>-</sup> + C <sub>6</sub> H <sub>6</sub> (major) C <sub>6</sub> H <sub>5</sub> NH <sup>-</sup> + H <sub>2</sub> SiNH (major) C <sub>6</sub> H <sub>5</sub> NH <sup>-</sup> + H <sub>2</sub> (minor)
CH <sub>3</sub> OSiH <sub>2</sub> NH <sup>-</sup> (3)	SiH <sub>2</sub> NH <sub>2</sub> <sup>-</sup> + CH <sub>2</sub> =O (major) CH <sub>3</sub> O <sup>-</sup> + H <sub>2</sub> SiNH (minor) HSiNH <sup>-</sup> + CH <sub>3</sub> OH (minor)
CH <sub>3</sub> SiF <sub>2</sub> NH <sup>-</sup> (4)	FSi(NH)CH <sub>2</sub> <sup>-</sup> + HF (major) SiF <sub>2</sub> NH <sup>-</sup> + CH <sub>3</sub> or CH <sub>3</sub> SiF <sub>2</sub> <sup>-</sup> + NH (minor)

acetate, we observe not only the major process just described for **1** and **2** with methyl formate, but a proton abstraction giving the enolate of methyl formate. Once again, the reactivity of anions **1–4** is a combination of that characteristic of simple amide ions and that caused by silicon substitution.

The reactions just described for anions **1–4** are strong evidence that the proposed structures are correct. The mechanistic schemes leading to products are reasonable in such structural terms. Furthermore, the similarity between the reactions of amides and these silamides indicates that the presence of silicon is often not the defining feature of their reactivity, but only a modifying influence.

#### Collision-Induced Dissociation (CID) Studies.

The CID products for the silamides (**1–4**) are presented in Table 5 and can be understood in terms of the structural assignments for these anions. An important dissociative process common to all the silamides **1–3** is represented in a general way by eq 3 (the analogous X<sup>-</sup> cleavage is not illustrated). In such a process, a group



attached to silicon is lost as an anion (R<sup>-</sup>) that can either escape the dissociation complex (1a) (e.g., **2** and **3**) or abstract a proton before the complex collapses (1b) (e.g., **1–3**). Anion **2** loses C<sub>6</sub>H<sub>5</sub><sup>-</sup> with no detectable loss of H<sup>-</sup>. Although the nature of our experimental setup makes it impossible to detect H<sup>-</sup> (*m/z* = 1), the small amount of C<sub>6</sub>H<sub>5</sub>NH<sup>-</sup> (plus H<sub>2</sub>) detected suggests that H<sup>-</sup> loss is minor. Because of the nearly identical basicities of C<sub>6</sub>H<sub>5</sub><sup>-</sup> and H<sup>-</sup>, however, we believe it is likely that both cleavage processes are occurring. A process analogous to that in eq 1 in which X<sup>-</sup> is cleaved explains the major CID product of **4**. Here a complex of [CH<sub>3</sub>SiF=NH···F<sup>-</sup>] forms before proton abstraction leads to FSiNHCH<sub>2</sub><sup>-</sup>.

In addition to the processes outlined in eq 3, SiH<sub>3</sub>NH<sup>-</sup> undergoes a minor amount of dissociation to SiH<sub>2</sub><sup>-</sup>. This may occur by silylene extrusion, a process quite common in the pyrolysis of organosilicon compounds.<sup>19,20</sup> Since

(19) Apeloig, Y. In *The Chemistry of Functional Groups*; Patai, S., Rappoport, Z., Eds.; John Wiley and Sons: New York, 1989; pp 57–225.

(20) Gordon, M. S.; Francisco, J. S.; Schlegel, H. B. In *Advances in Silicon Chemistry*; Larson, G. L., Ed.; JAI Press: Greenwich, CT, 1993; Vol. 2, pp 137–185.

Table 6. ΔG<sub>acid</sub><sup>o</sup> Values for Various Silamines (N–H)

silamine	ΔG <sub>acid</sub> <sup>o</sup> (in kcal/mol) <sup>a,b</sup>	bracketing acid <sup>c</sup> (protonates)	bracketing acid <sup>c</sup> (does not protonate)
SiH <sub>3</sub> NH <sub>2</sub>	368 ± 3	CH <sub>3</sub> CH <sub>2</sub> CN	CH <sub>3</sub> (CH <sub>2</sub> ) <sub>3</sub> OH
FSiH <sub>2</sub> NH <sub>2</sub>	366 ± 4	CH <sub>3</sub> CN	CH <sub>3</sub> (CH <sub>2</sub> ) <sub>5</sub> OH
C <sub>6</sub> H <sub>5</sub> SiH <sub>2</sub> NH <sub>2</sub>	366 ± 4	CH <sub>3</sub> CN	CH <sub>3</sub> (CH <sub>2</sub> ) <sub>5</sub> OH
CH <sub>3</sub> OSiH <sub>2</sub> NH <sub>2</sub>	368 ± 3	CH <sub>3</sub> CH <sub>2</sub> CN	CH <sub>3</sub> CH <sub>2</sub> CH <sub>2</sub> OH
CH <sub>3</sub> SiF <sub>2</sub> NH <sub>2</sub>	363 ± 3	(CH <sub>3</sub> CH <sub>2</sub> ) <sub>2</sub> CO	CH <sub>2</sub> FCH <sub>2</sub> OH

<sup>a</sup> The free energy change, ΔG<sub>acid</sub><sup>o</sup>, is commonly referred to as the acidity. <sup>b</sup> The acidity values reported are determined in relative terms from their ordering with the bracketing reference acids, which is known precisely. In absolute terms, the acidities depend on how accurately the acidities of the reference acids are known. This varies with the experimental method used in their determination. As a result, it is difficult to provide error limits on the accuracy of the data which are universally accepted. The absolute error limits reported here are consistent with our methodology and the reference acids used by us. <sup>c</sup> A “protonates” in the bracketing acid column signifies that the reference acid reacts with the corresponding silamide giving the silamine and the M – 1 of the reference acid; a “does not protonate” signifies that the acid listed does not so react with the silamide.

the electron affinities of NH<sub>2</sub> and SiH<sub>2</sub> are 17.8 and 25.9 kcal/mol,<sup>21</sup> dissociation to a complex of SiH<sub>2</sub> and NH<sub>2</sub><sup>-</sup> followed by electron transfer is a plausible route to SiH<sub>2</sub><sup>-</sup>. The methoxy-substituted silamide **3**, in losing formaldehyde, takes a dissociative path that the other silamides do not. This is a process we reported earlier in the CID of methoxy-substituted siloxide anions.<sup>22</sup> CH<sub>3</sub>SiF<sub>2</sub>NH<sup>-</sup> (**4**) takes still another dissociative path, although it is not clear what the products are since the resulting *m/z* is the same for both SiF<sub>2</sub>NH<sup>-</sup> and CH<sub>3</sub>SiF<sub>2</sub><sup>-</sup>. A path leading to SiF<sub>2</sub>NH<sup>-</sup> could follow the general outline of eq 1 by forming SiF<sub>2</sub>NH and CH<sub>3</sub><sup>-</sup>. The low electron affinity of CH<sub>3</sub><sup>-</sup> (1.8 kcal/mol)<sup>21</sup> and a presumed high electron affinity for SiF<sub>2</sub>NH would then give a reasonable picture of SiF<sub>2</sub>NH<sup>-</sup> formation. The small electron affinity of NH (8.6 kcal/mol)<sup>21</sup> suggests another possibility, namely that CH<sub>3</sub>SiF<sub>2</sub> and NH<sup>-</sup> form before electron transfer to give CH<sub>3</sub>SiF<sub>2</sub><sup>-</sup>. We have not tried to distinguish between these two minor products.

The somewhat different CID behavior of the four silamides is a reflection of their different structures. It is reasonable to assume that an anion such as SiH<sub>3</sub>NH<sup>-</sup>, having fewer locations to deposit excess energy, might, in addition to its loss of H<sup>-</sup>, dissociate by a unique process such as silylene extrusion. On the other hand, the other silamides with larger substituents dissociate in different ways because they have more places to deposit excess energy.<sup>14</sup>

**Acidity Studies.** The gas-phase acidities of many amines are known,<sup>4,6</sup> although values for only a few silamines have been reported.<sup>3</sup> The newly measured bracketed acidities of SiH<sub>3</sub>NH<sub>2</sub>, FSiH<sub>2</sub>NH<sub>2</sub>, C<sub>6</sub>H<sub>5</sub>SiH<sub>2</sub>NH<sub>2</sub>, CH<sub>3</sub>OSiH<sub>2</sub>NH<sub>2</sub>, and CH<sub>2</sub>SiF<sub>2</sub>NH<sub>2</sub> are presented in Table 6. The ΔG<sub>acid</sub><sup>o</sup> values for these silamides fall in the 363–368 kcal/mol range. Since gas-phase acidities are endergonic processes, a smaller magnitude of ΔG<sub>acid</sub><sup>o</sup> corresponds to a stronger acidity. The silylamines studied here are considerably stronger acids than typical amines (e.g., NH<sub>3</sub> and *t*-BuNH<sub>2</sub> with ΔG<sub>acid</sub><sup>o</sup> = 396 and 390 kcal/mol),<sup>4,5</sup> comparable to other simple silamines [e.g., (CH<sub>3</sub>)<sub>3</sub>SiNH<sub>2</sub> with ΔG<sub>acid</sub><sup>o</sup> = 371 kcal/mol]<sup>3</sup> and more weakly acidic than disilylamines

(21) Brinkman, E. A.; Wilbus, J. L.; Brauman, J. I. In *Negative Ions*; Esaulov, V. A., Ed.; Cambridge University Press: New York, 1993; pp 1–48.

(22) Damrauer, R.; Kremp, M. *Organometallics* **1990**, *9*, 999–1004.

[e.g.,  $((\text{CH}_3)_3\text{Si})_2\text{NH}$  with  $\Delta G_{\text{acid}}^\circ = 349$  kcal/mol].<sup>3</sup> Nevertheless, the effect of  $\beta$ -substitution on silion in the silamines is very small as is generally the case for other  $\beta$ -substitutions, for example, silanols.<sup>23,24</sup> A fluorine for hydrogen substitution in the silylamines makes  $\text{FSiH}_2\text{NH}_2$  a stronger acid by 2 kcal/mol than  $\text{SiH}_3\text{NH}_2$  while the same substitution in the silanols strengthens the acidity by 4 kcal/mol.<sup>23</sup> A  $\text{C}_6\text{H}_5$  for hydrogen substitution in the silamines strengthens the acidity by 2 kcal/mol; the same substitution in the silanols strengthens the acidity by 4 kcal/mol.<sup>26</sup> The effect of a methoxy substitution is small, with  $\text{CH}_3\text{OSiH}_2\text{NH}_2$  and  $\text{SiH}_3\text{NH}_2$  having the same acidity.<sup>23</sup> The closely corresponding silanols  $\text{CH}_3\text{O}(\text{CH}_3)_2\text{SiOH}$  and  $(\text{CH}_3)_3\text{SiOH}$  also have the same acidity. Perhaps surprisingly,  $\text{CH}_3\text{SiF}_2\text{NH}_2$  is a stronger acid than  $\text{SiH}_3\text{NH}_2$  by 5 kcal/mol while  $\text{CH}_3\text{SiF}_2\text{OH}$  is a 12 kcal/mol stronger acid than  $\text{SiH}_3\text{OH}$ .<sup>23</sup> These bracketing studies are made more difficult because of signal loss problems when using various alcohols as bracketing acids.

In earlier studies of the weakly acidic alkanes, we reported that  $\beta$ -methyl substitutions of alkanes had a larger acid strengthening effect than analogous substitutions in alcohols.<sup>25</sup> We suggested that the "much more strongly basic carbanions would be expected to make greater demands on methyl groups, which are postulated to stabilize anions by polarization".  $\beta$ -Methyl substitutions of amines have a similar acid strengthening effect to the analogous substitutions in alcohols.<sup>4,5</sup> The first  $\beta$ -methyl substitution increases the acidity by 3.9 kcal/mol, the second by 2.1 kcal/mol, and the third by 0.6 kcal/mol. The corresponding values for alkanes are 4.5, 2.7, and 4.0 kcal/mol, and for alcohols, 3.1, 1.9, and 1.0 kcal/mol.<sup>4</sup> Thus,  $\beta$ -substitution effects for silamines and silanols have similar sensitivities to those of simple amine and alcohols, although a full analysis is complicated in the silicon systems where longer bond distances attenuate polarizability effects.<sup>23,24</sup> As Grimm and Bartmess have recently reported, the effects of counterions in solution adds another level of complexity to the acidities of silamines.<sup>3</sup>

Finally, we return to the question of the relative acidity of Si-H and N-H. Since an experimental

determination of this is not readily made, we have examined the Si-H versus N-H acidity with Gaussian 92<sup>26</sup> using G2<sup>27</sup> computations on MP2/6-31+G(d,p) optimized structures for  $\text{SiH}_3\text{NH}_2$ ,  $[\text{SiH}_2\text{NH}]^-$ , and  $[\text{SiH}_3\text{NH}]^-$ . These demonstrate that Si-H is more weakly acidic in this compound by about 5 kcal/mol.<sup>28</sup> This is a reversal of the trend of  $\text{SiH}_3\text{CH}_3$  in which Si-H is more strongly acidic than C-H by about 12 kcal/mol<sup>28</sup> and contrasts with an earlier computational study.<sup>29</sup>

## Summary

Reactivity studies of anions 1-4 have been used to characterize their structures as  $\text{SiH}_3\text{NH}^-$  (1),  $\text{C}_6\text{H}_5\text{SiH}_2\text{NH}^-$  (2),  $\text{CH}_3\text{OSiH}_2\text{NH}^-$  (3), and  $\text{CH}_3\text{SiF}_2\text{NH}^-$  (4). The reactivity of anions 1-4 is generally similar to that of unsilylated amide ions; however, certain reactions have been shown to involve the substituted silicon in important ways. The CID behavior of these anions has been studied. The subtle structural features of the silamide anions are reflected in their complex behavior. The gas-phase acidities of  $\text{SiH}_3\text{NH}_2$ ,  $\text{FSiH}_2\text{NH}_2$ ,  $\text{C}_6\text{H}_5\text{SiH}_2\text{NH}_2$ ,  $\text{CH}_3\text{OSiH}_2\text{NH}_2$ , and  $\text{CH}_3\text{SiF}_2\text{NH}_2$  fall in a small range, indicating that  $\beta$ -substitution effects on silicon are small in much the same way that they are with substituted silanols.

**Acknowledgment.** We thank Joseph A. Hankin for expert experimental help in the last stage of this work and Christopher Hadad for expert help on the G2 computations. We also gratefully acknowledge the financial support of the National Science Foundation (CHE-8921522 and 9223037) and the donors of the Petroleum Research Fund, administered by the American Chemical Society.

OM940578F

(26) Gaussian 92, Revision G.2. M. J. Frisch, G. W. Trucks, M. Head-Gordon, P. M. W. Gill, M. W. Wong, J. B. Foresman, B. G. Johnson, H. B. Schlegel, M. A. Robb, E. S. Replogle, R. Gomperts, J. L. Andres, K. Raghavachari, J. S. Binkley, C. Gonzalez, R. L. Martin, D. J. Fox, D. J. Defrees, J. Baker, J. J. P. Stewart, and J. A. Pople, Gaussian, Inc., Pittsburgh, PA, 1992.

(27) G2: Curtiss, L. A.; Raghavachari, K.; Pople, J. A. *J. Chem. Phys.* **1991**, *94*, 7221.

(28) R. Damrauer, work in progress. A computational study of  $\text{SiH}_2\text{XY}$  probes various substituent effects on silicon. Substitution of X = H and F and Y =  $\text{CH}_3$ ,  $\text{NH}_2$ , and OH has shown unexpected substituent effects, particularly in terms of the almost complete invariance of Si-H acidity with substitution of X and Y.

(29) Hopkinson, A. C.; Lien, M. H. *J. Mol. Struct. (THEOCHEM)* **1983**, *92*, 153-166.

(23) Damrauer, R.; Simon, R.; Krempp, M. *J. Am. Chem.* **1991**, *113*, 4431-5.

(24) Gordon, M. S.; Damrauer, R.; Krempp, M. *J. Phys. Chem.* **1993**, *97*, 7820-7822.

(25) DePuy, C. H.; Gronert, S.; Barlow, S. E.; Bierbaum, V. M.; Damrauer, R. *J. Am. Chem. Soc.* **1989**, *111*, 1968-73.

# New Silyl-Substituted Cyclopentadienyl Titanium and Zirconium Complexes. X-ray Molecular Structures of $[\text{TiCl}_2\{\mu\text{-(OSiMe}_2\text{-}\eta^5\text{-C}_5\text{H}_4)\}]_2$ and $[\text{ZrCl}_2\{\mu\text{-}[(\eta^5\text{-C}_5\text{H}_4)\text{SiMe}_2\text{OSiMe}_2(\eta^5\text{-C}_5\text{H}_4)]\}]$

Santiago Ciruelos, Tomás Cuenca, Pilar Gómez-Sal,<sup>†</sup> Antonio Manzanero,<sup>†</sup> and Pascual Royo\*

Departamento de Química Inorgánica, Universidad de Alcalá, Campus Universitario, 28871 Alcalá de Henares, Spain

Received July 28, 1994<sup>®</sup>

We report the synthesis of 1-(chlorodimethylsilyl)-1-(trimethylsilyl)cyclopentadiene, **1**. The reaction of a toluene solution of **1** with one equivalent of  $\text{MCl}_4$  ( $\text{M} = \text{Ti}, \text{Zr}$ ) leads to the mono(cyclopentadienyl) derivatives  $[\text{MCl}_3(\eta^5\text{-C}_5\text{H}_4\text{SiMe}_2\text{Cl})]$  [ $\text{M} = \text{Ti}$  (**2**);  $\text{M} = \text{Zr}$  (**3**)] in 76 and 87% yields, respectively. The same reaction with  $\text{ZrCl}_4$  in a  $\text{Zr/Cp}$  molar ratio 1:2 in refluxing methylene dichloride yields the dicyclopentadienyl derivative  $[\text{ZrCl}_2(\eta^5\text{-C}_5\text{H}_4\text{SiMe}_2\text{Cl})_2]$ , **4**, whereas the related titanium compound cannot be synthesized by this method. These mono- and bis(cyclopentadienyl) complexes are very moisture sensitive and react with water to give different oxo complexes. Reaction of one equivalent of water with  $[\text{TiCl}_3(\eta^5\text{-C}_5\text{H}_4\text{SiMe}_2\text{Cl})]$  in toluene takes place with elimination of  $\text{HCl}$ , resulting in formation of the dinuclear titanium methylsiloxane derivative  $[\text{TiCl}_2\{\mu\text{-(OSiMe}_2\text{-}\eta^5\text{-C}_5\text{H}_4)\}]_2$ , **5**, in a quantitative yield, which by further addition of one equivalent of water gives the mononuclear compound  $[\text{TiCl}_2\{\text{OSiMe}_2\text{OSiMe}_2(\eta^5\text{-C}_5\text{H}_4)\}]$ , **6**, in very low yield. However the best procedure to obtain **6** (in 45% yield) is the direct reaction of  $[\text{TiCl}_3(\eta^5\text{-C}_5\text{H}_4\text{SiMe}_2\text{Cl})]$  with two equivalents of water. The analogous reaction of  $[\text{ZrCl}_2(\eta^5\text{-C}_5\text{H}_4\text{SiMe}_2\text{Cl})_2]$  with one equivalent of water proceeds to give  $[\text{ZrCl}_2\{\mu\text{-(}\eta^5\text{-C}_5\text{H}_4\text{)SiMe}_2\text{OSiMe}_2(\eta^5\text{-C}_5\text{H}_4)\}]$ , **7**. Alkylation of  $[\text{TiCl}_3(\eta^5\text{-C}_5\text{H}_4\text{SiMe}_2\text{Cl})]$  with  $\text{Mg}(\text{CH}_2\text{C}_6\text{H}_5)_2(\text{THF})_2$  leads to the tribenzyl derivative  $[\text{Ti}(\text{CH}_2\text{C}_6\text{H}_5)_3(\eta^5\text{-C}_5\text{H}_4\text{SiMe}_2\text{Cl})]$ , **8**, and alkylation of  $[\text{TiCl}_2\{\mu\text{-(OSiMe}_2\text{-}\eta^5\text{-C}_5\text{H}_4)\}]_2$  with  $\text{MgClMe}$  and  $\text{Mg}(\text{CH}_2\text{C}_6\text{H}_5)_2(\text{THF})_2$  allows the isolation of the oxoalkyl complexes  $[\text{TiR}_2\{\mu\text{-(OSiMe}_2\text{-}\eta^5\text{-C}_5\text{H}_4)\}]_2$  [ $\text{R} = \text{Me}$ , **9**;  $\text{R} = \text{CH}_2\text{C}_6\text{H}_5$ , **10**]. Reaction of  $[\text{MCl}_3(\eta^5\text{-C}_5\text{H}_4\text{SiMe}_2\text{Cl})]$  with  $\text{LiN}(\text{SiMe}_3)_2$  gives the amido complex  $[\text{TiCl}_2\{\text{N}(\text{SiMe}_3)_2(\eta^5\text{-C}_5\text{H}_4\text{SiMe}_2\text{Cl})\}]$ , **11**, whereas a similar reaction with  $\text{LiNH}^t\text{Bu}$  takes place with simultaneous elimination of  $\text{HCl}$  to give the cyclic amido pendant cyclopentadienyl complex  $[\text{TiCl}_2\{\text{N}^t\text{BuSiMe}_2(\eta^5\text{-C}_5\text{H}_4)\}]$ , **12**. The molecular structures of  $[\text{TiCl}_2\{\mu\text{-(OSiMe}_2\text{-}\eta^5\text{-C}_5\text{H}_4)\}]_2$  and  $[\text{ZrCl}_2\{\mu\text{-(}\eta^5\text{-C}_5\text{H}_4\text{)SiMe}_2\text{OSiMe}_2(\eta^5\text{-C}_5\text{H}_4)\}]$  have been determined by X-ray diffraction methods. Complex **5** is a dimer formed by two  $[\text{Me}_2\text{-SiCpTiCl}_2]$  fragments bonded by two oxygen bridges, connecting the silicon and titanium atoms from different units. **5** crystallizes in monoclinic space group  $P2_1/n$  with  $a = 9.461(7)$ ,  $b = 10.926(1)$ ,  $c = 10.507(3)$  Å,  $\beta = 95.20(2)^\circ$ , and  $V = 1081(1)$  Å<sup>3</sup> for  $Z = 2$ . The molecular structure of **7** corresponds to a typical bent dicyclopentadienyl system. Complex **7** crystallizes in the space group  $P2_1/c$  with  $a = 13.479(4)$ ,  $b = 8.654(1)$ ,  $c = 15.343(5)$  Å,  $\beta = 97.18(2)^\circ$ , and  $V = 1775(2)$  Å<sup>3</sup> for  $Z = 4$ .

## Introduction

$\eta^5$ -Cyclopentadienyl derivatives of group 4 elements play an important role in structural, synthetic, and catalytic organometallic chemistry. Replacement of one or more cyclopentadienyl ring hydrogens has been shown to result in significant changes in both steric and electronic effects at the metal center.

Attachment of metal complexes that are homogeneous catalysts to organic polymers and inorganic supports<sup>1</sup> is an area of increasing interest in organometallic chemistry, as they combine the most advantageous properties of the homogeneous and heterogeneous catalysis. Polysiloxanes have also been investigated as

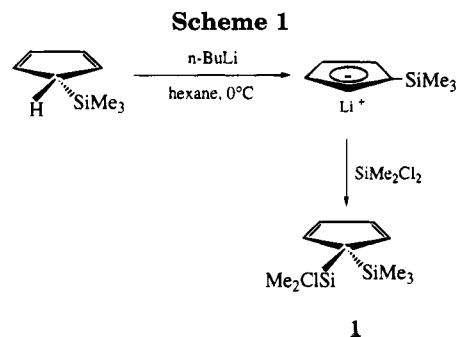
potential supports for homogeneous catalysts.<sup>2</sup> Recently there has been growing interest in the development of catalytic systems based on supported cyclopentadienyl ligands. Cyclopentadienyl ligands are specially attractive as anchoring groups since the metal is strongly bound by the  $\eta^5$ -coordination. Good candidates for this

(1) (a) Hartley, F. R., Vezze, P. N. *Adv. Organomet. Chem.*, **1977**, *15*, 189. (b) Murrell in J. J. Burton and R. L. Garten (Eds.), *Advanced Materials in Catalysis*, Academic Press, New York, **1977**. (c) Prueett, R. L. *Adv. Organomet. Chem.*, **1979**, *17*, 1. (d) James, B. R. *Adv. Organomet. Chem.*, **1979**, *17*, 319. (e) Pittman, C. U. in P. Hodge and D. C. Sherrington (Eds.), *Polymer-Supported Reactions in Organic Synthesis*, Wiley, New York, **1980**. (f) Akelah, A. *Synthesis*, **1981**, 413. (g) Bailey, D. C., Langer, S. H. *Chem. Rev.*, **1981**, *81*, 109. (h) Akelah, A., Sherrington, D. C. *Chem. Rev.*, **1981**, *81*, 557. (i) Klein, B., Kaziuskas, R. J., Wrighton, M. S. *Organometallics*, **1982**, *1*, 1338. (j) Booth, B. L., Ofunne, G. C., Stacey, C., Tait, P. J. T. *J. Organomet. Chem.*, **1986**, *315*, 143.

(2) Curtis, M. D., D'Errico, J. J., Duffy, D. N., Epstein, P. S., Bell, L. G. *Organometallics*, **1983**, *2*, 1808.

<sup>†</sup> X-ray diffraction studies.

<sup>®</sup> Abstract published in *Advance ACS Abstracts*, November 1, 1994.



proposal could be the silylated cyclopentadienyl derivatives, similar to those previously reported.<sup>3</sup> In this paper we report synthetic procedures to prepare mono- and bis(cyclopentadienyl) derivatives of titanium and zirconium with the monosubstituted (chlorodimethylsilyl)cyclopentadienyl group. The synthesis of the cyclopentadienyl ligand ( $C_5H_4(SiMe_2Cl)(SiMe_3)$ , **1**, the mono(cyclopentadienyl) derivatives [ $MCl_3(\eta^5-C_5H_4SiMe_2Cl)$ ] ( $M = Ti$ , **2**;  $M = Zr$ , **3**) and the bis(cyclopentadienyl) complex [ $ZrCl_2(\eta^5-C_5H_4SiMe_2Cl)_2$ ], **4**, is described. The alkyl complex [ $Ti(CH_2C_6H_5)_3(\eta^5-C_5H_4SiMe_2Cl)$ ], **8**, the amido complexes [ $TiCl_2\{N(SiMe_3)_2(\eta^5-C_5H_4SiMe_2Cl)\}$ ], **11**, and [ $TiCl_2\{N^tBuSiMe_2(\eta^5-C_5H_4)\}$ ], **12**, and the methylsiloxane derivatives [ $TiCl_2\{\mu-(OSiMe_2-\eta^5-C_5H_4)\}_2$ ], **5**, [ $TiCl_2\{OSiMe_2OSiMe_2-(\eta^5-C_5H_4)\}$ ], **6**, [ $ZrCl_2\{\mu-[(\eta^5-C_5H_4)SiMe_2OSiMe_2(\eta^5-C_5H_4)]\}$ ], **7**, and [ $TiR_2\{\mu-(OSiMe_2-\eta^5-C_5H_4)\}_2$ ] ( $R = Me$ , **9**;  $R = CH_2C_6H_5$ , **10**) are also reported, and the crystal structures of **5** and **7** have been determined by X-ray diffraction methods.

## Results and Discussion

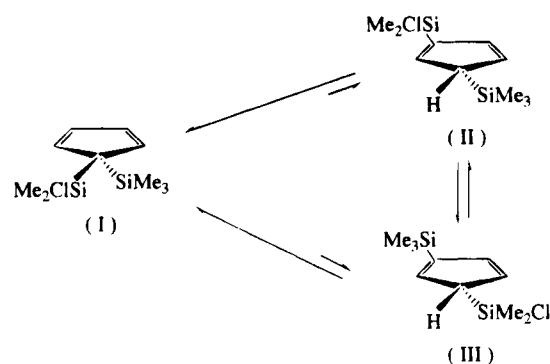
### Synthesis of Mono- and Bis(cyclopentadienyl) Complexes 1–4.

The reaction of a solution of 1-(trimethylsilyl)cyclopenta-2,4-diene in hexane with *n*-BuLi at 0 °C permits us to obtain a suspension of the white insoluble lithium salt, which after addition of dichlorodimethylsilane reacted to yield a colorless liquid, soluble in hexane (Scheme 1), that could be purified by distillation ( $65\text{ }^\circ\text{C}/1 \times 10^{-2}\text{ mmHg}$ ) and stored in the dark under an inert atmosphere for several months (72% yield).

This liquid was identified as 1-(chlorodimethylsilyl)-1-(trimethylsilyl)cyclopentadiene, **1**, by NMR spectroscopy. The  $^1H$  NMR spectrum ( $CDCl_3$  and  $C_6D_6$ ) of the resulting liquid shows resonances assignable to **1** (isomer I in Figure 1) (see Experimental Section).

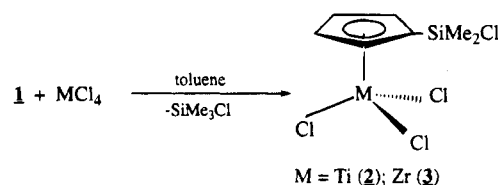
Other signals due to trimethylsilyl and chlorodimethylsilyl protons are observed at  $\delta -0.04$  and  $\delta 0.58$  ( $CDCl_3$ ), respectively, along with other weak and broad signals at ca.  $\delta 3$ , corresponding to  $sp^3-C$  bonded protons. This NMR behavior is indicative of the presence of an equilibrium<sup>4</sup> between the three isomers (I, II, and III) shown in Figure 1. The relative intensities associated with these resonances allow us to predict that isomer I is present in a ratio of 95% with respect to the other two isomers II and III.

Compound **1** reacts with one equivalent of  $TiCl_4$  at room temperature and  $ZrCl_4$  at 100 °C in toluene to give the mono(cyclopentadienyl) derivatives [ $MCl_3(\eta^5-C_5H_4-$

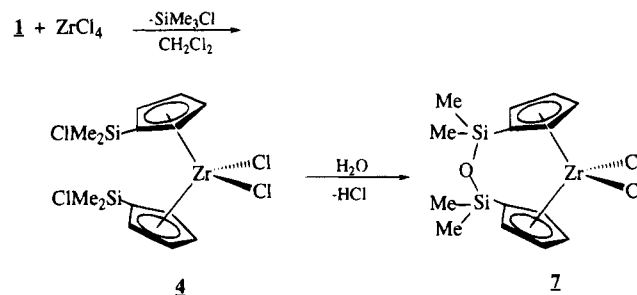


**Figure 1.** Equilibrium between the three possible isomers of **1**.

### Scheme 2



### Scheme 3



$SiMe_2Cl]$  [ $M = Ti$ , **2**;  $M = Zr$ , **3**] with elimination of  $SiMe_3Cl$  (Scheme 2). The high selectivity for  $SiMe_3Cl$  rather than  $SiMe_2Cl_2$  elimination is probably based on the lower affinity of the silicon bonded ring carbon atom for the attacking electrophile, due to the presence of the more electronegative chloro substituent. Yellow crystals of **2** were isolated in 76% yield by cooling a hexane solution to  $-30\text{ }^\circ\text{C}$ , whereas **3** was isolated as white crystals in 87% yield, after recrystallization from toluene/hexane of the solid obtained by cooling a hexane solution to  $-30\text{ }^\circ\text{C}$ .

The  $^1H$  and  $^{13}C$  NMR spectra for **2** and **3** show the presence of resonances for two methyl groups bonded to silicon, and an AA'BB' spin system is observed for the cyclopentadienyl protons. Broad  $^1H$  NMR signals observed for **3** are similar to those of  $(ZrCl_3\text{Cp})_x$ , indicating that a similar oligomeric or polymeric structure<sup>5</sup> can be proposed for this monocyclopentadienyl zirconium derivative.

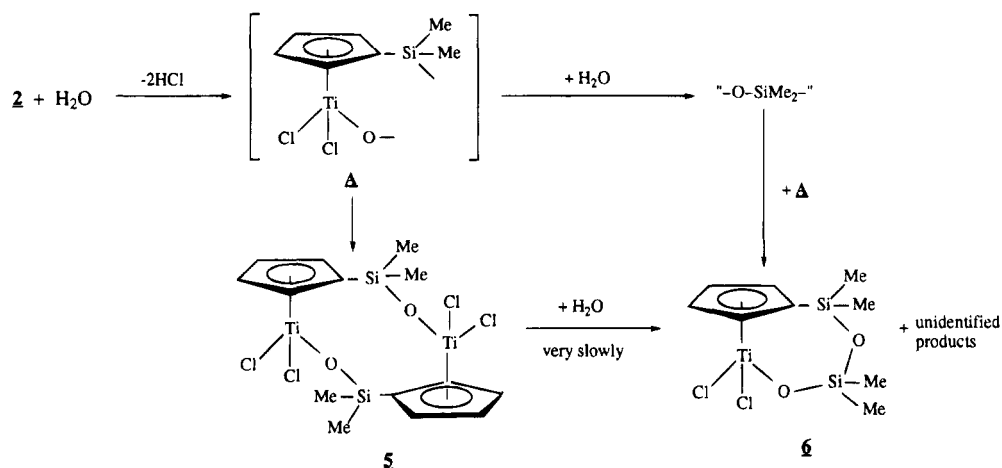
When the same reaction between **1** and  $ZrCl_4$  in a  $Zr/Cp$  molar ratio of 1/2 was carried out in refluxing methylene dichloride, the bis(cyclopentadienyl) derivative [ $ZrCl_2(\eta^5-C_5H_4SiMe_2Cl)_2$ ], **4**, was isolated (Scheme 3). Brown crystals of **4** were formed by cooling a dichloromethane solution to  $-20\text{ }^\circ\text{C}$  and recrystallized from toluene/hexane in 74% yield. However, the related bis(cyclopentadienyl) titanium complex could not be

(3) Winter, C. H., Zhou, X. X., Dobbs, D. A., Heeg, M. J. *Organometallics*, **1991**, *10*, 210.

(4) (a) Jutz, P., Sauer, R. *J. Organomet. Chem.*, **1973**, *50*, C29. (b) Siemeling, U. *J. Organomet. Chem.*, **1992**, *429*, C14.

(5) Wells, N. J., Huffmann, J. C., Caulton, K. G. *J. Organomet. Chem.*, **1981**, *213*, C17.

Scheme 4

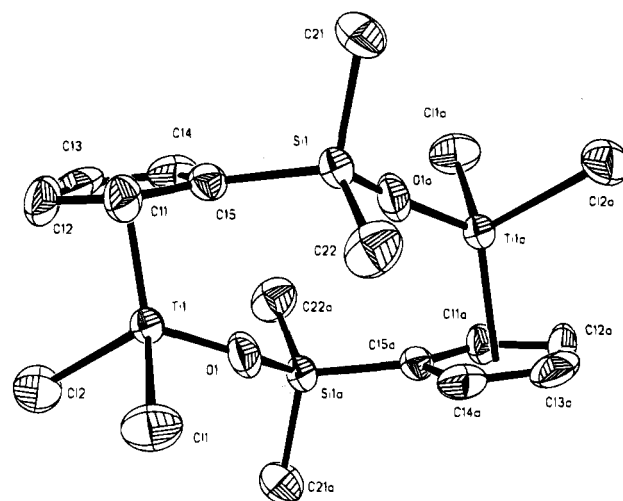


synthesized, as this reaction with  $\text{TiCl}_4$  only affords<sup>6</sup> the monocyclopentadienyl compound **2**.

These mono- and bis(cyclopentadienyl) complexes were found to be very moisture sensitive and react immediately with traces of water; therefore, they have to be stored under rigorously dry conditions. They are soluble in aromatic hydrocarbons, methylene dichloride and chloroform but insoluble in alkanes, with the exception of **2**, which is partially soluble in hexane.

**Synthesis of Oxocomplexes 5–7.** Complexes **2–4** have two different types of chlorine bonds that could be involved in hydrolysis, i.e. the chlorine bonded to silicon and those bonded to the metal. We were particularly interested in comparing the reactivity of both M–Cl bonds with water, and the subsequent reactivity of the products, in order to obtain information about the way to achieve selective or simultaneous hydrolysis of these bonds. Selective hydrolysis of the Si–Cl bond would be desirable in order to attach these complexes to acidic inorganic oxides as supports,<sup>1,2</sup> that can be used as heterogeneous catalysts for the oligo- or polymerization of olefins. Simultaneous hydrolysis of both Si–Cl and M–Cl bonds would lead to complexes with pendant cyclopentadienyl ligands, that combine the stability of the  $\eta^5$ -coordinated cyclopentadienyl ligand and the terminal anionic alkoxide coordinated to the high Lewis acidic metal center.

Addition of one equivalent of water to a toluene solution of the titanium compound **2** produced the evolution of HCl, and complex **5** was obtained as a yellow crystalline solid in a quantitative yield, by cooling the solution to  $-20^\circ\text{C}$ . The same complex **5** was also formed when only  $1/2$  equivalent of water was used, leaving  $1/2$  equivalent of unreacted starting complex **2**, indicating that both Si–Cl and Ti–Cl bonds are simultaneously hydrolyzed. However, the formation of the oxygen bridge is not an intramolecular reaction, as this would lead to a mononuclear four-membered Cp–Si–O–Ti cyclic species. Complex **5** was characterized as the dinuclear titanium compound (Scheme 4), which contains the oxygen atom bridging the silicon and the titanium atoms of two different units to form an eight-membered ring, if the Cp is considered as one member of the titanium–Cp–silicon–oxygen–titanium–Cp–



**Figure 2.** Ortep view of molecular structure of **5** with the atom-numbering scheme.

silicon–oxygen ring. This formulation is in agreement with the mass spectrum and the  $^1\text{H}$  NMR ( $\text{CDCl}_3$  and  $\text{C}_6\text{D}_6$ ) spectrum, which shows one singlet for the methylsilyl protons and two pseudotriplets corresponding to an AA'BB' spin system, for the cyclopentadienyl protons. Crystals of **5** suitable for X-ray diffraction were grown by slow cooling of a toluene–hexane solution to  $-30^\circ\text{C}$ . The molecular structure of **5**, obtained by X-ray diffraction, is shown in Figure 2, with the atomic labeling scheme. Final atomic coordinates and equivalent isotropic thermal parameters for non-hydrogen atoms are displayed in Table 1. Selected bond distances and angles are given in Table 2.

The molecular structure consists of a dinuclear compound formed by two fragments related by an inversion center. Dimerization is produced by the interaction of two  $[\text{Me}_2\text{SiCpTiCl}_2]$  units bonded by two oxygen atoms which connect one silicon and one titanium atoms from different units.

The coordination around the titanium atom corresponds to a pseudo-three-legged piano-stool structure similar to that found for complexes of the type  $\text{TiCl}_2\text{-Cp(X)}$ .<sup>7</sup> If the centroid of the silyl-substituted ring is

(6) (a) Cardoso, A. M., Clark, R. J. H., Moorhouse, S. *J. Chem. Soc. Dalton Trans.*, **1980**, 1156. (b) Hidalgo, G., Mena, M., Palacios, F., Royo, P., Serrano, R. *J. Organomet. Chem.*, **1988**, 340, 37.

(7) (a) Rogers, R. D., Benning, M. M., Kurihara, L. K., Moriarty, K. J., Rausch, M. D. *J. Organomet. Chem.*, **1985**, 293, 51. (b) Mena, M., Pellinghelli, M. A., Royo, P., Serrano, R., Tiripicchio, A. *J. Chem. Soc., Chem. Commun.*, **1986**, 1118.

**Table 1. Positional Parameters and Their Estimated Standard Deviations for 5**

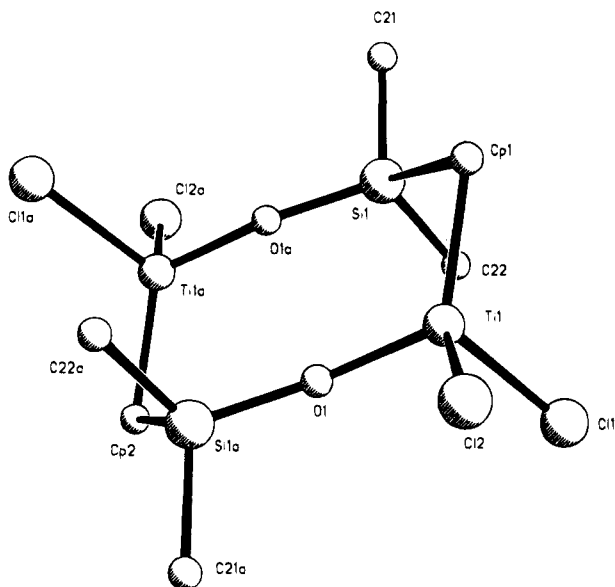
atom	x	y	z	B <sup>a</sup> (Å <sup>2</sup> )
Ti(1)	0.62148(3)	0.16861(3)	0.15107(3)	2.217(5)
Si(1)	0.61975(5)	0.05464(4)	-0.17760(4)	2.535(8)
Cl(1)	0.84357(5)	0.10047(6)	0.19970(6)	4.28(1)
Cl(2)	0.57657(7)	0.26053(6)	0.33583(5)	4.32(1)
O(1)	0.5157(2)	0.0355(1)	0.1538(1)	3.39(3)
C(11)	0.7191(2)	0.2683(2)	-0.0213(2)	3.01(3)
C(12)	0.6644(3)	0.3607(2)	0.0519(2)	3.82(4)
C(13)	0.5158(3)	0.3435(2)	0.0485(2)	4.01(4)
C(14)	0.4800(2)	0.2395(2)	-0.0268(2)	3.33(3)
C(15)	0.6068(2)	0.1889(2)	-0.0698(2)	2.45(3)
C(21)	0.5972(3)	0.1086(3)	-0.3452(2)	4.56(5)
C(22)	0.7887(3)	-0.0272(2)	-0.1419(3)	4.39(5)

<sup>a</sup> Isotropic equivalent displacement parameter is defined as  $(4/3)[a^2B(1,1) + b^2B(2,2) + c^2B(3,3) + ab(\cos \gamma)B(1,2) + ac(\cos \beta)B(1,3) + bc(\cos \alpha)B(2,3)]$ .

**Table 2. Selected Bond Distances (Å) and Bond Angles (deg) for Compound 5<sup>a</sup>**

Ti(1)–Cl(1)	2.244(1)	Ti(1)–Cl(2)	2.260(1)
Ti(1)–O(1)	1.767(1)	Ti(1)–C(11)	2.371(2)
Ti(1)–C(12)	2.395(2)	Ti(1)–C(13)	2.370(2)
Ti(1)–C(14)	2.330(2)	Ti(1)–C(15)	2.323(2)
Si(1)–O(1)	1.653(1)	Si(1)–C(15)	1.864(2)
Si(1)–C(21)	1.851(2)	Si(1)–C(22)	1.840(2)
C(11)–C(12)	1.396(2)	C(11)–C(15)	1.430(2)
C(12)–C(13)	1.416(4)	C(13)–C(14)	1.407(3)
C(14)–C(15)	1.431(2)	Ti(1)–Cp(1)	2.026
Cl(1)–Ti(1)–Cl(2)	101.36(2)	Cl(1)–Ti(1)–O(1)	104.09(5)
Cl(2)–Ti(1)–O(1)	101.57(5)	Ti(1)–O(1)–Si(1)	160.2(1)
Si(1)–C(15)–C(11)	127.3(1)	Si(1)–C(15)–C(14)	126.8(1)

<sup>a</sup> Numbers in parentheses are estimated standard deviations in the least significant digits. Cp(1) is the centroid of C(11), C(12), C(13), C(14), C(15).

**Figure 3.** View of central core of **5**. Cp1 and Cp2 are the centroid of cyclopentadienyl rings.

considered as a coordination site bonded to Ti, the central core of the dimeric structure appears as an eight-membered cycle, with a "chair conformation", as shown in Figure 3.

The formation of this cycle plays an important role in the disposition of the rest of the molecule. In fact, one of the interesting features is the position of the Ti atom with respect to the Cp-ring. The Ti–Cp(centroid) distance is 2.026 Å, larger than those found in  $[(TiCl_3)_2\{\mu-$

$(Me_2Si)_2(\eta^5-C_5H_5)_2\}]$  (2.004 Å)<sup>8</sup> or  $[TiCl_2\{O(CH_2)_3(\eta^5-C_5Me_4)\}]$  (2.015 Å),<sup>9</sup> but similar to those found in the fulvalene complex  $[(TiCl_2)_2(\mu-O)\{\mu-(\eta^5-\eta^5-C_{10}H_8)\}]$  (2.029 Å).<sup>10</sup> Another observed feature is the partial loss of the  $\eta^5$ -character of the Cp ligand, as shown by the different Ti–C distances, ranging from the shorter 2.323(2) Å for Ti–C15 (bonded to Si) to the larger 2.395(2) Å for Ti–C12. The C–C distances in the Cp ring also show slight differences ranging from 1.396(2) to 1.431(2) Å, in contrast with the situation in  $[(TiCl_3)_2\{\mu-(Me_2Si)_2(\eta^5-C_5H_5)_2\}]$  and  $[TiCl_2\{O(CH_2)_3(\eta^5-C_5Me_4)\}]$ ,<sup>9b</sup> where the  $\eta^5$ -character is retained. However, the Cp ring is planar and perpendicular to the plane defined by the Ti, C15, and Si atoms, which divides this Cp ring into two symmetrical moieties. The rest of the ligands bonded to Ti and the two chlorine atoms and the oxygen atoms define another plane almost parallel to the Cp plane with an angle of only 3°.

The Si atom is almost located in the Cp plane, with a distance to this plane of 0.06 Å, as expected for a Si–C<sub>sp</sub><sup>2</sup> bond. The distance from the Si atom to the plane formed by the oxygen and the two chlorine atoms on the same face of the metal, is 2.840 Å avoiding the intramolecular interaction that would give a mononuclear species. The Ti–O–Si angle (160.2°) is larger than that found in  $[TiCl_2\{O(CH_2)_3(\eta^5-C_5Me_4)\}]$ <sup>9b</sup> for the C–O–Ti angle (146.1°), corresponding to a more open eight-membered cycle with the cyclopentadienyl alkoxide ligand in comparison with the six-membered ring of the Teuben complex. Another difference between complex **5** and the Teuben complex is the closer linearity of the Ti–O–Si angle due to the stronger Si–O  $\pi$  bonding with the vacant 3d silicon orbitals, which is absent in the C–O–Ti system. However, the Ti–O distance, 1.767(1) Å, is the same in both compounds, indicating a partial Ti–O double-bond interaction. It is known that the maximum  $\pi$  interaction in the Ti–O bond corresponds to angles of 180°, but there exist many important examples showing that this relation is not always accomplished.<sup>11</sup> This distance is slightly shorter than that found in the fulvalene complex  $[(TiCl_2)_2(\mu-O)\{\mu-(\eta^5-\eta^5-C_{10}H_8)\}]$  (1.811 Å, average)<sup>10</sup> with a Ti–O–Ti unit. The Si–O distance (1.653(1) Å), is slightly larger than that found in siloxanes (mean value 1.63 Å)<sup>12</sup> and larger than the Si–O distance in the zirconium compound  $[Zr(\eta^5-C_5H_5)_2(\mu-OSiPh_2O)]_2$  (1.611 Å, average).<sup>13</sup> This behavior confirms the competition between silicon and titanium for  $\pi$ -bonding with the bridged oxygen atom, which is more favored for the Ti–O bond. Therefore, this Ti–O bond is found to be shorter in the Ti–O–Si unit than in the Ti–O–Ti unit.

(8) Cano, A., Cuenca, T., Gómez-Sal, P., Royo, B., Royo, P. *Organometallics*, **1994**, *13*, 1688.

(9) (a) Shapiro, P. J., Bunel, E., Schaefer, W. P., Bercaw, J. E. *Organometallics*, **1990**, *9*, 867. (b) Fandos R., Meetsma, A., Teuben, J. H. *Organometallics*, **1991**, *10*, 59. (c) Rieger, B. *J. Organomet. Chem.*, **1991**, *420*, C17. (d) Hughes, A. K., Meetsma, A., Teuben, J. H. *Organometallics*, **1993**, *12*, 1936.

(10) Alvaro, L. M., Cuenca, T., Flores, J. C., Royo, P., Pellinghelli, M. A., Tiripicchio, A. *Organometallics*, **1992**, *11*, 3301.

(11) Ciruelos, S., Cuenca, T., Flores, J. C., Gómez-sal, P., Royo, P. *Organometallics* **1993**, *12*, 944.

(12) Wells, A. F. "Structural Inorganic Chemistry", 3rd. ed.; Clarendon Press: Oxford, **1962**.

(13) Samuel, E., Harrod, J., McGlinchey, M. J., Cabestaing, C., Robert, F. *Inorg. Chem.*, **1994**, *33*, 1292.

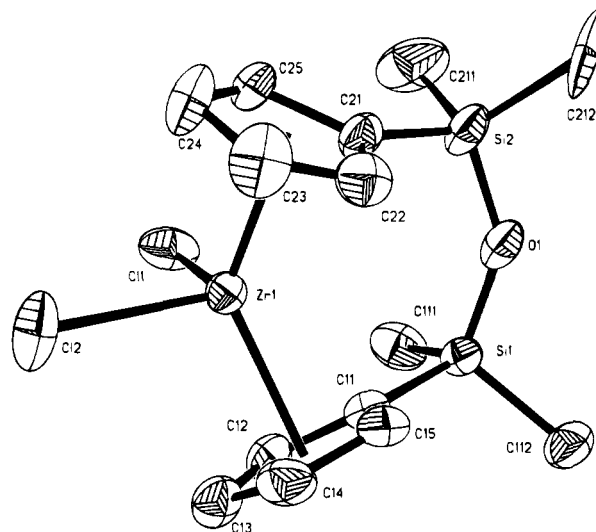
The Ti–Cl distances are 2.244(1) and 2.260(1) Å, in the range of mono(cyclopentadienyl) derivatives,<sup>10</sup> slightly larger than that found in [(TiCl<sub>3</sub>)<sub>2</sub>{μ-[(Me<sub>2</sub>Si)<sub>2</sub>(η<sup>5</sup>-C<sub>5</sub>H<sub>3</sub>)<sub>2</sub>]}] but slightly shorter than in [TiCl<sub>2</sub>{O(CH<sub>2</sub>)<sub>3</sub>(η<sup>5</sup>-C<sub>5</sub>Me<sub>4</sub>)}], due probably to the oxygen competition. The disposition of these ligands is alternated with respect to the Cp ring.

Addition of an excess of water to a toluene solution of **2** led to a solution which contained a mixture of different compounds, as shown by its <sup>1</sup>H NMR spectrum. However, complex **6** could be easily separated from this mixture in a 45% yield, as a yellow crystalline solid, because it is the only component that crystallizes on cooling a toluene-hexane solution of this mixture to –20 °C. Very low yields of complex **6** are also obtained together with other unidentified products, when a toluene solution of **5** is left to the open air for a period of time, by addition of a second equivalent of water or by reaction of a toluene solution of **5** with aqueous HCl. Therefore, complex **5** is resistant to hydrolysis, that takes place very slowly leading to complex **6**, which is the main product when an excess of water is added to complex **2**, preventing the formation of **5**.

This behavior can be explained (see Scheme 4) by assuming that simultaneous hydrolysis of both Si–Cl and Ti–Cl bonds in complex **2** takes place with elimination of HCl, leading to an intermediate fragment, which in the presence of an excess of water liberates the –SiMe<sub>2</sub>–O– fragment that couples to give **6**, whereas in the absence of water it dimerizes to give **5**. Complex **6** was characterized by its elemental analysis, mass spectrum, and <sup>1</sup>H, <sup>13</sup>C, and <sup>29</sup>Si NMR spectroscopy. The mass spectrum agrees with the formulation of **6** as a mononuclear compound, [TiCl<sub>2</sub>{OSiMe<sub>2</sub>OSiMe<sub>2</sub>(η<sup>5</sup>-C<sub>5</sub>H<sub>4</sub>)}], formed by a new six membered ring system (Ti–Cp–Si–O–Si–O) if Cp is considered as one of the members. In agreement with this formulation, the cyclopentadienyl protons appear as two pseudotriplets, whereas two singlets at δ 0.18 and δ 0.42 (CDCl<sub>3</sub>) are observed for the methyl–silyl protons with an intensity ratio of 3:3:1:1 with respect to the cyclopentadienyl signals. Two resonances are also observed for the methyl–silyl carbon atoms in the <sup>13</sup>C and for the two silicon atoms in the <sup>29</sup>Si NMR spectra, respectively.

The relative stability of the cycle could explain why **5** prefers a dinuclear disposition whereas **6** presents a mononuclear structure. As shown by the X-ray molecular structure of complex **5**, the long distance between the Ti center and the oxygen bonded to the silicon atom, coplanar with the cyclopentadienyl ring, prevents the formation of a mononuclear species, which would give a too greatly constrained four-membered ring, less stable than the eight-membered ring that leads to the preferred dinuclear disposition. However, **6** prefers a mononuclear disposition by formation of a stable six-membered ring. Teuben et al. have observed the stability of the six-membered ring Ti–Cp–C–C–C–O in the titanium cyclopentadienyl alkoxide [TiCl<sub>2</sub>{O(CH<sub>2</sub>)<sub>3</sub>(η<sup>5</sup>-C<sub>5</sub>Me<sub>4</sub>)}],<sup>9b</sup> in which the bidentate ligand is flexible enough to produce little steric constraint.

The reaction of complex **3** with one equivalent of water under the same conditions described for the titanium compound gave a white solid, insoluble in all the common solvents indicating its polymeric nature.



**Figure 4.** Ortep view of molecular structure of **7** with the atom numbering scheme.

Its analytical composition corresponds to the expected oxo compound [ZrCl<sub>2</sub>(η<sup>5</sup>-C<sub>5</sub>H<sub>4</sub>SiMe<sub>2</sub>O)]<sub>2</sub>, which could not be structurally characterized due to its lack of solubility.

The results observed in the reactions of **2** and **3** with water allow us to conclude that the reactivity of the Si–Cl bond, in this type of mono(cyclopentadienyl) complex, is very similar to the reactivity of one of the M–Cl bonds, so that the selective hydrolysis of one of these bonds is not possible in these compounds.

However, this selectivity could probably be easier for bis(cyclopentadienyl)-type complexes. The reaction of the bis(cyclopentadienyl) zirconium compound **4** with one equivalent of water gave a colorless crystalline solid (Scheme 3). The proton NMR spectra (CDCl<sub>3</sub> and C<sub>6</sub>D<sub>6</sub>) show the expected singlet for the methyl protons and two pseudotriplets for the cyclopentadienyl protons with an intensity ratio of 6:2:2, respectively. The infrared spectrum clearly shows the unit “ZrCl<sub>2</sub>”. These data together with the elemental analysis and the mass spectrum are in agreement with the formulation proposed for compound **7** (Scheme 3) as a tetramethyldisiloxane-bridged bis(cyclopentadienyl) dichloride complex. Single crystals of this compound have been obtained, and the X-ray diffraction study confirmed the proposed structure. Similar bis(cyclopentadienyl)titanium and -zirconium complexes have been obtained by reacting the lithium or sodium salt of 1,3-bis(cyclopentadienyl)-tetramethyldisiloxane and poly(cyclopentadienylmethylsiloxane) with MCl<sub>4</sub>.<sup>2,14</sup>

The X-ray crystal structure of compound **7** is shown in Figure 4 with the atomic labeling scheme. Final atomic parameters for non-hydrogen atoms are displayed in Table 3. Selected bond distances and bond angles are given in Table 4.

The molecular structure of **7** is a typical bent bis(cyclopentadienyl) system, similar to that reported previously for compounds with free or bridged cyclopentadienyl rings.<sup>15,16</sup> The structure of this zirconium

(14) (a) Wang, Y., Zhong, X., Wang, H., Yas, X. *Huaxue Xuebao* **1991**, *49*(11), 1107. (*Chem. Abstr.*, **1991**, *116*, 129129s). (b) Wang, Y., Zhong, X. *Youji Huaxue* **1992**, *12*(3), 286. (*Chem. Abstr.*, **1992**, *117*, 171616u).

(15) (a) Prout, K., Cameron, T. S., Forder, R. A., Critchley, S. R., Denton, B., Rees, G. V. *Acta Crystallogr.*, **1974**, *B30*, 2290. (b) Clearfield, A., Warner, D. K., Saldarriaga-Molina, C. H., Ropal, R., Bernal I. *Can. J. Chem.*, **1975**, *53*, 1622.



**Table 3. Positional Parameters and Their Estimated Standard Deviations for 7**

atom	x	y	z	B <sup>a</sup> (Å <sup>2</sup> )
Zr(1)	0.19851(1)	-0.09717(2)	0.17960(1)	2.151(4)
Si(1)	0.37998(4)	-0.15768(6)	0.38917(4)	2.37(1)
Si(2)	0.23196(5)	0.11286(7)	0.40237(5)	3.16(1)
Cl(1)	0.33396(5)	0.07341(7)	0.15212(5)	4.05(1)
Cl(2)	0.12819(5)	-0.1467(1)	0.02752(4)	4.56(1)
O(1)	0.3064(1)	-0.0325(2)	0.4286(1)	3.15(3)
C(11)	0.3102(1)	-0.2474(2)	0.2892(2)	2.43(4)
C(12)	0.3459(1)	-0.2755(2)	0.2077(2)	2.77(4)
C(13)	0.2740(2)	-0.3568(3)	0.1523(2)	3.23(4)
C(14)	0.1919(2)	-0.3829(2)	0.1996(2)	3.33(5)
C(15)	0.2145(2)	-0.3201(2)	0.2832(2)	2.74(4)
C(21)	0.1481(2)	0.0701(2)	0.29960(2)	2.62(4)
C(22)	0.0750(2)	-0.0479(3)	0.2855(2)	3.15(4)
C(23)	0.0223(2)	-0.0333(3)	0.2018(2)	3.92(5)
C(24)	0.0581(2)	0.0989(3)	0.1624(2)	3.89(5)
C(25)	0.1338(2)	0.1624(2)	0.2218(2)	3.12(4)
C(111)	0.4938(2)	-0.0630(3)	0.3592(2)	4.23(6)
C(112)	0.4116(2)	-0.3102(3)	0.4715(2)	3.64(5)
C(211)	0.3036(3)	0.2889(3)	0.3862(3)	6.22(8)
C(212)	0.1522(3)	0.1389(4)	0.4910(2)	6.09(7)

<sup>a</sup> Anisotropically refined atoms are given in the form of the isotropic equivalent displacement parameter refined as  $(4/3)[a^2B(1,1) + b^2B(2,2) + c^2B(3,3) + ab(\cos \gamma)B(1,2) + ac(\cos \beta)B(1,3) + bc(\cos \alpha)B(2,3)]$ .

**Table 4. Selected Bond Distances (Å) and Bond Angles (deg) for Compound 7**

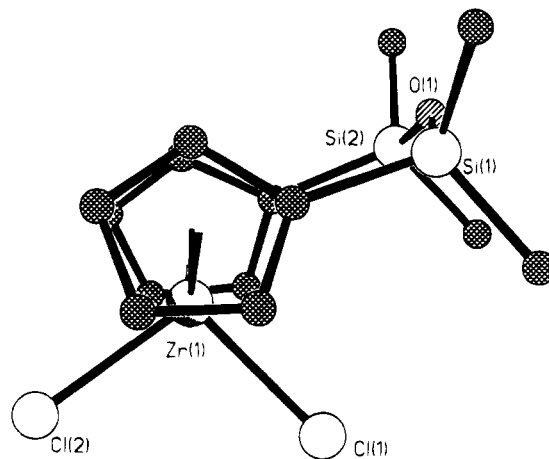
Zr(1)–Cl(1)	2.4256(7)	Zr(1)–Cl(2)	2.4443(7)
Zr(1)–C(11)	2.480(2)	Zr(1)–C(12)	2.511(2)
Zr(1)–C(13)	2.523(2)	Zr(1)–C(14)	2.495(2)
Zr(1)–C(15)	2.492(2)	Zr(1)–C(21)	2.495(2)
Zr(1)–C(22)	2.504(2)	Zr(1)–C(23)	2.504(2)
Zr(1)–C(24)	2.531(2)	Zr(1)–C(25)	2.523(2)
Si(1)–O(1)	1.635(1)	Si(1)–C(11)	1.865(2)
Si(1)–C(111)	1.847(3)	Si(1)–C(112)	1.839(2)
Si(2)–O(1)	1.627(2)	Si(2)–C(21)	1.866(2)
Si(2)–C(211)	1.837(3)	Si(2)–C(212)	1.850(3)
Zr(1)–Cp(1)	2.202	Zr(1)–Cp(2)	2.208
Cl(1)–Zr(1)–Cl(2)	98.71(3)	Si(1)–O(1)–Si(2)	143.5(1)
O(1)–Si(1)–C(11)	108.24(8)	O(1)–Si(2)–C(21)	110.24(9)
Cl(1)–Zr(1)–Cp(1)	106.7	Cl(1)–Zr(1)–Cp(2)	106.2
Cl(2)–Zr(1)–Cp(1)	104.9	Cl(2)–Zr(1)–Cp(2)	105.0
Cp(1)–Zr(1)–Cp(2)	130.9		

<sup>a</sup> Numbers in parentheses are estimated standard deviations in the least significant digits. Cp(1) is the centroid of C(11), C(12), C(13), C(14), C(15), and Cp(2) is the centroid of C(21), C(22), C(23), C(24), C(25).

compound is comparable with that previously reported for the similar titanium derivative.<sup>2</sup>

The two cyclopentadienyl rings are bonded by the Si–O–Si chain. The oxygen atom is out of the reflection plane defined by the zirconium and chlorine atoms, with a distance to the plane of 0.052(2) Å.

The most important feature in this structure is the disposition of the Si–O–Si bridge, which is long enough to allow the Cp rings to be located with an angle between the Cp planes of 51.1°, smaller than that found in the double-*ansa*-bridged complex [ZrCl<sub>2</sub>{(η<sup>5</sup>-C<sub>5</sub>H<sub>3</sub>)-(SiMe<sub>2</sub>)<sub>2</sub>(η<sup>5</sup>-C<sub>5</sub>H<sub>3</sub>)}] (69.6(1)°)<sup>8</sup> and in the mono-*ansa*-bridged derivative [ZrCl<sub>2</sub>{(η<sup>5</sup>-C<sub>5</sub>H<sub>4</sub>)SiMe<sub>2</sub>(η<sup>5</sup>-C<sub>5</sub>H<sub>4</sub>)}]<sup>16</sup> (56.8°), but comparable to those reported for other compounds containing free cyclopentadienyl rings. Accordingly, the Cp(centroid)–Zr–Cp(centroid) angle is more open, 130.9°, than those in the examples mentioned above. In this way, it is possible to introduce the Zr atom between the Cp rings and maintain the same distances for the Zr–Cp(centroid) (2.202 and 2.208

**Figure 5.** Alternative view of molecular structure of 7, showing the disposition of the ligand.

Å for both Cp), and for the normal to the Cp plane (2.194 and 2.208 Å). Thus, the Zr–C(Cp) distances are very similar, with a maximum difference of 0.04 Å, keeping the η<sup>5</sup>-coordination.

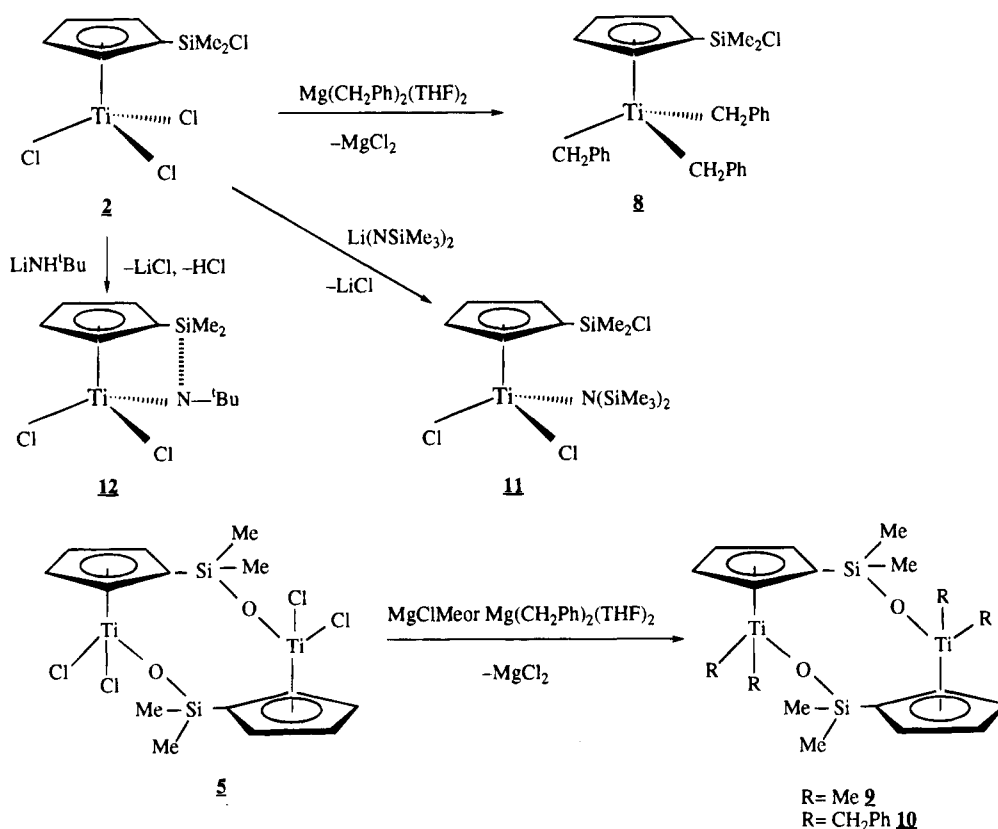
The Si–O–Si bond angle of 143.5 (1)° and the Si–O bond distances (1.635(1) and 1.627(2) Å) are similar to those observed in hexamethyldisiloxane.<sup>17</sup> Another important structural feature to notice is the conformation of the bridge that, as in the related titanium compound,<sup>2</sup> is not symmetrically placed with respect to the Cl–Zr–Cl angle but shows instead the disposition presented in Figure 5. Due to this wedging of the ring, the minimum C–C distance between the rings corresponds to C22–C15, whereas the distance C11–C21 is 3.526 Å.

This lack of symmetry affects the Zr–Cl distances, which are slightly different (Zr–Cl1, 2.4256(7) Å, and Zr–Cl2, 2.4443(7) Å) due to the different effect of the siloxo group. Both rings are located in an eclipsed configuration.

**Synthesis of Alkyl Complexes.** Reaction of complex 2 with 1.5 equivalents of Mg(CH<sub>2</sub>C<sub>6</sub>H<sub>5</sub>)<sub>2</sub>(THF)<sub>2</sub> in hexane at room temperature led to the tribenzyl derivative [Ti(CH<sub>2</sub>C<sub>6</sub>H<sub>5</sub>)<sub>3</sub>(η<sup>5</sup>-C<sub>5</sub>H<sub>4</sub>SiMe<sub>2</sub>Cl)], 8, which was isolated as red crystals in 86% yield from diethyl ether at -40 °C. The same compound was also obtained when an excess of the alkylating agent was used. The same reaction with 3 equivalents of MgClMe led to a yellow oil that spontaneously decomposed with evolution of methane to give a dark paramagnetic unidentified residue. The thermal decomposition was monitored by <sup>1</sup>H NMR spectroscopy in a sealed tube in the presence of ethyl benzoate and the formation of α-ethoxystyrene was detected, indicating the intermediate formation of a methylidenetitanium compound. The same behavior was also observed for complex 8 when heated to 80 °C with evolution of toluene and transfer of the benzylidene group to ethyl benzoate.

Alkylation of 5 with 4 equivalents of MgClMe or 2 equivalents of Mg(CH<sub>2</sub>C<sub>6</sub>H<sub>5</sub>)<sub>2</sub>(THF)<sub>2</sub> produced the tetramethyl and tetrabenzyl derivatives 9 and 10, respectively (Scheme 5). The same alkylations of complex 6 led to yellow and red oils, which could not be isolated

Scheme 5



as solids, that contained the expected methyl and benzyl complexes respectively, according to their  $^1\text{H}$  NMR spectra.

Compounds **8-10** were characterized by elemental analyses, mass spectrometry, and NMR spectroscopy. The  $^1\text{H}$  NMR spectrum of **8** in  $\text{C}_6\text{D}_6$  shows a singlet at  $\delta$  3.05 for the six equivalent protons of the benzyl methylene groups, whereas two doublets ( $J_{\text{H-H}} = 10$  Hz) are observed for the diastereotopic protons of the methylene groups bonded to the prochiral metal center in complex **10** and one singlet is observed at  $\delta$  0.75 due to the equivalent methyl groups in complex **9**.

**Synthesis of Amido Complexes.** As we have discussed above, both Si-Cl and M-Cl bonds are simultaneously involved in reactions with protic reagents such as water, whereas reactions with nucleophilic Grignard reagents take place selectively at the M-Cl bonds. In order to obtain additional information about this different reactivity, we decided to study the reactions of complex **2** with tertiary and secondary lithium amides.

Reaction of **2** with 1 equivalent of  $\text{LiN}(\text{SiMe}_3)_2$  in hexane at room temperature led to the amido complex  $[\text{TiCl}_2\{\text{N}(\text{SiMe}_3)_2\}(\eta^5\text{-C}_5\text{H}_4\text{SiMe}_2\text{Cl})]$ , **11**, which was isolated as orange crystals after cooling a hexane solution to  $-40$  °C. An analogous reaction of **2** with  $\text{LiNH}^t\text{Bu}$  took place with elimination of HCl and LiCl to give the constrained monomeric cyclic species  $[\text{TiCl}_2\{\text{N}^t\text{BuSiMe}_2(\eta^5\text{-C}_5\text{H}_4)\}]$ ,<sup>18</sup> **12**, containing the amido pendant cyclopentadienyl ligand in high yield (Scheme 5). Both

complexes were characterized by mass spectrometry and NMR spectroscopy (see Experimental Section).

### Experimental Section

All manipulations were performed under an inert atmosphere (dinitrogen or argon) using Schlenk and high vacuum line techniques or a VAC glove box Model HE 63P. Solvents were purified by distillation from an appropriate drying/deoxygenating agent (phosphorus pentoxide for dichloromethane, sodium for toluene and sodium/potassium alloy for hexane).  $\text{C}_5\text{H}_5\text{SiMe}_3$ ,<sup>19</sup>  $\text{Mg}(\text{CH}_2\text{Ph})_2(\text{THF})_2$ ,<sup>20</sup> and  $\text{LiN}(\text{SiMe}_3)_2$ <sup>21</sup> were prepared according to literature procedures. *n*-BuLi, *t*-BuNH<sub>2</sub>, MgClMe,  $\text{SiMe}_2\text{Cl}_2$ ,  $\text{TiCl}_4$ , and  $\text{ZrCl}_4$  (Aldrich) were obtained commercially. NMR spectra were recorded on a Varian Unity FT-300 and a Varian FT-500 Unity Plus instruments ( $^1\text{H}$  and  $^{13}\text{C}$  chemical shifts were referenced to  $\text{Me}_4\text{Si}$ ,  $\delta$  0 ppm, and  $^{29}\text{Si}$  chemical shifts were referenced to TMS external reference). IR spectra were performed (Nujol mulls) on a 883 Perkin-Elmer spectrophotometer. Mass spectra were recorded on a Hewlett-Packard 5890 spectrometer. Elemental C, H analyses were carried out on a Perkin-Elmer 240B microanalyzer.

**Synthesis of  $(\text{C}_5\text{H}_4)(\text{SiMe}_2\text{Cl})(\text{SiMe}_3)$ , **1**.** A 1.6 M solution of *n*-BuLi in hexane (3.75 mL, 6.00 mmol) was added dropwise, at 0 °C, to a solution of freshly distilled  $\text{C}_5\text{H}_5\text{SiMe}_3$  (1.00 mL, 0.83 g, 6.0 mmol) in 50 mL of hexane. The reaction mixture was slowly warmed to room temperature and stirred for 3 h. A white precipitate was formed which after filtration was washed with hexane ( $3 \times 20$  mL). To a suspension of this white solid in 50 mL of hexane was immediately added  $\text{SiMe}_2\text{Cl}_2$  (0.73 mL, 0.78 g, 6.02 mmol) at  $-10$  °C, and the reaction mixture was stirred for 5 h and warmed to room temperature. After filtration, the resulting solution was evaporated under

(18) (a) Stevens, J. C., Timmers, F. J., Wilson, D. R., Schmidt, G. F., Nickias, P. N., Rose, R. K., Knight, G. W., Lai, S., Eur. Pat. Appl. EP 416,815, 1991. (*Chem. Abstr.*, 1991, 115, 93163m). (b) Okuda, J. *Chem. Ber.*, 1990, 123, 1649.

(19) Abel, E. W., Dunster, M. O. *J. Organomet. Chem.*, 1971, 33, 161.

(20) Schrock R. R., *J. Organomet. Chem.*, 1976, 122, 209.

(21) Amonoo-Neizer, E. H., Shaw, R. A., Skovlin, D. O., Smith, B. C., *Inorg. Synth.*, 1966, 8, 19.

vacuum to give a yellow-orange oil. Distillation at 65 °C/1 × 10<sup>-2</sup> mmHg gave a colorless liquid which was characterized as **1** (1.00 g, 1.14 mL, 4.33 mmol, 72% yield) (*d* = 0.876 g/mL). <sup>1</sup>H NMR (300 MHz, CDCl<sub>3</sub>, 25 °C): δ 0.00 (s, 9H, SiMe<sub>3</sub>), 0.22 (s, 6H, SiMe<sub>2</sub>Cl), 6.54 (m, 2H, C<sub>5</sub>H<sub>4</sub>), 6.78 (m, 2H, C<sub>5</sub>H<sub>4</sub>). (300 MHz, C<sub>6</sub>D<sub>6</sub>, 25 °C): δ 0.01 (s, 9H, SiMe<sub>3</sub>), 0.12 (s, 6H, SiMe<sub>2</sub>Cl), 6.42 (m, 2H, C<sub>5</sub>H<sub>4</sub>), 6.65 (m, 2H, C<sub>5</sub>H<sub>4</sub>). <sup>13</sup>C NMR (75 MHz, CDCl<sub>3</sub>, 25 °C): δ -0.9 (q, <sup>1</sup>J<sub>C-H</sub> = 119 Hz, SiMe<sub>3</sub>), 1.6 (q, <sup>1</sup>J<sub>C-H</sub> = 121 Hz, SiMe<sub>2</sub>Cl), 58.2 [s, C<sub>ipso</sub>(C<sub>5</sub>H<sub>4</sub>)], 132.5, 134.7 [d, <sup>1</sup>J<sub>C-H</sub> = 165–169 Hz, C<sub>2</sub>-C<sub>5</sub>(C<sub>5</sub>H<sub>4</sub>)]. MS(EI) *m/z*: 230 (M<sup>+</sup>) (3%); 122 (M<sup>+</sup>-SiMe<sub>3</sub>Cl) (100%).

**Synthesis of TiCl<sub>3</sub>(η<sup>5</sup>-C<sub>5</sub>H<sub>4</sub>SiMe<sub>2</sub>Cl), **2**.** (C<sub>5</sub>H<sub>4</sub>)(SiMe<sub>2</sub>Cl)(SiMe<sub>3</sub>), **1** (1.11 mL, 0.97 g, 4.21 mmol), was added dropwise to a solution of TiCl<sub>4</sub> (0.46 mL, 0.79 g, 4.19 mmol) in toluene (40 mL). The reaction mixture was stirred for 2 days at room temperature. A change of color from orange to dark red was gradually observed. After evaporation under vacuum to dryness, an oil was obtained which was dissolved in hexane (60 mL). The resulting solution was concentrated and cooled to -30 °C to give a microcrystalline yellow solid which was characterized as **2**. (1.00 g, 3.21 mmol, 76% yield). Anal. Calcd. for C<sub>7</sub>H<sub>10</sub>Cl<sub>4</sub>SiTi: C, 26.95; H, 3.23. Found: C, 27.34; H, 3.39. <sup>1</sup>H NMR (300 MHz, CDCl<sub>3</sub>, 25 °C): δ 0.80 (s, 6H, SiMe<sub>2</sub>Cl), 7.10 (m, 2H, C<sub>5</sub>H<sub>4</sub>), 7.30 (m, 2H, C<sub>5</sub>H<sub>4</sub>). (300 MHz, C<sub>6</sub>D<sub>6</sub>, 25 °C): δ 0.47 (s, 6H, SiMe<sub>2</sub>Cl), 6.05 (m, 2H, C<sub>5</sub>H<sub>4</sub>), 6.45 (m, 2H, C<sub>5</sub>H<sub>4</sub>). <sup>13</sup>C NMR (75 MHz, CDCl<sub>3</sub>, 25 °C): δ 2.4 (q, <sup>1</sup>J<sub>C-H</sub> = 122 Hz, SiMe<sub>2</sub>Cl), 126.3, 129.1 [d, <sup>1</sup>J<sub>C-H</sub> = 178–179 Hz, C<sub>2</sub>-C<sub>5</sub>(C<sub>5</sub>H<sub>4</sub>)], 135.1 [s, C<sub>ipso</sub>(C<sub>5</sub>H<sub>4</sub>)]. MS(EI) *m/z*: 312 (M<sup>+</sup>) (7%); 242 (M<sup>+</sup>-2Cl) (35%).

**Synthesis of ZrCl<sub>3</sub>(η<sup>5</sup>-C<sub>5</sub>H<sub>4</sub>SiMe<sub>2</sub>Cl), **3**.** (C<sub>5</sub>H<sub>4</sub>)(SiMe<sub>2</sub>Cl)(SiMe<sub>3</sub>), **1** (0.85 mL, 0.74 g, 3.23 mmol), was added to a suspension of ZrCl<sub>4</sub> (0.75g, 3.22 mmol) in 15 mL of toluene. The Schlenk was connected to a bubbler and the reaction mixture was warmed slowly to 100 °C with vigorous stirring. As the temperature was raised the ZrCl<sub>4</sub> reacted and the formation of a brown solution was observed. The solution was filtered and cooled to -30 °C to give a white solid which was washed with cold hexane (2 × 20 mL). Recrystallization from toluene/hexane gave a microcrystalline white solid which was characterized as **3**. (1.00 g, 2.81 mmol, 87% yield). Anal. Calcd. for C<sub>7</sub>H<sub>10</sub>Cl<sub>4</sub>Zr: C, 23.67; H, 2.84. Found: C, 24.02; H, 3.06. <sup>1</sup>H NMR (300 MHz, CDCl<sub>3</sub>, 25 °C): δ 0.79 (s, 6H, SiMe<sub>2</sub>Cl), 6.99 (m, 2H, C<sub>5</sub>H<sub>4</sub>), 7.09 (m, 2H, C<sub>5</sub>H<sub>4</sub>). (300 MHz, C<sub>6</sub>D<sub>6</sub>, 25 °C): δ 0.50 (s, 6H, SiMe<sub>2</sub>Cl), 6.12 (m, 2H, C<sub>5</sub>H<sub>4</sub>), 6.39 (m, 2H, C<sub>5</sub>H<sub>4</sub>). <sup>13</sup>C{<sup>1</sup>H} NMR (75 MHz, C<sub>6</sub>D<sub>6</sub>, 25 °C): δ 124.0, 126.1 [C<sub>2</sub>-C<sub>5</sub>(C<sub>5</sub>H<sub>4</sub>)], (C<sub>ipso</sub>(C<sub>5</sub>H<sub>4</sub>) not observed). MS(EI) *m/z*: 354 (M<sup>+</sup>) (2%); 319 (M<sup>+</sup>-Cl) (28%).

**Synthesis of ZrCl<sub>2</sub>(η<sup>5</sup>-C<sub>5</sub>H<sub>4</sub>SiMe<sub>2</sub>Cl)<sub>2</sub>, **4**.** (C<sub>5</sub>H<sub>4</sub>)(SiMe<sub>2</sub>Cl)(SiMe<sub>3</sub>), **1** (1.49 mL, 1.31 g, 5.67 mmol) was added to a suspension of ZrCl<sub>4</sub> (0.66g, 2.83 mmol) in 50 mL of dichloromethane. The reaction mixture was refluxed with stirring for 4 days. ZrCl<sub>4</sub> gradually reacted and the formation of a brown solution was observed. After filtration the resulting solution was concentrated (10 mL) and cooled to -20 °C to give a brown solid which was washed with cold hexane (3 × 20 mL). Recrystallization from toluene/hexane gave a pale brown microcrystalline solid characterized as **4**. (1.00g, 2.09 mmol, 74% yield). Anal. Calcd. for C<sub>14</sub>H<sub>20</sub>Cl<sub>4</sub>Si<sub>2</sub>Zr: C, 35.21; H, 4.22. Found: C, 35.60; H, 4.57. <sup>1</sup>H NMR (300 MHz, CDCl<sub>3</sub>, 25 °C): δ 0.73 (s, 12H, SiMe<sub>2</sub>Cl), 6.59 (m, 4H, C<sub>5</sub>H<sub>4</sub>), 6.79 (m, 4H, C<sub>5</sub>H<sub>4</sub>). (300 MHz, C<sub>6</sub>D<sub>6</sub>, 25 °C): δ 0.67 (s, 12H, SiMe<sub>2</sub>Cl), 5.82 (m, 4H, C<sub>5</sub>H<sub>4</sub>), 6.37 (m, 4H, C<sub>5</sub>H<sub>4</sub>). <sup>13</sup>C{<sup>1</sup>H} NMR (75 MHz, C<sub>6</sub>D<sub>6</sub>, 25 °C): δ 116.8 [C<sub>ipso</sub>(C<sub>5</sub>H<sub>4</sub>)], 122.9, 127.0 [C<sub>2</sub>-C<sub>5</sub>(C<sub>5</sub>H<sub>4</sub>)]. MS(EI) *m/z*: 477 (M<sup>+</sup>) (5%), 407 (M<sup>+</sup>-2Cl) (94%).

**Synthesis of [TiCl<sub>2</sub>(η<sup>5</sup>-η<sup>1</sup>-C<sub>5</sub>H<sub>4</sub>SiMe<sub>2</sub>)(μ-O)]<sub>2</sub>, **5**.** Deoxygenated water (73 μL, 4.06 mmol) was added to a solution of TiCl<sub>3</sub>(η<sup>5</sup>-C<sub>5</sub>H<sub>4</sub>SiMe<sub>2</sub>Cl) **2** (1.26g, 4.04 mmol) in 50 mL of toluene. The reaction mixture was stirred for 15 h. The color of the solution changed to yellow orange. After filtration the resulting solution was concentrated (10 mL) and cooled to -20 °C to give a pale yellow microcrystalline solid which was characterized as **5**. Recrystallization from toluene/hexane at

-30 °C gave single crystals for X-ray diffraction. (1.00 g, 1.95 mmol, 96% yield). Anal. Calcd. for C<sub>14</sub>H<sub>20</sub>Cl<sub>4</sub>O<sub>2</sub>Si<sub>2</sub>Ti<sub>2</sub>: C, 32.71; H, 3.92. Found: C, 32.74; H, 4.04. <sup>1</sup>H NMR (300 MHz, CDCl<sub>3</sub>, 25 °C): δ 0.55 (s, 12H, SiMe<sub>2</sub>), 6.99 (m, 4H, C<sub>5</sub>H<sub>4</sub>), 7.05 (m, 4H, C<sub>5</sub>H<sub>4</sub>). (300 MHz, C<sub>6</sub>D<sub>6</sub>, 25 °C): δ 0.39 (s, 12H, SiMe<sub>2</sub>), 6.36 (m, 4H, C<sub>5</sub>H<sub>4</sub>), 6.64 (m, 4H, C<sub>5</sub>H<sub>4</sub>). <sup>13</sup>C{<sup>1</sup>H} NMR (75 MHz, CDCl<sub>3</sub>, 25 °C): δ 0.3 (SiMe<sub>2</sub>), 124.6, 126.5 [C<sub>2</sub>-C<sub>5</sub>(C<sub>5</sub>H<sub>4</sub>)], 131.6 [C<sub>ipso</sub>(C<sub>5</sub>H<sub>4</sub>)]. MS(EI) *m/z*: 499 (M<sup>+</sup>-CH<sub>3</sub>) (36%).

**Synthesis of TiCl<sub>2</sub>(η<sup>5</sup>-η<sup>1</sup>-C<sub>5</sub>H<sub>4</sub>SiMe<sub>2</sub>-O-SiMe<sub>2</sub>-O), **6**.** Deoxygenated water (242 μL, 13.9 mmol) was added, at room temperature, to a solution of TiCl<sub>3</sub>(η<sup>5</sup>-C<sub>5</sub>H<sub>4</sub>SiMe<sub>2</sub>Cl), **3** (2.09g, 6.70 mmol), in 50 mL of toluene. The reaction mixture was stirred for 24 h. After filtration the resulting solution was concentrated (10 mL) and cooled to -20 °C to give a pale green-yellow solid which was recrystallized from toluene/hexane at -20 °C giving a crystalline solid characterized as **6** (1.00g, 3.02 mmol, 45% yield). Anal. Calcd. for C<sub>9</sub>H<sub>16</sub>Cl<sub>2</sub>O<sub>2</sub>Si<sub>2</sub>Ti: C, 32.64; H, 4.87. Found: C, 32.95; H, 4.68. <sup>1</sup>H NMR (300 MHz, CDCl<sub>3</sub>, 25 °C): δ 0.18 (s, 6H, SiMe<sub>2</sub>), 0.42 (s, 6H, SiMe<sub>2</sub>), 6.76 (m, 2H, C<sub>5</sub>H<sub>4</sub>), 7.12 (m, 2H, C<sub>5</sub>H<sub>4</sub>). (300 MHz, C<sub>6</sub>D<sub>6</sub>, 25 °C): δ 0.03 (s, 6H, SiMe<sub>2</sub>), 0.12 (s, 6H, SiMe<sub>2</sub>), 6.26 (m, 2H, C<sub>5</sub>H<sub>4</sub>), 6.58 (m, 2H, C<sub>5</sub>H<sub>4</sub>). <sup>13</sup>C{<sup>1</sup>H} NMR (75 MHz, CDCl<sub>3</sub>, 25 °C): δ -0.2 (SiMe<sub>2</sub>), 0.0 (SiMe<sub>2</sub>), 128.4 [C<sub>ipso</sub>(C<sub>5</sub>H<sub>4</sub>)], 125.2, 125.1 [C<sub>2</sub>-C<sub>5</sub>(C<sub>5</sub>H<sub>4</sub>)]. <sup>13</sup>C NMR (75 MHz, C<sub>6</sub>D<sub>6</sub>, 25 °C): δ -0.4 (SiMe<sub>2</sub>), -0.3 (SiMe<sub>2</sub>), 128.9 [C<sub>ipso</sub>(C<sub>5</sub>H<sub>4</sub>)], 125.2, 125.1 [C<sub>2</sub>-C<sub>5</sub>(C<sub>5</sub>H<sub>4</sub>)]. <sup>29</sup>Si NMR (75 MHz, C<sub>6</sub>D<sub>6</sub>, 25 °C): δ -4.9 (SiMe<sub>2</sub>), -3.1 (SiMe<sub>2</sub>). MS(EI) *m/z*: 330 (M<sup>+</sup>) (3%), 315 (M<sup>+</sup>-CH<sub>3</sub>) (100%).

**Synthesis of Zr Cl<sub>2</sub> [(η<sup>5</sup>-η<sup>5</sup>-C<sub>5</sub>H<sub>4</sub>)<sub>2</sub>(μ-Me<sub>2</sub>SiOSiMe<sub>2</sub>)], **7**.** Deoxygenated water (47 μL, 2.61 mmol) was added to a solution of ZrCl<sub>2</sub>(η<sup>5</sup>-C<sub>5</sub>H<sub>4</sub>SiMe<sub>2</sub>Cl)<sub>2</sub>, **4** (1.25g, 2.62 mmol), in 50 mL of toluene. The reaction mixture was stirred at room temperature for 15 h. After filtration the resulting solution was concentrated (10 mL) and cooled to -20 °C to give a colorless solid. Recrystallization from toluene/hexane at -20 °C gave a white microcrystalline solid which was characterized as **7** (1.00g, 2.37 mmol, 91% yield). Anal. Calcd. for C<sub>14</sub>H<sub>20</sub>Cl<sub>2</sub>O<sub>2</sub>Si<sub>2</sub>Zr: C, 39.79; H, 4.77. Found: C, 39.59; H, 4.75. <sup>1</sup>H NMR (300 MHz, CDCl<sub>3</sub>, 25 °C): δ 0.37 (s, 12H, SiMe<sub>2</sub>), 6.54 (m, 4H, C<sub>5</sub>H<sub>4</sub>), 6.84 (m, 4H, C<sub>5</sub>H<sub>4</sub>). (300 MHz, C<sub>6</sub>D<sub>6</sub>, 25 °C): δ 0.23 (s, 12H, SiMe<sub>2</sub>), 6.27 (m, 4H, C<sub>5</sub>H<sub>4</sub>), 6.42 (m, 4H, C<sub>5</sub>H<sub>4</sub>). <sup>13</sup>C{<sup>1</sup>H} NMR (75 MHz, CDCl<sub>3</sub>, 25 °C): δ 0.8 (SiMe<sub>2</sub>), 117.1 [C<sub>ipso</sub>(C<sub>5</sub>H<sub>4</sub>)], 121.3, 125.5 [C<sub>2</sub>-C<sub>5</sub>(C<sub>5</sub>H<sub>4</sub>)]. MS(EI) *m/z*: 422 (M<sup>+</sup>) (6%), 417 (M<sup>+</sup>-CH<sub>3</sub>) (90%).

**Synthesis of Ti(CH<sub>2</sub>C<sub>6</sub>H<sub>5</sub>)<sub>3</sub>(η<sup>5</sup>-C<sub>5</sub>H<sub>4</sub>SiMe<sub>2</sub>Cl), **8**.** To a suspension of TiCl<sub>3</sub>(η<sup>5</sup>-C<sub>5</sub>H<sub>4</sub>SiMe<sub>2</sub>Cl), **2** (0.76g, 2.43 mmol), in 75 mL of hexane cooled to -60 °C was added dropwise a solution of Mg(CH<sub>2</sub>Ph)<sub>2</sub>(THF)<sub>2</sub> (2.56g, 7.30 mmol) in 30 mL of toluene. The reaction mixture was allowed to stir at room temperature for 3h, over which time it turned from yellow to dark red. After filtration the resulting solution was concentrated to 20 mL and cooled to -40 °C to give a dark red microcrystalline solid which was characterized as **8** (1.00g, 2.09 mmol, 86% yield). Anal. Calcd. for C<sub>28</sub>H<sub>31</sub>ClSiTi: C, 70.21; H, 6.52. Found: C, 70.56; H, 6.66. <sup>1</sup>H NMR (300 MHz, C<sub>6</sub>D<sub>6</sub>, 25 °C): δ 0.36 (s, 6H, SiMe<sub>2</sub>Cl), 3.05 (s, 6H, CH<sub>2</sub>Ph), 5.72 (m, 2H, C<sub>5</sub>H<sub>4</sub>), 6.10 (m, 2H, C<sub>5</sub>H<sub>4</sub>), 6.85–7.15 (m, Ph). <sup>13</sup>C NMR (75 MHz, C<sub>6</sub>D<sub>6</sub>, 25 °C): δ 3.0 (q, <sup>1</sup>J<sub>C-H</sub> = 119 Hz, SiMe<sub>2</sub>), 94.7 (t, <sup>1</sup>J<sub>C-H</sub> = 125 Hz, CH<sub>2</sub>Ph), 121.6, 121.9 [d, <sup>1</sup>J<sub>C-H</sub> = 173 Hz, C<sub>2</sub>-C<sub>5</sub>(C<sub>5</sub>H<sub>4</sub>)], 123.4, 127.2, 128.9 (d, <sup>1</sup>J<sub>C-H</sub> = 153–159 Hz, Ph), 148.6 (s, C<sub>ipso</sub>, Ph). (C<sub>ipso</sub> of C<sub>5</sub>H<sub>4</sub> not observed). MS(EI) *m/z*: 91 (C<sub>7</sub>H<sub>7</sub><sup>+</sup>, 100%).

**Synthesis of [TiMe<sub>2</sub>(η<sup>5</sup>-η<sup>1</sup>-C<sub>5</sub>H<sub>4</sub>SiMe<sub>2</sub>)(μ-O)]<sub>2</sub>, **9**.** To a suspension of [TiCl<sub>2</sub>(η<sup>5</sup>-η<sup>1</sup>-C<sub>5</sub>H<sub>4</sub>SiMe<sub>2</sub>)(μ-O)]<sub>2</sub>, **5** (1.67g, 3.25 mmol), in 100 mL of hexane, cooled to -60 °C, was added 4.33 mL of a 3M solution of MgCl<sub>2</sub> in THF (13.00 mmol) via syringe. After warming to 25 °C, the reaction mixture was allowed to stand for 5 h. The MgCl<sub>2</sub> formed was removed by filtration and the volume of the filtrate was reduced in vacuum to 20 mL and cooled to -60 °C. Yellow microcrystals were obtained and were characterized as **9** (1.00g, 2.31 mmol, 71% yield). Anal. Calcd. for C<sub>13</sub>H<sub>22</sub>O<sub>2</sub>Si<sub>2</sub>Ti<sub>2</sub>: C, 50.00; H, 7.46. Found: C, 49.53; H, 7.21. <sup>1</sup>H NMR (300 MHz, C<sub>6</sub>D<sub>6</sub>, 25 °C): δ

**Table 5.** Crystal and Experimental Data and Structure Refinement Procedures for Compounds **5** and **7**

	<b>5</b>	<b>7</b>
formula	C <sub>14</sub> H <sub>20</sub> O <sub>2</sub> Si <sub>2</sub> Cl <sub>4</sub> Ti <sub>2</sub>	C <sub>14</sub> H <sub>20</sub> O <sub>2</sub> Si <sub>2</sub> Cl <sub>2</sub> Zr
crystal habit	prismatic	prismatic
color	yellow	yellow
crystal size	0.20 × 0.12 × 0.15	0.3 × 0.20 × 0.15
symmetry	monoclinic <i>P</i> 2 <sub>1</sub> / <i>n</i>	monoclinic <i>P</i> 2 <sub>1</sub> / <i>c</i>
unit cell determination	least-squares fit from 25 reflns	
unit cell dimensions		
<i>a</i> , <i>b</i> , <i>c</i> , Å	9.461(7), 10.926(1), 10.507(3)	13.479(4), 8.654(1), 15.343(5)
β, deg	95.20(2)	97.18(2)
<i>V</i> , Å <sup>3</sup>	1081.8(6)	1775(1)
<i>Z</i>	2	4
<i>D</i> <sub>cal</sub> , g cm <sup>-3</sup>	1.578	1.581
<i>M</i> <sub>w</sub>	514.1	422.6
<i>F</i> (000)	520	856
μ, cm <sup>-1</sup>	13.443	10.386
scan mode	ω/2θ scans; θ <sub>max</sub> = 30°	ω/2θ scans; θ <sub>max</sub> = 30°
no. of reflections		
measured	3465	5666
independent observed	2803 <i>I</i> > 2σ( <i>I</i> ) criterion	4139 <i>I</i> > 2σ( <i>I</i> ) criterion
range of <i>hkl</i>	<i>h</i> -13 to 13; <i>k</i> 0 to 15; 0 to 14	<i>h</i> -19 to 19; <i>k</i> 0 to 12; 0 to 21
standard reflections	2 reflections every 120 min, no variation	
<i>R</i>	0.036	0.029
<i>R</i> <sub>w</sub>	0.065	0.054
max peak in final diff map, e/Å <sup>3</sup>	0.866	0.317
min peak in final diff map e/Å <sup>3</sup>	-0.544	-0.493
goodness of fit indicator	1.633	2.249
largest param shift/error	0.02	0.02

0.41 (s, 12H, SiMe<sub>2</sub>), 0.75 (s, 12H, TiMe), 6.13 (m, 4H, C<sub>5</sub>H<sub>4</sub>), 6.56 (m, 4H, C<sub>5</sub>H<sub>4</sub>). <sup>13</sup>C{<sup>1</sup>H} NMR (75 MHz, C<sub>6</sub>D<sub>6</sub>, 25 °C): δ 1.3 (SiMe<sub>2</sub>), 52.7 (TiMe), 118.7, 119.2 [C<sub>2</sub>-C<sub>5</sub> (C<sub>5</sub>H<sub>4</sub>)], 122.9 [C<sub>ipso</sub> (C<sub>5</sub>H<sub>4</sub>)]. MS(EI) *m/z* 417 (M<sup>+</sup>-CH<sub>3</sub>, 4%), 387 (M<sup>+</sup>-3CH<sub>3</sub>, 15%).

#### Synthesis of [Ti(CH<sub>2</sub>C<sub>6</sub>H<sub>5</sub>)<sub>2</sub>(η<sup>5</sup>-η<sup>1</sup>-C<sub>5</sub>H<sub>4</sub>SiMe<sub>2</sub>)(μ-O)]<sub>2</sub>, **10**.

To a suspension of [TiCl<sub>2</sub>(η<sup>5</sup>-η<sup>1</sup>-C<sub>5</sub>H<sub>4</sub>SiMe<sub>2</sub>)(μ-O)]<sub>2</sub>, **5** (0.90g, 1.75 mmol), in 100 mL of hexane, cooled to -60 °C, was added dropwise a solution of Mg(CH<sub>2</sub>Ph)<sub>2</sub>(THF)<sub>2</sub> (2.46g, 7.01 mmol) in 30 mL of toluene. The reaction mixture was allowed to stir at room temperature for 4h, turning from orange to dark red. After filtration over celite the resulting solution was concentrated to 20 mL and cooled to -40 °C to give a dark red microcrystalline solid which was characterized as **10** (1.00g, 1.36 mmol, 78% yield). Anal. Cald. for C<sub>42</sub>H<sub>48</sub>O<sub>2</sub>Si<sub>2</sub>Ti<sub>2</sub>: C, 68.47; H, 6.57. Found: C, 67.92; H, 6.88. <sup>1</sup>H NMR (300 MHz, C<sub>6</sub>D<sub>6</sub>, 25 °C): δ 0.31 (s, 12H, SiMe<sub>2</sub>), 2.54 (d, <sup>2</sup>J<sub>H-H</sub> = 10 Hz, 4H, CH<sub>2</sub>Ph), 2.74 (d, <sup>2</sup>J<sub>H-H</sub> = 10 Hz, 4H, CH<sub>2</sub>Ph), 5.79 (m, 4H, C<sub>5</sub>H<sub>4</sub>), 6.58 (m, 4H, C<sub>5</sub>H<sub>4</sub>), 6.93-7.18 (m, Ph). <sup>13</sup>C NMR (75 MHz, C<sub>6</sub>D<sub>6</sub>, 25 °C): δ 2.0 (q, <sup>1</sup>J<sub>C-H</sub> = 119 Hz, SiMe<sub>2</sub>), 82.7 (t, <sup>1</sup>J<sub>C-H</sub> = 125 Hz, CH<sub>2</sub>Ph), 121.7, 123.3 [d, <sup>1</sup>J<sub>C-H</sub> = 173 Hz, C<sub>2</sub>-C<sub>5</sub> (C<sub>5</sub>H<sub>4</sub>)], 124.2 (s, C<sub>ipso</sub>, C<sub>5</sub>H<sub>4</sub>), 122.7, 126.8, 128.6, (d, <sup>1</sup>J<sub>C-H</sub> = 153-159 Hz, Ph), 149.0 (s, C<sub>ipso</sub>, Ph). MS(EI) *m/z* 91 (C<sub>7</sub>H<sub>7</sub><sup>+</sup>, 100%).

#### Synthesis of TiCl<sub>2</sub>[N(SiMe<sub>3</sub>)<sub>2</sub>](η<sup>5</sup>-C<sub>5</sub>H<sub>4</sub>SiMe<sub>2</sub>Cl), **11**.

A mixture of TiCl<sub>3</sub>(η<sup>5</sup>-C<sub>5</sub>H<sub>4</sub>SiMe<sub>2</sub>Cl), **2** (0.98g, 3.14 mmol), and LiN(SiMe<sub>3</sub>)<sub>2</sub> (0.53g, 3.14 mmol) in 50 mL of hexane was stirred at room temperature for 10h and then filtered. The filtrate was concentrated under reduced pressure and cooled to -40 °C to give orange crystals which were characterized as **11**

(1.00g, 2.29 mmol, 73% yield). Anal. Cald. for C<sub>13</sub>H<sub>28</sub>Cl<sub>3</sub>NSi<sub>3</sub>-Ti: C, 35.74; H, 6.46; N, 3.21. Found: C, 36.06; H, 6.67; N, 3.29. <sup>1</sup>H NMR (300 MHz, C<sub>6</sub>D<sub>6</sub>, 25 °C): δ 0.25 (s, 18H, NSiMe<sub>3</sub>), 0.73 (s, 6H, SiMe<sub>2</sub>Cl), 6.21 (m, 2H, C<sub>5</sub>H<sub>4</sub>), 6.62 (m, 2H, C<sub>5</sub>H<sub>4</sub>). <sup>13</sup>C{<sup>1</sup>H} NMR (75 MHz, C<sub>6</sub>D<sub>6</sub>, 25 °C): δ 2.4 (SiMe<sub>2</sub>-Cl), 5.5 (NSiMe<sub>3</sub>), 118.9 [C<sub>2</sub>-C<sub>5</sub> (C<sub>5</sub>H<sub>4</sub>)]. (C<sub>ipso</sub> and another C<sub>2-5</sub> not observed). MS(EI) *m/z*: 437 (M<sup>+</sup>, 1%); 422 (M<sup>+</sup>-CH<sub>3</sub>, 6%), 262 [M<sup>+</sup>-CH<sub>3</sub>-NSi(Me<sub>3</sub>)<sub>2</sub>, 51%].

**Synthesis of TiCl<sub>2</sub>(η<sup>5</sup>-C<sub>5</sub>H<sub>4</sub>SiMe<sub>2</sub>-N<sup>t</sup>Bu), **12**.** A mixture of TiCl<sub>3</sub>(η<sup>5</sup>-C<sub>5</sub>H<sub>4</sub>SiMe<sub>2</sub>Cl), **2** (1.89g, 6.06 mmol), and LiNH<sup>t</sup>Bu (0.48g, 6.06 mmol) in 60 mL of hexane was stirred at room temperature overnight and then filtered. The filtrate was concentrated under reduced pressure and cooled to -30 °C to give an orange-brown solid. Recrystallization from toluene-hexane gave a microcrystalline solid whose analytical composition and NMR spectra were coincident with data reported<sup>18a</sup> for complex **12** (1.00g, 3.20 mmol, 53% yield).

**Crystal Structures of [TiCl<sub>2</sub>(η<sup>5</sup>-η<sup>1</sup>-C<sub>5</sub>H<sub>4</sub>SiMe<sub>2</sub>)(μ-O)]<sub>2</sub>, **5**, and ZrCl<sub>2</sub>[(η<sup>5</sup>-C<sub>5</sub>H<sub>4</sub>)<sub>2</sub>(μ-Me<sub>3</sub>SiOSiMe<sub>2</sub>)], **7**.** Crystallographic and experimental details of X-ray crystal structure determination are given in Table 5. Suitable crystals of **5** and **7** were mounted on an Enraf-Nonius CAD-4 automatic four-circle diffractometer with bisecting geometric and using graphite-oriented monochromator with Mo Kα radiation (λ(Mo Kα) = 0.710 73 Å). Data were collected at room temperature. Intensities were corrected for Lorentz and polarisation effects in the usual manner. No absorption or extinction corrections were made. The structures were solved by a combination of direct methods and Fourier synthesis and refined (on *F*) by full matrix least-squares calculations. All the non hydrogen atoms were refined anisotropically. In the last cycle of refinement the hydrogen atoms were introduced from geometric calculation refined one cycle isotropically and then fixed.

Final values of *R* = 0.036 and *R*<sub>w</sub> = 0.065 were obtained for compound **5** and *R* = 0.029 and *R*<sub>w</sub> = 0.054 for compound **7**, with *R*<sub>w</sub> = [Σ|w|*F*<sub>o</sub> - |*F*<sub>c</sub>|]<sup>2</sup>/Σ|w|*F*<sub>o</sub><sup>2</sup> and *w* = 4*F*<sub>o</sub><sup>2</sup>/[σ(*F*<sub>o</sub>)<sup>2</sup>].

Anomalous dispersion corrections and atomic scattering factors were taken from ref 22. Calculations were performed with the SDP package,<sup>23</sup> and the programs Multan<sup>24</sup> and Dirdif<sup>25</sup> on a Microvax II computer.

**Acknowledgment.** We are grateful to the DGICYT (Project PB-92-0178-C) for financial support. S.C. acknowledges the MEC, and A.M. acknowledges Universidad de Alcalá for fellowships.

**Supplementary Material Available:** Tables of hydrogen atom positional and isotropic thermal parameters, non-hydrogen atom anisotropic thermal parameters, and all bond distances and angles for **5** and **7** (14 pages). Ordering information is given on any current masthead page.

OM940607M

(22) *International Tables for X-Ray Crystallography*; Kynoch Press: Birmingham, U. K., 1974; Vol. IV.

(23) B. A. Frenz and Associates, Inc. SDP; Texas A&M and Enraf Nonius: College Station, TX 77840, and Delft, Holland, 1985.

(24) Main, P.; Fiske, S. E.; Hull, S. L.; Lessinger, L.; Germain, C.; Declercq, J. P.; Woolfson, M. M. MULTAN. Universities of York and Louvain, 1980.

(25) Beurkens, P. T.; Bossman, W. P.; Doesburg, H. M.; Could, R. O.; van der Hark, T. E. M.; Prick, P. A. J.; Noordik, J. H.; Beurkens, G.; Parthasarathu, V. DIRDIF Manual 82. Technical Report 1981-82; Crystallographic Laboratory: Toernooiveld, The Netherlands, 1981.

# Au-Ir and Hg-Ir Mixed-Metal Carbonyl Clusters. Synthesis, Characterization, and Solid State Structure of [Ir<sub>6</sub>(CO)<sub>15</sub>(AuPPh<sub>3</sub>)<sub>2</sub>] and [Ir<sub>6</sub>(CO)<sub>14</sub>(HgCl)<sub>2</sub>]<sup>2-</sup>

Alessandro Ceriotti, Roberto Della Pergola, and Luigi Garlaschelli\*

*Dipartimento di Chimica Inorganica, Metallorganica ed Analitica, via G. Venezian 21,  
20133 Milano, Italy*

Mario Manassero and Norberto Masciocchi\*

*Istituto di Chimica Strutturistica Inorganica, via G. Venezian 21, 20133 Milano, Italy*

Received July 13, 1994<sup>®</sup>

The neutral cluster [Ir<sub>6</sub>(CO)<sub>15</sub>(AuPPh<sub>3</sub>)<sub>2</sub>] has been obtained by reaction of [Ir<sub>6</sub>(CO)<sub>15</sub>]<sup>2-</sup> with [AuPPh<sub>3</sub>]<sup>+</sup>. It crystallizes in the triclinic space group *P*1 with cell constants *a* = 13.160(2) Å, *b* = 13.714(4) Å, *c* = 18.266(3) Å, α = 65.47(2)°, β = 110.93(2)°, γ = 112.07(1)°, *V* = 2699(2) Å<sup>3</sup>, and *Z* = 2. Data were collected at room temperature to a maximum 2θ = 54°. The final discrepancy indices were *R* = 0.032 and *R*<sub>w</sub> = 0.034 for 7217 independent reflections with *I* > 3σ(*I*). The structure was solved by direct methods. The iridium atoms of the cluster define an octahedral frame capped by one gold-phosphine group. The second AuPPh<sub>3</sub> unit spans one Ir-Au edge. The metal skeleton of C<sub>1</sub> symmetry is coordinated by twelve terminal and three edge-bridging carbonyl groups. The dianionic [Ir<sub>6</sub>(CO)<sub>14</sub>(HgCl)<sub>2</sub>]<sup>2-</sup> has been prepared from [Ir<sub>6</sub>(CO)<sub>15</sub>]<sup>2-</sup> and Hg<sub>2</sub>Cl<sub>2</sub>, HgCl<sub>2</sub> + Hg, or HgCl<sub>2</sub> in the presence of Na<sub>2</sub>CO<sub>3</sub>. The salt [PPh<sub>4</sub>]<sub>2</sub>[Ir<sub>6</sub>(CO)<sub>14</sub>(HgCl)<sub>2</sub>] crystallizes in the monoclinic space group *C*c with cell constants *a* = 10.257(2) Å, *b* = 46.848(4) Å, *c* = 14.639(3) Å, β = 107.83(2)°, *V* = 6696(4) Å<sup>3</sup>, and *Z* = 4. Data were collected at room temperature to a maximum 2θ = 50°. The final discrepancy indices were *R* = 0.037 and *R*<sub>w</sub> = 0.036 for 3619 independent reflections with *I* > 3σ(*I*). The metallic framework forms an octahedron of iridium atoms bearing, on four non-adjacent faces, two μ<sub>3</sub>-HgCl fragments and two μ<sub>3</sub>-CO groups. The chemical shift of the <sup>199</sup>Hg NMR was found at +1508 ppm, and suggests an anomalous oxidation state.

In recent papers we have described the syntheses and the chemical properties of mixed-metal clusters of formula [Ir<sub>6</sub>(CO)<sub>15</sub>ML]<sup>-</sup> [ML = CuNCMe (1),<sup>1</sup> AuPPh<sub>3</sub> (2),<sup>2</sup> and HgCl (3)<sup>2</sup>], obtained by the direct addition of electrophilic metal complexes to [Ir<sub>6</sub>(CO)<sub>15</sub>]<sup>2-</sup>. These anions showed very similar behavior and structures, with face capping ML groups. The main difference between them is the arrangement of the three bridging carbonyls, which shows enhanced face-bridging character in the sequence 1, 2 and 3, increasing the molecular symmetry in the solid state from C<sub>3</sub> to C<sub>3v</sub>.<sup>1,2</sup> These structural variations implied two different formal descriptions for the clusters: 1 and 2 were considered adducts of [Ir<sub>6</sub>(CO)<sub>15</sub>]<sup>2-</sup> with ML<sup>+</sup> fragments, retaining the ligand architecture of the parent dianion of D<sub>3</sub> symmetry; 3 was envisaged as a structural analogue of Ir<sub>6</sub>(CO)<sub>16</sub> (red isomer, *T<sub>d</sub>* point group),<sup>3</sup> where one μ<sub>3</sub>-CO is replaced by one HgCl<sup>-</sup> group, formally acting as a two electron donor.

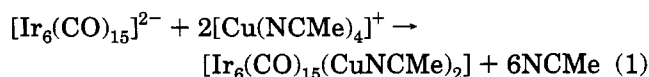
Moreover, the synthetic studies and the multinuclear NMR measurements showed that other species were formed when an excess of the heteroatom complex was added; these data prompted us to investigate the

systems further, resulting in the isolation of the new complexes [Ir<sub>6</sub>(CO)<sub>15</sub>{AuPPh<sub>3</sub>}<sub>2</sub>] (4) and [Ir<sub>6</sub>(CO)<sub>14</sub>-(HgCl)<sub>2</sub>]<sup>2-</sup> (5) which showed remarkable differences in the behavior of Hg and Au, confirming that the previous formalism has substantial support. The adduct [Ir<sub>6</sub>(CO)<sub>15</sub>{CuNCMe}<sub>2</sub>] (6) was obtained in solution, but was found to be too unstable to be crystallized.

## Results

The addition of [Cu(NCMe)<sub>4</sub>]<sup>+</sup>, [AuPPh<sub>3</sub>]<sup>+</sup> or HgCl<sub>2</sub> to [Ir<sub>6</sub>(CO)<sub>15</sub>]<sup>2-</sup> (molar ratio 1:1) in tetrahydrofuran (THF) at room temperature resulted in the fast formation of the monoanionic adducts [Ir<sub>6</sub>(CO)<sub>15</sub>CuNCMe]<sup>-</sup> (1), [Ir<sub>6</sub>(CO)<sub>15</sub>AuPPh<sub>3</sub>]<sup>-</sup> (2), and [Ir<sub>6</sub>(CO)<sub>15</sub>HgCl]<sup>-</sup> (3), which showed strikingly similar spectroscopic, structural, and chemical properties.<sup>1,2</sup> The same reactions were carried out with higher molar ratios between the monomeric complexes and the carbonyl cluster, searching for neutral derivatives.

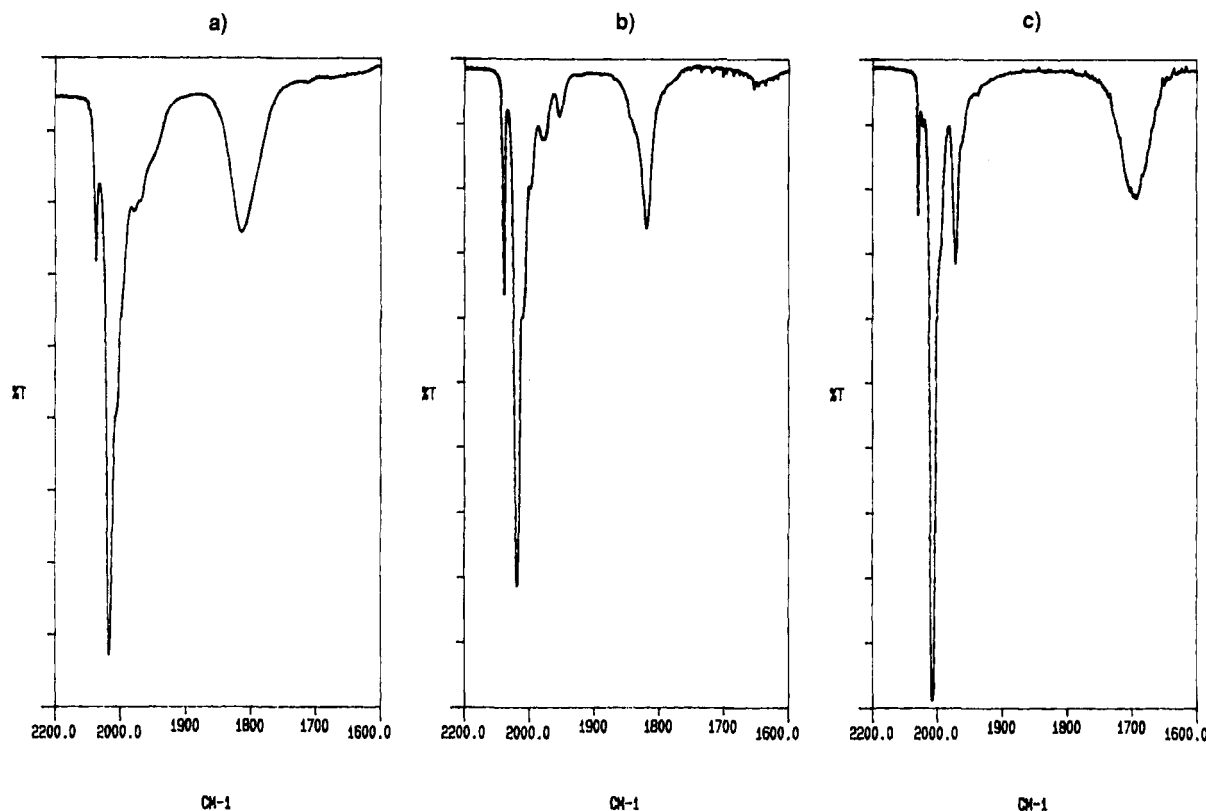
**Synthesis and Spectroscopic Characterization of [Ir<sub>6</sub>(CO)<sub>15</sub>(CuNCMe)<sub>2</sub>].** The reaction of [Ir<sub>6</sub>(CO)<sub>15</sub>]<sup>2-</sup> with [Cu(NCMe)<sub>4</sub>]<sup>+</sup> (molar ratio 1:2) in CH<sub>2</sub>Cl<sub>2</sub> produced a new species which was easily identified as [Ir<sub>6</sub>(CO)<sub>15</sub>-(CuNCMe)<sub>2</sub>], on the basis of the stoichiometry of reaction 1. The infrared spectrum of the product (ν<sub>CO</sub> in



<sup>®</sup> Abstract published in *Advance ACS Abstracts*, November 1, 1994.  
(1) Della Pergola, R.; Garlaschelli, L.; Demartin, F.; Manassero, M.; Masciocchi, N. *J. Organometal. Chem.*, **1992**, *436*, 241.

(2) Della Pergola, R.; Demartin, F.; Garlaschelli, L.; Manassero, M.; Martinengo, S.; Masciocchi, N.; Sansoni, M. *Organometallics*, **1991**, *10*, 2239.

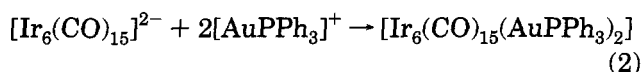
(3) Garlaschelli, L.; Martinengo, S.; Bellon, P. L.; Demartin, F.; Manassero, M.; Chiang, M. Y.; Wei, C. Y.; Bau, R. *J. Am. Chem. Soc.*, **1984**, *105*, 6664.



**Figure 1.** IR spectra of (a)  $[\text{Ir}_6(\text{CO})_{15}(\text{CuNCMe})_2]$  in  $\text{CH}_2\text{Cl}_2$ , (b)  $[\text{Ir}_6(\text{CO})_{15}(\text{AuPPh}_3)_2]$  in THF, and (c)  $(\text{PPh}_4)_2[\text{Ir}_6(\text{CO})_{14}(\text{HgCl})_2]$  in THF.

THF: 2075m, 2034vs, 1813m  $\text{cm}^{-1}$ , Figure 1a) closely resembles the spectrum of  $[\text{Ir}_6(\text{CO})_{15}(\text{AuPPh}_3)_2]$  (see later), and also that reported for  $[\text{Ru}_6\text{C}(\text{CO})_{16}(\text{CuNCMe})_2]$ ,<sup>4</sup> the coincidence of the infrared spectra strongly suggests very similar architectures between the three molecules. By analogy with  $[\text{Ru}_6\text{C}(\text{CO})_{16}(\text{CuNCMe})_2]$ ,<sup>4</sup> the two copper atoms are most likely within bonding distance of each other. Unfortunately, the Ir-Cu cluster was too unstable to be crystallized, and the characterization was limited to the IR data. Any attempt to grow crystals of **6** resulted in the transformation to  $\text{Ir}_6(\text{CO})_{16}$ <sup>3</sup> or **1**, depending on the conditions used. This instability is not surprising considering the efforts needed to obtain crystalline samples of **1**.

**Synthesis and Spectroscopic Data of  $[\text{Ir}_6(\text{CO})_{15}(\text{AuPPh}_3)_2]$ .** The addition of two moles of  $[\text{AuPPh}_3]^+$  onto  $[\text{Ir}_6(\text{CO})_{15}]^{2-}$  occurs only when a large excess of the cationic complex is used. Very similar results were obtained with solvent other than THF, such as 2-propanol or  $\text{CH}_2\text{Cl}_2$ . In the alcoholic solvent, the soluble potassium salt  $\text{K}_2[\text{Ir}_6(\text{CO})_{15}]$  was employed, according to eq 2. The cluster **4** was obtained as a microcrystalline



solid, which was isolated by filtration. A very large excess of gold was needed to obtain complete conversion even in  $\text{CH}_2\text{Cl}_2$ , where the  $[\text{AuPPh}_3]^+$  is less stabilized by solvation. The neutral cluster **4**, once formed, is fairly stable and can be crystallized from THF,  $\text{CH}_2\text{Cl}_2$ , or toluene, after precipitation with 2-propanol, with

comparable results. The capping groups are rapidly displaced when an excess of halide salts is added to the solution.<sup>2</sup>

The infrared spectrum of  $[\text{Ir}_6(\text{CO})_{15}(\text{AuPPh}_3)_2]$  shows bands at 2075m, 2036vs, 1978w, 1952w, 1819m  $\text{cm}^{-1}$ , in THF (Figure 1b). The <sup>31</sup>P NMR spectrum shows only one signal at 66.2 ppm ( $\text{CD}_2\text{Cl}_2$ , room temperature), which is slightly displaced to 64.9 ppm at  $-90^\circ\text{C}$ , indicating that the two phosphines are equivalent on the NMR time scale, even at low temperature. These findings are in contrast to the solid state structure, where the two phosphorus atoms are in different environments. The existence of several isomers is not unlikely, since for  $[\text{Ru}_6\text{C}(\text{CO})_{16}(\text{AuPMePh}_2)_2]$ <sup>5</sup> two different isomers in solution were observed by <sup>31</sup>P NMR; the isomer characterized by X-ray analysis showed two centrosymmetric edge-bridging gold atoms. However, **4** should be present in solution as a single isomer, different from that observed in the solid state; more probably, the two capping gold atoms are rapidly exchanging their site, even at  $-90^\circ\text{C}$ ; presumably, the  $\text{Au}_2(\text{PPh}_3)_2$  group oscillates between two adjacent faces of the octahedral iridium framework, as previously suggested for  $[\text{Ru}_6(\text{CO})_{16}\text{B}\{\text{Au}(\text{PPh}_3)_3\}_3]$ .<sup>6</sup>

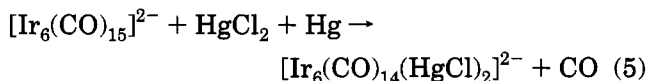
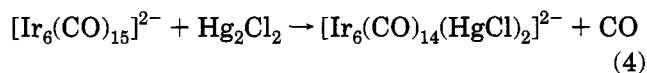
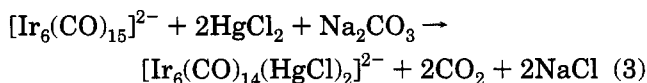
**Synthesis and Spectroscopic Data of  $[\text{Ir}_6(\text{CO})_{14}(\text{HgCl})_2]^{2-}$ .** The addition of a large excess of  $\text{HgCl}_2$  to  $[\text{Ir}_6(\text{CO})_{15}]^{2-}$  does not change the products of the reaction, and the monoadduct **3** is the only product which can always be detected. When a test reaction was carried out with  $\text{EtHgCl}$ , the formation of **3** was initially

(5) Bunkall, S. R.; Holden, H. D.; Johnson, B. F. G.; Lewis, J.; Pain, G. N.; Raithby, P. R.; Taylor, M. J. *J. Chem. Soc., Chem. Commun.*, **1984**, 25.

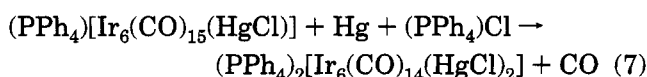
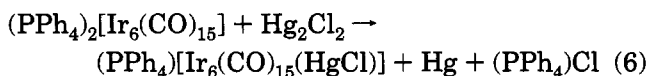
(6) Housecroft, C. E.; Matthews, D. M.; Waller, A.; Edwards, A. J.; Rheingold, A. L. *J. Chem. Soc., Dalton Trans.*, **1993**, 3057.

(4) Bradley, J. S.; Pruet, R. L.; Hill, E.; Ansell, G. B.; Leonowicz, M. E.; Modrick, M. A. *Organometallics*, **1982**, *1*, 748.

observed; however, after prolonged standing, small amounts of a more reduced species were formed. Eventually, this new cluster was isolated and was shown to be  $[\text{Ir}_6(\text{CO})_{14}(\text{HgCl})_2]^{2-}$  (**5**). The addition of the second Hg atom is thus accompanied by loss of CO and reduction of the cluster. Thereafter, three different successful methods of synthesis were devised, according to eqs 3–5.



All reactions are of a heterogeneous nature, since some of the reactants are insoluble in THF. Therefore they require more than 15 days to go to completeness, at room temperature; nevertheless they are very selective, and clean conversions to **5**, as the only carbonylic product, are obtained. The reactions proceed via the very rapid intermediate formation of **3**, which is then slowly transformed into the final product; in the case of reaction 4, the addition of the first  $\text{HgCl}^+$  group is allowed by the disproportionation of  $\text{Hg}_2\text{Cl}_2$ , with formation of elemental Hg and  $\text{Cl}^-$ , which can be clearly detected in the reaction vessel as a greyish residue; the step which follows can be considered as a ligand substitution:



The sequence represented by steps 6 and 7 can be effected by the successive addition of  $\text{HgCl}_2$  and Hg (eq 5), with identical results. The infrared spectrum of **5** in THF shows bands at 2057w, 2013vs, 1972m, 1697m,  $\text{br cm}^{-1}$  (Figure 1c), the band at lowest wavenumbers confirming the presence of face bridging carbonyls.

The  $^{199}\text{Hg}$  NMR spectrum was recorded, in THF at  $-90^\circ\text{C}$ , and showed a single peak at +1590 ppm. The signal could also be observed at room temperature at 1508 ppm, and is well outside the usual range for this nucleus (+500,  $-3500$  ppm).<sup>7</sup> This chemical shift should be compared with the value of  $-1168$  ppm found for **3**,<sup>2</sup> and strongly supports the hypothesis of an anomalous oxidation state of Hg in the cluster (see Discussion).

**Solid State Structure of  $[\text{Ir}_6(\text{CO})_{12}(\mu\text{-CO})_3(\text{AuPPh}_3)_2]$  (**4**).** The crystal structure of  $[\text{Ir}_6(\text{CO})_{15}(\text{AuPPh}_3)_2]$  consists of discrete neutral molecules held together by van der Waals contacts. A list of the relevant bond distances and angles appears in Table 1. The metal skeleton of **4** is based on a  $\text{Ir}_6$  octahedron [av. Ir–Ir = 2.803 Å (min 2.7498(6); max 2.9325(7) Å,

**Table 1. Selected Distances (Å) and Angles (deg) in  $[\text{Ir}_6(\text{CO})_{15}(\text{AuPPh}_3)_2]$  with Estimated Standard Deviations (Esd's) on the Last Figure in Parentheses<sup>a</sup>**

Metal–Metal			
Au(1)–Au(2)	2.8530(8)	Ir(2)–Ir(3)	2.7771(7)
Au(1)–Ir(1)	2.8313(6)	Ir(2)–Ir(5)	2.7657(7)
Au(1)–Ir(4)	2.9347(5)	Ir(2)–Ir(6)	2.8094(9)
Au(1)–Ir(5)	2.8327(9)	Ir(3)–Ir(4)	2.8081(9)
Au(2)–Ir(1)	2.6569(6)	Ir(3)–Ir(5)	2.7498(6)
Ir(1)–Ir(2)	2.760(1)	Ir(3)–Ir(6)	2.7694(7)
Ir(1)–Ir(4)	2.7849(7)	Ir(4)–Ir(5)	2.8582(9)
Ir(1)–Ir(5)	2.9325(7)	Ir(4)–Ir(6)	2.7810(7)
Ir(1)–Ir(6)	2.8422(5)		
Ir–C <sub>term</sub>			
Ir(1)–C(11)	1.90(1)	Ir(4)–C(41)	1.88(2)
Ir(1)–C(12)	1.90(2)	Ir(4)–C(42)	1.90(1)
Ir(2)–C(21)	1.91(2)	Ir(5)–C(51)	1.85(2)
Ir(2)–C(22)	1.88(1)	Ir(5)–C(52)	1.91(1)
Ir(3)–C(31)	1.87(1)	Ir(6)–C(61)	1.88(1)
Ir(3)–C(32)	1.87(2)	Ir(6)–C(62)	1.87(2)
Ir–Cb			
Ir(3)–Cb(1)	2.07(1)	Ir(6)–Cb(2)	2.29(2)
Ir(5)–Cb(1)	2.04(2)	Ir(4)–Cb(3)	2.01(1)
Ir(2)–Cb(2)	2.01(1)	Ir(6)–Cb(3)	2.15(2)
Other Distances			
C <sub>term</sub> –O <sub>term</sub> <sup>b</sup>	1.14	Au(1)–P(1)	2.293(4)
Cb–Ob <sup>b</sup>	1.16	Au(2)–P(2)	2.272(3)
Angles			
Ir(1)–Au(1)–Au(2)	55.73(2)	Ir(1)–Au(2)–Au(1)	61.72(2)
Ir(4)–Au(1)–Au(2)	111.09(2)	Ir(1)–Au(1)–P(1)	157.69(9)
Ir(4)–Au(1)–Ir(1)	57.73(2)	Ir(1)–Au(2)–P(2)	166.41(8)
Ir(5)–Au(1)–Au(2)	75.92(2)	Ir–C <sub>term</sub> –O <sub>term</sub> <sup>b</sup>	176
Ir(5)–Au(1)–Ir(1)	62.36(2)	Ir–Cb–Ob <sup>b</sup>	138.5
Ir(5)–Au(1)–Ir(4)	59.38(2)		

<sup>a</sup> Abbreviations for atoms in Tables 1–5: term = terminal; Ct = triple (face) bridging carbon; Ot = triple (face) bridging oxygen; Cb = double (edge) bridging carbon; Ob = double (edge) bridging oxygen. <sup>b</sup> Average values.

$Q^8 = 4.6$ ], capped on a triangular face by a  $\mu_3$ -AuPPh<sub>3</sub> ligand [av Au(1)–Ir = 2.86 Å]; another AuPPh<sub>3</sub> fragment bridges one of the Au–Ir edges [Au(1)–Au(2) = 2.8530(8) Å; Au(2)–Ir(1) = 2.6569(1) Å]. A set of twelve terminal (two on each iridium atom) and three edge-bridging carbonyl ligands complete the molecule, which is fully depicted, with partial labeling scheme, in Figure 2. Average bonding values are: Ir–C<sub>term</sub> 1.88; C<sub>term</sub>–O<sub>term</sub> 1.14; Ir–C<sub>br</sub> 2.10; C<sub>br</sub>–O<sub>br</sub> 1.16 Å; Ir–C<sub>term</sub>–O<sub>term</sub> 176; Ir–C<sub>br</sub>–O<sub>br</sub> 138° (term = terminal; br = bridging).

The nature, and geometry, of the  $\{\text{AuPPh}_3\}_2$  ligand in **4** can be interpreted on the basis of the strong "aurophilic attraction"<sup>10</sup> of two roughly linearly coordinating fragments [P(1)–Au(1)–Ir(1) = 157°; P(2)–Au(2)–Ir(1) = 166°], which, however, does not significantly affect the Au–P bond lengths [av. Au–P 2.28 Å in **4**; Au–P 2.272(3) in **2**].

**Solid State Structure of  $(\text{PPh}_4)_2[\text{Ir}_6(\text{CO})_{12}(\mu_3\text{-CO})_2(\text{HgCl})_2]$  (**5a**).** The crystal structure of  $[\text{PPh}_4]_2[\text{Ir}_6(\text{CO})_{14}(\text{HgCl})_2]$  consists of an ionic packing of cluster anions **5** and  $\text{PPh}_4^+$  cations; no anomalously short contacts are present. Relevant bond distances and angles are listed in Table 2. The metal cage of the

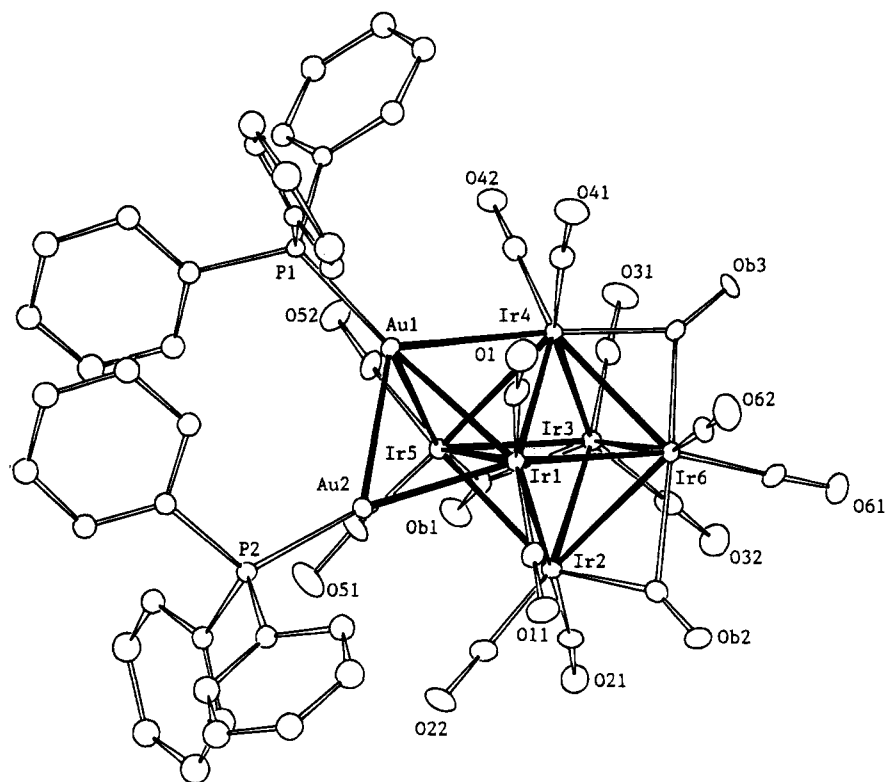
(8) The Q value measures the deviations of the M–M edges from the average value; it was introduced in Della Pergola, R.; Garlaschelli, L.; Martinengo, S.; Demartin, F.; Manassero, M.; Masciocchi, N.; Bau, R.; Zhao, D. *J. Organometal. Chem.*, **1990**, *396*, 385.

(9) A Fortran thermal-ellipsoid program for crystal structure illustration (Johnson, C. K. *ORTEP*; Oak Ridge National Laboratory: Oak Ridge, TN, 1971).

(10) Pyykkö, P.; Zhao, Y. *Angew. Chem. Int. Ed. Engl.*, **1991**, *30*, 604 and references therein.

(7) Granger, P. in *Transition Metal Nuclear Magnetic Resonance*, Pregosin, P. S. (ed.), Amsterdam, Elsevier, **1991**, p. 306–332.





**Figure 2.** ORTEP<sup>9</sup> drawing and atom-labeling scheme for  $[\text{Ir}_6(\text{CO})_{15}(\text{AuPPh}_3)_2]$ . Thermal ellipsoids are drawn at 30% probability. Carbonyl carbons are designated as the oxygens to which they are attached.

**Table 2.** Selected Distances (Å) and Angles (deg) in the Dianion  $[\text{Ir}_6(\text{CO})_{14}(\text{HgCl})_2]^{2-}$  with Estimated Standard Deviations (Esd's) on the Last Figure in Parentheses

Metal-Metal			
Ir(1)-Hg(1)	2.808(2)	Ir(1)-Ir(6)	2.754(2)
Ir(3)-Hg(1)	2.745(2)	Ir(2)-Ir(4)	2.768(2)
Ir(4)-Hg(1)	2.787(1)	Ir(2)-Ir(5)	2.748(2)
Ir(3)-Hg(2)	2.768(2)	Ir(2)-Ir(6)	2.754(2)
Ir(5)-Hg(2)	2.788(2)	Ir(3)-Ir(4)	2.899(2)
Ir(6)-Hg(2)	2.777(2)	Ir(3)-Ir(5)	2.825(2)
Ir(1)-Ir(2)	2.804(2)	Ir(3)-Ir(6)	2.846(2)
Ir(1)-Ir(3)	2.874(2)	Ir(4)-Ir(5)	2.746(2)
Ir(1)-Ir(4)	2.851(2)	Ir(5)-Ir(6)	2.947(2)
Ir-C <sub>term</sub>			
Ir(1)-C(11)	1.85(4)	Ir(4)-C(41)	1.96(3)
Ir(1)-C(12)	1.73(3)	Ir(4)-C(42)	1.80(3)
Ir(2)-C(21)	1.76(4)	Ir(5)-C(51)	1.89(4)
Ir(2)-C(22)	1.83(4)	Ir(5)-C(52)	1.83(4)
Ir(3)-C(31)	1.88(4)	Ir(6)-C(61)	1.85(3)
Ir(3)-C(32)	1.71(3)	Ir(6)-C(62)	1.89(4)
Ir-Ct			
Ir(1)-Ct(1)	2.01(3)	Ir(2)-Ct(2)	2.33(3)
Ir(2)-Ct(1)	2.29(3)	Ir(4)-Ct(2)	2.09(2)
Ir(6)-Ct(1)	2.06(3)	Ir(5)-Ct(2)	2.13(3)
Other Distances			
C-O <sub>term</sub> <sup>a</sup>	1.17	Hg(1)-Cl(1)	2.444(7)
Ct-Ot <sup>a</sup>	1.22	Hg(2)-Cl(2)	2.399(9)
Angles			
Ir(3)-Hg(1)-Ir(1)	62.33(5)	Ir(6)-Hg(2)-Ir(3)	61.76(5)
Ir(4)-Hg(1)-Ir(1)	61.28(5)	Ir(6)-Hg(2)-Ir(5)	63.96(5)
Ir(4)-Hg(1)-Ir(3)	63.20(4)	Ir-C <sub>term</sub> -O <sub>term</sub> <sup>a</sup>	171
Ir(5)-Hg(2)-Ir(3)	61.13(5)	Ir-Ct-Ot <sup>a</sup>	131.5

<sup>a</sup> Average values.

$[\text{Ir}_6(\text{CO})_{14}(\text{HgCl})_2]^{2-}$  anion is also based on an octahedron of iridium atoms [av. Ir-Ir = 2.818 Å (min 2.746(2); max 2.947(2) Å,  $Q^8 = 4.6$ ], which is capped in meta(1,3)<sup>11</sup> positions by two  $\mu_3$ -HgCl fragments [av Hg-Ir = 2.779 Å (min 2.768; max 2.808 Å)]. Twelve

terminal (two on each iridium atom) and two face-bridging carbonyl ligands complete the coordination around the metal cage. An ORTEP<sup>9</sup> drawing of the whole anion, with partial labeling scheme, is shown in Figure 3. Average bonding values are: Ir-C<sub>term</sub> 1.83; C<sub>term</sub>-O<sub>term</sub> 1.17; Ir-C<sub>br</sub> 2.15; C<sub>br</sub>-O<sub>br</sub> 1.22 Å; Ir-C<sub>term</sub>-O<sub>term</sub> 171; Ir-C<sub>br</sub>-O<sub>br</sub> 131° (term = terminal; br = bridging).

Comparison of homologous bond distances in **3** and **5** is very informative. Ir-Hg interactions are shortened, whereas Hg-Cl interactions are loosened; the same trend is observed in Ir-C and C-O distances, indicating (i) a stronger  $\pi$  back-donation effect in the dianion and (ii) the similar behavior of HgCl and CO in this context.<sup>2</sup>

## Discussion

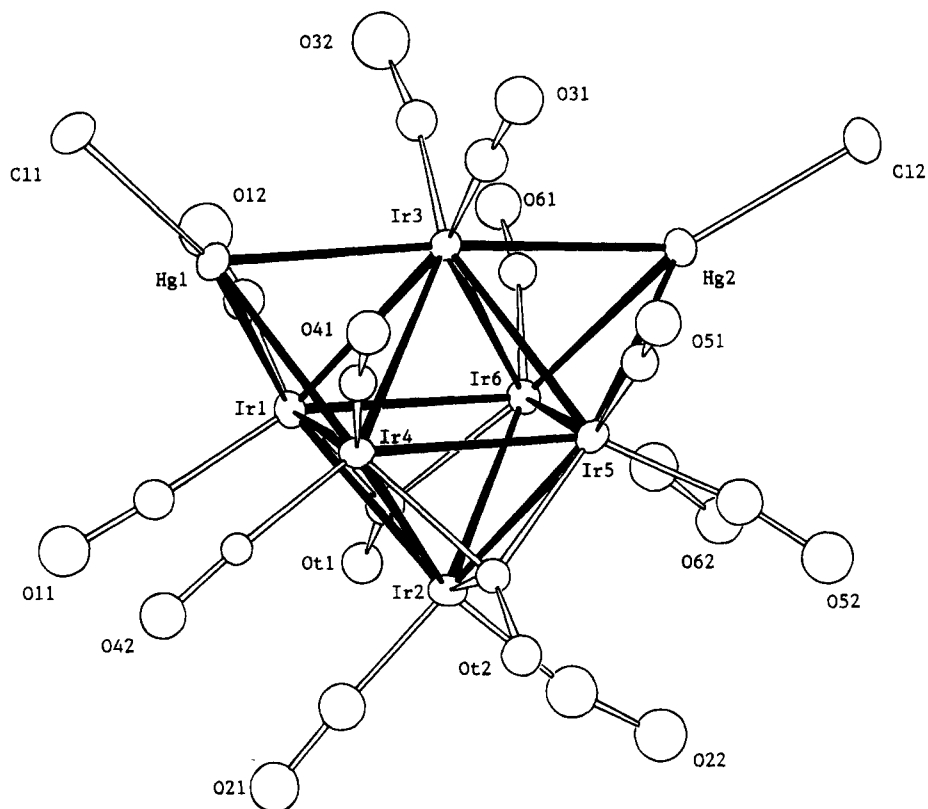
In the following discussion, we want to correlate the different geometries found in mono- and bicapped octahedral clusters.

Addition of a  $\mu_3$ -ML<sub>n</sub> fragment to an octahedral cluster frame (a in Scheme 1) generates a  $C_{3v}$  metal skeleton (b); **1**, **2**, and **3** are examples of this structure.

A further addition of a second metallic fragment can formally occur in three different modes: on using the nomenclature developed in ref 11, *trans*(1,4) ( $D_{3d}$ , c), *meta*(1,3) ( $C_{2v}$ , d), and *cis*(1,2) ( $C_{2v}$ , e) isomers can be formed. Octanuclear carbonyl clusters possessing a trans bicapped octahedral core are exemplified by  $\text{Ru}_6(\text{CO})_{18}[\text{Cu}(\text{C}_7\text{H}_8)]_2$ <sup>12</sup> and several carbido species of rhenium, such as  $[\text{Re}_8\text{C}(\text{CO})_{24}]^{2-}$ ,  $[\text{Re}_7\text{C}(\text{CO})_{21}\text{Pt}(\text{C}_4\text{H}_7)]^{2-}$ ,  $[\text{Re}_7\text{C}(\text{CO})_{21}\text{Ir}(\text{C}_2\text{H}_4)(\text{CO})]^{2-}$ ,  $[\text{Re}_7\text{C}(\text{CO})_{21}\text{Pd}(\text{C}_9\text{H}_9)]^{2-}$ , and

(11) Henly, T. J.; Shapley, J. R.; Rheingold, A. L. *J. Organometal. Chem.*, **1986**, *310*, 55.

(12) Ansell, G. B.; Modrick, M. A.; Bradley, J. S.; *Acta Cryst.*, **1984**, *C40*, 365.



**Figure 3.** ORTEP drawing and atom-labeling scheme for  $[\text{Ir}_6(\text{CO})_{14}(\text{HgCl})_2]^{2-}$ . Thermal ellipsoids are drawn at 30% probability. Carbonyl carbons are designated as the oxygens to which they are attached.

$[\text{Re}_7\text{C}(\text{CO})_{21}(\text{AuPPh}_3)]^{2-}$ ;<sup>11,13</sup> trigonal prisms bicapped on triangular faces are present in the  $[\text{Rh}_6\text{C}(\text{CO})_{15}(\text{ML})_2]$  family ( $M' = \text{Ag}$ ,  $L = \text{CH}_3\text{CN}$ ;  $M' = \text{Cu}$ ,  $\text{Ag}$ ,  $\text{Au}$ ,  $L = \text{PPh}_3$ ).<sup>14</sup>

The *meta*(1,3) bicapping process ideally leads to products possessing a metal skeleton of  $C_{2v}$  symmetry (d), such as those found in  $\text{Pt}_3\text{Ru}_5\text{C}(\text{CO})_{14}(\text{COD})_2$ ,<sup>15</sup>  $[\text{Os}_6\text{Pt}_2(\text{CO})_{17}(\text{COD})_2]$ ,<sup>16</sup>  $\text{Pd}_8(\text{CO})_8(\text{PMe}_3)_7$ ,<sup>17</sup> and in the  $[\text{Os}_8(\text{CO})_{22}]^{2-}$ ,<sup>18</sup>  $[\text{Re}_7\text{Ir}(\text{CO})_{23}]^{3-}$ <sup>19</sup> and  $[\text{Ir}_6(\text{CO})_{14}(\text{HgCl})_2]^{2-}$  anions. Products of *cis*(1,2) addition or clusters containing the metal cores (e) in Scheme 1, are still unknown; however, after a slight distortion the two capping metals can be shifted to within bonding distance of each other, leading to the metallic framework of  $[\text{Rh}_6\text{C}(\text{CO})_{13}(\text{AuPPh}_3)_2]$ <sup>20</sup> and  $[\text{Ru}_6\text{H}(\text{CO})_{16}\text{B}(\text{AuPPh}_3)_2]$ .<sup>6</sup> With different deformations the solid state structures (f) of  $[\text{Ru}_6\text{C}(\text{CO})_{16}(\text{CuL})_2]$ <sup>5</sup> and  $[\text{Ir}_6(\text{CO})_{15}(\text{AuPPh}_3)_2]$  can be attained, without breaking the M–M bond between the heterometal atoms. Considering the fluxional behavior

of the two  $\text{AuPPh}_3$  groups in 4, evidenced by <sup>31</sup>P NMR, this cluster can be conceived as having an average  $C_{2v}$  structure, i.e. (e) or even (g), where a formal  $\text{Au}_2(\text{PPh}_3)_2$  moiety bridges an Ir–Ir edge. This latter description would raise a strong analogy between the black ( $D_{2d}$ ) isomer of  $\text{Ir}_6(\text{CO})_{16}$ ,<sup>3</sup> possessing four symmetrically edge-bridging carbonyls, and compound 4, in which the two-electron donor  $\text{Au}_2(\text{PPh}_3)_2$  fragment formally substitutes one  $\mu$ -CO of the homoleptic cluster.

Finally, compounds 3 and 5 can also be correlated with the simple  $T_d$  geometry of the red isomer of  $\text{Ir}_6(\text{CO})_{16}$ ; as a matter of fact, substitution of  $\mu_3$ -carbonyls of the latter with one or two  $[\text{HgCl}]^-$  fragments leads to the structures of 3 and 5, respectively. In order to avoid a high separation of formal charge,  $[\text{Ir}_6(\text{CO})_{14}(\text{HgCl})_2]^-$ , as 3, should be better considered as an  $\text{Ir}_6(\text{CO})_{16}$  analogue, rather than as an adduct of two  $\text{HgCl}^+$  fragments to the (unknown)  $[\text{Ir}_6(\text{CO})_{14}]^{4-}$ .

Both views agree with electron-counting theories: according to the latter description, each  $[\text{HgCl}]^+$  capping group adds 12 electrons to the total number of CVE's (cluster valence electrons), but does not increase the number of filled skeletal orbitals, as required by the capping principle.<sup>21</sup> In the second case, the  $[\text{HgCl}]^-$  groups can be considered as nonconventional ligands donating two electrons each to the " $\text{Ir}_6(\text{CO})_{14}$ " fragment.

Indeed, EHMO calculations show that  $\text{HgCl}^-$  and CO groups are isolobal fragments, having a filled  $\sigma$  orbital and two empty  $\pi$  orbitals (suitable for back-donation) at comparable energy levels.<sup>22</sup> Moreover, the ability of Hg atoms to act as simple ligands in osmium carbonyl

(13) (a) Ma, L.; Wilson, S. R.; Shapley, J. R. *Inorg. Chem.*, **1990**, 29, 5133. (b) Henly, T. J.; Shapley, J. R.; Rheingold, A. L.; Geib, S. J. *Organometallics*, **1988**, 7, 441. (c) Henly, T. J.; Wilson, S. R.; Shapley, J. R. *Inorg. Chem.*, **1988**, 27, 2551. (d) Henly, T. J.; Shapley, J. R. *Organometallics*, **1989**, 8, 2729.

(14) (a) Albano, V. G.; Braga, D.; Martinengo, S.; Chini, P.; Sansoni, M.; Strumolo, D. *J. Chem. Soc., Dalton Trans.*, **1980**, 52. (b) Fumagalli, A.; Martinengo, S.; Albano, V. G.; Braga, D. *J. Chem. Soc., Dalton Trans.*, **1988**, 1237.

(15) Adams, R.; Wu, W. *J. Cluster Sci.*, **1991**, 2, 271.

(16) Couture, C.; Farrar, D. H.; Goudsmit, R. *J. Inorg. Chim. Acta*, **1984**, 89, L29.

(17) Bochmann, M.; Hawkins, I.; Hursthouse, M. B.; Short, R. L. *Polyhedron*, **1987**, 6, 1987.

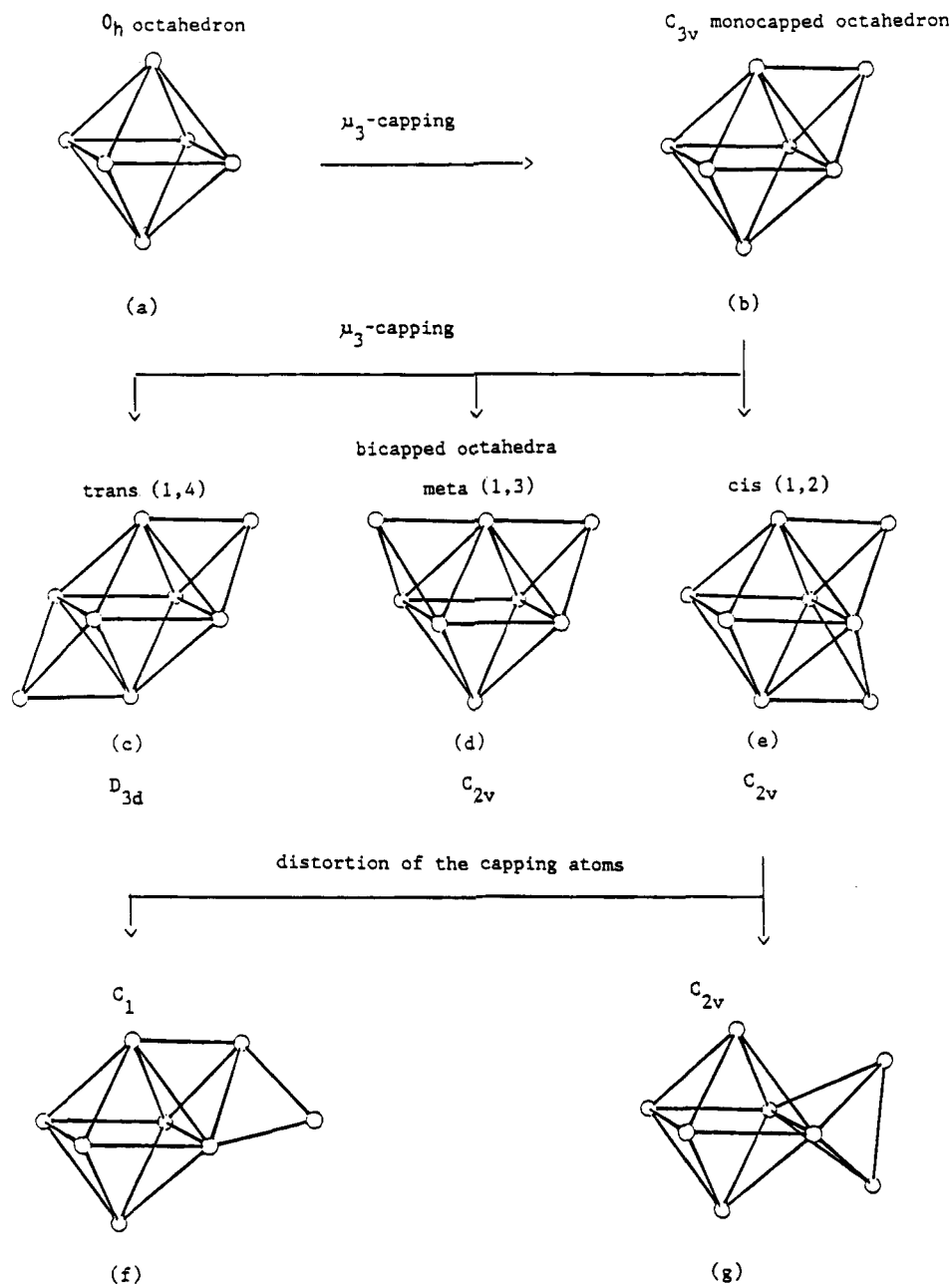
(18) Jackson, P. F.; Johnson, B. F. G.; Lewis, J.; Raithby, P. R. *J. Chem. Soc., Chem. Commun.*, **1980**, 60.

(19) Ma, L.; Wilson, S. R.; Shapley, J. R. *J. Am. Chem. Soc.*, **1994**, 116, 787.

(20) Fumagalli, A.; Martinengo, S.; Albano, V. G.; Braga, D.; Grepioni, F. *J. Chem. Soc., Dalton Trans.*, **1989**, 2343.

(21) (a) D. M. P. Mingos, *Acc. Chem. Res.*, **1984**, 17, 311. (b) D. M. P. Mingos, D. J. Wales, *Introduction to Cluster Chemistry*; Prentice-Hall International: Englewood Cliffs, NJ 1990.

## Scheme 1. Symmetry of Mono- and Bicapped Octahedra



clusters was recently invoked in order to rationalize their fluxional behavior.<sup>23</sup>

Unfortunately, very little data are known for the chemical shift of Hg bound to large clusters, and the value found for **5** cannot therefore be attributed great significance in supporting our proposal.<sup>7</sup> For sake of comparison, it should be noted that the chemical shift of HgCl groups bound to iridium in mononuclear organometallic compounds typically are in the negative range (-2000 to -3000 ppm).<sup>7</sup>

### Experimental Section

All the solvents were purified and dried by conventional methods and stored under nitrogen. All the reactions were carried out under an oxygen-free nitrogen atmosphere using the Schlenk-tube technique.<sup>24</sup>  $[\text{Ir}_6(\text{CO})_{15}]^{2-}$ ,<sup>25</sup>  $[\text{Cu}(\text{NCMe})_4]$ -

$\text{PF}_6$ ,<sup>26</sup> and  $\text{AuPPh}_3\text{Cl}$ <sup>27</sup> were prepared by the published methods. Infrared spectra (IR) were recorded on a Perkin-Elmer 781 grating spectrophotometer using calcium fluoride cells previously purged with  $\text{N}_2$ .

Samples for mass spectra were suspended in a matrix of *m*-nitrobenzyl alcohol and bombarded with a beam of Xe atoms at 70 keV with a VG Micromass machine and compared with computed theoretical isotope patterns; mass peaks refer to the most abundant isotopomers. Elemental analyses were carried out by the staff of Laboratorio di Analisi of the Dipartimento di Chimica Inorganica, Metallorganica e Analitica. <sup>31</sup>P and <sup>199</sup>Hg NMR spectra were recorded on a Bruker AC200 spectrometer, operating at 81.0 MHz for phosphorus and at 35.76 MHz for mercury and are reported in ppm downfield from the

(24) D. F. Shriver, M. A. Drezdson, in *The Manipulation of Air-sensitive Compounds*, 2nd ed.; Wiley: New York, 1986.

(25) Angoletta, M.; Malatesta, L.; Caglio, G. *J. Organometal. Chem.*, **1975**, *94*, 99.

(26) Kubas, G. J. *Inorg. Synth.*, **1979**, *19*, 311.

(27) Bruce, M. I.; Nicholson, B. K.; Shawkataly, O. B. *Inorg. Synth.*, **1989**, *26*, 325.

(22) CACAO, Mealli, C.; Proserpio, D. M. *J. Chem. Ed.*, **1990**, *67*, 399.

(23) Gade, L. H. *Angew. Chem. Int. Ed. Engl.*, **1993**, *32*, 24.

Table 3. Crystal Data and Data Collection Parameters

compd	4	5a
formula	C <sub>51</sub> H <sub>30</sub> Au <sub>2</sub> Ir <sub>6</sub> O <sub>15</sub> P <sub>2</sub>	C <sub>62</sub> H <sub>40</sub> Cl <sub>2</sub> Hg <sub>2</sub> Ir <sub>6</sub> O <sub>14</sub> P <sub>2</sub>
fw	2491.9	2696.2
cryst syst	triclinic	monoclinic
space group	P $\bar{1}$	Cc
a, Å	13.160(2)	10.257(2)
b, Å	13.714(4)	46.848(4)
c, Å	18.266(3)	14.639(3)
$\alpha$ , deg	65.47(2)	90
$\beta$ , deg	110.93(2)	107.83(2)
$\gamma$ , deg	112.07(1)	90
V, Å <sup>3</sup>	2699(2)	6696(4)
Z	2	4
D <sub>calcd</sub> , g cm <sup>-3</sup>	3.066	2.674
$\mu$ (Mo K $\alpha$ ), cm <sup>-1</sup>	202.06	165.85
min. trans. fact.	0.70	0.22
scan mode	$\omega$	$\omega$
$\omega$ -scan width, deg	1.2 + 0.35 tan $\theta$	1.2 + 0.35 tan $\theta$
$\theta$ -range, deg	3-27	3-25
octants of reciprocal space explored	$\pm h, \pm k, l$	$\pm h, k, l$
measd reflns	12197	6182
unique obsd reflns with $I > 3\sigma(I)$	7217	3619
final R and R <sub>w</sub> <sup>a</sup>	0.032, 0.034	0.037, 0.036
no. of variables	505	411

$$^a R = [\sum |F_o - k|F_c| / \sum F_o] \text{ and } R_w = [\sum w(F_o - k|F_c|)^2 / \sum wF_o^2]^{1/2}.$$

external standard (85% H<sub>3</sub>PO<sub>4</sub> in D<sub>2</sub>O for phosphorus and neat Me<sub>2</sub>Hg for mercury).<sup>2</sup>

**Preparation of [Ir<sub>6</sub>(CO)<sub>15</sub>(CuNCMe)<sub>2</sub>].** (PPh<sub>4</sub>)<sub>2</sub>[Ir<sub>6</sub>(CO)<sub>15</sub>] (90 mg; 40  $\mu$ mol), CH<sub>2</sub>Cl<sub>2</sub> (5 mL), [Cu(NCMe)<sub>4</sub>]PF<sub>6</sub> (30 mg; 80  $\mu$ mol) were placed in a Schlenk tube under nitrogen; infrared spectra showed complete conversion after 10 min stirring; cyclohexane (5 mL) was added and the colourless precipitate of (PPh<sub>4</sub>)PF<sub>6</sub> was eliminated by filtration. The red solution was layered with cyclohexane. On standing overnight, well shaped orange crystals of Ir<sub>6</sub>(CO)<sub>16</sub> and Cu metal were formed.

**Preparation of [Ir<sub>6</sub>(CO)<sub>15</sub>(AuPPh<sub>3</sub>)<sub>2</sub>] in 2-Propanol.** AuPPh<sub>3</sub>Cl (490 mg; 0.98 mmol) and THF (10 mL) were placed in a Schlenk tube. When the solid was dissolved, AgBF<sub>4</sub> (185 mg; 0.95 mmol) was added, causing the precipitation of AgCl which was allowed to settle for 10 min. K<sub>2</sub>[Ir<sub>6</sub>(CO)<sub>15</sub>] was dissolved with 2-propanol (30 mL) and filtered; the salt could not be weighed, since there were too large amounts of KCl present; it was estimated 350 mg (0.21 mmol). Small portions (2 mL each) of the solution of [AuPPh<sub>3</sub>]BF<sub>4</sub> were added, while monitoring the disappearance of [Ir<sub>6</sub>(CO)<sub>15</sub>]<sup>2-</sup> by infrared. When the reaction was complete, about one half of the solvent was evaporated *in vacuo*. The black solid was filtered, washed with 2-propanol (5 mL), and dried. It was then extracted with CH<sub>2</sub>Cl<sub>2</sub> and layered with 2-propanol.

**Preparation of [Ir<sub>6</sub>(CO)<sub>15</sub>(AuPPh<sub>3</sub>)<sub>2</sub>] in CH<sub>2</sub>Cl<sub>2</sub>.** A solution of [AuPPh<sub>3</sub>]BF<sub>4</sub> was prepared in a Schlenk tube under nitrogen with AuPPh<sub>3</sub>Cl (900 mg; 1.81 mmol), CH<sub>2</sub>Cl<sub>2</sub> (15 mL) and AgBF<sub>4</sub> (336 mg; 1.71 mmol). (NEt<sub>4</sub>)<sub>2</sub>[Ir<sub>6</sub>(CO)<sub>15</sub>] (350 mg; 0.19 mmol) was dissolved in CH<sub>2</sub>Cl<sub>2</sub> (15 mL), and small fractions of the first solution were added, monitoring the reaction by infrared. Total conversion was achieved after addition of 12 mL (molar ratio Ir<sub>6</sub>:Au = 1:7). The initially brown solution became red and, eventually, green. Addition of cyclohexane (15 mL) caused precipitation of colourless NEt<sub>4</sub>BF<sub>4</sub>, which was eliminated by filtration. The solution was dried, and the residue was dissolved in CH<sub>2</sub>Cl<sub>2</sub> and layered with 2-propanol. Yield 58%.

Anal. Calcd for C<sub>51</sub>H<sub>30</sub>Au<sub>2</sub>Ir<sub>6</sub>O<sub>15</sub>P<sub>2</sub>: C, 24.2; H, 1.2. Found: C, 24.26; H, 1.37.

FAB-MS (negative ions)  $m/z$ : 2037 [Ir<sub>6</sub>(CO)<sub>15</sub>AuPPh<sub>3</sub>]<sup>-</sup>; 2037 - 28x (x = 1-5) [Ir<sub>6</sub>(CO)<sub>15-x</sub>AuPPh<sub>3</sub>]<sup>-</sup>; the parent peak was never observed, either with electron impact or in the positive FAB region.

**Preparation of [Ir<sub>6</sub>(CO)<sub>14</sub>(HgCl<sub>2</sub>)<sub>2</sub>]<sup>2-</sup> from HgCl<sub>2</sub>.** (PPh<sub>4</sub>)<sub>2</sub>[Ir<sub>6</sub>(CO)<sub>15</sub>] (460 mg; 0.204 mmol), THF (20 mL), HgCl<sub>2</sub> (98 mg;

Table 4. Fractional Atomic Coordinates for [Ir<sub>6</sub>(CO)<sub>15</sub>(AuPPh<sub>3</sub>)<sub>2</sub>] (4) (Esd's in Parentheses)

atom	x/a	y/b	z/c
Au1	-0.31720(4)	0.49610(4)	0.25443(3)
Au2	-0.21608(4)	0.31816(4)	0.31209(4)
Ir1	-0.08140(4)	0.52205(4)	0.30067(3)
Ir2	0.01660(4)	0.55182(4)	0.17956(3)
Ir3	-0.05317(4)	0.74338(4)	0.07945(3)
Ir4	-0.15521(4)	0.71233(4)	0.20160(3)
Ir5	-0.21007(4)	0.54477(4)	0.12888(3)
Ir6	0.07365(4)	0.72841(4)	0.23976(3)
P1	-0.4943(2)	0.4568(3)	0.2716(2)
P2	-0.2936(3)	0.1316(3)	0.3417(2)
Ob1	-0.1758(9)	0.6135(9)	-0.0418(6)
Ob2	0.2513(7)	0.5968(8)	0.2894(7)
Ob3	0.0018(8)	0.9462(7)	0.1775(8)
O11	0.0806(9)	0.3837(9)	0.4106(7)
O12	-0.1260(9)	0.520(1)	0.4516(7)
O21	0.0956(8)	0.5828(9)	0.0313(7)
O22	0.000(1)	0.3056(8)	0.2412(9)
O31	-0.151(1)	0.9384(8)	-0.0278(7)
O32	0.1424(9)	0.848(1)	-0.0014(8)
O41	-0.198(1)	0.737(1)	0.3445(7)
O42	-0.3474(8)	0.8111(9)	0.0745(7)
O51	-0.263(1)	0.3268(8)	0.1033(8)
O52	-0.4430(8)	0.581(1)	0.0403(7)
O61	0.2756(8)	0.9097(8)	0.1850(7)
O62	0.1397(9)	0.716(1)	0.4189(7)
Cb1	-0.157(1)	0.628(1)	0.0209(9)
Cb2	0.164(1)	0.606(1)	0.2542(9)
Cb3	-0.022(1)	0.848(1)	0.192(1)
C11	0.021(1)	0.435(1)	0.3706(9)
C12	-0.115(1)	0.520(1)	0.3944(8)
C21	0.072(1)	0.574(1)	0.0890(9)
C22	0.007(1)	0.399(1)	0.218(1)
C31	-0.115(1)	0.863(1)	0.012(1)
C32	0.069(1)	0.808(1)	0.030(1)
C41	-0.185(1)	0.725(1)	0.290(1)
C42	-0.276(1)	0.773(1)	0.1251(9)
C51	-0.247(1)	0.407(1)	0.1170(9)
C52	-0.359(1)	0.563(1)	0.076(1)
C61	0.199(1)	0.841(1)	0.2045(8)
C62	0.114(1)	0.717(1)	0.3513(9)
C111	-0.604(1)	0.344(1)	0.2345(9)
C112	-0.574(1)	0.296(1)	0.1947(9)
C113	-0.654(1)	0.207(1)	0.170(1)
C114	-0.759(1)	0.169(1)	0.185(1)
C115	-0.787(1)	0.218(1)	0.224(1)
C116	-0.710(1)	0.312(1)	0.2478(9)
C121	-0.4995(9)	0.417(1)	0.3801(8)
C122	-0.593(1)	0.416(1)	0.3995(9)
C123	-0.595(1)	0.378(1)	0.484(1)
C124	-0.506(1)	0.344(1)	0.545(1)
C125	-0.409(1)	0.350(1)	0.525(1)
C126	-0.408(1)	0.385(1)	0.442(1)
C131	-0.5431(9)	0.582(1)	0.2168(8)
C132	-0.618(1)	0.598(1)	0.1396(9)
C133	-0.641(1)	0.703(1)	0.094(1)
C134	-0.588(1)	0.788(1)	0.130(1)
C135	-0.510(1)	0.769(1)	0.2088(9)
C136	-0.491(1)	0.669(1)	0.2483(9)
C211	-0.432(1)	0.080(1)	0.3634(9)
C212	-0.460(1)	0.147(1)	0.3911(9)
C213	-0.566(1)	0.108(1)	0.411(1)
C214	-0.640(1)	0.007(1)	0.404(1)
C215	-0.611(1)	-0.053(1)	0.377(1)
C216	-0.507(1)	-0.017(1)	0.3551(9)
C221	-0.311(1)	0.085(1)	0.2571(9)
C222	-0.406(1)	0.095(1)	0.1906(9)
C223	-0.415(1)	0.074(1)	0.120(1)
C224	-0.331(1)	0.038(1)	0.114(1)
C225	-0.236(1)	0.026(1)	0.181(1)
C226	-0.227(1)	0.046(1)	0.256(1)
C231	-0.206(1)	0.056(1)	0.4330(9)
C232	-0.118(1)	0.114(1)	0.484(1)
C233	-0.061(1)	0.048(1)	0.558(1)
C234	-0.085(1)	-0.067(1)	0.583(1)
C235	-0.171(1)	-0.123(1)	0.532(1)
C236	-0.230(1)	-0.061(1)	0.459(1)

**Table 5. Fractional Atomic Coordinates for the Anion  $[\text{Ir}_6(\text{CO})_{14}(\text{HgCl}_2)_2]^{2-}$  (5) (Esd's in Parentheses)**

atom	<i>x/a</i>	<i>y/b</i>	<i>z/c</i>
Hg1	0.0	0.14913(3)	0.0
Hg2	0.2484(2)	0.05208(3)	0.1863(1)
Ir1	0.0426(2)	0.14359(3)	0.1980(1)
Ir2	0.3139(2)	0.14387(3)	0.3188(1)
Ir3	0.1177(2)	0.09953(3)	0.0870(1)
Ir4	0.2663(2)	0.15307(3)	0.1245(1)
Ir5	0.3905(1)	0.10363(3)	0.2085(1)
Ir6	0.1623(2)	0.09430(3)	0.2879(1)
Cl1	-0.1217(8)	0.1637(2)	-0.1644(5)
Cl2	0.2913(9)	0.0017(2)	0.1887(6)
Ot1	0.074(2)	0.1384(5)	0.408(1)
Ot2	0.574(2)	0.1572(5)	0.245(1)
O11	-0.019(3)	0.2057(6)	0.214(2)
O12	-0.239(3)	0.1232(6)	0.150(2)
O21	0.314(2)	0.2029(6)	0.387(2)
O22	0.525(3)	0.1205(6)	0.491(2)
O31	0.208(2)	0.0801(5)	-0.083(2)
O32	-0.155(3)	0.0733(7)	0.023(2)
O41	0.345(2)	0.1506(5)	-0.064(2)
O42	0.263(2)	0.2149(5)	0.143(2)
O51	0.508(2)	0.0911(5)	0.043(2)
O52	0.632(3)	0.0762(6)	0.351(2)
O61	-0.092(2)	0.0602(5)	0.257(2)
O62	0.309(2)	0.0671(5)	0.478(2)
Ct2	0.107(3)	0.1321(7)	0.337(2)
Ct2	0.460(3)	0.1467(6)	0.224(2)
C11	0.015(3)	0.1825(8)	0.205(2)
C12	-0.123(3)	0.1304(7)	0.168(2)
C21	0.316(4)	0.1798(9)	0.355(2)
C22	0.452(4)	0.133(1)	0.426(3)
C31	0.176(3)	0.0892(8)	-0.019(2)
C32	-0.035(3)	0.0819(7)	0.047(2)
C41	0.317(3)	0.1536(7)	0.006(2)
C42	0.266(2)	0.1915(6)	0.129(2)
C51	0.463(3)	0.0939(7)	0.108(2)
C52	0.536(4)	0.0852(9)	0.292(3)
C61	0.011(3)	0.0709(7)	0.264(2)
C62	0.258(4)	0.0750(9)	0.403(3)

0.36 mmol) and  $\text{Na}_2\text{CO}_3 \cdot 10\text{H}_2\text{O}$  (77 mg; 0.27 mmol) were placed in a Schlenk tube under nitrogen. The reaction mixture was stirred vigorously for 12 days at room temperature. A black insoluble residue was slowly formed, while the colour of the clear solution turned red. Small amounts of  $\text{HgCl}_2$  and  $\text{Na}_2\text{CO}_3$  were then added, and the stirring continued for 5 more days. The disappearance of  $[\text{Ir}_6(\text{CO})_{15}\text{HgCl}]^-$  could be followed by monitoring the infrared band of the bridging carbonyls at  $1765\text{ cm}^{-1}$ . When the reaction was complete, the solution was cautiously filtered and dried *in vacuo*. The red residue was dissolved in  $\text{CH}_2\text{Cl}_2$  and layered with cyclohexane. Yield: 425 mg, 78%.

The cluster is well soluble in THF,  $\text{CH}_2\text{Cl}_2$ , and acetone. It decomposes when exposed to protic solvents, such as alcohols or water.

Anal. Calcd for  $\text{C}_{62}\text{H}_{40}\text{Cl}_2\text{Hg}_2\text{Ir}_6\text{P}_2\text{O}_{14}$ : C, 27.6; H, 1.5. Found: C, 28.2; H, 1.46. The compound is always impure with uncharacterized thin, colorless, needles.

The FAB-MS immediately recorded showed a broad, unresolved signal at  $m/z = 2008$ , corresponding to the parent peak. However, fast decomposition of the cluster with the matrix did not permit the recording of satisfactory spectra.

**Preparation of  $[\text{Ir}_6(\text{CO})_{14}(\text{HgCl}_2)_2]^{2-}$  from  $\text{Hg}_2\text{Cl}_2$ .**  $(\text{PPh}_3)_2[\text{Ir}_6(\text{CO})_{15}]$  (493 mg; 0.219 mmol), THF (20 mL), and  $\text{Hg}_2\text{Cl}_2$

(103 mg; 0.219 mmol) were placed in a Schlenk tube under nitrogen. A grey insoluble residue immediately formed, while the colour of the clear solution turned red. The reaction mixture was stirred vigorously for 15 days at room temperature. The product was treated as above described, with comparable yields (420 mg; 71%) and higher purity.

Anal. Calcd for  $\text{C}_{62}\text{H}_{40}\text{Cl}_2\text{Hg}_2\text{Ir}_6\text{P}_2\text{O}_{14}$ : C, 27.6; H, 1.5. Found: C, 27.33; H, 1.66.

**X-Ray Collections and Structural Refinements.** A summary of crystal data parameters and some experimental details are collected in Table 3. Crystals of the two compounds were mounted in arbitrary orientation on the tip of a glass fibre mounted onto a goniometer head. Diffraction data were collected on an Enraf-Nonius CAD4 automated diffractometer using Mo  $K\alpha$  radiation ( $\lambda = 0.71073\text{ \AA}$ ), equipped with a pyrolytic graphite crystal monochromator in the incident beam. Cell dimensions were obtained by the least-squares method on the setting angles of 25 intense reflections, randomly distributed in the reciprocal space, having  $9 < \theta < 11^\circ$ . Periodic measurements of three standard reflections revealed a crystal decay, on X-ray exposure, which was evaluated as null for **4** and 22% for **5a** (on *I*) at the end of data collection. Lorentz, polarization, decay and absorption corrections were applied, the latter performed with the empirical method described in ref 28.

The structures were solved by Direct Methods (MULTAN),<sup>29</sup> which succeeded in locating the metal atoms; the coordinates of the remaining non-hydrogen atoms were determined by successive least-squares refinements and difference Fourier maps. The refinements were carried out by full-matrix least squares with anisotropic temperature factors for Ir, Hg, Au, Cl, P and, for **4**, also for carbonyl atoms. Individual weights were given as:  $w = A/[\sigma^2(F_o) + BF_o^2]$ , with  $A = 1.3353$ ,  $1.0646$  and  $B = 0.000572$ ,  $0.000824$  for **4** and **5a**, respectively. Scattering factors, corrected for real and imaginary anomalous dispersion terms, were taken from ref 30; the contribution of the hydrogen atoms to the scattering factors was neglected. The absolute structure of the crystal of **5a** was tested by refining two inverted models; tabulated values refer to that having the lowest agreement discrepancy. All computations were performed on a Silicon Graphics Indigo computer, running IRIX 4.1, using SHELX.<sup>31</sup> The positional parameters for **4** and **5a** are listed in Tables 4 and 5, respectively.

**Acknowledgment.** We acknowledge the Ministero della Ricerca Scientifica for funding and the Consiglio Nazionale delle Ricerche for use of NMR equipments.

**Supplementary Material Available:** Tables of fractional atomic coordinates and isotropic thermal parameters and of all bond distances and angles for **4a** and **5a** (11 pages). Ordering information is given on any current masthead page.

OM940557L

(28) North, A. C. T.; Phillips, D. C.; Mathews, F. S.; Acta Cryst., Sect. A.: Cryst. Phys. Diff. Theor., Gen. Crystallogr. **1968**, A24, 351.

(29) Germain, G.; Main, P.; Woolfson, M. M. MULTAN, a system of computer programs for the automatic solution of crystal structures from X-ray diffraction data. Acta Crystallogr., **1971**, A27, 368.

(30) International Tables for X-Ray Crystallography; Kynoch Press: Birmingham, England, 1974; Vol. 4.

(31) Sheldrick, G. M. SHELX76, A program for crystal structure determination, University of Cambridge, 1976.

# Use of the 2,6-Bis[(dimethylamino)methyl]phenyl Ligand for the Study of Nucleophilic Substitution at Hexacoordinate Silicon Centers. Evidence Suggestive of a Heptacoordinate Silicon Transition State

Francis Carré, Claude Chuit, Robert J. P. Corriu,\* Alan Fanta,<sup>†</sup>  
Ahmad Mehdi, and Catherine Reyé

Laboratoire Hétérochimie et Amino-Acides CNRS, URA 1097, Université Montpellier II,  
Sciences et Techniques du Languedoc, Place E. Bataillon, 34095 Montpellier Cedex 5, France

Received July 7, 1994<sup>®</sup>

Two silicates bearing the potentially bis chelating ligand Ar = (C<sub>6</sub>H<sub>3</sub>(CH<sub>2</sub>NMe<sub>2</sub>)<sub>2</sub>-2,6) have been made with the objective of studying nucleophilic substitution reactions at hexacoordinate silicon. The X-ray crystal structure of the silicate [ArSi(O<sub>2</sub>C<sub>6</sub>H<sub>4</sub>-1,2)<sub>2</sub>]<sup>-</sup>PPN<sup>+</sup>, **3b**, has revealed that the anion exhibits slightly distorted octahedral geometry, with only one NMe<sub>2</sub> being coordinated to the silicon. Furthermore, the results of solution NMR studies of **3b** and [ArSiF<sub>4</sub>]<sup>-</sup>[K, 18-crown-6]<sup>+</sup>, **4**, are consistent with dynamic coordination, in which the NMe<sub>2</sub> groups are displacing each other through a heptacoordinate transition state and the central silicon atom is essentially hexacoordinated.

Initial experiments have indicated poor reactivity of hexafluorosilicate<sup>1</sup> and organopentafluorosilicates<sup>2,3</sup> toward Grignard reagents. However, further studies have confirmed the reactivity of hexacoordinate silicon complexes toward nucleophiles and have shown that this reactivity is highly dependent on the substituents around the silicon atom.<sup>4,5,6</sup> While hexacoordinate silicon species with Si-C bonds have been isolated<sup>7,8,9</sup> and often invoked as intermediates in the course of nucleophilic substitution at pentacoordinate silicon, the nature of the mechanism of nucleophilic displacement at hexacoordinate silicon compounds is unclear. Direct attack of a nucleophile at the silicon center with formation of a heptacoordinate intermediate (or transition state) is a possibility which deserves to be considered, especially since X-ray crystal structures of (4+3)<sup>10a,b</sup> and even (4+4)<sup>10b,11</sup> coordinate silicon compounds have been established.

<sup>†</sup> Present address: 3M Company, Bldg. 201-4N.01, St. Paul, MN 55144-1000.

<sup>®</sup> Abstract published in *Advance ACS Abstracts*, November 1, 1994.  
(1) Soshestvenskaya, E. M. *Zh. Obshch. Khim.* **1952**, *22*, 1122; *Chem. Abstr.* **1953**, *47*, 8030d.

(2) Müller, R. *Z. Chem.* **1965**, *5*, 220.  
(3) Tamao, K.; Mishima, M.; Yoshida, J.; Takahashi, M.; Ishida, N.; Kumada, M. *J. Organomet. Chem.* **1982**, *225*, 151.

(4) (a) Boudin, A.; Cerveau, G.; Chuit, C.; Corriu, R. J. P.; Reyé, C. *Angew. Chem., Int. Ed. Engl.* **1986**, *25*, 474. (b) Boudin, A.; Cerveau, G.; Chuit, C.; Corriu, R. J. P.; Reyé, C. *Organometallics* **1988**, *7*, 1165.

(5) Ray, D. J.; Laine, R. M.; Viney, C.; Robinson, T. R. *Polym. Prepr. (Am. Chem. Soc., Div. Polym. Chem.)* **1991**, *32*, 550.

(6) Brelière, C.; Corriu, R. J. P.; Royo, G.; Wong Chi Man, W. W. C.; Zwecker, J. *Organometallics* **1990**, *9*, 2633.

(7) Brelière, C.; Carré, F.; Corriu, R. J. P.; Poirier, M.; Royo, G.; Zwecker, J. *Organometallics* **1989**, *8*, 1831.

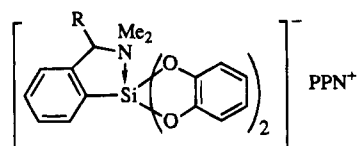
(8) Brelière, C.; Corriu, R. J. P.; Royo, G.; Zwecker, J. *Organometallics* **1989**, *8*, 1834.

(9) Carré, F.; Cerveau, G.; Chuit, C.; Corriu, R. J. P.; Reyé, C. *New J. Chem.* **1992**, *16*, 63.

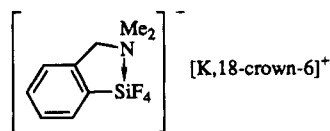
(10) (a) Brelière, C.; Carré, F.; Corriu, R. J. P.; Royo, G.; Wong Chi Man, M. *Organometallics* **1994**, *13*, 307. (b) We have adopted the nomenclature (4+n) to describe the geometry of compounds corresponding to capped tetrahedrons: four covalent bonds around the silicon atom + n coordinative interactions.

(11) Carré, F.; Chuit, C.; Corriu, R. J. P.; Mehdi, A.; Reyé, C. *Angew. Chem.* **1994**, *106*, 1152; *Angew. Chem., Int. Ed. Engl.* **1994**, *33*, 1097.

The structure of the silicate **1a**<sup>12</sup> exposed the quasi



**1 a** : R = H  
**b** : R = Me



**2**

octahedral geometry of the anion, and solution NMR studies of the silicate **2**<sup>13</sup> suggested an arrangement about the silicon atom consistent with an octahedral geometry. In this paper, dynamic NMR studies of silicates **3b** and **4**, in which heptacoordination at silicon can be achieved by chelation of both NMe<sub>2</sub> groups, as well as the determination of the X-ray structure of **3b** were completed. From these data, a mechanistic approach of nucleophilic displacement on anionic hexacoordinate silicon species will be proposed.

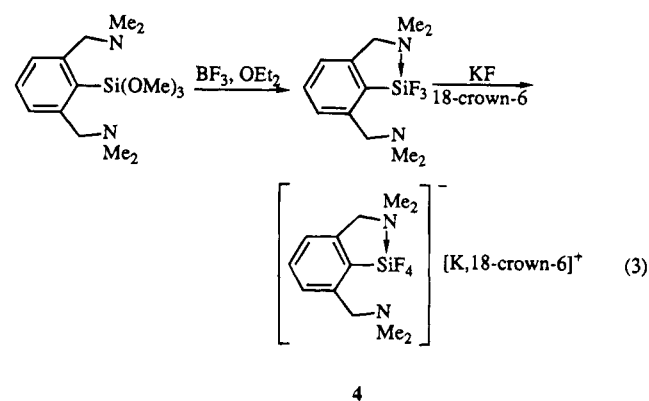
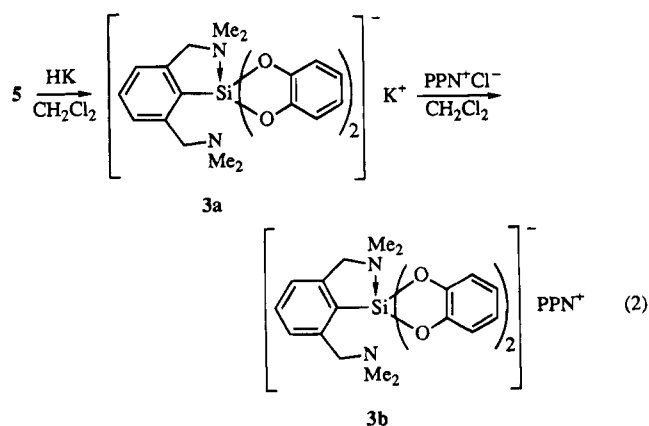
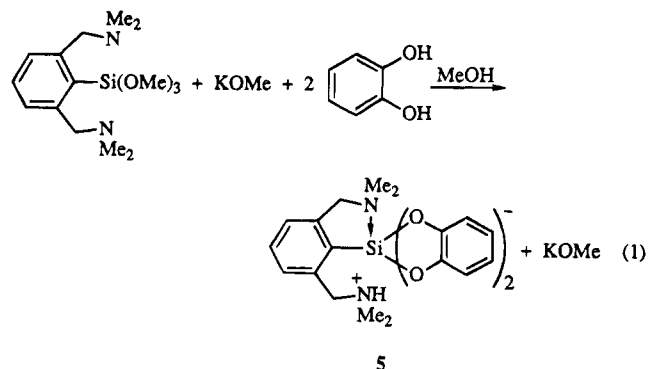
## Results and Discussion

**Synthesis of 3 and 4.** The preparation of **3a** was noteworthy in that it was not possible to synthesize it from the classical exchange reaction between catechol and [2,6-bis[(dimethylamino)methyl]phenyl]trimethoxysilane in methanol. The reaction produced zwitterion **5**<sup>14</sup> instead of the expected silane **3a** (eq 1). However, treatment of **5** with potassium hydride in CH<sub>2</sub>-

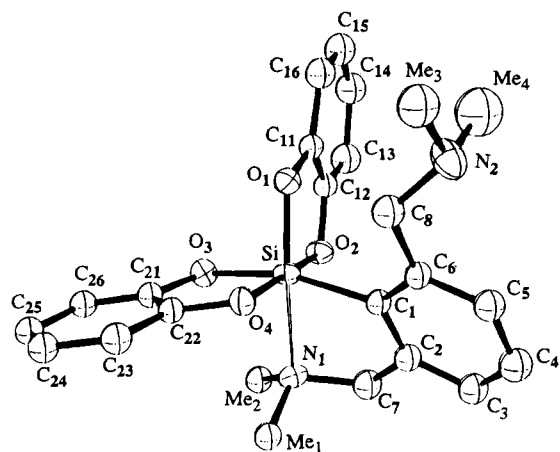
(12) Carré, F.; Cerveau, G.; Chuit, C.; Corriu, R. J. P.; Reyé, C. *Angew. Chem., Int. Ed. Engl.* **1989**, *28*, 489.

(13) Brelière, C.; Carré, F.; Corriu, R. J. P.; Douglas, W.; Poirier, M.; Royo, G.; Wong Chi Man, M. *Organometallics* **1992**, *11*, 1586.

$\text{Cl}_2$  resulted in **3a** quantitatively, which was transformed into **3b** by methathesis with bis(triphenylphosphoranylidene)ammonium chloride (PPNCl) (eq 2). Suitable crystals for X-ray structural analysis were grown from a saturated solution of **3b** in  $\text{CH}_2\text{Cl}_2/\text{Et}_2\text{O}$  cooled at  $-40^\circ\text{C}$ . Fluorosilicate **4** preparation was analogous to that of **2**<sup>13</sup> (eq 3). The silicate was air-stable and decomposed only slowly in solvent solutions open to the atmosphere.



**Structure of 3b in the Solid State.** The ORTEP drawing of **3b** is shown in Figure 1. Selected bond distances and angles are given in Table 1, and other crystallographic details are given in Tables 2 and 3. The X-ray structure determination of **3b** showed that the anion adopted a slightly distorted octahedral geometry with one dimethylamino group coordinated to the silicon atom ( $\text{Si}-\text{N}(1) = 2.173 \text{ \AA}$ ), while the second dimethylamino group was directed away from the silicon center ( $\text{Si}-\text{N}(2) = 4.792 \text{ \AA}$ ) without intermolecular bonding

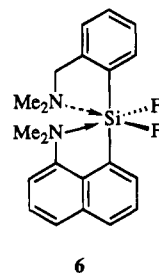


**Figure 1.** ORTEP drawing of the molecular structure of silicate **3b** showing the numbering scheme. The thermal ellipsoids and spheres are at the 30% probability level.

**Table 1.** Selected Interatomic Distances ( $\text{\AA}$ ) and Main Bond Angles (deg) in Silicate **3b**

Si-O1	1.767(5)	O1-Si-C1	100.5(3)
Si-O2	1.787(5)	O1-Si-O2	89.1(3)
Si-O3	1.795(5)	O1-Si-O3	94.2(3)
Si-O4	1.793(5)	O1-Si-O4	93.6(3)
Si-C1	1.954(7)	C1-Si-O2	95.8(3)
Si-N1	2.173(6)	O2-Si-O3	88.2(2)
Si-C8	3.464(9)	O3-Si-O4	86.6(2)
Si-N2	4.792(5)	O4-Si-C1	88.6(3)
O1-C11	1.338(9)	N1-Si-C1	81.0(3)
O2-C12	1.355(9)	N1-Si-O2	81.3(3)
C11-C12	1.360(11)	N1-Si-O3	85.3(3)
O3-C21	1.353(9)	N1-Si-O4	95.9(3)
O4-C22	1.345(8)	Si-C1-C6	128.8(5)
C21-C22	1.388(10)	Si-C1-C2	113.9(5)
C1-C2	1.394(10)	C1-C6-C8	122.8(7)
C1-C6	1.408(10)	C1-C2-C7	117.6(7)
O1-Si-N1	170.4(3)	C2-C7-N1	107.8(6)
O2-Si-O4	174.3(3)	C7-N1-Si	103.2(5)
O3-Si-C1	164.9(3)	C2-C1-C6	117.2(7)

interaction. Thus, the octahedral geometry previously found for complex **1a**<sup>12</sup> was maintained in **3b**. However, the octahedron was slightly more distorted with angles around the silicon atom being  $170.4^\circ$  (3),  $174.3^\circ$  (3), and  $164.9^\circ$  (3), whereas in **1a** they were  $167.3^\circ$  (4),  $172.6^\circ$  (3), and  $175.2^\circ$  (3), respectively. The dative Si-N bond in **1a**<sup>12</sup> was  $2.157 \text{ \AA}$ , which was not significantly different from that observed in **3b** ( $2.173 \text{ \AA}$ ). These values are short compared to those previously reported for the neutral hexacoordinate silicon compound **6**<sup>7</sup> ( $2.77$



and  $2.80 \text{ \AA}$ ). This is an illustration of the electrophilicity of the silicon atom in these derivatives, were the ligand

(15) Boudin, A.; Cerveau, G.; Chuit, C.; Corriu, R. J. P.; Reyé, C. *Bull. Chem. Soc. Jpn.* **1988**, *61*, 101.

(16) Handwerker, H.; Leis, C.; Probst, R.; Bissinger, P.; Grohmann, A.; Kiprof, P.; Herdtweck, E.; Blümel, J.; Auner, N.; Zybilla, C. *Organometallics* **1993**, *12*, 2162.

(14) Carré, F.; Chuit, C.; Corriu, R. J. P.; Mehdi, A.; Reyé, C. *J. Organomet. Chem.* **1993**, *446*, C6.



**Table 2. Summary of Crystal Data, Intensity Measurements, and Refinement**

formula	C <sub>61</sub> H <sub>59</sub> Cl <sub>2</sub> N <sub>3</sub> O <sub>4</sub> P <sub>2</sub> Si
cryst system	orthorhombic
space group	<i>P</i> 2 <sub>1</sub> 2 <sub>1</sub> 2 <sub>1</sub>
<i>a</i> , Å	9.9612(15)
<i>b</i> , Å	33.551(8)
<i>c</i> , Å	16.415(2)
vol, Å <sup>3</sup>	5486.2
mol wt	1059.1
<i>Z</i>	4
<sup>d</sup> calcd, g cm <sup>-3</sup>	1.282
<sup>d</sup> measd, g cm <sup>-3</sup>	1.28(1)
cryst size, mm <sup>3</sup>	0.32 × 0.45 × 0.50
cryst color	colorless
recryst solv	CH <sub>2</sub> Cl <sub>2</sub> /ether, 9:1
mp, °C	176–178
method of data collect	ω/θ
Radiant (graphite monochromated)	Mo Kα
μ, cm <sup>-1</sup>	2.44
2θ limits, deg	4–50
no. of unique reflns	8506
no. of obsd reflns	4405
final no. of variables	357
<i>R</i>	0.056
<i>R</i> <sub>w</sub>	0.060
residual electron density	0.71

geometry does not impose intramolecular coordination to the silicon center due to the freedom of motion allowed to the NMe<sub>2</sub> groups in the benzylic position.

**Dynamic NMR Studies of 3b in Solution.** The <sup>29</sup>Si NMR chemical shift of **3b** was in the range expected for a hexacoordinate bis(benzene-1,2-diolato)silicate with the resonance occurring at δ = -127.2 ppm in the

solid state and at δ = -129.4 in solution (CD<sub>2</sub>Cl<sub>2</sub>, 200 MHz), with that of **1a** being at δ = -121.2 ppm (CD<sub>2</sub>-Cl<sub>2</sub>). These values were markedly upfield with respect to that of the pentacoordinate phenylbis(benzene-1,2-diolato)silicate<sup>15</sup> (δ = -87.4 ppm in DMSO-*d*<sub>6</sub>). The <sup>1</sup>H NMR spectrum of **3b** was temperature dependent. At 295 K in CD<sub>2</sub>Cl<sub>2</sub>, the <sup>1</sup>H NMR spectrum of **3b** displayed a sharp signal for the twelve dimethylamino protons and a sharp signal for all the benzylic protons. Lowering the temperature of the NMR sample resulted in broadening and decoalescence of NMe<sub>2</sub> and methylene signals. At 183 K, the <sup>1</sup>H NMR spectrum of **3b** exhibited three single resonances for the dimethylamino groups. Two of these signals were assigned to one NMe<sub>2</sub> unit; the third was assigned to the other. The integration of these peaks gave a ratio of 1:1:2. At this temperature, both CH<sub>2</sub>N groups appeared as an AB pattern (Table 4). An estimation of the Gibbs free energy of activation from the coalescence temperature of the *N*-methyl signals gave Δ*G*<sup>‡</sup> = 46.4 kJ mol<sup>-1</sup> (*T*<sub>c</sub> = 203 K), and from the coalescence temperature of the CH<sub>2</sub>N signals Δ*G*<sup>‡</sup> = 42.2 kJ mol<sup>-1</sup> (*T*<sub>c</sub> = 223 K).

On the basis of the above observations, the following conclusions can be drawn. The magnetic equivalence of the two NMe<sub>2</sub> groups observed at room temperature can be interpreted in terms of a fluxional process involving the two NMe<sub>2</sub> units whereby fast exchange (on the NMR time scale) of one NMe<sub>2</sub> unit for the other at the hexacoordinate silicon center occurs. During this dissociative process there is simultaneously formation

**Table 3. Fractional Atomic Coordinates (×10<sup>4</sup>) and Isotropic Thermal Parameters (×10<sup>3</sup>)**

atom	<i>x/a</i>	<i>y/b</i>	<i>z/c</i>	<i>U</i> <sub>iso</sub>	atom	<i>x/a</i>	<i>y/b</i>	<i>z/c</i>	<i>U</i> <sub>iso</sub>
Si	2635(2)	1392.8(6)	7979(1)	<i>a</i>	C34	5754(10)	3709(3)	4786(6)	76(3)
O1	4403(5)	1408(1)	8062(3)	<i>a</i>	C35	5985(10)	4078(3)	4939(7)	79(3)
O2	2523(5)	1734(1)	8812(3)	<i>a</i>	C36	5305(9)	4276(3)	5606(5)	61(2)
O3	2451(5)	994(1)	8698(3)	<i>a</i>	C41	3323(7)	4780(2)	6765(4)	37(2)
O4	2657(5)	1016(1)	7205(3)	<i>a</i>	C42	4293(7)	5065(2)	6913(4)	37(2)
C1	2347(7)	1790(2)	7126(4)	39(2)	C43	4038(8)	5463(2)	6752(5)	50(2)
C2	1117(7)	1987(2)	7183(5)	47(2)	C44	2818(9)	5573(3)	6453(5)	58(2)
C3	710(9)	2273(3)	6616(5)	56(2)	C45	1815(9)	5293(3)	6297(5)	59(3)
C4	1525(10)	2372(3)	5992(5)	65(3)	C46	2091(8)	4890(2)	6451(5)	50(2)
C5	2776(9)	2183(2)	5908(5)	54(2)	C51	4745(7)	4237(2)	7802(4)	33(2)
C6	3173(7)	1885(2)	6459(5)	41(2)	C52	4419(8)	4457(2)	8502(5)	42(2)
C7	206(9)	1872(2)	7858(5)	57(2)	C53	5245(8)	4413(2)	9196(5)	53(2)
N1	462(6)	1440(2)	8052(4)	<i>a</i>	C54	6319(9)	4164(2)	9191(5)	53(2)
Me1	-251(8)	1193(2)	7448(5)	47(2)	C55	6645(9)	3953(2)	8478(5)	54(2)
Me2	-72(8)	1353(2)	8879(5)	50(2)	C56	5864(7)	3993(2)	7804(5)	44(2)
C8	4490(9)	1672(3)	6287(6)	57(2)	C61	909(7)	4087(2)	8578(4)	34(2)
N2	5497(8)	1915(2)	5890(5)	<i>a</i>	C62	790(7)	4497(2)	8459(5)	40(2)
Me3	6569(11)	1674(3)	5566(7)	83(3)	C63	259(8)	4743(2)	9063(5)	53(2)
Me4	6030(14)	2199(4)	6437(9)	125(5)	C64	-193(8)	4575(2)	9767(5)	51(2)
C11	4771(8)	1651(2)	8669(5)	41(2)	C65	-121(8)	4167(2)	9887(5)	54(2)
C12	3761(8)	1820(2)	9107(5)	42(2)	C66	468(7)	3923(2)	9308(5)	41(2)
C13	3965(10)	2065(3)	9798(6)	59(3)	C71	2561(7)	3394(2)	8160(4)	36(2)
C14	5372(10)	2129(3)	9981(6)	69(3)	C72	2636(8)	3045(2)	7710(5)	56(2)
C15	6343(10)	1985(3)	9553(6)	66(3)	C73	3592(9)	2763(3)	7915(6)	66(2)
C16	6109(9)	1742(3)	8876(5)	59(3)	C74	4468(9)	2815(3)	8533(5)	59(2)
C21	2339(8)	630(2)	8349(5)	41(2)	C75	4362(8)	3168(2)	8893(5)	51(2)
C22	2480(7)	647(2)	7508(4)	40(2)	C76	3440(8)	3452(2)	8808(4)	45(2)
C23	2389(7)	304(2)	7042(5)	46(2)	C81	93(7)	3550(2)	7303(5)	40(2)
C24	2143(8)	-56(2)	7437(5)	50(2)	C82	-272(10)	3657(3)	6515(6)	68(3)
C25	1974(8)	-72(2)	8281(5)	48(2)	C83	-1443(11)	3467(3)	6188(6)	75(3)
C26	2090(8)	279(2)	8742(5)	46(2)	C84	-2132(10)	3203(3)	6637(6)	72(3)
P1	3613(2)	4263.1(5)	6946(1)	<i>a</i>	C85	-1798(9)	3094(3)	7391(6)	69(3)
P2	1527(2)	3787.9(6)	7762(1)	<i>a</i>	C86	-656(8)	3273(2)	7744(5)	54(2)
N	2231(5)	4043(2)	7069(3)	34(1)	C	5499(11)	583(3)	6147(6)	84(3)
C31	4447(8)	4054(2)	6079(5)	40(2)	Cl 1	4673(3)	563(1)	5184(2)	108(1)
C32	4244(9)	3660(3)	5906(5)	56(2)	Cl 2a	7124(12)	450(4)	5846(8)	117(4)
C33	4940(11)	3471(3)	5235(6)	83(3)	Cl 2b	7266(8)	578(2)	6114(5)	131(3)

<sup>a</sup> The anisotropic thermal parameters for these atoms are given in Table 9 (supplementary material). The corresponding equivalent *U*<sub>iso</sub> values are 0.038(1), 0.048(3), 0.046(3), 0.043(3), 0.041(3), 0.047(4), 0.071(5), 0.032(1), and 0.034(1), respectively.

**Table 4.**  $^1\text{H}$  NMR Data of Hexacoordinated Anionic Silicate **3b**

	$T$ (K)	$\delta$ (ppm)
NCH <sub>3</sub>	293	2.40 (s, 12H)
	183	1.95 (s, 3H); 2.08 (s, 6H); 2.63 (s, 3H)
CH <sub>2</sub> N	293	3.76 (s, 4H)
	183	3.08 (d, 1H, $^2J(\text{H-H}) = 9.6$ Hz); 3.67 (d, 1H, $^2J(\text{H-H}) = 12$ Hz); 4.14 (d, 1H, $^2J(\text{H-H}) = 14$ Hz); 4.47 (d, 1H, $^2J(\text{H-H}) = 12$ Hz)

**Table 5.**  $^{19}\text{F}$ ,  $^{29}\text{Si}$ , and  $^1\text{H}$  NMR Data of Hexacoordinated Anionic Silicate **4**

nucleus	$T$ (K)	$\delta$ (ppm)
$^{29}\text{Si}$	293	-161.0 (quint, $^1J(\text{Si-F}) = 197.1$ Hz)
	183	-162.6 (ddt, $^1J(\text{Si-F}) = 217.5$ (SiX <sub>2</sub> ), 191.2 (SiY), 142.5 Hz (SiZ))
$^{19}\text{F}$	283	-118.2 (s)
	223	-119.1 (s, 2F); -122.1 (s, 1F); -130.1 (s, 1F)
$^1\text{H}$	293	2.30 (s, 12H, NCH <sub>3</sub> ); 3.70 (s, 4H, CH <sub>2</sub> N)
	183	2.10 (s, 6H, NCH <sub>3</sub> ); 2.27 (s, 6H, NCH <sub>3</sub> )

of one Si-N bond and cleavage of the other with rotation around the N-C bond and inversion at nitrogen. This dynamic N-Si-N coordination mode has been observed previously<sup>16</sup> on pentacoordinate silicon species.

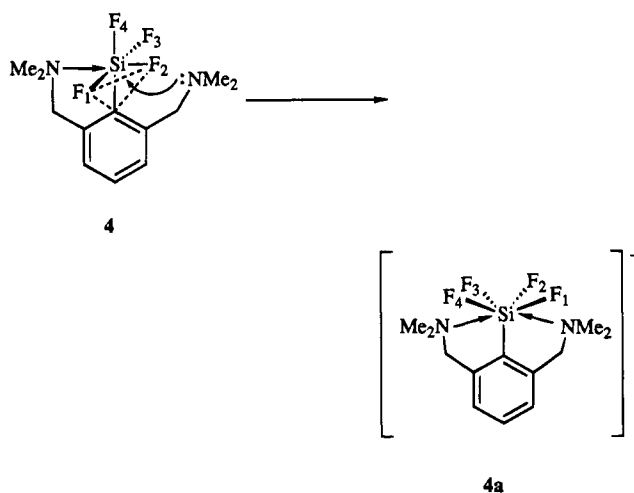
At 183 K this process slowed (on the NMR time scale), and the two NMe<sub>2</sub> units appeared dissociated such that one NMe<sub>2</sub> unit was away from the silicon center while the other was coordinated. This was the situation observed in the solid state. The free NMe<sub>2</sub> unit appeared as a singlet and the corresponding CH<sub>2</sub>N group appeared as an AB system because of the chirality at the silicon center. The chirality at the silicon atom also explained the diastereotopic nature of the methyls of the coordinate NMe<sub>2</sub> unit and the AB system of the corresponding CH<sub>2</sub>N group. These data imply that no isomerization occurred around the Si center. In contrast, an intramolecular nondissociative isomerization process had been observed on **1a** and **1b**<sup>12</sup> even at low temperature. This difference between **1a**, **1b**, and **3b** seems due to the dynamic N-Si-N coordination mode occurring on **3b** and hindering the isomerization.

**Dynamic NMR Studies of 4 in Solution.** At room temperature, the  $^{29}\text{Si}$  NMR spectrum of **4** in CD<sub>2</sub>Cl<sub>2</sub> showed a quintet centered at  $\delta = -161.0$  ppm due to coupling of the silicon atom with four equivalent fluorines resulting from intramolecular fluoride site exchange at this temperature. This chemical shift is in the range expected for hexacoordinate tetrafluorosilicates with the chemical shift of **2**<sup>13</sup> occurring at -160.1 ppm. At 183 K, the  $^{29}\text{Si}$  NMR spectrum of **4** showed a doublet of doublets of triplets centered at  $\delta = -162.6$  ppm corresponding to a SiX<sub>2</sub>YZ coupled system containing four fluorines, of which two are equivalent (Table 5). The  $^{29}\text{Si}$  NMR chemical shift of **4** is not significantly changed when **4** is cooled to 183 K ( $\delta = -162.6$  ppm).  $^{29}\text{Si}$ - $^{19}\text{F}$  coupling persists throughout the temperature range studied, which suggested that no intermolecular fluoride exchange occurred. Furthermore the  $^{29}\text{Si}$ - $^{19}\text{F}$  coupling constants at room temperature and at low temperature were close to those observed for **2**.<sup>13</sup> That was another indication of the hexacoordination at silicon regardless of the temperature.

The  $^{19}\text{F}$  NMR spectrum of **4** at 273 K showed a single resonance for the four magnetically equivalent fluorines, while at 193 K the  $^{19}\text{F}$  NMR spectrum became more

complicated: three distinct signals corresponding to an X<sub>2</sub>YZ system were observed. This finding was in accordance with the low-temperature  $^{29}\text{Si}$  NMR spectrum (Table 5).

At 273 K in CD<sub>2</sub>Cl<sub>2</sub>, the  $^1\text{H}$  NMR spectrum of **4** exhibited a sharp signal for the twelve dimethylamino protons and a sharp signal for the CH<sub>2</sub>N protons. As the temperature was decreased, the CH<sub>3</sub>N signal was split into two resonances of equal intensity. An estimation of  $\Delta G^\ddagger$ , calculated at  $T = 183$  K with a separation of the two methyl peaks of  $\Delta\nu = 42.5$  Hz, gave 38.5 kJ mol<sup>-1</sup>. From these NMR data, it can be concluded that **4** exhibited the same dynamic behavior as **3b**. At room temperature the equivalence of NMe<sub>2</sub> units observed in  $^1\text{H}$  NMR can also be interpreted as fast exchange (on the NMR time scale) of one NMe<sub>2</sub> unit for the other in the hexacoordinate silicon complex. The equivalence of fluorine atoms at room temperature observed in both  $^{19}\text{F}$  and  $^{29}\text{Si}$  NMR spectra can be explained by the formation of the symmetrical heptacoordinate intermediate (or transition state) **4a** in which all the  $^{19}\text{F}$  nuclei



are equivalent. The formation of **4a** results from attack of the noncoordinated NMe<sub>2</sub> group at the F<sub>1</sub>F<sub>2</sub>C (or F<sub>1</sub>F<sub>3</sub>C) face of the octahedron. Indeed, comparison of the NMR data of **4** and **2**<sup>13</sup> suggests an octahedral arrangement around the silicon atom in **4** with only one NMe<sub>2</sub> group coordinated to it, opposite one Si-F bond, as previously demonstrated for **2**.<sup>13</sup> This attack causes the fluorine atoms to adopt a symmetric rearrangement. At low temperature, the dynamic N-Si-N coordination mode becomes slow enough that the two NMe<sub>2</sub> groups appear separately by NMR with one coordinated to the silicon and the other uncoordinated. The coordinated group is not diastereotopic because of the symmetry of the hexacoordinate tetrafluorosilicate.

The potentially bis chelating 2,6-bis[(dimethylamino)methyl]phenyl ligand is an excellent tool for the study of nucleophilic substitution in hexacoordinate silicon compounds. In both models studied, displacement of one NMe<sub>2</sub> group by the other across the hexacoordinate silicon center can be observed by dynamic NMR studies. This movement mimics a nucleophilic attack on a hexacoordinate silicon center, and thus provides strong support for direct nucleophilic attack on a hexacoordinate silicon complex through a heptacoordinate transition state.

## Experimental Section

All the reactions were performed under a dry argon atmosphere using standard Schlenk techniques.  $^1\text{H}$ ,  $^{19}\text{F}$ , and  $^{29}\text{Si}$  NMR spectra were obtained using a Bruker 200-SY or a Bruker 250 AC spectrometer.  $^1\text{H}$  and  $^{29}\text{Si}$  chemical shifts were reported relative to  $\text{Me}_4\text{Si}$ , and  $^{19}\text{F}$  chemical shifts were relative to  $\text{CFCl}_3$ . Elemental analyses were performed by the centre de Microanalyse du CNRS.

**[2,6-Bis[(dimethylamino)methyl]phenyl]trimethoxysilane.** A solution of [2,6-bis[(dimethylamino)methyl]phenyl]lithium<sup>17</sup> (35 mmol) in ether (100 mL) was added dropwise at  $-10^\circ\text{C}$  to an ethereal solution (100 mL) of  $\text{ClSi}(\text{OMe})_3$  (35 mmol). The resulting mixture was stirred at room temperature for 5 h, filtered, and concentrated. The residue was distilled to give 6.9 g (63% yield) of a colorless oil: bp  $107\text{--}108^\circ\text{C}$  (0.25 mmHg);  $^1\text{H}$  NMR ( $\delta$  in  $\text{CDCl}_3$ ) 2.15 (s, 12H,  $\text{NMe}_2$ ), 3.55 (s, 9H,  $\text{OCH}_3$ ), 3.58 (s, 4H,  $\text{CH}_2\text{N}$ ), 7.25 (s, 3H, aromatic);  $^{29}\text{Si}$  NMR ( $\delta$  in  $\text{CDCl}_3$ )  $-53.8$ . Anal. Calcd for  $\text{C}_{15}\text{H}_{28}\text{N}_2\text{O}_3\text{Si}$ : C, 57.66; H, 9.03; N, 8.96. Found: C, 57.56; H, 8.93; N, 9.23.

**[2,6-Bis[(dimethylamino)methyl]phenyl]trifluorosilane.** Freshly distilled boron trifluoride etherate (5 mmol, 0.61 mL) was added dropwise to an ethereal solution (5 mL) of [2,6-bis[(dimethylamino)methyl]phenyl]trimethoxysilane (1.2 g, 3.8 mmol), and the reaction mixture was stirred for 10 min. The solvents were removed, and a foamy product was distilled to give 0.62 g (58% yield) of the expected product: bp  $142^\circ\text{C}$  (5 mmHg);  $^1\text{H}$  NMR ( $\delta$  in  $\text{CCl}_4$ ) 2.21 (s, 12H,  $\text{NMe}_2$ ), 3.54 (s, 4H,  $\text{CH}_2\text{N}$ ), 6.9–7.4 (m, 3H, aromatic);  $^{29}\text{Si}$  NMR ( $\delta$  in  $\text{CDCl}_3$ )  $-103.58$ . This product is very air-unstable, and no correct analysis was obtained.

**Potassium 18-Crown-6 [2,6-Bis[(dimethylamino)methyl]phenyl]tetrafluorosilicate (4).** To a dispersion of dry potassium fluoride (3.3 mmol, 0.193 g) in dry toluene (55 mL) was added 18-crown-6 ether (3.3 mmol) followed by a toluene solution (5 mL) of [2,6-bis[(dimethylamino)methyl]phenyl]trifluorosilane (3.3 mmol, 0.90 g). The mixture was stirred at room temperature, and after 2 days a precipitate was evident. The reaction mixture was filtered, and the precipitate was recrystallized from a THF/ $\text{Et}_2\text{O}$  mixture to give 1.62 g (82% yield) of colorless crystals of **4**: mp  $157\text{--}158^\circ\text{C}$ ;  $^1\text{H}$  NMR ( $\delta$  in  $\text{CD}_2\text{Cl}_2$ ) 2.30 (s, 12H,  $\text{N}(\text{CH}_3)_2$ ), 3.55 (s, 24H,  $\text{OCH}_2$ ), 3.70 (s, 4H,  $\text{CH}_2\text{N}$ ), 7.00 (s, 3H, aromatic). Anal. Calcd for  $\text{C}_{24}\text{H}_{43}\text{F}_4\text{N}_2\text{O}_6\text{SiK}$ : C, 48.14; H, 7.24; N, 4.68. Found: C, 47.91; H, 7.02; N, 4.91.

**Crystal Structure of Compound 3b: Crystal Preparation.** Crystals of compound **3b**<sup>14</sup> were grown by cooling a saturated dichloromethane/ether solution cooled at  $-40^\circ\text{C}$ . Colorless elongated blocks were produced. A block, approximately  $0.3 \times 0.45 \times 0.5$  mm, was sealed inside a Lindeman glass capillary and mounted on a Weissenberg camera. A monoclinic unit cell was first determined (19.1, 33.7, 10.5 Å;  $126.6^\circ$ ), which was later revealed to be an orthorhombic one, having the [101] direction parallel to the  $\phi$  axis of the diffractometer.

**X-ray Data Collection.** Data were collected at  $22^\circ\text{C}$  on a CAD-4 automated diffractometer with graphite-monochromatized  $\text{Mo K}\alpha$  radiation ( $\lambda = 0.71069$  Å). Lattice constants (Table 2) came from a least-squares refinement of 25 well-

defined reflections in the range  $19.5^\circ < 2\theta < 25^\circ$ . The intensities of three standard reflections were monitored after intervals of 60 min.; a 3% decrease in these check reflections was observed. Since the diffractometer operator was not fully confident in the  $\beta$  angle value, it was decided to collect a whole set of data ( $h,h:0,k;0,l$ ) to cope with the possibility of a structure determination in the monoclinic system. However, the examination of the data set collected established beyond doubt the orthorhombic symmetry of the lattice with space group  $P2_12_12_1$  (from the systematic absences). The structure amplitudes were obtained after decay correction and the usual Lorentz and polarization reductions. Only the reflections having  $\sigma(F)/F < 0.4$  were considered to be observed. No absorption corrections were made.

**Structure Determination and Refinement.** Direct methods (1980 version of the MULTAN program)<sup>18</sup> were used to solve the structure and to give the positions of the silicon and phosphorus atoms, along with the positions of the oxygen, carbon, and nitrogen atoms directly bound to silicon. These atomic positions were used to phase a Fourier map which gave the coordinates of the chlorine atoms ( $\text{CH}_2\text{Cl}_2$ ) and eight of the phenyl ring carbon atoms. Subsequent Fourier maps and difference Fourier syntheses revealed all the remaining non-hydrogen atoms. At this stage only the data set ( $h,0;0,k;0,l$ ) was used. After six cycles of least-squares refinement with isotropic thermal parameters to all atoms, the phosphorus, silicon, oxygen, and nitrogen atoms were refined anisotropically. Due to disorder in the  $\text{Cl}(2)$  atomic position the thermal parameters of both chlorine atoms were left isotropic. The conventional  $R$  factor was 0.080. The hydrogen atoms were positioned by calculation (SHELX-76 program)<sup>19</sup> and refinement converged to the  $R$  value of 0.061. An attempt to refine the opposite configuration of the molecule with the same data set established unambiguously that the present absolute configuration (displayed on Figure 1) is the correct one. Finally the second half of the data set ( $0,h;0,k;0,l$ ) was added to (but not merged into) the first one, and the refinement converged to the final  $R$  value of 0.056 along with a decrease in the  $\delta/\sigma$  ratios.

The final atomic coordinates are listed in Table 3. The labeling scheme is given in Figure 1. Typical bond lengths and main bond angles for the silicate anion are listed in Table 1.

**Acknowledgment.** We are grateful to R. Astier of the Laboratoire de Mesures Physiques (Université de Montpellier II) for help with X-ray data collection on a Nonius CAD-4 diffractometer.

**Supplementary Material Available:** Tables of interatomic distances in the anion, interatomic distances in the cation, bond angles concerning the whole determination structure, anisotropic thermal parameters (Si, P, O, and N atoms), and calculated hydrogen atom coordinates (Tables 6–10) (7 pages). Ordering information is given on any current masthead page.

OM9405347

(18) MULTAN-80, a system for computer programs for the automatic solution of crystal structures for X-ray diffraction data by P. Main, G. Germain, and M. M. Woolfson, Universities of York, England and Louvain, Belgium, 1980.

(19) SHELX-76, a program for crystal structure determination by G. M. Sheldrick, University of Cambridge, England, 1976.

(17) Jastrzebski, J. T. B. H.; van Koten, G.; Konijn, M.; Stam, C. H. *J. Am. Chem. Soc.* **1982**, *104*, 5490.

# Synthesis and Characterization of Ambient Temperature Stable Organopalladium(IV) Complexes, Including Aryl-, $\eta^1$ -Allyl-, Ethylpalladium(IV), and Pallada(IV)cyclopentane Complexes. Structures of the Poly(pyrazol-1-yl)borate Complexes $\text{PdMe}_3\{(\text{pz})_3\text{BH}\}$ and $\text{PdMe}_3\{(\text{pz})_4\text{B}\}$ and Three Polymorphs of $\text{PdMe}_2\text{Et}\{(\text{pz})_3\text{BH}\}$

Allan J. Canty,<sup>\*,†</sup> Hong Jin,<sup>†</sup> Andrew S. Roberts,<sup>†</sup> Brian W. Skelton,<sup>‡</sup> Peter R. Traill,<sup>†</sup> and Allan H. White<sup>‡</sup>

Department of Chemistry, University of Tasmania, Hobart, Tasmania 7001, Australia, and Department of Chemistry, University of Western Australia, Nedlands, W.A. 6009, Australia

Received July 14, 1994<sup>®</sup>

The palladium(II) complexes  $\text{PdMe}_2(\text{tmeda})$ ,  $\text{PdMePh}(\text{tmeda})$ , and  $\text{Pd}(\text{CH}_2\text{CH}_2\text{CH}_2\text{CH}_2)(\text{tmeda})$  ( $\text{tmeda}$  = tetramethylethylenediamine) react with potassium tris(pyrazol-1-yl)borate and organohalides  $\text{R}'\text{X}$  in acetone to form the octahedral palladium(IV) complexes  $\text{PdMeRR}''\{(\text{pz})_3\text{BH}\}$  ( $\text{R} = \text{Me}, \text{Ph}$ ) and  $\text{Pd}(\text{CH}_2\text{CH}_2\text{CH}_2\text{CH}_2)\text{R}''\{(\text{pz})_3\text{BH}\}$  ( $\text{R}'\text{X} = \text{MeI}, \text{EtI}, \text{PhCH}_2\text{Br}, \text{CH}_2=\text{CHCH}_2\text{I}$ ). The complexes are stable in the solid state and in solution at ambient temperature,  $\text{PdMe}_3\{(\text{pz})_3\text{BH}\}$  is more stable than the iodide salt of isoelectronic  $[\text{PdMe}_3\{(\text{pz})_3\text{CH}\}]^+$ , and the aryl- and  $\eta^1$ -propenylpalladium(IV) complexes are the first examples of aryl- and allylpalladium(IV) complexes that are stable above 0 °C. The tris(pyrazol-1-yl)borate ligand considerably enhances the stability of palladium(IV) complexes when compared with related neutral donor ligands. The ethylpalladium(IV) complexes have stabilities in solution similar to that of the most stable ethylpalladium(II) complexes reported. The complex  $\text{PdMe}_3\{(\text{pz})_4\text{B}\}$  (**2**) has been prepared, and structural studies of this complex and  $\text{PdMe}_2\text{R}''\{(\text{pz})_3\text{BH}\}$  [ $\text{R}'' = \text{Me}$  (**1**),  $\text{Et}$  (**3**)] completed, allowing the first comparison of structural parameters of ethylpalladium(II, IV) complexes and of  $\text{PdMe}_3\{(\text{pz})_3\text{BH}\}$  with the "isoelectronic" cation  $[\text{PdMe}_3\{(\text{pz})_3\text{CH}\}]^+$ . Three polymorphs of  $\text{PdMe}_2\text{Et}\{(\text{pz})_3\text{BH}\}$  were examined: complex **3a** is ordered, but the other polymorphs exhibit disordering in the conformation of the ethyl group (**3b**) and in the position of the ethyl group and one of the methyl groups (**3c**). Crystallographic data: for **1**, monoclinic, space group  $P2_1/c$ ,  $a = 16.559(16)$  Å,  $b = 7.859(4)$  Å,  $c = 13.774(15)$  Å,  $\beta = 118.88(8)^\circ$ ,  $Z = 4$ ,  $R = 0.032$ ,  $R_w = 0.043$ ; for **2**, monoclinic, space group  $P2_1/c$ ,  $a = 11.453(1)$  Å,  $b = 9.729(2)$  Å,  $c = 16.973(9)$  Å,  $\beta = 107.25(3)^\circ$ ,  $Z = 4$ ,  $R = 0.053$ ,  $R_w = 0.055$ ; for **3a**, monoclinic,  $P2_1/c$ ,  $a = 9.384(3)$  Å,  $b = 12.795(3)$  Å,  $c = 15.119(8)$  Å,  $\beta = 115.22(3)^\circ$ ,  $Z = 4$ ,  $R = 0.055$ ,  $R_w = 0.052$ ; for **3b**, orthorhombic,  $P2_12_12_1$ ,  $a = 13.955(3)$  Å,  $b = 13.152(18)$  Å,  $c = 9.047(6)$  Å,  $Z = 4$ ,  $R = 0.052$ ,  $R_w = 0.053$ ; for **3c**, tetragonal,  $P4_32_12$ ,  $a = 12.305(4)$  Å,  $c = 21.542(7)$  Å,  $Z = 8$ ,  $R = R_w = 0.035$ .

## Introduction

Synthetic, structural, and mechanistic aspects of organopalladium(IV) chemistry have developed rapidly since the initial report of the first hydrocarbyl complex

in 1986,  $\text{PdIME}_3(\text{bpy})$  ( $\text{bpy} = 2,2'$ -bipyridyl).<sup>1–6</sup> All complexes isolated to date contain bidentate or tripodal donor ligands, although evidence has been presented in support of the proposal that  $\text{PdBr}_2\text{H}(\text{Cy})(\text{PPh}_3)_2$  is present as one component in a solid obtained on heating  $\text{PdBr}_2(\text{PPh}_3)_2$  in cyclohexane.<sup>5</sup> Most of the complexes isolated have low stability, decomposing at or below

<sup>†</sup> University of Tasmania.

<sup>‡</sup> University of Western Australia.

<sup>®</sup> Abstract published in *Advance ACS Abstracts*, November 1, 1994.

(1) (a) Byers, P. K.; Canty, A. J.; Skelton, B. W.; White, A. H. *J. Chem. Soc., Chem. Commun.* **1986**, 1722. (b) Canty, A. J. *Acc. Chem. Res.* **1992**, *25*, 83, and references therein. (c) Canty, A. J.; Traill, P. R.; Skelton, B. W.; White, A. H. *J. Organomet. Chem.* **1992**, *433*, 213. (d) Byers, P. K.; Canty, A. J.; Honeyman, R. T.; Skelton, B. W.; White, A. H. *J. Organomet. Chem.* **1992**, *433*, 223. (e) Byers, P. K.; Canty, A. J.; Skelton, B. W.; Traill, P. R.; Watson, A. A.; White, A. H. *Organometallics* **1992**, *11*, 3085. (f) Canty, A. J. *Platinum Met. Rev.* **1993**, *37*, 2. (g) Bennett, M. A.; Canty, A. J.; Felixberger, J. K.; Rendina, L. M.; Sunderland, C.; Willis, A. C. *Inorg. Chem.* **1993**, *32*, 1951. (h) Canty, A. J.; Traill, P. R.; Colton, R.; Thomas, I. M. *Inorg. Chim. Acta* **1993**, *210*, 91. (i) Markies, B. A.; Canty, A. J.; Boersma, J.; van Koten, G. *Organometallics* **1994**, *13*, 2053. (j) Ducker-Benfer, C.; van Eldik, R.; Canty, A. J. *Organometallics* **1994**, *13*, 2412.

(2) (a) de Graaf, W.; Boersma, J.; Smeets, W. J. J.; Spek, A. L.; van Koten, G. *Organometallics* **1989**, *8*, 2907. (b) de Graaf, W.; Boersma, J.; van Koten, G. *Organometallics* **1990**, *9*, 1479. (c) Alsters, P. L.; Engel, P. F.; Hogerheide, M. P.; Copijn, M.; Spek, A. L.; van Koten, G. *Organometallics* **1993**, *12*, 1831.

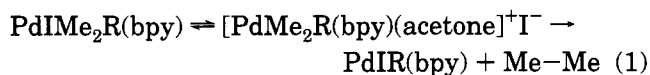
(3) (a) Catellani, M.; Chiusoli, G. P. *Gazz. Chim. Ital.* **1993**, *123*, 1. (b) Bocelli, G.; Catellani, M.; Ghelli, S. *J. Organomet. Chem.* **1993**, *458*, C12.

(4) van Asselt, R.; Rijnberg, E.; Elsevier, C. J. *Organometallics* **1994**, *13*, 706.

(5) Vedernikov, A. N.; Kuramshin, A. I.; Solomonov, B. N. *J. Chem. Soc., Chem. Commun.* **1994**, 121.

(6) Klaui, W.; Glaum, M.; Wagner, T.; Bennett, M. A. *J. Organomet. Chem.* **1994**, *472*, 355.

ambient temperature, facilitating kinetic studies of their decomposition that have revealed insights into C–C bond formation mechanisms of direct interest to potential roles for palladium(IV) in organic synthesis.<sup>1b</sup> Kinetic studies of the decomposition of PdMe<sub>3</sub>(bpy) in acetone, including a volume profile for the reaction, indicate that the major pathway for reductive elimination of ethane and formation of PdIme(bpy) proceeds via iodide dissociation (eq 1, R = Me) and that the inter-



mediate cation probably contains probably contains coordinated acetone [PdMe<sub>3</sub>(bpy)(acetone)]<sup>+</sup>.<sup>1j,7</sup>

For nitrogen donor tripod ligands coordinated to trimethylpalladium(IV), [PdMe<sub>3</sub>(L<sub>3</sub>-N,N',N'')]<sup>+</sup>X<sup>-</sup>, the stability of the complexes increases with increasing basicity of the ligands; e.g., complexes of bis(1-methylimidazol-2-yl)(pyridin-2-yl)methane are more stable than those of tris(pyrazol-1-yl)methane.<sup>8,9</sup>

In an attempt to gain further insight into these effects on stability, and to search for complexes that are stable at ambient temperature, we have investigated the synthesis and properties of palladium(IV) tris(pyrazol-1-yl)borate complexes, because poly(pyrazol-1-yl)borates are more basic than poly(pyrazol-1-yl)alkanes and the anticipated complexes "PdR<sub>3</sub>{(pz)<sub>3</sub>BH-N,N',N''}" are iso-electronic with [PdR<sub>3</sub>{(pz)<sub>3</sub>CH-N,N',N''}]<sup>+</sup>. We have found that the [(pz)<sub>3</sub>BH]<sup>-</sup> ligand has a remarkable ability to stabilize the higher oxidation state for palladium, allowing the isolation of a range of ambient temperature stable palladium(IV) complexes. These include palladium(IV)cyclopentane complexes, complexes containing η<sup>1</sup>-allyl and ethyl groups where the ethylpalladium(IV) complexes have stabilities comparable to the most stable ethylpalladium(II) complexes reported to date, and the first ambient temperature stable arylpalladium(IV) complexes and palladium(IV) complexes containing three different hydrocarbyl groups. Preliminary reports of parts of this work have appeared.<sup>10,11</sup>

## Experimental Section

The reagents PdMe<sub>2</sub>(tmeda)<sup>2a</sup> and PdMePh(tmeda)<sup>12</sup> and the palladium(II)cyclopentane complex Pd(C<sub>5</sub>H<sub>8</sub>)(tmeda)<sup>13</sup> were prepared as described. Solvents were dried and distilled, and all syntheses were carried out under nitrogen. Microanalyses were by the Central Science Laboratory, University of Tasmania, and NMR spectra were recorded with a Bruker AM 300 spectrometer, with chemical shifts given in ppm relative to Me<sub>4</sub>Si.

**Synthesis of Complexes. PdMe<sub>3</sub>{(pz)<sub>3</sub>BH} (1).** A solution of PdMe<sub>2</sub>(tmeda) (0.03 g, 0.12 mmol) and K[(pz)<sub>3</sub>BH] (0.03 g, 0.12 mmol) in acetone (10 mL) was stirred at 0 °C for 1 h.

(7) Byers, P. K.; Canty, A. J.; Crespo, M.; Puddephatt, R. J.; Scott, J. D. *Organometallics* **1988**, *7*, 1363.

(8) Byers, P. K.; Canty, A. J.; Skelton, B. W.; White, A. H. *Organometallics* **1990**, *9*, 826.

(9) Brown, D. G.; Byers, P. K.; Canty, A. J. *Organometallics* **1990**, *9*, 1231.

(10) Canty, A. J.; Traill, P. R. *J. Organomet. Chem.* **1992**, *435*, C8.

(11) Canty, A. J.; Honeyman, R. T.; Colton, R.; Skelton, B. W.; White, A. H. *J. Organomet. Chem.* **1994**, *471*, C8.

(12) Markies, B. A.; Canty, A. J.; de Graaf, W.; Boersma, J.; Janssen, M. D.; Hogerheide, M. P.; Smeets, W. J. J.; Spek, A. L.; van Koten, G. *J. Organomet. Chem.*, in press.

(13) (a) Diversi, P.; Ingrassio, G.; Lucherini, A.; Murtas, S. *J. Chem. Soc., Dalton Trans.* **1980**, 1633. (b) Diversi, P.; Ingrassio, G.; Lucherini, A. *Inorg. Synth.* **1983**, *22*, 167. (c) Canty, A. J.; Skelton, B. W.; Traill, P. R.; White, A. H. *Aust. J. Chem.* **1994**, *47*, 2119.

Iodomethane (0.017 g, 0.12 mmol) was added, the solution was stirred for 3 h at ambient temperature, and after centrifugation to precipitate a fine powder, the yellow solution was collected and evaporated to dryness under vacuum at 0 °C. The residue was extracted with diethyl ether, filtered, and evaporated to dryness. The solid obtained was recrystallized from diethyl ether/petroleum (bp 40–60 °C) to give a white crystalline product (0.037 g, 86%): <sup>1</sup>H NMR (CDCl<sub>3</sub>) δ 7.64 (d, 3, H3 or 5), 7.54 (d, 3, H3 or 5), 6.20 ("t", 3, H4), 1.38 (s, 9, PdMe); <sup>13</sup>C{<sup>1</sup>H} NMR (CDCl<sub>3</sub>) δ 138.3 (H3 or 5), 135.4 (C3 or 5), 105.5 (C4), 12.9 (PdMe). Anal. Calcd for C<sub>12</sub>H<sub>19</sub>BN<sub>6</sub>Pd: C, 39.5; H, 5.2; N, 23.0. Found: C, 39.8; H, 5.2; N, 23.0.

**PdMe<sub>3</sub>{(pz)<sub>4</sub>B} (2).** A solution of PdMe<sub>2</sub>(tmeda) (0.036 g, 0.14 mmol) and K[(pz)<sub>4</sub>B] (0.045 g, 0.14 mmol) in acetone (10 mL) was stirred at 40 °C for 1 h, and on lowering the temperature to ambient, iodomethane (0.02 g, 0.14 mmol) was added. The solution was stirred overnight, the solvent removed and the residue extracted with diethyl ether to give an orange solid. The solid was extracted with petroleum ether (2 × 5 mL, bp 40–60 °C) and evaporated to give the product as a white solid (61%): <sup>1</sup>H NMR (CDCl<sub>3</sub>) δ 8.03 (d, <sup>3</sup>J = 2.4 Hz, 1, H3 or 5 of uncoordinated pz), 7.96 (d(b), 1, H3 or 5 of uncoordinated pz), 7.66 (d, <sup>3</sup>J = 2.4 Hz, H3 or 5), 7.61 (d(b), 3, H3 or 5), 6.61 ("t"(b), 1, H4 of uncoordinated pz), 6.21 ("t"(b), 3, H4), 1.42 (s, 6, PdMe); <sup>13</sup>C{<sup>1</sup>H} NMR (CDCl<sub>3</sub>) δ 142 (C3 or 5 of uncoordinated pz), 139.2 (C3 or 5), 136.8 (C3 or 5 of uncoordinated pz), 133.3 (C3 or 5), 107.4 (C4 of uncoordinated pz), 105.9 (C4), 13.2 (PdMe). Anal. Calcd for C<sub>15</sub>H<sub>21</sub>BN<sub>6</sub>Pd: C, 41.8; H, 4.9; N, 26.0. Found: C, 42.4; H, 5.1; N, 25.9.

The following complexes were obtained by a procedure mostly similar to that for complex 1.

**PdMe<sub>2</sub>Et{(pz)<sub>3</sub>BH} (3):** iodoethane as reagent, crystallization from pentane, yield 80%; <sup>1</sup>H NMR (CDCl<sub>3</sub>) δ 7.70 (d(b), 2, H3 or 5 trans to Me), 7.66 (d(b), 1, H3 or 5 trans to Et), 7.63 (d(b), 2, H3 or 5 trans to Me), 7.54 (d(b), 1, H3 or 5 trans to Et), 6.23 ("t", 2, H4 trans to Me), 6.19 ("t", 1, H4 trans to Et), 2.42 (q, <sup>3</sup>J = 7.6 Hz, 2, PdCH<sub>2</sub>CH<sub>3</sub>), 1.42 (s, 6, PdMe), 1.09 (t, <sup>3</sup>J = 7.6 Hz, 3, PdCH<sub>2</sub>CH<sub>3</sub>); <sup>13</sup>C{<sup>1</sup>H} NMR (CDCl<sub>3</sub>) δ 138.6 (C3 or 5), 138.3 (C3 or 5), 135.5 (C3 or 5), 135.1 (C3 or 5), 105.5 (C4), 105.3 (C4), 28.9 (PdCH<sub>2</sub>CH<sub>3</sub>), 17.9 (PdMe), 15.6 (PdCH<sub>2</sub>CH<sub>3</sub>). Anal. Calcd for C<sub>13</sub>H<sub>21</sub>BN<sub>6</sub>Pd: C, 41.3; H, 5.6; N, 22.2. Found: C, 41.5; H, 5.9; N, 21.9.

**PdMe<sub>2</sub>(CH<sub>2</sub>Ph){(pz)<sub>3</sub>BH} (4):** benzyl bromide as reagent, crystallization from petroleum ether, yield 55%; <sup>1</sup>H NMR (CDCl<sub>3</sub>) δ 9.80 (d, <sup>3</sup>J = 2.3 Hz, 2, H3 or 5), 9.77 (d, <sup>3</sup>J = 2.0 Hz, 1, H3 or 5 trans to CH<sub>2</sub>Ph), 9.66 (d, <sup>3</sup>J = 2.0 Hz, 1, H3 or 5 trans to CH<sub>2</sub>Ph), 9.22 (m, 3, Ph(3–5)), 9.16 (m, 4, H3 or 5 trans to Me and Ph(2,6)), 8.33 ("t", 1, H4 trans to CH<sub>2</sub>Ph), 8.24 ("t", 2, H4 trans to Me), 3.54 (s, 2, PdCH<sub>2</sub>), 1.55 (s, 6, PdMe); <sup>13</sup>C{<sup>1</sup>H} NMR δ 146.7, 138.4, 135.4, 135.2, 130.1, 125.6, 105.5 (C4), 105.1 (C4), 36.1 (PdCH<sub>2</sub>), 18.5 (PdMe). Anal. Calcd for C<sub>18</sub>H<sub>23</sub>BN<sub>6</sub>Pd: C, 49.1; H, 5.3; N, 19.1. Found: C, 49.0; H, 5.5; N, 19.1.

**PdMe<sub>2</sub>(CH<sub>2</sub>CH=CH<sub>2</sub>){(pz)<sub>3</sub>BH} (5).** A procedure similar to that for 1 was followed except that oxidative addition with 2-propenyl iodide was carried out at –5 °C, and the complex was obtained by crystallization from petroleum ether, yield 71%: <sup>1</sup>H NMR ((CD<sub>3</sub>)<sub>2</sub>CO) δ 7.96 (d, <sup>3</sup>J = 2.1 Hz, H3 or 5 trans to Me), 7.93 (d, <sup>3</sup>J = 2.1 Hz, 1, H3 or 5 trans to allyl), 7.90 (d, <sup>3</sup>J = 2.1 Hz, 2, H3 or 5 trans to Me), 7.80 (d, <sup>3</sup>J = 2.1 Hz, 1, H3 or 5 trans to allyl), 6.24 ("t", 2, H4 trans to Me), 6.39 ("t", 1, H4 trans to allyl), 6.09 (m, PdCH<sub>2</sub>CHCH<sub>2</sub>), 5.34 (m, PdCH<sub>2</sub>CHCH<sub>2</sub> trans to CH), 5.15 (dd, <sup>2</sup>J = 9.9 Hz, <sup>3</sup>J = 1.2 Hz, 1, PdCH<sub>2</sub>CHCH<sub>2</sub> cis to CH), 3.20 (d, <sup>3</sup>J = 9 Hz, PdCH<sub>2</sub>), 1.61 (s, 6, PdMe); <sup>13</sup>C{<sup>1</sup>H} NMR δ 144.3, 143.7, 139.5 (C3 or 5), 139.3 (C3 or 5), 136.5 (C3 or 5), 136.3 (C3 or 5), 113.3 (PdCH<sub>2</sub>CHCH<sub>2</sub>), 106.3 (C4), 106.1 (C4), 34.6 (PdCH<sub>2</sub>), 18.2 (PdMe). Anal. Calcd for C<sub>14</sub>H<sub>21</sub>BN<sub>6</sub>Pd: C, 43.1; H, 5.4; N, 21.5. Found: C, 43.3; H, 5.6; N, 21.5.

**PdMePh{(pz)<sub>3</sub>BH} (6).** A solution of PdMePh(tmeda) (0.030 g, 0.095 mmol) and K[(pz)<sub>3</sub>BH] in acetone (5 mL) was stirred at 35 °C for 4 h. The solution was cooled to ambient temperature, iodomethane (50 μL) added, the solution stirred

Table 1. Specific Crystallographic Details

complex	PdMe <sub>3</sub> {(pz) <sub>3</sub> BH} (1)	PdMe <sub>3</sub> {(pz) <sub>4</sub> B} (2)	PdMe <sub>2</sub> Et{(pz) <sub>3</sub> BH} (3a)	PdMe <sub>2</sub> Et{(pz) <sub>3</sub> BH} (3b)	PdMe <sub>2</sub> Et{(pz) <sub>3</sub> BH} (3c)
formula	C <sub>12</sub> H <sub>19</sub> BN <sub>6</sub> Pd	C <sub>15</sub> H <sub>21</sub> BN <sub>6</sub> Pd	C <sub>13</sub> H <sub>21</sub> BN <sub>6</sub> Pd	C <sub>13</sub> H <sub>21</sub> BN <sub>6</sub> Pd	C <sub>13</sub> H <sub>21</sub> BN <sub>6</sub> Pd
space group	P2 <sub>1</sub> /c (No. 14)	P2 <sub>1</sub> /c (No. 14)	P2 <sub>1</sub> /c (No. 14)	P2 <sub>1</sub> 2 <sub>1</sub> 2 <sub>1</sub> (No. 19)	P4 <sub>3</sub> 2 <sub>1</sub> 2 (No. 96)
a (Å)	16.559(16)	11.453(1)	9.384(3)	13.955(3)	12.305(4)
b (Å)	7.859(4)	9.729(2)	12.795(3)	13.152(18)	
c (Å)	13.774(15)	16.973(9)	15.119(8)	9.047(6)	21.542(7)
β (deg)	118.88(8)	107.25(3)	115.22(3)		
V (Å <sup>3</sup> )	1570(3)	1806(1)	1642(1)	1660(3)	3262(2)
Z	4	4	4	4	8
mol wt	364.5	430.6	378.6	378.6	378.6
D <sub>calc</sub> (g cm <sup>-3</sup> )	1.54	1.58	1.53	1.51	1.54
crystal size (mm)	0.22 × 0.40 × 0.50	0.08 × 0.18 × 0.20	0.12 × 0.24 × 0.04	0.06 × 0.75 × 0.55	0.47 × 0.32 × 0.28
μ (cm <sup>-1</sup> )	10.7	8.9	11.3	11.2	11.4
F(000)	736	872	768	768	1536
2θ <sub>max</sub> (deg)	55	55	50	55	50
A* <sub>min,max</sub>	1.21, 1.38	1.07, 1.17	1.05, 1.14	1.07, 1.48	1.25, 1.40
N	3593	4149	2873	2166	1723
N <sub>o</sub>	3086	2683	1518	1470	1283
R	0.032	0.053	0.055	0.052	0.035
R <sub>w</sub>	0.043	0.055	0.052	0.053	0.035

for 2 min, and water (2 mL) added. The solvents were removed to give a white solid which was dissolved in ethanol (4 mL) and filtered, and water (4 mL) was added to precipitate a white solid. Ethanol was removed by rotary evaporation, and the resulting suspension was centrifuged to precipitate the product, which was washed with water, recentrifuged, collected, and dried under vacuum (0.029 g, 71%): <sup>1</sup>H NMR (CDCl<sub>3</sub>) δ 7.70 (m, 3H, H3 or 5), 7.62 (b, 1, H3 or H5), 7.24 (b, 2, H3 or 5), 7.03 and 6.96 (m(b), 5, Ph), 6.25 ("t", 1, H4), 6.15 ("t", 2, H4), 1.82 (2, 6, PdMe); <sup>13</sup>C{<sup>1</sup>H} NMR δ 140.0, 138.7, 136.9, 135.6, 135.2, 128.0 (Ph), 124.7 (Ph), 105.9 (C4), 105.7 (C4), 19.1 (PdMe). Anal. Calcd for C<sub>17</sub>H<sub>21</sub>BN<sub>6</sub>Pd: C, 47.9; H, 5.0; N, 19.7. Found: C, 47.8; H, 4.9; N, 19.6.

**PdMeEtPh{(pz)<sub>3</sub>BH} (7).** A procedure similar to that for **6** was followed, except that reaction with iodoethane was carried out at 55 °C, water was added at 45 °C until cloudiness occurred, and then iodomethane (100 μL) was added to convert any unreacted PdMePh(tmeda) to insoluble PdIPh(tmeda). Volatiles were removed on a vacuum line to give a white solid suspended in water. The product was extracted into diethyl ether, the diethyl ether layer was evaporated to dryness, the solid obtained was dissolved in acetone, and a solid precipitated with addition of water. Acetone was removed by rotary evaporation and the resulting suspension centrifuged to precipitate the product (84%): <sup>1</sup>H NMR (CDCl<sub>3</sub>) δ 7.72 (m, 3, H3 or 5), 7.66 (d, <sup>3</sup>J = 2.2 Hz, 1, H3 or 5), 7.31 (d(b), 1, H3 or 5), 7.17 (d(b), 1, H3 or 5), 7.00 (m(b), 5, Ph), 6.27 ("t", 1, H4), 6.19 ("t", 1, H4), 6.12 ("t", 1, H4), 2.83 (m, 2, PdCH<sub>2</sub>CH<sub>3</sub>), 1.81 (s, 3, PdMe), 0.99 (t, <sup>3</sup>J = 7.5 Hz, 3, PdCH<sub>2</sub>CH<sub>3</sub>); <sup>13</sup>C{<sup>1</sup>H} NMR: δ 140.7, 140.1, 139.1, 136.5, 135.7, 135.3, 134.9, 127.9 (Ph), 124.7 (Ph), 105.7 (C4), 105.5 (C4), 35.8 (PdCH<sub>2</sub>CH<sub>3</sub>), 21.7 (PdMe). Anal. Calcd for C<sub>15</sub>H<sub>23</sub>BN<sub>6</sub>Pd: C, 49.1; H, 5.3; N, 19.1. Found: C, 49.2; H, 5.4; N, 18.3.

**PdMe(CH<sub>2</sub>Ph)Ph{(pz)<sub>3</sub>BH} (8).** A procedure similar to that for **6** was followed using benzyl bromide (95%): <sup>1</sup>H NMR (CDCl<sub>3</sub>) δ 7.66 (d, <sup>3</sup>J = 2.4 Hz, 1, H3 or 5), 7.64 (d, <sup>3</sup>J = 2.2 Hz, 1, H3 or 5), 7.63 (d, <sup>3</sup>J = 2.2 Hz, 1, H3 or 5), 7.08 (d, <sup>3</sup>J = 2.0 Hz, 1, H3 or 5), 7.04 (m, 5, PdPh), 6.99 (d', 1, PdCH<sub>2</sub>Ph), 6.86 ("t", 2, PdCH<sub>2</sub>Ph), 6.78 (d', 2, PdCH<sub>2</sub>Ph), 6.56 (d, <sup>3</sup>J = 1.9 Hz, 1, H3 or 5), 6.09 ("t", 1, H4), 6.07 ("t", 1, H4), 6.01 ("t", 1, H4), 3.99 (d, <sup>2</sup>J = 8.2 Hz, 1, PdCHH), 3.89 (d, <sup>2</sup>J = 8.2 Hz, PdCHH), 1.97 (s, 3, PdMe); <sup>13</sup>C{<sup>1</sup>H} NMR δ 146.1, 140.3, 138.8, 136.5, 135.6, 135.2, 135.0, 130.4, 128.6, 128.0, 126.0, 124.9, 105.6 (C4), 105.5 (C4), 105.3 (C4), 43.1 (PdCH<sub>2</sub>Ph), 24.1 (PdMe). Anal. Calcd for C<sub>23</sub>H<sub>25</sub>BN<sub>6</sub>Pd: C, 54.9; H, 5.0; N, 16.7. Found: C, 54.8; H, 4.9; N, 16.3.

**PdMe(CH<sub>2</sub>CH=CH<sub>2</sub>)Ph{(pz)<sub>3</sub>BH} (9).** A procedure similar to that for **6** was followed, except that the oxidative addition reaction with 2-propenyl iodide was carried out at 0 °C, and workup of the solid used acetone/water (88%): <sup>1</sup>H NMR (CDCl<sub>3</sub>) δ 7.73 (d, <sup>3</sup>J = 2.2 Hz, 1, H3 or 5), 7.69 (m, 2, H3 or 5), 7.64 (d, <sup>3</sup>J = 2.2 Hz, 1, H3 or 5), 7.32 (b, 1, H3 or 5), 7.12 (d, <sup>3</sup>J = 1.8 Hz, 1, H3 or 5), 7.02 (m, Ph), 6.95 (m, Ph), 6.24

("t", 1, H4), 6.18 ("t", 1, H4), 6.11 ("t", 1, H4), 5.91 (m, 1, PdCH<sub>2</sub>CHCH<sub>2</sub>), 5.21 (d(b), 1, PdCH<sub>2</sub>CHCHH trans to CH), 5.02 (dd, <sup>3</sup>J = 9.9 Hz, <sup>2</sup>J = 2.3 Hz, PdCH<sub>2</sub>CHCHH cis to CH), 3.51 ("t", 1, PdCH<sub>2</sub>), 3.31 ("t", 1, PdCH<sub>2</sub>), 1.88 (s, PdMe); <sup>13</sup>C{<sup>1</sup>H} NMR δ 143.4, 140.5, 140.2, 139.4, 136.4, 135.8, 135.4, 135.1, 128.0 (Ph), 124.8 (Ph), 114.7 (PdCH<sub>2</sub>CHCH<sub>2</sub>), 105.7 (C4), 39.3 (PdCH<sub>2</sub>), 24.4 (PdMe). Anal. Calcd for C<sub>19</sub>H<sub>23</sub>BN<sub>6</sub>Pd: C, 50.4; H, 5.1; N, 18.6. Found: C, 50.4; H, 5.0; N, 18.5.

**Pd(C<sub>4</sub>H<sub>9</sub>)Me{(pz)<sub>3</sub>BH} (10).** A solution of Pd(C<sub>4</sub>H<sub>9</sub>)(tmeda) (0.06 g, 0.24 mmol) and K[(pz)<sub>3</sub>BH] (0.06 g, 0.24 mmol) in acetone (15 mL) was stirred at 0 °C for 2 h. Iodomethane (0.015 mL, 0.24 mmol) was added, and the solution was allowed to warm to ambient temperature and stirred for 4 h. On evaporation of solvent, the residue was extracted with diethyl ether and filtered to remove a yellow solid. The solution was evaporated to ~2 mL and cooled to -20 °C to give the product as a cream-colored solid (0.084 g, 90%): <sup>1</sup>H NMR (CDCl<sub>3</sub>) δ 7.78 (d, <sup>3</sup>J = 1.8 Hz, 1, H3 or 5 trans to Me), 7.64 (d, <sup>3</sup>J = 2.0 Hz, 3, H3 or 5), 7.44 (d, <sup>3</sup>J = 2.0 Hz, 2, H3 or 5), 6.20 ("t", <sup>3</sup>J = 3 Hz, 1, H4 trans to Me), 6.17 ("t", <sup>3</sup>J = 3 Hz, 2, H4), 3.16 (m, 2, PdCHH), 2.87 (m, 2, PdCHH), 1.78 (m, 4, CH<sub>2</sub>), 1.44 (s, 3, PdMe); <sup>13</sup>C{<sup>1</sup>H} NMR δ 138.9 (C3 or 5), 135.3 (C3 or 5), 105.3 (C4), 45.6 (PdCH<sub>2</sub>), 34.9 (CH<sub>2</sub>), 16.1 (PdMe). Anal. Calcd for C<sub>14</sub>H<sub>21</sub>BN<sub>6</sub>Pd: C, 43.0; H, 5.4; N, 21.5. Found: C, 43.0; H, 5.2; N, 20.5.

The following complexes were obtained by a procedure mostly similar to that for complex **10**.

**Pd(C<sub>4</sub>H<sub>9</sub>)Et{(pz)<sub>3</sub>BH} (11):** iodoethane as reagent, crystallization from pentane, yield 70%; <sup>1</sup>H NMR (CDCl<sub>3</sub>) δ 7.75 (d, <sup>3</sup>J = 1.8 Hz, 1, H3 or 5 trans to Et), 7.67 (d, <sup>3</sup>J = 1.8 Hz, 2, H3 or 5), 7.60 (d, <sup>3</sup>J = 1.8 Hz, 1, H3 or 5 or trans to Et), 7.51 (d, <sup>3</sup>J = 1.8 Hz, 2, H3 or 5), 6.18 ("t", 2, H4), 6.16 ("t", 1, H4 trans to Et), 3.20 (m, 2, PdCHH), 2.75 (m, 2, PdCHH), 2.40 (q, <sup>3</sup>J = 7.5 Hz, 2, PdCH<sub>2</sub>CH<sub>3</sub>), 1.79 (m, 4, CH<sub>2</sub>), 0.93 (t, <sup>3</sup>J = 7.5 Hz, 3, PdCH<sub>2</sub>CH<sub>3</sub>); <sup>13</sup>C{<sup>1</sup>H} NMR: δ 139.6 (C3 or 5), 139.0 (C3 or 5), 135.5 (C3 or 5), 135.1 (C3 or 5), 105.2 (C4), 47.6 (PdCH<sub>2</sub>CH<sub>2</sub>), 34.8 (PdCH<sub>2</sub>CH<sub>2</sub>), 30.4 (PdCH<sub>2</sub>CH<sub>3</sub>), 18.6 (PdCH<sub>2</sub>CH<sub>3</sub>). Anal. Calcd for C<sub>15</sub>H<sub>23</sub>BN<sub>6</sub>Pd: C, 44.5; H, 5.7; N, 20.8. Found: C, 44.6; H, 5.9; N, 20.5.

**Pd(C<sub>4</sub>H<sub>9</sub>)(CH<sub>2</sub>Ph){(pz)<sub>3</sub>BH} (12):** benzyl bromide as reagent, crystallization from pentane, yield 67%; <sup>1</sup>H NMR (CDCl<sub>3</sub>) δ 7.77 (d, <sup>3</sup>J = 2.0 Hz, 1, H3 or 5, pz trans to CH<sub>2</sub>Ph), 7.60 (d, <sup>3</sup>J = 2.2 Hz, 2, H3 or 5), 7.58 (d, <sup>3</sup>J = 2.0 Hz, 1, H3 or 5 trans to CH<sub>2</sub>Ph), 7.0-6.83 (m, 8, Ph and H3 or 5), 6.15 ("t", 1, H4 trans to CH<sub>2</sub>Ph), 6.01 ("t", <sup>3</sup>J = 3.0 Hz, 2, H4), 3.58 (s, 2, PdCH<sub>2</sub>Ph), 3.56 (m, 2, PdCHH), 2.85 (m, 2, PdCHH), 1.93 (m, 4, CH<sub>2</sub>); <sup>13</sup>C{<sup>1</sup>H} NMR: δ 146.9, 135.2, 139.0, 135.2, 129.9 (Ph), 128.4 (Ph), 125.3 (Ph), 105.2 (C4), 105.0 (C4), 49.6 (PdCH<sub>2</sub>), 39.0 (PdCH<sub>2</sub>Ph), 34.7 (CH<sub>2</sub>). Anal. Calcd for C<sub>20</sub>-H<sub>25</sub>BN<sub>6</sub>Pd: C, 51.5; H, 5.4; N, 18.0. Found: C, 51.5; H, 5.5; N, 17.9.

**Pd(C<sub>4</sub>H<sub>9</sub>)(CH<sub>2</sub>CH=CH<sub>2</sub>){(pz)<sub>3</sub>BH} (13):** oxidative addition of 2-propenyl iodide at -5 °C, crystallization from pentane,



**Table 2. Non-Hydrogen Atom Coordinates and Equivalent Isotropic Displacement Parameters for PdMe<sub>3</sub>{(pz)<sub>3</sub>BH} (1)**

atom	x	y	z	U <sub>eq</sub> (Å <sup>2</sup> )
Pd	0.16618(2)	0.22089(4)	0.21123(2)	0.0409(1)
C(a)	0.0834(3)	0.3159(6)	0.0570(3)	0.064(2)
C(b)	0.0746(3)	0.3166(7)	0.2555(4)	0.079(3)
C(c)	0.0874(3)	0.0083(6)	0.1626(3)	0.064(2)
B	0.3882(3)	0.2404(5)	0.3505(3)	0.041(2)
N(a1)	0.3501(2)	0.1460(3)	0.4183(2)	0.039(1)
N(a2)	0.2580(2)	0.1205(4)	0.3754(2)	0.045(1)
C(a3)	0.2472(3)	0.0353(5)	0.4522(3)	0.054(2)
C(a4)	0.3309(3)	0.0062(6)	0.5447(3)	0.060(2)
C(a5)	0.3956(3)	0.0786(5)	0.5208(3)	0.049(2)
N(b1)	0.3580(2)	0.1436(4)	0.2415(2)	0.039(1)
N(b2)	0.2672(2)	0.1196(3)	0.1681(2)	0.042(1)
C(b3)	0.2648(3)	0.0314(5)	0.0848(3)	0.054(2)
C(b4)	0.3519(3)	-0.0023(5)	0.1016(3)	0.059(2)
C(b5)	0.4102(3)	0.0706(5)	0.2024(3)	0.050(2)
N(c1)	0.3470(2)	0.4212(4)	0.3243(2)	0.043(1)
N(c2)	0.2544(2)	0.4450(4)	0.2670(3)	0.049(1)
C(c3)	0.2409(3)	0.6122(5)	0.2597(4)	0.065(2)
C(c4)	0.3235(4)	0.6975(5)	0.3122(4)	0.069(3)
C(c5)	0.3899(3)	0.5739(5)	0.3530(3)	0.053(2)

**Table 3. Non-Hydrogen Atom Coordinates and Equivalent Isotropic Displacement Parameters for PdMe<sub>3</sub>{(pz)<sub>4</sub>} (2)**

atom	x	y	z	U <sub>eq</sub> (Å <sup>2</sup> )
Pd	0.31895(5)	0.44420(5)	0.67790(3)	0.0388(2)
C(a)	0.3872(8)	0.2580(8)	0.6625(5)	0.064(3)
C(b)	0.1957(8)	0.3423(9)	0.7206(5)	0.060(3)
C(c)	0.4363(8)	0.4372(9)	0.7944(4)	0.063(3)
B	0.2658(7)	0.6968(7)	0.5469(4)	0.032(3)
N(a1)	0.2349(5)	0.7355(5)	0.6276(3)	0.033(2)
N(a2)	0.2493(5)	0.6471(6)	0.6906(3)	0.040(2)
C(a3)	0.2137(7)	0.7130(8)	0.7480(4)	0.045(3)
C(a4)	0.1768(7)	0.8432(8)	0.7228(4)	0.051(3)
C(a5)	0.1912(6)	0.8554(7)	0.6465(4)	0.043(3)
N(b1)	0.4014(5)	0.6544(5)	0.5682(3)	0.033(2)
N(b2)	0.4462(5)	0.5558(6)	0.6283(3)	0.041(2)
C(b3)	0.5610(7)	0.5357(8)	0.6313(4)	0.045(3)
C(b4)	0.5935(7)	0.6143(8)	0.5726(5)	0.051(3)
C(b5)	0.4900(7)	0.6866(7)	0.5329(4)	0.040(3)
N(c1)	0.1885(5)	0.5720(5)	0.5067(3)	0.032(2)
N(c2)	0.1964(5)	0.4553(6)	0.5520(3)	0.037(2)
C(c3)	0.1270(6)	0.3610(7)	0.5032(4)	0.041(3)
C(c4)	0.0740(7)	0.4163(7)	0.4255(4)	0.048(3)
C(c5)	0.1144(6)	0.5468(8)	0.4299(4)	0.041(2)
N(d1)	0.2416(5)	0.8222(6)	0.4916(3)	0.036(2)
N(d2)	0.1249(6)	0.8501(7)	0.4429(3)	0.053(3)
C(d3)	0.1297(9)	0.9793(8)	0.4184(5)	0.064(4)
C(d4)	0.2448(9)	1.0364(8)	0.4517(5)	0.061(4)
C(d5)	0.3118(7)	0.9354(8)	0.4989(4)	0.047(3)

yield 76%; <sup>1</sup>H NMR (CDCl<sub>3</sub>) δ 7.78 (d, <sup>3</sup>J = 2.0 Hz, 1, H3 or 5 trans to allyl), 7.68 (d, <sup>3</sup>J = 2.0 Hz, 2, H3 or 5), 7.62 (d, <sup>3</sup>J = 2.0 Hz, 1, H3 or 5 trans to allyl), 7.52 (d, <sup>3</sup>J = 2.0 Hz, 2, H3 or 5), 6.18 (m, 3, H4), 5.86 (m, 1, PdCH<sub>2</sub>CHCH<sub>2</sub>), 5.23 (dd, <sup>3</sup>J = 17 Hz, <sup>2</sup>J = 2.5 Hz, 1, PdCH<sub>2</sub>CHCHH trans to CH), 4.96 (dd, <sup>3</sup>J = 9.8 Hz, <sup>2</sup>J = 2.5 Hz, 1, PdCH<sub>2</sub>CHCHH cis to CH), 3.32 (m, 2, PdCHH), 3.07 (d, <sup>3</sup>J = 9 Hz, 2, PdCH<sub>2</sub>CHCH<sub>2</sub>), 2.76 (m, 2, PdCHH), 1.86 (m, 4, CH<sub>2</sub>); <sup>13</sup>C{<sup>1</sup>H} NMR δ 144.4, 139.8, 139.0, 135.5, 135.3, 112.6 (PdCH<sub>2</sub>CHCH<sub>2</sub>), 105.3 (C4), 105.2 (C4), 50.2 (PdCH<sub>2</sub>CH<sub>2</sub>), 37.7 (PdCH<sub>2</sub>CHCH<sub>2</sub>), 34.7 (CH<sub>2</sub>). Anal. Calcd for C<sub>16</sub>H<sub>23</sub>BN<sub>6</sub>Pd: C, 46.1; H, 5.6; N, 20.2. Found: C, 46.4; H, 5.7; N, 18.9.

**X-ray Structure Determinations.** For each complex, a unique data set was measured at 295 K using an Enraf-Nonius CAD-4 diffractometer operating in conventional 2θ-θ scan mode with monochromatic Mo Kα radiation (λ = 0.710 73 Å), yielding *N* independent reflections, *N*<sub>o</sub>, with *I* > 3σ(*I*) considered observed and used in the full matrix least-squares refinement after Gaussian absorption correction and solution

(14) Ibers, J. A.; Hamilton, W. C., Eds. *International Tables for X-Ray Crystallography*; Kynoch Press: Birmingham, England, 1974; Vol. 4.

(15) Hall, S. R.; Stewart, J. M. *The XTAL User's Manual*, Version 3.0; Universities of Western Australia and Maryland, 1990.

**Table 4. Non-Hydrogen Atom Coordinates and Equivalent Isotropic Displacement Parameters for PdMe<sub>2</sub>Et{(pz)<sub>3</sub>BH} (3a)**

atom	x	y	z	U <sub>eq</sub> (Å <sup>2</sup> )
Pd	0.8140(1)	0.65674(7)	0.26100(7)	0.0521(4)
C(a)	0.843(1)	0.5207(9)	0.2025(9)	0.078(7)
C(b)	1.014(1)	0.621(1)	0.3804(9)	0.090(7)
C(c)	0.959(2)	0.728(1)	0.208(1)	0.11(1)
C(d)	0.881(3)	0.783(2)	0.116(1)	0.19(2)
B	0.495(2)	0.744(1)	0.264(1)	0.060(7)
N(a1)	0.630(1)	0.8228(6)	0.3110(6)	0.049(4)
N(a2)	0.777(1)	0.8002(6)	0.3228(6)	0.052(4)
C(a3)	0.866(1)	0.881(1)	0.3703(9)	0.071(6)
C(a4)	0.774(2)	0.9566(9)	0.3877(9)	0.080(8)
C(a5)	0.626(2)	0.9176(9)	0.3501(8)	0.063(6)
N(b1)	0.468(1)	0.7213(6)	0.1591(7)	0.049(4)
N(b2)	0.585(1)	0.6862(7)	0.1393(6)	0.060(5)
C(b3)	0.522(2)	0.668(1)	0.0436(9)	0.070(6)
C(b4)	0.365(2)	0.6917(9)	-0.0006(8)	0.072(7)
C(b5)	0.333(1)	0.7248(8)	0.0761(9)	0.058(5)
N(c1)	0.541(1)	0.6396(6)	0.3208(6)	0.049(4)
N(c2)	0.671(1)	0.5862(6)	0.3274(6)	0.046(4)
C(c3)	0.678(2)	0.4986(9)	0.3753(8)	0.067(7)
C(c4)	0.554(2)	0.4937(9)	0.4018(9)	0.076(7)
C(c5)	0.470(1)	0.5827(9)	0.3654(8)	0.062(6)

**Table 5. Non-Hydrogen Atom Coordinates and Equivalent Isotropic Displacement Parameters for PdMe<sub>2</sub>Et{(pz)<sub>3</sub>BH} (3b)**

atom	x	y	z	U <sub>eq</sub> (Å <sup>2</sup> )
Pd	0.54445(7)	0.84129(6)	0.52319(9)	0.0678(3)
C(a)	0.456(1)	0.866(1)	0.712(1)	0.132(8)
C(b)	0.614(1)	0.973(1)	0.579(2)	0.113(6)
C(c)	0.645(2)	0.776(2)	0.656(2)	0.145(9)
C(d) <sup>a</sup>	0.686(3)	0.690(3)	0.594(5)	0.14(1)
C(d') <sup>a</sup>	0.620(5)	0.684(6)	0.723(9)	0.33(4)
B	0.469(1)	0.768(1)	0.204(1)	0.067(5)
N(a1)	0.5753(6)	0.7842(6)	0.197(1)	0.057(3)
N(a2)	0.6257(6)	0.8223(7)	0.3169(9)	0.060(3)
C(a3)	0.7154(8)	0.8276(9)	0.278(1)	0.072(5)
C(a4)	0.729(1)	0.799(1)	0.135(2)	0.085(6)
C(a5)	0.639(1)	0.7724(8)	0.085(1)	0.066(4)
N(b1)	0.4429(7)	0.6892(5)	0.322(1)	0.060(3)
N(b2)	0.4747(6)	0.7009(6)	0.459(1)	0.063(3)
C(b3)	0.4479(9)	0.6176(8)	0.533(1)	0.083(5)
C(b4)	0.404(1)	0.5512(8)	0.439(2)	0.093(6)
C(b5)	0.4034(9)	0.5987(9)	0.305(2)	0.079(5)
N(c1)	0.4192(7)	0.8719(7)	0.249(1)	0.075(4)
N(c2)	0.4391(8)	0.9145(7)	0.383(1)	0.083(4)
C(c3)	0.392(1)	1.0021(9)	0.381(2)	0.109(7)
C(c4)	0.339(1)	1.015(1)	0.255(2)	0.132(9)
C(c5)	0.361(1)	0.931(1)	0.166(2)	0.099(6)

<sup>a</sup> Site occupancy factors, 0.5.

of the structures by vector methods. Residuals *R* and *R*<sub>w</sub> are quoted on *F* at convergence (preferred hand, **3b**, **3c**); statistical weights derived from σ<sup>2</sup>(*I*) = σ<sup>2</sup>(*I*<sub>diff</sub>) + 0.0004σ<sup>4</sup>(*I*<sub>diff</sub>) were employed. Neutral atom complex scattering factors were used;<sup>14</sup> computation used the XTAL 3.0 program system implemented by Hall.<sup>15</sup> Crystal data, coordinates, and equivalent isotropic thermal parameters for the non-hydrogen atoms and geometries of the complexes are given in Tables 1–8, and views of the complexes are shown in Figures 1–3.

## Results and Discussion

**Synthesis and Characterization of Complexes.** The reagents PdMe<sub>2</sub>(tmeda)<sup>2a</sup> and PdMePh(tmeda)<sup>12</sup> and the pallada(II)cyclopentane complex Pd(C<sub>4</sub>H<sub>8</sub>)-(tmeda)<sup>13</sup> (tmeda = *N,N,N',N'*-tetramethylethylenediamine) were chosen as substrates for attempted synthesis of complexes containing [(pz)<sub>3</sub>BH]<sup>-</sup> because tmeda is known to be readily displaced by stronger donor ligands such as 2,2'-bipyridyl.<sup>1g,2a,6,12,13a,b</sup> Initial <sup>1</sup>H NMR studies of reactions indicated that displacement

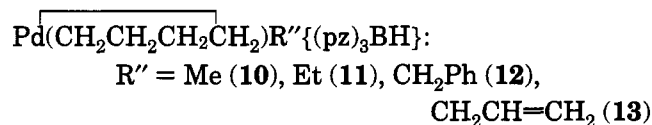
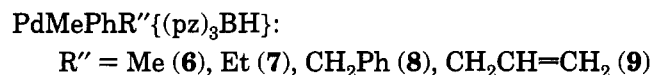
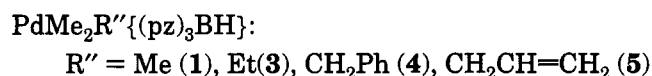
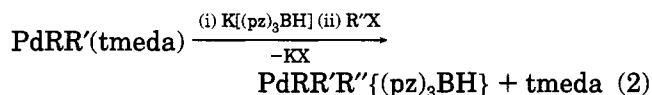


**Table 6. Non-Hydrogen Atom Coordinates and Equivalent Isotropic Displacement Parameters for PdMe<sub>2</sub>Et{(pz)<sub>3</sub>BH} (3c)**

atom	x	y	z	U <sub>eq</sub> (Å <sup>2</sup> )
Pd	0.60270(6)	0.20744(6)	0.51406(3)	0.0642(3)
C(a)	0.621(1)	0.354(1)	0.5565(6)	0.121(6)
C(b)	0.6115(9)	0.1439(9)	0.6016(4)	0.103(4)
C(c)	0.444(1)	0.222(2)	0.5258(9)	0.144(9)
C(d) <sup>a</sup>	0.382(3)	0.177(5)	0.533(3)	0.25(3)
C(d') <sup>a</sup>	0.618(3)	0.448(3)	0.518(2)	0.24(2)
B	0.7262(9)	0.1162(8)	0.3934(4)	0.068(4)
N(a1)	0.6543(5)	0.0273(5)	0.4201(3)	0.063(3)
N(a2)	0.5902(5)	0.0479(5)	0.4697(3)	0.062(2)
C(a3)	0.5330(7)	-0.0407(8)	0.4792(4)	0.080(4)
C(a4)	0.5593(9)	-0.1198(7)	0.4357(5)	0.090(4)
C(a5)	0.6365(8)	-0.0739(7)	0.3997(4)	0.076(4)
N(b1)	0.6552(5)	0.2132(6)	0.3749(3)	0.066(2)
N(b2)	0.5969(6)	0.2693(5)	0.4179(3)	0.068(3)
C(b3)	0.5399(8)	0.3432(8)	0.3870(5)	0.082(4)
C(b4)	0.5629(9)	0.3368(9)	0.3256(5)	0.092(5)
C(b5)	0.6331(8)	0.2548(8)	0.3186(4)	0.077(4)
N(c1)	0.8084(6)	0.1531(5)	0.4424(3)	0.068(3)
N(c2)	0.7764(6)	0.1953(5)	0.4970(3)	0.070(3)
C(c3)	0.8639(9)	0.2211(9)	0.5282(5)	0.089(4)
C(c4)	0.9552(9)	0.195(1)	0.4939(7)	0.117(6)
C(c5)	0.9170(9)	0.1514(8)	0.4414(6)	0.090(5)

<sup>a</sup> Site occupancy factor, 0.5.

of tmeda by [(pz)<sub>3</sub>BH]<sup>-</sup> occurs readily at 0 °C for PdMe<sub>2</sub>(tmeda) and Pd(C<sub>4</sub>H<sub>8</sub>)(tmeda), but that heating to ~35 °C is required for PdMePh(tmeda). Oxidative addition of organohalides to [PdMe<sub>2</sub>{(pz)<sub>3</sub>BH}]<sup>-</sup> or [Pd(C<sub>4</sub>H<sub>8</sub>){(pz)<sub>3</sub>BH}]<sup>-</sup> occurs at 0–25 °C, but ambient temperatures or above were generally required to observe reactions for [PdMePh{(pz)<sub>3</sub>BH}]<sup>-</sup>. Although temperatures required for synthesis were generally higher than the decomposition temperatures of most previously reported organopalladium(IV) complexes, a series of complexes were obtained in 55–95% yield (eq 2). Water



was rigorously excluded from all reactions, up to but not including the working up stage, as it has been established that the palladium(II) poly(pyrazol-1-yl)borate complexes [PdMeR{(pz)<sub>3</sub>BH}]<sup>-</sup> (R = Me, Ph) are susceptible to oxidation by water.<sup>11</sup>

Extensive attempts to obtain crystals suitable for a structural study were successful for PdMe<sub>3</sub>{(pz)<sub>3</sub>BH} (1) and PdMe<sub>2</sub>Et{(pz)<sub>3</sub>BH} (3) only, and the tetrakis(pyrazol-1-yl)borate complex PdMe<sub>3</sub>{(pz)<sub>4</sub>B} (2) was synthesized and crystallized to allow a comparison with 1.

<sup>1</sup>H and <sup>13</sup>C NMR spectra of the complexes are in accord with the formulations presented and may be readily assigned, e.g., occurrence of two pyrazole ring environments in 2:1 ratio for PdMe<sub>2</sub>R''{(pz)<sub>3</sub>BH} (R'' = Et, CH<sub>2</sub>Ph, CH<sub>2</sub>CH=CH<sub>2</sub>) and Pd(C<sub>4</sub>H<sub>8</sub>)R''{(pz)<sub>3</sub>BH}

**Table 7. Selected Bond Distances (Å) and Angles (deg) for PdMe<sub>3</sub>{(pz)<sub>3</sub>BH} (1) and PdMe<sub>3</sub>{(pz)<sub>4</sub>B} (2), and PdMe<sub>2</sub>Et{(pz)<sub>3</sub>BH} (3a–c)**

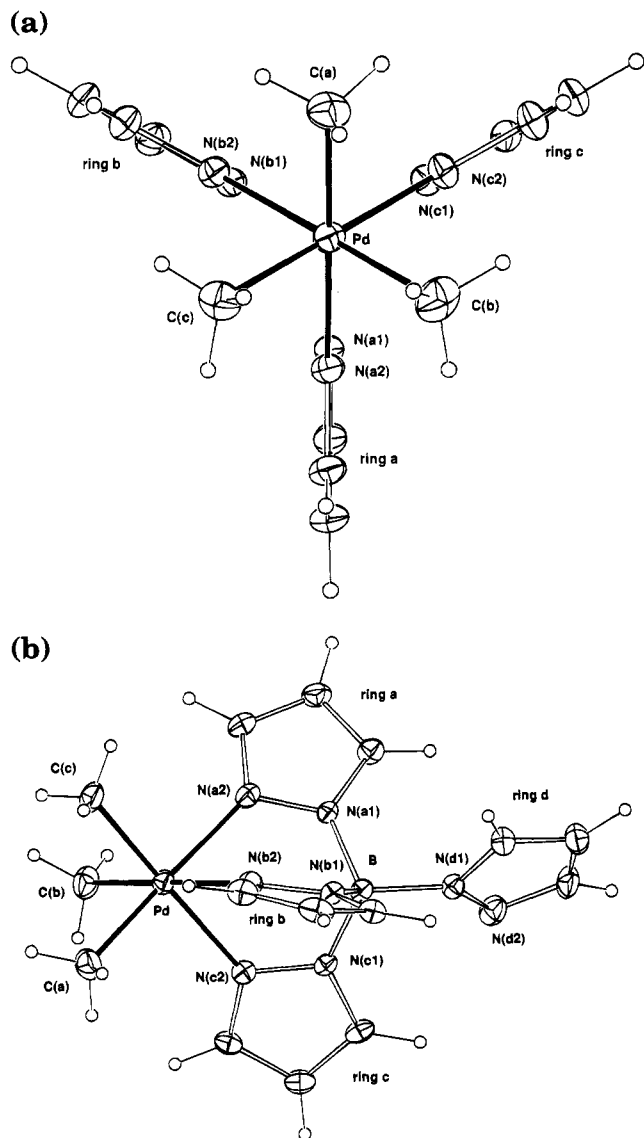
	PdMe <sub>3</sub> - {(pz) <sub>3</sub> BH} (1)	PdMe <sub>3</sub> - {(pz) <sub>4</sub> B} (2)	PdMe <sub>2</sub> Et{(pz) <sub>3</sub> BH}		
			3a	3b	3c
Bond Distances					
Pd–C(a)	2.034(4)	2.021(8)	2.02(1)	2.13(2)	2.04(1)
Pd–C(b)	2.032(7)	2.026(9)	2.03(1)	2.05(1)	2.045(9)
Pd–C(c)	2.024(5)	2.036(6)	2.06(2)	2.03(2)	1.97(2)
Pd–N(a2)	2.174(3)	2.164(6)	2.155(9)	2.198(9)	2.189(6)
Pd–N(b2)	2.178(4)	2.177(6)	2.183(7)	2.165(8)	2.208(6)
Pd–N(c2)	2.177(3)	2.184(4)	2.18(1)	2.17(1)	2.174(7)
C(a)–C(d')					1.42(4)
C(c)–C(d)			1.45(3)	1.39(5)	
C(c)–C(d')				1.40(8)	0.97(5)
B–N(a1)	1.545(6)	1.560(9)	1.54(2)	1.51(2)	1.52(1)
B–N(b1)	1.536(5)	1.542(9)	1.53(2)	1.53(2)	1.53(1)
B–N(c1)	1.542(5)	1.538(8)	1.54(2)	1.59(2)	1.53(1)
B–N(d1)		1.514(9)			
"Bite Distances" for the Poly(pyrazol-1-yl)borate Ligands					
N(a2)–N(b2)	2.900(9)	2.932(6)	2.97(1)	2.94(1)	2.945(9)
N(a2)–N(c2)	2.922(7)	2.941(5)	2.92(1)	2.93(1)	2.981(9)
N(b2)–N(c2)	2.936(7)	2.952(5)	2.90(1)	2.94(1)	2.934(10)
Bond Angles					
C(a)–Pd–C(b)	87.3(2)	86.8(4)	87.1(5)	87.1(6)	85.4(5)
C(a)–Pd–C(c)	87.5(2)	85.8(3)	88.9(7)	89.4(7)	88.5(8)
C(b)–Pd–C(c)	87.1(2)	88.0(3)	86.1(6)	83.4(7)	88.3(7)
N(a2)–Pd–N(b2)	84.7(1)	83.8(2)	86.3(3)	84.8(3)	84.1(2)
N(a2)–Pd–N(c2)	85.1(1)	84.5(2)	84.7(4)	84.4(4)	86.2(2)
N(b2)–Pd–N(c2)	85.4(1)	84.6(2)	83.3(3)	85.3(3)	84.1(3)
C(a)–Pd–N(a2)	178.4(2)	177.3(3)	178.3(5)	175.0(5)	177.4(5)
C(a)–Pd–N(b2)	93.9(2)	93.9(3)	92.7(4)	94.7(5)	96.8(4)
C(a)–Pd–N(c2)	94.0(2)	94.5(3)	93.9(5)	90.6(5)	91.5(5)
C(b)–Pd–N(a2)	94.0(2)	95.4(3)	93.9(4)	93.4(5)	93.6(3)
C(b)–Pd–N(b2)	178.5(1)	178.0(2)	174.1(5)	178.2(5)	177.4(3)
C(b)–Pd–N(c2)	93.8(2)	93.4(2)	90.8(5)	95.0(5)	94.4(4)
C(c)–Pd–N(a2)	93.4(1)	95.2(3)	92.6(6)	95.6(6)	93.9(7)
C(c)–Pd–N(b2)	93.7(2)	93.9(3)	99.8(5)	96.2(6)	93.3(6)
C(c)–Pd–N(c2)	178.3(1)	178.5(3)	175.7(5)	178.5(6)	177.3(7)
Pd–N(a2)–N(a1)	118.2(2)	117.8(4)	118.3(6)	116.3(6)	118.1(5)
Pd–N(a2)–C(a3)	135.5(3)	135.8(5)	135.7(9)	135.9(8)	135.6(6)
Pd–N(b2)–N(b1)	117.7(2)	119.1(4)	118.5(7)	119.9(6)	116.6(5)
Pd–N(b2)–C(b3)	136.2(2)	133.4(5)	135.2(9)	133.7(8)	136.4(6)
Pd–N(c2)–N(c1)	118.1(2)	120.7(4)	117.7(6)	118.5(7)	117.5(5)
Pd–N(c2)–C(c3)	135.6(3)	131.8(4)	135.0(9)	137(1)	134.8(6)
Pd–C(a)–C(d')					117(2)
Pd–C(c)–C(d)			116(1)	113(2)	139(4)
Pd–C(c)–C(d')				117(3)	
N(a1)–B–N(b1)	108.5(3)	109.5(4)	110(1)	111(1)	109.1(8)
N(a1)–B–N(c1)	108.7(4)	109.2(6)	109.4(8)	108.4(9)	109.6(7)
N(a1)–B–N(d1)		107.6(5)			
N(b1)–B–N(c1)	109.2(3)	107.5(5)	107(1)	108(1)	108.9(7)
N(b1)–B–N(d1)		110.3(6)			
N(c1)–B–N(d1)		112.7(4)			

**Table 8. Deviations (Å) of Palladium and Boron Atoms from the "C<sub>3</sub>N<sub>2</sub>" Mean Planes of Pyrazole Rings, and Angles (deg) between Planes<sup>a</sup>**

	PdMe <sub>3</sub> - {(pz) <sub>3</sub> BH} (1)	PdMe <sub>3</sub> - {(pz) <sub>4</sub> B} (2) <sup>b</sup>	PdMe <sub>2</sub> Et{(pz) <sub>3</sub> BH}		
			3a	3b	3c
Deviations					
Pd (ring a)	0.041(7)	0.00(1)	0.10(2)	0.15(2)	0.01(1)
Pd (ring b)	0.034(7)	0.45(1)	0.19(2)	0.03(2)	0.21(2)
Pd (ring c)	0.022(7)	0.16(1)	0.00(2)	0.21(2)	0.01(2)
B (ring a)	-0.012(7)	0.01(1)	-0.09(2)	-0.01(2)	-0.10(2)
B (ring b)	0.013(7)	0.07(1)	0.08(2)	-0.12(2)	0.07(2)
B (ring c)	0.026(8)	0.08(1)	-0.06(2)	0.06(3)	-0.03(2)
Angles					
rings a/b	119.0(2)	127.3(3)	127.5(6)	117.1(5)	112.3(4)
rings a/c	118.2(2)	124.2(3)	120.7(6)	115.5(6)	124.8(4)
rings b/c	122.3(2)	108.2(3)	111.4(6)	126.8(6)	122.8(4)

<sup>a</sup> χ<sup>2</sup> values for rings a–c, respectively: (1) 1.2, 0.3, 1.1; (2) 0.1, 13.1, 0.3, and for ring d 12.7; (3a) 0.2, 0.2, 0.4; (3b) 4.4, 8.7, 2.4; (3c) 0.3, 1.8, 1.7. <sup>b</sup> For ring d: Pd 1.29(2), B 0.33(1) Å, ring a/d 91.1(3), ring b/d 134.8(3), and ring c/d 142.5(3)<sup>o</sup>.

(R'' = Me, Et, CH<sub>2</sub>Ph, CH<sub>2</sub>CH=CH<sub>2</sub>), two pyrazole ring environments in 3:1 ratio for PdMe<sub>3</sub>{(pz)<sub>4</sub>B}, and three

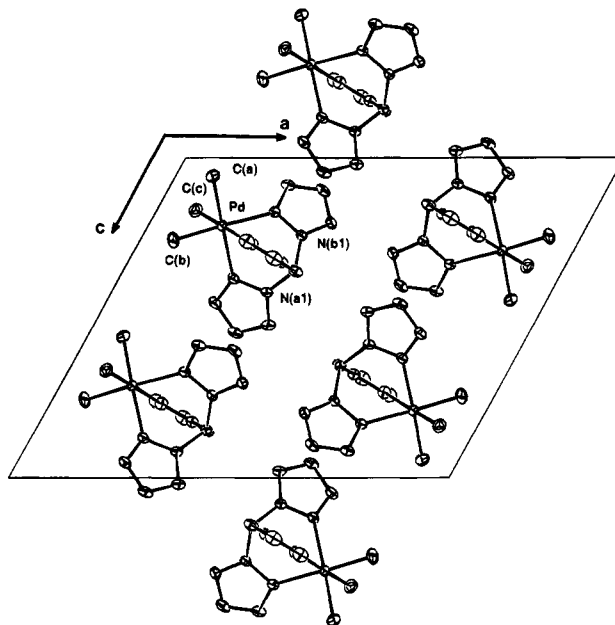


**Figure 1.** Molecular structures of (a, top) PdMe<sub>3</sub>{(pz)<sub>3</sub>BH} (1) illustrating the noncrystallographic  $C_{3v}$  symmetry and (b, bottom) PdMe<sub>3</sub>{(pz)<sub>4</sub>B} (2) illustrating the deviation (0.45 Å) of the palladium atom from the mean plane of pyrazole ring b. Thermal ellipsoids (20%) are shown for the non-hydrogen atoms, and hydrogen atoms (constrained at estimated positions) have been given an arbitrary radius of 0.1 Å.

pyrazole ring environments for PdMePhR''{(pz)<sub>3</sub>BH} (R'' = Et, CH<sub>2</sub>Ph, CH<sub>2</sub>CH=CH<sub>2</sub>). Replacement of methyl groups in PdMe<sub>3</sub>{(pz)<sub>3</sub>BH} by  $\eta^1$ -propenyl, benzyl, or phenyl groups results in a downfield shift for the remaining methyl resonance, as shown in Scheme 1a. The protons of the pallada(IV)cyclopentane rings are present as three resonances in 4:2:2 ratio. For these complexes, the protons closest to R'' in Pd(C<sub>4</sub>H<sub>8</sub>)R''{(pz)<sub>3</sub>BH}, H<sub>a</sub> in Scheme 1b, are expected to experience changes in chemical shift similar to that of the methyl groups in PdMe<sub>2</sub>R''{(pz)<sub>3</sub>BH}, allowing assignment of resonances as shown in Scheme 1b. Protons opposite to R'', H<sub>b</sub>, experience upfield shifts, in contrast to H<sub>a</sub>.

**X-ray Structural Studies.** Crystals of PdMe<sub>3</sub>{(pz)<sub>3</sub>BH} (1) and PdMe<sub>3</sub>{(pz)<sub>4</sub>B} (2) were obtained on dissolution in acetone followed by diffusion of diethyl ether vapor into the solution, and crystals of PdMe<sub>2</sub>Et{(pz)<sub>3</sub>BH} (3) formed from pentane.

Three crystalline forms of 3 were detected: complex 3a is ordered, but 3b has disordering of the methyl



**Figure 2.** Unit cell contents of PdMe<sub>3</sub>{(pz)<sub>3</sub>BH} (1) projected down  $b$ , illustrating the packing of molecules and showing views of the complex in a different orientation.

group of PdCH<sub>2</sub>CH<sub>3</sub> between two positions in equal proportions, and 3c has disorder in position between the ethyl group and one of the PdCH<sub>3</sub> groups in equal proportions (Figure 3). Disorder in complexes of tripod ligands is not unexpected, and recent examples include octahedral [PtPh<sub>2</sub>{(pz)<sub>3</sub>CH}][I][I<sub>3</sub>] which has an asymmetric unit containing one ordered cation and one disordered cation in which the position of the iodine and one of the phenyl groups is disordered.<sup>16</sup>

All of the complexes have octahedral geometry for palladium (Figures 1–3), and complexes 3b and 3c have geometries similar to those of the other complexes, but in view of the disorder, data for these complexes are generally excluded in detailed comparisons of geometries.

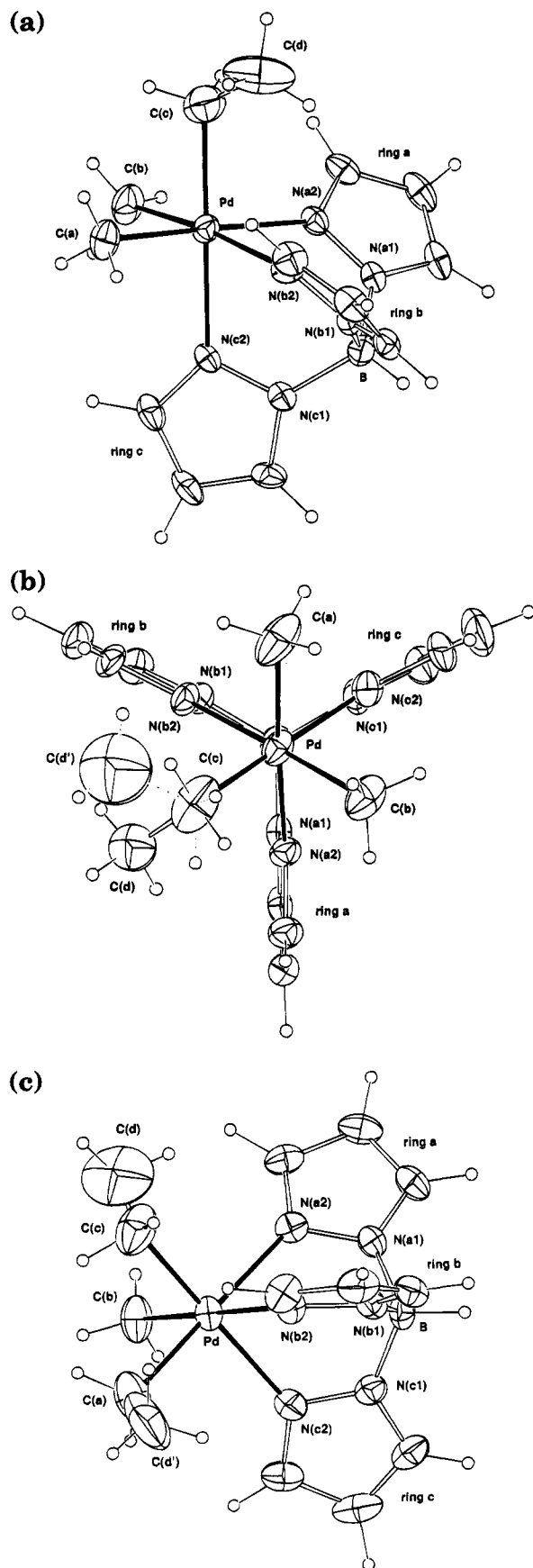
The trimethylpalladium(IV) complexes 1 and 2 (Figure 1) have bond lengths and angles at the palladium centre within 3 $\sigma$ , except for C(a)–Pd–C(b) [87.5(2)° in (1), 85.8(3)° in (2)] (Table 7). Complexes 1, 2, and 3a have C–Pd–C angles 85.8(3)–88.9(7)° and N–Pd–N chelate angles 83.3(3)–86.3(3)°, and complex 1 has noncrystallographic  $C_{3v}$  symmetry.

The palladium atoms in 1 and 3a–c lie within ~0.2 Å of the “C<sub>3</sub>N<sub>2</sub>” mean planes of coordinated pyrazole rings (Table 7), as found for the related cation [PdMe<sub>3</sub>{(pz)<sub>3</sub>CH}]<sup>+</sup>,<sup>8</sup> but for complex 2 the palladium atom lies 0.45(1) Å from the mean plane of ring b (Figure 1b). The larger deviation for the [(pz)<sub>4</sub>B]<sup>−</sup> complex appears to result from steric effects between ring d and the coordinated rings; steric interactions of this type between coordinated and uncoordinated rings of tridentate [B(pz)<sub>4</sub>]<sup>−</sup> have been documented recently in studies of complexes of group 2 metal ions.<sup>17</sup>

Complex 1 has average values of Pd–C and Pd–N about 0.02 and 0.03 Å shorter than those for isoelectronic [PdMe<sub>3</sub>{(pz)<sub>3</sub>CH}]<sup>+</sup>, but these differences are within 2 $\sigma$  and the bond lengths in the cation occur over

(16) Canty, A. J.; Honeyman, R. T.; Skelton, B. W.; White, A. H. *J. Organomet. Chem.* **1992**, *424*, 381.

(17) Sohrin, Y.; Kokusen, H.; Kihara, S.; Matsui, M.; Kushi, Y.; Shiro, M. *J. Am. Chem. Soc.* **1993**, *115*, 4128.



**Figure 3.** Molecular structures of  $\text{PdMe}_2\text{Et}\{(\text{pz})_3\text{BH}\}$  showing (a, top) the ordered structure of **3a** and disorder in (b, middle) the methyl positions of the ethyl group in **3b** and (c, bottom) in positions of the ethyl and methyl groups in **3c**.

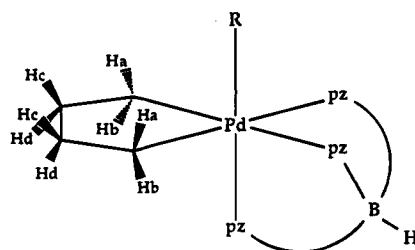
a wider range, Pd–C 2.036(11)–2.060(9) Å.<sup>8</sup> The  $\{(\text{pz})_3\text{BH}\}^-$  ligands in **1** and **3a** exhibit N–N “bite

**Scheme 1.**  $^1\text{H}$  NMR Chemical Shifts for (a) Methylpalladium(IV) Groups in  $\text{PdMeR}''\{(\text{pz})_3\text{BH}\}$  and (b) Pallada(IV)cyclopentane groups in  $\text{Pd}(\text{C}_4\text{H}_8)\text{R}\{(\text{pz})_3\text{BH}\}$

(a)  $\text{PdMe}_3 \sim \text{PdMe}_2\text{Et} < \text{PdMe}_2(\text{CH}_2\text{Ph}) < \text{PdMe}_2(\text{CH}_2\text{CH}=\text{CH}_2) <$   
1.38 1.42 1.55 1.61

$\text{PdMe}_2\text{Ph} \sim \text{PdMeEtPh} < \text{PdMePh}(\text{CH}_2\text{CH}=\text{CH}_2) < \text{PdMePh}(\text{CH}_2\text{Ph})$   
1.82 1.81 1.88 1.97

(b)



	Me	Et	$\text{CH}_2\text{CH}=\text{CH}_2$	$\text{CH}_2\text{Ph}$
Ha	3.16	3.20	3.32	3.56
Hb	2.87	2.75	2.76	2.85
Hc,d	1.78	1.79	1.86	1.93

distances” [2.90(1)–2.97(1) Å] (Table 7) similar to that of  $\text{PdMe}_3\{(\text{pz})_3\text{CH}\}$  [2.89(1)–2.92(1) Å], but form larger N–Pd–N bite angles, 83.3(3)–86.3(3)° compared with 8.17(3)–83.2(3)°. The larger angles appear to be directly attributable to B–N bond distances [1.53(2)–1.54(2) Å] that are longer than the analogous C–N bond distances [1.45(1)–1.48(1) Å]. The slightly more regular octahedral geometry of the  $\{(\text{pz})_3\text{BH}\}^-$  complexes compared to  $\text{PdMe}_3\{(\text{pz})_3\text{CH}\}$  is also reflected in Pd–N(n1)–C(n3) angles, which are  $\sim 2^\circ$  less in **1** and **3a** [135.0(9)–136.2(2)°] than in  $[\text{PdMe}_3\{(\text{pz})_3\text{CH}\}]^+$  [137.1(7)–138.2(6)°]. A similar trend in bite angles is found for  $\text{Pd}\{(\text{pz})_3\text{BH}-\text{N},\text{N}'\}_2$  [90.1(1)°] and  $[\text{Pd}\{(\text{pz})_3\text{CH}-\text{N},\text{N}'\}_2][\text{BF}_4]_2$  [87.4(5)°],<sup>18</sup> and in these complexes, angles closer to 90° are assumed to result from greater flexibility in the ligands when they are present as bidentates.

Complex **3** is the only ethylpalladium(IV) complex for which a crystal structure has been determined, and only two structures appear to have been published for palladium(II). These complexes, *trans*- $[\text{Pd}(\text{SPh})\text{Et}(\text{PMe}_3)_2]$ <sup>19a</sup> and *trans*- $[\text{PdBrEt}(\text{PMe}_3)_2]$ ,<sup>19b</sup> exhibit similar geometries for the ethylpalladium group, although they have smaller Pd–C–C angles, 107.6(6)° and 110.5(5)°, respectively, than that found for **3a**, 116(1)°.

**Stabilities of the Complexes.** All of the complexes are stable at ambient temperature and as suspensions in water. When heated in the solid state, they decompose to form black powders over wide temperature ranges, but the  $\text{PdMePhR}''$  complexes appear to be generally less stable than the  $\text{Pd}(\text{C}_4\text{H}_8)\text{R}''$  and  $\text{PdMe}_2\text{R}''$  complexes, and the least stable complexes in each group have  $\text{R}'' = \text{Et}$  or  $\text{CH}_2\text{CH}=\text{CH}_2$ . These stability trends are consistent with solution behavior, e.g., when studied by  $^1\text{H}$  NMR spectroscopy in toluene- $d_6$ , the complexes  $\text{PdMe}_2\text{R}''\{(\text{pz})_3\text{BH}\}$  and  $\text{Pd}(\text{C}_4\text{H}_8)\text{R}''\{(\text{pz})_3\text{BH}\}$  ( $\text{R}'' = \text{Et}$ ,  $\text{CH}_2\text{CH}=\text{CH}_2$ ) are stable to at least 80 °C, but  $\text{PdMe}$ -

(18) Canty, A. J.; Minchin, N. J.; Engelhardt, L. M.; Skelton, B. W.; White, A. H. *J. Chem. Soc., Dalton Trans.* **1986**, 645.

(19) (a) Osakada, Y.; Ozawa, Y.; Yamamoto, A. *Bull. Chem. Soc. Jpn.* **1991**, 64, 2002. (b) Osakada, Y.; Ozawa, Y.; Yamamoto, A. *J. Chem. Soc., Dalton Trans.* **1991**, 759.

PhEt{(pz)<sub>3</sub>BH} and PdMePh(CH<sub>2</sub>CH=CH<sub>2</sub>){(pz)<sub>3</sub>BH} decompose at 60–70 °C and ~25 °C, respectively, to give black solids. The nature of organic products from these decomposition reactions has not been ascertained.

A relatively small number of hydrocarbylpalladium(IV) complexes reported to date are stable at ambient temperature.<sup>1b,g,4,6</sup> Hydrocarbylpalladium(IV) chemistry is usually characterized by clean and facile reductive elimination reactions at low to moderate temperatures to form palladium(II) products, in particular phenylpalladium(IV) complexes; e.g., PdXMePh(CH<sub>2</sub>Ph)(bpy) (X = Br, I) decompose in both the solid state and solution at 0 °C to form PdX(CH<sub>2</sub>Ph)(bpy) and toluene.<sup>11</sup> However, the stabilities of the palladium(IV)cyclopentane and ethyl- and phenylpalladium(IV) complexes described here are similar to related diorganopalladium(II) analogues involving bidentate nitrogen donor ligands,<sup>12,13a,b,20</sup> e.g., the decomposition of Pd(C<sub>4</sub>H<sub>8</sub>)(bpy)<sup>13a</sup> and PdEt<sub>2</sub>(bpy)<sup>20</sup> has been studied in solution at 80 and 60 °C, respectively. Thus, with suitable choice of donor ligand systems, organopalladium(IV) complexes have stabilities comparable to that exhibited in well-established organopalladium(II) chemistry.

Although far fewer studies in organopalladium(IV) than organopalladium(II) chemistry have been reported to date, it appears that similar principles govern stabilities for “*cis*-PdR<sub>2</sub>” groups in square-planar palladium(II) and “*fac*-PdR<sub>3</sub>” groups in octahedral palladium(IV) complexes. Enhanced stability occurs for complexes containing polydentate ligands that have high donor ability and/or ability to adopt a conformation favoring

square-planar geometry for palladium(II) or octahedral geometry for palladium(IV), because these properties reduce tendencies toward donor group dissociation. For example, Pd(C<sub>4</sub>H<sub>8</sub>)(bpy) is more stable than Pd(C<sub>4</sub>H<sub>8</sub>)(tmeda) where bpy is more rigid than tmeda,<sup>13b</sup> and PdMe<sub>2</sub>(CH<sub>2</sub>Ph){(pz)<sub>3</sub>BH} is more stable than [PdMe<sub>2</sub>(CH<sub>2</sub>Ph){(pz)<sub>3</sub>CH}]X (X = Br, BF<sub>4</sub>)<sup>9</sup> where [(pz)<sub>3</sub>BH]<sup>-</sup> is a stronger donor than isoelectronic (pz)<sub>3</sub>CH and presents coordination geometries closer to octahedral. Similarly, although palladium(IV) appears to be stabilized by anionic “harder” nitrogen and oxygen<sup>6</sup> donor ligands, the “soft” thioether donor 1,4,7-trithiacyclononane (9S3) forms very stable complexes [PdMe<sub>3</sub>(9S<sub>3</sub>)]X (X = I, NO<sub>3</sub>),<sup>15</sup> and the high stability of these complexes may be related to the *fac*-9S3 group adopting a conformation in the complex which is very similar to that adopted by free 9S3.<sup>21</sup>

**Acknowledgment.** We thank the Australian Research Council for financial support, and Johnson Matthey Ltd. for generous loans of palladium chloride.

**Supplementary Material Available:** Listings of non-hydrogen atom thermal parameters, hydrogen atom parameters, and ligand geometry for the complexes (16 pages). Ordering information is given on any current masthead page.

OM9405192

(21) (a) Cooper, S. R.; Rawle, S. C. *Struct. Bonding* **1990**, 72, 1. (b) Blake, A. J.; Schroder, M. *Adv. Inorg. Chem.* **1990**, 35, 1. (c) Beech, J.; Cragg, P. J.; Drew, M. G. B. *J. Chem. Soc., Dalton Trans.* **1994**, 719.

(20) Sustmann, R.; Lau, J. *Chem. Ber.* **1986**, 119, 2531.

# Stable Arylpalladium Iodides and Reactive Arylpalladium Trifluoromethanesulfonates in the Intramolecular Heck Reaction

John M. Brown<sup>\*,†</sup> and Jesús J. Pérez-Torrente

*Dyson Perrins Laboratory, South Parks Road, Oxford OX1 3QY, United Kingdom*

Nathaniel W. Alcock and Howard J. Clase

*Department of Chemistry, University of Warwick, Coventry CV4 7AL, United Kingdom*

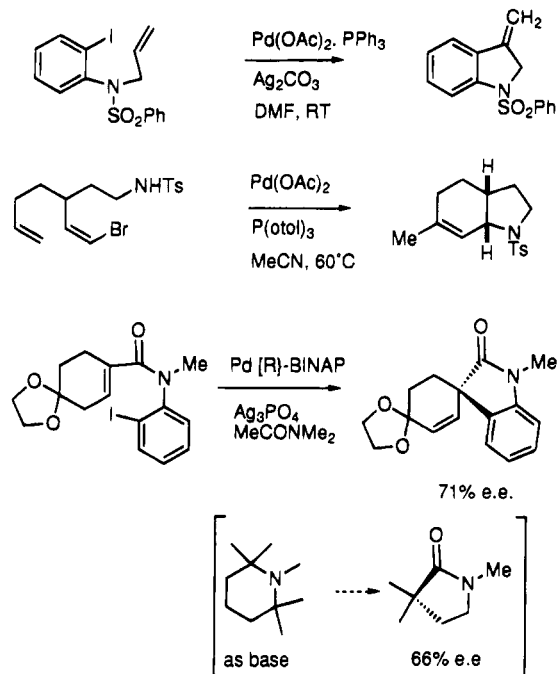
Received July 28, 1994<sup>⊗</sup>

The reactions of 1-iodo-2-(3-butenyl)benzene and of two side-chain ether analogs with [1,1'-bis(diphenylphosphino)ferrocene]( $\eta^2$ -cyclooctatetraene)palladium gave the expected ( $\eta^1$ -aryl)-( $\eta^1$ -iodo)palladium adducts, the 2-oxa-3-butenyl complex being characterized by X-ray crystallography. The alkene does not interact directly with palladium. Restricted rotation about the aryl–palladium bond was observed on the NMR time scale in all cases, since the methylene group(s) of the side chain were diastereotopic. The complexes were stable, but on treatment with silver trifluoromethanesulfonate in acetone at low temperature an unstable species was identified by  $^1\text{H}$  and  $^{31}\text{P}$  NMR in two of the three cases. Spectral observations were consistent with the formation and subsequent rearrangement of an intermediate along the pathway of an intramolecular Heck cyclisation with structure  $o\text{-C}_6\text{H}_4\text{OC}(\text{CH}_3)(\text{Pd}[\text{dppf}]\text{OTf})$ .

## 1. Introduction

Among palladium-catalyzed C–C bond-forming reactions, the Heck synthesis enjoys considerable current popularity because of its versatility and tolerance of functionality.<sup>1</sup> Recent developments include intramolecular examples leading to useful synthetic intermediates or targets,<sup>2</sup> the coupling of Heck reactions in tandem with other catalytic processes,<sup>3</sup> and both inter- and intramolecular asymmetric synthesis.<sup>2,4</sup> Synthetic application in this field has tended to run ahead of mechanistic understanding.<sup>5</sup> The intention of the present work was to make an initial contribution to understanding the catalytic cycle by characterizing likely intermediates using heteronuclear NMR techniques; such approaches have proved successful in their application to Pd-catalyzed cross-coupling<sup>6</sup> and other areas of homogeneous catalysis. Although the characterization of intermediates has not been completed at this stage, a general restricted rotation phenomenon has been delineated, underlining the tendency for arylpalladium complexes to prefer an orthogonal relationship between the coordination plane and the aromatic ring. Further, an unstable intermediate derived from the initial alkene

## Scheme 1



insertion product by a  $\beta$ -elimination and Pd–H readdition process has been identified.

## 2. Results and Discussion

**Synthesis of Complexes.** At the outset, the intention of the present work was to define the structure of intermediates in the Heck synthesis and the pathways available for their interconversion. In order to simplify the problem, an intramolecular reaction was selected. There have been many examples of the synthesis of

<sup>†</sup> Reprint requests by E-mail: bjm@vax.ox.ac.uk.

<sup>⊗</sup> Abstract published in *Advance ACS Abstracts*, November 1, 1994.

(1) Heck, R. F. *Org. React.* **1982**, *27*, 345.

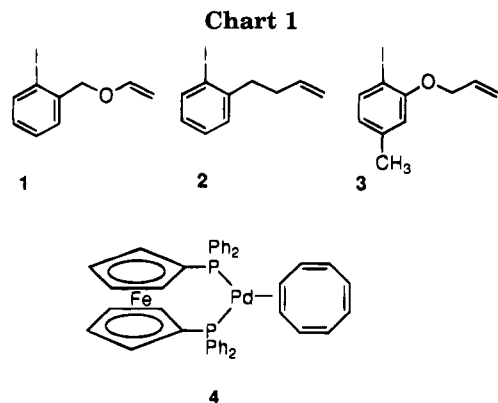
(2) Kondo, K.; Sodeoka, M.; Mori, M.; Shibasaki, M. *Synthesis* **1993**, 920. Ashimori, A.; Overman, L. E. *J. Org. Chem.* **1992**, *57*, 4571–4572.

(3) Burns, B.; Grigg, R.; Santhakumar, V.; Sridharan, V.; Stevenson, P.; Worakun, T. *Tetrahedron* **1992**, *48*, 7297.

(4) Ozawa, F.; Kubo, A.; Matsumoto, Y.; Hayashi, T.; Nishioka, E.; Yanagi, K.; Moriguchi, K. *Organometallics* **1993**, *12*, 4188–4196.

(5) For studies of acyl migration to coordinated alkenes: Daves, G. D., Jr.; Hallberg, A. *Chem. Rev.* **1989**, *89*, 1433–1445. Cf.: Ozawa, F.; Hayashi, T.; Koide, H.; Yamamoto, A. *J. Chem. Soc., Chem. Commun.* **1991**, 1469–1470. Dekker, G. P. C. M.; Elsevier, C. J.; Vrieze, K.; Van Leeuwen, P. W. N. M.; Roobeek, C. F. *J. Organomet. Chem.* **1992**, *430*, 357–372.

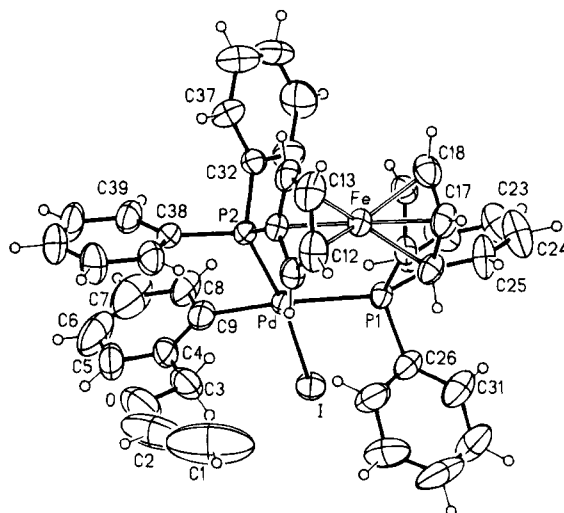
(6) Brown, J. M.; Cooley, N. A. *Organometallics* **1990**, *9*, 353–359.



5-ring heterocycles by the formal addition of an arylpalladium species to the double bond of an unsaturated *ortho* side chain.<sup>7</sup> When the alkene is three bonds removed from the aromatic ring, exocyclic ring closure occurs exclusively to give an indene or heterocyclic analog. Examples are shown in Scheme 1 which illustrates this point. It is significant to note that the initial product of reaction has an exocyclic double bond (as would be expected for formal Pd-Ar addition to the alkene) and that this is the sole product in the presence of silver carbonate as base, despite the fact that this is thermodynamically much less stable than the indole with an endocyclic double bond. The potential complexity of the reaction is indicated by the third example of Scheme 1, for which the preferred hand of product in an intramolecular Heck reaction depends on whether the base involved is  $\text{Ag}_3\text{PO}_4$  or 1,2,2,6,6-pentamethylpiperidine. The range of precedents recorded made this a suitable starting point, and accordingly the three aryl iodide precursors 1,<sup>8</sup> and 3<sup>9</sup> were synthesized.

In previously reported studies of the mechanism of cross-coupling,<sup>6</sup> palladium complexes of 1,1'-bis(diphenylphosphino)ferrocene have been successfully utilized. The putative first step in a catalytic Heck reaction is addition of the electrophile, normally an unsaturated iodide or trifluoromethanesulfonate, to a low-valent palladium species. Analogy with cross-coupling suggests that this is in the Pd(0) state. Zerovalent palladium complexes with a labile ligand and a cis-chelating diphosphine are difficult to isolate;<sup>10</sup> hence, the  $\eta^2$ -cyclooctatetraene complex 4 was prepared in solution in thf by reduction of the  $\text{P}_2\text{PdCl}_2$  precursor with dilithiocyclooctatetraene. The reaction of this alkene complex with alkenyl bromides gives first the direct alkene/alkene displacement product and subsequently the oxidative addition product derived from it; with alkenyl or aryl iodides only this  $\eta^1$ - $\eta^1$ -iodoalkyl complex is observed.<sup>11</sup>

After preparation of complex 4 in situ as a 0.02 M solution in thf, the iodide 1 was added directly at  $-78^\circ\text{C}$  and warmed to ambient temperature, whereupon the



**Figure 1.** ORTEP representation of the molecular structure of complex 5a. The atomic coordinates and isotropic thermal parameters are collected in Table 1 and selected bond distances and angles in Table 2.

color of the solution changed from dark red to orange. Workup gave a stable yellow solid in 81% yield which was recrystallized by slow diffusion of pentane/ $\text{Et}_2\text{O}$  into its thf solution, giving red-orange blocks of 5a suitable for X-ray analysis. The structure obtained is shown in Figure 1 and reveals a distorted-square-planar arrangement about the Pd atom; for example, the P-Pd-I angle is  $171.3^\circ$  and the P-Pd-C angle is  $172.6^\circ$  rather than the ideal  $180^\circ$ . The ligand bite angle is  $100.7^\circ$ , slightly larger than the typical value of  $98^\circ$  for the dppf ligand.<sup>12</sup> This enhanced angle is created by staggering the two ferrocenyl rings, while the Fc-P bonds are coplanar with their rings. The side-chain double bond shows a high degree of libration, particularly in the region of C1 and C2, but is remote from Pd with no significant bonding interaction. The bound aryl group is close to orthogonality with the mean square plane, a common feature of structurally related metal aryls. In the present case, there is substantial steric hindrance to positioning of the aryl group in the coordination plane, and this has consequences for the solution structures observed by NMR. Final atomic coordinates are given in Table 1 and selected bond lengths and angles in Table 2.

**Restricted Pd-Aryl Rotation.** Related complexes 6a and 7 were prepared by the same method used for complex 5a in 85% and 76% yields, respectively, and fully characterized. In all cases the  $^1\text{H}$  NMR spectra were informative. Taking first the vinyl ether complex 5a in  $\text{C}_6\text{D}_6$ , the benzylic  $\text{CH}_2$  was diastereotopic as a sharp AB quartet at 5.25 and 5.49 ppm (Figure 2), despite the lack of stereogenicity in the structure; the  $^{31}\text{P}$  NMR in thf appeared as a single AX quartet at 7.9 and 25.9 ppm. If rotation about the Pd-C bond is slow on the NMR time scale, the aromatic ring possesses planar chirality, and the enantiomers are interconverted by that rotation process. This requires slow rotation of the aryl-palladium bond on the NMR time scale, since rotation about that bond interconverts the enantiomers

(7) See, for example: Abramovitch, R. A.; Barton, D. H. R.; Finet, J.-P. *Tetrahedron* **1988**, *44*, 3039. Sakamoto, T.; Kondo, Y.; Uchiyama, M.; Yamanaka, H. *J. Chem. Soc., Perkin Trans. 1* **1993**, 1941.

(8) Beckwith, A. L. J.; Gara, W. B. *J. Chem. Soc., Perkin Trans. 2* **1975**, 795.

(9) Negishi, E.; Nguyen, T.; O'Connor, B.; Evans, J. M.; Silveira, A. *Heterocycles* **1989**, *28*, 55.

(10) But see: Krause, J.; Bonrath, W.; Porschke, K. R. *Organometallics* **1992**, *11*, 1158. Hodgson, M.; Parker, D.; Taylor, R. J.; Ferguson, G. *Organometallics* **1988**, *7*, 1761.

(11) Brown, J. M.; Guiry, P. J. *Inorg. Chim. Acta* **1994**, *220*, 249-261.

(12) Hayashi, T.; Kumada, M.; Higuchi, T.; Hirotsu, K. *J. Organomet. Chem.* **1987**, *334*, 195.

**Table 1.** Atom Coordinates ( $\times 10^4$ ) and Isotropic Thermal Parameters ( $\text{\AA}^2 \times 10^3$ )

atom	x	y	z	$U^a$
Pd	2380.9(4)	644.5(2)	2114.4(2)	33(1)*
I	2777.7(4)	-506.9(2)	1495.9(2)	49(1)*
Fe	3866.5(8)	2723.0(4)	2110.9(4)	38(1)*
P(1)	3255.1(14)	1250.0(7)	1266.5(7)	35(1)*
P(2)	1925.1(13)	1533.9(7)	2766.0(7)	33(1)*
O	4380(9)	-145(4)	3983(3)	106(3)*
C(1)	6452(18)	284(10)	3653(11)	216(13)*
C(2)	5661(17)	53(8)	4107(8)	155(9)*
C(3)	3789(9)	-50(4)	3344(3)	76(3)*
C(4)	2418(8)	-227(3)	3282(3)	64(3)*
C(5)	1919(14)	-658(5)	3722(5)	106(5)*
C(6)	612(14)	-853(6)	3612(7)	127(6)*
C(7)	-175(14)	-612(5)	3094(7)	119(6)*
C(8)	366(8)	-178(3)	2668(4)	65(3)*
C(9)	1627(7)	12(3)	2770(3)	51(2)*
C(10)	3099(5)	2222(3)	2818(3)	38(2)*
C(11)	4474(6)	2148(3)	2861(3)	46(2)*
C(12)	5053(7)	2798(4)	2919(3)	60(3)*
C(13)	4059(8)	3283(4)	2926(3)	61(3)*
C(14)	2859(6)	2949(3)	2865(3)	47(2)*
C(15)	3589(6)	2161(3)	1312(2)	37(2)*
C(16)	4841(6)	2487(3)	1340(3)	45(2)*
C(17)	4667(6)	3204(3)	13,69(3)	52(2)*
C(18)	3319(7)	3332(3)	1363(3)	54(2)*
C(19)	2643(6)	2692(3)	1318(3)	44(2)*
C(20)	2288(6)	1239(3)	500(3)	42(2)*
C(21)	1145(6)	857(3)	426(3)	44(2)*
C(22)	378(7)	884(4)	-138(3)	61(2)*
C(23)	733(9)	1282(4)	-631(3)	70(3)*
C(24)	1837(9)	1659(5)	-555(4)	84(4)*
C(25)	2638(8)	1647(4)	12(3)	63(3)*
C(26)	4851(6)	908(3)	1131(3)	47(2)*
C(27)	5647(7)	761(4)	1678(4)	70(3)*
C(28)	6925(9)	486(5)	1643(6)	95(4)*
C(29)	7278(10)	358(5)	1023(7)	105(5)*
C(29)	7278(10)	358(5)	1023(7)	105(5)*
C(30)	6493(10)	493(5)	500(5)	89(4)*
C(31)	5286(9)	769(4)	552(4)	72(3)*
C(32)	402(5)	1947(3)	2506(3)	38(2)*
C(33)	-195(6)	1793(4)	1917(3)	53(2)*
C(34)	-1312(7)	2149(5)	1701(4)	73(3)*
C(35)	-1798(7)	2658(4)	2071(5)	74(3)*
C(36)	-1241(7)	2796(4)	2649(4)	70(3)*
C(37)	-153(6)	2439(3)	2870(3)	52(2)*
C(38)	1758(6)	1360(3)	3610(3)	43(2)*
C(39)	590(7)	1063(4)	3790(3)	55(2)*
C(40)	514(8)	908(5)	4428(4)	73(3)*
C(41)	1536(10)	1030(5)	4865(3)	82(4)*
C(42)	2686(9)	1302(5)	4693(3)	76(3)*
C(43)	2778(7)	1471(4)	4060(3)	58(2)*
O(1s) <sup>b</sup>	3563(22)	6890(13)	117(12)	185(8)
C(1as) <sup>c</sup>	2309(28)	6703(15)	183(14)	55(7)
C(1bs) <sup>c</sup>	2258(33)	6985(18)	-187(17)	71(8)
C(2s) <sup>b</sup>	1533(26)	7375(15)	159(13)	128(8)
C(3as) <sup>c</sup>	2458(36)	7864(21)	343(18)	83(10)
C(3bs) <sup>c</sup>	2112(35)	7552(19)	664(18)	77(9)
C(4as) <sup>c</sup>	3830(33)	7569(19)	250(17)	79(9)
C(4bs) <sup>c</sup>	3334(60)	7030(36)	622(32)	117(22)

<sup>a</sup> Values marked with an asterisk are equivalent isotropic  $U$  values, defined as one-third of the trace of the orthogonalized  $U_{ij}$  tensor. <sup>b</sup> Occupancy 0.5. <sup>c</sup> Occupancy 0.25.

of **5a**. Recently,<sup>13</sup> a similar phenomenon was reported for the tmeda complex **8** in  $\text{CDCl}_3$ , although in MeOH the same compound was dynamic between 20 and 60 °C through a process involving coordination of the hydroxyl group and ionic dissociation of bromide. A range of Pt-aryl complexes also demonstrate restricted rotation.<sup>14</sup> In keeping with these observations, the same

**Table 2.** Selected Bond Distances ( $\text{\AA}$ ) and Angles (deg)

Pd-I	2.647(1)	O-C(2)	1.381(19)
Pd-P(1)	2.384(2)	O-C(3)	1.449(10)
Pd-P(2)	2.287(2)	C(1)-C(2)	1.387(28)
Pd-C(9)	2.055(7)	C(3)-C(4)	1.453(12)
P(1)-C(15)	1.810(6)	C(4)-C(5)	1.383(13)
P(2)-C(20)	1.834(6)	C(4)-C(9)	1.383(10)
P(1)-C(26)	1.821(7)	C(5)-C(6)	1.403(20)
P(2)-C(10)	1.805(6)	C(6)-C(7)	1.390(20)
P(2)-C(32)	1.812(6)	C(7)-C(8)	1.387(16)
P(2)-C(38)	1.838(6)	C(8)-C(9)	1.354(10)
I-Pd-P(1)	88.0	C(3)-C(4)-C(9)	120.0(7)
I-Pd-P(2)	171.2	C(5)-C(4)-C(9)	120.2(9)
P(1)-Pd-P(2)	100.7(1)	C(4)-C(5)-C(6)	117.2(10)
I-Pd-C(9)	84.6(2)	C(5)-C(6)-C(7)	122.2(12)
P(1)-Pd-C(9)	172.5(2)	C(6)-C(7)-C(8)	118.6(12)
P(2)-Pd-C(9)	86.6(2)	C(7)-C(8)-C(9)	119.6(9)
C(2)-O-C(3)	117.8(9)	Pd-C(9)-C(4)	119.9(5)
O-C(2)-C(1)	124.6(14)	Pd-C(9)-C(8)	117.9(5)
O-C(3)-C(4)	112.8(7)	C(4)-C(9)-C(8)	122.2(7)
C(3)-C(4)-C(5)	119.7(8)		

behavior was observed for both the butenyl complex **6a**, where both the  $\alpha$ - and  $\beta$ -methylenes are diastereotopic, and the allyloxy complex **7**, the relevant regions of their  $^1\text{H}$  NMR spectra being shown in Figure 2. A point of interest is that one of the two diastereotopic protons at the benzylic site in **7** exhibits a much stronger allylic coupling than the other, and also more pronounced homoallylic coupling, consistent with a well defined side-chain conformation in solution. As expected, the *trans*- $\text{PPh}_3$  complex **9** exhibits a singlet for the benzylic  $\text{CH}_2$ , since the symmetry plane orthogonal to the coordination plane renders the methylene hydrogens equivalent, irrespective of restricted rotation. The related 1-butenyl complex **10** showed similar behavior. Platinum complexes **5b** and **6b** were prepared in 85% and 80% yields, respectively, from the stable  $\eta^2$ -ethene complex **11**, by refluxing in thf for 3 h, followed by recrystallization.  $^1\text{H}$  NMR spectra very similar to those of their Pd analogs were obtained, with minor differences in chemical shift for the relevant diastereotopic proton pairs.

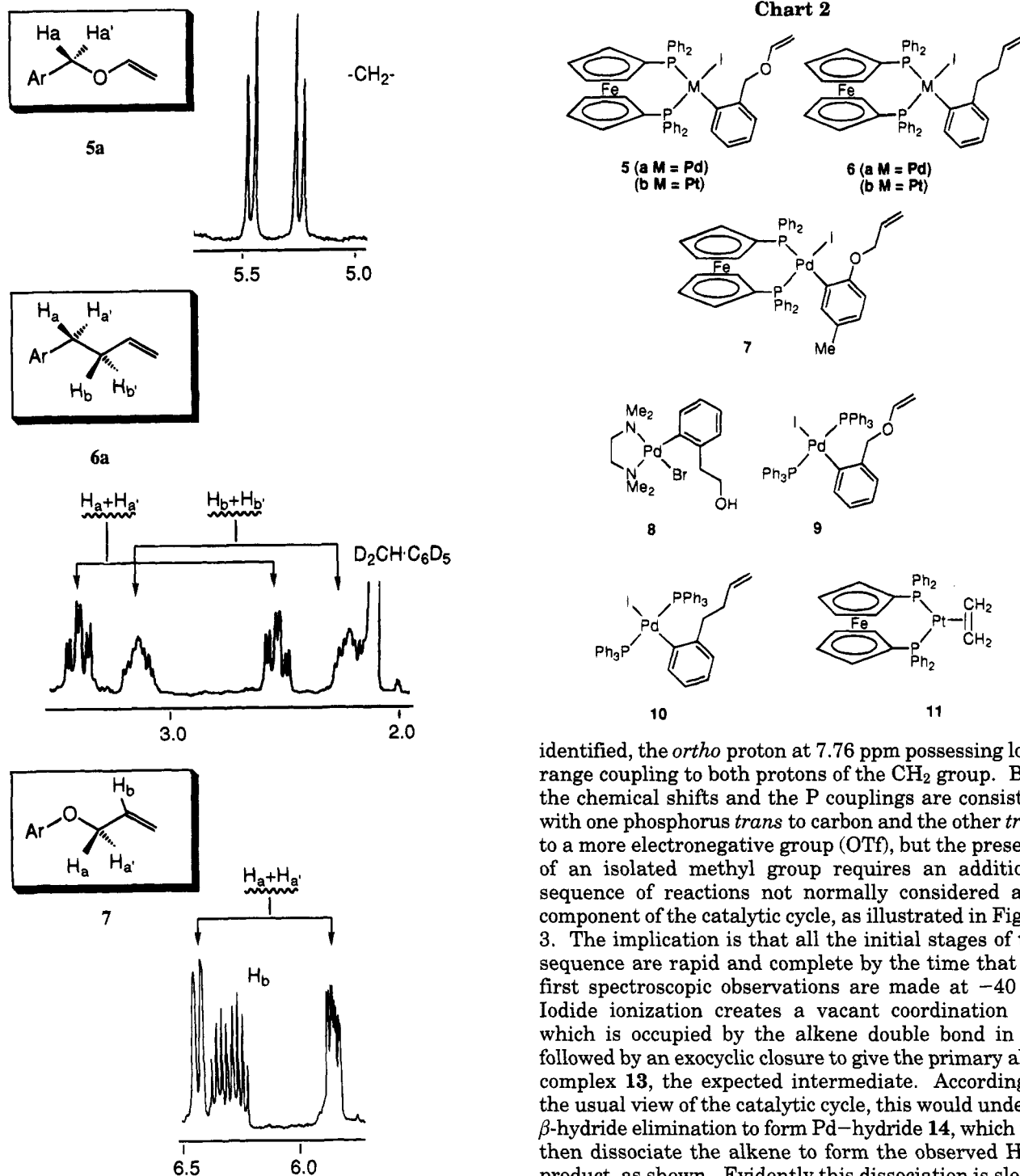
**Models for the Heck Reaction Pathway.** The aryl iodide complexes **5a**, **6a**, and **7** were all thermally stable and in the absence of forcing conditions exhibited no tendency for cyclization or other involvement of the double bond. Given that many Heck reactions are promoted by silver salts,<sup>15</sup> the effect on these model insertion step intermediates was investigated. Hence, reaction of complex **5a** with  $\text{AgOSO}_2\text{CF}_3$  in  $d_6$ -acetone at -78 °C caused instant precipitation of AgI which was removed by low-temperature Celite filtration. The  $^{31}\text{P}$  NMR spectrum at -30 °C or below demonstrated complete conversion to a single AX species at this temperature:  $\delta$  31.1 and 15.3 ppm ( $J = 51$  Hz). Broadening of the signals was observed above that temperature, and on brief warming to ambient and recooling loss of signal intensity was observed. Insight into the structure of this new species was obtained from the  $^1\text{H}$  NMR spectrum obtained at -20 °C. Two structures were anticipated from consideration of likely reaction pathways for a cationic complex produced in the  $\text{Ag}^+$ -induced step, namely the coordinated alkene complex **12** and cyclization product **13**, but the observed

(13) Alster, P. L.; Boersma, J.; Smeets, W. J. J.; Spek, A. L.; van Koten, G. *Organometallics* **1993**, *12*, 1639-1647.

(14) Alcock, N. W.; Brown, J. M.; Pérez-Torrente, J. J. *Tetrahedron Lett.* **1992**, *33*, 389-393; *Organometallics*, submitted for publication.

(15) Sato, Y.; Sodeoka, M.; Shibasaki, M. *J. Org. Chem.* **1989**, *54*, 4738. Abelman, M. M.; Oh, T.; Overman, L. E. *J. Org. Chem.* **1987**, *52*, 4130. Karabelas, K.; Hallberg, A. *J. Org. Chem.* **1986**, *51*, 5286.



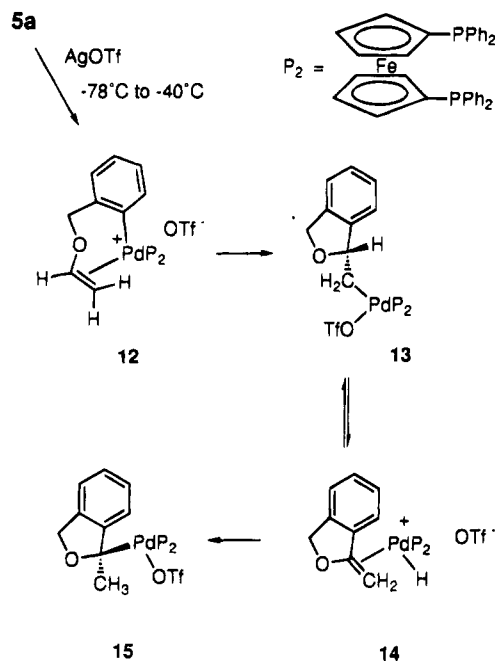


**Figure 2.**  $\text{CH}_2$  region of the  $^1\text{H}$  NMR spectra of complexes **5a**, **6a**, and **7**, demonstrating magnetic inequivalence.

spectrum is inconsistent with either of these. There is a inequivalent methylene group centered at 5.18 ppm ( $J_{\text{AB}} = 19$  Hz), with one of the pair partially obscured by a ferrocenyl signal, in which both protons possess two further couplings to phosphorus of 8 and 11 Hz. The only high-field signal is methyl group at 1.40 ppm, possessing coupling of 10.5 and 11.5 Hz to the two phosphorus nuclei. Signals associated with the vinyl group of the original alkene are absent. It was established via a COSY experiment that there is no detectable coupling between the  $\text{CH}_2$  and  $\text{CH}_3$  groups at 5.18 and 1.40 ppm; in the same experiment four contiguous aryl protons associated with the organic substrate were

identified, the *ortho* proton at 7.76 ppm possessing long-range coupling to both protons of the  $\text{CH}_2$  group. Both the chemical shifts and the P couplings are consistent with one phosphorus *trans* to carbon and the other *trans* to a more electronegative group (OTf), but the presence of an isolated methyl group requires an additional sequence of reactions not normally considered as a component of the catalytic cycle, as illustrated in Figure 3. The implication is that all the initial stages of this sequence are rapid and complete by the time that the first spectroscopic observations are made at  $-40$  °C. Iodide ionization creates a vacant coordination site which is occupied by the alkene double bond in **12**, followed by an exocyclic closure to give the primary alkyl complex **13**, the expected intermediate. According to the usual view of the catalytic cycle, this would undergo  $\beta$ -hydride elimination to form Pd-hydride **14**, which will then dissociate the alkene to form the observed Heck product, as shown. Evidently this dissociation is slower than Pd-H readdition to the alkene so that the more stable  $\eta^1$ -benzyl complex **15** is the first observed intermediate. Structure **15** fits the available spectroscopic data. Its propensity for decomposition by  $\beta$ -elimination would explain why attempts to obtain a pure sample were unsuccessful. Furthermore, attempts to characterize organic decomposition products were equivocal. While structure **15** is the most probable structure for the unstable intermediate, minor variations are also consistent with the data—for example, the coordinated triflate could be replaced by an acetone solvent molecule in **16**.<sup>16</sup> The high reactivity of complex **12** toward Pd-C insertion may be due to a number of factors, including

(16) Cf.: Seligson, A. L.; Trogler, W. C. *J. Am. Chem. Soc.* **1991**, *113*, 2520.



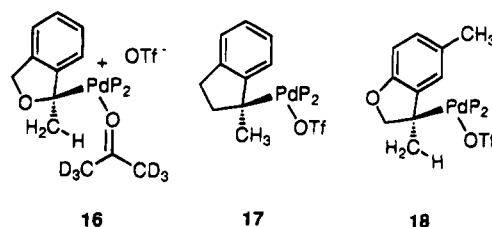
**Figure 3.** Reaction pathway from complex **5a** to the unstable intermediate **15** on reaction with AgOTf.

the favorable formation of a five-membered ring. In addition, the insertion step can be viewed as an electrophilic carbodepalladation, the electrophile being the ether-stabilized carbocation formed by addition of palladium to the terminal carbon of the alkene. The stoichiometric addition of an alkenyl bromide to norbornene promoted by Pd(0) under mild conditions had been noted.<sup>6</sup>

Under the same reaction conditions, the butenylaryl complex **6a** behaved similarly, although the purity and stability of the intermediate were both lower. Two coupled CH<sub>2</sub> groups are observed at  $\delta$  2.85 and 1.55 ppm, with further complexity arising from coupling to phosphorus. A CH<sub>3</sub> group with two equivalent phosphorus couplings is observed at 1.18 ppm. This new compound is assigned structure **17**, the cyclization step again being fast in both cases and leading to an intermediate of similar structure. The allyloxy complex **7** did not follow the same reaction pathway, and it proved impossible to characterize anything in that case. Notably, the related intermediate **18** could decompose directly to 3,5-dimethylbenzofuran. For the *trans*-PPh<sub>3</sub> complex **9**, reaction with AgOSO<sub>2</sub>CF<sub>3</sub> was slow and incomplete below -20 °C and did not lead to a clean characterizable species. In addition, the Pt complex **5b** did not yield useful information on treatment with AgOSO<sub>2</sub>CF<sub>3</sub> under the previously described conditions. The reaction occurred rapidly at -78 °C, but the first formed species was unstable and decomposed by multiple pathways.

**Significance of the Results.** With normal reactants, and conventional catalysts, the rate of turnover in catalytic Heck reactions is quite slow, so that reactions are typically carried out at 80–100 °C.<sup>1</sup> Many attempts have been made to facilitate reactivity, including the addition of phase-transfer catalysts,<sup>17</sup> conducting the reaction in water,<sup>18</sup> and the use of silver or thallium

### Chart 3



salts to promote the ionization of the Pd–I bond in the initial oxidative addition complex.<sup>15</sup> The use of aryl or vinyl triflates in place of halides as the electrophilic complex promises to permit the reaction to be conducted under milder conditions.<sup>4</sup> In view of the general sluggishness of catalysis, the high reactivity of complexes **5a** and **7** toward silver-ion promoted cyclization is surprising. It implies that the critical aryl–Pd insertion in the alkene is rapid at -40 °C and that the  $\beta$ -elimination step is sufficiently facile for intramolecular loss and readdition of Pd–H, giving the benzylpalladium complex inaccessible by direct reaction. It remains to be seen whether this intermediate **15** can be cleanly broken down to the alkene product by base and whether the Pd(0) species thus generated can be quantitatively recycled.

**Summary and Conclusions.** These experiments demonstrate that the pathway of the intramolecular Heck reaction can be simulated in a stoichiometric cycle, and in the absence of base (a normal component under catalytic conditions) an alkylpalladium complex **15** formed by elimination/readdition of palladium hydride is observable at sub-ambient temperature. The initial alkene complex and the first Pd alkyl formed by Pd–Ar addition to the coordinated alkene are evidently too transient to detect in this series. Access to a forward intermediate will permit further studies on the reaction mechanism to be carried out. Such studies will be the subject of future reports.

### 3. Experimental Section

**General Information.** All solvents were freshly distilled from standard drying agents and degassed by three freeze/thaw cycles before use. Organometallic reactions were carried out under dry argon by using Schlenk glassware and vacuum line techniques. Transfers were carried out with stainless steel cannulas under positive argon pressure. <sup>1</sup>H NMR spectra were recorded on a Varian Gemini 200 (200 MHz), a Bruker WH-300 (300 MHz), or a Bruker AM-500 (500 MHz) spectrometer and are referenced to residual protic solvents with chemical shifts being reported as  $\delta$  (ppm) from TMS. <sup>31</sup>P NMR spectra were recorded on a Bruker AM-250 spectrometer operating at 101.26 MHz using 85% H<sub>3</sub>PO<sub>4</sub> as external reference. Elemental analyses were performed by the Dyson Perrins Laboratory Analytical Service using a Carlo Erba 1106 elemental analyzer.

The starting materials [1,1'-bis(diphenylphosphino)ferrocene]palladium dichloride,<sup>19</sup> [1,1'-bis(diphenylphosphino)ferrocene]( $\eta^2$ -ethene)platinum (**11**),<sup>6</sup> and tetrakis(triphenylphosphine)palladium<sup>20</sup> were prepared by literature methods. Dilithium cyclooctatetraenide was prepared by the method of Katz and Garratt.<sup>21</sup>

(17) Jeffery, T. J. *Chem. Soc., Chem. Commun.* **1984**, 1287.

(18) Bumagin, N. A.; More, P. G.; Beletskaya, I. P. *J. Organomet. Chem.* **1989**, 371, 397.

(19) Hayashi, T.; Konishi, M.; Kobori, Y.; Kumada, M.; Higuchi, T.; Hirotsu, K. *J. Am. Chem. Soc.* **1984**, 106, 158.

(20) Coulson, D. R. *Inorg. Synth.* **1972**, 13, 121.

(21) Katz, T. J.; Garratt, P. J. *J. Am. Chem. Soc.* **1964**, 86, 4876.

**Preparation of *o*-Iodobenzyl Vinyl Ether (1).** The compound was prepared from 2-iodobenzyl alcohol by following a procedure similar to that given in the literature.<sup>8</sup> The crude product was distilled in a Kugelrohr apparatus: bp 80 °C, 0.3 mmHg (lit.<sup>9</sup> bp 82–83 °C, 0.8 mmHg). Yield: 70%.

**Preparation of 1-Iodo-2-(3-butenyl)benzene (2).** To a stirred solution of 2-iodobenzyl bromide (5.0 g, 0.017 mol) (prepared by metathesis of the commercially available 2-iodobenzyl chloride with a large excess of NaBr) in THF (60 mL) at –10 °C was added allylmagnesium bromide (18.5 mL, 1.0 M, 0.018 mol) by syringe over a period of 10 min. A white precipitate was immediately formed. After 5 h of stirring at ambient temperature, saturated ammonium chloride solution (10 mL) and water (20 mL) were added and the mixture was extracted with diethyl ether (2 × 20 mL). The ethereal layer was washed with water and brine, dried over anhydrous MgSO<sub>4</sub>, and concentrated under vacuum to give a yellow oil. The product was obtained as a yellow liquid by Kugelrohr distillation (100 °C at 0.3 mmHg); lit.<sup>8</sup> 130–132 °C, 19 mmHg. Yield: 92%.

**Preparation of 1-(Allyloxy)-2-iodo-4-methylbenzene (3).**<sup>9</sup> The compound was synthesized from 2-iodo-4-methylphenol<sup>22</sup> and allyl bromide on a 0.076 mol scale by following the literature procedure for the preparation of allyl aryl ethers:<sup>23</sup> bp 125–127 °C, 0.3 mmHg. Yield: 89%. <sup>1</sup>H NMR (200 MHz, CDCl<sub>3</sub>): 7.63 (d, 1H), 7.08 (dd, 1H), 6.71 (d, 1H) (aryl), 6.08 (m, 1H, –CH=CH<sub>2</sub>), 5.52 (dd, 1H, *J* = 18, 2 Hz, –CH=CH<sub>2</sub>), 5.32 (dd, 1H, *J*<sub>HH</sub> = 12, 2 Hz, –CH=CH<sub>2</sub>), 4.58 (br d, 2H, OCH<sub>2</sub>–), 2.23 (s, 3H, –CH<sub>3</sub>).

**Synthesis of the Complexes [(dppf)Pd(I)(R)]: R = *o*-(C<sub>6</sub>H<sub>4</sub>)CH<sub>2</sub>OCH=CH<sub>2</sub> (5a), *o*-(C<sub>6</sub>H<sub>4</sub>)CH<sub>2</sub>CH<sub>2</sub>CH=CH<sub>2</sub> (6a), *m*-CH<sub>3</sub>(C<sub>6</sub>H<sub>4</sub>)-*o*-OCH<sub>2</sub>CH=CH<sub>2</sub> (7).** A solution of dilithium cyclooctatetraenide (1.53 cm<sup>3</sup>, 0.26 M in diethyl ether, 0.41 mmol) was added dropwise over a period of 5 min to a stirred suspension of [(dppf)PdCl<sub>2</sub>] (0.30 g, 0.41 mmol) in THF (20 mL) at –78 °C to give a dark red solution in 15 min. Then, the appropriate *o*-iodoaryl species (1–3) (0.41 mmol) was added and the mixture was warmed slowly to room temperature (3 h) to give an orange solution. The solvent was removed under vacuum and the yellow residue extracted with toluene (15 mL) and then centrifuged in order to remove LiCl. Concentration of the clear orange solution under vacuum to ca. 2 mL and slow addition of cold hexane (20 mL) gave the complexes **5a**, **6a**, and **7** as yellow solids which were collected by filtration, washed with cold hexane, and dried under vacuum.

**[(dppf)Pd(I)(*o*-(C<sub>6</sub>H<sub>4</sub>)CH<sub>2</sub>OCH=CH<sub>2</sub>)] (5a).** Yield: 81%. Anal. Calcd for C<sub>44</sub>H<sub>37</sub>FeIOP<sub>2</sub>Pd: C, 56.08; H, 4.05. Found: C, 55.96; H, 4.13. <sup>1</sup>H NMR (300 MHz, C<sub>6</sub>D<sub>6</sub>): 8.30 (m, 4H), 7.70 (m, 2H), 7.46 (m, 1H), 7.30–6.91 (m, 9H), 6.88 (m, 4H), 6.69 (m, 4H) (ferrocenyl and aryl residues), 6.61 (dd, 1H, –CH=CH<sub>2</sub>), 5.49, 5.25 (2H, AB q, *J* = 12 Hz, –CH<sub>2</sub>O), 4.81 (s, 1H, Cp), 4.69 (dd, 1H, *J* = 1.4, 1.5 Hz, –CH=CH<sub>2</sub>), 4.32 (s, 1H, Cp), 4.14 (dd, 1H, *J* = 7, 1.5 Hz, –CH=CH<sub>2</sub>), 4.03 (s, 1H), 3.94 (s, 1H), 3.71 (s, 1H), 3.63 (s, 2H), 3.55 (s, 1H) (Cp). <sup>31</sup>P NMR (250 MHz, thf/D<sub>2</sub>O): 25.9 (d), 7.9 (d) (*J*<sub>P–P</sub> = 34 Hz).

**[(dppf)Pd(I)(*o*-(C<sub>6</sub>H<sub>4</sub>)CH<sub>2</sub>CH<sub>2</sub>CH=CH<sub>2</sub>)] (6a).** Yield: 85%. Anal. Calcd for C<sub>44</sub>H<sub>39</sub>FeIOP<sub>2</sub>Pd: C, 57.51; H, 4.27. Found: C, 57.32; H, 4.25. <sup>1</sup>H NMR (300 MHz, *d*<sub>8</sub>-toluene): 8.40 (m, 2H), 8.20 (m, 2H), 7.93 (m, 2H), 7.53 (m, 1H), 7.33–6.89 (m, 10H), 6.83 (m, 2H), 6.65 (m, 4H), 6.50 (m, 1H) (ferrocenyl and aryl residues), 6.20 (m, 1H, –CH=CH<sub>2</sub>), 5.37 (dd, 1H, *J* = 17, 2 Hz, –CH=CH<sub>2</sub>), 5.20 (dd, 1H, *J* = 11, 2 Hz, –CH=CH<sub>2</sub>), 5.05 (s, 1H), 4.10 (s, 2H), 3.92 (s, 1H), 3.75 (s, 1H), 3.69 (s, 1H), 3.64 (s, 1H), 3.56 (s, 1H) (Cp), 3.66 (td, 1H, Ar–CH<sub>2</sub>–), 3.11 (m, 1H, –CH<sub>2</sub>–), 2.51 (td, 1H, Ar–CH<sub>2</sub>–), 2.20 (m, 1H, –CH<sub>2</sub>–). <sup>31</sup>P NMR (250 MHz, thf/D<sub>2</sub>O): 25.4 (d), 9.4 (d) (*J*<sub>P–P</sub> = 35 Hz).

**[(dppf)Pd(I)(*m*-CH<sub>3</sub>(C<sub>6</sub>H<sub>4</sub>)-*o*-OCH<sub>2</sub>CH=CH<sub>2</sub>)] (7).**<sup>24</sup> Yield: 76%. Anal. Calcd for C<sub>44</sub>H<sub>39</sub>FeIOP<sub>2</sub>Pd: C, 56.52; H, 4.20. Found: C, 55.43; H, 4.73. <sup>1</sup>H NMR (300 MHz, *d*<sub>8</sub>-toluene): 8.37 (m, 2H), 8.26 (m, 2H), 7.70 (m, 2H), 7.68–7.00 (m, 13H), 6.90 (m, 2H), 6.75 (m, 2H) (ferrocenyl and aryl residues), 6.39 (d, 1H, OCH<sub>2</sub>–), 6.20 (m, 1H, –CH=CH<sub>2</sub>), 5.93 (m, 1H, OC–H<sub>2</sub>–), 5.52 (dd, 1H, *J* = 17, 1.8 Hz, –CH=CH<sub>2</sub>), 5.27 (dd, 1H, *J* = 10, 1.8 Hz, –CH=CH<sub>2</sub>), 5.01 (s, 1H), 4.35 (s, 2H), 4.08 (s, 1H), 4.00 (s, 1H), 3.69 (s, 2H), 3.57 (s, 1H) (Cp), 1.97 (s, 3H, –CH<sub>3</sub>). <sup>31</sup>P NMR (250 MHz, thf/D<sub>2</sub>O): 26.6 (d), 8.2 (d) (*J*<sub>P–P</sub> = 31 Hz).

**Synthesis of [(dppf)Pt(I)(*o*-(C<sub>6</sub>H<sub>4</sub>)CH<sub>2</sub>OCH=CH<sub>2</sub>)] (5b).** To a solution of [(dppf)Pt(η<sup>2</sup>-ethene)] (0.1 g, 0.128 mmol) in THF (10 mL) was added *o*-iodobenzyl vinyl ether (1; 0.041 g, 0.154 mmol). The mixture was refluxed for 3 h to give an orange solution. The solvent was removed under vacuum, and then acetone (2 mL) was added. Slow addition of diethyl ether (5 mL) and pentane (10 mL) affords the complex as an orange microcrystalline solid which was filtered, washed with pentane and dried in vacuo (0.109 g, 85%). Anal. Calcd for C<sub>43</sub>H<sub>37</sub>FeIOP<sub>2</sub>Pt: C, 51.15; H, 3.69. Found: C, 51.07; H, 3.86. <sup>1</sup>H NMR (300 MHz, C<sub>6</sub>D<sub>6</sub>): 8.41 (m, 2H), 8.30 (m, 2H), 7.70 (m, 2H), 7.51 (m, 1H), 7.30 (m, 4H), 7.26–6.85 (m, 9H), 6.78 (m, 4H) (ferrocenyl and aryl residues), 6.67 (dd, 1H, –CH=CH<sub>2</sub>), 5.43 (2H, AB, q, *J*<sub>AB</sub> = 12 Hz, –CH<sub>2</sub>O), 4.80 (s, 1H, Cp), 4.74 (dd, 1H, *J*<sub>H–H</sub> = 14, 1.4 Hz, –CH=CH<sub>2</sub>), 4.53 (s, 1H, Cp), 4.19 (dd, 1H, *J* = 7, 1.4 Hz, –CH=CH<sub>2</sub>), 4.05 (s, 1H), 4.02 (s, 1H), 3.72 (s, 1H), 3.65 (s, 2H), 3.61 (s, 1H), (Cp). <sup>31</sup>P NMR (250 MHz, thf/D<sub>2</sub>O): 13.6 (d, dd, *J*<sub>Pt–P</sub> = 4163 Hz, *J*<sub>P–P</sub> = 16 Hz), 10.6 (d, dd, *J*<sub>Pt–P</sub> = 1746 Hz).

**Synthesis of [(dppf)Pt(I)(*o*-(C<sub>6</sub>H<sub>4</sub>)CH<sub>2</sub>CH<sub>2</sub>CH=CH<sub>2</sub>)] (6b).** The complex was prepared from [(dppf)Pt(η<sup>2</sup>-ethene)] (0.060 g, 0.077 mmol) and 1-iodo-2-(3-butenyl)benzene (2; 0.026 g, 0.1 mmol), by a procedure identical with that given for **6a**, as an orange microcrystalline solid (0.062 g, 80%). Anal. Calcd for C<sub>44</sub>H<sub>39</sub>FeIP<sub>2</sub>Pt: C, 52.45; H, 3.90. Found: C, 52.40; H, 4.15. <sup>1</sup>H NMR (300 MHz, C<sub>6</sub>D<sub>6</sub>): 8.43 (m, 2H), 8.26 (m, 2H), 7.93 (m, 2H), 7.65 (m, 1H), 7.35–6.76 (m, 13H), 6.66 (m, 4H) (ferrocenyl and aryl residues), 6.28 (m, 1H, –CH=CH<sub>2</sub>), 5.41 (d, 1H, *J* = 17 Hz, –CH=CH<sub>2</sub>), 5.23 (d, 1H, *J* = 10 Hz, –CH=CH<sub>2</sub>), 5.12 (s, 1H), 4.17 (s, 1H), 4.05 (s, 1H), 3.86 (s, 1H), 3.73 (s, 1H), 3.64 (s, 1H), 3.59 (s, 1H), 3.57 (s, 1H) (Cp), 3.52 (dt, 1H, –CH<sub>2</sub>CH<sub>2</sub>–), 3.30 (m, 1H, –CH<sub>2</sub>CH<sub>2</sub>–), 2.59 (dt, 1H, –CH<sub>2</sub>CH<sub>2</sub>–), 2.35 (m, 1H, –CH<sub>2</sub>CH<sub>2</sub>–). <sup>31</sup>P NMR (250 MHz, thf/D<sub>2</sub>O): 13.1 (d, dd, *J*<sub>Pt–P</sub> = 4228 Hz, *J*<sub>P–P</sub> = 15 Hz), 10.0 (d, dd, *J*<sub>Pt–P</sub> = 1716 Hz).

**Synthesis of [(PPh<sub>3</sub>)<sub>2</sub>Pd(I)(*o*-(C<sub>6</sub>H<sub>4</sub>)CH<sub>2</sub>OCH=CH<sub>2</sub>)] (9).** To a solution of [Pd(PPh<sub>3</sub>)<sub>4</sub>] (0.2 g, 0.173 mmol) in THF (10 mL) was added *o*-iodobenzyl vinyl ether (1; 0.049 g, 0.19 mmol). The mixture was stirred for 2 h to give a pale yellow solution. Evaporation of the solvent under vacuum to ca. 1 mL and slow addition of MeOH (10 mL) gave the complex as a yellow microcrystalline solid, which was filtered, washed with MeOH, and vacuum-dried (0.140 g, 91%). Anal. Calcd for C<sub>45</sub>H<sub>39</sub>IOP<sub>2</sub>Pd: C, 60.65; H, 4.41. Found: C, 60.50; H, 4.53. <sup>1</sup>H NMR (300 MHz, CDCl<sub>3</sub>): 7.47 (m, 12H), 7.35–7.20 (m, 18H) (PPh<sub>3</sub> ligands), 6.83 (d, 1H), 6.49 (t, 1H), 6.42 (d, 1H), 6.25 (t, 1H) (aryl ligand), 5.97 (dd, 1H, –CH=CH<sub>2</sub>), 4.44 (s, 2H, –CH<sub>2</sub>O), 4.13 (dd, 1H, *J* = 14, 1.7 Hz, –CH=CH<sub>2</sub>), 3.94 (dd, 1H, *J* = 7, 1.7 Hz, –CH=CH<sub>2</sub>). <sup>31</sup>P NMR (250 MHz, thf/D<sub>2</sub>O): 23.5 (s).

**Synthesis of [(PPh<sub>3</sub>)<sub>2</sub>Pd(I)(*o*-(C<sub>6</sub>H<sub>4</sub>)CH<sub>2</sub>CH<sub>2</sub>CH=CH<sub>2</sub>)] (10).** The complex was synthesized from [Pd(PPh<sub>3</sub>)<sub>4</sub>] (0.1 g, 0.086 mmol) and 4-(*o*-iodophenyl)but-1-ene (1c; 0.051 g, 0.2 mmol); workup as above gave the compound as a yellow microcrystalline solid (0.069 g, 90%). Anal. Calcd for C<sub>46</sub>H<sub>41</sub>IOP<sub>2</sub>Pt: C, 62.14; H, 4.64. Found: C, 61.81; H, 4.66. <sup>1</sup>H NMR (300 MHz, CD<sub>2</sub>Cl<sub>2</sub>): 7.58–7.16 (m, 30H, PPh<sub>3</sub> ligands), 6.88 (d, 1H), 6.51 (t, 1H), 6.28 (t, 1H), 6.22 (d, 1H) (aryl ligand), 5.7 (m, 1H, –CH=CH<sub>2</sub>), 4.97–4.90 (m, 2H, *J* = ca. 17, 10, 1.5

(22) Kometani, T.; Watt, D. S.; Ji, T. *Tetrahedron Lett.* **1985**, 26, 2043.

(23) White, W. N.; Gwynn, D.; Schlitt, R.; Girard, C.; Fife, W. J. *Am. Chem. Soc.* **1958**, 80, 3271.

Table 3. Crystallographic Data for 5a

mol formula	C <sub>43</sub> H <sub>37</sub> OPdFeI <sup>1/4</sup> C <sub>4</sub> H <sub>10</sub> O <sup>1/4</sup> C <sub>4</sub> H <sub>8</sub> O
<i>M<sub>r</sub></i>	957.5
crys syst	monoclinic
crys size (mm)	0.45 × 0.44 × 0.25
space group	<i>P</i> 2 <sub>1</sub> / <i>c</i>
<i>a</i> (Å)	10.320(3)
<i>b</i> (Å)	19.499(5)
<i>c</i> (Å)	21.150(5)
β (deg)	94.61(2)
<i>V</i> (Å <sup>3</sup> )	4242(2)
<i>Z</i>	4
<i>D<sub>c</sub></i> (g cm <sup>-3</sup> )	1.44
<i>T</i> (K)	290
diffractometer	Nicolet P2 <sub>1</sub>
radiation; λ (Å)	Mo Kα; 0.710 69
μ (cm <sup>-1</sup> )	15.9
scan method	ω-2θ
2θ(max) (deg)	50
no. of unique rflns	7510
no. of obsd rflns	5958
criterion for observn	<i>I</i> > 2σ( <i>I</i> )
no. of params refined	474
<i>S</i> (goodness of fit)	0.98
Δσ <sub>max</sub>	0.9
<i>R</i>	0.042
<i>R<sub>w</sub></i>	0.050
residual electron density	+1.1/-0.4

Hz, -CH=CH<sub>2</sub>), 2.51 (m, 2H, Ar-CH<sub>2</sub>-), 1.65 (m, 2H, -CH<sub>2</sub>-). <sup>31</sup>P NMR (250 MHz, CH<sub>2</sub>Cl<sub>2</sub>/D<sub>2</sub>O): 21.9 (s).

**Reaction of 5a and 6a with Silver Trifluoromethanesulfonate.** Solid silver trifluoromethanesulfonate (0.044 g, 0.172 mmol) was added to a solution of [(dppf)Pd(I)(*o*-(C<sub>6</sub>H<sub>4</sub>)CH<sub>2</sub>-OCH=CH<sub>2</sub>)] (5a; 0.184 g, 0.172 mmol) in a 1:1 mixture of THF and acetone (6 mL) at -78 °C. The mixture was stirred for 1 h at this temperature and then filtered through Celite at -78 °C to give a clear orange solution containing complex 15. <sup>31</sup>P NMR (250 MHz, thf/acetone/D<sub>2</sub>O, -40 °C): 31.1 (d), 15.3 (d) (*J*<sub>P-P</sub> = 5.1 Hz). A sample for proton NMR was similarly obtained using *d*<sub>6</sub>-acetone as solvent. <sup>1</sup>H NMR (500 MHz, *d*<sub>6</sub>-acetone, -20 °C): 7.77 (m, 3H, dppf and aryl ligand), 7.68-7.48 (set of m, 14H, aryl), 7.34 (m, 3H, aryl), 7.03 (m, 1H, aryl), 6.78 (m, 2H, ferrocenyl), 6.59 (m, 1H, aryl), 5.16 (m, 2H, -CH<sub>2</sub>O (see text)), 5.11 (s, 1H), 4.80 (s, 1H), 4.60 (s, 2H), 4.34 (s, 1H), 4.29 (s, 1H), 3.84 (s, 1H), 3.34 (s, 1H) (Cp), 1.40 (dd, 3H, *J*<sub>H-P</sub> = 10.5, 11.7 Hz, -CH<sub>3</sub>).

In a similar way, reaction of [(dppf)Pd(I)(*o*-(C<sub>6</sub>H<sub>4</sub>)CH<sub>2</sub>CH<sub>2</sub>-CH=CH<sub>2</sub>)] (6a; 0.2 mmol scale) with AgOSO<sub>2</sub>CF<sub>3</sub> gave an orange solution of complex 18. <sup>1</sup>H NMR (500 MHz, *d*<sub>6</sub>-acetone, -20 °C): 7.85-7.10 (set of m, 20H, aryl residues), 7.05 (m, 1H, aryl), 6.83 (m, 2H, dppf), 6.52 (m, 1H, aryl), 5.03 (s, 1H), 4.74 (s, 1H), 4.70 (s, 1H), 4.68 (s, 1H), 4.33 (s, 1H), 4.30 (s, 1H), 3.68 (s, 1H), 3.47 (s, 1H) (Cp), 2.85 (m, 2H, -CH<sub>2</sub>-), 1.53 (m, 2H, -CH<sub>2</sub>-), 1.18 (t, 3H, *J*<sub>H-P</sub> = 11 Hz, -CH<sub>3</sub>). <sup>31</sup>P NMR (250 MHz, thf-acetone/D<sub>2</sub>O, -40 °C): 33.4 (d), 18.0 (d) (*J*<sub>P-P</sub> = 56 Hz).

(24) This compound was less pure than others in the series and did not analyze satisfactorily despite several attempts.

**Crystal Structure Determination.** Suitable orange crystals for X-ray structure determination were obtained by slow diffusion of a diethyl ether-pentane mixture into a saturated solution of the complex in THF at -15 °C. Crystal data collection parameters are summarized in Table 3. Data were collected with a Nicolet P2<sub>1</sub> four-circle diffractometer in the ω-2θ mode. The maximum 2θ was 50° with scan range +1.3° (2θ) around the Kα<sub>1</sub>-Kα<sub>2</sub> angles, scan speed 5-29° min<sup>-1</sup>, depending on the intensity of a 2 s prescan; backgrounds were measured at each end of the scan for 0.25 of the scan time. *hkl* ranges were: 0-12, 0-23, and -25 to +25. Three standard reflections were monitored every 200 reflections and showed no change during data collection. Unit cell dimensions and standard deviations were obtained by a least-squares fit to 15 reflections (25 < 2θ < 27°). Intensity data were corrected for absorption effects (by the Gaussian method); minimum and maximum transmission factors were 0.66 and 0.78.

Heavy atoms were located by the Patterson interpretation section of SHELXTL and the light atoms then found on successive Fourier syntheses. One partially occupied disordered solvent molecule was located; it was modeled as a 50:50 mixture of the two ethers, sharing the same oxygen and one carbon site, with a total occupancy of 0.5. All significant residual peaks were in the vicinity of this solvent, indicating that the description of the molecule was not perfect. Anisotropic temperature factors were used for all non-H atoms, apart from solvent atoms. Hydrogen atoms were given fixed isotropic temperature factors; *U* = 0.07 Å<sup>2</sup>. Those defined by the molecular geometry were inserted at calculated positions and not refined (omitted on the solvent molecule). A weighting scheme of the form *w* = 1/(σ<sup>2</sup>(*F*) + *gF*<sup>2</sup>) with *g* = 0.0043 was used and shown to be satisfactory by a weight analysis. All calculations were performed on a DEC Microvax-II computer using SHELXTL PLUS.<sup>25</sup> Scattering factors in the analytical form and anomalous dispersion factors were taken from ref 26.

**Acknowledgment.** We thank Johnson-Matthey for the loan of Pd and Pt salts and the Spanish Ministry of Education for a Fellowship (to J.J.P.-T).

**Supplementary Material Available:** Text giving additional details on the X-ray structure determination and lists of anisotropic thermal parameters, H-atom coordinates, and bond lengths and angles (8 pages). Ordering information is given on any current masthead page. Additional data are available from the Cambridge Crystallographic Centre, comprising H-atom coordinates, thermal parameters, and all bond lengths and angles.

OM940604+

(25) Sheldrick, G. M. *SHELXTL User's Manual*; Nicolet: Madison, WI, 1983, 1986.

(26) *International Tables for X-Ray Crystallography*; Kynoch Press: Birmingham, U.K., 1974; Vol. IV (present distributor Kluwer Academic Publishers, Dordrecht, The Netherlands).

# Density Functional Study of C-H and O-H Activation and Methanol Oxidation by Chromyl Chloride

Tom Ziegler\* and Jian Li

Department of Chemistry, University of Calgary, Calgary, Alberta, Canada T2N 1N4

Received July 19, 1994<sup>®</sup>

Calculations based on density functional theory (DFT) have been carried out on the activation of the C-H and O-H bonds in methanol by  $\text{CrCl}_2\text{O}_2$  (**1a**). Two modes of activation were considered. The first was the abstraction of hydrogen by  $\text{CrCl}_2\text{O}_2$  represented by the reactions (i):  $\text{CH}_3\text{OH} + \mathbf{1a} \rightarrow \text{Cl}_2(\text{O})\text{Cr-OH}$  (**1b**) +  $\text{OCH}_3$  and (ii):  $\text{CH}_3\text{OH} + \mathbf{1a} \rightarrow \text{Cl}_2(\text{O})\text{Cr-OH}$  (**1b**) +  $\text{CH}_2\text{OH}$ . The two reactions were found to be endothermic by 41 kcal/mol (i) and 34 kcal/mol (ii), respectively. The second mode involves addition of the O-H and C-H  $\sigma$ -bonds to a Cr-O multiple bond of **1a** leading to (iii):  $\text{Cl}_2(\text{O})(\text{OH})\text{Cr-OCH}_3$  (**1e**) and (iv):  $\text{Cl}_2(\text{O})(\text{OH})\text{Cr-CH}_2\text{OH}$  (**1f**). The calculated endothermicities were 8 kcal/mol for (iii) and 23 kcal/mol for (iv). It is concluded that (ii) and (iv) are feasible pathways for C-H activation whereas only (iii) is available for O-H activation. The activation processes (i-iv) constitute possible first steps in the oxidation of methanol by **1a**. Other possible steps of importance for the oxidation were investigated. They include the decomposition of the addition products (v):  $\mathbf{1e} \rightarrow \text{CrCl}_2(\text{OH})_2 + \text{H}_2\text{CO}$  -9 kcal/mol and (vi):  $\mathbf{1f} \rightarrow \text{CrCl}_2(\text{OH})_2 + \text{H}_2\text{CO}$  -18 kcal/mol as well as the capture of the radicals produced in the abstraction reactions (vii):  $\text{OCH}_3 + \mathbf{1a} \rightarrow \text{Cl}_2\text{O}_2\text{-Cr-OCH}_3$  (**1c**) -9 kcal/mol and (viii):  $\text{CH}_2\text{OH} + \mathbf{1a} \rightarrow \text{Cl}_2(\text{O})\text{CrO-CH}_2\text{OH}$  (**1d**) -36 kcal/mol. Fully optimized structures are provided for **1a** to **1f**. It is concluded that oxidation of methanol by  $\text{CrCl}_2\text{O}_2$  (ix):  $\text{CrCl}_2\text{O}_2 + \text{CH}_3\text{OH} \rightarrow \text{CrCl}_2(\text{OH})_2 + \text{H}_2\text{CO}$  is endothermic by 5 kcal/mol and most likely proceeds by addition of the O-H bond (iii) followed by decomposition to  $\text{CH}_2\text{O}$  (v). The strength of the  $\text{Cl}_2(\text{O})\text{CrO-H}$  bond is crucial for the C-H and O-H activation by **1a**. The  $\text{Cl}_2(\text{O})\text{CrO-H}$  bond energy has been compared to the O-H bond strengths in other hydroxy metal complexes. The following values were obtained:  $D(\text{O}_2\text{CrO-H}) = 81$  kcal/mol;  $D(\text{Cl}_2(\text{O})\text{CrO-H}) = 66$  kcal/mol;  $D(\text{O}_2\text{OHCrO}^- \text{-H}) = 56$  kcal/mol;  $D(\text{O}_3\text{MnO}^- \text{-H}) = 63$  kcal/mol and  $D(\text{O}_3\text{RuO-H}) = 64$  kcal/mol.

## I. Introduction

High oxidation state chromium(VI)  $d^0$ -oxo compounds such as chromic acid, chloro-chromate, chromium trioxide and chromyl chloride are used widely to oxidize alkanes, alkenes, alcohols, diols, aldehydes and ketones<sup>1</sup> in organic synthesis. Mechanistic studies of the oxidation reactions were first carried out experimentally by Westheimer,<sup>2</sup> Wiberg<sup>1a</sup> and others<sup>1</sup> in the 1960's. More recent experimental investigations have been conducted by Cook and Mayer<sup>3</sup> as well as Lee<sup>4</sup> et al. Molecular orbital methods have also been applied to the oxidation studies. Rappé<sup>5</sup> and Goddard employed the Generalized Valence Bond (GVB) method in an investigation of alkane, alcohol and alkene oxidation by chromyl chloride

and molybdenyl chloride. Other theoretical studies are due to Yamaguchi<sup>6</sup> et al. as well as Jørgensen<sup>7</sup> and Schiøtt.

It is the general consensus that the initial key step in oxidation by transition-metal oxides involves an activation of either a C-H or an O-H bond. The activation is considered to take place in one of two ways as illustrated in Schemes 1 and 2, where the oxidation of  $\text{CH}_3\text{OH}$  by chromyl chloride,  $\text{CrCl}_2\text{O}_2$ , is used as an example.

The activation mode in Scheme 1 involves the abstraction of a hydrogen atom by  $\text{CrCl}_2\text{O}_2$ , **1a**, from a O-H, **R1**, or C-H, **R2**, bond leading to  $\text{CrCl}_2(\text{O})\text{OH}$ , **1b**, and either of the radicals  $\text{OCH}_3$ , **R1**, or  $\text{CH}_2\text{OH}$ , **R2**. The radicals can react further with another  $\text{CrCl}_2\text{O}_2$  molecule to generate, **R3**,  $\text{Cl}_2(\text{O})_2\text{Cr-OCH}_3$ , **1c**, in the case of  $\text{OCH}_3$  or, **R4**,  $\text{Cl}_2\text{OCr-O-CH}_2\text{OH}$ , **1d**, in the case of  $\text{CH}_2\text{OH}$ . The species **1c** and **1d** might subsequently

<sup>®</sup> Abstract published in *Advance ACS Abstracts*, November 1, 1994.

(1) (a) Wiberg, K. B. in *Oxidation in Organic Chemistry* Part A; Wiberg, K. B., Eds.; Academic Press: New York, 1965. (b) Ley, S. V.; Madin, A. in *Comprehensive Organic Synthesis*; Trost, B. N.; Fleming, I.; Eds.; Pergamon: Oxford, 1991. (c) Cainelli, G.; Cardillo, G. *Chromium Oxidation in Organic Chemistry*; Springer-Verlag: Berlin, 1984. (d) Freeman, F. in *Organic Synthesis by Oxidation with Metal Compounds*; Mijs, W. I.; de Jonge, C. R. H. I., Eds.; Plenum: New York, 1986. (e) Muzart, J. *Chem. Rev.* **1992**, *92*, 113. (f) Sharpless, K. B.; Akashi, K. *J. Am. Chem. Soc.* **1975**, *97*, 5927. (g) Scott, S. L.; Bakac, A.; Espenson, J. H. *J. Am. Chem. Soc.* **1992**, *114*, 4205.

(2) Westheimer, F. H.; Chang, Y. W. *J. Phys. Chem.* **1959**, *63*, 438.

(3) Cook, G. K.; Mayer, J. M. *J. Am. Chem. Soc.* **1994**, *116*, 1855.

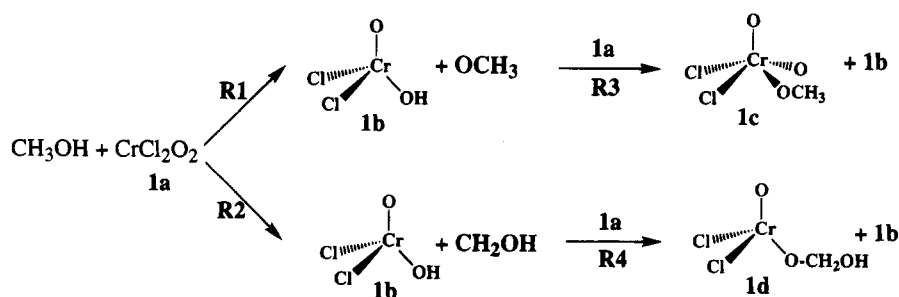
(4) (a) Lee, D. G.; Chen, T. *J. Org. Chem.* **1991**, *56*, 5341. (b) Lee, D. G.; Chen, T. *J. Am. Chem. Soc.* **1993**, *115*, 11231.

(5) (a) Rappé, A. K.; Goddard III, W. A. *Nature (London)* **1980**, *285*, 311. (b) Rappé, A. K.; Goddard III, W. A. *J. Am. Chem. Soc.* **1980**, *102*, 5114. (c) Rappé, A. K.; Goddard III, W. A. in *Potential Energy Surfaces and Dynamics Calculations*; Truhlar, D. G. Ed.; Plenum: New York, 1981. (d) Rappé, A. K.; Goddard III, W. A. *J. Am. Chem. Soc.* **1982**, *104*, 448. (e) Rappé, A. K.; Goddard III, W. A. *J. Am. Chem. Soc.* **1982**, *104*, 3287.

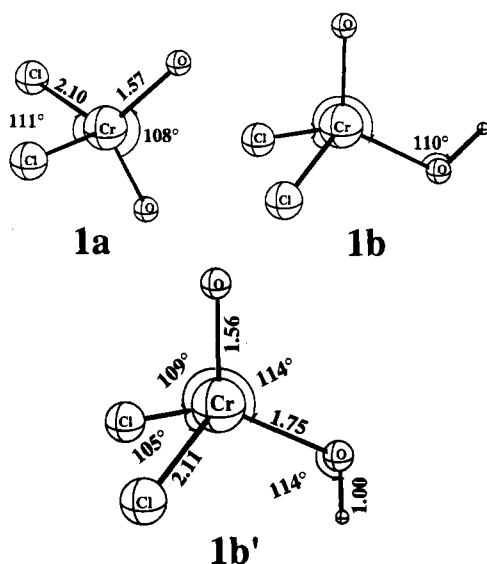
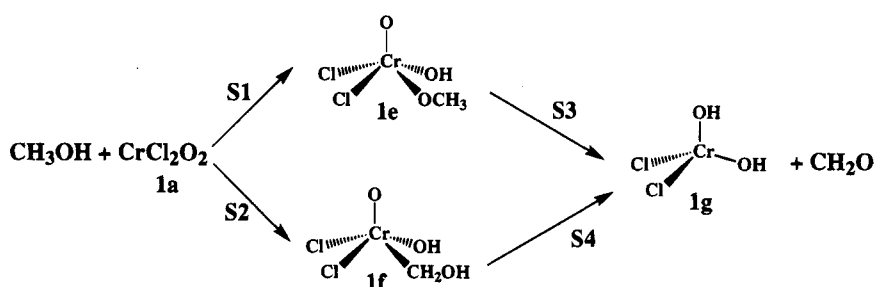
(6) Yamaguchi, K.; Tekahara, Y.; Fueno, T. in *Applied Quantum Chemistry*; Smith, V. H.; Schaefer III, H. F.; Morokuma, K., Eds.; D. Reidel: Dordrecht, 1986.

(7) Jørgensen, K. A.; Schiøtt, B. *Chem. Rev.* **1990**, *90*, 1483.

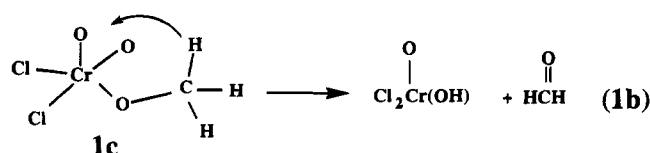
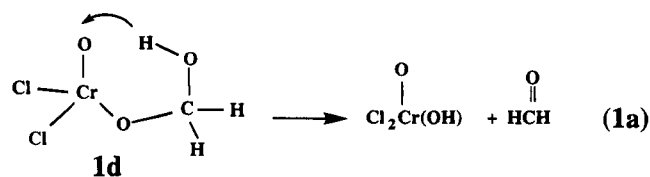
Scheme 1



Scheme 2



decompose into oxidized products<sup>8a</sup> as illustrated in eq 1.



The alternative activation mode is illustrated in Scheme 2. Here the O-H or C-H bonds are added to

the Cr-O linkage to produce respectively the methoxy complex **1e**, **S1**, or the hydroxymethyl complex **1f**, **S2**. A subsequent hydrogen transfer from the methoxy group, **1e**, or the hydroxymethyl ligand, **1f**, to the oxygen of the remaining Cr-O multiple bond, in respectively **S3** and **S4** of Scheme 2, produce  $\text{H}_2\text{CO}$  and the hydroxy complex, **1g**.

The way in which alcohols and other organic molecules are oxidized by  $\text{CrCl}_2\text{O}_2$  and related metal complexes might well be more complex than outlined above, and we shall in the following consider a few alternative routes. However, it is in general assumed that the initial step either consists of a hydrogen abstraction<sup>1a,2,3</sup>, Scheme 1, or an addition<sup>4,5</sup> of an O-H or a C-H bond to the M-O linkage. The preferred mode might very well depend on the nature of the oxidant.

The objective of the present study is to investigate the reaction enthalpies for the initial steps suggested in Schemes 1 and 2 as well as the subsequent decomposition reactions of eqs 1a and 1b. We shall begin by presenting some of the key thermodynamic data in section IIIA. The thermochemistry for the reactions in Schemes 1 and 2 are subsequently discussed in sections IIIB and IIIC, respectively. Considerations will also be given to the electronic and molecular structure for some of the species involved in the two schemes as well as eqs 1a and 1b. We present finally in section IIID a discussion of the strength and formal bond order of the Cr-O links in  $\text{CrCl}_2\text{O}_2$  and  $\text{CrCl}_4\text{O}$ , since the formal bond order of a M-O link has been associated with its ability to activate C-H and O-H bonds in a previous study by Rappé<sup>5</sup> and Goddard.

## II. Computational Details

All the calculations were carried out by using the density functional package A-MOL. This program was developed by Baerends<sup>9</sup> et al. and vectorized by Ravenek.<sup>10</sup> The numerical

(8) (a) Rócek, J.; Westheimer, F. H.; Eschenmoser, A.; Moldovanyi, L.; Schreiber, J. *Helv. Chim. Acta* **1962**, *45*, 2554. (b) Stavropoulos, P.; Bryson, N.; Youinou, M.-T.; Osborn, J. A. *Inorg. Chem.* **1990**, *29*, 1807.

(9) Baerends, E. J.; Ellis, D. E.; Ros, P. *Chem. Phys.* **1973**, *2*, 41.

(10) Ravenek, W. in *Algorithms and Applications on Vector and Parallel Computers*; te Riele, H. J. J.; Dekker, T. J.; van de Vorst, H. A., Eds.; Elsevier: Amsterdam, 1987.

integration procedure applied for the calculations is due to te Velde<sup>11</sup> et al. An uncontracted triple- $\zeta$  STO basis set was used for the  $ns$ ,  $np$ ,  $nd$ ,  $(n+1)s$  and  $(n+1)p$  orbitals of chromium, manganese and ruthenium. For carbon ( $2s, 2p$ ), chlorine ( $3s, 3p$ ), oxygen ( $2s, 2p$ ) and hydrogen ( $1s$ ), double- $\zeta$  basis sets were employed and augmented by an extra polarization function.<sup>12</sup> The inner cores of chromium and manganese ( $1s2s2p$ ), ruthenium ( $1s2s2p3s3p3d$ ), carbon ( $1s$ ) and oxygen ( $1s$ ) as well as chlorine ( $1s2s2p$ ) were treated by the frozen-core approximation<sup>9</sup>. A set of auxiliary  $s$ ,  $p$ ,  $d$ ,  $f$  and  $g$  STO functions was introduced in order to fit the molecular density and Coulomb potential accurately in each SCF-cycle.<sup>13</sup> All the geometries were optimized at the local density approximation (LDA) level<sup>14</sup> by the method due to Versluis<sup>15</sup> and Ziegler. The energy differences were calculated by including Becke's nonlocal exchange correction<sup>16</sup> and Perdew's nonlocal correlation correction<sup>17</sup> as perturbations based on the LDA density, LDA/NL. The validity of such a procedure has been investigated extensively.<sup>18</sup>

The calculated bond energies (BE) were analyzed by the Extended Transition State method (ETS).<sup>19</sup> The ETS method considers the bond between the fragments A and B in A-B as given by

$$BE = -[\Delta E_{\text{steric}} + \Delta E_{\text{orb-int}} + \Delta E_{\text{prep}} + \Delta E_{\text{prom}}] - [\Delta E_{\text{int}} + \Delta E_{\text{prep}} + \Delta E_{\text{prom}}] \quad (2a)$$

The first term,  $\Delta E_{\text{steric}}$ , is the steric interaction energy between A and B. It can be written as

$$\Delta E_{\text{steric}} = \Delta E_{\text{el}} + \Delta E_{\text{Pauli}} \quad (2b)$$

where  $\Delta E_{\text{el}}$  is the, usually attractive, electrostatic Coulomb interaction between A and B, whereas  $\Delta E_{\text{Pauli}}$  is the Pauli repulsion due to the destabilizing two-orbital four-electron interactions between occupied orbitals on A and B. The term  $\Delta E_{\text{int}}$  represents the stabilizing interaction between occupied and virtual orbitals on A and B, and  $\Delta E_{\text{prep}}$  takes into account deformations of A and B as the two fragments are combined into A-B. The term  $\Delta E_{\text{prom}}$  includes energies required to promote the fragments A and B from their ground states to their valence states. This term will only be used in connection with the Cr-O bond energy discussed in section III.D.

### III. Results and Discussion

**A. Strengths of O-H Bonds Formed by Metal-Oxo Compounds.** It is clear from Schemes 1 and 2 that the ability of  $\text{Cl}_2\text{CrO}_2$  and other oxo-metal complexes to form strong O-H bonds is of crucial importance<sup>3</sup> for their role as oxidizing agents in organic

**Table 1. Geometrical Parameters for  $d^0$  Oxo-Complexes and Methanol<sup>a</sup>**

molecule	calculated	experimental
$\text{CrCl}_2\text{O}_2$ (1a)	1.565(Cr-O), 2.098(Cr-Cl)	1.581(Cr-O), 2.126(Cr-Cl)
	108.6(OCrO), 111.6(ClCrCl)	108.7(OCrO), 113.0(ClCrCl) <sup>b</sup>
$\text{CH}_3\text{OH}$	1.415(C-O), 1.102(C-H)	1.425(C-O), 1.094(C-H)
	0.979(O-H), 108.4(COH)	0.945(O-H), 108.5(COH)
	110.0(OCH)	110.3(OCH) <sup>c</sup>
$\text{CrO}_3$	1.586 (Cr-O)	
$\text{HCrO}_4^-$	1.612(Cr-O), 1.840(Cr-OH)	1.637–1.648, <sup>e</sup> 1.65 <sup>f</sup>
$\text{MnO}_4^-$	1.604(Mn-O)	1.61 (Mn-O) <sup>g</sup>
$\text{RuO}_4$	1.709 (Ru-O)	1.705 (Ru-O) <sup>h</sup>

<sup>a</sup> Bond lengths in Ångstroms, and bond angles in degree. <sup>b</sup> Reference 20. <sup>c</sup> Reference 21. <sup>d</sup> Reference 21. <sup>e</sup> Crystallographic data for  $\text{K}_2\text{CrO}_4$ .<sup>23a</sup> <sup>f</sup> Reference 23. <sup>g</sup> Reference 24. <sup>h</sup> Reference 25.

synthesis. Preferably, the O-H bond formed in the hydroxy-metal complex should be comparable to the O-H or C-H bonds broken in the organic molecules. We have examined a number of oxo-metal systems and calculated the O-H bond dissociation energies in the corresponding hydroxy-metal complexes. The purpose of this investigation has been to supplement the sparse experimental data on O-H bond energies in hydroxy-metal complexes, and compare the calculated values with estimates for the organic C-H and O-H bonds. We shall in addition supply optimized structures for the oxo-metal and hydroxy-metal complexes involved.

Table 1 provides optimized structures for the investigated  $\text{CrO}_3$ ,  $\text{Cl}_2\text{CrO}_2$ ,  $\text{MnO}_4^-$ ,  $\text{O}_2\text{Cr}(\text{OH})\text{O}^-$  and  $\text{RuO}_4$   $d^0$  oxo complexes. The optimized bond distances and angles compare fairly well with available experimental<sup>20–25</sup> data. The error for the M-O bond distances in  $\text{CrO}_2\text{Cl}_2$ ,  $\text{MnO}_4^-$ ,  $\text{CrO}_2(\text{OH})_2$ , and  $\text{RuO}_4$  are within 0.02 Å. Experimental data are not available for  $\text{CrO}_3$ . The favorable comparison between experiment and calculations in Table 1 would indicate that the level of DFT theory applied here is adequate for structure optimizations within the class of molecules under investigation. We have also optimized the structure for  $\text{MnO}_4^{2-}$  in order to ensure that we can predict M-O distances for  $d^1$  complexes. Our Mn-O distance of 1.658 Å is in good agreement with the experimental<sup>24</sup> estimate of 1.66 Å.

The O-H bond energies for the hydroxy-metal compounds as well as the C-H and O-H bond strengths for methanol are summarized in Table 2. The calculated C-H and O-H bond strengths for methanol are in good agreement with experiment.<sup>26</sup> This is to be expected based on previous experience<sup>18</sup> with calculations on organic molecules. In particular, Becke has in a series of seminal papers<sup>27</sup> shown that the DFT method used here provides as accurate estimates of bond energies in

(20) Marsden, C. J.; Hedberg, L.; Hedberg, K. *Inorg. Chem.* **1982**, *21*, 1115.

(21) *Landolt-Börnstein* New Series, Group II, Vol. 7; Callomon, J. H.; Hirota, E.; Kuchitsu, K.; Lafferty, W. J.; Maki, A. G.; Pote, C. S., Eds.; Springer-Verlag: Berlin, 1976.

(22) Byström, A.; Wilhelmi, K. A. *Acta Chem. Scand.* **1950**, *4*, 1131.

(23) (a) Toriumi, K.; Saito, Y. *Acta Cryst. B* **1978**, *34*, 3149. (b) Krebs, B.; Hasse, K. D. *Acta Cryst. B* **1976**, *32*, 1334.

(24) Kálman, A. *J. Chem. Soc. A* **1971**, 1851.

(25) Seip, H. M. in *Molecular Structure by Diffraction Methods*, Sims, A.; Sutton, L. E., Eds.; Vol. 1, Part 1; The Chemical Society: London, 1973.

(26) *Handbook of Chemistry and Physics*, 73rd Edition; Lide, D. R., Ed.; CRC Press: Boca Raton, 1992.

(27) (a) Becke, A. D. *J. Chem. Phys.* **1993**, *98*, 1372. (b) Becke, A. D. *J. Chem. Phys.* **1993**, *98*, 5648.

(11) (a) Boerrigter, P. M.; te Velde, G.; Baerends, E. J. *Int. J. Quant. Chem.* **1987**, *33*, 87. (b) te Velde, G.; Baerends, E. J. *J. Comp. Phys.* **1992**, *99*, 84.

(12) (a) Snijders, G. J.; Baerends, E. J.; Vernooijs, P. *At. Nucl. Data Tables* **1982**, *26*, 483. (b) Vernooijs, P.; Snijders, G. J.; Baerends, E. J. *Slater Type Basis Functions for the Whole Periodic System*; Internal Report: Free University of Amsterdam, The Netherlands, 1981.

(13) Krijin, J.; Baerends, E. J. *Fit Functions in the HFS-methods*; Internal Report: Free University of Amsterdam, The Netherlands, 1984.

(14) Vosko, S. H.; Wilk, L.; Nusair, M. *Can. J. Phys.* **1980**, *58*, 1200.

(15) Verluis, L.; Ziegler, T. *J. Chem. Phys.* **1988**, *88*, 322.

(16) Becke, A. D. *Phys. Rev. A* **1988**, *38*, 2398.

(17) (a) Perdew, J. P. *Phys. Rev. Lett.* **1985**, *55*, 1655. (b) Perdew, J. P. *Phys. Rev. B* **1986**, *33*, 8822. (c) Perdew, J. P.; Wang, Y. *Phys. Rev. B* **1986**, *33*, 8800.

(18) (a) Ziegler, T. *Chem. Rev.* **1991**, *91*, 651. (b) Ziegler, T. *Pure Appl. Chem.* **1991**, *63*, 873. (c) Ziegler, T.; Verluis, L. *Adv. Chem. Ser.* **1992**, *No. 230*, 75. (d) Ziegler, T.; Tschinke, T. *ACS Symp. Ser.* **1990**, *No. 428*, 277.

(19) (a) Ziegler, T.; Rauk, A. *Theor. Chim. Acta* **1977**, *46*, 1. (b) Ziegler, T. in *Metal-Ligand Interactions: from Atoms, to Clusters, to Surfaces*; Salahub, D. R.; Russo, N., Eds.; NATO ASI C378; Kluwer Academic Publishers: Dordrecht, **1992**.



Table 2. Calculated O-H and C-H Bond Strengths<sup>a</sup>

$\Delta E_{\text{prep}}$	bond strength		Decomposition <sup>e,f</sup>			
	calc <sup>d</sup>	exp <sup>c</sup>	$\Delta E_{\text{int}}$	$\Delta E_{\text{steric}}$	$\Delta E_{\text{orb-int}}$	
H-CH <sub>2</sub> OH	101	94±2 <sup>b</sup>				
CH <sub>3</sub> O-H	108	104±1 <sup>b</sup>				
O <sub>2</sub> CrO-H	81		-89	167	-256	8
Cl <sub>2</sub> Cr(O)(O-H)	66		-79	167	-245	13
O <sub>2</sub> Cr(OH)(O-H) <sup>-</sup>	56		-76	163	-239	20
O <sub>3</sub> MnO-H <sup>-</sup>	63	83 <sup>c</sup>	-78	156	-234	15
O <sub>3</sub> RuO-H	64		-85	159	-244	21

<sup>a</sup> Energies in kcal/mol. <sup>b</sup> Reference 26. These are  $\Delta H_{298}$  values. <sup>c</sup> Reference 3 gives 80 kcal/mol. More recent value (private communication by same authors) is 83 kcal/mol. Both values correspond to  $\Delta H_{298}$ . <sup>d</sup> The theoretical values are electronic enthalpies,  $\Delta E_{\text{e}}$ . For a comparison with the experimental  $\Delta H_{298}$  values one would have to add vibrational zero point energy corrections as well as thermal corrections. The theoretical  $\Delta H_{298}$  estimate should be 2–5 kcal/mol lower than the theoretical  $\Delta E_{\text{e}}$  values, where the lower limit apply to the hydroxy-metal complexes. <sup>e</sup>  $\Delta E_{\text{int}} = \Delta E_{\text{steric}} + \Delta E_{\text{orb-int}}$ . <sup>f</sup>  $\Delta E_{\text{orb-int}} = -[\Delta E_{\text{int}} + \Delta E_{\text{prep}}]$ .

organic molecules as the highest level of *ab initio* theory based on the G2-scheme due to Pople<sup>28</sup> et al.

Following an approach developed by Bordwell<sup>29</sup> et al., Cook and Mayer<sup>3</sup> have estimated the O-H bond strengths for  $\text{MnO}_3(\text{OH})^-$  from redox potentials and  $\text{pK}_a$  values, Table 2. Their estimated value of 83 kcal/mol for the O-H bond energy in  $\text{MnO}_3(\text{OH})^-$  is much larger than the value of 63 kcal/mol obtained by the LDA/NL scheme, Table 2. We are at the moment not able to account for this discrepancy. The size of the deviation is surprising since the LDA/NL scheme applied here has provided accurate estimates of bond energies involving hydrogen in organic complexes<sup>18,27</sup> as well as transition metal complexes.<sup>18,19b</sup>

An ETS decomposition analysis<sup>19</sup> of the O-H bond energies is also included in Table 2. The ETS scheme writes according to eq 2a the total bond dissociation energy, BE, as a sum of the total interaction energy between the fragments A and B,  $-\Delta E_{\text{int}}$ , and the energy required,  $-\Delta E_{\text{prep}}$ , to distort the fragments from their geometries in the free state to the structures they adopt in the final compound A-B. It is remarkable that the interaction energies,  $-\Delta E_{\text{int}}$ , between hydrogen and the different oxo-metal fragments are quite similar.

A single orbital in each of the hydroxy-metal complexes is basically responsible for the O-H bond. The O-H bonding orbitals for  $\text{Cl}_2\text{Cr}(\text{O})(\text{OH})$  and  $\text{O}_2\text{Cr}(\text{OH})$  are depicted in Figure 1. The plots reveal that the hydrogen atom is embedded in the positive lobe of one of the oxygen  $\pi$ -type lone-pair orbitals. The  $-\Delta E_{\text{int}}$  term is seen to be ~5 kcal/mol smaller for the two charged species primarily as a result of the orbital interaction contribution  $-\Delta E_{\text{orb-int}}$ . The interaction between hydrogen and the  $\text{d}^0$  oxo-species involves the formation of the bonds shown in Figure 1 as well as the formal transfer of an electron from hydrogen to a d-based metal orbital in the resulting  $\text{d}^1$  hydroxy-metal complex. It is the electron transfer that is less favorable in the case of the negatively charged species.

The preparation energy,  $\Delta E_{\text{prep}}$ , diminish the total bond strength, BE, by 8–21 kcal/mol, Table 2, according to our calculations. The preparation process is first of all associated with a stretch of one M-O bond to form

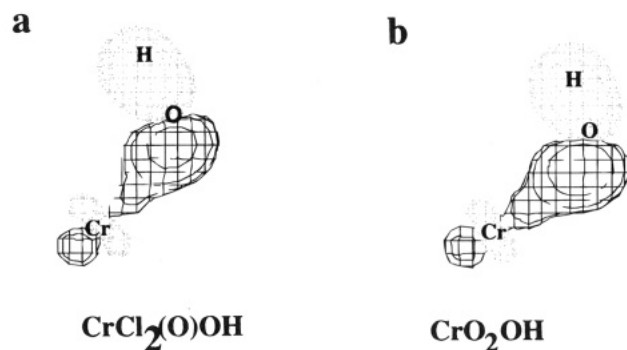
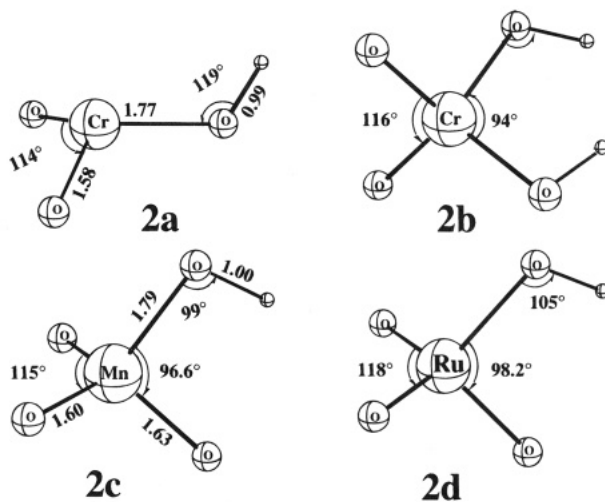
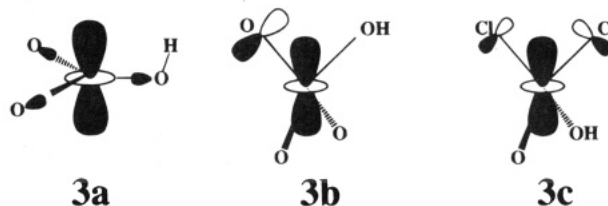


Figure 1. Bonding orbitals corresponding to the O-H bond in (a)  $\text{Cl}_2\text{Cr}(\text{O})(\text{OH})$  and (b)  $\text{O}_2\text{CrOH}$ .

the M-OH link. This stretch contributes to  $\Delta E_{\text{prep}}$  with nearly the same amount in the different species. There is in addition a reorganization of the remaining part of the complex. The reorganization consists of a distortion of the O-M-O and Cl-M-Cl bond angles as well as a modest elongation of one or more of the M-O or M-Cl bonds adjacent to the hydroxy ligand. The reorganization is associated with the occupation of a metal-based d-orbital as the  $\text{d}^1$  hydroxy complex is formed, and its contribution to  $\Delta E_{\text{prep}}$  varies. The optimized geometries for the  $\text{d}^1$  hydroxy metal-complexes are given in structures 1b, 2a, 2b, 2c, and 2d for  $\text{Cl}_2\text{Cr}(\text{O})(\text{OH})$ ,  $\text{O}_2\text{CrOH}$ ,  $\text{O}_2\text{Cr}(\text{OH})_2^-$ ,  $\text{O}_3\text{MnOH}^-$ , and  $\text{O}_3\text{RuOH}$ , respectively.



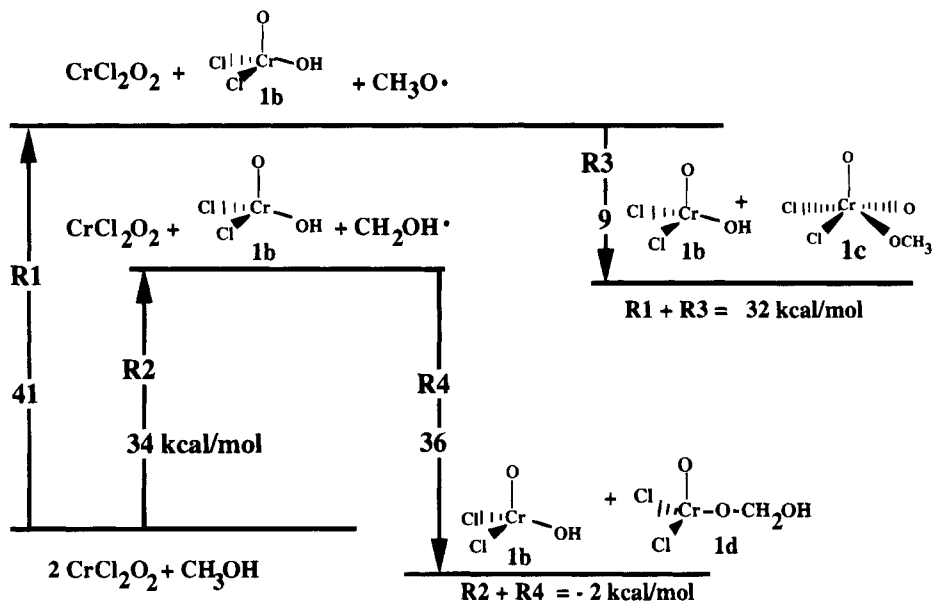
The  $\text{Cr}(\text{O})_2(\text{OH})$  species has the single electron situated in a  $\text{d}_{z^2}$  orbital, 3a. The orbital is weakly sigma anti-bonding but lacks any anti-bonding  $\pi$ -interactions due to symmetry. The weakly anti-bonding interactions



results in only a modest reorganization, and a small contribution to  $\Delta E_{\text{prep}}$ . In total  $\Delta E_{\text{prep}}$  for  $\text{O}_2\text{CrOH}$  amounts to 8 kcal. The modest size of  $\Delta E_{\text{prep}}$  makes the O-H bond in  $\text{O}_2\text{CrOH}$  stronger than the O-H bond in any of the other hydroxy-metal species. We calculate the O-H bond energy for  $\text{O}_2\text{CrOH}$  to be 81 kcal/mol.

(28) Pople, J. A.; Head-Gordon, M.; Fox, D. J.; Raghavachari, K.; Curtiss, L. A. *J. Chem. Phys.* **1989**, *90*, 5622.

(29) (a) Bordwell, F. G.; Chen, J. P.; Harrelson Jr., J. A. *J. Am. Chem. Soc.* **1988**, *110*, 1229. (b) Zhang, X. M.; Bordwell, F. G. *J. Am. Chem. Soc.* **1992**, *114*, 9787.



**Figure 2.** Energetics for steps **R1** to **R4** of Scheme 1. All energies in kcal/mol.

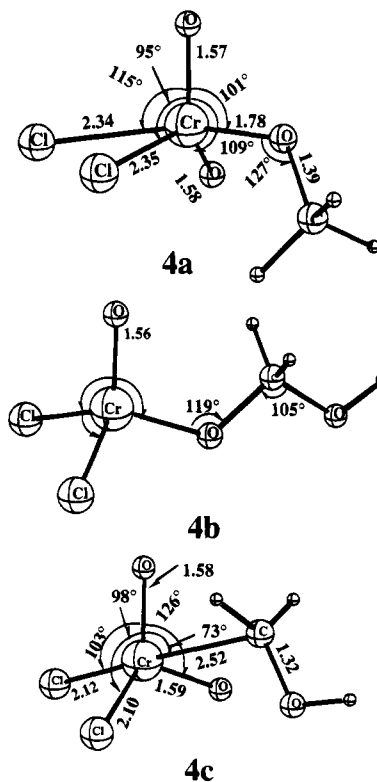
The singly occupied d-orbital in  $\text{O}_3\text{RuOH}$ , **3b**, as well as  $\text{O}_2\text{Cr}(\text{OH})_2^-$  and  $\text{O}_3\text{MnOH}^-$  is  $d_{z^2}$  based with a strong anti-bonding  $\pi$ -interaction(s) involving oxygen. It corresponds to one of the e-components in the tetrahedral crystal field splitting of the d many-fold. The anti-bonding interaction(s) will lead to elongation(s) of the M-O bond(s) involved and a considerable contribution to  $\Delta E_{\text{prep}}$ . We calculate the O-H bond energies to be 56 kcal/mol, 63 kcal/mol and 64 kcal/mol for  $\text{O}_2\text{Cr}(\text{OH})(\text{O}-\text{H})^-$ ,  $\text{O}_3\text{MnO}-\text{H}^-$  and  $\text{O}_3\text{RuO}-\text{H}$ , respectively. Thus, all three bonds are considerably weaker than in  $\text{O}_2\text{CrOH}$  due to the larger  $\Delta E_{\text{prep}}$  contribution, Table 2. In **2c** and **2d** the anti-bonding interaction involves only a single  $\pi$ -orbital on the unique oxygen, **3b**. The corresponding unique M-O bond is as a consequence elongated compared to the two equivalent M-O bonds.

The  $\text{Cl}_2\text{OCrOH}$  system has the single electron in a  $d_{z^2}$  orbital, **3c**. This orbital is weakly anti-bonding with respect to the chlorine  $\pi$ -orbitals. The anti-bonding  $\pi$ -interaction is not so strong as in **3b** since the chlorine  $\pi$ -orbitals form smaller overlaps with  $d_{z^2}$  than oxygen. It is thus understandable that the  $\Delta E_{\text{prep}}$  contribution of 13 kcal/mol as well as the O-H bond energy of 66 kcal/mol are intermediate between the corresponding values in  $\text{O}_2\text{CrOH}$  on the one hand and  $\text{O}_2\text{Cr}(\text{OH})(\text{O}-\text{H})^-$ ,  $\text{O}_3\text{MnO}-\text{H}^-$ ,  $\text{O}_3\text{RuO}-\text{H}$  on the other, Table 2. The Cr=O bond in **1b** is not elongated compared to the Cr-O bonds in **1a** since only chlorine  $\pi$ -orbitals are involved in the anti-bonding orbital **3c**. In fact, the Cr-O bond in **1b** is contracted by .01 Å compared to the corresponding bonds in **1a**.

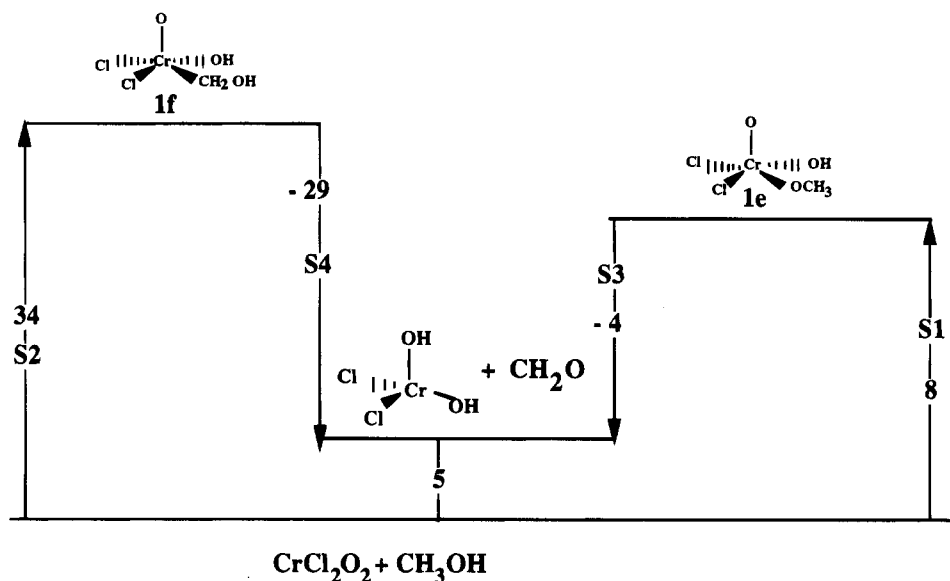
**B. Activation of Methanol by Hydrogen Abstraction.** The calculated O-H bond dissociation energy in  $\text{Cl}_2\text{Cr}(\text{O})\text{OH}$  together with the O-H and C-H bond strengths of methanol, Table 2, allow us to estimate the total reaction enthalpy for the first abstraction steps in Scheme 1 as 41 kcal/mol, **R1**, and 34 kcal/mol, **R2**, respectively. The step **R2** leading to **1b** and  $\text{CH}_2\text{OH}$  is more facile than the abstraction step **R1** producing **1b** and  $\text{OCH}_3$  because the C-H methanol bond is weaker than the O-H methanol bond. The energetics for steps **R1** and **R2** are recorded in Figure 2.

The organic radicals  $\text{OCH}_3$  and  $\text{CH}_2\text{OH}$  generated in

**R1** and **R2** can undergo a number of reactions<sup>3</sup>. We are interested in the capture of these radicals by another  $\text{Cl}_2\text{CrO}_2$  molecule, **R3** and **R4** of Scheme 1. The reaction between  $\text{Cl}_2\text{CrO}_2$  and  $\text{CH}_3\text{O}$ , **R3**, results in the square pyramidal five coordinated complex **4a**, (**1c**), with an oxygen in the axial position and the  $\text{OCH}_3$  group attached directly to chromium through the methoxy oxygen. The reaction enthalpy for **R3** is only -9 kcal/mol, testifying to a weak bond between  $\text{OCH}_3$  and the already coordinatively saturated chromium center with a formal oxidation number of VII. An alternative configuration with  $\text{OCH}_3$  bound to an oxygen on  $\text{Cl}_2\text{CrO}_2$  was found to be even less stable.



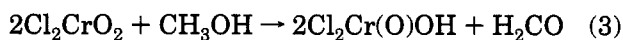
The reaction between  $\text{CH}_2\text{OH}$  and  $\text{Cl}_2\text{CrO}_2$ , **R4**, can



**Figure 3.** Energetics for steps **S1** to **S4** of Scheme 2. All energies in kcal/mol.

lead to the product **4b**, (**1d**), in which  $\text{CH}_2\text{OH}$  is bound through an oxygen on  $\text{CrCl}_2\text{CrO}_2$  or directly to the chromium atom, **4c**. The formation of **4b** from  $\text{CH}_2\text{OH}$  and  $\text{CrCl}_2\text{CrO}_2$  is favorable with a reaction enthalpy of  $-36$  kcal/mol, whereas the formation of **4c** is unfavorable with a reaction enthalpy of  $6$  kcal/mol. The stability of **4b** stems primarily from the relatively strong  $\text{Cl}_2(\text{O})\text{CrO}-\text{CH}_2\text{OH}$  bond which has about half the strength of the corresponding  $\text{Cl}_2(\text{O})\text{CrO}-\text{H}$  bond, Table 2. Thus the  $\text{OCH}_3$  radical is seen to bind directly to the metal center whereas the  $\text{CH}_2\text{OH}$  radical binds through an oxygen atom.

It follows from Figure 2 that the activation of the C-H bond in methanol leading to **4b**, (**1d**), along the steps **R2** and **R4** is favorable with an over-all reaction enthalpy of  $-2$  kcal/mol. The product **4b** can further decompose to **1b** and formaldehyde according to eq 1a, thus completing the total oxidation process of methanol:



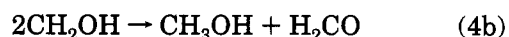
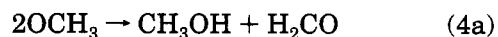
We find that the decomposition of **1d** according to eq 1a is endothermic by  $10$  kcal/mol. In eq 1a the loss of a strong O-H bond ( $\sim 104$  kcal/mol) and a weaker Cr-O-C bond ( $\sim 36$  kcal/mol) is compensated for by the formation of the Cr-O-H bond ( $\sim 66$  kcal/mol) and a C=O double bond ( $\sim 60-70$  kcal/mol).

We find further that the total reaction enthalpy for the process in eq 3 is  $3$  kcal/mol. The over-all barrier for **R2**+**R4** is likely to come from **R2**, the hydrogen abstraction step for which the reaction enthalpy is calculated to be  $29$  kcal/mol, Figure 2. This value is very close to the experimental barrier of  $27$  kcal/mol observed<sup>3</sup> for oxidation of cyclohexane by  $\text{CrCl}_2\text{CrO}_2$ . In this process the initial step is postulated<sup>3</sup> to be the abstraction of hydrogen from a C-H bond by  $\text{CrCl}_2\text{CrO}_2$ . However we have not been able to estimate the kinetic barrier for the abstraction reaction.

The alternative route involving the steps **R1** and **R3** is thermodynamically unfavorable by  $32$  kcal/mol. This route has in addition a barrier of at least  $41$  kcal/mol on account of the step **R1** which involves the activation of the O-H alcohol bond via abstraction of hydrogen by  $\text{CrCl}_2\text{CrO}_2$ . It is thus not likely that the combination **R1**

+ **R3** is of importance in the oxidation of alcohols by  $\text{CrCl}_2\text{CrO}_2$ , although **1c**, (**4a**), formed in **R3** of Scheme 2 can decompose to the oxidized product  $\text{H}_2\text{CO}$  as shown in eq 1b. The reaction (1b) was calculated to be exothermic by  $29$  kcal/mol. In eq 1b the loss of a strong O-H bond ( $\sim 104$  kcal/mol) and a very weak Cr-O $\text{CH}_3$  bond ( $\sim 9$  kcal/mol) is compensated for by the formation of the Cr-O-H bond ( $\sim 66$  kcal/mol) and a C=O double bond ( $\sim 60-70$  kcal/mol). The process in eq 1b is more favorable than the elimination reaction in eq 1a since the Cr-O $\text{CH}_3$  bond of  $9$  kcal/mol is weaker than the Cr-O-C bond of  $36$  kcal/mol.

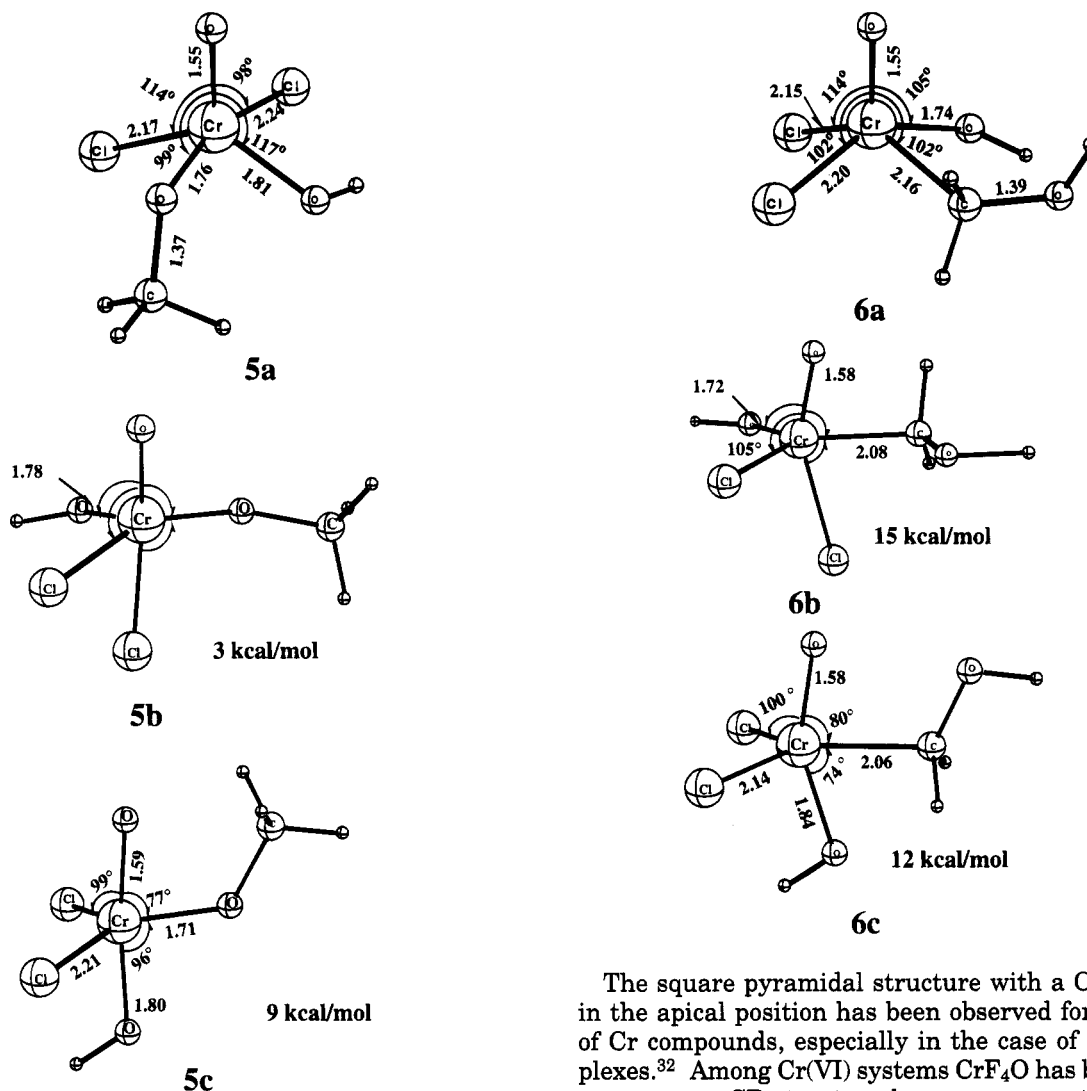
It should be mentioned that the reactions between the two organic radicals to produce formaldehyde



are favorable with reaction enthalpies of  $-65$  kcal/mol and  $-79$  kcal/mol for (4a) and (4b), respectively. However, it is not likely that the concentration of either  $\text{OCH}_3$  or  $\text{CH}_2\text{OH}$  is large enough to facilitate such a route.

We shall in the next section turn to a discussion of an alternative mechanism, Scheme 2, by which the C-H as well as O-H alcohol bonds can be activated by addition to a M-O linkage.

**C. Activation of Methanol by  $[2_\pi + 2_\sigma]$  addition.** The activation of O-H and C-H bonds by a  $[2_\pi + 2_\sigma]$  addition to the M-O link is illustrated in Scheme 2 as **S1** and **S2**, respectively. Addition of the O-H bond, **S1**, results in the five coordinated methoxy complex **1e**. The addition process is mildly endothermic with a reaction enthalpy of  $8$  kcal/mol, Figure 3. The five coordinated species **1e** could conceivably adopt either a square pyramidal (SP) or a trigonal bipyramidal (TB) conformation. The optimized structure of lowest energy, **5a**, has a SP conformation with oxygen in the apical position. This is the conformation adopted by most five coordinated oxy complexes of the chromium triad. Alternative TP structures with chlorine, **5b**, or OH, **5c**, trans to an oxygen atom in the axial positions were  $3$  kcal/mol and  $9$  kcal/mol higher in energy.



The addition of a C-H bond, **S2**, requires 23 kcal/mol, Figure 3, and results in the five coordinated hydroxymethyl complex **1f**. The most stable conformation for the hydroxymethyl complex is again a SP structure, **6a**, with oxygen in the apical position. Alternative TP structures with chlorine, **6b**, or OH, **6c**, in the axial positions trans to an oxygen atom were 15 kcal/mol and 12 kcal/mol higher in energy.

Experimental structures are not known for the five coordinated species studied here. However, the optimized Cr-O bond distances in **5a-c** and **6a-c** are all in the range, 1.55–1.58 Å, observed experimentally for related chromium-oxo systems.<sup>30</sup> The sum of the ionic radii for Cr(VI) and O(-II) is given by 1.9 Å, which is close to the calculated Cr-O single bond distances of between 1.72 Å and 1.84 Å. The calculated Cr(VI)-C single bond distances are in the range of 2.06–2.16 Å. Experimental Cr(VI)-C distances are not available for related systems. The observed Cr(IV)-C bond lengths in a number of CrR<sub>4</sub> compounds<sup>31</sup> are between 2.01 Å and 2.07 Å.

(30) (a) Nugent, W. A.; Mayer, J. M. *Metal-Ligand Multiple Bonds*, John Wiley and Sons: New York, 1988. (b) Mayer, J. M. *Inorg. Chem.* **1988**, *27*, 3899. (c) Colton, R. *Coord. Chem. Rev.* **1988**, *90*, 1; **1985**, *62*, 85; **1984**, *58*, 245; **1984**, *57*, 189. (d) Cielak-Golonka, M. *Coord. Chem. Rev.* **1991**, *109*, 223.

(31) Kirtley, S. W. in *Comprehensive Organometallic Chemistry*; Wilkinson, G.; Stone, F. G. A., Eds.; Vol. 3, Pergamon: Oxford, 1982.

The square pyramidal structure with a Cr-oxo bond in the apical position has been observed for a number of Cr compounds, especially in the case of Cr(V) complexes.<sup>32</sup> Among Cr(VI) systems CrF<sub>4</sub>O has been shown to possess a SP structure by measurements based on IR spectroscopy.<sup>33</sup>

Either of the products **5a** (**1e**) and **6a** (**1f**) can decompose by way of a hydrogen transfer to the oxygen atom involved in the remaining Cr-O multiple bond, thus producing H<sub>2</sub>CO and the d<sup>2</sup> complex CrCl<sub>2</sub>(OH)<sub>2</sub>, **S3** and **S4** of Scheme 2. We calculate **S3** to be exothermic by 4 kcal/mol, Figure 3, whereas **S4** has an exothermicity of 29 kcal/mol. For the over-all process



we find a slight endothermicity of 5 kcal/mol. Our calculations indicate in addition, Figure 3, that the route **S1+S3** with O-H activation is more attractive than the **S2+S4** path with C-H activation since **S1** requires 8 kcal/mol as opposed to 23 kcal/mol for **S2**. The difference between **S1** and **S2** can be attributed to a difference in the Cr-OCH<sub>3</sub> and Cr-CH<sub>2</sub>OH bond strengths. We calculate the Cr-OCH<sub>3</sub> bond energy of **5a** to be 33 kcal/mol whereas the Cr-CH<sub>2</sub>OH bond strength in **6a** only is 11 kcal/mol.

The factors responsible for the weak Cr-OCH<sub>3</sub> and Cr-CH<sub>2</sub>OH bonds have been studied by applying the ETS

(32) (a) Cotton, F. A.; Wilkinson, G. *Advanced Inorganic Chemistry*, 5rd Edition; John Wiley and Sons: New York, 1988. (b) Mitewa, M.; Bontchev, P. R. *Coord. Chem. Rev.* **1985**, *61*, 241.

(33) Hope, E. J.; Jones, P. J.; Levason, W.; Ogden, J. S.; Tajik, M.; Turff, J. W. *J. Chem. Soc. Dalton Trans.* **1985**, 529.

**Table 3.** Calculated Cr-C and Cr-O Bond Strengths<sup>a</sup> in **5a**, **6a**, and **1b**

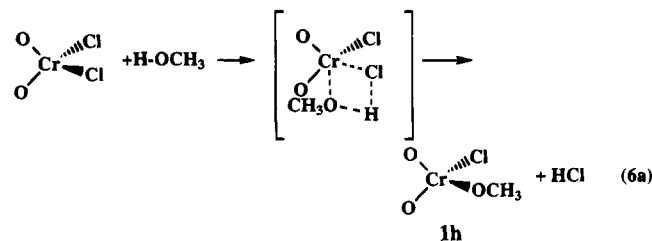
	bond strength <sup>c</sup>	$\Delta E_{\text{int}}^b$	$\Delta E_{\text{steric}}$	$\Delta E_{\text{orb-int}}$	$\Delta E_{\text{prep}}$
$\text{Cl}_2\text{Cr}(\text{O})(\text{OH})\text{-OCH}_3$	33	-57	73	-130	$21^d + 3^e$
$\text{Cl}_2\text{Cr}(\text{O})(\text{OH})\text{-CH}_2\text{OH}$	11	-40	54	-94	$24^d + 5^e$
$\text{Cl}_2\text{Cr}(\text{O})\text{-OH}$	82	-98	74	-172	$16^d$

<sup>a</sup> Energies in kcal/mol. <sup>b</sup>  $\Delta E_{\text{int}} = \Delta E_{\text{steric}} + \Delta E_{\text{orb-int}}$ . <sup>c</sup> Bond strength =  $-\Delta E_{\text{int}} + \Delta E_{\text{prep}}$ . <sup>d</sup> Relaxation energy metal fragment. <sup>e</sup> Relaxation energy for  $\text{OCH}_3$  and  $\text{CH}_2\text{OH}$ .

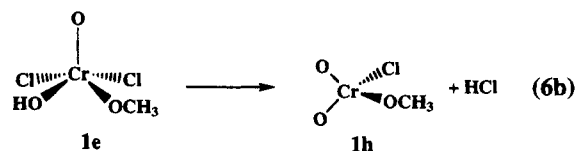
decomposition analysis of eq 2. The ETS results are shown in Table 3 where we also include a decomposition of the strong  $\text{Cl}_2\text{Cr}(\text{O})\text{-OH}$  bond for comparison. It is clear that the stabilizing  $-\Delta E_{\text{orb-int}}$  contribution to the  $\text{Cr-OCH}_3$  and  $\text{Cr-CH}_2\text{OH}$  bond energies is much smaller than the contribution from  $-\Delta E_{\text{orb-int}}$  to the  $\text{Cl}_2\text{Cr}(\text{O})\text{-OH}$  bond energy. Essentially, fewer d-orbitals are of the right symmetry to provide sizable  $\sigma$ -overlaps with the four equatorial ligands in **5a** and **6a** than with the four ligands in the tetrahedral  $\text{Cl}_2\text{Cr}(\text{O})\text{OH}$  complex. Another factor is the preparation energy  $\Delta E_{\text{prep}}$ . The  $\text{Cl}_2\text{Cr}(\text{O})(\text{OH})$  frameworks in **5a** and **6a** are distorted considerably in comparison to the framework, **1b**, of the isolated  $\text{Cl}_2\text{Cr}(\text{O})(\text{OH})$  complex in order to accommodate a fifth ligand. The distortion energy  $\Delta E_{\text{prep}}$  amounts to 27 kcal/mol and 29 kcal/mol for **5a** and **6a**, respectively.

The present set of calculations indicate that the oxidation of methanol by  $\text{CrCl}_2\text{O}_2$  could take place by O-H activation in the form of a  $[2\pi + 2\sigma]$  addition of the O-H bond to the Cr-O linkage. The routes based on C-H activation by hydrogen abstraction, **R2** of Scheme 1, or  $[2\pi + 2\sigma]$  addition of the C-H bond to the Cr-O linkage, **S2** of Scheme 2, are not likely with endothermicities of 29 kcal/mol and 34 kcal/mol, respectively. However, the paths based on C-H activation might be of importance in the oxidation of hydrocarbons by  $\text{CrCl}_2\text{O}_2$ .

One could imagine several alternative routes leading to methanol oxidation. The O-H bond might add to the Cr-Cl rather than the Cr-O linkage in a  $[2\sigma + 2\sigma]$   $\sigma$ -bond metathesis reaction leading to HCl and the methoxy complex **1h** as shown in eq 6a. This process is feasible

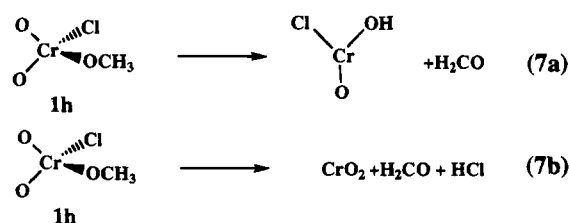


with a reaction enthalpy of 6 kcal/mol. The methoxy complex **1h** could alternatively be formed from **1e** by a hydrogen transfer between the methoxy group and an oxygen in one of the Cr-O multiple bonds as shown in eq 6b. The last step is exothermic by 8 kcal/mol.



The methoxy complex **1h** can decompose to formaldehyde by a transfer of hydrogen according to eq 7a or

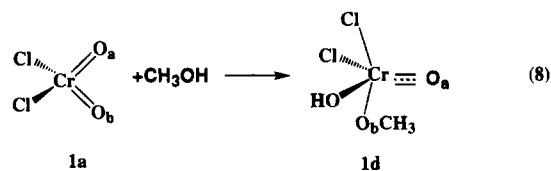
by the elimination of HCl according to eq 7b. We



calculate both of these steps to be rather endothermic with 30 kcal/mol for eq 7a and 92 kcal/mol for eq 7b. Mechanisms based on HCl elimination have some merits since Osborne<sup>8b</sup> et al. have observed the formation of methoxy complexes such as **1h**. However, it appears that the available routes to aldehyde from **1h** are too endothermic. The high endothermicity is partly due to the fact that the Cr-OCH<sub>3</sub> bond in the four coordinated methoxy-complex **1h** is much stronger than the Cr-OCH<sub>3</sub> bond in the five coordinated species **1e**. We have also examined routes involving C-H activation and HCl elimination. These routes are even less favorable.

Rappé and Goddard<sup>5</sup> have carried out GVB calculations on the energetics of steps **S1** and **S2** using ethanol as the substrate. They found that the formation of the ethoxy complex analogous to **5a** is endothermic by 5 kcal/mol whereas the formation of the ethylhydroxy species similar to **6a** is exothermic by 2 kcal/mol. In addition Rappé and Goddard found that the homolytic cleavage of the Cr-OC<sub>2</sub>H<sub>5</sub> bond was exothermic by 4 kcal/mol whereas the homolytic Cr-CHOHCH<sub>3</sub> bond cleavage was thermo-neutral. The results obtained by Rappé and Goddard differ from those reported here. However, it seems that the calculated energetics in the GVB study was based on assumed structures rather than optimized geometries as in the present investigation.

**D. Strengths of Chromium-Oxygen Double and Triple Bonds.** Rappé and Goddard<sup>5</sup> have pointed out that  $[2\sigma + 2\pi]$  addition reactions of the type shown in eq 8 are helped by significant changes in the chromium-oxygen bond orders. They emphasised the importance



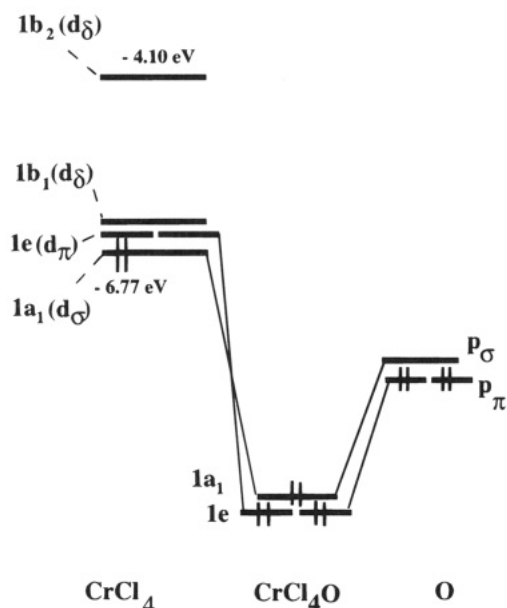
of the spectator oxo group in  $\text{CrCl}_2\text{O}_2$  and the difference between dioxo and monooxo bonds. Rappé and Goddard found from an analysis of the GVB wavefunctions that the Cr-oxo bonds in the dioxo complex  $\text{CrCl}_2\text{O}_2$  are double bonds, **1b**, like C=O bonds in carbon dioxide while the Cr-oxo bond in the monooxo methoxy complex, **1d**, is a strong triple bond like the C≡O bond in carbon monoxide. The  $\pi$ -contributions to the bond strengths of the Cr=O double bond in **1a** and the Cr≡O triple bond in **1d** are 51 and 82 kcal/mol, respectively, according to the bond strength calculation scheme used by Rappé and Goddard. This difference could serve as a driving force for addition processes of the type shown in eq 8.

We have carried out calculations on the  $\text{Cl}_2(\text{O})\text{Cr-O}$  and  $\text{Cl}_4\text{Cr-O}$  bond energies with the help of the ETS

**Table 4.** Cr-O Bond Strengths and Their Decompositions<sup>a</sup>

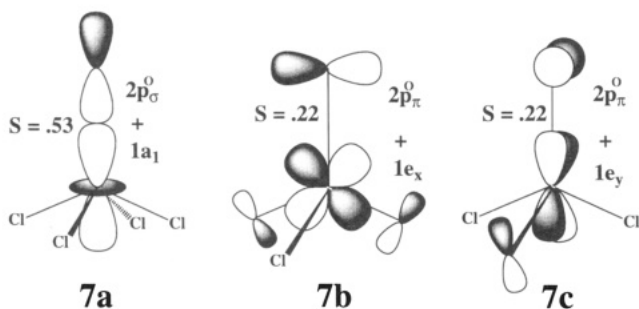
	bond strength	$\Delta E_{\text{int}}$	$\Delta E_{\text{steric}}$	$\Delta E_{\text{orb-int}}$	$\Delta E_{\text{prep}}$	$\Delta E_{\text{prom}}$
CrCl <sub>4</sub> -O	113	-174	166	-340	22	30 <sup>d</sup> + 9 <sup>e</sup>
CrCl <sub>2</sub> (O)-O	123	-176	170	-346	12	30 <sup>d</sup> + 11 <sup>f</sup>

<sup>a</sup> Energies in kcal/mol. <sup>b</sup>  $\Delta E_{\text{int}} = \Delta E_{\text{steric}} + \Delta E_{\text{orb-int}}$ . <sup>c</sup> Bond strength =  $-\Delta E_{\text{int}} + \Delta E_{\text{prep}} + \Delta E_{\text{prom}}$ . <sup>d</sup> Promotion energy from the O(<sup>3</sup>P) ground state to the O(1s<sup>2</sup>2s<sup>2</sup>2p<sup>4</sup>) oxygen valence configuration. <sup>e</sup> Promotion energy from the triplet ground state to the singlet valence state of CrCl<sub>4</sub>. <sup>f</sup> Promotion energy from the triplet ground state to the singlet valence state of CrCl<sub>2</sub>O.

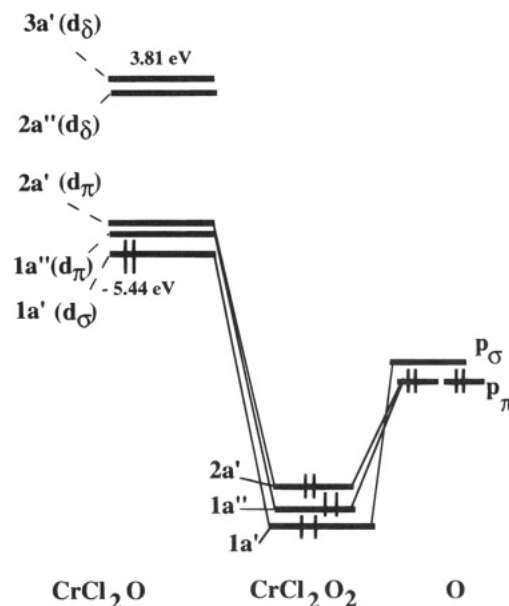
**Figure 4.** Diagram for the interaction between the singlet fragments O and CrCl<sub>4</sub> in CrCl<sub>4</sub>O.

method and full geometry optimization, Table 4. We find that the Cr=O bond strengths for CrCl<sub>2</sub>O<sub>2</sub> and CrCl<sub>4</sub>O are 123 and 113 kcal/mol, respectively. The bond energies are with respect to the oxygen O(<sup>3</sup>P)-ground states and the triplet ground states of the metal fragments. These values are comparable to the experimental<sup>34</sup> Cr-O bond strength of 124 kcal/mol for the diatomic CrO molecule. Thus, our calculations would indicate that the Cl<sub>2</sub>(O)Cr-O bond in **1a** actually is stronger than the Cr-O bond of Cl<sub>4</sub>CrO, in contrast to the arguments put forward by Rappé and Goddard.

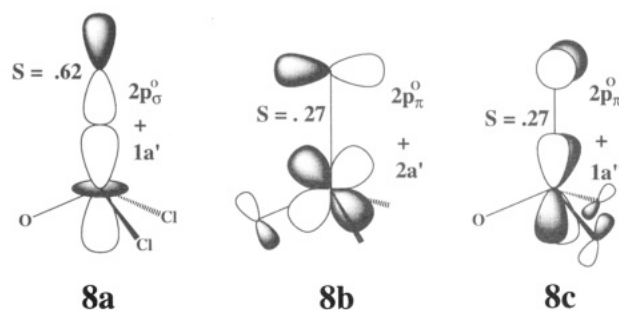
One can view the Cr-O bond in CrCl<sub>4</sub>O as formed from the interaction between the two singlet fragments O[<sup>1</sup>p<sub>π</sub><sup>4</sup>] and CrCl<sub>4</sub> [1a<sub>1</sub><sup>2</sup>], see Figure 4. Both fragments have a set of two π-orbitals and one σ-orbital which can form one σ-bond, **7a**, and two π-bonds, **7b–7c**. This simple



orbital analysis conforms well with the bond order of three assigned by Rappé and Goddard to the Cr-O

**Figure 5.** Diagram for the interaction between the singlet fragments O and CrCl<sub>2</sub>O in CrCl<sub>2</sub>O<sub>2</sub>.

linkage in Cl<sub>4</sub>CrO. The same authors assigned an order of two to the Cr-O bond in CrCl<sub>2</sub>O<sub>2</sub>. However, if one view the Cr-O bond in CrCl<sub>2</sub>O<sub>2</sub> as formed from the interaction between the two singlet fragments O[<sup>1</sup>p<sub>π</sub><sup>4</sup>] and CrOCl<sub>2</sub>[(1a')<sup>2</sup>], see Figure 5, a total of three bonding orbitals, **8a** (σ), **8b** (π) and **8c** (π), are formed, just as in the case of Cl<sub>4</sub>CrO. Thus, it is not easy from the simple



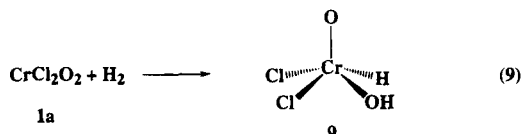
bonding analyses of the Cr-O linkage in CrCl<sub>2</sub>O<sub>2</sub> to assign a bond order of two. In fact our analysis would indicate that the Cr-O bonds qualitatively are the same in Cl<sub>4</sub>CrO and CrCl<sub>2</sub>O<sub>2</sub> with one σ- and two π-components. We don't feel that it is of much use to assign bond orders to the Cr-O links in Cl<sub>4</sub>CrO and CrCl<sub>2</sub>O<sub>2</sub>. It is more informative to look at the Cr-O bonding interactions, Figures 4 and 5, if one wants to assess the relative strengths of the two Cr-O links.

The ETS decomposition finds the steric repulsion,  $\Delta E_{\text{steric}}$ , as well as the orbital interaction,  $\Delta E_{\text{orb-int}}$ , to be quite similar for the Cl<sub>2</sub>(O)Cr-O and Cl<sub>4</sub>Cr-O bonds, Table 4, with identical values for the sum,  $\Delta E_{\text{int}}$ . We find that the ratio between the contribution from the σ-bond components **7a**, **8a** and the π-bond components, **7b+7c/8b+8c** to  $\Delta E_{\text{orb-int}}$  is roughly 5 to 1 in both **1a** and **1d**. The only difference between **1a** and **1d** is in  $\Delta E_{\text{prep}}$ , which is 10 kcal/mol larger for CrCl<sub>4</sub>O than for CrCl<sub>2</sub>O<sub>2</sub>. The larger preparation energy for CrCl<sub>4</sub>O is related to the substantial geometry change in the CrCl<sub>4</sub> fragments as it takes up its shape in the SP based Cl<sub>4</sub>-CrO complex with a coordinatively saturated chromium center.

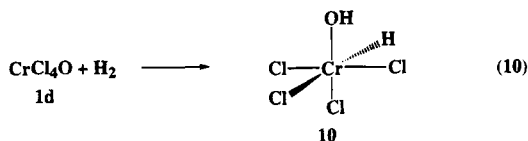
(34) Glidewell, C. *Inorg. Chim. Acta* **1977**, *24*, 149.

Ogden and coworkers have been able to determine the Cr-O stretching frequencies in  $\text{CrF}_4\text{O}^{33}$  and  $\text{CrF}_2\text{O}_2^{35}$  as 1028 and 1016(s)/1006(a)  $\text{cm}^{-1}$ , respectively, by low temperature matrix isolation techniques. This would indicate that the Cr-O bond strengths are similar in the two compounds. Sanderson has developed a scheme to calculate bond energies based on experimental heats of formation and electronegativities.<sup>36</sup> The W=O bond strength obtained by Sanderson for  $\text{WCl}_4\text{O}$  and  $\text{WCl}_2\text{O}_2$  in the gas-phase are 195.4 and 194.8 kcal/mol, respectively, again indicating that the two types of bonds are quite similar in strength.

Goddard<sup>5</sup> and Rappé found from GVB calculations that the hydrogenation of **1a**



is exothermic with  $\Delta G = -7$  kcal/mol, whereas the hydrogenation of **1d**



is endothermic with  $\Delta G = 71$  kcal/mol. They attributed this difference to a stronger Cr-O bond in **1d**. We have calculated the electronic reaction enthalpies,  $\Delta E$ , for the two reactions, and find them to be very similar with  $\Delta E_9 = -18.3$  kcal/mol and  $\Delta E_{10} = -21.5$  kcal/mol. Again our calculations do not support the notion that the Cr-O bond in **1d** should be stronger than the Cr-O bond in **1a**. We should note that the two Cr-Cl bond trans to hydrogen and OH are very long, 2.3 Å, and that  $\text{CrCl}_2(\text{OH})\text{H} + \text{Cl}_2$  only is 2 kcal/mol above **10** in energy.

(35) Hope, E. G.; Levason, W.; Ogden, J. S.; Tajik, M.; Turff, J. W. *J. Chem. Soc. Dalton Trans.* **1986**, 1587.

(36) Sanderson, R. T. *Inorg. Chem.* **1986**, *25*, 3518.

#### IV. Concluding Remarks

We have carried out DFT based calculations on the activation of the O-H and C-H bonds in methanol by  $\text{CrCl}_2\text{O}_2$ . It is shown that activation by hydrogen abstraction, Scheme 1, only is feasible for the weaker C-H bond whereas both bonds can be activated by a  $[2\sigma+2\pi]$  addition to Cr-O, Scheme 2. It is further suggested that oxidation of methanol by  $\text{CrCl}_2\text{O}_2$  involves O-H addition to the Cr-O bond, **R1** of Scheme 2, followed by hydrogen transfer from the methoxy-group to the oxygen of the remaining Cr-O multiple bond, **R3** of Scheme 2.

The strength of the  $\text{Cl}_2(\text{O})\text{CrO-H}$  bond is crucial for the C-H and O-H activation. The  $\text{Cl}_2(\text{O})\text{CrO-H}$  bond energy has been compared to the O-H bond strengths in other hydroxy metal complexes. The following values were obtained:  $D(\text{O}_2\text{CrO-H}) = 81$  kcal/mol;  $D(\text{Cl}_2(\text{O})\text{CrO-H}) = 66$  kcal/mol;  $D(\text{O}_2\text{OHCrO}^-\text{-H}) = 56$  kcal/mol;  $D(\text{O}_3\text{-MnO}^-\text{-H}) = 63$  kcal/mol and  $D(\text{O}_3\text{RuO}^-\text{-H}) = 64$  kcal/mol. The relative strength of the O-H bonds has been correlated to the amount of anti-bonding character in the d-based orbital holding the single electron in the  $d^1$  hydroxy complexes.

We have examined the strengths of the Cr-O bonds in di- and mono-oxo compounds. The Cr-O bond energies in  $\text{CrCl}_2\text{O}_2$  and  $\text{CrCl}_4\text{O}$  are 123 and 113 kcal/mol, respectively. An analysis further indicates that the Cr-O bonds qualitatively are the same in  $\text{Cl}_4\text{CrO}$  and  $\text{CrCl}_2\text{O}_2$  with one  $\sigma$ - and two  $\pi$ -components.

**Acknowledgment.** We thank the Natural Sciences and Engineering Research Council of Canada (NSERC) for financial support. J.L. thanks NSERC for an International Fellowship. Professor J. M. Mayer (University of Washington) has contributed to this work with many suggestions. This work was supported in part by the donors of the Petroleum Research Fund, administered by the American Chemical Society (ACS-PRF No. 27023-AC3). The University of Calgary is acknowledged for access to the IBM-6000/RISC facilities.

OM940566U



# Trends in Structure and Bonding of Fischer Type Chromium Carbenes and Silylenes. A Density Functional Study

Heiko Jacobsen and Tom Ziegler\*

Department of Chemistry, University of Calgary, 2500 University Drive N.W.,  
Calgary, Alberta, Canada T2N 1N4

Received July 11, 1994<sup>⊗</sup>

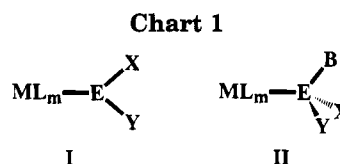
Density functional calculations were performed on a variety of carbene and silylene complexes involving the chromium pentacarbonyl fragment  $(\text{CO})_5\text{Cr}=\text{ER}_2$ , with  $\text{ER}_2 = \text{CH}_2$ ,  $\text{CF}_2$ ,  $\text{CCl}_2$ ,  $\text{CMe}_2$ ,  $\text{CMe}(\text{OMe})$ ,  $\text{SiH}_2$ ,  $\text{SiF}_2$ ,  $\text{SiCl}_2$ ,  $\text{SiMe}_2$ , and  $\text{SiMe}(\text{OMe})$ . Further, a calculation on the base-stabilized silylene complex  $(\text{CO})_5\text{Cr}=\text{Si}(\text{OPH}_3)\text{Cl}_2$  has been included. A bond analysis reveals that, compared with carbene compounds, silylene complexes form only weak  $\pi$  bonds with the metal center. Consequences for the coordination chemistry of silylene complexes as well as their reaction chemistry are discussed.

## Introduction

The concept of a double bond between transition metals and carbon constitutes one of the important elements in the field of organometallic chemistry. The notion of a metal–carbon double bond was first brought forward by Fischer and Maasböl<sup>1</sup> in 1964. They suggested that the product of the reaction between  $\text{LiMe}$  and  $\text{W}(\text{CO})_6$ , followed by protonation and subsequent treatment with  $\text{CH}_2\text{N}_2$ , should be formulated as  $(\text{CO})_5\text{W}=\text{CMe}(\text{OMe})$ . The chemistry of transition metal carbenes<sup>2</sup> developed rapidly, and these compounds have been established as valuable species in organic syntheses<sup>3</sup> as well as in catalytic processes.<sup>4</sup>

The field of the higher homologues of Fischer carbenes was pioneered by Marks<sup>5</sup> in the early seventies. Up to now, a larger number of germylene, stannylene, and even plumbylene systems have been structurally characterized.<sup>6,7</sup> Several modes of complexation are observed, two of which are displayed in Chart 1. We follow the notation of Petz<sup>6a</sup> and denote the structures as type I and type II complexes, respectively.

In these arrangements,  $\text{ML}_m$  represents the transition metal fragment, E is a group XIV element, X and Y represent  $\sigma$ -bonded substituents, and B stands for a neutral Lewis base molecule. Structures of type I complexes with  $\text{E} = \text{Ge}$ ,  $\text{Sn}$  reveal a trigonal planar coordination around the divalent E center in the solid state. The M–E bond lengths are noticeably shortened compared to known M–E single bonds. An example of analogous type I and type II stannylene complexes<sup>6a</sup>



indicates an increase of the M–E bond length by about 10 pm under complexation of the Lewis base. For the type II compound  $(t\text{-C}_4\text{H}_9)_2\text{SnCr}(\text{CO})_5\text{-C}_5\text{H}_5\text{N}$ , Brice and Cotton<sup>8</sup> describe the coordination around the tin center as an intermediate between a planar  $\text{SnCrC}_2$  group with pyridine approaching perpendicularly and a tetrahedral  $\text{SnCrC}_2\text{N}$  group.

In contrast to germylene and its higher analogues, the area of transition metal silylene chemistry has been developed rather recently and represents a field of ongoing research activity.<sup>9</sup> In 1987, the cationic<sup>10</sup> and neutral<sup>11</sup> type II coordination compounds of silylenes were discovered. In the following years, Zybilla and co-workers prepared a broad variety of base-stabilized silylene type II complexes<sup>12</sup> with the low-valent metal fragments  $\text{Fe}(\text{CO})_4$  and  $\text{Cr}(\text{CO})_5$ . All these complexes are structurally well characterized, and for several of the compounds the solid state structures have been determined. Also a few type I silylene complexes have been identified.<sup>12b,13</sup> Very recently, the first structure of a cationic type I silylene complex has been reported.<sup>13b</sup>

The reaction chemistry of the heavier carbene analogues is still in an early process of development<sup>6,9</sup> and not too many transformations involving silylene, germylene, and stannylene complexes are known in the literature. Most of the reactions deal with the modification of the  $\text{E}(\text{B})\text{XY}$  unit of type II complexes. However, Zybilla and co-workers reported the interesting Sila–

<sup>⊗</sup> Abstract published in *Advance ACS Abstracts*, November 15, 1994.

(1) Fischer, E. O.; Maasböl, A. *Angew. Chem., Int. Ed. Engl.* **1964**, *3*, 580.

(2) Dötz, K. H.; Fischer, H.; Hofmann, P.; Kreissl, F. R.; Schubert, U.; Weiss, K. *Transition Metal Carbene Complexes*; Verlag Chemie: Weinheim, Germany, 1983.

(3) Dötz, K. H. *Pure Appl. Chem.* **1983**, *55*, 1689. (b) Dötz, K. H. *Angew. Chem., Int. Ed. Engl.* **1984**, *23*, 587. (c) Brookhart, M.; Studabaker, W. B. *Chem. Rev.* **1987**, *87*, 411. (d) Hegedus, L. S. *Pure Appl. Chem.* **1990**, *62*, 691. (e) Schmalz, H. G. *Angew. Chem., Int. Ed. Engl.* **1994**, *33*, 303.

(4) Grubbs, R. H. In *Comprehensive Organometallic Chemistry*; Wilkinson, G., Stone, F. G. A., Abel, E. W., Eds.; Pergamon Press: Oxford, U.K., 1982; Vol. 8.

(5) Marks, T. J. *J. Am. Chem. Soc.* **1971**, *93*, 7090.

(6) (a) Petz, W. *Chem. Rev.* **1986**, *86*, 1019. (b) Lappert, M. S.; Rowe, R. S. *Coord. Chem. Rev.* **1990**, *100*, 267.

(7) Tokitoh, N.; Manmaru, K.; Okazaki, R. *Organometallics* **1994**, *13*, 167.

(8) Brice, M. D.; Cotton, F. A. *J. Am. Chem. Soc.* **1973**, *95*, 4529.

(9) Zybilla, C. *Top. Curr. Chem.* **1991**, *160*, 1.

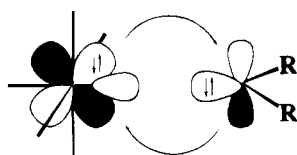
(10) Straus, D. A.; Tilley, T. D.; Rheingold, A. L.; Geib, S. J. *J. Am. Chem. Soc.* **1987**, *109*, 5872.

(11) Zybilla, C.; Müller, G. *Angew. Chem., Int. Ed. Engl.* **1987**, *26*, 669.

(12) (a) Zybilla, C.; Müller, G. *Organometallics* **1988**, *7*, 1368. (b) Leis, C.; Wilkinson, D. L.; Handwerker, H.; Zybilla, C.; Müller, G. *Organometallics* **1992**, *11*, 514. (c) Handwerker, H.; Paul, M.; Riede, J.; Zybilla, C. *J. Organomet. Chem.* **1993**, *459*, 151.

(13) (a) Leis, C.; Lachmann, H.; Müller, G.; Zybilla, C. *Polyhedron* **1991**, *10*, 1163. (b) Grumbine, S. K.; Tilley, T. D.; Arnold, F. P.; Rheingold, A. L. *J. Am. Chem. Soc.* **1994**, *116*, 5495.

Scheme 1



Wittig reaction<sup>12b</sup> of  $(\text{CO})_5\text{Cr}=\text{SiMe}_2$  with dimethyl carbonate, yielding  $(\text{CO})_5\text{Cr}=\text{C}(\text{OMe})_2$  and hexamethyltrisiloxane,  $[\text{Me}_2\text{SiO}]_3$ .

Calculations on Fischer type carbenes possessing a fully saturated coordination sphere provide a formidable task for computational chemistry. The first computations reported for the complexes  $(\text{CO})_5\text{Cr}=\text{CXY}$  ( $\text{X} = \text{OMe}, \text{NH}_2, \text{Y} = \text{Me}, \text{OEt}, \text{Ph}$ ;  $\text{X} = \text{NMe}_2, \text{Y} = \text{Me}, \text{Ph}$ ;  $\text{X} = \text{SMe}, \text{Y} = \text{Me}$ ) have been performed using the Fenske–Hall method.<sup>14</sup> On the basis of the result of a population analysis, qualitative trends in  $\sigma$ -donor as well as  $\pi$ -acceptor contributions from the various ligands were evaluated. During the eighties, Fischer type complexes with transition metal carbonyl fragments became accessible for *ab initio* calculations. In 1981, Spangler<sup>15</sup> and co-workers reported the electronic structure and the optimized  $\text{Ni}=\text{CH}_2$  bond length of  $(\text{CO})_3\text{NiCH}_2$ . Two years later, Nakatsuji and co-workers<sup>16a</sup> presented studies on the Fischer type compounds  $(\text{CO})_5\text{Cr}=\text{CMe}(\text{OMe})$  and  $(\text{CO})_4\text{Fe}=\text{CMe}(\text{OMe})$ , providing  $\text{M}=\text{C}$  bond energies and optimized  $\text{M}=\text{C}$  bond distances. These authors also investigated the silylene compound<sup>16b</sup>  $\text{Cr}(\text{CO})_5\text{SiH}(\text{OH})$ , demonstrating the possible existence of a transition metal silylene complex. In their classical work on transition metal carbenes, Taylor and Hall<sup>17</sup> made an essential contribution to the understanding of the nature of the bond in Fischer carbenes. The metal–carbon double bond is best described as  $\sigma/\pi$  dative interactions between two singlet fragments, as shown in Scheme 1. Recently, Márquez and Fernández Sanz<sup>18</sup> presented fully optimized SCF geometries of the molybdenum complexes  $(\text{CO})_5\text{Mo}=\text{EH}_2$  ( $\text{E} = \text{C}, \text{Si}, \text{Ge}, \text{Sn}$ ). They also employed the CASSCF method to get accurate values for the  $\text{Mo}=\text{E}$  bond distances and bond energies. Furthermore, MNDO calculations on chromium-based Fischer-type complexes of the type  $(\text{CO})_5\text{Cr}=\text{EX}_2$  ( $\text{E} = \text{C}, \text{Si}, \text{Ge}, \text{Sn}, \text{Pb}$ ;  $\text{X} = \text{H}, \text{Cl}$ ) have been performed by Abronin<sup>19</sup> and co-workers.

Approximate density functional theory (DFT) has been proven to be a powerful computational tool in determining the structures and energetics of transition metal complexes.<sup>20</sup> Thus, DFT seems to be the method of choice for careful investigation of the structures and bonding in Fischer type complexes. In connection with the generalized transition method, accurate total bond-

ing energies<sup>21,22</sup> are available, and the bond energy can be analyzed in terms of steric as well as orbital interactions.<sup>23</sup> Our studies were prompted not only by the recent developments in the field of silylene chemistry<sup>9–13</sup> but also by the continued interest in an understanding of the physical properties of Fischer carbenes.<sup>24</sup> In our first effort,<sup>25a</sup> we investigated the role of the transition metal  $\text{M}$  as well as of the main group element  $\text{E}$  on the bonding in complexes of the type  $(\text{CO})_5\text{M}=\text{EH}_2$ . We further discussed the influence of nonlocal corrections and relativistic effects on geometries and bond energies of carbene complexes,<sup>25b</sup> in order to judge the quality of our theoretical model.

The present work deals with the influence of the modification of the  $\text{R}$  substituent in  $\text{ER}_2$  carbene and silylene systems. In contrast to the early Fenske–Hall studies, we will base our selection of ligands on experimentally known silylene ligands rather than on typical Fischer type carbenes. We further present calculations on a “real life” Fischer carbene. It is still an interesting question how well DFT is able to handle the molecular structures of these challenging and rather complex molecules. Finally, we investigate one silylene type II compound. To our knowledge, so far no theoretical studies have been reported on this type of complexes. We hope to provide new insight into the different coordination as well as reaction chemistry of silylene complexes compared to their carbon analogues.

### Computational Details

The calculations in this work are based on approximate density functional theory within the local density approximation<sup>26</sup> (LDA) in the parametrization of Vosko, Wilk, and Nusair.<sup>27</sup> The exchange factor,  $\alpha_{\text{ex}}$ , was given the usual value of  $2/3$ . Bond energies were evaluated by adding Becke's nonlocal exchange correction<sup>28</sup> as well as Perdew's inhomogeneous gradient correction for correlation<sup>29</sup> as a perturbation (LDA/NL). In a more sophisticated approach, the before mentioned corrections were added self-consistently<sup>30</sup> (NL–SCF).

We utilized the AMOL program package for density functional calculations, which was developed by Baerends<sup>31</sup> and co-workers. The numerical integration scheme employed was that of te Velde<sup>32</sup> and co-workers. A triple  $\zeta$ -STO basis<sup>33</sup> was used to describe the  $ns, np, nd, (n+1)s$ , and  $(n+1)p$  shells of

(14) (a) Block, T. F.; Fenske, R. F.; Casey, C. P. *J. Am. Chem. Soc.* **1976**, *98*, 441. (b) Block, T. F.; Fenske, R. F. *J. Organomet. Chem.* **1977**, *139*, 235.

(15) Spangler, D.; Wendoloski, J. J.; Dupuis, M.; Chen, M. M. L.; Schaefer, H. F., III. *J. Am. Chem. Soc.* **1981**, *103*, 3985.

(16) (a) Nakatsuji, H.; Ushio, J.; Han, S.; Yonezawa, T. *J. Am. Chem. Soc.* **1983**, *105*, 426. (b) Nakatsuji, H.; Ushio, J.; Yonezawa, T. *J. Organomet. Chem.* **1983**, *258*, C1.

(17) Taylor, T. E.; Hall, M. B. *J. Am. Chem. Soc.* **1984**, *106*, 1576.

(18) Márquez, A.; Fernández Sanz, J. *J. Am. Chem. Soc.* **1992**, *114*, 2903.

(19) Abronin, I. A.; Avdyuhina, N. A.; Morozova, L. V.; Magomedov, G. K.-I. *J. Mol. Struct.* **1991**, *228*, 19.

(20) (a) Ziegler, T. *Pure Appl. Chem.* **1991**, *28*, 1271. (b) Ziegler, T. *Chem. Rev.* **1991**, *91*, 651.

(21) Ziegler, T.; Rauk, A.; Baerends, E. J. *Theor. Chim. Acta* **1977**, *43*, 261.

(22) Ziegler, T.; Rauk, A. *Theor. Chim. Acta* **1977**, *46*, 1.

(23) (a) Baerends, E. J.; Rozendaal, A. *NATO ASI* **1986**, *C176*, 159.

(b) Ziegler, T. *NATO ASI* **1991**, *C378*, 367.

(24) (a) Gandler, J. P.; Bernasconi, C. F. *Organometallics* **1989**, *8*, 2282. (b) Bernasconi, C. F.; Stronach, M. W. *J. Am. Chem. Soc.* **1993**, *115*, 1341. (c) Bernasconi, C. F.; Sun, W. *J. Am. Chem. Soc.* **1993**, *115*, 12526. (d) Bernasconi, C. F.; Flores, F. X.; Gandler, J. R.; Leyes, A. E. *Organometallics* **1994**, *13*, 2186.

(25) (a) Jacobsen, H.; Ziegler, T. *Inorg. Chem.*, submitted for publication. (b) Jacobsen, H.; Schreckenbach, G.; Ziegler, T. *J. Phys. Chem.* **1994**, *98*, 11406.

(26) (a) Gunnarsson, O.; Lundquist, I. *Phys. Rev.* **1974**, *B10*, 1319.

(b) Gunnarsson, O.; Lundquist, I. *Phys. Rev.* **1976**, *B13*, 4274.

(27) Vosko, S. J.; Wilk, M.; Nusair, M. *Can. J. Phys.* **1980**, *58*, 1200.

(28) (a) Becke, A. *J. Chem. Phys.* **1986**, *84*, 4524. (b) Becke, A. *J. Chem. Phys.* **1988**, *88*, 1053. (c) Becke, A. *Phys. Rev.* **1988**, *A38*, 3098.

(29) (a) Perdew, J. P. *Phys. Rev.* **1986**, *B33*, 8822. (b) Perdew, J. P. *Phys. Rev.* **1986**, *B34*, 7406.

(30) (a) Fan, L.; Ziegler, T. *J. Chem. Phys.* **1991**, *94*, 6057. (b) Fan, L. Ph.D. Thesis, University of Calgary, 1992.

(31) (a) Baerends, E. J.; Ellis, D. E.; Ros, P. E. *Chem. Phys.* **1973**, *2*, 41. (b) Baerends, E. J. Ph.D. Thesis, Vrije Universiteit Amsterdam, 1975.

(32) teVelde, G.; Baerends, E. J. *J. Comp. Phys.* **1992**, *99*, 84.

(33) (a) Snijders, G. J.; Baerends, E. J. Vernoijis, P. *At. Nucl. Data Tabl.* **1982**, *26*, 483. (b) Vernoijis, P.; Snijders, G. J.; Baerends, E. J. *Slater Type Basis Functions for the Whole Periodic Table*; Internal Report; Vrije Universiteit: Amsterdam, 1981.

Cr. For H, a double  $\zeta$ -STO basis<sup>33</sup> was extended by one 2p-STO polarization function. The *ns* and *np* orbitals of the remaining main group elements were described by a double  $\zeta$ -STO basis,<sup>33</sup> augmented by one (*n* + 1)d-STO polarization function for second row elements, and one *nd*-STO polarization function for higher row elements. Electrons in lower shells were treated within the frozen core approximation as outlined by Baerends and co-workers. An auxiliary set<sup>34</sup> of *s*, *p*, *d*, *f*, and *g* type STO functions, centered on all nuclei, was used to fit the molecular density as well as present Coulomb and exchange potentials accurately in each SCF cycle. The geometry optimization procedure was based on a method developed by Versluis and Ziegler.<sup>34</sup>

## Results and Discussion

We will begin our discussion with a short introduction to our method of bond energy decomposition. Since we already presented a detailed account of the bond analysis for Fischer complexes,<sup>25a</sup> we restrict ourselves to a concise description.

We analyze the Cr=E bond energy in (CO)<sub>5</sub>Cr=ER<sub>2</sub> complexes by considering the bond-forming reaction between the chromium pentacarbonyl fragment and the ER<sub>2</sub> moiety:



The energy associated with reaction 1 is called the bond-snapping energy BE<sub>snap</sub>. It can be decomposed into two main components, namely the steric repulsion term  $\Delta E^0$  and the electronic interaction term  $\Delta E_{\text{int}}$ :

$$\text{BE}_{\text{snap}} = -[\Delta E^0 + \Delta E_{\text{int}}] \quad (2)$$

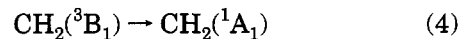
$\Delta E^0$  is in most cases dominated by the contribution of the so-called Pauli repulsion, which is directly related to the two-orbital three or four electron interactions between occupied orbitals on both fragments. Whereas  $\Delta E^0$  is mostly destabilizing in nature, the term  $\Delta E_{\text{int}}$  introduces the attractive orbital interactions between occupied and virtual orbitals on the two fragments. We will picture the bond as an interaction of two singlet fragments, as shown in Scheme 1. It has been argued<sup>25a</sup> that for carbene complexes with low-valent, late transition metals this bond description is most appropriate, even if the ER<sub>2</sub> ligand has a triplet ground state.

The bond energy BE is obtained when the bond-snapping energy is corrected by the preparation energy  $\Delta E_{\text{prep}}$ :

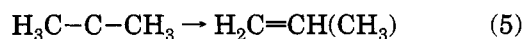
$$\text{BE} = \text{BE}_{\text{snap}} - \Delta E_{\text{prep}} \quad (3)$$

Since the equilibrium geometry of the fragments usually differs from their arrangement in the framework of the final molecule, a small geometric preparation energy is required to get the fragments ready for bonding interaction. Further, the fragments have to have the electronic valence configuration, necessary for formation of the bond. The (CO)<sub>5</sub>Cr fragment and most of the ER<sub>2</sub> ligands that we will encounter, namely CF<sub>2</sub>, CCl<sub>2</sub>, CMe(OMe), SiH<sub>2</sub>, SiF<sub>2</sub>, SiCl<sub>2</sub>, SiMe<sub>2</sub>, and SiMe(OMe), possess a singlet ground state and thus do not require an

electronic preparation. One of the exceptions is the methylene ligand, which needs to be electronically promoted:



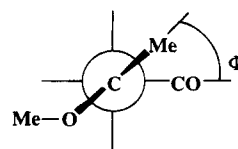
The triplet-singlet splitting of CH<sub>2</sub> which is associated with reaction 4 amounts to 38 kJ/mol.<sup>37</sup> Considering the (Me)<sub>2</sub>C ligand, we found that on the LDA/NL level of theory the triplet state is about 10 kJ/mol more stable than the singlet state. However, for this molecule one might further consider the following isomerization reaction:



A 1,2-H-shift transforms dimethylmethylene into methylethylene, a process which we have calculated to be favorable by 289 kJ/mol. This value is comparable with the intrinsic  $\pi$  bond strength in ethylene,  $D_{\pi}(\text{C}_2\text{H}_4) = 312$  kJ/mol.<sup>38</sup> It will depend on the definition of the reference state whether the Cr=C bond in (CO)<sub>5</sub>Cr=CMe<sub>2</sub> is to be considered as stable or not.

Martinho Simões and Beauchamp<sup>39</sup> differentiate between metal-ligand bond dissociation enthalpies and metal-ligand bond enthalpy terms. For the latter, the molecule dissociates into the starred fragments which have the same configuration as in the initial complex and which are not allowed to relax. However, only dissociation enthalpies are experimentally accessible, whereas the determination of the enthalpy terms requires the aid of calculations. They further argue that bond strengths are better described by bond enthalpy terms rather than by bond dissociation enthalpies. The concept of bond enthalpy terms is closely related to our bond snapping energy BE<sub>snap</sub>. The remaining differences due to zero point energy as well as to thermal corrections can be expected to be rather small. In the following, we will mainly use bond-snapping energies BE<sub>snap</sub> as a measure for M=E bond strengths, and we only occasionally refer to the corrected bond energies BE.

**Complexes (CO)<sub>5</sub>Cr=CMe(OMe) and (CO)<sub>5</sub>Cr=SiMe(OMe).** We have chosen (CO)<sub>5</sub>Cr=CMe(OMe) as the simplest model of a "real life" Fischer carbene complex. This compound was reported by Fischer and Maasböl<sup>40</sup> in 1967. We performed a full geometry optimization on the LDA as well as NL-SCF level of theory. Most crystal structures of Fischer carbenes show the ligand to adapt a staggered conformation *S* with respect to the transition metal.<sup>41</sup> We thus provided a starting geometry with a rotation angle  $\Phi = 45^\circ$ , as defined as follows:



Regarding the local orientation of the Me-C-OMe ligand, we have chosen a *trans* rather than a *cis* arrangement. This is in accord with the known structures of the closely related molecules (CO)<sub>5</sub>Cr=CMe(OEt)<sup>42a</sup> and (CO)<sub>5</sub>Cr=CPh(OMe).<sup>42b</sup> The optimized structures are displayed in **1a**, and all bond distances

(34) Krijn, J.; Baerends, E. J. *Fitfunctions in the HFS Method*, Internal Report; Vrije Universiteit: Amsterdam, 1984.

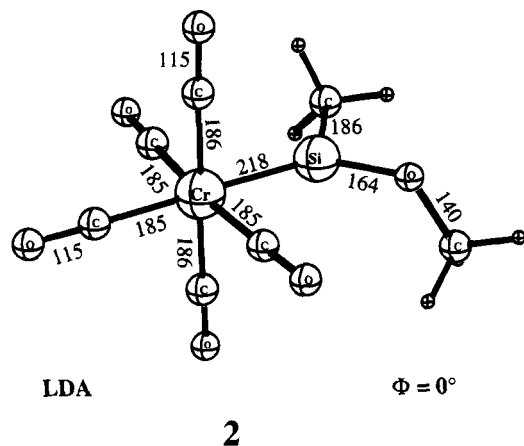
(35) Versluis, L.; Ziegler, T. *J. Chem. Phys.* **1988**, *88*, 322.

(36) Márquez, A.; Fernández Sanz, J. *J. Am. Chem. Soc.* **1992**, *114*, 10019.



the  $(\text{CO})_5\text{Cr}=\text{CMe}(\text{OMe})$  system,  $\text{BE}_{\text{snap}}(\text{LDA})$  value falls short by 12–13 kJ/mol, compared to  $\text{BE}_{\text{snap}}(\text{NL-SCF})$ .

The optimized LDA structure for  $(\text{CO})_5\text{Cr}=\text{SiMe}(\text{OMe})$  is displayed in **2**. We only observe minor changes



in the chromium pentacarbonyl fragment, compared to  $(\text{CO})_5\text{Cr}=\text{CMe}(\text{OMe})$ . It is of interest that for  $(\text{CO})_5\text{Cr}=\text{SiMe}(\text{OMe})$  the Cr–Si bond length is 2 pm shorter as compared to  $(\text{CO})_5\text{Cr}=\text{SiH}_2$ ,  $d_{\text{Cr-Si}} = 200$  pm. We will return to this point in the next section. The bond-snapping energy amounts to  $\text{BE}_{\text{snap}} = 260$  kJ/mol, with contributions from steric repulsion and orbital interaction as  $\Delta E^0 = 165$  kJ/mol and  $\Delta E_{\text{int}} = -425$  kJ/mol. Thus, the Cr=Si bond strength is only 40 kJ/mol weaker than the Cr=C analogue. Nakatsuji and co-workers<sup>16b</sup> have reported the Cr=Si bond to be 63 kJ/mol weaker than the corresponding Cr=C link. It is, however, not obvious why the reaction and coordination chemistry of silylene complexes is so significantly different from that of their carbene analogues. To get a better understanding of this problem, we will now study a variety of carbene and silylene ligands, and analyze the bonding according to  $\sigma$  and  $\pi$  bond contributions.

**Substituent Variation in  $(\text{CO})_5\text{Cr}=\text{CR}_2$  and  $(\text{CO})_5\text{Cr}=\text{SiR}_2$  Complexes.** We optimized the geometries of the Fischer type complexes  $(\text{CO})_5\text{Cr}=\text{ER}_2$ , with  $\text{ER}_2 = \text{CH}_2, \text{CF}_2, \text{CCl}_2, \text{CMe}_2, \text{SiH}_2, \text{SiF}_2,$  and  $\text{SiCl}_2$  and  $\text{SiMe}_2$ . The substituents methyl and chloride were chosen since corresponding type II silylene complexes with these ligands are experimentally known and structural characterized.<sup>12b</sup> We included the fluoride-substituted ligands since a variety of halocarbene complexes including  $\text{L}_n\text{M}=\text{CF}_2$  and  $\text{L}_n\text{M}=\text{CCl}_2$  have been studied.<sup>43</sup> The calculations were performed at the LDA level of theory with the  $\text{ER}_2$  ligand in an eclipsed conformation. Selected structural parameters and values for  $\Delta E^0$ ,  $\Delta E_{\text{int}}$ , and  $\text{BE}_{\text{snap}}$  are presented in Table 2.

Considering the Cr=E distances, we observe that the distances of the calculated carbene ligands vary over a range of 7 pm, whereas the largest difference of two silylene–metal bonds only amounts to 3 pm. We also note that all silylene ligands provide similar contributions in  $\Delta E^0$ , whereas for the carbene ligands a larger variation in  $\Delta E^0$  is found. We recall that the steric repulsion term is mainly determined by the influence of the Pauli repulsion term. Compared to the 1s core of carbon, silicon possesses an extended electronic core

**Table 2.** Selected Optimized Bond Distances and LDA/NL Bond Energies for Various  $(\text{CO})_5\text{Cr}=\text{ER}_2$  Systems

$\text{ER}_2$ for $(\text{CO})_5\text{Cr}=\text{ER}_2$	Bond distances <sup>a</sup>		bond energies <sup>b</sup>		
	$d(\text{Cr}=\text{E})$	$d(\text{Cr}-\text{CO})_{\text{ax}}$	$\Delta E^0$	$\Delta E_{\text{int}}$	$\text{BE}_{\text{snap}}$
$\text{CH}_2$	188	189	113	-469	356
$\text{CF}_2$	190	187	135	-348	213
$\text{CCl}_2$	193	188	141	-372	231
$\text{CMe}_2$	193	188	88	-390	302
$\text{SiH}_2$	220	186	157	-414	257
$\text{SiF}_2$	218	184	166	-353	187
$\text{SiCl}_2$	220	185	172	-360	188
$\text{SiMe}_2$	221	185	162	-439	277

<sup>a</sup> Distances in pm. <sup>b</sup> Energies in kJ/mol.

including p orbitals. Thus, for the  $\text{SiR}_2$  ligands the silicon center causes the major contribution to the term  $\Delta E^0$ . Small changes in the electronic effects then lead to small variations in the calculated Cr–Si bond length. For the carbene ligands, on the other hand, the substituents provide the major contribution to  $\Delta E^0$ . This is one of the reason for the variation in the calculated Cr=C bond lengths. The especially short Cr=CH<sub>2</sub> bond is also a result of electronic interaction, due to the fact that for the excited singlet methylene the acceptor orbital at carbon provides a better energetic match with the 3d donor orbitals of the metal fragment.<sup>25a</sup>

At first, it might be puzzling that the larger  $\text{CMe}_2$  ligand is associated with the smaller value for  $\Delta E^0$  (Table 2). However, one has to keep in mind that  $\Delta E^0$  also depends on the Cr=E separation. This structural parameter in turn is determined by the balance between  $\Delta E^0$  and  $\Delta E_{\text{int}}$ . The  $\text{CH}_2$  ligand undergoes a very strong electronic interaction with the  $\text{Cr}(\text{CO})_5$  fragment. Thus, shortening of the Cr=C bond effectively strengthens the Cr=C bond, with the enhanced electronic interaction overcoming the increase in  $\Delta E^0$ . The Cl-substituted  $\text{ER}_2$  ligands are associated with the largest value of  $\Delta E^0$ , since only Cl, compared to the other systems, has an extended eight electron core.

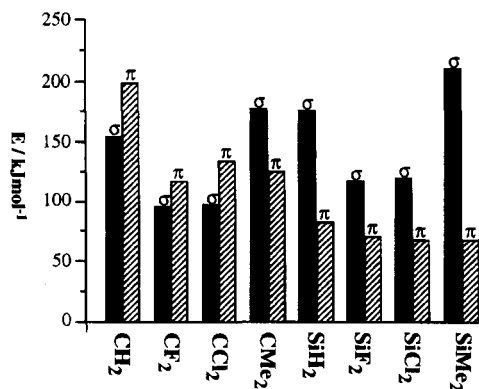
Another interesting structural parameter is the distance between the axial CO group and the chromium center. The LDA value for the Cr–C bond length in chromium hexacarbonyl amounts to 187 pm. Thus, for the carbene complexes one finds that the bond distance  $d_{(\text{Cr}-\text{CO})_{\text{ax}}}$  is slightly elongated, whereas for the silylene complexes this bond is slightly shortened compared to  $\text{Cr}(\text{CO})_6$ . This *trans* effect might be the first indicator for differences in bonding between  $\text{CR}_2$  and  $\text{SiR}_2$  ligands, suggesting that silylenes form weaker  $\pi$  bonds.

All ligands under investigation seem to form stable bonds with the chromium pentacarbonyl fragment. The bond strength of  $\text{CMe}_2$  is comparable to that of the  $\text{CMe}(\text{OMe})$  ligand. Compared to the alkyl-substituted systems, the halo ligands form significantly weaker bonds.

To our knowledge, the experimentally available metal carbene bond dissociation enthalpies are limited to three  $\text{Mn}(\text{CO})_5\text{CXY}$  molecules:  $D[\text{Mn}(\text{CO})_5^+=\text{CH}_2] = 401 \pm 31$  kJ/mol,  $D[\text{Mn}(\text{CO})_5^+=\text{CHF}] = 356 \pm 25$  kJ/mol, and  $D[\text{Mn}(\text{CO})_5^+=\text{CF}_2] = 332 \pm 12$  kJ/mol. All of these results were obtained by photoionization mass spectrometry.<sup>44</sup> The positive charge of the manganese complexes will have a significant influence on the  $\text{Mn}=\text{CR}_2$  bond dissociation enthalpies, and we cannot compare our calculated bond energies for the neutral

(43) Brothers, P. J.; Roper, W. R. *Chem. Rev.* **1988**, *88*, 1293.

(44) Stevens, A. E. Ph.D. Thesis, California Institute of Technology, 1981.



**Figure 1.** Reduced  $\sigma$  bond strengths and  $\pi$  bond strengths for various  $(\text{CO})_5\text{Cr}=\text{ER}_2$  complexes.

chromium carbenes with the experimental results. We might, however, compare the effect of fluorination, that is  $\Delta[D(\text{Mn}=\text{CH}_2), D(\text{Mn}=\text{CF}_2)]$ , and  $\Delta[\text{BE}(\text{Cr}=\text{CH}_2), \text{BE}(\text{Cr}=\text{CF}_2)]$ . Since we compare with bond dissociation enthalpies rather than with bond enthalpy terms, we have to correct our  $\text{BE}_{\text{snap}}$  values to bond energies  $\text{BE}$ , according to eq 3. The geometric preparation energies for  $(\text{CO})_5\text{Cr}=\text{CH}_2$  and  $(\text{CO})_5\text{Cr}=\text{CF}_2$  amount to 10 and 4 kJ/mol, respectively. We further correct  $\text{BE}(\text{Cr}=\text{CH}_2)$  with the experimental value for the triplet-singlet splitting of methylene. Thus, we obtain  $\Delta[\text{BE}(\text{Cr}=\text{CH}_2), \text{BE}(\text{Cr}=\text{CF}_2)] = 99$  kJ/mol. This result is in good agreement with the experimental value of  $\Delta[D(\text{Mn}=\text{CH}_2), D(\text{Mn}=\text{CF}_2)] = 69 \pm 43$  kJ/mol.

**Assignment of  $\sigma$  and  $\pi$  Bond Strengths.** In order to obtain values for the  $\sigma$  as well as the  $\pi$  component of the  $\text{Cr}=\text{E}$  double bond, we make use of the fact that we can decompose our electronic interaction energy due to different symmetry contributions:

$$\Delta E_{\text{int}} = \sum_{\Gamma} \Delta E_{\text{int}}^{\Gamma} \quad (6)$$

Here,  $\Gamma$  represents the different irreducible representations of the point group of the molecule. We can associate the different  $\Delta E_{\text{int}}^{\Gamma}$  terms from the right side of eq 6 with the intrinsic  $\sigma$  and  $\pi$  bond strengths,  $D_{\sigma, \text{int}}$  and  $D_{\pi, \text{int}}$ , respectively. Orbitals that have the plane of the  $\text{ER}_2$  ligands as a nodal plane contribute to  $D_{\pi, \text{int}}$ . Similarly, orbitals that lie in the plane of the  $\text{ER}_2$  ligand donate to  $D_{\sigma, \text{int}}$ . Thus, we can break down  $\Delta E_{\text{int}}$  into only two terms as

$$\Delta E_{\text{int}} = -[D_{\sigma, \text{int}} + D_{\pi, \text{int}}] \quad (7)$$

We can further combine  $D_{\sigma, \text{int}}$  and  $\Delta E^0$  to the so-called reduced intrinsic  $\sigma$  bond strength<sup>25a</sup>  $D'_{\sigma, \text{int}}$ :

$$D'_{\sigma, \text{int}} = D_{\sigma, \text{int}} - \Delta E^0 \quad (8)$$

We now are able to analyze our bond-snapping energy  $\text{BE}_{\text{snap}}$  or the  $\text{Cr}=\text{E}$  bond strength according to  $\sigma$  and  $\pi$  contributions as

$$\text{BE}_{\text{snap}} = D'_{\sigma, \text{int}} + D_{\pi, \text{int}} \quad (9)$$

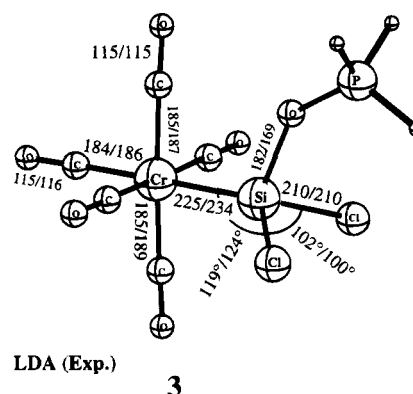
The results of our analysis are presented in Figure 1. We will first discuss the trends observed for the carbene ligands.  $\text{CH}_2$  possesses by far the strongest  $\pi$  bond with  $D_{\pi, \text{int}} = 198$  kJ/mol. The other carbene ligands possess  $\pi$  bond strengths around 120 kJ/mol. This can be

understood by noting that the F, Cl, and Me substituents can donate electrons into the empty p orbital at the carbon center. This substituent donation competes with the back-donation for the metal fragment, with the consequence that substituted carbene ligands form weaker  $\pi$  bonds than methylene itself. Further, we see that, with the exception of the  $\text{CMe}_2$  ligand, all investigated carbene ligands show a higher  $\pi$  bond than  $\sigma$  bond strength. This is in accord with the common notion that electron-withdrawing substituents enhance the ability of  $\pi$  acceptance, whereas alkyl substituents increase the capacity for  $\sigma$  donation.

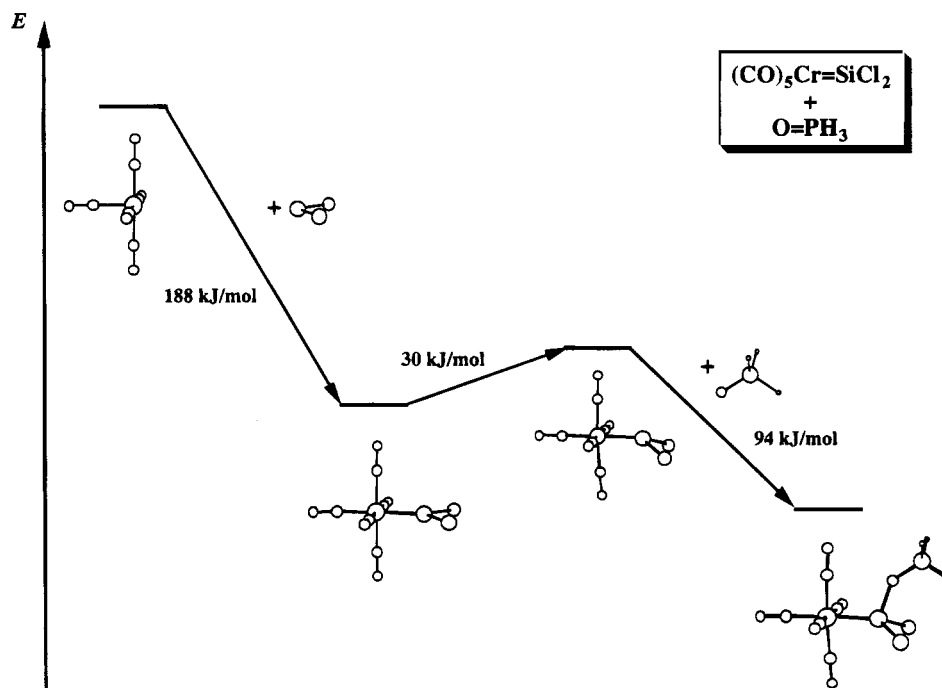
If we now turn to the silylene systems, we find that all systems possess only a weak  $\pi$  bond around 70 kJ/mol. The  $\sigma$  component contributes the major part to the bonding interaction. In general, we can state that the different bond strengths of the  $\text{ER}_2$  ligands are determined by the variation in  $D'_{\sigma, \text{int}}$  rather than in  $D_{\pi, \text{int}}$ . For both the series of ligands we obtain a similar ranking of  $D'_{\sigma, \text{int}}$ ,  $\text{EMe}_2 > \text{EH}_2 > \text{ECl}_2 \approx \text{EF}_2$ .

The fact that silylene systems possess only a weak  $\pi$  bond holds an explanation why these species follow a trend to form Lewis base adducts and to undergo type II complexation. In the next section, we will analyze a Lewis base adduct in more detail.

**Type II Complex  $(\text{CO})_5\text{Cr}=\text{SiCl}_2\text{-OPH}_3$ .** We have chosen  $(\text{CO})_5\text{Cr}=\text{SiCl}_2\text{-OPH}_3$  as a model compound of a type II silylene complex. The solid state structure of the related compound  $(\text{CO})_5\text{Cr}=\text{SiCl}_2\text{-HMPA}$  (HMPA = hexamethylphosphoric triamide) has been reported by Zybilla and co-workers.<sup>12b</sup> The optimized structural parameters together with experimental values are presented in 3. The calculated geometric arrangements



of the  $(\text{CO})_5\text{Cr}$  fragments and the  $\text{SiCl}_2$  ligand are in good agreement with the crystal structure. However, two structural parameters do not provide a good agreement between experiment and theory. First, the calculated  $\text{Cr}-\text{Si}$  bond length is 9 pm shorter than in the crystal structure. If we employ a nonlocal correction of 5 pm, as established for the  $(\text{CO})_5\text{Cr}=\text{CMe}(\text{OMe})$  molecule, our  $\text{Cr}-\text{Si}$  distance comes close to the experimental result. However, comparing the  $\text{Cr}-\text{Si}$  distance in the corresponding type I and type II complexes, we find a bond elongation under Lewis base addition of 5 pm. This is only half the value found for a pair of analogous type I/type II stannylenes.<sup>6a</sup> The other structural parameter that is in disagreement with the experiment is the  $\text{Si}-\text{O}$  separation. Our result is 13 pm too long compared to experiment.



**Figure 2.** Bond analysis for  $(\text{CO})_5\text{Cr}=\text{SiCl}_2$  and its Lewis base adduct  $(\text{CO})_5\text{Cr}=\text{SiCl}_2\text{-OPH}_3$ .

An explanation for the poor agreement in the Si–O bond lengths might be found in the difference of Lewis base strength of our model compound  $\text{OPH}_3$  and the experimentally employed  $\text{OP}(\text{N}(\text{Me})_2)_3$ . Since the Lewis adduct bond is relatively weak, differences in Lewis base strength might well have major consequences on the Si–O distance. Thus, if  $\text{OP}(\text{N}(\text{Me})_2)_3$  is a stronger donor than  $\text{OPH}_3$ , we can expect to find a shorter Si–O for the triamide. Consequently, this should lead to longer Cr–Si bond, since the  $\pi$  bond character of the metal–silicon bond is decreased. This would also provide a reason why our theoretically obtained bond elongation is smaller than the experimental value. To support our argument, we analyze the energies of the O-based donor orbitals for  $\text{OPH}_3$  and  $\text{OP}(\text{NH}_2)_3$  as a measure for the Lewis base strength. We find that the donating orbital for the triamide is 0.16 eV higher in energy than for  $\text{OPH}_3$ . The  $\text{OP}(\text{NH}_2)_3$  donor orbital provides a better energetic match for the acceptor orbital of the  $(\text{CO})_5\text{Cr}=\text{SiCl}_2$  fragment. Thus, a phosphoric triamide can indeed be considered as a somewhat stronger Lewis base than phosphine oxide.

In Figure 2, we present a bond analysis for the  $(\text{CO})_5\text{Cr}=\text{SiCl}_2\text{-OPH}_3$  molecule. We begin with the interaction of  $(\text{CO})_5\text{Cr}$  with  $\text{SiCl}_2$  to form the type I complex  $(\text{CO})_5\text{Cr}=\text{SiCl}_2$ . This process is favored by 188 kJ/mol, with a  $\pi$  contribution of  $D_{\pi,\text{int}} = 68$  kJ/mol. In the next step we provide the system for Lewis base addition. The bond elongation as well as the pyramidalization of the silicon center requires on energy of 30 kJ/mol. The addition of the Lewis base finally stabilizes the system by 94 kJ/mol. We see that the final step not only overcomes the 30 kJ/mol of preparation energy but could also compensate for the complete loss of the Cr=Si  $\pi$  bond.

### Concluding Remarks

The main difference between carbene and silylene ligands has been established in the very weak  $\pi$  bond strength of the latter. Lewis donation can favorably

compete with  $\pi$  bonding and as a consequence silylene complexes show a high tendency for type II complexation. Bulky substituents at the silylene ligands are required to protect the reactive Cr=Si  $\pi$  bond. However, a compromise has to be found between steric protection of the silicon center and steric repulsion with the metal fragment.

The Sila–Wittig reaction of  $(\text{CO})_5\text{Cr}=\text{SiCl}_2$  with  $\text{OC}(\text{OMe})_2$  has been proposed to proceed as a two step reaction. Experimental evidence clearly excludes a reaction mechanism in the sense of a concerted [2 + 2] cycloaddition.<sup>12b</sup> Our calculation support this notion and suggest that the polar addition of  $\text{OC}(\text{OMe})_2$  to the silylene complex initializes the formation of the product  $(\text{CO})_5\text{Cr}=\text{C}(\text{OMe})_2$ .

Although the  $\pi$  bond in silylene type I complexes is weak, our calculations indicate that those compounds form reasonably strong M–Si bonds and might be isolated without a stabilizing base. This has recently been demonstrated with the synthesis of  $[\text{Cp}^*(\text{PMe}_3)_2\text{-Ru}=\text{SiMe}_2]^+$ , for which the first crystal structure of a base-free silylene complex without  $\pi$ -donor stabilization has been obtained.<sup>13b</sup> The main features of this compound are a planar dimethylsilene ligand as well as the shortest Si–Ru bond reported so far. The results of Fenske–Hall calculations<sup>13b</sup> on the model compound  $[\text{Cp}(\text{PMe}_3)_2\text{Ru}=\text{SiH}_2]^+$  indicate a loss of electron density at the silylene ligand under coordination to the metal. This again is consistent with the fact that  $\text{SiR}_2$  ligands form weak  $\pi$  bonds and have mainly to be considered as  $\sigma$  donors.

**Acknowledgment.** This investigation was supported by the Natural Sciences and Engineering Research Council of Canada (NSERC) and by the donors of the Petroleum Research Fund, administered by the American Chemical Society (ACS-PRF No. 27023-AC3). Access to the IBM 6000 RISC computing facilities at the University of Calgary is acknowledged.



# Organic Syntheses via Transition Metal Complexes. 75.<sup>1</sup> Phosphinonaphthalenes and Phosphinoindenes by Cyclization of Alkynyl Carbene Complexes (M = Cr, W)

Rudolf Aumann,\* Beate Jasper, and Roland Fröhlich

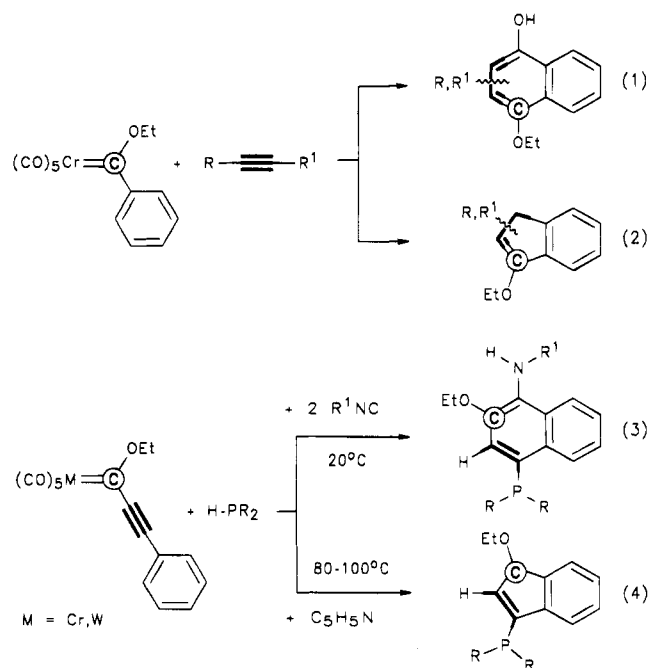
Organisch-Chemisches Institut der Universität Münster, Orleans-Ring 23,  
D-48149 Münster, Germany

Received July 5, 1994<sup>®</sup>

1-Amino-2-ethoxy-4-phosphinonaphthalenes **6a,b** (>90% yields) are obtained from (phenylalkynyl)carbene complexes  $(\text{CO})_5\text{M}=\text{C}(\text{OEt})-\text{C}\equiv\text{C}-\text{Ph}$  (M = Cr, W) **1** by a novel two-step carbene/alkyne benzannulation. The first step involves the formation of (*E*)-(2-phenyl-2-phosphinoethenyl)carbene complexes  $(\text{CO})_5\text{M}=\text{C}(\text{OEt})-\text{CH}=\text{C}(\text{Ph})-\text{PR}_2$  (*E*)-**3a-c** by 3-addition of secondary phosphines  $\text{HPR}_2$  (R = *t*-Bu, *c*-C<sub>6</sub>H<sub>11</sub>) **2a,b** to **1**. A subsequent addition of isocyanides R<sup>1</sup>NC (R = *t*-Bu, *c*-C<sub>6</sub>H<sub>11</sub>) **4a,b** to (*E*)-**3a-c** yields ketene imine complexes  $(\text{CO})_5\text{M}[\text{R}^1\text{N}=\text{C}=\text{C}(\text{OEt})-\text{CH}=\text{C}(\text{Ph})-\text{PR}_2]$  **A** by the insertion of **4** into the M=C bond of **3**. (Metal-free) ketene imines are generated from **A** by ligand displacement with **4** and cyclize spontaneously to **6**. Thermolysis of (*E*)-**3a-c** affords  $(\text{CO})_5\text{M}$  phosphinoindene complexes **9** and **10**. Reaction of **9** or **10** with pyridine yields phosphinoindenes **12** and pyridine complexes  $(\text{CO})_5\text{M}(\text{C}_5\text{H}_5\text{N})$  **11**. **10a**, C<sub>24</sub>H<sub>29</sub>CrO<sub>6</sub>P, was characterized by X-ray diffraction. It crystallizes in space group *P* $\bar{1}$  No. 2 with cell parameters *a* = 9.412(1) Å, *b* = 11.455(2) Å, *c* = 11.962(2) Å,  $\alpha$  = 89.10(1)°,  $\beta$  = 79.09(1)°,  $\gamma$  = 88.60(1)°, *Z* = 2, *R*<sub>1</sub> = 0.063, and *wR*<sup>2</sup> = 0.117.

Benzannulation reactions of (arylcabene)chromium complexes with alkynes have gained wide application in synthetic organic chemistry.<sup>2</sup> The so-called Dötz reaction involves the insertion of a C≡C into a Cr=C bond and leads to the formation of 1,4-dioxynaphthalenes (Scheme 1, eq 1). Indenes may be obtained as side products (Scheme 1, eq 2).<sup>2,3</sup> Intramolecular Dötz-type cyclizations of (alkynylcarbene)chromium complexes are governed by sterical restrictions.<sup>4</sup> Reactions of this type are achieved only when the reacting groups are tethered properly.<sup>5</sup> We report here on a carbene/alkyne benzannulation, which is different from the Dötz-type reaction. It requires two steps: a Michael addition of a protic nucleophile to a (2-aryalkynyl)carbene complex  $(\text{CO})_5\text{M}=\text{C}(\text{OEt})-\text{C}\equiv\text{C}-\text{Ar}$  (M = Cr, W) and the cyclization of the Michael adduct by the addition of an isocyanide. First examples of this reaction comprise the formation of 1,4-

## Scheme 1. Benzannulation and Formation of Indenes via the Arylcabene/Alkyne (Dötz Reaction) vs the (1-Aryalkynyl)carbene Complex Route



diamino-2-ethoxynaphthalenes by subsequent addition of a secondary amine and an isocyanide to a (phenylalkynyl)carbene complex  $(\text{CO})_5\text{M}=\text{C}(\text{OEt})-\text{C}\equiv\text{C}-\text{Ph}$  (M = Cr, W).<sup>6</sup> This novel type carbene/alkyne benzannulation is complementary to the Dötz reaction with regard to its regiochemistry, and insofar as heterosubstituents

<sup>®</sup> Abstract published in *Advance ACS Abstracts*, November 1, 1994.  
(1) Part 74: Aumann, R.; Jasper, B.; Läge, M.; Krebs, B. *Chem. Ber.*, in press.

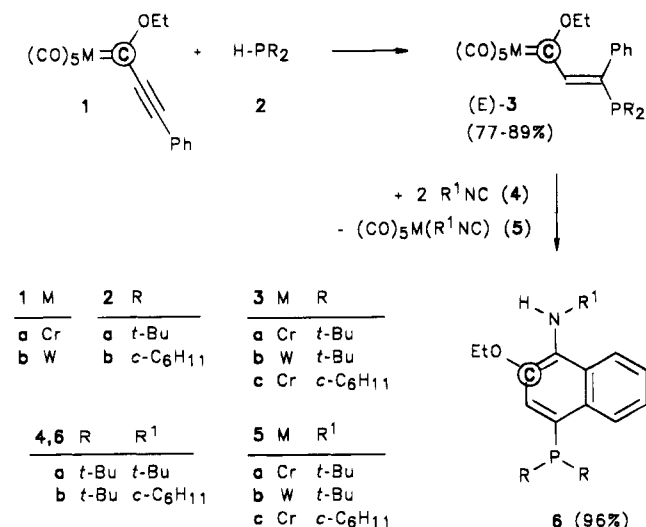
(2) Reviews: (a) Dötz, K. H. *Angew. Chem.* **1984**, *96*, 573–594; *Angew. Chem., Int. Ed. Engl.* **1984**, *23*, 587–608. (b) Wulff, W. D. *Adv. Met. Org. Chem.* **1988**, *1*, 209–393. (c) Dötz, K. H. *New J. Chem.* **1990**, *14*, 433. (d) Dötz, K. H. In *Organometallics in Organic Synthesis: Aspects of a Modern Interdisciplinary Field*; tom Dieck, H., de Meijere, A., Eds.; Springer: Berlin, 1988, p 85 ff. List of syntheses: (e) Wulff, W. D.; Bauda, W. E.; Kaesler, R. W.; Lankford, P. J.; Miller, R. A.; Murray, C. K.; Yang, D. C. *J. Am. Chem. Soc.* **1990**, *112*, 3642–3659. (f) Dötz, K. H.; Popall, M. *Chem. Ber.* **1988**, *121*, 665–672.

(3) (a) Dötz, K. H.; Pruskil, I.; Schubert, U.; Ackermann, K. *Chem. Ber.* **1983**, *116*, 2337–2343.

(4) Dötz, K. H.; Schäfer, T.; Kroll, F.; Harms, K. *Angew. Chem.* **1992**, *104*, 1257–1259; *Angew. Chem., Int. Ed. Engl.* **1992**, *31*, 1236–1238.

(5) (a) Semmelhack, M. F.; Bozell, J. J.; Keller, L.; Sato, T.; Spiess, E. J.; Wulff, W.; Zask, T. *Tetrahedron* **1985**, *41*, 5803–5812. (b) Anderson, B. A.; Bao, J.; Brandvold, T. A.; Challener, C. A.; Wulff, W. D.; Xu, Y.-C.; Rheingold, A. L. *J. Am. Chem. Soc.* **1993**, *115*, 10671–10687. (c) Chelain, E.; Goumont, R.; Hamon, L.; Parlier, A.; Rudler, M.; Rudler, H.; Daran, J.-C.; Vaisserman, J. *Am. Chem. Soc.* **1992**, *114*, 8088–8098. (d) Harvey, D. F.; Brown, M. F. *Tetrahedron Lett.* **1990**, *31*, 5223–5226. (e) Harvey, D. F.; Brown, M. F. *J. Am. Chem. Soc.* **1990**, *112*, 7806–7807. (f) Balzer, B. L.; Cazanoue, M.; Finn, M. G. *J. Am. Chem. Soc.* **1992**, *114*, 8735–8736. (g) Dötz, K. H.; Schäfer, T. O.; Harms, K. *Synthesis* **1992**, 146.

(6) (a) Aumann, R. *Chem. Ber.* **1993**, *126*, 1867–1872. (b) Aumann, R.; Jasper, B.; Goddard, R.; Krüger, C. *Chem. Ber.* **1994**, *127*, 717–724.

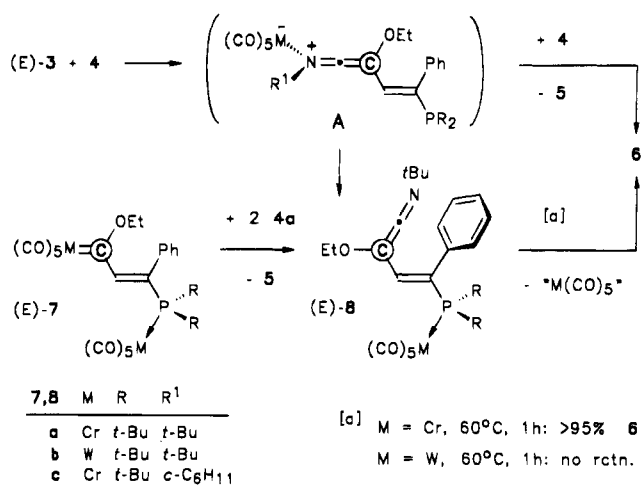
**Scheme 2. 1-Amino-4-phosphinonaphthalenes from (Arylalkynyl)carbene Complexes**


other than those based on oxygen are introduced at 1- and 4-positions of the six-membered ring.

We have extended our studies to the formation of 1-amino-2-ethoxy-4-phosphinonaphthalenes by the stepwise addition of secondary phosphines and isocyanides to (arylalkynyl)carbene complexes (Scheme 1, eq 3). We also report on the generation of phosphinoindenes from such compounds (Scheme 1, eq 4).

**Phosphinonaphthalenes 6.** The first step of the cyclization of an (arylalkynyl)carbene complex  $(\text{CO})_5\text{M}=\text{C}(\text{OEt})-\text{C}\equiv\text{C}-\text{Ph}$  **1** requires the addition of a protic nucleophile NuH to the alkyne unit in a *syn* fashion, by which an arylalkenyl carbene complex  $(\text{CO})_5\text{M}=\text{C}(\text{OEt})-\text{CH}=\text{C}(\text{Nu})\text{Ph}$  **3** of (*E*) configuration is generated. The (*E*) configuration is the stereochemical prerequisite for the subsequent cyclization. Thus, the stereochemistry of the 3-addition of NuH to **1** is crucial. Depending on the type of nucleophile involved, its addition to **1** may be highly stereoselective in one or the other direction.<sup>7</sup> The stereodifferentiation apparently results from different protonation sites of the zwitterionic  $(\text{CO})_5\text{M}^-[\text{C}(\text{OEt})=\text{C}(\text{Ph})\text{NuH}^+]$  and anionic allene-type intermediates  $(\text{CO})_5\text{M}[\text{C}(\text{OEt})=\text{C}(\text{Ph})\text{Nu}]^-$ ,<sup>1</sup> which are formed as the primary adducts of NuH and its conjugate base Nu<sup>-</sup>, respectively, to **1**.<sup>7i</sup> For the present case, the addition of a secondary phosphine H-PR<sub>2</sub> **2** to **1** is stereochemically uniform and leads to (2-phosphino-2-arylethenyl)carbene complexes (*E*)-**3a-c** of proper (*E*) configuration (Scheme 2) in 77–89% chemical yields (R = *tert*-Bu, *c*-C<sub>6</sub>H<sub>11</sub>).<sup>1</sup> Side reactions comprise the formation of small amounts of binuclear complexes (*E*)-**7** (Scheme 3).<sup>1</sup>

The alkenylcarbene complexes (*E*)-**3a-c** react with isocyanides **4a,b** under mild conditions and afford 1-amino-2-ethoxy-4-phosphinonaphthalenes **6a,b** in 96% yields (Scheme 2). The key step of this reaction consists

**Scheme 3. Ketene Imine Complexes A and (E)-8 as Key Intermediates**


in the insertion of an isocyanide **4** into the M=C bond of (*E*)-**3** with formation of a ketene imine complex **A** (Scheme 3).<sup>6,8,9</sup> Subsequently, **A** takes up a further equivalent of **4** and yields an isocyanide complex **5** by displacement of the ketene imine ligand. The latter cyclizes spontaneously at 20 °C to the naphthalene **6**. Ketene imine complexes (*E*)-**8a,c**, which are coordination isomers of **A**, are more stable thermally than **A**, due to steric hindrance of the cyclization step by the bulkiness of the  $(\text{CO})_5\text{MP}(\text{tert-Bu})_2$  unit. These compounds are generated by addition of 2 equiv of **4a** to the binuclear complexes (*E*)-**7a,c**<sup>1</sup> and could be characterized spectroscopically at 20 °C. The cyclization of (*E*)-**8a,c** to naphthalenes **6** requires heating to 60 °C in order to induce the disengagement of the  $(\text{CO})_5\text{M}$  moiety from the phosphorus atom. Thus, naphthalenes **6** are obtained from both, compounds **A** and their coordination isomers (*E*)-**8**, though different reaction temperatures are required.

**Phosphinoindenes 9, 10, and 12.** Indenes are formed on reaction of arylcarbene complexes with alkynes as side products of the Dötz reaction.<sup>2,3</sup> A different approach to the synthesis of indenes from carbene complexes is based on the cyclization of the C<sub>5</sub> skeleton of the (2-aryl-1-alkynyl)carbene ligand of **1**.

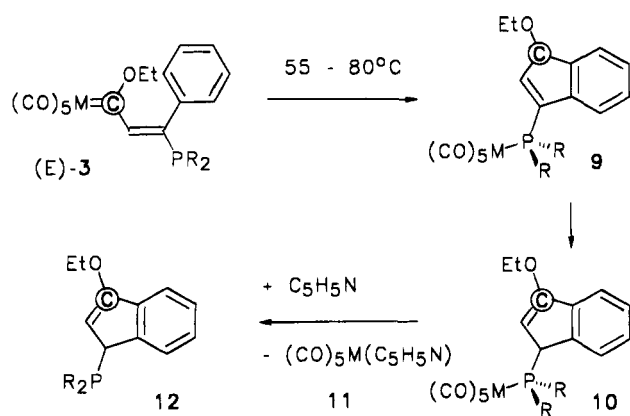
Phosphinoindenes **12** are generated together with pyridine complexes  $(\text{CO})_5\text{M}(\text{C}_5\text{H}_5\text{N})$  **11** in two steps, by the addition of secondary phosphines **2** to **1**, which leads to the formation of (2-phosphinoethenyl)carbene complexes (*E*)-**3** (Scheme 2) and the thermolysis of (*E*)-**3** in the presence of pyridine at 80–100 °C (Scheme 4; M = Cr, W; > 90% yields). Complexes **11** are removed most conveniently and almost quantitatively from the reaction mixture by crystallization from heptane at –15 °C, under which conditions compounds **12** are accumulated in the mother liquor.

The cyclization of (*E*)-**3** to **12** involves the formation of phosphino complexes **9** and **10** as intermediate products (Scheme 4). Compounds **9** are generated from (*E*)-**3**, supposedly by an attack of the carbene carbon atom at the aromatic ring.<sup>10</sup> A zwitterionic species **B**

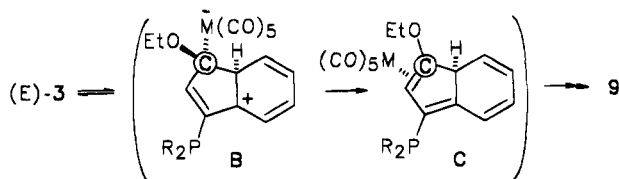
(7) (a) Fischer, E. O.; Kreissl, F. R. *J. Organomet. Chem.* **1972**, *35*, C47. (b) Fischer, E. O.; Kalder, H. *J. Organomet. Chem.* **1977**, *131*, 57. (c) Duetsch, M.; Stein, F.; Lackmann, R.; Pohl, E.; Herbst-Irmer, R.; de Meijere, A. *Chem. Ber.* **1992**, *125*, 2051. (d) Aumann, R.; Hinterding, P. *Chem. Ber.* **1992**, *125*, 2765. (e) Aumann, R.; Hinterding, P. *Chem. Ber.* **1993**, *126*, 421. (f) Camps, F.; Llebaria, A.; Moretó, J. M.; Ricart, S.; Viñas, S.; Ros, J.; Yáñez, R. *J. Organomet. Chem.* **1991**, *401*, C17. (g) Aumann, R.; *Chem. Ber.* **1992**, *125*, 2773. (h) Wang, S. L. B.; Wulff, W. D. *J. Am. Chem. Soc.* **1990**, *112*, 4550. (i) Aumann, R.; Jasper, B.; Läge, M.; Krebs, B. *Organometallics* **1994**, *13*, 3502.

(8) Review on this reaction type: Aumann, R. *Angew. Chem.* **1988**, *100*, 1512–1524; *Angew. Chem. Int. Ed. Engl.* **1988**, *27*, 1456–1467.  
(9) (a) Merlic, C. A.; Burns, E.; Xu, S.; Chen, Y. *J. Am. Chem. Soc.* **1992**, *114*, 8722–8724. (b) Merlic, C. A.; Burns, E. E. *Tetrahedron Lett.* **1993**, *34*, 5401.

**Scheme 4. Cyclization of (2-Phosphinoethenyl)carbene Complexes (*E*)-3 (M = Cr, W) with Formation of Phosphino Indenes 12 via 9 and 10**



3,9-12 M R  
 a Cr *t*-Bu  
 b W *t*-Bu  
 c Cr *c*-C<sub>6</sub>H<sub>11</sub>



may be formed initially and rearrange fast to an olefin complex **C**. The (CO)<sub>5</sub>M moiety of **C** could migrate to the phosphorus atom without losing contact to the indene skeleton. A (suprafacial) 1,5 hydrogen shift of the rearranged product may finally lead to **9**. The chromium complex **9a** can be isolated. It forms an isomer **9'a** in solution at 80 °C, while the tungsten complex **9b** remains unchanged for several hours even at 100 °C. <sup>1</sup>H NMR spectra of **9a** and **9'a** may be closely similar to each other with respect to the chemical shifts and the proton coupling pattern except for the vicinal couplings <sup>3</sup>J(P,2-H), which amount to 5.5 and 2.5 Hz, respectively. The different coupling constants may be attributed to the influence of conformational effects, for which Karplus-like curves have been established in the case of phosphine oxides and related compounds.<sup>11</sup>

The product composition resulting from the thermolysis of **3a-c** in the presence of equivalent amounts of pyridine was analyzed by <sup>1</sup>H NMR measurements (C<sub>6</sub>D<sub>6</sub>, 360 MHz) under different reaction conditions (Table 1). In the multi-step rearrangement sequence from (*E*)-**3** to **10**, the M(CO)<sub>5</sub> unit is not trapped by pyridine and therefore appears to remain in close contact to the indene ligand. We conclude that the isomerization of the rotamers **9a** and **9'a** might be initiated by a shift of the metal moiety from the phosphorus atom to the C=C bond of the indene skeleton and a rotation/inversion of the (slightly tilted) *Pt*-Bu<sub>2</sub> unit. This process may require less energy than

(10) More commonly, indene formation is viewed as occurring via a dissociation of carbon monoxide, a subsequent electrocyclic ring closure to a metalcyclohexadiene intermediate, a reductive elimination, and a metal-mediated hydrogen shift (see ref 2).

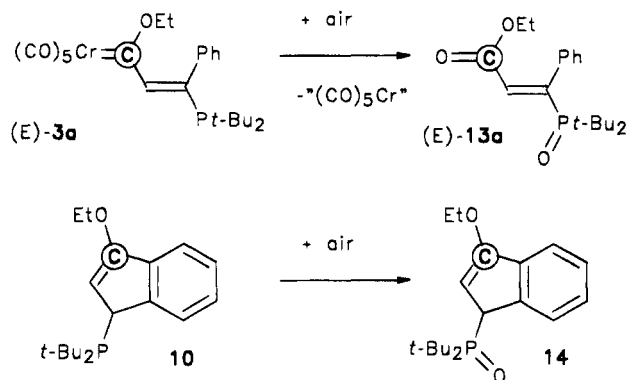
(11) Mavel, G. *Annu. Rep. NMR Spectrosc.* **1973**, 5b, 1-350.

**Table 1. Product Ratio of Indenes 9-12 Formed on Thermolysis of 3 under Different Reaction Conditions**

starting material	M	R	yield <sup>a</sup> (%)	reaction condns		9:9':10:12
				time (h)	temp (°C)	
<b>3a</b>	Cr	<i>t</i> -Bu	>90	3	60	4:1:0:0
<b>3a</b>	Cr	<i>t</i> -Bu	>90	3	80	0:0:1:0
<b>3a</b>	Cr	<i>t</i> -Bu	>90	3	80 (+C <sub>5</sub> H <sub>5</sub> N)	0:0:0:1
<b>3b</b>	W	<i>t</i> -Bu	>90	35	55	1:0:0:0
<b>3b</b>	W	<i>t</i> -Bu	>90	1	80	2:0:1:0
<b>3b</b>	W	<i>t</i> -Bu	>90	10	80	0:0:1:0
<b>3b</b>	W	<i>t</i> -Bu	>90	8	80 (+C <sub>5</sub> H <sub>5</sub> N)	0:0:0:1
<b>3c</b>	Cr	<i>c</i> -C <sub>6</sub> H <sub>11</sub>	>90	2	80	8:0:1:0
<b>3c</b>	Cr	<i>c</i> -C <sub>6</sub> H <sub>11</sub>	>90	2	100	0:0:1:0

<sup>a</sup> Total yield of indenenes according to <sup>1</sup>H NMR spectra. <sup>b</sup> Product ratio of corresponding indenenes.

**Scheme 5. Oxidation of Phosphinoindenenes and (2-Phosphinoethenyl)carbene Complexes**

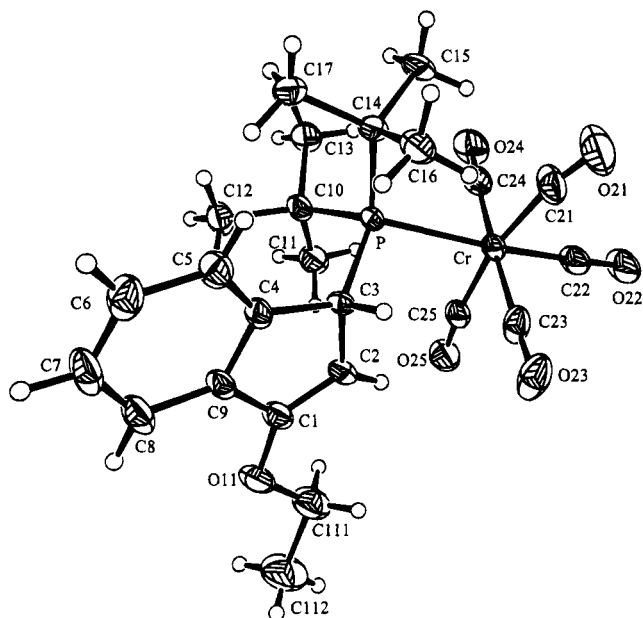


the dissociation of the P-Cr bond. A rearrangement simply by rotation of the C3-P bond of **9/9'** apparently is strongly hindered by the bulkiness of both the M(CO)<sub>5</sub> and the *tert*-butyl groups. The rearrangement of **9/9'** to **10** involves a metal-mediated (supposed intramolecular) 1,3 hydrogen shift and is observed at elevated reaction temperatures only (Table 1). The elimination of a pyridine complex **11** leads concomitantly to the generation of **12**.

**Oxidation of Phosphines 3 and 12.** It is important to note that compounds **12** are readily oxidized in solution on exposure to air within a few hours to the corresponding phosphine oxide **14** (Scheme 5). (2-Phosphinoethenyl)carbene complexes, e.g., (*E*)-**3a**, are stable in the solid state but decompose in solution under the influence of oxygen by formation of the phosphono acrylate, e.g., (*E*)-**13a**.

**Crystal Structure Analysis of Indene 10a.** Figure 1 shows the molecular structure and Tables 2 and 3 show the experimental data for the crystal structure of **10a**. The Cr-P distance [2.525(2) Å] is significantly longer than it is in compounds of type (*E*)-**7** (Scheme 3) [M = Cr, R = Ph, Cr-P 2.409(8)].<sup>1,12</sup> The coordination geometry at the phosphorus atom corresponds to a slightly distorted tetrahedral structure, with angles ranging from 105.7(2) to 116.7(2) Å. The Cr(CO)<sub>5</sub> moiety and the hydrogen atom 3-H are arranged *syn* to each other, in line with expectations, if **10** were generated from **9** by an intramolecular metal-induced 1,3 hydrogen shift (see above).

(12) For a compilation of more data, see: Jelinek-Fink, H.; Duessler, E. N.; Paine, R. T. *Acta Crystallogr.* **1987**, C43, 635-636.



**Figure 1.** View of the molecular structure of **10a** with selected bond distances (Å) and angles (deg): Cr–P 2.525(2), P–C3 1.893(5), P–C10 1.906(5), P–C14 1.903(6), Cr–P–C3 107.1(2), C10–P–C14 108.9, C3–C2 1.508(7), C3–C4 1.523(7), C2–C1 1.345(7), C4–C9 1.404(7), C1–C9 1.430(8), C1–O11 1.359(6), C10–P–C14 108.9(3), C3–P–Cr 107.1(2), C3–P–C10 106.3(2), C3–P–C14 105.7(2), C14–P–Cr 111.6(2), C10–P–Cr 116.7(2).

**Table 3.** Atomic Coordinates ( $\times 10^4$ ) and Equivalent Isotropic Displacement Parameters ( $\text{Å}^2 \times 10^3$ ) for **10a**<sup>a</sup>

	<i>x</i>	<i>y</i>	<i>z</i>	<i>U</i> (eq)
Cr	1310(1)	2466(1)	8972(1)	50(1)
C(21)	1775(7)	3550(7)	10006(6)	76(2)
O(21)	1889(6)	4237(6)	10669(5)	120(2)
C(22)	-469(8)	2532(6)	9912(5)	64(2)
O(22)	-1576(5)	2571(5)	10529(4)	94(2)
C(23)	797(7)	3782(6)	8126(6)	58(2)
O(23)	397(6)	4540(5)	7651(5)	90(2)
C(24)	1713(7)	1145(7)	9839(6)	62(2)
O(24)	1854(6)	339(5)	10386(4)	91(2)
C(25)	461(7)	1532(6)	8007(5)	51(2)
O(25)	-197(5)	1044(4)	7450(4)	69(1)
P	3818(2)	2299(1)	7771(1)	36(1)
C(10)	4485(6)	773(5)	7282(4)	42(2)
C(11)	3236(7)	102(5)	6989(5)	55(2)
C(12)	5716(7)	773(5)	6238(5)	54(2)
C(13)	5000(7)	92(5)	8248(5)	60(2)
C(14)	5221(6)	2985(5)	8497(4)	41(1)
C(15)	5035(7)	2575(6)	9734(5)	56(2)
C(16)	4958(6)	4311(5)	8470(5)	53(2)
C(17)	6805(6)	2722(5)	7939(5)	56(2)
C(1)	3251(7)	2677(5)	4683(5)	47(2)
O(11)	2611(5)	2328(4)	3820(3)	61(1)
C(111)	1107(9)	2056(7)	4120(6)	79(2)
C(112)	564(10)	1823(8)	3052(7)	126(4)
C(2)	2683(6)	2762(4)	5799(5)	41(1)
C(3)	3803(6)	3198(4)	6431(4)	37(1)
C(4)	5085(6)	3381(5)	5462(5)	39(1)
C(5)	6394(7)	3919(5)	5414(5)	50(2)
c(6)	7364(7)	3995(5)	4378(6)	59(2)
C(7)	6990(8)	3586(6)	3396(6)	62(2)
C(8)	5675(8)	3129(5)	3416(5)	54(2)
C(9)	4722(7)	3036(5)	4432(5)	42(1)

<sup>a</sup> *U*(eq) is defined as one-third of the trace of the orthogonalized *U*<sub>ij</sub> tensor.

**Table 2.** Crystal Data and Structure Refinement for **10a**

identification code	AUM_151
empirical formula	C <sub>24</sub> H <sub>29</sub> CrO <sub>6</sub> P
fw	496.44
temp (K)	223(2) K
wavelength (Å)	0.71073 Å
cryst syst	triclinic
space group	<i>P</i> $\bar{1}$ (No. 2)
unit cell dimens	
<i>a</i> (Å)	9.412(1)
<i>b</i> (Å)	11.455(2)
<i>c</i> (Å)	11.962(2)
$\alpha$ (deg)	89.10(1)
$\beta$ (deg)	79.09(1)
$\gamma$ (deg)	88.60(1)
vol (Å <sup>3</sup> )	1265.9(3)
<i>Z</i>	2
density (calcd) (mg/m <sup>3</sup> )	1.302
abs coeff (mm <sup>-1</sup> )	0.550
<i>F</i> (000)	520
cryst size (mm)	0.2 × 0.2 × 0.15
$\Theta$ range for data collection	2.53–26.31°
index ranges	0 ≤ <i>h</i> ≤ 11, -14 ≤ <i>k</i> ≤ 14, -14 ≤ <i>l</i> ≤ 14
no. of reflns colld	5469
no. of ind reflns	5141 [ <i>R</i> (int) = 0.058]
refinement method	full-matrix least squares on <i>F</i> <sup>2</sup>
data/restraints/params	5137/0/296
goodness of fit on <i>F</i> <sup>2</sup>	1.001
final <i>R</i> indices [ <i>I</i> > 2σ( <i>I</i> )]	<i>R</i> <sub>1</sub> = 0.063, <i>wR</i> <sup>2</sup> = 0.117
<i>R</i> indices (all data)	<i>R</i> <sub>1</sub> = 0.231, <i>wR</i> <sup>2</sup> = 0.171
largest diff peak and hole (eÅ <sup>-3</sup> )	
diffractometer	Enraf-Nonius CAD4
programs used	SHELX-86, SHELX-93, ORTEX

## Experimental Section

All operations were performed under argon. Solvents were dried by distillation from sodium/benzophenone. <sup>1</sup>H NMR and <sup>13</sup>C NMR spectra were obtained with Bruker WM 300 spectrometer. Multiplicities were determined by DEPT. Chemical shifts refer to δ<sub>TMS</sub> = 0.00 ppm. Other analyses: IR Digilab FTS 45; MS, Finnigan MAT 312; elemental analysis, Perkin-

Elmer 240 elemental analyser; melting points uncorrected; column chromatography, Merck Kieselgel 100. TLC, Merck DC-Alufolien Kieselgel 60 F 254. *R<sub>f</sub>* values refer to TLC tests.

**1-(*tert*-Butylamino)-4-(di-*tert*-butylphosphino)-2-ethoxynaphthalene (**6a**) and [(*E*)-*N*-(*tert*-Butyl)-4-(di-*tert*-butylphosphino)-2-ethoxy-4-phenyl-1,3-butadien-1-imine, P–Cr]pentacarbonylchromium [(*E*)-**8a**] from Chromium Complex (**E**)-**3a**.**

(a) **NMR experiment.** To 50 mg (0.10 mmol) of (3-*di-tert*-butylphosphino-1-ethoxy-3-phenyl-propenylidene)pentacarbonylchromium [(*E*)-**3a**]<sup>1</sup> in 1 mL of C<sub>6</sub>D<sub>6</sub> and hexamethylbenzene as an internal standard is added 16 mg (0.20 mmol) of *tert*-butyl isocyanide (**4a**) at 20 °C. The initially red solution turns yellow within 1 min. NMR measurements (360 MHz) indicate the presence of a 2:1:2:1 mixture of **6a**, (*E*)-**8a**, (CO)<sub>5</sub>Cr(*t*-BuNC) (**5a**), and unreacted **4a**. After 1 h at 60 °C, the signals of (*E*)-**8a** have disappeared, and signals expected for a 3:3 mixture of **6a** and **5a** are observed. (*E*)-**8a** is hydrolyzed on silica gel and therefore cannot be isolated by chromatography.

(b) **Preparation of 6a.** To 248 mg (0.50 mmol) of (*E*)-**3a** in 3 mL of cyclohexane is added 83 mg (1.00 mmol) of *tert*-butyl isocyanide (**4a**) with vigorous stirring at 20 °C. The mixture is heated to 60 °C for 1 h to complete the conversion of (*E*)-**8a** into **6a**. Chromatography on silica gel with pentane/dichloromethane (4:1) yields colorless **5a** (125 mg, identified by IR and by comparison of the TLC with authentic material); elution with dichloromethane/pentane (1:1) affords pale yellow **6a** [*R<sub>f</sub>* = 0.4 in dichloromethane/pentane (1:1), 185 mg, 96%, colorless crystals from pentane, mp 104 °C].

**6a:** <sup>1</sup>H NMR (C<sub>6</sub>D<sub>6</sub>): δ 9.35 [1H, dd, <sup>3</sup>*J* = 7 Hz, <sup>3</sup>*J*(P,H) = 7, 5-H], 8.62 [1H, d, <sup>3</sup>*J* = 7 Hz, 8-H], 7.76 [1H, d, <sup>3</sup>*J*(P,H) = 2 Hz, 3-H], 7.29 and 7.05 (1H each, dd, <sup>3</sup>*J* = 7 and 7 Hz each, 6-H and 7-H), 3.92 (2H, q, OCH<sub>2</sub>), 3.59 (1H, s broad, NH), 1.27 (9H, *Nt*-Bu), 1.20 (18H, *Pt*-Bu<sub>2</sub>), 1.23 (3H, t, CH<sub>3</sub>, Et). <sup>13</sup>C NMR (C<sub>6</sub>D<sub>6</sub>): δ 149.8 (C<sub>q</sub>, C2), 137.0 [C<sub>q</sub>, <sup>2</sup>*J*(P,C) = 26 Hz, C4], 134.8 [C<sub>q</sub>, <sup>3</sup>*J*(C,P) = 7 Hz, C1], 132.4 (C<sub>q</sub>, C9), 130.8 [C<sub>q</sub>,

$^1J(\text{C,P}) = 24 \text{ Hz}$ , C10], 127.9 [CH,  $^2J(\text{C,P}) = 37 \text{ Hz}$ , C3]; 126.6, 125.2, 124.1 (CH each, C6–C8), 121.5 [CH,  $^3J(\text{C,P}) = 4 \text{ Hz}$ , C5], 64.8 (OCH<sub>2</sub>), 56.0 (NMe<sub>3</sub>), 33.4 [Cq,  $^1J(\text{P,C}) = 22 \text{ Hz}$ , PCMe<sub>3</sub>], 31.8 (CH<sub>3</sub>, Nt-Bu), 30.0 [CH<sub>3</sub>,  $^2J(\text{C,P}) = 15 \text{ Hz}$ , Pt-Bu], 15.6 (CH<sub>3</sub>, Et). IR (diffuse reflection): 3330 cm<sup>-1</sup> [ $\nu(\text{N-H})$ ]. MS (70 eV), *m/e* (%): 388 (40) [M<sup>+</sup> + 1], 387 (50) [M<sup>+</sup>], 330 (50), 274 (100) [M<sup>+</sup> - *tert*-Bu - Me<sub>2</sub>C=CH<sub>2</sub>], 218 (40), 190 (10). Anal. Calcd for C<sub>24</sub>H<sub>38</sub>NOP (387.6): C, 74.38; H, 9.88; N, 3.61. Found: C, 74.43; H, 9.75; N, 3.52.

(*E*)-**8a**:  $^1\text{H NMR}$  (C<sub>6</sub>D<sub>6</sub>):  $\delta$  7.30 and 7.08 (2:3H, m each, 4-Ph), 7.10 [1H, d,  $^3J(\text{P,H}) = 8 \text{ Hz}$ , 3-H], 3.18 (2H, q, 2-OCH<sub>2</sub>), 1.18 [18H,  $^3J(\text{C,P}) = 12 \text{ Hz}$ , Pt-Bu<sub>2</sub>], 1.05 (9H, Nt-Bu), 0.71 (3H, t, CH<sub>3</sub>, Et).  $^{13}\text{C NMR}$  (C<sub>6</sub>D<sub>6</sub>):  $\delta$  222.6 [Cq, 1C,  $^2J(\text{P,C}) = 4 \text{ Hz}$ , *trans*-CO, (CO)<sub>5</sub>Cr], 219.1 [Cq, 4C,  $^2J(\text{P,C}) = 11 \text{ Hz}$ , *cis*-CO, (CO)<sub>5</sub>Cr], 191.8 (Cq, C1), 155.8 [Cq,  $^1J(\text{P,C}) = 86 \text{ Hz}$ , C4], 141.0 [CH,  $^2J(\text{P,C}) = 26 \text{ Hz}$ , C3], 137.1 [Cq,  $^2J(\text{P,C}) = 32 \text{ Hz}$ , *i*C, 4-Ph]; 128.8, 127.7, 125.3 (2:1:2, CH each, 4-Ph); 113.1 [Cq,  $^3J(\text{P,C}) = 18 \text{ Hz}$ , C2], 67.5 (OCH<sub>2</sub>), 61.4 (Cq, NMe<sub>3</sub>), 33.0 [Cq,  $^1J(\text{P,C}) = 22 \text{ Hz}$ , PCMe<sub>3</sub>], 31.3 (CH<sub>3</sub>, Nt-Bu), 31.0 (CH<sub>3</sub>, Pt-Bu<sub>2</sub>), 14.8 (CH<sub>3</sub>, Et).

**1-(*tert*-Butylamino)-4-(di-*tert*-butylphosphino)-2-ethoxynaphthalene (6a) from Tungsten Complex (*E*)-**3b**.** To 63 mg (0.10 mmol) of (3-di-*tert*-butylphosphino-1-ethoxy-3-phenylpropenylidene)pentacarbonyltungsten [(*E*)-**3b**]<sup>1</sup> in 1 mL of C<sub>6</sub>D<sub>6</sub> is added 16 mg (0.10 mmol) of *tert*-butyl isocyanide (**4a**) at 20 °C. The initially red solution turns yellow within 1 min.  $^1\text{H NMR}$  measurements (360 MHz) indicate that a clean conversion into a 1:1 mixture of **6a** and (CO)<sub>5</sub>W(*t*-BuNC) (**5b**) has occurred.

(*E*)-*N*-(*tert*-Butyl)-4-(di-*tert*-butylphosphino)-2-ethoxy-4-phenyl-1,3-butadien-1-imine, P-Cr]pentacarbonylchromium [(*E*)-**8a**] from (*E*)-**7a** and Its Conversion to **6a**. To 34 mg (0.05 mmol) of (*E*)-**7a**<sup>1</sup> in 1 mL of C<sub>6</sub>D<sub>6</sub> is added 8 mg (0.10 mmol) of **4a**. The initially red solution turns yellow immediately and shows  $^1\text{H}$  and  $^{13}\text{C NMR}$  spectra that are identical with those of (*E*)-**8a** and **5a**. After 1 h at 60 °C, a complete conversion of (*E*)-**8a** into **6a** is indicated by the  $^1\text{H NMR}$  spectrum.

(*E*)-*N*-(*tert*-Butyl)-4-(di-*tert*-butylphosphino)-2-ethoxy-4-phenyl-1,3-butadien-1-imine, P-Cr]pentacarbonylchromium [(*E*)-**8b**] from (*E*)-**7b** and Its Conversion to **6a**. To 48 mg (0.05 mmol) of (*E*)-**7b**<sup>1</sup> in 1 mL of C<sub>6</sub>D<sub>6</sub> is added 8 mg (0.10 mmol) of **4a**. The initially red solution turns yellow immediately and shows  $^1\text{H NMR}$  signals of (*E*)-**8b** and **5b**. Compound (*E*)-**8b** is stable at 60 °C for at least 1 h according to  $^1\text{H NMR}$  spectra. After 1 h at 100 °C, a partial conversion (10–20%) of (*E*)-**8b** into **6a** is observed.

(*E*)-**8b**:  $^1\text{H NMR}$  (C<sub>6</sub>D<sub>6</sub>):  $\delta$  7.35, and 7.03 (2:3H, m each, 4-Ph), 7.22 [1H, d,  $^3J(\text{P,H}) = 8 \text{ Hz}$ , 3-H], 3.28 (2H, q, 2-OCH<sub>2</sub>), 1.18 [18H,  $^4J(\text{C,P}) = 12 \text{ Hz}$ , Pt-Bu<sub>2</sub>], 1.07 (9H, Nt-Bu), 0.65 (3H, t, CH<sub>3</sub>, Et).

**4-(Di-*tert*-butylphosphino)-1-(cyclohexylamino)-2-ethoxynaphthalene (6b).** To 248 mg (0.50 mmol) of (3-di-*tert*-butylphosphino-1-ethoxy-3-phenylpropenylidene)pentacarbonylchromium [(*E*)-**3a**] in 3 mL of cyclohexane is added 109 mg (1.00 mmol) of cyclohexyl isocyanide (**4b**) with vigorous stirring at 20 °C. The mixture is heated to 60 °C for 1 h in order to guarantee a complete conversion of the ketene imine complex of type (*E*)-**8** into **6b**. Chromatography on silica gel with pentane/dichloromethane (4:1) yields colorless **5c** (140 mg, identified by IR and by comparison on TLC with authentic material) and with dichloromethane/pentane (1:1) pale yellow **6b** [*R*<sub>f</sub> = 0.4 in dichloromethane/pentane (1:1), 210 mg, 96%, colorless crystals from pentane, mp 104 °C). Alternatively, **6b** is obtained by the addition of 109 mg (1.00 mmol) of **4b** to 314 mg (0.50 mmol) of (3-di-*tert*-butylphosphino-1-ethoxy-3-phenylpropenylidene)pentacarbonyltungsten [(*E*)-**3b**] at 20 °C in a smooth reaction, as is indicated by the  $^1\text{H NMR}$  spectrum.

**6b**:  $^1\text{H NMR}$  (C<sub>6</sub>D<sub>6</sub>):  $\delta$  9.43 [1H, dd,  $^3J = 7 \text{ Hz}$ ,  $^3J(\text{P,H}) = 7, 5\text{-H}$ ], 8.35 (1H, d,  $^3J = 7 \text{ Hz}$ , 8-H), 7.82 [1H, d,  $^3J(\text{P,H}) = 2 \text{ Hz}$ , 3-H], 7.38 (2H, m, 6-H and 7-H), 3.95 (2H, q, OCH<sub>2</sub>), 3.45 (1H, s broad, NH), 3.25 (1H, m, NCH); 2.00, 1.55, 1.30–0.80

(11H, m, 5 CH<sub>2</sub>, C<sub>6</sub>H<sub>11</sub>), 1.28 [18H, d,  $^3J(\text{P,H}) = 14 \text{ Hz}$ , averaged signals of Pt-Bu<sub>2</sub>], 1.23 (3H, t, CH<sub>3</sub>, Et).  $^{13}\text{C NMR}$  (CDCl<sub>3</sub>):  $\delta$  145.4 (Cq, C2), 136.0 [Cq,  $^2J(\text{P,C}) = 26 \text{ Hz}$ , C4], 133.3 (Cq, C1), 128.5 [CH,  $^2J(\text{C,P}) = 37 \text{ Hz}$ , C3], 128.6 [Cq,  $^3J(\text{P,C}) = 7 \text{ Hz}$ , C9], 126.9 [Cq,  $^1J(\text{C,P}) = 24 \text{ Hz}$ , C10]; 124.5, 123.1, 123.0, 122.9 (CH each, C6 to C8), 121.5 [CH,  $^3J(\text{C,P}) = 4 \text{ Hz}$ , C5], 66.8 (OCH<sub>2</sub>), 57.0 (CH N); 34.6, 26.0, and 25.2 (2:1, CH<sub>2</sub> each, Cy); 32.7 [Cq,  $^1J(\text{P,C}) = 22 \text{ Hz}$ , PCMe<sub>3</sub>], 29.7 [6 CH<sub>3</sub>, d, dynamically broadened,  $^2J(\text{C,P}) = 15 \text{ Hz}$ , Pt-Bu<sub>2</sub>], 15.2 (CH<sub>3</sub>, Et). IR (diffuse reflection): 3344 cm<sup>-1</sup> [ $\nu(\text{N-H})$ ]. MS (70 eV), *m/e* (%): 413 (40) [M<sup>+</sup>], 356 (30), 300 (100) [M - 2 *t*-Bu]. Anal. Calcd for C<sub>26</sub>H<sub>40</sub>NOP (413.6): C, 75.51; H, 9.75; N, 3.39. Found: C, 75.55; H, 9.70; N, 3.34.

**[1-(Di-*tert*-butylphosphino)-3-ethoxyindene, P-Cr]pentacarbonylchromium (10a) and [3-(Di-*tert*-butylphosphino)-1-ethoxyindene, P-Cr]pentacarbonylchromium (9a and 9a').** A 248 mg (0.50 mmol) sample of (3-(di-*tert*-butylphosphino)-1-ethoxy-3-phenylpropenylidene)pentacarbonylchromium [(*E*)-**3a**] in 2.5 mL of dry benzene is heated to 60 °C for 3 h. According to  $^1\text{H NMR}$  spectra, (*E*)-**3a** is consumed completely and a 4:1 mixture of **9a** and **9a'** is formed. **9a** was isolated by crystallization from pentane at -15 °C [*R*<sub>f</sub> = 0.4 in dichloromethane/pentane (1:3), 150 mg, 60%], while **9a'** is accumulated in the mother liquor. Heating of a benzene solution of (*E*)-**3a** (or of **9a** and **9a'**) for 3 h to 80 °C yields mainly **10a** [*R*<sub>f</sub> = 0.4 in dichloromethane/pentane (1:10), yellow crystals from pentane at -45 °C, mp 102 °C, dec].

**10a**:  $^1\text{H NMR}$  (C<sub>6</sub>D<sub>6</sub>):  $\delta$  7.81, 7.56, 7.12, 7.04 (1H each; d, d, dd, dd;  $^3J = 8 \text{ Hz}$  each, 4-H–7-H); 5.81 [1H, dd,  $^3J(\text{P,H}) = 3 \text{ Hz}$ ,  $^3J = 2 \text{ Hz}$ , 2-H], 4.35 [1H, dd,  $^2J(\text{P,H}) = 8 \text{ Hz}$ ,  $^3J = 2 \text{ Hz}$ , 1-H], 3.95, and 3.80 (1H each, m each, diastereotopic OCH<sub>2</sub>), 1.23, 1.05 [9H each, d each,  $^3J(\text{P,H}) = 12 \text{ Hz}$  each, diastereotopic *t*-Bu], 1.15 (3H, t, CH<sub>3</sub>, Et).  $^{13}\text{C NMR}$  (C<sub>6</sub>D<sub>6</sub>):  $\delta$  221.8 [Cq, 1C,  $^2J(\text{P,C}) = 6 \text{ Hz}$ , *trans*-CO, (CO)<sub>5</sub>Cr], 219.1 [Cq, 4C,  $^2J(\text{P,C}) = 11 \text{ Hz}$ , *cis*-CO, (CO)<sub>5</sub>Cr], 157.5 [Cq, d,  $^3J(\text{P,C}) = 8 \text{ Hz}$ , C3], 143.8 [Cq, d,  $^2J(\text{P,C}) = 8 \text{ Hz}$ , C8], 142.6 (Cq, C9); 127.7, 126.6, 126.5, and 120.6 (CH each, C4–C7); 103.8 [CH, d,  $^2J(\text{P,C}) = 4 \text{ Hz}$ , C2], 66.4 (OCH<sub>2</sub>), 51.2 (CH, C1), 40.0, and 38.9 (Cq each, diastereotopic PCMe<sub>3</sub>), 31.5, and 30.8 (CH<sub>3</sub> each, diastereotopic Pt-Bu<sub>2</sub>), 15.8 (CH<sub>3</sub>, Et). IR (hexane), cm<sup>-1</sup> (%): 2056.2 (30), 1982.6 (5), 1928.0 (100) [ $\nu(\text{C=O})$ ]. MS (70 eV), *m/e* (%): 496 (20) [M<sup>+</sup>], 468 (10), 440 (5), 412 (30), 384 (25), 356 (60) [M<sup>+</sup> - 5CO], 314 (50), 304 (50) [356 - Cr], 272 (50), 248 (50), 247 (50), 159 (90), 131 (100) [indenone]. Anal. Calcd for C<sub>24</sub>H<sub>29</sub>CrO<sub>6</sub>P (496.5): C, 58.06; H, 5.89. Found: C, 58.23; H, 5.97.

**9a**:  $^1\text{H NMR}$  (C<sub>6</sub>D<sub>6</sub>):  $\delta$  8.18, 7.40, 7.21, 7.03 (1H each; d, d, dd, dd;  $^3J = 8 \text{ Hz}$  each, 4-H–7-H); 6.87 [1H, dd,  $^3J(\text{P,H}) = 5.5 \text{ Hz}$ ,  $^3J = 2 \text{ Hz}$ , 2-H], 5.03 (1H, d,  $^3J = 2 \text{ Hz}$ , 1-H), 3.28, and 3.15 (1H each, m each, diastereotopic OCH<sub>2</sub>), 1.20 (18H, 2 *t*-Bu), 1.15 (3H, t, CH<sub>3</sub>, Et).  $^{13}\text{C NMR}$  (C<sub>6</sub>D<sub>6</sub>):  $\delta$  222.6 [Cq, 1C,  $^2J(\text{P,C}) = 6 \text{ Hz}$ , *trans*-CO, (CO)<sub>5</sub>Cr], 219.1 [Cq, 4C,  $^2J(\text{P,C}) = 11 \text{ Hz}$ , *cis*-CO, (CO)<sub>5</sub>Cr], 147.3 (CH, C2), 143.8 [Cq,  $^1J(\text{P,C}) = 20 \text{ Hz}$ , C3], 143.6 (Cq, C8), 139.1 [Cq,  $^1J(\text{P,C}) = 9 \text{ Hz}$ , C9]; 128.4, 126.9, 125.4, 124.7 [CH each, C4–C7]; 83.0 [CH,  $^3J(\text{P,C}) = 4 \text{ Hz}$ , C1], 62.0 (OCH<sub>2</sub>), 38.8 and 38.6 [Cq each,  $^1J(\text{P,C}) = 15 \text{ Hz}$  each, PCMe<sub>3</sub>], 31.9 and 31.8 (3 CH<sub>3</sub> each, Pt-Bu), 16.5 (CH<sub>3</sub>, Et). IR (hexane), cm<sup>-1</sup> (%): 2057.7 (20), 1972.0 (5), 1941.2 (80), 1926.5 (100) [ $\nu(\text{C=O})$ ]. MS (70 eV), *m/e* (%): 496 (5) [M<sup>+</sup>], 412 (5), 384 (5), 356 (30) [M<sup>+</sup> - 5CO], 320 (30) [ligand + O?], 304 (10) [356 - Cr], 291 (20) [320 - Et], 247 (60) [304 - *t*Bu], 159 (95), 131 (100) [indenone]. Anal. Calcd for C<sub>24</sub>H<sub>29</sub>CrO<sub>6</sub>P (496.5): C, 58.06; H, 5.89. Found: C, 58.18; H, 5.94.

**9a'**:  $^1\text{H NMR}$  (C<sub>6</sub>D<sub>6</sub>):  $\delta$  7.94, 7.48, 7.23, 7.08 (1H each; d, d, dd, dd;  $^3J = 8 \text{ Hz}$  each, 4-H–7-H); 6.73 [1H, dd,  $^3J(\text{P,H}) = 2.5 \text{ Hz}$ ,  $^3J = 2 \text{ Hz}$ , 2-H], 5.14 (1H, d,  $^3J = 2 \text{ Hz}$ , 1-H), 3.39 and 3.25 (1H each, m each, diastereotopic OCH<sub>2</sub>), 1.25 (18H, 2 *t*-Bu), 1.11 (3H, t, CH<sub>3</sub>, Et).  $^{13}\text{C NMR}$  (C<sub>6</sub>D<sub>6</sub>):  $\delta$  219.1 and 218.1 [Cq each, d each,  $^2J(\text{P,C}) = 8.5 \text{ Hz}$  each, (CO)<sub>5</sub>Cr], 143.8 (CH, C2), 143.0 [Cq,  $^1J(\text{P,C}) = 18 \text{ Hz}$ , C3], 142.9 (Cq, C8), 142.0 (Cq, C9) = 9 Hz, C9]; 128.6, 127.8, 126.2, 123.8 [CH each, C4–

C7]; 84.0 [CH,  $^3J(P,C) = 8$  Hz, C1], 62.2 (OCH<sub>2</sub>), 39.4 and 38.6 (Cq each, diastereotopic PCMe<sub>3</sub>), 30.8 and 33.0 (3 CH<sub>3</sub> each, Pt-Bu), 16.5 (CH<sub>3</sub>, Et).

**[1-(Di-*tert*-butylphosphino)-3-ethoxyindene, P-W]pentacarbonylchromium (10b) and [3-(Di-*tert*-butylphosphino)-1-ethoxyindene, P-W]pentacarbonylchromium (9b) by Thermolysis of (E)-3b.** Thermolysis of [3-(di-*tert*-butylphosphino)-1-ethoxy-3-phenylpropenylidene]pentacarbonylchromium [(E)-3b] in an inert solvent leads to mixtures of varying composition, depending on the reaction conditions.

**(a) NMR Experiments.** A <sup>1</sup>H NMR spectrum of a solution of 32 mg (0.01 mmol) (E)-3b in 1 mL of C<sub>6</sub>D<sub>6</sub> after 35 h at 55 °C shows signals of 9b only. For different product composition, see Table 1.

**(b) Preparation of 9b.** A 314 mg (0.50 mmol) sample of (E)-3b in 3 mL of heptane is heated for 35 h to 55 °C. Chromatography on silica gel with pentane/dichloromethane (3:1) yields colorless 9b [*R*<sub>f</sub> = 0.4 in pentane/dichloromethane (3:1), 285 mg, 91%, pale yellow crystals, mp 98 °C].

**(c) Preparation of 10b.** A 314 mg (0.50 mmol) sample of (E)-3b in 3 mL of heptane is heated for 10 h to 80 °C. Chromatography on silica gel with pentane/dichloromethane (3:1) yields colorless 10b [*R*<sub>f</sub> = 0.4 in pentane/dichloromethane (3:1), 270 mg, 86%, pale yellow crystals, mp 140 °C, dec) and yellow 9b.

**10b:** <sup>1</sup>H NMR (C<sub>6</sub>D<sub>6</sub>): δ 7.87 (1H, d,  $^3J = 7.5$  Hz, 8-H), 7.56 (1H, dd,  $^3J = 7$  Hz,  $^4J = 1.5$  Hz, 4-H), 7.12 (1H, dd,  $^3J = 7.5$ , 7.5 Hz, 5-H), 7.05 (1H, ddd,  $^3J = 7$ , 7.5 Hz,  $^4J = 1.5$ , 6-H), 5.78 [1H, dd,  $^3J(P,H) = 3$  Hz,  $^3J = 2$  Hz, 2-H], 4.40 [1H, dd,  $^2J(P,H) = 8$  Hz,  $^3J = 2$  Hz, 1-H], 3.93 and 3.80 (1H each, m each, diastereotopic OCH<sub>2</sub>), 1.21 and 1.06 [9H each, d each,  $^3J(P,H) = 13$  Hz each, diastereotopic Pt-Bu<sub>2</sub>], 0.95 (3H, t, CH<sub>3</sub>, Et). <sup>13</sup>C NMR (C<sub>6</sub>D<sub>6</sub>): δ 199.8 [4C, d,  $^3J(P,C) = 6$  Hz, *cis*-CO, (CO)<sub>5</sub>W], 198.0 [1C, d,  $^3J(P,C) = 11$  Hz, *trans*-CO, (CO)<sub>5</sub>W], 157.5 [Cq, d,  $^3J(P,C) = 6$  Hz, C3], 142.3 [Cq, d,  $^2J(P,C) = 7$  Hz, C8], 141.4 (Cq, C9); 128.8, 128.6, 127.0, 119.8 (CH each, C4-C7); 103.8 (CH, C2), 65.8 (OCH<sub>2</sub>), 51.2 (CH,  $^1J(P,C) = 7$  Hz, C1), 40.0 and 39.0 [Cq each,  $^1J(P,C) = 6$  and 7 Hz, diastereotopic PCMe<sub>3</sub>], 31.6 and 31.4 (CH<sub>3</sub> each, diastereotopic Pt-Bu<sub>2</sub>), 15.0 (CH<sub>3</sub>, Et). MS (70 eV), <sup>184</sup>W, *m/e* (%): 628 (20) [M<sup>+</sup>], 488 (20) [M<sup>+</sup> - 5CO], 304 (30) [488 - W], 247 (30), 191 (30), 159 (80), 131 (100). IR (hexane), cm<sup>-1</sup> (%): 2067.3 (20), 1936.0 (100) [ν(C=O)]. Anal. Calcd for C<sub>24</sub>H<sub>29</sub>O<sub>6</sub>PW (628.3): C, 45.88; H, 4.65. Found: C, 45.97; H, 4.55.

**9b:** <sup>1</sup>H NMR (C<sub>6</sub>D<sub>6</sub>): δ 8.17, 7.40, 7.19, 7.01 (1H each; d, d, dd, dd; 4-H-7-H); 6.87 [2-H, dd,  $^3J(P,H) = 6$  Hz,  $^3J = 2$  Hz, 2-H], 5.05 (1H, d,  $^3J = 2$  Hz, 1-H), 3.30 and 3.25 (1H each, m each, diastereotopic OCH<sub>2</sub>), 1.25 and 1.20 (9H each, d each,  $^3J(P,H) = 14$  Hz each, diastereotopic Pt-Bu<sub>2</sub>), 1.15 (3H, t, CH<sub>3</sub>, Et). <sup>13</sup>C NMR (C<sub>6</sub>D<sub>6</sub>): δ 218.6 [Cq, 4C,  $^2J(P,C) = 8$  Hz, *cis*-CO, (CO)<sub>5</sub>W], 198.3 [Cq, 1C,  $^2J(P,C) = 21$  Hz, *trans*-CO, (CO)<sub>5</sub>W], 147.5 [CH,  $^2J(P,C) = 6$  Hz, C2], 143.8 (Cq, C8), 143.6 [Cq,  $^1J(P,C) = 17$  Hz, C3], 138.5 [Cq,  $^2J(P,C) = 15$  Hz, C9]; 128.3, 126.9, 126.2, 124.7 [CH each, C4-C7]; 83.0 [CH,  $^3J(P,C) = 9$  Hz, C1], 62.0 (OCH<sub>2</sub>), 38.3 and 38.1 [Cq each,  $^1J(P,C) = 14$  Hz each, diastereotopic PCMe<sub>3</sub>], 31.3 and 31.1 [CH<sub>3</sub> each,  $^2J(P,C) = 14$  Hz, diastereotopic CMe<sub>3</sub>], 16.3 (CH<sub>3</sub>, Et). IR (hexane), cm<sup>-1</sup> (%): 2067.7 (20), 1973.2 (5), 1940.2 (90), 1925.7 (100) [ν(C=O)]. MS (70 eV), <sup>184</sup>W, *m/e* (%): 628 (20) [M<sup>+</sup>], 572 (5), 516 (20), 488 (20) [M<sup>+</sup> - 5CO], 304 (30) [488 - W], 247 (30), 191 (60), 163 (40), 57 (100). Anal. Calcd for C<sub>24</sub>H<sub>29</sub>O<sub>6</sub>PW (628.3): C, 45.88; H, 4.65. Found: C, 46.12; H, 4.63.

**[3-(Dicyclohexylphosphino)-1-ethoxyindene, P-Cr]pentacarbonylchromium (9c) and [1-(Dicyclohexylphosphino)-3-ethoxyindene, P-Cr]pentacarbonylchromium (10c).** A 274 mg (0.50 mmol) sample of [3-dicyclohexylphosphino)-1-ethoxy-3-phenylpropenylidene]pentacarbonylchromium [(E)-3c] in 4 mL of heptane is heated for 2 h to 80 °C. The <sup>1</sup>H NMR spectra indicate a clean conversion of (E)-3c into a 8:1 mixture of 9c and 10c. After 2 h at 100 °C, compound 10c is observed as the only product.

**10c:** <sup>1</sup>H NMR (C<sub>6</sub>D<sub>6</sub>): δ 7.61, 7.21, 7.12, 7.02 (1H each; d, d, dd, dd;  $^3J = 8$  Hz each, 4-H-7-H); 5.50 [1H, dd,  $^3J(P,H) = 3$  Hz,  $^3J = 2$  Hz, 2-H], 4.15 [1H, dd,  $^2J(P,H) = 8$  Hz,  $^3J = 2$  Hz, 1-H], 3.80 and 3.65 (1H each, m each, diastereotopic OCH<sub>2</sub>), 2.30 and 2.25 [1H each, d each,  $^3J(P,H) = 12$  Hz each, diastereotopic CHP, Cy]; 1.85, 1.66, 1.52, 1.20 (2:8:8:2, m each, CH<sub>2</sub>, Cy), 1.05 (3H, t, CH<sub>3</sub>, Et). <sup>13</sup>C NMR (C<sub>6</sub>D<sub>6</sub>): δ 222.8 [Cq, 1C,  $^2J(P,C) = 6$  Hz, *trans*-CO, (CO)<sub>5</sub>Cr], 219.0 [Cq, 4C,  $^2J(P,C) = 13$  Hz, *cis*-CO, (CO)<sub>5</sub>Cr], 158.6 [Cq, C3], 142.5 [Cq, d,  $^2J(P,C) = 8$  Hz, C8], 141.1 (Cq, C9); 127.6, 126.4, 125.0, and 120.2 (CH each, C4-C7); 100.0 [CH, d,  $^2J(P,C) = 4$  Hz, C2], 65.6 (OCH<sub>2</sub>), 45.7 (CH, C1), 39.3 and 39.1 (CH each, diastereotopic CHP); 38.5, 36.6, 36.4, 35.3, 35.2 (CH<sub>2</sub> each, 2 Cy); 14.9 (CH<sub>3</sub>, Et). IR (hexane), cm<sup>-1</sup> (%): 2056.0 (30), 1982.6 (5), 1928.0 (100) [ν(C=O)]. MS (70 eV), *m/e* (%): 548 (20) [M<sup>+</sup>], 520 (10), 464 (40), 436 (30), 409 (50), 408 (60) [M<sup>+</sup> - 5CO], 356 (30) [408 - Cr], 327 (50) [356 - Et], 245 (30) [327 - C<sub>6</sub>H<sub>10</sub>], 131 (100). Anal. Calcd for C<sub>28</sub>H<sub>33</sub>CrO<sub>6</sub>P (548.5): C, 61.31; H, 6.06. Found: C, 61.44; H, 6.28.

**9c:** <sup>1</sup>H NMR (C<sub>6</sub>D<sub>6</sub>): δ 7.72, 7.30, 7.21, 7.13 (1H each; d, d, dd, dd;  $^3J = 8$  Hz each, 4-H-7-H); 7.02 [1H, dd,  $^3J(P,H) = 5.5$  Hz,  $^3J = 2$  Hz, 2-H], 5.00 (1H, d,  $^3J = 2$  Hz Hz, 1-H), 3.26 and 3.16 (1H each, m each, diastereotopic OCH<sub>2</sub>), 2.60 (2H, m, diastereotopic CHP); 2.10, 1.80, 1.60, 1.20 (4:6:6:4, CH<sub>2</sub> of Cy); 1.05 (3H, t, Et). IR (hexane), cm<sup>-1</sup> (%): 2056.7 (20), 1974.3 (5), 1925.2 (100) [ν(C=O)].

**1-(Di-*tert*-butylphosphino)-3-ethoxyindene (12) from (E)-3a or (E)-3b.** **(a) NMR experiment.** A 25 mg (0.05 mmol) sample of [3-(di-*tert*-butylphosphino)-1-ethoxy-3-phenylpropenylidene]pentacarbonylchromium [(E)-3a] in 1 mL of C<sub>6</sub>D<sub>6</sub>, 5 mg (0.05 mmol) of pyridine, and hexamethylbenzene as an internal standard is heated to 80 °C for 2 h. The <sup>1</sup>H NMR spectrum indicates a clean conversion of (E)-3a into 12 (>90%) and (CO)<sub>5</sub>Cr(C<sub>6</sub>H<sub>5</sub>N) 11a [δ = 7.91, 6.55, and 6.02, 2:1:2H, m each]. A 32 mg (0.05 mmol) sample of [3-(di-*tert*-butylphosphino)-1-ethoxy-3-phenylpropenylidene]pentacarbonylchromium [(E)-3b] and 5 mg of pyridine at 80 °C for 8 h give 12 (>90%) and (CO)<sub>5</sub>W(C<sub>6</sub>H<sub>5</sub>N) 11b [δ = 8.05, 6.95 and 6.04, 2:1:2H, m each].

**(b) Preparation of 12.** A 248 mg (0.50 mmol) sample (E)-3a in 4 mL of heptane and 45 mg (0.50 mmol) of pyridine is heated for 1.5 h to 80 °C. 11a forms yellow crystals at -15 °C, which are removed by centrifugation after 12 h. 12 separates from pentane at -45 °C in yellowish crystals, mp 88 °C. Solutions of 12 are sensitive to oxidation by air.

**12:** <sup>1</sup>H NMR (C<sub>6</sub>D<sub>6</sub>): δ 7.92, 7.68, 7.20 (1:1:2H, m each, 4-H-7-H); 5.56 (1H, d,  $^3J = 2$  Hz, 2-H), 3.84 (2H, m, diastereotopic OCH<sub>2</sub>), 3.70 [1H, dd,  $^2J(P,H) = 2$  Hz,  $^3J = 2$  Hz, 1-H], 1.29 and 0.93 [9H each, d each,  $^3J(P,H) = 11$  Hz each, diastereotopic *t*-Bu], 1.21 (3H, t, CH<sub>3</sub>, Et). <sup>13</sup>C NMR (C<sub>6</sub>D<sub>6</sub>): δ 157.8 (Cq, C3), 148.1 [Cq, d,  $^2J(P,C) = 16$  Hz, C8], 138.9 [Cq, d,  $^3J(P,C) = 4$  Hz, C9]; 126.6, 126.1, 125.2, 119.1 (CH each, C4-C7); 103.5 [CH, d,  $^2J(P,C) = 4$  Hz, C2], 65.3 (OCH<sub>2</sub>), 43.0 [CH, d,  $^1J(P,C) = 43$  Hz, C1], 34.1 and 32.3 [Cq each, d each,  $^1J(P,C) = 32$  and 26 Hz, diastereotopic PCMe<sub>3</sub>], 30.8 and 30.2 [CH<sub>3</sub> each, d each,  $^2J(P,C) = 14$  and 13 Hz, diastereotopic P(CMe<sub>3</sub>)], 14.9 (CH<sub>3</sub>, Et). MS (70 eV), *m/e* (%): 304 (10) [M<sup>+</sup>], 247 (80) [M - *t*-Bu], 191 (50), 159 (100) [M - *t*-Bu<sub>2</sub>P], 131 (100). Anal. Calcd for C<sub>19</sub>H<sub>29</sub>OP (304.4): C, 74.97; H, 9.60. Found: C, 74.75; H, 9.36.

**1-(Di-*tert*-butylphosphino)-3-ethoxyindene (14) by Oxidation of 12 on Air.** A 30 mg (0.10 mmol) sample of 1-di-*tert*-butylphosphino-3-ethoxyindene (12) in 1 mL of C<sub>6</sub>D<sub>6</sub> and hexamethylbenzene as an internal standard is exposed to air for 30 h at 20 °C. The <sup>1</sup>H NMR spectrum indicates that a clean conversion into 14 (>90%) has occurred. 14 separates from pentane at -45 °C in yellowish crystals. <sup>1</sup>H NMR (C<sub>6</sub>D<sub>6</sub>): δ 8.63, 7.71, 7.20 (1:1:2H, m each, 4-H-7-H); 5.16 [1H, dd,  $^3J = 2$  Hz,  $^3J(P,H) = 2$  Hz, 2-H], 4.06 [1H, dd,  $^2J(P,H) = 22$  Hz,  $^3J = 2$  Hz, 1-H], 3.85 (2H, m, diastereotopic OCH<sub>2</sub>), 1.55 and 1.10 [9H each, d each,  $^3J(P,H) = 25$  Hz each, diastereotopic *t*-Bu], 1.21 (3H, t, CH<sub>3</sub>, Et). <sup>13</sup>C NMR (C<sub>6</sub>D<sub>6</sub>): δ 154.3 (Cq, C3), 143.2

[Cq, d,  $^2J(\text{P},\text{C}) = 4$  Hz, C8], 136.0 (Cq, C9); 127.4, 126.8, 124.8, 118.4 (CH each, C4–C7); 97.4 (CH, C2), 64.9 (OCH<sub>2</sub>), 45.5 [CH, d,  $^1J(\text{P},\text{C}) = 33$  Hz, C1], 38.1 and 37.0 [Cq each, d each,  $^1J(\text{P},\text{C}) = 37, 33$  Hz, diastereotopic PCMe<sub>3</sub>], 30.6 and 27.2 [CH<sub>3</sub> each, d each,  $^2J(\text{P},\text{C}) = 11$  Hz, diastereotopic P(CMe<sub>3</sub>)], 14.6 (CH<sub>3</sub>, Et). IR (diffuse reflection), cm<sup>-1</sup> (%): = 1176 (100) [(C–O) and/or (P=O)]. MS (70 eV), *m/e* (%): 320 (10) [M<sup>+</sup>], 291 (10) [M – Et], 159 (100) [M – *t*-Bu<sub>2</sub>PO], 131 (50) [150 – CO]. Anal. Calcd for C<sub>19</sub>H<sub>29</sub>O<sub>2</sub>P (320.4): C, 74.97; H, 9.60. Found: C, 75.00; H, 9.75.

**(*E*)-Ethyl 3-(di-*tert*-butylphosphono)propenoate [(*E*)-13] by Oxidation of (*E*)-3a on Air.** A 25 mg (0.05 mmol) sample of [3-(di-*tert*-butylphosphino)-1-ethoxy-3-phenylpropenyldene]pentacarbonylchromium [(*E*)-3a] in 1 mL of C<sub>6</sub>D<sub>6</sub> and hexamethylbenzene as an internal standard is exposed to air for 30 h at 20 °C. The mixture is centrifuged, and a <sup>1</sup>H NMR spectrum is taken from the supernatant solution, which indicates a clean conversion of (*E*)-3a into (*E*)-13 (>90%). Compound (*E*)-13 separates from pentane at –45 °C in yellowish crystals, mp 87 °C. <sup>1</sup>H NMR (C<sub>6</sub>D<sub>6</sub>): δ 7.20, 7.05,

and 7.00 (2:1:2H, m each, Ph); 7.20 [1H, d,  $^3J(\text{P},\text{H}) = 15$  Hz, 2-H], 3.96 (2H, q, OCH<sub>2</sub>), 1.17 [18H, d,  $^2J(\text{P},\text{H}) = 13$  Hz, Pt-Bu<sub>2</sub>], 0.68 (3H, t, CH<sub>3</sub>, Et). MS (70 eV), *m/e* (%): 337 (10) [M<sup>+</sup> + 1], 279 (5) [M – *t*-Bu], 263 (5), 251 (70) [279 – H<sub>2</sub>C=CH<sub>2</sub>], 195 (100) [251 – C<sub>4</sub>H<sub>8</sub>], 57 (40), 41 (50). IR (diffuse reflection), cm<sup>-1</sup> (%): = 1728 (100) [(C=O)], 1165 (100) [(C–O) and/or (P=O)]. Anal. Calcd for C<sub>19</sub>H<sub>29</sub>O<sub>3</sub>P (336.4): C, 67.84; H, 8.69. Found: C, 67.93; H, 8.80.

**Acknowledgment.** This work was supported by the Volkswagen-Stiftung and the Fonds der Chemischen Industrie.

**Supplementary Material Available:** For 10a, tables of crystal data and details of data collection, interatomic distances and angles, final thermal parameters, and hydrogen positional parameters (8 pages). Ordering information is given on any current masthead page.

OM9405246



**[*cis,cis,trans*-RuCl<sub>2</sub>(CO)<sub>2</sub>{Ph<sub>2</sub>P(CH<sub>2</sub>CH<sub>2</sub>O)<sub>n</sub>CH<sub>2</sub>CH<sub>2</sub>PPh<sub>2</sub>-*P,P'*}]<sub>m</sub>**  
**(*n* = 4, 5; *m* = 1, 2, ...) Metallacrown Ethers. X-ray**  
**Crystal Structures of**  
***cis,cis,trans*-RuCl<sub>2</sub>(CO)<sub>2</sub>{Ph<sub>2</sub>P(CH<sub>2</sub>CH<sub>2</sub>O)<sub>4</sub>CH<sub>2</sub>CH<sub>2</sub>PPh<sub>2</sub>-*P,P'*}**,  
**a Complex Which Exhibits Rotational Isomers in the**  
**Solid State, and [*cis,cis,trans*-RuCl<sub>2</sub>(CO)<sub>2</sub>-**  
**{ $\mu$ -Ph<sub>2</sub>P(CH<sub>2</sub>CH<sub>2</sub>O)<sub>4</sub>CH<sub>2</sub>CH<sub>2</sub>PPh<sub>2</sub>-*P,P'*}]<sub>2</sub>, an Unusual**  
**Dimetallacrown Ether**

Gary M. Gray,\* Ashima Varshney, and Christina H. Duffey

*Department of Chemistry, The University of Alabama at Birmingham, 242-OB15 UAB Station, Birmingham, Alabama 35294, and Department of Chemistry, Samford University, Birmingham, Alabama 35229*

Received August 16, 1994<sup>⊗</sup>

The reactions of Ph<sub>2</sub>P(CH<sub>2</sub>CH<sub>2</sub>O)<sub>n</sub>CH<sub>2</sub>CH<sub>2</sub>PPh<sub>2</sub> (*n* = 4, 5) ligands with RuCl<sub>2</sub>(CO)<sub>3</sub>(THF) give a variety of complexes of the type [*cis,cis,trans*-RuCl<sub>2</sub>(CO)<sub>2</sub>{Ph<sub>2</sub>P(CH<sub>2</sub>CH<sub>2</sub>O)<sub>n</sub>CH<sub>2</sub>CH<sub>2</sub>PPh<sub>2</sub>-*P,P'*}]<sub>m</sub>. Multinuclear NMR and IR spectroscopic studies indicate that the major product in each reaction is the mononuclear (*m* = 1) complex in which the Ph<sub>2</sub>P(CH<sub>2</sub>CH<sub>2</sub>O)<sub>n</sub>CH<sub>2</sub>CH<sub>2</sub>PPh<sub>2</sub> ligand spans two trans positions. The minor products are polynuclear (*m* = 2, 3, ...) complexes in which each Ph<sub>2</sub>P(CH<sub>2</sub>CH<sub>2</sub>O)<sub>n</sub>CH<sub>2</sub>CH<sub>2</sub>PPh<sub>2</sub> ligand bridges two rutheniums. X-ray crystal structures of *cis,cis,trans*-RuCl<sub>2</sub>(CO)<sub>2</sub>{Ph<sub>2</sub>P(CH<sub>2</sub>CH<sub>2</sub>O)<sub>4</sub>CH<sub>2</sub>CH<sub>2</sub>PPh<sub>2</sub>-*P,P'*}, **4a**, (monoclinic space group *P*2<sub>1</sub>/*n*, *a* = 10.194(1), *b* = 22.907(3), *c* = 15.259(2) Å; β = 92.46(1)°; *V* = 3560.0(8) Å<sup>3</sup>; *Z* = 4) and [*cis,cis,trans*-RuCl<sub>2</sub>(CO)<sub>2</sub>{ $\mu$ -Ph<sub>2</sub>P(CH<sub>2</sub>CH<sub>2</sub>O)<sub>4</sub>CH<sub>2</sub>CH<sub>2</sub>PPh<sub>2</sub>-*P,P'*}]<sub>2</sub>(CH<sub>3</sub>)<sub>2</sub>CO, **4b**·(CH<sub>3</sub>)<sub>2</sub>CO, (monoclinic space group *P*2<sub>1</sub>/*a*, *a* = 18.976(3), *b* = 22.076(5), *c* = 10.426(8) Å; β = 111.64(1)°; *V* = 4060(1) Å<sup>3</sup>; *Z* = 4) confirm these conclusions. The monomeric **4a** is a rare example of an octahedral complex with a trans-spanning bis(phosphine) ligand. Two different rotamers of **4a** are observed in the solid state. In the major rotamer the trans-spanning ligand passes between one chloride and one carbonyl while in the minor rotamer the trans-spanning ligand passes between the two chlorides. The dimeric **4b** is the first example of a dimetallacrown ether. The trans phosphines in **4b** cause the formation of two, distinct metallacrown ether sites separated by a chloride and a carbonyl ligand on each ruthenium.

### Introduction

One of the most interesting classes of metallomacrocycles<sup>1</sup> are the metallacrown ethers, formed by chelation of R<sub>2</sub>PX(CH<sub>2</sub>CH<sub>2</sub>O)<sub>n</sub>CH<sub>2</sub>CH<sub>2</sub>XPR<sub>2</sub> (R = Ph, O-alkyl; X = -, O; *n* ≥ 3) ligands to transition metals.<sup>2-6</sup> These metallacrown ethers readily coordinate hard metal

cations, and the stabilities of the alkali metal cation complexes depend upon the relative sizes of the cation and the metallacrown ether cavity.<sup>2,4,6</sup> Cations bound to the metallacrown ethers can interact with the oxygen lone pairs of the carbonyl ligands in *cis*-Mo(CO)<sub>4</sub>{R<sub>2</sub>PX(CH<sub>2</sub>CH<sub>2</sub>O)<sub>n</sub>CH<sub>2</sub>CH<sub>2</sub>XPR<sub>2</sub>-*P,P'*} metallacrown ethers. Coordination of Li<sup>+</sup> activates the carbonyl ligands of *cis*-Mo(CO)<sub>4</sub>{R<sub>2</sub>PO(CH<sub>2</sub>CH<sub>2</sub>O)<sub>2</sub>CH<sub>2</sub>CH<sub>2</sub>OPR<sub>2</sub>-*P,P'*} metallacrown ethers toward nucleophilic attack by alkyl- and aryllithium reagents.<sup>2</sup> Coordination of Hg<sup>2+</sup> catalyzes the *cis* to *trans* isomerization of the *cis*-Mo(CO)<sub>4</sub>{Ph<sub>2</sub>P(CH<sub>2</sub>CH<sub>2</sub>O)<sub>4</sub>CH<sub>2</sub>CH<sub>2</sub>PPh<sub>2</sub>-*P,P'*} metallacrown ether.<sup>6</sup> These results suggest that hard metal ion complexes of metallacrown ethers could be used to activate a variety of bifunctional ligands, such as carbonyls, that can coordinate to both metal centers. This property could be quite useful in the design of catalysts for reactions involving such ligands.

The phosphorus-donor groups are *cis* coordinated in all reported metallacrown ethers except *trans*-Mo(CO)<sub>4</sub>{Ph<sub>2</sub>P(CH<sub>2</sub>CH<sub>2</sub>O)<sub>4</sub>CH<sub>2</sub>CH<sub>2</sub>PPh<sub>2</sub>-*P,P'*}, **1**.<sup>5</sup> The chelate

\* To whom correspondence should be addressed at The University of Alabama at Birmingham.

<sup>⊗</sup> Abstract published in *Advance ACS Abstracts*, November 1, 1994.  
 (1) This class of complexes has recently been reviewed: van Veggel, F. C. J. M.; Werblom, W.; Reinhoudt, D. N. *Chem. Reviews* **1994**, *94*, 279.

(2) (a) Powell, J.; Kuskis, A.; May, C. J.; Nyberg, S. C.; Smith, S. J. *J. Am. Chem. Soc.* **1981**, *103*, 5941. (b) Powell, J.; Nyberg, S. C.; Smith, S. J. *Inorg. Chim. Acta* **1983**, *76*, L75. (c) Powell, J.; Ng, K. S.; Ng, W. W.; Nyberg, S. C. *J. Organomet. Chem.* **1983**, *243*, C1. (d) Powell, J.; Gregg, M.; Kuskis, A.; Meindl, P. *J. Am. Chem. Soc.* **1983**, *105*, 1064. (e) Powell, J.; Gregg, M. R.; Kuskis, A.; May, C. J.; Smith, S. J. *Organometallics* **1989**, *8*, 2918. (f) Powell, J.; Kuskis, A.; May, C. J.; Meindl, P. E.; Smith, S. J. *Organometallics* **1989**, *8*, 2933. (g) Powell, J.; Gregg, M. R.; Meindl, P. E. *Organometallics* **1989**, *8*, 2942. (h) Powell, J.; Lough, A.; Wang, F. *Organometallics* **1992**, *11*, 2289.

(3) (a) Alcock, N. W.; Brown, J. M.; Jeffery, J. C. *J. Chem. Soc., Chem. Commun.* **1974**, 829. (b) Alcock, N. W.; Brown, J. M.; Jeffery, J. C. *J. Chem. Soc., Dalton Trans.* **1976**, 583. (c) Thewissen, D. H. W.; Timmer, K.; Noltes, J. G.; Marsman, J. W.; Laine, R. M. *Inorg. Chim. Acta* **1985**, *97*, 143. (d) Timmer, K.; Thewissen, D. H. W. *Inorg. Chim. Acta* **1985**, *100*, 235. (e) Timmer, K.; Thewissen, H. M. D.; Marsman, J. W. *Recl. Trav. Chim. Pays-Bas* **1988**, *107*, 248.

(4) (a) Varshney, A.; Gray, G. M. *Inorg. Chem.* **1991**, *30*, 1748. (b) Varshney, A.; Webster, M. L.; Gray, G. M. *Inorg. Chem.* **1992**, *31*, 2580.

(5) Gray, G. M.; Duffey, C. H. *Organometallics* **1994**, *13*, 1542.

(6) Gray, G. M.; Duffey, C. H. *Organometallics*, in press.

Table 1.  $^{31}\text{P}$  and Phenyl  $^{13}\text{C}$  NMR Data<sup>a</sup>

no.	P		ipso		ortho		meta		para
	$\delta(^{31}\text{P})$ (ppm)	$\delta(^{13}\text{C})$ (ppm)	$ J(\text{PC}) $ (Hz)	$\delta(^{13}\text{C})$ (ppm)	$ J(\text{PC}) $ (Hz)	$\delta(^{13}\text{C})$ (ppm)	$ J(\text{PC}) $ (Hz)	$\delta(^{13}\text{C})$ (ppm)	
1 <sup>b</sup>	32.57 s	139.48 aq	34 <sup>d</sup>	131.70 aq	11 <sup>f</sup>	128.28 bs		129.16 s	
2 <sup>c</sup>	-21.68 s	138.17 d	12 <sup>e</sup>	132.68 d	18 <sup>g</sup>	128.56 d	12 <sup>h</sup>	128.41 s	
3 <sup>c</sup>	-21.69 s	138.29 d	12 <sup>e</sup>	132.71 d	17 <sup>g</sup>	128.58 d	10 <sup>h</sup>	128.41 s	
4a	9.74 s	132.74 aq	47 <sup>d</sup>	132.55 aq	8 <sup>f</sup>	128.74 aq	8 <sup>f</sup>	130.79 s	
4b	13.43 s	131.02 aq	45 <sup>d</sup>	132.85 aq	8 <sup>f</sup>	128.52 bs		130.71 s	
4d	14.77 s	j		132.93 bs		128.43 bs		130.70 s	
5a	11.16 s	131.85 aq	46 <sup>d</sup>	132.63 aq	10 <sup>f</sup>	128.71 bs		130.81 s	

<sup>a</sup> b = broad, s = singlet, d = doublet, aq = apparent quintet. <sup>b</sup> Data from ref 5. <sup>c</sup> Data from ref 3a. <sup>d</sup>  $|^1J(\text{PC}) + ^3J(\text{PC})|$ . <sup>e</sup>  $|^1J(\text{PC})|$ . <sup>f</sup>  $|^2J(\text{PC}) + ^4J(\text{PC})|$ . <sup>g</sup>  $|^2J(\text{PC})|$ . <sup>h</sup>  $|^3J(\text{PC})|$ . <sup>i</sup>  $|^3J(\text{PC}) + ^5J(\text{OC})|$ . <sup>j</sup> Not observed.

Table 2. Aliphatic and Carbonyl  $^{13}\text{C}$  NMR Data<sup>a</sup>

no.	C1		C2		C3, C4, C5, C6	CO	
	$\delta(^{13}\text{C})$ (ppm)	$ J(\text{PC}) $ (Hz)	$\delta(^{13}\text{C})$ (ppm)	$ J(\text{PC}) $ (Hz)	$\delta(^{13}\text{C})$ (ppm)	$\delta(^{13}\text{C})$ (ppm)	$ J(\text{PC}) $ (Hz)
1 <sup>b</sup>	34.38 aq	22 <sup>d</sup>	66.96 aq	12 <sup>f</sup>	71.07 s, 71.03 s, 70.24 s	210.59 t	8
2 <sup>c</sup>	28.73 d	12 <sup>e</sup>	68.53 d	26 <sup>g</sup>	70.58 s, 70.53 s, 70.10 s		
3 <sup>c</sup>	28.73 d	13 <sup>e</sup>	68.49 d	25 <sup>g</sup>	70.55 s, 70.51 s, 70.51 s, 70.07 s		
4a	27.05 aq	29 <sup>d</sup>	65.18 s		70.46 s, 69.98 s, 69.07 s	191.67 t	11
4b	24.54 aq	27 <sup>d</sup>	66.01 s		70.61 s, 70.44 s, 69.95 s	192.23 t	11
4d	24.13 aq	27 <sup>d</sup>	66.05 s		70.43 s, 70.36 s, 69.86 s	192.25 t	11
5a	25.47 aq	28 <sup>d</sup>	65.54 s		70.97 s, 70.69 s, 69.89 s, 69.69 s	191.94 t	11

<sup>a</sup> b = broad, s = singlet, d = doublet, t = triplet, aq = apparent quintet. <sup>b</sup> Data from ref 5. <sup>c</sup> Data from ref 3a. <sup>d</sup>  $|^1J(\text{PC}) + ^3J(\text{PC})|$ . <sup>e</sup>  $|^1J(\text{PC})|$ . <sup>f</sup>  $|^2J(\text{PC}) + ^4J(\text{PC})|$ . <sup>g</sup>  $|^2J(\text{PC})|$ .

ring in **1** has very different solution and solid state conformations from those of the chelate rings in the metallacrown ethers with cis phosphorus-donor groups. In addition, the  $\text{Mo}(\text{CO})_4$  group in **1** freely rotates within the chelate ring making this complex a 'molecular gyroscope'. Both these properties suggest that metallacrown ethers with trans-coordinated phosphorus-donor groups (trans-metallacrown ethers) could exhibit properties that are quite different from those with cis-coordinated phosphorus-donor groups (cis-metallacrown ethers).

In this paper, we report the results of our studies of the reactions of  $\text{RuCl}_2(\text{CO})_3(\text{THF})$  with  $\text{Ph}_2\text{P}(\text{CH}_2\text{CH}_2\text{O})_n\text{CH}_2\text{CH}_2\text{PPh}_2$  ( $n = 4$  (**2**),  $5$  (**3**)). These reactions yield a variety of trans-metallacrown ethers, and these have been characterized by multinuclear NMR and IR spectroscopy. The insights that these spectroscopic studies provide into the solution structures of these metallacrown ethers are discussed. X-ray structures of the major product and one of the minor products from the reaction of  $\text{RuCl}_2(\text{CO})_3(\text{THF})$  with  $\text{Ph}_2\text{P}(\text{CH}_2\text{CH}_2\text{O})_4\text{CH}_2\text{CH}_2\text{PPh}_2$  have also been determined and are presented.

### Experimental Section

The  $^{31}\text{P}\{^1\text{H}\}$  and  $^{13}\text{C}\{^1\text{H}\}$  NMR spectra were recorded on a GE NT-300, multinuclear NMR spectrometer. The  $^{31}\text{P}$  NMR spectra were referenced to external 85%  $\text{H}_3\text{PO}_4$ , and the  $^{13}\text{C}$  NMR spectra were referenced to internal  $\text{SiMe}_4$ . The  $^{31}\text{P}$  and  $^{13}\text{C}$  NMR data for the complexes are given in Tables 1 and 2 with positive chemical shifts downfield from those of the references. Infrared spectra of KBr disks of the complexes were run on a Nicolet IR44 spectrometer. Elemental analyses were carried out by Atlantic Microlab, Inc., Norcross, GA.

All free ligands, tetrahydrofuran (THF) and diethyl ether were handled under high purity nitrogen, and all reactions and recrystallizations were carried out under high purity nitrogen. The solid products were air stable. All solvents were of reagent grade and were used as received except for diethyl ether and THF which were distilled from sodium-benzophenone. All starting materials were reagent grade and were used as received. The deuterated solvents were opened and handled under a nitrogen atmosphere at all times. The  $\text{Ph}_2\text{P}(\text{CH}_2\text{O})_n\text{CH}_2\text{CH}_2\text{PPh}_2$  ( $n = 4$  (**2**),  $5$  (**3**)) ligands<sup>4a</sup> and  $\text{RuCl}_2(\text{CO})_3(\text{THF})$ <sup>7</sup> were prepared using literature procedures.

$[\text{cis,cis,trans-Ru}(\text{CO})_2\text{Cl}_2\{\text{Ph}_2\text{P}(\text{CH}_2\text{CH}_2\text{O})_4\text{CH}_2\text{CH}_2\text{PPh}_2\text{-P,P'}\}]_m$  (**4**). Solutions of 1.00 g (3.05 mmol) of  $\text{RuCl}_2(\text{CO})_3(\text{THF})$  in 500 mL of dichloromethane and 1.85 g (3.23 mmol) of **2** in 500 mL of dichloromethane were added dropwise and simultaneously to 1000 mL of dichloromethane over a period of 5 h. The reaction mixture was then stirred for an additional 18 h after which it was evaporated to dryness to yield 2.56 g (100%) of crude **4** as a white foam. The  $^{31}\text{P}$  NMR (chloroform- $d_1$ ) of the material contained four singlets at 9.71 (**4a**, major), 13.42 (**4b**, minor), 14.35 (**4c**, very minor) and 14.77 (**4d**, minor) ppm. A portion of the material (0.80 g) was chromatographed on silica gel. Elution with a 3:1 mixture of ethyl acetate-hexanes yielded **4a** (0.46 g, 58%). Next, elution with a 4:1 mixture of ethyl acetate-hexanes initially yielded **4b** (0.13 g, 16%) and then a mixture of **4b**, **4c** and **4d**. Finally, elution with a 10:1 mixture of ethyl acetate-methanol yielded pure **4d** (0.07 g, 9%). Each fraction that contained a single component was triturated with hexanes to give the compounds as analytically pure white powders (mp 203–205 °C for **4a**, 192–195 °C for **4b**, 90–95 °C for **4d**). Anal. Calcd for  $\text{C}_{36}\text{H}_{40}\text{Cl}_2\text{O}_6\text{P}_2\text{Ru}$ : C, 53.86; H, 4.99%. Found for **4a**: C, 53.65; H, 5.09%. Found for **4b**: C, 53.56; H, 5.06%. Found for **4d**: C, 53.62; H, 5.13%. IR (KBr):  $\nu(\text{CO})$  2058, 1995  $\text{cm}^{-1}$ , **4a**; 2058, 1995  $\text{cm}^{-1}$ , **4b**; 2058, 1995  $\text{cm}^{-1}$ , **4d**.

$[\text{cis,cis,trans-Ru}(\text{CO})_2\text{Cl}_2\{\text{Ph}_2\text{P}(\text{CH}_2\text{CH}_2\text{O})_5\text{CH}_2\text{CH}_2\text{PPh}_2\text{-P,P'}\}]_m$  (**5**). Using the procedure for the preparation of crude **4**, 0.10 g (0.32 mmol) of **3** and 0.10 g (0.30 mmol) of  $\text{RuCl}_2(\text{CO})_3(\text{THF})$  were reacted to yield a white waxy residue. A  $^{31}\text{P}$  NMR spectrum of the material in chloroform- $d_1$  had singlets at 11.17 (**5a**, major), 13.99 (**5b**, minor) and 14.75 (**5c**, minor). The residue was chromatographed on silica gel. Elution with a 2:1 mixture of ethyl acetate-hexanes yielded 0.20 g (74%) of analytically pure **5a** (mp 280 °C). Anal. Calcd for  $\text{C}_{38}\text{H}_{44}\text{Cl}_2\text{O}_7\text{P}_2\text{Ru}$ : C, 53.91; H, 5.24%. Found: C, 54.49; H, 5.32%. IR (KBr):  $\nu(\text{CO})$  2058, 1997  $\text{cm}^{-1}$ .

(7) We originally reported that this complex was  $[\text{Ru}(\text{CO})_3\text{Cl}_2] \cdot 0.75\text{THF}$  based upon analytical results. (Reddy, V. V. S.; Whitten, J. E.; Redmill, K. A.; Varshney, A.; Gray, G. M. *J. Organomet. Chem.* **1989**, *372*, 207). We have now obtained a crystal structure of this complex (Duffey, C. H.; Gray, G. M. Unpublished results) which indicates that the correct formula is as shown in the text. The difference in formulas most likely is due to loss of THF during drying of the analytical sample.

**X-ray Structure Determination of 4a and 4b(CH<sub>3</sub>)<sub>2</sub>CO.** A colorless, needlelike crystal of **4a** was grown by slowly diffusing hexanes into a dichloromethane/methanol solution of the complex. A colorless, blocky crystal of **4b**(CH<sub>3</sub>)<sub>2</sub>CO was grown by slowly diffusing acetone into a dichloromethane solution of **4b**. The crystals were mounted on glass fibers with epoxy cement, and the cell constants were obtained from least-squares refinement of 25 reflections with  $25 \leq \theta \leq 35^\circ$  for **4a** and  $12 \leq \theta \leq 16^\circ$  for **4b**(CH<sub>3</sub>)<sub>2</sub>CO. All measurements were carried out on an Enraf-Nonius CAD4 diffractometer at 23 °C using graphite-monochromated Cu K $\alpha$  radiation ( $\lambda = 1.5418$  Å) for **4a** and at 22 °C using graphite-monochromated Mo K $\alpha$  radiation ( $\lambda = 0.71073$  Å) for **4b**(CH<sub>3</sub>)<sub>2</sub>CO. Data were collected by  $\omega$ - $2\theta$  scans for both crystals. No decay correction was applied to the data for **4a**, but an empirical absorption correction was applied. Both linear decay and empirical absorption corrections were applied to the data for **4b**(CH<sub>3</sub>)<sub>2</sub>CO.

Both structures were solved by heavy-atom methods and refined by a full-matrix least squares procedure that minimized  $w(|F_o| - |F_c|)^2$  where  $w = 1/\sigma^2(F_o)$  using the Crystals programs in the MolEN package of programs from Enraf-Nonius. The structure of **4a** was disordered due to rotational isomerism that exchanged one carbonyl and one chloride ligand. The sum of the occupancies of the chloride and carbonyls in the two sites were set equal to one, the occupancy of the chloride in one site was linked to that of the carbonyl in the other site and the occupancies were refined. The polyether chains in **4b**(CH<sub>3</sub>)<sub>2</sub>CO were quite mobile and gave poor bond lengths when freely refined. In order to obtain a reasonable structure, the C-C bond lengths were restrained to 1.54 Å and the C-O bond lengths were restrained to 1.43 Å during the refinement. This did not materially affect the R factors and did result in reasonable bond angles. All hydrogen atoms in both structures were placed in calculated positions (C-H = 0.96 Å,  $U_{\text{iso}}(\text{H}) = 1.3U_{\text{iso}}(\text{C})$ ) and were ridden on the heavy atoms to which they were attached. Both data sets were weighed using a non-Poisson scheme. A secondary extinction correction was applied to each set of data,<sup>9</sup> and the extinction coefficients were refined. In the last stage of the refinement for each structure, no parameter varied by more than 0.01 of its standard deviation, and the final difference Fourier map had no interpretable peaks. Heavy atom scattering factors were taken from the compilations of Cromer and Weber,<sup>9</sup> and those for hydrogen were taken from the *International Tables for X-Ray Crystallography*, Vol. IV.<sup>10</sup> Corrections for anomalous dispersion were taken from the compilations of Cromer and Lieberman<sup>11</sup> and applied to chlorine, phosphorus and ruthenium. Data for the X-ray structure analyses are given in Table 3. Positional parameters for **4a** are given in Table 4, and those for **4b**(CH<sub>3</sub>)<sub>2</sub>CO are given in Table 5. Values of selected bond lengths for **4a** are given in Table 6, and those for **4b**(CH<sub>3</sub>)<sub>2</sub>CO are given in Table 7. Values of selected bond angles for **4a** are given in Table 8, and those for **4b**(CH<sub>3</sub>)<sub>2</sub>CO are given in Table 9. Values of selected torsion angles for both structures and for **1** are given in Table 10. Tables of hydrogen atomic positional parameters, thermal parameters, torsion angles and least squares planes for **4a** and **4b** are available as supplementary material. ORTEP<sup>12</sup> drawings of the major and minor rotamers of **4a** are given in Figures 1 and 2, and that for **4b**(CH<sub>3</sub>)<sub>2</sub>CO is given in Figure 3.

## Results and Discussion

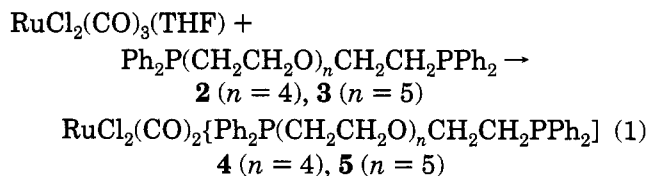
### Syntheses and Solution Conformations of the RuCl<sub>2</sub>(CO)<sub>2</sub>{Ph<sub>2</sub>P(CH<sub>2</sub>CH<sub>2</sub>O)<sub>n</sub>CH<sub>2</sub>CH<sub>2</sub>PPh<sub>2</sub>} Com-

**Table 3. Data Collection and Structure Solution and Refinement Parameters for 4a and 4b**

	<b>4a</b>	<b>4b</b> (CH <sub>3</sub> ) <sub>2</sub> CO
formula	C <sub>36</sub> H <sub>40</sub> Cl <sub>2</sub> O <sub>6</sub> P <sub>2</sub> Ru	C <sub>39</sub> H <sub>46</sub> Cl <sub>2</sub> O <sub>7</sub> P <sub>2</sub> Ru
MW	802.64	860.72
space group	<i>P</i> 2 <sub>1</sub> / <i>n</i>	<i>P</i> 2 <sub>1</sub> / <i>a</i>
<i>a</i> (Å)	10.194(1)	18.976(3)
<i>b</i> (Å)	22.907(3)	22.076(5)
<i>c</i> (Å)	15.259(2)	10.426(8)
$\beta$ (deg)	92.46(1)	111.64(1)
<i>V</i> (Å <sup>3</sup> )	3560.0(8)	4060.(1)
<i>Z</i>	4	4
<i>d</i> <sub>calc</sub> (g/cm <sup>3</sup> )	1.497	1.408
cryst dimens, mm	0.11 × 0.10 × 0.21	0.37 × 0.34 × 0.50
<i>h</i> <sub>max</sub> , <i>h</i> <sub>min</sub>	12, 0	24, -24
<i>k</i> <sub>max</sub> , <i>k</i> <sub>min</sub>	28, 0	0, -28
<i>l</i> <sub>max</sub> , <i>l</i> <sub>min</sub>	19, -19	13, 0
radiation ( $\lambda$ (Å))	Cu K $\alpha$ (1.54184)	Mo K $\alpha$ (0.71073)
temp (°C)	22	22
abs coeff (cm <sup>-1</sup> )	62.890	6.324
$\theta$ (limits (deg))	0.1-74	0.1-27.5
decay corr	none	linear
decay (%)		6.9
abs corr	empirical	empirical
<i>T</i> <sub>max</sub> , <i>T</i> <sub>min</sub> (%)	99.6, 84.8	99.9, 94.6
refl measd	8036	10 073
scan width (deg)	1.34	1.35
refl with $I \geq n\sigma(I)$	4310 ( <i>n</i> = 3)	4305 ( <i>n</i> = 2)
no. of variables	423	461
function minimized	$w( F_o  -  F_c )^2$	$w( F_o  -  F_c )^2$
weighing scheme	non-Poisson ( $w = 1/\sigma^2(F_o)$ )	non-Poisson ( $w = 1/\sigma^2(F_o)$ )
instrumental uncertainty factor	0.03	0.02
secondary extinction corr type	Zachariasen	Zachariasen
minimized extinction coeff	$7.608 \times 10^{-8}$	$2.867 \times 10^{-8}$
<i>R</i> , % <sup>a</sup>	7.13	5.58
<i>R</i> <sub>w</sub> (%) <sup>b</sup>	8.68	6.04
GOF <sup>c</sup>	1.324	1.972
max, min resid electron density (e/Å <sup>3</sup> )	1.057, -0.287	0.721, -0.140
max shift/error	0.01	0.01

<sup>a</sup>  $R = \sum(|F_o| - |F_c|)/\sum|F_o|$ . <sup>b</sup>  $R_w = \sum w(|F_o| - |F_c|)^2/\sum w|F_o|^2$ . <sup>c</sup> GOF =  $[\sum w(|F_o| - |F_c|)^2/n - m]^{0.5}$ .

**plexes.** In contrast to the reactions of the Ph<sub>2</sub>P(CH<sub>2</sub>CH<sub>2</sub>O)<sub>n</sub>CH<sub>2</sub>CH<sub>2</sub>PPh<sub>2</sub> (*n* = 4 (**2**), 5 (**3**)) ligands with Mo(CO)<sub>4</sub>(norbornadiene) and PtCl<sub>2</sub>(1,5-cyclooctadiene) in 1:1 ratios, which yield single products,<sup>4</sup> the reactions of these ligands with RuCl<sub>2</sub>(CO)<sub>3</sub>(THF) in 1:1 ratios under similar conditions yield a variety of products (eq 1). Elemental analyses of the crude reaction mixtures



indicate that all of these products have empirical formulas of the type RuCl<sub>2</sub>(CO)<sub>2</sub>{Ph<sub>2</sub>P(CH<sub>2</sub>CH<sub>2</sub>O)<sub>n</sub>CH<sub>2</sub>CH<sub>2</sub>PPh<sub>2</sub>} (*n* = 4 (**4**), 5 (**5**)). The various products do not interconvert as indicated by the fact that the <sup>31</sup>P NMR spectra of the mixture did not vary with either temperature or concentration and by the fact that the major components and some of the minor components could be separated by column chromatography on silica gel.

Each of the RuCl<sub>2</sub>(CO)<sub>2</sub>{Ph<sub>2</sub>P(CH<sub>2</sub>CH<sub>2</sub>O)<sub>n</sub>CH<sub>2</sub>CH<sub>2</sub>PPh<sub>2</sub>} complexes have identical ruthenium coordination geometries with cis carbonyls, cis chlorides and trans phosphines as shown by their IR and <sup>31</sup>P and <sup>13</sup>C NMR spectra (Tables 1 and 2). The IR spectrum of each

(8) Zachariasen, W. H. *Acta Crystallogr.* **1963**, *16*, 1139.

(9) Cromer, D. T.; Waber, D. T. *Acta Crystallogr.* **1965**, *18*, 104.

(10) *International Tables for Crystallography*; Hahn, T., Ed.; The Kynoch Press: Birmingham, U.K., 1974; Vol. IV, p 72.

(11) Cromer, D. T.; Lieberman, D. J. *J. Chem. Phys.* **1970**, *53*, 1891.

(12) Johnson, C. K. *ORTEP II. Report ORNL-5138*. Oak Ridge National Laboratory: Oak Ridge, TN, 1976.

**Table 4. Positional Parameters and Isotropic Thermal Factors ( $\text{\AA}^2$ ) for 4a<sup>a</sup>**

atom	x	y	z	B <sup>a</sup>
Ru	0.58941(6)	0.52967(3)	0.75769(4)	2.15(1)
Cl1	0.7932(2)	0.5718(1)	0.7086(2)	3.34(4)
Cl2	0.6528(4)	0.5260(2)	0.9125(3)	4.29(7)*
Cl2'	0.4986(7)	0.5273(3)	0.6141(5)	3.2(1)*
P1	0.4982(2)	0.62620(9)	0.7759(1)	2.16(4)
P2	0.6808(2)	0.43447(9)	0.7334(2)	2.49(4)
O1	0.5492(7)	0.7107(3)	0.5487(5)	4.5(2)
O2	0.7721(8)	0.6840(3)	0.4291(5)	5.1(2)
O3	0.835(1)	0.5342(4)	0.4268(5)	6.1(2)
O4	0.8076(7)	0.4133(3)	0.4880(4)	3.7(1)
O5	0.3393(7)	0.4745(3)	0.8153(5)	4.3(2)
O6	0.503(1)	0.5382(5)	0.5705(8)	5.1(3)*
O6'	0.695(3)	0.532(1)	0.955(2)	5.1(6)*
C1	0.4672(9)	0.6670(4)	0.6741(5)	2.7(2)
C2	0.5882(9)	0.6885(4)	0.6309(6)	3.4(2)
C3	0.637(1)	0.7495(5)	0.5130(9)	5.5(3)
C4	0.768(1)	0.7264(5)	0.4971(9)	5.5(3)
C5	0.767(1)	0.6275(5)	0.4554(8)	6.0(3)
C6	0.798(1)	0.5854(5)	0.3850(8)	5.3(3)
C7	0.851(1)	0.4837(5)	0.3722(7)	4.1(2)
C8	0.9025(9)	0.4356(5)	0.4306(6)	3.4(2)
C9	0.800(1)	0.4443(4)	0.5680(6)	3.5(2)
C10	0.6977(9)	0.4128(4)	0.6195(6)	3.0(2)
C11	0.3376(8)	0.6239(4)	0.8238(6)	2.5(2)
C12	0.3280(9)	0.6023(5)	0.9091(6)	3.6(2)
C13	0.207(1)	0.5942(5)	0.9443(6)	3.6(2)
C14	0.093(1)	0.6087(5)	0.8975(8)	4.3(2)
C15	0.1011(9)	0.6290(5)	0.8131(8)	4.6(3)
C16	0.2208(9)	0.6361(5)	0.7773(7)	3.5(2)
C17	0.5887(8)	0.6788(4)	0.8449(6)	2.6(2)
C18	0.5282(9)	0.7317(4)	0.8658(6)	3.1(2)
C19	0.599(1)	0.7727(4)	0.9174(6)	3.2(2)
C20	0.725(1)	0.7600(4)	0.9479(7)	3.6(2)
C21	0.783(1)	0.7084(5)	0.9287(8)	4.2(2)
C22	0.719(1)	0.6681(4)	0.8747(7)	3.8(2)
C23	0.8411(9)	0.4176(3)	0.7868(6)	2.7(2)
C24	0.888(1)	0.3593(4)	0.7814(7)	3.9(2)
C25	1.008(1)	0.3460(5)	0.8231(9)	5.1(3)
C26	1.084(1)	0.3873(5)	0.8635(8)	4.8(3)
C27	1.040(1)	0.4440(5)	0.8690(8)	4.5(2)
C28	0.9192(9)	0.4591(4)	0.8299(7)	3.5(2)
C29	0.5757(8)	0.3766(4)	0.7739(6)	2.5(2)
C30	0.507(1)	0.3375(5)	0.7192(7)	5.0(3)
C31	0.426(1)	0.2960(5)	0.7570(9)	6.8(3)
C32	0.412(1)	0.2919(5)	0.8437(8)	5.3(3)
C33	0.479(1)	0.3314(5)	0.8982(7)	4.6(2)
C34	0.559(1)	0.3734(5)	0.8629(6)	3.9(2)
C35	0.432(1)	0.4957(4)	0.7932(6)	3.2(2)
C36	0.533(1)	0.5351(6)	0.6307(9)	3.3(2)*
C36'	0.659(3)	0.531(1)	0.884(2)	3.0(5)*

<sup>a</sup> Starred *B* values are for atoms that were refined isotropically. Anisotropically refined atoms are given in the form of the isotropic equivalent displacement parameter defined as  $(4/3)[a^2B(1,1) + b^2B(2,2) + c^2B(3,3) + ab(\cos \gamma)B(1,2) + ac(\cos \beta)B(1,3) + bc(\cos \alpha)B(2,3)]$ .

complex has two equally intense bands at approximately 1995 and 2058  $\text{cm}^{-1}$  indicating that the carbonyls in each of the complexes are cis-coordinated.<sup>13</sup> The <sup>13</sup>C NMR spectrum of each complex has a single 1:2:1 triplet for the two carbonyls at approximately 192 ppm with a relatively small  $|^2J(\text{PC})|$  of approximately 11 Hz. This demonstrates that the carbonyls are chemically equivalent and are cis to both phosphines.<sup>13</sup> Each complex also has a single <sup>31</sup>P NMR resonance indicating that the phosphines are chemically equivalent.

The above data suggests that the reactions shown in

(13) (a) Lindner, E.; Schober, U.; Fawzi, R.; Hiller, W.; Englert, U.; Wegner, P. *Chem. Ber.* **1987**, *120*, 1621. (b) Reddy, V. V. S. R.; Whitten, J. E.; Redmill, K. A.; Varshney, A.; Gray, G. M. *J. Organomet. Chem.* **1989**, *372*, 207. (c) Lindner, E.; Karle, B. *Chem. Ber.* **1990**, *123*, 1469. (d) Lindner, E.; Mockel, A.; Mayer, H. A.; Fawzi, R. *Chem. Ber.* **1992**, *125*, 1363. (e) Lindner, E.; Mockel, A.; Mayer, H. A.; Kuhlbauch, H.; Fawzi, R.; Steimann, M. *Inorg. Chem.* **1993**, *32*, 1266.

**Table 5. Positional Parameters and Isotropic Thermal Factors ( $\text{\AA}^2$ ) for 4b-(CH<sub>3</sub>)<sub>2</sub>CO<sup>a</sup>**

atom	x	y	z	B <sup>a</sup>
Ru	0.22681(3)	0.07645(3)	0.00749(6)	4.08(1)
Cl1	0.2518(1)	0.00032(9)	-0.1402(2)	5.46(5)
Cl2	0.1715(1)	0.0017(1)	0.1115(2)	7.86(6)
P1	0.10206(9)	0.08849(9)	-0.1677(2)	3.96(4)
P2	-0.3453(1)	-0.0498(1)	-0.1860(2)	4.48(5)
O1	-0.0708(3)	0.0502(3)	-0.3333(8)	8.9(2)
O2	-0.1664(4)	0.1474(3)	-0.4275(7)	11.5(3)
O3	-0.2993(3)	0.1729(3)	-0.3448(7)	8.3(2)
O4	-0.4267(3)	0.1013(3)	-0.3953(6)	8.5(2)
O5	0.2964(3)	0.1737(3)	-0.1051(6)	6.9(2)
O6	0.1903(3)	0.1646(3)	0.1933(6)	8.9(2)
C1	0.0565(4)	0.0154(3)	-0.2078(8)	5.7(2)
C2	-0.0155(5)	0.0077(4)	-0.337(1)	9.4(3)
C3	-0.1389(5)	0.0451(4)	-0.453(1)	9.4(4)
C4	-0.1960(5)	0.0881(4)	-0.426(1)	12.5(4)
C5	-0.1748(6)	0.1877(5)	-0.327(1)	12.8(5)
C6	-0.2544(5)	0.2158(5)	-0.384(1)	10.9(4)
C7	-0.3734(5)	0.1968(4)	-0.374(1)	10.3(4)
C8	-0.4182(4)	0.1548(4)	-0.314(1)	9.4(3)
C9	-0.4344(4)	0.0516(4)	-0.3140(8)	6.8(2)
C10	-0.3576(4)	0.0314(4)	-0.2071(8)	5.8(2)
C11	0.0454(3)	0.1378(3)	-0.1051(7)	4.3(2)
C12	0.0006(4)	0.1161(4)	-0.0375(8)	6.5(2)
C13	-0.0346(4)	0.1561(5)	0.0227(8)	9.2(3)
C14	-0.0247(5)	0.2183(4)	0.0178(9)	8.9(3)
C15	0.0195(5)	0.2394(5)	-0.0490(8)	8.2(3)
C16	0.0544(4)	0.1994(4)	-0.1090(9)	6.2(2)
C17	0.0936(3)	0.1209(3)	-0.3331(6)	3.7(2)
C18	0.0288(4)	0.1498(3)	-0.4163(7)	4.6(2)
C19	0.0215(4)	0.1705(3)	-0.5449(7)	5.4(2)
C20	0.0798(4)	0.1643(4)	-0.5911(7)	6.0(2)
C21	0.1451(4)	0.1352(3)	-0.5108(7)	5.0(2)
C22	0.1530(4)	0.1140(3)	-0.3809(6)	4.1(2)
C23	0.4309(3)	0.0736(3)	0.1624(7)	4.5(2)
C24	0.4339(4)	0.0699(4)	0.0314(7)	5.5(2)
C25	0.5009(4)	0.0809(4)	0.0113(9)	7.3(2)
C26	0.5653(4)	0.0972(4)	0.1193(9)	7.5(3)
C27	0.5638(4)	0.1010(4)	0.2509(9)	7.2(3)
C28	0.4972(4)	0.0898(4)	0.2712(8)	5.8(2)
C29	0.3541(3)	0.0792(4)	0.3558(6)	4.8(2)
C30	0.3423(4)	0.0415(4)	0.4531(7)	6.8(2)
C31	0.3452(4)	0.0679(5)	0.5785(8)	7.8(3)
C32	0.3615(4)	0.1279(5)	0.6040(8)	8.4(3)
C33	0.3719(4)	0.1642(5)	0.5064(8)	7.6(3)
C34	0.3680(4)	0.1388(4)	0.3835(8)	6.2(2)
C35	0.2694(4)	0.1372(3)	-0.0630(7)	4.3(2)
C36	0.2042(4)	0.1305(4)	0.1217(8)	6.2(2)
O7	0.8469(4)	0.2328(4)	0.1868(8)	12.1(3)
C37	0.7521(7)	0.1752(6)	0.022(1)	17.9(6)
C38	0.7936(5)	0.1977(5)	0.151(1)	9.6(3)
C39	0.7673(8)	0.1812(7)	0.253(1)	25.9(7)

<sup>a</sup> Anisotropically refined atoms are given in the form of the isotropic equivalent displacement parameter defined as  $(4/3)[a^2B(1,1) + b^2B(2,2) + c^2B(3,3) + ab(\cos \gamma)B(1,2) + ac(\cos \beta)B(1,3) + bc(\cos \alpha)B(2,3)]$ .

**Table 6. Selected Bond Lengths ( $\text{\AA}$ ) for 4a**

Ru-Cl1	2.438(2)	O1-C3	1.39(1)
Ru-Cl2	2.424(4)	O2-C4	1.42(2)
Ru-Cl2'	2.343(7)	O2-C5	1.36(1)
Ru-P1	2.420(2)	O3-C6	1.38(1)
Ru-P2	2.406(2)	O3-C7	1.44(1)
Ru-C35	1.88(1)	O4-C8	1.43(1)
Ru-C36	2.00(1)	O4-C9	1.42(1)
Ru-C36'	2.02(3)	O5-C35	1.13(1)
P1-C1	1.829(9)	O6-C36	0.96(2)
P1-C11	1.822(8)	O6'-C36'	1.14(4)
P1-C17	1.824(9)	C1-C2	1.51(1)
P2-C10	1.82(1)	C3-C4	1.47(2)
P2-C23	1.836(9)	C5-C6	1.49(2)
P2-C29	1.828(9)	C7-C8	1.50(1)
O1-C2	1.39(1)	C9-C10	1.51(1)

eq 1 yield mixtures of monomers and oligomers. The minor products of each reaction appear to be oligomers as demonstrated by the fact that their <sup>31</sup>P NMR

**Table 7. Selected Bond Lengths (Å) for 4b·(CH<sub>3</sub>)<sub>2</sub>CO**

Ru—C11	2.440(2)	O2—C4	1.43(1) <sup>a</sup>
Ru—C12	2.417(3)	O2—C5	1.43(1) <sup>a</sup>
Ru—P1	2.413(2)	O3—C6	1.43(1) <sup>a</sup>
Ru—P1	2.404(3)	O3—C7	1.43(1) <sup>a</sup>
Ru—C35	1.853(8)	O4—C8	1.43(1) <sup>a</sup>
Ru—C36	1.843(9)	O4—C9	1.43(1) <sup>a</sup>
P1—C1	1.807(7)	O5—C35	1.13(1)
P1—C11	1.811(8)	O6—C36	1.16(1)
P1—C17	1.819(7)	C1—C2	1.53(1) <sup>b</sup>
P2—C10	1.811(8)	C3—C4	1.54(1) <sup>b</sup>
P2—C23	1.809(8)	C5—C6	1.54(1) <sup>b</sup>
P2—C29	1.834(7)	C7—C8	1.54(1) <sup>b</sup>
O1—C2	1.42(1) <sup>a</sup>	C9—C10	1.538(9) <sup>b</sup>
O1—C3	1.431(9) <sup>a</sup>		

<sup>a</sup> C—O distances were constrained to 1.43 Å. <sup>b</sup> C—C distances were constrained to 1.54 Å.

**Table 8. Selected Bond Angles (deg) for 4a**

C11—Ru—C12	96.8(1)	C35—Ru—C36	95.3(5)
C11—Ru—C12'	91.7(2)	C35—Ru—C36'	90.0(9)
C11—Ru—P1	90.58(8)	Ru—P1—C1	115.0(3)
C11—Ru—P2	88.34(8)	Ru—P1—C11	112.1(3)
C11—Ru—C35	178.5(3)	Ru—P1—C17	118.8(3)
C11—Ru—C36	83.7(4)	Ru—P2—C10	116.6(3)
C11—Ru—C36'	91.1(9)	Ru—P2—C23	117.8(3)
C12—Ru—P1	90.4(1)	Ru—P2—C29	111.6(3)
C12—Ru—P2	91.7(1)	C2—O1—C3	115.0(8)
C12—Ru—C35	84.3(3)	C4—O2—C5	115.6(9)
C12—Ru—C36	178.0(4)	C6—O3—C7	116.9(9)
C12'—Ru—P1	89.4(2)	C8—O4—C9	114.3(7)
C12'—Ru—P2	88.6(2)	P1—C1—C2	115.1(6)
C12'—Ru—C35	87.3(3)	O1—C2—C1	107.8(7)
C12'—Ru—C36'	177.2(9)	O1—C3—C4	116(1)
P1—Ru—P2	177.70(8)	O2—C4—C3	115(1)
P1—Ru—C35	90.5(3)	O2—C5—C6	113(1)
P1—Ru—C36	87.6(4)	O3—C6—C5	106(1)
P1—Ru—C36'	90.2(9)	O3—C7—C8	107.0(8)
P2—Ru—C35	90.6(3)	O4—C8—C7	113.6(8)
P2—Ru—C36	90.2(4)	O4—C9—C10	105.8(8)
P2—Ru—C36'	91.9(9)	P2—C10—C9	117.4(6)

**Table 9. Selected Bond Angles (deg) for 4b·(CH<sub>3</sub>)<sub>2</sub>CO**

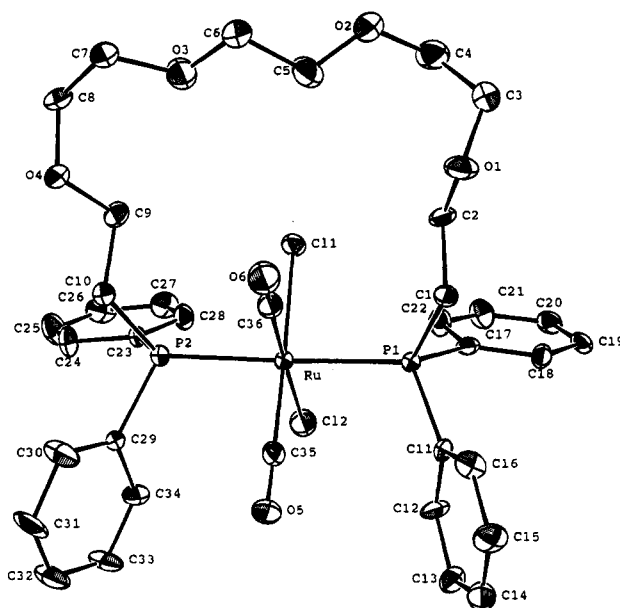
C11—Ru—C12	91.74(8)	Ru—P2—C10	112.2(2)
C11—Ru—P1	87.88(7)	Ru—P2—C23	117.0(2)
C11—Ru—P2	88.62(7)	Ru—P2—C29	112.8(2)
C11—Ru—C35	91.9(2)	C2—O1—C3	111.4(7)
C11—Ru—C36	176.5(3)	C4—O2—C5	114.4(9)
C12—Ru—P1	87.01(7)	C6—O3—C7	109.8(7)
C12—Ru—P2	85.52(7)	C8—O4—C9	107.3(7)
C12—Ru—C35	176.3(2)	P1—C1—C2	119.8(6)
C12—Ru—C36	84.8(3)	O1—C2—C1	109.4(8)
P1—Ru—P2	171.65(8)	O1—C3—C4	105.4(8)
P1—Ru—C35	94.0(2)	O2—C4—C3	104.9(8)
P1—Ru—C36	91.2(2)	O2—C5—C6	109.3(8)
P2—Ru—C35	93.7(2)	O3—C6—C5	103.2(8)
P2—Ru—C36	91.8(2)	O3—C7—C8	109.8(7)
C35—Ru—C36	91.6(4)	O4—C8—C7	102.4(8)
Ru—P1—C1	109.2(2)	O4—C9—C10	112.1(6)
Ru—P1—C11	109.9(2)	P2—C10—C9	114.9(5)
Ru—P1—C17	118.7(2)		

coordination chemical shifts ( $\delta^{31}\text{P}$  complex —  $\delta^{31}\text{P}$  ligand) (**4b**, 35.11 ppm; **4c**, 36.03 ppm; **4d**, 36.45 ppm; **5b**, 35.68 ppm; **5c**, 36.44 ppm) are similar to those of *cis,cis,trans*-Ru(CO)<sub>2</sub>Cl<sub>2</sub>{Ph<sub>2</sub>P(CH<sub>2</sub>CH<sub>2</sub>O)<sub>2</sub>CH<sub>3</sub>-P}<sub>2</sub> (**6**, 36.00 ppm).<sup>13b</sup> This similarity is due to the fact that bridging bis(phosphine) ligands in oligomeric complexes can adopt conformations similar to those of monodentate phosphine ligands.<sup>14</sup> The major products for each reaction appear to be monomers with trans-spanning Ph<sub>2</sub>P(CH<sub>2</sub>CH<sub>2</sub>O)<sub>n</sub>CH<sub>2</sub>CH<sub>2</sub>PPh<sub>2</sub> ligands as demonstrated by the fact that their <sup>31</sup>P NMR coordination chemical

**Table 10. Selected Torsion Angles (deg) for 4a, 4b·(CH<sub>3</sub>)<sub>2</sub>CO, and 1<sup>a</sup>**

	4a	4b·(CH <sub>3</sub> ) <sub>2</sub> CO	1 <sup>a</sup>
C11—Ru—P1—C1	67.3(3)	53.5(3)	
C11—Ru—P2—C10	-71.1(3)	-46.1(3)	
Ru—P1—C1—C2	-71.7(7)	-166.5(6)	65.5(4)
Ru—P2—C10—C9	69.4(7)	176.6(5)	-65.3(4)
C3—O1—C2—C1	158.8(8)	179.6(7)	-166.4(5)
C2—O1—C3—C4	61(1)	173.5(7)	-61.5(8)
C5—O2—C4—C3	-95(1)	-141.2(9)	157.9(7)
C4—O2—C5—C6	-169(1)	-83(1)	-177.8(6)
C7—O3—C6—C5	171(1)	172.2(8)	168.9(6)
C6—O3—C7—C8	175(1)	-172.1(8)	173.9(5)
C9—O4—C8—C7	-86(1)	153.5(7)	82.8(5)
C8—O4—C9—C10	-178.3(7)	-78.8(8)	178.4(4)
P1—C1—C2—O1	171.2(6)	-55.3(9)	-173.4(3)
O1—C3—C4—O2	68(1)	67(1)	-50.5(9)
O2—C5—C6—O3	159(1)	88(1)	142.4(6)
O3—C7—C8—O4	71(1)	-66.7(9)	-79.6(5)
O4—C9—C10—P2	170.8(6)	-139.4(6)	-173.5(3)

<sup>a</sup> Data from ref 5. Numbering is identical except Ru should be replaced with Mo.

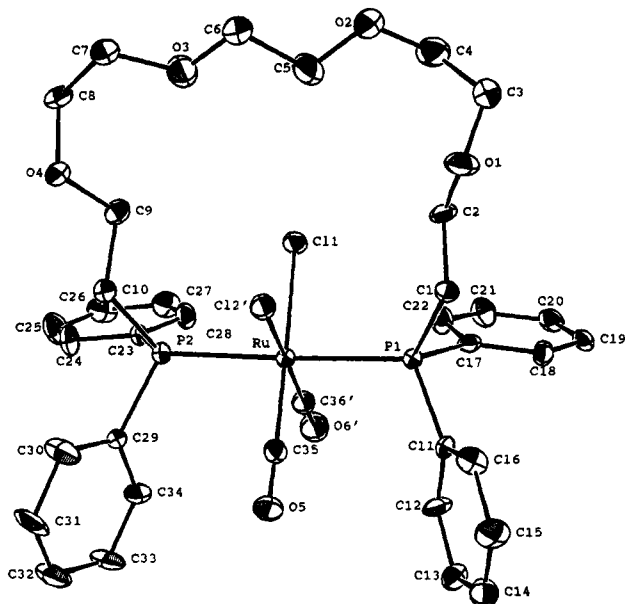


**Figure 1.** ORTEP<sup>12</sup> drawing of the molecular structure of the major rotamer of **4a**. Thermal ellipsoids are drawn at the 50% probability level, and hydrogen atoms are omitted for clarity.

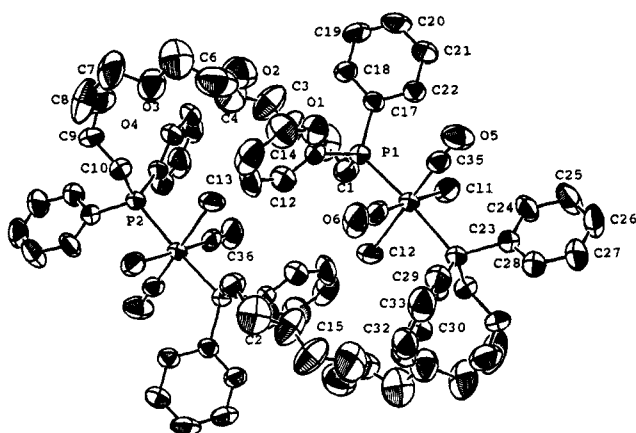
shifts (**4a**, 31.42 ppm; **5a**, 32.85 ppm), are smaller than that of **6**. This difference is due to the fact that trans-spanning bis(phosphine) ligands cannot adopt conformations similar to those of monodentate phosphine ligands.<sup>14</sup> These conclusions are supported by the X-ray crystal structures of **4a** and **4b** discussed below, and by the fact that the longer ligand, **3**, gives a higher yield of the monomeric product, **5a**.

The variations in chemical shifts of the *ipso*, *ortho*, *meta*, and *para* phenyl and the C1 and C2 methylene <sup>13</sup>C NMR resonances are also consistent with the assignment of the solution structures of the RuCl<sub>2</sub>(CO)<sub>2</sub>{Ph<sub>2</sub>P(CH<sub>2</sub>CH<sub>2</sub>O)<sub>n</sub>CH<sub>2</sub>CH<sub>2</sub>PPh<sub>2</sub>} complexes made in the previous paragraph. The chemical shifts of these resonances are similar for **4b** and **4d**, in which the Ph<sub>2</sub>P(CH<sub>2</sub>CH<sub>2</sub>O)<sub>4</sub>CH<sub>2</sub>CH<sub>2</sub>PPh<sub>2</sub> ligands are bridging, but are significantly different from those for **4a**, in which the same ligand is trans-spanning. The chemical shifts of these resonances for **5a**, in which the longer Ph<sub>2</sub>P(CH<sub>2</sub>CH<sub>2</sub>O)<sub>5</sub>CH<sub>2</sub>CH<sub>2</sub>PPh<sub>2</sub> ligand is trans-spanning, are in-

(14) Hill, W. E.; Minahan, D. M. A.; Taylor, J. G.; McAuliffe, C. A. *J. Am. Chem. Soc.* **1982**, *104*, 6001.



**Figure 2.** ORTEP<sup>12</sup> drawing of the molecular structure of the minor rotamer of **4a**. Thermal ellipsoids are drawn at the 50% probability level, and hydrogen atoms are omitted for clarity.



**Figure 3.** ORTEP<sup>12</sup> drawing of the molecular structure of **4b**. Thermal ellipsoids are drawn at the 50% probability level, and hydrogen atoms are omitted for clarity.

intermediate between those for **4a**, on the one hand, and those for **4b** and **4d**, on the other.

Although the complexes in this study are the first octahedral complexes observed to form both monomers with trans-spanning bis(phosphine) ligands and oligomers with bridging bis(phosphine) ligands, it is well established that such mixtures are formed when bis(phosphine) ligands react with square-planar platinum-group metal (Rh(I), Ir(I), Pd(II), and Pt(II)) precursors.<sup>14,15</sup> However, the behavior of the <sup>31</sup>P NMR

coordination chemical shifts is quite different for the two types of complexes. In the square planar complexes, the coordination chemical shifts from trans-coordination of bidentate ligands increase as the length of the ligand decreases,<sup>14</sup> but the opposite trend is observed for **4a** and **5a**. This suggests that the additional cis ligands in octahedral complexes cause the conformations of trans-spanning ligands in these complexes to be different from those of trans-spanning ligands in square planar complexes.

A final point of interest is that a single <sup>13</sup>C NMR resonance is observed for the carbonyl ligands in both **4a** and **5a**. This suggests that the RuCl<sub>2</sub>(CO)<sub>2</sub> group moves freely within the chelate ring to average the environments of the two carbonyl ligands because the chemical shifts of carbonyl resonances in transition metal complexes are quite sensitive to asymmetry in the phosphine ligands.<sup>15</sup> The rotation of the RuCl<sub>2</sub>(CO)<sub>2</sub> around the P–Ru–P axis is strongly supported by the fact that two rotamers of **4a** are observed in the solid state, as discussed below. The carbonyl <sup>13</sup>C NMR resonance of **4a** does not broaden as much as does that of *trans*-Mo(CO)<sub>4</sub>{Ph<sub>2</sub>P(CH<sub>2</sub>CH<sub>2</sub>O)<sub>4</sub>CH<sub>2</sub>CH<sub>2</sub>PPh<sub>2</sub>-*P,P'*}, **1**,<sup>5</sup> as the temperature is lowered from 21 °C to –80 °C. This suggests that the barrier to rotation about the P–M–P axis is somewhat lower in **4a** than in **1**. The lower rotation barrier in **4a** could be due to the fact that the carbonyl ligands in **4a** can be averaged by rotating the RuCl<sub>2</sub>(CO)<sub>2</sub> group so that the trans-spanning ligand moves over the smaller chlorides but not over the larger carbonyl ligands. This is not possible in **1**.

**X-ray Crystal Structure of *cis,cis,trans*-RuCl<sub>2</sub>(CO)<sub>2</sub>{Ph<sub>2</sub>P(CH<sub>2</sub>CH<sub>2</sub>O)<sub>4</sub>CH<sub>2</sub>CH<sub>2</sub>PPh<sub>2</sub>-*P,P'*}, **4a**.** The X-ray crystal structure of **4a** has been determined. The ruthenium has an octahedral coordination geometry with a trans-spanning Ph<sub>2</sub>P(CH<sub>2</sub>CH<sub>2</sub>O)<sub>4</sub>CH<sub>2</sub>CH<sub>2</sub>PPh<sub>2</sub> ligand, *cis* carbonyl ligands and *cis* chloride ligands consistent with the NMR data. Two rotamers of the RuCl<sub>2</sub>(CO)<sub>2</sub> group relative to the trans-spanning ligand are observed, and ORTEP drawings of the major and minor rotamers of **4a** are shown in Figures 1 and 2. In the major rotamer (~70%), the trans-spanning ligand passes between one carbonyl and one chloride while in the minor rotamer (~30%), the trans-spanning ligand passes between the two chlorides. There is no evidence of the third rotamer in which the trans-spanning ligand would pass between the two carbonyls. The relative abundances of the two rotamers are consistent with a statistical occupancy of the sites.

The presence of rotamers in the crystal structure of **4a** may be due to the fact that rotation about the P–Ru–P bond to generate the two different rotamers does not affect the orientation of the phenyls and the trans-spanning polyether chain. Because these are the outermost portions of the molecule, the rotamers would have the same shapes and could cocrystallize. However, if this is the case, it is somewhat surprising that the third rotamer, in which the trans-spanning ligand passes between the two carbonyls, is not observed. It is possible that this rotamer is not observed because, when the trans-spanning ligand is between two larger carbonyl ligands, it adopts a different and less stable conformation that prevents cocrystallization with the other two rotamers. This hypothesis is supported by the fact that conformation of the trans-spanning ligand

(15) (a) March, F. C.; Mason, R.; Thomas, K. M.; Shaw, B. L. *J. Chem. Soc., Chem. Commun.* **1975**, 584. (b) Pryde, A.; Shaw, B. L.; Weeks, B. J. *J. Chem. Soc., Dalton Trans.* **1976**, 322. (c) Appleton, T. G.; Bennett, M. A.; Tompkins, B. I. *J. Chem. Soc., Dalton Trans.* **1976**, 439. (d) Sanger, A. R. *J. Chem. Soc., Dalton Trans.* **1977**, 120. (e) Alcock, N. W.; Brown, J. M.; Jeffery, J. C. *J. Chem. Soc., Dalton Trans.* **1977**, 888. (f) Sanger, A. R. *J. Chem. Soc., Dalton Trans.* **1977**, 1971. (g) Al-Salem, N. A.; Empsall, H. D.; Markham, R.; Shaw, B. L.; Weeks, B. J. *J. Chem. Soc., Dalton Trans.* **1979**, 1972. (h) Hill, W. E.; McAuliffe, C. A.; Niven, I. E.; Parrish, R. V. *Inorg. Chim. Acta* **1980**, *38*, 273. (i) Crocker, C.; Errington, J.; Markham, R.; Moulton, C. J.; Odell, K. J.; Shaw, B. L. *J. Am. Chem. Soc.* **1980**, *102*, 4373. (j) Hill, W. E.; Minahan, D. M. A.; McAuliffe, C. A. *Inorg. Chem.* **1983**, *22*, 3382.

(16) Gray, G. M.; Redmill, K. A. *Inorg. Chem.* **1985**, *24*, 1279.

in **4a** is quite different from that of the identical ligand in **1** as indicated by torsion angles (Table 10) that differ by as much as  $60^\circ$ .

**X-ray Crystal Structure of [*cis,cis,trans*-RuCl<sub>2</sub>(CO)<sub>2</sub>{ $\mu$ -Ph<sub>2</sub>P(CH<sub>2</sub>CH<sub>2</sub>O)<sub>4</sub>CH<sub>2</sub>CH<sub>2</sub>PPh<sub>2</sub>-P,P'}], **4b**.** The X-ray crystal structure of **4b** has been determined and shown to be a cyclic dimer. An ORTEP drawing of the structure is shown in Figure 3. Consistent with the NMR data, each Ru has an octahedral coordination geometry with trans, bridging Ph<sub>2</sub>P(CH<sub>2</sub>CH<sub>2</sub>O)<sub>4</sub>CH<sub>2</sub>CH<sub>2</sub>PPh<sub>2</sub> ligands, cis carbonyl ligands and cis chloride ligands. The bond lengths and angles about the Ru are similar to those observed in **4a** with the largest difference in the P–Ru–P angles (**4b**:  $171.65(8)^\circ$ ; **4a**:  $177.70(8)^\circ$ ). This is consistent with the fact that the <sup>31</sup>P NMR coordination chemical shift of **4b** was larger than that of **4a** which suggested that the phosphorus environments were different in the two complexes.

The most interesting feature of this structure is that the trans coordination of the bridging bis(phosphine) ligands results in two, separate metallacrown ether sites. Because each ruthenium is octahedral and the molecule crystallizes around an inversion center, both a chloride and a carbonyl ligand stick into the cavity and separate these two sites. This results in a Ru–Ru distance of  $9.1961(9)$  Å indicating that there is no interaction between the two ruthenium centers. These

cavities are enclosed by the phenyl groups on P1 and P2 that are located above and below the cavities. This conformation suggests that it may be possible to coordinate a hard metal cation to each of these sites to form tetrametallic complexes. It may also be possible to bridge a bidentate ligand between the two rutheniums to generate a more rigid dimetallacrown ether. Such complexes could exhibit unusual catalytic activities and selectivities.

**Acknowledgment.** The authors thank the donors of the Petroleum Research Fund, administered by the American Chemical Society, for partial support of this research, Johnson Mathey for a generous loan of RuCl<sub>3</sub>·*n*H<sub>2</sub>O, and Dale C. Smith, Jr., for helpful discussions. A.V. thanks the Graduate School of the University of Alabama at Birmingham for a Graduate Fellowship.

**Supplementary Material Available:** Tables of X-ray crystallographic data for **4a** and **4b** including hydrogen coordinates and *B* values, anisotropic thermal parameters, complete bond lengths and angles, torsion angles, and least squares planes (16 pages). Ordering information is given on any current masthead page.

OM940650+



**Size-Selective Reactions of**  
***cis*-Mo(CO)<sub>4</sub>{Ph<sub>2</sub>P(CH<sub>2</sub>CH<sub>2</sub>O)<sub>*n*</sub>CH<sub>2</sub>CH<sub>2</sub>PPh<sub>2</sub>-*P,P'*}** (*n* = 4, 5)  
**Metallacrown Ethers with Mercury(II) Salts.**  
**Crystal Structure of *cis*-Mo(CO)<sub>4</sub>-**  
**{*μ*-Ph<sub>2</sub>P(CH<sub>2</sub>CH<sub>2</sub>O)<sub>5</sub>CH<sub>2</sub>CH<sub>2</sub>PPh<sub>2</sub>-*P,P',O,O',O'',O''',O''''*}.HgCl<sub>2</sub>,**  
**an Unusual Bimetallic Complex Containing a**  
**Molecular Cleft**

Gary M. Gray\* and Christina H. Duffey

*Department of Chemistry, The University of Alabama at Birmingham, UAB Station,  
 Birmingham, Alabama 35294*

*Received May 31, 1994*<sup>⊗</sup>

The reactions of mercury(II) salts with *cis*-Mo(CO)<sub>4</sub>{Ph<sub>2</sub>P(CH<sub>2</sub>CH<sub>2</sub>O)<sub>*n*</sub>CH<sub>2</sub>CH<sub>2</sub>PPh<sub>2</sub>-*P,P'*} (*n* = 5 (1), 4 (2)) metallacrown ethers are surprisingly complex, and the product depends upon the size of the metallacrown ether ring and the anion in the mercury(II) salt. The reaction of HgCl<sub>2</sub> and 1 gives the bimetallic metallacrown ether complex, *cis*-Mo(CO)<sub>4</sub>{*μ*-Ph<sub>2</sub>P(CH<sub>2</sub>CH<sub>2</sub>O)<sub>5</sub>CH<sub>2</sub>CH<sub>2</sub>PPh<sub>2</sub>-*P,P',O,O',O'',O''',O''''*}.HgCl<sub>2</sub>, 3, because the metallacrown ether ring is sufficiently large to accommodate the Hg<sup>2+</sup>. The X-ray crystal structure of 3 (triclinic space group *P*1̄, *a* = 10.387(2) Å, *b* = 13.0359(7) Å, *c* = 17.710(3) Å, α = 69.401(7)°, β = 81.32(1)°, γ = 87.15(1)°; *V* = 2218.8 Å<sup>3</sup>; *Z* = 2; *R* = 5.82; *R<sub>w</sub>* = 7.19; GOF = 1.996 for 497 parameters and 7737 out of 9505 unique reflections) has been determined. The coordination environment of the Hg<sup>2+</sup> is a hexagonal bipyramid with one missing equatorial ligand, axial chlorides, and equatorial ether oxygens. The open coordination site points toward the molybdenum, and the Mo–Hg distance is 6.8854(6) Å. In contrast, the reaction of HgCl<sub>2</sub> and 2 results in the isomerization of 2 to *trans*-Mo(CO)<sub>4</sub>{Ph<sub>2</sub>P(CH<sub>2</sub>CH<sub>2</sub>O)<sub>4</sub>CH<sub>2</sub>CH<sub>2</sub>PPh<sub>2</sub>-*P,P'*}, 4. The Hg<sup>2+</sup>, which is too large to fit in the metallacrown ether ring in 2, catalyzes this isomerization, perhaps via coordination to the metallacrown ether and a lone pair on one of the carbonyl oxygens. Finally, the reaction of Hg(NO<sub>3</sub>)<sub>2</sub>·H<sub>2</sub>O and 1 results in the oxidation of the molybdenum carbonyl complex and the formation of a Hg<sup>2+</sup> complex of Ph<sub>2</sub>P(CH<sub>2</sub>CH<sub>2</sub>O)<sub>5</sub>CH<sub>2</sub>CH<sub>2</sub>PPh<sub>2</sub>. This mercury complex is not formed when Hg(NO<sub>3</sub>)<sub>2</sub>·H<sub>2</sub>O is stirred with Ph<sub>2</sub>P(CH<sub>2</sub>CH<sub>2</sub>O)<sub>5</sub>CH<sub>2</sub>CH<sub>2</sub>PPh<sub>2</sub> indicating that the metallacrown ether is required for the reaction to occur.

### Introduction

Metallacrown ethers are formed when R<sub>2</sub>PX(CH<sub>2</sub>-CH<sub>2</sub>O)<sub>*n*</sub>CH<sub>2</sub>CH<sub>2</sub>XPR<sub>2</sub> (*R* = Ph, O-alkyl; *X* = -, O; *n* ≥ 3) ligands chelate transition metals.<sup>1–4</sup> These complexes are of interest because they contain both a transition metal complex, which may catalyze a variety of organic reactions, and a crown ether, which may act as a phase-transfer catalyst. Studies of these metallacrown ethers have shown that they, like the crown ethers, are capable

of coordinating alkali metal cations and that the stabilities of the resulting complexes depend upon the relative sizes of the cation and the metallacrown ether cavity.<sup>1,3</sup> These studies have also shown that carbonyl ligands in metallacrown ether complexes are activated toward nucleophilic attack by organolithium reagents when the cavity is of the appropriate size to bind the Li<sup>+</sup>.<sup>1</sup>

Little is known about the conformational changes that occur when these metallacrown ethers bind hard metal cations because no X-ray crystal structures of such complexes have been reported. In addition, nothing is known about the abilities of the metallacrown ether complexes to bind heavy metal cations such as Hg<sup>2+</sup>. In this paper, we report the results of a synthetic and NMR spectroscopic study of the reactions of Hg<sup>2+</sup> salts with metallacrown ethers of the type *cis*-Mo(CO)<sub>4</sub>{Ph<sub>2</sub>P(CH<sub>2</sub>CH<sub>2</sub>O)<sub>*n*</sub>CH<sub>2</sub>CH<sub>2</sub>PPh<sub>2</sub>-*P,P'*} (*n* = 5 (1) or *n* = 4 (2)). We also report the X-ray crystal structure of *cis*-Mo(CO)<sub>4</sub>{*μ*-Ph<sub>2</sub>P(CH<sub>2</sub>CH<sub>2</sub>O)<sub>5</sub>CH<sub>2</sub>CH<sub>2</sub>PPh<sub>2</sub>-*P,P',O,O',O'',O''',O''''*}.HgCl<sub>2</sub>, 3, and discuss the significance of this structure.

### Experimental Section

All manipulations were carried out under a atmosphere of nitrogen. The solvents were of reagent grade and were used

<sup>⊗</sup> Abstract published in *Advance ACS Abstracts*, November 15, 1994.

(1) (a) Powell, J.; Kuksis, A.; May, C. J.; Nyberg, S. C.; Smith, S. J. *J. Am. Chem. Soc.* **1981**, *103*, 5941. (b) Powell, J.; Nyberg, S. C.; Smith, S. J. *Inorg. Chim. Acta* **1983**, *76*, L75. (c) Powell, J.; Ng, K. S.; Ng, W. W.; Nyberg, S. C. *J. Organomet. Chem.* **1983**, *243*, C1. (d) Powell, J.; Gregg, M.; Kusksis, A.; Meindl, P. *J. Am. Chem. Soc.* **1983**, *105*, 1064. (e) Powell, J.; Gregg, M. R.; Kusksis, A.; May, C. J.; Smith, S. J. *Organometallics* **1989**, *8*, 2918. (f) Powell, J.; Kusksis, A.; May, C. J.; Meindl, P. E.; Smith, S. J. *Organometallics* **1989**, *8*, 2933. (g) Powell, J.; Gregg, M. R.; Meindl, P. E. *Organometallics* **1989**, *8*, 2942. (h) Powell, J.; Lough, A.; Wang, F. *Organometallics* **1992**, *11*, 2289.

(2) (a) Alcock, N. W.; Brown, J. M.; Jeffery, J. C. *J. Chem. Soc., Chem. Commun.* **1974**, 829. (b) Alcock, N. W.; Brown, J. M.; Jeffery, J. C. *J. Chem. Soc., Dalton Trans.* **1976**, 583. (c) Thewissen, D. H. W.; Timmer, K.; Noltes, J. G.; Marsman, J. W.; Laine, R. M. *Inorg. Chim. Acta* **1985**, *97*, 143. (d) Timmer, K.; Thewissen, D. H. W. *Inorg. Chim. Acta* **1985**, *100*, 235. (e) Timmer, K.; Thewissen, H. M. D.; Marsman, J. W. *Recl. Trav. Chim. Pays-Bas* **1988**, *107*, 248.

(3) (a) Varshney, A.; Gray, G. M. *Inorg. Chem.* **1991**, *30*, 1748. (b) Varshney, A.; Webster, M. L.; Gray, G. M. *Inorg. Chem.* **1992**, *31*, 2580.

(4) Gray, G. M.; Duffey, C. H. *Organometallics*, in press.

Table 1. NMR Data for the Metallacrown Ethers and their HgCl<sub>2</sub> Complexes

compd	P		C1		C2		C3-C6
	$\delta(^{31}\text{P})$ (ppm)	$ ^1J(\text{HgP}) $ (Hz)	$\delta(^{13}\text{C})$ (ppm)	$ J(\text{PC}) $ (Hz)	$\delta(^{13}\text{C})$ (ppm)	$ J(\text{PC}) $ (Hz)	$\delta(^{13}\text{C})$ (ppm)
1 <sup>a</sup>	20.44 s		32.87 aq	20 <sup>c</sup>	66.94 bs		69.96 s, 70.34 s, 70.47 s, 70.47 s
2 <sup>a</sup>	20.11 s		31.32 aq	15 <sup>c</sup>	67.71 bs		70.16 s, 70.25 s, 70.65 s
3 <sup>b</sup>	21.20 s		32.28 aq	13 <sup>c</sup>	67.33 bs		69.91 s, 69.91 s, 70.02 s, 70.07 s
4 <sup>b</sup>	32.54 s						
5 <sup>b</sup>	27.83 sd	9861	27.37 d	37 <sup>d</sup>	64.53 bs		70.00 s, 70.07 s, 70.07 s, 70.30 s
6 <sup>a</sup>	20.11 s		31.22 aq	15 <sup>c</sup>	67.57 aq	9 <sup>e</sup>	69.81 s, 69.99 s, 69.99 s, 69.99 s

<sup>a</sup> Data from ref 3a. <sup>b</sup> Data from this work. <sup>c</sup>  $|^1J(\text{PC}) + ^3J(\text{P}'\text{C})|$ . <sup>d</sup>  $|^1J(\text{PC})|$ . <sup>e</sup>  $|^2J(\text{PC}) + ^4J(\text{P}'\text{C})|$ .

as received. Literature procedures were used to prepare *cis*-Mo(CO)<sub>4</sub>{Ph<sub>2</sub>P(CH<sub>2</sub>CH<sub>2</sub>O)<sub>n</sub>CH<sub>2</sub>CH<sub>2</sub>PPh<sub>2</sub>-*P,P'*} (*n* = 5 (1), 4 (2)).<sup>3a</sup>

The <sup>31</sup>P{<sup>1</sup>H}, <sup>13</sup>C{<sup>1</sup>H}, and <sup>1</sup>H NMR spectra were recorded on a GE NT-300, wide-bore, multinuclear NMR spectrometer. The <sup>31</sup>P NMR spectra were referenced to external 85% phosphoric acid, and the <sup>13</sup>C and <sup>1</sup>H NMR spectra were referenced to internal tetramethylsilane. Chemical shifts that are downfield from those of the reference compounds are reported as positive. The <sup>31</sup>P and aliphatic <sup>13</sup>C NMR data for the complexes are given in Table 1. Infrared spectra of dilute dichloromethane solutions of the carbonyl complexes in a 0.2 mm KBr solution cell were run on a Nicolet IR44 FTIR spectrometer. The background for these measurements was pure dichloromethane in the same cell. Elemental analyses of the compounds were performed by Atlantic Microlab, Inc., Norcross, GA.

*cis*-Mo(CO)<sub>4</sub>{ $\mu$ -Ph<sub>2</sub>P(CH<sub>2</sub>CH<sub>2</sub>O)<sub>5</sub>CH<sub>2</sub>CH<sub>2</sub>PPh<sub>2</sub>-*P,P'*, *O,O',O'',O''',O''''*}-HgCl<sub>2</sub>, **3**. A mixture of 0.176 g (0.213 mmol) of **1** and 0.301 g (1.11 mmol) of HgCl<sub>2</sub> in 3 mL of chloroform-*d*<sub>1</sub> was stirred at ambient temperature for 4 h and then filtered through diatomaceous earth. The filtrate was allowed to stand in the dark for 2 days and then refiltered. This filtrate was evaporated to dryness to give a quantitative yield of crude **3**. Recrystallization from a dichloromethane-methanol mixture yielded analytically pure **3**. Anal. Calc (found) for C<sub>40</sub>H<sub>44</sub>Cl<sub>2</sub>HgO<sub>8</sub>MoP<sub>2</sub>: C, 58.11 (58.26); H, 5.36 (5.42). <sup>1</sup>H NMR (CDCl<sub>3</sub>):  $\delta$  7.507 and 7.352 (Ph, m, 5H);  $\delta$  3.652 (C5 and C6 methylenes; m, 4H), 3.578 (C4 methylene; m, 2H), 3.405 (C3 methylene; m, 2), 3.274 (C2 methylene, t,  $|^3J(\text{HH})| = 7.6$  Hz, 2H), 2.805 (C1 methylene, t,  $|^3J(\text{HH})| = 7.6$  Hz, 2H). IR [ $\nu(\text{CO})$ ] (CH<sub>2</sub>Cl<sub>2</sub>): 2022 m, 1919 sh, 1909 s, 1886 sh cm<sup>-1</sup>.

**Reaction of *cis*-Mo(CO)<sub>4</sub>{Ph<sub>2</sub>P(CH<sub>2</sub>CH<sub>2</sub>O)<sub>4</sub>CH<sub>2</sub>CH<sub>2</sub>PPh<sub>2</sub>-*P,P'*}, **2**, and HgCl<sub>2</sub>.** A mixture of 0.098 g (0.129 mmol) of **2** and 0.170 g (0.626 mmol) of HgCl<sub>2</sub> in 2.0 mL of chloroform-*d*<sub>1</sub> was stirred in the dark at ambient temperature for 70 h. The mixture was then filtered through a 0.2  $\mu\text{m}$  syringe filter. The residue was washed with two, 0.50 mL portions of chloroform-*d*<sub>1</sub>, and these were also filtered through the syringe filter and combined with the reaction mixture. A quantitative <sup>31</sup>P NMR spectrum was taken of the filtrate. This spectrum contained a singlet at 20.19 ppm due to **1** and a singlet at 32.54 ppm due to *trans*-Mo(CO)<sub>4</sub>{Ph<sub>2</sub>P(CH<sub>2</sub>CH<sub>2</sub>O)<sub>4</sub>CH<sub>2</sub>CH<sub>2</sub>PPh<sub>2</sub>-*P,P'*}, **4**, in a 46.3 to 53.7 ratio (from integration).

**Reaction of *cis*-Mo(CO)<sub>4</sub>(Ph<sub>2</sub>PMe)<sub>2</sub> and HgCl<sub>2</sub>.** The reaction of 0.078 g (0.129 mmol) of *cis*-Mo(CO)<sub>4</sub>(Ph<sub>2</sub>PMe)<sub>2</sub> and 0.170 g (0.626 mmol) of HgCl<sub>2</sub> in 2.0 mL of chloroform-*d*<sub>1</sub> was carried out using the procedure described for the reaction of **2** and HgCl<sub>2</sub>. A quantitative <sup>31</sup>P NMR spectrum of the filtrate contained a singlet at 15.44 ppm due to *cis*-Mo(CO)<sub>4</sub>(Ph<sub>2</sub>PMe)<sub>2</sub> and a singlet at 28.49 ppm due to *trans*-Mo(CO)<sub>4</sub>(Ph<sub>2</sub>PMe)<sub>2</sub> in a 79.2 to 20.8 ratio (from integration).

**Reaction of *cis*-Mo(CO)<sub>4</sub>{Ph<sub>2</sub>P(CH<sub>2</sub>CH<sub>2</sub>O)<sub>5</sub>CH<sub>2</sub>CH<sub>2</sub>PPh<sub>2</sub>-*P,P'*}, **2**, and Hg(NO<sub>3</sub>)<sub>2</sub>·H<sub>2</sub>O.** A mixture of 0.20 g (0.24 mmol) of **1** and 0.425 g (1.24 mmol) of Hg(NO<sub>3</sub>)<sub>2</sub>·H<sub>2</sub>O in 25 mL of dichloromethane was stirred at ambient temperature for 24 h. During this time, the color of the solution changed from

colorless to yellow to dark brown to beige and a beige solid precipitated. The reaction mixture was then filtered, and the filtrate evaporated to dryness to yield 0.126 g of a foamy white solid, **5**, which appeared to be a Hg(NO<sub>3</sub>)<sub>2</sub> complex of the Ph<sub>2</sub>P(CH<sub>2</sub>CH<sub>2</sub>O)<sub>5</sub>CH<sub>2</sub>CH<sub>2</sub>PPh<sub>2</sub> ligand on the basis of its <sup>31</sup>P and <sup>13</sup>C NMR spectra.

**X-ray Structure Determination of 3.** A colorless, needle-like crystal of **3** was grown by slowly diffusing hexanes into a THF solution of the complex. The crystal was mounted on a glass fiber with epoxy cement, and the cell constants were obtained from least-squares refinement of 25 reflections with 25  $\leq \theta \leq 35^\circ$ . All measurements were carried out at 23 °C on an Enraf-Nonius CAD4 diffractometer using graphite monochromated Cu K $\alpha$  radiation ( $\lambda = 1.5418 \text{ \AA}$ ).

Data were collected by  $\omega$ -2 $\theta$  scans. The crystal decayed 12.3% during the data collection, and a linear decay correction was applied. An analytical absorption correction (using the Crystal and Abscor programs) was also applied to the data. Of the 9505 independent reflections measured, 7737 had  $I > 3\sigma(I)$  and were used for structure solution and refinement.

The structure was solved by heavy-atom methods and refined by a full-matrix least squares procedure that minimized  $w(|F_o| - |F_c|)^2$ , where  $w = 1/\sigma^2(F_o)$ , using the MolEN package of programs. All non-hydrogen atoms were refined anisotropically. The hydrogen atoms were placed in calculated positions (C-H = 0.96  $\text{\AA}$ ,  $U_{\text{iso}}(\text{H}) = 1.3U_{\text{iso}}(\text{C})$ ) and were not refined. Data were weighted using a non-Poisson scheme. A secondary extinction correction was applied to the data,<sup>5</sup> and the extinction coefficient was refined. In the last stage of the refinement no parameter varied by more than 0.01 of its standard deviation, and the final difference Fourier map had no interpretable peaks. Atomic scattering factors were taken from the compilations of Cromer and Weber,<sup>6</sup> and those for H were taken from the ref 7. Corrections for anomalous dispersion were taken from the compilations of Cromer and Lieberman<sup>8</sup> and applied to chlorine, mercury, molybdenum, and phosphorus. Data for the X-ray structure analyses are given in Table 2. Positional parameters are given in Table 3. Values of selected bond lengths and angles and torsion angles are given in Tables 4-6. Tables of hydrogen atomic positional and thermal parameters, thermal parameters, torsion angles, and least squares planes are available as supplementary material. An ORTEP<sup>9</sup> drawing of the molecule is given in Figure 1.

## Results and Discussion

Previous studies of *cis*-Mo(CO)<sub>4</sub>{Ph<sub>2</sub>P(CH<sub>2</sub>CH<sub>2</sub>O)<sub>n</sub>-CH<sub>2</sub>CH<sub>2</sub>PPh<sub>2</sub>-*P,P'*} (*n* = 5 (1), 4 (2)) metallacrown ethers have shown that **1** weakly coordinates to Li<sup>+</sup> and

(5) Zachariasen, W. H. *Acta Crystallogr.* **1963**, *16*, 1139.

(6) Cromer, D. T.; Weber, D. T. *Acta Crystallogr.* **1965**, *18*, 104.

(7) *International Tables for Crystallography*; Hahn, T., Ed.; Kynoch Press: Birmingham, U.K., 1974; Vol. IV, p 72.

(8) Cromer, D. T.; Lieberman, D. J. *J. Chem. Phys.* **1970**, *53*, 1891.

(9) Johnson, C. K. *ORTEP II*. Report ORNL-5138; Oak Ridge National Laboratory: Oak Ridge, TN, 1976.

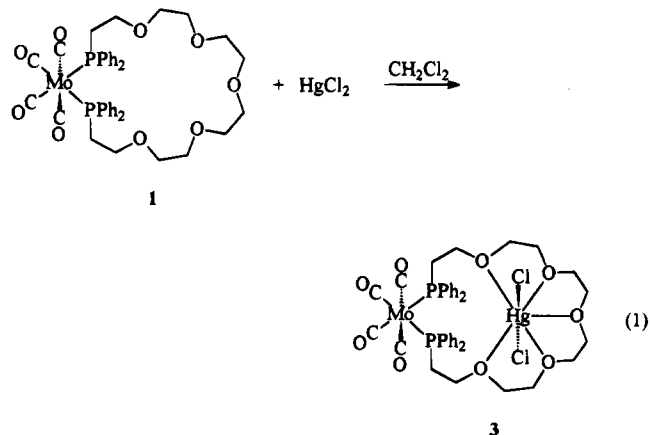
**Table 2. Data Collection and Structure Solution and Refinement Parameters for 3**

formula	C <sub>40</sub> H <sub>44</sub> Cl <sub>2</sub> HgMoO <sub>9</sub> P <sub>2</sub>
MW	1098.18
space group	P $\bar{1}$
<i>a</i> (Å)	10.387(2)
<i>b</i> (Å)	13.0359(7)
<i>c</i> (Å)	17.710(3)
$\alpha$ (deg)	69.401(7)
$\beta$ (deg)	81.32(1)
$\gamma$ (deg)	87.15(1)
<i>V</i> (Å <sup>3</sup> )	2218.8
<i>Z</i>	2
<i>d</i> <sub>calc</sub> (g/cm <sup>3</sup> )	1.644
cryst diamens (mm)	0.13 × 0.17 × 0.70
<i>h</i> <sub>max</sub> , <i>h</i> <sub>min</sub>	12, 0
<i>k</i> <sub>max</sub> , <i>k</i> <sub>min</sub>	-16, 16
<i>l</i> <sub>max</sub> , <i>l</i> <sub>min</sub>	-21, 21
$\lambda$ (Å)	1.541 84
temp (°C)	23
abs coeff (cm <sup>-1</sup> )	111.825
$\theta$ limits (deg)	0.1–74
decay corr	linear
decay (%)	12.3
abs corr	analytical
<i>T</i> <sub>max</sub> , <i>T</i> <sub>min</sub> (%)	38.46, 5.83
reflms measd	9505
scan width (deg)	1.34
reflms with <i>I</i> ≥ 3 $\sigma$ ( <i>I</i> )	7737
no. of variables	497
function minimized	$w( F_o  -  F_c )^2$
weighting scheme	non-Poisson ( $w = 1/\sigma^2(F_o)$ )
instrumental uncertainty factor	0.03
secondary extinction corr type	Zacharisen
minimized extinction coeff	$1.995 \times 10^{-6}$
<i>R</i> (%)	5.82
<i>R</i> <sub>w</sub> (%)	7.19
GOF <sup>c</sup>	1.996
max, min resid electron density (e/Å <sup>3</sup> )	3.109, -0.175
max shift/error	0.01

<sup>a</sup>  $R = \sum(|F_o| - |F_c|)/\sum|F_o|$ . <sup>b</sup>  $R_w = \sum w(|F_o| - |F_c|)^2/\sum w|F_o|^2$ . <sup>c</sup> GOF =  $[\sum w(|F_o| - |F_c|)^2/n - m]^{0.5}$ .

strongly coordinates to Na<sup>+</sup> but that **2** strongly coordinates to Li<sup>+</sup> and weakly coordinates to Na<sup>+</sup>.<sup>3a</sup> Because Na<sup>+</sup> and Hg<sup>2+</sup> have similar ionic radii (for coordination number 6: Na<sup>+</sup>, 1.16 Å, and Hg<sup>2+</sup>, 1.16 Å),<sup>10</sup> we expected that **1** would strongly bind Hg<sup>2+</sup> but that **2** would not. This picture, however, is much too simplistic.

**Reaction of *cis*-Mo(CO)<sub>4</sub>{Ph<sub>2</sub>P(CH<sub>2</sub>CH<sub>2</sub>O)<sub>5</sub>CH<sub>2</sub>-CH<sub>2</sub>PPh<sub>2</sub>-*P,P'*}, **1**, and HgCl<sub>2</sub>.** The reaction of **1** with HgCl<sub>2</sub> in dichloromethane, shown in eq 1, yields only



the bimetallic complex, *cis*-Mo(CO)<sub>4</sub>{ $\mu$ -Ph<sub>2</sub>P(CH<sub>2</sub>CH<sub>2</sub>O)<sub>5</sub>-CH<sub>2</sub>CH<sub>2</sub>PPh<sub>2</sub>-*P,P',O,O',O'',O''',O''''*}-HgCl<sub>2</sub>, **3**. This complex is quite stable in solution and can be recrystallized.

**Table 3. Positional Parameters and Isotropic Thermal Factors (Å<sup>2</sup>) for 3<sup>a</sup>**

atom	<i>x</i>	<i>y</i>	<i>z</i>	<i>B</i>
Hg	0.33142(3)	0.58858(2)	0.67593(2)	3.733(6)
Mo	0.06877(5)	1.02894(4)	0.77377(3)	2.576(9)
Cl2	0.1926(3)	0.5003(2)	0.7910(1)	6.05(6)
P1	0.2349(2)	0.8943(1)	0.84785(9)	2.62(3)
P2	-0.0437(2)	0.8863(1)	0.73701(9)	2.78(3)
O1	-0.1089(7)	1.2231(5)	0.6893(4)	7.0(2)
O2	0.2031(6)	1.2104(4)	0.8132(4)	5.9(1)
O3	0.2650(8)	1.0859(7)	0.6102(4)	8.3(2)
O4	-0.1272(6)	1.0081(5)	0.9345(4)	5.7(1)
O5	0.4733(5)	0.6686(4)	0.7860(3)	3.5(1)
O6	0.5579(6)	0.4760(4)	0.7473(3)	4.4(1)
O7	0.4390(6)	0.4195(4)	0.6315(3)	4.8(1)
O8	0.1972(6)	0.5082(4)	0.5741(3)	4.9(1)
O9	0.0908(5)	0.6996(4)	0.5990(3)	3.8(1)
C1	-0.0459(8)	1.1481(6)	0.7190(5)	4.2(2)
C2	0.1559(8)	1.1436(6)	0.7994(4)	3.9(2)
C3	0.1965(8)	1.0624(6)	0.6689(5)	4.3(2)
C4	-0.0586(7)	1.0103(6)	0.8778(4)	3.6(1)
C5	0.3048(6)	0.7905(5)	0.8039(4)	3.2(1)
C7	0.5720(7)	0.5960(6)	0.8189(4)	3.8(1)
C8	0.6408(8)	0.5518(6)	0.7565(5)	4.2(2)
C9	0.620(1)	0.4190(7)	0.6959(5)	5.4(2)
C10	0.524(1)	0.3504(7)	0.6834(5)	5.9(2)
C11	0.347(1)	0.3626(6)	0.6077(5)	5.3(2)
C12	0.285(1)	0.4404(7)	0.5420(5)	5.1(2)
C13	0.144(1)	0.5944(7)	0.5139(5)	5.1(2)
C14	0.0356(9)	0.6459(7)	0.5544(5)	5.6(2)
C15	-0.0070(7)	0.7501(6)	0.6389(4)	4.1(2)
C16	0.0604(7)	0.8144(6)	0.6780(4)	3.6(1)
C17	0.3782(6)	0.9720(5)	0.8445(4)	2.9(1)
C18	0.4751(7)	0.9991(6)	0.7775(4)	3.7(1)
C19	0.5794(7)	1.0632(6)	0.7712(5)	4.5(2)
C20	0.5911(8)	1.1027(6)	0.8320(6)	4.8(2)
C21	0.4929(9)	1.0796(6)	0.8980(4)	4.7(2)
C22	0.3868(8)	1.0159(6)	0.9052(4)	4.1(2)
C23	0.1971(6)	0.8094(5)	0.9555(4)	3.0(1)
C24	0.2902(7)	0.7704(6)	1.0073(4)	3.7(1)
C25	0.2567(9)	0.7040(7)	1.0877(4)	4.4(2)
C26	0.1272(9)	0.6773(7)	1.1186(5)	4.8(2)
C27	0.0344(8)	0.7121(6)	1.0688(5)	4.5(2)
C28	0.0671(7)	0.7771(6)	0.9876(4)	3.5(1)
C29	-0.1229(7)	0.7764(5)	0.8255(4)	3.2(1)
C30	-0.0794(8)	0.6706(6)	0.8522(5)	4.2(2)
C31	-0.1314(9)	0.5952(7)	0.9262(5)	5.5(2)
C32	-0.232(1)	0.6245(8)	0.9754(5)	5.6(2)
C33	-0.2784(9)	0.7294(7)	0.9490(5)	4.9(2)
C34	-0.2265(7)	0.8065(6)	0.8753(4)	3.7(2)
C35	-0.1699(6)	0.9352(5)	0.6700(4)	3.1(1)
C36	-0.2795(7)	0.8745(6)	0.6776(4)	3.4(1)
C37	-0.3655(7)	0.9109(7)	0.6205(4)	4.3(2)
C38	-0.3459(8)	1.0109(7)	0.5570(5)	4.8(2)
C39	-0.2363(8)	1.0691(7)	0.5493(4)	4.5(2)
C40	-0.1481(7)	1.0338(6)	0.6052(4)	3.7(1)

<sup>a</sup> Anisotropically refined atoms are given in the form of the isotropic equivalent displacement parameter defined as  $(4/3)[a^2B(1,1) + b^2B(2,2) + c^2B(3,3) + ab(\cos \gamma)B(1,2) + ac(\cos \beta)B(1,3) + bc(\cos \alpha)B(2,3)]$ .

The shift in the <sup>31</sup>P NMR resonance of **1** upon coordination of the HgCl<sub>2</sub> is in the opposite direction and approximately twice as large as the shift that occurs upon coordination of NaBPh<sub>4</sub> to **1** to form *cis*-Mo(CO)<sub>4</sub>{ $\mu$ -Ph<sub>2</sub>P(CH<sub>2</sub>CH<sub>2</sub>O)<sub>5</sub>CH<sub>2</sub>CH<sub>2</sub>PPh<sub>2</sub>-*P,P',O,O',O'',O''',O''''*}-NaBPh<sub>4</sub>, **6**.<sup>3a</sup> The shifts in the methylene <sup>13</sup>C NMR resonances of **1** upon coordination of the HgCl<sub>2</sub> are in the same directions as those observed upon coordination of NaBPh<sub>4</sub> to **1** but are of somewhat different magnitudes. These differences are not surprising given the different coordination geometries preferred by Hg<sup>2+</sup> and Na<sup>+</sup> and the flexibility of the metallacrown ether ring in **1**.

Table 4. Selected Bond Lengths (Å) for **3**

Hg—C11	2.281(2)	O2—C2	1.13(1)
Hg—C12	2.276(2)	O3—C3	1.12(1)
Hg—O5	3.085(6)	O4—C4	1.132(9)
Hg—O6	2.921(6)	O5—C6	1.434(9)
Hg—O7	2.727(6)	O5—C7	1.408(8)
Hg—O8	2.921(7)	O6—C8	1.41(1)
Hg—O9	3.078(5)	O6—C9	1.43(1)
Mo—P1	2.558(2)	O7—C10	1.42(1)
Mo—P2	2.557(2)	O7—C11	1.43(1)
Mo—C1	1.969(8)	O8—C12	1.43(1)
Mo—C2	1.999(9)	O8—C13	1.405(9)
Mo—C3	2.036(7)	O9—C14	1.42(1)
Mo—C4	2.046(7)	O9—C15	1.417(9)
P1—C5	1.854(7)	C5—C6	1.484(9)
P1—C17	1.823(7)	C7—C8	1.49(1)
P1—C23	1.830(6)	C9—C10	1.46(2)
P2—C16	1.842(8)	C11—C12	1.46(1)
P2—C29	1.826(5)	C13—C14	1.50(1)
P2—C35	1.841(7)	C15—C16	1.51(1)
O1—C1	1.16(1)		

Table 5. Selected Bond Angles (deg) for **3**

C11—Hg—C12	169.41(9)	Mo—P1—C5	118.0(3)
C11—Hg—O5	88.5(1)	Mo—P1—C17	102.6(3)
C11—Hg—O6	92.4(1)	Mo—P1—C23	103.6(3)
C11—Hg—O7	88.2(1)	Mo—P2—C16	102.6(3)
C11—Hg—O8	92.4(1)	Mo—P2—C29	100.8(3)
C11—Hg—O9	88.2(1)	Mo—P2—C35	103.6(3)
C12—Hg—O5	86.1(1)	C6—O5—C7	112.0(5)
C12—Hg—O6	92.3(1)	C8—O6—C9	113.1(6)
C12—Hg—O7	102.4(1)	C10—O7—C11	114.6(6)
C12—Hg—O8	93.1(1)	C12—O8—C13	113.7(6)
C12—Hg—O9	87.4(1)	C14—O9—C15	110.9(6)
O5—Hg—O6	57.4(1)	P1—C5—C6	117.9(5)
O6—Hg—O7	60.8(2)	O5—C6—C5	108.4(6)
O7—Hg—O8	61.4(2)	O5—C7—C8	109.8(6)
O8—Hg—O9	56.2(2)	O6—C8—C7	108.4(6)
P1—Mo—P2	94.57(5)	O6—C9—C10	109.4(8)
P1—Mo—C1	172.2(3)	O7—C10—C9	108.4(6)
P1—Mo—C2	86.7(2)	O7—C11—C12	109.3(7)
P1—Mo—C3	88.5(2)	O8—C12—C11	109.5(7)
P1—Mo—C4	94.1(2)	O8—C13—C14	108.9(6)
P2—Mo—C1	93.2(3)	O9—C14—C13	108.1(7)
P2—Mo—C2	178.4(2)	O9—C15—C16	107.6(6)
P2—Mo—C3	89.9(3)	P2—C16—C15	117.2(5)
P2—Mo—C4	94.5(2)		

Table 6. Selected Torsional Angles (deg) for **3** and Hg(CH<sub>3</sub>CH<sub>2</sub>O(CH<sub>2</sub>CH<sub>2</sub>O)<sub>4</sub>CH<sub>2</sub>CH<sub>3</sub>-O,O',O'',O''',O''''Cl<sub>2</sub>, **9**

<b>3</b>		<b>9<sup>a</sup></b>	
C7—O5—C6—C5	-176.2(6)	C3—O1—C2—C1	-170
C6—O5—C7—C8	-174.3(6)	C2—O1—C3—C4	171
O9—O6—C8—C7	-173.2(5)	C5—O2—C4—C3	170
C8—O6—C9—C10	-174.6(6)	C4—O2—C5—C6	-174
C11—O7—C10—C9	174.4(7)	C7—O3—C6—C5	-176
C10—O7—C11—C12	-168.1(7)	C6—O3—C7—C8	-179
C13—O8—C12—C11	172.9(8)	C9—O4—C8—C7	178
C12—O8—C13—C14	169.3(7)	C8—O4—C9—C10	177
C15—O9—C14—C13	180.0(6)	C11—O5—C10—C9	-178
C14—O9—C15—C16	-174.6(6)	C10—O5—C11—C12	-80
O5—C7—C8—O6	-73.1(7)	O1—C3—C4—O2	-77
O6—C9—C10—O7	71.9(8)	O2—C5—C6—O3	72
O7—C11—C12—O8	-72.2(9)	O3—C7—C8—O4	-71
O8—C13—C14—O9	68.2(8)	O4—C9—C10—O5	73

<sup>a</sup> Data from ref 14b.

The X-ray crystal structure of **3** is shown in Figure 1 and contains a number of interesting features. The coordination geometry of the molybdenum is a distorted octahedron similar to that observed in other *cis*-Mo(CO)<sub>4</sub>(P-donor ligand)<sub>2</sub> complexes. The P1—Mo—P2 angle (94.57(5)°) is similar to those in *cis*-Mo(CO)<sub>4</sub>{Ph<sub>2</sub>P(CH<sub>2</sub>CH<sub>2</sub>O)<sub>3</sub>CH<sub>2</sub>CH<sub>2</sub>PPh<sub>2</sub>-P,P'}, **7** (93.78(2)°),<sup>3a</sup> and *cis*-PtCl<sub>2</sub>{Ph<sub>2</sub>P(CH<sub>2</sub>CH<sub>2</sub>O)<sub>3</sub>CH<sub>2</sub>CH<sub>2</sub>PPh<sub>2</sub>-P,P'}, **8** (99.03(6)°).<sup>3b</sup> This suggests that the metallacrown ether

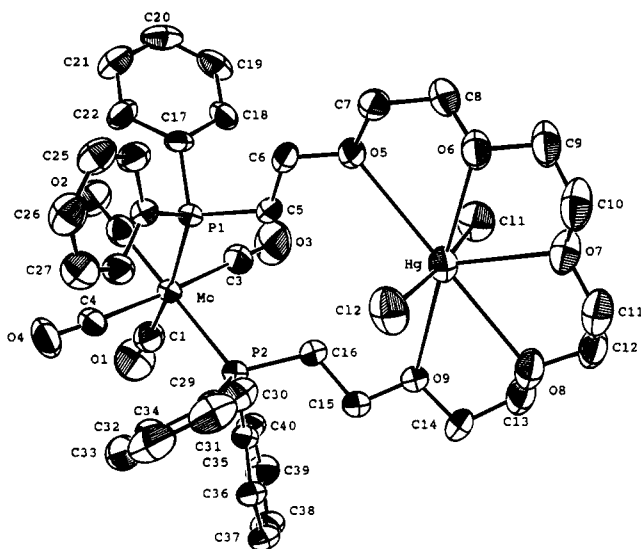


Figure 1. ORTEP drawing of the molecular structure of **3**. Thermal ellipsoids are drawn at the 50% probability level, and hydrogens are omitted for clarity.

ring in **2** is sufficiently flexible that coordination of HgCl<sub>2</sub> does not greatly perturb the coordination environment of the molybdenum.

The coordination environment of the Hg<sup>2+</sup> ion is unusual. The Hg<sup>2+</sup> is coordinated to all five oxygens in the metallacrown ether and to both chlorides. The oxygens are in a nearly planar arrangement (largest deviations from the least squares plane through the five oxygens are 0.141(6) Å for O7 and -0.107(6) Å for O8). The chlorides are trans to each other, and the mercury-chloride bonds are perpendicular to the least squares plane through the five ether oxygens. Because the O—Hg—O angles are all close to 60° and not 72°, the coordination environment of the Hg<sup>2+</sup> is better described as a hexagonal bipyramid with a missing equatorial ligand than as the more common pentagonal bipyramid.

The open coordination site in the hexagonal bipyramid is pointed toward the molybdenum. This, together with the Mo—Hg bond distance of 6.8854(6) Å, suggests that it might be possible to bridge a ligand between the metals in bimetallic, metallacrown ether complexes. One difficulty with this is that the protons on C5 and C16 are pointed into the cavity between the Mo and the Hg (distances (Å): H5—H16, 2.719; H5—H16', 3.178; H5'—H16, 2.184; H5'—H16', 3.322) and would interfere with a ligand bridging between the two metals. However, it seems likely that this could be avoided by rotation about the Mo—P bonds. This occurs rapidly in solution as indicated by the equivalence of the phenyl groups on the phosphines and thus should not introduce a great deal of strain into the molecule.

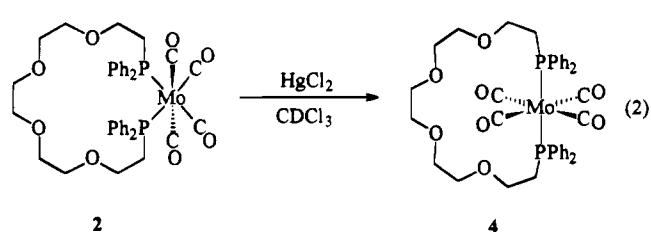
The asymmetric coordination environment of the Hg<sup>2+</sup> ion in **3** is unlike that observed for Hg<sup>2+</sup> coordinated to crown ethers and azacrown ethers. With larger crown ethers such as 1,4,10,13-tetraoxa-7,16-diazacyclooctadecane and 18-crown-6, the Hg<sup>2+</sup> coordinates in the center of the crown with the ether oxygens symmetrically arranged around the Hg<sup>2+</sup> and with trans monodentate anionic ligands.<sup>11</sup> With smaller crown ethers such as 15-crown-5, the Hg<sup>2+</sup> is too small to fit

(11) (a) Malmsten, L.-A. *Acta Crystallogr.* **1979**, *B35*, 1702. (b) Paige, C. R.; Richardson, M. F. *Can. J. Chem.* **1984**, *62*, 332. (c) Drew, M. G. B.; Lee, K. C.; Mok, K. F. *Inorg. Chim. Acta* **1989**, *155*, 39.

into the crown and coordinates above the crown with *cis* monodentate anionic ligands.<sup>12</sup> Very similar behavior is also observed in Pb<sup>2+</sup> crown ethers complexes.<sup>13</sup>

The Hg<sup>2+</sup> coordination environment in **3** closely resembles that in complexes with linear ethylene oxide oligomers.<sup>14</sup> This resemblance is seen in the similarity of the torsion angles for equivalent bonds in **3** and in Hg(CH<sub>3</sub>CH<sub>2</sub>O(CH<sub>2</sub>CH<sub>2</sub>O)<sub>4</sub>CH<sub>2</sub>CH<sub>3</sub>-O,O',O'',O''',O''''-Cl<sub>2</sub>, **9**, shown in Table 6. The only major difference in these angles is between that for C14-O9-C15-C16 in **3** and that for C10-O5-C11-C12 in **9**, and this is to be expected because the polyether is cyclic in **3** and acyclic in **9**. This striking similarity in torsion angles suggests that presence of the large transition metal complex in the ring allows metallacrown ethers to adopt a larger variety of coordination modes than can the crown ethers and therefore resemble the open chain polyethers in this regard.

**Reaction of *cis*-Mo(CO)<sub>4</sub>{Ph<sub>2</sub>P(CH<sub>2</sub>CH<sub>2</sub>O)<sub>4</sub>CH<sub>2</sub>-CH<sub>2</sub>PPh<sub>2</sub>-P,P'}**, **2**, and HgCl<sub>2</sub>. In contrast to the above results, when a chloroform-*d*<sub>1</sub> solution of **2** is stirred with excess HgCl<sub>2</sub> in the dark at ambient temperature, *trans*-Mo(CO)<sub>4</sub>{Ph<sub>2</sub>P(CH<sub>2</sub>CH<sub>2</sub>O)<sub>4</sub>CH<sub>2</sub>CH<sub>2</sub>-PPh<sub>2</sub>-P,P'}, **4**, is formed, as shown in eq 2. This

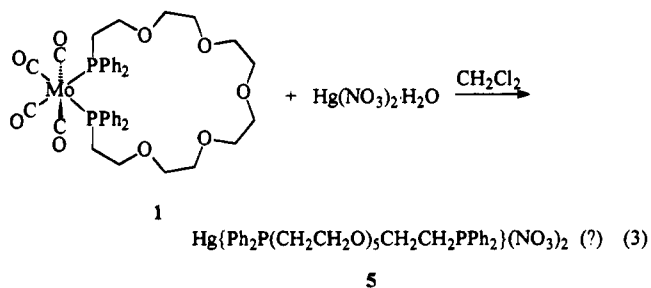


isomerization is 53.7% complete after 70 h in the presence of HgCl<sub>2</sub> but does not occur to any appreciable extent during this time if HgCl<sub>2</sub> is not present. We recently reported that this reaction occurs very slowly in the dark (15% isomerization after 24 days at 5 °C) and rapidly when **1** is irradiated with UV light (12 min at 21 °C).<sup>4</sup>

In order to better understand the mechanism of this isomerization, we carried out a similar isomerization of *cis*-Mo(CO)<sub>4</sub>(Ph<sub>2</sub>PMe)<sub>2</sub> to *trans*-Mo(CO)<sub>4</sub>(Ph<sub>2</sub>PMe)<sub>2</sub> in chloroform-*d*<sub>1</sub> solution in the presence of HgCl<sub>2</sub>. This isomerization also occurs but at a much lower rate than the isomerization of **2** to **4**. This suggests that the Hg<sup>2+</sup> facilitates the loss of the carbonyl by binding to the lone pair on the oxygen and weakening the metal carbon bonds as demonstrated by Shriver with a variety of Lewis acids and metal carbonyl complexes.<sup>15</sup> The increased rate of the isomerization of **2** to **4** by HgCl<sub>2</sub> could result from initial binding of the HgCl<sub>2</sub> to the metallacrown ether in **2** followed by coordination of a carbonyl oxygen to the Hg<sup>2+</sup>. The crystal structure of *cis*-Mo(CO)<sub>4</sub>{μ-Ph<sub>2</sub>P(CH<sub>2</sub>CH<sub>2</sub>O)<sub>5</sub>CH<sub>2</sub>CH<sub>2</sub>PPh<sub>2</sub>-P,P',O,O',O'',O''',O''''}·HgCl<sub>2</sub>, **3**, discussed above, suggests that bridging of a carbonyl between the Mo and the Hg<sup>2+</sup> in these complexes is possible. The proposed mecha-

nism is similar, in many respects, to the mechanism suggested by Powell for the activation of carbonyls to attack by alkyl- and aryllithiums in related metallacrown ethers.<sup>1</sup>

**Reaction of *cis*-Mo(CO)<sub>4</sub>{Ph<sub>2</sub>P(CH<sub>2</sub>CH<sub>2</sub>O)<sub>5</sub>CH<sub>2</sub>-CH<sub>2</sub>PPh<sub>2</sub>-P,P'}**, **2**, and Hg(NO<sub>3</sub>)<sub>2</sub>·H<sub>2</sub>O. In an attempt to synthesize a Hg<sup>2+</sup> complex with less strongly coordinating anions, Hg(NO<sub>3</sub>)<sub>2</sub>·H<sub>2</sub>O was added to a dichloromethane solution of **1**. This caused the color of the solution to change from colorless to deep brown and finally to beige and a beige solid to precipitate from the solution. A <sup>31</sup>P NMR spectrum of the methylene chloride soluble portion of the reaction mixture contained a single resonance that was a superimposed singlet and doublet. The relative intensities of the singlet and doublet and magnitude of the coupling constant indicated that the diphenylphosphino groups in the Ph<sub>2</sub>P(CH<sub>2</sub>CH<sub>2</sub>O)<sub>5</sub>CH<sub>2</sub>CH<sub>2</sub>PPh<sub>2</sub> ligand were coordinated to mercury. This suggests that the nitrate oxidized the molybdenum, hence the color change, allowing the diphenylphosphino groups of the Ph<sub>2</sub>P(CH<sub>2</sub>CH<sub>2</sub>O)<sub>5</sub>CH<sub>2</sub>CH<sub>2</sub>PPh<sub>2</sub> ligand to coordinate to the mercury, as shown in eq 3. The formulation for the product is supported



by the presence of resonances for all the ligand carbons and the absence of carbonyl resonances in its <sup>13</sup>C NMR spectrum and by the absence of C≡O stretches in its IR spectrum. This formulation is also supported by the fact that no reaction is observed when the Ph<sub>2</sub>P(CH<sub>2</sub>CH<sub>2</sub>O)<sub>5</sub>CH<sub>2</sub>CH<sub>2</sub>PPh<sub>2</sub> ligand is stirred with Hg(NO<sub>3</sub>)<sub>2</sub>·H<sub>2</sub>O in dichloromethane, indicating that the metallacrown ether is needed as a template for this reaction to occur. The only problem with this explanation is that all of the <sup>13</sup>C NMR resonances of the Ph<sub>2</sub>P(CH<sub>2</sub>CH<sub>2</sub>O)<sub>5</sub>CH<sub>2</sub>CH<sub>2</sub>PPh<sub>2</sub> ligand appear to be doublets, suggesting that only one phosphorus is coordinated to each Hg<sup>2+</sup>. However, these doublets could also result if |<sup>2</sup>J(PP')| is small, which would be the case if the complex is fluxional. Unfortunately, we have been unable to either purify or crystallize this material to prove the exact nature of the product.

## Conclusions

The reactions of Hg<sup>2+</sup> salts with the *cis*-Mo(CO)<sub>4</sub>-{Ph<sub>2</sub>P(CH<sub>2</sub>CH<sub>2</sub>O)<sub>*n*</sub>CH<sub>2</sub>CH<sub>2</sub>PPh<sub>2</sub>-P,P'} (*n* = 4, 5) metallacrown ethers are surprisingly complex. The nature of the product depends on the size of the metallacrown ether and the reactivity of the anions. The size-selective reactions of the metallacrown ethers with Hg<sup>2+</sup> are particularly fascinating because it might be possible to employ them in sensors for Hg<sup>2+</sup> and related anions.

The coordination environment of the Hg<sup>2+</sup> in *cis*-Mo(CO)<sub>4</sub>{μ-Ph<sub>2</sub>P(CH<sub>2</sub>CH<sub>2</sub>O)<sub>5</sub>CH<sub>2</sub>CH<sub>2</sub>PPh<sub>2</sub>-P,P',O,O',O'',O''',O''''}·HgCl<sub>2</sub> is a hexagonal bipyramid with

(12) Byriel, K. A.; Dunster, K. R.; Gahan, L. R.; Kennard, C. H. L.; Latten, J. L. *Inorg. Chim. Acta* **1992**, *196*, 35.

(13) Byriel, K. A.; Dunster, K. R.; Gahan, L. R.; Kennard, C. H. L.; Latten, J. L.; Swann, I. L. *Polyhedron* **1992**, *10*, 1205.

(14) (a) Iwamoto, R. *Bull. Chem. Soc. Jpn.* **1973**, *46*, 1115. (b) Iwamoto, R. *Bull. Chem. Soc. Jpn.* **1973**, *46*, 1115. (c) Iwamoto, R. *Bull. Chem. Soc. Jpn.* **1973**, *46*, 1123.

(15) Shriver, D. F. *J. Organomet. Chem.* **1975**, *94*, 25 and references therein.

an empty equatorial site pointing toward the molybdenum. This is quite interesting because it suggests that it should be possible to bridge a bifunctional ligand, such as carbon monoxide or carbon dioxide, between the two metals in these complexes. This type of bridging may be the reason that  $\text{HgCl}_2$  catalyzes the isomerization of *cis*- $\text{Mo}(\text{CO})_4\{\text{Ph}_2\text{P}(\text{CH}_2\text{CH}_2\text{O})_4\text{CH}_2\text{CH}_2\text{PPh}_2P,P'\}$  much more rapidly than it does the isomerization of *cis*- $\text{Mo}(\text{CO})_4(\text{Ph}_2\text{PMe})_2$ . In bimetallic metallocrown ethers containing Pt-group metal complexes, such bridging

could give rise to catalytic activities and selectivities that are quite different from those of monometallic Pt-group metal complex catalysts.

**Supplementary Material Available:** Tables listing positional and thermal parameters for hydrogens, temperature factors, bond lengths, bond angles, torsion angles, and least squares planes for **3** (10 pages). Ordering information is given on any current masthead page.

OM940409V

# Biological Recognition of Enantiomeric Silanes: Syntheses and Antimuscarinic Properties of Optically Active (2-Aminoethyl)cyclohexyl(hydroxymethyl)phenylsilanes and Related Quaternary Ammonium Derivatives<sup>||</sup>

Reinhold Tacke,<sup>\*,†</sup> Dirk Reichel,<sup>†</sup> Martin Kropfgans,<sup>†</sup> Peter G. Jones,<sup>‡</sup>  
Ernst Mutschler,<sup>§</sup> Jan Gross,<sup>§</sup> Xue Hou,<sup>⊥</sup> Magali Waelbroeck,<sup>⊥</sup> and  
Günter Lambrecht<sup>§</sup>

*Institut für Anorganische Chemie, Universität Karlsruhe, Engesserstrasse, Geb. 30.45, D-76128 Karlsruhe, Germany, Institut für Anorganische und Analytische Chemie, Technische Universität Braunschweig, Postfach 3329, D-38023 Braunschweig, Germany, Pharmakologisches Institut für Naturwissenschaftler, Biozentrum Niederursel, Universität Frankfurt, Marie-Curie-Strasse 9, Geb. N 260, D-60439 Frankfurt, Germany, and Laboratoire de Chimie Biologique et de la Nutrition, Faculté de Médecine et de Pharmacie, Université Libre de Bruxelles, Route de Lennik 808, B-1070 Bruxelles, Belgium*

Received August 19, 1994<sup>®</sup>

The racemic (2-aminoethyl)cyclohexyl(hydroxymethyl)phenylsilanes [*rac*-Ph(*c*-Hex)Si(CH<sub>2</sub>-OH)CH<sub>2</sub>CH<sub>2</sub>NR<sub>2</sub>] *rac*-**5a** (NR<sub>2</sub> = pyrrolidino), *rac*-**5b** (NR<sub>2</sub> = piperidino), and *rac*-**5c** (NR<sub>2</sub> = hexamethylenimino) were synthesized by a five-step synthesis starting from *rac*-Ph(*c*-Hex)-Si(CH<sub>2</sub>Cl)OMe. The (*R*)- and (*S*)-enantiomers of **5a–c** were obtained by resolution of *rac*-**5a–c** using the antipodes of *O,O'*-di-*p*-toluoyltartaric acid as resolving agents (resolution by fractional crystallization of diastereomeric salts). The enantiomeric purities of the resolved antipodes of **5a–c** were determined to be ≥98% ee (<sup>1</sup>H NMR) and ≥97% ee (<sup>13</sup>C NMR), respectively (NMR experiments using chiral shift reagents). Reaction of the pure (*R*)- and (*S*)-enantiomers of **5a–c** with methyl iodide gave the pure (*R*)- and (*S*)-enantiomers of the respective quaternary ammonium derivatives **6a–c**. The absolute configuration of (*R*)-**6b** was determined by single-crystal X-ray diffraction. The crystal data for this compound are as follows: C<sub>21</sub>H<sub>36</sub>INOSi, space group *P*2<sub>1</sub>2<sub>1</sub>2<sub>1</sub>, *a* = 890.5(3) pm, *b* = 916.2(2) pm, *c* = 2719.4(7) pm, *V* = 2.2187(11) nm<sup>3</sup>, *T* = -130 °C, *Z* = 4, *R*(*F*) = 0.0210. On the basis of the experimentally established absolute configuration of (*R*)-**6b**, the absolute configurations of all the other aforementioned optically active silicon compounds could be assigned by chemical and optical correlations. The pure (*R*)- and (*S*)-enantiomers of **5a–c** and **6a–c** were studied for their affinities for muscarinic M1, M2, M3, and M4 receptors by functional pharmacological experiments (M1, rabbit vas deferens; M2, guinea-pig atria; M3, guinea-pig ileum) and radioligand binding experiments (M1, human NB-OK 1 cells; M2, rat heart; M3, rat pancreas; M4, rat striatum). According to these studies, the (*R*)-enantiomers of **5a–c** and **6a–c** exhibited higher affinities for all four muscarinic receptor subtypes than their corresponding (*S*)-antipodes. The greatest difference (44-fold, M1 receptors) between the enantiomers was observed for 1-[2-[cyclohexyl(hydroxymethyl)phenylsilyl]ethyl]-1-methylhexamethyleniminium iodide (**6c**). The highest receptor selectivity was observed for (*R*)-**6c** at M1/M2 receptors (20-fold) and at M1/M3 receptors (6.9-fold). The potent M1-selective antagonist (*R*)-**6c** is considered to be an interesting lead for the development of new receptor-selective muscarinic antagonists.

## Introduction

During the past decade, we have developed a variety of highly potent and selective silicon-based muscarinic antagonists.<sup>1</sup> The racemic silanols, hexahydro-sila-difenidol<sup>1c,f,g,i,j,l</sup> (HHSiD; *rac*-**1**) and *p*-fluoro-hexahydro-sila-difenidol<sup>1g,i–k</sup> (*p*-F-HHSiD; *rac*-**2**), are the most

prominent drugs obtained in these studies. Both compounds are commercially available and are used worldwide as selective tools for the classification of muscarinic receptor subtypes. The related silanols, sila-procyclo-dine<sup>1a,b,d–f,l</sup> (**3**) and sila-tricyclamol iodide<sup>1e,f</sup> (**4**), are also potent and selective muscarinic antagonists, the (*R*)-enantiomers being more potent than the corresponding (*S*)-antipodes.<sup>1b,e</sup>

In the course of our structure–activity relationship studies of silicon-based muscarinic antagonists of this particular formula type, we have synthesized the enantiomers of the related (hydroxymethyl)silanes **5a–c** and their corresponding quaternary ammonium derivatives

<sup>||</sup> Dedicated to Professor Dr. Klaus Rühlmann on the occasion of his 65th birthday.

\* Author to whom correspondence should be addressed.

† University of Karlsruhe.

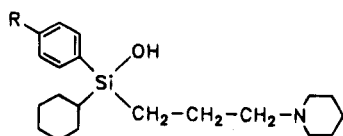
‡ Technical University of Braunschweig.

§ University of Frankfurt.

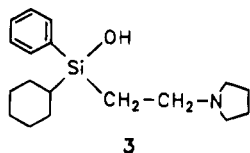
⊥ Free University of Brussels.

® Abstract published in *Advance ACS Abstracts*, November 1, 1994.

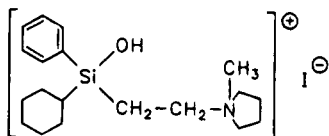




1: R = H, 2: R = F



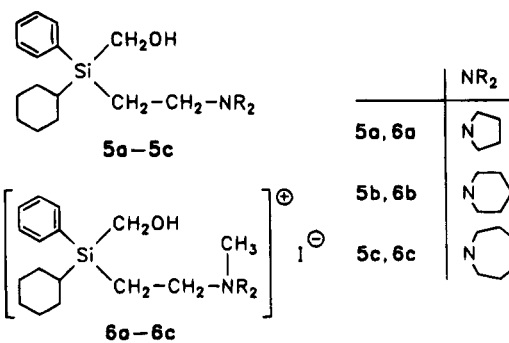
3



4

**6a-c** and have investigated the antimuscarinic properties of these compounds. Instead of the SiOH group of the above-mentioned silanols, compounds **5a-c** and **6a-c** contain a SiCH<sub>2</sub>OH unit. The aim of these studies was (i) to contribute to the chemistry of optically active silicon compounds and (ii) to obtain more information about the stereoselectivity of muscarinic receptor binding.<sup>2-4</sup> Optically active silanols, such as the enantiomers of **3** and **4**, racemize in aqueous solution and are therefore unsuitable for pharmacological stereoselectivity studies.<sup>1e</sup> In contrast, the related (hydroxymethyl)silanes **5a-c** and **6a-c** were expected to be configurationally stable and therefore to be useful tools for the stereochemical characterization of muscarinic receptor binding. Here we report on the synthesis of the pure enantiomers of **5a-c** and **6a-c** and their

pharmacological characterization at muscarinic M<sub>1</sub>, M<sub>2</sub>, M<sub>3</sub>, and M<sub>4</sub> receptors. The studies presented here were carried out as part of our systematic investigations in bioorganosilicon chemistry.<sup>5</sup>



## Results and Discussion

**Syntheses.** The preparation of the (*R*)- and (*S*)-enantiomers of the title compounds **5a-c** and **6a-c** is based on the synthesis of the racemic silanes *rac*-**5a-c**, followed by their resolution into the respective (*R*)- and (*S*)-enantiomers and subsequent transformation of the latter compounds into the (*R*)- and (*S*)-enantiomers of the ammonium derivatives **6a-c**.

The racemic compounds *rac*-**5a-c** and their quaternary ammonium derivatives *rac*-**6a-c** were synthesized according to Scheme 1, starting from *rac*-(chloromethyl)cyclohexyl(phenyl)methoxysilane<sup>1d</sup> (*rac*-**7**). In the first step, the methoxysilane *rac*-**7** was transformed into the corresponding vinylsilane *rac*-**8** by reaction with vinylmagnesium bromide in THF (yield 91%). Subsequent reaction with sodium acetate in DMF gave the (acetoxymethyl)silane *rac*-**9** (yield 92%), which was converted into the corresponding (hydroxymethyl)silane *rac*-**10** by reduction with lithium aluminum hydride in diethyl ether followed by hydrolysis with hydrochloric acid (yield 92%). *O*-Silylation of *rac*-**10** with chlorotrimethylsilane in *n*-pentane in the presence of triethylamine

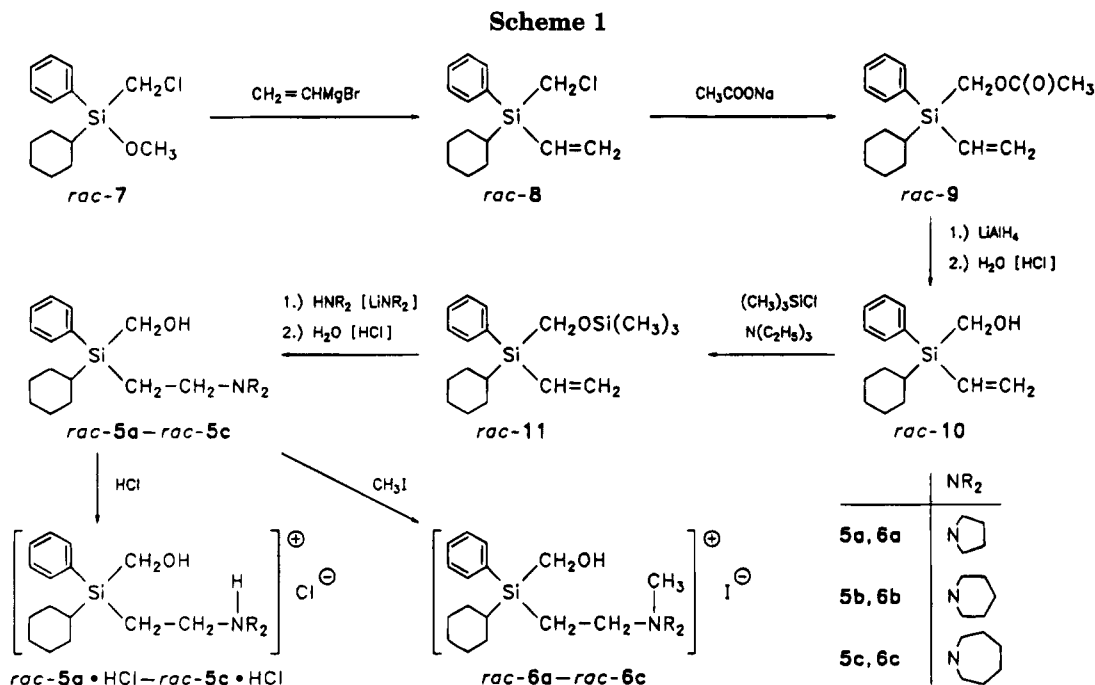
(1) Selected publications on silicon-based muscarinic antagonists: (a) Tacke, R.; Strecker, M.; Lambrecht, G.; Moser, U.; Mutschler, E. *Liebigs Ann. Chem.* **1983**, 922-930. (b) Sheldrick, W. S.; Linoh, H.; Tacke, R.; Lambrecht, G.; Moser, U.; Mutschler, E. *J. Chem. Soc., Dalton Trans.* **1985**, 1743-1746. (c) Tacke, R.; Linoh, H.; Zilch, H.; Wess, J.; Moser, U.; Mutschler, E.; Lambrecht, G. *Liebigs Ann. Chem.* **1985**, 2223-2228. (d) Tacke, R.; Pikies, J.; Linoh, H.; Rohr-Aehle, R.; Gönne, S. *Liebigs Ann. Chem.* **1987**, 51-57. (e) Tacke, R.; Linoh, H.; Ernst, L.; Moser, U.; Mutschler, E.; Sarge, S.; Cammenga, H. K.; Lambrecht, G. *Chem. Ber.* **1987**, *120*, 1229-1237. (f) Waelbroeck, M.; Tastenoy, M.; Camus, J.; Christophe, J.; Strohmman, C.; Linoh, H.; Zilch, H.; Tacke, R.; Mutschler, E.; Lambrecht, G. *Br. J. Pharmacol.* **1989**, *98*, 197-205. (g) Lambrecht, G.; Feifel, R.; Wagner-Röder, M.; Strohmman, C.; Zilch, H.; Tacke, R.; Waelbroeck, M.; Christophe, J.; Boddeke, H.; Mutschler, E. *Eur. J. Pharmacol.* **1989**, *168*, 71-80. (h) Tacke, R.; Linoh, H.; Rafeiner, K.; Lambrecht, G.; Mutschler, E. *J. Organomet. Chem.* **1989**, *359*, 159-168. (i) Waelbroeck, M.; Camus, J.; Tastenoy, M.; Mutschler, E.; Strohmman, C.; Tacke, R.; Lambrecht, G.; Christophe, J. *Eur. J. Pharmacol. Mol. Pharmacol. Sect.* **1991**, *206*, 93-103. (j) Lambrecht, G.; Feifel, R.; Moser, U.; Wagner-Röder, M.; Choo, L. K.; Camus, J.; Tastenoy, M.; Waelbroeck, M.; Strohmman, C.; Tacke, R.; Rodrigues de Miranda, J. F.; Christophe, J.; Mutschler, E. *Trends Pharmacol. Sci. Suppl.* **1989**, *10*, 60-64. (k) Tacke, R.; Mahner, K.; Strohmman, C.; Forth, B.; Mutschler, E.; Friebel, T.; Lambrecht, G. *J. Organomet. Chem.* **1991**, *417*, 339-353. (l) Waelbroeck, M.; Camus, J.; Tastenoy, M.; Lambrecht, G.; Mutschler, E.; Kropfgans, M.; Sperlich, J.; Wiesenberger, F.; Tacke, R.; Christophe, J. *Br. J. Pharmacol.* **1993**, *109*, 360-370. (m) Tacke, R.; Pikies, J.; Wiesenberger, F.; Ernst, L.; Schomburg, D.; Waelbroeck, M.; Christophe, J.; Lambrecht, G.; Gross, J.; Mutschler, E. *J. Organomet. Chem.* **1994**, *466*, 15-27. (n) Waelbroeck, M.; Camus, J.; Tastenoy, M.; Feifel, R.; Mutschler, E.; Tacke, R.; Strohmman, C.; Rafeiner, K.; Rodrigues de Miranda, J. F.; Lambrecht, G. *Br. J. Pharmacol.* **1994**, *112*, 505-514. (o) Tacke, R.; Kropfgans, M.; Tafel, A.; Wiesenberger, F.; Sheldrick, W. S.; Mutschler, E.; Egerer, H.; Rettenmayr, N.; Gross, J.; Waelbroeck, M.; Lambrecht, G. *Z. Naturforsch., B* **1994**, *49*, 898-910.

(2) Reviews on optically active silicon compounds: (a) Corriu, R. J. P.; Guérin, C. *Adv. Organomet. Chem.* **1982**, *20*, 265-312. (b) Corriu, R. J. P.; Guérin, C.; Moreau, J. J. E. *Top. Stereochem.* **1984**, *15*, 43-198.

(3) Recent publications on optically active silicon compounds (silicon atom as the center of chirality): (a) Terunuma, D.; Kato, M.; Kamei, M.; Uchida, H.; Ueno, S.; Nohira, H. *Bull. Chem. Soc. Jpn.* **1986**, *59*, 3581-3587. (b) Tacke, R.; Becker, B. *Main Group Met. Chem.* **1987**, *10*, 169-197. (c) Larson, G. L.; Prieto, J. A.; Ortiz, E. *Tetrahedron* **1988**, *44*, 3781-3790. (d) Syldatk, C.; Stoffregen, A.; Brans, A.; Fritsche, K.; Andree, H.; Wagner, F.; Hengelsberg, H.; Tafel, A.; Wuttke, F.; Zilch, H.; Tacke, R. In *Enzyme Engineering 9*; Blanch, H. W., Klivanov, A. M., Eds.; *Ann. N. Y. Acad. Sci.*, vol. 542; The New York Academy of Sciences: New York, 1988; pp 330-338. (e) Terunuma, D.; Yamamoto, N.; Kizaki, H.; Nohira, H. *Nippon Kagaku Kaishi* **1990**, 451-456. (f) Djerourou, A.-H.; Blanco, L. *Tetrahedron Lett.* **1991**, *32*, 6325-6326. (g) Tacke, R.; Brakmann, S.; Wuttke, F.; Fooladi, J.; Syldatk, C.; Schomburg, D. *J. Organomet. Chem.* **1991**, *403*, 29-41. (h) Tacke, R.; Brakmann, S.; Kropfgans, M.; Strohmman, C.; Wuttke, F.; Lambrecht, G.; Mutschler, E.; Proksch, P.; Schiebel, H.-M.; Witte, L. In *Frontiers of Organosilicon Chemistry*; Bassindale, A. R., Gaspar, P. P., Eds.; The Royal Society of Chemistry: Cambridge, 1991; pp 218-228. (i) Tacke, R.; Wuttke, F.; Henke, H. *J. Organomet. Chem.* **1992**, *424*, 273-280. (j) Yamamoto, K.; Kawanami, Y.; Miyazawa, M. *J. Chem. Soc., Chem. Commun.* **1993**, 436-437. (k) Tacke, R.; Reichel, D.; Günther, K.; Merget, S. *Z. Naturforsch., B*, submitted. (l) See also refs 1b and 1c.

(4) Reviews on stereoselectivity of muscarinic receptor binding: (a) Waelbroeck, M.; Tastenoy, M.; Camus, J.; Feifel, R.; Mutschler, E.; Strohmman, C.; Tacke, R.; Lambrecht, G.; Christophe, J. *Trends Pharmacol. Sci. Suppl.* **1989**, *10*, 65-69. (b) Casy, A. F. *The Steric Factor in Medicinal Chemistry: Dissymmetric Probes of Pharmacological Receptors*; Plenum Press: New York, London, 1993; pp 287-325.

(5) Review on bioorganosilicon chemistry: Tacke, R.; Linoh, H. In *The Chemistry of Organic Silicon Compounds, Part 2*; Patai, S., Rappoport, Z., Eds.; Wiley & Sons: Chichester, 1989; pp 1143-1206.



yielded the corresponding *O*-trimethylsilyl derivative *rac*-11 (yield 84%). Treatment of the vinylsilane *rac*-11 with a mixture of pyrrolidine and its lithium amide in THF, followed by hydrolysis with hydrochloric acid and subsequent workup with aqueous KOH, gave the corresponding (2-pyrrolidinoethyl)silane *rac*-5a (82%), which was then transformed into its hydrochloride *rac*-5a · HCl by reaction with hydrogen chloride in diethyl ether (yield 89%). The related (2-piperidinoethyl)silane *rac*-5b and (2-hexamethyleniminoethyl)silane *rac*-5c and their corresponding hydrochlorides *rac*-5b · HCl and *rac*-5c · HCl were obtained by analogous syntheses [yields 89% (*rac*-5b), 85% (*rac*-5c), 91% (*rac*-5b · HCl), and 90% (*rac*-5c · HCl)]. The quaternary ammonium compounds *rac*-6a–c were synthesized in the last step by reaction of the amines *rac*-5a–c with methyl iodide in acetone [yields 91% (*rac*-6a), 91% (*rac*-6b), and 90% (*rac*-6c)].

Compounds *rac*-5a and *rac*-8–11 were isolated as colorless liquids, whereas *rac*-5b,c, *rac*-5a–c · HCl, and *rac*-6a–c were obtained as colorless crystalline solids. The identity of these hitherto unknown compounds was established by elemental analyses (C, H, N), NMR-spectroscopic studies (<sup>1</sup>H, <sup>13</sup>C, and <sup>29</sup>Si NMR), and mass-spectrometric investigations (EI MS and FD MS, respectively).

The (*R*)- and (*S*)-enantiomers of 5a–c · HCl were obtained by resolution of *rac*-5a–c using the antipodes of *O,O'*-di-*p*-toluoyltartaric acid as resolving agents, followed by reaction of the respective enantiomerically pure (*R*)- and (*S*)-enantiomers of 5a–c with hydrogen chloride in diethyl ether (Scheme 2) (yields 9–12%; for details, see Experimental Section). Reaction of the purified antipodes of 5a–c · HCl with aqueous NaOH gave the pure (*R*)- and (*S*)-enantiomers of 5a–c (yields 84–92%). The pure antipodes of the quaternary ammonium derivatives 6a–c were obtained by reaction of the respective (*R*)- and (*S*)-enantiomers of 5a–c with methyl iodide in acetone (yields 67–85%).

With the exception of (*R*)-5a and (*S*)-5a (colorless oily liquids), the aforementioned optically active silicon

compounds were isolated as colorless crystalline solids. The identity of the (*R*)- and (*S*)-enantiomers of 5a–c, 5a–c · HCl, and 6a–c was established by elemental analyses (C, H, Cl, I, N), NMR-spectroscopic studies (<sup>1</sup>H, <sup>13</sup>C, and <sup>29</sup>Si NMR), and mass-spectrometric investigations (EI MS and FD MS, respectively). In addition, (*R*)-6b was structurally characterized by a single-crystal X-ray diffraction study. The determination of the absolute configurations and enantiomeric purities of the optically active compounds is described in the two following chapters. As the enantiomers of 5a–c and 6a–c were found to be configurationally stable under physiological conditions, they could be used to study the stereoselectivity of muscarinic receptor binding (see Pharmacological Studies).

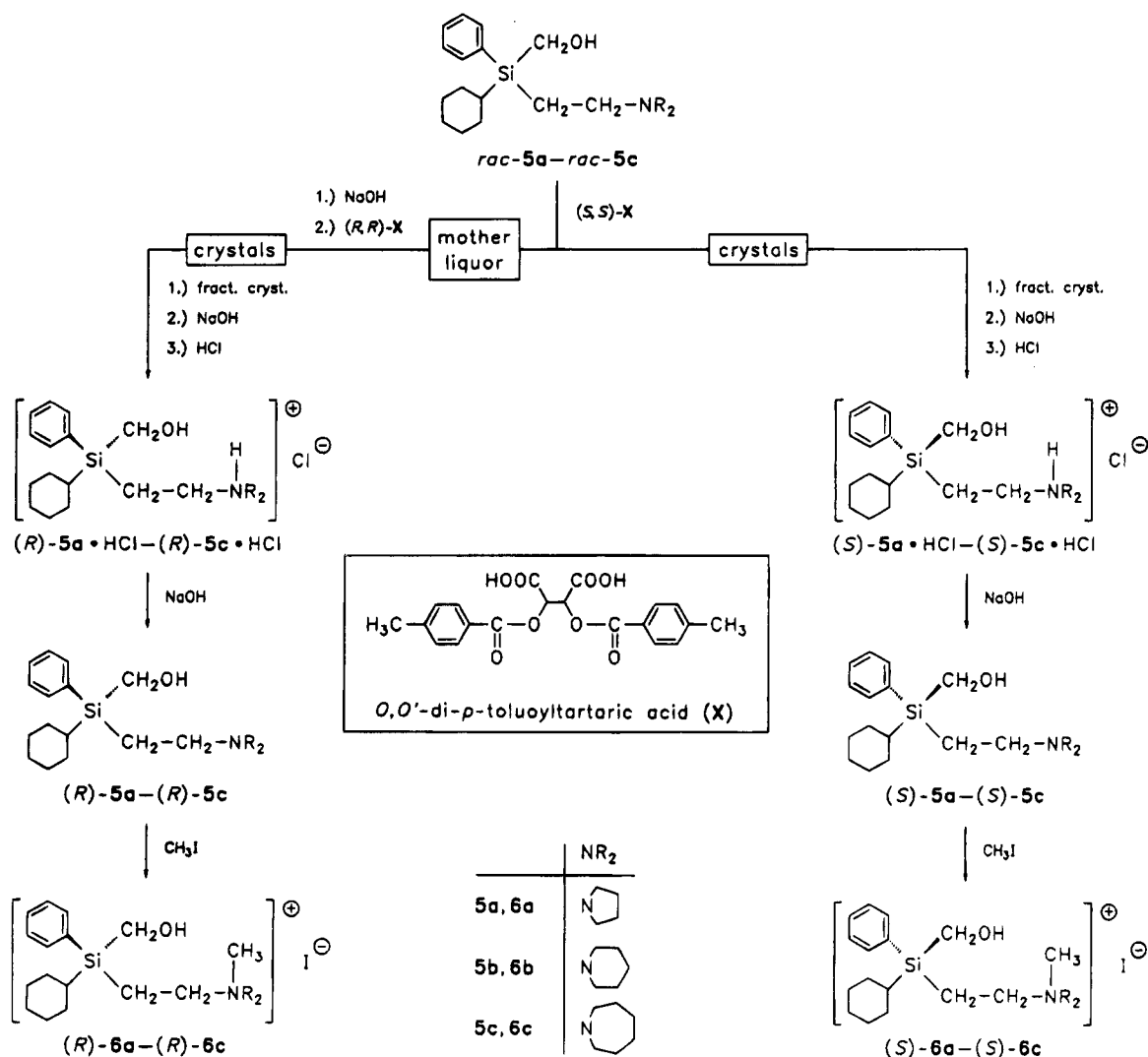
#### Determination of the Absolute Configurations.

The absolute configuration of the levorotatory enantiomer of 6b was determined by single-crystal X-ray diffraction. The crystal data and experimental parameters used for this study are given in Table 1; the structure of the cation of (–)-6b in the crystal is shown in Figure 1. According to this crystal structure analysis, (–)-6b (optical rotation measured for a solution in CHCl<sub>3</sub> at 546 nm) is the (*R*)-enantiomer. As the *N*-methylation of 5b with methyl iodide [(–)-5b → (–)-6b; (+)-5b → (+)-6b] and the conversion of 5b · HCl into 5b [(+)-5b · HCl → (–)-5b; (–)-5b · HCl → (+)-5b] do not affect the configuration at the silicon atom, assignment of the absolute configurations of (–)-5b [→ (*R*)], (+)-5b [→ (*S*)], (+)-5b · HCl [→ (*R*)], and (–)-5b · HCl [→ (*S*)] could also be made. Based on the unequivocally established configurations of the (*R*)- and (*S*)-enantiomers of 5b, 5b · HCl, and 6b, the absolute configurations of the antipodes of 5a, 5c, 5a · HCl, 5c · HCl, 6a, and 6c could be easily assigned by optical correlations (comparison of the signs of the respective optical rotations, measured in CHCl<sub>3</sub>; see Experimental Section).

#### Determination of the Enantiomeric Purities.

The enantiomeric purities of the (*R*)- and (*S*)-enantiomers of 5a–c were determined by NMR experiments using the chiral shift reagents (–)-2,2,2-trifluoro-1-(9-

Scheme 2



anthryl)ethanol [(-)-TFAE] ( $^1\text{H}$  NMR) and (+)-tris[3-(2,2,3,3,4,4,4-heptafluoro-1-hydroxybutylidene)-*d*-camphorato]europium(III) [(+)-Eu(hfc)<sub>3</sub>] ( $^{13}\text{C}$  NMR). As shown for **5b** in Figure 2, the enantiomers of this silane can be clearly discriminated by NMR spectroscopy and therefore quantitatively determined by integration of their characteristic resonance signals. Analogous NMR spectra (not shown) were obtained for **5a** and **5c**. According to this method, the enantiomeric purities of the resolved antipodes of **5a-c** were determined to be  $\geq 98\%$  ee ( $^1\text{H}$  NMR) and  $\geq 97\%$  ee ( $^{13}\text{C}$  NMR), respectively. As the reactions **5a-c**  $\rightarrow$  **5a-c**  $\cdot$  HCl and **5a-c**  $\rightarrow$  **6a-c** do not affect the absolute configuration at the silicon atom, the same enantiomeric purities can be assumed for the antipodes of **5a-c**  $\cdot$  HCl and **6a-c**. Thus, the (*R*)- and (*S*)-enantiomers of **5a-c**, **5a-c**  $\cdot$  HCl, and **6a-c** prepared in this study were almost enantiomerically pure.

**Pharmacological Studies.** The pure (*R*)- and (*S*)-enantiomers of **5a-c** and **6a-c** were studied for their affinities for muscarinic M<sub>1</sub>, M<sub>2</sub>, M<sub>3</sub>, and M<sub>4</sub> receptors by functional pharmacological experiments (M<sub>1</sub>, M<sub>2</sub>, M<sub>3</sub>) and radioligand binding experiments (M<sub>1</sub>, M<sub>2</sub>, M<sub>3</sub>, M<sub>4</sub>). The results of these investigations are summarized in Tables 2–4 and Figures 3 and 4.

All compounds concentration-dependently antagonized the 4-F-PyMcN<sup>+</sup>-induced inhibition of the neuro-

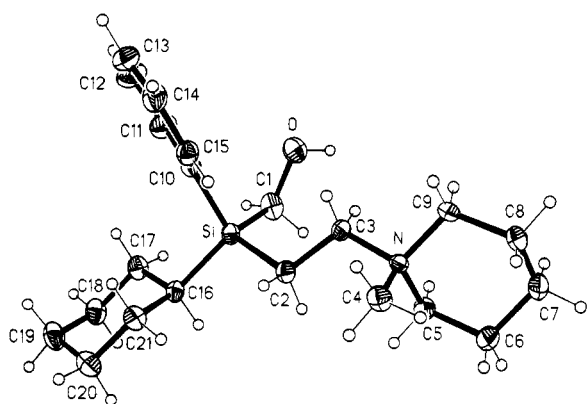
genic twitch contraction in rabbit vas deferens (M<sub>1</sub> receptors). Furthermore, they inhibited the negative inotropic responses in guinea-pig atria and ileal contractions (M<sub>2</sub> and M<sub>3</sub> receptors, respectively) mediated by arecaidine propargyl ester. The (*R*)- and (*S*)-enantiomers of **5a-c** and **6a-c** produced parallel shifts of the agonist concentration–response curves without changes in basal tension or maximum agonist responses. Arunlakshana–Schild plots were linear over the antagonist concentration range examined, and the slopes of the regression lines were not significantly different from unity. In addition, all the competition curves (not shown) obtained in binding studies were compatible with the existence of a single receptor subtype; the Hill coefficients were not different from unity. Thus, all compounds studied exhibited an apparently competitive antagonism at M<sub>1</sub>–M<sub>3</sub> receptors in functional studies and at M<sub>1</sub>–M<sub>4</sub> receptors in binding experiments.

The  $\text{pK}_i$  values of the (*R*)- and (*S*)-enantiomers of **5a-c** and **6a-c** obtained in binding studies at M<sub>1</sub>–M<sub>3</sub> receptors correspond reasonably to the respective antimuscarinic potencies ( $\text{pA}_2$  values) determined in functional experiments at M<sub>1</sub>, M<sub>2</sub>, and M<sub>3</sub> receptors (Tables 2 and 3). The binding affinities of the (*R*)-enantiomers of **5a-c** and **6a-c** to M<sub>4</sub> receptors in rat striatum were always lower than those found at M<sub>1</sub> receptors in NB-OK 1 cells, but higher than those obtained at M<sub>2</sub> and

**Table 1.** Crystal Data and Experimental Parameters for the Crystal Structure Analysis of (*R*)-**6b**

empirical formula	C <sub>21</sub> H <sub>36</sub> INOSi
formula mass, g mol <sup>-1</sup>	473.5
collection T, °C	-130
λ(Mo Kα), pm	71.073
cryst syst	orthorhombic
space group	P2 <sub>1</sub> 2 <sub>1</sub> 2 <sub>1</sub>
a, pm	890.5(3)
b, pm	916.2(2)
c, pm	2719.4(7)
V, nm <sup>3</sup>	2.2187(11)
Z	4
D(calcd), Mg m <sup>-3</sup>	1.418
μ(Mo Kα), mm <sup>-1</sup>	1.506
F(000)	976
cryst dimens, mm	0.58 × 0.42 × 0.35
θ range, deg	3.16–27.57
index ranges	-11 ≤ h ≤ 11, -11 ≤ k ≤ 0, -35 ≤ l ≤ 35
no. of coll reflns	8210
no. of indep reflns	5129
R <sub>int</sub>	0.0208
no. of reflns used	5128
no. of params	229
absorption correction	ψ scans, transmissions 0.67–0.87
S <sup>a</sup>	1.060
R(F) <sup>b</sup> [I > 2σ(I)]	0.0210
R <sub>w</sub> (F <sup>2</sup> ) <sup>c</sup>	0.0468
max/min res electron dens, e nm <sup>-3</sup>	+447/-385

<sup>a</sup>  $S = \{\sum[w(F_o^2 - F_c^2)^2]/(n - p)\}^{1/2}$ ;  $n$  = no. of reflections;  $p$  = no. of parameters. <sup>b</sup>  $R(F) = \sum||F_o| - |F_c||/\sum|F_o|$ . <sup>c</sup>  $R_w(F^2) = \{\sum[w(F_o^2 - F_c^2)^2]/\{\sum[w(F_o^2)^2]\}^{1/2}$ .



**Figure 1.** Structure of the cation of (*R*)-**6b** in the crystal (ORTEP plot, probability level 50%), showing the atomic numbering scheme. Selected bond distances (pm) and angles (deg): Si–C(1), 188.2(2); Si–C(2), 188.8(2); Si–C(10), 187.7(2); Si–C(16), 188.5(2); C(1)–O, 142.8(3); C(1)–Si–C(2), 109.30(10); C(1)–Si–C(10), 106.99(11); C(1)–Si–C(16), 111.13(10); C(2)–Si–C(10), 111.47(10); C(2)–Si–C(16), 107.40(10); C(10)–Si–C(16), 110.57(9); Si–C(1)–O, 110.4(2). The cation and anion of (*R*)-**6b** are connected by a hydrogen bond of the type O–H···I [O···I, 345.0(2) pm].

M3 receptors (except for compounds **5a** and **5b** at M3 receptors).

In general, the (*R*)-enantiomers (eutomers) exhibited higher affinities at all four muscarinic receptor subtypes than the corresponding (*S*)-enantiomers (distomers) (Tables 2–4; Figures 3 and 4). In addition, in most cases the (*R*)-enantiomers showed higher receptor selectivities. The rank order of the functional stereoselectivity ratios (Table 4) of compounds **5a–c** were M3 > M1 ≥ M2, whereas the quaternary ammonium derivatives **6a–c** had the order M1 ≥ M3 > M2 due to the large increase in stereoselectivity at M1 receptors

by *N*-methylation. The greatest difference between the enantiomers was found for compound **6c** (44-fold, M1 receptors).

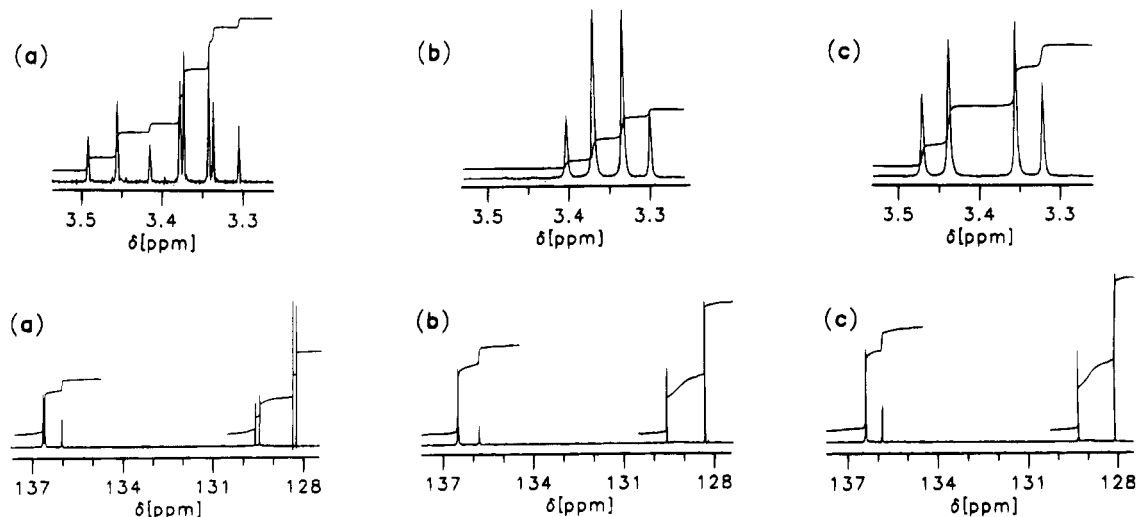
*N*-Methylation of the (*R*)-enantiomers of **5a–c** increased the affinity for functional M1, M2, and M3 receptors up to 65-fold [(*R*)-**5c** → (*R*)-**6c**], the increase being consistently highest at M1 receptors and lowest at M3 receptors. Thus, *N*-methylation of (*R*)-**5a–c** changed the receptor selectivity pattern from M3 ≥ M1 > M2 to M1 > M3 > M2. The highest receptor selectivity was observed for (*R*)-**6c** at M1/M2 receptors (20-fold) and at M1/M3 receptors (6.9-fold). This compound represents a potent M1-selective antagonist and is considered to be an interesting lead for the development of new receptor-selective muscarinic antagonists.

## Conclusions

The results described in this paper clearly demonstrate that enantiomeric silanes generally may differ in their biological properties. As shown for the title compounds, biological recognition of chiral silicon compounds (with the silicon atom as the center of chirality) may be reflected, for example, by different pharmacological potencies and selectivities of the respective antipodes. Since biologically active organosilicon compounds have a great potential of application as agrochemicals and drugs,<sup>5</sup> for future developments in this field extensive studies of the stereochemistry of chiral silicon compounds are necessary. In particular, the development of new preparative methods for the synthesis of enantiomerically pure chiral silanes is of great importance. In most cases (as in this study), optically active silicon compounds have been obtained by (i) classical resolution of the respective racemic mixtures via fractional crystallization of appropriate diastereomeric derivatives and (ii) stereoselective chemical transformations of the resolved enantiomers. As alternative methods, we have started to investigate (i) stereoselective biotransformations of suitable racemic or prochiral organosilicon substrates (see refs 3b,d,g,h and 5) and (ii) chromatographic racemate resolutions (see ref 3k). The development of efficient asymmetric chemical syntheses of enantiomerically pure chiral silicon compounds represents a further challenge.

## Experimental Section

**General Procedures.** All syntheses were carried out under dry nitrogen. The solvents used were dried according to standard procedures and stored under nitrogen. Melting points (uncorrected) were determined with a Leitz Laborlux S microscope, equipped with a heater (Leitz, Model M 350). <sup>1</sup>H and <sup>13</sup>C NMR spectra were recorded at room temperature on a Bruker AM-400 (<sup>1</sup>H, 400.1 MHz; <sup>13</sup>C, 100.6 MHz), Bruker AMX-300 (<sup>1</sup>H, 300.1 MHz; <sup>13</sup>C, 75.5 MHz), or Bruker AC-250 NMR spectrometer (<sup>1</sup>H, 250.1 MHz; <sup>13</sup>C, 62.9 MHz). <sup>29</sup>Si NMR spectra were recorded on a Bruker AC-250 NMR spectrometer operating at 49.7 MHz. Chemical shifts (ppm) were determined relative to internal CHCl<sub>3</sub> (<sup>1</sup>H, δ 7.25), CDCl<sub>3</sub> (<sup>13</sup>C, δ 77.05), and TMS (<sup>29</sup>Si, δ 0). Assignment of the <sup>13</sup>C NMR data was supported by DEPT experiments. Mass spectra were obtained with a Varian MAT-711 mass spectrometer (EI MS, 70 eV; FD MS, 11 kV, CH<sub>3</sub>OH as solvent); the selected *m/z* values given refer to the isotopes <sup>1</sup>H, <sup>12</sup>C, <sup>14</sup>N, <sup>16</sup>O, <sup>28</sup>Si, <sup>35</sup>Cl, and <sup>127</sup>I. Optical rotations were measured with a Perkin-Elmer polarimeter, Model 241; CHCl<sub>3</sub> served as solvent



**Figure 2.** Quantitative determination of the enantiomeric purities of the antipodes of **5b**: Characteristic  $^1\text{H}$  and  $^{13}\text{C}$  NMR partial spectra of the (*R*)- and (*S*)-enantiomers of **5b** in the presence of (–)-TFAE ( $^1\text{H}$  NMR; above) or (+)-Eu(hfc)<sub>3</sub> ( $^{13}\text{C}$  NMR; below) [(a) racemic mixture; (b) pure (*R*)-enantiomer obtained by preparative resolution; (c) pure (*S*)-enantiomer obtained by preparative resolution]. For details, see the Experimental Section.

**Table 2.** Affinities ( $pA_2$  Values) and Slopes of Arunlakshana–Schild Plots (in Parentheses) for the (*R*)- and (*S*)-Enantiomers of **5a–c** and **6a–c** at Muscarinic M1 Receptors in Rabbit Vas Deferens (RVD), M2 Receptors in Guinea-Pig Atria (GPA), and M3 Receptors in Guinea-Pig Ileum (GPI) as Well as Receptor Selectivities of These Compounds

compd	$pA_2$ values <sup>a</sup>			selectivity ratios <sup>b</sup>		
	RVD (M1)	GPA (M2)	GPI (M3)	M1/M2	M1/M3	M3/M2
( <i>R</i> )- <b>5a</b>	7.13 ± 0.02 (1.00 ± 0.04)	6.68 ± 0.02 (0.99 ± 0.04)	7.62 ± 0.04 (1.07 ± 0.06)	2.8	0.3	8.7
( <i>R</i> )- <b>5b</b>	7.39 ± 0.05 (1.14 ± 0.12)	6.76 ± 0.04 (0.85 ± 0.06)	7.32 ± 0.03 (0.91 ± 0.08)	4.3	1.2	3.6
( <i>R</i> )- <b>5c</b>	7.35 ± 0.04 (1.01 ± 0.07)	6.74 ± 0.03 (0.96 ± 0.05)	7.55 ± 0.04 (1.02 ± 0.06)	4.1	0.6	6.5
( <i>R</i> )- <b>6a</b>	8.67 ± 0.03 (1.03 ± 0.06)	7.98 ± 0.03 (1.05 ± 0.05)	8.38 ± 0.04 (1.00 ± 0.06)	4.9	2.0	2.5
( <i>R</i> )- <b>6b</b>	9.09 ± 0.06 (0.98 ± 0.10)	8.21 ± 0.01 (0.98 ± 0.02)	8.65 ± 0.05 (0.98 ± 0.07)	7.6	2.8	2.8
( <i>R</i> )- <b>6c</b>	9.16 ± 0.05 (0.84 ± 0.07)	7.86 ± 0.05 (0.91 ± 0.07)	8.32 ± 0.04 (1.03 ± 0.07)	20	6.9	2.9
( <i>S</i> )- <b>5a</b>	6.49 ± 0.04 (0.91 ± 0.08)	6.22 ± 0.03 (0.90 ± 0.05)	6.32 ± 0.04 (1.19 ± 0.09)	1.9	1.5	1.3
( <i>S</i> )- <b>5b</b>	6.53 ± 0.04 (1.18 ± 0.09)	6.26 ± 0.03 (1.11 ± 0.06)	6.15 ± 0.02 (1.03 ± 0.06)	1.9	2.4	0.8
( <i>S</i> )- <b>5c</b>	7.20 ± 0.03 (1.04 ± 0.05)	6.43 ± 0.04 (0.95 ± 0.06)	7.18 ± 0.04 (0.98 ± 0.07)	5.9	1.1	5.6
( <i>S</i> )- <b>6a</b>	7.46 ± 0.03 (0.97 ± 0.06)	7.44 ± 0.03 (0.98 ± 0.05)	7.08 ± 0.03 (1.00 ± 0.05)	1.1	2.4	0.4
( <i>S</i> )- <b>6b</b>	7.74 ± 0.04 (1.12 ± 0.07)	7.57 ± 0.05 (1.01 ± 0.07)	7.36 ± 0.03 (1.03 ± 0.06)	1.5	2.4	0.6
( <i>S</i> )- <b>6c</b>	7.52 ± 0.04 (0.97 ± 0.07)	6.98 ± 0.04 (0.95 ± 0.08)	7.03 ± 0.03 (0.98 ± 0.05)	3.5	3.1	1.1

<sup>a</sup> The parameters given represent the mean ± se ( $n = 3-4$ ). <sup>b</sup>  $K_D$  ratios ( $pA_2 = -\log K_D$ ) are given as a measure of the receptor selectivity; these values were calculated from the antilogs of the differences between the respective  $pA_2$  values.

{purified by dynamic drying on an  $\text{Al}_2\text{O}_3$  column [50 g  $\text{Al}_2\text{O}_3$  (Merck, 1077)/100 mL  $\text{CHCl}_3$ ] and subsequent distillation}.

**Preparation of *rac*-Cyclohexyl(hydroxymethyl)phenyl(2-pyrrolidinoethyl)silane (*rac*-**5a**).** A 1.6 M solution of *n*-butyllithium in *n*-hexane (20.0 mL, 32.0 mmol of *n*-BuLi) was added dropwise at 50 °C over 15 min to a stirred solution of pyrrolidine (6.70 g, 94.2 mmol) in THF (100 mL). After stirring at 50 °C for 30 min, a solution of *rac*-**11** (10.0 g, 31.4 mmol) in THF (100 mL) was added dropwise over 30 min. The resulting mixture was stirred at 50 °C for 3 h, cooled to room temperature, and then cautiously mixed with 2.0 M hydrochloric acid (250 mL). After stirring at room temperature for

**Table 3.** Affinities ( $pK_i$  Values) for the (*R*)- and (*S*)-Enantiomers of **5a–c** and **6a–c** Obtained in Binding Studies on Homogenates of Human NB-OK 1 Cells (M1 Receptors), as Well as Rat Heart (M2 Receptors), Rat Pancreas (M3 Receptors), and Rat Striatum (M4 Receptors)<sup>a</sup>

comps	$pK_i$ values			
	human NB-OK 1 cells (M1)	rat heart (M2)	rat pancreas (M3)	rat striatum (M4)
( <i>R</i> )- <b>5a</b> / <i>(S)</i> - <b>5a</b>	7.8/6.8	6.5/6.2	7.3/6.6	7.3/6.6
( <i>R</i> )- <b>5b</b> / <i>(S)</i> - <b>5b</b>	7.8/6.9	6.6/6.3	7.4/6.7	7.2/6.5
( <i>R</i> )- <b>5c</b> / <i>(S)</i> - <b>5c</b>	7.9/7.4	6.8/6.6	7.4/7.0	7.7/7.1
( <i>R</i> )- <b>6a</b> / <i>(S)</i> - <b>6a</b>	8.6/7.5	7.4/6.8	7.7/6.6	8.0/7.0
( <i>R</i> )- <b>6b</b> / <i>(S)</i> - <b>6b</b>	8.9/7.9	7.9/7.3	7.9/7.0	8.5/7.4
( <i>R</i> )- <b>6c</b> / <i>(S)</i> - <b>6c</b>	8.4/7.5	7.7/7.0	7.7/6.9	8.2/7.2

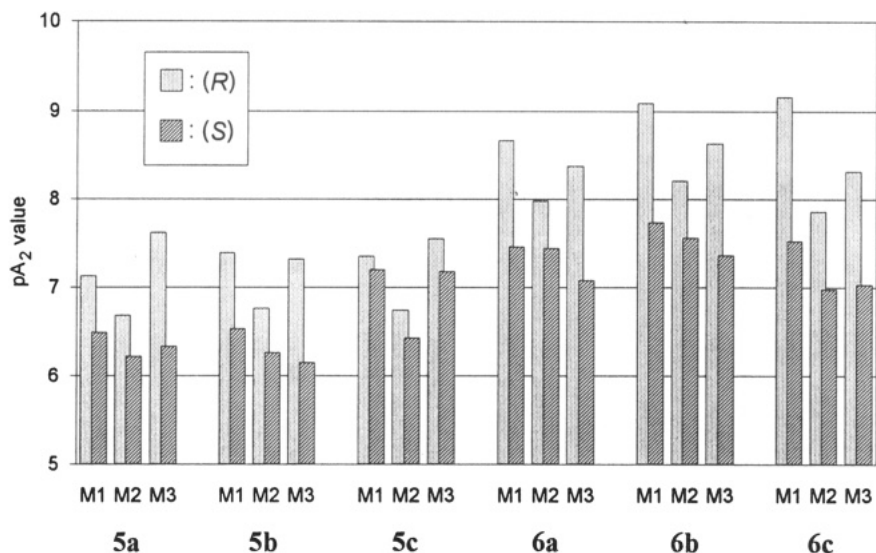
<sup>a</sup> All the experiments were repeated three times in duplicate. The standard deviations of the  $pK_i$  values were generally close to ±0.10, and always lower than ±0.15.

**Table 4.** Stereoselectivities of the (*R*)- and (*S*)-Enantiomers of **5a–c** and **6a–c** at Muscarinic M1 Receptors in Rabbit Vas Deferens (RVD), M2 Receptors in Guinea-Pig Atria (GPA), and M3 Receptors in Guinea-Pig Ileum (GPI)

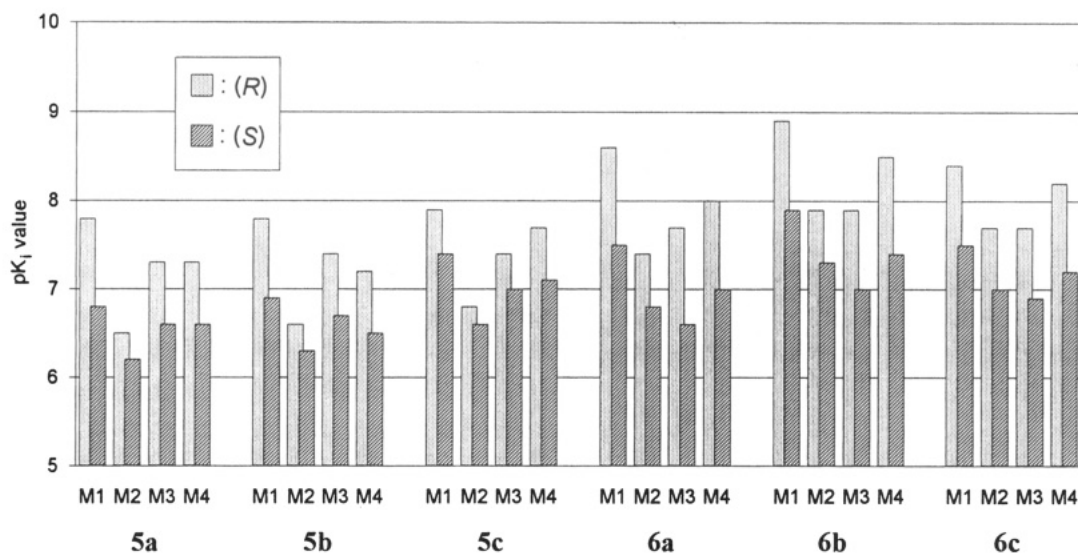
comps	stereoselectivities <sup>a</sup>		
	RVD (M1)	GPA (M2)	GPI (M3)
( <i>R</i> )- <b>5a</b> / <i>(S)</i> - <b>5a</b>	4.4	2.9	20
( <i>R</i> )- <b>5b</b> / <i>(S)</i> - <b>5b</b>	7.2	3.2	15
( <i>R</i> )- <b>5c</b> / <i>(S)</i> - <b>5c</b>	1.4	2.0	2.3
( <i>R</i> )- <b>6a</b> / <i>(S)</i> - <b>6a</b>	16	3.5	20
( <i>R</i> )- <b>6b</b> / <i>(S)</i> - <b>6b</b>	22	4.4	20
( <i>R</i> )- <b>6c</b> / <i>(S)</i> - <b>6c</b>	44	7.6	20

<sup>a</sup> These values are the antilogs of the differences between the respective  $pA_2$  values.

30 min, diethyl ether (250 mL) and 6.0 M aqueous KOH solution (100 mL) were added. The organic phase was separated and the aqueous layer extracted with diethyl ether (3 × 200 mL). After drying of the combined organic extracts over anhydrous  $\text{Na}_2\text{SO}_4$ , the solvent was removed under reduced pressure and the residue purified by Kugelrohr distillation (170 °C/0.01 Torr) to give *rac*-**5a** in 82% yield as an oily liquid (8.19 g, 25.8 mmol).  $^1\text{H}$  NMR (300.1 MHz,  $\text{CDCl}_3$ ):  $\delta$  0.85–1.3 and 1.55–1.85 (m, 17 H,  $\text{SiCH}_2\text{C}$ ,  $\text{SiCHC}_2$ ,  $\text{CCH}_2\text{C}$ ), 2.35–2.7 (m, 6 H,  $\text{NCH}_2\text{C}$ ), 3.60 ( $\delta_A$ ) and 3.63 ( $\delta_B$ ) (AB System,  $J_{AB} = 14.9$  Hz, 2 H,  $\text{SiCH}_2\text{O}$ ), 6.7 (br s, 1 H, OH), 7.45–7.55 (m, 5 H,  $\text{SiC}_6\text{H}_5$ ).  $^{13}\text{C}$  NMR (75.5 MHz,  $\text{CDCl}_3$ ):  $\delta$  11.5 ( $\text{SiCH}_2\text{C}$ ), 23.2 (2 C) ( $\text{CCH}_2\text{C}$ ), 23.4 (C-1,  $\text{SiC}_6\text{H}_{11}$ ), 26.7 ( $\text{CCH}_2\text{C}$ ), 27.50 ( $\text{CCH}_2\text{C}$ ), 27.54 ( $\text{CCH}_2\text{C}$ ), 27.9 ( $\text{CCH}_2\text{C}$ ), 28.0



**Figure 3.** Affinity profiles ( $pA_2$  values) of the (*R*)- and (*S*)-enantiomers of **5a–c** and **6a–c** at muscarinic M1 receptors in rabbit *vas deferens*, M2 receptors in guinea-pig atria, and M3 receptors in guinea-pig ileum.



**Figure 4.** Affinity profiles ( $pK_i$  values) of the (*R*)- and (*S*)-enantiomers of **5a–c** and **6a–c** at muscarinic M1 receptors in human NB-OK 1 cells, M2 receptors in rat heart, M3 receptors in rat pancreas, and M4 receptors in rat striatum.

(CCH<sub>2</sub>C), 49.2 (SiCH<sub>2</sub>O), 5.10 (SiCCH<sub>2</sub>N), 53.7 (2 C) (NCH<sub>2</sub>C, NC<sub>4</sub>H<sub>5</sub>), 127.7 (C-3/C-5, SiC<sub>6</sub>H<sub>5</sub>), 129.0 (C-4, SiC<sub>6</sub>H<sub>5</sub>), 134.4 (C-1, SiC<sub>6</sub>H<sub>5</sub>), 134.5 (C-2/C-6, SiC<sub>6</sub>H<sub>5</sub>). EI MS:  $m/z$  317 (3, M<sup>+</sup>) 84 (100, CH<sub>2</sub>=NC<sub>4</sub>H<sub>5</sub><sup>+</sup>). Anal. Calcd for C<sub>19</sub>H<sub>31</sub>NOSi (M<sub>r</sub> = 317.5): C, 71.87; H, 9.84; N, 4.41. Found: C, 71.7; H, 10.0; N, 4.3.

**Preparation of (*R*)-Cyclohexyl(hydroxymethyl)phenyl(2-pyrrolidinoethyl)silane [(*R*)-5a].** A 2.0 M aqueous NaOH solution (1.0 mL, 2.00 mmol of NaOH) was added to a mixture composed of an aqueous solution (30 mL) of (*R*)-**5a** · HCl (302 mg, 853 μmol) and diethyl ether (30 mL). After stirring for 5 min, the organic phase was separated and the aqueous layer extracted with diethyl ether (3 × 30 mL). The combined organic extracts were dried over anhydrous Na<sub>2</sub>SO<sub>4</sub>, and the solvent was removed under reduced pressure and the residue dried *in vacuo* to give (*R*)-**5a** in 88% yield as an oily liquid (238 mg, 750 μmol). The NMR and MS data of the product were identical with those obtained for *rac*-**5a**. [ $\alpha$ ]<sub>D</sub><sup>20</sup><sub>546</sub> = -1.7 (CHCl<sub>3</sub>, *c* = 1.0). Anal. Calcd for C<sub>19</sub>H<sub>31</sub>NOSi (M<sub>r</sub> = 317.5): C, 71.87; H, 9.84; N, 4.41. Found: C, 71.8; H, 9.9; N, 4.4.

**Preparation of (*S*)-Cyclohexyl(hydroxymethyl)phenyl(2-pyrrolidinoethyl)silane [(*S*)-5a].** This compound was prepared from (*S*)-**5a** · HCl (312 mg, 881 μmol) analogously to the synthesis of (*R*)-**5a** and isolated in 92% yield as an oily

liquid (257 mg, 809 μmol). The NMR and MS data of the product were identical with those obtained for *rac*-**5a**. [ $\alpha$ ]<sub>D</sub><sup>20</sup><sub>546</sub> = +1.7 (CHCl<sub>3</sub>, *c* = 1.0). Anal. Calcd for C<sub>19</sub>H<sub>31</sub>NOSi (M<sub>r</sub> = 317.5): C, 71.87; H, 9.84; N, 4.41. Found: C, 71.7; H, 10.0; N, 4.3.

**Preparation of *rac*-Cyclohexyl(hydroxymethyl)phenyl(2-piperidinoethyl)silane (*rac*-5b).** This compound was prepared analogously to the synthesis of *rac*-**5a** by addition of piperidine to the vinyl group of *rac*-**11** (10.0 g, 31.4 mmol). After Kugelrohr distillation (180 °C/0.01 Torr) and crystallization of the distillate at room temperature, *rac*-**5b** was isolated in 89% yield as a white crystalline solid (9.29 g, 28.0 mmol); mp 89–90 °C. <sup>1</sup>H NMR (400.1 MHz, CDCl<sub>3</sub>): δ 0.9–1.0, 1.0–1.3, 1.3–1.5, and 1.5–1.8 (m, 19 H, SiCH<sub>2</sub>C, SiCHC<sub>2</sub>, CCH<sub>2</sub>C), 2.1–2.6 (m, 6H, NCH<sub>2</sub>C), 3.61 (δ<sub>A</sub>) and 3.64 (δ<sub>B</sub>) (AB system, *J*<sub>AB</sub> = 14.9 Hz, 2 H, SiCH<sub>2</sub>O), 6.5 (br s, 1 H, OH), 7.3–7.6 (m, 5 H, SiC<sub>6</sub>H<sub>5</sub>). <sup>13</sup>C NMR (100.6 MHz, CDCl<sub>3</sub>): δ 9.6 (SiCH<sub>2</sub>C), 23.6 (C-1, SiC<sub>6</sub>H<sub>11</sub>), 24.2 (CCH<sub>2</sub>C), 25.2 (2 C) (CCH<sub>2</sub>C), 26.8 (CCH<sub>2</sub>C), 27.59 (CCH<sub>2</sub>C), 27.63 (CCH<sub>2</sub>C), 28.0 (CCH<sub>2</sub>C), 28.1 (CCH<sub>2</sub>C), 49.1 (SiCH<sub>2</sub>O), 54.0 (SiCCH<sub>2</sub>N), 54.4 (2 C) (NCH<sub>2</sub>C, NC<sub>5</sub>H<sub>10</sub>), 127.8 (C-3/C-5, SiC<sub>6</sub>H<sub>5</sub>), 129.1 (C-4, SiC<sub>6</sub>H<sub>5</sub>), 134.6 (3 C) (C-1/C-2/C-6, SiC<sub>6</sub>H<sub>5</sub>). EI MS:  $m/z$  331 (5, M<sup>+</sup>), 98 (100, CH<sub>2</sub>=NC<sub>5</sub>H<sub>10</sub><sup>+</sup>). Anal. Calcd for C<sub>20</sub>H<sub>33</sub>NOSi (M<sub>r</sub> = 331.6): C, 72.45; H, 10.03; N, 4.22. Found: C, 72.6; H, 10.2; N, 4.2.



**Preparation of (*R*)-Cyclohexyl(hydroxymethyl)phenyl(2-piperidinoethyl)silane [(*R*)-5b].** This compound was prepared from (*R*)-5b · HCl (342 mg, 929 μmol) analogously to the synthesis of (*R*)-5a and isolated in 87% yield as a white crystalline solid (269 mg, 811 μmol); mp 84–85 °C. The NMR and MS data of the product were identical with those obtained for *rac*-5b. [ $\alpha$ ]<sub>D</sub><sup>20</sup><sub>546</sub> = -4.3 (CHCl<sub>3</sub>, *c* = 1.0). Anal. Calcd for C<sub>20</sub>H<sub>33</sub>NOSi (M<sub>r</sub> = 331.6): C, 72.45; H, 10.03; N, 4.22. Found: C, 72.2; H, 10.3; N, 4.2.

**Preparation of (*S*)-Cyclohexyl(hydroxymethyl)phenyl(2-piperidinoethyl)silane [(*S*)-5b].** This compound was prepared from (*S*)-5b · HCl (390 mg, 1.06 mmol) analogously to the synthesis of (*R*)-5a and isolated in 86% yield as a white crystalline solid (302 mg, 911 μmol); mp 84–85 °C. The NMR and MS data of the product were identical with those obtained for *rac*-5b. [ $\alpha$ ]<sub>D</sub><sup>20</sup><sub>546</sub> = +4.3 (CHCl<sub>3</sub>, *c* = 1.0). Anal. Calcd for C<sub>20</sub>H<sub>33</sub>NOSi (M<sub>r</sub> = 331.6): C, 72.45; H, 10.03; N, 4.22. Found: C, 72.4; H, 10.3; N, 4.2.

**Preparation of *rac*-Cyclohexyl(2-hexamethyleniminoethyl)(hydroxymethyl)phenylsilane (*rac*-5c).** This compound was prepared analogously to the synthesis of *rac*-5a by addition of hexamethylenimine to the vinyl group of *rac*-11 (10.0 g, 31.4 mmol). After Kugelrohr distillation (190 °C/0.01 Torr) and crystallization of the distillate at room temperature, *rac*-5c was isolated in 85% yield (9.23 g, 26.7 mmol) as a white crystalline solid; mp 54–55 °C. <sup>1</sup>H NMR (400.1 MHz, CDCl<sub>3</sub>): δ 0.9–1.0, 1.0–1.3, and 1.5–1.8 (m, 21 H, SiCH<sub>2</sub>C, SiCHC<sub>2</sub>, CCH<sub>2</sub>C), 2.4–2.7 (m, 6 H, NCH<sub>2</sub>C), 3.62 (δ<sub>A</sub>) and 3.65 (δ<sub>B</sub>) (AB system, J<sub>AB</sub> = 14.9 Hz, 2 H, SiCH<sub>2</sub>O), 6.6 (br s, 1 H, OH), 7.25–7.6 (m, 5 H, SiC<sub>6</sub>H<sub>5</sub>). <sup>13</sup>C NMR (100.6 MHz, CDCl<sub>3</sub>): δ 10.4 (SiCH<sub>2</sub>C), 23.6 (C-1, SiC<sub>6</sub>H<sub>11</sub>), 26.6 (2 C) (CCH<sub>2</sub>C), 26.7 (3 C) (CCH<sub>2</sub>C), 27.60 (CCH<sub>2</sub>C), 27.62 (CCH<sub>2</sub>C), 28.0 (CCH<sub>2</sub>C), 28.1 (CCH<sub>2</sub>C), 49.1 (SiCH<sub>2</sub>O), 53.0 (SiCCH<sub>2</sub>N), 55.8 (2 C) (NCH<sub>2</sub>C, NC<sub>6</sub>H<sub>12</sub>), 127.8 (C-3/C-5, SiC<sub>6</sub>H<sub>5</sub>), 129.0 (C-4, SiC<sub>6</sub>H<sub>5</sub>), 134.6 (C-2/C-6, SiC<sub>6</sub>H<sub>5</sub>), 134.7 (C-1, SiC<sub>6</sub>H<sub>5</sub>). EI MS: *m/z* 345 (6, M<sup>+</sup>), 112 (100, CH<sub>2</sub>=NC<sub>6</sub>H<sub>12</sub><sup>+</sup>). Anal. Calcd for C<sub>21</sub>H<sub>35</sub>NOSi (M<sub>r</sub> = 345.6): C, 72.98; H, 10.21; N, 4.05. Found: C, 73.3; H, 10.2; N, 4.2.

**Preparation of (*R*)-Cyclohexyl(2-hexamethyleniminoethyl)(hydroxymethyl)phenylsilane [(*R*)-5c].** This compound was prepared from (*R*)-5c · HCl (306 mg, 801 μmol) analogously to the synthesis of (*R*)-5a and isolated in 84% yield as a white crystalline solid (233 mg, 674 μmol); mp 50–51 °C. The NMR and MS data of the product were identical with those obtained for *rac*-5c. [ $\alpha$ ]<sub>D</sub><sup>20</sup><sub>546</sub> = -3.4 (CHCl<sub>3</sub>, *c* = 1.0). Anal. Calcd for C<sub>21</sub>H<sub>35</sub>NOSi (M<sub>r</sub> = 345.6): C, 72.98; H, 10.21; N, 4.05. Found: C, 72.8; H, 10.4; N, 4.1.

**Preparation of (*S*)-Cyclohexyl(2-hexamethyleniminoethyl)(hydroxymethyl)phenylsilane [(*S*)-5c].** This compound was prepared from (*S*)-5c · HCl (381 mg, 997 μmol) analogously to the synthesis of (*R*)-5a and isolated in 86% yield as a white crystalline solid (297 mg, 859 μmol); mp 50–51 °C. The NMR and MS data of the product were identical with those obtained for *rac*-5c. [ $\alpha$ ]<sub>D</sub><sup>20</sup><sub>546</sub> = +3.4 (CHCl<sub>3</sub>, *c* = 1.0). Anal. Calcd for C<sub>21</sub>H<sub>35</sub>NOSi (M<sub>r</sub> = 345.6): C, 72.98; H, 10.21; N, 4.05. Found: C, 72.9; H, 10.4; N, 4.1.

**Preparation of *rac*-1-{2-[Cyclohexyl(hydroxymethyl)phenylsilyl]ethyl}pyrrolidinium Chloride (*rac*-5a · HCl).** A 3.1 M ethereal HCl solution (1.0 mL, 3.10 mmol of HCl) was added at room temperature to a stirred solution of *rac*-5a (500 mg, 1.57 mmol) in diethyl ether (50 mL). After stirring at room temperature for 15 min, the solvent and excess HCl were removed under reduced pressure. The solid residue was dried *in vacuo* and then recrystallized from acetone/diethyl ether (diffusion of diethyl ether *via* the gas phase into a solution of the product in acetone at room temperature) to give *rac*-5a · HCl in 89% yield as a colorless crystalline solid (495 mg, 1.40 mmol); mp 149–150 °C. <sup>1</sup>H NMR (400.1 MHz, CDCl<sub>3</sub>): δ 0.9–1.2, 1.4–1.7, and 1.9–2.1 (m, 17 H, SiCH<sub>2</sub>C, SiCHC<sub>2</sub>, CCH<sub>2</sub>C), 2.7–2.9, 3.0–3.15, 3.2–3.4, and 3.6–3.7 (m, 7 H, NCH<sub>2</sub>C, OH), 3.78 (s, 2 H, SiCH<sub>2</sub>O), 7.3–7.5 (m, 5 H, SiC<sub>6</sub>H<sub>5</sub>), 11.4 (br s, 1 H, NH). <sup>13</sup>C NMR (100.6 MHz, CDCl<sub>3</sub>): δ 7.7

(SiCH<sub>2</sub>C), 23.28 (C-1, SiC<sub>6</sub>H<sub>11</sub>), 23.33 (2 C) (CCH<sub>2</sub>C), 26.5 (CCH<sub>2</sub>C), 27.35 (CCH<sub>2</sub>C), 27.37 (CCH<sub>2</sub>C), 27.7 (CCH<sub>2</sub>C), 27.8 (CCH<sub>2</sub>C), 50.0 (SiCH<sub>2</sub>O), 52.4 (NCH<sub>2</sub>C), 52.5 (NCH<sub>2</sub>C), 52.6 (NCH<sub>2</sub>C), 128.2 (C-3/C-5, SiC<sub>6</sub>H<sub>5</sub>), 129.7 (C-4, SiC<sub>6</sub>H<sub>5</sub>), 132.4 (C-1, SiC<sub>6</sub>H<sub>5</sub>), 134.4 (C-2/C-6, SiC<sub>6</sub>H<sub>5</sub>). EI MS: *m/z* 317 (7, M<sub>Basse</sub><sup>+</sup>), 84 (100, CH<sub>2</sub>=NC<sub>4</sub>H<sub>8</sub><sup>+</sup>). Anal. Calcd for C<sub>19</sub>H<sub>32</sub>ClNOSi (M<sub>r</sub> = 354.0): C, 64.46; H, 9.11; N, 3.96. Found: C, 64.3; H, 9.0; N, 4.0.

**Preparation of (*R*)-1-{2-[Cyclohexyl(hydroxymethyl)phenylsilyl]ethyl}pyrrolidinium Chloride [(*R*)-5a · HCl].** The combined mother liquors [enriched with (*R*)-5a · (*S,S*)-*O,O'*-di-*p*-toluoyltartaric acid] collected in the several steps of the resolution of *rac*-5a [see preparation of (*S*)-5a · HCl] were concentrated under reduced pressure, and the solid residue was suspended in water (200 mL). After addition of diethyl ether (200 mL) and 2.0 M aqueous NaOH solution (40 mL), the resulting mixture was stirred at room temperature for 15 min, the organic phase separated, and the aqueous layer extracted with diethyl ether (3 × 150 mL). After drying of the combined organic extracts over anhydrous Na<sub>2</sub>SO<sub>4</sub>, the solvent was removed under reduced pressure and the residue dried *in vacuo* to yield a mixture of (*R*)-5a and (*S*)-5a [strongly enriched with (*R*)-5a] (6.85 g, 21.6 mmol). A boiling solution of this product in acetone (70 mL) was added to a filtered solution of (*R,R*)-*O,O'*-di-*p*-toluoyltartaric acid (8.33 g, 21.6 mmol) in boiling acetone (330 mL). After cooling of this mixture to room temperature and keeping it undisturbed for 60 h, the crystals that formed (10.1 g) were filtered off and then subjected to a 7-fold fractional crystallization following the procedure described for the preparation of (*S*)-5a · HCl. The product<sup>6</sup> (1.08 g) finally obtained by this method was transformed into crude (*R*)-5a (448 mg, 1.41 mmol) and then further into (*R*)-5a · HCl following the procedure described for the preparation of (*S*)-5a · HCl. Compound (*R*)-5a · HCl was isolated in 9% yield [related to (*R*)-5a in the racemic mixture of 5a] as a colorless crystalline solid (503 mg, 1.42 mmol); mp 131–132 °C. The NMR and MS data of the product were identical with those obtained for *rac*-5a · HCl. [ $\alpha$ ]<sub>D</sub><sup>20</sup><sub>546</sub> = +0.7 (CHCl<sub>3</sub>, *c* = 1.0). Anal. Calcd for C<sub>19</sub>H<sub>32</sub>ClNOSi (M<sub>r</sub> = 354.0): C, 64.46; H, 9.11; N, 3.96; Cl, 10.01. Found: C, 64.8; H, 9.3; N, 4.1; Cl, 10.0.

**Preparation of (*S*)-1-{2-[Cyclohexyl(hydroxymethyl)phenylsilyl]ethyl}pyrrolidinium Chloride [(*S*)-5a · HCl].** (*S,S*)-*O,O'*-Di-*p*-toluoyltartaric acid (11.7 g, 30.3 mmol) was dissolved in boiling acetone (470 mL). The hot solution was filtered and then added to a solution of *rac*-5a (9.60 g, 30.2 mmol) in boiling acetone (100 mL). The resulting mixture was cooled to room temperature and then kept undisturbed for 60 h to yield 16.6 g of a crystalline solid. The crystals were isolated by filtration and then subjected to a 7-fold fractional crystallization from acetone. For this purpose, the boiling saturated solution of the crystals in acetone was filtered and then allowed to cool slowly to room temperature over ca. 6 h (slow cooling in a water bath, starting at 55 °C). After keeping the mixture at room temperature for a further 48 h, the crystals formed were isolated by filtration and then subjected to the next crystallization step. In the case of the first three fractional crystallization steps, the crystals of a second precipitate (obtained by removal of the solvent of the filtrate under reduced pressure and crystallization of the resulting residue from boiling acetone in the same manner as described above) were collected as well, whereas in the four following fractional crystallization steps only the primary precipitate was isolated. The product<sup>6</sup> (1.29 g) finally obtained by this procedure was suspended in a mixture of water (100 mL) and diethyl ether (100 mL), followed by addition of 2.0 M aqueous NaOH solution (3.0 mL). After stirring at room temperature for 10 min, the organic phase was separated and the aqueous layer extracted with diethyl ether (3 × 100 mL). The combined organic

(6) According to <sup>1</sup>H and <sup>13</sup>C NMR studies (data not given), this product is the respective *O,O'*-di-*p*-toluoyl hydrogen tartrate containing ca. 1 mol equiv of acetone.



extracts were dried over anhydrous  $\text{Na}_2\text{SO}_4$ , and the solvent was removed under reduced pressure and the residue dried *in vacuo* to yield crude (*S*)-**5a** as an oily liquid (547 mg, 1.72 mmol). After dissolving this product in diethyl ether (100 mL), 3.1 M ethereal HCl solution (1.0 mL, 3.10 mmol of HCl) was added at room temperature and the resulting mixture stirred for 10 min. The solvent and excess HCl were removed under reduced pressure, and the solid residue was dried *in vacuo* and then recrystallized from acetone/diethyl ether (diffusion of diethyl ether *via* the gas phase into a solution of the product in acetone at room temperature) to give (*S*)-**5a**·HCl in 10% yield [related to (*S*)-**5a** in the racemic mixture of **5a**] as a colorless crystalline solid (556 mg, 1.57 mmol); mp 131–132 °C. The NMR and MS data of the product were identical with those obtained for *rac*-**5a**·HCl.  $[\alpha]_{546}^{20} = -0.7$  ( $\text{CHCl}_3$ ,  $c = 1.0$ ). Anal. Calcd for  $\text{C}_{19}\text{H}_{32}\text{ClNOSi}$  ( $M_r = 354.0$ ): C, 64.46; H, 9.11; N, 3.96; Cl, 10.01. Found: C, 64.8; H, 9.4; N, 3.9; Cl, 10.0.

**Preparation of *rac*-1-[2-(Cyclohexyl(hydroxymethyl)phenylsilyl)ethyl]piperidinium Chloride (*rac*-**5b**·HCl).** This compound was prepared from *rac*-**5b** (500 mg, 1.51 mmol) analogously to the synthesis of *rac*-**5a**·HCl and isolated in 91% yield as a colorless crystalline solid (507 mg, 1.38 mmol); mp 169–170 °C.  $^1\text{H}$  NMR (400.1 MHz,  $\text{CDCl}_3$ ):  $\delta$  0.9–1.25, 1.25–1.3, 1.35–1.9, and 2.0–2.2 (m, 19 H,  $\text{SiCH}_2\text{C}$ ,  $\text{SiCH}_2\text{C}_2$ ,  $\text{CCH}_2\text{C}$ ), 2.4–2.6, 2.9–3.0, 3.1–3.3, and 3.4–3.6 (m, 6 H,  $\text{NCH}_2\text{C}$ ), 3.1 (br s, 1 H, OH), 3.83 (s, 2 H,  $\text{SiCH}_2\text{O}$ ), 7.3–7.5 (m, 5 H,  $\text{SiC}_6\text{H}_5$ ), 11.2 (br s, 1 H, NH).  $^{13}\text{C}$  NMR (100.6 MHz,  $\text{CDCl}_3$ ):  $\delta$  5.7 ( $\text{SiCH}_2\text{C}$ ), 22.3 ( $\text{CCH}_2\text{C}$ ), 22.8 (2 C) ( $\text{CCH}_2\text{C}$ ), 23.3 (C-1,  $\text{SiC}_6\text{H}_{11}$ ), 26.6 ( $\text{CCH}_2\text{C}$ ), 27.4 (2 C) ( $\text{CCH}_2\text{C}$ ), 27.7 ( $\text{CCH}_2\text{C}$ ), 27.80 ( $\text{CCH}_2\text{C}$ ), 50.2 ( $\text{SiCH}_2\text{O}$ ), 51.8 ( $\text{NCH}_2\text{C}$ ), 52.5 ( $\text{NCH}_2\text{C}$ ), 54.5 ( $\text{NCH}_2\text{C}$ ), 128.2 (C-3/C-5,  $\text{SiC}_6\text{H}_5$ ), 129.8 (C-4,  $\text{SiC}_6\text{H}_5$ ), 132.4 (C-1,  $\text{SiC}_6\text{H}_5$ ), 134.5 (C-2/C-6,  $\text{SiC}_6\text{H}_5$ ). EI MS:  $m/z$  331 (4,  $M_{\text{Base}}^+$ ), 98 (100,  $\text{CH}_2=\text{NC}_5\text{H}_{10}^+$ ). Anal. Calcd for  $\text{C}_{20}\text{H}_{34}\text{ClNOSi}$  ( $M_r = 368.0$ ): C, 65.27; H, 9.31; N, 3.81. Found: C, 65.3; H, 9.5; N, 3.8.

**Preparation of (*R*)-1-[2-(Cyclohexyl(hydroxymethyl)phenylsilyl)ethyl]piperidinium Chloride [(*R*)-**5b**·HCl].** The combined mother liquors [enriched with (*R*)-**5b**·(*S,S*)-*O,O'*-di-*p*-toluoyltartaric acid] collected in the several steps of the resolution of *rac*-**5b** [see preparation of (*S*)-**5b**·HCl] were concentrated under reduced pressure, and the solid residue was suspended in water (200 mL). After addition of diethyl ether (200 mL) and 2.0 M aqueous NaOH solution (40 mL), the resulting mixture was stirred at room temperature for 15 min, the organic phase separated, and the aqueous layer extracted with diethyl ether (3 × 150 mL). After drying of the combined organic extracts over anhydrous  $\text{Na}_2\text{SO}_4$ , the solvent was removed under reduced pressure and the residue dried *in vacuo* to yield a mixture of (*R*)-**5b** and (*S*)-**5b** [strongly enriched with (*R*)-**5b**] (7.32 g, 22.1 mmol). A boiling solution of this product in acetone (75 mL) was added to a filtered solution of (*R,R*)-*O,O'*-di-*p*-toluoyltartaric acid (8.53 g, 22.1 mmol) in boiling acetone (1.3 L). After cooling of this mixture to room temperature and keeping it undisturbed for 60 h, the crystals that formed (12.7 g) were filtered off and then subjected to a 7-fold fractional crystallization following the procedure described for the preparation of (*S*)-**5b**·HCl. The product<sup>6</sup> (1.29 g) finally obtained by this method was transformed into crude (*R*)-**5b** (560 mg, 1.69 mmol) and then further into (*R*)-**5b**·HCl following the procedure described for the preparation of (*S*)-**5b**·HCl. Compound (*R*)-**5b**·HCl was isolated in 10% yield [related to (*R*)-**5b** in the racemic mixture of **5b**] as a colorless crystalline solid (567 mg, 1.54 mmol); mp 153–154 °C. The NMR and MS data of the product were identical with those obtained for *rac*-**5b**·HCl.  $[\alpha]_{546}^{20} = +7.9$  ( $\text{CHCl}_3$ ,  $c = 1.0$ ). Anal. Calcd for  $\text{C}_{20}\text{H}_{34}\text{ClNOSi}$  ( $M_r = 368.0$ ): C, 65.27; H, 9.31; N, 3.81; Cl, 9.63. Found: C, 65.4; H, 9.6; N, 3.8; Cl, 9.6.

**Preparation of (*S*)-1-[2-(Cyclohexyl(hydroxymethyl)phenylsilyl)ethyl]piperidinium Chloride [(*S*)-**5b**·HCl].** (*S,S*)-*O,O'*-Di-*p*-toluoyltartaric acid (11.7 g, 30.3 mmol) was

dissolved in boiling acetone (1.75 L). The hot solution was filtered and then added to a solution of *rac*-**5b** (10.0 g, 30.2 mmol) in boiling acetone (100 mL). The resulting mixture was cooled to room temperature and then kept undisturbed for 60 h to yield 19.4 g of a crystalline solid. The crystals were isolated by filtration and then subjected to a 7-fold fractional crystallization from acetone. For this purpose, the boiling saturated solution of the crystals in acetone was filtered and then allowed to cool slowly to room temperature over ca. 6 h (slow cooling in a water bath, starting at 55 °C). After keeping the mixture at room temperature for a further 48 h, the crystals formed were isolated by filtration and then subjected to the next crystallization step. In the case of the first three fractional crystallization steps, the crystals of a second precipitate (obtained by removal of the solvent of the filtrate under reduced pressure and crystallization of the resulting residue from boiling acetone in the same manner as described above) were collected as well, whereas in the four following fractional crystallization steps only the primary precipitate was isolated. The product<sup>6</sup> (1.52 g) finally obtained by this procedure was suspended in a mixture of water (100 mL) and diethyl ether (100 mL), followed by addition of 2.0 M aqueous NaOH solution (3.0 mL). After stirring at room temperature for 10 min, the organic phase was separated and the aqueous layer extracted with diethyl ether (3 × 100 mL). The combined organic extracts were dried over anhydrous  $\text{Na}_2\text{SO}_4$ , and the solvent was removed under reduced pressure and the residue dried *in vacuo* to yield crude (*S*)-**5b** as a white crystalline solid (658 mg, 1.98 mmol). After dissolving this product in diethyl ether (100 mL), 3.1 M ethereal HCl solution (1.0 mL, 3.10 mmol of HCl) was added at room temperature and the resulting mixture stirred for 10 min. The solvent and excess HCl were removed under reduced pressure, and the solid residue was dried *in vacuo* and then recrystallized from acetone/diethyl ether (diffusion of diethyl ether *via* the gas phase into a solution of the product in acetone at room temperature) to give (*S*)-**5b**·HCl in 12% yield [related to (*S*)-**5b** in the racemic mixture of **5b**] as a colorless crystalline solid (655 mg, 1.78 mmol); mp 153–154 °C. The NMR and MS data of the product were identical with those obtained for *rac*-**5b**·HCl.  $[\alpha]_{546}^{20} = -7.9$  ( $\text{CHCl}_3$ ,  $c = 1.0$ ). Anal. Calcd for  $\text{C}_{20}\text{H}_{34}\text{ClNOSi}$  ( $M_r = 368.0$ ): C, 65.27; H, 9.31; N, 3.81; Cl, 9.63. Found: C, 65.4; H, 9.6; N, 3.8; Cl, 9.6.

**Preparation of *rac*-1-[2-(Cyclohexyl(hydroxymethyl)phenylsilyl)ethyl]hexamethyleniminium Chloride (*rac*-**5c**·HCl).** This compound was prepared from *rac*-**5c** (500 mg, 1.45 mmol) analogously to the synthesis of *rac*-**5a**·HCl and isolated in 90% yield as a colorless crystalline solid (498 mg, 1.30 mmol); mp 163–164 °C.  $^1\text{H}$  NMR (300.1 MHz,  $\text{CDCl}_3$ ):  $\delta$  0.8–1.2, 1.3–1.8, and 1.9–2.2 (m, 21 H,  $\text{SiCH}_2\text{C}$ ,  $\text{SiCH}_2\text{C}_2$ ,  $\text{CCH}_2\text{C}$ ), 2.7–3.1 and 3.1–3.5 (m, 7H,  $\text{NCH}_2\text{C}$ , OH), 3.82 (s, 2 H,  $\text{SiCH}_2\text{O}$ ), 7.25–7.6 (m, 5 H,  $\text{SiC}_6\text{H}_5$ ), 11.1 (br s, 1 H, NH).  $^{13}\text{C}$  NMR (62.9 MHz,  $\text{CDCl}_3$ ):  $\delta$  6.2 ( $\text{SiCH}_2\text{C}$ ), 23.3 (C-1,  $\text{SiC}_6\text{H}_{11}$ ), 23.6 (2 C) ( $\text{CCH}_2\text{C}$ ), 26.5 (3 C) ( $\text{CCH}_2\text{C}$ ), 27.4 (2 C) ( $\text{CCH}_2\text{C}$ ), 27.7 (2 C) ( $\text{CCH}_2\text{C}$ ), 49.9 ( $\text{SiCH}_2\text{O}$ ), 53.0 ( $\text{NCH}_2\text{C}$ ), 53.7 ( $\text{NCH}_2\text{C}$ ), 54.9 ( $\text{NCH}_2\text{C}$ ), 128.1 (C-3/C-5,  $\text{SiC}_6\text{H}_5$ ), 129.7 (C-4,  $\text{SiC}_6\text{H}_5$ ), 132.5 (C-1,  $\text{SiC}_6\text{H}_5$ ), 134.4 (C-2/C-6,  $\text{SiC}_6\text{H}_5$ ). EI MS:  $m/z$  345 (5,  $M_{\text{Base}}^+$ ), 112 (100,  $\text{CH}_2=\text{NC}_6\text{H}_{12}^+$ ). Anal. Calcd for  $\text{C}_{21}\text{H}_{36}\text{ClNOSi}$  ( $M_r = 382.1$ ): C, 66.02; H, 9.50; N, 3.67. Found: C, 66.2; H, 9.8; N, 3.7.

**Preparation of (*R*)-1-[2-(Cyclohexyl(hydroxymethyl)phenylsilyl)ethyl]hexamethyleniminium Chloride [(*R*)-**5c**·HCl].** The combined mother liquors [enriched with (*R*)-**5c**·(*S,S*)-*O,O'*-di-*p*-toluoyltartaric acid] collected in the several steps of the resolution of *rac*-**5c** [see preparation of (*S*)-**5c**·HCl] were concentrated under reduced pressure, and the solid residue was suspended in water (200 mL). After addition of diethyl ether (200 mL) and 2.0 M aqueous NaOH solution (40 mL), the resulting mixture was stirred at room temperature for 15 min, the organic phase separated, and the aqueous layer extracted with diethyl ether (3 × 150 mL). After drying of the combined organic extracts over anhydrous  $\text{Na}_2\text{SO}_4$ , the

solvent was removed under reduced pressure and the residue dried *in vacuo* to yield a mixture of (*R*)-**5c** and (*S*)-**5c** [strongly enriched with (*R*)-**5c**] (7.21 g, 20.9 mmol). A boiling solution of this product in acetone (75 mL) was added to a filtered solution of (*R,R*)-*O,O'*-di-*p*-toluoyltartaric acid (8.06 g, 20.9 mmol) in boiling acetone (1.2 L). After cooling of this mixture to room temperature and keeping it undisturbed for 60 h, the crystals formed (13.1 g) were filtered off and then subjected to a 7-fold fractional crystallization following the procedure described for the preparation of (*S*)-**5c**·HCl. The product<sup>6</sup> (1.20 g) finally obtained by this method was transformed into crude (*R*)-**5c** (532 mg, 1.54 mmol) and then further into (*R*)-**5c**·HCl following the procedure described for the preparation of (*S*)-**5c**·HCl. Compound (*R*)-**5c**·HCl was isolated in 9% yield [related to (*R*)-**5c** in the racemic mixture of **5c**] as a colorless crystalline solid (512 mg, 1.34 mmol); mp 133–134 °C. The NMR and MS data of the product were identical with those obtained for *rac*-**5c**·HCl. [ $\alpha$ ]<sub>D</sub><sup>20</sup><sub>546</sub> = +7.0 (CHCl<sub>3</sub>, *c* = 1.0). Anal. Calcd for C<sub>21</sub>H<sub>36</sub>ClNOSi (M<sub>r</sub> = 382.1): C, 66.02; H, 9.50; N, 3.67; Cl, 9.28. Found: C, 66.0; H, 9.7; N, 3.7; Cl, 9.3.

**Preparation of (*S*)-1-[2-[Cyclohexyl(hydroxymethyl)phenylsilyl]ethyl]hexamethyleniminium Chloride [(*S*)-**5c**·HCl].** (*S,S*)-*O,O'*-Di-*p*-toluoyltartaric acid (11.6 g, 30.0 mmol) was dissolved in boiling acetone (1.75 L). The hot solution was filtered and then added to a solution of *rac*-**5c** (10.4 g, 30.1 mmol) in boiling acetone (100 mL). The resulting mixture was cooled to room temperature and then kept undisturbed for 60 h to yield 20.6 g of a crystalline solid. The crystals were isolated by filtration and then subjected to a 7-fold fractional crystallization from acetone. For this purpose, the boiling saturated solution of the crystals in acetone was filtered and then allowed to cool slowly to room temperature over ca. 6 h (slow cooling in a water bath, starting at 55 °C). After keeping the mixture at room temperature for a further 48 h, the crystals that formed were isolated by filtration and then subjected to the next crystallization step. In the case of the first three fractional crystallization steps, the crystals of a second precipitate (obtained by removal of the solvent of the filtrate under reduced pressure and crystallization of the resulting residue from boiling acetone in the same manner as described above) were collected as well, whereas in the four following fractional crystallization steps only the primary precipitate was isolated. The product<sup>6</sup> (1.35 g) finally obtained by this procedure was suspended in a mixture of water (100 mL) and diethyl ether (100 mL), followed by addition of 2.0 M aqueous NaOH solution (3.0 mL). After stirring at room temperature for 10 min, the organic phase was separated and the aqueous layer extracted with diethyl ether (3 × 100 mL). The combined organic extracts were dried over anhydrous Na<sub>2</sub>SO<sub>4</sub>, and the solvent was removed under reduced pressure and the residue dried *in vacuo* to yield crude (*S*)-**5c** as a white crystalline solid (591 mg, 1.71 mmol). After dissolving of this product in diethyl ether (100 mL), 3.1 M ethereal HCl solution (1.0 mL, 3.10 mmol of HCl) was added at room temperature and the resulting mixture stirred for 10 min. The solvent and excess HCl were removed under reduced pressure, and the solid residue was dried *in vacuo* and then recrystallized from acetone/diethyl ether (diffusion of diethyl ether *via* the gas phase into a solution of the product in acetone at room temperature) to give (*S*)-**5c**·HCl in 10% yield [related to (*S*)-**5c** in the racemic mixture of **5c**] as a colorless crystalline solid (601 mg, 1.57 mmol); mp 133–134 °C. The NMR and MS data of the product were identical with those obtained for *rac*-**5c**·HCl. [ $\alpha$ ]<sub>D</sub><sup>20</sup><sub>546</sub> = -7.0 (CHCl<sub>3</sub>, *c* = 1.0). Anal. Calcd for C<sub>21</sub>H<sub>36</sub>ClNOSi (M<sub>r</sub> = 382.1): C, 66.02; H, 9.50; N, 3.67; Cl, 9.28. Found: C, 66.1; H, 9.7; N, 3.7; Cl, 9.3.

**Preparation of *rac*-1-[2-[Cyclohexyl(hydroxymethyl)phenylsilyl]ethyl]-1-methylpyrrolidinium Iodide (*rac*-**6a**).** Methyl iodide (2.23 g, 15.7 mmol) was added to a solution of *rac*-**5a** (500 mg, 1.57 mmol) in acetone (50 mL) and the resulting mixture stirred at room temperature for 21 h. After

removal of the solvent and excess methyl iodide under reduced pressure, the solid residue was dried *in vacuo* and then recrystallized from acetone/diethyl ether (diffusion of diethyl ether *via* the gas phase into a solution of the product in acetone at room temperature) to give *rac*-**6a** in 91% yield as a colorless crystalline solid (660 mg, 1.44 mmol); mp 142–143 °C. <sup>1</sup>H NMR (250.1 MHz, CDCl<sub>3</sub>): δ 1.0–1.8 and 2.1–2.3 (m, 17 H, SiCH<sub>2</sub>C, SiCHC<sub>2</sub>, CCH<sub>2</sub>C), 3.1 (br s, 1 H, OH), 3.15 (s, 3 H, NCH<sub>3</sub>), 3.35–3.55, 3.55–3.75, and 3.8–4.0 (m, 6 H, NCH<sub>2</sub>C), 3.86 (s, 2 H, SiCH<sub>2</sub>O), 7.3–7.55 (m, 5 H, SiC<sub>6</sub>H<sub>5</sub>). <sup>13</sup>C NMR (62.9 MHz, CDCl<sub>3</sub>): δ 6.1 (SiCH<sub>2</sub>C), 21.8 (2 C) (CCH<sub>2</sub>C), 23.3 (C-1, SiC<sub>6</sub>H<sub>11</sub>), 26.5 (CCH<sub>2</sub>C), 27.4 (2 C) (CCH<sub>2</sub>C), 27.70 (CCH<sub>2</sub>C), 27.73 (CCH<sub>2</sub>C), 48.3 (NCH<sub>3</sub>), 48.7 (SiCH<sub>2</sub>O), 62.2 (NCH<sub>2</sub>C), 63.3 (NCH<sub>2</sub>C), 63.7 (NCH<sub>2</sub>C), 128.3 (C-3/C-5, SiC<sub>6</sub>H<sub>5</sub>), 129.8 (C-4, SiC<sub>6</sub>H<sub>5</sub>), 132.5 (C-1, SiC<sub>6</sub>H<sub>5</sub>), 134.4 (C-2/C-6, SiC<sub>6</sub>H<sub>5</sub>). FD MS: *m/z* 332 (100, M<sub>cation</sub><sup>+</sup>). Anal. Calcd for C<sub>20</sub>H<sub>34</sub>INOSi (M<sub>r</sub> = 459.5): C, 52.28; H, 7.46; N, 3.05. Found: C, 52.7; H, 7.8; N, 3.1.

**Preparation of (*R*)-1-[2-[Cyclohexyl(hydroxymethyl)phenylsilyl]ethyl]-1-methylpyrrolidinium Iodide [(*R*)-**6a**].** This compound was prepared analogously to the synthesis of *rac*-**6a** by addition of methyl iodide (184 mg, 1.30 mmol) to a solution of (*R*)-**5a** (210 mg, 661 μmol) in acetone (40 mL). (*R*)-**6a** was isolated in 71% yield as a colorless crystalline solid (216 mg, 470 μmol); mp 135–136 °C [recrystallization by diffusion of diethyl ether *via* the gas phase into a solution of the product in ethyl acetate/acetone (1/5, v/v) at room temperature]. The NMR and MS data of the product were identical with those obtained for *rac*-**6a**. [ $\alpha$ ]<sub>D</sub><sup>20</sup><sub>546</sub> = -5.6 (CHCl<sub>3</sub>, *c* = 1.0). Anal. Calcd for C<sub>20</sub>H<sub>34</sub>INOSi (M<sub>r</sub> = 459.5): C, 52.28; H, 7.46; N, 3.05; I, 27.62. Found: C, 52.4; H, 7.5; N, 3.0; I, 27.8.

**Preparation of (*S*)-1-[2-[Cyclohexyl(hydroxymethyl)phenylsilyl]ethyl]-1-methylpyrrolidinium Iodide [(*S*)-**6a**].** This compound was prepared analogously to the synthesis of *rac*-**6a** by addition of methyl iodide (207 mg, 1.46 mmol) to a solution of (*S*)-**5a** (231 mg, 728 μmol) in acetone (40 mL). (*S*)-**6a** was isolated in 67% yield as a colorless crystalline solid (225 mg, 490 μmol); mp 135–136 °C [recrystallization by diffusion of diethyl ether *via* the gas phase into a solution of the product in ethyl acetate/acetone (1/5, v/v) at room temperature]. The NMR and MS data of the product were identical with those obtained for *rac*-**6a**. [ $\alpha$ ]<sub>D</sub><sup>20</sup><sub>546</sub> = +5.6 (CHCl<sub>3</sub>, *c* = 1.0). Anal. Calcd for C<sub>20</sub>H<sub>34</sub>INOSi (M<sub>r</sub> = 459.5): C, 52.28; H, 7.46; N, 3.05; I, 27.62. Found: C, 52.6; H, 7.7; N, 3.0; I, 27.7.

**Preparation of *rac*-1-[2-[Cyclohexyl(hydroxymethyl)phenylsilyl]ethyl]-1-methylpiperidinium Iodide (*rac*-**6b**).** This compound was prepared analogously to the synthesis of *rac*-**6a** by addition of methyl iodide (860 mg, 6.06 mmol) to a solution of *rac*-**5b** (1.00 g, 3.02 mmol) in acetone (100 mL). *rac*-**6b** was isolated in 91% yield as a colorless crystalline solid (1.30 g, 2.75 mmol); mp 141–142 °C. <sup>1</sup>H NMR (250.1 MHz, CDCl<sub>3</sub>): δ 0.95–1.5 and 1.5–2.0 (m, 19 H, SiCH<sub>2</sub>C, SiCHC<sub>2</sub>, CCH<sub>2</sub>C), 3.1 (br s, 1 H, OH), 3.14 (s, 3 H, NCH<sub>3</sub>), 3.35–3.65 and 3.85–4.05 (m, 6 H, NCH<sub>2</sub>C), 3.87 (s, 2 H, SiCH<sub>2</sub>O), 7.3–7.55 (m, 5 H, SiC<sub>6</sub>H<sub>5</sub>). <sup>13</sup>C NMR (62.9 MHz, CDCl<sub>3</sub>): δ 4.1 (SiCH<sub>2</sub>C), 20.1 (2 C) (CCH<sub>2</sub>C), 20.8 (CCH<sub>2</sub>C), 23.4 (C-1, SiC<sub>6</sub>H<sub>11</sub>), 26.5 (CCH<sub>2</sub>C), 27.5 (2 C) (CCH<sub>2</sub>C), 27.7 (CCH<sub>2</sub>C), 27.8 (CCH<sub>2</sub>C), 47.2 (NCH<sub>3</sub>), 48.7 (SiCH<sub>2</sub>O), 59.8 (NCH<sub>2</sub>C), 60.3 (NCH<sub>2</sub>C), 61.9 (NCH<sub>2</sub>C), 128.3 (C-3/C-5, SiC<sub>6</sub>H<sub>5</sub>), 129.9 (C-4, SiC<sub>6</sub>H<sub>5</sub>), 132.5 (C-1, SiC<sub>6</sub>H<sub>5</sub>), 134.4 (C-2/C-6, SiC<sub>6</sub>H<sub>5</sub>). FD MS: *m/z* 346 (100, M<sub>cation</sub><sup>+</sup>). Anal. Calcd for C<sub>21</sub>H<sub>36</sub>INOSi (M<sub>r</sub> = 473.5): C, 53.27; H, 7.66; N, 2.96. Found: C, 53.3; H, 7.7; N, 3.0.

**Preparation of (*R*)-1-[2-[Cyclohexyl(hydroxymethyl)phenylsilyl]ethyl]-1-methylpiperidinium Iodide [(*R*)-**6b**].** This compound was prepared analogously to the synthesis of *rac*-**6a** by addition of methyl iodide (177 mg, 1.25 mmol) to a solution of (*R*)-**5b** (205 mg, 618 μmol) in acetone (40 mL). (*R*)-**6b** was isolated in 82% yield as a colorless crystalline solid (239 mg, 505 μmol); mp 164–165 °C. The NMR and MS data

of the product were identical with those obtained for *rac*-**6b**.  $[\alpha]_{546}^{20} = -5.9$  (CHCl<sub>3</sub>, *c* = 1.0). Anal. Calcd for C<sub>21</sub>H<sub>36</sub>INOSi (M<sub>r</sub> = 473.5): C, 53.27; H, 7.66; N, 2.96; I, 26.80. Found: C, 53.3; H, 7.7; N, 3.0; I, 26.7.

**Preparation of (S)-1-[2-(Cyclohexyl(hydroxymethyl)phenylsilyl)ethyl]-1-methylpiperidinium Iodide [(S)-6b].** This compound was prepared analogously to the synthesis of *rac*-**6a** by addition of methyl iodide (184 mg, 1.30 mmol) to a solution of (S)-**5b** (215 mg, 648 μmol) in acetone (40 mL). (S)-**6b** was isolated in 82% yield as a colorless crystalline solid (252 mg, 532 μmol); mp 164–165 °C. The NMR and MS data of the product were identical with those obtained for *rac*-**6b**.  $[\alpha]_{546}^{20} = +5.9$  (CHCl<sub>3</sub>, *c* = 1.0). Anal. Calcd for C<sub>21</sub>H<sub>36</sub>INOSi (M<sub>r</sub> = 473.5): C, 53.27; H, 7.66; N, 2.96; I, 26.80. Found: C, 53.4; H, 7.8; N, 2.9; I, 26.8.

**Preparation of *rac*-1-[2-(Cyclohexyl(hydroxymethyl)phenylsilyl)ethyl]-1-methylhexamethyleniminium Iodide (*rac*-6c).** This compound was prepared analogously to the synthesis of *rac*-**6a** by addition of methyl iodide (830 mg, 5.85 mmol) to a solution of *rac*-**5c** (1.00 g, 2.89 mmol) in acetone (100 mL). *rac*-**6c** was isolated in 90% yield as a colorless crystalline solid (1.27 g, 2.60 mmol); mp 149–150 °C. <sup>1</sup>H NMR (250.1 MHz, CDCl<sub>3</sub>): δ 1.0–2.0 (m, 21 H, SiCH<sub>2</sub>C, SiCHC<sub>2</sub>, CCH<sub>2</sub>C), 3.1 (br s, 1 H, OH), 3.15 (s, 3 H, NCH<sub>3</sub>), 3.25–3.6 and 3.85–4.0 (m, 6 H, NCH<sub>2</sub>C), 3.88 (s, 2 H, SiCH<sub>2</sub>O), 7.3–7.55 (m, 5 H, SiC<sub>6</sub>H<sub>5</sub>). <sup>13</sup>C NMR (62.9 MHz, CDCl<sub>3</sub>): δ 5.1 (SiCH<sub>2</sub>C), 22.0 (CCH<sub>2</sub>C), 22.1 (CCH<sub>2</sub>C), 23.4 (C-1, SiC<sub>6</sub>H<sub>11</sub>), 26.5 (CCH<sub>2</sub>C), 27.3 (2 C) (CCH<sub>2</sub>C), 27.5 (2 C) (CCH<sub>2</sub>C), 27.7 (CCH<sub>2</sub>C), 27.8 (CCH<sub>2</sub>C), 48.7 (SiCH<sub>2</sub>O), 50.0 (NCH<sub>3</sub>), 63.3 (NCH<sub>2</sub>C), 63.5 (NCH<sub>2</sub>C), 64.1 (NCH<sub>2</sub>C), 128.3 (C-3/C-5, SiC<sub>6</sub>H<sub>5</sub>), 129.9 (C-4, SiC<sub>6</sub>H<sub>5</sub>), 132.5 (C-1, SiC<sub>6</sub>H<sub>5</sub>), 134.4 (C-2/C-6, SiC<sub>6</sub>H<sub>5</sub>). FD MS: *m/z* 360 (100, M<sup>+</sup><sub>cation</sub>). Anal. Calcd for C<sub>22</sub>H<sub>38</sub>INOSi (M<sub>r</sub> = 487.5): C, 54.20; H, 7.86; N, 2.87. Found: C, 53.7; H, 7.7; N, 3.0.

**Preparation of (R)-1-[2-(Cyclohexyl(hydroxymethyl)phenylsilyl)ethyl]-1-methylhexamethyleniminium Iodide [(R)-6c].** This compound was prepared analogously to the synthesis of *rac*-**6a** by addition of methyl iodide (164 mg, 1.16 mmol) to a solution of (R)-**5c** (200 mg, 579 μmol) in acetone (40 mL). (R)-**6c** was isolated in 85% yield as a colorless crystalline solid (239 mg, 490 μmol); mp 176–177 °C. The NMR and MS data of the product were identical with those obtained for *rac*-**6c**.  $[\alpha]_{546}^{20} = -1.7$  (CHCl<sub>3</sub>, *c* = 1.0). Anal. Calcd for C<sub>22</sub>H<sub>38</sub>INOSi (M<sub>r</sub> = 487.5): C, 54.20; H, 7.86; N, 2.87; I, 26.03. Found: C, 54.3; H, 8.0; N, 2.9; I, 26.2.

**Preparation of (S)-1-[2-(Cyclohexyl(hydroxymethyl)phenylsilyl)ethyl]-1-methylhexamethyleniminium Iodide [(S)-6c].** This compound was prepared analogously to the synthesis of *rac*-**6a** by addition of methyl iodide (204 mg, 1.44 mmol) to a solution of (S)-**5c** (250 mg, 723 μmol) in acetone (40 mL). (S)-**6c** was isolated in 83% yield as a colorless crystalline solid (294 mg, 603 μmol); mp 176–177 °C. The NMR and MS data of the product were identical with those obtained for *rac*-**6c**.  $[\alpha]_{546}^{20} = +1.7$  (CHCl<sub>3</sub>, *c* = 1.0). Anal. Calcd for C<sub>22</sub>H<sub>38</sub>INOSi (M<sub>r</sub> = 487.5): C, 54.20; H, 7.86; N, 2.87; I, 26.03. Found: C, 54.6; H, 8.0; N, 3.0; I, 26.0.

**Preparation of *rac*-(Chloromethyl)cyclohexyl(methoxy)phenylsilane (*rac*-7).** Synthesis was as described in ref 1d.

**Preparation of *rac*-(Chloromethyl)cyclohexyl(phenyl)vinylsilane (*rac*-8).** A 1.0 M solution of vinylmagnesium bromide in THF (200 mL, 200 mmol of CH<sub>2</sub>=CHMgBr) was added dropwise at room temperature over 70 min to a stirred solution of *rac*-**7** (43.0 g, 160 mmol) in THF (200 mL). After heating under reflux for 6 h and stirring at room temperature for 14 h, a saturated aqueous NH<sub>4</sub>Cl solution (300 mL) was added to the reaction mixture at 0 °C. The organic phase was separated and the aqueous layer extracted with diethyl ether (4 × 200 mL). After drying of the combined organic extracts over anhydrous Na<sub>2</sub>SO<sub>4</sub> and removal of the solvent under reduced pressure, the residue was distilled *in vacuo* (Vigreux column) to give *rac*-**8** in 91% yield as a colorless liquid (38.6

g, 146 mmol); bp 101 °C/0.01 Torr. <sup>1</sup>H NMR (400.1 MHz, CDCl<sub>3</sub>): δ 1.2–1.4 and 1.7–1.9 (m, 11 H, SiC<sub>6</sub>H<sub>11</sub>), 3.17 (s, 2 H, SiCH<sub>2</sub>Cl), 5.95 (dd, *J*<sub>gem</sub> = 5.9 Hz, *J*<sub>trans</sub> = 18.2 Hz, 1 H, SiCH=CHH), 6.29 (dd, *J*<sub>gem</sub> = 5.9 Hz, *J*<sub>cis</sub> = 14.9 Hz, 1 H, SiCH=CHH), 6.34 (dd, *J*<sub>cis</sub> = 14.9 Hz, *J*<sub>trans</sub> = 18.2 Hz, 1 H, SiCH=CH<sub>2</sub>), 7.4–7.7 (m, 5 H, SiC<sub>6</sub>H<sub>5</sub>). <sup>13</sup>C NMR (100.6 MHz, CDCl<sub>3</sub>): δ 22.9 (C-1, SiC<sub>6</sub>H<sub>11</sub>), 26.7, 26.8, 27.3 (2 C), 27.91, and 27.94 (CCH<sub>2</sub>C, SiCH<sub>2</sub>Cl), 127.9 (C-3/C-5, SiC<sub>6</sub>H<sub>5</sub>), 129.7 (C-4, SiC<sub>6</sub>H<sub>5</sub>), 131.5 (SiCH=CH<sub>2</sub>), 132.7 (C-1, SiC<sub>6</sub>H<sub>5</sub>), 135.0 (C-2/C-6, SiC<sub>6</sub>H<sub>5</sub>), 136.4 (SiCH=CH<sub>2</sub>). EI MS: *m/z* 264 (5, M<sup>+</sup>), 215 (67, M<sup>+</sup> - CH<sub>2</sub>Cl), 181 (18, M<sup>+</sup> - C<sub>6</sub>H<sub>11</sub>), 133 (100, C<sub>8</sub>H<sub>9</sub>-Si<sup>+</sup>). Anal. Calcd for C<sub>15</sub>H<sub>21</sub>ClSi (M<sub>r</sub> = 264.9): C, 68.02; H, 7.99. Found: C, 68.1; H, 8.1.

**Preparation of *rac*-(Acetoxymethyl)cyclohexyl(phenyl)vinylsilane (*rac*-9).** A mixture of *rac*-**8** (15.0 g, 56.7 mmol) and sodium acetate (4.65 g, 56.7 mmol) in DMF (65 mL) was stirred under reflux for 5 h. The mixture was cooled to room temperature, the precipitate filtered off, and the solvent removed under reduced pressure. The residue was distilled *in vacuo* (Vigreux column) to give *rac*-**9** in 92% yield as a colorless liquid (15.1 g, 52.3 mmol); bp 110 °C/0.01 Torr. <sup>1</sup>H NMR (400.1 MHz, CDCl<sub>3</sub>): δ 1.1–1.3 and 1.7–1.9 (m, 11 H, SiC<sub>6</sub>H<sub>11</sub>), 2.02 (s, 3 H, CCH<sub>3</sub>), 4.17 (δ<sub>A</sub>) and 4.19 (δ<sub>B</sub>) (AB system, *J*<sub>AB</sub> = 14.5 Hz, 2 H, SiCH<sub>2</sub>O), 5.88 (dd, *J*<sub>gem</sub> = 5.3 Hz, *J*<sub>trans</sub> = 18.6 Hz, 1 H, SiCH=CHH), 6.21 (dd, *J*<sub>gem</sub> = 5.3 Hz, *J*<sub>cis</sub> = 14.7 Hz, 1 H, SiCH=CHH), 6.28 (dd, *J*<sub>cis</sub> = 14.7 Hz, *J*<sub>trans</sub> = 18.6 Hz, 1 H, SiCH=CH<sub>2</sub>), 7.35–7.65 (m, 5 H, SiC<sub>6</sub>H<sub>5</sub>). <sup>13</sup>C NMR (100.6 MHz, CDCl<sub>3</sub>): δ 20.8 (CCH<sub>3</sub>), 23.3 (C-1, SiC<sub>6</sub>H<sub>11</sub>), 26.7 (CCH<sub>2</sub>C), 27.4 (2 C) (CCH<sub>2</sub>C), 27.9 (2 C) (CCH<sub>2</sub>C), 53.3 (SiCH<sub>2</sub>O), 127.8 (C-3/C-5, SiC<sub>6</sub>H<sub>5</sub>), 129.5 (C-4, SiC<sub>6</sub>H<sub>5</sub>), 131.6 (SiCH=CH<sub>2</sub>), 132.8 (C-1, SiC<sub>6</sub>H<sub>5</sub>), 134.8 (C-2/C-6, SiC<sub>6</sub>H<sub>5</sub>), 136.0 (SiCH=CH<sub>2</sub>), 171.7 (CO). EI MS: *m/z* 261 (8, M<sup>+</sup> - CH=CH<sub>2</sub>), 211 (12, M<sup>+</sup> - C<sub>6</sub>H<sub>5</sub>), 205 (100, M<sup>+</sup> - C<sub>6</sub>H<sub>11</sub>), 133 (60, C<sub>8</sub>H<sub>9</sub>Si<sup>+</sup>). Anal. Calcd for C<sub>17</sub>H<sub>24</sub>O<sub>2</sub>Si (M<sub>r</sub> = 288.5): C, 70.78; H, 8.39. Found: C, 70.7; H, 8.3.

**Preparation of *rac*-(Cyclohexyl(hydroxymethyl)phenyl(vinyl)silane (*rac*-10).** A solution of *rac*-**9** (36.4 g, 126 mmol) in diethyl ether (300 mL) was added dropwise at -30 °C over 2 h to a stirred suspension of lithium aluminum hydride (9.57 g, 252 mmol) in diethyl ether (500 mL). The mixture was stirred at -30 °C for 30 min and then added in 20-mL portions (-30 °C) to ice-cold 18% hydrochloric acid (1.0 L). The organic phase was separated and the aqueous layer extracted with diethyl ether (4 × 500 mL). After drying of the combined organic extracts over anhydrous Na<sub>2</sub>SO<sub>4</sub> and removal of the solvent under reduced pressure, the residue was distilled *in vacuo* (Vigreux column) to give *rac*-**10** in 92% yield as a colorless liquid (28.7 g, 116 mmol); bp 105 °C/0.01 Torr. <sup>1</sup>H NMR (400.1 MHz, CDCl<sub>3</sub>): δ 1.1 (br s, 1 H, OH), 1.1–1.4 and 1.6–1.9 (m, 11 H, SiC<sub>6</sub>H<sub>11</sub>), 3.79 (s, 2 H, SiCH<sub>2</sub>O), 5.93 (dd, *J*<sub>gem</sub> = 5.4 Hz, *J*<sub>trans</sub> = 18.7 Hz, 1 H, SiCH=CHH), 6.25 (dd, *J*<sub>gem</sub> = 5.4 Hz, *J*<sub>cis</sub> = 14.9 Hz, 1 H, SiCH=CHH), 6.32 (dd, *J*<sub>cis</sub> = 14.9 Hz, *J*<sub>trans</sub> = 18.7 Hz, 1 H, SiCH=CH<sub>2</sub>), 7.35–7.65 (m, 5 H, SiC<sub>6</sub>H<sub>5</sub>). <sup>13</sup>C NMR (100.6 MHz, CDCl<sub>3</sub>): δ 23.1 (C-1, SiC<sub>6</sub>H<sub>11</sub>), 26.8 (CCH<sub>2</sub>C), 27.6 (2 C) (CCH<sub>2</sub>C), 27.9 (CCH<sub>2</sub>C), 28.0 (CCH<sub>2</sub>C), 51.7 (SiCH<sub>2</sub>O), 127.9 (C-3/C-5, SiC<sub>6</sub>H<sub>5</sub>), 129.5 (C-4, SiC<sub>6</sub>H<sub>5</sub>), 132.2 (SiCH=CH<sub>2</sub>), 133.4 (C-1, SiC<sub>6</sub>H<sub>5</sub>), 135.0 (C-2/C-6, SiC<sub>6</sub>H<sub>5</sub>), 136.1 (SiCH=CH<sub>2</sub>). EI MS: *m/z* 246 (2, M<sup>+</sup>), 215 (52, M<sup>+</sup> - CH<sub>2</sub>OH), 163 (74, M<sup>+</sup> - C<sub>6</sub>H<sub>11</sub>), 133 (100, C<sub>8</sub>H<sub>9</sub>Si<sup>+</sup>). Anal. Calcd for C<sub>15</sub>H<sub>22</sub>O<sub>2</sub>Si (M<sub>r</sub> = 246.4): C, 73.11; H, 9.00. Found: C, 73.1; H, 9.0.

**Preparation of *rac*-(Cyclohexyl(phenyl)(trimethylsilyloxy)methyl)vinylsilane (*rac*-11).** A solution of chlorotrimethylsilane (52.2 g, 480 mmol) in *n*-pentane (270 mL) was added dropwise at -30 °C over 100 min to a stirred solution of *rac*-**10** (29.6 g, 120 mmol) and triethylamine (13.0 g, 128 mmol) in *n*-pentane (430 mL). The solution was allowed to warm up to room temperature and then stirred for 19 h. The precipitate was filtered off, the solvent removed under reduced pressure, and the residue distilled *in vacuo* (Vigreux column) to give *rac*-**11** in 84% yield as a colorless liquid (32.3 g, 101 mmol); bp 86 °C/0.01 Torr. <sup>1</sup>H NMR (400.1 MHz, CDCl<sub>3</sub>): δ

**Table 5. Atomic Coordinates ( $\times 10^4$ ) and Equivalent Isotropic Displacement Parameters ( $\text{pm}^2 \times 10^{-1}$ ) for (R)-6b**

atom	x	y	z	$U(\text{eq})^a$
I	2892.4(2)	9270.0(2)	4778.5(1)	31.6(1)
Si	2224.9(7)	5109.1(6)	3853.7(2)	19.7(1)
O	-783(2)	5079(2)	4049.7(7)	45.1(5)
C(1)	391(3)	6094(3)	3945.5(9)	31.8(5)
C(2)	3139(2)	4790(2)	4470.6(7)	22.7(4)
C(3)	2122(2)	4031(2)	4836.2(6)	19.5(3)
N	2666(2)	4032(2)	5369.3(6)	16.1(3)
C(4)	4187(2)	3347(3)	5394.8(8)	25.3(5)
C(5)	2695(3)	5586(2)	5560.1(7)	24.4(4)
C(6)	3013(3)	5653(3)	6105.6(7)	32.3(5)
C(7)	1876(3)	4763(3)	6396.6(8)	34.4(6)
C(8)	1836(3)	3199(3)	6214.1(8)	28.0(5)
C(9)	1553(2)	3145(2)	5661.7(8)	22.2(4)
C(10)	1782(2)	3342(2)	3535.9(7)	22.1(4)
C(11)	765(3)	3316(3)	3143.6(9)	31.6(5)
C(12)	437(3)	2034(3)	2898.0(10)	40.3(6)
C(13)	1085(3)	733(3)	3042.0(9)	36.2(5)
C(14)	2068(3)	718(3)	3434.3(8)	31.1(4)
C(15)	2417(2)	2012(2)	3675.8(8)	24.4(5)
C(16)	3565(2)	6232(2)	3473.4(7)	20.9(4)
C(17)	2858(3)	6710(2)	2985.9(7)	26.3(4)
C(18)	3922(3)	7625(3)	2675.9(8)	30.4(5)
C(19)	5378(3)	6817(3)	2578.6(9)	33.7(6)
C(20)	6114(3)	6348(3)	3058.5(9)	32.7(5)
C(21)	5057(2)	5451(2)	3378.6(8)	25.8(5)

<sup>a</sup> The equivalent isotropic displacement parameter  $U(\text{eq})$  is defined as one-third of the trace of the orthogonalized  $U_{ij}$  tensor.

0.10 (s, 9 H, SiCH<sub>3</sub>), 1.1–1.4 and 1.7–1.9 (m, 11 H, SiC<sub>6</sub>H<sub>11</sub>), 3.69 (s, 2 H, SiCH<sub>2</sub>O), 5.58 (dd,  $J_{\text{gem}} = 5.1$  Hz,  $J_{\text{trans}} = 19.2$  Hz, 1 H, SiCH=CHH), 6.20 (dd,  $J_{\text{gem}} = 5.1$  Hz,  $J_{\text{cis}} = 14.9$  Hz, 1 H, SiCH=CHH), 6.32 (dd,  $J_{\text{cis}} = 14.9$  Hz,  $J_{\text{trans}} = 19.2$  Hz, 1 H, SiCH=CH<sub>2</sub>), 7.35–7.7 (m, 5 H, SiC<sub>6</sub>H<sub>5</sub>). <sup>13</sup>C NMR (100.6 MHz, CDCl<sub>3</sub>):  $\delta$  -0.8 (SiCH<sub>3</sub>), 23.3 (C-1, SiC<sub>6</sub>H<sub>11</sub>), 27.0 (CCH<sub>2</sub>C), 27.6 (2 C) (CCH<sub>2</sub>C), 28.1 (CCH<sub>2</sub>C), 28.2 (CCH<sub>2</sub>C), 51.5 (SiCH<sub>2</sub>O), 127.6 (C-3/C-5, SiC<sub>6</sub>H<sub>5</sub>), 129.2 (C-4, SiC<sub>6</sub>H<sub>5</sub>), 133.0 (SiCH=CH<sub>2</sub>), 134.6 (C-1, SiC<sub>6</sub>H<sub>5</sub>), 135.1 (C-2/C-6, SiC<sub>6</sub>H<sub>5</sub>), 135.3 (SiCH=CH<sub>2</sub>). EI MS:  $m/z$  318 (1, M<sup>+</sup>), 235 (99, M<sup>+</sup> - C<sub>6</sub>H<sub>11</sub>), 133 (100, C<sub>8</sub>H<sub>9</sub>Si<sup>+</sup>). Anal. Calcd for C<sub>18</sub>H<sub>30</sub>O<sub>2</sub>Si<sub>2</sub> (M<sub>r</sub> = 318.6): C, 67.86; H, 9.49. Found: C, 67.8; H, 9.5.

**Crystal Structure Analysis of (R)-6b.** Intensities were measured with monochromatized Mo K $\alpha$  radiation on a Stoe STADI-4 diffractometer equipped with a Siemens LT-2 low-temperature attachment. The structure was solved by the heavy-atom method and refined anisotropically on  $F^2$  (program SHELXL-93, G. M. Sheldrick, University of Göttingen). Hydrogen atoms were included with a riding model except for methyl or hydroxyl H (rigid groups). The absolute configuration was determined by an  $x$  refinement;<sup>7</sup>  $x$  refined to -0.028-(12). For further details, see Table 1. The atomic coordinates and equivalent isotropic displacement parameters for (R)-6b are listed in Table 5; the atomic numbering scheme is given in Figure 1. Tables of anisotropic thermal parameters, atomic coordinates for the hydrogen atoms, and complete lists of bond distances and angles are provided as supplementary material.

**NMR-Spectroscopic Determination of the Enantiomeric Purities of the Antipodes of 5a-c.** The enantiomeric purities of the (R)- and (S)-enantiomers of 5a-c were determined by NMR experiments using the chiral shift reagents (-)-2,2,2-trifluoro-1-(9-anthryl)ethanol [(-)-TFAE] (<sup>1</sup>H

NMR) and (+)-tris[3-(2,2,3,3,4,4,4-heptafluoro-1-hydroxybutylidene)-*d*-camphorato]europium(III) [(+)-Eu(hfc)<sub>3</sub>] (<sup>13</sup>C NMR). (-)-TFAE and (+)-Eu(hfc)<sub>3</sub> were purchased from Sigma and Aldrich, respectively. The NMR spectra were recorded at room temperature on a Bruker AM-400 NMR spectrometer operating at 400.1 MHz (<sup>1</sup>H) and 100.6 MHz (<sup>13</sup>C), respectively. The composition of the samples used for the <sup>1</sup>H NMR experiments was as follows: 30.2  $\mu\text{mol}$  of 5a-c, 152  $\mu\text{mol}$  of (-)-TFAE, 0.5 mL of CDCl<sub>3</sub>. The composition of the samples used for the <sup>13</sup>C NMR experiments was as follows: 90.5  $\mu\text{mol}$  of 5a-c, 45.2  $\mu\text{mol}$  of (+)-Eu(hfc)<sub>3</sub>, 0.5 mL of CDCl<sub>3</sub>.

**Functional Pharmacological Studies.** As a measure of affinity, pA<sub>2</sub> values of the pure (R)- and (S)-enantiomers of 5a-c and 6a-c were determined at muscarinic M1 receptors in rabbit vas deferens [1-[4-[(4-fluorophenyl)carbamoyloxy]-2-butyn-1-yl]-1-methylpyrrolidinium tosylate (4-F-PyMcN<sup>+</sup>) as agonist], M2 receptors in guinea-pig atria, and M3 receptors in guinea-pig ileum (arecaidine propargyl ester as agonist) according to published procedures.<sup>18</sup> Concentration-response curves of the agonists were constructed in the absence and in the presence of the antagonists [(R)- and (S)-enantiomers of 5a-c and 6a-c]. Dose ratios calculated from the respective EC<sub>50</sub> values of the agonists were used to perform a Schild analysis.<sup>8</sup> Since the Arunlakshana-Schild plots of all the compounds investigated were linear and the slopes of the regression lines were not significantly different from unity, pA<sub>2</sub> values were estimated as the intercept on the abscissa scale by fitting to the data the best straight line with a slope of unity (constrained plot).<sup>9</sup> The pA<sub>2</sub> values given in Table 2 correspond to -log K<sub>D</sub> values (K<sub>D</sub> = dissociation constant of the antagonist-receptor complex).

**Radioligand Binding Studies.** Radioligand binding studies of the pure (R)- and (S)-enantiomers of 5a-c and 6a-c were carried out with homogenates of human NB-OK 1 neuroblastoma cells (M1 receptors), as well as with homogenates of rat heart (M2 receptors), rat pancreas (M3 receptors), and rat striatum (M4 receptors). The radioligand was [<sup>3</sup>H]-N-methylscopolamine (0.24–1.0 nM). Data of the binding experiments were analyzed by an iterative curve fitting procedure. Dissociation constants (K<sub>i</sub> values) of the (R)- and (S)-enantiomers of 5a-c and 6a-c were determined from IC<sub>50</sub> values obtained from competition curves. The pK<sub>i</sub> values given in Table 3 correspond to -log K<sub>i</sub> values. For more experimental details, see ref 1f,i.

**Acknowledgment.** This work was supported by the Volkswagen-Stiftung (R.T.), the Fonds der Chemischen Industrie (G.L., R.T.), the Fonds de la Recherche Scientifique Médical (M.W.), and the Bayer AG, Germany (R.T.).

**Supplementary Material Available:** Tables of anisotropic thermal parameters, atomic coordinates for the hydrogen atoms, and complete lists of bond distances and angles for (R)-6b (6 pages). Ordering information is given on any current masthead page.

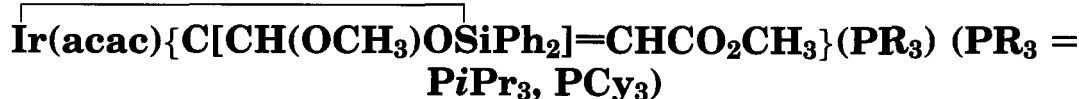
OM940667S

(8) Arunlakshana, O.; Schild, H. O. *Br. J. Pharmacol.* **1959**, *14*, 48–85.

(9) Tallarida, R. J.; Murray, R. B. *Manual of Pharmacologic Calculations with Computer Programs*; Springer: Berlin, 1986.

(7) Flack, H. D. *Acta Crystallogr. Ser. A* **1983**, *39*, 876–881.

# Addition of H<sub>2</sub>SiPh<sub>2</sub> to Ir(acac)(η<sup>2</sup>-CH<sub>3</sub>O<sub>2</sub>C–C≡C–CO<sub>2</sub>CH<sub>3</sub>)(PR<sub>3</sub>): Synthesis and Characterization of



Miguel A. Esteruelas,\* Fernando J. Lahoz, Enrique Oñate, Luis A. Oro, and  
Laura Rodríguez

*Departamento de Química Inorgánica, Instituto de Ciencia de Materiales de Aragón,  
Universidad de Zaragoza-Consejo Superior de Investigaciones Científicas,  
50009 Zaragoza, Spain*

Received August 5, 1994<sup>®</sup>

The complexes Ir(acac)(cyclooctene)(PR<sub>3</sub>) (PR<sub>3</sub> = PiPr<sub>3</sub> (2), PCy<sub>3</sub> (3)), which are prepared by reaction of Ir(acac)(cyclooctene)<sub>2</sub> (1) with the corresponding phosphine, react with carbon monoxide and acetylenedicarboxylic methyl ester to give Ir(acac)(CO)(PR<sub>3</sub>) (PR<sub>3</sub> = PiPr<sub>3</sub> (4), PCy<sub>3</sub> (5)) and Ir(acac)(η<sup>2</sup>-CH<sub>3</sub>O<sub>2</sub>C–C≡C–CO<sub>2</sub>CH<sub>3</sub>)(PR<sub>3</sub>) (PR<sub>3</sub> = PiPr<sub>3</sub> (6), PCy<sub>3</sub> (7)). The reactions of 6 and 7 with H<sub>2</sub>SiPh<sub>2</sub> afford Ir(acac){C[CH(OCH<sub>3</sub>)OSiPh<sub>2</sub>]=CHCO<sub>2</sub>CH<sub>3</sub>}(PR<sub>3</sub>) (PR<sub>3</sub> = PiPr<sub>3</sub> (8), PCy<sub>3</sub> (9)). The X-ray crystal structure analysis of 9 (monoclinic, space group P2<sub>1</sub>/c with a = 21.408(1) Å, b = 10.246(1) Å, c = 18.983(1) Å, and β = 106.89(1)°) reveals that the bonding situation in the Ir–Si–O sequence could be described as an intermediate state between metal–silylene stabilized by an oxygen base and a tetrahedral silicon.

## Introduction

The mechanisms of type Chalk–Harrod and their variants employ conventional oxidative addition, insertion, and reductive elimination steps to explain the hydrosilylation of olefins and alkynes.<sup>1</sup> The design of new catalysts requires a basic knowledge of the leading factors of these elementary steps. In this respect, the reactions of π-olefin<sup>2</sup> and π-alkyne<sup>3</sup> transition metal complexes with silanes are of great interest.

We have previously reported that square-planar complexes of the types Ir(OR')(COD)(PR<sub>3</sub>)<sup>4</sup> (COD = 1,5-cyclooctadiene) and Ir(η<sup>1</sup>-OC(O)CH<sub>3</sub>)(TFB)(PR<sub>3</sub>)<sup>5</sup> (TFB

= tetrafluorobenzobarrelene) react with tertiary silanes (HSiR''<sub>3</sub>) to give the dihydridosilyl derivatives IrH<sub>2</sub>–(SiR''<sub>3</sub>)(diolefin)(PR<sub>3</sub>), which have been found to promote silicon–carbon bond formation in hydrosilylation and dehydrogenative silylation of olefins<sup>6</sup> and alkynes.<sup>5</sup> Furthermore, we have observed that the reactions of Ir(η<sup>1</sup>-OC(O)CH<sub>3</sub>)(TFB)(PR<sub>3</sub>) with H<sub>2</sub>SiPh<sub>2</sub> afford IrH<sub>2</sub>{Si(OC(O)CH<sub>3</sub>)Ph<sub>2</sub>}(TFB)(PR<sub>3</sub>) (PR<sub>3</sub> = PiPr<sub>3</sub>, PCy<sub>3</sub>, PPh<sub>3</sub>), which are the first iridium compounds containing an acetoxysilyl ligand.<sup>5</sup>

As a continuation of our work in this field, we have now prepared the complexes Ir(acac)(η<sup>2</sup>-CH<sub>3</sub>O<sub>2</sub>C–C≡C–CO<sub>2</sub>CH<sub>3</sub>)(PR<sub>3</sub>) (PR<sub>3</sub> = PiPr<sub>3</sub>, PCy<sub>3</sub>) and investigated their reactivity toward H<sub>2</sub>SiPh<sub>2</sub>. As a result of this study, we have isolated the derivatives Ir(acac){C[CH(OCH<sub>3</sub>)OSiPh<sub>2</sub>]=CHCO<sub>2</sub>CH<sub>3</sub>}(PR<sub>3</sub>) (PR<sub>3</sub> = PiPr<sub>3</sub>, PCy<sub>3</sub>), which are the first examples of compounds containing a chelate silylvinyl ligand. In this paper, we report the synthesis and characterization of these (silylvinyl)iridium(III) complexes.

## Results and Discussion

On treatment with PiPr<sub>3</sub> and PCy<sub>3</sub>, the bis(cyclooctene)iridium complex 1 (Scheme 1) affords the phos-

<sup>®</sup> Abstract published in *Advance ACS Abstracts*, November 1, 1994.

(1) (a) Chalk, A. J.; Harrod, J. F. *J. Am. Chem. Soc.* **1965**, *87*, 16. (b) Schroeder, M.; Wrighton, M. S. *J. Organomet. Chem.* **1977**, *128*, 345. (c) Dickers, H. M.; Haszeldine, R. N.; Mather, A. P.; Parish, R. V. *J. Organomet. Chem.* **1978**, *161*, 91. (d) Randolph, C. L.; Wrighton, M. S. *J. Am. Chem. Soc.* **1986**, *108*, 3366. (e) Seitz, F.; Wrighton, M. S. *Angew. Chem., Int. Ed. Engl.* **1988**, *27*, 289. (f) Ojima, I.; Clos, N.; Donovan, R. J.; Ingallina, P. *Organometallics* **1990**, *9*, 3127. (g) Esteruelas, M. A.; Oro, L. A.; Valero, C. *Organometallics* **1991**, *10*, 462. (h) Duckett, S. B.; Perutz, R. N. *Organometallics* **1992**, *11*, 90. (i) Esteruelas, M. A.; Herrero, J.; Oro, L. A. *Organometallics* **1993**, *12*, 2377.

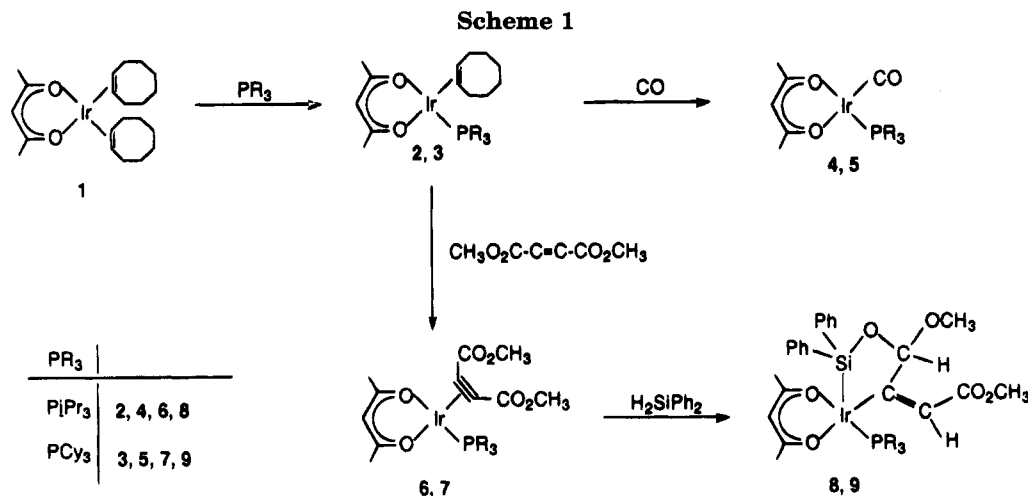
(2) (a) Haddleton, D. M.; Perutz, R. N. *J. Chem. Soc., Chem. Commun.* **1985**, 1372. (b) Bentz, P. O.; Ruiz, J.; Mann, B. E.; Spencer, C. M.; Maitlis, P. M. *J. Chem. Soc., Chem. Commun.* **1985**, 1374. (c) Ruiz, J.; Bentz, P. O.; Mann, B. E.; Spencer, C. M.; Taylor, B. F.; Maitlis, P. M. *J. Chem. Soc., Dalton Trans.* **1987**, 2709. (d) Duckett, S. B.; Haddleton, D. M.; Jackson, S. A.; Perutz, R. N.; Poliakov, M.; Upmacis, R. K. *Organometallics* **1988**, *7*, 1526. (e) Tanke, R. S.; Crabtree, R. H. *J. Chem. Soc., Chem. Commun.* **1990**, 1056. (f) Duckett, S. B.; Perutz, R. N. *J. Chem. Soc., Chem. Commun.* **1991**, 28.

(3) (a) Glockling, F.; Hooton, K. A. *J. Chem. Soc. A* **1967**, 1066. (b) Eaborn, C.; Metham, T. N.; Pidcock, A. *J. Organomet. Chem.* **1973**, *63*, 107. (c) Kiso, Y.; Tamao, K.; Kumada, M. *J. Organomet. Chem.* **1974**, *76*, 105. (d) Eaborn, C.; Metham, T. N.; Pidcock, A. *J. Organomet. Chem.* **1977**, *131*, 377. (e) Yamashita, H.; Tanaka, M.; Goto, M. *Organometallics* **1993**, *12*, 988.

(4) (a) Fernández, M. J.; Esteruelas, M. A.; Oro, L. A.; Apreda, M. C.; Foces-Foces, C.; Cano, F. H. *Organometallics* **1987**, *6*, 1751. (b) Fernández, M. J.; Esteruelas, M. A.; Covarrubias, M.; Oro, L. A.; Apreda, M. C.; Foces-Foces, C.; Cano, F. H. *Organometallics* **1989**, *8*, 1158.

(5) Esteruelas, M. A.; Nürnberg, O.; Oliván, M.; Oro, L. A.; Werner, H. *Organometallics* **1993**, *12*, 3264.

(6) (a) Fernández, M. J.; Esteruelas, M. A.; Jiménez, M. S.; Oro, L. A. *Organometallics* **1986**, *5*, 1519. (b) Oro, L. A.; Fernández, M. J.; Esteruelas, M. A.; Jiménez, M. S. *J. Mol. Catal.* **1986**, *37*, 151.



phine derivatives **2** and **3** in good yield. The reactions proceed at room temperature and do not lead to the displacement of the second olefin even if an excess of phosphine is used. The complexes **2** and **3**, which are yellow air-sensitive solids, are stable for 1 week if kept under argon at  $-20\text{ }^{\circ}\text{C}$ . The cyclooctene ligand of **2** and **3** is easily displaced by stronger  $\pi$ -acceptor ligands such as carbon monoxide and acetylenedicarboxylic methyl ester. By passing a slow stream of carbon monoxide through toluene solutions of **2** and **3**, the carbonyl complexes **4**<sup>7</sup> and **5** are formed. Similarly, treatment of hexane suspensions of **2** and **3** with stoichiometric amounts of acetylenedicarboxylic methyl ester affords **6** and **7** as orange solids in 76 and 73% yield, respectively.

The presence of the  $\pi$ -alkyne ligand in **6** and **7** can be inferred from the IR and  $^1\text{H}$  and  $^{13}\text{C}\{^1\text{H}\}$  NMR spectra of these compounds. The IR spectra show strong absorptions at 1820 (**6**) and 1860 (**7**)  $\text{cm}^{-1}$ , which are characteristic of  $\nu(\text{C}\equiv\text{C})$  vibrations. The  $^1\text{H}$  NMR spectra in benzene- $d_6$  contain singlets at about 3.5 ppm, due to the methyl groups of the acetylenedicarboxylic methyl ester. In the  $^{13}\text{C}\{^1\text{H}\}$  NMR spectra, the acetylenic carbon atoms appear at about 74 ppm as doublets with P–C coupling constants of 4 Hz. Singlets at 14.9 and 4.5 ppm, in the  $^{31}\text{P}\{^1\text{H}\}$  NMR spectra, are also characteristic of the new derivatives **6** and **7**, respectively.

Complexes **6** and **7** react with the stoichiometric amount of diphenylsilane, in hexane at room temperature to give after 12 h yellow solids in 41 and 53% yield. The IR and  $^1\text{H}$ ,  $^{13}\text{C}\{^1\text{H}\}$ , and  $^{31}\text{P}\{^1\text{H}\}$  spectra of these solids suggest that the products obtained from these reactions are the silylvinyl complexes **8** and **9** (Scheme 1), which are a result of a net transformation involving addition of one Si–H bond across the C=O and another across the alkyne triple bond.

The IR spectra in Nujol of both complexes show two strong  $\nu(\text{CO})$  absorptions between 1565 and 1520  $\text{cm}^{-1}$ , indicating that the acetylacetonato ligands are coordinated in a  $\eta^2$ -oxygen bonding mode.<sup>8</sup> Furthermore, bands at about 1700, 1580, and 1020  $\text{cm}^{-1}$  which can be assigned to the vibrations  $\nu(\text{C}=\text{O})$ ,  $\nu(\text{C}=\text{C})$ , and

$\nu(\text{Si}-\text{O})$  of the silylvinyl ligands, are also observed. The proposal that the oxygen atom of the carbonyl group of the silylvinyl ligands does not coordinate to the iridium atom of both compounds is strongly supported by the values of the stretching frequency of the  $\nu(\text{C}=\text{O})$  bonds.

The  $^1\text{H}$  and  $^{13}\text{C}\{^1\text{H}\}$  NMR spectra of **8** and **9** suggest that these compounds have a rigid structure in solution at room temperature. Thus, the  $^1\text{H}$  NMR spectra of both complexes show two singlets at 1.8 and 1.1 ppm, indicating that the methyl groups of the acetylacetonato ligands are chemically inequivalent. Two singlets are also observed for the  $\text{OCH}_3$  groups, at 4.0 and 3.4 ppm. The  $\text{CH}=\text{C}$  and  $\text{CHO}_2$  protons appear as singlets at about 6.7 ppm. In agreement with the  $^1\text{H}$  NMR spectra, the  $^{13}\text{C}\{^1\text{H}\}$  NMR spectra contain a resonance for each carbonyl and methyl group of the acetylacetonato ligands (see Experimental Section). In addition, the resonances corresponding to the vinylic and  $\text{CHO}_2$  carbon atoms of the silylvinyl ligands should be mentioned. The vinylic carbon atom directly linked to the iridium center in both complexes appears at about 177 ppm, as a doublet with a P–C coupling constant of 7 Hz, while the  $\text{CH}=\text{C}$  carbon atoms are observed at 123.6 (**8**) and 124.2 (**9**) ppm as singlets. Similar chemical shifts have been found for related vinylic carbon atoms.<sup>9</sup> The  $\text{CHO}_2$  resonances appear at 107.5 (**8**) and 107.7 (**9**) ppm. Singlets at 1.8 (**8**) and  $-9.4$  (**9**) ppm, in the  $^{31}\text{P}\{^1\text{H}\}$  NMR spectra, are also characteristic of these compounds.

In five-coordinate complexes of  $d^6$  electron configuration, the ground state geometry can be trigonal bipyramidal or square pyramidal. So, in order to determine the coordination polyhedron around the iridium atom and to get additional information on the bonding parameters of **8** and **9**, a single-crystal X-ray diffraction analysis of **9** was carried out.

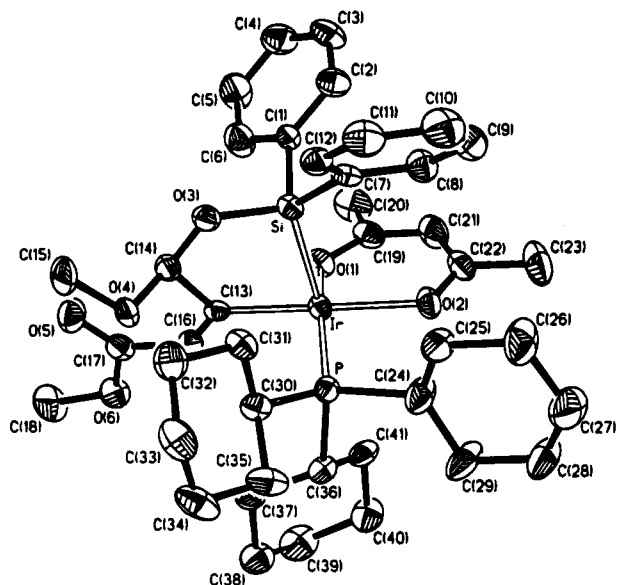
An ORTEP drawing of the molecule of **9** is presented in Figure 1. Selected bond distances and angles are listed in Table 1. The iridium atom is coordinated in a distorted square-pyramidal arrangement. The basis of the pyramid is defined by the oxygens of the acac ligand, the P atom of the phosphine, and the vinylic C(13) atom, showing significant deviations from the calculated least-squares plane: 0.139(4), 0.135(5), 0.016(2), and 0.228(5) Å, respectively. The metal is also out of this

(7) The synthesis of the carbonyl complex **4** has been previously reported. See: Papenfuhs, B.; Mahr, N.; Werner, H. *Organometallics* **1993**, *12*, 4244.

(8) Oro, L. A.; Carmona, D.; Esteruelas, M. A.; Foces-Foces, C.; Cano, F. H. *J. Organomet. Chem.* **1986**, *307*, 83.

(9) (a) Werner, H.; Esteruelas, M. A.; Otto, H. *Organometallics* **1986**, *5*, 2295. (b) Poulton, J. T.; Sigalas, M. P.; Eisenstein, O.; Caulton, K. G. *Inorg. Chem.* **1993**, *32*, 5490.





**Figure 1.** ORTEP diagram of  $\text{Ir}(\text{acac})\{\text{C}[\text{CH}(\text{OCH}_3)\text{OSiPh}_2]=\text{CHCO}_2\text{CH}_3\}(\text{PCy}_3)$  (**9**); 50% thermal ellipsoids are shown.

**Table 1.** Selected Bond Lengths (Å) and Angles (deg) for  $\text{Ir}(\text{acac})\{\text{C}[\text{CH}(\text{OCH}_3)\text{OSiPh}_2]=\text{CHCO}_2\text{CH}_3\}(\text{PCy}_3)$  (**9**)

Bond Lengths			
Ir-P	2.294(1)	O(4)-C(15)	1.429(9)
Ir-Si	2.264(2)	C(13)-C(14)	1.537(8)
Ir-O(1)	2.076(4)	C(13)-C(16)	1.347(8)
Ir-O(2)	2.111(5)	C(16)-C(17)	1.465(9)
Ir-C(13)	2.018(6)	O(5)-C(17)	1.208(8)
Si-O(3)	1.656(4)	O(6)-C(17)	1.360(8)
O(3)-C(14)	1.428(7)	O(6)-C(18)	1.439(10)
O(4)-C(14)	1.399(6)		
Bond Angles			
P-Ir-Si	103.38(5)	Si-Ir-O(2)	103.2(1)
P-Ir-O(1)	163.0(1)	Si-Ir-C(13)	79.2(2)
P-Ir-O(2)	89.6(1)	O(1)-Ir-O(2)	87.0(2)
P-Ir-C(13)	95.0(2)	O(1)-Ir-C(13)	87.5(2)
Si-Ir-O(1)	93.6(1)	O(2)-Ir-C(13)	174.2(2)
Ir-Si-O(3)	105.2(2)	O(3)-Si-C(1)	106.0(2)
Ir-Si-C(1)	110.0(2)	O(3)-Si-C(7)	109.2(2)
Ir-Si-C(7)	117.7(2)	C(1)-Si-C(7)	108.2(3)
Si-O(3)-C(14)	115.7(3)	Ir-C(13)-C(16)	120.0(4)
O(3)-C(14)-O(4)	108.7(4)	C(13)-C(16)-C(17)	128.0(5)
O(3)-C(14)-C(13)	111.6(5)	O(5)-C(17)-O(6)	121.4(6)
O(4)-C(14)-C(13)	110.0(4)	O(5)-C(17)-C(16)	129.1(6)
Ir-C(13)-C(14)	120.9(4)	O(6)-C(17)-C(16)	109.5(5)
C(14)-C(13)-C(16)	118.7(5)		

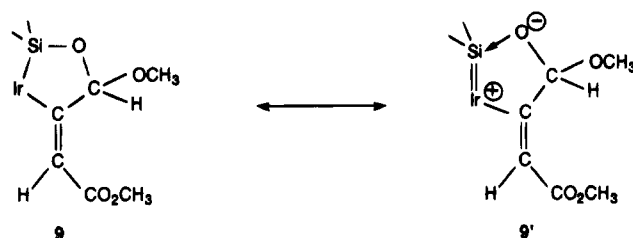
coordination plane, being shifted toward the apical position by 0.2372(3) Å. The Si atom, which occupies the apex, is also displaced toward the C(13) atom as a result of the ring constraint ( $\text{Si}-\text{Ir}-\text{C}(13) = 79.2(2)^\circ$ ).

The Ir-Si distance of 2.264(2) Å is significantly shorter than those determined previously for the six-coordinate iridium(III) complexes  $\text{IrH}_2(\text{SiEt}_3)(\text{COD})(\text{AsPh}_3)$  (2.414(2) Å),<sup>4a</sup>  $\text{IrH}_2(\text{SiMe}_2\text{Ph})(\text{CO})\{\text{P}(p\text{-tol})_3\}_2$  (2.414(2) Å),<sup>10</sup>  $\text{IrH}(\text{SiMe}_2\text{Cl})(\text{CO})(\text{dppe})$  (dppe = 1,2-bis(diphenylphosphino)ethane) (2.396(2) Å),  $\text{IrH}(\text{SiEtF}_2)_2(\text{CO})(\text{dppe})$  (2.360(10) Å),<sup>11</sup> and  $\text{IrH}(\text{Ph}_2\text{SiC}_6\text{H}_4)(\text{PMe}_3)_3$  (2.404(3) Å).<sup>12</sup> However, it is similar to those found in the complexes  $\text{IrHCl}(\text{SiMeCl}_2)(\text{P}i\text{Pr}_3)_2$  (2.235(5) Å)<sup>13</sup> and

(10) Rappoli, B. J.; Janik, T. S.; Churchill, M. R.; Thompson, J. S.; Atwood, J. D. *Organometallics* **1988**, *7*, 1939.

(11) Hays, M. K.; Eisenberg, R. *Inorg. Chem.* **1991**, *30*, 2623.

**Scheme 2**



$\text{IrCl}_2(\text{SiMeCl}_2)(\text{PMe}_3)_3$  (2.299(5) Å),<sup>14</sup> where it has been proposed that the high electron density of the iridium center and the  $\pi$ -accepting properties of  $\text{SiMeCl}_2$  ligand lead to a considerable back donation of  $d$  electron density to an acceptor orbital on silicon.

The short Ir-Si bond distance in **9**, which could be a reflection of the situation of the Si atom in the apical position of the metal coordination sphere with no *trans* ligand present, seems to suggest that for an adequate description of the bonding situation a second silylene resonance form such as **9'** (Scheme 2) may be considered.

This proposal is also supported by the Ir-Si-C(7) bond angle ( $117.2(2)^\circ$ ), which is close to the value expected for an  $\text{sp}^2$ -hybridized silicon. However, the Si-O(3) bond length (1.656(4) Å) lies in the upper part of the range of distances oxygen-tetrahedral silicon,<sup>15</sup> suggesting that the silylene character is minimal. The real bonding situation in complex **9** could be described as an intermediate state between a metal-silylene stabilized by an oxygen base and a tetrahedral silicon.

The Ir-C(13) distance (2.018(6) Å) is shorter than the Ir-C distances found in the iridium(III) complexes  $\text{IrH}(\text{CH}=\text{CH}_2)\text{Cl}(\eta^1\text{-}i\text{Pr}_2\text{PCH}_2\text{CH}_2\text{OCH}_3)_2$  (2.059(6) Å)<sup>18</sup> and  $\text{IrH}(\text{CH}=\text{CH}_2)(\eta^5\text{-C}_5\text{H}_5)(\text{PMe}_3)$  (2.054(4) Å),<sup>19</sup> but almost identical with that of the complex  $[\text{IrH}\{\text{C}(\text{COOCH}_3)=\text{CH}_2\}(\text{Hpz})(\text{PPh}_3)_2]\text{BF}_4$  (Hpz = pyrazole; 2.02(2) Å).<sup>20</sup> The C(13)-C(16) bond length (1.347(8) Å) compares well with the corresponding bond length in olefins (ca. 1.32 Å)<sup>21</sup> and supports the vinyl-metal formulation.

The reactions of **6** and **7** with  $\text{H}_2\text{SiPh}_2$  to give **8** and **9** merit further comment. Scheme 3 illustrates two plausible reaction routes that allow the formation of **8** and **9** to be rationalized. Path a involves the initial

(12) Aizenberg, M.; Milstein, D. *Angew. Chem., Int. Ed. Engl.* **1994**, *33*, 317.

(13) Yamashita, H.; Kawamoto, A. M.; Tanaka, M.; Goto, M. *Chem. Lett.* **1990**, 2107.

(14) Zlota, A. A.; Frolow, F.; Milstein, D. *J. Chem. Soc., Chem. Commun.* **1989**, 1826.

(15) Si-O single bonds in compounds of tetrahedral silicon normally fall in the range 1.63-1.66 Å,<sup>16</sup> whereas metal-silylene complexes stabilized by neutral oxygen bases have Si-O distances of about 1.74 Å.<sup>17</sup>

(16) Wiberg, N.; Wagner, G.; Müller, G.; Reide, J. *J. Organomet. Chem.* **1984**, *271*, 381.

(17) (a) Straus, D. A.; Tilley, T. D. *J. Am. Chem. Soc.* **1987**, *109*, 5872. (b) Ueno, K.; Tobita, H.; Shimoi, M.; Ogino, H. *J. Am. Chem. Soc.* **1988**, *110*, 4092. (c) Zybilla, C.; Müller, G. *Organometallics* **1988**, *7*, 1368. (d) Straus, D. A.; Zhang, C.; Quimbata, G. E.; Grumbine, S. D.; Heyn, R. H.; Tilley, T. D.; Rheingold, A. L.; Geib, S. J. *J. Am. Chem. Soc.* **1990**, *112*, 2673. (e) Woo, L. K.; Smith, D. A.; Young, Jr. V. G. *Organometallics* **1991**, *10*, 3977.

(18) Schulz, M.; Werner, H. *Organometallics* **1992**, *11*, 2790.

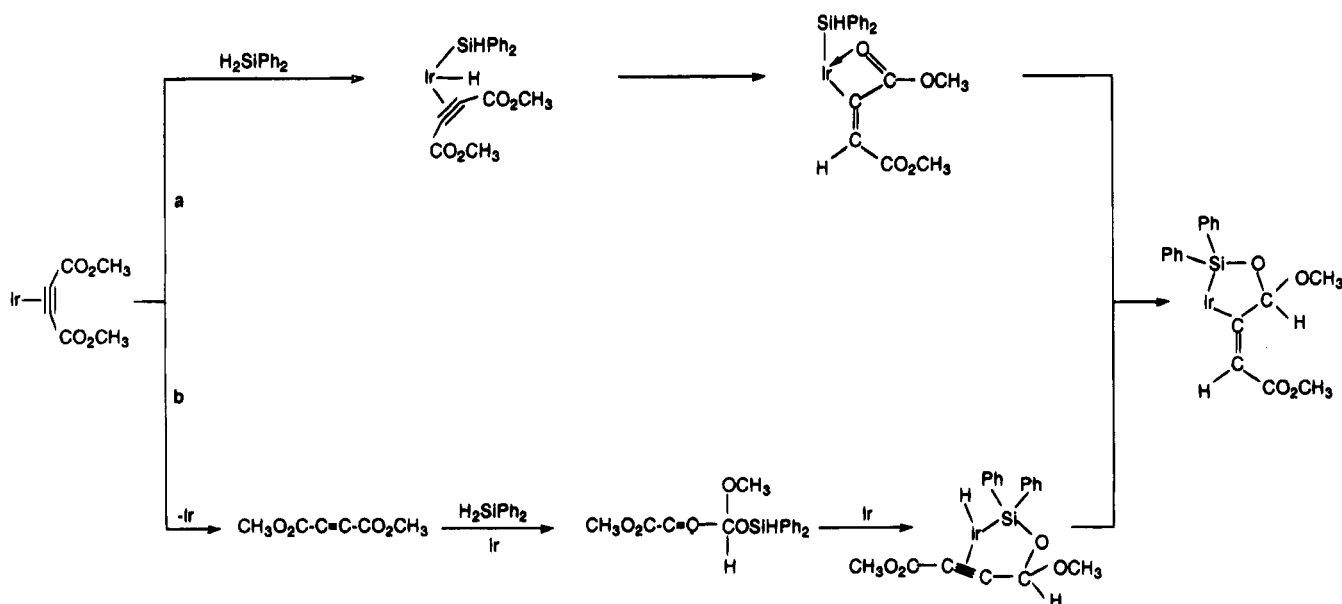
(19) (a) Stoutland, P. O.; Bergman, R. G. *J. Am. Chem. Soc.* **1985**, *107*, 4581. (b) Stoutland, P. O.; Bergman, R. G. *J. Am. Chem. Soc.* **1988**, *110*, 5732.

(20) Esteruelas, M. A.; García, M. P.; Martín, M.; Nürnberg, O.; Oro, L. A.; Werner, H. *J. Organomet. Chem.* **1994**, *466*, 249.

(21) Allen, F. H.; Kennard, O.; Watson, D. G.; Brammer, L.; Orpen, A. G.; Taylor, R. *J. Chem. Soc., Perkin Trans. 2* **1987**, 51.



Scheme 3



oxidative addition of the silane to the iridium(I) starting compounds to give hydride- $\pi$ -alkyne intermediates, which evolve, by insertion of the alkyne into the metal-hydrido bond, to (diphenylsilyl)-(vinyl)-iridium(III) species. The subsequent hydrosilylation of the carbonyl group of the ester at the  $\alpha$ -carbon atom of the vinyl ligand should afford **8** and **9**. Path b involves the initial dissociation of the alkyne, which undergoes selective hydrosilylation of the carbonyl group of one of the two esters.<sup>22</sup> The silane formed in this way reacts by oxidative addition to the metallic center. Subsequently, the insertion of the carbon-carbon triple bond into the iridium-hydrido bond should afford **8** and **9**.

When the mixtures of **6** and **7** with  $\text{H}_2\text{SiPh}_2$  were left to react for 20 min, the IR spectra of the obtained solids showed bands at 2120, 1715, and 1025  $\text{cm}^{-1}$  ( $\text{PiPr}_3$ ) and 2110, 1710, and 1015  $\text{cm}^{-1}$  ( $\text{PCy}_3$ ), which can be assigned to vibrations of Ir-H, C=O, and Si-O bonds, respectively. No  $\nu(\text{Si-H})$  absorptions were observed. This seems to suggest that path b is the main route in the formation of **8** and **9**. These solids could be intermedi-

ates of type  $\text{IrH}\{\eta^2\text{-C}(\text{CO}_2\text{CH}_3)=\text{C}(\text{OCH}_3)\text{OSiPh}_2\}$ . Unfortunately, characterization by NMR spectroscopy was not possible, because in benzene- $d_6$  solution they rapidly evolve to **8** and **9**.

### Concluding Remarks

The reactions of the complexes  $\text{Ir}(\text{acac})(\eta^2\text{-CH}_3\text{O}_2\text{C-C}\equiv\text{C-CO}_2\text{CH}_3)(\text{PR}_3)$  with  $\text{H}_2\text{SiPh}_2$  lead to  $\text{Ir}(\text{acac})\{\text{C}[\text{CH}(\text{OCH}_3)\text{OSiPh}_2]=\text{CHCO}_2\text{CH}_3\}(\text{PR}_3)$  ( $\text{PR}_3 = \text{PiPr}_3, \text{PCy}_3$ ), which are a result of a net transformation involving addition of one Si-H bond across the C=O and another across the alkyne triple bond. They are the first examples of compounds containing a chelate silylvinyl ligand. The X-ray diffraction analysis of the complex containing the tricyclohexylphosphine ligand

(22) Precedents for the hydrosilylation of the carbonyl group of  $\alpha$ - $\beta$ -unsaturated esters have been previously reported. See: (a) Ojima, I.; Kumagai, M.; Nagai, Y. *J. Organomet. Chem.* **1976**, *111*, 43. (b) Yamamoto, K.; Tabei, T. *J. Organomet. Chem.* **1992**, *428*, C1.

indicates that the bonding situation in the Ir-Si-O sequence could be described as an intermediate state between metal-silylene stabilized by an oxygen base and a tetrahedral silicon. The reactions of formation of these compounds, most probably, involve the initial hydrosilylation of the carbonyl group of one of the two esters of the alkyne.

### Experimental Section

**General Considerations.** All reactions were carried out under an argon atmosphere by using Schlenk tube techniques. Solvents were dried and purified by known procedures and distilled under argon prior to use. The starting complex  $\text{Ir}(\text{acac})(\text{cyclooctene})_2$  (**1**) was prepared by a published method.<sup>23</sup>

**Physical Measurements.** NMR spectra were recorded on a Varian 200 XL or on a Varian UNITY 300 spectrophotometer at room temperature. Chemical shifts are expressed in parts per million, upfield from  $\text{Si}(\text{CH}_3)_4$  ( $^{13}\text{C}\{^1\text{H}\}$ ,  $^1\text{H}$ ) and 85%  $\text{H}_3\text{PO}_4$  ( $^{31}\text{P}\{^1\text{H}\}$ ). Infrared spectra were recorded on a Perkin-Elmer 783 instrument. C and H analyses were carried out on a Perkin-Elmer 240 C microanalyzer.

**Preparation of  $\text{Ir}(\text{acac})(\text{cyclooctene})(\text{PiPr}_3)$  (**2**).** A suspension of **1** (100 mg, 0.20 mmol) in 10 mL of toluene was treated with  $\text{PiPr}_3$  (31  $\mu\text{L}$ , 0.20 mmol). After the mixture was stirred for 5 min at room temperature, the solution was filtered through Kieselguhr. The filtrate was concentrated to ca. 0.1 mL; addition of methanol caused the precipitation of a yellow solid. The solvent was decanted, and the solid was twice washed with methanol and then dried in vacuo. Yield: 80 mg (73%). Anal. Calcd for  $\text{C}_{22}\text{H}_{41}\text{IrO}_2\text{P}$ : C, 47.12; H, 7.36. Found: C, 46.90; H, 7.59. IR (Nujol,  $\text{cm}^{-1}$ ):  $\nu(\text{acac})$  1580, 1520.  $^1\text{H}$  NMR (300 MHz,  $\text{C}_6\text{D}_6$ ):  $\delta$  5.2 (s, 1 H, CH of acac); 3.0 (br, 2 H, HC=CH); 2.6-2.3 (m, 4 H, CHCH<sub>2</sub>); 2.0 (m, 4 H, CH<sub>2</sub>); 2.1 (m, 3 H, PCHCH<sub>3</sub>); 1.6 and 1.5 (both s, 6 H, CH<sub>3</sub> of acac); 1.4 (br, 4 H, CH<sub>2</sub>); 1.2 (dd, 18 H,  $J_{\text{P-H}} = 13$  Hz,  $J_{\text{H-H}} = 7$  Hz, PCHCH<sub>3</sub>).  $^{31}\text{P}\{^1\text{H}\}$  NMR (80 MHz,  $\text{C}_6\text{D}_6$ ):  $\delta$  33.4 (s).

**Preparation of  $\text{Ir}(\text{acac})(\text{cyclooctene})(\text{PCy}_3)$  (**3**).** The complex was prepared using the procedure described for **2**; starting with **1** (150 mg, 0.30 mmol) and  $\text{PCy}_3$  (82 mg, 0.16 mmol). Compound **3** was isolated as a yellow solid. Yield: 160 mg (80%). Anal. Calcd for  $\text{C}_{31}\text{H}_{54}\text{IrO}_2\text{P}$ : C, 54.60; H, 7.98. Found: C, 54.52; H, 8.27. IR (Nujol,  $\text{cm}^{-1}$ ):  $\nu(\text{acac})$  1580, 1520.

(23) Diversi, P.; Ingrassio, G.; Immirzi, A.; Porzio, W.; Zocchi, M. *J. Organomet. Chem.* **1977**, *125*, 253.

$^1\text{H}$  NMR (300 MHz,  $\text{C}_6\text{D}_6$ ):  $\delta$  5.2 (s, 1 H, CH of acac); 3.0 (br, 2 H, HC=CH); 2.6–2.4 (m, 4 H,  $\text{CHCH}_2$ ); 2.0 (m, 4 H,  $\text{CH}_2$ ); 1.7 and 1.6 (both s, 6 H,  $\text{CH}_3$  of acac); 2.2–1.2 (m, 37 H, Cy and  $\text{CH}_2$ ).  $^{31}\text{P}\{^1\text{H}\}$  NMR (80 MHz,  $\text{C}_6\text{D}_6$ ):  $\delta$  1.4 (s).

**Preparation of Ir(acac)(CO)(PiPr<sub>3</sub>) (4).** A slow stream of CO was passed for 5 min through a solution of **2** (110 mg, 0.20 mmol) in 10 mL of toluene. After the mixture was stirred for 15 min at room temperature, the solution was filtered through Kieselguhr. The filtrate was concentrated to ca. 0.1 mL; addition of hexane caused the precipitation of a greenish yellow solid. The solvent was decanted, and the solid was twice washed with hexane and then dried in vacuo. Yield: 64 mg (67%). Anal. Calcd for  $\text{C}_{15}\text{H}_{28}\text{IrO}_3\text{P}$ : C, 37.75; H, 5.88. Found: C, 37.34; H, 5.93. IR (Nujol,  $\text{cm}^{-1}$ ):  $\nu(\text{CO})$  1960,  $\nu(\text{acac})$  1580, 1525.  $^1\text{H}$  NMR (300 MHz,  $\text{C}_6\text{D}_6$ ):  $\delta$  5.2 (s, 1 H, CH of acac); 2.2 (m, 3 H,  $\text{PCHCH}_3$ ); 1.7 and 1.6 (both s, 6 H,  $\text{CH}_3$  of acac); 1.2 (dd, 18 H,  $J_{\text{P-H}} = 13$  Hz,  $J_{\text{H-H}} = 7$  Hz,  $\text{PCHCH}_3$ ).  $^{31}\text{P}\{^1\text{H}\}$  NMR (80 MHz,  $\text{C}_6\text{D}_6$ ):  $\delta$  35.8 (s).

**Preparation of Ir(acac)(CO)(PCy<sub>3</sub>) (5).** The complex was prepared using the procedure described for **4** starting with **3** (100 mg, 0.15 mmol). Compound **5** was isolated as a pale yellow solid. Yield: 76 mg (86%). Anal. Calcd for  $\text{C}_{24}\text{H}_{40}\text{IrO}_3\text{P}$ : C, 48.06; H, 7.62. Found: C, 48.42; H, 7.93. IR (Nujol,  $\text{cm}^{-1}$ ):  $\nu(\text{CO})$  1960,  $\nu(\text{acac})$  1585, 1520.  $^1\text{H}$  NMR (300 MHz,  $\text{C}_6\text{D}_6$ ):  $\delta$  5.3 (s, 1 H, CH of acac); 2.2–1.2 (m, 33 H, Cy); 1.7 and 1.6 (both s, 6 H,  $\text{CH}_3$  of acac).  $^{31}\text{P}\{^1\text{H}\}$  NMR (121.45 MHz,  $\text{C}_6\text{D}_6$ ):  $\delta$  25.4 (s).

**Preparation of Ir(acac)( $\eta^2\text{-CH}_3\text{O}_2\text{CC=CCO}_2\text{CH}_3$ )(PiPr<sub>3</sub>) (6).** A solution of **2** (110 mg, 0.20 mmol) in 15 mL of hexane was treated with  $\text{CH}_3\text{O}_2\text{CC=CCO}_2\text{CH}_3$  (24  $\mu\text{L}$ , 0.20 mmol). The mixture was stirred for 30 min at room temperature. An orange precipitate was formed. The solvent was decanted, and the solid was washed with hexane and then dried in vacuo. Yield: 88 mg (76%). Anal. Calcd for  $\text{C}_{20}\text{H}_{34}\text{IrO}_6\text{P}$ : C, 40.46; H, 5.77. Found: C, 40.71; H, 5.83. IR (Nujol,  $\text{cm}^{-1}$ ):  $\nu(\text{C=C})$  1820;  $\nu(\text{CO})$  1700, 1690;  $\nu(\text{acac})$  1580, 1515.  $^1\text{H}$  NMR (300 MHz,  $\text{C}_6\text{D}_6$ ):  $\delta$  5.1 (s, 1 H, CH of acac); 3.4 (s, 6 H,  $\text{CO}_2\text{CH}_3$ ); 2.3 (m, 3 H,  $\text{PCHCH}_3$ ); 1.8 and 1.6 (both s, 6 H,  $\text{CH}_3$  of acac); 1.1 (dd, 18 H,  $J_{\text{P-H}} = 14$  Hz,  $J_{\text{H-H}} = 7$  Hz,  $\text{PCHCH}_3$ ).  $^{31}\text{P}\{^1\text{H}\}$  NMR (121.45 MHz,  $\text{C}_6\text{D}_6$ ):  $\delta$  14.9 (s).  $^{13}\text{C}\{^1\text{H}\}$  NMR (75.45 MHz,  $\text{C}_6\text{D}_6$ ):  $\delta$  189.8 and 181.6 (both s, CO of acac); 154.7 (s,  $\text{COOCH}_3$ ); 101.4 (s, CH of acac); 74.18 (d,  $J_{\text{P-C}} = 4$  Hz,  $\text{C=C}$ ); 51.5 (s,  $\text{COOCH}_3$ ); 22.7 (d,  $J_{\text{P-C}} = 32$  Hz,  $\text{PCHCH}_3$ ); 26.0 (s,  $\text{CH}_3$  of acac); 19.1 (s,  $\text{PCHCH}_3$ ).

**Preparation of Ir(acac)( $\eta^2\text{-CH}_3\text{O}_2\text{CC=CCO}_2\text{CH}_3$ )(PCy<sub>3</sub>) (7).** The complex was prepared using the procedure described for **6** starting with **3** (120 mg, 0.18 mmol) and  $\text{CH}_3\text{O}_2\text{CC=CCO}_2\text{CH}_3$  (22  $\mu\text{L}$ , 0.18 mmol). Compound **7** was isolated as an orange solid. Yield: 105 mg (73%). Anal. Calcd for  $\text{C}_{29}\text{H}_{46}\text{IrO}_6\text{P}$ : C, 48.79; H, 6.49. Found: C, 48.80; H, 6.91. IR (Nujol,  $\text{cm}^{-1}$ ):  $\nu(\text{C=C})$  1860;  $\nu(\text{CO})$  1710;  $\nu(\text{acac})$  1590, 1515.  $^1\text{H}$  NMR (300 MHz,  $\text{C}_6\text{D}_6$ ):  $\delta$  5.1 (s, 1 H, CH of acac); 3.5 (s, 6 H,  $\text{CO}_2\text{CH}_3$ ); 2.2–1.2 (m, 33 H, Cy); 1.7 and 1.6 (both s, 6 H,  $\text{CH}_3$  of acac).  $^{31}\text{P}\{^1\text{H}\}$  NMR (121.45 MHz,  $\text{C}_6\text{D}_6$ ):  $\delta$  4.5 (s).  $^{13}\text{C}\{^1\text{H}\}$  NMR (75.45 MHz,  $\text{C}_6\text{D}_6$ ):  $\delta$  189.9 and 181.4 (both s, CO of acac); 154.7 (s,  $\text{COOCH}_3$ ); 101.6 (s, CH of acac); 74.0 (d,  $J_{\text{P-C}} = 3$  Hz,  $\text{C=C}$ ); 51.6 (s,  $\text{COOCH}_3$ ); 32.4 (d,  $J_{\text{P-C}} = 31$  Hz,  $\text{PCHCH}_2$ ); 29.7 (s,  $\text{CH}_2$ ); 28.0 (d,  $J_{\text{P-C}} = 10$  Hz,  $\text{PCHCH}_2$ ); 27.0 (s,  $\text{CH}_3$  of acac); 26.0 (s,  $\text{CH}_2$ ).

**Preparation of Ir(acac){C[CH(OCH<sub>3</sub>)OSiPh<sub>2</sub>]=CHCO<sub>2</sub>CH<sub>3</sub>}(PiPr<sub>3</sub>) (8).** A suspension of **6** (110 mg, 0.19 mmol) in 15 mL of hexane was treated with  $\text{H}_2\text{SiPh}_2$  (34.5  $\mu\text{L}$ , 0.19 mmol). The mixture was stirred for 12 h at room temperature. The solvent was decanted, and the pale yellow solid was washed with hexane and then dried in vacuo. Recrystallization from toluene–hexane gave pure **8**. Yield: 61 mg (41%). Anal. Calcd for  $\text{C}_{32}\text{H}_{48}\text{IrO}_6\text{PSi}$ : C, 49.40; H, 5.96. Found: C, 49.70; H, 5.50. IR (Nujol,  $\text{cm}^{-1}$ ):  $\nu(\text{CO})$  1710;  $\nu(\text{C=C})$  1590;  $\nu(\text{acac})$  1565, 1530;  $\nu(\text{Si-O})$  1020.  $^1\text{H}$  NMR (300 MHz,  $\text{C}_6\text{D}_6$ ):  $\delta$  8.2–6.9 (m, 10 H, Ph); 6.8 (s, 1 H, HC=C); 6.7 (s, 1 H,  $\text{CHO}_2$ ); 5.2 (s, 1 H, CH of acac); 4.0 and 3.4 (both s, 6 H,  $\text{COOCH}_3$ );

**Table 2. Atomic Coordinates ( $\times 10^4$ ;  $\times 10^5$  for Ir, P, and Si Atoms) and Equivalent Isotropic Displacement Coefficients ( $\text{\AA}^2 \times 10^3$ ;  $\times 10^4$  for Ir, P, and Si Atoms) for**

Ir(acac){C[CH(OCH <sub>3</sub> )OSiPh <sub>2</sub> ]=CHCO <sub>2</sub> CH <sub>3</sub> }(PCy <sub>3</sub> ) (9)				
atom	X/a	Y/b	Z/c	U <sub>eq</sub> <sup>a</sup>
Ir	22439(1)	62368(2)	-11487(1)	226(1)
P	29271(7)	54002(14)	-806(8)	240(5)
Si	20663(7)	45173(15)	-19311(8)	245(5)
O(1)	1666(2)	7492(4)	-1928(2)	31(1)
O(2)	1460(2)	6127(4)	-687(2)	33(1)
O(3)	2771(2)	4271(4)	-2107(2)	28(1)
O(4)	3822(2)	5029(4)	-1650(2)	29(1)
O(5)	3872(2)	7531(5)	-2490(2)	45(2)
O(6)	3870(2)	9362(5)	-1844(2)	44(2)
C(1)	1464(3)	4982(6)	-2839(3)	26(2)
C(2)	848(3)	4451(6)	-3099(3)	37(2)
C(3)	433(3)	4776(7)	-3775(3)	44(2)
C(4)	616(3)	5678(7)	-4223(4)	48(3)
C(5)	1228(3)	6226(8)	-3975(3)	51(3)
C(6)	1645(3)	5895(7)	-3285(4)	47(3)
C(7)	1787(3)	2950(5)	-1614(3)	25(2)
C(8)	1225(3)	2915(6)	-1388(3)	36(2)
C(9)	1016(3)	1788(7)	-1131(4)	47(3)
C(10)	1375(4)	658(7)	-1089(4)	51(3)
C(11)	1940(3)	670(7)	-1299(4)	43(3)
C(12)	2142(3)	1780(6)	-1566(3)	30(2)
C(13)	2954(2)	6513(5)	-1638(3)	21(2)
C(14)	3183(3)	5388(6)	-2038(3)	27(2)
C(15)	4117(3)	4250(7)	-2089(4)	46(3)
C(16)	3181(3)	7723(6)	-1690(3)	28(2)
C(17)	3664(3)	8128(6)	-2057(3)	32(2)
C(18)	4366(3)	9868(8)	-2143(4)	61(3)
C(19)	1051(3)	7666(6)	-2066(3)	36(2)
C(20)	746(3)	8540(7)	-2707(4)	53(3)
C(21)	662(3)	7135(7)	-1665(4)	43(2)
C(22)	872(3)	6459(6)	-1010(3)	36(2)
C(23)	388(3)	6078(7)	-606(4)	60(3)
C(24)	2477(4)	4636(7)	524(4)	47(3)
C(25)	2292(4)	3246(6)	379(4)	44(3)
C(26)	1841(4)	2730(7)	782(4)	57(3)
C(27)	1882(5)	3246(8)	1500(4)	73(4)
C(28)	2098(4)	4605(7)	1651(4)	51(3)
C(29)	2540(4)	5142(8)	1255(4)	69(4)
C(30)	3675(3)	4441(6)	-6(3)	27(2)
C(31)	3573(3)	3118(6)	-396(3)	29(2)
C(32)	4225(3)	2481(7)	-371(3)	40(2)
C(33)	4671(3)	2344(6)	423(4)	42(2)
C(34)	4756(3)	3639(7)	815(3)	45(2)
C(35)	4104(3)	4259(7)	787(3)	40(2)
C(36)	3258(3)	6938(5)	422(3)	26(2)
C(37)	3851(3)	7524(6)	261(3)	33(2)
C(38)	4060(3)	8755(7)	708(3)	44(2)
C(39)	3519(4)	9764(7)	580(4)	52(3)
C(40)	2902(3)	9196(6)	701(4)	42(3)
C(41)	2696(3)	7937(6)	261(3)	32(2)

<sup>a</sup> Equivalent isotropic  $U$  defined as one-third of the trace of the orthogonalized  $U_{ij}$  tensor.

2.2 (m, 3 H,  $\text{PCHCH}_3$ ); 1.8 and 1.0 (both s, 6 H,  $\text{CH}_3$  of acac); 1.1 (dd, 9 H,  $J_{\text{P-H}} = 13$  Hz,  $J_{\text{H-H}} = 7$  Hz,  $\text{PCHCH}_3$ ); 0.96 (dd, 9 H,  $J_{\text{P-H}} = 13$  Hz,  $J_{\text{H-H}} = 7$  Hz,  $\text{PCHCH}_3$ ).  $^{31}\text{P}\{^1\text{H}\}$  NMR (121.45 MHz,  $\text{C}_6\text{D}_6$ ):  $\delta$  1.8 (s).  $^{13}\text{C}\{^1\text{H}\}$  NMR (75.45 MHz,  $\text{C}_6\text{D}_6$ ):  $\delta$  185.8 and 183.2 (both s, CO of acac); 177.1 (d,  $J_{\text{P-C}} = 7$  Hz,  $\text{C=CH}$ ); 163.4 (s,  $\text{COOCH}_3$ ); 139.9 (d,  $J_{\text{P-C}} = 2$  Hz,  $\text{C}_{\text{ipso Ph}}$ ); 139.6 (d,  $J_{\text{P-C}} = 2$  Hz,  $\text{C}_{\text{ipso Ph}}$ ); 135.1 and 133.4 (both s,  $\text{C}_o \text{Ph}$ ); 129.2 and 127.8 (both s,  $\text{C}_p \text{Ph}$ ); 127.3 and 127.0 (both s,  $\text{C}_m \text{Ph}$ ); 123.6 (s,  $\text{C=CH}$ ); 107.5 (s,  $\text{CHO}_2$ ); 103.2 (s, CH of acac); 56.6 and 50.0 (both s,  $\text{COOCH}_3$ ); 27.2 (s,  $\text{CH}_3$  of acac); 25.2 (d,  $J_{\text{P-C}} = 30$  Hz,  $\text{PCHCH}_3$ ); 20.5 and 19.2 (both s,  $\text{PCHCH}_3$ ).

**Preparation of Ir(acac){C[CH(OCH<sub>3</sub>)OSiPh<sub>2</sub>]=CHCO<sub>2</sub>CH<sub>3</sub>}(PCy<sub>3</sub>) (9).** The complex was prepared using the procedure described for **8** by starting **7** (110 mg, 0.15 mmol) and  $\text{H}_2\text{SiPh}_2$  (28.5  $\mu\text{L}$ , 0.15 mmol). Compound **9** was isolated as a pale yellow solid. Yield: 73 mg (53%). Anal. Calcd for  $\text{C}_{41}\text{H}_{58}\text{IrO}_6\text{PSi}$ : C, 54.83; H, 6.50. Found: C, 54.63; H, 6.65. IR

**Table 3. Crystal Data and Data Collection and Refinement for Ir(acac){C[CH(OCH<sub>3</sub>)OSiPh<sub>2</sub>]=CHCO<sub>2</sub>CH<sub>3</sub>}(PCy<sub>3</sub>) (9)**

Crystal Data	
formula	C <sub>41</sub> H <sub>58</sub> IrO <sub>6</sub> PSi
mol wt	898.19
color and habit	light yellow, transparent prism
crystal size, mm	0.258 × 0.179 × 0.319
crystal syst	monoclinic
space group	<i>P</i> 2 <sub>1</sub> / <i>c</i> (No. 14)
<i>a</i> , Å	21.408(1)
<i>b</i> , Å	10.246(1)
<i>c</i> , Å	18.983(1)
$\beta$ , °	106.89(1)
<i>V</i> , Å <sup>3</sup>	3984.2(5)
<i>Z</i>	4
<i>D</i> <sub>calcd.</sub> , g cm <sup>-3</sup>	1.497
Data Collection and Refinement	
diffractometer	4-circle Siemens-STOE AED
$\lambda$ (Mo K $\alpha$ ) Å; technique	0.71073, bisecting geometry
monochromator	graphite oriented
$\mu$ , mm <sup>-1</sup>	3.45
scan type	$\omega/2\theta$
2 $\theta$ range, deg	3 ≤ 2 $\theta$ ≤ 50
temperature (K)	200
no. of data collect	7668
no. of unique data	6996 ( <i>R</i> <sub>int</sub> 0.026)
no. of obsd data	5272 ( <i>F</i> <sub>o</sub> ≥ 4.0 $\sigma$ ( <i>F</i> <sub>o</sub> ))
no. of params refined	452
<i>R</i> , <i>R</i> <sub>w</sub> <sup>a</sup>	0.0332, 0.0312

$$^a R = \sum ||F_o| - |F_c|| / \sum |F_o|; R_w = [\sum \{w(|F_o| - |F_c|)^2\} / \sum |F_o|^2]^{0.5}; w^{-1} = \sigma^2(F_o) + 0.000153(F_o)^2.$$

(Nujol, cm<sup>-1</sup>):  $\nu$ (CO) 1705;  $\nu$ (C=C) 1580;  $\nu$ (acac) 1560, 1520;  $\nu$ (Si-O) 1020. <sup>1</sup>H NMR (300 MHz, C<sub>6</sub>D<sub>6</sub>):  $\delta$  8.2–6.9 (m, 10 H, Ph); 6.8 (s, 1 H, HC=C); 6.7 (s, 1 H, CHO<sub>2</sub>); 5.2 (s, 1 H, CH of acac); 4.0 and 3.4 (both s, 6 H, COOCH<sub>3</sub>); 2.2–1.2 (m, 33 H, Cy); 1.8 and 1.1 (both s, 6 H, CH<sub>3</sub> of acac). <sup>31</sup>P{<sup>1</sup>H} NMR (121.45 MHz, C<sub>6</sub>D<sub>6</sub>):  $\delta$  -9.4 (s). <sup>13</sup>C{<sup>1</sup>H} NMR (75.45 MHz, C<sub>6</sub>D<sub>6</sub>):  $\delta$  186.0 and 183.3 (both s, CO of acac); 177.9 (d, *J*<sub>P-C</sub> = 7 Hz, C=CH); 163.5 (s, COOCH<sub>3</sub>); 140.4 (d, *J*<sub>P-C</sub> = 2 Hz, C<sub>ipso</sub> Ph); 139.6 (d, *J*<sub>P-C</sub> = 2 Hz, C<sub>ipso</sub> Ph); 135.4 and 133.6 (both s, C<sub>o</sub> Ph); 129.1 and 127.8 (both s, C<sub>p</sub> Ph); 127.4 and 127.1 (both s, C<sub>m</sub> Ph); 124.2 (s, C=CH); 107.7 (s, CHO<sub>2</sub>); 103.2 (s, CH of acac); 57.1 and 50.1 (both s, COOCH<sub>3</sub>); 35.4 (d, *J*<sub>P-C</sub> = 29 Hz, CH<sub>2</sub>CHP); 32.9 (s, CH<sub>2</sub>); 30.4 (s, CH<sub>2</sub>); 27.7 (d, *J*<sub>P-C</sub> = 10 Hz, CH<sub>2</sub>CHP); 27.5 (d, *J*<sub>P-C</sub> = 11 Hz, CH<sub>2</sub>CHP); 27.3 (s, CH<sub>3</sub> of acac); 26.6 (s, CH<sub>2</sub>).

**X-Ray Structure Analysis of Ir(acac){C[CH(OCH<sub>3</sub>)OSiPh<sub>2</sub>]=CHCO<sub>2</sub>CH<sub>3</sub>}(PCy<sub>3</sub>) (9).** Crystals suitable for an X-ray diffraction experiment were obtained by slow diffusion

of hexane into a concentrated solution of **9** in THF. Atomic coordinates and *U*<sub>eq</sub> values are listed in Table 2. A summary of crystal data, intensity collection procedure, and refinement data is reported in Table 3. The prismatic crystal studied was glued on a glass fiber and mounted on a Siemens-STOE AED-2 diffractometer. Cell constants were obtained from the least-squares fit of the setting angles of 58 reflections in the range 20 ≤ 2 $\theta$  ≤ 41°. The 7668 recorded reflections were corrected for Lorentz and polarization effects. Three orientation and intensity standards were monitored every 55 min of measuring time; no variation was observed. Reflections were also corrected for absorption by a semiempirical method ( $\Psi$ -scan).<sup>24</sup>

The structure was solved by Patterson (Ir atom) and conventional Fourier techniques. Refinement was carried out by full-matrix least squares with initial isotropic thermal parameters. Anisotropic thermal parameters were used in the last cycles of refinement for all non-hydrogen atoms. Hydrogen atoms were located from difference Fourier maps and included in the refinement (some of them in calculated positions, C–H = 0.96 Å) riding on carbon atoms with a common isotropic thermal parameter. Atomic scattering factors, corrected for anomalous dispersion for Ir, Si, and P, were taken from ref 25. The function minimized was  $\sum w(|F_o| - |F_c|)^2$  with the weight defined as  $w = 1/(\sigma^2|F_o| + 0.000153|F_o|^2)$ . Final *R* and *R*<sub>w</sub> values were 0.0332 and 0.0312. All calculations were performed by use of the SHELXTL-PLUS system of computer programs.<sup>26</sup>

**Acknowledgment.** We thank the DGICYT (Project PB 92-0092, Programa de Promoción General del Conocimiento) and EU (Project, Selective Processes and Catalysis Involving Small Molecules) for financial support. E.O. thanks the DGA (Diputación General de Aragón) for a grant. L. R. thanks the Spanish Government for a grant (Programa de Formación Científica para Iberoamérica).

**Supplementary Material Available:** Tables of anisotropic thermal parameters, atomic coordinates for hydrogen atoms, experimental details of the X-ray study, bond distances and angles, selected least-squares planes and interatomic distances (14 pages). Ordering information is given on any current masthead page.

OM940623J

(24) North, A. C. T.; Phillips, D. C.; Mathews, F. S. *Acta Crystallogr.* **1986**, *A24*, 351.

(25) *International Tables for X-Ray Crystallography*; Kynoch Press: Birmingham, England, 1974; Vol. IV.

(26) Sheldrick, G. M. *SHELXTL-PLUS*; Siemens Analytical X-ray Instruments, Inc.: Madison, WI, 1990.

# Synthesis of Stable ( $\eta^4$ -Vinylallene)iron Tricarbonyl Complexes: Preparation, Fluxionality, and X-ray Crystal Structure Analysis

Charles E. Kerr and Bruce E. Eaton\*

Department of Chemistry, Washington State University, Pullman, Washington 99164-4630

James A. Kaduk

Amoco Corporation, Naperville, Illinois

Received August 16, 1994<sup>⊙</sup>

Some of the first examples of air stable  $\eta^4$ -vinylallene- $\text{Fe}(\text{CO})_3$  complexes have been prepared by photochemical reaction of  $\text{Fe}(\text{CO})_5$  and vinylallenes. A high degree of diastereofacial selectivity was observed for iron coordination and the  $\pi$ -facial preference confirmed by X-ray crystallography. Comparison of NMR data ( $^1\text{H}$  and  $^{13}\text{C}$ ) for  $\eta^4$ -vinylallene- $\text{Fe}(\text{CO})_3$  complexes and  $\eta^4$ -isoprene- $\text{Fe}(\text{CO})_3$  revealed many similarities but some important differences that may be attributed to different polarization of these conjugated  $\pi$ -systems. Consistent with these differences the  $\eta^4$ -vinylallene- $\text{Fe}(\text{CO})_3$  complexes showed significantly higher  $\Delta G^\ddagger$  for interconversion of the carbonyl ligands as compared to  $\eta^4$ -isoprene- $\text{Fe}(\text{CO})_3$ . The X-ray data rule out intra- or intermolecular contacts as the cause of the increased barrier to carbonyl isomerization. The data clearly indicate that the central allene carbon is strongly backbonding to the iron center, which may account for observed NMR and X-ray results.

## Introduction

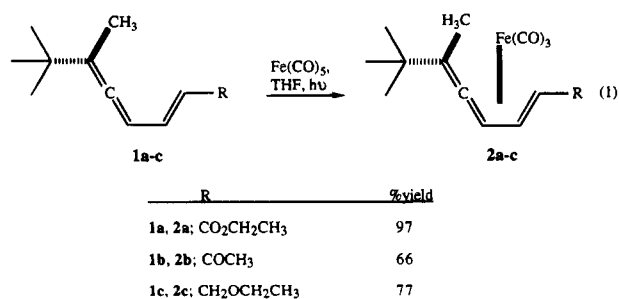
A wide array of  $\eta^2$ -allene-transition-metal complexes have been prepared and their structures studied.<sup>1</sup> In contrast very few examples of conjugated vinylallenes coordinated to transition metals have been reported.<sup>2</sup> Preparation of  $\eta^4$ -vinylallene- $\text{Fe}(\text{CO})_3$  complexes had been accomplished previously by treatment of the corresponding  $\eta^4$ -vinylketene- $\text{Fe}(\text{CO})_3$  complexes with stabilized Wittig reagents.<sup>2b</sup> It was of interest to probe the chemistry of these "high energy" ligands and determine if any stable complexes could be prepared by simple complexation of  $\text{Fe}(\text{CO})_3$ , a method that in contrast to the Wittig reaction of vinylketenes might allow for the inclusion of a wide array of hydrocarbon substituents at the terminal allene carbons.

In addition, previously it had been shown that conjugated diallenes,<sup>3</sup> allenyl ketones<sup>4</sup> and allenyl imines<sup>5</sup> react with CO and catalytic amounts of iron carbonyls to give [4 + 1] cycloaddition products. The stereoselectivity of those cycloaddition reactions was attributed to a high degree of diastereofacial selectivity on coordination of the iron to one face of the allene  $\pi$ -system. Herein we describe a highly diastereoselective synthesis of ( $\eta^4$ -vinylallene)iron- $\text{Fe}(\text{CO})_3$  complexes, related to the putative intermediates in the proposed [4 + 1] cycloaddition mechanisms.

The fluxionality of these new ( $\eta^4$ -vinylallene)iron tricarbonyl complexes was also examined by variable temperature NMR revealing significant differences in the dynamic behavior of the carbonyl ligands as compared to their  $\eta^4$ -diene counterparts. An X-ray crystallographic study was performed to unambiguously determine the facial preference of iron coordination and to better understand the nature of the bonding in these air-stable complexes.

## Results and Discussion

Using the method of Nakanishi,<sup>6</sup> the desired vinylallenes could be prepared in good yield starting from allenyl aldehydes.<sup>7</sup> Treatment of the vinylallenes with  $\text{Fe}_2(\text{CO})_9$  failed to give complete conversion. The best yields were obtained when the vinylallenes were treated with  $\text{Fe}(\text{CO})_5$  under 350 nm irradiation (eq 1). After



careful isolation under air-free conditions it was found that complex **2a** was in fact very robust and could be stored in the air at ambient temperature for several days without any detectable decomposition. The rela-

(6) Nakanishi, K.; Yudd, A. P.; Crouch, R. K.; Olson, G. I.; Cheung, H.-C.; Govindjee, R.; Ehbrey, T. G.; Patel, D. J. *J. Am. Chem. Soc.* **1976**, *98*, 236.

(7) Clinet, J. C.; Linstrumelle, G. *Nouveau J. Chim.* **1977**, *1*, 373.

<sup>⊙</sup> Abstract published in *Advance ACS Abstracts*, November 1, 1994.  
(1) Bowden, F. L.; Giles, R. *Coord. Chem. Rev.* **1976**, *20*, 81 and references cited therein.

(2) (a) Trifonov, L. S.; Orahovats, A. S.; Prewo, R.; Heimgartner, H. *Helv. Chim. Acta.* **1988**, *71*, 551. (b) Hill, L.; Saberi, S. P.; Slawin, A. M. Z.; Thomas, S. E.; Williams, D. J. *J. Chem. Soc., Chem. Commun.* **1991**, 1290. (c) Saberi, S. P.; Thomas, S. E. *J. Chem. Soc., Perkin Trans. 1* **1992**, 259.

(3) Eaton, B. E.; Rollman, B.; Kaduk, J. A. *J. Am. Chem. Soc.* **1992**, *114*, 6245.

(4) Sigman, M. S.; Kerr, C. E.; Eaton, B. E. *J. Am. Chem. Soc.* **1993**, *115*, 7545.

(5) Sigman, M. S.; Eaton, B. E. *J. Org. Chem.*, in press.

**Table 1.** Selected  $^1\text{H}$  and  $^{13}\text{C}$  NMR Data for Vinylallenes of the Corresponding Iron Carbonyl Complexes

	1a/2a	1b/2b	1c/2c	3/4
$^1\text{H}$ Chemical shifts ( $\delta$ ):				
H <sup>1</sup>	5.76/1.25	5.92/1.24	5.56/1.34	5.04/-0.22
H <sup>2</sup>	7.21/5.68	6.88/5.70	6.08/4.98	6.35/4.72
H <sup>3</sup>	5.64/4.46	5.64/4.48	5.72/4.48	
H <sub>3</sub> C <sup>6</sup>	1.47/1.85	1.50/1.89	1.56/1.92	
<i>t</i> -Bu	0.85/0.79	0.89/0.85	0.95/0.86	
$^1\text{H}$ Coupling constants (Hz):				
H <sup>1</sup> - H <sup>2</sup>	15.4/8.0	15.7/8.1	15.3/8.5	17.4/8.5
H <sup>2</sup> - H <sup>3</sup>	11.0/4.7	10.8/4.8	10.4/4.5	
H <sup>3</sup> - H <sub>3</sub> C <sup>6</sup>	2.6/1.4	2.7/1.7	2.7/1.6	
$^{13}\text{C}$ Chemical Shifts ( $\delta$ ):				
C <sup>1</sup>	119.6/47.9	129.1/55.3	127.7/61.6	113.5/38.0
C <sup>2</sup>	143.2/89.9	141.4/88.4	129.4/88.9	140.0/84.8
C <sup>3</sup>	93.2/68.9	93.6/69.3	93.9/66.3	142.5/103.2
C <sup>4</sup>	208.6/152.2	208.9/152.5	204.3/153.2	116.9/43.8
C <sup>5</sup>	110.6/133.8	110.6/133.8	109.7/132.4	
C <sup>6</sup>	14.4/20.7	14.4/20.8	14.9/20.7	
<i>t</i> -Bu	28.9/29.6	28.9/29.6	29.2/29.7	

tive stability of the complexes in air was  $2\mathbf{a} \geq 2\mathbf{b} \gg 2\mathbf{c}$ . Complex  $2\mathbf{c}$  decomposed in air after several minutes and was handled and stored in an argon atmosphere.

In all cases the substituents on the terminal allene carbons were methyl and *tert*-butyl. Excellent diastereoselectivity of iron coordination was observed. In all examples only one diastereomer was isolated as determined by  $^1\text{H}$  NMR (Table 1).

**NMR Analysis.** The assignments for the  $^1\text{H}$  resonances were made on the basis of COSY NMR experiments. To make assignment of the  $^{13}\text{C}$  NMR resonances HETCOR experiments were performed on both free vinylallene ligands and iron complexes.

What is the best structural description of these vinylallene- $\text{Fe}(\text{CO})_3$  complexes? Are the vinylallenes strictly  $\eta^4$ -bound to the iron and how do they compare to 1,3-diene- $\text{Fe}(\text{CO})_3$  complexes? We begin the analysis by comparing the resonances for the free vinylallene ligands ( $1\mathbf{a}-\mathbf{c}$ ) with the relevant isoprene ( $3$ ) proton resonances. The endo proton H<sup>1</sup> resonance is at lower field for all the vinylallenes studied as compared to  $3$ . Regardless of whether the group R on the vinyl allene was electron withdrawing or donating, the H<sup>1</sup> chemical shift was 0.5 to 0.8 ppm higher than for  $3$ . The internal proton H<sup>2</sup> (6.35 ppm) of isoprene is difficult to compare to the vinylallenes because of the methyl group at C<sup>3</sup>, but the vinylallenes  $1\mathbf{a}-\mathbf{c}$  span a range (7.21–6.08) that includes the frequency observed for  $3$ .

Larger differences exist between  $1\mathbf{a}-\mathbf{c}$  and  $3$  in their  $^{13}\text{C}$  NMR spectra. On average C<sup>1</sup> is shifted down field for  $1\mathbf{a}-\mathbf{c}$  as compared to  $3$ . Both the  $^{13}\text{C}$  NMR resonances C<sup>1</sup> and C<sup>2</sup> appear to be changed by the substituent R, perhaps due to changes in polarization about the vinylallene  $\pi$ -system. The resonance most notably different for  $1\mathbf{a}-\mathbf{c}$  versus  $3$  is C<sup>3</sup>, which is shifted ca.

49 ppm. This is undoubtedly the effect of the sp carbon C<sup>4</sup> in  $1\mathbf{a}-\mathbf{c}$ . These data suggest that conjugated vinylallenes are different from conjugated dienes in the way their  $\pi$ -systems are polarized and that vinylallenes may adopt other bonding interactions with  $\text{Fe}(\text{CO})_3$ .

The complexes  $2\mathbf{a}-\mathbf{c}$  and  $4$  show some similarity in their  $^1\text{H}$  and  $^{13}\text{C}$  NMR spectra. Beginning with the  $^1\text{H}$  NMR data, as seen for  $\eta^4$ -1,3-diene- $\text{Fe}(\text{CO})_3$  structures, the chemical shift of the endo proton H<sup>1</sup> (Table 1) is shifted upfield > 4 ppm on iron coordination while the H<sup>2</sup> and H<sup>3</sup> protons are shifted between 1 and 2 ppm upfield. The allenyl H<sup>3</sup> proton is virtually at the same chemical shift for all the complexes studied and is upfield 0.44 to 0.46 ppm as compared to the internal proton H<sup>2</sup> in the isoprene complex, possibly indicating more electron density at this location in the vinylallene complexes. All CH<sub>3</sub> groups of  $2\mathbf{a}-\mathbf{c}$  are shifted > 0.4 ppm downfield on complexation of  $\text{Fe}(\text{CO})_3$  indicating that they are positioned within the deshielding region of the iron and/or the carbonyl ligands. For both isoprene and the vinylallene complexes the  $^1\text{H}-^1\text{H}$  couplings are decreased by approximately 50%. This decrease in  $^1\text{H}-^1\text{H}$  coupling is consistent with iron backbonding into the antibonding  $\pi^*$ -orbital of the ligand. A small but measurable coupling is still present between the CH<sub>3</sub> groups and the allenyl H<sup>3</sup>-proton of  $2\mathbf{a}-\mathbf{c}$  indicating that there is electronic communication through the allenyl  $\pi$ -system accounting for the presence of a 5-bond coupling. Consistent with iron coordination anti to the less sterically hindered  $\pi$ -face of the allene, the resonance of the *t*-butyl group is shifted only slightly (0.09–0.04 ppm) upfield.

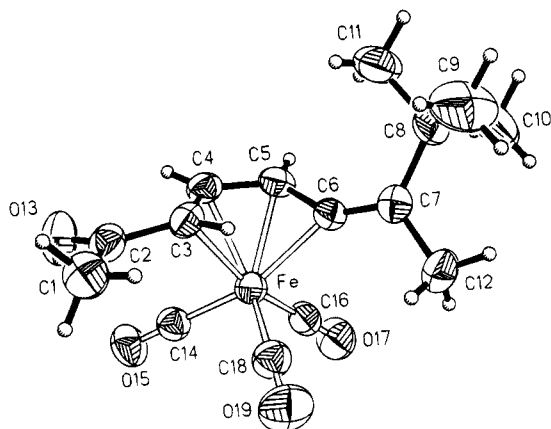
The  $^{13}\text{C}$  NMR data shows some interesting differences between the complexes  $2\mathbf{a}-\mathbf{c}$  and  $4$ . First, the resonance assigned to C<sup>1</sup> is shifted 5–24 ppm downfield for the complexed vinylallenes  $2\mathbf{a}-\mathbf{c}$  relative to  $4$ . Interestingly, the order of the magnitude of downfield shift is strongly affected by the group R, where ester ( $2\mathbf{a}$ ) < ketone ( $2\mathbf{b}$ ) < ether ( $2\mathbf{c}$ ). The internal carbon, C<sup>2</sup> of  $2\mathbf{a}-\mathbf{c}$  all have a chemical shift very similar to the corresponding carbon in complex  $4$ . In contrast, C<sup>3</sup> of  $2\mathbf{a}-\mathbf{c}$  is shifted approximately 34–37 ppm upfield as compared to  $4$ . Notably, the central allene carbon in all the vinylallene complexes, for which there is no counterpart in the isoprene complex, is shifted upfield more than 50 ppm on coordination of  $\text{Fe}(\text{CO})_3$ , consistent with a change in hybridization because of extensive back-bonding into the allene  $\pi$ -system. Concomitant with this shift of the central carbon of the allenes, the terminal carbon is shifted to lower field, possibly due to the electron withdrawing effect of the metal.

In contrast to  $4$ , all of the complexes  $2\mathbf{a}-\mathbf{c}$  show slow exchange of the carbonyl ligands. Variable temperature  $^{13}\text{C}$  NMR experiments revealed a trend in the coalescence temperature for the different substituents R attached to C<sup>1</sup> of the vinylallene (Table 2). The energy barrier to interconversion of carbonyl ligands in the vinylallene complexes  $2\mathbf{a}-\mathbf{c}$  increases with the degree of electron withdrawing character of the R group. For the vinylallene- $\text{Fe}(\text{CO})_3$  complexes studied  $\Delta G^\ddagger$  is 20–25 kJ/mol higher than for isoprene- $\text{Fe}(\text{CO})_3$  ( $4$ ), representing a difference in  $T_c$  of between 80–100 °C. It was of interest to determine if this higher barrier to interconversion of carbonyl ligands was because of steric, electronic or coordinating interactions of the

**Table 2.**  $^{13}\text{C}$  NMR Coalescence Temperature and Chemical Shift Data of Carbonyl Ligands of **2a**, **2b**, **2c**, and **4** in Toluene- $d_8$ 

	<b>2a</b>	<b>2b</b>	<b>2c</b>	<b>4</b>
$\Delta G^\ddagger$ (kJ/mol)/ $T_c$ (K)	83.3(1)/333	86.3(1)/342	78.3(1)/314	57.7(1)/234
chem shift ( $\delta$ ) <sup>a</sup>	209.1	209.6	211.2	211.8
chem shifts <sup>b</sup> ( $\delta$ )	206.2	205.5	209.0	210.2
	209.5	209.4	210.8	215.9
	214.9	215.5	216.1	

<sup>a</sup> At coalescence. <sup>b</sup> Below coalescence.  $\Delta G^\ddagger$  (kJ/mol) =  $9.62RT_c(10.32 + \log T_c/k_c)$ ,  $k_c = (\pi\Delta\nu/2)^{-1/2} \text{ s}^{-1}$ , where  $\Delta\nu$  is the difference between resonances.

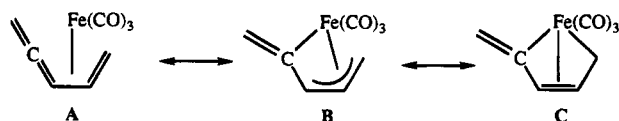
**Figure 1.** Ortep plot of the X-ray crystal structure of **2b**.**Table 3.** Selected Bond Lengths (Å) and Angles (deg) for **2b**

C1–C2	1.499(6)	C1–C2–C3	117.6(3)
C2–C3	1.470(5)	C1–C2–O13	120.8(4)
C2–O13	1.222(5)	C3–C2–O13	121.5(4)
C3–C4	1.419(5)	C2–C3–C4	121.2(3)
C4–C5	1.398(5)	C3–C4–C5	118.4(3)
C5–C6	1.418(5)	C4–C5–C6	115.4(3)
C6–C7	1.324(5)	C5–C6–C7	144.9(4)
C7–C8	1.538(5)	C6–C7–C8	122.1(3)
C7–C12	1.513(6)	C6–C7–C12	120.5(3)
Fe–C3	2.136(3)	C8–C7–C12	117.3(3)
Fe–C4	2.050(3)	C14–Fe–C16	90.5(2)
Fe–C5	2.071(4)	C14–Fe–C18	101.6(2)
Fe–C6	2.042(3)	C16–Fe–C18	98.3(2)
Fe–C14	1.811(4)	Fe–C14–O15	177.3(3)
Fe–C16	1.781(4)	Fe–C16–O17	178.3(4)
Fe–C18	1.793(4)	Fe–C18–O19	179.6(3)

substituent R. In addition, we wanted more definitive structural information on how the iron was bound to the vinylallene, including the selectivity of  $\pi$ -face coordination. Fortunately, we were able to crystallize **2b** and perform an X-ray crystal structure analysis.

**X-ray Crystal Structure Analysis 2b.** The crystal structure consists of discrete molecules of complex **2b** (Figure 1). Selected bond lengths and angles are provided in Table 3. The bond distances and angles of the ends of the vinylallene ligand fall within normal ranges for  $\eta^4$ -diene- $\text{Fe}(\text{CO})_3$  complexes. There are several structural features in the center of the complexed ligand that are significantly different.

The Fe–C vinylallene distances [2.136(3), 2.050(3), 2.071(4) and 2.042(3) Å] are similar to the average Fe–C distance of 2.09(6) Å, obtained from X-ray studies on 163  $\eta^4$ -diene- $\text{Fe}(\text{CO})_3$  complexes.<sup>8</sup> The Fe–CO dis-

**Figure 2.** Three resonance forms of vinylallene- $\text{Fe}(\text{CO})_3$  complexes.

tances of 1.781(4), 1.811(4) and 1.793(4) Å are also close to the average value of 1.81(9) Å observed in the diene complexes. The orientation of the vinylallene in **2b** with respect to the carbonyl ligands is very similar to that observed in several  $\eta^4$ -diene- $\text{Fe}(\text{CO})_3$  complexes having a conjugated carbonyl group.<sup>9</sup> The Fe–C–O angles [177.3(3), 178.3(4) and 179.6(3)°] are very close to linear. Both the molecular and crystal structure data rule out coordination or steric interaction of the carbonyl oxygen O13 as the cause of the slow interconversion of the carbonyl ligands. O13 is not oriented toward the Fe in the molecule, nor to the Fe in an adjacent molecule. The closest intermolecular contacts for O13 are 2.75 Å, too far away to account for the slow interconversion of the CO ligands.

Taken together the NMR and X-ray data suggest that it is best to view vinylallene- $\text{Fe}(\text{CO})_3$  complexes **2a–c** as  $\pi$ -bound but with a significant degree of  $\sigma$ -character between the iron and central allene carbon as shown by resonance structures **A** and **B** of Figure 2. The X-ray data rule out any significant contribution from resonance contributor **C** because the terminal vinyl carbon is close to  $\text{sp}^2$  hybridized and the vinylallene iron–carbon distances are all very similar. The iron appears to have little interaction with the terminal allene  $\pi$ -bond since this bond length is on the order of a typical C–C double bond.

**Conclusions.** The  $\eta^4$ -vinylallene- $\text{Fe}(\text{CO})_3$  complexes of this study are air-stable when electron-withdrawing carbonyl groups are in conjugation with the vinylallene. They can be prepared easily by treating the vinylallenes with  $\text{Fe}(\text{CO})_5$  and irradiating at 350 nm. The complexation of iron occurs preferentially to the  $\pi$ -face of the vinylallene ligand that is anti with respect to the *tert*-butyl group. On complexation of  $\text{Fe}(\text{CO})_3$ , vinylallenes show changes in chemical shift and  $\text{H}^1$ – $\text{H}^1$  coupling similar to those observed in  $\eta^4$ -isoprene- $\text{Fe}(\text{CO})_3$ . In contrast to known  $\eta^4$ -diene- $\text{Fe}(\text{CO})_3$  complexes, the CO ligands of  $\eta^4$ -vinylallene- $\text{Fe}(\text{CO})_3$  complexes show slow exchange by  $^{13}\text{C}$  NMR. One explanation is that the apparent strong interaction of the iron with the central allene carbon distorts the geometry of the vinylallene complexes so that they are not exclusively  $\pi$ -bound but possess a significant amount of  $\sigma$  character, thereby increasing the barrier for interconversion of the CO ligands. The structure of **2b** does show a significant rehybridization from  $\text{sp}$  to  $\text{sp}^2$  of the central allene carbon consistent with strong back-bonding from the iron into the allene  $\pi$ -system. X-ray

(8) Allen, F. H.; Davies, J. E.; Galloy, J. J.; Johnson, O.; Kennard, O.; Macrae, C. F.; Mitchell, E. M.; Smith, J. M.; Watson, D. G. *J. Chem. Inf. Comp. Sci.* **1991**, *31*, 187.

(9) Mason, R.; Robertson, G. B. *J. Chem. Soc. A.* **1970**, 1229. (b) Messenger, J. C.; Toupet, L. *Acta Cryst.* **1986**, *B42*, 371. (c) Morey, J.; Gree, D.; Mosset, P.; Toupet, L.; Gree, R. *Tetrahedron Lett.* **1987**, *28*, 2959. (d) Balde, L.; Rodier, N.; Bidaux, N.; Brion, J. D.; Le Baut, G. *Acta Cryst.* **1988**, *C44*, 1394. (e) Adams, C. M.; Ceroni, G.; Hafner, A.; Kalchauer, H.; von Philipsborn, W.; Prewo, R.; Schwenk, A. *Helv. Chim. Acta* **1988**, *71*, 1116. (f) Le Gall, T.; Lellouche, J.-P.; Toupet, L.; Beaucourt, J.-P. *Tetrahedron Lett.* **1989**, *30*, 6517. (g) Rohde, W.; Fischer, J.; De Cian, A. *J. Organomet. Chem.* **1990**, *393*, C25. (h) Benvenegun, T.; Martelli, J.; Gree, R.; Toupet, L. *Tetrahedron Lett.* **1990**, *31*, 3145.



crystal structure analysis did not reveal steric or coordinating interactions for either the carbonyl or CO ligands that could account for the relatively slow exchange of the CO ligands.

### Experimental Section

All reactions and manipulations were conducted under a dry argon atmosphere either using an inert atmosphere glovebox or standard Schlenk techniques. The Wittig<sup>6</sup> reagents and 4,5,5-trimethylhexa-2,3-dienal<sup>7</sup> were prepared as described in the literature. The silica gel used was 230–400 mesh ASTM. Vacuum distillations, and freeze/pump/thaw cycles were performed on a vacuum line (<1 μmHg). A minimum of three freeze/pump/thaw cycles were used when degassing samples. Irradiations were performed using a Rayonet photochemical reactor (350 nm, 10 bulbs). NMR data was acquired on a Bruker AMX (300 MHz <sup>1</sup>H). Infrared data was acquired from a Perkin-Elmer 1600 FTIR. Mass spectral data were obtained from the departmental facility at Washington State University. Elemental analysis was obtained from Desert Analytics, Tuscon, AZ. Melting points were recorded on a Mel-Temp apparatus and are uncorrected.

**Ethyl-6,7,7-trimethylocta-2,4,5-trienoate (1a).** Sodium hydride (1.5 g, 63 mmol) and THF (75 mL dried over Na/K/benzophenone) were placed in a flask under argon and cooled to 0 °C. Triethylphosphonoacetate (11.54 mL, 57.1 mmol) was added gradually. Evolution of hydrogen gas was observed. The mixture was stirred for 15 m and added to 4,5,5-trimethylhexa-2,3-dienal (7.5 mL, 51.9 mmol) and stirred at ambient temperature for 12 h. The reaction mixture was submitted to standard aqueous work up using diethyl ether. The ether layer was concentrated and applied to silica gel using ether as eluant. Removal of the ether followed by short-path vacuum distillation gave 8.44 g (78%) of **1a** pale yellow oil. <sup>1</sup>H NMR (300 MHz; CDCl<sub>3</sub>) δ 0.96 (s, 9H), 1.17 (t, *J* = 7.1 Hz, 3H), 1.62 (d, *J* = 2.5 Hz, 3H), 4.07 (q, *J* = 7.1 Hz, 2H), 5.71 (d, *J* = 15.4 Hz, 1H), 5.74 (dq, *J* = 11.0, 2.5 Hz, 1H), 7.04 (dd, *J* = 15.4, 11 Hz, 1H); <sup>13</sup>C {<sup>1</sup>H} (75 MHz; CDCl<sub>3</sub>) δ 14.01, 14.10, 28.64, 33.49, 59.72, 92.47, 110.23, 118.39, 143.39, 166.48, 208.41; IR (neat) 1941.5, 1719.8 cm<sup>-1</sup>; MS *m/z* (M<sup>+</sup>) 208. HRMS *m/z* for C<sub>13</sub>H<sub>20</sub>O<sub>2</sub> calcd 208.1463, found 208.1478.

**7,8,8-Trimethylnona-3,5,6-triene-2-one (1b).** 1-Triphenylphosphoranylidene-2-propanone (8.7 g, 27 mmol), *p*-dioxane (150 mL freshly distilled from K/benzophenone) and 4,5,5-trimethylhexa-2,3-dienal (3.0 mL, 20.8 mmol) were combined under argon and refluxed for 20 h. The dioxane was removed under reduced pressure. After precipitation of the triphenylphosphine oxide from pentane and filtration of the solvent was removed by reduced pressure. Fractional vacuum distillation gave 1.93 g (75%) of **1b** a pale yellow oil. <sup>1</sup>H NMR (300 MHz; CDCl<sub>3</sub>) δ 0.91 (s, 9H), 1.58 (d, *J* = 2.7 Hz, 3H), 2.07 (s, 3H), 5.69 (dq, *J* = 10.8, 2.6 Hz, 1H), 5.92 (d, *J* = 15.6 Hz, 1H), 6.83 (dd, *J* = 10.8, 15.7 Hz, 1H); <sup>13</sup>C {<sup>1</sup>H} (75 MHz; CDCl<sub>3</sub>) δ 14.0, 26.7, 28.6, 33.4, 92.8, 110.26, 128.0, 142.4, 197.34, 208.92; IR (neat) 1939.6, 1663.2 cm<sup>-1</sup>; MS *m/z* (M<sup>+</sup>) 178. HRMS *m/z* for C<sub>12</sub>H<sub>18</sub>O, calcd 178.1358, found 178.1374.

**6,7,7-Trimethylocta-2,4,5-triene-1-ol. 1a** (500 μL, 2.23 mmol) was dissolved in THF (25 mL distilled from NaK/benzophenone) and cooled to 0 °C pending addition of DIBAL (11.1 mL, 1M in THF, 11.1 mmol). After addition, the reaction was allowed to warm to ambient temperature and stirred for 20 h. Workup by extraction with ether/HCl, followed by concentration of the organic residue gave a yellow oil. The product was dried with MgSO<sub>4</sub> in dichloromethane to yield 350 mg (94%) of 6,7,7-trimethylocta-2,4,5-triene-1-ol as a colorless oil. <sup>1</sup>H NMR (300 MHz; CDCl<sub>3</sub>) δ .99 (s, 9H), 1.64 (d, *J* = 2.7 Hz, 3H), 3.37 (s, 1H), 4.04 (dd, *J* = 6.0, .9 Hz, 2H), 5.7 (m, 2H), 5.97 (ddt, *J* = 15.4, 10.3, 1.3 Hz, 1H); <sup>13</sup>C {<sup>1</sup>H} (75 MHz; CDCl<sub>3</sub>) δ 14.51, 28.26, 33.34, 62.44, 92.90, 109.22, 128.49, 128.62, 203.76; IR (neat) 3322.4, 1944.9 cm<sup>-1</sup>; MS *m/z* (M<sup>+</sup>) 166. HRMS *m/z* for C<sub>11</sub>H<sub>18</sub>O, calcd 166.1358, found 166.1346.

**1-Ethoxy-6,7,7-trimethylocta-2,4,5-triene (1c).** 6,7,7-Trimethylocta-2,4,5-trien-1-ol (2 mL, 10.48 mmol), THF (90 mL distilled from Na/K benzophenone) and 90 mL hexanes (freshly distilled from K) were combined and cooled to 0 °C. Butyllithium (7.4 mL, 1.5M in hexanes, 11.1 mmol) was added dropwise at 0 °C. The reaction mixture turned yellow immediately, then gradually turned green over several minutes. After 10 m DMSO (45 mL, distilled off CaH<sub>2</sub>) were added, followed by bromoethane (3.95 mL, 52.40 mmol). The reaction mixture was then allowed to warm to ambient temperature and stirred for 21 h. After standard aqueous work up the residue was vacuum distilled to give 1.85 g (91%) of **1c** as a pale yellow oil. <sup>1</sup>H NMR (300 MHz; CDCl<sub>3</sub>) δ 1.01 (s, 9H), 1.18 (t, *J* = 7 Hz, 3H), 1.66 (d, *J* = 2.7 Hz, 3H), 3.45 (q, *J* = 7 Hz, 2H), 3.94 (dd, *J* = 6.3, 1.2 Hz, 2H), 5.64 (dtd, *J* = 15.3, 6.3, 0.3 Hz, 1H), 5.69 (dq, *J* = 10.4, 2.7 Hz, 1H), 6.01 (ddt, *J* = 15.3, 10.3, 0.3 Hz, 1H); <sup>13</sup>C {<sup>1</sup>H} (75 MHz; CDCl<sub>3</sub>) δ 14.73, 15.11, 28.94, 33.57, 65.39, 70.95, 92.99, 109.58, 126.07, 130.36, 204.09; IR (neat) 1945.1, 1644.1, 1461.5 cm<sup>-1</sup>; MS *m/z* (M<sup>+</sup>) 194. HRMS *m/z* for C<sub>13</sub>H<sub>22</sub>O, calcd 194.1671; found 194.1675.

**( $\eta^4$ -Ethyl-6,7,7-trimethylocta-2,4,5-trienoate)iron tricarbonyl (2a).** Ethyl-6,7,7-trimethylocta-2,4,5-trienoate (177 mg, 85 μmol) was placed in a vacuum Schlenk tube and freeze-pump-thawed. The tube was charged with Fe(CO)<sub>5</sub> (223 μL, 1.70 mmol, 2 equiv) and THF (5 mL distilled from Na/K benzophenone) were added. The reaction bomb was then irradiated at 350 nm with stirring for 24 h. The resulting mixture was washed into a flask with ether and concentrated onto silica gel. The crude product was eluted from the silica with ether and concentrated. The residue was then eluted with benzene through a pasteur filter pipette of silica gel yielding 287 mg (97%) of **2a** as an amber oil. <sup>1</sup>H NMR (300 MHz; C<sub>6</sub>D<sub>6</sub>) δ 0.79 (s, 9H), .93(t, *J* = 7.1 Hz, 3H), 1.25 (d, *J* = 8.1 Hz, 1H), 1.85 (d, *J* = 1.4 Hz, 3H), 3.91 (AA'X, 2H), 4.46 (m, 1H), 5.68 (dd, *J* = 4.7, 7.9 Hz, 1H); <sup>13</sup>C {<sup>1</sup>H} (75 MHz; C<sub>6</sub>D<sub>6</sub>) δ 14.17, 20.66, 29.57, 36.84, 47.91, 60.42, 68.97, 89.88, 133.77, 152.17, 171.41, 205.94, 209.25, 214.36; IR (neat) 2058, 1980.2, 1706.6 cm<sup>-1</sup>. Anal. Calcd for C<sub>16</sub>H<sub>20</sub>O<sub>5</sub>Fe: C, 55.19; H, 5.79; Fe, 16.04. Found C, 55.17; H, 5.64; Fe, 15.92; MS *m/z* (M<sup>+</sup>) 348.

**( $\eta^4$ -7,8,8-Trimethylnona-3,5,6-triene-2-one)iron tricarbonyl (2b).** 7,8,8-Trimethylnona-3,5,6-trien-2-one (208 mg, 1.17 mmol) and THF (10 mL distilled from Na/K benzophenone) were combined and freeze-pump-thawed. Iron pentacarbonyl (750 μL, 5.7 mmol) was added and the solution irradiated for 5 h at 350 nm. The resultant mixture was concentrated onto silica gel. The dried residue was added to the top of a pad of silica gel and the product was eluted with 1:1 benzene:pentane. The concentrated eluent was eluted through a pasteur pipet of silica gel, first with benzene, then again with ether as the eluant. Removal of solvent gave 244 mg (66%) of **2b** as an orange oil. Crystallization from pentane gave amber crystals (Mp 55.5–58 °C, vacuum sealed capillary); <sup>1</sup>H NMR (300 MHz; C<sub>6</sub>D<sub>6</sub>) δ 0.85 (s, 9H), 1.24 (d, *J* = 8.1 Hz, 1H), 1.68 (s, 3H), 1.89 (s, 3H), 4.48 (m, 1H), 5.70 (dd, *J* = 8.0, 4.8 Hz, 1H); <sup>13</sup>C {<sup>1</sup>H} (75 MHz; C<sub>6</sub>D<sub>6</sub>) δ 20.70, 29.04, 29.62, 36.90, 55.31, 69.33, 88.40, 133.65, 152.33, 201.01, 205.2, 209.2, 215.4; IR (neat) 2057.1, 1982.1, 1679.0 cm<sup>-1</sup>. MS *m/z* (M<sup>+</sup>) 318. HRMS *m/z* for C<sub>15</sub>H<sub>18</sub>O<sub>4</sub>Fe, calcd 318.0559, found 318.0532.

**( $\eta^4$ -1-Ethoxy-6,7,7-trimethylocta-2,4,5-triene)iron tricarbonyl (2c).** 1-Ethoxy-6,7,7-trimethylocta-2,4,5-triene (171 mg, 879 μmol) was freeze-pump-thawed and THF (from 10 mL Na/K benzophenone) and Fe(CO)<sub>5</sub> (578 μL, 4.39 mmol) were added. After 18 h irradiation at 350 nm, the reaction mixture was concentrated onto silica gel. The crude product was eluted with ether, concentrated, and then purified by column chromatography (1:10 hexanes:toluene, flash silica) to yield **2c** 294 mg (77%). <sup>1</sup>H NMR (300 MHz; C<sub>6</sub>D<sub>6</sub>) δ 0.86 (s, 9H), 1.03 (t, *J* = 6.99 Hz, 3H), 1.34 (m, 1H), 1.92 (d, *J* = 1.63 Hz, 3H), 3.14 (m, 2H), 3.22 (m, 2H), 4.48 (m, 1H), 4.98 (dd, *J* = 4.5, 8.5 Hz, 1H); <sup>13</sup>C {<sup>1</sup>H} (75 MHz; C<sub>6</sub>D<sub>6</sub>) δ 15.22, 20.69,



29.73, 36.80, 61.63, 66.26, 66.39, 71.08, 88.98, 132.42, 153.18, 210; IR (neat) 2044.2, 1962.4  $\text{cm}^{-1}$ ; MS  $m/z$  ( $M^+$ ) 334. HRMS  $m/z$  for  $\text{C}_{16}\text{H}_{22}\text{O}_4\text{Fe}_1$ , calcd 334.0867, found 334.0864.

**X-ray Crystal Structure Analysis.** A clear yellow crystal approximately  $0.75 \times 0.58 \times 0.38$  mm was wedged in a 0.3 mm capillary and optically centered on a Nicolet/Siemens R3m single crystal diffractometer. The dimensions of the primitive monoclinic unit cell were determined from the setting angles of 23 strong reflections having  $25 < 2\theta < 32^\circ$ . The refined lattice parameters, derived from a Rietveld refinement<sup>10</sup> of a powder sample mixed with NIST 640b Si internal standard are as follows:  $a = 10.7875(8)$ ,  $b = 13.1067(13)$ ,  $c = 11.5274(10)$  Å, and  $\beta = 95.598(5)^\circ$ . A search of the Crystal Data database yielded no plausible hits.

The details of the data collection are reported in supplementary material. Both  $\omega$  and  $2\theta/\omega$  scans indicated that the crystal was of high quality. The intensities of four check reflections varied by  $\pm 1\%$  during data collection. An empirical absorption correction, derived from  $\psi$ -scans of 15 strong reflections well-distributed in reciprocal space, was applied. The maximum and minimum transmission were 0.268 and 0.227. The systematic absences unambiguously determined the space group to be  $P2_1/c$ .

Data processing was carried out using the SHELXTL Plus, version 3.4 system of programs (Nicolet Instrument Corp.). The structure was solved by direct methods, which indicated the position of the iron atom, 6 carbons and three oxygens. The remaining heavy atoms were located by difference Fourier techniques. The hydrogen atoms were included in the calculated positions.

(10) Larson, A. C.; Von Dreele, R. B. GSAS, The General Structure Analysis System; Los Alamos National Laboratory, Feb 1993 version.

All non-hydrogen atoms were refined anisotropically. All C–H distances were fixed at 0.96 Å. A common isotropic displacement coefficient was refined for the three vinyl hydrogens. The methyl groups were treated as rigid bodies. A common isotropic displacement coefficient was refined for the hydrogens on C1 and C12, and another common thermal parameter for the *tert*-butyl hydrogens on C9, C10 and C11 (Figure 1). The final refinement of 184 variables using 2135 observations yielded the residuals  $R = 0.0427$  and  $wR = 0.0545$ . The  $R$  factor expected from counting statistics is 0.0198. The atomic coordinates and the equivalent isotropic displacement coefficients of the heavy atoms, bond angles, bond lengths, anisotropic displacement coefficients and the observed and calculated structure factors are reported in supplementary material.

**Acknowledgment.** Support from the donors of the Petroleum Research Fund and a Grant-in-Aid from Washington State University is gratefully appreciated. NMR data were obtained from the WSU NMR Center supported in part by the NIH (Grant RR0631401) and NSF (Grant CHE-9115282). Special thanks to Matt Sigman for preparation of this manuscript.

**Supplementary Material Available:** X-ray crystal structure determination data for **2a** including tables of solution and refinement parameters, atomic coordinates, bond lengths, bond angles, and isotropic and anisotropic displacement coefficients and stereo ORTEP plots (10 pages). Ordering information is given on any current masthead page.

OM9406512

# Monomeric Alkyl and Hydride Derivatives of Zinc Supported by Poly(pyrazolyl)hydroborato Ligation: Synthetic, Structural, and Reactivity Studies

Adrian Looney, Runyu Han, Ian B. Gorrell, Mark Cornebise, Keum Yoon, and Gerard Parkin\*

Department of Chemistry, Columbia University, New York, New York 10027

Arnold L. Rheingold

Department of Chemistry, University of Delaware, Newark, Delaware 19716

Received September 1, 1994<sup>®</sup>

A series of monomeric four-coordinate monoalkyl zinc complexes  $[\text{Tp}^{\text{Bu}^t}]\text{ZnR}$  ( $[\text{Tp}^{\text{Bu}^t}] = \text{tris}(3\text{-tert-butylpyrazolyl})\text{hydroborato}$ ;  $\text{R} = \text{Me}, \text{Et}$ ) and  $[\text{Tp}^{\text{Me}_2}]\text{ZnMe}$  ( $[\text{Tp}^{\text{Me}_2}] = \text{tris}(3,5\text{-dimethylpyrazolyl})\text{hydroborato}$ ) has been prepared by metathesis of  $\text{R}_2\text{Zn}$  with  $\text{Tl}[\text{Tp}^{\text{Bu}^t}]$  and  $\text{Tl}[\text{Tp}^{\text{Me}_2}]$ , respectively, while the three-coordinate zinc alkyl derivatives  $[\text{Bp}^{\text{Bu}^t}]\text{ZnR}$  ( $[\text{Bp}^{\text{Bu}^t}] = \text{bis}(3\text{-tert-butylpyrazolyl})\text{hydroborato}$ ;  $\text{R} = \text{Me}, \text{Et}, \text{Bu}^t$ ) have been synthesized by the reactions of  $\text{R}_2\text{Zn}$  with  $\text{Tl}[\text{Bp}^{\text{Bu}^t}]$ . The monomeric zinc hydride derivative  $[\text{Tp}^{\text{Bu}^t}]\text{ZnH}$  has also been prepared by the reaction of  $\text{ZnH}_2$  with  $\text{Tl}[\text{Tp}^{\text{Bu}^t}]$ . The reactivities of  $[\text{Tp}^{\text{Bu}^t}]\text{ZnH}$  and  $[\text{Tp}^{\text{Bu}^t}]\text{ZnR}$  toward a variety of substrates have been investigated, giving rise to a series of derivatives  $[\text{Tp}^{\text{Bu}^t}]\text{ZnX}$  ( $\text{X} = \text{O}_2\text{CH}, \text{O}_2\text{CMe}, \text{C}_2\text{Ph}, \text{SH}, \text{OSiMe}_3, \text{Cl}, \text{Br}, \text{I}$ ). The Zn-C bonds of the three-coordinate complexes  $[\text{Bp}^{\text{Bu}^t}]\text{ZnR}$  ( $\text{R} = \text{Me}, \text{Et}$ ) are cleaved by  $\text{H}_2\text{O}$  to give the cyclic hydroxo trimer  $\{[\text{Bp}^{\text{Bu}^t}]\text{Zn}(\mu\text{-OH})\}_3$  and by  $\text{MeCO}_2\text{H}$  to give  $[\text{Bp}^{\text{Bu}^t}]\text{Zn}(\eta^2\text{-O}_2\text{CMe})$ .  $\text{Me}_2\text{CO}$ ,  $\text{MeCHO}$ , and  $(\text{CH}_2\text{O})_n$  insert into the B-H bond of  $[\text{Bp}^{\text{Bu}^t}]\text{ZnR}$ , in preference to the Zn-R bond, to give the complexes  $\{\text{HB}(\text{OR}')(\text{3-Bu}^t\text{pz})_2\}\text{ZnR}$  ( $\text{R}' = \text{Me}, \text{Et}, \text{Pr}^i$ ). The molecular structures of  $[\text{Tp}^{\text{Me}_2}]\text{ZnMe}$ ,  $[\text{Tp}^{\text{Me}_2}]_2\text{Zn}$ ,  $[\text{Tp}^{\text{Bu}^t}]\text{ZnH}$ ,  $[\text{Tp}^{\text{Bu}^t}]\text{Zn}(\eta^1\text{-O}_2\text{CMe})$ ,  $[\text{Tp}^{\text{Bu}^t}]\text{ZnNCS}$ ,  $[\text{Bp}^{\text{Bu}^t}]\text{ZnBu}^t$ , and  $\{[\text{Bp}^{\text{Bu}^t}]\text{Zn}(\mu\text{-OH})\}_3$  have been determined by X-ray diffraction.  $[\text{Tp}^{\text{Me}_2}]\text{ZnMe}$  is orthorhombic, *Pcmn* (No. 62),  $a = 7.831(2) \text{ \AA}$ ,  $b = 13.376(4) \text{ \AA}$ ,  $c = 18.877(4) \text{ \AA}$ ,  $V = 1977(1) \text{ \AA}^3$ , and  $Z = 4$ .  $[\text{Tp}^{\text{Me}_2}]_2\text{Zn}$  is triclinic,  $P\bar{1}$  (No. 2),  $a = 8.806(1) \text{ \AA}$ ,  $b = 10.195(2) \text{ \AA}$ ,  $c = 10.800(2) \text{ \AA}$ ,  $\alpha = 63.46(2)^\circ$ ,  $\beta = 85.11(2)^\circ$ ,  $\gamma = 79.63(1)^\circ$ ,  $V = 853(1) \text{ \AA}^3$ , and  $Z = 1$ .  $[\text{Tp}^{\text{Bu}^t}]\text{ZnH}$  is monoclinic, *Pn* (No. 7),  $a = 8.262(1) \text{ \AA}$ ,  $b = 15.465(2) \text{ \AA}$ ,  $c = 9.696(2) \text{ \AA}$ ,  $\beta = 100.76(2)^\circ$ ,  $V = 1217(1) \text{ \AA}^3$ , and  $Z = 2$ .  $[\text{Tp}^{\text{Bu}^t}]\text{Zn}(\eta^1\text{-O}_2\text{CMe})$  is orthorhombic, *P2<sub>1</sub>cn* (No. 33),  $a = 10.433(1) \text{ \AA}$ ,  $b = 15.832(2) \text{ \AA}$ ,  $c = 19.292(3) \text{ \AA}$ ,  $V = 3186(1) \text{ \AA}^3$ , and  $Z = 4$ .  $[\text{Tp}^{\text{Bu}^t}]\text{ZnNCS}$  is monoclinic, *P2<sub>1</sub>/n* (No. 14),  $a = 9.703(2) \text{ \AA}$ ,  $b = 17.001(4) \text{ \AA}$ ,  $c = 16.582(3) \text{ \AA}$ ,  $\beta = 95.08(1)^\circ$ ,  $V = 2725(1) \text{ \AA}^3$ , and  $Z = 4$ .  $[\text{Bp}^{\text{Bu}^t}]\text{ZnBu}^t$  is monoclinic, *P2<sub>1</sub>/n* (No. 14),  $a = 14.912(7) \text{ \AA}$ ,  $b = 8.556(2) \text{ \AA}$ ,  $c = 18.482(5) \text{ \AA}$ ,  $\beta = 112.86(3)^\circ$ ,  $V = 2173(2) \text{ \AA}^3$ , and  $Z = 4$ .  $\{[\text{Bp}^{\text{Bu}^t}]\text{Zn}(\mu\text{-OH})\}_3$  is orthorhombic, *Pc2<sub>1</sub>n* (No. 33),  $a = 12.302(2) \text{ \AA}$ ,  $b = 20.057(6) \text{ \AA}$ ,  $c = 22.110(2) \text{ \AA}$ ,  $V = 5455(2) \text{ \AA}^3$ , and  $Z = 4$ .

## Introduction

Organozinc complexes are presently used extensively in both organic and organometallic syntheses.<sup>1,2</sup> In particular, organozinc reagents offer valuable alternatives to the corresponding magnesium and lithium reagents in terms of both their reactivity and selectivity. However, in contrast to dialkylmagnesium reagents, in which the Mg centers are typically four-coordinate and tetrahedral (both in the solid state and as solvated derivatives in solution), dialkylzinc complexes exist as

monomeric two-coordinate linear molecules. In view of the different structures of dialkylmagnesium and dialkylzinc complexes, it is of some interest to compare the reactivity of isostructural organomagnesium and organozinc complexes. Such studies would thereby allow a comparison of the intrinsic reactivity of Zn-C and Mg-C bonds. We have recently described the use of the sterically-demanding tris(3-*tert*-butylpyrazolyl)hydroborato ligand,  $[\text{Tp}^{\text{Bu}^t}]$ ,<sup>3,4</sup> to provide a well-defined coordination environment for a series of four-coordinate monomeric magnesium alkyl derivatives  $[\text{Tp}^{\text{Bu}^t}]\text{MgR}$ .<sup>5</sup>

<sup>®</sup> Abstract published in *Advance ACS Abstracts*, November 1, 1994.

(1) (a) Boersma, J. In *Comprehensive Organometallic Chemistry*; Wilkinson, G., Stone, F. G. A., Abel, E. W., Eds.; Pergamon Press: Oxford, U.K., 1982; Vol. 2, pp 823-862. (b) Coates, G. E.; Green, M. L. H.; Wade, K. *Organometallic Compounds. Volume I: The Main Group Elements*, 3rd ed.; Methuen: London, 1967. (c) Elschenbroich, C.; Salzer, A. *Organometallics: A Concise Introduction*, 2nd ed.; VCH: New York, 1992.

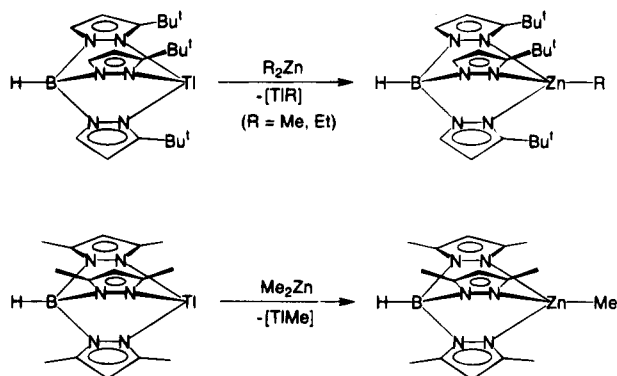
(2) (a) Miginiac, L. In *The Chemistry of the Metal-Carbon Bond*; Hartley, F. R., Patai, S., Eds.; Wiley: New York, 1985; Vol. 3, Chapter 2. (b) Furukawa, J.; Kawabata, N. *Adv. Organomet. Chem.* **1974**, *12*, 83-134. (c) Erdik, E. *Tetrahedron* **1992**, *48*, 9577-9648.

(3) Trofimenko, S.; Calabrese, J. C.; Thompson, J. S. *Inorg. Chem.* **1987**, *26*, 1507-1514.

(4) The nomenclature adopted here for tris(pyrazolyl)hydroborato ligands is based on that described by Trofimenko. Thus, the tris(pyrazolyl)hydroborato ligands are represented by the abbreviation Tp, with the 3- and 5-alkyl substituents listed, respectively, as superscripts.

(5) (a) Han, R.; Looney, A.; Parkin, G. *J. Am. Chem. Soc.* **1989**, *111*, 7276-7278. (b) Han, R.; Parkin, G. *J. Am. Chem. Soc.* **1990**, *112*, 3662-3663. (c) Han, R.; Parkin, G. *Organometallics* **1991**, *10*, 1010-1020. (d) Han, R.; Parkin, G. *J. Am. Chem. Soc.* **1992**, *114*, 748-757.

Scheme 1



Here we report that the tris(3-*tert*-butylpyrazolyl)hydroborato ligand also permits the isolation of the corresponding monomeric zinc alkyl and hydride derivatives [Tp<sup>Bu<sup>t</sup></sup>]ZnR and [Tp<sup>Bu<sup>t</sup></sup>]ZnH. Furthermore, we also describe the use of the bis(3-*tert*-butylpyrazolyl)hydroborato ligand, [Bp<sup>Bu<sup>t</sup></sup>],<sup>3</sup> to stabilize monomeric three-coordinate zinc alkyls [Bp<sup>Bu<sup>t</sup></sup>]ZnR. Some of this work has been previously communicated.<sup>6</sup>

## Results and Discussion

**Syntheses, Characterization, and Reactivity of the Four-Coordinate Zinc Alkyl Complexes [Tp<sup>Bu<sup>t</sup></sup>]ZnR and [Tp<sup>Me<sub>2</sub></sup>]ZnR.** Our recent studies have demonstrated that the sterically demanding tris(3-*tert*-butylpyrazolyl)hydroborato ligand, [Tp<sup>Bu<sup>t</sup></sup>],<sup>3</sup> provides a well-defined coordination environment for investigating the chemistry of four-coordinate alkyl complexes of beryllium and magnesium.<sup>5,7</sup> The corresponding zinc alkyl derivatives [Tp<sup>Bu<sup>t</sup></sup>]ZnR (R = Me, Et) may also be readily prepared by metathesis of R<sub>2</sub>Zn with Tl[Tp<sup>Bu<sup>t</sup></sup>] (Scheme 1). The reaction is accompanied by the deposition of Tl due to decomposition of unstable [TlR], thereby providing an effective driving force for the reaction.<sup>8</sup> In addition to the bulky tris(3-*tert*-butylpyrazolyl)hydroborato ligand, [Tp<sup>Bu<sup>t</sup></sup>], the less sterically demanding tris(3,5-dimethylpyrazolyl)hydroborato ligand, [Tp<sup>Me<sub>2</sub></sup>], may be used to prepare the methyl derivative [Tp<sup>Me<sub>2</sub></sup>]ZnMe (Scheme 1), of which the magnesium analogue [Tp<sup>Me<sub>2</sub></sup>]MgMe has been previously synthesized.<sup>5,9</sup>

The complexes [Tp<sup>Bu<sup>t</sup></sup>]ZnR represent the first examples of zinc alkyl derivatives stabilized by an η<sup>3</sup>-tris(pyrazolyl)hydroborato ligand.<sup>6a</sup> Vahrenkamp has also utilized the tris(3,5-diphenylpyrazolyl)hydroborato and tris(3-arylpyrazolyl)hydroborato (aryl = phenyl, tolyl, anisyl) ligands to synthesize the complexes [Tp<sup>Ph<sub>2</sub></sup>]ZnR and [Tp<sup>Ar</sup>]ZnR (R = Me, Et, Bu<sup>t</sup>, Ph).<sup>10</sup> Furthermore, the cadmium analogues [Tp<sup>Bu<sup>t</sup></sup>]CdR<sup>11</sup> and [Tp<sup>Me<sub>2</sub></sup>]CdR<sup>12</sup> have also been recently prepared using a similar approach.

(6) (a) Gorrell, I. B.; Looney, A.; Parkin, G. *J. Chem. Soc., Chem. Commun.* **1990**, 220–222. (b) Gorrell, I. B.; Looney, A.; Parkin, G.; Rheingold, A. L. *J. Am. Chem. Soc.* **1990**, *112*, 4068–4069. (c) Han, R.; Gorrell, I. B.; Looney, A. G.; Parkin, G. *J. Chem. Soc., Chem. Commun.* **1991**, 717–719.

(7) Han, R.; Parkin, G. *Inorg. Chem.* **1993**, *32*, 4968–4970.

(8) Gilman, H.; Jones, R. G. *J. Am. Chem. Soc.* **1946**, *68*, 517–520.

(9) Han, R.; Parkin, G. *J. Organomet. Chem.* **1990**, *393*, C43–C46.

(10) (a) Alsfasser, R.; Powell, A. K.; Vahrenkamp, H. *Angew. Chem., Int. Ed. Engl.* **1990**, *29*, 898–899. (b) Alsfasser, R.; Powell, A. K.; Trofimenko, S.; Vahrenkamp, H. *Chem. Ber.* **1993**, *126*, 685–694.

(11) Looney, A.; Saleh, A.; Zhang, Y.; Parkin, G. *Inorg. Chem.* **1994**, *33*, 1158–1164.

(12) Reger, D. L.; Mason, S. S. *Organometallics* **1993**, *12*, 2600–2603.

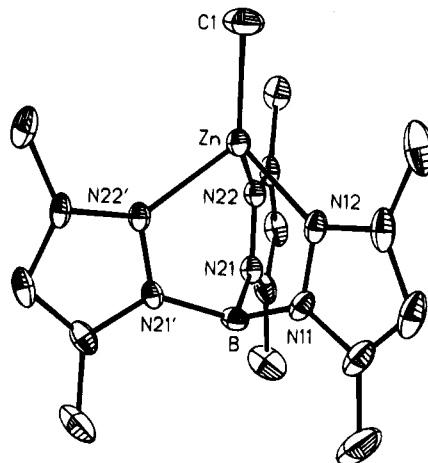


Figure 1. Molecular structure of [Tp<sup>Me<sub>2</sub></sup>]ZnMe.

Table 1. Selected Bond Lengths (Å) and Angles (deg) for [Tp<sup>Me<sub>2</sub></sup>]ZnMe

Zn–C(1)	1.981(8)	Zn–N(12)	2.048(6)
Zn–N(22)	2.056(4)	N(11)–N(12)	1.377(8)
N(21)–N(22)	1.364(6)	B–N(11)	1.540(12)
B–N(21)	1.545(7)		
C(1)–Zn–N(12)	123.6(4)	C(1)–Zn–N(22)	125.8(2)
N(12)–Zn–N(22)	90.5(2)	N(22)–Zn–N(22')	89.9(2)

Table 2. Comparison of Bond Lengths and Angles for [Tp<sup>R,R</sup>]MMe Complexes

	<i>d</i> (M–C)/Å	<i>d</i> (M–N)/Å <sup>a</sup>	N–M–C/deg <sup>a</sup>	ref
[Tp <sup>Me<sub>2</sub></sup> ]ZnMe	1.981(8)	2.053[10]	125[2]	this work
[Tp <sup>Ph</sup> ]ZnMe	1.950(4)	2.108[30]	126[2]	<i>b</i>
[Tp <sup>Bu<sup>t</sup></sup> ]ZnMe	1.971(4)	2.109[10]	125[2]	<i>c</i>
[Tp <sup>Bu<sup>t</sup></sup> ]MgMe	2.118(11)	2.135[10]	125[3]	<i>d</i>

<sup>a</sup> The number in parentheses indicates the range of bond lengths and angles. <sup>b</sup> Alsfasser, R.; Powell, A. K.; Trofimenko, S.; Vahrenkamp, H. *Chem. Ber.* **1993**, *126*, 685–694. <sup>c</sup> Yoon, K.; Parkin, G. *J. Am. Chem. Soc.* **1991**, *113*, 8414–8418. <sup>d</sup> Han, R.; Parkin, G. *Organometallics* **1991**, *10*, 1010–1020.

The molecular structures of the methyl derivatives [Tp<sup>Bu<sup>t</sup></sup>]ZnMe<sup>6a,13</sup> and [Tp<sup>Me<sub>2</sub></sup>]ZnMe (Figure 1) have been determined by X-ray diffraction, confirming the η<sup>3</sup>-coordination mode of the tris(pyrazolyl)hydroborato ligands. Selected bond lengths and angles for [Tp<sup>Me<sub>2</sub></sup>]ZnMe are presented in Table 1. The zinc centers are appropriately described as trigonally distorted tetrahedral, with average C–Zn–N and N–Zn–N bond angles of *ca.* 125 and 90°, respectively. The molecular structure of the derivative [Tp<sup>Ph</sup>]ZnMe has also been determined by Vahrenkamp, and average bond lengths and angles for these compounds are compared in Table 2.

Examination of Table 2 indicates the trend that the average Zn–N bond length increases very slightly as the steric bulk of the tris(pyrazolyl)hydroborato ligand increases.<sup>14</sup> Thus, the average Zn–N bond length of 2.053[10] Å in [Tp<sup>Me<sub>2</sub></sup>]ZnMe increases to 2.109[10] Å in [Tp<sup>Bu<sup>t</sup></sup>]ZnMe. The Zn–C bond lengths for the complexes [Tp<sup>Bu<sup>t</sup></sup>]ZnMe [1.981(8) Å] and [Tp<sup>Bu<sup>t</sup></sup>]ZnMe [1.971(4) Å] are close to, but slightly less than, the sum of the covalent radii of Zn and C (2.02 Å),<sup>15</sup> and are also in the range of known Zn–C bond lengths. For example,

(13) Yoon, K.; Parkin, G. *J. Am. Chem. Soc.* **1991**, *113*, 8414–8418.

(14) The cone angles of tris(pyrazolyl)hydroborato ligand increases from [Tp<sup>Me<sub>2</sub></sup>] (224°) to [Tp<sup>Bu<sup>t</sup></sup>] (244°). See ref 3.

(15) Pauling, L. *The Nature of The Chemical Bond*, 3rd ed.; Cornell University Press: Ithaca, NY, 1960; p 256.

Table 3. Terminal Zn–C Bond Lengths for R<sub>2</sub>Zn Complexes

R <sub>2</sub> Zn	d(Zn–C)/Å	ref
Me <sub>2</sub> Zn	1.930(2)	a
Et <sub>2</sub> Zn	1.950(2)	a
Pr <sup>n</sup> <sub>2</sub> Zn	1.952(3)	a
[c-Me <sub>2</sub> SiCH <sub>2</sub> SiMe <sub>2</sub> CH <sub>2</sub> SiMe <sub>2</sub> CH <sub>2</sub> ] <sub>2</sub> Zn	1.937(2)	b
[(Pr <sup>n</sup> O)SiMe <sub>2</sub> CH <sub>2</sub> ] <sub>2</sub> Zn	1.97[2]	c
[PhZn(μ-Ph)] <sub>2</sub>	1.946[5]	d
Zn{C <sub>6</sub> H <sub>3</sub> (CF <sub>3</sub> ) <sub>3</sub> } <sub>2</sub>	1.950[1]	e
Zn[2,4-Bu <sub>2</sub> C <sub>5</sub> H <sub>3</sub> ] <sub>2</sub>	1.969(8)	f
[(XMe <sub>2</sub> Si)(Me <sub>3</sub> Si) <sub>2</sub> C] <sub>2</sub> Zn		
X = Me	1.982(2)	g
X = CF <sub>3</sub> CO <sub>2</sub>	1.974(3)	h
X = MeO	1.980(4)	i
X = HO	1.968[3]	i
X = Cl	1.983(7)	j

<sup>a</sup> Almenningen, A.; Helgaker, T. U.; Haaland, A.; Samdal, S. *Acta Chem. Scand.* **1982**, A36, 159–156. <sup>b</sup> Westerhausen, M.; Rademacher, B. *J. Organomet. Chem.* **1993**, 443, 25–33. <sup>c</sup> Gais, H.-J.; Bülow, G.; Raabe, G. *J. Am. Chem. Soc.* **1993**, 115, 7215–7218. <sup>d</sup> Markies, P. R.; Schat, G.; Akkerman, O. S.; Bickelhaupt, F.; Smeets, W. J. J.; Spek, A. L. *Organometallics* **1990**, 9, 2243–2247. <sup>e</sup> Brooker, S.; Bertel, N.; Stalke, D.; Noltemeyer, M.; Roesky, H. W.; Sheldrick, G. M.; Edelmann, F. T. *Organometallics* **1992**, 11, 192–195. <sup>f</sup> Ernst, R. D.; Freeman, J. W.; Swepston, P. N.; Wilson, D. R. *J. Organomet. Chem.* **1991**, 402, 17–25. <sup>g</sup> Westerhausen, M.; Rademacher, B.; Poll, W. *J. Organomet. Chem.* **1991**, 421, 175–188. <sup>h</sup> Al-Juaid, S. S.; Eaborn, C.; Habtemariam, A.; Hitchcock, P. B.; Smith, J. D. *J. Organomet. Chem.* **1992**, 437, 41–45. <sup>i</sup> Aigbirhio, F. I.; Al-Juaid, S. S.; Eaborn, C.; Habtemariam, A.; Hitchcock, P. B.; Smith, J. D. *J. Organomet. Chem.* **1991**, 405, 149–160. <sup>j</sup> Cited in ref. i.

dialkylzinc complexes typically exhibit Zn–C bond lengths in the range 1.9–2.0 Å, as summarized in Table 3.

The Zn–C bond lengths in the complexes [Tp<sup>R,R'</sup>]ZnMe are also similar to those in the zinc ethyl derivatives (EtZn)<sub>2</sub>(μ-C<sub>20</sub>H<sub>28</sub>N<sub>4</sub>) (1.978[4] Å)<sup>16</sup> and [(EtZn)<sub>2</sub>{2-N(SiMe<sub>3</sub>)C<sub>5</sub>H<sub>3</sub>N-6-Me}]<sub>2</sub> (1.95[2] Å).<sup>17</sup> Moreover, the four-coordinate dialkyl derivatives Me<sub>2</sub>Zn[(CH<sub>2</sub>NMe)<sub>3</sub>]<sub>2</sub> [1.987(6) Å]<sup>18</sup> and Zn[(CH<sub>2</sub>)<sub>3</sub>NMe<sub>2</sub>]<sub>2</sub> [1.984(5) Å, X-ray; 1.991(6) Å, electron diffraction]<sup>19</sup> also have similar Zn–C bond lengths.

It is also worth noting that the Zn–C bond length of [Tp<sup>Bu<sup>t</sup></sup>]ZnMe [1.971(4) Å]<sup>13</sup> listed in Table 2 is longer than the value cited in the original report [1.890(10) Å].<sup>6a</sup> It is possible that the shorter value, which is anomalous compared to other Zn–CH<sub>3</sub> bond lengths (*vide supra*), is an artifact due to compositional disorder with an impurity (possibly [Tp<sup>Bu<sup>t</sup></sup>]ZnOH), since it is well documented that trace impurities may artificially influence apparent bond lengths as determined by single crystal X-ray diffraction.<sup>20</sup>

The Zn–C bond length in [Tp<sup>Bu<sup>t</sup></sup>]ZnMe [1.971(4) Å] may also be compared with the Mg–C bond length [2.118(11) Å] in the isostructural magnesium derivative, [Tp<sup>Bu<sup>t</sup></sup>]MgMe.<sup>5c</sup> As expected, the Zn–C bond length is slightly shorter than the Mg–C bond length,<sup>15</sup> and similar results have been observed in comparisons of other structurally related Mg and Zn alkyl derivatives. For example, the Zn–C bond length [1.957(5) Å] in the adduct (18-crown-6)ZnEt<sub>2</sub> is also shorter than the Mg–C

(16) Spek, A. L.; Jastrzebski, J. T. B. H.; van Koten, G. *Acta Crystallogr.* **1987**, C43, 2006–2007.

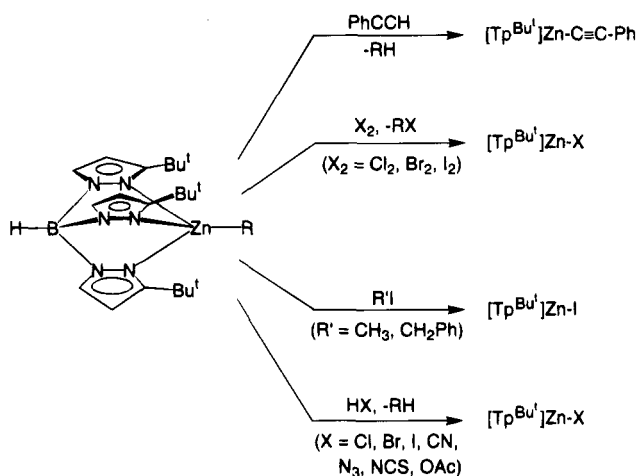
(17) Engelhardt, L. M.; Jacobsen, G. E.; Patalinghug, W. C.; Skelton, B. W.; Raston, C. L.; White, A. H. *J. Chem. Soc., Dalton Trans.* **1991**, 2859–2868.

(18) Hursthouse, M. B.; Motevalli, M.; O'Brien, P.; Walsh, J. R.; Jones, A. C. *Organometallics* **1991**, 10, 3196–3200.

(19) Dekker, J.; Boersma, J.; Fernholt, L.; Haaland, A.; Spek, A. L. *Organometallics* **1987**, 6, 1202–1206.

(20) (a) Parkin, G. *Acc. Chem. Res.* **1992**, 25, 455–460. (b) Parkin, G. *Chem. Rev.* **1993**, 93, 887–911.

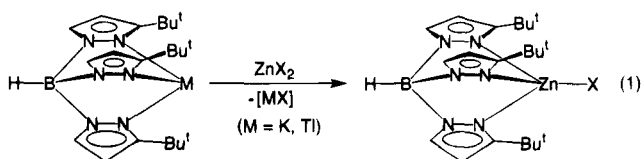
Scheme 2



bond length [2.104(2) Å] in the related complex, (18-crown-6)MgEt<sub>2</sub>.<sup>21</sup>

The alkyl derivatives [Tp<sup>Me<sub>2</sub></sup>]ZnMe, [Tp<sup>Bu<sup>t</sup></sup>]ZnMe, and [Tp<sup>Bu<sup>t</sup></sup>]ZnEt are soluble in hydrocarbon solvents and are characterized in solution by well-defined <sup>1</sup>H and <sup>13</sup>C NMR spectra (Table 4) which provide a useful spectroscopic handle for monitoring reactions. For example, in addition to resonances assignable to the tris(pyrazolyl)hydroborato ligand, the complex [Tp<sup>Bu<sup>t</sup></sup>]ZnMe is characterized by resonances attributable to the Zn–Me group at δ 0.54 ppm in the <sup>1</sup>H NMR spectrum and at δ –2.8 [q, <sup>1</sup>J<sub>C–H</sub> = 118 Hz] in the <sup>13</sup>C NMR spectrum.

The reactivity of the four-coordinate alkyl derivatives [Tp<sup>Bu<sup>t</sup></sup>]ZnR toward a number of reagents has been examined and is summarized in Scheme 2. Halogens (X<sub>2</sub>) rapidly cleave the Zn–C bond to eliminate RX and give the halide complex [Tp<sup>Bu<sup>t</sup></sup>]ZnX (X = Cl, Br, I). Protic reagents (HX) also readily cleave the Zn–R bond in [Tp<sup>Bu<sup>t</sup></sup>]ZnR to eliminate RH, with the concomitant formation of the corresponding [Tp<sup>Bu<sup>t</sup></sup>]ZnX derivative. Thus, the reactions of [Tp<sup>Bu<sup>t</sup></sup>]ZnR with hydrogen chloride, acetic acid, and phenylacetylene give [Tp<sup>Bu<sup>t</sup></sup>]ZnCl, [Tp<sup>Bu<sup>t</sup></sup>]Zn(η<sup>1</sup>-O<sub>2</sub>CMe) and [Tp<sup>Bu<sup>t</sup></sup>]ZnCCPh, respectively. Moreover, HX (X = Br, I, CN, N<sub>3</sub>, NCS), generated *in situ* by the treatment of Me<sub>3</sub>SiX with H<sub>2</sub>O, also reacts with [Tp<sup>Bu<sup>t</sup></sup>]ZnR to give [Tp<sup>Bu<sup>t</sup></sup>]ZnX. Trofimenko has previously synthesized [Tp<sup>Bu<sup>t</sup></sup>]ZnX (X = N<sub>3</sub>, NCS) by the reactions between K[Tp<sup>Bu<sup>t</sup></sup>] and ZnX<sub>2</sub>.<sup>3</sup> In a similar way, the complexes [Tp<sup>Bu<sup>t</sup></sup>]ZnX (X = Cl, Br, I, CN, O<sub>2</sub>CMe) may also be synthesized by metathesis of ZnX<sub>2</sub> with either K[Tp<sup>Bu<sup>t</sup></sup>] or Tl[Tp<sup>Bu<sup>t</sup></sup>] (eq 1). Furthermore, Vahrenkamp and Kläui have also independently used related methods for the synthesis of [Tp<sup>Ph<sub>2</sub></sup>]ZnX and [Tp<sup>Ar</sup>]ZnX derivatives.<sup>10,22</sup>



The molecular structures of the derivatives [Tp<sup>Bu<sup>t</sup></sup>]ZnX (X = Cl, Br, I),<sup>13</sup> [Tp<sup>Bu<sup>t</sup></sup>]ZnCN,<sup>23</sup> [Tp<sup>Bu<sup>t</sup></sup>]Zn(η<sup>1</sup>-O<sub>2</sub>CMe),

(21) Pajerski, A. D.; BergStresser, G. L.; Parvez, M.; Richey, H. G., Jr. *J. Am. Chem. Soc.* **1988**, 110, 4844–4845.

(22) Hartmann, F.; Kläui, W.; Kremer-Aach, A.; Mootz, D.; Strerath, A.; Wunderlich, H. Z. *Anorg. Allg. Chem.* **1993**, 619, 2071–2076.

(23) Yoon, K.; Parkin, G. *Inorg. Chem.* **1992**, 31, 1656–1662.

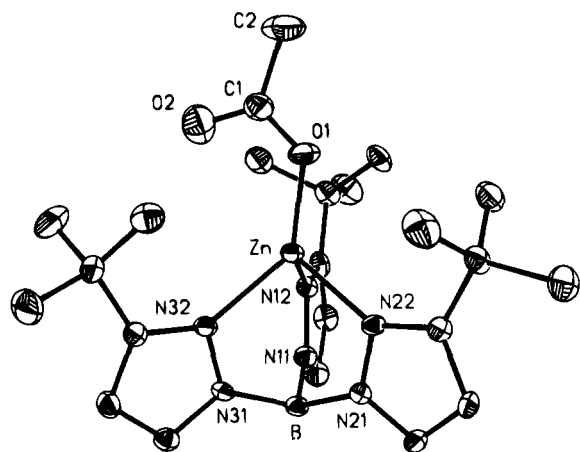


Figure 2. Molecular structure of  $[\text{Tp}^{\text{Bu}^t}]\text{Zn}(\eta^1\text{-O}_2\text{CMe})$ .

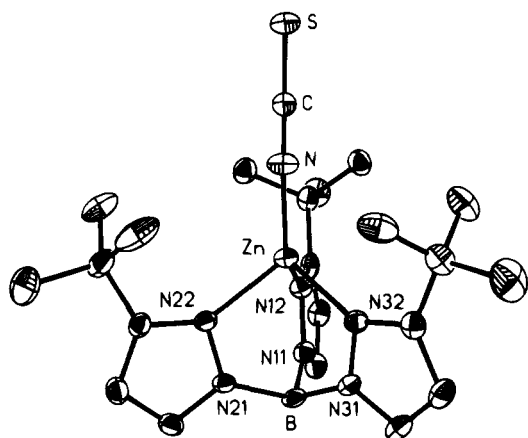


Figure 3. Molecular structure of  $[\text{Tp}^{\text{Bu}^t}]\text{ZnNCS}$ .

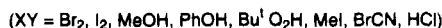
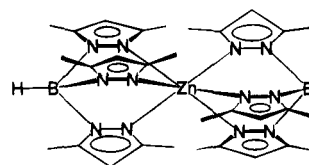
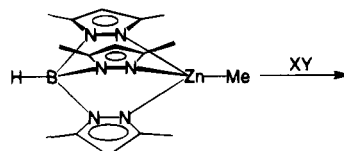
and  $[\text{Tp}^{\text{Bu}^t}]\text{ZnNCS}$  have been determined by X-ray diffraction, with the structures of  $[\text{Tp}^{\text{Bu}^t}]\text{Zn}(\eta^1\text{-O}_2\text{CMe})$  and  $[\text{Tp}^{\text{Bu}^t}]\text{ZnNCS}$  shown in Figures 2 and 3. Selected bond lengths and angles for  $[\text{Tp}^{\text{Bu}^t}]\text{Zn}(\eta^1\text{-O}_2\text{CMe})$  and  $[\text{Tp}^{\text{Bu}^t}]\text{ZnNCS}$  are presented in Tables 5 and 6.

The X-ray diffraction studies confirm that the acetate ligand in  $[\text{Tp}^{\text{Bu}^t}]\text{Zn}(\eta^1\text{-O}_2\text{CMe})$  is bound to zinc in a unidentate mode, with substantially different Zn–O separations of ca. 1.86 Å and 2.95 Å.<sup>24</sup> The structure of  $[\text{Tp}^{\text{Bu}^t}]\text{Zn}(\eta^1\text{-O}_2\text{CMe})$ , which is similar to that proposed for  $[\text{Tp}^{\text{Bu}^t}]\text{Mg}(\eta^1\text{-O}_2\text{CMe})$ ,<sup>5</sup> contrasts with that of the copper analogue  $[\text{Tp}^{\text{Bu}^t}]\text{Cu}(\eta^2\text{-O}_2\text{CMe})$  which has been proposed to exhibit bidentate coordination of the acetate ligand on the basis of the observed EPR spectrum.<sup>25,26</sup> Such a change in coordination mode for copper and zinc derivatives is to be anticipated on the basis of our recent structural studies on the nitrate derivatives  $[\text{Tp}^{\text{Bu}^t}]\text{M}(\text{NO}_3)$  (M = Co, Ni, Cu, Zn), for which the coordination mode of the nitrate ligand varies from unidentate for Zn to symmetric bidentate for Ni and Cu.<sup>27–29</sup>

It is of particular interest to compare the reactivity of  $[\text{Tp}^{\text{Bu}^t}]\text{ZnR}$  with that of the isostructural magnesium

derivative  $[\text{Tp}^{\text{Bu}^t}]\text{MgR}$ . In this regard, the rates of the reactions of  $[\text{Tp}^{\text{Bu}^t}]\text{ZnR}$  are significantly slower than those of the corresponding magnesium derivatives.<sup>5</sup> For example, although both  $[\text{Tp}^{\text{Bu}^t}]\text{ZnEt}$  and  $[\text{Tp}^{\text{Bu}^t}]\text{MgEt}$  react with  $\text{PhCH}_2\text{I}$  to give  $[\text{Tp}^{\text{Bu}^t}]\text{MI}$  (M = Zn, Mg), the half-lives of samples prepared under similar conditions are ca.  $2.3 \times 10^3$  h and 0.23 h at 100 °C, respectively, a factor of 4 orders of magnitude difference in reactivity. A similar difference in reactivity is observed in the reactions of  $[\text{Tp}^{\text{Bu}^t}]\text{ZnMe}$  and  $[\text{Tp}^{\text{Bu}^t}]\text{MgMe}$  toward  $\text{CO}_2$ . Thus, whereas  $[\text{Tp}^{\text{Bu}^t}]\text{MgMe}$  undergoes insertion of  $\text{CO}_2$  into the Mg–C bond at room temperature,<sup>30</sup> no reaction is observed between  $[\text{Tp}^{\text{Bu}^t}]\text{ZnMe}$  and  $\text{CO}_2$  at 140 °C, even though the expected product,  $[\text{Tp}^{\text{Bu}^t}]\text{Zn}(\eta^1\text{-O}_2\text{CMe})$ , has been prepared independently (*vide infra*).<sup>31</sup> Finally, whereas benzene solutions of the magnesium alkyl derivatives  $[\text{Tp}^{\text{Bu}^t}]\text{MgR}$  (R = Me, Et,  $\text{Pr}^i$ ,  $\text{Bu}^t$ ) react immediately with  $\text{O}_2$  at room temperature to give alkyl peroxy derivatives  $[\text{Tp}^{\text{Bu}^t}]\text{MgOOR}$ ,<sup>5,32</sup> solutions of the zinc derivative  $[\text{Tp}^{\text{Bu}^t}]\text{ZnEt}$  are stable toward  $\text{O}_2$  at 100 °C!

The reactivity of the less sterically demanding derivative  $[\text{Tp}^{\text{Me}_2}]\text{ZnMe}$  has also been investigated. This complex is indeed more reactive than  $[\text{Tp}^{\text{Bu}^t}]\text{ZnMe}$  toward a number of reagents, e.g.  $\text{Br}_2$ ,  $\text{I}_2$ , MeOH, PhOH,  $\text{Bu}^t\text{OOH}$ , MeI, BrCN, and HCl. However, in each case the major product of the reaction is the six-coordinate sandwich complex  $[\text{Tp}^{\text{Me}_2}]_2\text{Zn}$ , as a result of ligand redistribution (eq 2).<sup>33</sup> The facile formation of  $[\text{Tp}^{\text{Me}_2}]_2\text{Zn}$



Zn in the reactions of  $[\text{Tp}^{\text{Me}_2}]\text{ZnMe}$  is analogous to that observed for (i) the magnesium derivatives  $[\text{Tp}^{\text{Me}_2}]\text{MgR}$ ,<sup>5,9</sup> and (ii) the zinc alkyls  $\text{LOEtZnR}$  supported by the oxygen tripod ligand  $\text{LOEt} \equiv [\text{CpCo}\{\text{P}(\text{O})(\text{OEt})_2\}_3]$ .<sup>34</sup> Furthermore, the bis complex  $[\text{Tp}^{\text{Ph}}]_2\text{Zn}$  (and also  $[\text{Tp}^{\text{Ar}_2}]_2\text{Zn}$  derivatives) has also been observed independently by Vahrenkamp and Kläui to be a product of the reactions of  $[\text{Tp}^{\text{Ph}}]\text{ZnX}$  derivatives.<sup>10b,22</sup> Such observations again underscore the benefits associated with the bulky  $[\text{Tp}^{\text{Bu}^t}]$  ligand, the “tetrahedral enforcer”<sup>3</sup> nature of which effectively inhibits such reaction pathways.

(30) It should be noted that the reaction between  $[\text{Tp}^{\text{Bu}^t}]\text{MgMe}$  and  $\text{CO}_2$  is slow, but observable, at room temperature. However, at 80 °C the reaction takes place readily. See ref 5.

(31) It is worth noting that dialkylzinc compounds also do not react readily with carbon dioxide. However, in the presence of *N*-methylimidazole as a catalyst, insertion of  $\text{CO}_2$  into the Zn–C bond may occur. See ref 1a.

(32) In addition, the trimethylsilylmethyl derivative  $[\text{Tp}^{\text{Bu}^t}]\text{MgCH}_2\text{SiMe}_3$  reacts with  $\text{O}_2$  to give the trimethylsiloxy derivative: Han, R.; Parkin, G. *Polyhedron* **1990**, *9*, 2655–2657.

(33) In the absence of any reagent, solutions of  $[\text{Tp}^{\text{Me}_2}]\text{ZnMe}$  in benzene may be heated to 120 °C in a sealed tube for 12 h without significant decomposition.

(34) Looney, A.; Cornebise, M.; Miller, D.; Parkin, G. *Inorg. Chem.* **1992**, *31*, 989–992.

(24) The thioacetate derivative  $[\text{Tp}^{\text{Ph}}]\text{Zn}(\eta^1\text{-SC}(\text{O})\text{Me})$  also exhibits unidentate coordination with  $d(\text{Zn}–\text{S}) = 2.20$  Å and  $d(\text{Zn} \cdots \text{O}) = 2.92$  Å. See ref 10.

(25) Tolman, W. B. *Inorg. Chem.* **1991**, *30*, 4877–4880.

(26) Moreover, the related derivative  $[\text{Tp}^{\text{Pr}^2}]\text{Cu}(\eta^2\text{-O}_2\text{CC}_6\text{H}_4\text{Cl})$  has been structurally characterized by X-ray diffraction: Kitajima, N.; Fujisawa, K.; Mor-oka, Y. *J. Am. Chem. Soc.* **1990**, *29*, 357–358.

(27) Han, R.; Parkin, G. *J. Am. Chem. Soc.* **1991**, *113*, 9707–9708.

(28) Han, R.; Looney, A.; McNeill, K.; Parkin, G.; Rheingold, A. L.; Haggerty, B. S. *J. Inorg. Biochem.* **1993**, *49*, 105–121.

(29) Looney, A.; Han, R.; McNeill, K.; Parkin, G. *J. Am. Chem. Soc.* **1993**, *115*, 4690–4697.

Table 4. NMR Data<sup>a</sup>

type	assgnt	$\delta$ /ppm	coupling/Hz	type	assgnt	$\delta$ /ppm	coupling/Hz
<sup>1</sup> H NMR	$\eta^3$ -HB{C <sub>3</sub> N <sub>2</sub> H <sub>2</sub> C(CH <sub>3</sub> ) <sub>3</sub> } <sub>3</sub>	1.41	s	<sup>13</sup> C NMR	$\eta^3$ -HB{C <sub>3</sub> N <sub>2</sub> H <sub>2</sub> C(CH <sub>3</sub> ) <sub>3</sub> } <sub>3</sub>	30.7	q, <sup>1</sup> J <sub>C-H</sub> = 126 spt (partial res), <sup>3</sup> J <sub>C-H</sub> = 5
	$\eta^3$ -HB{C <sub>3</sub> N <sub>2</sub> H <sub>2</sub> C(CH <sub>3</sub> ) <sub>3</sub> } <sub>3</sub>	5.85	d, <sup>3</sup> J <sub>H-H</sub> = 2.2		$\eta^3$ -HB{C <sub>3</sub> N <sub>2</sub> H <sub>2</sub> C(CH <sub>3</sub> ) <sub>3</sub> } <sub>3</sub>	32.0	dct (partial res), <sup>2</sup> J <sub>C-H</sub> = 4
	1 H	7.36	d, <sup>3</sup> J <sub>H-H</sub> = 2.2		$\eta^3$ -HB{C <sub>3</sub> N <sub>2</sub> H <sub>2</sub> C(CH <sub>3</sub> ) <sub>3</sub> } <sub>3</sub>	102.0	d, <sup>1</sup> J <sub>C-H</sub> = 175
	$\eta^3$ -HB{C <sub>3</sub> N <sub>2</sub> H <sub>2</sub> C(CH <sub>3</sub> ) <sub>3</sub> } <sub>3</sub>	not obsd			1 C	135.2	d, <sup>1</sup> J <sub>C-H</sub> = 185
	ZnCH <sub>3</sub>	0.54	s		1 C	164.4	s
				ZnCH <sub>3</sub>	-2.8	q, <sup>1</sup> J <sub>C-H</sub> = 118	
<sup>1</sup> H NMR	$\eta^3$ -HB{C <sub>3</sub> N <sub>2</sub> H <sub>2</sub> C(CH <sub>3</sub> ) <sub>3</sub> } <sub>3</sub>	1.41	s	<sup>13</sup> C NMR	$\eta^3$ -HB{C <sub>3</sub> N <sub>2</sub> H <sub>2</sub> C(CH <sub>3</sub> ) <sub>3</sub> } <sub>3</sub>	30.9	q, <sup>1</sup> J <sub>C-H</sub> = 126
	$\eta^3$ -HB{C <sub>3</sub> N <sub>2</sub> H <sub>2</sub> C(CH <sub>3</sub> ) <sub>3</sub> } <sub>3</sub>	5.84	d, <sup>3</sup> J <sub>H-H</sub> = 2.2		$\eta^3$ -HB{C <sub>3</sub> N <sub>2</sub> H <sub>2</sub> C(CH <sub>3</sub> ) <sub>3</sub> } <sub>3</sub>	32.0	spt (partial res), <sup>3</sup> J <sub>C-H</sub> = 5
	1 H	7.36	d, <sup>3</sup> J <sub>H-H</sub> = 2.2		$\eta^3$ -HB{C <sub>3</sub> N <sub>2</sub> H <sub>2</sub> C(CH <sub>3</sub> ) <sub>3</sub> } <sub>3</sub>	102.0	dct (partial res), <sup>2</sup> J <sub>C-H</sub> = 4
	$\eta^3$ -HB{C <sub>3</sub> N <sub>2</sub> H <sub>2</sub> C(CH <sub>3</sub> ) <sub>3</sub> } <sub>3</sub>	not obsd			1 C	135.4	d, <sup>1</sup> J <sub>C-H</sub> = 176
	ZnCH <sub>2</sub> CH <sub>3</sub>	1.31	q, <sup>3</sup> J <sub>H-H</sub> = 8.0		1 C	164.7	d, <sup>2</sup> J <sub>C-H</sub> = 9
	ZnCH <sub>2</sub> CH <sub>3</sub>	1.96	t, <sup>3</sup> J <sub>H-H</sub> = 8.0		ZnCH <sub>2</sub> CH <sub>3</sub>	7.3	d, <sup>1</sup> J <sub>C-H</sub> = 184
					ZnCH <sub>2</sub> CH <sub>3</sub>	13.9	d, <sup>2</sup> J <sub>C-H</sub> = 6
					164.7	s	
					7.3	t, <sup>1</sup> J <sub>C-H</sub> = 116	
					13.9	q, <sup>2</sup> J <sub>C-H</sub> = 4	
						q, <sup>1</sup> J <sub>C-H</sub> = 123	
						t, <sup>2</sup> J <sub>C-H</sub> = 5	
<sup>1</sup> H NMR	$\eta^3$ -HB{C <sub>3</sub> N <sub>2</sub> H(CH <sub>3</sub> ) <sub>2</sub> } <sub>3</sub>	2.14	s	<sup>13</sup> C NMR	$\eta^3$ -HB{C <sub>3</sub> N <sub>2</sub> H(CH <sub>3</sub> ) <sub>2</sub> } <sub>3</sub>	12.3	q, <sup>1</sup> J <sub>C-H</sub> = 128
	$\eta^3$ -HB{C <sub>3</sub> N <sub>2</sub> H(CH <sub>3</sub> ) <sub>2</sub> } <sub>3</sub>	2.20	s		$\eta^3$ -HB{C <sub>3</sub> N <sub>2</sub> H(CH <sub>3</sub> ) <sub>2</sub> } <sub>3</sub>	12.9	q, <sup>1</sup> J <sub>H-H</sub> = 128
	$\eta^3$ -HB{C <sub>3</sub> N <sub>2</sub> H(CH <sub>3</sub> ) <sub>2</sub> } <sub>3</sub>	5.50	s		1 C	104.6	d, <sup>1</sup> J <sub>C-H</sub> = 173
	Zn-CH <sub>3</sub>	0.28	s		1 C	144.1	s
	$\eta^3$ -HB{C <sub>3</sub> N <sub>2</sub> H(CH <sub>3</sub> ) <sub>2</sub> } <sub>3</sub>	not obsd			1 C	148.6	s
				Zn-CH <sub>3</sub>	-16.7	q, <sup>1</sup> J <sub>C-H</sub> = 118	
<sup>1</sup> H NMR	$\eta^3$ -HB{C <sub>3</sub> N <sub>2</sub> H <sub>2</sub> C(CH <sub>3</sub> ) <sub>3</sub> } <sub>3</sub>	1.49	s	<sup>13</sup> C NMR	$\eta^3$ -HB{C <sub>3</sub> N <sub>2</sub> H <sub>2</sub> C(CH <sub>3</sub> ) <sub>3</sub> } <sub>3</sub>	30.9	q, <sup>1</sup> J <sub>C-H</sub> = 125
	$\eta^3$ -HB{C <sub>3</sub> N <sub>2</sub> H <sub>2</sub> C(CH <sub>3</sub> ) <sub>3</sub> } <sub>3</sub>	5.83	d, <sup>3</sup> J <sub>H-H</sub> = 2.2		$\eta^3$ -HB{C <sub>3</sub> N <sub>2</sub> H <sub>2</sub> C(CH <sub>3</sub> ) <sub>3</sub> } <sub>3</sub>	32.3	spt (partial res), <sup>3</sup> J <sub>C-H</sub> = 5
	1 H	7.34	d, <sup>3</sup> J <sub>H-H</sub> = 2.2		$\eta^3$ -HB{C <sub>3</sub> N <sub>2</sub> H <sub>2</sub> C(CH <sub>3</sub> ) <sub>3</sub> } <sub>3</sub>	101.9	s
	$\eta^3$ -HB{C <sub>3</sub> N <sub>2</sub> H <sub>2</sub> C(CH <sub>3</sub> ) <sub>3</sub> } <sub>3</sub>	not obsd			1 C	135.2	d, <sup>1</sup> J <sub>C-H</sub> = 175
	ZnH	5.36	s		1 C	164.1	d, <sup>2</sup> J <sub>C-H</sub> = 9
				1 C	135.2	d, <sup>1</sup> J <sub>C-H</sub> = 187	
				1 C	164.1	d, <sup>2</sup> J <sub>C-H</sub> = 6	
						s	
<sup>1</sup> H NMR	$\eta^3$ -HB{C <sub>3</sub> N <sub>2</sub> H <sub>2</sub> C(CH <sub>3</sub> ) <sub>3</sub> } <sub>3</sub>	1.45	s	<sup>13</sup> C NMR	$\eta^3$ -HB{C <sub>3</sub> N <sub>2</sub> H <sub>2</sub> C(CH <sub>3</sub> ) <sub>3</sub> } <sub>3</sub>	30.6	q, <sup>1</sup> J <sub>C-H</sub> = 126
	$\eta^3$ -HB{C <sub>3</sub> N <sub>2</sub> H <sub>2</sub> C(CH <sub>3</sub> ) <sub>3</sub> } <sub>3</sub>	5.81	d, <sup>3</sup> J <sub>H-H</sub> = 2.2		$\eta^3$ -HB{C <sub>3</sub> N <sub>2</sub> H <sub>2</sub> C(CH <sub>3</sub> ) <sub>3</sub> } <sub>3</sub>	32.1	spt (partial res), <sup>3</sup> J <sub>C-H</sub> = 5
	1 H	7.28	d, <sup>3</sup> J <sub>H-H</sub> = 2.2		$\eta^3$ -HB{C <sub>3</sub> N <sub>2</sub> H <sub>2</sub> C(CH <sub>3</sub> ) <sub>3</sub> } <sub>3</sub>	102.7	dct (partial res), <sup>2</sup> J <sub>C-H</sub> = 4
	$\eta^3$ -HB{C <sub>3</sub> N <sub>2</sub> H <sub>2</sub> C(CH <sub>3</sub> ) <sub>3</sub> } <sub>3</sub>	not obsd			1 C	136.2	d, <sup>1</sup> J <sub>C-H</sub> = 176
	ZnO <sub>2</sub> CH	8.91	s		1 C	165.6	d, <sup>2</sup> J <sub>C-H</sub> = 9
				ZnO <sub>2</sub> CH	166.7	d, <sup>1</sup> J <sub>C-H</sub> = 185	
						d, <sup>2</sup> J <sub>C-H</sub> = 8	
						s	
						d, <sup>1</sup> J <sub>C-H</sub> = 202	
<sup>1</sup> H NMR	$\eta^3$ -HB{C <sub>3</sub> N <sub>2</sub> H <sub>2</sub> C(CH <sub>3</sub> ) <sub>3</sub> } <sub>3</sub>	1.47	s	<sup>13</sup> C NMR	$\eta^3$ -HB{C <sub>3</sub> N <sub>2</sub> H <sub>2</sub> C(CH <sub>3</sub> ) <sub>3</sub> } <sub>3</sub>	30.5	q, <sup>1</sup> J <sub>C-H</sub> = 126
	$\eta^3$ -HB{C <sub>3</sub> N <sub>2</sub> H <sub>2</sub> C(CH <sub>3</sub> ) <sub>3</sub> } <sub>3</sub>	5.83	d, <sup>3</sup> J <sub>H-H</sub> = 2.2		$\eta^3$ -HB{C <sub>3</sub> N <sub>2</sub> H <sub>2</sub> C(CH <sub>3</sub> ) <sub>3</sub> } <sub>3</sub>	32.1	spt (partial res)
	1 H	7.31	d, <sup>3</sup> J <sub>H-H</sub> = 2.2		$\eta^3$ -HB{C <sub>3</sub> N <sub>2</sub> H <sub>2</sub> C(CH <sub>3</sub> ) <sub>3</sub> } <sub>3</sub>	102.6	<sup>3</sup> J <sub>C-H</sub> = 5
	$\eta^3$ -HB{C <sub>3</sub> N <sub>2</sub> H <sub>2</sub> C(CH <sub>3</sub> ) <sub>3</sub> } <sub>3</sub>	not obsd			$\eta^3$ -HB{C <sub>3</sub> N <sub>2</sub> H <sub>2</sub> C(CH <sub>3</sub> ) <sub>3</sub> } <sub>3</sub>	136.1	dct (partial res)
	ZnO <sub>2</sub> CCH <sub>3</sub>	2.25	s		1 C	165.2	<sup>2</sup> J <sub>C-H</sub> = 5
					1 C	177.0	d, <sup>1</sup> J <sub>C-H</sub> = 176
					ZnO <sub>2</sub> CCH <sub>3</sub>	23.1	d, <sup>2</sup> J <sub>C-H</sub> = 9
			ZnO <sub>2</sub> CCH <sub>3</sub>	177.0	d, <sup>1</sup> J <sub>C-H</sub> = 185		
					d, <sup>2</sup> J <sub>C-H</sub> = 7		
					s		
					q, <sup>1</sup> J <sub>C-H</sub> = 126		
					s		

Table 4 (Continued)

type	assgnt	$\delta$ /ppm	coupling/Hz	type	assgnt	$\delta$ /ppm	coupling/Hz
[Tp <sup>Bu</sup> ]ZnC <sub>2</sub> Ph							
<sup>1</sup> H NMR	$\eta^3$ -HB{C <sub>3</sub> N <sub>2</sub> H <sub>2</sub> C(CH <sub>3</sub> ) <sub>3</sub> } <sub>3</sub>	1.59	s	<sup>13</sup> C NMR	$\eta^3$ -HB{C <sub>3</sub> N <sub>2</sub> H <sub>2</sub> C(CH <sub>3</sub> ) <sub>3</sub> } <sub>3</sub>	30.9	q, <sup>1</sup> J <sub>C-H</sub> = 126 spt (partial res), <sup>3</sup> J <sub>C-H</sub> = 5
	$\eta^3$ -HB{C <sub>3</sub> N <sub>2</sub> H <sub>2</sub> C(CH <sub>3</sub> ) <sub>3</sub> } <sub>3</sub>	5.83	d, <sup>3</sup> J <sub>H-H</sub> = 2.2		$\eta^3$ -HB{C <sub>3</sub> N <sub>2</sub> H <sub>2</sub> C(CH <sub>3</sub> ) <sub>3</sub> } <sub>3</sub>	32.3	s
	1 H	7.31	d, <sup>3</sup> J <sub>H-H</sub> = 2.2		$\eta^3$ -HB{C <sub>3</sub> N <sub>2</sub> H <sub>2</sub> C(CH <sub>3</sub> ) <sub>3</sub> } <sub>3</sub>	102.2	d, <sup>1</sup> J <sub>C-H</sub> = 175 d, <sup>2</sup> J <sub>C-H</sub> = 9
	$\eta^3$ -HB{C <sub>3</sub> N <sub>2</sub> H <sub>2</sub> C(CH <sub>3</sub> ) <sub>3</sub> } <sub>3</sub>	not obsd			1 C	135.4	d, <sup>1</sup> J <sub>C-H</sub> = 185 d, <sup>2</sup> J <sub>C-H</sub> = 6
	ZnC <sub>2</sub> C <sub>6</sub> H <sub>5</sub>	7.78	m		1 C	164.9	s
	2 o-H	7.04 - 7.20	m		ZnC <sub>2</sub> Ph		
	2 m-H, 1 p-H				1 C	111.3	s
					1 C	112.7	
					ZnC <sub>2</sub> C <sub>6</sub> H <sub>5</sub>		
					1 ipso-C	128.4	s
					2 o-C	128.2	d, <sup>1</sup> J <sub>C-H</sub> = 188 d, <sup>2</sup> J <sub>C-H</sub> = 8
					2 m-C	131.8	d, <sup>1</sup> J <sub>C-H</sub> = 160 t, <sup>2</sup> J <sub>C-H</sub> = 7
					1 p-C	126.8	d, <sup>1</sup> J <sub>C-H</sub> = 160 t, <sup>2</sup> J <sub>C-H</sub> = 7
[Tp <sup>Bu</sup> ]ZnSH							
<sup>1</sup> H NMR	$\eta^3$ -HB{C <sub>3</sub> N <sub>2</sub> H <sub>2</sub> C(CH <sub>3</sub> ) <sub>3</sub> } <sub>3</sub>	1.49	s	<sup>13</sup> C NMR	$\eta^3$ -HB{C <sub>3</sub> N <sub>2</sub> H <sub>2</sub> C(CH <sub>3</sub> ) <sub>3</sub> } <sub>3</sub>	31.1	q, <sup>1</sup> J <sub>C-H</sub> = 126 spt (partial res), <sup>3</sup> J <sub>C-H</sub> = 5
	$\eta^3$ -HB{C <sub>3</sub> N <sub>2</sub> H <sub>2</sub> C(CH <sub>3</sub> ) <sub>3</sub> } <sub>3</sub>	5.81	d, <sup>3</sup> J <sub>H-H</sub> = 2.2		$\eta^3$ -HB{C <sub>3</sub> N <sub>2</sub> H <sub>2</sub> C(CH <sub>3</sub> ) <sub>3</sub> } <sub>3</sub>	32.2	dct (partial res), <sup>2</sup> J <sub>C-H</sub> = 4
	1 H	7.29	d, <sup>3</sup> J <sub>H-H</sub> = 2.2		$\eta^3$ -HB{C <sub>3</sub> N <sub>2</sub> H <sub>2</sub> C(CH <sub>3</sub> ) <sub>3</sub> } <sub>3</sub>	102.5	d, <sup>1</sup> J <sub>C-H</sub> = 176 d, <sup>2</sup> J <sub>C-H</sub> = 9
	$\eta^3$ -HB{C <sub>3</sub> N <sub>2</sub> H <sub>2</sub> C(CH <sub>3</sub> ) <sub>3</sub> } <sub>3</sub>	not obsd			1 C	135.7	d, <sup>1</sup> J <sub>C-H</sub> = 186 d, <sup>2</sup> J <sub>C-H</sub> = 6
	ZnSH	-0.52	s		1 C	165.4	s
[Tp <sup>Bu</sup> ]ZnOSiMe <sub>3</sub>							
<sup>1</sup> H NMR	$\eta^3$ -HB{C <sub>3</sub> N <sub>2</sub> H <sub>2</sub> C(CH <sub>3</sub> ) <sub>3</sub> } <sub>3</sub>	1.46	s	<sup>13</sup> C NMR	$\eta^3$ -HB{C <sub>3</sub> N <sub>2</sub> H <sub>2</sub> C(CH <sub>3</sub> ) <sub>3</sub> } <sub>3</sub>	31.0	q, <sup>1</sup> J <sub>C-H</sub> = 126 spt (partial res), <sup>3</sup> J <sub>C-H</sub> = 5
	$\eta^3$ -HB{C <sub>3</sub> N <sub>2</sub> H <sub>2</sub> C(CH <sub>3</sub> ) <sub>3</sub> } <sub>3</sub>	5.77	d, <sup>3</sup> J <sub>H-H</sub> = 2.2		$\eta^3$ -HB{C <sub>3</sub> N <sub>2</sub> H <sub>2</sub> C(CH <sub>3</sub> ) <sub>3</sub> } <sub>3</sub>	32.1	dct (partial res), <sup>2</sup> J <sub>C-H</sub> = 4
	1 H	7.25	d, <sup>3</sup> J <sub>H-H</sub> = 2.2		$\eta^3$ -HB{C <sub>3</sub> N <sub>2</sub> H <sub>2</sub> C(CH <sub>3</sub> ) <sub>3</sub> } <sub>3</sub>	102.0	d, <sup>1</sup> J <sub>C-H</sub> = 176 d, <sup>2</sup> J <sub>C-H</sub> = 9
	$\eta^3$ -HB{C <sub>3</sub> N <sub>2</sub> H <sub>2</sub> C(CH <sub>3</sub> ) <sub>3</sub> } <sub>3</sub>	not obsd			1 C	135.6	d, <sup>1</sup> J <sub>C-H</sub> = 186 d, <sup>2</sup> J <sub>C-H</sub> = 7
	ZnOSi(CH <sub>3</sub> ) <sub>3</sub>	0.56	s		1 C	164.9	s
					ZnOSi(CH <sub>3</sub> ) <sub>3</sub>	5.2	q, <sup>1</sup> J <sub>C-H</sub> = 117
[Bp <sup>Bu</sup> ]ZnMe							
<sup>1</sup> H NMR	$\eta^2$ -H <sub>2</sub> B{C <sub>3</sub> N <sub>2</sub> H <sub>2</sub> C(CH <sub>3</sub> ) <sub>3</sub> } <sub>2</sub>	1.21	s	<sup>13</sup> C NMR	$\eta^2$ -H <sub>2</sub> B{C <sub>3</sub> N <sub>2</sub> H <sub>2</sub> C(CH <sub>3</sub> ) <sub>3</sub> } <sub>2</sub>	31.1	q, <sup>1</sup> J <sub>C-H</sub> = 126
	$\eta^2$ -H <sub>2</sub> B{C <sub>3</sub> N <sub>2</sub> H <sub>2</sub> C(CH <sub>3</sub> ) <sub>3</sub> } <sub>2</sub>	5.76	d, <sup>3</sup> J <sub>H-H</sub> = 2.2		$\eta^2$ -H <sub>2</sub> B{C <sub>3</sub> N <sub>2</sub> H <sub>2</sub> C(CH <sub>3</sub> ) <sub>3</sub> } <sub>2</sub>	31.8	s
	1 H	7.29	d, <sup>3</sup> J <sub>H-H</sub> = 2.2		$\eta^2$ -H <sub>2</sub> B{C <sub>3</sub> N <sub>2</sub> H <sub>2</sub> C(CH <sub>3</sub> ) <sub>3</sub> } <sub>2</sub>	102.2	d, <sup>1</sup> J <sub>C-H</sub> = 175 d, <sup>2</sup> J <sub>C-H</sub> = 9
	$\eta^2$ -H <sub>2</sub> B{C <sub>3</sub> N <sub>2</sub> H <sub>2</sub> C(CH <sub>3</sub> ) <sub>3</sub> } <sub>2</sub>	not obsd			1 C	135.7	d, <sup>1</sup> J <sub>C-H</sub> = 185 d, <sup>2</sup> J <sub>C-H</sub> = 7
	ZnCH <sub>3</sub>	0.17	s		1 C	162.9	s
					ZnCH <sub>3</sub>	-10.9	q, <sup>1</sup> J <sub>C-H</sub> = 122
[Bp <sup>Bu</sup> ]ZnEt							
<sup>1</sup> H NMR	$\eta^2$ -H <sub>2</sub> B{C <sub>3</sub> N <sub>2</sub> H <sub>2</sub> C(CH <sub>3</sub> ) <sub>3</sub> } <sub>2</sub>	1.22	s	<sup>13</sup> C NMR	$\eta^2$ -H <sub>2</sub> B{C <sub>3</sub> N <sub>2</sub> H <sub>2</sub> C(CH <sub>3</sub> ) <sub>3</sub> } <sub>2</sub>	31.0	q, <sup>1</sup> J <sub>C-H</sub> = 126 spt (partial res), <sup>3</sup> J <sub>C-H</sub> = 5
	$\eta^2$ -H <sub>2</sub> B{C <sub>3</sub> N <sub>2</sub> H <sub>2</sub> C(CH <sub>3</sub> ) <sub>3</sub> } <sub>2</sub>	5.76	d, <sup>3</sup> J <sub>H-H</sub> = 2.2		$\eta^2$ -H <sub>2</sub> B{C <sub>3</sub> N <sub>2</sub> H <sub>2</sub> C(CH <sub>3</sub> ) <sub>3</sub> } <sub>2</sub>	31.7	s
	1 H	7.28	d, <sup>3</sup> J <sub>H-H</sub> = 2.2		$\eta^2$ -H <sub>2</sub> B{C <sub>3</sub> N <sub>2</sub> H <sub>2</sub> C(CH <sub>3</sub> ) <sub>3</sub> } <sub>2</sub>	102.1	d, <sup>1</sup> J <sub>C-H</sub> = 175 d, <sup>2</sup> J <sub>C-H</sub> = 9
	$\eta^2$ -H <sub>2</sub> B{C <sub>3</sub> N <sub>2</sub> H <sub>2</sub> C(CH <sub>3</sub> ) <sub>3</sub> } <sub>2</sub>	not obsd			1 C	135.6	d, <sup>1</sup> J <sub>C-H</sub> = 186 d, <sup>2</sup> J <sub>C-H</sub> = 8
	ZnCH <sub>2</sub> CH <sub>3</sub>	1.62	t, <sup>3</sup> J <sub>H-H</sub> = 8.2		1 C	162.7	s
	ZnCH <sub>2</sub> CH <sub>3</sub>	0.98	t, <sup>3</sup> J <sub>H-H</sub> = 8.2		ZnCH <sub>2</sub> CH <sub>3</sub>	12.5	q, <sup>1</sup> J <sub>C-H</sub> = 125 t, <sup>2</sup> J <sub>C-H</sub> = 5
					ZnCH <sub>2</sub> CH <sub>3</sub>	2.3	t, <sup>1</sup> J <sub>C-H</sub> = 121 q (partial res), <sup>2</sup> J <sub>C-H</sub> = 4 q (partial res), <sup>2</sup> J <sub>C-H</sub> = 4



Table 4 (Continued)

type	assgnt	$\delta$ /ppm	coupling/Hz	type	assgnt	$\delta$ /ppm	coupling/Hz
<b>[Bp<sup>Bu</sup>]<sup>+</sup>ZnBu<sup>-</sup></b>							
<sup>1</sup> H NMR	$\eta^2$ -H <sub>2</sub> B{C <sub>3</sub> N <sub>2</sub> H <sub>2</sub> C(CH <sub>3</sub> ) <sub>3</sub> } <sub>2</sub>	1.22	s	<sup>13</sup> C NMR	$\eta^2$ -H <sub>2</sub> B{C <sub>3</sub> N <sub>2</sub> H <sub>2</sub> C(CH <sub>3</sub> ) <sub>3</sub> } <sub>2</sub>	31.0	q, <sup>1</sup> J <sub>C-H</sub> = 126
	$\eta^2$ -H <sub>2</sub> B{C <sub>3</sub> N <sub>2</sub> H <sub>2</sub> C(CH <sub>3</sub> ) <sub>3</sub> } <sub>2</sub>				$\eta^2$ -H <sub>2</sub> B{C <sub>3</sub> N <sub>2</sub> H <sub>2</sub> C(CH <sub>3</sub> ) <sub>3</sub> } <sub>2</sub>	31.7	s
	1 H	5.73	d, <sup>3</sup> J <sub>H-H</sub> = 2.2		$\eta^2$ -H <sub>2</sub> B{C <sub>3</sub> N <sub>2</sub> H <sub>2</sub> C(CH <sub>3</sub> ) <sub>3</sub> } <sub>2</sub>		
	1 H	7.26	d, <sup>3</sup> J <sub>H-H</sub> = 2.2		1 C	102.2	d, <sup>1</sup> J <sub>C-H</sub> = 175
	$\eta^2$ -H <sub>2</sub> B{C <sub>3</sub> N <sub>2</sub> H <sub>2</sub> C(CH <sub>3</sub> ) <sub>3</sub> } <sub>2</sub>	not obsd			1 C	135.8	d, <sup>1</sup> J <sub>C-H</sub> = 185
	ZnC(CH <sub>3</sub> ) <sub>3</sub>	1.54	s		1 C	162.4	s
					ZnC(CH <sub>3</sub> ) <sub>3</sub>	33.2	q, <sup>1</sup> J <sub>C-H</sub> = 123
					ZnC(CH <sub>3</sub> ) <sub>3</sub>	22.6	s
<b>{[Bp<sup>Bu</sup>]<sup>+</sup>Zn(<math>\mu</math>-OH)}<sub>2</sub></b>							
<sup>1</sup> H NMR	$\eta^2$ -H <sub>2</sub> B{C <sub>3</sub> N <sub>2</sub> H <sub>2</sub> C(CH <sub>3</sub> ) <sub>3</sub> } <sub>2</sub>	1.29	s	<sup>13</sup> C NMR	$\eta^2$ -H <sub>2</sub> B{C <sub>3</sub> N <sub>2</sub> H <sub>2</sub> C(CH <sub>3</sub> ) <sub>3</sub> } <sub>2</sub>	31.4	q, <sup>1</sup> J <sub>C-H</sub> = 126
	$\eta^2$ -H <sub>2</sub> B{C <sub>3</sub> N <sub>2</sub> H <sub>2</sub> C(CH <sub>3</sub> ) <sub>3</sub> } <sub>2</sub>				$\eta^2$ -H <sub>2</sub> B{C <sub>3</sub> N <sub>2</sub> H <sub>2</sub> C(CH <sub>3</sub> ) <sub>3</sub> } <sub>2</sub>	31.8	spt (partial res), <sup>3</sup> J <sub>C-H</sub> = 4
	1 H	5.84	d, <sup>3</sup> J <sub>H-H</sub> = 2.2		$\eta^2$ -H <sub>2</sub> B{C <sub>3</sub> N <sub>2</sub> H <sub>2</sub> C(CH <sub>3</sub> ) <sub>3</sub> } <sub>2</sub>		
	1 H	7.46	d, <sup>3</sup> J <sub>H-H</sub> = 2.2		$\eta^2$ -H <sub>2</sub> B{C <sub>3</sub> N <sub>2</sub> H <sub>2</sub> C(CH <sub>3</sub> ) <sub>3</sub> } <sub>2</sub>		
	$\eta^2$ -H <sub>2</sub> B{C <sub>3</sub> N <sub>2</sub> H <sub>2</sub> C(CH <sub>3</sub> ) <sub>3</sub> } <sub>2</sub>	not obsd			1 C	101.8	d, <sup>1</sup> J <sub>C-H</sub> = 175
	ZnOH <sup>p</sup>	2.25	s		1 C	136.8	d, <sup>1</sup> J <sub>C-H</sub> = 185
					1 C	163.6	s
<b>{HB(OMe)(3-Bu<sup>p</sup>pz)<sub>2</sub>}ZnEt</b>							
<sup>1</sup> H NMR	HB(OCH <sub>3</sub> ){C <sub>3</sub> N <sub>2</sub> H <sub>2</sub> C(CH <sub>3</sub> ) <sub>3</sub> } <sub>2</sub>	1.28	s	<sup>13</sup> C NMR	HB(OCH <sub>3</sub> ){C <sub>3</sub> N <sub>2</sub> H <sub>2</sub> C(CH <sub>3</sub> ) <sub>3</sub> } <sub>2</sub>	30.8	q, <sup>1</sup> J <sub>C-H</sub> = 125
	H(OCH <sub>3</sub> )B{C <sub>3</sub> N <sub>2</sub> H <sub>2</sub> C(CH <sub>3</sub> ) <sub>3</sub> } <sub>2</sub>				HB(OCH <sub>3</sub> ){C <sub>3</sub> N <sub>2</sub> H <sub>2</sub> C(CH <sub>3</sub> ) <sub>3</sub> } <sub>2</sub>	31.8	spt (partial res), <sup>3</sup> J <sub>C-H</sub> = 5
	1 H	5.81	d, <sup>3</sup> J <sub>H-H</sub> = 2.2		HB(OCH <sub>3</sub> ){C <sub>3</sub> N <sub>2</sub> H <sub>2</sub> C(CH <sub>3</sub> ) <sub>3</sub> } <sub>2</sub>		
	1 H	7.32	d, <sup>3</sup> J <sub>H-H</sub> = 2.2		1 C	101.9	d, <sup>1</sup> J <sub>C-H</sub> = 174
	HB(OCH <sub>3</sub> ){C <sub>3</sub> N <sub>2</sub> H <sub>2</sub> C(CH <sub>3</sub> ) <sub>3</sub> } <sub>2</sub>	not obsd			1 C	133.3	d, <sup>1</sup> J <sub>C-H</sub> = 184
	Hb(OCH <sub>3</sub> ){C <sub>3</sub> N <sub>2</sub> H <sub>2</sub> C(CH <sub>3</sub> ) <sub>3</sub> } <sub>2</sub>	3.24	s		1 C	162.2	s
	ZnCH <sub>2</sub> CH <sub>3</sub>	1.73	t, <sup>3</sup> J <sub>H-H</sub> = 8.0		HB(OCH <sub>3</sub> ){C <sub>3</sub> N <sub>2</sub> H <sub>2</sub> C(CH <sub>3</sub> ) <sub>3</sub> } <sub>2</sub>	61.9	q, <sup>1</sup> J <sub>C-H</sub> = 141
	ZnCH <sub>2</sub> CH <sub>3</sub>	0.97	q, <sup>3</sup> J <sub>H-H</sub> = 8.0		ZnCH <sub>2</sub> CH <sub>3</sub>	13.2	m, <sup>2</sup> J <sub>C-H</sub> = 4
					ZnCH <sub>2</sub> CH <sub>3</sub>	-0.1	q, <sup>1</sup> J <sub>C-H</sub> = 124
					ZnCH <sub>2</sub> CH <sub>3</sub>		t, <sup>2</sup> J <sub>C-H</sub> = 5
					ZnCH <sub>2</sub> CH <sub>3</sub>		t, <sup>1</sup> J <sub>C3-H</sub> = 119
					ZnCH <sub>2</sub> CH <sub>3</sub>		q, <sup>2</sup> J <sub>C-H</sub> = 4
<b>{HB(OEt)(3-Bu<sup>p</sup>pz)<sub>2</sub>}ZnEt</b>							
<sup>1</sup> H NMR	HB(OCH <sub>2</sub> CH <sub>3</sub> ){C <sub>3</sub> N <sub>2</sub> H <sub>2</sub> C(CH <sub>3</sub> ) <sub>3</sub> } <sub>2</sub>	1.29	s	<sup>13</sup> C NMR	HB(OCH <sub>2</sub> CH <sub>3</sub> ){C <sub>3</sub> N <sub>2</sub> H <sub>2</sub> C(CH <sub>3</sub> ) <sub>3</sub> } <sub>2</sub>	30.8	q, <sup>1</sup> J <sub>C-H</sub> = 126
	H(OCH <sub>2</sub> CH <sub>3</sub> )B{C <sub>3</sub> N <sub>2</sub> H <sub>2</sub> C(CH <sub>3</sub> ) <sub>3</sub> } <sub>2</sub>				HB(OCH <sub>2</sub> CH <sub>3</sub> ){C <sub>3</sub> N <sub>2</sub> H <sub>2</sub> C(CH <sub>3</sub> ) <sub>3</sub> } <sub>2</sub>	31.8	spt (partial res), <sup>3</sup> J <sub>C-H</sub> = 5
	1 H	5.81	d, <sup>3</sup> J <sub>H-H</sub> = 2.2		HB(OCH <sub>2</sub> CH <sub>3</sub> ){C <sub>3</sub> N <sub>2</sub> H <sub>2</sub> C(CH <sub>3</sub> ) <sub>3</sub> } <sub>2</sub>		
	1 H	7.32	d, <sup>3</sup> J <sub>H-H</sub> = 2.2		1 C	101.7	d, <sup>1</sup> J <sub>C-H</sub> = 174
	HB(OCH <sub>2</sub> CH <sub>3</sub> ){C <sub>3</sub> N <sub>2</sub> H <sub>2</sub> C(CH <sub>3</sub> ) <sub>3</sub> } <sub>2</sub>	not obsd			1 C	133.1	d, <sup>1</sup> J <sub>C-H</sub> = 184
	HB(OCH <sub>2</sub> CH <sub>3</sub> ){C <sub>3</sub> N <sub>2</sub> H <sub>2</sub> C(CH <sub>3</sub> ) <sub>3</sub> } <sub>2</sub>	3.52	spt, <sup>3</sup> J <sub>H-H</sub> = 7.0		1 C	162.2	s
	HB(OCH <sub>2</sub> CH <sub>3</sub> ){C <sub>3</sub> N <sub>2</sub> H <sub>2</sub> C(CH <sub>3</sub> ) <sub>3</sub> } <sub>2</sub>	1.17	d, <sup>3</sup> J <sub>H-H</sub> = 7.0		1 C	61.9	d, <sup>1</sup> J <sub>C-H</sub> = 141
	ZnCH <sub>2</sub> CH <sub>3</sub>	1.79	t, <sup>3</sup> J <sub>H-H</sub> = 8.0		HB(OCH <sub>2</sub> CH <sub>3</sub> ){C <sub>3</sub> N <sub>2</sub> H <sub>2</sub> C(CH <sub>3</sub> ) <sub>3</sub> } <sub>2</sub>	16.8	spt, <sup>2</sup> J <sub>C-H</sub> = 4
	ZnCH <sub>2</sub> CH <sub>3</sub>	1.01	q, <sup>3</sup> J <sub>H-H</sub> = 8.0		ZnCH <sub>2</sub> CH <sub>3</sub>	13.1	q, <sup>1</sup> J <sub>C-H</sub> = 124
					ZnCH <sub>2</sub> CH <sub>3</sub>	0.77	t, <sup>2</sup> J <sub>C-H</sub> = 5
					ZnCH <sub>2</sub> CH <sub>3</sub>		t, <sup>1</sup> J <sub>C-H</sub> = 119
					ZnCH <sub>2</sub> CH <sub>3</sub>		q, <sup>2</sup> J <sub>C-H</sub> = 4
<b>{HB(OPr<sup>i</sup>)(3-Bu<sup>p</sup>Pz)<sub>2</sub>}ZnEt</b>							
<sup>1</sup> H NMR	HB(OCH(CH <sub>3</sub> ) <sub>2</sub> ){C <sub>3</sub> N <sub>2</sub> H <sub>2</sub> C(CH <sub>3</sub> ) <sub>3</sub> } <sub>2</sub>	1.29	s	<sup>13</sup> C NMR	HB(OCH(CH <sub>3</sub> ) <sub>2</sub> ){C <sub>3</sub> N <sub>2</sub> H <sub>2</sub> C(CH <sub>3</sub> ) <sub>3</sub> } <sub>2</sub>	30.8	q, <sup>1</sup> J <sub>C-H</sub> = 126
	H(OCH(CH <sub>3</sub> ) <sub>2</sub> )B{C <sub>3</sub> N <sub>2</sub> H <sub>2</sub> C(CH <sub>3</sub> ) <sub>3</sub> } <sub>2</sub>				HB(OCH(CH <sub>3</sub> ) <sub>2</sub> ){C <sub>3</sub> N <sub>2</sub> H <sub>2</sub> C(CH <sub>3</sub> ) <sub>3</sub> } <sub>2</sub>	31.7	spt (partial res), <sup>3</sup> J <sub>C-H</sub> = 5
	1 H	5.81	d, <sup>3</sup> J <sub>H-H</sub> = 2.2		HB(OCH(CH <sub>3</sub> ) <sub>2</sub> ){C <sub>3</sub> N <sub>2</sub> H <sub>2</sub> C(CH <sub>3</sub> ) <sub>3</sub> } <sub>2</sub>		
	1 H	7.32	d, <sup>3</sup> J <sub>H-H</sub> = 2.2		1 C	101.6	d, <sup>1</sup> J <sub>C-H</sub> = 174
	HB(OCH(CH <sub>3</sub> ) <sub>2</sub> ){C <sub>3</sub> N <sub>2</sub> H <sub>2</sub> C(CH <sub>3</sub> ) <sub>3</sub> } <sub>2</sub>	not obsd			1 C	132.7	d, <sup>1</sup> J <sub>C-H</sub> = 184
	HB(OCH(CH <sub>3</sub> ) <sub>2</sub> ){C <sub>3</sub> N <sub>2</sub> H <sub>2</sub> C(CH <sub>3</sub> ) <sub>3</sub> } <sub>2</sub>	3.92	spt, <sup>3</sup> J <sub>H-H</sub> = 6.2		1 C	161.9	s
	HB(OCH(CH <sub>3</sub> ) <sub>2</sub> ){C <sub>3</sub> N <sub>2</sub> H <sub>2</sub> C(CH <sub>3</sub> ) <sub>3</sub> } <sub>2</sub>	1.11	d, <sup>3</sup> J <sub>H-H</sub> = 6.2		1 C	69.4	d, <sup>1</sup> J <sub>C-H</sub> = 141
	ZnCH <sub>2</sub> CH <sub>3</sub>	1.81	t, <sup>3</sup> J <sub>H-H</sub> = 8.0		HB(OCH(CH <sub>3</sub> ) <sub>2</sub> ){C <sub>3</sub> N <sub>2</sub> H <sub>2</sub> C(CH <sub>3</sub> ) <sub>3</sub> } <sub>2</sub>	24.2	spt, <sup>2</sup> J <sub>C-H</sub> = 4
	ZnCH <sub>2</sub> CH <sub>3</sub>	1.00	q, <sup>3</sup> J <sub>H-H</sub> = 8.0		ZnCH <sub>2</sub> CH <sub>3</sub>	13.2	q, <sup>1</sup> J <sub>C-H</sub> = 126
					ZnCH <sub>2</sub> CH <sub>3</sub>	1.84	m, <sup>2</sup> J <sub>C-H</sub> = 5
					ZnCH <sub>2</sub> CH <sub>3</sub>		q, <sup>1</sup> J <sub>C-H</sub> = 124
					ZnCH <sub>2</sub> CH <sub>3</sub>		t, <sup>2</sup> J <sub>C-H</sub> = 5
					ZnCH <sub>2</sub> CH <sub>3</sub>		t, <sup>1</sup> J <sub>C-H</sub> = 119
					ZnCH <sub>2</sub> CH <sub>3</sub>		q, <sup>2</sup> J <sub>C</sub>

Table 4 (Continued)

type	assgnt	$\delta$ /ppm	coupling/Hz	type	assgnt	$\delta$ /ppm	coupling/Hz
$[\text{Bp}^{\text{Bu}}]\text{Zn}(\eta^2\text{-O}_2\text{CCH}_3)$							
$^1\text{H}$ NMR	$\text{H}_2\text{B}\{\text{C}_3\text{N}_2\text{H}_2\text{C}(\text{CH}_3)_3\}_2$	1.31	s	$^{13}\text{C}$ NMR	$\text{H}_2\text{B}\{\text{C}_3\text{N}_2\text{H}_2\text{C}(\text{CH}_3)_3\}_2$	30.6	q, $^1J_{\text{C-H}} = 126$
	$\text{H}_2\text{B}\{\text{C}_3\text{N}_2\text{H}_2\text{C}(\text{CH}_3)_3\}_2$				$\text{H}_2\text{B}\{\text{C}_3\text{N}_2\text{H}_2\text{C}(\text{CH}_3)_3\}_2$	31.6	s
	1 H	5.28	d, $^3J_{\text{H-H}} = 2.2$		$\text{H}_2\text{B}\{\text{C}_3\text{N}_2\text{H}_2\text{C}(\text{CH}_3)_3\}_2$		
	1 H	7.47	d, $^3J_{\text{H-H}} = 2.2$		1 C	102.3	d, $^1J_{\text{C-H}} = 175$
	$\text{H}_2\text{B}\{\text{C}_3\text{N}_2\text{H}_2\text{C}(\text{CH}_3)_3\}_2$	not obsd					d, $^2J_{\text{C-H}} = 9$
	$\text{Zn}(\eta^2\text{-O}_2\text{CCH}_3)$	2.06	s		1 C	136.8	d, $^1J_{\text{C-H}} = 185$
$[\text{Tp}^{\text{Me}_2}]_2\text{Zn}$							
$^1\text{H}$ NMR	$\eta^3\text{-HB}\{\text{C}_3\text{N}_2\text{H}(\text{CH}_3)_2\}_3$	1.63	s	$^{13}\text{C}$ NMR	$\eta^3\text{-HB}\{\text{C}_3\text{N}_2\text{H}(\text{CH}_3)_2\}_3$	12.2	q, $^1J_{\text{C-H}} = 128$
	$\eta^3\text{-HB}\{\text{C}_3\text{N}_2\text{H}(\text{CH}_3)_2\}_3$	2.29	s		$\eta^3\text{-HB}\{\text{C}_3\text{N}_2\text{H}(\text{CH}_3)_2\}_3$	12.9	q, $^1J_{\text{C-H}} = 129$
	$\eta^3\text{-HB}\{\text{C}_3\text{N}_2\text{H}(\text{CH}_3)_2\}_3$	5.69	s		$\eta^3\text{-HB}\{\text{C}_3\text{N}_2\text{H}(\text{CH}_3)_2\}_3$		
	$\eta^3\text{-HB}\{\text{C}_3\text{N}_2\text{H}(\text{CH}_3)_2\}_3$	not obsd			1 C	105.1	d, $^1J_{\text{C-H}} = 170$
					1 C	143.1	s
					1 C	149.1	s

<sup>a</sup> In  $\text{C}_6\text{D}_6$ . Abbreviations: s = singlet, d = doublet, t = triplet, q = quartet, spt = septet, dct = dectet, m = multiplet. <sup>b</sup>  $^2\text{H}$  NMR for  $\text{ZnOD}$ :  $\delta$  2.23 (s).

Table 5. Selected Bond Lengths (Å) and Angles (deg) for  $[\text{Tp}^{\text{Bu}}]\text{Zn}(\eta^1\text{-O}_2\text{CMe})$ 

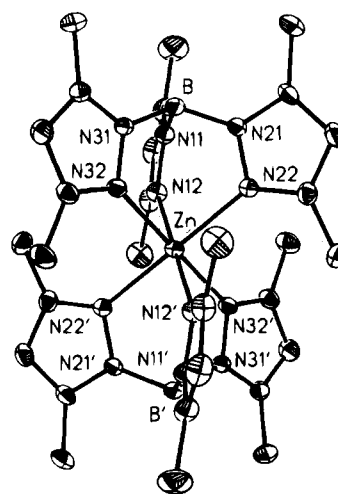
Zn-O(1)	1.859(6)	Zn-N(12)	2.061(5)
Zn-N(22)	2.075(5)	Zn-N(32)	2.108(6)
O(1)-C(1)	1.241(12)	O(2)-C(1)	1.225(13)
C(1)-C(2)	1.480(15)	N(11)-N(12)	1.364(9)
N(21)-N(22)	1.368(8)	N(31)-N(32)	1.368(8)
B-N(11)	1.548(10)	B-N(21)	1.522(10)
B-N(31)	1.539(10)		
N(12)-Zn-O(1)	122.1(3)	N(22)-Zn-O(1)	115.6(3)
N(32)-Zn-O(1)	129.2(2)	N(12)-Zn-N(22)	92.1(2)
N(12)-Zn-N(32)	97.0(3)	N(22)-Zn-N(32)	91.4(3)
Zn-O(1)-C(1)	122.7(6)	O(1)-C(1)-O(2)	122.0(9)
O(1)-C(1)-C(2)	116.6(9)	O(2)-C(1)-C(2)	121.1(10)

Table 6. Selected Bond Lengths (Å) and Angles (deg) for  $[\text{Tp}^{\text{Bu}}]\text{ZnNCS}$ 

Zn-N	1.893(4)	Zn-N(12)	2.041(3)
Zn-N(22)	2.027(3)	Zn-N(32)	2.029(3)
N-C	1.164(6)	C-S	1.586(5)
N(11)-N(12)	1.374(5)	N(21)-N(22)	1.378(4)
N(31)-N(32)	1.369(4)	B-N(11)	1.541(6)
B-N(21)	1.548(6)	B-N(31)	1.535(5)
N-Zn-N(12)	120.5(1)	N-Zn-N(22)	123.1(1)
N-Zn-N(32)	121.7(1)	N(12)-Zn-N(22)	94.4(1)
N(12)-Zn-N(32)	95.8(1)	N(22)-Zn-N(32)	94.3(1)
Zn-N-C	171.4(4)	N-C-S	179.7(4)

$[\text{Tp}^{\text{Me}_2}]_2\text{Zn}$  may also be prepared directly by the reaction of  $\text{K}[\text{Tp}^{\text{Me}_2}]$  with  $\text{ZnCl}_2$ , and its molecular structure has been determined by X-ray diffraction (Figure 4). Selected bond lengths and angles are listed in Table 7. The structure of  $[\text{Tp}^{\text{Me}_2}]_2\text{Zn}$  is closely related to that of the magnesium analogue  $[\text{Tp}^{\text{Me}_2}]_2\text{Mg}$ .<sup>9</sup> In marked contrast, however, the related  $[\text{Tp}^{\text{Ph}}]_2\text{Zn}$  complex does not exhibit an analogous structure. Specifically, the potentially tridentate  $[\text{Tp}^{\text{Ph}}]$  ligand acts only as a bidentate ligand in  $[\eta^2\text{-Tp}^{\text{Ph}}]_2\text{Zn}$ ,<sup>22</sup> so that the complex adopts only a four-coordinate pseudotetrahedral geometry, rather than the six-coordinate octahedral geometry adopted by  $[\text{Tp}^{\text{Me}_2}]_2\text{Zn}$ . The Zn-N bond lengths in the four-coordinate complex  $[\eta^2\text{-Tp}^{\text{Ph}}]_2\text{Zn}$  are also slightly shorter (2.013[6] Å) than in the octahedral derivative (2.17[3] Å). It is also worth noting that the four-coordinate structure of  $[\eta^2\text{-Tp}^{\text{Ph}}]_2\text{Zn}$  contrasts with the structure of  $[\text{Tp}^{\text{Ph}}]_2\text{Fe}$ , in which the Fe is octahedrally coordinated.<sup>35</sup>

**Synthesis, Characterization, and Reactivity of  $[\text{Tp}^{\text{Bu}}]\text{ZnH}$ .** In contrast to dialkylzinc derivatives

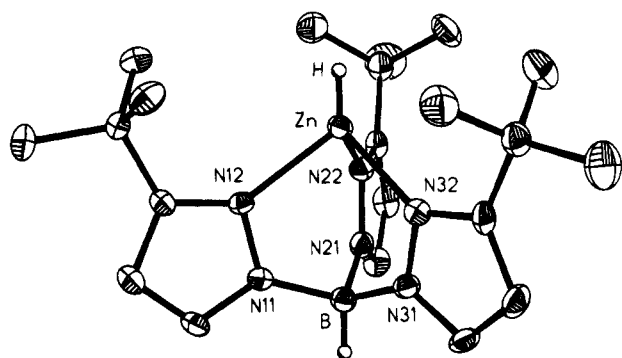
Figure 4. Molecular structure of  $[\text{Tp}^{\text{Me}_2}]_2\text{Zn}$ .Table 7. Selected Bond Lengths (Å) and Angles (deg) for  $[\text{Tp}^{\text{Me}_2}]_2\text{Zn}$ 

Zn-N(12)	2.187(3)	Zn-N(22)	2.183(2)
Zn-N(32)	2.146(2)	N(11)-N(12)	1.372(2)
N(21)-N(22)	1.373(2)	N(31)-N(32)	1.374(3)
B-N(11)	1.538(4)	B-N(21)	1.539(3)
B-N(31)	1.546(4)		
N(12)-Zn-N(22)	87.2(1)	N(12)-Zn-N(32)	85.9(1)
N(22)-Zn-N(32)	86.1(1)	N(12)-Zn-N(12')	180.0
N(22)-Zn-N(12')	92.8(1)	N(32)-Zn-N(12')	94.1(1)
N(12)-Zn-N(22')	92.8(1)	N(22)-Zn-N(22')	180.0
N(32)-Zn-N(22')	93.9(1)	N(22)-Zn-N(32')	93.9(1)
N(12)-Zn-N(32')	94.1(1)	N(32)-Zn-N(32')	180.0

which exist as two-coordinate monomeric species, zinc hydride is a polymeric material that is insoluble in most organic solvents.<sup>36</sup> By analogy with the use of the tris(pyrazolyl)hydroborato ligand to support the monomeric zinc alkyl derivatives described above, it was anticipated that the zinc hydride complex  $[\text{Tp}^{\text{Bu}}]\text{ZnH}$  could also be synthesized. Indeed,  $[\text{Tp}^{\text{Bu}}]\text{ZnH}$  is readily prepared by metathesis of  $\text{ZnH}_2$  with  $\text{Ti}[\text{Tp}^{\text{Bu}}]$  (eq 3). As with the reactions between  $\text{ZnR}_2$  and  $\text{Ti}[\text{Tp}^{\text{Bu}}]$ , the decomposition

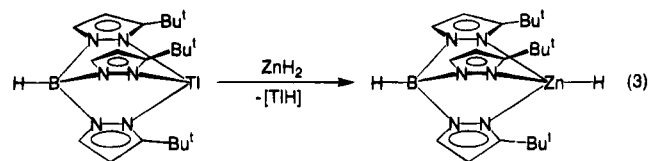
(35) Eichorn, D. M.; Armstrong, W. H. *Inorg. Chem.* **1990**, *29*, 3607-3612.

(36) De Koning, A. J.; Boersma, J.; van der Kerk, G. J. M. J. *Organomet. Chem.* **1980**, *186*, 159-172.



**Figure 5.** Molecular structure of  $[\text{Tp}^{\text{Bu}^t}]\text{ZnH}$ . (The hydride ligand was not located and is illustrated in an idealized position.)

of putative  $[\text{TiH}]$  provides an effective driving force for the reaction.



Zinc hydride derivatives are rare and are typically oligomeric.<sup>36,37</sup> For example, some zinc hydride derivatives include  $[\text{HZnN}(\text{Me})\text{CH}_2\text{CH}_2\text{NMe}_2]_2$ ,<sup>38</sup>  $[\text{HZnO}(\text{Bu}^t)]_4$ ,<sup>39</sup>  $[\text{HZnO}(\text{CH}_2)_2\text{NMe}_2]_2$ ,<sup>40</sup> and  $[\text{RZnH}(\text{NC}_5\text{H}_5)]_3$  ( $\text{R} = \text{Et}$ ,  $\text{Ph}$ ).<sup>41</sup> Of these derivatives, the only other structurally characterized zinc hydride complex is dimeric  $[\text{HZnN}(\text{Me})\text{CH}_2\text{CH}_2\text{NMe}_2]_2$ .<sup>38</sup>

The molecular structure of  $[\text{Tp}^{\text{Bu}^t}]\text{ZnH}$  has been determined by X-ray diffraction (Figure 5), which clearly identifies its monomeric nature.  $[\text{Tp}^{\text{Bu}^t}]\text{ZnH}$  is the first structurally-characterized monomeric zinc hydride derivative of which we are aware, and the synthetic methodology has also been applied to the synthesis of the terminal beryllium and cadmium hydride derivatives,  $[\text{Tp}^{\text{Bu}^t}]\text{BeH}$ <sup>42,43</sup> and  $[\text{Tp}^{\text{Bu}^t}]\text{CdH}$ .<sup>44</sup> Selected bond lengths and angles for  $[\text{Tp}^{\text{Bu}^t}]\text{ZnH}$  are presented in Table 8. The hydrogen atom bound to zinc in  $[\text{Tp}^{\text{Bu}^t}]\text{ZnH}$  was not located by the X-ray diffraction study; however, the expected axial location of the hydride ligand is clearly suggested by the trigonal coordination of the tris(3-*tert*-butylpyrazolyl)hydroborato ligand illustrated in Figure 5. Furthermore, evidence for the presence of the hydride ligand is provided by NMR and

(37) (a) De Koning, A. J.; Boersma, J.; van der Kerk, G. J. M. *J. Organomet. Chem.* **1980**, *195*, 1–12. (b) Ashby, E. C.; Goel, A. B. *Inorg. Chem.* **1981**, *20*, 1096–1101. (c) De Koning, A. J.; Boersma, J.; van der Kerk, G. J. M. *Tetrahedron Lett.* **1977**, 2547–2548.

(38) (a) Bell, N. A.; Coates, G. E. *J. Chem. Soc. A* **1968**, 823–826. (b) Bell, N. A.; Moseley, P. T.; Shearer, H. M. M.; Spencer, C. B. *J. Chem. Soc., Chem. Commun.* **1980**, 359–360. (c) Bell, N. A.; Moseley, P. T.; Shearer, H. M. M.; Spencer, C. B. *Acta Crystallogr.* **1980**, *B36*, 2950–2954.

(39) Neils, T. L.; Burlitch, J. M. *Inorg. Chem.* **1989**, *28*, 1607–1609. (40) Goeden, G. V.; Caulton, K. G. *J. Am. Chem. Soc.* **1981**, *103*, 7354–7355.

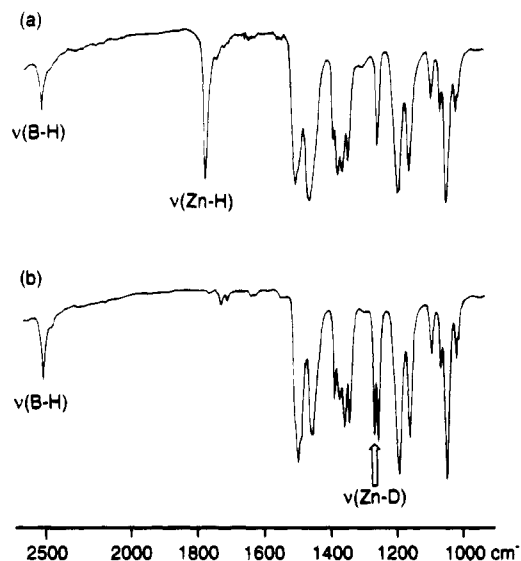
(41) De Koning, A. J.; Boersma, J.; van der Kerk, G. J. M. *J. Organomet. Chem.* **1978**, *155*, C5–C7. (42) Han, R.; Parkin, G. *Inorg. Chem.* **1992**, *31*, 983–988.

(43) The first terminal beryllium hydride complex to be structurally characterized by X-ray diffraction was the dimer  $[(\text{Me}_2\text{NCH}_2\text{CH}_2\text{NMe})\text{BeH}]_2$ . (a) Bell, N. A.; Coates, G. E.; Schneider, M. L.; Shearer, H. M. M. *J. Chem. Soc., Chem. Commun.* **1983**, 828–829. (b) Bell, N. A.; Coates, G. E.; Schneider, M. L.; Shearer, H. M. M. *Acta Crystallogr.* **1984**, *C40*, 608–610.

(44) (a) Reger, D. L.; Mason, S. S.; Rheingold, A. L. *J. Am. Chem. Soc.* **1993**, *115*, 10406–10407. (b) Reger, D. L.; Mason, S. S.; Rheingold, A. L. *J. Am. Chem. Soc.* **1994**, *116*, 2233.

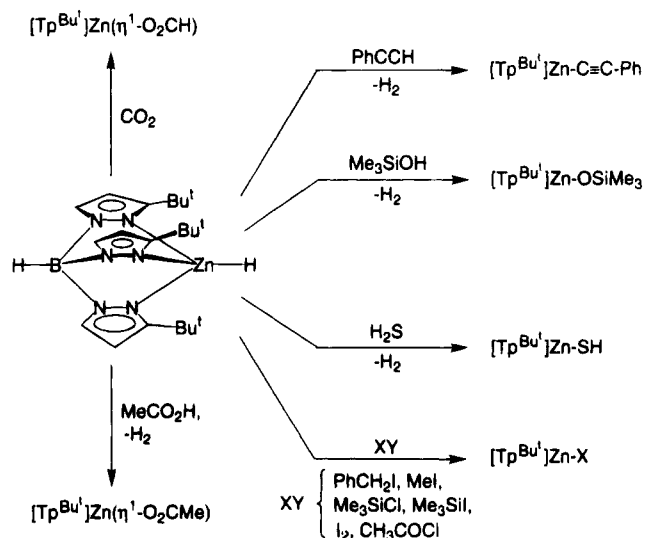
**Table 8.** Selected Bond Lengths (Å) and Angles (deg) for  $[\text{Tp}^{\text{Bu}^t}]\text{ZnH}$

Zn–N(12)	2.078(5)	Zn–N(22)	2.089(6)
Zn–N(32)	2.079(5)	N(11)–N(12)	1.371(7)
N(21)–N(22)	1.359(8)	N(31)–N(32)	1.348(9)
B–N(11)	1.549(9)	B–N(21)	1.541(9)
N(31)B–	1.556(10)		
N(12)–Zn–N(22)	90.2(2)	N(12)–Zn–N(32)	91.7(2)
N(22)–Zn–N(32)	92.3(2)		



**Figure 6.** IR spectra of (a)  $[\text{Tp}^{\text{Bu}^t}]\text{ZnH}$  and (b)  $[\text{Tp}^{\text{Bu}^t}]\text{ZnD}$ .

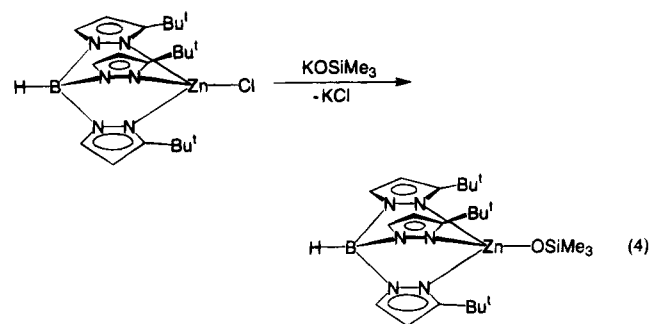
**Scheme 3**



IR studies. For example, the hydride resonance is observed at  $\delta$  5.36 ppm in the  $^1\text{H}$  NMR spectrum, an assignment that has been confirmed by the  $^2\text{H}$  NMR spectrum of the isotopomer  $[\text{Tp}^{\text{Bu}^t}]\text{ZnD}$ . Similarly,  $\nu$ -(Zn–H) is observed as a strong absorption at  $1770\text{ cm}^{-1}$  in the IR spectrum, which shifts to  $1270\text{ cm}^{-1}$  ( $\nu_{\text{H}}/\nu_{\text{D}} = 1.39$ ) upon deuterium substitution, as shown in Figure 6.

The zinc–hydride functionality in  $[\text{Tp}^{\text{Bu}^t}]\text{ZnH}$  is reactive toward a number of substrates, as summarized in Scheme 3. Thus, protic reagents ( $\text{HX} = \text{H}_2\text{S}$ ,  $\text{Me}_3\text{SiOH}$ ,  $\text{MeCO}_2\text{H}$ ,  $\text{PhC}\equiv\text{CH}$ ) react at the Zn–H bond to give  $[\text{Tp}^{\text{Bu}^t}]\text{ZnX}$  and  $\text{H}_2$ . The complex  $[\text{Tp}^{\text{Bu}^t}]\text{ZnOSiMe}_3$  may also be prepared independently by the reaction of

[Tp<sup>Bu<sup>t</sup></sup>]-ZnCl with KOSiMe<sub>3</sub> (eq 4). The Zn-H bond also

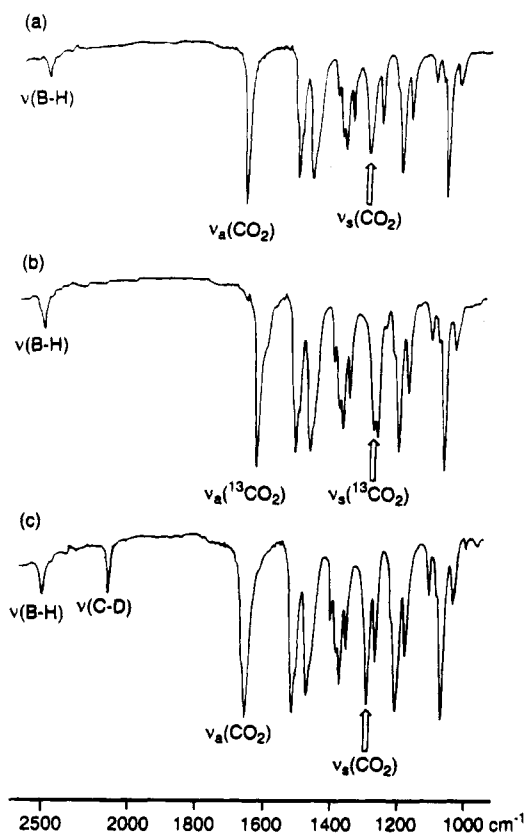


undergoes metathesis with a variety of halide derivatives. For example, [Tp<sup>Bu<sup>t</sup></sup>]-ZnH reacts with MeI and PhCH<sub>2</sub>I to give [Tp<sup>Bu<sup>t</sup></sup>]-ZnI and CH<sub>4</sub> and RH (R = Me, PhCH<sub>2</sub>). The reactions between [Tp<sup>Bu<sup>t</sup></sup>]-ZnH and RI, which occur at room temperature, were observed to be more facile than those of the corresponding alkyl derivatives [Tp<sup>Bu<sup>t</sup></sup>]-ZnR. The source of the hydrogen in the RH products was confirmed as the Zn-H group by the reaction of [Tp<sup>Bu<sup>t</sup></sup>]-ZnD with RI. [Tp<sup>Bu<sup>t</sup></sup>]-ZnH also reacts with MeCOCl, Me<sub>3</sub>SiX (X = Cl, I) and I<sub>2</sub> to give [Tp<sup>Bu<sup>t</sup></sup>]-ZnX (X = Cl, I).

The Zn-H group in [Tp<sup>Bu<sup>t</sup></sup>]-ZnH undergoes clean insertion of CO<sub>2</sub> at 50 °C to give the η<sup>1</sup>-formate derivative, [Tp<sup>Bu<sup>t</sup></sup>]-Zn(η<sup>1</sup>-O<sub>2</sub>CH). It is noteworthy that, as described above, the methyl derivative [Tp<sup>Bu<sup>t</sup></sup>]-ZnCH<sub>3</sub> does not react with CO<sub>2</sub> under similar conditions. The formate derivative [Tp<sup>Bu<sup>t</sup></sup>]-Zn(η<sup>1</sup>-O<sub>2</sub>CH) has been characterized by NMR and IR spectroscopy. The formate moiety of [Tp<sup>Bu<sup>t</sup></sup>]-Zn(η<sup>1</sup>-O<sub>2</sub>CH) is observed as a singlet at δ 8.91 ppm in the <sup>1</sup>H NMR spectrum and as a doublet at 166.7 ppm (<sup>1</sup>J<sub>C-H</sub> = 202 Hz) in the <sup>13</sup>C NMR spectrum. Although the molecular structure of [Tp<sup>Bu<sup>t</sup></sup>]-Zn(η<sup>1</sup>-O<sub>2</sub>CH) has not been determined by X-ray diffraction, the complex is characterized as an η<sup>1</sup>- rather than η<sup>2</sup>-formate derivative by analogy with the acetato complex [Tp<sup>Bu<sup>t</sup></sup>]-Zn(η<sup>1</sup>-O<sub>2</sub>CMe) (*vide supra*), and also on the basis of the stretching frequencies of the ν<sub>asym</sub>(CO<sub>2</sub>) (1655 cm<sup>-1</sup>) and ν<sub>sym</sub>(CO<sub>2</sub>) (1290 cm<sup>-1</sup>) absorptions in the IR spectrum. The absorptions associated with the formate group have been identified by the shifts observed for the isotopomers [Tp<sup>Bu<sup>t</sup></sup>]-Zn(η<sup>1</sup>-O<sub>2</sub><sup>13</sup>CH) and [Tp<sup>Bu<sup>t</sup></sup>]-Zn(η<sup>1</sup>-O<sub>2</sub>CD) (Figure 7). Most notably, the large difference between ν<sub>sym</sub>(CO<sub>2</sub>) and ν<sub>asym</sub>(CO<sub>2</sub>) (Δν = 365 cm<sup>-1</sup>) is very diagnostic of η<sup>1</sup>-coordination.<sup>45</sup>

The insertion of CO<sub>2</sub> into the Zn-H bond of [Tp<sup>Bu<sup>t</sup></sup>]-ZnH contrasts with the inertness of the alkyls [Tp<sup>Bu<sup>t</sup></sup>]-ZnR toward CO<sub>2</sub>. However, the Zn-H moiety is inert (at 120 °C and 1 atm) toward insertion of ethylene to give the ethyl derivative [Tp<sup>Bu<sup>t</sup></sup>]-ZnEt. Such an observation is presumably a reflection of kinetic factors since the ethyl derivative is stable under these conditions.

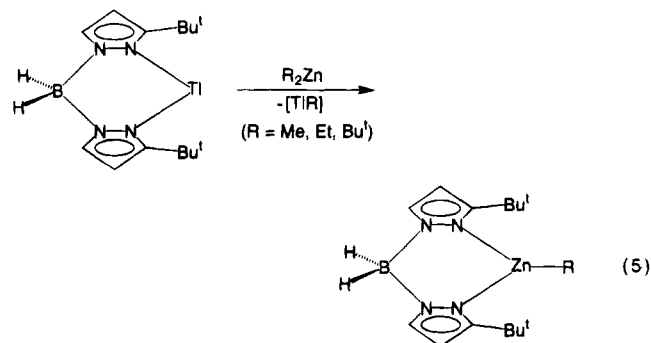
**Synthesis, Characterization, and Reactivity of the Three-Coordinate Zinc Alkyl Derivatives [Bp<sup>Bu<sup>t</sup></sup>]-ZnR.** The above studies have demonstrated the use of the tris(3-*tert*-butylpyrazolyl)hydroborato ligand to provide a well-defined environment for the study of four-coordinate alkyl and hydride derivatives of zinc. In order to investigate changes in reactivity of the Zn-C bond upon lowering the coordination number at the metal from four to three, we have utilized the cor-



**Figure 7.** IR spectra of (a) [Tp<sup>Bu<sup>t</sup></sup>]-Zn(η<sup>1</sup>-O<sub>2</sub>CH), (b) [Tp<sup>Bu<sup>t</sup></sup>]-Zn(η<sup>1</sup>-O<sub>2</sub><sup>13</sup>CH), and (c) [Tp<sup>Bu<sup>t</sup></sup>]-Zn(η<sup>1</sup>-O<sub>2</sub>CD).

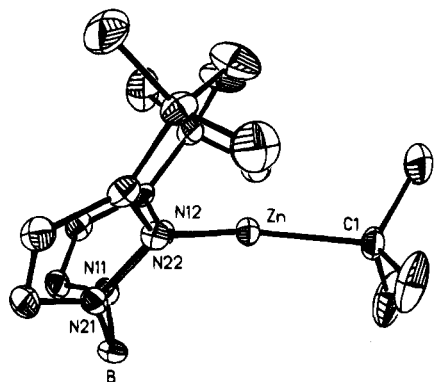
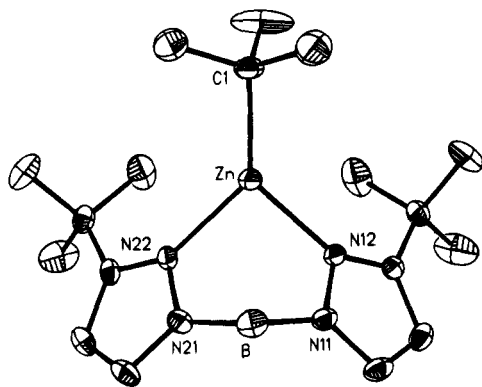
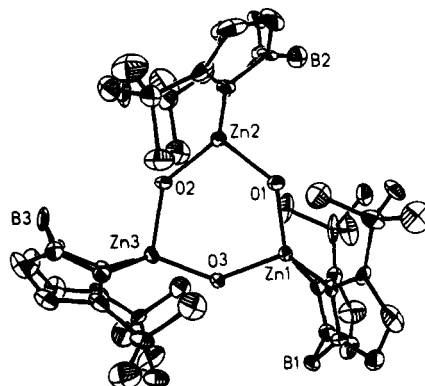
responding bidentate bis(3-*tert*-butylpyrazolyl)hydroborato ligand, [Bp<sup>Bu<sup>t</sup></sup>].

By analogy with the complexes [Tp<sup>Bu<sup>t</sup></sup>]-ZnR, the three-coordinate zinc alkyl derivatives [Bp<sup>Bu<sup>t</sup></sup>]-ZnR (R = Me, Et, Bu<sup>t</sup>) are readily prepared by metathesis of R<sub>2</sub>Zn with the thallium derivative Tl[Bp<sup>Bu<sup>t</sup></sup>] (eq 5). The molecular



structure of the *tert*-butyl derivative [Bp<sup>Bu<sup>t</sup></sup>]-ZnBu<sup>t</sup> has been determined by an X-ray diffraction study (Figures 8 and 9), and selected bond lengths and angles are listed in Table 9. The zinc center may be described as distorted trigonal planar, with the bond angles N(12)-Zn-N(22) = 94.3(2)°, N(12)-Zn-C(1) = 132.2(3)°, and N(22)-Zn-C(1) = 132.7(3)°. The sum of the three bond angles at zinc is 359.2(8)°, clearly indicating a high degree of coplanarity. Three coordination is quite rare for zinc compared to four-coordinate, although in recent years the number of such complexes has begun to increase quite rapidly.<sup>46</sup> Some specific examples of three-coordinate organozinc complexes include (i) {(Me<sub>3</sub>Si)<sub>2</sub>(Ph)P(NSiMe<sub>3</sub>)<sub>2</sub>}ZnPh,<sup>47</sup> (ii) [Zn(CH<sub>2</sub>CMe<sub>3</sub>)<sub>3</sub>]<sup>-</sup>, [Zn(CH<sub>2</sub>SiMe<sub>3</sub>)<sub>3</sub>]<sup>-</sup>, and [Zn(CH<sub>2</sub>SiMe<sub>3</sub>)<sub>2</sub>Ph]<sup>-</sup>,<sup>48</sup> (iii) [(Me<sub>3</sub>-Si)<sub>2</sub>CH]<sub>2</sub>Zn[η<sup>1</sup>-(MeNCH<sub>2</sub>)<sub>3</sub>] and [Zn{CH(SiMe<sub>3</sub>)<sub>2</sub>}<sub>3</sub>]<sup>-</sup>,<sup>49</sup>

(45) Monomeric carboxylato complexes with Δν values greater than 200 cm<sup>-1</sup> invariably have unidentate coordination: Deacon, G. B.; Phillips, R. J. *Coord. Chem. Rev.* **1980**, *33*, 227-250.

Figure 8. Molecular structure of  $[\text{Bp}^{\text{Bu}^t}]\text{ZnBu}^t$ .Figure 9. Molecular structure of  $[\text{Bp}^{\text{Bu}^t}]\text{ZnBu}^t$ .Figure 10. Molecular structure of  $\{[\text{Bp}^{\text{Bu}^t}]\text{Zn}(\mu\text{-OH})\}_3$ .Table 9. Selected Bond Lengths (Å) and Angles (deg) for  $[\text{Bp}^{\text{Bu}^t}]\text{ZnBu}^t$ 

Zn-C(1)	1.995(7)	Zn-N(12)	2.040(5)
Zn-N(22)	2.045(6)	C(1)-C(2)	1.486(15)
C(1)-C(3)	1.495(13)	C(1)-C(4)	1.501(11)
N(11)-N(12)	1.367(8)	N(21)-N(22)	1.377(8)
B-N(11)	1.547(10)	B-N(21)	1.541(12)
C(1)-Zn-N(12)	132.2(3)	C(1)-Zn-N(22)	132.7(3)
N(12)-Zn-N(22)	94.3(2)	Zn-C(1)-C(2)	108.6(5)
Zn-C(1)-C(3)	114.7(5)	Zn-C(1)-C(4)	109.7(6)
C(2)-C(1)-C(3)	107.2(9)	C(2)-C(1)-C(4)	108.8(7)
C(3)-C(1)-C(4)	107.7(8)		

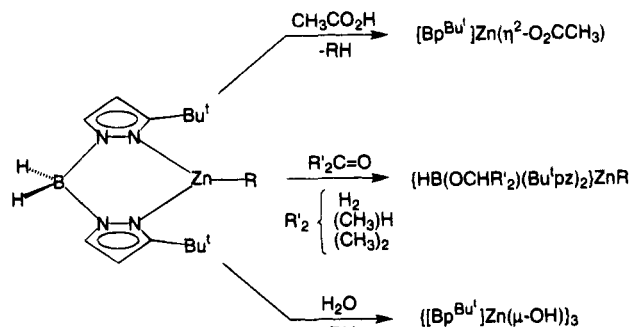
(iv)  $[\text{Zn}(\text{CH}_2\text{SiMe}_3)(\mu\text{-OC}_6\text{H}_2\text{Bu}^t_3)_2]$ ,  $[\text{Zn}(\text{CH}_2\text{SiMe}_3)(\mu\text{-SCPh}_3)_2]$ ,  $[\text{Zn}(\text{CH}_2\text{SiMe}_3)(\mu\text{-OC}_6\text{H}_2\text{Bu}^t_3)_3]$ , and  $[\text{Zn}(\text{CH}_2\text{SiMe}_3)(\mu\text{-OC}_6\text{H}_2\text{Pr}^i_3)_3]$ ,<sup>50</sup> and (v)  $[\text{ZnEt}(\mu\text{-OC}_6\text{H}_3\text{Bu}^t_2)_2]$ .<sup>51-53</sup>

(46) Recent examples of non-organometallic three-coordinate zinc complexes include  $[\text{Zn}\{\text{S}(\text{C}_6\text{HMe}_4)_3\}]_2$ ,<sup>46a</sup>  $[\text{Zn}(\mu\text{-OC}_6\text{H}_2)_2\{\text{N}(\text{SiMe}_3)_2\}]_2$ ,<sup>46b</sup>  $[\text{Zn}\{\mu\text{-S}(\text{C}_6\text{H}_2\text{Bu}^t_3)\}\{\text{S}(\text{C}_6\text{H}_2\text{Bu}^t_3)\}]_2$ ,<sup>46c</sup>  $[\text{Zn}\{\text{S}(\text{C}_6\text{H}_2\text{Bu}^t_3)\}\{\text{L}\}]_2$ ,<sup>46d</sup>  $[\text{Zn}\{\mu\text{-P}(\text{SiMe}_3)_2\}\{\text{P}(\text{SiMe}_3)_2\}]_2$ ,<sup>46e</sup>  $[\text{Zn}\{\mu\text{-TeSi}(\text{SiMe}_3)_3\}\{\text{TeSi}(\text{SiMe}_3)_3\}]_2$ ,<sup>46f</sup>  $[\text{Zn}(\text{SC}_6\text{H}_2\text{Bu}^t_3)_2(\text{OEt}_2)]_2$ ,<sup>46g</sup>  $[\text{Zn}_2(\text{Bu}^t_2\text{P})_2(\text{OH})(\mu\text{-OH})_2]$ ,<sup>46h</sup>  $[\text{Zn}(\text{FeCp}(\text{CO})_2)_3]$ ,<sup>46i</sup> and  $[\eta^2\text{-R}_2\text{N}(\text{Ph})\text{P}(\text{NR})_2]\text{ZnPh}$ .<sup>46j</sup> (a) Gruff, E. S.; Koch, S. A. *J. Am. Chem. Soc.* **1989**, *111*, 8762-8763. (b) Goel, S. C.; Chiang, M. Y.; Buhro, W. E. *Inorg. Chem.* **1990**, *29*, 4646-4652. (c) Bochmann, M.; Bwembya, G.; Grinter, R.; Lu, J.; Webb, K. J.; Williamson, D. J.; Hursthouse, M. B.; Mazid, M. *Inorg. Chem.* **1993**, *32*, 532-537. (d) Bochmann, M.; Bwembya, G. C.; Grinter, R.; Powell, A. K.; Webb, K. J.; Hursthouse, M. B.; Malik, K. M. A.; Mazid, M. A. *Inorg. Chem.* **1994**, *33*, 2290-2296. (e) Goel, S. C.; Chiang, M. Y.; Buhro, W. E. *J. Am. Chem. Soc.* **1990**, *112*, 5636-5637. (f) Bonasia, P. J.; Arnold, J. *Inorg. Chem.* **1992**, *31*, 2508-2514. (g) Power, P. P.; Shoner, S. C. *Angew. Chem., Int. Ed. Engl.* **1990**, *29*, 1403-1404. (h) Arif, A. M.; Cowley, A. H.; Jones, R. A.; Koschmieder, S. U. *J. Chem. Soc., Chem. Commun.* **1987**, 1319-1320. (i) Petersen, R. B.; Ragosta, J. M.; Whitwell, G. E., II; Burlitch, J. M. *Inorg. Chem.* **1983**, *22*, 3407-3415. (j) Romanenko, V. D.; Shul'gin, V. F.; Skopenko, V. V.; Markovskii, L. N. *Zh. Obshchei Khim.* **1984**, *54*, 2791-2792; *J. General Chem. (Engl. Transl.)* **1985**, 2501-2502.

(47) Chernega, A. N.; Antipin, M. Y.; Struchkov, Y. T.; Romanenko, V. D. *Koord. Chim.* **1989**, *15*, 894-901.

(48) Purdy, A. P.; George, C. F. *Organometallics* **1992**, *11*, 1955-1959.

Scheme 4



The three-coordinate alkyl derivatives  $[\text{Bp}^{\text{Bu}^t}]\text{ZnR}$  are also well characterized by  $^1\text{H}$  and  $^{13}\text{C}$  NMR spectroscopy in solution. For example,  $[\text{Bp}^{\text{Bu}^t}]\text{ZnMe}$  exhibits resonances attributable to the Zn-Me group at  $\delta$  1.41 and 30.7 (q,  $^1J_{\text{C-H}} = 126$  Hz) in the  $^1\text{H}$  and  $^{13}\text{C}$  NMR spectra, respectively.

The reactivity of  $[\text{Bp}^{\text{Bu}^t}]\text{ZnR}$  is summarized in Scheme 4. The Zn-C bonds are readily cleaved by the protic reagents  $\text{H}_2\text{O}$  and  $\text{MeCO}_2\text{H}$  to give the hydroxo  $\{[\text{Bp}^{\text{Bu}^t}]\text{Zn}(\mu\text{-OH})\}_3$  and acetato  $[\text{Bp}^{\text{Bu}^t}]\text{Zn}(\eta^2\text{-O}_2\text{CMe})$  derivatives, respectively. The molecular structure of the hydroxo derivative  $\{[\text{Bp}^{\text{Bu}^t}]\text{Zn}(\mu\text{-OH})\}_3$  has been determined to be a cyclic trimer by X-ray diffraction (Figure 10), and selected bond lengths and angles are given in Table 10. The molecule exhibits approximate  $C_{3h}$  symmetry, with each hydroxo group bridging two zinc centers. Although the X-ray structure determination did not reveal the location of the hydroxo hydrogen atoms, convincing evidence for their presence is provided by the  $\nu(\text{O-H})$  absorption at  $3611\text{ cm}^{-1}$  in the IR spectrum. This assignment has been confirmed by the observation of the shifts observed for the isotopomer

(49) Westerhausen, M.; Rademacher, B.; Schwarz, W. Z. *Anorg. Allg. Chem.* **1993**, *619*, 675-689.

(50) Olmstead, M. M.; Power, P. P.; Shoner, S. C. *J. Am. Chem. Soc.* **1991**, *113*, 3379-3385.

(51) Parvez, M.; BergStresser, G. L.; Richey, H. G., Jr. *Acta Crystallogr.* **1992**, *C48*, 641-644.

(52) Some older examples of three-coordinate organozinc derivatives include  $[\text{MeZn}(\mu\text{-NPh}_2)]_2$ ,<sup>52a</sup>  $[\text{Me}_2\text{N}(\text{CH}_2)_3\text{ZnWCp}(\text{CO})_3]$ ,<sup>52b</sup> and  $[(\text{Me}_2\text{PhSi})_3\text{CZn}(\mu\text{-OH})_2]$ .<sup>52c</sup> (a) Bell, N. A.; Shearer, H. M. M.; Spencer, C. B. *Acta Crystallogr.* **1983**, *C39*, 1182-1185. (b) Budzelaar, P. H. M.; Alberts-Jansen, H. J.; Mollema, K.; Boersma, J.; van der Kerk, G. J. M.; Spek, A. L.; Duisenberg, A. J. M. *J. Organomet. Chem.* **1983**, *243*, 137-148. (c) Al-Juaid, S. S.; Buttrus, N. H.; Eaborn, C.; Hitchcock, P. B.; Roberts, A. T. L.; Smith, J. D. S.; Sullivan, A. C. *J. Chem. Soc., Chem. Commun.* **1986**, 908-909.

(53) In the solid state, zinc exhibits three-coordination in the dialkyl  $\text{Zn}[(\text{CH}_2\text{SiMe}_2\text{OPr}^i)_2]$  due to an intermolecular Zn-O interaction [2.252(4) Å]. The C-Zn-C bond angle is  $152.3(3)^\circ$ ; Gais, H.-J.; Bülow, G.; Raabe, G. *J. Am. Chem. Soc.* **1993**, *115*, 7215-7218.

**Table 10. Selected Bond Lengths (Å) and Angles (deg) for  $\{[\text{Bp}^{\text{Bu}^t}]\text{Zn}(\mu\text{-OH})\}_3$** 

Zn(1)–O(1)	1.923(8)	Zn(1)–O(3)	1.957(10)
Zn(2)–O(1)	1.968(9)	Zn(2)–O(2)	1.888(9)
Zn(3)–O(2)	1.985(8)	Zn(3)–O(3)	1.917(10)
Zn(1)–N(12)	2.048(9)	Zn(1)–N(42)	2.054(11)
Zn(2)–N(22)	2.034(10)	Zn(2)–N(52)	2.022(11)
Zn(3)–N(32)	2.033(11)	Zn(3)–N(62)	2.035(11)
B(1)–N(11)	1.586(20)	B(1)–N(41)	1.554(22)
B(2)–N(21)	1.494(23)	B(2)–N(51)	1.554(22)
B(3)–N(31)	1.515(26)	B(3)–N(61)	1.613(24)
N(11)–N(12)	1.365(14)	N(21)–N(22)	1.376(17)
N(31)–N(32)	1.378(16)	N(41)–N(42)	1.325(17)
N(51)–N(52)	1.362(16)	N(61)–N(62)	1.374(16)
O(1)–Zn(1)–O(3)	103.6(4)	O(1)–Zn(1)–N(12)	118.9(4)
O(3)–Zn(1)–N(12)	112.1(4)	O(1)–Zn(1)–N(42)	122.1(4)
O(3)–Zn(1)–N(42)	105.5(4)	N(12)–Zn(1)–N(42)	94.3(4)
O(1)–Zn(2)–O(2)	104.0(4)	O(1)–Zn(2)–N(22)	108.5(4)
O(2)–Zn(2)–N(22)	119.2(4)	O(1)–Zn(2)–N(52)	109.0(4)
O(2)–Zn(2)–N(52)	121.1(4)	N(22)–Zn(2)–N(52)	94.4(4)
O(2)–Zn(3)–O(3)	102.0(4)	O(2)–Zn(3)–N(32)	109.3(4)
O(3)–Zn(3)–N(32)	120.1(4)	O(2)–Zn(3)–N(62)	107.3(4)
O(3)–Zn(3)–N(62)	124.1(4)	N(32)–Zn(3)–N(62)	93.4(4)
Zn(1)–O(1)–Zn(2)	135.3(5)	Zn(2)–O(2)–Zn(3)	137.2(5)
Zn(1)–O(3)–Zn(3)	137.5(4)		

**Table 11. Zn–O Bond Lengths of  $[\text{Zn}(\mu_2\text{-OH})\text{Zn}]$  Moieties**

	$d(\text{Zn}-\text{O})/\text{Å}$	ref
$\{[\text{Bp}^{\text{Bu}^t}]\text{Zn}(\mu\text{-OH})\}_3$	1.89(1)–2.02(1)	this work
$[(\text{Me}_2\text{PhSi})_3\text{CZn}(\mu\text{-OH})_2]$	1.899(9)	c
$\{[\text{Bu}^t\text{pz}]_3\text{Zn}\}_2(\mu\text{-OH})_2^{3+}$	1.91[1]	d
$[(\text{LH}_2)_2\text{Zn}_2(\mu\text{-OH})]^{+a}$	1.915(2)	e
$\{[(\text{Me}_3\text{tacn})\text{Zn}]_2(\mu\text{-OH})(\mu\text{-O}_2\text{CMe})_2\}$	1.996(4)	f
$[(\text{Me}_3\text{tacn})\text{Zn}(\mu\text{-OH})_2]^{2+}$	1.97[1]	f
$\{[\eta^4\text{-N}(\text{CH}_2\text{py})_3]\text{Zn}(\mu\text{-OH})_2\}^{2+}$	2.01[4]	g
$[\text{Zn}_2(\text{Bu}^t_2\text{P})_2(\text{OH})(\mu\text{-OH})_2]$	2.33[2] <sup>b</sup>	h

<sup>a</sup>  $\text{LH}_2 = 4,7\text{-bis}(2\text{-hydroxybenzyl})\text{-1-oxa-4,7-diazacyclononane}$ . <sup>b</sup> The terminal Zn–O bond length is 2.30(2) Å. <sup>c</sup> Al-Juaid, S. S.; Buttrus, N. H.; Eaborn, C.; Hitchcock, P. B.; Roberts, A. T. L.; Smith, J. D. S.; Sullivan, A. C. *J. Chem. Soc., Chem. Commun.* **1986**, 908–909. <sup>d</sup> Alsfasser, R.; Vahrenkamp, H. *Chem. Ber.* **1993**, *126*, 695–701. <sup>e</sup> Flassbeck, C.; Wieghardt, K.; Bill, E.; Butzlaff, C.; Trautwein, A. X.; Nuber, B.; Weiss, J. *Inorg. Chem.* **1992**, *31*, 21–26. <sup>f</sup> Chaudhuri, P.; Stockheim, C.; Wieghardt, K.; Deck, W.; Gregorzik, R.; Vahrenkamp, H.; Nuber, B.; Weiss, J. *Inorg. Chem.* **1992**, *31*, 1451–1457. <sup>g</sup> Murthy, N. N.; Karlin, K. D. *J. Chem. Soc., Chem. Commun.* **1993**, 1236–1238. <sup>h</sup> Arif, A. M.; Cowley, A. H.; Jones, R. A.; Koschmieder, S. U. *J. Chem. Soc., Chem. Commun.* **1987**, 1319–1320.

$\{[\text{Bp}^{\text{Bu}^t}]\text{Zn}(\mu\text{-OD})\}_3$  (2670  $\text{cm}^{-1}$ ). The Zn–OH moiety is also characterized by a resonance at 2.25 ppm in the  $^1\text{H}$  NMR spectrum.

The hydroxo bridge between each pair of zinc centers in the trimer  $\{[\text{Bp}^{\text{Bu}^t}]\text{Zn}(\mu\text{-OH})\}_3$  is slightly asymmetric. Thus, the lengths of the Zn–O bonds alternate in a short–long fashion around the  $\text{Zn}_3\text{O}_3$  ring, although the differences are small, *i.e.* the Zn(1)–O(1), Zn(2)–O(2) and Zn(3)–O(3) bonds average 1.91[2] Å, while Zn(1)–O(3), Zn(2)–O(1), and Zn(3)–O(2) bonds average 1.97–[2] Å. Notably, all these bridging Zn–OH interactions are longer than that in the monomeric terminal zinc hydroxo complex  $[\text{Tp}^{\text{Bu}^t,\text{Me}}]\text{ZnOH}$  [1.850(8) Å]<sup>54,55</sup> but comparable to the values reported for a number of complexes with hydroxo groups bridging two zinc centers, as summarized in Table 11. The data presented in Table 11 indicate that Zn–O bond lengths for hydroxo groups that bridge two zinc centers are typically of the order 1.89–2.01 Å. A notable exception, however, is the

(54) Alsfasser, R.; Trofimenko, S.; Looney, A.; Parkin, G.; Vahrenkamp, H. *Inorg. Chem.* **1991**, *30*, 4098–4100.

(55) The reference value for a pure single covalent Zn–O bond has been adopted to be 1.89 Å: Haaland, A. *Angew. Chem., Int. Ed. Engl.* **1989**, *28*, 992–1000.

complex  $[\text{Zn}_2(\text{Bu}^t_2\text{P})_2(\text{OH})(\mu\text{-OH})_2]$ , with Zn–O bond lengths (both terminal and bridging) which, as pointed out previously, are abnormally long (2.30–2.33 Å).<sup>46h</sup> It is plausible that the origin of the long Zn–O bond lengths in  $[\text{Zn}_2(\text{Bu}^t_2\text{P})_2(\text{OH})(\mu\text{-OH})_2]$  may be an artifact due to contamination, possibly with a chloride derivative.<sup>20</sup> Indeed, such a suggestion is reasonable since  $[\text{Zn}_2(\text{Bu}^t_2\text{P})_2(\text{OH})(\mu\text{-OH})_2]$  was prepared in only low yield by the reaction of  $\text{ZnCl}_2$  with  $\text{Bu}^t_2\text{PLi}$  and required the presence of adventitious water.

The above reactions with protic reagents are analogous to those of the four-coordinate complexes,  $[\text{Tp}^{\text{Bu}^t}]\text{ZnR}$ . However, whereas the tris(3-*tert*-butylpyrazolyl)hydroborato complexes  $[\text{Tp}^{\text{Bu}^t}]\text{ZnR}$  only show reactivity at the Zn–C bond, the bis(3-*tert*-butylpyrazolyl)hydroborato derivatives also exhibit reactivity at an additional site, namely the B–H bond. Thus, the bis(3-*tert*-butylpyrazolyl)hydroborato complexes,  $[\text{Bp}^{\text{Bu}^t}]\text{ZnR}$  (R = Me, Et), react with aldehydes and ketones,  $(\text{CH}_2\text{O})_n$ , MeCHO, and  $\text{Me}_2\text{CO}$ , to give the derivatives  $\{\text{HB}(\text{OR}')(\text{3-Bu}^t\text{pz})_2\}\text{ZnR}$  (R' = Me, Et, Pr<sup>i</sup>), as a result of insertion into the B–H bond. We have not yet determined whether the alkoxy substituents on boron are also coordinated to the zinc center, *i.e.*  $\{\eta^2\text{-HB}(\text{OR}')(\text{3-Bu}^t\text{pz})_2\}\text{ZnR}$  *vs*  $\{\eta^3\text{-HB}(\text{OR}')(\text{3-Bu}^t\text{pz})_2\}\text{ZnR}$ . Other bis(pyrazolyl)hydroborato metal complexes have also demonstrated the capability of reducing ketones to alcohols.<sup>56</sup> However, functionalized bis(pyrazolyl)hydroborato products were not isolated.

## Conclusion

In summary, the tris(pyrazolyl)hydroborato ligand system has allowed the isolation of monomeric four-coordinate zinc alkyl and hydride derivatives  $[\text{Tp}^{\text{Bu}^t}]\text{ZnR}$  (R = Me, Et),  $[\text{Tp}^{\text{Me}_2}]\text{ZnMe}$ , and  $[\text{Tp}^{\text{Bu}^t}]\text{ZnH}$ , while the bis(3-*tert*-butylpyrazolyl)hydroborato ligand system has allowed the isolation of monomeric three-coordinate zinc alkyl derivatives  $[\text{Bp}^{\text{Bu}^t}]\text{ZnR}$  (R = Me, Et, Bu<sup>t</sup>). The four-coordinate alkyl complexes are isostructural with the analogous magnesium derivatives, and comparison of the reactivity of the Zn–C and Mg–C bonds in these complexes provides good evidence for the intrinsic higher reactivity of the Mg–C *vs* the Zn–C bond. Comparison of the alkyl and hydride derivatives  $[\text{Tp}^{\text{Bu}^t}]\text{ZnR}$  and  $[\text{Tp}^{\text{Bu}^t}]\text{ZnH}$  indicates that the Zn–H bond exhibits higher reactivity than the Zn–C bond, especially with regards to insertion of  $\text{CO}_2$ . In contrast to the four-coordinate zinc alkyls  $[\text{Tp}^{\text{Bu}^t}]\text{ZnR}$ , the three-coordinate derivatives  $[\text{Bp}^{\text{Bu}^t}]\text{ZnR}$  exhibit two different sites of reactivity. Thus, the Zn–C bonds of  $[\text{Bp}^{\text{Bu}^t}]\text{ZnR}$  are the sites of reactivity with protic reagents such as  $\text{H}_2\text{O}$  and  $\text{MeCO}_2\text{H}$ , while the B–H bonds are the preferred sites of reactivity for insertion with ketones and aldehydes.

## Experimental Section

**General Considerations.** All manipulations were performed using a combination of glovebox, high-vacuum, and Schlenk techniques.<sup>57</sup> Solvents were purified and degassed by standard procedures.  $^1\text{H}$  and  $^{13}\text{C}$  NMR spectra were measured on Varian VXR 200, 300, and 400 spectrometers.

(56) Paolucci, G.; Cacchi, S.; Caglioti, L. *J. Chem. Soc., Perkin Trans. 1* **1979**, 1129–1131.

IR spectra were recorded as KBr pellets or Nujol mulls between KBr disks on a Perkin-Elmer 1420 spectrophotometer and are reported in  $\text{cm}^{-1}$ . Mass spectra were obtained on a Nermag R10-10 mass spectrometer using chemical ionization ( $\text{NH}_3$  or  $\text{CH}_4$ ) techniques. Elemental analyses were measured using a Perkin-Elmer 2400 CHN elemental analyzer.  $\text{ZnH}_2$ ,<sup>56</sup>  $\text{Me}_3\text{SiOH}$ ,<sup>58</sup>  $\text{Tl}[\text{Tp}^{\text{Bu}^t}]_3$ ,<sup>3</sup>  $\text{Tl}[\text{Tp}^{\text{Me}_2}]_3$ ,<sup>5c</sup>  $\text{K}[\text{Tp}^{\text{Me}_2}]_3$ ,<sup>59</sup>  $\text{Tl}[\text{Bp}^{\text{Bu}^t}]_3$ ,<sup>3</sup> and  $[\text{Tp}^{\text{Bu}^t}]\text{ZnNCS}$ <sup>3</sup> were prepared by the literature methods. NMR data are listed in Table 4.

**Synthesis of  $[\text{Tp}^{\text{Me}_2}]\text{ZnMe}$ .** A solution of excess  $\text{Me}_2\text{Zn}$  in decalin was added to a stirred suspension of  $\text{Tl}[\text{Tp}^{\text{Me}_2}]$  (1.00 g, 1.99 mmol) in THF (30 mL), resulting in the formation of a black precipitate. The volatile components were removed *in vacuo*, and the residue was extracted into benzene (*ca.* 30 mL). The mixture was filtered, the benzene removed *in vacuo*, and the product recrystallized from THF at  $-78^\circ\text{C}$ , giving  $[\text{Tp}^{\text{Me}_2}]\text{ZnMe}$  as a white solid (0.13 g, 17%). Anal. Calcd for  $[\text{Tp}^{\text{Me}_2}]\text{ZnMe}$ : C, 50.9; H, 6.7; N, 22.3. Found: C, 50.9; H, 6.7; N, 22.0. IR data: 2506 ( $\nu_{\text{B-H}}$ ).

**Synthesis of  $[\text{Tp}^{\text{Bu}^t}]\text{ZnMe}$ .** A solution of  $\text{Tl}[\text{Tp}^{\text{Bu}^t}]$  (0.5 g, 0.85 mmol) in THF (20 mL) was added dropwise to a solution of  $\text{Me}_2\text{Zn}$  in pentane (0.83 g, 0.87 mmol), resulting in the immediate formation of a black deposit of Tl metal. The mixture was stirred for 30 min at room temperature and filtered. The volatile components were removed from the filtrate under reduced pressure. The solid was extracted into pentane (20 mL) and filtered. The filtrate was concentrated to *ca.* 10 mL and placed at  $-78^\circ\text{C}$  giving a crop of colorless crystals of  $[\text{Tp}^{\text{Bu}^t}]\text{ZnMe}$ , which were isolated by filtration and dried *in vacuo* (150 mg, 38%). Anal. Calcd for  $[\text{Tp}^{\text{Bu}^t}]\text{ZnMe}$ : C, 57.3; H, 8.0; N, 18.2. Found: C, 56.6; H, 7.1; N, 17.2. IR data: 2505 ( $\nu_{\text{B-H}}$ ). MS:  $m/z$  461 ( $\text{M}^+ + 1$ ).

**Synthesis of  $[\text{Tp}^{\text{Bu}^t}]\text{ZnEt}$ .** A solution of  $\text{Tl}[\text{Tp}^{\text{Bu}^t}]$  (1.0 g, 1.7 mmol) in THF (30 mL) was added dropwise to a solution of  $\text{Et}_2\text{Zn}$  (1.4 g, 15% w/w in hexane, 1.7 mmol) in THF (10 mL) resulting in the formation of a black deposit of Tl metal. The mixture was stirred for 30 min at room temperature and filtered. The filtrate was concentrated to *ca.* 10 mL and placed at  $0^\circ\text{C}$  giving a crop of colorless crystals of  $[\text{Tp}^{\text{Bu}^t}]\text{ZnEt}$ , which were isolated by filtration and dried *in vacuo* (400 mg, 50%). Anal. Calcd for  $[\text{Tp}^{\text{Bu}^t}]\text{ZnEt}$ : C, 58.1; H, 8.3; N, 17.7. Found: C, 56.9; H, 8.2; N, 16.9. IR data: 2452 and 2480 ( $\nu_{\text{B-H}}$ ). MS:  $m/z$  475 ( $\text{M}^+ + 1$ ).

**Syntheses of  $[\text{Tp}^{\text{Bu}^t}]\text{ZnX}$  (X = Cl, Br, I, CN, NCS, O<sub>2</sub>CMe).** The complexes  $[\text{Tp}^{\text{Bu}^t}]\text{ZnX}$  were prepared by reaction of  $\text{K}[\text{Tp}^{\text{Bu}^t}]$  or  $\text{Tl}[\text{Tp}^{\text{Bu}^t}]$  with  $\text{ZnX}_2$  by a method analogous to that used for  $[\text{Tp}^{\text{Bu}^t}]\text{ZnN}_3$  and  $[\text{Tp}^{\text{Bu}^t}]\text{ZnNCS}$ ,<sup>3</sup> and a typical procedure is given for  $[\text{Tp}^{\text{Bu}^t}]\text{ZnCl}$ . A solution of  $\text{Tl}[\text{Tp}^{\text{Bu}^t}]$  (2.0 g, 3.42 mmol) in THF (40 mL) was added to a stirred suspension of  $\text{ZnCl}_2$  (0.56 g, 4.10 mmol) in THF (20 mL), resulting in the immediate formation of a white precipitate. The mixture was stirred for 1 h and filtered. The solvent was removed from the filtrate *in vacuo*, giving  $[\text{Tp}^{\text{Bu}^t}]\text{ZnCl}$  as a white solid (1.57 g, 96%).

Anal. Calcd for  $[\text{Tp}^{\text{Bu}^t}]\text{ZnCl}$ : C, 52.4; H, 7.1; N, 17.5. Found: C, 52.6; H, 7.0; N, 17.4. IR data: 2490 ( $\nu_{\text{B-H}}$ ). MS:  $m/z$  480 ( $\text{M}^+ + 1$ ).

Anal. Calcd for  $[\text{Tp}^{\text{Bu}^t}]\text{ZnBr}$ : C, 47.9; H, 6.5; N, 16.0. Found: C, 47.9; H, 6.4; N, 15.1. IR data: 2527 ( $\nu_{\text{B-H}}$ ). MS:  $m/z$  526 ( $\text{M}^+ + 1$ ).

Anal. Calcd for  $[\text{Tp}^{\text{Bu}^t}]\text{ZnI}$ : C, 44.0; H, 6.0; N, 14.7. Found: C, 44.2; H, 6.2; N, 14.4. IR data: 2519 ( $\nu_{\text{B-H}}$ ). MS:  $m/z$  572 ( $\text{M}^+ + 1$ ).

Anal. Calcd for  $[\text{Tp}^{\text{Bu}^t}]\text{ZnCN}$ : C, 55.9; H, 7.3; N, 20.7. Found: C, 56.2; H, 8.2; N, 20.6. IR data: 2520 ( $\nu_{\text{B-H}}$ ) and 2214 ( $\nu_{\text{C-N}}$ ). MS:  $m/z$  471 ( $\text{M}^+ + 1$ ).

Anal. Calcd for  $[\text{Tp}^{\text{Bu}^t}]\text{Zn}(\eta^1\text{-O}_2\text{CMe})$ : C, 54.6; H, 7.4; N, 16.6. Found: C, 54.6; H, 7.2; N, 16.2. IR data: 2480 ( $\nu_{\text{B-H}}$ ) and 1610 ( $\nu_{\text{asym CO}_2}$ ). MS:  $m/z$  505 ( $\text{M}^+ + 1$ ).

**Reaction of  $[\text{Tp}^{\text{Bu}^t}]\text{ZnEt}$  with  $\text{Cl}_2$  and  $\text{Br}_2$ .** A solution of  $[\text{Tp}^{\text{Bu}^t}]\text{ZnEt}$  (20 mg, 0.04 mmol) in *d*<sub>6</sub>-benzene (0.7 mL) was treated with  $\text{X}_2$  (X = Cl, Br, I). <sup>1</sup>H NMR spectroscopy demonstrated the formation of  $[\text{Tp}^{\text{Bu}^t}]\text{ZnX}$  and  $\text{EtX}$  after 1 day at room temperature.

**Reaction of  $[\text{Tp}^{\text{Bu}^t}]\text{ZnEt}$  with  $\text{Me}_3\text{SiX}/\text{H}_2\text{O}$  (X = Cl, Br, I, CN, N<sub>3</sub>, NCS).** A solution of  $[\text{Tp}^{\text{Bu}^t}]\text{ZnEt}$  (20 mg, 0.04 mmol) in *d*<sub>6</sub>-benzene (0.7 mL) was treated with a mixture of  $\text{Me}_3\text{SiX}/\text{H}_2\text{O}$  (X = Cl, Br, I, CN, N<sub>3</sub>, NCS). The reactions were monitored by <sup>1</sup>H NMR spectroscopy which demonstrated the formation of  $[\text{Tp}^{\text{Bu}^t}]\text{ZnX}$  and  $\text{C}_2\text{H}_6$ .

**Reaction of  $[\text{Tp}^{\text{Bu}^t}]\text{ZnMe}$  with HCl.** A solution of  $[\text{Tp}^{\text{Bu}^t}]\text{ZnMe}$  (20 mg, 0.04 mmol) in *d*<sub>6</sub>-benzene (0.7 mL) was treated with HCl (1 atm) at room temperature. The reaction was monitored by <sup>1</sup>H NMR spectroscopy which demonstrated the immediate formation of  $[\text{Tp}^{\text{Bu}^t}]\text{ZnCl}$ .

**Synthesis of  $[\text{Tp}^{\text{Bu}^t}]\text{ZnC}_2\text{Ph}$ .** A solution of  $[\text{Tp}^{\text{Bu}^t}]\text{ZnEt}$  (20 mg, 0.04 mmol) in *d*<sub>6</sub>-benzene (0.7 mL) was treated with  $\text{PhCCH}$  (0.05 mmol) and heated at  $70\text{--}80^\circ\text{C}$  for a period of days. The reaction was monitored by <sup>1</sup>H NMR spectroscopy which demonstrated the formation of  $[\text{Tp}^{\text{Bu}^t}]\text{ZnC}_2\text{Ph}$  and  $\text{C}_2\text{H}_6$ . Anal. Calcd for  $[\text{Tp}^{\text{Bu}^t}]\text{ZnC}_2\text{Ph}$ : C, 63.5; H, 7.3; N, 15.3. Found: C, 63.1; H, 7.4; N, 15.9. IR data: 2503 ( $\nu_{\text{B-H}}$ ). MS:  $m/z$  547 ( $\text{M}^+ + 1$ ).

**Reaction of  $[\text{Tp}^{\text{Bu}^t}]\text{ZnEt}$  with RI (R = Me,  $\text{PhCH}_2$ ).** A solution of  $[\text{Tp}^{\text{Bu}^t}]\text{ZnEt}$  (20 mg, 0.04 mmol) in *d*<sub>6</sub>-benzene (0.7 mL) was treated with RI (R = Me,  $\text{PhCH}_2$ ; 0.05 mmol) and heated at  $140^\circ\text{C}$  over a period of weeks. The reactions were monitored by <sup>1</sup>H NMR spectroscopy which demonstrated the slow formation of  $[\text{Tp}^{\text{Bu}^t}]\text{ZnI}$ .

**Reaction of  $[\text{Tp}^{\text{Bu}^t}]\text{ZnEt}$  with  $\text{MeCO}_2\text{H}$ .** A solution of  $[\text{Tp}^{\text{Bu}^t}]\text{ZnEt}$  (20 mg, 0.04 mmol) in *d*<sub>6</sub>-benzene (0.7 mL) was treated with  $\text{MeCO}_2\text{H}$  (2.8  $\mu\text{L}$ , 0.05 mmol) and left at room temperature. The reaction was monitored by <sup>1</sup>H NMR spectroscopy which demonstrated the formation of  $[\text{Tp}^{\text{Bu}^t}]\text{Zn}(\eta^1\text{-O}_2\text{CMe})$  and  $\text{C}_2\text{H}_6$ .

**Reactions of  $[\text{Tp}^{\text{Me}_2}]\text{ZnMe}$ .** A solution of  $[\text{Tp}^{\text{Me}_2}]\text{ZnMe}$  (*ca.* 10 mg) in *d*<sub>6</sub>-benzene (0.7 mL) was treated with a variety of reagents ( $\text{Br}_2$ ,  $\text{I}_2$ ,  $\text{MeOH}$ ,  $\text{PhOH}$ ,  $\text{Bu}^t\text{OOH}$ ,  $\text{MeI}$ ,  $\text{BrCN}$ ,  $\text{HCl}$ ) and monitored by <sup>1</sup>H NMR spectroscopy. In each case,  $[\text{Tp}^{\text{Me}_2}]\text{Zn}$  was observed to be a major product.

**Synthesis of  $[\text{Tp}^{\text{Me}_2}]\text{Zn}$ .** A solution of  $\text{K}[\text{Tp}^{\text{Me}_2}]$  (500 mg, 1.49 mmol) in THF (20 mL) was added to a stirred suspension of  $\text{ZnCl}_2$  (101 mg, 0.74 mmol) in THF (10 mL). The mixture was stirred overnight and the solvent removed *in vacuo*. The residue was extracted into  $\text{CH}_2\text{Cl}_2$  (30 mL) and the extract was washed with water. The solvent was removed from the  $\text{CH}_2\text{Cl}_2$  layer *in vacuo*, and the solid obtained was recrystallized from toluene at  $-78^\circ\text{C}$ . Yield of  $[\text{Tp}^{\text{Me}_2}]\text{Zn}$ : 173 mg (34%). Anal. Calcd for  $[\text{Tp}^{\text{Me}_2}]\text{Zn}$ : C, 54.6; H, 6.7; N, 25.5. Found: C, 54.7; H, 6.8; N, 25.9. IR data: 2506 ( $\nu_{\text{B-H}}$ ). MS:  $m/z$  659 ( $\text{M}^+ + 1$ ).

**Synthesis of  $[\text{Tp}^{\text{Bu}^t}]\text{ZnH}$ .** THF (50 mL) was added dropwise to a mixture of  $\text{Tl}[\text{Tp}^{\text{Bu}^t}]$  (1.0 g, 1.7 mmol) and  $\text{ZnH}_2$  (180 mg, 2.7 mmol), resulting in the immediate formation of a black deposit of Tl metal. The mixture was stirred for 30 h at room temperature and filtered. The filtrate was concentrated to *ca.* 10 mL and placed at  $0^\circ\text{C}$  giving colorless crystals. The crystals of  $[\text{Tp}^{\text{Bu}^t}]\text{ZnH}$  were isolated by filtration and dried *in vacuo* (0.10 g). Further crops of  $[\text{Tp}^{\text{Bu}^t}]\text{ZnH}$  were obtained from the mother liquor by a similar procedure. Total yield of  $[\text{Tp}^{\text{Bu}^t}]\text{ZnH}$ : 0.32 g (42%). Anal. Calcd for  $[\text{Tp}^{\text{Bu}^t}]\text{ZnH}$ : C, 56.3; H, 7.9; N, 18.9. Found: C, 55.9; H, 7.9; N, 19.2. IR: 2500 ( $\nu_{\text{B-H}}$ ), 1770 ( $\nu_{\text{Zn-H}}$ ). MS:  $m/z$  447 ( $\text{M}^+ + 1$ ).  $[\text{Tp}^{\text{Bu}^t}]\text{ZnD}$  was prepared analogously using  $\text{ZnD}_2$ . Yield of  $[\text{Tp}^{\text{Bu}^t}]\text{ZnD}$ : 40%. IR: 1270 ( $\nu_{\text{Zn-D}}$ ). MS:  $m/z$  448 ( $\text{M}^+ + 1$ ).

**Reaction of  $[\text{Tp}^{\text{Bu}^t}]\text{ZnH}$  with  $\text{CO}_2$ .** A solution of  $[\text{Tp}^{\text{Bu}^t}]\text{ZnH}$  (45 mg, 0.1 mmol) in benzene (1 mL) was treated with  $\text{CO}_2$  (1 atm) and heated at  $50^\circ\text{C}$  for 4 days. The volatile components were removed under reduced pressure giving

(57) (a) McNally, J. P.; Leong, V. S.; Cooper, N. J. *ACS Symp. Ser.* **1987**, No. 357, 6–23. (b) Burger, B. J.; Bercaw, J. E. *ACS Symp. Ser.* **1987**, No. 357, 79–97.

(58) George, P. D.; Sommer, L. H.; Whitmore, F. C. *J. Am. Chem. Soc.* **1953**, 75, 1585–1588.

(59) Trofimenko, S. *J. Am. Chem. Soc.* **1967**, 89, 6288–6294.



[Tp<sup>Bu<sup>t</sup></sup>]Zn( $\eta^1$ -O<sub>2</sub>CH) as a white solid (45 mg, 92%). Anal. Calcd for [Tp<sup>Bu<sup>t</sup></sup>]Zn( $\eta^1$ -O<sub>2</sub>CH): C, 53.7; H, 7.2; N, 17.1. Found: C, 53.1; H, 6.9; N, 16.4. IR: 2505 ( $\nu_{B-H}$ ), 1655 ( $\nu_{asym} CO_2$ ), 1290 ( $\nu_{sym} CO_2$ ). MS: *m/z* 491 ( $M^+ + 1$ ). [Tp<sup>Bu<sup>t</sup></sup>]Zn( $\eta^1$ -O<sub>2</sub><sup>13</sup>CH) and [Tp<sup>Bu<sup>t</sup></sup>]Zn( $\eta^1$ -O<sub>2</sub>CD) were prepared in a similar fashion using the appropriately labeled materials. IR data for [Tp<sup>Bu<sup>t</sup></sup>]Zn( $\eta^1$ -O<sub>2</sub><sup>13</sup>CH): 2505 ( $\nu_{B-H}$ ), 1620 ( $\nu_{asym}^{13}CO_2$ ), 1270 ( $\nu_{sym}^{13}CO_2$ ). IR data for [Tp<sup>Bu<sup>t</sup></sup>]Zn( $\eta^1$ -O<sub>2</sub>CD): 2510 ( $\nu_{B-H}$ ), 2120 ( $\nu_{C-D}$ ), 1645 ( $\nu_{asym} CO_2$ ), 1280 ( $\nu_{sym} CO_2$ ).

**Reaction of [Tp<sup>Bu<sup>t</sup></sup>]ZnH with C<sub>2</sub>H<sub>4</sub>.** A solution of [Tp<sup>Bu<sup>t</sup></sup>]ZnH (20 mg, 0.04 mmol) in *d*<sub>6</sub>-benzene (1 mL) was treated with C<sub>2</sub>H<sub>4</sub> (1 atm) and heated at 120 °C for about 20 days. No reaction was observed, except for slight decomposition of [Tp<sup>Bu<sup>t</sup></sup>]ZnH.

**Reaction of [Tp<sup>Bu<sup>t</sup></sup>]ZnH with H<sub>2</sub>S.** A solution of [Tp<sup>Bu<sup>t</sup></sup>]ZnH (40 mg, 0.09 mmol) in benzene (1 mL) was treated with H<sub>2</sub>S (1 atm) and left at room temperature for 1 h. The volatile components were removed under reduced pressure giving [Tp<sup>Bu<sup>t</sup></sup>]ZnSH as a white solid (40 mg, 93%). Anal. Calcd for [Tp<sup>Bu<sup>t</sup></sup>]ZnSH: C, 52.3; H, 7.4; N, 17.5. Found: C, 52.6; H, 7.3; N, 17.4. IR: 2500 ( $\nu_{B-H}$ ). MS: *m/z* 479 ( $M^+ + 1$ ).

**Reaction of [Tp<sup>Bu<sup>t</sup></sup>]ZnH with Me<sub>3</sub>SiOH.** A solution of [Tp<sup>Bu<sup>t</sup></sup>]ZnH (40 mg, 0.09 mmol) in benzene (1 mL) was treated with Me<sub>3</sub>SiOH (10  $\mu$ L), and heated at 70 °C for 3 days. The volatile components were removed under reduced pressure giving [Tp<sup>Bu<sup>t</sup></sup>]ZnOSiMe<sub>3</sub> as a white solid (45 mg, 93%). Anal. Calcd for [Tp<sup>Bu<sup>t</sup></sup>]ZnOSiMe<sub>3</sub>: C, 53.8; H, 8.1; N, 15.7. Found: C, 58.7; H, 7.3; N, 15.8. IR data: 2490 ( $\nu_{B-H}$ ).

**Reaction of [Tp<sup>Bu<sup>t</sup></sup>]ZnCl with KOSiMe<sub>3</sub>.** KOSiMe<sub>3</sub> (100 mg, 0.8 mmol) was added to a solution of [Tp<sup>Bu<sup>t</sup></sup>]ZnCl (250 mg, 0.5 mmol) in benzene (20 mL). The mixture was shaken at room temperature for 15 min and filtered. The colorless crystals were isolated and demonstrated to be [Tp<sup>Bu<sup>t</sup></sup>]ZnOSiMe<sub>3</sub> by <sup>1</sup>H NMR spectroscopy.

**Reaction of [Tp<sup>Bu<sup>t</sup></sup>]ZnH with MeCO<sub>2</sub>H.** A solution of [Tp<sup>Bu<sup>t</sup></sup>]ZnH (20 mg, 0.04 mmol) in benzene (1 mL) was treated with MeCO<sub>2</sub>H (0.05 mmol) and left at room temperature for 10 min. The reaction was monitored by <sup>1</sup>H NMR spectroscopy which demonstrated the formation of [Tp<sup>Bu<sup>t</sup></sup>]Zn( $\eta^1$ -O<sub>2</sub>CMe) and H<sub>2</sub>. Anal. Calcd for [Tp<sup>Bu<sup>t</sup></sup>]Zn( $\eta^1$ -O<sub>2</sub>CMe): C, 54.6; H, 7.4; N, 16.6. Found: C, 54.6; H, 7.2; N, 16.2.

**Reaction of [Tp<sup>Bu<sup>t</sup></sup>]ZnH with RX (R = Me, PhCH<sub>2</sub>).** A solution of [Tp<sup>Bu<sup>t</sup></sup>]ZnH (20 mg, 0.04 mmol) in *d*<sub>6</sub>-benzene (0.7 mL) was treated with RX (R = Me, PhCH<sub>2</sub>; 0.05 mmol) and left at room temperature. The reactions were monitored by <sup>1</sup>H NMR spectroscopy which demonstrated the formation of [Tp<sup>Bu<sup>t</sup></sup>]ZnI and RH (R = Me, PhCH<sub>2</sub>) over a period of days. The formation of [Tp<sup>Bu<sup>t</sup></sup>]ZnI and RD (CH<sub>3</sub>D, PhCH<sub>2</sub>D) was observed for the reaction of [Tp<sup>Bu<sup>t</sup></sup>]ZnD with RI.

**Reaction of [Tp<sup>Bu<sup>t</sup></sup>]ZnH with Me<sub>3</sub>SiX (X = Cl, I).** A solution of [Tp<sup>Bu<sup>t</sup></sup>]ZnH (20 mg, 0.04 mmol) in *d*<sub>6</sub>-benzene (1 mL) was treated with Me<sub>3</sub>SiX (X = Cl, I; 0.05 mmol) and heated at 70–80 °C for a period of days. The reactions were monitored by <sup>1</sup>H NMR spectroscopy which demonstrated the formation of [Tp<sup>Bu<sup>t</sup></sup>]ZnX (X = Cl, I).

**Reaction of [Tp<sup>Bu<sup>t</sup></sup>]ZnH with MeCOCl.** A solution of [Tp<sup>Bu<sup>t</sup></sup>]ZnH (20 mg, 0.04 mmol) in benzene (1 mL) was treated with MeCOCl (0.05 mmol) and left at room temperature for 1 day. The reaction was monitored by <sup>1</sup>H NMR spectroscopy which demonstrated the formation of [Tp<sup>Bu<sup>t</sup></sup>]ZnCl and MeCHO.

**Reaction of [Tp<sup>Bu<sup>t</sup></sup>]ZnH with I<sub>2</sub>.** A solution of [Tp<sup>Bu<sup>t</sup></sup>]ZnH (20 mg, 0.04 mmol) in *d*<sub>6</sub>-benzene (15 mL) was treated with I<sub>2</sub> (10 mg, 0.04 mol). The reaction was monitored by <sup>1</sup>H NMR spectroscopy which demonstrated the formation of [Tp<sup>Bu<sup>t</sup></sup>]ZnI immediately.

**Synthesis of [Bp<sup>Bu<sup>t</sup></sup>]ZnMe.** A solution of Me<sub>2</sub>Zn (2.5 g, 10% w/w in pentane, 2.6 mmol) was added dropwise to a solution of Tl[Bp<sup>Bu<sup>t</sup></sup>] (0.5 g, 1.1 mmol) in THF (15 mL), resulting in the formation of a black deposit of Tl metal. The mixture was stirred for 2 h at room temperature and filtered. The solvent was removed from the filtrate under reduced pressure, extracted into pentane (20 mL), and filtered. The filtrate was concentrated to *ca.* 10 mL and placed at 0 °C giving a crop of

colorless crystals. The crystals of [Bp<sup>Bu<sup>t</sup></sup>]ZnMe were isolated by filtration and dried *in vacuo* (200 mg, 54%). Anal. Calcd for [Bp<sup>Bu<sup>t</sup></sup>]ZnMe: C, 53.1 H, 8.0; N, 16.5. Found: C, 53.3; H, 7.6; N, 15.8. IR data: 2434 ( $\nu_{B-H}$ ). MS: *m/z* 339 ( $M^+ + 1$ ).

**Synthesis of [Bp<sup>Bu<sup>t</sup></sup>]ZnEt.** A solution of Et<sub>2</sub>Zn (4.5 g, 15% w/w in hexane, 5.5 mmol) was added dropwise to a solution of Tl[Bp<sup>Bu<sup>t</sup></sup>] (2.0 g, 4.3 mmol) in THF (30 mL), resulting in the immediate formation of a black deposit of Tl metal. The mixture was stirred for 30 min at room temperature and filtered. The solvent was removed from the filtrate under reduced pressure, extracted into pentane (30 mL), and filtered. The filtrate was concentrated to *ca.* 10 mL and placed at 0 °C giving a crop of colorless crystals of [Bp<sup>Bu<sup>t</sup></sup>]ZnEt. The crystals were isolated by filtration and dried *in vacuo* (800 mg, 53%). Anal. Calcd for [Bp<sup>Bu<sup>t</sup></sup>]ZnEt: C, 54.4; H, 8.3; N, 15.8. Found: C, 54.7; H, 7.8; N, 15.6. IR data: 2440 ( $\nu_{B-H}$ ). MS: *m/z* 353 ( $M^+ + 1$ ).

**Synthesis of [Bp<sup>Bu<sup>t</sup></sup>]ZnBu<sup>t</sup>.** A solution of Bu<sup>t</sup><sub>2</sub>Zn (8 mL, 0.2 M in pentane, 1.6 mmol) was added dropwise to a solution of Tl[Bp<sup>Bu<sup>t</sup></sup>] (0.5 g, 1.1 mmol) in THF (30 mL), resulting in the formation of a black deposit of Tl metal. The mixture was stirred for 1 h at room temperature and filtered. The solvent was removed from the filtrate under reduced pressure, extracted into pentane (20 mL), and filtered. The filtrate was concentrated to *ca.* 10 mL and placed at 0 °C giving a crop of colorless crystals of [Bp<sup>Bu<sup>t</sup></sup>]ZnBu<sup>t</sup>. The crystals were isolated by filtration and dried *in vacuo* (240 mg, 57%). Anal. Calcd for [Bp<sup>Bu<sup>t</sup></sup>]ZnBu<sup>t</sup>: C, 56.6 H, 8.7; N, 14.9. Found: C, 56.6; H, 8.4; N, 15.1. IR data: 2446 ( $\nu_{B-H}$ ). MS: *m/z* 381 ( $M^+ + 1$ ).

**Synthesis of {[Bp<sup>Bu<sup>t</sup></sup>]Zn( $\mu$ -OH)}<sub>3</sub>.** A solution of [Bp<sup>Bu<sup>t</sup></sup>]ZnEt (210 mg, 0.59 mmol) in THF (10 mL) was treated with H<sub>2</sub>O (11  $\mu$ L, 0.60 mmol). The mixture was stirred for 10 min at room temperature and filtered. The filtrate was removed under reduced pressure giving {[Bp<sup>Bu<sup>t</sup></sup>]Zn( $\mu$ -OH)}<sub>3</sub> (250 mg, 44%). Anal. Calcd for {[Bp<sup>Bu<sup>t</sup></sup>]Zn( $\mu$ -OH)}<sub>3</sub>: C, 49.2; H, 7.4; N, 16.4. Found: C, 50.1; H, 7.2; N, 15.9. IR data: 3611 ( $\nu_{O-H}$ ) and 2444 ( $\nu_{B-H}$ ). The isotopomer {[Bp<sup>Bu<sup>t</sup></sup>]Zn( $\mu$ -OD)}<sub>3</sub> was prepared by the corresponding reactions of [Bp<sup>Bu<sup>t</sup></sup>]ZnEt with D<sub>2</sub>O. IR data for {[Bp<sup>Bu<sup>t</sup></sup>]Zn( $\mu$ -OD)}<sub>3</sub>: 2670 ( $\nu_{O-D}$ ).

**Synthesis of {HB(OMe)(3-Bu<sup>t</sup>p<sub>z</sub>)<sub>2</sub>}ZnEt.** A solution of [Bp<sup>Bu<sup>t</sup></sup>]ZnEt (100 mg, 0.3 mmol) in benzene (1 mL) was treated with excess (CH<sub>2</sub>O)<sub>*n*</sub> and left at room temperature for 2 days. The mixture was filtered, and the volatile compounds were removed under reduced pressure giving {HB(OMe)(3-Bu<sup>t</sup>p<sub>z</sub>)<sub>2</sub>}ZnEt (*ca.* 90 mg, 78%). Anal. Calcd for {HB(OMe)(3-Bu<sup>t</sup>p<sub>z</sub>)<sub>2</sub>}ZnEt: C, 53.2; H, 8.1; N, 14.6. Found: C, 51.6; H, 7.8; N, 13.8. IR data: 2440 ( $\nu_{B-H}$ ). MS: *m/z* 383 ( $M^+ + 1$ ).

**Synthesis of {HB(OEt)(3-Bu<sup>t</sup>p<sub>z</sub>)<sub>2</sub>}ZnEt.** A solution of [Bp<sup>Bu<sup>t</sup></sup>]ZnEt (100 mg, 0.3 mmol) in benzene (1 mL) was treated with MeCHO (30  $\mu$ L, 0.53 mmol) and left at room temperature. The volatile compounds were removed under reduced pressure giving {HB(OEt)(3-Bu<sup>t</sup>p<sub>z</sub>)<sub>2</sub>}ZnEt (*ca.* 95 mg, 80%). Anal. Calcd for {HB(OEt)(3-Bu<sup>t</sup>p<sub>z</sub>)<sub>2</sub>}ZnEt: C, 54.4; H, 8.4; N, 14.1. Found: C, 53.6; H, 7.8; N, 14.2. IR data: 2440 ( $\nu_{B-H}$ ). MS: *m/z* 396 ( $M^+ + 1$ ).

**Synthesis of {HB(OPr<sup>*i*</sup>)(3-Bu<sup>t</sup>p<sub>z</sub>)<sub>2</sub>}ZnEt.** A solution of [Bp<sup>Bu<sup>t</sup></sup>]ZnEt (100 mg, 0.3 mmol) in benzene (1 mL) was treated with Me<sub>2</sub>CO (25  $\mu$ L, 0.44 mmol) and left at room temperature for several days. The volatile compounds were removed under reduced pressure giving {HB(OPr<sup>*i*</sup>)(3-Bu<sup>t</sup>p<sub>z</sub>)<sub>2</sub>}ZnEt (*ca.* 100 mg, 81%). Anal. Calcd for {HB(OPr<sup>*i*</sup>)(3-Bu<sup>t</sup>p<sub>z</sub>)<sub>2</sub>}ZnEt: C, 55.4; H, 8.6; N, 13.6. Found: C, 55.5; H, 8.5; N, 14.1. IR data: 2445 ( $\nu_{B-H}$ ). MS: *m/z* 411 ( $M^+ + 1$ ).

**Synthesis of [Bp<sup>Bu<sup>t</sup></sup>]Zn( $\eta^2$ -O<sub>2</sub>CMe).** A solution of [Bp<sup>Bu<sup>t</sup></sup>]ZnEt (100 mg, 0.3 mmol) in *d*<sub>6</sub>-benzene (0.7 mL) was treated with MeCO<sub>2</sub>H and left at room temperature for 1 day. The reaction was monitored by <sup>1</sup>H NMR spectroscopy which demonstrated the formation of [Bp<sup>Bu<sup>t</sup></sup>]Zn( $\eta^2$ -O<sub>2</sub>CMe). The volatile compounds were removed under reduced pressure giving [Bp<sup>Bu<sup>t</sup></sup>]Zn( $\eta^2$ -O<sub>2</sub>CMe) (*ca.* 80 mg, 70%). IR data: 2448 ( $\nu_{B-H}$ ) and 1580 ( $\nu_{CO_2}$ ). MS: *m/z* 383 ( $M^+ + 1$ ).

**X-ray Structure Determination of [Tp<sup>Me<sub>2</sub></sup>]ZnMe.** Crystal data, data collection, and refinement parameters for [Tp<sup>Me<sub>2</sub></sup>]-

Table 12. Crystal and Intensity Collection Data

	[Tp <sup>Me2</sup> ]ZnMe	[Tp <sup>Me2</sup> ] <sub>2</sub> Zn	[Tp <sup>Bu</sup> ]Zn(η <sup>1</sup> -OAc)(C <sub>6</sub> H <sub>6</sub> )	[Tp <sup>Bu</sup> ]ZnNCS	[Tp <sup>Bu</sup> ]ZnH	[Bp <sup>Bu</sup> ]ZnBu <sup>t</sup>	{[Bp <sup>Bu</sup> ]Zn(μ-OH)} <sub>3</sub>
formula	C <sub>16</sub> H <sub>23</sub> N <sub>6</sub> BZn	C <sub>30</sub> H <sub>44</sub> N <sub>12</sub> B <sub>2</sub> Zn	C <sub>29</sub> H <sub>43</sub> N <sub>6</sub> BO <sub>2</sub> Zn	C <sub>22</sub> H <sub>34</sub> N <sub>7</sub> SZn	C <sub>21</sub> H <sub>33</sub> N <sub>6</sub> BZn	C <sub>18</sub> H <sub>33</sub> N <sub>4</sub> BZn	C <sub>42</sub> H <sub>75</sub> N <sub>12</sub> O <sub>3</sub> B <sub>3</sub> Zn <sub>3</sub>
fw	377.6	659.8	583.90	494.0	447.7	381.7	1024.7
lattice	orthorhombic	triclinic	orthorhombic	monoclinic	monoclinic	monoclinic	orthorhombic
cell const							
<i>a</i> /Å	7.831(2)	8.806(1)	10.433(1)	9.703(2)	8.262(1)	14.912(7)	12.302(2)
<i>b</i> /Å	13.376(4)	10.195(2)	15.832(2)	17.001(4)	15.465(2)	8.556(2)	20.057(6)
<i>c</i> /Å	18.877(4)	10.800(2)	19.292(3)	16.582(3)	9.696(2)	18.482(5)	22.110(2)
<i>α</i> /deg	90.0	63.46(2)	90.0	90.0	90.0	90.0	90.0
<i>β</i> /deg	90.0	85.11(2)	90.0	95.08(1)	100.76(2)	112.86(3)	90.0
<i>γ</i> /deg	90.0	79.63(1)	90.0	90.0	90.0	90.0	90.0
<i>V</i> /Å <sup>3</sup>	1977(1)	853(1)	3186(1)	2725(1)	1217(1)	2173(2)	5455(2)
<i>Z</i>	4	1	4	4	2	4	4
radiation (λ/Å)	Mo Kα (0.710 73)	Mo Kα (0.710 73)	Mo Kα (0.710 73)	Mo Kα (0.710 73)	Mo Kα (0.710 73)	Mo Kα (0.710 73)	Mo Kα (0.710 73)
space group	<i>Pcmn</i> (No. 62)	<i>P</i> $\bar{1}$ (No. 2)	<i>P</i> <sub>21</sub> <i>cn</i> (No. 33)	<i>P</i> <sub>21</sub> <i>n</i> (No. 14)	<i>Pn</i> (No. 7)	<i>P</i> <sub>21</sub> <i>n</i> (No. 14)	<i>Pc</i> <sub>21</sub> <i>n</i> (No. 33)
<i>ρ</i> (calcd)/g cm <sup>-3</sup>	1.27	1.28	1.22	1.21	1.22	1.17	1.25
<i>μ</i> (Mo Kα)/cm <sup>-1</sup>	12.9	7.6	8.3	10.3	10.6	11.7	13.8
2θ range/deg	3–50	3–55	3–52	3–45	3–45	3–52	3–50
no. of data	1141 [ <i>F</i> > 6σ( <i>F</i> )]	3175 [ <i>F</i> > 6σ( <i>F</i> )]	2081 [ <i>F</i> > 6σ( <i>F</i> )]	2483 [ <i>F</i> > 6σ( <i>F</i> )]	2100 [ <i>F</i> > 6σ( <i>F</i> )]	1948 [ <i>F</i> > 6σ( <i>F</i> )]	2946 [ <i>F</i> > 5σ( <i>F</i> )]
no. of params	128	231	314	294	266	225	563
goodness of fit	1.39	1.37	1.38	1.20	1.55	1.21	1.20
<i>R</i>	0.0454	0.0391	0.0456	0.0386	0.0410	0.054	0.072
<i>R<sub>w</sub></i>	0.0580	0.0543	0.0548	0.0477	0.0589	0.0682	0.0637

ZnMe are summarized in Table 12. A single crystal of [Tp<sup>Me2</sup>]ZnMe was mounted in a glass capillary and placed on a Nicolet R3m diffractometer. The unit cell was determined by the automatic indexing of 25 centered reflections and confirmed by examination of the axial photographs. Intensity data were collected using graphite monochromated Mo Kα X-radiation (λ = 0.710 73 Å). Check reflections were measured every 100 reflections, and the data were scaled accordingly and corrected for Lorentz, polarization, and absorption effects. The structure was solved using direct methods and standard difference map techniques on a Data General NOVA 4 computer using SHELXTL.<sup>60</sup> Systematic absences were consistent with the space groups *Pcmn* (No. 62) or *Pc*<sub>21</sub>*n* (No. 33), but consideration of the *E*-value statistics suggested the choice *Pcmn* (No. 62). Hydrogens on carbon were included in calculated positions (*d*<sub>C-H</sub> = 0.96 Å; *U*<sub>iso</sub>(H) = 1.2*U*<sub>iso</sub>(C)).

**X-ray Structure Determination of [Tp<sup>Me2</sup>]<sub>2</sub>Zn.** Crystal data collection, and refinement parameters are summarized in Table 12, and the general procedure is as described for [Tp<sup>Me2</sup>]ZnMe. Systematic absences were consistent with the space groups *P*1 (No. 1) and *P* $\bar{1}$  (No. 2), but the structure was successfully solved in the centrosymmetric alternative *P* $\bar{1}$  (No. 2).

**X-ray Structure Determination of [Tp<sup>Bu</sup>]ZnH.** Crystal data, data collection, and refinement parameters are summarized in Table 12, and the general procedure is as described for [Tp<sup>Me2</sup>]ZnMe. Systematic absences were consistent with the space groups *Pn* (No. 7) and *P*<sub>21</sub>*n* (No. 13). Since the molecule possesses neither a 2-fold axis nor inversion center, the space group *Pn* (No. 7) was selected. Inversion of configuration indicated the correct absolute structure.

**X-ray Structure Determination of [Tp<sup>Bu</sup>]Zn(η<sup>1</sup>-O<sub>2</sub>-CMe)<sub>2</sub>C<sub>6</sub>H<sub>6</sub>.** Crystal data, data collection, and refinement parameters are summarized in Table 12, and the general procedure is as described for [Tp<sup>Me2</sup>]ZnMe. Systematic absences were consistent with the space groups *P*<sub>21</sub>*cn* (No. 33) and *Pcmn* (No. 62). The structure was successfully solved in

*P*<sub>21</sub>*cn* (No. 33), and inversion of configuration indicated the correct absolute structure. The centrosymmetric alternative was ruled out since the contents of the asymmetric unit were not related by a mirror plane.

**X-ray Structure Determination of [Tp<sup>Bu</sup>]ZnNCS.** Crystal data, data collection, and refinement parameters are summarized in Table 12, and the general procedure is as described for [Tp<sup>Me2</sup>]ZnMe. Systematic absences were consistent uniquely with the space group *P*<sub>21</sub>*n* (No. 14).

**X-ray Structure Determination of [Bp<sup>Bu</sup>]ZnBu<sup>t</sup>.** Crystal data, data collection, and refinement parameters are summarized in Table 12, and the general procedure is as described for [Tp<sup>Me2</sup>]ZnMe. Systematic absences were consistent uniquely with the space group *P*<sub>21</sub>*n* (No. 14).

**X-ray Structure Determination of {[Bp<sup>Bu</sup>]Zn(μ-OH)}<sub>3</sub>.** Crystal data, data collection, and refinement parameters are summarized in Table 12, and the general procedure is as described for [Tp<sup>Me2</sup>]ZnMe. Systematic absences were consistent with the space groups *Pc*<sub>21</sub>*n* (No. 33) and *Pcmn* (No. 62). The structure was successfully solved in *Pc*<sub>21</sub>*n* (No. 33), and inversion of configuration indicated the correct absolute structure. The centrosymmetric alternative was ruled out since the contents of the asymmetric unit were not related by a mirror plane.

**Acknowledgment.** Acknowledgment is made to the National Science Foundation (Grant CHE 93-00398) for support of this research. M.C. acknowledges support through the NSF REU Program at Columbia University.

**Supplementary Material Available:** Complete tables of atom coordinates, thermal parameters, bond distances and angles, and crystal data, data collection, and refinement parameters and ORTEP diagrams for [Tp<sup>Me2</sup>]ZnMe, [Tp<sup>Me2</sup>]<sub>2</sub>Zn, and [Tp<sup>Bu</sup>]ZnNCS (19 pages). Ordering information is given on any current masthead page. Tables for [Tp<sup>Bu</sup>]ZnH,<sup>6c</sup> [Tp<sup>Bu</sup>]Zn(η<sup>1</sup>-O<sub>2</sub>-CMe),<sup>6c</sup> [Bp<sup>Bu</sup>]ZnBu<sup>t</sup>,<sup>6b</sup> and {[Bp<sup>Bu</sup>]Zn(μ-OH)}<sub>3</sub><sup>6b</sup> were deposited with the original publications.

OM940694I

(60) Sheldrick, G. M. SHELXTL, An Integrated System for Solving, Refining and Displaying Crystal Structures from Diffraction Data; University of Göttingen, Göttingen, Federal Republic of Germany, 1981.

# Enthalpies of Reaction of ( $\eta^5$ -C<sub>5</sub>H<sub>5</sub>)Ru(cyclooctadiene)Cl with Tertiary Phosphine Ligands: Ligand Substitution as a Gauge for Metal Basicity and a Linear Correlation of Bond Length and Bond Enthalpy

Michèle E. Cucullu, Lubin Luo, and Steven P. Nolan\*

Department of Chemistry, University of New Orleans, New Orleans, Louisiana 70148

Paul J. Fagan, Nancy L. Jones,<sup>†</sup> and Joseph C. Calabrese

Central Research and Development, E. I. du Pont de Nemours & Co., Inc.,  
Experimental Station, P. O. Box 80328, Wilmington, Delaware 19880-0328

Received September 12, 1994<sup>®</sup>

The enthalpies of reaction of CpRu(COD)Cl (**1**) (Cp =  $\eta^5$ -C<sub>5</sub>H<sub>5</sub>; COD = cyclooctadiene) with a series of monodentate ligands, leading to the formation of CpRu(ER<sub>3</sub>)<sub>2</sub>Cl (E = P, As), have been measured by anaerobic solution calorimetry in THF at 30.0 °C. These reactions are rapid and quantitatively lead to the formation of the corresponding CpRu(ER<sub>3</sub>)<sub>2</sub>Cl complexes. The overall relative order of stability established for the preceding complexes is as follows: AsEt<sub>3</sub> < PPh<sub>3</sub> < PPh<sub>2</sub>Me < P(OPh)<sub>3</sub> < PEt<sub>3</sub> < P<sup>n</sup>Bu<sub>3</sub> < PPhMe<sub>2</sub> < PMe<sub>3</sub> < P(OMe)<sub>3</sub>. Comparisons with other organometallic systems providing insights into factors influencing the Ru–L bond disruption enthalpies and metal basicity are discussed. Structural studies of two of these CpRu(ER<sub>3</sub>)<sub>2</sub>Cl complexes (ER<sub>3</sub> = AsEt<sub>3</sub> (**2**) and PEt<sub>3</sub> (**3**)) have also been performed. Data for **2**: monoclinic, C2/c; *a* = 30.549(5); *b* = 10.523(2); *c* = 13.503(3) Å;  $\alpha = \gamma = 90^\circ$ ;  $\beta = 103.71(2)^\circ$ ; *V* = 4217.1 Å<sup>3</sup>; *Z* = 8; *d*<sub>calcd</sub> = 1.656 g cm<sup>-3</sup>; *n*<sub>obsd</sub> = 5328; *R* = 0.032. Data for **3**: monoclinic, P2<sub>1</sub>/c; *a* = 13.553(1); *b* = 8.283(2); *c* = 19.359(3) Å;  $\beta = 109.74(1)^\circ$ ; *V* = 2045.5 Å<sup>3</sup>; *Z* = 4; *d*<sub>calcd</sub> = 1.422 g cm<sup>-3</sup>; *n*<sub>obsd</sub> = 5152; *R* = 0.030. A relationship between bond distances and relative bond energies is made possible by the present data. This correlation is good and represents a rare example of such a relationship.

## Introduction

Thermochemical studies performed on organometallic systems have gained recognition as an area of research that can provide important insights into reactivity and bonding patterns.<sup>1–4</sup> In spite of this recognition, the solution thermochemistry of systems such as those revolving around group 8 metal centers is an area where more information is needed.<sup>1a,b</sup> The scarcity of thermo-

chemical investigations on organoruthenium complexes is all the more noticeable when one considers the catalytic activities displayed by these compounds, which range from the ring opening and closing metatheses of olefins<sup>5</sup> to the recently reported ruthenium-catalyzed synthesis of formic acid in supercritical CO<sub>2</sub>.<sup>6</sup> In view of the limited number of thermochemical studies for group 8 metal centers,<sup>7–9</sup> it is not too surprising that investigations addressing the influence of ancillary ligand modification on the enthalpy of ligand substitution for such systems are virtually nonexistent.

<sup>†</sup> Permanent address: Department of Chemistry and Biochemistry, LaSalle University, Philadelphia, PA 19141.

<sup>®</sup> Abstract published in *Advance ACS Abstracts*, November 1, 1994.

(1) For leading references in this area, see: (a) Nolan, S. P. *Bonding Energetics of Organometallic Compounds*. In *Encyclopedia of Inorganic Chemistry*; J. Wiley and Sons: New York, 1994. (b) Hoff, C. D. *Prog. Inorg. Chem.* **1992**, *40*, 503–561. (c) Martinho Simões, J. A.; Beauchamp, J. L. *Chem. Rev.* **1990**, *90*, 629–688. (d) Marks, T. J., Ed. *Bonding Energetics in Organometallic Compounds*. *ACS Symp. Ser.* **1990**, *428*. (e) Marks, T. J., Ed. *Metal-Ligand Bonding Energetics in Organotransition Metal Compounds*. *Polyhedron Symp. Print* **1988**, *7*. (f) Skinner, H. A.; Connor, J. A. In *Molecular Structure and Energetics*; Liebman, J. F., Greenberg, A., Eds.; VCH: New York, 1987; Vol. 2, Chapter 6. (g) Skinner, H. A.; Connor, J. A. *Pure Appl. Chem.* **1985**, *57*, 79–88. (h) Pearson, R. G. *Chem. Rev.* **1985**, *85*, 41–59. (i) Mondal, J. U.; Blake, D. M. *Coord. Chem. Rev.* **1983**, *47*, 204–238. (j) Mansson, M. *Pure Appl. Chem.* **1983**, *55*, 417–426. (k) Pilcher, G.; Skinner, H. A. In *The Chemistry of the Metal–Carbon Bond*; Harley, F. R., Patai, S., Eds.; Wiley: New York, 1984; pp 43–90. (l) Connor, J. A. *Curr. Top. Chem.* **1977**, *71*, 71–110.

(2) See, for example: (a) Nolan, S. P.; Hoff, C. D.; Stoutland, P. O.; Newman, L. J.; Buchanan, J. M.; Bergman, R. G.; Yang, G. K.; Peters, K. G. *J. Am. Chem. Soc.* **1987**, *109*, 3143–3145 and references therein. (b) Nolan, S. P.; Lopez de la Vega, R.; Hoff, C. D. *Organometallics* **1986**, *5*, 2529–2537.

(3) (a) Nolan, S. P.; Porchia, M.; Marks, T. J. *Organometallics* **1991**, *10*, 1450–1457. (b) Nolan, S. P.; Stern, D.; Marks, T. J. *J. Am. Chem. Soc.* **1989**, *111*, 7844–7854.

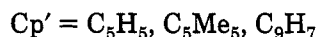
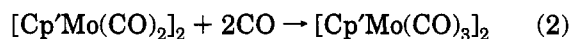
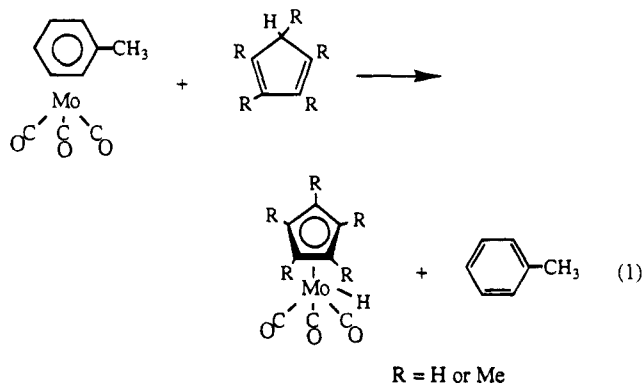
(4) (a) Nolan, S. P.; Stern, D.; Hedden, D.; Marks, T. J. In ref 1d, pp 159–174. (b) Nolan, S. P.; Lopez de la Vega, R.; Mukerjee, S. L.; Gonzalez, A. A.; Hoff, C. D. In ref 1e, pp 1491–1498. (c) Marks, T. J.; Gagné, M. R.; Nolan, S. P.; Schock, L. E.; Seyam, A. M.; Stern, D. L. *Pure Appl. Chem.* **1989**, *61*, 1665–1672. (d) Schock, L. E.; Marks, T. J. *J. Am. Chem. Soc.* **1988**, *110*, 7701–7715.

(5) (a) Novak, B. M.; Grubbs, R. H. *J. Am. Chem. Soc.* **1988**, *110*, 960–961. (b) Novak, B. M.; Grubbs, R. H. *J. Am. Chem. Soc.* **1988**, *110*, 7542–7543. (c) Nguyen, S. T.; Johnson, L. K.; Grubbs, R. H.; Ziller, J. W. *J. Am. Chem. Soc.* **1992**, *114*, 3974–3975. (d) Fu, G. C.; Nguyen, S. T.; Grubbs, R. H. *J. Am. Chem. Soc.* **1993**, *115*, 9856–9857. (e) Nguyen, S. T.; Grubbs, R. H.; Ziller, J. W. *J. Am. Chem. Soc.* **1993**, *115*, 9858–9859.

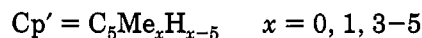
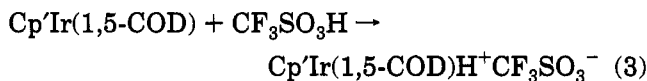
(6) Jessop, P. G.; Ikariya, T.; Noyori, R. *Nature* **1994**, *368*, 231–233.

(7) For solution calorimetric investigations of organogroup 8 complexes, see: (a) Nolan, S. P.; Martin, K. L.; Stevens, E. D.; Fagan, P. J. *Organometallics* **1992**, *11*, 3947–3953. (b) Luo, L.; Nolan, S. P. *Organometallics* **1992**, *11*, 3483–3486. (c) Luo, L.; Nolan, S. P. *Inorg. Chem.* **1993**, *32*, 2410–2415. (d) Luo, L.; Fagan, P. J.; Nolan, S. P. *Organometallics* **1993**, *12*, 3405–3411. (e) Luo, L.; Zhu, N.; Zhu, N.-J.; Stevens, E. D.; Nolan, S. P.; Fagan, P. J. *Organometallics* **1994**, *13*, 669–675. (f) Li, C.; Cucullu, M. E.; McIntyre, R. A.; Stevens, E. D.; Nolan, S. P. *Organometallics* **1994**, *13*, 3621–3627.

In fact, very little thermochemical information is available concerning the effects of ligand variation on enthalpies of reaction. Hoff and co-workers have probed ancillary ligand variation and thermodynamic effects in organomolybdenum complexes, examining enthalpies associated with the substitution/oxidative addition and ligand addition reactions illustrated in eqs 1 and 2.<sup>2b,10</sup>



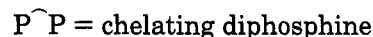
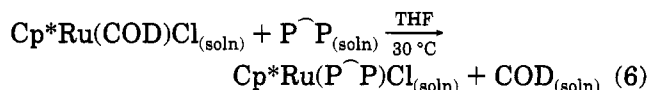
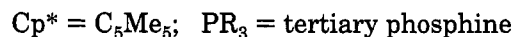
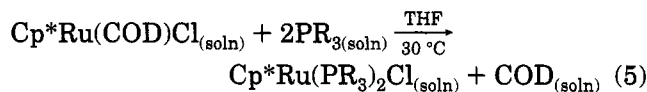
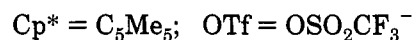
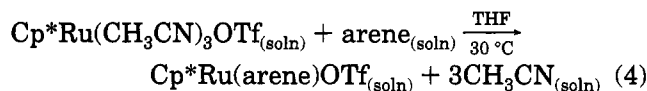
Sowa and Angelici have investigated the effects of ancillary ligand modification on the enthalpy of protonation of organoiridium complexes in order to gauge the basicity of the metal center.<sup>11</sup>



Lastly, Tilset and Parker have investigated the absolute metal-hydride bond dissociation enthalpy for transition metal hydrides, with little observed variation in M-H BDE associated with modifications of the ancillary ligation.<sup>12</sup>

In view of the dearth of thermodynamic information surrounding group 8 centered organometallic complexes and the importance of such species in catalysis,<sup>5,13</sup> we have recently been involved in the determination of enthalpies of ligand substitution reactions revolving

around these metal centers, using anaerobic solution calorimetry.<sup>7d-f</sup>



In order to gain insights into structural/bond strength influences, diffraction studies were performed on two organoruthenium complexes to allow the examination of bond length/bond disruption enthalpy correlation. This, to our knowledge, has not been examined extensively for organometallic complexes.<sup>13a,b</sup>

In the present study, we extend our solution thermochemical investigations to organoruthenium complexes bearing an ancillary Cp ligand and examine how the overall steric and electronic variations accompanying this change in ancillary ligation influence the thermodynamic stability of these complexes. Furthermore, structural investigations were carried out on two complexes in the present series that allow for a wider sampling of bond length variation with change in phosphine (or arsine) ancillary ligation. A combination of enthalpy data and structural results allows for the determination of a unique linear correlation existing between these two factors.

## Experimental Section

**General Considerations.** All manipulations involving organoruthenium complexes were performed under inert atmospheres of argon or nitrogen, using standard high-vacuum or Schlenk tube techniques, or in a Vacuum/Atmospheres glovebox containing less than 1 ppm oxygen and water. Ligands were purchased from Strem Chemicals or Aldrich and used as received. Solvents were dried and distilled under dinitrogen before use, employing standard drying agents.<sup>14</sup> Only materials of high purity as indicated by IR and NMR spectroscopies were used in the calorimetric experiments. NMR spectra were recorded using a Varian Gemini 300-MHz spectrometer. Calorimetric measurements were performed using a Calvet calorimeter (Setaram C-80), which was periodically calibrated using the TRIS reaction<sup>15</sup> or the enthalpy of solution of KCl in water.<sup>16</sup> The experimental enthalpies for these two standard reactions compared very closely to literature values. This calorimeter has been previously described,<sup>10a</sup> and typical procedures are described below. Experimental enthalpy data are reported with 95% confidence limits. Elemental analyses were performed by Oneida Research Services, Whitesboro, NY.

(14) Perrin, D. D.; Armarego, W. L. F. *Purification of Laboratory Chemicals*, 3rd ed.; Pergamon Press: New York, NY, 1988.

(15) Ojelund, G.; Wadsö, I. *Acta Chem. Scand.* **1968**, *22*, 1691-1699.

(16) Kilday, M. V. *J. Res. Natl. Bur. Stand. (U.S.)* **1980**, *85*, 467-481.

(8) (a) Mancuso, C.; Halpern, J. J. *Organomet. Chem.* **1992**, *428*, C8-C11. (b) Bryndza, H. E.; Fong, L. K.; Paciello, R. A.; Tam, W.; Bercaw, J. E. *J. Am. Chem. Soc.* **1987**, *109*, 1444-1456. (c) Collman, J. P.; McElwee-White, L.; Brothers, P. J.; Rose, E. *J. Am. Chem. Soc.* **1986**, *108*, 1332-1333.

(9) Calorimetric studies of coordination complexes have been reported for complexes of type  $[(\text{NH}_3)_5\text{RuOH}_2]^{2+}$ ; see, for example: (a) Wishart, J. F.; Taube, H.; Breslawer, K. L.; Isied, S. S. *Inorg. Chem.* **1986**, *25*, 1479-1481. (b) Wishart, J. F.; Taube, H.; Breslawer, K. L.; Isied, S. S. *Inorg. Chem.* **1984**, *23*, 2997-3001.

(10) (a) Nolan, S. P.; Hoff, C. D.; Landrum, J. T. *J. Organomet. Chem.* **1985**, *282*, 357-362. (b) Nolan, S. P.; Lopez de la Vega, R.; Hoff, C. D. *Inorg. Chem.* **1986**, *25*, 4446-4448.

(11) (a) Sowa, J. R., Jr.; Angelici, R. J. *J. Am. Chem. Soc.* **1991**, *113*, 2537-2544. (b) Rottink, M. K.; Angelici, R. J. *J. Am. Chem. Soc.* **1993**, *115*, 7267-7274.

(12) Tilset, M.; Parker, V. D. *J. Am. Chem. Soc.* **1989**, *111*, 6711-6717; **1990**, *112*, 2843.

(13) (a) Collman, J. P.; Hegedus, L. S.; Norton, J. R.; Finke, R. G. *Principles and Applications of Organotransition Metal Chemistry*, 2nd ed.; University Science: Mill Valley, CA, 1987. (b) Bennett, M. A.; Matheson, T. W. In *Comprehensive Organometallic Chemistry*; Wilkinson, G., Stone, F. G. A., Abel, E. W., Eds.; Pergamon Press: Oxford, England, 1982; Chapter 32.9. (c) Mitsudo, T.; Naruse, H.; Kondo, T.; Ozaki, Y.; Watanabe, Y. *Angew. Chem., Int. Ed. Engl.* **1994**, *33*, 580-581.

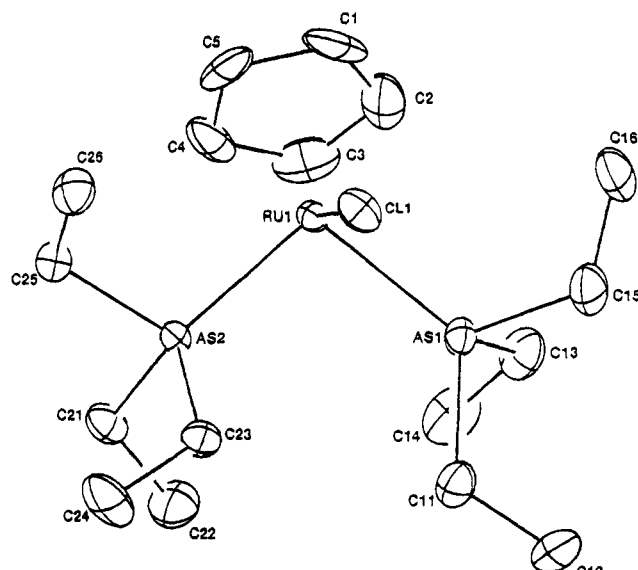
**Synthesis.** The compound CpRu(COD)Cl<sup>17</sup> was synthesized according to the reported literature procedure. The identity of the CpRu(PR<sub>3</sub>)<sub>2</sub>Cl (PR<sub>3</sub> = PPh<sub>3</sub>,<sup>18</sup> PMe<sub>3</sub>,<sup>19</sup> PPhMe<sub>2</sub>,<sup>20</sup> PPPh<sub>2</sub>Me,<sup>20</sup> P(OMe)<sub>3</sub>,<sup>20</sup> P(OPh)<sub>3</sub>,<sup>21</sup> P<sup>n</sup>Bu<sub>3</sub>)<sup>22</sup> complexes was ascertained by comparison with literature NMR spectroscopic data. Experimental synthetic procedures, leading to isolation of crystalline materials, for two previously unreported complexes are described below.

**CpRu(AsEt<sub>3</sub>)<sub>2</sub>Cl (2).** Under an inert atmosphere, a 25-mL flame-dried flask was charged with 270 mg (0.87 mmol) of CpRu(COD)Cl and 15 mL of dried THF. Then 300 μL (2.08 mmol) of AsEt<sub>3</sub> was slowly added to the solution, and this was stirred for 1 h. After this time, the solvent was removed under vacuum, and 10 mL of hexane was vacuum transferred to the cooled (-78 °C) flask containing the solid residue. The mixture was warmed up to 40 °C and stirred until all the solid had completely dissolved. The solution was then filtered and slowly cooled to -30 °C. Cold filtration afforded orange-red needles, which were washed with a small amount of hexane and dried in vacuum. This procedure affords an isolated yield of 340 mg (74%). <sup>1</sup>H-NMR (300 MHz, THF-*d*<sub>8</sub>, 25 °C): 1.14 (t, 18 H, -CH<sub>2</sub>CH<sub>3</sub>), 1.61 (m, 6 H, -CH<sub>2</sub>CH<sub>3</sub>), 1.92 (m, 6 H, -CH<sub>2</sub>CH<sub>3</sub>), 4.31 (s, 5H, Cp). Anal. Calcd for C<sub>17</sub>H<sub>35</sub>RuAs<sub>2</sub>Cl: C, 38.78; H, 6.71. Found: C, 39.05; H, 6.82.

**CpRu(PEt<sub>3</sub>)<sub>2</sub>Cl (3).** Under an inert atmosphere, a 25-mL flame-dried flask was charged with 200 mg (0.65 mmol) of CpRu(COD)Cl and 15 mL of dried THF. Then 210 μL (1.50 mmol) of PEt<sub>3</sub> was slowly added to the solution, which was stirred for 1 h. After this time, the solvent was removed under vacuum, and 10 mL of hexane was vacuum transferred to the cooled (-78 °C) flask containing the solid residue. The mixture was warmed up to about 40 °C and stirred until all the solid had completely dissolved. The solution was filtered and then slowly cooled to -30 °C. Cold filtration afforded orange-red needles, which were washed with a small amount of hexane and dried in vacuum. This procedure affords an isolated yield of 194 mg (68%). <sup>1</sup>H-NMR (300 MHz, THF-*d*<sub>8</sub>, 25 °C): 1.07 (m, 18 H, -CH<sub>2</sub>CH<sub>3</sub>), 1.58 (m, 6 H, -CH<sub>2</sub>CH<sub>3</sub>), 2.06 (m, 6 H, -CH<sub>2</sub>CH<sub>3</sub>), 4.45 (s, 5 H, Cp). Anal. Calcd for C<sub>17</sub>H<sub>35</sub>RuP<sub>2</sub>Cl: C, 46.57; H, 8.05. Found: C, 46.62; H, 7.79.

**<sup>1</sup>H NMR Titrations.** Prior to every set of calorimetric experiments involving a new ligand, an accurately weighed amount (±0.1 mg) of the organoruthenium complex was placed in a Wilmad screw-capped NMR tube fitted with a septum, and THF-*d*<sub>3</sub> was subsequently added. The solution was titrated with a solution of the ligand of interest by injecting the latter in aliquots through the septum with a microsyringe, followed by vigorous shaking. The reactions were monitored by <sup>1</sup>H NMR spectroscopy, and the reactions were found to be rapid, clean, and quantitative under experimental calorimetric conditions. These conditions are necessary for accurate and meaningful calorimetric results and were satisfied for all organoruthenium reactions investigated.

**Solution Calorimetry. (A) Calorimetric Measurement of Reaction Between CpRu(COD)Cl (1) and P(OMe)<sub>3</sub>.** The mixing vessels of the Setaram C-80 were cleaned, dried in an oven maintained at 120 °C, and then taken into the glovebox. A 30–40-mg sample of recrystallized CpRu(COD)Cl was



**Figure 1.** ORTEP of CpRu(AsEt<sub>3</sub>)<sub>2</sub>Cl (2) with ellipsoids drawn in at 50% probability.

accurately weighed into the lower vessel, which was closed and sealed with 1.5 mL of mercury. Four milliliters of a stock solution of P(OMe)<sub>3</sub> [5 mL of P(OMe)<sub>3</sub> in 25 mL of THF] was added, and the remainder of the cell was assembled, removed from the glovebox, and inserted in the calorimeter. The reference vessel was loaded in an identical fashion with the exception that no organoruthenium complex was added to the lower vessel. After the calorimeter had reached thermal equilibrium at 30.0 °C (about 2 h), the calorimeter was inverted, thereby allowing the reactants to mix. After the reaction had reached completion and the calorimeter had once again reached thermal equilibrium (ca. 2 h), the vessels were removed from the calorimeter. Conversion to CpRu(P(OMe)<sub>3</sub>)<sub>2</sub>Cl was found to be quantitative under these reaction conditions. Control reactions with Hg and no phosphine show no reaction. The enthalpy of reaction, -37.9 ± 0.1 kcal/mol, represents the average of five individual calorimetric determinations. This methodology represents a typical procedure involving all organometallic compounds and all reactions investigated in the present study.

**(B) Calorimetric Measurement of the Enthalpy of Solution of CpRu(COD)Cl (1) in THF.** In order to consider all species in solution, the enthalpy of solution of CpRu(COD)Cl had to be directly measured. This was performed by using a procedure similar to the one described above with the exception that no ligand was added to the reaction cell. This enthalpy of solution represents the average of five individual determinations and is 3.9 ± 0.1 kcal/mol.

**Structure Determination of CpRu(AsEt<sub>3</sub>)<sub>2</sub>Cl (2).** A rectangular orange plate, grown by slow cooling of a saturated THF solution, having approximate dimensions 0.38 × 0.05 × 0.46 mm was selected and mounted on the end of a glass fiber in a random orientation. This selected crystal was mounted on a Syntex R3 diffractometer, and data was collected using MoK $\alpha$  radiation at 173 K under a stream of cold nitrogen gas. Cell dimensions were determined by least-squares refinement of the measured setting angles of 25 reflections with 20° < 2 $\theta$  < 50°. The structure was solved using automated Patterson analysis and refined by full matrix least-squares techniques. Crystal data for 2 are summarized in Table 2, and selected bond distances and angles are listed in Table 3. Positional and equivalent isotropic thermal parameters are presented in Table 4. Figure 1 gives an ORTEP drawing of this molecule.

**Structure Determination of CpRu(PEt<sub>3</sub>)<sub>2</sub>Cl (3).** An orange wedge, grown from slow heptane diffusion through a saturated solution of THF, having approximate dimensions 0.20 × 0.17 × 0.46 mm was selected and mounted on the end

(17) Albers, M. O.; Robinson, D. J.; Shaver, A.; Singleton, E. *Organometallics* **1986**, *5*, 2199–2205.

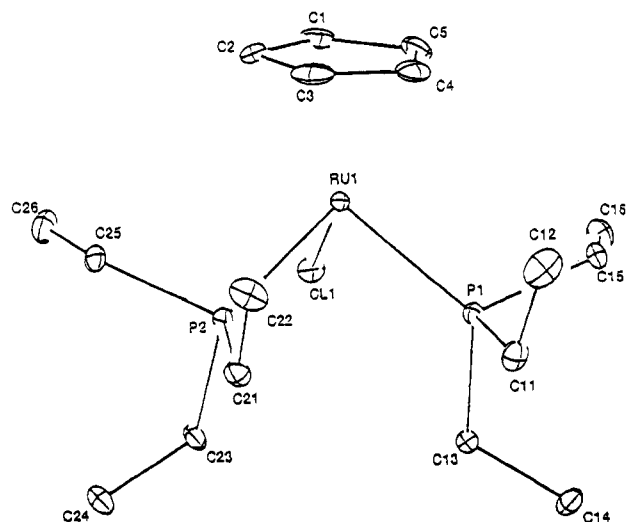
(18) Bruce, M. I.; Hameister, C.; Swincer, A. G.; Wallis, R. C. *Inorg. Synth.* **1982**, *21*, 78–84.

(19) (a) Treichel, P. M.; Komar, D. A. *Synth. React. Inorg. Met.-Org. Chem.* **1980**, *10*, 205–210. (b) Bruce, M. I.; Wong, F. S.; Skelton, B. W.; White, A. H. *J. Chem. Soc., Dalton Trans.* **1981**, 1398–1405. (c) Bruce, M. I.; Wong, F. S.; Skelton, B. W.; White, A. H. *J. Chem. Soc., Dalton Trans.* **1982**, 2203–2207.

(20) (a) Treichel, P. M.; Komar, D. A. *Synth. React. Inorg. Met.-Org. Chem.* **1984**, *14*, 383–400. (b) Bruce, M. I.; Cifuentes, M. P.; Snow, M. R.; Tiekink, R. T. *J. Organomet. Chem.* **1989**, *359*, 379–399.

(21) Bruce, M. I.; Humphrey, M. G.; Swincer, A. G.; Wallis, R. C. *Aust. J. Chem.* **1984**, *37*, 1747–1755.

(22) Lehmkuhl, H.; Mauermann, H.; Benn, R. *Liebigs Ann. Chem.* **1980**, 754–767.

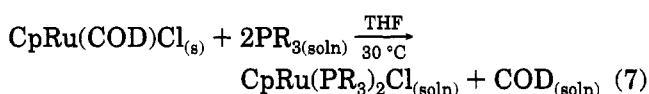


**Figure 2.** ORTEP of  $\text{CpRu}(\text{PEt}_3)_2\text{Cl}$  (**3**) with ellipsoids drawn in at 50% probability.

of a glass fiber in a random orientation. This selected crystal was mounted on a Syntex R3 diffractometer, and data was collected using  $\text{MoK}\alpha$  radiation at 173 K under a stream of cold nitrogen gas. Cell dimensions were determined by least-squares refinement of the measured setting angles of 25 reflections with  $20^\circ < 2\theta < 50^\circ$ . The structure was solved using direct methods (SHELXS) and refined by full matrix least-squares techniques. Crystal data for **3** are summarized in Table 5, and selected bond distances and angles are listed in Table 6. Positional and equivalent isotropic thermal parameters are presented in Table 7. Figure 2 gives an ORTEP drawing of this molecule.

## Results

A facile entryway into the thermochemistry of  $\text{CpRu}(\text{PR}_3)_2\text{Cl}$  complexes is made possible by the rapid and quantitative reaction of  $\text{CpRu}(\text{COD})\text{Cl}$  (**1**) with a variety of different phosphine ligands.<sup>17</sup>



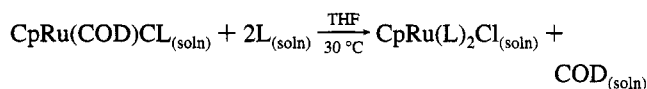
This type of phosphine binding reaction appears general and was found to be rapid and quantitative for all ligands calorimetrically investigated at  $30.0^\circ\text{C}$  in tetrahydrofuran. A compilation of phosphine and arsine ligands along with their respective enthalpies of reaction where all species are in solution are listed in Table 1.

Single-crystal structural studies were carried out on the two new complexes, **2** and **3**. Tables 2 and 7 give important bond distances and angles, and positional parameters are reported for both complexes along with appropriate ORTEP drawings (Figures 1 and 2).

## Discussion

The labile nature and relative thermodynamic stability of a number of metal–diene complexes are well known.<sup>13a</sup> Such complexes are often used to stabilize a catalytically active organometallic fragment. For example, the  $\text{Ni}(\text{COD})_2$  complex readily loses cyclooctadiene ligands to form nickel allyl complexes in the

**Table 1.** Enthalpies of Substitution (kcal/mol) in the Reaction  $\text{CpR}$



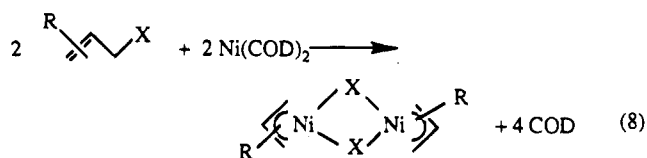
L	complex	$-\Delta H_{\text{rxn}}^a$
$\text{AsEt}_3$	$\text{CpRu}(\text{AsEt}_3)_2\text{Cl}$	19.4(0.2)
$\text{PPh}_3$	$\text{CpRu}(\text{PPh}_3)_2\text{Cl}$	22.9(0.4)
$\text{PPh}_2\text{Me}$	$\text{CpRu}(\text{PPh}_2\text{Me})_2\text{Cl}$	32.8(0.2)
$\text{P}(\text{OPh})_3$	$\text{CpRu}(\text{P}(\text{OPh})_3)_2\text{Cl}$	34.1(0.4)
$\text{PEt}_3$	$\text{CpRu}(\text{PEt}_3)_2\text{Cl}$	34.5(0.2)
$\text{P}^i\text{Bu}_3$	$\text{CpRu}(\text{P}^i\text{Bu}_3)_2\text{Cl}$	35.4(0.2)
$\text{PPhMe}_2$	$\text{CpRu}(\text{PPhMe}_2)_2\text{Cl}$	35.9(0.2)
$\text{PMe}_3$	$\text{CpRu}(\text{PMe}_3)_2\text{Cl}$	38.4(0.4)
$\text{P}(\text{OMe})_3$	$\text{CpRu}(\text{P}(\text{OMe})_3)_2\text{Cl}$	41.8(0.2)

<sup>a</sup> Enthalpy values are reported with 95% confidence limits.

**Table 2.** Summary of Crystallographic Data for  $\text{CpRu}(\text{AsEt}_3)_2\text{Cl}$  (**2**)

empirical formula	$\text{C}_{17}\text{H}_{35}\text{As}_2\text{ClRu}$
space group	$C2/c$
unit cell dimensions	
$a$ , Å	30.549 (5)
$b$ , Å	10.523 (2)
$c$ , Å	13.503 (3)
$\alpha$ , deg	90
$\beta$ , deg	103.71 (2)
$\gamma$ , deg	90
$V$ , Å <sup>3</sup>	4217.1
$Z$ , molecule/cell	8
density (calcd), g/cm <sup>3</sup>	1.656
$\mu(\text{Mo})$ , cm <sup>-1</sup>	39.62
monochromator	highly ordered graphite crystal
temp, K	173
abs corr	empirical ( $\psi$ -scan method)
diffractometer	Syntex R3
scan type	$\theta-2\theta$
data collected	$-39 \leq h \leq 39; 0 \leq k \leq 13; 0 \leq l \leq 17$
$2\theta$ range, deg	4.1–55.0
no. of collected reflns	3583
no. of indep reflns	3368
$R_F$ (obsd data), %	3.2
$R_wF$ , %	2.9
goodness of fit	1.05
number of variables	330

presence of allylic halides<sup>23</sup> (eq 8):



Another example is its involvement in the asymmetric isomerization of allylamines to enamines by Noyori and co-workers<sup>24</sup> who have used a  $[\text{Rh}(\text{COD})(\text{BINAP})]^+$  complex as catalyst precursor. The first step of the catalytic transformation involves substitution of solvent and/or substrate molecules for the outgoing COD ligand. The relative thermodynamic stability of these M–COD

(23) For reviews, see: (a) Semmelhack, M. F. *Org. React.* **1972**, *19*, 115–198. (b) Baker R. *Chem. Rev.* **1973**, *73*, 487–530. (c) Hegedus, L. S. *J. Organomet. Chem. Libr.* **1976**, *1*, 329–359. (d) Billington, D. C. *Chem. Soc. Rev.* **1985**, *14*, 93–120.

(24) (a) Noyori, R. *Science* **1990**, *248*, 1194–1199. (b) Noyori, R.; Takaya, H. *Acc. Chem. Res.* **1990**, *23*, 345–350. (c) Inoue, S.-I.; Takaya, H.; Tani, K.; Otsuka, S.; Sato, T.; Noyori, R. *J. Am. Chem. Soc.* **1990**, *112*, 4897–4905. (d) Otsuka, S.; Tani, K. *Synthesis* **1991**, 665–680. (e) Yamakawa, M.; Noyori, R. *Organometallics* **1992**, *11*, 3167–3169 and references therein.

**Table 3. Selected Bond Distances (Å) and Bond Angles (deg) for CpRu(AsEt<sub>3</sub>)<sub>2</sub>Cl (2)**

Bond Lengths <sup>a</sup>			
Ru(1)–Cl(1)	2.452(1)	C(25)–C(26)	1.515(6)
Ru(1)–As(1)	2.4125(7)	As(1)–C(11)	1.962(5)
Ru(1)–As(2)	2.4158(6)	As(1)–C(13)	1.968(5)
C(11)–C(12)	1.524(7)	As(1)–C(15)	1.963(5)
C(13)–C(14)	1.505(8)	As(2)–C(21)	1.949(4)
C(15)–C(16)	1.510(8)	As(2)–C(23)	1.953(4)
C(21)–C(22)	1.493(7)	As(2)–C(25)	1.958(4)
C(23)–C(24)	1.523(6)	Cp C–C(ave)	1.398(6)
Ru–Cp(cen)	1.811(5)	Ru–C(Cp ave)	2.166(5)
Bond Angles <sup>a</sup>			
Cl(1)–Ru(1)–As(1)	84.49(3)	As(2)–Ru(1)–C(4)	91.1(1)
Cl(1)–Ru(1)–As(2)	85.84(3)	As(2)–Ru(1)–C(5)	101.8(1)
As(1)–Ru(1)–As(2)	101.30(2)	C(11)–As(1)–C(13)	100.7(2)
Ru(1)–As(1)–C(11)	123.4(1)	C(11)–As(1)–C(15)	99.0(2)
Ru(1)–As(1)–C(13)	116.3(2)	C(13)–As(1)–C(15)	99.9(2)
Ru(1)–As(1)–C(15)	113.8(2)	C(21)–As(2)–C(23)	102.0(2)
Ru(1)–As(2)–C(21)	119.9(1)	C(21)–As(2)–C(25)	97.5(2)
Ru(1)–As(2)–C(23)	119.4(1)	C(23)–As(2)–C(25)	102.1(2)
Ru(1)–As(2)–C(25)	112.4(1)	As(1)–C(11)–C(12)	116.2(4)
As(2)–C(21)–C(22)	114.4(3)	As(1)–C(13)–C(14)	113.0(3)
As(2)–C(23)–C(24)	116.3(4)	As(1)–C(15)–C(16)	113.0(4)
As(2)–C(25)–C(26)	114.1(3)	As(1)–Ru(1)–Cp(cen)	124.2(2)
As(2)–Ru(1)–Cp(cen)	123.4(2)	Cl(1)–Ru(1)–Cp(cen)	126.3(2)

<sup>a</sup> Numbers in parentheses are the estimated standard deviations.

**Table 4. Fractional Coordinates (×10 000) and Isotropic Thermal Parameters for CpRu(AsEt<sub>3</sub>)<sub>2</sub>Cl (2)<sup>a</sup>**

atom	x	y	z	B (Å <sup>2</sup> )
Ru	1673.2(1)	1617.4(3)	1052.3(2)	1.4(1)
Cl1	1790.0(4)	1185.9(10)	-650.9(8)	2.3(1)
As1	1084.8(1)	3018.3(4)	164.3(3)	1.8(1)
As2	1282.7(1)	-396.3(3)	883.5(3)	1.5(1)
C1	2351(2)	2344(6)	1659(4)	3.9(2)
C2	2047(2)	3153(5)	1946(4)	3.7(2)
C3	1813(2)	2471(6)	2542(4)	3.7(2)
C4	1983(2)	1232(5)	2625(4)	3.4(1)
C5	2317(2)	1127(5)	2074(4)	3.2(1)
C11	500(2)	2414(5)	-637(4)	2.6(1)
C12	156(2)	3436(6)	-1083(5)	3.4(1)
C13	891(2)	4351(4)	990(4)	3.0(1)
C14	625(2)	3838(6)	1708(5)	3.7(2)
C15	1260(2)	4074(5)	-876(4)	3.0(1)
C16	1715(2)	4697(5)	-501(5)	3.8(2)
C21	893(2)	-811(4)	1790(4)	2.3(1)
C22	488(2)	22(6)	1669(5)	3.5(2)
C23	912(2)	-901(4)	-444(3)	2.1(1)
C24	737(2)	-2261(5)	-531(5)	3.6(2)
C25	1696(2)	-1838(4)	1232(4)	2.2(1)
C26	2035(2)	-1943(5)	581(4)	2.7(1)

<sup>a</sup> Numbers in parentheses are the estimated standard deviations.

bonding interactions has been observed in other organometallic systems.<sup>25</sup> Tolman and co-workers have studied, by solution calorimetry, phosphine and phosphite substitution reactions according to eq 9:<sup>26</sup>



As in the case of the Cp<sup>\*</sup>Ru(COD)Cl complex,<sup>7d</sup> the related CpRu(COD)Cl (1) complex was found to have a diene ligand that is weakly bound to the metal center. The labile nature of this diene ligand leads to the CpRu(COD)Cl complex being an efficient catalyst precursor; this emerging catalytic chemistry has recently been

(25) See, for example: Mukerjee, S. L.; Nolan, S. P.; Hoff, C. D.; de la Vega, R. *Inorg. Chem.* **1988**, *27*, 81–85.

(26) Tolman, C. A.; Reutter, D. W.; Seidel, W. C. *J. Organomet. Chem.* **1976**, *117*, C30–C33.

**Table 5. Summary of Crystallographic Data for CpRu(PEt<sub>3</sub>)<sub>2</sub>Cl (3)**

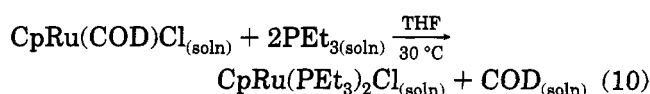
empirical formula	C <sub>17</sub> H <sub>35</sub> P <sub>2</sub> ClRu
space group	P2 <sub>1</sub> /c
unit cell dimensions	
a, Å	13.553(1)
b, Å	8.283(2)
c, Å	19.359(3)
α, deg	90
β, deg	109.74(1)
γ, deg	90
V, Å <sup>3</sup>	2045.5
Z, molecule/cell	4
density (calcd), g/cm <sup>3</sup>	1.422
μ(Mo), cm <sup>-1</sup>	10.32
monochromator	highly ordered graphite crystal
temp, K	173
abs corr	empirical (ψ-scan method)
diffractometer	Syntex R3
scan type	θ–2θ
data collected	–17 ≤ h ≤ 17; –10 ≤ k ≤ 0; 0 ≤ l ≤ 25
2θ range, deg	4.5–55.0
no. of collected reflns	5152
no. of indep reflns	3255
R <sub>F</sub> (obsd data), %	3.0
R <sub>wF</sub> , %	2.7
goodness of fit	0.94
number of variables	330

**Table 6. Selected Bond Distances (Å) and Bond Angles (deg) for CpRu(PEt<sub>3</sub>)<sub>2</sub>Cl (3)**

Bond Lengths <sup>a</sup>			
Ru(1)–Cl(1)	2.4502(8)	P(1)–C(15)	1.844(3)
Ru(1)–P(1)	2.2993(8)	P(2)–C(21)	1.847(3)
Ru(1)–P(2)	2.3080(9)	P(2)–C(23)	1.840(3)
P(2)–C(25)	1.845(6)	C(11)–C(12)	1.524(6)
C(13)–C(14)	1.529(4)	C(15)–C(16)	1.515(5)
C(21)–C(22)	1.515(5)	P(1)–C(11)	1.848(4)
C(23)–C(24)	1.524(5)	P(1)–C(13)	1.839(3)
C(25)–C(26)	1.522(5)	Cp C–C(ave)	1.404(6)
Ru–Cp(cen)	1.858(4)	Ru–C(Cp ave)	2.209(5)
Bond Angles <sup>a</sup>			
Cl(1)–Ru(1)–P(1)	90.43(3)	P(2)–Ru(1)–C(4)	128.4(1)
Cl(1)–Ru(1)–P(2)	90.50(3)	P(2)–Ru(1)–C(5)	158.6(1)
P(1)–Ru(1)–P(2)	94.71(3)	Ru(1)–P(1)–C(11)	120.5(1)
Ru(1)–P(1)–C(13)	117.6(1)	Ru(1)–P(1)–C(15)	111.8(1)
Ru(1)–P(2)–C(21)	120.9(1)	Ru(1)–P(2)–C(23)	118.1(1)
Ru(1)–P(2)–C(25)	112.2(1)	C(11)–P(1)–C(13)	100.8(2)
C(11)–P(1)–C(15)	100.3(2)	P(1)–C(11)–C(12)	116.5(3)
C(13)–P(1)–C(15)	103.2(2)	P(1)–C(13)–C(14)	117.6(2)
C(21)–P(2)–C(23)	100.9(2)	P(1)–C(15)–C(16)	115.4(3)
C(21)–P(2)–C(25)	99.5(2)	P(2)–C(21)–C(22)	115.5(3)
C(23)–P(2)–C(25)	102.2(2)	P(2)–C(23)–C(24)	117.3(3)
P(2)–C(25)–C(26)	114.6(2)	P(1)–Ru(1)–Cp(cen)	125.2(1)
P(2)–Ru(1)–Cp(cen)	126.1(1)	Cl(1)–Ru(1)–Cp(cen)	120.0(1)

<sup>a</sup> Numbers in parentheses are the estimated standard deviations.

reviewed.<sup>27</sup> The labile nature of the Ru–COD bond was exploited in the reaction shown in eq 10 and investigated by solution calorimetry.



$$\Delta H_{\text{rxn}} = -34.5 \pm 0.2 \text{ kcal/mol}$$

These reactions were found to be quantitative and rapid under the experimental calorimetric conditions. It is important to note that few thermodynamic data are available describing such systems. The magnitude of

(27) Butenschön, H. *Angew. Chem., Int. Ed. Engl.* **1994**, *33*, 636–638.



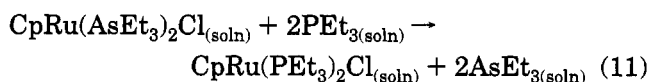
**Table 7. Fractional Coordinates ( $\times 10^4$ ) and Isotropic Thermal Parameters for  $\text{CpRu}(\text{PEt}_3)_2\text{Cl}$  (3)<sup>a</sup>**

atom	x	y	z	B ( $\text{\AA}^2$ )
Ru	7990.4(2)	293.9(3)	3106.0(1)	1.3(1)
Cl1	6736.2(6)	-1935.9(9)	2902.8(4)	2.0(1)
P1	7224.6(6)	1555.9(10)	3854.6(4)	1.6(1)
P2	6940.3(6)	1541.6(9)	2046.9(2)	1.4(1)
C1	9262(3)	-1540(5)	3259(2)	2.9(1)
C2	9299(3)	-458(6)	2724(3)	3.3(1)
C3	9493(3)	1101(5)	3057(2)	3.6(1)
C4	9575(3)	926(5)	3794(2)	3.3(1)
C5	9437(3)	-716(5)	3923(2)	2.9(1)
Cl1	7331(3)	3766(4)	3988(3)	2.6(1)
C12	8436(4)	4463(5)	4272(2)	3.9(2)
C13	5808(3)	1265(5)	3647(2)	2.2(1)
C14	5352(3)	1690(5)	4247(2)	2.6(1)
C15	7791(3)	869(4)	4814(2)	2.0(1)
C16	7608(3)	-892(5)	4945(2)	2.7(1)
C21	6678(3)	3765(4)	1973(3)	2.3(1)
C22	7923(3)	4610(6)	2128(2)	3.4(1)
C23	5537(3)	1027(5)	1701(2)	2.2(1)
C24	4906(3)	1561(5)	924(2)	2.5(1)
C25	7348(3)	1069(4)	1251(2)	2.1(1)
C26	7233(4)	-698(5)	1023(2)	3.1(1)

<sup>a</sup> Numbers in parentheses are the estimated standard deviations.

the thermodynamic forces behind catalytic and stoichiometric organoruthenium chemistry must be gauged in order to gain a better understanding of the factors controlling the stability of, for example, metal–diene interactions. Table 1 lists a variety of phosphine and arsine ligands readily able to substitute for COD in this system.

Arsine and phosphine ligands were investigated in view of their importance as catalyst modifiers.<sup>28</sup> As might be expected, in view of its steric bulk and weak electronic donating ability, the  $\text{AsEt}_3$  ligand is the most weakly bound ligand studied. A similar trend has been observed for  $(\text{AsEt}_3)_2\text{Fe}(\text{CO})_3$ <sup>7c</sup> and  $(\text{AsEt}_3)_2\text{Mo}(\text{CO})_4$ <sup>25</sup> complexes. The binding enthalpy of the arsine can be compared with that of its phosphine analog by simply taking the difference in enthalpies of reactions listed in Table 1. The reaction involving the phosphine ligand,  $\text{PEt}_3$ , displays an enthalpy 15.1 kcal/mol more exothermic than that of its arsenic relative.

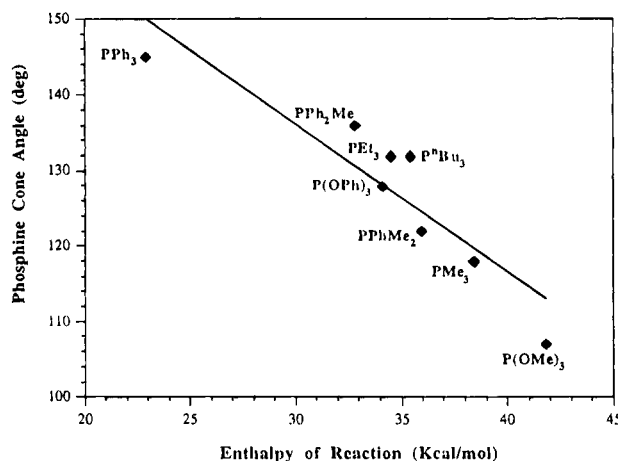


$$\Delta H_{\text{calcd}} = -15.1 \pm 0.4 \text{ kcal/mol}$$

This compares to an enthalpy difference of 12.2 kcal/mol for the  $\text{Cp}^*\text{Ru}(\text{L})_2\text{Cl}$  system.<sup>7d</sup> Similar enthalpy differences ( $12.4 \pm 0.3$  kcal/mol) have been observed in the *cis*- $(\text{L})_2\text{Mo}(\text{CO})_4$  complexes<sup>25</sup> ( $\text{L}$  = arsine and phosphine ligands). A recent study of the diaxial- $(\text{L})_2\text{Fe}(\text{CO})_3$  system<sup>7a,b</sup> also shows important similarities as far as the binding of arsenic *versus* phosphorus donors. Taking into consideration the estimated enthalpy of isomerization (axial–equatorial to diaxial) worth -5.4 kcal/mol, the difference in enthalpies of binding of  $\text{AsEt}_3$  *vs*  $\text{PEt}_3$  is calculated to be 12.5 kcal/mol in this iron system.

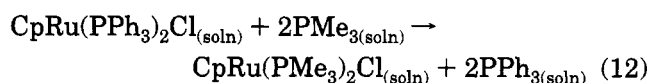
From the experimental data, it is now clear why the triphenylphosphine complex acts as a useful synthon in the isolation of bis(phosphine) complexes.<sup>18–22</sup> These

(28) Pignolet, L. H., Ed. *Homogeneous Catalysis with Metal Phosphine Complexes*; Plenum: New York, 1983.



**Figure 3.** Enthalpy of reaction *vs* phosphine cone angle for a series of tertiary phosphine ligands in the  $\text{CpRu}(\text{PR}_3)_2\text{Cl}$  system. Slope = -1.95;  $R = 0.91$ .

reactions are enthalpically driven; for a typical example, see eq 12. The ruthenium– $\text{PPh}_3$  is the weakest Ru–P



$$\Delta H_{\text{calcd}} = -14.5 \pm 0.6 \text{ kcal/mol}$$

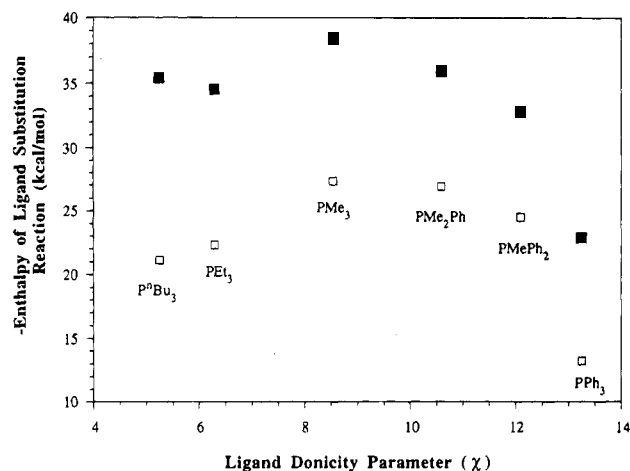
interaction found in the present study. Metal– $\text{PPh}_3$  interactions renowned for their thermodynamic weakness have found great use in catalysis. In this instance, we can estimate the difference in average Ru–P bond energy between the  $\text{PMe}_3$  and  $\text{PPh}_3$  to be on the order of 7.3 kcal/mol in tetrahydrofuran solution.

The data in Table 1 can be examined in terms of steric and electronic contributions to the enthalpy of reaction.<sup>26,29</sup> In view of the *cis* arrangement of phosphine ligands, steric factors might be expected, as in the related  $\text{Cp}^*$  system,<sup>7d</sup> to represent the predominant factor influencing the magnitude of the enthalpy of reaction. Since the steric factor has such a profound influence on the enthalpy of reaction, a direct relationship between the enthalpy of reaction and the phosphine cone angle was established (Figure 3), and the linear relationship emphasizes the major role played by steric effects in the present system. These results are in agreement with semiquantitative calculations.<sup>30</sup> In the present system, it appears, from the experimental enthalpy data, that trimethylphosphite leads to the formation of the most stable organoruthenium complex. This is not obvious even though similar high binding affinities of this ligand for transition metals have been observed previously.<sup>7d</sup> The relatively high affinity of ruthenium for phosphites can possibly be explained in terms of back donation from the metal into orbitals on the phosphite ligand (phosphorus–oxygen  $\sigma^*$  orbitals). Ruthenium(II)  $d^6$  is also known to be a strong back-bonding system.

Important insights are offered by a comparison between the present data and that of the  $\text{Cp}^*\text{Ru}(\text{PR}_3)_2\text{Cl}$  system. In both  $\text{Cp}$  and  $\text{Cp}^*$  systems the role of the

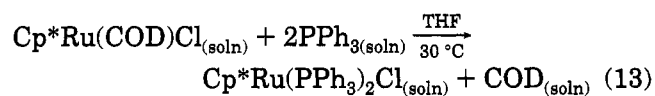
(29) (a) Tolman, C. A. *Chem. Rev.* **1977**, *77*, 313–348. (b) Manzer, L. E.; Tolman, C. A. *J. Am. Chem. Soc.* **1975**, *97*, 1955–1986.

(30) A treatment of the enthalpy data similar to the one already performed in ref 7d confirmed the major role of the steric component of the relationship initially discussed by Tolman in ref 29a.

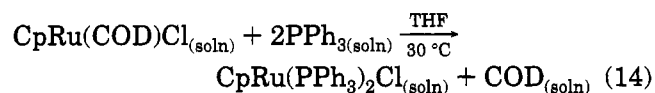


**Figure 4.** Enthalpy of reaction *vs* phosphine  $\chi$  values for a series of tertiary phosphine ligands in the Cp'Ru(PR<sub>3</sub>)<sub>2</sub>-Cl systems (Cp' = Cp and Cp\*).

phosphine steric factor is most important. Yet the difference in enthalpies of reaction between the two systems is based on differences in electronic features at the metal, resulting from a change of ancillary ligation (Cp *vs* Cp\*). Since Cp is less electron donating than Cp\*, the Cp system will be able to accommodate greater electron density from the incoming two-electron donor (higher electrophilicity), therefore leading to more exothermic enthalpies of ligand substitution. The electronic origin of this difference in enthalpy of reaction between the present Cp-based system and the Cp\*-based system can be further illustrated upon examination of  $\chi$  factors, used by Geiring and co-workers,<sup>31</sup> which express the donicity of the phosphine ligand. The ligand donicity remains constant while the accepting properties of the metal have been modified by the change in ancillary ligation (Cp to Cp\*). Herein lies the electronic difference between the two systems (Figure 4).



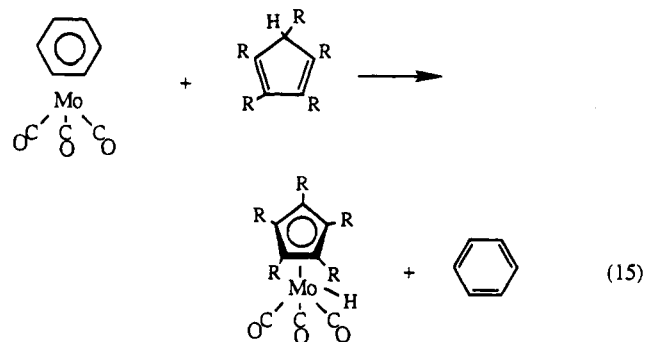
$$\Delta H_{\text{rxn}} = -18.1 \pm 0.2 \text{ kcal/mol}$$



$$\Delta H_{\text{rxn}} = -22.9 \pm 0.4 \text{ kcal/mol}$$

This difference in electronic properties at the metal center measures the change in metal basicity. Sowa and Angelici have investigated a series of iridium complexes and have observed a difference in enthalpies of protonation of 5.7 kcal/mol between CpIr(COD) and Cp\*Ir(COD) complexes.<sup>11</sup> In these experiments, H<sup>+</sup> proved to be more strongly bound to M-Cp\* by ca. 5 kcal/mol. This is in view of the increased electron density imparted by the better Cp\* donor. In the present ruthenium systems electron-donating phosphine groups are more strongly bound in the CpRu system. Both sets of experiments, although using different

approaches, relate information concerning the same fundamental characteristic, namely, metal basicity. Hoff and co-workers first demonstrated this difference in metal basicity between Cp and Cp\* in their thermochemical investigations of organomolybdenum complexes.<sup>10</sup>



$$R = \text{H}; \Delta H_{\text{rxn}} = -12.8 \text{ kcal/mol}$$

$$R = \text{Me}; \Delta H_{\text{rxn}} = -10.5 \text{ kcal/mol}$$

The enthalpy difference between ligand substitution reactions,  $-2.3$  kcal/mol, reflects the difference of metal basicity accompanying a change of the ancillary ligation. This difference is of the same order of magnitude as Angelici's enthalpies of protonation and the average difference in enthalpy of ligand substitution in the Cp *versus* Cp\* organoruthenium systems. Rottink and Angelici have also measured metal basicity differences in a related Cp'Ru(PPh<sub>3</sub>)<sub>2</sub>H system (Cp' = Cp and Cp\*) and found protonation to be 5.5 kcal/mol in favor of the Cp\*Ru(PPh<sub>3</sub>)<sub>2</sub>H complex.<sup>11b</sup> These researchers have also found differences in the related chloro complexes, Cp'Ru(PMe<sub>3</sub>)<sub>2</sub>Cl, on the order of 9.0 kcal/mol. This result can be compared directly with the present difference in enthalpies of ligand substitution in these two Cp'Ru(PR<sub>3</sub>)<sub>2</sub>Cl systems for PMe<sub>3</sub> ( $6.2 \pm 0.5$  kcal/mol).

Closer examination of the crystal structures of **2** and **3** reveals similar Ru-Cl bond distances of 2.452(1) and 2.4502(8) Å, respectively. The most noticeable variation between the two structures is the difference in the average Ru-E (E = As and P) distances, which are 2.4141(7) and 2.3036(9) Å. This difference in Ru-E distances can be qualitatively understood in terms of binding energy. The Ru-As interaction, being the weakest of the series examined, will possess the longest Ru-E bond distance (no corrections were applied for differences in atomic radii). Three other CpRu(PR<sub>3</sub>)<sub>2</sub>-Cl complexes (PR<sub>3</sub> = PMe<sub>3</sub>, P(OMe)<sub>3</sub>, and PPh<sub>3</sub>) have been structurally characterized previously.<sup>19b,20b</sup> A comparison involving all five complexes in terms of bond distances and bond angles (Table 8) suggests a linear relationship between bond enthalpy data and ruthenium-phosphine/arsine bond length information.<sup>32</sup> A graphic representation of the relationship is presented in Figure 5 and shows a good correlation ( $R = 0.94$ ) to exist in this system. A comparison between Cp- and Cp\*-based ruthenium complexes bearing similar arsine or phosphine ligands offers further insights into the

(32) Such a correlation is expected if no important variation in Ru-L<sub>n</sub> (L<sub>n</sub> = ancillary ligand) bond distance or L<sub>n</sub>-Ru-L<sub>n</sub> bond angle is present in these complexes. Studies aimed at probing the extent and reasons for such a correlation to exist in the present system are currently underway.

(31) (a) Liu, H.-Y.; Eriks, K.; Geiring, W. P. *Organometallics* **1990**, *9*, 1758-1766. (b) Fernandez, A. L.; Prock, A.; Geiring, W. P. *Organometallics* **1994**, *13*, 2767-2772.

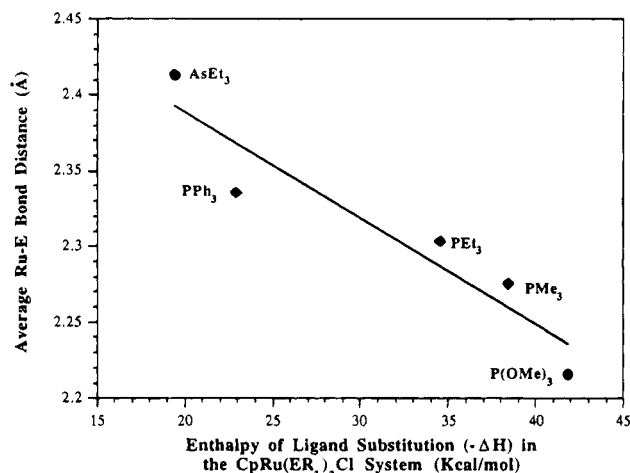
**Table 8.** Selected Bond Distances (Å) and Bond Angles (deg) for CpRu(ER<sub>3</sub>)<sub>2</sub>Cl Complexes

Bond Distances (Å)			
ER <sub>3</sub>	M–Cl	M–ER <sub>3</sub> (ave)	M–Cp
PMe <sub>3</sub> <sup>a,b</sup>	2.451(6)	2.326(6)	1.850(5)
PPh <sub>3</sub> <sup>a</sup>	2.453(2)	2.336(1)	1.847(4)
P(OMe) <sub>3</sub> <sup>c</sup>	2.393(3)	2.217(3)	1.953(4)
PEt <sub>3</sub> <sup>d</sup>	2.4502(8)	2.304(1)	1.858(4)
AsEt <sub>3</sub> <sup>d</sup>	2.452(1)	2.414(1)	1.811(5)

Bond Angles (deg)			
ER <sub>3</sub>	Cp(cen)M–Cl	Cl–M–E(ave)	E–M–E
PMe <sub>3</sub> <sup>a,b</sup>	123.6(2)	89.82(2)	94.7(2)
PPh <sub>3</sub> <sup>a</sup>	122.5(1)	89.73(4)	103.99(4)
P(OMe) <sub>3</sub> <sup>c</sup>	120.9(1)	93.4(1)	91.2(1)
PEt <sub>3</sub> <sup>d</sup>	120.0(1)	90.46(3)	94.71(3)
AsEt <sub>3</sub> <sup>d</sup>	126.3(2)	85.17(3)	101.30(2)

<sup>a</sup> See reference 19c. <sup>b</sup> Two independent molecules are found in this unit cell. <sup>c</sup> See reference 20b. <sup>d</sup> This work.



**Figure 5.** Enthalpy of ligand substitution reaction vs average Ru–E bond distance in the CpRu(ER<sub>3</sub>)<sub>2</sub>Cl system (E = As, P). Slope = –0.007; *R* = 0.94.

bond strength/bond length relationship. In the present system, the average Ru–As and Ru–P bond lengths cited above can be compared with distances of 2.445 and 2.321 Å for the related Cp\* complexes.<sup>33</sup> There appears to exist a correlation between bond length and magnitude of the enthalpies of substitution in both systems. Further structural studies are in progress in order to examine to what extent this relationship remains valid for these ruthenium systems.<sup>33</sup>

Trost and co-workers have recently reported on the catalytic role of CpRu(PPh<sub>3</sub>)<sub>2</sub>Cl as an efficient catalyst precursor in the ruthenium-catalyzed addition of allyl alcohols and acetylenes leading, in a simple synthetic route, to unsaturated ketones.<sup>34</sup> They have since reported that complex **1** can very easily perform such a

transformation, although using a different mechanistic route.<sup>35</sup> The utility of the ruthenium–COD complex (**1**) as a catalyst precursor can be understood in terms of relative bond dissociation enthalpies. The Ru–PPh<sub>3</sub> bond is on average 11.5 kcal/mol stronger than the Ru–olefin bond present in **1**. In view of the labile nature of the COD ligand in the present system and the catalytic activity of ruthenium complexes, **1** was found to be capable of mediating the catalytic isomerization and/or oligomerization of 1-hexene at 50 °C.<sup>36</sup>

## Conclusion

The labile nature of the COD ligand in CpRu(COD)–Cl was used to gain access to the thermochemistry of ligand substitution for monodentate arsine/phosphine/phosphite ligands. The enthalpy trend can be explained in terms of electronic and steric conditions to the enthalpy of reaction, with the steric constituent playing a major role. Reactions of monodentate ligands with **1** also show this reaction to be of synthetic use for isolation of complexes of formulation CpRu(L)<sub>2</sub>Cl. The increased exothermicity displayed by the CpRu(PR<sub>3</sub>)<sub>2</sub>Cl system over its Cp\* parent is taken as a gauge of the increased metal basicity on going from Cp to Cp\*, and for the first time, a gauge of metal basicity is obtained that relies exclusively on enthalpies of substitution reactions. A quantitative relationship is established between structural and thermodynamic parameters and displays a good correlation. The labile nature of the COD in **1** was used in catalytic tests and resulted in its assessment as an efficient catalyst precursor in the ruthenium-mediated oligomerization/isomerization of a terminal olefin. Further thermochemical, kinetic, mechanistic, and catalytic investigations focussing on this and related systems are present underway.

**Acknowledgment.** The donors of the Petroleum Research Fund, administered by the American Chemical Society; the Board of Regents of the Louisiana Education Quality Support Fund (LEQSF(RF/1993-96)-RD-A-47); and the National Science Foundation (CHE-9305492) are gratefully acknowledged for support of this research. We are also indebted to Aesar/Johnson-Matthey for the generous loan of ruthenium salts. We also wish to thank Dr. Charles H. Mahler and Professor Warren P. Geiring for helpful suggestions and discussions.

**Supplementary Material Available:** Tables of crystal and intensity data, atomic coordinates, selected distances and angles, anisotropic thermal displacement parameters, and hydrogen bond distances for **2** and **3** (8 pages). Ordering information is given on any current masthead page.

OM9407159

(33) Luo, L.; Li, C.; Cucullu, M. E.; Mahler, C. H.; Fagan, P. J.; Jones, N.; Nolan, S. P. Manuscript in preparation.

(34) Trost, B. M.; Dyker, G.; Kulawiec, R. J. *J. Am. Chem. Soc.* **1990**, *112*, 7809–7811.

(35) (a) Trost, B. M.; Martinez, J. A.; Kulawiec, R. J.; Indolese, A. F. *J. Am. Chem. Soc.* **1993**, *115*, 10402–10403. (b) Trost has also recently reported the catalytic use of **1** in a butenolide synthesis: Trost, B. M.; Müller, T. J. *J. Am. Chem. Soc.* **1994**, *116*, 4985–4986.

(36) For recent observation of such isomerization and oligomerization by a ruthenium complex, see: Carreno, R.; Chaudret, B.; Labroue, D.; Sabo-Etienne, S. *Organometallics* **1993**, *12*, 13–14.

# Thermal Fragmentation of Acyl Thiolato Complexes to Reactive Metal Sulfido Intermediates. Structure of $\text{Ru}(\eta^6\text{-SC}_3\text{Me}_3\text{COMe})(\text{PPh}_3)_2$

Qian Feng, Harald Krautscheid, Thomas B. Rauchfuss,\* Anton E. Skaugset, and Anne Venturelli

School of Chemical Sciences, University of Illinois, Urbana, Illinois 61801

Received February 18, 1994<sup>⊗</sup>

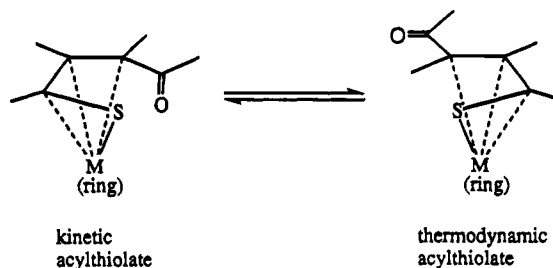
This study deals with the thermal decomposition of acylbutenethiolate ( $\text{SC}_3\text{Me}_3\text{COMe}$ ) complexes derived from the base hydrolysis of tetramethylthiophene complexes  $[(\text{ring})\text{M}(\text{C}_4\text{Me}_4\text{S})]^{2+}$  ( $\text{M} = \text{Ru}$ , ring = *p*-cymene,  $\text{C}_4\text{Me}_4\text{S}$ ;  $\text{M} = \text{Os}$ , ring = *p*-cymene;  $\text{M} = \text{Rh}$ , Ir, ring =  $\text{C}_5\text{Me}_5$ ). (cymene) $\text{Ru}(\text{SC}_3\text{Me}_3\text{COMe})$  (**1**) and  $(\text{C}_4\text{Me}_4\text{S})\text{Ru}(\text{SC}_3\text{Me}_3\text{COMe})$  undergo thermal fragmentation, affording tetramethylfuran and insoluble ruthenium sulfides. The thermal decomposition of both **1** and (cymene) $\text{Os}(\text{SC}_3\text{Me}_3\text{COMe})$  (**2**) follows first-order kinetics. Two intermediates were observed in the thermal decomposition of **2**. These intermediates are clusters containing inequivalent cymene groups as the only  $^1\text{H}$  NMR detectable ligands. The second, more stable, intermediate was isolated and identified as (cymene) $_3\text{Os}_3\text{S}_2$  (**4**). The complex  $\text{Ru}(\eta^6\text{-SC}_3\text{Me}_3\text{COMe})(\text{PPh}_3)_2$  (**5**) is obtained when **1** is thermolyzed in the presence of  $\text{PPh}_3$ . Crystallographic analysis confirmed the structure of **5**, in which the  $\eta^6$ -acyl thiolate is bound through the four carbon atoms as well as the O and S atoms. The formation of **5** is first order in [**1**]. At high  $[\text{PPh}_3]$  the rate is zero order in  $[\text{PPh}_3]$ , while at low  $[\text{PPh}_3]$  a bimolecular ( $[\text{PPh}_3][\text{Ru}]$ ) pathway is indicated. These results are explained in terms of a preequilibrium whereby the acyl thiolate in one isomeric form of **1** reversibly binds in an  $\eta^6$  mode. Thermal decompositions of  $(\text{C}_5\text{Me}_5)\text{M}(\text{SC}_3\text{Me}_3\text{COMe})$  ( $\text{M} = \text{Rh}$  (**6**), Ir (**7**)) occur unimolecularly to give tetramethylfuran and  $[(\text{C}_5\text{Me}_5)\text{MS}]_4$ . Thermolysis of **6** in the presence of  $\text{PPh}_3$  still gives tetramethylfuran, but the Rh product is spectroscopically identified as  $(\text{C}_5\text{Me}_5)_2\text{Ru}_2(\mu_2\text{-S})_2(\text{PPh}_3)$ .

## Introduction

The generation and study of reactive metal sulfido species provides insights into the conversion of small molecules to clusters. Two approaches have been described. In the first, coordinatively unsaturated metal sulfides are produced by desulfurization of sulfur-rich precursors, i.e. by changing the M/S ratio. For example, the desulfurization of  $(\text{C}_5\text{H}_5)_2\text{V}_2\text{S}_4$  with  $\text{PBU}_3$  gives a mixture of  $(\text{C}_5\text{H}_5)_4\text{V}_4\text{S}_4$  and  $(\text{C}_5\text{H}_5)_5\text{V}_5\text{S}_6$  clusters.<sup>1</sup> In a more controlled process the desulfurization of  $(\text{C}_5\text{Me}_5)_2\text{-Ru}_2\text{S}_4$  leads to  $(\text{C}_5\text{Me}_5)_2\text{Ru}_2\text{S}_2$ , which can be trapped with ligands such as CO and  $\text{R}_2\text{C}_2$ .<sup>2</sup> Alternatively, reactive metal sulfido intermediates have been generated via ligand dissociation. Bergman and co-workers have employed this method for the conversion of  $(\text{C}_5\text{-Me}_5)_2\text{ZrS}(\text{L})$  and  $(\text{C}_5\text{Me}_5)_2\text{M}_2\text{S}_2(\text{PR}_3)$  ( $\text{M} = \text{Rh}$ , Ir) to the highly reactive intermediates  $(\text{C}_5\text{Me}_5)_2\text{ZrS}^3$  and  $(\text{C}_5\text{-Me}_5)_2\text{M}_2\text{S}_2$ ,<sup>4</sup> respectively. In the present report we describe a new method for generating reactive metal sulfido intermediates via a unimolecular fragmentation of metal acyl thiolates.

It is useful to summarize what is known about the metal complexes of acyl thiolates, which can also be

## Scheme 1



- 1:  $\text{M} = \text{Ru}$ ; ring = cymene  
 2:  $\text{M} = \text{Os}$ ; ring = cymene  
 6:  $\text{M} = \text{Rh}$ ; ring =  $\text{C}_5\text{Me}_5$   
 7:  $\text{M} = \text{Ir}$ ; ring =  $\text{C}_5\text{Me}_5$

described as complexes of  $\alpha,\beta$ -unsaturated thiones (Scheme 1). The preparation of these complexes has been described in previous reports, and two new examples are reported in this paper.<sup>5-7</sup> The acyl thiolates are synthesized via the base hydrolysis of dicationic thiophene complexes.<sup>7</sup> This transformation effects the net addition of  $\text{O}^{2-}$  to the heterocycle and the formal reduction of the metal center by 2e. The acyl thiolate complexes are found to exist in either of two isomers, depending on the configuration of the carbon bearing the acyl (see Scheme 1). The kinetic isomer has the acyl

<sup>⊗</sup> Abstract published in *Advance ACS Abstracts*, November 15, 1994.

(1) Bolinger, C. M.; Darkwa, J.; Gammie, G.; Gammon, S. D.; Lyding, J. W.; Rauchfuss, T. B.; Wilson, S. R. *Organometallics* **1986**, *5*, 2386.

(2) Ogilvy, A. E.; Rauchfuss, T. B. *Organometallics* **1988**, *7*, 1884. Rauchfuss, T. B.; Rodgers, D. P. S.; Wilson, S. R. *J. Am. Chem. Soc.* **1986**, *108*, 3114.

(3) Carney, M. J.; Walsh, P. J.; Hollander, F. J.; Bergman, R. G. *Organometallics* **1992**, *11*, 761.

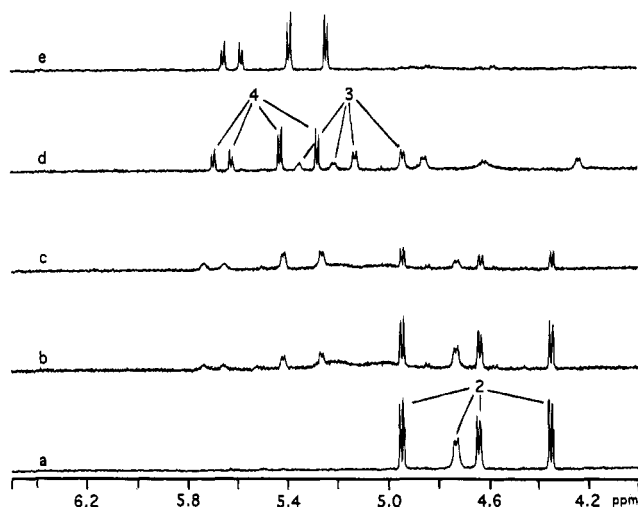
(4) Dobbs, D. A.; Bergman, R. G. *J. Am. Chem. Soc.* **1992**, *114*, 6908.

(5) Skaugset, A. E.; Rauchfuss, T. B.; Wilson, S. R. *Organometallics* **1990**, *9*, 2875.

(6) Skaugset, A. E.; Rauchfuss, T. B.; Wilson, S. R. *J. Am. Chem. Soc.* **1992**, *114*, 8521.

(7) Krautscheid, H.; Feng, Q.; Rauchfuss, T. B. *Organometallics* **1993**, *12*, 3273.

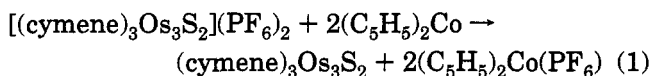




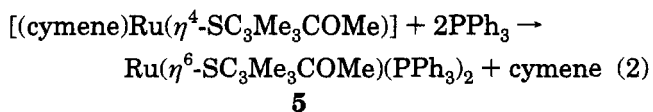
**Figure 3.** 400 MHz  $^1\text{H}$  NMR spectra for the thermolysis of (cymene) $\text{Os}(\eta^4\text{-SC}_3\text{Me}_3\text{COMe})$  (toluene- $d_8$  solution): (a)  $t = 0$  (75 °C); (b)  $t = 4.5$  h (75 °C); (c)  $t = 6.0$  h (75 °C); (d) sample in (c), recorded at 20 °C; (e) sample after heating at 75 °C for 20 h, recorded at 20 °C.

from the spectra in Figure 3 that **2** itself is dynamic, as seen for the corresponding ruthenium complex.<sup>7</sup>

Since **3** is formed at approximately the same rate as it decomposes, its solutions are always contaminated with **2**, **4**, or both. For this reason we decided to focus on the second intermediate **4**, which arises via the decomposition of **3**.  $^1\text{H}$  NMR spectra showed that the yield for **4** is  $\sim 25\%$ , which corresponds roughly to the ratio  $k_2/(k_2 + k_3)$ , less that amount which decomposes via the  $k_4$  pathway. Indeed, when the thermolysis was allowed to proceed until all **2** and **3** were consumed, we were able to isolate **4** as a dark green solid. Its field desorption mass spectrum showed a molecular ion envelope corresponding to (cymene) $_3\text{Os}_3\text{S}_2^+$ . Oxidation of **4** with HOTf gave the known red species [(cymene) $_3\text{Os}_3\text{S}_2$ ] $^{2+}$ .<sup>10</sup> Confirmatory evidence for the identity of **4** came from its independent synthesis by cobaltocene reduction of the known salt [(cymene) $_3\text{Os}_3\text{S}_2$ ](PF<sub>6</sub>)<sub>2</sub> (eq 1). The spectroscopic properties of (cymene) $_3\text{Os}_3\text{S}_2$  prepared in this way perfectly match those for **4**.



**Thermal Decomposition of (ring) $\text{Ru}(\text{SC}_3\text{Me}_3\text{COMe})$  (ring = cymene,  $\text{C}_4\text{Me}_4\text{S}$ ) in the Presence of  $\text{PPh}_3$ .** The thermal decomposition of **1** in the presence of  $\text{PPh}_3$  was investigated in an attempt to trap intermediates. When the reaction was conducted in warm toluene, free *p*-cymene and a compound analyzed as  $\text{Ru}(\eta^6\text{-SC}_3\text{Me}_3\text{COMe})(\text{PPh}_3)_2$  (**5**) formed (eq 2). The

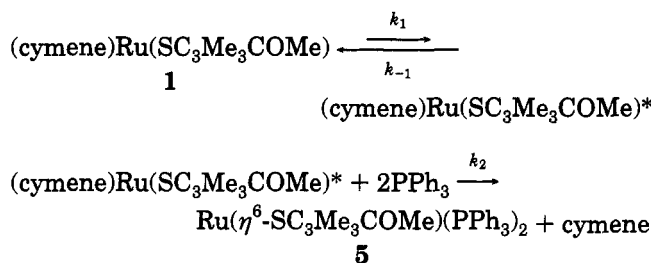


$^1\text{H}$  NMR spectrum of **5** showed four methyl signals, each of which appears as a doublet. The  $^{31}\text{P}\{^1\text{H}\}$  NMR spectrum consisted of two equally intense doublets. A series of selective as well as broad-band  $^1\text{H}\{^{31}\text{P}\}$  decou-

pling experiments showed that each of the phosphorus centers is coupled to a pair of methyl groups. The  $J(\text{P},\text{P}')$  value of 34 Hz indicates that the phosphine ligands are mutually *cis*. These NMR data are consistent with the results of a single-crystal structural analysis (see below). Solutions of  $(\text{C}_4\text{Me}_4\text{S})\text{Ru}(\text{SC}_3\text{Me}_3\text{COMe})$  and  $\text{PPh}_3$  react rapidly at room temperature to give **5**.

The progress of the reaction of **1** and  $\text{PPh}_3$  was monitored by  $^1\text{H}$  NMR spectroscopy at 70 °C in a  $\text{C}_6\text{D}_6$  solution. The sum of the concentrations of **1** and **5** remained constant, and no intermediates were observed. At high concentrations of  $\text{PPh}_3$  the rates were shown to be first order in **1** and independent of  $[\text{PPh}_3]$  ( $k_1 = 5.7 \times 10^{-5} \text{ s}^{-1}$ ,  $t_{1/2} = 3.4$  h). At lower  $\text{PPh}_3$  concentrations, the rate of the conversion of **1** to **5** was dependent on  $[\text{PPh}_3]$ . These results can be explained by invoking a two-step mechanism involving a metastable intermediate symbolized as (cymene) $\text{Ru}(\text{SC}_3\text{Me}_3\text{COMe})^*$  shown in Scheme 3. This scheme conforms to the conditions

### Scheme 3



of the steady-state approximation, which requires that [(cymene) $\text{Ru}(\text{SC}_3\text{Me}_3\text{COMe})^*$ ] be small and unchanging, leading to the rate equation (3). The special condition

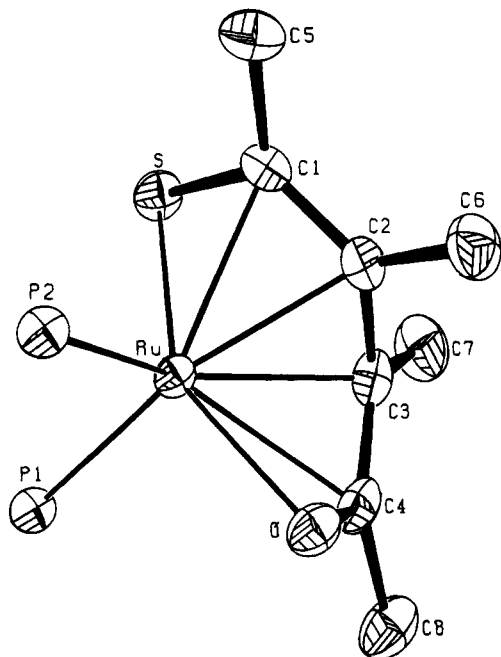
$$-\frac{d[\mathbf{1}]}{dt} = \frac{k_1[\mathbf{1}]}{1 + \frac{k_{-1}}{k_2[\text{PPh}_3]}} \quad (3)$$

of  $[\text{PPh}_3] = 2[\mathbf{1}]$  leads to the simplified integrated rate equation shown in eq 4 (see also Experimental Section). Plots of  $[\mathbf{1}]^{-1}$  vs  $(k_1t + \ln[\mathbf{1}])$  were shown to be linear.

$$\frac{1}{[\mathbf{1}]} = \frac{2k_2}{k_{-1}}(k_1t + \ln[\mathbf{1}]) + C \quad (4)$$

**Structure of  $\text{Ru}(\text{SC}_3\text{Me}_3\text{COMe})(\text{PPh}_3)_2$ .** As shown in Figure 4, the hydrocarbon ligand of **5** is coordinated to Ru in an  $\eta^6$  fashion with the two  $\text{PPh}_3$  ligands completing the coordination sphere. If the metal and the ligands are regarded as neutral, the thiolate ligand contributes six electrons and the metal attains an  $18e^-$  configuration. The  $\eta^6\text{-SC}_3\text{Me}_3\text{COMe}$  ligand consists of planar  $\text{SC}_2\text{Me}_2$  and  $\text{OC}_2\text{Me}_2$  subunits where the sum of the angles around C1 and C4 is 360°. The angle between these planes is 110.4°. The bond lengths of S–C1, C1–C2, C3–C4, and C4–O are intermediate between single and double bonds, while the C2–C3 bond, which links the two heteroallyl groups, is significantly longer (Table 1). These data suggest  $\pi$ -electron delocalization as expected for such a heteroallyl sys-

(10) Lockmeyer, J. R.; Rauchfuss, T. B.; Rheingold, A. L. *J. Am. Chem. Soc.* **1989**, *111*, 5733.



**Figure 4.** ORTEP plot of  $\text{Ru}(\eta^6\text{-SC}_3\text{Me}_3\text{COMe})(\text{PPh}_3)_2$  with thermal ellipsoids drawn at the 50% probability level.

**Table 1.** Important Bond Distances (Å) and Angles (deg) in  $\text{Ru}(\eta^6\text{-SC}_3\text{Me}_3\text{COMe})(\text{PPh}_3)_2$  (5)

Ru-S	2.394(9)	Ru-O	2.180(2)
Ru-C1	2.283(4)	Ru-C2	2.207(4)
Ru-C3	2.243(4)	Ru-C4	2.325(4)
S-C1	1.753(4)	C4-O	1.313(4)
C1-C2	1.399(5)	C2-C3	1.489(5)
C3-C4	1.389(6)		
O-C4-C8	115.6(3)	S-C1-C2	119.5(3)
S-C1-C5	118.0(3)	C2-C1-C5	122.4(3)
C3-C4-O	120.5(4)	C3-C4-C8	123.9(3)

tem.<sup>11</sup> The Ru-C distances indicate that C1-C4 atoms are coordinated to the Ru atom. The Ru-C4 distance is 0.08 Å longer than Ru-C3, which is in agreement with the case for the oxoallyl complex  $(\text{C}_5\text{H}_5)(\text{CO})_2\text{W}(\eta^3\text{-CH}_2\text{CONEt}_2)$ , in which the C-W distance for the central bond of 2.46 Å is 0.19 Å longer than  $C_{\text{term}}\text{-W}$ .<sup>12</sup> Also consistent with the  $\eta^3$ -oxoallyl formulation is the absence of any prominent bands in the  $\nu_{\text{C=O}}$  region. Finally, the  $^{13}\text{C}\{^1\text{H}\}$  NMR ( $\text{C}_6\text{D}_6$ ) spectrum does not show any peaks around 200 ppm typical of carbonyls. Overall, the coordination around Ru can be described as pseudotetrahedral with the S, C1, C2 and the C3, C4, O units as two vertices. In this way the complex is similar to  $\text{Ru}(\text{C}_3\text{H}_5)_2(\text{PPh}_3)_2$ <sup>13</sup> and  $\text{Ru}(\text{C}_4\text{H}_7)_2(\text{P}(\text{OMe})_3)_2$ .<sup>14</sup>

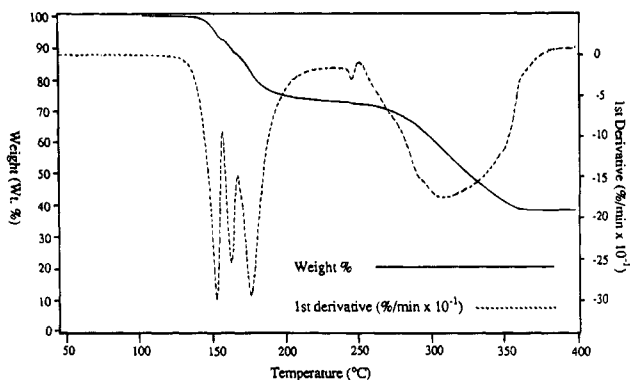
**Thermal Decomposition of  $(\text{C}_5\text{Me}_5)\text{M}(\text{SC}_3\text{Me}_3\text{COMe})$  (M = Rh, Ir).** Thermal decomposition of toluene solutions of  $(\text{C}_5\text{Me}_5)\text{Rh}(\text{SC}_3\text{Me}_3\text{COMe})$  (**6**) yielded tetramethylfuran and the cubane cluster  $(\text{C}_5\text{Me}_5)_4\text{Rh}_4\text{S}_4$ . The  $^1\text{H}$  NMR spectrum of the cluster exhibited only one singlet, consistent with its highly symmetrical structure featuring a  $\text{Rh}_4\text{S}_4$  core of idealized  $T_d$  symmetry. This cluster has previously been prepared by us via the

(11) (a) Robertson, G. B.; Whimp, P. O. *Inorg. Chem.* **1973**, *12*, 1740. (b) Holmgren, J. S.; Shapley, J. R.; Wilson, S. R.; Pennington, W. T. *J. Am. Chem. Soc.* **1986**, *108*, 508.

(12) Burkhardt, E. R.; Doney, J. J.; Bergman, R. G.; Heathcock, C. H. *J. Am. Chem. Soc.* **1987**, *109*, 2022.

(13) Smith, A. E. *Inorg. Chem.* **1972**, *11*, 2306.

(14) Marsh, R. A.; Howard, J.; Woodward, P. *J. Chem. Soc., Dalton Trans.* **1973**, 778.



**Figure 5.** Thermogravimetric analysis of  $(\text{C}_5\text{Me}_5)\text{Rh}(\eta^4\text{-SC}_3\text{Me}_3\text{COMe})$  (heating rate  $4^\circ\text{C}/\text{min}$ , under an He atmosphere).

reaction of  $(\text{C}_5\text{Me}_5)_2\text{Rh}_2\text{Cl}_4$  with  $(\text{Me}_3\text{Si})_2\text{S}$ ,<sup>15</sup> while Bergman and co-workers have isolated the mixed  $(\text{C}_5\text{Me}_5)_4\text{-Ir}_2\text{Rh}_2\text{S}_4$  cubane from the thermal decomposition of  $(\text{C}_5\text{Me}_5)_2\text{RhIrS}_2(\text{PMe}_3)$ .<sup>4</sup> The rate of decomposition of **6** in toluene- $d_8$  solution followed first-order kinetics over the temperature range  $80\text{--}100^\circ\text{C}$  (e.g.,  $k_1 = 4.55 \times 10^{-5} \text{ s}^{-1}$  at  $90^\circ\text{C}$ ). The temperature dependence of the rates over this admittedly small temperature range indicates a positive entropy of activation ( $\Delta S^\ddagger$ ) of  $\sim 44 \text{ J}/(\text{mol K})$ .

Solid-state thermolyses of **6** also proceeded well and allowed us to readily collect the volatile product. The  $^1\text{H}$  and  $^{13}\text{C}\{^1\text{H}\}$  NMR data for this compound compare well with literature values for tetramethylfuran,<sup>16</sup> and the identification was confirmed by high-resolution mass spectrometry. The thermal decomposition of  $(\text{C}_5\text{Me}_5)\text{-Rh}(\text{SC}_3\text{Me}(\text{CH}_2\text{D})_2\text{COMe})$ , derived from tetramethylthiophene specifically monodeuterated at the 3- and 4-methyl positions,<sup>6</sup> gave tetramethylfuran with one deuterium each in the the 3- and 4-positions. Thermogravimetric analysis showed that **6** decomposes in two stages (Figure 5). Between 150 and  $190^\circ\text{C}$ , 25% of the sample weight is lost; the elimination of tetramethylfuran should cause a weight loss of 32%. From 270 to  $350^\circ\text{C}$ , loss of an additional 34% of the sample weight occurs, leaving a residual 38%, compared to 34% the expected for  $\text{RhS}$ .

Thermal decomposition of toluene solutions of the iridium acyl thiolate **7** also afforded high yields of tetramethylfuran and the cluster. The  $^1\text{H}$  NMR data for the cluster compare well with literature values for  $(\text{C}_5\text{Me}_5)_4\text{Ir}_4\text{S}_4$ .<sup>4</sup> Final identification of the  $(\text{C}_5\text{Me}_5)_4\text{Ir}_4\text{-S}_4$  cubane was made by comparison to a specimen prepared by literature methods.<sup>9a</sup> The rate of decomposition in toluene- $d_8$  follows first-order kinetics at rates very similar to the rhodium case ( $k = 5.71 \times 10^{-5} \text{ s}^{-1}$  at  $90^\circ\text{C}$ ,  $t_{1/2} = 3.4 \text{ h}$ ).

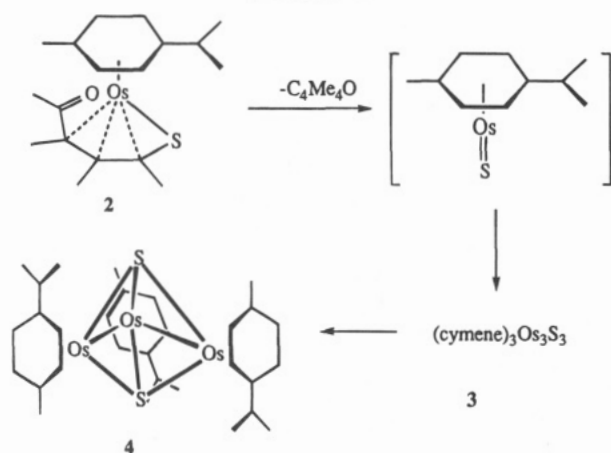
**Thermal Decomposition of  $(\text{C}_5\text{Me}_5)\text{Rh}(\text{SC}_3\text{Me}_3\text{COMe})$  in the Presence of  $\text{PPh}_3$ .** The rate of decomposition of the rhodium acyl thiolate **6** was unaffected by  $\text{PPh}_3$ . Sealed-tube  $^1\text{H}$  NMR experiments also demonstrated that the formation of tetramethylfuran was unaffected; however, we did not observe the formation of the cubane cluster. Independent studies demonstrated that the cubane cluster was unreactive toward excess  $\text{PPh}_3$  under similar reaction conditions.

(15) Lockemeyer, J. R.; Rauchfuss, T. B.; Venturelli, A. Unpublished results.

(16) Kiewiet, A.; de Wit, J.; Weringa, W. D. *Org. Magn. Reson.* **1974**, *6*, 461.



Scheme 4

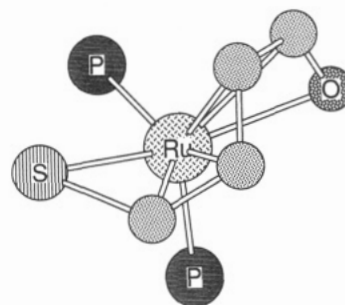


The fact that  $\text{PPh}_3$  blocks the formation of cubane but does not affect the rate of decomposition of **6** indicates that the  $\text{PPh}_3$  intercepts an intermediate subsequent to the rate-limiting step. Indeed, the  $^1\text{H}$  NMR spectrum of the reaction solution showed a strong singlet and a doublet ( $J_{\text{H}-^{103}\text{Rh}} = 3.2$  Hz), both centered at 1.55 ppm. The  $^{31}\text{P}\{^1\text{H}\}$  NMR spectrum consisted of one doublet at 58.2 ppm ( $J_{\text{Rh}-\text{P}} = 225$  Hz). These data compare favorably with those for  $(\text{C}_5\text{Me}_5)\text{Rh}(\text{PMe}_3)_2\text{S}_2\text{Ir}(\text{C}_5\text{Me}_5)$ ,<sup>4</sup> indicating that  $(\text{C}_5\text{Me}_5)\text{Rh}(\text{SC}_3\text{Me}_3\text{COMe})$  decomposes to give  $(\text{C}_5\text{Me}_5)_2\text{Rh}_2\text{S}_2$ , which can be intercepted by  $\text{PPh}_3$  to give  $(\text{C}_5\text{Me}_5)_2\text{Rh}_2\text{S}_2(\text{PPh}_3)$ .

### Discussion

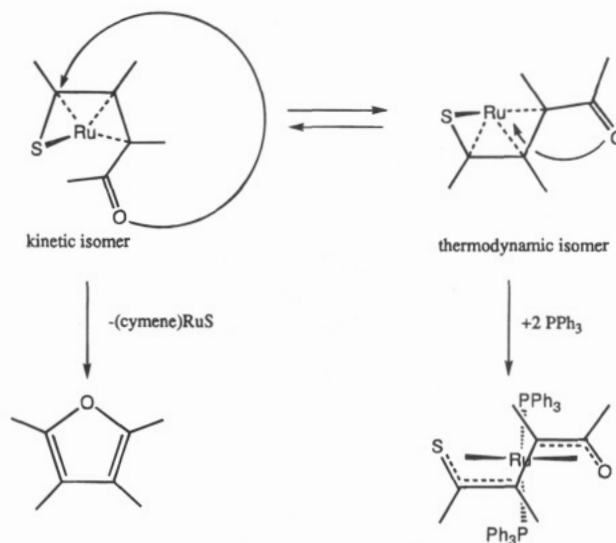
In this study we have examined the thermal fragmentation of acyl thiolate complexes of the type (ring) $\text{M}(\text{SC}_3\text{Me}_3\text{COMe})$ . While the (cymene)Ru derivative only gave insoluble materials, the thermolysis of the corresponding osmium compound, (cymene)Os( $\text{SC}_3\text{Me}_3\text{COMe}$ ) (**2**), proved very informative. Here it was established that the tetramethylfuran is indeed released prior to formation of the free cymene. Furthermore, two intermediates were observed, the second of which was identified as  $(\text{cymene})_3\text{Os}_3\text{S}_2$ . This species is more stable with respect to loss of cymene than the corresponding  $(\text{cymene})_3\text{Ru}_3\text{S}_2$ , which we had previously shown to decompose at room temperature.<sup>10</sup> Since the M:S ratio in the acyl thiolate is unity and it is otherwise in the isolated  $\text{Os}_3\text{S}_2$  cluster, it is proposed that the other intermediate (compound **3**) has an Os:S ratio of 1:1. Cluster **3** is proposed to arise via aggregation of the highly reactive entity (cymene)OsS (Scheme 4), a species we propose is structurally analogous to the imido complexes (cymene)Os(NR) (R = 2,6-dimethylphenyl, *tert*-butyl).<sup>17</sup> It is interesting that the Ru and Os compounds decompose to give trimetallic clusters while the Rh and Ir acyl thiolates give the cubane clusters.<sup>18</sup>

Attempts were made to intercept intermediates in these fragmentation processes by employing  $\text{PPh}_3$  as a trapping agent. For the Ru case,  $\text{PPh}_3$  completely changed the course of the reaction and no tetramethylfuran was generated. Instead we obtained the structurally unusual  $\eta^6$ -acyl thiolate complex **5**. The kinetics



**Figure 6.** Chem 3D view of the acyl thiolato ligand in  $\text{Ru}(\eta^6\text{-SC}_3\text{Me}_3\text{COMe})(\text{PPh}_3)_2$  showing that the ligand conformation corresponds to the thermodynamic isomer (see Scheme 1).

Scheme 5



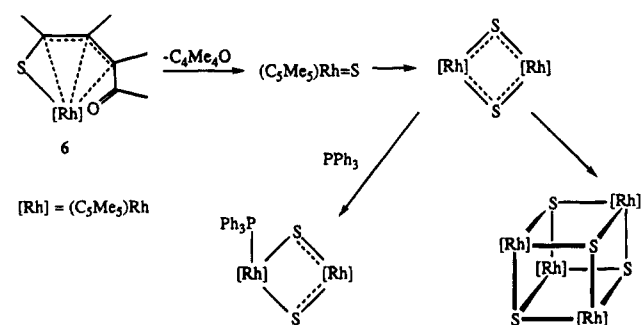
indicate that **1** exists in equilibrium with a reactive intermediate via a pathway that becomes rate limiting at high  $[\text{PPh}_3]$ . We propose that this unimolecular step involves the formation of  $(\eta^4\text{-cymene})\text{Ru}(\eta^6\text{-SC}_3\text{Me}_3\text{COMe})$ . The forward rate for this equilibration is far slower than the rate of isomerization of the acyl thiolate<sup>7</sup> and far faster than that for the unassisted thermal decomposition of (cymene)Ru( $\text{SC}_3\text{Me}_3\text{COMe}$ ). Insight into the nature of this pathway can be inferred from the crystal structure of **5**, which clearly arises from the thermodynamic isomer of the acyl thiolate (Figure 6). This result leads to a more global assessment of the reactivity of the acyl thiolates: the orientation of the carbonyl center determines the decomposition pathway. Thus, the carbonyl in the kinetic isomer is oriented correctly for cyclization, giving tetramethylfuran, while the carbonyl in the thermodynamic isomer cannot cyclize but instead binds to ruthenium to give the  $\eta^6$ -acyl thiolate complex which is trapped by  $\text{PPh}_3$  (Scheme 5).

The use of  $\text{PPh}_3$  allowed us to trap an intermediate in the thermal fragmentation of  $(\text{C}_5\text{Me}_5)\text{Rh}(\text{SC}_3\text{Me}_3\text{COMe})$  (**6**) (Scheme 6). Kinetic measurements show that trapping occurs after the rate-limiting step. The yield of the tetramethylfuran remained high, but no cubane cluster forms. Instead, we observed the formation of  $(\text{C}_5\text{Me}_5)_2\text{Rh}_2\text{S}_2(\text{PPh}_3)$ , a compound spectroscopically similar to  $(\text{C}_5\text{Me}_5)_2\text{IrRhS}_2(\text{PMe}_3)$ , a precursor to  $(\text{C}_5\text{Me}_5)_4\text{Ir}_2\text{Rh}_2\text{S}_4$ .<sup>4</sup> The formation of this compound implies that the cubane forms via the intermediacy of

(17) Michelman, R. I.; Andersen, R. A.; Bergman, R. G. *J. Am. Chem. Soc.* **1991**, *113*, 5100.

(18) We have never observed compounds of the type (arene) $_4\text{M}_4\text{S}_4$  for M = Ru, Os from reactions of [(cymene)MCl<sub>2</sub>]<sub>2</sub> with S<sup>2-</sup> sources.<sup>10</sup>

Scheme 6



$(\text{C}_5\text{Me}_5)_2\text{Rh}_2\text{S}_2$ . Analogous to the Ru and Os cases we propose that the precursor to this dirhodium species is  $(\text{C}_5\text{Me}_5)\text{RhS}$ .

### Experimental Section

**Materials and Methods.** The experiments were conducted by following protocols described in previous publications.<sup>6,7</sup> The preparations of  $(\text{C}_5\text{Me}_5)\text{Rh}(\text{SC}_3\text{Me}_3\text{COMe})$  (**7**),<sup>6</sup>  $(\text{C}_5\text{Me}_5)\text{Rh}(d_2\text{-SC}_3\text{Me}_3\text{COMe})$ ,<sup>6</sup>  $(\text{cymene})_3\text{Os}_3\text{S}_2(\text{PF}_6)_2$ ,<sup>10</sup> and (ring)Ru( $\text{SC}_3\text{Me}_3\text{COMe}$ ) (ring = cymene, tetramethylthiophene)<sup>7</sup> followed literature methods.  $[(\text{C}_5\text{Me}_5)\text{Ir}(\text{C}_4\text{Me}_4\text{S})](\text{CF}_3\text{SO}_3)_2$  was prepared from  $[(\text{C}_5\text{Me}_5)\text{IrCl}_2]_2$  analogously to the literature method for the  $\text{BF}_4^-$  salt.<sup>19</sup>

IR spectra were acquired using a Mattson Galaxy Series FTIR 3000 spectrometer. NMR spectra were collected on the General Electric instruments GN300NB and QE300 and the Varian spectrometers U400 and XL200. Field desorption and electron impact mass spectra were measured on a VG 70-VSE. Elemental analyses were performed by the University of Illinois Microanalytical Laboratory. Thermogravimetric analyses were measured by the University of Illinois Microanalytical Laboratory using a Perkin-Elmer Thermal Systems VII.

**Thermal Decomposition of  $(\text{cymene})\text{Ru}(\text{SC}_3\text{Me}_3\text{COMe})$ .** A solution of 50.6 mg (0.13 mmol) of **1** in 10 mL of toluene was heated at reflux for 12 h. The dark orange solution became colorless, and a fine gray powder formed. The volatile products were removed under vacuum. Anal. Found for the residue: C, 15.55; H, 3.09; Ru, 45.29; S, 13.64 (giving  $\text{C}_3\text{H}_7\text{-RuS}$ ). The thermal decomposition was conducted in toluene- $d_8$  at 95 °C and monitored by  $^1\text{H}$  NMR spectroscopy. The thermolysis resulted in the formation of 70–80% cymene and tetramethylfuran and the gray precipitate. The kinetics of the thermolysis of **1** were studied at 95 °C by integrated  $^1\text{H}$  NMR spectra recorded at 30 min to 1 h intervals. The rate of disappearance of one of the methyl singlets of **1** was measured vs an internal standard ( $\text{Ph}_2\text{CH}_2$ , singlet at 3.70 ppm) and was found to be first order ( $k = 3.5 \times 10^{-6} \text{ s}^{-1}$ ).

**Thermal Decomposition of  $(\text{C}_4\text{Me}_4\text{S})\text{Ru}(\text{SC}_3\text{Me}_3\text{COMe})$ .** A solution of 12 mg (30  $\mu\text{mol}$ ) of  $(\text{C}_4\text{Me}_4\text{S})\text{Ru}(\text{SC}_3\text{Me}_3\text{COMe})$  and biphenyl in 0.5 mL of  $\text{C}_6\text{D}_6$  was heated to 70 °C in a sealed tube. After 17 h, the decomposition was complete, as shown by  $^1\text{H}$  NMR spectroscopy. A dark solid precipitated and the solution became dark brown. On the basis of  $^1\text{H}$  NMR integrations, the yield of tetramethylthiophene was 100%, while the yield of tetramethylfuran was only 28%. After removal of the volatile material the residue was washed with hexane and dried under vacuum. Anal. Found: C, 38.79; H, 4.95; Ru, 31.04; S, 10.75.

**$(\text{cymene})\text{Os}(\text{C}_4\text{Me}_4\text{S})(\text{BF}_4)_2$ .** A slurry of 393 mg (2.02 mmol) of  $\text{AgBF}_4$  in 20 mL of  $\text{CH}_2\text{Cl}_2$  was treated with a solution of 380 mg (0.481 mmol) of  $[(\text{cymene})\text{OsCl}_2]_2$  in 20 mL of  $\text{CH}_2\text{Cl}_2$ . The reaction mixture was stirred for 2 h and then filtered to remove  $\text{AgCl}$ . The yellow filtrate of  $(\text{cymene})\text{Os}(\text{BF}_4)_2$  was treated dropwise with 300  $\mu\text{L}$  (291 mg, 2.08 mmol) of  $\text{C}_4\text{Me}_4\text{S}$ ,

resulting in a yellow precipitate. After 3 h, the solvent volume was reduced to 5 mL and the yellow solid was collected by filtration. The yellow precipitate was washed with ~3 mL of  $\text{CH}_2\text{Cl}_2$ . The solid was recrystallized from 4 mL of acetone by dilution with 7 mL of  $\text{CHCl}_3$ . Yield: 449 mg (73% yield).  $^1\text{H}$  NMR (acetone- $d_6$ ):  $\delta$  7.21 (d, 2H), 7.04 (d, 2H), 3.1 (sept, 1H), 2.67 (s, 6H), 2.60 (s, 6H), 2.56 (s, 3H), 1.40 (d, 6H). Anal. Calcd (found) for  $\text{C}_{18}\text{H}_{26}\text{B}_2\text{F}_8\text{OsS}$ : C, 33.87 (33.62); H, 4.11 (4.23).

**Preparation of  $(\text{cymene})\text{Os}(\text{SC}_3\text{Me}_3\text{COMe})$  (**2**).** A Schlenk flask was charged with 0.140 g (0.219 mmol) of solid  $[(\text{cymene})\text{Os}(\text{C}_4\text{Me}_4\text{S})(\text{BF}_4)_2]$ , and 18.26 mL of 0.030 M aqueous KOH solution (0.548 mmol) was added with stirring. The osmium salt initially dissolved. After 2 h, a yellow precipitate was observed in the solution. The reaction mixture was stirred for 12 h, and more precipitate was obtained. The volume of the solution was reduced to 10 mL under vacuum, and the yellow product was collected by filtration and washed with a few milliliters of  $\text{H}_2\text{O}$ . Recrystallization from acetone and  $\text{H}_2\text{O}$  gave yellow crystalline  $(\text{cymene})\text{Os}(\text{SC}_3\text{Me}_3\text{COMe})$  (**2**). Yield: 70 mg (67%).  $^1\text{H}$  NMR ( $\text{C}_6\text{D}_6$ ; 20 °C):  $\delta$  4.85 (d, 1H), 4.64 (br s, 2H), 4.25 (d, 1H), 2.38 (s, 3H), 2.20 (br s, 1H), 1.79 (s, 3H), 1.65 (s, 3H), 1.50 (s, 3H), 1.02 (br s, 6H). IR (KBr):  $\nu_{\text{CO}}$  1662  $\text{cm}^{-1}$ . Anal. Calcd (found) for  $\text{C}_{18}\text{H}_{26}\text{OOS}$ : C, 44.98 (44.33); H, 5.54 (5.50); S, 6.67 (6.38); Os, 25.81 (27.84).

**Thermal Decomposition of  $(\text{cymene})\text{Os}(\text{SC}_3\text{Me}_3\text{COMe})$ .** A yellow solution of 20.0 mg (0.042 mmol) of **2** in toluene- $d_8$  was sealed in a NMR tube under vacuum. After thermolysis for 10 h at 75 °C,  $^1\text{H}$  NMR spectroscopy showed that **4**, free cymene, and tetramethylfuran had formed. Filtration to remove the black solid and evaporation of the solution gave a dark green powder, which was identified by FD-MS as  $(\text{cymene})_3\text{Os}_3\text{S}_2$ . A toluene solution of **4** was treated with an excess of HOTf to give  $[(\text{cymene})_3\text{Os}_3\text{S}_2](\text{OTf})_2$  as a red oil, with its  $^1\text{H}$  NMR spectrum in acetone- $d_6$  matching that of the known  $(\text{cymene})_3\text{Os}_3\text{S}_2(\text{PF}_6)_2$ .<sup>10</sup>  $^1\text{H}$  NMR of **4** (toluene- $d_8$ , 20 °C): 5.69 (d, 2H), 5.62 (d, 2H), 5.42 (d, 2H), 5.27 (d, 2H), 2.22 (m, 2H), 2.11 (s, 3H), 1.89 (s, 6H), 1.19 (d, 6H), 1.14 (d, 12H). FD-MS:  $m/z$  1036.  $^1\text{H}$  NMR of  $(\text{cymene})_3\text{Os}_3\text{S}_2(\text{OTf})_2$  (acetone- $d_6$ ): 6.45 (m, 4H), 2.85 (m, 1H), 2.67 (s, 3H), 1.35 (s, 6H).

A solution of 7.6 mg (15.8  $\mu\text{mol}$ ) of **2** in 0.65 mL of toluene- $d_8$  was sealed in a NMR tube under vacuum with  $\text{Ph}_2\text{CH}_2$  as a standard. The sample was maintained at 95 °C, and integrated NMR spectra were recorded at 5–10 min intervals for 2 h, showing the disappearance of the methyl signal of **2** and formation of the methyl signals of **2** and  $(\text{cymene})_3\text{Os}_3\text{S}_2$  (**4**). The rate of disappearance of **2** was found to be first order with  $k_1 = 6.20 \times 10^{-4} \text{ s}^{-1}$ .  $^1\text{H}$  NMR of **3** (toluene- $d_8$ , 20 °C):  $\delta$  5.35 (br d, 2H), 5.20 (br d, 2H), 5.12 (d, 4H), 4.93 (d, 4H), 2.20 (m, 3H), 2.08 (observed by solvent), 1.93 (s, 6H), 1.28 (d, 6H), 1.19 (d, 12H).

The kinetics of these reactions were analyzed as follows. The rate for the loss of **2** is

$$d[\mathbf{2}]/dt = -k_1[\mathbf{2}] \quad (1a)$$

The rate equation for **3** is

$$d[\mathbf{3}]/dt = k_1[\mathbf{2}] - (k_2 + k_3)[\mathbf{3}] \quad (2a)$$

Dividing both sides of eq 2a by **[3]** gives

$$d[\mathbf{3}]/[\mathbf{3}]dt = k_1[\mathbf{2}]/[\mathbf{3}] - (k_2 + k_3) \quad (3a)$$

which can be rewritten as

$$[\mathbf{3}]/[\mathbf{3}] = k_1[\mathbf{2}]/[\mathbf{3}] - (k_2 + k_3) \quad (4a)$$

where  $[\mathbf{3}']$  is  $d[\mathbf{3}]/dt$ . Using the Cricket Graph III graphics program, we fitted our data for **[3]** vs  $t$  using a fourth-order polynomial. The time derivative of this polynomial was then taken as  $[\mathbf{3}']$ . A plot of  $[\mathbf{3}']/[\mathbf{3}]$  vs  $[\mathbf{2}]/[\mathbf{3}]$  gave a straight line

(19) Russell, M. J. H.; White, C.; Maitlis, P. M. *J. Chem. Soc., Dalton Trans.* 1978, 857.

with slope  $k_1 = 6.20 \times 10^{-4} \text{ s}^{-1}$  and an intercept  $(k_2 + k_3) = 9.23 \times 10^{-4} \text{ s}^{-1}$ .

Similarly, the rate equation for **4** is

$$d[4]/dt = k_2[3] - k_4[4] \quad (5a)$$

Dividing both sides of the above eq by [4] gives

$$d[4]/[4]dt = k_2[3]/[4] - k_4 \quad (6a)$$

Equation 6a can be rewritten as

$$[4]'/[4] = k_2[3]/[4] - k_4 \quad (7a)$$

A plot of  $[4]'/[4]$  vs  $[3]/[4]$  gave a straight line with slope  $k_2 = 3.32 \times 10^{-4} \text{ s}^{-1}$ ; therefore,  $k_3 = 5.98 \times 10^{-4} \text{ s}^{-1}$  was obtained from  $(k_2 + k_3) = 9.32 \times 10^{-4} \text{ s}^{-1}$ .

**(cymene)<sub>3</sub>Os<sub>3</sub>S<sub>2</sub> (4).** A slurry of 90 mg (67.8 μmol) of [(cymene)<sub>3</sub>Os<sub>3</sub>S<sub>2</sub>](PF<sub>6</sub>)<sub>2</sub> in 10 mL of benzene was treated with a solution of 28 mg (149 μmol) of (C<sub>5</sub>H<sub>5</sub>)<sub>2</sub>Co in 20 mL of benzene, resulting in a green slurry. After 5 h the green solution was filtered from the (C<sub>5</sub>H<sub>5</sub>)<sub>2</sub>CoPF<sub>6</sub> and the solvent was removed. The green solid was heated to 50 °C under vacuum for 3 h to remove any unreacted (C<sub>5</sub>H<sub>5</sub>)<sub>2</sub>Co. <sup>1</sup>H NMR (toluene-*d*<sub>8</sub>, 20 °C): 5.69 (d, 2H), 5.62 (d, 2H), 5.42 (d, 2H), 5.27 (d, 2H), 2.22 (m, 2H), 2.11 (s, 3H), 1.89 (s, 6H), 1.19 (d, 6H), 1.14 (d, 12H). UV-vis (CH<sub>3</sub>CN; λ, nm (log ε)): 340 (2.94), 504 (2.55), 616 (2.51). Anal. Calcd (found) for C<sub>30</sub>H<sub>42</sub>Os<sub>3</sub>S<sub>2</sub>: C, 34.74 (34.87); H, 4.08 (4.15); S, 6.18 (6.32).

**Ru(η<sup>6</sup>-SC<sub>3</sub>Me<sub>3</sub>COMe)(PPh<sub>3</sub>)<sub>2</sub> (5).** A solution of 110 mg (0.28 mmol) of **1** and 150 mg (0.57 mmol) of PPh<sub>3</sub> in 15 mL of toluene was heated to 70 °C. The orange color of the solution intensified, and after 24 h the solvent was evaporated under vacuum. The orange solid Ru(η<sup>6</sup>-SC<sub>3</sub>Me<sub>3</sub>COMe)(PPh<sub>3</sub>)<sub>2</sub> (**5**) was washed with hexane. Yield: 196 mg (90%). <sup>1</sup>H NMR (C<sub>6</sub>D<sub>6</sub>): δ 7.7 (m, 12H), 6.9 (m, 18H), 1.97 (d, *J* = 2.9 Hz, 3H), 1.41 (d, *J* = 2.9 Hz, 3H), 1.16 (d, *J* = 2.2 Hz, 3H), 0.96 (d, *J* = 3.8 Hz, 3H). <sup>13</sup>C{<sup>1</sup>H} NMR (CD<sub>2</sub>Cl<sub>2</sub>): δ 152.4 (s), 138.0 (d, *J* = 35.9 Hz), 134.6 (d, *J* = 10.7 Hz), 129.1 (m), 127.5 (m), 120.3 (d, *J* = 6.1 Hz), 106.4 (d, *J* = 6.9 Hz), 82.8 (d, *J* = 12.2 Hz), 23.6 (s), 19.0 (s), 13.4 (s), 8.0 (d, *J* = 1.5 Hz). <sup>31</sup>P{<sup>1</sup>H} NMR (C<sub>6</sub>D<sub>6</sub>): δ 53.4 (d, *J* = 34 Hz), 40.4 (d, *J* = 34 Hz). Anal. Calcd (found) for C<sub>44</sub>H<sub>42</sub>OP<sub>2</sub>RuS: C, 67.59 (67.01); H, 5.42 (5.24); P, 7.92 (7.78); Ru, 12.93 (11.15); S, 4.10 (4.46). FD-MS: *m/z* 782.

The rates of the conversion of **1** to **5** were investigated by <sup>1</sup>H NMR spectroscopy (C<sub>6</sub>D<sub>6</sub>) in vacuum-sealed NMR tubes. The samples were maintained at 70 °C, and integrated NMR spectra of the disappearance of the methyl signal of **1** were recorded at 15–30 min intervals for 7 h. The reactions were conducted in duplicate under the following initial conditions:

	expt i	expt ii
[1] <sub>0</sub> , M	0.02	0.02
[PPh <sub>3</sub> ] <sub>0</sub> , M	0.4	0.8

Both experiments gave the same linear plots of ln[1] vs *t* with the slope  $k_1 = 5.7 \times 10^{-5} \text{ s}^{-1}$ . Thus, the reaction is first order in **1** at high [PPh<sub>3</sub>].

For experiments where [PPh<sub>3</sub>]<sub>0</sub> < 0.1 M, plots of ln[1] vs *t* were not linear. A more complete test of the mechanism was based on a rate law developed from the steady-state approximation:

$$-\frac{d[1]}{dt} = \frac{k_1[1]}{1 + \frac{k_{-1}}{k_2[\text{PPh}_3]}} \quad (1b)$$

When [PPh<sub>3</sub>] = 2[1], the rate expression (1b) can be simplified as follows:

$$-\frac{d[1]}{dt} = \frac{k_1[1]}{1 + \frac{k_{-1}}{2k_2[1]}} = \frac{2k_1k_2[1]^2}{k_{-1} + 2k_2[1]} \quad (2b)$$

Equation 2b can be rewritten as

$$-(k_{-1} + 2k_2[1]) d[1] = 2k_1k_2[1]^2 dt \quad (3b)$$

Dividing both sides of eq 3b by  $k_2[1]^2$  gives

$$-\left[ \frac{k_{-1}}{k_2[1]^2} + \frac{2}{[1]} \right] d[1] = 2k_1 dt \quad (4b)$$

which upon integration and rearrangement gives

$$\frac{1}{[1]} = \frac{2k_2}{k_{-1}}(k_1t + \ln[1]) + C \quad (5b)$$

This model was tested by the reaction of benzene solutions of **1** (0.02 M) with 2 equiv of PPh<sub>3</sub> (0.04 M). The reaction was monitored by <sup>1</sup>H NMR spectroscopy at 70 °C. Plots of  $[1]^{-1}$  vs  $k_1t + \ln[1]$  were linear with a slope of  $2k_2/k_{-1}$  (=159.6 M<sup>-1</sup>) (Figure 7). This value can be substituted into eq 1b together with the value for  $k_1$  ( $5.7 \times 10^{-5} \text{ s}^{-1}$ ), giving the rate equation (6b). This equation defines conditions where the kinetics

$$-\frac{d[1]}{dt} = \frac{(5.7 \times 10^{-5})[1]}{1 + \frac{0.0125}{[\text{PPh}_3]}} \quad (6b)$$

should appear first order in [1], i.e. [PPh<sub>3</sub>] > 0.25 M. This is consistent with the results obtained above, in which the reactions of **1** with [PPh<sub>3</sub>]<sub>0</sub> = 0.4 or 0.8 M are first order in [1].

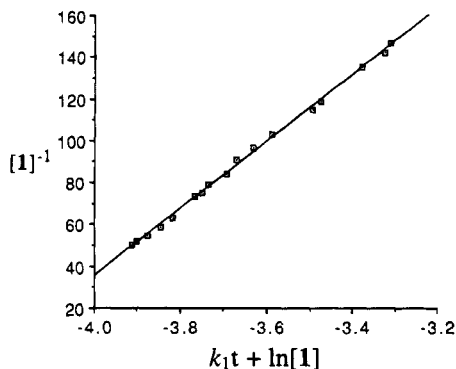
**Preparation of (C<sub>5</sub>Me<sub>5</sub>)Ir(SC<sub>3</sub>Me<sub>3</sub>COMe) (7).** A Schlenk flask was charged with 0.106 g (0.140 mmol) of solid [(C<sub>5</sub>Me<sub>5</sub>)Ir(C<sub>4</sub>Me<sub>4</sub>S)](OTf)<sub>2</sub> and 11.65 mL of 0.030 M aqueous KOH solution (0.350 mmol) was added with stirring. After 0.5 h, a yellow precipitate was observed in the solution. The reaction mixture was stirred for 24 h, and more precipitate was obtained. The yellow product collected by filtration was washed with 30 mL of H<sub>2</sub>O. The yellow solid was extracted into 20 mL of Et<sub>2</sub>O and filtered to remove KOTf. Recrystallization from acetone and H<sub>2</sub>O gave yellow crystalline **7**. Yield: 40 mg (60%). <sup>1</sup>H NMR (toluene-*d*<sub>8</sub>): δ 2.28 (br, s, 3H), 2.13 (s, 3H), 1.50 (s, 3H), 1.49 (s, 15H), 1.35 (s, 3H). <sup>13</sup>C{<sup>1</sup>H} NMR (C<sub>6</sub>D<sub>6</sub>): 203.40 (s), 91.16 (s), 90.27 (s), 86.01 (s), 62.65 (s), 27.09 (s), 22.00 (s), 20.92 (s), 13.63 (s), 8.70 (s). IR (KBr): ν<sub>CO</sub> 1672 cm<sup>-1</sup>. FAB-MS *m/z* 483 (M<sup>+</sup>). Anal. Calcd (found) for C<sub>18</sub>H<sub>27</sub>IrOS: C, 44.70 (44.84); H, 5.63 (5.78).

#### Thermal Decomposition of (C<sub>5</sub>Me<sub>5</sub>)Ir(SC<sub>3</sub>Me<sub>3</sub>COMe).

A solution of 0.711 g (1.47 mmol) of **7** in 10 mL of toluene was heated for ~10 h. Cooling the reaction mixture to room temperature produced red-black crystals of (C<sub>5</sub>Me<sub>5</sub>)<sub>4</sub>Ir<sub>4</sub>S<sub>4</sub>. Yield: 225 mg (59%). <sup>1</sup>H NMR (C<sub>6</sub>D<sub>6</sub>): δ 1.71 (s).<sup>4</sup> The kinetics of this decomposition reaction were monitored in toluene-*d*<sub>8</sub> by observing the disappearance of one of the methyl singlets of **7** in the <sup>1</sup>H NMR spectrum at 90 °C. The rate was found to be first order with  $k_1 = 5.7 \times 10^{-5} \text{ s}^{-1}$ .

#### Thermal Decomposition of (C<sub>5</sub>Me<sub>5</sub>)Rh(SC<sub>3</sub>Me<sub>3</sub>COMe).

A solution of 1.19 g (3.02 mmol) of **6** in 20 mL of toluene was heated to reflux. Over the course of ~12 h the red color of the solution changed to dark purple. The reaction solution was placed in a -20 °C freezer for 2 days followed by filtration to give purple-black crystals of (C<sub>5</sub>Me<sub>5</sub>)<sub>4</sub>Rh<sub>4</sub>S<sub>4</sub>. Yield: 573 mg (70%). <sup>1</sup>H NMR (C<sub>6</sub>D<sub>6</sub>): δ 1.72 (s). FD-MS: *m/z* 1080 (M<sup>+</sup>). Anal. Calcd (found) for C<sub>40</sub>H<sub>60</sub>Rh<sub>4</sub>S<sub>4</sub>: C, 44.45 (44.62); H, 5.60 (5.57); Rh, 38.09 (37.99); S, 11.87 (11.79).



**Figure 7.** Plot of  $[1]^{-1}$  vs  $k_1t + \ln[1]$ , where the slope is  $2k_2/k_{-1}$  ( $=159.6 \text{ M}^{-1}$ ).

A sample of 109 mg (0.28 mmol) of **6** was loaded into a Schlenk tube, and the tube was fitted with a tared trap. The sample was heated at 120 °C for 8 h under a nitrogen atmosphere. The system was then placed under vacuum, and a colorless product was condensed into the liquid-nitrogen-filled trap. Yield of tetramethylfuran ( $\text{C}_4\text{Me}_4\text{O}$ ): 27.2 mg (79%).  $^1\text{H}$  NMR of  $\text{C}_4\text{Me}_4\text{O}$  ( $\text{CCl}_4$ ):  $\delta$  2.09 (s, 6 H), 1.77 (s, 6 H).  $^{13}\text{C}\{^1\text{H}\}$  NMR of  $\text{C}_4\text{Me}_4\text{O}$  ( $\text{CCl}_4$ ):  $\delta$  142.86 (s), 113.70 (s), 10.87 (s), 7.96 (s). High-resolution EI-MS:  $m/z$  124.088 020 (calcd for  $\text{C}_8\text{H}_{12}\text{O}$   $m/z$  124.088 815). Thermolysis of  $(\text{C}_5\text{Me}_5)\text{Rh}(\text{d}_2\text{-SC}_3\text{Me}_3\text{COMe})$  gave the dideuteriotetramethylfuran 3,4-( $\text{CH}_2\text{D}$ )<sub>2</sub>-2,5- $\text{Me}_2\text{C}_4\text{O}$ .  $^1\text{H}$  NMR ( $\text{C}_6\text{D}_6$ ):  $\delta$  2.04 (s, 6 H), 1.70 (t, 4 H).

The kinetics of the thermolysis of **6** were determined from integrated  $^1\text{H}$  NMR spectra. The rate of disappearance of one of the methyl singlets of **6** was measured vs the internal standard  $\text{Ph}_2\text{CH}_2$  (3.70 ppm). The thermolyses were conducted at 80, 90, and 100 °C. The rate of disappearance of **6** was found to be first order with rate constants  $1.92 \times 10^{-5} \text{ s}^{-1}$  (80 °C),  $4.55 \times 10^{-5} \text{ s}^{-1}$  (90 °C), and  $6.50 \times 10^{-5} \text{ s}^{-1}$  (100 °C).

**Thermal Decomposition of  $(\text{C}_5\text{Me}_5)\text{Rh}(\text{SC}_3\text{Me}_3\text{COMe})$  in the Presence of  $\text{PPh}_3$ .** In a sealed NMR tube, a solution of 6.6 mg (16.7  $\mu\text{mol}$ ) of **6** and 11.1 mg (42.3  $\mu\text{mol}$ ) of  $\text{PPh}_3$  in toluene- $d_8$  was heated at 85 °C for 24 h. The  $^1\text{H}$  NMR spectrum showed that tetramethylfuran was formed, but  $(\text{C}_5\text{Me}_5)_4\text{Rh}_4\text{S}_4$  was not observed. The  $^1\text{H}$  NMR spectrum instead showed a superimposed singlet and doublet at 1.55 ppm ( $J_{\text{H-P}} = 3.2 \text{ Hz}$ ). The  $^{31}\text{P}\{^1\text{H}\}$  NMR spectrum consisted of one doublet at 58.2 ppm ( $J_{\text{P-Rh}} = 224 \text{ Hz}$ ),<sup>4</sup> and small amounts of  $\text{SPPH}_3$  (43.0 ppm) were also observed. This decomposition was monitored as follows: A toluene solution of **6** and 3 equiv of  $\text{PPh}_3$  in a sealed tube was heated to 90 °C in the NMR probe. The disappearance of **6** was found to be first order with a rate constant of  $3.5 \times 10^{-5} \text{ s}^{-1}$ . In the absence of  $\text{PPh}_3$ , the rate

constant was  $4.5 \times 10^{-5} \text{ s}^{-1}$ , suggesting that the decomposition of **6** is the rate-determining step. In a control experiment a refluxing toluene solution of  $(\text{C}_5\text{Me}_5)_4\text{Rh}_4\text{S}_4$  was shown to be unreactive toward 4 equiv of  $\text{PPh}_3$  after 3 days.

**Crystallographic Characterization of  $\text{Ru}(\eta^6\text{-SC}_3\text{Me}_3\text{COMe})(\text{PPh}_3)_2$ .** Orange-red, translucent crystals were obtained by layering a toluene solution with hexane. The crystal was mounted to a thin glass fiber using epoxy. Unit cell parameters were obtained from the least-squares fit of 25 reflections with  $9.5^\circ < 2\theta < 20^\circ$ . The space group  $P2_1/c$  (No. 14) was determined according to systematic absences and verified by successful refinement. Lorentz and polarization correction as well as numerical absorption correction were applied to the intensity data. The structure was solved by direct methods (SHELXS-86).<sup>20</sup> Correct positions for Ru, S, and P were deduced from the electron density map. Subsequent least-squares difference Fourier calculations (SHELX 76)<sup>21</sup> revealed positions for oxygen and all carbon atoms. The positions of the hydrogen atoms were calculated for idealized distances (0.96 Å) with common thermal parameters for each type of hydrogen. Anisotropic thermal parameters were used for all non-hydrogen atoms. Successful convergence was indicated by the maximum shift/error for the final refinement cycle. The highest peak in the final difference map was close to Ru.

**Acknowledgment.** This research was supported by the Division of Chemical Sciences, Office of Basic Energy Sciences, Office of Energy Research, Department of Energy, through Contract No. DOE DEFG02-90ER14146. H.K. thanks "Studienstiftung des deutschen Volkes" and BASF for a postdoctoral fellowship during the course of this research. A.V. is supported by the National Science Foundation through Grant No. CHE-92-12178.

**Supplementary Material Available:** Tables of data collection and refinement, bond angles and distances, thermal parameters, and atomic coordinates for **5** and text giving rate equations for the reaction of (cymene) $\text{Ru}(\text{SC}_3\text{Me}_3\text{COMe})$  and  $\text{PPh}_3$  (9 pages). Ordering information is given on any current masthead page.

OM940122Y

(20) (a) Stout, G. H.; Jensen, L. H. *X-Ray Structure Determination, a Practical Guide*; Macmillan: New York, 1968. (b) Sheldrick, G. M. SHELXS-86. In *Crystallographic Computing 3*; Sheldrick, G. M., Kruger, C., Goddard, R., Eds.; Oxford University Press: Oxford, U.K., 1985; pp 175-189.

(21) Sheldrick, G. M. SHELX-76, a Program for Crystal Structure Determination; University Chemical Laboratory, Cambridge, U.K., 1976.

# Reactions of a Cyclotrisilane with Olefins and Dienes: Evidence for an Equilibrium between Silylenes and a Cyclotrisilane<sup>†</sup>

Johannes Belzner,<sup>\*,‡</sup> Heiko Ihmels,<sup>‡</sup> Boris O. Kneisel,<sup>§</sup> Robert O. Gould,<sup>§,||</sup> and Regine Herbst-Irmer<sup>§</sup>

*Institut für Organische Chemie der Georg-August-Universität Göttingen, Tammannstrasse 2, D-37077 Göttingen, Germany, and Institut für Anorganische Chemie der Georg-August-Universität Göttingen, Tammannstrasse 4, D-37077 Göttingen, Germany*

Received May 17, 1994<sup>®</sup>

Various new siliranes were synthesized by reaction of the cyclotrisilane *cyclo*-(Ar<sub>2</sub>Si)<sub>3</sub> (Ar = 2-(Me<sub>2</sub>NCH<sub>2</sub>)C<sub>6</sub>H<sub>4</sub>; **1a**) with terminal and strained internal olefins under mild thermal conditions. The thermolysis of siliranes Ar<sub>2</sub>SiCH<sub>2</sub>CHR (**3a**, R = *n*-propyl; **3b**, R = *n*-butyl) indicated these compounds to be in a thermal equilibrium with cyclotrisilane **1a** and the corresponding alkene; this observation provides evidence for an equilibrium between the silylene Ar<sub>2</sub>Si: (**2a**) and cyclotrisilane **1a** and, moreover, proves that free silylenes are involved in silylene transfer reactions of **1a**. Reaction of **1a** with conjugated dienes resulted, presumably via vinylsiliranes, in the formation of the expected 1,4-cycloaddition products in high yield. The solid-state structures of silaindane **14** and silanorbornene **17a** were determined by single-crystal X-ray diffraction (**14**, monoclinic, C2/c, *a* = 36.255(7) Å, *b* = 8.877(2) Å, *c* = 14.966(2) Å, β = 109.60(1)°, *Z* = 8; **17a**, monoclinic, C2/c, *a* = 14.155(5) Å, *b* = 13.336(4) Å, *c* = 23.339(8) Å, β = 107.16(2)°, *Z* = 8).

## Introduction

In 1972, Lambert and Seyferth<sup>1</sup> reported the first isolation of stable siliranes (silacyclopropanes), which were synthesized by intramolecular closure of a C–C bond of acyclic precursors. Later it was demonstrated that siliranes also are formed by addition of thermally or photolytically generated silylenes to substituted olefins<sup>2</sup> and even ethene.<sup>3</sup> A major drawback of this method is the low stability of the siliranes under the conditions employed for silylene generation, which frequently gives rise to the isolation of isomerized compounds. This is especially true for the addition of silylenes to conjugated dienes: initially formed vinylsiliranes almost inevitably undergo subsequent rearrangements.<sup>4</sup> A third synthetically useful approach to

stable siliranes makes use of the reductive dehalogenation of dihalosilanes by lithium metal in the presence of olefins.<sup>2f,3,5</sup>

We have recently shown that cyclotrisilane **1a**<sup>6</sup> serves as an effective synthetic equivalent for silylene **2a**: it transfers all three of its silylene subunits to various unsaturated substrates such as ketones<sup>6</sup> or alkynes<sup>7</sup> under mild thermal conditions. It remained uncertain whether free silylenes are involved in these reactions. We now have investigated the reactivity of **1a** toward olefins, both to examine the aptitude of **1a** as a precursor for new siliranes and to obtain some insight into possible mechanisms of the unusual silylene transfer reactions of this cyclotrisilane.

## Results and Discussion

When **1a** was heated at 40 °C for 12 h with 1-pentene in C<sub>6</sub>D<sub>6</sub>, silirane **3a** was formed quantitatively, as shown by <sup>1</sup>H NMR spectroscopy using poly(dimethylsiloxane) as the internal integration standard. A large excess of olefin (>10 equiv per silylene unit of **1a**) was necessary in order to drive the reaction to completion. Furthermore, it was essential to perform this reaction in quite concentrated solution (>0.1 mol/L); otherwise, appreciable amounts of unidentified byproducts were formed. Even under these conditions, isolation of analytically pure silirane **3a** from the reaction mixture was impossible due to its thermal instability. Spectroscopically pure samples<sup>8</sup> of **3a** could be obtained by rapid removal of excess olefin and solvent in vacuo at room tempera-

<sup>†</sup> Dedicated to Prof. Dr. Wolfgang Lüttke on the occasion of his 75th birthday.

<sup>‡</sup> Institut für Organische Chemie der Georg-August Universität Göttingen.

<sup>§</sup> Institut für Anorganische Chemie der Georg-August Universität Göttingen.

<sup>||</sup> Permanent address: Department of Chemistry, West Mains Road, Edinburgh EH9 3JJ, Scotland.

<sup>®</sup> Abstract published in *Advance ACS Abstracts*, December 1, 1994.

(1) Lambert, R. L., Jr.; Seyferth, D. *J. Am. Chem. Soc.* **1972**, *94*, 9246.

(2) (a) Ishikawa, M.; Nakagawa, K.-I.; Kumada, M. *J. Organomet. Chem.* **1979**, *178*, 105. (b) Tortorelli, V. J.; Jones, M., Jr. *J. Am. Chem. Soc.* **1980**, *102*, 1425. (c) Seyferth, D.; Annarelli, D. C.; Duncan, D. P. *Organometallics* **1982**, *1*, 1288. (d) Tortorelli, V. J.; Jones, M., Jr.; Wu, S.-H.; Li, Z.-H. *Organometallics* **1983**, *2*, 759. (e) Ando, W.; Fujita, M.; Yoshida, H.; Sekiguchi, A. *J. Am. Chem. Soc.* **1988**, *110*, 3310. (f) Pae, D. H.; Xiao, M.; Chiang, M. Y.; Gaspar, P. P. *J. Am. Chem. Soc.* **1991**, *113*, 1281.

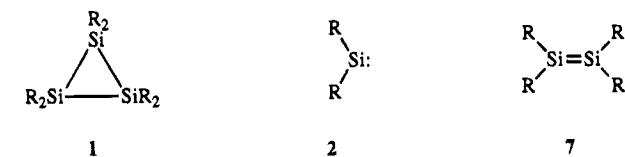
(3) Boudjouk, P.; Black, E.; Kumarathasan, R. *Organometallics* **1991**, *10*, 2095.

(4) For recent studies on the reactivity of silylenes with conjugated dienes, see: (a) Lei, D.; Hwang, R.-J.; Gaspar, P. P. *J. Organomet. Chem.* **1984**, *271*, 1. (b) Gaspar, P. P.; Lei, D. *Organometallics* **1986**, *5*, 1276. (c) Clarke, M. P.; Davidson, I. M. T. *J. Chem. Soc., Chem. Commun.* **1988**, 241. (d) Zhang, S.; Conlin, R. T. *J. Am. Chem. Soc.* **1991**, *113*, 4272.

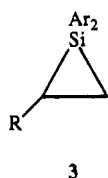
(5) Boudjouk, P.; Samaraweera, U.; Sooriyakumaran, R.; Chrisciel, J.; Anderson, K. R. *Angew. Chem.* **1988**, *100*, 1406; *Angew. Chem., Int. Ed. Engl.* **1988**, *27*, 1355.

(6) Belzner, J. *J. Organomet. Chem.* **1992**, *430*, C51.

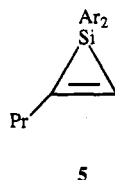
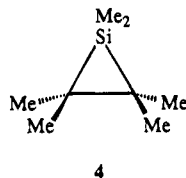
(7) Belzner, J.; Ihmels, H. *Tetrahedron Lett.* **1993**, 6541.



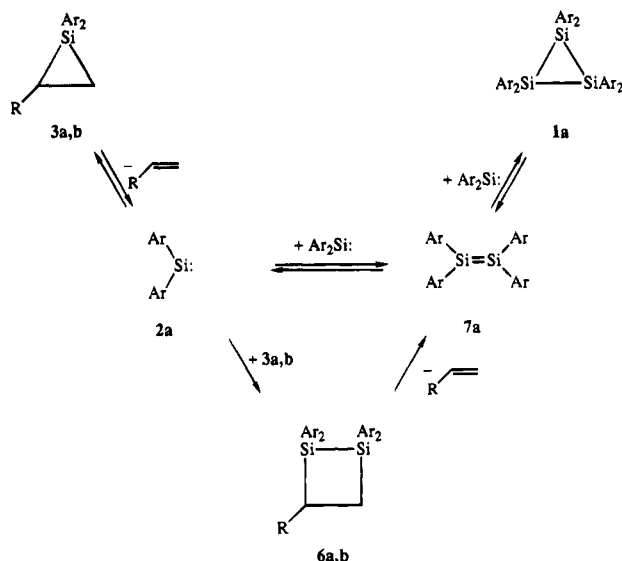
1a, 2a, 7a: R = 2-(Me<sub>2</sub>NCH<sub>2</sub>)C<sub>6</sub>H<sub>4</sub> (≡Ar)  
 1b, 2b, 7b: R = *t*-Bu  
 1c, 2c, 7c: R = H



3a, 6a: R = *n*-Pr  
 3b, 6b: R = *n*-Bu  
 3c, 6c: R = Ph



## Scheme 1



ture. Heating a concentrated solution of **3a**, which was prepared as described above, in C<sub>6</sub>D<sub>6</sub> for 5.5 h at 40 °C resulted in a mixture of **3a**, **1a**, and 1-pentene in a 1:1:3 ratio; this mixture could be converted back to **3a** by addition of excess olefin. Silirane **3b**, which was similarly prepared by reaction of **1a** with an excess of 1-hexene, exhibited an analogous partial retro reaction to cyclotrisilane **1a** and olefin. Both siliranes were obtained as highly air- and moisture-sensitive oils, which were identified mainly by their NMR spectra, especially the <sup>29</sup>Si NMR shift values, which fell into the high-field region typical for siliranes<sup>9</sup> (**3a**, δ -76.6; **3b**, δ -76.8) and proved the proposed cyclic structure unambiguously.

The thermal retro reaction of siliranes **3a** and **3b**, respectively, to cyclotrisilane **1a** and the corresponding olefin indicates an equilibrium that does not have any precedent in the chemistry of siliranes. A possible mechanistic pathway for this reversible reaction is represented in Scheme 1: the first step of the sequence is the extrusion of silylene **2a**, which could be trapped by addition to 1-pentyne, yielding quantitatively the known silirene **5**.<sup>7</sup> An analogous retro cleavage of a silirane is well-known from the pioneering studies on the reactivity of siliranes by Seyferth,<sup>2c,10</sup> which have unequivocally established an equilibrium between hexamethylsilirane (**4**) and dimethylsilylene: thermolysis of **4** resulted in formation of tetramethylethylene and dimethylsilylene, which polymerized, inserted into a Si-C bond of the starting silirane **4**, or could be intercepted by various trapping agents such as siloxanes, organosilicon hydrides, 2,3-dimethylbuta-1,3-diene, and alkynes. But whereas dimethylsilylene polymerizes in the absence of a trapping agent, **2a** trimerizes, presumably *via* disilene **7a** as intermediate, eventually

yielding cyclotrisilane **1a**.<sup>11</sup> An alternative, albeit less probable, mechanism cannot totally be ruled out: initially formed silylene **2a** could insert into a Si-C bond of the starting material to form 1,2-disilacyclobutane **6**; [2 + 2] cycloreversion of the four-membered ring again would lead to disilene **7a** as a precursor of **1a**. Both of the proposed mechanisms proceed through silylene **2a** as an intermediate. Because of the reversibility of the cyclotrisilane formation from **3a** and **3b**, the principle of microscopic reversibility applies to these reactions and we must conclude that in the reverse reaction, i.e., that of **1a** with olefins to form siliranes, silylene **2a** is involved as well.

This is the first time that an equilibrium between a cyclotrisilane, a disilene, and a silylene has been established, thus adding a third reaction mode to the known decomposition pathways of cyclotrisilanes.<sup>12</sup> In organotin chemistry, an analogous thermal equilibrium between cyclotristannane, distannene, and stannylene is well-known,<sup>13</sup> whereas in organosilicon chemistry it had been sought without success.<sup>14</sup> Only a few observations reported in the last number of years have given hints of the possibility of such an equilibrium. First, reductive dehalogenation of 1,2-dibromo-1,1,2,2-tetra-*tert*-butyldisilane led, depending on the reaction conditions, to the corresponding disilene **7b**, cyclotrisilane **1b**, or silylene **2b**, which was trapped by subsequent cycloaddition reactions.<sup>15</sup> The formation of compounds containing monosila or trisila units starting from a disilane may be due to silylene intermediates in these reactions but does not necessarily require the involvement of these species: it cannot be excluded that the initially formed disilene **7b** undergoes metal-mediated redistribution reactions *via* metal silyl compounds as

(11) Formation of a cyclotrisilane by addition of a silylene to a disilene was recently suggested by West: Gillette, G. R.; Noren, G.; West, R. *Organometallics* **1990**, *9*, 2925.

(12) Weidenbruch, M. *Comments Inorg. Chem.* **1986**, *5*, 247.

(13) (a) Masamune, S.; Sita, L. R. *J. Am. Chem. Soc.* **1985**, *107*, 6390. (b) Weidenbruch, M.; Schäfer, A.; Kilian, H.; Pohl, S.; Saak, W.; Marsmann, H. *Chem. Ber.* **1992**, *125*, 563.

(14) See, e.g.: Masamune, S.; Eriyama, Y.; Kawase, T. *Angew. Chem.* **1987**, *99*, 601; *Angew. Chem., Int. Ed. Engl.* **1987**, *26*, 584.

(15) (a) Weidenbruch, M.; Schäfer, A.; Thom, K. L. *Z. Naturforsch.* **1983**, *38B*, 1695. (b) Schäfer, A.; Weidenbruch, M.; Peters, K.; von Schnering, H. G. *Angew. Chem.* **1984**, *96*, 311; *Angew. Chem., Int. Ed. Engl.* **1984**, *23*, 302.

(8) The content of **1a** in such samples was shown by <sup>1</sup>H NMR spectroscopy to be less than 1%.

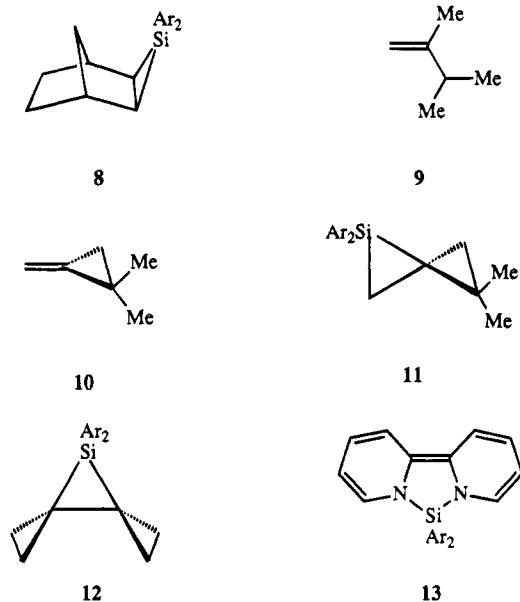
(9) Williams, E. A. In *The Chemistry of Organic Silicon Compounds*; Patai, S., Rappoport, Z., Eds.; Wiley: Chichester, U.K., 1989; p 511.

(10) (a) Seyferth, D.; Annarelli, D. C.; Vick, S. C.; Duncan, D. P. *J. Organomet. Chem.* **1980**, *201*, 179. (b) Seyferth, D.; Annarelli, D. C. *J. Am. Chem. Soc.* **1975**, *97*, 7162. (c) Seyferth, D.; Annarelli, D. C.; Vick, S. C. *J. Organomet. Chem.* **1984**, *272*, 123.

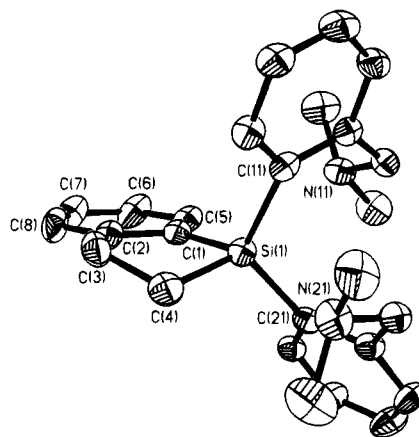


observed for various cyclic oligosilanes.<sup>16</sup> Second, an extremely bulky substituted disilene recently was reported to undergo silylene-like reactions.<sup>17</sup> Presumably the extreme steric bulk of the organic substituents in this disilene reduces the strength of the Si–Si double bond substantially. Finally, the ability of the 2-((dimethylamino)methyl)phenyl substituent to induce Si–Si bond cleavage in disilene **7a** by intramolecular coordination of the amino group to silicon finds support in *ab initio* calculations by Apeloig for the H<sub>2</sub>Si=SiH<sub>2</sub>/H<sub>2</sub>O interaction.<sup>18</sup> On the basis of these computational results, an equilibrium between disilene **7a**, which bears four potentially intramolecularly coordinating substituents, and the silylene **2a**, stabilized by intramolecular coordination, seems reasonable. It might be expected that such intramolecular coordination will substantially lower the activation energy for the formation of **2a** from **1a** and **7a**, respectively.<sup>19</sup>

**1a** did not react with unstrained internal olefins. Addition of **2a** to the C=C bond of *trans*-3-hexene, *trans*-stilbene, cyclooctene, cyclohexene, or cyclopentene was not observed. However, when the cyclopentene ring was part of a strained system as in norbornene, clean formation of tricyclic silirane **8** occurred. On the basis



of the <sup>1</sup>H and <sup>13</sup>C NMR data we assume the silirane ring in **8** adopts the *exo* configuration, which is in good agreement with the *exo* selectivity found for carbene attack on norbornene.<sup>20</sup> The same strategy that worked



**Figure 1.** Crystal structure of **14**. Hydrogen atoms are omitted for clarity; displacement ellipsoids are at the 50% probability level.

for norbornene, i.e., to increase the reactivity of the olefinic double bond by introduction of strain, was successful also with geminally disubstituted olefins. Whereas **9** did not form a silirane with **1a**, the methylenecyclopropane **10**, which is formally the ring-closure product of **9**, reacted with **1a** to give spiro[2.2]pentane **11**. Extending this methodology to bicyclic propylidene, whose enhanced reactivity toward carbenes is known as well,<sup>21</sup> allowed the synthesis of dispiro[2.0.2.1]-heptane **12** in quantitative yield. Decrease of strain, as realized in tetramethylethylene, resulted in complete suppression of the cycloaddition.

In contrast to **3a** and **3b**, **8** as well as **11** and **12** were thermally stable; no retro reaction to **1a** was observed at room temperature. Only at temperatures above 110 °C did **8** transfer its silylene unit to 2,2'-bipyridyl at a reasonable rate, giving the known<sup>6</sup> tricyclic system **13**.<sup>22</sup> Presumably the high strain energy of norbornene, which is formed in the course of the cleavage reaction, compared with that of normal olefins is responsible for the decreased silylene transfer reactivity of **8**.

The addition reaction of **2a** with styrene was more complex: stirring **1a** for 12 h at 40 °C with an excess of styrene led to quantitative formation of silindane **14**, whose structure was confirmed by X-ray analysis (Figure 1). When the reaction was monitored by means of <sup>1</sup>H NMR spectroscopy, the formation of an intermediate, **3c**, was observed, which was converted subsequently to **14**. So far, it has not been possible to find reaction conditions which allow the exclusive formation of **3c**.<sup>23</sup> On the basis of the characteristic <sup>29</sup>Si NMR shift  $\delta$  –82.5, as well as examination of <sup>1</sup>H NMR spectra of the reaction mixture, the structure of silirane **3c** was ascribed to this intermediate, which is formed by initial addition of **2a** to the olefinic double bond of styrene.

It has been assumed that silylene cycloaddition to conjugated dienes proceeds by a stepwise mechanism,

(16) Brough, L. F.; West, R. *J. Organomet. Chem.* **1980**, *194*, 139 and references cited therein.

(17) Tokitoh, N.; Suzuki, H.; Okazaki, R.; Ogawa, K. *J. Am. Chem. Soc.* **1993**, *115*, 10428.

(18) Apeloig, Y. In *Heteroatom Chemistry*; Block, E., Ed.; VCH: New York, 1990; p 27. For related calculations on silylenes, see: Gano, D. R.; Gordon, M. S.; Boatz, J. A. *J. Am. Chem. Soc.* **1991**, *113*, 6711.

(19) (a) Corriu, R.; Lanneau, G.; Priou, C.; Soulairol, F.; Auner, N.; Probst, R.; Conlin, R.; Tan, C. *J. Organomet. Chem.* **1994**, *466*, 55. (b) Conlin, R. T.; Laakso, D.; Marshall, P. *Organometallics* **1994**, *13*, 838.

(20) See for example: (a) Kropp, P. J.; Pienta, N. J.; Sawyer, J. A.; Polniaszek, R. P. *Tetrahedron* **1981**, *37*, 3229. (b) Jefford, C. W.; Mahajan, S.; Waslyn, J.; Waegell, B. *J. Am. Chem. Soc.* **1965**, *87*, 2183. (c) Sauer, R. R.; Sonnet, P. E. *Tetrahedron* **1965**, *20*, 1029. (d) Simmons, H. E.; Smith, R. D. *J. Am. Chem. Soc.* **1959**, *81*, 4256. (e) Moore, W. R.; Moser, W. R.; LaPrade, J. E. *J. Org. Chem.* **1963**, *28*, 2200.

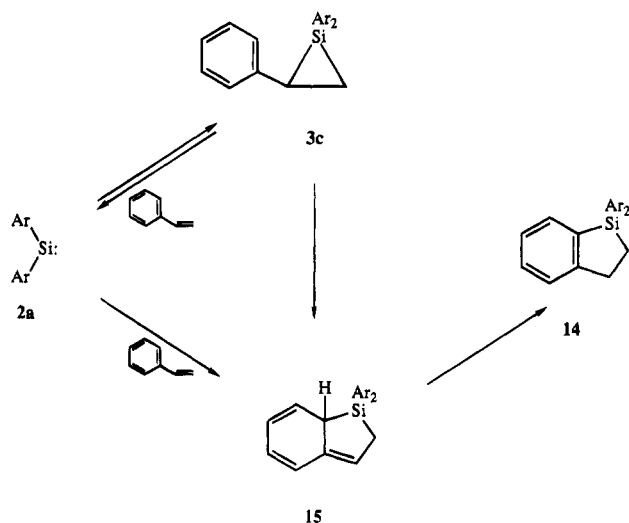
(21) See for example: (a) Fitjer, L.; Conia, J. M. *Angew. Chem.* **1973**, *85*, 349; *Angew. Chem., Int. Ed. Engl.* **1973**, *12*, 334. (b) Lukin, K. A.; Kuznetsova, T. S.; Kozhushkov, S. I.; Piven, V. A.; Zefirov, N. S. *Zh. Org. Khim.* **1988**, *24*, 1644.

(22) Similar compounds were shown by Weidenbruch to be the reaction products of photochemically generated **2b** with 2,2'-bipyridyl: (a) Weidenbruch, M.; Schäfer, A.; Marsmann, H. *J. Organomet. Chem.* **1988**, *354*, C12. (b) Weidenbruch, M.; Lesch, A.; Marsmann, H. *J. Organomet. Chem.* **1990**, *385*, C47.

(23) Very recently an analogous but stable phenyl-substituted silirane was obtained by cophotolysis of **1b** and 2-methylstyrene: Weidenbruch, M.; Kroke, E.; Marsmann, H.; Pohl, S.; Saak, W. *J. Chem. Soc., Chem. Commun.* **1994**, 1233.



Scheme 2



starting with 1,2-addition of the silylene to the C–C double bond, followed by subsequent rearrangement.<sup>24</sup> The transient existence of the initially formed vinylsilirane was proved indirectly by trapping experiments. Only recently, Conlin<sup>4d</sup> has succeeded in stabilizing such intermediates by reacting photolytically generated, bulky substituted silylenes with conjugated dienes. The resulting vinylsiliranes, which were contaminated with isomeric products, were identified unambiguously by means of NMR spectroscopy. Initial formation of the silirane **3c** also was observed in the reaction of **1a** with styrene, thus suggesting two different mechanistic pathways to **14** (Scheme 2). The silaindane either may be the product of a [1,3]-silyl migration<sup>25</sup> from initially formed **3c**, followed by irreversible rearomatization of intermediate **15**, which is the formal 1,4-addition product of **2a**, to the conjugated system, or it may be the result of a possibly reversible<sup>26</sup> 1,4-cycloaddition of **2a**, which originates from cycloreversion of silirane **3c** or directly from **1a**, to styrene, again yielding **15** as precursor of **14**. The second possibility appears to be less probable. Styrene is well-known to react with electron-deficient olefins as a 1,3-diene,<sup>27</sup> but this reaction mode was never observed for additions of carbenes<sup>28</sup> or other group 14 homologues to styrene or substituted styrenes. However, germynes have been reported to undergo concerted 1,4-cycloadditions with “normal” conjugated olefins such as 1,4-diphenyl-1,3-butadiene.<sup>29</sup>

(24) Gaspar, P. P. In *Reactive Intermediates*; Jones, M., Jr., Moss, R. A., Eds.; Wiley: New York, 1985; Vol. 3, p 333 and references cited therein.

(25) This shift may proceed in a concerted<sup>4c</sup> or stepwise<sup>4a</sup> fashion via diradical intermediates.

(26) Compare, e. g.: Lei, D.; Gaspar, P. P. *Organometallics* **1985**, *4*, 1471.

(27) Fringuelli, F.; Taticchi, A. *Dienes in the Diels-Alder Reaction*; Wiley: New York, 1990; and references cited therein.

(28) Compare, e. g.: Hoffmann, R. W.; Lilienblum, W.; Dittrich, B. *Chem. Ber.* **1974**, *107*, 3395.

(29) (a) Schriewer, M.; Neumann, W. P. *Angew. Chem.* **1981**, *93*, 1089; *Angew. Chem., Int. Ed. Engl.* **1981**, *20*, 1019. (b) Ma, E. C.-L.; Kobayashi, K.; Barzilai, M. W.; Gaspar, P. P. *J. Organomet. Chem.* **1982**, *224*, C13.

(30) Recently, rather incomplete NMR data for **16** were reported.<sup>19a</sup> The <sup>1</sup>H NMR shift values differ considerably from values found by us; we consider our data reported here to be correct.

(31) Hwang, R.-J.; Conlin, R. T.; Gaspar, P. P. *J. Organomet. Chem.* **1975**, *94*, C38.

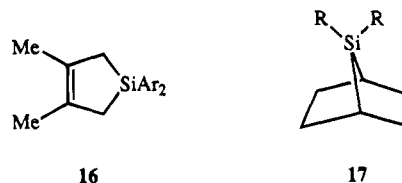
(32) Brook, A. G.; Baumegeger, A.; Lough, A. J. *Organometallics* **1992**, *11*, 310.

(33) Bondi, A. J. *Phys. Chem.* **1964**, *68*, 441.

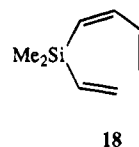
Table 1. Selected Bond Lengths (Å), Nonbonding Distances (Å), and Bond Angles (deg) in Silaindane **14**

Si(1)–C(1)	1.888(3)	Si(1)–C(4)	1.881(4)	Si(1)–C(11)	1.888(3)
Si(1)–C(21)	1.877(3)	C(1)–C(2)	1.392(5)	C(2)–C(3)	1.508(5)
C(3)–C(4)	1.533(5)				
Si(1)···N(11)	3.259(3)	Si(1)···N(21)	3.060(3)		
C(1)–Si(1)–C(4)	90.6(2)	C(1)–Si(1)–C(11)	112.8(1)		
C(4)–Si(1)–C(11)	109.9(2)	C(1)–Si(1)–C(21)	110.8(1)		
C(4)–Si(1)–C(21)	114.6(2)	C(11)–Si(1)–C(21)	115.6(2)		

When **1a** was stirred with 3 equiv of 2,3-dimethyl-1,3-butadiene at 40 °C for 12 h, silacyclopentene **16**<sup>30</sup> was formed quantitatively. In this case, the assumed



**17a**: R = 2-(Me<sub>2</sub>NCH<sub>2</sub>)C<sub>6</sub>H<sub>4</sub> (≡Ar)  
**17b**: R = Me

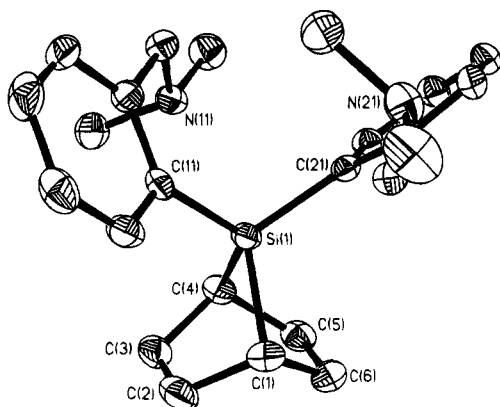


vinylsilirane intermediate could not be detected in the course of this cycloaddition. In comparison with the reluctance of the olefin **9** (vide supra) to react with **1a**, the activating influence of a conjugated double bond becomes rather evident. This seems to be true for cyclohexene and 1,3-cyclohexadiene as well: **2a** did not add to the isolated internal double bond of cyclohexene, whereas 7-silanorbornene **17a** was formed by reaction of **1a** with 1,3-cyclohexadiene without any side products. Comparison of this result with the outcome of the interaction of thermally generated dimethylsilylene with 1,3-cyclohexadiene, which resulted in a 1:1 mixture of the corresponding silanorbornene **17b** and the acyclic triene **18** in 20% yield,<sup>31</sup> once more points out the advantage of having precursors from which silylenes **2a** can be generated under mild conditions.

### Crystal Structures

Crystals of **14** suitable for X-ray structural analysis were obtained by crystallization from diethyl ether/pentane. Figure 1 shows the structure of **14**; selected interatomic distances and angles are listed in Table 1. Whereas atoms Si(1), C(1), C(2), and C(3) form an almost perfect plane (mean deviation 0.012 Å), C(4) is located 0.517 Å above this plane. Thus, the silacyclopentene ring in **14** adopts an envelope conformation, which is more strongly developed than that in a similar silaindane whose structure was reported recently by Brook.<sup>32</sup> The bonding geometry around silicon is that of distorted tetrahedron: the small endocyclic C(1)–Si(1)–C(4) angle (90.6(2)°) is in contrast with the widened exocyclic C(21)–Si(1)–C(11) angle (115.6(2)°). The Si(1)···N(11) and Si(1)···N(21) distances (3.259(3) and 3.060(3) Å, respectively) are shorter than the sum of the van der Waals radii of both elements (3.65 Å)<sup>33</sup> but significantly longer than the usual distance between

(34) Chuit, C.; Corriu, R. J. P.; Reye, C.; Young, J. C. *Chem. Rev.* **1993**, *93*, 1371.



**Figure 2.** Crystal structure of **17a**. Hydrogen atoms are omitted for clarity; displacement ellipsoids are at the 50% probability level.

silicon and nitrogen in hypercoordinated silicon compounds (ca. 2–3 Å).<sup>34</sup> This could indicate a weak coordination of nitrogen to silicon. However, this conclusion is questioned by the observation that the lone pairs of the amino groups are not oriented exactly toward the silicon center.

The structure of **17a** is shown in Figure 2; selected structural parameters are summarized in Table 2. The double bond is disordered over two positions (C(2)=C(3) and C(5)=C(6) bonds, respectively, resulting in bond lengths between single and double bonds. The occupation ratio refined to 7:3. Again, severe distortion of the tetrahedral geometry around the silicon center is obvious: the endocyclic C(1)–Si(1)–C(4) bond angle is reduced to 80.5(1)°, a phenomenon which finds its parallel in the structure of some 7-silanorbornadienes.<sup>35</sup> On the other hand, the exocyclic angles around silicon are significantly enlarged (up to 123.6(1)° for C(11)–Si(1)–C(4)). The widening of these angles allows one dimethylamino group to approach the silicon center, resulting in a Si(1)···N(11) distance of 2.918(2) Å. However, as in **14**, the missing exact orientation of the amino lone pair toward silicon argues against a significant Si···N interaction.

### Experimental Section

<sup>1</sup>H NMR and <sup>13</sup>C NMR spectra were recorded on a Bruker AM 250 (<sup>1</sup>H NMR, 250 MHz; <sup>13</sup>C NMR, 62.9 MHz). <sup>1</sup>H, <sup>1</sup>H and <sup>1</sup>H, <sup>13</sup>C COSY spectra were recorded on a Varian VXR-200 (200 MHz). C<sub>q</sub>, CH, CH<sub>2</sub>, and CH<sub>3</sub> were determined using the DEPT pulse sequence. <sup>29</sup>Si NMR spectra were recorded on a Bruker AMX 300 (59.6 MHz) using a refocused INEPT pulse sequence. Chemical shifts refer to δ<sub>TMS</sub> 0.0. Mass spectra were recorded on a Varian MAT CH7 and MAT 731; HRMS data were determined with a Varian MAT 311 A, using preselected ion peak matching at *R* ≈ 10 000 to be within ±2 ppm of the exact mass. Because of the high sensitivity of siliranes toward moisture and air, satisfactory mass spectra or elemental analyses could not be obtained in most cases. Mass spectra always showed, besides M<sup>+</sup>, the silirane contamination with hydrolysis product and corresponding fragments. Melting points are uncorrected. Elemental analyses were performed at Mikroanalytisches Labor der Georg-August-Universität Göttingen.

All manipulations were carried out under an inert argon atmosphere using carefully dried glassware. Solvents used were dried by refluxing over sodium and distilled immediately before use.

**Table 2.** Selected Bond Lengths (Å), Nonbonding Distances (Å), and Bond Angles (deg) in Silanorbornene **17a**

Si(1)–C(1)	1.917(3)	Si(1)–C(4)	1.908(2)	Si(1)–C(11)	1.886(3)
Si(1)–C(21)	1.883(2)				
		Si(1)···N(11)		2.918(2)	
C(1)–Si(1)–C(4)	80.5(1)	C(1)–Si(1)–C(11)		109.7(1)	
C(4)–Si(1)–C(11)	123.6(1)	C(1)–Si(1)–C(21)		114.5(1)	
C(4)–Si(1)–C(21)	114.8(1)	C(11)–Si(1)–C(21)		110.3(1)	

**1,1-Bis[2-((dimethylamino)methyl)phenyl]-2-*n*-propyl-1-silirane (3a).** To a solution of 45 mg (0.06 mmol) of **1a** in 0.4 mL of C<sub>6</sub>D<sub>6</sub> was added a 10-fold excess (about 0.07 mL) of 1-pentene. The solution was heated at 40 °C for 12 h. After the reaction was completed, solvent and excess alkene were removed in vacuo at room temperature. The remaining pale green oil was redissolved in C<sub>6</sub>D<sub>6</sub> to yield a solution of spectroscopically pure **3a**. The NMR spectra were determined within 30 min. <sup>1</sup>H NMR (C<sub>6</sub>D<sub>6</sub>): δ 0.60 (dd, <sup>3</sup>J<sub>trans</sub> = 7 Hz, <sup>2</sup>J = 11 Hz; 1 H, 3-H<sub>cis</sub>), 1.01 (t, <sup>3</sup>J = 7 Hz, 3 H, CH<sub>3</sub>), 1.18 (dd, <sup>3</sup>J<sub>cis</sub> = 11 Hz, <sup>2</sup>J = 11 Hz, 1 H, 3-H<sub>trans</sub>), 1.31–2.02 (m, 5 H, 2H-, propyl CH<sub>2</sub>), 1.80 (s, 6 H, NMe<sub>2</sub>), 1.83 (s, 6 H, NMe<sub>2</sub>), 3.18, 3.40 (AB system, <sup>2</sup>J = 13 Hz, 2 H, CH<sub>2</sub>N), 3.27 (s, 2 H, CH<sub>2</sub>N), 7.10–7.19 (m, 6 H, ar H), 7.92–7.98 (m; 2 H, ar H). <sup>13</sup>C NMR (C<sub>6</sub>D<sub>6</sub>): δ 5.3 (C-3), 14.4, 14.6 (CH<sub>3</sub>, C-2), 24.6, 35.7 (propyl CH<sub>2</sub>), 45.0, 45.1 (2 × NMe<sub>2</sub>), 64.6, 64.8 (2 × CH<sub>2</sub>N), 126.3 (ar CH), 126.6 (ar CH), 127.8 (ar CH), 128.0 (ar CH), 129.1 (ar CH), 129.2 (ar CH), 133.6 (ar C<sub>q</sub>), 135.7 (ar C<sub>q</sub>), 136.6 (ar CH), 137.4 (ar CH), 145.9 (ar C<sub>q</sub>), 146.7 (ar C<sub>q</sub>). <sup>29</sup>Si NMR (C<sub>6</sub>D<sub>6</sub>): δ –76.8.

**Thermolysis of 3a.** With 45 mg (0.05 mmol) of **1a** and 0.07 mL of 1-pentene in 0.4 mL of C<sub>6</sub>D<sub>6</sub> as starting materials, a solution of **3a** was prepared as described above. After rapid removal of solvent and excess alkene in vacuo at room temperature, 0.4 mL of C<sub>6</sub>D<sub>6</sub> was added to the residue; the content of starting materials **1a** and 1-pentene in this sample of **3a** was shown to be less than 1% by means of <sup>1</sup>H NMR spectroscopy. After poly(dimethylsiloxane) was added as internal integration standard, the solution was heated to 40 °C for 1 h. **1a** as well as 1-pentene were formed; the ratio **3a**:**1a**:1-pentene was spectroscopically determined to be 5:1:3. When the solution was heated to 40 °C for another 4.5 h, the ratio changed to 1:1:3.

**1,1-Bis[2-((dimethylamino)methyl)phenyl]-2-*n*-butyl-1-silirane (3b).** To a solution of 60 mg (0.07 mmol) of **1a** in 0.4 mL of C<sub>6</sub>D<sub>6</sub> was added 0.1 mL of 1-hexene. After the solution was heated for 3 h at 40 °C, the solvent and excess alkene were removed in vacuo at room temperature. The remaining oil was redissolved in C<sub>6</sub>D<sub>6</sub> to yield a solution of **3b** (97%, contaminated with 3% **1a**). <sup>1</sup>H NMR (C<sub>6</sub>D<sub>6</sub>): δ 0.62 (dd, <sup>3</sup>J<sub>trans</sub> = 7 Hz, <sup>2</sup>J = 10 Hz, 1 H, 3-H<sub>cis</sub>), 0.95 (t, <sup>3</sup>J = 7 Hz, 3 H, CH<sub>3</sub>), 1.12 (dd, <sup>3</sup>J<sub>cis</sub> = 12 Hz, <sup>2</sup>J = 10 Hz, 1 H, 3-H<sub>trans</sub>), 1.22–2.03 (m, 7 H, 2-H, butyl CH<sub>2</sub>), 1.81 (s, 6 H, NMe<sub>2</sub>), 1.83 (s, 6 H, NMe<sub>2</sub>), 3.20, 3.41 (AB system, <sup>2</sup>J = 13 Hz, 2 H, CH<sub>2</sub>N), 3.27 (s, 2 H, CH<sub>2</sub>N), 7.09–7.25 (m, 6 H, ar H), 7.94–7.98 (m, 2 H, ar H). <sup>13</sup>C NMR (C<sub>6</sub>D<sub>6</sub>): δ 5.4 (C-3), 14.5, 15.0 (CH<sub>3</sub>, C-2), 23.1, 33.2, 33.8 (butyl CH<sub>2</sub>), 45.0, 45.1 (2 × NMe<sub>2</sub>), 64.7, 64.9 (2 × CH<sub>2</sub>N), 126.2 (ar CH), 126.6 (ar CH), 127.8 (ar CH), 129.1 (ar CH), 129.2 (ar CH), 129.9 (ar CH), 133.6 (ar C<sub>q</sub>), 135.8 (ar C<sub>q</sub>), 136.6 (ar CH), 137.4 (ar CH), 145.9 (ar C<sub>q</sub>), 146.7 (ar C<sub>q</sub>). <sup>29</sup>Si NMR (C<sub>6</sub>D<sub>6</sub>): –76.6.

**Thermolysis of 3b.** With 60 mg (0.07 mmol) of **1a** and 0.1 mL of 1-hexene in 0.4 mL of C<sub>6</sub>D<sub>6</sub> as starting materials, a solution of **3b** was prepared as described above. After rapid removal of the solvent and the alkene in vacuo at room temperature, C<sub>6</sub>D<sub>6</sub> was added and the content of **1a** relative to **3b** was determined by <sup>1</sup>H NMR to be less than 3%. The solution was heated to 40 °C for 2 h, and the content of **3b** was found to be 15%. When the solution was left at room temperature for 12 h, the content of **1a** increased to 21%.

**1,1-Bis[2-((dimethylamino)methyl)phenyl]-2-phenyl-1-silirane (3c) and 2,3-Benzo-1,1-bis[2-((dimethylamino)-**

(35) Preut, H.; Mayer, B.; Neumann, W. P. *Acta Crystallogr.* **1983**, *C39*, 1118.

**methylphenyl]-1-silacyclopent-2-ene (14).** To a solution of 63 mg (0.07 mmol) of **1a** in 4 mL of toluene was added 0.2 mL of styrene. The solution was stirred at 40 °C for 1 h; **3c** could be identified in this reaction mixture in addition to starting materials and **14** by means of NMR spectroscopy. The solution was heated for another 11 h to 40 °C. After solvent and excess styrene were removed in vacuo, 85 mg of a spectroscopically pure, white solid was obtained. Recrystallization from ether/pentane (2:1) gave 44 mg (52%) of analytically pure **14**. **3c** (data incomplete due to partial signal overlap with starting materials and **14**). <sup>1</sup>H NMR (C<sub>6</sub>D<sub>6</sub>): δ 1.39 (dd, <sup>3</sup>J<sub>trans</sub> = 9 Hz, <sup>2</sup>J = 12 Hz, 1 H, 3-H<sub>cis</sub>), 2.63 (dd, <sup>3</sup>J<sub>trans</sub> = 9 Hz, <sup>3</sup>J<sub>cis</sub> = 11 Hz, 2 H, 2-H), 1.66 (s, 6 H, NMe<sub>2</sub>), 1.90 (s, 6 H, NMe<sub>2</sub>), 2.94 (B moiety of AB system, <sup>2</sup>J = 14 Hz). <sup>29</sup>Si NMR (C<sub>6</sub>D<sub>6</sub>): δ -82.5. **14**: mp 114–115 °C. <sup>1</sup>H NMR (CDCl<sub>3</sub>): δ 1.54 (dd, <sup>3</sup>J = 7 and 8 Hz, 2 H, 5-H), 1.83 (s, 12 H, NMe<sub>2</sub>), 3.20 (m, 6 H, CH<sub>2</sub>N, 4-H), 7.16–7.31 (m, 9 H, ar H), 7.69 (d, <sup>3</sup>J = 7 Hz, 2 H, ar H), 7.77 (d, <sup>3</sup>J = 7 Hz, 1 H, ar H). <sup>13</sup>C NMR (CDCl<sub>3</sub>): δ 12.9 (C-5), 31.7 (C-4), 45.1 (NMe<sub>2</sub>), 64.7 (CH<sub>2</sub>N), 125.2 (ar CH), 125.9 (ar CH), 126.4 (ar CH), 128.5 (ar CH), 128.8 (ar CH), 128.9 (ar CH), 134.6 (ar CH), 135.9 (ar C<sub>q</sub>), 136.0 (ar CH), 139.3 (ar C<sub>q</sub>), 145.2 (ar C<sub>q</sub>), 154.0 (ar C<sub>q</sub>). <sup>29</sup>Si NMR (C<sub>6</sub>D<sub>6</sub>): δ 2.5. MS (EI; 70 eV): *m/z* (relative intensity) 400 (M<sup>+</sup>, 1), 385 (M<sup>+</sup> - Me, 1), 297 (Ar<sub>2</sub>Si<sup>+</sup>, 2), 266 (M<sup>+</sup> - 134, 34), 57 (CHNMe<sub>2</sub><sup>+</sup>, 100). Anal. Calcd for C<sub>26</sub>H<sub>32</sub>N<sub>2</sub>Si: C, 77.95; H, 8.05; N, 6.99. Found: C, 78.03; H, 8.03; N, 6.94.

**1,1-Bis-[2-((dimethylamino)methyl)phenyl]-2-*n*-propyl-1-silirene (5).**<sup>7</sup> To a solution of 56 mg (0.15 mmol) of **3b** in 0.5 mL of C<sub>6</sub>D<sub>6</sub> in the presence of 0.2 mL of 1-pentene (to suppress retro reaction to **1a**) was added 0.2 mL of 1-pentyne, and the mixture was heated to 40 °C for 8 h. After evaporation of all volatile compounds in vacuo, silirene **5** remained as a <sup>1</sup>H NMR spectroscopically pure oil. Attempted further purification by distillation resulted in complete decomposition. <sup>1</sup>H NMR (C<sub>6</sub>D<sub>6</sub>): δ 1.03 (t, <sup>3</sup>J = 7 Hz, 3 H, CH<sub>3</sub>), 1.75–2.04 (m, 2 H, CH<sub>2</sub>), 1.94 (s, 12 H, NMe<sub>2</sub>), 2.67 (dt, <sup>3</sup>J = 7 Hz, <sup>4</sup>J = 1 Hz, 2 H, CH<sub>2</sub>), 3.28 (s, 4 H, CH<sub>2</sub>N), 7.07–7.21 (m, 6 H, ar H), 7.71 (dd, <sup>3</sup>J = 8 Hz, <sup>4</sup>J = 1 Hz, 2 H, ar H), 8.58 (t, <sup>4</sup>J = 1 Hz, 1 H, 3-H). <sup>13</sup>C NMR (C<sub>6</sub>D<sub>6</sub>): δ 14.6 (CH<sub>3</sub>), 21.5 (CH<sub>2</sub>), 38.7 (CH<sub>2</sub>), 45.3 (NMe<sub>2</sub>), 63.6 (CH<sub>2</sub>N), 126.8 (ar CH), 127.4 (ar CH), 128.9 (ar CH), 136.4 (ar CH), 138.5 (ar C<sub>q</sub>), 144.3 (ar C<sub>q</sub>), 147.9 (C-2), 180.5 (C-3, J<sub>C-H</sub> = 166 Hz). <sup>29</sup>Si NMR (C<sub>6</sub>D<sub>6</sub>): δ -106.3. MS (EI; 70 eV): *m/z* 364 (M<sup>+</sup>, 1). Anal. Calcd for C<sub>25</sub>H<sub>32</sub>N<sub>2</sub>Si: C, 75.77; H, 8.85. Found: C, 74.55; H, 8.82.

**exo-3,3-Bis[2-((dimethylamino)methyl)phenyl]-3-silatricyclo[3.2.1.0<sup>2,4</sup>]octane (8).** To a solution of 80 mg (0.09 mmol) of **1a** in 0.4 mL of C<sub>6</sub>D<sub>6</sub> was added 25 mg (0.27 mmol) of norbornene. The solution was heated for 4.5 h to 50 °C. After evaporation of solvent and remaining norbornene, **8** was obtained as a spectroscopically pure colorless oil. <sup>1</sup>H NMR (additional <sup>1</sup>H, <sup>1</sup>H and <sup>1</sup>H,<sup>13</sup>C COSY spectra; C<sub>6</sub>D<sub>6</sub>): δ 0.96–1.01 (m, 1 H, 8-H<sub>syn</sub>), 1.45–1.56 (m, 3 H, 8-H<sub>anti</sub>, 6,7-H<sub>endo</sub>), 1.76–2.01 (m, 4 H, 6,7-H<sub>exo</sub>, 2,4-H), 1.86 (s, 6 H, NMe<sub>2</sub>), 1.96 (s, 6 H, NMe<sub>2</sub>), 2.65–2.90 (broad s, 2 H, 1,5-H), 3.17 (s, 2 H, CH<sub>2</sub>N), 3.40–3.50 (broadened AB system, 2 H, CH<sub>2</sub>N), 6.95–6.99 (1 H, ar H), 7.10–7.20 (m, 5 H, ar H), 7.81 (dd, <sup>3</sup>J = 7 Hz, <sup>4</sup>J = 1 Hz, 1 H, ar H), 8.16–8.20 (m, 1 H, ar H). <sup>13</sup>C NMR (125.7 MHz, C<sub>6</sub>D<sub>6</sub>): δ 26.3 (broad, C-2,4), 34.3 (C-6,7), 36.4 (C-8), 40.1 (broad, C-1,5), 45.1 (NMe<sub>2</sub>), 45.2 (NMe<sub>2</sub>), 64.3 (CH<sub>2</sub>N), 64.7 (CH<sub>2</sub>), 126.0 (ar CH), 126.9 (ar CH), 127.1 (ar CH), 128.6 (ar CH), 128.9 (ar CH), 129.8 (ar CH), 134.7 (ar C<sub>q</sub>), 135.4 (ar C<sub>q</sub>), 136.4 (ar CH), 139.5 (ar CH), 146.1 (ar C<sub>q</sub>), 146.4 (ar C<sub>q</sub>). <sup>29</sup>Si NMR (C<sub>6</sub>D<sub>6</sub>): δ -77.3. HRMS: calcd for C<sub>25</sub>H<sub>34</sub>N<sub>2</sub>Si 390.2491, found 390.2491. Anal. Calcd for C<sub>25</sub>H<sub>34</sub>N<sub>2</sub>Si: C, 76.87; H, 8.77. Found: C, 75.70; H, 8.92.

**Thermolysis of 8 in the Presence of 2,2'-Bipyridyl.** To a solution of 211 mg (0.54 mmol) of **8** in 10 mL of xylene was added 84 mg (0.54 mmol) of 2,2'-bipyridyl. The solution was stirred for 12 h at 120 °C. After evaporation of the solvent the crude product was recrystallized from ether to give 63 mg (21%) of **13<sup>6</sup>** (mp 60–62 °C dec).

**Table 3. Summary of Crystal Data, Details of the Intensity Collection, and Least-Squares Refinement Parameters for Silaindane 14 and Silanorbornene 17a**

	14	17a
empirical formula	C <sub>26</sub> H <sub>32</sub> N <sub>2</sub> Si	C <sub>24</sub> H <sub>32</sub> N <sub>2</sub> Si
<i>M<sub>r</sub></i>	400.63	376.61
cryst size (mm)	0.7 × 0.6 × 0.3	0.7 × 0.7 × 0.5
cryst syst	monoclinic	monoclinic
space group	C2/c	C2/c
<i>a</i> (Å)	36.255(7)	14.155(5)
<i>b</i> (Å)	8.877(2)	13.336(4)
<i>c</i> (Å)	14.966(2)	23.339(8)
β (deg)	109.60(1)	107.16(2)
<i>V</i> (Å <sup>3</sup> )	4537(2)	4120(2)
<i>Z</i>	8	8
<i>D<sub>x</sub></i> (g cm <sup>-3</sup> )	1.173	1.188
μ (mm <sup>-1</sup> )	0.118	0.123
<i>F</i> (000)	1728	1632
2θ range (deg)	8 ≤ 2θ ≤ 45	8 ≤ 2θ ≤ 45
range of <i>hkl</i>	-38 ≤ <i>h</i> ≤ +38, -9 ≤ <i>k</i> ≤ +9, -7 ≤ <i>l</i> ≤ +16	-15 ≤ <i>h</i> ≤ +15, -12 ≤ <i>k</i> ≤ +14, -25 ≤ <i>l</i> ≤ +25
no. of rflns coll	4732	3565
no. of indep rflns	2881	2683
<i>R</i> (int)	0.0205	0.0437
no. of data	2876	2681
no. of params	266	249
<i>S</i>	1.103	1.131
<i>g</i> <sub>1</sub>	0.0554	0.0249
<i>g</i> <sub>2</sub>	13.5732	7.1883
<i>R</i> <sub>1</sub> ( <i>F</i> > 4σ( <i>F</i> ))	0.0515	0.0401
w <i>R</i> <sub>2</sub> (all data)	0.1552	0.0978
extinction coeff <i>x</i>		0.0013(2)
largest diff peak (e Å <sup>-3</sup> )	0.48	0.27
largest diff hole (e Å <sup>-3</sup> )	-0.48	-0.23

**1,1-Bis-[2-((dimethylamino)methyl)phenyl]-4,4-dimethyl-1-silaspiro[2.2]pentane (11).** To a solution of 70 mg of **1a** (0.08 mmol) in 4 mL of toluene was added 0.1 mL of **10**. The solution was stirred at 40 °C for 12 h. Solvent and alkene were removed in vacuo to give 90 mg of **11** as a spectroscopically pure, pale yellow oil. <sup>1</sup>H NMR (C<sub>6</sub>D<sub>6</sub>): δ 0.73, 1.13 (AX system, <sup>2</sup>J = 3 Hz, 2 H, 5-H), 0.88, 1.23 (AB system, <sup>2</sup>J = 10 Hz, 2 H, 2-H), 1.21 (s, 3 H, CH<sub>3</sub>), 1.39 (s, 3 H, CH<sub>3</sub>), 1.76 (s, 6 H, NMe<sub>2</sub>), 1.80 (s, 6 H, NMe<sub>2</sub>), 3.12, 3.27 (AB system, <sup>2</sup>J = 13 Hz, 2 H, CH<sub>2</sub>N), 3.21, 3.28 (AB system, <sup>2</sup>J = 13 Hz, 2 H, CH<sub>2</sub>N), 6.99–7.02 (m, 1 H, ar H), 7.13–7.23 (m, 5 H, ar H), 7.85–7.88 (m, 1 H, ar H), 8.09–8.13 (m, 1 H, ar H). <sup>13</sup>C NMR (C<sub>6</sub>D<sub>6</sub>): δ 8.1 (C-2), 20.2 (C-3, 4), 23.4 (CH<sub>3</sub>), 27.7 (CH<sub>3</sub>), 28.3 (C-5), 45.1 (NMe<sub>2</sub>), 45.4 (NMe<sub>2</sub>), 64.4 (CH<sub>2</sub>N), 64.6 (CH<sub>2</sub>N), 126.5 (ar CH), 126.9 (ar CH), 127.2 (ar CH), 128.4 (ar CH), 128.7 (ar CH), 129.3 (ar CH), 135.5 (ar CH), 135.9 (2 × ar C<sub>q</sub>), 137.1 (ar CH), 145.5 (ar C<sub>q</sub>), 145.6 (ar C<sub>q</sub>). <sup>29</sup>Si NMR (C<sub>6</sub>D<sub>6</sub>): δ -72.4. MS (EI; 70 eV): *m/z* (relative intensity) 376 (M<sup>+</sup>, 4), 363 (M<sup>+</sup> - Me, 16), 244 (M<sup>+</sup> - 134, 17). Anal. Calcd for C<sub>24</sub>H<sub>34</sub>N<sub>2</sub>Si: C, 76.13; H, 9.05. Found: C, 76.23; H, 9.25.

**7,7-Bis-[2-((dimethylamino)methyl)phenyl]-7-siladispiro[2.0.2.1]heptane (12).** To a solution of 112 mg (0.13 mmol) of **1a** in 0.4 mL of C<sub>6</sub>D<sub>6</sub> was added 31 mg (0.39 mmol) of bicyclopropylidene. The solution was heated to 50 °C for 7 h to give **12** quantitatively. <sup>1</sup>H NMR (C<sub>6</sub>D<sub>6</sub>): δ 0.67, 0.85 (m, AA'BB' system, 8 H, 1,2,5,6-H), 1.74 (s, 12 H, NMe<sub>2</sub>), 3.27 (s, 4 H, CH<sub>2</sub>N), 7.13–7.23 (m, 6 H, ar H), 8.07–8.11 (m, 2 H, ar H). <sup>13</sup>C NMR (C<sub>6</sub>D<sub>6</sub>): δ 8.3 (C-1,2,5,6), 10.9 (C-3,4), 45.3 (NMe<sub>2</sub>), 64.7 (CH<sub>2</sub>N), 126.7 (ar CH), 127.3 (ar CH), 129.0 (ar CH), 136.4 (ar C<sub>q</sub>), 136.6 (ar CH), 144.9 (ar C<sub>q</sub>). <sup>29</sup>Si NMR (C<sub>6</sub>D<sub>6</sub>): δ -75.6.

**1,1-Bis-[2-((dimethylamino)methyl)phenyl]-3,4-dimethyl-1-silacyclopent-3-ene (16).** To a solution of 51 mg (0.06 mmol) of **1a** in 5 mL of toluene was added 0.2 mL of 2,3-dimethyl-1,3-butadiene. The solution was stirred at 40 °C for 12 h. After removal of solvent and excess diene, 66 mg of **16** as a colorless, spectroscopically pure oil was obtained. The compound could be further purified by Kugelrohr distillation (125 °C/5 × 10<sup>-4</sup> mmHg) to yield 37 mg (57%) of **16** as a white

solid; mp 70 °C.  $^1\text{H}$  NMR ( $\text{CDCl}_3$ ):<sup>30</sup>  $\delta$  1.74 (broad s, 6 H,  $\text{CH}_3$ ), 1.84 (broad s, 16 H,  $\text{NMe}_2$ , 2,5-H), 3.15 (s, 4 H,  $\text{CH}_2\text{N}$ ), 7.25–7.30 (m, 6 H, ar H), 7.69 (d,  $^3J = 7$  Hz, 2 H, ar H).  $^1\text{H}$  NMR ( $\text{C}_6\text{D}_6$ ):  $\delta$  1.76 (s, 12 H,  $\text{NMe}_2$ ), 1.86 (s, 6 H,  $\text{CH}_3$ ), 1.99 (broad s, 4 H, 2,5-H), 3.12 (s, 4 H,  $\text{CH}_2\text{N}$ ), 7.17–7.28 (m, 6 H, ar H), 7.82–7.88 (m; 2 H, ar H).  $^{13}\text{C}$  NMR ( $\text{CDCl}_3$ ):  $\delta$  19.2 ( $\text{CH}_3$ ), 25.5 ( $\text{CH}_2$ ), 45.1 ( $\text{NMe}_2$ ), 64.5 ( $\text{CH}_2\text{N}$ ), 126.1 (ar CH), 128.3 (ar CH), 128.8 (ar CH), 130.4 (C-3,4), 135.7 (ar CH), 136.6 (ar  $\text{C}_q$ ), 145.3 (ar  $\text{C}_q$ ).  $^{29}\text{Si}$  NMR ( $\text{C}_6\text{D}_6$ ):  $\delta$  -2.3. MS (EI; 70 eV):  $m/z$  (relative intensity) 378 ( $\text{M}^+$ , 10), 363 ( $\text{M}^+ - \text{Me}$ , 4), 296 ( $\text{Ar}_2\text{Si}^+$ , 4), 281 ( $\text{Ar}_2\text{Si}^+ - \text{Me}$ , 100), 244 ( $\text{M}^+ - 134$ , 40). Anal. Calcd for  $\text{C}_{24}\text{H}_{34}\text{N}_2\text{Si}$ : C, 76.13; H, 9.05; N, 7.40. Found: C, 76.26; H, 9.15; N, 7.39.

**7,7-Bis-[2-((dimethylamino)methyl)phenyl]-7-sila-bicyclo[2.2.1]hept-2-ene (17).** To a solution of 58 mg (0.07 mmol) of **1a** in 4 mL of toluene was added 0.2 mL of 1,3-cyclohexadiene. The solution was stirred at 40 °C for 12 h. Solvent and excess diene were removed in vacuo, and 73 mg (99%) of **17** was obtained as a white, analytically pure solid; mp 100 °C.  $^1\text{H}$  NMR (250 MHz,  $\text{C}_6\text{D}_6$ ; additional  $^1\text{H}$ ,  $^1\text{H}$  COSY):  $\delta$  1.57 (broad d,  $^2J = 7$  Hz, 2 H, 5,6- $\text{H}_{\text{endo}}$ ), 1.79 (s, 6 H,  $\text{NMe}_2$ ), 1.88 (s, 6 H,  $\text{NMe}_2$ ), 2.17 (broad,  $^2J = 7$  Hz, 2 H, 5,6- $\text{H}_{\text{exo}}$ ), 2.45 (broad s, 2 H, 1,4-H), 3.09 (s, 2 H,  $\text{CH}_2\text{N}$ ), 3.13 (s, 2 H,  $\text{CH}_2\text{N}$ ), 6.45 (dd,  $^3J = 4$  Hz,  $^4J = 3$  Hz, 2 H, 2,3-H), 7.11–7.26 (m, 6 H, ar H), 7.72–7.76 (m, 1 H, ar H), 7.88–7.92 (m, 1 H, ar H).  $^{13}\text{C}$  NMR ( $\text{C}_6\text{D}_6$ ):  $\delta$  25.8 (C-5,6), 31.3 (C-1,4), 44.9 ( $\text{NMe}_2$ ), 64.6, 65.0 ( $2 \times \text{CH}_2\text{N}$ ), 125.6 (ar CH), 126.1 (ar CH), 128.3 (ar CH), 128.9 (ar CH), 129.3 (ar CH), 129.4 (ar CH), 133.8 (C-2,3), 134.6 (ar  $\text{C}_q$ ), 137.1 (ar  $\text{C}_q$ ), 137.7 (ar CH), 140.1 (ar CH), 145.7 (ar  $\text{C}_q$ ), 146.6 (ar  $\text{C}_q$ ).  $^{29}\text{Si}$  NMR ( $\text{C}_6\text{D}_6$ ):  $\delta$  19.0. MS (EI; 70 eV):  $m/z$  (relative intensity) 376 ( $\text{M}^+$ , 5), 296 ( $\text{Ar}_2\text{Si}^+$ , 7), 281 ( $\text{Ar}_2\text{Si}^+ - \text{Me}$ , 100), 238 ( $\text{Ar}_2\text{Si} - 58$ , 33). Anal. Calcd for  $\text{C}_{24}\text{H}_{32}\text{N}_2\text{Si}$ : C, 76.54; H, 8.56. Found: C, 76.49; H, 8.70.

**X-ray Structure Determination for 14 and 17a.** Crystal data, data collection, and least-squares parameters are summarized in Table 3. Data were collected at -120 °C on a STOE-Siemens-Huber four-circle diffractometer using graphite-monochromated Mo  $\text{K}\alpha$  radiation ( $\lambda = 0.71073$  Å). The structures were solved by direct methods.<sup>36</sup> All non-hydrogen atoms were refined anisotropically.<sup>37</sup> A riding model starting from calculated positions was employed for the hydrogen atoms. The structure was refined against  $F^2$  with the weighting scheme  $w^{-1} = \sigma^2(F_o^2) + (g_1P)^2 + g_2P$ , with  $P = (F_o^2 + 2F_c^2)/3$ . The  $R$  values were defined as  $R1 = \sum||F_o| - |F_c||/\sum|F_o|$  and  $wR2 = [\sum w(F_o^2 - F_c^2)^2/\sum wF_o^4]^{1/2}$ . For **17a** an extinction correction was applied:  $F_c^* = kF_c[1 + 0.001F_c^2\lambda^3/(\sin 2\theta)]^{-1/4}$ .

**Acknowledgment.** This work was supported by the Deutsche Forschungsgemeinschaft (financial support, fellowship to J.B.), the Fonds der Chemischen Industrie (financial support), the Friedrich-Ebert-Stiftung (fellowship to H.I.), and the Deutscher Akademischer Austauschdienst (fellowship to R.O.G.). We thank Dr. V. Belov, Dipl.-Chem. S. Bräse, and Dipl.-Chem. Th. Späth for samples of **10** and bicyclopropylidene, and cand.-chem. B. Geers for recording  $^1\text{H}$ ,  $^1\text{H}$  and  $^1\text{H}$ ,  $^{13}\text{C}$  COSY spectra.

**Supplementary Material Available:** For **14** and **17a**, tables of crystal data and refinement details, atomic coordinates, bond lengths and angles, anisotropic displacement parameters, and hydrogen atom coordinates (10 pages). Ordering information is given on any current masthead page.

OM940376J

(36) Sheldrick, G. M. *Acta Crystallogr.* **1990**, A46, 467.

(37) Sheldrick, G. M. *SHELXL-93, Program for Crystal Structure Refinement*; University of Göttingen: Göttingen, Germany, 1993.

# Experimental and Theoretical Studies of Gold(I) Complexes $\text{Au(L)}^+$ ( $\text{L} = \text{H}_2\text{O}, \text{CO}, \text{NH}_3, \text{C}_2\text{H}_4, \text{C}_3\text{H}_6, \text{C}_4\text{H}_6, \text{C}_6\text{H}_6, \text{C}_6\text{F}_6$ )

Detlef Schröder,<sup>\*,†</sup> Jan Hrušák,<sup>†</sup> Roland H. Hertwig,<sup>†</sup> Wolfram Koch,<sup>†</sup>  
Peter Schwerdtfeger,<sup>‡</sup> and Helmut Schwarz<sup>†</sup>

*Institut für Organische Chemie der Technischen Universität Berlin,  
D-10623 Berlin, Germany, and Computational Material Science and Engineering Research  
Centre, Department of Chemistry and the School of Engineering, University of Auckland,  
Private Bag 92019, Auckland, New Zealand*

Received July 6, 1994<sup>⊗</sup>

Radiative association enhances the formation of  $\text{Au(C}_6\text{F}_6)^+$  from bare  $\text{Au}^+$  ions and hexafluorobenzene in the low-pressure regime of a Fourier transform ion cyclotron resonance mass spectrometer. Due to the relatively small bond dissociation energy (BDE) of  $\text{Au}^+-\text{C}_6\text{F}_6$ , this complex can be used as a versatile precursor for the generation of other  $\text{Au(L)}^+$  complexes by ligand-exchange reactions. Ion/molecule reactions employing the bracketing technique provide a relative gold(I) cation affinity scheme for the various ligands L, i.e.  $\text{C}_6\text{F}_6 < \text{H}_2\text{O} < \text{CO} < \text{C}_2\text{H}_4 < \text{C}_6\text{H}_6 < \text{NH}_3 < \text{C}_3\text{H}_6 < \text{C}_4\text{H}_6$ . In addition, for some ligand pairs L/L' both the forward and reverse ligand exchange reactions were observed from which equilibrium data at room temperature were derived. For  $\text{Au(H}_2\text{O)}^+$ ,  $\text{Au(CO)}^+$ ,  $\text{Au(NH}_3)^+$ , and  $\text{Au(C}_2\text{H}_4)^+$  the absolute BDEs are evaluated by means of ab initio MO calculations at the MP2 level of theory, and the following gold(I) cation affinities are obtained: 39 kcal/mol ( $\text{L} = \text{H}_2\text{O}$ ), 50 kcal/mol (CO), 69 kcal/mol ( $\text{NH}_3$ ), and 73 kcal/mol ( $\text{C}_2\text{H}_4$ ), respectively. On the basis of a comparison of the experimental and computational findings, the absolute error of the calculated BDEs is estimated to be  $\pm 5$  kcal/mol. The unusually high BDE of  $\text{Au(C}_2\text{H}_4)^+$  of ca. 70 kcal/mol is further confirmed by the observation that ethene can replace not only a benzene molecule in  $\text{Au(C}_6\text{H}_6)^+$  in a slightly endothermic process but also the covalently bound iodine ligand in  $\text{AuI}^+$  to yield  $\text{Au(C}_2\text{H}_4)^+$ , setting a lower limit of 59 kcal/mol for  $\text{BDE(Au}^+-\text{C}_2\text{H}_4)$ . Finally, the relative gold(I) cation affinity scale is compared to findings for  $\text{M(L)}^+$  complexes of other transition metals.

Complexes of bare transition-metal cations with small ligands in the gas phase have attracted considerable interest within the last decade. Numerous experimental studies established accurate bond dissociation energies (BDEs) of  $\text{M(L)}^+$  complexes for the first-row transition-metal cations with a large variety of ligands.<sup>1</sup> In addition, nowadays theoretical results on these systems are available and found to be in reasonable agreement with the experimental findings, provided the correlation energy is taken into account appropriately.<sup>2</sup> In fact, in some cases the computational results prompted a revision of experimental figures.<sup>3</sup> So far, not much experimental effort has been undertaken to evaluate the thermochemistry of second- and third-row transition-metal ions.<sup>1</sup> Previous studies by Wilkins and co-workers<sup>4</sup> addressed the chemistry of bare  $\text{Au}^+$  with organic substrates, e.g. saturated and unsaturated hydrocarbons as well as monofunctionalized alkanes. A

particular feature of  $\text{Au}^+$  chemistry is due to the high ionization energy (IE) of the gold atom, which renders its chemistry quite different as compared to other transition-metal ions. For example, while most transition-metal cations dehydrate/dehydrohalogenate alkanols and haloalkanes, respectively, bare  $\text{Au}^+$  preferentially undergoes hydride transfer to yield neutral AuH together with the corresponding  $\alpha$ -cleavage products of the substrates, i.e. closed-shell organic ions.<sup>4</sup> In addition, heavy elements exhibit relativistic effects, which are most pronounced for gold.<sup>5</sup>

In this article we report combined experimental/computational studies of  $\text{Au(L)}^+$  complexes with some inorganic and organic ligands L.<sup>6</sup> The relative gold cation affinities of the various ligands as derived from bracketing experiments are supplemented by ab initio MO computations and compared to previous findings for other ligated transition-metal ions.

## Experimental and Computational Details

The experiments were performed with a Spectrospin CMS 47X Fourier transform ion cyclotron resonance (FTICR) mass spectrometer, which has been described in detail elsewhere.<sup>7</sup> In brief,  $\text{Au}^+$  ions were generated by laser desorption/laser

<sup>†</sup> Technischen Universität Berlin.

<sup>‡</sup> University of Auckland.

<sup>⊗</sup> Abstract published in *Advance ACS Abstracts*, November 15, 1994.

(1) Reviews: (a) Buckner, S. W.; Freiser, B. S. *Polyhedron* **1988**, *7*, 1583. (b) Freiser, B. S. *Chemtracts: Anal. Phys. Chem.* **1989**, *1*, 65. (c) Eller, K.; Schwarz, H. *Chem. Rev.* **1991**, *91*, 1121.

(2) (a) Tsipis, C. A. *Coord. Chem. Rev.* **1991**, *108*, 163. (b) Magnusson, E.; Moriarty, N. W. *J. Comput. Chem.* **1993**, *8*, 961.

(3) See for example: Sodupe, M.; Bauschlicher, C. W., Jr.; Langhoff, S. R.; Partridge, H. *J. Phys. Chem.* **1992**, *96*, 2118.

(4) (a) Weil, D. A.; Wilkins, C. L. *J. Am. Chem. Soc.* **1985**, *107*, 7316.

(b) Chowdhury, A. K.; Wilkins, C. L. *J. Am. Chem. Soc.* **1987**, *109*, 5336.

(5) Pyykkö, P. *Chem. Rev.* **1988**, *88*, 563.

(6) Theoretical studies of  $\text{Au(H}_2\text{O)}^+$  were reported in a preliminary communication: Hrušák, J.; Schröder, D.; Schwarz, H. *Chem. Phys. Lett.* **1994**, *225*, 416.

ionization<sup>8</sup> by focusing a beam of a Nd:YAG laser onto a pure gold target. The ions were extracted from the source and transferred to the analyzer cell by a system of electric potentials and lenses. The isolation of <sup>197</sup>Au<sup>+</sup> and all subsequent ion isolations were performed by using FERETS,<sup>9</sup> a computer-controlled ion ejection protocol which combines single-frequency pulses with frequency sweeps to optimize ion isolation. Au(L)<sup>+</sup> complexes were generated by reacting the ligands L with Au(C<sub>6</sub>F<sub>6</sub>)<sup>+</sup>, which was produced from Au<sup>+</sup> and a pulsed-in C<sub>6</sub>F<sub>6</sub>/Ar mixture, and subsequently thermalized by collisions with argon.<sup>10</sup> It is borne out in the experiments that thermalization of atomic Au<sup>+</sup> is not as efficient as for other transition-metal cations,<sup>10</sup> and more than 1000 collisions with argon were necessary for effective thermalization. Organic substrates were introduced *via* leak valves at pressures ranging from 2 × 10<sup>-9</sup> to 5 × 10<sup>-7</sup> mbar. Branching ratios and rate constants were derived from the analysis of the reaction kinetics, and the pseudo-first-order rate constants were converted to absolute rate constants by calibrating the pressure measurements<sup>11</sup> using rates of well-known ion/molecule processes;<sup>12</sup> the error of the absolute rate constants is estimated to be ±25%.<sup>10a</sup> If forward and backward ligand-exchange reactions were observed, a ca. 1:1 mixture of the respective neutrals L and L' was admitted to the FTICR cell. After the mass selection of Au(L)<sup>+</sup> and Au(L')<sup>+</sup> ions, generated as described above, the pressure and time dependence of the Au(L)<sup>+</sup>/Au(L')<sup>+</sup> ratios was monitored. With the knowledge of absolute pressures, these ratios are then converted to thermal equilibrium constants, K<sub>eq</sub>. As described in the following, the experimental error of K<sub>eq</sub> amounts to ±20%; however, due to systematic errors which are associated with the pressure measurement,<sup>10,11</sup> the absolute errors may well be larger.

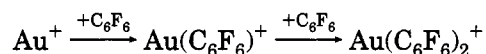
In the *ab initio* MO calculations we used the multielectron adjusted relativistic effective core potential (RECP),<sup>13</sup> augmented by additional diffuse and polarization functions, resulting in a [10s/8p/7d/1f]/(9s/5p/6d/1f) basis set for the gold atom.<sup>6</sup> For the other atoms we used the Dunning TZ2P basis sets with an additional f-polarization function (ζ = 1.85) for the carbon, nitrogen, and oxygen atoms, i.e. the contraction [10s/6p/2d/1f]/(5s/3p/2d/1f) and the [5s/2p/1d]/(3s/2p/1d) basis set for hydrogen atoms.<sup>14</sup> Full geometry optimizations have been performed by using standard procedures at the SCF and MP2 levels of theory. As has been demonstrated previously,<sup>6,15</sup> simple Au<sup>+</sup> compounds are reasonably described by this theoretical approach, and a further increase of the inclusion of correlation energy does not result in substantial changes in geometry and/or energy. All valence electrons were correlated in the perturbational treatment, and these calculations were performed in appropriate symmetries using the GAUSSIAN92-DFT program package.<sup>16</sup> All computations were per-

formed on either IBM/RS 6000 workstations or a CRAY-YMP computer. A complete theoretical treatment of basis set dependencies and relativistic effects, as well as various alternative computational approaches, will be published separately.<sup>17</sup>

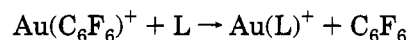
## Results and Discussion

Even at the low-pressure regime of the FTICR setup, thermalized Au<sup>+</sup> cations react with hexafluorobenzene (C<sub>6</sub>F<sub>6</sub>) to rapidly form the adduct complex Au(C<sub>6</sub>F<sub>6</sub>)<sup>+</sup>, indicating that the rovibrationally excited encounter complex Au(C<sub>6</sub>F<sub>6</sub>)<sup>+\*</sup> undergoes radiative stabilization.<sup>18</sup> Measurements of rate constants at different reactant pressures in the presence of argon as an additional third-body stabilization agent result in the following rate law for the association reaction of Au<sup>+</sup> with C<sub>6</sub>F<sub>6</sub>:  $k(p) = 1.5 \times 10^{-10} \text{ cm}^3 \text{ molecule}^{-1} \text{ s}^{-1} + (3 \times 10^{-20})p \text{ cm}^6 \text{ molecule}^{-2} \text{ s}^{-1}$ . In a secondary reaction, association to yield the corresponding bisadduct complex Au(C<sub>6</sub>F<sub>6</sub>)<sub>2</sub><sup>+</sup> is observed (Scheme 1). For convenience, C<sub>6</sub>F<sub>6</sub> was pulsed-in as a mixture with argon in order to allow rapid formation as well as thermalization of Au(C<sub>6</sub>F<sub>6</sub>)<sup>+</sup>. Thus, when the reagents were pumped-off, they did not affect the subsequent measurements.

### Scheme 1

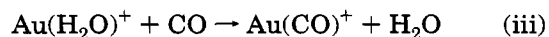
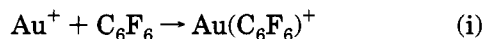


We were not able to determine the bond dissociation energy of the Au(C<sub>6</sub>F<sub>6</sub>)<sup>+</sup> so formed; however, as shown below, its BDE is relatively small. Therefore, this complex can be used as a suitable precursor for the generation of Au(L)<sup>+</sup> complexes with various other ligands by ligand-exchange reactions of the type



In addition, association to yield Au(C<sub>6</sub>F<sub>6</sub>)(L)<sup>+</sup> as well as subsequently Au(L)<sub>2</sub><sup>+</sup> was also observed.

Assuming that multiple collisions with argon effectively thermalize the Au(L)<sup>+</sup> complexes so formed, the occurrence of ligand exchange indicates that the BDE(Au<sup>+</sup>L) values or the particular ligands exceed BDE(Au<sup>+</sup>-C<sub>6</sub>F<sub>6</sub>). No exchange reactions were observed when Au(C<sub>6</sub>F<sub>6</sub>)<sup>+</sup> was reacted with N<sub>2</sub> and O<sub>2</sub>. For those ligands which undergo ligand exchange with Au(C<sub>6</sub>F<sub>6</sub>)<sup>+</sup>, the Au(L)<sup>+</sup> complexes so formed were subsequently mass-selected and reacted with other ligands L' to probe relative gold cation affinities, e.g.



(7) (a) Eller, K.; Schwarz, H. *Int. J. Mass Spectrom. Ion Processes* **1989**, *93*, 243. (b) Eller, K.; Zummack, W.; Schwarz, H. *J. Am. Chem. Soc.* **1990**, *112*, 621.

(8) (a) Freiser, B. S. *Talanta* **1985**, *32*, 697. (b) Freiser, B. S. *Anal. Chim. Acta* **1985**, *178*, 137.

(9) Forbes, R. A.; Laukien, F. H.; Wronka, J. *Int. J. Mass Spectrom. Ion Processes* **1988**, *83*, 23.

(10) (a) Schröder, D. Ph.D. Thesis, TU Berlin D83, 1993. (b) Schröder, D.; Fiedler, A.; Ryan, M. F.; Schwarz, H. *J. Phys. Chem.* **1994**, *98*, 68.

(11) The pressures were corrected for the relative sensitivity of the ion gauge for different gases. For details, see: (a) Nakao, F. *Vacuum* **1975**, *25*, 431. (b) Bartmess, J. E.; Georgiadis, R. M. *Vacuum* **1983**, *33*, 149.

(12) Examples of calibration reactions are described by: Lin, Y.; Ridge, D. P.; Munson, B. *Org. Mass Spectrom.* **1991**, *26*, 550.

(13) Schwerdtfeger, P.; Dolg, M.; Schwarz, W. H. E.; Bowmaker, G. A.; Boyd, P. D. W. *J. Chem. Phys.* **1989**, *91*, 1762.

(14) Huzinaga, S. *J. Chem. Phys.* **1965**, *42*, 1293.

(15) Veldkamp, A.; Frenking, G. *Organometallics* **1993**, *12*, 4613.

(16) Frisch, M. J.; Trucks, G. W.; Schlegel, H. W.; Gill, P. M. W.; Johnson, B. G.; Wong, M. W.; Foresman, J. B.; Robb, M. A.; Head-Gordon, M.; Replogle, E. S.; Gomperts, R.; Andres, J. L.; Raghavachari, K.; Binkley, J. S.; Gonzales, C.; Martin, R. L.; Fox, D. J.; Defrees, D. J.; Baker, J.; Stewart, J. J. P.; Pople, J. A. GAUSSIAN92-DFT, Rev. F.2; Gaussian Inc., Pittsburgh, PA, 1993.

(17) (a) Hrušák, J.; Hertwig, R. H.; Schröder, D.; Schwerdtfeger, P.; Koch, W.; Schwarz, H. *Organometallics*, in press. (b) Hrušák, J.; Hertwig, R. H.; Schröder, D.; Koch, W.; Schwarz, H. *Proc. Int. Congr. Quantum Chem.* **1994**, *8*, 350.

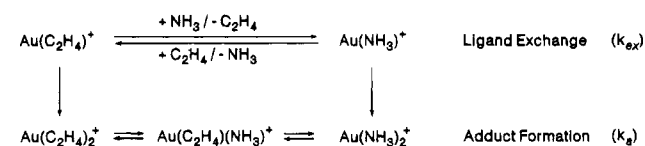
(18) (a) Dunbar, R. C. *Mass Spectrom. Rev.* **1992**, *11*, 309. (b) Dunbar, R. C.; Uechi, G. T.; Asamoto, B. *J. Am. Chem. Soc.* **1994**, *116*, 2466. (c) Thölmann, D.; McCormick, A.; McMahon, T. B. *J. Phys. Chem.* **1994**, *98*, 1156. (d) Stöckigt, D.; Schwarz, H. *Int. J. Mass Spectrom. Ion Processes*, in press.



**Table 1. Occurrence (+) or Nonoccurrence (-) of Ligand-Exchange Reactions  $\text{Au}(\text{L})^+ + \text{L}' \rightarrow \text{Au}(\text{L}')^+ + \text{L}$  for Various Ligands L and L'<sup>a</sup>**

Au(L) <sup>+</sup>	L'						
	H <sub>2</sub> O	CO	C <sub>2</sub> H <sub>4</sub>	C <sub>6</sub> H <sub>6</sub>	NH <sub>3</sub>	C <sub>3</sub> H <sub>6</sub>	C <sub>4</sub> H <sub>6</sub>
Au(C <sub>6</sub> F <sub>6</sub> ) <sup>+</sup>	+	+	+	+	+	+	+
Au(H <sub>2</sub> O) <sup>+</sup>	○	+	+	+	+	+	+
Au(CO) <sup>+</sup>	-	○	+	+	+	+	+
Au(C <sub>2</sub> H <sub>4</sub> ) <sup>+</sup>	-	-	○	+ <sup>b</sup>	+ <sup>b</sup>	+	+
Au(C <sub>6</sub> H <sub>6</sub> ) <sup>+</sup>	-	-	+ <sup>b</sup>	○	+ <sup>b</sup>	+	+
Au(NH <sub>3</sub> ) <sup>+</sup>	-	-	+ <sup>b</sup>	+ <sup>b</sup>	○	+ <sup>b</sup>	+
Au(C <sub>3</sub> H <sub>6</sub> ) <sup>+</sup>	-	-	-	-	+ <sup>b</sup>	○	+
Au(C <sub>4</sub> H <sub>6</sub> ) <sup>+</sup>	-	-	-	-	-	-	○

<sup>a</sup> The circles denote the rapid degenerate exchange reactions  $\text{Au}(\text{L})^+ + \text{L} \rightarrow \text{Au}(\text{L})^+ + \text{L}$ . For all ligand combinations, formation of the bisadduct complexes  $\text{Au}(\text{L})_2^+$  was observed as a secondary reaction. <sup>b</sup> For these ligand pairs forward and backward ligand-exchange reactions between  $\text{Au}(\text{L})^+$  and  $\text{Au}(\text{L}')^+$  were observed, if both neutral ligands were leaked simultaneously into the mass spectrometer. This observation indicates that for these ligands the difference of the gold(I) cation affinities of L and L' is <4 kcal/mol (see text).

**Scheme 2****Table 2. Equilibrium Constants ( $K_{\text{eq}}$ ) and Relative Abundances (%) of  $\text{Au}(\text{C}_2\text{H}_4)^+$  and  $\text{Au}(\text{NH}_3)^+$  as a Function of Partial Pressure  $p$  (mbar) and Reaction Time  $t_R$  (s)<sup>a</sup>**

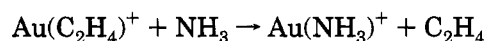
$p$		$t_R$	rel abund		$K_{\text{eq}}$
C <sub>2</sub> H <sub>4</sub>	NH <sub>3</sub>		Au(C <sub>2</sub> H <sub>4</sub> ) <sup>+</sup>	Au(NH <sub>3</sub> ) <sup>+</sup>	
$2.1 \times 10^{-8}$	$1.4 \times 10^{-8}$	10	3.2	100	0.021
$2.1 \times 10^{-8}$	$1.4 \times 10^{-8}$	20	2.9	100	0.019
$7.1 \times 10^{-8}$	$1.4 \times 10^{-8}$	5	8.0	100	0.016
$7.1 \times 10^{-8}$	$1.4 \times 10^{-8}$	10	8.3	100	0.017
$2.9 \times 10^{-7}$	$1.4 \times 10^{-8}$	5	48.5	100	0.023
$2.9 \times 10^{-7}$	$1.4 \times 10^{-8}$	10	49.0	100	0.024

<sup>a</sup> Prior to the reaction time a mixture of  $\text{Au}(\text{C}_2\text{H}_4)^+$  and  $\text{Au}(\text{NH}_3)^+$  was generated from  $\text{Au}^+$  and  $\text{C}_6\text{F}_6$  as described above, thermalized with pulsed-in argon, and preequilibrated for 15 s; then both ions were isolated in the FTICR cell. In terms of collision theory the ions undergo ca. 500 collisions with argon during thermalization and at least 15 collisions with ammonia and ethene, respectively. The intensities are normalized to  $\text{Au}(\text{NH}_3)^+ = 100\%$ . Naturally, adduct formation increases with pressure and reaction time; for example, for the entry in the last row the ratio  $\text{Au}(\text{NH}_3)^+/\text{Au}(\text{NH}_3)_2^+$  amounts to ca. 1:2.

This sequence of reactions enables us to determine a relative  $\text{Au}^+$  affinity scheme for the various ligands, i.e.  $\text{N}_2, \text{O}_2 < \text{C}_6\text{F}_6 < \text{H}_2\text{O} < \text{CO} < \text{C}_2\text{H}_4 < \text{C}_6\text{H}_6 < \text{NH}_3 < \text{C}_3\text{H}_6 < \text{C}_4\text{H}_6$  (Table 1). This ordering agrees well with the previous findings by Wilkins and co-workers,<sup>4</sup> who reported that benzene and also  $\text{CH}_3\text{CN}$  are more strongly bound to  $\text{Au}^+$  than  $\text{C}_2\text{H}_4$ .

In the case of the ligand pair  $\text{C}_2\text{H}_4$  and  $\text{NH}_3$  (Scheme 2), the rates  $k_a$  for the competitive formation of the adduct complexes  $\text{Au}(\text{C}_2\text{H}_4)_2^+$ ,  $\text{Au}(\text{C}_2\text{H}_4)(\text{NH}_3)^+$ , and  $\text{Au}(\text{NH}_3)_2^+$ , respectively, are much smaller than the rates of the ligand exchange reactions  $k_{\text{ex}}$ . Hence, it is possible to establish an equilibrium between  $\text{Au}(\text{C}_2\text{H}_4)^+$  and  $\text{Au}(\text{NH}_3)^+$  for certain  $\text{C}_2\text{H}_4/\text{NH}_3$  ratios (Table 2), which in turn enables one to evaluate the equilibrium constant  $K_{\text{eq}}$ . As can be seen from the time independence of the  $\text{Au}(\text{C}_2\text{H}_4)^+/\text{Au}(\text{NH}_3)^+$  ratios, the reaction time is sufficient to establish the equilibrium, and adduct formation does not affect the relative abundances. Furthermore,  $K_{\text{eq}}$  exhibits no distinct pressure

dependence; rather, the small spread of the  $K_{\text{eq}}$  values reflects the experimental uncertainties, the pressure measurement in particular. Given a thermal equilibrium between the two gold(I) complexes and assuming room temperature for the reactants,  $K_{\text{eq}}$  can be converted to  $\Delta\Delta G$  of the ligand-exchange reaction, leading to a value of  $-2.3 \pm 0.5$  kcal/mol<sup>19</sup> for the process



For the other ligand pairs studied, either the BDE differences were too large to attain equilibrium or rapid adduct formation obscures the otherwise straightforward conversion of ion signal intensities for the mono-ligand complexes to  $\Delta\Delta G$ . For example, if  $\text{Au}(\text{C}_3\text{H}_6)^+$  is reacted with a 1:1 mixture of ammonia and propene, association to bisligated complexes is so rapid that ligand exchange to yield  $\text{Au}(\text{NH}_3)^+$  amounts to only 5%. However, the occurrence of forward and backward ligand-exchange reactions was observed for the ligand pairs  $\text{L}/\text{L}' = \text{C}_2\text{H}_4/\text{C}_6\text{H}_6, \text{C}_6\text{H}_6/\text{NH}_3,$  and  $\text{NH}_3/\text{C}_3\text{H}_6$ , with the formation of  $\text{Au}(\text{L}')^+$  being favored when the partial pressures of L and L' are identical.

A principal shortcoming of the bracketing technique is that absolute values for the ligand binding energies can usually not be obtained by using this approach.<sup>20</sup> Wilkins and co-workers derived lower limits for BDE( $\text{Au}^+ - \text{H}_2\text{O}$ ) > 16 kcal/mol and BDE( $\text{Au}^+ - \text{C}_2\text{H}_4$ ) > 33 kcal/mol from the occurrence of ion/molecule reactions of  $\text{Au}^+$  with alcohols and alkanes.<sup>4</sup> However, this information is not very conclusive in that upper bounds have not been determined yet. More recently it has been demonstrated that for closed-shell gold compounds ab initio MO calculations can be performed with reasonable accuracy.<sup>6,15,21</sup> Therefore, we calculated the BDEs of  $\text{Au}(\text{H}_2\text{O})^+, \text{Au}(\text{CO})^+, \text{Au}(\text{C}_2\text{H}_4)^+,$  and  $\text{Au}(\text{NH}_3)^+$  at the MP2 level of theory using a relativistic effective core potential for the gold atom. In this article we refrain from a detailed discussion of the theoretical results with respect to basis set dependencies, different computational approaches, levels of correlation energy, and influences of relativistic effects;<sup>17</sup> rather, we will restrict the discussion to the structural and energetic aspects on the MP2 level of theory which will be compared with the experimental findings.

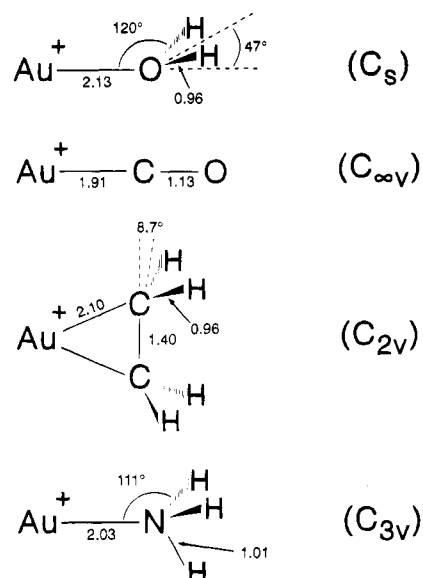
The optimized geometry of  $\text{Au}(\text{H}_2\text{O})^+$  (Figure 1) reveals a nonplanar structure, with the gold atom being located out of the H-O-H plane by 47°; the planar  $\text{C}_{2v}$ -symmetrical structure corresponds to a transition structure. BDE( $\text{Au}^+ - \text{H}_2\text{O}$ ) has been calculated to be 38.8 kcal/mol with respect to isolated  $\text{Au}^+$  and  $\text{H}_2\text{O}$  in their respective electronic ground states (Table 3).<sup>6</sup> The geometry-optimized structure of  $\text{Au}(\text{CO})^+$  and the BDE of 50.1 kcal/mol are in line with a recent computational

(19) The systematic errors are associated with the relative sensitivities of the ion gauge used (IMG 070, Balzers) for the various gases; for details, see ref 10a and 11.

(20) In some cases, lower and upper bounds are close to each other and permit a good estimate for the absolute BDEs. For a recent example concerning Au(I) compounds, see: (a) Schröder, D.; Hrušák, J.; Tornieporth-Oetting, I. C.; Klapötke, T. M.; Schwarz, H. *Angew. Chem., Int. Ed. Engl.* **1994**, *33*, 212. (b) Schwerdtfeger, P.; McFeaters, J. S.; Stephens, R. L.; Liddell, M. J.; Dolg, M.; Hess, B. A. *Chem. Phys. Lett.* **1994**, *218*, 362.

(21) (a) Reference 13. (b) Schwerdtfeger, P. *J. Am. Chem. Soc.* **1989**, *111*, 7261. (c) Schwerdtfeger, P.; Boyd, P. D. W.; Burrell, A. K.; Robinson, W. T.; Taylor, M. J. *Inorg. Chem.* **1990**, *29*, 3593. (d) For earlier work, see Ziegler, T.; Rauk, A. *Inorg. Chem.* **1979**, *18*, 1558.





**Figure 1.** Optimized geometries of  $\text{Au}(\text{H}_2\text{O})^+$ ,  $\text{Au}(\text{CO})^+$ ,  $\text{Au}(\text{C}_2\text{H}_4)^+$ , and  $\text{Au}(\text{NH}_3)^+$ , at the MP2-TZ2P+f level of theory (bond lengths in Å and angles in degrees).

**Table 3.** Symmetries, Bond Distances ( $r_{\text{Au-L}}$  in Å), Mulliken Charges ( $q_{\text{Au}}$ ) on the Gold Atom, and Bond Dissociation Energies (BDE in kcal/mol) for  $\text{Au}(\text{L})^+$  Complexes

	sym	$r_{\text{Au-L}}^a$	$q_{\text{Au}}$	BDE
$\text{Au}(\text{H}_2\text{O})^+{}^b$	$C_s$	2.13	0.86	38.8
$\text{Au}(\text{CO})^+$	$C_{\infty v}$	1.91	0.93	50.1
$\text{Au}(\text{C}_2\text{H}_4)^+$	$C_{2v}$	2.10	0.58	73.1
$\text{Au}(\text{NH}_3)^+$	$C_{3v}$	2.03	0.63	68.6

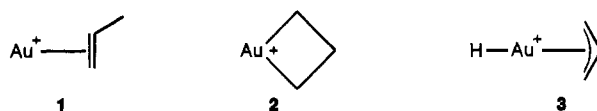
<sup>a</sup> The bond lengths refer to  $r_{\text{Au-O}}$ ,  $r_{\text{Au-C}}$ ,  $r_{\text{Au-C}}$ , and  $r_{\text{Au-N}}$ , respectively.

<sup>b</sup> The fully geometry-optimized structure of  $\text{Au}(\text{H}_2\text{O})^+$  is nonplanar; for details, see ref 6.

study,<sup>15</sup> the somewhat smaller bond lengths in the present work, as compared to the previous study,<sup>15</sup> has to be ascribed to the different basis sets used, i.e. Hay/Wadt ECP and 6-31G\*\* for the ligands versus TZ2P+f. The  $C_{2v}$ -symmetrical structure of  $\text{Au}(\text{C}_2\text{H}_4)^+$  agrees well with its description as a  $\pi$ -complex of ethene with the  $\text{Au}^+$  cation, in which the methylene groups are pyramidalized by 8.7°. Significant covalent contributions to the Au-C bonding are indicated by the lengthening of the C-C distance to 1.40 Å as compared to 1.33 Å in uncomplexed ethene. The computed BDE of  $\text{Au}(\text{C}_2\text{H}_4)^+$  amounts to 73.1 kcal/mol. Finally, the optimized geometry of  $\text{Au}(\text{NH}_3)^+$  exhibits  $C_{3v}$  symmetry with an almost unperturbed ammonia substrate and a BDE of 68.6 kcal/mol.

According to the computational results  $\text{Au}^+$  binds ethene more strongly than ammonia ( $\Delta E = 4.5$  kcal/mol), whereas the equilibrium data imply the opposite ( $\Delta\Delta G = -2.3$  kcal/mol). A possible reason for the discrepancy between the theoretical and experimental results might be due to entropy effects. However, a frequency analysis and the subsequent computation of  $\Delta\Delta G$  (298 K) do not resolve this discrepancy, since  $\Delta\Delta H$  and  $\Delta\Delta S$  precisely cancel each other, such that the computed  $\Delta\Delta G$  (298 K) also amounts to 4.5 kcal/mol. While one might doubt the magnitude as well as the precision of the experimental figure, the relative order of stabilities of the two complexes is unambiguous. Consequently, we are left with the conclusion that the calculated BDEs are associated with an absolute error

**Chart 1**



of at least 5 kcal/mol. With respect to the restricted basis set, and the limitations of the MP2 method in particular, an error of this magnitude is not unexpected at all.<sup>2b,13,17</sup>

Surprisingly, the BDEs of most ligands L to  $\text{Au}^+$  are significantly larger than for other transition-metal cations  $\text{M}^+$ . For example,  $\text{BDE}(\text{Au}^+-\text{C}_2\text{H}_4)$  is higher than those of most other known  $\text{M}(\text{C}_2\text{H}_4)^+$  complexes. In particular, the electronically related  $\text{Cu}(\text{C}_2\text{H}_4)^+$  and  $\text{Au}(\text{C}_2\text{H}_4)^+$  complexes exhibit BDEs of only 36 and 34 kcal/mol, respectively,<sup>3,22</sup> i.e. less than half of the value for gold. Furthermore, the magnitude of  $\text{BDE}(\text{Au}^+-\text{C}_2\text{H}_4)$  is on the order of that for cationic benzene complexes,<sup>1a,23</sup> which is in line with the experimental observation that the reaction of  $\text{Au}(\text{C}_2\text{H}_4)^+$  with benzene to yield  $\text{Au}(\text{C}_6\text{H}_6)^+$  and ethene is partially reversible.

The description of the structure of  $\text{Au}(\text{C}_2\text{H}_4)^+$  as an intact olefin complex<sup>24</sup> is further supported by the occurrence of ligand exchange reactions; in particular, the rapid degenerate exchange with  $\text{C}_2\text{D}_4$  to yield  $\text{Au}(\text{C}_2\text{D}_4)^+$  takes place without any evidence for H/D exchange processes. Similarly, the structure of  $\text{Au}(\text{C}_3\text{H}_6)^+$  should correspond to the genuine propene complex **1** (Chart 1). It is noteworthy that  $\text{BDE}(\text{Au}^+-\text{C}_3\text{H}_6)$  exceeds  $\text{BDE}(\text{Au}^+-\text{C}_6\text{H}_6)$ , although benzene may potentially serve as a  $\eta^6$  ligand. Chowdhury and Wilkins<sup>4b</sup> ascribed the absence of ligand exchange with benzene to an isomerization of the formal  $\eta^2$  complex  $\text{Au}(\text{C}_3\text{H}_6)^+$  (**1**), to yield the corresponding auracyclobutane **2**.<sup>25</sup> Furthermore, the absence of H/D exchange processes when  $\text{Au}(\text{C}_3\text{H}_6)^+$  is reacted with either  $\text{D}_2$  or  $\text{C}_2\text{D}_4$  led these authors to conclude that structure **3** does not participate. In order to solve this structural problem, we examined the secondary reactions of  $\text{Au}(\text{C}_3\text{H}_6)^+$ . (i) Upon reaction of  $\text{CH}_3\text{CH}_2\text{CD}_2\text{OH}$  with bare  $\text{Au}^+$  the labeled complex  $\text{Au}(\text{CH}_3\text{CH}=\text{CD}_2)^+$  is formed in reasonable yields.<sup>4a</sup> If this complex is reacted with unlabeled propene, besides adduct formation, rapid exchange to yield  $\text{Au}(\text{C}_3\text{H}_6)^+$  is observed; again, there is no evidence supporting the occurrence of H/D exchange processes. (ii) Similarly, the  $\text{C}_3\text{H}_6$  ligand in  $\text{Au}(\text{C}_3\text{H}_6)^+$  can be replaced by  $\text{NH}_3$  as well as butadiene to yield the corresponding  $\text{Au}(\text{L})^+$  complexes. These findings indicate that an intact propene substructure is present in  $\text{Au}(\text{C}_3\text{H}_6)^+$ ; thus, we conclude that **1** is formed in the experiment. The absence of ligand exchange with benzene, which was interpreted previously<sup>4b</sup> in terms of structure **2**, can simply be accounted for by the unusually high BDE of the propene complex **1**. For the sake of completeness we wish to stress that our mass-

(22) Guo, B. C.; Castleman, A. W., Jr. *Chem. Phys. Lett.* **1991**, *181*, 16.

(23) Willey, K. F.; Cheng, P. Y.; Bishop, M. B.; Duncan, M. A. *J. Am. Chem. Soc.* **1991**, *113*, 4721.

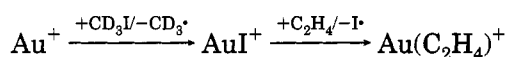
(24) For a survey of gold(I) olefin complexes in the condensed phase, see: Schmidbaur, H. *Gmelin Handbook*, Springer-Verlag: Berlin, 1980; *Au Organogold Compounds*, p 194.

(25) (a) Jacobson, D. B.; Freiser, B. S. *Organometallics* **1984**, *3*, 513. (b) van Koppen, P. A. M.; Bowers, M. T.; Beauchamp, J. L. *Organometallics* **1990**, *9*, 625. (c) Schultz, R. H.; Armentrout, P. B. *Organometallics* **1992**, *11*, 828.

spectrometric experiments cannot fully rule out that isomer **2** is also present. However, this would imply that structures **1** and **2** are in a rapid equilibrium. As a consequence, one would have to assume allylic C–H bond activation of **1** and subsequent H-transfer to the central carbon atom as well as formation of two Au–C bonds to yield **2**, with the allylic structure **3** as intermediate. Formation of **3** would imply not only that H/D exchange processes with labeled alkenes occur but also that dissociation to  $C_3H_5^+$  and neutral AuH (IE = 10.6 eV) is expected to take place. From the absence of these features we conclude that, most likely, **1** is formed exclusively in the experiment.

In order to confirm the order of magnitude for the BDE of  $Au(C_2H_4)^+$ , we performed an additional bracketing experiment in which  $AuI^+$  was reacted with ethene.  $AuI^+$  has been generated by reacting  $Au^+$  with  $CD_3I$ , indicating that BDE ( $Au^+–I$ ) exceeds 59 kcal/mol. Interestingly, the covalent iodine ligand is replaced quite rapidly by ethene ( $k_{ex} = 6.0 \cdot 10^{-10} \text{ cm}^3 \text{ molecules}^{-1} \text{ s}^{-1}$ ) with  $Au(C_2H_4)^+$  as the exclusive ionic product (Scheme 3). To the best of our knowledge, this reaction represents the *first* example for the substitution of a covalent ligand by a  $\pi$ -bonded one.<sup>26</sup>

### Scheme 3



As compared to the ligand binding energies of main-group as well as transition-metal cations, the ordering for  $Au^+$  differs significantly from that described previously for  $Li^+$ ,<sup>27</sup>  $Mg^+$ ,<sup>28</sup>  $Al^+$ ,<sup>29</sup>  $Mn^+$ ,<sup>30</sup>  $Cu^+$ ,<sup>31</sup> and  $Ni(c-C_5H_5)^+$ .<sup>32</sup> For example, the BDE( $Au^+–L$ ) values do not correlate with the corresponding proton affinities of the ligands,<sup>33</sup> as was observed for the other metal cations.<sup>27–32</sup> The most likely explanation for this deviation of  $Au^+$  involves the high IE of gold as well as the effects of  $s \rightarrow p$  and  $s \rightarrow d$  excitations as compared to its first- and second-row transition-metal congeners. Particularly, for gold(I) complexes the high IE will lead to significant electron transfer from the ligand to the metal cation, resulting in a relatively large covalent contribution to the bonding. In contrast, the nature of the binding for other cationic transition-metal complexes has been described as primarily electrostatic.<sup>2</sup> For the gold(I) complexes studied here, the charge transfer from the ligand to the gold atom is also borne out in the

(26) There exists one remotely related example in the literature; however, its details are not clear: Allison, J.; Ridge, D. P. *J. Am. Chem. Soc.* **1976**, *98*, 7445.

(27) (a) Staley, R. H.; Beauchamp, J. L. *J. Am. Chem. Soc.* **1975**, *97*, 5920. (b) Woodin, R. L.; Beauchamp, J. L. *J. Am. Chem. Soc.* **1978**, *100*, 501.

(28) Operti, L.; Tews, E. C.; Freiser, B. S. *J. Am. Chem. Soc.* **1988**, *110*, 5847.

(29) Uppal, J. S.; Staley, R. H. *J. Am. Chem. Soc.* **1982**, *104*, 1235.

(30) Uppal, J. S.; Staley, R. H. *J. Am. Chem. Soc.* **1982**, *104*, 1238.

(31) (a) Jones, R. W.; Staley, R. H. *J. Am. Chem. Soc.* **1980**, *102*, 3794. (b) Jones, R. W.; Staley, R. H. *J. Am. Chem. Soc.* **1982**, *104*, 2296. Also see: (c) Magnera, T. F.; David, D. E.; Stulik, D.; Orth, R. G.; Jonkman, H. T.; Michl, J. *J. Am. Chem. Soc.* **1989**, *111*, 5036. (d) El-Shall, M. S.; Schriver, K. E.; Whetten, R. L.; Meot-Ner (Mautner), M. *J. Phys. Chem.* **1989**, *93*, 7969.

(32) Corderman, R. R.; Beauchamp, J. L. *J. Am. Chem. Soc.* **1976**, *98*, 3998.

(33) For additional thermochemical data, see: (a) Lias, S. G.; Leibman, J. F.; Levin, R. D. *J. Phys. Chem. Ref. Data* **1984**, *13*, 695. (b) Lias, S. G.; Bartmess, J. E.; Liebman, J. F.; Holmes, J. L.; Levin, R. D.; Mallard, W. G. *J. Phys. Chem. Ref. Data* **1988**, *17*, Suppl. 1.

**Table 4.** Calculated and Estimated Bond Dissociation Energies (BDEs in kcal/mol) for  $Au(L)^+$  Complexes, Experimental Proton Affinities (PA in kcal/mol), and Ionization Energies (IE in eV) of the Ligands L

	BDE	PA(L) <sup>a</sup>	IE(L) <sup>b</sup>
$Au(H_2O)^+{}^c$	39	167	12.61
$Au(CO)^+$	50	142	14.01
$Au(C_2H_4)^+$	73	163	10.51
$Au(c-C_5H_5)^+$	≈70 <sup>c</sup>	181	9.25
$Au(NH_3)^+$	69	204	10.16
$Au(C_3H_6)^+$	>75 <sup>c</sup>	180	9.73
$Au(C_4H_6)^+$	>75 <sup>c</sup>	193	9.08

<sup>a</sup> The experimental data were taken from ref 33. <sup>b</sup> For comparison: IE(Au) = 9.225 eV. <sup>c</sup> Estimate derived from ion/molecule bracketing (see text).

charge distribution as derived from Mulliken population analysis (Table 3). Also, charge transfer causes the deviation from planarity in the case of  $Au(H_2O)^+$ , as analyzed in detail previously.<sup>6</sup> However, there exists no evident correlation between the IEs of the ligands and their corresponding gold cation affinity. Presumably, the unique feature of the gold(I) complexes is due to relativistic effects, which strengthen and shorten the bonds to the ligands. The precise nature and the origin of these effects are presently under investigation.<sup>17</sup>

Finally, in our study of gold(I) chemistry in the gas phase we hardly observe processes in which typical metal-mediated bond-activation processes occur. For example almost all transition-metal cations undergo condensation reactions with two or more butadiene molecules to yield higher hydrocarbons.<sup>1,34</sup> Although the  $Au^+$  cation clusters with butadiene to yield  $Au-(C_4H_6)_2^+$ , the product appears to be a simple dimeric complex without any evidence for C–C bond formation, consecutive dehydrogenation, olefin losses, etc. Similarly, in contrast to most other transition-metal cations, no H/D exchange processes are associated with  $Au^+$ -mediated dehydration or dehydrohalogenation of labeled alkanols or haloalkanes, respectively, as are reported to occur for alkali-metal cations.<sup>35</sup> In fact, none of the other reactants under study underwent chemical activation processes except for obvious charge transfer or hydride abstraction when thermochemically feasible. Thus, while gold(I) chemistry deserves interest with respect to relativistic effects on bonding, as far as catalysis is concerned, in the gas phase atomic  $Au^+$  seems to be quite inefficient.<sup>36,37</sup>

**Acknowledgment.** Continuous financial support was provided by the Deutsche Forschungsgemeinschaft and the Fonds der Chemischen Industrie. Furthermore, we are grateful to Degussa AG, Hanau, Germany, for the support of our “gold project”. Dipl.-Chem. Detlef Stöckigt is acknowledged for helpful discussions.

OM940527I

(34) Karrass, S.; Schröder, D.; Schwarz, H. *Chem. Ber.* **1992**, *125*, 751 and references cited therein.

(35) (a) Allison, J.; Ridge, D. P. *J. Am. Chem. Soc.* **1979**, *101*, 4998. (b) Prüsse, T.; Schwarz, H. *Organometallics* **1989**, *8*, 2856. (c) Eller, K. *Coord. Chem. Rev.* **1993**, *126*, 93.

(36) For a recent study on the inertness of gold(I) compounds in the condensed phase, see: Banaszak Holl, M. M.; Seidler, P. F.; Kowalczyk, S. P.; McFeely, F. R. *Inorg. Chem.* **1994**, *33*, 510.

(37) Puddephatt, R. J. *Polyhedron* **1994**, *13*, 1233.

# Activation of C–C and C–H Bonds of *cis*- and *trans*-1-Acetyl-2-methylcyclopropane by Bare Metal(I) Cations in the Gas Phase: Comparative Study of the First-Row Transition-Metal Ions Cr<sup>+</sup>–Cu<sup>+</sup>

Christoph A. Schalley, Detlef Schröder, and Helmut Schwarz\*

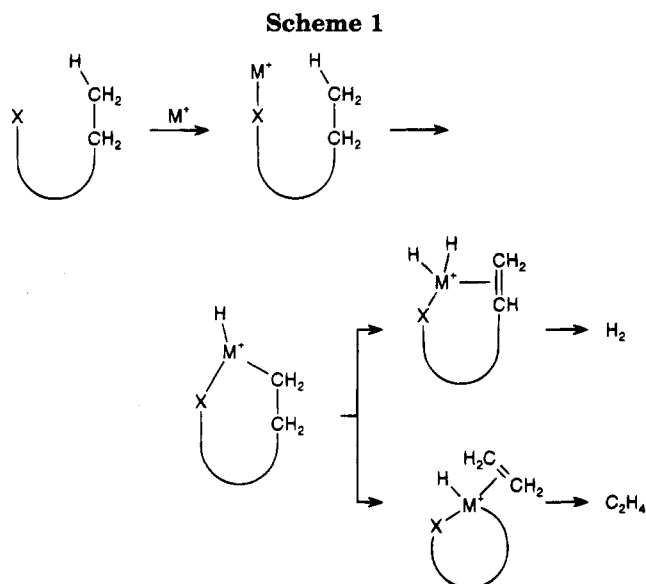
Institut für Organische Chemie der Technischen Universität Berlin, 10623 Berlin, Germany

Received June 13, 1994<sup>®</sup>

Stereochemical effects on transition-metal-mediated C–H and C–C bond activation are probed by examining unimolecular fragmentation reactions of 1-acetyl-2-methylcyclopropane/M<sup>+</sup> complexes (M = Cr<sup>+</sup>–Cu<sup>+</sup>) in the gas phase. Basically, three general reaction types can be distinguished: (i) metal-induced ring cleavage leading to losses of molecular hydrogen, ethene, and acetaldehyde (these C–H and C–C bond activation processes can be ascribed to remote functionalization of an acyclic hexenone/M<sup>+</sup> intermediate), (ii) insertion of the metal in an  $\alpha$ -C–C bond and subsequent decarbonylation to yield the corresponding olefin/M<sup>+</sup> complexes, and (iii) geminal C–C bond activation leading to the formation of metal carbene complexes as intermediates for M = Cr, Mn, Co, and Ni. These carbene complexes eventually give rise to unimolecular losses of ethene or propene. Direct C–H bond activation of the terminal methyl group is observed for none of the metals. Stereochemical differences for *cis* and *trans* isomers are only observed when the rate-determining steps for C–C bond activation leading to different products, i.e. remote functionalization and decarbonylation, compete directly with each other, and distinct stereochemical effects are observed for the Mn<sup>+</sup>, Fe<sup>+</sup>, and Cu<sup>+</sup> complexes. The experimental data and the trends within the late first-row transition metals are compared with previous findings and discussed in terms of activation barriers associated with C–C and C–H bond activation processes and thermodynamics.

## Introduction

While there have been numerous reports on the gas-phase chemistry of bare and partially ligated transition-metal ions with organic substrates,<sup>1</sup> detailed studies of the stereochemistry of C–H bond activation mediated by bare or ligated metal cations in the gas phase are scarce.<sup>2</sup> Carbonyl compounds may serve as a case in point, in that both the regio- and the stereochemistry of C–H and C–C bond activation by naked Fe<sup>+</sup> cations were examined in great detail.<sup>3</sup> In particular, the examination of unimolecular dissociations of metastable ketone/Fe<sup>+</sup> complexes provided detailed insight into the reaction mechanisms, rate-determining steps, and kinetic isotope effects associated with Fe<sup>+</sup>-mediated C–H and C–C bond activation in the gas phase.<sup>2f,3d–f</sup> In general, the studies revealed that these reactions,



involving the activation of ordinary C–H and C–C bonds, can be described in terms of the “remote functionalization” concept<sup>4</sup> (Scheme 1), provided one side chain bears at least three carbon atoms. Most interestingly, bare Fe(I) cations were also demonstrated to bring about diastereoselective C–H bond activation of acyclic ketones.<sup>2f,3f</sup>

With regard to the topic of stereochemistry in metal-mediated bond activation, the investigation of complexes

<sup>®</sup> Abstract published in *Advance ACS Abstracts*, November 15, 1994.

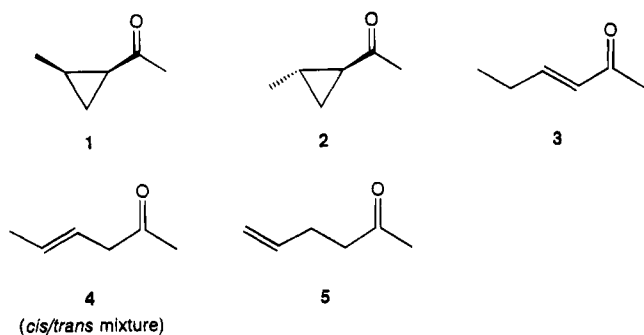
(1) For recent reviews see: (a) Eller, K.; Schwarz, H. *Chem. Rev.* **1991**, *91*, 1121. (b) Eller, K. *Coord. Chem. Rev.* **1993**, *126*, 93.

(2) (a) Nekrasov, Y. S.; Zagorevskii, D. V. *Org. Mass Spectrom.* **1991**, *26*, 733. (b) Prüsse, T.; Fiedler, A.; Schwarz, H. *Helv. Chim. Acta* **1991**, *74*, 43. (c) Seemeyer, K.; Prüsse, T.; Schwarz, H. *Helv. Chim. Acta* **1993**, *76*, 1632. (d) Seemeyer, K.; Prüsse, T.; Schwarz, H. *Helv. Chim. Acta* **1993**, *76*, 113. (e) Seemeyer, K.; Schwarz, H. *Helv. Chim. Acta* **1993**, *76*, 2384. (f) Schröder, D.; Schwarz, H. *J. Am. Chem. Soc.* **1993**, *115*, 8818. (g) Raabe, N.; Karrass, S.; Schwarz, H. *Chem. Ber.* **1994**, *127*, 261. (h) For a recent study of the gas-phase stereoselectivity in metal-free 1,2-elimination reactions, see: Rabasco, J. J.; Gronert, S.; Kass, S. R. *J. Am. Chem. Soc.* **1994**, *116*, 3133.

(3) (a) Burnier, R. C.; Byrd, G. D.; Freiser, B. S. *J. Am. Chem. Soc.* **1981**, *103*, 4360. (b) Grady, W. L.; Bursley, M. M. *Int. J. Mass Spectrom. Ion Processes* **1983**, *52*, 247. (c) Lombarski, M.; Allison, J. *Int. J. Mass Spectrom. Ion Processes* **1985**, *65*, 31. (d) Schröder, D.; Schwarz, H. *Chimia* **1989**, *43*, 317. (e) Schröder, D.; Schwarz, H. *J. Am. Chem. Soc.* **1990**, *112*, 5947. (f) Schröder, D. Ph.D. Thesis, Technische Universität Berlin D83, 1993.

(4) Schwarz, H. *Acc. Chem. Res.* **1989**, *22*, 282.

Chart 1



of *cis*- and *trans*-1-acetyl-2-methylcyclopropanes **1** and **2** (Chart 1) with bare transition-metal cations appears to be particularly promising, as the rigidity of these substrates confers a well-defined stereochemical relationship between the substituents. However, there are other features to be taken into account: the C–C bonds of the cyclopropyl backbone are weakened by the high ring-strain energy, while the cyclopropylic C–H bonds are strengthened and possess high bond dissociation energies in the range of 106 kcal/mol.<sup>5</sup> Due to these properties, the stereoisomeric cyclopropyl ketones **1** and **2** are likely not only to provide insight into some stereochemical details of metal-mediated reactions but also to serve as crucial test systems to further probe the concept of remote functionalization of C–H and C–C bonds. The study of unimolecular reactions of metastable ion complexes is ideally suited for this purpose, since they allow us to probe even the small energetic differences which result from stereochemical differences in the precursor molecules (e.g. *cis/trans* isomers) complexed to a bare metal cation.<sup>2b–g,3f</sup>

In a previous paper,<sup>6</sup> we reported in detail the reactions of metastable  $1/\text{Fe}^+$  and  $2/\text{Fe}^+$  complexes in the gas phase. By using a combination of tandem mass spectrometric methods and isotopic labeling techniques, we were able to provide evidence for the existence of two competing reaction channels being operative in the unimolecular fragmentation reactions of  $1/\text{Fe}^+$  and  $2/\text{Fe}^+$ . Briefly, the comparative study of the isotopologous  $\text{Fe}^+$  complexes of **1** and **2** (Chart 2) and the isomeric acyclic hexenone complexes  $3/\text{Fe}^+$ – $5/\text{Fe}^+$  demonstrated that one reaction channel (Scheme 2, path a) commences with a metal-induced ring cleavage leading eventually to the acyclic 3-hexen-2-one/ $\text{Fe}^+$  complex  $3/\text{M}^+$  ( $\text{M} = \text{Fe}$ ). The intermediate  $3/\text{Fe}^+$  serves as a branching point for the generation of the three main neutral products, i.e.  $\text{H}_2$ ,  $\text{C}_2\text{H}_4$ , and  $\text{CH}_3\text{CHO}$ , which are formed with similar intensities for the *cis* and *trans* isomers  $1/\text{Fe}^+$  and  $2/\text{Fe}^+$ ; consequently, path a is associated with a complete loss of stereochemical information. Hydrogen and ethene losses from  $3/\text{Fe}^+$  can be described in terms of the concept of remote functionalization, as depicted in Scheme 3 ( $\text{M} = \text{Fe}$ ). The metal-mediated  $\omega$ -C–H bond activation leads to  $7/\text{Fe}^+$ , which then, via a  $\beta$ -H shift and reductive elimination of  $\text{H}_2$ , gives rise to  $8/\text{Fe}^+$ . In competition,  $\beta$ -C–C bond cleavage, presumably via  $9/\text{Fe}^+$ , causes ethene loss to yield

$10/\text{Fe}^+$ . Loss of acetaldehyde ( $\Delta m = 44$ ) must not necessarily involve remote functionalization and can be accounted for by a partial isomerization of  $3/\text{Fe}^+$  to  $4/\text{Fe}^+$  or  $5/\text{Fe}^+$ ; from the last two complexes acetaldehyde can readily be formed via 1,4- or 1,2-elimination processes.

On the other hand,  $\text{Fe}^+$ -induced decarbonylation of **1** and **2** (Scheme 2, path b;  $\text{M} = \text{Fe}$ ) was shown<sup>6</sup> to commence with  $\alpha$ -C–C bond insertion, in analogy to the reaction of acetone with  $\text{Fe}^+$ ,<sup>3a,7</sup> to generate the intermediate  $6/\text{Fe}^+$ ; this species serves as a precursor for carbon monoxide loss. Most interestingly, in contrast to the eliminations of  $\text{H}_2$ ,  $\text{C}_2\text{H}_4$ , and  $\text{CH}_3\text{CHO}$ , the expulsion of carbon monoxide exhibits a distinct stereoselective effect, and the process is favored for the *trans* complex  $2/\text{Fe}^+$ . The observed stereochemical differences can be rationalized via the stereoselective formations of *cis*- and *trans*-3-allyl complexes  $6/\text{Fe}^+$  (Scheme 4,  $\text{M} = \text{Fe}$ ) in the course of the electrocyclic ring-opening process of the cyclopropyl backbone, where the formation of *trans*- $6/\text{Fe}^+$  is favored such that the decarbonylation of  $2/\text{Fe}^+$  is more abundant as compared to  $1/\text{Fe}^+$ . As a consequence, the subtle stereochemical differences between the *cis* and *trans* isomers  $1/\text{Fe}^+$  and  $2/\text{Fe}^+$  manifest themselves in the competition of the reaction channels in the unimolecular dissociation of the metastable complexes.

Here, we will present a more comprehensive, comparative study of the gas-phase reactions of **1** and **2** with late first-row transition-metal ions from  $\text{Cr}^+$  through  $\text{Cu}^+$ . As will be uncovered in the unimolecular fragmentation patterns, in addition to the reactions depicted for  $\text{M} = \text{Fe}$  in Schemes 2–4, some of the transition-metal ions induce quite remarkable processes, e.g. metal–carbene formations or losses of neutral metal fragments. Furthermore, the origin of distinct stereochemical effects for some metal complexes of the *cis/trans* isomers  $1/\text{M}^+$  and  $2/\text{M}^+$  as well as periodic trends are discussed and explained in terms of the internal energy content of the metastable ions in conjunction with the interplay of competing processes for the various metals.

## Experimental Section

The experiments were performed with a modified VG ZAB/HF/AMD 604 four-sector mass spectrometer of BEBE configuration (B stands for magnetic and E for electric sectors), which has been described previously.<sup>8</sup> In brief, the metal cations were generated from the substrates given in Table 1 and reacted in a chemical ionization (CI) source with the organic precursors of interest (Charts 1 and 2). Unfortunately, the measurements of  $\text{Ni}^+$  complexes could not be carried out using bis(cyclopentadienyl)nickel(II), bis(acetylacetonato)nickel(II), or bis(cycloocta-1,5-dienyl)nickel as substrates, because of isobaric interferences arising from these compounds. Therefore, the bis(hexafluoroacetylacetonato)nickel(II) complex ( $\text{Ni}(\text{hfac})_2$ ) has been used for the generation of  $\text{Ni}^+$  cations. Similarly,  $\text{Cu}^+$  had to be generated from  $(\text{Cu}(\text{hfac})_2)$ . In addition, instead of the isotopes  $^{58}\text{Ni}^+$  and  $^{63}\text{Cu}^+$ , complexes with the less abundant  $^{60}\text{Ni}^+$  and  $^{65}\text{Cu}^+$  isotopes had to be

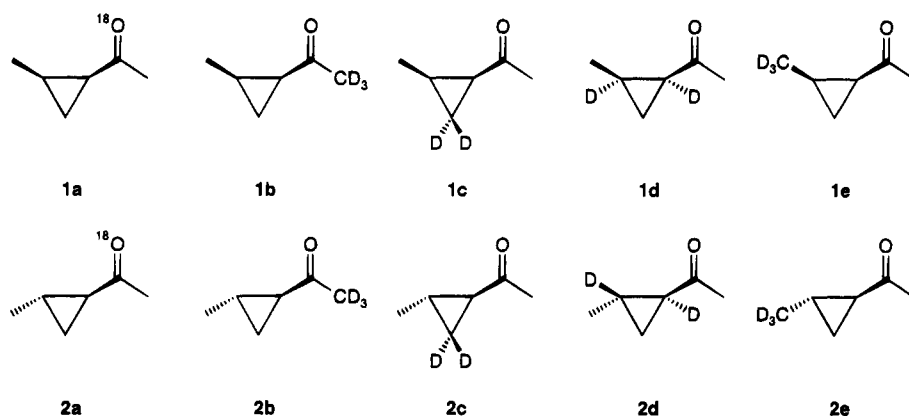
(5) (a) Ferguson, K. C.; Whittle, E. *Trans. Faraday Soc.* **1971**, *67*, 2618. (b) Baghal-Vajjoee, M. H.; Benson, S. W. *J. Am. Chem. Soc.* **1979**, *101*, 2838.

(6) Schalley, C. A.; Schröder, D.; Schwarz, H. *J. Am. Chem. Soc.*, in press.

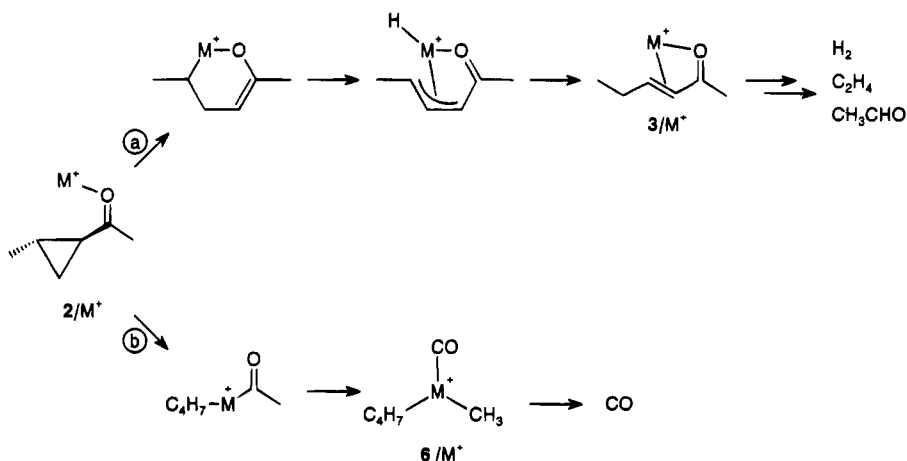
(7) (a) Halle, L. F.; Crowe, W. E.; Armentrout, P. B.; Beauchamp, J. L. *Organometallics* **1984**, *3*, 1694. (b) Sonnenfroh, D. M.; Farrar, J. M. *J. Am. Chem. Soc.* **1986**, *108*, 3521. (c) Schultz, R. H.; Armentrout, P. B. *J. Phys. Chem.* **1992**, *96*, 1662.

(8) (a) Srinivas, R.; Sülzle, D.; Weiske, T.; Schwarz, H. *Int. J. Mass Spectrom. Ion Processes* **1991**, *107*, 368. (b) Srinivas, R.; Sülzle, D.; Koch, W.; DePuy, C. H.; Schwarz, H. *J. Am. Chem. Soc.* **1991**, *113*, 5970.

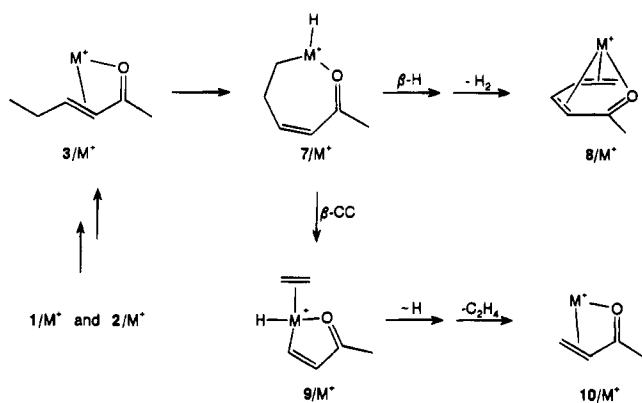
Chart 2



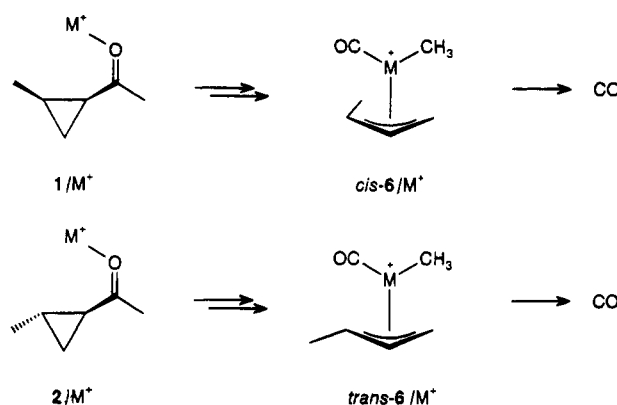
Scheme 2



Scheme 3



Scheme 4



studied, in order to avoid interferences from isobaric ions. In contrast to electron impact conditions, the relatively high pressure that prevails in the ion source during chemical ionization allows efficient cooling of the complexes generated.<sup>6</sup> Nevertheless, the metastable complexes must contain a certain amount of excess internal energy in order to undergo unimolecular dissociation within the time scale of the experiment.

The ketones were introduced *via* the heated septum inlet system (70 °C), and the mixture of ketone and metal precursor was subsequently ionized by a beam of electrons having 50–100 eV kinetic energy. The ions of interest were accelerated to 8 keV translational energy and mass-selected by means of B(1)/E(1) at a mass resolution of  $m/\Delta m = 2000$ –5000. Unimolecular fragmentations of metastable ions (MI) occurring in the field-free region preceding the second magnet were recorded by scanning B(2). For collisional activation (CA) experiments, mass-selected ions were collided with helium

(80% transmission). The CA spectra<sup>9</sup> are in line with the results reported below but are not pursued further in the present discussion. Therefore, the corresponding data are not given explicitly in this article; they are available from the authors upon request. The error of the relative intensities in MS/MS experiments does not exceed  $\pm 10\%$ .<sup>9</sup> Some MS/MS experiments<sup>10</sup> were performed with the complexes of unlabeled 1/M<sup>+</sup>–5/M<sup>+</sup> (M = Fe, Co)<sup>6,9</sup> by selecting the primary fragment ions by means of B(2), and the collision-induced fragmentations occurring in the subsequent field-free region were recorded by scanning E(2); these experiments will be referred to as MI/CA spectra. All spectra were accumulated

(9) Schalley, C. A. Diploma Thesis, Technische Universität Berlin, 1994.

(10) Busch, K. L.; Glish, G. L.; McLuckey, S. A. *Mass Spectrometry/Mass Spectrometry: Techniques and Applications of Tandem Mass Spectrometry*; VCH: Weinheim, Germany, 1988.

**Table 1. Precursors and Types of Inlet Systems Used for the Generation of Transition-Metal Ions  $M^+$  in the CI Source**

$M^+$	substrate	inlet syst (temp, °C)
Cr <sup>+</sup>	Cr(CO) <sub>6</sub>	direct (23)
Mn <sup>+</sup>	Cp'Mn(CO) <sub>3</sub> <sup>a</sup>	septum (70)
Fe <sup>+</sup>	Fe(CO) <sub>5</sub>	septum (70)
Co <sup>+</sup>	Co(CO) <sub>3</sub> NO	septum (70)
Ni <sup>+</sup> <sup>b</sup>	Ni(hfac) <sub>2</sub> <sup>c</sup>	direct (90)
Cu <sup>+</sup> <sup>b</sup>	Cu(hfac) <sub>2</sub> <sup>c</sup>	direct (45)

<sup>a</sup> Cp' = methylcyclopentadienyl. <sup>b</sup> To avoid interference with the hydrogen losses from heavier isotopologues, measurements have been carried out using the <sup>60</sup>Ni and <sup>65</sup>Cu isotopes, respectively. <sup>c</sup> hfac = hexafluoroacetylacetonate.

and on-line-processed with the AMD-Intectra data system; 5–30 scans were averaged to improve the signal-to-noise ratio.

All unlabeled and <sup>18</sup>O- and deuterium-labeled compounds (Chart 2) have been synthesized and purified by standard laboratory procedures and fully characterized by spectroscopic means as described in detail elsewhere.<sup>6,9</sup>

## Results and Discussion

The relative intensities of the decomposition products arising from unlabeled **1**/ $M^+$  and **2**/ $M^+$  are given in Table 2. These data reveal that, despite common features, the metal ions Cr<sup>+</sup> through Cu<sup>+</sup> give rise to different products. As far as product variety is concerned, Fe<sup>+</sup> seems to be the most selective metal ion in that only 5 products are formed; in contrast, the Cu<sup>+</sup> complexes give rise to more than 10 different products. Further, inspection of the data in Table 1 reveals the existence of a stereochemical effect for the metal complexes of **1** and **2** with  $M^+ = Mn^+, Fe^+, Cu^+$ , while for  $M^+ = Cr^+, Co^+, Ni^+$  intensity differences due to the stereochemistry of **1** and **2** are not observed.<sup>11</sup>

For comparative purposes, the complexes of the acyclic isomers **3–5** with  $M = Cr-Cu$  have also been included. As already noted,<sup>6</sup> for the Fe<sup>+</sup> complexes of **1** and **2** ring cleavage leading to **3**/Fe<sup>+</sup> is supported by the similarity of the MI spectra of **1**/Fe<sup>+</sup>, **2**/Fe<sup>+</sup>, and **3**/Fe<sup>+</sup>. We obtain similar results for the complexes of the other  $M^+$  ions examined here;<sup>9</sup> for the sake of brevity the corresponding data will not be given. A complete set of data is available from the authors upon request.

The unimolecular dissociations of the Fe<sup>+</sup> complexes have been discussed in detail elsewhere,<sup>6</sup> and a brief summary has also been given in the Introduction. For comparison, the data for both sets of stereoisomeric isotopologues are reproduced in Table 3; however, they will not be pursued further in the discussion. The reactions of Fe<sup>+</sup> with **1** and **2** (depicted in Schemes 2–4) may serve as a basis for the interpretation of the processes observed for the corresponding complexes of the other metal cations. In this paper, we will focus on the differences for the group VIII transition metals Co and Ni as well as for Cr, Mn, and Cu in comparison to the Fe<sup>+</sup> complexes.

**Complexes of **1** and **2** with Co<sup>+</sup> and Ni<sup>+</sup>.** Table 4 summarizes the data for the gas-phase reactions of Co<sup>+</sup> with the <sup>18</sup>O- and deuterium-labeled isotopologues of **2**. Since no significant *cis/trans* differences<sup>11</sup> are observed,

(11) A slightly different ethene/CO ratio is observed for the <sup>18</sup>O-labeled compounds **1a**/Co<sup>+</sup> (34/48) and **2a**/Co<sup>+</sup> (29/54) (values normalized to  $\Sigma = 100\%$ ). However, since these differences are within the experimental error limits, we refrain from drawing any conclusions from these data.

these data can be considered as being representative for both stereoisomers.

The intensities of the main fragmentation processes of the Co<sup>+</sup> complexes, i.e. dehydrogenation, ethene and carbon monoxide formation, and loss of acetaldehyde, differ from those observed for the Fe<sup>+</sup> complexes. The high amounts of ethene and CO losses, as compared to dehydrogenation, point to a lower activation barrier for the first two processes. Thus, for Co<sup>+</sup> (as well as for Ni<sup>+</sup>, see below) C–C bond activation is clearly favored over C–H bond activation. This observation is in line with previous findings, and similar trends have been reported for many reactions of group VIII transition-metal cations with numerous substrates.<sup>1</sup> In addition, formation of methane and water and consecutive losses of H<sub>2</sub> and H<sub>2</sub>O are observed as side reactions of low intensities; these will not be discussed further.

As compared to Fe<sup>+</sup>, the Co<sup>+</sup> complexes of labeled **1** and **2** reveal a similar distribution of isotopes for each group of neutral products. Therefore, we conclude that the unimolecular fragmentation reactions of the Fe<sup>+</sup> and Co<sup>+</sup> complexes follow the same mechanistic pathways. Ring cleavage yielding the acyclic **3**/Co<sup>+</sup> isomer is further supported by the fragmentations of authentic **3**/Co<sup>+</sup>, which are very similar to those of **1**/Co<sup>+</sup> and **2**/Co<sup>+</sup>, respectively. In addition, the MI/CA spectra of the ionic products due to ethene/CO losses from **1**/Co<sup>+</sup>–**5**/Co<sup>+</sup> are indistinguishable within experimental error. This indicates that identical products are formed after the expulsion of ethene and carbon monoxide, respectively, from the cyclopropyl ketone complexes as well as the acyclic isomers and, furthermore, strongly supports the operation of similar mechanisms for Fe<sup>+</sup> and Co<sup>+</sup>. Likewise, comparison of the MI/CA spectra of the ethene loss from **2a**/Co<sup>+</sup> with the CA spectrum<sup>12</sup> of an authentic methyl vinyl ketone/Co<sup>+</sup> complex reveals that the latter is indeed formed from **2**/Co<sup>+</sup> in the course of ethene loss.

In spite of these similarities, there is one striking difference in the reaction patterns of the Fe<sup>+</sup> and the Co<sup>+</sup> complexes: while expulsion of [D<sub>3</sub>]ethene ( $\Delta m = 31$ ) from the [D<sub>3</sub>]methyl-labeled complex **2e**/Fe<sup>+</sup> is negligible (Table 3), for **2e**/Co<sup>+</sup> the eliminations of [D<sub>3</sub>]ethene and [D<sub>2</sub>]ethene are observed with nearly the same intensities, whereas loss of [D<sub>1</sub>]ethene does not occur at all (Table 4). This isotope distribution immediately rules out simple H/D exchange processes with other positions in **2e**/Co<sup>+</sup>, since in the course of H/D exchange formation of [D<sub>3</sub>]ethene would invariably be accompanied by the expulsion of a [D<sub>1</sub>] isotopologue. Consequently, not only does ethene loss follow the remote functionalization mechanism (Scheme 3) but also a "carbene mechanism" is operative, as depicted in Scheme 5 ( $M = Co$ ). The ethylidene complex **11**/Co<sup>+</sup> rearranges *via* a hydrogen shift to **12**/Co<sup>+</sup>, from which ethene is extruded. This mechanistic picture agrees well with the low amount of [D<sub>1</sub>]ethene (arising from **2c**/Co<sup>+</sup> via the remote functionalization mechanism) and unlabeled ethene (formed *via* the carbene intermediate **11**/Co<sup>+</sup>). In line with the MI/CA results mentioned above, both mechanisms (Schemes 3 and 5) give rise to methyl vinyl ketone/Co<sup>+</sup> complexes, **10**/Co<sup>+</sup>, as ionic

(12) The CA spectra of the methyl vinyl ketone/ $M^+$  ( $M = Fe, Co$ ) complexes **10**/ $M^+$  were recorded at a reduced acceleration voltage, in order to ensure that these ions have the same kinetic energy as those produced by unimolecular ethene losses from **1a**/ $M^+$  and **2a**/ $M^+$ .

**Table 2.** Neutral Products Generated in the Unimolecular Decomposition Reactions of M<sup>+</sup> Complexes of 1-Acetyl-2-methylcyclopropanes **1** and **2**<sup>a</sup>

product	$\Delta m$ , amu	Cr <sup>+</sup>		Mn <sup>+</sup>		Fe <sup>+</sup>		Co <sup>+</sup>		Ni <sup>+</sup>		Cu <sup>+</sup>	
		1	2	1	2	1	2	1	2	1	2	1	2
H <sub>2</sub>	2	100	100	100	100	100	100	14	14	59	61	100	41
CH <sub>3</sub>	15			25	34							10	9
CH <sub>4</sub>	16	4	4					3	3	4	4	1	1
H <sub>2</sub> O	18	4	1	4	4	2	1	4	2	5	2	78	7
H <sub>2</sub> + H <sub>2</sub> O	20							2	2	2	1	1	1
CO/C <sub>2</sub> H <sub>4</sub>	28	8	8	58	68	43	76	100	100	100	100	86	100
CO + H <sub>2</sub>	30											1	1
C <sub>3</sub> H <sub>4</sub>	40			3	4								
C <sub>3</sub> H <sub>6</sub>	42	3	4	1	1								
CH <sub>3</sub> CHO	44			1	1	27	34	5	5	3	4		
C <sub>4</sub> H <sub>6</sub>	54			2	2								
MH	66											46	28
MCH <sub>3</sub>	80											32	30
ligand loss	98	1	2	6	11							3	2

<sup>a</sup> Intensities are given in percentages of the base peak. For the sake of clarity intensities less than 1% are omitted.

**Table 3.** Mass Differences ( $\Delta m$  in amu) Observed in the Unimolecular Decomposition Reactions of the Isotopologues of **1**/Fe<sup>+</sup> and **2**/Fe<sup>+</sup><sup>a</sup>

	$\Delta m$									
	-2	-3	-28	-29	-30	-31	-44	-45	-46	-47
<b>1</b> /Fe <sup>+</sup>	59		25				16			
<b>1a</b> /Fe <sup>+</sup>	62		11		11				16	
<b>1b</b> /Fe <sup>+</sup>	57		25							18
<b>1c</b> /Fe <sup>+</sup>	33	17	23	6			15	6		
<b>1d</b> /Fe <sup>+</sup>	35	17	13	13			21	1		
<b>1e</b> /Fe <sup>+</sup>	4	34	23		12	1	10	16		
<b>2</b> /Fe <sup>+</sup>	49		35				16			
<b>2a</b> /Fe <sup>+</sup>	50		11		23				16	
<b>2b</b> /Fe <sup>+</sup>	61		22							17
<b>2c</b> /Fe <sup>+</sup>	34	17	23	7			14	5		
<b>2d</b> /Fe <sup>+</sup>	34	17	20	11			17	1		
<b>2e</b> /Fe <sup>+</sup>	5	41	18		12	1	10	13		

<sup>a</sup> Intensities are expressed in  $\Sigma(\text{products}) = 100\%$ . Intensities less than 1% are omitted. In addition, minor losses of water are observed; see Table 2 ( $\Delta m = 18$ ).

**Table 4.** Mass Differences ( $\Delta m$  in amu) Observed in the Unimolecular Decomposition Reactions of the **2**/Co<sup>+</sup> Isotopologues<sup>a</sup>

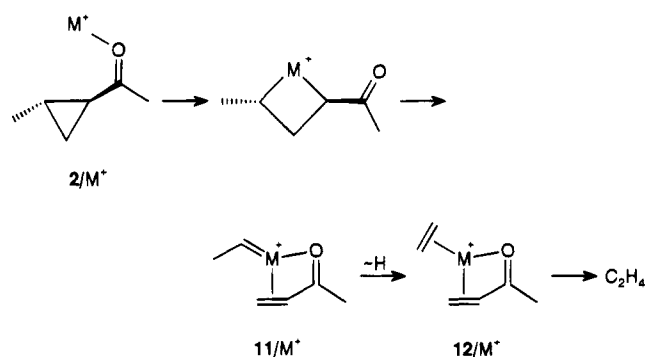
	$\Delta m$									
	-2	-3	-28	-29	-30	-31	-44	-45	-46	-47
<b>2</b> /Co <sup>+</sup>	12		84				4			
<b>2a</b> /Co <sup>+</sup>	12		29		54				5	
<b>2b</b> /Co <sup>+</sup>	13		82							5
<b>2c</b> /Co <sup>+</sup>	4	4	78	9			3	2		
<b>2d</b> /Co <sup>+</sup>	5	4	56	30			5			
<b>2e</b> /Co <sup>+</sup>	3	9	51		17	16	2	2		

<sup>a</sup> Intensities are expressed in  $\Sigma(\text{products}) = 100\%$ . Intensities less than 1% are omitted. The expulsions of methane and water and the consecutive losses of H<sub>2</sub>/H<sub>2</sub>O (Table 2) are not included, as these minor processes will not be discussed.

products. It should be mentioned that rearrangement processes of metal ethylenes to metal-olefin complexes have been postulated for the gas-phase reactions of methyl-substituted metallacyclobutanes<sup>13</sup> with Co<sup>+</sup> and Fe<sup>+</sup>. Likewise, unimolecular decarbonylation of propionic acid/Fe<sup>+</sup> complexes<sup>14</sup> leads to a methylcarbene/Fe(OH<sub>2</sub>)<sup>+</sup> complex, which subsequently rearranges to the corresponding ethene-ligated complex. Furthermore, a recent theoretical study<sup>15</sup> indicates that

(13) (a) Armentrout, P. B.; Halle, L. F.; Beauchamp, J. L. *J. Am. Chem. Soc.* **1981**, *103*, 6624. (b) Peake, D. A.; Gross, M. L.; Ridge, D. P. *J. Am. Chem. Soc.* **1984**, *106*, 4307.

(14) Schröder, D.; Zummack, W.; Schwarz, H. *J. Am. Chem. Soc.* **1994**, *116*, 5857.

**Scheme 5****Table 5.** Mass Differences ( $\Delta m$  in amu) Observed in the Unimolecular Decomposition Reactions of the **2**/<sup>60</sup>Ni<sup>+</sup> Isotopologues<sup>a,b</sup>

	$\Delta m$						
	-2	-3	-4	-28	-29	-30	-31
<b>2</b> /Ni <sup>+</sup>	38			62			
<b>2a</b> /Ni <sup>+</sup>	40			40		20	
<b>2b</b> /Ni <sup>+</sup>	37			63			
<b>2c</b> /Ni <sup>+</sup>	30	9	1	52	8		
<b>2d</b> /Ni <sup>+</sup>	27	8		44	21		
<b>2e</b> /Ni <sup>+</sup>	10	17	2	46	2	16	7

<sup>a</sup> Intensities are expressed in  $\Sigma(\text{products}) = 100\%$ . Only the main fragmentation reactions (i.e. dehydrogenation, ethene formation, and loss of carbon monoxide) are summarized here. <sup>b</sup> Since for the Ni<sup>+</sup> complexes no significant *cis/trans* differences are observed, only the data for the *trans* isotopomers are given as representative for both stereoisomers.

the isomerization barrier for free singlet methylcarbene is as low as 2.0 kcal/mol. Thus, we conclude that the rearrangement of the metal ethylidene to an ethene complex, i.e. **11**/Co<sup>+</sup> → **12**/Co<sup>+</sup>, is a facile process for the group VIII metal cations in general.

At first sight a comparison of the data given in Table 4 for the Co<sup>+</sup> complex cations with those summarized in Table 5 for the Ni<sup>+</sup> complexes reveals that the same mechanistic pathways are operative in the decomposition reactions of the complexes of both metal cations, though with different intensities. C–C bond activation is favored over dehydrogenation, but the amount of carbon monoxide generated from **1**/Ni<sup>+</sup> and **2**/Ni<sup>+</sup> is much lower as compared to the corresponding Co<sup>+</sup> complexes. As indicated by the [D<sub>1</sub>]ethene losses from **2e**/Ni<sup>+</sup>, H/D exchange processes have to be taken into

(15) Ma, B.; Schaefer, H. F. *J. Am. Chem. Soc.* **1994**, *116*, 3539.

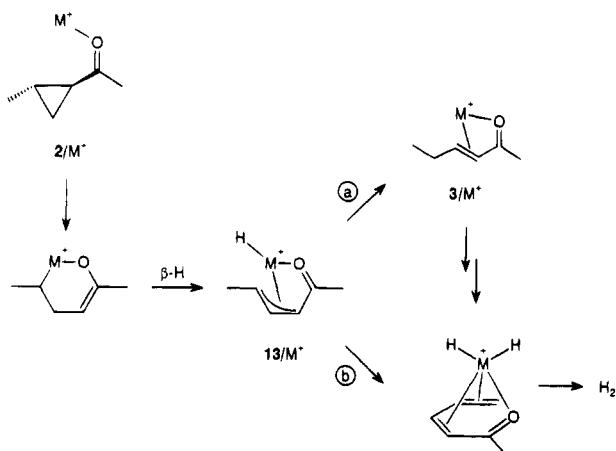


**Table 6. Mass Differences ( $\Delta m$  in amu) Observed in the Unimolecular Decomposition Reactions of the  $2/\text{Cr}^+$  Isotopologues<sup>a,b</sup>**

	$\Delta m$										
	-2	-3	-28	-29	-30	-31	-42	-43	-44	-45	$\text{Cr}^+$
$2/\text{Cr}^+$	88		7				3				2
$2a/\text{Cr}^+$	89		6				3				2
$2b/\text{Cr}^+$	85		9				5				1
$2c/\text{Cr}^+$	27	55	6	3					7		2
$2d/\text{Cr}^+$	74	15		5				4			2
$2e/\text{Cr}^+$	11	76			4	2				5	2

<sup>a</sup> Intensities are expressed in  $\Sigma(\text{products}) = 100\%$ . Intensities less than 1% are omitted. Since the methane and water losses are not discussed in detail, the corresponding data are omitted. <sup>b</sup> Since for the  $\text{Cr}^+$  complexes no significant *cis/trans* differences are observed, the data for the *trans* isotopomers are given as representative for both stereoisomers.

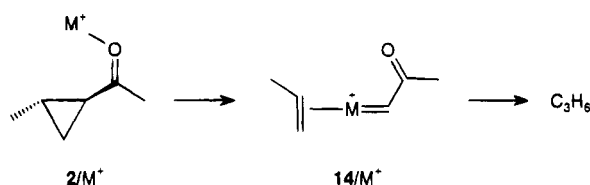
**Scheme 6**



account. Nevertheless, the rather high abundance of  $[\text{D}_3]$ ethene formation from  $2e/\text{Ni}^+$  cannot only be due to statistical H/D exchange processes. Therefore, the carbene mechanism as discussed for  $\text{Co}^+$  (Scheme 5) is also operative for the  $\text{Ni}^+$  complexes.

**Complexes of 1 and 2 with  $\text{Cr}^+$ .** The complexes of 1 and 2 with  $\text{Cr}^+$  exhibit some clear differences as compared to those with the group VIII transition metals (Table 6). For example, dehydrogenation corresponds to the by far most intense unimolecular fragmentation of  $1/\text{Cr}^+$  and  $2/\text{Cr}^+$ . Furthermore, in contrast to the group VIII metal complexes  $2c/\text{Cr}^+$  and  $2d/\text{Cr}^+$  do not exhibit the same  $\text{H}_2/\text{HD}$  ratio (Table 3); thus, for  $\text{Cr}^+$ -mediated dehydrogenation an alternative mechanism must be operative. Moreover, hydrogen atoms from the methylene group of the cyclopropyl ring (C(3)) contribute significantly to dehydrogenation. These findings can be rationalized by the mechanism depicted in Scheme 6. If path a, which leads from intermediate  $13/\text{M}^+$  to ring-opened  $3/\text{M}^+$ , is facile (and largely reversible) the hydrogen atoms attached originally to C(2)/C(3) will equilibrate prior to the remote functionalization. This holds true for the  $\text{Fe}^+$  complexes, as indicated by the same  $\text{H}_2/\text{HD}$  ratio for the two isotopomers  $2c/\text{Fe}^+$  and  $2d/\text{Fe}^+$ ; both precursors give rise to labeled 3-hexen-2-one/ $\text{Fe}^+$  intermediates bearing one deuterium atom at the ( $\omega - 1$ )-position of the side chain. In contrast, if the formation of  $3/\text{M}^+$  via step a is kinetically impeded,  $13/\text{M}^+$  may explore a different route by, for example, bypassing reaction a and following path b. This "direct" activation of the  $\omega$ -H atom in  $13/\text{M}^+$  will consequently result in a predominant loss of HD from  $2c/\text{Cr}^+$  and likewise in a higher intensity for the  $\text{H}_2$  loss from  $2d/$

**Scheme 7**



$\text{Cr}^+$ . This mechanism is also in keeping with the prevailing HD loss from  $2e/\text{Cr}^+$ . Presumably, the lifetime of the insertion intermediate is smaller for the  $\text{Cr}^+$  complexes as compared to the group VIII metal cations and, therefore, the direct route via is preferred for  $2/\text{Cr}^+$ .

As far as the minor fragmentation channels are concerned, the absence of  $\text{C}^{18}\text{O}$  loss ( $\Delta m = 30$ ) from the  $^{18}\text{O}$ -labeled complex  $2a/\text{Cr}^+$  reveals that decarbonylation does not interfere with ethene loss. From the observation of  $[\text{D}_1]$ - and  $[\text{D}_0]$ ethene losses from  $2c/\text{Cr}^+$  we conclude that at least two mechanisms are operative. One involves remote functionalization (Scheme 3,  $\text{M} = \text{Cr}$ ) via the intermediate  $3/\text{Cr}^+$ , and the other corresponds to the carbene mechanism (Scheme 5,  $\text{M} = \text{Cr}$ ). In keeping with this interpretation, only  $[\text{D}_1]$ ethene is generated from  $2d/\text{Cr}^+$ , whereas  $2c/\text{Cr}^+$  leads to losses of  $[\text{D}_0]$ - and  $[\text{D}_1]$ ethene and  $2e/\text{Cr}^+$  to losses of  $[\text{D}_2]$ - and  $[\text{D}_3]$ ethene, respectively.

The formation of carbene intermediates is not limited to ethene expulsion but is also involved in the loss of propene. As clearly shown by the data for the labeled complexes  $2c/\text{Cr}^+ - 2e/\text{Cr}^+$ , the  $\text{C}_3\text{H}_6$  moiety stems exclusively from the C(2)/C(3) positions of the cyclopropyl ring and the adjacent 2-methyl group. H/D exchange processes do not occur. These observations are easily rationalized in terms of the mechanism depicted in Scheme 7 ( $\text{M} = \text{Cr}$ ). Here,  $14/\text{Cr}^+$  is formed as a central intermediate, from which propene is lost eventually. The insertion of  $\text{Cr}^+$  in the C(1)-C(2) bond of the cyclopropyl ring can be rationalized in terms of thermodynamic arguments. The cyclopropylic C(1)-C(2) and C(1)-C(3) bonds are lengthened and weakened by conjugation with the carbonyl group,<sup>16</sup> such that C-C insertion of the metal ion is facilitated to some extent. Notably, only the  $\text{Cr}^+$  and  $\text{Mn}^+$  complexes give rise to this type of carbene mechanism, whereas the late-transition-metal cations from  $\text{Fe}^+$  through  $\text{Cu}^+$  do not mediate propene loss from  $2/\text{M}^+$ .

Methane and water losses are observed as side reactions. Due to the low intensities and some interferences the corresponding data cannot be deconvoluted exactly. Therefore, these reactions are not discussed here.<sup>9</sup> Last but not least, ligand detachment is observed for the  $\text{Cr}^+$  complexes of 1 and 2. Thus, the activation barriers for the decomposition reactions described above are of the same order of magnitude as the  $\text{Cr}^+$ -ligand bond dissociation energy.

**Complexes of 1 and 2 with  $\text{Mn}^+$ .** From the isotope distribution in the neutral fragments (Table 7) we can conclude that dehydrogenation and ethene formation

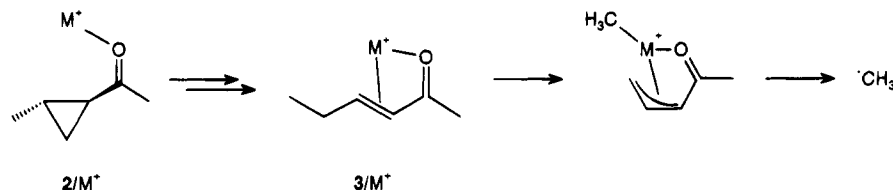
(16) (a) Hoffmann, R. *Tetrahedron Lett.* **1970**, 2907. (b) Dill, J. D.; Greenberg, A.; Liebman, J. F. *J. Am. Chem. Soc.* **1979**, *101*, 6814. (c) Clark, T.; Spitznagel, G. W.; Klose, R.; Schleyer, P. v. R. *J. Am. Chem. Soc.* **1984**, *106*, 4413. (d) Cremer, D.; Kraka, E. *J. Am. Chem. Soc.* **1985**, *107*, 3811. (e) Slee, T. S. In *Modern Models of Bonding and Delocalization*; Liebman, J. F., Greenberg, A., Eds.; VCH: New York, 1988.

Table 7. Mass Differences ( $\Delta m$  in amu) Observed in the Unimolecular Decomposition Reactions of the  $2/\text{Mn}^+$  Isotopologues<sup>a</sup>

	$\Delta m$											
	-2	-3	-4	-15	-16	-17	-18	-28	-29	-30	-31	$\text{Mn}^+$
$2/\text{Mn}^+$	47			16				32				5
$2a/\text{Mn}^+$	47			16				26		7		4
$2b/\text{Mn}^+$	45			18				32				5
$2c/\text{Mn}^+$	30	16	<1	13	4			10	19	2		6
$2d/\text{Mn}^+$	30	16	<1	15	2			7	24	2		4
$2e/\text{Mn}^+$	6	29	1			6	9	6	3	25	4	11

<sup>a</sup> Intensities are expressed in  $\Sigma(\text{products}) = 100\%$ . Intensities less than 1% are omitted (except for the  $\text{D}_2$  losses). Since the losses of methane, water, propene, and acetaldehyde and the formation of  $\text{Mn}(\text{CH}_3\text{CHO})^+$  are not discussed in detail, the corresponding data are omitted.

Scheme 8



follow the same mechanistic picture as outlined for the corresponding  $\text{Fe}^+$  complexes (Schemes 2 and 3). For example, the data for  $2c/\text{Mn}^+$  and  $2d/\text{Mn}^+$  are close to each other, as observed for the  $\text{Fe}^+$  complexes. Similarly, ethene expulsion overlaps with isobaric carbon monoxide loss as derived from  $\Delta m = 30$  for  $^{18}\text{O}$ -labeled  $2a/\text{Mn}^+$ . However, in contrast to the corresponding  $\text{Fe}^+$  complexes, the MI spectra of the acyclic isomers  $3/\text{Mn}^+$ ,  $4/\text{Mn}^+$ , and  $5/\text{Mn}^+$  are similar to each other, indicating a rapid migration of the double bond within the acyclic hexenone complexes. H/D exchange processes, following ring cleavage, also have to be taken into account for  $1/\text{Mn}^+$  and  $2/\text{Mn}^+$ , as revealed by the observed isotope distributions, e.g.  $\text{D}_2$  losses from  $2c/\text{Mn}^+ \rightarrow 2e/\text{Mn}^+$ ,  $[\text{D}_2]$ -ethene formation from  $2c/\text{Mn}^+ \rightarrow 2d/\text{Mn}^+$ , and  $[\text{D}_1]$ -ethene loss from  $2e/\text{Mn}^+$ .

In addition to the reaction pathways discussed so far, the  $\text{Mn}^+$  complexes undergo abundant loss of a methyl radical which stems predominantly from the terminal methyl group (see  $2e/\text{Mn}^+$ ,  $\Delta m = 18$ ), whereas the  $\alpha$ -methyl group is not involved (see  $2b/\text{Mn}^+$ ,  $\Delta m = 15$ ). However, the losses of  $\text{CH}_2\text{D}^{\bullet}$  ( $\Delta m = 16$ ) from  $2c/\text{Mn}^+$  and  $2d/\text{Mn}^+$  as well as  $\text{CHD}_2^{\bullet}$  from  $2e/\text{Mn}^+$  ( $\Delta m = 17$ ) indicate H/D exchange processes preceding dissociation. A plausible mechanism that accounts for the experimental findings involves initial formation of  $3/\text{Mn}^+$ , from which methyl loss may proceed *via* allylic C–C bond homolysis (Scheme 8). Similar allylic C–C bond activation processes have been reported for the fragmentations of alkene/ $\text{M}^+$ <sup>13,17</sup> and alkyne/ $\text{M}^+$ <sup>18</sup> complexes. However, in these examples the formation of radicals was avoided and rather followed by H-transfer from one ligand to the other, leading to reductive elimination of small alkanes as neutral products. In the present case, however, there is no accessible hydrogen atom that could be transferred easily without producing energetically demanding cumulene structures.

With regard to stereochemical features the  $\text{Mn}^+$  complexes exhibit clearly recognizable *cis/trans* differences. In particular, for the *trans* isomer,  $2/\text{Mn}^+$ , all

main fragmentation processes *except* dehydrogenation, i.e. methyl loss, formation of  $\text{CO}/\text{C}_2\text{H}_4$ , and ligand detachment, show enlarged intensities as compared to the *cis* isomer  $1/\text{Mn}^+$  (Table 2). In view of the fragmentation mechanisms outlined above, two arguments speak against a particular stereospecificity for the  $\text{Mn}^+$  complexes, e.g. selective formation of *cis*- or *trans*- $3/\text{Mn}^+$  from  $1/\text{Mn}^+$  and  $2/\text{Mn}^+$ , respectively. (i) Ring-opened  $3/\text{Mn}^+$  undergoes a fast isomerization of the double-bond position.<sup>9</sup> Since this is likely to be associated with *cis/trans* isomerization, complete loss of stereochemical information is expected. (ii) The “ $\alpha$ -insertion” channel, which leads to stereoselectivity in the case of the  $\text{Fe}^+$  complexes, is almost negligible for  $\text{Mn}^+$  complexes. Furthermore, the “ring cleavage/remote functionalization” channel dominating here has been shown not to be stereoselective for all metal ions discussed so far. Rather, as compared to  $1/\text{Mn}^+$ , the higher abundance of ligand detachment for the *trans* isomer clearly indicates an increased internal energy content of metastable  $2/\text{Mn}^+$  complexes monitored within the time window of the experiment. One may speculate that a possible origin for different internal energy contents in  $1/\text{Mn}^+$  and  $2/\text{Mn}^+$  is the different bond strengths of the metal–ligand bond for *cis* and *trans* complexes. However, this assumption can be excluded by using Cooks’ kinetic method.<sup>19</sup> The MI spectra of the mixed bis-(ligand) complexes  $1/2b/\text{Mn}^+$  and  $1b/2/\text{Mn}^+$  reveal a ca. 1:1 ratio for the losses of the *cis* and *trans* isomeric ketones; thus, their binding energies to  $\text{Mn}^+$  are identical within  $<\pm 1$  kcal/mol.

Consequently, the higher internal energy content of the *trans* isomers has to be rationalized differently. We suggest that the somewhat higher ring-strain energy of the *cis*-configured complexes, which is due to steric interactions of the 2-methyl group with the acetyl substituent, leads to a slightly faster decay of the  $1/\text{Mn}^+$  parent ions as compared to those of  $2/\text{Mn}^+$ . Thus,  $1/\text{Mn}^+$  ions reaching the field-free region preceding the second magnet in which the fragmentation is monitored will possess on average a lower ion internal energy content than the corresponding *trans* isomers. If this scenario holds true and we furthermore assume that

(17) (a) Hanratty, M.; Paulsen, C. M.; Beauchamp, J. L. *J. Am. Chem. Soc.* **1985**, *107*, 5074. (b) van Koppen, P. A. M.; Jacobson, D. B.; Illies, A.; Bowers, M. T.; Hanratty, M.; Beauchamp, J. L. *J. Am. Chem. Soc.* **1989**, *111*, 1991.

(18) MacMillan, D. K.; Gross, M. L.; Schulze, C.; Schwarz, H. *Organometallics* **1992**, *11*, 2079.

(19) For a general discussion of Cooks’ method and leading references, see: Brodbelt-Lustig, J. S.; Cooks, R. G. *Talanta* **1989**, *36*, 225.

**Table 8.** Mass Differences ( $\Delta m$  in amu) Observed in the Unimolecular Decomposition Reactions of the  $1^{65}\text{Cu}^+$  and  $2^{65}\text{Cu}^+$  Isotopologues<sup>a,b</sup>

	$\Delta m$											
	-2	-3	-4	-15	-18	-19	-28	-66	-67	-80	-83	$\text{Cu}^+$
<b>1</b> / $\text{Cu}^+$	28			3	22		24	13		9		1
<b>1b</b> / $\text{Cu}^+$	26				11	12	23	17			10	1
<b>1c</b> / $\text{Cu}^+$	12	11		3	18	1	23	12	7	12		1
<b>1d</b> / $\text{Cu}^+$	16	6		2	29		21	11	2	12		1
<b>1e</b> / $\text{Cu}^+$	5	16	1	2	15	12	23	11	3	12		1
<b>2</b> / $\text{Cu}^+$	19			4	3		46	13		14		1
<b>2b</b> / $\text{Cu}^+$	24				9	4	45	9			8	1
<b>2c</b> / $\text{Cu}^+$	9	9		4	4		46	8	6	13		1
<b>2d</b> / $\text{Cu}^+$	11	6		4	5	1	43	14	2	13		1
<b>2e</b> / $\text{Cu}^+$	4	11	1	4	1	2	47	12	2	16		1

<sup>a</sup> Intensities are expressed in  $\Sigma(\text{products}) = 100\%$ . Intensities less than 1% are omitted. <sup>b</sup> For the sake of clarity, only the main fragmentation reactions are included.

**Table 9.** Ionization Energies IE (eV) and Bond Dissociation Energies  $D$  (kcal/mol) for the  $\text{M}-\text{H}$  versus  $\text{M}^+-\text{H}$  and  $\text{M}-\text{CH}_3$  versus  $\text{M}^+-\text{CH}_3$  Bonds<sup>22</sup>

M	IE(MH)	$D(\text{M}^+-\text{H})$	$D(\text{M}-\text{H})$	IE(MCH <sub>3</sub> )	$D(\text{M}^+-\text{CH}_3)$	$D(\text{M}-\text{CH}_3)$
Cr	7.14	$32.5 \pm 2.2$	$41.1 \pm 3.1$	7.25	$30.1 \pm 1.9$	$41.1 \pm 6.9$
Mn	6.64	$48.6 \pm 3.3$	$30.1 \pm 4.1$	6.54	$51.0 \pm 1.9$	$30.1 \pm 4.1$
Fe	7.69	$49.8 \pm 1.4$	$45.7 \pm 3.1$	6.97	$57.9 \pm 1.9$	$37.1 \pm 6.9$
Co	7.81	$46.7 \pm 1.4$	$45.7 \pm 2.4$	7.71	$49.0 \pm 3.6$	$45.7 \pm 3.1$
Ni	8.44	$39.7 \pm 1.9$	$58.1 \pm 3.1$	8.09	$45.0 \pm 2.4$	$55.3 \pm 3.1$
Cu	9.42	$22.0 \pm 3.1$	$61.0 \pm 4.1$	8.96	$29.7 \pm 1.7$	$58.1 \pm 1.9$

dehydrogenation *via* remote functionalization is associated with the lowest activation barrier,<sup>20</sup> we expect that reactions with higher activation barriers are favored at the expense of dehydrogenation upon increase of the internal energy. This is indeed borne out in the experiment, in which the *cis/trans* differences can be ascribed to a decreasing intensity of dehydrogenation for the *trans* complexes.

As in the case of  $\text{Cr}^+$  complexes of **1** and **2**, the observation of facile ligand detachment from the  $\text{Mn}^+$  complexes indicates activation barriers for the other fragmentations comparable to the metal–ligand bond dissociation energy.

**Complexes of 1 and 2 with  $\text{Cu}^+$ .** The  $\text{Cu}^+$  complexes of **1** and **2** decompose *via* a manifold of reaction channels (Table 2). The most important ones correspond to dehydrogenation ( $\Delta m = 2$ ), losses of a methyl radical ( $\Delta m = 15$ ) and water ( $\Delta m = 18$ ), expulsion of carbon monoxide ( $\Delta m = 28$ ), losses of  $^{65}\text{CuH}$  ( $\Delta m = 66$ ) and  $^{65}\text{CuCH}_3$  ( $\Delta m = 80$ ), and ligand detachment ( $\Delta m = 98$ ). In addition, striking stereochemical effects seem to be operative. Unfortunately, the complexity of these reaction patterns made it difficult to derive a full mechanistic description of this system. Therefore, we will restrict our discussion to some basic conclusions that are based on the analysis of the isotopologues (Table 8).

Dehydrogenation follows by and large the mechanisms proposed above for the complexes of **1** and **2** with  $\text{Cr}^+$  (Scheme 6). Ring cleavage giving rise to  $3/\text{M}^+$  ( $\text{M} = \text{Cr}, \text{Cu}$ ) and subsequent dehydrogenation *via* remote functionalization competes with direct activation of an  $\omega$ -H atom in the intermediate  $13/\text{M}^+$ . This results in a higher abundance of the HD losses from **1c**/ $\text{Cu}^+$  and **2c**/ $\text{Cu}^+$ , as compared to those from **1d**/ $\text{Cu}^+$  and **2d**/ $\text{Cu}^+$ . However, the generation of  $\text{H}_2$  from **1e**/ $\text{Cu}^+$  and **2e**/ $\text{Cu}^+$  indicates that H/D exchange processes are operative once  $3/\text{Cu}^+$  is formed. Although dehydrogenation follows the remote functionalization mechanism to at least some extent, formation of ethene is not observed at all,

either by the “carbene route” or by remote functionalization, as evidenced from the absence of any fragments with  $\Delta m = 29-31$  for all isotopomers; therefore, we did not examine the  $^{18}\text{O}$ -labeled complexes **1a**/ $\text{Cu}^+$  and **2a**/ $\text{Cu}^+$ .

The loss of  $\text{CuH}$  quite likely involves allylic intermediates (such as **13**/ $\text{Cu}^+$ ), since the hydride structure is preformed. As allyl complexes are generated as intermediates during isomerization of the double-bond positions,<sup>6,13b,21</sup> one expects H/D exchange processes with the consequence that all positions of the cyclopropyl backbone are expected to participate, thus giving rise to the losses of  $\text{CuH}$  as well as  $\text{CuD}$ . This is indeed the case. Formation of neutral copper hydride is thermodynamically favored due to the rather high ionization energy (IE) of  $\text{CuH}$  on the one hand and the large  $\text{CuH}$  bond dissociation energy (BDE) as compared to the much lower BDE value given for the  $\text{Cu}^+-\text{H}$  bond (Table 9) on the other hand.<sup>22</sup> Since copper is the only metal included in this study which bears these unique features,<sup>23</sup> it can be easily understood why none of the other metals form a metal hydride or any other neutral metal fragments from their complexes with **1** or **2**.

In the formation of methyl radicals and of  $\text{CuCH}_3$  only the  $\alpha$ -methyl group is involved (see **1b**/ $\text{Cu}^+$  and **2b**/ $\text{Cu}^+$ , respectively). Presumably, both products arise *via*  $\alpha$ -insertion rather than allylic activation of the  $\omega$ -methyl group of ring-opened **3**/ $\text{Cu}^+$ , as was observed for the loss of  $\text{CH}_3$  from the  $\text{Mn}^+$  complexes. The intermediates **15**/ $\text{M}^+$  and **16**/ $\text{M}^+$  ( $\text{M} = \text{Cu}$ ) may well explain the expulsion of methyl radicals and of neutral  $\text{CuCH}_3$ , as well as decarbonylation. With respect to the loss of neutral  $\text{CuCH}_3$  the same thermochemical arguments apply as

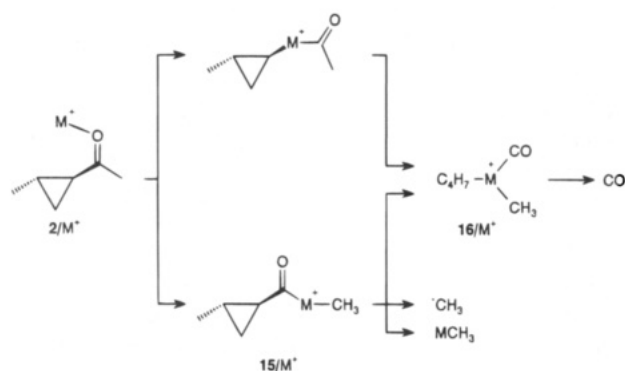
(20) (a) Schröder, D.; Eller, K.; Prüsse, T.; Schwarz, H. *Organometallics* **1991**, *9*, 2052. (b) Stöckigt, D.; Sen, S.; Schwarz, H. *Chem. Ber.* **1993**, *126*, 2553. (c) References 2f and 3d–f.

(21) Schwarz, J.; Schwarz, H. *Chem. Ber.* **1993**, *126*, 1257.

(22) Martinho Simões, J. A.; Beauchamp, J. L. *Chem. Rev.* **1990**, *90*, 629.

(23) Burmier, R. C.; Byrd, G. D.; Freiser, B. S. *Anal. Chem.* **1980**, *52*, 1641.

Scheme 9



**Table 10.** Data for the Unimolecular Decompositions of  $1/^{65}\text{Cu}^+$  and  $2/^{65}\text{Cu}^+$  after Subtraction of the Intensities of the Water Losses<sup>a</sup>

	$\Delta m$					Cu <sup>+</sup>
	-2	-15	-28	-66	-80	
1/Cu <sup>+</sup>	35	4	31	17	12	1
2/Cu <sup>+</sup>	20	4	47	13	15	1

<sup>a</sup> Intensities given are renormalized to  $\Sigma(\text{products}) = 100\%$ .

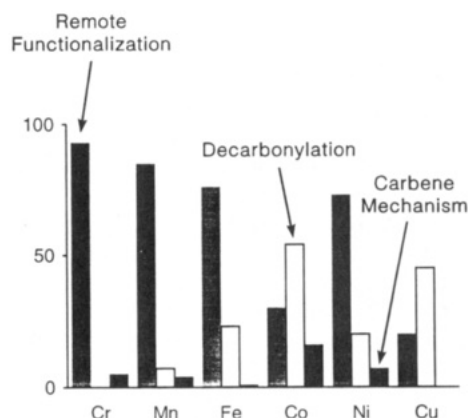
mentioned above for the discussion of the loss of CuH (Table 9). Obviously, the fact that losses of neutral metal fragments only occur for the Cu<sup>+</sup> complexes is due to the  $s^1d^{10}$  electronic configuration of neutral Cu being ideally suited for formation of one covalent bond, rendering hydride and methanide transfer from the substrate to the copper thermodynamically favorable.

Interestingly, the water losses reveal a drastically higher intensity for 1/Cu<sup>+</sup> as compared to 2/Cu<sup>+</sup>. However, the mechanism of water formation is by no means clear, and from the isotope distribution we only can conclude that hydrogen atoms from both methyl groups must be involved (1b/Cu<sup>+</sup> and 1e/Cu<sup>+</sup>; Table 8); a simple mechanistic picture involving enolization of the ketone and subsequent dehydration does not account for the experimental findings.<sup>23</sup>

The additional stereochemical influences on the other unimolecular decompositions of 1/Cu<sup>+</sup> versus 2/Cu<sup>+</sup> become more obvious when the percentages of the water losses are subtracted and the remaining fragments renormalized (Table 10). The intensities of dehydrogenation and CuH loss, i.e. the products arising from the "ring cleavage/remote functionalization" channel, are lower for the *trans* isomer, while the abundances of CO, CH<sub>3</sub>, and CuCH<sub>3</sub>, i.e. the products of the " $\alpha$ -insertion" channel, are higher. We recall that, for the Fe<sup>+</sup> complexes, CO loss is also clearly favored for the *trans* complex, and this has been explained in terms of different energy demands for the electrocyclic ring opening (Scheme 4). Similarly, this reasoning can account for the Cu<sup>+</sup> complexes of 1 and 2.

## Conclusions

Although the unimolecular decomposition reactions of the transition-metal complexes 1/M<sup>+</sup> and 2/M<sup>+</sup> reveal distinct features for each of the metal ions M<sup>+</sup> = Cr<sup>+</sup>–Cu<sup>+</sup> studied here, all main reactions can be categorized into three general reaction schemes: (i) metal-induced ring cleavage predominantly gives rise to H<sub>2</sub> and ethene *via* remote functionalization of acyclic 3/M<sup>+</sup>, (ii)  $\alpha$ -C–C bond insertion leads to carbon monoxide as neutral



**Figure 1.** Relative abundances of the three basic fragmentation channels for metastable  $2/M^+$  complexes for M = Cr–Cu. The first column represents the initial cleavage of the cyclopropyl backbone and subsequent remote functionalization, the second stands for  $\alpha$ -C–C bond activation next to the carbonyl group leading to consecutive decarbonylation, and the third column refers to the carbene mechanism; for details see text (data are extracted from Tables 3–8).

product, and (iii) carbene formation is observed for the Cr<sup>+</sup>, Mn<sup>+</sup>, Co<sup>+</sup>, and Ni<sup>+</sup> complexes, yielding ethene and propene, respectively. None of the metal cations investigated are capable of functionalizing directly the cyclopropyl backbone of 1 and 2 *via* remote functionalization of a  $\delta$ -C–H bond. Rather, initial C–C bond activation of the cyclopropyl backbone dominates the scene, until the acyclic isomeric 3/M<sup>+</sup> is formed, which can then be functionalized at positions remote from the carbonyl group. Within the group VIII transition-metal complexes of 1 and 2, respectively, the amount of C–C bond activation products reaches its maximum for the Co<sup>+</sup> complexes, while it decreases for the Fe<sup>+</sup> and Ni<sup>+</sup> complexes, which in turn show a higher abundance of C–H bond activation products.

With respect to the competition of the three basic pathways, i.e. remote functionalization, decarbonylation (paths a and b in Scheme 2), and the carbene mechanisms outlined in Schemes 5 and 7, the following conclusions can be derived from the present study (Figure 1). Except for Co<sup>+</sup> and Cu<sup>+</sup>, the initial ring cleavage of the cyclopropyl backbone followed by the remote functionalization mechanism corresponds to the dominating activation process for M = Cr, Mn, Fe, Ni. However, the examination of the isotopomers demonstrates the existence of subtle differences in that the rate-determining step of path a differs for the various metal cations. The direct activation of the functional group, i.e. decarbonylation, shows the opposite trend and reaches a maximum for the Co<sup>+</sup> complexes. Moreover, the efficient competition of decarbonylation with the remote functionalization path is the origin of the decreased remote functionalization for Co<sup>+</sup> and Cu<sup>+</sup>. As far as the Co<sup>+</sup> complexes are concerned, the prevailing direct C–C bond activation, which leads to decarbonylation, can be ascribed to a high stability of the insertion intermediate 6/Co<sup>+</sup> as compared to the other metal cations. For example, the sum of the bond dissociation energies of the dimethylmetal cations, M(CH<sub>3</sub>)<sub>2</sub><sup>+</sup>, is significantly higher for Co<sup>+</sup> (110 kcal/mol) as compared

to  $\text{Fe}^+$  and  $\text{Ni}^+$  (101 and  $>95$  kcal/mol, respectively).<sup>24,25</sup> Consequently, for  $2/\text{Co}^+$  the decarbonylation pathway will be energetically favored at the expense of the remote functionalization channel. On the other hand, for  $\text{Cu}^+$  the formation of an insertion intermediate with two covalent bonds is not feasible, since this would require an excitation of 3d electrons of  $\text{Cu}^+$  to the 4s or 4p manifold. Rather, for the  $\text{Cu}^+$  complexes initial C–C bond activation next to the carbonyl group may involve electron transfer from the acyl moiety to the  $\text{CuCH}_3$  fragment to yield a complex of the  $\text{C}_4\text{H}_7\text{CO}^+$  cation with neutral  $\text{CuCH}_3$ ; this scenario is further supported by the fact that indeed unimolecular loss of neutral  $\text{CuCH}_3$  from  $2/\text{Cu}^+$  is observed.<sup>23</sup> Moreover, since the remote functionalization pathway also involves insertion intermediates, but electron transfer from the remaining fragments is less facile as compared to an acyl group, the decarbonylation pathway gains in importance for  $2/\text{Cu}^+$ . With respect to the carbene mechanism we cannot interpret the relative abundances in terms of such simple thermodynamic and kinetic arguments. For example, for the metal cations under study the  $\text{M}^+ - \text{CH}_2$  binding energies reach a maximum for  $\text{M} = \text{Fe}$ ;<sup>24</sup> however, it is  $2/\text{Fe}^+$  in particular which hardly (or even not at all) follows this route. Presently, we are left with the assumption that the transition structures associated with the carbene route are energetically more demanding for  $\text{Fe}^+$  as compared to the other metals.

As far as the stereochemical features are concerned, we draw the following conclusions. The ring cleavage process, which leads to  $3/\text{M}^+$  and subsequent remote functionalization, does not occur stereospecifically. The only two metal cations which show large *cis/trans* differences are  $\text{Fe}^+$  and  $\text{Cu}^+$ . In both cases these differences can be ascribed to the efficiencies with which  $\alpha$ -C–C insertion reactions followed by formation of *cis*- and *trans*-3-allyl complexes take place. However, stereospecificity is only observed when the rate-determining steps (RDS) of the C–C bond activation leading either to subsequent rearrangement to 3-allyl complexes or decarbonylation directly compete with each other. Since it is well-known that C–C bond activation is facile for  $\text{Co}^+$  and  $\text{Ni}^+$ , it does not correspond to the RDS for these metals, and thus, these reactions are not stereospecific.<sup>11</sup> Likewise, the  $\text{Cr}^+$  complexes do not reveal *cis-trans* differences, since the predominant dehydrogenation prevents competition with other processes. For  $\text{Mn}^+$ , decarbonylation occurs and hence minor *cis-trans* differences are indeed observed.

(24) Armentrout, P. B.; Clemmer, D. E. In *Energetics of Organometallic Species*; Martinho Simões, J. A., Ed.; NATO ASI Series 367; Kluwer: Dordrecht, The Netherlands, 1992; p 321.

(25) For a theoretical study of  $\text{M}(\text{CH}_3)_2^+$  ( $\text{M} = \text{Sc-Cu}$ ), see: Rosi, M.; Bauschlicher, C. W., Jr.; Langhoff, S. R.; Partridge, H. *J. Phys. Chem.* **1990**, *94*, 8656.

From the observation of ligand detachment for the  $\text{Cr}^+$ ,  $\text{Mn}^+$ , and  $\text{Cu}^+$  complexes and its absence for the group VIII metals, we can derive some qualitative information about the barriers for C–H/C–C bond activation; these are of the same order of magnitude as the  $\text{M}^+ - \text{ligand}$  bond dissociation energies for the former and are clearly lower for the latter group. Although the binding energies of **2** to  $\text{M}^+$  have not been studied experimentally, the current knowledge of related systems<sup>26</sup> indicates that for  $\text{Cr}^+$  and  $\text{Mn}^+$  the observation of facile ligand detachment is also due to the low binding energies of these metal cations as compared to  $\text{Fe}^+$  through  $\text{Cu}^+$ . In fact, the relatively low binding energies of  $\text{Cr}^+$  and  $\text{Mn}^+$  to organic substrates have been associated with their electronic ground states ( $d^5$  and  $s^1d^5$ , respectively). In addition, thermodynamic grounds also account for the fact that loss of neutral metal fragments is only observed for the copper complexes  $1/\text{Cu}^+$  and  $2/\text{Cu}^+$ , respectively.

Finally, from the mechanisms outlined in this article we conclude that initial C–H bond activation of the 2-methyl group does not take place for the intact cyclopropane system. Even if this would occur due to the radicaloid nature<sup>27</sup> of cationic metal–carbon bonds, the cyclopropylmethyl radicals thus formed would undergo a rapid vinyl rearrangement.<sup>28</sup> Obviously, on geometric grounds direct C–H bond activation should occur much easier for the *cis* isomer,  $1/\text{M}^+$ , than for the *trans* isomer,  $2/\text{M}^+$ . However, neither the stereochemical features nor the isotope distribution provides any evidence for the operation of such a mechanism for all metal complexes studied. Thus, we conclude that for substituted cyclopropanes C–H bond activation at the  $\delta$ -position does not take place, in marked contrast to acyclic systems.<sup>1,4</sup>

**Acknowledgment.** Financial support by the Deutsche Forschungsgemeinschaft and the Fonds der Chemischen Industrie is acknowledged. We are grateful to Dipl.-Chem. Andreas Fiedler for helpful discussions and thank Katrin Schroeter and Robert Baumann for their efforts in the syntheses of labeled compounds.

OM940447E

(26) For experimental and theoretical values of the binding energies of  $\text{M}(\text{CO})^+$ ,  $\text{M}(\text{C}_2\text{H}_4)^+$ , and  $\text{M}(\text{C}_6\text{H}_6)^+$  for  $\text{M} = \text{Sc-Cu}$ , see: (a) Barnes, L. A.; Rosi, M.; Bauschlicher, C. W., Jr. *J. Chem. Phys.* **1990**, *93*, 609. (b) Sodupe, M.; Bauschlicher, C. W., Jr.; Langhoff, S. R.; Partridge, H. *J. Phys. Chem.* **1992**, *96*, 2118 (Addendum 5670). (c) Bauschlicher, C. W., Jr.; Partridge, H.; Langhoff, S. R. *J. Phys. Chem.* **1992**, *96*, 3273. (d) References 22 and 24. (e) See also: Tonkyn, R.; Ronan, M.; Weishaar, J. C. *J. Phys. Chem.* **1988**, *92*, 92.

(27) Schröder, D.; Fiedler, A.; Hrusák, J.; Schwarz, H. *J. Am. Chem. Soc.* **1992**, *114*, 1215.

(28) Griller, D.; Ingold, K. U. *Acc. Chem. Res.* **1980**, *13*, 317.

# <sup>19</sup>F Chemical Shifts of *m*- and *p*-Fluorophenyl Derivatives as a Probe of Metal–Ligand $\pi$ -Bonding

Russell S. Drago

Department of Chemistry, University of Florida, Gainesville, Florida 32611-2046

Received June 13, 1994<sup>®</sup>

Analysis of the <sup>19</sup>F chemical shifts of *m*-fluorophenyl derivatives of transition metal complexes establishes this measurement as a probe of metal electron density. The inductive  $\Delta E^X$  and  $\Delta C^X$  substituent constants are used to analyze the <sup>19</sup>F shifts of *m*-FC<sub>6</sub>H<sub>4</sub>–Pt–(PEt<sub>3</sub>)<sub>2</sub>–X complexes. An excellent data fit shows there is no indication of significant Pt–X back-bonding into X even when X is CN or C<sub>6</sub>H<sub>5</sub>.

## Introduction

In a recent article<sup>1</sup> it was shown that <sup>19</sup>F chemical shifts for a series of *m*-substituted fluorophenyl derivatives could be correlated with the  $3-\Delta E^X$  and  $3-\Delta C^X$  parameters<sup>2</sup> of the X-substituent. Since the shift reflects the electron-withdrawing and -releasing properties of the substituent, the correlation suggests that the *m*-fluorophenyl substituent attached to a metal complex may be a good probe of the influence that the coordination of ligands has on the electronic properties of metal centers. The 3-X substituent constants describe the inductive substituent influence on the electron density in the  $\sigma$  and  $\pi$  orbitals of the ring carbon to which they are attached. Since there is a node in the  $\pi$ -system between the carbon to which fluorine is attached and the meta carbon to which the 3-X substituent is attached, the substituent influence is transmitted by an inductive mechanism. The <sup>19</sup>F shift mirrors the change in electron density of the carbon attached to the substituent.

The *p*-substituted fluorophenyl derivatives showed a poor correlation of the <sup>19</sup>F shift with the  $4-\Delta E^X$  and  $4-\Delta C^X$  substituent constants. This was attributed<sup>1</sup> to a  $\pi$ -plus effect. This term signifies that mechanisms other than the normal conjugative electron density transmission of 4-X substituents to the para carbon are operative. In the normal 4-X conjugative interaction, the conjugative interaction of the substituent influences the total electron density on the para carbon attached to the reactive group. This change in electron density is transmitted to the reactive group from its attached carbon by a dominant  $\sigma$ -mechanism or is reflected in proportional changes in  $\sigma$ - and  $\pi$ -bonds of the para carbon to the reactive group. In cases where a spectral shift is measured instead of a reaction, the term "reactive group" encompasses the group undergoing the spectral transition.

The <sup>19</sup>F chemical shift is a  $\pi$ -plus system because it is more sensitive to the conjugative interactions of the substituent than described above as normal. This sensitivity results because the fluorine is directly conjugated to the substituent and because the *p*- $\pi$  orbital electron population on fluorine influences the chemical shift to a greater extent than the proportional changes

in electron density occurring in the fluorine  $\sigma$ -bond. In some cases, even though normal conjugative influences may be observed in the  $\sigma$ - and  $\pi$ -bonds for a particular reaction, the greater sensitivity of a different property to  $\pi$ -effects could lead to the  $\pi$ -plus mechanism. A second way in which the conjugative interaction can provide a  $\pi$ -plus contribution to the <sup>19</sup>F shifts is via the influence of substituent ring  $\pi$ -bonding on the energy of the  $\pi$ -orbitals. The paramagnetic contribution to the <sup>19</sup>F chemical shift arises from field induced mixing of the ground and excited states which is a function of  $1/\Delta E$ , where  $\Delta E$  is the energy difference of the ground state and the average energies of the empty molecular orbitals. As a result of these  $\pi$ -plus mechanisms, the <sup>19</sup>F shifts do not correlate with the 4-X substituent constants.

Metal complexes can be considered as substituents when bound to *meta*- and *para*-fluorophenyl. Different mechanisms for interaction of the metal with the *m*-fluorophenyl and *p*-fluorophenyl groups have led to the use of <sup>19</sup>F chemical shifts to probe  $\pi$ -back-bonding of ligands in metal complexes. In this article, <sup>19</sup>F chemical shifts of *meta*- and *para*-fluorophenyl probes bonded to a metal will be analyzed to reflect the changes in metal electron density resulting from coordination of X-groups directly to the metal. A very different conclusion concerning metal–ligand  $\pi$ -back-bonding results than from earlier literature interpretations of these measurements.

Analyses of the <sup>19</sup>F shifts will be carried out with the electrostatic-covalent substituent constant model.

$$\Delta\chi^X = d^E \Delta E^X + d^C \Delta C^X + \Delta\chi^H \quad (1)$$

In eq 1,  $\Delta E^X$  and  $\Delta C^X$  are the electrostatic-covalent analogues of Hammett  $\sigma$  values while the  $d^E$  and  $d^C$  parameters are interpreted as electrostatic and covalent components of  $\rho$ -values.

The  $\Delta E$  and  $\Delta C$  parameters are a unique set of substituent constants for they are directly related to the earlier  $E$  and  $C$  parameters used in the ECW equation (eq 2). Equations 3 and 4 show the relation of  $\Delta E^X$  and

$$\Delta\chi = E_A E_B + C_A C_B + W \quad (2)$$

$$E^X = E^H + s^E \Delta E^X \quad (3)$$

$\Delta C^X$  to the  $E$  and  $C$  parameters. In eqs 3 and 4,  $E^X$  and  $C^X$  are  $E$  and  $C$  values for the X-substituted

<sup>®</sup> Abstract published in *Advance ACS Abstracts*, November 15, 1994.

(1) Drago, R. S.; Zoltewicz, J. A. *J. Org. Chem.* **1994**, *59*, 2824.

(2) Drago, R. S.; Dadmun, A. P. *J. Am. Chem. Soc.* **1993**, *115*, 8592.



$$C^X = C^H + s^C \Delta C^X \quad (4)$$

compound and  $s^E$  and  $s^C$  indicate the sensitivity of the reactive center in a family of compounds to a substituent change. The  $s$ -values are set at one for the family of pyridine donors. For substituted phenols, the measured  $E_A$  and  $C_A$  values for several members of this family lead to  $s^E = -0.83$  and  $s^C = -0.23$ . The  $E_B^X$  and  $C_B^X$  or  $E_A^X$  and  $C_A^X$  values of eq 2 result for any X-substituted member of the family when the appropriate  $s$ ,  $\Delta E^X$ , and  $\Delta C^X$  values are substituted into eqs 3 and 4 along with  $E^H$  and  $C^H$ .

## Results and Discussion

**Fluorophenyl-Metal Systems.** The  $^{19}\text{F}$  chemical shifts of (*m*- and *p*-fluorophenyl)Pt[P(C<sub>2</sub>H<sub>5</sub>)<sub>3</sub>]<sub>2</sub>X provide the classic example<sup>4</sup> of the use of the fluorophenyl probes to infer metal-ligand  $\pi$ -back-bonding into X. The  $^{19}\text{F}$  chemical shifts of *m*- and *p*-FC<sub>6</sub>H<sub>4</sub>Pt[P(Et)<sub>3</sub>]<sub>2</sub>X are influenced<sup>3</sup> by the coordinating tendencies of the X group bound to platinum. Electron-releasing X ligands, decrease the partial positive charge on Pt making the ring carbon bound to platinum more carbanion-like. This in turn increases the shielding of the fluorine.<sup>3</sup> This trend is seen by comparing the experimental  $\delta(^{19}\text{F})$  values of the X = -CH<sub>3</sub> and -Cl compounds (Tables 1 and 2) for both the *m*- and *p*-fluorophenyl derivatives.

Cyanide is a strong coordinating ligand, and the small negative  $^{19}\text{F}$  value of the fluorophenyl derivatives when X is CN compared to that when X is chlorine was interpreted<sup>3</sup> as an indication of increased partial positive charge on Pt from metal-ligand  $\pi$ -back-bonding into the cyano group. In this article an alternative interpretation of  $^{19}\text{F}$  shifts will result.

***m*-FC<sub>6</sub>H<sub>4</sub>Pt(PEt<sub>3</sub>)<sub>2</sub>-X.** The analysis of  $^{19}\text{F}$  data for a coordinated fluorophenyl group requires a consideration of both the metal bonding to X and the metal bonding to the fluorophenyl group. First consider the data for the *m*-fluorophenyl derivatives in Table 1. The fluorine is attached to the benzene ring in the position meta to the Pt so there is a node in the  $\pi$ -system preventing a direct  $\pi$ -conjugative interaction of the phenyl-F  $\pi$ -bond with the  $p_z$  orbital of the carbon bound to the metal or to a potential Pt-phenyl  $\pi$ -bond. Since the  $^{19}\text{F}$  of the *m*-F phenyl ligand is mainly influenced by the  $\sigma$ -bonding of the *m*-fluorophenyl to platinum bond, it is a good probe of the electron withdrawal by X from the platinum center.

The platinum center is being modified by the bonding to X. The  $3-\Delta E^X$  and  $3-\Delta C^X$  substituent constants for the group, X, attached to platinum will be investigated as a measure of the  $\sigma$  inductive properties of the X group. If there were metal  $\pi$ -back-bonding into X or a lone pair donation from X into a metal, the metal reactivity would be incorrectly predicted by the  $3-\text{X}$  inductive, substituent constants.

When the  $3-\Delta E^X$  and  $3-\Delta C^X$  values<sup>3</sup> for the X ligands in Table 1 and the corresponding  $^{19}\text{F}$  chemical shifts are substituted into eq 1, eight simultaneous equations result. In the initial solution of these equations the iodo derivative was found to not fit well and missed in a direction suggestive of a steric effect; vide infra. When

**Table 1.**  $^{19}\text{F}$  Shielding in *m*-FC<sub>6</sub>H<sub>4</sub>-Pt(PEt<sub>3</sub>)<sub>2</sub>-X Complexes

X	$^{19}\text{F}_{\text{expt}}$	$^{19}\text{F}_{\text{calc3-X}}^b$ $^{19}\text{F}_{\text{calc4-X}}^c$	
		<i>m</i> -fluorophenyl <sup>a</sup>	
Cl	-2.50	-2.40	-2.96
Br	-2.34	-2.44	-3.06
I	-2.00	(-2.52)	(-3.00)
CN	-2.53	-2.53	-2.00
CH <sub>3</sub>	-4.26	-4.23	-3.78
SCN <sup>-</sup> (NCS <sup>-</sup> ) <sup>d</sup>	-1.90	-1.90 (-2.07) <sup>d</sup>	
OCN <sup>-</sup>	-2.48	-2.40	
C <sub>6</sub> H <sub>5</sub>	-3.72	-3.82	-3.35

<sup>a</sup> Data from ref 3. The iodo derivative was omitted from the data fit because of steric effects. It is not known if thiocyanate is bonded to sulfur or nitrogen. The data fit suggest nitrogen. In this article, the more shielded the  $^{19}\text{F}$ , the more negative the number. <sup>b</sup> The *m*-derivatives were calculated with  $\Delta\chi^X = -39.02(\pm 0.4)\Delta E_A + 7.09(\pm 0.1)\Delta C_A - 3.82(\pm 0.0)$ , using reported  $3-\Delta E$  and  $3-\Delta C$  values.  $\bar{x} = 0.06$  and the % fit is 3. <sup>c</sup> To examine conjugative interactions, the *m*-derivatives were calculated with  $\Delta\chi^X = -0.85(\pm 0.5)\Delta E_A + 0.00(\pm 0.01)\Delta C_A - 0.49(\pm 0.5)$ , using reported  $4-\Delta E$  and  $4-\Delta C$  values.  $\bar{v} = 0.05$  and the % fit is 28. <sup>d</sup> Values are fit for N bound and calculated in parentheses for S bound thiocyanate using reported  $\Delta E$  and  $\Delta C$  values. The N-bonded or S-bonded forms or a rapidly exchanging mixture fit the data well considering the uncertainty (see  $n$ -values) in these substituents.

this data point is omitted, the remaining seven equations produce an excellent data fit giving  $d_B^E = -39.02$ ,  $d_B^C = 7.09$ , and  $\Delta\chi^H = -3.82$  for the *m*-fluorophenyl probe. The  $\Delta\chi^H$  value corresponds to the value predicted for the platinum complex with X = H. The data fit is shown in Table 1 by comparing the column labeled  $^{19}\text{F}_{\text{calc3-X}}$  with the experimental values. *The  $\sigma$  inductive properties of the X-group attached to platinum accurately correlate the  $^{19}\text{F}$  shifts.* Thus, *m*-fluorophenyl shifts, which provide a measure of the electron density on platinum, indicate that the essential interaction of X with platinum for all the X groups in Table 1 is  $\sigma$  bonding. The mode of thiocyanate coordination is unknown, but it would fit if it were either sulfur or nitrogen bound.

The sign of  $d$  is determined by the signs of  $s^E$  and  $s^C$  for platinum and the signs of  $E_B^*$  and  $C_B^*$  for the fluorophenyl group.

$$d_B^E = s_A^E E_B^* \quad (5)$$

$$d_B^C = s_B^C C_B^* \quad (6)$$

The signs of  $d_B^E$  and  $d_B^C$  in the  $^{19}\text{F}$  fit<sup>1</sup> of a series of *m*-FC<sub>6</sub>H<sub>4</sub>X compounds with different substituent constants X is the same as that found here. These signs indicate that increasing the electrostatic character of the metal bond to the fluorophenyl group makes the meta carbon more carbanion-like which shields the fluorine and makes  $\delta$  more negative. The sign for  $d_B^C$  tells us that covalency in the bond of the metal to the fluorophenyl group deshields the fluorine and makes  $\delta$  less negative. This interpretation is in keeping with predictions of the influence of the meta carbon charge on both the electron population of the fluorine *p*-orbital and on its influence on the paramagnetic contribution to the  $^{19}\text{F}$  shift<sup>1</sup> from covalency.

In order to obtain a good fit, the iodo derivative was omitted. When the  $d^E$ ,  $d^C$ , and  $\Delta\chi^H$  parameters are used to calculate the value for this derivative, the calculated result is more negative than the experimental value. The more negative experimental value is consistent with

(3) Drago, R. S.; Dadmun, A. P. *J. Am. Chem. Soc.* **1994**, *116*, 1792.

(4) Parshall, G. W. *J. Am. Chem. Soc.* **1966**, *88*, 704.



the existence of a steric effect involving the ligands in the first coordination shell around the metal. Steric repulsion makes the platinum charge more positive than it would be if iodide were more strongly bound. The most interesting conclusion from this analysis is that there is no indication of any  $\pi$ -back-bonding when the X-group attached to platinum is cyano or phenyl.

To further probe the bonding of X to platinum, the  $4-\Delta E^X$  and  $4-\Delta C^X$  conjugative substituent constants of the X-groups bound to platinum were used to evaluate the shifts of the *meta*-fluorophenyl platinum complex. Though the 4-X substituent constants are not expected to be accurate measures of the Pt-X conjugative interactions, they should do better than the 3-X substituents if Pt-X  $\pi$ -back-bonding exists. The poor data fit for the *m*-fluorophenyl platinum complexes to the 4-X substituent constants is shown in Table 1 under the column labeled <sup>19</sup>F<sub>calc 4-X</sub>. Even with fewer known values of 4-X substituent constants, a poor fit results which provides further support for the conclusion that the X-group coordinated to Pt does not  $\pi$ -bond.

***p*-FC<sub>6</sub>H<sub>4</sub>Pt(Et<sub>3</sub>P)<sub>2</sub>X.** The <sup>19</sup>F shifts of *para*-fluorophenyl substituted platinum derivatives<sup>4</sup> will be considered next. The <sup>19</sup>F shift in the parafluoro group attached to Pt is fit to the 3-X substituent constants for the X groups attached to Pt. A poorer data fit results than for the *meta*-fluoro complexes even when X = I is

Table 2. <sup>19</sup>F Shielding in *p*-FC<sub>6</sub>H<sub>4</sub>-Pt(PEt<sub>3</sub>)<sub>2</sub>-X Complexes

X	<sup>19</sup> F <sub>expt</sub>	<sup>19</sup> F <sub>calc 3-X<sup>a</sup></sub>	X	<sup>19</sup> F <sub>expt</sub>	<sup>19</sup> F <sub>calc 3-X<sup>a</sup></sub>
Cl	-10.2	-10.0	CH <sub>3</sub>	-11.7	-11.5
Br	-10.0	-10.0	NSC <sup>-</sup> (SCN)	-9.2	-10.0 (-10.2)
I	-9.7	(-10.1)	OCN <sup>-</sup>	-10.2	-10.2
CN	-9.1	-9.1	C <sub>6</sub> H <sub>5</sub>	-10.9	-11.3
4-FC <sub>6</sub> H <sub>5</sub>	-10.8	-11.3			

<sup>a</sup> The *p*-derivatives were calculated with  $\Delta\chi^X = -6.49(\pm 2)\Delta E_B - 0.92(\pm 0.46)\Delta C_B - 11.2(\pm 0.0)$ , using reported 3- $\Delta E$  and 3- $\Delta C$  values for X. The  $\bar{x} = 0.26$  and the % fit is 11.

omitted because of the steric problem found in the *m*-fluorophenyl fit. The shift of the parafluoro group is very sensitive to even weak  $\pi$ -conjugation of X-groups. For example, 4-CH<sub>3</sub> hyperconjugation leads to a 4 ppm deviation in the <sup>19</sup>F shift of *p*-XC<sub>6</sub>H<sub>4</sub>F from that predicted with a 4-X substituent constant. The weak, direct  $\pi$  interaction of the X-group with the *para*-fluorophenyl group, is referred to as a  $\pi$ -plus contribution in the <sup>19</sup>F shifts. Electron density on the para carbon influences the <sup>19</sup>F shift by the normal conjugative and the  $\pi$ -plus mechanisms discussed earlier. This results in a crude relationship of the shift to the electron-withdrawing properties of the attached group. *The para-fluorophenyl group is a poorer probe of metal electron density than the meta-fluoro group.*

The deviations observed for the *p*-fluorophenyl platinum complexes are much smaller than those found in the <sup>19</sup>F fit of *p*-FC<sub>6</sub>H<sub>4</sub>X compounds. Thus, the extent of  $\pi$ -back-bonding of platinum into the fluorophenyl  $\pi$ -system is even less than the  $\pi$ -mixing involved in methyl hyperconjugation. The poor overlap and poor energy match of the platinum d-orbitals with the fluorophenyl  $\pi$ -system leads to little if any  $\pi$ -back-bonding into *p*-fluorophenyl which leads to a small  $\pi$ -plus effect in the <sup>19</sup>F shifts. In view of the extreme sensitivity of the *p*-fluorophenyl probe to  $\pi$ -plus contribution from electron density on the *para*-carbon, the

*p*-fluorophenyl is not as good a probe of electron density on the metal as the metafluorophenyl probe.

The final issue remaining concerns the greater shielding observed for the *p*-fluoro derivatives than for the *m*-fluoro derivatives. This results from the more effective transmission of the normal substituent influence through the  $\pi$ -system. The ring carbon bonded to a Pt-[Pt(Et)<sub>3</sub>]<sub>2</sub>-X substituent is carbanion like and this electron density is transmitted to the fluorine more effectively by the normal conjugative 4-X mechanism than by the 3-X inductive mechanism. In general, the 4-X substituent constants are larger in magnitude than the 3-X.

In summary, the <sup>19</sup>F shifts of the *m*-fluorophenyl derivatives provide the best indication of the electronic properties of the metal. These shifts show that the trend as X is varied is dominated by the metal-X  $\sigma$ -bonding interaction. There is no indication of metal to ligand  $\pi$ -back-bonding into cyanide. There is, however, indication of a steric effect with the iodo derivative. The steric effect causes the metal center to have an increased partial positive charge leading to a less negative experimental value for the <sup>19</sup>F resonance than predicted. These results suggest that <sup>19</sup>F chemical shifts of the meta and para fluorophenyl group can be a valuable probe for understanding organometallic chemistry. The former probes electron density on the group to which it is attached. The latter should give rise to a large  $\pi$ -plus contribution when metal  $\pi$ -back-bonding is significant. The data fit also demonstrates the remarkably broad scope of the  $\Delta E$  and  $\Delta C$  parameters by extending the type of system treated to substituents directly bound to Pt(II). The insights provided about the <sup>19</sup>F shifts in these systems were not obtained by other analyses. This success should encourage the application of the  $\Delta E$  and  $\Delta C$  substituent constant analyses in coordination and organometallic chemistry.

**FC<sub>6</sub>H<sub>4</sub>-Hg-X Complexes.** The next system to be analyzed involves a series of *meta*- and *para*-fluorophenyl mercury-X derivatives.<sup>5</sup> A limited number of X-groups have been studied. With limited substituents, the consistency of the data set with a  $\sigma$ -bonding interaction of X can be determined, but the absence of  $\pi$ -back-bonding is not firmly established. Only tentative values for the  $d^E$ ,  $d^C$ , and  $\Delta\chi^H$  parameter are obtained. The <sup>19</sup>F data for the *para*- and *meta*-fluorophenyl derivatives were fit using the 3-X substituents for the group bonded to mercury. The results are shown in Table 3. The

Table 3. <sup>19</sup>F Shifts For FC<sub>6</sub>H<sub>4</sub>-Hg-X Derivatives<sup>a</sup>

X	<i>m</i> -FC <sub>6</sub> H <sub>4</sub> <sup>-</sup>		<i>p</i> -FC <sub>6</sub> H <sub>4</sub> <sup>-</sup>	
	<sup>19</sup> F exp	<sup>19</sup> F calc <sup>b</sup>	<sup>19</sup> F exp	<sup>19</sup> F calc <sup>c</sup>
3-CH <sub>3</sub>	-0.31	-0.31	-0.24	-0.19
3-Br	2.08	2.08	2.78	2.78
3-C <sub>6</sub> H <sub>5</sub>	0.10	0.11	0.37	0.22
3-OH	1.32	1.32	1.11	1.32
3-CCl <sub>3</sub> <sup>d</sup>	1.53	1.54	2.30	2.28

<sup>a</sup> Data from ref 5. <sup>b</sup> Calculated with  $\Delta\chi^X = -26.75(\pm 0.05)\Delta E_B + 2.86(\pm 0.01)\Delta C_B + 0.22(\pm 0.0)$ . The  $\bar{x} = 0.010$  and the percent fit is better than 1%. <sup>c</sup> Calculated with  $\Delta\chi^X = -9.95(\pm 0.7)\Delta E_B - 2.50(\pm 0.18)\Delta C_B + 0.47(\pm 0.0)$ . The  $\bar{x} = 0.05$  and the percent fit is 2%.

excellent data fit of the metafluorophenyl derivative

suggests that the interaction of the X groups studied with mercury involves mainly  $\sigma$  bonding.

The parafluorophenyl data also gives a good fit with the 3-X substituent constants. The absence of a large  $\pi$ -plus contribution in the fit of the parafluorophenyl derivatives confirms the conclusion from the 3-fluorophenyl data that the X-substituents are only  $\sigma$  bonded.

**FC<sub>6</sub>H<sub>4</sub>-Co(DO-DOHpn)-X Complexes.** The <sup>19</sup>F chemical shift of *m*- and *p*-FC<sub>6</sub>H<sub>4</sub>-Co[(DO)(DOH)pn]-X complexes, (where DO-DOHpn is diacetylmonoxime-imino diacetylmonoximateiminopropane-1,3 and X is an anionic ligand) have been measured<sup>6</sup> to investigate the trans effect. The data are given in Table 4 along with the results of the data fit to eq 1.

**Table 4.** <sup>19</sup>F Shifts of *m*- and *p*-FC<sub>6</sub>H<sub>4</sub>-Co[(DO)-DOHpn]X<sup>a</sup>

X	<i>m</i> -fluorophenyl	
	<sup>19</sup> F <sub>exp</sub>	<sup>19</sup> F <sub>calc</sub> <sup>b</sup>
H <sub>3</sub> C <sup>-</sup>	-3.05	-3.05
OCN <sup>-</sup>	-0.98	-0.96
Br <sup>-</sup>	-0.68	-0.68
I <sup>-</sup>	-0.50	(-0.85)
NCS <sup>-</sup> (SCN <sup>-</sup> )	-0.52	-0.55 (-0.76)
X	<i>p</i> -fluorophenyl	
	<sup>19</sup> F <sub>exp</sub>	<sup>19</sup> F <sub>calc</sub> <sup>c</sup>
H <sub>3</sub> C <sup>-</sup>	-11.3	-11.3
<i>p</i> -FC <sub>6</sub> H <sub>4</sub> <sup>-</sup>	-10.6	-11.0
OCN <sup>-</sup>	-9.72	-9.66
Br <sup>-</sup>	-9.73	-9.69
I <sup>-</sup>	-9.73	-9.76
NCS <sup>-</sup> (SCN <sup>-</sup> )	-9.29	-9.37 (9.23)

<sup>a</sup> <sup>19</sup>F relative to C<sub>6</sub>H<sub>5</sub>F measured in (CH<sub>3</sub>)<sub>2</sub>SO. <sup>b</sup> Calculated with  $\Delta\chi^X = -17.31(\pm 0.2)\Delta E_B + 0.44(\pm 0.05)\Delta C_B - 2.52(\pm 0.0)$ .  $\bar{x} = 0.01$  and the % fit is 1. <sup>c</sup> Calculated with  $\Delta\chi^X = -33.41(\pm 1.2)\Delta E_B + 5.99(\pm 0.29)\Delta C_B - 10.91(\pm 0.0)$ .  $\bar{x} = 0.10$  and the % fit is 4.

The iodo derivative is well behaved in the *p*-fluorophenyl series but may be displaced by solvent in the *m*-fluorophenyl series. It was omitted from the data fit. The limited data set leads to tentative parameters but clearly shows the shifts for both the *m*-fluorophenyl and *p*-fluorophenyl derivatives of the compounds studied can be described with the 3- $\Delta E$  and 3- $\Delta C$  parameters of the -X group. No significant  $\pi$ -plus contribution is detected for the *p*-fluorophenylcobalt complexes. We can confidently state that these results do not support the literature<sup>6</sup> conclusions that there is extensive interaction of the cobalt with  $\pi$ -aryl ligands and that thiocyanate is a  $\pi$  donor ligand toward this complex.

**Fluorophenyl-M-B Systems.** The alkylcobaloximes, XCo(DMG)<sub>2</sub>L, contain a small, low oxidation state metal center and have been reported to  $\pi$ -back-bond into L when it is a phosphite ligand.<sup>7</sup> A series of <sup>19</sup>F shifts have been measured<sup>8</sup> for (*m*- and (*p*-fluorophenyl)cobaloxime adducts of various donors (B). To probe a  $\sigma$  donor interaction, this data is fit to the ECW equation (eq 7) using reported  $E_B$  and  $C_B$  parameters

$$\Delta\chi = E_A^*E_B + C_A^*C_B + W \quad (7)$$

**Table 5.** Fit of (*p*- and (*m*-Fluorophenyl)cobaloxime Donor B Adducts<sup>a</sup>

donor	<i>m</i> -FC <sub>6</sub> H <sub>5</sub>		<i>p</i> -FC <sub>6</sub> H <sub>5</sub>	
	exp	cal <sup>b</sup>	exp	cal <sup>c</sup>
4-CNC <sub>5</sub> H <sub>4</sub> N	-1.43	-1.38	-9.48	-9.21
C <sub>5</sub> H <sub>5</sub> N	-1.66	-1.71	-8.75	-9.44
4-CH <sub>3</sub> C <sub>5</sub> H <sub>4</sub> N	-1.75	-1.80		
4-NH <sub>2</sub> C <sub>5</sub> H <sub>4</sub> N	-2.05	-1.97	-10.0	-9.59
4-CH <sub>3</sub> C(O)NHC <sub>5</sub> H <sub>4</sub> N	-1.55	-1.65	-9.56	-9.39
CH <sub>3</sub> OH	-0.98	-0.98	-9.75	-9.73
(CH <sub>3</sub> ) <sub>2</sub> SO	-1.86	(-1.03)	-10.27	(-10.12)

<sup>a</sup> Data from ref 7. The  $E_B$  and  $C_B$  values for the substituted pyridine are calculated from  $\Delta E$  and  $\Delta C$  values.<sup>2,3</sup> The more negative the number the more shielded the fluorine. <sup>b</sup> <sup>19</sup>F chemical shift ppm, relative to internal FC<sub>6</sub>H<sub>5</sub>. Calculated with  $\Delta\chi^X = -0.72(\pm 0.20)E_B - 0.26(\pm 0.05)C_B - 0.48(\pm 0.12)$ .  $\bar{x} = 0.06$ , and the percent fit is 5. <sup>c</sup> <sup>19</sup>F chemical shift ppm, relative to internal FC<sub>6</sub>H<sub>5</sub>. Calculated with  $\Delta\chi^X = -1.13(\pm 0.50)E_B - 0.10(\pm 0.01)C_B - 7.77(\pm 0.30)$ .  $\bar{x} = 0.36$ , and the percent fit is 30.

for the donors.<sup>9</sup> The data fit for those bases in the  $E$  and  $C$  correlation are shown in Table 5. An excellent data fit is obtained for the *m*-fluorophenyl derivative. Substantial changes occur in the  $\pi^*$  energies of the substituted pyridines that have been studied and if  $\pi$ -back-bonding occurs it would vary over the series. Since the <sup>19</sup>F shifts are correlated with the  $\sigma$  donor,  $E_B$  and  $C_B$  parameters, we can conclude that  $\sigma$ -bonding is the principal interaction of the donors studied with the cobalt. The same electrostatic,  $E_B$ , and covalent,  $C_B$ , properties that determine enthalpies of interaction of these donors with various acceptors also determine the <sup>19</sup>F shifts. The enthalpies for the methylcobaloxime<sup>7</sup> acceptor have a large contribution from the covalency ( $E_A = 4.70$ ,  $C_A = 3.24$ ) with a  $C/E$  ratio of 0.69. The tentative parameters for the <sup>19</sup>F chemical shift, with a  $C^*/E^* = 0.36$ , suggest the shift is more dependent on the electrostatic properties of the base than the enthalpies are. The  $C_A^*/E_A^*$  ratio of 0.36 is large for a spectral probe.

Since the number and type of donor studied is limited, the conclusion to be drawn from the data fit is that there is no indication of metal to ligand  $\pi$ -back-bonding in the systems studied. The *m*-FC<sub>6</sub>H<sub>5</sub>Co(DH)<sub>2</sub>B system should be studied with more donors whose  $E_B$  and  $C_B$  values are known to establish that  $\pi$ -back-bonding into pyridine-type ligands does not occur and to establish this complex as a spectral probe. On the basis of the enthalpy fit to methylcobaloxime, it is anticipated that good  $\pi$ -back-bond acceptor ligands, e.g. CH<sub>3</sub>CN and P(OCH<sub>3</sub>)<sub>3</sub>, will lead to deviations in the <sup>19</sup>F fit.

The dimethyl sulfoxide adduct deviates from the fit. The  $E_B$  and  $C_B$  parameters are for oxygen-bonded dimethyl sulfoxide. The miss is consistent with other correlations that suggest dimethyl sulfoxide may be sulfur coordinated to the cobalt center.<sup>11</sup>

In contrast to the excellent  $\bar{x}$  for the data fit of the *m*-fluorophenyl adducts, the *p*-fluorophenyl derivatives give a poorer fit to the  $E_B$  and  $C_B$  of the coordinated donors. The deviations are not as large as those found<sup>1</sup> for  $\pi$ -plus contributions from the conjugative interaction of substituents in the 4-X fluorophenyl derivatives. The fit is consistent with a dominant  $\sigma$  interaction of the ligands with the cobalt.

(6) Hill, H. A. O.; Morallee, K. G.; Cernivez, F.; Pellizer, G. *J. Am. Chem. Soc.* **1972**, *94*, 277.

(7) Courtright, R. L.; Drago, R. S.; Nusz, J. A.; Nozari, M. *S. Inorg. Chem.* **1973**, *12*, 2809.

(8) Brown, K. L.; Lu, L.-Y. *Inorg. Chem.* **1981**, *20*, 4178.

(9) Drago, R. S. *Applications of Electrostatic-Covalent Models in Chemistry*; Surfside Scientific Publishers: P.O. Box 13413, Gainesville, FL, 1994.

(10) Drago, R. S. *Inorg. Chem.* **1990**, *29*, 1379.

(11) Drago, R. S. Submitted for publication.

The conclusions drawn from this analysis are consistent with the reported interpretation of the reactivity and spectroscopic properties of a series of XCo(DMG)<sub>2</sub>B complexes.<sup>7,11</sup> Very good  $\pi$ -acceptor ligands are necessary to obtain measurable contributions to bond strengths and equilibrium properties from  $\pi$ -back-bonding in this cobalt system.

**FC<sub>6</sub>H<sub>5</sub>BCl<sub>2</sub>-B Adducts.** The <sup>19</sup>F shifts upon coordination of a series of bases to 3- and 4-FC<sub>6</sub>H<sub>4</sub>-BCl<sub>2</sub> are reported.<sup>5</sup> Data for both sets of adducts are poorly fit. Steric effects are expected to be operative in these adducts and the poor fit is attributed to this problem. It is significant that a poor fit was obtained for this data set even though five experimental values were fit to three unknowns.

### Conclusions

The *meta*-fluorophenyl substituent constant is established as a probe of electron density on a metal complex. As such its <sup>19</sup>F shift can be used to probe the interaction of other ligands, X, with the metal to which the *m*-fluoro group is attached. The *p*-fluorophenyl substituent is a very sensitive probe of conjugative interactions of metal centers with this substituent. Good data fits to  $\Delta E$  and  $\Delta C$  are not expected, but the absence or existence of large  $\pi$ -plus contributions can provide information about  $\pi$ -back-bonding of the metal with the probe.

The number of donors studied in all of the systems analyzed in this article is limited. Even under these circumstances, the  $\Delta E$ - $\Delta C$  and the *ECW* analyses are shown to have utility in determining whether or not the data for the substituents studied provide experimental support for unusual effects (steric,  $\pi$ -back-bonding, nonspecific solvation, etc.) in organometallic chemistry. It is interesting to note that even with a limited number of systems, unusual effects are found in some of the data fits.

The parameters resulting from any fit of limited data should be considered tentative. Prediction of data for new donors should be limited to those whose  $C_B/E_B$  ratio or  $\Delta C/\Delta E$  ratio is in the range of those used in the data fits. The interpretation of the relative importance of covalent and electrostatic bond contributions from tentative parameters is not recommended.

### Calculations

**Substituent Constant Analyses.** Reported substituent constants are substituted into eq 1 along with the corresponding value of the <sup>19</sup>F shift ( $\Delta\chi$ ). A least squares minimization procedure is used to find the best fit  $d^E$ ,  $d^C$ , and  $\Delta\chi^H$  parameters. When omitting one substituent from the fit leads to a significant improvement in the fit of the remaining systems, it is omitted from the reported fit. The substituent constants for the deviating system is used to calculate  $\Delta\chi^X$  from the reported  $d^E$ ,  $d^C$ , and  $\Delta\chi^H$  parameters.

The addition of new data has led to the refinement<sup>12</sup> of several 3-X substituent constants reported previously.<sup>3</sup> The new values used in this study are listed in the order substituent/ $\Delta E/\Delta C/n$ : C<sub>6</sub>H<sub>5</sub>/0.011/0.058/0.3; SCN<sup>-</sup>/-0.110/-0.335/0.8; NCS<sup>-</sup>/-0.125/-0.442/0.6; OCN<sup>-</sup>/-0.099/-0.345/0.5; CCl<sub>3</sub>/-0.089/-0.372/0.8; *p*-FC<sub>6</sub>H<sub>4</sub>/0.004/0.035/0.5. All other parameters are those reported earlier.<sup>3</sup>

**Donor Adduct Analyses.** When the quantity being varied is a neutral base, the data are fit to eq 7. Reported values<sup>9</sup> of  $E_B$  and  $C_B$  are substituted into eq 7, and the least squares fit produces  $E_A^*$ ,  $C_A^*$ , and  $W$ .

OM940451Q

# Synthesis, Reactions, and $^{77}\text{Se}$ NMR Studies of $\eta^5$ -Selenophene Complexes of Chromium, Manganese, Ruthenium, and Iridium

Carter J. White and Robert J. Angelici\*

Department of Chemistry and Ames Laboratory,<sup>1</sup> Gilman Hall, Iowa State University, Ames, Iowa 50011

Moon-Gun Choi

Department of Chemistry, Yonsei University, Seoul 120-749, Korea

Received June 9, 1994<sup>®</sup>

The series of  $\eta^5$ -selenophene transition metal complexes ( $\eta^5$ -Seln)Cr(CO)<sub>3</sub> (**1-3**), [ $(\eta^5$ -Seln)Mn(CO)<sub>3</sub>]SO<sub>3</sub>CF<sub>3</sub> (**4-6**), [ $(\eta^5$ -Seln)RuCp\*]SO<sub>3</sub>CF<sub>3</sub> (**7-9**), and [ $(\eta^5$ -Seln)IrCp\*](BF<sub>4</sub>)<sub>2</sub> (**10-12**), where Seln = selenophene (Sel), 2-methylselenophene (2-MeSel), or 2,5-dimethylselenophene (2,5-Me<sub>2</sub>Sel), were synthesized and characterized by <sup>1</sup>H, <sup>13</sup>C, and <sup>77</sup>Se NMR and IR spectroscopy. The molecular structure of ( $\eta^5$ -2,5-Me<sub>2</sub>Sel)Cr(CO)<sub>3</sub> (**3**) was determined. Reactions of [ $(\eta^5$ -Sel)Mn(CO)<sub>3</sub>]SO<sub>3</sub>CF<sub>3</sub> (**4**) with nucleophiles (Nuc = H<sup>-</sup>, CN<sup>-</sup>) give the neutral addition products [(Sel-Nuc)Mn(CO)<sub>3</sub>] [Nuc = H<sup>-</sup>, Nuc = CN<sup>-</sup> (**4b**)] in which three carbon atoms and the Se are bonded to the Mn. The reaction of [ $(\eta^5$ -Sel)RuCp\*]SO<sub>3</sub>CF<sub>3</sub> (**7**) with H<sup>-</sup>, however, results in cleavage of the C-Se bond to form a butadiene selenide complex (( $\eta^5$ -SeCH=CHCH=CH<sub>2</sub>)RuCp\*) (**7a**). Still another type of product results from the reaction of [ $(\eta^5$ -2,5-Me<sub>2</sub>Sel)IrCp\*](BF<sub>4</sub>)<sub>2</sub> (**12**) with 2 equiv of H<sup>-</sup>; in this case, the H<sup>-</sup> acts as a reducing agent to give the ring-opened complex (C, Se-2,5-Me<sub>2</sub>Sel)IrCp\* (**12a**). All of these reactions are similar to those of the analogous  $\eta^5$ -thiophene complexes. The <sup>77</sup>Se NMR chemical shift values for the  $\eta^5$ -Seln ligands in complexes **1-12** fall within a range of 225 ppm; they are influenced by the metal and its ligands, the charge on the complex, and the number of methyl groups in the selenophene.

## Introduction

In studies of the mechanism(s) of thiophene (T) hydrodesulfurization (HDS), we and others have sought to understand how thiophene is bound to metal sites on the heterogeneous catalyst.<sup>2-4</sup> In HDS model organometallic complexes, thiophene is commonly known to coordinate either through the entire  $\pi$  system ( $\eta^5$ ) or through the sulfur atom [ $\eta^1(\text{S})$ ] only. Reactions of the  $\eta^5$  thiophene complexes have been linked to possible HDS mechanisms.<sup>5</sup> Thiophene has also been reported to coordinate to metals through a single C=C bond ( $\eta^2$ )<sup>6</sup> or through both C=C bonds ( $\eta^4$ ).<sup>7,8</sup>

Selenophene is a five-membered heterocyclic compound with a structure and chemistry similar to that of thiophene (Figure 1).<sup>9-12</sup> Our group has previously reported on the coordination of selenophenes (Seln) in

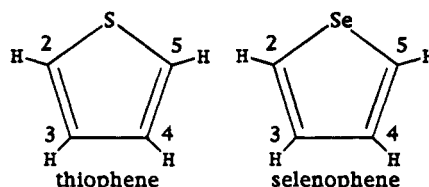
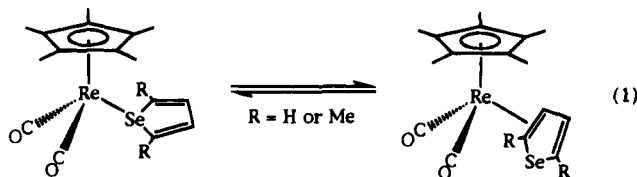


Figure 1. Structures and numbering of thiophene and selenophene.

the complexes Cp\*Re(CO)<sub>2</sub>(Seln).<sup>13,14</sup> In the electron-rich complex Cp\*Re(CO)<sub>2</sub>(Seln) (Cp\* =  $\eta^5$ -C<sub>5</sub>Me<sub>5</sub>), the selenophene (Sel) ligand is  $\eta^2$  coordinated through two of the carbons of Sel, while in the analogous 2,5-dimethylselenophene (2,5-Me<sub>2</sub>Sel) complex Cp\*(CO)<sub>2</sub>Re(2,5-Me<sub>2</sub>Sel), the ligand is coordinated through the Se atom. For the analogous 2-methylselenophene (2-MeSel) complexes, the  $\eta^1(\text{Se})$  and  $\eta^2$  isomers are in equilibrium (eq 1). Not only does the selenophene binding



mode depend on the number of methyl groups in the Seln, but the equilibrium amount of the  $\eta^1(\text{Se})$  isomer increases when the Cp\* ligand is replaced by the less electron-donating Cp ( $\eta^5$ -C<sub>5</sub>H<sub>5</sub>) in CpRe(CO)<sub>2</sub>(Seln).

<sup>®</sup> Abstract published in *Advance ACS Abstracts*, November 15, 1994.

(1) Ames Laboratory is operated for the U.S. Department of Energy by Iowa State University under Contract W-7405-Eng-82. This research was supported by the Office of Basic Energy Sciences, Chemical Sciences Division.

(2) Angelici, R. J. *Acc. Chem. Res.* **1988**, *21*, 387.

(3) Angelici, R. J. *Coord. Chem. Rev.* **1990**, *105*, 61.

(4) (a) Rauchfuss, T. B. *Prog. Inorg. Chem.* **1991**, *39*, 259. (b) Sanchez-Delgado, R. A. J. *Mol. Catal.* **1994**, *86*, 287.

(5) Angelici, R. J. In *Encyclopedia of Inorganic Chemistry*; King, R. B., Ed.; Wiley: New York, 1994; Vol. 3, pp 1433-1443.

(6) Cordone, R.; Harman, W. D.; Taube, H. *J. Am. Chem. Soc.* **1989**, *111*, 5969.

(7) Chen, J.; Angelici, R. J. *Organometallics* **1989**, *8*, 2277.

(8) Rauchfuss, T. B.; Ogilvy, A. E.; Skaugset, A. E. *Organometallics* **1989**, *8*, 2739.

(9) Magdesieva, N. N. *Farmakol. Toksikol. Prep. Selena, Mater. Simp.* **1967**, 41.

(10) Magdesieva, N. N. *Adv. Heterocycl. Chem.* **1970**, *12*, 1.

Lowering the electron density on Re favors the  $\eta^1(\text{Se})$  isomer, in which the Se acts as a two-electron donor to the Re. The  $\eta^2$  isomer becomes less favored in this case because the lower electron density on Re makes it less capable of  $\pi$  back-bonding to the olefin. In the analogous thiophene (Th) complexes,  $\text{Cp}^*\text{Re}(\text{CO})_2(\text{Th})$ , only the  $\eta^1(\text{S})$  isomer is observed regardless of the electron richness at the metal center or the methyl substitution in the thiophene.<sup>15,16</sup> The distinctly different  $^{77}\text{Se}$  chemical shifts of the  $\eta^1(\text{Se})$  and  $\eta^2$  isomers of the  $\text{Cp}^*\text{Re}(\text{CO})_2(\text{Seln})$  complexes suggest that  $^{77}\text{Se}$  NMR studies could be used to investigate the modes of selenophene binding on heterogeneous catalysts.

The only other known selenophene complexes are ( $\eta^5$ -Seln) $\text{Cr}(\text{CO})_3$  (Seln = selenophene, 2,5-dimethylselenophene), first reported by Öfele in 1966.<sup>17</sup> Recent  $^{13}\text{C}$  NMR studies of these complexes<sup>18</sup> show that the rotational barrier of the selenophene is higher than that of thiophene in the analogous complexes. The results suggest that selenophenes donate slightly more electron density to chromium than thiophenes do.

Although attempts to establish the mode of thiophene binding on HDS catalysts have not been successful, the existence of the NMR-active isotope  $^{77}\text{Se}$  (7.58% natural abundance) may make it possible to study selenophene binding to catalyst surfaces. Therefore, it is of interest to determine whether  $^{77}\text{Se}$  NMR spectroscopy is capable of distinguishing  $\eta^5$  coordination from  $\eta^1(\text{Se})$  coordination based on the chemical shift. In the investigations reported herein, we determine the  $^{77}\text{Se}$  NMR chemical shifts in the following series of complexes, ( $\eta^5$ -Seln) $\text{Cr}(\text{CO})_3$ , [ $(\eta^5$ -Seln) $\text{Mn}(\text{CO})_3$ ] $^+$ , [ $(\eta^5$ -Seln) $\text{RuCp}^*$ ] $^+$ , and [ $(\eta^5$ -Seln) $\text{IrCp}^*$ ] $^{2+}$  (where Seln = Sel, 2-MeSel, 2,5-Me<sub>2</sub>Sel), in which the metal, the charge on the complex, and the surrounding ligands are varied. The synthesis, characterization, and reaction chemistry of the new complexes are reported and compared to the previously studied thiophene analogs. In addition, the molecular structure of ( $\eta^5$ -2,5-Me<sub>2</sub>Sel) $\text{Cr}(\text{CO})_3$  determined by X-ray crystallography is compared with the recently published structure of the analogous  $\eta^5$ -thiophene complex ( $\eta^5$ -2,5-Me<sub>2</sub>T) $\text{Cr}(\text{CO})_3$ .<sup>18</sup>

## Experimental Section

**General Procedures.** All reactions and manipulations were carried out under an atmosphere of  $\text{N}_2$  using standard Schlenk techniques unless otherwise stated.<sup>19,20</sup> Solvents were reagent grade and dried under  $\text{N}_2$  by the following methods. Tetrahydrofuran (THF) and diethyl ether ( $\text{Et}_2\text{O}$ ) were distilled from Na/benzophenone. Hexanes,  $\text{CH}_2\text{Cl}_2$ , and MeCN were distilled from  $\text{CaH}_2$ . Acetone was dried with potassium carbonate and distilled. Nitromethane ( $\text{MeNO}_2$ ) was dried over  $\text{CaCl}_2$  and distilled. The solvents were used immediately

after distillation or were stored over 4 Å molecular sieves under  $\text{N}_2$ . The neutral alumina (Brockman, activity I, ~150 mesh) used for chromatography was deoxygenated at room temperature in high vacuum for 16 h, then deactivated with 5% (w/w)  $\text{N}_2$ -saturated water, and stored under  $\text{N}_2$ .

The  $^1\text{H}$  and  $^{13}\text{C}$  NMR spectra were recorded on either a Nicolet NT-300 MHz or a Varian VXR-300 MHz spectrometer with deuterated solvents as the internal locks and referenced to tetramethylsilane (TMS). The  $^{77}\text{Se}$  NMR spectra were recorded on the Varian VXR-300 spectrometer at room temperature and referenced to selenophene ( $\delta = 605.0$  ppm).<sup>21-23</sup> Electron-ionization mass spectra (EIMS) were performed on a Finnigan 4000 mass spectrometer. Fast atom bombardment (FAB) mass spectra were obtained using a Kratos MS-50 mass spectrometer. Infrared spectra were obtained on a Nicolet 710 FTIR spectrophotometer. Elemental analyses were performed by either Galbraith Laboratories, Inc., Knoxville, TN, or Desert Analytics, Tucson, AZ.

The following compounds were prepared by literature methods:  $\text{Cr}(\text{MeCN})_3(\text{CO})_3$ ,<sup>24</sup>  $\text{Mn}(\text{CO})_5(\text{OTf})$  ( $\text{OTf} = \text{SO}_3\text{CF}_3$ ),<sup>25</sup> [ $\text{Cp}^*\text{Ru}(\text{MeCN})_3$ ] $\text{OTf}$ ,<sup>26</sup> [ $\text{Cp}^*\text{IrCl}_2$ ] $_2$ ,<sup>27</sup> Sel,<sup>28,29</sup> 2-MeSel,<sup>30</sup> Me<sub>2</sub>-Sel.<sup>31</sup> All other compounds were purchased from commercial sources and used as received.

**( $\eta^5$ -Sel) $\text{Cr}(\text{CO})_3$  (1).** To prepare  $\text{Cr}(\text{MeCN})_3(\text{CO})_3$ , a solution of  $\text{Cr}(\text{CO})_6$  (1.10 g, 5.00 mmol) in freshly distilled MeCN (10 mL) was refluxed for 24 h under Ar. After the solution was cooled to room temperature, the solvent was removed under vacuum giving a very air-sensitive yellow solid which was redissolved in 5 mL of THF. Following the addition of selenophene (2.6 g, 20 mmol), the solution was refluxed for 10 min. The solution changed to a deep red color. After the solution was cooled to room temperature and the solvent removed under vacuum, the residue was dissolved in  $\text{CH}_2\text{Cl}_2$ /hexanes (1:9) and chromatographed on a neutral alumina column (2.2 × 30 cm). An initial yellow band was eluted with ether/hexanes (1:10). Then a red band was eluted with  $\text{Et}_2\text{O}$ ; it was collected, and the solvent was evaporated in vacuo to give the red crystalline solid product **1** (0.81 g, 61% based on  $\text{Cr}(\text{CO})_6$ ).  $^1\text{H}$  NMR  $\delta$  ( $\text{CDCl}_3$ ): 5.95 (m,  $J_{\text{H-Se}} = 18.8$  Hz, H(2), H(5)), 5.79 (m, H(3), H(4)).  $^{13}\text{C}$  NMR  $\delta$  ( $\text{CDCl}_3$ ): 91.82 (s, C(3), C(4)), 91.53 (s, C(2), C(5)), 233.03 (s, CO).  $^{77}\text{Se}$  NMR  $\delta$  ( $\text{CDCl}_3$ ): 152.3 (s). IR  $\nu(\text{CO})$   $\text{cm}^{-1}$  (hexanes): 1984 (s), 1918 (s), 1897 (s). Anal. Calcd for  $\text{C}_7\text{H}_4\text{O}_3\text{CrSe}$ : C, 31.48; H, 1.51. Found: C, 30.87; H, 1.27.

**( $\eta^5$ -2-MeSel) $\text{Cr}(\text{CO})_3$  (2).** This compound was prepared in the same manner as for **1** from  $\text{Cr}(\text{CO})_6$  (1.10 g, 5.00 mmol) and 2-MeSel (2.8 g, 15 mmol). **2** is an orange solid (0.91 g, 65% based on  $\text{Cr}(\text{CO})_6$ ).  $^1\text{H}$  NMR  $\delta$  ( $\text{CDCl}_3$ ): 5.79 (d,  $J_{\text{HH}} = 4.2$  Hz, H(5)), 5.75 (t,  $J_{\text{HH}} = 3.8$  Hz, H(4)), 5.46 (d,  $J_{\text{HH}} = 3.3$  Hz, H(3)), 2.37 (s,  $\text{CH}_3$ ).  $^{13}\text{C}$  NMR  $\delta$  ( $\text{CDCl}_3$ ): 113.77 (s, C(2)), 92.64 (s, C(4)), 92.59 (s, C(3)), 90.96 (s, C(5)), 18.09 (s,  $\text{CH}_3$ ), 233.2 (s, CO).  $^{77}\text{Se}$  NMR  $\delta$  ( $\text{CDCl}_3$ ): 186.1 (s). IR  $\nu(\text{CO})$   $\text{cm}^{-1}$  (hexanes): 1978 (s); 1912 (s); 1893 (s). Anal. Calcd for  $\text{C}_8\text{H}_6\text{O}_3\text{CrSe}$ : C, 34.18; H, 2.14. Found: C, 33.99; H, 2.11.

(21) McFarlane, H. C. E.; McFarlane, W. *NMR of Newly Accessible Nuclei*; Academic Press: New York, 1983; Vol. 2; pp 275-299.

(22) Baiwir, M. *Proceedings of the Fourth International Conference on the Organic Chemistry of Selenium and Tellurium*; 1983; pp 406-467.

(23) Christiaens, L.; Piette, J. L.; Laitem, L.; Baiwir, M.; Denoel, J.; Llabres, G. *Org. Magn. Reson.* **1976**, *8*, 354.

(24) Tate, D. P.; Knipple, W. R.; Angl, J. M. *Inorg. Chem.* **1962**, *1*, 433.

(25) Lesch, D. A.; Richardson, J. W.; Jacobson, R. A.; Angelici, R. J. *J. Am. Chem. Soc.* **1984**, *106*, 2901.

(26) Fagan, P. J.; Ward, M. D.; Calabrese, J. C. *J. Am. Chem. Soc.* **1989**, *111*, 1998.

(27) White, C.; Yates, A.; Maitlis, P. M. *Inorg. Synth.* **1992**, *29*, 230.

(28) Mohamand, S.; Bargon, J.; Waltman, R. J. *J. Org. Chem.* **1983**, *48*, 3544.

(29) Gronowitz, S.; Frejd, T.; Moberg-Ogard, A.; Tregre, L. *J. Heterocycl. Chem.* **1976**, *13*, 1319.

(30) Lumbroso, H.; Bertin, D. M.; Fringuelli, F.; Taticchi, A. *J. Chem. Soc., Perkin Trans.* **1977**, *2*, 775.

(31) Kharchenko, V. G.; Markushina, I. A.; Voronin, S. P. *Khim. Geterotsikl. Soedin. (Engl. Transl.)* **1982**, *18*, 418.

(11) Bird, C. W.; Cheeseman, G. W. H.; Hornfeldt, A. B. In *Comprehensive Heterocyclic Chemistry*; Katritzky, A. R., Rees, C. W., Eds.; Pergamon Press: New York, 1984; Vol. 4; pp 935-971.

(12) Hoernfeldt, A. B. *Adv. Heterocycl. Chem.* **1982**, *30*, 127.

(13) Choi, M. G.; Angelici, R. J. *J. Am. Chem. Soc.* **1990**, *112*, 7811.

(14) Choi, M. G.; Angelici, R. J. *J. Am. Chem. Soc.* **1991**, *113*, 5651.

(15) Choi, M. G.; Angelici, R. J. *J. Am. Chem. Soc.* **1989**, *111*, 8753.

(16) Choi, M. G.; Angelici, R. J. *Organometallics* **1991**, *10*, 2436.

(17) Öfele, K. *Chem. Ber.* **1966**, *99*, 1732.

(18) Sanger, M. J.; Angelici, R. J. *Organometallics* **1994**, *13*, 1821.

(19) Wayda, A. L.; Darensbourg, M. Y., Eds.; *Experimental Organometallic Chemistry: A Practicum in Synthesis and Characterization*; ACS Symposium Series 357; American Chemical Society: Washington, DC, 1987.

(20) Shriver, D. F.; Drezdson, M. A. *The Manipulation of Air Sensitive Compounds*, 2nd ed.; Wiley: New York, 1986.

**( $\eta^5$ -2,5-Me<sub>2</sub>SeI)Cr(CO)<sub>3</sub> (3).** This compound was prepared in the same manner as for **1** using Cr(CO)<sub>6</sub> (1.10 g, 5.00 mmol) and 2,5-Me<sub>2</sub>SeI (1.6 g, 10 mmol). **3** (0.77 g, 52% based on Cr(CO)<sub>6</sub>) was isolated as a red solid. <sup>1</sup>H NMR  $\delta$  (CDCl<sub>3</sub>): 5.39 (s, H(3), H(4)), 2.29 (s, CH<sub>3</sub>). <sup>13</sup>C NMR  $\delta$  (CDCl<sub>3</sub>): 113.55 (s, C(2), C(5)), 93.31 (s, C(3), C(4)), 18.11 (s, CH<sub>3</sub>), 233.9 (s, CO). <sup>77</sup>Se NMR  $\delta$  (CDCl<sub>3</sub>): 222.2 (s). IR  $\nu$ (CO) cm<sup>-1</sup> (hexanes): 1972 (s), 1905 (s), 1887 (s). Anal. Calcd for C<sub>9</sub>H<sub>8</sub>O<sub>3</sub>CrSe: C, 36.63; H, 2.73. Found: C, 36.58; H, 2.74.

**[( $\eta^5$ -SeI)Mn(CO)<sub>3</sub>](OTf) (4).** To a solution of Mn(CO)<sub>5</sub>(OTf) (0.0880 g, 0.250 mmol) in Et<sub>2</sub>O (50 mL) was added selenophene (0.16 g, 1.2 mmol); the solution was refluxed under N<sub>2</sub> in the dark for 48 h. The solution turned brown/red and a yellow precipitate formed. After filtration, the yellow precipitate was washed with Et<sub>2</sub>O (5 mL) once and hexanes (10 mL) twice and vacuum dried. The product **4** (0.0726 g, 68%) is a yellow crystalline powder. <sup>1</sup>H NMR  $\delta$  (CD<sub>3</sub>NO<sub>2</sub>): 7.32 (m, *J*<sub>H-Se</sub> = 18.3 Hz, H(2), H(5)), 6.98 (m, H(3), H(4)). <sup>13</sup>C NMR  $\delta$  (CD<sub>3</sub>NO<sub>2</sub>): 108.10 (s, C(3), C(4)), 101.55 (s, C(2), C(5)), 231.17 (s, CO). <sup>77</sup>Se NMR  $\delta$  (CD<sub>3</sub>NO<sub>2</sub>): 255.9 (s). IR  $\nu$ (CO) cm<sup>-1</sup> (CH<sub>3</sub>NO<sub>2</sub>): 2075 (s), 2016 (s), 2014 (sh). Anal. Calcd for C<sub>8</sub>H<sub>4</sub>O<sub>6</sub>MnSeSF<sub>3</sub>: C, 20.57; H, 0.86. Found: C, 21.28; H, 1.13.

**[( $\eta^5$ -2-MeSeI)Mn(CO)<sub>3</sub>](OTf) (5).** This synthesis was performed in the same manner as that for **4**; Mn(CO)<sub>5</sub>(OTf) (0.0880 g, 0.255 mmol) and 2-MeSeI (0.16 g, 1.1 mmol) were used. Pale yellow crystals of **5** (0.0783 g, 71%) were obtained. <sup>1</sup>H NMR  $\delta$  (CD<sub>3</sub>NO<sub>2</sub>): 6.91 (d, H(5)), 6.87 (t, H(4)), 6.68 (d, H(3)), 2.58 (s, CH<sub>3</sub>). <sup>13</sup>C NMR  $\delta$  (CD<sub>3</sub>NO<sub>2</sub>): 115.4 (s, C(2)), 106.1 (s, C(4)), 101.3 (s, C(3)), 100.6 (s, C(5)), 14.5 (s, CH<sub>3</sub>), 232.1 (s, CO). <sup>77</sup>Se NMR  $\delta$  (CD<sub>3</sub>NO<sub>2</sub>): 274.7 (s). IR  $\nu$ (CO) cm<sup>-1</sup> (CH<sub>3</sub>NO<sub>2</sub>): 2071 (s), 2009 (s).

**[( $\eta^5$ -2,5-Me<sub>2</sub>SeI)Mn(CO)<sub>3</sub>](OTf) (6).** This complex was prepared in the same manner as that for **4** from Mn(CO)<sub>5</sub>(OTf) (0.0880 g, 0.255 mmol) and 2,5-Me<sub>2</sub>SeI (0.16 g, 1.0 mmol). Pale yellow microcrystals of **6** (0.0871 g, 76%) were isolated after drying under vacuum. <sup>1</sup>H NMR  $\delta$  (CD<sub>3</sub>NO<sub>2</sub>): 6.45 (s, H(3), H(4)), 2.41 (s, CH<sub>3</sub>). <sup>13</sup>C NMR  $\delta$  (CD<sub>3</sub>NO<sub>2</sub>): 128.9 (s, C(2), C(5)), 100.1 (s, C(3), C(4)), 18.0 (s, CH<sub>3</sub>), 230.2 (s, CO). <sup>77</sup>Se NMR  $\delta$  (CD<sub>3</sub>NO<sub>2</sub>): 295.1 (s). IR  $\nu$ (CO) cm<sup>-1</sup> (CH<sub>3</sub>NO<sub>2</sub>): 2068 (s), 2003 (s). Anal. Calcd for C<sub>10</sub>H<sub>8</sub>O<sub>6</sub>MnSeSF<sub>3</sub>: C, 24.25; H, 1.63. Found: C, 24.63; H, 1.69.

**[Cp\*Ru( $\eta^5$ -SeI)](OTf) (7).** To a solution of [Cp\*Ru(MeCN)<sub>3</sub>](OTf) (0.100 g, 0.200 mmol) in CH<sub>2</sub>Cl<sub>2</sub> (10 mL) was added selenophene (0.16 g, 1.2 mmol); the solution was stirred at room temperature for 1 h. After filtration through Celite, the solution was concentrated to ~3 mL in vacuo. The product **7** was precipitated by slow addition of Et<sub>2</sub>O (20 mL), yielding a yellow crystalline powder (0.056 g, 55%). <sup>1</sup>H NMR  $\delta$  (acetone-*d*<sub>6</sub>): 6.39 (m, *J*<sub>H-Se</sub> = 17.8 Hz, H(2), H(5)), 5.94 (m, H(3), H(4)), 2.02 (s, CH<sub>3</sub>-Cp\*). <sup>13</sup>C NMR  $\delta$  (acetone-*d*<sub>6</sub>): 89.82 (s, C(3), C(4)), 87.31 (s, C(2), C(5)), 96.76 (s, C-Cp\*), 11.05 (s, CH<sub>3</sub>-Cp\*). <sup>77</sup>Se NMR  $\delta$  (CD<sub>3</sub>NO<sub>2</sub>): 211.9 (s). FAB/MS (CH<sub>2</sub>Cl<sub>2</sub>/3-nitrobenzyl alcohol matrix): *m/e* 369 (M<sup>+</sup>). The product was sometimes tan but was purified by adding a CH<sub>2</sub>Cl<sub>2</sub> solution of **7** onto a short column of neutral Al<sub>2</sub>O<sub>3</sub> (1.0  $\times$  5.0 cm). Elution with acetone gave a clean yellow product band that was collected. Removal of the solvent, under vacuum, and recrystallization of the residue from CH<sub>2</sub>Cl<sub>2</sub> layered with hexanes at -20 °C overnight gave yellow crystals of **7**.

**[Cp\*Ru( $\eta^5$ -2-MeSeI)](OTf) (8).** This synthesis was the same as that for **7** but using [Cp\*Ru(MeCN)<sub>3</sub>](OTf) (0.16 g, 0.31 mmol) and 2-MeSeI (0.16 g, 1.1 mmol). Pale yellow crystals of **8** (0.097 g, 58%) were obtained. <sup>1</sup>H NMR  $\delta$  (CDCl<sub>3</sub>): 6.51 (d, H(5)), 5.89 (t, H(4)), 5.71 (d, H(3)), 2.28 (s, CH<sub>3</sub>), 1.99 (s, CH<sub>3</sub>-Cp\*). <sup>13</sup>C NMR  $\delta$  (CDCl<sub>3</sub>): 103.9 (s, C(2)), 89.8 (s, C(4)), 88.6 (s, C(3)), 86.9 (s, C(5)), 15.9 (s, CH<sub>3</sub>), 95.6 (s, C-Cp\*), 10.9 (CH<sub>3</sub>-Cp\*). <sup>77</sup>Se NMR  $\delta$  (CD<sub>3</sub>NO<sub>2</sub>): 218.2 (s). FAB/MS (CH<sub>2</sub>Cl<sub>2</sub>/3-nitrobenzyl alcohol matrix): *m/e* 383 (M<sup>+</sup>). Anal. Calcd for C<sub>16</sub>H<sub>21</sub>RuSeSO<sub>3</sub>F<sub>3</sub>: C, 36.23; H, 3.99. Found: C, 36.25; H, 3.97.

**[Cp\*Ru( $\eta^5$ -2,5-Me<sub>2</sub>SeI)](OTf) (9).** This complex was prepared in the same manner as for **7** from [Cp\*Ru(MeCN)<sub>3</sub>](OTf)

(0.15 g, 0.29 mmol) and 2,5-Me<sub>2</sub>SeI (0.16 g, 1.0 mmol). Pale yellow microcrystals of **9** (0.096 g, 60%) were isolated after drying under vacuum. <sup>1</sup>H NMR  $\delta$  (CDCl<sub>3</sub>): 5.69 (s, H(3), H(4)), 2.26 (s, CH<sub>3</sub>), 1.96 (s, CH<sub>3</sub>-Cp\*). <sup>13</sup>C NMR  $\delta$  (CDCl<sub>3</sub>): 103.9 (s, C(2), C(5)), 89.4 (s, C(3), C(4)), 15.9 (s, CH<sub>3</sub>), 94.3 (s, C-Cp\*), 9.89 (s, CH<sub>3</sub>-Cp\*). <sup>77</sup>Se NMR  $\delta$  (CD<sub>3</sub>NO<sub>2</sub>): 219.8 (s). FAB/MS (CH<sub>2</sub>Cl<sub>2</sub>/3-nitrobenzyl alcohol matrix): *m/e* 397 (M<sup>+</sup>). Anal. Calcd for C<sub>17</sub>H<sub>23</sub>RuSeSO<sub>3</sub>F<sub>3</sub>: C, 37.50; H, 4.26. Found: C, 37.77; H, 4.32.

**[Cp\*Ir( $\eta^5$ -SeI)](BF<sub>4</sub>)<sub>2</sub> (10).** To a solution of [Cp\*IrCl<sub>2</sub>]<sub>2</sub> (0.44 g, 0.55 mmol) in acetone (5.0 mL) was added AgBF<sub>4</sub> (0.430 g, 2.21 mmol). The resulting mixture was stirred for 15 min and then filtered through Celite; the volume of the filtrate was then reduced to ~3 mL under vacuum. Selenophene (1.00 mL, 1.64 g, 12.2 mmol) was added, and the solution was gently heated at 50 °C for 5 min. After being cooled to room temperature, the solution was treated with Et<sub>2</sub>O (20 mL), which produced a gray-white solid. The solid was filtered from the solution and then redissolved in MeNO<sub>2</sub> (5 mL). The MeNO<sub>2</sub> solution was filtered to remove a black insoluble impurity; upon addition of Et<sub>2</sub>O (40 mL), the product **10** precipitated as a white solid. The product was separated by filtration and dried in vacuo, yielding 0.25 g (41%) of **10**. <sup>1</sup>H NMR  $\delta$  (CD<sub>3</sub>NO<sub>2</sub>): 7.99 (dd, *J*<sub>H-Se</sub> = 16.9 Hz, H(2), H(5)), 7.70 (dd, H(3), H(4)), 2.50 (s, CH<sub>3</sub>-Cp\*). <sup>13</sup>C NMR  $\delta$  (CD<sub>3</sub>NO<sub>2</sub>): 101.2 (s, C(3), C(4)), 100.3 (s, C(2), C(5)), 107.2 (s, C-Cp\*), 10.7 (s, CH<sub>3</sub>-Cp\*). <sup>77</sup>Se NMR  $\delta$  (CD<sub>3</sub>NO<sub>2</sub>): 371.2 (s). FAB/MS (3-nitrobenzyl alcohol matrix): *m/e* 547 (parent dication + BF<sub>4</sub><sup>-</sup>).

**[Cp\*Ir( $\eta^5$ -2-MeSeI)](BF<sub>4</sub>)<sub>2</sub> (11).** This compound was prepared from [Cp\*IrCl<sub>2</sub>]<sub>2</sub> (0.44 g, 0.55 mmol) and 2-MeSeI (1.5 g, 10 mmol) using the same method as described for **10**; it gives **11** as a white solid (0.220 g, 30.8%). <sup>1</sup>H NMR  $\delta$  (CD<sub>3</sub>NO<sub>2</sub>): 7.81 (d, H(5)), 7.55 (t, H(4)), 7.45 (d, H(3)), 2.76 (s, CH<sub>3</sub>), 2.45 (s, CH<sub>3</sub>-Cp\*). <sup>13</sup>C NMR  $\delta$  (CD<sub>3</sub>NO<sub>2</sub>): 120.7 (s, C(2)), 101.6 (s, C(4)), 100.8 (s, C(3)), 99.6 (s, C(5)), 16.2 (s, CH<sub>3</sub>), 106.8 (s, C-Cp\*), 10.6 (s, CH<sub>3</sub>-Cp\*). <sup>77</sup>Se NMR  $\delta$  (CD<sub>3</sub>NO<sub>2</sub>): 374.7 (s). Anal. Calcd for C<sub>15</sub>H<sub>21</sub>B<sub>2</sub>F<sub>8</sub>IrSe: C, 27.88; H, 3.28. Found: C, 27.54; H, 3.13.

**[Cp\*Ir( $\eta^5$ -2,5-Me<sub>2</sub>SeI)](BF<sub>4</sub>)<sub>2</sub> (12).** This compound was prepared in the same manner as **11** by use of [Cp\*IrCl<sub>2</sub>]<sub>2</sub> (0.44 g, 0.55 mmol) and 2,5-Me<sub>2</sub>SeI (1.40 g, 2.58 mmol). White solid **12** (0.359 g, 49.2%) was obtained. <sup>1</sup>H NMR  $\delta$  (CD<sub>3</sub>NO<sub>2</sub>): 7.31 (s, H(3), H(4)), 2.74 (s, CH<sub>3</sub>), 2.42 (s, CH<sub>3</sub>-Cp\*). <sup>13</sup>C NMR  $\delta$  (CD<sub>3</sub>NO<sub>2</sub>): 119.6 (s, C(3), C(4)), 100.8 (s, C(2), C(5)), 105.9 (C-Cp\*), 16.4 (s, CH<sub>3</sub>), 10.1 (CH<sub>3</sub>-Cp\*). <sup>77</sup>Se NMR  $\delta$  (CD<sub>3</sub>NO<sub>2</sub>): 379.8 (s). Anal. Calcd for C<sub>16</sub>H<sub>23</sub>B<sub>2</sub>F<sub>8</sub>IrSe: C, 29.11; H, 3.51. Found: C, 28.83; H, 3.53.

**Reaction of [( $\eta^5$ -SeI)Mn(CO)<sub>3</sub>](OTf) (4) with Hydride (H<sup>-</sup>) Sources. Method A. Reaction with NaBH<sub>4</sub>.** A solution of [( $\eta^5$ -SeI)Mn(CO)<sub>3</sub>](OTf) (**4**; 0.050 g, 0.12 mmol) in 10 mL of degassed deionized water was added all at once to an aqueous solution of 0.005 g (0.1 mmol) of NaBH<sub>4</sub> in 10 mL of degassed, deionized water. Immediately upon mixing, a yellow precipitate formed and gas was evolved. Extraction with hexanes (3  $\times$  10 mL) gave a bright yellow hexanes layer which was separated and dried over Na<sub>2</sub>SO<sub>4</sub>. After filtering, the yellow solution was chromatographed on an Al<sub>2</sub>O<sub>3</sub>/hexanes column (1  $\times$  15 cm). Elution with 5:1 hexanes/ether gave a bright yellow band that was collected, and the solvent was evaporated under vacuum to give bright yellow crystals. Yield (**4a**): 0.023 g (0.80 mmol) 69%. Elemental analyses were not possible because the crystals slowly decompose into a yellow/orange oil within 24 h. **4a** was characterized by the following spectra. <sup>1</sup>H NMR  $\delta$  (CDCl<sub>3</sub>): 6.95 (m, *J*<sub>H-Se</sub> = 17.4 Hz, H(5)), 6.02 (t, H(4)), 4.00 (dd, *J*<sub>H-Se</sub> = 11.7 Hz, H(2, endo)), 3.41 (m, H(3)), 3.07 (d, H(2, exo)). <sup>13</sup>C NMR  $\delta$  (CDCl<sub>3</sub>): 92.31 (s, C(4)), 77.24 (s, C(5)), 54.99 (s, C(3)), 50.17 (s, C(2)). <sup>77</sup>Se NMR  $\delta$  (CDCl<sub>3</sub>): -162.3 (s). IR  $\nu$ (CO) cm<sup>-1</sup> (hexanes): 2017 (s), 1940 (s), 1924 (s). EIMS *m/z*: 272 (M<sup>+</sup>), 244 (M<sup>+</sup> - CO), 216 (M<sup>+</sup> - 2CO), 188 (M<sup>+</sup> - 3CO), 133 (HSeI<sup>+</sup>).

**Method B. Reaction with Red-Al (Na[(CH<sub>3</sub>OC<sub>2</sub>H<sub>4</sub>)<sub>2</sub>-AlH<sub>2</sub>]).** A solution of 0.050 g (0.12 mmol) of [( $\eta^5$ -SeI)Mn(CO)<sub>3</sub>]-



(OTf) (4) in 10 mL of THF was cooled to 0 °C in an ice/water bath. To this stirred yellow solution was added all at once 0.175 mL of a 0.34 M Red-Al/THF (0.059 mmol) solution. After the resulting solution was allowed to warm to room temperature, the volatile components were removed under vacuum to give an orange/yellow oily solid. This was extracted with 2 × 10 mL of hexanes to give a bright yellow solution. Evaporation of the solution under vacuum gave a yellow oily solid (4a). Yield: 0.028 g (0.10 mmol) 91%. The  $^1\text{H}$ ,  $^{13}\text{C}$ , and  $^{77}\text{Se}$  NMR and IR spectra of this product were identical to those reported in the previous paragraph.

**Reaction of  $[(\eta^5\text{-Sel})\text{Mn}(\text{CO})_3](\text{OTf})$  (4) with NaCN.** A solution of  $[(\eta^5\text{-Sel})\text{Mn}(\text{CO})_3](\text{OTf})$  (4; 0.200 g, 0.24 mmol) in 10 mL of degassed deionized water was added all at once to an aqueous solution of 0.059 g (1.2 mmol) of NaCN in 10 mL of degassed, deionized water. Immediately upon mixing, a yellow/orange precipitate formed. Extraction with hexanes (3 × 10 mL) gave a bright yellow hexanes layer, which was separated and dried over  $\text{Na}_2\text{SO}_4$ ; the volatiles were removed from this solution under vacuum. The resulting yellow/orange oil was redissolved in hexanes and put onto a hexanes/ $\text{Al}_2\text{O}_3$  column (1 cm × 5 cm) which was eluted with ether to give a yellow band. This band was collected and evaporated under vacuum to give a yellow oil (4b; 0.021 g, 0.070 mmol, 29%).  $^1\text{H}$  NMR  $\delta$  (acetone- $d_6$ ): 7.05 (t,  $J_{\text{H-Se}} = 16.4$  Hz, H(5)), 6.28 (dd, H(4)), 4.86 (d,  $J_{\text{H-Se}} = 11.8$  Hz, H(2, endo)), 3.59 (m, H(3)).  $^{13}\text{C}$  NMR  $\delta$  (acetone- $d_6$ ): 92.75 (s, C(4)), 78.44 (s, C(5)), 52.13 (s, C(3)), 43.05 (s, C(2)).  $^{77}\text{Se}$  NMR  $\delta$  (acetone- $d_6$ ): 24.3 (s). IR  $\nu(\text{CO})$   $\text{cm}^{-1}$  (hexanes): 2028 (s), 1954 (vs), 1941 (s). EIMS  $m/z$ : 297 ( $\text{M}^+$ ), 271 ( $\text{M}^+ - \text{CN}$ ), 269 ( $\text{M}^+ - \text{CO}$ ).

**Reaction of  $[(\eta^5\text{-Sel})\text{RuCp}^*](\text{OTf})$  (7) with Red-Al ( $\text{Na}[(\text{CH}_3\text{OC}_2\text{H}_4\text{O})_2\text{AlH}_2]$ ).** To a suspension of 0.100 g (0.194 mmol) of  $[(\eta^5\text{-Sel})\text{RuCp}^*](\text{OTf})$  (7) in 20 mL of THF cooled to 0 °C in an ice/water bath was added all at once 0.060 mL (0.20 mmol) of a 3.4 M Red-Al/toluene solution. The solid quickly dissolved to give a yellow/orange solution. Evaporation under vacuum gave an orange oily solid that was extracted with ether (2 × 10 mL). The extracts were chromatographed on an  $\text{Al}_2\text{O}_3$ /hexanes column (1 cm × 5 cm) and eluted with ether to give a yellow band. The yellow band was collected and evaporated under vacuum to give the oily yellow solid 7a (0.055 g, 0.15 mmol, 77%). Due to its slow decomposition at room temperature, it was not possible to obtain elemental analyses.  $^1\text{H}$  NMR  $\delta$  ( $\text{CDCl}_3$ ): 6.38 (d,  $J_{\text{H-Se}} = 16.5$  Hz, H(5)), 5.68 (t, H(4)), 4.37 (m, H(3)), 2.72 (d, H(2, endo)), 2.53 (d, H(2, exo)), 1.86 (s, Cp\*).  $^{13}\text{C}$  NMR  $\delta$  ( $\text{CDCl}_3$ ): 97.9 (s, C(3)), 92.6 (s, C(4)), 90.4 (s, Cp\*), 89.0 (s, C(5)), 45.2 (s, C(2)), 10.6 (s,  $\text{CH}_3\text{-Cp}^*$ ).  $^{77}\text{Se}$  NMR  $\delta$  ( $\text{CDCl}_3$ ): 227.3 (s). EIMS exact mass calculated for  $\text{C}_{14}\text{H}_{20}\text{-}^{80}\text{Se}^{102}\text{Ru}$ : 369.97735. Found for  $\text{M}^+$ : 369.97737.

**Reaction of  $[(\eta^5\text{-2,5-Me}_2\text{Sel})\text{IrCp}^*](\text{OTf})_2$  (12) with Red-Al ( $\text{Na}[(\text{CH}_3\text{OC}_2\text{H}_4\text{O})_2\text{AlH}_2]$ ).** To a cooled (0 °C) suspension of 0.100 g (0.15 mmol) of  $[(\eta^5\text{-2,5-Me}_2\text{Sel})\text{IrCp}^*](\text{OTf})_2$  (12) in 10 mL of THF was added dropwise 1.00 mL (0.17 mmol) of a 0.17 M Red-Al ( $\text{Na}[(\text{CH}_3\text{OC}_2\text{H}_4\text{O})_2\text{AlH}_2]$ )/THF solution with stirring; an orange/red solution formed. After stirring for 1 h at 0 °C, the volatile components were evaporated under vacuum giving a red oily solid. Extraction with hexanes (3 × 10 mL) was followed by chromatography on an  $\text{Al}_2\text{O}_3$ /hexanes (1 cm × 10 cm) column using a 10% THF/hexanes eluent; this gave a deep red band that was collected. Solvent evaporation under vacuum gave the product 12a (0.013 g, 0.026 mmol, 17% yield), which was isolated as a deep red oily solid.  $^1\text{H}$  NMR  $\delta$  ( $\text{CDCl}_3$ ): 7.59 (d, H(3)), 7.49 (d, H(4)), 3.26 (s,  $\text{CH}_3$ ), 2.84 (s,  $\text{CH}_3$ ), 1.87 (s,  $\text{CH}_3\text{-Cp}^*$ ).  $^{13}\text{C}$  NMR  $\delta$  ( $\text{CDCl}_3$ ): 134.9 (s), 132.1 (s), 129.8 (s), 123.3 (s), 8.5 (s,  $\text{CH}_3$ ), 8.4 (s,  $\text{CH}_3$ ), 90.7 (s, Cp\*), 10.4 (s,  $\text{CH}_3\text{-Cp}^*$ ).  $^{77}\text{Se}$  NMR  $\delta$  ( $\text{CDCl}_3$ ): 905.4 (s).

**X-ray Structure Determination of  $(\eta^5\text{-2,5-Me}_2\text{Sel})\text{Cr}(\text{CO})_3$  (3).** A single crystal of 3 suitable for X-ray diffraction was obtained by vapor diffusion of hexanes into a saturated  $\text{Et}_2\text{O}$  solution of 3 at -20 °C. The single crystal was mounted

Table 1. Crystal and Data Collection Parameters for  $(\eta^5\text{-2,5-Me}_2\text{Sel})\text{Cr}(\text{CO})_3$ (3)

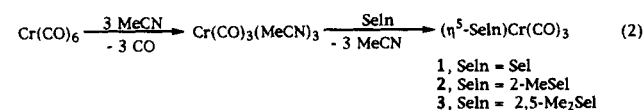
formula	$\text{CrSeC}_9\text{H}_8\text{O}_3$
fw	295.12
space group	$P2_1/c$
$a$ , Å	6.741(1)
$b$ , Å	12.534(3)
$c$ , Å	12.557(3)
$\alpha$ , deg	90.00
$\beta$ , deg	102.55(2)
$\gamma$ , deg	90.00
$V$ , Å <sup>3</sup>	1035.6(25)
$Z$	4
$D_{\text{calc}}$ , $\text{g/cm}^3$	1.893
crystal size, mm	$0.16 \times 0.22 \times 0.05$
$\mu(\text{Mo K}\alpha)$ , $\text{cm}^{-1}$	45.4
data collection instrument	Enraf-Nonius CAD4
radiation (monochromated in incident beam)	Mo K $\alpha$ ( $\lambda = 0.71073$ Å)
orientation reflcns, no., range ( $2\theta$ )	25, $17.8 < 2\theta < 35.0$
temp, °C	22.0(10)
scan method	$\theta$ - $2\theta$
data col range, $2\theta$ , deg	4.0–45.0
no data collected	3883
no unique data, total	1988
with $F^2 > 3\sigma(F^2)$	947
no. of params refined	128
trans factors, max, min ( $\psi$ scans)	0.998, 0.620
$R^a$	0.024
$R_w^b$	0.030
quality of fit indicator <sup>c</sup>	0.81
largest shift/esd, final cycle	0.00
largest peak, $\text{e}/\text{Å}^3$	0.36(8)

<sup>a</sup>  $R = \sum(|F_o| - |F_c|)/\sum|F_o|$ . <sup>b</sup>  $R_w = [\sum\omega(|F_o| - |F_c|)^2/\sum\omega|F_o|^2]^{1/2}$ ;  $\omega = 1/\sigma^2(|F_o|)$ . <sup>c</sup> Quality of fit,  $[\sum\omega(|F_o| - |F_c|)^2/(N - N_{\text{parameters}})]^{1/2}$ .

on the end of a glass fiber. Cell constants were determined from a list of reflections found by an automated search routine. Pertinent data collection and reduction information are given in Table 1. Lorentz and polarization corrections were applied. A correction based on decay in the standard reflection of 4.8% was applied to the data. An absorption correction was also made on the basis of a series of  $\Psi$  scans. The positions of the Cr and Se atoms were determined by interpretation of the Patterson map. All remaining non-hydrogen atoms were found in one successive difference Fourier map. All non-hydrogen atoms were refined with anisotropic displacement parameters. After the least squares converged, all hydrogen atoms were found in a difference Fourier map. These were placed into the model with isotopic temperature factors set equal to 1.3 times the isotropic equivalent of the attached atom. The hydrogen positions were not refined. Systematic trends in the  $F_o/F_c$  suggested that an extinction correction be included in the final least-squares fit. Bond distances and angles are presented in Table 2, and an ORTEP drawing of 3 is given in Figure 2. The final positional and thermal parameters are listed in Table 3.

## Results and Discussion

**Synthesis and Characterization of the  $\eta^5\text{-Seln}$  Complexes.** The complexes  $(\eta^5\text{-Seln})\text{Cr}(\text{CO})_3$  were prepared previously by reaction of  $\text{Cr}(\text{CO})_3(\text{py})_3$  with selenophenes.<sup>17</sup> Using this method, the yields were low (0–25%) and in our hands highly dependent on the careful manipulation and purification of the very air sensitive  $\text{Cr}(\text{CO})_3(\text{py})_3$  intermediate complex. The reactions (eq 2) of  $\text{Cr}(\text{CO})_3(\text{MeCN})_3$  with selenophenes are



more straight forward and give higher yields of  $(\eta^5\text{-}$



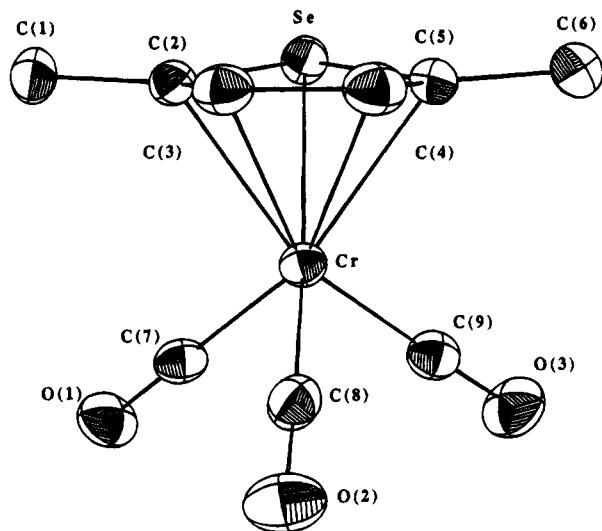
**Table 2.** Bond Distances (Å)<sup>a</sup> and Angles (deg)<sup>a</sup> for (η<sup>5</sup>-2,5-Me<sub>2</sub>SeI)Cr(CO)<sub>3</sub> (3)

atoms	distance	atoms	distance
Cr—Se	2.488(5)	Se—C(5)	1.912(7)
Cr—C(2)	2.218(6)	C(1)—C(2)	1.500(7)
Cr—C(3)	2.199(4)	C(2)—C(3)	1.364(7)
Cr—C(4)	2.202(6)	C(3)—C(4)	1.409(8)
Cr—C(5)	2.232(4)	C(4)—C(5)	1.386(8)
Cr—C(7)	1.829(6)	C(5)—C(6)	1.507(5)
Cr—C(8)	1.822(6)	C(7)—O(1)	1.151(8)
Cr—C(9)	1.835(6)	C(8)—O(2)	1.145(8)
Se—C(2)	1.899(8)	C(9)—O(3)	1.150(9)

atoms	angle	atoms	angle
C(2)—Se—C(5)	86.9(3)	C(1)—C(2)—C(3)	128.8(5)
C(2)—C(3)—C(4)	116.2(4)	C(6)—C(5)—C(4)	129.7(4)
C(3)—C(4)—C(5)	116.0(4)	Cr—C(7)—O(1)	178.2(5)
Se—C(2)—C(1)	120.0(4)	Cr—C(8)—O(2)	178.3(6)
Se—C(5)—C(6)	120.1(3)	Cr—C(9)—O(3)	176.7(6)
Se—C(5)—C(4)	109.6(4)	C(7)—Cr—C(9)	92.7(2)
Se—C(2)—C(3)	110.8(4)	C(7)—Cr—C(8)	89.7(2)
		C(8)—Cr—C(9)	86.5(3)

<sup>a</sup> Numbers in parentheses are estimated standard deviations in the least significant digits.

**Figure 2.** ORTEP Drawing of (η<sup>5</sup>-2,5-Me<sub>2</sub>SeI)Cr(CO)<sub>3</sub> (3).**Table 3.** Positional and Thermal Parameters for (η<sup>5</sup>-2,5-Me<sub>2</sub>SeI)Cr(CO)<sub>3</sub> (3)

atom	x	y	z	B <sup>a</sup> (Å <sup>2</sup> )
Cr	0.50022(1)	0.20323(6)	0.33291(5)	2.83(1)
Se	0.86397(7)	0.19014(4)	0.43137(4)	3.62(1)
C(1)	0.7793(7)	-0.0172(4)	0.3195(4)	4.6(1)
C(2)	0.7586(6)	0.1017(4)	0.3093(4)	3.3(1)
C(3)	0.6932(7)	0.1616(4)	0.2177(4)	3.7(1)
C(4)	0.6987(7)	0.2731(4)	0.2323(4)	4.1(1)
C(5)	0.7707(6)	0.3089(4)	0.3382(4)	3.7(1)
C(6)	0.8083(7)	0.4211(4)	0.3809(5)	5.4(1)
C(7)	0.3967(7)	0.3011(4)	0.4134(4)	3.8(1)
C(8)	0.2733(7)	0.2132(4)	0.2251(4)	3.5(1)
C(9)	0.3770(6)	0.0914(4)	0.3859(4)	3.5(1)
O(1)	0.3321(5)	0.3648(3)	0.4626(3)	5.68(9)
O(2)	0.1280(5)	0.2170(3)	0.1580(3)	5.12(9)
O(3)	0.2934(5)	0.0203(3)	0.4140(3)	5.20(9)

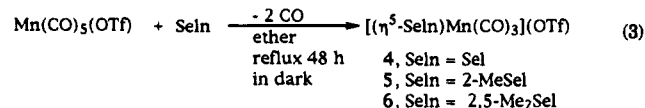
<sup>a</sup> Anisotropically refined atoms are given in the form of the isotropic equivalent displacement parameter defined as follows (<sup>1</sup>/<sub>3</sub>[a<sup>2</sup>B(1,1) + b<sup>2</sup>B(2,2) + c<sup>2</sup>B(3,3) + ab(cos γ)B(1,2) + ac(cos β)B(1,3) + bc(cos α)B(2,3)]).

Seln)Cr(CO)<sub>3</sub>. The pure moderately air stable red (η<sup>5</sup>-Seln)Cr(CO)<sub>3</sub> complexes **1**, **2**, and **3** are obtained in yields between 50 and 70%. The advantage of using this method over the direct reaction of Cr(CO)<sub>6</sub> with the Seln

ligand is that smaller amounts of the ligand are required to obtain the desired product in reasonable yield.

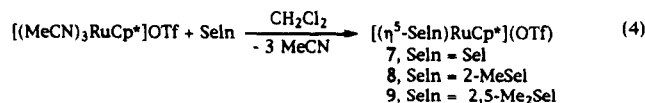
The <sup>1</sup>H, <sup>13</sup>C, and <sup>77</sup>Se NMR spectral data for **1** are given in Table 4. The <sup>1</sup>H NMR chemical shift values are similar to those reported previously;<sup>17,18</sup> however, the fine structure is resolved better and gives coupling constants between protons on adjacent carbons (*J*<sub>H-H</sub> = 2.5 Hz) and protons on carbons across the ring (*J*<sub>H-H</sub> = 2.0 Hz). Coupling of protons in the 2,5-position to the <sup>77</sup>Se (7.58% natural abundance) nucleus is observed in the satellite peaks, which give a two bond coupling constant of <sup>2</sup>*J*<sub>H-Se</sub> = 18.8 Hz; the Se satellite peaks are also used to definitively assign the resonances for protons H(2) and H(5). The <sup>1</sup>H NMR resonances for the analogous thiophene complex (η<sup>5</sup>-T)Cr(CO)<sub>3</sub> in CDCl<sub>3</sub> [δ 5.59 (m, H(3),H(4)), 5.37 (m, H(2),H(5))] are slightly upfield (0.2–0.3 ppm) of those of **1** in CDCl<sub>3</sub> [δ 5.95 (m, H(2), H(5)), 5.79 (m, H(3), H(4))].

The compounds [(η<sup>5</sup>-Seln)Mn(CO)<sub>3</sub>]OTf (**4**, **5**, and **6**) are isostructural and isoelectronic with the chromium complexes **1**–**3**. Due to the limited availability of the selenophene ligands, **4**–**6** were prepared (eq 3) using



only a 4-fold excess of the Seln ligand, rather than the large excess of thiophenes (Th) used in the synthesis of the thiophene complexes [(η<sup>5</sup>-Th)Mn(CO)<sub>3</sub>]OTf.<sup>25</sup> The product is totally insoluble in the ether solvent and can be isolated directly as the pure compound. The reaction must be protected from direct exposure to light to prevent the formation of unidentified side products. Yields of **4**–**6** vary from 20 to 80%. Key factors in obtaining high yields are preventing exposure to light during the long reflux period, moderate reaction temperatures, and using high-purity starting materials and solvents. In the <sup>1</sup>H NMR spectrum (Table 4), the selenophene protons in **4** are slightly downfield (~0.2 ppm) as compared with those in the analogous thiophene complex, [(η<sup>5</sup>-T)Mn(CO)<sub>3</sub>]<sup>+</sup> [δ 6.90 (H(2), H(5)), 6.77 (H(3), H(4))].<sup>25</sup>

Syntheses of the compounds [(η<sup>5</sup>-Seln)RuCp\*]OTf (**7**, **8**, and **9**) are accomplished by the same method (eq 4)



used for the previously reported thiophene complexes [(η<sup>5</sup>-Th)RuCp\*]OTf.<sup>33,34</sup> As was the case for **1** and **4**, the <sup>1</sup>H NMR resonances of the Seln in **7** (Table 4) are slightly deshielded as compared with those in the analogous thiophene compound [(η<sup>5</sup>-T)RuCp\*]<sup>+</sup> in acetone-*d*<sub>6</sub> [δ 6.22 (m, H(3), H(4)), 6.19 (m, H(2), H(5)), 2.07 (s, Cp\*)].<sup>33</sup>

(32) Mangini, A.; Taddei, F. *Inorg. Chim. Acta* **1968**, *2*, 12.

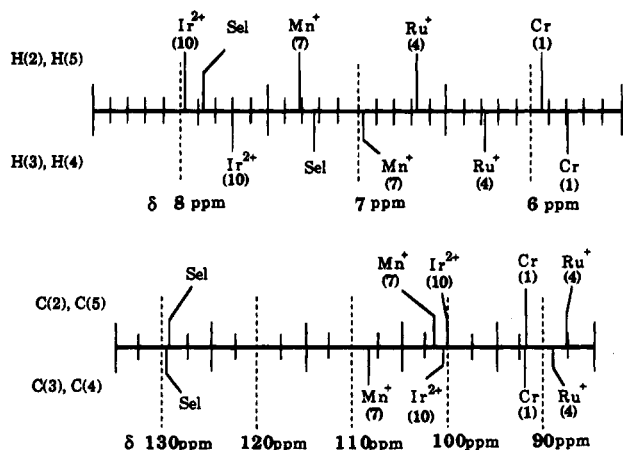
(33) Hachgenei, J. W.; Angelici, R. J. *J. Organomet. Chem.* **1968**, *355*, 359.

(34) Spies, G. H.; Angelici, R. J. *Organometallics* **1987**, *6*, 1897.

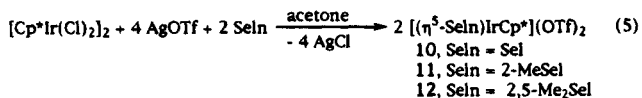
**Table 4.** Spectroscopic Data for  $\eta^5$ -Coordinated Selenophene (Sel) in  $(\eta^5\text{-Sel})\text{Cr}(\text{CO})_3$  (1),  $(\eta^5\text{-Sel})\text{Mn}(\text{CO})_3^+$  (4),  $(\eta^5\text{-Sel})\text{RuCp}^*]^+$  (7), and  $(\eta^5\text{-Sel})\text{IrCp}^*]^2+$  (10)

compd (solvent)	$^1\text{H}$ NMR ( $\delta$ in ppm)	$^{13}\text{C}$ NMR ( $\delta$ in ppm)	$^{77}\text{Se}$ NMR ( $\delta$ in ppm)	IR ( $\text{cm}^{-1}$ )
1 ( $\text{CDCl}_3$ )	5.95 (m, H(2), H(5)) <sup>a</sup>	91.53 (s, C(2), C(5))	152.3	1984 (s)
	5.79 (m, H(3), H(4))	91.82 (s, C(3), C(4)) 233.03 (CO)		1918 (s) 1897 (s)
4 ( $\text{CD}_3\text{NO}_2$ )	7.32 (s, H(2), H(5)) <sup>b</sup>	101.55 (s, C(2), C(5))	255.9	2075 (s)
	6.98 (s, H(3), H(4))	108.10 (s, C(3), C(4)) 231.17 (CO)		2016 (s) 2014 (sh)
7 (acetone- $d_6$ )	6.39 (m, H(2), H(5)) <sup>c</sup>	87.31 (s, C(2), C(5))	211.9	n/a <sup>e</sup>
	5.94 (m, H(3), H(4))	89.82 (s, C(3), C(4))		
10 ( $\text{CD}_3\text{NO}_2$ )	2.02 (s, $\text{CH}_3\text{-Cp}^*$ )	96.76 ( $\text{Cp}^*$ ), 11.05 ( $\text{Cp}^*$ )	371.2	
	7.99 (dd, H(2), H(5)) <sup>d</sup>	100.3 (s, C(2), C(5))		
	7.70 (dd, H(3), H(4))	101.2 (s, C(3), C(4)) 107.2 ( $\text{Cp}^*$ ), 10.7 ( $\text{Cp}^*$ )		
Sel ( $\text{CDCl}_3$ )	2.50 (s, $\text{CH}_3\text{-Cp}^*$ )	129.4 (s, C(2), C(5))	605.0	n/a
	7.88 (d, H(2), H(5))	130.4 (s, C(3), C(4))		

<sup>a</sup>  $J_{\text{H-Se}} = 18.8$  Hz. <sup>b</sup>  $J_{\text{H-Se}} = 18.3$  Hz. <sup>c</sup>  $J_{\text{H-Se}} = 17.8$  Hz. <sup>d</sup>  $J_{\text{H-Se}} = 16.9$  Hz. <sup>e</sup> Not applicable.

**Figure 3.**  $^1\text{H}$  and  $^{13}\text{C}$  NMR chemical shifts of selenophene in complexes 1, 4, 7, and 10.

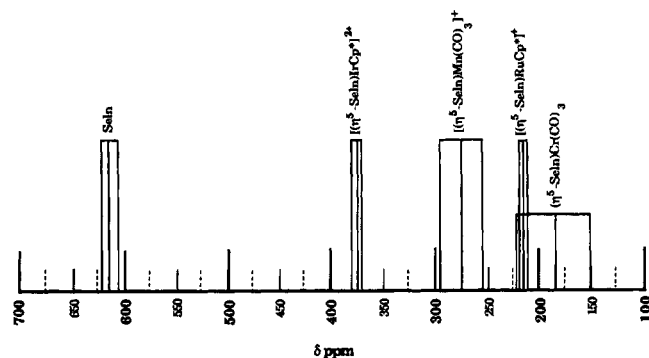
Selenophene compounds of the type  $(\eta^5\text{-Sel})\text{IrCp}^*](\text{BF}_4)_2$  (10, 11, and 12) are prepared by the same method (eq 5) used for the thiophene analogs.<sup>35,36</sup> These com-



plexes are isolated as white air-stable solids in yields of 41–49%. The  $^1\text{H}$  NMR chemical shift values for the Sel ligand in 10 (Table 4) are slightly downfield of those of the thiophene analog  $(\eta^5\text{-T})\text{IrCp}^*]^2+$  in  $\text{CD}_3\text{NO}_2$  [ $\delta$  7.60 (m, H(3), H(4)), 7.55 (m, H(2), H(5)), 2.50 (s,  $\text{Cp}^*$ )].<sup>36</sup>

**Comparison of the  $^1\text{H}$ ,  $^{13}\text{C}$ , and  $^{77}\text{Se}$  NMR Spectra of 1, 4, 7, and 10.** In all of these complexes, the H(2) and H(5) protons are assigned to the  $^1\text{H}$  NMR peaks that exhibit satellites due to  $^1\text{H}\text{-}^{77}\text{Se}$  coupling. These coupling constants,  $J_{\text{H-Se}}$ , are in a narrow range, 16.9–18.8 Hz (Table 4). No coupling between  $^{77}\text{Se}$  and the protons on C(3) and C(4) is observed in any of the complexes. Peaks in the  $^{13}\text{C}$  NMR spectra of the complexes are assigned (Table 4) to the Sel ring carbon atoms based on HETCOR spectra and making use of the proton assignments.

As is evident in Figure 3,  $^1\text{H}$  chemical shifts of both the H(2), H(5) and H(3), H(4) protons move upfield as

**Figure 4.**  $^{77}\text{Se}$  NMR chemical shift data for  $\eta^5$ -Sel complexes (1–12).

expected with decreasing positive charge on the complex:  $10 < 7 < 4 < 1$ . Only the +2 complex (10), has chemical shifts lower than those of the free Sel. The higher chemical shifts of the Sel in complexes 7, 4, and 1 is commonly observed when arene and thiophene<sup>18,25,32</sup> ligands are  $\pi$  bound in complexes with 0 and +1 charges.

Since  $^{13}\text{C}$  NMR chemical shifts are more sensitive to factors other than complex charge, it is not surprising that chemical shift values (Figure 3) for both the C(2), C(5) and C(3), C(4) carbon atoms follow a somewhat different trend,  $7 < 10 < 1 < 4$ , than was observed in the  $^1\text{H}$  NMR spectra. Moreover, the coordinated carbons of Sel in all of the complexes are upfield of those in the free Sel. Such upfield shifts are normally observed in  $\pi$ -arene<sup>37</sup> and  $\pi$ -thiophene<sup>18,25</sup> complexes.

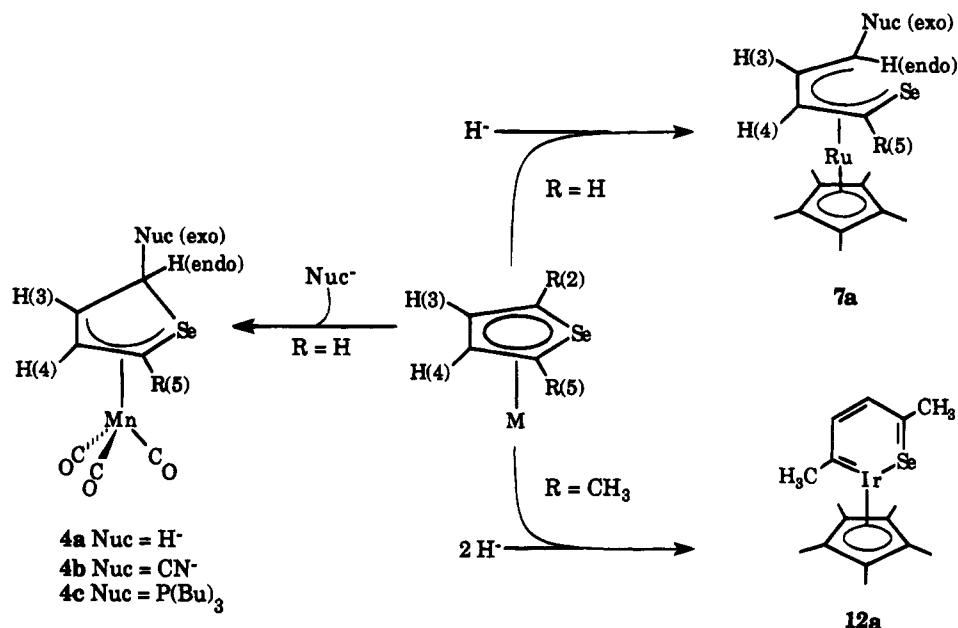
**$^{77}\text{Se}$  NMR Studies of  $\eta^5$ -Sel.** A goal of the studies described in this paper is to determine the usefulness of  $^{77}\text{Se}$  NMR spectroscopy for establishing the mode of selenophene binding in transition metal complexes and on catalyst surfaces. The  $^{77}\text{Se}$  nucleus has a natural abundance of 7.58% and a relative receptivity that is 2.98 times larger than  $^{13}\text{C}$ , with a chemical shift range of more than 3000 ppm.<sup>21</sup> The  $^{77}\text{Se}$  NMR chemical shift values of the  $\eta^5$ -Sel complexes are given in Table 4 and Figure 4. It is evident that the  $^{77}\text{Se}$  NMR signal moves downfield from the neutral complex (1), to the +1 charged complexes (4, 7) to the +2 charged complex (10). The chemical shift of the free selenophene ligand is further downfield than any of the complexes. Methyl substitution of the heterocyclic ring also affects the  $^{77}\text{Se}$

(35) Chen, J.; Daniels, L. M.; Angelici, R. J. *J. Am. Chem. Soc.* **1990**, *112*, 199.

(36) Huckett, S. C.; Miller, L. L.; Jacobson, R. A.; Angelici, R. J. *Organometallics* **1988**, *7*, 686.

(37) Mann, B. E.; Taylor, B. F.  *$^{13}\text{C}$  NMR Data for Organometallic Compounds*; Academic Press: London, 1981.

Scheme 1



chemical shift of the coordinated selenophene ring; increasing the number of methyl groups in the 2- and 5-positions causes the <sup>77</sup>Se chemical shift to move downfield. A similar trend occurs for the free ligands in CDCl<sub>3</sub>: Sel(δ 605) > 2-MeSel (δ 612) > 2,5-Me<sub>2</sub>Sel (δ 621).<sup>21,22</sup>

**Molecular Structure of (η<sup>5</sup>-2,5-Me<sub>2</sub>Se)Cr(CO)<sub>3</sub>.** The ORTEP drawing of (η<sup>5</sup>-2,5-Me<sub>2</sub>Se)Cr(CO)<sub>3</sub> (**3**) is given in Figure 2. The 2,5-Me<sub>2</sub>Se complex was chosen for the structural study in order to avoid the disorder previously found in the analogous thiophene complex (η<sup>5</sup>-T)Cr(CO)<sub>3</sub>.<sup>38</sup> The selenophene ring in **3** binds to the chromium tricarbonyl fragment through the selenium and the two C=C bonds each *trans* to a carbonyl ligand thereby giving pseudooctahedral coordination around the Cr. This is the same geometry found in both (η<sup>5</sup>-T)Cr(CO)<sub>3</sub><sup>38</sup> and (η<sup>5</sup>-2,5-Me<sub>2</sub>T)Cr(CO)<sub>3</sub>.<sup>18</sup> The selenophene ring is slightly bent, with the selenium atom out of the plane of the four carbon atoms (C(2), C(3), C(4), and C(5)) by 0.162(3) Å. The dihedral angle between the plane of the ring carbons (C(2), C(3), C(4), and C(5)) and the C(2)–Se–C(5) plane is 6.7(0.6)°. This angle is larger by 2.2(8)° than the corresponding angle in the sulfur-containing analog (η<sup>5</sup>-2,5-Me<sub>2</sub>T)Cr(CO)<sub>3</sub>. Other dihedral angles for thiophene rings are reported for the following complexes: Ru(Me<sub>4</sub>T)<sub>2</sub><sup>2+</sup> (5.0(0.5)° and 3.7(1.5)°); {[η<sup>5</sup>-Me<sub>4</sub>T]RuCl<sub>3</sub>S]<sup>+</sup> (11.8(1.9)°, 13.4(1.9)°, and 13.7(1.9)°).<sup>39</sup> The C–Se bond distances [1.899(8) and 1.912(7) Å] in the 2,5-Me<sub>2</sub>Se ring in **3** are slightly longer than that [1.855(7) Å] in free selenophene.<sup>11</sup> The C–Se distances in **3** are ~0.15 Å longer than the C–S distances in (η<sup>5</sup>-2,5-Me<sub>2</sub>T)Cr(CO)<sub>3</sub> due to the larger size of the selenium heteroatom. The ring C–C bond distances in the coordinated 2,5-Me<sub>2</sub>Se are, within experimental error, the same as in (η<sup>5</sup>-2,5-Me<sub>2</sub>T)Cr(CO)<sub>3</sub>. The Cr–Se bond [2.488(5) Å] in **3** is 0.113(5) Å longer than the Cr–S bond [2.3757(6) Å] in (η<sup>5</sup>-2,5-Me<sub>2</sub>T)Cr(CO)<sub>3</sub>, again presumably due to the larger size of Se. The Cr–Se distances in Cr(CO)<sub>4</sub>(CN(Et)<sub>2</sub>)-

(SeC<sub>6</sub>H<sub>4</sub>F)<sup>40</sup> [2.562(2) Å] and [CrCp(NO)(μ<sub>2</sub>-SeC<sub>6</sub>H<sub>5</sub>)<sub>2</sub>]<sup>41</sup> [2.45(1) Å] are longer and shorter, respectively, than that in **3**. The carbonyl Cr–C and C=O bond distances in **3** and (η<sup>5</sup>-2,5-Me<sub>2</sub>T)Cr(CO)<sub>3</sub> are the same within experimental error.

**Reactions of η<sup>5</sup>-Sel Complexes.** Previously, it was reported<sup>2,25</sup> that the η<sup>5</sup>-thiophene ligand in (η<sup>5</sup>-T)Mn(CO)<sub>3</sub><sup>+</sup> is attacked at the 2-position by a hydride donor [BH<sub>4</sub><sup>-</sup>, HFe(CO)<sub>4</sub><sup>-</sup>] to give the product (η<sup>4</sup>-T-H)Mn(CO)<sub>3</sub> in which three carbons and the sulfur are coordinated to the Mn. The same reaction of [(η<sup>5</sup>-Sel)Mn(CO)<sub>3</sub>]<sup>+</sup> (**4**) with 1 equiv of NaBH<sub>4</sub> or Red-Al as the hydride source gives the analogous product (η<sup>4</sup>-Sel-H)Mn(CO)<sub>3</sub> (**4a**), which is isolated in 80–90% (Scheme 1). The <sup>1</sup>H NMR spectrum of **4a** in CDCl<sub>3</sub> contains signals for the five hydrogens on the ring as follows: δ 6.95 (m, *J*<sub>H–Se</sub> = 17.4 Hz, H(5)), 6.02 (t, H(4)), 4.00 (dd, *J*<sub>H–Se</sub> = 11.7 Hz, H(2, endo)), 3.41 (m, H(3)), 3.07 (d, H(2, exo)). Assignments of these resonances were made by comparison of the data with those previously reported for (η<sup>4</sup>-T-H)Mn(CO)<sub>3</sub> in acetone-*d*<sub>6</sub> (not in CDCl<sub>3</sub> as originally reported<sup>25</sup>): δ 6.42 (s, H(5)), 5.89 (s, H(4)), 3.79 (d, H(2, endo)), 3.30 (s, H(3)), 3.29 (d, H(2, exo)). Coupling of <sup>77</sup>Se to H(2, endo) (<sup>2</sup>*J*<sub>H–Se</sub> = 11.7 Hz) and H(5) (<sup>2</sup>*J*<sub>H–Se</sub> = 17.4 Hz) indicates that the ring C–Se bonds remain intact. Coupling is not seen between <sup>77</sup>Se and H(2, exo) presumably due to the angle between the atoms. Integration of the <sup>2</sup>H NMR spectrum of the product resulting from the reaction of **4** with NaBD<sub>4</sub> shows a 6.4:1.0 ratio of products resulting from exo and endo attack. In the corresponding reaction of [(η<sup>5</sup>-T)Mn(CO)<sub>3</sub>]<sup>+</sup> with NaBD<sub>4</sub> the ratio of exo to endo attack was 3.6:1.0.<sup>42</sup> It is interesting to note that the <sup>77</sup>Se NMR signal for **4a** occurs at δ –162 ppm, which is more than 400 ppm upfield from that of complex **4**. This is the highest upfield resonance that we have seen for any of the selenophene complexes; metal organoselenides (NaSeMe

(40) Fischer, H.; Fischer, E. O.; Himmelreich, D.; Cai, R.; Schubert, U.; Ackermann, K. *Chem. Ber.* **1981**, *114*, 3220.

(41) Rott, J.; Guggolz, E.; Rettenmeier, A.; Ziegler, M. L. Z. *Naturforsch., Teil B* **1982**, *37*, 13.

(42) Hockett, S. C.; Sauer, N. N.; Angelici, R. J. *Organometallics* **1987**, *6*, 591.

(38) Bailey, M. F.; Dahl, L. F. *Inorg. Chem.* **1965**, *4*, 1306.

(39) Lockemeyer, J. R.; Rauchfuss, T. B.; Rheingold, A. L.; Wilson, S. R. *J. Am. Chem. Soc.* **1989**, *111*, 8828.

$\delta -332$ , NaSeEt  $\delta -150$ )<sup>21,22</sup> have chemical shifts in this range. The electron impact mass spectrum of **4a** shows a parent ion peak ( $M^+$ ) at  $m/z = 272.0$ . The reaction of **4a** with  $(Ph)_3C^+$  in  $CH_2Cl_2$  results in the loss of  $H^-$  to give back complex **4** in quantitative yield.

Other nucleophiles ( $CN^-$ ,  $PR_3$  for  $R = Me, n-Bu$ ) also react (Scheme 1) with **4** giving addition products that have spectral characteristics comparable to those of the known thiophene analogs.<sup>25</sup> The reaction of **4** with NaCN, carried out in the same manner as described for the analogous reaction of  $(\eta^5-T)Mn(CO)_3^+$  with NaCN, gives a yellow oil (**4b**) after evaporation under vacuum. The  $^1H$  NMR spectrum of **4b** in acetone- $d_6$  [ $\delta$  7.05 (t, H(5)), 6.28 (dd, H(4)), 4.86 (d, H(2, endo)), 3.59 (m, H(3))], contains complex second-order coupling of the ring protons. The resonances for H(2, endo) and H(5) show  $^{77}Se$  satellites with coupling constants of 11.8 and 16.4 Hz, respectively. The chemical shifts of these peaks are similar to those of the structurally characterized complex  $(\eta^4-T-CN)Mn(CO)_3$  in acetone- $d_6$  [ $\delta$  6.67 (s, H(5)), 6.13 (s, H(4)), 4.88 (s, H(2)), 3.56 (s, H(3))]; the peaks in this spectrum were broad, probably because of  $Mn^{2+}$  impurities, such that second-order coupling was not observed. The  $^{13}C$  NMR spectrum of **4b** in acetone- $d_6$  [ $\delta$  92.75 (s, C(4)), 78.44 (s, C(5)), 52.13 (s, C(3)), 43.05 (s, C(2))] also closely resembles that of the thiophene analog  $(\eta^4-T-CN)Mn(CO)_3$  in acetone- $d_6$  ( $\delta$  93.08, 69.89, 53.10, 50.77). An upfield shift of 231 ppm for the Sel-CN ligand in **4b** ( $\delta$  24.3) is observed in the  $^{77}Se$  NMR spectrum when compared to the chemical shift of the starting material **4** ( $\delta$  255.9). Thus, the NMR results suggest that **4b** is  $(\eta^4-Sel-CN)Mn(CO)_3$  in which the  $CN^-$  nucleophile has added to the 2-exo position of Sel (Scheme 1). Comparison of the IR spectrum of **4b** [ $\nu(CO)$  (hexanes): 2028 (s), 1954 (vs), 1941 (s)  $cm^{-1}$ ] with that of  $(\eta^4-T-CN)Mn(CO)_3$  [ $\nu(CO)$  (hexanes): 2029 (s), 1957 (vs), 1945 (vs)  $cm^{-1}$ ] also supports this assignment. In addition, the electron impact mass spectrum of **4b** contains a parent ion peak ( $M^+$ )  $m/z = 297$ .

Reactions of trialkylphosphines ( $PR_3$  for  $R = Me, n-Bu$ ) with (arene) $Mn(CO)_3^+$  complexes have been previously reported<sup>33,43</sup> to give the phosphonium ring adducts (arene- $PR_3$ ) $Mn(CO)_3^+$  that were not sufficiently stable to be isolated. The analogous reaction of **4** with  $P(n-Bu)_3$  gave  $(\eta^4-Sel-PBu_3)Mn(CO)_3^+$  (**4c**), which decomposed upon attempted isolation. The  $^1H$  NMR spectrum of **4c** in acetone- $d_6$  [ $\delta$  6.85 (s, H(5)), 6.20 (s, H(4)), 4.91 (s, H(2, endo)), 3.40 (s, H(3)), 1.97 (m), 1.46 (m), 0.965 (m)] and the IR spectrum in MeCN [ $\nu(CO)$ : 2019 (vs), 1938 (s), 1923 (s)  $cm^{-1}$ ] are very similar to those previously reported for  $(\eta^4-T-PBu_3)Mn(CO)_3^+$ .<sup>25</sup> The  $^{77}Se$  NMR spectrum of **4c** shows a doublet at  $\delta -60$  ( $J_{Se-P} = 5$  Hz) due to the coupling of  $^{77}Se$  to  $^{31}P$ . Other basic phosphines such as  $PMe_3$  and  $PEt_3$  react like  $P(n-Bu)_3$  to give phosphine adducts that could also not be isolated.

In contrast to the simple addition reaction of hydride to the thiophene in  $[(\eta^5-T)Mn(CO)_3]^+$ , hydride addition at C(2) in  $[(\eta^5-T)RuCp]^+$  results in cleavage of a C-S bond.<sup>33,34,44</sup> The analogous reaction of  $[(\eta^5-Sel)RuCp]^+$  (**7**) with hydride  $[Na[(H_3COC_2H_4O)_2AlH_2]]$  also causes C-Se bond cleavage to give the complex (Se-

$CH=CHCH=CH_2$ ) $RuCp^*$  (**7a**) in 30% yield (Scheme 1). The  $^1H$  NMR spectrum of **7a** in  $CDCl_3$  shows five resonances assignable to the protons of the coordinated selenide/diene ligand [ $\delta$  6.38 (d,  $J_{H-Se} = 17.5$  Hz, H(5)), 5.68 (t, H(4)), 4.37 (m, H(3)), 2.72 (d, H(2, endo)), 2.53 (d, H(2, exo)) and 1.85 (s, Me- $Cp^*$ )]. This spectrum is very similar to that of the thiophene analog  $(SC-H=CHCH=CH_2)RuCp^*$ .<sup>33</sup> Cleavage of the C(2)-Se bond is indicated by the lack of coupling of either the endo or exo proton at C(2) to  $^{77}Se$ . However, coupling is observed between the proton on C(5) and  $^{77}Se$ , with  $J_{H-Se}$  (16.5 Hz) approximately the same as that ( $J_{H-Se} = 17.4$  Hz) for the proton on C(5) in **4a**. In the  $^{13}C$  NMR spectrum of **7a** there are four resonances at  $\delta$  97.9 (s, C(3)), 92.6 (s, C(4)), 89.0 (s, C(5)) and 45.2 (s, C(2)) assignable to the carbons of the cleaved ring. The EI mass spectrum of **7a** contains a peak for the parent ion  $M^+$ .

The reaction of  $[(\eta^5-2,5-Me_2T)IrCp^*]^{2+}$  with  $Na[(CH_3OC_2H_4O)_2AlH_2]$  or the reducing agent  $Cp_2Co$  gives the neutral complex  $(\eta^4-2,5-Me_2T)IrCp^*$ , in which the  $\eta^4-2,5-Me_2T$  ligand is coordinated to the metal only through the four carbon atoms.<sup>7</sup> This  $\eta^4$  complex rearranges in the presence of base to give the ring-opened product  $(C,S-2,5-Me_2T)IrCp^*$  in which the Ir is inserted into a C-S bond to give a planar six-membered ring.<sup>7,35</sup> The analogous reaction of  $[(\eta^5-2,5-Me_2Sel)IrCp^*]^{2+}$  (**12**) with 2 equiv of  $Na[(CH_3OC_2H_4O)_2AlH_2]$  gives the ring-opened complex  $(C,Se-2,5-Me_2Sel)IrCp^*$  (**12a**) (Scheme 1) as the only isolable product in low yield (17%). The  $^1H$  NMR spectrum of **12a** in  $CDCl_3$  contains two deshielded proton resonances at  $\delta$  7.59 (d) and 7.49 (d), two methyl resonances at  $\delta$  3.26 (s) and 2.84 (s), and a singlet resonance for the  $Cp^*$  ligand at  $\delta$  1.87. This spectrum is almost identical to that of  $(C,S-2,5-Me_2T)IrCp^*$ , which has a planar six-membered  $\pi$ -delocalized ring that has been described as an iridathiabenzene.<sup>35</sup> The  $^{13}C$  NMR spectrum of **12a** in  $CDCl_3$  exhibits four carbon resonances at  $\delta$  134.9, 132.1, 129.8, and 123.3, which are characteristic of aromatic carbon atoms. Complex **12a** has an unusual  $^{77}Se$  NMR chemical shift ( $\delta$  905), which is substantially downfield of the resonance of unbound selenophene ( $\delta$  605) or the starting material **12** ( $\delta$  371). This downfield chemical shift is similar to that ( $\delta$  976) of the aromatic six-membered heterocyclic seleninium

cation  $(\overline{SeCHCHCHCHCH})^+$ .<sup>45</sup> This similarity in  $^{77}Se$  NMR chemical shift further supports the description of the six-membered ring in **12a** as a delocalized  $\pi$  system, making **12a** an iridaselenabenzene compound. The  $^1H$ ,  $^{13}C$ , and  $^{77}Se$  NMR data therefore suggest that **12a** has a structure containing a planar six-membered ring analogous to that established for the sulfur analog  $(C,S-2,5-Me_2T)IrCp^*$ .

## Conclusions

The synthesis of several new  $\eta^5$ -Seln transition metal complexes (**1-12**) has been undertaken so that a comparison of the spectroscopic and chemical properties could be made with the known  $\eta^5$ -Th complexes. The  $^1H$  and  $^{13}C$  NMR and IR spectroscopic data for the  $\eta^5$ -Seln complexes (**1-12**) are very similar to those of the analogous  $\eta^5$ -Th complexes. Reactions of the  $\eta^5$ -Seln

(43) Sweigart, D. A.; Kane-Maguire, L. A. P. *J. Chem. Soc., Chem. Commun.* **1976**, 13.

(44) Hachgenei, J. W.; Angelici, R. J. *Angew. Chem., Int. Ed. Engl.* **1987**, *26*, 909.

(45) Sandor, P.; Radics, L. *Org. Magn. Reson.* **1981**, *16*, 148.

ligand in **4**, **7**, and **12** with nucleophiles give the same types of products that are formed in the corresponding reactions of the analogous  $\eta^5$ -Th complexes. Differences between the structures of  $(\eta^5\text{-}2,5\text{-Me}_2\text{Se})\text{Cr}(\text{CO})_3$  and  $(\eta^5\text{-}2,5\text{-Me}_2\text{T})\text{Cr}(\text{CO})_3$  are mostly due to the larger size of the Se as compared to S. The  $^{77}\text{Se}$  chemical shifts of these  $\eta^5$ -Seln complexes all fall within the region between  $\delta$  375 and 150, the more positive the charge on the complex the more downfield the  $^{77}\text{Se}$  signal. The observation that the  $^{77}\text{Se}$  NMR chemical shifts fall within a range of only 225 ppm for a series of complexes with different metals, ligands, and ionic charges suggests that  $^{77}\text{Se}$  NMR spectroscopy may be a useful

probe for detecting  $\eta^5$ -selenophene binding on HDS catalytic surfaces.

**Acknowledgment.** The authors thank Dr. Victor G. Young, Jr., of the ISU Molecular Structure Laboratory for solving the molecular structure of **3**. We also thank Johnson-Mathey, Inc. for the generous loan of  $\text{RuCl}_3$  and  $\text{IrCl}_3$ .

**Supplementary Material Available:** Tables of displacement parameters ( $U$ s), hydrogen atom coordinates and displacement parameters, and least-squares planes (5 pages). Ordering information is given on any current masthead page.

OM940439Y

# Reactions of Rhodium Porphyrins with Lactones, Silanes, and Stannanes

Tadashi Mizutani,\* Tetsuya Uesaka, and Hisanobu Ogoshi\*

Department of Synthetic Chemistry and Biological Chemistry, Faculty of Engineering,  
Kyoto University, Yoshida, Sakyo-ku, Kyoto 606-01, Japan

Received June 3, 1994<sup>⊗</sup>

(2,3,7,8,12,13,17,18-Octaethylporphyrinato)rhodium(I) (Rh<sup>I</sup>OEP) cleaved the alkyl–oxygen bond of four-membered-ring and five-membered-ring lactones ( $\beta$ -propiolactone (**1**),  $\beta$ -butyrolactone (**2**), and  $\gamma$ -butyrolactone (**3**)) at room temperature to regioselectively yield ( $\omega$ -carboxyalkyl)Rh<sup>III</sup>OEP. [ $\{\text{Rh}^{\text{II}}\text{OEP}\}_2$ ] reacted with R<sup>1</sup><sub>2</sub>R<sup>2</sup>MH (**8**, M = Si, R<sup>1</sup> = R<sup>2</sup> = Et; **9**, M = Si, R<sup>1</sup> = R<sup>2</sup> = Ph; **10**, M = Si, R<sup>1</sup> = Me, R<sup>2</sup> = Ph; **11**, M = Si, R<sup>1</sup> = Me, R<sup>2</sup> = OEt; **16**, M = Sn, R<sup>1</sup> = R<sup>2</sup> = Bu; **17**, M = Sn, R<sup>1</sup> = R<sup>2</sup> = Ph) to yield Rh<sup>III</sup>(MR<sup>1</sup><sub>2</sub>R<sup>2</sup>)OEP. These alkyl-, silyl-, and stannylrhodium complexes of OEP were characterized by <sup>1</sup>H, <sup>13</sup>C, <sup>29</sup>Si, and <sup>119</sup>Sn NMR, IR, UV–vis, and mass spectroscopy. (triethylsilyl)Rh<sup>III</sup>OEP crystallizes in the monoclinic space group C2/c with unit cell dimensions  $a = 17.14(8)$  Å,  $b = 14.94(5)$  Å,  $c = 31.22(5)$  Å, and  $\beta = 103.5(2)^\circ$ ; the density is 1.28 g/cm<sup>3</sup> for  $Z = 8$ . The porphyrin plane is almost planar, and the rhodium metal resides on the plane. The Rh–Si distance is 2.32(1) Å, and all the eight ethyl groups on the pyrroles are directed toward the triethylsilyl group. The present method has proved to be a facile way to prepare bimetallic rhodium complexes of porphyrin.

Rhodium–porphyrin complexes are of interest for their diverse reactivities depending on the oxidation state of the rhodium metal.<sup>1,2</sup> Similar reactions were found to take place with both Rh porphyrin and Co porphyrin. The Rh porphyrin has been studied as a model of the vitamin B<sub>12</sub> coenzyme.<sup>3</sup> Rh(I) porphyrin, for example, is nucleophilic and undergoes numerous nucleophilic substitution and addition reactions such as conjugated addition to the  $\alpha,\beta$ -unsaturated carbonyl compounds<sup>2</sup> and cleavage of three- or four-membered cyclic ethers.<sup>4</sup> A Rh(II) porphyrin dimer undergoes radical reactions with olefins and acetylenes.<sup>5</sup> Wayland et al.<sup>6</sup> reported that (tetramesitylporphyrinato)rhodium(II) can cleave a C–H bond of methane. A Rh(III) porphyrin is electrophilic. It reacts with organolithium compounds<sup>2</sup> and acts as a Lewis acid catalyst.<sup>7</sup> These reactions, especially those forming a Rh–C bond, are useful for prediction of possible elementary reactions taking place in Co–C species derived from vitamin B<sub>12</sub>, since the similarity between the reactivity of the Rh(II) porphyrin and the Co(II) porphyrin has been noticed.<sup>8</sup> Recently, insertion reactions of carbenes catalyzed by rhodium(III) porphyrins have attracted much

interest.<sup>9</sup> In this paper we report that a nucleophilic Rh(I) porphyrin reacts with a four- or five-membered ring lactone at the alkoxide carbon to give ( $\omega$ -carboxyalkyl)Rh<sup>III</sup>OEP. Also, the Rh<sup>II</sup>OEP dimer reacts with hydrosilane or hydrostannane to give (trialkylsilyl)Rh<sup>III</sup>OEP or (trialkylstannyl)Rh<sup>III</sup>OEP, respectively.

## Results and Discussion

**Reaction of Rhodium(I) Octaethylporphyrin with Lactones.** Reactions of Rh<sup>I</sup>OEP with four-, five-, and six-membered ring lactones and ethyl acetate (as a representative of a linear ester) were performed at room temperature under Ar (Scheme 1). Products and yields of the reactions are summarized in Table 1. Four- and five-membered-ring lactones gave alkyl–rhodium complexes, while the six-membered-ring lactone and ethyl acetate did not. Therefore, the ring size of the lactone is one of the important factors in the limitation of this reaction. The strain energies are 8.8 kcal/mol for **3** and 11.2 kcal/mol for **4** (calorimetry),<sup>10a</sup> 7.3 kcal/mol for **3** and 10.0 kcal/mol for **4** (ab initio, HF/6-31G\*),<sup>10a</sup> and 8.70 kcal/mol for **3** and 10.36 kcal/mol for **4** (MM3).<sup>10b</sup> These data indicate that the six-membered-ring lactone (**4**) is more strained than the five-membered-ring lactone (**3**) by 1.7–2.7 kcal/mol. The difference in strain energy alone, therefore, cannot account for the difference in reactivity.

The second important result is the regioselectivity of the reaction. In the reaction, the alkyl–oxygen bond of lactone is cleaved in preference to the acyl–oxygen

<sup>⊗</sup> Abstract published in *Advance ACS Abstracts*, November 1, 1994.

(1) Guilard, R.; Kadish, K. M. *Chem. Rev.* **1988**, *88*, 1121.

(2) Ogoshi, H.; Setsune, J.; Omura, T.; Yoshida, Z. *J. Am. Chem. Soc.* **1975**, *97*, 6461.

(3) For examples of reactions of Co–porphyrins, see: (a) Ogoshi, H.; Kikuchi, Y.; Yamaguchi, T.; Toi, H.; Aoyama, Y. *Organometallics* **1987**, *6*, 2175. (b) Setsune, J.-i.; Ishimaru, Y.; Moriyama, T.; Kitao, T. *J. Chem. Soc., Chem. Commun.* **1991**, 555. (c) Gridnev, A. A.; Ittel, S. D.; Fryd, M.; Wayland, B. B. *J. Chem. Soc., Chem. Commun.* **1993**, 1010. (d) Gridnev, A. A.; Ittel, S. D.; Fryd, M.; Wayland, B. B. *Organometallics* **1993**, *12*, 4871.

(4) Ogoshi, H.; Setsune, J.; Yoshida, Z. *J. Organomet. Chem.* **1980**, *185*, 95.

(5) (a) Ogoshi, H.; Setsune, J.; Yoshida, Z. *J. Am. Chem. Soc.* **1977**, *99*, 3869. (b) Paonessa, R. S.; Thomas, N. C.; Halpern, J. *J. Am. Chem. Soc.* **1985**, *107*, 4333.

(6) Sherry, A. E.; Wayland, B. B. *J. Am. Chem. Soc.* **1990**, *112*, 1259.

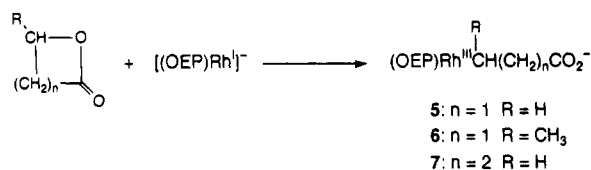
(7) Aoyama, Y.; Yamagishi, A.; Tanaka, Y.; Toi, H.; Ogoshi, H. *J. Am. Chem. Soc.* **1987**, *109*, 4735.

(8) Brown, K. L. In *B<sub>12</sub>*; Dolphin, D., Ed.; Wiley: New York, 1982; Vol. I, p 245.

(9) (a) Callot, H. J.; Metz, F.; Piechocki, C. *Tetrahedron* **1982**, *38*, 2365. (b) Maxwell, J. L.; Brown, K. C.; Bartley, D. W.; Kodadek, T. *Science* **1992**, *256*, 1544.

(10) (a) Wiberg, K. B.; Waldron, R. F. *J. Am. Chem. Soc.* **1991**, *113*, 7697. (b) Allinger, N. L.; Zhu, Z. S.; Chen, K. *J. Am. Chem. Soc.* **1992**, *114*, 6120.

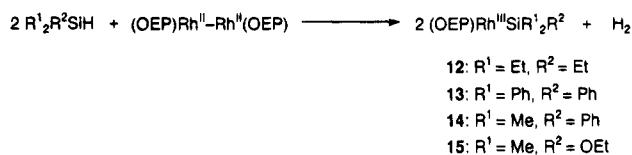
Scheme 1

Table 1. Reactions of Rh<sup>I</sup>OEP with Lactones

Substrate	Product	Yield (%)
	(OEP)Rh <sup>III</sup> CH <sub>2</sub> CH <sub>2</sub> CO <sub>2</sub> H 5	72
	(OEP)Rh <sup>III</sup> CH(CH <sub>3</sub> )CH <sub>2</sub> CO <sub>2</sub> H 6	68
	(OEP)Rh <sup>III</sup> CH <sub>2</sub> CH <sub>2</sub> CH <sub>2</sub> CO <sub>2</sub> H 7	45
	No reaction	
AcOEt	No reaction	

bond. Spectroscopic data of the product obtained from Rh<sup>I</sup>OEP and  $\beta$ -butyrolactone showed that the Rh atom is not bonded to the carbonyl carbon (C1) but bonded to the alkoxide carbon (C3). The <sup>1</sup>H NMR signal at  $\delta$  -6.42 ppm exhibits a coupling constant of  $J = 2.8$  Hz besides the vicinal H-H coupling, which can be ascribed to the coupling between <sup>1</sup>H and <sup>103</sup>Rh. If the rhodium were bonded to the carbonyl carbon, the expected chemical shift of the signal in the highest magnetic field would be close to -3.77 ppm, which is the chemical shift of the proton  $\beta$  to the Rh atom of [Rh<sup>III</sup>{CO(CH<sub>2</sub>)<sub>4</sub>CH<sub>3</sub>}-OEP] in CDCl<sub>3</sub>.<sup>11</sup> Therefore, the signal appearing at -6.47 ppm is assignable to the proton  $\alpha$  to the Rh atom. The <sup>13</sup>C NMR signal at  $\delta$  6.76 ppm recorded with complete <sup>1</sup>H decoupling exhibits a coupling constant of  $J = 27.9$  Hz, which can be ascribed to the coupling between <sup>13</sup>C and <sup>103</sup>Rh. The <sup>1</sup>H-<sup>13</sup>C HSQC spectrum indicated that the two signals noted above (<sup>1</sup>H and <sup>13</sup>C) are correlated and that the hydrogen and the carbon noted above are directly bonded to each other. The IR spectrum showed a peak at 1706 cm<sup>-1</sup>, which is ascribed to the C=O stretching of the carboxyl group. All these data are consistent with structure 5. It is noteworthy that the reaction is readily completed at room temperature. This can be ascribed to the high nucleophilicity of the Rh(I) porphyrin. The observed regioselectivity is similar to that observed for thiol,<sup>12</sup> selenium,<sup>13</sup> silicon,<sup>14</sup> and other<sup>15</sup> nucleophiles in their reactions with

Scheme 2

Table 2. Reactions of [Rh<sup>II</sup>OEP]<sub>2</sub> with Silanes

substrate	product	yield (%)	<sup>29</sup> Si NMR	
			$\delta$ (ppm)	$J_{Si-Rh}$ (Hz)
Et <sub>3</sub> SiH (8)	Rh <sup>III</sup> (SiEt <sub>3</sub> )OEP (12)	54	51.98	29.3
Ph <sub>3</sub> SiH (9)	Rh <sup>III</sup> (SiPh <sub>3</sub> )OEP (13)	65	11.56	35.7
Me <sub>2</sub> PhSiH (10)	Rh <sup>III</sup> (SiPhMe <sub>2</sub> )OEP (14)	44	28.30	30.2
(EtO)Me <sub>2</sub> SiH (11)	Rh <sup>III</sup> (SiMe <sub>2</sub> (OEt))OEP (15)	42	37.24	30.5

lactones.<sup>16</sup> In these reactions, a tendency is observed that "soft" nucleophiles attack the alkyl carbon to give alkyl-oxygen cleavage.<sup>13c,15b</sup> On the basis of these results, we suggest that the rhodium(I) porphyrin is a soft nucleophile.

**Reaction of Rhodium(I) Octaethylporphyrin with Lactams.** Reactions of [Rh<sup>I</sup>OEP] with lactams ( $\beta$ -propiolactam,  $\gamma$ -butyrolactam,  $\delta$ -valerolactam, and 1-methyl-2-pyrrolidinone) were also investigated. In contrast to lactones, no formation of alkyl-rhodium complexes was detected using <sup>1</sup>H NMR. The nucleophilic ring opening reaction is thus sensitive to the differences in leaving group structures (-CO<sub>2</sub><sup>-</sup> vs -CONH<sup>-</sup>).

**Reaction of Rh<sup>II</sup>OEP Dimer with Organosilanes.** The reaction of Rh complexes with organosilanes is interesting because some Rh complexes constitute an important group of the hydrosilylation catalyst. The development of versatile preparative methods of transition-metal-silicon complexes is thus desired. By using the metalloradical reactivity<sup>17</sup> of the Rh<sup>II</sup>OEP dimer, the preparation of silylrhodium complexes was explored.<sup>18</sup> Hydrosilanes reacted with the Rh<sup>II</sup>OEP dimer smoothly to give silylrhodium complexes of OEP (Scheme 2). The products, yields, and <sup>29</sup>Si NMR data (chemical shifts  $\delta$  and coupling constants <sup>1</sup>J<sub>Si-Rh</sub>) are listed in Table 2. The <sup>29</sup>Si NMR chemical shifts of the starting silanes were 0.15 ppm (8), -17.75 ppm (9), and -17.50 ppm (10).<sup>13</sup> Therefore, the <sup>29</sup>Si chemical shift displacements upon rhodium-silicon bond formation ranged from 30 to 50 ppm, which is characteristic of the chemical shift displacement of <sup>29</sup>Si bonded to a transition metal.<sup>19</sup> These NMR data indicate that triethylsilane (8), triphenylsilane (9), dimethylphenylsilane (10), and dimethylethoxysilane reacted with [Rh<sup>II</sup>OEP]<sub>2</sub> to form (trialkylsilyl)rhodium complexes.<sup>20</sup> Because the yields of 8 and 9 exceed 50% on the basis of [Rh<sup>II</sup>OEP]<sub>2</sub>, both Rh

(14) Kolb, M.; Barth, J. *Synth. Commun.* **1981**, *11*, 763.(15) (a) Ali, S. M.; Chapleo, C. B.; Finch, M. A. W.; Roberts, S. M.; Woolley, G. T.; Cave, R. J.; Newton, R. F. *J. Chem. Soc., Perkin Trans. I* **1980**, 2093. (b) Arnold, L. D.; Kalantar, T. H.; Vederas, J. C. *J. Am. Chem. Soc.* **1985**, *107*, 7105.(16) For a review on ester cleavage via S<sub>N</sub>2-type dealkylation. see: McMurry, J. *Org. React.* **1976**, *24*, 187.(17) Paonessa, R. S.; Thomas, N. C.; Halpern, J. *J. Am. Chem. Soc.* **1985**, *107*, 4333.(18) For examples of the reaction of silanes and transition metal complexes, see: (a) Baay, Y. L.; MacDiarmid, A. G. *Inorg. Chem.* **1969**, *8*, 986. (b) Sisak, A.; Ungvary, F.; Marko, L. *Organometallics* **1986**, *5*, 1019.(19) Marsmann, H. In *<sup>29</sup>Si-NMR Spectroscopic Results*; Diehl, P., Fluck, E., Kosfeld, R., Eds.; Springer-Verlag: Berlin, 1981; pp 66-235.(11) Ogoshi, H.; Setsune, J.; Nanbo, Y.; Yoshida, Z. *J. Organomet. Chem.* **1978**, *159*, 329.(12) Plieninger, H. *Chem. Ber.* **1950**, *83*, 265.(13) (a) Miyoshi, N.; Ishii, H.; Murai, S.; Sonoda, N. *Chem. Lett.* **1979**, 873. (b) Scarborough, R. M., Jr.; Toder, B. H.; Smith, A. B., III *J. Am. Chem. Soc.* **1980**, *102*, 3904. (c) Liotta, D.; Sunay, U.; Santiesteban, H.; Markiewicz, W. *J. Org. Chem.* **1981**, *46*, 2605.



Scheme 3

18: R = *n*-Bu

19: R = Ph

Table 3. Reactions of [(OEP)Rh<sup>II</sup>]<sub>2</sub> with Stannanes

substrate	product	yield (%)	<sup>119</sup> Sn NMR	
			δ (ppm)	J <sub>119Sn-103Rh</sub> (Hz)
<i>n</i> -Bu <sub>3</sub> SnH (16)	Rh <sup>III</sup> (SnBu <sub>3</sub> )OEP (18)	49	118.3	314.2
Ph <sub>3</sub> SnH (17)	Rh <sup>III</sup> (SnPh <sub>3</sub> )OEP (19)	44	-121.6	412.9

Table 4. Crystal Data for (OEP)RhSiEt<sub>3</sub> (12)

formula	C <sub>42</sub> H <sub>59</sub> N <sub>4</sub> SiRh
fw	750.95
space group	C2/c
<i>a</i> , Å	17.14(8)
<i>b</i> , Å	14.94(5)
<i>c</i> , Å	31.22(5)
β, deg	103.5(2)
<i>V</i> , Å <sup>3</sup>	7774(43)
<i>Z</i>	8
ρ(calcd), g/cm <sup>3</sup>	1.28
temp, °C	-120
cryst dimens, mm	0.25 × 0.25 × 0.25
radiation	graphite-monochromated Mo Kα radiation, 12 kW rotating anode generator
linear abs coeff, cm <sup>-1</sup>	5.0
detector aperture, mm	9.0 (horiz), 13.0 (vert)
scan type	ω-2θ
scan rate, deg/min	16.0 (in ω)
2θ limits, deg	0.0 < 2θ < 60.4
no. of rflns measd	12 149 total, 11 779 unique
no. of rflns used	9548
no. of variables	601
<i>R</i>	0.063
<i>R</i> <sub>w</sub>	0.078

atoms of [Rh<sup>II</sup>OEP]<sub>2</sub> are incorporated in the rhodium-silyl complexes.

Similarly, hydrostannanes react with the Rh(II) dimer to afford stannyl-rhodium complexes of OEP (Scheme 3). The products and <sup>119</sup>Sn NMR data are listed in Table 3. Coupling constants of 300–400 Hz were observed in the <sup>119</sup>Sn NMR spectra of the stannyl-rhodium complexes, supporting the notion that a direct bond between Rh and Sn exists in the product.<sup>21,22</sup>

Rh<sup>III</sup>(SiEt<sub>3</sub>)OEP crystallizes in the monoclinic space group *C*/2*c* with eight porphyrin molecules per unit cell. Crystal data, positional parameters, and intramolecular distances and angles are listed in Tables 4–7. The porphyrin is almost planar, and the rhodium atom resides on the plane (Figure 1). The displacement of the Rh atom from the least-squares plane of four nitrogen atoms was 0.090 Å, which is comparable to those of similar rhodium porphyrins ((OEP)RhMe, 0.051 Å;<sup>23</sup> (OEP)RhCHO, 0.080 Å;<sup>24</sup> (OEP)RhH, 0.010 Å;<sup>24</sup>

(20) For an example of a compound having a Rh–Si bond, see: Bennett, M. A.; Patmore, D. *J. Inorg. Chem.* **1971**, *10*, 2387.

(21) Coupling constants <sup>1</sup>J<sub>103Rh-119Sn</sub> of 102–615 Hz were reported for stannyl-rhodium complexes; see: (a) Ruiz, J.; Spencer, C. M.; Mann, B. E.; Taylor, B. F.; Maitlis, P. M. *J. Organomet. Chem.* **1987**, *325*, 253. (b) Fridalga, L.; Garralda, M. A.; Hernandez, R.; Ibarlucea, L. *Inorg. Chim. Acta* **1993**, *207*, 121. (c) Calton, L.; Weber, R. *Inorg. Chem.* **1993**, *32*, 4169.

(22) The phenyl group on stannanes causes upfield shifts of the <sup>119</sup>Sn chemical shifts. For example, chemical shifts of <sup>119</sup>Sn are -164.5 (Ph<sub>3</sub>SnH), -91.4 (Bu<sub>3</sub>SnH), -85.5 ((Ph<sub>3</sub>Sn)<sub>2</sub>O), and 82.0 ((Bu<sub>3</sub>Sn)<sub>2</sub>O), see: Wrackmeyer, B. In *Annual Reports on NMR Spectroscopy*; Webb, G. A. Ed.; Academic Press: London, 1985; Vol. 16, p 73.

(23) Takenaka, A.; Syal, S. K.; Sasada, Y.; Omura, T.; Ogoshi, H.; Yoshida, Z. *Acta Crystallogr., Sect. B: Struct. Crystallogr. Cryst. Chem.* **1976**, *B32*, 62.

(24) Jones, N. L.; Carroll, P. J.; Wayland, B. B. *Organometallics* **1986**, *5*, 33.

Table 5. Positional Parameters for Non-Hydrogen Atoms of 12

atom	<i>x</i>	<i>y</i>	<i>z</i>	<i>B</i> (eq), Å <sup>2</sup>
Rh(1)	0.09209(2)	-0.00455(2)	0.341049(9)	1.73(1)
Si(1)	0.04240(7)	-0.00308(7)	0.40394(4)	2.35(2)
N(1)	-0.0185(2)	0.0151(2)	0.3010(1)	1.8(1)
N(2)	0.1107(2)	0.1296(2)	0.3449(1)	1.9(1)
N(3)	0.2068(2)	-0.0248(2)	0.3760(1)	2.1(1)
N(4)	0.0775(2)	-0.1388(2)	0.3326(1)	2.0(1)
C(1)	-0.0726(2)	-0.0491(2)	0.2822(1)	1.9(1)
C(2)	-0.1452(2)	-0.0071(2)	0.2566(1)	2.1(1)
C(3)	-0.1332(2)	0.0827(2)	0.2605(1)	2.1(1)
C(4)	-0.0541(2)	0.0963(2)	0.2885(1)	1.9(1)
C(5)	-0.0193(2)	0.1787(2)	0.3002(1)	2.2(1)
C(6)	0.0573(2)	0.1948(2)	0.3263(1)	2.2(1)
C(7)	0.0930(2)	0.2826(2)	0.3368(1)	2.5(1)
C(8)	0.1684(2)	0.2690(3)	0.3616(1)	2.4(1)
C(9)	0.1793(2)	0.1738(3)	0.3665(1)	2.2(1)
C(10)	0.2488(2)	0.1319(3)	0.3887(1)	2.4(1)
C(11)	0.2618(2)	0.0399(3)	0.3936(1)	2.3(1)
C(12)	0.3362(2)	-0.0015(3)	0.4177(1)	2.6(1)
C(13)	0.3246(2)	-0.0920(3)	0.4140(1)	2.8(1)
C(14)	0.2440(2)	-0.1053(3)	0.3877(1)	2.3(1)
C(15)	0.2088(2)	-0.1882(3)	0.3753(1)	2.4(1)
C(16)	0.1322(2)	-0.2040(2)	0.3504(1)	2.1(1)
C(17)	0.0977(2)	-0.2918(2)	0.3389(1)	2.2(1)
C(18)	0.0221(2)	-0.2783(2)	0.3136(1)	2.1(1)
C(19)	0.0099(2)	-0.1828(2)	0.3098(1)	2.0(1)
C(20)	-0.0592(2)	-0.1407(2)	0.2863(1)	2.0(1)
C(21)	-0.2192(2)	-0.0557(3)	0.2325(1)	2.5(1)
C(22)	-0.2755(3)	-0.0810(4)	0.2617(2)	4.1(2)
C(23)	-0.1906(2)	0.1564(3)	0.2427(1)	2.5(1)
C(24)	-0.2373(3)	0.1879(4)	0.2748(2)	3.7(2)
C(25)	0.0496(3)	0.3691(3)	0.3228(2)	3.4(2)
C(26)	-0.0063(4)	0.3951(4)	0.3519(3)	5.1(3)
C(27)	0.2291(3)	0.3372(3)	0.3833(2)	3.2(2)
C(28)	0.2330(4)	0.3485(4)	0.4317(2)	4.6(2)
C(29)	0.4073(3)	0.0492(3)	0.4437(2)	3.2(2)
C(30)	0.3948(4)	0.0810(5)	0.4874(2)	4.8(3)
C(31)	0.3802(3)	-0.1654(3)	0.4343(2)	3.7(2)
C(32)	0.3634(6)	-0.2000(6)	0.4764(3)	6.2(4)
C(33)	0.1384(3)	-0.3780(3)	0.3555(2)	2.8(2)
C(34)	0.1325(4)	-0.4005(4)	0.4019(2)	4.4(2)
C(35)	-0.0410(3)	-0.3475(3)	0.2957(1)	2.5(1)
C(36)	-0.0986(3)	-0.3621(4)	0.3248(2)	3.7(2)
C(37)	-0.066(1)	0.0480(9)	0.3906(4)	13.3(8)
C(38)	-0.1074(8)	0.044(1)	0.4265(7)	16(1)
C(39)	0.0989(6)	0.083(1)	0.4481(2)	31(1)
C(41)	0.040(1)	-0.1138(6)	0.4283(5)	15.9(8)
C(42)	-0.0221(8)	-0.165(1)	0.4298(8)	27(2)

(OEP)RhCONH(xylyl), 0.072 Å<sup>25</sup>). The Rh–Si distance was 2.32(1) Å. All the ethyl groups on the porphyrin periphery are directed toward the triethylsilyl group. The crystal packing indicates that the aromatic part of the molecule is in contact with the aromatic part of the next molecule and the aliphatic part is in contact with the aliphatic part of the next molecule (Figure 2). This intermolecular interaction mode accounts for the fact that all the ethyl groups are pointed in the same direction.

Both the silyl and the stannyl complexes of the rhodium porphyrin are relatively stable. These results indicate that the present method provides a facile way to prepare bimetallic rhodium complexes of porphyrin.

## Experimental Section

**General Procedures.** <sup>1</sup>H and <sup>13</sup>C NMR spectra were obtained using a JEOL A-500 spectrometer, a JEOL GX-400 spectrometer, or a JEOL JNM FX 90Q FT NMR spectrometer, and chemical shifts are reported relative to internal Me<sub>4</sub>Si.

(25) Poszmik, G.; Carroll, P. J.; Wayland, B. B. *Organometallics* **1993**, *12*, 3410.

**Table 6. Intramolecular Distances Involving the Non-Hydrogen Atoms of 12<sup>a</sup>**

Rh(1)–Si(1)	2.32(1)	C(7)–C(25)	1.50(6)
Rh(1)–N(1)	2.03(3)	C(8)–C(9)	1.44(5)
Rh(1)–N(2)	2.03(3)	C(8)–C(27)	1.50(6)
Rh(1)–N(3)	2.04(3)	C(9)–C(10)	1.38(5)
Rh(1)–N(4)	2.03(3)	C(10)–C(11)	1.40(6)
Si(1)–C(37)	2.0(1)	C(11)–C(12)	1.46(5)
Si(1)–C(39)	2.0(1)	C(12)–C(13)	1.37(6)
Si(1)–C(41)	1.82(7)	C(12)–C(29)	1.50(6)
N(1)–C(1)	1.37(4)	C(13)–C(14)	1.45(5)
N(1)–C(4)	1.37(4)	C(13)–C(31)	1.49(6)
N(2)–C(6)	1.37(5)	C(14)–C(15)	1.39(5)
N(2)–C(9)	1.38(5)	C(15)–C(16)	1.38(5)
N(3)–C(11)	1.37(5)	C(16)–C(17)	1.45(5)
N(4)–C(16)	1.37(5)	C(17)–C(33)	1.50(5)
N(4)–C(19)	1.38(5)	C(18)–C(19)	1.44(5)
C(1)–C(20)	1.39(5)	C(19)–C(20)	1.39(5)
C(2)–C(3)	1.36(5)	C(21)–C(22)	1.52(7)
C(2)–C(21)	1.50(5)	C(23)–C(24)	1.50(7)
C(3)–C(4)	1.44(5)	C(25)–C(26)	1.52(8)
C(3)–C(23)	1.49(5)	C(27)–C(28)	1.50(7)
C(4)–C(5)	1.38(5)	C(29)–C(30)	1.51(8)
C(5)–C(6)	1.39(5)	C(31)–C(32)	1.5(1)
C(6)–C(7)	1.45(5)	C(33)–C(34)	1.51(8)
C(7)–C(8)	1.36(5)	C(35)–C(36)	1.50(7)
C(37)–C(38)	1.5(2)		
C(41)–C(42)	1.3(2)		

<sup>a</sup> Distances are in angstroms. Estimated standard deviations in the least significant figure are given in parentheses.

<sup>29</sup>Si NMR spectra were recorded on a JEOL A-500 spectrometer operating at 100 MHz with NOE-eliminated complete <sup>1</sup>H decoupling. Chemical shifts are reported relative to internal Me<sub>4</sub>Si. UV-vis spectra were recorded on either a Hitachi U-3410 spectrometer or a Hewlett-Packard 8452 diode array spectrophotometer with a thermostated cell compartment. Mass spectra were obtained with a JEOL JMS DX-300 mass spectrometer. High-resolution mass spectra were recorded on a JEOL JMS SX-102A instrument. Thin-layer chromatography (TLC) was performed on either Merck Kieselgel 60 F<sub>254</sub> or DC-Alufolien aluminium oxide 60 F<sub>254</sub> neutral (type E). Single-crystal X-ray diffraction was performed on a Rigaku AFC7R diffractometer.

**Materials.** Octaethylporphyrin (OEP) was prepared according to the published method.<sup>26</sup> [Rh<sup>III</sup>(OEP)] was prepared by treating OEP with Rh<sub>2</sub>(CO)<sub>8</sub>, followed by oxidation with I<sub>2</sub>. [Rh<sup>II</sup>OEP]<sub>2</sub> was prepared according to the published method.<sup>27</sup>

[Rh<sup>III</sup>(CH<sub>2</sub>CH<sub>2</sub>CO<sub>2</sub>H)OEP] (**5**). [Rh<sup>III</sup>I(OEP)] (11.4 mg, 14.9 μmol) was dissolved in dry and degassed ethanol at 50 °C, and NaBH<sub>4</sub> (2.6 mg, 68.7 μmol) in 0.5 M aqueous NaOH (2 mL) was added under Ar. The solution turned from red to deep orange. After it was stirred at 50 °C for 1 h under Ar, the solution was cooled to room temperature, and β-propiolactone (**1**; 0.1 mL, 1.59 mmol) was added. The color changed immediately to orange. After the solution was stirred for 30 min, the ethanol was evaporated under reduced pressure. The residue was washed with water and dried. The product was recrystallized from THF–MeOH; yield 6.8 mg (72%). <sup>1</sup>H NMR (Me<sub>2</sub>SO-*d*<sub>6</sub>, 500 MHz): δ 10.05 (s, 4H, meso), 4.08 (q, *J* = 14 Hz, *J* = 7.8 Hz, 8H, CH<sub>2</sub>CH<sub>3</sub>), 4.03 (q, *J* = 14 Hz, *J* = 7.8 Hz, 8H, CH<sub>2</sub>CH<sub>3</sub>), 1.85 (t, *J* = 7.8 Hz, 24H, CH<sub>2</sub>CH<sub>3</sub>), –4.60 (t, *J* = 8.7 Hz, 2H, RhCH<sub>2</sub>CH<sub>2</sub>CO<sub>2</sub>H), –6.42 (td, *J* = 8.7 Hz, *J*<sub>H–Rh</sub> = 2.8 Hz, 2H, RhCH<sub>2</sub>CH<sub>2</sub>CO<sub>2</sub>H), IR (KBr): 3400–2500, 2964, 2931, 2869, 1703, 1274, 1021 cm<sup>–1</sup>. UV-vis (CHCl<sub>3</sub>): λ<sub>max</sub> (log ε) 386.4 (0.77), 392.8 (0.80), 509.9 (0.084), 542.9 (0.27). FAB MS (*m*-nitrobenzyl alcohol matrix): *m/z* 708 (M<sup>+</sup>, 100). HRMS: calcd for C<sub>39</sub>H<sub>49</sub>N<sub>4</sub>O<sub>2</sub>Rh 708.291, found 708.297.

[Rh<sup>III</sup>(CH<sub>2</sub>CH<sub>2</sub>CH<sub>2</sub>CO<sub>2</sub>H)OEP] (**7**). Yield: 45%. <sup>1</sup>H NMR (Me<sub>2</sub>SO-*d*<sub>6</sub>, 500 MHz): δ 10.01 (s, 4H, meso), 4.06 (q, *J* = 14 Hz, *J* = 7.7 Hz, 8H, CH<sub>2</sub>CH<sub>3</sub>), 4.00 (q, *J* = 14 Hz, *J* = 7.7 Hz,

**Table 7. Intramolecular Bond Angles Involving the Non-Hydrogen Atoms of 12<sup>a</sup>**

Si(1)–Rh(1)–N(1)	92.6(9)	Rh(1)–N(4)–C(19)	127(2)
Si(1)–Rh(1)–N(2)	91.4(9)	C(16)–N(4)–C(19)	106(3)
Si(1)–Rh(1)–N(3)	93(1)	N(1)–C(1)–C(2)	110(3)
Si(1)–Rh(1)–N(4)	93.5(9)	N(1)–C(1)–C(20)	125(3)
N(1)–Rh(1)–N(2)	90(1)	C(2)–C(1)–C(20)	125(3)
N(1)–Rh(1)–N(3)	175(1)	C(1)–C(2)–C(3)	107(3)
N(1)–Rh(1)–N(4)	90(1)	C(1)–C(2)–C(21)	125(3)
N(2)–Rh(1)–N(3)	90(1)	C(3)–C(2)–C(21)	128(3)
N(2)–Rh(1)–N(4)	175(1)	C(2)–C(3)–C(4)	107(3)
N(3)–Rh(1)–N(4)	90(1)	C(2)–C(3)–C(23)	128(4)
Rh(1)–Si(1)–C(37)	110(2)	C(4)–C(3)–C(23)	124(3)
Rh(1)–Si(1)–C(39)	113(2)	N(1)–C(4)–C(3)	110(3)
Rh(1)–Si(1)–C(41)	113(3)	N(1)–C(4)–C(5)	125(3)
C(37)–Si(1)–C(39)	100(7)	C(3)–C(4)–C(5)	125(3)
C(37)–Si(1)–C(41)	109(6)	C(4)–C(5)–C(6)	127(4)
C(39)–Si(1)–C(41)	111(7)	N(2)–C(6)–C(5)	125(3)
Rh(1)–N(1)–C(1)	127(2)	N(2)–C(6)–C(7)	110(3)
Rh(1)–N(1)–C(4)	126(2)	C(5)–C(6)–C(7)	125(4)
C(1)–N(1)–C(4)	107(3)	C(6)–C(7)–C(8)	107(3)
Rh(1)–N(2)–C(6)	127(3)	C(6)–C(7)–C(25)	124(4)
Rh(1)–N(2)–C(9)	127(3)	C(8)–C(7)–C(25)	129(4)
C(6)–N(2)–C(9)	106(3)	C(7)–C(8)–C(9)	107(3)
Rh(1)–N(3)–C(11)	127(3)	C(7)–C(8)–C(27)	129(4)
Rh(1)–N(3)–C(14)	127(3)	C(9)–C(8)–C(27)	124(4)
C(11)–N(3)–C(14)	106(3)	Rh(1)–N(4)–C(16)	127(2)
N(2)–C(9)–C(8)	110(3)	C(18)–C(17)–C(33)	129(4)
N(2)–C(9)–C(10)	124(4)	C(17)–C(18)–C(19)	107(3)
C(8)–C(9)–C(10)	125(4)	C(17)–C(18)–C(35)	128(4)
C(9)–C(10)–C(11)	127(4)	C(19)–C(18)–C(35)	125(3)
N(4)–C(19)–C(18)	110(3)	C(18)–C(19)–C(20)	125(3)
N(4)–C(19)–C(20)	125(3)	C(1)–C(20)–C(19)	127(3)
N(3)–C(11)–C(10)	125(4)	C(2)–C(21)–C(22)	114(4)
N(3)–C(11)–C(12)	110(3)	C(3)–C(23)–C(24)	113(4)
C(10)–C(11)–C(12)	125(4)	C(12)–C(29)–C(30)	112(4)
C(11)–C(12)–C(13)	106(3)	C(13)–C(31)–C(32)	113(5)
C(11)–C(12)–C(29)	124(4)	Si(1)–C(37)–C(38)	115(10)
C(13)–C(12)–C(29)	129(4)	C(17)–C(33)–C(34)	113(4)
C(12)–C(13)–C(14)	107(4)	C(18)–C(35)–C(36)	113(4)
C(12)–C(13)–C(31)	129(4)	Si(1)–C(41)–C(42)	129(12)
C(14)–C(13)–C(31)	125(4)	C(16)–C(17)–C(33)	124(4)
N(3)–C(14)–C(13)	111(3)	C(7)–C(25)–C(26)	113(4)
N(3)–C(14)–C(15)	124(3)	C(8)–C(27)–C(28)	113(4)
C(13)–C(14)–C(15)	125(4)	N(4)–C(16)–C(17)	110(3)
C(14)–C(15)–C(16)	127(4)	C(15)–C(16)–C(17)	125(3)
N(4)–C(16)–C(15)	125(4)	C(16)–C(17)–C(18)	107(3)

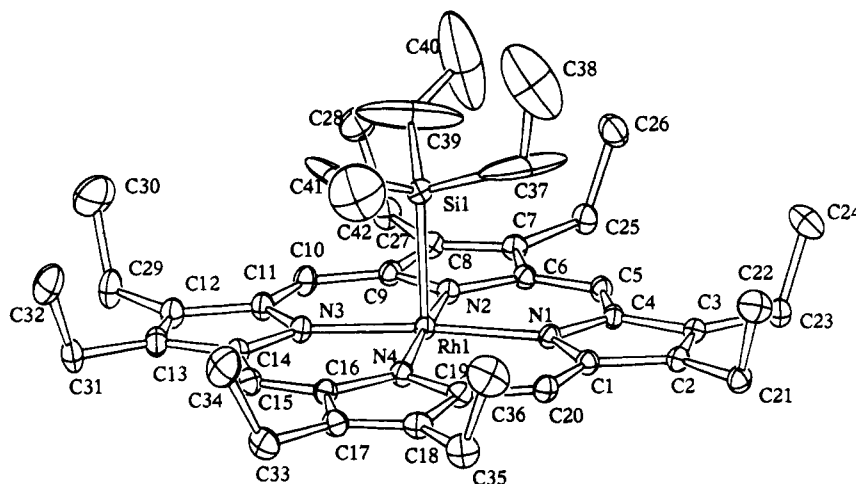
<sup>a</sup> Angles are in degrees. Estimated standard deviations in the least significant figure are given in parentheses.

8H, CH<sub>2</sub>CH<sub>3</sub>), 1.83 (t, *J* = 7.7 Hz, 24H, CH<sub>2</sub>CH<sub>3</sub>), –1.22 (t, *J* = 8.0 Hz, 2H, RhCH<sub>2</sub>CH<sub>2</sub>CH<sub>2</sub>CO<sub>2</sub>H), –4.93 (quintet, *J* = 7.8 Hz, 2H, RhCH<sub>2</sub>CH<sub>2</sub>CH<sub>2</sub>CO<sub>2</sub>H), –6.47 (td, *J* = 8.0 Hz, *J*<sub>H–Rh</sub> = 1.8 Hz, 2H, RhCH<sub>2</sub>CH<sub>2</sub>CH<sub>2</sub>CO<sub>2</sub>H). <sup>13</sup>C NMR (125 MHz, THF-*d*<sub>8</sub>): δ 172.16 (s, COOH), 142.21 (s, pyrrole α), 141.23 (s, pyrrole β), 99.09 (s, meso), 31.81 (s, α-C to carboxy), 22.10 (s, β-C to carboxy), 20.42 (s, CH<sub>2</sub>CH<sub>3</sub>), 18.95 (s, CH<sub>2</sub>CH<sub>3</sub>), 6.76 (d, *J*<sub>C–Rh</sub> = 27.9 Hz, γ-C to carboxy). IR (KBr): 3300–2500, 2962, 2929, 2868, 1706, 1274, 1019 cm<sup>–1</sup>. UV-vis (CHCl<sub>3</sub>): λ<sub>max</sub> (log ε) 385.8 (1.067), 391.8 (1.12), 509.6 (0.12), 542.6 (0.39). FAB MS (*m*-nitrobenzyl alcohol matrix): *m/z* 722 (M<sup>+</sup>, 100). HRMS: calcd for C<sub>40</sub>H<sub>51</sub>N<sub>4</sub>O<sub>2</sub>Rh 722.307, found 722.306.

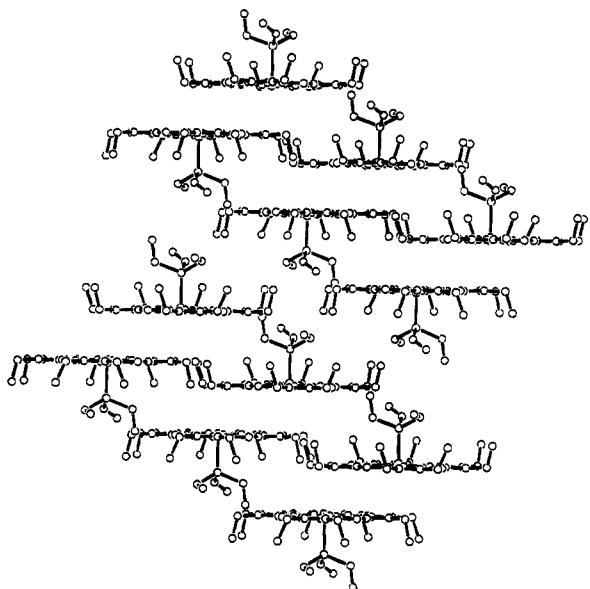
[Rh<sup>III</sup>{CH(CH<sub>3</sub>)CH<sub>2</sub>CO<sub>2</sub>H}OEP] (**6**). Yield: 68%. <sup>1</sup>H NMR (CDCl<sub>3</sub>, 500 MHz): δ 10.05 (s, 4H, meso), 3.92–4.18 (m, 16H, CH<sub>2</sub>CH<sub>3</sub>), 1.89 (t, *J* = 7.7 Hz, 24H, CH<sub>2</sub>CH<sub>3</sub>), –3.76 (dd, *J* = 14.7 Hz, *J* = 11.9 Hz, 1H, RhCH(CH<sub>3</sub>)CH<sub>2</sub>CO<sub>2</sub>H), –4.55 (dd, *J* = 14.7 Hz, *J* = 3.0 Hz, 1H, RhCH(CH<sub>3</sub>)CH<sub>2</sub>CO<sub>2</sub>H), –4.78 to –4.68 (m, 1H, RhCH(CH<sub>3</sub>)CH<sub>2</sub>CO<sub>2</sub>H), –4.94 (d, *J* = 6.1 Hz, 3H, RhCH(CH<sub>3</sub>)CH<sub>2</sub>CO<sub>2</sub>H). <sup>13</sup>C NMR (125 MHz, CDCl<sub>3</sub>): δ 170.03 (s, COOH), 141.83 (s, pyrrole α), 140.39 (s, pyrrole β), 99.25 (s, meso), 37.48 (s, α-C to carboxy), 19.76 (s, CH<sub>2</sub>CH<sub>3</sub>), 18.45 (s, CH<sub>2</sub>CH<sub>3</sub>), 18.18 (s, CH<sub>3</sub>), 17.11 (d, *J*<sub>C–Rh</sub> = 31.2 Hz, β-C to carboxy). IR (KBr): 2963, 2930, 2869, 1699, 1274, 1020 cm<sup>–1</sup>. UV-vis (benzene): λ<sub>max</sub> (log ε) 386.6 (1.23), 510.4 (0.12), 542.7 (0.37). FAB MS (*m*-nitrobenzyl alcohol matrix): *m/z*

(26) Whitlock, H. W.; Hanauer, R. *J. Org. Chem.* **1968**, *33*, 2169.

(27) Setsune, J.; Yoshida, Z.; Ogoshi, H. *J. Chem. Soc., Perkin Trans. I* **1982**, 983.



**Figure 1.** ORTEP drawing of  $\text{Rh}^{\text{III}}(\text{SiEt}_3)\text{OEP}$  showing thermal ellipsoids at the 30% probability level.



**Figure 2.** Crystal packing of  $\text{Rh}^{\text{III}}(\text{SiEt}_3)\text{OEP}$  in the direction of the *b* axis of the unit cell.

722 ( $\text{M}^+$ , 100). HRMS: calcd for  $\text{C}_{40}\text{H}_{51}\text{N}_4\text{O}_2\text{Rh}$  722.307, found 722.310.

**Reaction of  $[\text{Rh}^{\text{II}}\text{OEP}]_2$  with Triethylsilane (General Procedure).** To 53.4 mg of  $[\text{Rh}^{\text{II}}\text{OEP}]_2$  in dry degassed benzene (15 mL) was added triethylsilane (**8**; 0.66 mL, 4.1 mmol). The brown solution turned orange-red. The mixture was stirred at room temperature under Ar for 12 h. After the solvent was removed under reduced pressure, the residue was purified by column chromatography on silica gel (benzene:hexane = 1:2) to yield  $\text{Et}_3\text{SiRh}^{\text{III}}\text{OEP}$ ; yield 33.8 mg (54% based on  $[\text{Rh}^{\text{II}}\text{OEP}]_2$ ). The product was further purified by recrystallization from  $\text{CHCl}_3$ -hexane.

**$\text{Rh}^{\text{III}}(\text{SiEt}_3)\text{OEP}$  (**12**).** Yield: 54%. TLC:  $R_f$  0.46 ( $\text{SiO}_2$ , benzene:hexane = 1:5).  $^1\text{H}$  NMR ( $\text{CDCl}_3$ , 500 MHz):  $\delta$  9.93 (s, 4H, meso), 3.99 (q,  $J = 7.6$  Hz, 16H,  $\text{CH}_2\text{CH}_3$ ), 1.87 (t,  $J = 7.6$  Hz, 24H,  $\text{CH}_2\text{CH}_3$ ), -1.59 (t,  $J = 8.0$  Hz, 9H,  $\text{SiCH}_2\text{CH}_3$ ), -3.80 (q,  $J = 7.9$  Hz, 6H,  $\text{SiCH}_2\text{CH}_3$ ).  $^{13}\text{C}$  NMR (125 MHz,  $\text{C}_6\text{D}_6$ ):  $\delta$  141.63 (s, pyrrole  $\alpha$ -C), 141.32 (s, pyrrole  $\beta$ -C), 100.06 (s, porphyrin meso), 20.27 (s,  $\text{CH}_2\text{CH}_3$ ), 18.71 (s,  $\text{CH}_2\text{CH}_3$ ), 5.52 (s,  $\text{SiCH}_2\text{CH}_3$ ), 2.83 (s,  $\text{SiCH}_2\text{CH}_3$ ).  $^{29}\text{Si}$  NMR ( $\text{CDCl}_3$ , 100 MHz):  $\delta$  51.98 (d,  $J_{\text{Si-Rh}} = 29.3$  Hz). IR (KBr): 2962, 2928, 2867, 1449, 1377, 1273, 1017, 994, 956, 845, 693  $\text{cm}^{-1}$ . UV-vis (benzene):  $\lambda_{\text{max}}$  (log  $\epsilon$ ) 393.4 (1.30), 509.6 (0.091), 542.2 (0.353). FAB MS (*m*-nitrobenzyl alcohol matrix):  $m/z$  750 ( $\text{M}^+$ , 100). HRMS: calcd for  $\text{C}_{42}\text{H}_{59}\text{N}_4\text{SiRh}$  750.356, found 750.360.

**$\text{Rh}^{\text{III}}(\text{SiPh}_3)\text{OEP}$  (**13**).** Yield: 65%. TLC:  $R_f$  0.30 ( $\text{SiO}_2$ , benzene:hexane = 1:3).  $^1\text{H}$  NMR ( $\text{CDCl}_3$ , 500 MHz):  $\delta$  9.73 (s, 4H, meso), 6.69 (tt,  $J = 7.3$  Hz,  $J = 1.2$  Hz, 3H, 4'-H of Ph), 6.34 (dd,  $J = 7.3$  Hz,  $J = 7.9$  Hz, 6H, 3'-H of Ph), 4.13 (dd,  $J = 7.9$  Hz,  $J = 1.2$  Hz, 6H, 2'-H of Ph), 3.82-3.95 (m, 16H,  $\text{CH}_2\text{CH}_3$ ), 1.85 (t,  $J = 7.9$  Hz, 24H,  $\text{CH}_2\text{CH}_3$ ).  $^{29}\text{Si}$  NMR ( $\text{CDCl}_3$ , 100 MHz):  $\delta$  11.56 (d,  $J_{\text{Si-Rh}} = 35.7$  Hz). IR (KBr): 3075, 3045, 2961, 2928, 2867, 1448, 1274, 1059, 1021, 962, 698, 567  $\text{cm}^{-1}$ . UV-vis ( $\text{CHCl}_3$ ):  $\lambda_{\text{max}}$  (log  $\epsilon$ ) 544.2 (0.23), 508.8 (0.06), 393.3 (0.38), 380.5 (0.56). FAB MS (*m*-nitrobenzyl alcohol matrix):  $m/z$  894 ( $\text{M}^+$ , 100). HRMS: calcd for  $\text{C}_{54}\text{H}_{59}\text{N}_4\text{SiRh}$  894.356, found 894.360.

**$\text{Rh}^{\text{III}}(\text{SiPhMe}_2)\text{OEP}$  (**14**).** Yield: 44%. TLC:  $R_f$  0.29 ( $\text{SiO}_2$ , benzene:hexane = 1:5).  $^1\text{H}$  NMR ( $\text{C}_6\text{D}_6$ , 500 MHz, chemical shift relative to  $\text{C}_6\text{H}_6$  7.20 ppm):  $\delta$  10.0 (s, 4H, meso), 6.71 (t,  $J = 7.3$  Hz, 1H, 4'-H of Ph), 6.39 (dd,  $J = 7.3$  Hz,  $J = 7.9$  Hz, 2H, 3'-H of Ph), 4.21 (d,  $J = 8.0$  Hz, 2H, 2'-H of Ph), 3.6-3.96 (m, 16H,  $\text{CH}_2\text{CH}_3$ ), 1.90 (t,  $J = 7.9$  Hz, 24H,  $\text{CH}_2\text{CH}_3$ ), -3.61 (s, 6H,  $\text{SiCH}_3$ ).  $^{29}\text{Si}$  NMR ( $\text{CDCl}_3$ , 100 MHz):  $\delta$  28.30 (d,  $J_{\text{Si-Rh}} = 30.2$  Hz). IR (KBr): 3046, 2961, 2927, 2866, 1458, 1379, 1273, 1233, 1018, 959, 808  $\text{cm}^{-1}$ . UV-vis (benzene):  $\lambda_{\text{max}}$  (log  $\epsilon$ ) 541.8 (0.42), 508.8 (0.11), 394.2 (1.34). FAB MS (*m*-nitrobenzyl alcohol matrix):  $m/z$  770 ( $\text{M}^+$ , 100). HRMS: calcd for  $\text{C}_{44}\text{H}_{55}\text{N}_4\text{SiRh}$  770.325, found 770.329.

**$\text{Rh}^{\text{III}}(\text{SiOEtMe}_2)\text{OEP}$  (**15**).** Yield: 42%. TLC:  $R_f$  0.15 ( $\text{SiO}_2$ , benzene:hexane = 1:2).  $^1\text{H}$  NMR ( $\text{CDCl}_3$ , 500 MHz):  $\delta$  9.90 (s, 4H, meso), 3.90-3.98 (m, 16H,  $\text{CH}_2\text{CH}_3$ ), 1.81 (t,  $J = 7.7$  Hz, 24H,  $\text{CH}_2\text{CH}_3$ ), -0.14 (q,  $J = 7.0$  Hz, 2H,  $\text{SiOCH}_2\text{CH}_3$ ), -0.43 (t,  $J = 7.0$  Hz, 3H,  $\text{SiOCH}_2\text{CH}_3$ ), -4.17 (s, 6H,  $\text{SiCH}_3$ ).  $^{29}\text{Si}$  NMR ( $\text{CDCl}_3$ , 100 MHz):  $\delta$  37.24 (d,  $J_{\text{Si-Rh}} = 30.5$  Hz). IR (KBr): 2961, 2926, 2865, 1453, 1377, 1265, 1234, 1107, 1058, 1018, 957, 845, 811  $\text{cm}^{-1}$ . UV-vis ( $\text{CHCl}_3$ ):  $\lambda_{\text{max}}$  (log  $\epsilon$ ) 541.4 (0.25), 509.3 (0.07), 391.0 (1.06). FAB MS (*m*-nitrobenzyl alcohol matrix):  $m/z$  738 ( $\text{M}^+$ , 100). HRMS: calcd for  $\text{C}_{40}\text{H}_{55}\text{N}_4\text{OSiRh}$  738.320, found 738.313.

**$\text{Rh}^{\text{III}}(\text{SnBu}_3)\text{OEP}$  (**18**).** To a solution of  $[\text{Rh}^{\text{II}}\text{OEP}]_2$  (26.4 mg, 121  $\mu\text{mol}$ ) in degassed benzene (6 mL) was added tributyltin hydride (0.12 mL, 446  $\mu\text{mol}$ ) under Ar. After the mixture was stirred for 21 h at room temperature, the benzene was distilled off and the residue was purified by a short column of silica gel (benzene:hexane = 1:2) to give **18** (18.8 mg, 49%). TLC:  $R_f$  0.60 ( $\text{SiO}_2$ , benzene:hexane = 1:3).  $^1\text{H}$  NMR ( $\text{C}_6\text{D}_6$ , 500 MHz, chemical shift relative to  $\text{C}_6\text{H}_6$  7.20 ppm):  $\delta$  10.07 (s, 4H, meso), 3.94 (q,  $J = 7.7$  Hz, 16H,  $\text{CH}_2\text{CH}_3$ ), 1.93 (t,  $J = 7.7$  Hz, 24H,  $\text{CH}_2\text{CH}_3$ ), 0.48-0.52 (br s, 9H,  $\text{SnCH}_2\text{CH}_2\text{CH}_2\text{CH}_3$ ), 0.46 to -0.50 (m, 6H,  $\text{SnCH}_2\text{CH}_2\text{CH}_2\text{CH}_3$ ), -0.76 to -0.60 (m, 6H,  $\text{SnCH}_2\text{CH}_2\text{CH}_2\text{CH}_3$ ), -2.54 to -2.38 (m, 6H,  $\text{SnCH}_2\text{CH}_2\text{CH}_2\text{CH}_3$ ).  $^{13}\text{C}$  NMR (125 MHz,  $\text{C}_6\text{D}_6$ , chemical shift relative to  $\text{C}_6\text{D}_6$  128 ppm):  $\delta$  141.63 (s, pyrrole  $\alpha$ -C), 141.56 (s, pyrrole  $\beta$ -C), 99.92 (s, porphyrin meso), 27.14 (s,  $\text{SnCH}_2\text{CH}_2\text{CH}_2\text{CH}_3$ ), 26.92 (s,  $\text{SnCH}_2\text{CH}_2\text{CH}_2\text{CH}_3$ ), 20.00 (s,  $\text{CH}_2\text{CH}_3$ ),

18.66 (s, CH<sub>2</sub>CH<sub>3</sub>), 13.35 (s, SnCH<sub>2</sub>CH<sub>2</sub>CH<sub>2</sub>CH<sub>3</sub>), 7.47 (s, SnCH<sub>2</sub>CH<sub>2</sub>CH<sub>2</sub>CH<sub>3</sub>). <sup>119</sup>Sn NMR (CDCl<sub>3</sub>, 186 MHz): δ 118.32 (d, *J*<sub>Sn-Rh</sub> = 314.2 Hz). IR (KBr): 2959, 2926, 2866, 1448, 1375, 1272, 1144, 1110, 1058, 1019, 993, 958, 843 cm<sup>-1</sup>. UV-vis (benzene): λ<sub>max</sub> (log ε) 381.4 (0.86), 298.7 (0.48), 509.1 (0.083), 541.1 (0.28). FAB MS (*m*-nitrobenzyl alcohol matrix): *m/z* 925 (M<sup>+</sup>, 100). HRMS: calcd for C<sub>48</sub>H<sub>71</sub>N<sub>4</sub>RhSn 926.376, found 926.378.

**Rh<sup>III</sup>(SnPh<sub>3</sub>)OEP (19).** Yield: 44%. TLC *R<sub>f</sub>* 0.57 (SiO<sub>2</sub>, benzene:hexane = 1:2). <sup>1</sup>H NMR (C<sub>6</sub>D<sub>6</sub>, 500 MHz, chemical shift relative to C<sub>6</sub>H<sub>6</sub> 7.20 ppm): δ 9.94 (s, 4H, meso), 6.77 (tt, *J* = 7.3 Hz, 1.2 Hz, 3H, 4'-H of Ph), 6.55 (dd, *J* = 7.3 Hz, 7.4 Hz, 6H, 3'-H of Ph), 4.93 (dd, *J* = 7.4 Hz, 1.2 Hz, 6H, 2'-H of Ph), 3.80–3.93 (m, 16H, CH<sub>2</sub>CH<sub>3</sub>), 1.88 (t, *J* = 7.6 Hz, 24H, CH<sub>2</sub>CH<sub>3</sub>). <sup>119</sup>Sn NMR (CDCl<sub>3</sub>, 186 MHz): δ -121.57 (d, *J*<sub>Sn-Rh</sub> = 412.9 Hz). IR (KBr): 3059, 3046, 2964, 2929, 2866, 1447, 1376, 1273, 1145, 1059, 1021, 996, 962, 845, 727, 698 cm<sup>-1</sup>. UV-vis (benzene): λ<sub>max</sub> (log ε) 386.6 (1.09), 510.2 (0.073), 543.4 (0.27). FAB MS (*m*-nitrobenzyl alcohol matrix): *m/z* 986 (M<sup>+</sup>, 100). HRMS: calcd for C<sub>54</sub>H<sub>59</sub>N<sub>4</sub>RhSn 986.282, found 986.290.

**X-ray Structure Determination of Rh<sup>III</sup>(SiEt<sub>3</sub>)OEP.** Purple crystals of Rh<sup>III</sup>(SiEt<sub>3</sub>)OEP were obtained by recrystallization from CHCl<sub>3</sub>-hexane. Details of the crystal data, data collection, and data refinement are listed in Table 4. The structure was solved by direct methods<sup>28</sup> and expanded using Fourier techniques.<sup>29</sup>

**Acknowledgment.** We thank Dr. T. Kondo of the Division of Energy and Hydrocarbon Chemistry and H. Takagi for help in the X-ray crystallographic study and T. Kobatake for the measurements of mass spectra. We thank Anthony English of the Massachusetts Institute of Technology for proofreading the manuscript. This work was supported by a Grant-in-Aid for Specially Promoted Research (No. 04101003) from the Ministry of Education, Science, and Culture of Japan.

**Supplementary Material Available:** Tables of all bond distances and angles, anisotropic thermal parameters, torsion or conformation angles, and least-squares planes for **12** (17 pages). Ordering information is given on any current masthead page.

OM940427C

(28) Sheldrick, G. M. SHELXS86. In *Crystallographic Computing 3*; Sheldrick, G. M., Kruger, C., Goddard, R., Eds.; Oxford University Press: Oxford, U.K., 1985; pp 175–189.

(29) DIRDIF92: Beurskens, P. T.; Admiraal, G.; Beurskens, G.; Bosman, W. P.; Garcia-Granda, S.; Gould, R. O.; Smits, J. M. M.; Smykalla, C. Technical Report of the Crystallography Laboratory; University of Nijmegen, Nijmegen, The Netherlands, 1992.

# Dimethylsilyl and Ethylsilyl Cations: A Detailed Study of the $\text{SiC}_2\text{H}_7^+$ Potential Energy Surface

A. E. Ketvirtis, D. K. Bohme, and A. C. Hopkinson\*

Department of Chemistry, York University, Downsview, Ontario, Canada M3J 1P3

Received June 17, 1994<sup>®</sup>

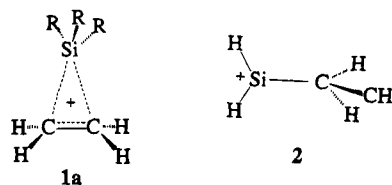
*Ab initio* molecular orbital calculations on stable isomers and on transition structures associated with the  $\text{SiC}_2\text{H}_7^+$  potential energy hypersurface are presented. All critical points below the energies of dissociation into  $\text{SiH}^+$  + ethane and into  $\text{SiH}_3^+$  + ethylene have been obtained by gradient optimizations with the split valence-shell basis set 6-31G(d,p), both at the SCF level of theory and with inclusion of electron correlation energy to second-order Møller–Plesset (MP2) perturbation theory. The dimethylsilyl cation, which was found to be at the global minimum on the surface at both levels of theory, was optimized subsequently at MP2/6-311G(d,p). All structures at critical points on the surfaces at both levels of theory were characterized by harmonic frequency calculations, from which zero-point vibrational energies also were obtained. Vibrational frequencies of the dimethylsilyl cation and of the next lowest energy isomer,  $\text{H}_3\text{CH}_2\text{CSiH}_2^+$ , obtained at MP2/6-31G(d,p), also are reported. Isomers of  $\text{SiC}_2\text{H}_7^+$  which contain fewer Si–H bonds tend to be lower in energy. The inclusion of electron correlation with the same basis set reduces the number of minima on the surface from 5 to 4 and reduces all of the barriers to interconversion between all stable isomers with the exception of that between the two lowest isomers. The latter value increases from 26.6 to 41.9 kcal mol<sup>-1</sup>. This topological feature has permitted the proposal of detailed mechanisms to rationalize hydrogen–deuterium exchange reactions observed elsewhere in the gas phase.

The chemistry of organosilicon compounds has been of considerable interest, both computationally and experimentally, for many years.<sup>1,2</sup> The circumstellar envelope of the carbon star IRC + 10216 has been found to contain molecules such as SiC,  $\text{SiC}_2$ , and  $\text{SiC}_4$ .<sup>3</sup> To date, no organosilicon species which include hydrogen have been detected; however, due to the relative abundance of hydrogen in the universe, it is probable that such species exist. Over the last decade, a vast literature has accumulated on the chemistry of organosilicon compounds. During this time, both theoretical and experimental techniques have improved enormously and both have made large contributions to our understanding of the structure and chemistry of small organosilicon compounds. Recent computational studies have been performed on cations of the formulas  $\text{SiC}_2\text{H}_n^+$  ( $n = 2, 4^4$  and  $n = 1, 3, 5^5$ ) in connection with previous gas-phase experimental research involving these ions in the SIFT (selected ion flow tube) apparatus.<sup>6</sup> These com-

putational studies have provided detailed information about thermodynamic stabilities of isomers of a given formula, about barriers to the interconversion of these isomers, and about the geometries of stable ions and of the transition structures to their interconversion.

The  $\text{SiC}_2\text{H}_7^+$  energy surface is of particular interest as it is the smallest cation in which it is possible to study the effects of both  $\alpha$ - and  $\beta$ -silyl substituents in saturated carbocations. It also permits comparison of the relative stabilities of isomeric alkyl and silyl cations.<sup>7</sup>

In early high-pressure and tandem mass spectrometric studies on the reaction of  $\text{SiH}_3^+$  with ethylene, Lampe and co-workers noted a “persistent-sticky complex”,  $\text{SiC}_2\text{H}_7^+$ , which added a further two ethylene molecules.<sup>8</sup> From this reactivity they concluded that the initial  $\pi$ -adduct, **1a** ( $R = \text{H}$ ), rearranged to the ethylsilyl cation **2** and that addition of further ethylene molecules occurred by insertion into the Si–H bonds of **2**, terminating in the triethylsilyl cation,  $\text{Si}(\text{C}_2\text{H}_5)_3^+$ .



Much of the subsequent gas-phase work has involved the experimentally more convenient  $\text{Si}(\text{CH}_3)_3$  group. The adduct formed from the addition of  $\text{Si}(\text{CH}_3)_3^+$  to  $\text{H}_2\text{C}=\text{CH}_2$  loses ethylene in bimolecular displacement reactions,<sup>9</sup> and high-energy collisional activation experi-

<sup>®</sup> Abstract published in *Advance ACS Abstracts*, November 15, 1994.

(1) (a) Grev, R. S.; Schaefer, H. F., III. *J. Chem. Phys.* **1984**, *80*, 3552. (b) Sadlej, A. J.; Diercksen, G. H. F.; Oddershede, J.; Sabin, J. R. *Chem. Phys.* **1988**, *122*, 297. (c) Martin, J. M. L.; François, J. P.; Gijbels, R. *J. Chem. Phys.* **1990**, *92*, 6655. (d) Langhoff, S. R.; Bauschlicher, C. W., Jr. *J. Chem. Phys.* **1990**, *93*, 42.

(2) (a) Sanford, R. F. *Astrophys. J.* **1950**, *111*, 362. (b) Kleman, B. *Astrophys. J.* **1956**, *123*, 162.

(3) (a) Cernicharo, J.; Gottlieb, C. A.; Guelin, M.; Thaddeus, P.; Vrtilek, J. M. *Astrophys. J.* **1989**, *341*, L25. (b) Thaddeus, P.; Cummins, S. E.; Linke, R. A. *Astrophys. J.* **1984**, *283*, L45. (c) Ohishi, M.; Kaifu, N.; Kawaguchi, K.; Murakami, A.; Saito, S.; Yamamoto, S.; Ishikawa, S.; Fujita, Y.; Shiratori, Y.; Irvine, W. M. *Astrophys. J.* **1989**, *345*, L83.

(4) Ketvirtis, A. E.; Bohme, D. K.; Hopkinson, A. C. *J. Mol. Struct. THEOCHEM* **1994**, *313*, 1.

(5) Ketvirtis, A. E.; Bohme, D. K.; Hopkinson, A. C. *J. Phys. Chem.*, in press.

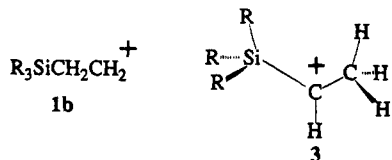
(6) Wlodek, S.; Fox, A.; Bohme, D. K. *J. Am. Chem. Soc.* **1991**, *113*, 4461.

(7) Hopkinson, A. C.; Lien, M. H. *J. Org. Chem.* **1981**, *46*, 998.

(8) (a) Mayer, T. M.; Lampe, F. W. *J. Phys. Chem.* **1974**, *78*, 2433.

(b) Allen, W. N.; Lampe, F. W. *J. Am. Chem. Soc.* **1977**, *99*, 6816.

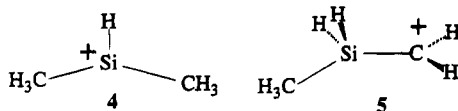
ments on the  $(\text{CH}_3)_3\text{SiC}_2\text{H}_4^+$  ion, derived from  $(\text{CH}_3)_3\text{SiCH}_2\text{CH}_2\text{OC}_6\text{H}_5$ , have shown the two  $\text{CH}_2$  groups to be equivalent.<sup>10</sup> Protonation of trimethylvinylsilane,  $(\text{CH}_3)_3\text{SiCH}=\text{CH}_2$ , produces an ion that has behavior identical to that of the adduct formed from  $\text{Si}(\text{CH}_3)_3^+$  plus  $\text{H}_2\text{C}=\text{CH}_2$ , leading to the conclusion that protonation occurs on the carbon adjacent to silicon, formally generating a  $\beta$ -silyl substituted primary carbocation, **1b** ( $\text{R} = \text{CH}_3$ ).<sup>11</sup> Protonation on the terminal carbon atom



of trimethylvinylsilane, which would produce the  $\alpha$ -silyl substituted ethyl cation, **3**, does not occur. The proton affinity of trimethylvinylsilane,  $(199 \pm 2) \text{ kcal mol}^{-1}$ , is much higher than that of ethylene ( $162.6 \text{ kcal mol}^{-1}$ ) and is similar to those of styrene and of tetramethylethylene, both molecules containing groups which are strongly stabilizing in carbocations.<sup>12</sup>

*Ab initio* molecular orbital calculations on isomers of  $\text{SiC}_2\text{H}_7^+$  have shown the cyclic structure **1a** to be preferred over **1b**, and the  $\beta$ -silyl group has been shown to stabilize the ethyl cation by  $\sim 38 \text{ kcal mol}^{-1}$ .<sup>13</sup> For  $\text{R} = \text{H}$ , MP2/6-31G(d)//HF/3-21G calculations have shown **1a** to be only  $5.5 \text{ kcal mol}^{-1}$  above **2** and **1b** to be not at a minimum.<sup>14a</sup> Structure **3** is considerably higher in energy than **2** (by  $31.0 \text{ kcal mol}^{-1}$ ) and also may not be at a minimum.<sup>14</sup>

As in carbocation chemistry, secondary silyl cations are usually more stable than primary ions, and therefore, ion **4** would be expected to be at the global



minimum on the  $\text{SiC}_2\text{H}_7^+$  potential energy surface. Gas-phase  $^{13}\text{C}$  labeling studies have shown  $\text{Si}(\text{CH}_3)_3^+$  to isomerize to  $\text{Si}(\text{C}_2\text{H}_5)(\text{CH}_3)\text{H}^+$  prior to the loss of ethylene, and a similar reaction is believed to occur between  $\text{Si}(\text{CH}_3)_2\text{H}^+$ , ion **4**, and  $\text{Si}(\text{C}_2\text{H}_5)\text{H}_2^+$ , ion **2**.<sup>15b,c</sup> This rearrangement requires either the intermediacy of the primary carbocation **5**, formed by a 1,2-hydride shift from  $\text{CH}_3$  (in **4**) to  $\text{Si}^+$ , or the simultaneous (dyotropic) migration of H and  $\text{CH}_3$  through transition structure **6**.

(9) (a) Wojtyniak, A. C. M.; Stone, J. A. *Int. J. Mass Spec. Ion Proc.* **1986**, *74*, 59. (b) Li, Y.; Stone, J. A. *J. Am. Chem. Soc.* **1989**, *111*, 5586.

(10) Ciommer, B.; Schwarz, H. *J. Organomet. Chem.* **1983**, *244*, 319.

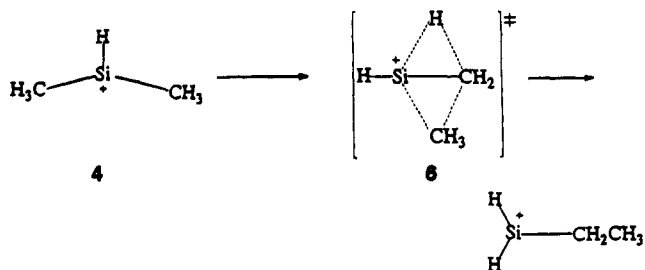
(11) Hajdasz, D.; Squires, R. *J. Chem. Soc., Chem. Commun.* **1988**, 1212.

(12) Eaborn, C.; Feichtmayr, F.; Horn, M.; Murrell, J. N. *J. Organomet. Chem.* **1974**, *77*, 39.

(13) Wierschke, S. G.; Chandrasekhar, J.; Jorgensen, W. L. *J. Am. Chem. Soc.* **1985**, *107*, 1496.

(14) (a) Apeloig, Y.; Karni, M.; Stanger, A.; Schwarz, H.; Drewello, T.; Czekay, G. *J. Chem. Soc., Chem. Commun.* **1987**, 989. (b) Drewello, T.; Burgers, P. C.; Zummack, W.; Apeloig, Y.; Schwarz, H. *Organometallics* **1990**, *9*, 1161.

(15) (a) Reuter, K. A.; Jacobson, D. B. *Organometallics* **1989**, *8*, 1126. (b) Bakhtiar, R.; Holznagel, C. M.; Jacobson, D. B. *J. Am. Chem. Soc.* **1992**, *114*, 3227. (c) Bakhtiar, R.; Holznagel, C. M.; Jacobson, D. B. *Organometallics* **1993**, *12*, 621. (d) Bakhtiar, R.; Holznagel, C. M.; Jacobson, D. B. *Organometallics* **1993**, *12*, 880.



There has been no reported *ab initio* molecular orbital study of **4** or of the transition structures for the interconversion of ions **1**–**5**. Here we report an *ab initio* study of the  $\text{SiC}_2\text{H}_7^+$  potential energy surface using structure optimization both at SCF and at MP2 levels of theory.

## Computational Methods

*Ab initio* molecular orbital calculations were performed using the GAUSSIAN suite of programs.<sup>16</sup> All structures were optimized at both the SCF/6-31G(d,p)<sup>17</sup> and MP2(full)/6-31G(d,p)<sup>17,18</sup> levels of theory using gradient techniques.<sup>19</sup> The structure which was found to exist at the global minimum on the MP2 surface was optimized subsequently at the MP2(full)/6-311G(d,p)<sup>17e,20</sup> level of theory. Transition structures were obtained either with the eigenvector-following (EF)<sup>21</sup> method or the CALCALL<sup>16</sup> algorithm. All critical points were characterized by harmonic frequency calculations both at SCF/6-31G(d,p) and at MP2(full)/6-31G(d,p), and the intrinsic reaction coordinate (IRC) method was used to establish which two minima were associated with each transition structure.<sup>22</sup> For all critical points on the MP2 surface other than that at the global minimum, single-point calculations at the MP2(full)/6-311G(d,p) level of theory were performed. Bond lengths and bond angles which involve heavy (non-hydrogen) atoms, as well as those which involve migrating hydrogen atoms, are reported.

(16) (a) Frisch, M. J.; Trucks, G. W.; Head-Gordon, M.; Gill, P. M. W.; Foresman, J. B.; Johnson, B. G.; Schlegel, H. B.; Robb, M. A.; Replogle, E. S.; Gomperts, R.; Andres, J. L.; Raghavachari, K.; Binkley, J. S.; Gonzalez, C.; Martin, R. L.; Fox, D. J.; DeFrees, D. J.; Baker, J.; Stewart, J. J. P.; Pople, J. A. GAUSSIAN 92, Revision C.4, Gaussian, Inc. Pittsburgh, PA, 1992. (b) Frisch, M. J.; Head-Gordon, M.; Trucks, G. W.; Foresman, J. B.; Schlegel, H. B.; Raghavachari, K.; Robb, M.; Binkley, J. S.; Gonzalez, C.; DeFrees, D. J.; Fox, D. J.; Whiteside, R. A.; Seeger, R.; Melius, C. F.; Baker, J.; Martin, R. L.; Kahn, L. R.; Stewart, J. J. P.; Topiol, S.; Pople, J. A. GAUSSIAN 90, Revision J, Gaussian, Inc., Pittsburgh, PA, 1990. (c) Frisch, M. J.; Binkley, J. S.; Schlegel, H. B.; Raghavachari, K.; Melius, C. F.; Martin, R. L.; Stewart, J. J. P.; Bobrowicz, F. W.; Rohlfing, C. M.; Kahn, L. R.; DeFrees, D. J.; Seeger, R.; Whiteside, R. A.; Fox, D. J.; Fleuder, E. M.; Pople, J. A. GAUSSIAN 86, Carnegie-Mellon Quantum Chemistry Publishing Unit, Carnegie-Mellon University, Pittsburgh, PA, 1984.

(17) (a) Hehre, W. J.; Ditchfield, R.; Pople, J. A. *J. Chem. Phys.* **1972**, *56*, 2257. (b) Hariharan, P. C.; Pople, J. A. *Theor. Chim. Acta* **1973**, *72*, 6250. (c) Gordon, M. S. *Chem. Phys. Lett.* **1980**, *76*, 163. (d) Francl, M. M.; Pietro, W. J.; Hehre, W. J.; Binkley, J. S.; Gordon, M. S.; DeFrees, D. J.; Pople, J. A. *J. Chem. Phys.* **1982**, *77*, 3654. (e) Frisch, M. J.; Pople, J. A.; Binkley, J. S. *J. Chem. Phys.* **1984**, *80*, 3265.

(18) (a) Møller, C.; Plesset, M. S. *Phys. Rev.* **1934**, *46*, 618. (b) Binkley, J. S.; Pople, J. A. *Int. J. Quant. Chem.* **1975**, *9*, 229.

(19) Schlegel, H. B. *J. Comp. Chem.* **1982**, *3*, 214.

(20) (a) Krishnan, R.; Binkley, J. S.; Seeger, R.; Pople, J. A. *J. Chem. Phys.* **1980**, *72*, 650. (b) McLean, A. D.; Chandler, G. S. *J. Chem. Phys.* **1980**, *72*, 5639.

(21) (a) Baker, J. *J. Comp. Chem.* **1986**, *7*, 385. (b) Baker, J. *J. Comp. Chem.* **1987**, *8*, 563. (c) Simons, J.; Jorgensen, P.; Taylor, H.; Ozment, J. *J. Phys. Chem.* **1983**, *87*, 2745. (d) Cerjan, C. J.; Miller, W. H. *J. Chem. Phys.* **1981**, *75*, 2800. (e) Bannerjee, A.; Adams, N.; Simons, J.; Shepard, R. *J. Phys. Chem.* **1985**, *89*, 52.

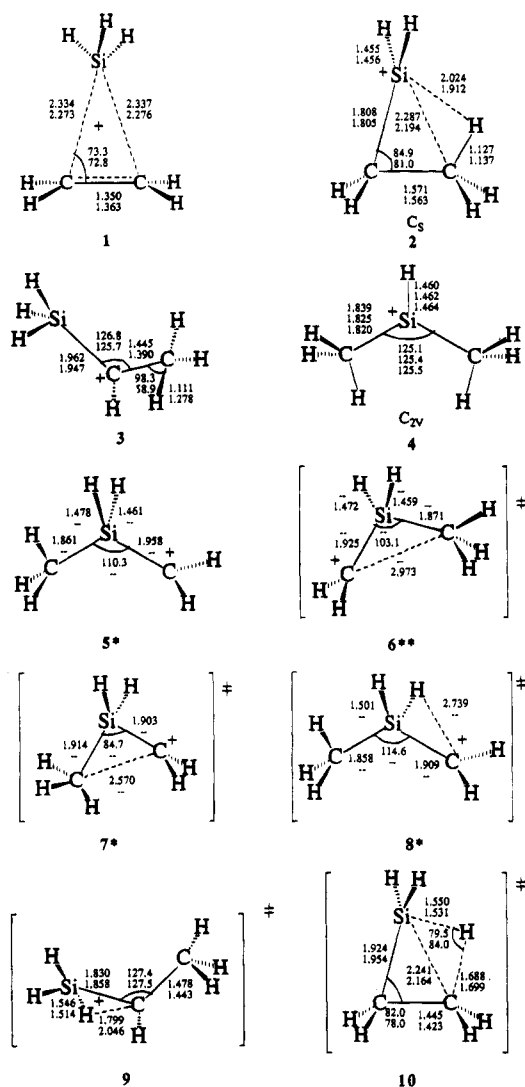
(22) Gonzalez, C.; Schlegel, H. B. *J. Chem. Phys.* **1989**, *90*, 2154.

(23) Krishnan, R.; Frisch, M. J.; Pople, J. A. *J. Chem. Phys.* **1980**, *72*, 4244.

Table 1. Total Energies (hartrees) for SiC<sub>2</sub>H<sub>7</sub><sup>+</sup> Isomers and Transition Structures<sup>a</sup>

ion	RHF/6-31G(d,p)	ZPE <sup>b</sup>	MP2(full)/6-31G(d,p)	ZPE <sup>c</sup>	MP2(full)/6-311G(d,p)
1	-368.439 43 (+23.2)	47.0	-368.828 09 (+26.5)	49.1	-369.020 07 (+26.5)
2	-368.445 01 (+20.6)	47.9	-368.840 00 (+17.8)	49.3	-369.034 23 (+17.8)
3	-368.415 30 (+36.5)	45.2	-368.793 76 (+45.1)	46.2	-368.986 77 (+44.5) <sup>e</sup>
4	-368.477 46 (0)	47.7	-368.869 50 (0)	48.6	-369.061 52 <sup>d</sup> (0)
5	-368.402 36 (+45.0)	45.6			
6			-368.768 74 (+61.1)	46.5	-368.960 30 (+61.4)
7	-368.399 43 (+47.2)	45.9			
8	-368.401 94 (+45.1)	45.4			
9	-368.404 47 (+43.5)	45.4	-368.784 55 (+50.3)	45.6	-368.977 79 (+49.5)
10	-368.415 59 (+37.8)	46.7	-368.809 31 (+36.7)	47.5	-369.003 55 (+35.3) <sup>e</sup>
SiH <sup>+</sup> + C <sub>2</sub> H <sub>6</sub>	-368.372 83 (+61.8)	43.8	-368.751 37 (+69.7)	44.2	-368.947 05 <sup>d</sup> (+67.4)
SiH <sub>3</sub> <sup>+</sup> + C <sub>2</sub> H <sub>4</sub>	-368.376 41 (+62.9)	47.2	-368.758 20 (+69.5)	48.3	-368.949 96 <sup>d</sup> (+69.7)

<sup>a</sup> Relative energies in kcal mol<sup>-1</sup> using scaled zero-point energies from SCF level calculations, except where zero-point energy has been obtained from MP2 level calculations, are listed in parentheses. <sup>b</sup> Zero-point energy from RHF/6-31G(d,p) in kcal mol<sup>-1</sup>, scaled by a factor of 0.89,<sup>28</sup> except where specified otherwise. <sup>c</sup> Zero-point energy from MP2(full)/6-31G(d,p) in kcal mol<sup>-1</sup>, scaled by a factor of 0.93.<sup>29</sup> <sup>d</sup> Optimized at MP2(full)/6-311G(d,p). <sup>e</sup> At MP2(fc)/6-311G(2df,2p) total energies (hartrees) are -368.886 46 for **3** and -368.877 62 for **10**.



\* Structures 5, 7, and 8 do not exist at the MP2 level of theory.

\*\* Structure 6 does not exist at the SCF level of theory.

**Figure 1.** Optimized structural parameters. Bond lengths are in angstroms, and bond angles are in degrees. Upper values are at SCF/6-31G(d,p), and lower values are at MP2-(full)/6-31G(d,p). Structures **5**, **7**, and **8** do not exist at the MP2 level of theory. Structure **6** does not exist at the SCF level of theory.

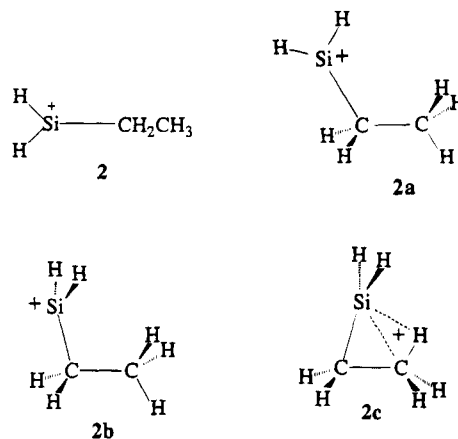
## Results and Discussion

**Details of the SiC<sub>2</sub>H<sub>7</sub><sup>+</sup> Potential Energy Surface.** Structural details for the ions 1–10 are given in Figure

1. On the SCF potential energy surface, ions 1–5 all are at minima, although the barriers to the rearrangements of the two highest energy isomers, **3** and **5**, are low (see Figure 2). We were, however, unable to locate a stable geometric analogue for structure **5** when electron correlation was included in the calculation.

Structure **4**, the dimethylsilyl cation, has been found to be at the global minimum on both the SCF and the MP2 surfaces. This result is consistent with the trend observed for other SiC<sub>2</sub>H<sub>n</sub><sup>+</sup> surfaces (Table 1) in which isomers which contain as many hydrogen atoms bonded to carbon (rather than to silicon) as possible tend to be more stable than are other isomers.<sup>4,5</sup>

It should be noted that there are three different conformational isomers associated with the skeletal structure depicted by ion **2** on the SCF surface.



Each of these rotamers exists at a local minimum at SCF/6-31G(d,p) and, in order of increasing energy, they are ranked **2a** < **2b** < **2c**. However, **2a**, **2b**, and **2c** are only 2.1 kcal mol<sup>-1</sup> apart in energy at this level of theory and there are negligible barriers to their interconversion. At MP2/6-31G(d,p), **2b** collapses into **2c** without a barrier, and the latter is 2.6 kcal mol<sup>-1</sup> more stable than **2a**. It should be noted as well that the Si–C–C bond angle in **2c** at MP2 is 81.0°; that of **2a** is 116.5°; thus, the reversal of stabilities of **2a** and **2c** between the SCF and MP2 levels of theory can be justified on the grounds that post-SCF level calculations tend to favor more nonclassical structures than do SCF-level optimizations. While **2c** cannot be considered a cyclic structure, there is, nevertheless, more interaction between the silicon atom and the carbon to which it is not



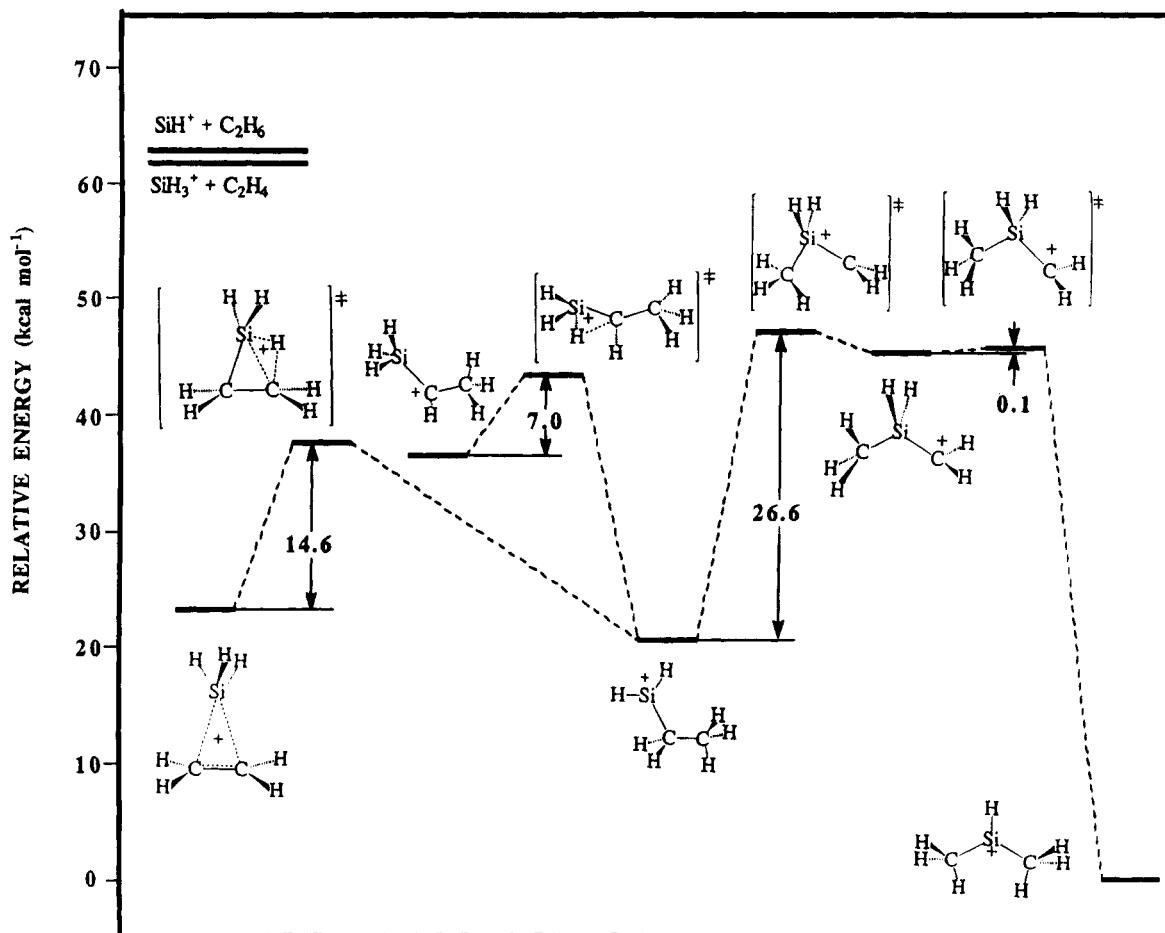


Figure 2. Potential energy surface as optimized at SCF/6-31G(d,p).

(formally) bonded than is the case in **2a** (as is shown in

Table 2. Harmonic Vibrational Frequencies ( $\text{cm}^{-1}$ ) and Intensities ( $\text{km/mol}$ ) for Structures **2** and **4** on the  $\text{SiC}_2\text{H}_7^+$  Surface from MP2(full)/6-31G(d,p) Calculations<sup>c</sup>

4 ( $C_{2v}$ ) <sup>a</sup>			2 ( $C_s$ ) <sup>b</sup>		
freq	intensity	sym	freq	intensity	sym
3265.3	13.7	a <sub>1</sub>	3319.7	22.4	a''
3264.6	5.9	b <sub>2</sub>	3303.5	7.2	a''
3195.7	28.0	b <sub>1</sub>	3230.2	13.0	a'
3194.2	0.0	a <sub>2</sub>	3206.3	10.0	a'
3112.9	3.7	a <sub>1</sub>	2708.4	77.1	a'
3111.0	66.2	b <sub>2</sub>	2479.0	17.0	a''
2429.7	34.4	a <sub>1</sub>	2430.2	8.8	a'
1474.4	24.3	b <sub>1</sub>	1612.3	14.3	a'
1470.7	15.7	a <sub>1</sub>	1511.8	5.5	a'
1462.7	0.0	a <sub>2</sub>	1472.9	10.9	a'
1457.9	3.6	b <sub>2</sub>	1455.7	7.6	a''
1361.5	5.6	a <sub>1</sub>	1211.6	13.0	a'
1354.1	92.9	b <sub>2</sub>	1196.2	7.2	a''
985.4	158.8	b <sub>2</sub>	1031.6	10.6	a'
924.4	73.6	a <sub>1</sub>	991.8	76.8	a'
880.0	88.2	b <sub>1</sub>	956.5	12.5	a''
838.4	29.5	b <sub>2</sub>	955.1	29.2	a'
672.8	1.0	a <sub>1</sub>	861.9	25.4	a''
659.7	1.7	b <sub>2</sub>	741.0	7.8	a'
641.0	0.0	a <sub>2</sub>	713.3	56.4	a'
481.2	12.0	b <sub>1</sub>	556.6	6.6	a''
226.3	4.3	a <sub>1</sub>	501.4	4.4	a''
50.0	0.4	b <sub>1</sub>	372.8	66.1	a'
34.7	0.0	a <sub>2</sub>	241.4	0.7	a''

<sup>a</sup> ZPE = 48.6 kcal mol<sup>-1</sup>, <sup>b</sup> ZPE = 49.3 kcal mol<sup>-1</sup>, <sup>c</sup> Frequencies have not been scaled, but ZPE has been scaled by a factor of 0.93.

the Mayer bond order<sup>24</sup> analyses of these two conformers). Furthermore, there is a noteworthy interaction between the Si atom and the eclipsing H atom of the neighboring methyl group (Mayer bond order = 0.091), an interaction which does not exist in **2a**. In addition, there are substantial differences in the bond orders associated with the C–C and C–H bonds of the two conformers. For example, the C–C bond order in **2a** is 0.925; that of **2c** is 0.849. As well, the C–H bond orders in the methyl group of **2c** have distinctly different values; those associated with the out-of-plane hydrogen atoms are small (0.930) relative to their counterparts in **2a** (0.966) but are large compared to the in-plane methyl C–H bond of **2c** (0.873). Thus, it is evident that all bonds associated with the  $\beta$ -carbon of **2c** are weak relative to their analogues in **2a**. This depletion of electron density associated with these bonds is accompanied by the existence of significant through-space

interactions between Si and the  $\beta$ -C and between Si and H of the adjacent methyl group. Due to the differences in the relative energies of these rotamers at SCF and at MP2, we include only the most stable conformer at

(24) Mayer, I. *Int. J. Quant. Chem.* **1986**, *29*, 477.

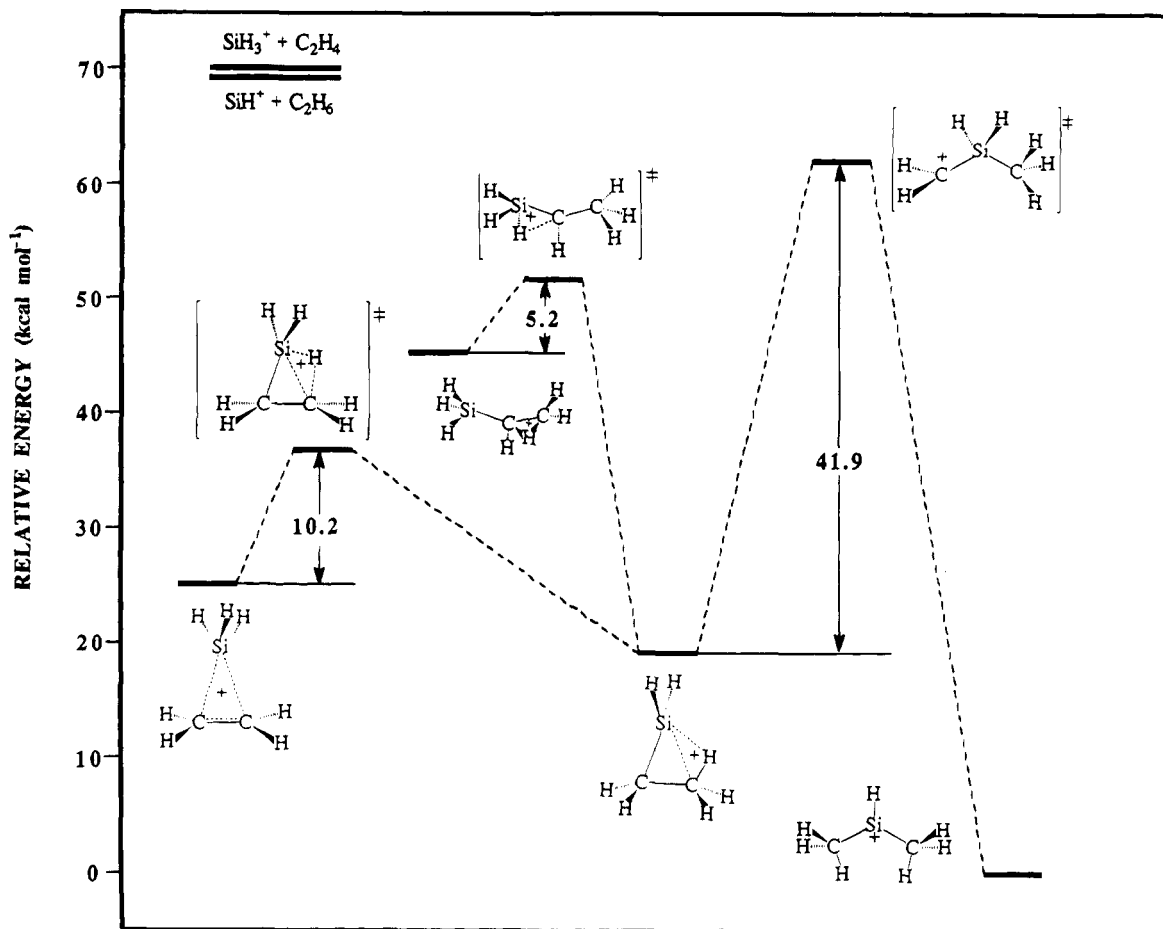


Figure 3. Potential energy surface as optimized at MP2/6-31G(d,p).

each level of theory in the energy level diagrams shown in Figures 2 and 3. Geometric parameters for only conformer **2c** are given in Figure 1.

One also may note the differences in bond orders associated with the  $\alpha$ -carbons of the two conformers. The two equivalent C-H bonds of **2a** (Mayer bond order = 0.919) are weaker than their counterparts in **2c** (0.934). These results suggest that charge delocalization in **2a**, from  $\text{CH}_2$  to  $\text{Si}^+$ , occurs to a greater extent than in **2c**.

When electron correlation is included, the surface reduces to four minima, with ion **2** being  $19.2 \text{ kcal mol}^{-1}$  above **4**, with ion **1** being  $25.2 \text{ kcal mol}^{-1}$  above **4**, and with ion **3** being  $45.1 \text{ kcal mol}^{-1}$  above **4**. As suggested by the early gas-phase results of Lampe and co-workers,<sup>8</sup> the barrier for conversion of **1** into **2** is quite low,  $14.6 \text{ kcal mol}^{-1}$  at SCF/6-31G(d,p) and  $10.2 \text{ kcal mol}^{-1}$  at MP2(full)/6-31G(d,p). This trend toward a lower isomerization barrier, as well as a trend toward a greater thermodynamic stability of **2** vis-à-vis **1** on inclusion of electron correlation (see Figures 2 and 3), suggest that **2** should be considerably more abundant than **1** in the gas phase.

The largest barrier is for the interconversion of the two lowest energy species, ions **2** and **4**, and at MP2/6-31G(d,p), this value ( $41.9 \text{ kcal mol}^{-1}$ ) is quite substantial, as suggested by Fourier transform mass spectrometry.<sup>15c</sup> These two ions have different gas-phase reactions with methanol and with ethene- $d_4$ ; such experiments have been used to show that these ions isomerize slowly unless activated by collision.<sup>15c</sup>

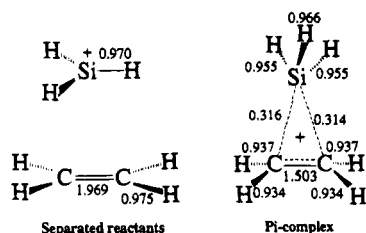
The interconversion of ions **2** and **4** is involved in the most dramatic topological difference between the SCF and MP2 surfaces. At the former level of theory, this interconversion is a two-stage process involving the intermediacy of ion **5**, as well as two transition structures (**7** and **8**). The higher barrier which must be surmounted, that for the conversion of **2** into **5** (through **7**), is  $26.6 \text{ kcal mol}^{-1}$  above **2**. At the MP2 level, **5** collapses into **4** without a barrier, and the critical points associated with structures **7**, **5**, and **8** coalesce into a single transition structure (**6**). This significant topological change is accompanied by a large increase in the barrier to interconversion of **2** and **4**, to  $41.9 \text{ kcal mol}^{-1}$ . This substantial barrier indicates the formation of a transition structure which is rather diffuse in geometry, as may be inferred by the existence of Si-C bond lengths ( $1.871$  and  $1.925 \text{ \AA}$ ) which are longer than that obtained experimentally for silaethane ( $1.867 \text{ \AA}$ ).<sup>25</sup> Therefore, the energy lowering caused by the inclusion of electron correlation is greater in the case of minima **2** and **4** than is the case for transition structure **6** at MP2.

The geometry of transition structure **6** is instructive in the context of the proposed dyotropic isomerization process between **2** and **4**.<sup>15c</sup> The suggested transition structure involves a hydrogen atom and a methyl group, both of which are depicted as bridging the remaining Si-C bond. However, it is evident from Figure 1 that **6** is considerably different in geometry. In our computed

(25) Hehre, W. J.; Radom, L.; Schleyer, P. v. R.; Pople, J. A. *Ab Initio Molecular Orbital Theory*; John Wiley & Sons: New York, 1986.

transition structure, the methyl group has completed its migration from C to Si, whereas the H atom, which must move in the opposite direction, still is firmly bonded to silicon. We have verified by the use of an IRC analysis that **6** interconverts **2** and **4**, and a subsequent attempt at obtaining a transition structure with a geometry more reminiscent of that proposed previously<sup>15c</sup> has been unsuccessful. Clearly then the dyotropic isomerization between **2** and **4** proceeds in an asynchronous fashion.

Ion **1**, created formally from the addition of  $\text{SiH}_3^+$  to ethylene, contains long Si–C distances, and the C–C bond distance is slightly longer than an experimental double bond length of ethylene (1.339 Å)<sup>25</sup> at both levels of theory. The weak Si–C interactions also are apparent from the Mayer bond orders (shown below). The long Si–C distances can be attributed to the donation of a  $\pi$ -electron pair from ethylene to the empty p-orbital of the electron deficient Si of the  $\text{SiH}_3^+$  group. However, unlike in the case of the formation of ground state  $\text{SiC}_2\text{H}_4^+$  ( $^2B_2$ ) from the addition of  $\text{Si}^+$  ( $^2P$ ) to ethylene, there is no back-donation of electrons from  $\text{SiH}_3^+$  to the  $\pi^*$  LUMO of ethylene in the formation of **1**. As a result, a three-center, two-electron bonding arrangement is created in **1**; thus, less than full Si–C bonds are created, and the resulting Si–C distances are much greater than what would be considered "normal" for an Si–C bond. The inclusion of electron correlation in the optimization of **1** has the effect of shortening the C–Si distances and of lengthening the C–C separation. These geometric changes are consistent with the tendency of post-SCF wave functions to give better descriptions of nonclassical structures than SCF-level wave functions. Clearly, there exist interactions between the Si atom and the carbons in **1**, but as is shown by the Mayer bond order<sup>24</sup> analysis



this ion should be considered more correctly to be a  $\pi$ -complex than a genuine three-membered ring.

Despite the long C–Si distance associated with this  $\pi$ -complex, the binding energy of **1** is 43.2 kcal mol<sup>-1</sup> when compared to the separated  $\text{SiH}_3^+$  + ethylene. This binding energy is considerably greater than that of the trimethylated cation **1a** (R = CH<sub>3</sub>) (23 kcal mol<sup>-1</sup> at "corrected" HF/6-31G(d)//HF/3-21G).<sup>14a</sup> This difference in binding energies is attributed to the greater intrinsic stability of the trimethylsilyl cation arising from the delocalization of charge onto the methyl groups.

Ion **3**, an  $\alpha$ -silyl substituted ethyl cation as optimized at SCF/6-31G(d,p), lies 36.5 kcal mol<sup>-1</sup> above **4**. However, the structure of **3** undergoes substantial modification on reoptimization at MP2(full)/6-31G(d,p). At this level, the optimized structure contains one hydrogen atom which bridges the two carbon atoms. In this way, ion **3** undergoes structural changes similar to those of the ethyl cation<sup>26</sup> on proceeding from SCF to post-SCF levels of theory. The structure of **3**, as well, is remi-

niscent of that of a high-energy isomer of  $\text{SiC}_2\text{H}_5^+$ , as has been reported elsewhere.<sup>5</sup>

Ion **3** is a further illustration of the well-established trend in which post-SCF level optimizations tend to favor nonclassical structures, such as cyclic ions. However, as can be seen in Figures 2 and 3, the barrier for the conversion of **3** to **2** is 7.0 kcal mol<sup>-1</sup> at SCF/6-31G(d,p), and this is reduced to 5.2 kcal mol<sup>-1</sup> at MP2/6-31G(d,p). Despite the large difference in the position of the bridging H atom in structure **3** as optimized at the SCF and MP2 levels, the overall barrier to rearrangement of **3** is only slightly reduced by the inclusion of electron correlation (from 7.0 kcal mol<sup>-1</sup>). Inclusion of additional polarization functions has been found to be necessary for a satisfactory description of some particularly electron-deficient hydrogen-bridged cations,<sup>27</sup> and we therefore examined structures **3** and **10** at a considerably higher level of theory, MP2 (frozen core)/6-311G(2df,2p). The results of this extension were consistent with our findings at MP2(full)/6-31G(d,p). Ion **3** is still at a local minimum, **10** is a transition structure, and both structures are almost identical to those obtained at MP2/6-31G(d,p). The barrier for the conversion of **3** and **2** is reduced slightly, to 4.9 kcal mol<sup>-1</sup>. Further extension of the basis set and recovery of more correlation energy may lead to further small reductions in the barrier. However, it seems probable that **3** will be at a local minimum at all levels of theory but the barrier to its rearrangement is sufficiently low to prevent it from being an observable species in room-temperature gas-phase chemistry.

Comparison of the SCF-optimized geometries and the MP2-optimized geometries for transition structure **10** (for the interconversion of **1** and **2**) and for transition structure **9** (for the isomerization of **3**  $\rightarrow$  **2**) shows increases in Si–C bond lengths and decreases in C–C bond lengths on inclusion of electron correlation. As well, the Si–C–C angle in **10** is observed to decrease markedly (from 82.0 to 78.0°) on inclusion of electron correlation. These structural differences are consistent with a shift in the geometry of the transition structures toward the higher energy isomer in each case on proceeding from SCF-level optimizations to MP2-level optimizations. These geometric changes can be justified easily on considering the fact that the differences in the energies of **1** and **2**, and of **3** and **2**, in turn, are greater at the MP2 level (where **2** is the more stable isomer of each pair). The Hammond postulate<sup>28</sup> predicts that the transition structure should be closer in geometry to the higher energy isomer; thus, shifts in the transition structure geometries of **10** and of **9** toward **1** and **3**, respectively, are not unexpected.

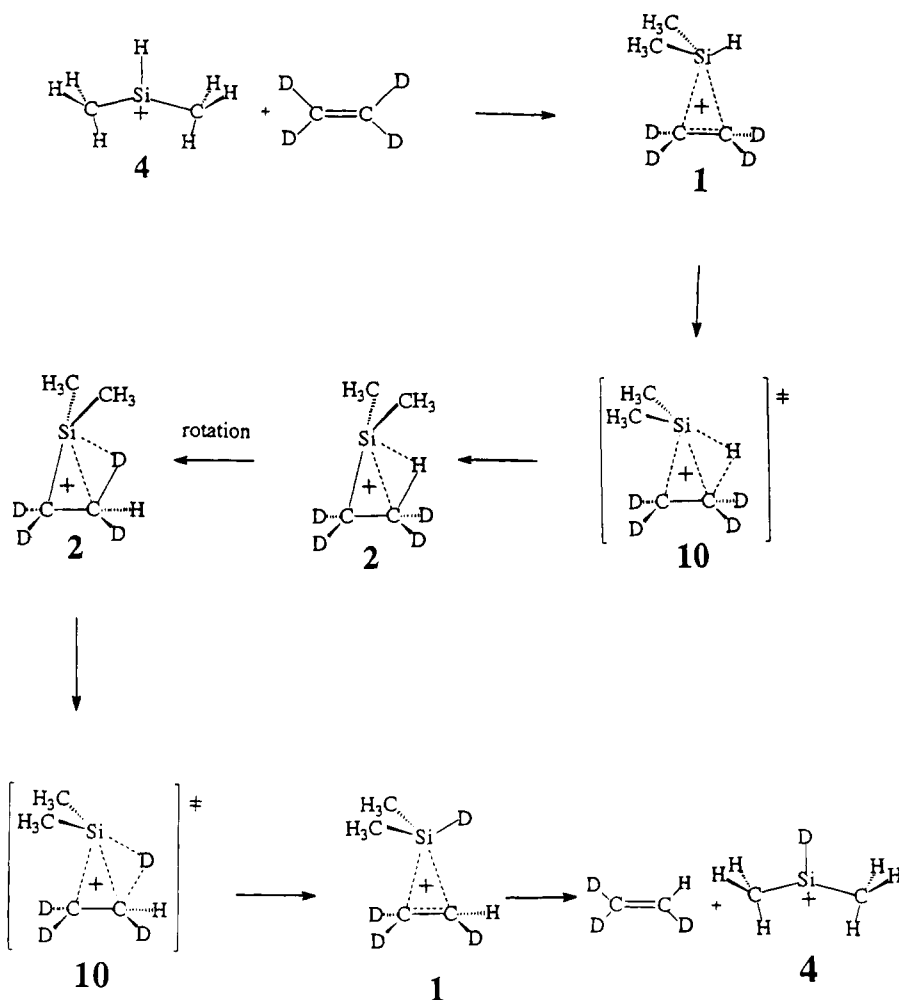
**Mechanistic Consequences.** The observed characteristics of the  $\text{SiC}_2\text{H}_7^+$  potential energy hypersurface have significant implications for the interpretation of results obtained from gas-phase experimental work. The existence of a large barrier to the interconversion of **2** and **4** suggests strongly that both isomers exist as stable species in the gas phase at normal temperatures. This result confirms the hypothesis made from the results of experimental observations that isomerization of these

(26) Raghavachari, K.; Whiteside, R. A.; Pople, J. A.; Schleyer, P. v. R. *J. Am. Chem. Soc.* **1981**, *103*, 5649.

(27) Glukhovtsev, M. N.; Schleyer, P. v. R.; Hommes, N. J. R. v. E.; Carneiro, J. W. de M.; Koch, W. *J. Comput. Chem.* **1993**, *14*, 285.

(28) Hammond, G. S. *J. Am. Chem. Soc.* **1955**, *77*, 334.

Scheme 1



two species "should have a considerable barrier".<sup>15b</sup> Experiments also have been performed on these two  $\text{SiC}_2\text{H}_7^+$  isomers using FTMS in an attempt to distinguish between them on the basis of their reactions with ethylene- $d_4$  and with  $^{13}\text{C}_2\text{H}_4$ , studies from which one H/D exchange for species 4 (to form  $\text{H}_3\text{CSiDCH}_3^+$ ) and seven H/D exchanges for structure 2 were reported.<sup>15c</sup>

The results of our computational study of the  $\text{SiC}_2\text{H}_7^+$  potential energy hypersurface yield greater mechanistic insight into these reactions than are obtained from experimental studies alone. Scheme 1 illustrates a plausible mechanism for the single H/D exchange observed in the reaction of 4 with ethylene- $d_4$ , in a scheme analogous to that proposed previously.<sup>15a,b</sup> The reaction may proceed via electrophilic attack of the positively-charged Si on ethylene- $d_4$ , to form a structure analogous to 1, but with two methyl groups replacing hydrogen atoms on silicon. This step may be followed by a 1,2-H shift, from Si to C, to form a dimethyl analogue to ion 2. Free rotation about the C-C single bond may allow the formation of a rotamer in which a deuterium atom, rather than a hydrogen atom, eclipses the silicon of the  $\text{Si}(\text{CH}_3)_2^+$  moiety, upon which a 1,2-D migration and subsequent elimination of  $\text{D}_2\text{C}=\text{CDH}$ , in reverse order to the process described above, regenerates the dimethylsilyl cation but with a deuterium atom bonded to silicon.

Scheme 2 provides a more detailed rationalization of the mechanism for seven H/D exchanges in the reaction

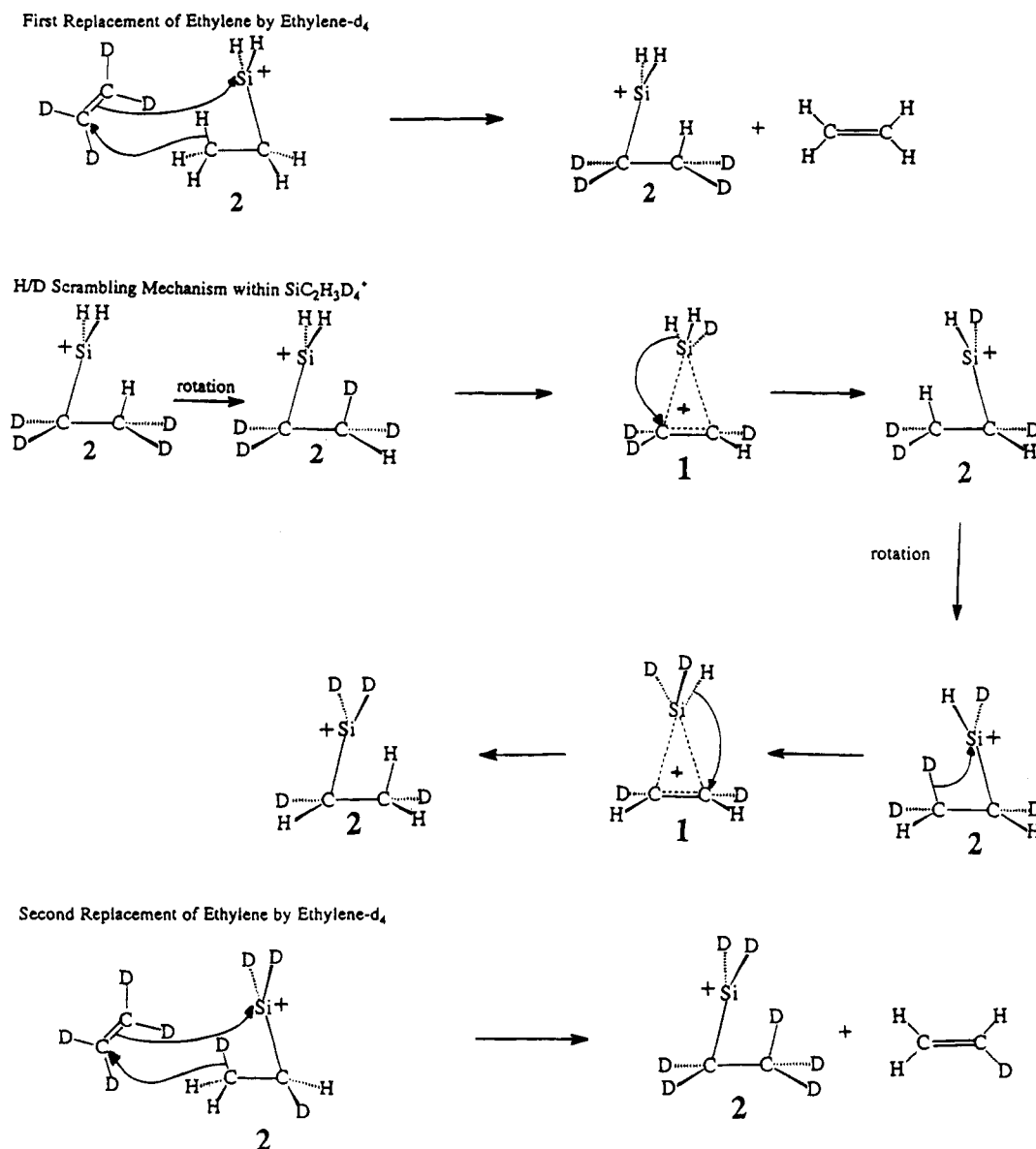
of 2 with ethylene- $d_4$ . This process is more complicated than that discussed in Scheme 1 because it involves internal H/D scrambling between Si and C of a given "intermediate"  $\text{SiC}_2\text{H}_n\text{D}_{7-n}$  species. It must be noted, as well, that, as our proposed pathway involves the intermediacy of species 1 as well as a series of 1,2-H<sup>-</sup> shifts and 1,2-D<sup>-</sup> shifts, it differs in this respect from that proposed previously, in which the existence of a species with the structure of 1 in gas-phase experimental studies was not considered.<sup>15c</sup>

**Vibrational Frequencies.** As the two lowest energy isomers on the  $\text{SiC}_2\text{H}_7^+$  surface are separated by a high-energy barrier, it is probable that both ions 2 and 4 will be observable in the gas phase at room temperature. Here we report the harmonic vibrational frequencies as obtained at MP2(full)/6-31G(d,p) on each of these two isomers, as well as the intensities, the symmetry assignments, and the scaled (by 0.93)<sup>29</sup> zero-point vibrational energies, in the hope that this information may be of use to experimental chemists who wish to study these ions spectroscopically.

## Conclusions

Structural isomers associated with critical points on the  $\text{SiC}_2\text{H}_7^+$  potential energy hypersurface have been investigated by *ab initio* MO theory. Our results

Scheme 2



reinforce the observations made for other organosilicon cationic surfaces that isomers on a given surface with fewer H atoms bonded to Si (as opposed to being bonded to C) tend to have the lowest electronic energies. The existence of a large energy barrier to the isomerization of structures **2** and **4**, calculated to be  $42 \text{ kcal mol}^{-1}$  and estimated experimentally to be  $\sim 35 \text{ kcal mol}^{-1}$ ,<sup>15d</sup> supports the postulate of Jacobson and coworkers<sup>15c</sup> and provides strong evidence for the presence of both isomers in the gas phase. By contrast, the existence of a small, but not insignificant, barrier ( $10 \text{ kcal mol}^{-1}$ , the same as the value estimated experimentally<sup>15d</sup>) to the interconversion of **1** and **2** may have important experimental ramifications in another sense. As Jacobson's group did not consider the possibility of the existence of species **1** in its gas-phase experiments but,

as illustrated in Schemes 1 and 2, the mechanisms of H/D exchanges may proceed through such an isomer, it is conceivable that what was observed may, in fact, have been a mixture of **1** and **2**. Further experimental verification, however, is required before any conclusions can be made about the mechanism.

**Acknowledgment.** We thank Steve Quan for technical assistance and Chris Rodriguez for insightful discussions. We thank Professor I. G. Csizmadia for giving us access to the Monstergauss program for calculations of Mayer bond indices. Continued financial support from the Natural Sciences and Engineering Research Council of Canada is much appreciated.

OM940477H

# Cyclometalated Platinum(II) Compounds with Fluorinated Iminic Ligands: Synthesis and Reactivity Tuning. Crystal Structures of the Compounds [PtMe(RCH=NCH<sub>2</sub>C<sub>6</sub>H<sub>5</sub>)(PPh<sub>3</sub>)] (R = 2,3,4-C<sub>6</sub>HF<sub>3</sub> and 2,3-C<sub>6</sub>H<sub>2</sub>F<sub>2</sub>)

Margarita Crespo\*

Departament de Química Inorgànica, Universitat de Barcelona, Diagonal 647, 08028 Barcelona, Spain

Xavier Solans and Mercè Font-Bardía

Departament de Cristal·lografia, Mineralogia i Dipòsits Minerals, Universitat de Barcelona, Martí i Franqués s/n, 08028 Barcelona, Spain

Received June 13, 1994<sup>®</sup>

[Pt<sub>2</sub>Me<sub>4</sub>(μ-SMe<sub>2</sub>)<sub>2</sub>] (1) reacts with fluorinated imines ArCH=NCH<sub>2</sub>C<sub>6</sub>H<sub>5</sub> (2; Ar = 2,3,4-C<sub>6</sub>H<sub>2</sub>F<sub>2</sub>, 2,4,5-C<sub>6</sub>H<sub>2</sub>F<sub>3</sub>, 2,3-C<sub>6</sub>H<sub>3</sub>F<sub>2</sub>) to yield the C,N-cyclometalated platinum(II) compounds [PtMe(RCH=NCH<sub>2</sub>C<sub>6</sub>H<sub>5</sub>)(SMe<sub>2</sub>)] (3) by *ortho* metalation with loss of methane. Complexes 3 react with triphenylphosphine to give cyclometalated compounds [PtMe(RCH=NCH<sub>2</sub>C<sub>6</sub>H<sub>5</sub>)(PPh<sub>3</sub>)] (4). For R = 2,4,5-C<sub>6</sub>HF<sub>3</sub>, an excess of PPh<sub>3</sub> produces metallacycle cleavage, and [PtMe(RCH=NCH<sub>2</sub>C<sub>6</sub>H<sub>5</sub>)(PPh<sub>3</sub>)<sub>2</sub>] (5) is formed with the imine acting as a [C<sup>-</sup>] unidentate ligand. Similarly, reactions of the previously reported compounds [PtMe{RCH=NCH<sub>2</sub>(2-C<sub>6</sub>H<sub>4</sub>Cl)}(SMe<sub>2</sub>)] (R = 3,5-C<sub>6</sub>H<sub>2</sub>F<sub>2</sub>, 2-C<sub>6</sub>H<sub>3</sub>F, 5-C<sub>6</sub>H<sub>3</sub>F) with PPh<sub>3</sub> produce the cyclometalated compounds 4. When an excess of PPh<sub>3</sub> is used, compounds 5 are obtained only if there is a fluorine atom adjacent to platinum (F<sup>5</sup>). 3–5 were characterized by elemental analyses and NMR spectroscopy, and [PtMe(2,3,4-C<sub>6</sub>HF<sub>3</sub>CH=NCH<sub>2</sub>C<sub>6</sub>H<sub>5</sub>)(PPh<sub>3</sub>)] (4a) and [PtMe(2,3-C<sub>6</sub>H<sub>2</sub>F<sub>2</sub>CH=NCH<sub>2</sub>C<sub>6</sub>H<sub>5</sub>)(PPh<sub>3</sub>)] (4c) were characterized crystallographically. 4a crystallizes in the monoclinic space group *P*2<sub>1</sub>/*c*, with *a* = 12.475(3) Å, *b* = 21.642(5) Å, *c* = 10.497(2) Å, β = 96.92(2)°, and *Z* = 4. 4c crystallizes in the triclinic space group *P*1̄, with *a* = 12.031(2) Å, *b* = 13.757(2) Å, *c* = 9.768(2) Å, α = 72.91(2)°, β = 114.91(1)°, γ = 104.20(2)°, and *Z* = 2. Structural and NMR parameters for compounds 4 are discussed in relation to the observed reactivity of these compounds.

## Introduction

Cyclometalated compounds have been extensively studied because of their potential utility in organic synthesis, and a number of synthetic approaches have been investigated.<sup>1</sup> Although organopalladium cyclometalated compounds have been the most studied, there are several classical examples of platinum complexes with *ortho*-metalated nitrogen donor ligands.<sup>2</sup> Recent reports of platinum(II) cyclometalated compounds concern their photochemical and electrochemical properties.<sup>3,4</sup> Moreover, there is an increasing interest in platinum(II) and even platinum(IV) compounds with either bidentate (C,N)<sup>5</sup> or terdentate (N,C,N' or C,N,N')<sup>6</sup> ligands. [Pt<sub>2</sub>Me<sub>4</sub>(μ-SMe<sub>2</sub>)<sub>2</sub>] has been shown to be a good substrate for the synthesis of cyclometalated platinum

compounds containing bidentate (C,N) or terdentate (C,N,N') ligands. For instance, platinum(II) compounds of the types [PtMe(C,N,N')]<sup>7</sup> and [PtMe(C,N)(SMe<sub>2</sub>)]<sup>8</sup> have been obtained under mild conditions by intramolecular C–H bond activation, followed by reductive elimination of the methane. Analogous reactions for C–X bonds (X = Br, Cl, F) have given platinum(IV) cyclometalated compounds such as [PtMe<sub>2</sub>X(C,N,N')]<sup>7,9</sup> or [PtMe<sub>2</sub>X(C,N)(SMe<sub>2</sub>)]<sup>8,10</sup>

In this paper we report the synthesis and reactivity of new cyclometalated platinum(II) compounds containing fluorinated iminic ligands of the type C<sub>6</sub>F<sub>x</sub>H<sub>5-x</sub>

(5) (a) Chattopadhyay, S.; Sinha, C.; Basu, P.; Chakravorty, A. *Organometallics* **1991**, *10*, 1135. (b) Newkome, G. R.; Theriot, K. J.; Fronczek, F. R.; Villar, B. *Organometallics* **1989**, *8*, 2523.

(6) (a) Canty, A. J.; Honeyman, R. T. *J. Organomet. Chem.* **1990**, *387*, 247. (b) Canty, A. J.; Honeyman, R. T.; Skelton, B. W.; White, A. H. *J. Organomet. Chem.* **1990**, *389*, 277. (c) Constable, E. C.; Henney, R. P. G.; Leese, T. A.; Tocher, D. A. *J. Chem. Soc., Chem. Commun.* **1990**, 513. (d) Wehman-Ooyevaar, I. C. M.; Kapteijn, G. M.; Grove, D. M.; Smeets, W. J. J.; Spek, A. L.; van Koten, G. *J. Chem. Soc., Dalton Trans.* **1994**, 703.

(7) Anderson, C. M.; Crespo, M.; Jennings, M. C.; Lough, A. J.; Ferguson, G.; Puddephatt, R. J. *Organometallics* **1991**, *10*, 2672.

(8) Crespo, M.; Martinez, M.; Sales, J.; Solans, X.; Font-Bardía, M. *Organometallics* **1992**, *11*, 1288.

(9) Anderson, C. M.; Crespo, M.; Ferguson, G.; Lough, A. J.; Puddephatt, R. J. *Organometallics* **1992**, *11*, 1177.

(10) (a) Crespo, M.; Martinez, M.; Sales, J. *J. Chem. Soc., Chem. Commun.* **1992**, 822. (b) Crespo, M.; Martinez, M.; Sales, J. *Organometallics* **1993**, *12*, 4297.

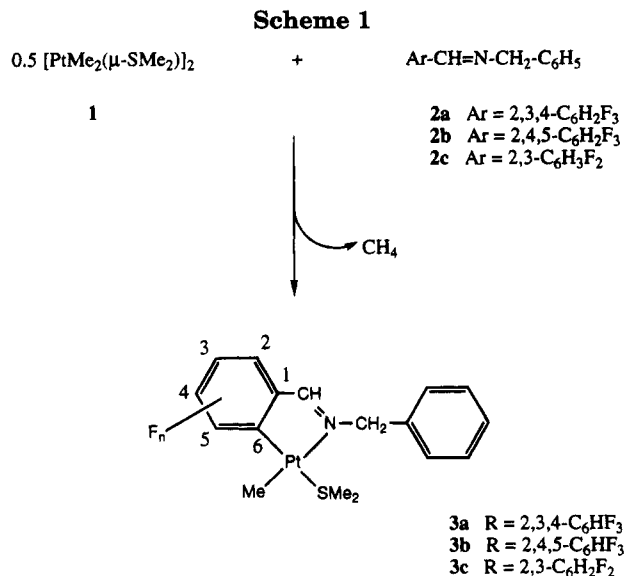
<sup>®</sup> Abstract published in *Advance ACS Abstracts*, November 1, 1994.

(1) (a) Omae, I. *Coord. Chem. Rev.* **1988**, *83*, 137. (b) Omae, I. *Chem. Rev.* **1979**, *79*, 287.

(2) (a) Cope, A. C.; Siekman, R. W. *J. Am. Chem. Soc.* **1965**, *87*, 3272. (b) Elder, R. C.; Crucea, R. D.; Morrison, R. F. *Inorg. Chem.* **1976**, *5*, 1623. (c) Cope, A. C.; Friedrich, E. C. *J. Am. Chem. Soc.* **1968**, *90*, 909.

(3) (a) Maestri, M.; Sandrini, D.; von Zelewsky, A.; Deuschel-Cornioley, C. *Inorg. Chem.* **1991**, *30*, 2476. (b) Minghetti, G.; Pilo, M.; Sanna, G.; Seeberg, R.; Stoccoro, S.; Laschi, F. *J. Organomet. Chem.* **1993**, *452*, 257. (c) Maestri, M.; Deuschel-Cornioley, C.; von Zelewsky, A. *Coord. Chem. Rev.* **1991**, *111*, 117.

(4) von Zelewsky, A.; Suckling, A. P.; Stoeckli-Evans, H. *Inorg. Chem.* **1993**, *32*, 4585.



CH=NCH<sub>2</sub>C<sub>6</sub>H<sub>5</sub>. We have recently studied<sup>10</sup> the reaction of several fluorinated iminic ligands with [Pt<sub>2</sub>Me<sub>4</sub>(μ-SMe<sub>2</sub>)<sub>2</sub>] (1); C-F bond activation has been achieved not only for pentafluorophenyl derivatives but also for trifluorinated ligands containing fluorine substituents in the two *ortho* positions such as 2,4,6- and 2,3,6-C<sub>6</sub>H<sub>2</sub>F<sub>3</sub>CH=NCH<sub>2</sub>C<sub>6</sub>H<sub>5</sub>. However, no reaction has been observed for the ligand 2,6-C<sub>6</sub>H<sub>3</sub>F<sub>2</sub>CH=NCH<sub>2</sub>C<sub>6</sub>H<sub>5</sub>. Thus, the presence of at least three fluorine atoms seems necessary to produce C-F bond activation. In order to ascertain whether the presence of two fluorines in *ortho* positions is also a requirement for C-F bond activation, we tested the reaction of trifluorinated ligands containing just one fluorine atom in an *ortho* position such as 2,3,4- and 2,4,5-C<sub>6</sub>H<sub>2</sub>F<sub>3</sub>CH=NCH<sub>2</sub>C<sub>6</sub>H<sub>5</sub> (2a,b, respectively). For these ligands, both C-H and C-F bond activations are plausible in principle.

Previous work with related ligands has shown that the presence of a fluorine atom adjacent to the position to be activated can be decisive in the selectivity of this process. For instance, it has been reported<sup>10</sup> that the ligand 3-C<sub>6</sub>H<sub>4</sub>FCH=NCH<sub>2</sub>(2-C<sub>6</sub>H<sub>4</sub>Cl) (2f) reacts with [Pt<sub>2</sub>Me<sub>4</sub>(μ-SMe<sub>2</sub>)<sub>2</sub>] via an *ortho*-metalation process in which the C-H bond having a vicinal fluorine atom is exclusively activated. For this reason, we also tested the difluorinated ligand 2,3-C<sub>6</sub>H<sub>3</sub>F<sub>2</sub>CH=NCH<sub>2</sub>C<sub>6</sub>H<sub>5</sub> (2c). It is interesting to note that chelate-assisted oxidative addition of C-F bonds to tungsten(0) has been successfully extended to monofluoro- and difluoro-substituted aromatic rings of suitably designed ligands.<sup>11</sup>

## Results

**Preparation of Platinum(II) Cyclometalated Compounds.** The reaction of [Pt<sub>2</sub>Me<sub>4</sub>(μ-SMe<sub>2</sub>)<sub>2</sub>] (1) with ligands 2a-c in acetone yielded the cyclometalated platinum(II) compounds [PtMe(RCH=NCH<sub>2</sub>C<sub>6</sub>H<sub>5</sub>)(SMe<sub>2</sub>)] (3; R = 2,3,4-C<sub>6</sub>HF<sub>3</sub>, 2,4,5-C<sub>6</sub>HF<sub>3</sub>, 2,3-C<sub>6</sub>H<sub>2</sub>F<sub>2</sub>) by *ortho* metalation with loss of methane, as shown in Scheme 1. The reaction is analogous to that reported for less fluorinated derivatives such as the ligands 2d-g depicted in Chart 1 and consists of an intramolecular

activation of the C-H bond followed by elimination of methane to produce compounds 3. The reactions were monitored by <sup>1</sup>H NMR, and in all cases only one compound was formed. C-F bond activation was not observed, even when an electron-withdrawing fluorine substituent was present in a position adjacent to the *ortho*-fluorine, as in ligands 2a,c.

Thus, when both C-F and C-H are present in the *ortho* positions of the aromatic ring, exclusive activation of the latter takes place. This finding may be related to the higher energy of the C-F bond compared to the C-H bond.<sup>12</sup> C-F bond activation has been reported<sup>10</sup> to occur in the presence of weaker C-X (X = H, Cl, Br) bonds for systems where activation of C-X bonds would produce a metallacycle that does not contain the C=N group, such as ligands 2h-j (Chart 1). However, in the present system, both C-H and C-F bond activations would lead to five-membered metallacycles containing the iminic functionality.

The results reported in this paper, together with others previously obtained, are summarized in Chart 1 and show that C-F bond activation is produced only if the aryl ring contains at least three fluorine atoms, with two of them in *ortho* positions (2h-l); when these requirements are not fulfilled, either no reaction occurs (2m) or C-H bond activation takes place (2a-f).

Compounds 3 were characterized by elemental analysis and <sup>1</sup>H, <sup>13</sup>C, and <sup>19</sup>F NMR spectra. In the <sup>1</sup>H NMR, the resonance of the methyl group bound to platinum appears as a pseudotriplet due to the coupling with <sup>195</sup>Pt and coupling constant values (<sup>2</sup>J(HPt) = ca. 80 Hz) are characteristic for platinum(II) compounds with methyl *trans* to N.<sup>13</sup> The resonance due to the iminic proton is also coupled with <sup>195</sup>Pt (<sup>3</sup>J(HPt) = ca. 50 Hz), thus showing the coordination of the ligand to platinum through the iminic nitrogen. For 3b, both the methyl hydrogens and the methyl carbon are coupled with F<sup>5</sup>, thus revealing a through-space interaction. In the <sup>19</sup>F NMR spectra, the resonances due to two (3c) or three (3a,b) aromatic fluorine atoms appear and the couplings with <sup>195</sup>Pt are sensitive to the position of the fluorine in the ring, while the values of the coupling constants with other fluorine or hydrogen atoms in the aryl ring are in good agreement with the values reported in the literature.<sup>14</sup>

**Reactions with Triphenylphosphine.** The reactions of compounds 3 with triphenylphosphine were studied, and the results are summarized in Scheme 2. Compounds 3a,c reacted with PPh<sub>3</sub> in a 1:1 molar ratio in acetone solution to yield the cyclometalated compounds [PtMe(2,3,4-C<sub>6</sub>HF<sub>3</sub>CH=NCH<sub>2</sub>C<sub>6</sub>H<sub>5</sub>)(PPh<sub>3</sub>)] (4a) and [PtMe(2,3-C<sub>6</sub>H<sub>2</sub>F<sub>2</sub>CH=NCH<sub>2</sub>C<sub>6</sub>H<sub>5</sub>)(PPh<sub>3</sub>)] (4c), which result from a displacement reaction of SMe<sub>2</sub> for PPh<sub>3</sub>. These compounds are yellow solids which were characterized by elemental analysis, IR, and <sup>1</sup>H, <sup>19</sup>F, and <sup>31</sup>P NMR spectra. The presence of PPh<sub>3</sub> coordinated to platinum is confirmed by IR and <sup>1</sup>H and <sup>31</sup>P NMR spectra, while no signals are obtained for SMe<sub>2</sub> in the <sup>1</sup>H NMR. Both the methyl and the iminic groups are

(12) Benson, S. W. *Thermochemical Kinetics*; Wiley: New York, 1976.

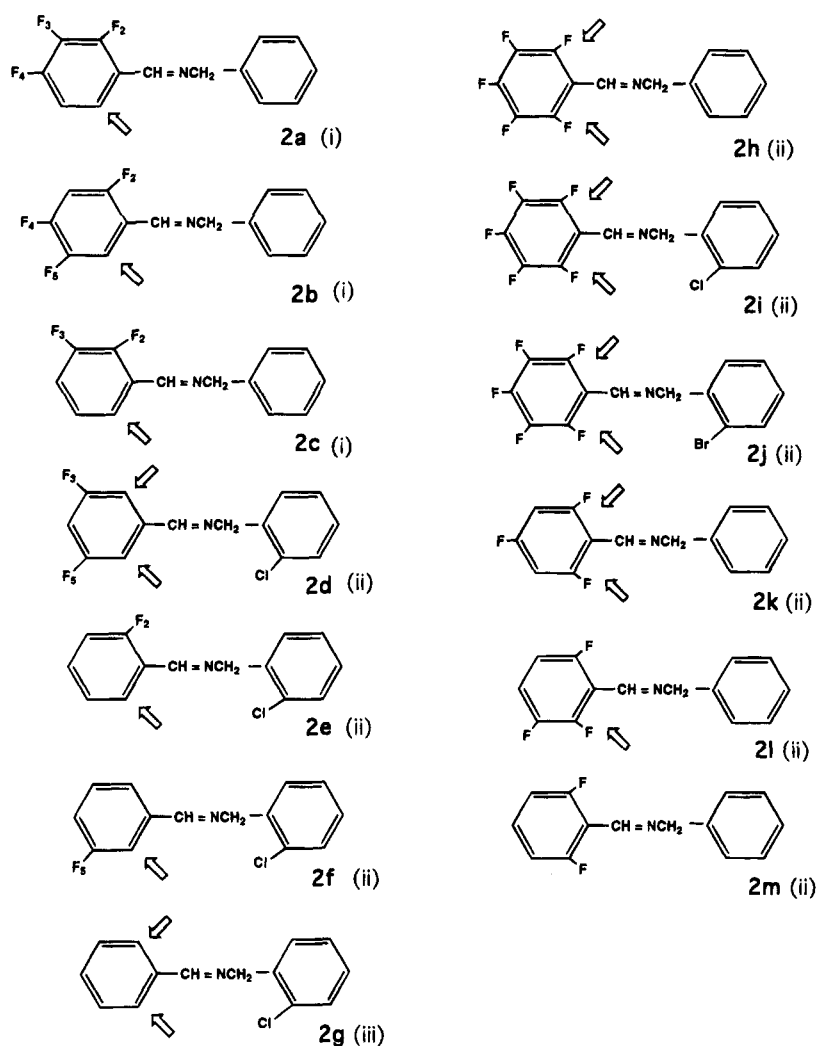
(13) Crespo, M.; Puddephatt, R. J. *Organometallics* 1987, 6, 2548.

(14) (a) Paudler, W. W. In *Nuclear Magnetic Resonance: General Concepts and Applications*; Wiley: New York, 1987. (b) Crocker, C.; Goodfellow, R. J.; Gimeno, J.; Usón, R. *J. Chem. Soc., Dalton Trans.* 1977, 1448.

(11) (a) Lucht, B. L.; Poss, M. J.; King, M. A.; Richmond, T. G. *J. Chem. Soc., Chem. Commun.* 1991, 400. (b) Richmond, T. G. *Coord. Chem. Rev.* 1990, 195, 221.



Chart 1



↗ denotes the activated bond upon reaction with (1)

(i) this work; (ii) ref. 10; (iii) ref. 17

coupled with  $^{195}\text{Pt}$  and the values of the coupling constants are similar to those obtained for compounds **3**. The methyl group appears as a doublet due to coupling with the phosphorus atom. Compounds **4a,c** were also characterized crystallographically.

Compound **3b**, however, under similar reaction conditions, gave  $[\text{PtMe}(2,4,5\text{-C}_6\text{HF}_3\text{CH}=\text{NCH}_2\text{C}_6\text{H}_5)(\text{PPh}_3)_2]$  (**5b**), together with decomposition products such as platinum(0) and uncoordinated imine. Compound **5b**, best obtained from reaction of **3b** with 2 equiv of  $\text{PPh}_3$ , is a white solid which was characterized by elemental analysis, IR, and  $^1\text{H}$ ,  $^{19}\text{F}$ ,  $^{31}\text{P}$ , and  $^{195}\text{Pt}$  NMR spectra. Spectral evidence points to the presence of the iminic ligand acting in a monodentate fashion through the aryl carbon, as shown in Scheme 2. The presence of two coordinated  $\text{PPh}_3$  ligands is confirmed by the relative intensities of the signals in the  $^1\text{H}$  NMR spectrum. The methyl resonance appears as a doublet of doublets; this pattern arises from coupling to two nonequivalent phosphorus atoms. The value of the coupling constant with platinum (smaller than for compound **3** or **4**) is consistent with the presence of a phosphine ligand in a position *trans* to the methyl group. Furthermore, the

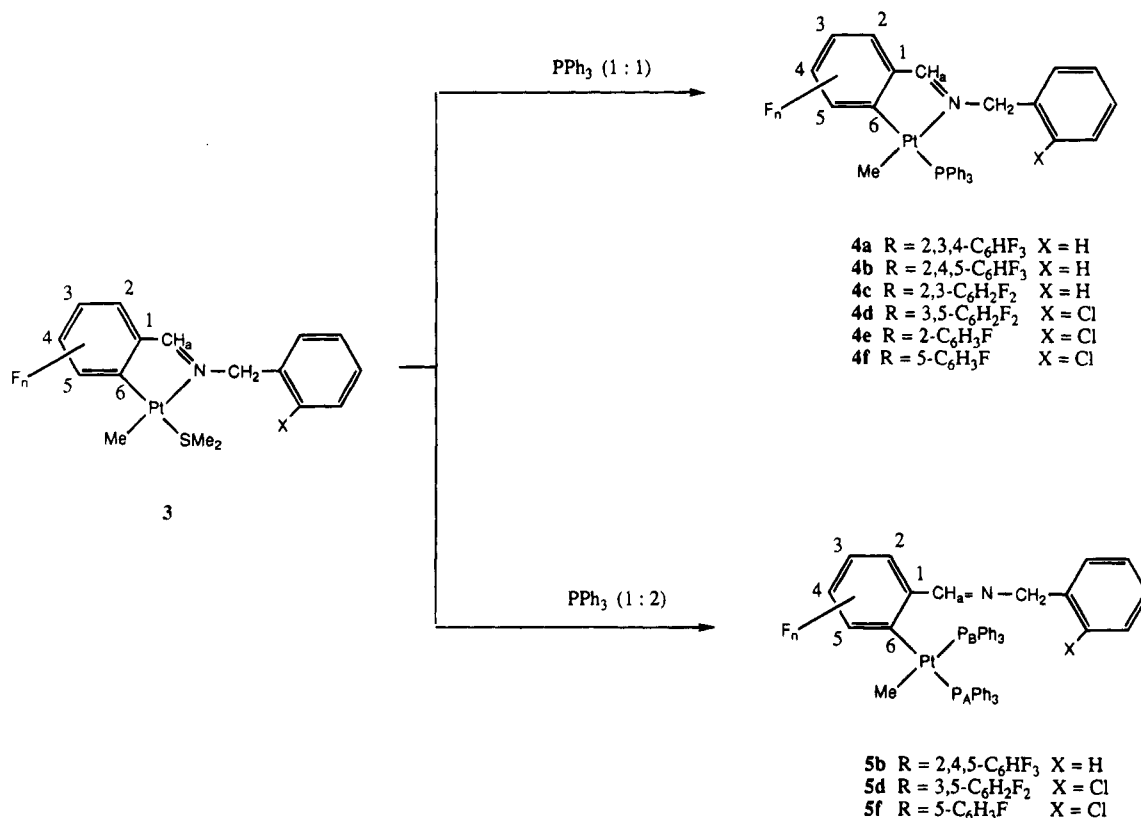
iminic nitrogen is not coupled with  $^{195}\text{Pt}$  and the methylene resonance appears as an *AB* quartet. The  $^{31}\text{P}$  NMR spectra show two sets of resonances due to the nonequivalent phosphorus atoms, both coupled with platinum.

In the  $^{19}\text{F}$  NMR spectrum, a dramatically large value (464 Hz) is obtained for  $^3J(\text{F}^5\text{-Pt})$  in comparison to the values for cyclometalated compounds **3b** (140 Hz) and **4b** (87 Hz). Analogous values have been reported in the literature<sup>15</sup> for the fluorine in *ortho* positions in (pentafluorophenyl)platinum(II) complexes. This large coupling constant in compound **5b** may arise from a perpendicular orientation of the aryl group to the coordination plane. Consistently, the methyl group does not couple with the fluorine in position 5 of the aryl group, thus precluding an interaction as observed in **3b** and **4b**.

Both  $^3J(\text{F-Pt})$  and  $^1J(\text{P-Pt})$  values for compound **5b** were confirmed within experimental error by the  $^{195}\text{Pt}$  NMR spectrum.  $\delta(^{195}\text{Pt})$  values are well within the

(15) (a) Forniés, J.; Fortunó, J. C.; Gómez, M. A.; Menjón, B.; Herdtweck, E. *Organometallics* **1993**, *12*, 4368. (b) Casas, J. M.; Forniés, J.; Martín, A.; Menjón, B. *Organometallics* **1993**, *12*, 4376.

Scheme 2



range expected for organoplatinum(II) compounds with phosphine ligands.<sup>16</sup>

When the reaction of compound **3b** with PPh<sub>3</sub> was carried out in acetone in the molar ratio 1:0.8, a mixture of **4b** and **5b** was formed, from which **4b** was isolated in a pure form. NMR parameters for this compound are analogous to those obtained for **4a,c**, except that the methyl group appears as a doublet of doublets due to coupling with both phosphorus and fluorine F<sup>5</sup> nuclei.

Attempts to obtain the corresponding compounds **5a,c** were unsuccessful, since the reaction of **3a** or **3c** with an excess of PPh<sub>3</sub> yields **4a** or **4c**, which do not react further with PPh<sub>3</sub>. That is, for compounds **3a,c**, the metallacycle is not cleaved upon reaction with PPh<sub>3</sub>. This behavior is analogous to that reported for [PtMe{C<sub>6</sub>H<sub>4</sub>CH=NCH<sub>2</sub>(2-C<sub>6</sub>H<sub>4</sub>Cl)}(PPh<sub>3</sub>)].<sup>17</sup>

The reaction of palladacycles with phosphines has been widely studied,<sup>18</sup> and depending on the nature of the cycle and the basicity of the nitrogen donor atom, cleavage of the metal–nitrogen bond may be achieved. However, in this system, a difference in reactivity toward PPh<sub>3</sub> is observed for metallacycles of the same nature and it can only be attributed to the different substituents in the aryl ring. In particular, the presence of a fluorine atom in the position adjacent to the Pt–C(aryl) bond (F<sup>5</sup>) seems to be decisive.

In order to confirm this suggestion, we studied the reactions with PPh<sub>3</sub> of monofluoro- and difluoro-substituted compounds such as **3d–f**, previously obtained. The results are shown in Scheme 2. **3e**, which

does not contain a fluorine atom in the position adjacent to the Pt–C(aryl) bond, reacted with only 1 equiv of PPh<sub>3</sub>, even when an excess of phosphine was used. Compounds **3d** and **3f**, which do contain a fluorine substituent in such a position, reacted with 2 equiv of PPh<sub>3</sub> to yield compounds **5d,f** with cleavage of the metallacycle. Compounds **4d,f** were easily obtained from reaction with 1 equiv of PPh<sub>3</sub>. A lower tendency to cleave the metallacycle is observed for less fluorinated compounds, **3d** and **3f**, than for the trifluorinated compound **3b**. On the other hand, the presence of a chlorine atom in the benzyl ring for compounds **3d–f** does not seem to be relevant.

NMR parameters for compounds **4d–f** and **5d,f**, reported in the Experimental Section, are similar to those described above for compounds **4** and **5**. <sup>195</sup>Pt and <sup>19</sup>F NMR spectra of compound **5d** are shown in Figure 1.

The <sup>1</sup>J(P–Pt) parameters for compounds **4** are larger when a fluorine atom is present in position 5 of the aryl ring (compounds **4b,d,f**). These values increase gradually as the total number of fluorine atoms in the ring increases. A similar trend is observed for compounds **4a,c,e**, although values are smaller. As a whole, <sup>1</sup>J(P–Pt) values decrease according to the sequence Ar = 2,4,5-C<sub>6</sub>HF<sub>3</sub> > 3,5-C<sub>6</sub>H<sub>2</sub>F<sub>2</sub> > 5-C<sub>6</sub>H<sub>3</sub>F > 2,3,4-C<sub>6</sub>HF<sub>3</sub> > 2,3-C<sub>6</sub>H<sub>2</sub>F<sub>2</sub> > 2-C<sub>6</sub>H<sub>3</sub>F > C<sub>6</sub>H<sub>4</sub>. It is illustrative to note that <sup>1</sup>J(P–Pt) for **4a**, containing the trifluorinated aryl group 2,3,4-C<sub>6</sub>HF<sub>3</sub>, is smaller (<sup>1</sup>J(P–Pt) = 2387 Hz) than for **4f**, containing the monofluorinated aryl group 5-C<sub>6</sub>H<sub>3</sub>F (<sup>1</sup>J(P–Pt) = 2479 Hz).

The increase in <sup>1</sup>J(P–Pt) values with increasing fluorination of the ring is consistent with a decrease in the *trans* influence of the aryl ring. <sup>1</sup>J(P–Pt) values can be rationalized in terms of the Fermi contact

(16) Benn, R.; Reinhard, R. D.; Rufinska, A. *J. Organomet. Chem.* **1985**, *282*, 291.

(17) Crespo, M.; Font-Bardía, M.; Solans, X. *J. Organomet. Chem.*, submitted for publication.

(18) Albert, J.; Gómez, M.; Granell, J.; Sales, J. *Organometallics* **1990**, *9*, 1405.

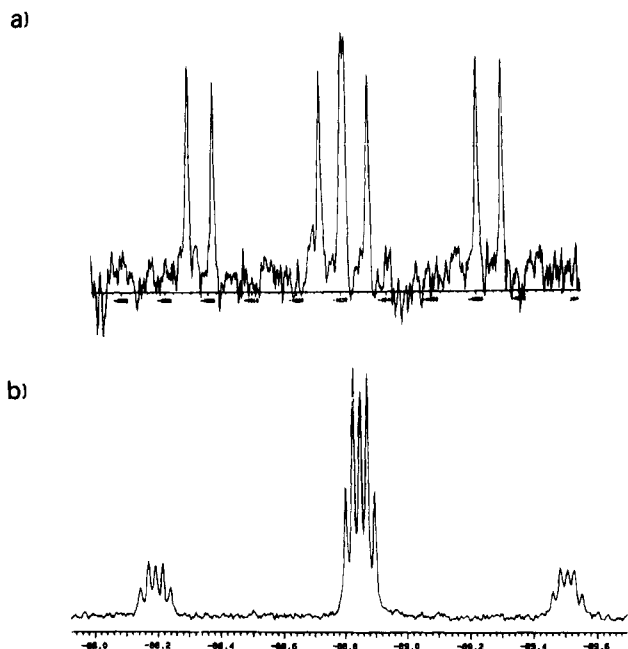


Figure 1. (a)  $^{195}\text{Pt}$  NMR spectrum of **5d**. (b)  $^{19}\text{F}$  NMR spectrum of **5d** ( $\text{F}_5$  region).

expression, which relates  $J$  to the electron density at the coupled nuclei.<sup>19</sup> The large inductive effect of fluorine substituents reduces the electron density on platinum, thus contracting the d orbitals and reinforcing the platinum–ligand bond in the *trans* position. The inductive effect must be more important for the fluorine  $\text{F}^5$  in a position *ortho* to the platinum.

For compounds **5**, values of  $^1J(\text{P}_A\text{--Pt})$  ( $\text{P}_A$  *trans* to aryl) follow the expected trend with increasing fluorination; however, no consistent trend is found for  $^1J(\text{P}_B\text{--Pt})$  values ( $\text{P}_B$  *cis* to aryl).

For compounds **5**, a downfield shift of the iminic proton ( $\delta$  9.00–9.52 ppm) related to compounds **4** is observed. As reported in the literature for several platinum compounds,<sup>20</sup> this shift implies a close vicinity between platinum and hydrogen atoms and can be explained by the existence of the weak three-center–four-electron interaction  $\text{C--H}\cdots\text{Pt}$ <sup>21</sup> rather than by the paramagnetic anisotropy of the metal. On the other hand, the large  $^3J(\text{F}^5\text{--Pt})$  values could be indicative of a  $\text{Pt}\cdots\text{F}^5$  interaction. These two observations suggest apical  $\text{Pt}\cdots\text{H}$  and  $\text{Pt}\cdots\text{F}^5$  interactions in the formally square-planar compounds **5**. A similar situation has been detected crystallographically for a related palladium compound.<sup>22</sup>

**Structures of Compounds 4a and 4c.** The crystal structures are composed of discrete molecules separated by van der Waals distances. Crystallographic data are given in the Experimental Section, atomic coordinates are in Tables 1 and 2, and selected bond distances and angles are listed in Tables 3 and 4. The structures are

Table 1. Atomic Coordinates ( $\times 10^4$ ) with Esd's in Parentheses for the Non-Hydrogen Atoms of **4a**

	x	y	z
Pt	4052(1)	1208(1)	2389(1)
P	2364(2)	914(1)	1454(2)
N	4467(5)	2051(4)	1469(6)
F(1)	7540(6)	1087(4)	6100(7)
F(2)	8311(6)	2178(4)	5403(7)
F(3)	7245(5)	2777(3)	3317(7)
C(1)	5473(6)	1430(5)	3431(7)
C(2)	6069(8)	1139(5)	4486(10)
C(3)	7015(7)	1420(7)	5101(10)
C(4)	7408(9)	1913(6)	4779(11)
C(5)	6853(11)	2256(7)	3709(12)
C(6)	5919(7)	1990(6)	3075(9)
C(7)	5317(7)	2306(5)	1976(8)
C(8)	3920(7)	2301(4)	230(8)
C(9)	4000(7)	1869(5)	-876(8)
C(10)	3193(8)	1879(4)	-1889(7)
C(11)	3328(12)	1482(8)	-2971(12)
C(12)	4206(16)	1143(10)	-2993(18)
C(13)	5034(13)	1103(6)	-1928(13)
C(14)	4926(7)	1533(6)	-933(8)
C(15)	3995(8)	361(4)	3389(8)
C(16)	2429(6)	150(4)	629(7)
C(17)	1841(9)	-356(5)	868(9)
C(18)	2022(9)	-904(7)	197(11)
C(19)	2697(10)	-871(6)	-791(11)
C(20)	3279(10)	-355(7)	-968(14)
C(21)	3175(8)	136(5)	-306(11)
C(22)	1519(7)	1377(5)	274(9)
C(23)	1036(11)	1156(5)	-942(11)
C(24)	346(8)	1577(7)	-1718(12)
C(25)	136(8)	2119(6)	-1385(15)
C(26)	638(12)	2351(7)	-226(13)
C(27)	1249(7)	1929(6)	602(9)
C(28)	1379(7)	798(5)	2607(9)
C(29)	329(8)	662(7)	2254(11)
C(30)	-434(9)	604(8)	3090(13)
C(31)	-84(9)	743(7)	4349(10)
C(32)	925(13)	891(8)	4783(15)
C(33)	1684(8)	945(5)	3859(10)

shown in Figure 2 and 3 and confirm the geometry predicted from spectroscopic studies. In particular, the  $\text{C}=\text{N}$  group is *endo* to the cycle and the methyl group is *trans* to the nitrogen atom. In both compounds, the coordination sphere of platinum is square planar with a tetrahedral distortion. The following displacements (A) are observed from the least-squares plane of the coordination sphere for **4a**: Pt, -0.001; P, 0.077; N, -0.086; C(1), 0.105; C(15), -0.094. Displacements for **4c** are as follows: Pt, 0.017; P, 0.084; N, -0.111; C(1), 0.116; C(15), -0.107. The metallacycles are approximately planar; the largest deviation from the mean plane determined by the five atoms is -0.022 Å for C(1) in **4a** and 0.029 Å for C(1) in **4c**. The angle between the metallacycle and the coordination planes is 4.6° for **4a** and 5.3° for **4c**.

The angles between adjacent atoms in the coordination sphere of platinum lie in the range 107.4(2)–78.4(4)° for **4a** and 98.5(2)–77.5(2)° for **4c**, the smallest angles corresponding to the metallacycle. Pt–N and Pt–C(aryl) bond lengths in **4a,c** are well within the range of values obtained for cyclometalated platinum(II),<sup>23,24</sup> platinum(IV),<sup>5,7,8,25</sup> and palladium(II)<sup>26</sup> com-

(19) Pregosin, P. S.; Kunz, R. W. In  $^{31}\text{P}$  and  $^{13}\text{C}$  NMR of Transition Metal Phosphine Complexes; Diehl, P., Fluck, E., Kosfeld, R., Eds.; Springer-Verlag: Berlin, 1979; pp 42–45.

(20) (a) Albinati, A.; Pregosin, P. S.; Wombacher, F. *Inorg. Chem.* **1990**, *29*, 1812. (b) Albinati, A.; Anklin, C. G.; Ganazzoli, F.; Rüegg, H.; Pregosin, P. S. *Inorg. Chem.* **1987**, *26*, 503. (c) Albinati, A.; Arz, C.; Pregosin, P. S. *Inorg. Chem.* **1987**, *26*, 508.

(21) Brammer, L.; Charnock, J. M.; Goggin, P. L.; Goodfellow, R. J.; Orpen, A. G.; Koetzle, T. F. *J. Chem. Soc., Dalton Trans.* **1991**, 1789.

(22) Albert, J.; Granell, J.; Moragas, R.; Sales, J.; Solans, X. *J. Organomet. Chem.*, submitted for publication.

(23) (a) Stoccoro, S.; Cinellu, M. A.; Zucca, A.; Minghetti, G.; Demartin, F. *Inorg. Chim. Acta* **1994**, *215*, 17. (b) Cauty, A. J.; Minchin, N. J.; Patrick, J. M.; White, A. H. *J. Chem. Soc., Dalton Trans.* **1983**, 1253.

(24) Navarro-Ranninger, C.; López-Solera, I.; Alvarez-Valdés, A.; Rodríguez-Ramos, J. H.; Massagué, J. R.; García-Ruano, J. L.; Solans, X. *Organometallics* **1993**, *12*, 4104.

**Table 2. Atomic Coordinates ( $\times 10^4$ ) with Esd's in Parentheses for the Non-Hydrogen Atoms of 4c**

	x	y	z
Pt	3206(1)	2222(1)	103(1)
P	2054(1)	3431(1)	-1797(2)
F(1)	6189(4)	-1333(3)	4399(5)
F(2)	4432(4)	-1463(3)	1570(6)
N	2630(4)	1026(4)	-1165(6)
C(1)	4295(6)	1126(4)	1623(10)
C(2)	5234(6)	1172(5)	3117(8)
C(3)	5908(7)	396(7)	4025(9)
C(4)	5618(6)	-527(6)	3496(8)
C(5)	4726(6)	-540(6)	2034(8)
C(6)	4089(5)	268(6)	1188(7)
C(7)	3156(6)	229(6)	-384(8)
C(8)	1683(6)	1014(6)	-2746(8)
C(9)	739(5)	19(5)	-2800(7)
C(10)	-276(7)	-65(7)	-2466(8)
C(11)	-1123(7)	-976(7)	-2564(11)
C(12)	-920(9)	-1713(6)	-2975(10)
C(13)	104(10)	-1628(7)	-3331(9)
C(14)	910(7)	-796(5)	-3237(8)
C(15)	3787(8)	3091(6)	1722(10)
C(16)	2488(6)	3841(6)	-3459(7)
C(17)	2002(7)	4691(7)	-4715(9)
C(18)	2337(9)	4963(5)	-5901(10)
C(19)	3222(8)	4510(6)	-5987(9)
C(20)	3762(8)	3779(8)	-4865(10)
C(21)	3372(7)	3390(5)	-3527(8)
C(22)	386(6)	2970(5)	-2510(8)
C(23)	-415(6)	3032(6)	-3994(8)
C(24)	-1649(6)	2652(7)	-4446(11)
C(25)	-2122(8)	2207(8)	-3359(13)
C(26)	-1348(7)	2117(6)	-1783(10)
C(27)	-98(6)	2514(7)	-1397(9)
C(28)	2130(6)	4670(6)	-1436(8)
C(29)	3227(6)	5332(5)	-1095(9)
C(30)	3395(7)	6196(7)	-653(11)
C(31)	2424(9)	6523(8)	-582(13)
C(32)	1328(10)	5839(8)	-767(13)
C(33)	1154(7)	4973(6)	-1273(10)

pounds. Von Zelewsky has reported that Pt-N and Pt-C bond lengths are similar for platinum(II) and platinum(IV) complexes due to the similar radii of square-planar Pt(II) and octahedral Pt(IV).<sup>4</sup> Moreover, Navarro-Ranninger has reported similar M-C and M-N bond distances for palladium(II) and platinum(II) cyclometalated compounds.<sup>24</sup> The iminic bond distances are within the range observed for analogous cyclometalated palladium(II)<sup>26</sup> and platinum(II)<sup>24</sup> compounds.

A comparative study of structural features for the platinum(II) compounds **4a,c** and the previously reported platinum(II) [PtMe(C<sub>6</sub>H<sub>4</sub>CH=NCH<sub>2</sub>(2-C<sub>6</sub>H<sub>4</sub>Cl))-(PPh<sub>3</sub>)] (**4g**) and platinum(IV) [PtMe<sub>2</sub>Cl(2-C<sub>6</sub>H<sub>3</sub>Cl-CH=NCH<sub>2</sub>C<sub>6</sub>H<sub>5</sub>)(PPh<sub>3</sub>)] (**6**) compounds is reported in Table 5. An analysis of these values reveals that Pt-N and Pt-P bond lengths for fluorinated compounds **4a,c** are longer and shorter, respectively, than for **4g**. However, no significant differences in these parameters are found between **4a** and **4c**. Similarly, Pt-Me, *cis* to C(aryl), bond distances are longer for **4a,c** than for **4g**. These results suggest that the electron-withdrawing ability of the fluorinated rings produces stronger Pt-P bonds in *trans*, and weaker Pt-N and Pt-Me bonds in

**Table 3. Selected Bond Lengths (Å) and Angles (deg) for Compound 4a**

Bond Lengths			
P-Pt	2.303(2)	C(6)-C(1)	1.40(2)
N-Pt	2.156(8)	C(3)-C(2)	1.412(14)
C(1)-Pt	2.026(8)	C(4)-C(3)	1.24(2)
C(15)-Pt	2.118(9)	C(5)-C(4)	1.45(2)
C(16)-P	1.873(9)	C(6)-C(5)	1.396(14)
C(22)-P	1.826(10)	C(2)-C(1)	1.406(13)
C(28)-P	1.843(9)	C(7)-C(6)	1.467(14)
C(3)-F(1)	1.371(14)	C(8)-N	1.495(10)
C(4)-F(2)	1.360(11)	C(9)-C(8)	1.502(14)
C(5)-F(3)	1.31(2)	C(7)-N	1.256(11)
Bond Angles			
N-Pt-P	107.4(2)	F(1)-C(3)-C(2)	114.8(12)
C(1)-Pt-P	172.5(2)	C(3)-C(4)-F(2)	124.4(11)
C(1)-Pt-N	78.4(4)	C(3)-C(4)-C(5)	119.0(10)
C(15)-Pt-P	83.6(3)	F(2)-C(4)-C(5)	116.5(10)
C(15)-Pt-N	168.1(3)	F(3)-C(5)-C(6)	121.7(13)
C(15)-Pt-C(1)	91.0(4)	F(3)-C(5)-C(4)	121.4(10)
C(16)-P-Pt	110.6(2)	C(6)-C(5)-C(4)	116.8(12)
C(22)-P-Pt	124.1(3)	C(5)-C(6)-C(1)	124.4(11)
C(22)-P-C(16)	103.0(4)	C(5)-C(6)-C(7)	120.1(12)
C(28)-P-Pt	113.9(3)	C(1)-C(6)-C(7)	115.5(8)
C(28)-P-C(16)	104.6(5)	N-C(7)-C(6)	117.0(10)
C(28)-P-C(22)	98.3(4)	C(9)-C(8)-N	112.5(7)
C(7)-N-Pt	114.7(6)	C(10)-C(9)-C(8)	118.6(9)
C(8)-N-Pt	125.9(5)	C(14)-C(9)-C(8)	119.8(7)
C(8)-N-C(7)	118.9(8)	C(17)-C(16)-P	124.9(7)
C(2)-C(1)-Pt	131.7(8)	C(21)-C(16)-P	113.8(6)
C(6)-C(1)-Pt	114.2(7)	C(27)-C(22)-P	118.2(7)
C(6)-C(1)-C(2)	114.1(8)	C(23)-C(22)-P	124.7(8)
C(3)-C(2)-C(1)	120.1(11)	C(33)-C(28)-P	118.1(7)
C(4)-C(3)-C(2)	125.6(12)	C(29)-C(28)-P	123.4(8)
C(4)-C(3)-F(1)	119.5(10)		

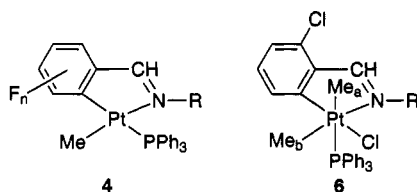
**Table 4. Selected Bond Lengths (Å) and Angles (deg) for Compound 4c**

Bond Lengths			
P-Pt	2.299(2)	C(6)-C(1)	1.302(9)
N-Pt	2.153(5)	C(3)-C(2)	1.358(11)
C(1)-Pt	2.051(7)	C(4)-C(3)	1.421(12)
C(15)-Pt	2.046(8)	C(5)-C(4)	1.381(10)
C(16)-P	1.805(6)	C(6)-C(5)	1.360(10)
C(22)-P	1.837(6)	C(2)-C(1)	1.429(10)
C(28)-P	1.814(7)	C(7)-C(6)	1.479(8)
C(4)-F(1)	1.330(8)	C(8)-N	1.485(8)
C(5)-F(2)	1.387(9)	C(9)-C(8)	1.548(9)
C(7)-N	1.275(9)		
Bond Angles			
N-Pt-P	98.5(2)	C(3)-C(4)-F(1)	120.2(6)
C(1)-Pt-P	173.8(2)	C(5)-C(4)-F(1)	122.7(6)
C(1)-Pt-N	77.5(2)	C(5)-C(4)-C(3)	117.1(7)
C(15)-Pt-P	92.5(2)	C(4)-C(5)-F(2)	115.7(6)
C(15)-Pt-N	167.3(3)	C(6)-C(5)-F(2)	122.6(6)
C(15)-Pt-C(1)	92.1(3)	C(6)-C(5)-C(4)	121.3(7)
C(16)-P-Pt	112.2(3)	C(5)-C(6)-C(1)	124.4(6)
C(22)-P-Pt	113.0(2)	C(7)-C(6)-C(1)	115.9(7)
C(22)-P-C(16)	106.6(3)	C(7)-C(6)-C(5)	119.5(7)
C(28)-P-Pt	120.5(2)	C(6)-C(7)-N	117.3(6)
C(28)-P-C(16)	100.0(3)	C(9)-C(8)-N	112.2(6)
C(28)-P-C(22)	102.9(3)	C(10)-C(9)-C(8)	121.0(7)
C(7)-N-Pt	113.0(4)	C(14)-C(9)-C(8)	119.7(6)
C(8)-N-Pt	128.1(5)	C(17)-C(16)-P	121.9(5)
C(8)-N-C(7)	118.8(5)	C(21)-C(16)-P	120.5(6)
C(2)-C(1)-Pt	128.3(5)	C(23)-C(22)-P	127.9(6)
C(6)-C(1)-Pt	116.1(5)	C(27)-C(22)-P	115.6(5)
C(6)-C(1)-C(2)	115.6(6)	C(29)-C(28)-P	120.5(5)
C(3)-C(2)-C(1)	123.3(7)	C(33)-C(28)-P	123.8(5)
C(4)-C(3)-C(2)	118.2(6)		

*cis*. We are tentative, however, about drawing conclusions from these structural values, since the differences in bond lengths are small and may be attributed to packing effects rather than to electronic effects. For instance, for *trans*-[PtX(C<sub>6</sub>H<sub>4</sub>Y)(PEt<sub>3</sub>)<sub>2</sub>] (X = Cl, Br, Y = *p*-NMe<sub>2</sub>, *p*-CF<sub>3</sub>, *p*-CO<sub>2</sub>Me, H, *m*-CN, *m*-NMe<sub>2</sub>) elec-

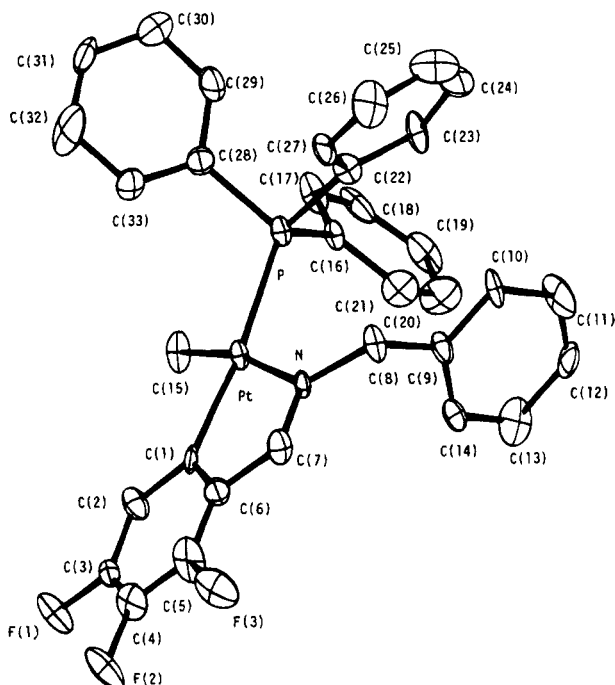
(25) (a) van Koten, G.; Terheiden, J.; van Beek, J. A. M.; Wehman-Ooyevaar, I. C. M.; Muller, F.; Stam, C. H. *Organometallics* **1990**, *9*, 903. (b) van Beek, J. A. M.; van Koten, G.; Wehman-Ooyevaar, I. C. M.; Smeets, W. J. J.; van der Sluis, P.; Spek, A. L. *J. Chem. Soc., Dalton Trans.* **1991**, 883.

(26) Albert, J.; Ceder, R. M.; Gómez, M.; Granell, J.; Sales, J. *Organometallics* **1992**, *11*, 1536.

**Table 5.** Bond Distances (Å) and Bond Angles (deg) for Cyclometalated Platinum(II) (4) and Platinum(IV) (6) Compounds of *N*-Benzylidenebenzylamines

compd <sup>a</sup>	Pt-CH <sub>3</sub>	Pt-C <sub>aryl</sub>	Pt-N	Pt-P	C=N	NPtC <sub>aryl</sub>
[PtMe(C <sub>6</sub> HF <sub>5</sub> CH=NR)(PPh <sub>3</sub> )] (4a)	2.118(9)	2.026(8)	2.156(8)	2.303(2)	1.256(11)	78.4(4)
[PtMe(C <sub>6</sub> H <sub>2</sub> F <sub>2</sub> CH=NR)(PPh <sub>3</sub> )] (4c)	2.046(8)	2.051(7)	2.153(5)	2.299(2)	1.275(9)	77.5(2)
[PtMe(C <sub>6</sub> H <sub>4</sub> CH=NR)(PPh <sub>3</sub> )] (4g) <sup>b</sup>	2.010(12)	1.973(10)	2.090(7)	2.334(3)	1.307(14)	79.3(5)
[PtMe <sub>2</sub> Cl(C <sub>6</sub> H <sub>3</sub> ClCH=NR)(PPh <sub>3</sub> )] (6) <sup>c</sup>	2.097(10) <sup>d</sup> 2.048(9) <sup>e</sup>	2.027(10)	2.152(7)	2.431(2)	1.291(11)	80.4(4)

<sup>a</sup> 4a, 4c, and 6, R = CH<sub>2</sub>C<sub>6</sub>H<sub>5</sub>; 4g, R = CH<sub>2</sub>(2-C<sub>6</sub>H<sub>4</sub>Cl). <sup>b</sup> Taken from ref 17. <sup>c</sup> Taken from ref 8. <sup>d</sup> Me<sub>a</sub>. <sup>e</sup> Me<sub>b</sub>.

**Figure 2.** View of the structure of 4a.

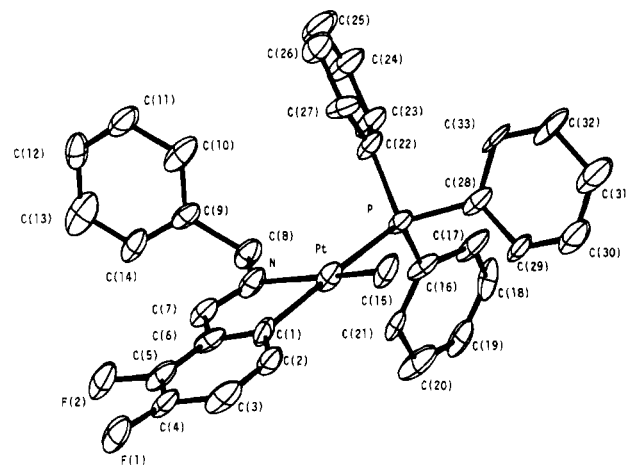
tronic effects of the substituents do not cause observable changes in the Pt-P bond lengths, although changes in <sup>1</sup>J(Pt-P) were observed.<sup>27</sup>

### Discussion

The results show that in [PtMe(RCH=NCH<sub>2</sub>C<sub>6</sub>H<sub>5</sub>)(SMe<sub>2</sub>)] the metallacycle can be cleaved by an excess of PPh<sub>3</sub> only if there is a fluorine atom in a position adjacent to the Pt-C(aryl) bond (position 5), irrespective of the fluorination of the ring, which is not decisive.

Unfortunately, no crystal structures of compounds 4 or 5 containing fluorine F<sup>5</sup> were obtained. However, spectroscopic data for these compounds are informative of the combined effects leading to a higher reactivity for *ortho*-platinated compounds bearing a fluorine adjacent to platinum.

The study of <sup>1</sup>J(P-Pt) values for compounds 4 reported in the previous section show that the electron-withdrawing ability of the aryl ring is more sensitive to the presence of a fluorine atom adjacent to platinum

**Figure 3.** View of the structure of 4c.

than to the total fluorination of the ring. This suggests that the presence of fluorine F<sup>5</sup> modifies the electronic distribution in the coordination sphere of platinum. Furthermore, the basicity of the iminic nitrogen decreases and, as a result, cleavage of the Pt-N bond occurs more readily.

On the other hand, steric repulsion between the methyl group and F<sup>5</sup> may account for the easier formation of compounds 5 when fluorine F<sup>5</sup>, adjacent to platinum, is present. The chelating nature of the iminic ligand in compounds 4 implies that F<sup>5</sup> should be in the coordination plane and, as reported above, it is coupled with the methyl group. Molecular models for compound 4b, based on the crystal structure of compound 4a, give a C...F distance of 2.617 Å. An analogous value (C...F = 2.773 Å) has been found in the molecular structure of CpRh(PMe<sub>3</sub>)(η<sup>2</sup>-C<sub>6</sub>F<sub>6</sub>),<sup>28</sup> and this value has been taken as an indication of a short contact between the methyl group and the fluorine, which are close enough for the van der Waals radii to overlap. Formation of compounds 5 with cleavage of the metallacycle would relieve the steric crowding in the coordination sphere of platinum.

It seems surprising that platinum(IV) metallacycles containing a pentafluorophenyl group such as [PtMe<sub>2</sub>F(C<sub>6</sub>F<sub>4</sub>CH=NCH<sub>2</sub>C<sub>6</sub>H<sub>5</sub>)(SMe<sub>2</sub>)] could not be cleaved

(28) Belt, S. T.; Helliwell, M.; Jones, W. D.; Partridge, M. G.; Perutz, R. N. *J. Am. Chem. Soc.* **1993**, *115*, 1429.

(29) Schmülling, M.; Ryabov, A. D.; van Eldik, R. *J. Chem. Soc., Chem. Commun.* **1992**, 1609.

with  $\text{PPh}_3$ .<sup>8</sup> This could be explained by the higher affinity of platinum(IV) for nitrogen donor ligands when compared to platinum(II). It is also worth noticing that, in octahedral platinum(IV) compounds, apical  $\text{Pt} \cdots \text{F}$  and  $\text{Pt} \cdots \text{H}$  interactions, as described for compounds **5** in the previous section, would be hindered. Although the main driving forces for the cleavage of the metallacycle are the stereoelectronic effects arising from the presence of  $\text{F}^5$ , the weak apical interactions may also account for the easy formation of compounds **5**.

### Conclusions

The reaction of  $[\text{Pt}_2\text{Me}_4(\mu\text{-SMe}_2)_2]$  (**1**) with di- or trifluorinated iminic ligands containing both C–F and C–H bonds in *ortho* positions produces exclusively C–H bond activation.

We have reported elsewhere<sup>10</sup> that the presence of a fluorine atom adjacent to the C–H bond to be activated in the iminic ligand is decisive in the selectivity of the metallacycle formation. The results reported here show that the position adjacent to the Pt–C(aryl) bond in platinum(II) metallacycles is also strategical in the *cis*-stabilization effect of the aryl group. Thus, the electronic and steric effects arising from the presence of a fluorine atom in this position have a more important effect on reactivity than the increase in fluorination.

For both platinum(II) and palladium(II), five-membered *endo* metallacycles are among the most stable. Nevertheless, platinacycles can be cleaved under mild conditions, provided that a fluorine atom is present in position 5. It has been shown that the reactivity of platinum(II) and palladium(II) complexes can be tuned by steric or electronic effects;<sup>27</sup> the results reported in this paper are a further example of reactivity tuning in platinum compounds.

### Experimental Section

<sup>1</sup>H, <sup>31</sup>P{<sup>1</sup>H}, <sup>19</sup>F, <sup>13</sup>C, and <sup>195</sup>Pt NMR spectra were recorded by using Varian Gemini 200 (<sup>1</sup>H, 200 MHz), Bruker WP80SY (<sup>31</sup>P, 32.4 MHz), and Varian XL 300FT (<sup>19</sup>F, 282.2 MHz; <sup>13</sup>C, 75.43 MHz; <sup>31</sup>P, 121.4 MHz; <sup>195</sup>Pt, 64.19 MHz) spectrometers and are referenced to  $\text{SiMe}_4$  (<sup>1</sup>H, <sup>13</sup>C),  $\text{H}_3\text{PO}_4$  (<sup>31</sup>P),  $\text{CCl}_3\text{F}$  (<sup>19</sup>F), and  $\text{H}_2\text{PtCl}_6$  in  $\text{D}_2\text{O}$  (<sup>195</sup>Pt).  $\delta$  values are given in ppm and *J* values in Hz. Microanalyses were performed by the Institut de Química Bio-Orgànica de Barcelona (CSIC) and by the Serveis Científic-Tècnics de la Universitat de Barcelona.

**Preparation of Compounds.** The complex  $[\text{Pt}_2\text{Me}_4(\mu\text{-SMe}_2)_2]$  (**1**) was prepared by the literature method.<sup>30</sup>

Compounds **2** were prepared by reaction of 5 mmol of the corresponding aldehyde with an equimolecular amount of the benzylamine in ethanol. The mixture was refluxed for 2 h, and the solvent was removed in a rotary evaporator to yield yellow oils.

**2,3,4-C<sub>6</sub>H<sub>2</sub>F<sub>3</sub>CHNCH<sub>2</sub>C<sub>6</sub>H<sub>5</sub> (2a).** <sup>1</sup>H NMR ( $\text{CDCl}_3$ ):  $\delta$  4.87 [s, CH<sub>2</sub>], 8.63 [s, CHN] {7.01 [m], 7.81 [m], 7.33 [m], aromatics}. <sup>19</sup>F NMR ( $\text{CDCl}_3$ ):  $\delta$  -137.17 [dd, <sup>3</sup>*J*(F<sup>2</sup>F<sup>3</sup>) = 21, <sup>4</sup>*J*(F<sup>2</sup>F<sup>4</sup>) = 9, F<sup>2</sup>], -149.50 [dt, <sup>4</sup>*J*(F<sup>4</sup>F<sup>3</sup>) = 21, <sup>4</sup>*J*(F<sup>4</sup>F<sup>2</sup>) = <sup>3</sup>*J*(F<sup>4</sup>H<sup>5</sup>) = 9, F<sup>4</sup>], -167.42 [dt, <sup>3</sup>*J*(F<sup>2</sup>F<sup>3</sup>) = <sup>3</sup>*J*(F<sup>4</sup>F<sup>3</sup>) = 21, <sup>4</sup>*J*(F<sup>3</sup>H<sup>5</sup>) = 6, F<sup>3</sup>].

**2,4,5-C<sub>6</sub>H<sub>2</sub>F<sub>3</sub>CHNCH<sub>2</sub>C<sub>6</sub>H<sub>5</sub> (2b).** <sup>1</sup>H NMR ( $\text{CDCl}_3$ ):  $\delta$  4.85 [s, CH<sub>2</sub>], 8.60 [s, CHN] {6.96 [m], 7.33 [m], 7.90 [m], aromatics}. <sup>19</sup>F NMR ( $\text{CDCl}_3$ ):  $\delta$  -130.25 [td, <sup>4</sup>*J*(F<sup>2</sup>F<sup>4</sup>) = <sup>3</sup>*J*(F<sup>2</sup>H) = 15, <sup>5</sup>*J*(F<sup>2</sup>F<sup>5</sup>) = 6, F<sup>2</sup>], -135.62 [dt, <sup>3</sup>*J*(F<sup>4</sup>F<sup>5</sup>) = 21, <sup>5</sup>*J*(F<sup>5</sup>F<sup>2</sup>) = <sup>4</sup>*J*(F<sup>5</sup>H<sup>3</sup>) = 6, F<sup>5</sup>], -148.35 [m, F<sup>4</sup>].

**2,3-C<sub>6</sub>H<sub>3</sub>F<sub>2</sub>CHNCH<sub>2</sub>C<sub>6</sub>H<sub>5</sub> (2c).** <sup>1</sup>H NMR ( $\text{CDCl}_3$ ):  $\delta$  4.87 [s, CH<sub>2</sub>], 8.63 [s, CHN] {7.01 [m], 7.33 [m], 7.81 [m], aromatics}.

<sup>19</sup>F NMR ( $\text{CDCl}_3$ ):  $\delta$  -145.32 [dt, *J*(FF) = 18, *J*(FH) = 6], -153.72 [dt, *J*(FF) = 18, *J*(FH) = 6].

Compounds **3** were prepared by reaction of 100 mg (0.17 mmol) of  $[\text{Pt}_2\text{Me}_4(\mu\text{-SMe}_2)_2]$  (**1**) with 0.35 mmol of the corresponding imine in acetone. The mixture was stirred for 16 h, and the solvent was removed in a rotary evaporator. The residue was washed in hexane and recrystallized in acetone/hexane to yield yellow-orange solids, which were filtered and washed with hexane.

**[PtMe(2,3,4-C<sub>6</sub>HF<sub>3</sub>CHNCH<sub>2</sub>C<sub>6</sub>H<sub>5</sub>)(SMe<sub>2</sub>) (3a).** Yield: 70 mg (77%). Mp: 141 °C dec. Anal. Calcd for  $\text{C}_{17}\text{H}_{18}\text{F}_3\text{NSPt}$ : C, 39.24; H, 3.49; N, 2.69. Found: C, 39.17; H, 3.63; N, 2.58. <sup>1</sup>H NMR (acetone-*d*<sub>6</sub>):  $\delta$  0.80 [s, <sup>2</sup>*J*(HPt) = 82, Me], 1.97 [s, <sup>3</sup>*J*(HPt) = 30, SMe<sub>2</sub>], 5.29 [s, <sup>3</sup>*J*(HPt) = 13, CH<sub>2</sub>], 9.10 [s, <sup>3</sup>*J*(HPt) = 56, CHN] {7.15 [m], 7.31 [m], aromatics}. <sup>19</sup>F NMR (acetone-*d*<sub>6</sub>):  $\delta$  -173.71 [td, <sup>5</sup>*J*(F<sup>3</sup>Pt) = 10, <sup>3</sup>*J*(F<sup>3</sup>F<sup>2</sup>) = <sup>3</sup>*J*(F<sup>3</sup>F<sup>4</sup>) = 19, <sup>4</sup>*J*(F<sup>3</sup>H<sup>5</sup>) = 7, F<sup>3</sup>], -141.62 [dd, <sup>4</sup>*J*(F<sup>2</sup>Pt) = 46, <sup>3</sup>*J*(F<sup>2</sup>F<sup>3</sup>) = 19, <sup>4</sup>*J*(F<sup>2</sup>F<sup>4</sup>) = 7, F<sup>2</sup>], -133.86 [m, <sup>4</sup>*J*(F<sup>4</sup>Pt) = 58, <sup>3</sup>*J*(F<sup>4</sup>F<sup>3</sup>) = 19, <sup>3</sup>*J*(F<sup>4</sup>H) = 11, <sup>4</sup>*J*(F<sup>4</sup>F<sup>2</sup>) = 7, F<sup>4</sup>]. <sup>13</sup>C NMR (acetone-*d*<sub>6</sub>):  $\delta$  -12.73 [s, <sup>1</sup>*J*(CPT) = 791, Me], 19.69 [s, SMe<sub>2</sub>], 62.96 [s, CH<sub>2</sub>], 114.78 [d, <sup>2</sup>*J*(CF) = 9, <sup>2</sup>*J*(CPT) = 97, C<sup>5</sup> in C<sub>6</sub>HF<sub>3</sub>] {128.10 [s], 128.35 [s], 129.19 [s], aryl carbons in C<sub>6</sub>H<sub>5</sub>}, 138.33 [s, C<sup>6</sup> in C<sub>6</sub>HF<sub>3</sub>], 169.55 [s, <sup>2</sup>*J*(CPT) = 82, CHN].

**[PtMe(2,4,5-C<sub>6</sub>HF<sub>3</sub>CHNCH<sub>2</sub>C<sub>6</sub>H<sub>5</sub>)(SMe<sub>2</sub>) (3b).** Yield: 75 mg (83%). Mp: 145 °C dec. Anal. Calcd for  $\text{C}_{17}\text{H}_{18}\text{F}_3\text{NSPt}$ : C, 39.24; H, 3.49; N, 2.69. Found: C, 39.45; H, 3.70; N, 2.62. <sup>1</sup>H NMR (acetone-*d*<sub>6</sub>):  $\delta$  1.15 [d, <sup>2</sup>*J*(HPt) = 80, <sup>5</sup>*J*(HF<sub>5</sub>) = 6, Me], 1.94 [s, <sup>3</sup>*J*(HPt) = 33, SMe<sub>2</sub>], 5.25 [s, <sup>3</sup>*J*(HPt) = 13, CH<sub>2</sub>], 9.18 [s, <sup>3</sup>*J*(HPt) = 55, CHN] {6.8 [m], 7.31 [m], aromatics}. <sup>19</sup>F NMR (acetone-*d*<sub>6</sub>):  $\delta$  -130.78 [td, <sup>3</sup>*J*(F<sup>5</sup>Pt) = 140.4, <sup>3</sup>*J*(F<sup>5</sup>F<sup>4</sup>) = <sup>5</sup>*J*(F<sup>5</sup>F<sup>2</sup>) = 18, <sup>4</sup>*J*(F<sup>5</sup>H<sup>3</sup>) = 6, F<sup>5</sup>], -129.65 [dt, <sup>4</sup>*J*(F<sup>4</sup>Pt) = 128, <sup>3</sup>*J*(F<sup>4</sup>F<sup>5</sup>) = 18, <sup>4</sup>*J*(F<sup>4</sup>F<sup>2</sup>) = <sup>3</sup>*J*(F<sup>4</sup>H) = 6, F<sup>4</sup>], -120.62 [dd, <sup>4</sup>*J*(F<sup>2</sup>Pt) = 67, <sup>5</sup>*J*(F<sup>2</sup>F<sup>5</sup>) = 18, <sup>4</sup>*J*(F<sup>2</sup>F<sup>4</sup>) = 6, F<sup>2</sup>]. <sup>13</sup>C NMR (acetone-*d*<sub>6</sub>):  $\delta$  -22.18 [d, <sup>4</sup>*J*(CF) = 17, <sup>1</sup>*J*(CPT) = 715, Me], 19.82 [s, SMe<sub>2</sub>], 63.20 [s, CH<sub>2</sub>], 101.041 [t, <sup>2</sup>*J*(CF) = 24, C<sup>3</sup> in C<sub>6</sub>HF<sub>3</sub>] {128.75 [s], 128.97 [s], 129.90 [s], aryl carbons in C<sub>6</sub>H<sub>5</sub>}, 139.13 [s, <sup>1</sup>*J*(CPT) = 1064, C<sup>6</sup> in C<sub>6</sub>HF<sub>3</sub>], 171.23 [s, <sup>2</sup>*J*(CPT) = 83, CHN].

**[PtMe(2,3-C<sub>6</sub>H<sub>2</sub>F<sub>2</sub>CHNCH<sub>2</sub>C<sub>6</sub>H<sub>5</sub>)(SMe<sub>2</sub>) (3c).** Yield: 70 mg (80%). Mp: 159 °C dec. Anal. Calcd for  $\text{C}_{17}\text{H}_{18}\text{F}_2\text{NSPt}$ : C, 40.69; H, 3.81; N, 2.79. Found: C, 39.58; H, 3.97; N, 2.65. <sup>1</sup>H NMR (acetone-*d*<sub>6</sub>):  $\delta$  0.84 [s, <sup>2</sup>*J*(HPt) = 82, Me], 1.97 [s, <sup>3</sup>*J*(HPt) = 28, SMe<sub>2</sub>], 5.29 [s, <sup>3</sup>*J*(HPt) = 13, CH<sub>2</sub>], 9.15 [s, <sup>3</sup>*J*(HPt) = 56, CHN], 7.30 [m, aromatics]. <sup>19</sup>F NMR (acetone-*d*<sub>6</sub>):  $\delta$  -145.81 [dd, <sup>4</sup>*J*(F<sup>2</sup>Pt) = 49, <sup>3</sup>*J*(F<sup>2</sup>F<sup>3</sup>) = 18, <sup>4</sup>*J*(F<sup>2</sup>H) = 6, F<sup>2</sup>], -151.29 [m, <sup>3</sup>*J*(F<sup>3</sup>F<sup>2</sup>) = 18, <sup>3</sup>*J*(F<sup>3</sup>H<sup>4</sup>) = 12, <sup>4</sup>*J*(F<sup>3</sup>H<sup>5</sup>) = 6, F<sup>3</sup>]. <sup>13</sup>C NMR (acetone-*d*<sub>6</sub>):  $\delta$  -13.30 [s, <sup>1</sup>*J*(CPT) = 797, Me], 19.56 [s, SMe<sub>2</sub>], 63.01 [s, CH<sub>2</sub>], 120.28 [d, <sup>2</sup>*J*(CF) = 15, <sup>2</sup>*J*(CPT) = 87, C<sup>5</sup> in C<sub>6</sub>HF<sub>3</sub>] {128.05 [s], 128.36 [s], 129.16 [s], aryl carbons in C<sub>6</sub>H<sub>5</sub>} {131.49 [s], 138.45 [s], aryl carbons} 170.02 [s, <sup>2</sup>*J*(CPT) = 87, CHN].

**4a** was prepared by reaction of 50 mg (0.096 mmol) of **3a** with an equimolar amount of  $\text{PPh}_3$  in acetone. The mixture was stirred at room temperature for 2 h. On addition of hexane, yellow crystals were formed, and they were collected by filtration, washed with hexane, and dried *in vacuo*. **4c–f** were prepared by an analogous procedure from the corresponding compounds **3**. Compound **4b** was best obtained by crystallization from the reaction mixture of **3b** with less than the equimolar amount of  $\text{PPh}_3$ . Suitable crystals for crystallographic analyses of **4a, c** were grown by slow evaporation from an acetone–hexane solution.

**5b** was prepared by reaction of 50 mg (0.096 mmol) of **3b** with 2 equiv of  $\text{PPh}_3$  in acetone. Within 1 h, the color of the solution faded and a white precipitate was formed. After addition of hexane, the white solid was collected by filtration, washed with hexane, and dried *in vacuo*. Compounds **5d, f** were prepared by an analogous procedure from the corresponding compounds **3**.

**[PtMe(2,3,4-C<sub>6</sub>HF<sub>3</sub>CHNCH<sub>2</sub>C<sub>6</sub>H<sub>5</sub>)(PPh<sub>3</sub>) (4a).** Yield: 50 mg (72%). Mp: 182 °C dec. Anal. Calcd for  $\text{C}_{33}\text{H}_{27}\text{F}_3\text{NPt}$ : C, 55.00; H, 3.78; N, 1.94. Found: C, 55.07; H, 3.77; N, 1.93. <sup>1</sup>H NMR (acetone-*d*<sub>6</sub>):  $\delta$  0.61 [d, <sup>2</sup>*J*(HPt) = 83, <sup>3</sup>*J*(HP) = 7,

(30) Scott, J. D.; Puddephatt, R. J. *Organometallics* **1983**, *2*, 1643.

Me], 4.38 [s,  $^3J(\text{HPt}) = 10$ , CH<sub>2</sub>], 8.80 [s,  $^3J(\text{HPt}) = 56$ , CHN] {6.80 [m], 7.19 [m], 7.42 [m], 7.60 [m], aromatics}.  $^{19}\text{F}$  NMR (acetone-*d*<sub>6</sub>):  $\delta -172.67$  [td,  $^3J(\text{F}^3\text{F}^2) = ^3J(\text{F}^3 - \text{F}^2) = 19$ ,  $^4J(\text{F}^3\text{H}^5) = 7$ , F<sup>3</sup>],  $-141.62$  [dt,  $^4J(\text{F}^2\text{Pt}) = 51$ ,  $^3J(\text{F}^2\text{F}^3) = 19$ ,  $^4J(\text{F}^2\text{F}^4) = ^5J(\text{F}^2\text{H}^5) = 7$ , F<sup>2</sup>],  $-133.43$  [m,  $^4J(\text{F}^4\text{Pt}) = 69$ , F<sup>4</sup>].  $^{31}\text{P}$  NMR (acetone):  $\delta 28.66$  [s,  $^1J(\text{PPt}) = 2387$ ].

[PtMe(2,4,5-C<sub>6</sub>H<sub>3</sub>HF<sub>3</sub>CHNCH<sub>2</sub>C<sub>6</sub>H<sub>5</sub>)(PPh<sub>3</sub>)<sub>2</sub>] (4b). Mp: 197 °C dec. Anal. Calcd for C<sub>33</sub>H<sub>27</sub>F<sub>3</sub>NPt: C, 55.00; H, 3.78; N, 1.94. Found: C, 54.98; H, 3.76; N, 1.85.  $^1\text{H}$  NMR (acetone-*d*<sub>6</sub>):  $\delta 0.99$  [dd,  $^2J(\text{HPt}) = 87$ ,  $^3J(\text{HP}) = 9$ ,  $^5J(\text{HF}^5) = 6$ , Me], 4.27 [s,  $^3J(\text{HPt}) = 11$ , CH<sub>2</sub>], 8.82 [s,  $^3J(\text{HPt}) = 54$ , CHN].  $^{19}\text{F}$  NMR (acetone-*d*<sub>6</sub>):  $\delta -120.78$  [m,  $^4J(\text{F}^2\text{Pt}) = 63$ ,  $^4J(\text{F}^2\text{F}^4) = 10$ ,  $^5J(\text{F}^2\text{F}^5) = 20$ ,  $^3J(\text{F}^2\text{H}) = 8$ , F<sup>2</sup>],  $-129.11$  [m,  $^4J(\text{F}^4\text{Pt}) = 104$ ,  $^3J(\text{F}^4\text{F}^5) = 20$ ,  $^4J(\text{F}^4\text{F}^2) = ^3J(\text{F}^4\text{H}) = 10$ ,  $^6J(\text{F}^4\text{H}^a) = 5$ , F<sup>4</sup>],  $-130.94$  [m,  $^3J(\text{F}^5\text{Pt}) = 87$ ,  $^3J(\text{F}^5\text{F}^4) = ^5J(\text{F}^5\text{F}^2) = 20$ ,  $^4J(\text{F}^5\text{H}^3) = ^5J(\text{F}^5\text{Me}) = 6$ , F<sup>5</sup>].  $^{31}\text{P}$  NMR (acetone):  $\delta 27.16$  [s,  $^1J(\text{PPt}) = 2651$ ].

[PtMe(2,3-C<sub>6</sub>H<sub>2</sub>F<sub>2</sub>CHNCH<sub>2</sub>C<sub>6</sub>H<sub>5</sub>)(PPh<sub>3</sub>)<sub>2</sub>] (4c). Yield: 57 mg (81%). Mp: 189 °C dec. Anal. Calcd for C<sub>33</sub>H<sub>28</sub>F<sub>2</sub>NPt: C, 56.41; H, 4.02; N, 1.99. Found: C, 56.42; H, 3.99; N, 1.98.  $^1\text{H}$  NMR (acetone-*d*<sub>6</sub>):  $\delta 0.65$  [d,  $^2J(\text{HPt}) = 83$ ,  $^3J(\text{HP}) = 7$ , Me], 4.40 [s,  $^3J(\text{HPt}) = 10$ , CH<sub>2</sub>], 8.82 [s,  $^3J(\text{HPt}) = 56$ , CHN] {6.85 [m], 7.19 [m], 7.41 [m], 7.61 [m], aromatics}.  $^{19}\text{F}$  NMR (acetone-*d*<sub>6</sub>):  $\delta -146.47$  [dt,  $^4J(\text{F}^2\text{Pt}) = 38$ ,  $^5J(\text{F}^2\text{F}^3) = 19$ ,  $^3J(\text{F}^2\text{H}) = 7$ , F<sup>2</sup>],  $-150.49$  [m,  $^3J(\text{F}^2\text{F}^3) = 19$ ,  $^3J(\text{F}^3\text{H}_4) = 11$ ,  $^4J(\text{F}^3\text{H}) = 5$ , F<sup>3</sup>].  $^{31}\text{P}$  NMR (acetone):  $\delta 29.18$  [s,  $^1J(\text{PPt}) = 2294$ ].

[PtMe(3,5-C<sub>6</sub>H<sub>2</sub>F<sub>2</sub>CHNCH<sub>2</sub>(2-C<sub>6</sub>H<sub>4</sub>Cl))(PPh<sub>3</sub>)<sub>2</sub>] (4d). Yield: 46.0 mg (70%). Mp: 162 °C dec. Anal. Calcd for C<sub>33</sub>H<sub>27</sub>ClF<sub>2</sub>NPt: C, 53.77; H, 3.69; N, 1.90. Found: C, 53.88; H, 3.81; N, 1.86.  $^1\text{H}$  NMR (acetone-*d*<sub>6</sub>):  $\delta 1.01$  [dd,  $^2J(\text{HPt}) = 83$ ,  $^3J(\text{HP}) = 9$ ,  $^5J(\text{HF}^5) = 6$ , Me], 4.29 [s,  $^3J(\text{HPt})$  as shoulders, CH<sub>2</sub>], 8.57 [s,  $^3J(\text{HPt}) = 54$ , CHN] {6.75 [m], 7.17 [m], 7.41 [m], 7.67 [m], aromatics}.  $^{19}\text{F}$  NMR (acetone-*d*<sub>6</sub>):  $\delta -94.55$  [m,  $^3J(\text{F}^5\text{Pt}) = 62$ , F<sup>5</sup>],  $-121.26$  [m, F<sup>3</sup>].  $^{31}\text{P}$  NMR (acetone):  $\delta 28.00$  [s,  $^1J(\text{PPt}) = 2549$ ].

[PtMe(2-C<sub>6</sub>H<sub>3</sub>FCHNCH<sub>2</sub>(2-C<sub>6</sub>H<sub>4</sub>Cl))(PPh<sub>3</sub>)<sub>2</sub>] (4e). Yield: 49.9 mg (72%). Mp: 167 °C dec. Anal. Calcd for C<sub>33</sub>H<sub>28</sub>ClFNPt: C, 55.12; H, 3.92; N, 1.95. Found: C, 55.51; H, 3.90; N, 2.02.  $^1\text{H}$  NMR (acetone-*d*<sub>6</sub>):  $\delta 0.75$  [d,  $^2J(\text{HPt}) = 83$ ,  $^3J(\text{HP}) = 8$ , Me], 4.44 [s,  $^3J(\text{HPt}) = 10$ , CH<sub>2</sub>], 8.75 [s,  $^3J(\text{HPt}) = 55$ , CHN] {6.75 [m], 7.25 [m], 7.44 [m], 7.69 [m], aromatics}.  $^{19}\text{F}$  NMR (acetone-*d*<sub>6</sub>):  $\delta -119.92$  [dd,  $^4J(\text{F}^2\text{Pt}) = 46$ ,  $^3J(\text{F}^2\text{H}^3) = 15$ ,  $^4J(\text{F}^2\text{H}^4) = 9$ , F<sup>2</sup>].  $^{31}\text{P}$  NMR (acetone):  $\delta 28.97$  [s,  $^1J(\text{PPt}) = 2246$ ].

[PtMe(5-C<sub>6</sub>H<sub>3</sub>FCHNCH<sub>2</sub>(2-C<sub>6</sub>H<sub>4</sub>Cl))(PPh<sub>3</sub>)<sub>2</sub>] (4f). Yield: 45.0 mg (65%). Mp: 177 °C dec. Anal. Calcd for C<sub>33</sub>H<sub>28</sub>ClFNPt: C, 55.12; H, 3.92; N, 1.95. Found: C, 54.90; H, 3.89; N, 1.91.  $^1\text{H}$  NMR (acetone-*d*<sub>6</sub>):  $\delta 1.02$  [dd,  $^2J(\text{HPt}) = 84$ ,  $^3J(\text{HP}) = 9$ ,  $^5J(\text{HF}^5) = 7$ , Me], 4.29 [s,  $^3J(\text{HPt}) = 11$ , CH<sub>2</sub>], 8.55 [s,  $^3J(\text{HPt}) = 55$ , CHN], {7.19 [m], 7.39 [m], 7.65 [m], aromatics}.  $^{19}\text{F}$  NMR (acetone-*d*<sub>6</sub>):  $\delta -98.29$  [m,  $^3J(\text{F}^5\text{Pt}) = 63$ , F<sup>5</sup>].  $^{31}\text{P}$  NMR (acetone):  $\delta 28.09$  [s,  $^1J(\text{PPt}) = 2479$ ].

[PtMe(2,4,5-C<sub>6</sub>H<sub>3</sub>HF<sub>3</sub>CHNCH<sub>2</sub>C<sub>6</sub>H<sub>5</sub>)(PPh<sub>3</sub>)<sub>2</sub>] (5b). Yield: 80 mg (85%). Mp: 110–115 °C dec. Anal. Calcd for C<sub>51</sub>H<sub>42</sub>F<sub>3</sub>NP<sub>2</sub>Pt: C, 62.32; H, 4.31; N, 1.42. Found: C, 61.80; H, 4.20; N, 1.38.  $^1\text{H}$  NMR (acetone-*d*<sub>6</sub>):  $\delta 0.23$  [dd,  $^2J(\text{HPt}) = 63$ ,  $^3J(\text{HP}_A) = 8$ ,  $^3J(\text{HP}_B) = 6$ , Me] {4.84 (d), 5.02 (d),  $^2J(\text{HH}) = 14$ , CH<sub>2</sub>, AB pattern}, 9.00 [s, CHN], 6.34 [m, C<sub>6</sub>H<sub>5</sub>F<sub>3</sub>] {7.06 [m], 7.24 [m], 7.36 [m], aromatics}.  $^{19}\text{F}$  NMR (acetone-*d*<sub>6</sub>):  $\delta -120.17$  [m,  $^3J(\text{F}^5\text{Pt}) = 464$ , F<sup>5</sup>],  $-121.28$  [m,  $^5J(\text{F}^2\text{F}^5) = 18$ ,  $^4J(\text{F}^2\text{F}^4) = 11$ ,  $^3J(\text{F}^2\text{H}^3) = 7$ , no Pt satellites, F<sup>2</sup>],  $-137.53$  [m,  $^4J(\text{F}^4\text{Pt}) = 114$ ,  $^3J(\text{F}^4\text{F}^5) = 34$ ,  $^4J(\text{F}^4\text{F}^2) = ^3J(\text{F}^4\text{H}^3) = 10$ ,  $^5J(\text{F}^4\text{H}^a) = 4$ , F<sup>4</sup>].  $^{31}\text{P}$  NMR (acetone):  $\delta 25.69$  [m,  $^1J(\text{P}_A\text{Pt}) = 2379$ , P<sub>A</sub>], 25.39 [d,  $^1J(\text{P}_B\text{Pt}) = 1972$ ,  $^2J(\text{P}_A\text{P}_B) = 16$ , P<sub>B</sub>].  $^{195}\text{Pt}$  NMR (acetone):  $\delta -4633.02$  [m,  $^1J(\text{Pt}-\text{P}_A) = 24.30$ ,  $^1J(\text{Pt}-\text{P}_B) = 1970$ ,  $^3J(\text{Pt}-\text{F}^5) = 444$ ,  $^4J(\text{Pt}-\text{F}^4) = 111$ ].

[PtMe(3,5-C<sub>6</sub>H<sub>2</sub>F<sub>2</sub>CHNCH<sub>2</sub>(2-C<sub>6</sub>H<sub>4</sub>Cl))(PPh<sub>3</sub>)<sub>2</sub>] (5d). Yield: 70 mg (75%). Mp: 147 °C dec. Anal. Calcd for C<sub>51</sub>H<sub>42</sub>ClF<sub>2</sub>NP<sub>2</sub>Pt: C, 61.29; H, 4.23; N, 1.40. Found: C, 60.81; H, 4.27; N, 1.35.  $^1\text{H}$  NMR (acetone-*d*<sub>6</sub>):  $\delta 0.25$  [dd,  $^2J(\text{HPt}) = 64$ ,  $^3J(\text{HP}_A) = 8$ ,  $^3J(\text{HP}_B) = 7$ , Me] {4.81 (d), 4.95 (d),  $^2J(\text{HH})$

Table 6. Crystallographic Data and Details of the Refinements for Compounds 4a,c

	4a	4c
formula	C <sub>33</sub> H <sub>27</sub> F <sub>3</sub> NPt	C <sub>33</sub> H <sub>28</sub> F <sub>2</sub> NPt
fw	720.67	702.66
cryst syst	monoclinic	triclinic
space group	P2 <sub>1</sub> /c	P $\bar{1}$
a, Å	12.475(3)	12.031(2)
b, Å	21.642(5)	13.757(2)
c, Å	10.497(2)	9.768(2)
$\alpha$ , deg	90	72.91(2)
$\beta$ , deg	96.92(2)	114.91(1)
$\gamma$ , deg	90	104.20(2)
V, Å <sup>3</sup>	2813.4(11)	1387.7(7)
D <sub>c</sub> , g cm <sup>-3</sup>	1.703	1.681
Z	4	2
F(000)	1412.0	688.0
cryst size, mm <sup>3</sup>	0.1 × 0.1 × 0.2	0.1 × 0.1 × 0.2
$\mu(\text{Mo K}\alpha)$ , cm <sup>-1</sup>	53.49	54.14
$\lambda(\text{Mo K}\alpha)$ , Å	0.710 69	0.710 69
T, K	293	298
no. of rflns collected	5140	5677
R	0.048	0.031
R <sub>w</sub> (F <sup>2</sup> )	0.112	0.078
no. of refined params	354	346
max shift/esd	0.1	0.1
max and min diff peaks, e Å <sup>-3</sup>	+1.7 and -1.3	+0.4 and -0.4

= 15, CH<sub>2</sub>, AB pattern], 9.50 [s, CHN], 6.10 [m, C<sub>6</sub>H<sub>2</sub>F<sub>2</sub>] {7.00 [m], 7.15 [m], 7.35 [m], aromatics}.  $^{19}\text{F}$  NMR (acetone-*d*<sub>6</sub>):  $\delta -88.85$  [m,  $^3J(\text{F}^5\text{Pt}) = 371$ ,  $^4J(\text{F}^5\text{P}) = 13$ ,  $^3J(\text{F}^5\text{H}^4) = ^4J(\text{F}^5\text{F}^3) = 7$ , F<sup>5</sup>],  $-124.72$  [m, F<sup>2</sup>].  $^{31}\text{P}$  NMR (acetone):  $\delta 24.16$  [t,  $^1J(\text{P}_A-\text{Pt}) = 2234$ ,  $^2J(\text{P}_A\text{P}_B) = ^4J(\text{P}_A\text{F}^5) = 14$ , P<sub>A</sub>], 23.07 [d,  $^1J(\text{P}_B\text{Pt}) = 1928$ ,  $^2J(\text{P}_A\text{P}_B) = 14$ , P<sub>B</sub>].  $^{195}\text{Pt}$  NMR (acetone):  $\delta -4630.59$  [m,  $^1J(\text{Pt}-\text{P}_A) = 2238$ ,  $^1J(\text{Pt}-\text{P}_B) = 1916$ ,  $^3J(\text{Pt}-\text{F}^5) = 371$ ].

[PtMe(5-C<sub>6</sub>H<sub>3</sub>FCHNCH<sub>2</sub>(2-C<sub>6</sub>H<sub>4</sub>Cl))(PPh<sub>3</sub>)<sub>2</sub>] (5f). Yield: 50 mg (53%). Mp: 152 °C dec. Anal. Calcd for C<sub>51</sub>H<sub>43</sub>ClFNP<sub>2</sub>Pt: C, 62.41; H, 4.42; N, 1.40. Found: C, 61.98; H, 4.20; N, 1.41.  $^1\text{H}$  NMR (acetone-*d*<sub>6</sub>):  $\delta 0.26$  [dd,  $^2J(\text{HPt}) = 65$ ,  $^3J(\text{HP}_A) = 9$ ,  $^3J(\text{HP}_B) = 6$ , Me] {4.81 (d), 4.94 (d),  $^2J(\text{HH}) = 15$ , CH<sub>2</sub>, AB pattern}, 9.52 [s,  $^3J(\text{HPt}) = 9$ , CHN] {6.60 (m), 6.30 (m), C<sub>6</sub>H<sub>3</sub>F} {7.06 [m], 7.24 [m], 7.36 [m], aromatics}.  $^{19}\text{F}$  NMR (acetone-*d*<sub>6</sub>):  $\delta -92.51$  [m,  $^3J(\text{F}^5\text{Pt}) = 377$ ,  $^4J(\text{F}^5\text{P}) = 13$ ,  $^3J(\text{F}^5\text{H}^4) = 6$ , F<sup>5</sup>].  $^{31}\text{P}$  NMR (acetone):  $\delta 24.13$  [t,  $^1J(\text{P}_A\text{Pt}) = 2175$ ,  $^2J(\text{P}_A\text{P}_B) = ^4J(\text{P}_A\text{F}^5) = 14$ , P<sub>A</sub>], 23.17 [d,  $^1J(\text{P}_B\text{Pt}) = 1930$ ,  $^2J(\text{P}_A\text{P}_B) = 14$ , P<sub>B</sub>].  $^{195}\text{Pt}$  NMR (acetone):  $\delta -4627.20$  [m,  $^1J(\text{Pt}-\text{P}_A) = 2202$ ,  $^1J(\text{Pt}-\text{P}_B) = 1930$ ,  $^3J(\text{Pt}-\text{F}^5) = 377$ ].

**X-ray Structure Analysis. Data Collection.** Prismatic crystals (0.1 × 0.1 × 0.2 mm) were selected and mounted on a Philips PW-1100 diffractometer (4a) or an Enraf-Nonius CAD4 diffractometer (4c). Unit cell parameters were determined from automatic centering of 25 reflections (8° ≤ θ ≤ 12°, 4a; 12° ≤ θ ≤ 21°, 4c) and refined by the least-squares method. Intensities were collected with graphite-monochromatized Mo Kα radiation, using the ω/2θ scan technique. For 4a, 5271 reflections were measured in the range 2° ≤ θ ≤ 30°; 5140 were independent reflections, and 5089 were assumed as observed by applying the condition I ≥ 2σ(I). For 4c, 5677 reflections were measured in the range 2° ≤ θ ≤ 30°, 3925 of which were assumed as observed by applying the condition I ≥ 2.5σ(I). Three reflections were measured every 2 h as orientation and intensity controls; significant intensity decay was not observed. Lorentz-polarization and absorption corrections were made. Further details are given in Table 6.

**Structure Solution and Refinement.** The structures were solved by Patterson synthesis, using the SHELXS computer program,<sup>31</sup> and refined by the full-matrix least-squares method, with the SHELXL93<sup>32</sup> computer program.

The function minimized was  $\sum w(|F_o| - |F_c|)^2$ , where  $w = (\sigma^2(F_o) + (0.1254P)^2 + 2.1781P)^{-1}$  for 4a and  $w = (\sigma^2(F_o) +$

(31) Sheldrick, G. M. *Acta Crystallogr.* 1990, A46, 467.

(32) Sheldrick, G. M. SHELX93: A computer program for crystal structure refinement; University of Gottingen, Germany, 1993.



$(0.2530P)^2 + 17.055P)^{-1}$  for **4c** and  $P = (F_o^2 + 2F_c^2)/3$ .  $f$ ,  $f'$ , and  $f''$  were taken from ref 33. All H atoms were computed and refined with an overall isotropic temperature factor, using a riding model. The final  $R$  factors, the number of refined parameters, and the maximum and minimum peaks in the final difference synthesis are given in Table 6.

**Acknowledgment.** We thank Drs. J. Albert and J. Granell for kindly providing a manuscript of their recent

---

(33) *International Tables of X-Ray Crystallography*; Kynoch Press: Birmingham, U.K., 1974; Vol. IV, pp 89–100, 149.

work. We acknowledge financial support from the DGICYT (Ministerio de Educación y Ciencia, Spain, project PB 93-0804) and a loan of  $K_2PtCl_4$  from Johnson Matthey Inc.

**Supplementary Material Available:** Tables of hydrogen coordinates, anisotropic thermal parameters, least-squares planes and atomic deviations, and all bond lengths and angles (12 pages). Ordering information is given on any current masthead page.

OM940453A

# Synthesis and Evaluation of the Bonding Properties toward Rhodium(I) of 2,5-Bis[3-(diphenylphosphino)propyl]thiophene: A New Versatile Ligand with $\eta^2$ , $\eta^3$ , and $\eta^7$ Modes of Bonding

Marie Alvarez, Noël Lugan, Bruno Donnadieu, and René Mathieu\*

Laboratoire de Chimie de Coordination du CNRS, UPR 8241, lié par conventions à l'Université Paul Sabatier et à l'Institut National Polytechnique, 205 route de Narbonne, 31077 Toulouse Cedex, France

Received June 14, 1994<sup>®</sup>

The new ligand 2,5-bis[3-(diphenylphosphino)propyl]thiophene (**2**) has been synthesized in four steps from thiophene, and its bonding capabilities with Rh(I) have been evaluated. With (COD)Rh(acac) in the presence of perchloric acid, the complex [(COD)Rh(**2**)](ClO<sub>4</sub>) (**3**) has been obtained but its low solubility suggests a polymeric structure. The 1,5-cyclooctadiene ligand is displaced by CO, leading to complexes that are in equilibrium, depending on the partial pressure of CO. Under a CO atmosphere, only the complex [Rh(CO)<sub>3</sub>(**2**)](ClO<sub>4</sub>) (**4**) is present in solution and its spectroscopic data are consistent with a trigonal-bipyramidal structure in which the two phosphorus atoms are in axial positions. Progressive decarbonylation causes the formation of [Rh(CO)<sub>2</sub>(**2**)](ClO<sub>4</sub>) as a mixture of cis (**5**) and trans (**6**) isomers (ligand **2** being bidentate through the phosphorus atoms) and of [Rh(CO)(**2**)](ClO<sub>4</sub>) (**7**), in which **2** is tridentate binding through the two phosphorus atoms and the sulfur of the thiophene ring. Complete decarbonylation of **7** is achieved through refluxing in acetone solution and leads to [Rh(**2**)](ClO<sub>4</sub>) (**8**). The structure of [Rh(**2**)]<sup>+</sup> has been established by an X-ray structure determination of the [Rh(**2**)](BPh<sub>4</sub>) salt (**8'**). Crystallographic data for **8'**: monoclinic *C*<sub>2h</sub><sup>5</sup>-*P*2<sub>1</sub>/*n*, *a* = 11.261(2) Å, *b* = 15.886(4) Å, *c* = 29.986(4) Å;  $\beta$  = 96.70(2)°; *V* = 5149 Å<sup>3</sup>, *Z* = 4; *R* = 0.0527, *R*<sub>w</sub> = 0.0586 for 4254 observations and 595 variable parameters. The cation consists of a rhodium atom  $\pi$  bound to the thiophene ring and bound to the two phosphorus atoms of ligand **2**.

## Introduction

In a recent publication we showed that the newly synthesized ligand, 2,5-bis[2-(diphenylphosphino)ethyl]thiophene (**1**) was a tridentate ligand binding through phosphorus and the sulfur atoms, for metals like Mo(0), Co(I), or Rh(I), generating complexes with a variety of geometries.<sup>1</sup> Moreover, the metal–sulfur bond is not labile in these complexes, an unexpected result considering that the sulfur atom in the thiophene ring is a weak nucleophile.<sup>2</sup> We have proposed that the tenacity of this bond is the consequence of constraints imposed by the short ethylene chain between the phosphorus atom and the thiophene ring.

In this study, our goal was to develop a new class of polydentate ligands with weak metal–ligand bonds which may be cleaved reversibly to open a coordination site on the metal to induce catalytic activity. This property is observed for some polydentate ligands that combine phosphorus with oxygen donor atoms.<sup>3</sup> For this reason, we decided to extend the length of the chain between the phosphorus atom and the thiophene ring and turned to the synthesis of 2,5-bis[3-(diphenylphosphino)propyl]thiophene (**2**).

In this paper, we relate the synthesis of ligand **2** and the results concerning the evaluation of its bonding

properties toward Rh(I), which show that this lengthening induces, as expected, a weakening of the Rh–S bond and allows ligand **2** to use  $\eta^2$  to  $\eta^7$  modes of bonding to the Rh(I) center. The evaluation of the catalytic activity of similar complexes of Rh(I) with ligands **1** and **2** toward hydroformylation of 1-hexene is also presented.

## Results and Discussion

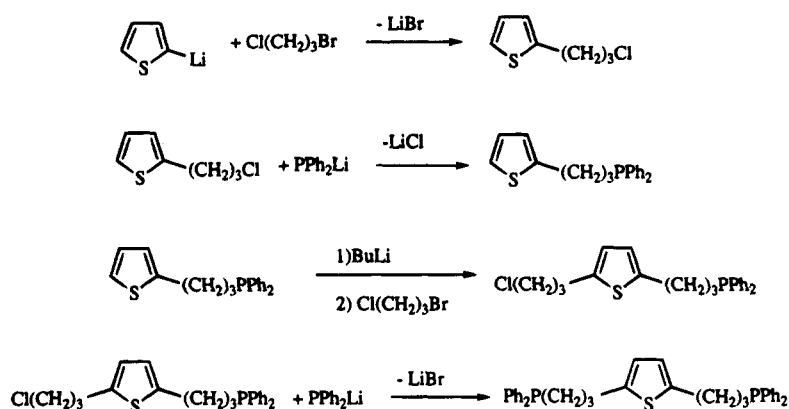
**(a) Synthesis of 2,5-Bis[3-(diphenylphosphino)propyl]thiophene.** Ligand **2** is synthesized in four steps from 2-lithiothiophene, as shown in Scheme 1. In the first step, the 2-lithio salt reacts with 1-bromo-3-chloropropane, leading to 2-(3-chloropropyl)thiophene. In the second step, reaction with PPh<sub>2</sub>Li allows the isolation of 2-[3-(diphenylphosphino)propyl]thiophene. Subsequent reactions with BuLi and 1-bromo-3-chloropropane lead to the formation of 2-[3-(diphenylphosphino)propyl]-5-(3-chloropropyl)thiophene, whose reaction with PPh<sub>2</sub>Li leads to ligand **2**, an air-stable white powder, with 49% overall yield from the starting thiophene.

**Evaluation of the Bonding Modes of **2** in Cationic Rh(I) Complexes.** To have a direct comparison with ligand **1**, we have continued to use the family of cationic complexes [Rh(COD)L<sub>2</sub>]<sup>+</sup>, which are easily obtained and which are good starting materials for the synthesis of carbonyl derivatives.<sup>4</sup>

<sup>®</sup> Abstract published in *Advance ACS Abstracts*, November 15, 1994.  
 (1) Alvarez, M.; Lugan, N.; Mathieu, R. *Inorg. Chem.* **1993**, *32*, 5652.  
 (2) (a) Angelici, R. J. *Acc. Chem. Res.* **1988**, *21*, 387. (b) Angelici, R. J. *Coord. Chem. Rev.* **1990**, *105*, 27. (c) Rauchfuss, T. B. *Prog. Inorg. Chem.* **1991**, *39*, 259.  
 (3) Bader, A.; Lindner, E. *Coord. Chem. Rev.* **1991**, *108*, 27.

(4) Schrock, R. R.; Osborn, A. J. *J. Am. Chem. Soc.* **1971**, *93*, 2397.

Scheme 1



When (COD)Rh(acac) is treated in THF with a slight excess of perchloric acid (see safety note below) and then with 1 equiv of **2**, immediate formation of a yellow precipitate, **3**, is observed. This complex is insoluble in all common solvents, suggesting a polymeric structure. This insolubility precludes any NMR measurements, but chemical analysis is consistent with the formula  $\{[\text{Rh}(\text{COD})(\mathbf{2})][\text{ClO}_4]\}_n$  for **3**.

When a suspension of **3** in dichloromethane is saturated with carbon monoxide, the yellow solid gradually disappears, giving a yellow solution. Monitoring the reaction by infrared spectroscopy shows the presence of a weak band at  $2072\text{ cm}^{-1}$  and of two strong bands at  $2030$  and  $2013\text{ cm}^{-1}$ . This spectrum is very similar to the spectrum of  $[\text{Co}(\text{CO})_3(\mathbf{1})]^+$  and is consistent with a trigonal-bipyramidal structure in which the asymmetry of the ligand induces the splitting of the  $E'$  mode expected for a  $D_{3h}$  symmetry group for the molecule and a weak activity for the infrared-inactive  $A'_1$  mode of vibration.<sup>5</sup> This hypothesis is confirmed by the  $^{31}\text{P}\{^1\text{H}\}$  NMR spectrum of the same solution: a doublet is observed at  $28.7\text{ ppm}$  ( $J(\text{Rh}-\text{P}) = 80.5\text{ Hz}$ ), with a coupling constant characteristic of  $[\text{Rh}(\text{CO})_3(\text{PR}_3)_2]^+$  complexes.<sup>6</sup> Moreover, the  $^1\text{H}$  NMR spectrum shows, besides the resonances due to free 1,5-cyclooctadiene, a singlet at  $6.79\text{ ppm}$  due to the protons of the thiophene ring and three multiplets due to the methylene groups. From these observations we propose that the action of carbon monoxide has induced the transformation of **3** into  $[\text{Rh}(\text{CO})_3(\mathbf{2})][\text{ClO}_4]$  (**4**) in which the two phosphorus atoms are in the axial positions of a trigonal bipyramid.

In order to evaluate the possible modes of bonding of ligand **2**, the solution of **4** was decarbonylated either by bubbling nitrogen into the solution or by evaporating the solvent under vacuum. Initial results showed that several products were present, depending the reaction conditions. This decarbonylation reaction was analyzed by the simultaneous use of IR and NMR spectroscopies at different stages of decarbonylation.

After the solvent from the solution of **4** has been evaporated under vacuum, IR spectroscopy of the residue shows the presence of two strong absorptions at  $2035$  and  $2020\text{ cm}^{-1}$  and one of medium intensity at  $1993\text{ cm}^{-1}$ . The  $^{31}\text{P}\{^1\text{H}\}$  NMR spectrum shows the presence of three complexes in about a 1:1:1 ratio, with

a doublet at  $26\text{ ppm}$  ( $J(\text{Rh}-\text{P}) = 133\text{ Hz}$ ) (**5**), a doublet at  $23\text{ ppm}$  ( $J(\text{Rh}-\text{P}) = 106\text{ Hz}$ ) (**6**), and a doublet at  $20\text{ ppm}$  ( $J(\text{Rh}-\text{P}) = 110\text{ Hz}$ ) (**7**).

Renewed evaporation of the solution and its prolonged standing under vacuum lead to a new mixture characterized in IR spectroscopy by a strong band at  $2020\text{ cm}^{-1}$ , a weak band at  $2035\text{ cm}^{-1}$ , and a medium intensity band at  $1993\text{ cm}^{-1}$ . The  $^{31}\text{P}\{^1\text{H}\}$  NMR spectrum shows that only two complexes **5** and **7** are present, **7** being the major product.

To complete the decarbonylation reaction, the dichloromethane solution was refluxed for 1 h. In the IR spectrum only the absorption at  $2020\text{ cm}^{-1}$  remains, and in the  $^{31}\text{P}\{^1\text{H}\}$  NMR spectrum **7** is still present but a new resonance is observed: a doublet at  $33\text{ ppm}$  ( $J(\text{Rh}-\text{P}) = 205\text{ Hz}$ ) (**8**). Prolonged heating of the solution or refluxing in acetone leads to the complete disappearance of **7** and to the unique presence of **8**, which shows no IR absorption in the CO stretching region. Bubbling carbon monoxide through a solution of **8** in dichloromethane regenerates complex **4**.

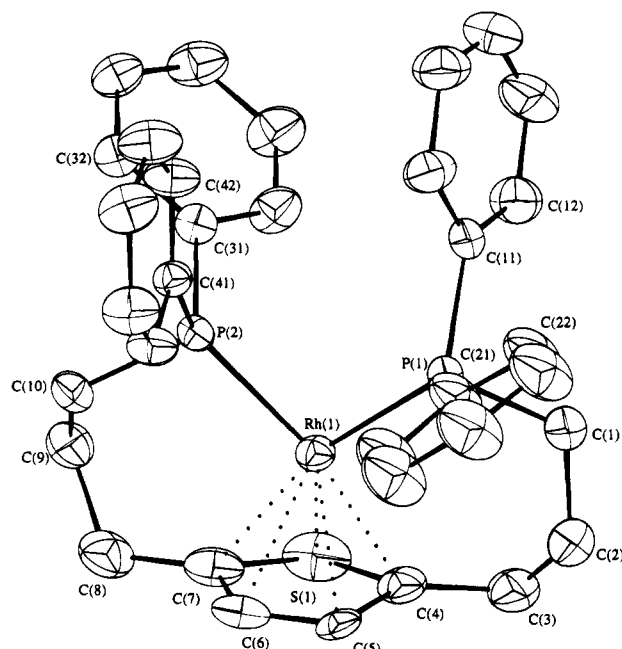
These observations show that ligand **2** has a greater flexibility than ligand **1** in its coordination to rhodium(I) and that the lengthening of the methylene chain between the phosphorus and the thiophene ring has allowed a situation where only the two phosphines are bound to the metal (e.g., complex **4**), a situation not encountered with complexes of ligand **1**.

The similarity of the spectroscopic data for complex **7** ( $\nu(\text{CO}) = 2020\text{ cm}^{-1}$ ,  $\delta^{31}\text{P} = 20\text{ ppm}$ ,  $J(\text{Rh}-\text{P}) = 110\text{ Hz}$ ) and that for the complex  $[\text{Rh}(\text{CO})(\mathbf{1})][\text{ClO}_4]$  ( $\nu(\text{CO}) = 2020\text{ cm}^{-1}$ ,  $\delta^{31}\text{P} = 8.3\text{ ppm}$ ,  $J(\text{Rh}-\text{P}) = 111.6\text{ Hz}$ )<sup>1</sup> indicates that these complexes have similar structures: **7** is a square-planar complex, the ligand being tridentate through the two phosphines and the sulfur atom of the thiophene ring and the carbonyl group being trans to the sulfur atom.

The identification of the complexes **5** and **6** is less straightforward, but information can be derived from the chronology of their formation and from their spectroscopic data. As they appear during the first steps of the decarbonylation of **4** and disappear during the formation of **7**, a monocarbonyl complex, they can be identified as dicarbonyl complexes. On this basis, the characterization of **6** is straightforward as this complex gives one IR absorption at  $2035\text{ cm}^{-1}$  and its  $^{31}\text{P}\{^1\text{H}\}$  NMR spectrum shows a coupling constant of  $J(\text{Rh}-\text{P}) = 106\text{ Hz}$ . These data are similar to the data observed for the  $[\text{Rh}(\text{CO})_2(\text{PR}_3)_2]^+$  complexes with a square-planar

(5) Adams, D. M. *Metal-Ligand and Related Vibrations*; Edward Arnold Ltd.: London, 1967; p 105.

(6) Lindner, E.; Wang, Q.; Mayer, H. A.; Fawzi, R.; Steimann, M. *Organometallics* **1993**, *12*, 1865.



**Figure 1.** ORTEP drawing of the cationic part of **8'** showing the numbering scheme.

structure and in which the CO ligands are in trans position.<sup>6</sup> In this situation, the ligand **2** is  $\eta^2$  bound to rhodium by the two phosphorus atoms in trans positions.

Complex **5** is characterized by two IR-active bands at 2035 and 1993  $\text{cm}^{-1}$ , which is consistent with a cis dicarbonyl complex. However, the value of the coupling constant  $J(\text{Rh}-\text{P}) = 133 \text{ Hz}$  in its  $^{31}\text{P}\{^1\text{H}\}$  NMR spectrum excludes a situation in which ligand **2** is  $\eta^3$  bound. Indeed, for the  $[\text{Rh}(\text{CO})_2(\mathbf{1})]^+$  complex  $J(\text{Rh}-\text{P}) = 90.3 \text{ Hz}$ <sup>1</sup> and similar low  $J(\text{Rh}-\text{P})$  values are also observed for other pentacoordinated  $[\text{Rh}(\text{CO})_2(\text{PR}_3)_3]^+$  compounds,<sup>7</sup> but in the case of  $[\text{Rh}(\text{CO})_2(\text{diphos})]^+$  compounds  $J(\text{Rh}-\text{P})$  values of 120 Hz are observed.<sup>8</sup> We thus propose for **5** a square-planar structure in which the ligand **2** is  $\eta^2$  bound to rhodium by the two phosphorus atoms in cis positions. These results demonstrate further that **2** is a very flexible ligand.

The completely decarbonylated complex has been fully characterized by an X-ray crystal structure determination on crystals of **8'** obtained after replacing the perchlorate anion by the tetraphenylborate anion. A perspective view of the molecule is given in Figure 1 along the labeling scheme. Bond lengths and angles of interest are gathered in Table 1.

It appears that the lengthening of the carbon chain between the phosphorus and the thiophene ring in ligand **2** has allowed the ring to participate in  $\pi$  bonding, leading to a structure similar to that observed for the complex  $[\text{Rh}(\eta^5\text{-C}_5\text{H}_4\text{S})(\text{PPh}_3)_2][\text{PF}_6]$ .<sup>9</sup> Comparison of bond lengths between the two structures shows that the main effect of the presence of the propyl chain between thiophene and the phosphorus atoms is the shortening of the rhodium-sulfur bond (2.567(3) Å in  $[\text{Rh}(\eta^5\text{-C}_5\text{H}_4\text{S})(\text{PPh}_3)_2][\text{PF}_6]$ ). This is likely to be due to an electronic effect of the substituents on the ring, as in

**Table 1.** Selected Bond Lengths (Å) and Angles (deg) for  $[\text{Rh}(\mathbf{1})][\text{BPh}_4] (\mathbf{8}')^a$

Bond Lengths			
Rh(1)–P(1)	2.235(2)	C(3)–C(4)	1.48(1)
Rh(1)–S(1)	2.504(3)	C(4)–C(5)	1.413(7)
Rh(1)–C(4)	2.221(7)	C(5)–C(6)	1.306(8)
Rh(1)–C(5)	2.275(6)	C(6)–C(7)	1.394(8)
Rh(1)–C(6)	2.307(7)	P(2)–C(10)	1.832(7)
Rh(1)–P(2)	2.251(2)	P(2)–C(31)	1.836(7)
Rh(1)–C(7)	2.261(8)	P(2)–C(41)	1.818(7)
P(1)–C(1)	1.832(9)	C(7)–C(8)	1.47(1)
P(1)–C(11)	1.826(8)	C(8)–C(9)	1.51(1)
P(1)–C(21)	1.83(1)	C(9)–C(10)	1.52(1)
S(1)–C(4)	1.763(7)	B(1)–C(51)	1.64(1)
S(1)–C(7)	1.724(7)	B(1)–C(61)	1.66(1)
C(1)–C(2)	1.50(1)	B(1)–C(71)	1.65(1)
C(2)–C(3)	1.49(2)	B(1)–C(81)	1.66(1)
Bond Angles			
P(1)–Rh(1)–P(2)	99.49(7)	Rh(1)–P(2)–C(31)	118.2(2)
Rh(1)–P(1)–C(1)	109.7(3)	C(10)–P(2)–C(31)	101.1(3)
Rh(1)–P(1)–C(11)	121.6(3)	Rh(1)–P(2)–C(41)	119.9(2)
C(1)–P(1)–C(11)	102.0(4)	C(10)–P(2)–C(41)	102.3(3)
Rh(1)–P(1)–C(21)	115.0(3)	C(31)–P(2)–C(41)	105.2(3)
C(1)–P(1)–C(21)	102.1(5)	S(1)–C(7)–C(6)	111.3(6)
C(11)–P(1)–C(21)	104.2(4)	Rh(1)–C(7)–C(8)	128.0(6)
C(4)–S(1)–C(7)	92.0(4)	S(1)–C(7)–C(8)	125.6(6)
P(1)–C(1)–C(2)	117.1(7)	C(6)–C(7)–C(8)	121.6(7)
C(1)–C(2)–C(3)	118.0(10)	C(7)–C(8)–C(9)	114.5(7)
C(2)–C(3)–C(4)	115.7(8)	C(8)–C(9)–C(10)	114.4(8)
Rh(1)–C(4)–C(3)	125.1(6)	P(2)–C(10)–C(9)	113.9(6)
S(1)–C(4)–C(3)	126.8(7)	C(51)–B(1)–C(61)	109.6(6)
S(1)–C(4)–C(5)	103.4(5)	C(51)–B(1)–C(71)	108.5(6)
C(3)–C(4)–C(5)	128.2(8)	C(61)–B(1)–C(71)	111.9(6)
C(4)–C(5)–C(6)	120.6(7)	C(51)–B(1)–C(81)	111.2(6)
C(5)–C(6)–C(7)	110.0(7)	C(61)–B(1)–C(81)	108.3(6)
Rh(1)–P(2)–C(10)	107.4(3)	C(71)–B(1)–C(81)	107.3(6)

<sup>a</sup> Estimated standard deviations in parentheses.

the ( $\eta^5$ -2,5-dimethylthiophene)(cyclooctadiene)Rh[BF<sub>4</sub>] compound recently described,<sup>10</sup> where the rhodium-sulfur bond length (2.467(3) Å) is similar to the length found in our complex.

In conclusion, this study of the reactivity of **3** toward carbon monoxide provides evidence for the great flexibility of ligand **2**. The longer carbon chain between the phosphorus atoms and the thiophene ring allows, compared to ligand **1**, ligand **2** to accommodate situations in which it can be either bidentate through the two phosphorus atoms in cis or trans positions on a square-planar complex or hexadentate through  $\pi$  coordination of the thiophene ring and coordination of the two phosphorus atoms. Like ligand **1**, **2** can also be tridentate through the two phosphorus and the sulfur atom of the thiophene ring. These observations are summarized in Scheme 2.

To determine whether the different bonding capabilities of ligands **1** and **2** have some impact on the catalytic activities of their complexes, we checked the behavior of complexes  $[\text{Rh}(\text{COD})(\mathbf{1})][\text{ClO}_4]$  (**9**) and  $[\text{Rh}(\text{COD})(\mathbf{2})][\text{ClO}_4]$  (**3**) as catalysts in the hydroformylation of 1-hexene. Under the same reaction conditions (20 bar of a 1:1 CO/H<sub>2</sub> mixture, 1-hexene/catalyst ratio of 200, 3NET<sub>3</sub>/Rh, CH<sub>2</sub>Cl<sub>2</sub> as solvent), which have not been optimized, after 6 h at 50 °C, 39% conversion of 1-hexene is observed with complex **9** as catalyst and 88% with complex **3**. The linear/branched ratio for the resulting aldehydes is 2.2 in the first case and 2.6 in the second case (mean of two experiments). From these results, it appears that the substitution of ligand **1** by the more

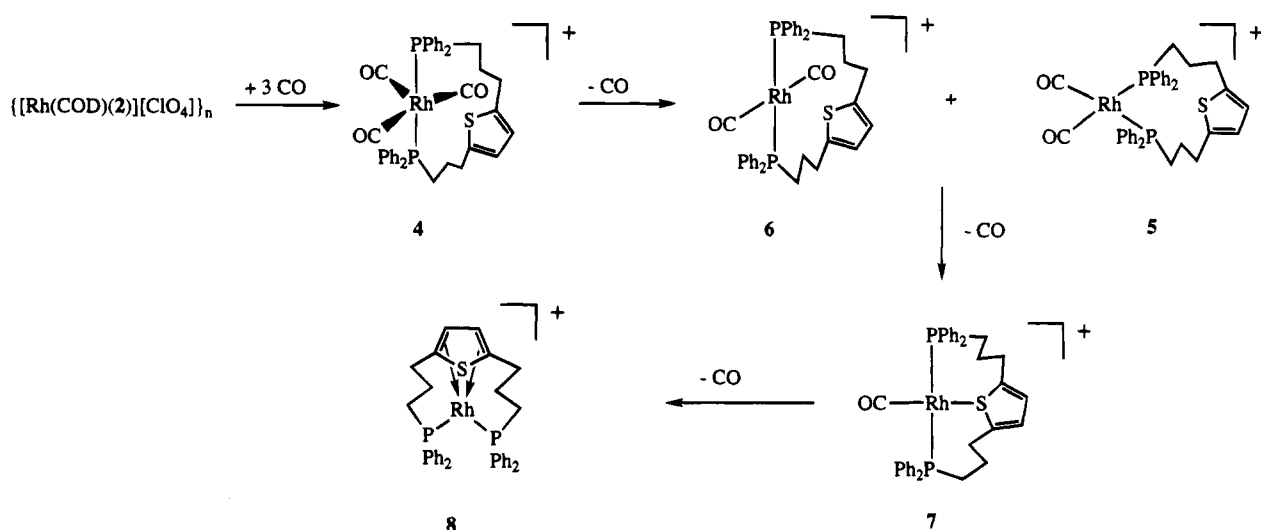
(7) Johnston, G. G.; Baird, M. C. *Organometallics* **1989**, *8*, 1894.

(8) Fairlie, D. P.; Bosnich, B. *Organometallics* **1988**, *7*, 936.

(9) Sanchez-Delgado, R. A.; Marquez-Silva, R. L.; Puga, J.; Tiripichio, A.; Tiripichio Camellini, M. *J. Organomet. Chem.* **1986**, *316*, C35.

(10) Polam, J. R.; Porter, L. C. *Organometallics* **1993**, *12*, 3504.

Scheme 2



labile ligand **2** increases the efficiency of the catalyst by a factor greater than 2.

### Experimental Section

All reactions were performed under a nitrogen atmosphere with use of standard Schlenk techniques. Elemental analyses were performed in our laboratory for C, H, and S.  $\text{PPh}_2\text{H}^{11}$  and  $(\text{COD})\text{Rh}(\text{acac})^{12}$  have been prepared according to published procedures.

**Safety Note!** Perchlorate salts of metal complexes with organic ligands are potentially explosive. Only small amounts of material should be prepared, and these should be handled with great caution.

**Synthesis of the 2,5-Bis[3-(diphenylphosphino)propyl]thiophene Ligand **2**.** This compound was synthesized in four steps from thiophene.

**(a) Synthesis of the 2-(3-Chloropropyl)thiophene.** To a stirred solution of 4 mL (49.9 mmole) of thiophene in 20 mL of THF at  $-60^\circ\text{C}$  was slowly added 31.25 mL (50 mmol) of a solution of BuLi, 1.6 M in hexane. The solution was then stirred and the temperature was raised to  $-40^\circ\text{C}$ . Then 4.95 mL of 1-bromo-3-chloropropane was slowly added. The temperature was increased to room temperature, and the solution was stirred for 15 h. The solvents were then evaporated under vacuum, and the residue was dissolved in 50 mL of diethyl ether. This solution was washed two times with 50 mL of water, and the ether solution was then dried over sodium sulfate. After filtration of the ether solution and elimination of ether under vacuum, 6.18 g of 2-(3-chloropropyl)thiophene was recovered as a pale yellow oil (77%) which was used without further purification.  $^1\text{H}$  NMR ( $\text{CDCl}_3$  solution, 200 MHz): 7.18 (m, 1H), 6.93 (m, 1H), 6.84 (m, 1H), 3.57 (t,  $J = 6.4$  Hz, 2H), 3.02 (t,  $J = 6.4$  Hz, 2H), 2.13 ppm (q,  $J = 6.4$  Hz, 2H).

**(b) Synthesis of the 2-[3-(Diphenylphosphino)propyl]thiophene.** To the 6.18 g of 2-(3-chloropropyl)thiophene (38.5 mmol) dissolved in 50 mL of THF was slowly added at  $0^\circ\text{C}$   $\text{PPh}_2\text{Li}$  (synthesized from 38.5 mmol of  $\text{PPh}_2\text{H}$  and 38.5 mmol of BuLi in 37 mL of THF). The solution was stirred for 2 h and then evaporated to dryness under vacuum. The residue was dissolved in 50 mL of diethyl ether, and the solution was washed two times with 50 mL of water and then dried over sodium sulfate. After filtration of this solution and evaporation of the solvent, recrystallization of the residue from methanol led to 10.75 g of the product as a white powder (90%).  $^1\text{H}$  NMR ( $\text{CDCl}_3$  solution, 200 MHz): 7.43–7.29 (m, 10H), 7.10

Table 2. Experimental Data for the X-ray Study of  $8\text{-Me}_2\text{CO}$

formula	$\text{C}_{61}\text{H}_{60}\text{BOP}_2\text{RhS}$
fw	1016.88
crystal system	monoclinic
space group	$C_{2h}^5 - P2_1/n$
$a$ , Å	11.261(2)
$b$ , Å	15.886(4)
$c$ , Å	28.986(4)
$\beta$ , deg	96.70(2)
$V$ , Å <sup>3</sup>	5149(2)
$Z$	4
$\rho_{\text{calcd}}$ , g·cm <sup>-3</sup>	1.312
$t$ , °C	22
radiation	Mo K $\alpha$ , $\lambda(\text{Mo K}\alpha_1) = 0.7093$ Å
linear abs coeff, cm <sup>-1</sup>	4.649
absorption correction, min–max	0.98–1.0
scan mode	$\omega/2\theta$
$2\theta$ limit, deg	2–48
no. of unique data used in final refinement, $F_o^2 > 3\sigma(F_o^2)$	4254
final no. of variables	594
$R$ (on $F_o$ , $F_o^2 > 3\sigma(F_o^2)$ ) <sup>a</sup>	0.0527
$R_w$ (on $F_o$ , $F_o^2 > 3\sigma(F_o^2)$ ) <sup>b</sup>	0.0586

<sup>a</sup>  $R = \sum ||F_o| - |F_c|| / \sum |F_o|$ . <sup>b</sup>  $R_w = [\sum w(|F_o| - |F_c|)^2 / \sum w|F_o|^2]^{1/2}$ , unit weights.

(m, 1H), 6.89 (m, 1H), 6.75 (m, 1H), 2.95 (t,  $J = 7.2$  Hz, 2H), 2.13 (m, 2H), 1.86 ppm (m, 2H).  $^{31}\text{P}\{^1\text{H}\}$  NMR ( $\text{CDCl}_3$  solution, 32.4 MHz):  $-17.5$  ppm.

**(c) Synthesis of 2-[3-(Diphenylphosphino)propyl]-5-(3-chloropropyl)thiophene.** To the 10.75 g of 2-[3-(diphenylphosphino)propyl]thiophene (34.6 mmol) in 50 mL of THF cooled at  $0^\circ\text{C}$  was slowly added 21.6 mL (34.6 mmole) of 1.6 M BuLi, and the solution was stirred for 1 h at this temperature. To this solution was slowly added 3.4 mL of 1-bromo-3-chloropropane (34.6 mmol). The solution was stirred for 2 h at  $0^\circ\text{C}$  and then for 2 h at room temperature. The solvents were removed under vacuum and the residue was dissolved in 50 mL of diethyl ether. The solution was washed with  $2 \times 50$  mL of water and then dried over sodium sulfate. After filtration of this solution and evaporation of the solvent under vacuum 12.72 g of a yellow oil was obtained (95%).  $^1\text{H}$  NMR ( $\text{CDCl}_3$  solution, 200 MHz): 7.53–7.32 (m, 10H), 6.61 (AB system,  $J_{AB} = 3.1$  Hz, 1H), 6.57 (AB system,  $J_{AB} = 3.1$  Hz, 1H), 3.57 (t,  $J = 6.4$  Hz, 2H), 2.97 (t,  $J = 7.1$  Hz, 2H), 2.90 (t,  $J = 7.4$  Hz, 2H), 2.13 (m, 4H), 1.83 ppm (m, 2H).  $^{31}\text{P}\{^1\text{H}\}$  NMR ( $\text{CDCl}_3$  sol., 32.4 MHz):  $-16.7$  ppm.

**(d) Synthesis of **2**.** To the 12.72 g of 2-[3-(diphenylphosphino)propyl]-5-(3-chloropropyl)thiophene (32.9 mmol) dissolved in 50 mL of THF and cooled to  $0^\circ\text{C}$  was slowly added 32.9 mmol of  $\text{PPh}_2\text{Li}$  in 36 mL of THF (synthesized from

(11) Gee, W.; Shaw, R. A.; Smith, B. C. *Inorg. Synth.* **1967**, *9*, 19.

(12) Sinou, D.; Kagan, H. B. *J. Organomet. Chem.* **1976**, *114*, 325.

PPh<sub>2</sub>H and BuLi). The solution was stirred for 2 h at room temperature and then the THF was eliminated under vacuum. The residue was dissolved in 50 mL of diethyl ether, and the solution was washed with 2 × 50 mL of water. The solution was dried over magnesium sulfate. After filtration of this solution and elimination of the solvent under vacuum, recrystallization of the residue from methanol gave 13.15 g (74.5%) of **2** as white crystals. <sup>1</sup>H NMR (CDCl<sub>3</sub> solution, 200 MHz): 7.44–7.24 (m, 20H), 6.51 (s, 2H), 2.85 (t, *J* = 7.2 Hz, 4H), 2.10 (m, 4H), 1.79 ppm (m, 4H). <sup>13</sup>C{<sup>1</sup>H} NMR (CDCl<sub>3</sub> solution, 20.1 MHz): 141.7 (C(2), C(5), C<sub>4</sub>H<sub>2</sub>S), 138.1 (d, *J*(P–C) = 13.2 Hz, Ph), 132.1 (d, *J*(P–C) = 18.5 Hz, Ph), 128 (Ph), 127.7 (C(3), C(4), C<sub>4</sub>H<sub>2</sub>S), 123.3 (Ph), 30.8 (d, *J*(P–C) = 13.5 Hz, CH<sub>2</sub>–CH<sub>2</sub>CH<sub>2</sub>PPh<sub>2</sub>), 27.3 (d, *J*(P–C) = 17 Hz, CH<sub>2</sub>CH<sub>2</sub>CH<sub>2</sub>PPh<sub>2</sub>), 26.8 ppm (d, *J*(P–C) = 11.8 Hz, CH<sub>2</sub>CH<sub>2</sub>CH<sub>2</sub>PPh<sub>2</sub>). <sup>31</sup>P{<sup>1</sup>H} NMR (CDCl<sub>3</sub> solution, 32.4 MHz): –16.9 ppm. Anal. Calcd for C<sub>34</sub>H<sub>34</sub>P<sub>2</sub>S: C, 76.10; H, 6.39; S, 5.97. Found: C, 75.82; H, 6.18; S, 5.85.

**Synthesis of [(COD)Rh(2)][ClO<sub>4</sub>]<sub>n</sub> (3).** See safety note above. To 0.3 g (1 mmol) of (COD)Rh(acac) dissolved in 3.5 mL of THF was added 0.99 mmol of HClO<sub>4</sub>. This solution was stirred for 15 min and then 0.505 g (0.94 mmol) of **2** dissolved in 6 mL of THF was added, and the solution was stirred for 2 h. A yellow precipitate appeared, and the solution was then filtered. The precipitate was washed with acetone and dried under vacuum; 0.637 g of **3** as a yellow powder was isolated (80%). Anal. Calcd for C<sub>42</sub>H<sub>46</sub>ClO<sub>4</sub>P<sub>2</sub>RhS: C, 59.57; H, 5.48; S, 3.79. Found: C, 59.60; H, 5.52; S, 3.91.

**Synthesis of [(CO)<sub>3</sub>Rh(2)][ClO<sub>4</sub>] (4).** See safety note above. Carbon monoxide was bubbled for 30 min through a suspension of 0.25 g of **3** in 10 mL of dichloromethane. The solid rapidly dissolved giving a yellow solution. **4** was unstable in the absence of CO and was characterized by IR + NMR spectroscopy. IR ν(CO) (CH<sub>2</sub>Cl<sub>2</sub> solution): 2072 (w), 2030 (s), 2013 (s) cm<sup>-1</sup>. <sup>1</sup>H NMR (CD<sub>2</sub>Cl<sub>2</sub> solution, 200 MHz): 7.90–7.30 (m, 20H), 6.79 (s, 2H), 3.57 (m, 4H), 2.72 (m, 4H), 1.88

ppm (m, 4H). <sup>31</sup>P{<sup>1</sup>H} NMR (CD<sub>2</sub>Cl<sub>2</sub> solution, 32.4 MHz): 28.7 ppm, (*J*(Rh–P) = 80.5 Hz).

**Synthesis of [Rh(2)][ClO<sub>4</sub>] (8).** See safety note above. This reaction was conducted in the same way as for **4** except that at the end of the reaction the solution was evaporated to dryness. The residue was dissolved in 15 mL of acetone, and the solution was refluxed for 45 min. The product was recrystallized from an acetone/hexane mixture giving 0.18 g of **8** as orange crystals (80%). <sup>1</sup>H NMR (CD<sub>2</sub>Cl<sub>2</sub> solution, 200 MHz): 7.27–7.24 (m, 20H), 6.53 (s, 2H), 2.72 (m, 4H), 2.0 (m, 4H), 1.69 ppm (m, 4H). <sup>13</sup>C{<sup>1</sup>H} NMR (CDCl<sub>3</sub> solution, 20.1 MHz): 136.2, 135.2 (m), 133.5 (m), 130.7 (m), 128.4 (m), 125.8 (m), 122(Ph), 100.5 (d, *J*(Rh–C) = 4.7 Hz, C(2), C(5), C<sub>4</sub>H<sub>2</sub>S), 99.1 (d, *J*(Rh–C) = 3.5 Hz, C(3), C(4), C<sub>4</sub>H<sub>2</sub>S), 27.7 (t, *J*(P–C) = 14.6 Hz, CH<sub>2</sub>CH<sub>2</sub>CH<sub>2</sub>PPh<sub>2</sub>), 27.3 (s, CH<sub>2</sub>CH<sub>2</sub>CH<sub>2</sub>PPh<sub>2</sub>), 24.3 ppm (t, *J*(P–C) = 2.7 Hz, CH<sub>2</sub>CH<sub>2</sub>CH<sub>2</sub>PPh<sub>2</sub>). <sup>13</sup>C NMR (CDCl<sub>3</sub> solution, 20.1 MHz): 99.1 (dd, *J*(Rh–C) = 3.5 Hz, *J*(C–H) = 180 Hz; C(3), C(4), C<sub>4</sub>H<sub>2</sub>S). <sup>31</sup>P{<sup>1</sup>H} NMR (CDCl<sub>3</sub> solution, 32.4 MHz): 33.8 ppm, *J*(Rh–P) = 205 Hz. Anal. Calcd for C<sub>34</sub>H<sub>34</sub>ClO<sub>4</sub>P<sub>2</sub>RhS: C, 55.26; H, 4.64; S, 4.34. Found: C, 55.32; H, 4.85; S, 4.12.

**Synthesis of [Rh(2)][BPh<sub>4</sub>] (8').** See safety note above. To a solution of 0.17 g of **8** in 3 mL of dichloromethane was added 0.118 g of NaBPh<sub>4</sub> dissolved in 3 mL of methanol. The solution was stirred for 30 min at room temperature and then evaporated to dryness. Recrystallization from an acetone/hexane mixture gave 0.17 g of **8'** as orange crystals. Anal. Calcd for **8'**·(CH<sub>3</sub>)<sub>2</sub>CO: C<sub>61</sub>H<sub>66</sub>BOP<sub>2</sub>RhS: C, 72.05; H, 5.95; S, 3.15. Found: C, 71.96; H, 5.97; S, 3.35.

**Catalytic Experiments.** All catalytic runs were performed in a home-built stainless steel autoclave equipped with gas and liquid inlets, a heating device, and magnetic stirring. Gas chromatography analyses were performed on an Intersmat IGC 120 FL gas chromatograph, with flame ionization detector, fitted with a 3 m × 1/8 in. column (10% Carbowax 20M in Chromosorb W 80/100 mesh), and using N<sub>2</sub> as carrier gas.

Table 3. Fractional Atomic Coordinates and Isotropic or Equivalent Temperature Factors (Å<sup>2</sup> × 100)<sup>a</sup>

atom	<i>x/a</i>	<i>y/b</i>	<i>z/c</i>	<i>U</i> <sub>eq</sub> <sup>b</sup>	atom	<i>x/a</i>	<i>y/b</i>	<i>z/c</i>	<i>U</i> <sub>eq</sub> <sup>b</sup>
Rh(1)	0.12981(5)	0.86050(4)	0.09579(2)	0.0407	C(44)	-0.0954(9)	0.6338(6)	0.2286(3)	0.0685
P(1)	0.2338(2)	0.7405(1)	0.09712(7)	0.0491	C(45)	-0.1392(8)	0.6709(6)	0.1874(3)	0.0647
S(1)	0.1719(2)	0.9963(2)	0.0569(1)	0.0780	C(46)	-0.0820(7)	0.7387(5)	0.1705(3)	0.0537
C(1)	0.3302(9)	0.7413(7)	0.0504(3)	0.0728	C(41)	0.0221(6)	0.7712(4)	0.1944(2)	0.0408
C(2)	0.277(1)	0.7737(8)	0.0038(4)	0.0868	B(1)	0.4001(8)	0.2440(6)	0.0711(3)	0.0476
C(3)	0.2562(9)	0.8659(8)	-0.0013(3)	0.0800	C(52)	0.6149(7)	0.2005(5)	0.1118(3)	0.0503
C(4)	0.1635(6)	0.9014(5)	0.0252(2)	0.0536	C(53)	0.6952(7)	0.1453(6)	0.1353(3)	0.0654
C(5)	0.0409(5)	0.8801(5)	0.0220(2)	0.0392	C(54)	0.6619(8)	0.0672(5)	0.1483(3)	0.0603
C(6)	-0.0295(7)	0.9170(5)	0.0485(3)	0.0564	C(55)	0.5455(9)	0.0445(5)	0.1376(3)	0.0634
P(2)	0.0883(1)	0.8629(1)	0.16990(6)	0.0372	C(56)	0.4638(8)	0.1007(5)	0.1147(3)	0.0595
C(7)	0.0320(6)	0.9810(5)	0.0741(3)	0.0607	C(51)	0.4957(7)	0.1808(4)	0.1007(2)	0.0414
C(8)	-0.0294(9)	1.0390(6)	0.1032(3)	0.0725	C(62)	0.4017(7)	0.1322(5)	0.0013(2)	0.0514
C(9)	0.0053(9)	1.0287(5)	0.1548(3)	0.0639	C(63)	0.3788(8)	0.1053(6)	-0.0440(3)	0.0657
C(10)	-0.0261(7)	0.9437(5)	0.1739(3)	0.0525	C(64)	0.3354(7)	0.1610(6)	-0.0782(3)	0.0589
C(12)	0.4526(8)	0.7414(8)	0.1535(3)	0.0765	C(65)	0.3128(7)	0.2416(6)	-0.0661(3)	0.0618
C(13)	0.5288(9)	0.7206(9)	0.1922(4)	0.0935	C(66)	0.3355(7)	0.2672(5)	-0.0198(3)	0.0539
C(14)	0.493(1)	0.6695(8)	0.2248(4)	0.0886	C(61)	0.3795(6)	0.2138(5)	0.0160(3)	0.0473
C(15)	0.380(1)	0.6404(7)	0.2205(3)	0.0782	C(72)	0.5194(8)	0.3801(5)	0.0451(3)	0.0628
C(16)	0.3031(9)	0.6596(5)	0.1814(3)	0.0659	C(73)	0.5653(9)	0.4606(6)	0.0524(4)	0.0787
C(11)	0.3386(7)	0.7107(5)	0.1473(3)	0.0514	C(74)	0.5474(9)	0.5058(6)	0.0906(4)	0.0722
C(22)	0.196(1)	0.5679(6)	0.0829(4)	0.0784	C(75)	0.4828(8)	0.4702(6)	0.1225(4)	0.0683
C(23)	0.129(1)	0.4971(7)	0.0720(4)	0.0892	C(76)	0.4368(7)	0.3900(5)	0.1144(3)	0.0582
C(24)	0.007(1)	0.5032(7)	0.0637(5)	0.0955	C(71)	0.4519(6)	0.3412(4)	0.0768(3)	0.0448
C(25)	-0.047(1)	0.5807(6)	0.0629(4)	0.0920	C(82)	0.2597(8)	0.2304(6)	0.1387(3)	0.0671
C(26)	0.022(1)	0.5507(6)	0.0738(4)	0.0809	C(83)	0.1533(9)	0.2380(6)	0.1584(3)	0.0711
C(21)	0.1442(9)	0.6460(6)	0.0838(3)	0.0694	C(84)	0.0510(8)	0.2564(6)	0.1301(4)	0.0706
C(32)	0.1827(7)	0.9130(5)	0.2600(3)	0.0509	C(85)	0.0546(7)	0.2680(6)	0.0836(4)	0.0693
C(33)	0.2706(8)	0.9411(5)	0.2932(3)	0.0601	C(86)	0.1613(7)	0.2606(5)	0.0636(3)	0.0553
C(34)	0.3829(8)	0.9548(6)	0.2815(3)	0.0694	C(81)	0.2690(7)	0.2426(5)	0.0917(3)	0.0494
C(35)	0.4085(8)	0.9410(7)	0.2372(3)	0.0725	C(101)	0.793(1)	0.4186(9)	0.1656(5)	0.1046
C(36)	0.3198(7)	0.9119(6)	0.2045(3)	0.0616	C(201)	0.739(1)	0.4095(8)	0.2100(5)	0.0971
C(31)	0.2057(6)	0.8985(4)	0.2150(2)	0.0436	C(301)	0.701(2)	0.327(1)	0.2191(7)	0.1727
C(42)	0.0661(8)	0.7321(5)	0.2348(3)	0.0560	O(101)	0.718(1)	0.4656(8)	0.2345(5)	0.1604
C(43)	0.008(1)	0.6637(6)	0.2520(3)	0.0710					

<sup>a</sup> Estimated standard deviations in parentheses. <sup>b</sup> *U*<sub>eq</sub> = 1/3 trace *U*.

Mesitylene was used as internal standard. The experimental conditions were as follows: 1-hexene (20 mmol), the complex (0.1 mmol), CH<sub>2</sub>Cl<sub>2</sub> (16 mL), mesitylene (1.5 mL), NEt<sub>3</sub> (0.04 mL), H<sub>2</sub> (10 atm), and CO (10 atm), 50 °C.

**X-ray Diffraction Studies.** Crystals of **8'** suitable for X-ray diffraction were obtained through recrystallization from hexane/acetone solutions at 0 °C. Data were collected on an Enraf-Nonius CAD4 diffractometer at 22 °C. Cell constants were obtained by the least-squares refinement of the setting angles of 25 reflections in the range 24° < 2θ(Mo Kα1) < 28°. The space group was determined by careful examination of systematic extinctions in the listing of the measured reflections. Data reductions were carried out using the CRYSTALS crystallographic computing package.<sup>13</sup> The intensities were corrected from absorption by using DIFABS program.<sup>14</sup> Table 2 presents further crystallographic information.

The structures were solved by using SHELXS-86 program,<sup>15</sup> which revealed the position of Rh, S, and P atoms. All remaining non-hydrogen atoms were located by the usual combination of full-matrix least-squares refinement and difference electron density syntheses by using the CRYSTALS program.<sup>13</sup> A molecule of acetone for each molecule of **8'** was

(13) Watkin, D. J.; Carruthers, J. R.; Betteridge, P. W. *CRYSTALS, An Advanced Crystallographic Program System*; Oxford, U.K., 1988.

(14) Walker, N.; Stuart, D. *Acta Crystallogr.* **1983**, *39*, 158.

found in the crystal lattice. Atomic scattering factors were taken from the usual tabulations.<sup>16</sup> Anomalous dispersion terms for Rh, S, and P atoms were included in  $F_c$ .<sup>17</sup> All non-hydrogen atoms were allowed to vibrate anisotropically. All the hydrogen atoms were set in idealized position (C–H = 0.98 Å). Scattering factors for the hydrogen atoms were taken from Stewart et al.<sup>18</sup> Final atomic coordinates for non-hydrogen atoms are given in Table 3.

**Supplementary Material Available:** Table S1, anisotropic thermal parameters for **8'**, and Table S2, hydrogen positions for **8'** (4 pages). Ordering information is given on any current masthead page.

OM940456N

(15) Sheldrick, G. M. *SHELXS-86, Programm for Crystal Structure Solution*; University of Göttingen: Göttingen, Federal Republic of Germany, 1986.

(16) Cromer, D. T.; Waber, J. T. *International Tables for X-ray Crystallography*; Kynoch Press: Birmingham, England, 1974; Vol. 4, Table 22B.

(17) Cromer, D. T.; Waber, J. T. In *International Tables for X-ray Crystallography*; Kynoch Press: Birmingham, England, 1975; Vol. 4, Table 2.3.1.

(18) Stewart, R. F.; Davidson, E. R.; Simpson, W. T. *J. Chem. Phys.* **1965**, *42*, 3175.



# Synthesis, Structures, and Reactivity of (R<sub>6</sub>-acen)ZrR'<sub>2</sub> and (R<sub>6</sub>-acen)Zr(R')<sup>+</sup> Complexes (R = H, F; R' = CH<sub>2</sub>CMe<sub>3</sub>, CH<sub>2</sub>Ph)

Erik B. Tjaden, Dale C. Swenson, and Richard F. Jordan\*

Department of Chemistry, University of Iowa, Iowa City, Iowa 52242

Jeffrey L. Petersen

Department of Chemistry, West Virginia University, Morgantown, West Virginia 26506

Received July 12, 1994<sup>⊙</sup>

The synthesis, structures, and reactivity of neutral and cationic Zr(IV) alkyl complexes incorporating acen and hexafluoroacen ligands are described. Alkane elimination reactions of H<sub>2</sub>(R<sub>6</sub>-acen) (**6a**, R = F; **6b**, R = H) and ZrR'<sub>4</sub> afford (R<sub>6</sub>-acen)ZrR'<sub>2</sub> (**11a**, R = F, R' = CH<sub>2</sub>CMe<sub>3</sub>; **11b**, R = H, R' = CH<sub>2</sub>CMe<sub>3</sub>; **12**, R = F, R' = CH<sub>2</sub>Ph) in high yield. **11a** has been characterized by X-ray diffraction: space group *P* $\bar{1}$ , *a* = 12.280(3) Å, *b* = 12.731(3) Å, *c* = 8.825(3) Å,  $\alpha$  = 96.66(2)°,  $\beta$  = 97.21(2)°,  $\gamma$  = 76.68(2)°, *V* = 1327(1) Å<sup>3</sup>, *Z* = 2, *R* = 0.042, *R*<sub>w</sub> = 0.049. **11a** adopts a trigonal prismatic structure with a twisted F<sub>6</sub>-acen ligand and a large angle (129.9(2)°) between the neopentyl groups. Solution NMR data for **11a,b** and **12** are in accord with similar structures. The reaction of **11a,b** with [HNMe<sub>2</sub>Ph][B(C<sub>6</sub>F<sub>5</sub>)<sub>4</sub>] yields cationic amine adducts [(R<sub>6</sub>-acen)Zr(CH<sub>2</sub>CMe<sub>3</sub>)(NMe<sub>2</sub>Ph)][B(C<sub>6</sub>F<sub>5</sub>)<sub>4</sub>] (**13a**, R = F; **13b**, R = H). Similarly, the reaction of **11a** with [HNEt<sub>2</sub>Ph][B(C<sub>6</sub>F<sub>5</sub>)<sub>4</sub>] yields [(F<sub>6</sub>-acen)Zr(CH<sub>2</sub>CMe<sub>3</sub>)(NEt<sub>2</sub>Ph)][B(C<sub>6</sub>F<sub>5</sub>)<sub>4</sub>] (**14**). However, the reaction of **11a** with [HNMePh<sub>2</sub>][B(C<sub>6</sub>F<sub>5</sub>)<sub>4</sub>] in benzene yields the base-free complex [(F<sub>6</sub>-acen)Zr(CH<sub>2</sub>CMe<sub>3</sub>)] [B(C<sub>6</sub>F<sub>5</sub>)<sub>4</sub>] (**15**). Complex **14** decomposes in CH<sub>2</sub>Cl<sub>2</sub> to [NEt<sub>2</sub>Ph(CH<sub>2</sub>Cl)] [B(C<sub>6</sub>F<sub>5</sub>)<sub>4</sub>] (**18**), an unusual chloride-bridged dinuclear cation [{"(F<sub>6</sub>-acen)Zr(CH<sub>2</sub>CMe<sub>3</sub>)<sub>2</sub>(μ-Cl)] [B(C<sub>6</sub>F<sub>5</sub>)<sub>4</sub>] (**19**), and free NEt<sub>2</sub>Ph in 1:1:1.3 ratio. It is proposed that this reaction proceeds via nucleophilic attack of NEt<sub>2</sub>Ph on the CH<sub>2</sub>Cl<sub>2</sub> ligand of an intermediate (F<sub>6</sub>-acen)Zr(CH<sub>2</sub>CMe<sub>3</sub>)(CH<sub>2</sub>Cl)<sub>2</sub><sup>+</sup> solvent adduct (formed by NEt<sub>2</sub>Ph dissociation from **14**), followed by trapping of the resulting (F<sub>6</sub>-acen)Zr(CH<sub>2</sub>CMe<sub>3</sub>)Cl (**17**) by a second equivalent of **14**. **13a** is stable toward this process because the amine does not dissociate extensively. Direct chloride abstraction from CH<sub>2</sub>Cl<sub>2</sub> is not observed; base-free **15** is very stable in CH<sub>2</sub>Cl<sub>2</sub>. **13a** has been characterized by X-ray diffraction: space group = *C2/c*, *a* = 39.707(4) Å, *b* = 11.226(1) Å, *c* = 30.045(3) Å,  $\beta$  = 126.667(9)°, *V* = 10742.6(22) Å<sup>3</sup>, *Z* = 8, *R* = 0.0608, *R*<sub>w</sub> = 0.0880. The (F<sub>6</sub>-acen)Zr(CH<sub>2</sub>CMe<sub>3</sub>)(NMe<sub>2</sub>Ph)<sup>+</sup> cation of **13a** adopts a distorted octahedral structure with a more planar F<sub>6</sub>-acen ligand (vs that in **11a**) and a large angle (144.7(2)°) between the neopentyl and amine ligands. **13a** and **15** react with Lewis bases to yield [(F<sub>6</sub>-acen)Zr(CH<sub>2</sub>CMe<sub>3</sub>)(L)<sub>n</sub>] [B(C<sub>6</sub>F<sub>5</sub>)<sub>4</sub>] adducts (*n* = 1, PMe<sub>2</sub>-Ph (**22**); *n* = 2, L = PMe<sub>3</sub> (**21**), CH<sub>3</sub>CN (**24**)). **13a** inserts CO, yielding a η<sup>2</sup>-acyl cation [(F<sub>6</sub>-acen)Zr{η<sup>2</sup>-C(=O)CH<sub>2</sub>CMe<sub>3</sub>}(NMe<sub>2</sub>Ph)] [B(C<sub>6</sub>F<sub>5</sub>)<sub>4</sub>] (**25**, two isomers). **13a** also reacts with 2 equiv of benzophenone to yield an alkoxide ketone complex [(F<sub>6</sub>-acen)Zr(OCPh<sub>2</sub>CH<sub>2</sub>CMe<sub>3</sub>)(O=CPh<sub>2</sub>)] [B(C<sub>6</sub>F<sub>5</sub>)<sub>4</sub>] (**26**). Neither **13a** nor **15** reacts with ethylene or 2-butyne in the absence of Al cocatalysts.

## Introduction

Cationic d<sup>0</sup> Cp<sub>2</sub>M(R)<sup>+</sup> (M = Ti, Zr, Hf) complexes have been utilized in a variety of catalytic processes, including Ziegler–Natta olefin polymerization.<sup>1</sup> These species are highly reactive because (i) the cationic d<sup>0</sup> metal center is very electrophilic, (ii) the polarized M–C bonds are inherently reactive, and (iii) the bent metallocene structure restricts coordination of substrates/ligands to sites which are cis to the M–R group. These properties lead to a rich insertion and σ-bond metathesis chemis-

try. Additionally, (iv) the steric, electronic and chirality properties of the metal center may be tailored by modifying the Cp ligands with substituents and linking groups. To probe the generality of these catalyst design concepts, and to develop new families of tunable catalysts, we are exploring the chemistry of new d<sup>0</sup> metal alkyl species which incorporate properties i–iv in non-Cp<sub>2</sub>M ligand environments.<sup>2–5</sup> In an initial approach, we demonstrated that (N<sub>4</sub>-macrocycle)M(R)<sup>+</sup> (N<sub>4</sub>-macrocycle = Me<sub>3</sub>-taa, Me<sub>4</sub>-taen; M = Zr, Hf) species display

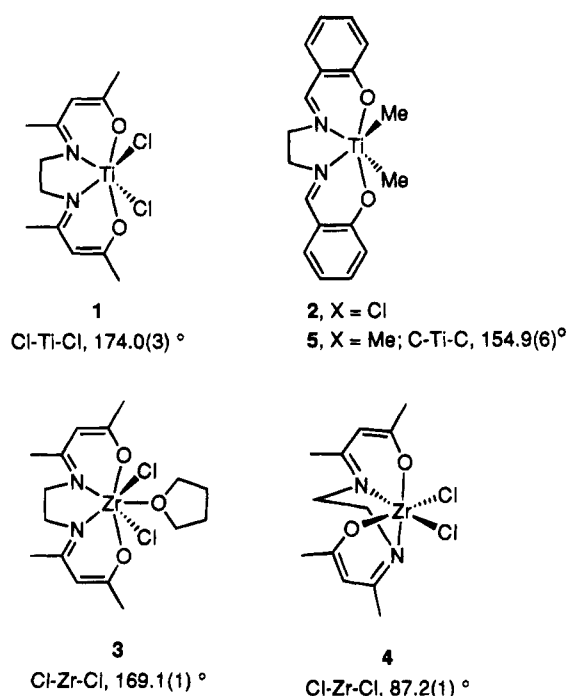
(2) For (N<sub>4</sub>-macrocycle)MR'<sub>2</sub> and (N<sub>4</sub>-macrocycle)M(R')<sup>+</sup> (M = group 4) complexes, see: (a) Uhrhammer, R.; Black, D. G.; Gardner, T. G.; Olsen, J. D.; Jordan, R. F. *J. Am. Chem. Soc.* **1993**, *115*, 8493. (b) Yang, C. H.; Ladd, J. A.; Goedken, V. L. *J. Coord. Chem.* **1988**, *18*, 317. (c) Floriani, C.; Ciurli, S.; Chiesi-Villa, A.; Guastini, C. *Angew. Chem., Int. Ed. Engl.* **1987**, *26*, 70. (d) DeAngelis, S.; Solari, E.; Gallo, E.; Chiesi-Villa, A.; Floriani, C.; Rizzoli, C. *Inorg. Chem.* **1992**, *31*, 2520. (e) Cotton, F. A.; Czuchajowska, J. *Polyhedron* **1990**, *21*, 2553.

<sup>⊙</sup> Abstract published in *Advance ACS Abstracts*, December 1, 1994.  
(1) (a) Jordan, R. F. *Adv. Organomet. Chem.* **1991**, *32*, 325. (b) Jordan, R. F.; Bradley, P. K.; LaPointe, R. E.; Taylor, D. F. *New J. Chem.* **1990**, *14*, 505. (c) Jordan, R. F. *J. Chem. Educ.* **1988**, *65*, 285. (d) Guram, A. S.; Jordan, R. F. In *Comprehensive Organometallic Chemistry*, 2nd ed.; in press.

electrophilic behavior, including alkyne insertion, ethylene polymerization, and ligand C–H activation.<sup>2a</sup> Here we describe related cationic species based on acen ligands.

Acen, salen and other tetradentate Schiff base ligands have been used throughout the transition metal series.<sup>6</sup> An important recent advance in this area is Jacobsen's development of enantioselective olefin epoxidation catalysts based on chiral Mn(III) salen complexes.<sup>7</sup> Schiff base complexes of early metals have also been prepared.<sup>8,9</sup> Floriani has described the syntheses and structures of (acen)TiCl<sub>2</sub> (1) and (salen)TiCl<sub>2</sub> (2)<sup>8c–e</sup> and (N<sub>2</sub>O<sub>2</sub>-chelate)MCl<sub>2</sub>(THF)<sub>n</sub> (N<sub>2</sub>O<sub>2</sub>-chelate = salen, salophen, acen; M = Zr, Hf; n = 0, 1)<sup>8b</sup> complexes (Chart 1). The six coordinate Ti complexes 1 and 2 exhibit planar N<sub>2</sub>O<sub>2</sub>-chelate cores and trans chloride ligands (e.g. Cl–Ti–Cl angle = 174.0(3)° for 1). The stereochemistry of the Zr and Hf complexes depends on the flexibility of the Schiff base ligand and the coordination number of the metal. The seven coordinate complex (acen)ZrCl<sub>2</sub>(THF) (3) adopts a pentagonal bipyramidal structure in which the trans chloride ligands (Cl–Zr–Cl, 169.1(1)°) occupy apical sites, and the THF is *cis* to

Chart 1



(3) For (N<sub>4</sub>-porphyrin)MX<sub>2</sub> (M = group 4) complexes, see: (a) Brand, H.; Arnold, J. *Organometallics* **1993**, *12*, 3655. (b) Brand, H.; Arnold, J. *J. Am. Chem. Soc.* **1992**, *114*, 2266. (c) Arnold, J.; Hoffman, C. G. *J. Am. Chem. Soc.* **1990**, *112*, 8620. (d) Kim, H.-J.; Whang, D.; Kim, K.; Do, Y. *Inorg. Chem.* **1993**, *32*, 360. (e) Ryu, S.; Whang, D.; Kim, J.; Yeo, W.; Kim, K. *J. Chem. Soc., Dalton Trans.* **1993**, 205. (f) Shibata, K.; Aida, T.; Inoue, S. *Chem. Lett.* **1992**, 1173. (g) Shibata, K.; Aida, T.; Inoue, S. *Tetrahedron Lett.* **1992**, *33*, 1077. (h) Schaverien, C. J.; Orpen, A. G. *Inorg. Chem.* **1991**, *30*, 4968.

(4) For (RO)<sub>2</sub>MX<sub>2</sub> (M = group 4) complexes, see: (a) Lubben, T. V.; Wolczanski, P. T.; Van Duyne, G. G. *Organometallics* **1984**, *3*, 977. (b) Latesky, S. L.; McMullen, A. K.; Niccolai, G. P.; Rothwell, I. P. *Organometallics* **1985**, *4*, 902. (c) Chesnut, R. W.; Durfee, L. D.; Fanwick, P. E.; Rothwell, I. P. *Polyhedron* **1987**, *6*, 2019. (d) Schaverien, C. J.; van der Linden, A. J. *Polym. Prepr. (Am. Chem. Soc., Div. Polym. Chem.)* **1994**, *35*, 672.

(5) For (NR<sub>2</sub>)<sub>2</sub>MX<sub>2</sub> (M = group 4) complexes, see: (a) Lappert, M. F.; Power, P. P.; Sanger, A. R.; Srivastava, R. C. *Metal and Metalloid Amides*; Ellis Horwood Limited: Chichester, England, 1980; Chapter 8. (b) Andersen, R. A. *Inorg. Chem.* **1979**, *18*, 2928. (c) Bruger, H.; Kluess, C. J. *Organomet. Chem.* **1976**, *108*, 69. (d) Cowdell, R. T.; Fowles, G. W. A.; Walton, R. A. *J. Less-Common Met.* **1963**, *5*, 386.

(6) (a) Garnovskii, A. D.; Nivorozhkin, A. L.; Minkin, V. I. *Coord. Chem. Rev.* **1993**, *126*, 1. (b) Calligaris, M.; Randaccio, L. In *Comprehensive Coordination Chemistry*; Wilkinson, G.; Gillard, R. D.; McCleverty, J. A., Eds.; Pergamon: Oxford, 1987; Vol. 2, Chapter 20.1, p 715. (c) Calligaris, M.; Nardin, G.; Randaccio, L. *Coord. Chem. Rev.* **1972**, *7*, 385. (d) Hennig, H. Z. *Chem.* **1971**, *11*, 81. (e) Holm, R. H.; Everett, G. W.; Chakravorty, A. *Prog. Inorg. Chem.* **1966**, *7*, 83.

(7) (a) Zhang, W.; Loebach, J. L.; Wilson, S. R.; Jacobsen, E. N. *J. Am. Chem. Soc.* **1990**, *112*, 2801. (b) Jacobsen, E. N.; Zhang, W.; Guler, M. L. *J. Am. Chem. Soc.* **1991**, *113*, 6703. (c) Zhang, W.; Jacobsen, E. N. *J. Org. Chem.* **1991**, *56*, 2296.

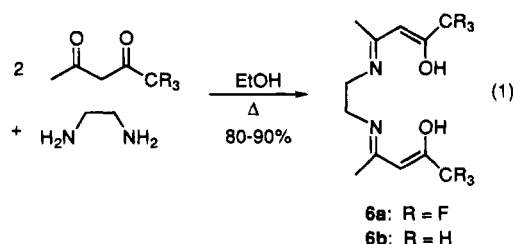
(8) For group 4 metal Schiff base complexes, see: (a) Solari, E.; Floriani, C.; Chiesi-Villa, A.; Rizzoli, C. *J. Chem. Soc., Dalton Trans.* **1992**, 367. (b) Cobrazza, F.; Solari, E.; Floriani, C.; Chiesi-Villa, A.; Guastini, C. *J. Chem. Soc., Dalton Trans.* **1990**, 1335. (c) Dell'Amico, G.; Marchetti, F.; Floriani, C. *J. Chem. Soc., Dalton Trans.* **1982**, 2197. (d) Mazzanti, M.; Rosset, J. M.; Floriani, C.; Chiesi-Villa, A.; Guastini, C. *J. Chem. Soc., Dalton Trans.* **1989**, 953. (e) Floriani, C. *Polyhedron* **1989**, *8*, 1717. (f) Gilli, G.; Cruickshank, D. W. J.; Beddocks, R. C.; Mills, O. S. *Acta Crystallogr., Sect. B* **1972**, *28*, 1889.

(9) For group 5 metal Schiff base complexes, see: (a) Rosset, J. M.; Floriani, C.; Mazzanti, M.; Chiesi-Villa, A.; Guastini, C. *Inorg. Chem.* **1990**, *29*, 3991. (b) Floriani, C.; Mazzanti, M.; Ciurli, S.; Chiesi-Villa, A.; Guastini, C. *J. Chem. Soc., Dalton Trans.* **1988**, 1361. (c) Gambarotta, S.; Mazzanti, M.; Floriani, C.; Chiesi-Villa, A.; Guastini, C. *Inorg. Chem.* **1986**, *25*, 2308. (d) Gambarotta, S.; Mazzanti, M.; Floriani, C.; Chiesi-Villa, A.; Guastini, C. *J. Chem. Soc., Chem. Commun.* **1985**, 829. (e) Teleb, S. M.; Sadeek, S. A.; Nour, E. M. *Spectrosc. Lett.* **1993**, *26*, 169. (f) Khuhawar, M. Y.; Soomro, A. I. *J. Chem. Soc. Pak.* **1992**, *14*, 206. (g) Pandeya, K. B.; Khare, D. *J. Indian Chem. Soc.* **1992**, *69*, 522. (h) Bencini, A.; Benelli, C.; Dei, A.; Gatteschi, D. *Inorg. Chem.* **1985**, *24*, 695. (i) Kuska, H. A.; Yang, P.-H. *Inorg. Chem.* **1977**, *16*, 1938. (j) Tandon, J. P.; Gupta, S. R.; Prasad, R. N. *Acta Chim. Acad. Sci. Hung.* **1975**, *86*, 33. (k) Murray, K. S.; Simm, G. R.; West, B. O. *Aust. J. Chem.* **1973**, *26*, 991.

both chlorides (average Cl–Zr–O<sub>THF</sub>, 95.5(1)°) in the open sector of the equatorial plane. In contrast, the six coordinate complex (acen)ZrCl<sub>2</sub> (4) adopts a distorted octahedral structure with a nonplanar acen ligand and *cis* chlorides (Cl–Zr–Cl, 87.2(1)°).

Despite the availability of these (N<sub>2</sub>O<sub>2</sub>-chelate)MCl<sub>2</sub>(THF)<sub>n</sub> complexes, alkyl derivatives are rare. Floriani found that the alkylation chemistry of (salen)TiCl<sub>2</sub> (2) is highly dependent on the nature of the alkylating agent and solvent.<sup>8a</sup> The reaction of 2 with MeLi in nonpolar aromatic solvents yields the thermally unstable dimethyl derivative *trans*-(salen)TiMe<sub>2</sub> (5), which is structurally analogous to 2 (C–Ti–C, 154.9(6)°, Chart 1). However, the use of the Grignard reagents leads to alkylation at a salen imine carbon or formation of reduced Ti(III) products, depending on the polarity of the solvent.

The objectives of the present study were to develop efficient syntheses of (N<sub>2</sub>O<sub>2</sub>-chelate)MR<sub>2</sub> and (N<sub>2</sub>O<sub>2</sub>-chelate)M(R)<sup>+</sup> (M = group 4 metal) complexes, and to compare the reactivity of the (N<sub>2</sub>O<sub>2</sub>-chelate)M(R)<sup>+</sup> cations with that of Cp<sub>2</sub>M(R)<sup>+</sup> and (N<sub>4</sub>-macrocyclic)M(R)<sup>+</sup> species. Tetradentate Schiff base ligands provide a promising alternative to cyclopentadienyl and N<sub>4</sub>-macrocyclic ligands because they are easily synthesized (eq 1),<sup>10</sup> their steric and electronic properties are readily



6a: R = F  
6b: R = H

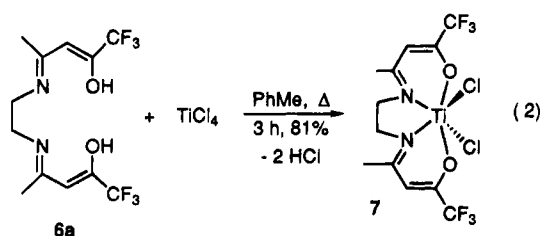
(10) (a) Liu, H. Y.; Scharbert, B.; Holm, R. H. *J. Am. Chem. Soc.* **1991**, *113*, 9530. (b) McCarthy, P. J.; Hovey, R. J.; Ueno, K.; Martell, A. E. *J. Am. Chem. Soc.* **1955**, *77*, 5820.

modified, and chiral versions are available.<sup>7,11</sup> Replacement of two nitrogen functions of an  $N_4$ -macrocyclic ligand with two oxygen functions should decrease the electron donor ability and increase the metal electrophilicity in the resulting complexes. Our initial studies have focused on  $(\text{acn})Zr(R)^+$  cations. We anticipated that the flexibility of the acn ligand (Chart 1) would allow such species to coordinate one or two additional ligands/substrates *cis* to the potentially reactive Zr-R group. For  $(\text{acn})MX_2$  systems, a nonplanar  $N_2O_2$ -chelate core forces the X substituents into a *cis* configuration (e.g. 4). Conversely, a more planar  $N_2O_2$ -chelate core forces the X substituents into a *trans* configuration, but allows coordination of an additional ligand in the open sector of the  $N_2O_2$ -chelate core *cis* to both X groups (e.g. 3). We have utilized both acn (referred to here as  $H_6\text{-acn}$ ) and the more electron-withdrawing analog  $F_6\text{-acn}$ , in which the alkoxide methyl groups are fluorinated (eq 1).

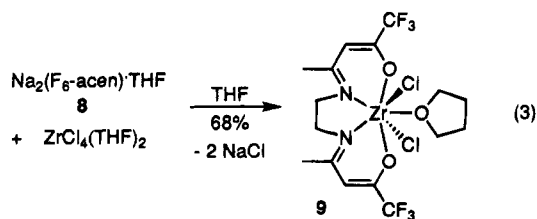
## Results and Discussion

**Synthesis and Attempted Alkylation of  $(R_6\text{-acn})MCl_2(\text{THF})_n$  ( $R = H, F$ ;  $M = Ti, Zr$ ;  $n = 0, 1$ ) Complexes.** We first attempted to generate  $(R_6\text{-acn})MR'_2$  complexes via alkylation of the corresponding dihalides. The dichloride  $(H_6\text{-acn})ZrCl_2(\text{THF})$  (3) was prepared previously by Floriani,<sup>8b</sup> and the  $(F_6\text{-acn})Ti$  and  $(F_6\text{-acn})Zr$  analogues were prepared by similar routes.

The addition of  $H_2(F_6\text{-acn})$  (6a) to  $TiCl_4$  in toluene results in the liberation of HCl and the formation of  $(F_6\text{-acn})TiCl_2$  (7), which is isolated as red crystals by recrystallization from cold  $CH_2Cl_2$ /pentane (eq 2). Dichloride



7 is assigned a *trans* structure based on the solid state structures of 1, 2, and 5 (Chart 1).<sup>8d,e</sup> The  $NCH_2CH_2N$  resonance ( $\delta$  3.96) in the  $^1H$  NMR spectrum appears as a sharp singlet which is consistent with a *trans* structure. Slow addition of a THF solution of  $Na_2(F_6\text{-acn})\cdot\text{THF}$  (8) to  $ZrCl_4(\text{THF})_2$  affords  $(F_6\text{-acn})ZrCl_2(\text{THF})$  (9) as an off-white powder in good yield (eq 3).



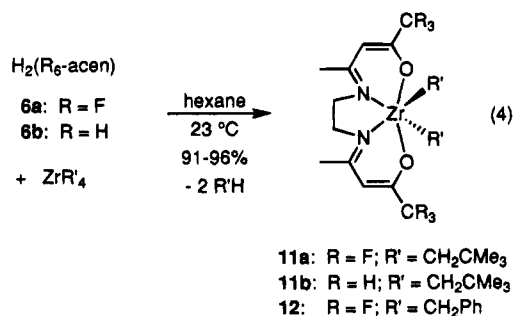
These conditions are required to inhibit the formation of the bis(ligand) complex  $(F_6\text{-acn})_2Zr$  (10). Eight-

coordinate complexes related to 10 have been reported previously.<sup>11a,12,13</sup> Dichloride 9 is soluble and stable in  $CH_2Cl_2$  and benzene, and is structurally analogous to  $(\text{acn})ZrCl_2(\text{THF})$  (3).<sup>8b</sup> The  $^1H$  NMR spectrum exhibits a sharp singlet ( $\delta$  3.98) for the  $NCH_2CH_2N$  backbone and two multiplets ( $\delta$  4.29, 1.99) for the coordinated THF, consistent with a pentagonal bipyramidal structure containing apical chloride ligands and an equatorial THF ligand.

The reaction of 7 with MeLi in toluene afforded a mixture of products which could not be separated or characterized. Presumably, this mixture contains *cis* and *trans*  $(F_6\text{-acn})TiMe_2$  isomers, as well as an alkyl migration product. Dichloride 7 does not react with  $MgMe_2$  or  $ZnMe_2$ . Attempted alkylations of  $(\text{salen})ZrCl_2(\text{THF})$ ,<sup>8b</sup> 3 and 9 with alkyllithium reagents (MeLi,  $Me_3SiCH_2Li$  and  $Me_3CCH_2Li$ ) in benzene/toluene were also unsuccessful. The dichlorides were consumed in these reactions, but the NMR spectra of the isolated materials indicated that complex product mixtures were formed. Attempted alkylation of 3 and 9 with  $MgMe_2$  yielded only unreacted dichlorides.

**Synthesis of  $(R_6\text{-acn})ZrR'_2$  ( $R = F, H$ ;  $R' = CH_2CMe_3, CH_2Ph$ ) Complexes by Alkane Elimination.** Because the  $(R_6\text{-acn})ZrR'_2$  complexes were not available via alkylation of the corresponding dichloride complexes, we pursued alternative synthetic approaches. Alkane elimination reactions between  $MR'_4$  ( $M = Ti, Zr, Hf$ ) species and protic reagents have been exploited in the syntheses of a variety of  $d^0$  alkyl complexes.<sup>2a,4,14</sup> We explored this route despite the limitation that  $R'$  is usually restricted to bulky alkyls (e.g.,  $-CH_2SiMe_3$ ,  $-CH_2Ph$ ,  $-CH_2CMe_3$ ).<sup>14,15</sup>

The addition of solid  $H_2(R_6\text{-acn})$  (6a,b) to  $ZrR'_4$  ( $R' = CH_2CMe_3, CH_2Ph$ ) in pentane/hexane results in alkane elimination and precipitation of the desired  $(R_6\text{-acn})ZrR'_2$  complexes 11a,b and 12 in high yield (eq 4).



These compounds are obtained as yellow to orange-red solids, and are soluble and stable in benzene,  $CH_2Cl_2$  and THF. These dialkyls appear to be more resistant to metal to ligand alkyl migrations than  $(\text{salen})TiR'_2$ .<sup>8a</sup>

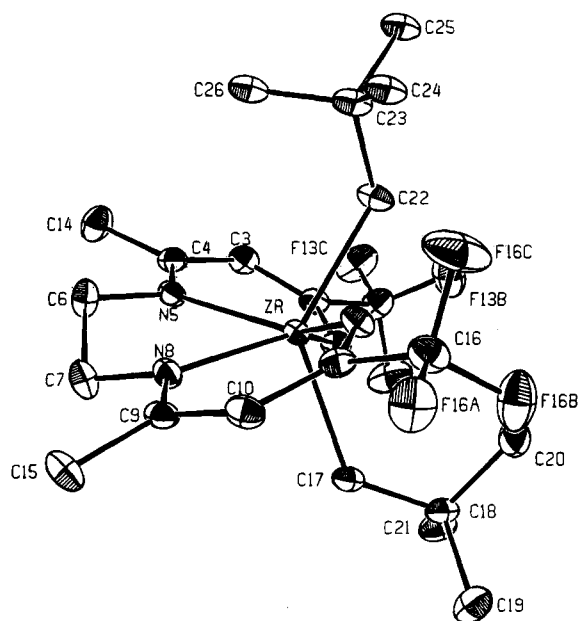
(11) (a) Illingsworth, M. L.; Cleary, B. P.; Jensen, A. J.; Schwartz, L. J.; Rheingold, A. L. *Inorg. Chim. Acta* 1993, 207, 147. (b) Khuhawar, M. Y. *J. Chem. Soc. Pak.* 1985, 7, 239. (c) Black, D. G.; Douglas, M.; Jordan, R. F., unpublished results.

(12) For  $(N_2O_2\text{-chelate})_2Zr$  complexes, see: (a) Archer, R. D.; Day, R. O.; Illingsworth, M. L. *Inorg. Chem.* 1979, 18, 2908. (b) Biradar, N. S.; Locker, A. L. *J. Karnatak Univ.* 1972, 17, 1.

(13) For  $(N_4\text{-porphyrin})_2M$  complexes, see: Kim, K.; Lee, W. S.; Kim, H.-J.; Cho, S.-H.; Girolami, G. S.; Gorlin, P. A.; Suslick, K. S. *Inorg. Chem.* 1991, 30, 2652.

(14) Collier, M. R.; Lappert, M. F.; Pearce, R. *J. Chem. Soc., Dalton Trans.* 1973, 445.

(15) (a) Zucchini, U.; Albizzati, E.; Giannini, U. *J. Organomet. Chem.* 1971, 26, 357. (b) Davidson, P. J.; Lappert, M. F.; Pearce, R. *J. Organomet. Chem.* 1973, 57, 269.



**Figure 1.** Structure of  $(F_6\text{-acen})Zr(\text{CH}_2\text{CMe}_3)_2$  (**11a**).

and  $(N_4\text{-macrocycle})ZrR_2$  complexes.<sup>16</sup> This process may be disfavored in  $(R_6\text{-acen})ZrR_2$  complexes by the less electrophilic and more crowded imine carbons and the stronger M–C bonds.

**Solid State Structure of  $(F_6\text{-acen})Zr(\text{CH}_2\text{CMe}_3)_2$  (**11a**).** An X-ray diffraction study was performed on **11a** to determine the solid state structures of the dialkyls. Single crystals of **11a** suitable for X-ray diffraction were grown from toluene layered with pentane at  $-35^\circ\text{C}$ . An ORTEP view is shown in Figure 1. Crystallographic details, atom coordinates, and key bond distances and angles are listed in Tables 1–3.

Complex **11a** adopts a monomeric elongated trigonal prismatic structure. The  $F_6\text{-acen}$  ligand is moderately twisted such that the molecule has approximate  $C_2$  symmetry. The dihedral angle between the two six membered chelate rings of **11a** ( $41.8(2)^\circ$ ) is considerably smaller than that in *cis*-(*acen*) $ZrCl_2$  (**4**,  $60.1(2)^\circ$ ), and, accordingly, the C–Zr–C angle ( $129.9(2)^\circ$ ) in **11a** is much larger than the Cl–Zr–Cl angle ( $87.2(1)^\circ$ ) in **4**. The C–Zr–C angle in **11a** is smaller than the Cl–Zr–Cl angle ( $169.1(1)^\circ$ ) in the seven-coordinate complex **3**. However, the C–Zr–C angle in **11a** is substantially larger than those in  $(N_4\text{-macrocycle})ZrR_2$  and  $Cp_2ZrR_2$  complexes ( $85\text{--}95^\circ$ ) in which the alkyl ligands are *cis*.<sup>2a,c,17</sup> The Zr–N distances in **11a** (average  $2.33(4)$  Å) are in the range for **3** (average  $2.32(3)$  Å) and **4** (average  $2.25(4)$  Å). Comparison of these data to  $Zr^{IV}$ –N distances in other complexes (e.g.  $Cp_2Zr(\eta^2\text{-pyridyl})(PMe_3)^+$  ( $2.21$  Å),  $(Cp_2Zr(\eta^2\text{-CH}_2\text{CH}_2\text{py})^+$  ( $2.30$

Å),  $Cp_2Zr(\text{pyrrolyl})_2$  (average  $2.17$  Å) suggests that N–Zr  $\pi$ -d interactions are not important.<sup>18</sup> The Zr–O distances (average  $2.13(3)$  Å) are longer and the Zr–O–C angles (average  $132.0(2)^\circ$ ) are smaller than those in both **3** (average  $2.05(3)$  Å; average  $137.9(1)^\circ$ ) and **4** (average  $2.01(3)$  Å; average  $134.2(2)^\circ$ ). These data are consistent with the expected weaker donor ability of the alkoxide function of  $F_6\text{-acen}^{2-}$  vs  $H_6\text{-acen}^{2-}$ . The small Zr–O–C angles indicate that the oxygen atoms are nearly  $sp^2$  hybridized and function as formal 4 electron ( $\sigma, \pi$ ) donors in these systems. For comparison, shorter Zr–O distances and larger Zr–O–C angles are observed in alkoxide/aryloxo complexes such as  $(Ar'O)Zr(\text{CH}_2\text{Ph})_3$  ( $1.942(9)$  Å;  $165.7(9)^\circ$ )<sup>4b</sup> and  $(\text{triox})_2ZrCl_3\text{-Li}(\text{OEt})_2$  (average  $1.89(7)$  Å; average  $169.0(7)^\circ$ ).<sup>4a</sup> The nearly linear alkoxide/aryloxo ligands are viewed as formal 6-electron ( $\sigma, \pi, \pi$ ) donors, or Cp equivalents in these cases.<sup>4</sup> Complex **11a** and analogous  $(R_6\text{-acen})ZrR_2$  complexes are thus best described as 16-electron species.

**Solution Structures of  $(R_6\text{-acen})ZrR_2$  Complexes.** The  $^1\text{H}$  NMR spectra of **11a,b** and **12** exhibit singlets for the  $N\text{CH}_2\text{CH}_2\text{N}$  and  $Zr\text{CH}_2$  hydrogens (**11a**,  $\delta$  2.76, 0.59; **11b**,  $\delta$  3.02, 0.49; **12**,  $\delta$  2.57, 2.25). It is likely that the solution structures of these compounds are analogous to the solid state structure of **11a** but that rapid inversion of the 5-membered chelate ring results in effective  $C_{2v}$  symmetry on the NMR time scale. Static structures with *cis* alkyl ligands (c.f. **4**, Chart I) would exhibit AB patterns for the diastereotopic  $Zr\text{CH}_2$  groups and multiplets for the inequivalent  $N\text{CH}_2\text{CH}_2\text{N}$  hydrogens. The  $Zr\text{CH}_2$   $J_{\text{CH}}$  values for neopentyl complexes **11a** ( $109.8$  Hz) and **11b** ( $112.5$  Hz) are in the low end of the range observed for normal  $sp^3$  carbons bonded to electrophilic metal centers. Neopentyl ligands distorted by  $\alpha$ -agostic interactions commonly exhibit lower  $J_{\text{CH}}$  ( $Zr\text{CH}_2$ ) values ( $\leq 100$  Hz).<sup>19,20,21</sup> The  $Zr\text{CH}_2$   $J_{\text{CH}}$  value for dibenzyl complex **12** ( $125.3$  Hz) is consistent with a normal benzyl structure;  $\eta^2$ -benzyl ligands typically exhibit larger  $J_{\text{CH}}$  ( $Zr\text{CH}_2$ ) values ( $> 130$  Hz).<sup>22</sup>

**Synthesis of  $[(R_6\text{-acen})Zr(\text{CH}_2\text{CMe}_3)(NMe_2\text{Ph})\text{-}[B(C_6F_5)_4]]$  ( $R = F, H$ ) Complexes.** Neutral  $Cp_2MR_2$  ( $M = \text{Ti}, Zr, \text{Hf}$ ) complexes have been converted to  $Cp_2M(R)(L)_n^+$  ( $L =$  Lewis base,  $n = 0\text{--}2$ ) cations<sup>1</sup> by M–R protonolysis with  $\text{HNR}_3^+$  reagents,<sup>21a,23</sup> M–R

(18) (a) Jordan, R. F.; Taylor, D. F.; Baenziger, N. C. *Organometallics* **1990**, *9*, 1546. (b) Bynum, R. V.; Hunter, W. E.; Rogers, R. D.; Atwood, J. L. *Inorg. Chem.* **1980**, *19*, 2368. (c) Moore, E. J.; Straus, D. A.; Armantrout, J.; Santarsiero, B. D.; Grubbs, R. H.; Bercaw, J. E. *J. Am. Chem. Soc.* **1983**, *105*, 2068.

(19) Reviews: (a) Brookhart, M.; Green, M. L. H.; Wong, L. *Prog. Inorg. Chem.* **1988**, *36*, 1. (b) Crabtree, R. H.; Hamilton, D. G. *Adv. Organomet. Chem.* **1988**, *28*, 299. (c) Ginzburg, A. S. *Russ. Chem. Rev.* **1988**, *57*, 1175. (d) See also: Cotton, F. A.; Luck, R. L. *Inorg. Chem.* **1989**, *28*, 3210.

(20) For  $\alpha$ -agostic M–CH<sub>3</sub> complexes, see: (a) Dawoodi, Z.; Green, M. L. H.; Mtetwa, V. S. B.; Prout, K.; Schultz, A. J.; Williams, J. M.; Koetzle, T. F. *J. Chem. Soc., Dalton Trans.* **1986**, 1629. (b) den Haan, K. H.; de Boer, J. L.; Teuben, J. H.; Smeets, W. J. J.; Spek, A. L. *J. Organomet. Chem.* **1987**, *327*, 31. (c) Green, M. L. H.; Hughes, A. K.; Popham, N. A.; Stephens, A. H. H.; Wong, L. *J. Chem. Soc., Dalton Trans.* **1992**, *12*, 3077.

(21) (a) Guo, Z.; Swenson, D. C.; Jordan, R. F. *Organometallics* **1994**, *13*, 1424. (b) Poole, A. D.; Williams, D. N.; Kenwright, A. M.; Gibson, V. C.; Clegg, W.; Hockless, C. R.; O'Neil, P. A. *Organometallics* **1993**, *12*, 2549. (c) Mena, M.; Pellighelli, M. A.; Royo, P.; Serrano, R.; Tiripicchio, A. *J. Chem. Soc., Dalton Trans.* **1986**, 1118. (d) Bruno, J. W.; Smith, G. M.; Marks, T. J.; Fair, C. K.; Schultz, A. J.; Williams, J. M. *J. Am. Chem. Soc.* **1986**, *108*, 40. (e) den Haan, K. H.; de Boer, J. L.; Teuben, J. H. *Organometallics* **1986**, *5*, 1726. (f) Jeske, G.; Schock, L. E.; Swepston, P. N.; Schumann, H.; Marks, T. J. *J. Am. Chem. Soc.* **1985**, *107*, 8103. (g) Cayias, J. Z.; Babiain, E. A.; Hrnrcir, D. C. *J. Chem. Soc., Dalton Trans.* **1986**, 2743. (h) van der Heijden, H.; Gal, A. W.; Pasman, P.; Orpen, A. G. *Organometallics* **1985**, *4*, 1847.

(16) (a) Thermally induced benzyl migration from Zr to a ligand imine carbon occurs in  $(\text{salen})Zr(\text{CH}_2\text{Ph})_2$  and  $(N_4\text{-macrocycle})Zr(R)_2$  species benzene or toluene solution. These reactions are promoted by donor solvents. Gardner, T. G.; Black, D. G.; Douglas, M.; Jordan, R. F., unpublished results. (b) Floriani observed  $\text{Me}^-$  attack at a ligand imine carbon upon addition of  $\text{MeMgBr}$  to  $(\text{Me}_4\text{-taa})ZrCl_2$  at low temperature in THF.<sup>2c</sup>

(17) (a) Cardin, D. J.; Lappert, M. F.; Raston, C. L. *Chemistry of Organo-Zirconium and -Hafnium Compounds*; Ellis Horwood, Ltd.: West Sussex, U.K., 1986; Chapter 4, pp 68–75. (b) Erker, G.; Kruger, C.; Muller, G. *Adv. Organomet. Chem.* **1985**, *24*, 1. (c) Hunter, W. E.; Hrnrcir, D. C.; Bynum, R. V.; Penttila, R. A.; Atwood, J. L. *Organometallics* **1983**, *2*, 750. (d) Erker, G.; Dorf, U.; Czisch, P.; Petersen, J. L. *Organometallics* **1986**, *5*, 668. (e) Gambarotta, S.; Strologo, S.; Floriani, C.; Chiesa-Villa, A.; Guastini, C. *Inorg. Chem.* **1985**, *24*, 654.

Table 1. Summary of Crystallographic Data for  $(F_6\text{-acen})\text{Zr}(\text{CH}_2\text{CMe}_3)_2$  (11a) and  $[F_6\text{-acen})\text{Zr}(\text{CH}_2\text{CMe}_3)(\text{NMe}_2\text{Ph})][\text{B}(\text{C}_6\text{F}_5)_4]$  (13a)

	11a	13a
empirical formula	$\text{C}_{22}\text{H}_{34}\text{F}_6\text{N}_2\text{O}_2\text{Zr}$	$\text{C}_{49}\text{H}_{34}\text{BF}_{26}\text{N}_3\text{O}_2\text{Zr}\cdot 0.5\text{C}_6\text{H}_5\text{Cl}$
fw	563.74	1349.10
cryst size (mm)	$0.44 \times 0.28 \times 0.17$	$0.20 \times 0.36 \times 0.54$
cryst color	orange	orange
$T$ (K)	120	295(2)
space group	$P\bar{1}$	$C2/c$
$a$ (Å)	12.280(3)	39.707(4)
$b$ (Å)	12.731(3)	11.226(1)
$c$ (Å)	8.825(3)	30.045(3)
$\alpha$ (deg)	96.66(2)	90
$\beta$ (deg)	97.21(2)	126.667(9)
$\gamma$ (deg)	76.68(2)	90
$V$ (Å <sup>3</sup> )	1327(1)	10742.6(22)
$Z$	2	8
$d_{\text{calcd}}$ (g/cm <sup>3</sup> )	1.41	1.668
cell dimen determ	40 reflns; $23^\circ < 2\theta < 28^\circ$	24 reflns; $20^\circ < 2\theta < 28^\circ$
$\lambda$ (Mo K $\alpha$ radiation, Å)	0.7107	0.7107
scan type	$\omega/\theta = 1$	$\omega$
scan limit (deg)	$4^\circ < 2\theta < 50^\circ$	$3.5^\circ < 2\theta < 50.0^\circ$
scan speed (deg/min)	1.43–6.67	2.00–5.00
$\omega$ scan range (deg)	$0.90 + \tan(\theta)$	variable
data collected $h; k; l$	–14, 3; –15, 15; –10, 10	–37, 47; 0, 13; –35, 0
no. of total reflns	5244	9604
no. of unique reflns	4486	9396
$R_{\text{int}}$	0.033	0.0426
obsd data criteria	$I > 3\sigma(I)$	$I > 2\sigma(I)$
no. of reflns used	3242	4584
max decay cor factor	1.026	1.07
$\mu$ , cm <sup>–1</sup>	4.66	3.65
max empirical abs cor	1.17	1.26
structure soln method	direct methods	Patterson/Fourier
refinement <sup>a</sup>	all non-H anisotropic, disordered <sup>t</sup> butyl C isotropic, neopentyl methylene H isotropic, all other H set at calcd positions	all non-H anisotropic, all H at calcd positions
tot. no. of params	311	793
$R$	0.042	0.0608
$R_w$	0.049	0.0880
weighting coefficients: P, Q <sup>a</sup>	0.02, 1.0	0.03, 0
SDOWU <sup>b</sup>	1.60	0.995
max resid density (e/Å <sup>3</sup> )	0.83	0.295

<sup>a</sup>  $W = [\sigma_F^2 + (PF)^2 + Q]^{-1}$ . <sup>b</sup> Standard deviation of unit weight.

Table 2. Selected Bond Distances and Angles for  $(F_6\text{-acen})\text{Zr}(\text{CH}_2\text{CMe}_3)_2$  (11a)

Zr–O(1)	2.124(3)	O(1)–C(2)	1.313(6)
Zr–O(12)	2.139(3)	O(12)–C(11)	1.300(6)
Zr–N(5)	2.347(4)	N(5)–C(4)	1.321(6)
Zr–N(8)	2.320(4)	N(8)–C(9)	1.331(6)
Zr–C(17)	2.283(4)	C(2)–C(3)	1.373(6)
Zr–C(22)	2.323(5)	C(3)–C(4)	1.447(7)
F(13A)–C(13)	1.343(5)	C(9)–C(10)	1.435(6)
F(13B)–C(13)	1.361(6)	C(10)–C(11)	1.375(7)
F(13C)–C(13)	1.350(6)	C(17)–C(18)	1.548(6)
F(16A)–C(16)	1.336(6)	C(22)–C(23)	1.542(6)
F(16B)–C(16)	1.362(6)	C(2)–C(13)	1.527(7)
F(16C)–C(16)	1.331(6)		
C(6)–C(7)	1.526(8)		
C(11)–C(16)	1.533(6)		
O(1)–Zr–O(12)	139.8(1)	N(5)–Zr–C(17)	122.7(1)
O(1)–Zr–N(5)	77.3(1)	N(5)–Zr–C(22)	98.2(1)
O(1)–Zr–N(8)	139.0(1)	N(8)–Zr–C(17)	91.0(2)
O(1)–Zr–C(17)	81.6(1)	N(8)–Zr–C(22)	130.9(1)
O(1)–Zr–C(22)	80.6(1)	C(17)–Zr–C(22)	129.9(2)
O(12)–Zr–N(5)	140.4(1)	Zr–O(1)–C(2)	130.5(2)
O(12)–Zr–N(8)	78.3(1)	Zr–O(12)–C(11)	133.5(3)
O(12)–Zr–C(17)	84.2(1)	Zr–N(5)–C(4)	128.2(3)
O(12)–Zr–C(22)	80.2(1)	Zr–N(8)–C(9)	127.9(3)
N(5)–Zr–N(8)	73.2(1)	Zr–C(17)–C(18)	128.1(3)
Zr–C(22)–C(23)	124.7(3)		

oxidative cleavage with  $\text{Cp}_2\text{Fe}^+$  or  $\text{Ag}^+$  reagents,<sup>22d,e,24</sup> and alkyl abstraction with  $\text{Ph}_3\text{C}^+$  or  $\text{B}(\text{C}_6\text{F}_5)_3$ .<sup>23c,25</sup> Among these methods, the protonolysis approach gave the best results with  $(R_6\text{-acen})\text{ZrR}'_2$  compounds. To

minimize reactions and interactions of the anion with the electrophilic metal cations and to increase solubility,  $\text{B}(\text{C}_6\text{F}_5)_4^-$  was used as the counterion.<sup>23e</sup>

Protonolysis of  $(R_6\text{-acen})\text{Zr}(\text{CH}_2\text{CMe}_3)_2$  (11a, R = F; 11b, R = H) with  $[\text{HNMe}_2\text{Ph}][\text{B}(\text{C}_6\text{F}_5)_4]$  in  $\text{CH}_2\text{Cl}_2$  affords the cationic amine adducts  $[(R_6\text{-acen})\text{Zr}(\text{CH}_2\text{CMe}_3)_2]^+$ .

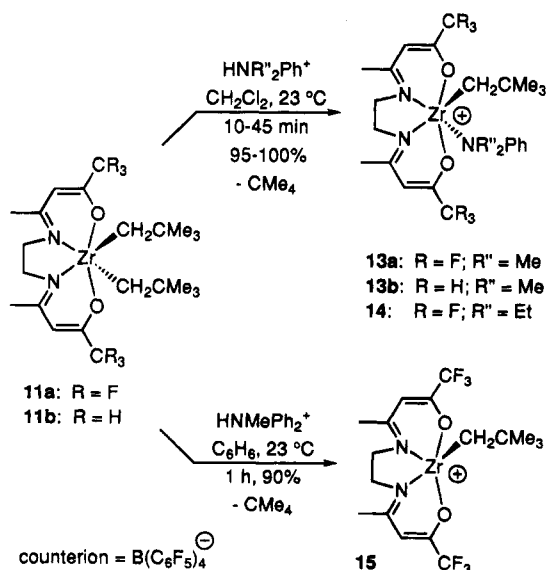
(22) (a) Hughes, A. K.; Meetsma, A.; Teuben, J. H. *Organometallics* **1993**, *12*, 1936. (b) Dryden, N. H.; Legzdins, P.; Trotter, J.; Yee, V. C. *Organometallics* **1991**, *10*, 2857. (c) Crowther, D. J.; Jordan, R. F.; Baenziger, N. C. *Organometallics* **1990**, *9*, 2574. (d) Jordan, R. F.; LaPointe, R. E.; Baenziger, N.; Hinch, G. D. *Organometallics* **1990**, *9*, 1539. (e) Jordan, R. F.; LaPointe, R. E.; Bajgur, C. S.; Echols, S. F.; Willet, R. J. *Am. Chem. Soc.* **1987**, *109*, 4111. (f) Latesky, S. L.; McMullen, A. K.; Niccolai, G. P.; Rothwell, I. P.; Huffman, J. C. *Organometallics* **1985**, *4*, 902.

(23) (a) Bochmann, M.; Wilson, L. M. *J. Chem. Soc., Chem. Commun.* **1986**, 1610. (b) Lin, Z.; Le Marechal, J.; Sabat, M.; Marks, T. J. *J. Am. Chem. Soc.* **1987**, *109*, 4127. (c) Turner, H. W.; Hlatky, G. G. *Eur. Pat. Appl.* 0 277 003, 1988. (d) Hlatky, G. G.; Turner, H. W.; Eckman, R. R. *J. Am. Chem. Soc.* **1989**, *111*, 2728. (e) Turner, H. W. *Eur. Pat. Appl.* 0 277 004, 1988. (f) Hlatky, G. G.; Eckman, R. R.; Turner, H. W. *Organometallics* **1992**, *11*, 1413. (g) Eshius, J. J. W.; Tan, Y. Y.; Meetsma, A.; Teuben, J. H.; Renkema, J.; Evens, G. G. *Organometallics* **1992**, *11*, 362. (h) Eshius, J. J. W.; Tan, Y. Y.; Renkema, J.; Teuben, J. H. *J. Mol. Catal.* **1990**, *62*, 277. (i) Amorose, D. M.; Lee, R. P.; Petersen, J. L. *Organometallics* **1991**, *10*, 2191. (j) Horton, A. D.; Orpen, A. G. *Organometallics* **1991**, *10*, 3910. (k) Bochmann, M.; Jagger, A. J.; Nicholls, J. C. *Angew. Chem., Int. Ed. Engl.* **1990**, *29*, 780. (l) Horton, A. D.; Frijns, J. H. G. *Angew. Chem., Int. Ed. Engl.* **1991**, *30*, 1152. (m) Grossman, R. B.; Doyle, R. A.; Buchwald, S. L. *Organometallics* **1991**, *10*, 1501. (n) Bochmann, M.; Lancaster, S. J. *J. Organomet. Chem.* **1992**, *434*, C1. (o) Ewen, J. A.; Edler, M. J.; Jones, R. L.; Haspelslagh, L.; Atwood, J. L.; Bott, S. G.; Robinson, K. *Makromol. Chem., Macromol. Symp.* **1991**, *48/49*, 253.

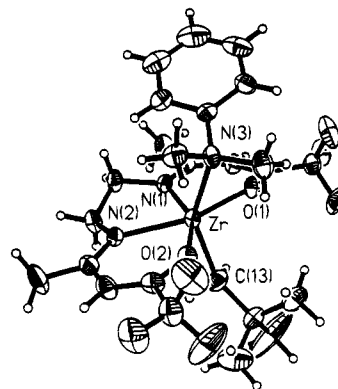
**Table 3. Atomic Coordinates and Isotropic Thermal Parameters (Å<sup>2</sup>) for (F<sub>6</sub>-acen)Zr(CH<sub>2</sub>CMe<sub>3</sub>)<sub>2</sub> (11a)**

atom	x	y	z	B <sup>a</sup> (Å <sup>2</sup> )
Zr	0.73092(4)	0.26191(3)	0.42514(5)	1.660(7)
F(13A)	0.6327(3)	0.6382(2)	0.2926(4)	4.44(8)
F(13B)	0.7576(3)	0.5397(3)	0.1535(4)	4.84(8)
F(13C)	0.8059(3)	0.6574(2)	0.3329(4)	4.55(7)
F(16A)	0.6379(2)	-0.1434(2)	0.2355(4)	3.54(6)
F(16B)	0.6079(3)	-0.0149(2)	0.0882(4)	4.33(7)
F(16C)	0.7768(3)	-0.1018(3)	0.1490(5)	5.77(8)
O(1)	0.7026(2)	0.4256(2)	0.3742(4)	2.04(6)
O(12)	0.7282(2)	0.1047(2)	0.3113(4)	2.12(6)
N(5)	0.8168(3)	0.3443(3)	0.6453(4)	2.03(7)
N(8)	0.7205(3)	0.1651(3)	0.6280(4)	2.08(7)
C(2)	0.7651(4)	0.4975(3)	0.4118(5)	2.20(9)
C(3)	0.8441(4)	0.5009(3)	0.5358(6)	2.38(9)
C(4)	0.8638(4)	0.4286(4)	0.6562(6)	2.35(9)
C(6)	0.8349(4)	0.2825(4)	0.7827(6)	2.8(1)
C(7)	0.7365(4)	0.2275(4)	0.7798(6)	2.8(1)
C(9)	0.6786(3)	0.0771(4)	0.6234(5)	2.23(9)
C(10)	0.6627(4)	0.0091(3)	0.4846(6)	2.36(9)
C(11)	0.6904(3)	0.0234(3)	0.3434(5)	2.04(9)
C(13)	0.7407(4)	0.5842(4)	0.2988(6)	3.1(1)
C(14)	0.9388(4)	0.4590(4)	0.7986(6)	3.4(1)
C(15)	0.6451(4)	0.0435(4)	0.7672(6)	3.0(1)
C(16)	0.6790(4)	-0.0603(4)	0.2060(6)	2.6(1)
C(17)	0.5404(3)	0.2934(4)	0.3676(5)	2.15(9)
C(18)	0.4705(3)	0.3326(3)	0.2181(6)	2.21(9)
C(19)	0.3607(4)	0.2871(4)	0.1864(7)	3.5(1)
C(20)	0.5395(4)	0.2943(4)	0.0810(6)	3.3(1)
C(21)	0.4359(4)	0.4569(4)	0.2309(6)	3.0(1)
C(22)	0.8720(4)	0.2453(4)	0.2658(6)	2.59(9)
C(23)	0.9874(4)	0.1658(4)	0.2830(6)	2.7(1)
C(24)	0.9747(9)	0.0574(9)	0.184(1)	3.7(2)*
C(25)	1.0827(9)	0.2038(9)	0.228(1)	3.5(2)*
C(26)	1.025(1)	0.145(1)	0.456(2)	4.8(3)*
C(24')	0.9842(8)	1.0472(7)	0.258(1)	2.4(2)*
C(25')	1.0590(8)	1.1924(8)	0.158(1)	3.0(2)*
C(26')	1.042(1)	1.193(1)	0.442(1)	4.1(2)*
C(23')	0.9874	1.1657	0.2830	4*

<sup>a</sup> Starred values denote atoms that were refined isotropically. *B* values for anisotropically refined atoms are given in the form of the isotropic equivalent displacement parameter defined as  $(4/3)[a^2B(1,1) + b^2B(2,2) + c^2B(3,3) + ab(\cos \gamma)B(1,2) + ac(\cos \beta)B(1,3) + bc(\cos \alpha)B(2,3)]$ .

**Scheme 1**

CMe<sub>3</sub>(NMe<sub>2</sub>Ph)][B(C<sub>6</sub>F<sub>5</sub>)<sub>4</sub>] (**13a**, R = F; **13b**, R = H) in high yields (Scheme 1). Complexes **13a,b** are deposited as sparingly soluble oils when generated in benzene/toluene. The fluorinated complex **13a** retains coordinated NMe<sub>2</sub>Ph upon crystallization and is stable in CH<sub>2</sub>Cl<sub>2</sub> (>24 h). In contrast, the nonfluorinated analog

**Figure 2.** Structure of the (F<sub>6</sub>-acen)Zr(CH<sub>2</sub>CMe<sub>3</sub>)(NMe<sub>2</sub>-Ph)<sup>+</sup> cation of **13a**.

**13b** decomposes upon attempted isolation and exhibits limited stability in CH<sub>2</sub>Cl<sub>2</sub> (<24 h).

**Solid State Structure of [(F<sub>6</sub>-acen)Zr(CH<sub>2</sub>CMe<sub>3</sub>)(NMe<sub>2</sub>Ph)][B(C<sub>6</sub>F<sub>5</sub>)<sub>4</sub>] (**13a**).** An X-ray diffraction study was performed on **13a** to determine the solid state structures of the alkyl cations. Single crystals of **13a** suitable for X-ray diffraction were grown at 23 °C from CH<sub>2</sub>Cl<sub>2</sub> layered with chlorobenzene. An ORTEP view of the (F<sub>6</sub>-acen)Zr(CH<sub>2</sub>CMe<sub>3</sub>)(NMe<sub>2</sub>Ph)<sup>+</sup> cation is shown in Figure 2. Crystallographic details, key bond distances and angles, and atomic coordinates are listed in Tables 1, 4 and 5.

Complex **13a** crystallizes as discrete cations and anions. The (F<sub>6</sub>-acen)Zr(CH<sub>2</sub>CMe<sub>3</sub>)(NMe<sub>2</sub>Ph)<sup>+</sup> cation adopts a distorted octahedral structure. The F<sub>6</sub>-acen ligand in **13a** adopts a more planar conformation than in (F<sub>6</sub>-acen)Zr(CH<sub>2</sub>CMe<sub>3</sub>)<sub>2</sub> (**11a**) as assessed by the dihedral angles between the 6-membered chelate rings (7.8 vs 41.8° for **13a**). The C–Zr–N<sub>amine</sub> angle (144.7(2)°) is significantly larger than the C–Zr–C angle in **11a** (129.9(2)°). The Zr–N<sub>F<sub>6</sub>-acen</sub> distances (average 2.28(4) Å) are similar to those in **11a** (average 2.33(4) Å). The Zr–N<sub>amine</sub> distance (2.441(4) Å) is somewhat elongated compared to the Zr–N<sub>F<sub>6</sub>-acen</sub> distances as expected on electronic grounds and is comparable to Zr–N distances in related Zr(IV) compounds containing neutral N-donor ligands (e.g. Cp\*<sub>2</sub>Zr(η<sup>2</sup>-OCCH<sub>2</sub>)(py) 2.403 Å,<sup>18c</sup> (Me<sub>4</sub>-taen)ZrCl<sub>2</sub>(NHMe<sub>2</sub>) 2.497 Å.<sup>11c</sup> The Zr–O distances (average 2.05(3) Å) are slightly shorter and the Zr–O–C angles (average 135.0(3)°) are slightly

(24) For [Cp<sub>2</sub>Fe]<sup>+</sup>, see: (a) Jordan, R. F.; Bajgur, C. S.; Willet, R.; Scott, B. *J. Am. Chem. Soc.* **1986**, *108*, 7410. (b) Alelyunas, Y. W.; Jordan, R. F.; Echols, S. F.; Borkowsky, S. L.; Bradley, P. K. *Organometallics* **1991**, *10*, 1406. (c) Borkowsky, S. L.; Jordan, R. F.; Hinch, G. D. *Organometallics* **1991**, *10*, 1268. (d) Tjaden, E. B.; Casty, G. L.; Stryker, J. M. *J. Am. Chem. Soc.* **1993**, *115*, 9814. For [Ag]<sup>+</sup>, see: (e) Jordan, R. F.; Dasher, W. E.; Echols, S. F. *J. Am. Chem. Soc.* **1986**, *108*, 1718. (f) Jordan, R. F.; Bajgur, C. S.; Dasher, W. E.; Rheingold, A. L. *Organometallics* **1987**, *6*, 1041. (g) Beverwijk, C. D. M.; van der Kerk, G. J. M.; Leusink, A. J.; Noltes, J. G. *Organomet. Chem. Rev. A* **1970**, *5*, 215. (h) Crowther, D. J.; Borkowsky, S. L.; Swenson, D.; Meyer, T. Y.; Jordan, R. F. *Organometallics* **1993**, *12*, 215. (i) Roddick, D. M.; Heyn, R. H.; Tilley, T. D. *Organometallics* **1989**, *8*, 324. (j) Borkowsky, S. L.; Baenziger, N. C.; Jordan, R. F. *Organometallics* **1993**, *12*, 486. For other 1 electron oxidants, see: (k) Burk, M. J.; Tumas, W.; Ward, M. D.; Wheeler, D. R. *J. Am. Chem. Soc.* **1990**, *112*, 6133.

(25) For Ph<sub>3</sub>C<sup>+</sup>, see: (a) Straus, D. A.; Zhang, C.; Tilley, T. D. *J. Organomet. Chem.* **1989**, *369*, C13. (b) Chien, J. C. W.; Tsai, W.; Rausch, M. D. *J. Am. Chem. Soc.* **1991**, *113*, 8570. (c) Ewen, J. A.; Elder, M. J. *Makromol. Chem., Macromol. Symp.* **1993**, *66*, 179. (d) Bochmann, M.; Lancaster, S. J. *Organometallics* **1993**, *12*, 633. (e) Razavi, A.; Thewalt, U. *J. Organomet. Chem.* **1993**, *45*, 111. For B(C<sub>6</sub>F<sub>5</sub>)<sub>3</sub>, see: (f) Yang, X.; Stern, C. L.; Marks, T. J. *J. Am. Chem. Soc.* **1991**, *113*, 3623. (g) Rodewald, S. R.; Jordan, R. F. *J. Am. Chem. Soc.* **1994**, *116*, 4491.

**Table 4.** Selected Bond Distances (Å) and Angles (deg) for  $[(F_6\text{-acen})Zr(CH_2CMe_3)(NMe_2Ph)][B(C_6F_5)_4]$  (**13a**)

Zr—O(1)	2.059(4)	Zr—O(2)	2.047(3)
Zr—N(1)	2.277(4)	Zr—N(2)	2.279(4)
Zr—N(3)	2.441(4)	Zr—C(13)	2.175(5)
O(1)—C(1)	1.293(6)	O(2)—C(8)	1.295(6)
N(1)—C(3)	1.307(6)	N(2)—C(6)	1.307(6)
N(1)—C(4)	1.484(6)	N(2)—C(5)	1.478(6)
C(1)—C(9)	1.519(7)	C(8)—C(12)	1.528(8)
C(1)—C(2)	1.336(7)	C(7)—C(8)	1.332(7)
C(2)—C(3)	1.435(7)	C(6)—C(7)	1.437(7)
C(3)—C(10)	1.503(7)	C(6)—C(11)	1.511(7)
C(4)—C(5)	1.476(7)	N(3)—C(20)	1.462(6)
N(3)—C(19)	1.495(6)	N(3)—C(18)	1.505(6)
F(1)—C(9)	1.340(6)	F(4)—C(12)	1.271(8)
F(2)—C(9)	1.306(7)	F(5)—C(12)	1.306(7)
F(3)—C(9)	1.307(7)	F(6)—C(12)	1.344(8)
C(13)—C(14)	1.515(7)	C(14)—C(15)	1.471(9)
C(14)—C(17)	1.480(8)	C(14)—C(16)	1.493(9)
O(1)—Zr—O(2)	125.50(14)	O(1)—C(1)—C(9)	112.0(5)
O(1)—Zr—N(1)	79.71(14)	O(2)—C(8)—C(12)	113.2(6)
O(1)—Zr—N(2)	154.70(14)	C(2)—C(1)—C(9)	121.7(5)
O(1)—Zr—C(13)	86.1(2)	C(7)—C(8)—C(12)	120.3(6)
O(1)—Zr—N(3)	76.43(14)	C(1)—C(2)—C(3)	125.4(5)
O(2)—Zr—N(1)	154.48(14)	C(8)—C(7)—C(6)	124.6(5)
O(2)—Zr—N(2)	79.72(14)	N(1)—C(3)—C(2)	121.9(5)
O(2)—Zr—C(13)	89.2(2)	N(2)—C(6)—C(7)	123.2(5)
O(2)—Zr—N(3)	77.0(2)	N(1)—C(3)—C(10)	123.1(5)
N(1)—Zr—N(2)	75.0(2)	N(2)—C(6)—C(11)	122.5(5)
N(1)—Zr—C(13)	97.3(2)	C(2)—C(3)—C(10)	114.9(5)
N(1)—Zr—N(3)	109.2(2)	C(7)—C(6)—C(11)	114.4(5)
N(2)—Zr—C(13)	97.4(2)	C(5)—C(4)—N(1)	111.0(4)
N(2)—Zr—N(3)	111.52(14)	C(4)—C(5)—N(2)	112.5(4)
C(13)—Zr—N(3)	144.7(2)	F(1)—C(9)—C(1)	112.8(5)
C(14)—C(13)—Zr	135.2(4)	F(4)—C(12)—C(8)	114.4(6)
C(1)—O(1)—Zr	133.7(3)	F(2)—C(9)—C(1)	112.9(5)
C(8)—O(2)—Zr	136.3(4)	F(5)—C(12)—C(8)	114.0(6)
C(3)—N(1)—C(4)	117.7(4)	F(3)—C(9)—C(1)	111.4(5)
C(6)—N(2)—C(5)	116.4(4)	F(6)—C(12)—C(8)	109.8(6)
C(3)—N(1)—Zr	129.3(4)	F(1)—C(9)—F(2)	106.4(5)
C(6)—N(2)—Zr	129.2(4)	F(4)—C(12)—F(5)	109.6(7)
C(4)—N(1)—Zr	113.0(3)	F(1)—C(9)—F(3)	105.9(5)
C(5)—N(2)—Zr	113.4(3)	F(4)—C(12)—F(6)	105.6(7)
C(18)—N(3)—Zr	112.7(3)	F(2)—C(9)—F(3)	107.0(6)
C(19)—N(3)—Zr	110.7(3)	F(5)—C(12)—F(6)	102.6(6)
C(20)—N(3)—Zr	103.2(3)	C(13)—C(14)—C(15)	111.1(6)
C(18)—N(3)—C(19)	106.9(4)	C(13)—C(14)—C(16)	110.1(6)
C(18)—N(3)—C(20)	109.5(4)	C(13)—C(14)—C(17)	111.3(6)
C(19)—N(3)—C(20)	114.1(4)	C(15)—C(14)—C(16)	108.6(7)
O(1)—C(1)—C(2)	126.3(5)	C(15)—C(14)—C(17)	108.9(7)
O(2)—C(8)—C(7)	126.5(6)	C(16)—C(14)—C(17)	106.7(6)

larger than those in **11a** (average 2.13(3) Å; average 132.0(2)°), indicating a stronger Zr—O interaction in the cation.

**Solution Behavior of 13a,b.** The ambient temperature  $^1\text{H}$  NMR spectrum of **13a** exhibits singlets for the  $ZrCH_2$  ( $\delta$  1.12) and  $F_6\text{-acen}$  ligand  $CH_3$  ( $\delta$  2.37) and methine ( $\delta$  6.20) groups, and a multiplet for the  $NCH_2CH_2N$  backbone ( $\delta$  3.85). The amine *p*-phenyl resonance ( $\delta_H$  7.20) is strongly deshielded and the  $NCH_3$  resonance ( $\delta_H$  2.86) is slightly shifted versus the corresponding free amine resonances ( $\delta$  6.71, 2.95).<sup>26</sup> The  $F_6\text{-acen}$  and  $ZrCH_2CMe_3$  resonances do not shift or broaden significantly when the temperature is lowered to  $-80^\circ\text{C}$ . However, the amine resonances broaden at  $-40^\circ\text{C}$  and then sharpen at  $-80^\circ\text{C}$ , but do not shift significantly over this temperature range. To probe the origin of these effects, the variable temperature  $^1\text{H}$  NMR

spectrum of a solution of **13a** containing ca. 0.2 equiv of excess  $NMe_2Ph$  was examined in a separate experiment. At  $-80^\circ\text{C}$ , separate resonances for free and coordinated amine are observed; these resonances broaden and coalesce ( $T_{\text{coal}}(NCH_3)$  ca.  $-40^\circ\text{C}$ ) as the temperature is raised. At ambient temperature a single set of amine resonances is observed. Collectively, these results establish that (i) in solution, **13a** adopts a structure similar to that in the solid state in which the sides of the  $F_6\text{-acen}$  ligand are equivalent and the neopentyl and  $NMe_2Ph$  ligands are nearly trans as indicated in Scheme 1, and (ii) **13a** undergoes rapid amine exchange above ca.  $-40^\circ\text{C}$ . However, the extent of amine dissociation must be small as the  $F_6\text{-acen}$  ligand and neopentyl resonances do not shift with temperature or added  $NMe_2Ph$ .<sup>27</sup>

The  $ZrCH_2$   $J_{CH}$  value (107.9 Hz) of **13a** is slightly smaller than that of neutral analog **11a**, but is not small enough to indicate substantial distortion of the neopentyl ligand. There is no evidence from the  $^{19}\text{F}$  NMR spectrum for significant cation/anion interactions in **13a**.

The  $^1\text{H}$  and  $^{13}\text{C}$  NMR properties of **13b** are similar to those of **13a**. However, the amine *p*-phenyl resonance ( $\delta_H$  6.99) is less shifted from the corresponding free amine resonance ( $\delta$  6.71) than that for **13a** ( $\delta_H$  7.20). As the temperature is lowered, the amine resonances broaden and shift further from those of free amine (to  $\delta_{p\text{-Ph}} = 7.05$ ;  $\delta_{NMe} = 2.67$  at  $-80^\circ\text{C}$ ). Therefore, the structure of **13b** is analogous to that of **13a** (i.e., the neopentyl and  $NMe_2Ph$  ligands are trans), the amine is more labile than in **13a** (slow  $NMe_2Ph$  exchange limit is not observed at  $-80^\circ\text{C}$ ), and the extent of  $NMe_2Ph$  dissociation increases significantly between  $-80$  and  $+23^\circ\text{C}$ .<sup>28</sup>

The stability of amine adduct **13a** suggests that the  $(F_6\text{-acen})Zr(CH_2CMe_3)^+$  cation is more electrophilic than  $(N_4\text{-macrocycle})Zr(R)^+$  and  $Cp_2Zr(R)^+$  species. The  $(N_4\text{-macrocycle})Zr(R)^+$  species do not coordinate  $NMe_2Ph$ .<sup>2a</sup> Sterically open  $(C_5R_5)_2Zr(Me)^+$  species generated through protonolysis of  $(C_5R_5)_2ZrMe_2$  with  $HNMe_2Ph^+$  weakly coordinate  $NMe_2Ph$ .<sup>23l,m</sup> Attempted isolation of these amine adducts yielded complex mixtures containing <1 equiv of  $NMe_2Ph$  per Zr. The greater lability of the amine in **13b** vs **13a** suggests that the nonfluorinated cation  $(H_6\text{-acen})Zr(CH_2CMe_3)^+$  is less electrophilic than  $(F_6\text{-acen})Zr(CH_2CMe_3)^+$ .

**Synthesis and Characterization of  $[(F_6\text{-acen})Zr-(CH_2CMe_3)(amine)_n][B(C_6F_5)_4]$  ( $n = 0, 1$ ) Complexes.** To prepare the base-free cation  $(F_6\text{-acen})Zr(CH_2CMe_3)^+$ , we investigated the reactions of **11a** with bulkier and more acidic ammonium reagents (versus  $HNMe_2Ph^+$ ), anticipating that bulky, weakly basic amines would be less likely to bind to Zr.

Protonolysis of **11a** with the bulky ammonium reagent  $[HNEt_2Ph][B(C_6F_5)_4]$  in  $CH_2Cl_2$  affords  $NET_2Ph$  adduct **14** (100%, NMR, Scheme 1). As anticipated on the basis of steric effects, this reaction is qualitatively slower than the reaction of **11a** with  $HNMe_2Ph^+$  (45 min vs 10 min, respectively). Complex **14** is less stable in

(26)  $^1\text{H}$  NMR ( $CD_2Cl_2$ ) for  $NMe_2Ph$ . At  $23^\circ\text{C}$ :  $\delta$  7.23 (t,  $J = 7.5$  Hz, 2H, *m*-Ph), 6.75 (d,  $J = 7.6$  Hz, 2H, *o*-Ph), 6.71 (t,  $J = 7.2$  Hz, 1H, *p*-Ph), 2.95 (s, 6H,  $NMe$ ). At  $-80^\circ\text{C}$ :  $\delta$  7.19 (t,  $J = 7.5$  Hz, 2H, *m*-Ph), 6.67 (d,  $J = 7.3$  Hz, 2H, *o*-Ph), 6.64 (t,  $J = 7.4$  Hz, 1H, *p*-Ph), 2.88 (s, 6H,  $NMe$ ).

(27) Amine exchange of **13a** may proceed via a dissociative mechanism involving a  $(F_6\text{-acen})Zr(CH_2CMe_3)(CH_2Cl_2)_n^+$  intermediate, or via an associative mechanism catalyzed by traces of free amine present in solution (e.g. from decomposition of **13a**).

(28) The concentrations of **13a** and **13b** in the variable temperature experiments were similar, ranging from 0.08 to 0.12 M.



**Table 5.** Atomic Coordinates ( $\times 10^4$ ) and Isotropic Thermal Parameters ( $\text{\AA}^2 \times 10^3$ ) for  $[(F_6\text{-acen})Zr(\text{CH}_2\text{CMe}_3)(\text{NMe}_2\text{Ph})][\text{BC}_6\text{F}_5)_4]$  (**13a**)<sup>a</sup>

	x	y	z	U(eq)		x	y	z	U(eq)
Zr	1281(1)	2277(1)	581(1)	40(1)	C(33)	3856(2)	269(6)	2456(2)	48(2)
O(1)	1886(1)	1938(3)	1265(1)	48(1)	C(34)	3814(2)	1408(6)	2587(3)	59(2)
O(2)	799(1)	2825(4)	602(1)	54(1)	C(35)	3588(2)	2228(6)	2176(3)	62(2)
N(1)	1593(1)	1885(4)	161(2)	42(1)	C(36)	3401(2)	1905(6)	1635(3)	58(2)
N(2)	760(1)	2489(4)	-344(2)	44(1)	C(37)	3451(2)	745(5)	1535(2)	46(2)
N(3)	1525(1)	4205(4)	1047(2)	47(1)	C(38)	3182(2)	-1903(4)	1507(2)	38(1)
F(1)	2859(1)	477(3)	2026(1)	78(1)	C(39)	3075(2)	-2079(5)	1863(2)	47(2)
F(2)	2707(1)	2073(4)	2247(2)	102(2)	C(40)	2679(2)	-2244(6)	1713(3)	56(2)
F(3)	2395(1)	482(4)	2163(2)	111(2)	C(41)	2350(2)	-2208(6)	1162(3)	62(2)
F(4)	199(2)	2559(5)	808(2)	157(2)	C(42)	2423(2)	-2033(5)	777(3)	58(2)
F(5)	-203(1)	3733(4)	148(2)	114(2)	C(43)	2832(2)	-1897(5)	954(2)	46(2)
F(6)	370(1)	4327(5)	836(2)	122(2)	C(44)	4039(2)	-2346(5)	2255(2)	40(1)
C(1)	2200(2)	1377(5)	1337(2)	42(1)	C(45)	4008(2)	-3479(6)	2408(2)	48(2)
C(2)	2243(2)	1086(5)	943(2)	49(2)	C(46)	4342(2)	-4139(6)	2829(2)	51(2)
C(3)	1959(2)	1411(5)	368(2)	45(1)	C(47)	4736(2)	-3673(6)	3114(2)	57(2)
C(4)	1336(2)	2277(6)	-427(2)	57(2)	C(48)	4795(2)	-2579(6)	2974(2)	58(2)
C(5)	884(2)	2102(6)	-697(2)	59(2)	C(49)	4454(2)	-1960(5)	2549(2)	50(2)
C(6)	362(2)	2711(6)	-597(2)	55(2)	F(7)	3503(1)	-3676(3)	11159(1)	57(1)
C(7)	187(2)	3027(5)	-309(3)	64(2)	F(8)	3723(1)	-4195(3)	459(1)	70(1)
C(8)	404(2)	3061(5)	240(3)	55(2)	F(9)	4098(1)	-2517(3)	232(1)	83(1)
C(9)	2541(2)	1111(6)	1946(3)	58(2)	F(10)	4257(1)	-319(3)	701(1)	72(1)
C(10)	2124(2)	1210(6)	35(2)	72(2)	F(11)	4049(1)	209(3)	1356(1)	57(1)
C(11)	44(2)	2649(7)	-1221(2)	97(3)	F(12)	4083(1)	-480(3)	2898(1)	72(1)
C(12)	184(2)	3374(7)	503(3)	73(2)	F(13)	3995(1)	1695(3)	3121(2)	93(1)
C(13)	1147(2)	444(5)	660(2)	68(2)	F(14)	3543(1)	3339(3)	2304(2)	97(1)
C(14)	1067(2)	-208(6)	1030(3)	61(2)	F(15)	3174(1)	2702(3)	1228(2)	88(1)
C(15)	1204(4)	-1457(8)	1109(5)	229(7)	F(16)	3238(1)	494(3)	984(1)	62(1)
C(16)	1301(2)	379(9)	1585(3)	141(4)	F(17)	3383(1)	-2030(3)	2421(1)	65(1)
C(17)	617(2)	-177(9)	797(4)	158(4)	F(18)	2605(1)	-2398(3)	2090(2)	89(1)
C(18)	1194(2)	5157(5)	754(2)	64(2)	F(19)	1949(1)	-2365(4)	991(2)	98(1)
C(19)	1649(2)	4123(6)	1624(2)	75(2)	F(20)	2103(1)	-1988(4)	235(1)	88(1)
C(20)	1872(2)	4493(4)	1020(2)	44(1)	F(21)	2875(1)	-1717(3)	547(1)	61(1)
C(21)	2291(2)	4507(5)	1484(3)	64(2)	F(22)	3628(1)	-4026(3)	2144(1)	60(1)
C(22)	2600(2)	4721(6)	1419(4)	87(3)	F(23)	4290(1)	-5246(3)	2954(1)	72(1)
C(23)	2508(3)	4922(7)	909(4)	98(3)	F(24)	5071(1)	-4299(4)	3530(1)	91(1)
C(24)	2096(3)	4935(6)	454(4)	92(3)	F(25)	5183(1)	-2119(4)	3241(2)	102(1)
C(25)	1776(2)	4727(5)	500(3)	64(2)	F(26)	4530(1)	-874(3)	2431(1)	65(1)
B	3662(2)	-1521(6)	1744(3)	41(2)	C(50)	5403(9)	3383(14)	2812(11)	62(8)
C(26)	3756(2)	-1702(5)	1273(2)	36(1)	C(51)	5338(8)	2166(16)	2734(9)	66(8)
C(27)	3687(2)	-2806(6)	1023(2)	41(1)	C(52)	4933(9)	1716(7)	2422(11)	82(8)
C(28)	3797(2)	-3093(5)	678(2)	50(2)	C(53)	4594(8)	2482(15)	2188(9)	71(6)
C(29)	3987(2)	-2244(6)	565(2)	51(2)	C(54)	4660(9)	3699(17)	2266(10)	88(10)
C(30)	4058(2)	-1152(6)	793(2)	49(2)	C(55)	5070(11)	4148(8)	2578(14)	63(8)
C(31)	3949(2)	-904(5)	1142(2)	40(1)	Cl	5835(1)	4144(4)	3190(2)	104(1)
C(32)	3675(2)	-124(5)	1924(2)	39(1)					

<sup>a</sup> U(eq) is defined as one-third of the trace of the  $U_{ij}$  tensor.

chlorinated solvents than **13a**; e.g., **14** undergoes significant decomposition in  $\text{CH}_2\text{Cl}_2$  within 3 h at 23 °C. The  $^1\text{H}$  and  $^{13}\text{C}$  NMR data ( $\text{CD}_2\text{Cl}_2$ ) for **14** are similar to those for **13a,b**, suggesting that **14** adopts a similar structure. The  $\text{NET}_2\text{Ph}$  *p*-phenyl resonance ( $\delta_{\text{H}}$  7.05) is deshielded from that of free  $\text{NET}_2\text{Ph}$  ( $\delta_{\text{H}}$  6.63) indicating that the amine is at least partially coordinated in  $\text{CD}_2\text{Cl}_2$ .

Protonolysis of **11a** with  $[\text{HNMePh}_2][\text{B}(\text{C}_6\text{F}_5)_4]$  in benzene yields the base-free complex **15** (90% NMR, 80% isolated, Scheme 1). Complex **15** precipitates as an oily yellow solid which does not retain the bulky  $\text{NMePh}_2$ . Complex **15** is soluble in  $\text{C}_6\text{H}_6$  at high dilution (ca.  $10^{-4}$  M). Protonolysis of **11a** with  $\text{HNMePh}_2^+$  also occurs cleanly in  $\text{CD}_2\text{Cl}_2$  at a rate which is qualitatively comparable to the rate of protonolysis of **11a** by  $\text{HNMe}_2\text{Ph}^+$  (<10 min, 23 °C). Thus the increased acidity of  $\text{HNMePh}_2^+$  ( $\text{p}K_{\text{a}}$  0.86,  $\text{H}_2\text{O}$ ) vs  $\text{HNMe}_2\text{Ph}^+$  ( $\text{p}K_{\text{a}}$  5.16) compensates for the increased bulk.<sup>29</sup> Base-free **15** is surprisingly stable in  $\text{CH}_2\text{Cl}_2$  showing little or no

decomposition after 2 days in solution at room temperature, and retains <1 equiv of  $\text{CH}_2\text{Cl}_2$  upon isolation.

Complex **15** has been characterized by  $^1\text{H}$ ,  $^{13}\text{C}$ , and  $^{19}\text{F}$  NMR studies and elemental analysis. The  $^1\text{H}$  NMR spectrum (ambient temperature,  $\text{CD}_2\text{Cl}_2$ ) contains a strongly deshielded singlet ( $\delta$  1.88) for the  $\text{ZrCH}_2$  group, singlets for the  $\text{F}_6\text{-acen}$   $\text{CH}_3$  ( $\delta$  2.47) and methine ( $\delta$  6.39) groups, and a multiplet for the  $\text{NCH}_2\text{CH}_2\text{N}$  ( $\delta$  4.06) backbone, indicating that the sides of the  $\text{F}_6\text{-acen}$  ligand are equivalent but the faces are not. This is confirmed by the  $^{13}\text{C}$  and  $^{19}\text{F}$  NMR spectra. The NMR spectra of **15** do not change significantly over the range +23 to -60 °C. These results suggest that, in solution, **15** adopts either a *trans*-( $\text{F}_6\text{-acen}$ ) $\text{Zr}(\text{R})(\text{L})^+$  ( $\text{L}$  = solvent<sup>30</sup> or counterion) structure analogous to those of amine adducts **13a,b** and **14** or a square pyramidal, five-coordinate structure analogous to that of (*acen*)/Ti-(*mesityl*).<sup>8e</sup> Low temperature NMR experiments de-

(30) The  $\text{CH}_2\text{Cl}_2$  ligand of  $\text{CpRe}(\text{NO})(\text{PPh}_3)(\text{ClCH}_2\text{Cl})^+$  was detected by  $^{13}\text{C}\{^1\text{H}\}$  NMR spectroscopy at -85 °C ( $\delta_{\text{C}}$  78.3). See: Fernandez, J. M.; Gladysz, J. A. *Organometallics* **1989**, *9*, 207 and references therein for other metal- $\text{CH}_2\text{Cl}_2$  complexes.

signed to probe this issue further were inconclusive and hindered by the poor solubility of **15** in  $CD_2Cl_2$  below  $-60\text{ }^\circ\text{C}$ .

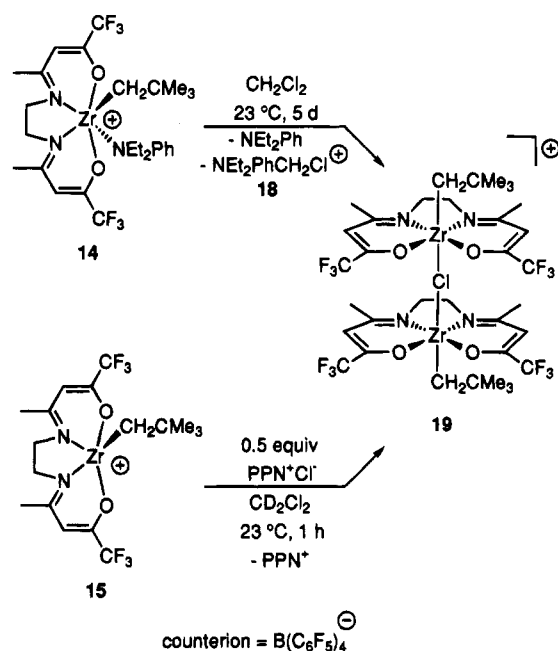
The ambient temperature  $^1\text{H}$  NMR spectrum of **15** generated *in situ* (and thus containing 1 equiv of  $\text{NMePh}_2$ ) is the superposition of spectra of isolated **15** and free  $\text{NMePh}_2$ , indicating that  $\text{NMePh}_2$  does not coordinate. However, low temperature  $^1\text{H}$  NMR spectroscopy establishes that the  $\text{NMePh}_2$  does coordinate below ca.  $-20\text{ }^\circ\text{C}$ , forming  $(F_6\text{-acen})Zr(\text{CH}_2\text{CMe}_3)(\text{NMePh}_2)^+$  (**16**). For example, at  $-60\text{ }^\circ\text{C}$ , the  $\text{ZrCH}_2$  resonance ( $\delta_{\text{H}}$  1.39) is strongly shielded relative to that of **15** ( $\delta_{\text{H}}$  1.88) and the  $\text{NCH}_2\text{CH}_2\text{N}$  resonance appears as two multiplets ( $\delta_{\text{H}}$  3.80, 3.52) rather than one ( $\delta_{\text{H}}$  4.06). Furthermore, the amine *p*-phenyl resonance is deshielded by ca. 0.2 ppm, and the slightly broadened  $\text{NMePh}_2$  signal is shielded by ca. 0.2 ppm vs the corresponding free  $\text{NMePh}_2$  resonances.<sup>31</sup>

**Stability and Fate of  $[(F_6\text{-acen})Zr(\text{CH}_2\text{CMe}_3)(\text{amine})_n][B(\text{C}_6\text{F}_5)_4]$  ( $n = 0, 1$ ) Complexes in  $\text{CH}_2\text{Cl}_2$ .** As noted above, the stability order of  $(F_6\text{-acen})Zr(\text{CH}_2\text{CMe}_3)(\text{L})^+$  complexes in  $\text{CH}_2\text{Cl}_2$  is **16** ( $\text{L} = \text{NMePh}_2$ ; exists as base-free **15** at  $23\text{ }^\circ\text{C}$ ) > **13a** ( $\text{L} = \text{NMe}_2\text{Ph}$ ) > **14** ( $\text{L} = \text{NEt}_2\text{Ph}$ ). This order was surprising because we had anticipated that  $(F_6\text{-acen})Zr(\text{CH}_2\text{CMe}_3)(\text{L})_n^+$  species would decompose to  $(F_6\text{-acen})Zr(\text{CH}_2\text{CMe}_3)\text{Cl}$  (**17**) by halide abstraction from  $\text{CH}_2\text{Cl}_2$ , a process which we expected to be promoted by increased amine lability. Furthermore, attempts to generate **17** by alternate routes were unsuccessful and indicated that this species is unstable toward ligand exchange/disproportionation reactions.<sup>32</sup> To probe these phenomena further, the decomposition of **14** was investigated in detail.

The decomposition of **14** in  $\text{CH}_2\text{Cl}_2$  (5 d,  $23\text{ }^\circ\text{C}$ ) yields  $\text{NEt}_2\text{Ph}(\text{CH}_2\text{Cl})^+$  (**18**) and an unusual chloride-bridged dinuclear cation  $\{(F_6\text{-acen})Zr(\text{CH}_2\text{CMe}_3)\}_2(\mu\text{-Cl})^+$  (**19**) (as the  $B(\text{C}_6\text{F}_5)_4^-$  salts), and free  $\text{NEt}_2\text{Ph}$  in 1:1:1.3 ratio (Scheme 2). Chloromethylammonium salt **18** was isolated by exposure of the reaction mixture to air to decompose the organometallic species, followed by extraction with toluene and recrystallization from cold  $\text{CH}_2\text{Cl}_2$ /pentane. The  $^1\text{H}$  NMR spectrum of **18** exhibits a lowfield  $\text{NCH}_2\text{Cl}$  resonance ( $\delta$  5.28; compare to  $[\text{ClCH}_2\text{NEt}_3]\text{Cl}$   $\delta$  5.68),<sup>33</sup> a complex multiplet ( $\delta_{\text{H}}$  3.91) for the diastereotopic  $\text{NCH}_2\text{CH}_3$  hydrogens, and two multiplets for the phenyl hydrogens a 3:2 ratio ( $\delta_{\text{H}}$  7.71, 7.43). The  $^{13}\text{C}$  NMR spectrum of **18** confirms the presence of the  $B(\text{C}_6\text{F}_5)_4^-$  counterion. Additionally, the  $\text{NCH}_2\text{Cl}$   $^{13}\text{C}$  resonance appears as a triplet ( $\delta_{\text{C}}$  64.0) with an unusually large  $J_{\text{CH}}$  value (169.4), as expected for an  $\text{sp}^3$  carbon bonded to electron-withdrawing chloride and quaternary nitrogen substituents.

The identity of **19** was confirmed by independent generation via addition of 0.5 equiv  $[\text{PPN}]\text{Cl}$  to base-

## Scheme 2



free **15** (100%, NMR, Scheme 2). Complex **19** could not be isolated completely free of **18** or  $[\text{PPN}][B(\text{C}_6\text{F}_5)_4]$  and was therefore characterized spectroscopically. The  $^1\text{H}$  NMR spectrum of **19** exhibits broad singlets for the  $\text{ZrCH}_2$  ( $\delta$  1.40) and  $\text{NCH}_2\text{CH}_2\text{N}$  ( $\delta$  3.87) groups and sharp singlets for the  $F_6\text{-acen}$  methyl and methine groups. The  $\text{ZrCH}_2$  resonance appears at  $\delta$  119.0 ( $J_{\text{CH}}$  105.0 Hz) in the  $^{13}\text{C}$  NMR spectrum. Integration of the  $^{19}\text{F}$  NMR spectrum (with correction for the presence of  $[\text{PPN}][B(\text{C}_6\text{F}_5)_4]$  quantified by the  $^1\text{H}$  NMR spectrum) establishes that the  $(F_6\text{-acen})Zr/B(\text{C}_6\text{F}_5)_4^-$  ratio is 2:1, consistent with the proposed structure. Complex **19** is related to the  $\mu\text{-oxo}$  species  $\{(H_6\text{-acen})\text{TiCl}_2\}_2(\mu\text{-O})$  characterized by Floriani.<sup>8d</sup>

Although  $\text{NEt}_3$  is converted to  $[\text{ClCH}_2\text{NEt}_3]\text{Cl}$  after standing in  $\text{CH}_2\text{Cl}_2$  solution for 3 days ( $23\text{ }^\circ\text{C}$ ),  $\text{NEt}_2\text{Ph}$  does not with  $\text{CD}_2\text{Cl}_2$  after 9 days ( $23\text{ }^\circ\text{C}$ ). Furthermore as noted above, base-free **15** is stable in  $\text{CH}_2\text{Cl}_2$  for extended periods of time. Therefore, the formation of **18** and **19** by reaction of **14** in  $\text{CH}_2\text{Cl}_2$  likely involves nucleophilic attack of  $\text{NEt}_2\text{Ph}$  on a  $\text{Zr}-\text{CH}_2\text{Cl}_2$  adduct, as indicated in the generalized Scheme 3. In this scheme, the labile amine adduct  $(F_6\text{-acen})Zr(R)(\text{NR}'_3)^+$  (e.g. **14**) formed by protonolysis is in equilibrium with the  $(F_6\text{-acen})Zr(R)(\text{CH}_2\text{Cl}_2)_n^+$  solvent adduct (**20**). Coordination of  $\text{CH}_2\text{Cl}_2$  to the electrophilic metal cation activates it for nucleophilic attack.  $\text{S}_{\text{N}}2$  displacement of  $(F_6\text{-acen})Zr(R)\text{Cl}$  (**17**) by amine yields  $\text{NR}'_3(\text{CH}_2\text{Cl})^+$ . Complex **17** reacts with a second  $(F_6\text{-acen})Zr(R)^+$  cation to afford **19** and free amine. This process should yield a 1:1:1 ratio of **18**, **19**, and amine (observed 1:1:1.3).

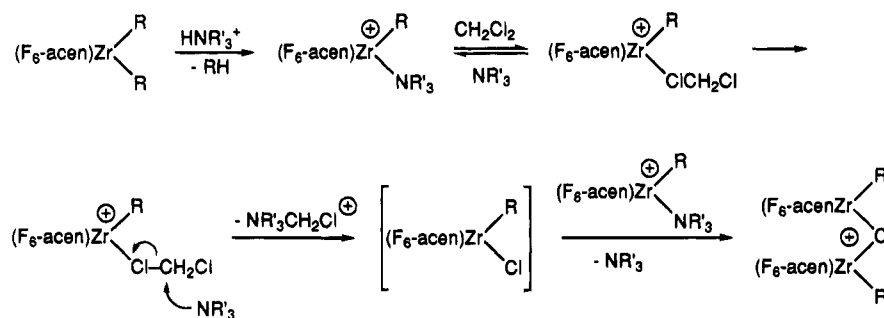
The stability of  $[(F_6\text{-acen})Zr(\text{CH}_2\text{CMe}_3)(\text{amine})]^+$  species in  $\text{CH}_2\text{Cl}_2$  thus depends on the Lewis basicity and nucleophilicity of the amine. The relatively basic  $\text{NMe}_2\text{Ph}$  does not dissociate significantly from **13a** in  $\text{CH}_2\text{Cl}_2$ ; as a result, the concentration of the  $\text{CH}_2\text{Cl}_2$  adduct is small and decomposition is slow. In contrast, the bulky, weakly basic  $\text{NMePh}_2$  is completely dissociated from **16** in  $\text{CH}_2\text{Cl}_2$  at  $23\text{ }^\circ\text{C}$ . However,  $\text{NMePh}_2$  is also a very weak nucleophile so decomposition is slow. The Lewis basicity and nucleophilicity of  $\text{NEt}_2\text{Ph}$  are inter-

(31)  $^1\text{H}$  NMR ( $\text{CD}_2\text{Cl}_2$ ) for  $\text{NMePh}_2$ . At  $23\text{ }^\circ\text{C}$ :  $\delta$  7.27 (t,  $J = 7.5$  Hz, 4H, *m*-Ph), 7.02 (d,  $J = 7.2$  Hz, 4H, *o*-Ph), 6.95 (t,  $J = 7.3$  Hz, 2H, *p*-Ph), 3.30 (s, 3H *NMe*).

(32) The reaction of  $(F_6\text{-acen})Zr(\text{CH}_2\text{CMe}_3)^+$  (**15**) with  $[\text{NMe}_4]\text{Cl}$  in  $\text{CD}_2\text{Cl}_2$  yields a mixture of  $(F_6\text{-acen})Zr(\text{CH}_2\text{CMe}_3)_2$  (**11a**),  $(F_6\text{-acen})_2\text{Zr}$  (**10**), and other soluble and insoluble Zr compounds. Similar product mixtures were obtained from reactions of **11a** with 1 equiv of  $[\text{HNEt}_3]\text{Cl}$  or 1 equiv of  $\text{HCl}$  (g). The reaction of **11a** with  $[\text{HNEt}_3]\text{Cl}$  in THF yields a mixture of **11a**,  $(F_6\text{-acen})Zr\text{Cl}_2(\text{THF})$  (**9**), **10** and other soluble Zr compounds.

(33) (a) Wright, D. A.; Wulfe, C. A. *J. Org. Chem.* **1970**, *35*, 4252. For other  $[\text{ClCH}_2\text{NR}_3]\text{Cl}$  species, see: (b) Willey, G. R.; Ravindran, M.; Drew, M. G. B. *Inorg. Chim. Acta* **1991**, *188*, 159. (c) Bohme, H.; Hilp, M.; Koch, L.; Ritter, E. *Chem. Ber.* **1971**, *104*, 2018.

Scheme 3



mediate versus  $\text{NMe}_2\text{Ph}$  and  $\text{NMePh}_2$ , and only in the case of **14** is the proper combination of amine lability and nucleophilicity required by Scheme 3 obtained.<sup>34</sup> Base-free cation **15** (which likely exists as  $(\text{F}_6\text{-acen})\text{Zr}(\text{CH}_2\text{CMe}_3)(\text{CH}_2\text{Cl}_2)_n^+$  (**20**) in  $\text{CH}_2\text{Cl}_2$ ) is stable in  $\text{CH}_2\text{Cl}_2$  due to the absence of nucleophilic species.

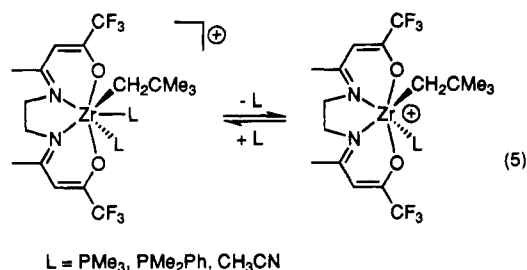
Processes related to that proposed in Scheme 3 have been observed in other systems. Crabtree reported that the methyl iodide adduct  $\text{IrH}_2(\text{Ime})_2(\text{PPh}_3)_2^+$  rapidly methylates tertiary amines, and Gladysz found that  $\text{CpRe}(\text{NO})(\text{PPh}_3)(\text{IR})^+$  species react rapidly with  $\text{PPh}_3$  to afford  $\text{Ph}_3\text{PR}^+$  salts, demonstrating that alkyl halides are activated for nucleophilic attack by coordination to electrophilic metal cations.<sup>35,36</sup> More recently, Crabtree and Faller have found that cationic  $\text{Fe}(\text{II})$  and  $\text{Ru}(\text{II})$  halocarbon complexes alkylate a wide range of nucleophiles, and Powell has reported that  $\text{CpRu}(\text{CO})(\text{PPh}_3)(\text{IR})^+$  cations react rapidly with fluoride sources to yield fluoroalkanes.<sup>37,38</sup> The formation of dinuclear halide bridged species  $(\text{L}_n\text{M})_2(\mu\text{-X})^+$  via reaction of  $\text{L}_n\text{MX}$  with  $\text{L}_2\text{M}(\text{L}')^+$  ( $\text{L}' = \text{halocarbon}$  or labile ligand) has been observed in several of these systems.

**Ligand Exchange Reactions of  $(\text{F}_6\text{-acen})\text{Zr}(\text{CH}_2\text{CMe}_3)(\text{amine})_n^+$  Complexes.** Addition of excess  $\text{PMe}_3$  to in situ generated  $(\text{F}_6\text{-acen})\text{Zr}(\text{CH}_2\text{CMe}_3)(\text{NMe}_2\text{Ph})^+$  (**13**) results in amine displacement and the formation of bis(phosphine) adduct **21** (Scheme 4).<sup>39</sup> Complex **21** is isolated as a thermally unstable yellow powder which decomposes when exposed to high vacuum ( $10^{-4}$  Torr, ca. 12 h), presumably via loss of  $\text{PMe}_3$ .

The low temperature ( $-80^\circ\text{C}$ )  $^{31}\text{P}\{^1\text{H}\}$  NMR spectrum of **21** displays two mutually coupled doublets ( $\delta -24.1, -35.5$ ;  $J_{\text{PP}} = 12.0$  Hz), indicative of two inequivalent  $\text{PMe}_3$  ligands. The low temperature ( $-80^\circ\text{C}$ )

$^1\text{H}$  NMR spectrum contains singlets for the  $\text{F}_6\text{-acen}$   $\text{CH}_3$  ( $\delta$  2.32) and methine ( $\delta$  6.12) groups, a broad doublet for the  $\text{ZrCH}_2$  ( $\delta$  1.08,  $J_{\text{PH}} = 5.0$  Hz) group, and two multiplets ( $\delta$  4.18, 3.53) for the  $\text{NCH}_2\text{CH}_2\text{N}$  backbone. Additionally, two doublets ( $\delta_{\text{H}} 1.24$ ,  $J_{\text{PH}} = 6.8$  Hz;  $\delta_{\text{H}} 0.70$ ,  $J_{\text{PH}} = 7.0$  Hz) are observed for the inequivalent  $\text{PMe}_3$  ligands. These data are consistent with a pentagonal bipyramidal structure in which the  $\text{PMe}_3$  ligands occupy axial and equatorial sites as indicated in Scheme 4. This structure is closely related to that of  $(\text{H}_6\text{-acen})\text{-ZrCl}_2(\text{THF})$  (**3**, Chart 1) and related complexes characterized by Floriani.

Complex **21** undergoes rapid (NMR time scale)  $\text{PMe}_3$  exchange above  $-10^\circ\text{C}$ . At this temperature the  $^{31}\text{P}\{^1\text{H}\}$  NMR spectrum coalesces to a broad singlet ( $-29.0$ ). In the  $^1\text{H}$  NMR spectrum, the  $\text{PMe}_3$  resonances collapse to a broad singlet ( $\delta$  1.05) and the  $\text{ZrCH}_2$  doublet collapses to a singlet ( $\delta$  1.22). Interestingly, the  $\text{NCH}_2\text{CH}_2\text{N}$  resonances do not change with temperature; even under conditions of fast  $\text{PMe}_3$  exchange ( $T > -10^\circ\text{C}$ ), two multiplets ( $\delta$  4.26, 3.64) are observed for the backbone. This indicates that the  $\text{PMe}_3$  ligands undergo site exchange between one axial and an equatorial site only; i.e., exchange of the neopentyl group between the two axial sites does not accompany the  $\text{PMe}_3$  exchange (eq 5).



(34) It is also possible that the steric properties of the amine influence the regioselectivity of amine attack on  $(\text{F}_6\text{-acen})\text{Zr}(\text{CH}_2\text{CMe}_3)(\text{CH}_2\text{Cl}_2)^+$ . The smaller  $\text{NMe}_2\text{Ph}$  may attack at Zr to re-form amine adduct **13a**, while the larger  $\text{NEt}_2\text{Ph}$  may be restricted to more remote attack at coordinated  $\text{CH}_2\text{Cl}_2$ , leading to decomposition. However, the observation that  $\text{NMe}_2\text{Ph}$  complex **13b** is unstable in  $\text{CH}_2\text{Cl}_2$  argues against this analysis. While the decomposition of **13b** was not studied in detail, it is likely that the greater lability of the coordinated amine (vs fluorinated analogue **13b**) promotes decomposition via Scheme 3.

(35) Burk, M. J.; Segmuller, B.; Crabtree, R. H. *Organometallics* **1987**, *6*, 2241.

(36) (a) Winter, C. H.; Arif, A. M.; Gladysz, J. A. *J. Am. Chem. Soc.* **1987**, *109*, 7560. (b) Winter, C. H.; Veal, W. R.; Garner, C. M.; Arif, A. M.; Gladysz, J. A. *J. Am. Chem. Soc.* **1989**, *111*, 4766. (c) Winter, C. H.; Arif, A. M.; Gladysz, J. A. *Organometallics* **1989**, *8*, 219. (d) Igau, A.; Gladysz, J. A. *Polyhedron* **1991**, *10*, 1903.

(37) Kulawiec, R. J.; Faller, J. W.; Crabtree, R. H. *Organometallics* **1990**, *9*, 745 and references therein.

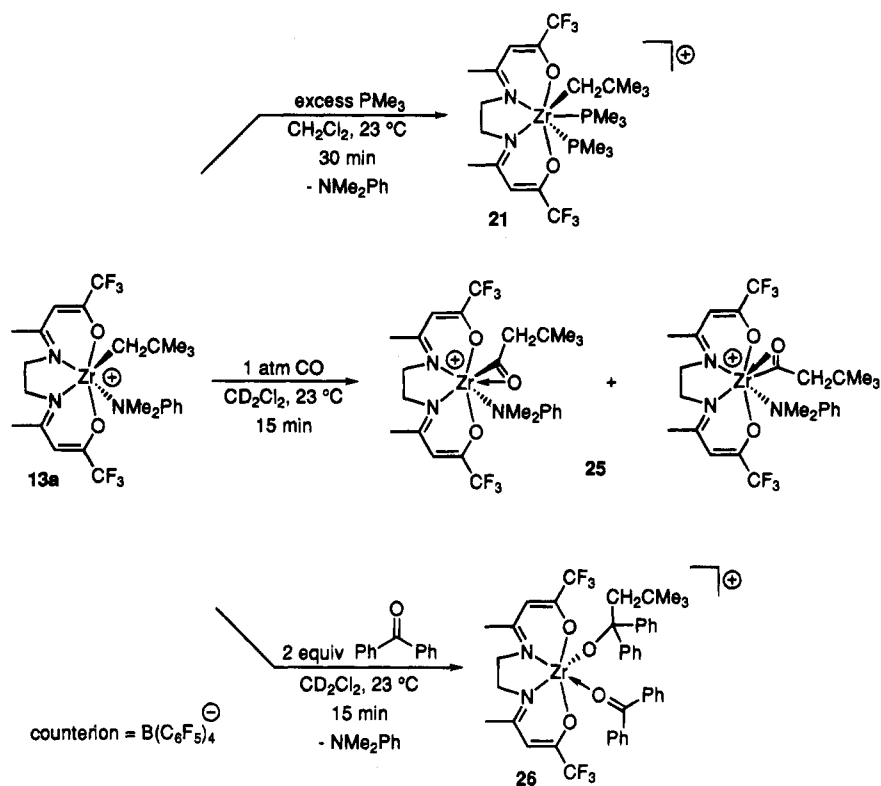
(38) Powell, J.; Horvath, M. J. *Organometallics* **1993**, *12*, 4067.

(39) Similarly, addition of excess THF to **13a** affords  $[(\text{F}_6\text{-acen})\text{Zr}(\text{CH}_2\text{CMe}_3)(\text{THF})_2][\text{B}(\text{C}_6\text{F}_5)_4]$ .  $^1\text{H}$  NMR ( $\text{CD}_2\text{Cl}_2$ ):  $\delta$  6.20 (s, 2H, CH), 4.18 (br m, 2H,  $\text{NCH}_2$ ), 3.78 (m, 8H, THF), 3.77 (br m, 2H,  $\text{NCH}_2$ ), 2.39 (s, 6H,  $\text{CH}_3$ ), 1.90 (m, 8H, THF), 1.17 (s, 2H,  $\text{Zr-CH}_2$ ), 0.78 (s, 9H,  $\text{CMe}_3$ ).

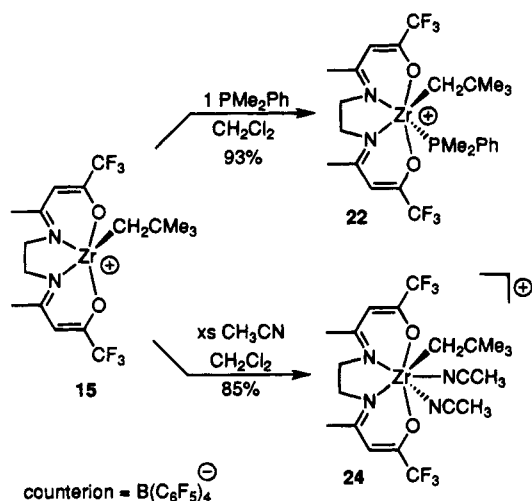
A more stable mono-phosphine complex  $(\text{F}_6\text{-acen})\text{Zr}(\text{CH}_2\text{CMe}_3)(\text{PMe}_2\text{Ph})^+$  (**22**) was prepared by reaction of **13a** or **15** with 1 equiv of  $\text{PMe}_2\text{Ph}$  (Scheme 5). The low temperature ( $-80^\circ\text{C}$ )  $^1\text{H}$  and  $^{31}\text{P}\{^1\text{H}\}$  NMR spectra for **22** are consistent with a trans structure, analogous to the structures of amine adducts **13a,b** and **14**. Singlets are observed for the  $\text{ZrCH}_2$  ( $\delta_{\text{H}} 1.09$ ),  $\text{F}_6\text{-acen}$  ligand  $\text{CH}_3$  ( $\delta_{\text{H}} 2.28$ ), and methine ( $\delta_{\text{H}} 6.23$ ) groups, and two multiplets ( $\delta_{\text{H}} 3.87, 3.41$ ) are observed for the  $\text{NCH}_2\text{CH}_2\text{N}$  hydrogens. The  $^{31}\text{P}\{^1\text{H}\}$  NMR spectrum contains a sharp singlet at  $\delta -11.6$ . These spectra do not change significantly when the temperature is increased to  $23^\circ\text{C}$ .

Addition of excess  $\text{PMe}_2\text{Ph}$  to **22** yields  $(\text{F}_6\text{-acen})\text{Zr}(\text{CH}_2\text{CMe}_3)(\text{PMe}_2\text{Ph})_2^+$  (**23**) which is structurally analo-

Scheme 4



Scheme 5



gous to bis( $\text{PMe}_3$ ) adduct **21**. This species undergoes rapid, reversible  $\text{PMe}_2\text{Ph}$  dissociation above ca.  $-40^\circ\text{C}$  by a mechanism analogous to that for  $\text{PMe}_3$  exchange of **21**.<sup>40</sup>

Treatment of **15** with excess  $\text{CH}_3\text{CN}$  affords  $(\text{F}_6\text{-acen})\text{Zr}(\text{CH}_2\text{CMe}_3)(\text{CH}_3\text{CN})_2^+$ , **24**, in high yield (Scheme 5). The low temperature ( $-90^\circ\text{C}$ )  $^1\text{H}$  NMR spectrum of **24** contains singlets for the  $\text{ZrCH}_2$  ( $\delta$  0.94),  $\text{F}_6\text{-acen}$   $\text{CH}_3$  (2.26), and methine (6.01) groups, and two multiplets ( $\delta$  4.07, 3.65) for the  $\text{NCH}_2\text{CH}_2\text{N}$  backbone. Additionally, two singlets ( $\delta$  2.34, 2.04) are observed for the inequivalent  $\text{CH}_3\text{CN}$  ligands. These data establish a pentagonal bipyramidal structure for **24**, analogous

to that of bis phosphine adducts **21** and **23**. Above  $-60^\circ\text{C}$ , the  $\text{CH}_3\text{CN}$  resonances collapse to one singlet ( $\delta_{\text{H}}$  2.20); however, the other resonances do not change significantly as the temperature is raised to  $23^\circ\text{C}$ . These results indicate that  $\text{CH}_3\text{CN}$  dissociation is rapid and reversible above ca.  $-60^\circ\text{C}$  (eq 5) but that the extent of dissociation is small. There is no evidence for  $\text{CH}_3\text{CN}$  insertion into the  $\text{Zr}-\text{CH}_2\text{CMe}_3$  bond in this system.

**Insertion Reactions of 13a and 15.** The reaction of *in situ* generated **13a** with CO (1 atm,  $\text{CD}_2\text{Cl}_2$ ) yields a bright red acyl complex **25** as a mixture of two isomers (Scheme 4). The isomers are initially formed in a 3.5:1 ratio, but after several hours, the isomeric ratio approaches unity and decomposition begins, resulting in the formation of  $[\text{ClCD}_2\text{NMe}_2\text{Ph}][\text{B}(\text{C}_6\text{F}_5)_4]$ .<sup>41</sup> Attempted isolation of **25** was unsuccessful. Key  $^1\text{H}$  NMR data for the major isomer include a deshielded singlet ( $\delta_{\text{H}}$  2.69) for the acyl  $\text{CH}_2$  group, singlets for the  $\text{F}_6\text{-acen}$   $\text{CH}_3$  ( $\delta$  2.27) and methine ( $\delta$  5.92) groups, and two multiplets ( $\delta$  4.22, 4.00) for the  $\text{NCH}_2\text{CH}_2\text{N}$  hydrogens. The  $^{13}\text{C}$  NMR ( $-50^\circ\text{C}$ ) spectrum displays a lowfield acyl carbon resonance ( $\delta$  312.0) characteristic of an  $\eta^2$ -acyl bonding mode.<sup>42</sup>  $^1\text{H}$  and  $^{13}\text{C}$  NMR data for the minor isomer are similar, although the acyl carbon resonance was not observed. These data are consistent with the pentagonal bipyramidal structures shown in Scheme 4, which differ in orientation of the  $\eta^2$ -acyl ligand. This isomerism is analogous to the "O-inside"/"O-outside" isomerism observed in  $\text{Cp}_2\text{M}(\eta^2\text{-acyl})\text{X}$  species.<sup>43</sup> The  $\nu_{\text{CO}}$  bands could not be conclusively identified in the IR spectrum

(40) Under conditions of slow exchange between the bis( $\text{PMe}_2\text{Ph}$ ) adduct **23** and mono( $\text{PMe}_2\text{Ph}$ ) adduct **22**, the  $\text{ZrCH}_2$   $^1\text{H}$  NMR resonance of **22** appears as a singlet. This suggests that the lack of observable  $J_{\text{FH}}$  coupling of the  $\text{ZrCH}_2$  resonance of solutions of pure **22** at  $-80^\circ\text{C}$  results from a small  $J_{\text{FH}}$  value rather than rapid  $\text{PMe}_2\text{Ph}$  exchange.

(41) Slow formation of  $[\text{NMe}_2\text{Ph}(\text{CD}_2\text{Cl})][\text{B}(\text{C}_6\text{F}_5)_4]$  is also observed when 1-pentyne, 2-butyne, and vinyltrimethylsilane are added to amine adduct **13a**.  $^1\text{H}$  NMR ( $\text{CD}_2\text{Cl}_2$ ):  $\delta$  7.69 (m, 3H, Ph), 7.52 (m, 2H, Ph), 3.65 (s, 6H,  $\text{NMe}_2$ ),  $\text{NCD}_2\text{Cl}$  not observed.

(42) Durfee, L. D.; Rothwell, I. P. *Chem. Rev.* **1988**, *88*, 1059.

(43) Erker, G. *Acc. Chem. Res.* **1984**, *17*, 103.

due to interference from the  $F_6$ -acen absorbances. The insertion of CO is not reversible in this system.

The addition of CO to a  $CD_2Cl_2$  solution of base-free **15** results in a complex mixture which has not been characterized. It is possible that  $(F_6\text{-acen})Zr(\text{acyl})(CO)^+$  species, analogous to the  $Cp_2Zr(\text{acyl})(CO)^+$  complexes formed by carbonylation of  $Cp_2Zr(R)^+$ , are generated.<sup>44</sup>

The reaction of in situ generated **13a** with 2 equivalents of benzophenone yields the alkoxide ketone complex  $(F_6\text{-acen})Zr(OCPh_2CH_2CMe_3)(O=CPh_2)^+$  (**26**, ca. 95%, NMR, Scheme 4). The  $NMe_2Ph$  coproduct is removed upon workup (benzene washes). Interestingly, the reaction of **13a** with 1 equiv of benzophenone yields a 1:1 mixture of **26** and unreacted **13a**. This suggests that  $NMe_2Ph$  is the preferred ligand for  $(F_6\text{-acen})Zr(CH_2CMe_3)^+$ , while benzophenone is the preferred ligand for  $(F_6\text{-acen})Zr(OCPh_2CH_2CMe_3)^+$ . This phenomenon can be rationalized in terms of the relative hardness of the metal centers and ligands; i.e., replacement of the alkyl ligand of  $(F_6\text{-acen})Zr(CH_2CMe_3)^+$  by the hard alkoxide in  $(F_6\text{-acen})Zr(OCPh_2CH_2CMe_3)^+$  increases the hardness of the metal center and results in a preference for binding the hard ketone ligand rather than the softer amine. The formation of a 1:1 mixture of **26** and **13a** may also be rationalized by postulating that **26** is formed by insertion of a bis ketone complex intermediate. Treatment of **26** with 1 equiv of THF does not result in benzophenone displacement.

The  $^1H$  NMR spectrum of **26** displays singlets for the alkoxide  $CH_2$  ( $\delta$  2.50),  $F_6$ -acen  $CH_3$  ( $\delta$  2.02) and methine ( $\delta$  5.78) groups, and two multiplets ( $\delta$  3.40, 3.20) for the  $NCH_2CH_2N$  backbone. The aromatic region of the spectrum is complex, but integration establishes that two equivalents of benzophenone are incorporated in **26**. The  $^{13}C$  NMR spectrum contains resonances for the coordinated  $Ph_2C=O$  ( $\delta$  206.3, vs  $\delta$  195 for free  $Ph_2CO$ ) and the  $ZrOC$  ( $\delta$  93.1) carbons. These data establish that the alkoxide and ketone ligands are trans, as indicated in Scheme 4. The  $\nu_{CO}$  band for the coordinated benzophenone could not be identified due to interference by the  $F_6$ -acen ligand bands.

Neither  $NMe_2Ph$  adduct **13a** nor base-free cation **15** reacts with 2-butyne in  $CD_2Cl_2$  at 23 °C. The reaction of **15** with 1-pentyne yields an orange solution which contains neopentane (100%). This presumably results from  $\sigma$ -bond metathesis; however, the expected organometallic product  $(F_6\text{-acen})Zr(C\equiv CCH_2CH_2CH_3)^+$  could not be identified.<sup>41</sup> Similarly, **13** and **15** are unreactive with ethylene. However, in the presence of small amounts of  $AlR'_3$  co-catalysts (2 and 1 equiv, respectively), both species are moderately active ethylene polymerization catalysts. These reactions will be discussed in more detail in a separate contribution.<sup>45</sup>

## Conclusions

Alkane elimination reactions of  $H_2(R_6\text{-acen})$  ( $R = H, F$ ) and  $ZrR'_4$  compounds ( $R' = CH_2CMe_3, CH_2Ph$ ) afford  $(R_6\text{-acen})ZrR'_2$  complexes cleanly in high yield. This approach circumvents the problems associated with alkylation of  $(R_6\text{-acen})ZrCl_2$  complexes. Protonolysis of  $(R_6\text{-acen})ZrR'_2$  with  $HNR_3^+$  reagents (anion =  $B(C_6F_5)_4^-$ ) yields  $(R_6\text{-acen})Zr(R')(NR_3)^+$  amine adducts or base-free

$(R_6\text{-acen})Zr(R')^+$  species depending on Lewis basicity of the amine. In particular, the reaction of  $(F_6\text{-acen})Zr(CH_2CMe_3)_2$  (**11a**) with  $HNMe_2Ph^+$  yields  $(F_6\text{-acen})Zr(CH_2CMe_3)(NMe_2Ph)^+$  (**13a**) while reaction with the more acidic and bulkier  $HNMePh_2^+$  yields base-free  $(F_6\text{-acen})Zr(CH_2CMe_3)^+$  (**15**). Ligand substitution reactions of **13a** provide access to a variety of  $(F_6\text{-acen})Zr(CH_2CMe_3)(L)_n^+$  cations ( $n = 2, L = PMe_3, CH_3CN, THF; n = 1$  or  $2, L = PMe_2Ph$ ).

The structures of these  $(R_6\text{-acen})Zr$  alkyls are variable due to the flexibility of the acen ligands. The dialkyl complex  $(F_6\text{-acen})Zr(CH_2CMe_3)_2$  (**11a**) adopts a trigonal prismatic structure with a twisted  $F_6$ -acen conformation; the  $C-Zr-C$  angle ( $129.9(2)^\circ$ ) is intermediate between cis and trans angles in octahedral complexes. The structure of the cationic amine complex **13a** features a more planar  $F_6$ -acen ligand and a large  $C-Zr-N_{amine}$  angle ( $144.7(3)^\circ$ ). Spectroscopic data for seven-coordinate  $(F_6\text{-acen})Zr(CH_2CMe_3)(L)_2^+$  species ( $L = PMe_3, PMe_2Ph, CH_3CN, THF$ ) are consistent with pentagonal bipyramidal structures in which the neopentyl group occupies an apical site and the near-planar  $F_6$ -acen ligand occupies equatorial sites.

Neutral  $(R_6\text{-acen})Zr(R')_2$  and cationic  $(R_6\text{-acen})Zr(R')(L)^+$  complexes are best described as 16-electron species. The metrical parameters for **11a** and **13a** indicate that the  $F_6$ -acen oxygens are  $sp^2$  hybridized and function as 4-electron donors, and the  $F_6$ -acen nitrogens function as 2-electron donors. Accordingly, the base-free cation  $(F_6\text{-acen})Zr(CH_2CMe_3)^+$  (**15**) is a 14-electron complex and exhibits electrophilic behavior as expected for such an unsaturated species. Cation **15** coordinates one or two Lewis bases (amines, phosphines, and nitriles) forming isolable 16- or 18-electron species, and also activates  $CH_2Cl_2$  for nucleophilic attack by  $NET_2Ph$  via formation of a transient  $(F_6\text{-acen})Zr(CH_2CMe_3)(CH_2Cl)_2^+$  species (**20**). The  $S_N2$  displacement of  $(R_6\text{-acen})Zr(R')Cl$  from  $CH_2Cl_2$  adducts of type **20** is the principal decomposition pathway for  $(R_6\text{-acen})Zr(R')(L)_n^+$  cations in  $CH_2Cl_2$  solvent, rather than direct chloride abstraction. Thus base-free **15** is stable in  $CH_2Cl_2$  in the absence of nucleophilic species.<sup>46</sup>

Cationic  $(F_6\text{-acen})Zr(CH_2CMe_3)(amine)_n^+$  species ( $n = 0, 1$ ) react with CO and benzophenone to afford the expected insertion products, but do not insert ethylene or alkynes in the absence of aluminum alkyl cocatalysts. Thus these systems are less reactive than  $Cp_2Zr(R)^+$  and  $(N_4\text{-macrocycle})Zr(R)^+$  cations which polymerize olefins and insert/oligomerize alkynes. The reactivity properties of **13a** and **15** may reflect structural effects. Coordination of bulky substrates such as ethylene or alkynes to **15** may yield  $(F_6\text{-acen})Zr(CH_2CMe_3)\text{-}(substrate)^+$  adducts (substrate = ethylene, alkyne) with large substrate-Zr-R angles similar to that observed for **13a** ( $R-Zr-NMe_2Ph$  angle  $144.7^\circ$ ); in such cases, migratory insertion is not expected to be favored. The higher insertion reactivity of CO and benzophenone may reflect the higher inherent reactivity of these smaller, polar substrates, or the formation of seven-coordinate  $(F_6\text{-acen})Zr(CH_2CMe_3)(L)\text{-}(substrate)^+$  intermediates with acute  $R-Zr\text{-}substrate$  angles. Of course, it is also possible that **13a** and **15** do not insert ethylene or alkynes simply because they do not coordinate these

(44) Guo, Z.; Swenson, D. C.; Guram, A. S.; Jordan, R. F. *Organometallics* **1994**, *13*, 766.

(45) Tjaden, E.; Jordan, R. F. Manuscript in preparation.

(46) The low nucleophilicity of  $B(C_6F_5)_4^-$  probably contributes significantly to the stability of **15**.

substrates. However, the strong amine binding in these systems suggests that their Lewis acidity is comparable to that of  $Cp_2M(R)^+$  and  $(N_4\text{-macrocycle})M(R)^+$  cations.

### Experimental Section

**General Data.** All manipulations were performed using standard Schlenk or high vacuum techniques, or directly in a Vacuum Atmospheres drybox. Benzene, benzene- $d_6$ , toluene, tetrahydrofuran, tetrahydrofuran- $d_8$ , hexane, and pentane were distilled from Na/benzophenone ketyl. Chlorobenzene and dichloromethane were distilled from  $CaH_2$ , and dichloromethane- $d_2$  was distilled from  $P_2O_5$ .  $PMe_3$  and  $PMe_2Ph$  were distilled from Na or 4 Å molecular sieves.  $NMe_2Ph$  and  $NET_2Ph$  were distilled from  $CaH_2$ . Benzophenone was recrystallized from hexane and dried under high vacuum ( $10^{-4}$  Torr) for 12 h. Ethylene (Matheson, Polymer grade) and carbon monoxide (Air Products, CP grade) were used as received.  $^1H$  (360 MHz),  $^{13}C$  (gated decoupled, 90 MHz),  $^{31}P$  (146 MHz) and  $^{11}B$  (115 MHz) NMR spectra were recorded on a Bruker AMX-360 spectrometer, and the  $^{19}F$  (282 MHz) NMR spectra were recorded on a Bruker AM-300 spectrometer. NMR spectra were recorded at 23 °C unless noted otherwise. X-ray structural analyses were performed on Enraf-Nonius CAD-4 (11a) and Siemens P4 (13a) diffractometers. Elemental analyses were performed by E + R Microanalytical Laboratory, Inc.

The following compounds were prepared by literature methods:  $ZrR_4$  ( $R$  = benzyl, neopentyl) complexes,<sup>15</sup> **6a,b**,<sup>10</sup>  $Li[B(C_6F_5)_4]$ ,<sup>47</sup>  $(salen)ZrCl_2(THF)$ , and  $(acen)ZrCl_2(THF)$ .<sup>8b</sup>

**[HNMe<sub>2</sub>Ph][B(C<sub>6</sub>F<sub>5</sub>)<sub>4</sub>].** An aqueous (100 mL) solution of  $[HNMe_2Ph]Cl$  (1.90 g, 12.1 mmol) was added to an aqueous (100 mL) suspension of  $Li[B(C_6F_5)_4]$  (7.85 g, 11.4 mmol) at 0 °C via cannula transfer (20 min). The resulting white slurry was stirred for 15 min. The solid was allowed to settle and the liquid phase removed by cannula filtration. The solid was washed with water ( $3 \times 50$  mL) and dried under vacuum at 60 °C for 9 h. The solid was dissolved in THF (40 mL) and filtered and the pale yellow filtrate concentrated *in vacuo*. Pentane (50 mL) and  $Et_2O$  (25 mL) were added to afford an oily white suspension which was concentrated *in vacuo*. This process was repeated until a flocculent white solid was obtained. The solid was collected by vacuum filtration and dried under vacuum at 60 °C for 48 h. Yield: 5.85 g, 7.30 mmol, 64%.  $^1H$  NMR (THF- $d_8$ ):  $\delta$  10.6 (br s, 1H, NH), 7.60 (m, 5H, Ph), 3.38 (s, 6H, CH<sub>3</sub>).

**[HNEt<sub>2</sub>Ph][B(C<sub>6</sub>F<sub>5</sub>)<sub>4</sub>].** Preparation is similar to that for  $[HNMe_2Ph][B(C_6F_5)_4]$ . Yield: 55%.  $^1H$  NMR (THF- $d_8$ ):  $\delta$  10.40 (br, 1H, NH), 7.62 (m, 5H, Ph), 3.72 (br dq,  $J = 15.5, 7.2$  Hz, 4H, NCH<sub>2</sub>), 1.18 (t,  $J = 7.2$  Hz, 6H, CH<sub>3</sub>).  $^{13}C$  NMR ( $CD_2Cl_2$ ):  $\delta$  148.5 (d,  $J_{CF} = 239.4$  Hz,  $B(C_6F_5)_4^-$ ), 138.6 (dt,  $J_{CF} = 243.9, 13.5$  Hz,  $B(C_6F_5)_4^-$ ), 136.7 (d,  $J_{CF} = 243.0$  Hz,  $B(C_6F_5)_4^-$ ), 132.5 (dt,  $J = 164.7, 6.3$  Hz, *p*-Ph), 132.0 (dd,  $J = 165.6, 8.1$  Hz, *o*-Ph), 131.1 (s, *i*-Ph), 124.5 (br,  $B(C_6F_5)_4^-$ ), 121.4 (dt,  $J = 160.2, 7.2$  Hz, *m*-Ph), 56.5 (t,  $J = 145.4$  Hz, NCH<sub>2</sub>), 11.1 (qt,  $J = 129.0, 3.2$  Hz, CH<sub>3</sub>).

**[HNMePh<sub>2</sub>][B(C<sub>6</sub>F<sub>5</sub>)<sub>4</sub>].** Solid  $[HNMePh_2]Cl$  (1.71 g, 7.78 mmol) was added to a dichloromethane (60 mL) suspension of  $Li[B(C_6F_5)_4]$  (7.75 g, 11.3 mmol) at 23 °C and the resulting white slurry stirred for 2.5 h. The slurry was filtered and the insolubles washed with dichloromethane (15 mL). The pale yellow filtrate was concentrated *in vacuo*. Pentane (50 mL) was added to afford a white oily suspension and the volatiles were removed *in vacuo*. The off-white solid was dissolved in toluene (200 mL) and filtered and the filtrate concentrated *in vacuo*. Dichloromethane (15 mL) and hexane (55 mL) were added to afford a white suspension which was concentrated *in vacuo* and cooled to -35 °C. The solid was collected by vacuum filtration and dried under vacuum at 110 °C for 7 d. Yield: 5.29 g, 6.12 mmol, 79%.  $^1H$  NMR ( $CD_2Cl_2$ ):  $\delta$  8.61 (s, 1H, NH), 7.65 (m, 6H, Ph), 7.41 (m, 4H, Ph), 3.84 (s, 3H, CH<sub>3</sub>).

$^{13}C$  NMR ( $CD_2Cl_2$ ):  $\delta$  148.4 (d,  $J_{CF} = 239.4$  Hz,  $B(C_6F_5)_4^-$ ), 140.9 (s, *i*-Ph), 138.6 (d,  $J_{CF} = 243.9$  Hz,  $B(C_6F_5)_4^-$ ), 136.7 (d,  $J_{CF} = 243.3$  Hz,  $B(C_6F_5)_4^-$ ), 132.4 (dt,  $J = 164.7, 6.3$  Hz, *p*-Ph), 132.0 (d,  $J = 162.9$  Hz, *o*-Ph), 124.0 (br,  $B(C_6F_5)_4^-$ ), 121.0 (d,  $J = 163.8$  Hz, *m*-Ph), 48.0 (q,  $J = 146.6$  Hz, CH<sub>3</sub>).

**(F<sub>6</sub>-acen)TiCl<sub>2</sub> (7).** A toluene (15 mL) solution of  $TiCl_4$  (0.340 g, 1.79 mmol) was added via cannula transfer to a toluene (7 mL) suspension of  $H_2(F_6\text{-acen})$ , **6a** (0.500 g, 1.50 mmol). The orange slurry was heated to reflux for 3 h to afford a dark red suspension. The volatiles were removed *in vacuo*. The resulting red solid was dissolved in  $CH_2Cl_2$  (30 mL) and filtered. The volatiles removed *in vacuo* to afford an orange-red powder. Yield: 0.548 g, 1.22 mmol, 81%. Recrystallization from cold  $CH_2Cl_2$ /pentane yielded analytically pure red crystals.  $^1H$  NMR ( $CD_2Cl_2$ ):  $\delta$  6.10 (s, 2H, CH), 3.96 (s, 4H, NCH<sub>2</sub>), 2.31 (s, 6H, CH<sub>3</sub>).  $^{13}C$  NMR ( $CD_2Cl_2$ ):  $\delta$  169.8 (s, CN), 156.8 (q,  $J_{CF} = 33.3$  Hz, CO), 118.9 (qd,  $J_{CF} = 276.3$  Hz,  $J = 2.7$  Hz, CF<sub>3</sub>), 109.4 (d,  $J = 166.5$  Hz, CH), 53.3 (t,  $J = 140.8$  Hz, NCH<sub>2</sub>), 23.1 (qd,  $J = 129.2, 2.7$  Hz, CH<sub>3</sub>);  $^{19}F$  NMR ( $CD_2Cl_2$ )  $\delta$  -73.8 (s, CF<sub>3</sub>). Anal. Calcd for  $C_{12}H_{12}Cl_2F_6N_2O_2Zr$ : C, 32.10; H, 2.69; N, 6.24. Found: C, 32.33; H, 2.69; N, 6.20.

**Na<sub>2</sub>(F<sub>6</sub>-acen)·THF (8).** Solid NaH (0.110 g, 4.58 mmol) was added slowly to a THF (50 mL) solution of **6a** (0.500 g, 1.50 mmol) at 23 °C resulting in the evolution of  $H_2$ . The reaction mixture was diluted with THF (25 mL) and stirred for 7 h. The slurry was heated to reflux for 1 h, cooled, and filtered. The volatiles were removed *in vacuo* from the pale yellow filtrate to afford an off-white solid, which was dried under vacuum for 3 h. Yield: 0.647 g, 1.44 mmol, 96%.  $^1H$  NMR ( $CD_2Cl_2$ ):  $\delta$  5.03 (s, 2H, CH), 3.57 (m, 4H, THF), 3.47 (s, 4H, NCH<sub>2</sub>), 1.83 (s, 6H, CH<sub>3</sub>), 1.75 (m, 4H, THF).  $^{13}C\{^1H\}$  NMR ( $CD_2Cl_2$ ):  $\delta$  166.5 (s, CN), 156.4 (q,  $J_{CF} = 28.0$  Hz, CO), 122.5 (q,  $J_{CF} = 281.7$  Hz, CF<sub>3</sub>), 96.1 (s, CH), 68.0 (s, THF), 52.5 (s, NCH<sub>2</sub>), 25.8 (s, THF), 20.0 (s, CH<sub>3</sub>).

**(F<sub>6</sub>-acen)ZrCl<sub>2</sub>(THF) (9).** A THF solution (35 mL) of  $Na_2(F_6\text{-acen})\cdot THF$  (**8**, 0.350 g, 0.781 mmol) was added dropwise (15 min) to a THF suspension (5 mL) of  $ZrCl_4(THF)_2$  (0.303 g, 0.803 mmol) at 23 °C, affording a pale yellow slurry which was stirred for 3.5 h. Dilution with dichloromethane (25 mL) and filtration yielded a pale yellow filtrate. Hexane (10 mL) was added and the resulting pale yellow, cloudy mixture was cooled to -35 °C and filtered. The volatiles were removed *in vacuo* to afford a pale yellow solid. Yield: 0.300 g, 0.531 mmol, 68%. Recrystallization from toluene at -35 °C yielded analytically pure white crystals containing 0.41 equiv of toluene (determined by NMR).  $^1H$  NMR ( $CD_2Cl_2$ ):  $\delta$  5.96 (s, 2H, CH), 4.29 (m, 4H, THF), 3.98 (s, 4H, NCH<sub>2</sub>), 2.25 (s, 6H, CH<sub>3</sub>), 1.99 (m, 4H, THF).  $^{13}C$  NMR ( $CD_2Cl_2$ ):  $\delta$  172.1 (s, CN), 156.5 (q,  $J_{CF} = 33.3$  Hz, CO), 120.0 (qd,  $J_{CF} = 278.1$  Hz,  $J = 1.8$  Hz, CF<sub>3</sub>), 103.7 (d,  $J = 165.6$  Hz, CH), 72.8 (t,  $J = 150.7$  Hz, THF), 52.7 (t,  $J = 139.1$  Hz, NCH<sub>2</sub>), 25.8 (t,  $J = 133.4$  Hz, THF), 23.9 (qd,  $J = 128.3, 2.9$  Hz, CH<sub>3</sub>).  $^{19}F$  NMR ( $CD_2Cl_2$ ):  $\delta$  -72.9 (s, CF<sub>3</sub>). Anal. Calcd for  $C_{16}H_{20}Cl_2F_6N_2O_2Zr \cdot 0.41\text{toluene}$ : C, 37.63; H, 3.90; N, 4.65. Found: C, 37.37; H, 3.73; N, 4.82.

**(F<sub>6</sub>-acen)<sub>2</sub>Zr (10).** Solid **8** (0.120 g, 0.268 mmol) and  $ZrCl_4(THF)_2$  (0.050 g, 0.130 mmol) were combined in an NMR tube. Dichloromethane- $d_2$  (ca. 0.6 mL) was added to the solids via vacuum transfer at -78 °C. The tube was frozen at -196 °C and flame-sealed under vacuum and then allowed to thaw to ambient temperature to afford an off-white solution with a white precipitate. Following NMR analysis, the suspension was filtered to afford a pale yellow filtrate. The volatiles were removed *in vacuo* yielding an off-white powder. Yield: 0.0902 g, 0.120 mmol, 92%.  $^1H$  NMR ( $CD_2Cl_2$ ):  $\delta$  5.47 (s, 2H, CH), 3.93 (s, 4H, NCH<sub>2</sub>), 3.71 (m, 6H, free THF), 2.12 (s, 6H, CH<sub>3</sub>), 1.84 (m, 6H, free THF).  $^{13}C$  NMR ( $CD_2Cl_2$ ):  $\delta$  165.6 (s, CN), 154.5 (q,  $J_{CF} = 33.3$  Hz, CO), 120.4 (q,  $J_{CF} = 278.1$  Hz, CF<sub>3</sub>), 100.7 (d,  $J = 163.8$  Hz, CH), 51.4 (t,  $J = 137.8$  Hz, NCH<sub>2</sub>), 22.9 (q,  $J = 128.5$  Hz, CH<sub>3</sub>). Anal. Calcd for  $C_{24}H_{24}F_{12}N_4O_4Zr$ : C, 38.35; H, 3.22; N, 7.45. Found: C, 38.30; H, 3.21; N, 7.32.

**(F<sub>6</sub>-acen)Zr(CH<sub>2</sub>CMe<sub>3</sub>)<sub>2</sub> (11a).** Solid **6a** (0.705 g, 2.12 mmol) was added (5 min) to a pentane solution (20 mL) of  $Zr$ -

(47) Massey, A. G.; Park, A. J. *J. Organomet. Chem.* **1964**, *2*, 245.



(CH<sub>2</sub>CMe<sub>3</sub>)<sub>4</sub> (0.800 g, 2.12 mmol) at 23 °C, affording a yellow-orange slurry which was stirred for 1.5 h. The slurry was concentrated *in vacuo* and cooled to -35 °C. The yellow-orange powder was collected by vacuum filtration and washed with cold pentane (15 mL). Yield: 1.13 g, 2.00 mmol, 95%. Recrystallization from toluene layered with pentane at -35 °C yielded analytically pure, orange-red cube shaped crystals, one of which was selected for an X-ray diffraction study. <sup>1</sup>H NMR (C<sub>6</sub>D<sub>6</sub>): δ 5.85 (s, 2H, CH), 2.76 (s, 4H, NCH<sub>2</sub>), 1.32 (s, 6H, CH<sub>3</sub>), 1.17 (s, 18H, CMe<sub>3</sub>), 0.59 (s, 4H, ZrCH<sub>2</sub>). <sup>13</sup>C NMR (C<sub>6</sub>D<sub>6</sub>): δ 174.9 (s, CN), 161.9 (qd, J<sub>CF</sub> = 33.3 Hz, J = 1.8 Hz, CO), 120.7 (qd, J<sub>CF</sub> = 278.1 Hz, J = 1.8 Hz, CF<sub>3</sub>), 99.6 (d, J = 163.8 Hz, CH), 88.6 (t, J = 109.8 Hz, ZrCH<sub>2</sub>), 53.0 (t, J = 137.3 Hz, NCH<sub>2</sub>), 35.7 (s, CMe<sub>3</sub>), 34.3 (qm, J = 122.9 Hz, CMe<sub>3</sub>), 23.3 (qd, J = 127.8, 3.1 Hz, CH<sub>3</sub>). <sup>19</sup>F NMR (C<sub>6</sub>D<sub>6</sub>): δ -72.1 (s). Anal. Calcd for C<sub>22</sub>H<sub>34</sub>F<sub>6</sub>N<sub>2</sub>O<sub>2</sub>Zr: C, 46.87; H, 6.08; N, 4.97. Found: C, 46.68; H, 5.97; N, 5.01.

(H<sub>6</sub>-acen)Zr(CH<sub>2</sub>CMe<sub>3</sub>)<sub>2</sub> (11b). Solid H<sub>2</sub>(H<sub>6</sub>-acen) (6b, 1.16 g, 5.17 mmol) was added (5 min) to a pentane solution (40 mL) of Zr(CH<sub>2</sub>CMe<sub>3</sub>)<sub>4</sub> (1.94 g, 5.16 mmol) at 23 °C, affording a yellow slurry which was stirred for 40 min. The slurry was concentrated *in vacuo* and cooled to -35 °C. The yellow powder was collected by vacuum filtration and washed with cold pentane (15 mL). Yield: 2.15 g, 4.71 mmol, 91%. Recrystallization from toluene layered with pentane at -35 °C yielded an analytically pure, yellow crystalline solid. <sup>1</sup>H NMR (C<sub>6</sub>D<sub>6</sub>): δ 5.32 (s, 2H, CH), 3.02 (s, 4H, NCH<sub>2</sub>), 2.19 (s, 6H, CH<sub>3</sub>), 1.54 (s, 6H, CH<sub>3</sub>), 1.25 (s, 18H, CMe<sub>3</sub>), 0.49 (s, 4H, ZrCH<sub>2</sub>). <sup>13</sup>C NMR (C<sub>6</sub>D<sub>6</sub>): δ 180.3 (br s, CN), 171.0 (s, CO), 102.0 (d, J = 158.4 Hz, CH), 82.8 (t, J = 112.5 Hz, ZrCH<sub>2</sub>), 52.7 (t, J = 135.5 Hz, NCH<sub>2</sub>), 35.4 (s, CMe<sub>3</sub>), 35.0 (qm, J = 122.7 Hz, CMe<sub>3</sub>), 25.4 (qd, J = 126.2, 1.3 Hz, CH<sub>3</sub>), 23.1 (qd, J = 126.6, 4.0 Hz). Anal. Calcd for C<sub>22</sub>H<sub>40</sub>N<sub>2</sub>O<sub>2</sub>Zr: C, 57.97; H, 8.85; N, 6.15. Found: C, 58.09; H, 8.70; N, 6.34.

(F<sub>6</sub>-acen)Zr(CH<sub>2</sub>Ph)<sub>2</sub> (12). Hexane (15 mL) was added to solid 6a (0.728 g, 2.19 mmol) and Zr(CH<sub>2</sub>Ph)<sub>4</sub> (1.00 g, 2.19 mmol) at 23 °C, affording an orange slurry which was stirred for 12 h with the exclusion of light. The orange solid was collected by vacuum filtration, washed with hexane (2 × 5 mL) and dried under vacuum (6 h). Yield: 1.27 g, 1.10 mmol, 96%. Recrystallization from toluene layered with hexanes at -35 °C yielded an analytically pure, orange-red crystalline solid. <sup>1</sup>H NMR (C<sub>6</sub>D<sub>6</sub>): δ 6.72 (t, J = 7.6 Hz, 4H, *m*-Ph), 6.54 (t, J = 7.3 Hz, 2H, *p*-Ph), 6.33 (d, J = 7.3 Hz, 4H, *o*-Ph), 5.76 (s, 2H, CH), 2.57 (s, 4H, NCH<sub>2</sub>), 2.25 (s, 4H, ZrCH<sub>2</sub>), 1.21 (s, 6H, CH<sub>3</sub>). <sup>13</sup>C NMR (THF-*d*<sub>8</sub>): δ 170.0 (s, CN), 155.6 (qd, J<sub>CF</sub> = 32.4 Hz, J = 2.7 Hz, CO), 147.6 (s, *i*-Ph), 128.1 (ddd, J = 153.4, 8.1, 1.8 Hz, *m*-Ph), 127.5 (dm, J = 153.9 Hz, *o*-Ph), 121.3 (qd, J<sub>CF</sub> = 278.1 Hz, J = 1.8 Hz, CF<sub>3</sub>), 121.0 (dt, J = 155.7, 7.2 Hz, *p*-Ph), 102.7 (d, J = 162.9 Hz, CH), 64.6 (t, J = 125.3 Hz, ZrCH<sub>2</sub>), 52.3 (t, J = 137.4 Hz, NCH<sub>2</sub>), 23.8 (qd, J = 127.8, 3.2 Hz, CH<sub>3</sub>). <sup>19</sup>F NMR (C<sub>6</sub>D<sub>6</sub>): δ -72.8 (s). Anal. Calcd for C<sub>26</sub>H<sub>26</sub>F<sub>6</sub>N<sub>2</sub>O<sub>2</sub>Zr: C, 51.73; H, 4.34; N, 4.64. Found: C, 51.85; H, 4.34; N, 4.88.

[(F<sub>6</sub>-acen)Zr(CH<sub>2</sub>CMe<sub>3</sub>)(NMe<sub>2</sub>Ph)][B(C<sub>6</sub>F<sub>5</sub>)<sub>4</sub>] (13a). Dichloromethane (10 mL) was added to solid (F<sub>6</sub>-acen)Zr(CH<sub>2</sub>CMe<sub>3</sub>)<sub>2</sub> (11, 0.208 g, 0.369 mmol) and [HNMe<sub>2</sub>Ph][B(C<sub>6</sub>F<sub>5</sub>)<sub>4</sub>] (0.295 g, 0.368 mmol) at 23 °C, affording an orange-yellow solution which was stirred for 25 min. The volatiles were removed *in vacuo* to afford an orange crystalline solid. Yield: 0.463 g, 0.358 mmol, 97%. Recrystallization from dichloromethane layered with chlorobenzene and toluene at -35 °C yielded an analytically pure, orange-yellow crystalline solid. Yield: 0.300 g, 0.232 mmol, 65%. Single crystals suitable for X-ray diffraction were obtained by slow crystallization at 23 °C from dichloromethane layered with chlorobenzene. <sup>1</sup>H NMR (CD<sub>2</sub>Cl<sub>2</sub>): δ 7.32 (t, J = 7.6 Hz, 2H, *m*-Ph), 7.20 (t, J = 7.4 Hz, 1H, *p*-Ph), 6.79 (d, J = 8.0 Hz, 2H, *o*-Ph), 6.20 (s, 2H, CH), 3.85 (m, 4H, NCH<sub>2</sub>), 2.86 (s, 6H, NMe<sub>2</sub>Ph), 2.37 (s, 6H, CH<sub>3</sub>), 1.12 (s, 2H, ZrCH<sub>2</sub>), 0.82 (s, 9H, CMe<sub>3</sub>). <sup>13</sup>C NMR (CD<sub>2</sub>Cl<sub>2</sub>): δ 179.9 (s, CN), 154.4 (q, J<sub>CF</sub> = 35.1 Hz, CO), 148.5 (dm, J<sub>CF</sub> = 243.9 Hz, B(C<sub>6</sub>F<sub>5</sub>)<sub>4</sub>-), 146.2 (br s, *i*-Ph), 138.6 (dm, J<sub>CF</sub>

= 242.1 Hz, B(C<sub>6</sub>F<sub>5</sub>)<sub>4</sub>-), 136.7 (dm, J<sub>CF</sub> = 238.5 Hz, B(C<sub>6</sub>F<sub>5</sub>)<sub>4</sub>-), 130.7 (dd, J = 162.0, 8.1 Hz, *m*-Ph), 127.6 (d, J = 163.8 Hz, *p*-Ph), 124.1 (br, B(C<sub>6</sub>F<sub>5</sub>)<sub>4</sub>-), 119.5 (q, J<sub>CF</sub> = 279.0 Hz, J = 1.8 Hz, CF<sub>3</sub>), 119.2 (dm, J = 156.6 Hz, *o*-Ph), 119.1 (t, J = 107.9 Hz, ZrCH<sub>2</sub>), 105.2 (d, J = 168.3 Hz, CH), 53.3 (t, J = 140.3 Hz, NCH<sub>2</sub>), 46.5 (qm, J = 144.3 Hz, NMe<sub>2</sub>Ph), 39.3 (s, CMe<sub>3</sub>), 31.5 (qm, J = 123.1 Hz, CMe<sub>3</sub>), 25.2 (qd, J = 129.5, 2.9 Hz, CH<sub>3</sub>). <sup>19</sup>F NMR (CD<sub>2</sub>Cl<sub>2</sub>): δ -75.1 (s, 6F, CF<sub>3</sub>), -135.8 (br s, 8F, B(C<sub>6</sub>F<sub>5</sub>)<sub>4</sub>-), -166.3 (t, J<sub>FF</sub> = 20.3 Hz, 4F, B(C<sub>6</sub>F<sub>5</sub>)<sub>4</sub>-), -170.2 (m, 8F, B(C<sub>6</sub>F<sub>5</sub>)<sub>4</sub>-). Anal. Calcd for C<sub>49</sub>H<sub>34</sub>BF<sub>26</sub>N<sub>3</sub>O<sub>2</sub>Zr: C, 45.52; H, 2.65; N, 3.25. Found: C, 45.35; H, 2.49; N, 3.17.

[(H<sub>6</sub>-acen)Zr(CH<sub>2</sub>CMe<sub>3</sub>)(NMe<sub>2</sub>Ph)][B(C<sub>6</sub>F<sub>5</sub>)<sub>4</sub>] (13b). Dichloromethane-*d*<sub>2</sub> (0.5 mL) was vacuum transferred at -78 °C into an NMR tube containing solid 11b (0.0565 g, 0.124 mmol) and [HNMe<sub>2</sub>Ph][B(C<sub>6</sub>F<sub>5</sub>)<sub>4</sub>] (0.0993 g, 0.124 mmol). The tube was frozen at -196 °C and flame sealed under vacuum. The tube was warmed to 23 °C and shaken to afford a yellow homogeneous solution. <sup>1</sup>H and <sup>13</sup>C NMR spectra were obtained. Following NMR analysis, the tube was cracked open and the contents transferred to a vial. The volatiles were removed *in vacuo* to afford a yellow powder. Yield: 0.120 g, 0.101 mmol, 81%. Attempted recrystallization from cold CH<sub>2</sub>Cl<sub>2</sub>/toluene resulted in decomposition. <sup>1</sup>H NMR (CD<sub>2</sub>Cl<sub>2</sub>): δ 7.29 (t, J = 7.8 Hz, 2H, *m*-Ph), 6.99 (t, J = 7.2 Hz, 1H, *p*-Ph), 6.83 (d, J = 8.1 Hz, 2H, *o*-Ph), 5.80 (br s, 2H, CH), 3.78 (br s, 4H, NCH<sub>2</sub>), 2.80 (s, 6H, NMe<sub>2</sub>Ph), 2.20 (br s, 6H, CH<sub>3</sub>), 2.15 (br s, 6H, CH<sub>3</sub>), 1.09 (s, 2H, ZrCH<sub>2</sub>), 0.86 (s, 9H, CMe<sub>3</sub>). <sup>1</sup>H NMR (-40 °C, CD<sub>2</sub>Cl<sub>2</sub>): δ 7.25 (t, J = 7.5 Hz, 2H, *m*-Ph), 6.96 (t, J = 7.3 Hz, 1H, *p*-Ph), 6.79 (d, J = 8.3 Hz, 2H, *o*-Ph), 5.58 (s, 2H, CH), 3.65 (m, 4H, NCH<sub>2</sub>), 2.71 (s, 6H, NMe<sub>2</sub>Ph), 2.12 (s, 6H, CH<sub>3</sub>), 2.10 (s, 6H, CH<sub>3</sub>), 0.74 (s, 9H, CMe<sub>3</sub>), 0.70 (s, 2H, ZrCH<sub>2</sub>). <sup>13</sup>C NMR (CD<sub>2</sub>Cl<sub>2</sub>): δ 179.1 (s, CN), 176.6 (s, CO), 149.0 (s, *i*-Ph), 148.6 (d, J<sub>CF</sub> = 240.3 Hz, B(C<sub>6</sub>F<sub>5</sub>)<sub>4</sub>-), 138.6 (d, J<sub>CF</sub> = 243.9 Hz, B(C<sub>6</sub>F<sub>5</sub>)<sub>4</sub>-), 136.7 (d, J<sub>CF</sub> = 243.9 Hz, B(C<sub>6</sub>F<sub>5</sub>)<sub>4</sub>-), 129.7 (dd, J = 157.5, 8.1 Hz, *m*-Ph), 124.4 (br, B(C<sub>6</sub>F<sub>5</sub>)<sub>4</sub>-), 120.1 (d, J = 164.7 Hz, *p*-Ph), 115.2 (d, J = 155.7 Hz, *o*-Ph), 107.1 (d, J = 161.1 Hz, CH), 104.6 (t, J = 106.2 Hz, ZrCH<sub>2</sub>), 52.4 (t, J = 138.1 Hz, NCH<sub>2</sub>), 42.7 (q, J = 133.6 Hz, NMe<sub>2</sub>Ph), 37.7 (s, CMe<sub>3</sub>), 33.4 (q, J = 123.6 Hz, CMe<sub>3</sub>), 24.3 (q, J = 127.5 Hz, CH<sub>3</sub>), 24.0 (q, J = 128.3 Hz, CH<sub>3</sub>).

[(F<sub>6</sub>-acen)Zr(CH<sub>2</sub>CMe<sub>3</sub>)(NEt<sub>2</sub>Ph)][B(C<sub>6</sub>F<sub>5</sub>)<sub>4</sub>] (14). Dichloromethane-*d*<sub>2</sub> (0.5 mL) was vacuum transferred at -78 °C into an NMR tube containing solid 11a (0.0618 g, 0.110 mmol) and [HNEt<sub>2</sub>Ph][B(C<sub>6</sub>F<sub>5</sub>)<sub>4</sub>] (0.0910 g, 0.110 mmol). The mixture was frozen at -196 °C and the tube flame-sealed under vacuum. The tube was warmed to 23 °C affording an orange solution which became green within 45 min. Analysis by NMR spectroscopy showed quantitative formation of 14 with no visible decomposition. <sup>1</sup>H NMR (CD<sub>2</sub>Cl<sub>2</sub>): δ 7.31 (t, J = 7.5 Hz, 2H, *m*-Ph), 7.05 (t, J = 6.3 Hz, 1H, *p*-Ph), 6.74 (d, J = 8.0 Hz, 2H, *o*-Ph), 6.28 (s, 2H, CH), 3.79 (m, 4H, NCH<sub>2</sub>), 3.34 (q, J = 7.1 Hz, 4H, NCH<sub>2</sub>CH<sub>3</sub>), 2.36 (s, 6H, CH<sub>3</sub>), 1.21 (br s, 2H, ZrCH<sub>2</sub>), 1.12 (t, J = 7.1 Hz, 6H, NCH<sub>2</sub>CH<sub>3</sub>), 0.92 (s, 12H, CMe<sub>4</sub>), 0.81 (br s, 9H, CMe<sub>3</sub>). <sup>13</sup>C NMR (CD<sub>2</sub>Cl<sub>2</sub>): δ 179.5 (s, CN), 158.7 (q, J<sub>CF</sub> = 36.0 Hz, CO), 148.6 (dm, J<sub>CF</sub> = 239.4 Hz, B(C<sub>6</sub>F<sub>5</sub>)<sub>4</sub>-), 143.8 (s, *i*-Ph), 138.6 (dt, J<sub>CF</sub> = 243.9 Hz, J = 13.5 Hz, B(C<sub>6</sub>F<sub>5</sub>)<sub>4</sub>-), 136.7 (d, J<sub>CF</sub> = 244.8 Hz, B(C<sub>6</sub>F<sub>5</sub>)<sub>4</sub>-), 131.1 (dd, J = 159.3, 8.1 Hz, *m*-Ph), 124.5 (d, J = 161.1 Hz, *p*-Ph), 124.1 (br, B(C<sub>6</sub>F<sub>5</sub>)<sub>4</sub>-), 119.5 (q, J<sub>CF</sub> = 279.0 Hz, CF<sub>3</sub>), 118.1 (d, J = 160.2 Hz, *o*-Ph), 117.1 (t, J = 107.1 Hz, ZrCH<sub>2</sub>), 105.7 (d, J = 167.4 Hz, CH), 52.9 (t, J = 140.1 Hz, NCH<sub>2</sub>), 45.7 (tq, J = 137.9, 4.0 Hz, NCH<sub>2</sub>CH<sub>3</sub>), 39.5 (s, CMe<sub>3</sub>), 32.8 (q, J = 121.0 Hz, CMe<sub>3</sub>), 25.2 (q, J = 129.3 Hz, CH<sub>3</sub>), 10.5 (q, J = 126.3 Hz, NCH<sub>2</sub>CH<sub>3</sub>).

[(F<sub>6</sub>-acen)Zr(CH<sub>2</sub>CMe<sub>3</sub>)]<sub>2</sub>[B(C<sub>6</sub>F<sub>5</sub>)<sub>4</sub>] (15). Benzene (20 mL) was added to solid 11a (1.02 g, 1.81 mmol) and [HNMePh]<sub>2</sub>[B(C<sub>6</sub>F<sub>5</sub>)<sub>4</sub>] (1.56 g, 1.81 mmol) at 23 °C, affording an orange-yellow oily solution from which a yellow solid precipitated after 1 h. The filtrate was decanted and the solid was washed with benzene (2 × 5 mL) and pentane (5 × 10 mL) and dried *in vacuo* (5 h) to afford a yellow powder. Yield: 1.68 g, 1.44 mmol, 80%. <sup>1</sup>H NMR (CD<sub>2</sub>Cl<sub>2</sub>): δ 6.39 (s, 2H, CH), 4.06 (m,



4H, NCH<sub>2</sub>), 2.47 (s, 6H, CH<sub>3</sub>), 1.88 (s, 2H, ZrCH<sub>2</sub>), 1.01 (s, 9H, CMe<sub>3</sub>). <sup>13</sup>C NMR (CD<sub>2</sub>Cl<sub>2</sub>): δ 181.5 (s, CN), 157.5 (q, *J*<sub>CF</sub> = 37.8 Hz, CO), 148.5 (d, *J*<sub>CF</sub> = 239.4 Hz, B(C<sub>6</sub>F<sub>5</sub>)<sub>4</sub><sup>-</sup>), 138.6 (dm, *J*<sub>CF</sub> = 243.9 Hz, B(C<sub>6</sub>F<sub>5</sub>)<sub>4</sub><sup>-</sup>), 136.7 (d, *J*<sub>CF</sub> = 244.8 Hz, B(C<sub>6</sub>F<sub>5</sub>)<sub>4</sub><sup>-</sup>), 124.2 (br, B(C<sub>6</sub>F<sub>5</sub>)<sub>4</sub><sup>-</sup>), 118.8 (q, *J*<sub>CF</sub> = 276.3 Hz, CF<sub>3</sub>), 113.1 (tm, *J* = 109.8 Hz, ZrCH<sub>2</sub>), 108.1 (d, *J* = 169.2 Hz, CH), 52.1 (t, *J* = 142.0 Hz, NCH<sub>2</sub>), 38.3 (s, CMe<sub>3</sub>), 32.9 (q, *J* = 124.2 Hz, CMe<sub>3</sub>), 24.3 (q, *J* = 129.8 Hz, CH<sub>3</sub>). <sup>19</sup>F NMR (CD<sub>2</sub>Cl<sub>2</sub>): δ -76.5 (s, 6F, CF<sub>3</sub>), -135.9 (s, 8F, B(C<sub>6</sub>F<sub>5</sub>)<sub>4</sub><sup>-</sup>), -166.2 (t, *J*<sub>FF</sub> = 19.7 Hz, 4F, B(C<sub>6</sub>F<sub>5</sub>)<sub>4</sub><sup>-</sup>), -170.2 (s, 8F, B(C<sub>6</sub>F<sub>5</sub>)<sub>4</sub><sup>-</sup>). Anal. Calcd for C<sub>41</sub>H<sub>23</sub>BF<sub>26</sub>N<sub>2</sub>O<sub>2</sub>Zr: C, 42.03; H, 1.98; N, 2.39. Found: C, 41.89; H, 1.98; N, 2.17.

[NMe<sub>2</sub>Ph(CH<sub>2</sub>Cl)]<sub>2</sub>[B(C<sub>6</sub>F<sub>5</sub>)<sub>4</sub>] (18). Dichloromethane (8 mL) was added to solid 11a (0.419 g, 0.743 mmol) and [HNMe<sub>2</sub>Ph]<sub>2</sub>[B(C<sub>6</sub>F<sub>5</sub>)<sub>4</sub>] (0.617 g, 0.744 mmol). The solution was allowed to stand at ambient temperature for 10 days, with the color changing from yellow to green. The volatiles were removed *in vacuo* to afford a green oily residue. In the air, the material was dissolved in CH<sub>2</sub>Cl<sub>2</sub> and filtered through a plug of wet Celite. The volatiles were removed *in vacuo* and the greenish residue repeatedly triturated with toluene (200 mL). The toluene fractions were recrystallized from cold CH<sub>2</sub>Cl<sub>2</sub>/pentane to afford off-white needles of 18. <sup>1</sup>H NMR (CD<sub>2</sub>Cl<sub>2</sub>): δ 7.71 (m, 3H, Ph), 7.43 (m, 2H, Ph), 5.28 (s, 2H, NCH<sub>2</sub>Cl), 3.91 (m, 4H, NCH<sub>2</sub>CH<sub>3</sub>), 1.21 (t, *J* = 7.2 Hz, 6H, CH<sub>3</sub>). <sup>13</sup>C NMR (CD<sub>2</sub>Cl<sub>2</sub>): δ 148.5 (d, *J*<sub>CF</sub> = 238.5 Hz, B(C<sub>6</sub>F<sub>5</sub>)<sub>4</sub><sup>-</sup>), 139.2 (br s, *i*-Ph), 138.6 (d, *J*<sub>CF</sub> = 244.8 Hz, B(C<sub>6</sub>F<sub>5</sub>)<sub>4</sub><sup>-</sup>), 136.6 (d, *J*<sub>CF</sub> = 245.7 Hz, B(C<sub>6</sub>F<sub>5</sub>)<sub>4</sub><sup>-</sup>), 132.4 (dt, *J* = 165.6, 7.2 Hz, *p*-Ph), 132.1 (dd, *J* = 162.0, 7.2 Hz, *o*-Ph), 124.2 (br, B(C<sub>6</sub>F<sub>5</sub>)<sub>4</sub><sup>-</sup>), 121.0 (d, *J* = 159.3 Hz, *m*-Ph), 64.0 (t, *J* = 169.4 Hz, NCH<sub>2</sub>Cl), 58.9 (t, *J* = 145.5 Hz, NCH<sub>2</sub>CH<sub>3</sub>), 8.1 (q, *J* = 129.2 Hz, CH<sub>3</sub>). Anal. Calcd for C<sub>65</sub>H<sub>17</sub>BClF<sub>20</sub>N: C, 47.89; H, 1.95; N, 1.60. Found: C, 47.74; H, 1.88; N, 1.74.

{[(F<sub>6</sub>-acen)Zr(CH<sub>2</sub>CMe<sub>3</sub>)<sub>2</sub>(μ-Cl)]<sub>2</sub>}[B(C<sub>6</sub>F<sub>5</sub>)<sub>4</sub>] (19). Solid [PPN]Cl (0.0614 g, 0.107 mmol) was added (2 min) to a dichloromethane (7 mL) solution of 15 (0.251 g, 0.214 mmol) at 25 °C. The resulting yellow solution was stirred for 15 min. The volatiles were removed *in vacuo* to afford a yellow oily residue which foamed into a solid. <sup>1</sup>H, <sup>13</sup>C, and <sup>19</sup>F NMR were obtained showing complex 19 (100%, NMR) and [PPN]<sub>2</sub>[B(C<sub>6</sub>F<sub>5</sub>)<sub>4</sub>]. Attempted separation of the two components via crystallization was unsuccessful; in the best case a sample of 19 containing 20% [PPN]<sub>2</sub>[B(C<sub>6</sub>F<sub>5</sub>)<sub>4</sub>] was obtained. <sup>1</sup>H NMR (CD<sub>2</sub>Cl<sub>2</sub>): δ 6.40 (s, 4H, CH), 3.86 (br s, 8H, NCH<sub>2</sub>), 2.36 (s, 12H, CH<sub>3</sub>), 1.48 (br s, 4H, ZrCH<sub>2</sub>), 0.67 (s, 18H, CMe<sub>3</sub>). <sup>13</sup>C NMR (CD<sub>2</sub>Cl<sub>2</sub>): δ 174.2 (s, CN), 154.1 (q, *J*<sub>CF</sub> = 35.1 Hz, CO), 148.5 (d, *J*<sub>CF</sub> = 237.6 Hz, B(C<sub>6</sub>F<sub>5</sub>)<sub>4</sub><sup>-</sup>), 138.6 (dt, *J*<sub>CF</sub> = 243.9, 13.5 Hz, B(C<sub>6</sub>F<sub>5</sub>)<sub>4</sub><sup>-</sup>), 136.6 (d, *J*<sub>CF</sub> = 243.9 Hz, B(C<sub>6</sub>F<sub>5</sub>)<sub>4</sub><sup>-</sup>), 124.3 (br, B(C<sub>6</sub>F<sub>5</sub>)<sub>4</sub><sup>-</sup>), 119.7 (qd, *J*<sub>CF</sub> = 277.2 Hz, *J* = 2.7 Hz, CF<sub>3</sub>), 119.0 (t, *J* = 105.3 Hz, ZrCH<sub>2</sub>), 109.0 (d, *J* = 167.4 Hz, CH), 52.6 (t, *J* = 140.0 Hz, NCH<sub>2</sub>), 40.0 (s, CMe<sub>3</sub>), 32.9 (q, *J* = 123.8 Hz, CMe<sub>3</sub>), 24.3 (q, *J* = 129.1 Hz, CH<sub>3</sub>); <sup>19</sup>F NMR (CD<sub>2</sub>Cl<sub>2</sub>) δ -75.2 (s, 12F, CF<sub>3</sub>), -136.0 (s, 8F, B(C<sub>6</sub>F<sub>5</sub>)<sub>4</sub><sup>-</sup>), -166.5 (t, *J*<sub>FF</sub> = 19.7 Hz, 4F, B(C<sub>6</sub>F<sub>5</sub>)<sub>4</sub><sup>-</sup>), -170.4 (br s, 8F, B(C<sub>6</sub>F<sub>5</sub>)<sub>4</sub><sup>-</sup>).

[(F<sub>6</sub>-acen)Zr(CH<sub>2</sub>CMe<sub>3</sub>)<sub>2</sub>(PMe<sub>2</sub>Ph)]<sub>2</sub>[B(C<sub>6</sub>F<sub>5</sub>)<sub>4</sub>] (21). Dichloromethane (10 mL) was added via vacuum transfer at -196 °C to solid 11a (0.117 g, 0.207 mmol) and [HNMe<sub>2</sub>Ph]<sub>2</sub>[B(C<sub>6</sub>F<sub>5</sub>)<sub>4</sub>] (0.166 g, 0.207 mmol). The flask was warmed to 23 °C and the resulting yellow homogeneous solution stirred for 10 min. The solution was frozen at -196 °C, and PMe<sub>3</sub> (0.600 mmol) was added via vacuum transfer. The flask was warmed to 23 °C and the resulting yellow homogeneous solution stirred for 1 h. The volatiles were removed *in vacuo* to afford an oily yellow solid. The solid was washed with benzene (5 × 10 mL) and dried under vacuum for 3 h to afford a thermally unstable yellow powder. Yield: 0.240 g, 0.181 mmol, 88%. Attempted recrystallization from cold CH<sub>2</sub>Cl<sub>2</sub>/toluene resulted in decomposition. <sup>1</sup>H NMR (CD<sub>2</sub>Cl<sub>2</sub>): δ 6.18 (s, 2H, CH), 4.27 (m, 2H, NCH<sub>2</sub>), 3.65 (m, 2H, NCH<sub>2</sub>), 2.40 (s, 6H, CH<sub>3</sub>), 1.27 (s, 2H, ZrCH<sub>2</sub>), 1.08 (br d, *J*<sub>PH</sub> = 5.5 Hz, 18H, PMe<sub>3</sub>), 0.83 (s, 9H, CMe<sub>3</sub>). <sup>1</sup>H NMR (-80 °C, CD<sub>2</sub>Cl<sub>2</sub>): δ 6.12 (s, 2H, CH), 4.18 (m, 2H, NCH<sub>2</sub>), 3.53 (m, 2H, NCH<sub>2</sub>), 2.32 (s, 6H, CH<sub>3</sub>), 1.24

(d, *J*<sub>PH</sub> = 6.8 Hz, 9H, PMe<sub>3</sub>), 1.08 (br d, *J*<sub>PH</sub> = 5.0 Hz, 2H, ZrCH<sub>2</sub>), 0.70 (d, *J*<sub>PH</sub> = 7.0 Hz, 9H, PMe<sub>3</sub>), 0.69 (s, 9H, CMe<sub>3</sub>). <sup>13</sup>C NMR (CD<sub>2</sub>Cl<sub>2</sub>): δ 174.2 (s, CN), 155.6 (q, *J*<sub>CF</sub> = 34.2 Hz, CO), 148.5 (d, *J*<sub>CF</sub> = 239.4 Hz, B(C<sub>6</sub>F<sub>5</sub>)<sub>4</sub><sup>-</sup>), 138.6 (dm, *J*<sub>CF</sub> = 243.9 Hz, B(C<sub>6</sub>F<sub>5</sub>)<sub>4</sub><sup>-</sup>), 136.7 (dm, *J*<sub>CF</sub> = 242.1 Hz, B(C<sub>6</sub>F<sub>5</sub>)<sub>4</sub><sup>-</sup>), 124.5 (br, B(C<sub>6</sub>F<sub>5</sub>)<sub>4</sub><sup>-</sup>), 119.8 (q, *J*<sub>CF</sub> = 279.0 Hz, CF<sub>3</sub>), 104.4 (d, *J* = 166.5 Hz, CH), 101.9 (t, *J* = 108.0 Hz, ZrCH<sub>2</sub>), 52.9 (t, *J* = 138.6 Hz, NCH<sub>2</sub>), 37.8 (s, CMe<sub>3</sub>), 33.6 (q, *J* = 123.4 Hz, CMe<sub>3</sub>), 24.8 (qd, *J* = 128.9, 2.6 Hz, CH<sub>3</sub>), 12.0 (br q, *J* = 128.7, PMe<sub>3</sub>); <sup>31</sup>P{<sup>1</sup>H} NMR (-80 °C, CD<sub>2</sub>Cl<sub>2</sub>) δ -24.1 (d, *J* = 12.8 Hz), -35.5 (d, *J* = 11.2 Hz).

[(F<sub>6</sub>-acen)Zr(CH<sub>2</sub>CMe<sub>3</sub>)(PMe<sub>2</sub>Ph)]<sub>2</sub>[B(C<sub>6</sub>F<sub>5</sub>)<sub>4</sub>] (22). A dichloromethane (3 mL) solution of PMe<sub>2</sub>Ph (0.0218 g, 0.158 mmol) was added to a dichloromethane (6 mL) solution of 15 (0.171 g, 0.146 mmol) at 23 °C. The yellow-orange solution was stirred for 30 min. Pentane (10 mL) was added resulting in the formation of a red-orange oil. The mixture was stored at -35 °C for 12 h. The oil was separated by decantation, washed with pentane (2 × 10 mL), and dried under vacuum for 5 h to afford an orange solid. Yield: 0.179 g, 0.137 mmol, 93%. <sup>1</sup>H NMR (CD<sub>2</sub>Cl<sub>2</sub>): δ 7.42 (m, 3H, Ph), 7.17 (t, *J* = 8.0 Hz, 2H, Ph), 6.16 (s, 2H, CH), 3.99 (m, 2H, NCH<sub>2</sub>), 3.51 (m, 2H, NCH<sub>2</sub>), 2.28 (s, 6H, CH<sub>3</sub>), 1.42 (d, *J* = 6.4 Hz, 6H, PMe<sub>2</sub>-Ph), 1.26 (s, 2H, ZrCH<sub>2</sub>), 0.78 (s, 9H, CMe<sub>3</sub>). <sup>1</sup>H NMR (-80 °C, CD<sub>2</sub>Cl<sub>2</sub>): δ 7.34 (m, 3H, Ph), 7.02 (m, 2H, Ph), 6.23 (s, 2H, CH), 3.87 (m, 2H, NCH<sub>2</sub>), 3.40 (m, 2H, NCH<sub>2</sub>), 2.28 (s, 6H, CH<sub>3</sub>), 1.49 (d, *J* = 7.9 Hz, 6H, PMe<sub>2</sub>Ph), 1.09 (s, 2H, ZrCH<sub>2</sub>), 0.60 (s, 9H, CMe<sub>3</sub>). <sup>13</sup>C NMR (CD<sub>2</sub>Cl<sub>2</sub>): δ 175.3 (s, CN), 156.2 (q, *J*<sub>CF</sub> = 35.1 Hz, CO), 148.5 (d, *J*<sub>CF</sub> = 242.1 Hz, B(C<sub>6</sub>F<sub>5</sub>)<sub>4</sub><sup>-</sup>), 138.6 (d, *J*<sub>CF</sub> = 244.8 Hz, B(C<sub>6</sub>F<sub>5</sub>)<sub>4</sub><sup>-</sup>), 136.7 (d, *J*<sub>CF</sub> = 243.0 Hz, B(C<sub>6</sub>F<sub>5</sub>)<sub>4</sub><sup>-</sup>), 134.1 (br s, *i*-Ph), 130.5 (br d, *p*-Ph), 130.2 (d, *J* = 157.5 Hz, *o*-Ph), 129.4 (d, *J* = 162.0 Hz, *m*-Ph), 128.7 (br, B(C<sub>6</sub>F<sub>5</sub>)<sub>4</sub><sup>-</sup>), 119.7 (q, *J*<sub>CF</sub> = 277.2 Hz, CF<sub>3</sub>), 107.4 (t, *J* = 107.6 Hz, ZrCH<sub>2</sub>), 104.8 (d, *J* = 166.5 Hz, CH), 53.0 (t, *J* = 138.8 Hz, NCH<sub>2</sub>), 38.2 (s, CMe<sub>3</sub>), 33.1 (q, *J* = 123.5 Hz, CMe<sub>3</sub>), 24.8 (q, *J* = 128.8 Hz, CH<sub>3</sub>), 10.9 (q, *J* = 135.1 Hz, PMe<sub>2</sub>Ph). <sup>19</sup>F NMR (CD<sub>2</sub>Cl<sub>2</sub>): δ -75.2 (s, 6F, CF<sub>3</sub>), -135.9 (br s, 8F, B(C<sub>6</sub>F<sub>5</sub>)<sub>4</sub><sup>-</sup>), -166.4 (t, 4F, *J*<sub>FF</sub> = 20.3 Hz, B(C<sub>6</sub>F<sub>5</sub>)<sub>4</sub><sup>-</sup>), -170.2 (m, 8F, B(C<sub>6</sub>F<sub>5</sub>)<sub>4</sub><sup>-</sup>). <sup>31</sup>P{<sup>1</sup>H} NMR (-80 °C, CD<sub>2</sub>Cl<sub>2</sub>): δ -11.6 (s). Anal. Calcd for C<sub>49</sub>H<sub>34</sub>BF<sub>26</sub>N<sub>2</sub>O<sub>2</sub>Zr: C, 44.93; H, 2.62; N, 2.14. Found: C, 44.74; H, 2.33; N, 2.33.

[(F<sub>6</sub>-acen)Zr(CH<sub>2</sub>CMe<sub>3</sub>)(PMe<sub>2</sub>Ph)]<sub>2</sub>[B(C<sub>6</sub>F<sub>5</sub>)<sub>4</sub>] (23). <sup>1</sup>H NMR (-80 °C, CD<sub>2</sub>Cl<sub>2</sub>): δ 7.54 (m, 6H, Ph), 6.78 (m, 4H, Ph), 5.83 (s, 2H, CH), 3.99 (m, 2H, NCH<sub>2</sub>), 3.40 (m, 2H, NCH<sub>2</sub>), 2.06 (s, 6H, CH<sub>3</sub>), 1.60 (d, *J*<sub>PH</sub> = 5.7 Hz, 6H, PMe<sub>2</sub>Ph), 1.18 (s, 2H, ZrCH<sub>2</sub>), 0.78 (d, *J*<sub>PH</sub> = 5.5 Hz, 6H, PMe<sub>2</sub>Ph), 0.64 (s, 9H, CMe<sub>3</sub>). <sup>31</sup>P{<sup>1</sup>H} NMR (-80 °C, CD<sub>2</sub>Cl<sub>2</sub>): δ -18.5 (d, *J*<sub>PP</sub> = 8.8 Hz), -23.5 (d, *J*<sub>PP</sub> = 9.0 Hz).

[(F<sub>6</sub>-acen)Zr(CH<sub>2</sub>CMe<sub>3</sub>)(NCMe<sub>2</sub>)<sub>2</sub>][B(C<sub>6</sub>F<sub>5</sub>)<sub>4</sub>] (24). Acetonitrile (0.3 mL) was added to a dichloromethane solution (6 mL) of 15 (0.203 g, 0.173 mmol) at 23 °C and the bright yellow solution stirred for 45 min. Hexane (10 mL) was added to precipitate a yellow solid, and the slurry was cooled to -35 °C. The solid was collected by vacuum filtration, washed with hexane (2 × 5 mL), and dried under vacuum (5 h) to afford a yellow powder. Yield: 0.185 g, 0.148 mmol, 85%. <sup>1</sup>H NMR (CD<sub>2</sub>Cl<sub>2</sub>): δ 6.12 (s, 2H, CH), 4.17 (m, 2H, NCH<sub>2</sub>), 3.80 (m, 2H, NCH<sub>2</sub>), 2.35 (s, 6H, CH<sub>3</sub>), 2.19 (s, 6H, CH<sub>3</sub>CN), 1.25 (s, 2H, ZrCH<sub>2</sub>), 0.82 (s, 9H, CMe<sub>3</sub>); <sup>1</sup>H NMR (-90 °C, CD<sub>2</sub>Cl<sub>2</sub>) δ 6.01 (s, 2H, CH), 4.07 (m, 2H, NCH<sub>2</sub>), 3.65 (m, 2H, NCH<sub>2</sub>), 2.34 (s, 3H, CH<sub>3</sub>CN), 2.26 (s, 6H, CH<sub>3</sub>), 2.04 (s, 3H, CH<sub>3</sub>CN), 0.94 (s, 2H, ZrCH<sub>2</sub>), 0.64 (s, 9H, CMe<sub>3</sub>). <sup>13</sup>C NMR (CD<sub>2</sub>Cl<sub>2</sub>): δ 174.1 (s, CN), 156.3 (q, *J*<sub>CF</sub> = 35.1 Hz, CO), 148.5 (d, *J*<sub>CF</sub> = 237.6 Hz, B(C<sub>6</sub>F<sub>5</sub>)<sub>4</sub><sup>-</sup>), 138.5 (d, *J*<sub>CF</sub> = 244.8 Hz, B(C<sub>6</sub>F<sub>5</sub>)<sub>4</sub><sup>-</sup>), 136.7 (d, *J*<sub>CF</sub> = 243.8 Hz, B(C<sub>6</sub>F<sub>5</sub>)<sub>4</sub><sup>-</sup>), 124.2 (br, B(C<sub>6</sub>F<sub>5</sub>)<sub>4</sub><sup>-</sup>), 119.9 (q, *J* = 9.9 Hz, CH<sub>3</sub>CN), 119.7 (q, *J*<sub>CF</sub> = 279.0 Hz, CF<sub>3</sub>), 104.1 (d, *J* = 166.5 Hz, CH), 98.7 (t, *J* = 108.2 Hz, ZrCH<sub>2</sub>), 52.8 (t, *J* = 138.5 Hz, NCH<sub>2</sub>), 37.1 (s, CMe<sub>3</sub>), 33.6 (q, *J* = 123.4 Hz, CMe<sub>3</sub>), 24.3 (qd, *J* = 129.0, 2.9 Hz, CH<sub>3</sub>), 2.0 (q, *J* = 137.1, CH<sub>3</sub>CN). <sup>19</sup>F NMR (CD<sub>2</sub>Cl<sub>2</sub>): δ -77.0 (s, 6F, CF<sub>3</sub>), -135.8 (s, 4F, B(C<sub>6</sub>F<sub>5</sub>)<sub>4</sub><sup>-</sup>), -166.4 (t, *J*<sub>FF</sub> = 19.7 Hz, 4F, B(C<sub>6</sub>F<sub>5</sub>)<sub>4</sub><sup>-</sup>), -170.3 (s,

8F, B(C<sub>6</sub>F<sub>5</sub>)<sub>4</sub><sup>-</sup>). Anal. Calcd for C<sub>45</sub>H<sub>29</sub>BF<sub>26</sub>N<sub>4</sub>O<sub>2</sub>Zr: C, 43.11; H, 2.33; N, 4.47. Found: C, 43.25; H, 2.33; N, 4.24.

[(F<sub>8</sub>-acen)Zr{η<sup>2</sup>-C(=O)CH<sub>2</sub>CMe<sub>3</sub>}(NMe<sub>2</sub>Ph)][B(C<sub>6</sub>F<sub>5</sub>)<sub>4</sub>] (25). Dichloromethane-*d*<sub>2</sub> (0.5 mL) was vacuum transferred at -78 °C into an NMR tube containing solid 11a (0.0454 g, 0.0805 mmol) and [HNMe<sub>2</sub>Ph][B(C<sub>6</sub>F<sub>5</sub>)<sub>4</sub>] (0.0645 g, 0.0805 mmol). The tube was warmed to 23 °C and shaken (10 min) to afford an orange-yellow homogeneous solution. The tube was frozen at -196 °C, exposed to CO (1 atm), and carefully allowed to warm to 23 °C, affording a bright red solution. <sup>1</sup>H NMR (CD<sub>2</sub>Cl<sub>2</sub>, major isomer only): δ 7.32 (t, *J* = 7.3 Hz, 2H, *m*-Ph), 7.16 (t, *J* = 7.3 Hz, 1H, *p*-Ph), 6.94 (d, *J* = 7.5 Hz, 2H, *o*-Ph), 5.92 (s, 2H, CH), 4.22 (m, 2H, NCH<sub>2</sub>), 4.00 (m, 2H, NCH<sub>2</sub>), 2.80 (s, 6H, NMe<sub>2</sub>Ph), 2.69 (s, 2H, C(O)CH<sub>2</sub>), 2.27 (s, 6H, CH<sub>3</sub>), 1.09 (s, 9H, CMe<sub>3</sub>). <sup>13</sup>C NMR (-50 °C, CD<sub>2</sub>Cl<sub>2</sub>): δ 312.0 (s, ZrC(O)), 175.5 (s, CN), 153.9 (q, *J*<sub>CF</sub> = 35.1 Hz, CO), 147.7 (d, *J*<sub>CF</sub> = 238.5 Hz, B(C<sub>6</sub>F<sub>5</sub>)<sub>4</sub><sup>-</sup>), 147.4 (s, *i*-Ph), 137.9 (d, *J*<sub>CF</sub> = 243.0 Hz, B(C<sub>6</sub>F<sub>5</sub>)<sub>4</sub><sup>-</sup>), 136.0 (d, *J*<sub>CF</sub> = 244.8 Hz, B(C<sub>6</sub>F<sub>5</sub>)<sub>4</sub><sup>-</sup>), 129.0 (dd, *J* = 161.1, 7.2 Hz, Ph), 126.0 (d, *J* = 162.9 Hz, Ph), 123.1 (br, B(C<sub>6</sub>F<sub>5</sub>)<sub>4</sub><sup>-</sup>), 119.3 (d, *J* = 156.6 Hz, Ph), 118.8 (q, *J*<sub>CF</sub> = 277.2 Hz, CF<sub>3</sub>), 104.0 (d, *J* = 166.5 Hz, CH), 57.0 (t, *J* = 129.2 Hz, CH<sub>2</sub>), 52.5 (t, *J* = 140.4 Hz, NCH<sub>2</sub>), 45.0 (q, *J* = 138.0 Hz, NMe<sub>2</sub>Ph), 30.7 (s, CMe<sub>3</sub>), 29.4 (q, *J* = 125.5 Hz, CMe<sub>3</sub>), 24.6 (q, *J* = 129.2 Hz, CH<sub>3</sub>).

[(F<sub>8</sub>-acn)Zr(OCPh<sub>2</sub>CH<sub>2</sub>CMe<sub>3</sub>)(O=CPh<sub>2</sub>)][B(C<sub>6</sub>F<sub>5</sub>)<sub>4</sub>] (26). Dichloromethane (15 mL) was added to solid 11a (0.209 g, 0.370 mmol) and [HNMe<sub>2</sub>Ph][B(C<sub>6</sub>F<sub>5</sub>)<sub>4</sub>] (0.296 g, 0.370 mmol) at 23 °C, affording an orange solution which was stirred for 10 min. Solid benzophenone (0.135 g, 0.740 mmol) was added, resulting in a bright red solution which was stirred for 35 min.

The volatiles were removed *in vacuo* to afford a red-brown oily residue, which was washed with benzene (10 mL) and pentane (10 mL). The resulting red oil foamed into an orange solid when dried under vacuum (4 h). Attempted recrystallization from cold CH<sub>2</sub>Cl<sub>2</sub>/toluene resulted in decomposition. <sup>1</sup>H NMR (CD<sub>2</sub>Cl<sub>2</sub>): δ 7.80 (t, *J* = 7.3 Hz, 2H, Ph), 7.64 (d, *J* = 7.3 Hz, 4H, Ph), 7.53 (t, *J* = 7.5 Hz, 4H, Ph), 7.28 (m, 4H, Ph), 7.22 (m, 6H, Ph), 5.78 (s, 2H, CH), 3.43 (m, 2H, NCH<sub>2</sub>), 3.27 (m, 2H, NCH<sub>2</sub>), 2.50 (s, 2H, CH<sub>2</sub>), 2.02 (s, 6H, CH<sub>3</sub>), 0.76 (s, 9H, CMe<sub>3</sub>). <sup>13</sup>C NMR (CD<sub>2</sub>Cl<sub>2</sub>): δ 206.3 (s, Ph<sub>2</sub>C=O), 176.3 (s, CN), 157.1 (q, *J*<sub>CF</sub> = 33.3 Hz, CO), 148.5 (d, *J*<sub>CF</sub> = 238.5 Hz, B(C<sub>6</sub>F<sub>5</sub>)<sub>4</sub><sup>-</sup>), 146.6 (s, *i*-Ph<sub>2</sub>C=O), 138.6 (d, *J*<sub>CF</sub> = 243.0 Hz, B(C<sub>6</sub>F<sub>5</sub>)<sub>4</sub><sup>-</sup>), 136.8 (d, *J*<sub>CF</sub> = 244.8 Hz, B(C<sub>6</sub>F<sub>5</sub>)<sub>4</sub><sup>-</sup>), 136.7 (d, *J* = 159.3 Hz, Ph), 134.8 (t, *J* = 7.2 Hz, *i*-Ph), 132.6 (dt, *J* = 163.8, 7.2 Hz, Ph), 129.4 (dd, *J* = 164.2, 7.2 Hz, Ph), 128.3 (d, *J* = 158.4 Hz, Ph), 127.8 (d, *J* = 160.2 Hz, Ph), 172.1 (d, *J* = 156.6 Hz, Ph), 124.5 (br, B(C<sub>6</sub>F<sub>5</sub>)<sub>4</sub><sup>-</sup>), 119.3 (q, *J*<sub>CF</sub> = 277.2 Hz, CF<sub>3</sub>), 104.3 (d, *J* = 165.6 Hz, CH), 93.1 (s, ZrOC), 53.4 (t, *J* = 122.0 Hz, OC(Ph)<sub>2</sub>CH<sub>2</sub>), 51.8 (t, *J* = 141.7 Hz, NCH<sub>2</sub>), 31.8 (s, CMe<sub>3</sub>), 31.2 (q, *J* = 120.3 Hz, CMe<sub>3</sub>), 23.6 (q, *J* = 128.9 Hz, CH<sub>3</sub>).

**Supplementary Material Available:** Tables of complete bond distances and angles, anisotropic thermal parameters and hydrogen atom coordinates for 11a and 13a and hydrogen atom bond distances and angles, least-squares planes, and torsional angles for 11a (21 pages). Ordering information is given on any current masthead page.

OM940553G

# Radical Processes in the Reduction of Nitrobenzene Promoted by Iron Carbonyl Clusters. X-ray Crystal Structures of $[\text{Fe}_3(\text{CO})_9(\mu_3\text{-NPh})]^{2-}$ , $[\text{HFe}_3(\text{CO})_9(\mu_3\text{-NPh})]^-$ , and the Radical Anion $[\text{Fe}_3(\text{CO})_{11}]^-$

Fabio Ragaini,<sup>†</sup> Jeong-Sup Song, David L. Ramage, and Gregory L. Geoffroy\*

Department of Chemistry, The Pennsylvania State University,  
University Park, Pennsylvania 16802

Glenn A. P. Yap and Arnold L. Rheingold

Department of Chemistry, University of Delaware, Newark, Delaware 19716

Received July 20, 1994<sup>®</sup>

The halides  $\text{Cl}^-$ ,  $\text{Br}^-$ , and  $\text{I}^-$  and the pseudo-halide  $\text{NCO}^-$  react with  $\text{Fe}_3(\text{CO})_{12}$  (**1**) in aprotic solvents to induce a disproportionation reaction yielding the radical anion  $[\text{Fe}_3(\text{CO})_{11}]^-$  (**3**). This species has been fully characterized by single-crystal X-ray diffraction studies of its  $\text{PPh}_4^+$  and  $\text{PPN}^+$  salts, although the latter was disordered. Crystal data for  $\text{PPh}_4^+\cdot\mathbf{3}$ :  $\text{C}_{35}\text{H}_{20}\text{Fe}_3\text{O}_{11}\text{P}$ , monoclinic,  $P2_1/n$ ,  $a = 11.313(2)$ ,  $b = 12.966(3)$ , and  $c = 23.682(5)$  Å,  $\beta = 91.380(9)^\circ$ ,  $V = 3472.8(9)$  Å<sup>3</sup>,  $Z = 4$ ,  $R(F) = 6.73\%$ . In contrast to other related  $\text{Fe}_3$  carbonyl clusters, the structures show that the anion has one semibridging CO and ten terminal CO ligands. Cluster **3** also forms upon reaction of  $[\text{Fe}_3(\text{CO})_{11}]^{2-}$  with  $\text{ArNO}_2$ , and it disproportionates under a CO atmosphere to yield  $\text{Fe}(\text{CO})_5$  and  $[\text{Fe}_3(\text{CO})_{11}]^{2-}$ . The mixed-metal cluster  $\text{Fe}_2\text{-Ru}(\text{CO})_{12}$  also reacts with  $[\text{PPN}]\text{Cl}$  to yield  $[\text{PPN}][\text{Fe}_2\text{Ru}(\text{Cl})(\text{CO})_{10}]$ , a reaction which is similar to that previously observed for  $\text{Ru}_3(\text{CO})_{12}$ . Reaction of  $[\text{Fe}_3(\text{CO})_{11}]^-$  with  $\text{PhNO}$  and  $\text{PhNO}_2$  yields a mixture of clusters which, after workup, gives azo- and azoxybenzene. When  $\text{Cl}_5\text{C}_6\text{-NO}_2$  was used in place of  $\text{PhNO}_2$ , the cluster  $[\text{Fe}_3(\text{CO})_9(\mu_3\text{-NC}_6\text{Cl}_5)]^{2-}$  (**5**) was obtained together with other products. Cluster **5** can be protonated by  $\text{HBF}_4$  to yield  $[\text{HFe}_3(\text{CO})_9(\mu_3\text{-NC}_6\text{Cl}_5)]^-$  (**6**). The non-chlorinated analogue of **5**,  $[\text{PPh}_4]_2[\text{Fe}_3(\text{CO})_9(\mu_3\text{-NPh})]\cdot 2\text{CH}_2\text{Cl}_2$  ( $\text{PPh}_4\cdot\mathbf{8}\cdot 2\text{CH}_2\text{-Cl}_2$ ), has been characterized by an X-ray diffraction study. Crystal data for  $\text{PPh}_4\cdot\mathbf{8}\cdot 2\text{CH}_2\text{-Cl}_2$ :  $P2_1$ ,  $a = 13.065(3)$ ,  $b = 18.114(4)$ , and  $c = 13.618(3)$  Å,  $\beta = 98.93(2)^\circ$ ,  $Z = 2$ ,  $R(F) = 6.94\%$ ,  $R(wF) = 7.30\%$ . The cluster  $[\text{HFe}_3(\text{CO})_{11}]^-$  (**2**) has been found to react with  $\text{PhNO}$  and  $\text{ArNO}_2$  by an initial electron-transfer process to form  $[\text{HFe}_3(\text{CO})_9(\mu_3\text{-NPh})]^-$  (**7**), with  $\text{PhNO}$  giving higher yields. This species has been crystallographically characterized as its  $\text{PPN}^+$  salt: Crystal data for  $\text{PPN}\cdot\mathbf{7}$ :  $P2_1/c$ ,  $a = 15.03(3)$ ,  $b = 21.22(3)$ , and  $c = 16.12(3)$  Å,  $\beta = 106.71(2)^\circ$ ,  $Z = 4$ ,  $R(F) = 10.05\%$ ,  $R(wF) = 11.34\%$ . Cluster **7** reacts with  $\text{PhNO}$  in the presence of radical activators to yield azo- and azoxybenzene. The use of 2-Me-C<sub>6</sub>H<sub>4</sub>NO in this reaction gave only symmetrical azo- and azoxyarenes, implying that these products do not derive from a coupling of the imido fragment in **7** with free  $\text{ArNO}$ . Cluster **7** reacts with water to yield aniline in the presence of  $[\text{Cp}_2\text{Fe}][\text{PF}_6]$  but not in its absence. Competition experiments show that **7** is not a kinetically significant intermediate in the phase-transfer-catalyzed reduction of  $\text{ArNO}_2$  by  $\text{Fe}_3(\text{CO})_{12}$  and imply that radical intermediates are also involved in this reaction.

## Introduction

Reduction and carbonylation of organic nitro compounds are reactions of significant potential synthetic and industrial interest, since many products can be obtained from nitro compounds and CO in a single step, including amines, amides, oximes, ureas, carbamates, isocyanates, and indoles.<sup>1</sup> Many different complexes

have been reported to promote or to catalyze reduction and carbonylation of nitro compounds, with the most efficient metals being palladium, rhodium, and ruthenium. Only limited attention has been given to the study of iron complexes as promoters for these reactions.<sup>2-5</sup> Several iron compounds are known to promote the stoichiometric reduction of nitro compounds,<sup>2-4</sup> but few

<sup>†</sup> On leave from the Dipartimento di Chimica Inorganica, Metallorganica e Analitica and CNR Center, Milano, Italy.

<sup>®</sup> Abstract published in *Advance ACS Abstracts*, December 1, 1994.

(1) Cenini, S.; Pizzotti, M.; Crotti, C. Metal Catalyzed Deoxygenation Reactions by Carbon Monoxide of Nitroso and Nitro Compounds. In *Aspects of Homogeneous Catalysis*; Ugo, R., Ed.; D. Reidel: Dordrecht, The Netherlands, 1988; Vol. 6; pp 97-198.

(2) (a) des Abbayes, H.; Alper, H. *J. Am. Chem. Soc.* **1977**, *99*, 98. (b) Alper, H.; Gopal, M. *J. Chem. Soc., Chem. Commun.* **1980**, 821. (c) Alper, H.; Paik, H.-N. *Nouv. J. Chim.* **1978**, *2*, 245. (d) Alper, H.; Des Roches, D.; des Abbayes, H. *Angew. Chem., Int. Ed. Engl.* **1977**, *16*, 41.

(3) NGuini Effa, J.-B.; Djebaili, B.; Lieto, J.; Aune, J.-P. *J. Chem. Soc., Chem. Commun.* **1983**, 408.

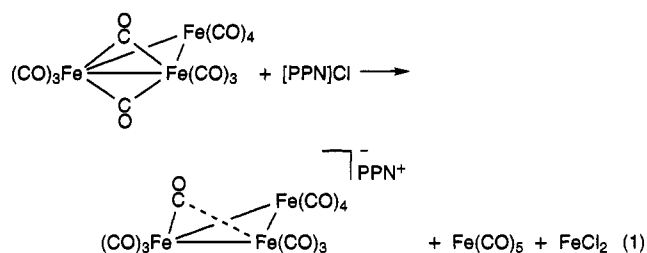
catalytic processes have been reported.<sup>5</sup> Despite the apparent lower efficiency of iron-based catalysts, their use is of interest due to the comparative cost advantage of iron compared to the other metals commonly employed as catalysts for these reactions. Since little is known about the mechanism by which nitro and nitroso compounds react with iron carbonyls, we have initiated an investigation in this area, using  $\text{Fe}_3(\text{CO})_{12}$  (**1**) and  $[\text{HFe}_3(\text{CO})_{11}]^-$  (**2**) as starting compounds. As alkylammonium halides have been shown to be efficient cocatalysts in the related  $\text{Ru}_3(\text{CO})_{12}$ -catalyzed carbonylation of nitrobenzene,<sup>6</sup> we have also investigated the reactivity of  $\text{Fe}_3(\text{CO})_{12}$  with  $[\text{PPN}]\text{X}$  salts ( $\text{X} = \text{Cl}^-$ ,  $\text{Br}^-$ ,  $\text{I}^-$ ,  $\text{NCO}^-$ ;  $\text{PPN}^+ = (\text{PPh}_3)_2\text{N}^+$ ). As described herein, this has led to the isolation of the radical anion cluster  $[\text{Fe}_3(\text{CO})_{11}]^{\cdot-}$  (**3**) as  $\text{PPN}^+$  or  $\text{PPh}_4^+$  salts, both of which have been crystallographically characterized.

The full characterization of  $[\text{Fe}_3(\text{CO})_{11}]^{\cdot-}$  is of significance in itself, since numerous studies in recent years have demonstrated the importance of free-radical processes in organometallic chemistry, including a number of catalytic reactions known or proposed to involve radical intermediates.<sup>7</sup> However, few of these intermediates have been definitively characterized, and because of their elusive nature it has seldom proven possible to conduct detailed investigations of their chemical behavior. One of the radical anions that has been invoked in a number of reactions is  $[\text{Fe}_3(\text{CO})_{11}]^{\cdot-}$ . This cluster radical anion has been observed during the reaction of  $\text{Fe}_3(\text{CO})_{12}$  with nitro- and nitrosoparaffins under conditions similar to those used for  $\text{Fe}_3(\text{CO})_{12}$ -catalyzed carbonylation of these reagents.<sup>8</sup> The anion  $[\text{Fe}_3(\text{CO})_{11}]^{\cdot-}$  has also been invoked as a key intermediate in the electron-transfer-catalyzed substitution reactions of  $\text{Fe}_3(\text{CO})_{12}$ .<sup>9,10</sup> This anion has been claimed to form in a number of ways, including reduction of  $\text{Fe}(\text{CO})_5$  and  $\text{Fe}_3(\text{CO})_{12}$ ,<sup>11,12</sup> oxidation of the anion  $[\text{Fe}_3(\text{CO})_{11}]^{2-}$  (**4**),<sup>11</sup> electron transfer between  $\text{Fe}_3(\text{CO})_{12}$  and  $[\text{Fe}_3(\text{CO})_{11}]^{2-}$ ,<sup>13</sup> disproportionation of  $\text{Fe}_3(\text{CO})_{12}$  induced by strong bases

and basic solvents such as DMF,<sup>14–16</sup> and  $^{60}\text{Co}$  radiolysis of  $\text{Fe}_3(\text{CO})_{12}$  and  $[\text{HFe}_3(\text{CO})_{11}]^-$ .<sup>11c,17</sup> Although it appears to have been isolated on two occasions,<sup>13</sup> it has only been characterized by its EPR data<sup>11</sup> and even that has been disputed.<sup>12</sup> The isolation and characterization of  $[\text{Fe}_3(\text{CO})_{11}]^{\cdot-}$  should now make possible detailed explorations of the mechanistic and reaction chemistry of this important species. In this paper, we also report the results of an investigation of the reactivity of  $[\text{Fe}_3(\text{CO})_{11}]^{\cdot-}$  with nitro and nitroso organic compounds. Part of the results reported herein have been previously communicated in a preliminary form.<sup>18</sup>

## Results and Discussion

**Synthesis of  $[\text{Fe}_3(\text{CO})_{11}]^{\cdot-}$  (**3**).** Alkylammonium halides are known to strongly enhance the activity of  $\text{Ru}_3(\text{CO})_{12}$  as catalyst for the carbonylation of nitro organic compounds to the corresponding carbamates.<sup>6a</sup> Although the reactions of halides with  $\text{Ru}_3(\text{CO})_{12}$  are now well understood,<sup>19,20</sup> the corresponding reactivity of  $\text{Fe}_3(\text{CO})_{12}$  (**1**) with halides has not been well developed.<sup>21</sup> We have found that  $[\text{Ph}_4\text{P}]\text{Cl}$  and the  $[\text{PPN}]^+$  salts of  $\text{Cl}^-$ ,  $\text{Br}^-$ ,  $\text{I}^-$ , and  $\text{NCO}^-$  react with **1** to induce a disproportionation reaction to form the radical anion  $[\text{Fe}_3(\text{CO})_{11}]^{\cdot-}$  (**3**),  $\text{Fe}(\text{CO})_5$ , and  $\text{FeX}_n$  salts as principal products, e.g., eq 1. Trace amounts of other anionic



clusters have also been observed, among which the most

(4) (a) Landesberg, J. M.; Katz, L.; Olsen, C. *J. Org. Chem.* **1972**, *37*, 930. (b) Boldrini, G. P.; Umani-Ronchi, A.; Panunzio, M. *J. Organomet. Chem.* **1979**, *171*, 85.

(5) (a) Knifton, J. F. *J. Org. Chem.* **1976**, *41*, 1200. (b) Cann, K.; Cole, T.; Slegier, W.; Pettit, R. *J. Am. Chem. Soc.* **1978**, *100*, 3969. (c) Alper, H.; Hashem, K. E. *J. Am. Chem. Soc.* **1981**, *103*, 6514. (d) Kmiecik, J. E. *J. Org. Chem.* **1965**, *30*, 2014.

(6) (a) Cenini, S.; Crotti, C.; Pizzotti, M.; Porta, F. *J. Org. Chem.* **1988**, *53*, 1243. (b) Han, S.-H.; Song, J.-S.; Macklin, P. D.; Nguyen, S. T.; Geoffroy, G. L.; Rheingold, A. L. *Organometallics* **1989**, *8*, 2127.

(7) (a) Chanon, M.; Julliard, M.; Poite, J. C., Eds. *Paramagnetic Organometallic Species in Activation/Selectivity, Catalysis*; NATO ASI Series C257; Kluwer Academic Publishers: Dordrecht, The Netherlands, 1989. (b) Trogler, W. C., Ed. *Organometallic Radical Processes*; Journal of Organometallic Chemistry Library 22; Elsevier: Amsterdam, 1990. (c) Chanon, M. *Acc. Chem. Res.* **1987**, *20*, 214. (d) Julliard, M.; Chanon, M. *Chem. Rev.* **1983**, *83*, 425. (e) Tyler, D. F. *Prog. Inorg. Chem.* **1988**, *36*, 125.

(8) Belousov, Yu. A.; Kolosova, T. A. *Polyhedron* **1987**, *6*, 1959.

(9) Bruce, M. I.; Hambley, T. W.; Nicholson, B. K. *J. Chem. Soc., Dalton Trans.* **1983**, 2385.

(10) Luo, F.-H.; Yang, S.-R.; Li, C.-S.; Duan, J.-P.; Cheng, C.-H. *J. Chem. Soc., Dalton Trans.* **1991**, 2435.

(11) (a) Krusic, P. J. *Int. Conf. EPR Spectrosc.* **1978**. (b) Krusic, P. J.; San Filippo, J., Jr.; Hutchinson, B.; Hance, R. L.; Daniels, L. M. *J. Am. Chem. Soc.* **1981**, *103*, 2129. (c) Morton, J. R.; Preston, K. F.; Charland, J.-P.; Krusic, P. J. *J. Mol. Struct.* **1990**, *223*, 115.

(12) Dawson, P. A.; Peake, B. M.; Robinson, B. H.; Simpson, J. *Inorg. Chem.* **1980**, *19*, 465.

(13) (a) Chini, P. *J. Organomet. Chem.* **1980**, *200*, 37. (b) Furuya, F. R.; Gladfelter, W. L. *J. Chem. Soc., Chem. Commun.* **1986**, 129.

(14) Babain, V. N.; Belousov, Yu. A.; Gumenyuk, V. V.; Salimov, R. M.; Materikova, R. B.; Kochetkova, N. S. *J. Organomet. Chem.* **1983**, *241*, C41.

(15) Yang, S. L.; Li, C. S.; Cheng, C. H. *J. Chem. Soc., Chem. Commun.* **1987**, 1872.

(16) Other studies in these laboratories have shown that phosphinimines,  $\text{R}_3\text{P}=\text{NR}'$ , efficiently induce disproportionation of  $\text{Fe}_3(\text{CO})_{12}$  to form  $[\text{Fe}_3(\text{CO})_{11}]^{\cdot-}$  as the  $[\text{R}_3\text{P}-\text{NHR}']^+$  salt: Nguyen, S. T.; Mirkin, C. A.; Ragaini, F.; Geoffroy, G. L. Unpublished results.

(17) Peake, B. M.; Symons, M. C. R.; Wyatt, J. L. *J. Chem. Soc., Dalton Trans.* **1983**, 1171.

(18) Ragaini, F.; Ramage, D. L.; Song, J.-S.; Geoffroy, G. L.; Rheingold, A. L. *J. Am. Chem. Soc.* **1993**, *115*, 12183.

(19) (a) Han, S.-H.; Geoffroy, G. L.; Dombeck, B. D.; Rheingold, A. L. *Inorg. Chem.* **1988**, *27*, 4355. (b) Lavigne, G.; Kaesz, H. D. *J. Am. Chem. Soc.* **1984**, *106*, 4647. (c) Lavigne, G.; Lugan, N.; Bonnet, J.-J. *Inorg. Chem.* **1987**, *26*, 2345. (d) Rivomanana, S.; Lavigne, G.; Lugan, N.; Bonnet, J.-J. *Organometallics* **1991**, *10*, 2285. (e) Lavigne, G.; Lugan, N.; Kalck, P.; Soulié, J. M.; Lerouge, O.; Saillard, J. Y.; Halet, J. F. *J. Am. Chem. Soc.* **1992**, *114*, 10669. (f) Cenini, S.; Pizzotti, M.; Crotti, C.; Ragaini, F.; Porta, F. *J. Mol. Catal.* **1988**, *49*, 59. (g) Chin-Choy, T.; Harrison, W. T. A.; Stucky, G. D.; Keder, N.; Ford, P. C. *Inorg. Chem.* **1989**, *28*, 2028. (h) Lillis, J.; Rokicki, A.; Chin, T.; Ford, P. C. *Inorg. Chem.* **1983**, *32*, 5040.

(20) For recent reviews, see: (a) Ford, P. C.; Rokicki, A. *Adv. Organomet. Chem.* **1988**, *28*, 139. (b) Lavigne, G.; Kaesz, H. D. In *Metal Clusters in Catalysis*; Gates, B., Guzzi, L., Knözinger, H., Eds.; Elsevier: Amsterdam, 1986; Chapter 4, pp 43–88. (c) Lavigne, G. In *The Chemistry of Metal Cluster Complexes*; Shriver, D., Adams, R. D., Kaesz, H. D., Eds.; VCH: New York, 1990; Chapter 5, pp 201–303.

(21) In ref 19a, it was noted that  $\text{Fe}_3(\text{CO})_{12}$  reacted with  $[\text{PPN}]\text{I}$  in refluxing THF to form  $[\text{PPN}][\text{HFe}_3(\text{CO})_{11}]$  and  $[\text{PPN}][\text{Fe}(\text{CO})_4]$ , but the presence of 5–10% MeOH in commercial  $\text{Fe}_3(\text{CO})_{12}$  is likely responsible for those results which differ from those reported herein.

abundant was  $[\text{PPN}]_2[\text{Fe}_4(\text{CO})_{13}]$ .<sup>22</sup> These disproportionation reactions occur in thoroughly dried THF,  $\text{CH}_2\text{Cl}_2$ , and  $\text{Et}_2\text{O}$  solvents, with the latter found to be best for isolation of the product, since all other byproducts are insoluble in this solvent except for  $\text{Fe}(\text{CO})_5$ , which is easily removed by evaporation. The reaction with  $[\text{PPN}]\text{Cl}$  is much faster in THF ( $\sim 10$  min) than in  $\text{Et}_2\text{O}$  ( $\sim 1.5$  h), which is likely due to the limited solubility of  $[\text{PPN}]\text{Cl}$  in the latter solvent. The reactions with  $[\text{PPN}]\text{Br}$  and  $[\text{PPN}]\text{I}$  were slower than the corresponding reaction with  $[\text{PPN}]\text{Cl}$  when run in THF ( $\sim 30$  and  $75$  min, respectively) but proceeded at comparable rates in  $\text{Et}_2\text{O}$ . The lower nucleophilicity of  $\text{Br}^-$  and  $\text{I}^-$  in nonprotic solvents like THF or ether, with respect to  $\text{Cl}^-$ , it most likely compensated in this case by the higher solubility of the corresponding PPN salts. The yields for the reactions in  $\text{Et}_2\text{O}$  were comparable for all the anions and were near 50% in each case (see Experimental Section).

The residue from the reaction of  $\text{Fe}_3(\text{CO})_{12}$  with  $[\text{PPN}]\text{NCO}$ , after extraction with THF, was shown to contain the  $[\text{PPN}]^+$  salt of the known<sup>23</sup> anion  $[\text{Fe}(\text{NCO})_4]^-$  by comparison of its IR spectra (Nujol mull,  $\nu_{\text{NCO}} = 2189$   $\text{cm}^{-1}$ ;  $\text{MeNO}_2$ ,  $\nu_{\text{NCO}} = 2195$   $\text{cm}^{-1}$ ) to those reported<sup>23</sup> and by the presence of a molecular ion for the anion at  $M^- = 224$  in its negative ionization FAB mass spectrum. The identification of  $\text{FeCl}_2$  in the residue from the reaction of  $\text{Fe}_3(\text{CO})_{12}$  with  $[\text{PPN}]\text{Cl}$  was less certain, but the presence of a shoulder at  $494$   $\text{cm}^{-1}$  on the  $499$   $\text{cm}^{-1}$   $[\text{PPN}]^+$  peak in the KBr IR spectrum of the tan residue compares to the  $493.2$   $\text{cm}^{-1}$  band reported for  $\text{FeCl}_2$ .<sup>24</sup> This shoulder is not observed in the KBr IR spectrum of pure  $[\text{PPN}]\text{Cl}$ .

By running the disproportionation reaction under various solvent and concentration conditions, we observed an inhibiting effect by small amounts of CO, such as those which are formed during the reaction itself. This effect was only observed when the reaction was run in  $\text{Et}_2\text{O}$  with a high concentration of the reagents (1 g of  $\text{Fe}_3(\text{CO})_{12}$  in 100 mL of  $\text{Et}_2\text{O}$ ) and was particularly evident when  $[\text{PPh}_4]\text{Cl}$  was used. Under these conditions, the reaction stopped completely after consumption of about half of the reagents, but it could be started again by bubbling nitrogen through the solution. Under the same conditions, but using  $[\text{PPN}]\text{Cl}$  instead of  $[\text{PPh}_4]\text{Cl}$ , the reaction only slowed, taking several hours to reach completion, but it did not completely stop. Even in this case, however, it was possible to appreciably increase the rate of the reaction by bubbling nitrogen through the solution at regular intervals of time.<sup>25</sup> This effect was not noted when the reaction was conducted in THF or  $\text{CH}_2\text{Cl}_2$ , which is likely due to the higher solubility of the alkylammonium salts in these solvents. Although our data are not sufficient to indicate a specific mechanism for the formation of  $[\text{Fe}_3(\text{CO})_{11}]^-$ , it is clear from the CO inhibiting effect that one of the earliest stages of the reaction must be

the formation of a complex from which the halide ligand can be displaced by CO to re-form  $\text{Fe}_3(\text{CO})_{12}$ . From the reactivity data and by analogy with the corresponding reactions of  $\text{Ru}_3(\text{CO})_{12}$ ,<sup>19,20</sup> this complex is likely to be  $[\text{Fe}_3(\text{X})(\text{CO})_{11}]^-$  ( $\text{X} = \text{Cl}, \text{Br}, \text{I}, \text{NCO}$ ). The presence of a larger amount of CO (1 atm) induced different reactivity, as described below.

The  $[\text{PPN}]^+$  and  $[\text{PPh}_4]^+$  salts of the radical anion  $[\text{Fe}_3(\text{CO})_{11}]^-$  (**3**) are stable in the crystalline state under  $\text{N}_2$  for several days, but THF solutions decompose over the course of 1–2 days to yield  $[\text{PPN}][\text{HF}_3(\text{CO})_{11}]$  (**PPN-2**),<sup>26</sup>  $\text{Fe}(\text{CO})_5$ , and  $[\text{PPN}]_2[\text{Fe}_4(\text{CO})_{13}]$ .<sup>22,27</sup> The anion **2** likely forms via hydrogen atom abstraction from THF, a conclusion supported by the observation that its formation was completely suppressed when  $[\text{Fe}_3(\text{CO})_{11}]^-$  was allowed to decompose in benzene solution, whereas the two other products were still formed.

Addition of CO (1 atm) to solutions of  $[\text{Fe}_3(\text{CO})_{11}]^-$  induced its immediate disproportionation to form mainly  $\text{Fe}(\text{CO})_5$  and  $[\text{Fe}_3(\text{CO})_{11}]^{2-}$  (**4**).<sup>28</sup> The same two products were also obtained when  $\text{Fe}_3(\text{CO})_{12}$  was allowed to react with halides under a CO atm, although the intermediate formation of  $[\text{Fe}_3(\text{CO})_{11}]^-$  was not directly observed in this latter reaction. The disappearance of  $\text{Fe}_3(\text{CO})_{12}$  was  $\sim 3$  times faster when the halide reactions were performed under a CO atm. This rate acceleration contrasts with the inhibition of the reaction by low amounts of CO and suggests the involvement of an autocatalytic reaction in which the initially formed radical anion **3** reacts with CO to yield radical species of lower nuclearity which readily transfer an electron either to  $\text{Fe}_3(\text{CO})_{12}$ , regenerating **3**, or to another molecule of **3**, generating  $[\text{Fe}_3(\text{CO})_{11}]^{2-}$ .<sup>29</sup> The first possibility should be most favored until almost all of the starting  $\text{Fe}_3(\text{CO})_{12}$  has been consumed, and under a CO atm only a small amount of halide is needed to initiate an autocatalytic reaction which eventually consumes all of the starting cluster.

The EPR signal obtained from  $[\text{PPN}][\text{Fe}_3(\text{CO})_{11}]$ , (**PPN-3**)  $\{g(\text{THF}, -78^\circ\text{C}) = 2.0489\}$  compares well with data previously reported for radical anion  $[\text{Fe}_3(\text{CO})_{11}]^-$ .<sup>11</sup> In its IR spectrum, **3** shows only terminal carbonyl bands [ $\nu_{\text{CO}}(\text{THF}) = 2057$  (vw), 2017 (w), 1984 (vs), 1966 (ms), 1933 (mw), 1922 (w, sh)  $\text{cm}^{-1}$ ], and the spectrum is identical to the spectra produced upon reacting together equimolar amounts of  $[\text{PPN}]_2[\text{Fe}_3(\text{CO})_{11}]$  and  $\text{Fe}_3(\text{CO})_{12}$  and upon oxidation of  $[\text{Fe}_3(\text{CO})_{11}]^{2-}$ , routes which have been used previously to prepare **3**.<sup>11,13</sup> The absence of an IR band in the region characteristic of bridging CO's is in accord with the solid state structure described below which shows 10 terminal carbonyls and 1 weakly semibridging CO (see Figure 1).

(26) (a) Dahl, L. F.; Blount, J. F. *Inorg. Chem.* **1965**, *4*, 1373. (b) Hodali, H. A.; Arcus, C.; Shriver, D. F. *Inorg. Synth.* **1980**, *20*, 218.

(27) Although no other product was observed by IR, some non-carbonyl compound is probably formed, since additional CO is necessary to complete the disproportionation of  $[\text{Fe}_3(\text{CO})_{11}]^-$  into  $\text{Fe}(\text{CO})_5$  and  $[\text{Fe}_4(\text{CO})_{13}]^{2-}$ .

(28) (a) Lo, F. Y.-K.; Longoni, G.; Chini, P.; Lower, L. D.; Dahl, L. F. *J. Am. Chem. Soc.* **1980**, *102*, 7691. (b) Hodali, H. A.; Shriver, D. F. *Inorg. Synth.* **1980**, *20*, 222.

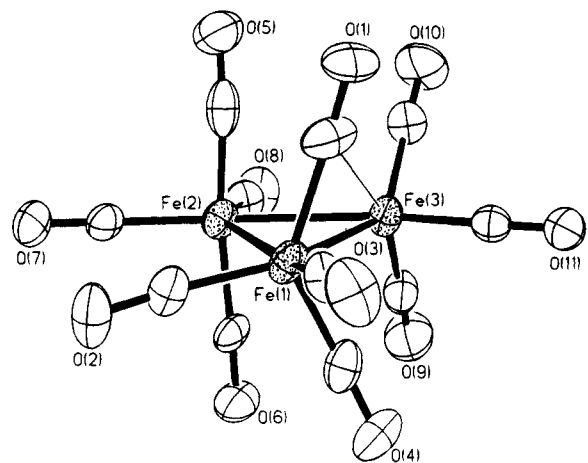
(29) (a) For related reactions see refs 9, 10, and 15. In ref 15, reaction of  $\text{Fe}_3(\text{CO})_{12}$  with CO to yield  $\text{Fe}(\text{CO})_5$  was reported to be catalyzed by an electron-transfer path and  $[\text{Fe}_3(\text{CO})_{11}]^-$  was detected by EPR, along with  $[\text{Fe}_3(\text{CO})_{12}]^-$  and  $[\text{Fe}_2(\text{CO})_8]^-$ . (b)  $[\text{Fe}_3(\text{CO})_{11}]^-$  can be produced upon reduction of  $\text{Fe}_3(\text{CO})_{12}$  in the absence of CO since under these conditions insufficient CO is released in the transformation of  $[\text{Fe}_3(\text{CO})_{12}]^-$  into  $[\text{Fe}_3(\text{CO})_{11}]^-$  to induce further fragmentation of the latter species.

(22) Whitmire, K.; Ross, J.; Cooper, C. B., III; Shriver, D. F. *Inorg. Synth.* **1982**, *21*, 66.

(23) Forster, D.; Goodgame, D. M. L. *J. Chem. Soc.* **1965**, 262.

(24) Jacox, M. E.; Milligan, D. E. *J. Chem. Phys.* **1969**, *51*, 4143.

(25) Continuous bubbling of  $\text{N}_2$  through the solution during the entire reaction led to irreproducible results, since much of the  $\text{Et}_2\text{O}$  solvent evaporated under these conditions and had to be readded periodically. Also, evaporation of the solvent caused a marked decrease in the temperature of the solution. This inhibiting effect by CO was also clearly observed when the weak base  $\text{R}_3\text{P}=\text{NR}'$  was used to induce the disproportionation of  $\text{Fe}_3(\text{CO})_{12}$  (see ref 16).



**Figure 1.** ORTEP drawing of  $[\text{PPh}_4][\text{Fe}_3(\text{CO})_{11}](\text{PPh}_4 \cdot 3)$  with thermal ellipsoids drawn at the 30% probability level.

### X-ray Crystal Structure of $[\text{PPh}_4][\text{Fe}_3(\text{CO})_{11}]$ .

Despite the high reactivity of  $[\text{Fe}_3(\text{CO})_{11}]^-$ , X-ray-quality crystals of its  $[\text{PPN}]^+$  and  $[\text{PPh}_4]^+$  salts were obtained by slow diffusion of pentane into  $-70^\circ\text{C}$   $\text{Et}_2\text{O}$  solutions of the salts. Both salts were characterized by X-ray diffraction studies, although the  $[\text{PPN}]^+$  salt was disordered and produced a lower quality structure (see supplementary material). An ORTEP drawing of the  $[\text{Fe}_3(\text{CO})_{11}]^-$  anion in the  $[\text{PPh}_4]^+$  salt is shown in Figure 1, and the relevant crystallographic data are set out in Tables 1 and 2. Unlike the related  $\text{Fe}_3$  carbonyl clusters  $\text{Fe}_3(\text{CO})_{12}$ ,<sup>30</sup>  $[\text{Fe}_3(\text{CO})_{11}]^{2-}$ ,<sup>28</sup> and  $[\text{HF}_3(\text{CO})_{11}]^-$ <sup>26</sup> which display 2-fold symmetry and have bridging CO's,  $[\text{Fe}_3(\text{CO})_{11}]^-$  is without symmetry and possesses only a very weakly semibridging CO. The semibridged Fe(1)–Fe(3) bond distance of 2.503(2) Å is significantly shorter than the Fe(1)–Fe(2) and Fe(2)–Fe(3) distances, which are more typical of Fe–Fe single bond values.<sup>30</sup> The CO groups at Fe(2) are arranged in the expected axial (5, 6) and equatorial (7, 8) arrangements. However, the presence of the unsymmetrical bridge has caused a tilting of CO(1) away from an axial position toward Fe(3), while the nearly equatorial plane for CO(2) and CO(3) is twisted so as to bring CO(1) closer and CO(4) further from Fe(3). The geometry at Fe(3) is roughly trigonal bipyramidal. The absence of a full bridging CO ligand was unexpected. It is generally considered that an increase in the negative charge on a cluster leads to an increased tendency for carbonyl ligands to display a bridging coordination mode. However, in the structure of  $[\text{Fe}_3(\text{CO})_{11}]^-$  the opposite trend is observed with respect to  $\text{Fe}_3(\text{CO})_{12}$ , which, at least in the solid state, has two bridging carbonyl ligands. It is to be noted that the "normal" tendency is again observed with the dianion  $[\text{Fe}_3(\text{CO})_{11}]^{2-}$ , which has two bridging and one semibridging CO ligands.

Overall, the determined structure is in excellent agreement with that proposed on the basis of a single-crystal EPR study of PPN·3 doped into crystals of  $[\text{PPN}][\text{HF}_3(\text{CO})_{11}]$ ,<sup>11c</sup> which, along with EPR studies of <sup>57</sup>Fe-enriched **3**, led to the conclusion that the unpaired electron was localized on a single iron atom.<sup>11</sup> This is a remarkable feature since unpaired spin density is usually considered to be quite delocalized over several

**Table 1.** Crystallographic Data for  $[\text{PPh}_4][\text{Fe}_3(\text{CO})_{11}](\text{PPh}_4 \cdot 3)$ ,  $[\text{PPN}][\text{HF}_3(\text{CO})_9(\mu_3\text{-NPh})]$  (PPN·7), and  $[\text{PPh}_4]_2[\text{Fe}_3(\text{CO})_9(\mu_3\text{-NPh})] \cdot 2\text{CH}_2\text{Cl}_2$  ( $\text{PPh}_4 \cdot 8 \cdot 2\text{CH}_2\text{Cl}_2$ )

	PPh <sub>4</sub> ·3	PPN·7	PPh <sub>4</sub> ·8·2CH <sub>2</sub> Cl <sub>2</sub>
(a) Crystal Parameters			
formula	C <sub>35</sub> H <sub>20</sub> Fe <sub>3</sub> O <sub>11</sub> P	C <sub>51</sub> H <sub>36</sub> Fe <sub>3</sub> N <sub>2</sub> O <sub>9</sub> P <sub>2</sub>	C <sub>65</sub> H <sub>49</sub> Cl <sub>4</sub> Fe <sub>3</sub> NO <sub>9</sub> P <sub>2</sub>
fw	815.0	1050.3	1247.64
cryst sys	monoclinic	monoclinic	monoclinic
space group	<i>P</i> 2 <sub>1</sub> / <i>n</i>	<i>P</i> 2 <sub>1</sub> / <i>c</i>	<i>P</i> 2 <sub>1</sub>
<i>a</i> , Å	11.313(2)	15.03(3)	13.065(3)
<i>b</i> , Å	12.966(3)	21.22(3)	18.114(4)
<i>c</i> , Å	23.682(5)	16.12(3)	13.618(3)
β, deg	91.380(9)	106.71(2)	98.93(2)
<i>V</i> , Å <sup>3</sup>	3472.8(9)	4922(15)	3184(1)
<i>Z</i>	4	4	2
<i>D</i> (calcd)	1.559	1.417	1.301
μ(Mo Kα), cm <sup>-1</sup>	13.42	9.94	5.10
temp, K	213	296	295
size, mm	0.12 × 0.32 × 0.58	0.10 × 0.20 × 0.40	0.30 × 0.34 × 0.36
color	burgundy	red	deep red
<i>T</i> (max)/ <i>T</i> (min)	1.21	1.10	1.16
(b) Data Collection			
diffractometer	Siemens R3m/V	Siemens R3m/V	Nicolet P3
monochromator		graphite	
wavelength, Å		0.710 73	
radiation		Mo Kα	
scan method		ω	
scan limits, deg	4–55	4–45	4–45
data collected	±14, +16, +30	±16, +22, +17	±15, +20, +15
( <i>h</i> , <i>k</i> , <i>l</i> )			
rflns collcd	8537	6687	4865
indpdt rflns	7974	6419	4298
obs rflns	3410 ( <i>n</i> = 5)	2791 ( <i>n</i> = 4)	3133 ( <i>n</i> = 4)
( <i>F</i> <sub>o</sub> ≥ <i>σ</i> ( <i>F</i> <sub>o</sub> ))			
std rflns		3 std/197 rflns	
var in stds, %	1–2	1–2	<1
(c) Refinement			
<i>R</i> ( <i>F</i> ), %	6.73	10.05	6.94
<i>R</i> ( <i>wF</i> ), %	8.05	11.34	7.30
GOF	1.37	2.07	1.84
Δσ(max)	0.41	0.004	0.02
Δ(ρ), eÅ <sup>-3</sup>	1.96	1.32	0.76
<i>N</i> <sub>o</sub> / <i>N</i> <sub>v</sub>	8.5	9.1	6.5

$$^a R(F) = \sum(|F_o| - |F_c|) / \sum|F_o|; R(wF) = \sum(w^{1/2}(|F_o| - |F_c|)) / (\sum(w^{1/2}|F_o|));$$

$$\text{GOF} = [\sum w(|F_o| - |F_c|)^2 / (N_o - N_v)]^{1/2}.$$

**Table 2.** Selected Bond Lengths and Angles for  $[\text{PPh}_4][\text{Fe}_3(\text{CO})_{11}](\text{PPh}_4 \cdot 3)$

Bond Lengths (Å)			
Fe(1)–Fe(2)	2.685(2)	Fe(1)–Fe(3)	2.503(2)
Fe(2)–Fe(3)	2.630(2)	Fe(1)–C(1)	1.885(12)
Fe(3)–C(1)	2.488(11)	C(1)–O(1)	1.34(13)
Bond Angles (deg)			
Fe(2)–Fe(1)–Fe(3)	60.8(1)	Fe(1)–Fe(2)–Fe(3)	56.2(1)
Fe(1)–Fe(3)–Fe(2)	63.0(1)	Fe(3)–Fe(1)–C(1)	67.4(4)
Fe(2)–Fe(1)–C(1)	88.1(3)	Fe(1)–C(1)–O(1)	168.1(10)
Fe(3)–C(1)–O(1)	122.8(9)		

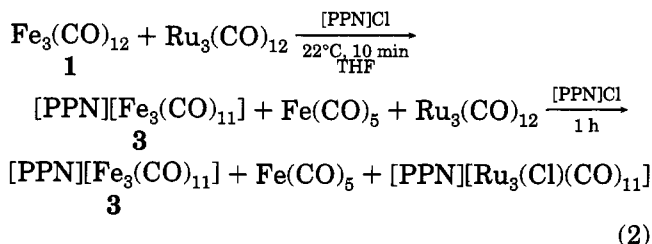
atoms in a metal cluster. By comparison, the related, but likely more symmetrical, radical anion cluster  $[\text{Fe}_3(\text{CO})_{12}]^-$  showed no indication of charge localization.<sup>11b</sup> The crystallographic results presented here combined with these EPR data<sup>11</sup> suggest that in  $[\text{Fe}_3(\text{CO})_{11}]^-$  the unpaired electron is likely localized on the unique trigonal bipyramidal Fe(CO)<sub>3</sub> center {Fe(3) in Figure 1}.

**Comparison of the Reactivity of  $\text{Fe}_3(\text{CO})_{12}$ ,  $\text{Ru}_3(\text{CO})_{12}$ , and  $\text{Fe}_2\text{Ru}(\text{CO})_{12}$  with  $[\text{PPN}]\text{Cl}$ .** Now that the separate reactions of  $[\text{PPN}]\text{Cl}$  with  $\text{Ru}_3(\text{CO})_{12}$ <sup>19,20</sup> and  $\text{Fe}_3(\text{CO})_{12}$  are well understood, it is of interest to compare the relative reactivity of these two clusters with each other and with the mixed-metal

(30) (a) Cotton, F. A.; Troup, J. M. *J. Am. Chem. Soc.* **1974**, *96*, 4155.  
(b) Braga, D.; Farrugia, L.; Grepioni, F.; Johnson, B. F. G. *J. Organomet. Chem.* **1994**, *464*, C39.

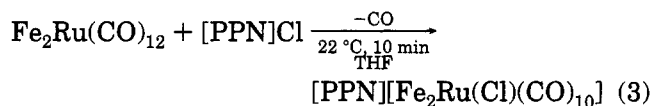


cluster  $\text{Fe}_2\text{Ru}(\text{CO})_{12}$ .<sup>31</sup> When a mixture of  $\text{Fe}_3(\text{CO})_{12}$  and  $\text{Ru}_3(\text{CO})_{12}$  was allowed to react with  $[\text{PPN}]\text{Cl}$  in THF, the results shown in eq 2 were obtained, which



show that at room temperature mixtures of these two clusters react independently with chloride and that  $\text{Fe}_3(\text{CO})_{12}$  reacts faster than does  $\text{Ru}_3(\text{CO})_{12}$ . After 10 min, IR analysis indicated that all of the  $\text{Fe}_3(\text{CO})_{12}$  had been consumed with the formation of  $[\text{Fe}_3(\text{CO})_{11}]^-$  and  $\text{Fe}(\text{CO})_5$  but the  $\text{Ru}_3(\text{CO})_{12}$  was largely unchanged. However, upon continued stirring,  $\text{Ru}_3(\text{CO})_{12}$  reacted with chloride to produce  $[\text{Ru}_3(\text{Cl})(\text{CO})_{11}]^-$  which then slowly converted to  $[\text{Ru}_3(\mu\text{-Cl})(\text{CO})_{10}]^-$ , in accord with the literature.<sup>19a,g</sup>

Reaction of  $\text{Fe}_2\text{Ru}(\text{CO})_{12}$  with  $[\text{PPN}]\text{Cl}$  in THF yielded a new cluster believed to be  $[\text{PPN}][\text{Fe}_2\text{Ru}(\text{Cl})(\text{CO})_{10}]$  on the basis of its IR and negative ionization FAB mass spectra and of its elemental analysis (eq 3). This



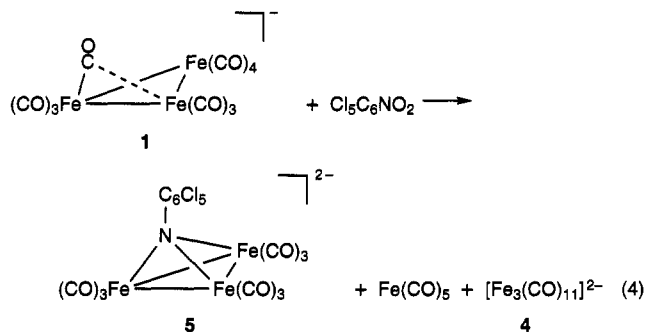
reaction closely parallels the known reactivity of  $\text{Ru}_3(\text{CO})_{12}$  with  $[\text{PPN}]\text{Cl}$ <sup>19,20</sup> but differs significantly from the above-described reaction of  $\text{Fe}_3(\text{CO})_{12}$  with chloride. No evidence was obtained for the formation of radical species in the combination of  $\text{Fe}_2\text{Ru}(\text{CO})_{12}$  with  $[\text{PPN}]\text{Cl}$ ,<sup>32</sup> indicating that the formation of a radical anion cluster is peculiar to  $\text{Fe}_3(\text{CO})_{12}$  within this general cluster family.

**Reactivity of  $[\text{Fe}_3(\text{CO})_{11}]^-$  with Nitro and Nitroso Organic Compounds.** It is known that the dianion  $[\text{Fe}_3(\text{CO})_{11}]^{2-}$  readily forms upon reduction of  $\text{Fe}_3(\text{CO})_{12}$  (**1**) by  $\text{OH}^-$  or by disproportionation of **1** induced by strong bases<sup>14,28</sup> under conditions similar to those employed during the catalytic carbonylation of  $\text{PhNO}_2$  to methyl phenylcarbamate by  $\text{Fe}_3(\text{CO})_{12}/\text{CH}_3\text{O}^-$ .<sup>5c</sup> The dianion  $[\text{Fe}_3(\text{CO})_{11}]^{2-}$  has also been suggested to form during the phase-transfer-catalyzed reduction of nitro aromatic compounds to the corresponding anilines by  $\text{Fe}_3(\text{CO})_{12}/\text{OH}^-$ .<sup>2a,c,d</sup> An EPR study of the reaction of the dianion  $[\text{Fe}_3(\text{CO})_{11}]^{2-}$  with  $\text{PhNO}$  and  $\text{PhNO}_2$  has previously indicated the formation of the radical anion  $[\text{Fe}_3(\text{CO})_{11}]^-$  and other products.<sup>8</sup> However, since EPR is such a sensitive technique for detecting minute quantities of radical species, it could be argued that  $[\text{Fe}_3(\text{CO})_{11}]^-$  is formed only in very small amounts during the aforementioned reaction. To test if  $[\text{Fe}_3(\text{CO})_{11}]^-$  is formed in significant quantities under these conditions, we performed the reaction of  $[\text{Me}_3\text{NCH}_2\text{Ph}]_2[\text{Fe}_3(\text{CO})_{11}]$  (**Me**<sub>3</sub>NCH<sub>2</sub>Ph-**4**) with excess

$\text{PhNO}_2$  in THF.<sup>33</sup> Although the reaction was complex, IR analysis indicated that the radical anion  $[\text{Fe}_3(\text{CO})_{11}]^-$  was clearly the dominant product during the first few reaction minutes.

Having thus shown that  $[\text{Fe}_3(\text{CO})_{11}]^-$  (**3**) is formed in relevant amounts under conditions similar to those used in different reducing systems, it is now important to understand the nature of its reactions with nitro and nitroso organic compounds. It was observed that reaction of  $\text{PhNO}$  or  $\text{PhNO}_2$  in THF with pure **PPN-3** or with the solution obtained by mixing  $\text{Fe}_3(\text{CO})_{12}$  with  $[\text{PPN}]\text{Cl}$ , led to the formation of a mixture of clusters and  $\text{Fe}(\text{CO})_5$ . Chromatography of this mixture on silica gel led to the isolation of azo- and azoxybenzene in low yields. However, these two organic compounds are not direct products of the reaction, since they were not found in the hexane extract of the reaction residue before chromatography. Also isolated after chromatography were  $\text{Fe}_3(\text{CO})_{12}$  and  $[\text{PPN}][\text{HF}_3(\text{CO})_{11}]$  as the major iron-containing products.

In order to obtain more stable products from the above described reactions, we turned to the use of pentachloronitrobenzene in place of unsubstituted nitrobenzene. This approach was partly successful, although the reaction was still found to be extremely sensitive to even minor variations in the experimental conditions (THF or  $\text{Et}_2\text{O}$  solvent; rate of reagent addition and concentrations;  $\text{PPN}^+$  or  $\text{PPh}_4^+$  cations). Apart from  $\text{Fe}(\text{CO})_5$ , which always formed in large amounts, one product which formed under nearly all conditions was a new carbonyl cluster (**5**), which is proposed on the basis of evidenced described below to be the dianion  $[\text{Fe}_3(\text{CO})_9(\mu_3\text{-NC}_6\text{Cl}_5)]^{2-}$  with a  $\mu_3$ -imido ligand (eq 4). This species



was insoluble in  $\text{Et}_2\text{O}$  but was soluble in THF in which it showed IR bands at 1995 (w), 1929 (vs), 1898 (m), and 1871 (w). The pattern of this spectrum is very similar to that of  $\text{Fe}_3(\text{CO})_{10}(\mu_3\text{-NPh})$ ,<sup>34</sup> but the most intense band is shifted by more than  $100 \text{ cm}^{-1}$  to lower frequencies in **5** and the absorption at  $1736 \text{ cm}^{-1}$  in the spectrum of  $\text{Fe}_3(\text{CO})_{10}(\mu_3\text{-NPh})$  which is attributed to a triply-bridging CO is missing in the spectrum of **5**. The IR band pattern was also nearly superimposable on the spectrum of an independently synthesized sample of  $[\text{Me}_3\text{NCH}_2\text{Ph}]_2[\text{Fe}_3(\text{CO})_9(\mu_3\text{-O})]$ ,<sup>35</sup> although all of the IR bands of **5** were shifted to lower frequencies by about  $5 \text{ cm}^{-1}$ . An even better agreement exists between the IR

(33) The trimethylbenzylammonium salt of **4** was used instead of the corresponding  $\text{PPN}^+$  or  $\text{PPh}_4^+$  salts because the last two are nearly insoluble in THF.

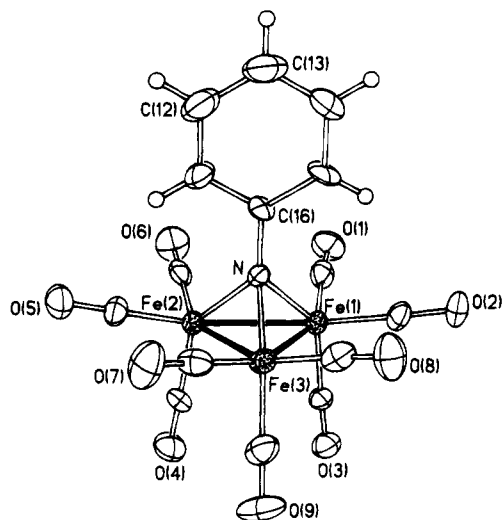
(34) Andrews, M. A.; Kaesz, H. D. *J. Am. Chem. Soc.* **1979**, *101*, 7255.

(35) Ceriotti, A.; Resconi, L.; Demartin, F.; Longoni, G.; Manassero, M.; Sansoni, M. *J. Organomet. Chem.* **1983**, *249*, C35.

(31) Yawney, D. B. W.; Stone, F. G. A. *J. Chem. Soc. A* **1969**, 502.

(32) During the first minutes of the reaction, formation of an intermediate product was observed by IR, which then disappeared yielding  $[\text{Fe}_2\text{Ru}(\text{Cl})(\text{CO})_{10}]^-$ . This cluster is suggested to be  $[\text{Fe}_2\text{Ru}(\text{Cl})(\text{CO})_{11}]^-$  by analogy with the corresponding reactions of  $\text{Ru}_3(\text{CO})_{12}$ .<sup>19g</sup>





**Figure 2.** ORTEP drawing of  $[\text{PPh}_4]_2[\text{Fe}_3(\text{CO})_9(\mu_3\text{-NPh})] \cdot 2\text{CH}_2\text{Cl}_2$  ( $\text{PPh}_4 \cdot 8 \cdot 2\text{CH}_2\text{Cl}_2$ ) with thermal ellipsoids drawn at the 30% probability level.

frequencies of **5** (in THF) and those reported for  $[\text{Et}_4\text{N}]_2[\text{Fe}_3(\text{CO})_9(\mu_3\text{-S})]$  in acetone.<sup>36</sup> In the  $^{13}\text{C}$  NMR spectrum of **5**, signals for the  $-\text{NC}_6\text{Cl}_5$  group were observed at  $\delta$  143.5, 131.5, and 116.9 (THF- $d_6$ ), with the fourth expected resonance probably obscured by the more intense signals of the  $\text{PPN}^+$  cation. These resonances compare to the  $\delta$  147.9, 136.5, 133.7, and 124.9 ( $\text{CD}_2\text{-Cl}_2$ ) resonances of  $\text{Cl}_5\text{C}_6\text{NO}_2$ . These various spectroscopic data strongly suggest for **5** the formulation  $[\text{Fe}_3(\text{CO})_9(\mu_3\text{-NC}_6\text{Cl}_5)]^{2-}$ . Despite an intense effort, **5** could not be obtained in an analytically pure form as either  $\text{PPN}^+$  or  $\text{PPh}_4^+$  salts. An impurity was always present, apparently  $[\text{Fe}_4(\text{CO})_{13}]^{2-}$  (see also later), which was indicated in the IR spectrum of **5** by a variable intensity shoulder at  $1945\text{ cm}^{-1}$  on the  $1929\text{ cm}^{-1}$  band.

Further support for the proposed formulation of **5** as  $[\text{Fe}_3(\text{CO})_9(\mu_3\text{-NC}_6\text{Cl}_5)]^{2-}$  comes from its protonation reactions. Treatment of **5** with  $\text{HBF}_4$  in THF, followed by evaporation of the solvent and extraction with  $\text{Et}_2\text{O}$ , afforded a new cluster **6**, whose IR band pattern ( $\nu_{\text{CO}}$  (THF) = 2048 (w), 2010 (s), 1981 (vs), 1963 (ms), 1645 (m), 1914 (w)  $\text{cm}^{-1}$ ) was nearly superimposable on the spectrum of  $[\text{HFe}_3(\text{CO})_9(\mu_3\text{-NPh})]^-$  (**7**; see later), although the bands were shifted  $\sim 5\text{ cm}^{-1}$  to higher energy in **6**. The negative ionization FAB mass spectrum of  $\text{PPN} \cdot \mathbf{6}$  showed a parent peak at  $M^- = 684$  with an isotopic intensity pattern in excellent agreement with that calculated for  $[\text{HFe}_3(\text{CO})_9(\mu_3\text{-NC}_6\text{Cl}_5)]^-$ . THF extraction of the residue obtained after the initial  $\text{Et}_2\text{O}$  extraction showed the presence of a mixture of clusters, among which  $[\text{Fe}_4(\text{CO})_{13}]^{2-}$  was identified as the predominant species by comparison of its IR spectrum with that of an independently synthesized sample.<sup>22</sup>

Although X-ray-quality crystals of **5** could not be obtained, its structure is likely similar to that of the corresponding non-chlorinated analogue  $[\text{PPh}_4]_2[\text{Fe}_3(\text{CO})_9(\mu_3\text{-NPh})]$  ( $\text{PPh}_4 \cdot \mathbf{8}$ ), which was serendipitously obtained in these laboratories and was structurally characterized (see Figure 2 and below). A few crystals of this latter compound formed during recrystallization

of the reaction mixture resulting from addition of methoxide ion to  $\text{Fe}_3(\text{CO})_{10}(\mu_3\text{-NPh})$ .<sup>37</sup> The formation of dianionic  $\mu_3$ -imido  $\text{Fe}_3$  clusters such as **5** or **8** is unprecedented, although many neutral or monoanionic trinuclear iron,<sup>34,38</sup> ruthenium,<sup>6b,39</sup> and osmium<sup>40</sup> clusters having one or two capping imido groups have been reported.

As previously mentioned, the reaction of  $[\text{Fe}_3(\text{CO})_{11}]^{+}$  with  $\text{Cl}_5\text{C}_6\text{NO}_2$  is extremely sensitive to the experimental conditions. In addition to  $[\text{Fe}_3(\text{CO})_9(\mu_3\text{-NC}_6\text{Cl}_5)]^{2-}$  (**5**), several other carbonyl clusters formed in irreproducible yields and were not characterized. The position of the IR bands of these compounds indicates that at least some are dianionic, and one compound which could be identified is  $[\text{Fe}_3(\text{CO})_{11}]^{2-}$  (**4**). This cluster was obtained in the highest yields by slowly adding dropwise an  $\text{Et}_2\text{O}$  solution of  $\text{Cl}_5\text{C}_6\text{NO}_2$  to an  $\text{Et}_2\text{O}$  solution of  $[\text{PPh}_4][\text{Fe}_3(\text{CO})_{11}]$  ( $\text{PPh}_4 \cdot \mathbf{3}$ ), with only about a third of the stoichiometric amount of  $\text{Cl}_5\text{C}_6\text{NO}_2$  required to consume all of **3**. However, only a very small amount of **4** was produced when  $\text{PPN} \cdot \mathbf{3}$  was used instead of  $\text{PPh}_4 \cdot \mathbf{3}$ , all other conditions being similar. The observation of **4** in these reactions raised the possibility that  $[\text{Fe}_3(\text{CO})_9(\mu_3\text{-NC}_6\text{Cl}_5)]^{2-}$  (**5**) could derive from the reaction of  $\text{Cl}_5\text{C}_6\text{NO}_2$  with **4**, rather than directly from **3**. However, it was observed that the direct reaction of  $\text{Cl}_5\text{C}_6\text{NO}_2$  with  $\text{Me}_3\text{NCH}_2\text{Ph} \cdot \mathbf{4}$  gave in the initial stages essentially only formation of **3**. Only after most of the starting **4** was consumed, did the concentration of **3** decrease. Thus, **5** does not derive directly from **4** but must be obtained through a more complex pathway.

**Reactions of  $[\text{HFe}_3(\text{CO})_{11}]^-$  (**2**) with  $\text{PhNO}$  and  $\text{PhNO}_2$ .** In addition to  $\text{Fe}_3(\text{CO})_{12}$ , another iron complex that has been often used as a reducing agent for organic nitro compounds is  $[\text{HFe}_3(\text{CO})_{11}]^-$  (**2**). This cluster is known to promote the reduction of nitrobenzene to aniline both directly<sup>4b</sup> and when supported on organic polymers.<sup>3</sup> It has also been suggested to be formed and to be the active reductant in several systems in which  $\text{Fe}_3(\text{CO})_{12}$  was used as the iron source.<sup>2,4a</sup> The anion  $[\text{HFe}_3(\text{CO})_{11}]^-$  has also been reported to react with nitrobenzene to afford  $[\text{HFe}_3(\text{CO})_9(\mu_3\text{-NPh})]^-$  in poor yields,<sup>34</sup> but this product was not well characterized in that study.

Since reactions of nitro and nitroso organic compounds have been shown in several cases to proceed through an intermediate electron-transfer process,<sup>8,41</sup> we decided to investigate if this was the case for the reactions of  $[\text{HFe}_3(\text{CO})_{11}]^-$ . To avoid any uncertainty connected with the use of EPR spectroscopy to detect

(37) Song, J.-S.; Geoffroy, G. L. Unpublished results.

(38) (a) Clegg, W.; Sheldrick, G. M.; Stalke, D.; Bhaduri, S.; Khwaja, H. K. *Acta Crystallogr.* **1984**, *C40*, 2045. (b) Aime, S.; Gervasio, G.; Milone, L.; Rossetti, R.; Stanghellini, P. L. *J. Chem. Soc., Dalton Trans.* **1978**, 534. (c) Williams, G. D.; Whittle, R. R.; Geoffroy, G. L.; Rheingold, A. L. *J. Am. Chem. Soc.* **1987**, *109*, 3936. (d) Bockman, T. M.; Wang, Y.; Kochi, J. K. *New J. Chem.* **1988**, *12*, 387. (e) Song, J.-S.; Han, S.-H.; Nguyen, S. T.; Geoffroy, G. L.; Rheingold, A. L. *Organometallics* **1990**, *9*, 2386.

(39) Bruce, I. M.; Cifuentes, M. P.; Humphrey, M. G. *Polyhedron* **1991**, *10*, 277 and references therein.

(40) (a) Smeieja, J. A.; Gladfelter, W. L. *Inorg. Chem.* **1986**, *25*, 2667. (b) Ramage, D. L.; Geoffroy, G. L.; Rheingold, A. L.; Haggerty, B. S. *Organometallics* **1992**, *11*, 1242.

(41) (a) Sherlock, S. J.; Boyd, D. C.; Moasser, B.; Gladfelter, W. L. *Inorg. Chem.* **1991**, *30*, 3626. (b) Kunin, A. G.; Noiro, M. D.; Gladfelter, W. L. *J. Am. Chem. Soc.* **1989**, *111*, 2739. (c) Ragaini, F.; Cenini, S.; Demartin, F. *J. Chem. Soc., Chem. Commun.* **1992**, 1467. (d) Ragaini, F.; Cenini, S.; Demartin, F. *Organometallics* **1994**, *13*, 1178. (e) Berman, R. S.; Kochi, J. K. *Inorg. Chem.* **1980**, *19*, 248.

(36) Markó, L.; Takács, J.; Papp, S.; Markó-Monostory, B. *Inorg. Chim. Acta* **1980**, *45*, L189. (b) The corresponding Se and Te analogues have been recently reported and their crystal structures solved: Bachman, R. E.; Whitmire, K. H. *Inorg. Chem.* **1994**, *33*, 2527.



**Table 3. Selected Bond Lengths and Angles for [PPN][HF<sub>3</sub>(CO)<sub>9</sub>(μ<sub>3</sub>-NPh)] (PPN-7)**

Bond Lengths (Å)			
Fe(1)–Fe(2)	2.559(7)	Fe(1)–N(1)	1.918(15)
Fe(1)–Fe(3)	2.498(7)	Fe(2)–N(1)	1.914(18)
Fe(2)–Fe(3)	2.487(7)	Fe(3)–N(1)	1.908(15)
Bond Angles (deg)			
Fe(1)–Fe(2)–Fe(3)	59.3(2)	Fe(1)–N(1)–Fe(3)	81.5(6)
Fe(1)–Fe(3)–Fe(2)	61.8(2)	Fe(1)–N(1)–Fe(2)	83.8(7)
Fe(2)–Fe(1)–Fe(3)	58.9(2)	Fe(2)–N(1)–Fe(3)	81.2(7)
N(1)–Fe(1)–Fe(2)	48.0(5)	N(1)–Fe(2)–Fe(3)	49.3(5)
N(1)–Fe(1)–Fe(3)	49.1(5)	N(1)–Fe(2)–Fe(1)	48.2(4)
N(1)–Fe(3)–Fe(1)	49.4(4)	N(1)–Fe(3)–Fe(2)	49.5(6)

**Table 4. Selected Bond Lengths and Angles for [PPh<sub>4</sub>]<sub>2</sub>[Fe<sub>3</sub>(CO)<sub>9</sub>(μ<sub>3</sub>-NPh)]·2CH<sub>2</sub>Cl<sub>2</sub> (PPh<sub>4</sub>·8·2CH<sub>2</sub>Cl<sub>2</sub>)**

Bond Lengths (Å)			
Fe(1)–Fe(2)	2.515(2)	Fe(1)–N	1.923(10)
Fe(1)–Fe(3)	2.517(3)	Fe(2)–N	1.911(11)
Fe(2)–Fe(3)	2.508(3)	Fe(3)–N	1.909(11)
Bond Angles (deg)			
Fe(1)–Fe(2)–Fe(3)	60.1(1)	Fe(1)–N–Fe(3)	82.1(4)
Fe(1)–Fe(3)–Fe(2)	60.1(1)	Fe(1)–N–Fe(2)	82.0(4)
Fe(2)–Fe(1)–Fe(3)	59.8(1)	Fe(2)–N–Fe(3)	82.1(4)
N–Fe(1)–Fe(2)	48.8(3)	N–Fe(2)–Fe(3)	48.9(3)
N–Fe(1)–Fe(3)	48.7(3)	N–Fe(2)–Fe(1)	49.2(3)
N–Fe(3)–Fe(1)	49.2(3)	N–Fe(3)–Fe(2)	49.0(3)

shown in Figures 2 and 3, respectively, and the relevant crystallographic data are set out in Tables 1–4. Each of the anions consists of a triangle of Fe atoms capped by a μ<sub>3</sub>-NPh ligand and with each iron atom additionally coordinated with three CO ligands. In **7**, the Fe(1)–Fe(2) vector is bridged by a hydride ligand which was located by difference Fourier analysis and fixed. The Fe(1)–Fe(2) distance of 2.559(7) Å is longer than the 2.492 Å average of the Fe(1)–Fe(3) and Fe(2)–Fe(3) distances, consistent with the hydride ligand bridging this bond. In **8**, the Fe–Fe distances average 2.513 Å. Excluding the hydride-bridged Fe–Fe bond in **7**, all of the Fe–Fe distances in both anions are significantly shorter than the average Fe–Fe distance in Fe<sub>3</sub>(CO)<sub>12</sub> (2.639 Å)<sup>30</sup> but are similar to the 2.484 Å average Fe–Fe distance in [Fe<sub>3</sub>(CO)<sub>9</sub>(μ<sub>3</sub>-O)]<sup>2-</sup><sup>35</sup> and the 2.453 average Fe–Fe bonding distances in Fe<sub>3</sub>(CO)<sub>9</sub>(μ<sub>3</sub>-NPh)<sub>2</sub>.<sup>38a</sup> The Fe–N distances in **7** and **8** each average 1.914 Å which are shorter than the 1.946 Å average Fe–N distance in doubly-bridged Fe<sub>3</sub>(CO)<sub>9</sub>(μ<sub>3</sub>-NPh)<sub>2</sub>.<sup>38a</sup> The similarity of the Fe–N distances in these two compounds indicates that the presence of the hydride ligand in **7** does not significantly weaken the adjacent Fe–N bonds.

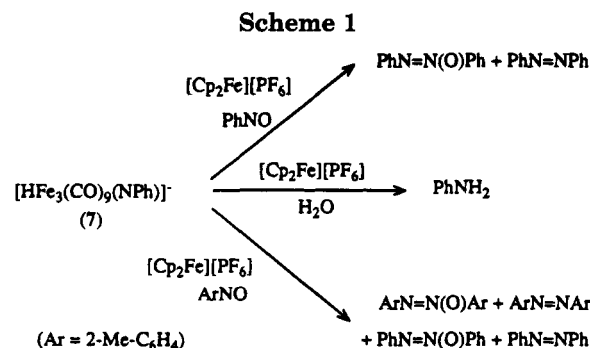
**Reactivity of [HF<sub>3</sub>(CO)<sub>9</sub>(μ<sub>3</sub>-NPh)]<sup>-</sup> (**7**) with ArNO and Water.** It was noted above that azo- and azoxybenzene were observed as byproducts during the reaction of [HF<sub>3</sub>(CO)<sub>11</sub>]<sup>-</sup> (**2**) with PhNO. Since the major organometallic product of this reaction is [HF<sub>3</sub>(CO)<sub>9</sub>(μ<sub>3</sub>-NPh)]<sup>-</sup> (**7**), we considered the possibility that the azo- and azoxybenzene could be produced via reaction of the excess PhNO present with this species. The reaction of **7** with PhNO was thus investigated under a variety of conditions with monitoring by IR and gas chromatography. First it was observed that addition of a 1.1:1 molar amount of PhNO (either as a solid or dissolved in THF) to a solution of **7** in THF gave an immediate reaction which was complete in less than 20 min and which consumed only a part of the added PhNO. Approximately equimolar amounts of azo- and azoxybenzene were formed in this reaction. However,

only a very small decrease in the intensity of the IR bands of **7** was observed, and a small amount of an insoluble dark material was formed. The reaction stopped completely after the first ~20 min, and no variation in the concentration of the reagents was observed over the further course of several hours, despite the fact that most of the starting **7** and PhNO were still present. Addition of further aliquots of PhNO gave the same effect. Part of the newly added PhNO was immediately consumed, but the reaction then stopped again. As more PhNO was added, the percentage of azoxybenzene in the product decreased in favor of azoxybenzene, which eventually became the only observable product (by GC) at later stages of the process.

It was further observed that after the reaction had stopped in one of the intermediate stages described above, it could be started again by adding small amounts of a one-electron oxidant such as AgBF<sub>4</sub> or [Cp<sub>2</sub>Fe][PF<sub>6</sub>]. The latter was found to be more efficient, and about 9 equiv of PhNO was consumed per 1 equiv of [Cp<sub>2</sub>Fe][PF<sub>6</sub>]. Some **7** also decomposed to yield an insoluble dark product, but the amount of **7** which reacted was much lower than the amount of PhNO consumed and appeared similar to the equivalents of added [Cp<sub>2</sub>Fe][PF<sub>6</sub>]. The fact that [Cp<sub>2</sub>Fe][PF<sub>6</sub>] is acting as an oxidant was confirmed by the detection of ferrocene in the gas chromatogram of the reaction mixture. However, an exact ratio of the amount of **7** consumed to the amount of [Cp<sub>2</sub>Fe][PF<sub>6</sub>] added could not be determined due to the uncertainty in the measurement of the absorbance of the IR bands of **7** compared to the higher precision of the gas chromatographic analysis. In separate experiments, it was shown that no reaction at all occurred between [Cp<sub>2</sub>Fe][PF<sub>6</sub>] and PhNO under similar reaction conditions except with no **7** present. As long as carefully dried solvents and glassware were used in the above reactions, no aniline was detected, although this species did form in small amounts if trace water was present. In the presence of a large amount of water in a two-phase system, [Cp<sub>2</sub>Fe][PF<sub>6</sub>] was ineffective as an oxidant.

We interpret the above observations as indicating that **7** and PhNO do not react with each other, at least at room temperature, in the absence of some "activator". The [Cp<sub>2</sub>Fe][PF<sub>6</sub>] experiments indicate that this activator is an oxidizing agent which presumably abstracts an electron from [HF<sub>3</sub>(CO)<sub>9</sub>(μ<sub>3</sub>-NPh)]<sup>-</sup> (**7**) to form highly reactive organometallic products which react with several equivalents of PhNO to form azo- and azoxybenzene. The reactivity observed after each addition of PhNO in the absence of an intentionally added oxidizing agent may be attributed to the presence of oxidizing impurities in the PhNO reactant or the admission of adventitious oxidizing agent during the addition step. The reaction stops once these impurities have been consumed and the organometallic compounds derived from the oxidation of **7** have decomposed to unreactive insoluble products.

We have considered the possibility that some or all of the azo- and azoxybenzene formed in the above reactions could derive from coupling of the phenylimido fragment in [HF<sub>3</sub>(CO)<sub>9</sub>(μ<sub>3</sub>-NPh)]<sup>-</sup> (**7**) with free PhNO. As a test for this possibility, we reacted **7** with 2-Me-C<sub>6</sub>H<sub>4</sub>NO to see if the mixed derivatives 2-Me-C<sub>6</sub>H<sub>4</sub>N=NPh and 2-Me-C<sub>6</sub>H<sub>4</sub>N(O)=NPh would form.

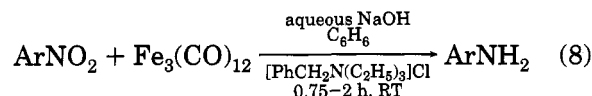


The reaction proceeded as in the case of PhNO, with several additions of small amounts of  $[\text{Cp}_2\text{Fe}][\text{PF}_6]$  being necessary to drive the reaction to completion. GC-MS analysis of the organic products showed the formation of all of the *symmetrical* azo- and azoxy derivatives ( $\text{PhN}=\text{NPh}$ ,  $\text{PhN}(\text{O})=\text{NPh}$ , 2-Me- $\text{C}_6\text{H}_4\text{N}=\text{NC}_6\text{H}_4$ -2-Me, and 2-Me- $\text{C}_6\text{H}_4\text{N}(\text{O})=\text{NC}_6\text{H}_4$ -2-Me) but only a trace of 2-Me- $\text{C}_6\text{H}_4\text{N}=\text{NPh}$  ( $\sim 0.3\%$  with respect to  $\text{PhN}(\text{O})=\text{NPh}$ ), and no mixed azoxybenzene was produced. This result clearly implies that the azo- and azoxyarene products *do not* derive from coupling of the imido fragment with free nitrosoarene. The reaction is clearly more complex, but our data are insufficient to assess the details, except to imply that radical intermediates are involved.<sup>43</sup> The results described in this section are summarized in Scheme 1.

Having described the reactivity of  $[\text{HFe}_3(\text{CO})_9(\mu_3\text{-NPh})]^-$  (**7**) with nitrosobenzenes, we can now analyze in more detail the reaction of  $[\text{HFe}_3(\text{CO})_{11}]^-$  (**2**) with PhNO. As noted above, the evidence indicates that reaction of **2** with PhNO proceeds through an intermediate electron-transfer process, and some radical clusters must be formed initially. We have also shown that radical clusters are also implicated in the formation of azo- and azoxybenzene from **7** and PhNO and that azo- and azoxybenzene are formed even in the reaction of **2** with PhNO. The effect of slowly adding PhNO *versus* adding it all at once for **2** is opposite that for **7**. For **2**, addition of PhNO all at once causes an increase in its consumed amount and a decrease in the yield of **7**, whereas for preformed **7** the reaction rapidly stops after consumption of only a small amount of PhNO. A larger amount reacts when the addition is slow. This suggests that the formation of azo- and azoxybenzene from **2** does not derive from a following reaction of **7** but that it is promoted by some radical complexes before the final formation of the stable diamagnetic product (Scheme 2). In this reaction scenario, trapping of a radical cluster by free PhNO to generate azo- or azoxybenzene would be in competition with radical pair cage collapse to yield **7**, thus explaining the selectivity effect observed. It should be noted that the reactions on the right side of the scheme consume more PhNO and do not produce **7**. A decrease in the concentration of PhNO in solution is also proposed to favor reduction by CO with respect to oxidation of an iron center. Dissolution of CO into solution is in fact much too slow to be relevant for a reaction that is complete in a few minutes. This effect of the rate of addition of PhNO closely parallels that reported by Pettit *et al.*,<sup>5b</sup> who noted that the  $\text{Fe}(\text{CO})_5$ -

promoted reduction of nitrobenzene by  $\text{CO}/\text{H}_2\text{O}$  ( $P_{\text{CO}} = 1700$  psi) to aniline can be run in a catalytic way with respect to the iron compound provided PhNO<sub>2</sub> is added slowly (10–12 h) to the reaction vessel. An explanation similar to that discussed herein was given for that effect. Our observation of a low efficiency of an atmospheric pressure of CO in preventing iron oxidation is also in agreement with the previously reported fact that the yield of aniline in the phase-transfer-catalyzed reduction of PhNO<sub>2</sub> by  $\text{Fe}_3(\text{CO})_{12}$  was even lower when the reaction was run under CO rather than under a nitrogen atmosphere.<sup>2c</sup>

**Examination of the Role of  $[\text{HFe}_3(\text{CO})_9(\mu_3\text{-NPh})]^-$  (**7**) in the Reduction of PhNO<sub>2</sub> to PhNH<sub>2</sub> Promoted by Iron Clusters.** The cluster anion  $[\text{HFe}_3(\text{CO})_9(\mu_3\text{-NPh})]^-$  (**7**) (although originally represented with a terminal rather than a triply bridging imido group) has been proposed to be an intermediate in the phase-transfer-catalyzed reduction of substituted nitrobenzenes to the corresponding anilines by  $\text{Fe}_3(\text{CO})_{12}$  (eq 8).<sup>2a,c</sup> This cluster was also directly observed by IR



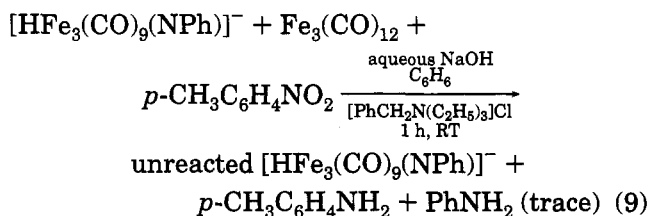
during the reaction when  $[\text{HFe}_3(\text{CO})_{11}]^-$  (**2**) supported over a poly(styrene-divinylbenzene) membrane functionalized with  $-\text{NR}_3^+$  groups was used as a reducing agent for nitrobenzene.<sup>3</sup> However, the experimental conditions of this latter procedure are very different from those of the previous one, since the reaction was performed by passing a gas stream of PhNO<sub>2</sub> over the solid support containing **2**.

Isolation of **7** in a pure form allowed us to test its involvement in these reactions. The surprising finding was that **7** was completely unreactive under the same experimental conditions in which the phase-transfer-catalyzed reduction of  $\text{ArNO}_2$  by  $\text{Fe}_3(\text{CO})_{12}$  was performed. This is in accord with the fact that protonation of **7** would be necessary to induce further reaction, but **7** is an extremely weak base. It had been previously reported that **7** can be protonated by phosphoric acid to yield  $\text{H}_2\text{Fe}_3(\text{CO})_9(\mu_3\text{-NPh})$ .<sup>34</sup> In the course of this study, we have verified that such a strong acid is required to effect this reaction, and even a medium-strength acid such as  $\text{CF}_3\text{COOH}$  is completely ineffective in protonating **7**. Thus it is extremely unlikely that protonation of **7** occurs under the basic conditions used in the reduction of  $\text{ArNO}_2$ .

Since we have shown that **7** can be activated by radical species and that radicals are formed during the

(43) Formation of mixed azoxybenzenes has been previously observed by one of us in related reactions of several mononuclear systems.<sup>41d</sup>

reactions of  $[\text{HFe}_3(\text{CO})_{11}]^-$  (**2**) and  $[\text{Fe}_3(\text{CO})_{11}]^{2-}$  (**4**) with  $\text{ArNO}_2$ , it may be argued that **7** is indeed an intermediate in the reduction of  $\text{ArNO}_2$  and that it is then activated by radicals formed at other stages of the reaction. To test this hypothesis, we reacted **7** and  $\text{Fe}_3(\text{CO})_{12}$  together with *p*-Me-C<sub>6</sub>H<sub>4</sub>NO<sub>2</sub> under phase-transfer-catalyzed conditions similar to those previously reported.<sup>2a</sup> Whereas *p*-Me-C<sub>6</sub>H<sub>4</sub>NO<sub>2</sub> was completely converted to *p*-Me-C<sub>6</sub>H<sub>4</sub>NH<sub>2</sub>, cluster **7** was recovered almost quantitatively, and only a very small amount of aniline was found among the products (eq 9).



We thus conclude that **7** is not a kinetically relevant intermediate in the phase-transfer-catalyzed reduction of  $\text{ArNO}_2$  by  $\text{Fe}_3(\text{CO})_{12}$ , although it is possible that it is involved in a secondary pathway. Concerning the role of  $[\text{HFe}_3(\text{CO})_{11}]^-$  (**2**), our data do not allow a definitive conclusion. The observed reactivity for **2** implies that it could be an intermediate in the reduction of nitrobenzene. However, it has been proposed that  $[\text{Fe}_3(\text{CO})_{11}]^{2-}$  (**4**) is an intermediate in the formation of **2** from  $\text{Fe}_3(\text{CO})_{12}$ ,<sup>2a,c,d,44</sup> and since **4** reacts quickly with  $\text{ArNO}_2$  to generate  $[\text{Fe}_3(\text{CO})_{11}]^-$  (**3**), it is possible that **2** is not formed in the presence of  $\text{ArNO}_2$  and that the reaction proceeds through **4** and **3**. Protonation of one reaction intermediate (likely a nitrogen-containing cluster) by water could then occur at a later stage in the process. It should be noted that formation of the N-H bond does not need to occur by a direct protonation. Since some of the radical cluster involved are surely neutral species, they should be easily attacked by  $\text{OH}^-$  present in the reaction medium, ultimately yielding  $\text{CO}_2$  and a hydride ligand, which may later transfer to nitrogen. The reaction pathways involving **2** or **3** and **4** are not mutually exclusive, and both may operate under the usual reaction conditions.

We now turn to the possible involvement of  $[\text{HFe}_3(\text{CO})_9(\mu_3\text{-NPh})]^-$  (**7**) in the gas-solid phase reduction of  $\text{PhNO}_2$  by  $[\text{HFe}_3(\text{CO})_{11}]^-$  (**2**) supported over an organic polymer.<sup>3</sup> In this case, formation of **7** during the reduction was observed by IR. As the reported data on this reaction are limited, only a few comments are possible. Formation of **7** would probably be favored by the gas-solid reaction conditions which prevent the separation of the initially formed radical pair. The proton source for further reaction was proposed to be some unknown impurities in the polymer.<sup>3</sup> As the acidity of these impurities is not known, no pathway can be ruled out, but the earlier noted low basicity of **7** suggests that radical intermediates may be involved even in this case.

### Concluding Remarks

One aim of this work was to draw a comparison of the reactivity of nitro and nitroso aromatic compounds

with  $\text{Fe}_3(\text{CO})_{12}$  and the corresponding ruthenium and osmium clusters, including the effect of halide promoters. Despite the fact that many similarities exist between the behavior of ruthenium<sup>6b</sup> and osmium<sup>40b</sup> compounds, the reactivity of  $\text{Fe}_3(\text{CO})_{12}$  has often been found to be very different. This is immediately evident from the reaction of  $\text{Fe}_3(\text{CO})_{12}$  with halides which gives the radical anion cluster **3**, which has no parallel in ruthenium or osmium chemistry where instead halide-substituted diamagnetic clusters are formed.<sup>19,20,45</sup> Even the mixed-metal cluster  $\text{Fe}_2\text{Ru}(\text{CO})_{12}$  reacts in a way similar to its homometallic ruthenium and osmium analogues.

As previously noted,  $[\text{Fe}_3(\text{CO})_{11}]^-$  (**3**) has been shown to be involved in a number of reactions, and its isolation and full characterization in this study now makes it possible to explore more extensively its reactivity. In this paper we have only studied the reactions of **3** with nitro and nitroso aromatic compounds. These reactions have been shown to be extremely complex and to depend significantly on slight variations of the experimental conditions. Although some of the products could be isolated and characterized, the reactions appear to be too complex and not readily amenable to a complete mechanistic study. Many different competing pathways are surely operating, and their predominance seems to be linked to slight differences in the concentrations and solubilities of the relevant complexes. Given these problems, extrapolation of these data to the actual experimental conditions in which catalytic and stoichiometric carbonylation and reduction of nitrobenzene are performed should be carried out only with extreme caution, since the actual concentrations of **3** and other species during these reactions are not known.

A similar, although somewhat less pronounced, problem was encountered in the study of the reactivity of  $[\text{HFe}_3(\text{CO})_{11}]^-$  (**2**). The formation of radicals and their relevance at several stages of the reaction appears to be extremely important in this system also. In a previous paper,<sup>38c</sup> some of us had shown that oxidation by air or by  $[\text{Cp}_2\text{Fe}]^+$  of several iron clusters of the types  $[\text{Fe}_3(\mu_3\text{-NPh})_2(\text{CO})_8(\text{C}(\text{O})\text{R})]^-$  or  $\text{Fe}_3(\mu_3\text{-NPh})_2(\text{CO})_8(\text{C}(\text{OEt})\text{Ph})$  greatly enhanced their reactivity. In the course of the present work, we have extended the examination of the effects of radical formation on complexes such as  $[\text{HFe}_3(\mu_3\text{-NPh})(\text{CO})_9]^-$  (**7**) that are related to those formed or proposed to form under the experimental conditions commonly employed for the reduction and carbonylation of aromatic nitro compounds, and we have also conducted competition experiments to test the kinetic relevance of the radical processes in these reactions. The data obtained quite strongly support the proposal that, although different paths may be operating in competition with each other, many of the intermediates in the reactions are radical species and the corresponding diamagnetic compounds are completely inert under the same conditions. Some diamagnetic species may eventually be formed and then activated by oxidation, but at least in the case of the phase-transfer-catalyzed reduction of aromatic nitro compounds by  $\text{Fe}_3(\text{CO})_{12}$ , this does not appear to be a kinetically relevant pathway.

The reactions between nitro or nitroso organic com-

(44) Hieber, W.; Brendel, G. *Z. Anorg. Allg. Chem.* **1957**, *289*, 338.

(45) Zuffa, J. L.; Kivi, S. J.; Gladfelter, W. L. *Inorg. Chem.* **1969**, *28*, 1888.

pounds and several complexes have been previously shown to proceed initially through electron transfer from the complex to the organic molecule.<sup>8,41</sup> However, the products of these reactions, at least in the cases in which it has been possible to characterize them, are diamagnetic complexes, and the importance of radical processes during the further steps of the reduction have not been explored. This is the first time that such radical processes have been shown to be relevant to the reduction of nitrobenzene.<sup>46</sup> Although the fact that radical processes are important in the reactions of iron complexes does not imply that this is the case also for the compounds of other metals, it does suggest that their importance even in other cases may have been underestimated. For example, preliminary work in these laboratories have shown that the ruthenium imido cluster  $\text{Ru}_3(\text{CO})_{10}(\mu_3\text{-NPh})$  can be oxidized to its corresponding radical cation and that this latter species displays strongly enhanced reactivity.<sup>47</sup>

### Experimental Section

Unless otherwise specified, all reactions and manipulations were performed under a prepurified  $\text{N}_2$  atmosphere using standard Schlenk apparatus, cannula techniques, and magnetic stirring. All glassware was kept in an oven for at least 2 h and then evacuated on a vacuum line immediately before use. Solvents were dried by standard procedures. Compounds **1**,<sup>48</sup> **PPN-2**,<sup>26b</sup> **PPh<sub>4</sub>-2**,<sup>26b</sup> **Et<sub>4</sub>N-2**,<sup>4b</sup> **PPN-4**,<sup>28b</sup>  $[\text{PPN}][\text{Fe}_4(\text{CO})_{13}]$ ,<sup>22</sup>  $\text{Fe}_2\text{Ru}(\text{CO})_{12}$ ,<sup>31</sup> and  $[\text{Cp}_2\text{Fe}][\text{PF}_6]$ <sup>49</sup> were synthesized by methods reported in the literature or by slight modifications thereof. The salts  $[\text{PPN}]\text{Br}$ ,  $[\text{PPN}]\text{I}$ , and  $[\text{PPN}]\text{NCO}$  were prepared from  $[\text{PPN}]\text{Cl}$  by metathesis according to literature methods<sup>60</sup> and were dried at 140 °C overnight prior to use. All other organic compounds were commercial products and were used as received.  $[\text{PPh}_4]\text{Cl}$  was stored and weighed in a glovebox. Gas chromatographic analyses were performed on a Perkin-Elmer 8420 capillary gas chromatograph equipped with a PSS 255 column. Whenever possible,  $R_i$  values ( $R_i$  = response factor, relative to hexamethylbenzene as an internal standard) were determined by the use of solutions of known concentrations of the compounds. For the few cases in which the compound was not available in large amount (substituted azo and azoxy compounds), an approximate  $R_i$  was estimated by comparison of the measured  $R_i$  values for the unsubstituted azo- and azoxybenzene, nitrobenzene, nitrosobenzene, and aniline with those of the corresponding available substituted compounds. GC-MS analyses were conducted on a Hewlett Packard 5890 gas chromatograph, equipped with a 5971 A mass selective detector. NMR spectra were recorded on a Bruker AM-300 spectrometer. EPR spectra were recorded on a Varian EPR spectrometer. Elemental analyses were performed by Schwartzkop Microanalytical Laboratories, Woodside, NY.

**Synthesis of  $[\text{PPN}][\text{Fe}_3(\text{CO})_{11}]$  (PPN-3).**  $\text{Fe}_3(\text{CO})_{12}$  (**1**) (200 mg, 0.4 mmol) and  $[\text{PPN}]\text{Cl}$  (230 mg, 0.4 mmol) were placed in a 50 mL Schlenk flask, and  $\text{Et}_2\text{O}$  (20 mL) was added. The reaction was followed by IR until complete disappearance of the 2049  $\text{cm}^{-1}$  band of **1** (~1.5 h). The solution was then

(46) In ref 8, several radical species were observed by EPR and were suggested as intermediates in the reduction of aliphatic nitro compounds. However, since the reactions were analyzed only by EPR, all diamagnetic species, including the final organic products, could not be observed and the kinetic relevance of the observed processes to the total reaction is not obvious.

(47) Song, J.-S. Ph.D. Thesis, The Pennsylvania State University, 1990.

(48) McFarlane, W.; Wilkinson, G. *Inorg. Synth.* **1965**, *8*, 181.

(49) Yang, E. S.; Chan, M.-S.; Wahl, A. C. *J. Phys. Chem.* **1975**, *79*, 2049.

(50) Martinsen, A.; Songstad, J. *Acta Chem. Scand.* **1977**, *A31*, 645.

filtered through a pad of Celite and evaporated to dryness under vacuum, affording analytically pure PPN-3 as a purple microcrystalline material (216 mg, 50% yield with respect to **1**). IR analysis of the distillate from the reaction mixture, condensed in a Schlenk flask immersed in liquid nitrogen, showed the presence of  $\text{Fe}(\text{CO})_5$  in ~20% yield, as estimated from the intensity of the 2017  $\text{cm}^{-1}$  band of  $\text{Fe}(\text{CO})_5$  measured in the absorbance mode and compared to a calibration obtained by measuring the absorbance of this band in several solutions containing known amounts of  $\text{Fe}(\text{CO})_5$ . The reaction was also performed on larger amounts (1 g of  $\text{Fe}_3(\text{CO})_{12}$ ) with similar results, but the yield was somewhat lower unless  $\text{N}_2$  was bubbled periodically through the solution. Similar procedures were used for the reactions of **1** with  $[\text{PPN}]\text{Br}$ ,  $[\text{PPN}]\text{I}$ , and  $[\text{PPh}_4]\text{Cl}$ .

**PPN-3.** IR (THF:  $\nu_{\text{CO}}$  = 2057 (vw), 2017 (w), 1984 (vs), 1966 (ms), 1933 (mw), 1922 (w, sh)  $\text{cm}^{-1}$ . EPR (THF, -78 °C):  $g$  = 2.0489. Anal. Calcd for  $\text{C}_{47}\text{H}_{30}\text{Fe}_3\text{NO}_{11}\text{P}_2$ : C, 55.66; H, 2.98; N, 1.38. Found: C, 55.06; H, 3.14; N, 1.45.

**Reaction of  $\text{Fe}_3(\text{CO})_{12}$  with  $[\text{PPN}]\text{NCO}$ . Identification of  $[\text{PPN}][\text{Fe}(\text{NCO})_4]$ .** Solid  $[\text{PPN}]\text{NCO}$  (61 mg, 0.11 mmol) was added to a THF (50 mL) solution of  $\text{Fe}_3(\text{CO})_{12}$  (**1**) (50.0 mg, 0.099 mmol) after which the solution changed from dark green to dark purple in less than 5 min. An IR band at 2197  $\text{cm}^{-1}$  for coordinated NCO was observed in the IR spectrum of the reaction mixture. The solvent was removed under vacuum, leaving a purple residue which was extracted with  $\text{Et}_2\text{O}$  (100 mL) affording a purple solution and a golden brown residue. The solvent was evaporated from the purple solution under vacuum leaving PPN-3 (28 mg, 0.028 mmol, 28%) after freezing pentane over the oily residue and thawing three times. The golden brown residue was extracted with THF (50 mL) giving a brown solution and a tan powder. IR analysis of the solution indicated the presence of at least two anionic carbonyl compounds and at least one compound with a coordinated NCO ligand ( $\nu_{\text{NCO}}$  = 2190  $\text{cm}^{-1}$ ). The tan powder was determined to be  $[\text{PPN}][\text{Fe}(\text{NCO})_4]$ <sup>23</sup> by the sharp  $\nu_{\text{NCO}}$  peak in its IR spectrum and the absence of other bands assignable to iron carbonyl ligands or to free  $\text{NCO}^-$  and by its mass spectrum. [IR (KBr):  $\nu_{\text{NCO}}$  = 2189  $\text{cm}^{-1}$ . IR ( $\text{MeNO}_2$ ):  $\nu_{\text{NCO}}$  = 2195  $\text{cm}^{-1}$ . MS (FAB, 18-crown-6/tetraglyme matrix),  $M^-$  = 224 (calcd 224)].

**Reaction of  $[\text{PPN}][\text{Fe}_3(\text{CO})_{11}]$  (PPN-3) with CO.** The purple salt  $[\text{PPN}][\text{Fe}_3(\text{CO})_{11}]$  (100 mg, 0.1 mmol) was placed in a 50 mL Schlenk flask under a CO atmosphere, and THF (10 mL) was added. An orange-brown precipitate immediately started to form as  $[\text{PPN}][\text{Fe}_3(\text{CO})_{11}]$  dissolved. After 5 min the solution was almost colorless, and its IR spectrum indicated only the presence of  $\text{Fe}(\text{CO})_5$ . The suspension was evaporated under vacuum, and the orange solid was washed with THF (20 mL). Only a very small amount of the solid dissolved in THF, giving a very pale orange solution with IR bands at 2020 (vw), 1996 (vw), 1964 (w), and 1936 (w). The solid remaining after the THF washing (73 mg) was dissolved in  $\text{CH}_3\text{CN}$ , and the IR spectrum of this solution showed the predominant presence of  $[\text{Fe}_3(\text{CO})_{11}]^{2-}$ , which was confirmed by protonation with  $\text{CF}_3\text{COOH}$  to afford  $[\text{HFe}_3(\text{CO})_{11}]^-$ .

**Reaction of a  $\text{Fe}_3(\text{CO})_{12}/\text{Ru}_3(\text{CO})_{12}$  Mixture with  $[\text{PPN}]\text{-Cl}$ .** To a solution of  $\text{Fe}_3(\text{CO})_{12}$  (33 mg, 0.066 mmol) and  $\text{Ru}_3(\text{CO})_{12}$  (21 mg, 0.033 mmol) in THF (30 mL) was added  $[\text{PPN}]\text{Cl}$  (57 mg, 0.1 mmol). The solution was stirred for 10 min, during which time it changed color from dark green to purple. The IR spectrum at this point showed carbonyl bands attributed to a mixture of  $[\text{Fe}_3(\text{CO})_{11}]^-$ ,  $\text{Fe}(\text{CO})_5$ , and  $\text{Ru}_3(\text{CO})_{12}$ . After stirring for 1 h, all the  $\text{Ru}_3(\text{CO})_{12}$  had disappeared and IR bands attributable to  $[\text{Ru}_3(\text{Cl})(\text{CO})_{11}]^-$ <sup>19g</sup> were observed.

**Reaction of  $\text{Fe}_2\text{Ru}(\text{CO})_{12}$  with  $[\text{PPN}]\text{Cl}$ .** To a solution of  $\text{Fe}_2\text{Ru}(\text{CO})_{12}$  (55 mg, 0.1 mmol) in THF (50 mL) was added  $[\text{PPN}]\text{Cl}$  (57 mg, 0.1 mmol) in  $\text{CH}_2\text{Cl}_2$  (1 mL), followed by stirring for 10 min. During this time the purple solution became dark brown. The resulting solution was filtered



through a pad of Celite, and the solvent was evaporated under vacuum to leave a dark brown solid. This solid was washed with Et<sub>2</sub>O (50 mL) and recrystallized from hexane/CH<sub>2</sub>Cl<sub>2</sub> at -20 °C to yield [PPN][Fe<sub>2</sub>Ru(μ-Cl)(CO)<sub>10</sub>] as a brown microcrystalline solid (58 mg, 54% yield). IR (THF): ν<sub>CO</sub> = 2073 (w), 2023 (sh), 2014 (vs), 1987 (s), 1970 (m), 1963 (m), 1953 (m), 1796 (w) cm<sup>-1</sup>. MS (FAB<sup>-</sup>): *m/e* 528.6. Anal. Calcd for C<sub>46</sub>H<sub>30</sub>ClFe<sub>2</sub>NO<sub>10</sub>P<sub>2</sub>Ru: C, 51.78; H, 2.83; N, 1.31. Found: C, 51.89; H, 3.09; N, 1.31.

**Reaction of [Me<sub>3</sub>NCH<sub>2</sub>Ph]<sub>2</sub>[Fe<sub>3</sub>(CO)<sub>11</sub>] with Cl<sub>5</sub>C<sub>6</sub>NO<sub>2</sub>.** The salt [Me<sub>3</sub>NCH<sub>2</sub>Ph]<sub>2</sub>[Fe<sub>3</sub>(CO)<sub>11</sub>] (380 mg, 0.49 mmol) was placed in a 50 mL Schlenk flask and dissolved in THF (15 mL). In a separate Schlenk tube, Cl<sub>5</sub>C<sub>6</sub>NO<sub>2</sub> (173 mg, 0.59 mmol) was dissolved in THF (12 mL, affording a 0.049 M solution), and 3 mL of this solution was added to the [Fe<sub>3</sub>(CO)<sub>11</sub>]<sup>2-</sup> solution. A gradual decrease of the intensity of the IR bands due to [Fe<sub>3</sub>(CO)<sub>11</sub>]<sup>2-</sup> was observed during the first 20 min, with a corresponding increase of the bands of [Fe<sub>3</sub>(CO)<sub>11</sub>]<sup>-</sup>. A small band attributed to Fe(CO)<sub>5</sub> also appeared at 2018 cm<sup>-1</sup>. After 20 min the reaction stopped, and an additional 3 mL of the Cl<sub>5</sub>C<sub>6</sub>NO<sub>2</sub> solution was added. A further increase in the intensity of the IR bands due to [Fe<sub>3</sub>(CO)<sub>11</sub>]<sup>-</sup> occurred, but several overlapping absorptions also appeared and an insoluble residue formed. Further additions of the nitro compound led to a decrease in the absorptions of [Fe<sub>3</sub>(CO)<sub>11</sub>]<sup>-</sup>, accompanied by the formation of a complex mixture of products among which only Fe(CO)<sub>5</sub> could be identified with certainty. The reaction between [Me<sub>3</sub>NCH<sub>2</sub>Ph]<sub>2</sub>[Fe<sub>3</sub>(CO)<sub>11</sub>] and PhNO<sub>2</sub> was performed in a similar way, except that a 3-fold molar excess of PhNO<sub>2</sub> was immediately added at the beginning of the reaction.

**Reaction of [PPN][Fe<sub>3</sub>(CO)<sub>11</sub>] with PhNO and PhNO<sub>2</sub>.** The salt [PPN][Fe<sub>3</sub>(CO)<sub>11</sub>] (418 mg, 0.412 mmol) was dissolved in THF (200 mL), PhNO (48.5 mg, 0.453 mmol) was added, and the solution was stirred for 20 min during which time the solution turned from a dark purple to a dark brown. The THF solvent and Fe(CO)<sub>5</sub> were removed under vacuum, and the reaction mixture was chromatographed on a silica gel column using CH<sub>2</sub>Cl<sub>2</sub> as eluent to give green and red bands, both of which contained azo- and azoxybenzene (by TLC vs authentic samples). The green band contained mainly Fe<sub>3</sub>(CO)<sub>12</sub> (by IR), and the red band contained [PPN][HFe<sub>3</sub>(CO)<sub>11</sub>] (by IR, <sup>1</sup>H NMR, and FAB mass spectra). Further chromatography on silica gel preparative TLC plates led to the isolation of azobenzene (4.3 mg, 0.024 mmol, 11% yield) and azoxybenzene (3.8 mg, 0.019 mmol, 8% yield), which were identified by their R<sub>f</sub> values on silica gel TLC strips as well as by their <sup>1</sup>H NMR spectra. The reaction between [PPN][Fe<sub>3</sub>(CO)<sub>11</sub>] and PhNO<sub>2</sub> was performed similarly, but 2 h was necessary to complete the reaction. Azo- and azoxybenzene were again identified by TLC analysis of the reaction mixture, although no attempt was made to quantitatively recover them.

**Synthesis of [PPN]<sub>2</sub>[Fe<sub>3</sub>(CO)<sub>9</sub>(μ<sub>3</sub>-NC<sub>6</sub>Cl<sub>5</sub>)] (PPN-5).** The salt [PPN][Fe<sub>3</sub>(CO)<sub>11</sub>] (800 mg, 0.79 mmol) was placed in a three necked 100 mL flask equipped with a gas inlet, an equilibrated dropping funnel, and a septum. The upper neck of the funnel was also closed with a septum. THF (50 mL) was added to the flask, and to the funnel was added a solution of Cl<sub>5</sub>C<sub>6</sub>NO<sub>2</sub> (233 mg, 0.79 mmol) in THF (10 mL). This solution was slowly added to the flask over 3 h, after which time the pale red solution, containing Fe(CO)<sub>5</sub> as the predominant product (by IR), was filtered through a frit and the residue was washed with Et<sub>2</sub>O (2 × 20 mL). THF extraction of the residue (3 × 20 mL) gave a brown solution which was evaporated under vacuum to give a brown solid (376 mg) which contained mainly [PPN]<sub>2</sub>[Fe<sub>3</sub>(CO)<sub>9</sub>(μ<sub>3</sub>-NC<sub>6</sub>Cl<sub>5</sub>)] (PPN-5), although an impurity showing an IR band at 1945 cm<sup>-1</sup> was present. Attempts to eliminate this impurity were only partially successful. Further extraction with CH<sub>3</sub>CN of the residue remaining after the THF extraction afforded an orange-brown solution showing in the IR spectrum bands at 1997 (w), 1931 (vs), 1900 (m), and 1874 (w) cm<sup>-1</sup>, which were

similar, but not coincident, with those of [Fe<sub>3</sub>(CO)<sub>9</sub>(μ<sub>3</sub>-NC<sub>6</sub>Cl<sub>5</sub>)]<sup>2-</sup> (5) in the same solvent. This product was not obtained reproducibly and was not further investigated.

**PPN-5.** IR (THF): ν<sub>CO</sub> = 1995 (w), 1929 (vs), 1898 (ms), 1871 (w) cm<sup>-1</sup>. <sup>13</sup>C NMR (THF-d<sub>6</sub>): 143.5, 131.5, 116.9 ppm (signals are also present due to the PPN cation).

**Protonation of [PPN]<sub>2</sub>[Fe<sub>3</sub>(CO)<sub>9</sub>(μ<sub>3</sub>-NC<sub>6</sub>Cl<sub>5</sub>)] (PPN-5) with HBF<sub>4</sub>.** An impure sample of PPN-5 (see preceding reaction; 280 mg) was placed in a 50 mL Schlenk flask, and THF (8 mL) was added. To a separate Schlenk tube containing THF (3 mL) was added HBF<sub>4</sub>·2Et<sub>2</sub>O (50 μL). A few drops of this solution were added immediately to the PPN-5 solution, and an IR spectrum showed the disappearance of 5 and the formation of a new compound. The solution was dried under vacuum, and the residue was extracted with Et<sub>2</sub>O (8 mL). The ether extract contained a cluster identified as [PPN][HFe<sub>3</sub>(CO)<sub>9</sub>(μ<sub>3</sub>-NC<sub>6</sub>Cl<sub>5</sub>)] (PPN-6) on the basis of the similarity of its IR spectrum with that of [PPN][HFe<sub>3</sub>(CO)<sub>9</sub>(μ<sub>3</sub>-NPh)] (PPN-7) and by the isotopic pattern of the parent peak in its mass spectrum. The residue after extraction with Et<sub>2</sub>O was redissolved in THF. An IR spectrum of this solution showed largely [Fe<sub>4</sub>(CO)<sub>13</sub>]<sup>2-</sup> (ν<sub>CO(max)</sub> = 1945 cm<sup>-1</sup>) as evidenced by comparison with the IR spectrum of an authentic sample, but a weak absorption at 1970 cm<sup>-1</sup> was also present.

**PPN-6.** IR (THF): ν<sub>CO</sub> = 2048 (w), 2019 (s), 1981 (vs), 1963 (ms), 1945 (m), 1914 (w) cm<sup>-1</sup>. MS (FAB<sup>-</sup>, calculated intensities for the isotopic peaks of [HFe<sub>3</sub>(CO)<sub>9</sub>(μ<sub>3</sub>-NC<sub>6</sub>Cl<sub>5</sub>)]<sup>-</sup> and experimental intensities relative to the parent peak in parentheses): M<sup>-</sup> = 280 (0.11, 0.15), 282 (0.70, 0.69), 283 (0.17, 0.16), 284 (1, 1), 285 (0.24, 0.24), 286 (0.64, 0.66), 287 (0.15, 0.18), 288 (0.22, 0.19).

**Reaction of [Et<sub>4</sub>N][HFe<sub>3</sub>(CO)<sub>11</sub>] (Et<sub>4</sub>N-2) with PhNO in the Presence of Ac<sub>2</sub>O.** To a solution of Et<sub>4</sub>N-2 (130 mg, 0.21 mmol) and PhNO (21 mg, 0.20 mmol) in THF (50 mL) was added acetic anhydride (1 mL). The solution was stirred for 1 h, during which time the purple solution turned to dark brown. The solvent was removed under vacuum, and the residue was chromatographed on Florisil using 1:1 pentane/CH<sub>2</sub>Cl<sub>2</sub> as eluent to yield PhN(OAc)Ac (12 mg, 0.062 mmol, 31% yield) and PhNHAc (15 mg, 0.11 mmol, 57% yield).

**Reaction of [Et<sub>4</sub>N][HFe<sub>3</sub>(CO)<sub>11</sub>] (Et<sub>4</sub>N-2) with *p*-MeOC<sub>6</sub>H<sub>4</sub>NO<sub>2</sub> in the Presence of Ac<sub>2</sub>O.** To a solution of Et<sub>4</sub>N-2 (130 mg, 0.21 mmol) and *p*-MeOC<sub>6</sub>H<sub>4</sub>NO<sub>2</sub> (31 mg, 0.20 mmol) in THF (50 mL) was added 5 mL of acetic anhydride. The solution was stirred for 12 h, and the solvent was removed under vacuum. The residue was chromatographed on Florisil using 1:1 pentane/CH<sub>2</sub>Cl<sub>2</sub> as eluent to yield *p*-MeOC<sub>6</sub>H<sub>4</sub>N(OAc)Ac (4 mg, 0.018 mmol, 9% yield; IR (KBr) 1765 (s), 1715 (s), 1602 (m) cm<sup>-1</sup>; MS (EI) *m/e* 223; <sup>1</sup>H NMR (CDCl<sub>3</sub>) δ 7.17 (d, 2H), 6.99 (d, 2H), 3.83 (s, 3H, CH<sub>3</sub>O), 2.21 (s, 3H, OC(O)-CH<sub>3</sub>), 2.04 (s, 3H, NC(O)CH<sub>3</sub>) and *p*-MeOC<sub>6</sub>H<sub>4</sub>NHAc (9 mg, 0.055 mmol, 27% yield).

**Synthesis of [PPN][HFe<sub>3</sub>(CO)<sub>9</sub>(μ<sub>3</sub>-NPh)] (PPN-7) by Reaction of [PPN][HFe<sub>3</sub>(CO)<sub>11</sub>] (PPN-2) with PhNO.** To a three necked 250 mL flask equipped with a gas inlet, a graduated equilibrated addition funnel, and a septum were added PPN-2 (624 mg, 0.61 mmol) and hexamethylbenzene (250 mg) as a GC internal standard. The latter is not necessary if the reaction is performed only to synthesize PPN-7. The upper neck of the addition funnel was also closed with a septum. The whole apparatus was evacuated and filled with CO three times, and then THF (100 mL) was added to the flask. To the addition funnel was added a solution of PhNO (525 mg, 4.9 mmol) in THF (25 mL). This solution was added dropwise over the course of several hours, and the reaction course was monitored by IR and GC analysis. The reaction was complete after 6 h and after the addition of 19.1 mL of the PhNO solution. This volume corresponds to the addition of 402 mg of PhNO, but GC analysis of the solution after the end of the reaction evidenced the presence of 70 mg of unreacted PhNO. Thus the amount of PhNO effectively reacted is 332 mg, corresponding to 5.0 mmol/mmol of



[ $\text{HFe}_3(\text{CO})_{11}$ ]<sup>-</sup> (**2**). GC analysis also showed the presence of azobenzene (54.8 mg) and azoxybenzene (144.6 mg) in 22% and 47% yields, respectively, with respect to the reacted PhNO. GC analysis during the reaction showed that all of the azobenzene was formed during the first 1 h of reaction. GC analysis of the starting PhNO showed that neither azo- nor azoxybenzene were present as impurities in this compound. During the reaction a dark precipitate was also formed. The solution, containing PPN-7, was filtered through a pad of Celite, eliminating the dark precipitate, and dried under vacuum, affording an oil which was triturated with hexane (3 × 100 mL) until it became a brown powder (390 mg, 75% crude yield). This material is sufficiently pure for most purposes, although it can be recrystallized from 2-propanol (80/0 °C) to afford a brown microcrystalline solid.

**PPN-7.** IR (THF):  $\nu_{\text{CO}}$  = 2046 (w), 2005 (s), 1974 (vs), 1959 (ms), 1941 (mw), 1900 (w, br)  $\text{cm}^{-1}$ .  $^1\text{H}$  NMR ( $\text{CDCl}_3$ ): -20.5 ppm. MS (FAB<sup>-</sup>, calculated intensities for the isotopic peaks of [ $\text{HFe}_3(\text{CO})_9(\mu_3\text{-NPh})$ ]<sup>-</sup> and experimental intensities relative to the parent peak in parentheses):  $M^-$  = 508 (0.01, 0.02), 510 (0.19, 0.19), 511 (0.04, 0.05), 512 (1, 1), 513 (0.25, 0.25), 514 (0.06, 0.06). Anal. Calcd for  $\text{C}_{51}\text{H}_{36}\text{N}_2\text{P}_2\text{O}_9\text{Fe}_3$ : C, 58.3; H, 3.4; N, 2.7. Found: C, 57.9; H, 3.1; N, 2.7.

**Reaction of [PPN][ $\text{HFe}_3(\text{CO})_9(\mu_3\text{-NPh})$ ] (PPN-7) with  $\text{ArNO}$ . (a)  $\text{Ar} = \text{Ph}$ . To a 100 mL Schlenk flask was added PPN-7 (300 mg, 0.29 mmol), PhNO (34.3 mg, 0.31 mmol), and hexamethylbenzene (50 mg, GC internal standard). The flask was evacuated and filled with CO three times, after which THF (30 mL) was added. Samples were periodically withdrawn for GC analysis, and additional PhNO was added after 130 min (182 mg, 1.7 mmol). The time profile for the formation of azobenzene and azoxybenzene is as follows: 20 min reaction, azobenzene (8.5 mg), azoxybenzene (9.8 mg); 80 min reaction, azobenzene (8.7 mg), azoxybenzene (10.4 mg); 133 min reaction, azobenzene (11.3 mg), azoxybenzene (32.7 mg); 250 min, azobenzene (12.5 mg), azoxybenzene (39.4 mg); 16.2 h, azobenzene (12.7 mg), azoxybenzene (40.2 mg). At this point [ $\text{Cp}_2\text{Fe}$ ][ $\text{PF}_6$ ] (0.024 mmol) was added and GC monitoring continued [after 5 min, azobenzene (12.4 mg), azoxybenzene (60.3 mg); after 3 h, azobenzene (13.0 mg), azoxybenzene (61.6 mg); this amount of azoxybenzene corresponded to 4.5 mol/mol of added [ $\text{Cp}_2\text{Fe}$ ][ $\text{PF}_6$ ]]. Similar behavior was observed upon further additions of [ $\text{Cp}_2\text{Fe}$ ][ $\text{PF}_6$ ], but bubbling oxygen through the solution was ineffective in promoting the reaction. During the reaction, a decrease of the intensity of the IR bands of **7** occurred, but no new IR bands were observed and a dark precipitate formed.**

(b)  $\text{Ar} = 2\text{-Me-C}_6\text{H}_4$ . The salt PPN-7 (50 mg, 0.048 mmol) and hexamethylbenzene (18 mg, GC internal standard) were placed in a Schlenk tube under a CO atmosphere, and THF (10 mL) was added. The solution was left to stir for 10 min to allow for saturation with CO, after which time 2-Me- $\text{C}_6\text{H}_4\text{NO}$  (20.6 mg, 0.19 mmol) was added. The reaction was followed analogous to that in the preceding section upon adding 10, 20, and 40 mg of [ $\text{Cp}_2\text{Fe}$ ][ $\text{PF}_6$ ] after 1, 4, and 9 h, respectively. After the second addition of [ $\text{Cp}_2\text{Fe}$ ][ $\text{PF}_6$ ], the IR spectrum of the solution showed complete disappearance of the original absorptions and new absorptions at higher frequencies. After the third addition, only very weak bands were present in the IR spectrum of the solution. GC analysis of the solution at the end of the reaction showed the presence of 2-Me- $\text{C}_6\text{H}_4\text{NO}$  (2.34 mg), 2-Me- $\text{C}_6\text{H}_4\text{NH}_2$  (0.12 mg), 2-Me- $\text{C}_6\text{H}_4\text{N}=\text{NC}_6\text{H}_4$ -2-Me (0.52 mg), 2-Me- $\text{C}_6\text{H}_4\text{N}(\text{O})=\text{NC}_6\text{H}_4$ -2-Me (10.8 mg), PhNH<sub>2</sub> (0.08 mg), PhN=NPh (0.93 mg), and PhN(O)=NPh (1.57 mg). Only a trace amount of 2-Me- $\text{C}_6\text{H}_4\text{N}=\text{NPh}$  (~0.005 mg, at the limits of detectability by GC-MS) was detected, but no mixed azoxy compounds were formed.

**Attempted Reaction of [PPN][ $\text{HFe}_3(\text{CO})_9(\mu_3\text{-NPh})$ ] (PPN-7) under Phase-Transfer Conditions.** To a 50 mL Schlenk flask was added PPN-7 (155 mg, 0.15 mmol), [ $\text{Et}_3\text{NCH}_2\text{Ph}$ ][Cl] (22 mg, 0.097 mmol), and THF (5 mL). After dissolution of the cluster, 5 mL of a 1 M aqueous solution of

NaOH was added, and the mixture was vigorously stirred. The conditions are as close as possible to those reported in ref 2c, except that THF was used as a solvent in place of benzene, given the very low solubility of PPN-7 in benzene. The use of THF as the solvent does not appreciably alter the reaction course, as evidenced by the experiment described in the following paragraph. No reaction was observed over the course of 12 h by IR and GC analysis, even after addition of [ $\text{Cp}_2\text{Fe}$ ][ $\text{PF}_6$ ] (10 mg, 0.03 mmol).

**Reaction of  $\text{Fe}_3(\text{CO})_{12}$ , [PPN][ $\text{HFe}_3(\text{CO})_9(\mu_3\text{-NPh})$ ] (PPN-7), and 4-Me- $\text{C}_6\text{H}_4\text{NO}_2$  under Phase-Transfer Conditions.** To a Schlenk tube was added  $\text{Fe}_3(\text{CO})_{12}$  (48.0 mg, 0.095 mmol), PPN-7 (50.0 mg, 0.047 mmol), 4-Me- $\text{C}_6\text{H}_4\text{NO}_2$  (13.1 mg, 0.095 mmol), [ $\text{Et}_3\text{NCH}_2\text{Ph}$ ][Cl] (22.0 mg, 0.097 mmol), hexamethylbenzene (9.5 mg, GC internal standard), THF (5 mL), and 1 M NaOH (in  $\text{H}_2\text{O}$ , 5 mL). After 1 h, GC analysis of the organic layer showed complete consumption of 4-Me- $\text{C}_6\text{H}_4\text{NO}_2$  and the formation of 4-toluidine (8.7 mg,  $8.1 \times 10^{-2}$  mmol) and aniline (0.23 mg,  $2.5 \times 10^{-3}$  mmol). No azo or azoxy compounds were detected. The IR spectrum of the solution showed that the intensity of the bands of **7** was virtually unchanged, but  $\text{Fe}_3(\text{CO})_{12}$  had completely disappeared and new bands at 1940 (s, br) and 1878 (m, br) were present.

**Reaction of [PPN][ $\text{HFe}_3(\text{CO})_9(\mu_3\text{-NPh})$ ] (PPN-7) with [ $\text{Cp}_2\text{Fe}$ ][ $\text{PF}_6$ ] and  $\text{H}_2\text{O}$ .** The salt PPN-7 (20 mg, 0.019 mmol) was placed in a Schlenk tube and dissolved in THF (2 mL), and water (10  $\mu\text{L}$ ) and [ $\text{Cp}_2\text{Fe}$ ][ $\text{PF}_6$ ] (20 mg, 0.06 mmol) were added. After 1 h, GC and GC-MS analysis of the reaction solution showed the formation of aniline.

**X-ray Crystallographic Analysis of [PPh<sub>4</sub>][ $\text{Fe}_3(\text{CO})_{11}$ ] (PPh<sub>4</sub>-3), [PPN][ $\text{HFe}_3(\text{CO})_9(\mu_3\text{-NPh})$ ] (PPN-7), and [PPh<sub>4</sub>]<sub>2</sub>[ $\text{Fe}_3(\text{CO})_9(\mu_3\text{-NPh})$ ]<sub>2</sub>·2CH<sub>2</sub>Cl<sub>2</sub> (PPh<sub>4</sub>-8·2CH<sub>2</sub>Cl<sub>2</sub>).** Crystal, data collection, and refinement parameters are collected in Table 1. All crystals were mounted on fine glass fibers with epoxy cement. In all cases, but especially so for PPN-7, the specimens diffracted weakly and broadly. Learned-profile routines were used to improve the measurement of weak reflections. Crystals of PPN-7 displayed a thin tabular habit which in most instances occurred in stacks. A microscalpel constructed from a flake of glass was used to separate the tablets.

The unit-cell parameters were each obtained from the angular settings of the least squares fit of 25 reflections ( $20^\circ \leq 2\theta \leq 25^\circ$ ). Photographic evidence and the observed diffraction symmetry indicated  $2/m$  Laue symmetry for all three. For PPh<sub>4</sub>-3 and PPN-7 systematic absences allowed the unambiguous assignment of the space groups  $P2_1/n$  and  $P2_1/c$ , respectively. For PPh<sub>4</sub>-8·2CH<sub>2</sub>Cl<sub>2</sub>, either  $P2_1$  or  $P2_1/m$  were indicated. The noncentrosymmetric alternative was chosen due to the absence of molecular mirror-plane symmetry and the chemically well-behaved results of refinement. The enantiomorph was tested by the Rogers method;  $\eta$  refined to 1.10(9), indicating that the hand reported is correct. Despite some specimens with irregular shapes, no corrections for absorption were deemed necessary on the basis of the maximum/minimum transmission ratios near unity.

All structures were solved by direct methods. For PPh<sub>4</sub>-3, all non-hydrogen atoms were anisotropically refined. Phenyl rings were constrained to rigid, planar hexagons, and hydrogen atoms were treated as idealized contributions. For PPN-7, only the Fe, O, and N atoms were anisotropically refined. Ligand hydrogen atoms were ignored. Despite the low-quality data for this compound, difference maps consistently indicated the presence of a H-atom bridging the longest Fe-Fe bond. It was included as a fixed contribution but not refined. To conserve data, common C-O and Fe-C bond distance parameters were refined to 1.165(9) and 1.730(9) Å, respectively. For PPh<sub>4</sub>-8·2CH<sub>2</sub>Cl<sub>2</sub>, all non-hydrogen atoms except for those associated with the cation were anisotropically refined. The phenyl rings were constrained to rigid, planar hexagons.

The structure of PPN-3 was also determined. The anion is structurally identical to that found for PPh<sub>4</sub>-3, but the iron triangle shows a minor contribution (11%) of a "star of David"

disorder pattern. PPN·3:  $C_{47}H_{30}Fe_3NO_{11}P_2$ , monoclinic,  $I2/a$ ,  $a = 17.686(4) \text{ \AA}$ ,  $b = 14.066(3) \text{ \AA}$ ,  $c = 36.610(7) \text{ \AA}$ ,  $\beta = 93.82(3)^\circ$ ,  $V = 9087(5) \text{ \AA}^3$ ,  $Z = 8$ ,  $R(F) = 10.33\%$ . Additional data on PPN·3 are included in the supplementary material.

All computations used various releases of SHELXTL software (G. Sheldrick) as distributed by Nicolet and Siemens XRD (Madison, WI).

**Acknowledgment.** We thank the U.S. Department of Energy, Office of Basic Energy Sciences, for support of this work, and F.R. acknowledges the Italian Consiglio Nazionale delle Ricerche for a fellowship which

permitted his stay in Pennsylvania. We also thank Prof. A. Ceriotti for the communication of unpublished results.

**Supplementary Material Available:** Lists of atomic positional and  $U(eq)$  parameters, bond lengths, bond angles, and anisotropic thermal parameters for  $[PPh_4][Fe_3(CO)_{11}]$ ,  $[PPN][Fe_3(CO)_{11}]$ ,  $[PPN][HFe_3(CO)_9(\mu_3-NPh)]$ , and  $[PPh_4]_2[Fe_3(CO)_9(\mu_3-NPh)] \cdot 2CH_2Cl_2$  and an ORTEP drawing for  $[PPN][Fe_3(CO)_{11}]$  (29 pages). Ordering information is given on any current masthead page.

OM940577N

**Platinum(II) Aminophosphine– and  
Amidophosphine–Phosphinite Complexes: Synthesis,  
Structure, and Use in Catalytic Asymmetric  
Hydroformylation of Styrene. Crystal Structure of  
[(S)-1-(Diphenylphosphino)-2-(((diphenylphosphino)oxy)-  
methyl)pyrrolidine]dichloroplatinum(II)**

Saïd Naïli, Jean-François Carpentier, Francine Agbossou, and André Mortreux\*

*Laboratoire de Catalyse Hétérogène et Homogène, Groupe de Chimie Organique Appliquée,  
URA CNRS 402, Ecole Nationale Supérieure de Chimie de Lille, B.P. 108,  
59652 Villeneuve d'Ascq Cedex, France*

Guy Nowogrocki and Jean-Pierre Wignacourt

*Laboratoire de Cristallographie et de Physicochimie du Solide, URA CNRS 452, Ecole  
Nationale Supérieure de Chimie de Lille, B.P. 108, 59652 Villeneuve d'Ascq Cedex, France*

Received July 19, 1994<sup>®</sup>

The optically active complexes [PtCl<sub>2</sub>(AMPP)] (**2a–g**; AMPP = aminophosphine– and amidophosphine–phosphinite chelates derived from (S)-2-(hydroxymethyl)pyrrolidine and (S)-2-(hydroxymethyl)-5-pyrrolidinone) have been prepared in high yields from the corresponding ligands (**1a–g**) and Pt(COD)Cl<sub>2</sub> (COD = 1,5-cyclooctadiene). The structure of [PtCl<sub>2</sub>((S)-Ph,Ph-ProNOP)] [(S)-1-(diphenylphosphino)-2-(((diphenylphosphino)oxy)methyl)pyrrolidine]dichloroplatinum(II), (**2a**) has been determined. The compound crystallizes in the orthorhombic space group *P*2<sub>1</sub>2<sub>1</sub>2<sub>1</sub> with *a* = 10.933(6) Å, *b* = 15.646(10) Å, *c* = 16.512(4) Å, and *Z* = 4. The platinum atom has a *cis* square-planar coordination, with angular distortions due to steric factors. <sup>1</sup>H, <sup>13</sup>C{<sup>1</sup>H}, and <sup>31</sup>P{<sup>1</sup>H} NMR spectra of the complexes are also reported. Complexes **2a–g** in combination with SnCl<sub>2</sub>·2H<sub>2</sub>O catalyze the asymmetric hydroformylation of styrene into (S)-2-phenylpropanal with quite slow catalytic rates (100 turnovers in 15–200 h). Various branched/normal (*b/n*) ratios (0.4–0.8) and enantiomeric excess (*ee*) values (40–56%) were obtained. The results suggest that the catalytic activity of the [PtCl<sub>2</sub>(AMPP)] complexes is mainly affected by the aminophosphine moiety of the ligand (highest catalytic activities observed with *N*-diphenylphosphino substituents), whereas the enantioselectivity depends on the nature of the phosphinite part (best optical yields observed with (dicyclohexylphosphino)oxy substituents).

### Introduction

Catalytic asymmetric hydroformylation of olefins is a process of great interest for the preparation of enantiomerically pure aldehydes, useful as building blocks for the synthesis of many biologically active compounds.<sup>1</sup> Platinum–tin and rhodium catalysts modified by chiral phosphines and diphosphines have been mostly used as the catalysts.<sup>1,2</sup> In spite of relatively high enantioselectivities, platinum–tin based catalysts exhibit several disadvantages, mainly low reaction rates and poor

branched to normal regioselectivities for the desired chiral products. In contrast, until recently, rhodium based systems showed good catalytic activities and regioselectivities but suffered from relatively poor enantioselectivities. This last point has been greatly improved by the use of new chiral phosphine–phosphite<sup>3</sup> and binucleating tetraphosphine ligands.<sup>4</sup>

We have extensively studied the synthesis and the catalytic applications of easily accessible ligands, the aminophosphine–phosphinites (abbreviated AMPP). Their high efficiency in transition metal complex catalyzed asymmetric processes such as hydrogenation of dehydroamino acids<sup>5</sup> and activated keto compounds<sup>6</sup> over rhodium- and ruthenium-based catalysts, and the

<sup>®</sup> Abstract published in *Advance ACS Abstracts*, December 15, 1994.

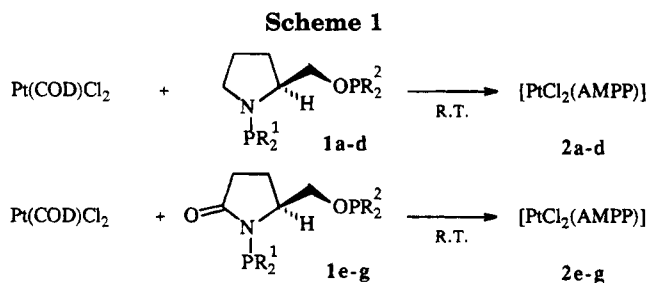
(1) For recent reviews, see: (a) Botteghi, C.; Paganelli, S.; Schionato, A.; Marchetti, M. *Chirality* **1991**, *3*, 355. (b) Stille, J. K. In *Comprehensive Organic Synthesis*; Trost, B. M., Fleming, I., Semmelhack, M. F., Eds.; Pergamon Press: Oxford, England, 1991; p 927. (c) Consiglio, G. In *Catalytic Asymmetric Synthesis*; Ojima, I., Ed.; VCH: New York, 1993; p 273. (d) Noyori, R. In *Asymmetric Catalysis in Organic Synthesis*; Wiley: New York, 1994; p 162.

(2) (a) Consiglio, G.; Pino, P. *Top. Curr. Chem.* **1982**, *105*, 77. (b) Parrinello, G.; Stille, J. K. *J. Am. Chem. Soc.* **1987**, *109*, 7122. (c) Gladioli, S.; Pinna, L. *Tetrahedron: Asymmetry* **1990**, *1*, 693. (d) Stille, J. K.; Su, H.; Brecht, P.; Parrinello, G.; Hegedus, L. S. *Organometallics* **1991**, *10*, 1183. (e) Consiglio, G.; Nefkens, S. C. A.; Borer, A. *Organometallics* **1991**, *10*, 2046. (f) Toth, I.; Guo, I.; Hanson, B. E. *Organometallics* **1993**, *12*, 848. (g) Kollar, L.; Kegl, T.; Bakos, J. J. *Organomet. Chem.* **1993**, *453*, 155.

(3) (a) Sakai, N.; Mano, S.; Nozaki, K.; Takaya, H. *J. Am. Chem. Soc.* **1993**, *115*, 1993. (b) Sakai, N.; Nozaki, K.; Takaya, H. *J. Chem. Soc., Chem. Commun.* **1994**, 395. (c) Higashizima, T.; Sakai, N.; Nozaki, K.; Takaya, H. *Tetrahedron Lett.* **1994**, *35*, 2023.

(4) Stanley, G. G. Abstracts of Papers Presented at the 15th Conference on Catalysis of Organic Reactions, Phoenix, AZ, May 2–5, 1994.

(5) (a) Cesarotti, E.; Chiesa, A.; Ciani, G.; Sironi, A. *J. Organomet. Chem.* **1983**, *251*, 79. (b) Pracejus, G.; Pracejus, H. *J. Mol. Catal.* **1984**, *24*, 227. (c) Karim, A.; Mortreux, A.; Petit, F. *J. Organomet. Chem.* **1986**, *312*, 375. (d) Pavlov, V. A.; Klabunovskii, E. I.; Struchkov, Y. T.; Voloboev, A. A.; Yanovsky, A. I. *J. Mol. Catal.* **1988**, *44*, 217.



1 - 2	R <sup>1</sup>	R <sup>2</sup>
a	Phenyl	Phenyl
b	Cyclohexyl	Phenyl
c	Phenyl	Cyclohexyl
d	Cyclohexyl	Cyclohexyl
e	Phenyl	Phenyl
f	Cyclohexyl	Cyclohexyl
g	Cyclopentyl	Cyclopentyl

formation of carbon-carbon bonds during nickel-<sup>7</sup> and palladium-catalyzed<sup>8</sup> coupling reactions has been reported. These ligands have also proven their ability for the asymmetric hydroformylation of styrene on rhodium and platinum-tin catalytic systems.<sup>9</sup> Thus, we sought to extend our studies to other AMPP ligands. Here, we wish to report the synthesis and the characterization of platinum(II) complexes chelated by aminophosphine- and amidophosphine-phosphinite ligands derived from (*S*)-proline and (*S*)-pyroglutamic acid. The catalytic properties of these compounds have been evaluated in the asymmetric hydroformylation of styrene.

## Results and Discussion

**Synthesis and Characterization.** The complexes  $[\text{PtCl}_2(\text{AMPP})]$  (**2a-g**; AMPP = aminophosphine- and amidophosphine-phosphinites derived from (*S*)-2-(hydroxymethyl)pyrrolidine and (*S*)-2-(hydroxymethyl)-5-pyrrolidinone) were prepared through reaction of  $\text{Pt}(\text{COD})\text{Cl}_2$  and the corresponding ligand (**1a-g**) (Scheme 1).

All the reactions proceeded very readily at room temperature and were almost quantitative. When acetone was used as solvent, a white precipitate of complexes **2a-g** was gradually formed, whereas in dichloromethane, the solution usually remained homogeneous. In both solvents, no side products were detected by  $^{31}\text{P}\{^1\text{H}\}$  NMR spectroscopy of the crude reaction mixture (see below). In contrast to the free ligands, which are quite air sensitive,<sup>10</sup> complexes **2a-g** are stable off-white solids and can be stored in air over long periods of time. Moreover, in solution, with care-

fully degassed mixtures, we observed only a slow decomposition of the complexes due to the formation of phosphine oxides, thus indicating a strong coordination of the ligands to the platinum moiety.

The new complexes **2a-g** have been characterized by  $^{31}\text{P}\{^1\text{H}\}$  NMR spectroscopy (Table 1). A typical spectrum of  $[\text{PtCl}_2((S)\text{-Ph,Ph-ProNOP})]$  (**2a**) is illustrated in Figure 1. The  $^{31}\text{P}\{^1\text{H}\}$  NMR spectrum of the free ligand (*S*)-Ph,Ph-ProNOP (**1a**) consists of two singlets at  $\delta$  46.1 and 113.7 ppm, assigned to the diphenylphosphino groups coordinated to nitrogen and oxygen, respectively.<sup>11</sup> In the platinum complex **2a** (Figure 1), the  $-\text{NPPH}_2$  and  $-\text{OPPh}_2$  resonances consist of two sets of doublets of similar intensity due to coupling between the two phosphorus atoms ( $^2J(\text{P,P}) = 13.8$  Hz) and two doublets of doublets constituting the  $^{195}\text{Pt}$  satellites ( $J(\text{Pt,P(N)}) = 4026$  Hz,  $J(\text{Pt,P(O)}) = 3956$  Hz). The  $-\text{NPPH}_2$  resonance is only 5.8 ppm upfield ( $\delta$  51.9 ppm) from that of the free ligand, whereas the  $-\text{OPPh}_2$  signal shifted 32.2 ppm downfield ( $\delta$  81.5 ppm). Such chemical shift trends are observed for all the complexes. Nevertheless, this behavior is more pronounced with basic ligands, especially those where the phosphorus atom of the P(N) residue is substituted by cyclohexyl groups and, to a lesser extent, by cyclopentyl groups (compare ligands and complexes **b**, **d**, **f**, and **g**).

The 400 MHz  $^1\text{H}$  NMR spectrum of **2a** (see Experimental Section) is complex due to the presence of enantiotopic protons and of strongly coupled spin systems ( $^1\text{H}$ ,  $^{31}\text{P}$ ,  $^{195}\text{Pt}$ ). Nevertheless, the absence of overlapping multiplets allows an assignment of individual proton resonances on the basis of the literature,<sup>11</sup> and this reveals significant shifts of 2-H and 3-H of the coordinated ligand relative to free (*S*)-Ph,Ph-ProNOP.<sup>11</sup>

**Crystal Structure of 2a.** Slow recrystallization from dichloromethane of the crude complex **2a** afforded colorless crystals which proved to be suitable for X-ray investigation. Data were collected on a crystal of **2a**, as summarized in Table 4. A view of the molecule is depicted in Figure 2, together with the numbering scheme adopted. Table 2 lists fractional atomic coordinates and Table 3 selected bond lengths, bond angles, and deviations from the mean plane  $\text{Pt}-\text{Cl}-\text{Cl}-\text{P(N)}-\text{P(O)}$ . The coordination geometry of the platinum atom is close to square planar. The metal-phosphorus bonds ( $\text{Pt}-\text{P(O)} = 2.214(2)$  Å;  $\text{Pt}-\text{P(N)} = 2.238(2)$  Å) are similar to those found in the previously reported complexes containing the (*S*)-Ph,Ph-ProNOP moiety,<sup>5a,d,8,12</sup> except that the  $\text{Pt}-\text{P(O)}$  bond is somewhat shortened (2.214 Å in this complex *vs.* 2.242–2.303 Å in the literature). Both chlorine atoms are located at the same distances from Pt ( $\text{Pt}-\text{Cl} = 2.342(2)$  and  $2.343(2)$  Å) with similar  $\text{Cl}-\text{Pt}-\text{P}$  angles ( $\text{Cl}-\text{Pt}-\text{P(O)} = 86.0(2)^\circ$ ;  $\text{Cl}-\text{Pt}-\text{P(N)} = 90.0(1)^\circ$ ), thus indicating that the two diphenylphosphino moieties induce almost the same hindrance on the square plane. Nevertheless, the orientation of the phenyl rings are different. Those bonded to P(O) are almost symmetrically disposed from each side of the mean square plane (out-of-plane dis-

(6) (a) Hatat, C.; Kokel, N.; Mortreux, A.; Petit, F. *Tetrahedron Lett.* **1990**, *31*, 4139. (b) Roucoux, A.; Agbossou, F.; Mortreux, A.; Petit, F. *Tetrahedron: Asymmetry* **1993**, *4*, 2279. (c) Hapiot, F.; Agbossou, F.; Mortreux, A. *Tetrahedron: Asymmetry* **1994**, *5*, 515.

(7) (a) Buono, G.; Siv, C.; Peiffer, G.; Triantaphylides, C.; Denis, P.; Mortreux, A.; Petit, F. *J. Org. Chem.* **1985**, *50*, 1782. (b) Suisse, I.; Bricout, H.; Mortreux, A. *Tetrahedron Lett.* **1994**, *35*, 413.

(8) Cesarotti, E.; Grassi, M.; Prati, L.; Demartin, F. *J. Chem. Soc., Dalton Trans.* **1991**, 2073.

(9) (a) Mutez, S.; Mortreux, A.; Petit, F. *Tetrahedron Lett.* **1988**, *29*, 1911. (b) Pottier, Y.; Mortreux, A.; Petit, F. *J. Organomet. Chem.* **1989**, *370*, 333.

(10) All the ligands described are air-sensitive. Nevertheless, compounds **1a** and **1e** degrade slower than fully or partially alkylated ligands.

(11) Cesarotti, E.; Grassi, M.; Prati, L. *J. Chem. Soc., Dalton Trans.* **1989**, 161.

(12) (a) Cesarotti, E.; Prati, L.; Sironi, A.; Ciani, G.; White, C. *J. Chem. Soc., Dalton Trans.* **1987**, 1149. (b) Cesarotti, E.; Grassi, M.; Prati, L.; Demartin, F. *J. Organomet. Chem.* **1989**, *370*, 407. (c) Baldovino, C.; Cesarotti, E.; Prati, L.; Demartin, F. *Gazz. Chim. Ital.* **1992**, *122*, 475.

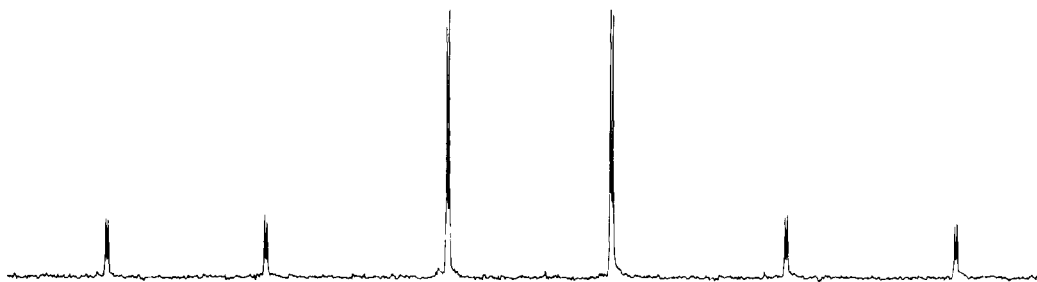


Figure 1. <sup>31</sup>P{<sup>1</sup>H} NMR spectrum of [PtCl<sub>2</sub>((*S*)-Ph,Ph-ProNOP)] (**2a**) (CD<sub>2</sub>Cl<sub>2</sub>, 32.4 MHz).

Table 1. <sup>31</sup>P{<sup>1</sup>H} NMR Data (32.44 MHz, CD<sub>2</sub>Cl<sub>2</sub>, 298 K) for Ligands **1a–g** and Complexes **2a–g**

ligand	δ(P(N)) (ppm)	δ(P(O)) (ppm)	complex	δ(P(N)) (ppm)	δ(P(O)) (ppm)	J(P–P) (Hz)	J(Pt–P(N)) (Hz)	J(Pt–P(O)) (Hz)
<b>1a</b>	46.1	113.7	<b>2a</b>	51.9	81.5	13.8	4026	3956
<b>1b</b>	53.9	113.4	<b>2b</b>	77.6	74.2	7.9	4140	3989
<b>1c</b>	46.6	147.7	<b>2c</b>	50.9	124.9	7.9	4137	3931
<b>1d</b>	53.9	146.5	<b>2d</b>	77.1	125.5	7.0	4060	3928
<b>1e</b>	37.7	117.6	<b>2e</b>	50.5	80.8	13.8	4108	3814
<b>1f</b>	58.8	151.0	<b>2f</b>	83.9	112.4	6.9	4104	3785
<b>1g</b>	59.7	146.1	<b>2g</b>	72.3	121.0	4.1	4030	3943

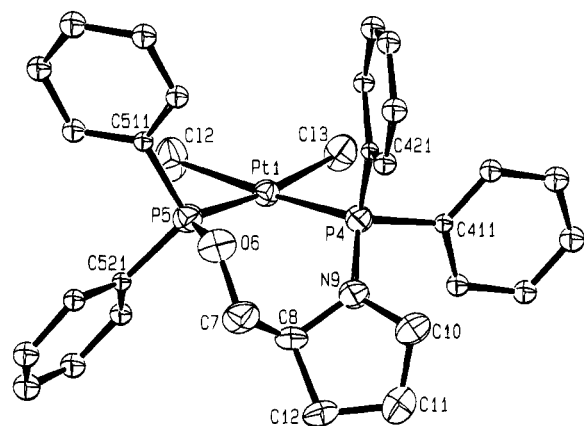


Figure 2. ORTEP drawing for complex **2a** (50% probability ellipsoids).

placements  $-1.275$  and  $1.620$  Å, respectively), whereas the phenyl rings bound to P(N) are unsymmetrically displaced (out-of-plane displacements  $-0.374$  and  $1.673$  Å, respectively). An important widening of the P(N)–Pt–P(O) bond angle ( $95.3(1)^\circ$ ) is observed, inducing by a common "reverse scissoring effect" the decrease of the trans Cl–Pt–Cl bond angle ( $88.4(1)^\circ$ ). The increased P(N)–Pt–P(O) bond angle is ascribed to the rigidity of the seven-membered metallacycle fused with the proline cycle. This metallacycle is in a boat-type conformation, with the oxygen atom in the mean plane as usually observed in (*S*)-Ph,Ph-ProNOP complexes.<sup>5a,d,8,12</sup>

#### Enantioselective Hydroformylation of Styrene.

The aminophosphine–phosphinite complexes of platinum(II) **2a–g** were used along with SnCl<sub>2</sub>·2H<sub>2</sub>O as a cocatalyst in the asymmetric hydroformylation of styrene. Reactions were carried out under classical reaction conditions (Table 5) to give a mixture of the branched (2-phenylpropanal) and the normal (3-phenylpropanal) regioisomers (Scheme 2). The branched to normal ratios (*b/n*) were generally low, the best result being obtained with complex **2e** (0.8). As usually observed, ethylbenzene was formed along with the hydroformylation products during the course of the reaction. Nevertheless, this side reaction remained marginal, except with [PtCl<sub>2</sub>((*S*)-Cp,Cp-oxoProNOP)] (**2g**), which gave 30% of ethylbenzene.<sup>13</sup>

Table 2. Atomic Coordinates for [PtCl<sub>2</sub>((*S*)-Ph,Ph-ProNOP)] (**2a**)

atom	<i>x/a</i>	<i>y/b</i>	<i>z/c</i>	<i>U</i> <sub>eq</sub> , Å <sup>2</sup>
Pt(1)	0.21195(2)	0.06481(2)	0.09579(2)	0.0278(1)
Cl(2)	0.0252(2)	0.1062(2)	0.1534(2)	0.0541(7)
Cl(3)	0.3109(2)	0.1570(1)	0.1864(1)	0.0449(5)
P(4)	0.3935(2)	0.0223(1)	0.0477(1)	0.0313(5)
P(5)	0.1034(2)	-0.0276(1)	0.0241(1)	0.0336(5)
O(6)	0.1783(6)	-0.0897(3)	-0.0357(4)	0.043(2)
C(7)	0.2241(9)	-0.0592(6)	-0.1137(5)	0.045(2)
C(8)	0.2945(8)	0.0224(5)	-0.1065(4)	0.037(2)
N(9)	0.3999(5)	0.0147(5)	-0.0514(4)	0.041(1)
C(10)	0.5139(9)	0.0039(8)	-0.988(7)	0.056(3)
C(11)	0.4871(9)	0.0571(9)	-0.1750(7)	0.068(3)
C(12)	0.3511(9)	0.0493(8)	-0.1909(5)	0.051(3)
C(411)	0.5261(8)	0.0896(5)	0.0712(5)	0.038(2)
C(412)	0.5408(9)	0.1613(7)	0.0225(7)	0.055(3)
C(413)	0.647(1)	0.2138(7)	0.0366(7)	0.062(3)
C(414)	0.729(1)	0.1921(8)	0.0963(8)	0.070(4)
C(415)	0.711(1)	0.1208(8)	0.1432(8)	0.077(4)
C(416)	0.6076(9)	0.0681(7)	0.1308(7)	0.059(2)
C(421)	0.4312(7)	-0.0797(4)	0.0925(5)	0.037(2)
C(422)	0.479(1)	-0.1460(7)	0.0502(7)	0.062(3)
C(423)	0.509(1)	-0.2225(8)	0.0871(8)	0.071(4)
C(424)	0.491(1)	-0.2350(8)	0.1680(7)	0.060(3)
C(425)	0.441(1)	0.1668(8)	0.2136(8)	0.070(3)
C(426)	0.4115(9)	0.0900(6)	0.1761(6)	0.050(3)
C(511)	-0.0158(8)	0.0414(5)	-0.0412(5)	0.042(2)
C(512)	-0.0366(9)	0.1012(7)	-0.0470(7)	0.056(3)
C(513)	-0.122(1)	0.1335(8)	-0.1002(8)	0.068(3)
C(514)	-0.185(1)	0.0781(9)	0.1511(9)	0.091(5)
C(515)	-0.167(1)	0.0077(9)	-0.1448(8)	0.075(4)
C(516)	-0.0812(9)	0.0398(6)	-0.0874(7)	0.054(3)
C(521)	0.0350(8)	-0.1083(5)	0.0878(6)	0.044(2)
C(522)	-0.092(1)	-0.1050(7)	0.1016(8)	0.064(3)
C(523)	-0.145(1)	-0.1688(8)	0.1541(8)	0.073(4)
C(524)	-0.074(1)	-0.2330(9)	0.1845(9)	0.073(4)
C(525)	0.055(1)	0.2355(8)	0.1700(8)	0.071(4)
C(526)	0.106(1)	-0.1737(7)	0.1191(7)	0.061(3)

The activity of the catalytic system involving these aminophosphine–phosphinite ligands was unusually low ( $0.05$ – $6.7$  h<sup>-1</sup>). Nevertheless, the catalytic rate was strongly dependent on the nature of the ligand. Thus, in the case of (*S*)-2-(hydroxymethyl)pyrrolidine-derived complexes (**2a–d**), higher reaction rates were obtained from complexes bearing *N*-diphenylphosphino-substituted ligands, *i.e.* **2a** ( $2.8$  h<sup>-1</sup>) and **2c** ( $2.6$  h<sup>-1</sup>). These

(13) Similar hydroformylation catalyzed by **2g** at 80 °C for 12 h resulted in 96% conversion of styrene with a decrease of the selectivity into ethylbenzene down to 24%; normal and branched aldehydes were obtained in 52% and 24% selectivity (56% ee), respectively.

**Table 3.** Selected Bond Distances (Å), Bond Angles (deg), and Deviations from the Pt(1)–Cl(2)–Cl(3)–P(4)–P(5) Mean Plane (Å)<sup>a</sup>

(a) Bond Distances			
Pt(1)–Cl(2)	2.342(2)	Pt(1)–Cl(3)	2.343(2)
Pt(1)–P(4)	2.238(2)	Pt(1)–P(5)	2.214(2)
P(4)–N(9)	1.643(7)	P(5)–O(6)	1.609(6)
P(4)–C(411)	1.832(9)	P(5)–C(511)	1.813(9)
P(4)–C(421)	1.807(7)	P(5)–C(521)	1.807(9)
N(9)–C(10)	1.482(12)	O(6)–C(7)	1.462(10)
C(10)–C(11)	1.537(17)	C(7)–C(8)	1.495(12)
C(11)–C(12)	1.515(14)	C(8)–N(9)	1.473(10)
C(12)–C(8)	1.582(12)		
(b) Bond Angles			
Cl(2)–Pt(1)–Cl(3)	88.4(1)	P(4)–Pt(1)–P(5)	95.3(1)
Cl(3)–Pt(1)–P(4)	90.0(1)	P(5)–Pt(1)–Cl(2)	86.0(2)
Pt(1)–P(4)–N(9)	114.4(5)	Pt(1)–P(5)–O(6)	116.8(5)
Pt(1)–P(4)–C(411)	117.1(6)	Pt(1)–P(5)–C(511)	117.9(6)
Pt(1)–P(4)–C(421)	108.6(5)	Pt(1)–P(5)–C(521)	111.5(6)
C(411)–P(4)–C(421)	103.9(7)	C(511)–P(5)–C(521)	107.5(9)
C(411)–P(4)–N(9)	102.6(8)	C(511)–P(5)–O(6)	102.6(7)
C(421)–P(4)–N(9)	109.5(8)	C(521)–P(5)–O(6)	98.4(7)
P(4)–N(9)–C(10)	124.8(1.3)	C(11)–C(12)–C(8)	104.7(1.2)
P(4)–N(9)–C(8)	125.2(1.1)	C(12)–C(8)–C(7)	111.0(1.3)
C(10)–N(9)–C(8)	110.0(1.2)	C(12)–C(8)–N(9)	105.0(1.0)
N(9)–C(10)–C(11)	102.1(1.3)	C(8)–C(7)–O(6)	112.7(1.2)
C(10)–C(11)–C(12)	106.6(1.4)	C(7)–O(6)–P(5)	121.1(1.0)
(c) Deviations from the Mean Plane			
Pt(1)	–0.067	C(8)	–1.874(8)
Cl(2)	–0.008(3)	C(7)	–1.110(9)
Cl(3)	0.041(2)	C(411)	–0.374(9)
P(4)	–0.007(2)	C(421)	1.673(8)
P(5)	0.040(2)	C(511)	–1.275(9)
O(6)	0.096(6)	C(521)	1.620(9)
N(9)	–1.066(8)		

$$^a 0.07355x - 0.70831y + 0.70206z - 0.62881 = 0.$$

**Table 4.** Crystallographic Data for [PtCl<sub>2</sub>((S)-Ph,Ph-ProNOP)] (2a)

Crystal Data	
formula	C <sub>29</sub> H <sub>29</sub> Cl <sub>2</sub> NOP <sub>2</sub> Pt
mol wt	735.49
color and habit	colorless prism
space group	P2 <sub>1</sub> 2 <sub>1</sub> 2 <sub>1</sub>
cryst syst	orthorhombic
a, Å	10.933(6)
b, Å	15.646(10)
c, Å	16.512(4)
V, Å <sup>3</sup>	2824
θ range for acc cell, deg	6–20
Z	4
d <sub>calcd</sub> , g cm <sup>–3</sup>	1.730
F(000)	1439
μ(Mo Kα), cm <sup>–1</sup>	53.00
Data Collection and Refinement	
temp, K	298
θ range, deg	2–30
scan type	ω/2θ
cryst size, mm	0.120 × 0.180 × 0.240
no. of data collected	6752
no. of unique data	5726
hkl range	–14, 14; 0, 20; 0, 21
R <sub>merge</sub>	0.0255
std reflns	(205); (332); (125)
observability criterion n, I > nσ(I)	3
no. of data in refinement	5452
no. of refined params	205
final R	0.037
R <sub>w</sub>	0.041

complexes led to almost identical activities, indicating a rather low influence of the phosphinite moiety as long as the nitrogen is substituted by a diphenylphosphino group. The introduction of cyclohexyl substituents at P(N) resulted in a considerable decrease of the catalytic activity (runs 2 and 4): thus, the lowest activity was

observed in the case of complex **2d** (0.05 h<sup>–1</sup>), in which both phosphorus atoms are substituted by cyclohexyl groups. A similar trend was observed for the complexes chelated by ligands derived from (S)-2-(hydroxymethyl)-5-pyrrolidinone, *i.e.* **2e** (6.7 h<sup>–1</sup>) and **2f** (0.44 h<sup>–1</sup>). Furthermore, the introduction of a 5-oxo function in the pyrrolidine cycle has a beneficial effect on the catalytic activity of the platinum complexes, since, for instance, the time required for total conversion of styrene is halved between [PtCl<sub>2</sub>((S)-Ph,Ph-ProNOP)] (**2a**) and [PtCl<sub>2</sub>((S)-Ph,Ph-oxoProNOP)] (**2e**) (run 1 *vs* run 5 and run 4 *vs* run 6). It is noteworthy that some black platinum deposit was usually observed at the end of the reaction with ProNOP-derived complexes (**2a–d**). This deposit was not observed for 5-oxoProNOP-derived complexes (**2e–g**). Moreover, in the case of **2e**, <sup>31</sup>P NMR spectra of the catalytic system (**2e** + SnCl<sub>2</sub>) recorded before and after catalysis were unchanged. These results show that the catalytic activity of [PtCl<sub>2</sub>(AMPP)] complexes is mainly controlled by the aminophosphine moiety of the ligand and suggest that the reaction rate increases with the reduction of the electron density on the P(N) atom. This detrimental effect of basic ligands on both rhodium- and platinum-catalyzed hydroformylation has already been reported.<sup>14</sup>

The regioselectivity of hydroformylation was only slightly affected by the nature of the ligand. Although all the (S)-2-(hydroxymethyl)pyrrolidine-derived ligands gave almost similar selectivities into the branched aldehyde (37–40%), these are only slightly higher than those obtained from oxo derivatives (29–33%). In each case, the prevailing enantiomer had the *S* configuration. Complexes **2a** and **2b**, both bearing –OPPh<sub>2</sub> functions, afforded 2-phenylpropanal in 40–42% ee, whereas the presence of cyclohexyl substituents at the phosphinite function (complex **2c**) resulted in an increased enantiomeric excess of up to 55%. This indicates that the phosphinite moiety of the ligand has a stronger influence than the aminophosphine residue toward enantioselectivity of [PtCl<sub>2</sub>(AMPP)] complexes. This possibility is supported by the fact that both [PtCl<sub>2</sub>((S)-Ph,Ph-ProNOP)] (**2a**) and [PtCl<sub>2</sub>((S)-Ph,Ph-oxoProNOP)] (**2e**) gave nearly the same enantiomeric excesses (42 and 40%, respectively). Similarly, complexes **2c** and **2f**, in which both P(O) moieties are substituted by cyclohexyl groups, led to almost identical enantiomeric excesses (55 and 56%, respectively). The results obtained with cyclopentyl substituents are intermediate between those with phenyl and cyclohexyl groups (runs 5–7).

## Conclusion

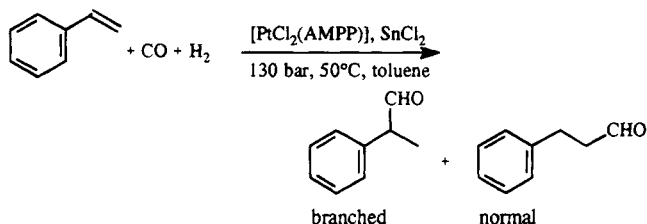
The formation of the platinum(II) aminophosphine–phosphinite complexes described in this study can be readily and cleanly achieved. These compounds, which are very stable under ordinary conditions, catalyze the asymmetric hydroformylation of styrene. Unfortunately, the catalytic activities are very low and the enantioselectivities are only moderate compared to the latest results reported.<sup>3,4</sup> Nevertheless, our results confirm that the aminophosphine and the phosphinite moieties may have different influences on the catalytic properties of the complexes, as already observed during asymmetric hydrogenation processes.<sup>6</sup> Future develop-

Table 5. Asymmetric Hydroformylation of Styrene Catalyzed by Complexes 2a-g<sup>a</sup>

run no.	complex	time <sup>b</sup> (h)	conversion <sup>c</sup> (mol %)	aldehyde n/b <sup>d</sup> (mol %)	hydrogenat <sup>e</sup> (mol %)	ee <sup>f</sup> (%) (config)
1	2a	36	100	59/39	2	42 (S)
2	2b	70	100	52/40	8	40 (S)
3	2c	38	100	62/37	1	55 (S)
4	2d	200	10	54/38	8	nd <sup>g</sup>
5	2e	15	100	68/29	3	40 (S)
6	2f	160	70	62/33	4	56 (S)
7	2g	70	90	47/22	30	47 (S)

<sup>a</sup> Conditions: Temperature, 50 °C; P, 130 atm; H<sub>2</sub>/CO, 1.5; Pt/Sn/styrene, 1/1/100; solvent, toluene. <sup>b</sup> Optimized reaction times in the case of total conversion of styrene. <sup>c</sup> Styrene conversion. <sup>d</sup> Selectivities into 3- and 2-phenylpropanal determined by GLC analysis. <sup>e</sup> Selectivities into ethylbenzene determined by GLC analysis. <sup>f</sup> See Experimental Section. <sup>g</sup> Not determined.

Scheme 2



ments include the design of new ligands and extension of this study to different olefins.

## Experimental Section

**General Considerations.** All reactions were carried out under a dry dinitrogen atmosphere using standard Schlenk techniques. Toluene and diethyl ether were distilled from sodium/benzophenone ketyl. Acetone and dichloromethane were distilled from potassium carbonate and calcium hydride, respectively. Dried solvents were degassed prior to use. The starting compounds Pt(COD)Cl<sub>2</sub><sup>15</sup> and aminophosphine-phosphinite ligands 1a-g<sup>5a,6</sup> were prepared according to literature methods. Styrene was freshly distilled under dinitrogen before use.

Elemental analyses were performed by Laboratoires Wolff, Clichy, France. NMR spectra were recorded at room temperature in CD<sub>2</sub>Cl<sub>2</sub> on Bruker AM-400 (<sup>1</sup>H, 400.1 MHz; <sup>13</sup>C{<sup>1</sup>H}, 100.6 MHz) and WP-80 spectrometers (<sup>31</sup>P{<sup>1</sup>H}, 32.4 MHz). Proton and carbon chemical shifts were referenced internally using the residual solvent resonances relative to tetramethylsilane (δ 0 ppm). Phosphorus chemical shifts were referenced to external 85% H<sub>3</sub>PO<sub>4</sub> (δ 0 ppm). MS (FAB<sup>+</sup>) mass spectra of platinum complexes were obtained in 3-nitrobenzyl alcohol/1,3,5-trichlorobenzene (80/20) v/v matrices by using a CONCEPT II H-H spectrometer (Kratos Analytical Ltd.). The compositions of the catalytic reaction mixtures were determined by GLC analysis with a Delsi 30 gas instrument equipped with a flame ionization detector using a 25 m × 0.25 mm CPSil 5-CB fused silica capillary column. Optical rotations were measured on a Perkin-Elmer 241 polarimeter.

**[(S)-1-(Diphenylphosphino)-2-(((diphenylphosphino)oxy)methyl)pyrrolidine]dichloroplatinum(II) (2a).** Pt(COD)Cl<sub>2</sub> (0.374 g, 1 mmol) was dissolved in acetone (15 mL), and a solution of (S)-Ph,Ph-ProNOP (1a; 0.469 g, 1 mmol) in acetone (5 mL) was added dropwise over 5 min. A white precipitate was gradually formed. After 1 h of stirring at room temperature, the solvent was evaporated under vacuum and the residue was washed with Et<sub>2</sub>O (10 mL) and high-vacuum-dried to give 0.70 g (95%) of complex 2a as a white powder. Anal. Calcd for C<sub>29</sub>H<sub>29</sub>Cl<sub>2</sub>NOP<sub>2</sub>Pt: C, 47.35; H, 3.97; N, 1.90. Found: C, 47.48; H, 4.00; N, 1.91. <sup>1</sup>H NMR: δ 1.31 (m, 1 H, 3-H), 1.66 (m, 1 H, 4-H), 1.81 (m, 1 H, 4-H), 1.97 (m, 1 H, 3-H), 2.57 (m, 1 H, 5-H), 2.97 (m, 1 H, 5-H), 3.32 (m, 1 H, 1-H), 3.63 (m, 1 H, 1-H), 4.75 (m, 1 H, 2-H), 7.10–7.83 (m, 20 H, PPh<sub>2</sub>).

(15) Drew, D.; Doyle, J. R.; Shaver, A. G. *Inorg. Synth.* **1972**, *13*, 47.

<sup>13</sup>C{<sup>1</sup>H} NMR: δ 27.0 (C-4), 28.6 (C-3), 50.4 (C-5), 60.3 (C-2), 70.8 (C-1), 128.3–135.5 (PPh<sub>2</sub>). <sup>31</sup>P{<sup>1</sup>H} NMR: see Table 1.

**[(S)-1-(Dicyclohexylphosphino)-2-(((diphenylphosphino)oxy)methyl)pyrrolidine]-dichloroplatinum(II) (2b).** Pt(COD)Cl<sub>2</sub> (0.374 g, 1 mmol) and (S)-Cy,Ph-ProNOP (1b; 0.482 g, 1 mmol) were reacted in a procedure analogous to that given for 2a. A similar workup gave 0.72 g (96%) of complex 2b as a white solid. Anal. Calcd for C<sub>29</sub>H<sub>41</sub>Cl<sub>2</sub>NOP<sub>2</sub>Pt: C, 46.59; H, 5.53; N, 1.88. Found: C, 46.38; H, 5.56; N, 1.98. MS (FAB<sup>+</sup>; *m/z* (isotopic mass)): 712 [PtCl((S)-Cy,Ph-ProNOP), M - Cl]. <sup>1</sup>H NMR: δ 0.98–2.08 (m, 24 H, Cy H + 3-H + 4-H), 2.60 (m, 1 H, 5-H), 3.11 (m, 3 H, Cy H + 5-H), 3.45 (m, 1 H, 1-H), 3.54 (m, 1 H, 1-H), 4.44 (m, 1 H, 2-H), 7.12–8.02 (m, 10 H, PPh<sub>2</sub>). <sup>13</sup>C{<sup>1</sup>H} NMR: δ 25.2–31.2 (CH<sub>2</sub> Cy, C-3, C-4), 36.7 (CH Cy, *J*(C,P) = 45 Hz), 41.2 (CH Cy, *J*(C,P) = 37 Hz), 46.6 (C-5), 58.8 (C-2), 67.2 (C-1), 128.1–134.9 (PPh<sub>2</sub>). <sup>31</sup>P{<sup>1</sup>H} NMR: see Table 1.

The other complexes (2c–g) were prepared in the same way in almost quantitative yields from the corresponding ligands. All these compounds showed similar characteristics and were essentially characterized by <sup>31</sup>P{<sup>1</sup>H} NMR spectroscopy, which gave evidence of their purity (see Table 1). Their <sup>1</sup>H and <sup>13</sup>C{<sup>1</sup>H} NMR spectra are complex due to the presence of overlapping multiplets and highly coupled systems. The <sup>1</sup>H and <sup>13</sup>C{<sup>1</sup>H} NMR data of [PtCl<sub>2</sub>((S)-Cp,Cp-oxoProNOP)] (2g) are reported below.

**[(S)-1-(Dicyclopentylphosphino)-2-(((dicyclopentylphosphino)oxy)methyl)-5-pyrrolidinone]dichloroplatinum(II) (2g).** <sup>1</sup>H NMR: δ 1.51–2.45 (m, 36 H), 2.69 (m, 1 H), 2.88 (m, 1 H, *J* = 2.3 and 9.5 Hz), 3.02 (dd, 1 H, *J* = 4.9 and 7.3 Hz), 3.33 (sext (virt), 1 H, *J* = 8.9 Hz), 3.72 (m, 1 H), 4.18 (m, 1 H), 4.36 (m, 1 H). <sup>13</sup>C{<sup>1</sup>H} NMR: δ 25.5–32.7 (CH<sub>2</sub> Cp, C-3, C-4), 39.7–42.9 (CH Cp), 59.1 (C-2), 69.4 (C-1), 179.3 (C=O).

**Crystal Structure of 2a.** Suitable crystals were obtained as colorless prisms by slow recrystallization from dichloromethane. The crystal selected was mounted for data collection on an Enraf-Nonius CAD4 diffractometer, as summarized in Table 4. The intensities of 3 representative reflections which were measured after every 2 h remained constant throughout data collection, indicating crystal and electronic stability. Data were corrected for Lorentz and polarization effects but not (since the crystal was small and approximately equidimensioned) for absorption. The atomic coordinates of the platinum atom were deduced from the Patterson function, and the positions of chlorine, phosphorus, oxygen, nitrogen, and carbon atoms were identified from successive difference-Fourier syntheses. All positional and thermal parameters were refined with SHELX-76.<sup>16</sup> The atomic scattering factors for neutral atoms, as well as the anomalous dispersion correction coefficients, were taken from ref 17. The hydrogen atoms could have been identified but were not included in the refinement process. The phenyl carbon atoms were kept isotropic, and the anisotropic refinement of the non-phenyl atoms yielded a final *R* = 0.037 and *R*<sub>w</sub> = 0.041, with *w* = 1/[σ<sup>2</sup>(*F*) + 0.00369*F*<sup>2</sup>] in the final stages.

(16) Sheldrick, G. SHELX-76, System of Crystallographic Computer Programs, University of Cambridge, Cambridge, England, 1976.

(17) Cromer, D. T. *International Tables for X-ray Crystallography*; Kynoch Press: Birmingham, England, 1974; Vol. IV.



**Catalytic Asymmetric Hydroformylations.** All catalytic reactions were conducted in a magnetically stirred and double-walled 50 mL stainless steel reactor. In a typical experiment, a solution of the cocatalyst  $\text{SnCl}_2 \cdot 2\text{H}_2\text{O}$  (0.1 mmol) and of the platinum complex (0.1 mmol) in toluene (10 mL) was introduced in the reactor under dinitrogen. Then, styrene (10 mmol) and the internal standard (*n*-decane) were introduced. The reactor was sealed, pressurized to 130 atm with  $\text{CO}/\text{H}_2$  (2/3), and heated to 50 °C. The reaction was monitored by GLC analysis of aliquots of the reaction mixture. After total consumption of styrene, the reactor was cooled to room temperature and depressurized. The pale yellow solution was analyzed by GLC to determine the selectivities of hydroformylated (branched and normal) products and ethylbenzene. Pentane was added to the crude reaction mixture to precipitate the catalyst. The resulting solid was filtered off, and the remaining solution was then fractionally distilled under vacuum. The optical purity of 2-phenylpropanal was determined by polarimetry on the basis of  $[\alpha]_{\text{D}}^{21} = +315.8^\circ$  (*c* 1.5, benzene) for (*S*)-2-phenylpropanal.<sup>18</sup> The enantiomeric excess

values reported in Table 5 are based on at least three reproducible runs. The estimated accuracy of the enantiomeric excess values is  $\pm 3\%$ .

**Acknowledgment.** This study was supported by the CNRS and SIPSY Co. We thank Dr. B. Mouchel and Dr. G. Ricart for NMR and mass spectrometry assistance. We are indebted to Prof. A. Welch for helpful discussions and for assistance in preparing the manuscript.

**Supplementary Material Available:** Tables of non-phenyl carbon atom anisotropic thermal parameters, phenyl carbon atom isotropic thermal parameters, and all bond distances and angles for **2a** (35 pages). Ordering information is given on any current masthead page.

OM9405706

(18) Consiglio, G.; Pino, P.; Flowers, L. I. *J. Chem. Soc., Chem. Commun.* **1983**, 93.

# Addition Reactions of CpMo(NO)(=CXMe<sub>3</sub>) (X = H, D) Complexes with Heteroatom–Hydrogen Bonds

Peter Legzdins,\* John E. Veltheer, and Michelle A. Young

Department of Chemistry, The University of British Columbia,  
Vancouver, British Columbia, Canada V6T 1Z1

Raymond J. Batchelor and Frederick W. B. Einstein\*

Department of Chemistry, Simon Fraser University,  
Burnaby, British Columbia, Canada V5A 1S6

Received July 20, 1994<sup>®</sup>

A mechanistic study of the thermal decomposition of CpMo(NO)(CD<sub>2</sub>CMe<sub>3</sub>)<sub>2</sub> in solution provides clear evidence for the formation of CpMo(NO)(=CDCMe<sub>3</sub>). This transient 16-electron neopentylidene complex, either  $\alpha$ -protio or  $\alpha$ -deuterio, reacts with the heteroatom–hydrogen bonds of amines and alcohols (EHR; R = alkyl, aryl; E = NH, O) to form neopentyl amide and alkoxide complexes of the general form CpMo(NO)(CH<sub>2</sub>CMe<sub>3</sub>)(ER). The solid-state molecular structure of CpMo(NO)(CH<sub>2</sub>CMe<sub>3</sub>)(NH-*p*-tolyl) (**4**) has been determined as a representative three-legged piano-stool molecule in this class. Crystals of **4** are monoclinic, space group *P*2<sub>1</sub>/*c*, with *a* = 11.243(2) Å, *b* = 9.632(2) Å, *c* = 16.845(3) Å,  $\beta$  = 99.74(1)°, and *Z* = 4; *R*<sub>F</sub> = 0.031 for 2213 data with *I*<sub>0</sub> ≥ 2.5σ(*I*<sub>0</sub>). The pyridine-trapped complexes CpMo(NO)(=CXMe<sub>3</sub>)(py) (X = H, **2**; X = D, **2-d**) function as stable synthetic precursors to CpMo(NO)(=CXMe<sub>3</sub>) and can thus be derivatized to CpMo(NO)(CXHCMe<sub>3</sub>)(ER) complexes (ER = NHR, OR, SCMe<sub>3</sub>, OC(O)Me) when reacted with amines, alcohols, thiols, or carboxylic acids, respectively. Reactions with bifunctional reagents produce bimetallic complexes. Thus, treatment of CpMo(NO)(=CHCMe<sub>3</sub>) with neopentyl glycol, hydroquinone, and water provides [CpMo(NO)(CH<sub>2</sub>CMe<sub>3</sub>)<sub>2</sub>(μ-X)] complexes (X = OCH<sub>2</sub>CMe<sub>2</sub>CH<sub>2</sub>O, OC<sub>6</sub>H<sub>4</sub>O, O, respectively). Labeling studies demonstrate that these conversions involve the addition of the heteroatom–hydrogen bonds to the Mo=C linkage of CpMo(NO)(=CHCMe<sub>3</sub>) in a stereoselective manner rather than protonolysis of the initial dialkyl reagent. The most plausible mechanism for these addition reactions involves initial formation of the EHR adducts CpMo(NO)(=CHCMe<sub>3</sub>)-(EHR), followed by subsequent syn E–H addition across the Mo=C linkage.

## Introduction

In our laboratories we have recently been investigating the synthesis and characterization of Cp'M(NO)R<sub>2</sub> complexes (Cp' = Cp, Cp\*; M = Mo, W; R = alkyl, aryl).<sup>1</sup> In general, these bis(hydrocarbyl) 16-valence-electron complexes are reasonably thermally stable at room temperature either as solids or in solution.<sup>2,3</sup> This stability reflects both the nonbonding nature of the metal-centered LUMO<sup>4</sup> of these complexes and their kinetic inertness toward decomposition. An exception to this generalization is CpMo(NO)(CH<sub>2</sub>CMe<sub>3</sub>)<sub>2</sub>, which is thermally sensitive and decomposes to CpMo(NO)(=CHCMe<sub>3</sub>), at 16-electron neopentylidene complex, and neopentane.<sup>5</sup> The neopentylidene complex may be trapped by a variety of Lewis bases, and we have characterized several 18-electron adduct complexes of the type CpMo(NO)(=CHCMe<sub>3</sub>)L (L = Lewis base).<sup>6</sup> In

this paper, we present full details of our mechanistic investigations into the formation of CpMo(NO)(=CHCMe<sub>3</sub>) by the first-order thermal decomposition of CpMo(NO)(CH<sub>2</sub>CMe<sub>3</sub>)<sub>2</sub>, a process that involves intramolecular  $\alpha$ -hydrogen elimination of neopentane. This behavior is typical of Schrock-type alkylidene complexes which are usually derived via alkane loss from precursors containing *cis*-dialkyl ligands.<sup>7</sup> Even though the 16-electron neopentylidene complex CpMo(NO)(=CHCMe<sub>3</sub>) exists only transiently, its characteristic chemical reactivity can be investigated. In this report we specifically address the characteristic reactivity of CpMo(NO)(=CHCMe<sub>3</sub>) and demonstrate that the complex behaves like a Schrock alkylidene in terms of polarization of its M=C bond but is less reactive toward nonpolar substrates. We also show that the alkylidene complex adds heteroatom–hydrogen bonds, E–H (E = N, O, S), across its Mo=C linkage in a stereoselective manner.

## Experimental Section

All reactions and subsequent manipulations were performed under anaerobic and anhydrous conditions using an atmo-

<sup>®</sup> Abstract published in *Advance ACS Abstracts*, November 15, 1994.

(1) Legzdins, P.; Veltheer, J. E. *Acc. Chem. Res.* **1993**, *26*, 41.  
(2) Legzdins, P.; Rettig, S. J.; Sánchez, L. *Organometallics* **1988**, *7*, 2394.

(3) Dryden, N. H.; Legzdins, P.; Rettig, S. J.; Veltheer, J. E. *Organometallics* **1992**, *11*, 2583.

(4) (a) For Mo see: Legzdins, P.; Rettig, S. J.; Sánchez, L.; Bursten, B. E.; Gatter, M. G. *J. Am. Chem. Soc.* **1985**, *107*, 1411. (b) For W see: Bursten, B. E.; Cayton, R. H. *Organometallics* **1987**, *6*, 2004.

(5) Legzdins, P.; Rettig, S. J.; Veltheer, J. E. *J. Am. Chem. Soc.* **1992**, *114*, 6922.

(6) Legzdins, P.; Rettig, S. J.; Veltheer, J. E.; Batchelor, R. J.; Einstein, F. W. B. *Organometallics* **1993**, *12*, 3575.

(7) Schrock, R. R. *Acc. Chem. Res.* **1979**, *12*, 98.

sphere of prepurified argon. Unless specified otherwise, reactions were effected in cylindrical, thick-walled glass reactors equipped with greaseless stopcocks. General procedures routinely employed in our laboratories have been described in detail previously.<sup>3</sup>

The organometallic precursors used in this work, CpMo(NO)(CX<sub>2</sub>CMe<sub>3</sub>)<sub>2</sub> (X = H, **1**; X = D, **1-d**) and CpMo(NO)(=CHCMe<sub>3</sub>)(py) (**2**), were prepared according to their published procedures.<sup>6</sup> (Me<sub>3</sub>CCH<sub>2</sub>)<sub>2</sub>Mg $\cdot$ x(dioxane) was also prepared by its published procedure.<sup>5</sup> Me<sub>3</sub>CNH<sub>2</sub> (Aldrich) was vacuum-transferred from CaH<sub>2</sub>. Mesitylene (MCB) was dried over CaCl<sub>2</sub> and degassed in vacuo.<sup>9</sup> All other reagents, i.e. (*p*-tol)-NH<sub>2</sub> (Aldrich; *p*-tol = *p*-tolyl), neopentyl glycol (2,2-dimethyl-1,3-propanediol, Eastman Kodak), hydroquinone (1,4-dihydroxybenzene, Mallinckrodt), acetic acid (glacial, Fisher), succinimide (Aldrich), *p*-cresol (Aldrich), *t*-BuSH (Aldrich), phenol (Mallinckrodt), Ph<sub>3</sub>SiOH (Aldrich), Ph<sub>2</sub>SiH<sub>2</sub> (Aldrich), Me<sub>2</sub>CO (BDH), PhCHO (Aldrich), and PhCCH (Aldrich), were used as received.

The column chromatography material used during this work was alumina (80–200 mesh, Fisher neutral, Brockman activity I). Filtrations were performed through Celite 545 diatomaceous earth (Fisher) that had been oven-dried and cooled in vacuo.

**Generation of CpMo(NO)(CH<sub>2</sub>CMe<sub>3</sub>)<sub>2</sub> (**1**) for Preparative Purposes.** In a typical experiment (0.5–5 mmol scale), THF (10 mL/mmol) was vacuum-transferred onto an equimolar mixture of CpMo(NO)Cl<sub>2</sub> and (Me<sub>3</sub>CCH<sub>2</sub>)<sub>2</sub>Mg $\cdot$ x(dioxane) at –78 °C. The stirred reaction mixture was warmed to –40 °C over 1 h to ensure complete reaction. The final red solution of the bis(neopentyl) complex ( $\nu_{\text{NO}}$  1608 cm<sup>-1</sup>) was taken almost to dryness in vacuo at 0 °C. The oily red residue was suspended in Et<sub>2</sub>O (25 mL/mmol), and the red suspension was filtered through a column of chilled (0 °C) alumina. The filtrate was immediately used in further reactions. The yield of CpMo(NO)(CH<sub>2</sub>CMe<sub>3</sub>)<sub>2</sub> (**1**) based on CpMo(NO)Cl<sub>2</sub> was found to be approximately 55%.<sup>6</sup>

**Preparation of CpMo(NO)(=CDCMe<sub>3</sub>)(py) (**2-d**).** CpMo(NO)(CD<sub>2</sub>CMe<sub>3</sub>)<sub>2</sub> (**1-d**; 100 mg, 0.294 mmol) and pyridine (45 mg, 0.569 mmol) were combined in the reaction vessel, Et<sub>2</sub>O (20 mL) was added, and the mixture was stirred for 45 °C for 4 h. The final amber reaction mixture was taken to a brown oil in vacuo. Pentane (20 mL) was added to the oil, and the mixture was stirred at ambient temperature for 30 min. The solvent was removed in vacuo, the remaining yellow-brown powder was dissolved in Et<sub>2</sub>O (20 mL), and the solution was filtered through Celite (2 × 2 cm). The filtrate was concentrated under reduced pressure and was then cooled at –30 °C overnight to induce the deposition of yellow-brown crystals of **2-d** (48 mg, 48% yield). Drying of these crystals in vacuo resulted in their becoming slightly discolored, probably due to their losing some of the coordinated pyridine.

Anal. Calcd for C<sub>15</sub>H<sub>20</sub>N<sub>2</sub>OMo: C, 52.95; H, 5.92; N, 8.23. Found: C, 52.02; H, 5.96; N, 8.09. IR (Nujol):  $\nu_{\text{NO}}$  1532 (vs), 1545 (br, vs) cm<sup>-1</sup>. <sup>1</sup>H NMR (C<sub>6</sub>D<sub>6</sub>):  $\delta$  8.27 (d, 2H, pyridine protons,  $J_{\text{HH}} = 1.5$  Hz), 6.65 (t, 1H, pyridine proton,  $J_{\text{HH}} = 7.9$  Hz), 6.23 (t, 2H, pyridine protons,  $J_{\text{HH}} = 5.8$  Hz), 5.50 (s, 5H, C<sub>5</sub>H<sub>5</sub>), 1.50 (s, 9H, C(CH<sub>3</sub>)<sub>3</sub>). <sup>2</sup>H NMR (C<sub>6</sub>D<sub>6</sub>, 40 MHz):  $\delta$  13.61. Low-resolution mass spectrum (probe temperature 120 °C): *m/z* 343 (P<sup>+</sup>).

**Preparation of CpMo(NO)(CH<sub>2</sub>CMe<sub>3</sub>)(NHR) (R = CMe<sub>3</sub> (**3**), *p*-tol (**4**)).** The reactions leading to **3** and **4** were conducted in a similar manner. A sample of CpMo(NO)(CH<sub>2</sub>CMe<sub>3</sub>)<sub>2</sub> (from 2 mmol of CpMo(NO)Cl<sub>2</sub>) in Et<sub>2</sub>O (50 mL) was prepared in the usual manner. The red solution was treated with an excess of amine introduced either as a solid (*p*-tol)-NH<sub>2</sub>, 600 mg) or by vacuum transfer (Me<sub>3</sub>CNH<sub>2</sub>, ~1 mL), and the mixture was stirred for 8 h in the dark at 15 °C. The final

reaction mixture (brown for **3**, orange for **4**) was taken to dryness, and the excess amine was removed in vacuo. Exposure to dynamic vacuum (5 × 10<sup>-3</sup> mmHg) for several hours at ambient temperature was necessary to sublime all excess (*p*-tol)NH<sub>2</sub> from **4**. CpMo(NO)(CH<sub>2</sub>CMe<sub>3</sub>)(NHCMe<sub>3</sub>) (**3**) was recrystallized from pentane as amber needles in 56% yield. Complex **4**, CpMo(NO)(CH<sub>2</sub>CMe<sub>3</sub>)(NH-*p*-tol), was recrystallized from Et<sub>2</sub>O as orange blocks (33% yield).

**Complex 3.** Anal. Calcd for C<sub>14</sub>H<sub>26</sub>N<sub>2</sub>OMo: C, 50.30; H, 7.84; N, 8.38. Found: C, 50.60; H, 7.79; N, 8.10. IR (Nujol):  $\nu_{\text{NO}}$  1554 (br, vs) cm<sup>-1</sup>. <sup>1</sup>H NMR (C<sub>6</sub>D<sub>6</sub>):  $\delta$  8.92 (br s, 1H, NH), 5.22 (s, 5H, C<sub>5</sub>H<sub>5</sub>), 2.16 (d, 1H, CH<sub>2</sub>,  $J_{\text{HH}} = 11.8$  Hz), 1.61 (d, 1H, CH<sub>2</sub>,  $J_{\text{HH}} = 11.8$  Hz), 1.30 (s, 18H, 2 × C(CH<sub>3</sub>)<sub>3</sub>). <sup>13</sup>C NMR (C<sub>6</sub>D<sub>6</sub>):  $\delta$  102.55 (C<sub>5</sub>H<sub>5</sub>), 68.00 (NHC(CH<sub>3</sub>)<sub>3</sub>), 46.16 (CH<sub>2</sub>), 36.20 (CH<sub>2</sub>C(CH<sub>3</sub>)<sub>3</sub>), 34.24, 32.75 (2 × C(CH<sub>3</sub>)<sub>3</sub>). Low-resolution mass spectrum (probe temperature 180 °C): *m/z* 335 (P<sup>+</sup> – H).

**Complex 4.** Anal. Calcd for C<sub>17</sub>H<sub>24</sub>N<sub>2</sub>OMo: C, 55.44; H, 6.57; N, 7.61. Found: C, 55.25; H, 6.49; N, 7.70. IR (Nujol):  $\nu_{\text{NO}}$  1548 (s), 1563 (sh) cm<sup>-1</sup>. Ratio of isomers 1:1. <sup>1</sup>H NMR (C<sub>6</sub>D<sub>6</sub>):  $\delta$  10.49, 9.84 (br s, 2H, 2 × NH), 7.37, 6.96, 6.81, 6.38 (d, 8H, 2 × *H*<sub>ortho</sub> and 2 × *H*<sub>meta</sub>,  $J_{\text{HH}} = 7.4$  or 9.3 Hz), 5.14, 5.12 (s, 10H, 2 × C<sub>5</sub>H<sub>5</sub>), 2.26 (2 superimposed doublets, 1H each, CH<sub>anti</sub>,  $J_{\text{HH}} = 12.9$  Hz), 2.08, 2.05 (s, 6H, 2 × *p*-CH<sub>3</sub>), 1.82 (d, 1H, CH<sub>syn</sub>,  $J_{\text{HH}} = 10.8$  Hz), 1.67 (d, 1H, CH<sub>syn</sub>,  $J_{\text{HH}} = 11.1$  Hz), 1.32, 1.28 (s, 18H, 2 × C(CH<sub>3</sub>)<sub>3</sub>). <sup>13</sup>C NMR (C<sub>6</sub>D<sub>6</sub>):  $\delta$  153.56, 153.15 (2 × C<sub>ipso</sub>), 133.59, 133.29 (2 × C<sub>para</sub>), 130.08, 129.42 (2 × C<sub>ortho</sub>), 119.80, 119.65 (2 × C<sub>meta</sub>), 103.25, 103.07 (2 × C<sub>5</sub>H<sub>5</sub>), 57.42, 55.18 (2 × CH<sub>2</sub>), 37.52, 36.89 (2 × CMe<sub>3</sub>), 34.05, 33.99 (2 × C(CH<sub>3</sub>)<sub>3</sub>), 20.85 (2 × *p*-CH<sub>3</sub>). Low-resolution mass spectrum (probe temperature 200 °C): *m/z* 370 (P<sup>+</sup>).

**Alternative Preparation of Complexes 3 and 4.** A 30 mg sample of CpMo(NO)(=CHCMe<sub>3</sub>)(py) (**2**) in C<sub>6</sub>D<sub>6</sub> (0.8 mL) in an NMR tube was treated either with solid (*p*-tol)NH<sub>2</sub> (9.5 mg, 1.0 equiv) or with vacuum-transferred Me<sub>3</sub>CNH<sub>2</sub> (excess). The contents of the tube were shaken and then left to stand for 24 h at room temperature, whereupon the once amber solutions appeared red. The excess Me<sub>3</sub>CNH<sub>2</sub> was removed in vacuo. The <sup>1</sup>H NMR spectra of the final reaction mixtures revealed the quantitative conversion of the pyridine complex into **3** or **4**. Signals due to free pyridine ( $\delta$  8.55 (2H), 7.31 (2H), 6.95 (1H) ppm) were also evident in the spectra.

**Generation of CpMo(NO)(CHDCMe<sub>3</sub>)(NHCMe<sub>3</sub>) (**3-d**).** An excess of NH<sub>2</sub>CMe<sub>3</sub> was vacuum-transferred onto CpMo(NO)(=CDCMe<sub>3</sub>)(py) (**2-d**) (10 mg) dissolved in C<sub>6</sub>D<sub>6</sub> (0.8 mL) in an NMR tube. The reaction mixture became red while being heated at 45 °C for 1 h. The excess NH<sub>2</sub>CMe<sub>3</sub> was removed in vacuo. The <sup>1</sup>H NMR spectrum of the residue dissolved in C<sub>6</sub>D<sub>6</sub> confirmed the quantitative conversion of the pyridine complex to **3-d**, signals due to free pyridine also being evident. **3-d** was also obtained by the vacuum transfer of NH<sub>2</sub>CMe<sub>3</sub> onto CpMo(NO)(CD<sub>2</sub>CMe<sub>3</sub>)<sub>2</sub> (**1-d**; 20 mg) dissolved in C<sub>6</sub>D<sub>6</sub> (0.8 mL) in an NMR tube and then heating as described above. Both methods afforded the same product complex (<sup>1</sup>H NMR (C<sub>6</sub>D<sub>6</sub>)  $\delta$  8.92 (br s, 1H, NH), 5.21 (s, 5H, C<sub>5</sub>H<sub>5</sub>), 1.59 (s, 1H, CHD), 1.30 (s, 18H, 2 × C(CH<sub>3</sub>)<sub>3</sub>); <sup>2</sup>H NMR (C<sub>6</sub>D<sub>6</sub>, 40 MHz)  $\delta$  2.12). Prolonged heating or leaving the reaction mixture in C<sub>6</sub>D<sub>6</sub> overnight resulted in further reaction of the product complex.

**Preparation of CpMo(NO)(CHDCMe<sub>3</sub>)(NH-*p*-tolyl) (**4-d**).** In a drybox, solid CpMo(NO)(CD<sub>2</sub>CMe<sub>3</sub>)<sub>2</sub> (**1-d**) (100 mg, 0.296 mmol) and solid (*p*-tol)NH<sub>2</sub> (100 mg, 0.935 mmol, 3.16 equiv) were weighed into the reaction vessel. Et<sub>2</sub>O (10 mL) was vacuum-transferred onto the solids to obtain a red solution which over the course of 24 h turned dark orange while being stirred. The orange solution was taken to dryness, and excess amine was removed by sublimation at room temperature. The remaining orange solid was extracted with Et<sub>2</sub>O (15 mL); the extracts were filtered through Celite (1 × 2 cm), concentrated in vacuo, and crystallized over 1 week at –30 °C. Orange crystals of **4-d** (74 mg, 68% yield) were isolated by removing the mother liquor with a pipet.

(8) Dryden, N. H.; Legzdins, P.; Trotter, J.; Yee, Y. C. *Organometallics* **1991**, *10*, 2857.

(9) Perrin, D. D.; Armarego, W. L. F.; Perrin, D. R. *Purification of Laboratory Chemicals*, 3rd ed.; Pergamon Press: Oxford, U.K., 1988.

Ratio of isomers 1:1. <sup>1</sup>H NMR (C<sub>6</sub>D<sub>6</sub>): δ 10.48, 9.83 (br s, 2H, 2 × NH), 7.36, 6.97, 6.81, 6.38 (d, 8H, 2 × H<sub>ortho</sub> and 2 × H<sub>meta</sub>), J<sub>HH</sub> = 8.1 Hz), 5.14, 5.12 (s, 10H, 2 × C<sub>5</sub>H<sub>5</sub>), 2.08, 2.05 (s, 6H, 2 × *p*-CH<sub>3</sub>), 1.78, 1.63 (br s, 2H, 2 × CHD), 1.32, 1.28 (s, 18H, 2 × C(CH<sub>3</sub>)<sub>3</sub>). <sup>2</sup>H NMR (C<sub>6</sub>H<sub>6</sub>, 40 MHz): δ 2.32 (br s, CHDCMe<sub>3</sub>). Low-resolution mass spectrum (probe temperature 200 °C): *m/z* 371 (P<sup>+</sup>).

**Alternative Preparation of Complex 4-d.** CpMo(NO)(=CDCMe<sub>3</sub>)(py) (**2-d**; 5 mg) and (*p*-tol)NH<sub>2</sub> (1.5 mg, 1.0 equiv) were reacted in a manner similar to that described above for the generation of CpMo(NO)(CHDCMe<sub>3</sub>)(NHCM<sub>3</sub>) (**3-d**) to obtain a C<sub>6</sub>D<sub>6</sub> solution of the desired complex.

**Generation of CpMo(NO)(CH<sub>2</sub>CMe<sub>3</sub>)(NH-*o*-tol) (5).** Samples of CpMo(NO)(=CHCMe<sub>3</sub>)(py) (**2**; 30 mg) and (*o*-tol)NH<sub>2</sub> (9.5 mg, 1.0 equiv) were weighed into an NMR tube. C<sub>6</sub>D<sub>6</sub> (0.8 mL) was added to the tube, and the contents were shaken. After 1 week at ambient temperature, the once amber solution appeared red, and a <sup>1</sup>H NMR spectrum of the reaction mixture revealed the quantitative conversion of the pyridine complex to **5**.

Ratio of isomers 1.7:1. <sup>1</sup>H NMR (C<sub>6</sub>D<sub>6</sub>): δ 10.58 (br s, 1H, NH major), 9.90 (br s, 1H, NH minor), 7.20, 6.91, 6.72 (m, aryl protons of both isomers), 5.21 (s, 5H, C<sub>5</sub>H<sub>5</sub> minor), 5.17 (s, 5H, C<sub>5</sub>H<sub>5</sub> major), 2.41 (two superimposed d, one methylene of each CH<sub>2</sub> major and minor, J<sub>HH</sub> = 9.5 Hz), 1.75 (d, 1H, CH<sub>2</sub> major), second minor CH is obscured, 1.71 (s, 3H, *o*-CH<sub>3</sub> major), 1.60 (s, 3H, *o*-CH<sub>3</sub> minor), 1.38 (s, 9H, C(CH<sub>3</sub>)<sub>3</sub> major), 1.31 (s, 9H, C(CH<sub>3</sub>)<sub>3</sub> minor).

**Generation of CpMo(NO)(CH<sub>2</sub>CMe<sub>3</sub>)(NC(O)CH<sub>2</sub>CH<sub>2</sub>C(O)) (6).** In a drybox, CpMo(NO)(=CHCMe<sub>3</sub>)(py) (10 mg, 0.029 mmol) and succinimide (3 mg, 1 equiv) were weighed into an NMR tube. C<sub>6</sub>D<sub>6</sub> (0.8 mL) was added to the tube, and the contents were shaken for 5 min. After that time a <sup>1</sup>H NMR spectrum of the reaction mixture revealed the quantitative conversion of the pyridine complex of **6**. Signals due to free pyridine were also evident in the spectrum. Over the course of several days at room temperature the neopentyl succinimate complex **6** decomposed completely to a variety of Cp-containing products. Hence, no effort was made to isolate complex **6**.

<sup>1</sup>H NMR (C<sub>6</sub>D<sub>6</sub>): δ 5.25 (s, 5H, C<sub>5</sub>H<sub>5</sub>), 4.56 (d, 1H, CH<sub>2</sub>, J<sub>HH</sub> = 9.6 Hz), 1.90 (s, 4H, succinimide CH<sub>2</sub>), 1.27 (s, 9H, C(CH<sub>3</sub>)<sub>3</sub>), 0.41 (d, 1H, CH<sub>2</sub>, J<sub>HH</sub> = 9.6 Hz).

**Preparation of CpMo(NO)(CH<sub>2</sub>CMe<sub>3</sub>)(OPh) (7).** A solution of CpMo(NO)(CH<sub>2</sub>CMe<sub>3</sub>)<sub>2</sub> (from 1 mmol of CpMo(NO)Cl<sub>2</sub>) in Et<sub>2</sub>O (25 mL) was prepared as described above. The red solution was cannulated into a reaction vessel containing PhOH (250 mg, 2.5 equiv). The resulting solution was stirred in the dark for 12 h, after which time the solvent and excess phenol were removed in vacuo (8 h at room temperature). The residual red oil was dissolved in hexanes (20 mL) and filtered through Celite (1 × 2 cm). The filtrate was concentrated slightly and then maintained at -30 °C for 1 week in a freezer. The red oil which settled was separated from the hexanes mother liquor via cannulation. The oil (~90 mg, ~25% yield) was dried overnight in vacuo.

Anal. Calcd for C<sub>16</sub>H<sub>21</sub>N<sub>2</sub>O<sub>2</sub>Mo: C, 54.09; H, 5.96; N, 3.94. Found: C, 54.32; H, 6.08; N, 4.00. IR (Nujol): ν<sub>NO</sub> 1608–1588 (v br, vs) cm<sup>-1</sup>. <sup>1</sup>H NMR (C<sub>6</sub>D<sub>6</sub>): δ 7.65–6.59 (3 br m, 5H, Ph), 5.19 (s, 5H, C<sub>5</sub>H<sub>5</sub>), 3.51 (d, 1H, CH<sub>2</sub>, J<sub>HH</sub> = 10.2 Hz), 1.41 (d, 1H, CH<sub>2</sub>, J<sub>HH</sub> = 10.2 Hz), 1.15 (s, 9H, C(CH<sub>3</sub>)<sub>3</sub>). <sup>13</sup>C{<sup>1</sup>H} NMR (C<sub>6</sub>D<sub>6</sub>): δ 129.69, 122.39, 117.74, 108.93 (C<sub>aryl</sub>), 104.58 (C<sub>5</sub>H<sub>5</sub>), 77.08 (CH<sub>2</sub>), 39.16 (C(CH<sub>3</sub>)<sub>3</sub>), 33.28 (C(CH<sub>3</sub>)<sub>3</sub>).

**Preparation of CpMo(NO)(CH<sub>2</sub>CMe<sub>3</sub>)(OC<sub>6</sub>H<sub>4</sub>-*p*-Me) (8).** In a glovebox CpMo(NO)(=CHCMe<sub>3</sub>)(py) (100 mg, 0.294 mmol) and *p*-cresol (32 mg, 1.0 equiv) were weighed into the reaction vessel. The vessel was removed from the box, and benzene (10 mL) was vacuum-transferred onto the solids. Over the course of 1 h at room temperature a color change of the stirred mixture from orange to red occurred. The final reaction mixture was taken to dryness in vacuo and was extracted with Et<sub>2</sub>O (10 mL). The extract was filtered through Celite (2 × 2

cm), concentrated in vacuo, and then maintained at -30 °C overnight in a freezer. In total, three fractions of red crystals (96 mg, 88% yield) were isolated by cannulation after repeated concentrations and crystallizations.

Anal. Calcd for C<sub>17</sub>H<sub>23</sub>N<sub>2</sub>O<sub>2</sub>Mo: C, 55.28; H, 6.29; N, 3.79. Found: C, 55.32; H, 6.29; N, 3.85. IR (Nujol): ν<sub>NO</sub> 1612 (vs) cm<sup>-1</sup>. <sup>1</sup>H NMR (C<sub>6</sub>D<sub>6</sub>): δ 7.25 (m, 2H, H<sub>ortho</sub>), 7.03 (m, 2H, H<sub>meta</sub>), 5.21 (s, 5H, C<sub>5</sub>H<sub>5</sub>), 3.43 (d, 1H, CH<sub>2</sub>, J<sub>HH</sub> = 10.8 Hz), 2.12 (s, 3H, *p*-CH<sub>3</sub>), 1.47 (d, 1H, CH<sub>2</sub>, J<sub>HH</sub> = 10.8 Hz), 1.18 (s, 9H, C(CH<sub>3</sub>)<sub>3</sub>). <sup>13</sup>C{<sup>1</sup>H} NMR (C<sub>6</sub>D<sub>6</sub>): δ 131.90, 130.13, 117.42 (C<sub>aryl</sub>), 104.61 (C<sub>5</sub>H<sub>5</sub>), 75.07 (CH<sub>2</sub>), 39.10 (C(CH<sub>3</sub>)<sub>3</sub>), 33.36 (C(CH<sub>3</sub>)<sub>3</sub>), 20.72 (*p*-CH<sub>3</sub>). Low-resolution mass spectrum (probe temperature 100 °C): *m/z* 371 (P<sup>+</sup>), 314 (P<sup>+</sup> - CMe<sub>3</sub>).

**Generation of CpMo(NO)(CHDCMe<sub>3</sub>)(OC<sub>6</sub>H<sub>4</sub>-*p*-Me) (8-d).** Samples of CpMo(NO)(=CDCMe<sub>3</sub>)(py) (**2-d**; 10 mg) and *p*-cresol (3 mg, 1.0 equiv) were reacted in a manner similar to that described above for the generation of CpMo(NO)(CHDCMe<sub>3</sub>)(NHCM<sub>3</sub>) (**3-d**). Alternatively, *p*-cresol (6 mg, 1.0 equiv) could be added to a sample of CpMo(NO)(CD<sub>2</sub>CMe<sub>3</sub>)<sub>2</sub> (**1-d**; 20 mg) dissolved in C<sub>6</sub>D<sub>6</sub> (0.8 mL) in an NMR tube and heated. Both methods afforded the same product complex. <sup>1</sup>H NMR (C<sub>6</sub>D<sub>6</sub>): δ 7.25 (m, 2H, H<sub>ortho</sub>), 7.04 (m, 2H, H<sub>meta</sub>), 5.21 (s, 5H, C<sub>5</sub>H<sub>5</sub>), 2.08 (s, 3H, *p*-CH<sub>3</sub>), 1.45 (s, 1H, CHD), 1.19 (s, 9H, C(CH<sub>3</sub>)<sub>3</sub>). <sup>2</sup>H NMR (C<sub>6</sub>H<sub>6</sub>, 40 MHz): δ 3.43 (br s, CHDCMe<sub>3</sub>).

**Preparation of CpMo(NO)(CH<sub>2</sub>CMe<sub>3</sub>)(OSiPh<sub>3</sub>) (9).** In a glovebox CpMo(NO)(=CHCMe<sub>3</sub>)(py) (102 mg, 0.300 mmol) and Ph<sub>3</sub>SiOH (83 mg, 1.0 equiv) were weighed into a reaction vessel. Benzene (20 mL) was vacuum-transferred onto the solids. The reaction mixture was then warmed to room temperature and stirred for 1.5 h. Over the course of the reaction a color change from amber to dark red-brown occurred. The solvent was removed from the final mixture in vacuo, and the residue was extracted with Et<sub>2</sub>O (2 × 25 mL). The extracts were filtered through Celite (1 × 4 cm), and the filtrate was concentrated under reduced pressure to incipient precipitation. Well-defined red blocks of **9** (121 mg, 75% yield) formed overnight and were isolated by cannulation.

Anal. Calcd for C<sub>28</sub>H<sub>31</sub>N<sub>2</sub>O<sub>2</sub>SiMo: C, 62.55; H, 5.82; N, 2.61. Found: C, 62.63; H, 5.76; N, 2.47. IR (Nujol): ν<sub>NO</sub> 1607 (v br) cm<sup>-1</sup>. <sup>1</sup>H NMR (C<sub>6</sub>D<sub>6</sub>): δ 7.78 (m, 6H, Ph), 7.15 (m, 9H, Ph), 5.07 (s, 5H, C<sub>5</sub>H<sub>5</sub>), 3.79 (d, 1H, CH<sub>2</sub>, J<sub>HH</sub> = 9.9 Hz), 1.01 (s, 9H, C(CH<sub>3</sub>)<sub>3</sub>), 0.99 (d, 1H, CH<sub>2</sub>, J<sub>HH</sub> = 9.9 Hz). <sup>13</sup>C{<sup>1</sup>H} NMR (C<sub>6</sub>D<sub>6</sub>): δ 137.51, 135.74, 129.96, 128.15 (C<sub>aryl</sub>), 104.29 (C<sub>5</sub>H<sub>5</sub>), 83.29 (CH<sub>2</sub>), 39.57 (C(CH<sub>3</sub>)<sub>3</sub>), 33.13 (C(CH<sub>3</sub>)<sub>3</sub>). Low-resolution mass spectrum (probe temperature 150 °C): *m/z* 539 (P<sup>+</sup>), 482 (P<sup>+</sup> - CMe<sub>3</sub>).

**Preparation of [CpMo(NO)(CH<sub>2</sub>CMe<sub>3</sub>)<sub>2</sub>(μ-OC<sub>6</sub>H<sub>4</sub>O)] (10).** A solution of CpMo(NO)(CH<sub>2</sub>CMe<sub>3</sub>)<sub>2</sub> (from 1 mmol of CpMo(NO)Cl<sub>2</sub>) in Et<sub>2</sub>O (25 mL) was generated in the usual manner. The red solution was cannulated into a reaction vessel containing hydroquinone (165 mg, 1.5 mmol, ~3 equiv). The solution was stirred in the dark for 6 h until the reaction mixture consisted of a deep red solution over a black precipitate. The final mixture was taken to dryness, and the residue was extracted with Et<sub>2</sub>O (3 × 30 mL). The combined extracts were filtered through Celite (2 × 5 cm). The red filtrate was concentrated in vacuo and then maintained at -30 °C for 1 week in a freezer. The red crystals (105 mg, 33% yield based on CpMo(NO)Cl<sub>2</sub>) that had formed were isolated by cannulation and dried in vacuo.

Anal. Calcd for C<sub>26</sub>H<sub>36</sub>N<sub>2</sub>O<sub>4</sub>Mo<sub>2</sub>: C, 49.38; H, 5.74; N, 4.43. Found: C, 49.49; H, 5.73; N, 4.28. IR (Nujol): ν<sub>NO</sub> 1595 (vs) cm<sup>-1</sup>; 845, 825, 805 (s) cm<sup>-1</sup>. <sup>1</sup>H NMR (C<sub>6</sub>D<sub>6</sub>): δ 7.34 (br s, 4H, C<sub>6</sub>H<sub>4</sub>), 5.21 (s, 10H, C<sub>5</sub>H<sub>5</sub>), 3.40 (d, 2H, CH<sub>2</sub>, J<sub>HH</sub> = 10.2 Hz), 1.50 (d, 2H, CH<sub>2</sub>, J<sub>HH</sub> = 10.2 Hz), 1.18 (s, 18H, C(CH<sub>3</sub>)<sub>3</sub>). <sup>13</sup>C{<sup>1</sup>H} NMR (C<sub>6</sub>D<sub>6</sub>): δ 118.05 (C<sub>ortho</sub>), 104.66 (C<sub>5</sub>H<sub>5</sub>), 74.57 (CH<sub>2</sub>), 38.98 (C(CH<sub>3</sub>)<sub>3</sub>), 33.36 (C(CH<sub>3</sub>)<sub>3</sub>); C<sub>180</sub> not observed.

**Preparation of [CpMo(NO)(CH<sub>2</sub>CMe<sub>3</sub>)<sub>2</sub>(μ-OCH<sub>2</sub>CMe<sub>2</sub>CH<sub>2</sub>O)] (11).** In a glovebox CpMo(NO)(CHCMe<sub>3</sub>)(py) (320 mg, 0.941 mmol) and neopentyl glycol (49 mg, 0.50 equiv) were weighed into a reaction vessel. The vessel was removed from

the box, benzene (20 mL) was vacuum-transferred onto the solids, and the mixture was stirred. Over the course of 3 days at room temperature a color change from orange to maroon occurred. The final reaction mixture was taken to dryness in vacuo, and the residue was extracted with pentane (25 mL). The extract was filtered through Celite (2 × 2 cm), concentrated in vacuo, and then maintained at -30 °C for several hours. After this time a brown precipitate was separated from the solution by cannulation, and the red solution was returned to the freezer. The desired complex precipitated overnight as a red powder. The red powder was recrystallized from pentane to obtain **11** (149 mg, 50% yield) as an analytically pure red solid.

Anal. Calcd for  $C_{25}H_{42}N_2O_4Mo_2$ : C, 47.92; H, 6.77; N, 4.47. Found: C, 47.94; H, 6.86; N, 4.44. IR (Nujol):  $\nu_{NO}$  1598 (br, s)  $cm^{-1}$ ; 811, 799 (s)  $cm^{-1}$ .  $^1H$  NMR ( $C_6D_6$ ):  $\delta$  5.40 (s, 5H,  $C_5H_5$ ), 5.37 (s, 5H,  $C_5H_5$ ), 4.99 (m, 2H), 4.75 (m, 2H), 2.86 (m, 2H), 1.63 (m, 2H), 1.28 (s, 9H,  $C(CH_3)_3$ ), 1.27 (s, 9H,  $C(CH_3)_3$ ), 0.94 (s, 3H,  $C(CH_3)_2$ ), 0.91 (s, 3H,  $C(CH_3)_2$ ).  $^{13}C\{^1H\}$  NMR ( $C_6D_6$ ):  $\delta$  104.86 ( $C_5H_5$ ), 104.82 ( $C_5H_5$ ), 90.66 ( $OCH_2$ ), 90.30 ( $OCH_2$ ), 63.80 ( $MoCH_2$ ), 63.13 ( $MoCH_2$ ), 40.93 ( $CMe_3$ ), 40.60 ( $CMe_3$ ), 37.99 ( $CMe_2$ ), 33.61 (2 ×  $C(CH_3)_3$ ), 21.58 ( $C(CH_3)_2$ ), 21.51 ( $C(CH_3)_2$ ). Low-resolution mass spectrum (probe temperature 100 °C):  $m/z$  555 ( $P^+$  -  $CHCMe_3$ ).

**Preparation of [CpMo(NO)(CH<sub>2</sub>CMe<sub>3</sub>)<sub>2</sub>(μ-O) (12).** CpMo(NO)(=CHCMe<sub>3</sub>)(py) (180 mg, 0.529 mmol) was treated with water (0.5 mL, excess) in benzene (20 mL). Over the course of 2 h at room temperature the stirred reaction mixture became red-brown. The final mixture was then taken to dryness in vacuo, and Et<sub>2</sub>O (20 mL) was used to extract the brown residue. The red-brown extract was filtered through Celite (2 × 5 cm), concentrated in vacuo, and then maintained at -30 °C for several days. Black-red, air-stable crystals of **12** (100 mg, 70% yield) were isolated by removing the mother liquor via cannula and were dried in vacuo for several hours.

Anal. Calcd for  $C_{20}H_{32}N_2O_3Mo_2$ : C, 44.46; H, 5.97; N, 5.18. Found: C, 44.46; H, 5.99; N, 5.20. IR (Nujol):  $\nu_{NO}$  1599, 1575 (vs)  $cm^{-1}$ ; 839, 804 (m)  $cm^{-1}$ .  $^1H$  NMR ( $C_6D_6$ ):  $\delta$  5.37, 5.30 (two s, 10H,  $C_5H_5$ ), 3.01, 2.72, 1.98, 1.65 (four d, 8H,  $CH_2$ ,  $J_{HH} = 11.4$  Hz), 1.29, 1.25 (two s, 18H,  $C(CH_3)_3$ ).  $^{13}C\{^1H\}$  NMR ( $C_6D_6$ ):  $\delta$  104.98, 104.75 (2 ×  $C_5H_5$ ), 65.83, 64.97 (2 ×  $CH_2$ ), 33.98 (2 ×  $C(CH_3)_3$ ),  $C(CH_3)_3$  not observed. Low-resolution mass spectrum (probe temperature 120 °C):  $m/z$  540 ( $P^+$ ), 262 ( $CpMo(NO)(CH_2CMe_3)^+$ ).

**Preparation of CpMo(NO)(CH<sub>2</sub>CMe<sub>3</sub>)(SCMe<sub>3</sub>) (13).** CpMo(NO)(=CHCMe<sub>3</sub>)(py) (273 mg, 0.803 mmol) in benzene (20 mL) was treated with an excess of 2-methyl-2-propanethiol introduced by vacuum transfer. The reaction mixture was stirred for 1 h until it was deep red, and the solvent and excess thiol were then removed in vacuo. The red residue was extracted with pentane (2 × 10 mL). The extracts were filtered through Celite (1 × 3 cm), concentrated in vacuo, and then maintained at -30 °C overnight. Deep red crystals of **13** were isolated by filtration, and the remaining mother liquor was concentrated and cooled to obtain a second crop of CpMo(NO)(CH<sub>2</sub>CMe<sub>3</sub>)(SCMe<sub>3</sub>) (total 205 mg, 73% yield).

Anal. Calcd for  $C_{14}H_{25}NOSMo$ : C, 47.85; H, 7.19; N, 3.99. Found: C, 47.98; H, 7.12; N, 3.96. IR (Nujol):  $\nu_{NO}$  1631 (s), 1608 (sh)  $cm^{-1}$ .  $^1H$  NMR ( $C_6D_6$ ):  $\delta$  5.15 (s, 5H,  $C_5H_5$ ), 3.05 (d, 1H,  $CH_2$ ,  $J_{HH} = 10.2$  Hz), 1.78 (s, 9H,  $CH_2C(CH_3)_3$ ), 1.24 (s, 9H,  $SC(CH_3)_3$ ), 0.79 (d, 1H,  $CH_2$ ,  $J_{HH} = 10.2$  Hz).  $^{13}C\{^1H\}$  NMR ( $C_6D_6$ ):  $\delta$  101.81 (s,  $C_5H_5$ ), 70.94 (s,  $CH_2$ ), 39.21 (s,  $CH_2C(CH_3)_3$ ), 35.14, 33.72 (s, 2 ×  $C(CH_3)_3$ ). Low-resolution mass spectrum (probe temperature 120 °C):  $m/z$  353 ( $P^+$ ), 295 ( $P^+$  -  $CMe_3$ ).

**Generation of CpMo(NO)(CHDCMe<sub>3</sub>)(SCMe<sub>3</sub>) (13-d).** An excess of HSCMe<sub>3</sub> was vacuum-transferred onto CpMo(NO)(=CHCMe<sub>3</sub>)(py) (**2-d**; 10 mg) in an NMR tube, and the reaction was effected in a manner identical with that described above for the generation of CpMo(NO)(CHDCMe<sub>3</sub>)(NHCMe<sub>3</sub>) (**3-d**) to obtain **13-d**.  $^1H$  NMR ( $C_6D_6$ ):  $\delta$  5.15 (s, 5H,  $C_5H_5$ ),

**Table 1. Crystallographic Data for the Structure Determination of CpMo(NO)(*p*-NHC<sub>6</sub>H<sub>4</sub>Me)(CH<sub>2</sub>CMe<sub>3</sub>)**

formula	MoON <sub>2</sub> C <sub>17</sub> H <sub>24</sub>	cryst syst	monoclinic
fw	368.33	space group	<i>P</i> 2 <sub>1</sub> / <i>c</i>
<i>a</i> (Å) <sup>a</sup>	11.243(2)	$\rho_c$ (g cm <sup>-3</sup> )	1.361
<i>b</i> (Å)	9.632(2)	$\lambda$ (Mo K $\alpha_1$ ) (Å)	0.709 30
<i>c</i> (Å)	16.845(3)	$\mu$ (Mo K $\alpha$ ) (cm <sup>-1</sup> )	7.1
$\beta$ (deg)	99.74(1)	min-max 2 $\theta$ (deg)	4-50
<i>V</i> (Å <sup>3</sup> )	1797.9	transmiss <sup>b</sup>	0.816-0.903
<i>Z</i>	4	cryst dimens (mm)	0.17 × 0.32 × 0.35
<i>R</i> <sub>F</sub> <sup>c</sup>	0.031	<i>R</i> <sub>wF</sub> <sup>d</sup>	0.036

<sup>a</sup> Cell dimensions were determined from 25 reflections ( $36^\circ \leq 2\theta \leq 40^\circ$ ). <sup>b</sup> The data were corrected for the effects of absorption. <sup>c</sup>  $R_F = \sum(|F_o| - |F_c|)/\sum|F_o|$ , for 2213 data ( $I_o \geq 2.5\sigma(I_o)$ ). <sup>d</sup>  $R_{wF} = [\sum(w(|F_o| - |F_c|)^2)/\sum(wF_o^2)]^{1/2}$  for 2213 data ( $I_o \geq 2.5\sigma(I_o)$ );  $w = [\sigma(F_o)^2 + 0.0001F_o^2]^{-1}$ .

1.77 (s, 9H,  $CH_2C(CH_3)_3$ ), 1.22 (s, 9H,  $SC(CH_3)_3$ ), 0.79 (br s, 1H, *CHD*).  $^2H$  NMR ( $C_6H_6$ , 40 MHz):  $\delta$  3.05 (br s,  $CHDCMe_3$ ).

**Preparation of CpMo(NO)(CH<sub>2</sub>CMe<sub>3</sub>)( $\eta^2$ -OC(O)Me) (14).** CpMo(NO)(=CHCMe<sub>3</sub>)(py) (150 mg, 0.441 mmol) in benzene (20 mL) was treated with glacial acetic acid (290  $\mu$ L, 0.5 mmol) dropwise via a microsyringe. The color of the reaction mixture faded from dark orange to yellow as the acetic acid was added. The reaction mixture was stirred for 30 min to ensure complete reaction. The solvent and excess acid were then removed in vacuo. The residue was extracted with pentane (2 × 10 mL). The extracts were filtered through Celite (1 × 3 cm), concentrated in vacuo, and then maintained at -30 °C overnight. Pale orange crystals of **14** (114 mg, 81% yield) were isolated by removing the mother liquor with a pipet.

Anal. Calcd for  $C_{12}H_{19}NO_3Mo$ : C, 44.86; H, 5.97; N, 4.36. Found: C, 45.06; H, 6.13; N, 4.37. IR (Nujol):  $\nu_{NO}$  1612 (s br), 1530, 1426 ( $\nu_{CO}$ )  $cm^{-1}$ .  $^1H$  NMR ( $C_6D_6$ ):  $\delta$  5.14 (s, 5H,  $C_5H_5$ ), 2.73 (d, 1H,  $CH_2$ ,  $J_{HH} = 12.0$  Hz), 1.80 (d, 1H,  $CH_2$ ,  $J_{HH} = 12.0$  Hz), 1.56 (s, 3H,  $CH_3$ ), 1.33 (s, 9H,  $C(CH_3)_3$ ).  $^{13}C\{^1H\}$  NMR ( $C_6D_6$ ):  $\delta$  188.21 (*CO*), 104.21 ( $C_5H_5$ ), 66.98 ( $CH_2$ ), 38.87 ( $C(CH_3)_3$ ), 33.92 ( $C(CH_3)_3$ ), 23.01 ( $CH_3$ ). Low-resolution mass spectrum (probe temperature 120 °C):  $m/z$  323 ( $P^+$ ).

**Other Reactions.**  $Ph_2SiH_2$ ,  $Me_2CO$ ,  $PhCHO$ , and  $PhCCH$  all failed to react with CpMo(NO)(CHCMe<sub>3</sub>)(py) at room temperature, as judged by  $^1H$  NMR spectroscopy of appropriate reaction mixtures in  $C_6D_6$ . Over the course of several days at room temperature the formation of [CpMo(NO)(CHCMe<sub>3</sub>)<sub>2</sub>] could be observed, but it has been previously established that this bimetallic complex forms directly from the pyridine adduct in the absence of any added ligand.<sup>6</sup>

**X-ray Crystallographic Analysis of CpMo(NO)(CH<sub>2</sub>CMe<sub>3</sub>)(NH-*p*-tol) (4).** A crystal of **4** was mounted in a capillary tube under an argon atmosphere. Data were recorded at ambient temperature on an Enraf-Nonius CAD4F diffractometer using graphite-monochromatized Mo K $\alpha$  radiation. Unit-cell dimensions were determined from 25 well-centered reflections ( $36^\circ \leq 2\theta \leq 40^\circ$ ). Two intensity standards were measured for every 1 h of exposure time and declined systematically by 3% during the course of the measurements. The data were corrected for absorption by the Gaussian integration method, and corrections were carefully checked against measured  $\psi$  scans. Data reduction included corrections for intensity scale variation and for Lorentz and polarization effects.

Crystallographic details are summarized in Table 1. Final fractional atomic coordinates for the non-hydrogen atoms and for H(20) are listed in Table 2. The structure was solved from the Patterson map by the heavy-atom method. After the non-hydrogen atoms had been located and refined, an electron-density difference map showed evidence for anisotropic thermal motion for the non-hydrogen atoms and revealed the locations of some of the hydrogen atoms, in particular the anilide hydrogen, H(20).

Anisotropic thermal parameters for all non-hydrogen atoms were included in the refinement. Extreme anisotropy of the refined thermal motion for the methyl carbon atoms of the

**Table 2. Atomic Coordinates and Isotropic or Equivalent Isotropic Temperature Factors (Å<sup>2</sup>) for the Non-Hydrogen Atoms (plus H(20)) of CpMo(NO)(*p*-NHC<sub>6</sub>H<sub>4</sub>Me)(CH<sub>2</sub>CMe<sub>3</sub>)**

atom	<i>x/a</i>	<i>y/b</i>	<i>z/c</i>	<i>U</i> <sub>iso</sub>
Mo	0.39333(3)	0.20762(3)	0.22677(2)	0.053
O	0.3369(2)	-0.0273(3)	0.3276(1)	0.065
N(1)	0.3630(3)	0.0762(3)	0.2923(2)	0.054
N(2)	0.5612(3)	0.2502(4)	0.2719(2)	0.059
C(1)	0.2473(5)	0.1515(7)	0.1136(3)	0.087
C(2)	0.3535(6)	0.0814(5)	0.1082(2)	0.080
C(3)	0.4413(5)	0.1781(5)	0.0963(2)	0.077
C(4)	0.3903(4)	0.3067(5)	0.0949(2)	0.071
C(5)	0.2714(5)	0.2922(6)	0.1058(3)	0.085
C(6) <sup>a</sup>	0.314(1)	0.375(1)	0.289(1)	0.073
C(7) <sup>a</sup>	0.1982(8)	0.3782(9)	0.3249(6)	0.070
C(8) <sup>a</sup>	0.0861(7)	0.367(1)	0.2599(5)	0.106
C(9) <sup>a</sup>	0.1911(8)	0.260(2)	0.3844(8)	0.080
C(10) <sup>a</sup>	0.190(1)	0.514(1)	0.3691(7)	0.115
C(26) <sup>b</sup>	0.296(3)	0.376(2)	0.275(3)	0.073
C(27) <sup>b</sup>	0.188(2)	0.353(2)	0.318(1)	0.070
C(28) <sup>b</sup>	0.096(2)	0.252(2)	0.269(1)	0.106
C(29) <sup>b</sup>	0.235(2)	0.276(4)	0.396(2)	0.080
C(30) <sup>b</sup>	0.121(2)	0.488(2)	0.328(2)	0.115
C(11)	0.6430(3)	0.2187(3)	0.3425(2)	0.053
C(12)	0.7661(4)	0.2298(4)	0.3437(3)	0.067
C(13)	0.8449(4)	0.2030(5)	0.4139(3)	0.076
C(14)	0.8066(4)	0.1625(4)	0.4838(2)	0.064
C(15)	0.6841(3)	0.1532(4)	0.4817(2)	0.059
C(16)	0.6030(3)	0.1801(3)	0.4128(2)	0.057
C(17)	0.8942(4)	0.1336(5)	0.5596(3)	0.086
H(20)	0.593(4)	0.294(4)	0.244(2)	0.07(1)

<sup>a</sup> Site occupancy 0.675(9). <sup>b</sup> Site occupancy 1.0 - 0.675(9) = 0.325.

neopentyl group, as well as evidence from further difference maps, led to this entire group (C(6)–C(10), H(61)–H(103) and C(26)–C(30), H(261)–H(303)) being modeled as unequally disordered between two orientations which differ principally in the rotation about the bond between the quaternary and secondary carbon atoms. This model was developed with the use of geometric restraints. It finally included one set of anisotropic thermal parameters for each pair of carbon atoms and a constrained relative occupancy parameter for the groups. Some soft restraints were retained to stabilize the final cycles of refinement with respect to the unresolved atom pairs.

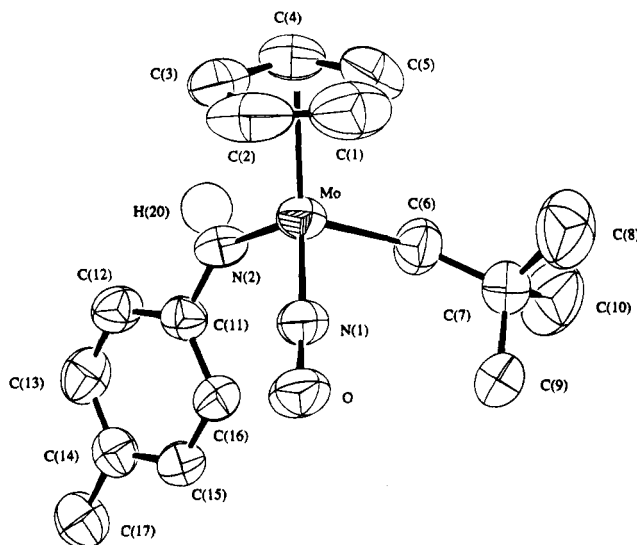
Hydrogen atoms for the neopentyl, cyclopentadienyl, and aryl groups were included at calculated positions (C–H = 0.95 Å). In subsequent cycles of refinement the coordinate shifts for these hydrogen atoms were linked with those of their respectively bound carbon atoms. Two sets of three half-occupancy hydrogen atoms, calculated at fully staggered relative orientations for methyl group C(17), were included as well. The entire ensemble was refined as a rigid group. This treatment accounted for the electron density in the region better than an ordered arrangement. No nonbonded contacts less than the appropriate sums of van der Waals radii were observed between methyl group C(17) and the disordered neopentyl groups. Soft restraints maintaining axial symmetry of this methyl group about the C(14)–C(17) bond were retained in the final cycles of refinement. A single parameter was refined for the net isotropic thermal motion for each of the following groups: H(1)–H(5); H(12)–H(16); H(61), H(62), H(261), and H(262); H(71)–H(103) and H(271)–H(303); H(171)–H(176). Independent coordinates and an isotropic thermal parameter were refined for H(20).

The final full-matrix least-squares refinement involved 218 parameters, 2213 data ( $I_o \geq 2.5\sigma(I_o)$ ), and 32 restraints. An empirical weighting scheme based on counting statistics was applied such that  $w(|F_o| - |F_c|)^2$  was nearly constant as a function of both  $|F_o|$  and  $(\sin \theta)/\lambda$ . The refinement converged at  $R = 0.031$  and  $R_w = 0.036$ . The programs used for absorption corrections, data reduction, structure solution, refinement, and plot generation were from the NRCVAX Crystal Structure System.<sup>10</sup> Final refinement was made using

**Table 3. Selected Metrical Parameters for Complex 4**

Bond Lengths, Å (Esd)			
N(2)–H(20)	0.76(4)	Mo–N(2)	1.955(3)
Mo–C(6)	2.190 <sup>a</sup>	N(1)–O	1.221(3)
Mo–N(1)	1.751(3)		
Bond Angles, deg (Esd)			
C(6)–Mo–N(1)	95.3(5)	Mo–N(2)–H(20)	113.3(32)
N(1)–Mo–N(2)	100.6(1)	Mo–N(2)–C(11)	137.1(3)
N(2)–Mo–C(6)	96.0(5)	C(11)–N(2)–H(20)	109.5(32)
Mo–C(6)–C(7)	130.4 <sup>a</sup>	Mo–N(1)–O	170.2(3)

<sup>a</sup> Parameter restrained during refinement.



**Figure 1.** ORTEP diagram of CpMo(NO)(CH<sub>2</sub>CMe<sub>3</sub>)(NH-*p*-tol) (**4**). Ellipsoids of 50% probability are shown for the non-hydrogen atoms. Hydrogen atoms other than H(20) have been omitted for clarity.

CRYSTALS.<sup>11</sup> Complex scattering factors for neutral atoms<sup>12</sup> were used in the calculation of structure factors. Selected bond lengths and angles are provided in Table 3. A view of the solid-state molecular structure of complex **4** is shown in Figure 1. Anisotropic thermal parameters, complete tables of bond lengths and bond angles (including those involving hydrogen atoms), torsion angles, intermolecular contacts, and least-squares planes are included as supplementary material.

**Kinetic Measurements of the Conversion of CpMo(NO)(CD<sub>2</sub>CMe<sub>3</sub>)<sub>2</sub> (1-*d*<sub>4</sub>) to CpMo(NO)(=CDCMe<sub>3</sub>).** Solid CpMo(NO)(CD<sub>2</sub>CMe<sub>3</sub>)<sub>2</sub> and the appropriate quantity of trapping ligand were weighed into a volumetric flask in a drybox. Dissolution into the appropriate solvent was quickly effected. The volumetric flask was shaken, and an aliquot was transferred to a 1.00-cm UV–vis spectrophotometer cell equipped with a 4-mm Teflon stopcock. The concentration of the trapping ligand was sufficiently high so that all runs were effectively conducted under pseudo-first-order conditions. The cell was quickly removed from the drybox and placed in a cell holder in a Hewlett-Packard 8542A diode array spectrometer. The temperature of the cell holder was maintained constant ( $\pm 0.1$  °C) by a Haake W19 temperature bath equipped with a Haake D8 temperature controller. The solution was left unstirred and allowed to equilibrate with the spectrometer temperature for 300 s. Spectra were then recorded at regular intervals, and data were collected for at least 3 half-lives. The absorbance values at infinity were determined experimentally

(10) Gabe, E. J.; LePage, Y.; Charland, J.-P.; Lee, F. L.; White, P. S. *J. Appl. Chem.* **1989**, *22*, 384.

(11) Watkin, D. J.; Carruthers, J. R.; Betteridge, P. W. *CRYSTALS*; Chemical Crystallography Laboratory, University of Oxford: Oxford, England, 1984.

(12) *International Tables for X-ray Crystallography*; Kynoch Press: Birmingham, England, 1975; Vol. IV, p 99.



by allowing certain runs to proceed for at least 10 half-lives. The measured infinity values were always within 0.1 of computer-optimized infinity values. For example, the infinity value for run 4 was measured to be 0.130, whereas the calculated value for  $A_\infty$  was optimized to 0.1299. The observed rate constants ( $k_{\text{obs}}$ ) were then calculated from plots of  $\ln(A_t - A_\infty)$  versus time (in seconds). Values of  $\Delta H^\ddagger$  and  $\Delta S^\ddagger$  were determined from Eyring plots of  $\ln(k_{\text{obs}}/T)$  versus  $1/T$ , where  $\Delta H^\ddagger = -R(\text{slope})$  and  $\Delta S^\ddagger = R[\text{intercept} - \ln(k_B/h)]$  and  $R$ ,  $k_B$ , and  $h$  are the gas constant, Boltzmann's constant, and Planck's constant, respectively.

## Results and Discussion

In general, 16-electron  $\text{Cp}'\text{M}(\text{NO})\text{R}_2$  complexes are thermally stable at 20 °C when isolated in analytically pure form.<sup>1-3</sup> However, as the electron deficiency of these complexes increases, so too does their thermal sensitivity. Since we have been unable to isolate the most thermally sensitive and most Lewis acidic compounds in this class, namely the  $\text{CpMo}(\text{NO})(\text{aryl})_2$  species, we have not been able to effect a systematic study of their thermal decomposition. The next most thermally sensitive class of these nitrosyl complexes involves the related molybdenum dialkyl complexes  $\text{CpMo}(\text{NO})(\text{alkyl})_2$ .<sup>3</sup> As it turns out, the most thermally sensitive, yet isolable,  $\text{Cp}'\text{M}(\text{NO})\text{R}_2$  complex, namely  $\text{CpMo}(\text{NO})(\text{CH}_2\text{CMe}_3)_2$ , is also the one that decomposes the most cleanly.

**Sources of  $\text{CpMo}(\text{NO})(=\text{CHCMe}_3)$  and  $\text{CpMo}(\text{NO})(=\text{CDCMe}_3)$ .** We have recently reported the synthesis and characterization of the  $\text{CpMo}(\text{NO})(\text{CX}_2\text{CMe}_3)_2$  ( $\text{X} = \text{H}$  (**1**),  $\text{D}$  (**1-d<sub>4</sub>**)) complexes and their reactions with Lewis bases.<sup>6</sup> Complex **1** can be prepared, but due to its propensity to decompose thermally to  $\text{CpMo}(\text{NO})(=\text{CHCMe}_3)$ , it must be used immediately in further derivatization reactions. On the other hand, **1-d<sub>4</sub>** can be crystallized and stored at -30 °C without decomposition. It thus serves as a reasonably stable source of the  $\alpha$ -deuteriocarbene complex  $\text{CpMo}(\text{NO})(=\text{CDCMe}_3)$ . Of the Lewis-base carbene adducts that we prepared previously, only the pyridine adduct  $\text{CpMo}(\text{NO})(=\text{CHCMe}_3)(\text{py})$  (**2**) shows any degree of substitutional lability. Consequently, we now use this adduct as a stable, storable source of the  $\alpha$ -protiocarbene complex  $\text{CpMo}(\text{NO})(=\text{CHCMe}_3)$ .

**Kinetic Studies.** With a reasonable amount of chemical evidence for the transient existence of  $\text{CpMo}(\text{NO})(=\text{CHCMe}_3)$  now being available,<sup>5,6</sup> a kinetic investigation of the trapping reactions forming  $\text{CpMo}(\text{NO})(=\text{CHCMe}_3)\text{L}$  species seemed in order. However, the thermal instability of  $\text{CpMo}(\text{NO})(\text{CH}_2\text{CMe}_3)_2$  makes a kinetic analysis of its thermal decomposition rather difficult. For example, the air-sensitive complex decomposes thermally quite substantially in the time required to get a sample into a drybox. It thus seemed to us that the logical next step was to use its tetra- $\alpha$ -deuterio analogue (**1-d<sub>4</sub>**), since it should show a substantial kinetic isotope effect if  $\alpha$ -H abstraction is a mechanistic path to the transient carbene species.<sup>13</sup> As it turns out, **1-d<sub>4</sub>** is indeed markedly more thermally

(13) Three attempts were made to determine the kinetic isotope effect for this system, but difficulty in handling samples of the nondeuterated dialkyl complex gave unreliable and nonreproducible measurements. The three values of  $k_H/k_D$  that were determined were 4, 7, and 11. It is worth pointing out that isotope effects of approximately 6 are typically observed in  $d^0$  systems.<sup>15</sup>

**Table 4. Monitored Peak UV-Vis Data for  $\text{CpMo}(\text{NO})(\text{CD}_2\text{CMe}_3)_2$  in Various Solvents**

solvent	$\lambda$ (nm)	$\epsilon$ ( $\text{M}^{-1} \text{cm}^{-1}$ )
$\text{CH}_2\text{Cl}_2$	472	390
$\text{Et}_2\text{O}$	484	391
hexanes	490	391
THF	482	393
mesitylene	486	380

**Table 5. Thermal Decomposition Reactions of **1-d<sub>4</sub>** in the Presence of Phosphines in  $\text{CH}_2\text{Cl}_2$ <sup>a</sup>**

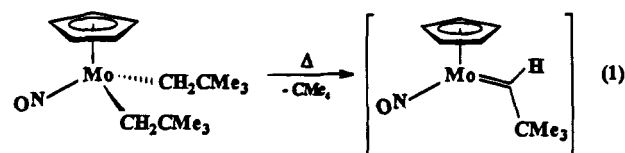
run no.	trapping ligand	[ligand] (M)	amt of ligand (equiv)	$10^4 k_{\text{obs}}$ ( $\text{s}^{-1}$ )
1	$\text{PPh}_2\text{Me}$	$5.994 \times 10^{-3}$	3.56	2.785
2	$\text{PPh}_2\text{Me}$	$8.831 \times 10^{-3}$	5.24	2.514
3	$\text{PPh}_2\text{Me}$	$1.712 \times 10^{-2}$	10.17	2.891
4	$\text{PPh}_2\text{Me}$	$2.298 \times 10^{-2}$	13.64	2.898
5	$\text{PPh}_3$	$1.093 \times 10^{-2}$	6.49	2.930
6	$\text{P}(p\text{-tol})_3$	$1.456 \times 10^{-2}$	9.00	2.935

<sup>a</sup>  $[\text{CpMo}(\text{NO})(\text{CD}_2\text{CMe}_3)_2] = 1.684 \times 10^{-3} \text{ M}$ .

stable than its perhydro congener, and it was thus used in all kinetic investigations. The increased thermal stability of **1-d<sub>4</sub>** is consistent with the view that its primary pathway for thermal decomposition involves  $\alpha$ -H(D) elimination as the rate-determining step. Since the dialkyl complex  $\text{CpMo}(\text{NO})(\text{CD}_2\text{CMe}_3)_2$  is red and its phosphine adducts are yellow, this kinetic study was conducted using UV-vis spectroscopy to monitor the progress of various conversions.  $\text{CpMo}(\text{NO})(\text{CD}_2\text{CMe}_3)_2$  exhibits a band at  $\sim 470$ – $490$  nm in its UV-vis spectra (Table 4), whereas  $\text{CpMo}(\text{NO})(=\text{CDCMe}_3)\text{L}$  complexes show no features in their UV-vis spectra above 400 nm.

**Variation of Ligand and Ligand Concentration.** The formation of  $\text{CpMo}(\text{NO})(=\text{CDCMe}_3)$  from **1-d<sub>4</sub>** is rate-determining. Thus, thermolysis of  $\text{CpMo}(\text{NO})(\text{CD}_2\text{CMe}_3)_2$  in the presence of trapping ligands, L, is clearly first-order in the complex and zero-order in L. The decomposition of  $1.684 \times 10^{-3} \text{ M}$  solutions of **1-d<sub>4</sub>** in  $\text{CH}_2\text{Cl}_2$  at 40 °C in the presence of 3.56, 5.24, 10.17, or 13.64 equiv of  $\text{PPh}_2\text{Me}$ , 6.49 equiv of  $\text{PPh}_3$ , or 9.00 equiv of  $\text{P}(p\text{-tol})_3$  affords  $k_{\text{obs}}$  values of  $(2.83 \pm 0.16) \times 10^{-4} \text{ s}^{-1}$  (all six experiments are tabulated in Table 5). A typical set of spectra and a typical plot are shown in Figure 2.

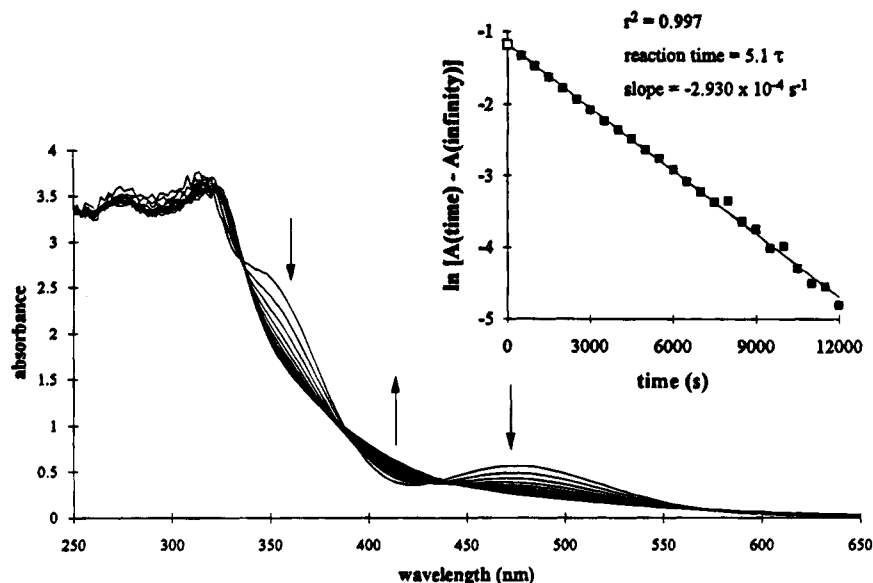
Since the reaction to form adducts of  $\text{CpMo}(\text{NO})(=\text{CHCMe}_3)$  is independent of the nature or concentration of the trapping ligand, an intramolecular elimination of neopentane via an  $\alpha$ -H abstraction reaction as the rate-determining step is strongly indicated as the mechanistic path to the key neopentylidene nitrosyl intermediate (eq 1). The transient neopentylidene



complex has a very short lifetime and in solution is quickly trapped by available phosphine. This conclusion is substantiated by the observation of an isosbestic point in both IR and UV-vis spectral monitoring of these thermolysis reactions.<sup>14</sup>

(14) Ebsworth, E. A. V.; Rankin, D. W. H.; Craddock, S. *Structural Methods in Inorganic Chemistry*; Blackwell Scientific: Oxford, U.K., 1987; p 276.





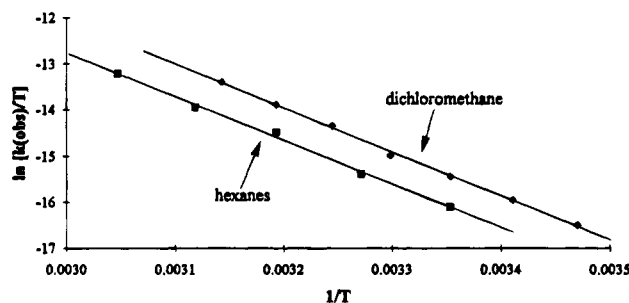
**Figure 2.** Absorption spectral changes for the thermolysis of  $\text{CpMo}(\text{NO})(\text{CD}_2\text{CMe}_3)_2$  in  $\text{CH}_2\text{Cl}_2$  in the presence of 6.49 equiv of  $\text{PPh}_3$  (run 5). Inset: First-order log plot of data (at 472 nm).

**Table 6.** Selected Rate Constants as a Function of Temperature in Various Solvents

solvent	temp ( $^\circ\text{C}$ )	$k_{\text{obs}}$ ( $\text{s}^{-1}$ )	$\ln(k_{\text{obs}}/T)$
$\text{CH}_2\text{Cl}_2$	25.0	$5.856 \times 10^{-5}$	-15.44
	40.0	$2.912 \times 10^{-4}$	-13.89
$\text{Et}_2\text{O}$	25.0	$2.920 \times 10^{-5}$	-16.14
	40.0	$1.515 \times 10^{-4}$	-14.54
hexanes	25.0	$3.010 \times 10^{-5}$	-16.11
	40.0	$1.610 \times 10^{-4}$	-14.48
THF	25.0	$2.491 \times 10^{-5}$	-16.30
	40.0	$1.409 \times 10^{-4}$	-14.61
mesitylene	25.0	$2.757 \times 10^{-5}$	-16.20
	40.0	$1.619 \times 10^{-4}$	-14.48

**Variation of Temperature.** To gain some insight into the nature of the transition state during the generation of  $\text{CpMo}(\text{NO})(=\text{CDCMe}_3)$ , a kinetic analysis at various temperatures was conducted. Measurements were carried out in five solvents under identical chemical conditions. In all 27 runs (summarized in Table 6) the concentration of **1-d<sub>4</sub>** was maintained at  $3.558 \times 10^{-3}$  M (30.0 mg in 25 mL). The trapping ligand used was  $\text{PPh}_2\text{Me}$  (concentration  $2.490 \times 10^{-2}$  M; 124.7 mg in 25 mL, 7.0 equiv).

When rates at one temperature (25  $^\circ\text{C}$ ) are compared, the reaction is clearly fastest in dichloromethane. The other four solvents show very similar rate constants. Thus, if  $k_{\text{obs}}(\text{THF})$  is arbitrarily set at 100, then the rate increases as  $\text{THF}$  (100) < mesitylene (111) <  $\text{Et}_2\text{O}$  (117) < hexanes (121) <  $\text{CH}_2\text{Cl}_2$  (235) at 25  $^\circ\text{C}$ . At 40  $^\circ\text{C}$ , the order changes slightly to  $\text{THF}$  (100) <  $\text{Et}_2\text{O}$  (108) < hexanes (114) < mesitylene (115) <  $\text{CH}_2\text{Cl}_2$  (207). Thus, within the experimental errors of the measurements, dichloromethane doubles the rates for reaction 1, but the rates are nearly independent of all other solvents used in this study. These results may be compared to those observed by Schrock in related studies of some Ta systems for which he found rate constants at room temperature to increase as  $\text{Et}_2\text{O}$  (100) < pentane (200) < benzene (400) <  $\text{CHCl}_3$  and  $\text{CH}_2\text{Cl}_2$  (1500).<sup>15</sup> In both systems halogenated solvents seem to be promoters of  $\alpha$ -H abstraction reactions, but the exact role the solvent



**Figure 3.** Representative Eyring plots for the conversion of  $\text{CpMo}(\text{NO})(\text{CD}_2\text{CMe}_3)_2$  to  $\text{CpMo}(\text{NO})(=\text{CDCMe}_3)$  in hexanes and  $\text{CH}_2\text{Cl}_2$ .

**Table 7.** Activation Parameters Derived from Eyring Plots

run nos.	solvent	$\Delta H^\ddagger$ (kJ/mol)	$\Delta S^\ddagger$ (J/(mol K)) <sup>a</sup>	$\Delta G^\ddagger_{298}$ (kJ/mol)
7-13	$\text{CH}_2\text{Cl}_2$	79.2	-60.1 [-14.4]	97.1
14-18	$\text{Et}_2\text{O}$	81.4	-58.9 [-14.1]	99.0
19-23	hexanes	78.5	-68.1 [-16.3]	98.8
24-28	THF	78.9	-68.1 [-16.3]	99.2
29-33	mesitylene	73.7	-84.0 [-20.1]	98.7

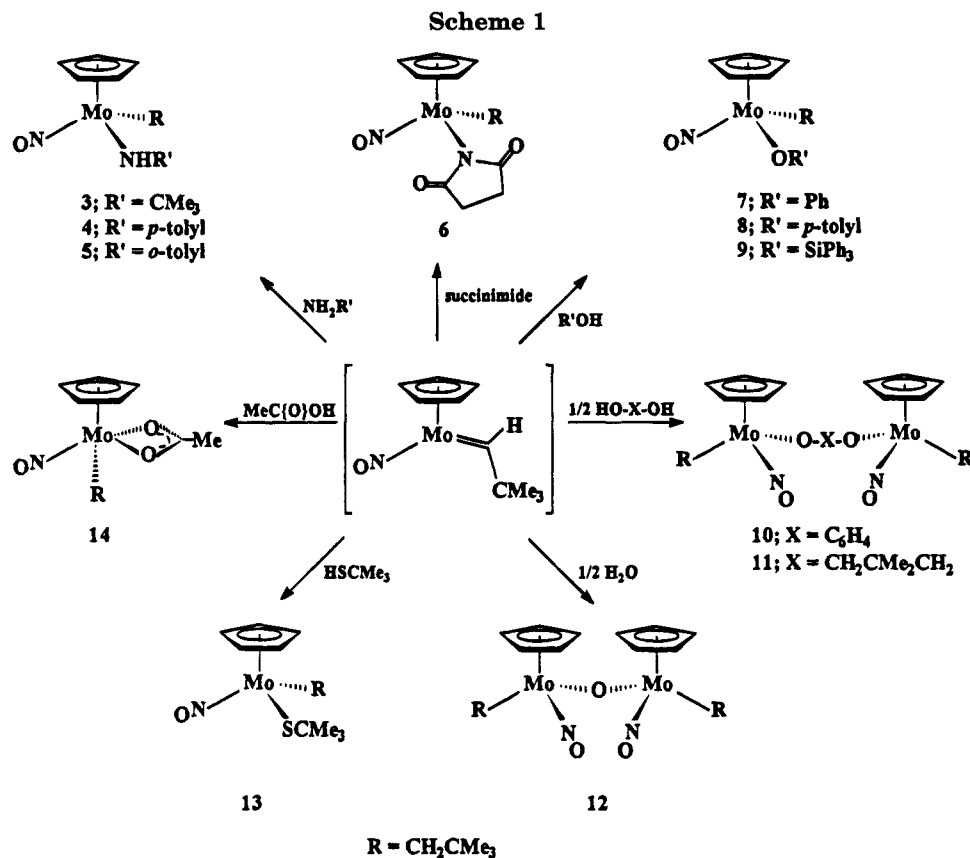
<sup>a</sup>  $\Delta S^\ddagger$  value in brackets is in eu.

plays remains to be ascertained. Conversion of selected data in Table 6 to Eyring plots is shown in Figure 3, and the respective activation parameters for all solvents are compiled in Table 7. It may be noted at this point that kinetic measurements were also attempted in  $\text{CHCl}_3$ , benzene, and toluene, but these three solvents are reactive toward  $\text{CpMo}(\text{NO})(=\text{CDCMe}_3)$  once it is formed.

Consideration of the thermolysis data leads to two conclusions. First, in all cases the entropy of activation is negative, thereby implying a highly ordered transition state.<sup>15</sup> Second, since both  $\Delta H^\ddagger$  and  $\Delta S^\ddagger$  do not vary appreciably with solvent, it appears that the intramolecular expulsion of neopentane in this reaction is not particularly affected by the solvent and that there is a negligible difference in charge separation between the ground state and the transition state for the reaction.

**Nature of  $\text{CpMo}(\text{NO})(=\text{CHCMe}_3)$ .** The exceptional reactivity of the transient carbene complex  $\text{CpMo}(\text{NO})(=\text{CHCMe}_3)$  can be viewed as being reflective of both

(15) Wood, C. D.; McLain, S. J.; Schrock, R. R. *J. Am. Chem. Soc.* **1979**, *101*, 3210.



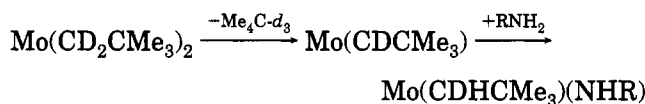
its coordinative and electronic unsaturation. The formation of adducts of this compound converts the 5-coordinate, 16-electron complex to a more stable 6-coordinate, 18-electron species. On the basis of steric grounds it is not unreasonable to expect that free CpMo(NO)(=CHCMe<sub>3</sub>) is a potent Lewis acid, given that its dialkyl precursor, CpMo(NO)(CH<sub>2</sub>CMe<sub>3</sub>)<sub>2</sub>, is Lewis acidic.<sup>1,6</sup>

**Reaction Chemistry of CpMo(NO)(=CHCMe<sub>3</sub>). Addition Reactions with Molecules Containing E–H Bonds (E = N, O, S).** In order to learn more about the chemical nature of the M=C linkage in the transient CpMo(NO)(=CHCMe<sub>3</sub>) complex, we exposed this compound to a variety of organic reagents. Unlike Fischer carbene or Schrock alkylidene complexes, CpMo(NO)(=CHCMe<sub>3</sub>) shows little or no reactivity with olefins, acetylenes, and ketones but is very reactive toward substrates with accessible heteroatom–hydrogen bonds capable of functioning simultaneously as a Lewis base and a Brønsted acid. Substrates (EHR) containing E–H bonds add stereoselectively across the Mo=C double bond of CpMo(NO)(=CHCMe<sub>3</sub>) to produce complexes of the general type CpMo(NO)(CH<sub>2</sub>CMe<sub>3</sub>)(ER), most likely via adducts of the type CpMo(NO)(=CHCMe<sub>3</sub>)(EHR) (vide infra). These chemical transformations are collected in Scheme 1, and identical products result from the reactions of either CpMo(NO)(CH<sub>2</sub>CMe<sub>3</sub>)<sub>2</sub> or CpMo(NO)(=CHCMe<sub>3</sub>)(py) with EHR. In the next paragraphs we consider specific EHR reactants in turn.

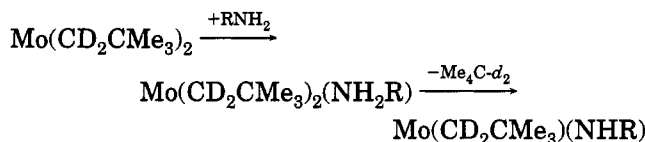
**Amines.** As indicated in Scheme 1, the reactions of CpMo(NO)(CH<sub>2</sub>CMe<sub>3</sub>)<sub>2</sub> with primary alkyl- or arylamines, RNH<sub>2</sub>, produce alkyl- or arylamido complexes of the type CpMo(NO)(CH<sub>2</sub>CMe<sub>3</sub>)(NHR') (R' = CMe<sub>3</sub> (**3**), *p*-tol (**4**), *o*-tol (**5**)).<sup>16</sup> Complex **3** is produced as a single

geometrical isomer, but complexes **4** and **5** form as 1:1 and 1.7:1 mixtures of geometrical isomers, respectively (see Experimental Section), probably resulting from hindered rotation about the multiple Mo–amide linkage (vide infra).<sup>17</sup> In order to determine whether these products arise from protonolysis of the dialkyl complex or NH addition across the Mo=C bond in CpMo(NO)(=CHCMe<sub>3</sub>), control experiments using the deuterated starting material were conducted. The reaction of CpMo(NO)(CD<sub>2</sub>CMe<sub>3</sub>)<sub>2</sub> with (*p*-tol)NH<sub>2</sub> affords CpMo(NO)(CHDCMe<sub>3</sub>)(NH-*p*-tol) (**4-d**), thereby confirming that the mechanism of the reaction proceeds via the carbene complex (route A, Mo = CpMo(NO)) and not via direct protonolysis of an alkyl ligand (route B), which would lead to CpMo(NO)(CD<sub>2</sub>CMe<sub>3</sub>)(NH-*p*-tol) (**4-d**).

route A:



route B:



The other interesting aspect of the reactions of amines with CpMo(NO)(=CDCMe<sub>3</sub>) is that they are stereose-

(16) Related Cp\*–containing alkyl amide complexes have been prepared by metathesis reactions of amines and Cp\*M(NO)(R)Cl: Legzdins, P.; Rettig, S. J.; Ross, K. J. *Organometallics* **1993**, *12*, 2103.

(17) We have also observed the existence of such geometrical isomers in related CpW(NO)(amido)(aryl) complexes: Legzdins, P.; Ross, K. J. Unpublished observations.

lective. Consequently, treatment of CpMo(NO)(CD<sub>2</sub>CMe<sub>3</sub>)<sub>2</sub> or CpMo(NO)(CDCMe<sub>3</sub>)(py) with Me<sub>3</sub>CNH<sub>2</sub> produces a single product complex, **3-d**. This complex, CpMo(NO)(CDHCMe<sub>3</sub>)(NHCMe<sub>3</sub>), has chiral centers at Mo and the alkyl carbon. Hence, in principle, it may be formed in two diastereomeric pairs of enantiomers (*R,S/S,R* and *R,R/S,S*), but experimentally we find that it is formed as only one pair of enantiomers which probably exists as a racemic mixture.

Treatment of a C<sub>6</sub>D<sub>6</sub> solution of CpMo(NO)(=CHCMe<sub>3</sub>)(py) (**2**) with a secondary amine such as succinimide results in the rapid formation of CpMo(NO)-(CH<sub>2</sub>CMe<sub>3</sub>)(NC(O)CH<sub>2</sub>CH<sub>2</sub>C(O)) (**6**) in quantitative yield. This complex, however, decomposes over the course of hours at room temperature and converts to numerous products, as judged by <sup>1</sup>H NMR spectroscopy.

**X-ray Crystallographic Analysis of Complex 4.** Due to the complicated nature of the NMR spectra of complexes **4** and **5**, an X-ray crystallographic analysis of one of these compounds was performed. Complex **4**, CpMo(NO)(CH<sub>2</sub>CMe<sub>3</sub>)(NH-*p*-tol), was chosen since it readily forms X-ray-quality crystals from Et<sub>2</sub>O. The complex is monomeric, its solid-state molecular structure being shown in Figure 1. The internal metrical parameters for the CpMo(NO)(CH<sub>2</sub>CMe<sub>3</sub>) fragment (Table 3) resemble those found in CpMo(NO)(CD<sub>2</sub>CMe<sub>3</sub>)<sub>2</sub> (**1-d**),<sup>6</sup> The anilide hydrogen atom, H(20), lies in the plane defined by Mo–N(2)–C(11) (deviation from the plane 0.03(4) Å), as expected<sup>18</sup> for a planar amide ligand which is providing three electrons to the 15-valence-electron CpMo(NO)(CH<sub>2</sub>CMe<sub>3</sub>) fragment. The Mo–N(2) bond length of 1.955(3) Å appears to be typical for a Mo–NHR linkage.<sup>19</sup> The large Mo–N(2)–C(11) bond angle of 137.1(3)° is also consistent with Mo–N multiple bonding being present in this molecule. These structural aspects of amide ligands are often encountered with coordinatively unsaturated metal complexes in which the amide lone pair is delocalized into an appropriate metal-centered acceptor orbital.<sup>17,20</sup>

The most obvious difference between this structure and that possessed by its parent bis(neopentyl) complex (**1-d**) occurs within the bond angles in the legs of the piano stool. As we have recently discussed in some detail,<sup>1</sup> the bond angles about the metal centers in 16-electron alkyl and aryl complexes, Cp\*M(NO)R<sub>2</sub>, are substantially different. For the complex **1-d** these angles are 97.5(1), 98.3(3), and 111.5(2)°. In the structure of complex **4** the analogous angles are more similar to each other (i.e. 95.3(5), 100.6(1), and 96.0(5)°). Evidently, the ability of the amide ligand to donate extra electron density to the Mo center satisfies some of the electron deficiency inherent in CpMo(NO)-(CD<sub>2</sub>CMe<sub>3</sub>)<sub>2</sub> and effectively negates any open coordination position between the alkyl and amide linkages. Consequently, the angle between the two neopentyl groups in **1-d** is 111.5(1)°, whereas the angle between the neopentyl and anilide groups in **4** is only 96.0(5)°.

(18) Buhro, W. E.; Zwick, B. D.; Georgiou, S.; Hutchinson, J. P.; Gladysz, J. A. *J. Am. Chem. Soc.* **1988**, *110*, 2427.

(19) (a) For example, the average Mo–amide bond length in Mo<sub>2</sub>(OCMe<sub>3</sub>)<sub>4</sub>(PhNH)<sub>2</sub>(PhNH<sub>2</sub>)<sub>2</sub> is 1.97 Å; see: Chisholm, M. H.; Parkin, I. P.; Streib, W. E.; Folting, K. S. *Polyhedron* **1991**, *10*, 2309. (b) This length in [HB(Me<sub>2</sub>pz)<sub>3</sub>]Mo(NH-*n*-Bu)<sub>2</sub> is 1.94 Å; see: Obaidi, N. A.; Hamor, T. A.; Jones, C. J.; McCleverty, J. A.; Paxton, K. J. *Chem. Soc., Dalton Trans.* **1986**, 1525.

(20) Lappert, M. F.; Power, P. P.; Sanger, A. R.; Srivastava, R. C. *Metal and Metalloid Amides*; Wiley: New York, 1980.

The Nujol-mull IR spectra of both **1-d** and **4** are also consistent with these structural observations, since the observed values of ν<sub>NO</sub> for these materials are 1623 and 1548 cm<sup>-1</sup>, respectively, the spatially constricted complex **4** being the weaker Lewis acid by a substantial margin. The above evidence thus indicates that the amide ligand can donate significant amounts of π-electron density to the Mo atom. Multiple-bond character in the Mo–N linkage probably accounts for the two rotational isomers of the complex observed in the room-temperature NMR spectra of complex **4** (vide supra). Furthermore, the planarity of the amide ligand in this complex rules out slow inversion at N as a cause for the existence of two isomers. A variable-temperature NMR study of **4** reveals only line broadening (80 °C in C<sub>6</sub>D<sub>6</sub>) and then decomposition of the compound before any coalescence of signals is observed.

**Alcohols.** Formal addition of the O–H bond of PhOH, *p*-MeC<sub>6</sub>H<sub>4</sub>OH, or Ph<sub>3</sub>SiOH across the Mo=C double bond of CpMo(NO)(=CHCMe<sub>3</sub>) affords the alkoxy alkyl complexes CpMo(NO)(CH<sub>2</sub>CMe<sub>3</sub>)(OPh) (**7**), CpMo(NO)(CH<sub>2</sub>CMe<sub>3</sub>)(OC<sub>6</sub>H<sub>4</sub>-*p*-Me) (**8**), and CpMo(NO)(CH<sub>2</sub>CMe<sub>3</sub>)(OSiPh<sub>3</sub>) (**9**), respectively. Since *p*-cresol reacts with CpMo(NO)(=CDCMe<sub>3</sub>) to afford just one pair of enantiomers of **8-d**, these additions also apparently occur stereoselectively. The phenoxy complex is a red oil at room temperature, but it may be purified by deposition from hexanes at low temperatures. The cresolate complex is a solid which can be easily crystallized from diethyl ether. Complex **7** was synthesized by allowing **1** to thermally decompose in the presence of phenol, whereas complexes **8** and **9** were synthesized by direct addition of cresol or triphenylsilanol to the neopentylidene pyridine adduct **2**. These last two reactions are quantitative in C<sub>6</sub>D<sub>6</sub>, as judged by the NMR spectra of appropriate reaction mixtures, and are complete in less than 1 h at room temperature. The fact that complexes **7–9** are thermally stable indicates that our previously unsuccessful attempts<sup>21</sup> to synthesize CpMo(NO)(R)(OR') complexes were more reflective of the metathesis methodology employed rather than the inherent instability of the product complexes. It may also be noted here that Schrock has shown previously that Cp\*WMe<sub>3</sub>(=CH<sub>2</sub>) reacts with C<sub>6</sub>F<sub>5</sub>OH to give Cp\*WMe<sub>4</sub>(OC<sub>6</sub>F<sub>5</sub>).<sup>22</sup> Osborn has also demonstrated that Mo(NR)(=CHCMe<sub>3</sub>)(CH<sub>2</sub>CMe<sub>3</sub>)<sub>2</sub> reacts with C<sub>6</sub>F<sub>5</sub>OH to produce Mo(NR)(CH<sub>2</sub>CMe<sub>3</sub>)<sub>3</sub>(OC<sub>6</sub>F<sub>5</sub>).<sup>23</sup> Similarly, W(C<sub>6</sub>H<sub>4</sub>CH<sub>2</sub>NMe<sub>2</sub>)(=CHSiMe<sub>3</sub>)(CH<sub>2</sub>SiMe<sub>3</sub>)(=NPh) reacts with *tert*-butyl alcohol to yield W(C<sub>6</sub>H<sub>4</sub>CH<sub>2</sub>NMe<sub>2</sub>)(CH<sub>2</sub>SiMe<sub>3</sub>)<sub>2</sub>(=NPh)(OCMe<sub>3</sub>) but reacts with HOSiPh<sub>3</sub> to produce the new alkylidene complex W(C<sub>6</sub>H<sub>4</sub>CH<sub>2</sub>NMe<sub>2</sub>)(=CHSiMe<sub>3</sub>)(=NPh)(OSiPh<sub>3</sub>).<sup>24</sup> This replacement of an alkyl group by the weakly π-donating triphenylsiloxy group has also been observed by Osborn et al.<sup>23</sup>

Addition of one O–H bond of hydroquinone (1,4-dihydroxybenzene) across the Mo=C bond of CpMo(NO)(=CHCMe<sub>3</sub>) generated in situ results in the production

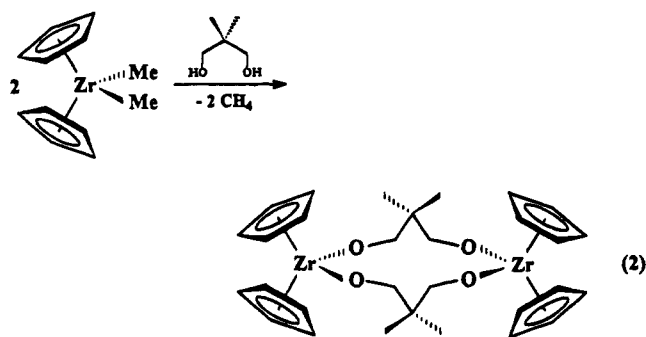
(21) Lundmark, P. J. Ph.D. Dissertation, The University of British Columbia, 1993.

(22) Liu, A. H.; Murray, R. C.; Dewan, J. C.; Santarsiero, B. D.; Schrock, R. R. *J. Am. Chem. Soc.* **1987**, *109*, 4282.

(23) Ehrefeld, D.; Kress, J.; Moore, B. M.; Osborn, J. A.; Schoettel, G. *J. Chem. Soc., Chem. Commun.* **1987**, 129.

(24) Van der Schaaf, P. A.; Grove, D. M.; Smeets, W. J. J.; Spek, A. L.; van Koten, G. *Organometallics* **1993**, *12*, 3955.

of the bimetallic complex  $[\text{CpMo}(\text{NO})(\text{CH}_2\text{CMe}_3)_2(\mu\text{-OC}_6\text{H}_4\text{O})]$  (**10**). NMR spectroscopy indicates that both ends of this molecule are magnetically equivalent. The reaction leading to **10** occurs in the presence of excess hydroquinone, but no monomeric  $\text{CpMo}(\text{NO})(\text{CH}_2\text{CMe}_3)(\text{OC}_6\text{H}_4\text{OH})$  species can be isolated from the final reaction mixture. Evidently, the OH bond in this putative intermediate complex is considerably more reactive than are the OH bonds of the diol reagent. In a similar manner, the addition of neopentyl glycol to **2** results in the formation of the analogous bimetallic complex **11** (Scheme 1). Interestingly, work by Stephan<sup>25</sup> has shown that treatment of  $\text{Cp}_2\text{ZrMe}_2$  with neopentyl glycol does not afford the cyclic bis(alkoxide) complex but rather a bimetallic complex with two bridging dialkoxy ligands (eq 2).



Our experimental results are consistent with the existence of  $\text{Mo}-\text{CH}_2\text{CMe}_3$  bonds in the alkoxo alkyl complexes that are stable to alcohols. For instance, treatment of a  $\text{CpMo}(\text{NO})(\text{CH}_2\text{CMe}_3)(\text{OR})$  complex with an excess of ROH does not lead to the formation of  $\text{CpMo}(\text{NO})(\text{OR})_2$  under ambient conditions.

**Water.** Treatment of the pyridine adduct **2** with water leads to the bridging oxo complex  $[\text{CpMo}(\text{NO})(\text{CH}_2\text{CMe}_3)_2(\mu\text{-O})]$  (**12**) (Scheme 1). Crystals of **12** are air-stable, red, and diamagnetic. NMR spectra of complex **12** indicate that it exists as a mixture of isomers (1:1 ratio), a feature that we have found for other complexes of the general type  $[\text{Cp}'\text{Mo}(\text{NO})\text{R}]_2(\mu\text{-O})$ , which are formed by direct hydrolysis of  $\text{Cp}'\text{Mo}(\text{NO})\text{-R}_2$  complexes.<sup>26</sup>

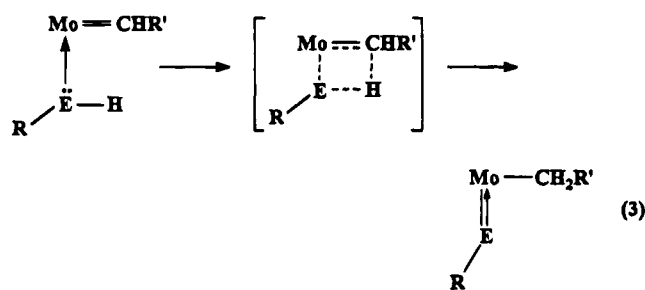
**Thiol.** Treatment of the pyridine adduct **2** with 2-methyl-2-propanethiol results in the rapid formation of the neopentyl thiolate complex  $\text{CpMo}(\text{NO})(\text{CH}_2\text{CMe}_3)(\text{SCMe}_3)$  (**13**; 100% by  $^1\text{H}$  NMR; 72% isolated yield) in a manner completely analogous to that of the neopentyl alkoxide complexes considered above. Again, this addition proceeds stereoselectively since the analogous reaction of  $\text{CpMo}(\text{NO})(=\text{CDCMe}_3)$  with an excess of  $\text{HSCMe}_3$  affords a single pair of enantiomers of the product complex **13-d**. Complex **13** probably has a molecular structure similar to that possessed by  $\text{CpW}(\text{NO})(\text{CH}_2\text{SiMe}_3)(\text{SCH}_2\text{SiMe}_3)$ , which we have previously prepared by the insertion of elemental sulfur into  $\text{CpW}(\text{NO})(\text{CH}_2\text{SiMe}_3)_2$ .<sup>27</sup>

**Acetic Acid.** The reaction of complex **2** with acetic acid is instantaneous and quantitative, and the transformation is accompanied by a color change from amber

to pale yellow. The acetate complex formed (**14**) is stable to the presence of excess acetic acid, a fact which again shows the resistance of the  $\text{Mo}-\text{CH}_2\text{CMe}_3$  bond to protonolysis (vide supra).<sup>28</sup> Complex **14** is formulated as containing an  $\eta^2\text{-OC}(\text{O})\text{Me}$  group (Scheme 1) because of the difference between the symmetric and asymmetric stretching modes of the CO moieties in its Nujol-mull IR spectrum. These two bands at 1426 and 1530  $\text{cm}^{-1}$  are separated by 104  $\text{cm}^{-1}$ , which is well within the range normally associated with bidentate carboxylate ligands.<sup>29</sup>

**Carbon and Silicon Acids and Related Compounds.** The carbene complex **2** is unreactive toward  $\text{PhCHO}$ ,  $\text{Me}_2\text{CO}$ , or  $\text{PhCCH}$ . Like their carbon analogues, Si-H bonds also fail to react with **2**. Since the  $\text{p}K_a$  of phenylacetylene ( $\sim 29$ , DMSO)<sup>30</sup> is much lower than that of amines which do react with **2** (vide supra), it clearly indicates that formation of a Lewis-base-Lewis-acid adduct is paramount to the eventual formation of addition products. This point is discussed further in the next section.

**Mechanistic Considerations.** In the light of the results discussed in the preceding sections, the most plausible mechanistic pathway for the reactions outlined in Scheme 1 is shown in eq 3. Previous work has shown



that the pyridine ligand of complex **2** is readily substituted by Lewis bases such as  $\text{PMe}_3$ .<sup>6</sup> Since  $\text{E}-\text{H}$  ( $\text{E} = \text{C}, \text{Si}$ ) bonds fail to react with **2**, it appears that initial formation of a Lewis-base-Lewis-acid adduct (on the left in eq 3) either by trapping of  $\text{CpMo}(\text{NO})(=\text{CHCMe}_3)$  or by displacement of pyridine from **2** is essential for the formation of the addition products  $\text{CpMo}(\text{NO})(\text{CH}_2\text{CMe}_3)(\text{ER})$ . Monitoring of the reaction of  $\text{CpMo}(\text{NO})(=\text{CHCMe}_3)(\text{py})$  with  $\text{Ph}_3\text{SiOH}$  by low-temperature NMR spectroscopy fails to reveal the presence of any intermediate species such as the putative alcohol complex  $\text{CpMo}(\text{NO})(=\text{CHCMe}_3)(\text{O}(\text{H})\text{SiPh}_3)$ . Nevertheless, we favor the base exchange followed by proton transfer (possibly via a four-center transition state) on the basis of our prior studies.

**Related Research Efforts.** Addition reactions of nucleophilic carbene complexes with acids such as  $\text{HCl}$  have been reported.<sup>31</sup> However, similar transformations with covalent heteroatom-hydrogen bonds are relatively rare. In addition to the chemistry presented in

(28) Legzdins, P.; Rettig, S. J.; Ross, K. J. Submitted for publication.

(29) (a) Darensbourg, D. J.; Grottsch, G.; Wiegrefe, P.; Rheingold, A. *Inorg. Chem.* **1987**, *26*, 3827. (b) Coutts, R. S. P.; Wailes, P. C. *Aust. J. Chem.* **1967**, *20*, 1579.

(30) Lowry, K. S.; Richardson, T. H. *Mechanism and Theory in Organic Chemistry*; Harper and Row: New York, 1987.

(31) Hill, A. F.; Roper, W. R.; Waters, J. M.; Wright, A. H. *J. Am. Chem. Soc.* **1983**, *105*, 5939.

(25) Stephan, D. W. *Organometallics* **1990**, *9*, 2718.

(26) Legzdins, P.; Lundmark, P. J.; Phillips, E. C.; Rettig, S. J.; Veltheer, J. E. *Organometallics* **1992**, *11*, 2991.

(27) Evans, S. V.; Legzdins, P.; Rettig, S. J.; Sánchez, L.; Trotter, J. *Organometallics* **1987**, *6*, 7.

this paper, the best studied other example comes from the Bergman group, who showed that Cp\*Ir(PMe<sub>3</sub>)(=CH<sub>2</sub>) reacts with phenols, primary alcohols, succinimide, and 2-methyl-2-propanethiol to afford alkoxide, hydride, amide, and thiolate methyl complexes, respectively.<sup>32</sup> Interestingly, CO<sub>2</sub> also reacts with Cp\*Ir(PMe<sub>3</sub>)(=CH<sub>2</sub>) to form an addition product, Cp\*Ir(PMe<sub>3</sub>)(CH<sub>2</sub>C(O)O), but olefins and acetylenes fail to give addition products. Thus, both Cp\*Ir(PMe<sub>3</sub>)(=CH<sub>2</sub>) and CpMo(NO)(=CHCMe<sub>3</sub>)(py) have a very polar M=C bond and are very nucleophilic at C<sub>α</sub>.

An interesting reaction which is the reverse of that observed in our chemistry occurs with Fischer carbene complexes. Thus, (CO)<sub>5</sub>Cr(=C(Ph)OMe) reacts with R<sub>3</sub>M-H (M = Si, Ge, Sn) to produce (CO)<sub>5</sub>Cr(C(H)(Ph)OMe)(MR<sub>3</sub>) complexes which upon treatment with Lewis bases (L) convert to (CO)<sub>5</sub>CrL and R<sub>3</sub>M-C(H)(Ph)OMe.<sup>33</sup> The mechanistic path for these conversions is believed to be dominated by associative nucleophilic attack of hydride at the carbene carbon.

### Conclusion

The synthetic methods presented in this paper are potentially of considerable utility. For instance, we have previously been unable to prepare *perhydrocyclopentadienyl* amide and alkoxide complexes via metathesis reactions from the CpMo(NO)Cl<sub>2</sub> precursor because of its propensity to be reduced by MOR and MNHR salts (M = Li, Na, K).<sup>21,34</sup> The reduction potential of CpMo(NO)Cl<sub>2</sub> in CH<sub>2</sub>Cl<sub>2</sub> is -100 mV vs SCE, whereas the

analogous potential of the Cp\* derivative is -350 mV.<sup>35</sup> Consequently, the above-mentioned salts are less likely to reduce Cp\* starting materials, and so the syntheses of Cp\*Mo(NO)(ER)<sub>2</sub> (E = O, NH) are much easier than the syntheses of CpM(NO)(ER)<sub>2</sub> complexes.<sup>16,36</sup> Furthermore, the preparations of alkyl amide and alkoxide complexes, CpMo(NO)(CH<sub>2</sub>CMe<sub>3</sub>)(ER), are limited by the considerable difficulty in generating pure CpMo(NO)(CH<sub>2</sub>CMe<sub>3</sub>)Cl.<sup>1</sup> Thus, the extension of this methodology is probably most important for reactants of very high pK<sub>a</sub> (such as amines), since the alkali-metal salts of these compounds are extremely potent nucleophiles and/or reducing agents.

**Acknowledgment.** We are grateful to the Natural Sciences and Engineering Research Council of Canada for support of this work in the form of grants to P.L. and F.W.B.E. We also thank the University of British Columbia for the award to M.A.Y. of a University Graduate Fellowship.

**Supplementary Material Available:** A complete table of rate constants for reaction 1 effected in various solvents at different temperatures and tables of hydrogen atom coordinates, anisotropic thermal parameters, all bond lengths and bond angles, torsion angles, additional crystallographic data, and least-squares planes for complex 4 (9 pages). Ordering information is given on any current masthead page.

OM940576V

(34) Legzdins, P.; Ross, K. J. Unpublished observations.

(35) Legzdins, P.; Reina, R.; Shaw, M. J.; Batchelor, R. J.; Einstein, F. W. B. *Organometallics* **1993**, *12*, 1029.

(36) Legzdins, P.; Lundmark, P. J.; Rettig, S. J. *Organometallics* **1993**, *12*, 3545.

(32) Klein, D. P.; Bergman, R. G. *J. Am. Chem. Soc.* **1989**, *111*, 3079.

(33) Dötz, K. H. *Angew. Chem., Int. Ed. Engl.* **1984**, *23*, 587.

# Polysilylation of Naphthalene Revisited: Synthesis and Structural Study of 1,2,3,5,6,7-Hexakis(trimethylsilyl)-1,2,3,5,6,7-hexahydronaphthalene<sup>†</sup>

Micheline Grignon-Dubois\*

Laboratoire de chimie organique et organométallique, Université Bordeaux I,  
351 Cours de la Libération, 33405 Talence-Cedex, France

Michel Laguerre and Michel Saux

Laboratoire de chimie analytique, Faculté de Pharmacie, Université Bordeaux II,  
3 Place de la Victoire, 33076 Bordeaux, France

Received July 26, 1994<sup>®</sup>

Revisiting the reductive polysilylation of naphthalene using Me<sub>3</sub>SiCl/Mg/HMPT reagent, we have shown that the reaction was not correctly interpreted. The hexasilylated product **2** previously described has been reformulated as **6** on the basis of NMR data and X-ray study. In addition, a molecular mechanics study of both **2** and **6** allowed understanding of the polysilylation process.

## Introduction

Reductive silylation of naphthalene **1** with an excess of Me<sub>3</sub>SiCl/Mg/HMPT reagent has been previously reported to give a hexasilylated derivative in 20–30% yield.<sup>1</sup> The *s-cis* dienic structure **2** (Figure 1) has been ascribed to this compound on the basis of the UV spectra and mechanistic considerations. We have recently shown that silylation of quinoline<sup>2</sup> and isoquinoline<sup>3</sup> also lead to hexasilylated derivatives, but in these cases we obtained the *s-trans* dienic structures **3–5** (Figure 1) as demonstrated by NMR and X-ray studies. These results and the fact that the physical chemistry data reported for **2** seemed to us more in accordance with a *s-trans* dienic skeleton prompted us to reinvestigate this reaction. We now present evidence for the reformulation of **2** and a rationale for the silylation process based on structural parameters and molecular mechanics calculations (MM3).<sup>4</sup>

## Results and Discussion

The silylation has been conducted as reported in ref 1, excepting in the Me<sub>3</sub>SiCl quantity used (7 equiv versus naphthalene instead of 6 equiv), and the temperature and reaction time (85 °C for 24 h instead of 100 °C during 72–96 h). These modifications allowed us to increase the yield from 20–30% to 42%. Our sample shows the same spectroscopic and physicochemical data as previously reported<sup>1</sup> (see Experimental

Section). In particular, it exhibits the same 116 °C melting point (EtOH) and a 273 nm λ<sub>max</sub> in UV. We assigned it the *s-trans* dienic structure **6** (Figure 1), which is in better agreement with the NMR data and the UV spectra. These conclusions were supported by a single-crystal X-ray analysis. An ORTEP drawing of **6** is shown in Figure 2. Bond lengths, valence and dihedral angles, and Si···Si distances are given in Tables II–IV (supplementary material) and Figure 3. In the solid state, **6** exhibits a nonplanar dienic linkage with a dihedral angle of 156.3° leading to a curved shape of the carbon frame. The molecule is symmetric about a C<sub>2</sub> axis orthogonal to the plane of the skeleton and passing through the middle of the C4a–C8a bond. This symmetry is well demonstrated by the superimposition of the two cyclohexene moieties, which leads to a rms of 0.02 Å (methyl groups excluded). Four silicons are positioned on the *exo* side (Si1 and Si5 in the axial position and Si3 and Si7 in the equatorial) and two on the *endo* side (Si2 and Si6 in axial). They can be classified in two equivalent groups of three, which are positioned alternatively up and down on each six-membered ring (Figure 3). Their location determined an almost equilateral triangle, due to the similarity of the Si···Si distance values (average 4.426 Å). The 5.19 Å distance between Si1 and Si5 shows that they are only slightly interacting despite their *cis*-diaxial relationship, which is certainly responsible for the curved shape of the skeleton. Indeed, only one H···H and one C···C nonbonding distance for these silyl groups are shorter than the sum of the van der Waals radii<sup>5a</sup> (respectively 1.92 and 3.77 Å long). This is the same for the vicinal silicon groups Si6 and Si7, for which the shortest 3.98 Å C···C distance is very close to the 4 Å normal minimal value.<sup>5a</sup> Only Si2 and Si3 led to a noticeable steric hindrance with a 3.76 Å measured C···C distance. An

\* To whom correspondence should be addressed (tel. 56846286; fax 56846646).

<sup>†</sup> Dedicated to Norbert Duffaut, a pioneer in organosilicon chemistry, who initiated French research in this field.

<sup>®</sup> Abstract published in *Advance ACS Abstracts*, December 1, 1994.

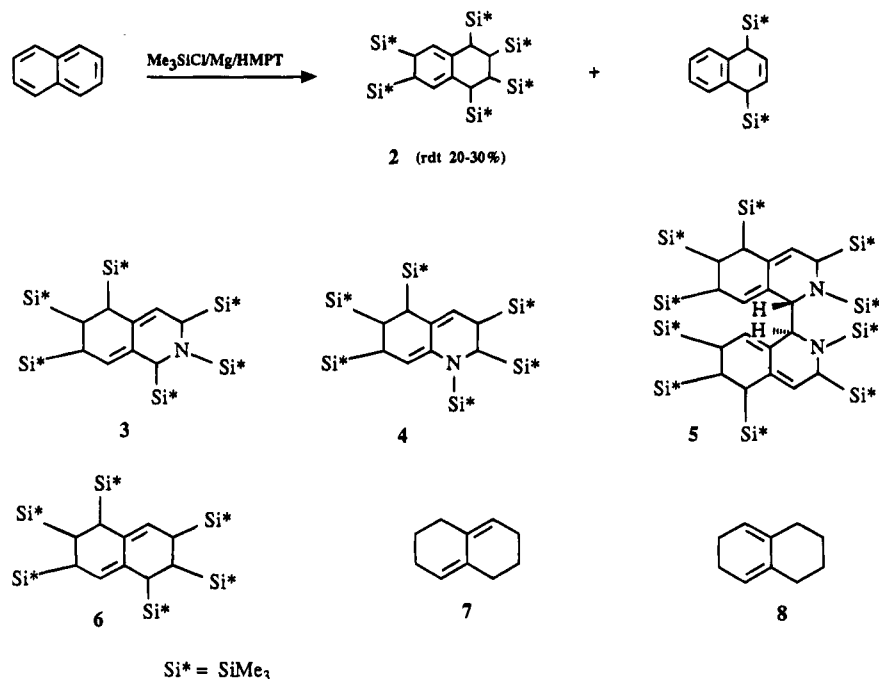
(1) (a) Dunogues, J.; Calas, R.; Biran, C.; Duffaut, N. *J. Organomet. Chem.* **1965**, *30*, 943. (b) Laguerre, M.; Dunoguès, J.; Calas, R. *Tetrahedron Lett.* **1981**, *22*, 1227.

(2) Grignon-Dubois, M.; Fialeix, M.; Rezzonico, B. *Can. J. Chem.* **1990**, *68*, 2153.

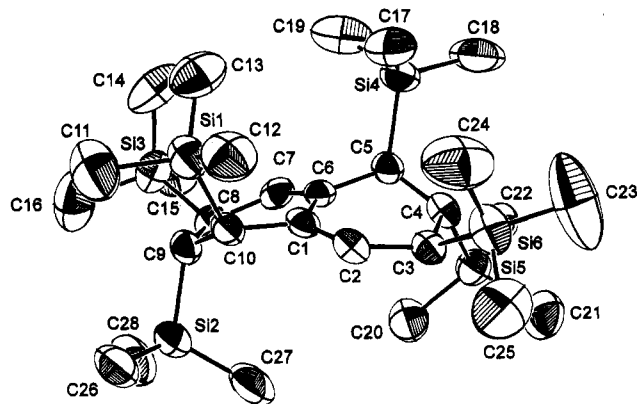
(3) Grignon-Dubois, M.; Fialeix, M.; Léger, J.-M. *Can. J. Chem.* **1993**, *71*, 754.

(4) Allinger, N. L.; Yuh, Y. H.; Lii, J. H. *J. Am. Chem. Soc.* **1989**, *111*, 8551.

(5) (a) Bock, H.; Ruppert, K.; Näther, C.; Havlas, Z.; Herrmann, H.-F.; Arad, C.; Göbel, I.; John, A.; Meuret, J.; Nick, S.; Rauschenbach, A.; Seitz, W.; Vaupel, T.; Solouki, B. *Angew. Chem., Int. Ed. Engl.* **1992**, *31*, 550 and references therein. (b) Allen, F. H.; Kennard, O.; Watson, D. G.; Brammer, L.; Orpeen, A. G.; Taylor, R. *J. Chem. Soc., Perkin Trans. 2* **1987**, 51.



**Figure 1.** *s-cis* and *s-trans* dienic linkages obtained (or postulated for **2**) from naphthalene, quinoline, and isoquinoline.



**Figure 2.** ORTEP drawing of compound **6** showing the atom-numbering scheme. (Hydrogen atoms have been omitted for clarity.)

additional packing analysis of the crystal lattice reveals very weak van der Waals contacts, which is in accordance with the observed low stability of the crystal under X-ray (see Experimental Section). Steric hindrance leads to opening of the C–C–Si valence angles and lengthening of all the Si–C<sub>ring</sub> bonds (average 1.902 Å), as depicted in Figure 3. As a consequence, some important closings of the Si–C–H angles are observed. The C–C bonds in allylic positions only slightly deviate from the 1.506 Å normal value, whereas those in homoallylic positions are considerably longer (1.560 Å).<sup>5</sup> It is worth noting that these last values are related to the shorter Si···Si distances as we previously observed with *gem*-disilyl derivatives,<sup>6</sup> which also shows the influence of steric hindrance on bond lengths.

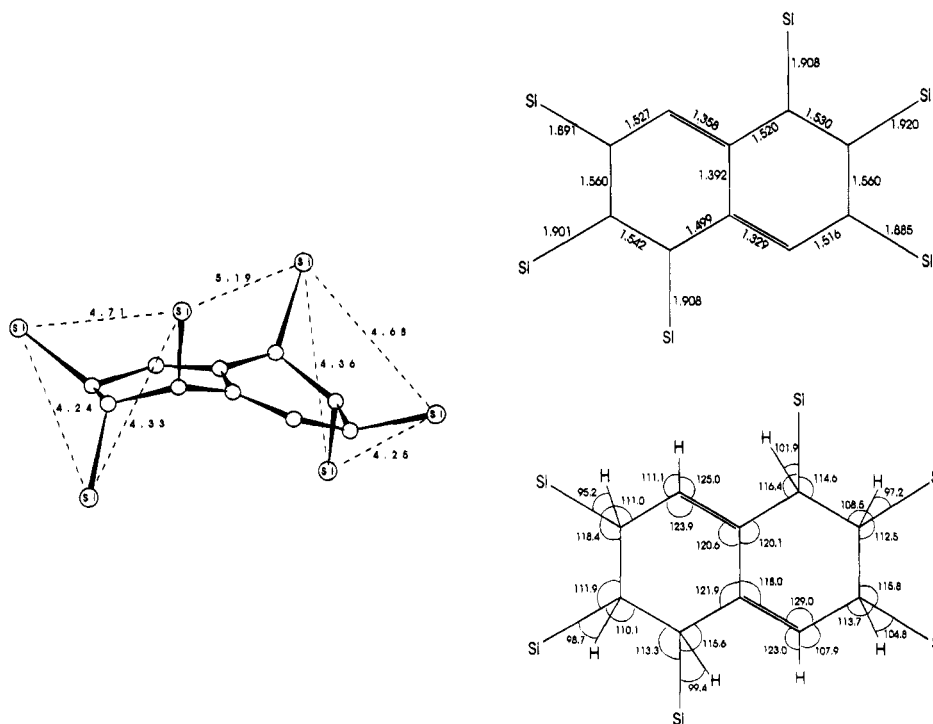
Spectroscopic data of **6** lead to the following comments. <sup>1</sup>H NMR data and UV spectra had been previously reported for 1,2,3,5,6,7- (**7**) and 1,2,3,4,6,7-hexahydronaphthalene (**8**),<sup>7</sup> which respectively present

a *s-cis* and *s-trans* structure as in **2** and **6** (Figure 1). In particular, comparison of the UV  $\lambda_{\max}$  values, 237 nm (14 600) for **7**, 263 nm (4830) for **8**, and 273 nm (13 500) for the hexasilylated compound, had led the previous authors<sup>1</sup> to assign it the *s-cis* structure as in **8**. In fact, the important magnitude difference of the  $\epsilon$  values seems more in accordance with a *s-trans* structure, and the silicon group, are not without influence on the  $\lambda_{\max}$  value. In order to demonstrate the effect of a trimethylsilyl group in allylic position, we have measured the  $\lambda_{\max}$  in 3-(trimethylsilyl)cyclopentene, for which we found 208 nm. Comparison of this value to the 173 nm calculated value in cyclopentene (see Experimental Section) clearly shows the bathochromic effect of an allylic trimethylsilyl group linked to a cyclene. It has not been possible to calculate the  $\lambda_{\max}$  values in **2** and **6**, the silicon atom not being parametrized. In order to obtain a better evaluation of the contribution of the silicon groups in **6**, we have calculated the  $\lambda_{\max}$  of its twisted carbon framework. The 236 nm calculated value, which can be compared to the measured values reported in literature<sup>7,8</sup> for **7** (242 nm,  $\epsilon = 17\,400$ , or 237 nm,  $\epsilon = 14\,600$ ), shows that the slight torsion of the dienic linkage (156.3°) has only a weak effect on the  $\lambda_{\max}$ . From these results, absorption could be estimated around 390 nm for **2** and 360 nm for **6** (four allylic silyl groups in each molecule). In fact, the X-ray structure of **6** shows that only the two C1–Si and C5–Si bonds are in a perfect perpendicular orientation versus the double bond, which leads to a maximum stabilizing  $\pi$  interaction.<sup>9</sup> Considering this structural feature, the 273 nm  $\lambda_{\max}$  value appears in good accordance with both the dienic twisting and a double bathochromic effect of the silicon. Concerning the <sup>1</sup>H NMR data, it is worth noting that both relative chemical shifts and <sup>3</sup>J coupling

(6) Laguerre, M.; Grignon-Dubois, M. *J. Mol. Struct.* **1994**, *319*, 167.  
 (7) Marvel, E. N.; Kaple, G.; Delphey, J.; Platt, N.; Polston, N.; Tashiro, J. *Tetrahedron* **1973**, *29*, 3797.

(8) Hückel, W.; Krauss, W. *J. Liebigs Ann.* **1962**, *654*, 49.  
 (9) (a) Weidner, U.; Schweig, A. *Angew. Chem., Int. Ed. Engl.* **1972**, *11*, 146. (b) Unwalla, R. J.; Profeta, S., Jr.; Cartledge, F. K. *J. Org. Chem.* **1988**, *53*, 5658.





**Figure 3.** Shortest Si...Si nonbonding distances (Å) and important valence bond angles (deg) and bond distances (Å).

constants for **6** are in good agreement with those reported for **4** and **7** but not **8**.<sup>2,7</sup>

In order to have a better idea of the conformational behavior of **6** without the crystal packing effect, we performed a molecular mechanics study. In particular, it appears interesting to examine angle valence deformations and conformational preferences due to steric hindrance among the six silyl groups. The MM3 force field<sup>4</sup> was chosen as giving the best results after comparison between crystallographic and computational structures built *ex nihilo* for several polysilylated compounds. Indeed, to check the accuracy of this force field toward highly distorted polysilylated derivatives, we have calculated the 1,2,3,4,5,6-hexakis(trimethylsilyl)benzene molecule, whose X-ray structure has been described by Sakurai et al.<sup>10</sup> It is worth noting that even in this extreme case, we found a rms of 0.2 Å if one considers the superimposition of all the silicons and aromatic carbons. The optimized structure obtained for **6** has been compared to its X-ray structure. Superimposition of all the heavy atoms led to a rms value of 0.066 Å, showing that the conformation in the crystal is very close to the lowest energy one. This is well demonstrated by the dienic twisting angles, which are respectively 23.7 and 22.8°. In order to systematically explore the conformational space of **2** and **6**, we performed both a stochastic dynamics simulation<sup>11</sup> and a Monte Carlo conformational search<sup>12</sup> starting from the X-ray structure for **6** and a local minimum for **2**. The comparison of the calculated energy values shows that **6** (97.6 kJ/mol) is more stable than **2** (121.5 kJ/mol). This difference is essentially due to the greater van der Waals contribution in **2**. Monte Carlo calculations

performed on **7** and **8** have confirmed that the *s-trans* structure (10.43 kJ/mol) is more stable than the *s-cis* isomer (42.11 kJ/mol). Both **2** and **6** present four silyl groups in allylic positions. Comparison of the lowest-energy conformers of **6** showed that two C1-Si and C5-Si bonds are in a perfect perpendicular orientation versus the double bond, which leads to a maximum stabilizing  $\pi$  interaction.<sup>9</sup> In contrast, this arrangement is no longer possible for **2**, due to the presence of four successive silicon groups on the same cycle. In this case, only the C1-Si bond can adopt a similar, but less favorable (84°), orientation.

From a mechanistic point of view, this conformational study of hexasilylated regioisomers shows that the double-1,2,3-substituted arrangement, which avoids severe spatial hindrance, is thermodynamically more favorable than the 1,2,3,4,6,7-one. Indeed, the former geometry allows arrangement of all the bulky silyl groups alternatively above and below the ring plane with only *trans* axial-axial or axial-equatorial interaction. This is not possible when four silyl groups are borne by the same ring, which leads to overcrowding due to a vicinal *trans*-diequatorial relationship. This conclusion is exemplified by the results we previously obtained with quinoline<sup>2</sup> and isoquinoline,<sup>3</sup> demonstrating that reductive silylation of two-fused six-membered aromatic rings follows the same general route described in Figure 4. Actually, the 1,2,6,7-tetrasilyl intermediate had been isolated in the case of naphthalene.<sup>1b</sup> Concerning the stereochemistry of the three disilylation steps, examination of the X-ray structure of **6** shows that the two 1,2-additions are *trans*, whereas the last 1,4-addition is *cis*. In the case of quinoline, we came to the same conclusion on the basis of <sup>1</sup>H NMR analysis.<sup>2</sup> To fully rationalize these results, a study associating MM3 calculations and X-ray and NMR data is now in progress for a series of polysilylated derivatives.

(10) Sakurai, H.; Ebata, K.; Kabuto, C.; Sekiguchi, A. *J. Am. Chem. Soc.* **1990**, *112*, 1799.

(11) van Gunsteren, W. F.; Berendsen, H. J. C. *Mol. Simul.* **1988**, *1*, 173.

(12) (a) Chang, G.; Guida, W. C.; Still, W. C. *J. Am. Chem. Soc.* **1989**, *111*, 4379. (b) Saunders, M.; Houk, K. N.; Wu, Y.-D.; Still, W. C.; Lipton, M.; Chang, G.; Guida, W. C. *J. Am. Chem. Soc.* **1990**, *112*, 1419.

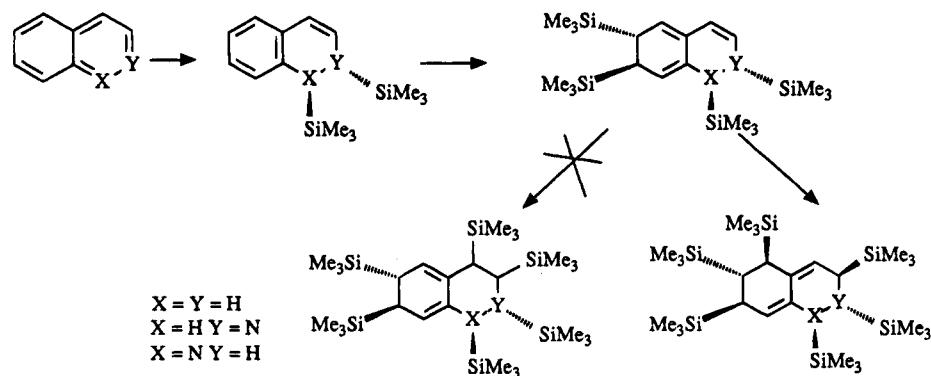


Figure 4. General pathway of the reductive hexasilylation of naphthalene and its heterocyclic analogues.

### Experimental Section

Melting points were determined on a Mettler capillary apparatus and are uncorrected. IR spectra were obtained on a Perkin-Elmer 457 spectrophotometer. UV spectra were recorded on a Varian DMS 90 (double beam) apparatus. A base line correction program was performed before each run. The  $^1\text{H}$  and  $^{13}\text{C}$  NMR spectra were recorded on a Bruker AM 250 spectrometer ( $\text{CDCl}_3$  solutions, TMS as internal standard), and  $^{29}\text{Si}$  NMR spectra, on a Bruker AC 200. Mass spectra were measured on an AEI MS 12 spectrometer. Elemental analyses were performed by service central d'analyse du CNRS (F-69390 Vernaison, France).

**Materials.** Unless specified otherwise, reagent-grade chemicals were used as received. HMPA (Aldrich) was degassed before use by an ultrasonic cleaning bath. Trimethylchlorosilane was distilled from magnesium powder prior to use. Reductive silylation was carried out under an argon atmosphere by employing vacuum line techniques.

**Silylation of Naphthalene.** To a vigorously stirred suspension of magnesium (1.59 g;  $6.6 \times 10^{-2}$  mol) in HMPA (65 mL) and freshly distilled trimethylchlorosilane (21.4 g; 198 mmol), a solution of naphthalene (3.84 g; 30 mmol) dissolved in HMPA (10 mL) was added dropwise within 0.5 h. During addition, the temperature was kept at  $85^\circ\text{C}$ . The mixture was then stirred for 24 h at this temperature and then cooled to room temperature. Addition of 50 mL of cyclohexane led to precipitation of the  $\text{MgCl}_2/2\text{HMPT}$  complex, which was filtered off. After evaporation of the solvent, the crude product was distilled under reduced pressure, providing 1,4-bis(trimethylsilyl)-1,4-dihydronaphthalene as a colorless liquid (bp  $82^\circ\text{C}$  (0.2 mmHg), 2.3 g, 28%). The remaining yellow viscous oil (10.4 g) was crystallized from ethanol to give **6** as yellowish crystals (7.2 g; 42%).

**NMR Data for 1,1-Bis(trimethylsilyl)-1,4-dihydronaphthalene.**  $^1\text{H}$  ( $\text{CDCl}_3$ , 250 MHz): 0.0 (s, 18 H), 3.0 (d, 2 H,  $J$  1.6 Hz), 5.6 (d, 2 H,  $J$  1.6 Hz), 6.9–7.0 (m, 4 H).  $^{13}\text{C}$  ( $\text{CDCl}_3$ , 62.9 MHz):  $\text{SiMe}_3$ , -2.04; CH, 34.04, 123.6, 124.8, 128.0; C, 135.3.  $^{29}\text{Si}$  ( $\text{CDCl}_3$ , 39.73 MHz): 3.54.

**Structural Data for Compound 6.** Mp  $116^\circ\text{C}$  (capillary), lit.<sup>1</sup> mp  $116^\circ\text{C}$ . UV ( $\text{C}_6\text{H}_{12}$ ):  $\lambda_{\text{max}}$  273 nm (13 500).  $^1\text{H}$  ( $\text{CDCl}_3$ , 250 MHz): -0.03 (s, 9 H), 0.06 (s, 9 H), 0.12 (s, 9 H), 1.27 (d, 1 H,  $J$  0.8 Hz), 1.85 (broad s, 2 H), 5.24 (d, 1 H, 2.7 Hz).  $^{13}\text{C}$  ( $\text{CDCl}_3$ , 62.9 MHz):  $\text{SiMe}_3$ , -2.4, -0.6, -0.4; CH, 15.7, 25.7, 30.1, 121.15; C, 129.2.  $^{29}\text{Si}$  ( $\text{CDCl}_3$ , 39.73 MHz): 3.4; 4.15; 4.9. Anal. Calcd for  $\text{C}_{28}\text{H}_{52}\text{Si}_6$ : C, 59.28; H, 11.02; Si, 29.70. Found: C, 59.02; H, 11.23; Si, 29.21.

**X-ray Crystallography of Compound 6.** A prismatic single crystal of  $\text{C}_{28}\text{H}_{52}\text{Si}_6$  (fw = 567.32) having approximate dimensions of  $0.25 \times 0.25 \times 0.30$  mm was obtained at room temperature from ethanol solution and mounted on a glass fiber in a random orientation. The intensity data collection was performed at  $25^\circ\text{C}$  on an Enraf-Nonius CAD-4 diffractometer. The data were measured with the  $\omega/2\theta$  scan technique and a variable scanning rate, using graphite-monochromated Cu K $\alpha$  radiation. A total of 3967 reflections were collected, of

Table 1. Positional and Thermal Parameters and Their Estimated Standard Deviations

atom	<i>x</i>	<i>y</i>	<i>z</i>	<i>B</i> ( $\text{\AA}^2$ ) <sup>a</sup>
Si1	0.2425(2)	0.0683(5)	0.8714(1)	9.7(1)
Si2	0.4839(2)	-0.0064(5)	0.8549(2)	9.6(1)
Si3	0.3496(3)	-0.3565(6)	0.8598(2)	10.4(2)
Si4	0.0725(2)	-0.1299(5)	0.6671(1)	9.6(1)
Si5	0.2541(2)	-0.361(5)	0.5800(1)	8.4(1)
Si6	0.1485(2)	0.3012(5)	0.6343(2)	10.0(2)
C1	0.2706(5)	0.033(1)	0.7579(4)	6.4(4)
C2	0.2564(5)	0.147(1)	0.7263(4)	6.2(4)
C3	0.2198(6)	0.154(1)	0.6588(4)	6.4(4)
C4	0.1905(5)	0.017(1)	0.6284(4)	6.7(4)
C5	0.1834(5)	-0.098(1)	0.6690(4)	6.8(4)
C6	0.2467(5)	-0.088(1)	0.7296(4)	6.2(4)
C7	0.2860(6)	-0.196(1)	0.7561(4)	6.5(4)
C8	0.3575(6)	-0.208(1)	0.8138(4)	7.7(4)
C9	0.3758(6)	-0.074(1)	0.8474(4)	7.3(4)
C10	0.3127(5)	0.038(1)	0.8247(4)	7.0(4)
C11	0.3006(9)	0.062(2)	0.9485(6)	19.3(7)
C12	0.1951(8)	0.230(2)	0.8536(6)	12.6(6)
C13	0.1602(8)	-0.048(2)	0.8606(6)	14.4(6)
C14	0.247(1)	-0.382(2)	0.8667(6)	19.1(8)
C15	0.3711(8)	-0.499(2)	0.8231(6)	11.3(5)
C16	0.425(2)	-0.354(2)	0.9335(7)	22(1)
C17	0.0301(7)	0.002(2)	0.7003(6)	13.4(6)
C18	0.0104(8)	-0.155(3)	0.5929(6)	29(1)
C19	0.0687(8)	-0.280(2)	0.7061(8)	15.1(6)
C20	0.3604(7)	-0.071(2)	0.6274(5)	12.0(5)
C21	0.2585(9)	0.088(2)	0.5274(5)	12.3(6)
C22	0.2119(8)	-0.186(2)	0.5380(5)	12.2(5)
C23	0.081(2)	0.292(2)	0.5623(9)	34(1)
C24	0.0859(9)	0.339(2)	0.6790(9)	18.2(8)
C25	0.210(1)	0.453(2)	0.6402(7)	16.7(7)
C26	0.5127(7)	0.116(2)	0.9140(6)	11.8(6)
C27	0.4836(7)	0.071(2)	0.7860(6)	15.5(7)
C28	0.5618(8)	-0.140(2)	0.8761(7)	15.9(7)

<sup>a</sup> *B* values for anisotropically refined atoms are given in the form of the isotropic equivalent displacement parameter defined as  $(4/3)[a^2B(1,1) + b^2B(2,2) + c^2B(3,3) + ab(\cos \gamma)B(1,2) + ac(\cos \beta)B(1,3) + bc(\cos \alpha)B(2,3)]$ .

which 3922 were unique and not systematically absent; 2123 were used for calculation ( $F \geq 3\sigma(F)$ ). The intensities were corrected for Lorentz and polarization effects but not for absorption. As for many polysilylated derivatives, the crystals proved to be unstable under X-ray radiation. In the first experiment, after a total exposure time of 75 h, the total loss in intensity was 41.1%. A second crystal was chosen and measured but did not result in improved data. This fact explains the large *B* factors for some methyl groups (C11, C14, C16, C18, C23).

The structure was solved by direct methods using the MULTAN 80 program<sup>13</sup> for electron density synthesis. Block-diagonal matrix least-squares refinements were performed for a scale factor and positional and anisotropic thermal parameters of the non-hydrogen atoms. The hydrogen atoms were included in the calculations and refined with isotropic thermal parameters. The function minimized was  $\sum w(|F_o| - |F_c|)^2$ , and

the weight  $w$  is defined as  $4F_o^2/\sigma^2(F_o)^2$ . The scattering factors used for non-hydrogen atoms were taken from ref 14, and those for hydrogen atoms, from Stewart et al.<sup>15</sup> All calculations were performed on a MicroVax computer using the MolEN program.<sup>16</sup> Atomic parameters are given in Table 1. The molecule and its atom numbering scheme are shown in Figure 2.

**X-ray Crystal Structure Data for 6:** Monoclinic, space group  $P2_1/c$ ,  $a = 17.077(4)$  Å,  $b = 10.102(3)$  Å,  $c = 23.832(7)$  Å,  $\beta = 109.05(2)^\circ$ ,  $V = 3886(1)$  Å<sup>3</sup>,  $Z = 4$ ,  $D_x = 0.970$  g cm<sup>-3</sup>,  $\mu = 21.3$  cm<sup>-1</sup>, no. of variables = 555,  $R = 0.081$ ,  $R_w = 0.072$ , and  $S = 1.17$ .

**Electronic Spectral Calculations.** The UV spectra were calculated according the ZINDO/S method of M. Zerner, as implemented in HyperChem Version 3 for Windows (Autodesk, Inc.). Configuration interaction was first calculated with the Hamiltonian AM1, RHF spin pairing, total charge = 0, and spin multiplicity = 1 for lowest state. Then the UV spectral calculations were performed using the following overlap weighting factors: 1.267 for  $\sigma-\sigma^{17}$  and 0.585 for  $\pi-\pi$ .<sup>18</sup> The accuracy of the calculations was checked versus  $\lambda_{max}$  of cyclohexene (found, 182 nm; calc, 174.4 nm) and 1,2-dimethylcyclohexene (found, 194 nm; calc, 186.8 nm). Under these conditions the following results were obtained: cyclopentene, 172.99 nm; **7**, 269.15, oscillator strength 0.36 (measured 263 nm, 4830);<sup>5</sup> **8**, 239.46, oscillator strength 1.048 (measured 237 nm, 14 600,<sup>8</sup> or 242 nm, 17 400;<sup>7</sup> *s-trans* dienic framework in the crystalline conformation of **6**, 235.87 nm, oscillator strength 0.888.

**Molecular Modeling.** Calculations were performed on a SGI Indigo platform running Macromodel version 3.5 (Columbia University, New York).<sup>19</sup> Conformational minima were found using the modified MM3\* (91) force field as implemented

in the program.<sup>4</sup> X-ray structures were minimized to a final rms gradient  $\leq 0.005$  kJ/(mol·Å) via the truncated Newton conjugate gradient (TNCG) method (1000 cycles).

**Stochastic Dynamics Simulation.** This variant of molecular dynamic (forces from the force field are increased by frictional and random forces, which simulate some of the properties of a solvent medium) is implemented in MacroModel.<sup>11</sup> The MM3\* (91) force field was chosen. The kinetic energy was increased from 300 to 900 K with a bath constant of 0.2 ps. A total time of run of 50 ps (time step 1 fs) was chosen, one conformer was sampled each 1 ps and minimized with the truncated Newton conjugate gradient method (TNCG, 1000 cycles, rms  $\leq 0.005$  kJ/(mol·Å)), and all the unique (heavy atoms only) conformers within a 50 kJ energy range were reported and classed by ascending energy. The run used the minimized X-ray conformation as starting geometry for **6** and a local minimum for **2**.

**Monte Carlo-Style Conformational Search.** This program has been used as implemented in MacroModel.<sup>12</sup> The automatic setup has been selected, i.e., single bonds variable, chiral center set, flexible ring opened, and 1000 steps made per input structure in a 50 kJ energy range. Each conformer was fully minimized (TNCG, 1000 cycles, rms,  $\leq 0.005$  kJ/(mol·Å)). The least-used structures were used as starting geometries only if their energies were within the energetic window (50 kJ/mol of the lowest energy structure yet found).

For **6**, 47 conformers were found, but due to equivalencies of the methyl groups borne by silicon atoms, only 11 truly different classes of conformers were reported from 97.58 to 118.3 kJ/mol, the first one being the X-ray structure.

For **2**, 44 conformers were found, but as above, only 9 truly different classes were reported from 121.5 to 139.9 kJ/mol.

The *s-cis* and *s-trans* nonsilylated dienes **7** and **8** were treated as above, resulting in two conformers (10.43–11.04 kJ/mol) with **7** and four conformers (42.11–55.62 kJ/mol) with **8**.

**Supplementary Material Available:** Tables of bond distances, bond angles, torsion angles, hydrogen positional and thermal parameters, anisotropic thermal parameters, and least-squares planes (17 pages). Ordering information is given on any current masthead page.

OM9405955

(19) Macromodel (Mohamadi, F.; Richards, N. G. J.; Guida, W. C.; Liskamp, R.; Lipton, M.; Cauffield, C.; Chang, G.; Hendrickson, T.; Still, W. C. *J. Comput. Chem.* **1990**, *11*, 441).

(13) Main, P.; Hull, S. E.; Lessinger, L.; Germain, G.; Declercq, J.-P.; Woolfson, M. M. MULTAN 80: A System of Computer Programs for the Automatic Solution of Crystal Structures from X-Ray Diffraction Data. Univs of York, England, and Louvain, Belgium, 1978.

(14) *International Tables for X-ray Crystallography*; Kynoch Press: Birmingham, England, 1974; Vol. IV. (Present distributor: D. Reidel, Dordrecht, The Netherlands.)

(15) Stewart, R. F.; Davidson, E. R.; Simpson, W. T. *J. Chem. Phys.* **1965**, *42*, 3175.

(16) MolEN is an interactive structure solution procedure (Enraf-Nonius, Delft, The Netherlands, 1990).

(17) Ridley, J. E.; Zerner, M. C. *Theor. Chim. Acta* **1976**, *42*, 223.

(18) Del Bene, J.; Jaffe, H. H. *J. Chem. Phys.* **1968**, *48*, 1807.

# Structures and Bond Energies of the Transition-Metal Carbonyls $M(\text{CO})_5$ ( $M = \text{Fe, Ru, Os}$ ) and $M(\text{CO})_4$ ( $M = \text{Ni, Pd, Pt}$ )<sup>1</sup>

Andreas W. Ehlers and Gernot Frenking\*

Fachbereich Chemie, Philipps-Universität Marburg, Hans-Meerwein-Strasse,  
D-35032 Marburg, Germany

Received July 26, 1994<sup>®</sup>

The equilibrium geometries of the transition-metal carbonyls  $M(\text{CO})_n$  ( $M = \text{Fe, Ru, Os}$ ;  $n = 4, 5$ ) and  $M(\text{CO})_n$  ( $M = \text{Ni, Pd, Pt}$ ;  $n = 3, 4$ ) are calculated at the MP2 level using effective core potentials for the metals and 6-31G(d) basis sets for C and O. The first ligand dissociation energies of the saturated metal carbonyls are theoretically predicted using the coupled cluster theory (CCSD(T)) approach. The calculated dissociation energies  $\Delta H^{298}$  ( $\text{Fe}(\text{CO})_5$ , 46.5 kcal/mol;  $\text{Ru}(\text{CO})_5$ , 30.9 kcal/mol;  $\text{Os}(\text{CO})_5$ , 42.4 kcal/mol;  $\text{Ni}(\text{CO})_4$ , 24.4 kcal/mol;  $\text{Pd}(\text{CO})_4$ , 9.6 kcal/mol;  $\text{Pt}(\text{CO})_4$ , 13.0 kcal/mol) indicate that the second-row transition elements have the weakest carbonyl bond.

## 1. Introduction

The accurate determination of thermochemical data for transition-metal complexes is a difficult problem for experimental and theoretical methods.<sup>2</sup> In a recent publication we have shown that the metal–ligand bond lengths and first dissociation energies of  $\text{Mo}(\text{CO})_6$  and  $\text{W}(\text{CO})_6$  are predicted with excellent accuracy at the CCSD(T)/MP2 level of theory using effective core potentials for the metals and moderate basis sets for C and O.<sup>3</sup> The calculated Cr–CO bond length of  $\text{Cr}(\text{CO})_6$  was slightly too short and the bond energy too high.<sup>3</sup> Here we report our results for the pentacarbonyls of the group 8 elements  $M(\text{CO})_5$  ( $M = \text{Fe, Ru, Os}$ ) and the tetracarbonyls of the group 10 elements  $M(\text{CO})_4$  ( $M = \text{Ni, Pd, Pt}$ ) using the same theoretical method as in our previous study.<sup>3</sup>

## 2. Methods

The geometries are optimized at the MP2<sup>4</sup> level using an effective core potential (ECP) and a (441/2111/ $N - 11$ ) split-valence basis set for the metals, which is derived from the (55/5/ $N$ ) minimal basis set optimized by Hay and Wadt<sup>5</sup> ( $N = 5, 4, 3$  for the first-, second-, and third-row transition metals, respectively). The ECPs are derived from nonrelativistic atom calculations of the first-row transition elements (Cr, Fe, Ni) and relativistic calculations of the second- and third-row transition elements (Mo, W, Ru, Os, Pd, Pt). A 6-31G(d) all-electron basis set is used for C and O.<sup>6</sup> This basis set combination is denoted BS II. The dissociation energies are calculated using coupled-cluster theory with singles and

doubles and a noniterative estimate of triple substitutions (CCSD(T)).<sup>7</sup> Zero-point vibrational energies (ZPEs) are calculated at the Hartree–Fock level. The geometries have been calculated using the program TURBOMOLE.<sup>8</sup> For the CCSD(T) calculations the program ACES II<sup>9</sup> was employed.

As in our previous study of  $M(\text{CO})_6$  compounds,<sup>3</sup> we did not correct the calculated dissociation energies for the basis set superposition error (BSSE). There are two types of errors in calculations using a truncated basis set, i.e. the BSSE and the basis set incompleteness error (BSIE). These two errors have opposite sign. Both errors can, in principle, be corrected by saturating the basis set. Correcting for the BSSE would leave the BSIE uncorrected. We think that for a comparison with experimental values directly calculated results should be used rather than estimated data.

## 3. Results and Discussion

Table 1 shows the theoretically predicted and experimentally observed equilibrium geometries of the metal carbonyls. The theoretical and experimental first dissociation energies are shown in Table 2. The calculated and experimental bond energies for the hexacarbonyls  $M(\text{CO})_6$  are given for comparison.

The theoretically predicted geometry of  $\text{Fe}(\text{CO})_5$  at the MP2/II level has Fe–CO bonds which are clearly too short. In particular, the axial Fe–CO bond is calculated to be significantly shorter (1.688 Å) than is experimentally observed (Table 1). This is because the Hartree–Fock wave function is a very poor approximation for the electronic structure of  $\text{Fe}(\text{CO})_5$ .<sup>10</sup> The calculations predict that the axial Fe–C bonds are shorter than the

<sup>®</sup> Abstract published in *Advance ACS Abstracts*, December 1, 1994.  
(1) Theoretical Studies of Organometallic Compounds. 10. Part 9: Böhme, M.; Frenking, G.; Reetz, M. T. *Organometallics* 1994, 13, 4237.  
(2) (a) Salahub, D. R.; Zerner, M. C., Eds. *The Challenge of d and f Electrons: Theory and Computation*; ACS Symposium Series 349; American Chemical Society, Washington, DC, 1989. (b) Marks, T. J., Ed. *Bonding Energetics in Organometallic Compounds*; ACS Symposium Series 428; American Chemical Society: Washington, DC, 1990.  
(3) (a) Ehlers, A. W.; Frenking, G. *J. Am. Chem. Soc.* 1994, 116, 1514. (b) Ehlers, A. W.; Frenking, G. *J. Chem. Soc., Chem. Commun.* 1993, 1710.  
(4) (a) Møller, C.; Plesset, M. S. *Phys. Rev.* 1934, 46, 618. (b) Binkley, J. S.; Pople, J. A. *Int. J. Quantum Chem.* 1975, 9, 229.  
(5) Hay, P. J.; Wadt, W. R. *J. Chem. Phys.* 1985, 82, 299.  
(6) Hehre, W. J.; Ditchfield, R.; Pople, J. A. *J. Chem. Phys.* 1972, 56, 2257.

(7) (a) Cizek, J. *J. Chem. Phys.* 1966, 45, 4256. (b) Pople, J. A.; Krishnan, R.; Schlegel, H. B.; Binkley, J. S. *Int. J. Quantum Chem.* 1978, 14, 545. (c) Bartlett, R. J.; Purvis, G. D. *Int. J. Quantum Chem.* 1978, 14, 561. (d) Purvis, G. D.; Bartlett, R. J. *J. Chem. Phys.* 1982, 76, 1910. (e) Purvis, G. D.; Bartlett, R. J. *J. Chem. Phys.* 1987, 86, 7041.  
(8) (a) Häser, M.; Ahlrichs, R. *J. Comput. Chem.* 1989, 10, 104. (b) Ahlrichs, R.; Bär, M.; Häser, M.; Horn, H.; Kölmel, C. *Chem. Phys. Lett.* 1989, 162, 165. (c) Horn, H.; Weiss, H.; Häser, M.; Ehrig, M.; Ahlrichs, R. *J. Comput. Chem.* 1991, 12, 1058. (d) Häser, M.; Almlöf, J.; Feyereisen, M. W. *Theor. Chim. Acta* 1991, 79, 115.  
(9) An ab initio program written by: Stanton, J. F.; Gauss, J.; Watts, J. D.; Lauderdale, W. J.; Bartlett, R. J. ACES II; University of Florida, Gainesville, FL, 1991.

Table 1. Calculated and Experimental Bond Lengths (Å) of the Metal Carbonyls

	sym	state	$r_{M-C1}$	$r_{M-C2}$	$r_{C1-O1}$	$r_{C2-O2}$	method	ref
Fe(CO) <sub>5</sub> <sup>a</sup>	<i>D</i> <sub>3h</sub>	<sup>1</sup> A <sub>1</sub> '	1.688	1.766	1.176	1.166	MP2	this work
			1.877	1.847			MCPF	10b
			1.798	1.836			CCI	10a
			1.77	1.79			DFT	16
			1.807	1.827	1.152	1.152	exptl	11
			1.811(2)	1.803(2)	1.117(2)	1.133(3)	exptl	12
Ru(CO) <sub>5</sub> <sup>a</sup>	<i>D</i> <sub>3h</sub>	<sup>1</sup> A <sub>1</sub> '	1.943	1.952	1.162	1.165	MP2	this work
			1.95	1.96			DFT	16
			1.941(13)	1.961(13)	1.126(9)	1.127(10)	exptl	14
			1.963	1.945	1.163	1.168	MP2	this work
Os(CO) <sub>5</sub> <sup>a</sup>	<i>D</i> <sub>3h</sub>	<sup>1</sup> A <sub>1</sub> '	1.98	1.99			DFT	16
			1.982(20)	1.937(19)	1.130(52)	1.131(35)	exptl	15
			1.726	1.713	1.170	1.178	MP2	this work
			1.951	1.904	1.161	1.171	MP2	this work
Fe(CO) <sub>4</sub> <sup>b</sup>	<i>C</i> <sub>2v</sub>	<sup>1</sup> A <sub>1</sub>	1.942	1.909	1.165	1.172	MP2	this work
			1.801		1.162		MP2	this work
Ru(CO) <sub>4</sub> <sup>c</sup>	<i>C</i> <sub>2v</sub>	<sup>1</sup> A <sub>1</sub>	1.831			CCSD(T)	26	
Os(CO) <sub>4</sub> <sup>d</sup>	<i>T</i> <sub>d</sub>	<sup>1</sup> A <sub>1</sub>	1.873				MP2	27
			1.817(2)		1.127(3)		exptl	12
			1.825(2)		1.122(2)		exptl	25
			2.013		1.157		MP2	this work
			2.032				MP2	27
			1.966		1.160		MP2	this work
Pd(CO) <sub>4</sub>	<i>T</i> <sub>d</sub>	<sup>1</sup> A <sub>1</sub>	2.100				MP2	27
			1.796		1.163		MP2	this work
Pt(CO) <sub>4</sub>	<i>T</i> <sub>d</sub>	<sup>1</sup> A <sub>1</sub>	1.981		1.158		MP2	this work
			1.935		1.161		MP2	this work
Ni(CO) <sub>3</sub>	<i>D</i> <sub>3h</sub>	<sup>1</sup> A <sub>1</sub> '						
Pd(CO) <sub>3</sub>	<i>D</i> <sub>3h</sub>	<sup>1</sup> A <sub>1</sub> '						
Pt(CO) <sub>3</sub>	<i>D</i> <sub>3h</sub>	<sup>1</sup> A <sub>1</sub> '						

<sup>a</sup> The first bond length refers to the axial bond and the second to the equatorial bond. <sup>b</sup> Calculated bond angle  $\alpha(C_1-Fe-C_1') = 170.0^\circ$ ,  $\alpha(C_2-Fe-C_2') = 135.9^\circ$ . <sup>c</sup> Calculated bond angle  $\alpha(C_2-Ru-C_1') = 179.4^\circ$ ,  $\alpha(C_2-Ru-C_2') = 137.4^\circ$ . <sup>d</sup> Calculated bond angle  $\alpha(C_1-Os-C_1') = 157.0^\circ$ ,  $\alpha(C_2-Os-C_2') = 138.9^\circ$ .

Table 2. Calculated and Experimental First Dissociation Energies (kcal/mol)

	this work			other			exptl $\Delta H^{298}$
	$\Delta E$	$\Delta H^a$	$\Delta H^{298}$	$\Delta E$ - (MCPF)	$\Delta E$ - (CCSD(T))	$\Delta E$ - (DFT) <sup>d</sup>	
Cr(CO) <sub>6</sub>	45.8	43.2	45.3	32.7 <sup>i</sup>	42.7 <sup>i</sup>	35.1 (46.2)	36.8 ± 2 <sup>b</sup>
Mo(CO) <sub>6</sub>	40.4	38.2	40.3			28.4 (39.7)	40.5 ± 2 <sup>b</sup>
W(CO) <sub>6</sub>	48.0	45.7	47.8			33.9 (43.7)	46.0 ± 2 <sup>b</sup>
Fe(CO) <sub>5</sub>	46.9	44.4	46.5	39 ± 5 <sup>h</sup>		44.2	41 ± 2 <sup>b</sup>
Ru(CO) <sub>5</sub>	30.9	28.8	30.9			22.1	27.6 ± 0.4 <sup>c</sup>
Os(CO) <sub>5</sub>	42.9	40.3	42.4			23.5	30.6 ± 0.3 <sup>c</sup>
Ni(CO) <sub>4</sub>	23.6	22.3	24.4	24 <sup>f</sup>	29.8 <sup>e</sup>	25.3	25 ± 2 <sup>d</sup> 22–24 <sup>e</sup>
Pd(CO) <sub>4</sub>	7.8	7.5	9.6			6.5	
Pt(CO) <sub>4</sub>	12.1	10.9	13.0			9.1	

<sup>a</sup> Reference 16. Values in parentheses are from ref 34. <sup>b</sup> Reference 20. <sup>c</sup> Reference 21. <sup>d</sup> Reference 31. <sup>e</sup> Reference 32. <sup>f</sup> Reference 33. <sup>g</sup> Reference 26. <sup>h</sup> Reference 10b. <sup>i</sup> Reference 22, activation barrier for associative-dissociative mechanism (see text). <sup>j</sup> Reference 10c.

equatorial Fe–C bonds. The question about the relative bond lengths of the axial and equatorial Fe–CO bonds has not definitely been answered as yet. In a gas-phase electron diffraction study<sup>11</sup> the average Fe–CO<sub>eq</sub> distance (1.827 Å) was reported to be *longer* than the axial value Fe–CO<sub>ax</sub> (1.807 Å). However, the refinement model used to interpret the electron diffraction results constrained the axial and equatorial C–O distances to be equal.<sup>11</sup> A very recent X-ray diffraction analysis of the low-temperature crystals showed that the equatorial Fe–CO bonds are slightly *shorter* (1.803 Å) than the axial Fe–CO bonds (1.811 Å) and that the axial and equatorial C–O distances are different ( $r_{ax}(C-O) = 1.117$  Å,  $r_{eq}(C-O) = 1.133$  Å).<sup>12</sup> From the vibrational spectra and force constants of Fe(CO)<sub>5</sub> it was concluded

that the equatorial Fe–CO bonds should be shorter than the axial Fe–CO bonds.<sup>13</sup> Previous calculations at the MCPF level of theory<sup>10b</sup> predict that the axial Fe–CO bonds should be longer than the equatorial bonds. The opposite result was obtained at the CCI level using natural orbitals as reference functions.<sup>10a</sup> However, the C–O bond lengths were constrained to be the same in these calculations.<sup>10a</sup> The conflicting results of theory and experiment<sup>10–13</sup> indicate that the relative bond lengths of the axial and equatorial Fe–CO bonds are uncertain.

The situation is different for Ru(CO)<sub>5</sub> and Os(CO)<sub>5</sub>. Table 1 shows that the theoretically predicted M–CO bond lengths are in excellent agreement with the results obtained from gas-phase electron diffraction. Theory and experiment agree that the axial Ru–CO bonds are slightly *shorter* than the equatorial Ru–CO bonds, while the axial Os–CO bonds are *longer* than the equatorial Os–CO bonds. The differences between the absolute values of the theoretical and experimental M–CO distances are within the experimental error range. Since the experimental results from the electron diffraction measurements were derived using different refinement models considering different axial and equatorial C–O bond lengths, we think that the results are reliable.<sup>14,15</sup> It is remarkable that the calculations at the MP2/II level give the correct (opposite) order of the relative M–CO bond lengths of Ru(CO)<sub>5</sub> and Os(CO)<sub>5</sub>. Previous calculations using density functional theory predict that the equatorial M–CO bonds of Ru(CO)<sub>5</sub> and Os(CO)<sub>5</sub> should be longer than the axial M–CO bonds.<sup>16</sup>

Table 1 shows the optimized geometries for the lowest

(10) (a) Lüthi, H. P.; Siegbahn, P. E. M.; Almlöf, J. *J. Phys. Chem.* **1985**, *89*, 2156. (b) Barnes, L. A.; Rosi, M.; Bauschlicher, C. W. *J. Chem. Phys.* **1991**, *94*, 2031. (c) Barnes, L. A.; Liu, B.; Lindh, R. *J. Chem. Phys.* **1993**, *98*, 3978.

(11) Beagley, B.; Schmidling, D. G. *J. Mol. Struct.* **1974**, *22*, 466.

(12) Braga, D.; Grepioni, F.; Orpen, A. G. *Organometallics* **1993**, *12*, 1481.

(13) Jones, L. H.; McDowell, R. S.; Goldblatt, M.; Swanson, B. I. *J. Chem. Phys.* **1972**, *57*, 2050.

(14) Huang, J.; Hedberg, K.; Davis, H. B.; Pomeroy, R. K. *Inorg. Chem.* **1990**, *29*, 3923.

(15) Huang, J.; Hedberg, K.; Pomeroy, R. K. *Organometallics* **1988**, *7*, 2049.

lying ( $^1A_1$ ) singlet state of the tetracarbonyls of Fe, Ru, and Os. Experimental studies have indicated that  $\text{Fe}(\text{CO})_4$  has a triplet ground state,<sup>17</sup> while  $\text{Ru}(\text{CO})_4$  and  $\text{Os}(\text{CO})_4$  probably have a singlet ground state.<sup>18,19</sup> Because we are mainly interested in the spin-allowed dissociation mechanism, we calculated only the singlet states of the carbonyls. The optimized structures have  $C_{2v}$  symmetry with two long M–CO bonds, which form a rather wide angle of nearly  $180^\circ$  (Table 1). The shorter M–CO bonds have angles between  $135$  and  $140^\circ$ . A similar structure has been calculated for the  $^1A_1$  excited state of  $\text{Fe}(\text{CO})_4$  by Barnes et al.<sup>10b</sup>

The calculated first dissociation energy of  $\text{Fe}(\text{CO})_5$  relative to the  $^1A_1$  singlet state of  $\text{Fe}(\text{CO})_4$  ( $\Delta H^{298} = 46.5$  kcal/mol) is higher than the experimental value of  $41 \pm 2$  kcal/mol.<sup>20</sup> This is not surprising, because the optimized geometry of  $\text{Fe}(\text{CO})_5$  has Fe–CO bonds that are too short. The calculated first dissociation energy of  $\text{Ru}(\text{CO})_4$  ( $\Delta H^{298} = 30.9$  kcal/mol) is in reasonable agreement with the experimentally determined activation enthalpy  $\Delta H^\ddagger = 27.6 \pm 0.4$  kcal/mol for the substitution reaction of  $\text{Ru}(\text{CO})_5$  with triphenylphosphine in cyclohexane as a solvent, which proceeds via a dissociative mechanism.<sup>21</sup> The activation enthalpy for CO substitution of  $\text{Os}(\text{CO})_5$  has been determined as  $\Delta H^\ddagger = 30.6 \pm 0.3$  kcal/mol.<sup>22</sup> The calculations predict  $\Delta H^{298} = 42.4$  kcal/mol, which is significantly higher than the observed activation enthalpy. However, the measured activation entropy for the CO substitution reaction of  $\text{Os}(\text{CO})_5$  is more than 10 times lower ( $\Delta S^\ddagger = 1.33 \pm 0.03$  cal/(mol K)) than for  $\text{Ru}(\text{CO})_5$  ( $\Delta S^\ddagger = 15.2 \pm 1.3$  cal/(mol K)) and  $\text{Fe}(\text{CO})_5$  ( $\Delta S^\ddagger = 18$  cal/(mol K)), "indicating perhaps the Os–CO bond is not completely broken in the transition state for the reaction".<sup>22</sup> This is a strong indication that the observed CO substitution reaction of  $\text{Os}(\text{CO})_5$  follows an  $S_N2$ -type associative/dissociative mechanism, rather than an  $S_N1$ -type dissociative mechanism. A similar change in the reaction mechanism has been observed for carbonyl complexes of group 6 elements. Mechanistic studies of substitution reactions show that chromium carbonyl complexes follow a dissociative/associative mechanism, while the CO substitution of carbonyl complexes of molybdenum and tungsten takes place via association/dissociation.<sup>23</sup> The activation barrier for CO substitution of  $\text{W}(\text{CO})_6$  was measured as 39.7 kcal/mol,<sup>24</sup> while gas-phase laser pyrolysis studies show that the first dissociation energy is  $46.0 \pm 2$  kcal/mol.<sup>20</sup> We believe that the experimental value  $\Delta H^\ddagger = 30.6 \pm 0.3$  kcal/mol<sup>22</sup> for  $\text{Os}(\text{CO})_5$  is the activation barrier for an associative/dissociative substitution reac-

tion. The calculations predict that the first dissociation energy of  $\text{Os}(\text{CO})_5$  is significantly higher ( $\Delta H^{298} = 42.4$  kcal/mol).

The calculated Ni–CO bond length of  $\text{Ni}(\text{CO})_4$  (1.801 Å) is slightly shorter than the experimentally observed values (gas phase,<sup>25</sup> 1.825 Å; solid state,<sup>12</sup> 1.817 Å). A good agreement is also found between the calculated Ni–CO bond length at the CCSD(T)<sup>26</sup> level and the experimental values (Table 1). There are no experimental values for the M–CO distances of  $\text{Pd}(\text{CO})_4$  and  $\text{Pt}(\text{CO})_4$  known to us. Because of the excellent agreement between the calculated and experimental M–CO bond length values for  $\text{Mo}(\text{CO})_6$ ,  $\text{W}(\text{CO})_6$ ,<sup>3</sup>  $\text{Ru}(\text{CO})_5$ , and  $\text{Os}(\text{CO})_5$  (Table 1), we think that the predicted M–CO bond lengths for  $\text{Pd}(\text{CO})_4$  (2.013 Å) and  $\text{Pt}(\text{CO})_4$  (1.966 Å) should be correct within  $\pm 0.02$  Å. Previous calculations<sup>27</sup> at the MP2 level using ECPs for the metals gave significantly longer bonds for the tetracarbonyls of the group 10 elements (Table 1). However, these calculations employed the large-core ECP, which has only the  $[n]s$  and  $[n-1]d$  electrons in the valence sphere<sup>28</sup> and a 4-31G basis set for C and O.<sup>27</sup> It has been shown that better results are obtained when the  $[n-1]s^2$  and  $[n-1]p^6$  electrons are included in the valence sphere.<sup>29</sup>

The tricarbonyls  $M(\text{CO})_3$  of the group 10 transition metals are calculated with a  $D_{3h}$  equilibrium geometry. This is in agreement with the analysis of matrix IR spectra of  $\text{Ni}(\text{CO})_3$  and  $\text{Pd}(\text{CO})_3$ , which indicate that the tricarbonyls possess probably a trigonal-planar  $D_{3h}$  geometry.<sup>30</sup>

The theoretically predicted first dissociation energy of  $\text{Ni}(\text{CO})_4$  ( $\Delta H^{298} = 24.4$  kcal/mol) is in good agreement with the experimental values of  $25 \pm 2$  kcal/mol<sup>31</sup> and 22–24 kcal/mol.<sup>32</sup> A similar value (24 kcal/mol) has been calculated at the MCP level,<sup>33</sup> while the CCSD(T) result<sup>26</sup> (29.8 kcal/mol) is too high. The calculated bond energies for  $\text{Pd}(\text{CO})_4$  ( $\Delta H^{298} = 9.6$  kcal/mol) and  $\text{Pt}(\text{CO})_4$  ( $\Delta H^{298} = 13.0$  kcal/mol) are much lower. The relative weakness of the M–CO bonds of the higher homologues of the  $M(\text{CO})_4$  series is in agreement with the low stability of these compounds. While  $\text{Ni}(\text{CO})_4$  is stable at ambient temperatures,  $\text{Pd}(\text{CO})_4$  and  $\text{Pt}(\text{CO})_4$  have only been isolated in a low-temperature matrix.<sup>30</sup> The analysis of the vibrational spectra of the tetracarbonyls<sup>30b</sup> gave force constants for the M–CO bond stretching mode of 1.80, 0.82, and 1.28 mdyn/Å for  $\text{Ni}(\text{CO})_4$ ,  $\text{Pd}(\text{CO})_4$ , and  $\text{Pt}(\text{CO})_4$ , which is in qualitative agreement with the calculated bond strength.

Table 2 allows a comparison between the theoretically predicted and experimentally observed first dissociation

(16) Ziegler, T.; Tschinke, V.; Ursenbach, C. *J. Am. Chem. Soc.* **1987**, *109*, 4825.

(17) Poliakoff, M.; Turner, J. J. *J. Chem. Soc., Dalton Trans.* **1974**, 70, 93.

(18) (a) Bogdan, P.; Weitz, E. *J. Am. Chem. Soc.* **1989**, *111*, 3136.

(b) Bogdan, P.; Weitz, E. *J. Am. Chem. Soc.* **1990**, *112*, 639.

(19) Ziegler, T. *Inorg. Chem.* **1986**, *25*, 2721.

(20) Lewis, K. E.; Golden, D. M.; Smith, G. P. *J. Am. Chem. Soc.* **1984**, *106*, 3905.

(21) Hug, R.; Poë, A. J.; Chawla, S. *Inorg. Chim. Acta* **1980**, *38*, 121.

(22) Shen, J.-K.; Gao, Y.-C.; Shi, Q.-Z.; Basolo, F. *Inorg. Chem.* **1989**, *28*, 4304.

(23) Wieland, S.; van Eldik, R. *Organometallics* **1991**, *10*, 3110.

(24) (a) Angelici, R. J. *Organomet. Chem. Rev. A* **1968**, *3*, 173. (b) Covey, W. D.; Brown, T. L. *Inorg. Chem.* **1973**, *12*, 2820. (c) Centini, G.; Gambino, O. *Atti. Accad. Sci. Torino, Cl. Sci. Fis., Mat. Nat.* **1963**, *97*, 1197. (d) Werner, H. *Angew. Chem., Int. Ed. Engl.* **1968**, *7*, 930.

(e) Graham, J. R.; Angelici, R. J. *Inorg. Chem.* **1967**, *6*, 2082. (f) Werner, H.; Prinz, R. *Chem. Ber.* **1960**, *99*, 3582. (g) Werner, H.; Prinz, R. *J. Organomet. Chem.* **1966**, *5*, 79.

(25) Hedberg, L.; Iijima, T.; Hedberg, K. *J. Chem. Phys.* **1979**, *70*, 3224.

(26) Blomberg, M. R. A.; Siegbahn, P. E. M.; Lee, T. J.; Rendell, A. P.; Rice, J. E. *J. Chem. Phys.* **1991**, *95*, 5898.

(27) Rohlfing, C. M.; Hay, P. J. *J. Chem. Phys.* **1985**, *83*, 4641.

(28) Hay, P. J.; Wadt, W. R. *J. Chem. Phys.* **1985**, *82*, 270.

(29) Jonas, V.; Frenking, G.; Reetz, M. T. *J. Comput. Chem.* **1992**, *13*, 919.

(30) (a) Kündig, P.; Moskovits, M.; Ozin, G. A. *Can. J. Chem.* **1972**, *50*, 3587. (b) Kündig, E. P.; McIntosh, D.; Moskovits, M.; Ozin, G. A. *J. Am. Chem. Soc.* **1973**, *95*, 7234.

(31) Stevens, A. E.; Feigerle, C. S.; Lineberger, W. C. *J. Am. Chem. Soc.* **1982**, *104*, 5026.

(32) (a) Basolo, F. *Chem. Br.* **1969**, *5*, 505. (b) Day, J. P.; Basolo, F.; Pearson, R. G. *J. Am. Chem. Soc.* **1968**, *90*, 6927. (c) Turner, J. J.; Simpson, M. B.; Poliakoff, M.; Maier, W. B., III. *J. Am. Chem. Soc.* **1983**, *105*, 3898.

(33) Blomberg, M. R. A.; Brandemark, U. B.; Siegbahn, P. E. M.; Wennerberg, J.; Bauschlicher, C. W. *J. Am. Chem. Soc.* **1988**, *110*, 6650.

energies of the saturated carbonyls of the transition elements of groups 6, 8, and 10. The only other complete set of theoretical bond energies are the DFT results by Ziegler et al.,<sup>16</sup> which are also shown in Table 2. The calculated dissociation energies for the carbonyls of the second- and third-row transition metals by Ziegler<sup>16</sup> are significantly lower than our ECP results. The bond energies of the hexacarbonyls  $M(\text{CO})_6$  ( $M = \text{Cr}, \text{Mo}, \text{W}$ ) have recently been recalculated by Ziegler<sup>34</sup> using newly developed DFT methods, which include nonlocal corrections and relativistic effects. The new values are in much better agreement with our values (see the DFT values in Table 2, given in parentheses). We think that a recalculation of the pentacarbonyls and

tetracarbonyls might also lead to a better agreement with the ECP results. The theoretically predicted first CO dissociation energies for the transition metals of the second and third rows reported here should be correct within  $\pm 3$  kcal/mol.

**Acknowledgment.** We thank Prof. Tom Ziegler for a preprint of ref 34. This work has been financially supported by the Deutsche Forschungsgemeinschaft and the Fonds der Chemischen Industrie. We thank Dr. Jürgen Gauss for a copy of the program ACES II and Prof. Reinhard Ahlrichs for the program TURBO-MOLE. Excellent service by the computer centers of the HRZ Marburg and HHRZ Darmstadt is gratefully acknowledged.

---

(34) Li, J.; Schreckenbach, G.; Ziegler, T. *J. Phys. Chem.*, in press.

OM940592S



# Synthetic, Structural, Mechanistic, and Theoretical MO Studies of the Alkali-Metal Chemistry of Dibenzylamine and Its Transformation to 1,3-Diphenyl-2-azaallyl Derivatives

Philip C. Andrews,<sup>†</sup> David R. Armstrong,<sup>†</sup> Daniel R. Baker,<sup>†</sup> Robert E. Mulvey,<sup>\*,†</sup> William Clegg,<sup>‡</sup> Lynne Horsburgh,<sup>‡</sup> Paul A. O'Neil,<sup>‡</sup> and David Reed<sup>§</sup>

Department of Pure and Applied Chemistry, University of Strathclyde, Glasgow, G1 1XL U.K., and Departments of Chemistry, University of Newcastle, Newcastle upon Tyne, NE1 7RU U.K., and University of Edinburgh, Edinburgh, EH9 3JJ U.K.

Received July 26, 1994<sup>⊗</sup>

Dibenzylamido anions ((PhCH<sub>2</sub>)<sub>2</sub>N<sup>-</sup>) can be transformed into 1,3-diphenyl-2-azaallyl anions ({PhC(H)-N<sup>-</sup>-C(H)Ph}<sup>-</sup>) by the assistance of PMDETA-((Me<sub>2</sub>NCH<sub>2</sub>CH<sub>2</sub>)<sub>2</sub>NMe) complexed Li<sup>+</sup>, Na<sup>+</sup>, or K<sup>+</sup> cations. The heavier alkali-metal cations give only the trans,trans conformation of the azaallyl anion, in contrast to the lighter Li<sup>+</sup> cation, which yields two crystalline conformers, the trans,trans and an unknown species. Ab initio MO geometry optimizations on model Li and Na complexes intimate that it is the relative tightness of the contact ion pair structures which dictates this distinction with Li<sup>+</sup> having more influence on the conformation and stability of the anion than Na<sup>+</sup>, which forms a much looser contact ion pair more akin to the "free" anion. On the basis of kinetic <sup>1</sup>H NMR studies, combined with X-ray crystallographic data, the amido → azaallyl conversion can be explained in terms of a two-step process involving β-elimination of a metal hydride followed by hydride metalation of the produced imine PhCH<sub>2</sub>N=C(H)Ph. This process appears to be initiated by deaggregation of the metallodibenzylamine to an intermediate monomeric structure, accomplished by solvation. The nature and degree of solvation required depend on the particular M<sup>+</sup> cation involved. Three new crystal structures are revealed in the course of this study. All are based on familiar four-membered (N-M)<sub>2</sub> rings, but whereas the sodium complex [{(PhCH<sub>2</sub>)<sub>2</sub>NNa·TMEDA}<sub>2</sub>] and the lithium complex [{(PhCH<sub>2</sub>)<sub>2</sub>NLi·THF}<sub>2</sub>] are both discrete dimers, unique [{(PhCH<sub>2</sub>)<sub>2</sub>NLi]<sub>2</sub>(dioxane)}<sub>∞</sub>], isolated as its toluene hemisolvate, is a polymer composed of linked dimeric units and so is the first dibenzylamido alkali-metal species to have an infinitely extended structure.

## Introduction

Over the past decade, dibenzylamine ((PhCH<sub>2</sub>)<sub>2</sub>NH), a nitrogen acid, has played a significant part in the rational development of lithium amide chemistry. Compounds belonging to this class constitute one of the major tools of contemporary organic synthesis, primarily as strong selective deprotonating agents.<sup>1</sup> (Dibenzylamido)lithium, [{(PhCH<sub>2</sub>)<sub>2</sub>NLi]<sub>n</sub>}, has contrastingly found use as a nitrogen nucleophile in the aminolysis of esters, producing high yields of the resulting organic amides.<sup>2</sup> However, the most instructive findings to date involving this ligand have been structural rather than synthetic. To begin with, the crystal structure of the unsolvated lithio derivative provided direct evidence of the cyclic, low-oligomeric (in this case, trimeric) constitution of certain lithium amides, while comparison with the dimeric, solvated structures of [{(PhCH<sub>2</sub>)<sub>2</sub>NLi·OEt<sub>2</sub>]<sub>2</sub>] and [{(PhCH<sub>2</sub>)<sub>2</sub>NLi·HMPA}<sub>2</sub>] illustrated the competing

effects of aggregation and complexation.<sup>3</sup> From structural characterization of the lithium amidomagnesiates [{(PhCH<sub>2</sub>)<sub>2</sub>N]<sub>4</sub>Li<sub>2</sub>Mg] and [{(PhCH<sub>2</sub>)<sub>2</sub>N]<sub>3</sub>LiMgpy}, we learned that the stoichiometries and coordination geometries are largely dictated by the state (solvated or unsolvated) of the Li<sup>+</sup> cations for both steric and electronic reasons.<sup>4</sup> Another intermetallic dibenzylamide, this time combining Li<sup>+</sup> and Na<sup>+</sup>, established for the first time that the ladder motif is a structural option for a mixed-alkali-metal composition.<sup>5</sup> Collectively these structures testify to the coordinative versatility of the dibenzylamido ligand, as they show that its anionic N center can bond terminally, or bridge in μ<sub>2</sub> or μ<sub>3</sub> styles, to metal centers.

Besides these simple coordinative distinctions, there exists another facet of alkali-metal dibenzylamide chemistry. Under the mediation of a Na<sup>+</sup> counterion complexed by tridentate PMDETA ((Me<sub>2</sub>NCH<sub>2</sub>CH<sub>2</sub>)<sub>2</sub>NMe) the amido anion ((PhCH<sub>2</sub>)<sub>2</sub>N<sup>-</sup>) is observed to convert to the 2-azaallyl formulation [PhC(H)-N<sup>-</sup>-C(H)Ph]<sup>-</sup>.<sup>6,7</sup> Resonance-stabilized anions of this type are valuable

<sup>†</sup> University of Strathclyde.

<sup>‡</sup> University of Newcastle.

<sup>§</sup> University of Edinburgh.

<sup>⊗</sup> Abstract published in *Advance ACS Abstracts*, December 1, 1994.

(1) (a) Wakefield, B. J. *Organolithium Methods*; Academic Press: London, 1987. (b) Brandsma, L.; Verkruijse, H. *Preparative Polar Organometallic Chemistry*; Springer-Verlag: Berlin, 1987; Vol. 1.

(2) Yang, K.-W.; Cannon, J. G.; Rose, J. G. *Tetrahedron Lett.* **1970**, 21, 1791.

(3) Barr, D.; Clegg, W.; Mulvey, R. E.; Snaith, R. *J. Chem. Soc., Chem. Commun.* **1984**, 285.

(4) Clegg, W.; Henderson, K. W.; Mulvey, R. E.; O'Neil, P. A. *J. Chem. Soc., Chem. Commun.* **1994**, 769.

(5) Baker, D. R.; Mulvey, R. E.; Clegg, W.; O'Neil, P. A. *J. Am. Chem. Soc.* **1993**, 115, 6472.

(6) Andrews, P. C.; Armstrong, D. R.; Mulvey, R. E.; Reed, D. J. *Am. Chem. Soc.* **1988**, 110, 5235.

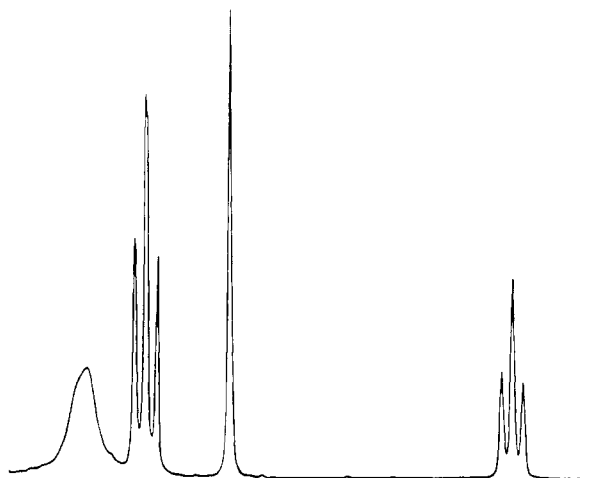
components for assembling nitrogen heterocycles, made via cycloaddition reactions with assorted anionophiles (e.g., olefins, allenes).<sup>8</sup> Often marked by high stereoselectivity, the cycloadditions can be achieved either inter- or intramolecularly.<sup>9</sup>

What prompts this amido  $\rightarrow$  azaallyl transformation, and how is it effected? These previously unanswered questions fueled the detailed NMR spectroscopic and X-ray crystallographic investigation reported herein, from which it has emerged that the transformation can now be rationalized in terms of a two-step mechanism involving  $\beta$ -elimination of a metal hydride, followed by hydride metalation. Also, it has been established that the  $\text{Li}^+$  and  $\text{K}^+$  congeners can undergo the same transformation, though, as in the  $\text{Na}^+$  case, the process is delicate, being critically dependent on the nature and degree of solvation of the  $\text{M}^+$  cation. However, the identity of the  $\text{M}^+$  cation is important, as the  $\text{Li}^+$  system yields two distinct crystalline azaallyl conformers, whereas the other systems yield only one. To attempt to understand this distinction, an ab initio MO theoretical study was carried out on different model azaallyl conformations.

## Results and Discussion

**Syntheses and NMR Spectroscopic Data. 1. Sodium Compounds.** Previously it was known that the dibenzylamido anion ( $(\text{PhCH}_2)_2\text{N}^-$ ) could either remain intact or be converted to the azaallyl anion ( $\text{PhC(H)}^-\text{N}^-\text{C(H)Ph}^-$ ), in the presence of a  $\text{Na}^+$  counterion.<sup>6,7</sup> The former situation occurs on reacting the precursor amine with an equimolar amount of  $\text{Bu}^n\text{Na}$  in hexane solution, the product being the red powdery solid (dibenzylamido)sodium,  $[\{(\text{PhCH}_2)_2\text{NNa}\}_n]$  (**1**). Its benzylic protons give rise to a singlet at  $\delta$  3.67 in the  $^1\text{H}$  NMR spectrum (in  $\text{C}_6\text{D}_6$  solution). Resonances in this region provide a marker with which to distinguish amido species from azaallyl modifications. Conversion to the azaallyl form takes place on adding the trinitrogen base PMDETA (1 equiv) to this reaction mixture. Characteristically dichroic (green by reflected light, red by transmitted), the product has the molecular formula  $[\{(\text{PhC(H)}^-\text{N}^-\text{C(H)Ph}^-)\text{Na}^+\cdot\text{PMDETA}\}]_n$  (**2**), the crystal structure of which has been reported.<sup>7</sup>

With the aim of growing crystals suitable for X-ray diffraction study, we further examined toluene solutions of **1**, exploiting its moderate arene solubility. Though unsuccessful, these attempts did uncover that repeatedly heating and then cooling such toluene solutions induces the formation and precipitation of some 2-azaallyl product, which can be identified by its  $^1\text{H}$  NMR fingerprint. This consists of four signals located at the low-frequency end of the aromatic region, a broad singlet, a triplet, a sharper singlet, and a triplet, in order of decreasing chemical shift, associated with the *ortho* H, *meta* H,  $\text{PhC(H)}$ , and *para* H, respectively (an example is shown in Figure 1). This pattern, corresponding to the trans,trans conformation (dynamic on the NMR time scale), appears to be independent of the particular  $\text{M}^+$  cation to which it is attached. Further proof of the thermal induction of the conversion process



**Figure 1.**  $^1\text{H}$  NMR "fingerprint" associated with the 1,3-diphenyl-2-azaallyl anion.

was obtained by a melting point determination: the red solid **1** is observed to change to a dichroic melt at 89–91  $^\circ\text{C}$ .

The influence of solvation of the  $\text{Na}^+$  cation was studied in greater detail by monitoring the effects of adding different Lewis bases to solutions of **1**. TMEDA ( $\text{Me}_2\text{NCH}_2\text{CH}_2\text{NMe}_2$ ), in contrast to PMDETA, can only offer (at most) a bidentate chelating bridge to a metal ion, as demonstrated in the recent crystal structure report of the monobenzyl-substituted sodium amide  $[\{(\text{PhCH}_2(\text{Me})\text{NNa}\cdot\text{TMEDA})_2\}]^{10}$  and in various other alkali-metal complexes.<sup>11</sup> The crystalline product grown from an equimolar 1/TMEDA mixture,  $[\{(\text{PhCH}_2)_2\text{NNa}\cdot\text{TMEDA}\}_2]$  (**3**), also exhibits this mode of chelation, but more significantly, it retains the amido functional group originally present in **1**; i.e., no conversion to the azaallyl form occurs. The benzylic units are visible in the  $^1\text{H}$  NMR spectrum of a  $\text{C}_6\text{D}_6$  solution of **3**, appearing at  $\delta$  4.48, which represents a shift to higher frequency of 0.81 ppm compared to that in unsolvated **1**. Thus, overall, TMEDA ligation of the  $\text{Na}^+$  center causes a substantial deshielding of the benzylic protons. No definite structural information is available on the unsolvated compound, but the crystal structure of complex **3** (discussed below and shown in Figure 6) was determined. Significantly, the intact dibenzylamido units are found in a dimeric arrangement, as opposed to the monomeric arrangement which accommodates the azaallyl group in **2**. Where these structures do coincide is in having tetracoordinated  $\text{Na}^+$  centers. Hence, the loss of denticity in switching from PMDETA to TMEDA is balanced by a gain in association (from monomer to dimer). This prompts the following question: "Is deaggregation to a monomeric state a prerequisite to the formation of the azaallyl entity?" Rerunning the  $^1\text{H}$  NMR spectrum of **3** in the coordinating solvent  $\text{C}_4\text{D}_8\text{O}$  ( $\text{THF}-d_8$ ) showed that the complex had been quantita-

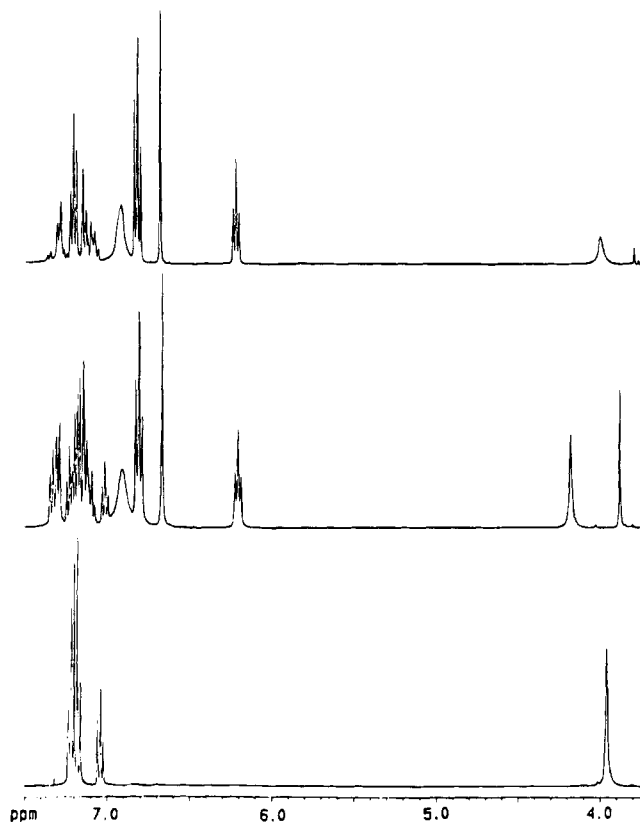
(7) Andrews, P. C.; Mulvey, R. E.; Clegg, W.; Reed, D. *J. Organomet. Chem.* **1990**, *386*, 287.

(8) For a review, see: Kauffmann, T. *Angew. Chem.* **1974**, *86*, 715; *Angew. Chem., Int. Ed. Engl.* **1974**, *13*, 627.

(9) Pearson, W. H.; Walters, M. A.; Oswell, K. D. *J. Am. Chem. Soc.* **1986**, *108*, 2769.

(10) Andrews, P. C.; Armstrong, D. R.; Clegg, W.; MacGregor, M.; Mulvey, R. E. *J. Chem. Soc., Chem. Commun.* **1991**, 497.

(11) Reviews of alkali-metal organic structures: (a) Setzer, W.; Schleyer, P. v. R. *Adv. Organomet. Chem.* **1985**, *24*, 353. (b) Schade, C.; Schleyer, P. v. R. *Adv. Organomet. Chem.* **1987**, *27*, 169. (c) Seebach, D. *Angew. Chem.* **1988**, *100*, 1685; *Angew. Chem., Int. Ed. Engl.* **1988**, *27*, 1624. (d) Boche, G. *Angew. Chem.* **1989**, *101*, 286; *Angew. Chem., Int. Ed. Engl.* **1989**, *28*, 277. (e) Mulvey, R. E. *Chem. Soc. Rev.* **1991**, *20*, 167. (f) Gregory, K.; Schleyer, P. v. R.; Snaith, R. *Adv. Inorg. Chem.* **1991**, *37*, 47. (g) Williard, P. G. In *Comprehensive Organic Synthesis*; Pergamon Press: Oxford, U.K., 1991; Vol. 1, 1. (h) Weiss, E. *Angew. Chem.* **1993**, *105*, 1565; *Angew. Chem., Int. Ed. Engl.* **1993**, *32*, 1501.



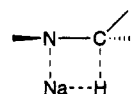
**Figure 2.**  $^1\text{H}$  NMR ( $\text{THF-}d_6$ ,  $25^\circ\text{C}$ ) kinetic study of  $[\{(\text{PhCH}_2)_2\text{NNa}\cdot\text{THF}\}_n]$  (**5**): (Bottom) time = 0; (middle) time = 24 h; (top) time = 1 week.

tively transformed to the azaallyl form, as evidenced by the appearance of its fingerprint signals and by the total lack of a benzylic  $\text{CH}_2$  signal. Given the small quantity of solid needed for this measurement, the sodium amide is effectively swamped by THF molecules. To establish whether this conversion could be stoichiometrically controlled, a solution of the TMEDA complex **3** (10 mmol) was treated with a limited amount of THF (3 mL). Slow cooling of this solution produced a large crop of dichroic crystals identified as the mixed, dual-donor species  $[\{\text{PhC}(\text{H})=\text{N}^-\text{C}(\text{H})\text{Ph}\}^-\text{Na}^+\cdot\text{TMEDA}\cdot\text{THF}]$  (**4**). Clearly, therefore, the TMEDA/THF combination mimics the role of PMDETA in **2**, confirming that fulfillment of the coordinative requirements of a monomeric structure is a prerequisite to the occurrence of the amido  $\rightarrow$  azaallyl conversion. More information was gleaned from hexane solutions of **1** containing THF exclusively. Low concentrations of THF (e.g., 1.6 mL/10 mmol of **1**) afforded red crystalline blocks of the 1/1 amido/THF complex  $[\{(\text{PhCH}_2)_2\text{NNa}\cdot\text{THF}\}_n]$  (**5**). A simple kinetic study (Figure 2) revealed that dissolving freshly prepared **5** in a donor medium ( $\text{THF-}d_6$ ) and immediately recording its  $^1\text{H}$  NMR spectrum at first encouraged the retention of the amido character, as witnessed by the  $\text{PhCH}_2$  singlet and Ph multiplets at  $\delta$  3.96 and 7.20/7.04, respectively. However, after 24 h these signals had diminished, while the azaallyl fingerprint had appeared, as had another set of signals belonging to neither the amido nor the azaallyl entities. From relative integrals it can be estimated that at this stage 44% of the amide has been fully converted to the azaallyl product, and another 44% has been partially converted to an intermediate species, leaving 12% unchanged. When this spectrum is rerun repeatedly, the amido  $\rightarrow$  azaallyl conversion is found to level off so

that after 1 week a plot of the percentage conversion against time showed the maximum conversion to be about 60%. Higher concentrations of THF (e.g., 4 mL/10 mmol of **1**) in the reaction mixture pushed the process past the amido complex stage to ultimately yield dichroic crystals of the tris(THF)-solvated azaallyl  $[\{\text{PhC}(\text{H})=\text{N}^-\text{C}(\text{H})\text{Ph}\}^-\text{Na}^+\cdot 3\text{THF}]$  (**6**). Thus, as before, a 3-fold donor atom coordination of the  $\text{Na}^+$  cation accompanies, or directs, the conversion to the delocalized N-centered anion.

Having established the importance of a tris-solvated  $\text{Na}^+$  center to the conversion process, the next consideration is the identity of the intermediate observed in the kinetic NMR study of **5**. The singlet located at  $\delta$  4.17 (Figure 2) provides a pointer, belonging as it does to the benzylic  $\text{CH}_2$  region. All the remaining resonances are grouped together in the aromatic region, close to and partly overlapping the amido (Ph) signals, though significantly they appear at slightly higher frequencies than the azaallyl resonances. The imine *N*-benzylidenebenzylamine,  $\text{PhCH}_2\text{N}=\text{C}(\text{H})\text{Ph}$ , was considered but dismissed on the grounds of markedly different chemical shifts (e.g., its benzylic  $\text{CH}_2$  occurs at  $\delta$  4.75) and of the lack of a  $\text{N}=\text{CH}$  signal (which in the imine occurs at  $\delta$  8.37, whereas the highest signal found here occurs at  $\delta$  7.35). It is more likely, given the similarity between this set of signals and that belonging to the (dibenzylamido)sodium-associated complex **5**, that the unknown is another (dibenzylamido)sodium species, of a different aggregation, though its precise nature cannot be stated with any certainty.

Whatever the active species (monomer or not), it must itself go through an intermediate (the imine,  $\text{PhCH}_2\text{N}=\text{C}(\text{H})\text{Ph}$ ), but in a process too fast to detect by NMR spectroscopic means, prior to forming the azaallyl product. Moreover, to balance the reaction stoichiometry, formation of this imine from sodium dibenzylamide would require the concomitant formation of  $\text{NaH}$  (which may or may not be solvated by THF). This event, in turn, might explain why a monomeric setup may be pivotal to the conversion process, as it is well documented that  $\beta$ -hydride eliminations from alkali-metal organyls are stereospecific processes which, by definition, require transition states with fixed stereochemistries.<sup>12</sup> Kinetic studies of the decomposition of alkylolithiums (e.g.,  $\text{Bu}^n\text{Li}$ ,  $\text{Oct}^n\text{Li}$ ) into  $\text{LiH}$  and the appropriate olefin<sup>13</sup> point toward four-center cyclic transition states, which in this case would correspond to

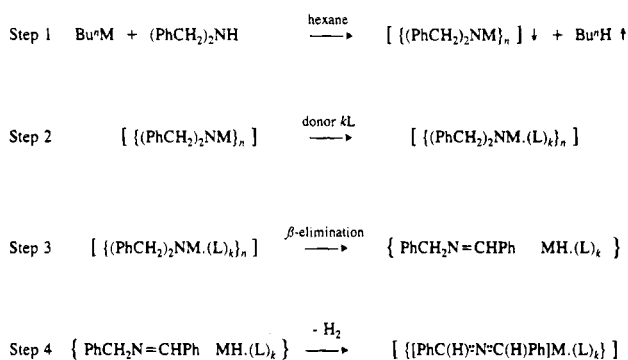


The irreversible, unimolecular  $\beta$ -hydride eliminations involved in such decompositions are thermally induced, and moreover, the rate-determining step appears to concern fully aggregated (hexameric) alkylolithiums. The amido  $\rightarrow$  azaallyl conversion (and by implication the elimination of  $\text{NaH}$ ) can also be thermally driven, but more importantly, associated (dimeric) sodium dibenzylamide structures (e.g., as shown in Figure 6) can be compelled to undergo this transformation at much lower

(12) Davidson, P. J.; Lappert, M. F.; Pearce, R. *Chem. Rev.* **1976**, *76*, 219. (b) Glaze, W. H.; Lin, J.; Felton, E. G. *J. Org. Chem.* **1966**, *31*, 2643. (c) Houk, K. N.; Rondan, N. G.; Schleyer, P. v. R.; Kaufmann, E.; Clark, T. *J. Am. Chem. Soc.* **1985**, *107*, 2821.

(13) Finnegan, R. A.; Kutta, H. W. *J. Org. Chem.* **1965**, *30*, 4138.

## Scheme 1



temperatures (e.g., ambient) by placing a third donor atom on the  $\text{Na}^+$  centers to promote cleavage of the  $(\text{NNa})_2$  ring.

Logically, the final step in the conversion process involves hydride metalation of the intermediate imine to form both the azaallyl product and dihydrogen. Scheme 1 lists all four stages in the mechanism for the conversion of dibenzylamine to the metal azaallyl complex. The final step is a known chemical reaction, recently exploited by Floriani et al., who generated the potassium analogue  $[(\text{PhC}(\text{H})=\text{N}=\text{C}(\text{H})\text{Ph})-\text{K}^+(\text{18-crown-6})]$  from an imine/KH/crown ether mixture.<sup>14</sup> Significantly, this preparation required 12 h at reflux temperature. Clearly, therefore, dibenzylamine is superior as a source of the 2-azaallyl anion, as it produces this anion almost immediately at ambient temperature. Though the potassium complex was merely used for this purpose (specifically to transfer the anion to a zirconium center), it was isolated and the resulting X-ray crystallographic study revealed a monomeric contact ion pair arrangement akin to that of **2**. For completeness, to confirm that NaH could similarly deprotonate the imine to generate the azaallyl species, we reacted such mixtures in the presence of PMDETA and of TMEDA/THF. Both preparations were successful, giving the expected dichroic products **2** and **4**, respectively, though only in very modest yields, reflecting the comparative inertness of and, linked to this, the poor solubility of the ionic hydride. This conflicts with the facile production of the azaallyl entities via the dibenzylamine route, which is seemingly quantitative. The key difference is that the hydride metalation step occurs in situ in the latter case, and so solubility problems are circumvented. Furthermore, the in situ NaH may be activated either by Lewis base solvation or by remaining attached to the imine produced simultaneously.

**2. Lithium Compounds.** Mixtures of (dibenzylamido)lithium and the donor solvent HMPA or  $\text{Et}_2\text{O}$  had previously been examined in some detail, but these only produced simple Lewis acid–Lewis base complexes with intact amido groups<sup>3</sup> and gave no hint of possible azaallyl products. In light of the new developments, we subjected the lithium amide to a selection of donor solvents similar to that used in the sodium work. We also studied the lithiation of the imine  $\text{PhCH}_2\text{N}=\text{C}(\text{H})\text{Ph}$ .

THF had the same effect as  $\text{Et}_2\text{O}$ , deaggregating the trimeric lithium amide to a dimeric complex,  $[(\text{PhCH}_2)_2\text{NLi} \cdot \text{THF}]_2$  (**7**), whose crystal structure is shown in Figure 7. The amount of excess THF present in the

reaction mixture did not appear to have any bearing on the nature of the product, but 10 molar equiv was necessary to completely dissolve the pink (dibenzylamido)lithium suspension in hexane. Retention of the  $(\text{PhCH}_2)_2\text{N}$  group was confirmed by the benzylic  $\text{CH}_2$  resonance at  $\delta$  3.71 in the  $^1\text{H}$  NMR spectrum of a  $\text{C}_4\text{D}_8\text{O}$  ( $\text{THF}-d_8$ ) solution. When the temperature was raised, the pink crystals of **7** melted at 135–137 °C to a red liquid, with no sign of a dichroic hue, suggesting that the amido character is retained (i.e. it does not convert to an azaallyl form).

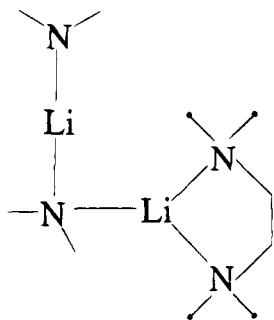
Switching from THF to polydentate 1,4-dioxane promotes the joining up of the discrete O-complexed  $(\text{NLi})_2$  rings into a polymeric chain structure of formula  $[[(\text{PhCH}_2)_2\text{NLi}]_2(\text{dioxane})]_n$ , isolated as its toluene hemisolvate **8**. Characterization was achieved by means of a crystal structure determination (Figures 8 and 9) and NMR spectroscopic studies. The bridging role played by the donor results in a 2/1 lithium amide/donor ratio overall in the structure, corresponding to the initial stoichiometry used in the reaction mixture (i.e., 0.5 molar equiv of dioxane/equiv of lithium amide, though dilute solutions (1 mmol of amide in 30 mL of toluene) were necessary to obtain crystals of **8** and to avoid the rapid precipitation of a powdery form). However, this reaction proved to be sensitive to a change in stoichiometry with an excess of dioxane (10 molar equiv) producing the donor-rich, crystalline variant  $[(\text{PhCH}_2)_2\text{NLi} \cdot 2(\text{dioxane})]_n$  (**9**). Distinguishable from **8** by the relative integrals of the benzylic and dioxane resonances on the  $^1\text{H}$  NMR spectrum and by its lower melting point (86–88 °C; cf. dec. at 260 °C), these crystals are notably less stable, degrading to an oil after 1 day of storage in an argon-filled glovebox, whereas **8** is stable indefinitely. For this reason the crystal structure of **9** could not be ascertained, though the above characteristics point toward an oligomeric structure, in which case the instability could be connected to dioxane molecules having one ligating end (terminally attached to  $\text{Li}^+$ ) and one unligating end. Whatever the precise structure, it is certain that amido character is maintained and that there is no azaallyl formation.

Treating the lithium amide with excess TMEDA gave  $[(\text{PhCH}_2)_2\text{NLi}]_2 \cdot \text{TMEDA}$  (**10**), a red crystalline complex with the same 2/1 acceptor/donor stoichiometry displayed by **8**. Therefore, as was the case with THF and dioxane, solvation by TMEDA fails to disrupt the amido character of the anionic ligand. If we draw comparisons to the sodium work, this failure is not unexpected given the empirical formula of **10**, which, to have an integral number of donor molecules, requires dimeric (or higher associated) amido units and not monomeric units which appear essential to azaallyl formation. Though the structure of **10** has not yet been determined, it may be relevant that its 2/1  $\text{Li}^+/\text{TMEDA}$  stoichiometry fits another structural type referred to as an open dimer (see Figure 3), recently established for the lithio (TMEDA) derivative of 2,2,6,6-tetramethylpiperidine.<sup>15</sup>

The complexed lithium amide structures proved more resilient than sodium congeners to variations in the quantity of donor solvent present, presumably as a consequence of the greater strength of NLi ring bonds versus NNa ones. This is particularly apparent when a mixed TMEDA/THF medium is considered. Whereas

(14) Veya, P.; Floriani, C.; Chiesi-Villa, A.; Guastini, C. *J. Chem. Soc., Chem. Commun.* **1991**, 991.

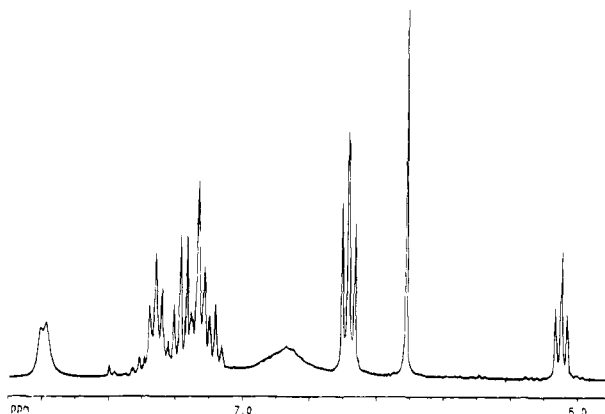
(15) Williard, P. G.; Liu, Q.-Y. *J. Am. Chem. Soc.* **1993**, *115*, 3380.



**Figure 3.** Idealized general structure of the open dimer adopted by TMEDA solvates of some lithium amides.

this combination causes the sodium amide to convert to the tris(solvated) azaallyl derivative **4** containing both TMEDA and THF ligands, in contrast, the lithium amide remains as such due to the smaller  $\text{Li}^+$  center being merely monosolvated (by a THF molecule); i.e., the mixture produces the same dimeric complex (**7**) as produced in THF alone, with TMEDA playing no part in complex formation. This preference for THF over TMEDA, which is also observed in solution when the solid TMEDA complex **10** is dissolved in  $\text{C}_4\text{D}_8\text{O}$  ( $\text{THF}-d_8$ ), could be indicative of an energetic preference for the closed-ring dimer over an open-ring alternative.<sup>16</sup> Moreover, it is clear that aggregation (dimerization) is more important than solvation in this lithium system, as monosolvated dimers dominate in donor-rich media, with no evidence of bis-solvated (whether by two THF molecules or one TMEDA) monomers. THF being less sterically demanding obviously fits the exocyclic coordination site at  $\text{Li}^+$  in this dimeric  $(\text{NLi})_2$  ring structure better than does TMEDA. Analogous TMEDA-solvated dimers, which would formally contain four-coordinate  $\text{Li}^+$  centers, are rare, though they can occur with small and/or flat amido substituents as typified by  $[\{\text{Ph}(\text{Me})\text{NLi}\cdot\text{TMEDA}\}_2]$ .<sup>17</sup> Bulkier ligands, on the other hand, force the adoption of monomeric arrangements with formally three-coordinate  $\text{Li}^+$  centers, as demonstrated in  $[\text{Bu}^t_3\text{C}_6\text{H}_2(\text{H})\text{NLi}\cdot\text{TMEDA}]$ .<sup>18</sup>

It was decided to investigate the effect of the triamine PMDETA, in the expectation that dimerization (of any type) could no longer be sustained due to the increased steric requirement involved. Accordingly, 1 molar equiv of PMDETA was added to a hexane solution of (dibenzylamido)lithium, which was then heated gently. Slow cooling of the resulting deep red solution to ambient temperature afforded a large crop of purple-red crystals speckled with dichroic flakes. This crop was clearly a mixture; the dichroism suggested azaallyl formation, confirmed by a  $^1\text{H}$  NMR spectrum (Figure 4), which showed no benzylic  $\text{CH}_2$  resonance and from which the crystals were formulated as  $[\{\text{PhC}(\text{H})\text{N}^-\text{C}(\text{H})\text{Ph}\}^- \text{Li}^+\text{PMDETA}]$  (**11**), though the two distinct isomers **11A** and **11B** could be distinguished. More specifically, the clutch of four signals characteristic of the (trans,trans) 2-azaallyl ligand is clearly visible between  $\delta$  6.95 and 6.08 (assigned to **11A**) as are the four lower frequency signals between  $\delta$  2.37 and 2.10 due to complexed PMDETA. In addition, a clutter of multiplets lies toward the high-frequency end of the aromatic region



**Figure 4.**  $^1\text{H}$  NMR ( $\text{THF}-d_8$ ,  $40^\circ\text{C}$ ) of  $[\{\text{PhC}(\text{H})\text{N}^-\text{C}(\text{H})\text{Ph}\}^- \text{Li}^+\text{PMDETA}]_n$  (**11**) showing clearly the presence of the two isomeric forms **11A** and **11B**.

(in the range  $\delta$  7.7–7.1), assigned to **11B**. Significantly, combining the relative integrals of **11A** and **11B** and comparing this total to the relative integral of the PMDETA signals give a 1/1  $\text{PhC}(\text{H})\text{NC}(\text{H})\text{Ph}/\text{PMDETA}$  stoichiometric ratio. Repeating this preparation several times always gave the same mixed product, though the relative proportions of **11A** and **11B** varied slightly. However, the overall  $\text{PhC}(\text{H})\text{NC}(\text{H})\text{Ph}/\text{PMDETA}$  stoichiometry remained constant at 1/1. Clearly, irrespective of the identity of **11B**, which as yet remains to be established, the amido  $\rightarrow$  azaallyl conversion had taken place, initiated by PMDETA completely deaggregating the lithium amide to a monomeric form primed for  $\beta$ -hydride elimination.<sup>19</sup> In this respect the lithium and sodium systems are in parity. Of course, where they differ is in the fact that only one azaallyl conformer (trans,trans) crystallizes in the latter case, as established by an X-ray analysis of **2**, whereas the former system yields two distinct crystalline conformers (**11A** and **11B**). Bracketing the alkali metals together as mere counterions " $\text{M}^+$ " is clearly erroneous in this case. Hence, this example illustrates why it is important to consider each alkali metal individually in synthetic applications seemingly concerning "anions".<sup>20</sup>

To establish whether or not this cocrystallization phenomenon was specific to the dibenzylamido pathway, a 1/1/1 mixture of  $\text{Bu}^n\text{Li}$ , the imine  $\text{PhCH}_2\text{N}=\text{C}(\text{H})\text{Ph}$ , and PMDETA was examined. The deeply colored complex produced by this lithiation reaction (though not involving PMDETA) has incidentally been proposed as an indicator for the standardization of organolithium reagents in ether or hydrocarbon media.<sup>21</sup> Performing our lithiation at low temperature ( $-78^\circ\text{C}$ ) in hexane and warming the solution to ambient temperature before introducing PMDETA also produced a mixture of **11A** and **11B** (as well as  $\text{Bu}^n\text{H}$ ), which, as in the previous case, could not be separated to allow them to be characterized by X-ray diffraction. The overall yield of **11** was high, but more importantly, the relative percentage of **11A** to **11B** was found to be approximately 50/50 based on the integration in the  $^1\text{H}$  NMR spectrum. Significantly, however, when PMDETA is present at the outset of the reaction (i.e., added directly to the cold  $\text{Bu}^n$ -

(16) For a discussion on effects of TMEDA vs those of THF in alkali-metal systems see: Collum, D. B. *Acc. Chem. Res.* **1992**, *25*, 448.

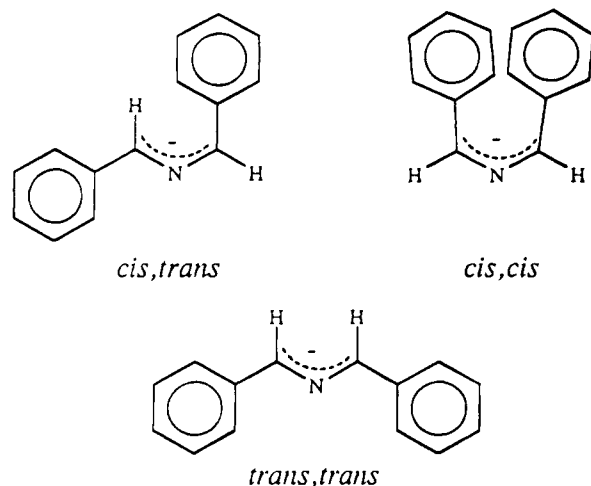
(17) Barr, D.; Clegg, W.; Mulvey, R. E.; Snaith, R.; Wright, D. S. *J. Chem. Soc., Chem. Commun.* **1987**, 716.

(18) Fjeldberg, T.; Hitchcock, P. B.; Lappert, M. F.; Thorne, A. J. *J. Chem. Soc., Chem. Commun.* **1984**, 822.

(19) For related LiH eliminations see: Richey, H. G., Jr.; Erickson, W. F. *J. Org. Chem.* **1983**, *48*, 4349.

(20) For a review of the effect of the gegenion on the structures and stabilities of alkali-metal compounds, see: Lambert, C.; Schleyer, P. v. R. *Angew. Chem., Int. Ed. Engl.* **1994**, *33*, 1129.

(21) Duhamel, L.; Plaquevent, J.-C. *J. Org. Chem.* **1979**, *44*, 3404.



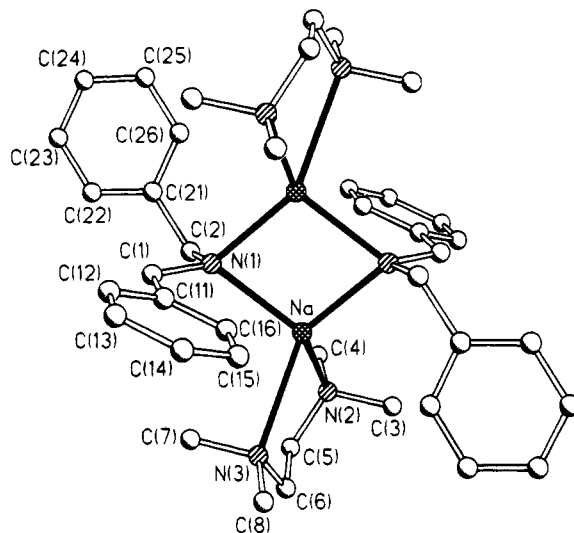
**Figure 5.** Idealized conformations of the 1,3-diphenyl-2-azaallyl anion.

Li/imine mixture), the ratio changes to approximately 90/10. Metalation in this case is presumably via "Bu<sup>n</sup>-Li-PMDETA", suggesting that sterically and/or electronically a complexed Li<sup>+</sup>-PMDETA cation acts more like a Na<sup>+</sup> cation than a "free" Li<sup>+</sup> cation, since it gives the trans,trans conformer (11A) predominately. Two distinct types of PMDETA are not evident from variable-temperature <sup>1</sup>H NMR studies of 11, which is perhaps understandable given that 11A and 11B differ in conformation (of the anion) only and that in both isomers PMDETA will probably be found in its normal tridentate manner to a Li<sup>+</sup> center attached to the azaallyl C-N-C unit via the central N atom. Idealized conformations of the anion are shown in Figure 5.

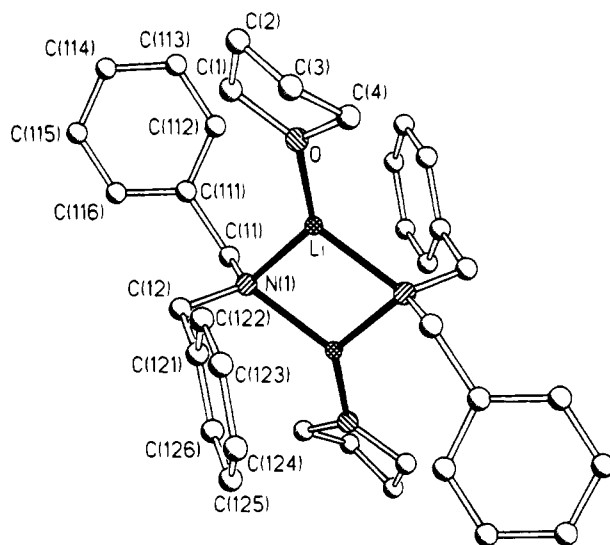
**3. Potassium Compounds.** Having established that both Li and Na can facilitate the amido → azaallyl conversion and having found significant differences between these systems, we decided to extend and complete our experimental survey by examining the effect of the larger K<sup>+</sup> cation.

Reaction of a 1/1 molar mixture of dibenzylamine and Bu<sup>n</sup>K with 2 molar equiv of PMDETA afforded a large crop of needlelike crystals. Their dichroic (green/red) appearance suggested an azaallyl formulation, and this was definitely confirmed by <sup>1</sup>H NMR spectroscopic studies, which revealed them to be [[PhC(H)<sup>-</sup>N<sup>-</sup>C(H)Ph]<sup>-</sup>K<sup>+</sup>·2PMDETA] (12). Note that in agreement with the reaction stoichiometry the complex contains two solvent molecules per metal center. This "excess" donor solvent was necessary to completely solubilize an apolar (hexane) solvent suspension of the intermediate amide [{(PhCH<sub>2</sub>)<sub>2</sub>NK}]<sub>n</sub> (13). The stoichiometric solvation present in 12 proved insufficient to render the compound arene-soluble, in contrast to what is often the case with organic derivatives of the smaller alkali metals; therefore, its solution <sup>1</sup>H NMR spectrum had to be run in polar C<sub>4</sub>D<sub>8</sub>O (THF-*d*<sub>8</sub>).

All three alkali-metal cations (Li<sup>+</sup>, Na<sup>+</sup>, K<sup>+</sup>) can thus bring about the dibenzylamido → azaallyl transformation. What does differ, of course, and why each alkali-metal system should be individually assessed, is the number of ligating centers required to enforce a monomeric state, given that we are dealing with homoleptic systems. This general point is exemplified here by the fact that one PMDETA ligand is adequate for Na<sup>+</sup>, whereas K<sup>+</sup> needs two such ligands, in keeping with their relative sizes. Complex 12 was examined by X-ray



**Figure 6.** Molecular structure of [(PhCH<sub>2</sub>)<sub>2</sub>NNa·TMEDA]<sub>2</sub> (3) with atomic labeling scheme. Hydrogen atoms have been omitted.

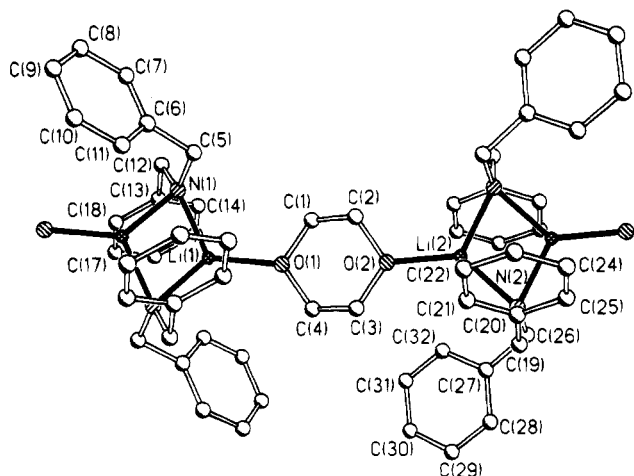


**Figure 7.** Molecular structure of [(PhCH<sub>2</sub>)<sub>2</sub>NLi·THF]<sub>2</sub> (7) with atomic labeling scheme. Hydrogen atoms have been omitted.

diffraction, but an accurate structure could not be obtained due to poor crystal quality. However, it was possible to make out its monomer (contact ion pair) arrangement and bis(PMDETA) solvation. Aggregation would not have been expected in any event, given the precedent set by monomeric [[PhC(H)<sup>-</sup>N<sup>-</sup>C(H)Ph]<sup>-</sup>K<sup>+</sup>·(18-crown-6)], discussed earlier.<sup>14</sup> The only structural aspect open to debate is whether the K<sup>+</sup> center in 12 binds to both types of atoms in the C-N-C linkage, as found in the crown analogue, or whether it binds to the central N alone. Given the multiple nature of the C-N-C bonds and the close proximity of the C and N atoms therein, the former option is preferred.

**X-ray Crystallographic Studies.** Three new crystal structures have been determined during the course of this work. Two of them, the sodium complex [(PhCH<sub>2</sub>)<sub>2</sub>NNa·TMEDA]<sub>2</sub> (3) and the lithium complex [(PhCH<sub>2</sub>)<sub>2</sub>NLi·THF]<sub>2</sub> (7), are discretely dimeric (Figures 6 and 7, respectively), while the third, [(PhCH<sub>2</sub>)<sub>2</sub>NLi]<sub>2</sub>(dioxane)<sub>∞</sub>, isolated as its toluene hemisolvate 8, exists as a polymer made up of two distinct dimeric units (Figures 8 and 9). Here the difference in aggrega-





**Figure 8.** Molecular structure of  $[[[(\text{PhCH}_2)_2\text{NLi}]_2\text{-(dioxane)}]_n]$  (**8**) in its toluene hemisolvate with atomic labeling scheme.

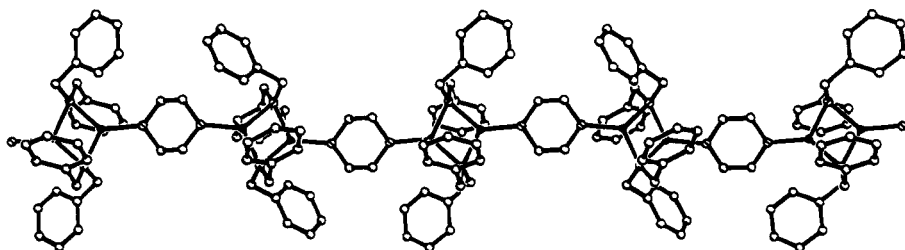
tion state is due to the bifunctionality of 1,4-dioxane, which facilitates its monodentate, bridging role. TMEDA can also assume this role, but it is more commonly found in a bidentate, terminal role as in **3**. Table 1 compares selected dimensions of the complexed  $(\text{NM})_2$  four-membered rings of **3**, **7**, and **8**. As is usual for aza-alkali-metal rings, they are rhomboidal with acute angles at N and obtuse angles at M, with the latter being greater for  $\text{Li}^+$  ( $103.04(12)^\circ$  in **7**;  $105.8^\circ$  (mean) in **8**) than for  $\text{Na}^+$  ( $97.44(6)^\circ$ ). Due to crystallographic symmetry impositions, all these rings are strictly planar. Buckling the ring as in the related monobenzyl amide  $[\{\text{PhCH}_2(\text{Me})\text{NNa}^+\text{TMEDA}\}_2]^{10}$  causes only slight changes in its dimensions (i.e., N–Na bond length (mean)  $2.37 \text{ \AA}$ , cf.  $2.40 \text{ \AA}$  in **3**; bond angle at N  $80.8^\circ$ , cf.  $82.4^\circ$ ; bond angle at Na  $96.7^\circ$ , cf.  $97.4^\circ$ ). Of greater significance is the closer, more symmetrical approach of TMEDA (N–Na bond lengths  $2.496$  and  $2.511 \text{ \AA}$  (mean  $2.504 \text{ \AA}$ ), cf.  $2.489$  and  $2.678 \text{ \AA}$  (mean  $2.584 \text{ \AA}$ ) in **3**) which signifies that the dibenzyl units sterically shield the  $\text{Na}^+$  cation more so than the benzyl methyl units. Four-coordinate overall, the  $\text{Na}^+$  cation occupies an extremely distorted tetrahedral site (range of  $\text{NNa}^+\text{N}$  angles  $71\text{--}139^\circ$ , mean  $110.2^\circ$ ). Not surprisingly, the smaller  $\text{Li}^+$  centers can only attain coordination numbers of 3 in their dimeric setups, bonding to a single monodentate O donor ligand. The  $\text{Li}^+$  geometries are pyramidal, but only marginally so, as evidenced by the sums of their bond angles (i.e.,  $356.7^\circ$  in **7**;  $352.6$  and  $358.9^\circ$  in **8**). There are no significant differences in the bond lengths involving the  $\text{Li}^+$  centers (i.e., (mean) N–Li  $2.043$  and  $1.983 \text{ \AA}$ , O–Li  $1.915$  and  $1.924 \text{ \AA}$ , for **7** and **8**, respectively), and when these are compared with corresponding bond lengths in the previously reported ether and HMPA complexes of (dibenzylamido)lithium, the O–Li bond lengths follow the order HMPA ( $1.850$

$\text{\AA}$ )  $<$  THF  $\approx$  dioxane  $<$  ether ( $2.009 \text{ \AA}$ ). Clearly this trend is in keeping with the stereochemistries about the ligating O atoms, as HMPA is the least restricted, having an essentially linear P=O–Li linkage, and the cyclic ethers THF and dioxane are similar to each other in this regard, whereas the branched, acyclic nature of ether makes it the most sterically crowded. Benzyl-amido substituents are inherently flexible ligands, as regards the direction and tilt of their phenyl rings, but are relatively inflexible in the way they bridge to the metal centers in these dimeric rings. An exception is the endocyclic MNM' angle, which is mainly dictated by the relative size of the alkali metal M: the larger  $\text{Na}^+$  cation widens this by about  $5\text{--}10^\circ$  compared to that in the  $(\text{NLi})_2$  rings (i.e.,  $82.56^\circ$  for **3**; cf.  $76.96^\circ$  for **7** and  $74.6$  and  $73.8^\circ$  for **8**). However, irrespective of the particular alkali metal attached, the anionic N atoms adopt four-coordinate, distorted-tetrahedral (mean bond angles  $109.3$ ,  $108.9$ , and  $107.8^\circ$  in **3**, **7**, and **8**, respectively) geometries, and the C–N–C bond angles are all similar ( $108.4$ ,  $109.5$ , and  $109.8$  (mean), respectively).

The unique feature of **8** is its polymeric association. To link up the dimeric  $(\text{NLi})_2$  units into infinite chains, the dioxane molecule adopts a chair conformation. Its four carbon atoms reside in a plane, while the two ligating oxygen atoms lie above and below this plane. The oxygen atoms have a three-coordinated distorted-triangular geometry. The O(1), Li(1), C(1), and C(4) atoms are approximately coplanar, as are the O(2), Li(2), C(2), and C(3) atoms. Within these units the smallest bond angles occur inside the ether ring (C(4)O(1)C(1),  $110.3^\circ$ ; C(3)O(2)C(2),  $110.4^\circ$ ; cf.  $129.6$ ,  $119.1$ ,  $128.7$ , and  $119.2$  for C(4)O(1)Li(1), C(1)O(1)Li(1), C(3)O(2)Li(2), and C(2)O(2)Li(2), respectively). A similar pattern was recently observed in the alkylaluminum amide  $[\{\text{Me}_2\text{Al}[\text{N}(\text{SiMe}_3)_2]\}_2\text{-(dioxane)}]$  with an endocyclic C–O–C angle of  $111.4^\circ$ .<sup>22</sup>

**Theoretical Calculations.** Ab initio MO geometry optimizations<sup>23</sup> were performed at the SCF level using the 6-31G basis set.<sup>24</sup>

Figure 5 shows the idealized conformations (trans,trans; cis,trans; cis,cis) of the free 1,3-diphenyl-2-azaallyl anion. Simply by inspection, one would anticipate the first- and third-named isomers to be the most and least stable, respectively, as a consequence of the relative proximities of their phenyl substituents. Calculations confirm this is the case. Being considerably distorted from the idealized geometry and having a relative energy over  $18 \text{ kcal mol}^{-1}$  less favorable than that of the trans,trans isomer, the cis,cis isomer is clearly unrealistic and does not warrant further discussion. Intermediate in stability with a relative energy of  $6.4 \text{ kcal mol}^{-1}$ , the cis,trans optimized ( $C_s$ ) structure is planar, like its trans,trans ( $C_{2v}$ ) counterpart. Both therefore closely resemble their idealized representations in appearance. Delocalization is marginally more

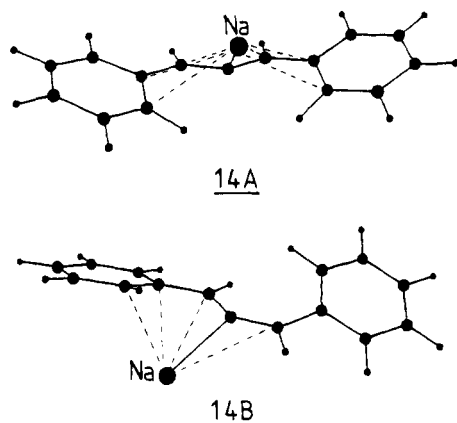


**Figure 9.** Polymeric chain structure of **8**.



**Table 1.** Selected Dimensions of the Complexed (NM)<sub>2</sub> Four-Membered Rings of Compounds[{(PhCH<sub>2</sub>)<sub>2</sub>NNa·TMEDA}]<sub>2</sub> (3), [(PhCH<sub>2</sub>)<sub>2</sub>NLi·THF]<sub>2</sub> (7), and [[(PhCH<sub>2</sub>)<sub>2</sub>NLi]<sub>2</sub>(dioxane)]<sub>∞</sub> (8)

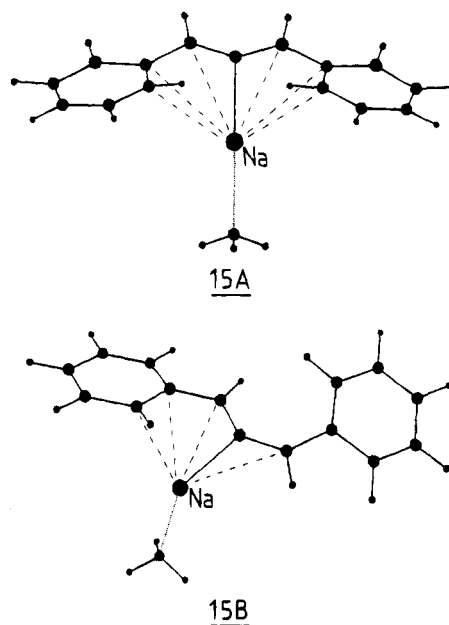
	3	7	8
N-M (Å)	Na-N(1) 2.397(2) Na-N(1a) 2.412(2)	Li-N(1) 2.028(3) Li-N(1a) 2.058(3)	Li(1)-N(1) 1.939(7) Li(1)-N(1a) 2.037(7) Li(2)-N(2) 1.978(7) Li(2)-N(2b) 1.978(7)
N-M-N (deg)	N(1)-Na-N(1a) 97.44(6)	N(1)-Li-N(1a) 103.04(12)	N(1)-Li(1)-N(1a) 105.4(3) N(2)-Li(2)-N(2b) 106.2(3)
M-N-M (deg)	Na-N(1)-Na(a) 82.56(6)	Li-N(1)-Li(1a) 76.96(12)	Li(1)-N(1)-Li(1a) 74.6(3) Li(2)-N(2)-Li(2b) 73.8(3)

**Figure 10.** Ab initio structures of unsolvated (1,3-diphenyl-2-azaallyl)sodium models. Here, and in Figures 11–14, short metal–carbon contacts are represented by broken lines.

efficient in the trans,trans arrangement, as evidenced by the lower charge on the central N atom (−0.48 e, cf. −0.54 e). There are also differences, mostly minor, in bond lengths and bond angles, a significant example being the azaallyl C–N–C bond angle, which is wider (135.3°, cf. 126.5°) in the cis,trans structure to offset increased steric crowding.

Calculations on the contact (anion–cation) pair structures (cation = Na<sup>+</sup> or Li<sup>+</sup>) are now discussed for each cation in turn.

**1. Sodium Models.** The relative stabilities of the trans,trans and cis,trans conformations remain the same (energy difference 5.3 kcal mol<sup>−1</sup>) in the presence of the larger, more polarizable Na<sup>+</sup> cation. Disruption of the p<sub>π</sub>–p<sub>π</sub> orbital overlap dominates here, at the expense of metal–anion bonding, for the preferred structure (14A) has (overall) longer and weaker, though more, Na<sup>+</sup>–anion interactions than 14B (Figure 10). In the former case, the anion hapticity is η<sup>7</sup> (bond lengths: N–Na, 2.248 Å; C<sub>α</sub>–Na (×2), 2.964 Å; C<sub>ipso</sub>–Na (×2), 3.083 Å; C<sub>ortho</sub>–Na (×2), 2.819 Å), whereas in the latter case this decreases to η<sup>4</sup> (N–Na, 2.271 Å; C<sub>α</sub>–Na, 2.595 Å; C<sub>ipso</sub>–Na, 2.626 Å; C<sub>ortho</sub>–Na, 2.590 Å) or η<sup>5</sup> if the long C<sub>α</sub>–Na contact (3.205 Å) is included. Note that short metal···H(C) contacts present in these calculated structures are disregarded, as it is taken that the bonding is primarily metal–C based and that these short contacts arise because of the close attachment of the H atoms (which carry a positive charge!) to the C atoms. Other notable features of 14A are the small metal–anion incline (37.1°) (i.e., the dihedral angle between the N–Na slope and the CNC plane), compared to 50.1° in the crystal structure of 2, and the perceptible tilt (19°) of the phenyl rings out of the CNC plane

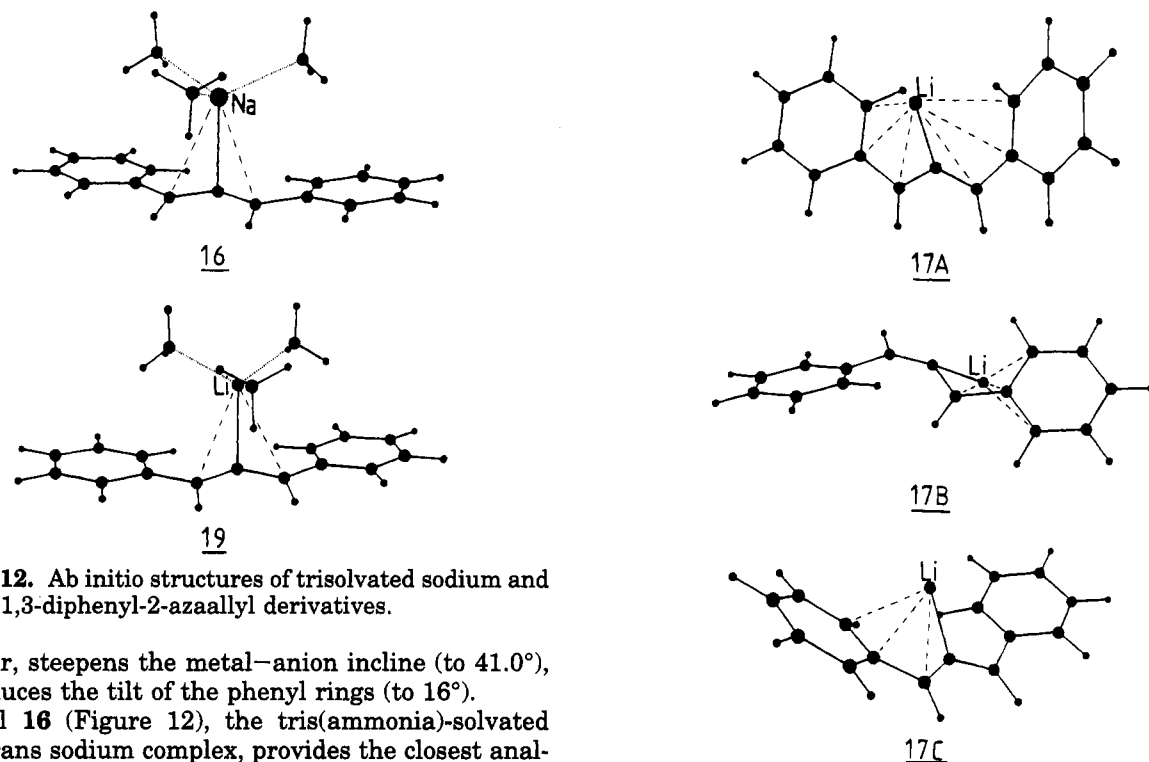
**Figure 11.** Ab initio structures of monosolvated (1,3-diphenyl-2-azaallyl)sodium models.

toward the centrally disposed Na<sup>+</sup> cation. Forcing the metal to lie in the same plane as the trans,trans anion (between Ph rings) results in a loss in stability of 13.3 kcal mol<sup>−1</sup>, advertising the N atom's preference for a pyramidal geometry over a planar one, in its interaction with the metal.

Solvation is taken into consideration in models 15A and 15B (Figure 11) with each Na<sup>+</sup> cation solvated by a single ammonia molecule. Again, the trans,trans conformer is energetically preferred, by a similar margin (5.4 kcal mol<sup>−1</sup>). The energy gain on solvation is 21.0 kcal mol<sup>−1</sup>, due to the formation of the N–Na dative bond (length 2.399 Å; NNa-N bond angle 155.9°). Corresponding values for the cis,trans conformer are 20.8 kcal mol<sup>−1</sup>, 2.404 Å, and 132.8°, respectively. The asymmetric anion in this structure (15B) binds to the solvated cation in a η<sup>4</sup> arrangement (N–Na, 2.311 Å; C<sub>α</sub>–Na, 2.628 Å; C<sub>ipso</sub>–Na, 2.684 Å; C<sub>ortho</sub>–Na, 2.675 Å) or in a η<sup>5</sup> arrangement if the long C<sub>α</sub>–Na contact (3.203 Å) is included. In contrast, 15A displays a looser η<sup>7</sup> interaction (N–Na, 2.279 Å; C<sub>α</sub>–Na (×2), 2.980 Å; C<sub>ipso</sub>–Na (×2), 3.149 Å; C<sub>ortho</sub>–Na (×2), 2.936 Å), if the long ipso carbon–metal separations are included. Comparison with 14A reveals that, as expected, solvation weakens and loosens the polyhapto anion–cation con-

(23) Dupuis, M.; Spangler, D.; Wendolowski, J. NRCC Software Catalog, Vol. 1, Program No. QG01 (GAMESS), Daresbury, U.K. (b) Guest, M. F.; Fantucci, P.; Harrison, R. J.; Kendrick, J.; van Lenthe, J. H.; Schoeffel, K.; Sherwood, P. GAMESS-UK; CFS Ltd., 1993.

(24) Hehre, W. J.; Ditchfield, R.; Pople, J. A. *J. Chem. Phys.* **1972**, *56*, 2257. (b) Hariharan, P. C.; Pople, J. A. *Theor. Chim. Acta* **1973**, *28*, 213.



**Figure 12.** Ab initio structures of trisolvated sodium and lithium 1,3-diphenyl-2-azaallyl derivatives.

tact pair, steepens the metal–anion incline (to  $41.0^\circ$ ), and reduces the tilt of the phenyl rings (to  $16^\circ$ ).

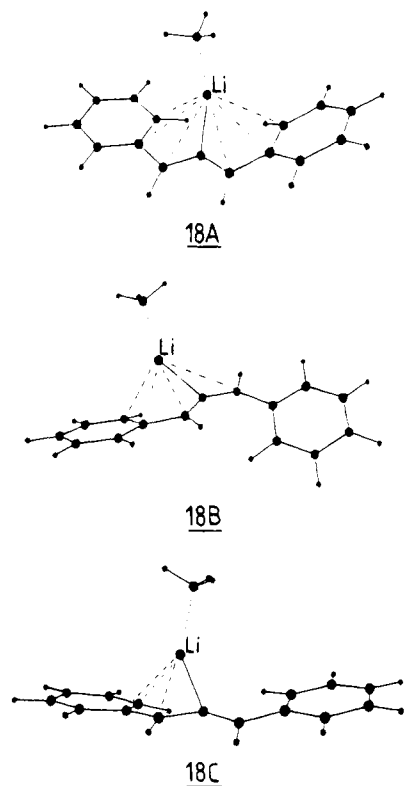
Model **16** (Figure 12), the tris(ammonia)-solvated trans,trans sodium complex, provides the closest analogy to the crystal structure of the PMDETA solvate **2**. However, the three model monodentate ligands are clearly more efficient at solvating, and are more compactly organized about the metal center than the sole tridentate ligand. This is reflected in a substantial elongation of the (anion) N–Na bond (length  $2.501 \text{ \AA}$ ; cf.  $2.384 \text{ \AA}$  in **2**<sup>7</sup>) and an exaggerated metal–anion incline ( $77.8^\circ$ ; cf.  $50.1^\circ$  in **2**). Rarely can the actual solvating ligands used in the synthetic experiments be considered theoretically, as the number of atomic orbitals usually has to be restricted in a calculated structure (since  $\text{NH}_3$  or  $\text{H}_2\text{O}$  molecules have fewer, they are often used to simulate the solvent molecules); therefore, such differences between real and theoretical solvates are to be expected. On account of the extra solvation in **16**, the tilt of the phenyl rings ( $8.2^\circ$ ) becomes less significant compared to that in **15A**.

**2. Lithium Models.** The experimental survey implied that there is an approximately equal chance of the 2-azaallyl anion adopting either the trans,trans or unknown form when it is in contact with the smaller, less polarizable  $\text{Li}^+$  cation in the absence of solvation. On the other hand, the trans,trans conformer forms exclusively with  $\text{Na}^+$ . At the simplest level, this suggests that in the latter case the contact ion pair is loose, effectively approaching the “free” anion, whereas in the former case, the contact ion pair is much tighter to the extent that the metal ion now exerts a much greater influence on the stability of the anion. Hence, in effect, the close attachment of the  $\text{Li}^+$  cation reduces the energetic preference for the trans,trans conformation over other possible conformations. The relative energies of the calculated structures strongly support this idea. Model **17A**, the trans,trans  $\text{Li}^+$  ( $C_s$ ) structure, is more stable than **17B**, the cis,trans ( $C_1$ ) counterpart, but by a mere  $1.7 \text{ kcal}$  (Figure 13). This is in contrast with the much larger differentials of  $6.4$  and  $5.3 \text{ kcal}$  found for the free anion and  $\text{Na}^+$  complex analogs, respectively. Interestingly, however, model **17A** is not the most stable arrangement. Model **17C** (Figure 13), another trans,trans structure but an asymmetrical one

**Figure 13.** Ab initio structures of unsolvated (1,3-diphenyl-2-azaallyl)lithium models.

with the  $\text{Li}^+$  cation oriented toward, and thus strongly interacting with, one side of the anion, has the lowest energy of all,  $1.9 \text{ kcal}$  more favorable than **17A**. This  $\text{Li}^+$  cation makes four short contacts (to N,  $1.944 \text{ \AA}$ ; to  $C_\alpha$ ,  $2.163 \text{ \AA}$ ; to  $C_{\text{ipso}}$ ,  $2.250 \text{ \AA}$ ; to  $C_{\text{ortho}}$ ,  $2.265 \text{ \AA}$ ) with the shortest contact to the remote side of the anion being considerably longer ( $C_\alpha$ ,  $3.048 \text{ \AA}$ ). In relation to the CNC plane, the metal is inclined at an angle of  $31.9^\circ$ .

On monosolvation, the energy gap between the  $C_s$  trans,trans structure (**18A**) and cis,trans (**18B**) minima (Figure 14) increases (to  $2.9 \text{ kcal}$ ), but not significantly so. In the favored structure (**18A**) the anion assumes a  $\eta^7$  mode toward the metal (bond lengths: to N,  $1.955 \text{ \AA}$ ; to  $C_\alpha$ ,  $C_{\alpha'}$ ,  $2.738 \text{ \AA}$ ; to  $C_{\text{ortho}}$ ,  $C_{\text{ortho}'}$ ,  $2.693 \text{ \AA}$ ; to  $C_{\text{ipso}}$ ,  $C_{\text{ipso}'}$ ,  $2.932 \text{ \AA}$ ), which is inclined at an angle of  $29.1^\circ$  toward the CNC plane. As in the analogous Na model (**15A**), the phenyl rings tilt out of this plane in the direction of the metal center, at an angle of  $20^\circ$ . Solvation in **18A** provides an additional stability of  $27.5 \text{ kcal mol}^{-1}$  when compared against the unsolvated analog **17A**, due to the formation of the (ammonia) N–Li bond (length  $2.031 \text{ \AA}$ ). Significantly, however, as in the unsolvated series **17A–C**, again the lowest minimum of all (by  $1.4 \text{ kcal mol}^{-1}$ ; cf. **18A**) is an asymmetric variant of the trans,trans structure (**18C**, Figure 14) in which the lithium coordination is biased toward one side of the anion. The  $\text{Li}^+$  cation interacts strongly with the (anionic) N ( $1.985 \text{ \AA}$ ),  $C_\alpha$  ( $2.269 \text{ \AA}$ ),  $C_{\text{ipso}}$  ( $2.354 \text{ \AA}$ ), and  $C_{\text{ortho}}$  ( $2.357 \text{ \AA}$ ) as well as with  $\text{NH}_3$  (N–Li,  $2.036 \text{ \AA}$ ), while the nearest C ( $C_{\alpha'}$ ) of the remote side of the anion lies  $3.035 \text{ \AA}$  away from the metal. As a result, the C–N bonds of the central CNC unit (bond angle  $127.3^\circ$ ) are inequivalent, being  $1.361$  and  $1.290 \text{ \AA}$ . The longer bond involves the  $C_\alpha$  atom strongly attached to the  $\text{Li}^+$  center. Lying  $36.6^\circ$  out of the CNC plane, the  $\text{Li}^+$  center's attraction for one side of the anion can be gauged by a comparison of the  $C_\alpha\text{NLi}$  and  $C_{\alpha'}\text{NLi}$  bond angles, which are  $83.2$  and  $134.7^\circ$ , respectively. It is significant that



**Figure 14.** Ab initio structures of monosolvated (1,3-diphenyl-2-azaallyl)lithium models.

this asymmetrical bridging is exclusive to Li; corresponding Na models when freely optimized always reverted to the  $C_s$  trans,trans arrangements (e.g., **14A** and **15A**). To convert a trans,trans structure to a cis,trans alternative requires rotation of one of the PhC(H) units about the N–C axis. With Li having two inequivalent N–C “axes” in **18C**, the implication is that there will be two distinct energy barriers, depending on which PhC(H) unit (metal coordinated or metal noncoordinated) is rotated, i.e., a lower and a higher one. Irrespective of which half of the anion is involved, rotation should be distinctly easier than in the Na structure, where both PhC(H) units would have the same energy barrier to rotation because of the symmetrical nature of the CNC metal bridge. Hence, it should be easier to form the two conformers (the trans,trans and cis,trans) in the Li case, though whether the cis,trans species is produced in the synthetic experiments is still open to debate.

The tris(ammonia) solvate **19** (Figure 12) provides some indication of the likely structure of the crystalline trans,trans Li PMDETA solvate **11A**, for which no crystal structure is available. It also enables a comparison to be made with **16**, from which the influence of the identity of the metal cation ( $\text{Li}^+$  or  $\text{Na}^+$ ) in the structure can be ascertained. In both cases, the ammonia ligands form shorter bonds to the metal cation (2.119/2.129 Å in **19**; 2.459/2.470 Å in **16**) than do the central nitrogen atoms of the CNC linkages (2.327 Å in **19**; 2.501 Å in **16**). Solvation by PMDETA would not be as efficient as that achieved by the less sterically inhibited ammonia molecules. Therefore, the cation–anion separations are overestimated in the calculated structures (by approximately 5%, when the (anion) N–Na bond length in **16** is compared with that in crystalline **2** (2.384 Å)). Size dictates that  $\text{Li}^+$  cations are more strongly solvated than  $\text{Na}^+$  cations. Here, the

respective total enthalpies of solvation are 57.7 and 50.6 kcal mol<sup>-1</sup>, which corresponds to 19.2 and 16.9 kcal mol<sup>-1</sup>, respectively, per ammonia molecule. Geometrically, the complexes are very similar in the vicinity of the cation–anion attachment. For **19**, the cation–anion inclination angle is 77.9°, the CNC bond angle is 127.2°, and the tilt of the phenyl rings toward the cation is 9.0°. Corresponding dimensions in **16** are 77.8, 127.7, and 8.2°, respectively. This finding is consistent with the experimental NMR data of the lithium (**11A**) and sodium (**2**) complexes, which give essentially identical <sup>1</sup>H spectra. The similarity extends to the anion hapticity ( $\eta^3$ ), as aside from the central N, the cations interact with the pair of equivalent  $C_q$  atoms (bond lengths: for  $\text{Li}^+$ , 2.780 Å; for  $\text{Na}^+$ , 2.934 Å) but not with the  $C_{ortho}$  atoms, which lie 3.758 and 3.783 Å away, respectively. However, in reality, these latter atoms lie significantly closer to the metal center (e.g., 3.133 Å in the crystalline  $\text{Na}^+$  complex **2**), due to the poorer solvating power of the sterically bulkier PMDETA ligand.

The conclusion of this theoretical part of the study is that it is the tightness of the metal–anion contact pair (greater for  $\text{Li}^+$  than  $\text{Na}^+$ ) and, linked to this, the ability of the stronger interacting metal center to lean toward one particular side of the anion, which offers the possibility of a second stable anion conformation in addition to the symmetrical trans,trans one—the preferred choice in the absence of a metal cation.

## Experimental Section

All manipulations were carried out under an argon atmosphere using standard Schlenk techniques. Solvents were distilled from an appropriate drying agent prior to use. All chemicals were obtained from Aldrich with the exception of  $\text{Bu}^n\text{Na}^{25}$  and  $\text{Bu}^n\text{K}^{26}$  which were synthesized according to reported methods. <sup>1</sup>H and <sup>13</sup>C NMR spectra were recorded on a Bruker AMX400 spectrometer operating at 400 and 100.6 MHz, respectively. Products **1–13** were all shown to be air- and moisture-sensitive but were stable (with the exception of **9**) indefinitely when stored under argon. Notably, the product yields reported are first-batch figures (based upon consumption of the starting metalating reagent) with a view to obtaining single crystals suitable for X-ray diffraction and are not optimized.

**Preparation of [(PhCH<sub>2</sub>)<sub>2</sub>NNa]<sub>n</sub> (**1**).** Dibenzylamine (1.92 mL, 10 mmol) was added dropwise to a chilled, stirred suspension of  $\text{Bu}^n\text{Na}$  (0.80 g, 10 mmol) in hexane (~8 mL). Warming to room temperature deposited a red solid, which was washed with chilled hexane and dried in vacuo. Yield: 1.71 g, 78%. Mp: 89–91 °C to a dichroic melt. Anal. Calcd for  $\text{C}_{14}\text{H}_{14}\text{NNa}$ : C, 76.7; H, 6.4; N, 6.5; Na, 10.5. Found: C, 75.8; H, 6.3; N, 6.8; Na, 10.9. <sup>1</sup>H NMR (benzene-*d*<sub>6</sub>, 25 °C) in ppm:  $\delta$  7.29–7.07 (m, *o*-, *m*-, *p*-H, 10H), 3.67 (s, PhCH<sub>2</sub>, 4H).

**Preparation of [[PhC(H)=N–C(H)Ph]<sup>-</sup>Na<sup>+</sup>PMDETA] (**2**).** Freshly prepared **1** (2.19 g, 10 mmol) was stirred in hexane (~8 mL). Dropwise addition of PMDETA (2.08 mL, 10 mmol) and toluene (~5 mL) completely dissolved the red precipitate with gentle heating. Cooling the deep purple solution to room temperature afforded a large crop of red-green dichroic needles which were washed with chilled toluene and dried in vacuo. Yield: 1.76 g, 45%. Mp: 169 °C to a dichroic melt. Anal. Calcd for  $\text{C}_{23}\text{H}_{35}\text{N}_4\text{Na}$ : C, 70.8; H, 9.0; N, 14.4; Na, 5.9. Found: C, 71.1; H, 8.6; N, 13.9; Na, 5.9. <sup>1</sup>H NMR (THF-*d*<sub>8</sub>, 25 °C) in ppm:  $\delta$  7.04 (br s, *o*-H, 4H), 6.95 (t, *m*-H, 4H), 6.79 (s, PhCH, 2H), 6.34 (t, *p*-H, 2H); PMDETA signals 2.53 and 2.45 (t, NCH<sub>2</sub>, 4H), 2.31 (s, NCH<sub>3</sub>, 12H), 2.24 (s,

(25) Lochmann, L.; Pospisil, J.; Lim, D. *Tetrahedron Lett.* **1966**, 2, 257.

(26) Lochmann, L.; Lim, D. *J. Organomet. Chem.* **1971**, 28, 153.

$\text{NCH}_3$ , 3H).  $^{13}\text{C}$  NMR (THF- $d_8$ , 25 °C) in ppm:  $\delta$  144.27 (*ipso*-C), 127.91 (*m*-C), 117.50 (*o*-C), 114.35 (PhCH), 110.06 (*p*-C); PMDETA signals 57.42 and 55.48 ( $\text{CH}_2$ ), 44.76 ( $\text{CH}_3$ , terminal), 41.94 ( $\text{CH}_3$ , central).

**Preparation of  $[\{(\text{PhCH}_2)_2\text{NNA}\cdot\text{TMEDA}\}_2]$  (3).** Freshly prepared **1** (2.19 g, 10 mmol) was stirred in hexane (~8 mL). Dropwise addition of TMEDA (1.51 mL, 10 mmol) and toluene (~1 mL) with gentle heating completely dissolved the red precipitate. Cooling the red solution to room temperature afforded a large crop of red crystals which were washed with chilled toluene and dried in vacuo. Yield: 1.41 g, 42%. Mp: 83–84 °C to a red liquid. Anal. Calcd for  $\text{C}_{20}\text{H}_{30}\text{N}_3\text{Na}$ : C, 71.6; H, 9.0; N, 12.5; Na, 6.9. Found: C, 74.3; H, 8.4; N, 11.9; Na, 7.5.  $^1\text{H}$  NMR (benzene- $d_6$ , 25 °C) in ppm:  $\delta$  7.44 (d, *o*-H, 4H), 7.31 (t, *m*-H, 4H), 7.15 (t, *p*-H, 2H), 4.48 (br s,  $\text{PhCH}_2$ , 4H); TMEDA signals 1.93 (s,  $\text{CH}_2\text{N}$ , 4H), 1.83 (s,  $\text{NCH}_3$ , 12H).  $^{13}\text{C}$  NMR (benzene- $d_6$ , 25 °C) in ppm:  $\delta$  149.50 (*ipso*-C), 128.39 (*o*-C), 128.03 (*m*-C), 125.46 (*p*-C), 62.77 (PhCH $_2$ ); TMEDA signals 57.48 ( $\text{CH}_2$ ), 45.45 ( $\text{CH}_3$ ).

**Preparation of  $[\{(\text{PhCH}(\text{H})\text{-N-C(H)Ph})\text{-Na}^+\cdot\text{TMEDA}\cdot\text{THF}\}]$  (4).** Freshly prepared **1** (2.19 g, 10 mmol) was stirred in hexane (~8 mL). Dropwise addition of TMEDA (1.51 mL, 10 mmol) and THF (0.8 mL, 10 mmol) completely dissolved the red precipitate with gentle warming. Cooling the deep purple solution to room temperature afforded a large crop of red-green dichroic crystals which were washed with chilled toluene and dried in vacuo. Yield: 1.86 g, 46%. Mp: 120–122 °C to a dichroic melt. Anal. Calcd for  $\text{C}_{24}\text{H}_{36}\text{N}_3\text{ONa}$ : C, 71.1; H, 8.9; N, 10.4; Na, 5.7. Found: C, 71.0; H, 7.8; N, 4.3; Na, 6.1.  $^1\text{H}$  NMR (THF- $d_8$ , 25 °C) in ppm:  $\delta$  6.81 (br s, *o*-H, 4H), 6.78 (t, *m*-H, 4H), 6.64 (s, PhCH, 2H), 6.18 (t, *p*-H, 2H); TMEDA signals 2.29 (s,  $\text{CH}_2\text{N}$ , 4H), 2.12 (s,  $\text{NCH}_3$ , 12H); THF signals 3.60 (m,  $\alpha$ - $\text{CH}_2$ , 4H), 1.75 (m,  $\beta$ - $\text{CH}_2$ , 4H).  $^{13}\text{C}$  NMR (THF- $d_8$ , 25 °C) in ppm:  $\delta$  145.47 (*ipso*-C), 129.16 (*m*-C), 118.76 (*o*-C), 115.54 (PhCH), 111.43 (*p*-C); TMEDA signals 58.84 ( $\text{CH}_2$ ), 46.24 ( $\text{CH}_3$ ); THF signals 68.38 ( $\alpha$ - $\text{CH}_2$ ), 26.50 ( $\beta$ - $\text{CH}_2$ ).

**Preparation of  $[\{(\text{PhCH}_2)_2\text{NNA}\cdot\text{THF}\}_n]$  (5).** Freshly prepared **1** (2.19 g, 10 mmol) was stirred in hexane (~8 mL). Dropwise addition of THF (1.60 mL, 20 mmol) completely dissolved the red precipitate with gentle heating. Cooling the dark red solution to room temperature afforded a large crop of red crystals which were washed with chilled toluene and dried in vacuo. Yield: 1.19 g, 41%. Mp: 78–80 °C to a dichroic melt. Anal. Calcd for  $\text{C}_{18}\text{H}_{22}\text{NONa}$ : C, 74.2; H, 7.6; N, 4.8; Na, 7.9. Found: C, 73.9; H, 7.3; N, 4.9; Na, 8.2.  $^1\text{H}$  NMR (THF- $d_8$ , 25 °C) in ppm:  $\delta$  7.23–7.16 (m, *o*-, *m*-H, 8H), 7.04 (t, *p*-H, 2H), 3.96 (s,  $\text{PhCH}_2$ , 4H); THF signals 3.63 (m,  $\alpha$ - $\text{CH}_2$ , 4H), 1.77 (m,  $\beta$ - $\text{CH}_2$ , 4H).  $^{13}\text{C}$  NMR (THF- $d_8$ , 25 °C) in ppm:  $\delta$  149.93 (*ipso*-C), 128.78 (*o*-C), 128.41 (*m*-C), 125.42 (*p*-C), 63.51 (PhCH $_2$ ); THF signals 63.38 ( $\alpha$ - $\text{CH}_2$ ), 26.49 ( $\beta$ - $\text{CH}_2$ ).

**Preparation of  $[\{(\text{PhC}(\text{H})\text{-N-C(H)Ph})\text{-Na}^+\cdot 3\text{THF}\}]$  (6).** Freshly prepared **1** (2.19 g, 10 mmol) was stirred in hexane (~8 mL). Dropwise addition of excess THF (2.4 mL, 30 mmol) completely dissolved the red precipitate with gentle heating. Cooling the deep purple solution to 3 °C for 24 h afforded a large crop of red-green dichroic crystals which were washed with chilled toluene and dried in vacuo. Yield: 2.13 g, 49%. Mp: 62–64 °C to a dichroic melt. Anal. Calcd for  $\text{C}_{26}\text{H}_{38}\text{NO}_3\text{Na}$ : C, 72.1; H, 8.3; N, 3.2; Na, 5.3. Found: C, 71.0; H, 6.4; N, 3.3; Na, 5.0.  $^1\text{H}$  NMR (THF- $d_8$ , 25 °C) in ppm:  $\delta$  6.88 (br s, *o*-H, 4H), 6.79 (t, *m*-H, 4H), 6.34 (s, PhCH, 2H), 6.18 (t, *p*-H, 2H); THF signals 3.60 (m,  $\alpha$ - $\text{CH}_2$ , 4H), 1.77 (m,  $\beta$ - $\text{CH}_2$ , 4H).  $^{13}\text{C}$  NMR (THF- $d_8$ , 25 °C) in ppm:  $\delta$  145.49 (*ipso*-C), 129.12 (*m*-C), 121.66 (*o*-C), 115.50 (PhCH), 111.40 (*p*-C); THF signals 63.38 ( $\alpha$ - $\text{CH}_2$ ), 26.49 ( $\beta$ - $\text{CH}_2$ ).

**Preparation of  $[\{(\text{PhCH}_2)_2\text{NLi}\cdot\text{THF}\}_2]$  (7).** Dibenzylamine (1.92 mL, 10 mmol) was added dropwise to a chilled, stirred solution of  $\text{Bu}^n\text{Li}$  (10 mmol in hexane, 6.9 mL of a 1.45 M solution), which resulted in the formation of a pink solid. Addition of THF (8 mL, 100 mmol) completely dissolved the pink precipitate with gentle heating. Cooling the red solution to ambient temperature afforded a large crop of pink crystals

which were washed with chilled THF and dried in vacuo. Yield: 1.84 g, 67%. Mp: 135–137 °C to a red liquid. Anal. Calcd for  $\text{C}_{18}\text{H}_{22}\text{NOLi}$ : C, 78.6; H, 8.0; N, 5.1; Li, 2.6. Found: C, 78.6; H, 7.8; N, 6.1; Li, 2.3.  $^1\text{H}$  NMR (THF- $d_8$ , 25 °C) in ppm:  $\delta$  7.31–6.97 (m, *o*-, *m*-, *p*-H, 10H), 3.71 (s,  $\text{PhCH}_2$ , 4H); THF signals 3.63 (m,  $\alpha$ - $\text{CH}_2$ , 4H), 1.77 (m,  $\beta$ - $\text{CH}_2$ , 4H).  $^{13}\text{C}$  NMR (THF- $d_8$ , 25 °C) in ppm:  $\delta$  148.50 (*ipso*-C), 129.22 (*o*-C), 128.47 (*m*-C), 125.80 (*p*-C), 61.88 (PhCH $_2$ ); THF signals 68.29 ( $\alpha$ - $\text{CH}_2$ ), 26.43 ( $\beta$ - $\text{CH}_2$ ).

**Preparation of  $[\{(\text{PhCH}_2)_2\text{NLi}\}_2(\text{dioxane})_n]$  (8).** Dibenzylamine (1.92 mL, 10 mmol) was added dropwise to a chilled, stirred solution of  $\text{Bu}^n\text{Li}$  (10 mmol in hexane, 6.9 mL of a 1.45 M solution), which resulted in the formation of a pink solid. Dropwise addition of 1,4-dioxane (0.43 mL, 5 mmol) resulted in the formation of a red solid. Single crystals (red) were obtained by preparing **8** (in its toluene hemisolvate form) on a 1 mmol scale in 30 mL of toluene, heating to 100 °C, and cooling to room temperature over several hours. Both crystals and solid gave identical analyses. Yield: 0.26 g, 52% (crystals). Mp: >360 °C. Crystals do not melt below this temperature but turn from red to white above 250 °C. Anal. Calcd for  $\text{C}_{22}\text{H}_{36}\text{N}_2\text{O}_2\text{Li}$ : C, 77.7; H, 7.3; N, 5.7; Li, 2.8. Found: C, 79.0; H, 6.2; N, 5.8; Li, 2.9.  $^1\text{H}$  NMR (THF- $d_8$ , 25 °C) in ppm:  $\delta$  7.19–7.04 (m, *o*-, *m*-, *p*-H, 20H), 3.62 (s,  $\text{PhCH}_2$ , 8H); dioxane signal 3.56 (s,  $\text{OCH}_2$ , 8H); toluene signals 7.13 (m, *o*-, *m*-, *p*-H, 5H), 2.31 (s,  $\text{PhCH}_3$ , 3H). Integration indicates variable amounts of toluene in crystals, as this is easily lost when the product is dried in vacuo.  $^{13}\text{C}$  NMR (THF- $d_8$ , 25 °C) in ppm:  $\delta$  148.51 (*ipso*-C), 129.22 (*o*-C), 128.47 (*m*-C), 125.79 (*p*-C), 61.67 (PhCH $_2$ ); dioxane signal 67.87 ( $\text{OCH}_2$ ); toluene signals 138.27 (*ipso*-C), 129.62 (*o*-C), 128.90 (*m*-C), 126.03 (*p*-C), 21.51 (PhCH $_3$ ).

**Preparation of  $[\{(\text{PhCH}_2)_2\text{NLi}\cdot 2\text{dioxane}\}_n]$  (9).** Dibenzylamine (1.92 mL, 10 mmol) was added dropwise to a chilled, stirred solution of  $\text{Bu}^n\text{Li}$  (10 mmol in hexane, 6.9 mL of a 1.45 M solution). Dropwise addition of excess 1,4-dioxane (8.5 mL, 100 mmol) and toluene (~10 mL) completely dissolved the precipitate with gentle warming. Cooling the purple solution to room temperature afforded a large crop of pink crystalline flakes which were washed with chilled toluene and dried in vacuo. Yield: 2.16 g, 57%. Mp: 86–88 °C to a red liquid. Anal. Calcd for  $\text{C}_{22}\text{H}_{30}\text{NO}_4\text{Li}$ : C, 69.7; H, 7.9; N, 3.7; Li, 1.9. Found: C, 70.0; H, 7.6; N, 4.3; Li, 1.7.  $^1\text{H}$  NMR (THF- $d_8$ , 25 °C) in ppm:  $\delta$  7.16–7.09 (m, *o*-, *m*-, *p*-H, 10H), 3.58 (s,  $\text{PhCH}_2$ , 4H); dioxane signal 3.56 (s,  $\text{OCH}_2$ , 16H).  $^{13}\text{C}$  NMR (THF- $d_8$ , 25 °C) in ppm:  $\delta$  148.49 (*ipso*-C), 129.22 (*o*-C), 128.48 (*m*-C), 125.81 (*p*-C), 61.68 (PhCH $_2$ ); dioxane signal 67.88 ( $\text{OCH}_2$ ). Notably, **9** was stable only for a few days under argon before converting into a pink oil, although the oil retains the analytical makeup.

**Preparation of  $[\{(\text{PhCH}_2)_2\text{NLi}\}_2\text{TMEDA}\}_n]$  (10).** Dibenzylamine (1.92 mL, 10 mmol) was added dropwise to a chilled, stirred solution of  $\text{Bu}^n\text{Li}$  (10 mmol in hexane, 6.9 mL of a 1.45 M solution), which resulted in the formation of a pink precipitate. Dropwise addition of TMEDA (1.51 mL, 10 mmol) and toluene (~15 mL) completely dissolved the pink solid on gentle heating. Cooling the red solution to room temperature afforded a large crop of red crystals which were washed with chilled toluene and dried in vacuo. Yield: 2.56 g, 49%. Mp: 117–119 °C to a red liquid. Anal. Calcd for  $\text{C}_{34}\text{H}_{44}\text{N}_4\text{Li}_2$ : C, 78.2; H, 8.4; N, 10.7; Li, 2.7. Found: C, 78.9; H, 8.6; N, 7.3; Li, 2.9.  $^1\text{H}$  NMR (THF- $d_8$ , 25 °C) in ppm:  $\delta$  7.18–7.03 (m, *o*-, *m*-, *p*-H, 20H), 3.59 (s,  $\text{PhCH}_2$ , 8H); TMEDA signals 2.32 (br s,  $\text{CH}_2\text{N}$ , 4H), 2.17 (br s,  $\text{NCH}_3$ , 12H).  $^{13}\text{C}$  NMR (THF- $d_8$ , 25 °C) in ppm:  $\delta$  148.50 (*ipso*-C), 129.22 (*o*-C), 128.47 (*m*-C), 125.80 (*p*-C), 61.78 (PhCH $_2$ ); TMEDA signals 59.10 ( $\text{CH}_2$ ), 46.36 ( $\text{CH}_3$ ).

**Preparation of  $[\{(\text{PhC}(\text{H})\text{-N-C(H)Ph})\text{-Li}^+\cdot\text{PMDETA}\}_n]$  (11).** Dibenzylamine (1.92 mL, 10 mmol) was added dropwise to a chilled, stirred solution of  $\text{Bu}^n\text{Li}$  (10 mmol in hexane, 6.9 mL of a 1.45 M solution), which resulted in the precipitation of a pink solid. Dropwise addition of PMDETA (2.08 mL, 10 mmol) completely dissolved the pink solid. Cooling the deep

Table 2. Structure Determination Summary

	3	7	8
formula	C <sub>40</sub> H <sub>60</sub> N <sub>6</sub> Na <sub>2</sub>	C <sub>36</sub> H <sub>44</sub> Li <sub>2</sub> N <sub>2</sub> O <sub>2</sub>	C <sub>32</sub> H <sub>36</sub> Li <sub>2</sub> N <sub>2</sub> O <sub>2</sub> ·0.5C <sub>7</sub> H <sub>8</sub>
color, habit	red prism	red prism	red prism
cryst size (mm)	0.58 × 0.54 × 0.52	0.69 × 0.69 × 0.65	0.30 × 0.20 × 0.20
cryst syst	triclinic	monoclinic	triclinic
space group	<i>P</i> $\bar{1}$	<i>P</i> 2 <sub>1</sub> / <i>c</i>	<i>P</i> $\bar{1}$
<i>a</i> (Å)	9.674(3)	10.454(2)	8.910(6)
<i>b</i> (Å)	11.183(3)	17.534(3)	13.677(9)
<i>c</i> (Å)	11.373(3)	8.930(2)	14.888(10)
$\alpha$ (deg)	114.02(2)	90	65.69(4)
$\beta$ (deg)	111.952(8)	102.01(3)	78.31(4)
$\gamma$ (deg)	91.339(14)	90	80.27(3)
<i>V</i> (Å <sup>3</sup> )	1019.7(5)	1601.1(5)	1612(2)
<i>Z</i>	1	2	2
<i>fw</i>	670.92	550.61	540.58
density (calcd) (g/cm <sup>3</sup> )	1.093	1.142	1.114
abs coeff (mm <sup>-1</sup> )	0.083	0.069	0.067
<i>F</i> (000)	364	592	578
temp (K)	240	160	200
2 $\theta$ range (deg)	4–50	5–50	5–50
max indices <i>hkl</i>	11,13,13	12,20,10	10,16,17
no. of rflns collected	7103	4399	6703
no. of indep rflns	3604	2820	5703
weighting parameters <i>a, b</i>	0.0811, 0.1390	0.0419, 0.5645	0.0759, 1.6585
no. of params refined	222	209	391
<i>R<sub>w</sub></i> (all data)	0.1668	0.1392	0.2501
<i>R</i> (obsd data)	0.0546 (2162)	0.0477 (2335)	0.0604 (2809)
goodness of fit	1.059	1.062	1.039
max, min electron dens (e/Å <sup>3</sup> )	+0.20, -0.23	+0.25, -0.21	+0.24, -0.20

purple solution to room temperature afforded a large crop of microcrystalline product (purple-red crystals speckled with dichroic flakes) which was washed with chilled toluene and dried in vacuo. Yield: 1.23 g, 33%. Mp: 112–114 °C to a dichroic melt. Anal. Calcd for C<sub>23</sub>H<sub>35</sub>N<sub>4</sub>Li: C, 73.8; H, 9.4; N, 15.0; Li, 1.9. Found: C, 69.5; H, 9.9; N, 15.9; Li, 1.9. <sup>1</sup>H NMR (THF-*d*<sub>6</sub>, 40 °C) in ppm:  $\delta$  7.80–7.06 (m, *o*-, *m*-, *p*-H and PhCH, 12H), 6.93–6.84 (br s, *o*-H, 4H), 6.68 (t, *m*-H, 4H), 6.50 (s, PhCH, 2H), 6.03 (t, *p*-H, 2H); PMDETA signals 2.35 and 2.27 (dm, CH<sub>2</sub>CH<sub>2</sub>, 8H), 2.13 (s, NCH<sub>3</sub>, 6H), 2.10 (s, NCH<sub>3</sub>, 24H).

**Preparation of [(PhC(H)-N-C(H)Ph)-K<sup>+</sup>·2PMDETA]<sub>n</sub> (12).** Dibenzylamine (1.92 mL, 10 mmol) was added dropwise to a chilled, stirred suspension of Bu<sup>n</sup>K (0.96 g, 10 mmol) in hexane (~8 mL), which resulted in the precipitation of a purple solid. Dropwise addition of PMDETA (4.16 mL, 20 mmol) and toluene (~5 mL) completely dissolved the purple solid with gentle heating. Cooling the purple solution to room temperature afforded a large crop of red-green dichroic needles which were washed with chilled toluene and dried in vacuo. Yield: 1.62 g, 40%. Mp: 132–133 °C to a dichroic melt. Anal. Calcd for C<sub>32</sub>H<sub>58</sub>N<sub>7</sub>K: C, 66.3; H, 10.0; N, 16.9; K, 6.7. Found: C, 66.0; H, 9.3; N, 12.8; K, 5.3. <sup>1</sup>H NMR (THF-*d*<sub>6</sub>, 25 °C) in ppm:  $\delta$  7.06 (br s, *o*-H, 4H), 6.94 (t, *m*-H, 4H), 6.73 (s, PhCH, 2H), 6.31 (t, *p*-H, 2H); PMDETA signals 2.58 and 2.47 (t, NCH<sub>2</sub>, 8H), 2.36 (s, NCH<sub>3</sub>, 6H), 2.31 (s, NCH<sub>3</sub>, 24H). <sup>13</sup>C NMR (THF-*d*<sub>6</sub>, 25 °C) in ppm:  $\delta$  144.32 (*ipso*-C), 127.77 (*m*-C), 117.56 (*o*-C), 113.82 (*p*-C), 109.61 (PhCH); PMDETA signals 57.61 and 56.10 (CH<sub>2</sub>), 44.95 (CH<sub>3</sub> terminal), 42.01 (CH<sub>3</sub> central).

**Preparation of [(PhCH<sub>2</sub>)<sub>2</sub>NK]<sub>n</sub> (13).** Dibenzylamine (1.92 mL, 10 mmol) was added dropwise to a chilled stirred suspension of Bu<sup>n</sup>K (0.96 g, 10 mmol) in hexane (~8 mL), which resulted in the formation of a purple solid. This was washed with chilled toluene and dried in vacuo. Yield: 2.02 g, 86%. Mp: 266–268 °C to a dichroic melt. Anal. Calcd for C<sub>14</sub>H<sub>14</sub>NK: C, 71.5; H, 6.0; N, 6.0; K, 16.6. Found: C, 72.0; H, 6.8; N, 6.0; K, 15.5. <sup>1</sup>H NMR (benzene-*d*<sub>6</sub>, 25 °C) in ppm:  $\delta$  7.27–7.00 (m, *o*-, *m*-, *p*-H, 10H), 3.57 (s, PhCH<sub>2</sub>, 4H).

**X-ray Crystallography.** All measurements were made at reduced temperatures on a Stoe-Siemens diffractometer with

Table 3. Atomic Coordinates (×10<sup>4</sup>) and Equivalent Isotropic Displacement Parameters<sup>a</sup> (Å<sup>2</sup> × 10<sup>3</sup>) for 3

	<i>x</i>	<i>y</i>	<i>z</i>	<i>U</i> (eq)
Na	4475.2(10)	6216.2(9)	5947.3(9)	48.1(3)
N(1)	3738(2)	5129(2)	3437(2)	45.2(5)
N(2)	2996(2)	7018(2)	7398(2)	54.7(6)
N(3)	4440(3)	8796(2)	6587(2)	61.8(6)
C(1)	3882(3)	5636(2)	2503(2)	50.5(6)
C(11)	5461(3)	6360(2)	2950(2)	48.2(6)
C(12)	5854(3)	6533(3)	1960(3)	63.9(7)
C(13)	7264(4)	7202(3)	2315(4)	78.3(9)
C(14)	8341(4)	7743(3)	3700(4)	80.5(9)
C(15)	7994(3)	7590(3)	4701(3)	73.0(8)
C(16)	6566(3)	6904(3)	4328(3)	60.6(7)
C(2)	2126(3)	4613(2)	2946(3)	51.8(6)
C(21)	1375(3)	3409(2)	1497(3)	48.5(6)
C(22)	236(3)	3452(3)	358(3)	69.3(8)
C(23)	-382(4)	2357(4)	-969(3)	89.2(10)
C(24)	114(4)	1195(4)	-1176(4)	84.4(10)
C(25)	1216(4)	1116(3)	-46(4)	89.1(11)
C(26)	1844(3)	2216(3)	1269(3)	74.5(9)
C(3)	4045(4)	7231(3)	8796(3)	85.8(10)
C(4)	1640(4)	6051(4)	6912(4)	97.4(12)
C(5)	2562(4)	8266(3)	7403(4)	82.8(10)
C(6)	3799(4)	9267(3)	7637(3)	80.2(10)
C(7)	3341(4)	8564(3)	5184(3)	86.6(10)
C(8)	5755(4)	9810(3)	7054(4)	92.2(11)

<sup>a</sup> *U*(eq) is defined as one-third of the trace of the orthogonalized *U*<sub>ij</sub> tensor.

graphite-monochromated Mo K $\alpha$  radiation ( $\lambda = 0.71073$  Å) and a Cryostream cooler.<sup>27</sup> Crystallographic data are in Table 2. Cell parameters were refined in each case from 2 $\theta$  values (20–25°) of 32 reflections measured at  $\pm\omega$  to minimize systematic errors. Intensities were measured with  $\omega/\theta$  scans and an on-line profile fitting procedure.<sup>28</sup> No significant variation was observed for selected standard reflections monitored at regular intervals. No corrections were applied for absorption; extinction effects were also found to be negligible.

The structures were solved by automatic direct methods and refined by least-squares on *F*<sup>2</sup> values, all measured data being used. Disorder was successfully modeled for the THF ligands of 7 and the toluene solvent in 8. Hydrogen atoms were included

**Table 4. Selected Bond Lengths (Å) and Angles (deg) for 3<sup>a</sup>**

Na-N(1)	2.397(2)	Na-N(1a)	2.412(2)
Na-N(2)	2.489(2)	Na-N(3)	2.678(2)
N(1)-Na-N(1a)	97.44(6)	N(1)-Na-N(2)	132.53(8)
N(1a)-Na-N(2)	116.65(7)	N(1)-Na-N(3)	104.82(7)
N(1a)-Na-N(3)	138.64(9)	N(2)-Na-N(3)	71.26(7)
C(1)-N(1)-C(2)	107.8(2)	C(1)-N(1)-Na	130.9(2)
C(2)-N(1)-Na	99.82(13)	C(1)-N(1)-Na(a)	116.27(14)
C(2)-N(1)-Na(a)	118.2(2)	Na-N(1)-Na(a)	82.56(6)
C(3)-N(2)-C(4)	109.3(3)	C(3)-N(2)-C(5)	111.4(2)
C(4)-N(2)-C(5)	109.2(2)	C(3)-N(2)-Na	103.8(2)
C(4)-N(2)-Na	113.3(2)	C(5)-N(2)-Na	109.9(2)
C(8)-N(3)-C(7)	109.1(3)	C(8)-N(3)-C(6)	108.2(2)
C(7)-N(3)-C(6)	112.1(3)	C(8)-N(3)-Na	124.9(2)
C(7)-N(3)-Na	96.2(2)	C(6)-N(3)-Na	105.9(2)

<sup>a</sup> Symmetry transformation used to generate equivalent atoms: (a)  $-x + 1, -y + 1, -z + 1$ .

**Table 5. Atomic Coordinates ( $\times 10^4$ ) and Equivalent Isotropic Displacement Parameters<sup>a</sup> ( $\text{Å}^2 \times 10^3$ ) for 7**

	x	y	z	U(eq)
Li	4026(3)	10296.7(13)	430(3)	31.4(5)
N(1)	4733.5(13)	9221.8(7)	818(2)	35.9(3)
C(11)	3894(2)	8585.9(9)	179(2)	39.5(4)
C(111)	2683(2)	8472.1(8)	841(2)	33.8(4)
C(112)	1596(2)	8940.7(9)	403(2)	41.5(4)
C(113)	494(2)	8851.2(10)	1009(2)	46.8(5)
C(114)	449(2)	8284.5(11)	2080(2)	46.3(5)
C(115)	1518(2)	7814.8(10)	2530(2)	44.9(4)
C(116)	2621(2)	7906.3(9)	1922(2)	38.9(4)
C(12)	5296(2)	9071.3(9)	2416(2)	37.6(4)
C(121)	6331(2)	9658.5(9)	3026(2)	34.4(4)
C(122)	6031(2)	10330.1(9)	3716(2)	39.2(4)
C(123)	6983(2)	10871.1(10)	4254(2)	46.6(5)
C(124)	8262(2)	10751.1(11)	4106(2)	49.2(5)
C(125)	8576(2)	10093.9(12)	3416(2)	48.7(5)
C(126)	7619(2)	9556.0(10)	2872(2)	41.4(4)
O	2949.1(13)	10910.6(7)	1442(2)	50.3(4)
C(1)	2186(2)	10717.1(11)	2549(3)	49.9(5)
C(2)	1911(3)	11443(2)	3290(4)	85.7(9)
C(3)	2879(7)	11944(3)	3076(11)	73(2)
C(4)	2995(19)	11760(13)	1491(28)	77(5)
C(3A)	2237(7)	12070(2)	2144(9)	57(2)
C(4A)	3308(19)	11688(12)	1476(29)	68(3)

<sup>a</sup> U(eq) is defined as one-third of the trace of the orthogonalized  $U_{ij}$  tensor.

**Table 6. Selected Bond Lengths (Å) and Angles (deg) for 7<sup>a</sup>**

Li-O	1.915(3)	Li-N(1)	2.028(3)
Li-N(1a)	2.058(3)		
O-Li-N(1)	132.13(14)	O-Li-N(1a)	121.56(13)
N(1)-Li-N(1a)	103.04(12)	C(12)-N(1)-C(11)	109.49(13)
C(12)-N(1)-Li	113.35(13)	C(11)-N(1)-Li	118.36(13)
C(12)-N(1)-Li(a)	115.80(13)	C(11)-N(1)-Li(a)	119.79(13)
Li-N(1)-Li(a)	76.96(12)	C(4A)-O-C(1)	113.4(10)
C(1)-O-C(4)	103.6(9)	C(4A)-O-Li	111.9(9)
C(1)-O-Li	131.18(13)	C(4)-O-Li	123.9(8)

<sup>a</sup> Symmetry transformation used to generate equivalent atoms: (a)  $-x + 1, -y + 2, -z$ .

in calculated positions and refined isotropically with a riding model, except for the disordered solvent. Other atoms were refined anisotropically. The weighting scheme was of the form  $w^{-1} = \sigma^2(F_o^2) + (aP)^2 + bP$ , where  $P = (2F_o^2 + F_c^2)/3$ . Residuals are defined as  $R_w = \sum[w(F_o^2 - F_c^2)^2] / \sum[w(F_o^2)^2]^{1/2}$  for all data and conventional  $R = \sum||F_o| - |F_c|| / \sum|F_o|$  for reflections having  $F_o^2 > 2\sigma(F_o^2)$ , the latter for comparison with conventional refinements based on  $F$  values. Programs were standard Stoe control software, members of the SHELX family,<sup>29</sup> and locally written routines, running on personal computers and UNIX workstations.

(29) Sheldrick, G. M. *SHELXTL/PC Manual*; Siemens Analytical X-Ray Instruments, Inc.: Madison, WI, 1990; SHELXL-93, Program for Crystal Structure Refinement; University of Göttingen, Göttingen, Germany, 1993.

**Table 7. Atomic Coordinates ( $\times 10^4$ ) and Equivalent Isotropic Displacement Parameters<sup>a</sup> ( $\text{Å}^2 \times 10^3$ ) for 8**

	x	y	z	U(eq)
O(1)	2947(3)	3754(2)	1930(2)	53.0(7)
O(2)	1829(3)	1876(2)	3448(2)	54.2(7)
C(1)	1693(5)	3303(4)	1832(3)	61.5(12)
C(2)	1807(5)	2111(4)	2412(3)	63.4(12)
C(3)	3073(5)	2351(3)	3547(3)	53.9(11)
C(4)	2962(5)	3527(3)	2955(3)	56.9(11)
Li(1)	4079(7)	4740(5)	752(4)	48(2)
N(1)	3720(3)	4896(2)	-544(2)	42.6(7)
C(5)	3808(5)	3915(3)	-732(3)	50.9(10)
C(6)	4813(4)	3953(3)	-1692(3)	44.5(9)
C(7)	4231(5)	4321(3)	-2582(3)	52.8(10)
C(8)	5175(5)	4395(3)	-3463(3)	60.1(11)
C(9)	6731(6)	4080(4)	-3464(4)	65.4(12)
C(10)	7331(5)	3702(4)	-2586(4)	64.5(12)
C(11)	6380(5)	3650(3)	-1711(3)	55.8(11)
C(12)	2711(5)	5733(3)	-1161(3)	53.2(10)
C(13)	2261(5)	6650(3)	-825(3)	50.5(10)
C(14)	967(5)	6640(4)	-139(4)	69.2(13)
C(15)	512(7)	7478(6)	185(5)	94(2)
C(16)	1398(9)	8330(15)	-187(5)	99(2)
C(17)	2713(8)	8357(4)	-859(4)	89(2)
C(18)	3135(6)	7514(4)	-1185(3)	64.5(12)
Li(2)	618(8)	784(5)	4457(4)	48(2)
N(2)	531(3)	71(2)	5921(2)	42.6(7)
C(19)	2022(5)	-411(3)	6239(3)	58.1(11)
C(20)	2804(5)	-1106(3)	5699(3)	50.0(10)
C(21)	3724(5)	-687(4)	4787(3)	58.2(11)
C(22)	4427(5)	-1339(5)	4281(4)	82(2)
C(23)	4207(7)	-2410(5)	4694(6)	94(2)
C(24)	3284(7)	-2824(4)	5585(6)	92(2)
C(25)	2592(5)	-2183(4)	6079(4)	67.8(13)
C(26)	-313(5)	616(3)	6560(3)	51.8(10)
C(27)	359(4)	1613(3)	6445(3)	48.4(10)
C(28)	1165(5)	1637(4)	7138(3)	61.9(11)
C(29)	1798(5)	2564(4)	6991(4)	73.2(14)
C(30)	1631(6)	3478(4)	6161(4)	71.9(13)
C(31)	836(6)	3481(4)	5463(4)	67.1(13)
C(32)	214(5)	2558(3)	5603(3)	58.8(11)

<sup>a</sup> U(eq) is defined as one-third of the trace of the orthogonalized  $U_{ij}$  tensor.

**Table 8. Selected Bond Lengths (Å) and Angles (deg) for 8<sup>a</sup>**

O(1)-Li(1)	1.926(6)	O(2)-Li(2)	1.922(6)
Li(1)-N(1)	1.939(7)	Li(1)-N(1a)	2.037(7)
Li(2)-N(2)	1.978(7)	Li(2)-N(2b)	1.978(7)
C(1)-O(1)-C(4)	110.3(3)	C(1)-O(1)-Li(1)	119.1(3)
C(4)-O(1)-Li(1)	129.6(3)	C(3)-O(2)-C(2)	110.4(3)
C(3)-O(2)-Li(2)	128.7(3)	C(2)-O(2)-Li(2)	119.2(3)
O(1)-Li(1)-N(1)	118.9(3)	O(1)-Li(1)-N(1a)	128.3(3)
N(1)-Li(1)-N(1a)	105.4(3)	C(12)-N(1)-C(5)	109.9(3)
C(12)-N(1)-Li(1)	125.6(3)	C(5)-N(1)-Li(1)	118.0(3)
C(12)-N(1)-Li(1a)	115.1(3)	C(5)-N(1)-Li(1a)	106.9(3)
Li(1)-N(1)-Li(1a)	74.6(3)	O(2)-Li(2)-N(2)	132.5(3)
O(2)-Li(2)-N(2b)	120.2(3)	N(2)-Li(2)-N(2b)	106.2(3)
C(19)-N(2)-C(26)	109.7(3)	C(19)-N(2)-Li(2)	113.7(3)
C(26)-N(2)-Li(2)	120.4(3)	C(19)-N(2)-Li(2b)	117.5(3)
C(26)-N(2)-Li(2b)	118.1(3)	Li(2)-N(2)-Li(2b)	73.8(3)

<sup>a</sup> Symmetry transformations used to generate equivalent atoms: (a)  $-x + 1, -y + 1, -z$ ; (b)  $-x, -y, -z + 1$ .

Refined coordinates are given in Tables 3, 5, and 7 and selected bond lengths and angles in Tables 4, 6, and 8.

**Acknowledgment.** We thank the EPSRC for financial support and Professor C. L. Raston (Griffith University, Brisbane, Australia) for useful discussions.

**Supplementary Material Available:** Tables of bond lengths and angles, anisotropic displacement parameters, and hydrogen atom coordinates and isotropic displacement parameters for the crystal structures of 3, 7, and 8 (10 pages). Ordering information is given on any current masthead page.

OM940597P



# Cyclopentadienyldicarbonyliron Halides as Electrophiles: Reactions of $(\eta^5\text{-C}_5\text{H}_5)\text{Fe}(\text{CO})_2\text{I}$ with MeLi in the Presence of Monophosphines and Diphosphines

Lung-Shiang Luh,<sup>1a,b</sup> Uche B. Eke,<sup>1a,c</sup> and Ling-Kang Liu\*,<sup>1a,b</sup>

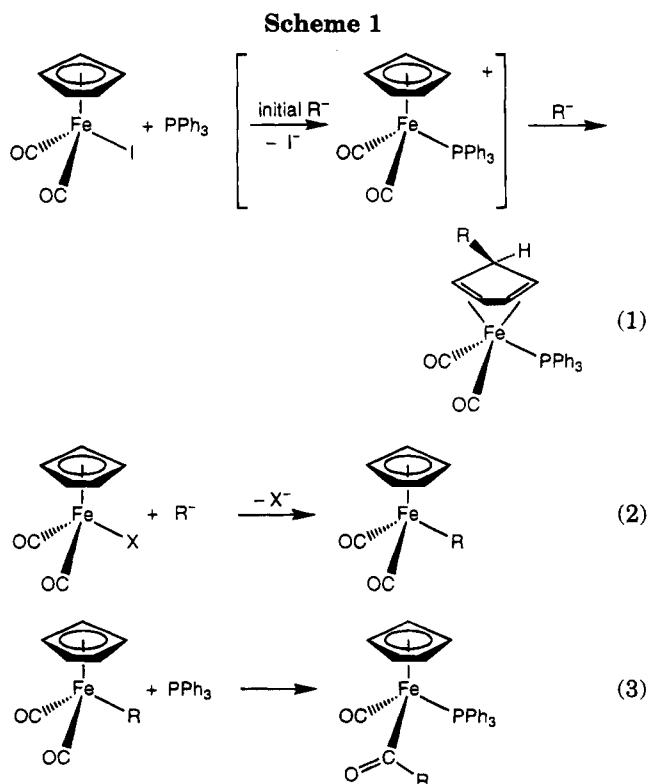
*Institute of Chemistry, Academia Sinica, Taipei, Taiwan 11529, Republic of China, Department of Chemistry, National Taiwan University, Taipei, Taiwan 10767, Republic of China, and Department of Chemistry, University of Ilorin, Ilorin, Nigeria*

Received August 26, 1994<sup>®</sup>

Treatment of equimolar amounts of  $(\eta^5\text{-C}_5\text{H}_5)\text{Fe}(\text{CO})_2\text{I}$  and  $\text{PR}_3$  in THF at  $-78^\circ\text{C}$  with slightly more than 1 molar equiv of MeLi produces mainly  $(\eta^4\text{-MeC}_5\text{H}_5)\text{Fe}(\text{CO})_2(\text{PR}_3)$  (**1-4**) for  $\text{PR}_3 = \text{PPh}_3, \text{PMePh}_2, \text{PMe}_2\text{Ph}, \text{PMe}_3$ , the yields increasing in the order  $\text{PMe}_3 < \text{PMePh}_2 < \text{PMe}_2\text{Ph} < \text{PPh}_3$ , parallel to the decreasing order of the  $\sigma$ -donating tendency and increasing cone angle. In the presence of  $\text{Ph}_2\text{PCH}_2\text{PPh}_2$  (=dppm) the reaction yields the unidentate complex  $(\eta^4\text{-MeC}_5\text{H}_5)\text{Fe}(\text{CO})_2(\eta^1\text{-dppm})$  (**5**). In the presence of  $\text{Ph}_2\text{P}(\text{CH}_2)_n\text{PPh}_2$  ( $n = 2$  (dppe), 3 (dppp), 4 (dppb)) the reaction yields the respective bridging  $[(\eta^4\text{-MeC}_5\text{H}_5)\text{Fe}(\text{CO})_2]_2(\mu, \eta^1:\eta^1\text{-Ph}_2\text{P}(\text{CH}_2)_n\text{PPh}_2)[(\eta^4\text{-MeC}_5\text{H}_5)\text{Fe}(\text{CO})_2]$  complexes **6-8**. Both complexes **2** and **6** have been investigated by X-ray structure analysis. The results indicate that the Me group is *exo* to the cyclopentadiene ring. The coordination geometry of Fe may be described as that of a distorted square pyramid with one CO placed at the apical position, phosphine in the basal plane *trans* to one of the double bonds, and the second CO ligand *trans* to the second double bond. A similar reaction of  $(\eta^5\text{-C}_5\text{H}_5)\text{Fe}(\text{CO})_2\text{I}$  with *n*-BuLi at  $-78^\circ\text{C}$  in the presence of dppe results in  $(\eta^4\text{-BuC}_5\text{H}_5)\text{Fe}(\text{CO})_2(\mu, \eta^1:\eta^1\text{-dppe})(\eta^4\text{-BuC}_5\text{H}_5)\text{Fe}(\text{CO})_2$  (**9**),  $(\eta^4\text{-BuC}_5\text{H}_5)\text{Fe}(\text{CO})_2(\mu, \eta^1:\eta^1\text{-dppe})(\eta^5\text{-C}_5\text{H}_5)\text{Fe}(\text{CO})\text{C}(\text{O})\text{Bu}$  (**10**), and  $(\eta^5\text{-C}_5\text{H}_5)\text{Fe}(\text{CO})\text{C}(\text{O})\text{Bu}(\mu, \eta^1:\eta^1\text{-dppe})(\eta^5\text{-C}_5\text{H}_5)\text{Fe}(\text{CO})\text{C}(\text{O})\text{Bu}$  (**11**) in 55%, 18%, and 1% yields, respectively.

## Introduction

The reactions of  $(\eta^5\text{-C}_5\text{H}_5)\text{Fe}(\text{CO})_2\text{X}$  ( $\text{X} = \text{Cl}, \text{Br}, \text{I}$ ) with  $\text{RLi}$  ( $\text{R} = \text{Me}, n\text{-Bu}, s\text{-Bu}, \text{Ph}$ ) in the presence of  $\text{PPh}_3$  at low temperature have been studied earlier.<sup>2</sup> The reaction pattern found is that of a facile three-component reaction which effectively changes the  $\eta^5\text{-C}_5\text{H}_5$  bonding mode in  $(\eta^5\text{-C}_5\text{H}_5)\text{Fe}(\text{CO})_2\text{X}$  to  $\eta^4\text{-RC}_5\text{H}_5$  bonding in  $(\eta^4\text{-RC}_5\text{H}_5)\text{Fe}(\text{CO})_2(\text{PPh}_3)$ . The *in situ* generated  $[(\eta^5\text{-C}_5\text{H}_5)\text{Fe}(\text{CO})_2]_2$  is believed to be the catalyst that assists conversion of the neutral complex  $(\eta^5\text{-C}_5\text{H}_5)\text{Fe}(\text{CO})_2\text{X}$  and  $\text{PPh}_3$  to the cation  $[(\eta^5\text{-C}_5\text{H}_5)\text{Fe}(\text{CO})_2\text{PPh}_3]^+$ , which in turn is immediately attacked by  $\text{RLi}$  from an *exo* position at the  $\text{C}_5\text{H}_5$  ring (Scheme 1, eq 1),<sup>2</sup> instead of sequential metal-halide exchange (eq 2)<sup>3</sup> and phosphine-assisted migratory insertion (eq 3).<sup>4</sup> In this report, the effects of the variation of the phosphine reactant in the three-component reaction are summarized.



## Results and Discussion

Treatment of equimolar amounts of  $(\eta^5\text{-C}_5\text{H}_5)\text{Fe}(\text{CO})_2\text{I}$  and  $\text{PR}_3$  in THF at  $-78^\circ\text{C}$  dropwise with slightly more than 1 molar equiv of MeLi produces  $(\eta^4\text{-MeC}_5\text{H}_5)\text{Fe}(\text{CO})_2(\text{PR}_3)$  (**1-4**) for  $\text{PR}_3 = \text{PPh}_3, \text{PMePh}_2, \text{PMe}_2\text{Ph}, \text{PMe}_3$ , often also with trace amounts of  $(\eta^5\text{-C}_5\text{H}_5)\text{Fe}(\text{CO})_2$ -

<sup>®</sup> Abstract published in *Advance ACS Abstracts*, November 15, 1994.

(1) (a) Academia Sinica. (b) National Taiwan University. (c) University of Ilorin.

(2) (a) Liu, L.-K.; Luh, L.-S. *Organometallics* **1994**, *13*, 2816. (b) Luh, L.-S.; Liu, L.-K. *Bull. Inst. Chem., Acad. Sin.* **1994**, *41*, 39.

(3) (a) Koerner von Gustorf, E. A.; Grevels, F.-W.; Fischler, I., Eds. *The Organic Chemistry of Iron*; Academic Press: New York, 1978; Vol. 1, p 352. (b) Davies, S. G. *Organotransition Metal Chemistry: Applications to Organic Synthesis*; Pergamon Press: Oxford, U.K., 1982; pp 24-25. (c) Pearson, A. J. *Metallo-organic Chemistry*; Wiley: Chichester, U.K., 1985; p 333. (d) Piper, T. S.; Wilkinson, G. *J. Inorg. Nucl. Chem.* **1956**, *3*, 104. (e) Li, H.-J.; Turnbull, M. M. *J. Organomet. Chem.* **1991**, *419*, 245. (f) Chukwu, R.; Hunter, A. D.; Santarsiero, B. D.; Bott, S. G.; Atwood, J. L.; Chassignac, J. *Organometallics* **1992**, *11*, 589. (g) Akita, M.; Terada, M.; Moro-Oka, Y. *Organometallics* **1992**, *11*, 1825.

(4) (a) Bibler, J. P.; Wojcicki, A. *Inorg. Chem.* **1966**, *5*, 889. (b) Butler, I. S.; Basolo, F.; Pearson, R. G. *Inorg. Chem.* **1967**, *6*, 2074. (c) Green, M.; Westlake, D. J. *J. Chem. Soc. A* **1971**, 367.



Me, <sup>5</sup>( $\eta^5$ -C<sub>5</sub>H<sub>5</sub>)Fe(CO)(PR<sub>3</sub>)C(O)Me,<sup>4,6,8,11</sup> [( $\eta^5$ -C<sub>5</sub>H<sub>5</sub>)Fe(CO)<sub>2</sub>]<sub>2</sub>,<sup>7</sup> and ( $\eta^5$ -C<sub>5</sub>H<sub>5</sub>)Fe(CO)(PR<sub>3</sub>)I.<sup>8</sup> The yields of products of ( $\eta^4$ -MeC<sub>5</sub>H<sub>5</sub>)Fe(CO)<sub>2</sub>(PR<sub>3</sub>) are in the range 34–78%, increasing in the order PMe<sub>3</sub> < PMePh<sub>2</sub> < PMe<sub>2</sub>Ph < PPh<sub>3</sub>, parallel to the order of decreasing  $\sigma$ -donating capability<sup>9</sup> and to the order of increasing cone angle<sup>10</sup> of the phosphine. The tendency is expected in terms of the reactive cation intermediate [( $\eta^5$ -C<sub>5</sub>H<sub>5</sub>)Fe(CO)<sub>2</sub>PR<sub>3</sub>]<sup>+</sup> reacting with the nucleophile RLi.<sup>2</sup> While steric effects may be more important than electronic effects in common PR<sub>3</sub> reactions, PR<sub>3</sub> is only involved in the three-component reaction during the conversion of ( $\eta^5$ -C<sub>5</sub>H<sub>5</sub>)Fe(CO)<sub>2</sub>X to [( $\eta^5$ -C<sub>5</sub>H<sub>5</sub>)Fe(CO)<sub>2</sub>PR<sub>3</sub>]<sup>+</sup>, the reactive cation intermediate, which then proceeds with ring alkylation on the side opposite to PR<sub>3</sub> and two bonds away. Hence, the electronic effects are favored. Replacing PPh<sub>3</sub> with PMe<sub>3</sub>, for example, decreases the electrophilicity of the cation toward RLi. Thus, the *exo* MeLi addition at the C<sub>5</sub>H<sub>5</sub> ring of [( $\eta^5$ -C<sub>5</sub>H<sub>5</sub>)Fe(CO)<sub>2</sub>PMe<sub>3</sub>]<sup>+</sup> is less favored than at [( $\eta^5$ -C<sub>5</sub>H<sub>5</sub>)Fe(CO)<sub>2</sub>PPh<sub>3</sub>]<sup>+</sup>. However, since PMe<sub>3</sub> is a better ligand than PPh<sub>3</sub> in phosphine substitution reactions, the reactive intermediate [( $\eta^5$ -C<sub>5</sub>H<sub>5</sub>)Fe(CO)<sub>2</sub>PMe<sub>3</sub>]<sup>+</sup> would be expected to accumulate, which is not observed experimentally. In the PMe<sub>3</sub> reaction, ( $\eta^5$ -C<sub>5</sub>H<sub>5</sub>)Fe(CO)-PMe<sub>3</sub>C(O)Me is isolated in 14.6% yield and [( $\eta^5$ -C<sub>5</sub>H<sub>5</sub>)Fe(CO)(PMe<sub>3</sub>)<sub>2</sub>]<sup>+</sup>I<sup>-</sup> is obtained as well in 15% yield, apparently at the expense of **4** as the CO alkylation and the PMe<sub>3</sub> substitution of CO in [( $\eta^5$ -C<sub>5</sub>H<sub>5</sub>)Fe(CO)<sub>2</sub>PMe<sub>3</sub>]<sup>+</sup> become competing reactions *vs* ring alkylation. As a general trend, going from PMe<sub>3</sub> to PMe<sub>2</sub>Ph to PMePh<sub>2</sub> to PPh<sub>3</sub>, the three-component reaction becomes progressively cleaner.

The difference in the back-donation from Fe core to CO ligands is reflected in the IR  $\nu_{CO}$  stretching frequencies. Two IR absorption bands are recorded for each ( $\eta^4$ -MeC<sub>5</sub>H<sub>5</sub>)Fe(CO)<sub>2</sub>(PR<sub>3</sub>) complex. The symmetric  $\nu_{CO}$  frequencies are 1958, 1962, 1962, and 1964 cm<sup>-1</sup> and the asymmetric ones are 1893, 1898, 1901, and 1904 cm<sup>-1</sup> for **4**, **3**, **2**, and **1**, respectively. Among the phosphines employed, PMe<sub>3</sub> and PPh<sub>3</sub> are respectively the most and least  $\sigma$ -donating, leading to the most and least electron-rich Fe cores for the corresponding complexes, and these are found to exhibit the lowest and highest IR stretching frequencies, respectively.

The <sup>31</sup>P NMR chemical shifts of free PMe<sub>3</sub>, PMePh<sub>2</sub>, PMe<sub>2</sub>Ph, and PPh<sub>3</sub> have been reported as  $\delta$  -62, -45,

Table 1. Observed and Calculated <sup>31</sup>P Chemical Shifts of Complexes 1–4

complex	$\Delta_{\text{obsd.}}$ , $\delta$	$\Delta_{\text{calcd.}}$ , $\delta$	diff, $\delta$
<b>1</b>	28.0	26.3	1.7
<b>2</b>	39.2	41.6	-2.4
<b>3</b>	56.8	56.9	-0.1
<b>4</b>	73.2	72.2	1.0

-26, and -8, respectively.<sup>12</sup> The <sup>31</sup>P NMR signals for the corresponding complexes **1–4** are  $\delta$  28.0, 39.2, 56.8, and 73.2, respectively. The coordination shifts are from 90 to 81  $\delta$  units downfield when the free PR<sub>3</sub> becomes coordinated in the ( $\eta^4$ -MeC<sub>5</sub>H<sub>5</sub>)Fe(CO)<sub>2</sub>(PR<sub>3</sub>) complexes. A regular variation in the chemical shift of the tertiary phosphine has been noted on stepwise substitution of the alkyl groups by other alkyl/aryl groups. The <sup>31</sup>P NMR chemical shift  $\Delta$  of a tertiary phosphine is given by the equation

$$\Delta = -62 + \sum_{n=1}^3 \sigma_n^p$$

where  $\sigma^p$  is the group contribution; e.g.,  $\sigma_{\text{Me}}^p = 0$ ,  $\sigma_{\text{Ph}}^p = 18$ .<sup>13</sup> The calculated chemical shifts are within 2  $\delta$  units from the observed chemical shifts. For the complexes ( $\eta^4$ -MeC<sub>5</sub>H<sub>5</sub>)Fe(CO)<sub>2</sub>(PR<sub>3</sub>), the <sup>31</sup>P NMR chemical shift  $\Delta$  also can be fit by least-squares methods into the following similar equation (deviations <2.4  $\delta$ ):

$$\Delta = 26.3 + 0.85 \sum_{n=1}^3 \sigma_n^p$$

employing the same  $\sigma^p$  for Me and Ph. Table 1 lists the observed and calculated <sup>31</sup>P shifts for complexes **1–4**. A multiplier of 0.85 is found necessary, indicating a smaller variation step for the complexes, different from that for the free phosphines. Apparently, the back-bonding of Fe to diene and CO ligands regulates Fe–P bonding electron density and accordingly the shielding of the P nucleus.

The results of the X-ray structure analysis of **2**, as shown in Figure 1, suggest that the nucleophilic addition of Me<sup>-</sup> is direct, without the Fe mediation, and the Me group is *exo* to the cyclopentadiene ring. The coordination geometry of Fe may be described as that of a distorted square pyramid with one CO placed at the apical position, PMePh<sub>2</sub> in the basal plane *trans* to one of the double bonds, and the second CO ligand *trans* to the second double bond. The diene atoms C3, C4, C5, and C6 are coplanar within 0.002(7) Å. The plane of C7, C8, Fe, C2, and O2 (deviations within 0.059(7) Å) is perpendicular to the plane of C3–C6, the interplanar angle being 85.2(2)°. That is, the planar diene skeleton is orthogonal to the plane made up of the unique C atom of the cyclopentadiene ring, the neighboring *exo*-C atom, Fe, and the apical CO group. A similar orthogonality has been evidenced in PPh<sub>3</sub> analogs: 86.4(1)° in ( $\eta^4$ -PhC<sub>5</sub>H<sub>5</sub>)Fe(CO)<sub>2</sub>(PPh<sub>3</sub>),<sup>2b</sup> 93.1 and 89.8° in the two independent molecules of ( $\eta^4$ -PhCH<sub>2</sub>C<sub>5</sub>H<sub>5</sub>)Fe(CO)<sub>2</sub>(PPh<sub>3</sub>),<sup>14</sup> and 90.6(2)° in ( $\eta^4$ -BuC<sub>5</sub>H<sub>5</sub>)Fe(CO)<sub>2</sub>(PPh<sub>3</sub>).<sup>2a</sup> The distance between C7 and the plane of C3–C6 is 0.570(9) Å. The three-atom plane of

(12) Gorenstein, D. G., Ed. *Phosphorus-31 NMR: Principles and Applications*; Academic Press: New York, 1984; p 24.

(13) (a) Grim, S. O.; McFarlane, W. *Nature (London)* **1965**, *208*, 995. (b) Grim, S. O.; McFarlane, W.; Davidoff, E. F. *J. Org. Chem.* **1967**, *32*, 781.

(14) Sim, G. A.; Woodhouse, D. I.; Knox, G. R. *J. Chem. Soc., Dalton Trans.* **1979**, 629.

(5) (a) Piper, T. S. *Naturwissenschaften* **1957**, *43*, 15. (b) Clifford, A. F. *J. Inorg. Nucl. Chem.* **1963**, *25*, 1065. (c) King, R. B.; Bisnette, M. B. *J. Organomet. Chem.* **1964**, *2*, 15. (d) Jordan, R. F.; Norton, J. R. *J. Am. Chem. Soc.* **1979**, *101*, 4853.

(6) (a) Miholova, D.; Vlcek, A. A. *J. Organomet. Chem.* **1982**, *240*, 413. (b) Folkes, C. R.; Rest, A. J. *J. Organomet. Chem.* **1977**, *136*, 355. (c) Gingell, A. C.; Rest, A. J. *J. Organomet. Chem.* **1975**, *99*, C27. (d) Brunner, H.; Schmidt, E. *J. Organomet. Chem.* **1972**, *36*, C18. (e) Stepowska, H.; Zamojski, A. *J. Organomet. Chem.* **1993**, *456*, 221. (f) Davies, S. G.; Smallridge, A. J. *J. Organomet. Chem.* **1990**, *397*, C13. (g) Herndon, J. W.; Wu, C.; Ammon, H. L. *J. Org. Chem.* **1988**, *53*, 2873. (h) Brookhart, M.; Liu, Y. *Organometallics* **1989**, *8*, 1572. (i) Groetsch, G.; Malisch, W. *J. Organomet. Chem.* **1983**, *246*, C42.

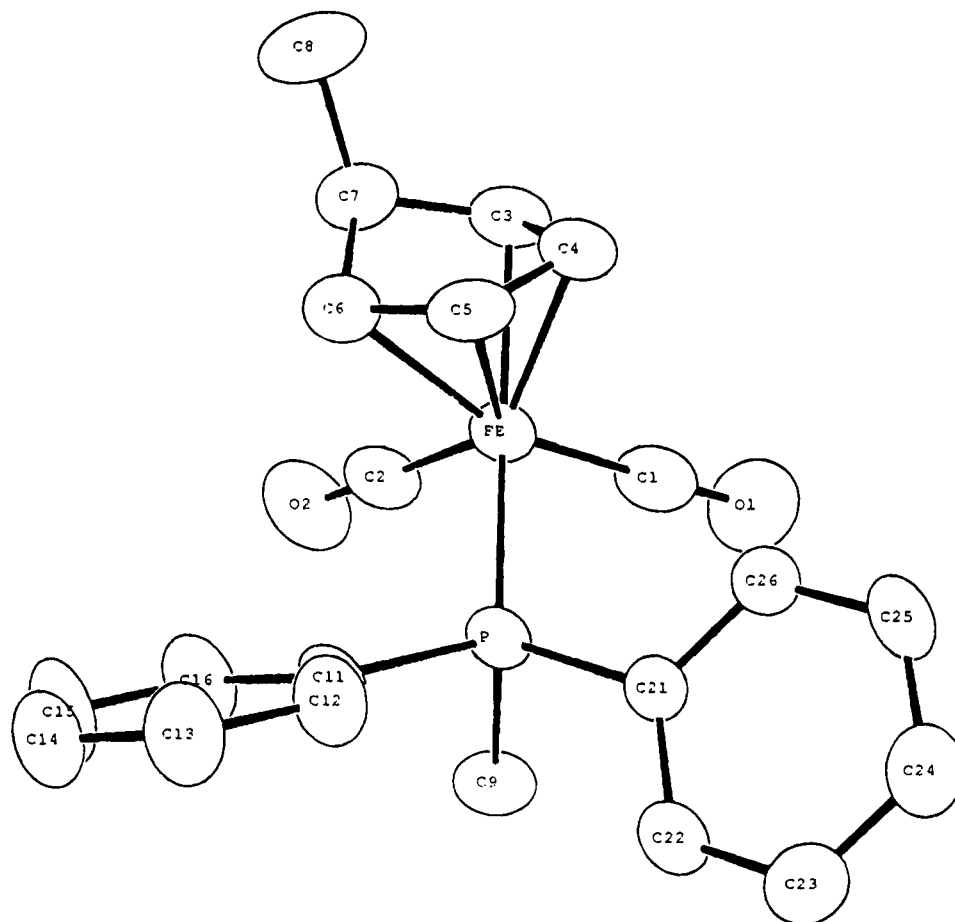
(7) (a) Adams, R. D.; Cotton, F. A. *J. Am. Chem. Soc.* **1973**, *95*, 6589. (b) Manning, A. R. *J. Chem. Soc. A* **1968**, 1319.

(8) Treichel, P. M.; Shubkin, R. L.; Barnett, K. W.; Reichard, D. *Inorg. Chem.* **1966**, *5*, 1177.

(9) (a) Atwood, J. D. *Inorganic and Organometallic Reaction Mechanism*; Wadsworth: Belmont, 1985; Chapter 4. (b) Lukehart, C. M. *Fundamental Transition Metal Organometallic Chemistry*; Wadsworth: Belmont, 1985; Chapter 3.

(10) Tolman, C. A. *Chem. Rev.* **1977**, *77*, 313.

(11) Treichel, P. M.; Komar, D. A. *J. Organomet. Chem.* **1981**, *206*, 77.



**Figure 1.** Molecular plot of complex **2** with atomic numbering sequences. The thermal ellipsoids are plotted at the 50% level. The H atoms are omitted for clarity. Selected bond lengths (Å): Fe–P, 2.202(2); Fe–C1, 1.749(6); Fe–C2, 1.768(6); Fe–C3, 2.111(5); Fe–C4, 2.050(5); Fe–C5, 2.051(4); Fe–C6, 2.113(5); O1–C1, 1.158(7); O2–C2, 1.147(7). Selected bond angles (deg): P–Fe–C1, 90.3(2); P–Fe–C2, 96.5(2); C1–Fe–C2, 102.9(2).

C3, C6, and C7 is tilted by  $34.2(4)^\circ$  away from Fe to the other side of the diene plane. In  $(\eta^4\text{-PhC}_5\text{H}_5)\text{Fe}(\text{CO})_2(\text{PPh}_3)$  the tilt is  $34.1^\circ$ , in  $(\eta^4\text{-PhCH}_2\text{C}_5\text{H}_5)\text{Fe}(\text{CO})_2(\text{PPh}_3)$  the tilts are  $34.7$  and  $32.9^\circ$ , and in  $(\eta^4\text{-BuC}_5\text{H}_5)\text{Fe}(\text{CO})_2(\text{PPh}_3)$  the tilt is  $34.9^\circ$ .

The Fe–P(PMePh<sub>2</sub>) length is 2.202(2) Å, seemingly shortened if compared with those of PPh<sub>3</sub> analogs; for example, Fe–P(PPh<sub>3</sub>) = 2.211(1) Å in  $(\eta^4\text{-BuC}_5\text{H}_5)\text{Fe}(\text{CO})_2(\text{PPh}_3)$ . Considering the Fe–P bond, the Me group of PMePh<sub>2</sub> is seen to be virtually *trans* to the centroid of the diene (torsion angle  $169.2(2)^\circ$ ). The average Fe–C(diene) lengths are 2.116(6) Å for the outer C atoms and 2.052(6) Å for the inner C atoms—the outer C atoms of the diene are slightly farther away. The Fe–C(CO) lengths are 1.745(7) Å for the basal CO and 1.773(7) Å for the apical CO—the basal CO is slightly less distant.

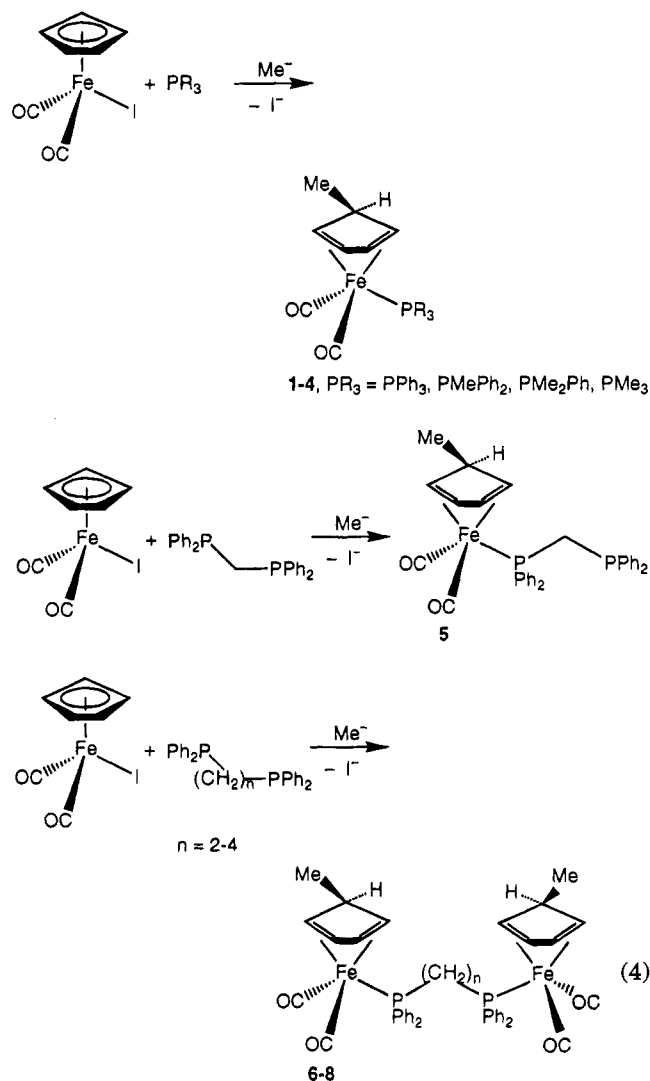
The extension from monophosphines to diphosphines gives interesting results. Considering the chelation effect, the  $\alpha,\omega$ -bis(diphenylphosphine)alkane, e.g., dppe, would be expected to prefer chelating at one metal atom to bridging between two metal atoms in the commonly studied ligand substitution reactions.<sup>15</sup> Nonetheless, in the three-component reactions of  $(\eta^5\text{-C}_5\text{H}_5)\text{Fe}(\text{CO})_2\text{I}$  with MeLi in the presence of  $\alpha,\omega$ -bis(diphenylphosphine)alkanes at low temperature, all diphosphines except dpmm give a bridged complex, linking two  $[(\eta^4\text{-MeC}_5\text{H}_5)\text{Fe}(\text{CO})_2]$

units as the major product (Scheme 2). For dpmm, there seems to be a high barrier to bring two  $[(\eta^4\text{-MeC}_5\text{H}_5)\text{Fe}(\text{CO})_2]$  units into close proximity, presumably steric in origin. The reaction of  $(\eta^5\text{-C}_5\text{H}_5)\text{Fe}(\text{CO})_2\text{I}$  with MeLi in the presence of dpmm yields the unidentate complex  $(\eta^4\text{-MeC}_5\text{H}_5)\text{Fe}(\text{CO})_2(\eta^1\text{-dpmm})$  (**5**) in 69% yield as the only ring-alkylation product. Complex **5** has one dangling PPh<sub>2</sub> group ready for further phosphine substitution reactions or phosphine-induced processes, which are presently under investigation. For dppe, dpmp, and dpmb, the isolated yields of  $[(\eta^4\text{-MeC}_5\text{H}_5)\text{Fe}(\text{CO})_2][\mu,\eta^1:\eta^1\text{-Ph}_2\text{P}(\text{CH}_2)_n\text{PPh}_2][(\eta^4\text{-MeC}_5\text{H}_5)\text{Fe}(\text{CO})_2]$  (**6–8** for  $n = 2\text{--}4$ ) are very good (53, 62, and 68%, respectively). The rate for the ring alkylation must therefore be orders of magnitude greater than any possible CO substitution. Since the compounds are very similar in the local bonding environment around Fe, the results of spectroscopic measurements of **5–8** are very similar and consistent with those of **2**.

Complex **6** has been investigated by a single-crystal X-ray diffraction study. Figure 2 shows the molecular plot of **6**, in which a bridging dppe links two  $[(\eta^4\text{-MeC}_5\text{H}_5)\text{Fe}(\text{CO})_2]$  units. Given four molecules in the unit cell of  $C2/c$  that has eight equivalent positions, only half of the molecule is crystallographically independent, the molecule being required to possess a  $C_2$  crystallographic symmetry. The Me group is on *exo* position on the cyclopentadiene ring. The coordination geometry around Fe is that of a distorted square pyramid with

(15) Cotton, F. A., Wilkinson, G., Eds. *Advanced Inorganic Chemistry*, 5th ed.; Wiley: New York, 1988; Section 2.4.

Scheme 2



one CO placed at the apical position,  $\text{PPh}_2(\text{CH}_2-)$  in the basal plane *trans* to one of the double bonds, and the second CO ligand *trans* to the second double bond. The diene of C2, C3, C4, and C5 is planar within 0.005(4) Å, making a dihedral angle of 89.0(1)° with the plane made up of C1, C6, Fe, C8, and O8 (deviations less than 0.006(4) Å). The distance between C1 and the diene plane is 0.586(5) Å. The three-atom plane of C1, C2, and C5 tilted by 34.9(3)° away from Fe. Considering the Fe–P bond, the  $-\text{CH}_2-$  group is seen to approach a *trans* position to the centroid of diene, the torsion angle of centroid–Fe–P– $\text{CH}_2$  being 163.4(1)°. The Fe–P length of 2.208(1) Å, the average Fe–C(diene) lengths of 2.106(5) and 2.051(5) Å for the outer and inner C atoms of diene, and the Fe–C(CO) lengths of 1.755(3) Å for basal CO and 1.768(3) Å for apical CO are seen to conform to the structural parameters of compound 2. The  $\text{PCH}_2\text{CH}_2\text{P}$  fragment is *trans* in conformation.

The reaction of  $(\eta^5\text{-C}_5\text{H}_5)\text{Fe}(\text{CO})_2\text{I}$  with BuLi in the presence of dppe yields products of both ring alkylation (major) and CO alkylation (Scheme 3). Much fewer substitution/deprotonation reactions take place when MeLi is replaced by *n*-BuLi in the three-component reaction. The product distribution of the three dppe-containing products isolated is as follows:  $(\eta^4\text{-BuC}_5\text{H}_5)\text{Fe}(\text{CO})_2(\mu, \eta^1: \eta^1\text{-dppe})(\eta^4\text{-BuC}_5\text{H}_5)\text{Fe}(\text{CO})_2$  (**9**; 55%),  $(\eta^4\text{-$

$\text{BuC}_5\text{H}_5)\text{Fe}(\text{CO})_2(\mu, \eta^1: \eta^1\text{-dppe})(\eta^5\text{-C}_5\text{H}_5)\text{Fe}(\text{CO})\text{C}(\text{O})\text{Bu}$  (**10**; 18%),  $(\eta^5\text{-C}_5\text{H}_5)\text{Fe}(\text{CO})\text{C}(\text{O})\text{Bu}(\mu, \eta^1: \eta^1\text{-dppe})(\eta^5\text{-C}_5\text{H}_5)\text{Fe}(\text{CO})\text{C}(\text{O})\text{Bu}$  (**11**; 1%).

Complex **9** shows IR  $\nu_{\text{CO}}$  bands of 1962 and 1899  $\text{cm}^{-1}$ , a  $^{31}\text{P}$  NMR chemical shift of  $\delta$  69.9, and  $^1\text{H}$  NMR shifts of  $\delta$  4.90, 2.53, and 2.34 (integration 2:1:2) for cyclopentadiene, indicative of the presence of two equivalent  $(\eta^4\text{-RC}_5\text{H}_5)\text{Fe}(\text{CO})_2(\text{PR}_3)$  fragments bridged by dppe. The spectroscopic data of complex **11** are typical of  $(\eta^5\text{-C}_5\text{H}_5)\text{Fe}(\text{CO})\text{C}(\text{O})\text{R}$  linked to a phosphine: the IR  $\nu_{\text{CO}}$  bands of 1907 and 1595  $\text{cm}^{-1}$ , a  $^1\text{H}$  NMR chemical shift of  $\delta$  4.34 for  $(\eta^5\text{-C}_5\text{H}_5)$  ring, and a  $^{31}\text{P}$  NMR chemical shift of  $\delta$  76.4. The molecular connectivity of complex **10** is readily derived from the spectroscopic data: the IR  $\nu_{\text{CO}}$  bands of 1903 and 1596  $\text{cm}^{-1}$ , the  $^1\text{H}$  NMR peak of  $\delta$  4.28, and the  $^{31}\text{P}$  NMR chemical shift of  $\delta$  76.0 are typical of a  $(\eta^5\text{-C}_5\text{H}_5)\text{Fe}(\text{CO})\text{C}(\text{O})\text{R}$  linked to a phosphine. In addition, the IR  $\nu_{\text{CO}}$  bands of 1962 and 1903 (overlapped)  $\text{cm}^{-1}$ , the  $^{31}\text{P}$  NMR chemical shift of  $\delta$  69.8, and the  $^1\text{H}$  NMR shifts of  $\delta$  4.90, 2.51, and 2.42 (integration 2:1:2) are indicative of the presence of a  $(\eta^4\text{-RC}_5\text{H}_5)\text{Fe}(\text{CO})_2(\text{PR}_3)$  fragment as well. Thus, for complex **10**, a dppe group linking two isomeric, butylated  $[(\text{C}_5\text{H}_5)\text{Fe}(\text{CO})_2]$  units has been established, one end in the form of  $(\eta^5\text{-C}_5\text{H}_5)\text{Fe}(\text{CO})\text{C}(\text{O})\text{Bu}$  and the other end in the form of  $(\eta^4\text{-BuC}_5\text{H}_5)\text{Fe}(\text{CO})_2$ .

The two  $\text{PPh}_2$  groups of dppe in the reaction of  $(\eta^5\text{-C}_5\text{H}_5)\text{Fe}(\text{CO})_2\text{I}$  with BuLi at low temperature hardly exhibit any neighboring effects, each proceeding independently with ring alkylation or CO alkylation, such that the three dppe-containing species being produced are in a statistical ratio. A simple calculation results in a ratio of (49–64):(14–16):1 for **9**:**10**:**11**, assuming each  $\text{PPh}_2$  group with the ring alkylation to be 7–8 times more favorable than the CO alkylation.

## Experimental Section

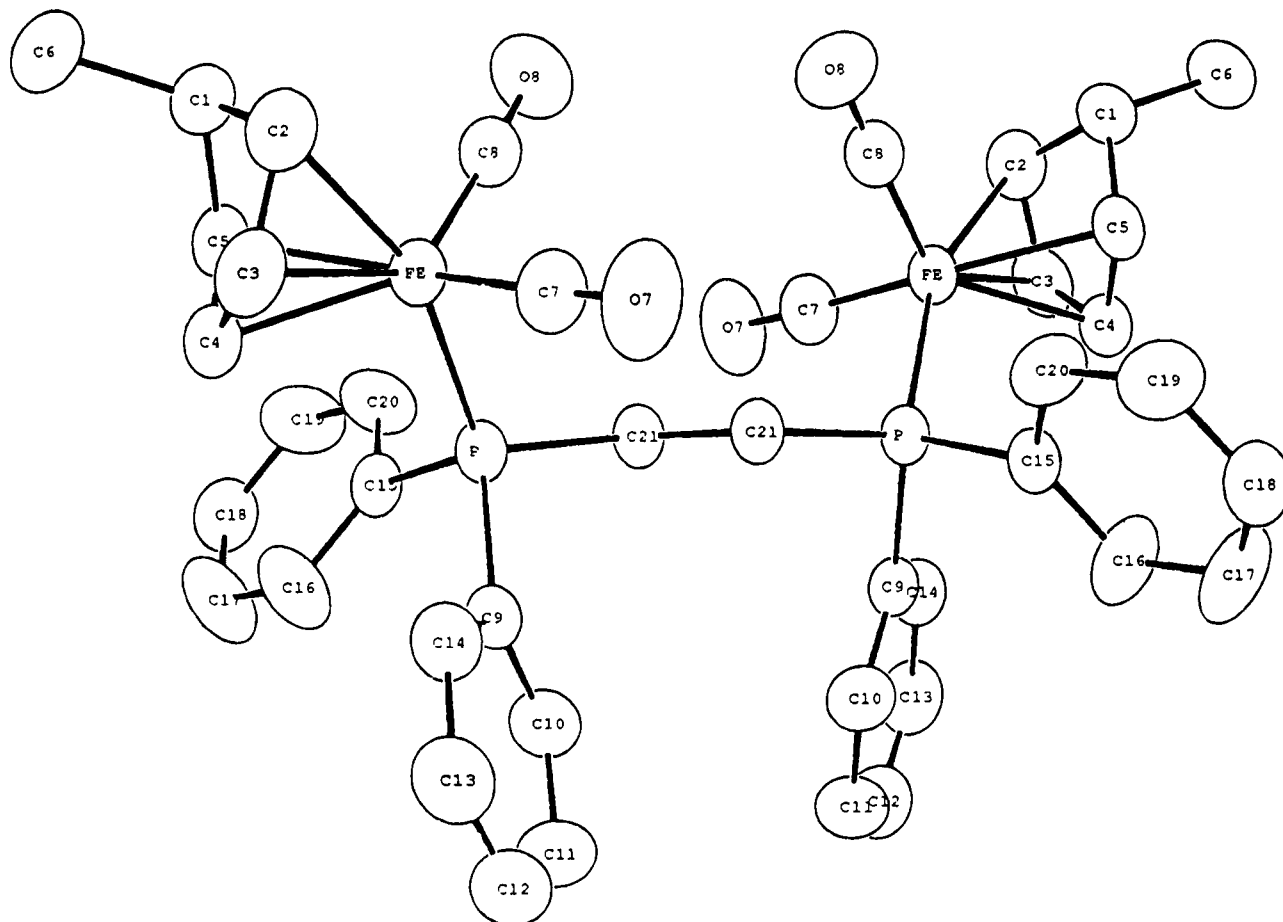
**General Considerations.** All manipulations were performed under an atmosphere of prepurified nitrogen with standard Schlenk techniques. All solvents were distilled from an appropriate drying agent.<sup>16</sup> Infrared spectra were recorded in  $\text{CH}_2\text{Cl}_2$  using  $\text{CaF}_2$  optics on a Perkin-Elmer 882 spectrophotometer. The  $^1\text{H}$  NMR and  $^{13}\text{C}$  NMR spectra were obtained on Bruker AC200/AC300 spectrometers, with chemical shifts reported in  $\delta$  values relative to the residual solvent resonance of  $\text{CDCl}_3$  ( $^1\text{H}$  7.24 ppm,  $^{13}\text{C}$  77.0 ppm). The  $^{31}\text{P}\{^1\text{H}\}$  NMR spectra were obtained on Bruker AC200/AC300 spectrometers using 85%  $\text{H}_3\text{PO}_4$  as an external standard ( $^{31}\text{P}$  0.00 ppm). The melting points (uncorrected) were determined on a Yanaco MPL melting-point apparatus.  $(\eta^5\text{-C}_5\text{H}_5)\text{Fe}(\text{CO})_2\text{I}$  was prepared according to the literature procedure.<sup>17</sup> Other reagents were obtained from commercial sources, e.g. Aldrich and Merck, and used without further purification.

Since essentially the same procedure was used in all experiments, the first reaction is given in detail to serve as a general one. For later experiments only the salient data, deviations from the general procedure, and product characterization data will be reported.

**Reaction of 1:1  $(\eta^5\text{-C}_5\text{H}_5)\text{Fe}(\text{CO})_2\text{I}$  and  $\text{PPh}_3$  with MeLi.**  $(\eta^5\text{-C}_5\text{H}_5)\text{Fe}(\text{CO})_2\text{I}$  (1.520 g, 5 mmol) and  $\text{PPh}_3$  (1.312 g, 5 mmol) were dissolved in THF (150 mL) and maintained at  $-78$

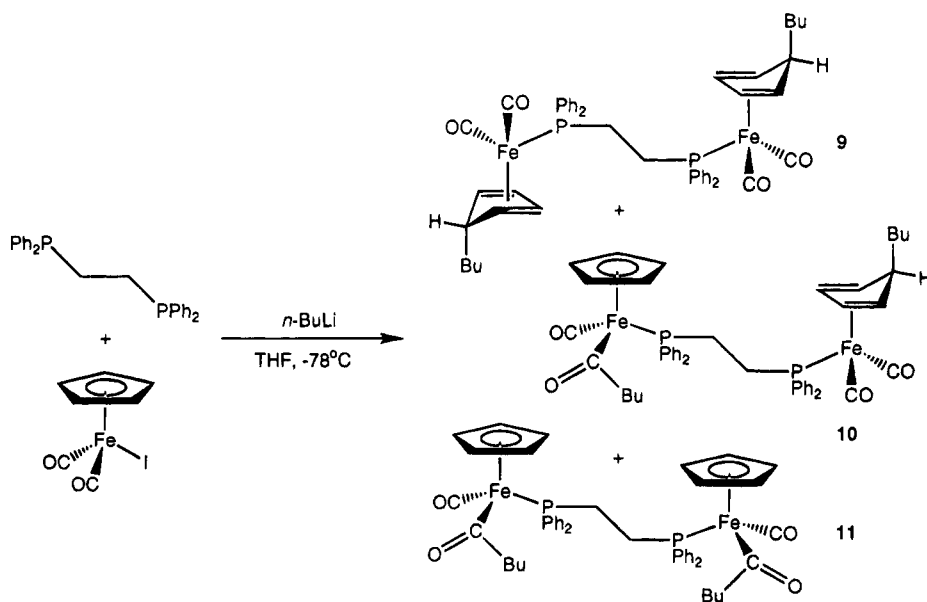
(16) Perrin, D. D.; Armarego, W. L. F.; Perrin, D. R. *Purification of Laboratory Chemicals*; Pergamon Press: Oxford, U.K., 1981.

(17) (a) Dombek, B. D.; Angelici, R. J. *Inorg. Chim. Acta* **1973**, *7*, 345. (b) Meyer, T. J.; Johnson, E. C.; Winterton, N. *Inorg. Chem.* **1971**, *10*, 1673. (c) *Inorg. Synth.* **1971**, *12*, 36. (d) *Inorg. Synth.* **1963**, *7*, 110.



**Figure 2.** Molecular plot of complex **6** with atomic numbering sequences. The thermal ellipsoids are plotted at the 50% level. The H atoms are omitted for clarity. Selected bond lengths (Å): Fe–P, 2.208(1); Fe–C2, 2.092(3); Fe–C3, 2.046(3); Fe–C4, 2.056(3); Fe–C5, 2.120(3); Fe–C7, 1.755(3); Fe–C8, 1.768(3); O7–C7, 1.151(4); O8–C8, 1.145(4). Selected bond angles (deg): P–Fe–C7, 93.4(1); P–Fe–C8, 99.0(1); C7–Fe–C8, 101.4(2).

### Scheme 3



°C. MeLi (1.6 M in ether, 3.75 mL, 6 mmol) in 30 mL of Et<sub>2</sub>O at –78 °C was added dropwise to the solution. The mixture was stirred for an additional 1 h before being warmed to room temperature and stirred overnight (3–4 h should be enough generally). The solution was quenched with water. The organic layer was combined with the benzene extracts of the water layer, dried over MgSO<sub>4</sub>, and then evaporated to dryness

under vacuum. The resulting oil-like concentrates were mixed well with 5 g of silica gel and 10 mL of CH<sub>2</sub>Cl<sub>2</sub> and then pumped dry before packing at the top of a SiO<sub>2</sub> column. Purification by column chromatography, with 1:10–1:7 EtOAc/*n*-hexane as eluent, gave, according to the order of appearance, four products: the yellow ( $\eta^5$ -MeC<sub>5</sub>H<sub>5</sub>)Fe(CO)<sub>2</sub>(PPh<sub>3</sub>)<sub>2</sub> (**1**; 77.8%), the orange ( $\eta^5$ -C<sub>5</sub>H<sub>5</sub>)Fe(CO)(PPh<sub>3</sub>)C(O)Me<sup>6</sup> (1.2%), a trace

amount of purple  $[(\eta^5\text{-C}_5\text{H}_5)\text{Fe}(\text{CO})_2]_2$ ,<sup>7</sup> and a trace amount of greenish  $(\eta^5\text{-C}_5\text{H}_5)\text{Fe}(\text{CO})_2(\text{PPh}_3)\text{I}$ .<sup>8</sup>

1: mp 131–133 °C; IR ( $\text{CH}_2\text{Cl}_2$ )  $\nu_{\text{CO}}$  1964 (s), 1904 (s)  $\text{cm}^{-1}$ ;  $^1\text{H}$  NMR ( $\text{CDCl}_3$ )  $\delta$  0.33 (d,  $^5J_{\text{PH}} = 6$  Hz, 3H, Me), 2.41 (b, 2H,  $-\text{CH}=\text{CHCHMe}-$ ), 2.72 (b, 1H,  $-\text{CH}=\text{CHCHMe}-$ ), 5.03 (b, 2H,  $-\text{CH}=\text{CHCHMe}-$ ), 7.32–7.42 (m, 15H, Ph);  $^{13}\text{C}$  NMR ( $\text{CDCl}_3$ )  $\delta$  28.2 (s, Me), 50.8 (s,  $-\text{CH}=\text{CHCHMe}-$ ), 57.6 (s,  $-\text{CH}=\text{CHCHMe}-$ ), 82.0 (s,  $-\text{CH}=\text{CHCHMe}-$ ), 128.0–136.7 (m, Ph), 219.8 (d,  $^2J_{\text{PC}} = 10.1$  Hz, CO);  $^{31}\text{P}$  NMR ( $\text{CDCl}_3$ )  $\delta$  73.2 (s); MS ( $m/z$ )  $\text{M}^+$  454 (parent ion). Anal. Calcd for  $\text{C}_{26}\text{H}_{23}\text{FeO}_2\text{P}$ : C, 68.74; H, 5.10. Found: C, 69.04; H, 5.19.

**Reaction of 1:1  $(\eta^5\text{-C}_5\text{H}_5)\text{Fe}(\text{CO})_2\text{I}$  and  $\text{PMePh}_2$  with MeLi.**  $(\eta^5\text{-C}_5\text{H}_5)\text{Fe}(\text{CO})_2\text{I}$  (0.608 g, 2 mmol),  $\text{PMePh}_2$  (0.400 g, 2 mmol), THF (50 mL), MeLi (1.6 M in  $\text{Et}_2\text{O}$ , 2.0 mL, 3.2 mmol diluted in 10 mL of  $\text{Et}_2\text{O}$ ). The final mixture was filtered and the solvent removed on a rotary evaporator. The residue was partitioned in  $\text{CH}_2\text{Cl}_2$  and cold  $\text{H}_2\text{O}$  (5.0 mL). The  $\text{CH}_2\text{Cl}_2$  layer was collected and dried with  $\text{MgSO}_4$ , and the solvent was removed, resulting in a residue. The latter was chromatographed using a silica gel column (dry packing, with 10% ethyl acetate in *n*-hexane as eluent). The first band yielded the yellow  $(\eta^4\text{-MeC}_5\text{H}_5)\text{Fe}(\text{CO})_2\text{PMePh}_2$  (**2**; 0.255 g, 65%). The product was recrystallized from a mixture of  $\text{CH}_2\text{Cl}_2$  and *n*-hexane to give crystals suitable for X-ray crystallography. The second band (brown) was only very minor and presumably was the CO-alkylated product as judged from spectroscopic data.

2: mp 96–97 °C; IR ( $\text{CH}_2\text{Cl}_2$ )  $\nu_{\text{CO}}$  1962 (vs), 1901 (vs)  $\text{cm}^{-1}$ ;  $^{31}\text{P}$  NMR ( $\text{CDCl}_3$ )  $\delta$  56.8;  $^1\text{H}$  NMR ( $\text{CDCl}_3$ )  $\delta$  7.36 (b, 10H, Ph), 5.02 (b, 2H,  $-\text{CH}=\text{CHCHMe}-$ ), 2.66 (b, 1H,  $-\text{CH}=\text{CHCHMe}-$ ), 2.42 (b, 2H,  $-\text{CH}=\text{CHCHMe}-$ ), 1.78 (d,  $^2J_{\text{PH}} = 9$  Hz, 3H, *PMe*), 0.33 (d,  $^5J_{\text{PH}} = 6$  Hz, 3H, Me);  $^{13}\text{C}$  NMR ( $\text{CDCl}_3$ )  $\delta$  19.5 (d,  $^1J_{\text{PC}} = 28.0$  Hz, *PMe*), 28.3 (s, Me), 51.1 (s,  $-\text{CH}=\text{CHCHMe}-$ ), 56.9 (s,  $-\text{CH}=\text{CHCHMe}-$ ), 81.4 (s,  $-\text{CH}=\text{CHCHMe}-$ ), 128.1–138.5 (m, Ph), 219.3 (d,  $^2J_{\text{PC}} = 14.0$  Hz, CO); MS ( $m/z$ )  $\text{M}^+$  392 (parent ion). Anal. Calcd for  $\text{C}_{21}\text{H}_{21}\text{FeO}_2\text{P}$ : C, 64.27; H, 5.41. Found: C, 64.32; H, 5.40.

**Reaction of 1:1  $(\eta^5\text{-C}_5\text{H}_5)\text{Fe}(\text{CO})_2\text{I}$  and  $\text{PMe}_2\text{Ph}$  with MeLi.**  $(\eta^5\text{-C}_5\text{H}_5)\text{Fe}(\text{CO})_2\text{I}$  (1.216 g, 4 mmol),  $\text{PMe}_2\text{Ph}$  (0.553 g, 4 mmol), THF (100 mL), MeLi (1.6 M in  $\text{Et}_2\text{O}$ , 3.0 mL, 4.8 mmol, diluted in 30 mL of  $\text{Et}_2\text{O}$ ). The final dark brown solution was cannulated and filtered through a short plug of alumina to remove the salts. The filtrate, a clear reddish brown solution, was evaporated to dryness under vacuum. The residue was extracted with *n*-hexane and passed through a bed of Celite before collection. The solvent was removed under vacuum to obtain an oil, which was redissolved in  $\text{CH}_2\text{Cl}_2$ , mixed with 3 g of nonactivated alumina, dry packed on top of a column of alumina, and chromatographed, with 10% ethyl acetate in *n*-hexane as eluent. One band separated on the column to give  $(\eta^4\text{-MeC}_5\text{H}_5)\text{Fe}(\text{CO})_2\text{PMe}_2\text{Ph}$  (**3**; 0.767 g, 58.0%) as a yellow oil after solvent removal. The *n*-hexane residue (a greenish oil) rapidly decomposed on the column during attempted purification.

3: viscous oil; IR ( $\text{CH}_2\text{Cl}_2$ )  $\nu_{\text{CO}}$  1962 (vs), 1898 (vs)  $\text{cm}^{-1}$ ;  $^{31}\text{P}$  NMR ( $\text{CDCl}_3$ )  $\delta$  39.2;  $^1\text{H}$  NMR ( $\text{CDCl}_3$ )  $\delta$  7.48–7.31 (m, 5H, Ph), 4.92 (b, 2H,  $-\text{CH}=\text{CHCHMe}-$ ), 2.65 (b, 1H,  $-\text{CH}=\text{CHCHMe}-$ ), 2.54–2.53 (m, 2H,  $-\text{CH}=\text{CHCHMe}-$ ), 1.53 (d,  $^2J_{\text{PH}} = 9$  Hz, 6H, *PMe*), 0.34 (d,  $^5J_{\text{PH}} = 6$  Hz, 3H, Me);  $^{13}\text{C}$  NMR ( $\text{CDCl}_3$ )  $\delta$  19.9 (d,  $^1J_{\text{PC}} = 27.3$  Hz, *PMe*), 28.4 (s, Me), 51.2 (s,  $-\text{CH}=\text{CHCHMe}-$ ), 56.1 (s,  $-\text{CH}=\text{CHCHMe}-$ ), 81.2 (s,  $-\text{CH}=\text{CHCHMe}-$ ), 128.2–139.2 (m, Ph), 219.1 (d,  $^2J_{\text{PC}} = 13.9$  Hz, CO); MS ( $m/z$ )  $\text{M}^+$  330 (parent ion). Anal. Calcd for  $\text{C}_{16}\text{H}_{15}\text{FeO}_2\text{P}$ : C, 58.16; H, 5.80. Found: C, 58.28; H, 5.78.

**Reaction of 1:1  $(\eta^5\text{-C}_5\text{H}_5)\text{Fe}(\text{CO})_2\text{I}$  and  $\text{PMe}_3$  with MeLi.**  $(\eta^5\text{-C}_5\text{H}_5)\text{Fe}(\text{CO})_2\text{I}$  (1.216 g, 4 mmol),  $\text{PMe}_3$  (0.304 g, 4 mmol), THF (100 mL), MeLi (1.6 M in  $\text{Et}_2\text{O}$ , 3.0 mL, 4.8 mmol, diluted in 30.0 mL of  $\text{Et}_2\text{O}$ ). The final dark brown solution was worked up according to the same procedure as in the  $\text{PMe}_2\text{Ph}$  reaction, except for elution with 20% ethyl acetate in *n*-hexane. Two bands separated on the column. After solvent removal, the first band (yellow) was purified by vacuum

distillation to a liquid-nitrogen trap to give  $(\eta^4\text{-MeC}_5\text{H}_5)\text{Fe}(\text{CO})_2\text{PMe}_3$  (**4**; 0.35 g, 34%) as a yellow solid. The second band (orange) yielded, after solvent removal and purification by sublimation,  $(\eta^5\text{-C}_5\text{H}_5)\text{Fe}(\text{CO})\text{C}(\text{O})\text{Me}(\text{PMe}_3)\text{I}$  (0.15 g, 14.6%) as an orange waxy compound. The *n*-hexane residue was purified by washing repeatedly with small portions of *n*-hexane to give brown solids of  $(\eta^5\text{-C}_5\text{H}_5)\text{Fe}(\text{CO})(\text{PMe}_3)_2\text{I}$  (0.16 g, 15%).

4: mp 51–52 °C; IR ( $\text{CH}_2\text{Cl}_2$ )  $\nu_{\text{CO}}$  1958 (vs), 1893 (vs)  $\text{cm}^{-1}$ ;  $^{31}\text{P}$  NMR ( $\text{CDCl}_3$ )  $\delta$  28.0;  $^1\text{H}$  NMR ( $\text{CDCl}_3$ )  $\delta$  4.99 (b, 2H,  $-\text{CH}=\text{CHCHMe}-$ ), 2.61 (b, 3H,  $-\text{CH}=\text{CHCHMe}-$ ), 1.22 (d,  $^2J_{\text{PH}} = 9$  Hz, 9H, *PMe*), 0.38 (d,  $^5J_{\text{PH}} = 6$  Hz, 3H, Me);  $^{13}\text{C}$  NMR ( $\text{CDCl}_3$ )  $\delta$  20.4 (d,  $^1J_{\text{PC}} = 26.5$  Hz, *PMe*), 28.4 (s, Me), 51.2 (s,  $-\text{CH}=\text{CHCHMe}-$ ), 55.2 (s,  $-\text{CH}=\text{CHCHMe}-$ ), 80.6 (s,  $-\text{CH}=\text{CHCHMe}-$ ), 218.8 (b, CO); MS ( $m/z$ )  $\text{M}^+$  1268 (parent ion). Anal. Calcd for  $\text{C}_{11}\text{H}_{11}\text{FeO}_2\text{P}$ : C, 46.18; H, 6.69. Found: C, 46.73; H, 6.42.

$(\eta^5\text{-C}_5\text{H}_5)\text{Fe}(\text{CO})\text{C}(\text{O})\text{Me}(\text{PMe}_3)$ : mp 80–81 °C (lit.<sup>11</sup> mp 71–73 °C); IR ( $\text{CH}_2\text{Cl}_2$ )  $\nu_{\text{CO}}$  1907 (vs), 1588 (s)  $\text{cm}^{-1}$ ;  $^{31}\text{P}$  NMR ( $\text{CDCl}_3$ )  $\delta$  43.0;  $^1\text{H}$  NMR ( $\text{CDCl}_3$ )  $\delta$  4.45 (s, 5H, Cp), 2.52 (s, 3H, Me), 1.34 (d,  $^2J_{\text{PH}} = 9$  Hz, 9H, *PMe*). Anal. Calcd for  $\text{C}_{11}\text{H}_{11}\text{FeO}_2\text{P}$ : C, 46.18; H, 6.69. Found: C, 46.73; H, 6.42.

$(\eta^5\text{-C}_5\text{H}_5)\text{Fe}(\text{CO})(\text{PMe}_3)_2\text{I}$ : mp >300 °C (lit.<sup>11</sup> mp 302–340 °C); IR ( $\text{CH}_2\text{Cl}_2$ )  $\nu_{\text{CO}}$  1963 (vs)  $\text{cm}^{-1}$ ;  $^{31}\text{P}$  NMR ( $\text{CDCl}_3$ )  $\delta$  27.3;  $^1\text{H}$  NMR ( $\text{CDCl}_3$ )  $\delta$  5.02 (s, 5H, Cp), 1.67 (b, 18H, *PMe*); MS ( $m/z$ )  $\text{M}^+$  301.

**Reaction of  $(\eta^5\text{-C}_5\text{H}_5)\text{Fe}(\text{CO})_2\text{I}$  and Diphosphine (=dppm, dppp, or dppb) with MeLi.**  $(\eta^5\text{-C}_5\text{H}_5)\text{Fe}(\text{CO})_2\text{I}$  (1.216 g, 4 mmol), diphosphine (dppm, 1.538 g, 4 mmol; dppp, 0.825 g, 2 mmol; dppb, 0.853 g, 2 mmol), THF (70 mL), MeLi (1.6 M in  $\text{Et}_2\text{O}$ , 3.0 mL, 4.8 mmol, diluted in 30 mL of  $\text{Et}_2\text{O}$ ). The final yellow solution was worked up in the same way as that in the  $\text{PMe}_2\text{Ph}$  reaction to yield three bands, the first band being yellow solids, after solvent removal, identified as  $(\eta^4\text{-MeC}_5\text{H}_5)\text{Fe}(\text{CO})_2(\eta^1\text{-dppm})$  (**5**; 1.60 g, 69.0%),  $(\eta^4\text{-MeC}_5\text{H}_5)\text{Fe}(\text{CO})_2(\mu, \eta^1\text{-}\eta^1\text{-dppp})(\eta^4\text{-MeC}_5\text{H}_5)\text{Fe}(\text{CO})_2$  (**7**; 0.99 g, 62.1%), and  $(\eta^4\text{-MeC}_5\text{H}_5)\text{Fe}(\text{CO})_2(\mu, \eta^1\text{-}\eta^1\text{-dppb})(\eta^4\text{-MeC}_5\text{H}_5)\text{Fe}(\text{CO})_2$  (**8**; 0.90 g, 67.5%) for dppm, dppp, and dppb, respectively. The second band was brown and was obtained in only trace amounts. For dppm and dppb, the second band could not be eluted from the column and the third band was hardly noticed. In the case of dppp, the second band yielded a trace amount of brown solid, conforming likely to  $(\eta^4\text{-MeC}_5\text{H}_5)\text{Fe}(\text{CO})_2(\mu, \eta^1\text{-}\eta^1\text{-dppp})(\eta^5\text{-C}_5\text{H}_5)\text{Fe}(\text{CO})\text{C}(\text{O})\text{Me}$  from spectroscopic characteristics. The third band was green and was obtained in too little quantity to be characterized unambiguously.

5: mp 91–92 °C; IR ( $\text{CH}_2\text{Cl}_2$ )  $\nu_{\text{CO}}$  1963 (vs), 1902 (vs)  $\text{cm}^{-1}$ ;  $^{31}\text{P}$  NMR ( $\text{CDCl}_3$ )  $\delta$  66.4 (d,  $^2J_{\text{PP}} = 81.7$  Hz), –25.6 (d,  $^2J_{\text{PP}} = 81.7$  Hz);  $^1\text{H}$  NMR ( $\text{CDCl}_3$ )  $\delta$  7.19–7.42 (m, 20H, Ph), 4.87 (b, 2H,  $-\text{CH}=\text{CHCHMe}-$ ), 3.0 (dd,  $^2J_{\text{PH}} = 7.7$  Hz,  $^2J_{\text{PH}} = 2.1$  Hz, 2H,  $\text{PCH}_2\text{P}$ ), 2.63 (b, 1H,  $-\text{CH}=\text{CHCHMe}-$ ), 2.28 (b, 2H,  $\text{CH}=\text{CHCHMe}-$ ), 0.27 (d,  $^5J_{\text{PH}} = 6$  Hz, 3H, Me);  $^{13}\text{C}$  NMR ( $\text{CDCl}_3$ )  $\delta$  28.1 (s, Me), 34.3 (dd,  $^1J_{\text{PC}} = 32.4$  Hz,  $^1J_{\text{PC}} = 19.9$  Hz,  $\text{PCH}_2\text{P}$ ), 51.0 (s,  $-\text{CH}=\text{CHCHMe}-$ ), 57.4 (s,  $-\text{CH}=\text{CHCHMe}-$ ), 81.9 (s,  $-\text{CH}=\text{CHCHMe}-$ ), 127.9–138.8 (m, Ph), 219.8 (dd,  $^2J_{\text{PC}} = 14.2$  Hz,  $^4J_{\text{PC}} = 1.8$  Hz, CO); MS ( $m/z$ )  $\text{M}^+$  1577. Anal. Calcd for  $\text{C}_{33}\text{H}_{30}\text{FeO}_2\text{P}_2$ : C, 68.75; H, 5.25. Found: C, 68.86; H, 5.21.

7: mp 61–62 °C; IR ( $\text{CH}_2\text{Cl}_2$ )  $\nu_{\text{CO}}$  1964 (vs), 1902 (vs)  $\text{cm}^{-1}$ ;  $^{31}\text{P}$  NMR ( $\text{CDCl}_3$ )  $\delta$  65.7;  $^1\text{H}$  NMR ( $\text{CDCl}_3$ )  $\delta$  7.30–7.26 (m, 20H, Ph), 4.81 (b, 4H,  $-\text{CH}=\text{CHCHMe}-$ ), 2.58 (b, 2H,  $-\text{CH}=\text{CHCHMe}-$ ), 2.25 (b, 4H,  $-\text{CH}=\text{CHCHMe}-$ ), 2.12–2.04 (m, 4H,  $-\text{PCH}_2\text{P}$ ), 1.49 (b, 2H,  $-\text{PCH}_2\text{CH}_2\text{P}$ ), 0.27 (d,  $^5J_{\text{PH}} = 6$  Hz, 6H, Me);  $^{13}\text{C}$  NMR ( $\text{CDCl}_3$ )  $\delta$  20.2 (s,  $\text{CH}_2\text{CH}_2\text{CH}_2$ ), 28.6 (s, Me), 35.2 (d,  $^1J_{\text{PC}} = 36.3$  Hz,  $\text{PCH}_2\text{P}$ ), 51.4 (s,  $-\text{CH}=\text{CHCHMe}-$ ), 57.5 (s,  $-\text{CH}=\text{CHCHMe}-$ ), 82.1 (s,  $-\text{CH}=\text{CHCHMe}-$ ), 128.6–137.2 (m, Ph), 219.9 (d,  $^2J_{\text{PC}} = 13.9$  Hz, CO); MS ( $m/z$ )  $\text{M}^+$  796 (parent ion). Anal. Calcd for  $\text{C}_{43}\text{H}_{42}\text{Fe}_2\text{O}_4\text{P}_2$ : C, 64.80; H, 5.32. Found: C, 65.33; H, 5.34.

8: mp 129–131 °C; IR ( $\text{CH}_2\text{Cl}_2$ )  $\nu_{\text{CO}}$  1961 (vs), 1900 (vs)  $\text{cm}^{-1}$ ;  $^{31}\text{P}$  NMR ( $\text{CDCl}_3$ )  $\delta$  66.2;  $^1\text{H}$  NMR ( $\text{CDCl}_3$ )  $\delta$  7.33–7.29 (m, 20H, Ph), 4.89 (b, 4H,  $-\text{CH}=\text{CHCHMe}-$ ), 2.64 (d,  $^4J_{\text{PH}} = 6$  Hz, 2H,  $-\text{CH}=\text{CHCHMe}-$ ), 2.30 (b, 4H,

–CH=CHCHMe–), 2.10–2.07 (m, 4H, –PCH<sub>2</sub>–), 1.50–1.26 (m, 4H, –PCH<sub>2</sub>CH<sub>2</sub>–), 0.29 (d, <sup>5</sup>J<sub>PH</sub> = 6 Hz, 6H, CH<sub>3</sub>); <sup>13</sup>C NMR (CDCl<sub>3</sub>) δ 25.6 (d, <sup>2</sup>J<sub>PC</sub> = 14.2 Hz, PCH<sub>2</sub>CH<sub>2</sub>–), 28.2 (s, Me), 32.5 (d, <sup>1</sup>J<sub>PC</sub> = 25.7 Hz, PCH<sub>2</sub>CH<sub>2</sub>–), 51.0 (s, –CH=CHCHMe–), 57.1 (s, –CH=CHCHMe–), 81.9 (s, –CH=CHCHMe–), 128.1–137.1 (m, Ph), 219.8 (d, <sup>2</sup>J<sub>PC</sub> = 14.1 Hz, CO); MS (*m/z*) M + 1 811. Anal. Calcd for C<sub>44</sub>H<sub>44</sub>Fe<sub>2</sub>O<sub>4</sub>P<sub>2</sub>: C, 65.20; H, 5.48. Found: C, 64.95; H, 5.80.

**Reaction of 1:1 (η<sup>5</sup>-C<sub>5</sub>H<sub>5</sub>)Fe(CO)<sub>2</sub>I and dppe with MeLi:** (η<sup>5</sup>-C<sub>5</sub>H<sub>5</sub>)Fe(CO)<sub>2</sub>I (1.520 g, 5 mmol), dppe (0.995 g, 2.5 mmol), THF (100 mL), MeLi (1.6 M, 3.75 mL, 6 mmol, diluted in 30 mL of Et<sub>2</sub>O). The column chromatography gave five compounds: the yellow (η<sup>5</sup>-C<sub>5</sub>H<sub>5</sub>)Fe(CO)<sub>2</sub>Me (3.7%)<sup>3</sup> and [(η<sup>4</sup>-MeC<sub>5</sub>H<sub>5</sub>)Fe(CO)<sub>2</sub>(μ,η<sup>1</sup>-dppe)](η<sup>4</sup>-MeC<sub>5</sub>H<sub>5</sub>)Fe(CO)<sub>2</sub> (**6**; 52.5%), the green (η<sup>4</sup>-MeC<sub>5</sub>H<sub>5</sub>)Fe(CO)<sub>2</sub>(μ,η<sup>1</sup>-dppe)(η<sup>5</sup>-C<sub>5</sub>H<sub>5</sub>)Fe(CO)I (2.3%), the orange (η<sup>4</sup>-MeC<sub>5</sub>H<sub>5</sub>)Fe(CO)<sub>2</sub>(μ,η<sup>1</sup>-dppe)(η<sup>5</sup>-C<sub>5</sub>H<sub>5</sub>)Fe(CO)C(O)Me (6.7%), and the purple [(η<sup>5</sup>-C<sub>5</sub>H<sub>5</sub>)Fe(CO)<sub>2</sub>]<sub>2</sub> (2.2%).<sup>7</sup> For complex **6**, crystals suitable for X-ray diffraction were grown from CH<sub>2</sub>Cl<sub>2</sub>/*n*-hexane by a slow evaporation method.

**6:** mp 187–188 °C; IR (CH<sub>2</sub>Cl<sub>2</sub>) ν<sub>CO</sub> 1962 (s), 1901 (s) cm<sup>-1</sup>; <sup>31</sup>P NMR (CDCl<sub>3</sub>) δ 70.2 (s); <sup>1</sup>H NMR (CDCl<sub>3</sub>) δ 7.25–7.31 (m, 10H, Ph), 4.90 (b, 2H, –CH=CHCHMe–), 2.66 (d, <sup>4</sup>J<sub>PH</sub> = 6 Hz, 1H, –CH=CHCHMe–), 2.29 (b, 2H, –CH=CHCHMe–), 2.09 (s, 2H, –PCH<sub>2</sub>–), 0.30 (d, <sup>5</sup>J<sub>PH</sub> = 6 Hz, 3H, Me); <sup>13</sup>C NMR (CDCl<sub>3</sub>): δ 27.1 (vt, <sup>1</sup>J<sub>PC</sub> = 13.3 Hz, –CH<sub>2</sub>–), 28.2 (s, Me), 51.0 (s, –CH=CHCHMe–), 57.4 (s, –CH=CHCHMe–), 82.1 (s, –CH=CHCHMe–), 128.6–136.9 (m, Ph), 219.9 (vt, <sup>2</sup>J<sub>PC</sub> = 6.8 Hz, CO); MS (*m/z*) M<sup>+</sup> 782 (parent ion). Anal. Calcd for C<sub>42</sub>H<sub>40</sub>Fe<sub>2</sub>O<sub>4</sub>P<sub>2</sub>: C, 64.48; H, 5.15. Found: C, 64.68; H, 5.25.

(η<sup>4</sup>-MeC<sub>5</sub>H<sub>5</sub>)Fe(CO)<sub>2</sub>(μ,η<sup>1</sup>-dppe)(η<sup>5</sup>-C<sub>5</sub>H<sub>5</sub>)Fe(CO)I: IR (CH<sub>2</sub>Cl<sub>2</sub>) ν<sub>CO</sub> 1962 (s), 1948 (sh), 1903 (s) cm<sup>-1</sup>; <sup>31</sup>P NMR (CDCl<sub>3</sub>) δ 70.4 (d, <sup>3</sup>J<sub>PP</sub> = 39 Hz), 66.4 (d, <sup>3</sup>J<sub>PP</sub> = 39 Hz); <sup>1</sup>H NMR (CDCl<sub>3</sub>) δ 7.23–7.33 (b, 20H, Ph), 5.01, 4.85 (s, 2H, –CH=CHCHMe–), 4.34 (s, 5H, Cp), 2.69 (b, 1H, –CH=CHCHMe–), 2.60, 2.30 (b, 4H, –PCH<sub>2</sub>–), 2.46, 2.03 (s, 2H, –CH=CHCHMe), 0.28 (b, 3H, Me); MS (*m/z*) M<sup>+</sup> 881 (parent ion). Anal. Calcd for C<sub>41</sub>H<sub>40</sub>Fe<sub>2</sub>O<sub>3</sub>P<sub>2</sub>: C, 66.53; H, 6.05. Found: C, 66.70; H, 5.83.

(η<sup>4</sup>-MeC<sub>5</sub>H<sub>5</sub>)Fe(CO)<sub>2</sub>(μ,η<sup>1</sup>-dppe)(η<sup>5</sup>-C<sub>5</sub>H<sub>5</sub>)Fe(CO)C(O)Me: mp 159–160 °C; IR (CH<sub>2</sub>Cl<sub>2</sub>) ν<sub>CO</sub> 1963 (s), 1905 (s), 1595 (w) cm<sup>-1</sup>; <sup>31</sup>P NMR (CDCl<sub>3</sub>) δ 75.9 (d, <sup>3</sup>J<sub>PP</sub> = 39.4 Hz); <sup>1</sup>H NMR (CDCl<sub>3</sub>) δ 7.18–7.37 (m, 20H, Ph), 4.95, 4.83 (b, 2H, –CH=CHCHMe–), 4.31 (s, 5H, Cp), 2.63 (b, 1H, –CH=CHCHMe–), 2.51 (s, 3H, COMe), 2.16, 2.04 (b, 2H, –CH=CHCHMe), 0.28 (d, <sup>5</sup>J<sub>PH</sub> = 15.0 Hz, 3H, Me); <sup>13</sup>C NMR (CDCl<sub>3</sub>) δ 25.3 (d, <sup>1</sup>J<sub>PC</sub> = 24.7 Hz, –CpFePCH<sub>2</sub>CH<sub>2</sub>P), 27.2 (d, <sup>1</sup>J<sub>PC</sub> = 22.0 Hz, –CpFePCH<sub>2</sub>CH<sub>2</sub>P), 28.2 (d, <sup>5</sup>J<sub>PC</sub> = 5.5 Hz, Me), 51.0 (s, COMe), 51.6 (d, <sup>3</sup>J<sub>PC</sub> = 4.8 Hz, –CH=CHCHMe–), 57.8 (s, –CH=CHCHMe–), 82.0 (d, <sup>2</sup>J<sub>PC</sub> = 4.9 Hz, –CH=CHCHMe–), 84.7 (s, Cp), 128.0–138.4 (m, Ph), 219.5 (d, <sup>2</sup>J<sub>PC</sub> = 14.0 Hz, CO), 220.0 (d, <sup>2</sup>J<sub>PC</sub> = 10.1 Hz, CO), 220.7 (s, CO), 275.3 (d, <sup>2</sup>J<sub>PC</sub> = 21.9 Hz, COMe); MS (*m/z*) M<sup>+</sup> 782 (parent ion). Anal. Calcd for C<sub>42</sub>H<sub>40</sub>Fe<sub>2</sub>O<sub>4</sub>P<sub>2</sub>: C, 64.48; H, 5.15. Found: C, 64.30; H, 5.01.

**Reaction of 1:1 (η<sup>5</sup>-C<sub>5</sub>H<sub>5</sub>)Fe(CO)<sub>2</sub>I and dppe with *n*-BuLi:** (η<sup>5</sup>-C<sub>5</sub>H<sub>5</sub>)Fe(CO)<sub>2</sub>I (1.520 g, 5 mmol), dppe (0.995 g, 2.5 mmol), THF (120 mL), *n*-BuLi (1.6 M, 3.75 mL, 6 mmol, diluted in 30 mL of *n*-hexane). The purification gave four compounds: the yellow (η<sup>4</sup>-BuC<sub>5</sub>H<sub>5</sub>)Fe(CO)<sub>2</sub>(μ,η<sup>1</sup>-dppe)(η<sup>4</sup>-BuC<sub>5</sub>H<sub>5</sub>)Fe(CO)<sub>2</sub> (**9**; 55%), the orange (η<sup>4</sup>-BuC<sub>5</sub>H<sub>5</sub>)Fe(CO)<sub>2</sub>(μ,η<sup>1</sup>-dppe)(η<sup>5</sup>-C<sub>5</sub>H<sub>5</sub>)Fe(CO)C(O)Bu (**10**; 18.0%), the purple [(η<sup>5</sup>-C<sub>5</sub>H<sub>5</sub>)Fe(CO)<sub>2</sub>]<sub>2</sub> (2.3%), and a trace amount of orange (η<sup>5</sup>-C<sub>5</sub>H<sub>5</sub>)Fe(CO)C(O)Bu(μ,η<sup>1</sup>-dppe)(η<sup>5</sup>-C<sub>5</sub>H<sub>5</sub>)Fe(CO)C(O)Bu (**11**; 1%).

**9:** mp 140–141 °C, IR (CH<sub>2</sub>Cl<sub>2</sub>) ν<sub>CO</sub> 1962 (s), 1899 (s) cm<sup>-1</sup>; <sup>31</sup>P NMR (CDCl<sub>3</sub>) δ 69.9 (s); <sup>1</sup>H NMR (CDCl<sub>3</sub>) δ 7.28–7.31 (m, 10H, Ph), 4.90 (b, 2H, –CH=CHCHBu–), 2.53 (b, 1H, –CH=CHCHBu–), 2.34 (b, 2H, –CH=CHCHBu–), 2.08 (b, 2H, –PCH<sub>2</sub>–), 0.47–1.08 (m, 9H, Bu); <sup>13</sup>C NMR (CDCl<sub>3</sub>) δ 14.0 (s, –CH<sub>2</sub>CH<sub>2</sub>CH<sub>2</sub>CH<sub>3</sub>), 22.7 (s, –CH<sub>2</sub>CH<sub>2</sub>CH<sub>2</sub>CH<sub>3</sub>), 26.5 (d, J<sub>PC</sub> = 30 Hz, –PCH<sub>2</sub>–), 28.3 (s, –CH<sub>2</sub>CH<sub>2</sub>CH<sub>2</sub>CH<sub>3</sub>), 43.0 (s,

**Table 2. Crystal Data and Refinement Details of Complexes 2 and 6**

	2	6
space group	<i>Pbca</i>	<i>C2/c</i>
<i>a</i> , Å	7.764(2)	10.659(2)
<i>b</i> , Å	16.704(3)	21.105(2)
<i>c</i> , Å	29.758(4)	16.972(2)
β, deg		99.54(1)
<i>V</i> , Å <sup>3</sup>	3859.2(11)	3765.1(8)
empirical formula	C <sub>21</sub> H <sub>21</sub> FeO <sub>2</sub> P	C <sub>42</sub> H <sub>40</sub> Fe <sub>2</sub> O <sub>4</sub> P <sub>2</sub>
<i>f</i> <sub>w</sub>	392.21	782.41
<i>Z</i>	8	4
<i>D</i> <sub>calc</sub> , g/cm <sup>3</sup>	1.350	1.380
μ, mm <sup>-1</sup>	0.90	0.89
λ, Å	0.710 69	0.710 69
2θ(max), deg	45	50
diffractometer	Nonius CAD-4	Nonius CAD-4
no. of unique reflns	2520	3306
no. of observns	1634 ( <i>I</i> <sub>net</sub> > 2.0σ( <i>I</i> <sub>net</sub> ))	2447 ( <i>I</i> <sub>net</sub> > 2.5σ( <i>I</i> <sub>net</sub> ))
transmission factors	0.892–0.994	0.946–0.998
no. of atoms	46	45
no. of params	226	226
weights	counting statistics	counting statistics
weight modifier	0.0001	0.0001
<i>R</i> <sup>a</sup>	0.032	0.031
<i>R</i> <sub>w</sub> <sup>b</sup>	0.039	0.036
GOF <sup>c</sup>	1.54	1.54
Δ/σ	0.002	0.001
<i>D</i> map, e/Å <sup>3</sup>	–0.230 to +0.210	–0.200 to +0.330

<sup>a</sup> *R* = Σ(*F*<sub>o</sub> – *F*<sub>c</sub>)/Σ(*F*<sub>o</sub>). <sup>b</sup> *R*<sub>w</sub> = [Σ(*w*(*F*<sub>o</sub> – *F*<sub>c</sub>)<sup>2</sup>)/Σ(*w**F*<sub>o</sub><sup>2</sup>)]<sup>1/2</sup>. <sup>c</sup> GOF = [Σ(*w*(*F*<sub>o</sub> – *F*<sub>c</sub>)<sup>2</sup>)/(no. of rflns – (no. of params))]<sup>1/2</sup>.

**Table 3. Final Atomic Fractional Coordinates for Non-H Atoms of 2**

atom	<i>x</i>	<i>y</i>	<i>z</i>	<i>B</i> <sub>iso</sub> , Å <sup>2</sup>
Fe	0.13266(8)	0.37791(4)	0.14468(2)	2.85(3)
P	0.18051(15)	0.24830(7)	0.13950(4)	2.78(5)
O1	0.1949(6)	0.3734(2)	0.2410(1)	7.1(3)
O2	0.4621(5)	0.4284(2)	0.1073(1)	5.9(2)
C1	0.1703(6)	0.3742(3)	0.2026(2)	4.1(2)
C2	0.3338(7)	0.4089(3)	0.1229(2)	3.7(2)
C3	–0.0060(6)	0.4865(3)	0.1411(2)	3.9(2)
C4	–0.1150(6)	0.4197(3)	0.1490(2)	3.8(2)
C5	–0.0984(6)	0.3685(3)	0.1117(2)	3.5(2)
C6	0.0193(6)	0.4056(3)	0.0820(2)	3.8(2)
C7	0.0213(7)	0.4945(3)	0.0914(2)	4.3(3)
C8	–0.1178(8)	0.5419(4)	0.0668(2)	6.5(3)
C9	0.3977(6)	0.2199(3)	0.1573(2)	4.2(3)
C11	0.1695(6)	0.2058(3)	0.0827(1)	3.0(2)
C12	0.0469(7)	0.1510(3)	0.0695(2)	3.9(2)
C13	0.0445(7)	0.1210(3)	0.0258(2)	4.6(3)
C14	0.1630(8)	0.1469(3)	–0.0046(2)	4.7(3)
C15	0.2842(8)	0.2022(3)	0.0078(2)	5.4(3)
C16	0.2871(7)	0.2323(3)	0.0509(2)	4.5(3)
C21	0.0434(6)	0.1806(3)	0.1722(1)	2.7(2)
C22	0.0785(6)	0.0993(3)	0.1749(2)	3.3(2)
C23	–0.0247(7)	0.0488(3)	0.1998(2)	4.0(3)
C24	–0.1656(7)	0.0790(3)	0.2222(2)	4.1(2)
C25	–0.2023(6)	0.1593(3)	0.2199(2)	3.9(2)
C26	–0.0972(6)	0.2103(3)	0.1951(2)	3.4(2)

–CH<sub>2</sub>CH<sub>2</sub>CH<sub>2</sub>CH<sub>3</sub>), 56.0 (s, –CH=CHCHBu–), 56.8 (s, –CH=CHCHBu–), 82.5 (s, –CH=CHCHBu–), 128.3–131.9 (m, Ph), 219.9 (b, CO); MS (*m/z*) M<sup>+</sup> 866 (parent ion). Anal. Calcd for C<sub>48</sub>H<sub>52</sub>Fe<sub>2</sub>O<sub>4</sub>P<sub>2</sub>: C, 66.53; H, 6.05. Found: C, 66.49; H, 6.33.

**10:** mp 60–61 °C; IR (CH<sub>2</sub>Cl<sub>2</sub>) ν<sub>CO</sub> 1962 (s), 1903 (s), 1596 (w) cm<sup>-1</sup>; <sup>31</sup>P NMR (CDCl<sub>3</sub>) δ 76.0 (d, <sup>3</sup>J<sub>PP</sub> = 36.3 Hz), 69.8 (d, <sup>3</sup>J<sub>PP</sub> = 36.3 Hz); <sup>1</sup>H NMR (CDCl<sub>3</sub>) δ 7.19–7.38 (m, 20H, Ph), 4.82, 4.90 (s, 2H, –CH=CHCHBu–), 4.29 (d, 5H, J<sub>PH</sub> = 1.2 Hz, Cp), 2.51 (b, 1H, –CH=CHCHBu–), 2.26, 2.42 (s, 2H, –CH=CHCHBu–), 0.50–3.00 (m, 22H, –PCH<sub>2</sub>CH<sub>2</sub>P–, –C(O)–Bu, –Bu); MS (*m/z*) M<sup>+</sup> 866 (parent ion). Anal. Calcd for C<sub>48</sub>H<sub>52</sub>Fe<sub>2</sub>O<sub>4</sub>P<sub>2</sub>: C, 66.53; H, 6.05. Found: C, 66.70; H, 5.83.

**11:** IR (CH<sub>2</sub>Cl<sub>2</sub>) ν<sub>CO</sub> 1907 (s), 1595 (w) cm<sup>-1</sup>; <sup>31</sup>P NMR



**Table 4. Final Atomic Fractional Coordinates for Non-H Atoms of 6**

atom	x	y	z	$B_{\text{iso}}, \text{\AA}^2$
Fe	0.07509(4)	0.09562(2)	0.13244(2)	2.83(2)
P	0.58109(7)	0.17911(3)	0.13517(4)	2.60(3)
O7	0.8451(2)	0.1161(1)	0.2924(1)	6.4(1)
O8	0.5288(3)	-0.0040(1)	0.1606(2)	6.4(1)
C1	0.7430(3)	0.0131(1)	0.0201(2)	3.9(1)
C2	0.8352(3)	0.0341(2)	0.0927(2)	4.2(2)
C3	0.8671(3)	0.0978(2)	0.0726(2)	4.0(1)
C4	0.7655(3)	0.1249(1)	0.0294(2)	3.5(1)
C5	0.6759(3)	0.0760(1)	0.0082(2)	3.3(1)
C6	0.8068(3)	-0.0087(2)	-0.0504(2)	5.2(2)
C7	0.7878(3)	0.1092(2)	0.2293(2)	4.0(1)
C8	0.5970(3)	0.0358(2)	0.1503(2)	3.9(1)
C9	0.6552(3)	0.2567(1)	0.1581(2)	3.0(1)
C10	0.5848(3)	0.3103(2)	0.1696(2)	4.2(1)
C11	0.6434(4)	0.3681(2)	0.1880(2)	5.4(2)
C12	0.7737(4)	0.3737(2)	0.1925(2)	5.5(2)
C13	0.8432(3)	0.3218(2)	0.1799(2)	4.8(2)
C14	0.7863(3)	0.2634(2)	0.1636(2)	3.8(1)
C15	0.4724(2)	0.1939(1)	0.0413(2)	2.7(1)
C16	0.4866(3)	0.2434(2)	-0.0084(2)	4.8(2)
C17	0.4055(4)	0.2503(2)	-0.0809(2)	5.7(2)
C18	0.3111(3)	0.2076(2)	-0.1041(2)	4.2(1)
C19	0.2956(3)	0.1588(2)	-0.0548(2)	5.2(2)
C20	0.3754(3)	0.1515(2)	0.0178(2)	4.6(2)
C21	0.4677(2)	0.1747(1)	0.2066(1)	2.8(1)

(CDCl<sub>3</sub>)  $\delta$  76.4 (s); <sup>1</sup>H NMR (CDCl<sub>3</sub>)  $\delta$  7.29 (b, 10H, Ph), 4.34 (b, 10H, Cp), 2.19 (b, 2H, -PCH<sub>2</sub>-), 0.80–1.24 (m, 9H, Bu).

**X-ray Structure Analysis.** The single-crystal X-ray diffraction measurements were performed on a Nonius CAD-4 automated diffractometer using graphite-monochromated Mo K $\alpha$  radiation. A total of 25 high-angle reflections were used in a least-squares fit to obtain accurate cell constants. Diffraction intensities were collected up to  $2\theta < 45^\circ$  using the  $\theta/2\theta$  scan technique, with background counts made for half the total scan time on each side of the peak. Three standard reflections, remeasured every 1 h, showed no significant decrease in intensity during data collection. The reflections with  $I_o > 2.0\sigma(I_o)$  or  $2.5\sigma(I_o)$  were judged as observations and

were used for solution and structure refinement. Data were corrected for Lorentz-polarization factors. An empirical absorption correction based on a series of  $\psi$  scans was applied to the data. The structure was solved by direct methods<sup>18</sup> and refined by a full-matrix least-squares routine<sup>19</sup> with anisotropic thermal parameters for all non-hydrogen atoms (weight =  $1/[\sigma(F_o)^2 + 0.0001(F_o)^2]$ ,  $\sigma(F_o)$  from counting statistics). All of the hydrogen atoms were placed isotropically at their calculated positions (C-H = 1.00 Å) and fixed in the calculations. Atomic scattering factor curves  $f_o$ ,  $\Delta f'$ , and  $\Delta f''$  of Fe, P, O, C, and  $f_o$  of H were taken from ref 20. For a summary of crystal data and refinement details, see Table 2. Selected bond distances and angles are given in the captions of Figures 1 and 2, respectively, with respective final atomic fractional coordinates given in Tables 3 and 4.

**Acknowledgment.** Partial financial support from the National Science Council of the ROC is acknowledged. We thank Mr. Y.-S. Wen and K.-J. Lin for their assistance with single-crystal X-ray diffraction data collection.

**Supplementary Material Available:** For the structures of **2** and **6**, listings of crystallographic data, positional and anisotropic thermal parameters, bond distances and angles, torsion angles, and least-squares planes (16 pages). Ordering information is given on any current masthead page.

OM940685+

(18) Main, P. In Sheldrick, G. M., Krueger, C., Goddard, R., Eds. *Crystallographic Computing 3: Data Collection, Structure Determination, Proteins and Databases*; Clarendon Press: Oxford, U.K., 1985; pp 206–215.

(19) (a) Gabe, E. J.; Le Page, Y.; White, P. S.; Lee, F. L. *Acta Crystallogr.* **1987**, *43A*, S294. (b) Gabe, E. J.; Le Page, Y.; Lee, F. L. In *Crystallographic Computing 3: Data Collection, Structure Determination, Proteins and Databases*; Sheldrick, G. M., Krueger, C., Goddard, R., Eds.; Clarendon Press: Oxford, U.K., 1985; pp 167–174.

(20) Ibers, J. A., Hamilton, W. C., Eds.; *International Tables for X-ray Crystallography*; Kynoch: Birmingham, U.K. (current distributor D. Reidel, Dordrecht, The Netherlands), 1974; Vol. 4, Tables 2.2A and 2.3.1D.



# Mixed-Valence Dirhenium Alkylidyne Complexes of the Type $[\text{Re}_2(\mu\text{-Cl})(\mu\text{-CO})(\equiv\text{CCH}_2\text{R})\text{Cl}_2(\text{L})(\mu\text{-dppm})_2]^{n+}$ ( $\text{R} = n\text{-Pr}, n\text{-Bu}; \text{L} = \text{CO}, \text{xylNC}; n = 0, 1$ ) Possessing Very Unsymmetrical Structures

David A. Kort, Keng-Yu Shih, Wengan Wu, Phillip E. Fanwick, and Richard A. Walton\*

Department of Chemistry, Purdue University, 1393 Brown Building, West Lafayette, Indiana 47907-1393

Received August 22, 1994<sup>®</sup>

A series of mixed-valence, unsymmetrical, dirhenium alkylidyne complexes of the type  $[(\text{L})\text{ClRe}(\mu\text{-Cl})(\mu\text{-CO})(\mu\text{-dppm})_2\text{Re}(\equiv\text{CCH}_2\text{R})\text{Cl}]\text{X}$  ( $\text{dppm} = \text{Ph}_2\text{PCH}_2\text{PPh}_2$ ;  $\text{L} = \text{CO}, \text{xylNC}$ ;  $\text{R} = n\text{-Pr}, n\text{-Bu}$ ;  $\text{X} = \text{PF}_6, \text{SO}_3\text{CF}_3$ ) have been formed via the ring-opening reactions of the 3-metallafuran complexes  $[\text{Re}_2(\mu\text{-Cl})(\mu\text{-COC}(\text{R})\text{CH})\text{Cl}_2(\text{L})(\mu\text{-dppm})_2]\text{X}$ . These paramagnetic complexes (one unpaired electron) can be reduced to their diamagnetic congeners  $(\text{L})\text{ClRe}(\mu\text{-Cl})(\mu\text{-CO})(\mu\text{-dppm})_2\text{Re}(\equiv\text{CCH}_2\text{R})\text{Cl}$ , which show well-defined  $^1\text{H}$  and  $^{31}\text{P}$  NMR spectra. X-ray crystallographic structure determinations have been carried out on representative members of the ionic and neutral sets of complexes, *viz.*,  $[\text{Re}_2(\mu\text{-Cl})(\mu\text{-CO})(\equiv\text{CCH}_2\text{-}n\text{-Bu})\text{Cl}_2(\text{CNxyl})(\mu\text{-dppm})_2]\text{SO}_3\text{CF}_3 \cdot 0.5\text{CH}_2\text{Cl}_2$  (**7d**) and  $\text{Re}_2(\mu\text{-Cl})(\mu\text{-CO})(\equiv\text{CCH}_2\text{-}n\text{-Pr})\text{Cl}_2(\text{CNxyl})(\mu\text{-dppm})_2 \cdot 2\text{CH}_2\text{Cl}_2$  (**8a**). The structures of the dirhenium units in these two compounds are essentially the same; the principal difference is the Re-Re distance, which increases from 2.817(2) Å in **7d** to 3.039(1) Å in **8a**. The Re≡C distances involving the alkylidyne ligands are typical for this type of unit (1.74(3) Å in **7d**; 1.70(1) Å in **8a**). Both complexes have a semibridging CO ligand, the Re-C distances being 1.93(3) and 2.57(4) Å in **7d** and 1.87(1) and 2.62(1) Å in **8a**. Crystal data for **7d**: space group *Pnma* (No. 62) with  $a = 24.482(5)$  Å,  $b = 15.377(3)$  Å,  $c = 17.904(4)$  Å,  $V = 6740(4)$  Å<sup>3</sup>, and  $Z = 4$ . The structure was refined to  $R = 0.056$  ( $R_w = 0.069$ ) for 2650 data with  $I > 3.0\sigma(I)$ . Crystal data for **8a**: space group *Pnma* (No. 62) with  $a = 24.383(4)$  Å,  $b = 15.420(3)$  Å,  $c = 17.614(3)$  Å,  $V = 6622(4)$  Å<sup>3</sup>, and  $Z = 4$ . The structure was refined to  $R = 0.034$  ( $R_w = 0.042$ ) for 3569 data with  $I > 3.0\sigma(I)$ .

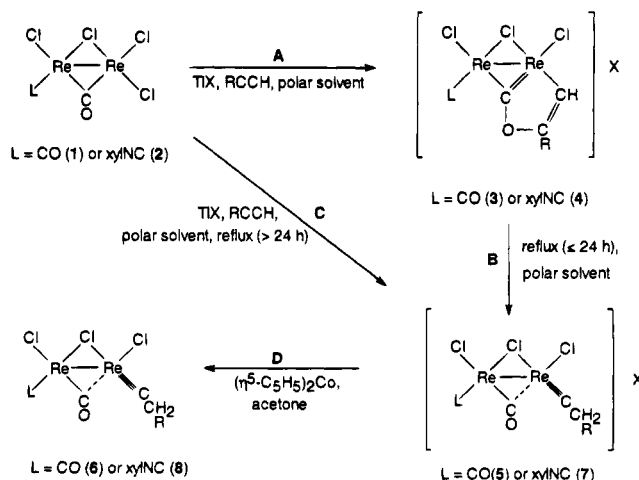
## Introduction

We have recently described<sup>1,2</sup> novel cases of CO-alkyne coupling in which the edge-sharing bioctahedral dicarbonyl complex  $\text{Re}_2(\mu\text{-Cl})(\mu\text{-CO})\text{Cl}_3(\text{CO})(\mu\text{-dppm})_2$  (**1**) and the analogous mixed carbonyl-isocyanide complex  $\text{Re}_2(\mu\text{-Cl})(\mu\text{-CO})\text{Cl}_3(\text{CNxyl})(\mu\text{-dppm})_2$  (**2**) react with terminal alkynes  $\text{RC}\equiv\text{CH}$  to generate 3-metallafuran complexes (Scheme 1, step A). These reductively coupled products ( $\text{L} = \text{CO}$  (**3**);  $\text{L} = \text{xylNC}$  (**4**)) can be reduced to their paramagnetic, neutral congeners  $\text{Re}_2(\mu\text{-Cl})(\mu\text{-COC}(\text{R})\text{CH})\text{Cl}_2(\text{L})(\mu\text{-dppm})_2$  by cobaltocene. Studies of the reactivities of these interesting 3-metallafuran complexes are currently being pursued, and we now describe in full detail their conversion to a new class of mixed-valence dirhenium alkylidyne complexes.<sup>3</sup>

## Experimental Section

**Starting Materials.** The compounds  $\text{Re}_2(\mu\text{-Cl})(\mu\text{-CO})\text{Cl}_3(\text{CO})(\mu\text{-dppm})_2$  (**1**),  $\text{Re}_2(\mu\text{-Cl})(\mu\text{-}^{13}\text{CO})\text{Cl}_3(^{13}\text{CO})(\mu\text{-dppm})_2$ ,  $\text{Re}_2(\mu\text{-Cl})(\mu\text{-CO})\text{Cl}_3(\text{CNxyl})(\mu\text{-dppm})_2$  (**2**),  $[\text{Re}_2(\mu\text{-Cl})(\mu\text{-COC}(\text{R})\text{CH})\text{Cl}_2(\text{L})(\mu\text{-dppm})_2]\text{X}$

**Scheme 1. Formation of 3-Metallafuran Complexes and Their Conversion to Dirhenium Alkylidyne Complexes (Anions X = PF<sub>6</sub> or O<sub>3</sub>SCF<sub>3</sub>)<sup>a</sup>**



<sup>a</sup> The  $\mu\text{-dppm}$  ligands are omitted for clarity.

$\text{Cl}_2(\text{CO})(\mu\text{-dppm})_2]\text{PF}_6$  ( $\text{R} = n\text{-Pr}$ , **3a**;  $\text{R} = n\text{-Bu}$ , **3b**),  $[\text{Re}_2(\mu\text{-Cl})(\mu\text{-COC}(\text{R})\text{CH})\text{Cl}_2(\text{CNxyl})(\mu\text{-dppm})_2]\text{PF}_6$  ( $\text{R} = n\text{-Pr}$ , **4a**;  $\text{R} = n\text{-Bu}$ , **4b**) and  $\text{Ti}(\text{SO}_3\text{CF}_3)$  were prepared according to literature procedures.<sup>2-6</sup> Alkynes were purchased from Aldrich Chemical Co. and were used without further purification. Solvents were obtained from commercial sources and deoxy-

<sup>®</sup> Abstract published in *Advance ACS Abstracts*, December 1, 1994.

(1) Shih, K.-Y.; Fanwick, P. E.; Walton, R. A. *J. Am. Chem. Soc.* **1993**, *115*, 9319.

(2) Shih, K.-Y.; Fanwick, P. E.; Walton, R. A. *Organometallics* **1994**, *13*, 1235.

(3) For a preliminary report of some of these results, see: Shih, K.-Y.; Fanwick, P. E.; Walton, R. A. *J. Chem. Soc., Chem. Commun.* **1994**, 861.

generated prior to use. Syntheses were performed using standard Schlenk techniques under an atmosphere of dry nitrogen.

**A. Synthesis of  $[\text{Re}_2(\mu\text{-Cl})(\mu\text{-CO})(\equiv\text{CCH}_2\text{R})\text{Cl}_2(\text{CO})(\mu\text{-dppm})_2]\text{X}$ .** (i) **R = *n*-Pr, X =  $\text{PF}_6$  (5a).** Procedure a. A mixture of **1** (0.050 g, 0.037 mmol) and  $\text{TiPF}_6$  (0.02 g, 0.057 mmol) in acetone (10 mL) was treated with 1-pentyne (0.07 mL) and heated at reflux for 24 h. The white precipitate of  $\text{TiCl}$  was filtered off and the green filtrate evaporated to dryness. The gray-green solid was extracted into ca. 2 mL of  $\text{CH}_2\text{Cl}_2$ , and the extract treated with diethyl ether (100 mL) to induce precipitation. The green product was filtered off, washed with diethyl ether ( $3 \times 5$  mL), and dried in vacuo; yield 0.021 g (37%).

**Procedure b.** A quantity of  $[\text{Re}_2(\mu\text{-Cl})(\mu\text{-COC}(n\text{-Pr})\text{CH})\text{Cl}_2(\text{CO})(\mu\text{-dppm})_2]\text{PF}_6$  (**3a**; 0.040 g, 0.026 mmol) in acetone (4 mL) was heated at reflux for 12 h. The green solution was then evaporated to dryness. The addition of ca. 1 mL of  $\text{CH}_2\text{Cl}_2$  to this green residue, followed by 40 mL of diethyl ether, precipitated the title compound **5a**. The solid was filtered off and washed with diethyl ether ( $3 \times 5$  mL); yield 0.020 g (50%). This same reaction may also be carried out with either acetonitrile or methanol as the reaction solvent.

(ii) **R = *n*-Pr, X =  $\text{SO}_3\text{CF}_3$  (5b).** A mixture of **1** (0.112 g, 0.084 mmol) and  $\text{Ti}(\text{SO}_3\text{CF}_3)$  (0.033 g, 0.093 mmol) in dichloromethane (10 mL) was treated with 1-pentyne (0.1 mL) and then with concentrated  $\text{HCl}$  (0.1 mL) and finally heated at reflux for 24 h. The white precipitate ( $\text{TiCl}$ ) was filtered off and the dark green filtrate evaporated to dryness. The green residue was extracted into ca. 2 mL of  $\text{CH}_2\text{Cl}_2$  and the extract then layered with 40 mL of diethyl ether to induce precipitation of the title compound. The dark green solid was filtered off, washed with diethyl ether ( $3 \times 5$  mL), and dried in vacuo; yield 0.059 g (46%). Anal. Calcd for  $\text{C}_{59}\text{H}_{55}\text{Cl}_5\text{F}_3\text{O}_5\text{P}_4\text{Re}_2\text{S}$  (i.e.,  $[\text{Re}_2\text{Cl}_3(\equiv\text{CCH}_2\text{-}n\text{-Pr})(\text{CO})_2(\mu\text{-dppm})_2]\text{SO}_3\text{CF}_3\text{-CH}_2\text{Cl}_2$ ): C, 44.10; H, 3.45. Found: C, 43.48; H, 3.36. The presence of lattice  $\text{CH}_2\text{Cl}_2$  was confirmed by  $^1\text{H}$  NMR spectroscopy.

(iii) **R = *n*-Bu, X =  $\text{PF}_6$  (5c).** Procedure a. The use of 1-hexyne (0.07 mL) and a procedure and workup similar to that described in section A(i), procedure a, produced the title compound; yield 0.018 g (30%).

**Procedure b.** The use of  $[\text{Re}_2(\mu\text{-Cl})(\mu\text{-COC}(n\text{-Bu})\text{CH})\text{Cl}_2(\text{CO})(\mu\text{-dppm})_2]\text{PF}_6$  (**3b**; 0.040 g, 0.026 mmol) and a procedure similar to that described in section A(i), procedure b, gave the title complex; yield 0.018 g (45%).

(iv) **R = *n*-Bu, X =  $\text{SO}_3\text{CF}_3$  (5d).** A mixture of **1** (0.128 g, 0.095 mmol) and  $\text{Ti}(\text{SO}_3\text{CF}_3)$  (0.035 g, 0.099 mmol) in dichloromethane (10 mL) was treated with 1-hexyne (0.1 mL), followed by concentrated  $\text{HCl}$  (0.1 mL), and then heated at reflux for 24 h. The title complex was isolated from the reaction mixture with the use of a procedure similar to that described in section A(ii); yield 0.106 g (73%). Anal. Calcd for  $\text{C}_{59.5}\text{H}_{56}\text{Cl}_4\text{F}_3\text{O}_5\text{P}_4\text{Re}_2\text{S}$  (i.e.,  $[\text{Re}_2\text{Cl}_3(\equiv\text{CCH}_2\text{-}n\text{-Bu})(\text{CO})_2(\mu\text{-dppm})_2]\text{SO}_3\text{CF}_3 \cdot 0.5\text{CH}_2\text{Cl}_2$ ): C, 45.28; H, 3.58. Found: C, 45.54; H, 3.56. The presence of a small amount of lattice  $\text{CH}_2\text{Cl}_2$  was confirmed by  $^1\text{H}$  NMR spectroscopy.

**B. Synthesis of  $[\text{Re}_2(\mu\text{-Cl})(\mu\text{-CO})(\equiv\text{CCH}_2\text{R})\text{Cl}_2(\text{CO})(\mu\text{-dppm})_2]$ .** (i) **R = *n*-Pr (6a).** Procedure a. A mixture of  $[\text{Re}_2(\mu\text{-Cl})(\mu\text{-CO})(\equiv\text{CCH}_2\text{-}n\text{-Pr})\text{Cl}_2(\text{CO})(\mu\text{-dppm})_2]\text{PF}_6$  (**5a**) and  $(\eta^5\text{-C}_5\text{H}_5)_2\text{Co}$  (0.007 g, 0.037 mmol) in acetone (5 mL) was stirred at room temperature for 2 h. The resulting green precipitate was filtered off and washed with diethyl ether ( $3 \times 5$  mL). The crude product was extracted into  $\text{CH}_2\text{Cl}_2$  (ca. 5 mL) and filtered through a glass frit. An excess of *n*-pentane (30 mL) was added to the filtrate, which was then chilled to  $0^\circ\text{C}$  for 1 h to yield the green title compound (**6a**); yield 0.025 g (70%).

(4) Cotton, F. A.; Daniels, L. M.; Dunbar, K. R.; Falvello, L. R.; Tetrick, S. M.; Walton, R. A. *J. Am. Chem. Soc.* **1985**, *107*, 3524.

(5) Cotton, F. A.; Dunbar, K. R.; Price, A. C.; Schwotzer, W.; Walton, R. A. *J. Am. Chem. Soc.* **1986**, *108*, 4843.

(6) Woodhouse, M. E.; Lewis, F. D.; Marks, T. J. *J. Am. Chem. Soc.* **1982**, *104*, 5586.

**Procedure b.** A mixture of **1** (0.100 g, 0.075 mmol) and  $\text{TiPF}_6$  (0.040 g, 0.057 mmol) in acetone (15 mL) and  $\text{CH}_2\text{Cl}_2$  (5 mL) was treated with 1-pentyne (0.08 mL) and heated at reflux for 24 h. The white precipitate ( $\text{TiCl}$ ) was filtered off and the green filtrate treated with  $(\eta^5\text{-C}_5\text{H}_5)_2\text{Co}$  (0.015 g, 0.079 mmol). This mixture was then stirred at room temperature for 2 h and the green solid filtered off and washed with diethyl ether ( $3 \times 5$  mL). This crude product was extracted into a minimum volume of  $\text{CH}_2\text{Cl}_2$  (ca. 10 mL), and an excess of *n*-pentane (ca. 50 mL) was added. This mixture was chilled to  $0^\circ\text{C}$  to induce crystallization; yield 0.049 g (48%). Anal. Calcd for  $\text{C}_{57}\text{H}_{53}\text{Cl}_3\text{O}_2\text{P}_4\text{Re}_2$ : C, 49.87; H, 3.90. Found: C, 49.23; H, 3.82.

(ii) **R = *n*-Bu (6b).** Procedure a. The use of  $[\text{Re}_2(\mu\text{-Cl})(\mu\text{-CO})(\equiv\text{CCH}_2\text{-}n\text{-Bu})\text{Cl}_2(\text{CO})(\mu\text{-dppm})_2]\text{PF}_6$  (**5c**; 0.04 g, 0.026 mmol) and a procedure analogous to that described in section B(i), procedure a, produced the title complex; yield 0.027 g (75%).

**Procedure b.** The use of 1-hexyne (0.08 mL) and a procedure and workup similar to that described in section B(i), procedure b, gave the title complex; yield 0.05 g (49%). Anal. Calcd for  $\text{C}_{60}\text{H}_{59}\text{Cl}_7\text{O}_2\text{P}_4\text{Re}_2$  (i.e.,  $[\text{Re}_2\text{Cl}_3(\equiv\text{CCH}_2\text{-}n\text{-Bu})(\text{CO})_2(\mu\text{-dppm})_2\text{CH}_2\text{Cl}_2]$ ): C, 46.29; H, 3.82. Found: C, 46.83; H, 3.75. The presence of lattice  $\text{CH}_2\text{Cl}_2$  was confirmed by  $^1\text{H}$  NMR spectroscopy.

**C. Synthesis of the  $^{13}\text{C}$ -Labeled Complex  $[\text{Re}_2(\mu\text{-Cl})(\mu\text{-CO})(\equiv\text{CCH}_2\text{-}n\text{-Pr})\text{Cl}_2(^{13}\text{CO})(\mu\text{-dppm})_2]$ .** This labeled complex was obtained starting from  $[\text{Re}_2(\mu\text{-Cl})(\mu\text{-}^{13}\text{CO})\text{Cl}_3(^{13}\text{CO})(\mu\text{-dppm})_2]$  (0.050 g, 0.037 mmol) by the use of the method in section B(i), procedure a, via the intermediacy of  $[\text{Re}_2(\mu\text{-Cl})(\mu\text{-}^{13}\text{CO})(\equiv\text{CCH}_2\text{-}n\text{-Pr})\text{Cl}_2(^{13}\text{CO})(\mu\text{-dppm})_2]\text{PF}_6$ ; yield 0.018 g (35%).

**D. Synthesis of  $[\text{Re}_2(\mu\text{-Cl})(\mu\text{-CO})(\equiv\text{CCH}_2\text{R})\text{Cl}_2(\text{CNxyl})(\mu\text{-dppm})_2]\text{X}$ .** (i) **R = *n*-Pr, X =  $\text{PF}_6$  (7a).** Procedure a. A mixture of **2** (0.100 g, 0.069 mmol) and  $\text{TiPF}_6$  (0.04 g, 0.114 mmol) in acetone (20 mL) was treated with 1-pentyne (0.08 mL) and heated at reflux for 24 h. The white precipitate ( $\text{TiCl}$ ) was filtered off and the green filtrate evaporated to dryness. The residue was extracted into  $\text{CH}_2\text{Cl}_2$  (ca. 2 mL) and excess diethyl ether (40 mL) added to induce precipitation. The green solid was filtered off, washed with diethyl ether (10 mL), and dried in vacuo; yield 0.050 g (45%). Anal. Calcd for  $\text{C}_{66}\text{H}_{64}\text{Cl}_5\text{F}_6\text{NOP}_5\text{Re}_2$  (i.e.,  $[\text{Re}_2\text{Cl}_3(\equiv\text{CCH}_2\text{-}n\text{-Pr})(\text{CO})(\text{CNxyl})(\mu\text{-dppm})_2]\text{PF}_6\text{-CH}_2\text{Cl}_2$ ): C, 46.47; H, 3.79. Found: C, 46.89; H, 3.83. The presence of a small amount of lattice  $\text{CH}_2\text{Cl}_2$  was confirmed by  $^1\text{H}$  NMR spectroscopy.

**Procedure b.** A solution of  $[\text{Re}_2(\mu\text{-Cl})(\mu\text{-COC}(n\text{-Pr})\text{CH})\text{Cl}_2(\text{CNxyl})(\mu\text{-dppm})_2]\text{PF}_6$  (**4a**; 0.040 g, 0.025 mmol) in  $\text{CH}_3\text{CN}$  (5 mL) was heated at reflux for 24 h. The resulting green solution was reduced to ca. 2 mL by evaporation and diethyl ether (40 mL) added to induce precipitation of the product. The green precipitate was filtered off, washed with diethyl ether (10 mL), and dried in vacuo; yield 0.012 g (30%).

(ii) **R = *n*-Pr, X =  $\text{SO}_3\text{CF}_3$  (7b).** A mixture of **2** (0.177 g, 0.123 mmol) and  $\text{Ti}(\text{SO}_3\text{CF}_3)$  (0.045 g, 0.127 mmol) in dichloromethane (10 mL) was treated with 1-pentyne (0.10 mL), followed by concentrated  $\text{HCl}$  (0.1 mL), and then heated at reflux for 24 h. The white precipitate ( $\text{TiCl}$ ) was filtered off and the dark green filtrate evaporated to dryness. The green solid was extracted into ca. 2 mL of  $\text{CH}_2\text{Cl}_2$  and the extract then layered with 40 mL of diethyl ether to induce precipitation of the title compound. The dark green solid was then filtered off, washed with diethyl ether ( $3 \times 5$  mL), and dried in vacuo; yield 0.141 g (70%). Anal. Calcd for  $\text{C}_{66.5}\text{H}_{63}\text{Cl}_4\text{F}_3\text{NO}_4\text{P}_4\text{Re}_2\text{S}$  (i.e.,  $[\text{Re}_2\text{Cl}_3(\equiv\text{CCH}_2\text{-}n\text{-Pr})(\text{CO})(\text{CNxyl})(\mu\text{-dppm})_2]\text{SO}_3\text{CF}_3 \cdot 0.5\text{CH}_2\text{Cl}_2$ ): C, 47.90; H, 3.81. Found: C, 47.74; H, 3.94. The presence of lattice  $\text{CH}_2\text{Cl}_2$  was confirmed by  $^1\text{H}$  NMR spectroscopy.

(iii) **R = *n*-Bu, X =  $\text{PF}_6$  (7c).** Procedure a. The use of 1-hexyne (0.08 mL) and a procedure similar to that described in section D(i), procedure a, gave the title complex; yield 0.052 g (46%). Anal. Calcd for  $\text{C}_{67}\text{H}_{66}\text{Cl}_5\text{F}_6\text{NOP}_5\text{Re}_2$  (i.e.,  $[\text{Re}_2\text{Cl}_3(\equiv\text{CCH}_2\text{-}n\text{-Bu})(\text{CO})(\text{CNxyl})(\mu\text{-dppm})_2]\text{PF}_6\text{-CH}_2\text{Cl}_2$ ): C, 46.79; H,

3.88. Found: C, 46.85; H, 3.90. The presence of a small amount of lattice  $\text{CH}_2\text{Cl}_2$  was confirmed by  $^1\text{H}$  NMR spectroscopy.

**Procedure b.** A quantity of  $[\text{Re}_2(\mu\text{-Cl})(\mu\text{-COC}(n\text{-Bu})\text{CH})\text{Cl}_2(\text{CNxyl})(\mu\text{-dppm})_2]\text{PF}_6$  (**4b**; 0.040 g, 0.025 mmol) in methanol (5 mL) was heated at reflux for 24 h. The resulting green solution was reduced to ca. 2 mL by evaporation and diethyl ether added (40 mL) to induce precipitation of the title compound. The green precipitate was filtered off, washed with diethyl ether (10 mL), and dried in vacuo; yield 0.018 g (45%).

**Procedure c.** A solution of  $[\text{Re}_2(\mu\text{-Cl})(\mu\text{-COC}(n\text{-Bu})\text{CH})\text{Cl}_2(\text{CNxyl})(\mu\text{-dppm})_2]\text{PF}_6$  (**4b**; 0.030 g, 0.019 mmol) in acetone (4 mL) was treated with 60% aqueous  $\text{HPF}_6$  (0.10 mL) and heated at reflux for 24 h. The resulting solution was reduced to ca. 2 mL by evaporation and diethyl ether added (50 mL) to induce precipitation. After a period of ca. 20 min, the gray-green solid was filtered off, washed with diethyl ether (10 mL), and dried in vacuo; yield 0.013 g (43%).

The analogous  $[\text{BF}_4]^-$  salt  $[\text{Re}_2(\mu\text{-Cl})(\mu\text{-CO})(\equiv\text{CCH}_2\text{-}n\text{-Bu})\text{Cl}_2(\text{CNxyl})(\mu\text{-dppm})_2]\text{BF}_4$  can be prepared by the use of a procedure similar to that described above, except that the 60% aqueous  $\text{HPF}_6$  is replaced by 0.10 mL of 85%  $\text{HBF}_4\cdot\text{Et}_2\text{O}$ .

(iv) **R = n-Bu, X =  $\text{SO}_3\text{CF}_3$  (7d).** A mixture of **2** (0.093 g, 0.064 mmol) and  $\text{Ti}(\text{SO}_3\text{CF}_3)_4$  (0.025 g, 0.071 mmol) in dichloromethane (10 mL) was treated with 1-hexyne (0.05 mL) and concentrated HCl (0.1 mL) and then heated at reflux for 24 h. The title complex was isolated from this reaction mixture through the use of a procedure analogous to that given in section D(ii); yield 0.071 g (67%). Anal. Calcd for  $\text{C}_{67.5}\text{H}_{65}\text{Cl}_4\text{F}_3\text{NO}_4\text{P}_4\text{Re}_2\text{S}$  (i.e.,  $[\text{Re}_2\text{Cl}_3(\equiv\text{CCH}_2\text{-}n\text{-Bu})(\text{CO})(\text{CNxyl})(\mu\text{-dppm})_2]\text{SO}_3\text{CF}_3\cdot 0.5\text{CH}_2\text{Cl}_2$ ): C, 48.22; H, 3.90. Found: C, 48.22; H, 4.01. The presence of lattice  $\text{CH}_2\text{Cl}_2$  was confirmed by  $^1\text{H}$  NMR spectroscopy.

**E. Synthesis of  $\text{Re}_2(\mu\text{-Cl})(\mu\text{-CO})(\equiv\text{CCH}_2\text{R})\text{Cl}_2(\text{CNxyl})(\mu\text{-dppm})_2$ .** (i) **R = n-Pr (8a).** **Procedure a.** A mixture of  $[\text{Re}_2(\mu\text{-Cl})(\mu\text{-CO})(\equiv\text{CCH}_2\text{-}n\text{-Pr})\text{Cl}_2(\text{CNxyl})(\mu\text{-dppm})_2]\text{PF}_6$  (0.04 g, 0.025 mmol) and  $(\eta^5\text{-C}_5\text{H}_5)_2\text{Co}$  (0.006 g, 0.032 mmol) in acetone (6 mL) was stirred at room temperature for 2 h. The resulting green precipitate was filtered off and washed with diethyl ether (3  $\times$  5 mL). This crude product was extracted into ca. 4 mL of  $\text{CH}_2\text{Cl}_2$ , and then filtered through a glass frit. Addition of diethyl ether (25 mL) to the solution and cooling it to 0  $^\circ\text{C}$  for 1 h yielded the green title compound; yield 0.026 g (71%). Anal. Calcd for  $\text{C}_{66}\text{H}_{64}\text{Cl}_5\text{NOP}_4\text{Re}_2$  (i.e.,  $\text{Re}_2\text{Cl}_3(\equiv\text{CCH}_2\text{-}n\text{-Pr})(\text{CO})(\text{CNxyl})(\mu\text{-dppm})_2\cdot\text{CH}_2\text{Cl}_2$ ): C, 49.80; H, 4.06. Found: C, 49.46; H, 4.16. The presence of a small amount of lattice  $\text{CH}_2\text{Cl}_2$  was confirmed by  $^1\text{H}$  NMR spectroscopy.

**Procedure b.** A mixture of **2** (0.100 g, 0.069 mmol) and  $\text{TiPF}_6$  (0.040 g, 0.057 mmol) in acetone (20 mL) was treated with 1-pentyne (0.08 mL) and heated at reflux for 24 h. The white precipitate ( $\text{TiCl}_4$ ) was filtered off and the green filtrate treated with  $(\eta^5\text{-C}_5\text{H}_5)_2\text{Co}$  (0.014 g, 0.074 mmol). This solution was stirred at room temperature for 2 h. The green title compound was filtered off and washed with diethyl ether (3  $\times$  5 mL). This crude product was recrystallized from  $\text{CH}_2\text{Cl}_2$  and diethyl ether; yield 0.041 g (40%).

(ii) **R = n-Bu (8b).** **Procedure a.** This complex was prepared from  $[\text{Re}_2(\mu\text{-Cl})(\mu\text{-CO})(\equiv\text{CCH}_2\text{-}n\text{-Bu})\text{Cl}_2(\text{CNxyl})(\mu\text{-dppm})_2]\text{PF}_6$  (**7c**; 0.04 g, 0.025 mmol) following a procedure analogous to that described in section E(i), procedure a; yield 0.025 g (67%). Anal. Calcd for  $\text{C}_{66}\text{H}_{64}\text{Cl}_5\text{NOP}_4\text{Re}_2$ : C, 53.27; H, 4.21. Found: C, 53.02; H, 4.38.

**Procedure b.** The use of 1-hexyne (0.08 mL) and a procedure analogous to that described in section E(i), procedure b, produced the title complex; yield 0.047 g (46%).

**Preparation of Single Crystals.** Crystals of  $[\text{Re}_2(\mu\text{-Cl})(\mu\text{-CO})(\equiv\text{CCH}_2\text{-}n\text{-Bu})\text{Cl}_2(\text{CNxyl})(\mu\text{-dppm})_2]\text{SO}_3\text{CF}_3\cdot 0.5\text{CH}_2\text{Cl}_2$  (**7d**) were obtained as dark brown plates by the diffusion of diisopropyl ether into a solution of **7d** in dichloromethane while suitable dark cubic crystals of composition  $\text{Re}_2(\mu\text{-Cl})(\mu\text{-CO})(\equiv\text{CCH}_2\text{-}n\text{-Pr})\text{Cl}_2(\text{CNxyl})(\mu\text{-dppm})_2\cdot 2\text{CH}_2\text{Cl}_2$  (**8a**) were grown

**Table 1. Crystallographic Data for  $[\text{Re}_2(\mu\text{-Cl})(\mu\text{-CO})(\equiv\text{CCH}_2\text{-}n\text{-Bu})\text{Cl}_2(\text{CNxyl})(\mu\text{-dppm})_2]\text{SO}_3\text{CF}_3\cdot 0.5\text{CH}_2\text{Cl}_2$  (**7d**) and  $\text{Re}_2(\mu\text{-Cl})(\mu\text{-CO})(\equiv\text{CCH}_2\text{-}n\text{-Pr})\text{Cl}_2(\text{CNxyl})(\mu\text{-dppm})_2\cdot 2\text{CH}_2\text{Cl}_2$  (**8a**)**

	<b>7d</b>	<b>8a</b>
chem formula	$\text{Re}_2\text{Cl}_3\text{SP}_4\text{F}_3\text{O}_4\text{NC}_{67.5}\text{H}_{65}$	$\text{Re}_2\text{Cl}_3\text{P}_4\text{ONC}_{67}\text{H}_{66}$
fw	1681.44	1645.75
space group	<i>Pnma</i> (No. 62)	<i>Pnma</i> (No. 62)
<i>a</i> , Å	24.482(5)	24.383(4)
<i>b</i> , Å	15.377(3)	15.420(3)
<i>c</i> , Å	17.904(4)	17.614(3)
<i>V</i> , Å <sup>3</sup>	6740(4)	6622(4)
<i>Z</i>	4	4
<i>T</i> , K	293	293
$\lambda$ , Å (Mo K $\alpha$ )	0.710 73	0.710 73
$\rho_{\text{calcd}}$ , g cm <sup>-3</sup>	1.657	1.650
$\mu$ (Mo K $\alpha$ ), cm <sup>-1</sup>	39.61	41.24
transmissn coeff	1.00–0.87	1.00–0.74
<i>R</i> <sup>a</sup>	0.056	0.034
<i>R</i> <sub>w</sub> <sup>b</sup>	0.069	0.042
GOF	1.649	1.228

<sup>a</sup>  $R = \sum ||F_o| - |F_c|| / \sum |F_o|$ . <sup>b</sup>  $R_w = \{ \sum w(|F_o| - |F_c|)^2 / \sum w|F_o|^2 \}^{1/2}$ ;  $w = 1/\sigma^2(|F_o|)$ .

by the diffusion of *n*-heptane into a dichloromethane solution of this complex.

**X-ray Crystallography.** The structures of **7d** and **8a** were determined at room temperature by the application of standard procedures. Each crystal used for data collection was mounted on a glass fiber in a random orientation. The basic crystallographic parameters for these two crystals are listed in Table 1. The cell constants were based on 25 reflections in the range  $9 < \theta < 19^\circ$  for **7d** and  $20 < \theta < 23^\circ$  for **8a**, measured by the computer-controlled diagonal slip method of centering. Three standard reflections were measured after every 5000 s of beam time during data collection, and there were no systematic variations in intensity. The data processing was performed on a microVAX II computer using the Enraf-Nonius MolEN structure determination package. Lorentz and polarization corrections were applied to both data sets, and an empirical absorption correction was applied in each case; for **7d** the method based on a series of  $\psi$  scans was used, while for **8a** the method used was that of Walker and Stuart.<sup>7</sup>

**7d** crystallized in the orthorhombic crystal system. The systematic absences in the data set were consistent with both the *Pna2*<sub>1</sub> and the *Pnma* space groups. Efforts to solve the structure in the space group *Pna2*<sub>1</sub> were unsuccessful. The centric space group was therefore assumed and subsequently confirmed by the successful solution and refinement of the structure. The structure was solved by a combination of direct methods (SHELX-86) and difference Fourier syntheses. The lattice was found to contain four formula units of the complex in the unit cell, and the cation and anion are thus required to contain crystallographic planes of symmetry. Due to an obscure disorder at the end of the six-member alkylidyne carbon chain, C(1)–C(6), the last carbon atom in this chain, C(6), could not be refined to convergence. It was thus refined with fixed parameters, and as a result, one of the carbon–carbon bond distances in this chain was extremely long (C(4)–C(5) = 1.74(9) Å). The carbon atoms in this alkylidyne chain and in the isocyanide ligand were refined isotropically, while the remaining non-hydrogen atoms were refined with anisotropic thermal parameters. For the triflate anion, atoms F(101), C(100), S, and O(1) were located on a mirror plane; the uniformly large anisotropic thermal parameters associated with the atoms of this anion reflect its rather high thermal motion, which may be a consequence of its relatively loose packing in the crystal. In the final stage of the structure analysis, half a dichloromethane molecule from the crystallization solvent was located; the solvent molecule was posi-

(7) Walker, N.; Stuart, D. *Acta Crystallogr., Sect. A: Found Crystalllogr.* **1983**, *A39*, 158.

tioned about a crystallographic mirror plane. It was included in the analysis and was satisfactorily refined anisotropically for its chlorine atoms (Cl(501) and Cl(502)) and isotropically for its carbon atom (C(500)). Corrections for anomalous scattering were applied to all anisotropically refined atoms.<sup>8</sup> Hydrogen atoms were not included in the calculations. The structure was refined in full-matrix least squares where the function minimized was  $\sum w = (|F_o| - |F_c|)^2$ , where  $w$  is the weighting factor defined as  $w = 1/\sigma^2(|F_o|)$ . The final residuals for **7d** were  $R = 0.056$  ( $R_w = 0.069$ ) and  $GOF = 1.649$ . The highest peak in the final difference Fourier was  $1.55 \text{ e}/\text{\AA}^3$ .

The structure of a crystal of **8a** was determined as described for **7d**. The structure was again solved satisfactorily in the centric space group  $Pnma$  with  $Z = 4$ ; the neutral dirhenium unit was required to possess a crystallographic plane of symmetry. All carbon atoms of the alkylidyne ligand refined satisfactorily with anisotropic thermal parameters. Two independent  $\text{CH}_2\text{Cl}_2$  solvent molecules were found to be present in the crystal lattice. Both are located about mirror planes, one having its  $\text{CCl}_2$  unit in the plane while the other has the  $\text{CCl}_2$  angle bisected by the plane. These molecules were refined with full occupancy factors, and all six non-hydrogen atoms were refined with anisotropic thermal parameters. Corrections for anomalous scattering were applied to all anisotropically refined atoms.<sup>8</sup> All hydrogen atoms, except those of the  $\text{CH}_2\text{Cl}_2$  molecules, were introduced at calculated positions ( $\text{C-H} = 0.95 \text{ \AA}$ ,  $B = 1.3B_s$ ), not refined but constrained to ride on their C atoms. The structure was refined in full-matrix least squares where the function minimized was  $\sum w = (|F_o| - |F_c|)^2$ , where  $w$  is the weighting factor defined as  $w = 1/\sigma^2(|F_o|)$ . The final residuals for **8a** were  $R = 0.034$  ( $R_w = 0.042$ ) and  $GOF = 1.228$ . The highest peak in the final difference Fourier was  $0.83 \text{ e}/\text{\AA}^3$ .

**Physical Measurements.** A Perkin-Elmer 1800 FTIR spectrometer was used to record the IR spectra of the compounds as mineral oil (Nujol) mulls. Electrochemical measurements were carried out on dichloromethane solutions that contained 0.1 M tetra-*n*-butylammonium hexafluorophosphate (TBAH) as supporting electrolyte.  $E_{1/2}$  values, determined as  $(E_{p,a} + E_{p,c})/2$ , were referenced to the silver/silver chloride (Ag/AgCl) electrode at room temperature and are uncorrected for junction potentials. Under our experimental conditions  $E_{1/2} = +0.47 \text{ vs Ag/AgCl}$  for the ferrocenium/ferrocene couple. Voltammetric experiments were performed with a BAS Inc. Model CV-27 instrument in conjunction with a BAS Model RXY recorder. The  $^{31}\text{P}\{^1\text{H}\}$  NMR spectra were obtained with use of a Varian XL-200A spectrometer operated at 80.98 MHz or a GE QE-300 spectrometer equipped with a multinuclear Quad probe operated at 121.5 MHz with 85%  $\text{H}_3\text{PO}_4$  as an external standard.  $^1\text{H}$  and  $^{13}\text{C}\{^1\text{H}\}$  NMR spectra were obtained on a GE QE-300 spectrometer operated at 300 and 75.61 MHz, respectively. Proton resonances were referenced internally to the residual protons in the incompletely deuteriated solvent. The  $^2\text{H}\{^1\text{H}\}$  NMR spectra were recorded (in  $\text{CH}_2\text{Cl}_2$ ) with the use of a Varian XL-200A spectrometer. Magnetic susceptibility measurements were carried out by the Evans method.<sup>9</sup> X-Band ESR spectra were recorded at ca.  $-160 \text{ }^\circ\text{C}$  with the use of a Varian E-109 spectrometer.

Elemental microanalyses were performed by Dr. H. D. Lee of the Purdue University Microanalytical Laboratory. Microanalyses of representative samples of the dirhenium alkylidyne complexes of types **5**–**8** were obtained.

## Results

When solutions of the 3-metallafuran complexes **3** and **4** ( $R = n\text{-Pr}$  or  $n\text{-Bu}$ ) are refluxed in polar solvents

**Table 2. Positional Parameters and Equivalent Isotropic Displacement Parameters ( $\text{\AA}^2$ ) for the Non-Phenyl Group Atoms of the Dirhenium Cation of **7d** and Their Estimated Standard Deviations<sup>a</sup>**

atom	x	y	z	B
Re(1)	0.15790(5)	1/4	0.91397(6)	3.40(2)
Re(2)	0.26294(5)	1/4	0.84973(6)	3.02(2)
Cl(1)	0.0632(3)	1/4	0.8877(5)	5.4(2)
Cl(2)	0.3119(3)	1/4	0.7310(4)	5.1(2)
Cl(B)	0.1777(3)	1/4	0.7760(4)	4.4(2)
P(1)	0.1530(2)	0.0881(3)	0.9141(3)	3.6(1)
P(2)	0.2667(2)	0.0907(3)	0.8478(2)	3.10(9)
O(10)	0.2716(8)	1/4	1.018(1)	5.2(5)
N	0.3841(8)	1/4	0.905(1)	3.6(5)
C(1)	0.157(1)	1/4	1.011(2)	4.7(6)*
C(2)	0.162(2)	1/4	1.090(2)	7.8(9)*
C(3)	0.115(2)	1/4	1.143(3)	14(2)*
C(4)	0.129(3)	1/4	1.233(4)	19(2)*
C(5)	0.060(3)	1/4	1.257(4)	16(2)*
C(6)	0.06443	1/4	1.34728	20*
C(10)	0.258(1)	1/4	0.957(1)	4.2(6)
C(12)	0.2216(7)	0.043(1)	0.921(1)	4.0(4)
C(20)	0.343(1)	1/4	0.888(2)	4.9(7)
C(601)	0.443(1)	1/4	0.921(2)	5.8(7)*
C(602)	0.453(2)	1/4	1.000(2)	9(1)*
C(603)	0.514(2)	1/4	1.018(3)	12(1)*
C(604)	0.541(2)	1/4	0.945(3)	12(1)*
C(605)	0.534(2)	1/4	0.876(3)	12(1)*
C(606)	0.474(2)	1/4	0.854(3)	11(1)*
C(621)	0.414(2)	1/4	1.055(2)	9(1)*
C(661)	0.460(2)	1/4	0.775(2)	8(1)*

<sup>a</sup> Anisotropically refined atoms are given in the form of the isotropic equivalent thermal parameter defined as  $(^{1/3}[a^2\beta(1,1) + b^2\beta(2,2) + c^2\beta(3,3) + ab(\cos \gamma)\beta(1,2) + ac(\cos \beta)\beta(1,3) + bc(\cos \alpha)\beta(2,3)])$ . Data for the phenyl group atoms of the dppm ligands, the atoms of the triflate anion, and the atoms of the lattice dichloromethane molecule are available as supplementary material. An asterisk denotes a value for an isotropically refined atom.

(acetone, methanol, and acetonitrile were used) for periods of up to 24 h, the dirhenium alkylidyne complexes of types **5** and **7** can be isolated in yields of 30–50% upon the addition of diethyl ether to the green reaction solutions (Scheme 1, step B). An alternative and more convenient procedure is to heat the reaction mixtures that are known to produce<sup>2</sup> the 3-metallafuran complexes **3** and **4** from the precursors **1** and **2** for periods in excess of 24 h (Scheme 1, step C). This strategy avoids the necessity of isolating the "intermediate" complexes **3** and **4** and gives **5** and **7** in isolated yields of 30–70%.

The complexes **5** and **7** display terminal  $\nu(\text{CN})_t$  or  $\nu(\text{CO})_t$  modes in their IR spectra at ca. 2150 and ca. 2035  $\text{cm}^{-1}$ , respectively, as well as a bridging  $\nu(\text{CO})_b$  mode close to 1800  $\text{cm}^{-1}$  (Table 6). The  $\nu(\text{P-F})$  mode of the  $[\text{PF}_6]^-$  anion is found at ca. 840  $\text{cm}^{-1}$  in the spectra of **5a**, **5c**, **7a**, and **7c**, while for the  $[\text{SO}_3\text{CF}_3]^-$  salts **5b**, **5d**, **7b**, and **7d**, there is a characteristic anion mode at ca. 1260  $\text{cm}^{-1}$ .

The cyclic voltammetric properties of solutions of all six complexes of types **5** and **7** in 0.1 M TBAH/ $\text{CH}_2\text{Cl}_2$  are very similar to one another (see Table 6). Each shows a reversible one-electron oxidation and a reversible one-electron reduction with  $i_{p,a} = i_{p,c}$  and  $\Delta E$  (i.e.,  $E_{p,a} - E_{p,c}$ ) = 60–70 mV at a sweep rate of 200 mV/s. The carbonyl-containing complexes **5a**–**5d** also show an irreversible reduction at  $E_{p,c}$  of ca.  $-1.8 \text{ V}$ . The two reversible processes are shifted to more negative potentials by between 360 and 240 mV on changing from  $L = \text{CO}$  (**5**) to  $L = \text{xylNC}$  (**7**); this reflects the greater  $\pi$ -acceptor properties of CO (compared to xylNC), which

(8) (a) Cromer, D. T. *International Tables for X-ray Crystallography*; Kynoch: Birmingham, England, 1974; Vol. IV, Table 2.3.1. (b) For the scattering factors used in the structure solution, see: Cromer, D. T.; Weber, J. T. in ref 8a, Table 2.2B.

(9) Evans, D. F. *J. Chem. Soc.* **1959**, 2003.

**Table 3. Positional Parameters and Equivalent Isotropic Displacement Parameters ( $\text{\AA}^2$ ) for the Non-Phenyl Group Atoms of the Dirhenium Molecule of **8a** and Their Estimated Standard Deviations<sup>a</sup>**

atom	x	y	z	B
Re(1)	0.23541(2)	1/4	0.15029(2)	2.162(8)
Re(2)	0.34833(2)	1/4	0.07724(2)	2.322(8)
Cl(1)	0.1938(1)	1/4	0.2785(2)	3.66(6)
Cl(2)	0.4457(1)	1/4	0.1030(2)	3.74(6)
Cl(B)	0.3249(1)	1/4	0.2179(1)	2.99(5)
P(1)	0.23353(8)	0.0938(1)	0.1466(1)	2.56(4)
P(2)	0.34841(8)	0.0933(1)	0.0766(1)	2.61(4)
O(12)	0.2291(3)	1/4	-0.0215(4)	4.1(2)
N(30)	0.1128(4)	1/4	0.1030(5)	3.9(2)
C(B)	0.2789(3)	0.0490(5)	0.0729(4)	2.7(2)
C(11)	0.2433(5)	1/4	0.0449(6)	3.2(2)
C(21)	0.3485(5)	1/4	-0.0195(6)	3.5(3)
C(22)	0.3427(6)	1/4	-0.1033(7)	5.4(4)
C(23)	0.3930(7)	1/4	-0.1478(8)	7.1(4)
C(24)	0.3921(9)	1/4	-0.230(1)	12.9(9)
C(25)	0.439(1)	1/4	-0.273(1)	16(1)
C(30)	0.1582(4)	1/4	0.1205(6)	2.8(2)
C(31)	0.0569(5)	1/4	0.0868(8)	5.0(3)
C(32)	0.0412(6)	1/4	0.011(1)	7.2(4)
C(33)	-0.0165(8)	1/4	-0.002(1)	11.3(7)
C(34)	-0.0514(7)	1/4	0.058(2)	14.9(9)
C(35)	-0.0353(6)	1/4	0.130(1)	10.2(7)
C(36)	0.0215(6)	1/4	0.149(1)	6.5(4)
C(321)	0.0810(8)	1/4	-0.0527(9)	8.4(5)
C(361)	0.0398(7)	1/4	0.227(1)	8.4(5)

<sup>a</sup> Anisotropically refined atoms are given in the form of the isotropic equivalent thermal parameter defined as  $(1/3)[a^2\beta(1,1) + b^2\beta(2,2) + c^2\beta(3,3) + ab(\cos \gamma)\beta(1,2) + ac(\cos \beta)\beta(1,3) + bc(\cos \alpha)\beta(2,3)]$ . Data for the phenyl group atoms of the dpmm ligands and the atoms of the lattice dichloromethane molecules are available as supplementary material.

**Table 4. Selected Bond Distances ( $\text{\AA}$ ) and Bond Angles (deg) for the Dirhenium Cation of **7d**<sup>a</sup>**

Distances			
Re(1)–Re(2)	2.817(2)	Re(2)–C(20)	2.08(4)
Re(1)–Cl(1)	2.366(8)	O(10)–C(10)	1.13(3)
Re(1)–Cl(B)	2.518(7)	N–C(20)	1.04(3)
Re(1)–P(1)	2.492(5)	N–C(601)	1.47(4)
Re(1)–C(1)	1.74(3)	C(1)–C(2)	1.41(5)
Re(1)–C(10)	2.57(4)	C(2)–C(3)	1.49(6)
Re(2)–Cl(2)	2.439(7)	C(3)–C(4)	1.64(8)
Re(2)–Cl(B)	2.469(8)	C(4)–C(5)	1.74(9)
Re(2)–P(2)	2.451(5)	C(5)–C(6)	1.60(7)
Re(2)–C(10)	1.93(3)		
Angles			
Re(2)–Re(1)–Cl(1)	144.4(2)	Cl(2)–Re(2)–C(10)	154(1)
Re(2)–Re(1)–Cl(B)	54.8(2)	Cl(2)–Re(2)–C(20)	79.7(9)
Re(2)–Re(1)–P(1)	92.5(1)	Cl(B)–Re(2)–P(2)	91.4(1)
Re(2)–Re(1)–C(1)	115(1)	Cl(B)–Re(2)–C(10)	119(1)
Cl(1)–Re(1)–Cl(B)	89.6(3)	Cl(B)–Re(2)–C(20)	166.8(9)
Cl(1)–Re(1)–P(1)	87.3(1)	P(2)–Re(2)–C(10)	90.9(1)
Cl(1)–Re(1)–C(1)	101(1)	P(2)–Re(2)–C(20)	88.2(1)
Cl(B)–Re(1)–P(1)	90.6(1)	C(10)–Re(2)–C(20)	74(1)
Cl(B)–Re(1)–C(1)	170(1)	Re(1)–Cl(B)–Re(2)	68.8(2)
P(1)–Re(1)–C(1)	89.9(1)	C(20)–N–C(601)	175(3)
Re(1)–Re(2)–Cl(2)	143.5(2)	Re(1)–C(1)–C(2)	174(3)
Re(1)–Re(2)–Cl(B)	56.4(2)	C(1)–C(2)–C(3)	125(4)
Re(1)–Re(2)–P(2)	92.3(1)	C(2)–C(3)–C(4)	117(6)
Re(1)–Re(2)–C(10)	62(1)	C(3)–C(4)–C(5)	93(5)
Re(1)–Re(2)–C(20)	136.8(9)	C(4)–C(5)–C(6)	101(5)
Cl(2)–Re(2)–Cl(B)	87.1(3)	Re(2)–C(10)–O(10)	160(3)
Cl(2)–Re(2)–P(2)	88.2(1)	Re(2)–C(20)–N	178(3)

<sup>a</sup> Numbers in parentheses are estimated standard deviations in the least significant digits.

results in a higher positive charge at the dirhenium core in the case of L = CO. The accessibility of the reduction ( $E_{1/2}(\text{red})$  in Table 6) has been shown by the reduction of **5** and **7** to their neutral congeners **6** and **8** through the use of cobaltocene as the reducing agent (Scheme

**Table 5. Selected Bond Distances ( $\text{\AA}$ ) and Bond Angles (deg) for **8a**<sup>a</sup>**

Distances			
Re(1)–Re(2)	3.0391(6)	Re(2)–C(21)	1.70(1)
Re(1)–Cl(1)	2.475(3)	Re(2)–C(11)	2.62(1)
Re(1)–Cl(B)	2.485(3)	O(12)–C(11)	1.22(1)
Re(1)–P(1)	2.409(2)	N(30)–C(30)	1.15(1)
Re(1)–C(11)	1.87(1)	N(30)–C(31)	1.39(2)
Re(1)–C(30)	1.95(1)	C(21)–C(22)	1.48(2)
Re(2)–Cl(2)	2.417(3)	C(22)–C(23)	1.46(2)
Re(2)–Cl(B)	2.542(3)	C(23)–C(24)	1.45(2)
Re(2)–P(2)	2.417(2)	C(24)–C(25)	1.37(3)
Angles			
Re(2)–Re(1)–Cl(1)	139.23(7)	Re(1)–Re(2)–Cl(B)	51.94(6)
Re(2)–Re(1)–Cl(B)	53.67(6)	Re(1)–Re(2)–P(2)	90.16(5)
Re(2)–Re(1)–P(1)	90.34(5)	Re(1)–Re(2)–C(21)	115.2(4)
Re(2)–Re(1)–C(11)	59.0(4)	Cl(2)–Re(2)–Cl(B)	92.2(1)
Re(2)–Re(1)–C(30)	139.4(3)	Cl(2)–Re(2)–P(2)	90.01(5)
Cl(1)–Re(1)–Cl(B)	85.6(1)	Cl(2)–Re(2)–C(21)	100.7(4)
Cl(1)–Re(1)–P(1)	90.95(5)	Cl(B)–Re(2)–P(2)	90.29(5)
Cl(1)–Re(1)–C(11)	161.7(4)	Cl(B)–Re(2)–C(21)	167.1(4)
Cl(1)–Re(1)–C(30)	81.4(3)	P(2)–Re(2)–P(2)	179.4(1)
Cl(B)–Re(1)–P(1)	91.69(5)	P(2)–Re(2)–C(21)	89.71(5)
Cl(B)–Re(1)–C(11)	112.7(4)	Re(1)–Cl(B)–Re(2)	74.39(7)
Cl(B)–Re(1)–C(30)	166.9(3)	Re(1)–C(11)–O(12)	158(1)
P(1)–Re(1)–P(1)	176.2(1)	Re(2)–C(21)–C(22)	174(1)
P(1)–Re(1)–C(11)	88.59(5)	C(21)–C(22)–C(23)	117(1)
P(1)–Re(1)–C(30)	88.54(5)	C(22)–C(23)–C(24)	122(2)
C(11)–Re(1)–C(30)	80.3(5)	C(23)–C(24)–C(25)	122(2)
Re(1)–Re(2)–Cl(2)	144.12(8)	Re(1)–C(30)–N(30)	180.0(9)

<sup>a</sup> Numbers in parentheses are estimated standard deviations in the least significant digits.

1, step D). This can be accomplished either by the treatment of samples of **5** and **7** with an acetone solution of  $(\eta^5\text{-C}_5\text{H}_5)_2\text{Co}$  or by the addition of cobaltocene to solutions of **5** and **7** that had been generated directly from **1** and **2**, respectively, via **3** and **4**.

The complexes of types **6** and **8**,  $\text{Re}_2(\mu\text{-Cl})(\mu\text{-CO})(\equiv\text{CCH}_2\text{R})\text{Cl}_2(\text{L})(\mu\text{-dpmm})_2$  (L = CO or xylNC), have  $\nu(\text{CO})$  and  $\nu(\text{CN})$  bands in their IR spectra (recorded as Nujol mulls) that are at frequencies lower than the corresponding modes in the spectra of **5** and **7** (Table 6). This reflects the increase in the extent of  $\text{Re} \rightarrow \text{CO}(\pi^*)$  and  $\text{Re} \rightarrow \text{CNxyl}(\pi^*)$  back-bonding in the more electron-rich neutral complexes **6** and **8**. The  $^{13}\text{C}$ -labeled complex  $\text{Re}_2(\mu\text{-Cl})(\mu\text{-}^{13}\text{CO})(\equiv\text{CCH}_2\text{-}n\text{-Pr})\text{Cl}_2(\text{CO})(\mu\text{-dpmm})_2$  shows the expected shift of the two  $\nu(\text{CO})$  bands to lower frequencies (1944 (s) and 1762 (m)  $\text{cm}^{-1}$ ) compared to what is observed with the  $^{12}\text{C}$ -labeled derivative **6a** (1987 (s) and 1804 (m)  $\text{cm}^{-1}$ ). The very close relationship between the pairs of **5**, **6** and **7**, **8** is further demonstrated by the cyclic voltammetric properties of these sets of complexes (Table 6). The only difference within each pair is that the reduced complexes (**6** and **8**) have processes at +0.29 and +0.03 V, respectively, that correspond to oxidations of the bulk complexes, whereas they are reductions in the case of **5** and **7** (Table 6).

The ionic species **5** and **7** are paramagnetic<sup>10,11</sup> and display only very broad peaks in their  $^1\text{H}$  NMR spectra. In contrast, their neutral congeners of types **6** and **8** are diamagnetic and exhibit well-defined  $^1\text{H}$  and  $^{31}\text{P}\{^1\text{H}\}$  NMR spectra, the latter having the appearance of AA'BB' patterns (Table 7). The room-temperature

(10) A magnetic moment determination on a chloroform solution of **7d** at room temperature by the Evans method<sup>9</sup> gave a value of  $\mu_{\text{eff}} = 1.8(\pm 0.1) \mu_{\text{B}}$ .

(11) A dichloromethane solution of **7c** (at  $-160^\circ\text{C}$ ) gave a broad anisotropic signal centered at  $g = 2.17$  showing Re hyperfine.

**Table 6. Electrochemical and Infrared Spectral Data for Alkylidyne Complexes of the Types  $[\text{Re}_2(\mu\text{-Cl})(\mu\text{-CO})(\equiv\text{CCH}_2\text{R})\text{Cl}_2(\text{L})(\mu\text{-dppm})_2]\text{X}$  and  $\text{Re}_2(\mu\text{-Cl})(\mu\text{-CO})(\equiv\text{CCH}_2\text{R})\text{Cl}_2(\text{L})(\mu\text{-dppm})_2$  (R = *n*-Pr, *n*-Bu; L = CO, xyINC; X = PF<sub>6</sub>, SO<sub>3</sub>CF<sub>3</sub>)**

complex	R	L	X	CV half-wave potentials, <sup>a</sup> V			IR spectra, <sup>b</sup> cm <sup>-1</sup>		
				$E_{1/2}(\text{ox})$	$E_{1/2}(\text{red})$	$E_{p,c}$	$\nu(\text{CN})_t$	$\nu(\text{CO})_t$	$\nu(\text{CO})_b$
5a	<i>n</i> -Pr	CO	PF <sub>6</sub>	+1.17(70)	+0.27(60)	-1.80		2036 (s)	1816 (m)
5b	<i>n</i> -Pr	CO	SO <sub>3</sub> CF <sub>3</sub>	+1.18(60)	+0.27(60)	-1.85		2038 (s)	1820 (m)
5c	<i>n</i> -Bu	CO	PF <sub>6</sub>	+1.18(70)	+0.28(70)	-1.85		2032 (s)	1831 (m, br)
5d	<i>n</i> -Bu	CO	SO <sub>3</sub> CF <sub>3</sub>	+1.19(60)	+0.26(70)	-1.80		2036 (s)	1814 (m)
6a	<i>n</i> -Pr	CO		+1.19(70)	+0.29(60) <sup>c</sup>	-1.84		1987 (s), 1963 (m, sh)	1804 (m)
6b	<i>n</i> -Bu	CO		+1.19(60)	+0.29(60) <sup>c</sup>	-1.85		1990 (s)	1804 (m)
7a	<i>n</i> -Pr	xyINC	PF <sub>6</sub>	+0.86(60)	+0.03(60)		2152 (s)		1826 (m, sh), 1802 (m)
7b	<i>n</i> -Pr	xyINC	SO <sub>3</sub> CF <sub>3</sub>	+0.86(60)	+0.01(60)		2150 (s)		1794 (m)
7c	<i>n</i> -Bu	xyINC	PF <sub>6</sub>	+0.82(60)	+0.02(60)		2155 (s)		~1820 (m, br)
7d	<i>n</i> -Bu	xyINC	SO <sub>3</sub> CF <sub>3</sub>	+0.85(70)	+0.00(70)		2150 (s)		1798 (m)
8a	<i>n</i> -Pr	xyINC		+0.86(60)	+0.03(60) <sup>c</sup>		2078 (s)		1785 (m)
8b	<i>n</i> -Bu	xyINC		+0.86(60)	+0.03(60) <sup>c</sup>		2078 (s)		1785 (m)

<sup>a</sup> Measured on 0.1 M TBAH/CH<sub>2</sub>Cl<sub>2</sub> solutions and referenced to the Ag/AgCl electrode with a scan rate ( $\nu$ ) of 200 mV/s at a Pt-bead electrode. Under our experimental conditions,  $E_{1/2} = +0.47$  V vs Ag/AgCl for the ferrocenium/ferrocene couple. In all cases,  $i_{p,a} \approx i_{p,c}$ . The  $E_{p,a} - E_{p,c}$  values (in mV) are given in parentheses. <sup>b</sup> IR spectra recorded as Nujol mulls. <sup>c</sup>  $E_{1/2}(\text{ox})$  value.

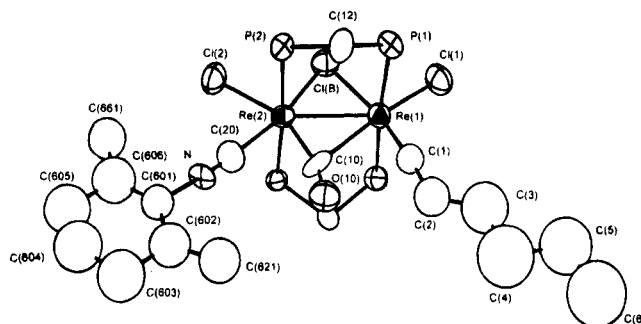
**Table 7. <sup>1</sup>H and <sup>31</sup>P{<sup>1</sup>H} NMR Spectral Data for the Diamagnetic Alkylidyne Complexes of the Type  $\text{Re}_2(\mu\text{-Cl})(\mu\text{-CO})(\equiv\text{CCH}_2\text{R})\text{Cl}_2(\text{L})(\mu\text{-dppm})_2$  (R = *n*-Pr, *n*-Bu; L = CO, xyINC)**

complex	R	L	<sup>1</sup> H NMR, <sup>a</sup> $\delta$	<sup>31</sup> P{ <sup>1</sup> H} NMR, <sup>b</sup> $\delta$
6a	<i>n</i> -Pr	CO	0.03 (m, 2 H), 0.40 (t, 3 H), <sup>c</sup> 0.47 (m, 4 H), <sup>c</sup> 3.39 (m, 2 H), <sup>d</sup> 4.19 (m, 2 H), <sup>d</sup> 6.90–7.90 (m, 40 H) <sup>e</sup>	-6.6, -12.8
6b	<i>n</i> -Bu	CO	0.05 (m, 2 H), 0.42 (p, 2 H), 0.64 (t, 3 H), <sup>c</sup> 0.77 (m, 4 H), <sup>c</sup> 3.40 (m, 2 H), <sup>d</sup> 4.20 (m, 2 H), <sup>d</sup> 6.90–7.90 (m, 40 H) <sup>e</sup>	-6.6, -13.0
8a	<i>n</i> -Pr	xyINC	0.07 (m, 2 H), 0.35 (t, 3 H), 0.42 (m, 4 H), ~2.15 (vbr, 6 H), 3.40 (m, 2 H), <sup>d</sup> 4.19 (m, 2 H), <sup>d</sup> 6.50–8.00 (m, 43 H) <sup>e</sup>	-6.7; -13.0
8b	<i>n</i> -Bu	xyINC	-0.02 (m, 2 H), 0.43 (m, 2 H), 0.64 (t, 3 H), <sup>c</sup> ~0.69 (vbr, 2 H), <sup>c</sup> 0.77 (m, 2 H), 1.79 (s, 6 H), 3.43 (m, 2 H), <sup>d</sup> 4.22 (m, 2 H), <sup>d</sup> 6.50–7.90 (m, 43 H) <sup>e</sup>	-4.6; -13.2

<sup>a</sup> Spectra were recorded in CD<sub>2</sub>Cl<sub>2</sub>. The appearance of the spectra and the relative intensities are indicated in parentheses: s, singlet; d, doublet; t, triplet; p, pentet; m, multiplet; vbr, very broad. <sup>b</sup> Spectra were recorded in CD<sub>2</sub>Cl<sub>2</sub> and have the appearance of AA'BB' patterns; the chemical shifts quoted are those of the center components of the two multiplets. <sup>c</sup> Overlapping multiplets. <sup>d</sup> Resonances of the CH<sub>2</sub> units of the dppm ligands. <sup>e</sup> Resonances of the phenyl ring protons.

<sup>13</sup>C{<sup>1</sup>H} spectrum of  $\text{Re}_2(\mu\text{-Cl})(\mu\text{-}^{13}\text{CO})(\equiv\text{CCH}_2\text{-}n\text{-Pr})\text{Cl}_2\text{-}^{13}\text{CO}(\mu\text{-dppm})_2$  (recorded in CD<sub>2</sub>Cl<sub>2</sub>) shows broad resonances at  $\delta = +183$  and  $\delta = +193$  that are assigned<sup>12</sup> to the terminal and bridging CO ligands, respectively, which are bound to a dirhenium unit. However, we did not observe the natural-abundance carbyne-carbon resonance even with the use of very long data acquisition times.

The structural identities of representative members of the two sets of complexes of types 5, 7 and 6, 8 were established by single-crystal X-ray structure analyses. An ORTEP representation of the structure of the dirhenium cation  $[\text{Re}_2(\mu\text{-Cl})(\mu\text{-CO})(\equiv\text{CCH}_2\text{-}n\text{-Bu})\text{Cl}_2(\text{CNxy})\text{-}(\mu\text{-dppm})_2]^+$ , present in the triflate salt 7d, is shown in Figure 1. The structure is that of a distorted edge-shared bioctahedron. Although two different batches of good-quality single crystals of the neutral dicarbonyl complex 6a were obtained from CHCl<sub>3</sub>/*n*-pentane and CH<sub>2</sub>Cl<sub>2</sub>/*n*-heptane, and two data sets were collected at +20 °C, a complete and satisfactory refinement of this complex was thwarted by a twofold disorder problem involving the terminal CO and alkylidyne ligands that is of a type we have encountered previously with other edge-shared bioctahedral dirhenium species that contain the trans  $\text{Re}_2(\mu\text{-dppm})_2$  unit.<sup>2,13</sup> However, a trans disposition of dppm ligands and the all-cis arrangement of chloride ligands within the  $[\text{Re}_2(\mu\text{-Cl})\text{-}(\mu\text{-CO})(\equiv\text{CCH}_2\text{-}n\text{-Bu})\text{Cl}_2(\mu\text{-dppm})_2]$  unit were shown to be present and the



**Figure 1.** ORTEP representation of the structure of the  $[\text{Re}_2(\mu\text{-Cl})(\mu\text{-CO})(\equiv\text{CCH}_2\text{-}n\text{-Bu})\text{Cl}_2(\text{CNxy})\text{-}(\mu\text{-dppm})_2]^+$  cation as present in complex 7d with the phenyl group atoms of the dppm ligands omitted. The thermal ellipsoids are drawn at the 50% probability level.

Re-Re distance found to be ca. 3.0 Å. After a number of attempts, a suitable crystal of composition  $\text{Re}_2(\mu\text{-Cl})(\mu\text{-CO})(\equiv\text{CCH}_2\text{-}n\text{-Pr})\text{Cl}_2(\text{CNxy})\text{-}(\mu\text{-dppm})_2 \cdot 2\text{CH}_2\text{Cl}_2$  (8a) was obtained and the structure was successfully solved. The ORTEP drawing of the structure of this dirhenium complex is shown in Figure 2. The important structural parameters for 7d and 8a are given in Tables 2–5. Full details of these structures are available as supplementary material.

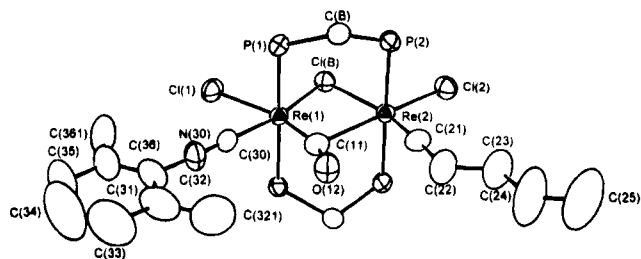
## Discussion

The conversion of the 3-metallafuran complexes of types 3 and 4 to the dirhenium alkylidyne complexes 5 and 7 as outlined in the reaction scheme (step B) represents a novel entry into rhenium alkylidyne chem-

(12) Cotton, F. A.; Daniels, L. M.; Dunbar, K. R.; Falvello, L. R.; Tetrick, S. M.; Walton, R. A. *J. Am. Chem. Soc.* **1985**, *107*, 3524.

(13) Esjornson, D.; Derringer, D. R.; Fanwick, P. E.; Walton, R. A. *Inorg. Chem.* **1989**, *28*, 2821.





**Figure 2.** ORTEP representation of the  $\text{Re}_2(\mu\text{-Cl})(\mu\text{-CO})(=\text{CCH}_2\text{-}n\text{-Pr})\text{Cl}_2(\text{CNxyI})(\mu\text{-dppm})_2$  molecule (**8a**) with the phenyl group atoms of the dppm ligands omitted. The thermal ellipsoids are drawn at the 50% probability level.

istry. This route contrasts, for example, with strategies used in the synthesis of the important mononuclear Re(VII) alkylidyne Schrock complexes, in which ancillary imido, alkoxide, and/or alkylidene ligands are also present,<sup>14</sup> the mononuclear hydrido-alkylidyne complexes of Re(VII) we have recently reported,<sup>15</sup> and the formally Re(V) alkylidyne complexes described by Pombeiro and co-workers.<sup>16</sup> While dirhenium alkylidyne complexes of other types are known,<sup>17</sup> this is the first alkylidyne chemistry to be developed using the electron-rich triple bond ( $\sigma^2\pi^4\delta^2\delta^{*2}$  configuration).

Although the paramagnetism of the complexes of types **5** and **7** precluded their characterization by NMR spectroscopy, the accessibility of their neutral, diamagnetic congeners **6** and **8** (Scheme 1, step D) enabled the  $^1\text{H}$  and  $^{31}\text{P}$  NMR spectra of this set of complexes to be obtained (Table 7). In all cases, the integrity of the alkyl chain of the alkylidyne ligands was confirmed, thereby establishing that the carbon chain of the parent alkyne (1-pentyne or 1-hexyne) was intact. The  $^{31}\text{P}\{^1\text{H}\}$  spectra, which have the appearance of AA'BB' patterns, are in accord with unsymmetrical dirhenium structures, as confirmed by X-ray structure determinations on crystals of the representative complexes **7d** and **8a** (Figures 1 and 2). The structures of the dirhenium units in these two complexes are very similar to one another; this is to be expected based upon the reversibility of the [5]/[6] and [7]/[8] redox couples as seen in the cyclic voltammograms of these complexes (Table 6). Both are edge-sharing bioctahedra in which one of the bridging ligands is an unsymmetrically bound CO ligand displaying quite disparate Re–C distances (1.93(3) and 2.57(4) Å for **7d**; 1.87(1) and 2.62(1) Å for **8a**). In each case, the longer of the two distances involves the formally higher valent Re center, i.e., the one bound to the alkylidyne ligand. The Re=C distances (1.74(3) Å for **7d**; 1.70(1) Å for **8a**) are at the short end of the range encountered for this

structural unit.<sup>14,15,16c</sup> The Re–Cl(bridging) bond that is trans to the Re=C unit is, as expected, the longest of the two Re–Cl distances (2.518(7) vs 2.469(8) Å in **7d**; 2.542(3) vs 2.485(3) Å in **8a**); this accords with the presence of a structural trans effect.

The most significant difference between the structures of **7d** and **8a** is the difference in the Re–Re distances (2.817(2) Å in **7d**; 3.039(1) Å in **8a**). While the shorter of the two Re–Re distances clearly signals the presence of a significant Re–Re interaction, the distance of 3.039(1) Å in **8a** is at the limit of what is normally considered the Re–Re bonding range. A comparison of the changes in the Re–Cl(B) and Re–CO distances between **7d** and **8a** is not profitable because of the relatively low precision of these parameters in the structure of **7d**.

In the case of the cationic dirhenium species that are present in complexes of types **5** and **7**, we can consider them to represent formally mixed-valence Re(III)–Re(IV) species. Their one-electron reduction to the neutral complexes **6** and **8** then gives rise to formally Re(II)–Re(IV) species. While the unsymmetrical nature of these complexes, in which the two Re centers are in such disparate ligand environments, complicates any detailed appraisal of the Re–Re bonding in these complexes, it is clear that the bonding scheme that has been derived for a more symmetrical edge-sharing bioctahedral species, in which there is no metal–ligand multiple bonding,<sup>18</sup> will not apply here. Specifically, in the present cases, two of the three d orbitals that would normally be available for Re–Re bonding are involved in forming the Re=C bond at the more highly “oxidized” Re center. This will leave two essentially nonbonding filled d orbitals at the “reduced” Re center for  $\pi$ -back-bonding to the cis xylNC and CO ligands. Accordingly, it seems reasonable to conclude, based on these arguments and the Re–Re bond distance data, that the **5**, **6** and **7**, **8** sets correspond to species in which the metal–metal bond orders are 0.5/0, rather than 1.5/1 and that the reductions **5** → **6** and **7** → **8** involve the addition of an electron to an antibonding metal-based orbital that is already partially filled in the dirhenium cations of **5** and **7**.

The decoupling reactions of the 2-metalated-3-metallafuran units  $\text{Re}(\mu\text{-COC}(\text{R})\text{CH})\text{Re}$  of **3** and **4** involve the net addition of a single hydrogen atom and are accompanied by a formal redox change from a  $\text{Re}_2(8^+)$  core in **3** and **4** to a  $\text{Re}_2(7^+)$  core in **5** and **7** (see Scheme 1). Since the products of types **5** and **7** are paramagnetic, we have not been able to follow the course of these reactions by NMR spectroscopy. However we did monitor these reactions using IR spectroscopy but found no evidence for the formation of intermediates.

A plausible mechanism could involve attack of  $\text{H}^+$  at the 5-position of the metallafuran ring (the carbon atom that has the R substituent) or at the oxygen atom, with concomitant ring opening and the formation of the dirhenium alkylidyne dicationic species  $[\text{Re}_2(\mu\text{-Cl})(\mu\text{-CO})(=\text{CCH}_2\text{R})\text{Cl}_2(\text{L})(\mu\text{-dppm})_2]^{2+}$ . Such dicationic species are potent one-electron oxidants (Table 6) and will therefore easily be reduced to the monocationic species **5** and **7** in the reaction medium. The involvement of  $\text{H}^+$  is supported by the observation that the addition of

(14) (a) Edwards, D. S.; Biondi, L. V.; Ziller, J. W.; Churchill, M. R.; Schrock, R. R. *Organometallics* **1983**, *2*, 1505. (b) Toreki, R.; Schrock, R. R. *J. Am. Chem. Soc.* **1990**, *112*, 2448. (c) Weinstock, I. A.; Schrock, R. R.; Davis, W. M. *J. Am. Chem. Soc.* **1991**, *113*, 135. (d) Toreki, R.; Schrock, R. R.; Vale, M. G. *J. Am. Chem. Soc.* **1991**, *113*, 3650. (e) Toreki, R.; Schrock, R. R.; Davis, W. M. *J. Am. Chem. Soc.* **1992**, *114*, 3367. (f) Toreki, R.; Vaughn, G. A.; Schrock, R. R.; Davis, W. M. *J. Am. Chem. Soc.* **1993**, *115*, 127.

(15) Leeaphon, M.; Fanwick, P. E.; Walton, R. A. *J. Am. Chem. Soc.* **1992**, *114*, 1890.

(16) (a) Almeida, S. S. P. R.; Frau'sto Da Silva, J. J. R.; Pombeiro, A. J. L. *J. Organomet. Chem.* **1993**, *450*, C7. (b) Carvalho, M. F. N. N.; Henderson, R. A.; Pombeiro, A. J. L.; Richards, R. L. *J. Chem. Soc., Chem. Commun.* **1989**, 1796. (c) Pombeiro, A. J. L.; Hills, A.; Hughes, D. L.; Richards, R. L. *J. Organomet. Chem.* **1988**, *352*, C5.

(17) For example, see: Casey, C. P.; Ha, Y.; Powell, D. R. *J. Am. Chem. Soc.* **1994**, *116*, 3424. This chemistry is accessed via the doubly bonded dirhenium complex  $[\text{Cp}^*\text{Re}(\text{CO})_2]$  and the enyne  $\text{HC}=\text{CC}(\text{CH}_3)=\text{CH}_2$ .

(18) Cotton, F. A.; Walton, R. A. *Multiple Bonds Between Metal Atoms*, 2nd ed.; Oxford University Press: Oxford, U.K., 1993; pp 593–600.



bases such as DBU and  $\text{NEt}_3$  to methanol or dichloromethane solutions of  $[\text{Re}_2(\mu\text{-Cl})(\mu\text{-COC}(n\text{-Pr})\text{CH})\text{Cl}_2(\text{CNxyl})(\mu\text{-dppm})_2]^+$  prevented the formation of  $[\text{Re}_2(\mu\text{-Cl})(\mu\text{-CO})(\equiv\text{CCH}_2\text{-}n\text{-Pr})\text{Cl}_2(\text{CNxyl})(\mu\text{-dppm})_2]^+$ .

The source of the additional hydrogen atom that is incorporated into the alkylidyne product can be the solvent, as shown by the reaction of  $[\text{Re}_2(\mu\text{-Cl})(\mu\text{-COC}(n\text{-Bu})\text{CH})\text{Cl}_2(\text{CNxyl})(\mu\text{-dppm})_2]\text{PF}_6$  (**4b**) with  $\text{CD}_3\text{OD}$  or  $\text{CH}_3\text{OD}$ , which leads to the incorporation of deuterium to give  $[\text{Re}_2(\mu\text{-Cl})(\equiv\text{CCHD-}n\text{-Bu})\text{Cl}_2(\text{CNxyl})(\mu\text{-dppm})_2]\text{PF}_6$  (**7c**). The  $^2\text{H}\{^1\text{H}\}$  NMR spectrum (recorded in  $\text{CH}_2\text{-Cl}_2$ ) of its analogous NMR-active reduced congener **8b** shows a single resonance at  $\delta +0.69$ . A comparison of the  $^1\text{H}$  NMR (Table 7) and  $^2\text{H}\{^1\text{H}\}$  NMR spectra of this product<sup>19</sup> shows that the deuterium label is incorporated exclusively at the  $\beta$ -carbon of the alkylidyne unit. However, integration of this signal in the  $^1\text{H}$  NMR spectrum shows that additional D incorporation has

(19) Decoupling experiments show conclusively that the assignments of the  $^1\text{H}$  NMR spectrum of the  $\equiv\text{CCH}_2\text{CH}_2\text{CH}_2\text{CH}_2\text{CH}_3$  unit in the diamagnetic, reduced complex **8b** (see Table 7) are as follows ( $\delta$  values are given in the same order as the atoms are in the alkyl chain):  $\delta +0.69, -0.02, +0.43, +0.77, \text{ and } +0.64$ .

occurred to give significant levels of  $\equiv\text{CCD}_2\text{-}n\text{-Bu}$ ; this D for H exchange must presumably occur during the formation of an unstable (and undetected) intermediate. We note that small amounts of water might be implicated as the source of hydrogen in the other solvent systems in which the 3-metallafuran to alkylidyne transformations can occur.

**Acknowledgment.** Support from the National Science Foundation, through Grants CHE91-07578 and CHE94-09932 to R.A.W. is gratefully acknowledged. We also thank the National Science Foundation for Grant CHE86-15556 for the purchase of the microVAX II computer and diffractometer.

**Supplementary Material Available:** Tables giving full details of the crystal data and data collection parameters (Tables S1 and S6), atomic positional parameters (Tables S2, S7, and S8), anisotropic thermal parameters (Tables S3 and S9), bond distances (Tables S4 and S10), and bond angles (Tables S5 and S11) for **7d** and **8a** (26 pages). Ordering information is given on any current masthead page.

OM940669C

# Oxygen-Atom Transfer from Nitrous Oxide to an Organonickel(II) Phosphine Complex. Syntheses and Reactions of New Nickel(II) Aryloxides and the Crystal Structure of $(\text{Me}_2\text{PCH}_2\text{CH}_2\text{PMe}_2)\text{Ni}(\text{O}-o\text{-C}_6\text{H}_4\text{CMe}_2\text{CH}_2)$

Kwangmo Koo,<sup>1a</sup> Gregory L. Hillhouse,<sup>\*,1a</sup> and Arnold L. Rheingold<sup>\*,1b</sup>

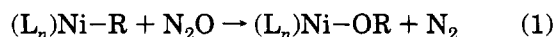
Searle Chemistry Laboratory, Department of Chemistry, The University of Chicago, Chicago, Illinois 60637, and the Department of Chemistry, University of Delaware, Newark, Delaware 19716

Received August 17, 1994<sup>®</sup>

Reaction of  $(\text{PMe}_3)_2\text{Ni}(\text{CH}_2\text{CMe}_2\text{-}o\text{-C}_6\text{H}_4)$  (**1**) with  $\text{N}_2\text{O}$  gives the oxametallacycle  $[(\text{PMe}_3)\text{Ni}(\text{O}-o\text{-C}_6\text{H}_4\text{CMe}_2\text{CH}_2)]_2$  (**2**) and  $\text{O}=\text{PMe}_3$ . Dimeric **2** reacts with CO to give the benzopyran  $\text{CH}_2\text{-CMe}_2\text{-}o\text{-C}_6\text{H}_4\text{OC(O)}$  (**3**) and with HCl to give 2-*tert*-butylphenol. The chelating ligands 2,2'-bipyridine (bipy), 1,10-phenanthroline (phen), and 1,2-bis(dimethylphosphino)ethane (dmpe) react with **2** to afford the monomeric aryloxide complexes  $(\text{bipy})\text{Ni}(\text{O}-o\text{-C}_6\text{H}_4\text{CMe}_2\text{CH}_2)$  (**4**),  $(\text{phen})\text{Ni}(\text{O}-o\text{-C}_6\text{H}_4\text{CMe}_2\text{CH}_2)$  (**5**), and  $(\text{dmpe})\text{Ni}(\text{O}-o\text{-C}_6\text{H}_4\text{CMe}_2\text{CH}_2)$  (**6**), respectively. Reaction of **4** or **5** with CO affords good yields of the lactone **3**. Treatment of **5** with  $\text{I}_2$  induces formal O,C-reductive elimination, giving 4,4-dimethyl-3,4-dihydrocoumarin,  $\text{O}-o\text{-C}_6\text{H}_4\text{CMe}_2\text{-CH}_2$  (**9**), in good yield. **6** has been characterized by single-crystal X-ray diffraction. **6** crystallizes from pentane solution in the monoclinic space group  $P2_1/n$  with  $a = 9.206(2)$  Å,  $b = 12.685(3)$  Å,  $c = 15.998(3)$  Å,  $\beta = 90.33(3)^\circ$ , and  $Z = 4$ . The least-squares refinement converged to  $R(F) = 4.04\%$  and  $R(wF) = 4.89\%$  for the 1989 unique data with  $F_o > 4.5\sigma(F_o)$ .

## Introduction

We have been exploring the use of nitrous oxide as an O-atom transfer reagent to organic ligands in transition-metal complexes. Our earlier studies concentrated on reactions of  $\text{N}_2\text{O}$  with group 4 metallocene derivatives,<sup>2</sup> especially alkyne complexes of Ti and Zr,<sup>3</sup> but recently we have extended the scope of our research to include late-metal complexes, particularly those of square-planar nickel(II) containing the  $\pi$ -acid coligands 2,2'-bipyridine (bipy) and 1,10-phenanthroline (phen).<sup>4</sup> In these latter studies, interesting transformations were effected, notably the oxidation of simple alkyl groups attached to Ni to give stable Ni alkoxides (eq 1).



Is a  $\pi$ -acid bipyridine (or phenanthroline) an essential component in activating the  $(\text{bipy})\text{NiR}_2$  complexes toward reactivity with  $\text{N}_2\text{O}$ ? In addressing this question, we have examined the reactivity of  $(\text{PMe}_3)_2\text{Ni}(\text{CH}_2\text{CMe}_2\text{-}$

$o\text{-C}_6\text{H}_4)$  (**1**)<sup>5</sup> with  $\text{N}_2\text{O}$  and report herein the results of our study of this system.

## Experimental Section

**General Considerations.** Reactions were carried out using standard high-vacuum and Schlenk techniques using dry, air-free solvents. NMR spectra were recorded in  $\text{C}_6\text{D}_6$  or  $\text{CD}_2\text{Cl}_2$  solutions at ambient temperature.  $^1\text{H}$  NMR spectra were recorded at 500 MHz using a General Electric  $\Omega$ -500 spectrometer;  $^{13}\text{C}\{^1\text{H}\}$  NMR spectra were recorded using a GE  $\Omega$ -500 or  $\Omega$ -300 spectrometer operating at 125.00 or 75.5 MHz, respectively.  $^{31}\text{P}\{^1\text{H}\}$  NMR spectra were recorded using a GE  $\Omega$ -500 operating at 202.5 MHz. Infrared spectra were recorded on a Nicolet 20SXB spectrometer in a Nujol mull with KBr plates. Electron impact mass spectra were recorded on a VG Analytical, LTD 70-70 EQ double focusing (EB) mass spectrometer. Elemental analyses were performed by Desert Analytics (Tucson, AZ). 2,2'-bipyridine (bipy) and 1,10-phenanthroline (phen) were purchased from Aldrich Chemical Co., and 1,2-bis(dimethylphosphino)ethane (dmpe) was purchased from Strem Chemical Co.  $(\text{PMe}_3)_2\text{Ni}(\text{CH}_2\text{CMe}_2\text{-}o\text{-C}_6\text{H}_4)$  (**1**) was prepared according to literature method.<sup>5</sup>

**Preparation of  $[(\text{PMe}_3)\text{Ni}(\text{O}-o\text{-C}_6\text{H}_4\text{CMe}_2\text{CH}_2)]_2$  (**2**).** A solution of **1** (0.22 g, 0.64 mmol) in benzene (10 mL) was stirred under an  $\text{N}_2\text{O}$  atmosphere at 55 °C for 3 d, the solution was filtered, and the filtrate was evaporated to dryness. The residue was extracted with 35 mL of *n*-hexane. The hexane solution was concentrated and cooled to -78 °C, to give **2** (0.10

(5) Carmona, E.; Palma, P.; Paneque, M.; Poveda, M. L.; Gutiérrez-Puebla, E.; Monge, A. *J. Am. Chem. Soc.* **1986**, *108*, 6424.

<sup>®</sup> Abstract published in *Advance ACS Abstracts*, December 1, 1994.  
(1) (a) The University of Chicago. (b) University of Delaware.  
(2) Vaughan, G. A.; Rupert, P. B.; Hillhouse, G. L. *J. Am. Chem. Soc.* **1987**, *109*, 5538.

(3) (a) Vaughan, G. A.; Hillhouse, G. L.; Lum, R. T.; Buchwald, S. L.; Rheingold, A. L. *J. Am. Chem. Soc.* **1988**, *110*, 7215. (b) Vaughan, G. A.; Sofield, C. D.; Hillhouse, G. L.; Rheingold, A. L. *J. Am. Chem. Soc.* **1989**, *111*, 5491. (c) Vaughan, G. A.; Hillhouse, G. L.; Rheingold, A. L. *J. Am. Chem. Soc.* **1990**, *112*, 7994.

(4) (a) Matsunaga, P. T.; Hillhouse, G. L.; Rheingold, A. L. *J. Am. Chem. Soc.* **1993**, *115*, 2075. (b) Matsunaga, P. T.; Mavropoulos, J. C.; Hillhouse, G. L. *Polyhedron* **1994**, *13*, in press.

g, 55%) as a yellow powder.  $^1\text{H}$  NMR ( $\text{C}_6\text{D}_6$ ):  $\delta$  7.56 (d, 2H, aryl), 7.26 (d, 2H, aryl), 7.11 (t, 2H, aryl), 6.85 (t, 2H, aryl), 1.58 (s, 12H,  $\text{CH}_3$ ), 0.57 (m, 4H,  $\text{CH}_2$ ), 0.53 (d, 18H,  $\text{PCH}_3$ ,  $^2J_{\text{HP}} = 9$  Hz).  $^{31}\text{P}\{^1\text{H}\}$  NMR ( $\text{C}_6\text{D}_6$ ):  $\delta$  -7.45.  $^{13}\text{C}\{^1\text{H}\}$  NMR ( $\text{C}_6\text{D}_6$ , 125.7 MHz):  $\delta$  161.0, 140.2, 126.7, 125.3, 119.6, 117.7, 35.7, 31.0, 29.9 (d,  $^2J_{\text{PC}} = 29$  Hz), 13.7 (d,  $^1J_{\text{PC}} = 29$  Hz). An analytical sample recrystallized from  $\text{C}_6\text{H}_6$ /hexane was solvated with  $1/2\text{C}_6\text{H}_6$ . Anal. Calcd for  $\text{C}_{23}\text{H}_{45}\text{P}_2\text{O}_2\text{Ni}_2$ : C, 57.6; H, 7.50. Found: C, 57.9; H, 7.62.

**Reaction of 2 with HCl.** To a solution of **2** (0.37 g, 0.65 mmol) in benzene (10 mL) was introduced an excess of anhydrous HCl. The solution was stirred at ambient temperature for 10 min, the solution was filtered, and the filtrate was evaporated to dryness using a rotary evaporator. The residue was dissolved in hexane and chromatographed on silica gel (eluent: hexane/ethyl acetate, 1:1) to give 2-*tert*-butylphenol (0.16 g, 81%). The product was identified by spectral comparison with an authentic sample.

**Preparation of 4,4-Dimethyl-2-oxo-2H-1-benzopyran (3).** A solution of **2** (0.20 g, 0.36 mmol) in benzene (10 mL) was stirred under a CO atmosphere at ambient temperature for 15 min, the solution was filtered, and the filtrate was evaporated to dryness using a rotary evaporator. The residue was dissolved in hexane and chromatographed on silica gel (eluent: hexane/ethyl acetate, 1:1) to give **3** (0.04 g, 67%).  $^1\text{H}$  NMR ( $\text{CD}_2\text{Cl}_2$ ):  $\delta$  7.33 (d, 1H, aryl), 7.25 (t, 1H, aryl), 7.15 (t, 1H, aryl), 7.03 (d, 1H, aryl), 2.63 (s, 2H,  $\text{CH}_2$ ), 1.37 (s, 6H,  $\text{CH}_3$ ).  $^{13}\text{C}\{^1\text{H}\}$  NMR ( $\text{CD}_2\text{Cl}_2$ , 125.7 MHz):  $\delta$  168.3 (C=O), 151.1 (aryl), 132.3 (aryl), 128.5 (aryl), 125.0 (aryl), 124.9 (aryl), 117.2 (aryl), 43.8 ( $\text{CH}_2$ ), 33.5 ( $\text{CMe}_2$ ), 27.7 ( $\text{CH}_3$ ). IR:  $\nu(\text{C}=\text{O})$  1775 (s)  $\text{cm}^{-1}$ . EIMS  $m/z$  176 ( $\text{M}^+$ ).

**Preparation of (bipy)Ni(O-*o*- $\text{C}_6\text{H}_4\text{CMe}_2\text{CH}_2$ ) (4).** To a cold solution of **2** (0.36 g, 0.66 mmol) in benzene (10 mL) was added 0.30 g of 2,2'-bipyridine (0.64 mmol). The reaction mixture was warmed to room temperature and stirred for 30 min, at which time the blue solution was filtered. The filtrate was dried in vacuo and washed with *n*-hexane (15 mL) to give crude **4** which was recrystallized from toluene/hexane as blue needles (0.20 g, 43%).  $^1\text{H}$  NMR ( $\text{C}_6\text{D}_6$ ):  $\delta$  9.45–6.18 (m, 12H, aryl), 2.11 (s, 2H,  $\text{CH}_2$ ), 1.92 (s, 6H,  $\text{CH}_3$ ).  $^{13}\text{C}\{^1\text{H}\}$  NMR ( $\text{C}_6\text{D}_6$ , 75.5 MHz):  $\delta$  148.2, 147.6, 136.4, 134.3, 126.5, 125.1, 120.6, 118.8, 114.8, 40.9, 35.1, 31.4 (due to the low solubility of **4** in  $\text{C}_6\text{D}_6$ , two of its aryl/bipy resonances were not observed). Anal. Calcd for  $\text{C}_{20}\text{H}_{20}\text{N}_2\text{NiO}$ : C, 66.2; H, 5.55; N, 7.71. Found: C, 66.0; H, 5.45; N, 7.51.

**Preparation of (phen)Ni(O-*o*- $\text{C}_6\text{H}_4\text{CMe}_2\text{CH}_2$ ) (5).** Using a procedure analogous to that described above for **4**, except that 1,10-phenanthroline was used instead of 2,2'-bipyridine, reaction of **2** (0.15 g, 0.26 mmol) with phen (0.1 g, 0.52 mmol) yielded **5** (0.18 g, 88%) as dark purple-blue powder.  $^1\text{H}$  NMR ( $\text{CDCl}_3$ ):  $\delta$  9.42–6.4 (m, 12H, aryl), 2.00 (s, 2H,  $\text{CH}_2$ ), 1.46 (s, 6H,  $\text{CH}_3$ ). Anal. Calcd for  $\text{C}_{22}\text{H}_{20}\text{N}_2\text{NiO}$ : C, 68.3; H, 5.21; N, 7.24. Found: C, 68.8; H, 5.22; N, 6.70. The  $^{13}\text{C}$  NMR spectrum of **5** was not obtained due to its low solubility in solvents with which it does not react over the time period needed to acquire carbon data.

**Preparation of (dmpe)Ni(O-*o*- $\text{C}_6\text{H}_4\text{CMe}_2\text{CH}_2$ ) (6).** Using a procedure analogous to that described above for **4**, except that 1,2-bis(dimethylphosphino)ethane was used instead of 2,2'-bipyridine, reaction of **2** (0.12 g, 0.21 mmol) with dmpe (70  $\mu\text{L}$ , 0.42 mmol) yielded **6** (0.09 g, 60%) as yellow powder.  $^1\text{H}$  NMR ( $\text{C}_6\text{D}_6$ ):  $\delta$  7.57 (d, 1H, aryl), 7.37 (t, 1H, aryl), 7.29 (d, 1H, aryl), 6.93 (t, 1H, aryl), 1.82 (s, 6H,  $\text{CH}_3$ ), 1.22 (m, 2H,  $\text{CH}_2$ ), 0.96 (d, 6H,  $\text{PCH}_3$ ,  $^2J_{\text{PH}} = 8$  Hz), 0.75 (m, 2H,  $\text{CH}_2$ ), 0.71 (d, 6H,  $\text{PCH}_3$ ,  $^2J_{\text{PH}} = 8$  Hz), 0.60 (m, 2H,  $\text{CH}_2$ ).  $^{13}\text{C}\{^1\text{H}\}$  NMR ( $\text{C}_6\text{D}_6$ , 125 MHz):  $\delta$  163.6, 138.2, 127.1, 125.2, 120.1, 114.2, 40.1 (dd,  $^1J_{\text{PC}} = 70$  Hz,  $^2J_{\text{PC}} = 24$  Hz), 35.1, 33.1 (d,  $^4J_{\text{PC}} = 7$  Hz), 30.1 (dd,  $^2J_{\text{PC}} = 25$  Hz,  $^1J_{\text{PC}} = 70$  Hz), 23.5 (dd,  $^2J_{\text{PC}}(\text{trans}) = 25$  Hz,  $^2J_{\text{PC}}(\text{cis}) = 11$  Hz), 11.9 (d,  $^1J_{\text{PC}} = 29$  Hz), 10.3 (d,  $^1J_{\text{PC}} = 15$  Hz).  $^{31}\text{P}\{^1\text{H}\}$  NMR ( $\text{C}_6\text{D}_6$ ):  $\delta$  35.1 (d,  $^2J_{\text{PP}} = 4$  Hz),

Table 1. Crystallographic Data for **6**

Crystal Parameters			
formula	$\text{C}_{16}\text{H}_{28}\text{NiOP}_2$	$V, \text{\AA}^3$	1868.1(6)
formula weight	357.0	$Z$	4
crystal system	monoclinic	cryst dimens, mm	$0.42 \times 0.42 \times 0.56$
space group	$P2_1/n$	cryst color	orange
$a, \text{\AA}$	9.206(2)	$D(\text{calc}), \text{g cm}^{-3}$	1.269
$b, \text{\AA}$	12.685(3)	$\mu(\text{Mo K}\alpha), \text{cm}^{-1}$	12.04
$c, \text{\AA}$	15.998(3)	temp, K	297
$\beta$ , deg	90.33(3)		
Data Collection			
diffractometer	Siemens Pr	rflns collected	3047
monochromator	graphite	indpt rflns	2935
radiation	Mo K $\alpha$	indpt obsvd rflns	1989
	$(\lambda = 0.71073 \text{\AA})$	$F_o \geq n\sigma(F_o)$ ( $n = 4.5$ )	
$2\theta$ scan range, deg	4.0–48.0	std. rflns std./rfln	3 std/197 rflns
data collected ( $h, k, l$ )	$\pm 10, +14, +18$	var in stds, %	<1
Refinement <sup>a</sup>			
$R(F)$ , %	4.04	$\Delta(\rho), \text{e \AA}^{-3}$	0.33
$R(wF)$ , %	4.89	$N_o/N_v$	10.9
$\Delta\sigma(\text{max})$	0.001	GOF	1.02

<sup>a</sup> Quantity minimized =  $\sum w\Delta^2$ ;  $R = \sum \Delta / \sum (F_o)$ ;  $R(w) = \sum \Delta w^{1/2} / \sum (F_o w^{1/2})$ ;  $\Delta = |F_o - F_c|$ .

23.7 (d,  $^2J_{\text{PP}} = 4$  Hz). Anal. Calcd for  $\text{C}_{16}\text{H}_{28}\text{NiOP}_2$ : C, 53.8; H, 7.09. Found: C, 54.0; H, 7.39.

**Reaction of 4 with CO.** Using a procedure analogous to that described above for **3**, a solution of **4** (0.32 g, 0.88 mmol) in benzene (20 mL) was stirred for 12 h under CO (1 atm). Workup and chromatography gave **3** (0.04 g, 58%).

**Reaction of 5 with CO.** Using a procedure analogous to that described above for **3**, a solution of **5** (0.08 g, 0.21 mmol) in benzene (20 mL) was stirred for 12 h under CO (1 atm). Workup and chromatography gave **3** (0.03 g, 82%).

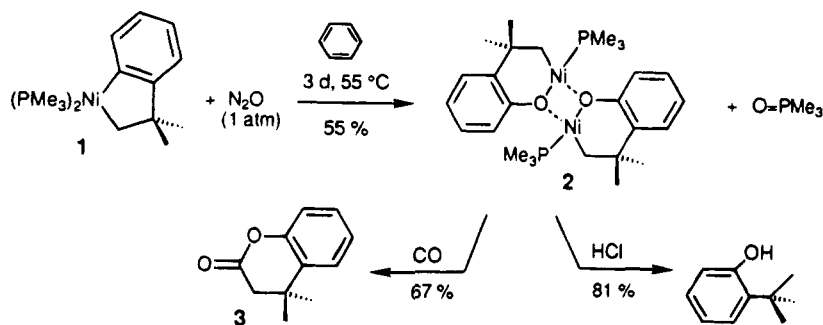
**Preparation of 4,4-Dimethyl-3,4-dihydrocoumarin (9).** To a solution of **5** (0.11 g, 0.27 mmol) in THF (20 mL) was added  $\text{I}_2$  (0.07 g, 0.27 mmol) under an Ar counterflow, causing an immediate color change from purple to dark yellow. The solution was stirred for 1 h at room temperature and then filtered. The filtrate was evaporated to dryness by using a rotary evaporator. The residue was extracted with ethyl acetate (30 mL), the extracts were concentrated, and chromatography on silica gel (eluent: *n*-hexane/ethyl acetate, 5:1) gave 4,4-dimethyl-3,4-dihydrocoumarin (**9**) (0.02 g, 55%).  $^1\text{H}$  NMR ( $\text{C}_6\text{D}_6$ ):  $\delta$  6.99 (t, 1H, aryl), 6.87 (d, 2H, aryl), 6.79 (t, 1H, aryl), 3.93 (s, 2H,  $\text{CH}_2$ ), 1.04 (s, 6H,  $\text{CH}_3$ ).  $^{13}\text{C}$  NMR ( $\text{C}_6\text{D}_6$ , 125.7 MHz):  $\delta$  159.9 (aryl), 136.7 (aryl), 127.8 (aryl), 122.4 (aryl), 120.8 (aryl), 110.1 (aryl), 84.2 ( $\text{CH}_2$ ), 41.7 ( $\text{CMe}_2$ ), 27.3 ( $\text{CH}_3$ ). EIMS  $m/z$  148 ( $\text{M}^+$ ).

**Crystallographic Studies on 6.** Crystal, data collection, and refinement parameters are given in Table 1. Suitable crystals of **6** were selected and mounted with epoxy cement to glass fibers. The unit-cell parameters were obtained by the least-squares refinement of the angular settings of 24 reflections ( $20^\circ \leq 2\theta \leq 25^\circ$ ). The systematic absences in the diffraction data for **6** are uniquely consistent for the space group  $P2_1/n$ . The structure was solved using direct methods, completed by subsequent difference Fourier syntheses and refined by full-matrix least-squares procedures. All non-hydrogen atoms were refined with anisotropic displacement coefficients. Hydrogen atoms were treated as idealized contributions. All software and sources of the scattering factors are contained in either the SHELXTL (5.1) or the SHELXTL PLUS (4.2) program libraries (G. Sheldrick, Siemens XRD, Madison, WI).

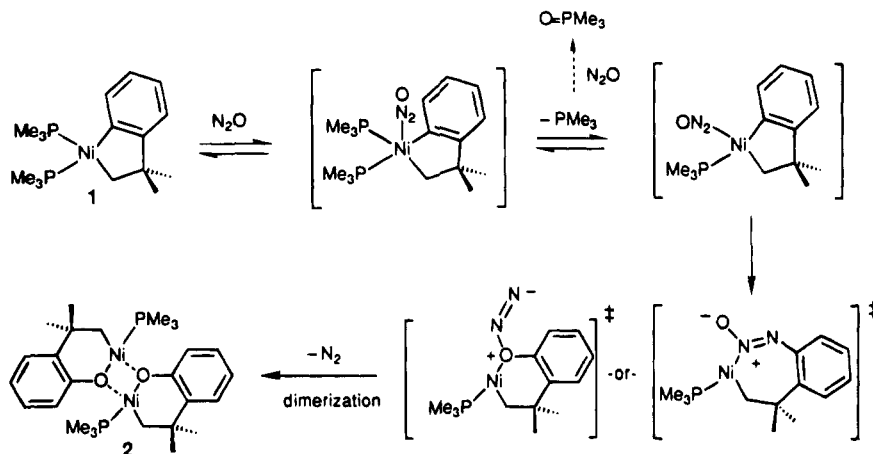
## Results and Discussion

Nitrous oxide reacts slowly, over a period of 3 days at 55  $^\circ\text{C}$ , with benzene solutions of  $(\text{PMe}_3)_2\text{Ni}(\text{CH}_2\text{CMe}_2-$

Scheme 1



Scheme 2



$o\text{-C}_6\text{H}_4$ ) (**1**)<sup>5</sup> to give  $[(\text{PMe}_3)_2\text{Ni}(\text{O}-o\text{-C}_6\text{H}_4\text{CMe}_2\text{CH}_2)]_2$  (**2**), a product resulting from insertion of an oxygen atom from  $\text{N}_2\text{O}$  into a Ni-C bond of **1** (see Scheme 1) and loss of  $\text{PMe}_3$  (as  $\text{O}=\text{PMe}_3$ ). The insertion reaction is regioselective, as judged by multinuclear NMR spectroscopy, and the site of insertion was determined to be at the Ni-aryl bond (not the Ni-alkyl linkage) by chemical methods: (i) reaction of **2** with anhydrous HCl gives 2-tert-butylphenol exclusively, and (ii) reaction of **2** with carbon monoxide gives only 4,4-dimethyl-2-oxo-2H-1-benzopyran (**3**). Moreover, a derivative of **2** has been characterized by crystallographic methods, and the structure confirms the atomic connectivity as depicted in Scheme 1 (*vide infra*). Formulation of **2** as a dimer follows from the 1:1 stoichiometric ratio of the  $\text{C}_{10}\text{H}_{12}\text{O}$  ligand to the  $\text{PMe}_3$  ligand and by analogy to other O-bridging dimeric products observed in reactions of **1**.<sup>5</sup>

The regiochemistry of O-insertion in the reaction of **1** with  $\text{N}_2\text{O}$  is consistent with observations of Carmona et al., concerning the regiochemistry in addition reactions of heterocumulenes ( $\text{CO}_2$ ,  $\text{CS}_2$ ,  $\text{COS}$ ,  $\text{PhNCS}$ ,  $\text{PhNCO}$ ,  $\text{ToI}(\text{N}(\text{C}(\text{O})\text{Ph})_2)$ ) with **1**.<sup>5,6</sup> This is in contrast to molecules *without* cumulated multiple bonds, like  $\text{CO}$  and  $\text{H}_2\text{CO}$ , which react by inserting into the Ni- $\text{CH}_2$  bond.<sup>5,6</sup> The observed regiochemistry in the  $\text{N}_2\text{O}$  reaction might therefore have mechanistic significance since it suggests (at least indirectly) that nitrous oxide reacts by inserting into the Ni-C bond as a heterocumulene (i.e.,  $\text{N}=\text{N}=\text{O}$ ) and not by simply delivering its oxygen atom in a stepwise atom-transfer process. A possible

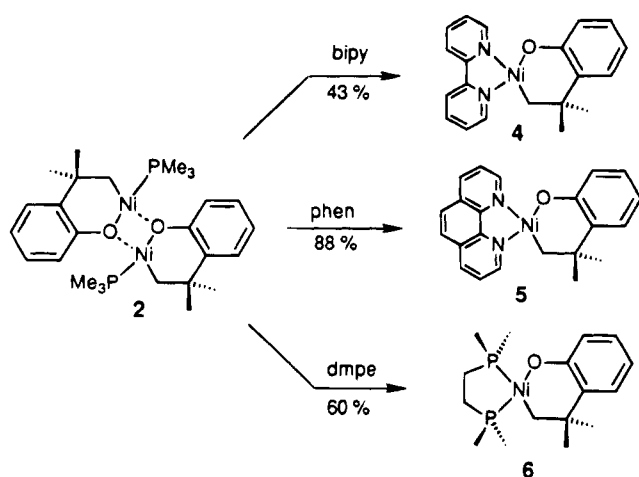
reaction sequence for  $\text{N}_2\text{O}$  consistent with mechanistic proposals made for the other heterocumulene insertions is outlined in Scheme 2; the regiochemistry of the insertion is controlled by the greater lability of the phosphine ligand trans to  $\text{CH}_2$ .<sup>6</sup> It is noteworthy that the  $\text{N}_2\text{O}$  oxidation of  $(\text{C}_5\text{Me}_5)_2\text{Zr}(\text{PhC}\equiv\text{CPh})$  to  $(\text{C}_5\text{Me}_5)_2\text{Zr}(\text{OCPh}=\text{CPh})$  was shown to proceed via an isolable  $\text{N}_2\text{O}$ -inserted intermediate similar to the one proposed in Scheme 2,  $(\text{C}_5\text{Me}_5)_2\text{Zr}(\text{N}(\text{O})\text{N}(\text{CPh})=\text{CPh})$ ,<sup>3b</sup> although the relevance of this electron-poor early-metal system to the electron-rich nickel complex **1** is debatable.

In the reaction of **1** with  $\text{N}_2\text{O}$ , it is somewhat surprising that not all of the  $\text{PMe}_3$  is oxidized to  $\text{O}=\text{PMe}_3$  (1 equiv of  $\text{PMe}_3$  remains in the product, **2**). In a control experiment it was found that free  $\text{PMe}_3$  is oxidized to  $\text{O}=\text{PMe}_3$  under the reaction conditions required for formation of **2** (3 d,  $55^\circ\text{C}$ ). This result suggests that the remaining  $\text{PMe}_3$  ligand in **2** is one that does not dissociate from Ni, and that  $\text{N}_2\text{O}$  preferentially oxidizes the Ni-C(aryl) bond over both the Ni-C(alkyl) bond as well as the coordinated  $\text{PMe}_3$  ligand.

Dimeric **2** reacts under mild conditions ( $20^\circ\text{C}$ , 30 min) with the chelating bidentate ligands 2,2'-bipyridine, 1,10-phenanthroline, and 1,2-bis(dimethylphosphino)ethane to afford the monomeric aryloxo complexes  $(\text{bipy})\text{Ni}(\text{O}-o\text{-C}_6\text{H}_4\text{CMe}_2\text{CH}_2)$  (**4**),  $(\text{phen})\text{Ni}(\text{O}-o\text{-C}_6\text{H}_4\text{CMe}_2\text{CH}_2)$  (**5**), and  $(\text{dmpe})\text{Ni}(\text{O}-o\text{-C}_6\text{H}_4\text{CMe}_2\text{CH}_2)$  (**6**), respectively (see Scheme 3). It is interesting that neither  $(\text{bipy})\text{Ni}(\text{CH}_2\text{CMe}_2-o\text{-C}_6\text{H}_4)$ <sup>6</sup> nor  $(\text{dmpe})\text{Ni}(\text{CH}_2\text{CMe}_2-o\text{-C}_6\text{H}_4)$ <sup>6</sup> reacts with nitrous oxide to give **4** or **6**, respectively, findings consistent with reported observations that

(6) Cámpora, J.; Gutiérrez, E.; Monge, A.; Palma, P.; Poveda, M. L.; Ruíz, C.; Carmona, E. *Organometallics* **1994**, *13*, 1728.

Scheme 3



(dmpe)Ni(CH<sub>2</sub>CMe<sub>2</sub>-*o*-C<sub>6</sub>H<sub>4</sub>) reacts much slower (and with differing reactivity) with heterocumulenes than does **1**.<sup>6</sup> We have previously noted that the metallacycles (bipy)Ni{(CH<sub>2</sub>)<sub>2</sub>C(CH<sub>2</sub>)C(CH<sub>2</sub>)CH<sub>2</sub>} and (bipy)Ni{(CH<sub>2</sub>)<sub>2</sub>C<sub>6</sub>H<sub>4</sub>}, both possessing sp<sup>2</sup>-hybridized ring carbons in the β-positions, show no reactivity toward N<sub>2</sub>O, whereas similar (bipy)Ni-metallacycles having sp<sup>2</sup>-hybridized ring carbons in the β-positions uniformly react with N<sub>2</sub>O to give O-transfer products.<sup>4b</sup> The fact that we can prepare **4** by an alternative route (i.e., from **2** + bipy) lends support to our earlier speculation that the lack of reactivity of N<sub>2</sub>O with (bipy)nickelacycles having sp<sup>2</sup>-β carbons might be a consequence of prohibitive rigidity in these systems, and flexibility in the metallacycle could be important in allowing distortions required to accommodate the incoming N<sub>2</sub>O substrate.<sup>4b</sup>

The structure of (dmpe)Ni(O-*o*-C<sub>6</sub>H<sub>4</sub>CMe<sub>2</sub>CH<sub>2</sub>) (**6**) has been determined by single-crystal X-ray diffraction methods on crystals grown from pentane solution. Pertinent crystallographic data are given in Table 1, and bond lengths and selected bond angles are given in Table 2. A perspective view of **6** along with the atom-labeling scheme is shown in Figure 1. Monomeric **6** adopts a square-planar geometry about Ni. The most significant feature of the structure is that it allows for the unambiguous identification of the site of O-atom insertion, i.e., at the Ni-C(aryl) bond and not at the Ni-C(aliphatic) bond. The salient metrical parameters found in **6** are very similar to the corresponding angles and distances found in the structure of the oxanickelacyclohexane complex (bipy)Ni{O(CH<sub>2</sub>)<sub>4</sub>} (**7**).<sup>4a</sup> The Ni(1)-O(1) bond in **6** (1.872(3) Å) is somewhat longer than the Ni-O bond in **7** (1.815(6) Å), whereas the Ni-C bond lengths in **6** and **7** are, within experimental error, the same (Ni(1)-C(1) = 1.936(5) Å in **6**). In both structures, the CH<sub>2</sub> group exerts a more pronounced trans lengthening influence than does the OR group: in **6**, Ni(1)-P(1) = 2.103(1) Å (trans to O) and Ni(1)-P(2) = 2.207(2) Å (trans to CH<sub>2</sub>), a difference (Δ) of 0.10 Å (in **7**, Δ = 0.05 Å). These trends are also manifested

in the structure of (PMe<sub>3</sub>)<sub>2</sub>Ni{OC(O)-*o*-C<sub>6</sub>H<sub>4</sub>CMe<sub>2</sub>CH<sub>2</sub>} (**8**), the product of the reaction of **1** with CO<sub>2</sub>, where Ni-O = 1.877(9), Ni-C = 1.96(1), and Δ = 0.15 Å.<sup>5</sup>

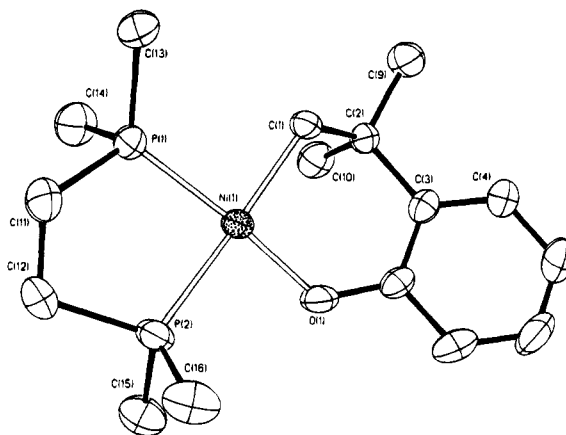


Figure 1. The molecular structure and atom-numbering scheme for (dmpe)Ni(O-*o*-C<sub>6</sub>H<sub>4</sub>CMe<sub>2</sub>CH<sub>2</sub>) (**6**). The hydrogen atoms have been omitted for clarity.

Table 2. Bond Lengths and Selected Bond Angles for **6**

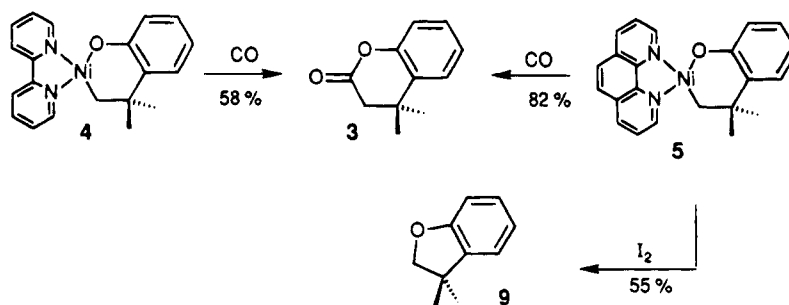
Bond Lengths (Å)			
Ni(1)-P(1)	2.103(1)	Ni(1)-P(2)	2.207(2)
Ni(1)-O(1)	1.872(3)	Ni(1)-C(1)	1.936(5)
P(1)-C(11)	1.830(5)	P(1)-C(13)	1.812(5)
P(1)-C(14)	1.802(6)	P(2)-C(12)	1.836(6)
P(2)-C(15)	1.801(6)	P(2)-C(16)	1.805(6)
O(1)-C(8)	1.316(6)	C(1)-C(2)	1.548(6)
C(2)-C(3)	1.524(6)	C(2)-C(9)	1.530(7)
C(2)-C(10)	1.536(7)	C(3)-C(4)	1.373(7)
C(3)-C(8)	1.422(6)	C(4)-C(6)	1.377(8)
C(5)-C(6)	1.370(10)	C(6)-C(7)	1.376(9)
C(7)-C(8)	1.396(7)	C(11)-C(12)	1.528(8)
Selected Bond Angles (deg)			
P(1)-Ni(1)-P(2)	87.6(1)	P(1)-Ni(1)-O(1)	173.5(1)
P(2)-Ni(1)-O(1)	88.6(1)	P(1)-Ni(1)-C(1)	89.9(1)
P(2)-Ni(1)-C(1)	173.9(1)	O(1)-Ni(1)-C(1)	94.4(2)
Ni(1)-O(1)-C(8)	127.2(3)	Ni(1)-C(1)-C(2)	115.8(3)
C(1)-C(2)-C(3)	110.5(4)	C(1)-C(2)-C(9)	108.2(4)
C(3)-C(2)-C(9)	111.5(4)	C(1)-C(2)-C(10)	109.3(4)
C(3)-C(2)-C(10)	109.4(4)	C(9)-C(2)-C(10)	107.9(4)
C(2)-C(3)-C(4)	122.2(4)	C(2)-C(3)-C(8)	119.6(4)
C(4)-C(3)-C(8)	118.2(4)	C(3)-C(4)-C(5)	122.5(5)
C(4)-C(5)-C(6)	119.5(6)	C(5)-C(6)-C(7)	120.0(5)
C(6)-C(7)-C(8)	121.4(4)	O(1)-C(8)-C(3)	123.9(4)
O(1)-C(8)-C(7)	117.7(4)	C(3)-C(8)-C(7)	118.4(4)

Like **2**, both **4** and **5** react with excess CO to give **3** (Scheme 4).<sup>7</sup> It is noteworthy that the transformations of Schemes 1 and 4, sequential addition of "O" and "CO" to give **3** from **1**, formally represent addition of the elements of CO<sub>2</sub>. However, the sense of addition is reversed from that of direct addition of CO<sub>2</sub> to **1**, where it is the C-atom of CO<sub>2</sub> that is attached to the aryl ring in **8**, not an O-atom as is the case in our work. This is an intriguing observation that highlights the opportunities for obtaining unique transformations by utilizing an atom-transfer reaction coupled with a secondary reaction. For example, reactions involving O-transfer from N<sub>2</sub>O coupled to addition of H<sub>2</sub> could give products significantly different from those obtained by reaction of the same systems with H<sub>2</sub>O.

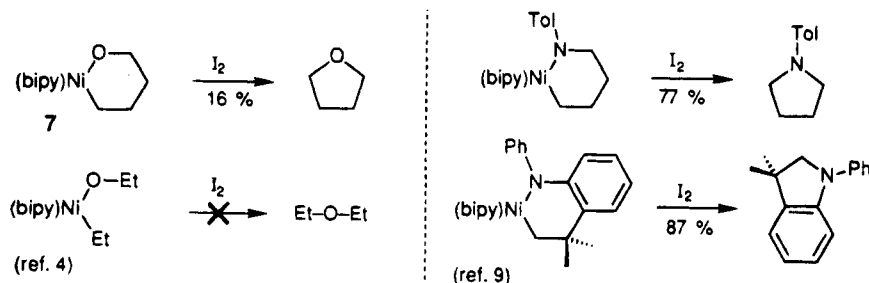
Reaction of I<sub>2</sub> with **5** results in formal reductive elimination with formation of a new O-C bond to give 4,4-dimethyl-3,4-dihydrocoumarin (**9**) in 55% yield (Scheme 4). Reductive elimination reactions that form

(7) For other examples of CO-insertion, reductive elimination reactions in related systems, see: (a) Kim, Y.-J.; Osakada, K.; Sugita, K.; Yamamoto, T.; Yamamoto, A. *Organometallics* **1988**, *7*, 2182. (b) Komiya, S.; Akai, Y.; Tanaka, K.; Yamamoto, T.; Yamamoto, A. *Organometallics* **1985**, *4*, 1130. (c) References 4 and 6.

Scheme 4



Scheme 5



C–X bonds, where X is a heteroatom, are exceedingly rare.<sup>8</sup> We have reported a few examples of such O,C-reductive eliminations in Ni(II) systems, but the yields are uniformly low (~15–20 %) and limited to cyclic derivatives (see Scheme 5).<sup>4</sup> The higher yield realized in the formation of **9** from **5** is an encouraging result that merits mechanistic investigation. It is noteworthy that similar reductive eliminations forming N–C bonds have been observed for related Ni(II) compounds (Scheme 5),<sup>9</sup> and these unusual elimination reactions might be a consequence of weak Ni–NR<sub>2</sub> and Ni–OR bonds in these electron-rich, late-metal complexes.

**Conclusions.** Nitrous oxide has been found to react slowly, in a regioselective way with (PMe<sub>3</sub>)<sub>2</sub>Ni(CH<sub>2</sub>-CMe<sub>2</sub>-o-C<sub>6</sub>H<sub>4</sub>) (**1**), a square-planar Ni(II) complex containing (i) two Ni–PMe<sub>3</sub> bonds, (ii) a Ni–C(aryl) bond, and (iii) a Ni–C(aliphatic) bond. The organometallic product, [(PMe<sub>3</sub>)Ni(O-o-C<sub>6</sub>H<sub>4</sub>CMe<sub>2</sub>CH<sub>2</sub>)]<sub>2</sub> (**2**), incorporates only one O-atom per Ni, and this appears as an O-insertion into the Ni–aryl bond. One equivalent of PMe<sub>3</sub> is oxidized to O=PMe<sub>3</sub>, and this probably occurs to a phosphine that has dissociated from the metal, i.e., the oxidation occurs outside of the Ni coordination

sphere. The observed regiochemistry of the O-insertion suggests, by analogy to literature precedent,<sup>6</sup> that N<sub>2</sub>O reacts by inserting into **1** as a heterocumulene, and not by simple direct O-transfer. Several monomeric derivatives of **2** have been prepared by reacting the dimer with chelating bidentate ligands, and the molecular structure of one such derivative, (dmpe)Ni(O-o-C<sub>6</sub>H<sub>4</sub>CMe<sub>2</sub>CH<sub>2</sub>) (**6**), has been determined by X-ray crystallography.

The 1,10-phenanthroline derivative (phen)Ni(O-o-C<sub>6</sub>H<sub>4</sub>CMe<sub>2</sub>CH<sub>2</sub>) (**5**) reacts with I<sub>2</sub> to effect formal O,C-reductive elimination to give the dihydrocoumarin **9** in good yield. Because of the unique nature of the reductive elimination to form a C–X bond in this and closely related systems,<sup>4,9</sup> we are actively investigating mechanistic details of this reaction.

**Acknowledgment.** We are grateful to the National Science Foundation for financial support of this research through a grant to G.L.H. (CHE-9200943) and to the government of South Korea for an Overseas Scholarship to K.K.

**Supplementary Material Available:** Tables of crystallographic details, atomic coordinates, bond angles and distances, anisotropic thermal parameters, and hydrogen atom coordinates (8 pages). Ordering information is given on any current masthead page.

OM940658J

(8) Collman, J. P.; Hegedus, L. S.; Norton, J. R.; Finke, R. G. *Principles and Applications of Organotransition Metal Chemistry*; University Science Books: Mill Valley, CA, 1987.

(9) Koo, K.; Hillhouse, G. L., unpublished results.

# Significance of Carbenoid Character during the Protonation of Four- and Five-Membered Diruthenacycles Formed from the Reaction of $\text{Ru}_2(\text{Me}_2\text{PCH}_2\text{PMe}_2)_2(\text{CO})_5$ with Dimethyl Acetylenedicarboxylate

Kimberly A. Johnson, Michael D. Vashon, Bahram Moasser, Bridget K. Warmka, and Wayne L. Gladfelter\*

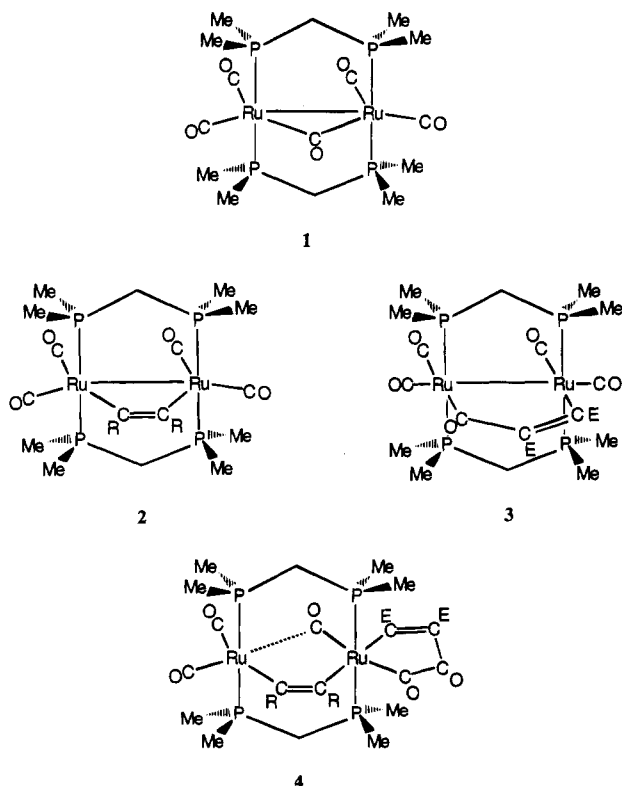
Department of Chemistry, University of Minnesota, Minneapolis, Minnesota 55455

Received August 23, 1994<sup>®</sup>

Protonation of the diruthenacyclobutene  $\text{Ru}_2(\text{dmpm})_2(\text{CO})_4[\mu\text{-}\eta^1\text{:}\eta^1\text{-C}_2(\text{CO}_2\text{Me})_2]$  (dmpm = bis(dimethylphosphino)methane) resulted in stereoselective formation of the chelated (*Z*)-alkenyl complex  $\{\text{Ru}_2(\text{dmpm})_2(\text{CO})_4[\text{C}_2(\text{H})(\text{CO}_2\text{Me})_2]\}[\text{BF}_4]$ , as determined by single-crystal X-ray crystallography ( $P2_12_12$  (No. 18) space group,  $a = 15.61(2)$  Å,  $b = 22.67(2)$  Å,  $c = 9.34(1)$  Å,  $V = 3308(5)$  Å<sup>3</sup>,  $Z = 4$ ). Protonation of the diruthenacyclopentenone  $\text{Ru}_2(\text{dmpm})_2(\text{CO})_4[\mu\text{-C}(\text{O})\text{C}_2(\text{CO}_2\text{Me})_2]$  occurs reversibly at the carbonyl oxygen of the bridging group, giving the corresponding diruthenacyclopentenol. The X-ray crystal structure of the solvated molecule [ $P2_1$  (No. 4) space group,  $a = 16.010(7)$  Å,  $b = 11.833(6)$  Å,  $c = 19.450(8)$  Å,  $\beta = 103.44(3)^\circ$ ,  $V = 3584(5)$  Å<sup>3</sup>,  $Z = 4$ ] and its unusual blue color suggest a highly delocalized  $\pi$ -system between the two metals. Reaction of the metal hydride  $[\text{HRu}_2(\text{dmpm})_2(\text{CO})_5][\text{BF}_4]$  with dimethyl acetylenedicarboxylate (DMAD) results in formation of a new C–H bond and a  $\sigma$ -bound (*E*)-alkenyl ligand. This same (*E*)-alkenyl product can also be formed by addition of CO to and alkene isomerization of the chelated (*Z*)-alkenyl complex  $\{\text{Ru}_2(\text{dmpm})_2(\text{CO})_4[\text{C}_2(\text{H})(\text{CO}_2\text{Me})_2]\}[\text{BF}_4]$ .

## Introduction

The formation of new C–C bonds by coupling CO and alkynes has been reported for several dinuclear metal complexes.<sup>1–14</sup> During studies of the reactivity of the electron-rich dinuclear ruthenium diphosphine complex  $\text{Ru}_2(\text{dmpm})_2(\text{CO})_5$  (**1**), we recently described the isolation and characterization of four- and five-membered dimetallacycles and an  $\alpha$ -ketoacyl complex that resulted from reaction of **1** with dimethyl acetylenedicarboxylate (DMAD).<sup>7</sup> Although these C–C bond-forming reactions proved facile, removal of the new organic moiety from the dimer was not observed. Reactions of these complexes with  $\text{H}^+$  appeared as a potential route to cleave the Ru–C bonds. In this paper we describe the results of protonating the complexes  $\text{Ru}_2(\text{dmpm})_2(\text{CO})_4[\mu\text{-C}(\text{O})\text{C}_2(\text{CO}_2\text{Me})_2]$  and  $\text{Ru}_2(\text{dmpm})_2(\text{CO})_4[\mu\text{-C}_2(\text{CO}_2\text{Me})_2]$



and reacting dimethyl acetylenedicarboxylate with  $[\text{HRu}_2(\text{dmpm})_2(\text{CO})_5]^+$ .

<sup>®</sup> Abstract published in *Advance ACS Abstracts*, December 1, 1994.

(1) Dyke, A. F.; Knox, S. A. R.; Morris, M. J.; Naish, P. J. *J. Chem. Soc., Dalton Trans.* **1983**, 1417.

(2) Knox, S. A. R. *Pure Appl. Chem.* **1984**, *56*, 81.

(3) Gracey, B. P.; Knox, S. A. R.; Macpherson, K. A.; Orpen, A. G.; Stobart, S. R. *J. Chem. Soc., Dalton Trans.* **1985**, 1935.

(4) Hogarth, G.; Kayser, F.; Knox, S. A. R.; Morton, D. A. V.; Orpen, A. G.; Turner, M. L. *J. Chem. Soc., Chem. Commun.* **1988**, 358.

(5) Shore, N. E. *Chem. Rev.* **1988**, *88*, 1081.

(6) Dickson, R. S. *Polyhedron* **1991**, *10*, 1995.

(7) Johnson, K. A.; Gladfelter, W. L. *Organometallics* **1992**, *11*, 2534.

(8) Garcia Alonso, F. J.; Riera, V.; Ruiz, M. A.; Tiripicchio, A.; Camellini, M. T. *Organometallics* **1992**, *11*, 370.

(9) Takats, J. *J. Cluster Sci.* **1992**, *3*, 479.

(10) Adams, R. D.; Chen, G.; Chen, L.; Wu, W.; Yin, J. *Organometallics* **1993**, *12*, 3431.

(11) Adams, R. D.; Chen, L.; Wu, W. *Organometallics* **1993**, *12*, 4112.

(12) Adams, R. D.; Chen, G.; Chen, L.; Yin, Y. *Organometallics* **1993**, *12*, 2644.

(13) Adams, R. D.; Chen, L.; Huang, M. *Organometallics* **1994**, *13*, 2696.

(14) Burn, M. J.; Kiel, G.-Y.; Seils, F.; Takats, J.; Washington, J. *J. Am. Chem. Soc.* **1989**, *111*, 6850.



Table 1. Summary of Spectroscopic Data

compd	$\nu_{\text{CO}}$ ( $\text{cm}^{-1}$ ; $\text{CH}_2\text{Cl}_2$ )	$^1\text{H}$ NMR (ppm; $\text{CD}_2\text{Cl}_2$ )	$^{31}\text{P}\{^1\text{H}\}$ NMR (ppm; $\text{CD}_2\text{Cl}_2$ )
5	2023 m, 1997 s, 1971 w, 1949 w, 1700 w, 1646 w	1.6 (s, 12H, Me), 1.73 (s, 12H, Me), 2.84 (m, 2H, $\text{CH}_2$ ), 2.97 (m, 2H, $\text{CH}_2$ ), 3.82 (s, 3H, OMe), 3.84 (s, 3H, OMe)	-3.0 (s, br)
6	2017 m, 1996 s, 1960 m, 1933 w, 1705 w, 1594 w, 1545 w ( $\nu_{\text{C}=\text{C}}$ )	1.72 (m, 24H, Me), 2.71 (m, 2H, $\text{CH}_2$ ), 2.96 (m, 2H, $\text{CH}_2$ ), 3.67 (s, 3H, OMe), 3.77 (s, 3H, OMe), 6.4 (s, 1H, vinyl)	aa'bb': $\delta_a$ 1.7, $\delta_b$ -2.6
8	2064 w, 2025 m, 1988 s, 1953 w, 1704 w, 1561 w ( $\nu_{\text{C}=\text{C}}$ )	1.61 (s, 12H, Me), 1.77 (s, 12H, Me), 2.4 (m, br, 2H, $\text{CH}_2$ ), 3.0 (m, br, 2H, $\text{CH}_2$ ), 3.63 (s, 3H, OMe), 3.78 (s, 3H, OMe), 6.1 (s, 1H, vinyl)	aa'bb': $\delta_a$ 0.82, $\delta_b$ 1.65 ( $J_{aa'} = 168$ , $J_{ab'} = 49$ , $J_{ab} = 21$ , $J_{a'b'} = 19$ , $J_{a'b} = 51$ , $J_{bb'} = 178$ Hz) <sup>a</sup>

<sup>a</sup> Values for the  $\delta$ 's and  $J$ 's were obtained by simulating the spectrum. The large (trans) P-P coupling constants represent the minimum values necessary to fit the spectrum.

Table 2. Summary of Crystallographic Data

	{Ru <sub>2</sub> (dmpm) <sub>2</sub> (CO) <sub>4</sub> [ $\mu$ -C(OH)C <sub>2</sub> (CO <sub>2</sub> Me) <sub>2</sub> ]}[BF <sub>4</sub> ]-CH <sub>2</sub> Cl <sub>2</sub> (5)	{Ru <sub>2</sub> (dmpm) <sub>2</sub> (CO) <sub>4</sub> [C(H)C <sub>2</sub> (CO <sub>2</sub> Me) <sub>2</sub> ]}[BF <sub>4</sub> ] <sup>1/2</sup> Et <sub>2</sub> O (6)
Crystal Parameters		
cryst syst	monoclinic	orthorhombic
space group	<i>P</i> 2 <sub>1</sub> (No. 4)	<i>P</i> 2 <sub>1</sub> 2 <sub>1</sub> 2 (No. 18)
formula	Ru <sub>2</sub> C <sub>22</sub> H <sub>37</sub> O <sub>9</sub> P <sub>4</sub> BF <sub>4</sub> Cl <sub>2</sub>	Ru <sub>2</sub> C <sub>22</sub> H <sub>40</sub> O <sub>8.5</sub> P <sub>4</sub> BF <sub>4</sub>
fw	929.27	853.39
<i>a</i> , Å	16.010(7)	15.61(2)
<i>b</i> , Å	11.833(6)	22.67(2)
<i>c</i> , Å	19.450(8)	9.34(1)
$\beta$ , deg	103.44(3)	90
<i>V</i> , Å <sup>3</sup>	3584(5)	3308(5)
<i>Z</i>	4	4
$\rho$ (calcd), g cm <sup>-3</sup>	1.722	1.713
temp, °C	-80	-116
abs coeff, cm <sup>-1</sup>	12.1	11.49
cryst dimens, mm	0.500 × 0.150 × 0.100	0.350 × 0.250 × 0.250
max-min abs cor factors, %	133-85	125-64
abs cor applied	empirical (DIFABS)	empirical (DIFABS)
Measurement of Intensity Data		
diffractometer	Enraf-Nonius CAD-4	
radiation	Mo K $\alpha$ ( $\lambda = 0.71073$ Å)	
monochromator	graphite cryst	
programs used	Texsan	
method of structure soln	Patterson	direct
scan type	$\omega$ -2 $\theta$	$\omega$ -2 $\theta$
scan range, deg	0-50	0-56
rfins measd	<i>h, k, l</i>	<i>hkl</i>
no. of unique rflns	6511	4466
no. of rflns used	4517	2387
cutoff	3 $\sigma$	3 $\sigma$
<i>R</i>	0.05	0.05
<i>R</i>	0.072	0.086
<i>R</i> <sub>w</sub>	0.087	0.105
error in observn of unit wt	2.10	2.79

## Experimental Section

**General Considerations.** Ru<sub>3</sub>(CO)<sub>12</sub> (Strem), bis(dimethylphosphino)methane (dmpm, Strem), tetrafluoroboric acid-diethyl ether complex (HBF<sub>4</sub>·Et<sub>2</sub>O, Aldrich), dimethyl acetylenedicarboxylate (DMAD, Aldrich), carbon monoxide (Air Products, CP grade, 99.3%), and <sup>13</sup>CO (Aldrich, 99%) were used without further purification. Ru<sub>2</sub>(dmpm)<sub>2</sub>(CO)<sub>5</sub>,<sup>15</sup> Ru<sub>2</sub>(dmpm)<sub>2</sub>(<sup>13</sup>CO)<sub>5</sub>, Ru<sub>2</sub>(dmpm)<sub>2</sub>(CO)<sub>4</sub>[ $\mu$ -C(O)C<sub>2</sub>(CO<sub>2</sub>Me)<sub>2</sub>],<sup>7</sup> Ru<sub>2</sub>(dmpm)<sub>2</sub>(CO)<sub>4</sub>[ $\mu$ -C<sub>2</sub>(CO<sub>2</sub>Me)<sub>2</sub>],<sup>15</sup> and [HRu<sub>2</sub>(dmpm)<sub>2</sub>(CO)<sub>5</sub>][BF<sub>4</sub>]<sup>15</sup> were prepared as previously reported. All <sup>13</sup>C-enriched materials were prepared using Ru<sub>2</sub>(dmpm)<sub>2</sub>(<sup>13</sup>CO)<sub>5</sub> (~60% enriched). Toluene, diethyl ether (Et<sub>2</sub>O), and hexane were dried by distillation from sodium benzophenone ketyl under nitrogen. Methylene chloride (CH<sub>2</sub>Cl<sub>2</sub>) was dried over calcium hydride and distilled under N<sub>2</sub> prior to use. All reactions were conducted under a nitrogen atmosphere using standard Schlenk techniques. Infrared spectra were obtained on a Mattson Polaris FTIR spectrometer. <sup>1</sup>H, <sup>13</sup>C, and <sup>31</sup>P NMR spectra were recorded on a Varian VXR-300 spectrometer. The <sup>31</sup>P NMR spectra were referenced to 85% H<sub>3</sub>PO<sub>4</sub> (external sample). Mass spectra were collected on a VG 7070E-HF instrument. Elemental analyses were performed by M-H-W Laboratories.

Table 1 contains a summary of the infrared and <sup>1</sup>H and <sup>31</sup>P-{<sup>1</sup>H} NMR spectroscopic data.

**Preparation of Ru<sub>2</sub>(dmpm)<sub>2</sub>(CO)<sub>4</sub>[ $\mu$ -C(OH)C<sub>2</sub>(CO<sub>2</sub>Me)<sub>2</sub>]-[BF<sub>4</sub>] (5).** Ru<sub>2</sub>(dmpm)<sub>2</sub>(CO)<sub>4</sub>[ $\mu$ -C(O)C<sub>2</sub>(CO<sub>2</sub>Me)<sub>2</sub>] (3; 0.056 g, 0.074 mmol) was charged to a 50 mL, three-neck flask equipped with a stirbar, gas adapter, and pressure-equalizing addition funnel then dissolved in CH<sub>2</sub>Cl<sub>2</sub> (10 mL). A CH<sub>2</sub>Cl<sub>2</sub> (5 mL) solution of HBF<sub>4</sub>·Et<sub>2</sub>O (25  $\mu$ L, 0.15 mmol) was added dropwise over 5 min. An immediate color change from orange to blue/green occurred, and after 10 min at room temperature the solution was blue. The solution was condensed to ~5 mL, and Et<sub>2</sub>O (8 mL) was added. When the mixture was cooled, air-stable blue-green needle-shaped crystals formed (yield 51 mg, 82%). <sup>13</sup>C{<sup>1</sup>H} NMR (CD<sub>2</sub>Cl<sub>2</sub>):  $\delta$  17.8 (m, CH<sub>3</sub>), 19.3 (m, CH<sub>3</sub>), 20.5 (m, CH<sub>3</sub>), 45.0 (quint,  $J_{\text{CP}} = 12.8$  Hz, CH<sub>2</sub>), 51.25 (s, OCH<sub>3</sub>), 149.7 (s, vinyl), 166.0 (s, C(O)OCH<sub>3</sub>), 179.2 (s, C(O)-OCH<sub>3</sub>), 189.9 (t,  $J_{\text{CP}} = 6.4$  Hz, CO), 191.2 (t,  $J_{\text{CP}} = 6.4$  Hz, CO), 207.4 (t,  $J_{\text{CP}} = 6.4$  Hz, 2 CO), 247.5 (t,  $J_{\text{CP}} = 8.6$  Hz, vinyl), 296.2 (t,  $J_{\text{CP}} = 4.2$  Hz, COH). Anal. Calcd for {HRu<sub>2</sub>(dmpm)<sub>2</sub>(CO)<sub>5</sub>[C<sub>2</sub>(CO<sub>2</sub>Me)<sub>2</sub>]}[BF<sub>4</sub>]: C, 29.86; H, 4.15; P, 14.69. Found: C, 29.74; H, 4.41; P, 14.46. FAB mass spectrum: (<sup>101</sup>Ru) *m/e* 758, int. 99%, [P]<sup>+</sup>; fragments observed, [P - *n*CO]<sup>+</sup>, where *n* = 1-4.

Table 3. Positional Parameters for  $\{\text{Ru}_2(\text{dmpm})_2(\text{CO})_4[\mu\text{-C}(\text{OH})\text{C}_2(\text{CO}_2\text{Me})_2]\}[\text{BF}_4]\cdot\text{CH}_2\text{Cl}_2$ 

atom	x	y	z	atom	x	y	z
Ru1A	0.1617(1)	0.2306(1)	-0.06282(9)	C12B	0.654(1)	0.431(2)	0.456(1)
Ru2A	0.3353(1)	0.2268(2)	0.0235(1)	O12B	0.643(1)	0.517(1)	0.4734(9)
P11A	0.1153(4)	0.1784(5)	0.0386(3)	C21B	0.954(1)	0.276(2)	0.567(1)
P12A	0.2144(4)	0.2906(5)	-0.1600(3)	O21B	1.024(1)	0.262(2)	0.594(1)
P21A	0.2885(4)	0.2348(7)	0.1299(3)	C22B	0.841(2)	0.456(3)	0.506(2)
P22A	0.3867(4)	0.2109(7)	-0.0802(3)	O22B	0.838(1)	0.551(2)	0.511(1)
C11A	0.048(1)	0.222(2)	-0.123(1)	C1B	0.698(1)	0.190(2)	0.606(1)
O11A	-0.020(1)	0.226(2)	-0.155(1)	C2B	0.813(1)	0.264(2)	0.323(1)
C12A	0.150(1)	0.392(2)	-0.038(1)	C3B	0.535(2)	0.298(2)	0.549(1)
O12A	0.140(1)	0.477(2)	-0.0205(9)	C4B	0.560(2)	0.070(2)	0.512(1)
C21A	0.448(2)	0.209(2)	0.076(1)	C5B	0.650(2)	0.314(2)	0.243(1)
O21A	0.520(1)	0.195(2)	0.107(1)	C6B	0.740(1)	0.489(2)	0.328(1)
C22A	0.341(1)	0.392(2)	0.022(1)	C7B	0.752(1)	0.417(2)	0.648(1)
O22A	0.341(1)	0.485(2)	0.0184(9)	C8B	0.863(2)	0.238(3)	0.695(1)
C1A	0.174(1)	0.253(2)	0.117(1)	C9B	0.959(2)	0.386(3)	0.397(2)
C2A	0.312(1)	0.214(2)	-0.165(1)	C10B	0.954(2)	0.144(3)	0.410(2)
C3A	0.115(2)	0.027(2)	0.062(1)	C13B	0.767(2)	0.053(2)	0.457(1)
C4A	0.003(2)	0.219(2)	0.034(1)	C14B	0.777(1)	-0.073(2)	0.458(1)
C5A	0.144(1)	0.279(2)	-0.248(1)	C15B	0.736(3)	-0.249(4)	0.402(2)
C6A	0.245(1)	0.439(2)	-0.163(1)	C16B	0.699(1)	0.106(2)	0.411(1)
C7A	0.329(2)	0.357(3)	0.184(2)	C17B	0.651(1)	0.050(2)	0.348(1)
C8A	0.314(2)	0.115(2)	0.188(1)	C18B	0.525(2)	-0.040(3)	0.293(2)
C9A	0.451(2)	0.082(2)	-0.083(1)	C19B	0.823(1)	0.120(2)	0.510(1)
C10A	0.465(2)	0.318(2)	-0.088(1)	O1B	0.825(1)	-0.128(2)	0.503(1)
C13A	0.255(2)	0.001(2)	-0.040(1)	O2B	0.726(1)	-0.125(2)	0.403(1)
C14A	0.263(2)	-0.126(2)	-0.045(1)	O3B	0.675(1)	0.048(2)	0.293(1)
C15A	0.216(2)	-0.290(3)	-0.109(2)	O4B	0.574(1)	0.011(1)	0.3523(8)
C16A	0.191(1)	0.064(2)	-0.079(1)	O5B	0.875(1)	0.058(2)	0.561(1)
C17A	0.131(1)	0.009(2)	-0.142(1)	B1Z	0.0172(6)	0.0608(9)	0.2336(5)
C18A	0.000(2)	-0.068(3)	-0.189(2)	F1Z	-0.026(1)	0.156(1)	0.243(1)
C19A	0.314(1)	0.058(2)	0.015(1)	F2Z	0.0967(8)	0.089(1)	0.2254(8)
O1A	0.315(1)	-0.183(2)	-0.003(1)	F3Z	-0.026(1)	0.005(1)	0.1751(6)
O2A	0.209(1)	-0.169(2)	-0.098(1)	F4Z	0.025(1)	-0.007(1)	0.2912(6)
O3A	0.148(1)	0.011(1)	-0.2009(8)	B1Y	0.500(1)	0.101(1)	0.7242(8)
O4A	0.060(1)	-0.024(1)	-0.1279(9)	F1Y	0.447(1)	0.183(2)	0.738(1)
O5A	0.368(1)	-0.009(2)	0.064(1)	F2Y	0.570(1)	0.149(2)	0.708(1)
Ru1B	0.6651(1)	0.2726(2)	0.4266(1)	F3Y	0.458(2)	0.037(2)	0.669(1)
Ru2B	0.8392(1)	0.2862(2)	0.5125(1)	F4Y	0.526(1)	0.035(2)	0.782(1)
P11B	0.6165(4)	0.2079(5)	0.5253(3)	C1X	0.199(2)	0.239(2)	0.361(1)
P12B	0.7171(4)	0.3373(6)	0.3303(3)	C11X	0.3084(5)	0.2231(8)	0.3902(5)
P21B	0.7866(4)	0.2840(6)	0.6148(3)	C12X	0.1744(6)	0.3733(8)	0.3205(4)
P22B	0.8912(4)	0.2726(8)	0.4094(3)	C1W	0.703(3)	0.175(4)	0.856(3)
C11B	0.552(1)	0.256(2)	0.369(1)	C11W	0.8050(8)	0.117(2)	0.871(1)
O11B	0.485(1)	0.254(2)	0.335(1)	C12W	0.708(1)	0.3150(9)	0.8299(7)

**Preparation of  $\text{Ru}_2(\text{dmpm})_2(\text{CO})_4[\text{C}_2(\text{H})(\text{CO}_2\text{Me})_2][\text{BF}_4]$  (6).**  $\text{Ru}_2(\text{dmpm})_2(\text{CO})_4[\text{C}_2(\text{CO}_2\text{Me})_2]$  (2; 0.03 g, 0.04 mmol) was charged to a 50 mL, three-neck flask equipped with a stirbar, gas adapter, and pressure-equalizing addition funnel and dissolved in  $\text{CH}_2\text{Cl}_2$  (10 mL). A  $\text{CH}_2\text{Cl}_2$  (5 mL) solution of  $\text{HBF}_4\cdot\text{Et}_2\text{O}$  (7.6  $\mu\text{L}$  of an 85% solution, 0.04 mol) was added dropwise over 5 min. The color of the solution changed slightly from pale yellow to yellow. The reaction mixture was stirred at room temperature for 30 min. Air-stable, solvated, yellow crystals were isolated (yield 26 mg, 80%) by condensing the solution to approximately half of the original volume and then adding  $\text{Et}_2\text{O}$  (10 mL).  $^{13}\text{C}\{^1\text{H}\}$  NMR ( $\text{CD}_2\text{Cl}_2$ ):  $\delta$  18.0 (m,  $\text{CH}_3$ ), 18.8 (m,  $\text{CH}_3$ ), 20.4 (m,  $\text{CH}_3$ ), 39.1 (quint,  $J_{\text{CP}} = 12.8$  Hz,  $\text{CH}_2$ ), 52.0 (s,  $\text{OCH}_3$ ), 55.2 (s,  $\text{OCH}_3$ ), 136.2 (t,  $J_{\text{CP}} = 5.5$  Hz,  $\text{RuC}=\text{C}$ ), 164.6 (s,  $\text{RuC}=\text{C}$ ), 170.9 (t,  $J_{\text{CP}} = 14$  Hz,  $\text{C}(\text{O})\text{OCH}_3$ ), 185.9 (t,  $J_{\text{CP}} = 8$  Hz, CO), 191.8 (s,  $\text{C}(\text{O})\text{OCH}_3$ ), 192.7 (t,  $J_{\text{CP}} = 9$  Hz, CO), 206.1 (t,  $J_{\text{CP}} = 13$  Hz, CO), 207.1 (t,  $J_{\text{CP}} = 13$  Hz, CO). FAB mass spectrum: ( $^{101}\text{Ru}$ )  $m/e$  730, int. 30%,  $[\text{P}]^+$ ; fragments observed,  $[\text{P} - n\text{CO}]^+$ , where  $n = 1-4$ .

**Reaction of  $[\text{HRu}_2(\text{dmpm})_2(\text{CO})_5][\text{BF}_4]$  (7) with  $\text{C}_2(\text{CO}_2\text{Me})_2$ .** 7 (0.06 g, 0.085 mmol) was charged to a 50 mL, three-neck flask equipped with a stirbar, gas adapter, and pressure-equalizing addition funnel and then dissolved in  $\text{CH}_2\text{Cl}_2$  (10 mL). A  $\text{CH}_2\text{Cl}_2$  (10 mL) solution of DMAD (10.5  $\mu\text{L}$ , 0.085 mmol) was added dropwise over 5 min. No color change was observed. An infrared spectrum of the solution after 1 h at room temperature showed complete reaction of the starting materials. A yellow powder was isolated (yield 52 mg, 73%) by slowly adding small portions of hexane until the solid

precipitated.  $^{13}\text{C}$  NMR ( $\text{CD}_2\text{Cl}_2$ , 75 MHz):  $\delta$  16.5 (br m,  $^1J_{\text{CH}} = 134$  Hz, 4  $\text{CH}_3$ ), 19.6 (br m,  $^1J_{\text{CH}} = 125$  Hz, 2  $\text{CH}_3$ ), 20.7 (br m,  $^1J_{\text{CH}} = 130$  Hz, 2  $\text{CH}_3$ ), 48.5 (tt,  $^1J_{\text{CH}} = 130$ ,  $^1J_{\text{CP}} = 14.8$  Hz,  $\text{CH}_2$ ), 50.8 (q,  $^1J_{\text{CH}} = 146$  Hz,  $\text{OCH}_3$ ), 51.2 (q,  $^1J_{\text{CH}} = 146$  Hz,  $\text{OCH}_3$ ), 124.6 (d,  $^1J_{\text{CH}} = 164$  Hz,  $\text{RuC}=\text{CH}$ ), 163.1 (m,  $^2J_{\text{CP}} = 3.5$  Hz,  $\text{RuC}=\text{CH}$ ), 176.0 (tdd,  $^2J_{\text{CP}} = 9.4$ ,  $^2J_{\text{CH}} = 1.9$ ,  $^3J_{\text{CH}} = 1.9$  Hz,  $\text{C}(\text{O})\text{OCH}_3$ ), 178.1 (dq,  $^3J_{\text{CH}} = 14.8$ ,  $^3J_{\text{CP}} = 4.0$  Hz,  $\text{C}(\text{O})\text{OCH}_3$ ), 188.6 (t,  $J_{\text{CP}} = 8.7$  Hz, CO), 209.6 (m, 2 CO), 210.9 (t,  $J_{\text{CP}} = 13.3$  Hz, 2 CO). Anal. Calcd for  $[\text{HRu}_2(\text{dmpm})_2(\text{CO})_5[\text{C}_2(\text{CO}_2\text{Me})_2][\text{BF}_4]$  (8): C, 29.82; H, 4.14. Found: C, 29.65; H, 4.37. FAB mass spectrum: ( $^{101}\text{Ru}$ )  $m/e$  759, int. 40%,  $[\text{P}]^+$ ; fragments observed,  $[\text{P} - n\text{CO}]^+$ , where  $n = 1-4$ .

**Carbonylation of 6.** An NMR tube was charged with 35 mg (0.04 mmol) of 6 and subsequently connected to a modified calibrated gas volume assembly. When the NMR tube was cooled to  $-78$  °C, 0.74 mL of  $\text{CD}_2\text{Cl}_2$  was condensed into the tube from a vacuum still. A valve on the apparatus was opened to a source of CO (1 atm) and then closed again. The lower portion of the NMR tube was immersed in liquid  $\text{N}_2$ , and after 15 min the tube was flame-sealed. The amount of dissolved CO was approximated (0.04 mmol) from integration of the  $^{13}\text{C}$  NMR signal at 184 ppm relative to C9 in the spectrum of the final product. The initial total pressure inside the tube at 25 °C was estimated to be 5 atm. When the sample was thawed and efficient mixing of the head space gas with the solution was ensured (54 mM), the tube was placed into the probe of the spectrometer and the first spectrum collected approximately 5 min after the sample was warmed to room temperature.

**Table 4. Bond Distances (Å) in**  
**[Ru<sub>2</sub>(dmpm)<sub>2</sub>(CO)<sub>4</sub>[μ-C(OH)C<sub>2</sub>(CO<sub>2</sub>Me)<sub>2</sub>][BF<sub>4</sub>]-CH<sub>2</sub>Cl<sub>2</sub>**

A. Metal-Metal and Metal-Ligand Distances			
Ru1A-Ru2A	2.894(3)	Ru1B-Ru2B	2.902(3)
Ru1A-P11A	2.347(7)	Ru1B-P11B	2.362(7)
Ru1A-P12A	2.351(6)	Ru1B-P12B	2.348(7)
Ru1A-C11A	1.93(2)	Ru1B-C11B	1.90(2)
Ru1A-C12A	1.99(2)	Ru1B-C12B	1.98(2)
Ru1A-C16A	2.07(2)	Ru1B-C16B	2.08(2)
Ru2A-P21A	2.360(7)	Ru2B-P21B	2.333(7)
Ru2A-P22A	2.358(7)	Ru2B-P22B	2.349(8)
Ru2A-C21A	1.87(3)	Ru2B-C21B	1.90(2)
Ru2A-C22A	1.96(2)	Ru2B-C22B	2.01(3)
Ru2A-C19A	2.03(2)	Ru2B-C19B	1.98(2)
B. Intraligand Distances			
P11A-C1A	1.83(2)	P11B-C1B	1.81(2)
P21A-C1A	1.81(2)	P21B-C1B	1.78(2)
P12A-C2A	1.83(2)	P12B-C2B	1.80(2)
P22A-C2A	1.80(2)	P22B-C2B	1.84(2)
C11A-O11A	1.12(3)	C11B-O11B	1.13(3)
C21A-O21A	1.18(3)	C21B-O21B	1.13(3)
C12A-O12A	1.09(3)	C12B-O12B	1.10(3)
C22A-O22A	1.09(3)	C22B-O22B	1.14(4)
C19A-C13A	1.42(3)	C19B-C13B	1.43(3)
C13A-C16A	1.35(3)	C13B-C16B	1.38(3)
C16A-C17A	1.52(3)	C16B-C17B	1.45(3)
C13A-C14A	1.51(4)	C13B-C14B	1.50(3)
C19A-O5A	1.39(3)	C19B-O5B	1.36(2)
C14A-O1A	1.22(3)	C14B-O1B	1.21(3)
C17A-O3A	1.23(3)	C17B-O3B	1.22(3)
C14A-O2A	1.29(3)	C14B-O2B	1.33(3)
C15A-O2A	1.45(4)	C15B-O2B	1.47(5)
C17A-O4A	1.30(3)	C17B-O4B	1.34(3)
C18A-O4A	1.44(3)	C18B-O4B	1.38(3)

**X-ray Crystallographic Studies.** Neither compound yielded high-quality crystals during any of the several attempts to obtain a sample for the single-crystal structural analysis. Thick blue crystals of **5** and yellow crystals of **6** were grown as described in the previous sections. Suitable crystals were removed directly from the supernatant and coated with a high-viscosity hydrocarbon, mounted on a fiber, and cooled to -80 °C for **5** and -116 °C for **6**. Several crystals of **6** were twinned; the final, irregularly shaped crystal chosen for complete data collection was slightly cracked, and the intensities were weak. A preliminary peak search of 25 centered reflections indicated that the crystal of **5** was monoclinic and that **6** was orthorhombic. The space group  $P2_1$  (No. 4) was chosen for **5** on the basis of the systematic absences ( $0k0 = 2n + 1$ ), packing considerations, and statistical analysis of intensity distribution. Following successful refinement of **5**, an examination of the structure revealed a pronounced pseudosymmetry. If the coordinates of molecule A were  $x$ ,  $y$ , and  $z$ , the coordinates of molecule B were approximately  $x + 0.5$ ,  $y + 0.05$ , and  $z + 0.5$ . That is, they were related by an approximate translation of 0.5, 0.05, 0.5. If the  $y$  translation were 0, rather than 0.05, the true unit cell would be half as large with  $a' = a$ ,  $b' = b$ , and  $c' = (a + c)/2$ . In this case the reflections  $h + l$  odd would have zero intensity. In fact, the reflections with  $h + l$  odd were much less intense than those with  $h + l$  even, but they were present. The unique space group  $P2_12_12_1$  (No. 18) was chosen for **6** on the basis of the systematic absences ( $h00$ ,  $h = 2n + 1$ ;  $0k0$ ,  $k = 2n + 1$ ). During data collection, no decay of intensity was observed in three check reflections for either crystal. Table 2 includes the details of the structural analyses.

Because the structure of **5** was acentric, there were not enough data to give all atoms anisotropic displacement parameters. Only the heavy atoms (Ru, P, and Cl) were refined anisotropically. For **6**, anisotropic temperature factors were used for all non-hydrogen atoms except C3, C5, C11, C13, C16, C21, and the solvent atoms (O1Z, C2Z, and C3Z). Attempts to model these atoms with anisotropic temperature factors were unsuccessful. Hydrogen atoms were included in the structure factor calculations for both structures in idealized

**Table 5. Bond Angles (deg) for**  
**[Ru<sub>2</sub>(dmpm)<sub>2</sub>(CO)<sub>4</sub>[μ-C(OH)C<sub>2</sub>(CO<sub>2</sub>Me)<sub>2</sub>][BF<sub>4</sub>]-CH<sub>2</sub>Cl<sub>2</sub>**

A. Ligand-Metal-Ligand Angles			
C11A-Ru1A-C12A	93.8(9)	C11B-Ru1B-C12B	97.2(9)
C11A-Ru1A-C16A	94.3(8)	C11B-Ru1B-C16B	93.7(8)
C11A-Ru1A-P11A	93.0(7)	C11B-Ru1B-P11B	90.0(8)
C11A-Ru1A-P12A	89.8(6)	C11B-Ru1B-P12B	91.6(8)
C11A-Ru1A-Ru2A	175.7(7)	C11B-Ru1B-Ru2B	177.2(7)
C12A-Ru1A-C16A	171.9(8)	C12B-Ru1B-C16B	168.8(7)
C12A-Ru1A-P11A	89.1(7)	C12B-Ru1B-P12B	89.7(7)
C12A-Ru1A-P12A	88.6(7)	C12B-Ru1B-P11B	90.1(7)
C12A-Ru1A-Ru2A	90.5(6)	C12B-Ru1B-Ru2B	85.6(6)
C16A-Ru1A-P12A	91.7(6)	C16B-Ru1B-P12B	92.5(6)
C16A-Ru1A-P11A	90.2(8)	C16B-Ru1B-P11B	87.4(6)
C16A-Ru1A-Ru2A	81.4(5)	C16B-Ru1B-Ru2B	83.5(5)
P12A-Ru1A-P11A	176.5(2)	P12B-Ru1B-P11B	178.5(2)
P12A-Ru1A-Ru2A	89.8(1)	P12B-Ru1B-Ru2B	88.3(2)
P11A-Ru1A-Ru2A	87.6(2)	P11B-Ru1B-Ru2B	90.2(1)
C21A-Ru2A-C19A	93(1)	C21B-Ru2B-C19B	93.2(9)
C21A-Ru2A-C22A	95(1)	C21B-Ru2B-C22B	94(1)
C21A-Ru2A-P22A	88.2(1)	C21B-Ru2B-P22B	88.6(7)
C21A-Ru2A-P21A	89.6(9)	C21B-Ru2B-P21B	91.4(7)
C21A-Ru2A-Ru1A	173.8(9)	C21B-Ru2B-Ru1B	172.9(8)
C19A-Ru2A-C22A	171.9(7)	C19B-Ru2B-C22B	172.5(9)
C19A-Ru2A-P22A	86.1(6)	C19B-Ru2B-P22B	88.7(6)
C19A-Ru2A-P21A	91.9(6)	C19B-Ru2B-P21B	86.7(6)
C19A-Ru2A-Ru1A	81.1(5)	C19B-Ru2B-Ru1B	80.0(5)
C22A-Ru2A-P22A	92.2(6)	C22B-Ru2B-P22B	90(1)
C22A-Ru2A-P21A	90.0(6)	C22B-Ru2B-P21B	94.4(9)
C22A-Ru2A-Ru1A	91.0(5)	C22B-Ru2B-Ru1B	92.6(8)
P22A-Ru2A-P21A	177.0(3)	P22B-Ru2B-P21B	175.5(3)
P22A-Ru2A-Ru1A	89.0(2)	P22B-Ru2B-Ru1B	89.3(2)
P21A-Ru2A-Ru1A	92.9(2)	P21B-Ru2B-Ru1B	90.1(2)
B. Intraligand Angles			
Ru1A-P11A-C1A	112.1(8)	Ru1B-P11B-C1B	115.9(8)
Ru1A-P12A-C2A	111.2(7)	Ru1B-P12B-C2B	111.8(7)
Ru2A-P21A-C1A	113.9(8)	Ru2B-P21B-C1B	111.4(8)
Ru2A-P22A-C2A	119.5(8)	Ru2B-P22B-C2B	118.7(8)
P11A-C1A-P21A	111(1)	P11B-C1B-P21B	114(1)
P12A-C2A-P22A	111(1)	P12B-C2B-P22B	108(1)
Ru1A-C16A-C13A	128(2)	Ru1B-C16B-C13B	122(1)
Ru2A-C19A-C13A	127(1)	Ru2B-C19B-C13B	128(1)
C19A-C13A-C16A	116(2)	C19B-C13B-C16B	118(2)
Ru1A-C11A-O11A	174(2)	Ru1B-C11B-O11B	176(2)
Ru1A-C12A-O12A	173(2)	Ru1B-C12B-O12B	176(2)
Ru2A-C21A-O21A	178(3)	Ru2B-C21B-O21B	174(2)
Ru2A-C22A-O22A	177(2)	Ru2B-C22B-O22B	170(3)

positions using  $d_{C-H} = 0.95$  Å and an isotropic temperature factor 20% greater than the  $B_{eq}$  value of the carbon to which they were bonded. The values of the atomic scattering factors used in the calculations were taken from the usual tabulations,<sup>16-18</sup> and the effects for anomalous dispersion were included for the non-hydrogen atoms. The positional parameters, bond distances, and bond angles are listed in Tables 3-5 for **5** and Tables 6-8 for **6**.

## Results

**Isolation and Spectroscopic Characterization of 5.** The protonation of **3** with  $\text{HBF}_4 \cdot \text{Et}_2\text{O}$  was conducted at room temperature in  $\text{CH}_2\text{Cl}_2$ . The rapid color change from orange to blue indicated the reaction occurred upon addition of the acid. Isolation of the product was accomplished by crystallization from a 1/1  $\text{CH}_2\text{Cl}_2/\text{Et}_2\text{O}$  solution. The mass spectrum and elemental analysis of the material were consistent with the molecular

(16) Cromer, D. T.; Waber, J. T. In *International Tables for X-Ray Crystallography*; Kynoch Press: Birmingham, England, 1974; Vol. IV, Table 2.

(17) Cromer, D. T. In *International Tables for X-Ray Crystallography*; Kynoch Press: Birmingham, England, 1974; Vol. IV, Table 2.

(18) Cromer, D. T.; Ibers, J. A. In *International Tables for X-Ray Crystallography*; Kynoch Press: Birmingham, England, 1974; Vol. IV, Table 2.

**Table 6. Positional Parameters for  $\{\text{Ru}_2(\text{dmpm})_2(\text{CO})_4[\text{C}_2(\text{H})(\text{CO}_2\text{Me})_2]\}[\text{BF}_4]^{1/2}\text{Et}_2\text{O}$** 

atom	x	y	z
Ru1	0.2182(1)	0.2056(1)	0.2664(2)
Ru2	0.3107(1)	0.1356(1)	0.4861(2)
P11	0.2945(5)	0.2876(4)	0.3530(6)
P12	0.1519(5)	0.1174(4)	0.1932(7)
P21	0.3272(4)	0.2204(3)	0.6314(6)
P22	0.2951(6)	0.0506(3)	0.3446(6)
C11	0.144(2)	0.212(1)	0.430(2)
O11	0.099(1)	0.214(1)	0.524(2)
C12	0.157(2)	0.253(2)	0.132(3)
O12	0.118(1)	0.281(1)	0.050(2)
C13	0.321(2)	0.185(1)	0.157(2)
O13	0.378(1)	0.173(1)	0.094(1)
C21	0.224(2)	0.111(1)	0.592(3)
O21	0.162(1)	0.097(1)	0.666(2)
C1	0.295(2)	0.289(1)	0.544(2)
C2	0.231(2)	0.058(1)	0.175(2)
C3	0.403(2)	0.295(1)	0.300(2)
C4	0.251(2)	0.359(2)	0.308(3)
C5	0.433(2)	0.232(1)	0.697(3)
C6	0.266(2)	0.220(2)	0.795(2)
C7	0.108(4)	0.114(2)	0.016(3)
C8	0.068(2)	0.089(3)	0.306(4)
C9	0.252(3)	-0.012(1)	0.440(3)
C10	0.389(3)	0.021(2)	0.266(4)
C14	0.399(2)	0.092(1)	0.611(3)
C15	0.377(2)	0.061(1)	0.745(3)
C16	0.372(2)	-0.028(2)	0.875(3)
C17	0.478(2)	0.092(1)	0.571(2)
C18	0.492(2)	0.127(1)	0.439(2)
C19	0.581(2)	0.158(1)	0.247(3)
O1	0.351(2)	0.0857(9)	0.853(2)
O2	0.387(2)	0.0041(8)	0.747(2)
O3	0.433(1)	0.1527(6)	0.384(1)
O4	0.571(1)	0.127(1)	0.387(2)
B1	0.838(3)	0.104(3)	0.104(5)
F1	0.753(2)	0.100(1)	0.092(3)
F2	0.862(2)	0.111(1)	0.230(2)
F3	0.866(2)	0.155(1)	0.035(3)
F4	0.875(2)	0.062(1)	0.027(3)
O1Z	0	0	0.769(9)
C2Z	-0.049(2)	0.040(1)	0.717(3)
C3Z	-0.051(2)	0.045(1)	0.576(2)

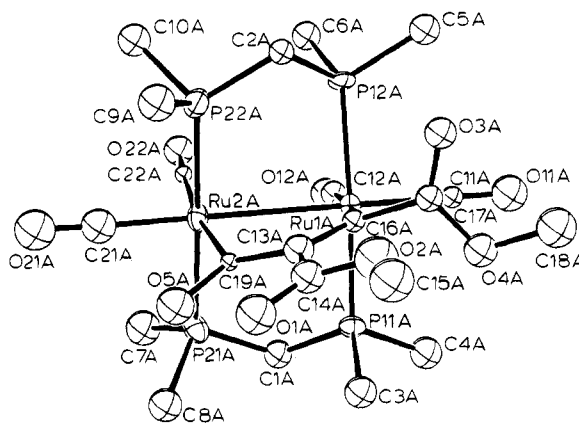
**Table 7. Bond Distances (Å) in  $\{\text{Ru}_2(\text{dmpm})_2(\text{CO})_4[\text{C}_2(\text{H})(\text{CO}_2\text{Me})_2]\}[\text{BF}_4]^{1/2}\text{Et}_2\text{O}$** 

A. Metal-Metal and Metal-Ligand Distances			
Ru1-Ru2	2.970(4)	Ru2-P21	2.367(8)
Ru1-P11	2.352(8)	Ru2-P22	2.351(8)
Ru1-P12	2.35(1)	Ru2-C21	1.78(3)
Ru1-C11	1.92(2)	Ru2-C14	2.05(3)
Ru1-C12	1.91(4)	Ru2-O3	2.17(2)
Ru1-C13	1.95(3)		
B. Intraligand Distances			
P11-C1	1.78(2)	P21-C1	1.83(3)
P12-C2	1.82(3)	P22-C2	1.89(2)
C11-O11	1.12(3)	C21-O21	1.22(3)
C12-O12	1.17(4)	C13-O13	1.11(3)
C14-C17	1.29(4)	C17-C18	1.48(3)
C18-O3	1.21(3)	C14-C15	1.48(4)
C15-O1	1.23(3)		

formula  $\{\text{Ru}_2(\text{dmpm})_2(\text{CO})_4[\text{C}(\text{OH})\text{C}_2(\text{CO}_2\text{Me})_2]\}[\text{BF}_4]$  (**5**). The infrared spectrum of **5** exhibited terminal metal carbonyl stretching energies from 2023 to 1949  $\text{cm}^{-1}$ , a shift of 30  $\text{cm}^{-1}$  to higher energy from the corresponding stretches in **3**, consistent with the change from a neutral to a cationic metal species. Also observed were stretches due to the ester carbonyls at 1700 and 1646  $\text{cm}^{-1}$  and a  $\nu_{\text{C-C}}$  band at 1530  $\text{cm}^{-1}$ . The singlet at 149.7 ppm in the  $^{13}\text{C}$  NMR spectrum was assigned to C13 (see Figure 1), and the two singlets at 166.0 and 179.24 ppm were assigned to two ester carbonyls. The multiplets at 189.9, 191.1, and 207.4 ppm were due to the metal carbonyls. The two downfield signals at 247.5 and 296.2

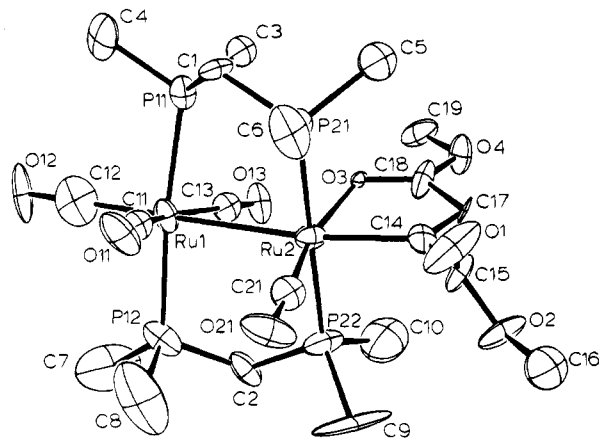
**Table 8. Bond Angles (deg) for  $\{\text{Ru}_2(\text{dmpm})_2(\text{CO})_4[\text{C}_2(\text{H})(\text{CO}_2\text{Me})_2]\}[\text{BF}_4]^{1/2}\text{Et}_2\text{O}$** 

A. Ligand-Metal-Ligand Angles			
C11-Ru1-C12	100(1)	C21-Ru2-C14	92(1)
C11-Ru1-C13	158(1)	C21-Ru2-O3	168(1)
C11-Ru1-P12	91.9(9)	C21-Ru2-P22	89(1)
C11-Ru1-P11	88.3(8)	C21-Ru2-P21	91(1)
C11-Ru1-Ru2	77.7(8)	C21-Ru2-Ru1	101(1)
C12-Ru1-C13	101(1)	C14-Ru2-O3	75(1)
C12-Ru1-P12	94(1)	C14-Ru2-P22	89.8(7)
C12-Ru1-P11	92(1)	C14-Ru2-P21	89.4(7)
C12-Ru1-Ru2	177.5(8)	C14-Ru2-Ru1	167.0(9)
C13-Ru1-P12	90.3(8)	O3-Ru2-P22	89.5(4)
C13-Ru1-P11	87.3(8)	O3-Ru2-P21	90.7(4)
C13-Ru1-Ru2	80.6(7)	O3-Ru2-Ru1	91.6(4)
P12-Ru1-P11	174.0(3)	P22-Ru2-P21	179.1(3)
P12-Ru1-Ru2	87.8(2)	P22-Ru2-Ru1	89.9(2)
P11-Ru1-Ru2	86.4(2)	P21-Ru2-Ru1	90.9(2)
B. Intraligand Angles			
Ru1-P11-C1	111(1)	Ru2-P21-C1	113.8(7)
Ru1-P12-C2	111(1)	Ru2-P22-C2	117(1)
Ru1-C11-O11	178(3)	Ru2-C21-O21	177(3)
Ru1-C12-O12	179(3)	Ru2-C14-C17	119(2)
Ru1-C13-O13	179(3)	Ru2-O3-C18	113(2)
P11-C1-P21	116(1)	P12-C2-P22	110(1)
C14-C17-C18	112(2)	O3-C18-C17	120(3)

**Figure 1.** ORTEP drawing of the cation portion of **5** showing the atom labels. Thermal ellipsoids are drawn at the 50% probability level.

ppm were assigned to the remaining vinyl carbon, C16, and the carbonyl carbon, C19, respectively. The downfield shift of these resonances suggested there was delocalization of the  $\pi$ -electron density resulting from metal-to-carbon multiple-bond character. These spectroscopic data were consistent with protonation at the carbonyl oxygen, O5. The  $^{31}\text{P}$  NMR spectrum exhibited a broad singlet at -3.0 ppm. We propose that the minor chemical differences between the two rutheniums reduce the chemical shifts between the phosphorus ligands to the point where they are nearly identical. The electronic absorption spectrum of **5** revealed absorption maxima at 600 (320), 400 (2100), and 321 nm (16 700  $\text{M}^{-1}\text{cm}^{-1}$ ).

**Structure of 5.** Single-crystal X-ray crystallography of **5** established that the structure consisted of well-separated cation, anion, and solvent units with two of each per asymmetric unit. As shown in Figure 1, the axial positions were occupied by the dmpm ligands. The equatorial plane contained four terminal carbonyl ligands and a three-carbon bridge in the same diruthenacyclopentenone arrangement found in **3**. The Ru1A-Ru2A distance of 2.894(3) Å (Ru1B-Ru2B = 2.902(3) Å) was shortened significantly from that of **3** (Ru1-Ru2 = 2.936(1) Å). The angle between the planes defined by P11-Ru1-P12-Ru2 and P21-Ru2-P22-Ru1 of 19.87°



**Figure 2.** ORTEP drawing of the cation portion of **6** showing the atom labels. Thermal ellipsoids are drawn at the 50% probability level.

indicated the ruthenium–phosphine framework was twisted in comparison to that in  $\text{Ru}_2(\text{dmpm})_2(\text{CO})_5$  (twist angle  $3.75^\circ$ );<sup>15</sup> however, it was identical with the corresponding twist angle in **3** of  $19.82^\circ$ .<sup>7</sup> The lengthening of the C19A–O5A distance from 1.23(3) Å in **3** to 1.39(3) Å (C19B–O5B = 1.36(2) Å) in **5** was consistent with the assignment of O5 as the site of protonation. The short Ru1A–C16A and Ru2A–C19A distances of 2.07(2) (Ru1B–C16B = 2.08(2) Å) and 2.03(2) Å (Ru2B–C19B = 1.98(2) Å), respectively, and the similarity between C19A–C13A and C13A–C16A distances of 1.42(3) Å (C19B–C13B = 1.43(3) Å) and 1.35(3) Å (C13B–C16B = 1.38(3) Å), respectively, suggested a delocalized  $\pi$ -system across these four bonds.

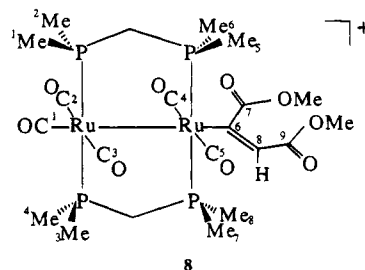
**Isolation and Spectroscopic Characterization of 6.** Protonation of **2** with  $\text{HBF}_4 \cdot \text{Et}_2\text{O}$  resulted in a subtle color change from pale yellow to yellow over a period of approximately 20 min. The mass spectrum and elemental analysis of the yellow, crystalline product were consistent with the molecular formula  $\{\text{Ru}_2(\text{dmpm})_2(\text{CO})_4[\text{C}_2\text{H}(\text{CO}_2\text{Me})_2]\}[\text{BF}_4]$  (**6**). The infrared spectrum of **6** displayed four terminal CO bands from 2018 to 1934  $\text{cm}^{-1}$ , ester stretches at 1704 and 1594  $\text{cm}^{-1}$ , and the  $\nu_{\text{C}=\text{C}}$  band at 1545  $\text{cm}^{-1}$ . The  $^1\text{H}$  NMR spectrum exhibited a singlet due to the vinyl proton at 6.4 ppm. In the  $^{13}\text{C}\{^1\text{H}\}$  NMR spectrum, the resonances at 185.9, 192.7, 206.1, and 207.1 ppm were assigned to the metal carbonyls by  $^{13}\text{C}\{^1\text{H}\}$  NMR of the  $^{13}\text{CO}$ -enriched material. By virtue of the chemical shifts, the multiplet at 136.2 ppm and the singlet at 164.6 ppm were assigned to the vinyl carbons C17 and C14, respectively (see Figure 2 for numbering). The metal-bound carbons of most  $\sigma$ -alkenyl complexes are usually located well downfield from the uncomplexed carbon.<sup>19</sup> The singlet at 191.8 ppm was assigned to the ester carbonyl carbon C15, which was deshielded slightly compared to C18 (170.9 ppm) due to complexation of the oxygen to the ruthenium.

**Structure of 6.** The structure of **6** (Figure 2) consisted of well-separated cation, anion, and solvent molecules. The connectivity of the cation portion of the molecule was found to be quite different from that of **2**. The equatorial ligands included four terminal CO's and a chelating five-membered metallacycle comprised of one Ru, the two vinyl carbons, and the carbonyl carbon and oxygen of one of the ester groups of the DMAD

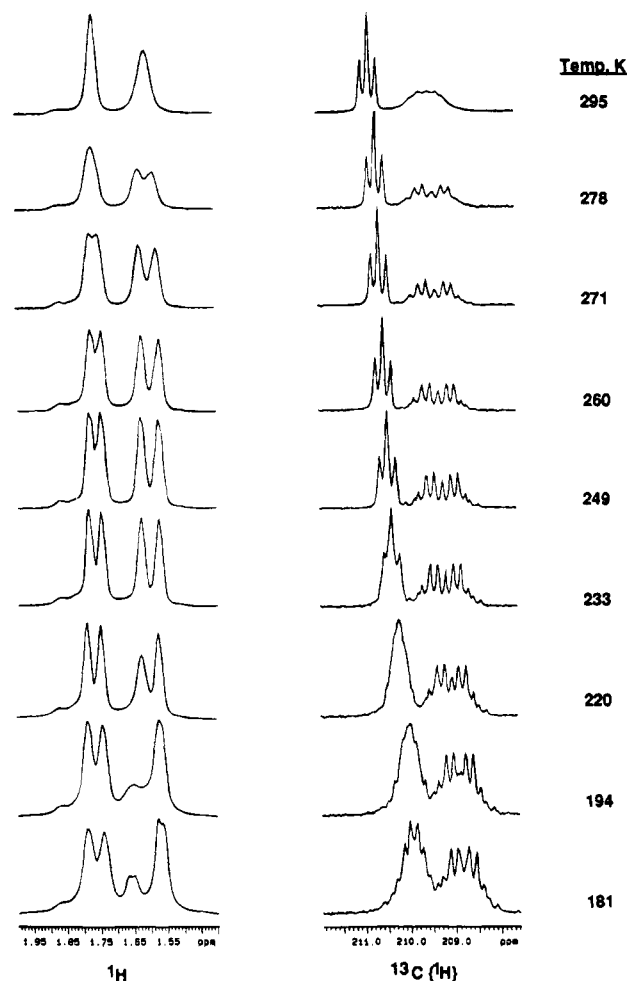
ligand. The axial positions were occupied by the diphosphine ligands. The Ru1–Ru2 bond distance of 2.970(4) Å was elongated in comparison to other structures reported for this system. The angle between the planes defined by P11–Ru1–P12–Ru2 and P21–Ru2–P22–Ru1 of  $35.2^\circ$  illustrated the severe twisting of the ruthenium–phosphine framework. The freedom to twist in **6** was due to the lack of a third bridging ligand across the metal–metal bond. The dmpm bridges were flexible enough such that, in the absence of a more rigid bridge, the molecule was free to adopt a nearly staggered conformation, minimizing electronic repulsion between the  $d\pi$  orbitals of adjacent metal centers as well as steric congestion due to 1,2-diaxial ligand interactions.<sup>20</sup>

The Ru2–C21 distance of 1.78(3) Å was somewhat shorter than that of the other carbonyl ligands (1.91(4)–1.95(3) Å), consistent with the weak trans influence of the ester ligand. The Ru2–C14 distance of 2.05(3) Å is typical for a Ru–C single bond. The C14–C17 and C17–C18 distances of 1.29(4) and 1.48(3) Å, respectively, indicated the  $\pi$  bond is localized between C14 and C17. The long Ru2–O3 distance of 2.17(2) Å and the C18–O3 distance of 1.21(3) Å suggested only a weak interaction exists between Ru2 and O3.

**Isolation and Solution Spectroscopic Characterization of 8.** The reaction of **7** with DMAD resulted in a color change from yellow to very pale yellow over a period of about 15 min. The product was isolated as a pale yellow powder, and the elemental analysis and mass spectral data established it as  $\{\text{Ru}_2(\text{dmpm})_2(\text{CO})_5[\text{C}_2\text{H}(\text{CO}_2\text{Me})_2]\}[\text{BF}_4]$  (**8**). The infrared spectrum of **8** displayed three CO terminal bands from 2024 to 1953  $\text{cm}^{-1}$ , an ester band at 1704  $\text{cm}^{-1}$ , and the  $\nu_{\text{C}=\text{C}}$  signal at 1561  $\text{cm}^{-1}$ . The  $^1\text{H}$  NMR spectrum contained a resonance located at 6.1 ppm assigned to the vinyl hydrogen. The methyl and methylene signals from the dmpm ligands were broadened, rendering the  $^{31}\text{P}$  coupling unresolvable. This broadening was also reflected in the  $^{13}\text{C}\{^1\text{H}\}$  NMR spectrum of the phosphine methyl multiplets. On the basis of the observed coupling to the vinyl hydrogen ( $J_{\text{CH}} = 164$  Hz), the singlet at 124.8 ppm in the  $^{13}\text{C}$  NMR spectrum was assigned to the carbon C8 (see below). As with compound **6**, the carbon bound to the ruthenium was shifted downfield to 163.1 ppm. The signals at 175.7 and 178.0 ppm both displayed C–H coupling to the three hydrogens of the methyl esters and were assigned to the ester carbonyl carbons. The 178.0 ppm resonance also displayed a 14.8 Hz coupling constant to the vinylic hydrogen, whereas the peak at 175.7 ppm exhibited a small, approximately 2 Hz, coupling to this hydrogen. This pattern of coupling constants defined the stereochemistry<sup>21</sup>



The resonance at 175.7 was a triplet due to long-range “W” carbon–phosphorus coupling. The location of the vinyl ligand in the position trans to the Ru–Ru bond was consistent with the spectroscopy and was similar



**Figure 3.** Variable-temperature  $^1\text{H}$  and  $^{13}\text{C}\{^1\text{H}\}$  NMR spectra for **8**.

to the location of the methyl and acetyl ligands in  $[\text{Ru}_2(\text{dmpm})_2(\text{CO})_5\text{Me}]^+$  and  $\{\text{Ru}_2(\text{dmpm})_2(\text{CO})_5[\text{C}(\text{O})\text{-Me}]\}^+$ .<sup>22</sup>

Compound **8** was found to be fluxional on the NMR time scale. Figure 3 shows the phosphine–methyl region of the  $^1\text{H}$  NMR spectrum and the  $^{13}\text{C}\{^1\text{H}\}$  NMR signals from four of the five carbonyl ligands. The methyl signals at 295 K were each integrated to 12 protons. Cooling the sample to 233 K resulted in gradual separation of these two broad bands into four signals. At 233 K, the four resonances represented the sets [1, 3], [2, 4], [5, 7], and [6, 8]. The corresponding  $^{13}\text{C}\{^1\text{H}\}$  NMR spectrum exhibited resolution of the broad multiplet at 295 K into overlapping multiplets for the (now different) carbonyls 4 and 5. Because the sample was only partly enriched (60%) with  $^{13}\text{CO}$ , the complex pattern that appeared by 233 K at 209 ppm resulted from the superposition of two spin systems. The species exhibiting the  $\text{trans-}^{13}\text{C}\text{-}^{13}\text{C}$  coupling accounted for 43% of the total intensity. This coupling was absent in the two  $^{13}\text{C}/^{12}\text{C}$  isotopomers, which accounted for 57% of the intensity. A complete modeling of the spectrum was not undertaken. The triplet at 210.5 ppm exhibited a slight broadening by 233 K, and the triplet at 188.6 (assigned to C1) was unchanged throughout the entire

temperature range. The fluxional process causing these spectral changes was proposed to be the rotation of the vinyl group about the Ru–C bond, which was hindered by the phosphine methyl groups.

Between 233 and 181 K a second set of spectral changes were observed. The  $^1\text{H}$  NMR spectrum showed all four peaks broadening at 220 K. The  $^1\text{H}$  NMR resonance located at 1.62 ppm significantly broadened by 194 K but then sharpened into a doublet by 181 K. The  $^{13}\text{C}\{^1\text{H}\}$  NMR spectrum showed the coalescence of the triplet at 210 ppm while additional changes occurred in the multiplet at 209 ppm. By 194 K the multiplet at 210 ppm began to be resolved while the multiplet at 209 ppm completely lost its center peak.

We have no convincing explanation for the lower energy process. With the absence of a third bridging ligand, however, we would predict that the  $\text{Ru}_2\text{P}_4$  framework of **8** would be twisted into a staggered conformation as was observed in the structure of **6**. The low-temperature process may represent rotation about the Ru–Ru bond that would interconvert the conformers present as a result of the twisting of the  $\text{Ru}_2\text{P}_4$  backbone.

Finally, we were also able to isolate **8** by the reaction of **6** with CO. When this reaction was conducted in a sealed NMR tube at approximately 5 atm of CO pressure, **6** smoothly transformed into **8** with no observable intermediates. A plot of  $\ln[\mathbf{6}]$  vs time was linear for 6 half-lives and yielded an observed rate constant of  $5.58 \times 10^{-4} \text{ s}^{-1}$ . The effect of CO pressure was not studied.

## Discussion

A summary of the protonations described in this paper, in addition to the synthetic reactions for preparing the starting materials, is shown in Scheme 1. The starting zerovalent diruthenium complex is the only species to yield an isolable metal hydride. At least formally, the oxidation state of each ruthenium increased in both **2** and **3** to +1, a fact that may contribute to the reduced basicity of the M–M bond.

The most notable physical change observed during any of the reactions is the blue color formed upon protonation of orange solutions of **3**. The electronic absorption spectrum indicates transitions at 600 (320), 400 (2100), and 321 nm ( $16\,700 \text{ M}^{-1} \text{ cm}^{-1}$ ). The dinuclear ruthenium complex  $[(\eta^5\text{-C}_5\text{H}_5)_2\text{Ru}(\text{CO})_2]_2$  exists in both the CO-bridged and nonbridged structures. The electronic absorption features in the spectrum of the unbridged isomer of  $[(\eta^5\text{-C}_5\text{H}_5)_2\text{Ru}(\text{CO})_2]_2$  appear at 330 (13 900) and 435 nm ( $1280 \text{ M}^{-1} \text{ cm}^{-1}$ ) and are assigned to the  $\sigma$  to  $\sigma^*$  and  $d\pi$  to  $\sigma^*$  transitions, respectively.<sup>23</sup> The intensity and wavelength of the absorption of **5** at 321 nm suggest its assignment to a  $\sigma$  to  $\sigma^*$  transition of the Ru–Ru bond. In addition, we assign the shoulder at 400 nm to the  $d\pi$  to  $\sigma^*$  transition. The blue color of the complex, however, is due to the 600 nm absorption and is unusual.

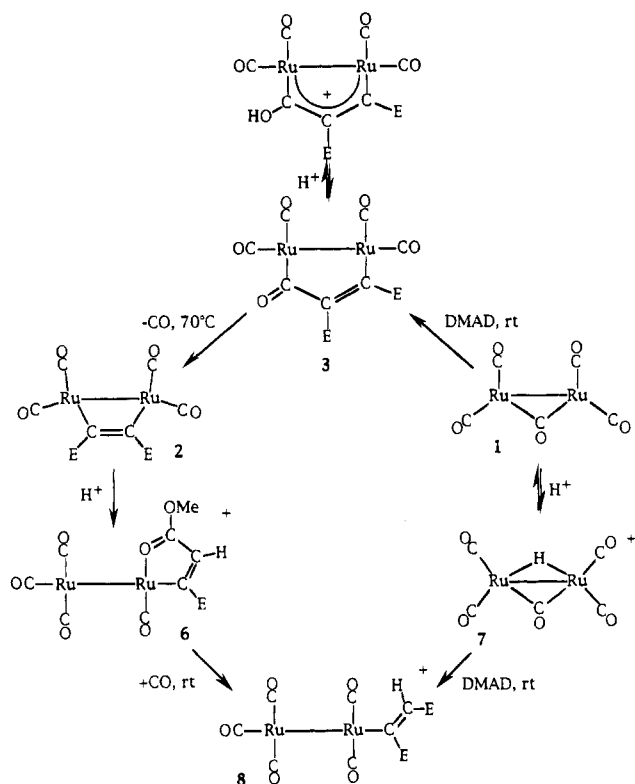
(20) Kullberg, M. L.; Lemke, F. R.; Powell, D. R.; Kubiak, C. P. *Inorg. Chem.* **1985**, *24*, 3589.

(21) Marshall, J. L. *Carbon-Carbon and Carbon-Proton NMR Couplings*; Verlag Chemie: Deerfield Beach, FL, 1983; Vol. 2, p 241.

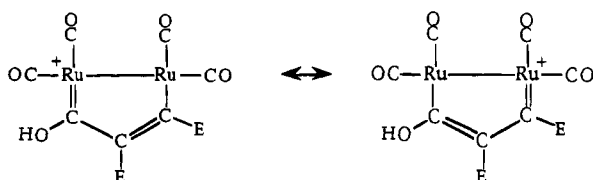
(22) Johnson, K. A.; Gladfelter, W. L. *Organometallics* **1990**, *9*, 2101.

(23) Abrahamson, H. B.; Palazzotto, M. C.; Reichel, C. L.; Wrighton, M. S. *J. Am. Chem. Soc.* **1979**, *101*, 4123.

## Scheme 1. Summary of Reactions



The two resonance hybrids of **5** that highlight the extended  $\pi$  system connecting the two metals are



These resonance hybrids are not degenerate due to the electronic differences between the  $-\text{OH}$  and  $-\text{COOMe}$  substituents located on carbons C19 and C16 (the metal-bound carbons). It is noteworthy that formal oxidation states of the two metals differ. One possible explanation of the electronic absorption feature at 600 nm is that it results from an intervalence charge-transfer transition that would have the effect of interconverting the resonance structures shown above. Alternatively, this absorption could be assigned to a  $\pi$  to  $\pi^*$  or an  $n(\text{d}\pi)$  to  $\pi^*$  transition involving a fully delocalized pentadienyl  $(\text{Ru}-\text{C}-\text{C}-\text{C}-\text{Ru})^+$  chromophore. The structural features discussed below favor the delocalized bonding model.

The reversible nature of the protonation was discovered when **5** was dissolved in THF. An infrared spectrum of the solution indicates that **3** forms, presumably by deprotonation by the anion. When this solution is concentrated to dryness, **5** is regenerated. This behavior is notably different from that observed during the protonation of related dimetallacyclopentenones.<sup>1,2,9</sup> The final products usually involve cleavage of the carbonyl carbon to alkyne carbon bond and produce a bridging alkenyl ligand. In one case an intermediate is isolated in which the proton is bound to the carbonyl carbon.<sup>1</sup> The protonation of **3** at the carbonyl oxygen is similar to the O-alkylation of a related mononuclear

rhenacyclobutenone, an observation explained by invoking substantial carbenoid character of the Re-C bond.<sup>24</sup>

Single-crystal X-ray crystallographic studies of both the neutral and protonated forms of the molecule allow an opportunity to observe the structural changes that occur upon protonation of **3**. Figure 4 shows the equatorial planes of compounds **3** and **5** (dmpm ligands omitted). The Ru1A-Ru2A distance of 2.894(3) Å (Ru1B-Ru2B = 2.902(3) Å) in **5** is shortened compared to the Ru1-Ru2 distance in **3** (2.936(1) Å). The distances between the metals and the carbons of the bridge also contracted upon protonation, suggesting an increase in the Ru-C multiple-bond character of this interaction. This is consistent with the downfield shift of the signals due to these carbons in the <sup>13</sup>C NMR spectrum. The contraction of the C19-C13 distance and the slight lengthening of the C13-C16 distance in **5** are consistent with the delocalization of the  $\pi$ -electrons described above. The lengthening of the C19A-O5A bond to 1.39(2) Å (C19B-O5B = 1.36(2) Å) is the primary evidence indicating that O5 is the site of protonation. It is interesting to note how the adjacent ester group has oriented itself to be coplanar with C19-O5 (angle between planes O5A-C19A-C13A and C13A-C14A-O1A 7.17°). Although the proton is not crystallographically located, we suggest that it lies somewhere between O5 and O1 and that hydrogen bonding may be responsible for the twist of the ester group. This may also contribute to the difficulty in locating the resonance for O-H in the <sup>1</sup>H NMR spectrum.

The two reactions that yield a new C-H bond are related to each other by switching the order of addition of the substrates (alkyne and H<sup>+</sup>) to Ru<sub>2</sub>(dmpm)<sub>2</sub>(CO)<sub>5</sub>. Formation of the metal hydride followed by alkyne addition results in stereoselective cis addition, whereas protonation of the preformed alkyne complex leads exclusively to the Z product. Although no intermediates were observed, alkyne coordination prior to migratory insertion is the most likely sequence for the formation of the (E)-alkenyl complex **8**.

While cis stereochemistry is the more common result of insertion of alkynes into mononuclear metal hydrides, similar reactions with di- and polynuclear metal complexes can lead to either cis or trans stereochemistry. With complexes containing the  $\mu$ - $\eta^2$ -alkyne bonding mode, e.g. Fe<sub>2</sub>( $\mu$ - $\eta^2$ -RCCR)(CO)<sub>6</sub> and Rh<sub>2</sub>( $\mu$ -H)<sub>2</sub>( $\mu$ - $\eta^2$ -RCCR)[P(O-*i*-Pr)<sub>3</sub>]<sub>4</sub>, trans addition predominates.<sup>25</sup> Dinuclear A-frame complexes, however, produce cis addition products.<sup>26-28</sup> Protonation of a cis-dimetallated complex of DMAD, Fe<sub>2</sub>(SMe)<sub>2</sub>(CO)<sub>6</sub>(DMAD), by Mathieu and co-workers also resulted in formation of a cis-alkene product via a mechanism involving initial attack of H<sup>+</sup> at one of the metal centers, forming the metal hydride.<sup>29</sup>

One of the two explanations of the trans stereochemistry resulting from the protonation of **2** is summarized in Scheme 2. Protonation on one of the carbonyls of **2** is aided by the electron-rich nature of the metals.

(24) Padolik, L. L.; Gallucci, J. C.; Wojcicki, A. *J. Am. Chem. Soc.* **1993**, *115*, 9986.

(25) Burch, R. R.; Shusterman, A. J.; Muetterties, E. L.; Teller, R. G.; Williams, J. M. *J. Am. Chem. Soc.* **1983**, *105*, 3546.

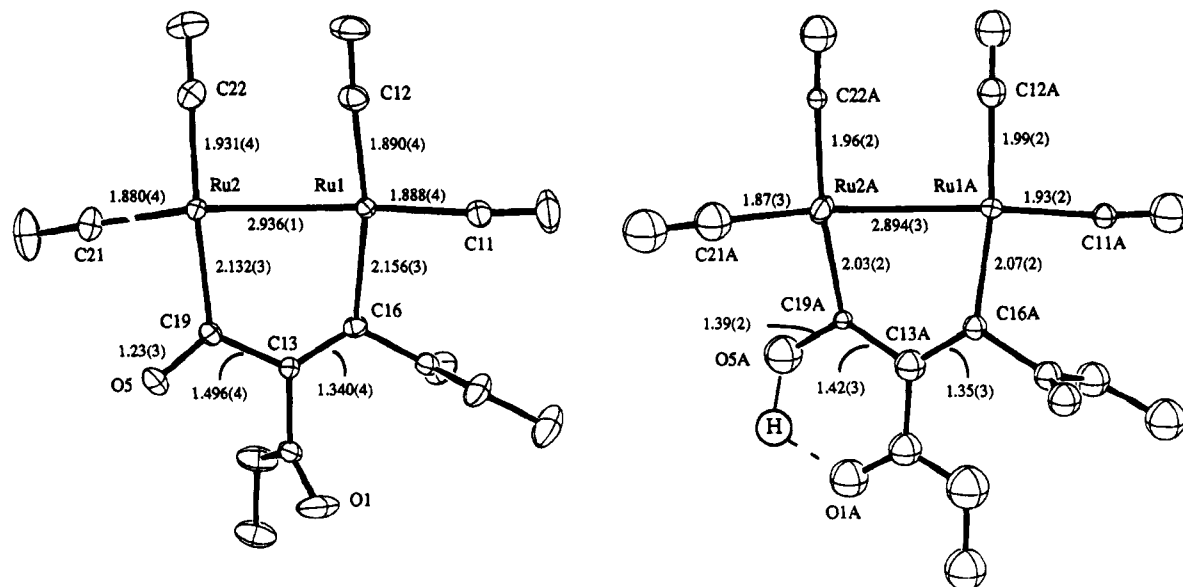
(26) Hommeltoft, S. I.; Berry, D. H.; Eisenberg, R. *J. Am. Chem. Soc.* **1986**, *108*, 5345.

(27) Vaartstra, B. A.; Cowie, M. *Organometallics* **1990**, *9*, 1594.

(28) Berry, D. H.; Eisenberg, R. *Organometallics* **1987**, *6*, 1796.

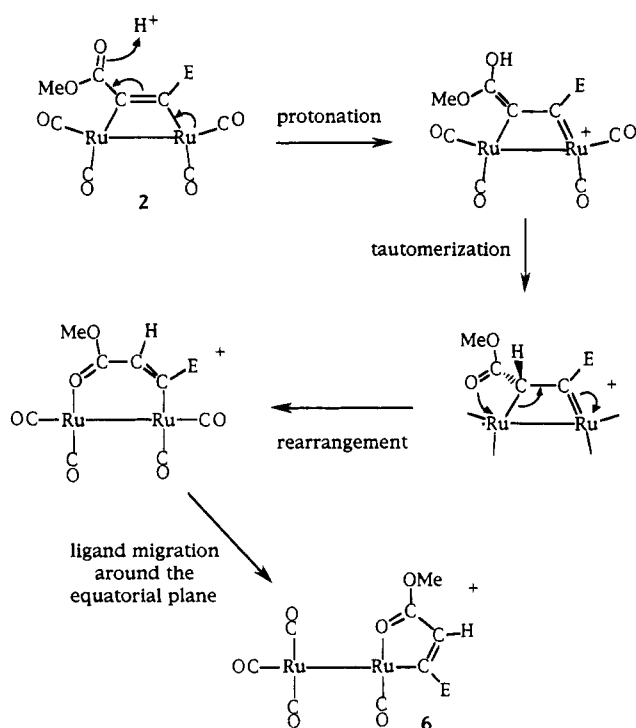
(29) Bonnet, J. J.; Mathieu, R.; Ibers, J. A. *Inorg. Chem.* **1980**, *19*, 2448.





**Figure 4.** ORTEP drawings of **3** (left) and the cation portion of **5** (right) showing the structural differences in the ligands of the equatorial plane (dmpm ligands omitted for clarity).

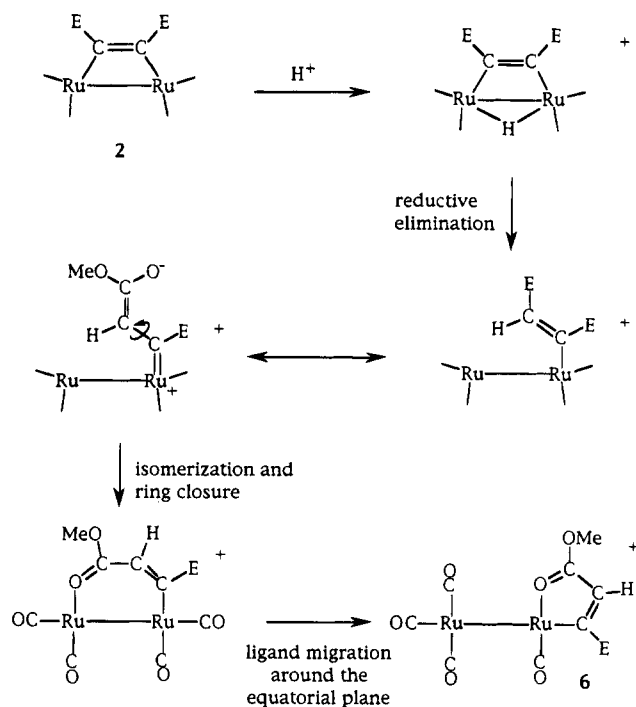
### Scheme 2. Trans Ru-H Addition via Ligand Protonation



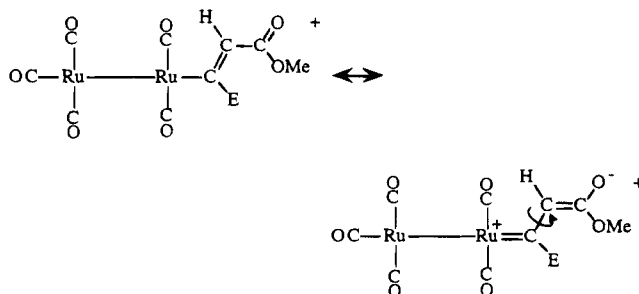
Tautomerization of this intermediate provides a path for the formation of the new C-H bond. Rearrangement of the complex could occur by substitution of the Ru-C with the Ru-O linkage. The stereochemistry would be established when rotation about the C-C bond occurs, allowing favorable  $\pi$ -overlap between the C orbital initially bound to Ru and the p orbital on the carbene carbon. The most favorable direction of rotation would bring the ester carbonyl oxygen toward (rather than away from) the ruthenium to form the Ru-O bond. This motion locks in the trans stereochemistry. The final migration of the ligands around the equatorial plane is likely to have a low energy barrier.

Compounds **6** and **8** differ by one CO ligand and the alkenyl stereochemistry. Anticipating the weakness of

### Scheme 3. Trans Ru-H Addition via Isomerization



the Ru-O bond in **6**, we observed its reaction with CO. Surprisingly, the alkenyl stereochemistry changed from *Z* to *E*, an isomerization that can be explained by the significance of the carbenoid resonance hybrid



The driving force controlling the stereochemistry in **8** is the reduced steric repulsion between the alkenyl ligand of the *E* isomer and the remaining ligands attached to the same ruthenium.

This facile isomerization allows us to propose (Scheme 3) an alternative mechanism for the formation of **6**. Protonation of the Ru–Ru bond followed by reductive elimination of the C–H bond would form an (*E*)- $\sigma$ -alkenyl complex which could isomerize to the *Z* isomer, a process that would be driven in the forward direction by chelation.

In all of the reactions described in this paper, the combination of the electron-rich nature of the Ru<sub>2</sub>(dmpm)<sub>2</sub> unit and the electron-poor alkyne enhances the

importance of carbenoid resonance forms which appear to dominate the reactivity of these metallacycles.

**Acknowledgment.** The research was supported by a grant (No. CHE-9021923) from the National Science Foundation. K.A.J. gratefully acknowledges fellowship support from the University of Minnesota, Department of Chemistry. We thank Doyle Britton for determining the crystal structures.

**Supplementary Material Available:** Lists of H atom positions, thermal parameters, and bond distances and angles for **5** and **6** (30 pages). Ordering information is given on any current masthead page.

OM9406759

# Borabenzene Derivatives. 22.<sup>1</sup> Synthesis of Boratabenzene Salts from 2,4-Pentadienylboranes. Structure of [NMe<sub>3</sub>Ph][C<sub>5</sub>H<sub>5</sub>BMe]

Gerhard E. Herberich,\* Bernd Schmidt, and Ulli Englert

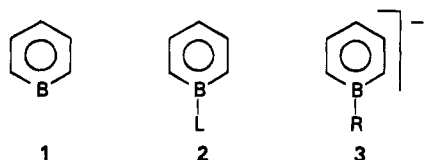
Institut für Anorganische Chemie, Technische Hochschule Aachen, D-52056 Aachen, Germany

Received August 12, 1994<sup>®</sup>

Borylation of potassium pentadienide with BCl(NR<sub>2</sub>)<sub>2</sub> and subsequent alcoholysis produce 2,4-pentadienylboranes C<sub>5</sub>H<sub>7</sub>B(NR<sub>2</sub>)<sub>2</sub> (**4a-c**: R = Me, Et, Pr<sup>i</sup>), C<sub>5</sub>H<sub>7</sub>B(OR)<sub>2</sub> (**4e,f**: R = Et, Bu<sup>t</sup>), and C<sub>5</sub>H<sub>7</sub>B(OCR<sub>2</sub>)<sub>2</sub> with 1,3,2-dioxaborolane rings (**4g,h**: R = H, Me) as mixtures of *E* and *Z* isomers. Metalation of **4a,b** in THF by lithium dialkylamides LiNR'<sub>2</sub> (R' = Me, Et, Pr<sup>i</sup>) in the presence of TMEDA results (i) in a nonproductive deborylation via primary attack at the boron center, (ii) in ring closure to produce boratabenzene salts [Li(TMEDA)][C<sub>5</sub>H<sub>5</sub>BNR<sub>2</sub>] (**10a,b**: R = Me, Et), and (iii) in substitution of *B*-dialkylamino groups when NR<sub>2</sub> is bulkier than NR'<sub>2</sub>. **10a** is obtained in 26.5% yield. Metalation of **4h** in THF by the sterically demanding lithium dialkylamides LDA and LiTMP affords a precipitate of the spiroborate [Li(THF)][C<sub>5</sub>H<sub>6</sub>B(OCMe<sub>2</sub>)<sub>2</sub>] (**13**) in 63% yield in equilibrium with the presumed isomer Li[C<sub>5</sub>H<sub>5</sub>BO(CMe<sub>2</sub>)<sub>2</sub>OH] (Li(**3g**)) in the THF solution. **13** can be transformed into boratabenzenes by several methods. (i) Treatment with Me<sub>3</sub>SiCl produces a 1:1 mixture of isomeric boracyclohexadienes C<sub>5</sub>H<sub>6</sub>BOCMe<sub>2</sub>CMe<sub>2</sub>OSiMe<sub>3</sub> (**15a**, 2,4-isomer; **15b**, 2,5-isomer) which, on subsequent low-temperature metalation, give Li[C<sub>5</sub>H<sub>5</sub>BO(CMe<sub>2</sub>)OSiMe<sub>3</sub>] (Li(**3h**)). (ii) Metalation of **13** at -78 °C affords Li<sub>2</sub>[C<sub>5</sub>H<sub>5</sub>BO(CMe<sub>2</sub>)O] (Li<sub>2</sub>(**3i**)) and, after treatment with Me<sub>3</sub>SiCl, the bora-2,4-cyclohexadiene (5-Me<sub>3</sub>Si)C<sub>5</sub>H<sub>5</sub>BOCMe<sub>2</sub>CMe<sub>2</sub>OSiMe<sub>3</sub> (**16**). (iii) Treatment of **13** with Al<sub>2</sub>Me<sub>6</sub> in toluene at -78 °C affords Li[C<sub>5</sub>H<sub>5</sub>BMe] (Li(**3b**)) in 79% yield as a white solid. This salt is also obtained from Li(**3h**) and Al<sub>2</sub>Me<sub>6</sub>. (iv) Addition of **15** to LiBu<sup>t</sup> in pentane/hexane produces Li[C<sub>5</sub>H<sub>5</sub>BBu<sup>t</sup>] (Li(**3c**)) in 53% yield. Combining strongly alkaline aqueous solutions of [NMe<sub>3</sub>Ph]I and Li(**3b**) affords [NMe<sub>3</sub>Ph][C<sub>5</sub>H<sub>5</sub>BMe] (**18**). **18** crystallizes in the monoclinic space group *P*2<sub>1</sub>/*n* with *a* = 935.4(1) pm, *b* = 1557.4(4) pm, *c* = 988.8(1) pm, β = 95.47(1)°, and *Z* = 4. The 1-methylboratabenzene ion of **18** displays nearly perfect C<sub>2v</sub> symmetry with intra-ring bond distances of 150.1, 138.8, and 139.2 pm (average) for B-C1 (B-C5), C1-C2 (C4-C5), and C2-C3 (C3-C4), respectively.

## Introduction

Borabenzene (borinine)<sup>3</sup> **1** is a highly reactive species.<sup>4</sup>



**2**: a, L = py; b, L = N<sub>2</sub>

**3**: a, R = Ph; b, R = Me; c, R = Bu<sup>t</sup>; d, R = NMe<sub>2</sub>;

e, R = NEt<sub>2</sub>; f, R = OMe; g, R = O(CMe<sub>2</sub>)<sub>2</sub>OH;

h, R = O(CMe<sub>2</sub>)<sub>2</sub>OSiMe<sub>3</sub>; i, R = O(CMe<sub>2</sub>)O<sup>-</sup>

According to quantum-chemical calculations<sup>5</sup> (MNDO,<sup>5a</sup> ab initio STO-3G and 4-31G,<sup>5b</sup> HF/6-31G\* and MP2/6-31G\*<sup>5c</sup>) **1** is a planar aromatic ring with a low-lying in-

plane σ\* orbital which is largely localized at the boron atom. **1** can be stabilized by uncharged Lewis bases, as in the borabenzene-pyridine adduct **2a**,<sup>6</sup> and an adduct with N<sub>2</sub> (**2b**) has been observed in matrix isolation experiments.<sup>4</sup> The stabilizing Lewis base may also be anionic, as in the 1-phenylboratabenzene ion (**3a**)<sup>7</sup> and its methyl analog (**3b**).<sup>8</sup> Other boratabenzene ions (**3c**,<sup>9</sup> **3f**)<sup>6</sup> have been mentioned in the literature but have remained uncharacterized. Furthermore, borabenzene rings **2** and boratabenzene ions **3**<sup>-</sup> may act as ligands to transition metals, both in sandwich-type complexes<sup>10,11</sup> and in triple-decker complexes.<sup>12</sup> Pertinent work up to 1985 has been reviewed.<sup>10</sup>

We set out recently to develop a new synthetic entry into borabenzene chemistry.<sup>2</sup> With piperylene (1,3-pentadiene) as the starting C<sub>5</sub> component, a metalation/

(6) Boese, R.; Finke, N.; Henkelmann, J.; Maier, G.; Paetzold, P.; Reisenauer, H. P.; Schmid, G. *Chem. Ber.* **1985**, *118*, 1644.

(7) Ashe, A. J., III; Shu, P. *J. Am. Chem. Soc.* **1971**, *93*, 1804.

(8) Herberich, G. E.; Becker, H. *J. Angew. Chem., Int. Ed. Engl.* **1975**, *14*, 184.

(9) Ashe, A. J., III; Meyers, E.; Shu, P.; von Lehmann, T.; Bastide, J. *J. Am. Chem. Soc.* **1975**, *97*, 6865.

(10) Herberich, G. E.; Ohst, H. *Adv. Organomet. Chem.* **1986**, *25*, 199.

(11) For more recent work see: (a) Herberich, G. E.; Klein, W.; Spaniol, T. P. *Organometallics* **1993**, *12*, 2660. (b) Maier, G.; Wolf, H.-J.; Boese, R. *Chem. Ber.* **1990**, *123*, 505.

(12) Herberich, G. E.; Englert, U.; Pubanz, D. *J. Organomet. Chem.* **1993**, *459*, 1.

<sup>®</sup> Abstract published in *Advance ACS Abstracts*, November 15, 1994.

(1) Part 21: See ref 2.

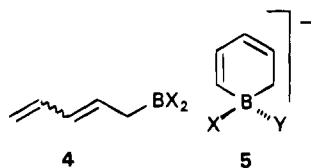
(2) Herberich, G. E.; Schmidt, B.; Englert, U.; Wagner, T. *Organometallics* **1993**, *12*, 2891.

(3) Nomenclature: *Pure Appl. Chem.* **1983**, *55*, 409.

(4) Maier, G.; Reisenauer, H. P.; Henkelmann, J.; Kliche, C. *Angew. Chem., Int. Ed. Engl.* **1988**, *27*, 295.

(5) (a) Raabe, G.; Heyne, E.; Schleker, W.; Fleischhauer, J. Z. *Naturforsch.* **1984**, *39A*, 678. (b) Raabe, G.; Schleker, W.; Heyne, E.; Fleischhauer, J. Z. *Naturforsch.* **1987**, *42A*, 352. (c) Cioslowski, J.; Hay, P. J. *J. Am. Chem. Soc.* **1990**, *112*, 1707.

borylation sequence can be used to synthesize bis-(dialkylamino)-2,4-pentadienylboranes **4a–c** and, by a subsequent alcoholysis step, dialkoxy-2,4-pentadienylboranes **4e–h**. The metalation of some of these compounds **4** leads to ring closure reactions with formation of borata-2,4-cyclohexadiene species **5**, which after further transformation afford a variety of boratabenzene species.



- 4: **a**, X = NMe<sub>2</sub>; **b**, X = NEt<sub>2</sub>; **c**, X = NPr<sup>i</sup><sub>2</sub>; **d**, X = OMe;  
**e**, X = OEt; **f**, X = OBu<sup>t</sup>; **g**, 2 X = OCH<sub>2</sub>CH<sub>2</sub>O;  
**h**, 2 X = OCM<sub>2</sub>CM<sub>2</sub>O; **i**, X = Ph; **j**, X = Pr  
**5**: **a**, X, Y = NMe<sub>2</sub>; **b**, X + Y = OCM<sub>2</sub>CM<sub>2</sub>O

The earlier synthetic methods, the tin route<sup>7</sup> and the cobaltocene route,<sup>8,13</sup> are difficult and laborious and have always remained the bottleneck in the further development of borabenzene chemistry. Our new synthetic approach is more efficient. As a consequence, many only slightly examined or unexplored aspects of borabenzene chemistry will become amenable to study in the future. In this paper we describe the new 2,4-pentadienylboranes **4**, their metalation chemistry, and new boracyclohexadienes and boratabenzene species.

## Results and Discussion

**2,4-Pentadienylboranes.** A few 2,4-pentadienylboranes **4** have been described previously (**4d**,<sup>14</sup> **4h**,<sup>15</sup> **4i**,<sup>16</sup> **4j**<sup>17</sup>). These compounds are best prepared from alkali-metal pentadienides<sup>18</sup> and a B<sub>1</sub> component, but more complicated (and less useful) methods have been used for the preparation of **4h**.<sup>15</sup>

Lithium pentadienide can be generated from 1,4-pentadiene with butyllithium in THF<sup>19</sup> but unfortunately not from the more readily available 1,3-pentadiene because of predominating ether cleavage<sup>20a</sup> and polymerization.<sup>19,20b</sup> The potassium compound can be obtained by kationation of 1,4-pentadiene with KNH<sub>2</sub> in NH<sub>3</sub><sup>21</sup> or, more conveniently, from 1,3-pentadiene with Lochmann–Schlosser base<sup>22</sup> or by treatment of the diene with elemental potassium in THF/NEt<sub>3</sub>.<sup>23</sup>

(13) (a) Herberich, G. E.; Greiss, G.; Heil, H. F. *Angew. Chem., Int. Ed. Engl.* **1970**, *9*, 805. (b) Herberich, G. E.; Greiss, G. *Chem. Ber.* **1972**, *105*, 3413.

(14) (a) Schlosser, M.; Rauchschalbe, G. *J. Am. Chem. Soc.* **1978**, *100*, 3258. (b) Bosshardt, H.; Schlosser, M. *Helv. Chim. Acta* **1980**, *63*, 2393. (c) Fujita, K.; Schlosser, M. *Helv. Chim. Acta* **1982**, *65*, 1258.

(15) Hoffmann, R. W.; Landmann, B. *Chem. Ber.* **1986**, *119*, 1039.

(16) Hutchings, M. G.; Paget, W. E.; Smith, K. *J. Chem. Res., Synop.* **1983**, *31*; *J. Chem. Res., Miniprint* **1983**, 342.

(17) Gurskii, M. E.; Gridnev, I. D.; Geiderikh, A. V.; Ignatenko, A. V.; Bubnov, Yu. N. *Organometallics* **1992**, *11*, 4056.

(18) Yasuda, H.; Nakamura, A. *J. Organomet. Chem.* **1985**, *285*, 15.

(19) Bates, R. B.; Gosselink, D. W.; Kaczynski, J. A. *Tetrahedron Lett.* **1967**, 199.

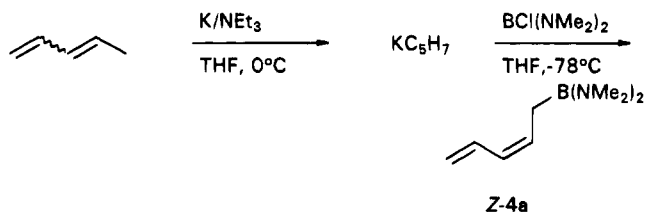
(20) (a) Maercker, A.; Theysohn, W. *Liebigs Ann. Chem.* **1971**, 746, 70. (b) Hsieh, H.; Tobolsky, A. V. *J. Polym. Sci.* **1957**, *25*, 245.

(21) Heizwolf, G. J.; Kloosterziel, H. *Recl. Trav. Chim. Pays-Bas* **1967**, *88*, 807.

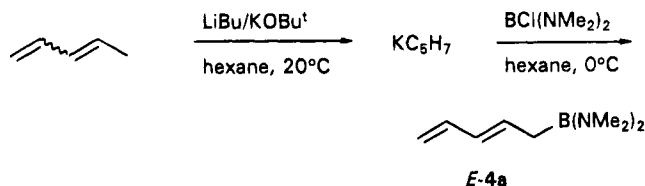
(22) Bahl, J. J.; Bates, R. B.; Gordon, B., III. *J. Org. Chem.* **1979**, *44*, 2290.

(23) Yasuda, H.; Ohnuma, Y.; Yamauchi, M.; Tani, H.; Nakamura, A. *Bull. Chem. Soc. Jpn.* **1979**, *52*, 2036.

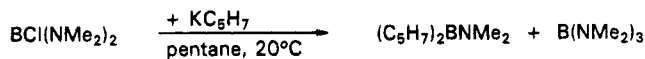
### Scheme 1



### Scheme 2



### Scheme 3



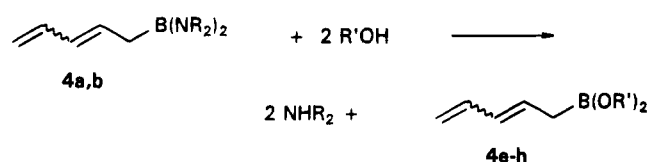
Since for the preparation of the boranes **4** high purity of the pentadienide is required, the direct reaction of 1,3-pentadiene with elemental potassium<sup>23</sup> and the kationation with Lochmann–Schlosser base<sup>22</sup> turned out to be the most useful for our purposes. Borylation with bis(dialkylamino)chloroboranes BCl(NR<sub>2</sub>)<sub>2</sub> (R = Me, Et, Pr<sup>i</sup>) produces the corresponding bis(dialkylamino)-2,4-pentadienylboranes **4a–c** as mixtures of *E* and *Z* isomers. The composition of these mixtures strongly depends on the reaction conditions. Although we have not investigated this aspect in detail, a few comments seem warranted.

When KC<sub>5</sub>H<sub>7</sub> is prepared by the Nakamura method<sup>23</sup> and when BCl(NMe<sub>2</sub>)<sub>2</sub> is added to a suspension of KC<sub>5</sub>H<sub>7</sub> in THF at –78 °C, the reaction predominantly produces the *Z* isomer (*Z*)-**4a** (Scheme 1). When, however, the KC<sub>5</sub>H<sub>7</sub> species is prepared with Lochmann–Schlosser base<sup>22</sup> and when the suspension of KC<sub>5</sub>H<sub>7</sub> in hexane is added to BCl(NMe<sub>2</sub>)<sub>2</sub> at 0 °C, the reaction affords mainly the *E* isomer (*E*)-**4a** (Scheme 2). Likewise, the closely related reaction of KC<sub>5</sub>H<sub>7</sub> with Me<sub>3</sub>SiCl produces the *E* isomeric product when hexane is used as reaction medium, while in THF the *Z* isomer is formed.<sup>24</sup> Rather surprisingly, when KC<sub>5</sub>H<sub>7</sub> is prepared by the Nakamura method and when a suspension of this compound in pentane is added to BCl(NMe<sub>2</sub>)<sub>2</sub> in pentane at 20 °C, an undesired dismutation comes into play and mainly produces B(NMe<sub>2</sub>)<sub>3</sub> and a mixture of stereoisomeric (dimethylamino)di-2,4-pentadienylboranes (Scheme 3).

The dialkoxy-2,4-pentadienylboranes **4e–h** can readily be obtained via alcoholysis of **4a** or **4b**. This method<sup>25</sup> is general and simple and gives excellent yields of **4e–h** as mixtures of *E* and *Z* isomers (Scheme 4). In the cases of the diols glycol and pinacol high dilution is necessary to avoid extensive formation of polymeric product. We note that **4d** has been obtained from KC<sub>5</sub>H<sub>7</sub> and BF(OMe)<sub>2</sub>.<sup>14a</sup>

(24) Yasuda, H.; Yamauchi, M.; Ohnuma, Y.; Nakamura, A. *Bull. Chem. Soc. Jpn.* **1981**, *54*, 1481.

(25) (a) Mikhailov, B. M.; Shchegoleva, T. A. *Izv. Akad. Nauk SSSR, Ser. Khim.* **1958**, 777; *Bull. Acad. Sci. USSR, Div. Chem. Sci. (Engl. Transl.)* **1958**, 753. (b) For the use of pinacol see also: Hoffmann, R. W.; Zeiss, H.-J. *Angew. Chem., Int. Ed. Engl.* **1979**, *18*, 306.

Scheme 4<sup>a</sup>

<sup>a</sup> Legend for 4: e, R' = Et; f, R' = Bu<sup>t</sup>; g, 2 R' = CH<sub>2</sub>CH<sub>2</sub>; h, 2 R' = CMe<sub>2</sub>CMe<sub>2</sub>.

The new 2,4-pentadienylboranes **4a–c,e–g** are all distillable liquids which are sensitive to air and water. They were mainly characterized by their NMR spectra. In the <sup>1</sup>H NMR spectra the coupling constant  $J_{23}$  amounts to 15 Hz for the *E* isomers and 11 Hz for the *Z* isomers. The signal for 4-H is always the lowest field signal; in addition, it shows a low-field shift of ca.  $\Delta\delta = 0.45$  for the *E* isomer relative to the *Z* isomer. The  $\delta(^{11}\text{B})$  shifts reflect the borane substitution pattern, as expected.<sup>26</sup> In the <sup>13</sup>C NMR spectra the chemical shifts are very similar to those of the stereoisomeric 1,3-pentadienes.<sup>27</sup> The signal for C-4 appears at  $\delta(^{13}\text{C})$  138 for the *E* isomers and at  $\delta(^{13}\text{C})$  132 for the *Z* isomers; this characteristic difference provides the most convenient distinction between the stereoisomers.

**Metalation of Bis(dialkylamino)-2,4-pentadienylboranes.** Simple organoboranes undergo quaternization at boron when treated with bases. In most structural situations quaternization is the low-energy-pathway reaction and deprotonation, mostly at the position  $\alpha$  to the boron, cannot compete. Occasionally some other reactions may also interfere, such as hydride transfer<sup>28</sup> from LiBu<sup>t</sup> and electron transfer<sup>29</sup> from the base.

The central theme of all metalation chemistry here is the suppression of the quaternization reaction. In principle, this can be achieved by means of steric and electronic substituent effects. In practice, the factors which govern the outcome of attempted metalation reactions turn out to be fairly complex. Rathke and Kow demonstrated the importance of steric protection of the boron center when they successfully metalated 9-bora-bicyclo[3.3.1]nonane derivatives with the bulky base lithium 2,2,6,6-tetramethylpiperidide (LiTMP).<sup>30</sup> The importance of electronic factors is evidenced by the smooth metalation of 1-phenylbora-2,5-cyclohexadiene with LiBu<sup>t</sup> in the very first report of an organoborane metalation by Ashe and Shu.<sup>7</sup> Extensive work by Matteson and his group on the metalation of dialkoxy-organoboranes for the first time demonstrated in detail the intricacies of the interplay of steric and electronic effects in these reactions.<sup>31</sup>

(26) (a) Nöth, H.; Wrackmeyer, B. In *NMR Basic Principles and Progress*; Diehl, P., Fluck, E., Kosfeld, R., Eds.; Springer-Verlag: Berlin, 1978; Vol. 14. (b) Wrackmeyer, B. *Annu. Rep. NMR Spectrosc.* **1988**, *20*, 61.

(27) Kalinowski, H.-O.; Berger, S.; Braun, S. *<sup>13</sup>C-NMR-Spektroskopie*; Georg Thieme Verlag: Stuttgart, Germany, 1984; p 117.

(28) (a) Corey, E. J.; Albonico, S. M.; Koelliker, U.; Schaaf, T. K.; Varma, R. K. *J. Am. Chem. Soc.* **1971**, *93*, 1491. (b) Brown, H. C.; Kramer, G. W.; Hubbard, J. C.; Krishnamurthy, S. *J. Organomet. Chem.* **1980**, *188*, 1.

(29) Pelter, A.; Singaram, B.; Williams, L.; Wilson, J. W. *Tetrahedron Lett.* **1983**, *24*, 623.

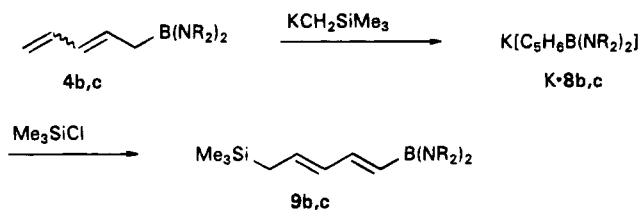
(30) (a) Rathke, M. W.; Kow, R. *J. Am. Chem. Soc.* **1972**, *94*, 6854. (b) Kow, R.; Rathke, M. W. *J. Am. Chem. Soc.* **1973**, *95*, 2715.

(31) (a) Matteson, D. S.; Moody, R. *J. Organometallics* **1982**, *1*, 20. (b) Matteson, D. S.; Arne, K. *Organometallics* **1982**, *1*, 280. (c) Matteson, D. S.; Majumdar, D. *Organometallics* **1983**, *2*, 230.

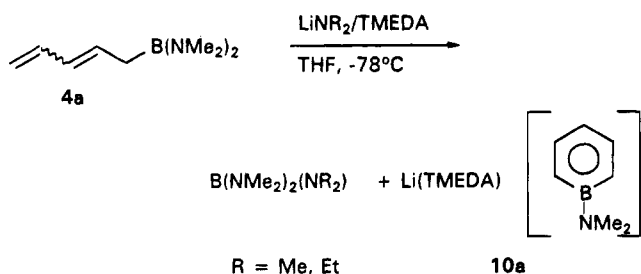
Scheme 5



Scheme 6



Scheme 7



Metalation of bis(dialkylamino)organoboranes has not been reported prior to this work. Electronic stabilization at the boron center by dialkylamino substituents is particularly efficient, rendering quaternization less favorable. Thus, B(NMe<sub>2</sub>)<sub>3</sub> and LiNMe<sub>2</sub> do coexist in THF solution without reaction.<sup>32</sup> The more Lewis acidic MeB(NMe<sub>2</sub>)<sub>2</sub> (**6**) and LiNMe<sub>2</sub> are in equilibrium with the borate Li[MeB(NMe<sub>2</sub>)<sub>3</sub>] (**7**) (Scheme 5), as observed by <sup>1</sup>H and <sup>11</sup>B NMR spectroscopy; the resulting borate **7** may be isolated as a white powder.<sup>32</sup>

**4b,c** react with KCH<sub>2</sub>SiMe<sub>3</sub> in cyclohexane<sup>33</sup> to give insoluble potassium pentadienides **K(8b,c)** (of unspecified stereochemistry). These were characterized as distillable trimethylsilyl derivatives **9b,c** (Scheme 6).<sup>2</sup> More common carbon bases such as LiBu<sup>t</sup> and Lochmann-Schlosser base mainly effected fast polymerization.

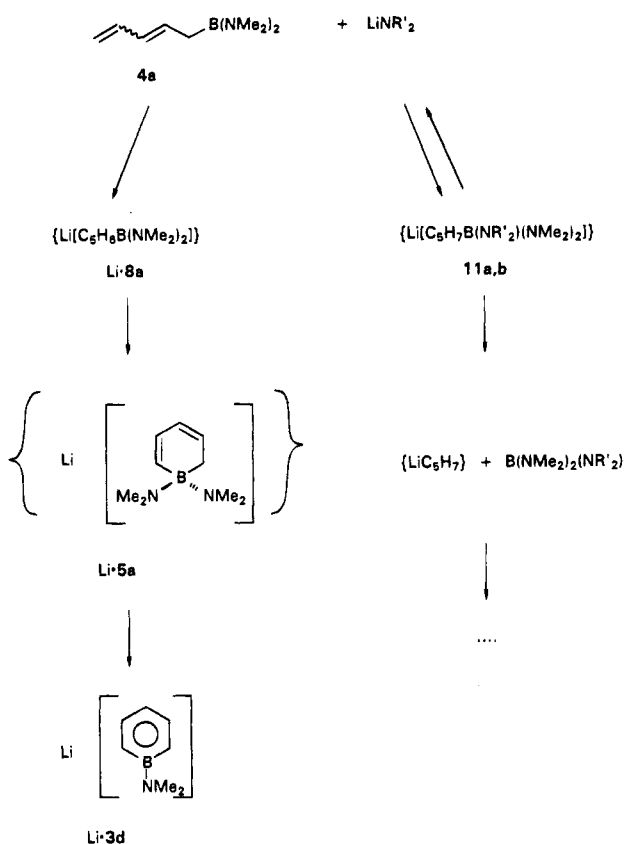
We have also studied the metalation of **4a–c** with lithium amides LiNR'<sub>2</sub> (R = Me, Et, Pr<sup>i</sup>) in THF and in the presence of tetramethylethylenediamine (TMEDA). When the dimethylamino compound **4a** is treated with LiNMe<sub>2</sub> or LiNEt<sub>2</sub>, two parallel reactions take place: formation of the 1-(dimethylamino)boratabenzene salt **10a** (≡[Li(TMEDA)](**3d**); 30%) and a nonproductive deborylation reaction with formation of B(NMe<sub>2</sub>)<sub>3</sub> (70%) or B(NMe<sub>2</sub>)<sub>2</sub>(NEt<sub>2</sub>), respectively (Scheme 7).

The combinations **4a,b**/LiNEt<sub>2</sub> and **4a,b**/excess LDA (LiNPr<sup>i</sup>) give analogous results. The rate of product formation decreases with increasing bulk of the *B*-dialkylamino group and of the attacking lithium amide, and no reaction takes place with the combinations **4c**/LiNEt<sub>2</sub> and **4c**/LDA. In the case of the combinations **4b,c**/LiNMe<sub>2</sub>, where the *B*-dialkylamino group is more voluminous than the amide LiNR'<sub>2</sub>, an exchange of the dialkylamino group takes place prior to ring closure and **10a** is formed subsequently. Similar observations were

(32) Herberich, G. E.; Fischer, A. Unpublished work.

(33) (a) Hartmann, J.; Schlosser, M. *Helv. Chim. Acta* **1976**, *59*, 453. (b) Zaidlewicz, M. *J. Organomet. Chem.* **1985**, *293*, 139.

Scheme 8



made for the metalation of 1-(dialkylamino)-2,5-dihydro-1H-boroles with lithium amides.<sup>34</sup>

In practice the isolation of the salts **10** requires separation from residual lithium amide. This separation works best when **4a** is metalated with LiNEt<sub>2</sub>. Both LiNMe<sub>2</sub> and LDA (which has to be used in large excess) cocrystallize with the product **10a**. For similar reasons the more soluble **10b** ( $\equiv [Li(TMEDA)](3e)$ ) has not been obtained in pure form.

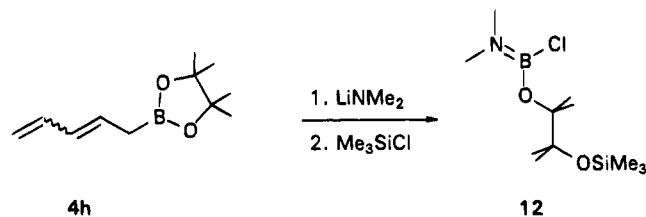
Our results may be interpreted along the lines of Scheme 8. When **4a** is treated with the lithium amide LiNR'<sub>2</sub>, a reversible quaternization is established, producing borates **11a,b**. The reversibility of this quaternization is in close analogy to Scheme 5 and allows for the exchange of amido groups: e.g., in the combination **4c**/LiNMe<sub>2</sub>. Deprotonation of **4a** produces the pentadienide Li(**8a**). This pentadienide is thought to undergo a spontaneous cyclization to give the borata-2,4-cyclohexadiene salt Li(**5a**), which in turn is transformed into the boratabenzene salt Li(**3d**), probably via a dequaternization with subsequent deprotonation. In NMR-tube experiments none of the postulated intermediates Li(**8a**) and Li(**5a**) can be seen; that is, the deprotonation of **4a** is rate-determining. The borates **11a,b** are less stable with respect to B–C bond heterolysis than the borate **7**. They decompose and produce lithium pentadienide and the observed boranes B(NMe<sub>2</sub>)<sub>3</sub> and B(NMe<sub>2</sub>)<sub>2</sub>(NEt<sub>2</sub>), respectively. The lithium pentadienide is not found and will presumably be protonated by the amines present in the reaction mixture and by ether cleavage of THF; when the reaction mixture is quenched with Me<sub>3</sub>SiCl, the volatiles contain Me<sub>3</sub>SiOCH=CH<sub>2</sub>.

(34) Herberich, G. E.; Hostalek, M.; Laven, R.; Boese, R. *Angew. Chem., Int. Ed. Engl.* **1990**, *29*, 317.

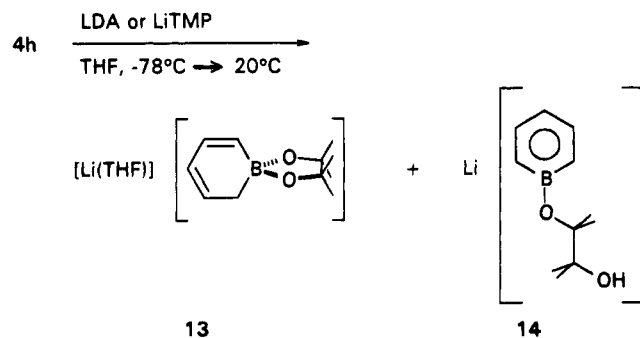
**Metalation of the 2-(2,4-Pentadienyl)dioxaborolane 4h.** Attempted metalation of the dialkoxy-2,4-pentadienylboranes **4e–h** met with no success in most experiments. The Lewis acidity of the boron in **4d–h** is higher than in the bis(dialkylamino) compounds **4a–c**. As a consequence, addition of the base at the boron center is more favorable and is the first step in a variety of undesired reactions. Carefully tuned steric effects can be used to remedy the situation.

When the bulky dioxaborolane **4h** is treated with LiNMe<sub>2</sub> in THF, addition at the boron center still takes place, and after the reaction mixture is quenched with Me<sub>3</sub>SiCl, the borane **12** was obtained as the main product (Scheme 9). This product gives evidence for two detrimental reactions: loss of the C<sub>5</sub> substituent and opening of the dioxaborolane ring.

Scheme 9



Scheme 10

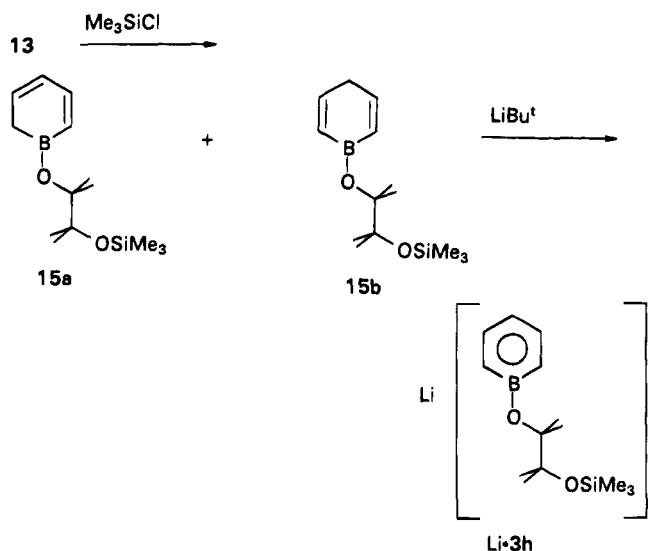


When **4h** is treated with the more voluminous base LDA or LiTMP in THF (but not in ether), metalation and subsequent ring closure are effected (Scheme 10). Two products are formed in high total yield (>80%): a boratacyclohexadiene salt which precipitates as a white solid (**13**,  $\equiv Li(THF)(5b)$ ) and a tautomeric boratabenzene salt (**14**,  $\equiv Li(3g)$ ) in the THF solution.

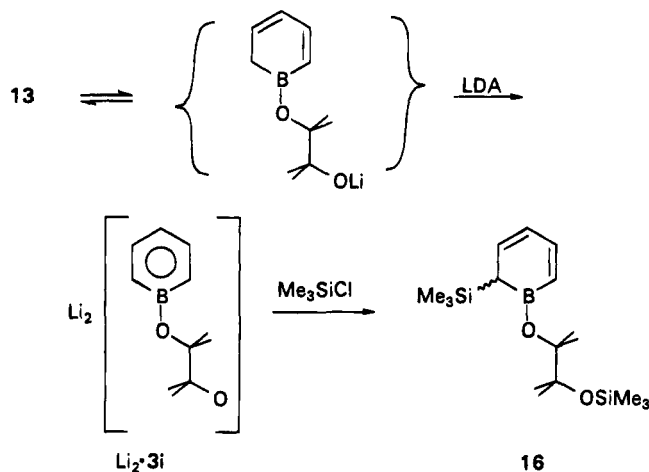
Both products are prone to decomposition. The spiroborate **13** can be isolated by filtration of the reaction mixture. It is soluble in acetone, and these solutions are sufficiently stable to allow a full identification of **13** by NMR spectroscopy. The filtrate shows only one <sup>11</sup>B NMR signal at  $\delta(^{11}B)$  35 which indicates the presence of a boratabenzene species; on attempted isolation of **14** more of the solid **13** is obtained, though of lower purity. This observation supports the assumption that the boratabenzene ion in question is indeed **3g**<sup>-</sup>.

The metalation of **4h** takes place in THF but not in the more poorly solvating diethyl ether. It is also essential to keep the temperature as low as possible during the metalation process to assure optimal chemoselectivity. Auxiliary bases such as TMEDA are of no influence. Finally we note that many details of our metalation experiments have close parallels in Matteison's work on the metalation of other dioxaborolanes.<sup>31</sup>

Scheme 11



Scheme 12



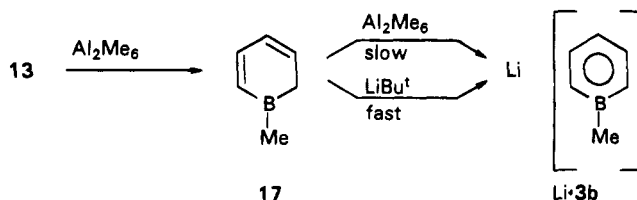
### Boratabenzene Salts via the Spiroborane 13.

Various attempts were made to transform the spiroborate **13** into boratabenzene species. Treatment of **13** with  $\text{Me}_3\text{SiCl}$  in pentane or in THF at  $-78^\circ\text{C}$  induces ring opening; the bora-2,4-cyclohexadiene **15a** and, surprisingly, the tautomeric bora-2,5-cyclohexadiene **15b** are formed in approximately equal amounts (Scheme 11). The mixture of the boracyclohexadienes **15** can be metalated with  $\text{LiBu}^t$  in pentane at  $-78^\circ\text{C}$  or with LDA in THF to produce **Li(3h)** in near-quantitative yield (Scheme 11).

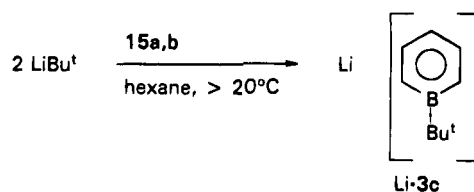
When the spiroborate **13** is metalated by LDA in THF, the doubly charged boratabenzene species  $\mathbf{3i}^{2-}$  is obtained in solution. As the acidity of piperylene is too low for deprotonation by lithium amides, we may safely assume that the spiroborate **13** is also inert to LDA; in other words, spontaneous opening of the dioxaborolane ring of the boratacyclohexadiene  $\mathbf{5b}^-$  will precede the metalation step. The salt  $\text{Li}_2(\mathbf{3i})$  can be isolated and characterized by NMR spectroscopy, while treatment with  $\text{Me}_3\text{SiCl}$  in situ affords the bora-2,4-cyclohexadiene **16** (Scheme 12). We note in passing that the two metalation steps  $\mathbf{4h} \rightarrow \mathbf{13} \rightarrow \mathbf{3i}^{2-}$  could not be combined, in our hands, into a one-pot preparation.

The preparation of lithium 1-methylboratabenzene **Li(3b)** is of particular interest. The reaction of the spiroborate **13** with methylolithium results mainly in

Scheme 13



Scheme 14



total degradation, producing (inter alia) trimethylborane; **Li(3b)** is only a minor product and can be identified by NMR spectroscopy. However, when **13** is treated with trimethylaluminum in  $\text{Et}_2\text{O}$ /toluene solution at  $-78^\circ\text{C}$ , a highly selective ring-opening reaction takes place and lithium 1-methylboratabenzene (**Li(3b)**) is obtained as a white powder in high yield. Monitoring the reaction by  $^{11}\text{B}$  NMR spectroscopy reveals the fast appearance of a signal at  $\delta(^{11}\text{B})$  70 which is slowly replaced with a new signal at  $\delta(^{11}\text{B})$  36. The first signal is assigned to 1-methylbora-2,4-cyclohexadiene (**17**) (cf.  $\delta(^{11}\text{B})$  73.8 for 1-propylbora-2-cyclohexene<sup>35</sup>), while the second signal belongs to **Li(3b)** (Scheme 13). When  $\text{LiBu}^t$  is added to the solution after the appearance of the first signal, the salt **Li(3b)** is formed within minutes because the metalation of **17** is very much faster with  $\text{LiBu}^t$  than with  $\text{Al}_2\text{Me}_6$ . **Li(3b)** can also be made from **Li(3h)** and  $\text{Al}_2\text{Me}_6$ , but this alternative is not recommended because it is less efficient synthetically.

Lithium 1-*tert*-butylboratabenzene (**Li(3c)**) is obtained when the boracyclohexadiene mixture **15** is added to *tert*-butyllithium in pentane/hexane without cooling (Scheme 14). Two steps are involved, a substitution at boron and a deprotonation reaction. The product of a primary deprotonation of **15** would be **Li(3h)** (cf. Scheme 11). We find that the alkoxy group of **Li(3h)** cannot be substituted by treatment with methylolithium or with *tert*-butyllithium at room temperature. This signifies that **Li(3h)** cannot be an intermediate here and that the substitution of the alkoxy group of **15** occurs as the first reaction step.

**Salt Metathesis in Aqueous Solution.** Attempts to crystallize the 1-methylboratabenzene species **Li(3b)** or to obtain a crystalline solvate of it with the help of chelating amines and ethers were largely unsuccessful. With 12-crown-4 crystals of a 1:1 solvate were obtained which afterwards were found to be disordered.

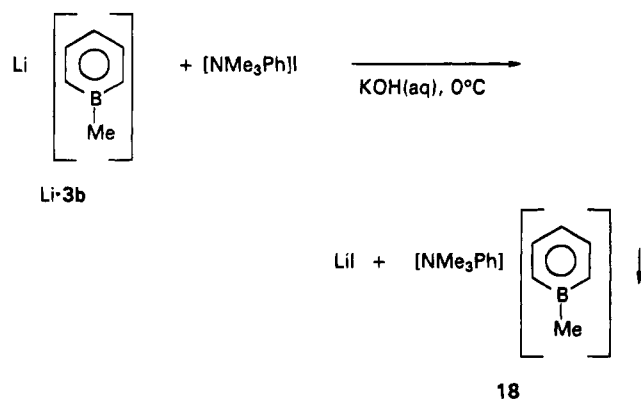
Since it is known that 1-phenylboratabenzene is a considerably weaker base in THF solutions than cyclopentadienide,<sup>36</sup> we turned to strongly alkaline aqueous (!) solutions. Combining alkaline solutions of trimethylphenylammonium iodide and of **Li(3b)** at  $0^\circ\text{C}$  instantaneously produced a precipitate of  $[\text{NMe}_3\text{Ph}][\text{C}_5\text{H}_5\text{BMe}]$  (**18**) in high yield (Scheme 15).

(35) Gurskii, M. E.; Gridnev, I. D.; Geiderikh, A. V.; Ignatenko, A. V.; Bubnov, Y. N. *Organometallics* **1992**, *11*, 4056.

(36) Sandford, H. F. Ph.D. Thesis, University of Michigan, 1979.



Scheme 15

Table 1. Selected  $^1\text{H}$  NMR Data for Boratabenzenes Li(3)

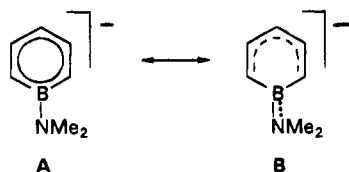
compd	$\delta(\text{H}2)$	$\delta(\text{H}3)$	$\delta(\text{H}4)$	$J_{23}$ , Hz	$J_{34}$ , Hz	R at boron
Li(3b)	6.47	7.28	6.18	9.8	7.0	Me
Li(3c)	6.36	7.05	5.92	10.2	6.9	Bu <sup>t</sup>
Li(3d)	5.65	7.04	5.50	10.7	6.7	NMe <sub>2</sub>
Li(3e)	5.63	7.05	5.50	11.0	6.7	NEt <sub>2</sub>
Li(3h)	5.67	6.99	5.66	10.2	6.8	OCMe <sub>2</sub> CMe <sub>2</sub> OSiMe <sub>3</sub>
Li(3i)	5.66	7.00	5.61	10.3	7.1	OCMe <sub>2</sub> CMe <sub>2</sub> O <sup>-</sup>

Table 2. Selected  $^{13}\text{C}$  and  $^{11}\text{B}$  Chemical Shift Data for Boratabenzenes Li(3)

compd	$\delta(\text{C}2)$	$\delta(\text{C}3)$	$\delta(\text{C}4)$	$\delta(^{11}\text{B})$	R at boron
Li(3b)	127	132.8	107.9	36	Me
Li(3c)	123	133.2	108.4	39	Bu <sup>t</sup>
Li(3d)	110	134.4	99.7	28	NMe <sub>2</sub>
Li(3e)	110	134.4	99.1	31	NEt <sub>2</sub>
Li(3h)	115	134.7	105.8	34	OCMe <sub>2</sub> CMe <sub>2</sub> OSiMe <sub>3</sub>
Li(3i)	115	134.6	104	34	OCMe <sub>2</sub> CMe <sub>2</sub> O <sup>-</sup>

**NMR Spectra of Boratabenzenes.** Known NMR data for boratabenzene ions are extremely limited (Li(3a),  $^1\text{H}$  and  $^{11}\text{B}$  NMR; Li(3b),  $^1\text{H}$  NMR).<sup>10</sup> Tables 1 and 2 give an overview of the data obtained in this work.

The proton chemical shifts  $\delta(^1\text{H})$  are found between those of benzene and LiCp ( $\delta(^1\text{H})$  5.59 in THF<sup>37</sup>) and show high charge densities in the positions para and ortho to the boron. The presence of the electropositive boron atom gives rise to a characteristic large  $^3J_{23}$  coupling constant.  $\pi$  interactions with the lone pair of the amino groups and, to a lesser extent, with the alkoxy groups cause a general high-field shift which indicates a reduced ring current effect. This effect is most pronounced for the ortho and para positions and may be interpreted in terms of resonance formulas **A** (predominating for 3b<sup>-</sup>) and **B** (predominating for 3d<sup>-</sup>; cf. the structure of 10a<sup>2</sup>) or in terms of the orbital coefficients of the boratabenzene HOMO.



The carbon chemical shifts  $\delta(^{13}\text{C})$  show little variation for the meta position as in monosubstituted benzenes. For the ortho and even more so for the para position they reflect high charge densities (cf.  $\delta(^{13}\text{C})$  103.6 for

Table 3. Atomic Coordinates of Non-Hydrogen Atoms for 18

atom	x	y	z	$U_{\text{eq}}^a$
N1	0.2334(2)	0.4110(1)	0.4659(2)	0.0363(4)
C1	0.1277(3)	0.2279(2)	1.1585(2)	0.0516(7)
C2	0.0913(3)	0.1633(2)	1.2455(2)	0.0553(7)
C3	0.1935(3)	0.1184(2)	1.3285(2)	0.0572(7)
C4	0.3390(3)	0.1387(2)	1.3287(2)	0.0572(7)
C5	0.3864(3)	0.2024(2)	1.2457(2)	0.0527(7)
C6	0.3290(4)	0.3266(2)	1.0530(3)	0.0787(9)
C10	0.2335(2)	0.4757(1)	0.5788(2)	0.0365(5)
C11	0.2551(2)	0.5610(1)	0.5472(2)	0.0420(6)
C12	0.2626(2)	0.6216(2)	0.6505(2)	0.0474(6)
C13	0.2466(3)	0.5973(2)	0.7823(2)	0.0530(7)
C14	0.2227(3)	0.5125(2)	0.8119(2)	0.0532(7)
C15	0.2152(3)	0.4504(2)	0.7098(2)	0.0455(6)
C16	0.2018(3)	0.3212(2)	0.5108(2)	0.0486(6)
C17	0.3789(2)	0.4108(2)	0.4137(2)	0.0431(6)
C18	0.1218(2)	0.4342(2)	0.3517(2)	0.0478(6)
B	0.2824(3)	0.2522(2)	1.1513(2)	0.0502(7)

<sup>a</sup> Equivalent isotropic  $U_{\text{eq}}$  defined as one-third of the trace of the orthogonalized  $U_{ij}$  tensor; in  $10^4 \text{ pm}^2$ .

Table 4. Selected Bond Distances and Bond Angles for 18

(a) Bond Distances (pm)			
N1–C10	150.3(2)	N1–C16	150.5(2)
N1–C17	150.1(2)	N1–C18	150.8(2)
C10–C11	138.4(2)	C10–C15	138.1(2)
C11–C12	138.8(2)	C14–C15	139.5(2)
C12–C13	138.0(2)	C13–C14	137.5(3)
C1–C2	138.8(2)	C4–C5	138.7(3)
C2–C3	138.8(3)	C3–C4	139.7(3)
C1–B	150.3(3)	C5–B	149.8(3)
C6–B	159.9(3)		
(b) Bond Angles (deg)			
C2–C1–B	120.4(1)	C4–C5–B	120.9(1)
C1–C2–C3	122.4(1)	C3–C4–C5	121.9(2)
C2–C3–C4	120.2(1)	C1–B–C5	114.3(2)
C1–B–C6	122.0(2)	C5–B–C6	123.7(2)

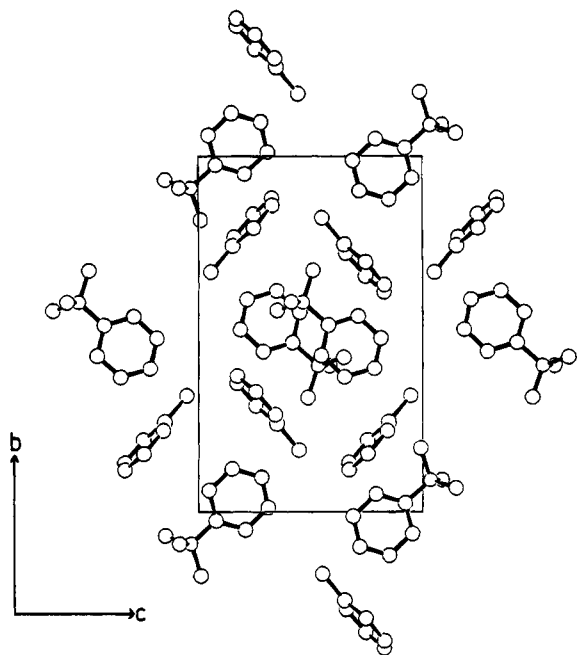
LiCp<sup>38</sup>) and a strong influence of the substituent at boron. With increasing  $\pi$  interaction between the  $p_z$  orbital at boron and the substituent lone pair, formula **B** gains favor, as seen from the high-field shifts for Li(3d–i). Coupling constants are reported for Li(3b,c) (see Experimental Section).

The only boron resonance documented so far for a boratabenzene species was that of the phenyl derivative Li(3a) ( $\delta(^{11}\text{B})$  28<sup>7</sup>). This chemical shift value is evidence for the delocalization of negative charge onto the boron.<sup>7</sup> Our data demonstrate again the importance of  $\pi$  interactions with the substituent at boron. Alkoxy substituents and (more strongly) dialkylamino groups effect marked high-field shifts. On this basis, especially in comparison to the methyl compound Li(3b), the phenyl group in Li(3a) is by no means an innocent substituent. The boron chemical shift data also indicate the importance of steric effects. Thus, Li(3c,e) show small but significant low-field shifts relative to Li(3b,d), respectively; this steric effect is also known for a number of other boron compounds.<sup>26</sup>

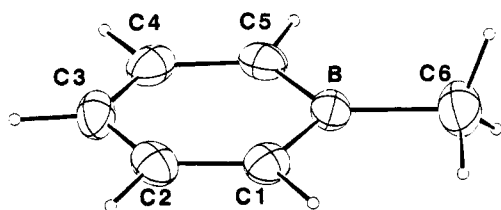
**Crystal Structure of [PhNMe<sub>3</sub>][C<sub>5</sub>H<sub>5</sub>BMe] (18).** The ammonium salt 18 could easily be crystallized from THF to give crystals suitable for a diffraction study. Atomic coordinates and selected bond lengths and bond angles for 18 are listed in Tables 3 and 4.

Crystalline 18 possesses the structure of an ionic solid. Cations and anions are arranged in alternating

(37) Ford, W. T. *J. Organomet. Chem.* 1971, 32, 27.(38) Fischer, P.; Stadelhofer, J.; Weidlein, J. *J. Organomet. Chem.* 1976, 116, 65.



**Figure 1.** Crystal packing of  $[\text{NMe}_3\text{Ph}][\text{C}_5\text{H}_5\text{BMe}]$  (**18**) as a projection onto the  $bc$  plane.



**Figure 2.** Thermal ellipsoid (30% probability) plot of the 1-methylboratabenzene ion in **18**. The alternative orientation of the methyl hydrogen atoms is omitted for clarity.

layers parallel to the  $ac$  plane and perpendicular to the long lattice constant  $b$ . The boratabenzene ions lie at approximate heights of  $y \approx 1/4$  and  $3/4$ , while the trimethylphenylammonium ions are at  $y \approx 0$  and  $1/2$ . Figure 1 illustrates the packing. The shortest van der Waals interactions between anions and cations are due to hydrogen-hydrogen contacts of the usual distance, close to 240 pm.

The 1-methylboratabenzene ion (Figure 2) displays near- $C_{2v}$  symmetry. The boratabenzene ring is almost perfectly planar (with a maximum deviation for atom C3 of 0.9(2) pm from the least-squares plane), and the averaged intra-ring distances amount to 150.1, 138.8, and 139.2 pm for B-C1 (B-C5), C1-C2 (C4-C5), and C2-C3 (C3-C4), respectively. These values reflect a high degree of delocalization within the ring. When the structure of **18** is compared to the known structures of borabenzene-pyridine **2a**<sup>6</sup> and of the *B*-(dimethylamino)boratabenzene salt  $[\text{Li}(\text{TMPDA})](\equiv \text{19}; \text{TMPDA} = N,N,N',N'$ -tetramethylpropylenediamine),<sup>2</sup> small but significant variations in the B-C ring distances are seen. These B-C distances are longer than in **2a** (148.2(4) and 146.5(4) pm)<sup>6</sup> and shorter than in **19** (150.6(1) and 152.5(2) pm).<sup>2</sup> These small differences reflect the different perturbations of the borabenzene ring which are exerted by the substituents at the B atom.

**Concluding Remarks.** The synthetic work presented in this paper should make boratabenzene salts

more widely available. Starting from 1 mol of elemental potassium, we obtain 100 mmol of **10a** in two steps or more than 150 mmol of **Li(3b)** in four steps. Thus, boratabenzenes should now be amenable to further study, especially in the fields of physical organic chemistry and organic reaction chemistry.

The *B*-dimethylamino derivative **19** was the first boratabenzene derivative to be characterized structurally.<sup>2</sup> The structure of the *B*-methyl compound **18** is now the second example and, quite importantly, the first structure of a boratabenzene with an innocent substituent at boron.

## Experimental Section

**General Procedures.** Reactions were carried out under an atmosphere of dinitrogen by means of conventional Schlenk techniques. Pentane and hexane were distilled from Na/K alloy, and THF was distilled from sodium benzophenone ketyl. Silica and alumina were heated under high vacuum at 300 °C prior to use. Alumina was deactivated (7% H<sub>2</sub>O, deoxygenated) after cooling. Melting points were measured in sealed capillaries and are uncorrected. Elemental analyses were performed at the Analytische Laboratorien, D-51647 Gummersbach, Germany.

NMR spectra were recorded on Bruker WP 80 PFT (<sup>1</sup>H, 80 MHz), Bruker WH 270 PFT (<sup>13</sup>C, 67.9 MHz; <sup>11</sup>B, 86.6 MHz), JEOL NM-PS-100 (<sup>11</sup>B, 32.08 MHz), and Varian Unity 500 spectrometers (<sup>1</sup>H, 500 MHz; <sup>13</sup>C, 125.7 MHz; <sup>11</sup>B, 160.4 MHz). Mass spectra were recorded on Varian MAT CH-5 and Finnigan MAT-95 spectrometers.

**Bis(dimethylamino)[(*E*)-2,4-pentadienyl]borane (*E*-**4a**).** Piperylene (32 mL, 0.32 mol) was added dropwise to a mixture of  $\text{KO}^t\text{Bu}$  (35.9 g, 0.32 mol) and  $\text{Li}^t\text{Bu}$  (1.6 M solution in hexane, 200 mL, 0.32 mol) in hexane (300 mL). After the mixture was stirred for 12 h at room temperature, the brown precipitate of  $\text{KC}_5\text{H}_7$  was filtered off and washed thoroughly with hexane (3 × 50 mL). The  $\text{KC}_5\text{H}_7$  was suspended in hexane (200 mL) and added in small portions to a solution of  $\text{BCl}(\text{NMe}_2)_2$  (36 mL, 0.22 mol) in hexane (500 mL) and THF (20 mL) at 0 °C. KCl was removed by filtration, and all volatiles were pumped off under vacuum. Distillation of the residue gave **4a** (22.8 g, 62%) as a colorless liquid: *E* isomer with ≤10% *Z* isomer; bp 72–75 °C/9 mbar.

**(*E*)-**4a**:** <sup>1</sup>H NMR (500 MHz,  $\text{CDCl}_3$ )  $\delta$  6.30 (ddd,  $J = 16.78, 10.38, 10.07$  Hz, 1H, 4-H), 5.98 (ddm,  $J = 14.95, 10.38$  Hz, 1H, 3-H), 5.77 (dt,  $J = 14.95, 7.63$ , 1H, 2-H), 4.99 (dm,  $J = 16.8$  Hz, 1H, 5-H-*trans*), 4.84 (dm,  $J = 10.07$  Hz, 1H, 5-H-*cis*), 2.66 (s, 12H,  $\text{NMe}_2$ ), 1.74 (d,  $J = 7.63$  Hz, 2H, 1-H); <sup>13</sup>C NMR (126 MHz,  $\text{CDCl}_3$ )  $\delta$  138.1, 134.7, and 129.8 (CH), 112.5 ( $\text{CH}_2=$ ), 39.4 ( $\text{NMe}_2$ ), 21 (br,  $\text{CH}_2\text{B}$ ); <sup>11</sup>B NMR (32 MHz,  $\text{CDCl}_3$ ,  $\text{BF}_3 \cdot \text{Et}_2\text{O}$  external)  $\delta$  33; MS (70 eV)  $m/z$  ( $I_{\text{rel}}$ ) 166 (15,  $\text{M}^+$ ), 100 (100,  $\text{M}^+ - \text{C}_5\text{H}_6$ ).

**Bis(dimethylamino)[(*Z*)-2,4-pentadienyl]borane (*Z*-**4a**).** Piperylene (220 mL, 2.2 mol) in THF (250 mL) was added to a mixture of elemental potassium (small pieces, 39.1 g, 1.0 mol),  $\text{NEt}_3$  (210 mL, 1.5 mol), and THF (800 mL) at -10 °C within 1.5 h. The mixture was stirred at 0 °C for 4 h and then at reflux temperature for 1.5 h to assure complete (!) consumption of the potassium. *Caution!* A runaway reaction may occur when the temperature is not carefully controlled in the early stages of the reaction. After the mixture was cooled to -78 °C,  $\text{BCl}(\text{NMe}_2)_2$  (135 mL, 0.83 mol) in THF (150 mL) was added dropwise with stirring. Workup as described for (*E*)-**4a** gave (*Z*)-**4a** (103.5 g, 75%) with varying admixtures (10–40%) of the *E* isomer.

**(*Z*)-**4a**:** <sup>1</sup>H NMR (500 MHz,  $\text{CDCl}_3$ )  $\delta$  6.76 (ddd,  $J = 16.78, 11.0, 10.08$  Hz, 1H, 4-H), 5.92 (ddm,  $J = 11.0, 11.0$  Hz, 1H, 3-H), 5.51 (dt,  $J = 11.0, 7.1$  Hz, 1H, 2-H), 5.13 (dd,  $J = 16.78$  Hz, 2.13 Hz, 1H, 5-H-*trans*), 5.02 (dm,  $J = 10.08$  Hz, 1H, 5-H-*cis*), 2.66 (s, 12H,  $\text{NMe}_2$ ), 1.84 (d,  $J = 7.1$  Hz, 2H, 1-H); <sup>13</sup>C

NMR (126 MHz, CDCl<sub>3</sub>) δ 132.8, 131.8, and 127.1 (CH), 115.2 (CH<sub>2</sub>=), 40.3 (NMe<sub>2</sub>), 17.5 (br, CH<sub>2</sub>B); <sup>11</sup>B NMR (32 MHz, CDCl<sub>3</sub>, BF<sub>3</sub>·Et<sub>2</sub>O external) δ 33; MS (70 eV) *m/z* (*I*<sub>rel</sub>) 166 (12, M<sup>+</sup>), 100 (100, M<sup>+</sup> - C<sub>5</sub>H<sub>5</sub>).

**Dismutation in the System BCl(NMe<sub>2</sub>)<sub>2</sub>/KC<sub>5</sub>H<sub>7</sub>.** A suspension of KC<sub>5</sub>H<sub>7</sub>, prepared from potassium (32.0 g, 0.82 mol) and piperylene (180.2 mL, 1.80 mol) as described above, was added to BCl(NMe<sub>2</sub>)<sub>2</sub> (90.3 g, 0.67 mol) in pentane (800 mL). Workup as for **4a** gave B(NMe<sub>2</sub>)<sub>3</sub> (34.2 g, 0.24 mol; bp 50 °C/25 mbar) and (C<sub>5</sub>H<sub>7</sub>)<sub>2</sub>B(NMe<sub>2</sub>) (44.0 g, 0.23 mol; bp 96–100 °C/8 mbar) with a total yield of 0.47 mol (70%).

(C<sub>5</sub>H<sub>7</sub>)<sub>2</sub>BNMe<sub>2</sub>: <sup>1</sup>H NMR (500 MHz, CDCl<sub>3</sub>) δ 6.30 (ddd, *J* = 17.09, 10.37, 10.07 Hz, 2H, 4-H), 5.98 (ddm, *J* = 14.96, 10.38 Hz, 2H, 3-H), 5.74 (dt, 14.96, 7.90, 0.61 Hz, 2H, 2-H), 5.00 (dm, *J* = 17.09 Hz, 2H, 5-H-*trans*), 4.86 (dm, *J* = 10.07 Hz, 2H, 5-H-*cis*), 2.77 (s, 6H, NMe<sub>2</sub>), 1.82 (d, *J* = 7.93 Hz, 4H, 1-H); <sup>13</sup>C NMR (126 MHz, CDCl<sub>3</sub>) δ 137.8, 133.6, and 130.5 (CH), 112.9 (CH<sub>2</sub>=), 39.5 (NMe<sub>2</sub>), 25.1 (br, CH<sub>2</sub>B); <sup>11</sup>B NMR (32 MHz, CDCl<sub>3</sub>, BF<sub>3</sub>·OEt<sub>2</sub> external) δ 43; MS (70 eV) *m/z* (*I*<sub>rel</sub>) 189 (5, M<sup>+</sup>), 122 (38, M<sup>+</sup> - C<sub>5</sub>H<sub>7</sub>), 55 (100, BNMe<sub>2</sub>H<sup>+</sup>).

**Synthesis of (E)-4b.** The procedure described for (E)-**4a** gave (E)-**4b** (57%): bp 83 °C/0.8 mbar.

(E)-**4b**: <sup>1</sup>H NMR (500 MHz, CDCl<sub>3</sub>) δ 6.29 (ddd, *J* = 17.09, 10.38, 10.38 Hz, 1H, 4-H), 5.98 (dd, *J* = 14.96, 10.38 Hz, 1H, 3-H), 5.78 (dt, *J* = 14.96, 7.50 Hz, 1H, 2-H), 4.97 (dd, *J* = 17.09, 1.83 Hz, 1H, 5-H-*trans*), 4.83 (dd, *J* = 10.38, 1.83 Hz, 1H, 5-H-*cis*), 1.71 (d, *J* = 7.63 Hz, 2H, CH<sub>2</sub>B), NMe<sub>2</sub> signals 2.97 (q, *J* = 7.02 Hz, 8H, NCH<sub>2</sub>) and 1.02 (t, *J* = 7.02 Hz, 12H, Me); <sup>13</sup>C NMR (67.9 MHz, CDCl<sub>3</sub>, -50 °C) δ 138.2, 135.5, and 130.1 (CH), 112.2 (CH<sub>2</sub>=), 21.6 (CH<sub>2</sub>B), NMe<sub>2</sub> signals 42.0 (NCH<sub>2</sub>) and 15.6 (Me); <sup>11</sup>B NMR (32 MHz, CDCl<sub>3</sub>, BF<sub>3</sub>·OEt<sub>2</sub> external) δ 34; MS (70 eV) *m/z* (*I*<sub>rel</sub>) 222 (3, M<sup>+</sup>), 155 (100, M<sup>+</sup> - C<sub>5</sub>H<sub>7</sub>).

**Synthesis of (E)-4c.** The procedure described for (E)-**4a** gave (E)-**4c** (29%): bp 95 °C/0.5 mbar.

(E)-**4c**: <sup>1</sup>H NMR (500 MHz, CDCl<sub>3</sub>) δ 6.33 (ddd, *J* = 16.79, 10.37, 10.07 Hz, 1H, 4-H), 5.95 (dd, *J* = 15.26, 10.07 Hz, 1H, 3-H), 5.85 (dt, *J* = 15.26, 7.02 Hz, 1H, 2-H), 4.97 (d, *J* = 16.78 Hz, 1H, 5-H-*trans*), 4.81 (d, *J* = 10.38 Hz, 1H, 5-H-*cis*), 1.96 (d, *J* = 7.02 Hz, 2H, CH<sub>2</sub>B), NPr<sub>2</sub> signals 3.51 (sept, *J* = 7.02 Hz, 4H, NCH) and 1.06 (d, *J* = 7.02 Hz, 24H, Me); <sup>13</sup>C NMR (67.9 MHz, CDCl<sub>3</sub>, -50 °C) δ 138.1, 137.8, and 129.5 (CH), 112.1 (CH<sub>2</sub>=), 26.4 (CH<sub>2</sub>B), NPr<sub>2</sub> signals 46.3 (NCH) and 24.4 (Me); <sup>11</sup>B NMR (32 MHz, CDCl<sub>3</sub>, BF<sub>3</sub>·OEt<sub>2</sub> external) δ 37; MS (70 eV) *m/z* (*I*<sub>rel</sub>) 279 (15, M<sup>+</sup> + 1), 211 (100, M<sup>+</sup> - C<sub>5</sub>H<sub>5</sub>).

**Alcoholysis of 4a with Primary Alcohols.** **4a** (10.0 g, 0.060 mol) was added to the primary alcohol (0.120 mol). The mixture was heated to 50 °C for 6 h to complete the reaction and then distilled to give **4e** (8.6 g, 85%; bp 71 °C/15 mbar) and **4f** (10.5 g, 78%; bp 74 °C/7 mbar), respectively.

(E)-**4e**: <sup>1</sup>H NMR (500 MHz, CDCl<sub>3</sub>) δ 6.31 (ddd, *J* = 17.09, 10.38, 10.38 Hz, 1H, 4-H), 6.00 (dd, *J* = 14.95, 10.38 Hz, 1H, 3-H), 5.79 (dt, *J* = 14.96, 7.63 Hz, 1H, 2-H), 5.02 (dm, *J* = 17.09 Hz, 1H, 5-H-*trans*), 4.89 (dm, *J* = 10.40 Hz, 1H, 5-H-*cis*), 1.74 (d, *J* = 7.63 Hz, 2H, 1-H), OEt signals 3.88 (q, *J* = 7.02 Hz, 4H, OCH<sub>2</sub>) and 1.19 (t, *J* = 7.02 Hz, 6H, Me); <sup>13</sup>C NMR (126 MHz, CDCl<sub>3</sub>) δ 137.6, 131.9, and 131.1 (CH), 113.5 (CH<sub>2</sub>=), 19 (br, CH<sub>2</sub>B), OEt signals 59.3 (OCH<sub>2</sub>) and 17.3 (Me); <sup>11</sup>B NMR (32 MHz, CDCl<sub>3</sub>, BF<sub>3</sub>·OEt<sub>2</sub> external) δ 30; MS (70 eV) *m/z* (*I*<sub>rel</sub>) 168 (25, M<sup>+</sup>), 101 (80, M<sup>+</sup> - C<sub>5</sub>H<sub>7</sub>), 45 (100, EtO<sup>+</sup>).

(E)-**4f**: <sup>1</sup>H NMR (500 MHz, CDCl<sub>3</sub>) δ 6.32 (ddd, *J* = 17.09, 10.69, 10.10 Hz, 1H, 4-H), 5.96 (ddm, *J* = 15.26, 10.07 Hz, 1H, 3-H), 5.82 (dt, *J* = 15.26, 7.63, 1H, 2-H), 4.99 (dm, *J* = 17.09 Hz, 1H, 5-H-*trans*), 4.85 (dm, *J* = 10.10 Hz, 1H, 5-H-*cis*), 1.73 (d, *J* = 7.63 Hz, 2H, 1-H), 1.31 (s, 18H, Bu<sup>t</sup>); <sup>13</sup>C NMR (126 MHz, CDCl<sub>3</sub>) δ 138.0, 134.2, and 129.9 (CH), 112.7 (CH<sub>2</sub>=), Bu<sup>t</sup> signals 72.9 (CMe<sub>3</sub>) and 30.6 (CMe<sub>3</sub>); <sup>11</sup>B NMR (32 MHz, CDCl<sub>3</sub>, BF<sub>3</sub>·OEt<sub>2</sub> external) δ 30; MS (70 eV) *m/z* (*I*<sub>rel</sub>) 224 (5, M<sup>+</sup>), 157 (5, M<sup>+</sup> - C<sub>5</sub>H<sub>7</sub>), 57 (100, Bu<sup>t</sup> +).

**Synthesis of 4g.** A solution of **4a** (15.0 g, 0.090 mol) in THF (140 mL) was added dropwise to ethylene glycol (5.6 g, 0.090 mol) in THF (260 mL) at room temperature. After the mixture was stirred for 12 h, the volatiles were removed under

reduced pressure. Distillation of the residue yielded (E/Z)-**4g** (8.8 g, 71%): bp 80 °C/14 mbar.

(E)-**4g**: <sup>1</sup>H NMR (500 MHz, CDCl<sub>3</sub>) δ 6.30 (ddd, *J* = 16.70, 10.70, 10.50 Hz, 1H, 4-H), 6.06 (ddm, *J* = 15.30, 10.50 Hz, 1H, 3-H), 5.77 (dt, *J* = 15.30, 7.60 Hz, 1H, 2-H), 5.18 (dm, *J* = 16.50 Hz, 1H, 5-H-*trans*), 5.08 (dm, *J* = 10.00 Hz, 1H, 5-H-*cis*), 4.19 (s, 4H, OCH<sub>2</sub>), 1.81 (d, *J* = 7.60 Hz, 2H, 1-H); <sup>13</sup>C NMR (126 MHz, CDCl<sub>3</sub>) δ 137.3, 130.3, and 127.4 (CH), 114.1 (CH<sub>2</sub>=), 65.6 (OCH<sub>2</sub>), 15.8 (br, CH<sub>2</sub>B); <sup>11</sup>B NMR (32 MHz, CDCl<sub>3</sub>, BF<sub>3</sub>·OEt<sub>2</sub> external) δ 34; MS (70 eV) *m/z* (*I*<sub>rel</sub>) 138 (95, M<sup>+</sup>), 67 (100, M<sup>+</sup> - C<sub>5</sub>H<sub>7</sub>).

(Z)-**4g**: <sup>1</sup>H NMR (500 MHz, CDCl<sub>3</sub>) δ 6.63 (dddd, *J* = 17.10, 11.00, 10.30, 1.1 Hz, 1H, 4-H), 6.03 (ddm, *J* = 10.50, 10.30 Hz, 1H, 3-H), 5.58 (dtm, *J* = 10.40, 8.10 Hz, 1H, 2-H), 5.04 (dm, *J* = 17.10 Hz, 1H, 5-H-*trans*), 4.91 (dm, *J* = 10.00 Hz, 1H, 5-H-*cis*), 4.19 (s, 4H, OCH<sub>2</sub>), 1.91 (d, *J* = 8.00 Hz, 2H, CH<sub>2</sub>B); <sup>13</sup>C NMR (126 MHz, CDCl<sub>3</sub>) δ 132.0, 131.8, and 129.2 (CH), 116.7 (CH<sub>2</sub>=), 65.6 (OCH<sub>2</sub>), 11.5 (br, CH<sub>2</sub>B); <sup>11</sup>B NMR and MS see (E)-**4g**.

**Synthesis of 4h.** A solution of **4a** (19.9 g, 0.12 mol) in THF (100 mL) was added dropwise to pinacol (14.0 g, 0.12 mol) in THF (150 mL) at room temperature. After the mixture was stirred for 12 h, the volatiles were removed in vacuo. Distillation of the residue gave (E/Z)-**4h** (18.8 g, 82%): bp 80 °C/10 mbar.

(E/Z)-**4h**: <sup>1</sup>H NMR (500 MHz, CDCl<sub>3</sub>) for *E* isomer δ 6.30 (ddd, *J* = 16.80, 10.0, 10.0 Hz, 1H, 4-H), 6.04 (ddm, *J* = 15.1, 10.0 Hz, 1H, 3-H), 5.76 (dtm, *J* = 15.1, 7.5, 1H, 2-H), 5.03 (dm, *J* = 16.8 Hz, 1H, 5-H-*trans*), 4.89 (dm, *J* = 10.0 Hz, 1H, 5-H-*cis*), 1.75 (d, *J* = 7.5 Hz, 2H, 1-H), and 1.24 (s, 12H, OCM<sub>2</sub>), for *Z* isomer δ 6.63 (dddd, *J* = 17.0, 11.0, 10.1, 1.1 Hz, 1H, 4-H), 6.01 (ddm, *J* = 11.0, 9.5 Hz, 1H, 3-H), 5.58 (dt, *J* = 9.5, 8.0 Hz, 1H, 2-H), 5.15 (dm, *J* = 17.0 Hz, 1H, 5-H-*trans*), 5.06 (dm, *J* = 10.0 Hz, 1H, 5-H-*cis*), 1.84 (d, *J* = 8.0 Hz, 2H, 1-H), 1.24 (s, 12H, OCM<sub>2</sub>); <sup>13</sup>C NMR (126 MHz, CDCl<sub>3</sub>) δ 137.5, 132.2, 131.7, 130.5, 129.1, and 127.6 (CH), 116.3 and 113.8 (CH<sub>2</sub>=), 83.4 (CM<sub>2</sub>), 24.8 (CMe<sub>2</sub>), 16.5 (br, CH<sub>2</sub>B), 12.0 (br, CH<sub>2</sub>B); <sup>11</sup>B NMR (32 MHz, CDCl<sub>3</sub>, BF<sub>3</sub>·Et<sub>2</sub>O external) δ 33; MS (70 eV) *m/z* (*I*<sub>rel</sub>) 194 (100, M<sup>+</sup>), 67 (80, M<sup>+</sup> - C<sub>5</sub>H<sub>5</sub>).

**Synthesis of [Li(TMEDA)][C<sub>5</sub>H<sub>5</sub>BNMe<sub>2</sub>] (10a).** LiNET<sub>2</sub> (73.9 g, 0.93 mol) was dissolved in THF (500 mL) and TMEDA (139 mL, 0.93 mol). A solution of **4a** (103.5 g, 0.623 mol) in THF (150 mL) was added dropwise with stirring at -78 °C. The mixture was then warmed to room temperature within 3 h, and stirring was continued for 12 h. After removal of the volatiles in vacuo hexane (400 mL) was added to precipitate a white powder consisting of LiNET<sub>2</sub> and **10a**, which was collected by filtration. Cooling of the filtrate to -30 °C for 12 h gave colorless crystals of **10a**. Extraction of the LiNET<sub>2</sub>/**10a** mixture with pentane gave a second crop of pure **10a** with a total yield of 40.1 g (26.5%): mp 82 °C.

**10a**: <sup>1</sup>H NMR (500 MHz, [D<sub>8</sub>]THF) δ 7.04 (dd, *J* = 10.68, 6.71 Hz, 2H, 3-/5-H), 5.65 (dd, *J* = 10.70, 0.92 Hz, 2H, 2-/6-H), 5.50 (tt, *J* = 6.70, 0.91 Hz, 1H, 4-H), 2.69 (s, 6H, NMe<sub>2</sub>), TMEDA signals 2.26 (s, 4H, NCH<sub>2</sub>) and 2.11 (s, 12H, NMe<sub>2</sub>); <sup>13</sup>C NMR (67.9 MHz, [D<sub>8</sub>]THF) δ 134.4 (C-3,5), ca. 110 (br, C-2,6), 99.7 (C-4), 39.6 (BNMe<sub>2</sub>), TMEDA signals 58.7 (NCH<sub>2</sub>) and 46.0 (NMe<sub>2</sub>); <sup>11</sup>B NMR (32 MHz, THF, BF<sub>3</sub>·Et<sub>2</sub>O external) δ 28.

**Synthesis of [Li(TMEDA)][C<sub>5</sub>H<sub>5</sub>BNMe<sub>2</sub>] (10b).** **4b** was treated with 2 equiv of LiNET<sub>2</sub> (or LDA) by the procedure described for **10a**. Removal of the volatiles yielded an oily residue consisting of **10b**, excess LiNET<sub>2</sub>, and some B(NEt<sub>2</sub>)<sub>3</sub>. Attempts to isolate pure **10b** by crystallization were not successful.

**10b**: <sup>1</sup>H NMR (500 MHz, [D<sub>8</sub>]THF) δ 7.05 (dd, *J* = 10.99, 6.72, 1.0 Hz, 2H, 3-/5-H), 5.63 (d, *J* = 10.99 Hz, 2H, 2-/6-H), 5.50 (tt, *J* = 6.72, 1.22 Hz, 1H, 4-H), NMe<sub>2</sub> signals 3.09 (q, 4H, NCH<sub>2</sub>) and 1.01 (t, 6H, Me), TMEDA signals 2.24 (s, 4H, NCH<sub>2</sub>) and 2.11 (s, 12H, NMe<sub>2</sub>); <sup>13</sup>C NMR (126 MHz, [D<sub>8</sub>]THF) δ 134.4 (C-3,5), ~110 (br, C-2,6), 99.1 (C-4), NMe<sub>2</sub> signals 43.9

(NCH<sub>2</sub>) and 16.3 (Me), TMEDA signals 58.0 (NCH<sub>2</sub>) and 46.0 (NMe<sub>2</sub>); <sup>11</sup>B NMR (32 MHz, THF, BF<sub>3</sub>·OEt<sub>2</sub> external) δ 31.

**Attempted Metalation of 4h with LiNMe<sub>2</sub>.** A solution of 4h (1.94 g, 10 mmol) in THF (5 mL) was added dropwise with stirring to LiNMe<sub>2</sub> (0.51 g, 10 mmol) in THF (10 mL) and TMEDA (1.5 mL, 10 mmol) at -78 °C. The mixture was then warmed to ambient temperature within 3 h, and stirring was continued for 12 h. After the temperature was lowered to -50 °C, Me<sub>3</sub>SiCl (2.5 mL, 20 mmol) was added. Then, after the mixture was warmed to room temperature, all volatiles were removed under reduced pressure. Hexane (20 mL) was added and a precipitate of LiCl was filtered off. After removal of the solvent the residue was heated in vacuo (24 mbar) to 120 °C, and 12 (1.9 g, 68%) was collected by condensation as a colorless liquid.

**12:** <sup>1</sup>H NMR (80 MHz, CDCl<sub>3</sub>) δ 2.54 (s, 3H, NMe<sub>2</sub>), 2.48 (s, 3H, NMe<sub>2</sub>), 1.16 (s, 6H, CMe<sub>2</sub>), 1.15 (s, 6H, CMe<sub>2</sub>), 0.05 (s, 9H, SiMe<sub>3</sub>); <sup>13</sup>C NMR (67.9 MHz, CDCl<sub>3</sub>) δ 81.7 and 78.2 (s, CMe<sub>2</sub>), 39.1 and 36.1 (NMe<sub>2</sub>), 24.8 and 24.4 (CMe<sub>2</sub>), 2.2 (SiMe<sub>3</sub>); <sup>11</sup>B NMR (32 MHz, CDCl<sub>3</sub>, BF<sub>3</sub>·OEt<sub>2</sub> external) δ 25.

**Metalation of 4h with LDA and Synthesis of 13.** LiBu (1.6 M solution, 62.5 mL, 0.10 mol) was added to diisopropylamine (14.0 mL, 0.10 mol) in THF (50 mL) at 0 °C. After the mixture was stirred for 0.5 h at ambient temperature, the solution was cooled to -78 °C and 4h (19.4 g, 0.10 mol) in THF (40 mL) was added dropwise within 30 min. While the deep red reaction mixture was slowly warmed to ambient temperature, a white precipitate formed. Stirring was continued for 12 h. Then the precipitate was collected by filtration, washed with pentane (3 × 10 mL), and dried under vacuum to yield pure 13 (17.0 g, 63%): mp 142 °C.

**13:** <sup>1</sup>H NMR (500 MHz, [D<sub>6</sub>]acetone) δ 6.13 (dd, *J* = 12.20, 5.00 Hz, 1H, 3-H), 5.92 (d, *J* = 12.20 Hz, 1H, 2-H), 5.85 (dt, 9.5, 4.60 Hz, 1H, 5-H), 5.62 (ddm, *J* = 9.5, 5.0, 2.1 Hz, 1H, 4-H), 1.19 (dd, *J* = 4.60, 2.14 Hz, 2H, 6-H), 1.09 (s, 6H, CMe<sub>2</sub>), 1.06 (s, 6H, CMe<sub>2</sub>), THF signals 3.63 (m, 4H, OCH<sub>2</sub>), 1.79 (m, 4H, CH<sub>2</sub>); <sup>13</sup>C NMR (126 MHz, [D<sub>6</sub>]acetone) δ 149.0 (br, CHB), 134.5, 131.4, and 125.4 (CH), 78.3 (CMe<sub>2</sub>), 26.3 and 26.1 (CMe<sub>2</sub>), signal for CH<sub>2</sub>B not found; <sup>11</sup>B NMR (32 MHz, [D<sub>6</sub>]acetone, BF<sub>3</sub>·OEt<sub>2</sub> external) δ 5.7.

**Reaction of 13 with Me<sub>3</sub>SiCl.** Me<sub>3</sub>SiCl (7.8 mL, 62.5 mmol) was added with stirring to a suspension of 13 (17.0 g, 62.5 mmol) in pentane (200 mL) at -78 °C. The reaction mixture was warmed to ambient temperature, and stirring was continued for 12 h. The white precipitate of LiCl was filtered off. After removal of the solvent the residue was heated under vacuum (10<sup>-3</sup> mbar) to 100 °C, and 15 (8.3 g, 50%) was collected by condensation as a colorless liquid.

**15a:** <sup>1</sup>H NMR (500 MHz, CDCl<sub>3</sub>) δ 7.13 (ddd, *J* = 12.20, 5.49, 0.91 Hz, 1H, 3-H), 6.26 (dt, *J* = 9.5, 4.3 Hz, 1H, 5-H), 6.14 (dd, 9.46, 5.50 Hz, 1H, 4-H), 6.10 (d, *J* = 12.20 Hz, 1H, 2-H), 1.87 (dd, *J* = 4.28, 1.84 Hz, 1H, 6-H), 1.35 (s, 6H, CMe<sub>2</sub>), 1.25 (s, 6H, CMe<sub>2</sub>), 0.09 (s, 9H, SiMe<sub>3</sub>); <sup>13</sup>C NMR (126 MHz, CDCl<sub>3</sub>) δ 148.6, 136.4, and 125.0 (CH), 129 (CHB), 81.0 and 78.4 (CMe<sub>2</sub>), 41 (br, CH<sub>2</sub>B), 25.0 and 24.0 (CMe<sub>2</sub>), 2.5 (SiMe<sub>3</sub>); <sup>11</sup>B NMR (87 MHz, CDCl<sub>3</sub>, BF<sub>3</sub>·OEt<sub>2</sub> external) δ 46; MS (70 eV) *m/z* (*I*<sub>rel</sub>) 266 (5, M<sup>+</sup>), 173 (15, CMe<sub>2</sub>CMe<sub>2</sub>OSiMe<sub>3</sub><sup>+</sup>), 131 (60, CMe<sub>2</sub>OSiMe<sub>3</sub><sup>+</sup>), 93 (90, C<sub>5</sub>H<sub>6</sub>BO<sup>+</sup>), 73 (100, SiMe<sub>3</sub><sup>+</sup>).

**15b:** <sup>1</sup>H NMR (500 MHz, CDCl<sub>3</sub>) δ 7.07 (dt, *J* = 12.51, 3.05 Hz, 1H, 3-H), 6.23 (dt, *J* = 12.51, 1.84 Hz, 1H, 2-H), 3.00 (tt, 3.05, 1.84 Hz, 2H, 4-H), 1.39 (s, 6H, CMe<sub>2</sub>), 1.28 (s, 6H, CMe<sub>2</sub>), 0.10 (s, 9H, SiMe<sub>3</sub>); <sup>13</sup>C NMR (126 MHz, CDCl<sub>3</sub>) δ 151.2 (C-3), 132 (br, C-2), 80.5 and 78.4 (CMe<sub>2</sub>), 25.0 and 23.7 (CMe<sub>2</sub>), 2.5 (SiMe<sub>3</sub>); <sup>11</sup>B NMR (87 MHz, CDCl<sub>3</sub>, BF<sub>3</sub>·OEt<sub>2</sub> external) δ 37; MS, see data for 15a.

**Synthesis of Li[C<sub>5</sub>H<sub>5</sub>BO(CMe<sub>2</sub>)<sub>2</sub>OSiMe<sub>3</sub>] (Li(3b)).** LiBu<sup>+</sup> (1.7 M solution in hexane, 10.3 mL, 17.5 mmol) was added dropwise with stirring to 15 (4.65 g, 17.5 mmol) in pentane (20 mL) at -78 °C. While the solution was warmed to ambient temperature, a white precipitate formed. The solid was isolated to give Li(3b) (4.28 g, 90 %): mp 153 °C.

**Li(3b):** <sup>1</sup>H NMR (500 MHz, [D<sub>8</sub>]THF) δ 6.99 (dd, *J* = 10.2, 6.8 Hz, 2H, 3-/5-H), 5.67 (d, *J* = 10.2 Hz, 2H, 2-/6-H), 5.66 (tm, *J* = 6.6 Hz, 1H, 4-H), 1.40 (s, 6H, CMe<sub>2</sub>), 1.39 (s, 6H, CMe<sub>2</sub>), 0.24 (s, 9H, SiMe<sub>3</sub>); <sup>13</sup>C NMR (126 MHz, [D<sub>8</sub>]THF) δ 134.7 (C-3,5), 115.3 (br, C-2,6), 105.8 (C-4), 84.1 and 78.4 (CMe<sub>2</sub>), 25.5 and 23.2 (CMe<sub>2</sub>), 2.9 (SiMe<sub>3</sub>); <sup>11</sup>B NMR (32 MHz, [D<sub>8</sub>]THF, BF<sub>3</sub>·OEt<sub>2</sub> external) δ 34.

**Metalation of 13 with LDA and Synthesis of Li<sub>2</sub>(3i).** A solution of LDA (0.79 g, 7.4 mmol) in THF (20 mL) was added dropwise to a suspension of the borate 13 (2.0 g, 7.4 mmol) in THF (20 mL) at -78 °C. The solution was warmed to room temperature, and stirring was continued for 2 h. Removal of all volatiles under reduced pressure yielded Li<sub>2</sub>(3i) (1.7 g, 82%), no melting point or decomposition ≤250 °C.

**Li<sub>2</sub>(3i):** <sup>1</sup>H NMR (80 MHz, [D<sub>8</sub>]THF) δ 7.00 (dd, *J* = 10.3, 7.1 Hz, 2H, 3-/5-H), 5.66 (d, *J* = 10.3 Hz, 2H, 2-/6-H), 5.61 (t, *J* = 7.1 Hz, 1H, 4-H), 1.39 (s, 6H, CMe<sub>2</sub>), 1.11 (s, 6H, CMe<sub>2</sub>), several lines are broadened when measured at 500 MHz but not when measured at 80 MHz, presumably due to dynamic association equilibria; <sup>13</sup>C NMR (126 MHz, [D<sub>8</sub>]THF) δ 134.6 (C-3,5), 115.5 (br, C-2,6), 104.5 (br, C-4), 81.7 (br) and 75.4 (CMe<sub>2</sub>), 29.5 (br) and 29.0 (br) (CMe<sub>2</sub>); <sup>11</sup>B NMR (160 MHz, [D<sub>8</sub>]THF, BF<sub>3</sub>·OEt<sub>2</sub> external) δ 34.1.

**Reaction of Li<sub>2</sub>(3i) with Me<sub>3</sub>SiCl. Preparation of 16.** Me<sub>3</sub>SiCl (2.5 mL, 20 mmol) was added to a solution of Li<sub>2</sub>(3i) at -78 °C, prepared from LDA (0.79 g, 7.4 mmol) and borate 13 (2.0 g, 7.4 mmol) as described above. The solution was warmed to room temperature, and the solvent was removed in vacuo. Pentane (20 mL) was added to the residue to precipitate LiCl, which was filtered off. Distillative workup of the filtrate gave 16 (2.0 g, 80%) as a colorless liquid: bp 96 °C/10<sup>-3</sup> mbar.

**16:** <sup>1</sup>H NMR (500 MHz, CDCl<sub>3</sub>) δ 7.16 (ddd, *J* = 12.20, 5.80, 1.1 Hz, 1H, 3-H), 6.46 (dd, *J* = 9.2, 5.2 Hz, 1H, 5-H), 6.20 (d, *J* = 12.2 Hz, 1H, 2-H), 6.12 (dd, *J* = 9.2, 5.8 Hz, 1H, 4-H), 2.40 (d, *J* = 5.2 Hz, 1H, 6-H), 1.36 (s, 6H, CMe<sub>2</sub>), 1.25 (s, 6H, CMe<sub>2</sub>), 0.09 (s, 9H, SiMe<sub>3</sub>), 0.01 (s, 9H, SiMe<sub>3</sub>); <sup>13</sup>C NMR (126 MHz, CDCl<sub>3</sub>) δ 148.0, 140.9, and 121.3 (C-3,4,5), 127.8 (br, C-2), 80.9 and 78.5 (CMe<sub>2</sub>), 41.5 (br, C-6), 25.5 and 25.0 (CMe<sub>2</sub>), 2.5 and -0.1 (SiMe<sub>3</sub>); <sup>11</sup>B NMR (32 MHz, CDCl<sub>3</sub>, BF<sub>3</sub>·OEt<sub>2</sub> external) δ 47; MS (70 eV) *m/z* (*I*<sub>rel</sub>) 338 (<5, M<sup>+</sup>), 207 (70, M<sup>+</sup> - CMe<sub>2</sub>OSiMe<sub>3</sub>), 131 (70, CMe<sub>2</sub>OSiMe<sub>3</sub><sup>+</sup>), 73 (100, SiMe<sub>3</sub><sup>+</sup>).

**Reaction of 13 with Al<sub>2</sub>Me<sub>6</sub> and Synthesis of Li[C<sub>5</sub>H<sub>5</sub>BMe] (Li(3b)).** Al<sub>2</sub>Me<sub>6</sub> (2.0 M AlMe<sub>3</sub> in toluene, 54 mL, 108 mmol) was added dropwise with stirring to a suspension of 13 (14.6 g, 54 mmol) in Et<sub>2</sub>O (70 mL) at -78 °C. The mixture was warmed to room temperature within 3 h, and stirring was continued for 24 h while the solid dissolved and a yellow solution formed. Upon removal of the Et<sub>2</sub>O under somewhat reduced pressure a precipitate forms, which is filtered off, washed with toluene (3 × 20 mL), and dried in vacuo for 12 h to remove the toluene, giving Li(3b) (4.15 g, 79%) as a white solid: no melting observed up to 250 °C.

**Li(3b):** <sup>1</sup>H NMR (500 MHz, [D<sub>8</sub>]THF) δ 7.28 (dd, *J* = 9.8, 7.0 Hz, 1H, 3-/5-H), 6.47 (d, *J* = 9.8 Hz, 1H, 2-/6-H), 6.18 (tm, *J* = 7.0 Hz, 1H, 4-H), 0.67 (s, 3H, BMe); <sup>13</sup>C NMR (67.9 MHz, [D<sub>8</sub>]THF) δ 132.8 (dd, *J* = 138.7, <sup>3</sup>*J* = 7.0 Hz, C-3,5), 127 (d, br, C-2,6), 107.9 (dt, *J* = 153.5, <sup>3</sup>*J* = 7.0 Hz, C-4), 4.4 (q, br, BMe); <sup>11</sup>B NMR (32 MHz, [D<sub>8</sub>]THF, BF<sub>3</sub>·OEt<sub>2</sub> external) δ 36.

**Synthesis of Li[C<sub>5</sub>H<sub>5</sub>BBu<sup>+</sup>] (Li(3c)).** A two-necked 50 mL flask, equipped with a reflux condenser and a dropping funnel, was charged with LiBu<sup>+</sup> (1.7 M in pentane, 8.0 mL, 13.6 mmol). Boracyclohexadiene 15 (1.80 g, 6.8 mmol) in hexane (10 mL) was added rapidly. The reaction mixture began to reflux and turned yellow, and a yellowish, partly solid precipitate formed. After the mixture was stirred for 2 h at ambient temperature and evaporated to dryness, the residue was washed with toluene (3 × 5 mL) to leave behind pure Li(3c) (0.50 g, 53%) as a white powder, no melting observed up to 250 °C.

**Li(3c):** <sup>1</sup>H NMR (80 MHz, [D<sub>8</sub>]THF) δ 7.05 (dd, *J* = 10.2, 6.9 Hz, 1H, 3-/5-H), 6.36 (d, *J* = 10.0 Hz, 1H, 2-/6-H), 5.92 (t, *J* = 6.9 Hz, 1H, 4-H), 1.00 (s, 9H, BBu<sup>+</sup>); <sup>13</sup>C NMR (67.9 MHz,

**Table 5. Crystallographic Data, Data Collection Parameters, and Refinement Parameters for 18**

formula	C <sub>15</sub> H <sub>22</sub> BN
fw	227.16
space group	P2 <sub>1</sub> /n (No. 14)
a, pm	935.4(1)
b, pm	1557.4(4)
c, pm	988.8(1)
β, deg	95.47(1)
V, nm <sup>3</sup>	1.4340(4)
Z	4
density (calc), g cm <sup>-3</sup>	1.052
cryst size, mm <sup>3</sup>	0.3 × 0.3 × 0.3
μ(Cu Kα), cm <sup>-1</sup> a	4.13
radiation (λ, pm)	Cu Kα (154.18)
temp, K	208
scan mode (2θ range, deg)	ω (10–148)
no. of unique rflns	2763
N <sub>o</sub> , no. of obsd rflns <sup>b</sup>	2178
N <sub>p</sub> , no. of params refined	255
R <sup>c</sup>	0.064
R <sub>w</sub> <sup>d</sup>	0.068 <sup>e</sup>
residual electron density, 10 <sup>-6</sup> e pm <sup>-3</sup>	0.15

<sup>a</sup> No absorption correction was applied. <sup>b</sup>  $I \geq 0.5\sigma(I)$ . <sup>c</sup>  $R = \sum ||F_o| - |F_c|| / \sum |F_o|$ . <sup>d</sup>  $R_w = [\sum w(|F_o| - |F_c|)^2 / \sum w|F_o|^2]^{1/2}$ . <sup>e</sup>  $w^{-1} = \sigma^2(F_o)$ .

[D<sub>8</sub>]THF) δ 133.2 (dd, <sup>1</sup>J = 146.3, <sup>3</sup>J = 7.8 Hz, C-3,5), 123 (d, br, <sup>1</sup>J = 120 Hz, C-2,6), 108.4 (dt, <sup>1</sup>J = 154.3, <sup>3</sup>J = 8.9 Hz, C-4), 32.7 (qsept, <sup>1</sup>J = 122.6, <sup>3</sup>J = 5.5 Hz, CMe<sub>3</sub>), CMe<sub>3</sub> not found; <sup>11</sup>B NMR (32 MHz, [D<sub>8</sub>]THF, BF<sub>3</sub>·OEt<sub>2</sub> external) δ 39.

**Synthesis of [NMe<sub>3</sub>Ph][C<sub>5</sub>H<sub>5</sub>BMe] (18).** Li(3b) (300 mg, 3.1 mmol) was quickly dissolved in an aqueous solution of KOH (20%, 10 mL) at 0 °C. A cold solution of [NMe<sub>3</sub>Ph]I (0.82 g, 3.1 mmol) in EtOH (5 mL) and aqueous KOH (5 mL) was kept ready and was poured into the solution of Li(3b). A white precipitate formed instantaneously. The solid was filtered off, sucked dry, and dried briefly under vacuum; it was then dissolved in THF (10 mL). Keeping the solution at -30 °C for 12 h afforded 18 (550 mg, 79%) as orange-yellow crystals; mp 116 °C. *Keeping the temperature of all solutions and reaction vessels at ≤0 °C is essential!*

18: <sup>1</sup>H NMR (500 MHz, [D<sub>8</sub>]THF) δ 7.01 (ddm, *J* = 10.0, 6.9 Hz, 2H, 3-/5-H), 6.26 (dm, *J* = 10.0 Hz, 2H, 2-/6-H), 5.95 (t, *J* = 6.9 Hz, 1H, 4-H), 0.52 (s, 3H, BMe), NMe<sub>3</sub>Ph signals 7.50 (dm, *J* = 8.85 Hz, 2H, H<sub>o</sub>), 7.45 (dd, *J* = 8.85, 7.02 Hz, 2H, H<sub>m</sub>), 7.40 (tm, *J* = 7.02 Hz, 1H, H<sub>p</sub>), and 3.04 (s, 9H, NMe<sub>3</sub>); <sup>13</sup>C NMR (126 MHz, [D<sub>8</sub>]THF) δ 133.3 (C-3,5), 128 (br, C-2,6), 109.5 (C-4), NMe<sub>3</sub>Ph signals 130.6 (C<sub>m</sub>), 130.2 (C<sub>p</sub>), 121.1, (C<sub>o</sub>), and 56.6 (NMe<sub>3</sub>), BMe and C<sub>i</sub> not found; <sup>11</sup>B NMR (160 MHz, [D<sub>8</sub>]THF, BF<sub>3</sub>·OEt<sub>2</sub> external) δ 35.1. Anal. Calcd for C<sub>15</sub>H<sub>22</sub>BN: C, 79.31; H, 9.76. Found: C, 79.45; H, 9.87.

**Crystal Structure Determination of 18.** The data collection was performed on an ENRAF-Nonius CAD4 diffractometer with Cu Kα radiation (graphite monochromator). Crystal data, data collection parameters, and refinement parameters are given in Table 5. The structure was solved by direct methods<sup>39</sup> and refined on structure factors with the SDP program system.<sup>40</sup> The hydrogen atoms of the methyl group C6 show rotational disorder around the B–C axis, and split positions with equal multiplicity were refined. In the final refinement, a correction for secondary extinction was applied to the calculated structure factors.<sup>41</sup>

**Acknowledgment.** This work was generously supported by the Deutsche Forschungsgemeinschaft, the Volkswagen-Stiftung, and the Fonds der Chemischen Industrie.

**Supplementary Material Available:** Tables of bond distances, anisotropic thermal parameters, and hydrogen atom coordinates for 18 (6 pages). Ordering information is given on any current masthead page.

OM940648I

(39) Sheldrick, G. M. SHELXS-86, Program for Crystal Structure Solution; University of Göttingen, Göttingen, Germany, 1986.

(40) Frenz, B. A. The ENRAF-Nonius CAD4 SDP – a real-time system for concurrent X-ray data collection and crystal structure determination. In *Computing in Crystallography*; Schenk, H., Olthoff-Hazekamp, R., van Koningsveld, H., Bassi, G. C., Eds.; Delft University Press: Delft, The Netherlands, 1978. SDP-PLUS, Version 1.1 (1984), and VAXSDP, Version 2.2 (1985), were also used.

(41) Zachariasen, W. H. *Acta Crystallogr.* **1963**, *16*, 1139.

# X-ray Structure, EXAFS Studies, and Fluxional Behavior of $\text{Ru}_3\text{Pt}(\mu\text{-H})(\mu_3\text{-COMe})(\text{CO})_{10}(\text{PR}_3)$

David Ellis, Louis J. Farrugia,\* and Peter Wiegeleben

Department of Chemistry, University of Glasgow, Glasgow G12 8QQ, U.K.

John G. Crossley, A. Guy Orpen,\* and Peter N. Waller

School of Chemistry, University of Bristol, Cantocks Close, Bristol BS8 1TS, U.K.

Received August 17, 1994<sup>®</sup>

Reaction of  $\text{Pt}(\text{PR}_3)(\text{nb})_2$  ( $\text{R} = \text{Cy}$  or  $i\text{Pr}$ ;  $\text{nb} = \text{bicyclo}[2.2.1]\text{hept-2-ene}$ ) with 1 mole equiv of  $\text{Ru}_3(\mu\text{-H})(\mu\text{-COMe})(\text{CO})_{10}$  (**1**) affords the title cluster  $\text{Ru}_3\text{Pt}(\mu\text{-H})(\mu_3\text{-COMe})(\text{CO})_{10}(\text{PR}_3)$  (**2a**,  $\text{R} = \text{Cy}$ ; **2b**,  $\text{R} = i\text{Pr}$ ) in ~50% yield. Crystal data for (**2a**): monoclinic, space group  $P2_1/c$ ,  $a = 19.1198(8)$  Å,  $b = 10.0226(7)$  Å,  $c = 19.8234(12)$  Å,  $\beta = 107.978(4)^\circ$ ,  $V = 3613.3(4)$  Å<sup>3</sup>,  $R(R_w) = 0.028$  (0.032) for 4897 independent, observed [ $I > 2.5\sigma(I)$ ] absorption corrected data. The metal framework consists of an essentially regular tetrahedron, with  $\text{Pt-Ru} = 2.760(1)\text{--}2.903(1)$  Å, and  $\text{Ru-Ru} = 2.754(1)\text{--}2.972(1)$  Å. The methoxymethylidyne ligand asymmetrically bridges the  $\text{Ru}_3$  face, with  $\text{Ru-C} = 1.973(6)\text{--}2.597(6)$  Å.  $\text{Pt}(\text{L}_{\text{III}})\text{-edge}$  and  $\text{Ru K-edge}$  EXAFS spectra on **2a** indicate that a similar structure is maintained in tetrahydrofuran solution. Two fluxional processes involving CO exchange are observed for **2b** by variable-temperature NMR spectroscopy. The lowest energy process results in complete equilibration of all Ru-bound CO ligands, and it is rapid at all accessible temperatures. A second, higher energy process results in complete CO scrambling.

## Introduction

Electron-counting procedures such as the polyhedral skeletal electron pair theory can adequately account for the structures of most carbonyl clusters of the transition metals in the periodic groups 14–18.<sup>1</sup> In the case of both homo<sup>2</sup> and hetero<sup>3</sup> platinum (and palladium) clusters, however, these rules are not always obeyed. In certain cases the Pt atom behaves as a “normal” transition metal, with a formal 18 electron count, while in other cases the clusters appear to be electron deficient, and the Pt atom formally has a 16 electron count.<sup>3</sup> A corollary is that in clusters that have the same electron count, differing metal core geometries may result. For instance, we have observed that the 60 cluster valence electron (CVE) species  $\text{Os}_3\text{Pt}(\mu\text{-H})_2(\text{CO})_{10}(\text{PR}_3)(\text{L})$  may have a tetrahedral<sup>4</sup> or nonplanar butterfly<sup>4a,5</sup> metal skeleton, depending on the nature of the two-electron donor ligand L. Braunstein *et al.*<sup>6</sup> have also reported that the 58 CVE clusters  $\text{M}_2\text{Pt}_2(\text{CO})_6(\text{PR}_3)_2\text{-Cp}_2$  ( $\text{M} = \text{Mo}, \text{W}$ ) adopt either planar-butterfly or tetrahedral geometries depending on the phosphine ligand, and in certain instances, both isomers coexist in solution. Recently we have shown by <sup>31</sup>P EXSY

studies<sup>7</sup> that these isomers of  $\text{Mo}_2\text{Pt}_2(\text{CO})_6(\text{PCy}_3)\text{Cp}_2$  exchange on the NMR time scale, with an activation barrier of ~78 kJ mol<sup>-1</sup>. Thus, for platinum-containing clusters, the energy difference between various skeletal geometries appears finely balanced. Indeed, in the case of  $\text{Pt}_3(\mu\text{-PPh}_2)(\text{Ph})(\text{PPh}_3)_3$ , merely the presence of different solvents of crystallization in the lattice is enough to induce substantial changes to the Pt–Pt distances.<sup>8</sup>

In order to examine the range of structures available in small hetero-platinum clusters, we have embarked on a program of synthesis and structural determination of a number of 60 CVE  $\text{Ru}_3\text{Pt}$  clusters. Stone *et al.*<sup>9</sup> had reported the synthesis of  $\text{Fe}_3\text{Pt}(\mu_3\text{-H})(\mu_3\text{-COMe})(\text{CO})_{10}(\text{PPh}_3)$  from the reaction of  $\text{Pt}(\text{PPh}_3)(\text{C}_2\text{H}_4)_2$  with  $\text{Fe}_3(\mu\text{-H})(\mu\text{-COMe})(\text{CO})_{10}$ . The analogous reaction of  $\text{Pt}(\text{PCy}_3)(\text{C}_2\text{H}_4)_2$  with  $\text{Os}_3(\mu\text{-H})(\mu\text{-COMe})(\text{CO})_{10}$  did not give the corresponding  $\text{Os}_3\text{Pt}$  cluster, but instead afforded the pentanuclear carbido species  $\text{Os}_3\text{Pt}_2(\mu\text{-H})(\mu_5\text{-C})(\mu\text{-OMe})(\text{CO})_{10}(\text{PCy}_3)_2$  as the sole isolable product.<sup>10</sup> In these studies, it was also stated<sup>9–11</sup> that treatment of  $\text{Ru}_3(\mu\text{-H})(\mu\text{-COMe})(\text{CO})_{10}$  (**1**) with  $\text{Pt}(\text{PPh}_3)(\text{C}_2\text{H}_4)_2$  did not afford any Ru–Pt clusters. We now report that reaction of  $\text{Pt}(\text{PR}_3)(\text{nb})_2$  ( $\text{R} = \text{Cy}$  or  $i\text{Pr}$ ) with **1** does indeed result in the high-yield formation of the desired product  $\text{Ru}_3\text{Pt}(\mu\text{-H})(\mu_3\text{-COMe})(\text{CO})_{10}(\text{PR}_3)$ .

<sup>®</sup> Abstract published in *Advance ACS Abstracts*, December 1, 1994.  
(1) (a) Mingos, D. M. P. *Acc. Chem. Res.* **1984**, *17*, 311. (b) Wade, K. *Adv. Inorg. Chem. Radiochem.* **1976**, *18*, 1. (c) Owen, S. M. *Polyhedron* **1988**, *7*, 253.

(2) Mingos, D. M. P.; Wardle, R. W. M. *Transition Met. Chem. (N.Y.)* **1985**, *10*, 441.

(3) Farrugia, L. J. *Adv. Organomet. Chem.* **1990**, *31*, 301.

(4) (a) Farrugia, L. J.; Green, M.; Hankey, D. R.; Murray, M.; Orpen, A. G.; Stone, F. G. A. *J. Chem. Soc., Dalton Trans.* **1985**, 177. (b) Ewing, P.; Farrugia, L. J. *Organometallics* **1989**, *8*, 1665.

(5) (a) Farrugia, L. J.; Howard, J. A. K.; Mitrprachachon, P.; Stone, F. G. A.; Woodward, P. J. *Chem. Soc., Dalton Trans.* **1981**, 162. (b) Farrugia, L. J. *Acta Crystallogr. Sect. C* **1991**, *C47*, 1310.

(6) Braunstein, P.; de Meric de Bellefon, C.; Bouaoud, S.-E.; Grandjean, D.; Halet, J.-F.; Saillard, J.-Y. *J. Am. Chem. Soc.* **1991**, *113*, 5282.

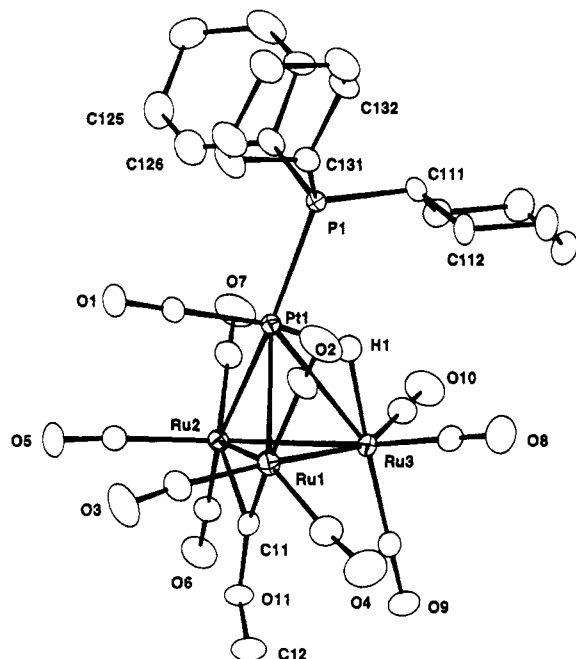
(7) Braunstein, P.; Farrugia, L. J.; Wiegeleben, P., unpublished results.

(8) (a) Bender, R.; Braunstein, P.; Tiripicchio, A.; Tiripicchio-Camellini, M. *Angew. Chem., Int. Ed. Engl.* **1985**, *24*, 861. (b) Taylor, N. J.; Chieh, P. C.; Carty, A. J. *J. Chem. Soc., Chem. Commun.* **1975**, 448.

(9) Green, M.; Mead, K. A.; Mills, R. M.; Salter, I. D.; Stone, F. G. A.; Woodward, P. J. *Chem. Soc., Chem. Commun.* **1982**, 51.

(10) Farrugia, L. J.; Miles, A. D.; Stone, F. G. A. *J. Chem. Soc., Dalton Trans.* **1985**, 2437.

(11) Salter, I. D. Ph.D. Thesis, University of Bristol, Bristol, U.K., 1983.



**Figure 1.** Molecular structure and atomic labeling scheme for cluster **2a**.

## Results and Discussion

There are now well-established strategies for heterometallic cluster synthesis.<sup>12</sup> One conceptually simple method of obtaining 60 CVE Ru<sub>3</sub>Pt clusters is to add a 12-electron Pt fragment such as "Pt(PR<sub>3</sub>)" to preformed 48-electron triruthenium clusters. The reagent that has been used successfully for the production of "Pt(PR<sub>3</sub>)" fragments in cluster synthesis is the bis(ethene) complex Pt(PR<sub>3</sub>)(C<sub>2</sub>H<sub>4</sub>)<sub>2</sub>.<sup>13</sup> The preparation of this complex from Pt(COD)Cl<sub>2</sub> involves several stages, including the isolation of Pt(COD)<sub>2</sub>. We now report that the complex Pt(PR<sub>3</sub>)(nb)<sub>2</sub> (nb = bicyclo[2.2.1]hept-2-ene), prepared *in situ* by treatment of Pt(nb)<sub>3</sub><sup>14</sup> with 1 mole equiv of phosphine, behaves in the same way as the ethene complex as a source of "Pt(PR<sub>3</sub>)". This is advantageous, since Pt(nb)<sub>3</sub> may be prepared in a single step in consistently high yield from Pt(COD)Cl<sub>2</sub>.<sup>14</sup> No attempt was made to isolate the monophosphine complex, although <sup>31</sup>P NMR showed the reaction mixture consisted primarily of a single platinum/phosphorus-containing species.<sup>15</sup> The reaction of Ru<sub>3</sub>(μ-H)(μ-COME)(CO)<sub>10</sub> (**1**) with Pt(PR<sub>3</sub>)(nb)<sub>2</sub> (R = Cy or 'Pr) affords the deep red clusters Ru<sub>3</sub>Pt(μ-H)(μ<sub>3</sub>-COME)(CO)<sub>10</sub>(PR<sub>3</sub>) (**2a**, R = Cy; **2b**, R = 'Pr) as the sole isolable heteronuclear products in ~50–60% yield. Both **2a** and **2b** were obtained as crystalline materials from hexane. The new complexes

(12) (a) Roberts, D. A.; Geoffroy, G. L. In *Comprehensive Organometallic Chemistry*; Wilkinson, G., Stone, F. G. A., Abel, E., Eds.; Pergamon: Oxford, U.K., 1982; Vol. 6, Chapter 40. (b) Geoffroy, G. L. In *Metal Clusters in Catalysis*; Gates, B. C., Guzzi, L., Knozinger, H., Eds.; Elsevier: New York, 1986; Chapter 1. (c) Adams, R. D. In *The Chemistry of Metal Cluster Complexes*; Shriver, D. F., Kaesz, H. D., Adams, R. D., Eds.; VCH: New York, 1990; Chapter 3. (d) Vahrenkamp, H. *Adv. Organomet. Chem.* **1983**, *22*, 169. (e) Stone, F. G. A. *Angew. Chem., Int. Ed. Engl.* **1984**, *23*, 89.

(13) (a) Stone, F. G. A. *Inorg. Chim. Acta* **1981**, *50*, 33. (b) Stone, F. G. A. *Acc. Chem. Res.* **1981**, *14*, 318.

(14) (a) Green, M.; Howard, J. A. K.; Spencer, J. L.; Stone, F. G. A. *J. Chem. Soc., Dalton Trans.* **1977**, 271. (b) Craswell, L. E.; Spencer, J. L. *Inorg. Synth.* **1990**, *28*, 126.

(15) For the reaction of Pt(nb)<sub>3</sub> with P<sup>i</sup>Pr<sub>3</sub> there are <sup>31</sup>P NMR signals at δ 56.8 (*J*(Pt–P) = 3449 Hz) ~80% of total intensity and also signals at δ 47.5, 45.9 (*J*(Pt–P) = 3266, 3182 Hz) ~20%.

**Table 1.** Final Positional Parameters (Fractional Coordinates)<sup>a</sup> and Isotropic Thermal Parameters<sup>b</sup> for Complex **2a**

	<i>x/a</i>	<i>y/b</i>	<i>z/c</i>	<i>U</i>
Pt	0.77831(1)	0.06013(2)	0.74306(1)	0.033
Ru(1)	0.83217(3)	0.15534(5)	0.88354(2)	0.044
Ru(2)	0.92646(2)	0.11964(5)	0.79047(2)	0.036
Ru(3)	0.83111(3)	0.33141(5)	0.77574(2)	0.042
P	0.67198(7)	0.01399(14)	0.64734(7)	0.035
O(1)	0.8187(3)	-0.2156(5)	0.7990(3)	0.078
O(2)	0.6674(3)	0.0815(7)	0.8508(3)	0.111
O(3)	0.8962(3)	-0.0520(6)	0.9967(3)	0.110
O(4)	0.8050(4)	0.3634(7)	0.9801(3)	0.137
O(5)	0.9962(3)	-0.1418(5)	0.8543(3)	0.073
O(6)	1.0744(3)	0.2388(6)	0.8023(3)	0.086
O(7)	0.8911(3)	0.0682(6)	0.6296(2)	0.095
O(8)	0.6992(3)	0.4841(6)	0.7905(3)	0.110
O(9)	0.9365(3)	0.5469(5)	0.8517(3)	0.089
O(10)	0.8416(3)	0.4233(6)	0.6334(3)	0.098
O(11)	0.9884(2)	0.2708(4)	0.9232(2)	0.061
C(1)	0.8045(3)	-0.1110(6)	0.7771(3)	0.052
C(2)	0.7275(4)	0.1071(8)	0.8566(3)	0.070
C(3)	0.8688(4)	0.0209(7)	0.9533(3)	0.064
C(4)	0.8184(4)	0.2824(8)	0.9459(4)	0.080
C(5)	0.9702(3)	-0.0460(7)	0.8284(3)	0.050
C(6)	1.0182(3)	0.1948(6)	0.7958(3)	0.054
C(7)	0.9003(3)	0.0815(7)	0.6881(3)	0.056
C(8)	0.7484(4)	0.4257(7)	0.7856(4)	0.065
C(9)	0.8971(4)	0.4649(7)	0.8237(4)	0.061
C(10)	0.8391(4)	0.3885(7)	0.6874(4)	0.063
C(11)	0.9293(3)	0.2144(6)	0.8795(3)	0.047
C(12)	0.9890(5)	0.3137(8)	0.9918(4)	0.089
C(111)	0.6219(3)	0.1614(6)	0.5999(3)	0.043
C(112)	0.5922(3)	0.2476(6)	0.6480(3)	0.061
C(113)	0.5536(4)	0.3737(8)	0.6109(4)	0.084
C(114)	0.6014(5)	0.4519(7)	0.5786(5)	0.089
C(115)	0.6277(5)	0.3675(8)	0.5277(4)	0.090
C(116)	0.6683(4)	0.2450(7)	0.5646(3)	0.061
C(121)	0.6949(3)	-0.0792(7)	0.5769(3)	0.059
C(122)	0.6337(4)	-0.1044(8)	0.5080(3)	0.070
C(123)	0.6620(6)	-0.1628(12)	0.4525(4)	0.130
C(124)	0.7138(6)	-0.2693(9)	0.4719(5)	0.107
C(125)	0.7745(5)	-0.2474(9)	0.5405(4)	0.095
C(126)	0.7456(5)	-0.1926(10)	0.5985(4)	0.116
C(131)	0.6003(3)	-0.0733(6)	0.6759(3)	0.049
C(132)	0.5248(3)	-0.0903(7)	0.6211(3)	0.060
C(133)	0.4685(4)	-0.1433(9)	0.6552(4)	0.085
C(134)	0.4940(4)	-0.2661(8)	0.6947(4)	0.084
C(135)	0.5672(4)	-0.2513(9)	0.7499(4)	0.086
C(136)	0.6238(4)	-0.2005(8)	0.7153(4)	0.087
H(1)	0.767(3)	0.208(5)	0.724(3)	0.06(2)

<sup>a</sup> ESDs in parentheses. <sup>b</sup> Å<sup>2</sup>, equivalent isotropic parameters *U*<sub>eq</sub> for anisotropic atoms. Equivalent isotropic *U*<sub>eq</sub> defined as one-third of the trace of the orthogonalized *U*<sub>ij</sub> tensor.

were characterized by spectroscopic methods, and a single crystal X-ray structural determination was carried out on **2a**.

**Crystal Structure Analysis of 2a.** The molecular structure and atomic labeling scheme is shown in Figure 1, and the atomic coordinates and important metrical parameters are given in Tables 1 and 2, respectively. The metal skeleton of **2a** approximates to a regular tetrahedron. The three Pt–Ru distances range from 2.760(1) to 2.903(1) Å, the longest being associated with the Pt(μ-H)Ru vector, Pt–Ru(3). Two of the Ru–Ru vectors, Ru(1)–Ru(3) = 2.767(1) Å and Ru(2)–Ru(3) = 2.754(1) Å are very similar in length, while the third distance Ru(1)–Ru(2) = 2.972(1) Å is significantly longer. To our knowledge the only other crystallographically characterized *tetrahedral* Ru<sub>3</sub>Pt clusters are the 60 CVE cluster Ru<sub>3</sub>Pt(μ-H)<sub>2</sub>(CO)<sub>10</sub>(COD) (**3**)<sup>16</sup> and

(16) Adams, R. D.; Li, Z.; Lii, J.-C.; Wu, W. *Inorg. Chem.* **1992**, *31*, 3445.



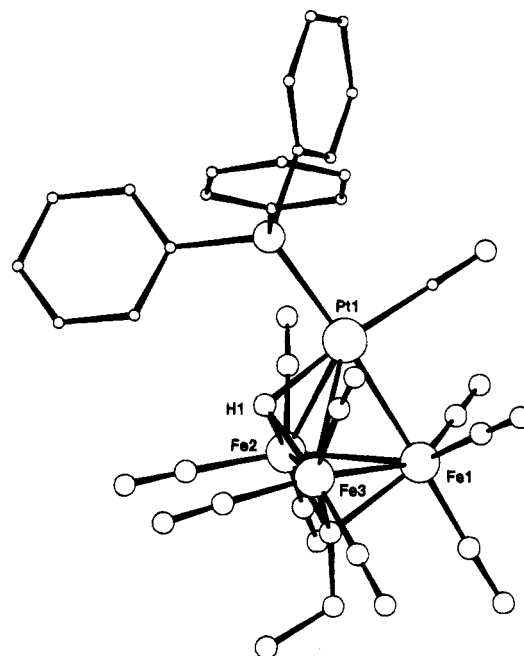
**Table 2. Important Bond Lengths (Å) and Bond Angles (deg) for Complex 2a**

Bond Lengths (Å)			
Pt–Ru(1)	2.821(1)	Pt–Ru(2)	2.760(1)
Pt–Ru(3)	2.903(1)	Pt–P	2.359(2)
Pt–C(1)	1.854(7)	Pt–H(1)	1.53(6)
Ru(1)–Ru(2)	2.972(1)	Ru(1)–Ru(3)	2.767(1)
Ru(1)–C(2)	1.965(8)	Ru(1)–C(3)	1.903(7)
Ru(1)–C(4)	1.850(8)	Ru(1)–C(11)	1.973(6)
Ru(2)–Ru(3)	2.754(1)	Ru(2)–C(5)	1.906(7)
Ru(2)–C(6)	1.882(7)	Ru(2)–C(7)	1.972(7)
Ru(2)–C(11)	1.990(6)	Ru(3)–C(8)	1.904(8)
Ru(3)–C(9)	1.883(7)	Ru(3)–C(10)	1.893(8)
Ru(3)–C(11)	2.597(6)	Ru(3)–H(1)	1.82(6)
P–C(111)	1.852(6)	P–C(121)	1.842(7)
P–C(131)	1.856(6)	O(11)–C(11)	1.321(8)
O(11)–C(12)	1.423(8)		
Bond Angle (deg)			
Ru(1)–Pt–Ru(2)	64.4(1)	Ru(1)–Pt–Ru(3)	57.8(1)
Ru(1)–Pt–P	145.3(1)	Ru(1)–Pt–C(1)	88.8(2)
Ru(1)–Pt–H(1)	84.2(20)	Ru(2)–Pt–Ru(3)	58.1(1)
Ru(2)–Pt–P	148.8(1)	Ru(2)–Pt–C(1)	86.7(2)
Ru(2)–Pt–H(1)	85.8(20)	Ru(3)–Pt–P	121.1(1)
Ru(3)–Pt–C(1)	138.5(2)	Ru(3)–Pt–H(1)	32.9(20)
P–Pt–C(1)	100.4(2)	P–Pt–H(1)	88.2(20)
C(1)–Pt–H(1)	171.4(20)	C(11)–O(11)–C(12)	120.6(6)
Ru(1)–C(11)–Ru(2)	97.2(3)	Ru(1)–C(11)–Ru(3)	73.1(2)
Ru(1)–C(11)–O(11)	136.6(5)	Ru(2)–C(11)–Ru(3)	72.4(2)
Ru(2)–C(11)–O(11)	124.7(5)	Ru(3)–C(11)–O(11)	126.1(4)

the 58 CVE species Ru<sub>3</sub>Pt(μ-H)(μ-PPH<sub>2</sub>)(CO)<sub>9</sub>(PCy<sub>3</sub>) (4)<sup>17</sup> and Ru<sub>3</sub>Pt(μ-H)(μ-C<sub>8</sub>H<sub>13</sub>)(CO)<sub>9</sub>(PCy<sub>3</sub>) (5).<sup>18</sup> All of these clusters have essentially regular tetrahedral metal skeletons, with the Pt–Ru bonds in the range 2.718(1)–2.895(2) Å and the Ru–Ru separations in the range 2.662(1)–2.950(1) Å. The differing nature of the bridging ligands, and the inherent unsaturation in the 58 CVE clusters 4<sup>17</sup> and 5,<sup>18</sup> adequately accounts for the spread in the metal–metal distances.

The asymmetry in the Ru–Ru distances in 2a is presumably due to the effect of the bridging methoxymethylidyne ligand. This moiety is best described as asymmetrically μ<sub>3</sub>-bonded, with the strongest interactions between C(11) and Ru(1) and Ru(2). The Ru(3)–C(11) distance of 2.597(6) Å is significantly longer than the other Ru–C(11) distances of 1.973(6) and 1.990(6) Å. The structure of the parent cluster 1 has been independently determined by Johnson *et al.*<sup>19</sup> and Churchill *et al.*<sup>20</sup> The methoxymethylidyne ligand in 1 is essentially a μ<sub>2</sub>-ligand, and both studies find that the three Ru–Ru distances are very similar, ranging from 2.803(2) to 2.821(2) Å in the Johnson *et al.* study<sup>19</sup> and from 2.816(1) to 2.838(1) Å in the work of Churchill *et al.*<sup>20</sup> As both ourselves<sup>21</sup> and Keister<sup>22</sup> have previously noted, the methoxymethylidyne ligand can exhibit a spectrum of interactions with a trimetallic cluster, ranging from μ<sub>2</sub>, through semi μ<sub>3</sub> to symmetric μ<sub>3</sub>-bonding.

The other point of interest in the structure of 2a concerns the orientation of the "T-shaped" Pt(μ-H)(CO)-



**Figure 2.** Molecular structure of Fe<sub>3</sub>(μ<sub>3</sub>-H)(μ<sub>3</sub>-COMe)(CO)<sub>10</sub>(PPh<sub>3</sub>) (6), drawn from coordinates obtained from the Cambridge Crystallographic Data Base.

(PR<sub>3</sub>) unit relative to the Ru<sub>3</sub> triangle. The atoms Pt, P, C(1), O(1), and H(1) are virtually coplanar (see Table 5 of the supplementary material), and lie in the molecular pseudomirror plane, such that the hydride ligand bridges the Pt–Ru(3) vector. The hydride appears to be more closely associated with the Pt center than with the Ru center, as judged by the Pt–H(1) distance of 1.53(6) Å compared with the Ru(3)–H(1) separation of 1.82(6) Å. The hydride position was obtained directly from a Fourier map, and this atom was refined without constraint, but it should be noted that the both the precision and accuracy are necessarily limited (the associated ESDs are quite high). Nevertheless, potential energy minimization calculations<sup>23</sup> indicate that the lowest energy site along this vector is at a position which is in very close agreement<sup>24</sup> with that obtained from the X-ray refinement. In addition, the asymmetry in the Pt(μ-H)Ru bridge is consistent with the fluxional behavior described below, in that the integrity of the Pt(μ-H)(CO)(PR<sub>3</sub>) unit is retained in the lowest energy process.

Most interestingly, the orientation of the Pt(μ-H)(CO)(PR<sub>3</sub>) unit in the analogous cluster Fe<sub>3</sub>Pt(μ<sub>3</sub>-H)(μ<sub>3</sub>-COMe)(CO)<sub>10</sub>(PPh<sub>3</sub>) (6),<sup>9</sup> shown in Figure 2, differs from that observed in 2a. It is related by a rotation of ~60° about the pseudo-C<sub>3</sub> axis of the Fe<sub>3</sub> triangle, and this results in the hydride ligand bridging a PtFe<sub>2</sub> face rather than a Pt–Fe edge. In cluster 6, the methoxymethylidyne ligand is closer to a symmetric μ<sub>3</sub>-ligand, although the C–Fe distance of 2.024(10) Å to the unique Fe atom is marginally longer than the other two Fe–C distances, 1.919(11) and 1.892(12) Å.<sup>9</sup> The relationship

(23) Orpen, A. G. *J. Chem. Soc., Dalton Trans.* 1980, 2509.

(24) The hydride position determined by HYDEX<sup>23</sup> is (0.7614, 0.2103, 0.7225) with Pt–H = 1.57 Å and Ru–H = 1.87 Å, while that obtained from the difference Fourier was (0.7663, 0.2146, 0.7174) with Pt–H = 1.62 Å and Ru–H = 1.83 Å. These positions are probably more realistic than that given in Table 1, which was obtained from the least-squares refinement.

(17) Powell, J.; Brewer, J. C.; Gulia, G.; Sawyer, J. F. *Inorg. Chem.*, 1989, 28, 4470.

(18) Farrugia, L. J.; MacDonald, N.; Peacock, R. D. *Acta Crystallogr. Sect. C* 1991, C47, 2561.

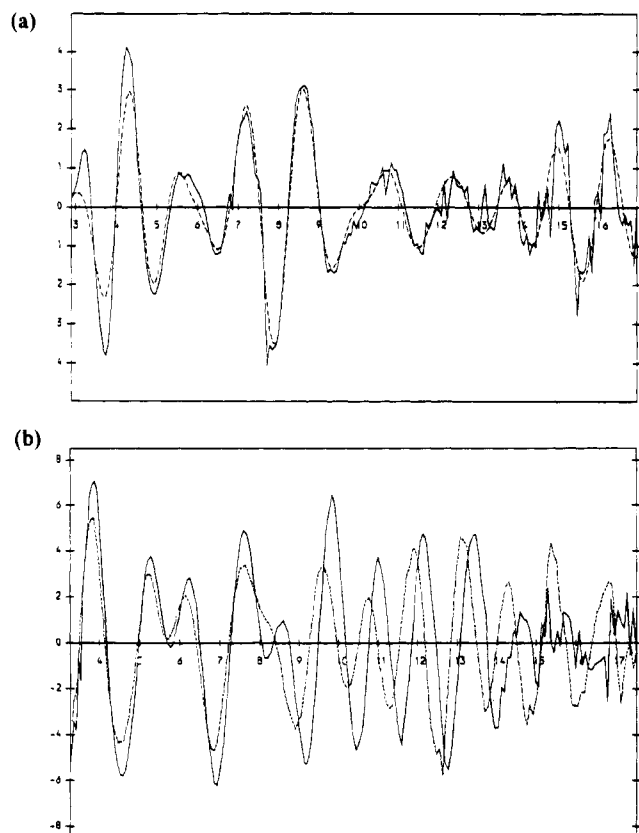
(19) Johnson, B. F. G.; Lewis, J.; Orpen, A. G.; Raithby, P. R.; Süss, G. *J. Organomet. Chem.* 1979, 173, 187.

(20) Churchill, M. R.; Beanan, L. R.; Wasserman, H. J.; Bueno, C.; Rahman, Z. A.; Keister, J. B. *Organometallics* 1983, 2, 1179.

(21) (a) Aitchison, A. A.; Farrugia, L. J. *Organometallics* 1986, 5, 1103. (b) Aitchison, A. A.; Farrugia, L. J. *Organometallics* 1987, 6, 819.

(c) Farrugia, L. J. *J. Organomet. Chem.* 1986, 310, 67.

(22) Keister, J. B. *Polyhedron* 1986, 7, 847.



**Figure 3.** (a) Calculated (---) versus experimental (—)  $k^3$ -weighted EXAFS spectra of **2a** (Pt  $L_{III}$ -edge) in THF solution at room temperature. (b) Experimental  $k^3$ -weighted Ru K-edge EXAFS spectra of **2a** as solid (—) and in THF solution (---).

between the structures of **2a** and **6** provides an insight into the fluxional behavior of **2** discussed below.

**EXAFS Studies on 2a.** In order to ascertain whether there were any differences between the metal skeleton of cluster **2** in the solid and solution phases, arising from the known "flexibility" of platinum clusters,<sup>2-8</sup> we resorted to the EXAFS technique which can provide such information. Platinum  $L_{III}$ -edge spectra were collected for THF solution (at room temperature, see Figure 3a) and solid samples (at both room temperature and low temperature, nominally 78 K) of **2a**. There are no significant differences between molecular dimensions determined from the models for these spectra (see Table 3). All distances agree reasonably with the crystallographically determined data, the largest deviation being for the Pt···O contact, which is  $\sim 0.06$  Å longer in the EXAFS models. This latter effect is perhaps due to the multiply scattered oxygen shell overlapping the metal-metal peaks, making accurate fitting difficult. However, inclusion of the oxygen, with multiple scattering corrections, does effect a large improvement of the model; the fit index is typically halved. A relatively large number of correlations between parameters of  $>0.5$  are observed (see Table 3), due to the overlapping shells at distances 2.7–3.1 Å.

These analyses therefore imply that there is little difference in the platinum environment between the solid and solution states. The different Pt–Ru distances (two short and one long) can be reliably differentiated. A model with only a single Pt–Ru contact had a fit index of 4.4, compared with a fit of 1.3 for a model having two

different Pt–Ru contacts. Attempts to include all three Pt–Ru contacts at different distances resulted in even more large correlations and a rather unstable refinement, although all three distances were in reasonable agreement with the crystallographic data.

Ruthenium K-edge spectra were collected for THF solution and solid samples (at room temperature) of **2a** and are shown in Figure 3b. The EXAFS spectra are somewhat different, as is reflected by the final models obtained; that for the solid has rather longer Ru–Ru distances, although the (average) Ru–Pt distance is similar for both. The Ru–Ru contacts however are apparently markedly reduced in the model for the solution data compared with that for the solid. The fact that there are two different Ru environments, and that the Ru···O, Ru···Ru, and Ru···Pt distances are all in the range 2.7–3.1 Å, is likely to make accurate fitting more difficult. Again there are high correlations between parameters, a problem that is increased if the model is made any more complex, e.g., splitting the average Ru–Pt shell into two shells leads to a model with 24 correlations of  $>0.5$  and an even more unstable refinement. Nevertheless, the different scattering characteristics of Pt and Ru do allow the separate metal contacts (Ru and Pt) to be refined. The difference between the EXAFS data for solution and solid phase data is surprising and should be treated with some scepticism. If real, this effect may be related to a more symmetrical structure being present in solution in the absence of packing effects which distort metal–metal distances in the solid state.

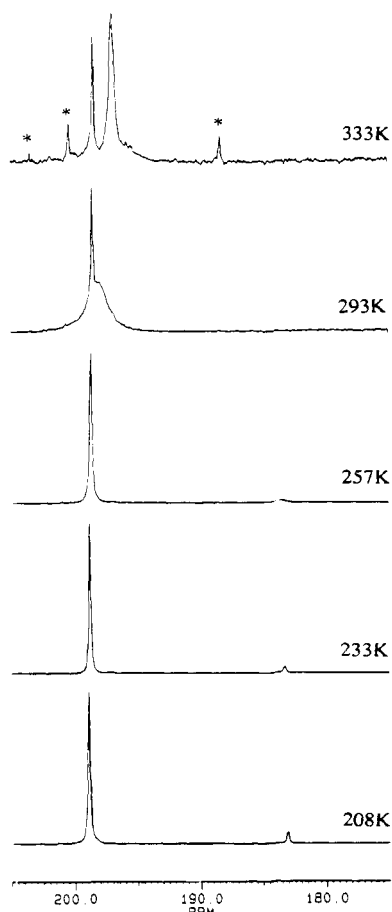
**Fluxional Behavior of 2b.** Figure 4 shows the variable-temperature  $^{13}\text{C}$  NMR spectra in the carbonyl region between 208 and 333 K of a  $^{13}\text{C}$ -enriched sample of **2b** ( $R = i\text{Pr}$ ) in  $\text{CD}_2\text{Cl}_2$ . The behavior of the signal due to the Pt-bound carbonyl ligand is shown in detail in Figure 5, while Figure 6 shows the  $^1\text{H}$  NMR spectra of the same sample in the hydride region. At the lowest temperature measured, all Ru-bound carbonyls are equivalent and give rise to a sharp singlet at  $\delta$  199.1. The line width does not increase significantly on cooling to 190 K, indicating that the process responsible for the scrambling of all nine Ru-bound CO ligands must have a very low activation barrier. The Pt-bound CO ligand appears as a doublet centered at  $\delta$  182.3 [ $J(^{31}\text{P}-\text{C}) = 4.9$  Hz] which is flanked by  $^{195}\text{Pt}$  satellites with a coupling of  $J(^{195}\text{Pt}-\text{C}) = 1534$  Hz (see Figure 5b). The high-frequency satellite appears as a shoulder on the resonance at  $\delta$  199.1. The Pt-bound carbonyl is also strongly coupled to the hydride ligand (Figure 5a), with  $J(^1\text{H}-\text{C}) = 33.2$  Hz. As the temperature is raised, the two signals at  $\delta$  199.1 and 182.2 broaden and coalesce, indicating intermetallic CO scrambling.

At 208 K, the hydride resonance (Figure 6a) appears as a doublet centered at  $\delta$  -14.71 with  $J(^{31}\text{P}-\text{H}) = 9.3$  Hz. The resonance is flanked by  $^{195}\text{Pt}$  satellites [ $J(^{195}\text{Pt}-\text{H}) = 558$ , not shown in Figure 6] and also by  $^{13}\text{C}$  satellites, with  $J(^{13}\text{C}-\text{H}) = 33.1$  Hz. At this temperature, there is only one resolved coupling to  $^{13}\text{C}$ , viz. to the CO ligand on the Pt atom, which is *trans* to the hydride. Couplings of a similar magnitude within Pt-( $\mu$ -H)(CO)( $\text{PR}_3$ ) groups have been observed in related

Table 3. Details of EXAFS Data Analysis for 2a

Pt environment									Ru environment						
Pt L <sub>III</sub> -edge EXAFS									Ru K-edge EXAFS						
XRD <sup>a</sup>		contact N (atom)	room temp solid		low temp solid		thf solution		XRD <sup>a</sup>		contact N (atom)	room temp solid		thf solution	
contact	R/Å		R/Å	σ/Å <sup>2</sup>	R/Å	σ/Å <sup>2</sup>	R/Å	σ/Å <sup>2</sup>	contact	R/Å		R/Å	σ/Å <sup>2</sup>	R/Å	σ/Å <sup>2</sup>
1 Pt-C	1.854	1 C	1.872(4) <sup>b</sup>	0.0048(6)	1.882(4)	0.0043(7)	1.874(4)	0.0052(7)	11 Ru-C	1.920*	3.67 C	1.931(3)	0.0092(4)	1.917(3)	0.0080(4)
1 Pt-P	2.359	1 P	2.338(3)	0.0085(5)	2.336(3)	0.0046(4)	2.345(3)	0.0068(6)	1 Ru-C	2.597		not fitted		not fitted	
1 Pt-Ru	2.760	2 Ru	2.786(3)	0.0117(4)	2.781(2)	0.0072(2)	2.786(3)	0.0115(4)	3 Ru-Pt	2.828*	1 Pt	2.871(28)	0.022(6)	2.882(3)	0.0058(5)
1 Pt-Ru	2.821														
1 Pt-Ru	2.903	1 Ru	2.927(4)	0.0073(5)	2.910(3)	0.0040(3)	2.919(4)	0.0068(4)	2 Ru-Ru	2.761*	0.67 Ru	2.803(3)	0.0048(3)	2.719(2)	0.0036(5)
1 Pt-O	2.989	1 O	3.058(9)	0.011(2)	3.051(7)	0.0041(3)	3.065(9)	0.010(2)	1 Ru-Ru	2.972	0.33 Ru	3.028(5)	0.0028(7)	2.924(11)	0.0030(4)
									11 Ru-O	3.033*	3.67 O	3.074(11)	0.033(2)	3.037(8)	0.027(2)
correlations between R and σ > 0.50			σ4-σ5 = 0.57		R3-R4 = 0.72		σ4-σ3 = 0.74					R5-R3 = 0.62		σ2-σ3 = 0.70	
			σ4-σ3 = 0.67		R4-R5 = 0.67		σ4-σ5 = 0.67					R5-σ2 = -0.53		σ2-R4 = 0.67	
			σ4-R5 = -0.60		R3-R5 = 0.58		R3-σ4 = -0.55					R3-σ4 = 0.55		σ4-σ3 = 0.92	
			σ4-R3 = -0.66		R5-σ4 = -0.56		R4-R3 = 0.83					R3-σ2 = -0.63		σ4-R2 = -0.84	
			R5-R3 = 0.77		R3-σ4 = -0.64		R4-R5 = 0.76					R4-R2 = -0.65		σ4-R3 = -0.90	
			R5-R4 = 0.75		σ4-σ5 = 0.50							R2-σ5 = 0.67		σ3-R2 = -0.75	
			σ3-σ5 = 0.63									σ4-σ2 = -0.71		σ3-R3 = -0.71	
			R3-R4 = 0.75											σ5-R4 = 0.53	
														σ5-R3 = 0.55	
														R2-R3 = 0.81	
k <sub>max</sub> (Å <sup>-1</sup> )			16.6		18.7		16.9					17.6		17.6	
R (%) <sup>c</sup>			13.1		12.6		13.8					8.0		7.8	
R' (%)			8.7		8.4		9.9					7.7		7.4	

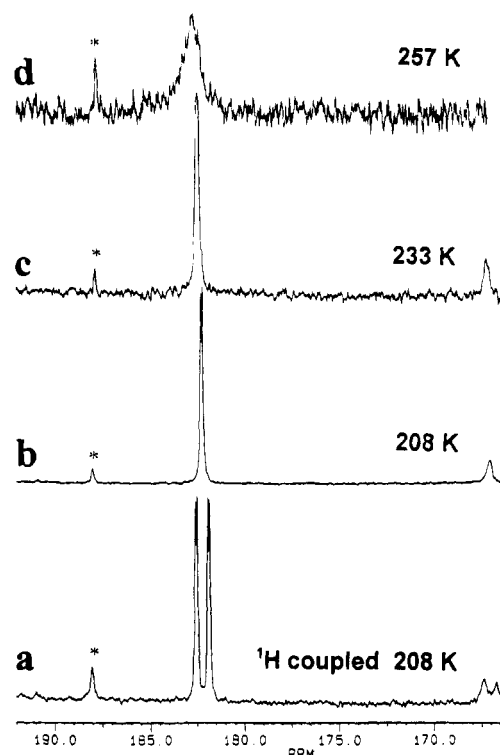
<sup>a</sup> XRD values are distances derived from the crystal structure determination; asterisk indicates averaged values. <sup>b</sup> The estimated standard deviation in the least significant digit as calculated by EXCURV90 model fitting is given in parentheses. We note that such estimates of precision are likely to be underestimates of accuracy and particularly so in cases of high correlation between parameters. <sup>c</sup> Residual indexes R and R' were calculated as follows:  $R = \frac{\sum_i \{k^3(\sum_j \chi_{ij}^{obs} - \chi_{ij}^{calc})\}^2}{\sum_i \{k^3 \chi_{ij}^{obs}\}^2}$ . R' was calculated as for R, with final model parameters, but with data Fourier filtered with  $r_{max} = 5.0 \text{ \AA}$  to remove noise.



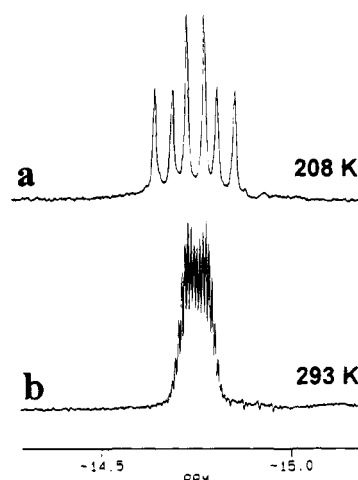
**Figure 4.** Variable-temperature  $^{13}\text{C}\{^1\text{H}\}$  NMR spectrum in the carbonyl region of cluster **2b**. Impurities due to decomposition are marked with an asterisk.

$\text{Os}_3\text{Pt}$  clusters.<sup>25</sup> The intensity of the  $^{13}\text{C}$  satellites indicates that the level of enrichment is  $\sim 50\%$ . On warming to 293 K, there is no change in the resonance position, but the coupling pattern becomes much more complicated. This is due to a further exchange process, which results in the complete carbonyl scrambling between Ru and Pt centers and which is also observed in the broadening and collapse of the  $^{13}\text{C}$  resonances shown in Figures 4 and 5. The complexity of the hydride signal at 293 K arises because this hydrogen now experiences an *averaged* coupling to all the  $^{13}\text{C}$  nuclei in individual molecules. Due to the relatively high level of  $^{13}\text{C}$  enrichment, the most abundant isotopomer is the one containing five  $^{13}\text{CO}$  ligands per molecule, and those isotopomers with four and six  $^{13}\text{CO}$  ligands have very similar abundances. The observed  $^1\text{H}$  signal thus consists of a doublet of sextets, superimposed on a doublet of quintets and a doublet of septets. Due to this complexity, we have not analyzed this multiplet in full, though it is clear that the *averaged*  $^{13}\text{C}$  coupling is  $\sim 3$  Hz.

Since we were unable to "freeze" out the fluxional motion, it is not possible to ascertain with certainty the CO exchange mechanisms. One possibility is a "merry-go-round" exchange, coupled with  $\text{Ru}(\text{CO})_3$  tripodal rotations. On the other hand, in view of our previous



**Figure 5.** Detail of the variable-temperature  $^{13}\text{C}\{^1\text{H}\}$  NMR spectrum of **2b** showing the signal for the Pt-bound carbonyl ligand. Impurities are marked with an asterisk. The high-frequency  $^{195}\text{Pt}$  satellite is obscured by the intense resonance at  $\delta$  199.1 from the Ru-bound carbonyls.



**Figure 6.** Variable-temperature  $^1\text{H}$  NMR spectrum in the hydride region. The  $^{195}\text{Pt}$  satellites are not shown.

study<sup>26</sup> on  $\text{Os}_3\text{Pt}(\mu\text{-H})_2(\text{CO})_9(\text{CNCy})(\text{PCy}_3)$ , it seems likely that a rapid rotation of the  $\text{Pt}(\mu\text{-H})(\text{CO})(\text{PR}_3)$  unit about the pseudo- $\text{C}_3$  axis of the  $\text{Ru}_3$  triangle occurs, which renders each Ru center chemically equivalent. This motion retains the stereochemical integrity of the  $\text{Pt}(\mu\text{-H})(\text{CO})(\text{PR}_3)$  unit, and it means that the hydride ligand alternately bridges an Ru–Pt edge and an  $\text{Ru}_2$ –Pt face. If such a motion is coupled with a rapid tripodal rotation of one or both of the chemically distinct  $\text{Ru}(\text{CO})_3$  groups, and a rapid rotation about the C–O bond of the COMe ligand,<sup>21</sup> then the complete scrambling of the Ru-bound CO ligands will result.

(25) (a) Ewing, P.; Farrugia, L. J.; Rycroft, D. S. *Organometallics* **1988**, *7*, 859. (b) Ewing, P.; Farrugia, L. J. *Organometallics* **1988**, *7*, 871.

(26) Farrugia, L. J. *Organometallics* **1989**, *8*, 2410.

EHMO calculations by Schilling and Hoffmann<sup>27</sup> have suggested that the rotation of the PtL<sub>3</sub> unit about the C<sub>3</sub> axis of an M<sub>3</sub> triangle (in this case a Ru<sub>3</sub> triangle) would have a low activation barrier. A comparison of the structures of **2a** and **6** (Figures 1 and 2) also suggests that such a rotation is possible, since they differ merely by a 60° rotation of the Pt( $\mu$ -H)(CO)(PR<sub>3</sub>) unit. Indeed cluster **6** may be viewed as a model for the transition state in the fluxional rotation in **2a**. Intriguingly, such a model would also suggest there is a "compensatory" motion of the methoxymethylidyne ligand, which is coupled to the Pt( $\mu$ -H)(CO)(PR<sub>3</sub>) rotation. This is of course required if the Pt( $\mu$ -H)(CO)(PR<sub>3</sub>) rotation is to be a degenerate process, since the methoxymethylidyne ligand is asymmetrically bonded to the Ru<sub>3</sub> face.

The exchange of the Pt-bound CO ligand with the other carbonyls, which occurs at temperatures at and above 293 K, may involve CO-bridging intermediates. A similar process has been previously observed for Os<sub>3</sub>-Pt( $\mu$ -H)<sub>2</sub>(CO)<sub>9</sub>(Pt-PCy<sub>3</sub>)(Os-PMe<sub>2</sub>Ph).<sup>28</sup> The spectrum at 333 K (Figure 4) shows a broad signal for the averaged environment of all 10 carbonyls at  $\delta$  196.5. This resonance is flanked on the high-frequency side by a sharp <sup>195</sup>Pt satellite, while the corresponding low-frequency satellite is only visible as a broad shoulder at 333 K. Unfortunately, the fast exchange spectrum could not be obtained due to sample decomposition. This behavior is due to the different effective chemical shifts for the averaging of the high- and low-frequency <sup>195</sup>Pt satellites and is commonly observed.<sup>25a,28</sup> The averaged <sup>195</sup>Pt coupling is 151 Hz.

## Experimental Section

General experimental techniques were as previously<sup>26</sup> described. NMR spectra were measured on a Bruker AM200. <sup>1</sup>H (201.3 MHz) and <sup>13</sup>C (50.32 MHz) spectra were referenced to internal solvent signals and are reported relative to SiMe<sub>4</sub>. <sup>31</sup>P (81.02 MHz) spectra are referenced to 85% H<sub>3</sub>PO<sub>4</sub>. The complexes Ru<sub>3</sub>( $\mu$ -H)( $\mu$ -COMe)(CO)<sub>10</sub><sup>19</sup> and Pt(nb)<sub>3</sub><sup>14</sup> were prepared by literature methods. The former complex was enriched with <sup>13</sup>CO by stirring at 90 °C under 1 atm of <sup>13</sup>CO for 12 h.

**Preparation of Ru<sub>3</sub>Pt( $\mu$ -H)( $\mu_3$ -COMe)(CO)<sub>10</sub>(PCy<sub>3</sub>) (**2a**).** To a stirred solution of Pt(nb)<sub>3</sub> (0.394 g, 0.828 mmol) in hexane (30 mL) was added PCy<sub>3</sub> (0.826 mmol). This solution was cooled to 0 °C, a solution of Ru<sub>3</sub>( $\mu$ -H)( $\mu$ -COMe)(CO)<sub>10</sub> (0.501 g, 0.803 mmol) was added, and the reaction mixture was allowed to warm to room temperature. Stirring was continued over 2 h, during which the solution changed from orange to deep red. Volatiles were removed under vacuum, and the residue was chromatographed on Florisil. The first band to elute with hexane was unreacted Ru<sub>3</sub>( $\mu$ -H)( $\mu$ -COMe)(CO)<sub>10</sub> as a yellow band (0.01 g, 2%). A second red band eluted with hexane/CH<sub>2</sub>-Cl<sub>2</sub> (4:1), which on removal of solvent and crystallization from hexane afforded Ru<sub>3</sub>Pt( $\mu$ -H)( $\mu_3$ -COMe)(CO)<sub>10</sub>(PCy<sub>3</sub>) (**2a**; 0.42 g, 0.42 mmol, 51%) as red crystals.

A similar reaction of **1** with Pt(nb)<sub>2</sub>(P<sup>i</sup>Pr<sub>3</sub>) afforded after workup complex **2b**.

**Characterization Data for 2a.** IR (hexane):  $\nu$ (CO) 2070 (w), 2046 (m), 2032 (s), 2022 (m), 1985 (m, sh), 1980 (s, br) 1968 cm<sup>-1</sup> (w). <sup>1</sup>H NMR (CDCl<sub>3</sub>, 298 K):  $\delta$  4.41 (s, 3H, Me), 2.40–1.10 (m, 33H, Cy), -14.43 (d, 1H, Pt( $\mu$ -H)Ru,  $J$ (P-H) = 9.4 Hz,  $J$ (<sup>195</sup>Pt-H) = 559 Hz). <sup>13</sup>C{<sup>1</sup>H} NMR (CDCl<sub>3</sub>,

**Table 4. Experimental Details of Crystallographic Study**

compound formula	C <sub>30</sub> H <sub>37</sub> O <sub>11</sub> PPtRu <sub>3</sub>
<i>M<sub>r</sub></i>	1102.88
space group	<i>P</i> 2 <sub>1</sub> / <i>c</i>
crystal system	monoclinic
<i>a</i> /Å	19.1198(8)
<i>b</i> /Å	10.0226(7)
<i>c</i> /Å	19.8234(12)
$\beta$ /deg	107.978(4)
<i>V</i> /Å <sup>-3</sup>	3613.3(4)
$\theta$ range for cell	17.5–20.8
<i>Z</i>	4
<i>D</i> <sub>calc</sub> /g cm <sup>-3</sup>	2.207
<i>F</i> (000)	2120
$\mu$ (MoK $\alpha$ )/cm <sup>-1</sup>	52.04
<i>T</i> /K	298
scan mode	$\theta/2\theta$
$\theta$ range/deg	2.1–25.0
crystal size/mm	0.1 × 0.2 × 0.33
range of transmission coeff corr.	0.84–1.17
no. of data collected	6986
no. of unique data	6368
<i>hkl</i> range	-22–0; 0–11; -23–23
<i>R</i> <sub>merge</sub>	0.030
standard reflections	(-3,1,-7) (8,1,-7) (2,-4,-5)
observability criterion <i>n I</i> > <i>n<math>\sigma</math>(I)</i>	2.5
no. of data in refinement	4897
no. of refined parameters	213
final <i>R</i>	0.028
<i>R</i> <sub>w</sub>	0.032
goodness of fit <i>S</i>	1.2
largest remaining feature in electron density map/e Å <sup>-3</sup>	+0.75 (max) -0.61 (min)
shift/ESD in last cycle	0.011 (mean) 0.091 (max)

298 K):  $\delta$  25.9 (s, 3C, Cy), 27.2 (d, 6C, Cy,  $J$ (P-C) = 11 Hz), 30.2 (6C, s, Cy), 36.7 (d, 3C, Cy,  $J$ (P-C) = 21 Hz), 71.3 (s, 1C, COCH<sub>3</sub>), 197 (br, 10C, averaged Pt-CO and Ru-CO signals), 197.2 (high-frequency <sup>195</sup>Pt satellite), 349.7 (d, 1C, COMe,  $J$ (P-C) = 2 Hz). <sup>31</sup>P{<sup>1</sup>H} NMR (CDCl<sub>3</sub>, 298 K):  $\delta$  71.7 (s,  $J$ (<sup>195</sup>Pt-P) = 2679 Hz). Anal. Calcd for C<sub>30</sub>H<sub>37</sub>O<sub>11</sub>PPtRu<sub>3</sub>; C, 34.10; H, 3.12. Found: C, 33.74, H, 3.23%.

**Characterization Data for 2b.** IR (hexane):  $\nu$ (CO) 2072 (w), 2046 (m), 2034 (s), 2024 (m), 1982 (s, br) 1965 cm<sup>-1</sup> (w, sh). <sup>1</sup>H NMR (CDCl<sub>3</sub>, 298 K):  $\delta$  4.42 (s, 3H, COMe), 2.55 (spt, 3H, CH,  $J$ (H-H) = 7.1 Hz), 1.30 (dd, 18H, CHMe<sub>2</sub>,  $J$ (P-H) = 15.1 Hz,  $J$ (H-H) = 7.1 Hz), -14.44 (d, 1H, Pt( $\mu$ -H)Ru,  $J$ (P-H) = 9.7 Hz,  $J$ (<sup>195</sup>Pt-H) = 558 Hz). <sup>13</sup>C{<sup>1</sup>H} (CDCl<sub>3</sub>, 298 K),  $\delta$  19.9 (s, 6C, CHMe<sub>2</sub>,  $J$ (Pt-C) = 15 Hz), 26.6 (d, 3C, CHMe<sub>2</sub>,  $J$ (P-C) = 22 Hz,  $J$ (Pt-C) = 26 Hz), 71.3 (s, 1C, COMe), 196–197 (br, CO), 349.6 (s, 1C, COMe). <sup>13</sup>C{<sup>1</sup>H} (CD<sub>2</sub>-Cl<sub>2</sub>, 208 K, <sup>13</sup>CO-enriched sample):  $\delta$  199.1 (s, 9C, Ru-CO), 182.3 (d, 1C, Pt-CO,  $J$ (P-C) = 4.9 Hz,  $J$ (<sup>195</sup>Pt-C) = 1534 Hz). <sup>31</sup>P{<sup>1</sup>H} (CD<sub>2</sub>-Cl<sub>2</sub>, 208 K):  $\delta$  80.3 (s, Pt-P,  $J$ (<sup>195</sup>Pt-P) = 2664 Hz). Anal. Calcd for C<sub>21</sub>H<sub>25</sub>O<sub>11</sub>PPtRu<sub>3</sub>; C, 25.67; H, 2.55. Found: C, 26.10, H, 2.27%.

**Crystal Structure Determination.** Details of data collection procedures and structure refinement are given in the Table 4. Crystals of **2a** were obtained as dark red prisms from hexane solution. A single crystal of suitable size was attached to a glass fiber using acrylic resin and mounted on a goniometer head in a general position. Data were collected on an Enraf-Nonius Turbo CAD4 diffractometer, running under CAD4-Express software and using graphite monochromated X-radiation ( $\lambda$  = 0.710 69 Å). Accurate unit cell dimensions were determined by refinement of the setting angles of 25 optimal high-angle reflections, which were flagged during data collection. Standard reflections were measured every 2 h during data collection, and no significant variations in intensity were noted. Lorentz polarization and absorption (DI-FABS<sup>29</sup>) corrections were applied. The structure was solved

(29) Walker, N.; Stuart, D. *Acta Crystallogr., Sect. A: Found. Crystallogr.* **1983**, *A39*, 158.

(30) *International Tables for X-Ray Crystallography*; Kynoch: Birmingham, U.K. 1974; Vol. 4.

(27) Schilling, B. E. R.; Hoffmann, R. *J. Am. Chem. Soc.* **1979**, *101*, 3456.

(28) Farrugia, L. J.; Rae, S. E. *Organometallics* **1991**, *10*, 3919.

for the metal atoms by Patterson methods. Subsequent difference syntheses gave all the other non-H atomic positions. All non-H atoms were allowed anisotropic thermal motion. Aliphatic hydrogen atoms were included at calculated positions (C-H = 0.96 Å) and were allowed to ride on their attached carbon atom. A common refined isotropic thermal parameter was used for all aliphatic hydrogen atoms. The hydridic hydrogen H(1) was observed in a difference Fourier map (height 0.72 e Å<sup>-3</sup>) and was subjected to unrestrained refinement, with isotropic thermal motion. Refinement was by full-matrix least squares, minimizing the function  $\sum w(|F_o| - |F_c|)^2$  and using the weighting scheme  $w = [\sigma^2(F_o)]^{-1}$ , which was judged to be satisfactory from analysis of the variances as functions of  $F_o$  and  $\sin(\theta)/\lambda$ . The standard deviations of observations  $\sigma(F_o)$  were estimated from counting statistics. Neutral atom scattering factors were taken from ref 30, with corrections for anomalous dispersion. All calculations were carried out on a DEC alpha-3000 workstation, using the Glasgow GX suite of programs.<sup>31</sup>

**EXAFS Measurements.** All EXAFS data were collected at the Daresbury synchrotron radiation source (SRS) on stations 7.1 and 9.2 in transmission mode, at the Ru K- and Pt L<sub>III</sub>-edges to 20 Å<sup>-1</sup> in  $k$ -space. The solid samples were diluted with boron nitride in order to achieve changes in  $\log(I_0/I)$  in the range 1–1.5 at the absorption edge. Solution samples were collected in cells of path length ~3 mm. Raw data were corrected for dark currents and converted to  $k$ -space (with EXCALIB<sup>32</sup>), and the background absorption was subtracted (with EXBACK<sup>32</sup>) to yield EXAFS functions  $\chi(k)$ . These spectra were truncated (at  $k_{\max}$ ; see Table 3) to remove the noisy high- $k$  data and Fourier filtered to remove features at distances below ~1.1 Å, but not to remove long-distance

features of the quasi-radial distribution function (*i.e.*, no further noise removal was attempted). Model fitting was carried out with EXCURV90,<sup>32</sup> using curved wave theory and allowing for multiple scattering to third order for linear and near-linear (M-C-O) atom arrangements. Only shells significant at the 95% level were included in the final models; *i.e.*, shells added to the model were only retained if they caused a reduction in the fit index of more than 4% of the previous value.<sup>33</sup> The number of independent parameters was held below  $2\Delta k\Delta r/\pi$ .<sup>34</sup> Details of the final models are listed in Table 3, which gives interatomic distances ( $R$ ), Debye-Waller factors ( $s$ ), and the coordination numbers, *i.e.*, the number of atoms in a given shell. *Ab initio* phase shifts and back-scattering factors using spherical wave theory were used throughout. The values used throughout for the proportion of adsorption leading to EXAFS (AFAC = 0.08) and the magnitude of inelastic effects modeled by an imaginary potential (VPI = -4.0 eV) were confirmed by fits to data previously reported.<sup>35</sup>

**Acknowledgment.** We thank the SERC for financial support, and PDRA funding (for D.E. and J.G.C.).

**Supplementary Material Available:** Tables of atomic parameters, anisotropic thermal parameters, bond lengths and bond angles, and least-squares plane deviations for **2a** (9 pages). Ordering information is given on any current mast-head page. Tables of observed and calculated structure factors are available on request (from L.J.F.).

OM940657R

(33) Joyner, R. W.; Martin, K. J.; Meehan, P. J. *Phys. C* **1987**, *20*, 4005.

(34) *X-ray Absorption Fine Structure*; Hasnain, S. S., Ed.; Wiley: New York, 1992; Chapter 15.

(35) Dent, A. J.; Farrugia, L. J.; Orpen, A. G.; Stratford, S. E. *J. Chem. Soc., Chem. Commun.* **1992**, 1456.

(31) Mallinson, P.; Muir, K. W. *J. Appl. Crystallogr.* **1985**, *18*, 51.

(32) Binstead, N.; Gurman, S. J.; Campbell, J. W., EXCALIB, EXBACK, and EXCURV 90, SERC Daresbury Laboratory Programs, 1990.

**Unusual Chloropalladation of  
1,2,3-Tri-*tert*-butyl-3-vinyl-1-cyclopropene To Give an  
 $\eta^3$ -(Chloromethyl)cyclobutenyl Ligand. Crystal and  
Molecular Structures of  
Di- $\mu$ -chlorobis[(1-3 $\eta$ )-4-*endo*-(chloromethyl)-  
1,2,3-tri-*tert*-butylcyclobutenyl]dipalladium and  
Tetra- $\mu$ -chlorobis[(1-3 $\eta$ )-4-*endo*-(chloromethyl)-  
1,2,3-tri-*tert*-butylcyclobutenyl]tripalladium**

Bernadette T. Donovan,<sup>1a</sup> Russell P. Hughes,<sup>\*,1a</sup> Paul P. Spara,<sup>1a</sup> and  
Arnold L. Rheingold<sup>1b</sup>

*Departments of Chemistry, Burke Chemistry Laboratory, Dartmouth College,  
Hanover, New Hampshire 03755-3564, and University of Delaware, Newark, Delaware 19716*

Received August 18, 1994<sup>®</sup>

Treatment of [PdCl<sub>2</sub>(PhCN)<sub>2</sub>] with 1.5 equiv of 1,2,3-tri-*tert*-butyl-3-vinyl-1-cyclopropene (**1**) afforded the dimeric  $\eta^3$ -cyclobutenyl compound **2**. Although the reaction required only a 1:1 ratio of **1** to [PdCl<sub>2</sub>(PhCN)<sub>2</sub>], use of only a slight excess of vinylcyclopropene in the initial reaction solution resulted in a mixture of **2** and the tripalladium compound **3**. Compound **2** converts to **3** in the presence of added [PdCl<sub>2</sub>(PhCN)<sub>2</sub>]. Solid state structures of **2** and **3** were determined by X-ray crystallography. **2**: monoclinic, *P*2<sub>1</sub>/*c*, *a* = 14.113(4) Å, *b* = 11.032(3) Å, *c* = 13.752(4) Å;  $\beta$  = 118.90(2)°, *V* = 1874.5(9) Å<sup>3</sup>, and *Z* = 2. **3**: monoclinic, *P*2<sub>1</sub>/*c*, *a* = 14.923(3) Å, *b* = 10.189(3) Å, *c* = 17.559(5) Å;  $\beta$  = 111.24(2)°, *V* = 2488(1) Å<sup>3</sup>, and *Z* = 2. Both complexes contain the same cyclobutenyl ligand  $\eta^3$ -bound to palladium, with a pendant chloromethyl group on its *endo* face. The mechanism of formation of the *endo*-(chloromethyl)cyclobutenyl ligand is discussed.

### Introduction

The thermal ring expansion of vinylcyclopropanes to give cyclopentenes is well-known.<sup>2</sup> Since the original observation of this rearrangement<sup>3</sup> several mechanistic investigations have been carried out, providing evidence that diradical pathways<sup>4</sup> and concerted ones<sup>5</sup> are possible. Transition metal complexes, including those of Fe(0), Ir(I), Ni(0), Ni(II), and Pd(0), are also known to promote this rearrangement.<sup>2</sup> The most likely mechanistic sequence involves binding of the transition metal to the vinyl group, cleavage of the C–C bond in the cyclopropane ring, and subsequent C–C bond formation to give the cyclopentene. A particularly illustrative example comes from the work of Brown on rhodium-promoted reactions of divinylcyclopropanes in which the stepwise nature of the ring expansion mechanism has been revealed.<sup>6</sup>

The ring expansions of the more highly unsaturated 3-vinyl-1-cyclopropene molecules to give five-membered ring cyclopentadienes or indenenes are also well-known<sup>7</sup> and can be achieved thermally<sup>7b</sup> or photochemically.<sup>7</sup> The photochemical transformations have been most thoroughly studied and appear to occur via diradical pathways.<sup>8</sup>

It has been demonstrated that ring expansion of the more highly unsaturated 3-vinyl-1-cyclopropanes to 1,3-cyclopentadienes can also be promoted by transition metal compounds.<sup>9a,b</sup> In contrast, six-membered ring 2,4-cyclohexadienones<sup>9a</sup> or their tautomeric phenol derivatives<sup>9b,c</sup> were isolated when certain vinylcyclopropanes were treated with CO-containing transition metal compounds. More recently, reactions between

(6) Aris, V.; Brown, J. M.; Conneely, J. A.; Golding, B. T.; Williamson, D. H. *J. Chem. Soc., Perkin Trans. 2* **1975**, 4–10. Alcock, N. W.; Brown, J. M.; Conneely, J. A.; Williamson, D. H. *J. Chem. Soc., Perkin Trans. 2* **1979**, 962–971.

(7) (a) Padwa, A. *Org. Photochem.* **1979**, *4*, 261–326, and references therein. (b) Breslow, R. In *Molecular Rearrangements*; de Mayo, Ed.; Wiley: New York, 1963; Part 1, p 236. (c) Zimmerman, H. E.; Hovey, M. C. *J. Org. Chem.* **1979**, *44*, 2331–2345. (d) Zimmerman, H. E.; Kreil, K. J. *J. Org. Chem.* **1982**, *47*, 2060–2075. (e) Zimmerman, H. E.; Fleming, S. A. *J. Org. Chem.* **1985**, *50*, 2539–2551.

(8) (a) Padwa, A.; Blacklock, T. J.; Getman, D.; Hatanaka, N.; Lorza, R. *J. Org. Chem.* **1978**, *43*, 1481–1492. (b) Zimmerman, H. E.; Aasen, S. M. *J. Org. Chem.* **1978**, *43*, 1493–1506.

(9) (a) Grabowski, N. A.; Hughes, R. P.; Jaynes, B. S.; Rheingold, A. L. *J. Chem. Soc., Chem. Commun.* **1986**, 1694. (b) Cho, S. H.; Liebeskind, L. S. *J. Org. Chem.* **1987**, *52*, 2631. (c) Semmelhack, M. F.; Ho, S.; Steigerwald, M.; Lee, M. C. *J. Am. Chem. Soc.* **1987**, *109*, 4397.

<sup>®</sup> Abstract published in *Advance ACS Abstracts*, December 1, 1994.

(1) (a) Dartmouth College. (b) University of Delaware.

(2) Hudlicky, T.; Kutchan, T. M.; Navqui, S. M. *Org. React.* **1985**, *33*, 247–335. Goldschmidt, Z.; Crammer, R. *Chem. Soc. Rev.* **1988**, *17*, 229–267. Salaün, J. In *The Chemistry of the Cyclopropyl Group*; Rappoport, Z., Ed.; John Wiley and Sons: New York, 1987; pp 809–878. Sarel, S. *Acc. Chem. Res.* **1978**, *11*, 204–211. Khusnutdinov, R. I.; Dzhemilev, U. M. *J. Organomet. Chem.* **1994**, *471*, 1–18.

(3) Neureiter, N. P. *J. Org. Chem.* **1959**, *24*, 2044–2046.

(4) See, for example: Reference 2. Willcott, M. R., III; Cargle, V. H. *J. Am. Chem. Soc.* **1969**, *91*, 4310–4311.

(5) See, for example: Reference 2. Gajewski, J. J.; Olson, L. P. *J. Am. Chem. Soc.* **1991**, *113*, 7432–7433. Gajewski, J. J.; Squicciarini, M. P. *J. Am. Chem. Soc.* **1989**, *111*, 6717–6728.

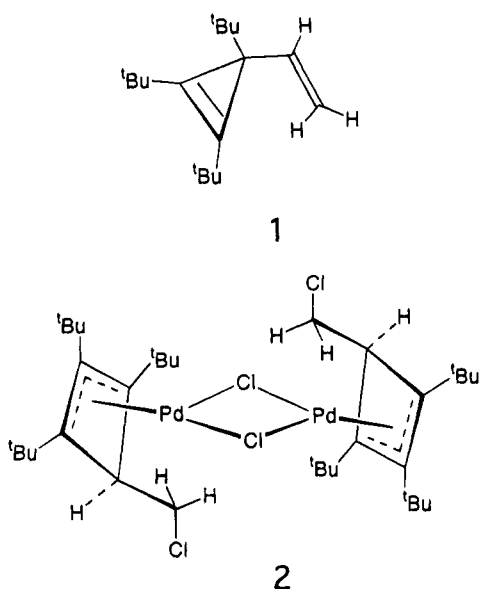


substituted vinylcyclopropenes and certain rhodium,<sup>10</sup> iridium,<sup>10</sup> and ruthenium<sup>11</sup> compounds have provided routes to organometallic complexes containing  $\eta^5$ -cyclopentadienyl ligands. The stepwise nature of the ring expansion reaction was established by the isolation of ring-opened 1,2,3,5- $\eta$ -pentadienediyl intermediates and subsequent stereochemical studies on their ring-closure reactions to give initially  $\eta^4$ -cyclopentadiene and, subsequently,  $\eta^5$ -cyclopentadienyl, ligands.<sup>12-14</sup> This chemistry has provided a novel route to a sterically congested cyclopentadienyl ligand containing three adjacent *tert*-butyl groups.<sup>15</sup>

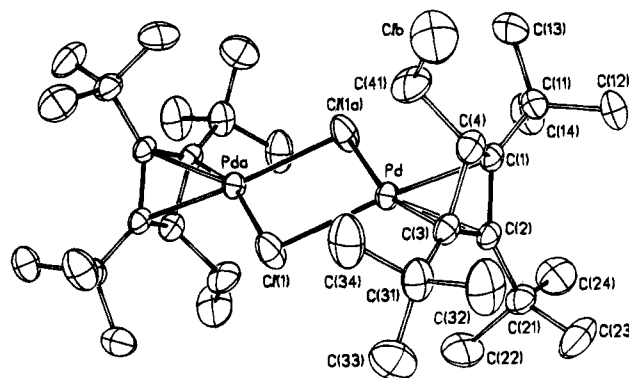
While the chloropalladation and concomitant ring opening of vinylcyclopropane and its substituted derivatives was discovered many years ago, early reports contained some erroneous structures and conclusions and only more recently has the detailed nature of this intriguing reaction been clarified.<sup>16</sup> For comparative purposes, we wished to investigate the corresponding chloropalladation of a vinylcyclopropene, and the surprising results are described herein.

## Results and Discussion

Reaction of  $[\text{PdCl}_2(\text{PhCN})_2]$  with 1.5 equiv of 1,2,3-tri-*tert*-butyl-3-vinyl-1-cyclopropene (**1**) in  $\text{CH}_2\text{Cl}_2$  solu-



tion at room temperature resulted in the initially orange solution becoming yellow. Removal of solvent under reduced pressure provided an oily yellow solid.  $^1\text{H}$  NMR analysis of the crude material showed the presence of only a single reaction product **2**, in addition to resonances for free benzonitrile and unreacted **1**. The presence of unreacted vinylcyclopropene in the crude reaction residue indicates the absence of any process



**Figure 1.** Molecular structure and atom numbering scheme for **2**. Thermal ellipsoids are drawn at the 40% probability level.

**Table 1.** Atomic Coordinates ( $\times 10^4$ ) and Isotropic Thermal Parameters ( $\text{\AA}^2 \times 10^3$ ) for **2**

	x	y	z	$U^a$
Pd	1170.4(2)	4981.4(2)	6342.5(2)	33.5(1)
Cl(1)	770.4(8)	5106(1)	4410.9(8)	58.8(5)
Cl(a)	2619(31)	1271(17)	7916(22)	71(6)
Cl(b)	3024(22)	1272(7)	8020(7)	93(4)
C(1)	1916(3)	4748(3)	8091(3)	33(1)
C(11)	1403(3)	4651(4)	8835(3)	45(2)
C(12)	2311(4)	4837(4)	10040(4)	60(2)
C(13)	951(4)	3370(5)	8747(4)	69(3)
C(14)	472(4)	5530(5)	8571(4)	66(2)
C(2)	2498(3)	5653(3)	7805(3)	33(1)
C(21)	2718(3)	7026(4)	7998(3)	45(2)
C(22)	2376(4)	7679(4)	6897(4)	75(3)
C(23)	3914(4)	7192(5)	8814(4)	76(3)
C(24)	2084(4)	7619(4)	8503(4)	73(3)
C(3)	2884(3)	4728(3)	7349(3)	35(1)
C(31)	3708(3)	4584(4)	6946(3)	50(2)
C(32)	4818(4)	4345(6)	7985(4)	79(3)
C(33)	3803(4)	5658(5)	6309(5)	75(3)
C(34)	3443(4)	3458(5)	6202(4)	74(3)
C(4)	2616(8)	3748(8)	7968(8)	41(2)
C(41)	2070(4)	2546(3)	7361(4)	62(3)

<sup>a</sup> Equivalent isotropic  $U$  defined as one-third of the trace of the orthogonalized  $U_{ij}$  tensor.

**Table 2.** Selected Bond Distances and Angles for **2**

(a) Bond Distances ( $\text{\AA}$ )			
Pd—Cl(1)	2.438(1)	C(1)—C(2)	1.462(6)
Pd—Cl(1a)	2.417(1)	C(2)—C(3)	1.435(6)
Pd—C(1)	2.123(4)	C(3)—C(4)	1.531(6)
Pd—C(2)	2.112(3)	C(1)—C(4)	1.546(6)
Pd—C(3)	2.146(3)	C(4)—C(41)	1.558(5)
Pd···C(4)	2.570(3)	C(41)—Cl(b)	1.852(17)
(b) Bond Angles (deg)			
Pd—Cl(1)—Pd(a)	94.7(1)	C(1)—C(2)—C(21)	135.7(4)
Cl(1)—Pd—Cl(1a)	85.3(1)	C(3)—C(2)—C(21)	133.2(4)
C(1)—C(2)—C(3)	90.8(3)	C(2)—C(3)—C(31)	138.9(4)
C(2)—C(3)—C(4)	90.7(4)	C(4)—C(3)—C(31)	124.4(3)
C(3)—C(4)—C(1)	84.2(3)	C(1)—C(4)—C(41)	119.2(4)
C(4)—C(1)—C(2)	89.1(3)	C(3)—C(4)—C(41)	119.7(4)
C(2)—C(1)—C(14)	138.0(3)	C(4)—C(41)—Cl(b)	109.2(5)
C(2)—C(1)—C(14)	124.3(3)		

whereby **1** undergoes any catalytic transformations by  $[\text{PdCl}_2(\text{PhCN})_2]$ .

After recrystallization of the reaction mixture from  $\text{CHCl}_3$ , yellow crystals of **2** were subjected to an X-ray diffraction study which revealed the solid state structure of the complex. An ORTEP of **2** is displayed in Figure 1. Table 1 lists atomic coordinates and isotropic thermal parameters for the structure determination, and Table 2 gives some selected bond distances and angles. The ORTEP reveals that **2** is a chloride-bridged dimeric Pd complex containing an  $\eta^3$ -cyclobutenyl ring bound to

(10) Egan, J. W.; Hughes, R. P.; Rheingold, A. L. *Organometallics* **1987**, *6*, 1578.

(11) Hughes, R. P.; Robinson, D. J. *Organometallics* **1989**, *8*, 1015.

(12) Donovan, B. T.; Egan, J. W.; Hughes, R. P.; Spara, P. P.; Trujillo, H. A.; Rheingold, A. L. *Isr. J. Chem.* **1990**, *30*, 351.

(13) Donovan, B. T.; Hughes, R. P.; Trujillo, H. A. *J. Am. Chem. Soc.* **1990**, *112*, 7076.

(14) Donovan, B. T.; Hughes, R. P.; Kowalski, A. S.; Trujillo, H. A.; Rheingold, A. L. *Organometallics* **1993**, *12*, 1038.

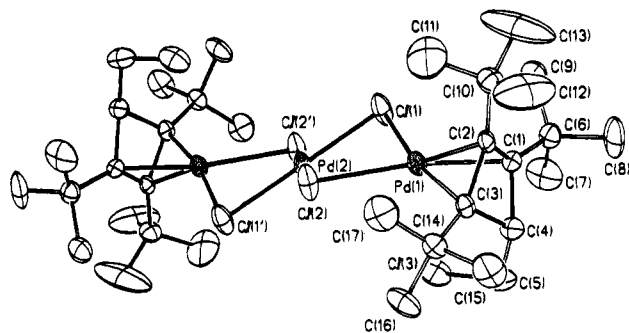
(15) Donovan, B. T.; Hughes, R. P.; Trujillo, H. A.; Rheingold, A. L. *Organometallics* **1992**, *11*, 64.

(16) Parra-Hake, M.; Rettig, M. F.; Williams, J. L.; Wing, R. M. *Organometallics* **1986**, *5*, 1032, and references cited therein.

each metal. The terminal vinylic methylene carbon atom of the original five-carbon vinylcyclopropene skeleton appears as a chloromethyl group bound to the cyclobutenyl ring on the same face as the palladium (i.e., the *endo* face of the ring). The cyclobutenyl ring skeleton has an  $\eta^3$ -allylic coordination of C(1)–C(2)–C(3) with an average Pd–C bond length of 2.13 Å. The Pd<sub>2</sub>Cl<sub>2</sub> rectangle is planar, and the plane of the allyl fragment is tilted 85.1° with respect to this plane. The sp<sup>3</sup> carbon of the ring, C(4), is bent out of the allyl ligand plane by 24.1° away from the metal, with a Pd–C(4) distance of 2.571 Å. A number of compounds similar to **2** may be found in the literature. Dahl and Oberhansli characterized di( $\mu$ -chloro)bis(1,2,3- $\eta^3$ -*exo*-ethoxycyclobutenyl)dipalladium(II),<sup>17a</sup> its *endo* isomer,<sup>17a</sup> and a related Ni(II) compound.<sup>17b</sup> The structural features of **2** are in good agreement with these compounds.

NMR data of CDCl<sub>3</sub> solutions of **2** are consistent with the solution structure being identical to that observed in the solid state. The plane of symmetry in the molecule is clear from the 2:1 ratio of the <sup>t</sup>Bu resonances at  $\delta$  1.31 (s, 36 H) and 1.49 (s, 18 H), and the triplet at 3.00 ppm (2 H, *J* = 3.0 Hz) and doublet at 4.20 ppm (4 H, *J* = 3.0 Hz) support the presence of the H and CH<sub>2</sub>-Cl fragments bound to the sp<sup>3</sup> carbon of the cyclobutenyl ring. The *endo* disposition of the chloromethyl substituent cannot be determined from solution NMR data, and we assume that the solid state structure is maintained.

Although **2** was the exclusive product from the reaction of [PdCl<sub>2</sub>(PhCN)<sub>2</sub>] with an excess of **1**, use of less than 1.5 equiv of **1** per equivalent of [PdCl<sub>2</sub>(PhCN)<sub>2</sub>] in the initial reaction solution resulted in a more complicated product mixture. When [PdCl<sub>2</sub>(PhCN)<sub>2</sub>] was allowed to react with 1.1 equiv of **1** in CH<sub>2</sub>Cl<sub>2</sub> solution at room temperature, only a subtle change in solution color from orange to lighter orange was noted after a 12 h reaction period. <sup>1</sup>H NMR analysis of the crude reaction mixture showed the presence of peaks for a second product, **3**, in addition to those for **2**, **1**, and free



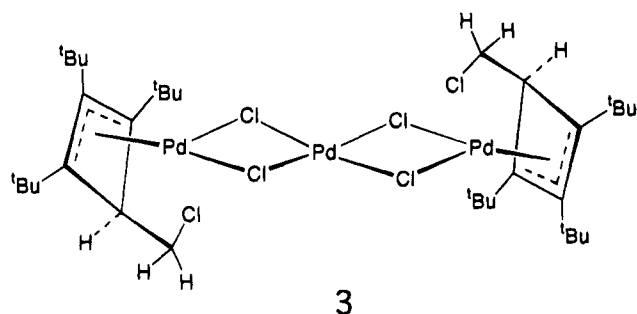
**Figure 2.** Molecular structure and atom numbering scheme for **3**, omitting two molecules of CHCl<sub>3</sub>. Pd(2) resides at a crystallographic inversion center. Thermal ellipsoids are drawn at the 40% probability level.

**Table 3.** Atomic Coordinates ( $\times 10^4$ ) and Isotropic Thermal Parameters ( $\text{\AA}^2 \times 10^3$ ) for **3**

	<i>x</i>	<i>y</i>	<i>z</i>	<i>U</i> <sup>a</sup>
Pd(1)	3376.8(4)	6748.0(6)	5539.4(4)	38.2(2)
Pd(2)	5000	5000	5000	43.7(4)
Cl(1)	4162(2)	6905(2)	4511(2)	68(1)
Cl(2)	3789(2)	4400(2)	5455(2)	66(1)
Cl(3)	5070(2)	7194(3)	6982(2)	75(1)
C(1)	2951(5)	8627(7)	5824(4)	36(3)
C(2)	2143(5)	7703(7)	5592(4)	34(3)
C(3)	2634(5)	6981(7)	6358(4)	36(3)
C(4)	3253(5)	8203(8)	6736(4)	43(4)
C(5)	4284(6)	8142(10)	7332(5)	66(4)
C(6)	3215(6)	9937(8)	5525(5)	48(3)
C(7)	4295(7)	10194(11)	5934(7)	94(6)
C(8)	2689(9)	10992(9)	5798(7)	97(7)
C(9)	3021(7)	10029(9)	4611(5)	70(4)
C(10)	1154(6)	7643(9)	4932(5)	53(3)
C(11)	960(10)	6362(15)	4506(10)	198(10)
C(12)	421(8)	7726(20)	5294(8)	173(10)
C(13)	978(9)	8608(18)	4282(10)	226(11)
C(14)	2404(5)	5862(8)	6835(5)	44(3)
C(15)	1846(8)	6448(10)	7339(6)	82(5)
C(16)	3335(7)	5288(9)	7428(6)	77(5)
C(17)	1861(8)	4715(10)	6324(6)	85(5)
Cs	1887(10)	3949(13)	3331(8)	112(7)
Cl(4)	2790(3)	3257(4)	3112(3)	144(3)
Cl(5)	1176(4)	4989(4)	2523(3)	149(2)
Cl(6)	1142(4)	2775(7)	3453(5)	271(5)

<sup>a</sup> Equivalent isotropic *U* defined as one-third of the trace of the orthogonalized *U*<sub>ij</sub> tensor.

displays an ORTEP of **3**; two molecules of CHCl<sub>3</sub> in the lattice are omitted for clarity. Atomic coordinates and isotropic thermal parameters are given in Table 3, and selected bond distances and angles are provided in Table 4. The ORTEP shows that **3** contains three Pd atoms linked by bridging chloride ligands. The compound contains  $\eta^3$ -cyclobutenyl rings identical to those observed in **2**. Once again the chloromethyl substituent is on the *endo* face of the four-membered ring, which shows  $\eta^3$ -allylic coordination of C(1)–C(2)–C(3) to Pd with an average bond distance of 2.12 Å. The Pd(1)–Cl(1)–Pd(2)–Cl(2) fragment is bent and has a dihedral angle [Cl(1), Pd(1), Cl(2)]–[Cl(1), Pd(2), Cl(2)] of 145.7(1)°. With the exception of this bent fragment, the principal difference between the solid state structures of **2** and **3** is the extra PdCl<sub>2</sub> fragment found in the latter. Incorporation of additional PdCl<sub>2</sub> units into such bridged species is not uncommon.<sup>18</sup> Whether or not the resultant Pd<sub>3</sub>Cl<sub>4</sub> bridge is planar or bent has been attributed to crystal packing forces.<sup>18</sup> Curiously, the



PhCN. The ratio of **2** to **3** was 4:1. The spectrum of **3** displayed singlets at 1.22 (36 H) and 1.54 ppm (18 H), a triplet at 3.08 ppm (2 H, *J* = 3.0 Hz), and a doublet at 4.08 ppm (4 H, *J* = 3.0 Hz). The similarity of this pattern to that of the <sup>1</sup>H NMR spectrum of **2** suggested that the structure of **3** was closely related, although it was not possible to deduce the exact structure of **3** from this information alone.

Fortunately, good-quality crystals of **3** could be obtained separately from **2**, since this compound is considerably less soluble than **2**. An X-ray crystallographic study revealed the solid state structure of **3**. Figure 2

(17) (a) Dahl, L. F.; Oberhansli, W. E. *Inorg. Chem.* **1965**, *4*, 629. (b) Dahl, L. F.; Oberhansli, W. E. *Inorg. Chem.* **1965**, *4*, 343.

(18) (a) Parra-Hake, M.; Rettig, M. F.; Wing, R. M. *Organometallics* **1983**, *2*, 1013, and references cited therein. (b) Bailey, P. M.; Kelley, E. A.; Maitlis, P. M. *J. Organomet. Chem.* **1978**, *144*, C52.

**Table 4. Selected Bond Distances and Angles for 3**

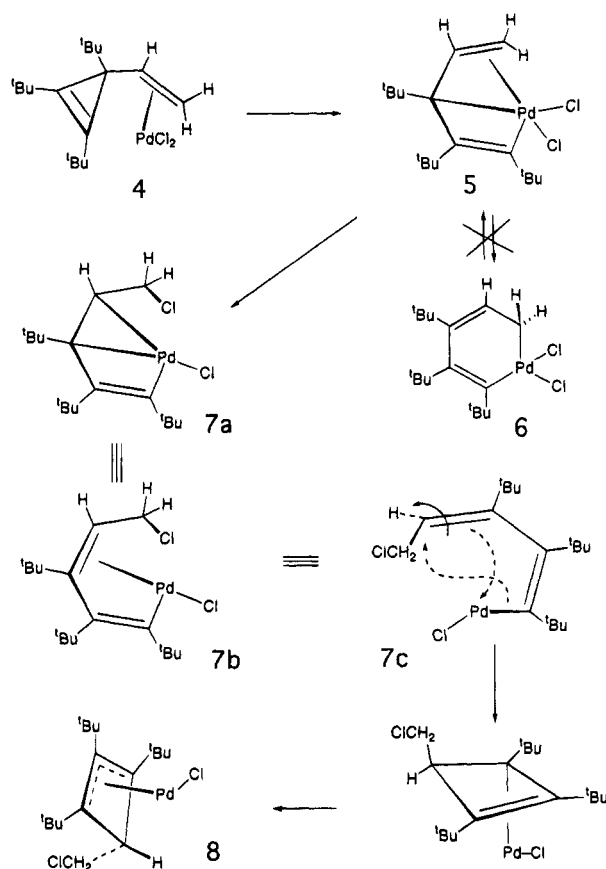
(a) Bond Distances (Å)			
Pd(1)–C(1)	2.132(8)	Pd(2)–Cl(2)	2.308(2)
Pd(1)–C(2)	2.114(8)	C(1)–C(2)	1.467(10)
Pd(1)–C(3)	2.122(9)	C(2)–C(3)	1.473(9)
Pd(1)–Cl(1)	2.488(3)	C(3)–C(4)	1.550(10)
Pd(1)–Cl(2)	2.487(2)	C(4)–C(1)	1.560(10)
Pd(1)···Cl(3)	2.893(2)	C(4)–C(5)	1.516(10)
Pd(2)–Cl(1)	2.300(2)	C(5)–Cl(3)	1.791(11)
(b) Bond Angles (deg)			
Cl(1)–Pd(2)–Cl(1')	180	C(1)–Pd(1)–C(2)	40.4(3)
Cl(2)–Pd(2)–Cl(2')	180	C(1)–Pd(1)–C(3)	57.9(3)
Cl(1)–Pd(2)–Cl(2)	88.0(1)	C(2)–Pd(1)–C(3)	40.7(3)
Cl(1)–Pd(2)–Cl(2')	92.0(1)	C(1)–C(2)–C(3)	88.9(5)
Cl(1)–Pd(1)–Cl(2)	80.0(1)	C(2)–C(3)–C(4)	90.7(5)
Cl(1)–Pd(1)–C(1)	111.7(2)	C(3)–C(4)–C(1)	82.9(5)
Cl(1)–Pd(1)–C(2)	130.5(2)	C(4)–C(1)–C(2)	90.5(6)
Cl(1)–Pd(1)–C(3)	169.4(2)	C(1)–C(4)–C(5)	124.3(8)
Cl(2)–Pd(1)–C(1)	168.0(2)	C(3)–C(4)–C(5)	124.1(7)
Cl(2)–Pd(1)–C(2)	133.1(2)	C(4)–C(5)–Cl(3)	114.3(6)
Cl(2)–Pd(1)–C(3)	110.4(2)		
(c) Dihedral Angle (deg)			
[Cl(1), Pd(1), Cl(2)]–[Cl(1), Pd(2), Cl(2)]			145.7(1)

chloromethyl substituent in **2** is oriented with the chlorine directed away from the palladium, whereas that in **3** has the chlorine located over the metal. We ascribe these differences in conformation to crystal packing forces. This interpretation is consistent with the observation of disorder in the CH<sub>2</sub>Cl group in **2**, with a 75%/25% occupancy. The major occupancy site is shown in Figure 1.

Treatment of solutions of pure **2** with additional [PdCl<sub>2</sub>(PhCN)<sub>2</sub>] resulted in rapid formation of **3**. Thus, unless an excess of vinylcyclopropene is used in the original reaction, the initially formed **2** presumably competes with free vinylcyclopropene for the additional "PdCl<sub>2</sub>" resulting in a mixture of products.

The overall reaction differs from other known transition metal promoted reactions of vinylcyclopropenes in that it affords a four-membered ring, rather than a six-membered metallacyclohexadiene, or a five-membered cyclopentadiene ring.<sup>9a,10–14</sup> The mechanism of this particular ring expansion reaction is rather intriguing in that the observed *endo* disposition of the chloromethyl substituent is difficult to explain on the basis of past precedent.<sup>10–14</sup> Based on these previous results, the mechanistic options outlined in Scheme 1 seem reasonable.

Binding of palladium to the vinyl group rather than the endocyclic olefin is assumed to give intermediate **4**, followed by insertion of palladium into the cyclopropene  $\sigma$ -bond to afford the pentadienediyl intermediate **5**. Rhodium analogues of **5** have been isolated and crystallographically characterized.<sup>12</sup> Isotopic labeling studies have illustrated unambiguously that a planar metallacyclohexadiene ring like **6** (Scheme 1) cannot be formed from this particular vinylcyclopropene **1**, due to the requirement that three *tert*-butyl groups would have to occupy contiguous carbon atoms in such a ring system.<sup>12,13</sup> Consequently, by analogy to previously characterized rhodium chemistry,<sup>13</sup> the subsequent chemistry of pentadienediyl ligands like that in **5** is expected to involve a stereospecific ring closure by *cis* addition of the Pd–C(=C) bond to the coordinated olefin to give a cyclopentadiene ligand. Clearly this does not occur. However, chloropalladation of coordinated olefins is well-known;<sup>18a</sup> addition of Pd–Cl to the coordinated olefin in **5** would afford the butadienyl–Pd intermediate

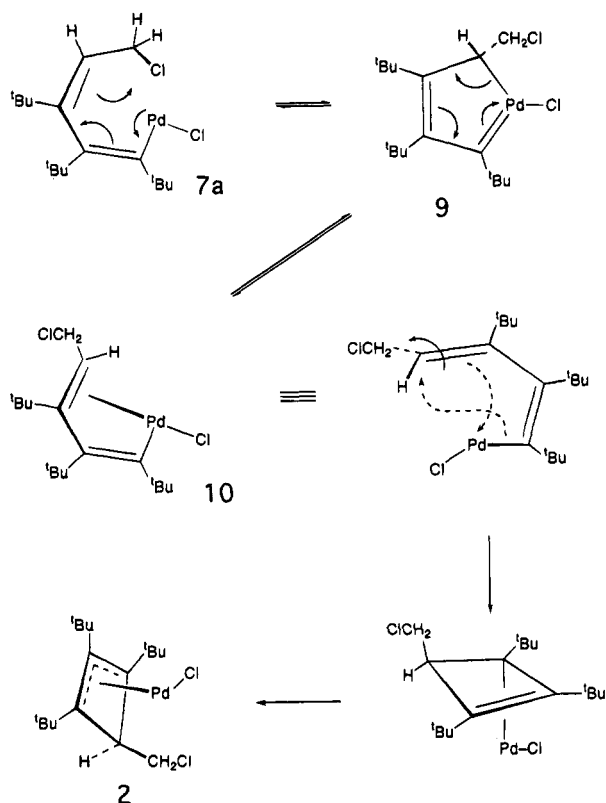
**Scheme 1**

**7**, which can be drawn as either canonical form **7a** or **7b**. Notably, by virtue of the required conformation of the coordinated olefin in **5**, the resultant chloromethyl substituent in **7** must be *trans* to the *tert*-butyl group, as shown in **7b**. The stereochemistry (and reversibility) of ring closure of butadienyl–palladium complexes to give cyclobutenyl complexes is well established in light of its significance in the palladium-promoted cyclooligomerization of alkynes.<sup>19</sup> Closure is known to be stereospecific and is usually discussed as a thermally allowed conrotatory electrocyclic closure, as predicted by the Woodward–Hoffman rules.<sup>19a,b</sup> As an aside, because the structures of butadienyl–Pd species are helical, with nonconjugated double bonds,<sup>19c</sup> as shown for **7c** (Scheme 1), and consequently a concerted electrocyclic reaction seems unlikely, we prefer to think of this reaction as a *cis* addition of the Pd–C  $\sigma$ -bond to the coordinated olefin as shown for **7c** and as demonstrated for pentadienediyl complexes.<sup>13</sup> Consequently, all such closure reactions must appear to be "conrotatory", regardless of ring size, as the olefin terminus must rotate as shown in **7c**. Such closure of **7** must afford the cyclobutenyl ligand with the chloromethyl group in the *exo* position. Consequently we discount the mechanism shown in Scheme 1.

The only way that an *endo*-chloromethyl group could be generated by this kind of pathway would be by a stereomutation of **7**, in the manner proposed by Maitlis for certain other butadienyl complexes,<sup>19b</sup> and as shown in Scheme 2. The metallacyclic flip, via intermediate **9**, can afford the required precursor **10** for generation

(19) (a) Jack, T. R.; May, C. J.; Powell, J. J. *Am. Chem. Soc.* **1978**, *100*, 5057. (b) Taylor, S. H.; Maitlis, P. M. *J. Am. Chem. Soc.* **1978**, *100*, 4700. (c) Bailey, P. M.; Taylor, S. H.; Maitlis, P. M. *J. Am. Chem. Soc.* **1978**, *100*, 4711.

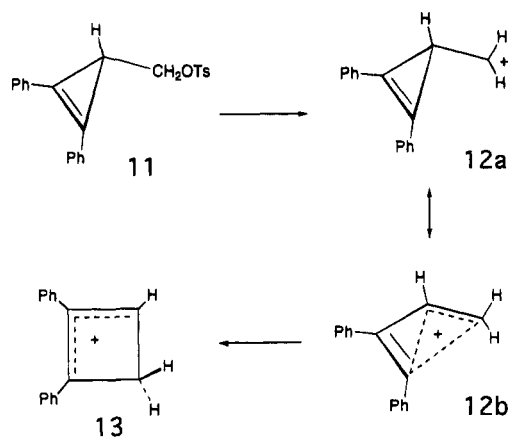
Scheme 2



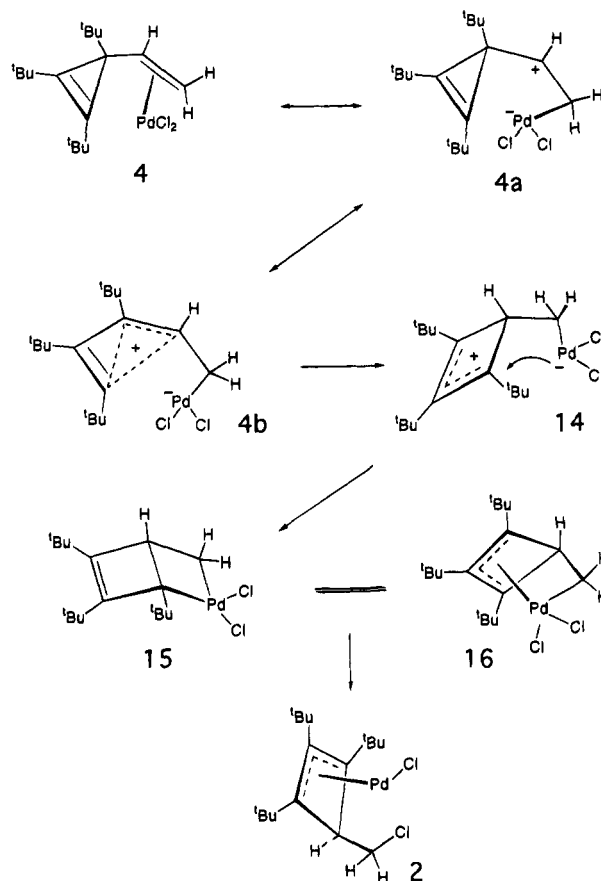
of the observed product **2**. This pathway requires formation of a high-energy metallacycle **9** in which three *tert*-butyl groups occupy positions on contiguous carbon atoms, and the required intermediate **10** requires forcing the chloromethyl group *cis* to a *tert*-butyl group prior to ring closure to give **2**. Alternatively, a direct alkyl-to-carbene migration in intermediate **9** would afford **2** directly.<sup>20</sup> In a planar metallacycle like **9**, this seems unlikely since overlap of the migrating alkyl carbon orbital with the  $\pi$ -orbital of the carbene ligand is zero; were **9** puckered, with the chloromethyl substituent exclusively in an equatorial position, such a mechanism would account for formation of **2**.<sup>20</sup> We feel that while these high-energy pathways might generate some of the observed *endo* product **2**, neither seems highly likely to be the exclusive pathway for cyclobutenyl ligand formation, given the optional lower energy route to isomer **8** shown in Scheme 1. We discount these mechanisms accordingly.

Abandonment of the mechanisms shown in Schemes 1 and 2, albeit for good reasons, requires us to propose a pathway based on another precedent, one that may challenge some of our previous assumptions of how the initial metal-promoted vinylcyclopropene ring opening occurs. Breslow has shown that solvolysis reactions of the cyclopropenylcarbinyl tosylate **11** (Scheme 3) do not proceed via trapping of the carbenium ion **12a**.<sup>21</sup> Instead, the barrier to loss of tosylate is lowered considerably by delocalization of developing positive charge at the CH<sub>2</sub> carbon atom into the Walsh C-C  $\sigma$ -orbitals of the cyclopropene ring as shown in **12b**. There is no stabilization available by conjugation with the endocyclic olefin. Furthermore, the activation barrier to rear-

Scheme 3



Scheme 4



angement of **12b** to the far more stable cyclobutenyl cation **13** is very low, with the result that the only products obtained in this reaction are those resulting from trapping of the cyclobutenyl cation **13**.<sup>21</sup> These observations suggest another way of thinking about the first formed olefin complex intermediate **4** as shown in Scheme 4. One resonance form for **4** is shown as **4a**. This is a cyclopropenylcarbinyl cation completely analogous to that shown in Scheme 3 as **12a**. Analogous delocalization of positive charge at the olefinic carbon atom into the  $\sigma$ -framework of the cyclopropenyl ring must be possible as shown in **4b**, and the barrier to rearrangement of **4b** to **14** should also be very small. Intramolecular trapping of **14** would afford **15** as shown, and reductive elimination of a C-Cl bond from **15**, or perhaps from its  $\eta^3$  form **16**, would yield the observed product **2** with the correct stereochemical disposition of the chloromethyl substituent.

(20) We are grateful to a reviewer for suggesting this pathway as an alternative mechanism.

(21) Breslow, R.; Lockhart, J.; Small, A. *J. Am. Chem. Soc.* **1962**, *84*, 2793.

This mechanism, with its organic precedent, provides an intriguing alternative, and certainly a more satisfying outcome, than those in Schemes 1 and 2. Experiments designed to probe for the intermediacy of intermediates analogous to **15** in other transition metal promoted reactions of vinylcyclopropenes are possible and are currently underway in our laboratory.

## Experimental Section

**General Procedures.** All manipulations were carried out using standard Schlenk techniques unless otherwise indicated, although the starting materials and products all appear to be air stable. Synthetic, crystallization, and NMR solvents were dried and then distilled under dinitrogen prior to use.  $\text{CH}_2\text{Cl}_2$  was dried over  $\text{P}_4\text{O}_{10}$ ,  $\text{CaH}_2$ , or  $\text{Na-Pb}$ . Benzene was dried over  $\text{K}$ , and  $\text{CDCl}_3$  over Linde 4 Å molecular sieves or  $\text{P}_4\text{O}_{10}$ . Petroleum ether (35–50 °C fraction) was purified by stirring over concentrated  $\text{H}_2\text{SO}_4$  for several days (in order to remove olefins), followed by washing successively with distilled water, 10% aqueous sodium carbonate solution, and again with distilled water. The solvent was dried with  $\text{MgSO}_4$ , then  $\text{Na}$  metal, and finally with  $\text{Na/K}$  alloy.

Palladium(II) chloride was obtained from Johnson Matthey Aesar-Alfa. The preparation of 1,2,3-tri-*tert*-butyl-3-vinyl-1-cyclopropene (**1**) has already been reported.<sup>12</sup>  $[\text{PdCl}_2(\text{PhCN})_2]$  was prepared by the literature method.<sup>22</sup>

$^1\text{H}$  (300 MHz) and  $^{13}\text{C}\{^1\text{H}\}$  (75 MHz) NMR data were obtained using a Varian Associates XL-300 spectrometer at 23 °C. All  $^1\text{H}$  and  $^{13}\text{C}$  chemical shifts are reported as parts per million downfield from tetramethylsilane. Infrared spectra were recorded on a Bio-Rad Digilab FTS-40 spectrophotometer. Melting points were determined using an Electrothermal capillary melting point apparatus and are uncorrected. Microanalyses were performed at Spang Microanalytical Laboratory, Eagle Harbor, MI.

**Preparation and Characterization of 2 and 3.** (a) **Isolation of Crystals of Tetrakis( $\mu$ -chloro)bis[1,2,3- $\eta^3$ -4-endo-(chloromethyl)-1,2,3-tri-*tert*-butylcyclobutenyl]tripalladium(II) (**3**).**  $\text{PdCl}_2(\text{PhCN})_2$  (0.337 g, 0.881 mmol) was dissolved in  $\text{CH}_2\text{Cl}_2$  (5 mL) in a Schlenk tube. A solution of **1** (0.207 g, 0.883 mmol) in  $\text{C}_6\text{H}_6$  (3 mL) was then layered on top of the orange  $\text{CH}_2\text{Cl}_2$  solution. This bilayered array was maintained while the Schlenk tube was allowed to stand at room temperature. Red-brown crystals formed at the interface of the two layers after 2.5 h, at which time the mixture was cannula filtered. These isolated crystals of **3** had the following spectral features:  $^1\text{H}$  NMR ( $\text{CDCl}_3$ ):  $\delta$  1.22 (s, 36 H,  $^t\text{Bu}$ ), 1.54 (s, 18 H,  $^t\text{Bu}$ ), 3.08 (t, 2 H,  $J = 3.0$  Hz, CH), 4.08 (d, 4 H,  $J = 3.0$  Hz,  $\text{CH}_2\text{Cl}$ ).  $^{13}\text{C}$  NMR ( $\text{CDCl}_3$ ):  $\delta$  29.9 (C6), 32.5 (C7), 32.6 (C3), 35.4 (C5), 44.9 (C8), 53.3 (C4), 101.9 (C1), 136.1 (C2). IR (KBr pellet): 2999 (sh), 2961, 2918, 2870, 1482, 1471, 1396, 1362, 1228, 738 ( $\text{cm}^{-1}$ ). Mp 180–182 °C (dec). The crystals were recrystallized from  $\text{CHCl}_3$  and were then subjected to an X-ray diffraction study.

(b) **Isolation of Crystals of Bis( $\mu$ -chloro)bis[1,2,3- $\eta^3$ -4-endo-(chloromethyl)-1,2,3-tri-*tert*-butylcyclobutenyl]dipalladium(II) (**2**).** Refrigeration of the mother liquor from part a (above) at –20 °C for 5 days afforded a mixture of yellow crystals of **2** and orange crystals which were apparently composed of a 1:1 mixture of **3** and **2**. The yellow and orange crystals were separated manually with the aid of a microscope. The yellow crystals (**2**) had the following spectral features:  $^1\text{H}$  NMR ( $\text{CDCl}_3$ ):  $\delta$  1.31 (s, 36 H,  $^t\text{Bu}$ ), 1.49 (s, 18 H,  $^t\text{Bu}$ ), 3.01 (t, 2 H,  $J = 3.0$  Hz CH), 4.21 (d, 4 H,  $J = 3.0$  Hz,  $\text{CH}_2\text{Cl}$ ).  $^{13}\text{C}\{^1\text{H}\}$  NMR:  $\delta$  29.9 (C34), 32.5 (C24), 32.6 (C21), 35.5 (C31), 44.3 (C41), 53.9 (C4), 101.7 (C1), 133.8 (C2). IR (KBr pellet): 2982 (sh), 2962, 2929, 2866, 2336, 2326, 1485, 1397, 1365, 1228, 751 ( $\text{cm}^{-1}$ ). Mp 170–174 °C (dec). Anal. Calcd for  $\text{C}_{34}\text{H}_{60}\text{Cl}_4\text{Pd}_2$ : C, 49.60; H, 7.27. Found: C, 49.51; H, 7.33.

The orange crystals presumably resulted from cocrystallization of **3** and **2** in a 1:1 ratio, as evidenced by their solution  $^1\text{H}$  NMR data ( $\text{CDCl}_3$ ), which was indistinguishable from that of a solution prepared from pure **3** and **2**:  $\delta$  1.22 (s, 36 H,  $^t\text{Bu}$ ), 1.31 (s, 36 H,  $^t\text{Bu}$ ), 1.49 (s, 18 H,  $^t\text{Bu}$ ), 1.54 (s, 18 H,  $^t\text{Bu}$ ), 3.00 (br s, 1 H, CH), 3.08 (br s, 1 H, CH), 4.08 (br s, 2 H,  $\text{CH}_2\text{Cl}$ ), 4.21 (d, 2 H,  $J = 2$  Hz,  $\text{CH}_2\text{Cl}$ ).

(c) **Details of X-ray Diffraction Study of 2.**  $[\text{C}_{17}\text{H}_{30}\text{Cl}_2\text{-Pd}]_2$ , yellow, monoclinic,  $P2_1/c$ ,  $a = 14.113(4)$ ,  $b = 11.032(3)$ ,  $c = 13.752(4)$  Å;  $\beta = 118.90(2)^\circ$ ,  $V = 1874.5(9)$  Å<sup>3</sup>,  $Z = 2$ ,  $D_{\text{calc}} = 1.46$  g  $\text{cm}^{-3}$ ,  $\mu$  (Mo  $K\alpha$ ) = 12.44  $\text{cm}^{-1}$ , and  $T = 293$  K. Of 4079 absorption-corrected reflections collected (Nicolet R3/ $\mu$  diffractometer,  $4^\circ \leq 2\theta \leq 52^\circ$ ), 3708 were independent ( $R_{\text{int}} = 3.65\%$ ) and 2583 were observed ( $F_o \geq 5\sigma F_o$ ). The Pd atom was located by a Patterson map. Very large thermal parameters for the C-bound Cl atom were interpreted as disorder over two sites, Cl(a), 25% and Cl(b), 75% occupancy. The sites are separated by  $\sim 0.5$  Å. Hydrogen atoms were idealized and isotropic, non-hydrogen atoms anisotropic:  $R_{\text{F}} = 3.45\%$ ,  $R(wF) = 3.98\%$ ,  $\text{GOF} = 1.248$ ,  $\Delta/\sigma$  max = 0.127,  $\Delta\rho_{\text{max}} = 1.01$  eÅ<sup>-3</sup> (Pd noise), data/parameter = 13.5. All computations used SHELXTL (5.1) software, G. Sheldrick, Nicolet XRD, Madison, WI.

(d) **Details of X-ray Diffraction Study of 3.**  $[\text{C}_{34}\text{H}_{60}\text{Cl}_6\text{-Pd}_3]_2\text{CHCl}_3$ , red-brown monoclinic,  $P2_1/c$ ,  $a = 14.923(3)$ ,  $b = 10.189(3)$ ,  $c = 17.559(5)$  Å;  $\beta = 111.24(2)^\circ$ ,  $V = 2488(1)$  Å<sup>3</sup>,  $D_{\text{calc}} = 1.655$  g  $\text{cm}^{-3}$ ,  $\mu$  (Mo  $K\alpha$ ) = 17.2  $\text{cm}^{-1}$ , and  $T = 293$  K. Of 4307 reflections collected (Nicolet R3m/ $\mu$  diffractometer,  $4^\circ \leq 2\theta \leq 48^\circ$ ), 3906 were independent and 2670 were observed ( $F_o \geq 3\sigma F_o$ ). Systematic absences in the diffraction data uniquely determined the space group. Corrections for absorption (empirical, six reflections, 10° steps) and decay were applied to the data. The structure was solved from a sharpened Patterson map. Two molecules of recrystallization solvent,  $\text{CHCl}_3$ , accompany each  $\text{Pd}_3$  complex in the lattice. All non-hydrogen atoms were refined with anisotropic thermal parameters, and all hydrogen atoms were treated as idealized isotropic contributions ( $d_{\text{CH}} = 0.96$  Å). All computations used SHELXTL (5.1) software (G. Sheldrick, Nicolet XRD, Madison, WI).

**Reaction of  $\text{PdCl}_2(\text{PhCN})_2$  with 1.5 Equiv of 1.** **1** (0.185 g, 0.79 mmol) was added to a solution of freshly prepared  $\text{PdCl}_2(\text{PhCN})_2$  (0.200 g, 0.52 mmol) in  $\text{CH}_2\text{Cl}_2$  (10 mL) at room temperature. The solution was allowed to stir for 12 h, during which time a color change from orange to yellow-amber was noted. Solvent was removed by reduced pressure, leaving a wet yellow solid.  $^1\text{H}$  NMR analysis of a  $\text{CDCl}_3$  solution of the crude residue showed the presence of **1**,  $\text{PhCN}$  ( $\delta$  7.65–7.43 (m,  $\text{PhCN}$ )), and the dipalladium product **2**. Resonances for the tripalladium complex were absent from the spectrum.

**Reaction of  $\text{PdCl}_2(\text{PhCN})_2$  with 1.1 Equiv of 1.** **1** (0.101 g, 0.431 mmol) was added to a solution of freshly prepared  $\text{PdCl}_2(\text{PhCN})_2$  (0.150 g, 0.391 mmol) in  $\text{CH}_2\text{Cl}_2$  (10 mL) at room temperature. During the 12 h reaction, the color of the initially orange solution lightened but did not become yellow. Solvent was removed by reduced pressure, leaving an oily orange solid. In addition to showing resonances for free  $\text{PhCN}$  and **1**,  $^1\text{H}$  NMR analysis of a  $\text{CDCl}_3$  solution of the crude residue revealed the presence of **2** and **3** in a ratio of 4:1.

**Acknowledgment.** We are grateful to the National Science Foundation for generous financial support of this work, and to Johnson Matthey Aesar/Alfa for a loan of palladium(II) chloride.

**Supplementary Material Available:** Tables of bond distances and bond angles for **2** and **3**, anisotropic thermal parameters and H atom coordinates and isotropic thermal parameters for **2**, and anisotropic thermal parameters for **3** (6 pages). Ordering information is given on any current masthead page.

# Structural Studies on Mesityluminum Addition Compounds

Mark S. Lalama, Jeff Kampf, David G. Dick, and John P. Oliver\*

Department of Chemistry, Wayne State University, Detroit, Michigan 48202

Received May 5, 1994<sup>®</sup>

Four mesityluminum derivatives,  $\text{Mes}_3\text{Al}(\text{4-picoline})(\text{C}_7\text{H}_8)_{0.5}$  (**1**),  $\text{EtMes}_2\text{Al}\cdot\text{THF}$  (**2**),  $\text{Mes}_2\text{ClAl}\cdot\text{THF}$  (**3**), and  $[\text{Mes}_2\text{Al}(\mu\text{-Cl})]_2$  (**4**) ( $\text{Mes} = 2,4,6\text{-trimethylphenyl}$ ), have been prepared and their structures determined by single crystal X-ray diffraction methods. Compound **1** crystallizes in the monoclinic space group  $C2/c$  (No. 15):  $a = 43.784(15)$  Å,  $b = 8.901(1)$  Å,  $c = 16.760(2)$  Å,  $\beta = 104.02(2)^\circ$ ,  $Z = 8$ ,  $R = 10$ , and  $R_w = 9.9$ . Compound **2** crystallizes in the orthorhombic space group  $P2_12_12_1$  (No. 19):  $a = 12.057(9)$  Å,  $b = 13.490(3)$  Å,  $c = 14.037(2)$  Å,  $Z = 4$ ,  $R = 5.4$ , and  $R_w = 3.9$ . The halide derivative **3** crystallizes in the primitive monoclinic space group  $P2_1/a$  (No. 14):  $a = 17.18(1)$  Å,  $b = 14.754(2)$  Å,  $c = 17.316(2)$  Å,  $\beta = 92.74(3)^\circ$ ,  $Z = 8$ ,  $R = 6.5$ , and  $R_w = 2.4$ . The base-free compound **4** exists as a dimer and crystallizes in the space group  $P2_1/c$  (No. 14):  $a = 12.288(2)$  Å,  $b = 15.824(3)$  Å,  $c = 9.095(2)$  Å,  $\beta = 108.43(2)^\circ$ ,  $Z = 4$ ,  $R = 5.4$ , and  $R_w = 5.9$ . The distortion associated with **1**, **2**, and **3** relative to the parent monomeric molecule,  $\text{Mes}_3\text{Al}$ , is discussed with respect to substitution of the mesityl group for the Cl and Et ligands.

## Introduction

Bulky substituents have been widely used in main group chemistry to stabilize highly reactive compounds or species with unique structures.<sup>1-6</sup> The synthesis of such compounds is of current interest due to their novel chemistry and structural features. For example, the halide complexes have been demonstrated to be valuable precursors to divalent Group 3 compounds.<sup>7-10</sup> We have established that  $\text{Mes}_3\text{Al}$  is a three-coordinate, monomeric molecule in which the mesityl group affords a very bulky unit with the ortho methyl groups providing significant steric hindrance/protection of the metal center and preventing formation of the commonly observed carbon-bridged aluminum dimer.<sup>3</sup> The molecule was shown to have an open pocket on either side of the aluminum atom which might accommodate a basic moiety. Seidel established that the THF adduct,  $\text{Mes}_3\text{Al}\cdot\text{THF}$ ,<sup>11</sup> can be formed, and our examination of its structure shows that the THF molecule binds directly to the aluminum.<sup>12</sup> The geometry of the resulting addition compound is distorted from that of other simple adducts. To further explore the effects of the base size and substitution on the geometry around the aluminum atom, we have prepared and structurally characterized

$\text{Mes}_3\text{Al}(\text{4-picoline})(\text{C}_7\text{H}_8)_{0.5}$  (**1**),  $\text{EtMes}_2\text{Al}\cdot\text{THF}$  (**2**),  $\text{Mes}_2\text{ClAl}\cdot\text{THF}$  (**3**), and  $[\text{Mes}_2\text{Al}(\mu\text{-Cl})]_2$  (**4**). The structural observations resulting from this work are discussed with respect to related Group 13 organometallic complexes containing sterically-demanding ligands.

## Experimental Section

**(A) General Procedures and Information.** The compounds under investigation are both air and water sensitive, so all reactions and manipulations were carried out using standard Schlenk line and glovebox techniques. Argon was purified by passing it through a series of columns containing Deox catalyst (Alfa), sodium hydroxide, and calcium chloride. All solvents used were dried using standard techniques,<sup>13</sup> and all glassware was oven dried. The alkyaluminum halides,  $\text{EtAlCl}_2$  (1.8 M solution in toluene),  $\text{MeAlCl}_2$  (1.0 M solution in hexane), 4-picoline, and 2-bromomesitylene were purchased from Aldrich and used as received.  $\text{Mes}_3\text{Al}$ ,  $\text{Mes}_2\text{Al}\cdot\text{THF}$ , and  $\text{MesMgBr}$  were prepared according to the literature methods.<sup>3,12</sup> Aluminum trichloride was purchased from EM Science and sublimed using a high-vacuum system prior to use. <sup>1</sup>H and <sup>13</sup>C NMR spectra were recorded on a General Electric QE 300 NMR or a Varian Gemini-300 spectrometer at ambient temperature. The proton chemical shifts were referenced to  $\text{C}_6\text{D}_5\text{H}$  ( $\delta = 7.15$  ppm), and the carbon resonances were referenced to  $\text{C}_6\text{D}_6$  ( $\delta = 128.0$  ppm). Elemental analyses on selected compounds were performed by Galbraith Laboratories, Knoxville, TN. Melting points were recorded on a Haake-Buchler apparatus in sealed capillaries and are reported uncorrected. Mass spectrometry data were obtained on a Kratos MS80 RFA mass spectrometer with electron impact ionization at 70 eV, and IR spectra were recorded as Nujol mulls on a Nicolet DX20 FTIR spectrometer.

**Synthesis of  $\text{Mes}_3\text{Al}(\text{4-picoline})(\text{C}_7\text{H}_8)_{0.5}$  (**1**).** The THF adduct of  $\text{Mes}_3\text{Al}$  (0.500 g, 1.09 mmol) was dissolved in 50 mL of toluene. A 0.11 mL (1.1 mmol) portion of 4-picoline was added at room temperature, and the mixture was stirred overnight. The resulting solution was concentrated, yielding a white product which was recrystallized from hot toluene: mp 169 °C dec; <sup>1</sup>H NMR ( $\text{C}_6\text{D}_6$ ,  $\delta$ , ppm) 1.37 (s, 3H, 4- $\text{CH}_3$ -

(13) Shriver, D. F.; Drezdon, M. A. *The Manipulation of Air-Sensitive Compounds*; John Wiley & Sons: New York, 1986.

<sup>®</sup> Abstract published in *Advance ACS Abstracts*, December 1, 1994.

- (1) Leman, J. T.; Barron, A. R. *Organometallics* **1989**, *8*, 2214.
- (2) Petrie, M. A.; Olmstead, M. M.; Hope, H.; Bartlett, R. A.; Power, P. P. *J. Am. Chem. Soc.* **1993**, *115*, 3221.
- (3) Jerius, J. T.; Hahn, J. M.; Rahman, A. F. M. M.; Mols, O.; Ilsley, W. H.; Oliver, J. P. *Organometallics* **1986**, *5*, 1812.
- (4) Ranaivonjatovo, H.; Escudie, J.; Couret, C.; Declercq, J.-P.; Dubourg, A.; Satgé, J. *Organometallics* **1993**, *12*, 1674.
- (5) Beachley, O. T., Jr.; Churchill, M. R.; Pazik, J. C.; Ziller, J. W. *Organometallics* **1986**, *5*, 1814.
- (6) Baines, K. M.; Cooke, J. A. *Organometallics* **1992**, *11*, 3487.
- (7) Uhl, W. Z. *Naturforsch.* **1988**, *43b*, 1113.
- (8) Pluta, C.; Pörschke, K.-R.; Krüger, C.; Hildenbrand, K. *Angew. Chem., Int. Ed. Engl.* **1993**, *32*, 388.
- (9) Uhl, W.; Vester, A.; Kaim, W.; Poppe, J. *J. Organomet. Chem.* **1993**, *454*, 9.
- (10) Wehmschulte, R. J.; Ruhlandt-Senge, K.; Olmstead, M. M.; Hope, H.; Sturgeon, B. E.; Power, P. P. *Inorg. Chem.* **1993**, *32*, 2983.
- (11) Seidel, W. Z. *Angew. Chem.* **1985**, *524*, 101.
- (12) De Mel, V. S. J.; Oliver, J. P. *Organometallics* **1989**, *8*, 827.

pyridine), 2.10 (s, 1.5H, PhCH<sub>3</sub>), 2.26 (s, 9H, *p*-Me of Mes), 2.44 (s, 18H, *o*-Me of Mes), 5.96 (d, 2H,  $J_{\text{H-H}} = 5$  Hz, *m*-H of 4-picoline), 6.89 (s, 6H, *m*-H of Mes), 6.99–7.13 (m, 2.5H, toluene), 8.41 (d, 2H,  $J_{\text{H-H}} = 5$  Hz, *o*-H of 4-picoline); <sup>13</sup>C{<sup>1</sup>H} NMR (C<sub>6</sub>D<sub>6</sub>, δ, ppm) 21.26 (*p*-Me of Mes), 25.94 (*o*-Me of Mes), 21.36 (Me-pyridine), 20.55 (PhMe), 125.06, 125.64, 128.32, 128.50, 129.27, 136.29, 146.18, 149.41, 150.24 (aryl).

**Synthesis of EtMes<sub>2</sub>Al·THF (2).** A solution of EtAlCl<sub>2</sub> in toluene (1.8 M, 58.2 mL, 103 mmol) was added dropwise to 2 equiv of the mesityl Grignard reagent at 0 °C. The reaction mixture was refluxed for 2 h and stirred overnight. The solvent was removed under vacuum and the crude product extracted twice with hot toluene (~300 mL). The volume of the toluene extract was reduced by 50%, resulting in the precipitation of a crude product identified primarily as magnesium salts. The supernatant was decanted and the toluene removed under vacuum, yielding a white solid which was washed with pentane. The solid was recrystallized from benzene at approximately 5 °C, collected, and identified as EtMes<sub>2</sub>Al·THF: yield, 75%; mp 166–169 °C; <sup>1</sup>H NMR (C<sub>6</sub>D<sub>6</sub>, δ, ppm) 0.50 (q, 2H, -CH<sub>2</sub>CH<sub>3</sub>), 1.07 (m, 4H, 3,4-H of THF), 1.21 (t, 3H, -CH<sub>2</sub>CH<sub>3</sub>), 2.25 (s, 6H, *p*-Me), 2.43 (s, 12H, *o*-Me), 3.57 (m, 4H, 2,5-H of THF), 6.85 (s, 4H, *m*-H); <sup>13</sup>C NMR (C<sub>6</sub>D<sub>6</sub>, δ, ppm) 7.02 (-CH<sub>2</sub>CH<sub>3</sub>), 10.65 (-CH<sub>2</sub>CH<sub>3</sub>), 21.28 (*p*-Me), 24.84 (THF), 25.50 (*o*-Me), 71.40 (THF), 127.69 (*m*-Ar), 136.22 (*p*-Ar), 145.39 (*o*-Ar), 147.06 (*ipso*-C). Anal. Calcd (found) for C<sub>24</sub>H<sub>35</sub>AlO: C, 78.65 (76.42); H, 9.63 (9.28).

**Synthesis of Mes<sub>2</sub>ClAl·THF (3).** A solution of AlCl<sub>3</sub> in THF was prepared by placing THF (~150 mL) in a flask which was then cooled to -78 °C. The AlCl<sub>3</sub> (13.30 g, 100 mmol) was added slowly with stirring. The solution was brought to room temperature and added dropwise to 2 equiv of the mesityl Grignard solution at 0 °C. After addition of the aluminum halide, the mixture was allowed to warm to room temperature and then was refluxed for 2 h and allowed to stir overnight. The solvent was removed under reduced pressure, and the remaining solid was extracted with warm toluene (~60 °C, ~800 mL). Concentration of this solution followed by addition of pentane yielded a white solid which was recrystallized from toluene at -20 °C and identified as Mes<sub>2</sub>ClAl·THF: yield, 70%; mp 155–159 °C; <sup>1</sup>H NMR (C<sub>6</sub>D<sub>6</sub>, δ, ppm) 1.01 (m, 4H, 3,4-H of THF), 2.22 (s, 6H, *p*-Me), 2.56 (s, 12H, *o*-Me), 3.67 (m, 4H, 2,5-H of THF), 6.85 (s, 4H, *m*-H); <sup>13</sup>C NMR (C<sub>6</sub>D<sub>6</sub>, δ, ppm) 20.90 (*p*-Me), 24.41 (THF), 25.37 (*o*-Me), 72.39 (THF), 127.88 (*m*-Ar), 137.18 (*p*-Ar), 142.90 (*ipso*-C), 145.41 (*o*-Ar). Anal. Calcd (found) for C<sub>22</sub>H<sub>30</sub>AlClO: C, 70.86 (69.75), H, 8.11 (8.11).

**Preparation of [Mes<sub>2</sub>Al(μ-Cl)]<sub>2</sub> (4).** Trimesitylaluminum (0.500 g, 1.30 mmol) was added to 0.5 equiv of AlCl<sub>3</sub> in benzene. The mixture was stirred overnight, during which time the trihalide disappeared. The solvent was removed under reduced pressure, and the residue was recrystallized from hexane at -20 °C: yield, 0.670 g, 57%; mp 160–161 °C; <sup>1</sup>H NMR (C<sub>6</sub>D<sub>6</sub>, δ, ppm) 2.10 (s, 6H, *p*-Me of Mes), 2.44 (s, 12H, *o*-Me of Mes), 6.67 (s, 4H, aryl of Mes); <sup>13</sup>C{<sup>1</sup>H} NMR (C<sub>6</sub>D<sub>6</sub>, δ, ppm) 21.19 (*p*-Me of Mes), 25.15 (*o*-Me of Mes), 127.38, 128.32, 139.30, 145.34 (aryl); IR (Nujol, ν, cm<sup>-1</sup>) 1603 (s), 1057 (m), 1027 (m), 951 (w), 845 (s), 614 (s), 541 (m); MS (EI, *m/e*, relative intensity) 549 (M<sup>+</sup> - Cl - Me - H, 0.1), 446 (M<sup>+</sup> - Mes - Cl, 0.5), 300 (Mes<sub>2</sub>AlCl, 14.5), 285 (Mes<sub>2</sub>AlCl - Me, 3.4), 265 (Mes<sub>2</sub>Al, 36.7), 181 (MesAlCl, 6.8).

**Synthesis of Mes<sub>2</sub>MeAl·THF (5).** A 1.0 M hexane solution of MeAlCl<sub>2</sub> (51.5 mL, 52 mmol) was added dropwise to 2 equiv of MesMgBr in THF at 0 °C. The reaction mixture was refluxed for 2 h and stirred overnight. The product was isolated using the procedure described for **3**: yield, 75%; mp 136–140 °C; <sup>1</sup>H NMR (C<sub>6</sub>D<sub>6</sub>, δ, ppm) -0.06 (s, 3H, AlCH<sub>3</sub>), 0.96 (m, 4H, THF), 2.27 (s, 6H, *p*-Me), 2.48 (s, 12H, *o*-Me), 3.50 (br, 4H, THF), 6.89 (s, 4H, *m*-H); <sup>13</sup>C NMR (C<sub>6</sub>D<sub>6</sub>, δ, ppm) -4.46 (AlCH<sub>3</sub>), 21.26 (*p*-Me), 24.75 (THF), 25.61 (*o*-Me), 71.52 (THF), 127.79 (*m*-Ar), 136.35 (*p*-Ar), 145.46 (*o*-Ar), 147.37 (*ipso*-C).

### (B) X-ray Data Collection and Structure Refinement.

Crystals of suitable quality were prepared using the procedures described above. Crystals of **1–4** were sealed in thin-walled glass capillaries under an argon atmosphere. Diffraction data for **1** and **4** were collected on a Nicolet P2<sub>1</sub> diffractometer using Mo Kα radiation. Data for **2** were collected on a Nicolet P3/V diffractometer using Cu radiation while data for **3** were obtained from a Nicolet R3 diffractometer using Mo Kα radiation. The initial orientation matrices were obtained from machine-centered reflections selected from rotation photographs. These data were used to determine the crystal systems. Rotation photographs around each axis were consistent with monoclinic (**1**, **3**, **4**) and orthorhombic (**2**) crystal systems. Ultimately, 25 high-angle reflections were used to determine the final cell constants and orientation matrices. Systematic absences indicated that **1** could belong to the space group C2/c or Cc. Wilson statistics suggested a centrosymmetric structure, and therefore the space group C2/c was chosen. The assignment of this space group was confirmed by successful refinement of the structure. The space groups P2<sub>1</sub>2<sub>1</sub>2<sub>1</sub>, P2<sub>1</sub>/a and P2<sub>1</sub>/c were unambiguously determined from systematic absences for **2**, **3**, and **4**, respectively. No absorption corrections were applied to the data since in all cases the absorption coefficients are small (1–8 cm<sup>-1</sup>). Three standard reflections were collected every 97 reflections, revealing that **1**, **2**, **3**, and **4** decayed 1, 3, 7, and 6%, respectively. Selected X-ray data and structural parameters are listed in Table 1.

For **2** and **3**, the data reduction was carried out using SHELXTL programs,<sup>14</sup> and the data refinement was performed with SHELX-76.<sup>15</sup> Structures **1** and **4** were refined using SHELXTL PC.<sup>16</sup> Scattering factors<sup>17</sup> for neutral non-hydrogen atoms were used and the data were corrected for Lorentz and polarization effects. Direct methods were used to determine the heavy atom positions for all four compounds. The remaining non-hydrogen atoms were located from successive difference Fourier map calculations. Full-matrix, least-squares refinement of positional and thermal parameters for non-hydrogen atoms was carried out by minimizing the function  $\sum (w|F_o| - |F_c|)^2$ . The methyl groups were treated as rigid rotors, with a C–H bond distance of 0.96 Å and H–C–H angles of 109.4°. Their isotropic thermal parameters were fixed either at 1.2 times the isotropic thermal parameter of the contiguous carbon atom (**2** and **3**) or at 0.08 Å<sup>2</sup> (**1** and **4**). All hydrogen atom positional parameters were allowed to ride with their parent carbon atoms during subsequent refinement.

In the final cycles of refinement in **1**, the Al and N atoms were refined anisotropically. All other atoms were refined isotropically because of the limited size of the data set. In **2**, **3**, and **4**, all non-hydrogen atoms were refined anisotropically. The asymmetric unit of **1** contains one independent molecule and one-half of a molecule of toluene in the asymmetric unit, the atoms of which occupy general positions. The toluene molecule was disordered and was located near the center of inversion. Its position was located from a difference Fourier map. It occupied two positions with interchange of the toluene methyl group. It was refined as a rigid group, with  $d_{\text{ring}} = 1.395 \pm 0.05$  Å and  $d_{\text{methyl}} = 0.96$  Å, with a 50% occupancy factor for the two orientations of the toluene. One and two independent molecules occur in the asymmetric units of **2** and **3**, respectively, and one-half of the dimer in the asymmetric unit of **4**. All observed reflections were used for the refinement of **1**, but three, six, and two reflections were excluded during the refinement of **2**, **3**, and **4**, respectively. The residual

(14) Sheldrick, G. M. *SHELXTL*; University of Göttingen: Göttingen, Federal Republic of Germany, 1978.

(15) Sheldrick, G. M. *SHELX-76*; University Chemical Laboratory: Cambridge, England, 1976.

(16) *SHELXTL PC*; Siemens Analytical X-Ray Instruments, Inc.: Madison, WI, 1990.

(17) *International Tables for X-ray Crystallography*; Kynoch: Birmingham, England, 1974; Vol. IV (present distributor, D. Reidel: Dordrecht).



**Table 1.** Selected Experimental Parameters for the X-ray Diffraction Study of Mes<sub>3</sub>Al(4-picoline)(C<sub>7</sub>H<sub>8</sub>)<sub>0.5</sub> (1), EtMes<sub>2</sub>Al·THF (2), Mes<sub>2</sub>ClAl·THF (3), and [Mes<sub>2</sub>Al(μ-Cl)]<sub>2</sub> (4)

	1	2	3	4
formula	C <sub>36.5</sub> H <sub>40</sub> NAl	C <sub>24</sub> H <sub>35</sub> OAl	C <sub>22</sub> H <sub>30</sub> OClAl	C <sub>18</sub> H <sub>22</sub> AlCl
mol wt	519.71	366.52	372.91	300.81
space group	C2/c (No. 15)	P2 <sub>1</sub> 2 <sub>1</sub> 2 <sub>1</sub> (No. 19)	P2 <sub>1</sub> /a (No. 14)	P2 <sub>1</sub> /c (No. 14)
a (Å)	43.784(15)	12.057(9)	17.18(1)	12.288(2)
b (Å)	8.901(1)	13.490(3)	14.754(2)	15.824(3)
c (Å)	16.760(2)	14.027(2)	17.316(2)	9.095(2)
β (deg)	104.02(2)	90.00	92.74(3)	108.43(2)
V (Å <sup>3</sup> )	6337(2)	2281(2)	4384(3)	1678.2(5)
Z	8	4	8	4
D <sub>calc</sub> (g/cm <sup>3</sup> )	1.089	1.067	1.130	1.191
radiation (Å)	Mo Kα	Cu Kα	Mo Kα	Mo Kα
2θ range (deg)	4.5–45.0	0–110	5–50	5–50
F(000) (electrons)	2232	800	1600	640
no. of data collected	4310	3297	7935	3201
no. of unique reflns	4172	2882	7074	2945
no. of obsd reflns	1875 (F <sub>o</sub> ≥ 4σF <sub>o</sub> )	2465 (F <sub>o</sub> ≥ 4σF <sub>o</sub> )	3396 (F <sub>o</sub> ≥ 3σF <sub>o</sub> )	1450 (F <sub>o</sub> ≥ 4σF <sub>o</sub> )
μ (cm <sup>-1</sup> )	0.88	8.04	2.18	2.69
refined variables	326	236	452	175
R <sup>a</sup>	0.10	0.0542 (0.0561) <sup>c</sup>	0.065	0.054
R <sub>w</sub> <sup>b</sup>	0.099	0.0391 (0.0405) <sup>c</sup>	0.024	0.059
max shift/esd	0.000	0.003	0.002	0.000

<sup>a</sup> R = Σ(|F<sub>o</sub>| - |F<sub>c</sub>|)/Σ|F<sub>o</sub>|. <sup>b</sup> R<sub>w</sub> = [Σw(|F<sub>o</sub>| - |F<sub>c</sub>|)<sup>2</sup>/Σw|F<sub>o</sub>|<sup>2</sup>]<sup>1/2</sup>. <sup>c</sup> Bracketed values are for the opposite enantiomer.

electron densities of 1–4 are of no chemical significance. Positional and thermal parameters of the non-hydrogen atoms are presented in Tables 2–5. Selected bond distances and angles are given in Table 6. Complete listings of crystal and X-ray data collection parameters, bond distances and angles, hydrogen atom parameters, and anisotropic thermal parameters are deposited as supplementary material.

## Results and Discussion

The monomeric aluminum compounds EtMes<sub>2</sub>Al·THF (2), Mes<sub>2</sub>ClAl·THF (3), and Mes<sub>2</sub>MeAl·THF (5) were prepared by reaction of the Grignard reagent, MesMgBr, in THF with EtAlCl<sub>2</sub>, AlCl<sub>3</sub>, and MeAlCl<sub>2</sub>, respectively. The chloro-bridged dimer [Mes<sub>2</sub>Al(μ-Cl)]<sub>2</sub> (4) was obtained through the exchange reaction of Mes<sub>3</sub>Al and AlCl<sub>3</sub> in benzene. The halide adduct 3 was prepared previously from MgMes<sub>2</sub> and AlCl<sub>3</sub>.<sup>11</sup> The picoline derivative Mes<sub>3</sub>Al(4-picoline)(C<sub>7</sub>H<sub>8</sub>)<sub>0.5</sub> (1) was obtained by the displacement of the THF in Mes<sub>3</sub>Al·THF by addition of 4-picoline. These five products are obtained in good yields and in pure form as colorless crystalline materials by recrystallization from hydrocarbon solvents. The adducts are readily characterized by their <sup>1</sup>H and <sup>13</sup>C NMR spectra. Integration of the <sup>1</sup>H NMR spectra reveal that 1:1 adducts are formed with THF and 4-picoline. The proton and carbon chemical shifts of the mesityl, ethyl, and methyl ligands occur in the expected regions. Coordination of THF is indicated by the large upfield shift of the 3,4-protons from 1.73 ppm in free THF to 0.96–1.07 ppm for 2, 3, and 5. This observation has been noted for several aluminum compounds containing halide, silyl, and organic ligands.<sup>18</sup> Large upfield shifts are also noted for the proton resonances of 1. The methyl group and ortho protons of 4-picoline move upfield by approximately 1.0 ppm to 1.37 and 5.96 ppm, respectively.

All of these compounds are sensitive to moisture and oxygen. They possess greater kinetic stability than the base-free compounds, and the mixed ligand derivatives 2, 3, and 5 can be isolated in reasonably pure form,

**Table 2.** Atomic Coordinates (×10<sup>4</sup>) and Isotropic Thermal Parameters (×10<sup>3</sup>) for the Non-Hydrogen Atoms of Mes<sub>3</sub>Al(4-picoline) (1)

Atom	x	y	z	U <sub>eq</sub> <sup>a</sup>
Al(1)	3841(1)	1731(4)	7931(2)	38(1)
N(1)	3675(2)	0(9)	7143(4)	37(4)
C(1)	4021(2)	3360(11)	7356(5)	34(3)
C(2)	4223(2)	4360(12)	7865(6)	38(3)
C(3)	4421(3)	5372(12)	7588(6)	47(3)
C(4)	4424(3)	5378(12)	6750(6)	45(3)
C(5)	4222(3)	4473(12)	6230(6)	44(3)
C(6)	4022(2)	3494(12)	6502(6)	39(3)
C(7)	4240(3)	4460(14)	8788(6)	57(3)
C(8)	4651(3)	6425(14)	6458(7)	70(4)
C(9)	3801(3)	2593(13)	5847(7)	58(3)
C(11)	3422(2)	2090(12)	8221(6)	38(3)
C(12)	3254(2)	3447(13)	8104(6)	44(3)
C(13)	2945(3)	3586(14)	8208(7)	63(4)
C(14)	2803(3)	2370(14)	8478(7)	61(4)
C(15)	2963(3)	1022(14)	8611(7)	62(4)
C(16)	3266(3)	867(12)	8486(6)	45(3)
C(17)	3385(3)	4862(13)	7799(7)	67(4)
C(18)	2469(3)	2504(18)	8590(9)	111(6)
C(19)	3406(3)	-693(12)	8667(7)	58(4)
C(21)	4196(2)	736(11)	8720(6)	37(3)
C(22)	4452(2)	45(12)	8470(6)	37(3)
C(23)	4664(3)	-880(13)	8956(6)	49(3)
C(24)	4651(2)	-1247(12)	9754(7)	47(3)
C(25)	4433(3)	-488(12)	10060(6)	45(3)
C(26)	4211(2)	445(12)	9572(6)	37(3)
C(27)	4505(3)	424(13)	7605(6)	54(3)
C(28)	4881(3)	-2348(13)	10278(7)	67(4)
C(29)	3990(2)	1285(12)	9993(6)	51(3)
C(31)	3817(2)	-1336(13)	7181(6)	40(3)
C(32)	3698(2)	-2513(12)	6654(6)	39(3)
C(33)	3423(3)	-2318(12)	6079(6)	42(3)
C(34)	3266(2)	-972(12)	6043(6)	43(3)
C(35)	3398(3)	130(12)	6593(6)	43(3)
C(36)	3293(3)	-3555(14)	5484(8)	79(4)
C(40) (Tol)	2482(3)	2585(24)	4405(5)	50
C(41) (Tol)	2747(3)	2892(25)	5031(7)	50
C(42) (Tol)	2729(3)	2811(25)	5853(6)	50
C(43) (Tol)	2457(4)	2245(27)	6039(6)	50
C(44) (Tol)	2210(3)	1712(23)	5414(8)	50
C(45) (Tol)	2228(4)	1826(25)	4590(7)	50
C(46) (Tol)	2483(4)	2864(26)	3497(6)	50

$$^a U_{eq} = \frac{1}{3} \sum_i \sum_j U_{ij} a_i^* a_j^* \bar{a}_i \bar{a}_j.$$

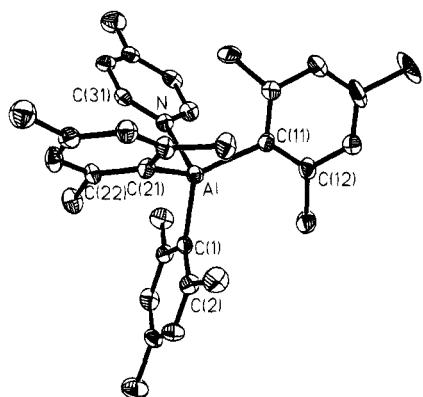
showing their stability toward redistribution of the organic groups. The compounds have slight solubility

(18) Sierra, M. L.; de Mel, V. S. J.; Oliver, J. P. *Organometallics* 1989, 8, 2312.

**Table 3. Atomic Coordinates and Isotropic Thermal Parameters for the Non-Hydrogen Atoms of EtMes<sub>2</sub>Al·THF (2)**

Atom	x	y	z	U <sub>eq</sub> <sup>a</sup>
Al1	0.5047(1)	0.36047(9)	0.11641(9)	0.0635(5)
C1	0.5094(5)	0.5036(3)	0.0784(3)	0.064(2)
C2	0.4154(4)	0.5385(4)	0.0281(3)	0.070(2)
C3	0.4090(5)	0.6346(4)	-0.0068(4)	0.084(2)
C4	0.4923(6)	0.7006(4)	0.0047(4)	0.085(2)
C5	0.5850(5)	0.6719(4)	0.0541(3)	0.081(2)
C6	0.5941(4)	0.5743(4)	0.0919(3)	0.071(2)
C7	0.3180(4)	0.4703(4)	0.0091(4)	0.109(3)
C8	0.4862(5)	0.8064(3)	-0.0348(3)	0.121(3)
C9	0.7006(4)	0.5473(4)	0.1449(4)	0.101(3)
C10	0.5183(4)	0.2646(3)	0.0064(3)	0.062(2)
C11	0.4819(5)	0.1654(4)	0.0145(4)	0.081(2)
C12	0.4923(5)	0.0971(4)	-0.0589(4)	0.096(3)
C13	0.5382(5)	0.1217(5)	-0.1426(4)	0.099(3)
C14	0.5772(5)	0.2165(4)	-0.1554(4)	0.089(2)
C15	0.5659(4)	0.2867(4)	-0.0803(4)	0.072(2)
C16	0.4298(5)	0.1313(4)	0.1089(4)	0.138(3)
C17	0.5484(6)	0.0462(4)	-0.2234(4)	0.171(4)
C18	0.6133(4)	0.3885(4)	-0.0987(3)	0.102(3)
C19	0.3900(4)	0.3413(4)	0.2163(3)	0.083(2)
C20	0.3683(5)	0.4251(5)	0.2768(4)	0.140(4)
O1	0.6369(3)	0.3202(3)	0.1842(2)	0.075(1)
C21	0.7317(4)	0.2670(4)	0.1442(4)	0.097(3)
C22	0.7881(5)	0.2192(5)	0.2265(5)	0.130(3)
C23	0.7561(6)	0.2772(7)	0.3080(4)	0.192(5)
C24	0.6478(5)	0.3203(5)	0.2881(4)	0.121(3)

$$^a U_{eq} = \frac{1}{3} \sum_i \sum_j U_{ij} a_i^* a_j^* \bar{a}_i \bar{a}_j.$$



**Figure 1.** ORTEP diagram of Mes<sub>3</sub>Al(4-picoline)(C<sub>7</sub>H<sub>8</sub>)<sub>0.5</sub> (1) with 30% thermal ellipsoids. The hydrogen atoms have been omitted for clarity. The lattice solvent molecule is not shown.

in hexane, moderate solubility in aromatic solvents, and high solubility in polar solvents.

The results of the crystallographic study show that the three addition compounds Mes<sub>3</sub>Al(4-picoline)-(C<sub>7</sub>H<sub>8</sub>)<sub>0.5</sub> (1), EtMes<sub>2</sub>Al·THF (2), and Mes<sub>2</sub>ClAl·THF (3) have structures comparable to those of other amine and ether trialkyl- and triarylaluminum adducts.<sup>19</sup> A more detailed analysis of each of these structures follows. In 1, a single molecular unit of Mes<sub>3</sub>Al(4-picoline) along with one-half of a molecule of toluene constitutes the asymmetric unit. The presence of the toluene has been confirmed by <sup>1</sup>H and <sup>13</sup>C NMR spectroscopy, but the coordinates for this molecule did not refine well. An ORTEP drawing of 1 is shown in Figure 1. The ORTEP diagrams for 2 and 3 are shown in Figures 2 and 3, respectively. The geometry around the Al atom in each

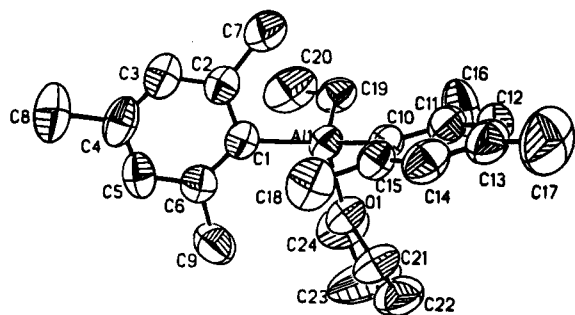
**Table 4. Atomic Coordinates and Isotropic Thermal Parameters for the Non-Hydrogen Atoms of Mes<sub>2</sub>ClAl·THF (3)**

Atom	x	y	z	U <sub>eq</sub> <sup>a</sup>
Al1	0.8566(1)	0.0287(1)	0.5943(1)	0.0632(9)
Cl1	0.9733(1)	0.0696(1)	0.64062(9)	0.0639(7)
C1	0.8673(4)	-0.1020(4)	0.5678(4)	0.055(3)
C2	0.8588(4)	-0.1418(5)	0.4932(4)	0.056(3)
C3	0.8841(4)	-0.2298(5)	0.4803(4)	0.064(3)
C4	0.9157(4)	-0.2836(5)	0.5385(5)	0.066(3)
C5	0.9196(4)	-0.2491(5)	0.6129(4)	0.069(3)
C6	0.8970(4)	-0.1607(5)	0.6273(4)	0.066(3)
C7	0.8206(4)	-0.0918(4)	0.4257(3)	0.089(4)
C8	0.9461(4)	-0.3781(4)	0.5212(4)	0.105(4)
C9	0.9010(4)	-0.1295(4)	0.7109(4)	0.104(4)
C10	0.7689(4)	0.0814(5)	0.6506(4)	0.064(3)
C11	0.7702(5)	0.1700(5)	0.6821(4)	0.068(4)
C12	0.7064(6)	0.2050(5)	0.7179(4)	0.075(4)
C13	0.6385(6)	0.1587(6)	0.7243(5)	0.086(4)
C14	0.6341(5)	0.0725(6)	0.6939(5)	0.090(4)
C15	0.6977(5)	0.0351(5)	0.6585(4)	0.075(4)
C16	0.8404(4)	0.2305(5)	0.6751(4)	0.104(4)
C17	0.5694(5)	0.2027(5)	0.7600(4)	0.129(5)
C18	0.6855(4)	-0.0612(5)	0.6276(4)	0.113(4)
O1	0.8520(3)	0.1007(3)	0.5039(3)	0.065(2)
C19	0.9183(4)	0.1216(5)	0.4552(4)	0.084(4)
C20	0.8814(6)	0.1692(7)	0.3866(5)	0.157(6)
C21	0.8030(6)	0.1891(7)	0.3999(6)	0.143(6)
C22	0.7805(4)	0.1464(5)	0.4708(5)	0.103(4)
Al2	0.8834(1)	0.1869(1)	0.0690(1)	0.0593(9)
Cl2	1.0076(1)	0.1516(1)	0.0863(1)	0.0724(8)
C23	0.8827(4)	0.3193(4)	0.0502(4)	0.055(3)
C24	0.8604(4)	0.3653(5)	-0.0185(4)	0.066(3)
C25	0.8718(4)	0.4587(5)	-0.0257(4)	0.072(4)
C26	0.9027(4)	0.5107(5)	0.0329(5)	0.072(4)
C27	0.9219(4)	0.4674(6)	0.1011(4)	0.078(4)
C28	0.9120(4)	0.3743(5)	0.1111(4)	0.063(3)
C29	0.8222(4)	0.3154(4)	-0.0877(4)	0.121(4)
C30	0.9163(4)	0.6115(4)	0.0232(4)	0.105(4)
C31	0.9331(4)	0.3327(4)	0.1899(4)	0.099(4)
C32	0.8091(4)	0.1303(5)	0.1389(4)	0.054(3)
C33	0.8193(4)	0.0443(5)	0.1729(4)	0.062(3)
C34	0.7644(5)	0.0061(5)	0.2195(4)	0.070(4)
C35	0.6961(5)	0.0498(6)	0.2338(4)	0.070(4)
C36	0.6840(5)	0.1333(5)	0.2000(4)	0.080(4)
C37	0.7390(5)	0.1738(5)	0.1544(4)	0.065(3)
C38	0.8912(4)	-0.0134(4)	0.1599(4)	0.102(4)
C39	0.6352(4)	0.0060(5)	0.2823(4)	0.115(4)
C40	0.7166(4)	0.2659(4)	0.1202(4)	0.098(4)
O2	0.8646(3)	0.1191(3)	-0.0232(3)	0.063(2)
C41	0.9205(4)	0.1023(5)	-0.0822(4)	0.094(4)
C42	0.8749(6)	0.0625(8)	-0.1474(5)	0.136(6)
C43	0.8055(7)	0.0243(7)	-0.1177(6)	0.161(7)
C44	0.7927(4)	0.0677(5)	-0.0441(5)	0.106(4)

$$^a U_{eq} = \frac{1}{3} \sum_i \sum_j U_{ij} a_i^* a_j^* \bar{a}_i \bar{a}_j.$$

of these can be described as a distorted tetrahedron. The six angles at the Al atom fall in the range of 94.2(4)–121.4(3)° for 1 and are similar to those observed in Mes<sub>3</sub>Al·THF,<sup>12</sup> which fall between 91.4 and 120.3°. In 2 and 3, where one of the Mes moieties has been replaced by an ethyl group or chlorine atom, the angles fall in the range of 97.4(2)–120.8(2)° for 2 and 98.6(2)–124.8(3)° for 3. This wide distribution of angles can be attributed to steric interactions between the mesityl groups or the other substituents bound to the aluminum. The C–Al–N, C–Al–O, and Cl–Al–O angles for 1, 2, and 3 are listed in Table 6. The average C–Al–N angle is 102°. In 2 the average of the C–Al–O angles is 103.5°, and in 3 the average value of the C–Al–O angles is 106.4°, but if the Cl–Al–O angles are included, the average ligand to oxygen angle becomes 103.4°. The corresponding C–Al–C and C–Al–O angles in Mes<sub>3</sub>Al·THF average 116.2 and 101.5°,<sup>12</sup> and those in (Me<sub>3</sub>Al)<sub>2</sub>C<sub>4</sub>H<sub>8</sub>O<sub>2</sub>,

(19) Oliver, J. P. In *The Chemistry of the Metal-Carbon Bond*; Hartley, F. R., Patai, S., Eds.; John Wiley: New York, 1985; Vol. 2, pp 789–826.

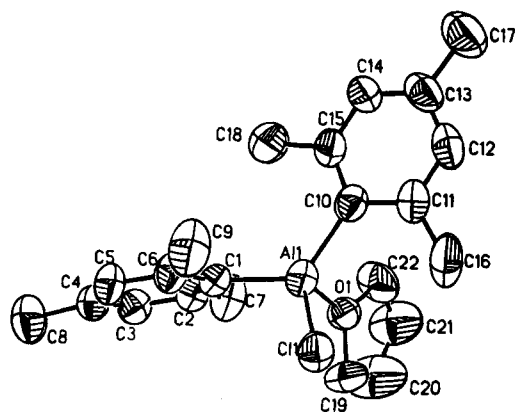


**Figure 2.** ORTEP diagram of EtMes<sub>2</sub>Al·THF (**2**) with 50% thermal ellipsoids. The hydrogen atoms have been omitted for clarity.

**Table 5.** Atomic Coordinates ( $\times 10^4$ ) and Isotropic Thermal Parameters ( $\times 10^3$ ) for the Non-Hydrogen Atoms of [Mes<sub>2</sub>Al( $\mu$ -Cl)]<sub>2</sub> (**4**)

Atom	x	y	z	$U_{eq}^a$
Al(1)	-1197(1)	119(1)	567(2)	36(1)
Cl(1)	539(1)	830(1)	898(1)	43(1)
C(1)	-2354(3)	921(3)	-672(5)	35(2)
C(2)	-2369(4)	1720(3)	12(5)	40(2)
C(3)	-3158(4)	2330(3)	-735(6)	46(2)
C(4)	-3952(4)	2184(3)	-2166(6)	49(2)
C(5)	-3960(3)	1401(3)	-2832(5)	45(2)
C(6)	-3195(3)	774(3)	-2126(5)	39(2)
C(7)	-1566(4)	1920(3)	1607(5)	55(2)
C(8)	-4796(4)	2878(4)	-2946(7)	76(3)
C(9)	-3311(4)	-77(3)	-2928(6)	62(2)
C(11)	-1389(3)	-525(3)	2317(5)	37(2)
C(12)	-480(3)	-932(3)	3456(5)	38(2)
C(13)	-697(4)	-1481(3)	4527(5)	44(2)
C(14)	-1795(4)	-1635(3)	4571(5)	43(2)
C(15)	-2682(4)	-1223(3)	3498(5)	45(2)
C(16)	-2511(3)	-680(3)	2386(5)	43(2)
C(17)	756(3)	-773(3)	3577(5)	54(2)
C(18)	-2017(5)	-2247(3)	5712(6)	63(2)
C(19)	-3574(4)	-298(4)	1253(7)	78(3)

$$^a U_{eq} = \frac{1}{3} \sum_i \sum_j U_{ij} a_i^* a_j^* \bar{a}_i \bar{a}_j.$$



**Figure 3.** ORTEP diagram of Mes<sub>2</sub>ClAl·THF (**3**) with 50% thermal ellipsoids. The hydrogen atoms have been omitted for clarity.

116.8 and 100.4°. The deviations between the smallest L–Al–L (94°) and the largest (125°) angles in **1**, **2**, and **3** are nearly the same (Table 6) and are similar to that in Mes<sub>3</sub>Al·THF.<sup>12</sup> Further, there is no pattern discernible in the distribution. These findings lead to the conclusion that the structures of addition compounds with two or three mesityl groups bound to the aluminum are determined by the steric requirements of the mesityl group. The sum of the L–Al–L angles (L = C, Cl)

provides a measure of the planarity of the L<sub>3</sub>Al unit. In **1**, **2**, and **3**, the sum is 347.8, 344.6, and 343.7° (av). These values are typical for aluminum addition compounds, with the small decrease indicating a small decrease in the steric interaction with substitution of Et or Cl for a Mes group.

The Al–C distances of **1**–**4** (Table 6) are in the range of 2.004–2.033 Å for the organic derivatives and 1.966 to 1.993 Å for those containing a chlorine atom and are typical of Al–C single bond lengths for a variety of organoaluminum compounds as noted earlier.<sup>3,21</sup> The average Al–Cl bond length in **3**, 2.206 Å, is longer by ~0.05 Å than that of MesAlCl<sub>2</sub>·THF<sup>21</sup> and ~0.05 Å longer than the bond in AlCl<sub>3</sub>·2THF<sup>22</sup> but is within the range expected for single Al–Cl bonds. The Al–N distance in **1** (2.045(8) Å) is similar to the Al–N distance in Me<sub>3</sub>Al·quinuclidine (2.06(1) Å),<sup>23</sup> but longer than the distances found in Me<sub>2</sub>Al·NMe<sub>3</sub> (2.02 Å),<sup>24</sup> Cs<sup>+</sup>·[Me<sub>3</sub>Al·N<sub>3</sub>]<sup>-</sup> (1.97(1) Å)<sup>25</sup> and Me<sub>3</sub>Al·NCCH<sub>3</sub> (2.02(1) Å).<sup>26</sup>

The Al–O distances in **2** and **3** are 1.934(4) and 1.894(5) Å (av) and are listed, along with Al–O distances for other adducts, in Table 7. The Al–O bond distances listed fall into three groups: those associated with trialkyl addition compounds with Al–O bond distances greater than 2.0 Å, those with aryl groups bound to aluminum which fall in the broad range of 1.9–1.97 Å and those with a halogen atom bound to aluminum with Al–O distances less than 1.9 Å. The Lewis acidity of the compounds follows this same pattern, with increasing acidity corresponding to decreasing Al–O bond length. On this basis, the increased Lewis acidity of **3** accounts for the shorter Al–O distance observed in this compound. The Al–O distance in MesAlCl<sub>2</sub>·THF, at 1.852(1) Å, is the shortest in the mesityl derivatives while (Trip)AlBr<sub>2</sub>·OEt<sub>2</sub> shows an Al–O distance of 1.865(11) Å.<sup>21</sup> The C–Al–O angle also appears to be correlated with the Lewis acidity of the aluminum derivative. As the acidity of the metal increases, the Al–O length decreases, and a corresponding increase in the C–Al–O angle is observed. Steric repulsion between the base and the mesityl groups does not affect the Al–O distance of ether adducts. In the adducts Me<sub>3</sub>Al·OMe<sub>2</sub><sup>27</sup> and (Me<sub>3</sub>Al)<sub>2</sub>p-dioxane,<sup>20</sup> the Al–O bond distances are 2.014(14) and 2.02(2) Å, respectively, while shorter distances are found for Bz<sub>3</sub>Al·OEt<sub>2</sub><sup>28</sup> (1.901(4) Å) and (*o*-Tol)<sub>3</sub>Al·OEt<sub>2</sub><sup>29</sup> (1.928(3) Å). In the mesityl derivatives Mes<sub>3</sub>Al·THF,<sup>12</sup> **2**, and **3**, the Al–O bond distances are 1.969(5), 1.934(4), and 1.898(5) Å, respectively.

The structural determination of **4** completes the series Mes<sub>2</sub>MCl (M = Al, Ga, In). An ORTEP diagram is

(21) Petrie, M. A.; Power, P. P.; Dias, H. V. R.; Ruhlandt-Senge, K.; Waggoner, K. M.; Wehmschulte, R. J. *Organometallics* **1993**, *12*, 1086.

(22) Cowley, A. H.; Cushner, M. C.; Davis, R. E.; Riley, P. E. *Inorg. Chem.* **1981**, *20*, 1179.

(23) Whitt, C. D.; Parker, L. M.; Atwood, J. L. *J. Organomet. Chem.* **1971**, *32*, 291.

(24) Atwood, J. L.; Milton, P. A. *J. Organomet. Chem.* **1973**, *52*, 275.

(25) Atwood, J. L.; Newberry, W. R. J., III. *J. Organomet. Chem.* **1975**, *87*, 1.

(26) Atwood, J. L.; Seale, S. K.; Roberts, D. H. *J. Organomet. Chem.* **1973**, *51*, 105.

(27) Haaland, A.; Samdal, S.; Stokkeland, O.; Weidlein, J. *J. Organomet. Chem.* **1977**, *134*, 165.

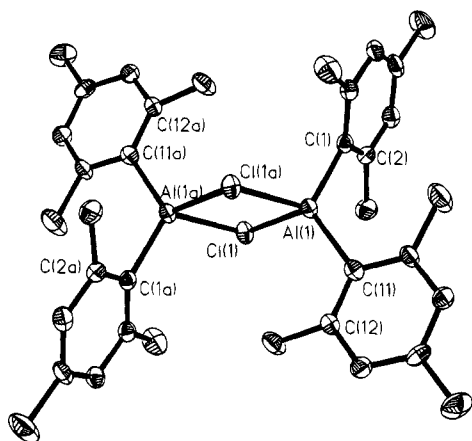
(28) Rahman, A. F. M. M.; Siddiqui, K. F.; Oliver, J. P. *J. Organomet. Chem.* **1987**, *319*, 161.

(29) Barber, M.; Liptak, D.; Oliver, J. P. *Organometallics* **1982**, *1*, 1307.

(20) Atwood, J. L.; Stucky, G. D. *J. Am. Chem. Soc.* **1967**, *89*, 5362.

**Table 6.** Selected Bond Distances (Å) and Angles (deg) for Mes<sub>3</sub>Al(4-picoline)(C<sub>7</sub>H<sub>8</sub>)<sub>0.5</sub> (1), EtMes<sub>2</sub>Al·THF (2), MesClAl·THF (3), and [Mes<sub>2</sub>Al(μ-Cl)]<sub>2</sub> (4)

Mes <sub>3</sub> Al(4-picoline)(C <sub>7</sub> H <sub>8</sub> ) <sub>0.5</sub> (1)	EtMes <sub>2</sub> Al·THF (2)	Mes <sub>2</sub> ClAl·THF (3)				[Mes <sub>2</sub> Al(μ-Cl)] <sub>2</sub> (4)			
		molecule 1		molecule 2					
Al-C1	2.005(11)	Al-C1	2.004(4)	Al1-C1	1.993(7)	Al2-C23	1.980(7)	Al1-C1	1.972(4)
Al-C11	2.033(12)	Al-C10	2.020(5)	Al1-C10	1.992(8)	Al2-C32	1.985(7)	Al1-C11	1.966(5)
Al-C19	1.990(10)	Al-C19	1.986(5)	Al1-C11	2.207(3)	Al2-C12	2.204(3)	Al1-C11	2.346(2)
Al-N	2.045(8)	Al-O	1.934(4)	Al1-O1	1.890(5)	Al2-O2	1.898(5)	Al1-C11A	2.315(2)
Cl-Al-C11	118.9(4)	C1-Al-C10	114.3(2)	C1-Al1-C10	124.8(3)	C23-Al2-C32	121.1(3)	C1-Al1-C11	123.1(2)
C1-Al-C21	107.8(4)	C1-Al-C19	109.5(2)	C10-Al1-C11	114.3(2)	C32-Al2-C12	117.7(2)	C11-Al1-C11A	85.2(1)
C11-Al-C21	121.1(4)	C10-Al-C19	120.8(2)	C1-Al1-C11	104.8(2)	C23-Al2-C12	104.7(2)	Al1-C11-A11A	94.8(1)
C1-Al-N	110.7(4)	C1-Al-O	112.2(2)	C1-Al1-O1	110.7(3)	C23-Al2-O2	112.5(3)		
C11-Al-N	94.2(4)	C10-Al-O	97.4(2)	C10-Al1-O1	100.5(3)	C32-Al2-O2	101.7(2)		
C21-Al-N	101.1(4)	C19-Al-O	101.0(2)	C11-Al1-O1	98.6(2)	C12-Al2-O2	96.6(2)		

**Figure 4.** ORTEP diagram of [Mes<sub>2</sub>Al(μ-Cl)]<sub>2</sub> (4) with 30% thermal ellipsoids. The hydrogen atoms have been omitted for clarity.**Table 7.** Structural Parameters of Aluminum Adducts as a Function of Lewis Acidity

Compound	C-Al-O (deg)	Al-O (Å)	Al-C (Å)
Mes <sub>3</sub> Al·OMe <sub>2</sub> <sup>a</sup>	98.7	2.014	1.973
(Me <sub>3</sub> Al) <sub>2</sub> ·p-dioxane <sup>b</sup>	100.4	2.02	1.97
Mes <sub>3</sub> Al·THF <sup>c</sup>	101.3	1.969	2.017
Ph <sub>2</sub> AlSi(SiMe <sub>3</sub> ) <sub>3</sub> ·THF <sup>d</sup>	103.2	1.927	1.985
EtMes <sub>2</sub> Al·THF <sup>e</sup>	103.5	1.934	2.012, 1.986 (Et)
( <i>o</i> -Tol) <sub>3</sub> Al·OEt <sub>2</sub> <sup>f</sup>	103.8	1.928	1.990
Bz <sub>3</sub> Al·OEt <sub>2</sub> <sup>g</sup>	105.6	1.901	1.986
Mes <sub>2</sub> ClAl·THF <sup>e</sup>	106.4	1.894	1.988
TripAlBr <sub>2</sub> ·OEt <sub>2</sub> <sup>h</sup>	107.6	1.865	1.976
MesAlCl <sub>2</sub> ·THF <sup>h</sup>	115.2	1.852	1.969

<sup>a</sup> Reference 27. <sup>b</sup> Reference 20. <sup>c</sup> Reference 12. <sup>d</sup> Reference 18. <sup>e</sup> This work. <sup>f</sup> Reference 29. <sup>g</sup> Reference 28. <sup>h</sup> Reference 21.

shown in Figure 4. Like the Ga and In analogues, 4 exists in the solid state as a dimer containing a planar Al<sub>2</sub>Cl<sub>2</sub> core. It is isomorphous with the gallium analogue.<sup>21</sup> The Al-Cl distances are 2.346(2) and 2.315(2) Å, and, like the Ga compound, the core is asymmetric. This feature has also been noted for [Trip<sub>2</sub>Al(μ-Br)]<sub>2</sub>.<sup>21</sup> [Mes<sub>2</sub>In(μ-Cl)]<sub>2</sub> displays equivalent In-Cl bonds.<sup>1</sup> The average Al-Cl distance of 4 (2.329) is longer than the single Al-Cl bond in compounds such as 3 (2.206(4) Å), EtCl<sub>2</sub>Al·P(SiMe<sub>3</sub>)<sub>3</sub> (2.114(4) and 2.156(4) Å), and *i*-Bu<sub>2</sub>ClAl·P(SiMe<sub>3</sub>)<sub>3</sub> (2.179(4) Å)<sup>30</sup> but comparable to the distances observed for the bridging halides such as those in [Me<sub>2</sub>Al(μ-Cl)]<sub>2</sub> (2.303 Å).<sup>31</sup> The endocyclic Al-Cl-Al and Cl-Al-Cl angles are 90.6 and 89.4° and the

exocyclic C-Al-C angle is 126.9°. The comparable endocyclic angles in the three compounds, [Mes<sub>2</sub>M(μ-Cl)]<sub>2</sub> (M = Al, Ga, and In), are 94.8, 95.9, and 96.5° (M-Cl-M) and 85.2, 84.1, and 83.5° (Cl-M-Cl), and the C-M-C angles are 122.7(2), 126.6(2), and 131.0°, respectively. In [Trip<sub>2</sub>Al(μ-Br)]<sub>2</sub>, the exocyclic angle is 130.0(4)°.<sup>21</sup> These observations indicate that the intramolecular interactions between the Ar groups in [Ar<sub>2</sub>M(μ-X)]<sub>2</sub> have very little effect on either the endo- or the exocyclic angles in these compounds.

There are four major factors which determine the stability of Group 13 addition compounds: the Lewis acidity of the metal, which follows the order Al > Ga > In; the modification of the Lewis acidity by the substituents bound to the metal, which decreases from X > Ar > R (X = halogen; Ar = aryl, R = alkyl); the basicity of the ligand; and the steric interactions, which include those on the metal and that between the incoming base and the substituents bound to the metal. In the present system, the adducts Mes<sub>3</sub>Al·OEt<sub>2</sub>, Mes<sub>3</sub>Al·THF, and Mes<sub>3</sub>Al·4-picoline increase in stability as a function of the basicity of the ligand. Diethyl ether and THF can be removed readily, while 4-picoline cannot be removed without additional decomposition of the compound. This order follows that expected for the bases. The heavier homologues Mes<sub>3</sub>Ga<sup>5</sup> and Mes<sub>3</sub>In<sup>1</sup> do not form stable adducts with Et<sub>2</sub>O or THF. Similarly, in the neopentyl series, Np<sub>3</sub>Al binds Et<sub>2</sub>O,<sup>32</sup> Np<sub>3</sub>Ga does not form a stable adduct with Et<sub>2</sub>O but does with THF,<sup>33</sup> and Np<sub>3</sub>In forms addition compounds only with very strong bases such as NMe<sub>3</sub>.<sup>34</sup> The latter sequence follows the order of acidity expected for the metals.

Study of the organoaluminum derivatives in the absence of a coordinating ligand provides additional insight into the steric interactions. The ability of these compounds to form dimeric or trimeric aggregates is well established. The stability of the dimer in the series [Ph<sub>2</sub>Al(μ-Ph)]<sub>2</sub> ≥ [(2-MeC<sub>6</sub>H<sub>4</sub>)<sub>2</sub>Al(μ-2MeC<sub>6</sub>H<sub>4</sub>)]<sub>2</sub> > Mes<sub>3</sub>Al decreases in the order shown, with Mes<sub>3</sub>Al observed only as a monomer. The observation that [Mes<sub>2</sub>Al(μ-Cl)]<sub>2</sub> and [Mes<sub>2</sub>Ga(μ-Cl)]<sub>2</sub> are dimeric with chlorine bridges supports the earlier suggestion that the steric interference that prevents dimerization occurs at the bridging site. With more sterically demanding ligands,

(30) Wells, R. L.; McPhail, A. T.; Self, M. F.; Laske, J. A. *Organometallics* **1993**, *12*, 3333.

(31) Brendhaugen, K.; Haaland, A.; Novak, D. P. *Acta Chem. Scand.* **1974**, *A28*, 45.

(32) Beachley, O. T., Jr.; Victoriano, L. *Organometallics* **1988**, *7*, 63.

(33) Beachley, O. T., Jr.; Pazik, J. C. *Organometallics* **1988**, *7*, 1516.

(34) Beachley, O. T., Jr.; Spiegel, E. F.; Kopasz, J. P.; Rogers, R. D. *Organometallics* **1989**, *8*, 1915.

such as those found in  $\text{Trip}_2\text{GaCl}^{21}$  and  $\text{Mes}^*_2\text{InBr}$ ,<sup>35</sup> the halide derivatives are monomeric, indicating that the bulky substituents interact, preventing bridge formation.

Study of the  $\text{Ar}_n\text{R}_{3-n}\text{Al}$  systems such as  $\text{Mes}_2\text{MeAl}$  and  $\text{Mes}_2\text{EtAl}$  is complicated by the exchange of groups and the possible formation of dimeric species with alkyl and/or aryl bridges. It is clear from the formation of the mixed species **2** and **5** stabilized by THF that mixed derivatives can be prepared.

In other compounds with bulky substituents, such as  $\text{Np}_3\text{Al}$  and  $(\text{Me}_3\text{SiCH}_2)_3\text{Al}$ , which are isostructural, the neopentyl derivative is monomeric,<sup>32</sup> while the (trimethylsilyl)methyl derivative is involved in a monomer-dimer equilibrium in solution.<sup>36</sup> Substitution of a hydride for one of the bulky substituents permits the

formation of an equilibrium between dimers and trimers for  $[\text{Np}_2\text{Al}(\mu\text{-H})]_n$ ,<sup>32</sup> and the formation of trimers for  $(\text{Me}_3\text{SiCH}_2)_2\text{AlH}$ .<sup>37</sup>

The mixed mesityl-alkyl derivatives remain to be studied, but with the reduced steric requirements of the methyl group, one may find associated species in solution.

**Supplementary Material Available:** Complete listings of crystal and X-ray data collection parameters, bond distances and angles, anisotropic thermal parameters for the non-hydrogen atoms, and atomic coordinates and isotropic thermal parameters for the hydrogen atoms (22 pages). Ordering information is given on any current masthead page.

OM940350S

---

(36) Nyathi, J. Z.; Ressler, J. M.; Smith, J. D. *J. Organomet. Chem.* **1974**, *70*, 35.

(37) Beachley, O. T., Jr.; Tessier-Youngs, C. *Organometallics* **1983**, *2*, 796.

---

(35) Rahbarnoochi, H.; Heeg, M. J.; Oliver, J. P. *Organometallics* **1994**, *13*, 2123.

# Synthesis and Molecular Structures of the First Example of Tellurolate Dimers, $[\text{Mes}_2\text{In}(\mu\text{-Te-}n\text{-Pr})]_2$ and $[\text{Mes}_2\text{In}(\mu\text{-TePh})]_2$ : Potential Precursors to Indium Chalcogenides

Hamid Rahbarnoohi, Rajesh Kumar, Mary Jane Heeg, and John P. Oliver\*

Department of Chemistry, Wayne State University, Detroit, Michigan 48202

Received September 7, 1994<sup>⊙</sup>

The reaction of trimesitylindium,  $\text{Mes}_3\text{In}$ , ( $\text{Mes} = 2,4,6\text{-trimethylphenyl}$ ) with the ditellurides,  $(n\text{-Pr})_2\text{Te}_2$  and  $\text{Ph}_2\text{Te}_2$ , yields the related organotellurolates,  $[\text{Mes}_2\text{In}(\mu\text{-Te-}n\text{-Pr})]_2$  (**1**) and  $[\text{Mes}_2\text{In}(\mu\text{-TePh})]_2$ , (**2**). **1** and **2** have been characterized by  $^1\text{H}$ ,  $^{13}\text{C}$ , and  $^{125}\text{Te}$  NMR spectroscopy, and their structures have been determined by single crystal X-ray diffraction techniques. The crystal structure parameters are: for **1**, space group,  $P\bar{1}$  (No. 2),  $a = 9.176(1) \text{ \AA}$ ,  $b = 10.687(1) \text{ \AA}$ ,  $c = 11.771(2) \text{ \AA}$ ,  $\alpha = 91.79(1)^\circ$ ,  $\beta = 109.97(1)^\circ$ ,  $\gamma = 99.68(1)^\circ$ ,  $V = 1064.5(2) \text{ \AA}^3$ ,  $Z = 2$ ,  $R (R_w) = 3.1 (3.0)\%$  based on 2776 ( $I > 2.0\sigma(I)$ ) observed reflections; and for **2**, space group,  $P2_1/c$  (No. 14),  $a = 8.778(1) \text{ \AA}$ ,  $b = 23.283(9) \text{ \AA}$ ,  $c = 11.278(2) \text{ \AA}$ ,  $\beta = 101.74(1)^\circ$ ,  $V = 2261(1) \text{ \AA}^3$ ,  $Z = 4$ ,  $R (R_w) = 3.1 (3.1)\%$  based on 2919 ( $I > 3.0\sigma(I)$ ) observed reflections. The central  $(\text{InTe})_2$  core of **1** and **2** is planar with *trans* orientation of the TeR groups.

## Introduction

Recent literature in the chemistry of heavier Group 13-15/16 organometallic compounds has been directed toward synthesis of their materials as precursors for MOCVD preparation of thin films. These studies include preparation of thin films of InS and GaS<sup>1,2</sup> and  $\text{R}_3 - n\text{In}(\text{SeR}')_n$  used to produce  $\text{In}_x\text{Se}_y$  films.<sup>3</sup> Almost all of the published work on these organometallic precursors describes thiolate and selenolate complexes of Group 13<sup>4-10</sup> with very little work on the tellurium derivatives.<sup>6,8,11-13</sup> In this paper we begin to address the preparation of the tellurium derivatives with a description of the synthesis and characterization of tellurolato complexes,  $[\text{Mes}_2\text{In}(\mu\text{-TeR})]_2$ , formed by the interaction of the dichalcogenide,  $(\text{RTe})_2$ , with trimesitylindium. Structural data obtained using single crystal X-ray diffraction is presented, and the nature of the compounds in solution has been studied with NMR spectroscopy.

## Experimental Section

**General Experimental Procedures.** All solvents were purified and dried by standard techniques.<sup>14</sup> Argon gas was purified by passing it through a series of columns containing Deox catalyst (Alfa), phosphorus pentoxide, and sodium hydroxide. The  $(n\text{-Pr})_2\text{Te}_2$  (Strem) and the  $\text{Ph}_2\text{Te}_2$  (Aldrich) were used as received. Trimesitylindium,  $\text{Mes}_3\text{In}$ , was prepared according to the published procedure.<sup>15</sup> The compounds are both oxygen and water sensitive so standard Schlenk line and glove box techniques were employed. All of the glassware used in the synthetic work was oven and/or flame dried.  $^1\text{H}$  and  $^{13}\text{C}$  NMR spectra were recorded on either a QE-300 or a GN-300 NMR General Electric spectrometer. The  $^{125}\text{Te}$  NMR spectra were recorded on a Bruker AC200 spectrometer. The  $^1\text{H}$  and  $^{13}\text{C}$  chemical shifts were referenced to benzene ( $\delta = 7.15$  for  $^1\text{H}$  and  $\delta = 128.00$  for  $^{13}\text{C}$ ) while  $^{125}\text{Te}$  chemical shifts were referenced to external  $\text{Me}_2\text{Te}$  in  $\text{CDCl}_3$ . Elemental analyses were performed by Galbraith Laboratories, Knoxville, TN. Melting points were recorded on a Haake-Buchler apparatus in sealed capillaries and are uncorrected. Mass spectra were run with a MS-80 AUTOCONSOLE (Kratos Analytical Instruments) mass spectrometer in the EI mode at 70 eV.

**Preparation of  $[\text{Mes}_2\text{In}(\mu\text{-Te-}n\text{-Pr})]_2$  (**1**).**  $(n\text{-Pr})_2\text{Te}_2$  (0.51 g, 1.50 mmol) was added to a solution of  $\text{Mes}_3\text{In}$  (0.71 g, 1.50 mmol) in hexane (ca. 100 mL). The solution was stirred for four days at room temperature. The yellow precipitate resulting from the reaction was separated from the filtrate and recrystallized from 40 mL of a hot solution of toluene and hexane in 3:1 ratio, giving colorless crystals. Yield 80%. mp: 234 °C. Anal. for  $\text{C}_{21}\text{H}_{29}\text{InTe}$  calcd (found): C, 48.15 (48.16); H, 5.58 (5.68).  $^1\text{H-NMR}$  ( $\text{C}_6\text{D}_6$ ,  $\delta$ , ppm): 2.14 (s, 6H, *p*- $\text{CH}_3$  of InMes), 2.69 (s, 12H, *o*- $\text{CH}_3$  of InMes), 6.77 (s, 4H, MesIn); 0.39 (t, 3H), 1.06 (m, 2H), 2.44 (t, 2H, Te-*n*Pr).  $^{13}\text{C}\{^1\text{H}\}\text{-NMR}$  ( $\text{C}_6\text{D}_6$ ,  $\delta$ , ppm): 21.1 (*p*- $\text{CH}_3$  of Mes), 27.1 (*o*- $\text{CH}_3$  of Mes), 127.7, 137.7, 138.7, 144.3, 145.5 (MesIn); 25.9, 15.7, 10.1 (*n*-PrTe). Mass spectral data (EI mode): peaks at 353, 342, 299, 213, 171, 119, 105, 91 *m/e* corresponding to fragments  $\text{Mes}_2\text{In}^{+}$ ,  $n\text{-Pr}_2\text{Te}_2^{+}$  and other rearrangement products or fragments.

(14) Shriver, D. F.; Drezdson, M. A. *The Manipulation of Air-Sensitive Compounds*; John Wiley & Sons: New York, 1986.

(15) Leman, J. T.; Barron, A. R. *Organometallics* 1989, 8, 2214.

\* Abstract published in *Advance ACS Abstracts*, December 1, 1994.

(1) MacInnes, A. N.; Power, M. B.; Barron, A. R. *Chem. Mater.* 1992, 4, 11.

(2) MacInnes, A. N.; Cleaver, W. M.; Barron, A. R.; Power, M. B.; Hepp, A. F. *Adv. Mater. Opt. Electron.* 1992, 1, 229.

(3) Gysling, H. J.; Wernberg, A. A.; Blanton, T. N. *Chem. Mater.* 1992, 4, 900.

(4) Oliver, J. P.; Kumar, R.; Taghiof, M. In *Coordination Chemistry of Aluminum*; Robinson, G. H., Ed.; VCH: New York, 1993; pp 167-195.

(5) Oliver, J. P.; Kumar, R. *Polyhedron* 1990, 9, 409.

(6) Cowley, A. H.; Jones, R. A.; Harris, P. R.; Atwood, D. A.; Contreras, L.; Burek, C. J. *Angew. Chem., Int. Ed. Engl.* 1991, 30, 1143.

(7) Power, M. B.; Ziller, J. W.; Barron, A. R. *Organometallics* 1992, 11, 2783.

(8) Power, M. B.; Ziller, J. W.; Tyler, A. N.; Barron, A. R. *Organometallics* 1992, 11, 1055.

(9) Beachley, O. T., Jr.; Lee, J. C., Jr.; Gysling, H. J.; Chao, S.-H. L.; Churchill, M. R.; Lake, C. H. *Organometallics* 1992, 11, 3144.

(10) Beachley, O. T., Jr.; Chao, S.-H. L.; Churchill, M. R.; Lake, C. H. *Organometallics* 1993, 12, 5025.

(11) Banks, M. A.; Beachley, O. T., Jr.; Gysling, H. J.; Luss, H. R. *Organometallics* 1990, 9, 1979.

(12) Uhl, W.; Layh, M.; Becker, G.; Klinkhammer, K. W.; Hildenbrand, T. *Chem. Ber.* 1992, 125, 1547.

(13) Merzweiler, K.; Rudolph, F.; Brands, L. Z. *Naturforsch.* 1992, 49b, 470.

**Table 1. Selected Experimental Parameters for the X-ray Diffraction Study of [Mes<sub>2</sub>In(μ-Te-*n*-Pr)]<sub>2</sub> (1) and [Mes<sub>2</sub>In(μ-TePh)]<sub>2</sub> (2)**

compound	[Mes <sub>2</sub> In(μ-Te- <i>n</i> -Pr)] <sub>2</sub> (1)	[Mes <sub>2</sub> In(μ-TePh)] <sub>2</sub> (2)
empirical formula	C <sub>21</sub> H <sub>29</sub> TeIn	C <sub>24</sub> H <sub>27</sub> TeIn
formula wt (amu)	523.88	557.90
space group	P1̄ (No. 2)	P2 <sub>1</sub> /c (No. 14)
<i>a</i> (Å)	9.176(1)	8.778(1)
<i>b</i> (Å)	10.687(1)	23.283(9)
<i>c</i> (Å)	11.771(2)	11.278(2)
α (deg)	91.79(1)	
β (deg)	109.97(1)	101.74(1)
γ (deg)	99.68(1)	
vol (Å <sup>3</sup> )	1064.4(2)	2261(1)
Z	2	4
dens. (calcd) (g cm <sup>-3</sup> )	1.642	1.642
radiation type	Mo Kα (λ = 0.71073 Å)	Mo Kα (λ = 0.71073 Å)
	graphite monochromator	graphite monochromator
temp (°C)	20	22
linear absn	24.52	23.07
coefficient (μ) (cm <sup>-1</sup> )		
$R = \frac{\sum(F_o - F_c)}{\sum F_o}$	3.1	3.1
$R_w = \frac{[\sum w(F_o - F_c)^2]}{[\sum w F_o^2]}^{1/2}$	3.0	3.1
$w^{-1} = \sigma^2(F_o) + 0.00005(F_o)^2$		

**Preparation of [Mes<sub>2</sub>In(μ-TePh)]<sub>2</sub> (2).** In a procedure similar to that for **1**, hexane was added to a mixture of Mes<sub>2</sub>In (0.75 g, 1.58 mmol) and Ph<sub>2</sub>Te<sub>2</sub> (0.65 g, 1.58 mmol). The solution was stirred for three days at room temperature. The yellow precipitate resulting from the reaction was separated from the filtrate and recrystallized from a hot solution of toluene and hexane (3:1), giving yellow crystals. Yield: 80%. mp: 153 °C dec. Anal. for C<sub>24</sub>H<sub>27</sub>InTe calcd (found): C, 51.67 (51.45); H, 4.88 (4.96). <sup>1</sup>H NMR (C<sub>6</sub>D<sub>6</sub>, δ, ppm): 2.11 (s, 6H, *p*-CH<sub>3</sub> of InMes), 2.54 (s, 12H, *o*-CH<sub>3</sub> of InMes), 6.45–7.2 (m, 5H, phenyl group) 6.64 (s, 4H, Mes); <sup>13</sup>C{<sup>1</sup>H} NMR (C<sub>6</sub>D<sub>6</sub>, δ, ppm): 21.1(*p*-CH<sub>3</sub> of Mes), 27.1 (*o*-CH<sub>3</sub> of Mes), 127.1, 127.8, 128.7, 137.7, 138.7, 144.3, 145.9 (PhTe + MesIn). <sup>125</sup>Te NMR (C<sub>6</sub>D<sub>6</sub>, δ, ppm): 106. Mass spectral data (EI mode): peaks at 353, 326, 311, 284, 246, 204, 154, 119, 105, 91 *m/e* dominated by Mes<sub>2</sub>In<sup>+</sup> and fragments of lower mass resulting from decomposition of the molecule under the conditions used.

**Attempted Synthesis of [Mes<sub>2</sub>In(μ-TeMes)]<sub>2</sub>.** The reaction of Mes<sub>2</sub>In (1.00 g, 2.12 mmol) with elemental tellurium (0.27 g, 2.12 mmol) was attempted in refluxing toluene under conditions used to prepare [Mes<sub>2</sub>In(μ-SeMes)]<sub>2</sub><sup>16</sup> and under more forcing conditions of refluxing mesitylene (bp 164 °C), but no reaction was observed after two days.

**X-ray Structure Determination of [Mes<sub>2</sub>In(μ-Te-*n*-Pr)]<sub>2</sub> (1) and [Mes<sub>2</sub>In(μ-TePh)]<sub>2</sub> (2).** X-ray quality crystals of **1** and **2** were grown using the procedures described in the Experimental Section. Suitable crystals were mounted in thin-walled capillary tubes in the dry box, plugged with grease, removed from the dry box, flame-sealed, mounted on a goniometer head and placed on a P2<sub>1</sub> (1) or P3/V (2) diffractometer for data collection. **1** was triclinic and assigned to the space group P1̄ (No. 2) based on successful refinement of the structure. **2** was monoclinic and assigned to P2<sub>1</sub>/c (No. 14) on the basis of systematic absences. Lattice constants were verified by axial photographs. Data reduction, structure solution, and full matrix least-squares refinement for **1** were carried out using SHELXTL PC.<sup>17</sup> Data reduction for **2** was carried out using the SHELXTL software.<sup>18</sup> Full-matrix least-squares refinement was carried out using SHELX-76.<sup>19</sup> Direct method routines produced acceptable solutions for the struc-

(16) Rahbarnoohi, H.; Kumar, R.; Heeg, M. J.; Oliver, J. P. Unpublished.

(17) SHELXTL PC; Siemens Analytical X-Ray Instruments, Inc.: Madison, WI, 1990.

(18) Sheldrick, G. M. SHELXTL; University of Göttingen: Göttingen, Federal Republic of Germany, 1978.

(19) Sheldrick, G. M. SHELX-76; University Chemical Laboratory: Cambridge, England, 1976.

**Table 2. Atomic Coordinates (×10<sup>4</sup>) and Isotropic Thermal Parameters (×10<sup>3</sup>) for the Non-Hydrogen Atoms of [Mes<sub>2</sub>In(μ-Te-*n*-Pr)]<sub>2</sub> (1)**

atom	<i>x</i>	<i>y</i>	<i>z</i>	U <sub>eq</sub> <sup>a</sup>
Te(1)	-1186(1)	1445(1)	232(1)	45(1)
In(1)	1622(1)	525(1)	1676(1)	43(1)
C(1)	3314(6)	2295(5)	1969(5)	42(2)
C(2)	4258(7)	2628(5)	1272(5)	49(3)
C(3)	5109(7)	3872(6)	1406(6)	59(3)
C(4)	5071(8)	4794(6)	2220(7)	63(3)
C(5)	4205(8)	4466(6)	2959(6)	62(3)
C(6)	3322(7)	3218(5)	2843(5)	51(3)
C(7)	4390(8)	1668(6)	374(6)	73(3)
C(8)	6027(10)	6134(7)	2357(8)	96(4)
C(9)	2406(9)	2932(6)	3674(6)	72(4)
C(10)	1572(7)	-650(5)	3134(5)	40(2)
C(11)	278(7)	-990(5)	3517(5)	46(2)
C(12)	349(8)	-1821(6)	4410(5)	57(3)
C(13)	1686(9)	-2338(6)	4956(5)	63(3)
C(14)	2947(8)	-1975(6)	4583(6)	60(3)
C(15)	2930(7)	-1152(5)	3702(5)	49(3)
C(16)	-1225(8)	-493(6)	2977(6)	63(3)
C(17)	1724(11)	-3235(8)	5916(7)	106(5)
C(18)	4378(8)	-835(6)	3344(6)	67(3)
C(19)	113(7)	2871(5)	-529(5)	53(3)
C(20)	-914(8)	3701(5)	-1318(6)	61(3)
C(21)	6(10)	4612(6)	-1901(7)	87(4)

$$^a U_{eq} = 1/3 \sum_i \sum_j U_{ij} a_i^* a_j^* \bar{a}_i \bar{a}_j.$$

**Table 3. Atomic Coordinates and Isotropic Thermal Parameters for the Non-Hydrogen Atoms of [Mes<sub>2</sub>In(μ-TePh)]<sub>2</sub> (2)**

atom	<i>x</i>	<i>y</i>	<i>z</i>	U <sub>eq</sub> <sup>a</sup>
Te1	0.31383(4)	0.45872(2)	0.55696(3)	0.0481(1)
In1	0.35329(4)	0.52856(2)	0.35073(3)	0.0464(1)
C1	0.2759(6)	0.6174(2)	0.3534(5)	0.048(2)
C2	0.1934(7)	0.6403(2)	0.4348(5)	0.056(2)
C3	0.1503(8)	0.6980(3)	0.4262(6)	0.072(3)
C4	0.1869(9)	0.7331(3)	0.3398(7)	0.079(3)
C5	0.2662(8)	0.7104(3)	0.2575(6)	0.074(3)
C6	0.3113(7)	0.6529(3)	0.2632(5)	0.059(2)
C7	0.1464(8)	0.6047(3)	0.5328(6)	0.077(3)
C8	0.137(1)	0.7954(3)	0.3308(8)	0.131(5)
C9	0.3982(9)	0.6301(3)	0.1702(6)	0.084(3)
C10	0.2774(6)	0.4731(2)	0.1945(4)	0.047(2)
C11	0.1196(6)	0.4621(2)	0.1634(5)	0.053(2)
C12	0.0610(7)	0.4276(3)	0.0633(6)	0.063(2)
C13	0.1559(8)	0.4039(3)	-0.0059(5)	0.064(2)
C14	0.3128(7)	0.4145(3)	0.0257(5)	0.062(2)
C15	0.3756(7)	0.4489(3)	0.1232(5)	0.058(2)
C16	0.0067(7)	0.4851(3)	0.2361(6)	0.071(3)
C17	0.0905(9)	0.3659(3)	-0.1131(6)	0.096(3)
C18	0.5500(7)	0.4591(3)	0.1513(6)	0.075(3)
C19	0.3285(7)	0.3738(2)	0.4936(6)	0.061(2)
C20	0.2736(9)	0.3303(3)	0.5553(7)	0.098(4)
C21	0.291(1)	0.2742(4)	0.520(1)	0.138(6)
C22	0.357(1)	0.2615(4)	0.424(1)	0.135(6)
C23	0.409(1)	0.3050(4)	0.3628(9)	0.121(5)
C24	0.3971(9)	0.3610(3)	0.3985(7)	0.084(3)

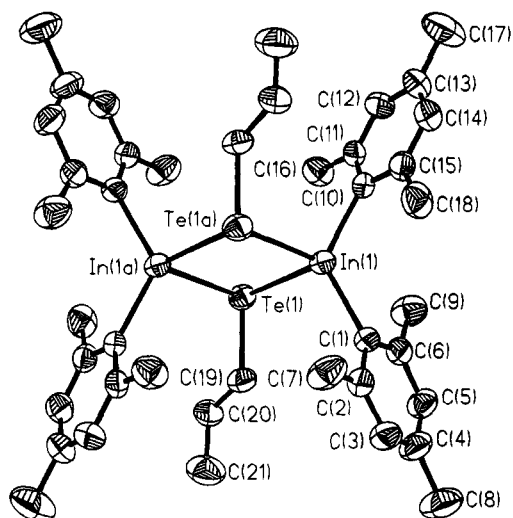
$$^a U_{eq} = 1/3 \sum_i \sum_j U_{ij} a_i^* a_j^* \bar{a}_i \bar{a}_j.$$

tures, yielding positions for some of the non-hydrogen atoms while other atoms were located during subsequent refinement. In each case the absorption corrections were semiempirical from ψ-scans, and no correction for secondary extinction was made. The hydrogen atom positions in all compounds were calculated and riding on the carbon atoms to which they were bound. Selected parameters from the crystal structure determinations are presented in Table 1. The atomic coordinates and isotropic thermal parameters for **1** and **2** are listed in Tables 2 and 3.

## Results and Discussion

**Syntheses.** The *n*-propyl and phenyl tellurolates of sterically-hindered mesitylindium, **1** and **2**, can be





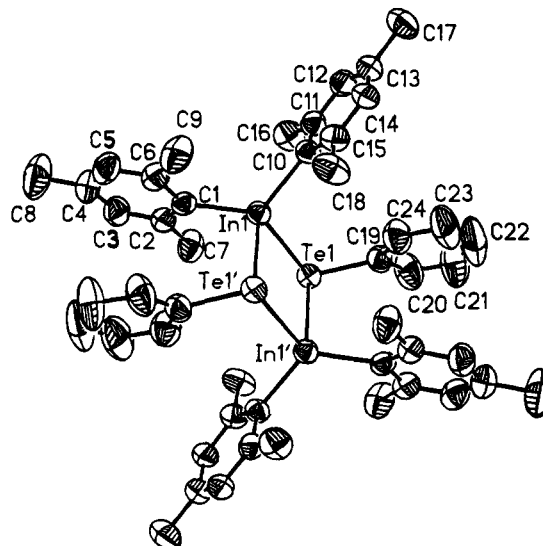
**Figure 1.** A diagram (50% thermal ellipsoids) of  $[\text{Mes}_2\text{In}(\mu\text{-Te-}n\text{-Pr})]_2$  (**1**) showing the atom labeling scheme. Hydrogen atoms have been omitted for clarity.

prepared at room temperature by reduction of the Te–Te bond of the dichalcogenides,  $\text{R}_2\text{Te}_2$  ( $\text{R} = n\text{-Pr, Ph}$ ) with  $\text{Mes}_3\text{In}$  in hexane. The reaction likely proceeds through formation of a weakly associated addition complex followed by a migration of groups, but the mechanism for this process has not been established. We made no attempt to isolate and identify the telluro ethers from these reactions due to their inherent toxicity and foul smell. An alternate path for the formation of these compounds by direct reaction of  $\text{Mes}_3\text{In}$  with elemental Te was explored, but no reaction was observed between  $\text{Mes}_3\text{In}$  and tellurium.

Under similar conditions the reaction of  $\text{Me}_3\text{In}$  with  $\text{Ph}_2\text{Te}_2$  resulted in mixtures of products which were insoluble in aromatic solvents (benzene, toluene) and the donor solvent THF and were not characterized further.

The tellurolato complexes,  $[\text{Mes}_2\text{In}(\mu\text{-TeR})]_2$ , are isolated as creamy-yellow solids which decompose slowly on contact with air and moisture. They show poor solubility in pentane and hexane but are fairly soluble in aromatic solvents such as benzene and toluene. They are thermally unstable in solution, decomposing in hot toluene to give an insoluble creamy-yellow solid. The chemical analyses are excellent. Mass spectral data obtained by direct insertion of the solid into a heated inlet were dominated by the  $\text{Mes}_2\text{In}^+$  fragment but showed other species derived from the parent molecule. No peak for the dimeric species was observed for either compound under the conditions used.

**Structure and Bonding in  $[\text{Mes}_2\text{In}(\mu\text{-Te-}n\text{-Pr})]_2$  (**1**) and  $[\text{Mes}_2\text{In}(\mu\text{-TePh})]_2$  (**2**).** The structures of **1** and **2** represent the first organoindium tellurolates to be reported. Diagrams of the molecular units for **1** and **2** are shown in Figures 1 and 2. Selected bond distances and bond angles are presented in Table 4. The asymmetric unit in **1** is a  $\text{Mes}_2\text{InTe-}n\text{-Pr}$  moiety which generates the dimeric molecule through the inversion center. The asymmetric unit for **2** is a  $\text{Mes}_2\text{InTePh}$  unit with a  $Z$  of 4 in the unit cell. Overall structural features such as aggregation, the planarity of the  $(\text{InTe})_2$  ring, and the *anti* orientation of the RTe ligands are very similar to those observed in other Group 13 derivatives. Two views of **1** are shown in diagram I (Figure 3); I-A



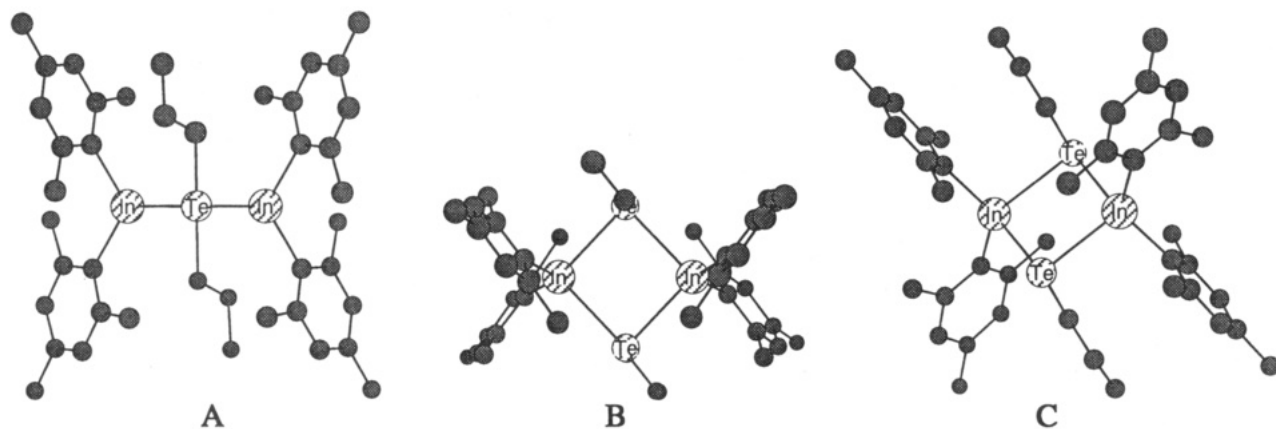
**Figure 2.** A diagram (50% thermal ellipsoids) of  $[\text{Mes}_2\text{In}(\mu\text{-TePh})]_2$  (**2**) showing the atom labeling scheme. Hydrogen atoms have been omitted for clarity.

**Table 4.** Selected Bond Distances (Å) and Bond Angles (deg) for  $[\text{Mes}_2\text{In}(\mu\text{-TeR})]_2$

	$[\text{Mes}_2\text{In}(\mu\text{-Te-}n\text{-Pr})]_2$ , <b>1</b>	$[\text{Mes}_2\text{In}(\mu\text{-TePh})]_2$ , <b>2</b>
In1–In1' (separation)	4.033(1)	4.030(1)
In1–Te1	2.906(1)	2.919(1)
In1–Te1'	2.911(1)	2.911(1)
In1–C1	2.170(5)	2.179(5)
In1–C10	2.163(6)	2.179(4)
Te1–In1–Te1'	92.2(1)	92.5(1)
In1–Te1–In1'	87.8(1)	87.5(1)
C1–In1–C10	122.1(2)	121.9(2)
In1–Te1–C	93.8(2)	103.0(2)
In1'–Te1–C	92.8(2)	95.2(2)
$\Sigma \angle \text{Te}$	274.4	285.7

is a view along the Te–Te vector, and I-B is perpendicular to the Te–Te vector. They show the relative orientations of the organic groups to the  $(\text{InTe})_2$  ring in the solid state. The shortest nonbinding interactions (3.2 to 3.4 Å) are between the *o*-methyl groups on the mesitylene rings and the indium atoms. All other distances are nearly 4 Å or greater, indicating no significant steric effects within the molecule. The organic groups on the Te atoms are twisted so that the plane described by the three carbon atoms is nearly parallel to the plane of the closest mesitylene group (I-C). The two mesitylene groups are rotated so that their planes are nearly perpendicular. The organic groups in **2** are oriented in a similar way. The geometry around Te is pyramidal ( $\Sigma \angle \text{Te} = 274.4^\circ$ ) in **1** and ( $\Sigma \angle \text{Te} = 285.7^\circ$ ) in **2**. The In1–Te1 and In1–Te1' bond distances are 2.906(1) and 2.911(1) Å for **1** and 2.919(1) and 2.911(1) Å for **2**. A slightly longer In–Te bond distance of 3.01 Å can be estimated from a sum of the ionic radii of  $\text{In}^{3+}$  and  $\text{Te}^{2-}$ . A shorter range of 2.839–2.898 Å for In–Te has been reported in cubane  $\{[\text{Cp}(\text{CO})_3\text{Mo}]_4\text{In}_4\text{Te}_4\}$ .<sup>13</sup> The C–Te bond distances of 2.115(6) and 2.178(6) Å are similar to those found in two- or three-coordinate bridging tellurium atoms in organotellurolates.<sup>11</sup> The In–C bond distances range from 2.163(6) to 2.179(5) Å and are comparable to those found in related organoindium compounds.<sup>15,20</sup> The C–In–C

(20) Leman, J. T.; Ziller, J. W.; Barron, A. R. *Organometallics* **1991**, *10*, 1766.



**Figure 3.**

angles are  $122.1(2)^\circ$  in **1** and  $121.9^\circ$  in **2** and, again, are comparable to those observed in other  $\text{Mes}_2\text{In}$  derivatives. A planar core is found in  $[\text{Mes}_2\text{In}(\mu\text{-Cl})_2]_2$ ,<sup>15</sup> but folded conformations are reported for  $[\text{Np}_2\text{In}(\mu\text{-SePh})_2]$ ,<sup>9</sup>  $\text{Np}_2\text{In}(\mu\text{-SePh})(\mu\text{-P-}t\text{-Bu}_2)\text{InNp}_2$  (Np = neopentyl),<sup>10</sup> and  $[\text{Mes}_2\text{In}(\mu\text{-I})_2]_2$ .<sup>15</sup>

### Conclusion

The dimesitylindium tellurolates have been prepared by the reaction of  $\text{Mes}_3\text{In}$  with dichalcogenides,  $\text{R}_2\text{Te}_2$ , under mild conditions. This synthetic route provides an alternative method to obtain these complexes, especially in those cases where the protic substrates,  $\text{REH}$ , are unstable. These derivatives are dimeric in the solid state. The bridging hetero atom of the central  $(\text{InTe})_2$  core is generally pyramidal with angles between the substituent groups approaching  $90^\circ$  as expected for systems using pure p orbitals. In comparison with the earlier chalcogens, we see decreasing angles between the substituents and increasing p-character in the order  $\text{S} < \text{Se} < \text{Te}$ . This structural feature is in contrast to those of the oxygen-bridged derivatives which generally adopt a planar configuration. The central ring is strictly planar with *trans* orientation of the bridging ligands. With the structural data available, it is very difficult to make any prediction about the conformation of the core. It seems reasonable to state that the packing

forces in the crystals may be partially responsible in determining the core geometry. Such dimers may serve as molecular precursors to their materials under OMCVD studies. In this context, our preliminary studies on the pyrolysis of  $[\text{Mes}_2\text{In}(\mu\text{-TePh})_2]$  (**2**) are very encouraging. Heating **2** at  $600^\circ\text{C}$  under dynamic vacuum yields a metallic film. Powder X-ray diffraction pattern on this material shows a mixture of various forms of indium telluride. The predominant product formed was  $\text{In}_2\text{Te}_3$  (JCPD, No. 33-1488). Other unidentified species were also present. Further studies on the suitability of these precursors to give binary materials are in progress.

**Acknowledgment** is made to the donors of the Petroleum Research Fund, administered by the American Chemical Society, for support of this research. Mike Fuerth, Department of Chemistry, University of Windsor, is acknowledged for providing the  $^{125}\text{Te}$  NMR spectrum.

**Supplementary Material Available:** Complete listings of bond distances and bond angles, anisotropic thermal parameters for the heavy atoms and hydrogen atom positional parameters (9 pages). See any current masthead page for ordering information.

OM940704F

# Reactions of Isocyanide-Substituted Dimanganese Carbonyl Complexes with Alkynes. Alkyne–Isocyanide Coupling and the Synthesis of Metalated N-Substituted Pyridines

Richard D. Adams\* and Mingsheng Huang

Department of Chemistry and Biochemistry, University of South Carolina,  
Columbia, South Carolina 29208

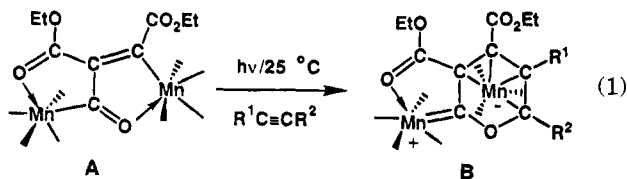
Received September 7, 1994<sup>®</sup>

When activated by Me<sub>3</sub>NO in the presence of MeCN, the compounds Mn<sub>2</sub>(CO)<sub>9</sub>(CNR) (**1a,b**; R = Me, Ph) react with MeO<sub>2</sub>CC≡CCO<sub>2</sub>Me to yield the new compounds Mn<sub>2</sub>(CO)<sub>8</sub>[μ-(MeO<sub>2</sub>C)C=C(CO<sub>2</sub>Me)C=NR] (**2a,b**; R = Me, Ph) in yields of 40% and 32%, respectively. Minor products, Mn<sub>2</sub>(CO)<sub>7</sub>(CNR)[μ-(MeO<sub>2</sub>C)C=C(CO<sub>2</sub>Me)C=O] (**3a,b**; R = Me, Ph) were also formed. Compound **2a** was characterized crystallographically. The structure shows that the isocyanide ligand was coupled to the alkyne, and the nitrogen atom is coordinated to one of the manganese atoms to form a five-membered cyclo-mangana enimine ring. One of the carboxylate groups is coordinated to the other manganese atom. The compounds Mn<sub>2</sub>(CO)<sub>7</sub>[μ-η<sup>4</sup>-CN(Me)CHCHC(CO<sub>2</sub>Me)C(CO<sub>2</sub>Me)] (**4a**), Mn<sub>2</sub>(CO)<sub>7</sub>[μ-η<sup>4</sup>-CN(Ph)CHCHC(CO<sub>2</sub>Me)C(CO<sub>2</sub>Me)] (**4b**), and Mn<sub>2</sub>(CO)<sub>7</sub>[μ-η<sup>4</sup>-CN(Me)CHC(CO<sub>2</sub>Me)C(CO<sub>2</sub>Me)C(CO<sub>2</sub>Me)] (**4c**) were prepared in yields of 27%, 32%, and 31%, respectively, by treatment of **2a,b** with C<sub>2</sub>H<sub>2</sub> and of **2a** with HC≡C(CO<sub>2</sub>Me) in the presence of UV irradiation. Compound **4a** was characterized crystallographically. This compound contains a metalated N-methylpyridine ring formed by a 1,4-cycloaddition of the alkyne to the enimine grouping in compound **2a**. One of the metal atoms was shifted to a π-bonding coordination involving four of the carbon atoms of the pyridine ring. Crystal data: for **2a** space group P2<sub>1</sub>/n, a = 10.981(4) Å, b = 11.425(2) Å, c = 16.780(5) Å, β = 92.00(3)°, Z = 4, 1526 reflections, R = 0.041; for **4a** space group P2<sub>1</sub>/n, a = 9.655(2) Å, b = 17.538(5) Å, c = 12.599(1) Å, β = 107.03(1)°, Z = 4, 1950 reflections, R = 0.033.

## Introduction

Metal-assisted coupling reactions between alkynes and CO have provided routes for the synthesis of a wide variety of new organic ligands<sup>1</sup> and new organic molecules.<sup>2</sup> Recent studies have shown that ligands formed by the coupling of alkynes to CO in the presence of dinuclear manganese carbonyl complexes frequently results in the formation of groupings in which the oxygen atom of the CO group is coordinated to one or both of the metal atoms.<sup>3–6</sup> This coordination can have a significant effect upon the subsequent reactivity of the

complex and the ligand grouping itself.<sup>7</sup> For example, we have recently shown that the metalated enone complex Mn<sub>2</sub>(CO)<sub>8</sub>[μ-(EtO<sub>2</sub>C)C=C(CO<sub>2</sub>Et)C=O] (**A**) will decarbonylate and add an alkyne in the presence of UV irradiation to yield complexes containing metalated pyran rings (e.g. Mn<sub>2</sub>(CO)<sub>7</sub>[μ-η<sup>4</sup>-COCR<sup>2</sup>CR<sup>1</sup>C(CO<sub>2</sub>Et)C(CO<sub>2</sub>Et)] (**B**)) by a 1,4-cycloaddition of alkynes to the enone grouping in **A** (eq 1).



Studies of the coupling of alkynes to isocyanides have been far fewer.<sup>8</sup> We have now found that the compounds Mn<sub>2</sub>(CO)<sub>9</sub>(CNR) (**1a,b**; R = Me, Ph) can be activated by treatment with Me<sub>3</sub>NO in the presence of NCMe toward reaction with MeO<sub>2</sub>CC≡CCO<sub>2</sub>Me. The principal products **2** obtained from these reactions contain cyclometalated enimine groupings formed by the

<sup>®</sup> Abstract published in *Advance ACS Abstracts*, December 1, 1994.

(1) (a) Dyke, A. F.; Knox, S. A. R.; Naish, P. J.; Taylor, G. E. *J. Chem. Soc., Dalton Trans.* **1982**, 1297. (b) Finimore, S. R.; Knox, S. A. R.; Taylor, G. E. *J. Chem. Soc., Dalton Trans.* **1982**, 1783. (c) Hogarth, G.; Kayser, F.; Knox, S. A. R.; Morton, D. A. V.; Orpen, A. G.; Turner, M. L. *J. Chem. Soc., Chem. Commun.* **1988**, 358. (d) Gracey, B. P.; Knox, S. A. R.; Macpherson, K. A.; Orpen, A. G.; Stobart, S. R. *J. Chem. Soc., Dalton Trans.* **1985**, 1935. (e) Dickson, R. S. *Polyhedron* **1991**, *10*, 1995. (f) Johnson, K. A.; Gladfelter, W. L. *Organometallics* **1992**, *11*, 2534. (g) Takats, J. *J. Cluster Sci.* **1992**, *3*, 479.

(2) (a) Shore, N. E. *Chem. Rev.* **1988**, *88*, 1081. (b) Colquhoun, H. M.; Thompson, D. J.; Twigg, M. V. *Carbonylation: Direct Synthesis of Carbonyl Compounds*; Plenum Press: New York, 1991. (c) Pino, P.; Braca, G. In *Organic Synthesis via Metal Carbonyls*; Wender, I., Pino, P., Eds.; Wiley: New York, 1977; Vol. 2, pp 420–516.

(3) (a) Adams, R. D.; Chen, G.; Chen, L.; Wu, W.; Yin, J. *Organometallics* **1993**, *12*, 3431. (b) Adams, R. D.; Chen, G.; Chen, L.; Wu, W.; Yin, J. *J. Am. Chem. Soc.* **1991**, *113*, 9406.

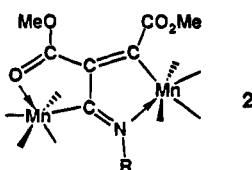
(4) Adams, R. D.; Chen, L.; Wu, W. *Organometallics* **1993**, *12*, 4112. (5) García Alonso, F. J.; Riera, V.; Ruiz, M. A.; Tiripicchio, A.; Camellini, M. T. *Organometallics* **1992**, *11*, 370.

(6) Derunov, V. V.; Shilova, O. S.; Batsanov, A. S.; Yannovskii, A. I.; Struchkov, Yu. T.; Kolobova, N. E. *Metalloorg. Khim.* **1991**, *4*, 1166.

(7) (a) Adams, R. D.; Chen, L.; Huang, M. *Organometallics* **1994**, *13*, 2696. (b) Adams, R. D.; Chen, L. *J. Am. Chem. Soc.* **1994**, *116*, 4467.

(8) (a) Singleton, E.; Oosthuizen, H. E. *Adv. Organomet. Chem.* **1983**, *22*, 209. (b) Otsuka, S.; Nakamura, A. *Adv. Organomet. Chem.* **1976**, *14*, 245. (c) Jautelat, M.; Ley, K. *Synthesis* **1970**, 593.

coupling of the alkyne to the isocyanide ligand and the coordination of the nitrogen atom to one of the manganese atoms.



Like compound **A**, these compounds also add a second alkyne in the presence of UV irradiation. These products contain metalated *N*-substituted pyridine ligands formed by a 1,4-cycloaddition of the alkyne to the enimine grouping in the compounds **2**. The results of this study are reported here.

### Experimental Section

Unless otherwise indicated, all reactions were carried out under an atmosphere of nitrogen. Hexane was freshly distilled over Na prior to use. MeCN and CH<sub>2</sub>Cl<sub>2</sub> solvents were dried over CaH<sub>2</sub>. HC≡CH was purchased from Union Carbide Inc.; HC≡CCO<sub>2</sub>Me (99%) and MeO<sub>2</sub>CC≡CCO<sub>2</sub>Me (99%) were purchased from Aldrich Co. and were used without further purification. Trimethylamine *N*-oxide dihydrate was dehydrated by using a Dean-Stark apparatus with benzene as the solvent prior to use. CNMe,<sup>9</sup> CNPh,<sup>9</sup> and Mn<sub>2</sub>(CO)<sub>9</sub>(NCMe)<sup>10</sup> were prepared by the reported procedures. UV irradiations were performed on solutions in Pyrex glassware by using an externally positioned 1000-W high-pressure mercury lamp purchased from Cooper Lighting, Vicksburg, MS. TLC separations were performed in air using silica gel (60 Å, F<sub>254</sub>) on plates (Whatman, 0.25 mm). IR spectra were recorded on a Nicolet 5DXB FT-IR spectrophotometer. <sup>1</sup>H NMR spectra were taken at 400 MHz on a Bruker Am-400 spectrometer. Elemental analyses were performed by Oneida Research Services Inc., Whitesboro, NY.

**Preparation of Mn<sub>2</sub>(CO)<sub>9</sub>(CNMe) (1a) and Mn<sub>2</sub>(CO)<sub>9</sub>(CNPh) (1b).** (a) Mn<sub>2</sub>(CO)<sub>9</sub>(CNMe). A solution of a 250.0-mg amount (0.62 mmol) of Mn<sub>2</sub>(CO)<sub>9</sub>(NCMe) and 38.9 μL (0.74 mmol) of CNMe in 200 mL of CH<sub>2</sub>Cl<sub>2</sub> was heated to reflux for 2 h. After the mixture was cooled to room temperature, the solvent was removed *in vacuo*, and the residue was isolated by column chromatography. Elution with a hexane/CH<sub>2</sub>Cl<sub>2</sub> (5/1) solvent mixture yielded 218.0 mg of yellow Mn<sub>2</sub>(CO)<sub>9</sub>(CNMe) (**1a**; 87%). It was spectroscopically identical in the IR to the compound with the same formula reportedly obtained from the reaction of Mn<sub>2</sub>(CO)<sub>10</sub> with CNMe.<sup>11</sup>

(b) Mn<sub>2</sub>(CO)<sub>9</sub>(CNPh). By a procedure similar to that described above, Mn<sub>2</sub>(CO)<sub>9</sub>(CNPh) was prepared in 88% yield from the reaction of Mn<sub>2</sub>(CO)<sub>9</sub>(NCMe) and CNPh. It was spectroscopically identical to the material with the same formula reportedly obtained from the reaction of MeMn(CO)<sub>5</sub> with CNPh.<sup>12</sup>

**Reaction of 1a with MeO<sub>2</sub>CC≡CCO<sub>2</sub>Me.** A 300.0-mg amount (0.74 mmol) of **1a** and a 67.3-mg amount (0.90 mmol) of Me<sub>3</sub>NO in 50 mL of MeCN was stirred at 25 °C for 30 min. The solvent was removed under vacuum, and the orange solid was redissolved in 50 mL of CH<sub>2</sub>Cl<sub>2</sub>. To this solution was added a 138.5-μL amount (1.12 mmol) of MeO<sub>2</sub>CC≡CCO<sub>2</sub>Me via a syringe. This solution was then stirred at 25 °C for 20 h. The solvent was removed by rotary evaporation, and the

product was isolated by chromatography over a silica gel column. This yielded 16.2 mg of unreacted **1a** (eluted with a hexane/CH<sub>2</sub>Cl<sub>2</sub> (4/1) solvent mixture) 155.1 mg of yellow Mn<sub>2</sub>(CO)<sub>8</sub>[μ-(MeO<sub>2</sub>C)C≡C(CO<sub>2</sub>Me)C≡NMe] (**2a**; 40% yield (eluted with a hexane/CH<sub>2</sub>Cl<sub>2</sub> (2/1) solvent mixture)) and 45.8 mg of orange Mn(CO)<sub>4</sub>[μ-(MeO<sub>2</sub>C)C≡C(CO<sub>2</sub>Me)C=O]Mn(CO)<sub>3</sub>(CNMe) (**3a**; 12% yield (eluted by a hexane/CH<sub>2</sub>Cl<sub>2</sub> (1/1) solvent mixture)). Spectral data for **2a**: IR (ν<sub>CO</sub> in hexane, cm<sup>-1</sup>) 2095 (w), 2080 (m), 2015 (vs), 1999 (s), 1960 (s), 1951 (m), 1724 (w, br), 1600 (w, br), 1548 (w, br); <sup>1</sup>H NMR (δ in CDCl<sub>3</sub>, ppm) 3.87 (s, 3H, OCH<sub>3</sub>), 3.83 (s, 3H, OCH<sub>3</sub>), 3.78 (s, 3H, NCH<sub>3</sub>). Anal. Calcd (found): C, 37.20 (37.05); H, 1.75 (1.41); N, 2.70 (2.69). Spectral data for **3a**: IR (ν<sub>CO,CN</sub> in hexane, cm<sup>-1</sup>) 2191 (w, br), 2090 (m), 2035 (vs), 2025 (s), 2014 (s), 2004 (s), 1976 (s), 1959 (s), 1918 (s), 1947 (s), 1724 (w, br), 1609 (m, br), 1542 (w, br); <sup>1</sup>H NMR (δ in CDCl<sub>3</sub>, ppm) 3.89 (s, 3H, OCH<sub>3</sub>), 3.84 (s, 3H, OCH<sub>3</sub>), 3.35 (s, 3H, NCH<sub>3</sub>). Anal. Calcd (found): C, 37.20 (36.19); H, 1.75 (1.77); N, 2.70 (2.78).

**Reaction of 1b with MeO<sub>2</sub>CC≡CCO<sub>2</sub>Me.** Using a procedure similar to that described above, a reaction of 370.0 mg (0.796 mmol) of **1b** with 1.5 equiv of MeO<sub>2</sub>CC≡CCO<sub>2</sub>Me yielded two new compounds: Mn<sub>2</sub>(CO)<sub>8</sub>[(MeO<sub>2</sub>C)C≡C(CO<sub>2</sub>Me)C≡NPh] (**2b**; 32% yield) and Mn(CO)<sub>4</sub>[(MeO<sub>2</sub>C)C≡C(CO<sub>2</sub>Me)C=O]Mn(CO)<sub>3</sub>(CNPh) (**3b**; 2% yield). Spectral data for **2b**: IR (ν<sub>CO</sub> in hexane, cm<sup>-1</sup>) 2003 (s), 2079 (m), 2011 (vs), 2005 (vs), 1996 (m), 1968 (s), 1723 (w, br), 1600 (w, br), 1541 (w, br); <sup>1</sup>H NMR (δ in CDCl<sub>3</sub>, ppm) 7.39–7.03 (m, 5H, Ph), 3.90 (s, 3H, OCH<sub>3</sub>), 3.86 (s, 3H, OCH<sub>3</sub>). Spectral data for **3b**: IR (ν<sub>CO,CN</sub> in hexane, cm<sup>-1</sup>) 2143 (w, br), 2090 (m), 2031 (vs), 2015 (s), 2006 (s), 1981 (s), 1960 (s), 1952 (s), 1724 (w, br), 1608 (m, br), 1524 (w, br); <sup>1</sup>H NMR (δ in CDCl<sub>3</sub>, ppm) 7.38 (m, 5H, Ph), 3.90 (s, 3H, OCH<sub>3</sub>), 3.87 (s, 3H, OCH<sub>3</sub>).

**Reaction of the Compounds 2 with Alkynes.** (a) **2a with HC≡CH.** A 50.0-mg (0.097-mmol) amount of **2a** was dissolved in 300 mL of hexane in a 500-mL Pyrex flask. The solution was purged with HC≡CH for 15 min and then exposed to UV light at 25 °C for 5 min. The solvent was then removed under vacuum, and the residue was separated by TLC using a hexane/CH<sub>2</sub>Cl<sub>2</sub> (1/1) solvent mixture. This yielded 2.2 mg of starting material and 13.6 mg of Mn<sub>2</sub>(CO)<sub>7</sub>[μ-η<sup>4</sup>-CN(Me)CHCHC(CO<sub>2</sub>Me)C(CO<sub>2</sub>Me)] (**4a**) in 27% yield. Spectra data for **4a**: IR (ν<sub>CO</sub> in hexane, cm<sup>-1</sup>) 2100 (w), 2021 (s), 2008 (m), 1953 (m), 1935 (m), 1921 (m), 1730 (w, br), 1577 (w, br); <sup>1</sup>H NMR (δ in CDCl<sub>3</sub>, ppm) 6.05 (d, <sup>3</sup>J<sub>H-H</sub> = 4.7 Hz, 1H, CH), 4.16 (d, <sup>3</sup>J<sub>H-H</sub> = 4.7 Hz, 1H, CH), 3.88 (s, 3H, OCH<sub>3</sub>), 3.73 (s, 3H, OCH<sub>3</sub>), 3.32 (s, 3H, NCH<sub>3</sub>). Anal. Calcd (found): C, 39.64 (39.34); H, 2.15 (2.15); N, 2.72 (2.76).

(b) **2b with HC≡CH.** Using a procedure similar to that described above, irradiation of a solution of 50.0 mg of **2b** in hexane with HC≡CH (slow purge) gave the compound Mn<sub>2</sub>(CO)<sub>7</sub>[μ-η<sup>4</sup>-CN(Ph)CHCHC(CO<sub>2</sub>Me)C(CO<sub>2</sub>Me)] (**4b**) in 32% yield. Spectral data for **4b**: IR (ν<sub>CO</sub> in hexane, cm<sup>-1</sup>) 2097 (w), 2016 (s), 2006 (m), 1968 (m), 1934 (m), 1921 (m), 1730 (w, br), 1577 (w, br); <sup>1</sup>H NMR (δ in CDCl<sub>3</sub>, ppm) 7.51–6.93 (m, 5H, Ph), 6.13 (d, <sup>3</sup>J<sub>H-H</sub> = 4.5 Hz, 1H, CH), 4.43 (d, <sup>3</sup>J<sub>H-H</sub> = 4.5 Hz, 1H, CH), 3.93 (s, 3H, OCH<sub>3</sub>), 3.76 (s, 3H, OCH<sub>3</sub>).

(c) **2a with HC≡CCO<sub>2</sub>Me.** A 20.0-mg amount (0.039 mmol) of **2a** and a 17.4-μL amount of HC≡CCO<sub>2</sub>Me were dissolved in 80 mL of hexane. The solution was exposed to UV light at 25 °C for 5 min. The solvent was then removed under vacuum, and the residue was separated by TLC using a hexane/CH<sub>2</sub>Cl<sub>2</sub> (1/1) solvent mixture to give 0.8 mg of unreacted starting material and 6.9 mg of orange Mn<sub>2</sub>(CO)<sub>7</sub>[μ-η<sup>4</sup>-CN(Me)CHC(CO<sub>2</sub>Me)C(CO<sub>2</sub>Me)C(CO<sub>2</sub>Me)] (**4c**) in 31% yield. Spectral data for **4c**: IR (ν<sub>CO</sub> in hexane, cm<sup>-1</sup>) 2101 (w), 2015 (s), 1958 (m), 1950 (m), 1934 (m), 1733 (w, br), 1716 (w, br), 1585 (w, br); <sup>1</sup>H NMR (δ in CDCl<sub>3</sub>, ppm) 6.58 (s, 1H, CH), 3.89 (s, 3H, OCH<sub>3</sub>), 3.76 (s, 6H, OCH<sub>3</sub>), 3.44 (s, 3H, NCH<sub>3</sub>).

(9) William, P. W.; George, W. G.; Ivar, K. U. *Angew. Chem., Int. Ed. Engl.* **1972**, *11*, 530.

(10) Koelle, U. J. *Organomet. Chem.* **1978**, *155*, 53.

(11) Grant, S.; Newman, J.; Manning, A. R. *J. Organomet. Chem.* **1975**, *96*, C11.

(12) Joshi, K. K.; Pauson, P. L.; Stubbs, W. H. *J. Organomet. Chem.* **1963**, *1*, 51.

**Table 1.** Crystallographic Data for Compounds **2a** and **4a**

	<b>2a</b>	<b>4a</b>
empirical formula	Mn <sub>2</sub> O <sub>12</sub> NC <sub>16</sub> H <sub>9</sub>	Mn <sub>2</sub> O <sub>11</sub> NC <sub>17</sub> H <sub>11</sub>
fw	517.12	515.15
cryst syst	monoclinic	monoclinic
lattice params		
<i>a</i> (Å)	10.981 (4)	9.655(2)
<i>b</i> (Å)	11.425(2)	17.538(5)
<i>c</i> (Å)	16.780(5)	12.599(1)
$\beta$ (deg)	92.00(3)	107.03(1)
<i>V</i> (Å <sup>3</sup> )	2103.9(9)	2039.9(6)
space group	<i>P</i> 2 <sub>1</sub> / <i>n</i> (No. 14)	<i>P</i> 2 <sub>1</sub> / <i>n</i> (No. 14)
<i>Z</i>	4	4
<i>D</i> <sub>calc</sub> , g/cm <sup>3</sup>	1.63	1.68
$\mu$ (Mo K $\alpha$ ) (cm <sup>-1</sup> )	12.62	12.98
temp (°C)	20	20
2 $\theta$ <sub>max</sub> (deg)	42.0	42.0
no. of obs rflns: total; <i>I</i> > 3 $\sigma$ ( <i>I</i> )	2409; 1526	2291; 1950
no. of variables	280	276
residuals: <sup>a</sup> <i>R</i> ; <i>R</i> <sub>w</sub>	0.041; 0.036	0.033; 0.040
goodness-of-fit indicator (GOF)	2.33	2.73
max shift in final cycle	0.00	0.06
largest peak in final diff map (e/Å <sup>3</sup> )	0.26	0.33
abs cor: max/min		empirical, 1.0/0.92

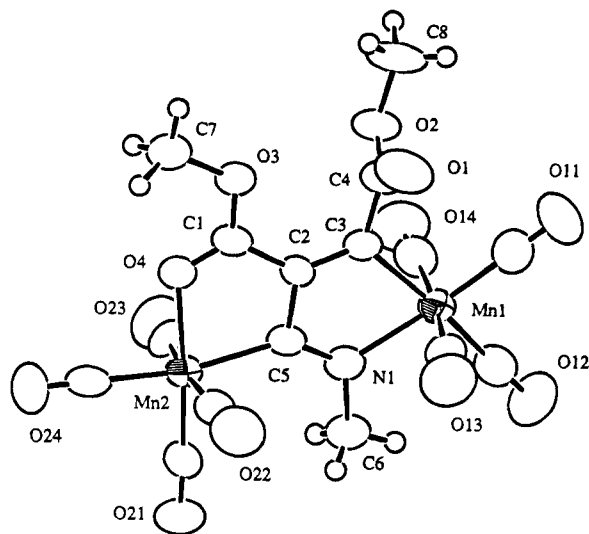
<sup>a</sup>  $R = \sum_{hkl} (|F_o| - |F_c|) / \sum_{hkl} |F_o|$ ;  $R_w = [\sum_{hkl} w(|F_o| - |F_c|)^2 / \sum_{hkl} w F_o^2]^{1/2}$ ,  $w = 1/\sigma^2(F_o)$ ;  $GOF = [\sum_{hkl} (|F_o| - |F_c|)^2 / \sigma(F_o)] / (n_{data} - n_{var})$ .

**Crystallographic Analysis.** Crystals of compounds **2a** and **4a** suitable for X-ray diffraction analysis were grown by slow evaporation of solvent from a solution in a hexane/CH<sub>2</sub>Cl<sub>2</sub> (1/1) solvent mixture at 25 °C. All crystals that were used in diffraction intensity measurements were mounted in thin-walled glass capillaries. Diffraction measurements were made on a Rigaku AFC6S fully automated four-circle diffractometer by using graphite-monochromated Mo K $\alpha$  radiation. The unit cells were determined and refined from 15 randomly selected reflections obtained by using the AFC6 automatic search, center, index, and least-squares routines. All data processing was performed on a Digital Equipment Corp. VAXstation 3520 computer by using the TEXSAN motif structure solving program library obtained from Molecular Structure Corp., The Woodlands, TX. Neutral atom scattering factors were calculated by the standard procedures.<sup>13a</sup> Anomalous dispersion corrections were applied to all non-hydrogen atoms.<sup>13b</sup> Lorentz/polarization (Lp) corrections were applied to the data for each structure. Full-matrix least-squares refinements minimized the function  $\sum_{hkl} w(|F_o| - |F_c|)^2$ , where  $w = 1/\sigma(F_o)^2$ ,  $\sigma(F_o) = \sigma(F_o^2)/2F_o$ , and  $\sigma(F_o^2) = [\sigma(I_{raw})^2 + (0.02I_{net})^2]^{1/2}/Lp$ . Both structures were solved by a combination of direct methods (MITHRIL) and difference Fourier syntheses. Crystal data and results of the analyses are listed in Table 1.

Both compounds crystallized in the monoclinic crystal system in the space group *P*2<sub>1</sub>/*n* which was identified uniquely from the patterns of systematic absences observed in the data. For both structures least-squares refinements were completed using anisotropic thermal parameters for all non-hydrogen atoms. The positions of all hydrogen atoms were calculated by assuming idealized geometries with C–H = 0.95 Å. The scattering contributions of calculated hydrogen atoms were added to the structure factor calculations, but their positions were not refined.

## Results

When they are treated with Me<sub>3</sub>NO in the presence of NCMe, the compounds Mn<sub>2</sub>(CO)<sub>9</sub>(CNR) (**1a,b**; R = Me, Ph) can be activated toward a subsequent reaction with the alkyne MeO<sub>2</sub>C≡CCO<sub>2</sub>Me. The principal products obtained from this sequence of reactions are

**Figure 1.** ORTEP diagram of Mn<sub>2</sub>(CO)<sub>8</sub>[μ-(MeO<sub>2</sub>C)C=C-(CO<sub>2</sub>Me)C=NMe] (**2a**) showing 50% probability thermal ellipsoids.**Table 2.** Positional Parameters and *B*(eq) Values for **2a**

atom	<i>x</i>	<i>y</i>	<i>z</i>	<i>B</i> (eq), Å <sup>2</sup>
Mn(1)	0.26983(12)	0.15771(11)	0.88986(08)	3.87(6)
Mn(2)	-0.16542(11)	0.25184(11)	0.83054(07)	3.65(6)
O(1)	0.2869(05)	0.4446(06)	1.0021(04)	6.4(4)
O(2)	0.3240(05)	0.4790(05)	0.8725(03)	4.7(3)
O(3)	0.0486(04)	0.5321(05)	0.8968(03)	4.3(3)
O(4)	-0.1049(05)	0.4201(04)	0.8553(03)	4.2(3)
O(11)	0.5134(06)	0.2155(06)	0.9604(04)	8.0(5)
O(12)	0.3601(06)	-0.0834(06)	0.8573(05)	9.4(5)
O(13)	0.1750(06)	0.1094(06)	1.0502(04)	7.8(4)
O(14)	0.3313(06)	0.2353(06)	0.7267(04)	7.1(4)
O(21)	-0.2755(06)	0.0222(05)	0.7988(04)	7.2(4)
O(22)	-0.1854(06)	0.1944(06)	1.0020(04)	7.3(4)
O(23)	-0.1107(06)	0.2701(06)	0.6576(04)	6.7(4)
O(24)	-0.4166(05)	0.3505(6)	0.8088(04)	8.0(4)
N(1)	0.0918(05)	0.1321(05)	0.8493(04)	3.8(4)
C(1)	0.0011(08)	0.4308(07)	0.8760(05)	3.8(5)
C(2)	0.0802(07)	0.3279(07)	0.8782(04)	3.1(4)
C(3)	0.1972(07)	0.3208(06)	0.9013(04)	3.2(4)
C(4)	0.2708(07)	0.4228(07)	0.9342(06)	4.1(5)
C(5)	0.0166(07)	0.2190(07)	0.8515(04)	3.3(4)
C(6)	0.0504(07)	0.0146(07)	0.8251(05)	5.1(5)
C(7)	-0.0350(07)	0.6306(07)	0.8945(05)	4.9(5)
C(8)	0.4024(08)	0.5766(08)	0.8980(06)	7.3(6)
C(11)	0.4201(09)	0.1944(08)	0.9333(05)	5.5(5)
C(12)	0.3229(08)	0.0059(08)	0.8706(06)	6.0(6)
C(13)	0.2135(08)	0.1250(07)	0.9896(06)	4.9(5)
C(14)	0.3100(07)	0.2046(07)	0.7891(06)	4.6(5)
C(21)	-0.2296(07)	0.1098(08)	0.8094(06)	5.2(5)
C(22)	-0.1810(07)	0.2199(07)	0.9368(06)	4.5(5)
C(23)	-0.1303(08)	0.2673(07)	0.7237(06)	4.4(5)
C(24)	-0.3207(08)	0.3143(07)	0.8177(06)	5.1(5)

the new compounds Mn<sub>2</sub>(CO)<sub>8</sub>[μ-(MeO<sub>2</sub>C)C=C(CO<sub>2</sub>Me)C=NR] (**2a,b**; R = Me, Ph) obtained in the yields of 40% and 32%, respectively. An accompanying minor product formulated as Mn<sub>2</sub>(CO)<sub>7</sub>(CNR)[μ-(MeO<sub>2</sub>C)C=C(CO<sub>2</sub>Me)C=O] (**3a,b**; R = Me, Ph) was also obtained in each respective reaction. Compound **2a** was characterized structurally by a single-crystal X-ray diffraction analysis, and an ORTEP drawing of its molecular structure is shown in Figure 1. Final atomic positional parameters are listed in Table 2. Selected interatomic distances and angles are given in Tables 3 and 4, respectively. The molecule contains a enimine grouping that was formed by the coupling of the isocyanide ligand to the alkyne. Formally, this group has been inserted into the metal–metal bond that exists

(13) (a) *International Tables for X-ray Crystallography*; Kynoch Press: Birmingham, England, 1975; Vol. IV, Table 2.2B, pp 99–101. (b) *Ibid.*, Table 2.3.1, pp 149–150.

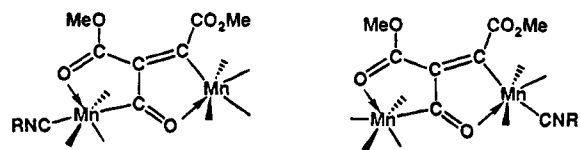
Table 3. Intramolecular Distances for 2a<sup>a</sup>

Mn(1)–N(1)	2.069(6)	O(2)–C(4)	1.367(9)
Mn(1)–C(3)	2.039(7)	O(2)–C(8)	1.463(9)
Mn(1)–C(11)	1.83(1)	O(3)–C(1)	1.311(8)
Mn(1)–C(12)	1.86(1)	O(3)–C(7)	1.452(8)
Mn(1)–C(13)	1.84(1)	O(4)–C(1)	1.209(8)
Mn(1)–C(14)	1.84(1)	O–C (av)	1.130(9)
Mn(2)–O(4)	2.071(5)	N(1)–C(5)	1.293(8)
Mn(2)–C(5)	2.052(8)	N(1)–C(6)	1.470(8)
Mn(2)–C(21)	1.799(9)	C(1)–C(2)	1.46(1)
Mn(2)–C(22)	1.83(1)	C(2)–C(3)	1.331(9)
Mn(2)–C(23)	1.86(1)	C(2)–C(5)	1.49(1)
Mn(2)–C(24)	1.85(1)	C(3)–C(4)	1.51(1)
O(1)–C(4)	1.173(9)		

<sup>a</sup> Distances are in angstroms. Estimated standard deviations in the least significant figure are given in parentheses.

in the dimanganese species **1a,b**. The nitrogen atom N(1) is coordinated to the manganese atom Mn(1), and the carbon C(5) is coordinated to the metal atom Mn(2). The Mn(1)–N(1) = 2.069(6) Å distance is slightly shorter than the corresponding distance of 2.078(3) Å found for the Mn–O distance in the metalated enone complex **A** shown in eq 1,<sup>7</sup> while the Mn(2)–C(5) distance (2.052(8) Å) is slightly longer than that found in compound **A** (1.954(7) Å). Formally, there is a double bond between the atoms C(2) and C(3) and C(5) and N(1), and this is reflected in the short bond distances (1.331(9) and 1.293(8) Å). The C(2)–C(5) distance is formally single at 1.49(1) Å. One of the carboxylate groups is coordinated to the manganese atom Mn(2) (Mn(2)–O(4) = 2.071(5) Å), and this results in the formation of a second five-membered ring which is similar to that found in **A**. The IR spectrum of **2a** shows two low-energy absorptions at 1600 and 1548 cm<sup>-1</sup>, which can be attributed to the stretching frequencies of the C=O of the coordinated carboxylate and C=N of the imine groups, respectively. Compound **2b** is believed to be structurally analogous to that of **2a**.

The minor products **3a,b** exhibit high-frequency absorptions at 2191 and 2143 cm<sup>-1</sup>, respectively, that are characteristic of coordinated isocyanide ligands, which indicates that the isocyanide has not been coupled to the alkyne in the formation of these products. However, the presence of two low-energy absorptions (1609, 1542 cm<sup>-1</sup> for **3a** and 1600, 1541 cm<sup>-1</sup> for **3b**) indicates the formation of a molecule with a structure similar to that of **A** and **2a**. Thus, these molecules are formulated as isocyanide-substituted derivatives of **A**. A variety of different isomers may exist depending upon which metal atom contains the isocyanide ligand



Possible isomers of 3a-b

and also at which site on a given metal atom the isocyanide ligand resides.

When the cyclometalated enimine complexes **2a,b** were irradiated in the presence of a slow purge with HC≡CH, the new compounds Mn<sub>2</sub>(CO)<sub>7</sub>[μ-η<sup>4</sup>-CN(Me)-CHCHC(CO<sub>2</sub>Me)C(CO<sub>2</sub>Me)] (**4a**) and Mn<sub>2</sub>(CO)<sub>7</sub>[μ-η<sup>4</sup>-CN(Ph)CHCHC(CO<sub>2</sub>Me)C(CO<sub>2</sub>Me)] (**4b**) were obtained

Table 4. Intramolecular Bond Angles for 2a<sup>a</sup>

N(1)–Mn(1)–C(3)	78.0(3)	C(3)–C(2)–C(5)	118.4(7)
O(4)–Mn(2)–C(5)	80.3(3)	Mn(1)–C(3)–C(2)	113.9(6)
Mn(2)–O(4)–C(1)	116.8(5)	Mn(1)–C(3)–C(4)	122.2(6)
Mn(1)–N(1)–C(5)	118.6(5)	C(2)–C(3)–C(4)	123.9(7)
Mn(1)–N(1)–C(6)	120.0(5)	O(1)–C(4)–O(2)	125.5(8)
C(5)–N(1)–C(6)	121.2(6)	O(1)–C(4)–C(3)	125.4(8)
O(3)–C(1)–O(4)	122.4(8)	O(2)–C(4)–C(3)	108.9(7)
O(3)–C(1)–C(2)	118.2(7)	Mn(2)–C(5)–N(1)	139.0(6)
O(4)–C(1)–C(2)	119.4(8)	Mn(2)–C(5)–C(2)	110.1(5)
C(1)–C(2)–C(3)	128.5(7)	N(1)–C(5)–C(2)	110.9(6)
C(1)–C(2)–C(5)	113.1(7)	Mn–C–O (av)	177.0(9)

<sup>a</sup> Angles are in degrees. Estimated standard deviations in the least significant figure are given in parentheses.

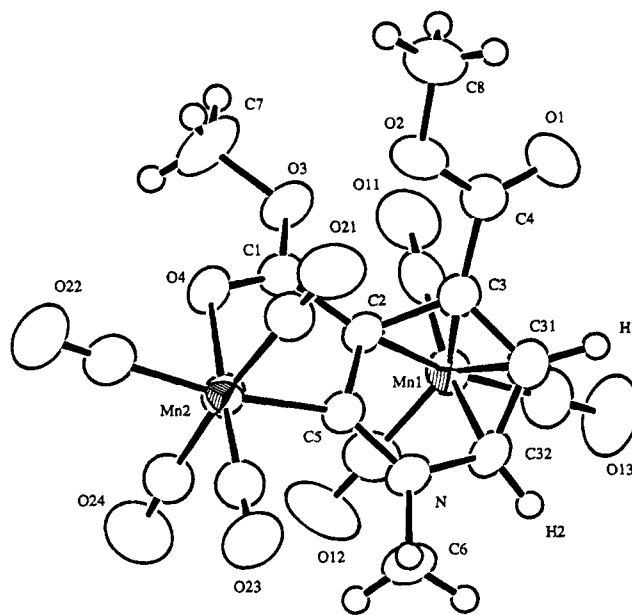


Figure 2. ORTEP diagram of Mn<sub>2</sub>(CO)<sub>7</sub>[μ-η<sup>4</sup>-CN(Me)-CHCHC(CO<sub>2</sub>Me)C(CO<sub>2</sub>Me)] (**4a**) showing 50% probability thermal ellipsoids.

in yields of 27% and 32%, respectively. Compound **4a** was characterized structurally by a single-crystal X-ray diffraction analysis, and an ORTEP diagram of its molecular structure is shown in Figure 2. Final atomic positional parameters are listed in Table 5. Selected bond distances and angles are listed in Tables 6 and 7, respectively. This compound contains a six-atom nitrogen-containing heterocycle that has a manganese atom at the 2-position, methoxycarbonyl groups at the 3- and 4-positions, and a methyl group on the nitrogen atom. It could be viewed as a substituted *N*-methylpyridine, but the ring is decidedly nonplanar. Four carbon atoms (C(2), C(3), C(31) and C(32)) coordinated to the manganese atom Mn(1) form one plane, while a second plane is formed by the atoms C(2), C(5), N, and C(32). The dihedral angle between the two planes is 42.6°. Carbon C(5) is formally a carbene center (Mn(2)–C(5) = 2.016(4) Å), and there is significant multiple bonding between the atoms C(5) and N (C(5)–N = 1.311(4) Å). Two distances (C(3)–C(31) and C(31)–C(32)) are significantly shorter than the others: 1.409(5) and 1.420(6) Å vs 1.462(5), 1.470(5), and 1.469(5) Å for C(2)–C(3), C(2)–C(5), and C(32)–N, respectively. One carboxylate group is coordinated to the manganese atom Mn(2) to form a five-membered ring (Mn(2)–O(4) = 2.087(3) Å). Structurally, compound **4a** is very similar to the com-

Table 5. Positional Parameters and  $B(\text{eq})$  Values for **4a**

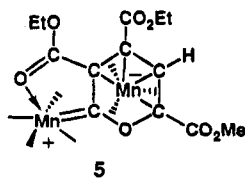
atom	x	y	z	$B(\text{eq}), \text{\AA}^2$
Mn(1)	0.59719(6)	0.18526(3)	0.64411(5)	2.94(3)
Mn(2)	0.17295(6)	0.09019(4)	0.73137(5)	3.07(3)
O(1)	0.7674(3)	-0.0099(2)	0.6942(3)	5.5(2)
O(2)	0.6028(3)	-0.0314(2)	0.7814(3)	4.8(1)
O(3)	0.6066(3)	0.1094(2)	0.8954(2)	4.1(1)
O(4)	0.3661(3)	0.1025(1)	0.8590(2)	3.4(1)
O(11)	0.8540(4)	0.2021(2)	0.8400(3)	5.5(2)
O(12)	0.4547(4)	0.3312(2)	0.6600(3)	6.8(2)
O(13)	0.7787(4)	0.2447(2)	0.5117(3)	6.9(2)
O(21)	0.2433(4)	-0.0730(2)	0.7032(2)	6.2(2)
O(22)	0.0269(4)	0.0504(2)	0.9036(3)	6.9(2)
O(23)	-0.0924(3)	0.0667(2)	0.5472(2)	5.4(2)
O(24)	0.1093(4)	0.2568(2)	0.7313(3)	6.8(2)
N	0.2948(3)	0.1367(2)	0.5388(2)	2.9(1)
C(1)	0.4740(4)	0.1067(2)	0.8252(3)	3.0(2)
C(2)	0.4610(4)	0.1109(2)	0.7078(2)	2.6(2)
C(3)	0.5603(4)	0.0708(2)	0.6589(3)	2.6(2)
C(4)	0.6575(4)	0.0069(2)	0.7118(3)	3.1(2)
C(5)	0.3083(4)	0.1165(2)	0.6416(3)	2.8(2)
C(6)	0.1590(4)	0.1500(2)	0.4523(3)	3.9(2)
C(7)	0.6215(5)	0.1025(3)	1.0119(3)	5.9(3)
C(8)	0.6891(6)	-0.0946(3)	0.8396(4)	6.1(3)
C(11)	0.7522(5)	0.1946(2)	0.7656(4)	3.7(2)
C(12)	0.5116(5)	0.2750(3)	0.6540(3)	4.1(2)
C(13)	0.7075(5)	0.2210(2)	0.5634(4)	4.2(2)
C(21)	0.2176(4)	-0.0120(3)	0.7156(3)	3.74(9)
C(22)	0.0814(5)	0.0662(3)	0.8374(4)	4.3(2)
C(23)	0.0104(5)	0.0768(2)	0.6197(4)	3.75(9)
C(24)	0.1346(5)	0.1940(3)	0.7353(4)	4.2(2)
C(31)	0.5368(4)	0.0890(2)	0.5461(3)	3.0(2)
C(32)	0.4291(4)	0.1459(2)	0.5077(3)	3.1(2)

Table 6. Intramolecular Distances for **4a**<sup>a</sup>

Mn(1)–C(2)	2.167(4)	O(2)–C(8)	1.449(5)
Mn(1)–C(3)	2.056(4)	O(3)–C(1)	1.327(5)
Mn(1)–C(11)	1.808(5)	O(3)–C(7)	1.438(5)
Mn(1)–C(12)	1.798(5)	O(4)–C(1)	1.237(5)
Mn(1)–C(13)	1.788(5)	O–C (av)	1.140(5)
Mn(1)–C(31)	2.073(4)	N–C(5)	1.311(4)
Mn(1)–C(32)	2.105(4)	N–C(6)	1.458(5)
Mn(2)–O(4)	2.087(3)	N–C(32)	1.469(5)
Mn(2)–C(5)	2.016(4)	C(1)–C(2)	1.450(5)
Mn(2)–C(21)	1.867(5)	C(2)–C(3)	1.462(5)
Mn(2)–C(22)	1.853(5)	C(2)–C(5)	1.470(5)
Mn(2)–C(23)	1.790(5)	C(3)–C(4)	1.488(5)
Mn(2)–C(24)	1.861(5)	C(3)–C(31)	1.409(5)
O(1)–C(4)	1.183(4)	C(31)–C(32)	1.420(6)
O(2)–C(4)	1.332(5)		

<sup>a</sup> Distances are in angstroms. Estimated standard deviations in the least significant figure are given in parentheses.

pond **5** formed by the addition of  $\text{HC}\equiv\text{CCO}_2\text{Me}$  to the enone complex **A** (eq 1).



On the basis of simple electron-counting procedures, complex **4a** is formally zwitterionic with a positive charge on Mn(2) and a negative charge on Mn(1). Compound **4b** is believed to be structurally analogous to **4a** with a phenyl group bonded to the nitrogen atom in the place of the methyl group in **4a**.

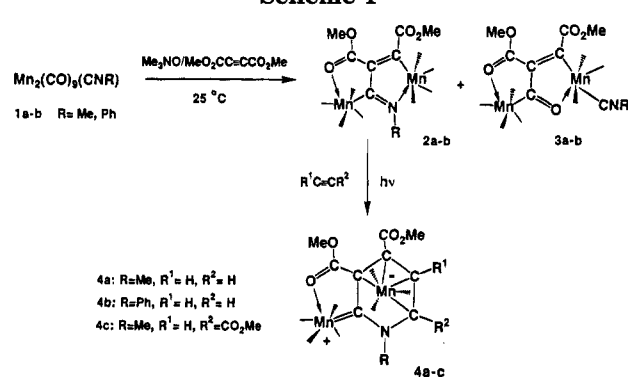
When **2a** was allowed to react with  $\text{HC}\equiv\text{CCO}_2\text{Me}$  in the presence of UV irradiation, the compound  $\text{Mn}_2(\text{CO})_7[\mu-\eta^4\text{-CN}(\text{Me})\text{CHC}(\text{CO}_2\text{Me})\text{C}(\text{CO}_2\text{Me})\text{C}(\text{CO}_2\text{Me})]$  (**4c**) was obtained in 31% yield. Compound **4c** is

Table 7. Intramolecular Bond Angles for **4a**<sup>a</sup>

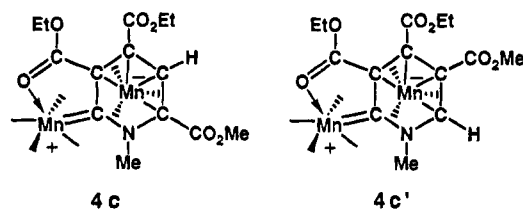
C(2)–Mn(1)–C(3)	40.4(1)	C(3)–C(2)–C(5)	117.8(3)
C(2)–Mn(1)–C(31)	68.6(1)	Mn(1)–C(3)–C(2)	73.9(2)
C(2)–Mn(1)–C(32)	72.4(1)	Mn(1)–C(3)–C(4)	132.2(3)
C(3)–Mn(1)–C(31)	39.9(1)	Mn(1)–C(3)–C(31)	70.7(2)
C(3)–Mn(1)–C(32)	69.0(2)	C(2)–C(3)–C(4)	125.3(3)
C(31)–Mn(1)–C(32)	39.7(2)	C(2)–C(3)–C(31)	112.7(3)
O(4)–Mn(2)–C(5)	80.1(1)	C(4)–C(3)–C(31)	121.1(3)
C(4)–O(2)–C(8)	116.0(3)	O(1)–C(4)–O(2)	123.3(4)
C(1)–O(3)–C(7)	117.7(3)	O(1)–C(4)–C(3)	125.9(4)
Mn(2)–O(4)–C(1)	113.2(2)	O(2)–C(4)–C(3)	110.8(3)
C(5)–N–C(6)	126.0(3)	Mn(2)–C(5)–N	136.3(3)
C(5)–N–C(32)	117.0(3)	Mn(2)–C(5)–C(2)	111.9(2)
C(6)–N–C(32)	117.0(3)	N–C(5)–C(2)	111.8(3)
O(3)–C(1)–O(4)	121.3(3)	Mn(1)–C(31)–C(3)	69.4(2)
O(3)–C(1)–C(2)	117.1(3)	Mn(1)–C(31)–C(32)	71.4(2)
O(4)–C(1)–C(2)	121.6(4)	C(3)–C(31)–C(32)	112.8(4)
Mn(1)–C(2)–C(1)	121.9(3)	Mn(1)–C(32)–N	110.3(2)
Mn(1)–C(2)–C(3)	65.7(2)	Mn(1)–C(32)–C(31)	68.9(2)
Mn(1)–C(2)–C(5)	111.5(2)	N–C(32)–C(31)	116.6(3)
C(1)–C(2)–C(3)	122.4(3)	Mn–C–O (av)	178.2(3)
C(1)–C(2)–C(5)	110.8(3)		

<sup>a</sup> Angles are in degrees. Estimated standard deviations in the least significant figure are given in parentheses.

Scheme 1



believed to be analogous to **4a,b**, but on the basis of its IR and <sup>1</sup>H NMR spectra alone, one is not able to distinguish between the two possible isomers **4c** and **4c'**.



However, in comparison with **5**, we prefer the structure **4c**, where the carboxylate substituent is located next to the heteroatom.

## Discussion

In our previous studies we showed that  $\text{Mn}_2(\text{CO})_9(\text{NCMe})$  reacts with  $\text{EtO}_2\text{CC}\equiv\text{CCO}_2\text{Et}$  by insertion of the alkyne into the metal–metal bond and coupling of one of the CO ligands to yield the metalated enone complex **A**.<sup>7</sup> Similarly, treatment of the isocyanide complexes  $\text{Mn}_2(\text{CO})_9(\text{CNR})$  (**1a,b**) with  $\text{Me}_3\text{NO}$  in NCMe followed by addition of  $\text{MeO}_2\text{CC}\equiv\text{CCO}_2\text{Me}$  has yielded the metalated enimine complexes **2a,b** by the insertion of the alkyne into the metal–metal bond and coupling to the CNR ligand (see Scheme 1). The presumed intermediate  $\text{Mn}_2(\text{CO})_9(\text{NCMe})(\text{CNR})$  is unstable, and we thus used it without isolation. We have

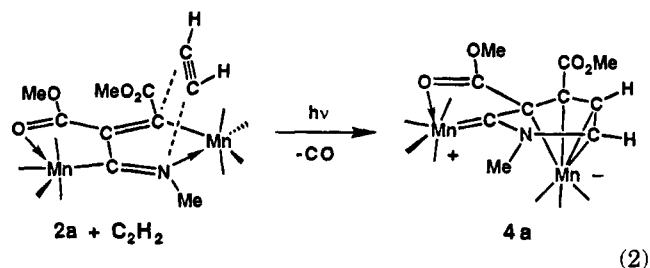


shown previously that the enone complexes are formed by the insertion of a CO ligand into a metal-carbon bond of a dimetalated olefin precursor complex.<sup>7</sup> Similarly, we propose that the coupling of the isocyanides to the alkyne occurs by the insertion of the isocyanide into the metal-carbon bond of an unobserved dimetalated olefin intermediate. Small amounts of the isocyanide-containing metalated enone complexes **3a,b** were also obtained in these reactions. The higher yields of the complexes **2a,b** relative to complexes **3a,b** is believed to be due to the greater ability of isocyanides to insert into the metal-carbon bond than is the case for CO. This tendency has been observed previously for isocyanide insertion into other types of metal-carbon bonds.<sup>14</sup>

In the metalated enone complexes the oxygen atom of the C=O group is coordinated to one of the metal atoms. We found the nitrogen atom of the C=NR group is coordinated to one of the metal atoms in a similar fashion. The coordination of the oxygen atom in the enone complexes provided a condition that facilitated a novel 4 + 2 cycloaddition of alkynes to these complexes to produce metalated pyrans (eq 1) that could subsequently be freed from the metal atoms by treatment with a mixture of CO and HCl gases.

Likewise, we have found that the addition of alkynes to the compounds **2a,b** in the presence of UV irradiation produces a similar 4 + 2 cycloaddition of the alkyne to the complexes to produce nitrogen-containing heterocycles in the form of the metalated N-substituted

pyridine complexes **4a,b** (eq 2). Solutions of **2a** and



$HC\equiv CH$  showed no evidence of reaction at room temperature over periods of up to 3.5 h. However, on exposure to UV irradiation the reactions were complete within 5 min. The irradiation almost certainly promotes the decarbonylation step, which may facilitate the alkyne coupling to the enimine grouping through an initial interaction of the alkyne with the metal atom.

We have attempted to remove and isolate the heterocycle by treatment with CO/HCl mixtures, but due to the very small quantities involved we have been unable to obtain complete characterizations of these compounds.

**Acknowledgment.** This research was supported by the Office of Basic Energy Science of the U.S. Department of Energy.

**Supplementary Material Available:** Tables of hydrogen atom positional parameters and anisotropic thermal parameters for **2a** and **4a** (5 pages). Ordering information is given on any current masthead page.

OM940703N

(14) (a) Adams, R. D.; Chodosh, D. F. *J. Am. Chem. Soc.* **1977**, *99*, 6544. (b) Yamamoto, Y.; Yamazaki, H. *Inorg. Chem.* **1974**, *13*, 2145.

# Ligand Substitution at 19-Electron Centers and the Indenyl Effect in Organometallic Radicals. Electrochemical CO Substitution in (Cyclopentadienyl)Fe(CO)<sub>3</sub><sup>+</sup> and (Indenyl)Fe(CO)<sub>3</sub><sup>+</sup>

K. A. Pevear, M. M. Banaszak Holl, G. B. Carpenter, A. L. Rieger, P. H. Rieger, and D. A. Sweigart\*

Department of Chemistry, Brown University, Providence, Rhode Island 02912

Received September 19, 1994<sup>®</sup>

Electrochemical reduction of ( $\eta^5$ -Cp)Fe(CO)<sub>3</sub><sup>+</sup> (**1**<sup>+</sup>) and ( $\eta^5$ -indenyl)Fe(CO)<sub>3</sub><sup>+</sup> (**2**<sup>+</sup>) in the presence of P- and As-donor nucleophiles (L) leads to rapid and efficient CO substitution by an electron-transfer-catalyzed (ETC) pathway to afford ( $\eta^5$ -Cp)Fe(CO)<sub>2</sub>L<sup>+</sup> and ( $\eta^5$ -indenyl)Fe(CO)<sub>2</sub>L<sup>+</sup>. The CO substitution may also be effected quantitatively and rapidly by using trace amounts of chemical reducing agents such as NEt<sub>3</sub> and Na/Pb. A detailed variable-temperature electrochemical study showed that the 19-electron radical **1** dissociates CO with a rate constant greater than 10<sup>3</sup> s<sup>-1</sup> at -112 °C in butyronitrile. In contrast, **2** is relatively stable, with  $k_{-CO}$  being at least 10<sup>6</sup> times less than that for **1**. Voltammetry with conventional electrodes and with microelectrodes under steady-state conditions allowed the mechanism of CO substitution in the 19-electron radicals **1** and **2** to be established as strictly dissociative. This fact, as well as the determination (from microelectrode steady-state experiments) that the rate of heterogeneous charge transfer for the process **2**<sup>+</sup> → **2** is fast while that for **2** → **2**<sup>-</sup> is slow, argues strongly that the indenyl ligand in **2** is  $\eta^5$ -bonded and not  $\eta^3$ -bonded as previously proposed. The results of extended Hückel MO calculations provide a simple explanation of the reduced reactivity of **2** in comparison to **1**, without the necessity of invoking ring slippage. The LUMO's of **1**<sup>+</sup> and **2**<sup>+</sup> contain a large amount of metal character, as was confirmed by an examination of the ESR spectrum of **2**. The LUMO's of **1**<sup>+</sup> and **2**<sup>+</sup> are both Fe-CO antibonding and have a similar amount of metal character but differ in that the LUMO of **2**<sup>+</sup> has a significant localization on the benzene ring of the indenyl ligand, with proportionately less localization on the CO ligands. Accordingly, the rate of dissociation of CO is much greater for **1** than for **2**. The origin of this effect can be traced to the presence of a low-lying  $\pi^*$  orbital in the indenyl anion that is predominantly localized on the benzene ring and which has the proper symmetry to interact with one of the two LUMO's on the Fe(CO)<sub>3</sub><sup>2+</sup> fragment. In effect, the indenyl ligand acts like an electron sink when **2**<sup>+</sup> is reduced, but this involves neither ring slippage to  $\eta^3$  bonding nor a diminution of electron density on the metal in comparison to that in **1**. The principal conclusion is that changing from cyclopentadienyl to indenyl ligands should greatly retard dissociative substitutions at 19e<sup>-</sup> centers (*inverse* "indenyl effect"), while, for *similar* reasons, substitutions should be accelerated at 18e<sup>-</sup> centers (A or D mechanism) and 17e<sup>-</sup> centers (A mechanism), in accordance with the well-known indenyl effect. Also reported in this study is the X-ray structure of [( $\eta^5$ -indenyl)Fe(CO)<sub>3</sub>]PF<sub>6</sub>: orthorhombic, space group *Pnma*, *a* = 9.7911(8) Å, *b* = 7.5975(11) Å, *c* = 19.909(2) Å, *Z* = 4, 1405 unique reflections, *R*<sub>1</sub> = 0.075, *wR*<sub>2</sub> = 0.204.

## Introduction

Organometallic radicals with 17 or 19 electrons about the metal generally show greatly enhanced reactivity in comparison to their 18-electron analogues.<sup>1,2</sup> A variety of stoichiometric and catalytic transformations of 18-electron complexes can be initiated by the *in situ* conversion to odd-electron species.<sup>1-5</sup> Seventeen-electron radicals may be generated by oxidation or, in the

case of polynuclear complexes, by photodissociation of a metal-metal bond.<sup>6-9</sup> However generated, 17-electron complexes often have sufficient stability to allow spectroscopic characterization. In the presence of appropriate nucleophiles they typically undergo rapid ligand substitution by an associative pathway.<sup>4</sup>

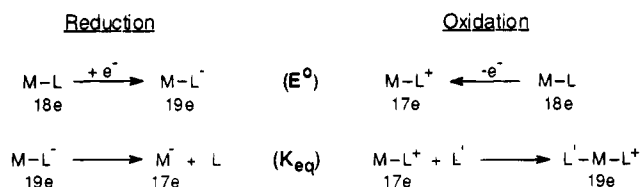
Perhaps the most obvious way to form a 19-electron complex is *via* reduction of an 18-electron precursor.

<sup>®</sup> Abstract published in *Advance ACS Abstracts*, November 15, 1994.  
(1) *Organometallic Radical Processes*; Troglor, W. C., Ed.; Elsevier: Amsterdam, 1990.

(2) (a) Tyler, D. R. *Prog. Inorg. Chem.* **1988**, *36*, 125. (b) Astruc, D. *Chem. Rev.* **1988**, *88*, 1189. (c) Baird, M. C. *Chem. Rev.* **1988**, *88*, 1217. (d) Tyler, D. R.; Mao, F. *Coord. Chem. Rev.* **1990**, *97*, 119. (e) Tyler, D. R. *Acc. Chem. Res.* **1991**, *24*, 325. (f) Kaim, W. *Coord. Chem. Rev.* **1987**, *76*, 187.

(3) (a) Bezems, G. J.; Rieger, P. H.; Visco, S. *J. Chem. Soc., Chem. Commun.* **1981**, 265. (b) Arewgoda, C. M.; Robinson, B. H.; Simpson, J. *J. Chem. Soc., Chem. Commun.* **1982**, 284. (c) Darchen, A.; Mahe, C.; Patin, H. *J. Chem. Soc., Chem. Commun.* **1982**, 243. (d) Arewgoda, M.; Rieger, P. H.; Robinson, B. H.; Simpson, J.; Visco, S. *J. Am. Chem. Soc.* **1982**, *104*, 5633. (e) Miholova, D.; Vlcek, A. A. *J. Organomet. Chem.* **1985**, *279*, 317. (f) Hinkelmann, K.; Mahlendorf, F.; Heinze, J.; Schacht, H.-T.; Field, J. S.; Vahrenkamp, H. *Angew. Chem., Int. Ed. Engl.* **1987**, *26*, 352.

Scheme 1

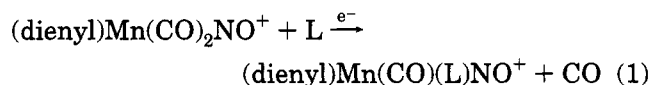


However, as shown in Scheme 1, ligand dissociation may accompany reduction and in order to "see" the 19-electron complex, the equilibrium constant ( $K_{\text{eq}}$ ) for the  $19e \leftrightarrow 17e$  interconversion must be small. This is more likely to occur as  $E^\circ$  becomes more positive; i.e., an easily reduced (electron poor)  $\text{M-L}$  complex is less likely to dissociate ligand  $\text{L}$  after reduction. It is also possible to generate 19-electron radicals by oxidation in the presence of a potential ligand ( $\text{L}'$ ). Again, the key step is the  $17e \leftrightarrow 19e$  interconversion, and one anticipates that the larger the  $E^\circ$ , the better, because a difficult to oxidize  $\text{M-L}$  will be more prone to bind another ligand (large  $K_{\text{eq}}$ ) after oxidation to  $\text{M-L}^+$ . However, there is a difficulty here in that ligand addition to  $\text{M-L}^+$  is often followed by a second spontaneous oxidation of  $\text{L}'\text{-M-L}^+$ , so that the only observed species is the 18-electron  $\text{L}'\text{-M-L}^{2+}$ . In other words, the disproportionation of  $\text{L}'\text{-M-L}^+$  to  $\text{L}'\text{-M-L}^{2+}$  and  $\text{M-L}$  (plus  $\text{L}'$ ) is exoergic. For this reason, it is normally preferable to utilize reduction chemistry in order to generate and study 19-electron complexes.

However formed, 19-electron complexes seem to be very reactive with respect to oxidation, ligand loss, and/or ligand substitution. For example, it is reported that  $\text{Mn}(\text{CO})_6$ ,  $\text{Mn}(\text{CO})_2(\eta^2\text{-dppe})_2$ , (mesitylene) $\text{W}(\text{CO})_3(\text{MeCN})^+$ , and  $\text{CpFe}(\text{CO})_2(\eta^1\text{-dppe})$  all dissociate a ligand with a half-life at room temperature of less than 1  $\mu\text{s}$ .<sup>5d,5f,5b</sup> Nineteen-electron complexes are often postu-

lated as intermediates or transition-state species, but due to their great reactivity, authentic examples are rare. For obvious reasons, it is usually assumed that ligand substitution at 19-electron centers is dissociative.<sup>2,3,5</sup> While this qualitative assumption is almost certainly correct, there is very little quantitative information available describing how reactivity depends on the nature of the metal and the nonreacting ligands. For example, the reactivity dependence on the metal within a given triad is unknown, although it seems probable that large rate differences exist with 19-electron complexes (*vide infra*). In this context, it has recently been found<sup>4i</sup> that the reactivity pattern for CO substitution at 17-electron centers within the chromium triad differs greatly from that found with analogous 18-electron complexes. Information of this sort should be relevant to the study of processes that have organometallic radicals as intermediates.

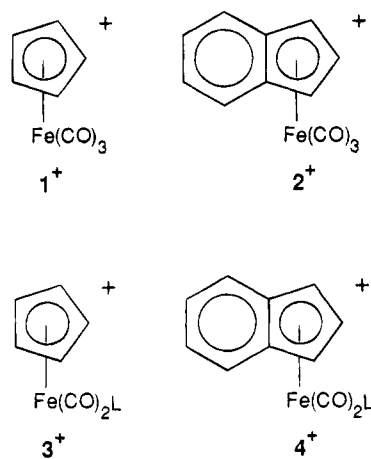
There have been three detailed mechanistic studies of ligand substitution in 19-electron complexes reported to date. In one study, it was shown<sup>10</sup> that the arene in  $\text{CpFe}(\text{arene})$  is replaced by phosphines via an associative pathway; it is likely that successive arene ring slippage occurs to avoid the formation of 21-electron intermediates. Another study concerned<sup>11</sup> dissociative CO substitution in  $\text{Co}(\text{CO})_3\text{L}_2$  ( $\text{L}_2$  is 2,3-bis(diphenylphosphino)maleic anhydride). In this case, however, recent ESR work showed<sup>12</sup> that only a few percent of the unpaired spin density is located on the metal, indicating that the molecule is in reality an 18-electron complex with a radical ligand. A third study dealt with CO substitution in  $(\text{MeCp})\text{Mn}(\text{CO})_2\text{NO}$  and  $(\text{indenyl})\text{Mn}(\text{CO})_2\text{NO}$ , which were found<sup>13</sup> to react by a strictly dissociative pathway. These 19-electron radicals<sup>14</sup> were generated as intermediates in the electron-transfer-catalyzed (ETC) CO substitution of the 18-electron cations according to eq 1 ( $\text{L}$  is a P-donor).



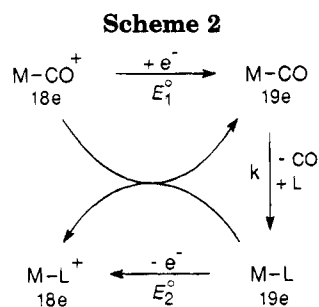
The rate of eq 1 was found to be greatly increased by adding a trace of reducing agent, in which case rapid and clean conversion to product occurred within a fraction of a second. Scheme 2 illustrates the mechanism for this ETC process, which was studied in detail by electrochemical techniques.<sup>13</sup> Reduction of  $\text{M-CO}^+$  yields the 19-electron  $\text{M-CO}$ , which rapidly substitutes a ligand to give  $\text{M-L}$ . In general,  $\text{M-L}$  is more easily oxidized than is  $\text{M-CO}$ , from which it follows that  $\text{M-L}$  formed during the reaction will react with  $\text{M-CO}^+$  in a disproportionation step to give  $\text{M-L}^+$  and regenerate  $\text{M-CO}$ . Alternatively, heterogeneous electron transfer from an electrode to  $\text{M-CO}^+$  leads to  $\text{M-L}$ , which then

- (4) (a) Fawcett, J. P.; Jackson, R. A.; Pöe, A. *J. Chem. Soc., Dalton Trans.* **1978**, 789. (b) Hershberger, J. W.; Klinger, R. J.; Kochi, J. K. *J. Am. Chem. Soc.* **1983**, *105*, 61. (c) Shi, Q.-Z.; Richmond, T. G.; Troglor, W. C.; Basolo, F. *J. Am. Chem. Soc.* **1984**, *106*, 71. (d) Herrinton, T. R.; Brown, T. L. *J. Am. Chem. Soc.* **1985**, *107*, 5700. (e) Turaki, N. N.; Huggins, J. M. *Organometallics* **1986**, *5*, 1703. (f) Basolo, F. *Polyhedron* **1990**, *9*, 1535. (g) Watkins, W. C.; Jaeger, T.; Kidd, C. E.; Fortier, S.; Baird, M. C.; Kiss, G.; Roper, G. C.; Hoff, C. D. *J. Am. Chem. Soc.* **1992**, *114*, 907. (h) Song, L.; Troglor, W. C. *J. Am. Chem. Soc.* **1992**, *114*, 3355. (i) Meng, Q.; Huang, Y.; Ryan, W. J.; Sweigart, D. A. *Inorg. Chem.* **1992**, *31*, 4051. (j) Poli, R.; Owens, B. E.; Linck, R. G. *Inorg. Chem.* **1992**, *31*, 662.
- (5) (a) Magnuson, R. H.; Meirowitz, R.; Zulu, S. J.; Giering, W. P. *Organometallics* **1983**, *2*, 460. (b) Kuchynka, D. J.; Amatore, C.; Kochi, J. K. *Inorg. Chem.* **1986**, *25*, 4087. (c) Donovan, B. T.; Geiger, W. E. *J. Am. Chem. Soc.* **1988**, *110*, 2335. (d) Kuchynka, D. J.; Kochi, J. K. *Inorg. Chem.* **1989**, *28*, 855. (e) Ryan, O. B.; Tilset, M.; Parker, V. D. *J. Am. Chem. Soc.* **1990**, *112*, 2618. (f) Zhang, Y.; Gosser, D. K.; Rieger, P. H.; Sweigart, D. A. *J. Am. Chem. Soc.* **1991**, *113*, 4062.
- (6) (a) Caspar, J. V.; Meyer, T. J. *J. Am. Chem. Soc.* **1980**, *102*, 7795. (b) Moore, B. D.; Simpson, M. B.; Poliakoff, M.; Turner, J. J. *J. Chem. Soc., Chem. Commun.* **1984**, 972. (c) Dixon, A. J.; Healy, M. A.; Poliakoff, M.; Turner, J. J. *J. Chem. Soc., Chem. Commun.* **1986**, 994.
- (7) (a) Dixon, A. J.; Gravelle, S. J.; van de Burgt, L. J.; Poliakoff, M.; Turner, J. J.; Weitz, E. *J. Chem. Soc., Chem. Commun.* **1987**, 1023. (b) Dixon, A. J.; George, M. W.; Hughes, C.; Poliakoff, M.; Turner, J. J. *J. Am. Chem. Soc.* **1992**, *114*, 1719.
- (8) (a) Goldman, A. S.; Tyler, D. R. *Inorg. Chem.* **1987**, *26*, 253. (b) Castellani, M. P.; Tyler, D. R. *Organometallics* **1989**, *8*, 2113.
- (9) (a) Wrighton, M. S.; Ginley, D. S. *J. Am. Chem. Soc.* **1975**, *97*, 4246. (b) Goldman, A. S.; Tyler, D. R. *Inorg. Chim. Acta* **1985**, *98*, L47. (c) Abrahamson, H. B.; Palazzotto, M. C.; Reichel, C. L.; Wrighton, M. S. *J. Am. Chem. Soc.* **1979**, *101*, 4123. (d) Stiegman, A. E.; Stieglitz, M.; Tyler, D. R. *J. Am. Chem. Soc.* **1983**, *105*, 6032. (e) Stiegman, A. E.; Tyler, D. R. *Inorg. Chem.* **1984**, *23*, 527. (f) Avey, A.; Tenhaeff, S. C.; Weakley, J. R.; Tyler, D. R. *Organometallics* **1991**, *10*, 3607. (g) Avey, A.; Tyler, D. R. *Organometallics* **1992**, *11*, 3856. (h) Scott, S. L.; Espenson, J. H.; Ahu, Z. *J. Am. Chem. Soc.* **1993**, *115*, 1789.

- (10) Ruiz, J.; Lacoste, M.; Astruc, D. *J. Am. Chem. Soc.* **1990**, *112*, 5471.
- (11) Mao, F.; Tyler, D. R.; Keszler, D. *J. Am. Chem. Soc.* **1989**, *111*, 130.
- (12) (a) Mao, F.; Tyler, D. R.; Rieger, A. L.; Rieger, P. H. *J. Chem. Soc., Faraday Trans.* **1991**, *87*, 3113. (b) Mao, F.; Tyler, D. R.; Bruce, M. R. M.; Bruce, A. E.; Rieger, A. L.; Rieger, P. H. *J. Am. Chem. Soc.* **1992**, *114*, 6418.
- (13) (a) Neto, C. C.; Kim, S.; Meng, Q.; Sweigart, D. A.; Chung, Y. K. *J. Am. Chem. Soc.* **1993**, *115*, 2077. (b) Huang, Y.; Neto, C. C.; Pevear, K. A.; Banaszak Holl, M. M.; Sweigart, D. A.; Chung, Y. K. *Inorg. Chim. Acta* **1994**, *226*, 53.
- (14) The 19-electron radical  $\text{CpRe}(\text{CO})_2\text{NO}$  was also generated but was found to be unreactive toward CO substitute on the CV time scale.



**Figure 1.** Numbering scheme for complexes studied.



returns an electron to the electrode, provided  $E_1^\circ > E_2^\circ$  (Scheme 2). Thus, the overall substitution reaction in eq 1 is catalytic in electrons whether the electron transfer is homogeneous or heterogeneous. The necessary conditions for efficient ETC catalysis are that the reduction potentials be in the order  $E^\circ(\text{M}-\text{CO}^+) > E^\circ(\text{M}-\text{L}^+)$  and that the 19-electron radicals  $\text{M}-\text{CO}$  and  $\text{M}-\text{L}$  be sufficiently stable with respect to decomposition so that there can be many turnovers. The former requirement applies to most reductions, because departing ligands are usually replaced by ones that increase the electron density on the metal. It follows that catalytic reductive activation of organometallics to ligand substitution should be common, whereas catalytic oxidative activation should be uncommon. It is possible that many substitution reactions of 18-electron complexes thought to occur by conventional associative or dissociative pathways in fact take place by an electron-transfer-catalyzed mechanism initiated by the presence of trace amounts of adventitious reductants or oxidants in solution.<sup>3,8,15,16</sup>

The (dienyl) $\text{Mn}(\text{CO})_2\text{NO}^+$  system nicely fulfilled the conditions for ETC substitution initiated by reduction and, furthermore, was particularly well suited for an examination by variable-temperature electrochemical techniques, with the result that the mechanistic details of CO substitution in the 19-electron intermediates could be quantitatively established. In the present paper, we describe an electrochemical investigation of reductively activated CO substitution in  $(\eta^5\text{-Cp})\text{Fe}(\text{CO})_3^+$  ( $1^+$ ) and  $(\eta^5\text{-indenyl})\text{Fe}(\text{CO})_3^+$  ( $2^+$ ). It is shown that, upon reduction,  $1^+$  very rapidly dissociates CO and dimerizes to  $[\text{CpFe}(\text{CO})_2]_2$ . In the presence of P-donor nucleophiles, the dimerization reaction is quenched and

an efficient ETC substitution occurs to afford  $(\eta^5\text{-Cp})\text{Fe}(\text{CO})_2\text{L}^+$  ( $3^+$ ) by the mechanism shown in Scheme 2. The indenyl complex  $2^+$  was chosen for study in order to determine if an "indenyl effect" operates in CO substitutions in 19-electron radicals. This effect is one example of the general idea that accessibility of a transition state through ring slippage in an associative process gets easier as the ligand conjugation increases. In comparison to a  $\text{C}_5\text{H}_5$  group, the benzene ring in  $\text{C}_9\text{H}_7$  allows for easier delocalization of electrons "freed" as the bonding to the metal slips from  $\eta^5$  to  $\eta^3$ . This results in a lower energy for  $\eta^3$  intermediates or activated complexes, with the result that the rate of associative ligand substitution increases.<sup>17</sup> This rate increase can be large; for example, (indenyl) $\text{Rh}(\text{CO})_2$  undergoes associative CO substitution about  $10^8$  times faster than does  $(\text{Cp})\text{Rh}(\text{CO})_2$ . The idea of ring slippage is well documented with the indenyl ligand. There exist a number of structural studies showing the indenyl group bonded in an  $\eta^3$  fashion with the benzene ring bent away from the  $\eta^3$ -allyl portion of the molecule by ca.  $20^\circ$ .<sup>18,19</sup>

Thus, it is clearly established that the indenyl group can slip and thereby facilitate associative ligand substitution at 18-electron centers. Interestingly, early studies of CO substitution reactions of (dienyl) $\text{Fe}(\text{CO})_2\text{I}$  and (dienyl) $\text{Mo}(\text{CO})_3\text{X}$  complexes suggest<sup>20</sup> that *dissociative* pathways also are faster when the dienyl ligand is  $\text{C}_9\text{H}_7$  as compared to  $\text{C}_5\text{H}_5$ . In these cases the rate acceleration is several orders of magnitude and was ascribed to an interaction between the metal and the benzene ring of the indenyl ligand that occurs in concert with CO dissociation; the necessity to form a high-energy 16-electron intermediate is alleviated to whatever extent this intramolecular nucleophilic assistance actually occurs. With the 19-electron complexes (dienyl) $\text{Mn}(\text{CO})_2\text{NO}$ , it was found<sup>13</sup> that the rate of CO dissociation is very similar when the dienyl group is  $\text{C}_5\text{H}_5$  or  $\text{C}_9\text{H}_7$ ; i.e., there is no "indenyl effect". In dramatic contrast to this behavior, it is shown herein that the radicals  $1$  and  $2$ , although apparently undergoing CO substitution by the same dissociative mechanism, differ in reactivity by more than a factor of  $10^6$ . Furthermore, the indenyl complex  $2$  is *slower* to react than is the cyclohexadienyl analogue  $1$ , so that there is an *inverse* indenyl effect in this case. It is suggested that this obtains because the indenyl group allows for a (relative) stabilization of the ground state of the 19-electron radical *without* the necessity of ring slippage, thereby increasing the activation energy of CO dissociation.

The present study describes the ETC process shown

(17) (a) Rerek, M. E.; Basolo, F. *Organometallics* **1983**, *2*, 372. (b) Ji, L.-N.; Rerek, M. E.; Basolo, F. *Organometallics* **1984**, *3*, 740. (c) Rerek, M. E.; Basolo, F. *J. Am. Chem. Soc.* **1984**, *106*, 5908. (d) Bang, H.; Lynch, T. J.; Basolo, F. *Organometallics* **1992**, *11*, 40. (e) Monti, D.; Bassetti, M. *J. Am. Chem. Soc.* **1993**, *115*, 4658.

(18) (a) Nesmeyanov, A. N.; Ustynyuk, N. A.; Makarova, L. G.; Andianov, V. G.; Struchkov, Y. T.; Andrae, S. *J. Organomet. Chem.* **1978**, *159*, 189. (b) Allen, S. R.; Baker, P. K.; Barnes, S. G.; Bottrill, M.; Green, M.; Orpen, A. G.; Williams, I. D.; Welch, A. *J. Chem. Soc., Dalton Trans.* **1983**, 927. (c) Faller, J. W.; Crabtree, R. H.; Habib, A. *Organometallics* **1985**, *4*, 929. (d) Merola, J. S.; Kacmarcik, R. T.; Van Engen, D. *J. Am. Chem. Soc.* **1986**, *108*, 329. (e) Kowaleski, R. M.; Rheingold, A. L.; Trogler, W. C.; Basolo, F. *J. Am. Chem. Soc.* **1986**, *108*, 2460.

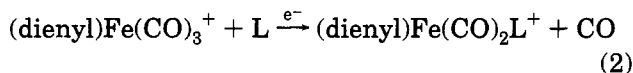
(19) Forschner, T. C.; Cutler, A. R.; Kullnig, R. K. *Organometallics* **1987**, *6*, 889.

(20) (a) White, C.; Mawby, R. *J. Inorg. Chim. Acta* **1970**, *4*, 261. (b) Hart-Davis, A. J.; White, C.; Mawby, R. *J. Inorg. Chim. Acta* **1970**, *4*, 441. (c) Jones, D. J.; Mawby, R. *J. Inorg. Chim. Acta* **1972**, *6*, 157.

(15) James, T. A.; McCleverty, J. A. *J. Chem. Soc. A* **1970**, 850.

(16) Butts, S. B.; Shriver, D. F. *J. Organomet. Chem.* **1979**, *169*, 191.

in eq 2, with major emphasis on the mechanistic aspects of the CO substitution reactions of the neutral 19-electron intermediates, **1** and **2**. Variable-temperature



voltammetric techniques were utilized, including steady-state voltammetry with microelectrodes (diameter  $\leq 10 \mu\text{m}$ ) at low scan rates (e.g., 20 mV/s). The steady-state method is attractive because it is relatively free of capacitive charging current and ohmic polarization effects that plague time-dependent voltammetric measurements in organic solvents.<sup>21</sup> Steady-state voltammetry with microelectrodes can be used to determine heterogeneous charge transfer rate constants that would be difficult or impossible to obtain with conventionally sized electrodes;<sup>22</sup> this procedure has been used to study electron transfer to **2**<sup>+</sup> and **2** (*vide infra*). The steady-state technique can also be used to study homogeneous reactions, although applications to organometallics are so far very few in number.<sup>23</sup> Herein it is demonstrated that microelectrodes can be successfully and conveniently applied in a quantitative manner to determine the rate of CO substitution in the radical **2**.

### Experimental Section

**Materials.** The complex  $[\text{CpFe}(\text{CO})_3]\text{PF}_6$  (**1**<sup>+</sup>) was synthesized according to a published procedure.<sup>24</sup> The substituted complex  $[\text{CpFe}(\text{CO})_2\text{PPh}_3]\text{PF}_6$  was made from  $\text{CpFe}(\text{CO})_2\text{I}$  as described in the literature.<sup>25</sup> During the course of this work we found, however, that this and other complexes of formula  $[\text{CpFe}(\text{CO})_2\text{L}]\text{PF}_6$  (**3**<sup>+</sup>; L = PPh<sub>3</sub>, P(OPh)<sub>3</sub>, P(OEt)<sub>3</sub>, PBu<sub>3</sub>, P(C<sub>2</sub>H<sub>4</sub>CN)<sub>3</sub>) are more easily synthesized in high yield by the following procedure: to a solution of  $[\text{CpFe}(\text{CO})_3]\text{PF}_6$  in acetonitrile is added 1 equiv of phosphine or phosphite (L). A trace of NEt<sub>3</sub> (1 mol % is sufficient) is added to the reaction mixture, and there is immediate and quantitative conversion to product **3**<sup>+</sup>, as may be conveniently verified by recording an IR spectrum.<sup>8a,25a,26</sup> After evaporation, the residue is dissolved in THF and the product precipitated by slow addition of hexanes. The indenyl complex  $[(\text{C}_9\text{H}_7)\text{Fe}(\text{CO})_3]\text{PF}_6$  (**2**<sup>+</sup>) was made from the dimer  $[(\text{C}_9\text{H}_7)\text{Fe}(\text{CO})_2]_2$  by a reported<sup>27</sup> method that was slightly modified by using an atmosphere of CO instead of N<sub>2</sub>. The conversion of **2**<sup>+</sup> to substituted

derivatives  $(\text{C}_9\text{H}_7)\text{Fe}(\text{CO})_3^+$  (**4**<sup>+</sup>, L = P-donor) occurs thermally.<sup>27</sup> As with **1**<sup>+</sup>, however, we found that the NEt<sub>3</sub>-catalyzed transformation of **2**<sup>+</sup> to **4**<sup>+</sup> is a clean and rapid reaction that is especially convenient for the preparation of **4**<sup>+</sup> *in situ*.

**Electrochemical Studies.** Voltammetric experiments were done under a blanket of nitrogen or carbon monoxide that was saturated with solvent. The electrolyte was 0.10 M Bu<sub>4</sub>NPF<sub>6</sub>, which was synthesized by metathesis of Bu<sub>4</sub>NBr and HPF<sub>6</sub>, recrystallized from CH<sub>2</sub>Cl<sub>2</sub>/hexanes, and dried under vacuum. The solvents used were CH<sub>2</sub>Cl<sub>2</sub> and MeCN, both of which were purchased in HPLC grade from Fisher Scientific (catalog numbers D143-1, D150-1, and A998-1). These solvents were found to be entirely suitable for use without additional "purification"; indeed, distillation gave no improvement in electrochemical behavior, as judged from the solvent potential window and, in the case of CH<sub>2</sub>Cl<sub>2</sub>, the chemical reversibility of the oxidation of (benzene)Cr(CO)<sub>3</sub>, a complex known<sup>28</sup> to be very sensitive to trace nucleophilic impurities. Voltammetry at low temperatures utilized a simple slush bath, with a thermocouple probe inserted into the electrochemical cell to monitor the temperature.

Cyclic voltammetry was done with EG&G 173/175/179 potentiostatic instrumentation. The working electrode was a 1 mm diameter platinum, gold, or glassy-carbon disk, and the counter electrode was a platinum wire. The reference was a Metrohm Ag/AgCl electrode filled with CH<sub>2</sub>Cl<sub>2</sub>/0.10 M Bu<sub>4</sub>NClO<sub>4</sub> and saturated with LiCl; this was separated from the test solution by a salt bridge containing 0.10 M Bu<sub>4</sub>NPF<sub>6</sub> in the solvent in use. Inlaid-disk microelectrodes were fabricated with platinum and gold wire of diameter 1–100  $\mu\text{m}$  as previously described.<sup>29</sup> Steady-state voltammetry with microelectrodes of diameter 10  $\mu\text{m}$  was performed in a Faraday cage using a two-electrode configuration in conjunction with a Keithley Model 427 current amplifier. Variable-temperature IR spectroelectrochemistry was done with an optically transparent thin-layer electrode (OTTE), the construction and use of which has been reported.<sup>30</sup> Bulk electrolyses were done with a platinum-basket working electrode and a platinum-mesh counter electrode, which was separated from the test solution by a salt bridge. Digital simulation of proposed mechanisms utilized the program DigiSim.<sup>31</sup> This program utilizes an efficient fast implicit finite difference algorithm and is able to simulate moderately complex mechanisms within a few minutes on a PC with a 486 chip. Data input includes an  $E^\circ$  value for each heterogeneous electron transfer step and an estimate of the rate constants for any homogeneous reactions. In agreement with experimental data, the relevant heterogeneous electron transfers were taken as Nernstian. The simulation results were found to be quite sensitive to the input values of the homogeneous CO dissociation rate constants, which were altered in a systematic manner

(21) (a) Wightman, R. M.; Wipf, D. O. *Electroanal. Chem.* **1989**, *15*, 267. (b) Baer, C. D.; Camaioni-Neto, C. A.; Sweigart, D. A.; Bond, A. M.; Mann, T. F.; Tondreau, G. A. *Coord. Chem. Rev.* **1989**, *93*, 1. (c) Bond, A. M.; Oldham, K. B.; Zoski, C. G. *Anal. Chim. Acta* **1989**, *216*, 177.

(22) Zhang, Y.; Baer, C. D.; Camaioni-Neto, C. A.; O'Brien, P.; Sweigart, D. A. *Inorg. Chem.* **1991**, *30*, 1682.

(23) (a) Zoski, C. G.; Sweigart, D. A.; Stone, N. J.; Rieger, P. H.; Mocellin, E.; Mann, T. F.; Mann, D. R.; Gosser, D. K.; Doeff, M. M.; Bond, A. M. *J. Am. Chem. Soc.* **1988**, *110*, 2109. (b) Amatore, C.; Pflüger, F. *Organometallics* **1990**, *9*, 2276.

(24) Gill, U. S.; Lee, C. C.; Sutherland, R. G. *Synth. React. Inorg. Met.-Org. Chem.* **1984**, *14*, 953.

(25) (a) Treichel, P. M.; Shubkin, R. L.; Barnett, K. W.; Reichard, D. *Inorg. Chem.* **1966**, *5*, 1177. (b) Reger, D. L.; Coleman, C. J. *Organomet. Chem.* **1977**, *131*, 153.

(26) (a) Davison, A.; Green, M. L. H.; Wilkinson, G. *J. Chem. Soc.* **1961**, 3172. (b) Grant, M. E.; Alexander, J. J. *J. Coord. Chem.* **1979**, *9*, 205.

(27) (a) Hammud, H. H.; Moran, G. M. *J. Organomet. Chem.* **1986**, *307*, 255. (b) Brown, D. A.; Fitzpatrick, N. J.; Glass, W. K.; Ahmed, H. A.; Cunningham, D.; McArdle, P. J. *Organomet. Chem.* **1993**, *455*, 157.

(28) Stone, N. J.; Sweigart, D. A.; Bond, A. M. *Organometallics* **1986**, *5*, 2553.

(29) Baer, C. D.; Stone, N. J.; Sweigart, D. A. *Anal. Chem.* **1988**, *60*, 188.

(30) (a) Bullock, J. P.; Boyd, D. C.; Mann, K. R. *Inorg. Chem.* **1987**, *26*, 3086. (b) Pike, R. D.; Alavosus, T. J.; Camaioni-Neto, C. A.; Williams, J. C.; Sweigart, D. A. *Organometallics* **1989**, *8*, 2631.

(31) (a) DigiSim 1.0 program, Bioanalytical Systems, Inc., West Lafayette, IN. (b) Rudolph, M.; Reddy, D. P.; Feldberg, S. W. *Anal. Chem.*, submitted for publication.

until the voltammetric shapes and current ratios closely matched the experimental ones. A reasonable estimate of the precision with which the CO dissociation rate constants were determined is  $\pm 20\%$ .

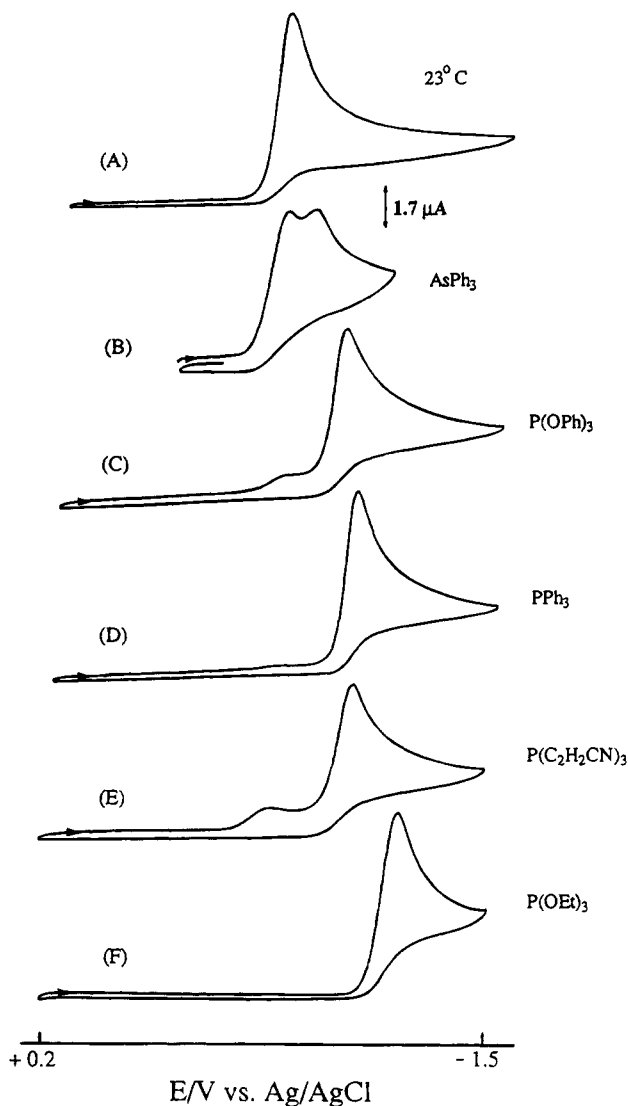
**Molecular Orbital Calculations.** Extended Hückel calculations were carried out on  $1^+$  and  $2^+$  using the CAChe set of computation programs developed by Tektronix. Molecules were constructed using the molecular editor, and bond distances and angles were adjusted to be in agreement with the known X-ray structure of  $[\text{CpFe}(\text{CO})_3]\text{PF}_6$ <sup>32a</sup> and  $[(\text{indenyl})\text{Fe}(\text{CO})_3]\text{PF}_6$  (*vide infra*). The Wolfberg–Helmholz proportionality constant was set to 2.0 in order to be consistent with Hoffmann's calculations on transition metal carbonyl fragments.<sup>32b</sup> Calculations were also performed on the fragment  $\text{Fe}(\text{CO})_3^{2+}$ , with results that agreed with the literature.<sup>32b</sup>

**Crystal Structure of  $[(\text{Indenyl})\text{Fe}(\text{CO})_3]\text{PF}_6$ .** A crystal of  $[2]\text{PF}_6$  was grown by diethyl ether diffusion into a MeCN solution. X-ray analysis was carried out using a Siemens P4 single-crystal diffractometer controlled by XSCANS software.  $\omega$  scans were used for data collection. Data reduction included profile fitting and an empirical absorption correction based on separate azimuthal scans for five reflections (maximum and minimum transmission 0.403 and 0.369). The structure was determined by Patterson methods and refined initially by use of programs in the SHELXTL 5.1 package. Final refinement on  $F^2$  was carried out using SHELXL 93 by G. M. Sheldrick. Non-hydrogen atoms were refined anisotropically, and hydrogen atoms were placed in theoretical positions. As a consequence of the relatively weak diffraction pattern and unresolved disorder in the  $\text{PF}_6^-$  anion, the accuracy of the analysis is less than is typical for small molecules.

**Electron Spin Resonance Studies.** ESR spectra were obtained with a Bruker ER-220D X-band spectrometer, equipped with a Bruker variable-temperature accessory, a Bruker gauss meter, a Systron-Donner microwave frequency counter, and an ASPECT-2000 computer.

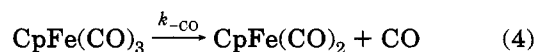
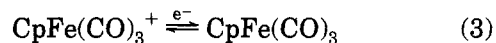
## Results and Discussion

**Reduction of  $\text{CpFe}(\text{CO})_3^+$  ( $1^+$ ).** An investigation of  $1^+$  by cyclic voltammetry showed its reduction (see Figure 2A) to be chemically irreversible under all conditions tried. These included scan rates up to 100 V/s at low temperatures in various solvents: MeCN ( $-43^\circ\text{C}$ ),  $\text{CH}_2\text{Cl}_2$  ( $-45^\circ\text{C}$ ), BuCN ( $-112^\circ\text{C}$ ). Changing the atmosphere from  $\text{N}_2$  to CO, even at  $-112^\circ\text{C}$ , had no effect on the CV. It was previously reported<sup>33</sup> that  $1^+$  forms  $[\text{CpFe}(\text{CO})_2]_2$  ( $\text{Fp}_2$ ) when reduced. We confirmed that reduction either by bulk electrolysis at a platinum electrode or by chemical reduction with  $\text{NEt}_3$  consumes one electron and cleanly converts  $1^+$  into  $\text{Fp}_2$ . The CVs of  $1^+$  gave a second reduction wave with a peak potential that exactly matched that found by us and others<sup>34</sup> for  $\text{Fp}_2$ , which implies that the dimer is formed



**Figure 2.** Cyclic voltammograms of 1.0 mM  $[\text{CpFe}(\text{CO})_3]\text{PF}_6$  in MeCN/0.10 M  $\text{Bu}_4\text{NPF}_6$  under  $\text{N}_2$  at  $23^\circ\text{C}$  in the presence of the indicated nucleophiles: (A) none; (B) 10 mM  $\text{AsPh}_3$ ; (C) 3.0 mM  $\text{P}(\text{OPh})_3$ ; (D) 2.0 mM  $\text{PPh}_3$ ; (E) 2.0 mM  $\text{P}(\text{C}_2\text{H}_4\text{CN})_3$ ; (F) 2.0 mM  $\text{P}(\text{OEt})_3$ . The working electrode was a 1 mm diameter platinum disk, and the scan rate was 0.50 V/s. All potentials are relative to ferrocene ( $E_{1/2} = 0.50$  V).

on the CV time scale, most likely after dissociation of CO from  $1$  as summarized in eqs 3–5. The dimerization



in eq 5 is known<sup>6a,b</sup> from photodissociation experiments with  $\text{Fp}_2$  to be extremely rapid, with  $k_{\text{D}}$  reported as  $3 \times 10^9 \text{ M}^{-1} \text{ s}^{-1}$  at room temperature. Using eqs 3–5 as a model, digital simulations show that  $k_{-\text{CO}}$  must be greater than  $10^3 \text{ s}^{-1}$  at  $-112^\circ\text{C}$  in order for the calculated CV to match the observed chemically irreversible CV obtained at that temperature in BuCN. The conclusion is that  $1$  very rapidly dissociates CO, even at  $-112^\circ\text{C}$ . It is interesting to note that a room-

(32) (a) Gress, M. E.; Jacobson, R. A. *Inorg. Chem.* **1973**, *12*, 1746.

(b) Elian, M.; Hoffmann, R. *Inorg. Chem.* **1975**, *14*, 1058.

(33) Dessy, R. E.; King, R. B.; Waldrop, M. J. *Am. Chem. Soc.* **1966**, *88*, 5112.

(34) (a) Davies, S. G.; Simpson, S. J.; Parker, V. D. *J. Chem. Soc., Chem. Commun.* **1984**, 352. (b) Bullock, J. P.; Palazotto, M. C.; Mann, K. R. *Inorg. Chem.* **1991**, *30*, 1284. (c) Dalton, E. F.; Ching, S.; Murray, R. W. *Inorg. Chem.* **1991**, *30*, 2642.

**Table 1.** Reduction Potentials of ( $\eta^5$ -Cp)Fe(CO) $_2$ L $^+$  ( $3^+$ ) and ( $\eta^5$ -indenyl)Fe(CO) $_2$ L $^+$  ( $4^+$ ) Complexes at 23 °C $^a$ 

complex	L	$E_p^b$	complex	L	$E_{1/2}^c$
1 $^+$	CO	-0.60	2 $^+$	CO	-0.26
3 $^+$	AsPh $_3$	-0.70	4 $^+$	AsPh $_3$	-0.5 $^d$
3 $^+$	P(OPh) $_3$	-0.90	4 $^+$	P(C $_2$ H $_4$ CN) $_3$	-0.53
3 $^+$	PPh $_3$	-0.94	4 $^+$	P(OPh) $_3$	-0.54
3 $^+$	P(C $_2$ H $_4$ CN) $_3$	-0.95	4 $^+$	PPh $_3$	-0.69
3 $^+$	P(OEt) $_3$	-1.11	4 $^+$	P(OMe) $_3$	-0.69
			4 $^+$	diphos	-0.71

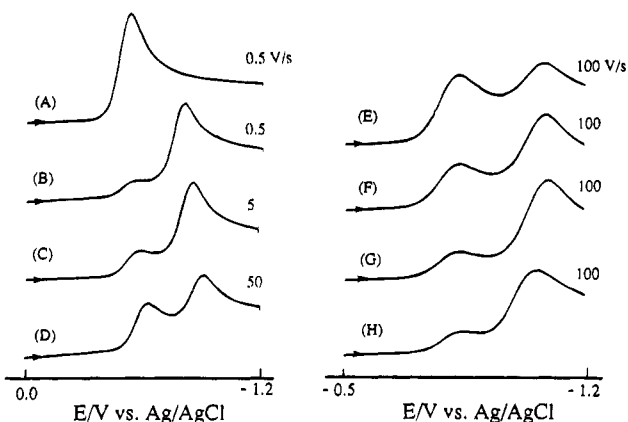
$^a$  All solutions contained Bu $_4$ NPF $_6$  at 0.10 M and electroactive complex as the PF $_6^-$  salt at 1.0 mM. All potentials are relative to ferrocene ( $E_{1/2} = +0.50$  V).  $^b$  These are peak potentials recorded in MeCN solvent at 0.50 V/s.  $^c$  The solvent was CH $_2$ Cl $_2$ .  $^d$  The reduction is chemically irreversible;  $E_{1/2}$  was estimated from the value of  $E_p$  at 0.5 V/s.

temperature value as great as 10 $^7$  s $^{-1}$  for  $k_{-CO}$  only requires a small activation energy for CO dissociation (e.g., 25 kJ).

Upon addition of a phosphine, phosphite, or arsine nucleophile, the CV of 1 $^+$  changed as indicated in Figure 2. The wave due to the reduction of 1 $^+$  almost completely vanished (except with AsPh $_3$ ), and a new wave appeared at a more negative potential. IR spectra recorded after the electrochemical experiments verified that no reaction had occurred in the bulk solution. This behavior suggested that CO substitution by nucleophile (L) had occurred by an ETC pathway to produce CpFe(CO) $_2$ L $^+$  ( $3^+$ ), which was responsible for the new reduction wave. In accordance with this interpretation, genuine samples of 3 $^+$  were found to be reduced at potentials identical with those in Figure 2. Furthermore, adding a trace of reducing agent (NEt $_3$ , Na/Pb, BH $_4^-$ ) to a solution of 1 $^+$  and L led to the immediate and quantitative formation of 3 $^+$ , as judged from IR spectra. Bulk electrolysis of 1 $^+$  in the presence of P-donors led to total conversion to 3 $^+$  after passage of less than 1 mol % of electrons; in most experiments ca. 0.1 mol % was sufficient. It is clear, therefore, that 1 $^+$  is converted to 3 $^+$  by an efficient ETC process. Indeed, we chose to use this chemistry for the simple and convenient synthesis of 3 $^+$  complexes (see Experimental Section). In this regard, it is pertinent to note a report $^8$  that CO substitution in CpFe(CO) $_2$ P(OEt) $_3^+$  by excess P(OEt) $_3$  is catalyzed by a chemical reducing agent (Cp $_2$ -Co), which suggests that an ETC pathway may be useful for multiple CO substitutions.

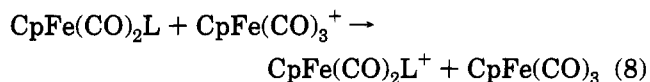
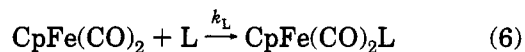
Table 1 lists the relevant reduction potential data for 1 $^+$  and 3 $^+$ . Some of these potentials were reported previously. $^{26b}$  As can be seen in Figure 2, 3 $^+$  is reduced in a chemically irreversible manner. Scanning to more negative potentials gave a wave corresponding to Fp $_2$ . Earlier work suggested $^{8,33}$  that 3 $^+$  (L = PPh $_3$ , P(OEt) $_3$ ) forms Fp $_2$  upon reduction, and we verified via bulk electrolysis that this is the case for CpFe(CO) $_2$ PPh $_3^+$ .

Figure 3 gives the voltammograms of 1 $^+$  in the presence of P(OPh) $_3$  as a function of scan rate, nucleophile concentration, and temperature. Curves B–E show that at fixed [P(OPh) $_3$ ] the ratio of the current due to 1 $^+$  to that due to 3 $^+$ ,  $i(1^+)/i(3^+)$ , increases markedly with scan rate. Curves E–G indicate that  $i(1^+)/i(3^+)$  decreases with increasing [P(OPh) $_3$ ]. Finally, curves E and H show that the current ratio decreases as the temperature is lowered. In these and all other experiments with 1 $^+$  in the presence of a nucleophile, including AsPh $_3$ , it was found that switching from N $_2$  to an atmosphere of CO had no effect on the voltammograms.



**Figure 3.** Voltammograms of 1.0 mM [CpFe(CO) $_3$ ]PF $_6$  in MeCN/0.10 M Bu $_4$ NPF $_6$  as a function of varying concentrations of P(OPh) $_3$  and scan rate. All experiments were at 23 °C except (H), which was at -45 °C. The values of [P(OPh) $_3$ ] (in mM units) were as follows: (A) 0; (B–E) 2.0; (F) 6.0; (G) 10; (H) 2.0. The working electrode was a platinum disk of diameter 1 mm for A–C and 100  $\mu$ m for D–H. All potentials are relative to ferrocene ( $E_{1/2} = 0.50$  V). Currents are normalized for display purposes.

The ETC substitution of CO by L in 1 $^+$  can be analyzed by reference to Scheme 2 or, more explicitly, by considering eqs 3–5 in conjunction with eqs 6–8. The



most striking experimental observation is the diminution or complete disappearance of the reduction wave due to 1 $^+$  when a nucleophile is present (Figure 2). This occurs because the reduction to CpFe(CO) $_3$  is followed by rapid substitution to give CpFe(CO) $_2$ L, which is oxidized at potentials near the reduction wave of 1 $^+$ . In addition, the disproportionation reaction given in eq 8 is highly favored and serves to remove 1 $^+$  from the vicinity of the electrode and thereby decrease the current. Of course, in order for  $i(1^+)$  to vanish, it is necessary for  $k_{-CO}$  to be sufficiently large. If  $k_{-CO}$  is large enough, then competition between eqs 5 and 6 determines the relative magnitude of  $i(1^+)$ , which will be nonzero to the extent that CpFe(CO) $_2$  ends up as the dimer Fp $_2$ . As noted above, the experimental results without nucleophile present showed that  $k_{-CO}$  is greater than 10 $^3$  at -112 °C. In the presence of nucleophile, digital simulations of the mechanism defined by eqs 3–8 indicate that it is possible for  $i(1^+)$  to vanish, provided  $k_L$  is sufficiently large, only if  $k_{-CO}$  is at least 10 $^4$  times the experimental scan rate. Precisely this behavior was observed with the nucleophile P(OEt) $_3$  at 100 V/s and 23 °C, from which we infer that  $k_{-CO} > 10^6$  s $^{-1}$ . Indeed, similar results from experiments at -45 °C imply that  $k_{-CO} > 3 \times 10^5$  s $^{-1}$  at this temperature. The conclusion is that dissociation of CO from CpFe(CO) $_3$  is extremely rapid, probably being greater than 10 $^7$  s $^{-1}$  at room temperature. Furthermore, the observed lack of any effect of excess CO on the CV's with or without nucleophile present means that even under conditions in



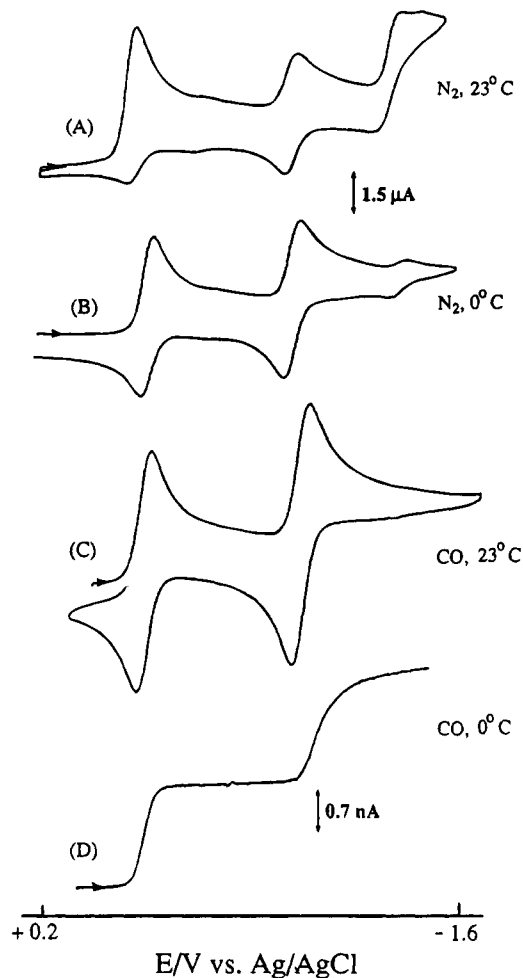
which the reverse of eq 4 could be expected to contribute, the net rate of CO dissociation remains large enough so that only "limiting" behavior is observed.

This establishes that  $k_{-CO}$  is large enough so that any nonzero value for  $i(1^+)$  cannot be attributed to "slow" CO dissociation from **1**. Rather, nonzero  $i(1^+)/i(3^+)$  ratios, as in Figure 3, indicate that dimerization ( $k_D$ ) and nucleophile addition ( $k_L$ ) compete. This competition is illustrated by curves E–G in Figure 3, which show  $i(1^+)/i(3^+)$  decreasing as the nucleophile concentration, and hence the rate of eq 6, increases. It may also be noted from curves B–E that  $i(1^+)/i(3^+)$  increases with scan rate. This is a consequence of the dimerization being *second* order in complex. Curves E and H show further that  $i(1^+)/i(3^+)$  decreases as the temperature is lowered at fixed scan rate and nucleophile concentration. From this observation, it may be inferred that  $k_D$  is more sensitive to temperature than is  $k_L$ , i.e.,  $\Delta H^\ddagger(k_D) > \Delta H^\ddagger(k_L)$ .

The ratio  $i(1^+)/i(3^+)$  was found to be nearly zero under many experimental conditions, from which it may be concluded that the rate of nucleophile addition to the 17-electron  $\text{CpFe}(\text{CO})_2$  (eq 6) must be very large and can easily dominate the dimerization rate. Since it is known<sup>6a,b</sup> that  $k_D$  is ca.  $10^9 \text{ M}^{-1} \text{ s}^{-1}$ , it is possible to determine  $k_L$  from an analysis of data typified by that in Figure 3. By matching of the experimental data to digital simulations of eqs 3–8 and using the assumption that  $k_D = 10^9 \text{ M}^{-1} \text{ s}^{-1}$ , the following reactivity order was obtained ( $k_L$  at 23 °C in units of  $\text{M}^{-1} \text{ s}^{-1}$  given in parentheses):  $\text{P}(\text{OEt})_3$  ( $> 10^9$ ),  $\text{PPh}_3$  ( $2 \times 10^8$ ),  $\text{P}(\text{OPh})_3$  ( $5 \times 10^7$ ),  $\text{P}(\text{C}_2\text{H}_4\text{CN})_3$  ( $3 \times 10^7$ ),  $\text{AsPh}_3$  ( $8 \times 10^5$ ). This reactivity order is typical for nucleophilic attack on an organometallic complex.<sup>35</sup> There are several values of  $k_L$  for eq 6 reported in the literature with which our results may be compared. Fast time-resolved IR spectroscopy following photolysis of  $\text{Fp}_2$  in the presence of  $\text{P}(\text{OMe})_3$  was used<sup>7</sup> to measure  $k_L$  as  $9 \times 10^8 \text{ M}^{-1} \text{ s}^{-1}$  for this nucleophile. Disproportionation of  $\text{Fp}_2$  with diphos present was interpreted<sup>8</sup> as occurring by a radical chain mechanism in which  $k_L$  for diphos addition to  $\text{CpFe}(\text{CO})_2$  to give  $\text{CpFe}(\text{CO})_2(\eta^1\text{-diphos})$  was estimated as  $3 \times 10^7 \text{ M}^{-1} \text{ s}^{-1}$ . Thus, reported values of  $k_L$  are comparable to those found in the present study and this lends credence to the proposed mechanistic scheme in which ligand substitution at the 19-electron  $\text{CpFe}(\text{CO})_3$  occurs by CO dissociation to give the 17-electron intermediate  $\text{CpFe}(\text{CO})_2$ , which is then trapped by nucleophile.

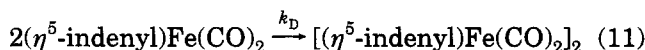
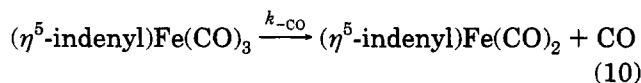
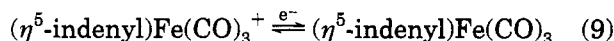
An alternative interpretation of the electrochemical data in terms of an associative mechanism for CO substitution in **1** (perhaps with a  $\eta^3\text{-Cp}$  ligand) is inconsistent with the observed rapid formation of  $\text{Fp}_2$ , with the results obtained with the indenyl analogue of **1**<sup>+</sup>, and with the results of MO calculations (*vide infra*).

**Reduction of (Indenyl)Fe(CO)<sub>3</sub><sup>+</sup> (2<sup>+</sup>).** The behavior of the indenyl complex **2**<sup>+</sup> contrasts sharply with that of the Cp analogue **1**<sup>+</sup>. Figure 4A shows that reduction at 23 °C under N<sub>2</sub> is characterized by two partially reversible couples ( $E_{1/2} = -0.26, -0.94 \text{ V}$ ) and a third irreversible one at  $E_p \approx -1.45 \text{ V}$ . Changing to an atmosphere of CO and/or lowering the temperature to 0 °C resulted in the virtual disappearance of the third reduction wave, while the first two became reversible



**Figure 4.** Cyclic voltammograms of 0.90 mM [(indenyl)Fe(CO)<sub>3</sub>]PF<sub>6</sub> in CH<sub>2</sub>Cl<sub>2</sub>/0.10 M Bu<sub>4</sub>NPF<sub>6</sub> under N<sub>2</sub> or CO at the indicated temperatures. Experiments A–C were at 0.50 V/s with a 1 mm diameter glassy-carbon-disk working electrode. Experiment D was at 20 mV/s with a 10 μm diameter gold electrode. All potentials are relative to ferrocene ( $E_{1/2} = 0.50 \text{ V}$ ).

one-electron couples (curves B and C). Experiments with the indenyl dimer [(indenyl)Fe(CO)<sub>2</sub>]<sub>2</sub> (**5**) showed that it is irreversibly reduced with  $E_p \approx -1.45 \text{ V}$ . We, therefore, ascribe the third wave in Figure 4A to the reduction of **5**, apparently formed as a decomposition product upon electron transfer to **2**<sup>+</sup>. Most likely, **5** is formed in much the same manner as  $\text{Fp}_2$  is formed from **1**, namely CO dissociation followed by dimerization (eqs 9–11). However, in contrast to the behavior of **1**, the



CO dissociation is readily inhibited and dimer formation quenched by the presence of an CO atmosphere or by a modest lowering of the temperature (or increase in scan rate). Under these conditions, **2** is relatively stable and undergoes reversible reduction to **2**<sup>-</sup> (*vide infra*) at  $E_{1/2} = -0.94 \text{ V}$ .

(35) Howell, J. A. S.; Burkinshaw, P. M. *Chem. Rev.* **1983**, *83*, 557.

Chemical reduction of  $2^+$  in  $\text{CH}_2\text{Cl}_2$  at  $23^\circ\text{C}$  by Na/Pb alloy gave the dimer **5** cleanly, as did reduction with an IR-OTTLE cell under the same conditions. However, an IR-OTTLE experiment at  $-20^\circ\text{C}$  showed that  $2^+$  is converted initially into a tricarbonyl species having IR bands at 2035 and 1957 (br)  $\text{cm}^{-1}$ . These IR bands match those previously assigned to the neutral (indenyl) $\text{Fe}(\text{CO})_3$  radical (**2**), which was detected<sup>36</sup> during photolysis of the dimer **5** in the presence of CO. Bulk electrolysis of  $2^+$  or **5** at  $-2\text{ V}$  under CO at  $0^\circ\text{C}$  led to formation of  $2^-$  ( $\nu_{\text{CO}}$  1952, 1890, 1869  $\text{cm}^{-1}$  in  $\text{CH}_2\text{Cl}_2$ ); this is known<sup>19</sup> complex that can be synthesized by the irreversible addition of CO to (indenyl) $\text{Fe}(\text{CO})_2^-$ . A structural study<sup>19</sup> showed that  $2^-$  is an 18-electron complex with a slipped ring, i.e.,  $(\eta^3\text{-indenyl})\text{Fe}(\text{CO})_3^-$ .

The electrochemical and IR experiments under CO or below  $0^\circ\text{C}$  show that  $2^+$  is reduced in two reversible 1-electron steps corresponding to the couples  $2^+/2$  and  $2/2^-$ . Since  $2^+$  is known to have an 18-electron  $\eta^5$ -indenyl structure and  $2^-$  is known to be an 18-electron  $\eta^3$ -indenyl complex, the obvious point of interest is the bonding mode in **2**. The much greater stability of **2** in comparison to **1** with respect to loss of CO suggests that **2** may contain a slipped  $\eta^3$ -indenyl ligand; i.e., it is a 17-electron complex. There is precedence for such a structure, namely,  $(\eta^3\text{-indenyl})(\eta^5\text{-indenyl})\text{V}(\text{CO})_2$ .<sup>18e</sup> Indeed, an  $\eta^3$ -indenyl structure has already been suggested for **2** by Wrighton et al.;<sup>36</sup> the basis of this assignment was the similarity of the IR  $\nu_{\text{CO}}$  bands of **2** and the 17-electron complex  $(\eta^3\text{-C}_3\text{H}_5)\text{Fe}(\text{CO})_3$ . As these authors noted, however, the similarity of the IR bands does not unambiguously prove that **2** has a slipped indenyl ring. In fact, a close examination of the IR frequencies indicates to us that the 19-electron structure is the more likely. The  $\nu_{\text{CO}}$  frequencies are slightly lower for **2** than for  $(\eta^3\text{-C}_3\text{H}_5)\text{Fe}(\text{CO})_3$ , which would not be expected if **2** were a 17-electron complex due to an anticipated "substituent" effect. Another observation relates to the change in  $\nu_{\text{CO}}$  for the  $2^+ \rightarrow 2$  transformation. The average  $\nu_{\text{CO}}$  value increases by  $80\text{ cm}^{-1}$ . This is less by about  $30\text{ cm}^{-1}$  than the change observed<sup>4i,37</sup> for the oxidation of (arene) $\text{Cr}(\text{CO})_3$  to the monocation, an  $18e^- \rightarrow 17e^-$  transformation. Accordingly, if  $2^- \rightarrow 2$  were an  $18e^- \rightarrow 17e^-$  process, it seems likely that  $\Delta\nu_{\text{CO}}$  would be greater than  $80\text{ cm}^{-1}$ . In any case we conclude that a reliable distinction between an  $\eta^3$ - and  $\eta^5$ -structure for **2** cannot be made from  $\nu_{\text{CO}}$  frequencies alone.

There are, however, two very good reasons to believe that **2** is a 19-electron complex and does not contain an  $\eta^3$ -indenyl group. The first reason relates to the mechanism of CO substitution in **2**, which will be shown below to be strictly dissociative. If **2** were a 17-electron complex, it would be expected to react by an associative mechanism.<sup>4</sup> The second argument in favor of **2** being a 19-electron complex is to be found in Figure 4D. This is a steady-state voltammogram obtained with a  $10\text{ }\mu\text{m}$  diameter gold microelectrode operating at  $20\text{ mV/s}$ . The two chemically reversible waves can be analyzed as previously described<sup>22</sup> to obtain an estimate of the rate of heterogeneous charge transfer. The first wave is characterized by  $E_{1/2} = -0.25\text{ V}$  and  $E_{1/4} - E_{3/4} = 55 \pm$

4 mV. The value of  $E_{1/4} - E_{3/4}$  indicates a Nernstian or electrochemically reversible charge transfer; i.e., the electron transfer is fast. The second wave is clearly broadened relative to the first and has  $E_{1/2} = -1.02\text{ V}$  and  $E_{1/4} - E_{3/4} = 115 \pm 10\text{ mV}$ . The  $E_{1/2}$  value for this  $2/2^-$  couple is shifted negative relative to the average of the cathodic and anodic peak potentials in the transient CV (curve C), and the  $E_{1/4} - E_{3/4}$  parameter is far from Nernstian. In fact, this parameter is near the anticipated<sup>22</sup> value for totally irreversible charge transfer; i.e., the electron transfer is slow. It is well documented<sup>38</sup> that ring slippage accompanying a redox process is often evidenced by a slow rate of electron transfer. The obvious interpretation in the present case is that the  $\eta^5 \rightarrow \eta^3$  slippage occurs upon the reduction of **2** to  $2^-$ ; i.e., **2** does not contain an  $\eta^3$ -indenyl ligand. It would be difficult indeed to explain the observed microelectrode results in terms of substantial molecular rearrangement in the Nernstian  $2^+ \rightarrow 2$  step while the  $2 \rightarrow 2^-$  step, which would then involve little rearrangement, is decidedly non-Nernstian. It may be added at this point that the voltammogram in Figure 4D nicely illustrates the advantages of microelectrodes over conventionally sized ones for the measurement of rates of charge transfer. It would be most difficult to eliminate ohmic polarization distortions from curve C to the extent necessary, and even then the  $2/2^-$  couple would probably be quasi-reversible electrochemically. Microelectrodes in the steady state domain are more sensitive to charge transfer effects and lead to much less distortion; indeed, the very fact that the  $2^+/2$  couple in Figure 4D is Nernstian is proof of the absence of ohmic distortion.

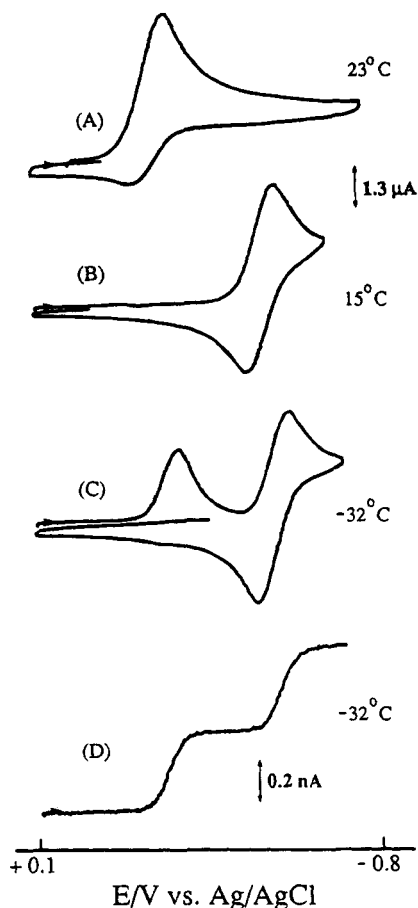
In the presence of P-donor nucleophiles (also  $\text{AsPh}_3$ ) it was found that  $2^+$  undergoes facile CO substitution by an ETC mechanism, in analogy to the behavior of  $1^+$  (*vide supra*). For example, a solution of  $2^+$  and  $\text{P}(\text{O}Ph)_3$  in  $\text{CH}_2\text{Cl}_2$  in the dark gave no reaction overnight but reacted immediately upon the addition of a trace of a dilute solution of  $\text{NET}_3$  to give  $(\text{indenyl})\text{Fe}(\text{CO})_2\text{P}(\text{O}Ph)_3^+$ . Other nucleophiles behaved similarly, except that thermal CO substitution would occasionally occur within 30 min without the intentional addition of a reducing agent. Such behavior was not reproducible and is probably due to adventitious reductants that initiate an ETC process. The considerably more positive  $E_{1/2}$  of  $2^+$  compared to that of  $1^+$  (Table 1) means that  $2^+$  should be more susceptible to trace reducing impurities, and this may account for the apparent<sup>27b</sup> greater ease of thermal substitution in  $2^+$ .

The electrochemical behavior of  $2^+$  in the presence of nucleophiles is typified by Figures 5 and 6. If we look first at Figure 5A,B, it can be seen that the reduction wave for  $2^+$  was completely suppressed by the addition of  $5\text{ mM P}(\text{O}Ph)_3$ . A new reversible couple appeared at a more negative potential, and this is assigned to  $4^+/4$ , which was verified by comparison to a genuine sample of  $4^+$ . (Table 1 provides a data summary for all nucleophiles studied.) Lowering the temperature below  $15^\circ\text{C}$  caused the reappearance of a wave due to  $2^+$ ; Figure 5C shows that at  $-32^\circ\text{C}$  the current ratio  $i(2^+)/i(4^+)$  is about 0.7. Significantly, increasing the nucleo-

(36) Wu, Y.-M.; Zou, C.; Wrighton, M. S. *J. Am. Chem. Soc.* **1987**, *109*, 5861.

(37) Meng, Q.; Huang, Y.; Ryan, W. J.; Sweigart, D. A., to be submitted for publication.

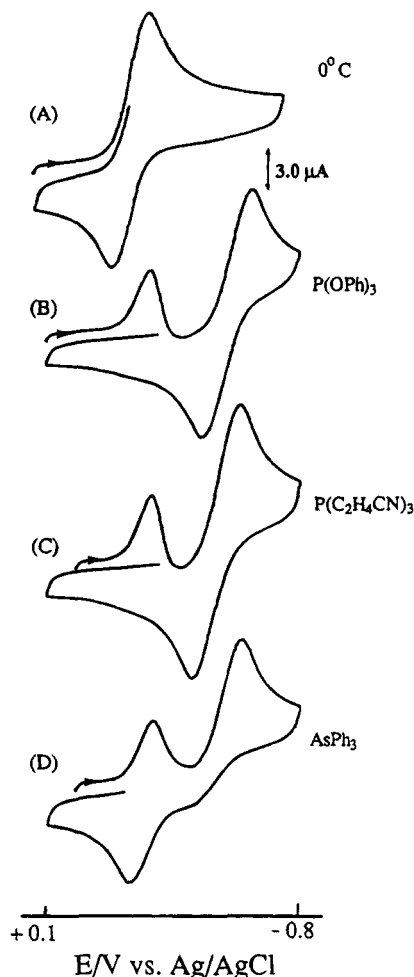
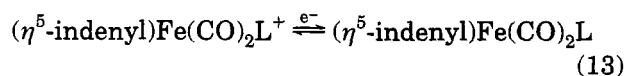
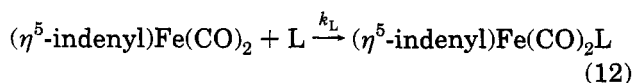
(38) (a) Nielson, R. M.; Weaver, M. J. *Organometallics* **1989**, *8*, 1636. (b) Merkert, J.; Nielson, R. M.; Weaver, M. J.; Geiger, W. E. *J. Am. Chem. Soc.* **1989**, *111*, 7084. (c) Pierce, D. T.; Geiger, W. E. *J. Am. Chem. Soc.* **1989**, *111*, 7636. (d) Pierce, D. T.; Geiger, W. E. *J. Am. Chem. Soc.* **1992**, *114*, 6063.



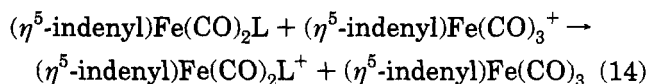
**Figure 5.** Cyclic voltammograms of 0.90 mM [(indenyl)-Fe(CO)<sub>3</sub>]PF<sub>6</sub> in CH<sub>2</sub>Cl<sub>2</sub>/0.10 M Bu<sub>4</sub>NPF<sub>6</sub> under N<sub>2</sub> at the indicated temperatures. Experiments B–D contained 5.0 mM P(OPh)<sub>3</sub>. For A–C the scan rate was 0.50 V/s with a 1 mm diameter glassy-carbon-disk working electrode. Experiment D was at 20 mV/s with a 10 μm diameter gold electrode. All potentials are relative to ferrocene ( $E_{1/2} = 0.50$  V).

phile concentration had no effect on the CV in curve C. The current ratio  $i(2^+)/i(4^+)$  was also found to increase as the scan rate increased at a fixed temperature. For example, the CV's for three nucleophiles at 5 V/s are shown in Figure 6. Note that the three CV's have very similar values of  $i(2^+)/i(4^+)$ . The electrochemical results obtained for the reduction of 2<sup>+</sup> in the presence of a variety of nucleophiles and under various conditions can be summarized as follows. (1) Switching from an atmosphere of N<sub>2</sub> to CO retarded the CO substitution ( $i(2^+)/i(4^+)$  increased), but only at low concentrations of nucleophile. (2) Under an N<sub>2</sub> atmosphere, the nucleophile concentration did not affect  $i(2^+)/i(4^+)$  for [Nu] ≥ 4 mM. (3) All nucleophiles gave nearly the same limiting value of  $i(2^+)/i(4^+)$  (e.g., see Figure 6).

These observations constitute strong evidence that (indenyl)Fe(CO)<sub>3</sub> (2) undergoes CO substitution by a dissociative pathway. The ETC mechanism proposed consists of eqs 9–14. This is identical with that



**Figure 6.** Cyclic voltammograms of 0.80 mM [(indenyl)-Fe(CO)<sub>3</sub>]PF<sub>6</sub> in CH<sub>2</sub>Cl<sub>2</sub>/0.10 M Bu<sub>4</sub>NPF<sub>6</sub> under N<sub>2</sub> at 0 °C and a scan rate of 5.0 V/s. Experiments B–D contained the indicated nucleophiles at a concentration of 4.0 mM. The working electrode was 1 mm diameter glassy carbon disk. All potentials are relative to ferrocene ( $E_{1/2} = 0.50$  V).



assigned to CpFe(CO)<sub>3</sub><sup>+</sup>, but with the important difference that the dimerization reaction (eq 11) can be ignored because no dimer (5) formed in any reductions of 2<sup>+</sup> with a nucleophile present.<sup>39</sup> According to this mechanism, the rate-determining step in the ETC substitution reaction 2<sup>+</sup> + L → 4<sup>+</sup> is CO dissociation from the 19-electron 2 to give the 17-electron intermediate (η<sup>5</sup>-indenyl)Fe(CO)<sub>2</sub>, which is rapidly trapped by L. Quite unlike the case with 1<sup>+</sup>, the CV's only show a nonzero current for  $i(2^+)$  when  $k_{-\text{CO}}$  is too small with respect to the experimental time scale to allow complete dissociation (e.g., Figure 5C). The dimerization step ( $k_D$ ) is not important and does not compete with nucleophile addition to the 17-electron intermediate after CO loss, again unlike the situation with the Cp system. The reason that all nucleophiles give essentially the same value of  $i(2^+)/i(4^+)$  and that the CV's are insensitive to nucleophile concentration is simply because the extent

(39) Alternatively, it is sufficient to note that the 2<sup>+</sup>/2 couple is chemically reversible under the experimental conditions of temperature and scan rate that were utilized in comparisons to digital simulations.

to which the substitution reaction occurs is controlled by the rate-determining CO dissociation.

In spite of the apparent differences exhibited by the voltammograms for the Cp and indenyl systems, the mechanism of CO substitution in the two 19-electron species, (dienyl)Fe(CO)<sub>3</sub>, is qualitatively the same, namely, dissociation of CO followed by nucleophile addition. Digital simulation of the mechanism defined by eqs 9–14 (omitting eq 11) accurately reproduced the CVs. The disproportionation reaction (eq 14) plays a dominant role in the chemistry observed. This can be inferred from the magnitude of *i*(2<sup>+</sup>) on the second cycle of multiple-scan CVs. For example, Figure 5C and Figure 6B,C show that *i*(2<sup>+</sup>) is zero on the second cycle. This occurs because eq 14 removes 2<sup>+</sup> from the electrode vicinity. Simulations indicate that the rate constant for eq 14 must be at least 10<sup>4</sup> M<sup>-1</sup> s<sup>-1</sup>. Happily, however, it is not necessary to more accurately define this constant because the first CV cycle, from which the rate data were extracted, is predicted to be relatively little influenced by eq 14. An analysis of the data with P(OPh)<sub>3</sub> as the nucleophile over the temperature range -45 to -3 °C gave the following activation parameters for *k*<sub>-CO</sub> from **2**: Δ*H*<sup>‡</sup> = 52 ± 5 kJ, Δ*S*<sup>‡</sup> = 0 ± 20 J K<sup>-1</sup>.

The rate constant for CO dissociation from **2** was also determined over the temperature range -42 to -26 °C via steady-state voltammetry with a 10 μm diameter gold microelectrode. Figure 5D shows the voltammogram obtained at -32 °C, which may be compared to its companion voltammogram in Figure 5C obtained under transient conditions with a 1 mm diameter electrode. The steady-state curve has two current plateaus for the same reason the transient one has two reduction waves. Both steady-state waves are electrochemically reversible, suggesting, as noted above, that the one-electron reduction of 2<sup>+</sup> and 4<sup>+</sup> occurs without ring slippage. The rate of the substitution reaction **2** + L → **4** is reflected in the relative currents of the steady-state waves. Digital simulations, when compared to experiment, gave activation parameters for *k*<sub>-CO</sub> essentially identical with those obtained from conventional CVs (*vide supra*). Thus, it may be concluded that microelectrodes in the steady-state mode can be usefully applied to yield simultaneous information about the rate of electron transfer and the rate of coupled homogeneous reactions.

In conclusion, the electrochemical studies have established that CO substitution is strictly dissociative and much more rapid in the 19-electron radicals **1** and **2** than in the respective 18-electron cations. In addition, it has been shown that **1** is at least 10<sup>6</sup> times more reactive than **2** with respect to CO dissociation (*k*<sub>-CO</sub>(**1**) > 10<sup>6</sup>*k*<sub>-CO</sub>(**2**)) and, as a consequence, CO substitution occurs much more slowly in the indenyl complex **2**. In other words, there is an *inverse* indenyl effect for CO substitution in **1** and **2**. This is perhaps surprising in view of the *similar* rates for CO dissociation from the 19-electron complexes (MeCp)Mn(CO)<sub>2</sub>NO and (indenyl)Mn(CO)<sub>2</sub>NO.<sup>13</sup> It may be noted that most of the studies of 1<sup>+</sup> were conducted in MeCN solvent, whereas reactions of 2<sup>+</sup> were done in CH<sub>2</sub>Cl<sub>2</sub>. Different solvents were used for solubility and incidental reasons. However, cross checks showed that the reaction rates reported in this study are *very* similar (in fact, identical within error) in both solvents.

Table 2. Summary of Crystal Structure Data for [(η<sup>5</sup>-indenyl)Fe(CO)<sub>3</sub>]PF<sub>6</sub>

formula	C <sub>12</sub> H <sub>7</sub> FeO <sub>3</sub> PF <sub>6</sub>
fw	400.00
space group	<i>Pnma</i> , orthorhombic
cryst dimens, mm	0.31 × 0.26 × 0.25
scan type	<i>ω</i>
temp, K	298(2)
<i>a</i> , Å	9.7911(8)
<i>b</i> , Å	7.5975(11)
<i>c</i> , Å	19.909(2)
<i>V</i> , Å <sup>3</sup>	1481.0(3)
<i>Z</i>	4
<i>ρ</i> <sub>calcd</sub> , g cm <sup>-3</sup>	1.794
<i>F</i> (000)	792
radiation	Mo Kα (0.710 73 Å)
<i>μ</i> , cm <sup>-1</sup>	12.02
2θ limits, deg	2.05–25.00
no. of reflns collected	1923
no. of indep reflns	1405
no. of variables	118
R1 <sup>a</sup>	0.075 ( <i>I</i> > 2σ( <i>I</i> ))
wR2 <sup>b</sup>	0.204
GOF	0.935 <sup>c</sup>

<sup>a</sup> R1 = Σ||*F*<sub>o</sub> - |*F*<sub>c</sub>||/Σ|*F*<sub>o</sub>|. <sup>b</sup> wR2 = [Σw(*F*<sub>o</sub><sup>2</sup> - *F*<sub>c</sub><sup>2</sup>)<sup>2</sup>/Σw*F*<sub>o</sub><sup>4</sup>]<sup>1/2</sup>. <sup>c</sup> Based on *F*<sup>2</sup>.

It seems likely that the inverse indenyl effect is a reflection of the more extensively conjugated π-system in 2<sup>+</sup> as compared to 1<sup>+</sup>, thus allowing for greater charge delocalization upon reduction to the 19-electron radical. In this manner **2** would be stabilized relative to **1**. This is somewhat analogous to the greater stability (with respect to decomposition) of (η<sup>4</sup>-naphthalene)Cr(CO)<sub>3</sub><sup>2-</sup> in comparison to (η<sup>4</sup>-benzene)Cr(CO)<sub>3</sub><sup>2-</sup>, in which the arene ring is known<sup>40</sup> to slip to η<sup>4</sup>-bonding when the neutral precursors are reduced by two electrons, thus maintaining an 18-electron count. The inverse indenyl effect described herein, however, refers to 19-electron species and does not involve ring slippage. The next section presents a simple molecular orbital interpretation of this phenomenon, together with an explanation for its absence in the manganese radical (indenyl)Mn(CO)<sub>2</sub>NO.

**Molecular Orbital Comparison of Complexes 1 and 2.** In order to better understand the reactivity order **1** ≫ **2**, extended Hückel calculations were performed on 1<sup>+</sup> and 2<sup>+</sup>. The geometry of 1<sup>+</sup> was obtained from a published X-ray structure.<sup>32a</sup> The bond lengths and angles for 2<sup>+</sup> were taken from the X-ray structure of [**2**]PF<sub>6</sub>, which was determined in the present study. Tables 2 and 3 and Figure 7 provide relevant crystallographic and structural data for 2<sup>+</sup>. The rotational position of the Fe(CO)<sub>3</sub> fragment is such that one of the highly linear Fe–C–O linkages eclipses the indenyl C(1) carbon. This results in a highly symmetrical structure with a mirror plane perpendicular to the indenyl ligand. The bond distances and angles in 2<sup>+</sup> are analogous to those found in studies of other indenyl complexes.<sup>27b,18e,41</sup> The principal structural features for 2<sup>+</sup> are a highly

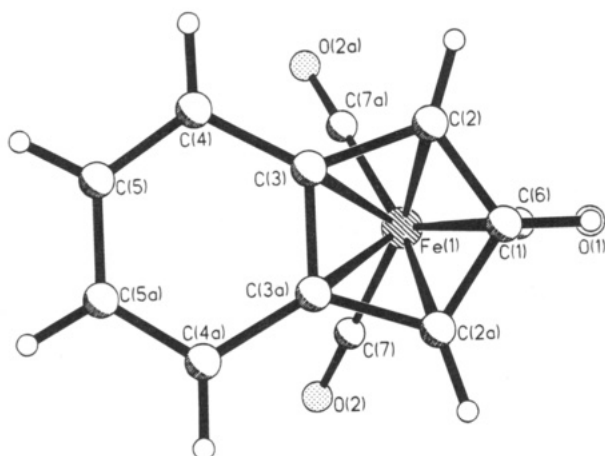
(40) (a) Rieke, R. D.; Henry, W. P.; Arney, J. S. *Inorg. Chem.* **1987**, *26*, 420. (b) Weay, H. G.; Butenschön, H. *Angew. Chem., Int. Ed. Engl.* **1990**, *29*, 1444.

(41) (a) Nesmeyanov, A. N.; Ustynyuk, N. A.; Makarova, L. G.; Andrianov, V. G.; Struchkov, Y. T.; Andrae, S.; Ustynyuk, Y. A.; Malyugina, S. G. *J. Organomet. Chem.* **1978**, *159*, 189. (b) Honan, M. B.; Atwood, J. L.; Bernal, I.; Herrmann, W. A. *J. Organomet. Chem.* **1979**, *179*, 403. (c) Allen, S. R.; Baker, P. K.; Barnes, S. G.; Bottrill, M.; Green, M.; Orpen, A. G.; Williams, I. D.; Welch, A. J. *J. Chem. Soc., Dalton Trans.* **1983**, 927. (d) Faller, J. W.; Crabtree, R. H.; Habib, A. *Organometallics* **1985**, *4*, 929.

**Table 3.** Selected Bond Lengths (Å) and Bond Angles (deg) for  $[(\eta^5\text{-indenyl})\text{Fe}(\text{CO})_3]\text{PF}_6^a$ 

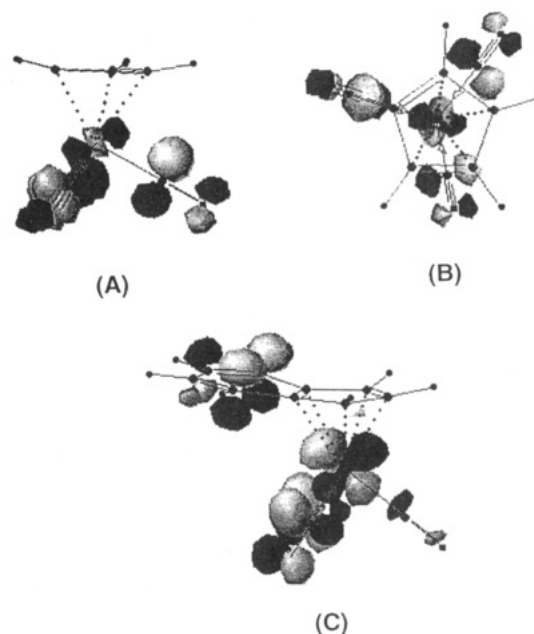
Bond Lengths			
Fe—C(1)	2.037(11)	O(2)—C(7)	1.121(11)
Fe—C(2)	2.086(8)	O(2a)—C(7a)	1.121(11)
Fe—C(2a)	2.086(8)	C(1)—C(2)	1.387(12)
Fe—C(3)	2.166(7)	C(1)—C(2a)	1.387(12)
Fe—C(3a)	2.166(7)	C(2)—C(3)	1.442(11)
Fe—C(6)	1.780(12)	C(3)—C(3a)	1.393(14)
Fe—C(7)	1.787(11)	C(3)—C(4)	1.435(11)
Fe—C(7a)	1.787(11)	C(4)—C(5)	1.332(12)
O(1)—C(6)	1.130(13)	C(5)—C(5a)	1.340(20)
Bond Angles			
C(7)—Fe—C(7a)	97.3(7)	C(7)—Fe—C(3a)	89.9(3)
C(7)—Fe—C(6)	93.6(4)	C(2)—C(1)—C(2a)	111.8(12)
C(6)—Fe—C(1)	88.7(5)	C(1)—C(2)—C(3)	105.8(9)
C(7)—Fe—C(2)	155.3(4)	C(3a)—C(3)—C(4)	119.4(5)
C(7a)—Fe—C(2)	94.7(4)	C(3a)—C(3)—C(2)	108.3(5)
C(1)—Fe—C(2)	39.3(3)	C(4)—C(3)—C(2)	132.3(8)
C(6)—Fe—C(2a)	107.2(4)	C(4)—C(3)—Fe	127.5(5)
C(2)—Fe—C(2a)	66.9(6)	C(5)—C(4)—C(3)	117.1(9)
C(6)—Fe—C(3)	146.8(4)	C(4)—C(5)—C(5a)	123.4(6)
C(1)—Fe—C(3)	64.8(4)	O(1)—C(6)—Fe	177.0(11)
C(2)—Fe—C(3)	39.6(3)	O(2)—C(7)—Fe	177.1(9)

<sup>a</sup> Symmetry transformation used to generate equivalent atoms labeled "a":  $x, -y + 1/2, z$ .

**Figure 7.** Structural drawing and atomic numbering scheme for  $(\eta^5\text{-indenyl})\text{Fe}(\text{CO})_3^+$ .

planar indenyl ligand (RMS deviation 0.009 Å) and an average Fe—C(ring) bond length of 2.11 Å.

The results of the MO calculations provide a simple explanation for the much reduced reactivity of **2** in comparison to **1**, without the necessity of invoking ring slippage. Figure 8 shows the LUMO's for  $1^+$  and  $2^+$ . In  $1^+$ , the LUMO (Figure 8A,B) is localized approximately equally on the metal and the CO ligands, with only a small contribution from the cyclopentadienyl atomic orbitals. Furthermore, the Fe—CO interaction in the LUMO is antibonding, thus accounting for the ready dissociation of CO upon reduction of  $1^+$ . In  $2^+$ , the LUMO (Figure 8C) is calculated to contain about the same amount of metal character as in  $1^+$ . However, there is a marked difference in that this LUMO is significantly localized on the benzene ring of the indenyl ligand, with a concomitant reduction in the contribution from the CO's. Thus, the LUMO on  $2^+$  is less Fe—CO antibonding than the LUMO on  $1^+$ , which is in accord with the observed reactivity order  $k_{-\text{CO}}(1) \gg k_{-\text{CO}}(2)$ . In effect, the indenyl complex, when reduced, is able to accommodate some of the electron density in the uncoordinated but conjugated benzene ring. This is electron density that would otherwise reside in the CO ligands

**Figure 8.** (A, B) Two views of the calculated LUMO for  $\text{CpFe}(\text{CO})_3^+$ . (C) The LUMO for  $(\text{indenyl})\text{Fe}(\text{CO})_3^+$ .

in an Fe—CO  $\pi^*$ -derived orbital. It is important to note that the MO calculations and the ESR spectrum of **2** (*vide infra*) indicate that **1** and **2** have a large fraction of the unpaired spin density on the metal and are best formulated as 19-electron complexes and not as  $(18 + \delta)$ -electron species.

The reason the LUMO's for  $1^+$  and  $2^+$  differ as they do can be traced to the presence of a low-lying  $\pi^*$  orbital in the indenyl anion that is mostly localized on the benzene ring and which has the proper symmetry to interact strongly with one of the two LUMO's on the  $\text{Fe}(\text{CO})_3^{2+}$  fragment. This interaction gives rise to the MO shown in Figure 8C. Note that this mechanism whereby the uncoordinated part of the indenyl ligand assumes "extra" electron density when  $2^+$  is reduced, and so in a sense acts as an "electron sink", does not entail slippage to  $\eta^3$  bonding. Obviously, the type of interaction just described for the indenyl system is unavailable to the cyclopentadienyl complex  $1^+$ . In a similar vein, it was noted above that CO dissociation from the 19-electron complexes  $(\text{MeCp})\text{Mn}(\text{CO})_2\text{NO}$  and  $(\text{indenyl})\text{Mn}(\text{CO})_2\text{NO}$  occurs at about the same rate. The lack of an inverse "indenyl effect" in this case can be easily understood on the basis of MO calculations,<sup>13b</sup> which indicate that the electron sink nature of the indenyl benzene ring is largely overshadowed by the accepting power of the NO ligand. As a result, the LUMO's of the two manganese complexes are virtually identical and have only minor localization on the dienyl ligands.

**ESR Spectrum of (Indenyl)Fe(CO)<sub>3</sub> (2).** In agreement with Wrighton et al.,<sup>36</sup> we found that the ESR spectrum of **2** in  $\text{CH}_2\text{Cl}_2/\text{C}_2\text{H}_4\text{Cl}_2$  solution at 230 K consists of a single line ( $g = 2.007$ ). Although no hyperfine structure was resolved, the peak-to-peak line width (3.9 G) could mask  $^1\text{H}$  couplings as large as 1 G; i.e., as much as one-fourth to half of the spin density could reside on the indenyl ligand without resolved hyperfine structure. The frozen solution at 110 K showed three features corresponding to a rhombic  $g$  matrix with components 1.986, 2.009, and 2.024; again,

no hyperfine structure was resolved. The departure of the  $g$  components from the free-electron value ( $g_e = 2.0023$ ) suggests a significant contribution of iron atomic orbitals to the singly occupied molecular orbital. The ESR results are thus entirely consistent with the conclusions of the extended Hückel calculations described above.

**Conclusions.** The present studies indicate that extending the conjugation of a dienyl ligand from cyclopentadienyl to indenyl can markedly influence the stability and reactivity of 19-electron complexes. The indenyl ligand exerts this effect due to the electron-accepting power of the uncoordinated benzene ring, which reduces metal-CO antibonding interactions. The result is increased stability and a reduced rate of CO dissociation. Thus, dissociative CO substitution reactions of the 19-electron complexes  $\text{CpFe}(\text{CO})_3$  and (indenyl) $\text{Fe}(\text{CO})_3$  differ greatly in rate, with the latter at least  $10^6$  times less reactive. Ironically, this *inverse* indenyl effect has the same origin as the *positive* effect seen with 18-electron systems, and probably also 17-electron ones. In the 17- and 18-electron systems, associative nucleophilic attack is facilitated by the electron sink nature of the indenyl ligand, which may in the extreme case slip to  $\eta^3$  bonding. In this way the energy of the activated complex is lowered and the rate increases. With 19-electron complexes, such as **2**, the indenyl ligand is performing its electron sink role in the ground state (*without ring slippage*), thereby stabilizing it with respect to CO dissociation. For this reason the activation energy for CO substitution is *increased* at 19-electron centers. The generalized conclusion is that

indenyl ligands will accelerate substitutions at  $18e^-$  centers (A or  $D^{20}$  mechanism) and  $17e^-$  centers (A mechanism) but inhibit substitutions at  $19e^-$  centers (D mechanism).

One may anticipate an effect analogous to that described herein whenever the conjugation in a  $\pi$ -hydrocarbon ligand is increased, e.g., replacing benzene by naphthalene or pyrrole by indole, etc. The 19-electron radical produced by reduction of the more highly conjugated complex should be relatively more stable with respect to CO dissociation and, therefore, less prone to rapid unproductive decomposition. This, in turn, suggests an increased potential for utilization in productive reactions, both catalytic and stoichiometric.

**Acknowledgment.** This work was supported by grants from the National Science Foundation (Grant Nos. CHE-8821588 and CHE-9400800). The X-ray equipment was purchased with assistance from grants from the National Science Foundation (Grant No. CHE-8206423) and the National Institutes of Health (Grant No. RR-06462). We are grateful to Professor Y. K. Chung of Seoul National University for very helpful discussions.

**Supplementary Material Available:** Tables of atomic coordinates, thermal parameters, bond lengths, and bond angles and a packing diagram for [(indenyl) $\text{Fe}(\text{CO})_3$ ] $\text{PF}_6$  (6 pages). Ordering information is given on any current masthead page.

OM940725+

# Facile Syntheses, Isomeric Structures, and Chemical Reactivity of Diruthenium(I) Complexes $[\text{Ru}_2(\text{CO})_4(\text{MeCN})_4\text{L}_2]\text{X}_2$ ( $\text{L} = \text{MeCN}$ , $\text{PPh}_3$ , $\text{PPh}_2(\text{allyl})$ , $\text{PMe}_3$ ; $\text{X}^- = \text{PF}_6^-$ , $\text{BF}_4^-$ ). A Convenient Route to 1,2-Diamides and 1,2-Dithiolates

Kom-Bei Shiu,\* Chien-Hsing Li, and Tsung-Jung Chan

Department of Chemistry, National Cheng Kung University,  
Tainan, Taiwan 701, Republic of China

Shie-Ming Peng and Ming-Chu Cheng

Department of Chemistry, National Taiwan University, Taipei, Taiwan 106, Republic of China

Sue-Lein Wang and Fen-Ling Liao

Department of Chemistry, National Tsing Hua University,  
Hsinchu, Taiwan 300, Republic of China

Michael Y. Chiang

Department of Chemistry, National Sun Yat-Sen University,  
Kaohsiung, Taiwan 804, Republic of China

Received September 9, 1994<sup>⊙</sup>

Alkylating agents such as  $\text{Et}_3\text{O}^+\text{X}^-$  ( $\text{X}^- = \text{PF}_6^-$  or  $\text{BF}_4^-$ ) readily remove the bridging acetate groups of  $[\text{Ru}_2(\text{CO})_4(\text{O}_2\text{CMe})_2\text{L}_2]$  at ambient temperature to give the versatile complexes  $[\text{Ru}_2(\text{CO})_4(\text{NCMe})_4\text{L}_2]\text{X}_2$  ( $\text{L} = \text{MeCN}$  (1),  $\text{PPh}_3$  (2),  $\text{PPh}_2(\text{allyl})$  (3), and  $\text{PMe}_3$  (4)). The crystal structures of 3 and 4 were determined by X-ray crystallography: [3][ $\text{BF}_4$ ]<sub>2</sub>,  $a = 20.292(6)$ ,  $b = 17.223(7)$ ,  $c = 15.186(3)$ ,  $\beta = 113.324(18)^\circ$ ,  $V = 4873(3) \text{ \AA}^3$ , monoclinic  $\text{C}2/c$ ,  $Z = 4$ , refined to  $R = 0.045$ ,  $R_w = 0.048$ , and  $\text{GOF} = 2.27$ . [4][ $\text{BF}_4$ ]<sub>2</sub>,  $a = 12.570(4)$ ,  $b = 14.251(5)$ ,  $c = 18.773(6) \text{ \AA}$ ,  $\beta = 104.96(3)^\circ$ ,  $V = 3251(9) \text{ \AA}^3$ , monoclinic  $\text{P}2_1/n$ ,  $Z = 4$ , refined to  $R = 0.044$ ,  $R_w = 0.044$ , and  $\text{GOF} = 1.53$ . Although 3 adopts a *trans*-staggered structure, 4 is in a *cis*-staggered geometry. The high reactivity of 1-4 is demonstrated via the cation-anion annihilation between  $2^{2+}$  and the doubly deprotonated anion,  $(\text{E}-\text{E})^{2-}$ , to give  $[\text{Ru}_2(\text{CO})_4\{\mu-\eta^2, \eta^2-(\text{E}-\text{E})\}(\text{PPh}_3)_2]$  ( $(\text{E}-\text{E})^{2-} = 1,2-(\text{NH})_2\text{C}_6\text{H}_4^{2-}$  (7); 2,3-( $\text{NH})_2\text{C}_{10}\text{H}_6^{2-}$  (8); 1,2-( $\text{NH})_2$ -4,5- $\text{Cl}_2\text{C}_6\text{H}_2^{2-}$  (9); 1,2-( $\text{NH})_2$ -4,5- $\text{Me}_2\text{C}_6\text{H}_2$  (10); 9,10-( $\text{NH})_2\text{C}_{14}\text{H}_8$  (11); and 1,2- $\text{S}_2\text{C}_6\text{H}_4^{2-}$  (12)). The structures of 7-12 were also confirmed by an X-ray single-crystal structure of 12:  $a = 11.155(1)$ ,  $b = 21.302(2)$ ,  $c = 10.183(2) \text{ \AA}$ ,  $\alpha = 93.65(1)$ ,  $\beta = 113.43(1)$ ,  $\gamma = 101.19(1)^\circ$ ,  $V = 2151.2(6) \text{ \AA}^3$ , triclinic  $\text{P}\bar{1}$ ,  $Z = 2$ , refined to  $R = 0.038$ ,  $R_w = 0.046$ , and  $\text{GOF} = 2.81$ . The Ru-Ru distances are 2.8647(11)  $\text{ \AA}$  in 3, 2.861(1)  $\text{ \AA}$  in 4, and 2.6767(5)  $\text{ \AA}$  in 12.

## Introduction

Multinuclear metal carbonyl complexes of doubly anionic difunctional ligands,  $(\text{E}-\text{E})^{2-}$ , prepared from heterocyclic compounds such as 1,2-diaminobenzene,<sup>1</sup> 1,2-bis(phenylphosphino)benzene,<sup>2</sup> 1,8-diaminonaphthalene,<sup>3</sup> or catechol<sup>4</sup> have recently been active areas of research, probably due to the related rich coordination chemistry, especially that involving *controlled* aggregation and/or fragmentation pathways<sup>5</sup> of the metal-

metal bonds. Recognition of the fact that dinuclear compounds can be either fragmented into mononuclear products or aggregated into tri- or higher-nuclear cluster compounds, mediated by the ligands, prompted us to find a facile approach, as shown below, to ligated dinuclear compounds. It involves acetate removal from  $[\text{Ru}_2(\text{CO})_4(\text{MeCO}_2)_2\text{L}_2]$  to form  $[\text{Ru}_2(\text{CO})_4(\text{MeCN})_4\text{L}_2]^{2+}$  and then cation-anion annihilation with  $(\text{E}-\text{E})^{2-}$  to readily give  $[\text{Ru}_2(\text{CO})_4\{\mu-\eta^2, \eta^2-(\text{E}-\text{E})\}\text{L}_2]$  (Scheme 1).

(3) (a) Andreu, P. L.; Cabeza, J. A.; Riera, V.; Robert, F.; Jeannin, Y. *J. Organomet. Chem.* **1989**, *372*, C15. (b) Cabeza, J. A.; Fernandez-Colinas, J. M.; Riera, V.; Pellinghelli, M. A.; Tiripicchio, A. *J. Chem. Soc., Dalton Trans.* **1991**, 371. (c) Cabeza, J. A.; Fernandez-Colinas, J. M.; Garcia-Granda, S.; Riera, V.; Maelen, J. F. V., *Inorg. Chem.* **1992**, *31*, 1233.

(4) (a) Connelly, N. G.; Manners, I.; Protheroe, J. R. C.; Whiteley, M. W. *J. Chem. Soc., Dalton Trans.* **1984**, 2713. (b) Bohle, D. S.; Christense, A. N.; Goodson, P. A. *Inorg. Chem.* **1993**, *32*, 4173. (c) Churchill, M. R.; Lake, C. H.; Paw, W.; Keister, J. B. *Organometallics* **1994**, *13*, 8. (d) Bohle, D. S.; Carron, K. T.; Christense, A. N.; Goodson, P. A.; Powell, A. K. *Organometallics* **1994**, *13*, 1355.

(5) Shriver, D. F.; Kaesz, H. D.; Adams, R. D. *The Chemistry of Metal Cluster Complexes*, VCH: New York, 1990; Chapters 3, 6.

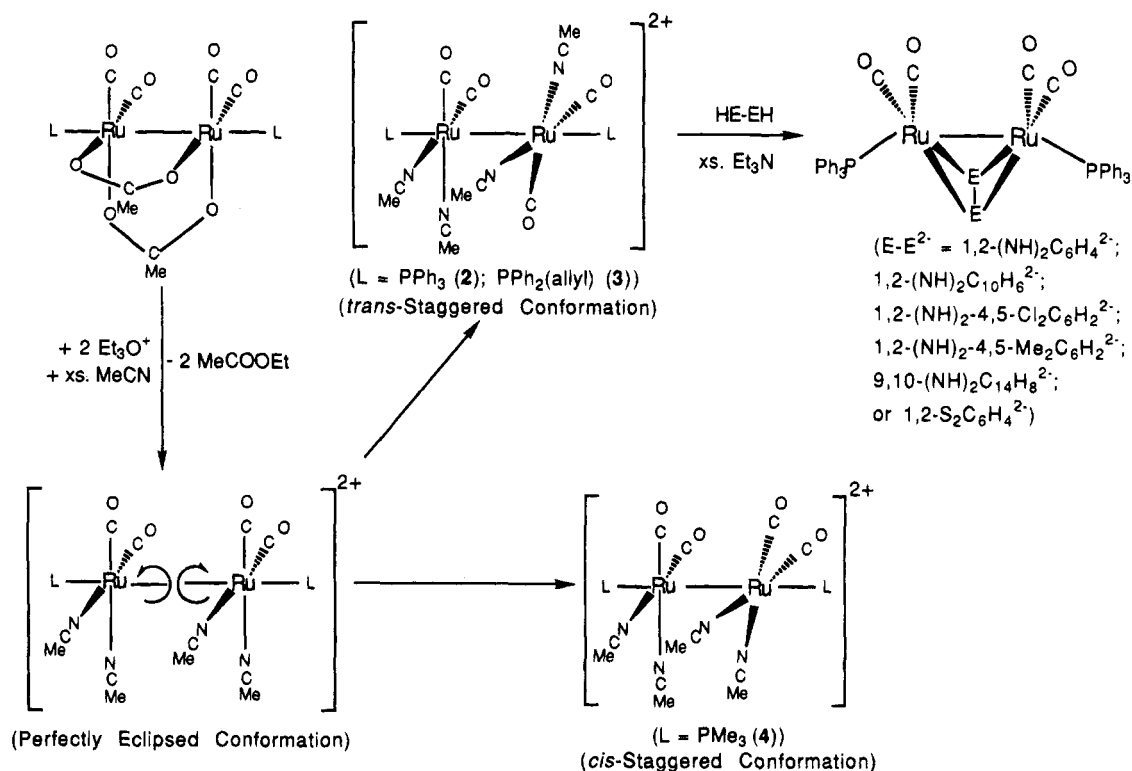
<sup>⊙</sup> Abstract published in *Advance ACS Abstracts*, December 1, 1994.

(1) (a) Anillo, A.; Riera, V.; Obeso-Rosete, R.; Font-Altaba, F.; Solans, X. *J. Organomet. Chem.* **1987**, *327*, C43. (b) Cabeza, J. A.; Riera, V.; Pellinghelli, M. A.; Tiripicchio, A. *J. Organomet. Chem.* **1989**, *376*, C23. (c) Garcia-Granda, S.; Obeso-Rosete, R.; Gonzalez, J. M. R.; Anillo, A. *Acta Crystallogr.* **1990**, *C46*, 2043. (d) Anillo, A.; Cabeza, J. A.; Obeso-Rosete, R.; Riera, V. *J. Organomet. Chem.* **1990**, *393*, 423. (e) Anillo, A.; Obeso-Rosete, R.; Pellinghelli, M. A.; Tiripicchio, A. *J. Chem. Soc., Dalton Trans.* **1991**, 2019.

(2) Soucek, M. D.; Clubb, C. C.; Kyba, E. P.; Price, D. S.; Scheuler, V. G.; Aldaz-Palacios, H. O.; Davis, R. E. *Organometallics* **1994**, *13*, 1120.



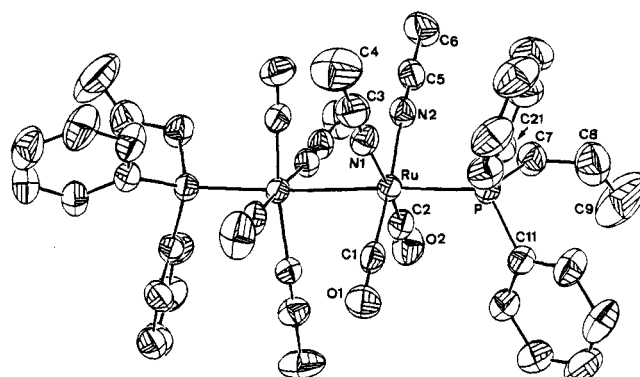
Scheme 1



## Results and Discussion

Partial or total removal of the acetate groups in dinuclear complexes such as  $[\text{M}_2(\text{O}_2\text{CMe})_4]$  ( $\text{M} = \text{Mo}$  or  $\text{Rh}$ ) by treatment of the complexes with strong acids or alkylating reagents is well-known in the literature.<sup>6</sup> We now report that the acetate-removal approach using alkylating reagents works equally well in metal carbonyl complexes of acetates such as  $[\text{Ru}_2(\text{CO})_4(\text{MeCO}_2)_2\text{L}_2]$  in the presence of a weakly coordinating solvent such as MeCN, giving  $[\text{Ru}_2(\text{CO})_4(\text{MeCN})_4\text{L}_2]\text{X}_2$  ( $\text{L} = \text{MeCN}$  (1),  $\text{PPh}_3$  (2),  $\text{PPh}_2(\text{allyl})$  (3), and  $\text{PMe}_3$  (4)) nearly quantitatively.

Following addition of an alkylating reagent to a solution of  $[\text{Ru}_2(\text{CO})_4(\text{MeCO}_2)_2\text{L}_2]$  in  $\text{CH}_2\text{Cl}_2$  and MeCN, three new carbonyl stretching bands and one shoulder having strong intensities (for 1–4) and two other new bands with medium intensities at 1758 and 1728  $\text{cm}^{-1}$  (probably due to ethyl acetate and related derivatives) were soon observed in the solution IR spectrum. The reaction is usually complete within 30 min. Longer or shorter time needed for a complete conversion appears dependent on the specific L used. The two acetate groups of  $[\text{Ru}_2(\text{CO})_4(\text{MeCO}_2)_2\text{L}_2]$  were first probably converted into ethyl acetate and then replaced quickly by the MeCN to give 1–4. Compounds [1][PF<sub>6</sub>]<sub>2</sub> and [2][PF<sub>6</sub>]<sub>2</sub> were reported in 1993 but prepared by a somewhat tedious procedure from  $[\text{Ru}_2(\text{CO})_6\text{Cl}_2]$ .<sup>7</sup>



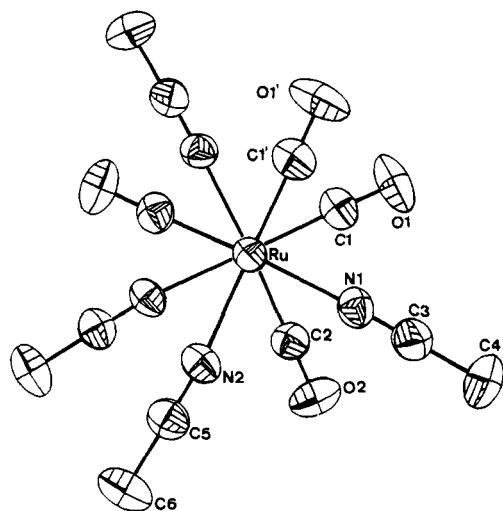
**Figure 1.** ORTEP representation with 50% probability ellipsoids of  $[\text{Ru}_2(\text{CO})_4(\text{MeCN})_4\{\text{PPh}_2(\text{allyl})\}_2]^{2+}$  ( $3^{2+}$ ).

Intrigued by the unexpected steric effect of propeller configurations of a  $\text{PPh}_3$  ligand to induce isomerism,<sup>8</sup> we determined the structures of  $[3][\text{BF}_4]_2$  (Figure 1) and  $[4][\text{BF}_4]_2$  (Figure 3) even though that of  $[2][\text{PF}_6]_2$  was reported previously.<sup>7</sup> Selected bond distances and angles are listed in Table 1. From Figures 1 and 3, it is quite obvious that the two phosphine ligands occupy positions *trans* to the Ru–Ru bond in  $3^{2+}$  and  $4^{2+}$  with the torsional angles  $\text{P}'\text{-Ru}'\text{-Ru-P} = 143.6(1)^\circ$  in  $3^{2+}$  and  $\text{P}(1)\text{-Ru}(1)\text{-Ru}(2)\text{-P}(2) = 178.7(1)^\circ$  in  $4^{2+}$ , although like  $2^{2+}$ , only  $3^{2+}$  contains a crystallographically imposed  $C_2$  axis. To our surprise, and in contrast to cations  $2^{2+}$  and  $3^{2+}$ , which are similar to each other in having a *trans*-staggered conformation (Figure 2), cation  $4^{2+}$  has a *cis*-staggered conformation (Figure 4), similar to the related triazolylborate complexes  $[\text{Ru}_2\{\text{HB}(\text{pz})_3\}_2(\text{CO})_4]$  (5) and  $[\text{Ru}\{\text{HB}(\text{tz})_3\}_2(\text{CO})_4]$  (6) ( $\text{pz} = 1\text{-pyrazolyl}$ ;  $\text{tz} = 1,2,4\text{-triazolyl}$ ).<sup>9</sup> The conformations observed in 3 and 4 can be achieved by rotating the two *cis*-Ru(CO)<sub>2</sub>

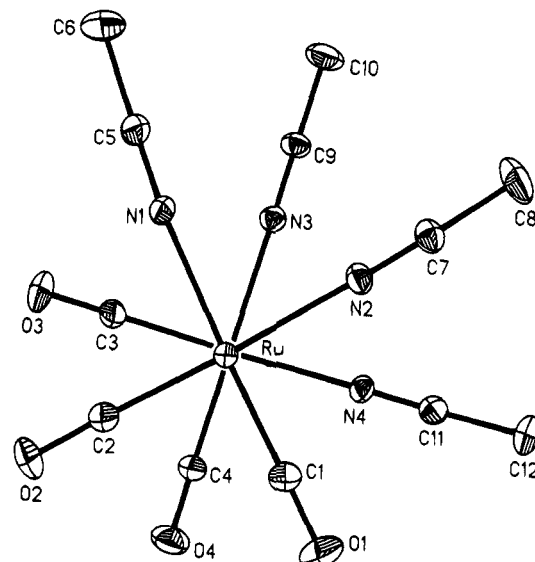
(6) (a) Pimblett, G.; Garner, C. D.; Clegg, W. *J. Coord. Chem.* **1974**, *3*, 255. (b) Mayer, J. M.; Abbot, E. H. *Inorg. Chem.* **1983**, *22*, 2774. (c) Telsler, J.; Drago, R. S. *Inorg. Chem.* **1984**, *23*, 1798. (d) Baranovskii, I. B.; Golubnichaya, M. A.; Dikareva, L. M.; Shchelokov, R. N. *Russ. J. Inorg. Chem.* **1984**, *29*, 872. (e) Cotton, F. A.; Reid, A. H.; Schwotzer, W. *Inorg. Chem.* **1985**, *24*, 3965. (f) Pimblett, G.; Garner, C. D.; Clegg, W. *J. Chem. Soc., Dalton Trans.* **1986**, 1257. (g) Baranovskii, I. B.; Golubnichaya, M. A.; Zhilyaev, A. N.; Shchelokov, R. N. *Sov. J. Coord. Chem.* **1988**, 369. (h) Dunbar, K. R. *J. Am. Chem. Soc.* **1988**, *110*, 8247.

(7) Klemper, W. G.; Bianxia, Z. *Inorg. Chem.* **1993**, *32*, 5821.

(8) Brunner, H.; Oeschey, R.; Nuber, B. *Angew. Chem., Int. Ed. Engl.* **1994**, *33*, 866.



**Figure 2.** Projection of cation  $3^{2+}$  down the Ru–Ru bond (two  $\text{PPh}_2(\text{allyl})$  groups have been omitted for clarity).



**Figure 4.** Projection of cation  $4^{2+}$  down the Ru–Ru bond (two  $\text{PMe}_3$  groups have been omitted for clarity).

**Table 1.** Selected Bond Lengths (Å) and Angles (deg) for 3, 4, and 12

Bond Lengths for 3			
Ru–Ru'	2.8647(11)	Ru–P	2.3843(18)
Ru–C(2)	1.848(8)	Ru–N(1)	2.102(6)
C(1)–O(1)	1.140(10)	C(2)–O(2)	1.142(9)
Ru–C(1)	1.855(8)	Ru–N(2)	2.100(5)

Bond Angles for 3			
P–Ru–C(1)	93.60(20)	P–Ru–C(2)	95.66(21)
P–Ru–N(1)	91.31(16)	P–Ru–N(2)	89.50(15)
P–Ru–Ru'	176.45(5)		

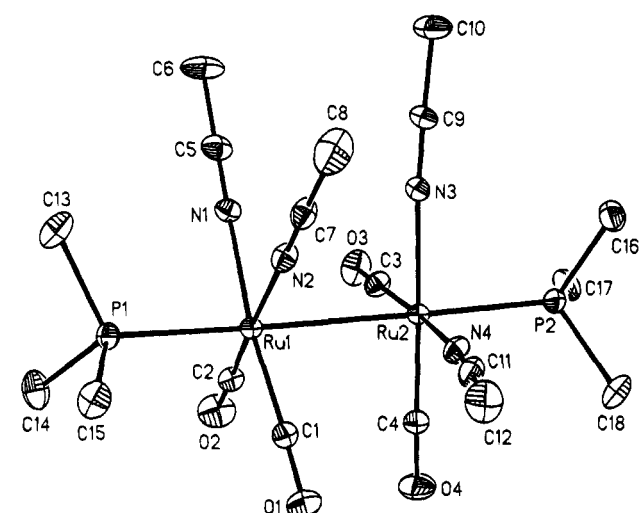
Bond Lengths for 4			
Ru(1)–Ru(2)	2.861(1)	Ru(1)–P(1)	2.383(2)
Ru(1)–C(2)	1.848(8)	Ru(1)–N(1)	2.105(6)
C(1)–O(1)	1.148(10)	C(2)–O(2)	1.153(10)
Ru(2)–C(3)	1.867(8)	Ru(2)–C(4)	1.854(8)
Ru(2)–N(4)	2.104(7)	C(3)–O(3)	1.136(11)
Ru(1)–C(1)	1.855(7)	Ru(1)–N(2)	2.107(6)
Ru(1)–N(2)	2.107(6)	Ru(2)–P(2)	2.381(2)
Ru(2)–P(2)	2.381(2)	Ru(2)–N(3)	2.097(6)
Ru(2)–N(3)	2.097(6)	C(4)–O(4)	1.146(10)

Bond Angles for 4			
P(1)–Ru(1)–C(1)	93.8(3)	P(1)–Ru(1)–C(2)	97.1(3)
P(1)–Ru(1)–N(1)	91.5(2)	P(1)–Ru(1)–N(2)	86.5(2)
P(2)–Ru(2)–C(3)	97.0(3)	P(2)–Ru(2)–C(4)	92.6(3)
P(2)–Ru(2)–N(3)	89.4(2)	P(2)–Ru(2)–N(4)	89.2(2)
P(1)–Ru(1)–Ru(2)	172.1(1)	P(2)–Ru(2)–Ru(1)	174.8(1)

Bond Lengths for 12			
Ru(1)–Ru(2)	2.6767(5)	Ru(1)–S(1)	2.433(1)
Ru(1)–P(1)	2.362(1)	Ru(1)–C(43)	1.869(5)
Ru(2)–S(1)	2.415(1)	Ru(2)–S(2)	2.430(1)
Ru(2)–C(45)	1.864(5)	Ru(2)–C(46)	1.827(5)
C(44)–O(2)	1.148(5)	C(45)–O(3)	1.152(6)
Ru(1)–S(2)	2.415(1)	Ru(1)–C(44)	1.866(5)
Ru(1)–C(44)	1.866(5)	Ru(2)–P(2)	2.365(1)
Ru(2)–P(2)	2.365(1)	C(43)–O(1)	1.144(5)
C(43)–O(1)	1.144(5)	C(46)–O(4)	1.162(7)

Bond Angles for 12			
Ru(1)–S(1)–Ru(2)	67.02(3)	Ru(1)–S(2)–Ru(2)	67.08(3)
P(1)–Ru(1)–Ru(2)	151.70(3)	P(2)–Ru(2)–Ru(1)	151.51(3)

( $\text{PPh}_3$ ) $_2$ ) ((E–E) $^{2-}$  = 1,2-(NH) $_2$ C $_6$ H $_4$  $^{2-}$  (**7**); 2,3-(NH) $_2$ -C $_{10}$ H $_6$  $^{2-}$  (**8**); 1,2-(NH) $_2$ -4,5-Cl $_2$ C $_6$ H $_2$  $^{2-}$  (**9**); 1,2-(NH) $_2$ -4,5-Me $_2$ C $_6$ H $_2$  (**10**); 9,10-(NH) $_2$ C $_{14}$ H $_8$  (**11**), and 1,2-S $_2$ C $_6$ H $_4$  $^{2-}$  (**12**)) in 85–95% yield. The synthesis of **7** was reported earlier, but with a lower yield, from carbonylation of [Ru{1,2-(NH) $_2$ C $_6$ H $_4$ }(PPh $_3$ ) $_3$ ], from a reaction between this compound and Cr(CO) $_6$ , or from that between [Ru(CO) $_3$ (PPh $_3$ ) $_2$ ] and 1,2-(NH) $_2$ C $_6$ H $_4$ .<sup>1</sup> Since the spectral data of **8**–**12** are quite similar to those of **7**, the structures of **8**–**12** are believed to be, like that of **7**, to have an almost perpendicular (E–E) plane. Indeed, confirmation was also provided by an X-ray diffraction study of **12** (Figure 5), which revealed a longer Ru–Ru bond length (2.6767(5) Å in **12** versus 2.560(1) Å in **7**).



**Figure 3.** ORTEP representation with 50% probability ellipsoids of [Ru $_2$ (CO) $_4$ (MeCN) $_4$ (PMe $_3$ ) $_2$ ] $^{2+}$  (**4** $^{2+}$ ).

groups of a perfectly eclipsed conformation away from each other to form a twist angle of 130.9° in **3** $^{2+}$  and 43.8° in **4** $^{2+}$  (Scheme 1). The Ru–Ru distance of 2.861(1) Å in **4** is the shortest one among all the reported values (2.8647(11) Å in **3**, 2.8731(8) Å in **2**,<sup>7</sup> 2.8688(7) Å in **6**, and 2.882(1) Å in **5**<sup>9</sup>). If the significantly shorter Ru–Ru bond length in **3** relative to that in **2**<sup>7</sup> is attributed to the smaller PPh $_2$ (allyl) (Tolman cone angle 140°)<sup>10</sup> relative to PPh $_3$  (Tolman cone angle 145°),<sup>11</sup> the nearly identical Ru–Ru bond lengths in **3** and **4** should be explained by considering both the steric (Tolman cone angle 118°)<sup>11</sup> and electronic<sup>12</sup> effects of PMe $_3$ . However, it is not presently known for sure whether the steric or the electronic effect is more important, determining the preferred conformation of the phosphine ligands in **2**–**4**.

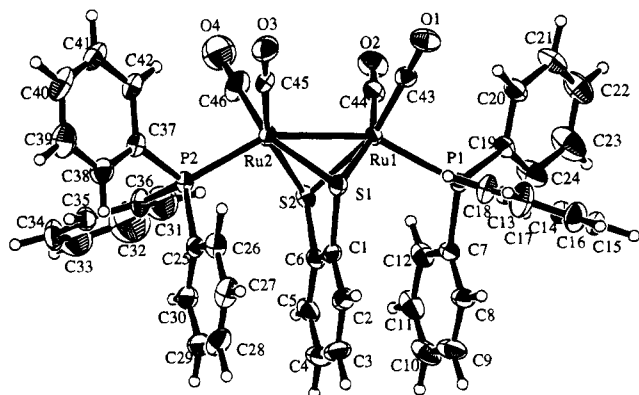
Reaction of **2** with various heterocyclic compounds, HE–EH, in the presence of excess Et $_3$ N, afforded the yellow crystalline dinuclear products [Ru $_2$ (CO) $_4$ (E–E)-

(9) (a) Steyn, M. M. d. V.; Singleton, E.; Hietkamp, S.; Liles, D. C. *J. Chem. Soc., Dalton Trans.* **1990**, 2991. (b) Shiu, K.-B.; Guo, W.-N.; Peng, S.-M.; Cheng, M.-C. *Inorg. Chem.* **1994**, *33*, 3010.

(10) Since the size of PPh $_2$ Et is similar to that of PPh $_2$ (allyl), the Tolman cone angle of 140° for PPh $_2$ Et is used for that of PPh $_2$ (allyl).<sup>11</sup>

(11) Tolman, C. A. *Chem. Rev.* **1977**, *77*, 313.

(12) In the related [Ru $_2$ (CO) $_4$ (MeCO) $_2$ L $_2$ ] system, it was found that a better electron donor may lengthen the Ru–Ru bond.<sup>13</sup>



**Figure 5.** ORTEP representation with 50% probability ellipsoids of **12**.

**Table 2.** Fractional Atomic Coordinates and  $B_{eq}$  for **3**

	x	y	z	$B_{eq},^a \text{ \AA}^2$
Ru	0.00037(3)	0.28703(3)	0.15587(4)	2.99(3)
P	0.00851(9)	0.28435(11)	0.00353(12)	3.39(8)
C1	0.0340(4)	0.3882(4)	0.1817(5)	4.1(4)
O1	0.0558(4)	0.4500(3)	0.1964(4)	6.8(4)
C2	0.0916(4)	0.2488(4)	0.2242(5)	3.9(4)
O2	0.1481(3)	0.2255(4)	0.2664(4)	5.9(3)
N1	-0.1065(3)	0.3257(3)	0.0933(4)	3.8(3)
C3	-0.1648(5)	0.3433(4)	0.0572(6)	4.7(4)
C4	-0.2402(5)	0.3647(6)	0.0111(8)	7.9(6)
N2	-0.0392(3)	0.1728(3)	0.1332(4)	3.8(3)
C5	-0.0544(4)	0.1089(5)	0.1243(5)	4.2(4)
C6	-0.0716(5)	0.0264(5)	0.1149(6)	6.3(5)
C7	0.0341(4)	0.1877(4)	-0.0249(6)	4.9(4)
C8	0.0495(6)	0.1806(6)	-0.1092(7)	7.5(7)
C9	0.1167(8)	0.1730(8)	-0.1029(13)	13.7(14)
C11	0.0756(4)	0.3468(4)	-0.0120(5)	3.8(4)
C12	0.1403(4)	0.3594(5)	0.0625(6)	5.5(5)
C13	0.1946(5)	0.3984(6)	0.0482(7)	6.9(6)
C14	0.1842(6)	0.4253(6)	-0.0406(9)	6.9(6)
C15	0.1195(6)	0.4149(6)	-0.1153(7)	6.8(6)
C16	0.0644(4)	0.3755(5)	-0.1023(6)	5.4(4)
C21	-0.0756(4)	0.3102(4)	-0.0935(5)	3.8(4)
C22	-0.1218(4)	0.2539(5)	-0.1502(6)	5.5(5)
C23	-0.1882(5)	0.2760(6)	-0.2186(7)	6.8(5)
C24	-0.2086(4)	0.3518(7)	-0.2289(7)	6.6(5)
C25	-0.1643(5)	0.4081(5)	-0.1725(7)	5.7(5)
C26	-0.0973(4)	0.3876(5)	-0.1035(5)	4.7(4)
B	0.6466(10)	0.4791(10)	0.1675(13)	8.6(10)
F1	0.5942(6)	0.4420(5)	0.1208(9)	19.7(8)
F2	0.6871(6)	0.5007(10)	0.1283(9)	24.0(13)
F3	0.6306(9)	0.5444(8)	0.1885(16)	26.4(20)
F4	0.6822(8)	0.4540(13)	0.2422(10)	30.1(16)

$^a B_{eq} = (8/3)\pi^2(U_{11}(aa^*)^2 + U_{22}(bb^*)^2 + U_{33}(cc^*)^2 + 2U_{12}aa^*bb^* \cos \gamma + 2U_{13}a^*c^* \cos \beta + 2U_{23}bb^*c^* \cos \alpha)$ .

If planes 1–3 are defined to include C(1)–C(6), C(7)–C(12), and C(25)–C(30) atoms, respectively, the angles formed by any two planes are 8.6° between planes 1 and 2, 2.4° between planes 1 and 3, and 6.3° between planes 2 and 3. In other words, the three phenyl planes are almost parallel to each other. Apparently, the specific propeller configuration of PPh<sub>2</sub>R (R = Ph or allyl) influences not only the structures of **2** and **3** but that of **12**. As with structure **7**,<sup>1</sup> structure **12** has the low Ru–S–Ru angles (67.02(3) and 67.08(3)°) and similar Ru–S distances (2.415(1), 2.415(1), 2.430(1), and 2.433(1) Å).

## Conclusions

Our investigation into the controlled aggregation and/or fragmentation pathways of metal–metal bonds has resulted in the synthesis of a variety of 1,2-diamides and -dithiolates and several novel molecular structures.

**Table 3.** Atomic Coordinates ( $\times 10^4$ ) and Equivalent Isotropic Displacement Coefficients ( $\text{\AA}^2 \times 10^3$ ) for **4**

	x	y	z	$U_{eq}^a$
Ru(1)	1688(1)	1850(1)	153(1)	28(1)
Ru(2)	3392(1)	1910(1)	-605(1)	29(1)
P(1)	285(2)	2030(1)	788(1)	35(1)
P(2)	4802(2)	2111(2)	-1228(1)	38(1)
F(1)	972(10)	6236(13)	1708(11)	219(10)
F(2)	1885(14)	5339(17)	1226(12)	253(12)
F(3)	2719(15)	6362(22)	2008(13)	316(16)
F(4)	1881(30)	5340(18)	2344(18)	345(22)
F(5)	6124(11)	3674(12)	1890(10)	205(9)
F(6)	6626(11)	3955(16)	871(7)	213(10)
F(7)	7808(12)	3362(18)	1775(11)	262(13)
F(8)	7178(23)	4722(16)	1665(17)	315(19)
O(1)	3498(6)	2355(6)	1486(4)	72(3)
O(2)	2146(7)	-179(4)	538(5)	75(3)
O(3)	2543(6)	70(5)	-1305(4)	68(3)
O(4)	4921(6)	861(5)	629(4)	72(3)
N(1)	514(6)	1548(4)	-842(3)	37(2)
N(2)	1395(5)	3265(5)	-162(4)	39(2)
N(3)	2306(5)	2660(5)	-1448(4)	38(2)
N(4)	3830(5)	3210(5)	-79(4)	40(2)
B(1)	1930(11)	5844(11)	1819(9)	75(5)
B(2)	6937(11)	3836(12)	1572(8)	74(5)
C(1)	2817(7)	2163(6)	970(5)	43(3)
C(2)	1981(7)	597(6)	371(5)	42(3)
C(3)	2852(7)	768(6)	-1039(5)	45(3)
C(4)	4318(7)	1259(6)	165(5)	43(3)
C(5)	-130(8)	1453(6)	-1378(5)	52(3)
C(6)	-969(12)	1359(10)	-2069(7)	88(5)
C(7)	1215(7)	4019(6)	-351(5)	44(3)
C(8)	1010(9)	4976(7)	-612(9)	82(5)
C(9)	1776(7)	3061(6)	-1947(4)	45(3)
C(10)	1130(9)	3582(9)	-2565(6)	73(4)
C(11)	3988(6)	3894(6)	234(5)	44(3)
C(12)	4107(9)	4766(7)	647(6)	64(4)
C(13)	-1041(7)	2383(8)	212(7)	65(4)
C(14)	-31(9)	1017(7)	1274(6)	63(4)
C(15)	616(8)	2916(6)	1507(6)	55(3)
C(16)	4587(8)	3079(7)	-1879(5)	55(3)
C(17)	5062(9)	1117(7)	-1756(6)	60(4)
C(18)	6126(8)	2377(9)	-596(7)	75(4)

$^a$  Equivalent isotropic  $U$  defined as one-third of the trace of the orthogonalized  $U_{ij}$  tensor.

The techniques that we have developed provide convenient routes to the synthesis of these materials and may be potentially applicable to a wide variety of other systems. Synthesis and reactivity of other diruthenium(I) complexes analogous to **1–4** and pyrolysis experiments of **7–12** in the presence or absence of other metal carbonyl complexes are in progress.

## Experimental Section

**General Comments.** All solvents were dried and purified by standard methods (ethers, paraffins, and arenes from potassium with benzophenone as indicator; halocarbons and acetonitrile from CaH<sub>2</sub> and alcohols from the corresponding alkoxide) and were freshly distilled under nitrogen immediately before use. All reactions and manipulations were carried out in standard Schlenk ware, connected to a switchable double method providing vacuum and nitrogen. Reagents were used as supplied by Aldrich. <sup>1</sup>H and <sup>31</sup>P NMR spectra were measured on a Bruker AMC-400 or a Varian Unity Plus-400 (<sup>1</sup>H, 400 MHz; <sup>31</sup>P, 162 MHz) NMR spectrometer. <sup>1</sup>H Chemical shifts ( $\delta$  in ppm,  $J$  in Hz) are defined as positive downfield relative to internal MeSi<sub>4</sub> (TMS) or the deuterated solvent, while <sup>31</sup>P chemical shifts are defined as positive downfield relative to external 85% H<sub>3</sub>PO<sub>4</sub>. The IR spectra, calibrated with polystyrene, were recorded on a Hitachi Model 270-30 instrument. The following abbreviations were used: s, strong; m, medium; w, weak. Microanalyses were carried out

Table 4. Atomic Coordinates and  $B_{eq}$  for 12

atom	x	y	z	$B_{eq}, \text{\AA}^2$
Ru(1)	0.41265(4)	0.19004(2)	0.53736(4)	2.619(8)
Ru(2)	0.60012(4)	0.30205(2)	0.63735(4)	2.923(9)
S(1)	0.3882(1)	0.28796(5)	0.4289(1)	3.01(3)
S(2)	0.6038(1)	0.21353(6)	0.4773(1)	3.41(3)
P(1)	0.2568(1)	0.10739(5)	0.3469(1)	2.73(3)
P(2)	0.7451(1)	0.39017(6)	0.6042(1)	2.98(3)
O(1)	0.2293(4)	0.2005(2)	0.6852(4)	5.6(1)
O(2)	0.5430(4)	0.1020(2)	0.7409(4)	5.8(1)
O(3)	0.4961(4)	0.3789(2)	0.8096(4)	6.1(1)
O(4)	0.8024(6)	0.2724(3)	0.9085(6)	9.1(1)
C(1)	0.4315(5)	0.2715(2)	0.2817(5)	3.3(1)
C(2)	0.3678(6)	0.2900(2)	0.1484(6)	4.6(1)
C(3)	0.4078(8)	0.2767(3)	0.0386(6)	6.0(2)
C(4)	0.5114(8)	0.2469(3)	0.0642(7)	6.2(2)
C(5)	0.5755(6)	0.2275(2)	0.1970(6)	4.8(1)
C(6)	0.5338(5)	0.2395(2)	0.3054(5)	3.5(1)
C(7)	0.3111(5)	0.0912(2)	0.2029(5)	3.3(1)
C(8)	0.2466(6)	0.1045(2)	0.0662(6)	4.3(1)
C(9)	0.2986(8)	0.0948(3)	-0.0366(7)	6.1(2)
C(10)	0.4140(8)	0.0728(3)	0.0002(8)	6.6(2)
C(11)	0.4788(7)	0.0599(3)	0.1372(8)	5.7(2)
C(12)	0.4299(6)	0.0697(2)	0.2399(6)	4.5(1)
C(13)	0.0872(4)	0.1195(2)	0.2485(5)	3.0(1)
C(14)	-0.0179(5)	0.0688(2)	0.1549(5)	4.0(1)
C(15)	-0.1441(5)	0.0793(3)	0.0782(6)	4.7(1)
C(16)	-0.1682(5)	0.1393(3)	0.0943(7)	5.6(2)
C(17)	-0.0668(6)	0.1890(3)	0.1873(7)	6.2(2)
C(18)	0.0610(5)	0.1793(2)	0.2636(6)	4.6(1)
C(19)	0.2200(5)	0.0282(2)	0.4003(5)	3.3(1)
C(20)	0.1909(6)	0.0247(3)	0.5205(6)	4.8(1)
C(21)	0.1586(7)	-0.0344(3)	0.5631(7)	6.3(2)
C(22)	0.1571(7)	-0.0904(3)	0.4898(9)	6.7(2)
C(23)	0.1847(8)	-0.0882(3)	0.3708(9)	8.2(2)
C(24)	0.2167(7)	-0.0292(3)	0.3258(7)	6.0(2)
C(25)	0.6762(5)	0.4144(2)	0.4267(5)	3.3(1)
C(26)	0.5666(5)	0.4425(2)	0.3899(6)	4.2(1)
C(27)	0.5075(6)	0.4590(3)	0.2543(7)	5.5(2)
C(28)	0.5531(7)	0.4457(3)	0.1525(7)	6.2(2)
C(29)	0.6568(7)	0.4169(3)	0.1836(7)	5.8(2)
C(30)	0.7204(5)	0.4013(2)	0.3201(6)	4.3(1)
C(31)	0.9259(9)	0.3180(4)	0.6165(9)	8.9(2)
C(32)	1.048(1)	0.3063(5)	0.620(1)	13.6(3)
C(33)	1.1493(9)	0.3576(4)	0.6301(9)	9.0(2)
C(34)	1.1344(6)	0.4167(3)	0.6462(7)	5.9(2)
C(35)	1.0134(5)	0.4280(2)	0.6363(6)	4.1(1)
C(36)	0.9088(5)	0.3783(2)	0.6215(6)	4.0(1)
C(37)	0.7932(5)	0.4662(2)	0.7272(5)	3.6(1)
C(38)	0.8172(6)	0.5267(3)	0.6870(6)	5.0(1)
C(39)	0.8584(7)	0.5834(3)	0.7868(8)	6.7(2)
C(40)	0.8729(6)	0.5787(3)	0.9249(8)	6.3(2)
C(41)	0.8500(6)	0.5203(3)	0.9676(6)	5.4(2)
C(42)	0.8099(5)	0.4639(2)	0.8704(6)	4.3(1)
C(43)	0.2980(5)	0.1968(2)	0.6278(5)	3.5(1)
C(44)	0.4913(5)	0.1350(2)	0.6632(5)	3.7(1)
C(45)	0.5383(5)	0.3503(2)	0.7452(5)	3.8(1)
C(46)	0.7259(6)	0.2837(3)	0.8012(6)	6.0(2)

$$^a B_{eq} = (\frac{8}{3})\pi^2(U_{11}(aa^*)^2 + U_{22}(bb^*)^2 + U_{33}(cc^*)^2 + 2U_{12}aa^*bb^* \cos \gamma + 2U_{13}aa^*c^* \cos \beta + 2U_{23}bb^*cc^* \cos \alpha).$$

by the staff of the Microanalytical Service of the Department of Chemistry, National Cheng Kung University.

**Synthesis of  $[\text{Ru}_2(\text{CO})_4(\text{MeCN})_2\text{L}_2]\text{X}_2$  (L = MeCN (1),  $\text{PPh}_3$  (2),  $\text{PPh}_2(\text{allyl})$  (3), and  $\text{PMe}_3$  (4);  $\text{X}^- = \text{PF}_6^-$ ,  $\text{BF}_4^-$ ).** The preparations of 1–4 are similar to each other. A typical procedure for 3 is described below. A mixture of  $[\text{Ru}_2(\text{CO})_4(\text{MeCO})_2\{\text{PPh}_2(\text{allyl})\}_2]^{14}$  (0.41 g, 0.46 mmol), MeCN (1 mL), and  $\text{CH}_2\text{Cl}_2$  (25 mL) was added dropwise to  $\text{Et}_3\text{O}^+\text{BF}_4^-$  (2 mL, 1.0 M solution in  $\text{CH}_2\text{Cl}_2$ ). The solution was stirred for 30 min at ambient temperature (ca. 28 °C), and volatiles were removed under vacuum to give an oily solid. MeOH (ca. 5 mL) was

then added, and the suspension was stirred for 10 min to destroy excess  $\text{Et}_3\text{O}^+\text{BF}_4^-$ . Filtration gave a yellow solid, which was then washed with  $\text{Et}_2\text{O}$  (2 mL) and dried under vacuum to give the pure product of  $[\mathbf{3}][\text{BF}_4]_2$  (0.63 g, 93%). Anal. Calcd for  $\text{C}_{42}\text{H}_{42}\text{B}_2\text{F}_4\text{N}_4\text{O}_4\text{P}_2\text{Ru}_2$ : C, 45.67; H, 3.83; N, 5.07. Found: C, 45.45; H, 3.80; N, 5.16.  $^1\text{H NMR}$  (25 °C,  $\text{CD}_3\text{CN}$ , 400 MHz):  $\delta$  2.11 (s, 12 H), 3.45 (m, 4 H), 4.97 (m, 2 H), 5.06 (m, 2 H), 5.58 (m, 2 H), 7.56 (m, 2 H).  $^{31}\text{P}\{^1\text{H}\}$  NMR (25 °C,  $\text{CD}_3\text{CN}$ , 162 MHz):  $\delta$  17.34. IR ( $\text{CH}_2\text{Cl}_2$ ):  $\nu_{\text{CN}}$ , 2296 w, 2260 w;  $\nu_{\text{CO}}$ , 2048 s, 2024 s, 1990 s, 1980 sh  $\text{cm}^{-1}$ . For  $[\mathbf{4}][\text{BF}_4]_2$ . Anal. Calcd for  $\text{C}_{18}\text{H}_{30}\text{B}_2\text{F}_4\text{N}_4\text{O}_4\text{P}_2\text{Ru}_2$ : C, 26.89; H, 3.76; N, 6.97. Found: C, 26.70; H, 3.81; N, 6.85.  $^1\text{H NMR}$  (25 °C,  $\text{CD}_3\text{CN}$ , 400 MHz):  $\delta$  1.65 (t,  $J_{\text{P,H}} = 4.8$  Hz, 18 H), 1.96 (s, 12 H).  $^{31}\text{P}\{^1\text{H}\}$  NMR (25 °C,  $\text{CD}_3\text{CN}$ , 162 MHz):  $\delta$  -9.99. IR ( $\text{CH}_2\text{Cl}_2$ ):  $\nu_{\text{CN}}$ , 2296 w, 2252 w;  $\nu_{\text{CO}}$ , 2044 s, 2016 s, 1974 s, 1954 sh  $\text{cm}^{-1}$ .

**Synthesis of  $[\text{Ru}_2(\text{CO})_4(\text{E}-\text{E})(\text{PPh}_3)_2] ((\text{E}-\text{E})^{2-} = 1,2\text{-(NH)}_2\text{C}_6\text{H}_4^{2-}$  (7); 2,3-(NH) $_2\text{C}_{10}\text{H}_6^{2-}$  (8); 1,2-(NH) $_2$ -4,5-Cl $_2$ -C $_6\text{H}_2^{2-}$  (9); 1,2-(NH) $_2$ -4,5-Me $_2\text{C}_6\text{H}_2$  (10); 9,10-(NH) $_2\text{C}_{14}\text{H}_8$  (11), and 1,2-S $_2\text{C}_6\text{H}_4^{2-}$  (12)).** The preparations of 7–12 are similar to each other. A typical procedure for 10 is described below. In a 100-mL Schlenk flask was dissolved  $[\mathbf{2}][\text{BF}_4]_2$  (0.168 g, 0.143 mmol) in 15 mL of MeCN at room temperature. 4,5-Dimethyl-1,2-phenylenediamine (0.039 g, 0.29 mmol) and 0.2 mL of  $\text{Et}_3\text{N}$  were added to the Ru solution. The mixture was then heated at 82 °C for 1 h and cooled to room temperature. After the volatiles were pumped off, the residue was dissolved in 15 mL of  $\text{CH}_2\text{Cl}_2$ , filtered through a bed of Celite 2 cm deep, added to 10 mL of MeOH, and concentrated to 10 mL, producing yellow microcrystals. Filtration through a medium frit gave the product **10** (0.16 g, 85%). Anal. Calcd for  $\text{C}_{48}\text{H}_{40}\text{N}_2\text{O}_4\text{P}_2\text{Ru}_2$ : C, 59.26; H, 4.14; N, 2.88. Found: C, 58.55; H, 4.12; N, 2.82.  $^1\text{H NMR}$  (25 °C,  $\text{CDCl}_3$ , 400 MHz):  $\delta$  1.37 (s, 6 H), 2.12 (s, 2 H), 4.64 (s, 2 H), 7.29 (m, 30 H).  $^{31}\text{P}\{^1\text{H}\}$  (25 °C,  $\text{CDCl}_3$ , 162 MHz):  $\delta$  28.15. IR ( $\text{CH}_2\text{Cl}_2$ ):  $\nu_{\text{CO}}$ , 2000 s, 1966 m, 1926 s  $\text{cm}^{-1}$ . For **6**. Anal. Calcd for  $\text{C}_{50}\text{H}_{36}\text{N}_2\text{O}_4\text{P}_2\text{Ru}_2$ : C, 60.48; H, 3.65; N, 2.82. Found: C, 60.46; H, 3.63; N, 2.74.  $^1\text{H NMR}$  (25 °C, acetone- $d_6$ , 400 MHz):  $\delta$  4.16 (s, 2 H), 5.31 (s, 2 H), 6.44 (m, 2 H), 6.58 (m, 2 H), 7.27 (m, 30 H).  $^{31}\text{P}\{^1\text{H}\}$  (25 °C, acetone- $d_6$ , 162 MHz):  $\delta$  34.15. IR ( $\text{CH}_2\text{Cl}_2$ ):  $\nu_{\text{CO}}$ , 2004 s, 1972 m, 1932 s  $\text{cm}^{-1}$ . For **7**. Anal. Calcd for  $\text{C}_{46}\text{H}_{34}\text{Cl}_2\text{N}_2\text{O}_4\text{P}_2\text{Ru}_2$ : C, 54.50; H, 3.38; N, 2.76. Found: C, 54.13; H, 3.35; N, 2.69.  $^1\text{H NMR}$  (25 °C, acetone- $d_6$ , 400 MHz):  $\delta$  3.96 (s, 2 H), 5.09 (s, 2 H), 7.37 (m, 30 H).  $^{31}\text{P}\{^1\text{H}\}$  (25 °C, acetone- $d_6$ , 162 MHz):  $\delta$  29.91. IR ( $\text{CH}_2\text{Cl}_2$ ):  $\nu_{\text{CO}}$ , 2012 s, 1974 m, 1936 s  $\text{cm}^{-1}$ . For **9**. Anal. Calcd for  $\text{C}_{64}\text{H}_{40}\text{N}_2\text{O}_4\text{P}_2\text{Ru}_2$ : C, 62.07; H, 3.86; N, 2.68. Found: C, 62.10; H, 3.84; N, 2.58.  $^1\text{H NMR}$  (25 °C, acetone- $d_6$ , 400 MHz):  $\delta$  4.12 (s, 2 H), 7.53 (d,  $J = 8.4$  Hz, 2 H), 8.02 (d,  $J = 8.4$  Hz, 2 H), 7.00–7.17 (m, 34 H).  $^{31}\text{P}\{^1\text{H}\}$  (25 °C,  $\text{CDCl}_3$ , 162 MHz):  $\delta$  29.73. IR ( $\text{CH}_2\text{Cl}_2$ ):  $\nu_{\text{CO}}$ , 2004 s, 1970 m, 1928 s  $\text{cm}^{-1}$ . For **10**. Anal. Calcd for  $\text{C}_{46}\text{H}_{34}\text{O}_4\text{P}_2\text{Ru}_2\text{S}_2$ : C, 56.44; H, 3.50. Found: C, 56.05; H, 3.53.  $^1\text{H NMR}$  (25 °C, acetone- $d_6$ , 400 MHz):  $\delta$  5.83 (m, 2 H), 6.03 (m, 2 H), 7.28 (m, 18 H), 7.40 (m, 12 H).  $^{31}\text{P}\{^1\text{H}\}$  (25 °C, acetone- $d_6$ , 162 MHz):  $\delta$  37.56. IR ( $\text{CH}_2\text{Cl}_2$ ):  $\nu_{\text{CO}}$ , 2016 s, 1982 m, 1950 s  $\text{cm}^{-1}$ .

**Single-Crystal X-ray Diffraction Studies of 3, 4, and 12.** Suitable single crystals were grown from  $\text{CH}_2\text{Cl}_2$ /hexane or  $\text{CH}_2\text{Cl}_2$ / $\text{Et}_2\text{O}$  at room temperature and chosen for the single-crystal structure determination. Atomic coordinates and equivalent isotropic displacement coefficients for **3**, **4**, and **12** are listed in Tables 2–4, respectively. The X-ray diffraction data were measured on a four-circle diffractometer. Intensities of three standard reflections were monitored every hour or every 50 reflection throughout the data measurement. The variation was less than 2%. For **3**, the structure was solved by heavy-atom method and refined by a full-matrix least-square procedure using NRCVAX.<sup>15</sup> For **4**, the structure was solved by direct methods and refined by a full-matrix least-

(13) Shiu, K.-B.; Peng, S.-M.; Cheng, M.-C. *J. Organomet. Chem.* **1993**, *452*, 143.

(14) Crooks, G. R.; Johnson, B. F. G.; Lewis, J.; Williams, I. G. *J. Chem. Soc. A* **1969**, 2761.

(15) Gabe, E. J.; Le Page, Y.; Charland, J.-P.; Lee, F. L.; White, P. S. *J. Appl. Crystallogr.* **1989**, *22*, 384.

Table 5. Crystal Data for 3, 4, and 12

compound	3	4	12
formula	$C_{42}H_{42}B_2F_8N_4O_4P_2Ru_2$	$C_{18}H_{30}B_2F_4N_4O_4P_2Ru_2$	$C_{46}H_{34}O_4P_2Ru_2S_2$
fw	1104.50	804.2	978.98
color, habit	orange rhomboid	yellow column	yellow needle
diffractometer used	Nonius CAD4	Siemens R3m/V	Rigaku AFC7S
space group	monoclinic, $P2_1/c$	monoclinic, $P2_1/n$	triclinic, $P\bar{1}$
$a$ , Å	20.292(6)	12.570(4)	11.151(1)
$b$ , Å	17.223(7)	14.251(5)	21.302(2)
$c$ , Å	15.186(3)	18.773(6)	10.183(2)
$\alpha$ , deg	90	90	93.65(1)
$\beta$ , deg	113.324(18)	104.96(3)	113.43(1)
$\gamma$ , deg	90	90	101.19(1)
$V$ , Å <sup>3</sup>	4873(3)	3251(9)	2151.2(6)
$Z$	4	4	2
$D_{\text{calcd}}$ , g cm <sup>-3</sup>	1.505	1.643	1.511
$\lambda$ (Mo K $\alpha$ ), Å	0.709 30	0.710 73	0.710 69
$F(000)$	2216	1592	984
unit cell detn			
no. $2\theta$ range, deg	25, 18–24	16, 13–23	25, 36–40
scan type	$\theta$ - $2\theta$	$\theta$ - $2\theta$	$\omega$ - $2\theta$
$2\theta$ range, deg	2–45	2.5–50	6–50
$h, k, l$ range	$\pm 21, 18, 16$	$\pm 14, 16, 21$	$13, \pm 25, \pm 11$
$\mu$ (Mo K $\alpha$ ), cm <sup>-1</sup>	7.43	11.02	9.2
cryst size, mm	$0.40 \times 0.45 \times 0.45$	$0.60 \times 0.28 \times 0.16$	$0.16 \times 0.16 \times 0.58$
transm factor	0.944–1.000	0.888–0.939	0.933–1.000
temp, K	298	296	297
no. of measd reflns	3177	6280	7990
no. of unique reflns	3176	5729	7562
no. of obsd reflns ( $N_o$ )	2764 ( $> 2\sigma$ )	3912 ( $> 3\sigma$ )	6344 ( $> 3\sigma$ )
$R$ , <sup>a</sup> $R_w$ , <sup>a</sup>	0.045, 0.048	0.044, 0.044	0.038, 0.046
GOF <sup>a</sup>	2.27	1.53	2.81
no. of ref params ( $N_p$ )	290	362	485
weighting scheme	unit weights	$[\sigma^2(F_o) + 0.0003F_o^2]^{-1}$	$[\sigma^2(F_o)]^{-1}$
$g$ (second ext coeff) $\times 10^4$	0.65(9)	0	0
$(\Delta\rho)_{\text{max}}$ , e Å <sup>-3</sup>	0.97	1.06	1.38
$(\Delta\rho)_{\text{min}}$ , e Å <sup>-3</sup>	-0.62	-0.71	-1.04

$$^a R = [\sum(|F_o| - |F_c|)/\sum|F_o|]. R_w = [\sum w(|F_o| - |F_c|)^2/\sum w|F_o|^2]^{1/2}. GOF = [\sum w(|F_o| - |F_c|)^2/(N_o - N_p)]^{1/2}.$$

square procedure using SHELXTL-PLUS.<sup>16</sup> For **12**, the structure was solved by direct methods and refined by a full-matrix least-square procedure using TEXSAN.<sup>17</sup> The other essential details of single-crystal data measurement and refinement are given in Table 5.

(16) Sheldrick, G. M. *SHELXTL-Plus Crystallographic System*, release 4.21; Siemens Analytical X-ray Instruments: Madison, WI, 1991.

(17) Crystal Structure Analysis Package, Molecular Structure Corp., TX, 1985, 1992.

**Acknowledgment** is made to the National Science Council of Republic of China for financial support of this research (Contract NSC84-2113-M006-010).

**Supplementary Material Available:** Tables of complete bond lengths and angles, anisotropic displacement coefficients, and hydrogen coordinates for **3**, **4**, and **12** (17 pages). Ordering information is given on any current masthead page.

OM940710B

# Unexpected Formation of 1,4-Disilacyclohexa-2,5-dienes in the Palladium-Catalyzed Reactions of Cl(SiMe<sub>2</sub>)<sub>3</sub>Cl with Acetylenes and Its Application to Polymer Synthesis

Yoshifumi Tanaka,<sup>†</sup> Hiroshi Yamashita,<sup>‡</sup> and Masato Tanaka<sup>\*,†,‡</sup>

National Institute of Materials and Chemical Research, Tsukuba, Ibaraki 305, Japan, and  
Department of Chemistry, University of Tsukuba, Tsukuba, Ibaraki 305, Japan

Received September 12, 1994<sup>®</sup>

Cl(SiMe<sub>2</sub>)<sub>3</sub>Cl (**1a**) reacts with 2 equiv of acetylenes RC≡CR' for (R, R') = (Ph, H), (Hex, H), (Ph(CH<sub>2</sub>)<sub>2</sub>, H), (NC(CH<sub>2</sub>)<sub>3</sub>, H), (Ph, Me), and (Ph, Ph) in the presence of palladium catalysts at 120–140 °C to give 1,4-disilacyclohexa-2,5-dienes in 82–20% yields along with the coproduct Me<sub>2</sub>SiCl<sub>2</sub>. Terminal acetylenes exhibit higher reactivities than internal acetylenes. PdCl<sub>2</sub>L<sub>2</sub> catalysts with L = P(aryl)<sub>3</sub> or AsPh<sub>3</sub> are efficient, while those with L = P(alkyl)<sub>3</sub> or PhCN are not effective. Use of X(SiMe<sub>2</sub>)<sub>3</sub>X (X = F, OMe) in place of **1a** produces very little 1,4-disilacyclohexa-2,5-diene. Possible involvement of silylene species in the catalysis is suggested by the reaction of **1a** with Pt(PEt<sub>3</sub>)<sub>3</sub>, which gives *cis*-(ClMe<sub>2</sub>Si)(Me<sub>3</sub>SiCl)Pt(PEt<sub>3</sub>)<sub>2</sub> (**9**), presumably via silyleneplatinum intermediates, and by the generation of dimethylsilylene in the thermolysis of **9**. Complex **9** is alternatively obtained in the reaction of ClMe<sub>2</sub>SiSiClMeSiMe<sub>3</sub> with Pt(PEt<sub>3</sub>)<sub>3</sub>. Reaction of **1a** with *m*-diprop-1-yn-1-ylbenzene gives a regular silicon polymer of low molecular weight consisting of alternating 1,4-disilacyclohexa-2,5-dien-2,5- or -2,6-ylene and *m*-phenylene units, most of the termini being 1,2-bis-(chlorodimethylsilyl)ethenyl groups. Similar reactions with *p*- and *m*-diethynylbenzene also give silicon polymers that contain 1,4-disilacyclohexa-2,5-dienylene and phenylene rings in the backbone.

## Introduction

Development of new catalysis for organosilane chemistry is a subject of current interest.<sup>1</sup> Addition of Si–Si bonds to organic unsaturated compounds in particular is an intriguing reaction in view of potential applications to polymer synthesis and to organic synthesis.<sup>2</sup> Previously we reported that Si–Si bonds of

fully organic di-, tri-, and polysilanes that usually were reluctant to react with acetylenes could undergo addition reactions cleanly when the Pd–P(OCH<sub>2</sub>)<sub>3</sub>Cet catalyst system was applied.<sup>2a,i</sup> As an alternative way to promote the reaction, introduction of electronegative groups onto silicon atoms appeared promising on the basis of our previous work.<sup>3</sup> The outcome of this approach with Cl(SiMe<sub>2</sub>)<sub>3</sub>Cl, however, was totally unexpected. The reaction of the trisilane with acetylenes readily took place as anticipated, but the major products were 1,4-disilacyclohexa-2,5-diene derivatives.<sup>4</sup> In this paper are reported the new catalysis, possible elemental reactions behind the catalysis, and its application to polymer synthesis.

## Results and Discussion

**Reaction of X(SiMe<sub>2</sub>)<sub>3</sub>X (X = Cl, F, OMe) with Phenylacetylene.** A 1,3-dichlorotrisilane, Cl(SiMe<sub>2</sub>)<sub>3</sub>Cl (**1a**), reacted with 2 equiv of phenylacetylene (**2a**) in the presence of a palladium catalyst to give a 1,4-disilacyclohexa-2,5-diene (**3a**) and its coproduct, Me<sub>2</sub>SiCl<sub>2</sub> (**4**), as the major products (eq 1). Thus, heating a mixture of **1a**, phenylacetylene (**2a**, 3 equiv), PdCl<sub>2</sub>(PPh<sub>3</sub>)<sub>2</sub> (1 mol % based on **1a**), and benzene at 120 °C for 1 h gave **3a** in a high yield (80% GC yield based on

(3) Yamashita, H.; Kobayashi, T.-a.; Hayashi, T.; Tanaka, M. *Chem. Lett.* **1990**, 1447.

(4) 1,4-Disilacyclohexa-2,5-dienes are known to be formed in the reactions of thermally generated silylene species with acetylenes. For instance, see: (a) Atwell, W. H.; Weyenberg, D. R. *J. Am. Chem. Soc.* **1968**, *90*, 3438 and references cited therein. (b) Barton, T. J.; Kilgour, J. A. *J. Am. Chem. Soc.* **1976**, *98*, 7746 and references cited therein. (c) Halevi, E. A.; West, R. *J. Organomet. Chem.* **1982**, *240*, 129 and references cited therein.

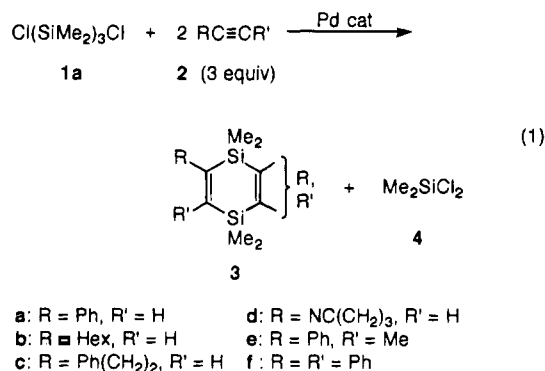
<sup>†</sup> University of Tsukuba.

<sup>‡</sup> National Institute of Materials and Chemical Research.

<sup>®</sup> Abstract published in *Advance ACS Abstracts*, November 1, 1994.

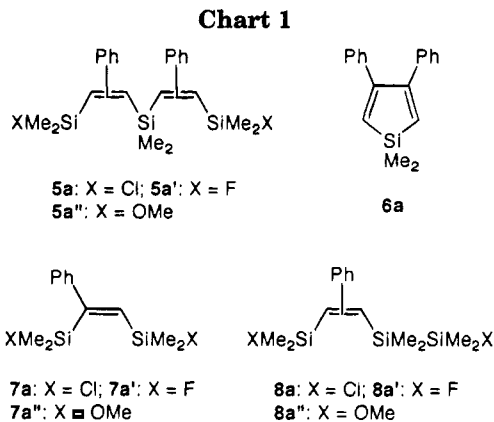
(1) For some catalytic reactions involving silicon–metal intermediates, see: Tilley, T. D. In *The Chemistry of Organic Silicon Compounds*; Patai, S., Rappoport, Z., Eds.; Wiley: Chichester, U.K., 1989; Chapter 24.

(2) For addition to acetylenes, see: (a) Sakurai, H.; Kamiyama, Y.; Nakadaira, Y. *J. Am. Chem. Soc.* **1975**, *97*, 931. (b) Okinoshima, H.; Yamamoto, K.; Kumada, M. *J. Organomet. Chem.* **1975**, *86*, C27. (c) Tamao, K.; Hayashi, T.; Kumada, M. *J. Organomet. Chem.* **1976**, *114*, C19. (d) Watanabe, H.; Kobayashi, M.; Higuchi, K.; Nagai, Y. *J. Organomet. Chem.* **1980**, *186*, 51. (e) Matsumoto, H.; Matsubara, I.; Kato, T.; Shono, K.; Watanabe, H.; Nagai, Y. *J. Organomet. Chem.* **1980**, *199*, 43. (f) Watanabe, H.; Kobayashi, M.; Saito, M.; Nagai, Y. *J. Organomet. Chem.* **1981**, *216*, 149. (g) Yamashita, H.; Catellani, M.; Tanaka, M. *Chem. Lett.* **1991**, 241. (h) Ito, Y.; Suginome, M.; Murakami, M. *J. Org. Chem.* **1991**, *56*, 1948. (i) Yamashita, H.; Tanaka, M. *Chem. Lett.* **1992**, 1547. (j) Finckh, W.; Tang, B.-Z.; Lough, A.; Manners, I. *Organometallics* **1992**, *11*, 2904. (k) Murakami, M.; Oike, H.; Sugawara, M.; Suginome, M.; Ito, Y. *Tetrahedron* **1993**, *49*, 3933. (l) Murakami, M.; Suginome, M.; Fujimoto, K.; Ito, Y. *Angew. Chem., Int. Ed. Engl.* **1993**, *32*, 1473. For some recent papers on addition to other unsaturated compounds, see: (m) Ishikawa, M.; Nishimura, Y.; Sakamoto, H.; Ono, T.; Ohshita, J. *Organometallics* **1992**, *11*, 483. (n) Tsuji, Y.; Lago, R. M.; Tomohiro, S.; Tsuneishi, H. *Organometallics* **1992**, *11*, 2353. (o) Hayashi, T.; Kobayashi, T.-a.; Kawamoto, A. M.; Yamashita, H.; Tanaka, M. *Organometallics* **1990**, *9*, 280. (p) Murakami, M.; Suginome, M.; Fujimoto, K.; Nakamura, H.; Andersson, P. G.; Ito, Y. *J. Am. Chem. Soc.* **1993**, *115*, 6487. (q) Ito, Y.; Suginome, M.; Matsuura, T.; Murakami, M. *J. Am. Chem. Soc.* **1991**, *113*, 8899. (r) Yamashita, H.; Reddy, N. P.; Tanaka, M. *Chem. Lett.* **1993**, 315. (s) Yamashita, H.; Reddy, N. P.; Tanaka, M. *Macromolecules* **1993**, *26*, 2143.



**1a** along with **4** (70%) (Table 1, run 1). Concentration of the reaction mixture followed by preparative TLC gave pure **3a** in 70% yield. The isolated **3a** showed satisfactory NMR, IR, and (HR)MS data. Compound **3a** was a mixture of two regioisomers with respect to the phenyl groups (the ratio of 2,5-/2,6-diphenyl (= 3,6-/3,5-dihydro) isomers = 20:80). In this reaction, the normally expected acetylene-insertion compound, a bis(2-silylethenyl)silane (**5a**), was formed only in low yield (8%), as were other byproducts such as a 1-silacyclopenta-2,4-diene (**6a**, 8%) and a 1,2-disilylethene, (ClMe<sub>2</sub>-Si)PhC=CH(SiMe<sub>2</sub>Cl) (**7a**, 18%) (Chart 1). Compound **5a** was a regioisomeric mixture comprising 1,7-dichloro-2,5-, -2,6-, and -3,5-diphenyl-1,4,7-trisilahepta-2,5-diene in about a 1:1:1 ratio. The yield and regioisomeric ratio of **5a** were estimated by GC analysis of the corresponding methylated compound (P1) after the reaction mixture had been treated with MeMgI. On the other hand, **6a** was nearly all one regioisomer, 3,4-diphenyl-1-silacyclopenta-2,4-diene. Compounds P1, **6a**, and **7a** were identified by comparison with authentic samples prepared separately.

Besides PdCl<sub>2</sub>(PPh<sub>3</sub>)<sub>2</sub>, other PdCl<sub>2</sub>L<sub>2</sub> complexes with L = triarylphosphines or AsPh<sub>3</sub> also catalyzed the foregoing reaction to give **3a** in good to moderate yields (Table 1, runs 2–7). The yields of **3a** were similar when PdCl<sub>2</sub>L<sub>2</sub> (L = PPh<sub>3</sub>, P(*p*-tolyl)<sub>3</sub>, or P(*p*-FC<sub>6</sub>H<sub>4</sub>)<sub>3</sub>) catalysts were used, although the yield of the byproduct **5a** was higher for L = P(*p*-tolyl)<sub>3</sub> (runs 1–3). Substitution of phenyl groups in PdCl<sub>2</sub>(PPh<sub>3</sub>)<sub>2</sub> by bulkier *o*-tolyl groups resulted in a decrease in the conversion of **1a** and the yield of **3a**, although it almost completely suppressed the formation of the byproducts **5a**, **6a**, and **7a** (runs 1 and 4–6). A similar result was obtained upon replacement of PPh<sub>3</sub> by AsPh<sub>3</sub> (runs 1 and 7). In contrast with triarylphosphines, trialkylphosphines and bidentate phosphines such as PMe<sub>3</sub>, PEt<sub>3</sub>, P<sup>*i*</sup>Bu<sub>3</sub>, dppb (1,4-bis(diphenylphosphino)butane), and dppf (1,1'-bis(diphenylphosphino)ferrocene) were ineffective in the present reaction (runs 8–12). The results indicate that phosphorus ligands with strong coordination ability are not favorable for promoting the reaction. A palladium catalyst without phosphine or arsine ligands, PdCl<sub>2</sub>(PhCN)<sub>2</sub>, also was not effective (run 13). In addition to the PdCl<sub>2</sub>L<sub>2</sub> catalysts, the Pd(dba)<sub>2</sub>-2P(OCH<sub>2</sub>)<sub>3</sub>CEt (dba = dibenzylideneacetone) system that was highly efficient in the simple insertion of **2a** into the Si–Si bonds of octamethyltrisilane<sup>2g</sup> also gave **3a** and **4** as the major products, albeit with a lower conversion of **1a** (run 14). Other group 10 metal complexes such as PtCl<sub>2</sub>(PPh<sub>3</sub>)<sub>2</sub> and NiCl<sub>2</sub>(PPh<sub>3</sub>)<sub>2</sub> were inactive under the present conditions (runs 15 and 16). Although the reaction rate



**Table 1.** Effect of Catalyst on the Reaction of Cl(SiMe<sub>2</sub>)<sub>3</sub>Cl (**1a**) with Phenylacetylene (**2a**)<sup>a</sup>

run	catalyst	conversion of <b>1a</b> (%)	yield <sup>b</sup> (%)					<b>3a</b> (A)/ <b>3a</b> (B) <sup>c</sup>
			<b>3a</b>	<b>4</b>	<b>5a</b>	<b>6a</b>	<b>7a</b>	
1	PdCl <sub>2</sub> (PPh <sub>3</sub> ) <sub>2</sub>	~100	80	70	8	8	18	20/80
2	PdCl <sub>2</sub> [P( <i>p</i> -tolyl) <sub>3</sub> ] <sub>2</sub>	93	64	49	18	7	20	22/78
3	PdCl <sub>2</sub> [P( <i>p</i> -FC <sub>6</sub> H <sub>4</sub> ) <sub>3</sub> ] <sub>2</sub>	97	78	62	9	4	16	22/78
4	PdCl <sub>2</sub> [PPh <sub>2</sub> ( <i>o</i> -tolyl)] <sub>2</sub>	93	80	68	6	0	10	23/77
5	PdCl <sub>2</sub> [PPh( <i>o</i> -tolyl)] <sub>2</sub>	84	79	67	4	1	7	26/74
6	PdCl <sub>2</sub> [P( <i>o</i> -tolyl)] <sub>3</sub>	52	25	23	0	0	1	28/72
7	PdCl <sub>2</sub> (AsPh <sub>3</sub> ) <sub>2</sub>	58	42	35	1	1	3	28/72
8	PdCl <sub>2</sub> (PMe <sub>3</sub> ) <sub>2</sub>	1	1	1	0	0	0	nc <sup>d</sup>
9	PdCl <sub>2</sub> (PEt <sub>3</sub> ) <sub>2</sub>	1	~0	1	0	0	0	
10	PdCl <sub>2</sub> (P <sup><i>i</i></sup> Bu <sub>3</sub> ) <sub>2</sub>	3	2	2	0	0	0	nc <sup>d</sup>
11	PdCl <sub>2</sub> (dppb) <sup>e</sup>	1	1	1	0	0	0	nc <sup>d</sup>
12	PdCl <sub>2</sub> (dppf) <sup>f</sup>	5	4	4	0	0	0	nc <sup>d</sup>
13	PdCl <sub>2</sub> (PhCN) <sub>2</sub>	16	4	14	1	0	0	nc <sup>d</sup>
14	Pd(dba) <sub>2</sub> -2P(OCH <sub>2</sub> ) <sub>3</sub> CEt <sup>g</sup>	42	36	28	2	2	9	22/78
15	PtCl <sub>2</sub> (PPh <sub>3</sub> ) <sub>2</sub>	0	0	0	0	0	0	
16	NiCl <sub>2</sub> (PPh <sub>3</sub> ) <sub>2</sub>	0	0	0	0	0	0	

<sup>a</sup> **1a**, 0.40 mmol; **2a**, 1.2 mmol; catalyst, 0.004 mmol; benzene, 0.1 mL; 120 °C; 1 h. <sup>b</sup> GC yield based on **1a**. <sup>c</sup> A, 3,6-dihydro isomer; B, 3,5-dihydro isomer. The ratios were estimated by GC. <sup>d</sup> Not checked. <sup>e</sup> dppb = 1,4-bis(diphenylphosphino)butane. <sup>f</sup> dppf = 1,1'-bis(diphenylphosphino)ferrocene. <sup>g</sup> dba = dibenzylideneacetone.

varied widely depending on the catalyst, the ratios of the regioisomers of **3a** (A/B) were always in the range of 2:8 to 3:7.

The effects of other reaction conditions were examined using the PdCl<sub>2</sub>(PPh<sub>3</sub>)<sub>2</sub> catalyst (Table 2). Lowering the temperature from 120 to 100 °C markedly slowed the reaction, while raising the temperature to 140 °C scarcely affected the product distribution (runs 1–3). Decreasing the ratio of **2a/1a** from 3 to 2 gave lower yields of **3a** and **4** with 16% recovery of **1a** (runs 2 and 4), although acetylene **2a** was consumed almost completely (~99% conversion).<sup>5</sup> Increasing the palladium concentration resulted in lower yields of **3a** and **4** with a tendency to increase **5a** (runs 4–8). Use of DME solvent in place of benzene caused little change of the product distribution (runs 4 and 9). In contrast, the more polar CH<sub>3</sub>CN significantly facilitated the formation of **5a** by suppressing the formation of other products (runs 4 and 10). The ratio of the regioisomers of **3a** (A/B) was not influenced so much by the reaction conditions, ranging from 2:8 to 3:7.

Different from **1a**, the corresponding fluoro- or methoxy-substituted trisilane, F(SiMe<sub>2</sub>)<sub>3</sub>F (**1b**) or MeO(SiMe<sub>2</sub>)<sub>3</sub>OMe (**1c**), gave hardly any 1,4-disilacyclohexa-2,5-diene **3a** under the same conditions as those used for **1a**. Thus, GC and GC-MS analyses of the reaction mixture obtained in the reaction of **1b** with **2a** showed formation of a bis(2-silylethenyl)silane (**5a'**, ~50% yield),

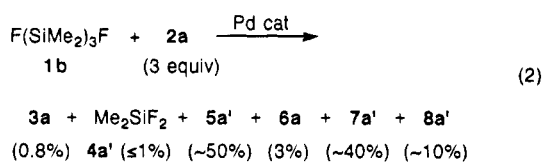


Table 2. Effects of Reaction Conditions on the Reaction of Cl(SiMe<sub>2</sub>)<sub>3</sub>Cl (1a) with Phenylacetylene (2a)<sup>a</sup>

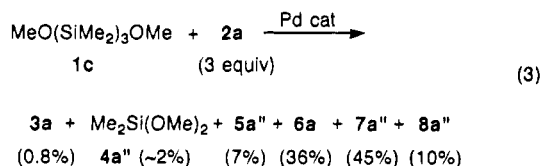
run	2a/1a	Pd cat (mol % <sup>b</sup> )	solvent	temp (°C)	conversion of 1a (%)	yield <sup>c</sup> (%)					3a(A)/3a(B) <sup>d</sup>
						3a	4	5a	6a	7a	
1	3	1	benzene	100	4	3	2	~0	1	1	nc <sup>e</sup>
2	3	1	benzene	120	~100	80	70	8	8	18	20/80
3	3	1	benzene	140	~100	80	66	7	8	21	22/78
4	2	1	benzene	120	84	61	42	6	7	17	19/81
5	2	0.5	benzene	120	75	64	44	6	4	15	19/81
6	2	2	benzene	120	99	56	41	10	4	13	18/82
7	2	4	benzene	120	96	45	35	7	8	19	22/78
8	2	8	benzene	120	98	46	32	20	7	17	29/71
9	2	1	DME <sup>f</sup>	120	92	66	47	8	7	18	18/82
10	2	1	CH <sub>3</sub> CN	120	~100	38	38	41	~0	9	17/83

<sup>a</sup> 1a, 0.40 mmol; 2a, 0.80–1.2 mmol; PdCl<sub>2</sub>(PPh<sub>3</sub>)<sub>2</sub>, 0.004–0.032 mmol; solvent, 0.1 mL; 100–140 °C; 1 h. <sup>b</sup> Based on 1a. <sup>c</sup> GC yield based on 1a. <sup>d</sup> A, 3,6-dihydro isomer; B, 3,5-dihydro isomer. The ratios were estimated by GC. <sup>e</sup> Not checked. <sup>f</sup> 1,2-Dimethoxyethane.

a 1,2-disilylethene (7a', ~40%), a (2-silylethenyl)disilane (8a', ~10%), and 6a (3%) along with much lower yields of 3a (0.8%) and difluorodimethylsilane (4a', ≤1%) (Chart 1; eq 2). Similarly, the reaction of 1c gave only



small quantities of 3a (0.8%) and dimethoxydimethylsilane (4a'', ~2%) and formed much larger amounts of 6a (36%), a 1,2-disilylethene (7a'', 45%), and by simple insertion compounds 5a'' (7%) and 8a'' (10%) (Chart 1; eq 3). The present reaction of 1c strikingly contrasted



(5) In every PdCl<sub>2</sub>(PPh<sub>3</sub>)<sub>2</sub>-catalyzed reaction of 1a with 2a, trimers of 2a (mainly two isomers (T1, T2), T1/T2 ≥ 10:1, trace–10% total yield) were observed by GC and/or GC-MS; GC-MS (EI, 70 eV): *m/z* (relative intensity) for T1, 306 (100, M<sup>+</sup>), 305 (18), 291 (21), 289 (25), 145 (17); for T2, 306 (100, M<sup>+</sup>), 289 (11), 228 (10), 226 (9). In addition, 2a underwent oligo- and polymerization under similar reaction conditions (2a, 1.2 mmol; PdCl<sub>2</sub>(PPh<sub>3</sub>)<sub>2</sub>, 0.004 mmol; benzene, 0.1 mL; 120 °C; 1 h) to form dimers (two isomers (D1, D2), D1/D2 = 1:~1), trimers (T1, T2 and other three isomers (T3–5), T1/T2/T3/T4/T5 = 100:14:10:6:4 by GC), and higher oligomers (*M<sub>w</sub>* ≤ 10<sup>3</sup> by GPC using polystyrene standards) in ≤0.5, ~10, and ~35% yields, respectively (45% conversion of 2a). GC-MS (EI, 70 eV): *m/z* (relative intensity) for D1, 204 (100, M<sup>+</sup>), 203 (96), 202 (63), 101 (35); for D2, 204 (100, M<sup>+</sup>), 203 (79), 202 (82), 101 (19); for T3, 306 (100, M<sup>+</sup>), 305 (30), 229 (37), 228 (28), 215 (25), 144 (28); for T4, 306 (100, M<sup>+</sup>), 305 (28), 229 (56), 228 (32); for T5, 306 (100, M<sup>+</sup>), 305 (25), 229 (31), 228 (31), 215 (34), 145 (24). Major isomers T1 and T2 were respectively assigned as 1,2,4- and 1,3,5-triphenylbenzene; GC retention times and GC-MS fragmentation patterns of T1 and T2 were in good agreement with those of authentic samples prepared by the Rh<sub>4</sub>(CO)<sub>12</sub>-catalyzed reaction of 2a,<sup>6d</sup> although the GC-MS data for 1,2,4-triphenylbenzene were not consistent with those reported for it that were obtained with a U catalyst.<sup>6e</sup> The other minor isomers, T3–5, seem to be linear trimers, although their structures have not been confirmed. These results indicate that oligo- and polymerization of 2a proceeds as a side reaction in the reaction of 1a with 2a.<sup>6</sup>

(6) For examples of palladium-catalyzed oligo- and/or polymerization of terminal acetylenes, see: (a) Odaira, Y.; Hara, M.; Tsutsumi, S. *Technol. Rep. Osaka Univ.* **1965**, *15*, 325. (b) Simionescu, C. I.; Percec, V.; Dumitrescu, S. *J. Polym. Sci. Polym. Chem. Ed.* **1977**, *15*, 2497. (c) Ishikawa, M.; Oshita, J.; Ito, Y.; Minato, A. *J. Organomet. Chem.* **1988**, *346*, C58. For examples of other transition metal-catalyzed oligo- and/or polymerizations of 2a, see: (d) Iwashita, Y.; Tamura, F. *Bull. Chem. Soc. Jpn.* **1970**, *43*, 1517. (e) Wen, T. C.; Chang, C. C.; Chuang, Y. D.; Chiu, J. P.; Chang, C. T. *J. Am. Chem. Soc.* **1981**, *103*, 4576. (f) Matsuda, T.; Mouri, T.; Higashimura, T. *Bull. Chem. Soc. Jpn.* **1980**, *53*, 1152.

Table 3. Reactions of Cl(SiMe<sub>2</sub>)<sub>3</sub>Cl (1a) with Acetylenes (2)<sup>a</sup>

run	2	Pd cat (mol % <sup>b</sup> )	temp (°C)	time (h)	conversion of 1a (%)	yield <sup>c</sup> (%)		3(A)/3(B) <sup>d</sup>
						3	4	
1	2a	1	120	1	~100	80 (70)	70	20/80
2	2b	1	120	1	99	50	41	27/73
3	2c	1	120	1	93	65 (57)	61	30/70
4	2d	1	120	1	~100	63	46	30/70
5	2e	1	120	1	20	18	12	nc <sup>e</sup>
6	2e	1	120	16	37	30	26	50/50
7	2e	8	120	1	64	42	47	nc <sup>e</sup>
8	2e	8	120	16	92	69	60	50/50
9	2f	1	120	1	2	nc <sup>e</sup>	2	
10	2f	10	140	18	70	(20)	58	

<sup>a</sup> 1a, 0.40 mmol; 2, 1.2 mmol; PdCl<sub>2</sub>(PPh<sub>3</sub>)<sub>2</sub>, 0.004–0.040 mmol; benzene, 0.1 mL; 120–140 °C; 1–18 h. <sup>b</sup> Based on 1a. <sup>c</sup> GC yield based on 1a. Figures in parentheses are isolated yields. <sup>d</sup> For 3a–d A, 3,6-dihydro isomer B, 3,5-dihydro isomer. For 3e: A, 2,5-dimethyl isomer; B, 2,6-dimethyl isomer. The ratios were estimated by GC and/or <sup>1</sup>H NMR. <sup>e</sup> Not checked.

with the previously reported result that 1c reacted with diphenylacetylene at 275 °C without palladium catalysts to give the corresponding 1,4-disilacyclohexa-2,5-diene, presumably via dimethylsilylene generated thermally from 1c.<sup>4a</sup>

**Reactions of 1a with Other Acetylenes.** Other terminal acetylenes, 1-octyne (2b), 4-phenyl-1-butyne (2c), and 5-hexynenitrile (2d), also reacted with 1a under the same conditions as those for 2a to give the corresponding 1,4-disilacyclohexa-2,5-dienes (3b–d) in 65–50% yields along with comparable amounts of 4 (eq 1; Table 3, runs 2–4). Likewise, an internal acetylene, 1-phenyl-1-propyne (2e), gave a 1,4-disilacyclohexa-2,5-diene (3e) in 69% yield, although a larger amount of the catalyst and a longer reaction time were required to obtain a better yield (runs 5–8). Products 3b–e were isolated by preparative TLC and/or preparative GC and were identified by NMR, IR, (HR)MS, and/or elemental analysis. Each compound of 3b–e was obtained as a mixture of two regioisomers with respect to the placement of substituents. For terminal acetylenes 3a–d, 2,6-disubstituted (= 3,5-dihydro) isomers were favorably formed, the ratios of 2,5-/2,6-disubstituted (= 3,6-/3,5-dihydro) isomers ranging from 2:8 to 3:7. On the other hand, the internal acetylene 2e gave 3e with a 1:1 isomer ratio. GC-MS of each reaction mixture indicated formation of byproducts such as a bis(2-silylethenyl)silane, a 1-silacyclopenta-2,4-diene, and/or a 1,2-disilylethene, which corresponded to 5a, 6a, and 7a, respectively, although their structures have not been unambiguously confirmed as yet (see Experimental Section). The reaction with sterically much bulkier 2f gave the corresponding 1,4-disilacyclohexa-2,5-diene 3f

only in a low yield (20%) even at a higher temperature of 140 °C (runs 9 and 10). Reactions of other acetylenes such as trimethylsilylacetylene, 3-(trimethylsiloxy)-1-propyne, ethyl propiolate, and dimethyl acetylenedicarboxylate resulted in complex mixtures; GC and GC-MS indicated that the yields of 1,4-disilacyclohexa-2,5-dienes were  $\leq 10\%$ .

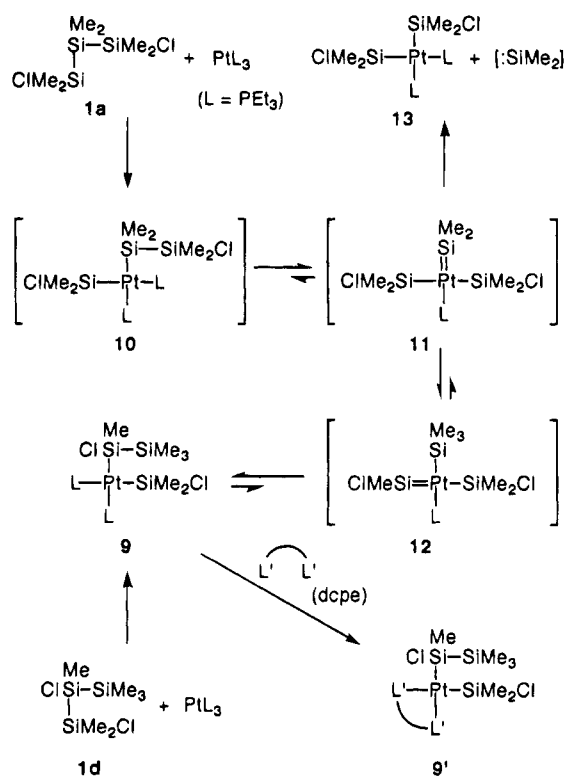
Although terminal acetylenes **2a-d** generally gave higher yields of **3** than internal acetylenes **2e** and **2f**, it usually was necessary to use them in excess (the ratio of **2/1a** = 3:1) because acetylene oligo- and polymerization take place as side reactions.<sup>5</sup> On the other hand, the reaction of an internal acetylene did not require use of an excess since the oligo- and polymerization proceeded hardly at all under the present conditions. In fact, in the reaction of **2e** under the conditions of run 8 in Table 3, lowering the ratio of **2e/1a** from 3:1 to 2:1 resulted in an even higher yield (90%) of **3e** based on the consumption of the acetylene (66%).

The 1,4-disilacyclohexa-2,5-dienes formed in the present reactions usually did not have chlorine atoms substituted at the silicon atoms. However, the reaction of **2e** gave a product whose GC-MS parent ion corresponded to that of 1-chloro-1,4-disilacyclohexa-2,5-diene (**3e'**), although its yield was less than 1%. Phenylation of **3e'** with PhLi resulted in better GC separation to reveal formation of mainly two isomeric phenylated compounds, **3e''(A)** and **3e''(B)**, corresponding to **3e'** in about a 1:1 GC ratio.

**Reaction of 1a or ClMe<sub>2</sub>SiSiClMeSiMe<sub>3</sub> with Pt(PET<sub>3</sub>)<sub>3</sub>.** A possible intermediate for the formation of **3** is a silylenepalladium species. Silyleneplatinum species were previously proposed as intermediates in the formation of **3f** in the platinum-catalyzed reaction of Me<sub>3</sub>SiSiMe<sub>2</sub>H with **2f**.<sup>7-9</sup> To gain supportive observations for silylenemetal species, **1a** (2 equiv) was treated with Pt(PET<sub>3</sub>)<sub>3</sub> in benzene-*d*<sub>6</sub> at 60 °C for 2 h. <sup>1</sup>H, <sup>13</sup>C, <sup>29</sup>Si, <sup>31</sup>P, and <sup>195</sup>Pt NMR of the reaction mixture revealed formation of *cis*-(ClMe<sub>2</sub>Si)(Me<sub>3</sub>SiClMeSi)Pt(PET<sub>3</sub>)<sub>2</sub> (**9**) in  $\geq 90\%$  yield along with free PET<sub>3</sub>. Addition of dcpe (1,2-bis(dicyclohexylphosphino)ethane) to the benzene-*d*<sub>6</sub> solution of **9** caused ligand exchange to give (ClMe<sub>2</sub>Si)(Me<sub>3</sub>SiClMeSi)Pt(dcpe) (**9'**, ~80% NMR yield) and liberated PET<sub>3</sub>. Complex **9** was alternatively obtained by the reaction of a 1,2-dichlorotrisilane, ClMe<sub>2</sub>SiSiClMeSiMe<sub>3</sub> (**1d**, 2 equiv), with Pt(PET<sub>3</sub>)<sub>3</sub> in a nearly quantitative NMR yield. These results and NMR spectral data (vide infra) proved the identities of **9** and **9'**, although their isolation in pure form has been unsuccessful to date.

Complex **9** shows two <sup>29</sup>Si NMR signals arising from the ClSi groups adjacent to the platinum at similar positions, 43.0 (<sup>2</sup>J<sub>PtSi</sub> = 70 Hz, <sup>1</sup>J<sub>PtSi</sub> = 1220 Hz) and 46.4 ppm (<sup>2</sup>J<sub>PtSi</sub> = 76 Hz, <sup>1</sup>J<sub>PtSi</sub> = 1361 Hz). On the other hand, the terminal Me<sub>3</sub>Si <sup>29</sup>Si signal appears at -11.6 ppm with <sup>3</sup>J<sub>PtSi</sub> = 9 Hz and <sup>2</sup>J<sub>PtSi</sub> = 131 Hz, which are much smaller than <sup>2</sup>J<sub>PtSi</sub> and <sup>1</sup>J<sub>PtSi</sub>. In <sup>31</sup>P NMR, the phosphorus signal is observed at 14.3 ppm with relatively small <sup>1</sup>J<sub>PtP</sub> value (1763 Hz), which is consistent

Scheme 1



with *cis* geometry of disilylbis(phosphino)platinum complexes.<sup>3,10</sup> In NMR the ligand phosphorus atoms are equivalent at room temperature, indicating that rapid ligand exchange is taking place. In agreement with this, <sup>31</sup>P NMR of the bidentate phosphine complex **9'**, in which the ligand exchange does not proceed so easily, displays two phosphorus signals at 69.2 and 72.9 ppm with <sup>2</sup>J<sub>PP</sub> = 17 Hz.

The formation of **9** is best rationalized by the reaction sequence outlined in Scheme 1 that involves oxidative addition of the Si-Si bond of **1a** to give (ClMe<sub>2</sub>Si)(ClMe<sub>2</sub>SiMe<sub>2</sub>Si)Pt(PET<sub>3</sub>)<sub>2</sub> (**10**),<sup>3,11</sup> 1,2-migration of the ClMe<sub>2</sub>-Si group of the disilanyl ligand leading to a silyleneplatinum species (ClMe<sub>2</sub>Si)<sub>2</sub>(Me<sub>2</sub>Si=)Pt(PET<sub>3</sub>) (**11**),<sup>12</sup> 1,3-migration of the methyl group in the ClMe<sub>2</sub>Si ligand providing (ClMe<sub>2</sub>Si)(Me<sub>3</sub>Si)(ClMeSi=)Pt(PET<sub>3</sub>) (**12**), and 1,2-migration of the Me<sub>3</sub>Si group resulting in **9**. The formation of **9** rather than **10** as the major product seems to be associated with thermodynamical stability of the SiSi-Pt bond; the Me<sub>3</sub>SiClMeSi-Pt bond is likely to be stronger than the ClMe<sub>2</sub>SiMe<sub>2</sub>Si-Pt bond in view of the electronegativity of the substituents at the silicon atoms adjacent to the platinum.<sup>13</sup>

In the absence of the extra phosphine, **9** was found to be readily transformed into *cis*-(ClMe<sub>2</sub>Si)<sub>2</sub>Pt(PET<sub>3</sub>)<sub>2</sub>

(10) Kobayashi, T.-a.; Hayashi, T.; Yamashita, H.; Tanaka, M. *Chem. Lett.* **1988**, 1411 and references cited therein.

(11) For other examples of oxidative addition of the Si-Si bonds of halogen-substituted noncyclic disilanes to platinum(0) or palladium(0) complexes, see: (a) Schmid, G.; Balk, H.-J. *Chem. Ber.* **1970**, *103*, 2240. (b) Glocking, F.; Houston, R. E. *J. Organomet. Chem.* **1973**, *50*, C31. (c) Eaborn, C.; Griffiths, R. W.; Pidcock, A. *J. Organomet. Chem.* **1982**, *225*, 331. (d) Murakami, M.; Yoshida, T.; Ito, Y. *Organometallics* **1994**, *13*, 2900.

(12) Generation of silylene species from oligosilylmetal complexes has been increasingly documented. For examples, see: (a) Tobita, H.; Wada, H.; Ueno, K.; Ogino, H. *Organometallics* **1994**, *13*, 2545 and references cited therein. (b) Pannell, K. H.; Brun, M.-C.; Sharma, H.; Jones, K.; Sharma, S. *Organometallics* **1994**, *13*, 1075 and references cited therein. (c) Tamao, K.; Tarao, Y.; Nakagawa, Y.; Nagata, K.; Ito, Y. *Organometallics* **1993**, *12*, 1113.

(7) Yamamoto, K.; Okinoshima, H.; Kumada, M. *J. Organomet. Chem.* **1971**, *27*, C31.

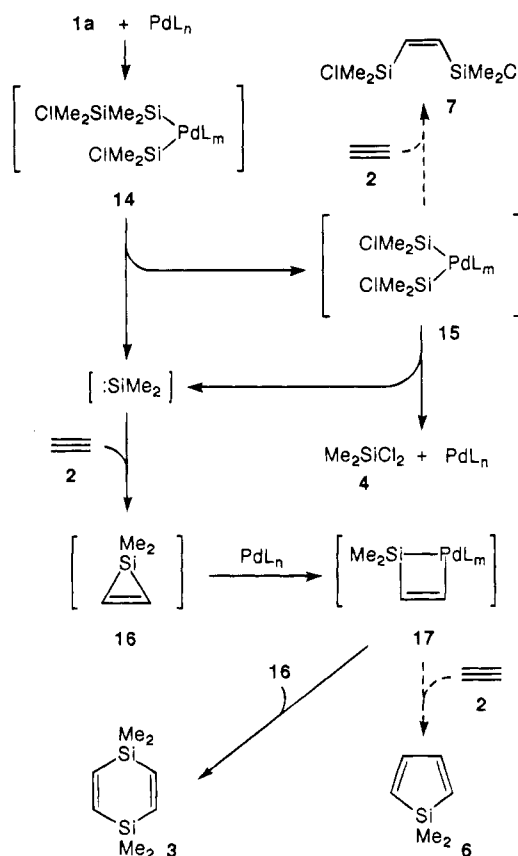
(8) Formation of 1,4-disilacyclohexa-2,5-dienes, presumably via silylene species, was observed in the palladium-catalyzed reactions of cyclooligosilanes with acetylenes as well: (a) Carlson, C. W.; West, R. *Organometallics* **1983**, *2*, 1801. (b) Ishikawa, M.; Fukui, T. *Chem. Express* **1987**, *2*, 623.

(9) See also: Yamashita, H.; Tanaka, M.; Goto, M. *Organometallics* **1992**, *11*, 3227.

(13) with release of a silylene species, presumably via the silyleneplatinum species **12** and **11**.<sup>12</sup> Thus, the solution of **9** obtained from **1a** and Pt(PET<sub>3</sub>)<sub>3</sub> was concentrated in vacuo at room temperature to remove the liberated PET<sub>3</sub>, and benzene-*d*<sub>6</sub> was added to the residue. NMR of the resulting mixture (~0.2 M Pt solution) showed formation of **13** in ~20% NMR yield with ~30% conversion of **9**. When the mixture was heated at 60 °C for 3 h, the yield of **13** was increased to ~75% with concomitant consumption of **9** (~90% conversion). The fate of the extruded :SiMe<sub>2</sub> unit is uncertain at the moment. However, several new <sup>1</sup>H NMR signals, the total intensity of which was in agreement with the **9** to **13** conversion, were observed in the 0.1–0.8 ppm region, indicative of the formation of polysilane and/or polysiloxane fragments. On the other hand, extrusion of the silylene species was significantly inhibited by free phosphine, as evidenced by the high-yield formation of **9** from **1a** and Pt(PET<sub>3</sub>)<sub>3</sub> and by the stability of **9** in the resulting solution, i.e., in the presence of extruded PET<sub>3</sub>. Furthermore, addition of PET<sub>3</sub> was found to suppress the conversion of **9** to **13**. Thus, after removal of volatiles from a reaction mixture of **1a** and Pt(PET<sub>3</sub>)<sub>3</sub>, benzene-*d*<sub>6</sub> was added (~0.1 M Pt). NMR measurement at this stage showed that ca. 40% of complex **9** had already been converted to **13**. PET<sub>3</sub> (1 equiv) was added to a portion of the benzene-*d*<sub>6</sub> solution, and the mixture was left standing at room temperature for 8 h, to result in only 10% additional conversion; i.e., ca. 50% of **9** still remained unconverted. On the other hand, a control experiment without addition of PET<sub>3</sub>, using the remainder of the benzene-*d*<sub>6</sub> solution, revealed 40% additional conversion to leave only 20% unconverted **9**.<sup>14</sup> This indicates that generation of dimethylsilylene requires dissociation of the phosphine ligand prior to the 1,2-migration of the silyl group leading to the formation of silyleneplatinum species.

**Mechanism.** The results obtained in the reaction of **1a** with Pt(PET<sub>3</sub>)<sub>3</sub> suggest that some silylene species are likely to be involved in the catalysis (Scheme 2). Thus, oxidative addition of **1a** to a palladium species followed by 1,2-migration of the disilanyl ClMe<sub>2</sub>Si group in the resulting (disilanyl)(silyl)palladium **14** would lead to the formation of a (dimethylsilylene)palladium species, which is able to generate dimethylsilylene along with a disilylpalladium, **15**. Reaction of the released dimethylsilylene with an acetylene would give a 1-silacycloprop-2-ene, **16**,<sup>4,15</sup> which could react with a palladium species to form a 1-pallada-2-silacyclobut-3-ene, **17**.<sup>16,17</sup> Reaction of **17** with **16** is likely to give the 1,4-disilacyclohexa-2,5-diene **3**,<sup>17a,b,18</sup> while reaction of **17** with a second acetylene molecule appears to afford the 1-silacyclopenta-2,4-diene byproduct **6**.<sup>2b,9,17a,c</sup> Compounds **3** and **6** may be formed partly by thermal

Scheme 2



reactions of **16**.<sup>19</sup> The formation of the 1-chloro-1,4-disilacyclohexa-2,5-diene **3e'** is also explained by incorporation of chloromethylsilylene, which is possibly generated from a (chlorosilylene)palladium species analogous to **12**. On the other hand, the disilylpalladium **15** is likely to give the 1,2-disilylethene byproduct **7** on the basis of the previous results that disilyl species of group 10 metals undergo equimolar reactions with acetylenes to give 1,2-disilylethene compounds.<sup>3,11d,20</sup> However, **15** is envisioned to be able to extrude another dimethylsilylene, since **1a** serves as a source of formally two silylene units in the catalysis. Indeed, we have found that the disilanyl(silyl)platinum **9** released two di-

(17) Species **17** is proposed as an intermediate in the dimerization of **16**<sup>17a</sup> and in the addition reaction of **16** to acetylenes<sup>17a,c</sup> in the presence of palladium catalysts. For examples of group 10 metal-catalyzed reactions, see: (a) Sakurai, H.; Kamiyama, Y.; Nakadaira, Y. *J. Am. Chem. Soc.* **1977**, *99*, 3879. (b) Ishikawa, M.; Sugisawa, H.; Kumada, M.; Higuchi, T.; Matsui, K.; Hirotsu, K. *Organometallics* **1982**, *1*, 1473 and references cited therein. (c) Seyferth, D.; Shannon, M. L.; Vick, S. C.; Lim, T. F. O. *Organometallics* **1985**, *4*, 57 and references cited therein.

(18) Catalytic<sup>17a,b</sup> or thermal<sup>19a,b</sup> dimerization of **16** that has a rather bulky substituent at each of the C=C carbon atoms seems to result in placing the bulky substituents at the 2- and 5-position rather than 2- and 6-position in the 1,4-disilacyclohexa-2,5-diene ring system. The regioselectivity is different from that observed in the present catalysts (Table 3). This might suggest a possibility of different routes for the formation of **3**.

(19) Thermal dimerization of **16**<sup>19a,b</sup> and addition of **16** to acetylenes<sup>19a,c</sup> are known, although thermal reactions seem to require severe conditions, as compared with catalytic reactions,<sup>19c</sup> and occasionally form considerable amounts of other products: (a) Ishikawa, M.; Fuchikami, T.; Kumada, M. *J. Organomet. Chem.* **1977**, *142*, C45. (b) Ishikawa, M.; Sugisawa, H.; Kumada, M.; Kawakami, H.; Yamabe, T. *Organometallics* **1983**, *2*, 974. (c) Seyferth, D.; Vick, S. C.; Shannon, M. L.; Lim, T. F. O.; Duncan, D. P. *J. Organomet. Chem.* **1977**, *135*, C37 and references cited therein.

(20) (a) Kiso, Y.; Tamao, K.; Kumada, M. *J. Organomet. Chem.* **1974**, *76*, 105. (b) Kobayashi, T.-a.; Hayashi, T.; Yamashita, H.; Tanaka, M. *Chem. Lett.* **1989**, 467. (c) Pan, Y.; Mague, J. T.; Fink, M. J. *Organometallics* **1992**, *11*, 3495.

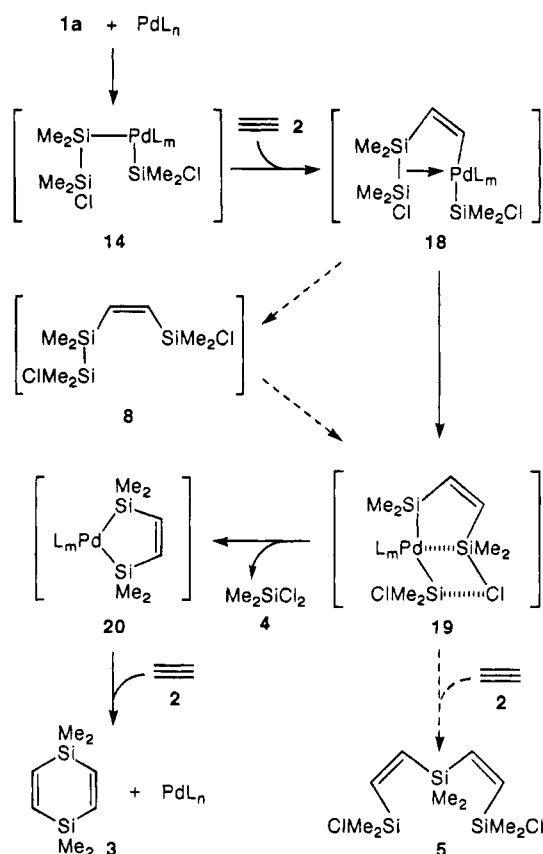
(13) Electronegative substituents at the silicon atoms are known to stabilize the Si–M (M = transition metal) bonds. For instance, see: Aylett, B. J. *Adv. Inorg. Chem. Radiochem.* **1982**, *25*, 1.

(14) The rate of decomposition seemed to be higher in more dilute solution.

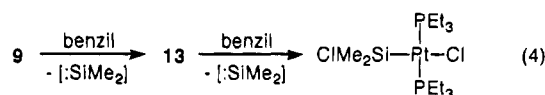
(15) For instance, see: (a) Conlin, R. T.; Gaspar, P. P. *J. Am. Chem. Soc.* **1976**, *98*, 3715. (b) Seyferth, D.; Annarelli, D. C.; Vick, S. C. *J. Am. Chem. Soc.* **1976**, *98*, 6382. (c) Seyferth, D.; Vick, S. C. *J. Organomet. Chem.* **1977**, *125*, C11. (d) Ishikawa, M.; Nakagawa, K.; Kumada, M. *J. Organomet. Chem.* **1977**, *131*, C15.

(16) We are unable to conclude whether the extruded silylene species is free or coordinated to a catalyst species. When a Si=Pd species is generated, it may react with an acetylene to form **17** directly without intervention of **16**.

Scheme 3



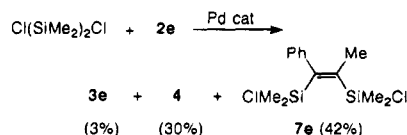
methylsilylene units successively upon treatment with a silylene trapping agent (benzil) to give *trans*-(ClMe<sub>2</sub>-Si)PtCl(PEt<sub>3</sub>)<sub>2</sub> in a high yield ( $\geq 80\%$ ) (eq 4).<sup>21,22</sup>



On the other hand, one can conceive an alternative route, which may explain the predominant formation of **3** and **4** more reasonably (Scheme 3). This reaction sequence is also initiated by the oxidative addition of **1a** to give the (disilanyl)(silyl)palladium **14**. Insertion of an acetylene<sup>23</sup> into the ClSi-Si-Pd bond rather than the ClSi-Pd bond<sup>13</sup> forms a (2-disilanylenehenyl)-(silyl)palladium, **18**. Reductive elimination of the

(21) The details will be reported separately.

(22) However, an attempt to obtain a 1,4-disilacyclohexa-2,5-diene by a palladium-catalyzed reaction of a 1,2-dichlorodisilane with an acetylene has not been so successful; the PdCl<sub>2</sub>(PPh<sub>3</sub>)<sub>2</sub>-catalyzed reaction of Cl(SiMe<sub>2</sub>)<sub>2</sub>Cl with **2e** (1 equiv) at 120 °C for 19 h gave **3e** only in 3% yield, which was much lower than that of 1,2-disilylene **7e** (42%), although **4** was also formed as a major product (30%) (89% conversion of the disilane).



This indicates that some acetylenes may not effectively trap the dimethylsilylene that might be extruded from disilylpalladium species like **15**. Formation of small amounts of 1,4-disilacyclohexa-2,5-diene byproducts was observed in the palladium-catalyzed double silylation of 1,4-bis(trimethylsilyl)buta-1,3-diyne with ClXMe<sub>2</sub>SiSiMe<sub>2</sub>Cl<sub>2</sub> (X = Cl, Me) as well: Kusumoto, T.; Hiyama, T. *Tetrahedron Lett.* **1987**, *28*, 1807.

Si-C=C-Si-Si linkage<sup>24</sup> followed (or assisted) by oxidative addition of the Si-Si bond to the palladium center provides a [(2-silylethenyl)silyl](silyl)palladium, **19**. Metathesis that extrudes **4** gives a 1-pallada-2,5-disilacyclohex-3-ene species, **20**, which finally undergoes insertion of a second acetylene molecule to end up with **3**.<sup>25</sup> Although there has been no direct evidence for Scheme 3, the formation of bis(2-silylethenyl)silane byproducts such as **5a** suggests that an intermediate species such as **19** is involved in the catalysis. In addition, a (2-silylethenyl)disilane compound, **8a** (Chart 1), which was possibly formed from **18** by reductive elimination, was observed only in the early stage of the reaction of **1a** with **2a**.<sup>26</sup> Furthermore, the difference in the yield of **3a** from **1a-c** might be rationalized by the postulated mechanism; **1b** and **1c** have much stronger and probably much less reactive Si-X (X = F, OMe) bonds than **1a**.<sup>27</sup> Therefore, metathesis corresponding to the conversion of species **19** to **20** is likely to be difficult for **1b** and **1c**, resulting in very low yields of **3a** (vide supra). Instead, **1b** and **1c** may prefer formation of **5a'** and **5a''**, respectively, from a species analogous to **19**; the ratio of the yield for **3a/5a'** in the reaction of **1b** was 0.8:~50, and that for **3a/5a''** in the reaction of **1c** was 0.8:7.

**Reactions of 1a with Diynes.** Diethynylbenzene was subjected to reaction, aiming at the synthesis of new silicon polymers consisting of 1,4-disilacyclohexa-2,5-dienylene and phenylene units.<sup>28</sup> When a mixture of **1a**, *p*-diethynylbenzene (**21**, 1 equiv), and PdCl<sub>2</sub>(PPh<sub>3</sub>)<sub>2</sub> (1 mol %) was heated in benzene at 120 °C for 6.5 h, a polymeric product was obtained as an insoluble brown solid (mp > 300 °C) (eq 5). Another reaction using a mixture of **21** (0.9 equiv) and **2a** (0.2 equiv), a stoichiometry which was expected to decrease the molecular weight and improve the solubility of the polymeric product, again gave an insoluble yellow-brown polymer (**22**, mp > 300 °C). The IR spectrum of **22** resembled that of **3a**, and elemental analysis of **22** nearly was in agreement with that calculated for the expected structure. In addition, the solid-state CP/MAS NMR spectrum of **22** clearly displayed the <sup>13</sup>C and <sup>29</sup>Si resonances

(23) Formation of Si-C=C-Pt species by acetylene insertion into the Si-Pt bond was demonstrated in the reactions of (halogeno)(silyl)platinum complexes: (a) Yamashita, H.; Tanaka, M.; Goto, M. *Organometallics* **1993**, *12*, 988. See also: (b) Chatt, J.; Eaborn, C.; Kapoor, P. N. *J. Organomet. Chem.* **1970**, *23*, 109.

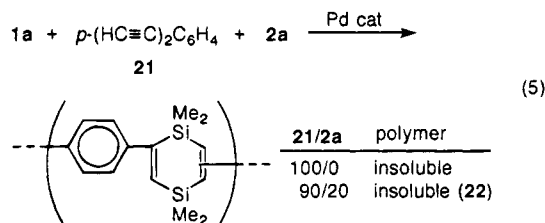
(24) Reductive elimination of the Si-C bond from an (alkyl)(silyl)-bis(phosphine)platinum was reported: Ozawa, F.; Hikida, T.; Hayashi, T. *J. Am. Chem. Soc.* **1994**, *116*, 2844.

(25) 1-Nickela-, -platina-, and -ferra-2,5-disilacyclohex-3-ene complexes are known to react with acetylenes to give 1,4-disilacyclohexa-2,5-diene compounds: (a) Liu, C.-s.; Cheng, C.-w. *J. Am. Chem. Soc.* **1975**, *97*, 6746. (b) Tanaka, M.; Uchimar, Y. *Bull. Soc. Chim. Fr.* **1992**, *129*, 667. (c) Sakurai, H.; Kobayashi, T.; Nakadaira, Y. *J. Organomet. Chem.* **1978**, *162*, C43.

(26) When the reaction of **1a** with **2a** under the conditions of run 1 in Table 1 was discontinued at 10 min, GC and GC-MS indicated formation of ClMe<sub>2</sub>SiRC=CR'SiMe<sub>2</sub>Cl ((R, R') = (Ph, H), (H, Ph), **8a**, 5% yield), along with **3a** (60%), **4** (46%), **5a** (5%), **6a** (4%), **7a** (8%), and recovered **1a** (29%). Compound **8a** was identified after the Si-Cl bonds were converted to Si-Me or Si-OMe bonds (see Experimental Section). On the other hand, **8a** was not found in the reaction for 1 h, indicating that **8a** had been converted into other products, possibly via **19**.

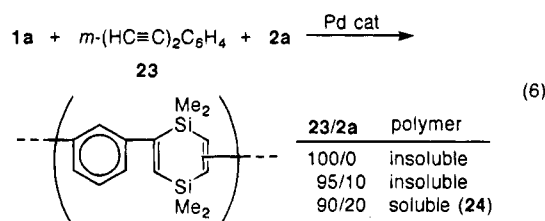
(27) The dissociation energy of the X-SiMe<sub>3</sub> bond increases in the order of X = Cl (~410 kJ/mol) < MeO (530) < F (590): Armitage, D. A. In *Comprehensive Organometallic Chemistry*; Wilkinson, G., Stone, F. G. A., Abel, E. W., Eds.; Pergamon: Oxford, U.K., 1982; Vol. 2, p 6.

(28) Thermally stable siloxane polymers containing 1,4-disilacyclohexa-2,5-diene rings were reported. See: Rhein, R. A. In *Silicon-Based Polymer Science*; Zeigler, J. M., Fearon, F. W. G., Eds.; Advances in Chemistry Series 224; American Chemical Society: Washington, DC, 1990; Chapter 19.



ascribable to the MeSi and aromatic CH moieties at positions similar to those for **3a**. These results strongly suggest the existence of 1,4-disilacyclohexa-2,5-dienylene and phenylene rings in the backbone, although **22** may possess other unidentified structures.<sup>29</sup> Thermogravimetric analysis (TGA) of **22** showed high thermal stability as anticipated from the structure; the 10% weight loss temperature under He (heating rate = 10 °C/min) was 473 °C.

The reaction of *m*-diethynylbenzene (**23**) in the absence or presence of **2a** (**23/2a** = 95:10) formed insoluble polymers as well (eq 6). However, use of an increased

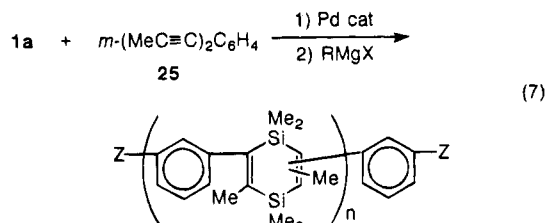


amount of **2a** (**23/2a** = 90:20) gave a soluble pale brown polymer (**24**) after the reaction mixture was treated with MeMgI, to convert the Si-Cl bonds of the products into Si-Me bonds, and reprecipitated with benzene-2-propanol. GPC measurement of **24** showed the  $M_w$  to be  $2.8 \times 10^4$  ( $M_w/M_n = 5.2$ ) with reference to the polystyrene standards. The <sup>1</sup>H, <sup>13</sup>C, and <sup>29</sup>Si NMR and IR spectra of **24** unambiguously showed the existence of 1,4-disilacyclohexa-2,5-dienylene and *m*-phenylene rings. In addition, the elemental analysis was also almost satisfactory for the expected structure, although **24** also may contain structurally unknown moieties as in the case of **22**.<sup>29</sup>

Internal acetylenes usually are more reluctant to undergo oligo- and/or polymerization than terminal acetylenes (vide supra). Therefore, diynes with internal acetylenic moieties seem to be better monomers for the above reaction. In fact, *m*-diprop-1-yn-1-ylbenzene (**25**), which did not polymerize to an appreciable extent under the present reaction conditions,<sup>30</sup> was found to react with **1a** to provide a polymer of the expected structure (eq 7). Thus, a mixture of **25** and **1a** (1 equiv) was heated in the presence of PdCl<sub>2</sub>(PPh<sub>3</sub>)<sub>2</sub> (8 mol %) at 120 °C for 16 h. Treatment of the reaction mixture with MeMgI for capping the Si-Cl bonds of the resulting

(29) In the reactions forming **22** and **24**, **1a** remained partly unreacted, while the acetylenes were nearly completely consumed (**1a** ≥ 13%, **21** ~ 0%, **2a** ~ 0%; **1a** = 26%, **23** ~ 0%, **2a** ~ 0%), indicating that some unidentified aromatic and/or vinylic structures arising from side reactions such as oligo- and polymerization of the ethynyl group itself<sup>9</sup> are also incorporated in the backbone of the produced polymers **22** and **24**. In fact, even without **1a** the diynes **21** and **23** gave insoluble polymeric black solids under similar reaction conditions. The quantities of the unidentified moieties in **22** and **24**, however, seem to be respectably small, judging from satisfactory elemental analysis and very high similarity of IR spectra between the polymers in question and **3a**, as compared with the diyne polymerization products.

(30) Diyne **25** could be recovered in ≥95% yield even after heating it with PdCl<sub>2</sub>(PPh<sub>3</sub>)<sub>2</sub> (8 mol %) in benzene at 120 °C for 16 h.



Z = -(YMe<sub>2</sub>Si)C=CMe(SiMe<sub>2</sub>Y) (= Z1) or

-C≡CMe (= Z2) (Z1/Z2 ≥ 9/1), n ≈ 4

**26**: Y = Cl; **26'**: Y = Me; **26''**: Y = *p*-MeOC<sub>6</sub>H<sub>4</sub>

polymer **26** followed by reprecipitation with THF/MeOH gave a pale brown solid, oligomeric *m*-phenylene(1,4-disilacyclohexa-2,5-dien-2,5- or -2,6-ylene) (**26'**; the ratio of 1,4-disilacyclohexa-2,5-dien-2,5/2,6-ylene units ≈ 9:10; the degree of polymerization n ≈ 4), in about 50% yield based on **25**. The <sup>1</sup>H, <sup>13</sup>C, and <sup>29</sup>Si NMR and IR spectra, the analytical data, and the GPC molecular weight of **26'** are well consistent with the proposed structure. On the basis of a comparison of its NMR with that of an authentic sample of (Me<sub>3</sub>Si)-PhC=CMe(SiMe<sub>3</sub>) (**27a**), the structures of the termini were mostly assigned to be 1,2-bis(trimethylsilyl)ethynyl (Z1) groups with a small portion of 1-propynyl (Z2) groups; the ratio of Z1/Z2 groups was estimated at more than 9:1.

Likewise, treatment of **26** with *p*-MeOC<sub>6</sub>H<sub>4</sub>MgBr gave a polymer, **26''**, with (*p*-MeOC<sub>6</sub>H<sub>4</sub>)Me<sub>2</sub>Si groups substituted at the termini, although **26''** has not been obtained in pure form. Identification of the terminal structure of **26''** was again based on a comparison with an authentic sample of (RMe<sub>2</sub>Si)PhC=CMe(SiMe<sub>2</sub>R) (**27b**, R = *p*-MeOC<sub>6</sub>H<sub>4</sub>). The formation of **26'** and **26''** clearly indicates that **26** has reactive Si-Cl bonds at the termini. This suggests a possibility of silicon polymer synthesis starting with **26** as a new building block, as such or after its reduction into the Si-H compound.

In conclusion, 1,4-disilacyclohexa-2,5-dienes are obtained in the palladium-catalyzed reactions of Cl-(SiMe<sub>2</sub>)<sub>3</sub>Cl with acetylenes. An investigation relevant to the mechanism has disclosed that skeletal rearrangement takes place in the reaction of the trisilene with Pt(PET<sub>3</sub>)<sub>3</sub> to give *cis*-(ClMe<sub>2</sub>Si)(Me<sub>3</sub>SiClMeSi)Pt(PET<sub>3</sub>)<sub>2</sub>, which then generates dimethylsilylene in the absence of the extra phosphine to provide *cis*-(ClMe<sub>2</sub>Si)<sub>2</sub>Pt-(PET<sub>3</sub>)<sub>2</sub>. The novel catalysis is applicable to the synthesis of new silicon polymers containing 1,4-disilacyclohexa-2,5-dienylene rings in the backbone.

## Experimental Section

<sup>1</sup>H, <sup>13</sup>C, <sup>29</sup>Si, <sup>31</sup>P, and/or <sup>195</sup>Pt NMR spectra in solution and solid state were measured on a Bruker ARX-300 instrument (300 MHz for <sup>1</sup>H, 75.5 MHz for <sup>13</sup>C, 59.6 MHz for <sup>29</sup>Si, 121.5 MHz for <sup>31</sup>P, and 64.5 MHz for <sup>195</sup>Pt). CDCl<sub>3</sub> was used as solvent unless otherwise noted. Chemical shifts in solution are referenced to Me<sub>4</sub>Si (0 ppm), CHCl<sub>3</sub> (7.25 ppm), or C<sub>6</sub>D<sub>5</sub>H (7.16 ppm) for <sup>1</sup>H NMR; CDCl<sub>3</sub> (77.0 ppm) or C<sub>6</sub>D<sub>6</sub> (128.0 ppm) for <sup>13</sup>C NMR; Me<sub>4</sub>Si (0 ppm) for <sup>29</sup>Si NMR; H<sub>3</sub>PO<sub>4</sub> (85% solution in D<sub>2</sub>O, 0 ppm) for <sup>31</sup>P NMR; Na<sub>2</sub>Pt<sub>2</sub>Cl<sub>6</sub> (saturated solution in D<sub>2</sub>O, 0 ppm) for <sup>195</sup>Pt NMR. Those in solid state are referenced to glycine (C=O, 176.46 ppm) for <sup>13</sup>C NMR and sodium 4,4-dimethyl-4-silapentanesulfonate (1.534 ppm) for <sup>29</sup>Si NMR. <sup>29</sup>Si NMR measurements in solution were performed

with an INEPT pulse sequence ( $\tau = 37$  ms,  $\Delta = 12$  ms).<sup>31</sup> <sup>13</sup>C and <sup>29</sup>Si NMR spectra in solid state were measured using a pulse program of cpseltics.x (CP/MAS with total sideband suppression). IR spectra were recorded on a JASCO FT/IR-5000 spectrometer. GC-MS spectra (EI, 70 eV) were measured on a Shimadzu QP-1000 or QP-5000 spectrometer. GC-HRMS measurements (EI, 70 eV) were performed on a JEOL DX-303 spectrometer. GC analyses were carried out with packed columns of OV-101 on Chromosorb WHP (1 or 3 m) and/or capillary CBP1-M25 (25 m) using internal standards. The column for preparative GC was OV-101 on Chromosorb WHP (1 m). Molecular weights of polymers were measured using polystyrene standards with a GPC system equipped with a Shimadzu LC-6A high-pressure pump, Shodex KF-801, KF-802, and KF-80M columns, and a GL Sciences Model 504R RI detector. TGA was carried out with a Shimadzu TG-30 system.

Every liquid starting material or solvent was dried with an appropriate drying agent such as sodium, CaH<sub>2</sub> or 4A molecular sieves and distilled under nitrogen or in vacuo. Cl(SiMe<sub>2</sub>)<sub>3</sub>Cl<sup>32</sup> and ClPhMeSiSiMe<sub>3</sub><sup>33</sup> were prepared according to the literature. ZnF<sub>2</sub>·4H<sub>2</sub>O, Pd(OAc)<sub>2</sub>, and CuI were purchased and were used as received. AlCl<sub>3</sub> and *p*-diethynylbenzene were sublimed in vacuo before use. PdCl<sub>2</sub>(PPh<sub>3</sub>)<sub>2</sub>,<sup>34</sup> PdCl<sub>2</sub>[P(*p*-tolyl)<sub>3</sub>]<sub>2</sub>,<sup>35</sup> PdCl<sub>2</sub>[P(*p*-FC<sub>6</sub>H<sub>4</sub>)<sub>3</sub>]<sub>2</sub>,<sup>36</sup> PdCl<sub>2</sub>[PPh<sub>2</sub>(*o*-tolyl)]<sub>2</sub>,<sup>35</sup> PdCl<sub>2</sub>[PPh(*o*-tolyl)]<sub>2</sub>,<sup>36</sup> PdCl<sub>2</sub>[P(*o*-tolyl)]<sub>3</sub>,<sup>36</sup> PdCl<sub>2</sub>(AsPh<sub>3</sub>)<sub>2</sub>,<sup>37</sup> PdCl<sub>2</sub>(PMe<sub>3</sub>)<sub>2</sub>,<sup>38</sup> PdCl<sub>2</sub>(dppb),<sup>39</sup> PdCl<sub>2</sub>(dppf),<sup>40</sup> PdCl<sub>2</sub>(PhCN)<sub>2</sub>,<sup>41</sup> Pd(dba)<sub>2</sub>,<sup>42</sup> PtCl<sub>2</sub>(PPh<sub>3</sub>)<sub>2</sub>,<sup>43</sup> and NiCl<sub>2</sub>(PPh<sub>3</sub>)<sub>2</sub><sup>44</sup> were synthesized by the reported procedures. PdCl<sub>2</sub>(PET<sub>3</sub>)<sub>2</sub><sup>45</sup> and PdCl<sub>2</sub>(P<sup>i</sup>Bu<sub>3</sub>)<sub>2</sub><sup>46</sup> were prepared by the reactions of PdCl<sub>2</sub>(PhCN)<sub>2</sub> with the corresponding phosphines (2 equiv).<sup>47</sup> P(OCH<sub>2</sub>)<sub>3</sub>CET was distilled in vacuo and recrystallized from hexane. PPh<sub>3</sub> and dcpo were recrystallized from ethanol. Pt(PET<sub>3</sub>)<sub>3</sub><sup>48a</sup> was prepared by heating Pt(PET<sub>3</sub>)<sub>4</sub><sup>48b</sup> in vacuo at around 60 °C for about 5 min.

**Preparation of F(SiMe<sub>2</sub>)<sub>3</sub>F (1b).** A mixture of **1a** (24 mmol) and ZnF<sub>2</sub>·4H<sub>2</sub>O (96 mmol) was stirred under nitrogen at 60 °C for 2 h.<sup>49</sup> Filtration (washing with pentane) followed by distillation gave **1b** (9.6 mmol, 40% yield) as a colorless oil. **1b**: bp 75–78 °C/48 mmHg (lit.<sup>50</sup> 82–83 °C/55 mmHg); <sup>1</sup>H NMR (C<sub>6</sub>D<sub>6</sub>)  $\delta$  0.11 (s, 6 H, FSiSiCH<sub>3</sub>), 0.27 (d, <sup>3</sup>J<sub>FH</sub> = 8.6

Hz, 12 H, FSiCH<sub>3</sub>); <sup>13</sup>C NMR (C<sub>6</sub>D<sub>6</sub>)  $\delta$  -8.0 (t, <sup>3</sup>J<sub>FC</sub> = 1.6 Hz, FSiSiC), 1.1 (d, <sup>2</sup>J<sub>FC</sub> = 12.2 Hz, FSiC); <sup>29</sup>Si NMR (C<sub>6</sub>D<sub>6</sub>)  $\delta$  -53.5 (t, <sup>2</sup>J<sub>Fsi</sub> = 26 Hz, SiSiF), 37.1 (dd, <sup>1</sup>J<sub>Fsi</sub> = 309 Hz, <sup>3</sup>J<sub>Fsi</sub> = ~3 Hz, SiF).

**Preparation of MeO(SiMe<sub>2</sub>)<sub>3</sub>OMe (1c).** MeOH (80 mmol) was added dropwise to a stirred mixture of **1a** (35 mmol), triethylamine (80 mmol), and benzene (30 mL) under nitrogen at 0 °C over 2 h, and the resulting mixture was stirred at room temperature for 1 h. Filtration followed by distillation (twice) gave **1c** (7.5 mmol, 22% yield) as a colorless oil. **1c**: bp 98 °C/34 mmHg (lit.<sup>51</sup> 79 °C/10 mmHg); <sup>1</sup>H NMR (C<sub>6</sub>D<sub>6</sub>)  $\delta$  0.21 (s, 6 H, OSiSiCH<sub>3</sub>), 0.27 (s, 12 H, OSiCH<sub>3</sub>), 3.30 (s, 6H, CH<sub>3</sub>O); <sup>13</sup>C NMR (C<sub>6</sub>D<sub>6</sub>)  $\delta$  -6.3 (OSiC), -0.4 (OSiSiC), 50.8 (OC); <sup>29</sup>Si NMR (C<sub>6</sub>D<sub>6</sub>)  $\delta$  -53.4 (OSiSi), 19.0 (OSi).

**Reactions of X(SiMe<sub>2</sub>)<sub>3</sub>X (1a, X = Cl; 1b, X = F; 1c, X = OMe) with Acetylenes.** Each reaction was carried out under nitrogen in a sealed glass tube (8 mm $\phi$ ). Typical examples of the reactions are shown below. As for the regioisomers of compound **3**, A and B, respectively, stand for the 3,6- and 3,5-dihydro isomers for **3a–d** and the 2,5- and 2,6-dimethyl isomers for **3e**. In the reactions of **2b–d** and **1b,c**, the ratios (quantities) of unidentified products were estimated by GC with a TCD detector.

**(a) Reaction of 1a with Phenylacetylene (2a).** A mixture of **1a** (0.40 mmol), phenylacetylene (**2a**, 1.2 mmol), PdCl<sub>2</sub>(PPh<sub>3</sub>)<sub>2</sub> (0.004 mmol), and benzene (0.1 mL) was heated at 120 °C for 1 h. GC and GC-MS analyses of the reaction mixture showed ~100% conversion of **1a** with formation of 1,1,4,4-tetramethyl-2,5- and -2,6-diphenyl-1,4-disilacyclohexa-2,6-diene (**3a**, two GC peaks, A/B = 20:80, 0.32 mmol, 80% yield based on **1a**), Me<sub>2</sub>SiCl<sub>2</sub> (**4**, 0.28 mmol, 70%), 1,7-dichloro-1,1,4,4,7,7-hexamethyl-2,5-, 2,6-, and -3,5-diphenyl-1,4,7-trisilahepta-2,5-diene (**5a**, one GC peak, 0.033 mmol, 8%), 1,1-dimethyl-3,4-diphenyl-1-silacyclopenta-2,4-diene (**6a**, 0.031 mmol, 8%), and 1,2-bis(chlorodimethylsilyl)-1-phenylethene (**7a**, 0.073 mmol, 18%). Concentration of the reaction mixture followed by preparative TLC (silica gel, hexane) gave **3a** (A/B = 20:80, 0.28 mmol, 70% yield) as a white solid. Recrystallization from hexane gave nearly pure **3a** (B).

In a separate reaction under the same conditions, the reaction mixture was poured into an ether (~2.5 mL) solution of MeMgI (~2.5 mmol), and the resulting mixture was refluxed overnight. Usual workup followed by GC analysis revealed almost complete consumption of **5a** and **7a** with formation of 1,1,1,4,4,7,7,7-octamethyl-2,5-, -2,6-, and -3,5-diphenyl-1,4,7-trisilahepta-2,5-diene (P1, three GC peaks A/B/C = 1:~1:~1, 0.033 mmol) and 1,2-bis(trimethylsilyl)-1-phenylethene (P2).

Another reaction under the same conditions was discontinued at 10 min. GC analysis showed recovery of **1a** (29%) and formation of **3a** (60%), **4** (46%), **5a** (5%), **6a** (4%), **7a** (8%), and 1,5-dichloro-1,1,4,4,5,5-hexamethyl-2- and -3-phenyl-1,4,5-trisilapent-2-ene (**8a**, one GC peak, 0.02 mmol, 5%). The reaction mixture was divided into two portions, which were treated with MeMgI (~4 mmol)/ether and MeOH (1 mmol)/Et<sub>3</sub>N (1 mmol), respectively. GC analyses showed conversion of **5a**, **7a**, and **8a** into the corresponding methyl and methoxy derivatives. In the methylation reaction, the products were P1 (vide supra, three GC peaks, A/B/C = 1:~1:~1), P2, and 1,1,1,4,4,5,5,5-octamethyl-2- and -3-phenyl-1,4,5-trisilapent-2-ene (P3, two GC peaks, A/B = ~2:1), while the methoxylation gave 1,7-dimethoxy-1,1,4,4,7,7-hexamethyl-2,5-, -2,6-, and -3,5-diphenyl-1,4,7-trisilahepta-2,5-diene (**5a''**, one GC peak), 1,2-bis(methoxydimethylsilyl)-1-phenylethene (**7a''**), and 1,5-dimethoxy-1,1,4,4,5,5-hexamethyl-2- and -3-phenyl-1,4,5-trisilapent-2-ene (**8a''**, one GC peak).

(31) Blinka, T. A.; Helmer, B. J.; West, R. *Adv. Organomet. Chem.* **1984**, *23*, 193.

(32) Kobayashi, T.; Pannell, K. H. *Organometallics* **1991**, *10*, 1960.

(33) Ishikawa, M.; Fuchikami, T.; Kumada, M. *J. Organomet. Chem.* **1978**, *162*, 223.

(34) King, A. O.; Negishi, E.-i.; Villani, F. J., Jr.; Silveira, A., Jr. *J. Org. Chem.* **1978**, *43*, 358.

(35) Sakakura, T.; Yamashita, H.; Kobayashi, T.-a.; Hayashi, T.; Tanaka, M. *J. Org. Chem.* **1987**, *52*, 5733.

(36) Neilan, J. P.; Laine, R. M.; Cortese, N.; Heck, R. F. *J. Org. Chem.* **1976**, *41*, 3455.

(37) Itatani, H.; Bailar, J. C., Jr. *J. Am. Oil Chem. Soc.* **1967**, *44*, 147.

(38) Evans, J. G.; Goggin, P. L.; Goodfellow, R. J.; Smith, J. G. *J. Chem. Soc. A* **1968**, 464.

(39) Tanaka, M.; Kobayashi, T.-a.; Sakakura, T. *Nippon Kagaku Kaishi* **1985**, 537.

(40) Hayashi, T.; Konishi, M.; Kumada, M. *Tetrahedron Lett.* **1979**, 1871.

(41) Doyle, J. R.; Slade, P. E.; Jonassen, H. B. *Inorg. Synth.* **1960**, *6*, 216.

(42) Ukai, T.; Kawazura, H.; Ishii, Y. *J. Organomet. Chem.* **1974**, *65*, 253.

(43) Hsu, C.-Y.; Leshner, B. T.; Orchin, M. *Inorg. Synth.* **1979**, *19*, 114.

(44) Cotton, F. A.; Faut, O. D.; Goodgame, D. M. L. *J. Am. Chem. Soc.* **1961**, *83*, 344.

(45) Mann, F. G.; Purdie, D. *J. Chem. Soc.* **1935**, 1549.

(46) mp 150.2–151.5 °C. Anal. Calcd for C<sub>24</sub>H<sub>54</sub>Cl<sub>2</sub>P<sub>2</sub>Fd: C, 49.53; H, 9.35. Found: C, 49.54; H, 9.35.

(47) Jenkins, J. M.; Verkade, J. G. *Inorg. Synth.* **1968**, *11*, 108.

(48) (a) Yoshida, T.; Matsuda, T.; Otsuka, S. *Inorg. Synth.* **1979**, *19*, 107. (b) Yoshida, T.; Matsuda, T.; Otsuka, S. *Inorg. Synth.* **1979**, *19*, 110.

(49) Tamao, K.; Okazaki, S.; Kumada, M. *J. Organomet. Chem.* **1978**, *146*, 87.

(50) Pitt, C. G. *J. Am. Chem. Soc.* **1969**, *91*, 6613.

(51) Atwell, W. H.; Weyenberg, D. R. *J. Organomet. Chem.* **1967**, *7*, 71.



The GC retention times and/or GC-MS fragmentation patterns of **6a**,<sup>9</sup> **7a**,<sup>52</sup> **P1**,<sup>2g</sup> **P2**,<sup>2g</sup> and **P3**<sup>2g</sup> were in good agreement with those of authentic samples prepared by literature reactions.

**3a**:<sup>53</sup> mp (B) 95–96 °C; <sup>1</sup>H NMR (A) δ 0.27 (s, 12 H, SiCH<sub>3</sub>), 6.78 (s, 2 H, =CH), 7.13–7.39 (m, 10 H, C<sub>6</sub>H<sub>5</sub>); <sup>1</sup>H NMR (B) δ 0.23 and 0.24 (each s, each 6 H, SiCH<sub>3</sub>), 6.71 (s, 2 H, =CH), 7.17–7.39 (m, 10 H, C<sub>6</sub>H<sub>5</sub>); <sup>13</sup>C NMR (A) δ 1.6 (SiCH<sub>3</sub>), 126.2 (*p*-C), 126.6 and 128.3 (*o*- and *m*-C), 145.5 (=CH), 146.3 (*ipso*-C), 160.6 (=CC); <sup>13</sup>C NMR (B) δ -1.2 and -0.6 (SiCH<sub>3</sub>), 126.3 (*p*-C), 126.5 and 128.1 (*o*- and *m*-C), 145.4 (=CH), 147.3 (*ipso*-C), 162.1 (=CC); <sup>29</sup>Si NMR (A) δ -21.8; <sup>29</sup>Si NMR (B) δ -24.0, -22.8; IR (KBr, A/B = 20:80) 1597 (m), 1485 (m), 1439 (m), 1267 (m), 1245 (s, SiMe), 882 (s), 864 (s), 832 (s), 779 (s), 762 (s), 723 (s), 700 (s), 545 (m), 518 (m), 480 (m) cm<sup>-1</sup>; GC-MS (A/B = 20:80) *m/z* (relative intensity) 320 (76, M<sup>+</sup>), 305 (100), 245 (11), 227 (14), 203 (32), 159 (18), 145 (20), 135 (22), 105 (14), 73 (53), 59 (11), 43 (29); GC-HRMS (A and B): calcd for C<sub>20</sub>H<sub>24</sub>Si<sub>2</sub>, 320.1416; found, 320.1414.

**5a**: GC-MS *m/z* (relative intensity) 355 (19, M<sup>+</sup> for <sup>35</sup>Cl-SiMe<sub>2</sub>Cl), 255 (41), 253 (100), 159 (23), 145 (17), 135 (97), 93 (16), 73 (14), 43 (12).

**5a'**: GC-MS *m/z* (relative intensity) 425 (2, M<sup>+</sup> - Me), 249 (100), 135 (17), 89 (44), 73 (11), 59 (33).

**7a'**: GC-MS *m/z* (relative intensity) 280 (2, M<sup>+</sup>), 265 (53), 250 (19), 233 (11), 219 (37), 163 (22), 151 (11), 145 (32), 135 (11), 133 (11), 105 (12), 89 (100), 73 (14), 59 (71), 43 (12).

**8a**: GC-MS *m/z* (relative intensity) 346 (0.2, M<sup>+</sup> for <sup>35</sup>Cl), 253 (38), 159 (18), 135 (100), 93 (13), 73 (22).

**8a'**: GC-MS *m/z* (relative intensity) 323 (2, M<sup>+</sup> - Me), 249 (100), 219 (11), 135 (20), 89 (38), 73 (20), 59 (40).

**(b) Reaction of 1b with 2a**. A mixture of **1b** (0.40 mmol), **2a** (1.2 mmol), PdCl<sub>2</sub>(PPh<sub>3</sub>)<sub>2</sub> (0.004 mmol), and benzene (0.1 mL) was heated at 120 °C for 1 h. GC and GC-MS analyses showed ~100% conversion of **1b** and formation of **3a** (0.003 mmol, 0.8%), difluorodimethylsilane (**4a'**, ≤0.004 mmol, ≤1%), 1,7-difluoro-1,1,4,4,7,7-hexamethyl-2,5-, -2,6-, and -3,5-diphenyl-1,4,7-trisilahepta-2,5-diene (**5a'**, three GC peaks, A/B/C = 9:17:16, ~0.2 mmol, ~50%), **6a** (0.011 mmol, 3%), **6a'** (an isomer of **6a**, ~0.06 mmol, ~15%), 1,2-bis(fluorodimethylsilyl)-1-phenylethene (**7a'**, ~0.16 mmol, ~40%), and 1,5-difluoro-1,1,4,4,5,5-hexamethyl-2- and -3-phenyl-1,4,5-trisilapent-2-ene (**8a'**, two GC peaks, A/B = 1:9, ~0.04 mmol, ~10%). In a separate reaction under identical conditions, a half portion of the reaction mixture was treated with MeOH (5 mmol)/Et<sub>3</sub>N (1 mmol) at room temperature for 10 min. GC showed partial conversion of **5a'**, **7a'**, and **8a'** (each ~30%) into the corresponding methoxy derivatives, **5a''**, **7a''**, and **8a''**.

**5a'**: GC-MS *m/z* (relative intensity) (A) 401 (0.6, M<sup>+</sup> - Me), 237 (84), 159 (23), 135 (100), 77 (21); (B) 416 (0.1, M<sup>+</sup>), 237 (100), 159 (18), 145 (10), 135 (97), 77 (17), 43 (10); (C) 401 (0.9, M<sup>+</sup> - Me), 339 (28), 321 (10), 320 (33), 305 (11), 247 (20), 237 (21), 159 (20), 145 (17), 135 (100), 77 (24), 73 (14), 43 (12).

**6a'**: GC-MS *m/z* (relative intensity) 262 (100, M<sup>+</sup>), 247 (59), 145 (26), 121 (32), 105 (38), 43 (42).

**7a'**:<sup>2c</sup> GC-MS *m/z* (relative intensity) 256 (24, M<sup>+</sup>), 241 (30), 179 (21), 178 (18), 163 (26), 160 (33), 159 (10), 145 (41), 139 (13), 135 (40), 83 (13), 77 (100), 49 (17), 47 (22).

**8a'**: GC-MS *m/z* (relative intensity) (A) 314 (0.2, M<sup>+</sup>), 237 (56), 159 (22), 135 (100), 77 (18), 73 (27); (B) 314 (2, M<sup>+</sup>), 237 (49), 159 (19), 135 (100), 77 (13), 73 (22), 43 (15).

**(c) Reaction of 1c with 2a**. A mixture of **1c** (0.40 mmol), **2a** (1.2 mmol), PdCl<sub>2</sub>(PPh<sub>3</sub>)<sub>2</sub> (0.004 mmol), and benzene (0.1 mL) was heated at 120 °C for 1 h. GC and GC-MS analyses showed ~100% conversion of **1c** and formation of **3a** (0.003

mmol, 0.8%), dimethoxydimethylsilane (**4a''**, ~0.008 mmol, ~2%), **5a''** (one GC peak, 0.026 mmol, 7%), **6a** (0.14 mmol, 36%), **7a''** (0.18 mmol, 45%), **8a''** (one GC peak, 0.040 mmol, 10%), and **P4**, whose GC-MS suggested an M<sup>+</sup> of 498 (**5a''** + SiMe<sub>2</sub>) (GC area ratio of **5a''**/**P4** = 1:~1).

**P4**: GC-MS *m/z* (relative intensity) 483 (2, M<sup>+</sup> - Me), 409 (100, M<sup>+</sup> - SiMe<sub>2</sub>OMe), 394 (49), 147 (29), 117 (18), 89 (67), 73 (54), 59 (59).

**(d) Reaction of 1a with 1-Octyne (2b)**. A mixture of **1a** (0.40 mmol), 1-octyne (**2b**, 1.2 mmol), PdCl<sub>2</sub>(PPh<sub>3</sub>)<sub>2</sub> (0.004 mmol), and benzene (0.1 mL) was heated at 120 °C for 1 h. GC and GC-MS analyses showed recovery of **1a** (1% and formation of 1,1,4,4-tetramethyl-2,5- and -2,6-dihexyl-1,4-disilacyclohexa-2,5-diene (**3b**, 0.20 mmol, 50% yield) and **4** (0.16 mmol, 41%) along with other byproducts, **6b** (one GC peak) and **7b** (GC area ratio of **3b**/**6b**/**7b** = 5:3:4). GC-MS parent ions of the latter two compounds and respectively corresponded to 1,1-dimethyl-1-sila-2,4-, -2,5-, and/or -3,4-dihexylcyclopenta-2,4-diene and 1,2-bis(chlorodimethylsilyl)oct-1-ene. Preparative GC of the reaction mixture gave **3b** (A/B = 27:73) as a colorless oil.

**3b**: <sup>1</sup>H NMR (A) δ 0.09 (s, 12 H, SiCH<sub>3</sub>), 0.88 (t, *J* = 6.4 Hz, 6 H, CH<sub>2</sub>CH<sub>3</sub>), 1.20–1.35 (m, 12 H, (CH<sub>2</sub>)<sub>3</sub>CH<sub>3</sub>), 1.35–1.47 (m, 4 H, =CCCH<sub>2</sub>), 2.17 (t, *J* = 7.6 Hz, 4 H, =CCH<sub>2</sub>), 6.35 (s, 2 H, =CH); <sup>1</sup>H NMR (B) δ 0.06 and 0.13 (each s, each 6 H, SiCH<sub>3</sub>), 0.88 (t, *J* = 6.4 Hz, 6H, CH<sub>2</sub>CH<sub>3</sub>), 1.20–1.35 (m, 12 H, (CH<sub>2</sub>)<sub>3</sub>CH<sub>3</sub>), 1.35–1.47 (m, 4 H, =CCCH<sub>2</sub>), 2.17 (t, *J* = 7.6 Hz, 4 H, =CCH<sub>2</sub>), 6.39 (s, 2 H, =CH); <sup>13</sup>C NMR (A) δ -1.2 (SiCH<sub>3</sub>), 14.1 (CH<sub>2</sub>CH<sub>3</sub>), 22.7, 28.5, 29.2, and 31.8 ((CH<sub>2</sub>)<sub>4</sub>CH<sub>3</sub>), 39.5 (=CCH<sub>2</sub>), 140.33 (=CH), 162.2 (=CC); <sup>13</sup>C NMR (B) δ -1.9 and -0.9 (SiCH<sub>3</sub>), 14.1 (CH<sub>2</sub>CH<sub>3</sub>), 22.7, 28.6, 29.2, and 31.8 ((CH<sub>2</sub>)<sub>4</sub>CH<sub>3</sub>), 39.3 (=CCH<sub>2</sub>), 140.27 (=CH), 161.9 (=CC); <sup>29</sup>Si NMR (A) δ -23.4; <sup>29</sup>Si NMR (B) δ -24.3, -24.1; IR (neat, A/B = 27:73) 1466 (m), 1404 (m), 1381 (m), 1247 (s, SiMe), 849 (s), 832 (s), 754 (m), 663 (m) cm<sup>-1</sup>; GC-MS (A/B = 27:73) *m/z* (relative intensity) 336 (51, M<sup>+</sup>), 321 (100), 279 (18), 266 (19), 262 (15), 251 (74), 182 (27), 181 (30), 168 (16), 167 (18), 141 (22), 109 (15), 97 (17), 85 (15), 83 (22), 73 (87), 59 (72), 43 (22); GC-HRMS (A and B): calcd for C<sub>20</sub>H<sub>40</sub>Si<sub>2</sub>, 336.2668; found, 336.2680.

**6b**: GC-MS *m/z* (relative intensity) 278 (7, M<sup>+</sup>), 208 (34), 207 (13), 193 (34), 166 (100), 165 (37), 151 (13), 139 (21), 138 (34), 137 (17), 123 (26), 109 (14), 97 (10), 95 (12), 83 (11), 73 (15), 59 (44), 43 (20), 41 (15).

**7b**: GC-MS *m/z* (relative intensity) 281 (4, M<sup>+</sup> - Me), 228 (6), 227 (6), 226 (8), 140 (5), 111 (13), 109 (5), 98 (100), 95 (15), 93 (36), 83 (10), 73 (7), 65 (5), 59 (13), 43 (9).

**(e) Reaction of 1a with 4-Phenyl-1-butyne (2c)**. A mixture of **1a** (0.40 mmol), 4-phenyl-1-butyne (**2c**, 1.2 mmol), PdCl<sub>2</sub>(PPh<sub>3</sub>)<sub>2</sub> (0.004 mmol), and benzene (0.1 mL) was heated at 120 °C for 1 h. GC and GC-MS analyses showed recovery of **1a** (7%) and formation of 1,1,4,4-tetramethyl-2,5- and -2,6-bis(2-phenylethyl)-1,4-disilacyclohexa-2,5-diene (**3c**, 0.26 mmol, 65% yield) and **4** (0.24 mmol, 61%) along with other byproducts, **6c** (two GC peaks, A/B = ~4:1) and **7c** (GC area ratio of **3c**/**6c**/**7c** = 10:4:5). GC-MS parent ions of **6c** and **7c**, respectively, corresponded to 1,1-dimethyl-2,4- and -2,5-, and/or -3,4-bis(2-phenylethyl)-1-silacyclopenta-2,4-diene and 1,2-bis(chlorodimethylsilyl)-4-phenylbut-1-ene. Concentration of the reaction mixture followed by preparative TLC (silica gel, hexane) gave **3c** (A/B = 30:70, 0.23 mmol, 57% yield) as a white solid. Recrystallization from hexane gave nearly pure **3c** (B).

**3c**: mp (B) 128–129 °C; <sup>1</sup>H NMR (A) δ 0.13 (s, 12 H, SiCH<sub>3</sub>), 2.44–2.78 (m, 8 H, CH<sub>2</sub>), 6.42 (s, 2 H, =CH), 7.15–7.32 (m, 10 H, C<sub>6</sub>H<sub>5</sub>); <sup>1</sup>H NMR (B) δ 0.09 and 0.17 (each s, each 6 H, SiCH<sub>3</sub>), 2.44–2.78 (m, 8 H, CH<sub>2</sub>), 6.49 (s, 2 H, =CH), 7.15–7.32 (m, 10 H, C<sub>6</sub>H<sub>5</sub>); <sup>13</sup>C NMR (A) δ -1.5 (SiCH<sub>3</sub>), 34.9 and 40.7 (CH<sub>2</sub>), 125.6 (*p*-C), 128.1 and 128.6 (*o*- and *m*-C), 140.6 (=CH), 142.3 (*ipso*-C), 160.9 (=CC); <sup>13</sup>C NMR (B) δ -2.2 and -1.0 (SiCH<sub>3</sub>), 35.0 and 40.6 (CH<sub>2</sub>), 125.7 (*p*-C), 128.2 and 128.4 (*o*- and *m*-C), 140.9 (=CH), 142.3 (*ipso*-C), 160.4 (=CC); <sup>29</sup>Si NMR (A) δ -22.9; <sup>29</sup>Si NMR (B) δ -23.9, -23.5; IR (KBr, B)

(52) Nagai, Y.; Watanabe, H.; Yoshibayashi, M. (Toshiba Silicone Co. Ltd). Jpn. Kokai Tokkyo Koho JP 79-88224 and 79-88225, 1979; *Chem. Abstr.* 1979, 91, P175513a, P175514b.

(53) Appler, H.; Neumann, W. P. *J. Organomet. Chem.* 1986, 314, 261.

(54) Watanabe, H.; Kobayashi, M.; Higuchi, K.; Nagai, Y. *J. Organomet. Chem.* 1980, 186, 51.



1603 (m), 1497 (m), 1454 (m), 1247 (s, SiMe), 978 (m), 886 (m), 859 (s), 839 (s), 814 (m), 774 (m), 750 (s), 702 (s), 667 (s), 542 (m)  $cm^{-1}$ ; GC-MS (A/B = 30:70)  $m/z$  (relative intensity) 376 (12,  $M^+$ ), 362 (13), 361 (37), 286 (17), 285 (57), 247 (19), 246 (30), 211 (13), 197 (14), 187 (15), 181 (26), 147 (30), 145 (24), 135 (26), 121 (13), 97 (12), 91 (33), 83 (18), 73 (100), 59 (50), 45 (14), 43 (20). Anal. (B) Calcd for  $C_{24}H_{32}Si_2$ : C, 76.53; H, 8.56. Found: C, 76.81; H, 8.71.

**6c:** GC-MS  $m/z$  (relative intensity) (A) 318 (22,  $M^+$ ), 227 (69), 225 (27), 214 (16), 213 (31), 199 (21), 185 (20), 167 (16), 145 (14), 135 (28), 121 (17), 91 (100), 59 (55), 43 (28); (B) 318 (33,  $M^+$ ), 227 (100), 199 (15), 185 (11), 173 (17), 145 (18), 135 (48), 121 (14), 91 (41), 73 (11), 59 (36), 43 (17).

**7c:** GC-MS  $m/z$  (relative intensity) 316 (3,  $M^+$  for  $^{35}Cl$ ), 223 (13), 188 (15), 187 (10), 173 (15), 129 (25), 128 (18), 97 (31), 95 (17), 93 (44), 91 (100), 65 (14), 59 (12).

**(f) Reaction of 1a with 5-Hexynenitrile (2d).** A mixture of **1a** (0.40 mmol), 5-hexynenitrile (**2d**, 1.2 mmol),  $PdCl_2(PPh_3)_2$  (0.004 mmol), and benzene (0.1 mL) was heated at 120 °C for 1 h. GC and GC-MS analyses showed ~100% conversion of **1a** and formation of 1,1,4,4-tetramethyl-2,5- and -2,6-bis(3-cyanopropyl)-1,4-disilacyclohexa-2,5-diene (**3d**, 0.25 mmol, 63% yield) and **4** (0.18 mmol, 46%) along with byproducts **5d'** (three GC peaks, A/B/C = 3:18:1), **6d** (one GC peak), **7d**, and **7d'** (GC area ratio of **3d/5d'/6d/7d/7d'** = 100:33:2:5:10). GC-MS analysis suggested **5d'** to be 3,6-, 3,7-, and 4,6-bis(3-cyanopropyl)-2,2,5,5,8,8-hexamethyl-1-oxa-2,5,8-trisilacycloocta-3,6-diene, a cyclosiloxane formed by hydrolysis of 1,7-dichloro-2,5-, -2,6-, and -3,5-bis(3-cyanopropyl)-1,1,4,4,7,7-hexamethyl-1,4,7-trisilahepta-2,5-diene. Compounds **6d**, **7d**, and **7d'** were respectively suggested by GC-MS to be 2,4-, 2,5-, and/or 3,4-bis(3-cyanopropyl)-1,1-dimehtyl-1-silacyclopenta-2,4-diene, 5,6-bis(chlorodimethylsilyl)-5-hexenenitrile, and 3-(3-cyanopropyl)-2,2,5,5-tetramethyl-1-oxa-2,5-disilacyclopent-3-ene (possibly formed by hydrolysis of **7d**). Preparative GC of the reaction mixture gave **3d** (A/B = 30:70) as a colorless oil.

**3d:**  $^1H$  NMR (A)  $\delta$  0.12 (s, 12 H,  $SiCH_3$ ), 1.81 (tt,  $J \approx 7.5$  and 7.2 Hz, 4 H,  $=CCCH_2$ ), 2.22–2.46 (m, 8 H,  $=CCH_2$  and  $CH_2CN$ ), 6.40 (s, 2 H,  $=CH$ );  $^1H$  NMR (B)  $\delta$  0.08 and 0.17 (each s, each 6 H,  $SiCH_3$ ), 1.81 (tt,  $J \approx 7.5$  and 7.2 Hz, 4 H,  $=CCCH_2$ ), 2.22–2.46 (m, 8 H,  $=CCH_2$  and  $CH_2CN$ ), 6.45 (s, 2 H,  $=CH$ );  $^{13}C$  NMR (A)  $\delta$  -1.5 ( $SiCH_3$ ), 16.6 (CCCN), 24.0 (CCN), 37.6 ( $=CC$ ), 119.6 (CN), 142.1 ( $=CH$ ), 158.3 ( $=CC$ );  $^{13}C$  NMR (B)  $\delta$  -2.1 and -1.2 ( $SiCH_3$ ), 16.6 (CCCN), 24.0 (CCN), 37.4 ( $=CC$ ), 119.6 (CN), 142.5 ( $=CH$ ), 158.4 ( $=CC$ );  $^{29}Si$  (A) NMR  $\delta$  -22.6;  $^{29}Si$  NMR (B)  $\delta$  -23.7, -23.1; IR (neat, A/B = 30:70) 2250 (m, CN), 1458 (m), 1427 (m), 1251 (s, SiMe), 1021 (m), 878 (s), 835 (s), 756 (m), 665 (s)  $cm^{-1}$ ; GC-MS (A/B = 30:70)  $m/z$  (relative intensity) 302 (4,  $M^+$ ), 287 (100), 234 (13), 209 (32), 194 (43), 136 (18), 83 (14), 73 (26), 59 (16), 43 (15). Anal. (A and B) Calcd for  $C_{18}H_{28}N_2Si_2$ : C, 63.52; H, 8.66; N, 9.26. Found: C, 63.04; H, 8.31; N, 8.93.

**5d':** GC-MS  $m/z$  (relative intensity) (A) 376 (3,  $M^+$ ), 361 (23), 207 (43), 152 (35), 151 (69), 136 (42), 117 (18), 98 (22), 97 (25), 83 (33), 73 (100), 59 (38), 45 (21), 43 (26); (B) 376 (2,  $M^+$ ), 361 (22), 210 (18), 152 (20), 151 (40), 136 (38), 131 (17), 117 (17), 98 (20), 97 (25), 83 (34), 73 (100), 59 (37), 45 (23), 43 (25); (C) 376 (9,  $M^+$ ), 361 (30), 347 (19), 243 (18), 210 (18), 151 (24), 136 (33), 131 (19), 117 (20), 98 (21), 97 (27), 83 (35), 73 (100), 59 (47), 58 (20), 45 (27), 43 (33).

**6d:** GC-MS  $m/z$  (relative intensity) 244 (19,  $M^+$ ), 229 (16), 190 (100), 188 (24), 176 (42), 109 (44), 95 (30), 84 (16), 83 (30), 69 (21), 67 (24), 59 (60), 55 (23), 53 (25), 43 (94).

**7d:** GC-MS  $m/z$  (relative intensity) 264 (16,  $M^+$  for  $^{35}Cl$ -Me), 186 (15), 136 (27), 95 (43), 93 (100), 83 (23), 65 (33), 63 (21), 43 (21).

**7d':** GC-MS  $m/z$  (relative intensity) 225 (6,  $M^+$ ), 210 (100), 198 (21), 193 (50), 170 (22), 158 (32), 157 (32), 133 (28), 118 (52), 117 (45), 83 (21), 73 (99), 59 (37), 45 (51), 43 (38).

**(g) Reaction of 1a with 1-Phenyl-1-propyne (2e).** A mixture of **1a** (0.40 mmol), 1-phenyl-1-propyne (**2e**, 1.2 mmol),  $PdCl_2(PPh_3)_2$  (0.032 mmol), and benzene (0.1 mL) was heated

at 120 °C for 16 h. GC and GC-MS analyses showed recovery of **1a** (8%) and formation of 1,1,2,4,4,5-hexamethyl-3,6-diphenyl- and 1,1,2,4,4,6-hexamethyl-3,5-diphenyl-1,4-disilacyclohexa-2,5-diene (**3e**, 0.28 mmol, 69% yield), **4** (0.24 mmol, 60%), and 1,2-bis(chlorodimethylsilyl)-1-methyl-2-phenylethene<sup>52</sup> (**7e**, 0.05 mmol, 13%). Compound **3e'**, whose GC-MS parent ion corresponded to 1-chloro-1,2,4,4,5-pentamethyl-3,6-diphenyl-, 1,2,4,4,6-pentamethyl-3,5-diphenyl-, and/or 1,3,4,4,5-pentamethyl-2,6-diphenyl-1,4-disilacyclohexa-2,5-diene, was also found in the reaction mixture (GC area ratio of **3e/3e'** = 6: $\leq$ 0.1). Concentration of the reaction mixture followed by preparative TLC (silica gel, hexane) gave **3e** (A/B = 50:50, 0.14 mmol, 36% yield) as a white solid. Recrystallization from hexane gave nearly pure **3e** (A).

In a separate reaction under similar conditions (**1a**, 0.40 mmol; **2e**, 1.2 mmol;  $PdCl_2(PPh_3)_2$ , 0.008 mmol; 120 °C; 24 h), the reaction mixture was poured into an ether (3 mL) solution of PhLi (~0.4 mmol) at -70 °C. The resulting mixture was stirred at room temperature for 1 h. Usual workup followed by GC and GC-MS analyses showed almost complete consumption of **3e'**, and a product (**3e''**, mainly two GC peaks, A/B = 1:~1) that was suggested by GC-MS to be the phenylated compound of **3e'** was instead found in the reaction mixture.

**3e:**<sup>4a</sup> mp (A) 127–129 °C;  $^1H$  NMR (A)  $\delta$  0.07 (s, 12 H,  $SiCH_3$ ), 1.61 (s, 6 H,  $=CCH_3$ ), 6.93–7.36 (m, 10 H,  $C_6H_5$ );  $^1H$  NMR (B)  $\delta$  -0.12 and 0.25 (each s, each 6 H,  $SiCH_3$ ), 1.63 (s, 6 H,  $=CCH_3$ ), 6.90–7.36 (m, 10 H,  $C_6H_5$ );  $^{13}C$  NMR (A)  $\delta$  -2.7 ( $SiCH_3$ ), 18.8 ( $=CCH_3$ ), 125.28 (*p*-C), 127.6 and 128.04 (*o*- and *m*-C), 143.57 and 149.8 ( $=CCH_3$  and *ipso*-C), 155.0 ( $=CC_6H_5$ );  $^{13}C$  NMR (B)  $\delta$  -3.0 and -2.3 ( $SiCH_3$ ), 18.6 ( $=CCH_3$ ), 125.25 (*p*-C), 127.6 and 128.01 (*o*- and *m*-C), 143.63 and 149.2 ( $=CCH_3$  and *ipso*-C), 155.6 ( $=CC_6H_5$ );  $^{29}Si$  NMR (A)  $\delta$  -22.8;  $^{29}Si$  NMR (B)  $\delta$  -24.8, -20.9; IR (KBr, A/B = 50:50) 1597 (m), 1483 (m), 1439 (m), 1245 (s, SiMe), 992 (m), 930 (m), 901 (m), 839 (s), 820 (s), 772 (s), 758 (s), 702 (s), 656 (m), 487 (m), 418 (m)  $cm^{-1}$ ; GC-MS (A/B = 50:50)  $m/z$  (relative intensity) 348 (77,  $M^+$ ), 333 (100), 217 (80), 159 (33), 135 (27), 105 (12), 97 (15), 73 (74), 59 (14), 45 (12), 43 (27); GC-HRMS (A and B): calcd for  $C_{22}H_{28}Si_2$ , 348.1730; found, 348.1731.

**3e':** GC-MS  $m/z$  (relative intensity) 368 (100,  $M^+$  for  $^{35}Cl$ ), 353 (84), 317 (13), 275 (35), 237 (39), 221 (20), 159 (59), 135 (28), 115 (18), 105 (33), 97 (23), 93 (31), 73 (17), 63 (21), 43 (72).

**3e'':** GC-MS  $m/z$  (relative intensity) (A) 410 (64,  $M^+$ ), 395 (55), 348 (100), 333 (21), 317 (34), 279 (40), 221 (30), 159 (47), 135 (49), 105 (44), 73 (24), 43 (28); (B) 410 (40,  $M^+$ ), 395 (30), 317 (15), 279 (24), 221 (19), 159 (23), 135 (100), 116 (29), 105 (24), 73 (19), 43 (28); GC-HRMS calcd for  $C_{27}H_{30}Si_2$ , 410.1886; found, 410.1881 (A) and 410.1874 (B).

**(h) Reaction of 1a with Diphenylacetylene (2f).** A mixture of **1a** (0.40 mmol), diphenylacetylene (**2f**, 1.2 mmol),  $PdCl_2(PPh_3)_2$  (0.04 mmol), and benzene (0.1 mL) was heated at 140 °C for 18 h. Cooling the reaction mixture to room temperature gave 1,1,4,4-tetramethyl-2,3,5,6-tetraphenyl-1,4-disilacyclohexa-2,5-diene (**3f**, 0.080 mmol, 20% yield) as white crystals. GC analysis of the supernatant solution showed recovery of **1a** (30%) and formation of **4** (0.23 mmol, 58% yield). NMR data of **3f** were in good agreement with the reported values.<sup>53</sup>

**Reaction of 1a with Pt(PET<sub>3</sub>)<sub>3</sub>.** A mixture of **1a** (0.32 mmol), Pt(PET<sub>3</sub>)<sub>3</sub> (0.16 mmol), and benzene-*d*<sub>6</sub> (0.25 mL) was heated under nitrogen in a sealed NMR tube at 60 °C for 2 h. NMR of the reaction mixture revealed formation of *cis*-(ClMe<sub>2</sub>-Si)(Me<sub>2</sub>SiClMeSi)Pt(PET<sub>3</sub>)<sub>2</sub> (**9**,  $\geq$ 90% yield).

In a separate reaction under similar conditions (**1a**, 0.62 mmol; Pt(PET<sub>3</sub>)<sub>3</sub>, 0.56 mmol; 60 °C; 2.5 h (no solvent)), pentane (0.5 mL) was added to the reaction mixture. Cooling the solution to -80 °C gave a yellow gummy solid. The supernatant solution was removed, and the residual solid was dried in vacuo at -80 °C. At room temperature the solid became a yellow viscous oil. Its NMR showed the existence of **9**, *cis*-

(ClMe<sub>2</sub>Si)<sub>2</sub>Pt(PEt<sub>3</sub>)<sub>2</sub><sup>3</sup> (**13**), and unreacted **1a** (**9/13/1a** ≈ 85:10:5). Further attempts to improve the purity of **9** by repeated reprecipitation resulted in decomposition of **9** to give increased amounts of **13**.

**9**: <sup>1</sup>H NMR (C<sub>6</sub>D<sub>6</sub>) δ 0.37 (s, 9 H, Si(CH<sub>3</sub>)<sub>3</sub>), 0.79–1.04 (m, 24 H, SiCl(CH<sub>3</sub>)<sub>2</sub> and PCCH<sub>3</sub>), 1.05 (t, <sup>4</sup>J<sub>PH</sub> ≈ 1.0 Hz, <sup>3</sup>J<sub>PH</sub> ≈ 29 Hz, 3 H, SiCl(CH<sub>3</sub>)Si(CH<sub>3</sub>)<sub>3</sub>), 1.63–1.91 (m, 12 H, PCH<sub>2</sub>); <sup>13</sup>C δ 0.8 (s, Si(CH<sub>3</sub>)<sub>3</sub>), 8.7 (s, <sup>3</sup>J<sub>PC</sub> = 16 Hz, PCC), 11.8 (t, <sup>3</sup>J<sub>PC</sub> = 4 Hz, <sup>2</sup>J<sub>PC</sub> = 71 Hz, SiCl(CH<sub>3</sub>)Si(CH<sub>3</sub>)<sub>3</sub>), 13.4 (t, <sup>3</sup>J<sub>PC</sub> = 6 Hz, <sup>2</sup>J<sub>PC</sub> = 97 Hz, SiCl(C<sup>a</sup>H<sub>3</sub>)(C<sup>b</sup>H<sub>3</sub>)), 14.0 (t, <sup>3</sup>J<sub>PC</sub> = 7 Hz, <sup>2</sup>J<sub>PC</sub> = 100 Hz, SiCl(C<sup>a</sup>H<sub>3</sub>)(C<sup>b</sup>H<sub>3</sub>)), 19.7 (d, <sup>1</sup>J<sub>PC</sub> = 12 Hz, <sup>2</sup>J<sub>PC</sub> = 20 Hz, PC<sup>a</sup>), 19.8 (d, <sup>1</sup>J<sub>PC</sub> = 12 Hz, <sup>2</sup>J<sub>PC</sub> = 20 Hz, PC<sup>b</sup>); <sup>29</sup>Si δ -11.6 (t, <sup>3</sup>J<sub>PSi</sub> = 9 Hz, <sup>2</sup>J<sub>PSi</sub> = 131 Hz, PtSiSi), 43.0 (t, <sup>2</sup>J<sub>PSi</sub> = 70 Hz, <sup>1</sup>J<sub>PSi</sub> = 1220 Hz, PtSi<sup>a</sup>Cl), 46.4 (t, <sup>2</sup>J<sub>PSi</sub> = 76 Hz, <sup>1</sup>J<sub>PSi</sub> = 1361 Hz, PtSi<sup>b</sup>Cl); <sup>31</sup>P δ 14.3 (s, <sup>1</sup>J<sub>PP</sub> = 1763 Hz); <sup>195</sup>Pt δ -4650 (t, <sup>1</sup>J<sub>PtP</sub> = 1763 Hz).

**Reaction of 9 with dcpe.** To dcpe (0.16 mmol) under nitrogen was added a reaction mixture obtained by the reaction of **1a** (0.32 mmol) with Pt(PEt<sub>3</sub>)<sub>3</sub> (0.16 mmol) in benzene-*d*<sub>6</sub> (0.25 mL) at 60 °C for 2 h (the yield of **9** was ≥90%). NMR of the resulting mixture showed almost complete conversion of **9** with formation of (ClMe<sub>2</sub>Si)(Me<sub>3</sub>SiClMeSi)Pt(dcpe) (**9'**, ~80% yield on the basis of <sup>31</sup>P NMR) and small amounts of unknown Pt(dcpe) species.

In a separate similar experiment, the reaction mixture obtained from dcpe (0.24 mmol) and a solution of **9** that was prepared by the reaction of **1a** (0.48 mmol) with Pt(PEt<sub>3</sub>)<sub>3</sub> (0.24 mmol) in benzene-*d*<sub>6</sub> (0.37 mL) at 60 °C for 3 h was concentrated in vacuo. Washing the residual solid with pentane (~0.5 mL) gave a pale yellow solid (~67 mg). Its <sup>1</sup>H NMR spectrum showed the existence of **9'** and unreacted **1a** (**9'/1a** ≈ 13:1), while its <sup>31</sup>P NMR spectrum displayed the signals of **9'** and an unknown Pt(dcpe) species X (69.7 (<sup>2</sup>J<sub>PP</sub> = 16 Hz, <sup>1</sup>J<sub>PtP</sub> = 1494 Hz), 73.0 ppm (<sup>2</sup>J<sub>PP</sub> = 16 Hz, <sup>1</sup>J<sub>PtP</sub> = 1530 Hz)) (**9'/X** = ~4:1). Attempted recrystallization of **9'** from pentane (large amounts) or benzene–pentane resulted in decomposition of **9'** to give PtCl<sub>2</sub>(dcpe)<sup>55</sup> and other unidentified products.

**9'**: <sup>13</sup>C NMR (C<sub>6</sub>D<sub>6</sub>) (for Si(CH<sub>3</sub>)<sub>3</sub>) δ 1.2 (s, <sup>3</sup>J<sub>PC</sub> = 8 Hz, Si(CH<sub>3</sub>)<sub>3</sub>), 11.5 (t, <sup>3</sup>J<sub>PC</sub> = 6 Hz, <sup>2</sup>J<sub>PC</sub> = 71 Hz, SiCl(CH<sub>3</sub>)Si(CH<sub>3</sub>)<sub>3</sub>), 13.1 (t, <sup>3</sup>J<sub>PC</sub> = 10 Hz, <sup>2</sup>J<sub>PC</sub> = 100 Hz, SiCl(C<sup>a</sup>H<sub>3</sub>)(C<sup>b</sup>H<sub>3</sub>)), 14.1 (t, <sup>3</sup>J<sub>PC</sub> = 11 Hz, <sup>2</sup>J<sub>PC</sub> = 106 Hz, SiCl(C<sup>a</sup>H<sub>3</sub>)(C<sup>b</sup>H<sub>3</sub>)); <sup>29</sup>Si δ -10.4 (d, <sup>3</sup>J<sub>PSi</sub> = 16 Hz, <sup>2</sup>J<sub>PSi</sub> = 145 Hz, PtSiSi), 52.6 (dd, <sup>2</sup>J<sub>PSi</sub> = 9 and 154 Hz, <sup>1</sup>J<sub>PSi</sub> = 1172 Hz, PtSi<sup>a</sup>Cl), 55.7 (dd, <sup>2</sup>J<sub>PSi</sub> = 11 and 169 Hz, <sup>1</sup>J<sub>PSi</sub> = 1324 Hz, PtSi<sup>b</sup>Cl); <sup>31</sup>P δ 69.2 (d, <sup>2</sup>J<sub>PP</sub> = 17 Hz, <sup>1</sup>J<sub>PtP</sub> = 1518 Hz), 72.8 (d, <sup>2</sup>J<sub>PP</sub> = 17 Hz, <sup>1</sup>J<sub>PtP</sub> = 1579 Hz); <sup>195</sup>Pt δ -5068 (dd, <sup>1</sup>J<sub>PtP</sub> = 1518 and 1579 Hz).

**Thermolysis of 9.** A benzene-*d*<sub>6</sub> solution of **9** obtained by the reaction of **1a** (0.18 mmol) with Pt(PEt<sub>3</sub>)<sub>3</sub> (0.17 mL) in benzene-*d*<sub>6</sub> (0.25 mL) at 60 °C for 3 h was concentrated in vacuo, and benzene-*d*<sub>6</sub> (~1 mL) was added to the residue. A portion of the solution (0.25 mL) was sealed in an NMR tube under nitrogen. Its NMR spectrum showed ~30% conversion of **9** with formation of **13** (~20% yield). When the solution was heated at 60 °C for 3 h, its NMR spectrum showed consumption of **9** (~90%) with formation of **13** (~75%) and other unidentified MeSi products, proton signals of which ranged from 0.1 to 0.8 ppm. The integral ratio of the MeSi proton signals of **13** to those of other MeSi products was about 2:1. NMR spectra of **13** were in agreement with those of the authentic sample.<sup>3</sup>

**Preparation of ClMe<sub>2</sub>SiSiClMeSiMe<sub>3</sub> (1d).** PhMe<sub>2</sub>SiCl (0.122 mol) was added dropwise to a stirred mixture of lithium (0.144 mol) and THF (150 mL) under argon at 0 °C over 1 h, and the resulting mixture was stirred at 0 °C overnight. The dark red supernatant solution of PhMe<sub>2</sub>SiLi that formed was added dropwise to a well-stirred THF (100 mL) solution of ClPhMeSiSiMe<sub>3</sub> (0.116 mol) at room temperature over 3 h. Usual workup followed by distillation gave PhMe<sub>2</sub>SiSiPhMeSiMe<sub>3</sub> (**1d'**, 0.083 mol, 71% yield) as a colorless oil. **1d'**: bp 131 °C/

0.25 mmHg; <sup>1</sup>H NMR δ 0.21 (s, 9 H, Si(CH<sub>3</sub>)<sub>3</sub>), 0.55 (s, 6 H, Si(CH<sub>3</sub>)<sub>2</sub>(C<sub>6</sub>H<sub>5</sub>)), 0.58 (s, 3 H, Si(CH<sub>3</sub>)Si(CH<sub>3</sub>)<sub>3</sub>); <sup>13</sup>C NMR δ -8.55 (Si(CH<sub>3</sub>)<sub>3</sub>), -2.7 and -2.6 (Si(CH<sub>3</sub>)<sub>2</sub>(C<sub>6</sub>H<sub>5</sub>)), -1.0 (Si(CH<sub>3</sub>)Si(CH<sub>3</sub>)<sub>3</sub>), 127.8 (*p*-C), 128.0 and 128.6 (*m*-C), 134.0 and 134.7 (*o*-C), 137.2 and 139.5 (*ipso*-C). Anal. Calcd for C<sub>18</sub>H<sub>28</sub>Si<sub>3</sub>: C, 65.78; H, 8.59. Found: C, 65.73; H, 8.73.

HCl gas (purity ≥99.7%) was passed through concentrated H<sub>2</sub>SO<sub>4</sub> solution and bubbled into a stirred mixture of **1d'** (0.076 mol), AlCl<sub>3</sub> (0.0075 mol), and CCl<sub>4</sub> (50 mL) at room temperature.<sup>32</sup> When the starting and monochlorinated trisilanes were consumed (monitored by GC), bubbling of HCl gas was stopped, and acetone (2 mL) was added to the solution. Evaporation of the solvent followed by distillation gave **1d** (0.060 mol, 79% yield) as a colorless oil. **1d**:<sup>56</sup> bp 73–75 °C/8 mmHg; <sup>1</sup>H NMR (C<sub>6</sub>D<sub>6</sub>) δ 0.15 (s, 9 H, Si(CH<sub>3</sub>)<sub>3</sub>), 0.42 and 0.45 (each s, each 3 H, Si(CH<sub>3</sub>)<sub>2</sub>(C<sub>6</sub>H<sub>5</sub>)), 0.51 (s, 3 H, Si(CH<sub>3</sub>)Si(CH<sub>3</sub>)<sub>3</sub>); <sup>13</sup>C NMR (C<sub>6</sub>D<sub>6</sub>) δ -2.4 (Si(CH<sub>3</sub>)<sub>3</sub>), -1.9, 1.5, and 2.2 (Si(CH<sub>3</sub>)Cl). Anal. Calcd for C<sub>6</sub>H<sub>18</sub>Cl<sub>2</sub>Si<sub>3</sub>: C, 29.37; H, 7.39. Found: C, 29.08; H, 7.06.

**Reaction of 1d with Pt(PEt<sub>3</sub>)<sub>3</sub>.** A mixture of **1d** (0.48 mmol), Pt(PEt<sub>3</sub>)<sub>3</sub> (0.24 mmol), and benzene-*d*<sub>6</sub> (0.25 mL) was heated under nitrogen in a sealed NMR tube at 60 °C for 4 h. NMR of the reaction mixture showed formation of **9** in a nearly quantitative yield.

**Reaction of Cl(SiMe<sub>2</sub>)<sub>2</sub>Cl with 2e.** A mixture of Cl(SiMe<sub>2</sub>)<sub>2</sub>Cl (0.60 mmol), **2e** (0.60 mmol), PdCl<sub>2</sub>(PPh<sub>3</sub>)<sub>2</sub> (0.048 mmol), and benzene (0.15 mL) was heated under nitrogen in a sealed glass tube at 120 °C for 18 h. GC and GC–MS analyses showed recovery of Cl(SiMe<sub>2</sub>)<sub>2</sub>Cl (11%) and **2e** (34%) along with formation of **3e** (0.009 mmol, 3% yield based on **2e**), **4** (0.18 mmol, 30%), and **7e** (0.25 mmol, 42%). Preparative GC gave **7e** as a colorless oil. **7e**:<sup>52</sup> <sup>1</sup>H NMR δ 0.39 and 0.74 (each s, each 6 H, SiCH<sub>3</sub>), 1.71 (s, 3 H, =CCH<sub>3</sub>), 6.85–7.36 (m, 5 H, C<sub>6</sub>H<sub>5</sub>); <sup>29</sup>Si NMR δ 13.5, 19.8; GC–MS *m/z* (relative intensity) 302 (8, M<sup>+</sup> for <sup>35</sup>Cl), 211 (17), 209 (47), 159 (22), 135 (16), 97 (10), 95 (35), 93 (100), 65 (13), 43 (10).

**Preparation of *m*-Diprop-1-yn-1-ylbenzene (25).** A mixture of *m*-dibromobenzene (36 mmol), propyne (~150 mmol), Pd(OAc)<sub>2</sub> (0.36 mmol), PPh<sub>3</sub> (0.72 mmol), CuI (0.18 mmol), and piperidine (45 mL) was stirred under nitrogen in a stainless steel autoclave (100 mL) at 110 °C for 12 h.<sup>57</sup> Usual workup followed by Kugelrohr distillation (86 °C, 0.4 mmHg) gave **25** (25 mmol, 71% yield) as a pale yellow oil. **25**: <sup>1</sup>H NMR δ 2.03 (s, 6 H, CH<sub>3</sub>), 7.15–7.42 (m, 4 H, C<sub>6</sub>H<sub>4</sub>); <sup>13</sup>C NMR δ 4.3 (CH<sub>3</sub>), 79.1 (CCH<sub>3</sub>), 86.2, (C≡CCH<sub>3</sub>), 124.1 (phenylene 1,3-C), 128.1 (phenylene 5-C), 130.6 (phenylene 4,6-C), 134.4 (phenylene 2-C); IR (neat) 2244 (m, C≡C), 1601 (s), 1479 (s), 893 (m), 795 (s, *m*-phenylene), 688 (s) cm<sup>-1</sup>; GC–MS *m/z* (relative intensity) 154 (100, M<sup>+</sup>), 153 (56), 152 (64), 151 (24), 115 (15), 76 (21), 63 (15), 51 (11).

**Reactions of 1a with Diynes.** Each reaction was carried out under nitrogen in a sealed glass tube. Typical examples of the reactions are shown below.

**(a) Reactions of 1a with *p*-Diethynylbenzene (21).** A mixture of **1a** (0.40 mmol), **21** (0.36 mmol), **2a** (0.08 mmol), PdCl<sub>2</sub>(PPh<sub>3</sub>)<sub>2</sub> (0.004 mmol), and benzene (0.1 mL) was heated at 120 °C for 6.5 h. An insoluble brown solid was observed in the resulting mixture. GC analysis of the supernatant solution showed recovery of **1a** (≥13%), **21** (~0%), and **2a** (~0%). Filtration of the reaction mixture followed by washing with benzene (1 mL × 2) gave a yellow-brown solid (**22**, 47 mg), which was insoluble in benzene, THF, and CHCl<sub>3</sub>.

**22**: mp >300 °C; IR (KBr) 1603 (m), 1493 (m), 1404 (m), 1249 (s, SiMe), 1017 (m), 868 (vs), 835 (vs), 770 (m), 694 (m), 661 (m) cm<sup>-1</sup>. Anal. Calcd for C<sub>14.6</sub>H<sub>18.6</sub>Si<sub>2</sub> (= 2 × Si(CH<sub>3</sub>)<sub>2</sub> + 0.9 × (HC≡C)<sub>2</sub>C<sub>6</sub>H<sub>4</sub> + 0.2 × C<sub>6</sub>H<sub>5</sub>C≡CH): C, 70.07; H, 7.49. Found: C, 69.16; H, 6.59. TGA of **22** under He at a 10 °C/min incremental rate showed that the 10% weight loss

(56) Einholz, W.; Gollinger, W.; Haubold, W. Z. *Naturforsch.* **1990**, *45b*, 25.

(57) For instance: Takahashi, S.; Kuroyama, Y.; Sonogashira, K.; Hagihara, N. *Synthesis* **1980**, 627.

(55) Hackett, M.; Whitesides, G. M. *J. Am. Chem. Soc.* **1988**, *110*, 1449.

temperature was 473 °C. The weight loss after heating to 900 °C was 28%.

A separate double scale reaction gave a larger amount of **22** (93 mg). Its solid-state NMR data are as follows:  $^{13}\text{C}$  NMR  $\delta$  -7 to 6 (br,  $\text{SiCH}_3$ ), 116–133 (br, *o*- and *m*-C), 133–152 (br, *p*-C);  $^{29}\text{Si}$  NMR  $\delta$  -25 to -20 (br, rings).

**(b) Reaction of 1a with *m*-Diethynylbenzene (23).** A mixture of **1a** (0.40 mmol), **23** (0.36 mmol), **2a** (0.08 mmol),  $\text{PdCl}_2(\text{PPh}_3)_2$  (0.004 mmol), and benzene (0.1 mL) was heated at 120 °C for 6.5 h. GC analysis of the resulting mixture showed recovery of **1a** (26%), **23** (~0%), and **2a** (~0%). The reaction mixture was poured into an ether (3 mL) solution of  $\text{MeMgI}$  (~4 mmol), and the resulting mixture was refluxed overnight. Usual workup (extraction with benzene) followed by reprecipitation with benzene/2-propanol (*v/v* = 1/10) gave a pale brown solid (**24**, ~20 mg).

**24:**  $M_w = 2.8 \times 10^4$  ( $M_w/M_n = 5.2$ );  $^1\text{H}$  NMR  $\delta$  -0.20 to 0.45 (br m,  $\text{SiCH}_3$ ), 6.50–6.82 (br m,  $\text{C}=\text{CH}$ ), 6.82–7.40 (br m,  $\text{C}_6\text{H}_4$ );  $^{13}\text{C}$  NMR  $\delta$  -1.1, -0.5, and 1.0 ( $\text{SiCH}_3$ ), 124.3–128.3 (phenylene 2-, 4,6-, and 5-C), 145.4 and 147.3 ( $=\text{CH}$  and phenylene 1,3-C), 162.3 ( $=\text{CC}_6\text{H}_4$ );  $^{29}\text{Si}$  NMR  $\delta$  -24.1, -22.8, and -21.9 (rings), -10.7 (small, probably  $=\text{CSiMe}_2$  of non-ring moieties); IR (KBr) 1591 (m), 1473 (m), 1406 (m), 1249 (s,  $\text{SiMe}$ ), 1089 (m), 1031 (m), 905 (m), 866 (vs), 835 (vs), 795 (s), 774 (s), 760 (s, *m*-phenylene), 700 (m), 663 (m)  $\text{cm}^{-1}$ . Anal. Calcd for  $\text{C}_{14.6}\text{H}_{18.6}\text{Si}_2$  ( $= 2 \times \text{Si}(\text{CH}_3)_2 + 0.9 \times (\text{HC}=\text{C})_2\text{C}_6\text{H}_4 + 0.2 \times \text{C}_6\text{H}_5\text{C}=\text{CH}$ ): C, 70.07; H, 7.49. Found: C, 69.40; H, 7.30.

**(c) Reaction of 1a with 25.** A mixture of **1a** (0.4 mmol), **25** (0.4 mmol),  $\text{PdCl}_2(\text{PPh}_3)_2$  (0.032 mmol), and benzene (0.1 mL) was heated in a sealed glass tube at 120 °C for 16 h. GC analysis of the resulting mixture showed recovery of **1a** (5%) and **25** (5%). The reaction mixture was poured into an ether (3 mL) solution of  $\text{MeMgI}$  (~4 mmol), and the resulting mixture was refluxed overnight. Usual workup (extraction with benzene) followed by reprecipitation with THF/MeOH (*v/v* = 1/10) gave a pale brown solid of a methylated polymer (**26'**) (63 mg, ~0.20 mmol monomer unit, ~50% yield based on **25**).

In a separate reaction under the same conditions, the reaction mixture was treated with *p*- $\text{MeOC}_6\text{H}_4\text{MgBr}$  (~4 mmol) in place of  $\text{MeMgI}$ . Similar workup followed by reprecipitation with THF/MeOH (*v/v* = 1/10) gave a pale yellow solid of an anisylated polymer (**26''**, 22 mg, ~0.08 mmol monomer unit, ~20%).  $^1\text{H}$  NMR of **26''** showed the existence of small amounts of impurities in the  $\text{SiMe}$  region of **26''** (the integral ratio of the  $\text{SiMe}$  proton signals of **26''**/impurities = ~9:1).

**26':** Softening temperature 132–148 °C;  $M_w = 3.0 \times 10^3$  ( $M_w/M_n = 2.2$ );  $^1\text{H}$  NMR  $\delta$  -0.17 to -0.01 (br m, disilacyclohexadien-2,6-ylene,  $\text{SiCH}^a_3$ ), -0.01 to 0.20 (br m, disilacyclohexadien-2,5-ylene and terminal  $\text{SiCH}^b_3$ ), 0.20–0.50 (br m, disilacyclohexadien-2,6-ylene and terminal  $\text{SiCH}^c_3$ ), 1.53–1.70 (br m,  $=\text{CCH}^d_3$ ), 2.03 and 2.05 (each s, terminal  $=\text{CCH}^e_3$ ), 6.35–7.80 (br m,  $\text{C}_6\text{H}_4$ ) (the integral ratio of  $\text{H}^a/\text{H}^b/\text{H}^c/\text{H}^d/\text{H}^e \approx 5:15:11:13:\leq 1$ ; the calculated ratio for **26'** (the ratio of 1,4-disilacyclohexa-2,5-dien-2,5/2,6-ylene units = 9:10; *n* = 4; the ratio of Z1/Z2 groups = 9:1) = 5:15:11:12:0.2);  $^{13}\text{C}$  NMR  $\delta$  -3.05, -2.97, -2.6, -2.5, and -2.1 (rings'  $\text{SiCH}_3$ ), 1.3 and 1.8 (terminal  $\text{SiCH}_3$ ), 4.3 (terminal  $\text{C}=\text{CCH}_3$ ), 18.6 and 18.7 (rings'

$\text{C}=\text{CCH}_3$ ), 22.6 (terminal  $\text{C}=\text{CCH}_3$ ), 80.0 (terminal  $\text{C}=\text{CCH}_3$ ), 85.5 (terminal  $\text{C}=\text{CCH}_3$ ), 123.6–132.2 (phenylene 2-, 4,6-, and 5-C), 143.0–143.8 and 148.9–149.9 ( $=\text{CCH}_3$  and phenylene 1,3-C), 155.2–156.0 ( $=\text{CC}_6\text{H}_4$ );  $^{29}\text{Si}$  NMR  $\delta$  -24.7, -22.9, and -21.0 (rings), -9.5 and -6.1 (terminal); IR (KBr) 2240 (vw,  $\text{C}=\text{C}$ ), 1591 (m), 1572 (m), 1470 (m), 1437 (m), 1406 (m), 1247 (s,  $\text{SiMe}$ ), 1085 (m), 922 (m), 901 (m), 835 (s), 764 (s, *m*-phenylene), 708 (m), 656 (m)  $\text{cm}^{-1}$ . Anal. Calcd for  $(\text{C}_{16}\text{H}_{22}\text{Si}_2)_n(\text{C}_{22.8}\text{H}_{42.4}\text{Si}_{3.6})_m$  (**26'**, *n* = 4; the ratio of Z1/Z2 groups = 9:1; FW = 1499.8): C, 69.51; H, 8.76. Found: C, 69.66; H, 8.47.

**26'':**  $M_w = 1.1 \times 10^4$  ( $M_w/M_n = 4.0$ ) (before reprecipitation  $M_w = 3.3 \times 10^3$  ( $M_w/M_n = 2.4$ ));  $^1\text{H}$  NMR  $\delta$  -0.28 to -0.03, -0.03 to 0.15, and 0.15–0.51 (each br m,  $\text{SiCH}_3$ ), 1.63 (br s,  $=\text{CCH}_3$ ), 2.03 and 2.05 (each s, terminal  $=\text{CCH}_3$ ), 3.75–3.88 (m,  $\text{OCH}_3$ ), 6.45–7.63 (br m,  $\text{C}_6\text{H}_4$ );  $^{29}\text{Si}$  NMR  $\delta$  -24.7, -22.9, and -21.0 (rings), -12.8 and -9.9 (terminal); IR (KBr) 2240 (vw,  $\text{C}=\text{C}$ ), 1731 (m), 1593 (m), 1506 (m), 1470 (m), 1441 (m), 1278 (m), 1247 (s,  $\text{SiMe}$ ), 1183 (m), 1110 (m), 1036 (m), 980 (m), 924 (m), 901 (m), 841 (s), 822 (s), 766 (s, *m*-phenylene), 710 (s), 656 (m)  $\text{cm}^{-1}$ .

**Preparation of  $(\text{RMe}_2\text{Si})\text{MeC}=\text{CPh}(\text{SiMe}_2\text{R})$  (**27a**, **R** = **Me**; **27b**, **R** = *p*- $\text{MeOC}_6\text{H}_4$ ).** A mixture of  $\text{Cl}(\text{SiMe}_2)_2\text{Cl}$  (0.60 mmol), **2e** (0.60 mmol),  $\text{PdCl}_2(\text{PPh}_3)_2$  (0.048 mmol), and benzene (0.15 mL) was heated in a sealed glass tube at 120 °C for 19 h. The reaction mixture containing **7e** was poured into an ether (3 mL) solution of  $\text{MeMgI}$  (~4 mmol), and the resulting mixture was refluxed overnight. Usual workup followed by preparative TLC (silica gel, hexane) and Kugelrohr distillation (140 °C, 16 mmHg) gave **27a** (0.25 mmol, 42% yield) as a colorless oil.

In a separate reaction under the same conditions, the reaction mixture was treated with *p*- $\text{MeOC}_6\text{H}_4\text{MgBr}$  (~4 mmol) in place of  $\text{MeMgI}$ . Usual workup (extraction with toluene) followed by preparative TLC (silica gel, hexane) gave an off-white solid of **27b** (24 mg, about 50% purity with impurities of  $(p\text{-MeOC}_6\text{H}_4)_2\text{SiMe}_2$  and  $[(p\text{-MeOC}_6\text{H}_4)_2\text{Me}_2\text{Si}]_2$ ).

**27a:**  $^{20a}^1\text{H}$  NMR  $\delta$  0.03 and 0.25 (each s, each 9 H,  $\text{SiCH}_3$ ), 1.55 (s, 3 H,  $=\text{CCH}_3$ ), 6.76–7.32 (m, 5 H,  $\text{C}_6\text{H}_5$ );  $^{13}\text{C}$  NMR  $\delta$  1.3 and 1.7 ( $\text{SiCH}_3$ ), 22.7 ( $=\text{CCH}_3$ ), 124.6 (*p*-C), 127.1 and 128.0 (*o*- and *m*-C), 147.5 and 149.9 ( $=\text{CCH}_3$  and *ipso*-C), 156.7 ( $=\text{CC}_6\text{H}_5$ );  $^{29}\text{Si}$  NMR  $\delta$  -9.4, -6.1; IR (neat) 1249 (s,  $\text{SiMe}$ ), 922 (m), 891 (m), 835 (vs), 779 (m), 756 (m), 702 (m)  $\text{cm}^{-1}$ ; GC-MS *m/z* (relative intensity) 262 (11,  $\text{M}^+$ ), 247 (13), 189 (15), 159 (18), 135 (27), 73 (100), 45 (18). Anal. Calcd for  $\text{C}_{15}\text{H}_{26}\text{Si}_2$ : C, 68.62; H, 9.98. Found: C, 68.48; H, 10.26.

**27b:**  $^1\text{H}$  NMR  $\delta$  0.05 and 0.20 (each s, each 6 H,  $\text{SiCH}_3$ ), 1.63 (s, 3 H,  $=\text{CCH}_3$ ), 3.81 (s, 6 H,  $\text{OCH}_3$ ), 6.50–7.48 (m, 13 H, rings' H);  $^{29}\text{Si}$  NMR  $\delta$  -12.7, -9.8; GC-MS *m/z* (relative intensity) 447 (5,  $\text{M}^+ + 1$ ), 338 (17), 251 (10), 165 (100).

**Acknowledgment.** We are grateful to Drs. Toshiaki Kobayashi and Teruyuki Hayashi for their partial contributions to the preliminary experiments. This work was partly supported by the British Council and the Ciba-Geigy Foundation (Japan) for the Promotion of Science.

OM9407130

# Concerted Multiple Dehydrogenation of Gas-Phase Saturated Cyclic C<sub>4</sub>-C<sub>8</sub> Hydrocarbons by Os<sup>+</sup>

Xinzhen Xiang and Fernando R. Tollens

Department of Chemistry, The Ohio State University, Columbus, Ohio 43210

Alan G. Marshall\*

National High Magnetic Field Laboratory and Department of Chemistry,  
Florida State University, Tallahassee, Florida 32306

Received October 4, 1994<sup>⊗</sup>

The gas-phase reactions of laser-generated Os<sup>+</sup> with various cycloalkanes, C<sub>5</sub>H<sub>10</sub>, C<sub>6</sub>H<sub>12</sub>, C<sub>7</sub>H<sub>14</sub>, C<sub>8</sub>H<sub>16</sub>, C<sub>6</sub>H<sub>10</sub>, C<sub>6</sub>H<sub>6</sub>, *cis*-1,2-dimethylhexane, and *cis*-1,3-dimethylhexane, have been examined by Fourier transform ion cyclotron resonance (FT-ICR) mass spectrometry. In contrast to many transition-metal ions, whose reactions with alkanes show extensive cleavage of C-C bonds, dehydrogenation is the major process in all reactions. No evidence of C-C insertion is found, and the carbon ring is left intact. Saturated cyclic hydrocarbons exposed to Os<sup>+</sup> undergo repeated dehydrogenation to form the complex ions (C<sub>n</sub>H<sub>n</sub>)Os<sup>+</sup>, which then react with another corresponding neutral hydrocarbon molecule to form [C<sub>n</sub>H<sub>n</sub>-Os-C<sub>n</sub>H<sub>n</sub>]<sup>+</sup>. The Os-ligand complex ions may be identified unambiguously from isotopic distributions. Reaction mechanisms for the various reaction pathways are proposed.

## Introduction

The gas-phase reactions of transition-metal ions have been studied intensively for the past two decades;<sup>1-14</sup> the chemistry of naked transition-metal ions or metal cluster ions with various hydrocarbons provides valuable insight into the mechanisms of condensed-phase reactions as well as the efficiencies of stoichiometric or catalytic processes in general.<sup>2</sup> Fourier transform ion cyclotron resonance mass spectrometry (FT-ICR/MS) has the capability of ultrahigh resolution, wide mass range, multistage MS/MS capability with a single mass spectrometer, simultaneous detection of all ions, long ion storage period, and relatively easy and accurate adjustment of ion kinetic energy.<sup>2-5,11,12,15-31</sup> These

features make FT-ICR/MS ideally suited for the study of gas-phase ion-molecule reaction chemistry.<sup>2,4,5,7-14,32-37</sup>

Among the transition metals, osmium holds special interest because it has catalytic value for dehydrogenation, hydrogenation,<sup>38</sup> and dehydroxylation reactions. Irikura *et al.*<sup>8</sup> have investigated the ion-molecule reactivities of OsO<sub>n</sub><sup>+</sup> (*n* = 0-4) with a number of hydrocarbons and small molecules. They observed cycloaddition with H<sub>2</sub>, bond metathesis, oxo transfer, and hydrogen atom abstraction. Although much investigation has been focused on catalytic surfaces,<sup>38</sup> there has been virtually no examination of the fundamental reactions in the gas phase between Os<sup>+</sup> and organic species, because Os<sup>+</sup> presents several difficulties for mass spectrometric analysis: (a) high mass resolving power is needed to distinguish the large number of isotopes of osmium; (b) Os<sup>+</sup> oxidizes readily, so that experiments are best conducted at very low pressure ( $\leq 10^{-8}$  Torr); (c) osmium does not form a simple stable volatile metal carbonyl (for ready gas-phase electron

\* To whom correspondence should be addressed.

⊗ Abstract published in *Advance ACS Abstracts*, December 1, 1994.

(1) Armentrout, P. B.; Beauchamp, J. L. *Acc. Chem. Res.* **1989**, *22*, 315-321.

(2) Eller, K.; Schwarz, H. *Chem. Rev.* **1991**, *91*, 1121-1177.

(3) Freiser, B. S. *Talanta* **1985**, *32*, 697-708.

(4) Freiser, B. S. *Chemtracts: Anal. Phys. Chem.* **1989**, *1*, 65-109.

(5) Freiser, B. S. In *Bonding Energetics in Organometallic Compounds*; Marks, T. J., Ed.; ACS Symposium Series 428; American Chemical Society: Washington, DC, 1990; pp 55-69.

(6) Hettich, R. L.; Freiser, B. S. *J. Am. Chem. Soc.* **1987**, *109*, 3537-3542.

(7) Huang, Y.; Wise, M. B.; Jacobson, D. B.; Freiser, B. S. *Organometallics* **1987**, *6*, 346-354.

(8) Irikura, K. K.; Beauchamp, J. L. *J. Am. Chem. Soc.* **1989**, *111*, 75-85.

(9) Jacobson, D. B.; Freiser, B. S. *J. Am. Chem. Soc.* **1983**, *105*, 5197-5206.

(10) Jacobson, D. B.; Freiser, B. S. *J. Am. Chem. Soc.* **1983**, *105*, 7492-9500.

(11) Nibbering, N. M. M. *Acc. Chem. Res.* **1990**, *23*, 279-285.

(12) Sharpe, P.; Richardson, D. E. *Coord. Chem. Rev.* **1989**, *93*, 59-85.

(13) Simões, J. A. M.; Beauchamp, J. L. *Chem. Rev.* **1990**, *90*, 629-688.

(14) Tolbert, M. A.; Beauchamp, J. L. *J. Am. Chem. Soc.* **1984**, *106*, 8117-8122.

(15) Ghaderi, S. *Ceram. Trans.* **1989**, *5*, 73-86.

(16) Gord, J. R.; Freiser, B. S. *Anal. Chim. Acta* **1989**, *225*, 11-24.

(17) Wanczek, K.-P. *Int. J. Mass Spectrom. Ion Processes* **1989**, *95*, 1-38.

(18) Wilkins, C. L.; Chowdhury, A. K.; Nuwaysir, L. M.; Coates, M. L. *Mass Spectrom. Rev.* **1989**, *8*, 67-92.

(19) Laude, D. A., Jr.; Hogan, J. D. *TM, Tech. Mess.* **1990**, *57*, 155-159.

(20) *Lasers in Mass Spectrometry*; Lubman, D. M., Ed.; Oxford University Press: New York, 1990.

(21) Campana, J. E. In *Proceedings of SPIE—Applied Spectroscopy in Material Science*; International Society for Optical Engineering: Bellingham, WA, 1991; pp 138-149.

(22) Marshall, A. G.; Grosshans, P. B. *Anal. Chem.* **1991**, *63*, 215A-229A.

(23) Nuwaysir, L. M.; Wilkins, C. L. In *Proceedings of SPIE—Applied Spectroscopy in Material Science*; International Society for Optical Engineering: Bellingham, WA, 1991; pp 112-123.

(24) Dunbar, R. C. *Mass Spectrom. Rev.* **1992**, *11*, 309-339.

(25) Jacoby, C. B.; Holliman, C. L.; Gross, M. L. In *Mass Spectrometry in the Biological Sciences: A Tutorial*; Gross, M. L., Ed.; Kluwer Academic: Dordrecht, The Netherlands, 1992; pp 93-116.

(26) Köster, C.; Kahr, M. S.; Castoro, J. A.; Wilkins, C. L. *Mass Spectrom. Rev.* **1992**, *11*, 495-512.

(27) Marshall, A. G.; Schweikhard, L. *Int. J. Mass Spectrom. Ion Processes* **1992**, *118/119*, 37-70.

(28) Schweikhard, L.; Alber, G. M.; Marshall, A. G. *Phys. Scr.* **1992**, *46*, 598-602.

ionization), as do many of the more accessible transition metals (e.g., Fe(CO)<sub>5</sub>). In this paper, we show that all of these difficulties may be overcome by use of Fourier transform ion cyclotron resonance mass spectrometry to examine the primary and secondary ion-molecule reaction products of laser-desorbed Os<sup>+</sup> with various cyclic (C<sub>5</sub>–C<sub>8</sub>) hydrocarbons in the gas phase, and we propose mechanisms for the major reactions.

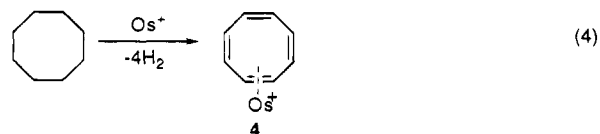
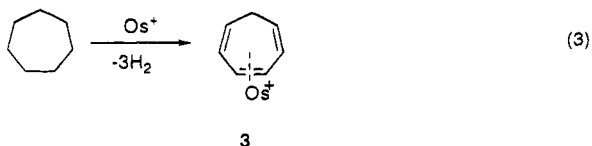
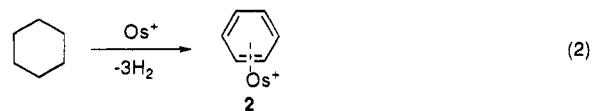
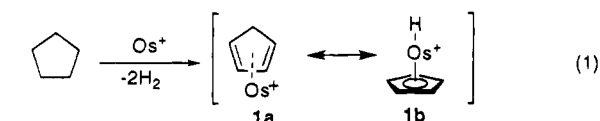
### Experimental Section

All hydrocarbons were obtained from Aldrich Chemical Co. (Milwaukee, WI). Each was introduced at a pressure of  $5 \times 10^{-7}$  Torr through a leak valve from a sample reservoir after degassing by several freeze-pump-thaw cycles on the foreline vacuum chamber of the instrument. Osmium ions were generated by laser desorption from osmium metal sponge with a Continuum Model YG-660A Nd:YAG laser operated at 1.064  $\mu\text{m}$ , at a power density of  $\sim 500$  MW/cm<sup>2</sup> ( $\sim 50$  mJ in  $\sim 10$  ns over a spot size  $\sim 1$  mm in diameter). A subsequent variable delay period allowed for thermal ion-molecule reactions to occur. Mass spectra were obtained on a standard Extrel/Millipore FTMS-2000 FT-ICR mass spectrometer (Extrel FTMS, Madison, WI) with dual 1.875-in. cubic ion traps centered in the bore of a superconducting magnet (3.0 T). The instrument was modified with CTI Corp. Helix CryoTorr 8 Cryopumps (1250 L s<sup>-1</sup> pumping speed for N<sub>2</sub>) rather than the usual diffusion pumps on both the source and analyzer sides of the dual trap, and both sides of the dual vacuum chamber were backed by a single 50 L s<sup>-1</sup> Leybold-Hereaus Model TMP-50 turbopump. The trapping voltage was typically 2 V. Broadband frequency-sweep excitation at a sweep rate of 1000 Hz  $\mu\text{s}^{-1}$  was followed by acquisition of a 16K time-domain transient signal which was digitized in direct mode at a Nyquist bandwidth of 2 MHz and padded with an additional 16K of zeroes before discrete Fourier transformation (without prior apodization).

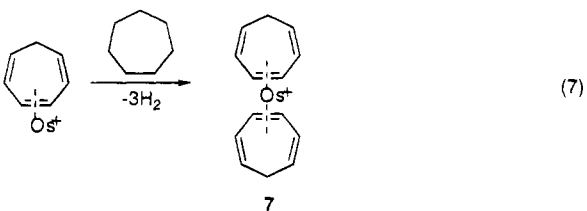
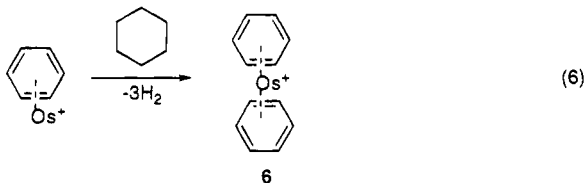
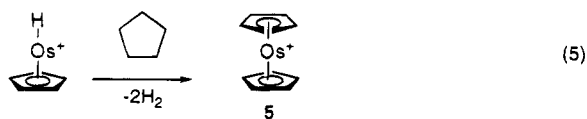
### Results and Discussion

**Reactions of Os<sup>+</sup> with Cyclic Alkanes C<sub>n</sub>H<sub>2n</sub> (n = 5–8).** The primary and secondary ion-molecule reactions of Os<sup>+</sup> with cyclic alkanes C<sub>n</sub>H<sub>2n</sub> (n = 5–8) are shown in eqs 1–7. Minor products appearing only after long reaction periods have been ignored. FT-ICR mass spectra at various reaction periods are shown in Figure 1.

primary reactions:



secondary reactions:



The reactivities of three of the four cyclic hydrocarbons are strikingly similar. Initially, the only process observed for C<sub>5</sub>H<sub>10</sub>, C<sub>6</sub>H<sub>12</sub>, and C<sub>7</sub>H<sub>14</sub> is multiple dehydrogenation, leading to formation of complexes which are well-described by ligands of stable aromatic (4n + 2 electrons) structure: ( $\eta$ -C<sub>5</sub>H<sub>5</sub>)OsH<sup>+</sup>, ( $\eta$ -C<sub>6</sub>H<sub>6</sub>)Os<sup>+</sup>, and ( $\eta$ -C<sub>7</sub>H<sub>7</sub>)Os<sup>+</sup> (see reactions 1–3). We see no evidence for ring-opening reactions by Os<sup>+</sup>, in contrast to Fe<sup>+</sup>, which has been observed to react with alkanes by means of both C–H and C–C bond insertions.<sup>10</sup> (Fe<sup>+</sup> does not cleave bonds in C<sub>5</sub> and C<sub>6</sub> rings<sup>10</sup> but does so in C<sub>7</sub> and C<sub>8</sub> rings.<sup>2</sup>) After longer reaction periods, the primary reaction products react further with another saturated cyclic hydrocarbon molecule to generate the adducts C<sub>10</sub>H<sub>10</sub>Os<sup>+</sup>, C<sub>12</sub>H<sub>12</sub>Os<sup>+</sup>, and C<sub>14</sub>H<sub>16</sub>Os<sup>+</sup>, which have the presumed structures ( $\eta$ -C<sub>5</sub>H<sub>5</sub>)<sub>2</sub>Os<sup>+</sup>, ( $\eta$ -C<sub>6</sub>H<sub>6</sub>)<sub>2</sub>Os<sup>+</sup>, and ( $\eta$ -C<sub>7</sub>H<sub>7</sub>)<sub>2</sub>Os<sup>+</sup> shown in reactions 5–7. These Os<sup>+</sup> reactions parallel those of La<sup>+</sup>, which forms C<sub>5</sub>H<sub>6</sub>La<sup>+</sup> and C<sub>10</sub>H<sub>10</sub>La<sup>+</sup> with cyclopentane and C<sub>6</sub>H<sub>6</sub>La<sup>+</sup> and C<sub>12</sub>H<sub>12</sub>La<sup>+</sup> with cyclohexane.<sup>7</sup> After an extended reaction period, products from C–C bond cleavage begin to appear.

In contrast, the larger ring compound C<sub>8</sub>H<sub>16</sub> exhibits noticeable ring cleavage to yield products such as C<sub>6</sub>H<sub>6</sub>Os<sup>+</sup> and C<sub>7</sub>H<sub>8</sub>Os<sup>+</sup>, although the most abundant product is still the dehydrogenated species: C<sub>8</sub>H<sub>8</sub>Os<sup>+</sup>. The difference between C<sub>8</sub>H<sub>16</sub> on the one hand and C<sub>5</sub>H<sub>10</sub>, C<sub>6</sub>H<sub>12</sub>, and C<sub>7</sub>H<sub>14</sub> on the other may be attributed to the

(29) Speir, J. P.; Gorman, G. S.; Amster, I. J. In *Mass Spectrometry in the Biological Sciences: A Tutorial*; Gross, M. L., Ed.; Kluwer Academic: Dordrecht, The Netherlands, 1992; pp 199–212.

(30) Buchanan, M. V.; Hettich, R. L. *Anal. Chem.* **1993**, *65*, 245A–259A.

(31) Schweikhard, L.; Marshall, A. G. *J. Am. Soc. Mass Spectrom.* **1993**, *4*, 433–452.

(32) Kiplinger, J. P.; Tollens, F. R.; Marshall, A. G.; Kobayashi, T.; Lagerwall, D. R.; Paquette, L. A.; Bartmess, J. E. *J. Am. Chem. Soc.* **1989**, *111*, 6914–6919.

(33) Irikura, K. K.; Beauchamp, J. L. *J. Am. Chem. Soc.* **1991**, *113*, 2767–2768.

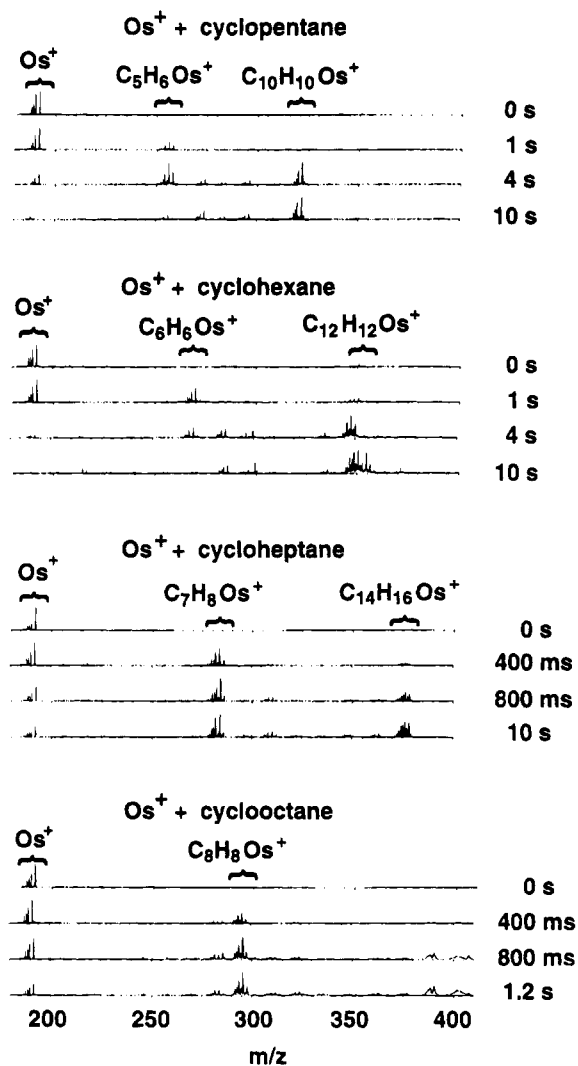
(34) Larson, B. S.; Ridge, D. P. *J. Am. Chem. Soc.* **1984**, *106*, 1912.

(35) Sunderlin, L. S.; Armentrout, P. B. *J. Am. Chem. Soc.* **1989**, *111*, 3845–3855.

(36) Dunbar, R. C.; Solooki, D.; Tessier, C. A.; Youngs, W. J.; Asamoto, B. *Organometallics* **1991**, *10*, 52–54.

(37) Stirk, K. M.; Kiminkinen, M.; Kenttämää, H. I. *Chem. Rev.* **1992**, *92*, 1649–1665.

(38) Dil'magambetov, S. N.; Dzhardamalieva, K. K.; Sokol'skii, D. V. *Khim. Khim. Tekhnol. (Alma-Ata)* **1978**, 199–206.

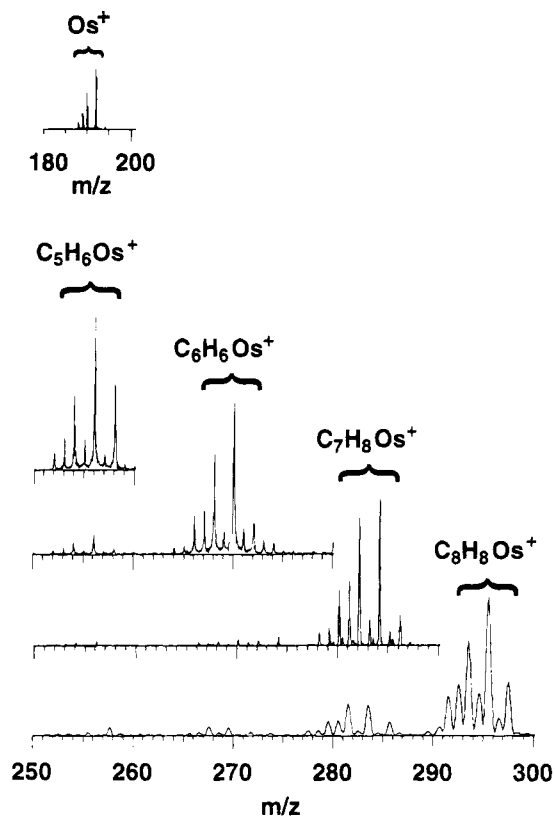


**Figure 1.** FT-ICR mass spectra of the products of the reaction of  $\text{Os}^+$  with cyclic alkanes  $\text{C}_n\text{H}_{2n}$  ( $n = 5-8$ ), after each of several stated reaction periods.

$4n$ -electron antiaromatic character (and thus lower stability) of  $\text{C}_8\text{H}_8\text{Os}^+$ . For example,  $\text{C}_8\text{H}_8\text{Os}^+$  may undergo carbon-carbon cleavage followed by elimination of  $\text{C}_2\text{H}_2$  to form  $\text{C}_6\text{H}_6\text{Os}^+$ . Alternatively (see Figure 2),  $\text{C}_8\text{H}_8\text{Os}^+$  may react with another  $\text{C}_8\text{H}_8$  neutral to form  $\text{C}_{16}\text{H}_{16}\text{Os}^+$ , which presumably has the sandwich structure  $(\eta\text{-C}_8\text{H}_8)_2\text{Os}^+$ .

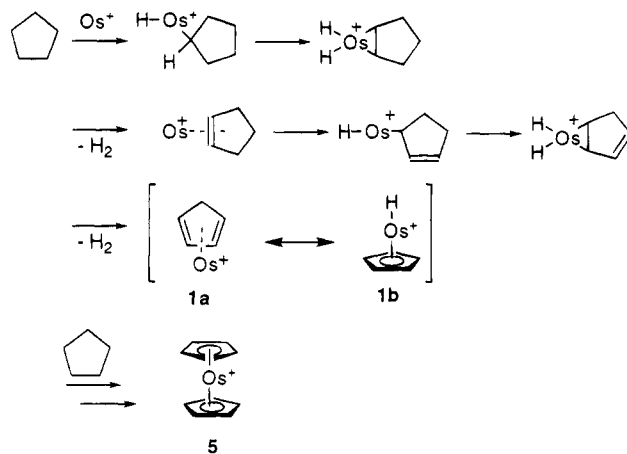
In some cases, the mass spectra are complicated by the isotopic distribution of osmium, leading to difficulty in distinguishing (e.g.)  $\text{C}_n\text{H}_m+2^{190}\text{Os}^+$  from  $\text{C}_n\text{H}_m^{192}\text{Os}^+$ , whose masses differ by only 0.0126 amu. Nevertheless, the appropriate osmium-ligand complex ion may be identified unambiguously in such cases from the isotopic abundance pattern. For example, Figure 2 shows experimental isotopic abundance multiplets for  $\text{C}_n\text{H}_n\text{Os}^+$ .

In principle, it is possible to tell whether  $\text{Os}^+$  ions are in their ground state or excited states before they react with neutrals. For ground-state  $\text{Os}^+$ , the  $\text{Os}^+$  concentration should decrease exponentially with reaction period, whereas for excited-state ions,  $\text{Os}^+$  concentration will vary nonexponentially with reaction period. Unfortunately, we were unable to make quantitative comparisons of  $\text{Os}^+$  concentration after different reaction periods, because the signal-to-noise ratio was limited (due in part to the large number of isotopes of



**Figure 2.** Experimental FT-ICR mass spectral isotopic abundance patterns of the products of the reaction of  $\text{Os}^+$  with cyclic alkanes  $\text{C}_n\text{H}_{2n}$  ( $n = 5-8$ ).

### Scheme 1



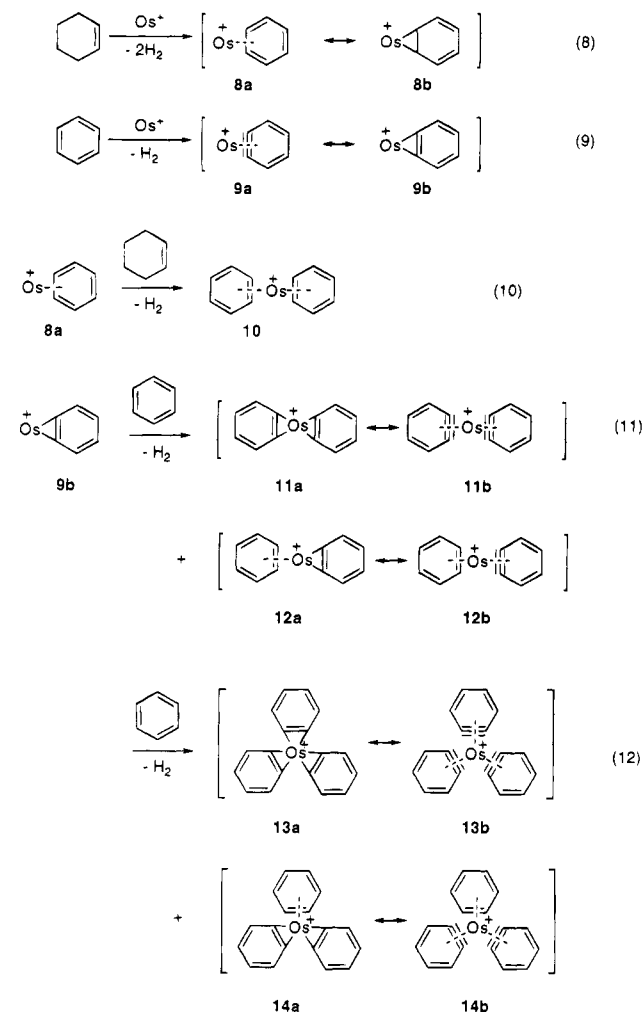
osmium) and the laser power was not sufficiently reproducible from one shot to the next.

The various reactions may be rationalized by C-H insertion followed by dehydrogenation, on the basis of the reaction between  $\text{Os}^+$  and  $\text{C}_5\text{H}_{10}$  as an odd-number carbon example (Scheme 1) and the reaction of  $\text{Os}^+$  and  $\text{C}_6\text{H}_{12}$  as an even-number carbon example (Scheme 2). (A similar mechanism has been proposed by Land *et al.*<sup>39</sup> for the *surface* reaction between platinum and cyclohexane, for which cyclohexene intermediates were detected by mass spectrometry.)  $\text{Os}^+$  first inserts into a C-H bond; the resulting Os-ligand complex then easily loses  $\text{H}_2$ . This process is repeated until a stable aromatic or maximally conjugated species is formed.

(39) Land, D. P.; Pettiette-Hall, C. L.; McIver, R. T. J.; Hemminger, J. C. *J. Am. Chem. Soc.* **1989**, *111*, 5970-5972.



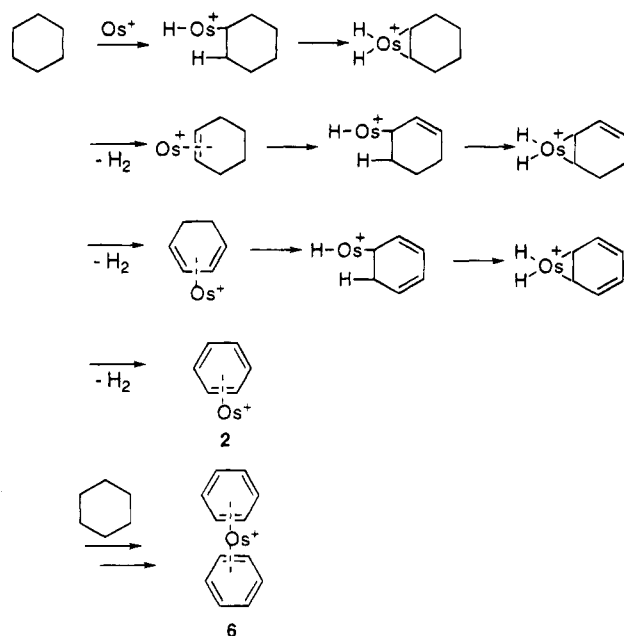
**Reactions of Os<sup>+</sup> with Unsaturated Cyclic Hydrocarbons.** If our analysis of the mechanism of reaction of Os<sup>+</sup> with *saturated* cyclic hydrocarbons is correct, then we should expect to see similar products from the reaction of Os<sup>+</sup> with *unsaturated* cyclic hydrocarbons. FT-ICR mass spectra for the reaction of Os<sup>+</sup> with cyclohexene and benzene, C<sub>6</sub>H<sub>10</sub> and C<sub>6</sub>H<sub>6</sub>, following each of several reaction periods are shown in Figure 3 (top). The reactivity of Os<sup>+</sup> toward cyclohexene is clearly similar to that with cyclohexane: we observe dehydrogenation exclusively, to give stable C<sub>6</sub>H<sub>6</sub>Os<sup>+</sup> (reaction 8),



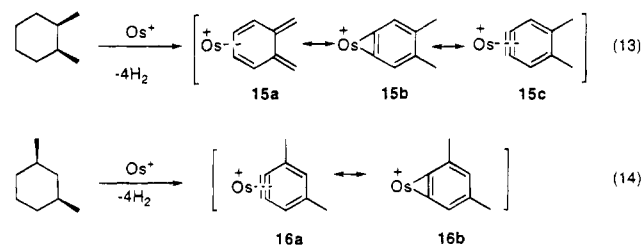
which further reacts with another molecule of cyclohexene (reaction 10) to form C<sub>12</sub>H<sub>12</sub>Os<sup>+</sup> (with the presumed structure (η-C<sub>6</sub>H<sub>6</sub>)<sub>2</sub>Os<sup>+</sup>). The sole product of the reaction of Os<sup>+</sup> with benzene (Figure 3, bottom) is C<sub>6</sub>H<sub>4</sub>Os<sup>+</sup> (reaction 9) rather than the direct adduct C<sub>6</sub>H<sub>6</sub>Os<sup>+</sup>, further corroborating that reaction of Os<sup>+</sup> with saturated cyclic hydrocarbons indeed proceeds by dehydrogenation rather than by direct attachment. In contrast, Hettich *et al.*<sup>6</sup> found that the major product for reaction of iron cluster ions (M = CuFe<sup>+</sup>, ScFe<sup>+</sup>, TiFe<sup>+</sup>, and Fe<sub>2</sub><sup>+</sup>) with benzene was C<sub>6</sub>H<sub>6</sub>M<sup>+</sup>, whereas NbFe<sup>+</sup> did not react with benzene. Finally, C<sub>6</sub>H<sub>4</sub>Os<sup>+</sup> reacts further (reactions 11, 12) with benzene to form C<sub>12</sub>H<sub>8</sub>Os<sup>+</sup> (presumably (C<sub>6</sub>H<sub>4</sub>)<sub>2</sub>Os<sup>+</sup>) and C<sub>12</sub>H<sub>10</sub>Os<sup>+</sup> and subsequently C<sub>18</sub>H<sub>12</sub>Os<sup>+</sup> and C<sub>18</sub>H<sub>14</sub>Os<sup>+</sup>.

**Reactions of Os<sup>+</sup> with Substituted Cyclohexanes.** To demonstrate how ring substituents affect the

Scheme 2



Os<sup>+</sup> chemistry, we reacted Os<sup>+</sup> with *cis*-1,2-dimethylcyclohexane and *cis*-1,3-dimethylcyclohexane, to yield the FT-ICR mass spectra shown in Figure 4. The products of the primary and secondary reactions are shown in reactions 13 and 14. The chemical formula of both 1,2-



dimethylcyclohexane and 1,3-dimethylcyclohexane is C<sub>8</sub>H<sub>16</sub>, the same as that of cyclooctane. Interestingly, the reactions of Os<sup>+</sup> with *cis*-1,2-dimethylcyclohexane, *cis*-1,3-dimethylcyclohexane, and cyclooctane are similar in that each loses 4 H<sub>2</sub> to yield C<sub>8</sub>H<sub>8</sub>Os<sup>+</sup>, which is relatively unstable and either dissociates to form noticeable amounts of C<sub>6</sub>H<sub>6</sub>Os<sup>+</sup> and C<sub>7</sub>H<sub>8</sub>Os<sup>+</sup> or reacts with another molecule of C<sub>8</sub>H<sub>16</sub> to form complex ions with two ligands.

In summary, saturated cyclic hydrocarbons exposed to Os<sup>+</sup> undergo exclusively C–H insertion to form the complex ions C<sub>n</sub>H<sub>n</sub>–Os<sup>+</sup>, which then react with another corresponding neutral hydrocarbon molecule to form [C<sub>n</sub>H<sub>n</sub>–Os–C<sub>n</sub>H<sub>n</sub>]<sup>+</sup> ions.

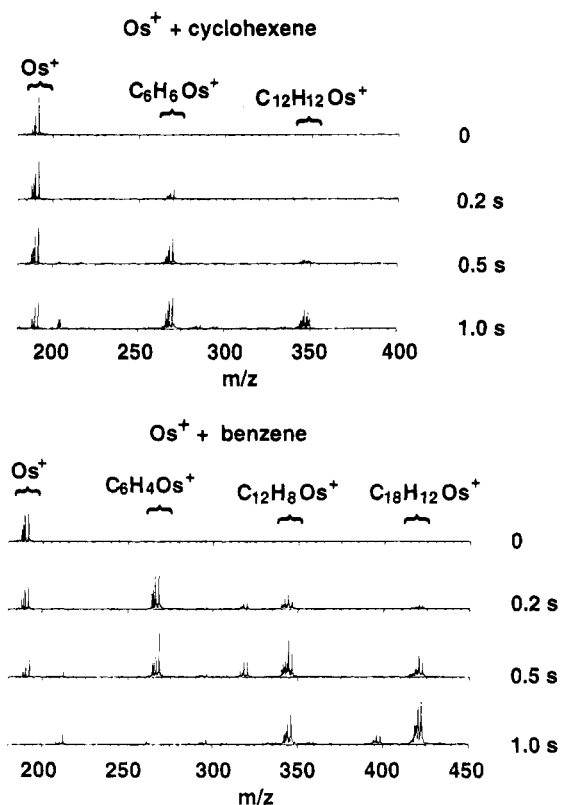
**Dehydrogenation of Benzene.** Perhaps the most novel feature of the present results is the observation of the dehydrogenation of benzene. Benzene itself is unreactive with Fe<sup>+</sup> (the group 8 congener of Os<sup>+</sup>) as well as with Ti<sup>+</sup>, V<sup>+</sup>, Cr<sup>+</sup>, Mn<sup>+</sup>, Fe<sup>+</sup>, Co<sup>+</sup>, Ni<sup>+</sup>, Cu<sup>+</sup>, Mo<sup>+</sup>, Ag<sup>+</sup>, and W<sup>+</sup>.<sup>2</sup> However, early-transition-metal ions (Sc<sup>+</sup>,<sup>5</sup> Nb<sup>+</sup>,<sup>40,41</sup> and Ta<sup>+</sup><sup>42,43</sup>) can dehydrogenate benzene.

(40) Buckner, S. W.; MacMahon, T. J.; Byrd, G. D.; Freiser, B. S. *Inorg. Chem.* **1989**, *28*, 351.

(41) Higashide, H.; Oka, T.; Kasatani, K.; Shinohara, H.; Sato, H. *Chem. Phys. Lett.* **1989**, *171*, 297.

(42) Wise, M. B.; Jacobson, D. B.; Freiser, B. S. *J. Am. Chem. Soc.* **1985**, *107*, 1590.





**Figure 3.** FT-ICR mass spectra of the products of the reaction of  $\text{Os}^+$  with cyclohexene and benzene after each of several stated reaction periods.

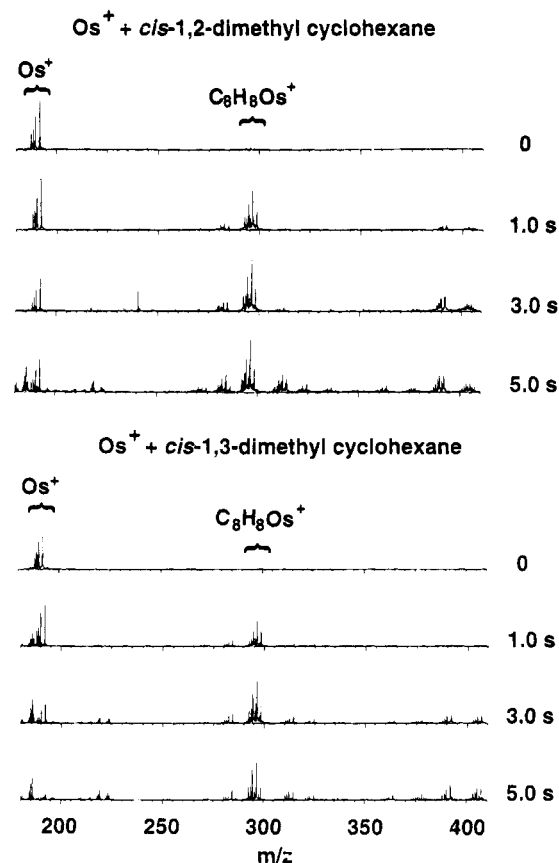
Moreover, neutral niobium clusters dehydrogenate benzene.<sup>44</sup> Finally,  $\text{Fe}^+$  reacts with alkyl halides to form polyphenylene complexes<sup>45-47</sup> of the type postulated here as products of the  $\text{Os}^+$  reaction with benzene.

**Acknowledgment.** This work was supported by the National Science Foundation (Grant No. CHE-90-

(43) Wise, M. B.; Jacobson, D. B.; Freiser, B. S. *J. Am. Chem. Soc.* **1985**, *107*, 6744.

(44) St. Pierre, R. J.; Chronister, E. L.; El-Sayed, M. *J. Phys. Chem.* **1987**, *91*, 5228.

(45) Bjarnason, A.; Taylor, J. W. *Organometallics* **1989**, *8*, 2020.



**Figure 4.** FT-ICR mass spectra of the products of the reaction of  $\text{Os}^+$  with *cis*-1,2-dimethylcyclohexane and *cis*-1,3-dimethylcyclohexane after each of several stated reaction periods.

21058), The Ohio State University, and the National High Magnetic Field Laboratory at Florida State University.

OM940770H

(46) Bjarnason, A.; Taylor, J. W. *Organometallics* **1990**, *9*, 1493.

(47) Huang, Y.; Freiser, B. S. *J. Am. Chem. Soc.* **1989**, *111*, 2387.

## Notes

## Aqueous Organometallic Chemistry: Phase-Transfer-Catalyzed Alkylation of Fischer Carbene Complexes<sup>†</sup>

Sk. Rasidul Amin and Amitabha Sarkar\*

*Division of Organic Chemistry (Synthesis), National Chemical Laboratory, Pune-411008, India*

Received May 16, 1994<sup>®</sup>

*Summary: Fischer carbene complexes can be conveniently alkylated, often with high diastereoselectivity, by reactive halides under biphasic conditions.*

### Introduction

Fischer carbene complexes of group VI transition metals have emerged as a versatile class of organometallic intermediates useful in organic synthesis<sup>1</sup> as testified by a large number of natural products that have been synthesized *via* Fischer carbene complexes. Several important applications include carbocyclic<sup>2</sup> and heterocyclic<sup>3</sup> annulation by thermal reactions, as well as photochemical CO insertions leading to  $\beta$ -lactams<sup>4</sup> and cyclobutanones.<sup>5</sup>

Since the most common route to these complexes involves reaction of organolithium or organomagnesium reagents with metal hexacarbonyl, sensitive functionalities are incompatible with such a procedure. Therefore, alkylation of the acidic  $\alpha$ -carbon is often a method of choice<sup>6</sup> to prepare functionalized Fischer carbene complexes. Alkylations are usually carried out in tetrahydrofuran using *n*-butyllithium as a base. However, certain limitations are encountered with this protocol. For instance, reactions are unsatisfactory if alkoxy-carbene complexes are not alkylated using primary triflates.<sup>7</sup> This disadvantage has been redressed partly by the use of aminocarbene complexes<sup>8</sup> or by replacement of a *cis*-CO ligand with a phosphine.<sup>7</sup> While

dialkylation may be achieved with reactive substrates,<sup>9</sup> alkylation of a secondary carbon center is often difficult.

A possible source of such difficulty could lie in the magnitude of nucleophilicity of the metal carbene anion. This is reminiscent of the task of alkylating aliphatic nitro compounds at the  $\alpha$ -carbon. The  $pK_a$  of the  $\alpha$ -methyl group of alkoxy-carbene complexes has been estimated by Casey<sup>6</sup> to be 8.0 in THF. Later, the  $pK_a$  of (methylmethoxycarbene)chromium complex was determined<sup>10</sup> in water-piperidine solvent mixture as 12.3, a value comparable to the  $pK_a$  of diethyl malonate or ethyl acetoacetate.<sup>11</sup> Water is known to modify the reactivity of various types of substances and the course of several reactions including organometallic ones.<sup>12a</sup> It was of interest, therefore, to explore whether alkylation of alkoxy-carbene complexes could be achieved efficiently in the presence of water.<sup>12b</sup>

In this paper, we describe a facile alkylation procedure for alkoxy-carbene complexes in a biphasic medium mediated by a phase-transfer catalyst. In particular, this procedure even allows efficient dialkylation with reactive electrophiles, and secondary centers can be alkylated in high yield. High diastereoselectivity has also been observed in certain reactions.

### Results and Discussion

When (methyl(benzyloxy)carbene)chromium complex **3** in dichloromethane was treated with excess methyl iodide in the presence of 50% aqueous NaOH and 10 mol % of tetrabutylammonium bromide at room temperature, the dialkylated product was obtained after overnight stirring in 64% yield as the sole product. The reaction was less efficient with ethyl iodide but proceeded satisfactorily with allyl and benzyl halides. The results are summarized in Table 1 and Schemes 1 and 2.

With methylcarbene complexes **1-6**, in all cases, the dialkylation product was observed as the only product.

(9) Alvarez, C.; Pacreau, A.; Parlier, A.; Rudler, H. *Organometallics* **1987**, *6*, 1057.

(10) Gandler, J. R.; Bernasconi, C. F. *Organometallics* **1989**, *8*, 2282.

(11) March, J. *Advanced Organic Chemistry: Reactions, Mechanisms and Structure*, 4th ed.; Wiley: New York, 1992; p 251.

(12) (a) Gyldenfeldt, F. V.; Marton, D.; Tagliavini, G. *Organometallics* **1994**, *13*, 906 and ref 1-10 therein. (b) For a recent example of O-alkylation of Fischer carbene complexes using tetraalkylammonium salts, see: Hoyer, T. R.; Chen, K.; Vyvyan, J. R. *Organometallics* **1993**, *12*, 2806.

<sup>†</sup> NCL Communication No. 5896.

<sup>®</sup> Abstract published in *Advance ACS Abstracts*, November 1, 1994.

(1) Wulff, W. D. *Comprehensive Organic Synthesis*; Trost, B. M., Fleming, I., Eds.; Pergamon Press: Oxford, England, 1991; Vol. 5, p 1065.

(2) (a) Dotz, K. H. *Angew. Chem., Int. Ed. Engl.* **1984**, *23*, 587. (b) Wulff, W. D. *Advances in Metal-Organic Chemistry*; Liebeskind, L. S., Ed.; JAI Press: Greenwich, CT, 1989; Vol. 1.

(3) (a) Dragisich, V.; Murray, C. K.; Warner, B. P.; Wulff, W. D.; Yang, D. C. *J. Am. Chem. Soc.* **1990**, *112*, 1251. (b) Grotjahn, D. B.; Dotz, K. H. *Synlett* **1991**, *11*, 381. (c) Rudler, H.; Audouin, M.; Chelain, E.; Denise, B.; Goumont, R.; Massoud, A.; Parlier, A.; Pacreay, A.; Rudler, M.; Yefsah, R.; Alvarez, C.; Delgado-reyes, F. *Chem. Soc. Rev.* **1991**, *20*, 503.

(4) Hegedus, L. S. *New Aspects of Organic Chemistry I*; Yoshida, Z., Shiba, T., Oshiro, T., Eds.; VCH: Kodansha, Japan, 1989; p 39.

(5) Soderberg, B. C.; Hegedus, L. S.; Sierra, M. A. *J. Am. Chem. Soc.* **1990**, *112*, 4364.

(6) (a) Casey, C. P. *Reactive Intermediates*; Wiley: New York, 1985; Vol. 3, p 109. (b) Casey, C. P. *Transition Metal Organometallics in Organic Synthesis*; Alper, H., Ed.; Academic Press: New York, 1976; Vol. 1, p 189.

(7) Xu, Y. C.; Wulff, W. D. *J. Org. Chem.* **1987**, *52*, 3263.

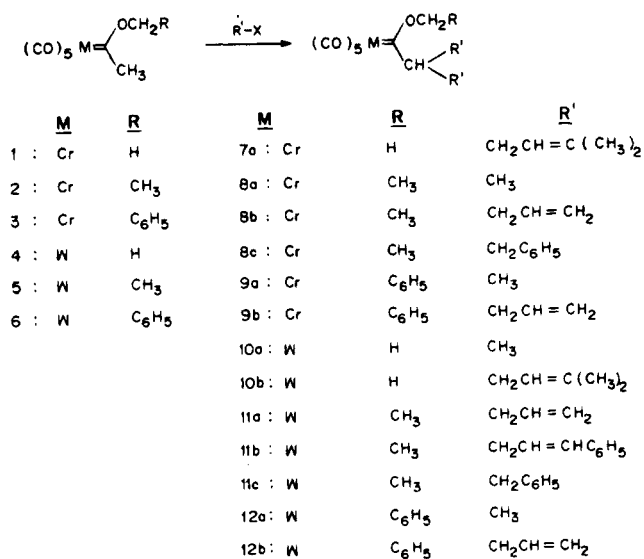
(8) Wulff, W. D.; Anderson, B. A.; Isaacs, L. D. *Tetrahedron Lett.* **1989**, *30*, 4061.

Table 1

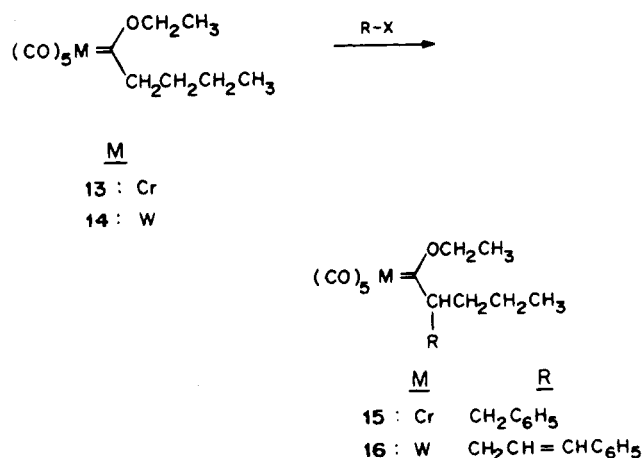
entry	substrate	electrophile <sup>a</sup>	time (h)	product	yield (%) <sup>b</sup>
1	1	(CH <sub>3</sub> ) <sub>2</sub> C=CHCH <sub>2</sub> Br	4	7a	73
2	2	CH <sub>3</sub> I	overnight	8a	64
3	2	CH <sub>2</sub> =CHCH <sub>2</sub> Br	3.5	8b	70 <sup>c</sup>
4	2	CH <sub>2</sub> =CHCH <sub>2</sub> Cl	3.5	8b	51
5	2	C <sub>6</sub> H <sub>5</sub> CH <sub>2</sub> Br	3	8c	56
6	2	C <sub>2</sub> H <sub>5</sub> I	overnight		<i>d</i>
7	3	CH <sub>3</sub> I	overnight	9a	64
8	3	CH <sub>2</sub> =CHCH <sub>2</sub> Br	3	9b	80
9	3	CH <sub>2</sub> =CHCH <sub>2</sub> Br	5	9b	48 <sup>e</sup>
10	4	CH <sub>3</sub> I	overnight	10a	58
11	4	(CH <sub>3</sub> ) <sub>2</sub> C=CHCH <sub>2</sub> Br	4	10b	70
12	5	CH <sub>2</sub> =CHCH <sub>2</sub> Br	3	11a	63
13	5	C <sub>6</sub> H <sub>5</sub> CH=CHCH <sub>2</sub> Cl	1.5	11b	56
14	5	C <sub>6</sub> H <sub>5</sub> CH <sub>2</sub> Br	3	11c	62
15	6	CH <sub>3</sub> I	overnight	12a	61
16	6	CH <sub>2</sub> =CHCH <sub>2</sub> Br	3.5	12b	78
17	13	C <sub>6</sub> H <sub>5</sub> CH <sub>2</sub> Br	4.5	15	67
18	14	C <sub>6</sub> H <sub>5</sub> CH=CHCH <sub>2</sub> Cl	2	16	69

<sup>a</sup> 2–5 equiv used in all cases. <sup>b</sup> Isolated yield after chromatography. <sup>c</sup> When 1 equiv of allyl bromide was used, 40% dialkylated and 10% monoalkylated products were obtained. <sup>d</sup> Poor yield (<15%) accompanied by extensive decomposition. <sup>e</sup> Reaction in benzene with K<sub>2</sub>CO<sub>3</sub>/18-crown-6.

Scheme 1

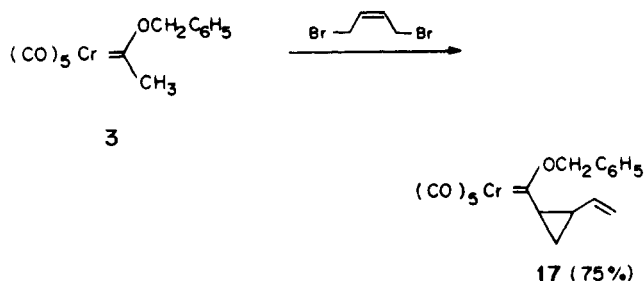


Scheme 2

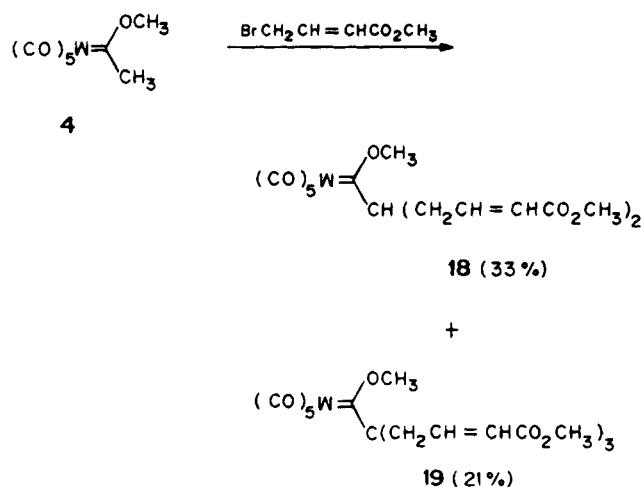


When 1 equiv of allyl bromide was used with complex **2**, the dialkylated product was obtained predominantly (40%) along with some monoalkylated product (10%), while 25% of the starting material was recovered

Scheme 3



Scheme 4



unchanged. This indicated that the secondary carbanion underwent alkylation faster than the primary one. Indeed, the alkylations of secondary carbanionic centers were achieved in high yield, as seen from the last entries of Table 1.

In order to effect cyclization, *cis*-1,4-dibromo-2-butene was chosen as an electrophile. As depicted in Scheme 3, a vinylcyclopropane, rather than a cyclopentene, was readily obtained as a single diastereomer (<sup>1</sup>H and <sup>13</sup>C NMR spectra) in high yield. The first nucleophilic substitution was followed by an intramolecular S<sub>N</sub>2' displacement. The stereochemistry of the product was tentatively deduced<sup>13</sup> from the coupling constants of vicinal protons (3.6 Hz) as *trans*.

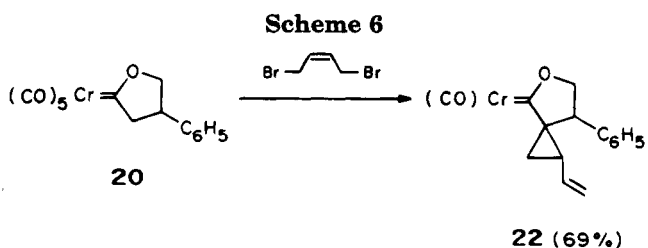
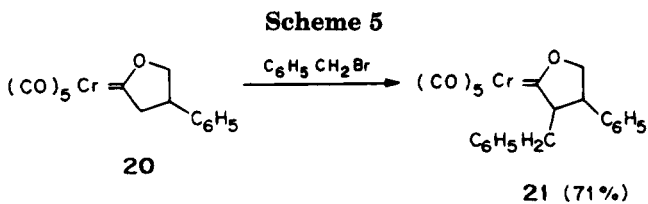
When methyl 3-bromocrotonate was used as the electrophile, di- and trialkylated products were obtained (Scheme 4). No cyclic product corresponding to alkylation followed by an intramolecular Michael addition was obtained.

Diastereoselectivity in such alkylations was studied with the cyclic carbene complex **20** reported by Casey.<sup>14</sup> Although the reaction shown in Scheme 5 was carried out at room temperature, only one diastereomer of the product **21** was obtained in 71% yield. The coupling constant (1.5 Hz) of the methine proton adjacent to the carbene carbon indicated the *trans*-relationship between vicinal substituents.

An interesting spiro-compound **22**, also a single diastereomer, was isolated when the substrate **20** was

(13) Jackman, L. M.; Sternhell, K. *Applications of Nuclear Magnetic Resonance Spectroscopy in Organic Chemistry*, 2nd ed.; Pergamon Press: Oxford, U.K., 1969; p 286.

(14) (a) Casey, C. P.; Anderson, R. L. *J. Organomet. Chem.* **1974**, *73*, C28. (b) Lattuada, L.; Licandro, E.; Maiorana, S.; Molinari, H.; Papagni, A. *Organometallics* **1991**, *10*, 807.



alkylated with *cis*-1,4-dibromo-2-butene (Scheme 6). A fast second alkylation leading to the cyclopropane could explain the high diastereoselectivity.

Thus, the biphasic reaction condition was found to be eminently suitable for functionalizing simpler Fischer carbene complexes by facile C–C bond formation. The origin of such facility of alkylation is, however, less clear. It was observed that the alkylation of the carbene complex **3** with allyl bromide proceeded in benzene with  $\text{K}_2\text{CO}_3$  as base and 18-crown-6 as the PTC, to give the diallylated product **9b** in 48% yield (accompanied by some decomposition). Although this yield was lower than that obtained (80%) with aqueous NaOH/dichloromethane, the fact that the reaction at all takes place in nonaqueous medium raises an interesting question about the exact role of water.

Recently it has been shown that “naked” enolates are reactive enough to generate acylmetalates which, in turn, can be converted to carbene complexes.<sup>15</sup> Thus, one may need to consider the role of ion-pairing in such reactions. The carbanion generated from a carbene complex by BuLi is likely to form an ion pair between lithium and oxygen (of CO) of considerable tightness. On the other hand, in the present procedure, the tetrabutylammonium counterion may not form an efficient ion pair and thus the carbanionic reactivity would be localized on the  $\alpha$ -carbon of the carbene complex. The same should be true if 18-crown-6 is used to capture potassium ions. The aminocarbene complexes, with  $\text{pK}_a$  of around 20.0 (see ref 16), cannot be alkylated at carbon under these biphasic conditions.<sup>17</sup>

### Summary

In summary, we have described a mild and facile C-alkylation procedure for Fischer carbene complexes that can provide diversely functionalized products. In view of the fact that these are important synthetic intermediates and are ester (or amide) equivalents, this practical protocol is likely to find extensive application in the future. However, simple primary halides are not strong enough electrophiles to be useful with this procedure.

(15) Veya, P.; Floriani, C.; Chiesi-Villa, A.; Rizzoli, C. *Organometallics* **1994**, *13*, 214.

(16) Anderson, B. A.; Wulff, W. D.; Rahm, A. *J. Am. Chem. Soc.* **1993**, *115*, 4602.

(17) It is possible to *N*-alkylate aminocarbene complexes under PTC conditions, an account of which will be reported in due course.

### Experimental Section

All reactions were performed under an inert atmosphere of argon, using freshly distilled, degassed solvents. Infrared spectra were recorded on a Perkin-Elmer 599B spectrometer in chloroform.  $^1\text{H}$  and  $^{13}\text{C}$  NMR spectra were taken either on a Bruker WH-90 or on a Bruker AC 200 spectrometer in  $\text{CDCl}_3$ . Chemical shifts are reported in  $\delta$  (ppm) relative to tetramethylsilane as internal reference. Elemental analyses of solid compounds were carried out on a Carlo-Erba 1100 automatic analyzer by Dr. S. Y. Kulkarni and his group at NCL. The liquid samples did not give satisfactory elemental analyses. Melting points in the Celsius scale were determined in open capillary tubes on a Thermo-nik Campbell melting point apparatus and are uncorrected.

Pentacarbonyl(methylmethoxycarbene)chromium(0),<sup>18</sup> pentacarbonyl(methylethoxycarbene)chromium(0),<sup>19</sup> pentacarbonyl(methyl(benzyloxy)carbene)chromium(0),<sup>20</sup> pentacarbonyl(*n*-butylethoxycarbene)chromium(0),<sup>19</sup> pentacarbonyl(methylmethoxycarbene)tungsten(0),<sup>18</sup> pentacarbonyl(methylethoxycarbene)tungsten(0),<sup>19</sup> pentacarbonyl(*n*-butylethoxycarbene)tungsten(0),<sup>19</sup> and pentacarbonyl(4-phenyl-2-oxacyclopentylidene)chromium(0)<sup>14b</sup> were prepared according to literature procedures.<sup>21</sup> All other reagents were obtained from Aldrich (Milwaukee, WI) and Loba Chemie (Bombay, India) and used without further purification.

**General Procedure for the Alkylation of Carbene Complexes. Method A.** The carbene complex (*n* mmol) and tetrabutylammonium bromide (0.1*n* mmol) in dichloromethane (15*n* mL) was treated with 50% aqueous NaOH and the halide (2–5*n* mmol). The mixture was stirred at room temperature under argon until the starting material was consumed (TLC). The reaction mixture was diluted with water, extracted with dichloromethane, dried, and concentrated under reduced pressure. The pure product was isolated by flash chromatography.

**Method B.** The carbene complex (*n* mmol), potassium carbonate, and 18-crown-6 (0.05*n* mmol) was treated with the halide (2–5*n* mmol). The pure product was isolated as described in method A.

**Complex 7a:** Orange oil. IR: 2050 (m), 1975 (sh), 1930 (s)  $\text{cm}^{-1}$ .

**Complex 8a:** Yellow solid (mp 39 °C). IR: 2060 (m), 1990 (sh), 1945 (s)  $\text{cm}^{-1}$ . Anal. Calcd for  $\text{C}_{11}\text{H}_{12}\text{CrO}_6$ : C, 45.20; H, 4.10. Found: C, 45.70; H, 4.40.

**Complex 8b:** Orange oil. IR: 2055 (m), 1985 (sh), 1945 (s)  $\text{cm}^{-1}$ .

**Complex 8c:** Orange oil. IR: 2055 (m), 1990 (sh), 1945 (s)  $\text{cm}^{-1}$ .

**Complex 9a:** Yellow solid (mp 52 °C). IR: 2080 (m), 2000 (sh), 1960 (s)  $\text{cm}^{-1}$ . Anal. Calcd for  $\text{C}_{16}\text{H}_{14}\text{CrO}_6$ : C, 54.24; H, 3.9. Found: C, 54.84; H, 4.49.

**Complex 9b:** Orange oil. IR: 2060 (m), 1990 (sh), 1950 (s)  $\text{cm}^{-1}$ .

**Complex 10a:** Yellow solid (mp 66 °C). IR: 2060 (m), 1980 (sh), 1930 (s)  $\text{cm}^{-1}$ . Anal. Calcd for  $\text{C}_{10}\text{H}_{10}\text{WO}_6$ : C, 29.27; H, 2.44. Found: C, 29.62; H, 2.47.

**Complex 10b:** Orange oil. IR: 2060 (m), 1980 (sh), 1920 (s)  $\text{cm}^{-1}$ .

**Complex 11a:** Orange oil. IR: 2080 (m), 1995 (sh), 1955 (s)  $\text{cm}^{-1}$ .

**Complex 11b:** Orange oil. IR: 2080 (m), 1995 (sh), 1950 (s)  $\text{cm}^{-1}$ .

**Complex 11c:** Orange oil. IR: 2085 (m), 2000 (sh), 1950 (s)  $\text{cm}^{-1}$ .

(18) Aumann, R.; Fischer, E. O. *Chem. Ber.* **1968**, *101*, 954.

(19) Darenbourg, M. Y.; Darenbourg, D. J. *Inorg. Chem.* **1970**, *9*, 32.

(20) Macomber, D. W.; Hung, M. H.; Madhukar, P.; Liang, M. *Organometallics* **1991**, *10*, 737.

(21) The substrates 1–6 were prepared according to the procedure described in ref 12b.

**Complex 12a:** Yellow solid (mp 60 °C). IR: 2090 (m), 2000 (sh), 1950 (s)  $\text{cm}^{-1}$ . Anal. Calcd for  $\text{C}_{16}\text{H}_{14}\text{WO}_6$ : C, 39.50; H, 2.88. Found: C, 39.73; H, 2.87.

**Complex 12b:** Red oil. IR: 2080 (m), 2000 (sh), 1955 (s)  $\text{cm}^{-1}$ .

**Complex 15:** Orange oil. IR: 2080 (m), 1995 (sh), 1950 (s)  $\text{cm}^{-1}$ .

**Complex 16:** Orange oil. IR: 2075 (m), 1985 (sh), 1940 (s)  $\text{cm}^{-1}$ .

**Complex 17:** Yellow solid (mp 65 °C). IR: 2060 (m), 1995 (sh), 1945 (s)  $\text{cm}^{-1}$ . Anal. Calcd for  $\text{C}_{18}\text{H}_{14}\text{CrO}_6$ : C, 57.14; H, 3.70. Found: C, 56.93; H, 3.94.

**Complex 18:** Red oil. IR: 2070 (m), 1980 (sh), 1920 (s), 1723 (s), 1657 (m)  $\text{cm}^{-1}$ .

**Complex 19:** Red oil. IR: 2069 (m), 1985 (sh), 1939 (s), 1731 (s), 1651 (m)  $\text{cm}^{-1}$ .

**Complex 21:** Yellow solid (mp 58 °C). IR: 2060 (m), 1985

(sh), 1940 (s)  $\text{cm}^{-1}$ . Anal. Calcd for  $\text{C}_{22}\text{H}_{16}\text{CrO}_6$ : C, 61.68; H, 3.74. Found: C, 61.27; H, 4.16.

**Complex 22:** Red oil. IR: 2065 (m), 1985 (sh), 1940 (s)  $\text{cm}^{-1}$ .

**Acknowledgment.** The authors thank Dr. S. Rajappa for his encouragement and support and Prof. T. R. Hoye of the University of Minnesota for sharing some of his unpublished results and helpful discussions. S.R.A. thanks CSIR, New Delhi, India, for a research fellowship.

**Supplementary Material Available:** Tables of  $^1\text{H}$  and  $^{13}\text{C}$  NMR spectral data and figures showing spectra of all new compounds (54 pages). Ordering information is given on any current masthead page.

OM940370U

# Highly Reactive Platinum(0) Carbene Intermediates in the Reactions of Diazo Compounds. A Fast Atom Bombardment Mass Spectrometric Study

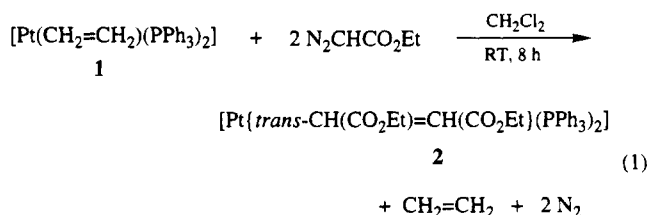
Roberta Bertani,<sup>†</sup> Rino A. Michelin,<sup>\*,‡</sup> Mirto Mozzon,<sup>‡</sup> Piero Traldi,<sup>§</sup>  
Roberta Seraglia,<sup>§</sup> Maria de Fatima Costa Guedes da Silva,<sup>||</sup> and  
Armando J. L. Pombeiro<sup>\*,||</sup>

Centro di Chimica e Tecnologia dei Composti Metallorganici degli Elementi di Transizione del CNR and Istituto di Chimica Industriale, Facoltà di Ingegneria, Università di Padova, Via F. Marzolo 9, 35131 Padova, Italy, Servizio di Spettrometria di Massa, Area della Ricerca, CNR, Corso Stati Uniti 4, 35100 Padova, Italy, and Centro de Química Estrutural, Complexo I, Instituto Superior Técnico, Av. Rovisco Pais, 1096 Lisbon codex, Portugal

Received March 14, 1994<sup>®</sup>

**Summary:** The reaction of  $[Pt(CH_2=CH_2)(PPh_3)_2]$  (**1**) with  $N_2CHCO_2Et$ , carried out directly in the FAB matrix and monitored by MS, leads to molecular ions corresponding to the species  $[Pt\{N_2C(H)CO_2Et\}(PPh_3)_2]$ ,  $[Pt\{C(H)CO_2Et\}(PPh_3)_2]$ , and  $[Pt\{C(H)CO_2Et\}(PPh_3)_2]_2$ , which are involved as intermediates in the formation of the final fumarate Pt(0) derivative  $[Pt\{trans-C(H)CO_2Et=C(H)CO_2Et\}(PPh_3)_2]$ . Chemical evidence of the intermediacy of a Pt(0) carbene stems from the fact that **1** is active in the cyclopropanation of styrene in the presence of  $N_2CHCO_2Et$ .

formation of the fumarate complex  $[Pt\{trans-CH(CO_2Et)=CH(CO_2Et)\}(PPh_3)_2]$  (**2**) (eq 1):<sup>5</sup>



## Introduction

While there has been considerable interest in the reactions of diazo compounds with transition metal centers to afford carbenes,<sup>1</sup> a relatively small number of investigations have been reported for zerovalent group 10 transition metal complexes.<sup>2</sup> The products of the latter reactions include diazoalkane complexes<sup>2b–e</sup> or derived species such as ketenimines<sup>2e</sup> or azines<sup>2f,g</sup> but no carbenes have been isolated or detected, in spite of being postulated as intermediates in some of the above-mentioned processes as well as in the catalytic cyclopropanation of olefins.<sup>1a,b,3</sup>

Our interest in the synthesis, chemistry, and electrochemistry of group 10 transition metal carbene complexes<sup>4</sup> led us recently to investigate the reaction of ethyl diazoacetate,  $N_2CHCO_2Et$ , with the Pt(0) complex  $[Pt(CH_2=CH_2)(PPh_3)_2]$  (**1**), which leads in solution to the

Although the formation of the olefin in complex **2** was suggested to proceed through the intermediacy of a Pt(0)–carbene (in view of the known coupling reactions of highly reactive carbenes to afford olefins<sup>6</sup>), no such intermediate was spectroscopically detected.

Following some promising results that we have recently obtained on ion–molecule reactions performed by mass spectrometry,<sup>7</sup> we thought it was of interest to study reaction 1 under fast atom bombardment (FAB) conditions since mass spectrometry, coupled with the mass-analyzed ion kinetic energy (MIKE) technique, allows the detection as well as the structural characterization of ionic species having lifetimes less than  $10^{-5}$  s. Furthermore, FAB conditions, being milder than those of electron impact (EI),<sup>8</sup> have been shown to be

(4) See, for example: Michelin, R. A.; Zanotto, L.; Braga, D.; Sabatino, P.; Angelici, R. *J. Inorg. Chem.* **1988**, *27*, 85. *Idem. Ibid.* **1988**, *27*, 93. Bertani, R.; Mozzon, M.; Michelin, R. A. *Inorg. Chem.* **1988**, *27*, 2809. Michelin, R. A.; Ros, R.; Guadalupi, G.; Bombieri, G.; Benetollo, F.; Chapuis, G. *Inorg. Chem.* **1989**, *28*, 840. Michelin, R. A.; Bertani, R.; Mozzon, M.; Zanotto, L.; Benetollo, F.; Bombieri, G. *Organometallics* **1990**, *9*, 1449. Zanotto, L.; Bertani, R.; Michelin, R. A. *Inorg. Chem.* **1990**, *29*, 3265. Bertani, R.; Mozzon, M.; Michelin, R. A.; Benetollo, F.; Bombieri, G.; Castilho, T. J.; Pombeiro, A. J. L. *Inorg. Chim. Acta* **1991**, *189*, 175. Bertani, R.; Mozzon, M.; Michelin, R. A.; Castilho, T. J.; Pombeiro, A. J. L. *J. Organomet. Chem.* **1992**, *431*, 117. Castilho, T. J.; Guedes da Silva, M. F. C.; Pombeiro, A. J. L.; Bertani, R.; Mozzon, M.; Michelin, R. A. In *Molecular Electrochemistry of Inorganic, Bioinorganic and Organometallic Compounds*; Pombeiro, A. J. L., McCleverty, J. A., Eds.; NATO ASI Series C385; Kluwer Academic Publishers: Dordrecht, Holland, 1993; p 345. Michelin, R. A.; Bertani, R.; Mozzon, M.; Benetollo, F.; Bombieri, G.; Silva, M. F. C. G.; Pombeiro, A. J. L. *Organometallics* **1993**, *12*, 2372.

(5) Silva, M. F. C. G.; Silva, J. J. R. F.; Pombeiro, A. J. L.; Bertani, R.; Michelin, R. A.; Mozzon, M.; Benetollo, F.; Bombieri, G.; *Inorg. Chim. Acta* **1993**, *214*, 85.

(6) Seitz, W. J.; Saha, A. K.; Hossain, M. M. *Organometallics* **1993**, *12*, 2604. (b) Woo, L. K.; Smith, D. A. *Organometallics* **1992**, *11*, 2344.

(7) (a) Bertani, R.; Mozzon, M.; Michelin, R. A.; Seraglia, R.; Traldi, P. *Org. Mass Spectrom.* **1992**, *27*, 1187. (b) Bertani, R.; Cecchetto, W.; Polloni, R.; Crociani, B.; Seraglia, R.; Traldi, P. *Inorg. Chim. Acta* **1990**, *174*, 61.

<sup>†</sup> Centro di Chimica e Tecnologia dei Composti Metallorganici degli Elementi di Transizione, CNR, Padova.

<sup>‡</sup> Istituto di Chimica Industriale, Università di Padova.

<sup>§</sup> Servizio di Spettrometria di Massa, Area della Ricerca, CNR, Padova.

<sup>||</sup> Instituto Superior Técnico, Lisbon.

<sup>®</sup> Abstract published in *Advance ACS Abstracts*, November 1, 1994.

(1) (a) Sutton, D. *Chem. Rev.* **1993**, *93*, 995. (b) Doyle, M. P. *Chem. Rev.* **1986**, *86*, 919. (c) Herrmann, W. A. *Angew. Chem., Int. Ed. Engl.* **1978**, *17*, 800. (d) Hillhouse, G. L.; Haymore, B. L. *J. Am. Chem. Soc.* **1982**, *104*, 1537 and references therein.

(2) (a) Schramm, K. D.; Ibers, J. A. *Inorg. Chem.* **1980**, *19*, 2441. (b) Nakamura, A.; Yoshida, T.; Cowie, M.; Otsuka, S.; Ibers, J. A. *J. Am. Chem. Soc.* **1977**, *99*, 2108. (c) Otsuka, S.; Nakamura, A.; Koyama, T.; Tatsumo, Y.; *Liebigs Ann. Chem.* **1975**, 626. (d) Otsuka, S.; Nakamura, A.; Koyama, T.; Tatsumo, Y. *J. Chem. Soc., Chem. Commun.* **1972**, 1105. (e) Yarrow, D. J.; Ibers, J. A.; Tatsumo, Y.; Otsuka, S. *J. Am. Chem. Soc.* **1973**, *95*, 8590. (f) Clemens, J.; Green, M.; Stone, F. G. A. *J. Chem. Soc., Dalton Trans.* **1973**, 1620. (g) Cardin, D. J.; Cetinkaya, B.; Cetinkaya, E.; Lappert, M. F. *Ibid.* **1973**, 514.

(3) Weiss, K. In *Transition Metal Carbene Complexes*; Verlag Chemie: Weinheim, 1983; p. 228.

quite suitable for the study of organometallic and coordination systems, which appear to be stable in the matrix.<sup>9</sup> We report herein a successful detection by FAB MS of a Pt(0)-carbene derivative as well as of other reactive species, which are likely to be involved in reaction 1. Furthermore, chemical evidence for the intermediacy of a zerovalent Pt-carbene species in reaction 1 is given also from experimental results in which **1** is shown to promote the cyclopropanation<sup>10</sup> of styrene in the presence of N<sub>2</sub>CHCO<sub>2</sub>Et.

### Experimental Section

[Pt(CH<sub>2</sub>=CH<sub>2</sub>)(PPh<sub>3</sub>)<sub>2</sub>] (**1**) was prepared by a published method,<sup>11</sup> whereas ethyl diazoacetate was used as purchased from Aldrich. Compound **2** was prepared as previously reported.<sup>5</sup> <sup>1</sup>H and <sup>13</sup>C NMR spectra were recorded on a AC 200 Bruker spectrometer.

In a separate experiment, reaction 1 was carried out in a NMR tube by reacting **1** (0.075 g, 0.013 mmol) and N<sub>2</sub>-CHCOOEt (210 μL, 0.199 mmol) in CD<sub>2</sub>Cl<sub>2</sub> (0.8 mL), and it was followed by <sup>1</sup>H and <sup>13</sup>C NMR at variable temperature in the range 223–278 K (see Results and Discussion).

All mass spectrometric measurements were performed on a VG ZAB 2F instrument.<sup>12</sup> Positive ion FAB mass spectra were obtained by bombarding 3-nitrobenzyl alcohol solutions of the samples with 8-keV Xe atoms.<sup>13</sup> Metastable transitions were detected by MIKE spectrometry.<sup>14a</sup> Collisionally induced decomposition mass-analyzed ion kinetic energy (CID MIKE) spectra were obtained with 8-keV ions colliding with air in the second field free region.<sup>14b</sup> Accurate mass measurements for all metal-containing fragment ions were obtained with the peak matching technique at 20 000 resolving power (10% valley definition). Nominal molecular masses were calculated using the mass 194 isotope of platinum. Precursor ion scans were obtained by B<sup>2</sup>/E = constant linked scans.<sup>15</sup>

Reaction 1 was performed under FAB conditions by initially mixing **1** (37.3 mg, 0.05 mmol) and N<sub>2</sub>CHCO<sub>2</sub>Et (119 μL, 0.100 mmol) with 3-nitrobenzyl alcohol (1.5 mL), placing the reaction mixture on the probe tip and then introducing it immediately into the source.

The cyclopropanation reaction was carried out according to the following procedure. Compound **1** (0.010 g, 0.013 mmol) was dissolved in 5 mL of CH<sub>2</sub>Cl<sub>2</sub>, and then, under stirring, styrene (0.500 g, 0.46 mmol) was added, followed by ethyl diazoacetate (100 μL, 0.084 mmol). The reaction mixture was stirred at ambient temperature for 24 h, and then the solvent was evaporated under reduced pressure to give an oil, which was treated with 1 mL of CH<sub>2</sub>Cl<sub>2</sub> and analyzed by GC/MS (on a QMD1000 instrument) using a PS 264 column, 25 m, 0.25 μm, from 100 to 250 °C, 10°/min. The GC/MS spectrum showed the presence of two peaks with retention times of 16.73 and 17.38 min in an abundance ratio of about 1:2 and both showing a molecular ion at *m/z* 190. They were identified by

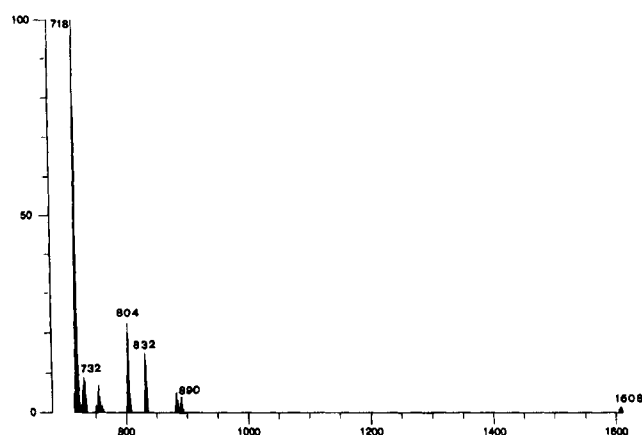


Figure 1. FAB MS spectrum of reaction 1.

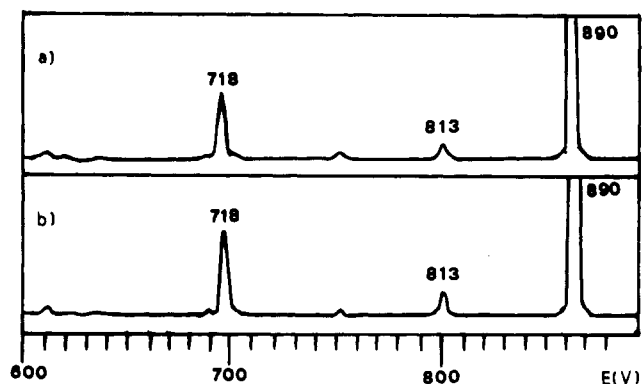


Figure 2. (a) MIKE spectrum of the molecular ion of **2**. (b) MIKE spectrum of ionic species at *m/z* 890 formed by running reaction 1 under FAB conditions.

comparison with the NBS mass spectra collection as *cis*- and *trans*-2-phenyl-1-cyclopropane (ethylcarboxylate esters), respectively. The conversion of ethyl diazoacetate to cyclopropanes was 20%. The <sup>1</sup>H NMR spectrum of the CD<sub>2</sub>Cl<sub>2</sub> solution confirmed the presence of both cyclopropanes identified by comparison with the known NMR spectral data.<sup>16</sup>

### Results and Discussion

Reaction 1 was run under FAB MS conditions (see Experimental Section), and the spectrum of the reaction mixture just introduced is reported in Figure 1. The spectrum shows the formation of ionic species at *m/z* 890 isobaric with the molecular ion of compound **2**. A comparison of the MIKE spectrum of M<sup>+</sup> of **2** (Figure 2a),<sup>17</sup> independently prepared according to reaction 1, with that of such ionic species (Figure 2b) reveals that they are identical, since both undergo a retrosynthetic process to yield [Pt(PPh<sub>3</sub>)<sub>2</sub>]<sup>+</sup> (*m/z* 718) and loss of a Ph<sup>•</sup> radical leading to the ions at *m/z* 813. CID MIKE spectra of the ions at *m/z* 890 are still identical and do not show the occurrence of further decomposition pathways. These results indicate that reaction 1, performed either under FAB conditions or in condensed phase, gives rise to the same product.

The FAB mass spectrum of the reaction mixture (Figure 1) also shows well-detectable ions at *m/z* 718,

(16) Nakamura, A.; Konishi, A.; Tatsumo, Y.; Otsuka, S. *J. Am. Chem. Soc.* **1978**, *100*, 3443.

(17) The FAB mass spectrum of **2** shows the molecular ion at *m/z* 890 (2%), ions at *m/z* 813 (4%) due to the loss of a Ph<sup>•</sup> radical, and ions at *m/z* 732 (see text) together with ions at *m/z* 718 (100%) originated by the loss of the fumarate ligand.

(8) Sharp, T. R.; White, M. R.; Davis, J. F.; Stang, P. J. *Org. Mass Spectrom.* **1984**, *19*, 107.

(9) Bruce, M. I.; Liddell, M. *Appl. Organomet. Chem.* **1987**, *1*, 191.

(10) (a) Doyle, M. P.; Griffin, J. H.; Bagheri, V.; Dorow, R. L. *Organometallics* **1984**, *3*, 53. (b) Brookhart, M.; Studabaker, W. B. *Chem. Rev.* **1987**, *87*, 411. (c) Seitz, W. J.; Saha, A. K.; Hossain, M. M. *Organometallics* **1993**, *12*, 2604.

(11) Nagel, U. *Chem. Ber.* **1982**, *115*, 1998.

(12) Morgan, R. P.; Beynon, J. H.; Bateman, R. H.; Green, B. N. *Int. J. Mass Spectrom. Ion Phys.* **1978**, *28*, 171.

(13) (a) Barber, M.; Bordoli, R. S.; Sedgwick, R. D.; Tyler, A. N. *J. Chem. Soc., Chem. Commun.* **1979**, 325. (b) Miller, J. M. *Adv. Inorg. Chem. Radiochem.* **1984**, *28*, 1. (c) Williams, D. H.; Findeis, A. F.; Naylar, S.; Gibson, B. V. *J. Am. Chem. Soc.* **1987**, *109*, 1980.

(14) (a) Cooks, R. J.; Beynon, J. H.; Caprioli, R. M.; Lester, G. R. *Metastable Ions*; Elsevier: Amsterdam, 1973. (b) Porter, C. J.; Benjan, J. H.; Ast, T. *Org. Mass Spectrom.* **1981**, *16*, 101.

(15) Bruins, A. R.; Jennings, K. R.; Evans, S. *Int. J. Mass Spectrom. Ion Phys.* **1978**, *26*, 395.





present in the MIKE spectrum of ions at  $m/z$  804 (Figure 3b) together with species originating from the retrosynthetic process at  $m/z$  718 and from the loss of  $\cdot\text{OCH}_2\text{CH}_3$  at  $m/z$  759.

It is worthwhile noting that the last step in the proposed mechanism of Scheme 1, i.e., the conversion of the dimer to the fumarate product, could not be confirmed by the MIKE data study owing to the low abundance of the ionic species at  $m/z$  1608, while the parent ion scan spectrum of ionic species at  $m/z$  890 shows a weak (signal-to-noise ratio 5:1) signal corresponding to the ions at  $m/z$  1608. Furthermore, such conversion is in agreement with the formation of olefin complexes from dinuclear carbene intermediates as reported for the synthesis of a Re-ethylene derivative from Re-methylene species.<sup>20</sup> Stable carbene dimers

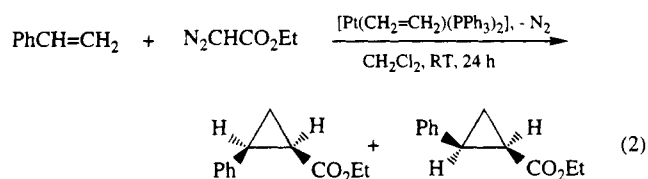
are also known: a  $(\eta\text{-C}_5\text{H}_5)$ -substituted  $\overline{\text{TiCH}_2\text{TiCH}_2}$  metallocycle was isolated from a reaction that generated  $(\eta\text{-C}_5\text{H}_5)_2\text{Ti}(\text{=CH}_2)$ <sup>20b</sup>, and an X-ray structure of  $(\eta\text{-C}_5\text{H}_5)_2[(\text{C}_2\text{H}_5)_3\text{AlCl}]\text{ZrCH}_2\text{CH}_2\text{Zr}[\text{AlCl}(\text{C}_2\text{H}_5)_3](\eta\text{-C}_5\text{H}_5)_2$ <sup>20c</sup> showed an arrangement of core atoms in which a full  $\text{CH}_2\text{-CH}_2$  bond is present, but some bonding of each zirconium to the  $\beta$   $\text{CH}_2$  remains.

The FAB MS and MIKE results do not provide any evidence of alternative mechanisms such as those involving any of the following intermediates, which were not detected:  $[\text{Pt}(\text{N}_2\text{CHCO}_2\text{Et})_2(\text{PPh}_3)_2]$  ( $m/z$  946),  $[\text{Pt}\{\text{C}(\text{H})\text{CO}_2\text{Et}\}(\text{N}_2\text{CHCO}_2\text{Et})(\text{PPh}_3)_2]$  ( $m/z$  918), and  $[\text{Pt}\{\text{C}(\text{H})\text{CO}_2\text{Et}\}_2(\text{PPh}_3)_2]$  ( $m/z$  890).<sup>22</sup>

The formation of the ionic species at  $m/z$  832, assigned to the molecular ion of the monoadduct  $[\text{Pt}(\text{N}_2\text{CHCO}_2\text{Et})(\text{PPh}_3)_2]^+$ , is supported also by <sup>13</sup>C NMR data. In fact, when reaction 1 in  $\text{CD}_2\text{Cl}_2$  was monitored at variable temperature (223–278 K), a resonance at  $\delta$  37.78 (triplet, <sup>3</sup> $J_{\text{PC}}$  12.56 Hz, <sup>2</sup> $J_{\text{CPt}}$  195.67 Hz) was detected. The value of <sup>2</sup> $J_{\text{CPt}}$ , which is close to those reported for nitrile Pt(II) complexes of the type  $[\text{PtCl}_2(\text{NCR})_2]$  (<sup>2</sup> $J_{\text{CPt}}$  ca. 230–280 Hz),<sup>23</sup> suggest an  $\eta^2$ -coordination mode of the diazo ligand. This type of

coordination has been proposed previously for other zerovalent diazo-Pd and -Pt complexes<sup>2a</sup> and has been confirmed by an X-ray analysis for the related Ni(0) species,  $[\text{Ni}(\text{diazofluorene})(\text{CN-}t\text{-Bu})_2]$ .<sup>2b</sup> However, in the latter studies as well as in the present investigation, no carbene intermediate could be spectroscopically detected, possibly as a result of its low concentration and/or high reactivity.

The formation of the carbene intermediate  $[\text{Pt}\{\text{C}(\text{H})\text{CO}_2\text{Et}\}(\text{PPh}_3)_2]$  was also substantiated chemically by observing the formation of cyclopropanes from styrene in the reaction mixture of  $[\text{Pt}(\text{CH}_2=\text{CH}_2)(\text{PPh}_3)_2]$  with  $\text{N}_2\text{CHCO}_2\text{Et}$  (eq 2), which is believed to involve coupling of the carbene with the olefin, as has been reported for several other transition metal-catalyzed cyclopropanation reactions of olefins:<sup>10</sup>



It is noteworthy that when reaction 2 is performed under FAB conditions, a less abundant formation of the fumarate derivative **2** is observed, accompanied by the well-detectable ionic species at  $m/z$  804 and 832 and by the appearance of new ionic species at  $m/z$  908. These last species correspond to the molecular ion of the carbene-olefin adduct  $[\text{Pt}\{\text{C}(\text{H})\text{CO}_2\text{Et}\}(\text{CH}_2=\text{CHPh})(\text{PPh}_3)_2]^+$ , which is reported to be a key intermediate in the catalytic cyclopropanation and also the meta-thesis of olefins and for which a metallocyclobutane structure is proposed.<sup>3</sup>

In conclusion, FAB mass spectrometry appears to be a technique particularly suitable for the detection of highly reactive species such as those described in the present study, which have short lifetimes and are present in low concentration. We are currently investigating the generality of these Pt(0)-promoted cyclopropanation reactions with diazo compounds as well as the role of the Pt(0)-carbene intermediates.

**Acknowledgments.** R.A.M. and A.J.L.P. thank CNR and JNICT, respectively, for partial support within their international cooperation program. R.A.M. also thanks CNR and MURST for financial support.

OM940193X

(23) Fracarollo, D.; Bertani, R.; Mozzon, M.; Belluco, U.; Michelin, R. A. *Inorg. Chim. Acta* **1992**, *201*, 15.

(22) As suggested by a reviewer, the formation of ionic species at  $m/z$  804 does not necessarily require the initial coordination of the diazo ester to the metal and subsequent  $\text{N}_2$  loss; it could be also explained by a FAB-induced loss of  $\text{N}_2$  from the free diazo compound to give the free carbene  $[(\text{CO}_2\text{Et})(\text{H})\text{C}]^+$ , which then reacts with  $[\text{Pt}(\text{PPh}_3)_2]^+$ . Such a reaction would be an ion-ion reaction, highly unfavored from the thermodynamic point of view; however, the possible presence of  $\text{:CHR}$  cannot rule out an ion-neutral reaction with  $[\text{Pt}(\text{PPh}_3)_2]^+$ . Furthermore, the FAB mass spectrum of free  $\text{N}_2\text{CHCO}_2\text{Et}$  (in either glycerol or *m*-nitrobenzyl alcohol as matrix) shows the presence of the molecular ion at  $m/z$  114 and of the carbene ion at  $m/z$  86, but not of the olefin  $\text{CO}_2\text{EtCH}=\text{CHCO}_2\text{Et}$  at  $m/z$  172. This finding indicates that the final Pt(0)-fumarate derivative is not formed by coordination of the preformed olefin to the  $[\text{Pt}(\text{PPh}_3)_2]^+$  species.

# [Co<sub>2</sub>Au<sub>2</sub>(CO)<sub>6</sub>(μ-dppm)<sub>2</sub>]: A 10-Membered Cycle Compound Including a Novel Co<sub>2</sub>Au<sub>2</sub> Z-Skew Frame Geometry

Angels Pons, Oriol Rossell, and Miquel Seco\*

Departament de Química Inorgànica, Universitat de Barcelona, Diagonal 647, 08028 Barcelona, Spain

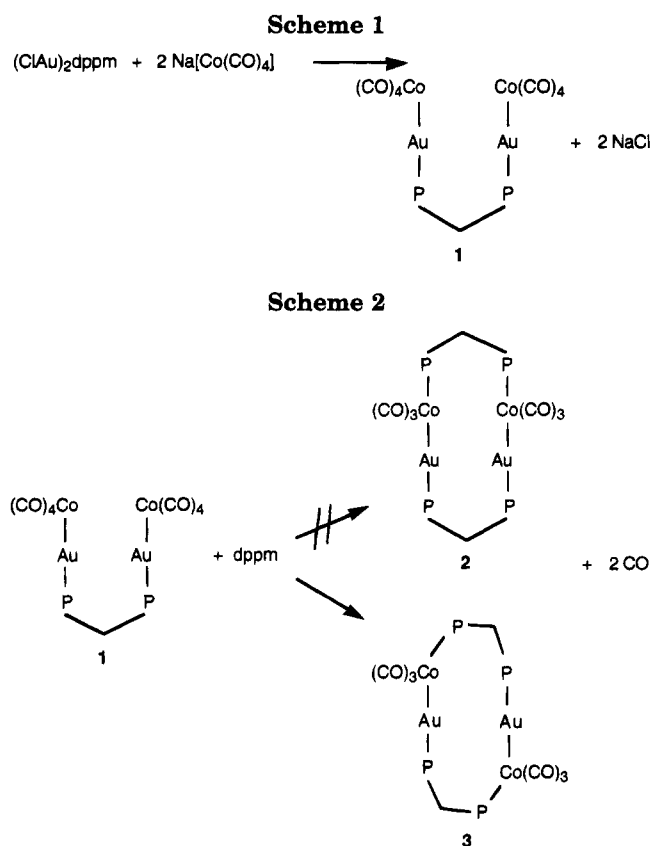
Aurea Perales

Departamento de Rayos X, Instituto Rocasolano, Serrano 119, 28006 Madrid, Spain

Received June 16, 1994<sup>®</sup>

**Summary:** The substitution of two carbonyl groups by a dppm ligand in the complex  $[(\text{CO})_4\text{CoAu}]_2(\text{dppm})$  (**1**) causes permutation in the metal skeleton sequence, giving the novel complex  $[\text{Co}_2\text{Au}_2(\text{CO})_6(\mu\text{-dppm})_2]$  (**3**) characterized by X-ray crystallography. Crystals of **3** are monoclinic, space group *Cc* with unit cell parameters of  $a = 18.834(1)$  Å,  $b = 16.257(1)$  Å,  $c = 20.366(2)$  Å,  $\beta = 112.350(3)^\circ$ ,  $Z = 4$ , and  $V = 6235(11)$  Å<sup>3</sup>. A mechanism for the formation of **3** is suggested.

The ability of bis(diphenylphosphinomethane) (dppm) to form bridged polynuclear complexes with new chemical and structural properties has led to increased interest in this and related ligands.<sup>1</sup> Particularly in the chemistry of mixed transition metal–gold clusters, it has been demonstrated that the use of the chelating digold phosphine cation  $[\text{Au}_2(\text{dppm})]^{2+}$  may force the two Au atoms to remain in relatively close contact in the final cluster or, alternatively, may allow the cluster to adopt a more open structure consisting of two independent metal cluster fragments linked by the phosphine. Examples of the first type include the nearly square  $[\text{Fe}_2\text{Au}_2(\text{CO})_8(\mu\text{-dppm})]_2$ <sup>2</sup> and of the second, the species  $[\{\text{Fe}_2\text{Au}(\text{CO})_6(\mu\text{-CO})(\mu\text{-PhC}=\text{CHPh})\}_2(\mu\text{-dppm})]_2$ ,<sup>3</sup>  $[\{\text{Fe}_3\text{Au}(\text{CO})_{10}(\mu\text{-CO})\}_2(\mu\text{-dppm})]_2$ ,<sup>4</sup> and  $[\{\text{Os}_4\text{AuH}_3(\text{CO})_{12}\}_2(\mu\text{-dppe})]_2$ .<sup>5,6</sup> All these facts prompted us to extend our studies to other transition metals, especially Co, due to the catalytic properties reported for its derivatives. Our main interest was to establish general routes for building square metal clusters, which have been much less studied than those displaying tetrahedral or butterfly geometry.



The colorless microcrystalline complex  $[(\text{CO})_4\text{CoAu}]_2(\text{dppm})$  (**1**), obtained by reaction of  $[(\text{ClAu})_2(\text{dppm})]$  with 2 equiv of  $\text{Na}[\text{Co}(\text{CO})_4]$  (Scheme 1), was thought to be an interesting precursor for tetranuclear  $\text{Co}_2\text{Au}_2$  derivatives, by substitution of two carbonyl ligands by a diphosphine ligand.

This strategy was supported by the fact that the reactions involving the substitution of a carbonyl group by a neutral ligand in  $[(\text{CO})_4\text{Co}-\text{M}]$  ( $\text{M} = \text{metal fragment}$ ) occur, without exception, in the CO ligand trans to the M fragment.<sup>7</sup> Consequently, **2** was anticipated to be the result of this reaction (Scheme 2). Surpris-

(7) Bryan, R. F.; Manning, A. R. *J. Chem. Soc., Chem. Commun.* **1968**, 1316. Ibers, J. A. *J. Organomet. Chem.* **1968**, *14*, 423. Stalick, J. K.; Ibers, J. A. *Ibid.* **1970**, *22*, 213. Norman, N. C.; Webster, P. M.; Farrugia, L. J. *Ibid.* **1992**, *430*, 205. Calderazzo, F.; Poli, R.; Pelizzi, G. *J. Chem. Soc., Dalton Trans.* **1984**, 2535. Bashkin, J.; Briant, C. E.; Mingos, D. M. P.; Wardle, R. W. M. *Transition Met. Chem.* **1985**, *10*, 113.

\* Abstract published in *Advance ACS Abstracts*, November 1, 1994.

(1) Chaudret, B.; Delavaux, B.; Poilblanc, R. *Coord. Chem. Rev.* **1988**, *86*, 191. Elliot, D. J.; Holah, D. G.; Hughes, A. N.; Magnuson, V. R.; Moser, I. M.; Puddephatt, R. J.; Xu, W. *Organometallics* **1991**, *10*, 3933. Aggarwal, R. P.; Connelly, N. G.; Crespo, M. C.; Dune, B. J.; Hopkins, P. M.; Orpen, A. G. *J. Chem. Soc., Dalton Trans.* **1992**, 655. Delaet, D. L.; del Rosario, R.; Fanwick, P. E.; Kubiak, C. P. *J. Am. Chem. Soc.* **1987**, *109*, 754. Braunstein, P.; de Méric de Bellefont, C.; Oswald, B.; Ries, M.; Lafranchi, M.; Tiripicchio, A. *Inorg. Chem.* **1993**, *32*, 1638. Alvarez, M. A.; García, M. E.; Riera, V.; Ruiz, M. A.; Bois, C.; Jeannin, Y. *Angew. Chem.* **1993**, *105*, 1232.

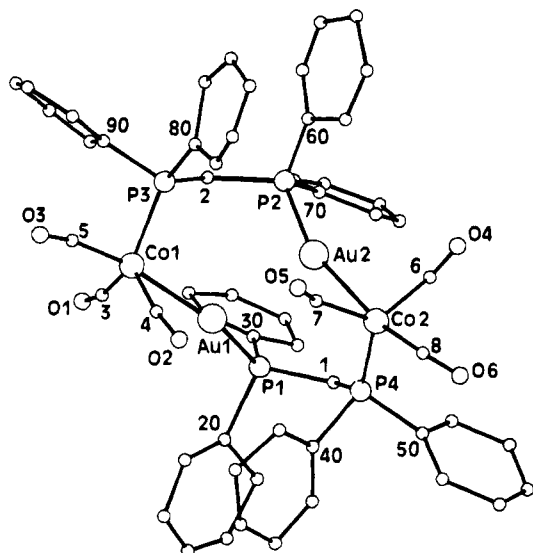
(2) Alvarez, S.; Rossell, O.; Seco, M.; Valls, J.; Pellinghelli, M. A.; Tiripicchio, A. *Organometallics* **1991**, *10*, 2309.

(3) Reina, R.; Rossell, O.; Seco, M.; Ros, J.; Yáñez, R.; Perales, A. *Inorg. Chem.* **1991**, *30*, 3973.

(4) Rossell, O.; Seco, M.; Reina, R.; Font-Bardía, M.; Solans, X. *Organometallics* **1994**, *13*, 2127.

(5) Amoroso, A. J.; Edwards, A. J.; Johnson, B. F. G.; Lewis, J.; Al-Mandhary, M. R.; Raithby, P. R.; Saharan, V. P.; Wong, W. T. *J. Organomet. Chem.* **1993**, *443*, C11.

(6) A similar bonding mode has been observed in the copper complex  $[\text{PPh}_4]_2[\{\text{Fe}_2(\text{CO})_8\}_2(\mu_4\text{-}\eta^2\text{-Cu}_2(\text{C}_7\text{H}_7\text{PCH}_2\text{CH}_2\text{PC}_7\text{H}_7))]$ : Deng, H.; Shore, S. G. *Organometallics* **1991**, *10*, 3486.



**Figure 1.** View of the molecular structure of the complex **3** together with the atomic numbering scheme.

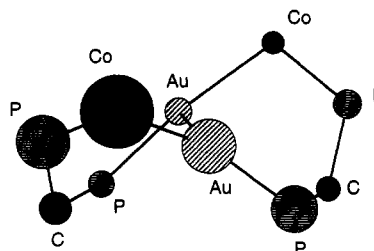
**Table 1.** Selected Bond Distances (Å) and Angles (deg) for **3**

Co(1)–Au(1)	2.552(17)	P(3)–C(2)	1.816(49)
Co(2)–Au(2)	2.453(16)	P(2)–C(2)	1.897(60)
P(1)–Au(1)	2.207(21)	Co(1)–C(3)	1.731(43)
P(2)–Au(2)	2.334(21)	Co(1)–C(4)	1.702(46)
P(3)–Co(1)	2.217(19)	Co(1)–C(5)	1.751(45)
P(4)–Co(2)	2.190(20)	Co(2)–C(6)	1.973(53)
P(1)–C(1)	1.811(65)	Co(2)–C(7)	1.901(51)
P(4)–C(1)	1.969(50)	Co(2)–C(8)	1.867(56)
Au(2)–Au(1)–Co(1)	104.8(4)	Au(2)–Co(2)–P(4)	95.7(7)
Au(1)–Au(2)–Co(2)	106.8(4)	Au(1)–Co(1)–P(3)	95.0(7)
Au(1)–Au(2)–P(2)	89.4(5)	Au(2)–Co(2)–C(8)	160.4(6)
Au(2)–Au(1)–P(1)	91.5(5)	Au(2)–Co(2)–C(7)	68.3(4)
Co(2)–Au(2)–P(2)	159.7(6)	Au(2)–Co(2)–C(6)	79.0(5)
Co(1)–Au(1)–P(1)	159.1(6)		

ingly, this reaction did not follow this pattern, and the final product was the compound  $[\text{Co}_2\text{Au}_2(\text{CO})_6(\mu\text{-dppm})_2]$  (**3**).

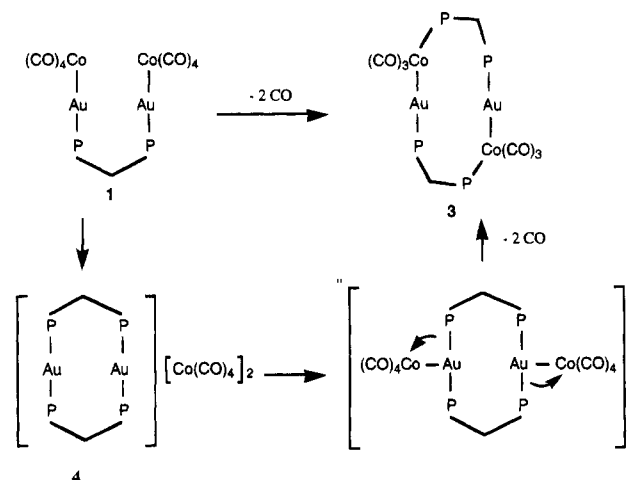
The structure of **3** is depicted in Figure 1, together with the atomic numbering scheme, while selected bond and angle parameters are listed in Table 1; it consists of a 10-atom cycle, containing the  $\text{Co}_2\text{Au}_2$  metal framework in an unprecedented Z-skew form, with the Co–Au bonds in reverse order to that expected. The four atoms are not coplanar, and the dihedral angle between the  $\text{Co}(1)\text{Au}(1)\text{Au}(2)$  and  $\text{Co}(2)\text{Au}(1)\text{Au}(2)$  planes is  $124.8^\circ$ . The geometry around each metal, ignoring the Au–Au interaction, can be described as distorted linear for the gold atoms and distorted trigonal bipyramidal for the cobalt atoms. Interestingly, the gold atoms show a short transannular  $\text{Au}\cdots\text{Au}$  contact ( $\text{Au}(1)\text{–Au}(2) = 2.977(10)$  Å), in good agreement with the tendency of this metal to give this type of interaction. This is achieved through  $5d^{10}\text{–}5d^{10}$  interactions based on a mixing with the 6s and 6p orbitals, whose energies are lowered by relativistic effects.<sup>8</sup>

A remarkable aspect of this 10-atom cycle is its highly distorted framework (Figure 2). This can be seen by comparing, for instance, the Au–P (2.207 and 2.334 Å)



**Figure 2.** View of the distorted 10-atom cycle of **3**.

**Scheme 3**



and Au–Co (2.453 and 2.552 Å) distances and in the nonlinearity of the Co–Au–P atom systems (Co–Au–P angles of  $159.7$  and  $159.1^\circ$ ), in contrast to that observed in the compound  $[\text{Fe}_2\text{Au}_2(\text{CO})_8(\text{dppm})]$ , in which the Fe–Au–P angles are nearly  $180^\circ$  ( $177.3$  and  $172.6^\circ$ ).<sup>2</sup>

Another interesting feature is the closely trigonal bipyramidal geometry around the cobalt, with a gold atom coordinated in an axial position (the  $\text{Au}(2)\text{–Co}(2)\text{–C}(8)$  angle is  $160.4(6)^\circ$ ) and with the phosphorus atom lying in an equatorial coordination site (the  $\text{Au}(2)\text{–Co}(2)\text{–P}(4)$  angle is  $95.7(7)^\circ$ ). On the other hand, the equatorial carbonyl ligands are bent toward the apical gold atoms (angles:  $\text{Au}(2)\text{–Co}(2)\text{–C}(7) = 68.3$  and  $\text{Au}(2)\text{–Co}(2)\text{–C}(6) = 79.0^\circ$ ). This bending, reported in other Au and Hg complexes,<sup>9</sup> has been described as the result of a partial electron density donation from the M–Au (or Hg)  $\sigma$  bond toward  $\pi^*(\text{CO})$  orbitals.

If we assume that the dppm ligand ensures the maintenance of a preformed geometry as a general strategy to make dinuclear building blocks, **3** demonstrates that this pattern is not followed in this four-metal system, and this has also been observed in other reactions with iron metal clusters.<sup>10</sup>

Although the pathway for the formation of **3** is still unclear, the following experimental observations allow us to suggest that shown in Scheme 3: **1** reacts with an equimolar amount of dppm in toluene at room temperature to give quantitatively the white crystalline solid **4**. According to its  $\nu(\text{CO})$  IR spectrum (a very strong band centered at  $1890\text{ cm}^{-1}$ ) and  $^{31}\text{P}$  NMR in  $\text{CH}_2\text{Cl}_2$  (a signal at  $\delta = 32$  ppm) along with its elemental

(8) Jiang, Y.; Alvarez, S.; Hoffmann, R. *Inorg. Chem.* **1985**, *24*, 749. Pyykkö, P.; Zhao, Y. *Angew. Chem. Int. Ed. Engl.* **1991**, *30*, 604. Dávila, R. M.; Elduque, A.; Grant, T.; Staples, R. J.; Fackler, J. P. *Inorg. Chem.* **1993**, *32*, 1749 and references therein.

(9) Usón, R.; Laguna, A.; Laguna, M.; Jones, P. G.; Sheldrick, G. M. *J. Chem. Soc., Dalton Trans.* **1981**, 366. Alvarez, S.; Ferrer, M.; Reina, R.; Rossell, O.; Seco, M.; Solans, X. *J. Organomet. Chem.* **1989**, *377*, 291.

(10) Braunstein, P.; Knorr, M.; Tiripicchio, A.; Tiripicchio Camellini, M. *Inorg. Chem.* **1992**, *31*, 3685.

analysis, **4** can be unambiguously formulated as  $[\text{Au}_2(\text{dppm})_2][\text{Co}(\text{CO})_4]_2$ , despite the fact that unfortunately we were not able to grow crystals for an X-ray structure determination. On the other hand, when a suspension of **4** in toluene was heated to 80 °C, the solution became yellow, and after addition of hexane, yellow crystals of **3** were obtained, as compared with an authenticated sample.

In conclusion, these results suggest that **3** can be formed in THF via the ionic intermediate **4**, not detected in this solvent, which would undergo an intramolecular reorganization involving the migration of phosphorus from the gold atom to  $\text{Co}(\text{CO})_4$  units, with concomitant loss of two carbonyl groups; (see Scheme 3). It is possible that the existence of  $\text{Au}\cdots\text{Au}$  contacts may favor this process. Experiments aimed at defining the factors which govern this type of reaction are in progress.

### Experimental Section

All manipulations were performed under an atmosphere of prepurified  $\text{N}_2$  with use of standard Schlenk techniques, and all solvents were distilled from appropriate drying agents. Elemental analyses of C and H were carried out at the Institut de Bio-Orgànica de Barcelona. Infrared spectra were recorded in THF solutions on an FT-IR 520 Nicolet spectrophotometer.  $^1\text{H}$  and  $^{31}\text{P}\{^1\text{H}\}$  NMR spectra were obtained on a Bruker WP 80SY spectrometer ( $\delta(85\% \text{H}_3\text{PO}_4) = 0.0$  ppm). The complex  $(\text{ClAu})_2(\text{dppm})$  was synthesized and isolated as a solid from  $\text{AuCl}(\text{tht})$ <sup>11</sup> solutions by adding the appropriate amount of the diphosphine.

**Preparation of  $[(\text{CO})_4\text{CoAu}]_2(\text{dppm})$  (**1**).** Solid  $(\text{ClAu})_2(\text{dppm})$  (1.4 g, 1.65 mmol) was added to a solution of  $\text{Na}[\text{Co}(\text{CO})_4]$  (0.64 g, 3.30 mmol) in tetrahydrofuran (100 mL) at 0 °C under a nitrogen atmosphere. The solution was stirred for 0.5 h and evaporated to dryness. The residual solid was extracted twice with toluene (2 × 25 mL), and after filtration, the solution was concentrated to 10 mL. The addition of 15 mL of hexane gave white microcrystals of **1**. Yield: 70%. IR (THF,  $\text{cm}^{-1}$ ):  $\nu(\text{CO})$  stretch 2052 s, 2023 m, 1978 s br, 1957 vs br.  $^{31}\text{P}\{^1\text{H}\}$  NMR (240 K, toluene,  $\delta$  (ppm)): 24.86 (s).  $^1\text{H}$  NMR (acetone- $d_6$ ,  $\delta$  (ppm)): 4.56 (t,  $\text{CH}_2\text{-P}$ ,  $J(\text{H,P}) = 12$  Hz). Anal. Calcd: C, 35.38; H, 1.98. Found: C, 35.41; H, 2.01.

**Preparation of  $[\text{Co}_2\text{Au}_2(\text{CO})_6(\mu\text{-dppm})_2]$  (**3**).** A solution of **1** (0.1 g, 0.089 mmol) in tetrahydrofuran (100 mL) at room temperature, under a nitrogen atmosphere, was treated with 0.034 g (0.089 mmol) of solid dppm. After 15 min of stirring, the mixture was evaporated to dryness. The residual solid was treated with 10 mL of dichloromethane and filtered, and after addition of 15 mL of methanol, bright yellow microcrystals of **3** were obtained in ca. 40–60% yield. IR (KBr,  $\text{cm}^{-1}$ ):  $\nu(\text{CO})$  stretch 1992 m, 1990 vs, 1912 m, 1896 s, 1872 m.

(11) Usón, R.; Laguna, A. *Organomet. Synth.* **1986**, 3, 324.

Table 2. Crystallographic Data for **3**

formula	$\text{C}_{36}\text{H}_{44}\text{Au}_2\text{Co}_2\text{O}_6\text{P}_4$		
$f_w$	1448.6	Z	4
space group	Cc	$D_{\text{calcd}}$ , $\text{gcm}^{-3}$	1.6754
$a$ , Å	18.834(1)	$\mu(\text{Mo K}\alpha)$ , $\text{cm}^{-1}$	57.815
$b$ , Å	16.257(1)	$T$ , °C	25
$c$ , Å	20.366(2)	$\lambda$ , $\text{cm}^{-1}$	0.7107
$\beta$ , deg	112.350(3)	R	0.065
$V$ , Å <sup>3</sup>	6235(11)		

$^{31}\text{P}\{^1\text{H}\}$  NMR (240 K,  $\text{CH}_2\text{Cl}_2$ ,  $\delta$  (ppm)): 57.2 (dd), 27.1 (dd,  $^{2+3}J(\text{P,P}) = 107$  Hz).  $^1\text{H}$  NMR ( $\text{CD}_2\text{Cl}_2$ ,  $\delta$  (ppm)): 3.50 (t, br,  $\text{CH}_2\text{-P}$ ,  $J(\text{H,P}) = 10.1$  Hz). Anal. Calcd: C, 46.43; H, 3.06. Found: C, 46.17; H, 3.13.

**Preparation of  $[\text{Au}_2(\mu\text{-dppm})_2][\text{Co}(\text{CO})_4]_2$  (**4**).** A solution of **1** (0.1 g, 0.09 mmol) in toluene (100 mL) at room temperature, under a nitrogen atmosphere, was treated with 0.035 g (0.09 mmol) of solid dppm. The solution was stirred for 0.5 h. The addition of 20 mL of hexane gave white microcrystals of **4**. Yield: 70%. IR (toluene,  $\text{cm}^{-1}$ ):  $\nu(\text{CO})$  stretch 1890 s.  $^{31}\text{P}\{^1\text{H}\}$  NMR (240 K,  $\text{CH}_2\text{Cl}_2$ ,  $\delta$  (ppm)): 32(s). Anal. Calcd: C, 46.25; H, 2.92. Found: C, 45.06; H, 2.84.

**X-ray Structure Determination.** A summary of the crystal data is given in Table 2. A prismatic orange-red crystal (0.18 × 0.16 × 0.11 mm) was sealed in a glass capillary tube and mounted on a Phillips PW 100 diffractometer. Cell parameters were calculated from accurate settings of 25 automatically centered reflections in the range of  $6 < \Theta < 14^\circ$ . Intensities were collected with graphite-monochromated Mo K $\alpha$  radiation ( $\mu = 48.122 \text{ cm}^{-1}$ ) operating in an  $\omega$ -2 $\Theta$  scan mode to  $\Theta_{\text{max}} = 25^\circ$  with a scan speed of  $0.05^\circ \text{ s}^{-1}$  and a scan width of  $1.50^\circ$ . Five thousand forty-five unique reflections were collected, of which 3709 with  $l > 3\sigma(l)$  were used in refinement. The structure was solved by the heavy-atom method and subsequent Fourier difference synthesis, which revealed the positions of all non-hydrogen atoms of the complex. An absorption correction was applied. All computations were performed on a VAX 6410 computer using the X-ray 76 system.<sup>12</sup> Refinements were carried out by least-squares methods. Hydrogen atoms in the phenyl rings were introduced in positions calculated with a C–H distance of 1.00 Å, each with a thermal parameter of the parent carbon atom. The final R value was 0.065.

**Acknowledgment.** Financial support was generously provided by the DGICYT (Project PB93-0766).

**Supplementary Material Available.** Tables of anisotropic thermal parameters and bond distances and angles (8 pages). Ordering information is given on any current masthead page.

OM940472K

(12) Stewart, J. M.; Machin, P. A.; Dickinson, C. W.; Ammon, H. L.; Heck, H.; Flack, H. Y. *The X-ray 76 System*. Technical Report TR446; Computer Science Center, University of Maryland: College Park, MD, 1976.

## Formation of a Cyclopentadienyl Arene Coordination Complex of Potassium in the Presence of THF and Aryloxy Ligands: Synthesis and Structure of $\{K[(\mu\text{-C}_5\text{H}_5)_2\text{Nd}(\mu\text{-O-C}_6\text{H}_3\text{Me}_2\text{-2,6})_2]\}_n$

William J. Evans, Mohammad A. Ansari, and Saeed I. Khan

*Organometallics*, 1995, 14 (1), 558-560 • DOI: 10.1021/om00001a077 • Publication Date (Web): 01 May 2002

Downloaded from <http://pubs.acs.org> on March 9, 2009

### More About This Article

---

The permalink <http://dx.doi.org/10.1021/om00001a077> provides access to:

- Links to articles and content related to this article
- Copyright permission to reproduce figures and/or text from this article

# Formation of a Cyclopentadienyl Arene Coordination Complex of Potassium in the Presence of THF and Aryloxy Ligands: Synthesis and Structure of $\{K[(\mu-C_5H_5)_2Nd(\mu-O-C_6H_3Me_2-2,6)_2]\}_n$

William J. Evans\* and Mohammad A. Ansari

Department of Chemistry, University of California, Irvine, Irvine, California 92717

Saeed I. Khan

Department of Chemistry and Biochemistry, University of California, Los Angeles, Los Angeles, California 90024

Received June 27, 1994<sup>®</sup>

**Summary:**  $KC_5H_5$  reacts with  $[Nd(OAr)_3(THF)_2]_2 \cdot 2THF$  ( $Ar = C_6H_3Me_2-2,6$ ), **1**, prepared from  $NdCl_3$  and  $NaOAr$  in THF, to form in high yield  $\{K[(\mu-C_5H_5)_2Nd(\mu-OAr)_2]\}_n$ , **2**, which crystallizes from THF/benzene. In **2**, the potassium is coordinated in a distorted tetrahedral arrangement by two cyclopentadienyl ring centroids and two aryloxy arene ring centroids with no close contacts to oxygen donor atoms (shortest  $K \cdots O$  distance is 4.4 Å). Neodymium has a distorted tetrahedral coordination environment formed by two  $C_5H_5$  ring centroids and two aryloxy oxygen atoms. All of the ligands are bridging and generate a two dimensional extended network. **2** crystallizes in the monoclinic space group  $P2_1/n$  with unit cell dimensions at 160 K of  $a = 9.827(2)$  Å,  $b = 15.637(4)$  Å,  $c = 16.166(4)$  Å,  $\beta = 95.96(1)^\circ$ ,  $V = 2470(1)$  Å<sup>3</sup>,  $Z = 4$ . Least squares refinement of the model based on 1959 reflections ( $|F_o| > 6\sigma(F_o)$ ) converged to  $R = 0.067$ .

## Introduction

Alkali metals commonly become incorporated into complexes of yttrium and the lanthanides via bridging interactions with anionic ligands.<sup>1,2</sup> A wide variety of bridges are known, but halide and oxygen donor ligands are the most common. We have recently shown that this type of heterometallic bridging can be quite useful in generating new types of coordination environments for yttrium and the lanthanides.<sup>3,4</sup> Hence, this bridging can be exploited to provide stabilization to ligand sets which normally would not generate readily isolable yttrium and lanthanide complexes.

We now report a case in which potassium becomes involved in extensive bridging interactions without interacting with any available oxygen donor ligands, i.e. this is a potassium aryloxy complex containing no K-O bonds. This demonstrates that the bridging and heteroatom stabilization capacity of potassium is quite flexible and should be more fully explored in ligand systems beyond those involving the usual electronegative donor atoms.

## Experimental Section

The syntheses and subsequent manipulations of the compounds described below were conducted with rigorous exclusion of air and moisture using standard Schlenk, vacuum line, and glovebox techniques. Solvents were dried and physical measurements obtained as previously described.<sup>5a</sup> Complexometric analysis of metal content was determined as previously described.<sup>5b</sup> CH analyses were determined on a Carlo Erba EA 1108 instrument.  $NaOC_6H_3Me_2-2,6$  was prepared as reported in the literature<sup>6</sup> using sublimed 2,6-dimethylphenol (Aldrich).

$[Nd(OC_6H_3Me_2-2,6)_3(THF)_2]_2 \cdot 2THF$ , **1**. **1** was prepared by a slight modification of the method used to prepare  $Y(OC_6H_3Me_2-2,6)_3(THF)_3$ .<sup>6</sup> In the glovebox,  $NdCl_3$  (2.00 g, 7.8 mmol) and  $NaOC_6H_3Me_2-2,6$  (3.37 g, 23.4 mmol) were added to a 100 mL round bottom flask containing 50 mL of THF and the mixture was stirred overnight. Removal of the solvent by rotary evaporation left a blue powder which was extracted with toluene and dried. The solid was redissolved in THF and the solvent was removed by rotary evaporation. The sample was dried at  $10^{-5}$  torr for 24 h to yield **1** as a blue crystalline powder (4.45 g, 74%). Anal. Calcd for  $C_{72}H_{102}O_{12}Nd_2$ : Nd, 19.92. Found: 20.6. IR (KBr,  $cm^{-1}$ ): 3000(s), 2920(s, br), 2860(s), 2840(s), 1590(m), 1580(m), 1560(w), 1430(w), 1310(w), 1300(s), 1250(s), 1090(m), 995(s), 985(m), 875(s), 830(s), 755(m), 745(m), 670(m), 595(m).

**1** crystallizes from THF at room temperature by slow evaporation in the glovebox in the space group  $P2_1/n$  with  $a = 12.658(4)$  Å,  $b = 18.844(6)$  Å,  $c = 15.714(5)$  Å,  $\beta = 115.15(7)^\circ$ ,  $V = 3393(1)$  Å<sup>3</sup>. **1** was characterized by X-ray diffraction, but unfortunately crystal decomposition occurred during data collection. Hence, although the final  $R$  factor based on 2100 reflections and 203 parameters is 6.9% and the temperature factors are reasonable, the distances and angles may not be reliable. The identity of the compound was established to be dimeric in the solid state (Figure 1) with each Nd ligated by two terminal aryloxy groups, two terminal THF molecules, and two bridging aryloxy ligands. There are also two THF molecules per dimer in the lattice. A summary of crystallographic data is given in the supplementary material.

$\{K[(\mu-C_5H_5)_2Nd(\mu-OC_6H_3Me_2-2,6)_2]\}_n$ , **2**. Addition of  $KC_5H_5$  (103 mg, 1.0 mmol) to **1** (362 mg, 0.25 mmol) in 10 mL of THF formed a cloudy blue suspension. The reaction mixture was stirred for 18 h and centrifuged. The supernatant was dried on a rotary evaporator to produce a pale blue solid. Recrystallization of this material from THF/benzene yielded **2** as blue irregularly shaped crystals (430 mg, 77%). Anal. Calcd for

<sup>®</sup> Abstract published in *Advance ACS Abstracts*, November 1, 1994.

(1) Evans, W. J.; Boyle, T. J.; Ziller, J. W. *Inorg. Chem.* **1992**, *31*, 1120-1122, and references therein.

(2) Schaverien, C. J. *Adv. Organomet. Chem.* **1994**, *36*, 283-362.

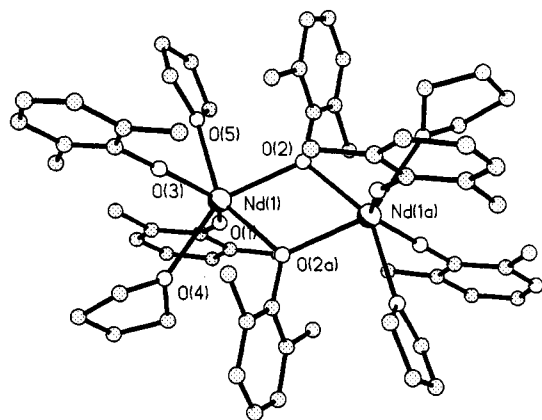
(3) Evans, W. J.; Boyle, T. J.; Ziller, J. W. *J. Organomet. Chem.* **1994**, *462*, 141-148.

(4) Evans, W. J.; Boyle, T. J.; Ziller, J. W. *J. Am. Chem. Soc.* **1993**, *115*, 5084-5092.

(5) (a) Evans, W. J.; Chamberlain, L. R.; Ulibarri, T. A.; Ziller, J. W. *J. Am. Chem. Soc.* **1988**, *110*, 6423-6432. (b) Atwood, J. L.; Hunter, W. E.; Wayda, A. L.; Evans, W. J. *Inorg. Chem.* **1981**, *20*, 4115-4119.

(6) Evans, W. J.; Olofson, J. M.; Ziller, J. W. *Inorg. Chem.* **1989**, *28*, 4308-4309.





**Figure 1.** Ball and stick diagram of  $[\text{Nd}(\text{OC}_6\text{H}_3\text{Me}_2\text{-}2,6)_3(\text{THF})_2]_2$ .

**Table 1.** Crystallographic Data for  $\{\text{K}[(\text{C}_5\text{H}_5)_2\text{Nd}(\text{OAr})_2]\}_n^a$

formula	$\text{NdKO}_2\text{C}_{26}\text{H}_{28}$	$V, \text{Å}^2$	2470(1)
mol wt	555.84	$Z$	4
crystal system	monoclinic	$D_{\text{calcd}}, \text{g cm}^{-3}$	1.49
space group	$P2_1/n$	temp, K	156
cell constants		abs coeff, $\mu, \text{cm}^{-1}$	22.94
$a, \text{Å}$	9.827(2)	transmission coeff min-max	0.87-1.06
$b, \text{Å}$	15.637(4)	$R_F, \%$	0.073
$c, \text{Å}$	16.166(4)	$R_{wF}, \%$	0.065
$\beta, \text{deg}$	95.96(1)	GOF	1.666

<sup>a</sup> Radiation for the structure was Mo K $\alpha$ ;  $\lambda = 0.7107 \text{ Å}$ .

$\text{C}_{26}\text{H}_{28}\text{O}_2\text{KNd}$ : Nd, 25.98, C, 56.19; H, 5.04. Found: Nd, 26.6; C, 54.24; H, 4.67. <sup>1</sup>H NMR (benzene- $d_6$ ):  $\delta$  7.66 (br,  $\nu_{1/2} = 480 \text{ Hz}$ ), 6.88 (br,  $\nu_{1/2} = 410 \text{ Hz}$ ), 5.40 (br,  $\nu_{1/2} = 150 \text{ Hz}$ ), -4.21 (br,  $\nu_{1/2} = 350 \text{ Hz}$ ). IR (KBr,  $\text{cm}^{-1}$ ): 3020(s), 2940(s br), 2900(s), 1586(w), 1424(m), 1280(s), 1236(m), 1090(m), 1050(w), 977(w), 916(w), 853(s), 843(w), 746(m), 691(m).

**X-ray Data Collection, Structure Determination, and Refinement for  $\{\text{K}[(\mu\text{-C}_5\text{H}_5)_2\text{Nd}(\mu\text{-OC}_6\text{H}_3\text{Me}_2\text{-}2,6)_2]\}_n$ , **2**.** A pale blue irregularly shaped crystal of approximate dimensions  $0.40 \times 0.35 \times 0.35 \text{ mm}$  was coated with Paratone oil, mounted on a glass fiber, and transferred onto a locally automated Picker diffractometer (Crystal Logic).<sup>7</sup> Accurate unit cell parameters and the orientation matrix were obtained by least-squares refinement of 20 reflections. Three standard reflections were monitored every 97 reflections which showed no significant variation throughout the data collection. Data were corrected for Lorentz and polarization effects, and a  $\varphi$ -scan procedure was used for an empirical absorption correction. A total of 3606 data were collected of which 1959 with  $|F_o| > 6\sigma(|F_o|)$  were subsequently used in the structure analysis.

The structure was solved in the monoclinic space group  $P2_1/n$  by Patterson methods, SHELX86,<sup>8</sup> and subsequent difference-Fourier maps. Idealized hydrogen atom positions were calculated ( $\text{C-H} = 0.95 \text{ Å}$ ) and included as fixed contributors in a riding model. A few carbon atoms turned nonpositive definite on anisotropic refinement thus in the final cycle all the carbon atoms were treated isotropically. The final refinement with 157 parameters converged to  $R = 0.073$  and  $R_w = 0.065$  and  $\text{GOF} = 1.666$ . Crystallographic details are given in Table 1. Important distances and angles are listed in Table 2.

## Results and Discussion

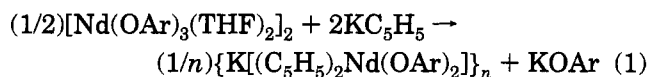
Recent studies of mixed ligand cyclopentadienyl alkoxide and aryloxy complexes of yttrium and the lanthanide metals (e.g. the bimetallic series  $[(\text{C}_5\text{R}_5)\text{Y}(\mu\text{-}$

**Table 2.** Selected Interatomic Bond Distances (Å) and Angles (deg) Involving the Non-Hydrogen Atoms for  $\{\text{K}[(\text{C}_5\text{H}_5)_2\text{Nd}(\text{OAr})_2]\}_n$

Bond Distances			
Nd-O(1)	2.206(12)	Nd-O(2)	2.194(11)
Nd-C(17)	2.75(5)	Nd-C(18)	2.79(2)
Nd-C(19)	2.79(2)	Nd-C(20)	2.81(7)
Nd-C(21)	2.79(3)	Nd-C(22)	2.81(2)
Nd-C(23)	2.79(2)	Nd-C(24)	2.80(2)
Nd-C(25)	2.82(2)	Nd-C(26)	2.78(2)
K-C(1)	3.55(2)	K-C(2)	3.39(2)
K-C(3)	3.20(2)	K-C(4)	3.17(2)
K-C(5)	3.35(2)	K-C(6)	3.56(2)
K..C(9A)	3.74(2)	K-C(10A)	3.52(2)
K-C(11A)	3.36(2)	K-C(12A)	3.53(2)
K..C(13A)	3.84(2)	K..C(14A)	3.93(2)
K-C(17B)	3.21(2)	K-C(18B)	3.02(2)
K-C(19B)	3.07(2)	K-C(20B)	3.29(2)
K-C(21B)	3.37(2)	K-C(22C)	3.09(2)
K-C(23C)	3.24(2)	K-C(24C)	3.30(2)
K-C(25C)	3.20(2)	K-C(26C)	3.09(2)
K-(Cp-cent)	2.95, 2.96	K-(arene-cent)	3.08, 3.39
Nd-(Cp-cent)	2.52, 2.54		
Angles			
O(1)-Nd-O(2)	97.0(4)	Nd-O(1)-C(1)	146.5(10)
Nd-O(2)-C(9)	162.8(12)	Cent-Nd-Cent	121.4

$\text{OCMe}_3)(\text{OCMe}_3)_2$  ( $\text{C}_5\text{R}_5 = \text{C}_5\text{H}_5, \text{C}_5\text{Me}_5, \text{C}_5\text{H}_4\text{Me}, \text{C}_5\text{H}_4\text{SiMe}_3, \text{indenyl}$ )<sup>9</sup> and the monometallic complex  $(\text{C}_5\text{Me}_5)\text{Y}[\text{OC}_6\text{H}_3(\text{CMe}_3)_2\text{-}2,6\text{-Me-}4]_2$ <sup>10</sup> have shown that such complexes can be precursors to reactive alkylalkoxide systems<sup>4</sup> and to species catalytically active for polymerization of alkenes.<sup>10</sup> Since the 2,6-dimethylphenoxide ligand can generate both monometallic and bimetallic complexes, i.e.,  $\text{Ln}(\text{OAr})_3(\text{THF})_3$  and  $[\text{Ln}(\text{OAr})_3(\text{THF})]_2$  ( $\text{Ar} = \text{C}_6\text{H}_3\text{Me}_2\text{-}2,6$ ),<sup>6</sup> we were interested in determining what mixed ligand complexes this aryloxy would support.

Reaction of 1 equivalent of  $\text{KC}_5\text{H}_5$  with  $[\text{Nd}(\text{OAr})_3(\text{THF})_2]_2$  in THF formed a ligand rearrangement product  $\{\text{K}[(\text{C}_5\text{H}_5)_2\text{Nd}(\text{OAr})_2]\}_n$ , **2**, in very low yield, which could be generated in high yield using the stoichiometry shown in eq 1. The identity of the blue paramagnetic



complex was established by a single crystal X-ray diffraction study which revealed an unusual structure.

The structure of **2** (Figure 2) is comprised of  $[(\text{C}_5\text{H}_5)_2\text{Nd}(\text{OAr})_2]^-$  anions connected into a two-dimensional layered structure by K cations bridged by arene and cyclopentadienyl rings. The most unusual structural feature of **2** is the coordination around potassium. Each potassium atom connects four different  $[(\text{C}_5\text{H}_5)_2\text{Nd}(\text{OAr})_2]^-$  anions and is surrounded by two bridging  $\text{C}_5\text{H}_5$  groups and two bridging arenes. Although there are several examples of alkali metal interactions with the arene and cyclopentadienyl rings,<sup>11-14</sup> to our knowledge

(9) Evans, W. J.; Boyle, T. J.; Ziller, J. W. *Organometallics*, **1993**, *12*, 3998-4009.

(10) (a) Schaverien, C. J.; Frijns, J. H. G.; Heeres, H. J.; Hende, J. R.; Teuben, J. H.; Spek, A. L. *J. Chem. Soc., Chem. Commun.* **1991**, 642-644. (b) Schaverien, C. J. *Organometallics*, **1994**, *13*, 69-82.

(11) Weiss, E. *Angew. Chem., Int. Ed. Engl.* **1993**, *32*, 1501-1670.

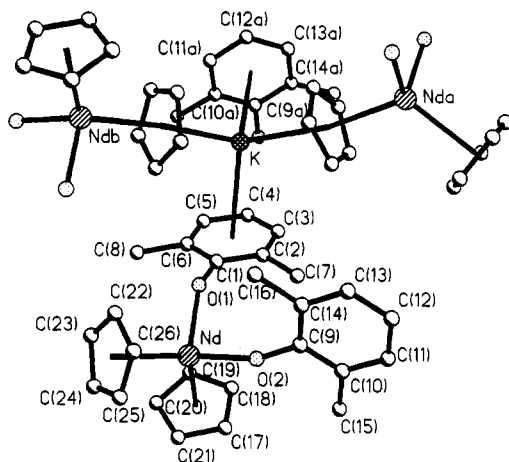
(12) Christian, S.; Schleyer, P. v. R. *Adv. Inorg. Chem.* **1987**, *27*, 169-278.

(13) Clark, D. L.; Watkin, J. G.; Huffman, J. C. *Inorg. Chem.* **1992**, *31*, 1554-1556.

(14) Schaverien, C. J.; van Mechelen, J. B. J. *Organometallics*, **1991**, *10*, 1704-1709.

(7) Modified by C. E. Strouse of the Department of Chemistry, University of California, Los Angeles.

(8) Sheldrick, G. M. *Acta Crystallogr.* **1990**, *A46*, 467-473.



**Figure 2.** Portion of the pseudo-two-dimensional extended structure of  $\{K[(\mu\text{-C}_5\text{H}_5)_2\text{Nd}(\mu\text{-C}_6\text{H}_3\text{Me}_2\text{-}2,6)]_n\}_n$ , **2**.

there is no example of both kinds of interactions in the same molecule. More remarkable is the fact that there are no close potassium-oxygen contacts even though the product is formed in THF and contains aryloxide ligands. Hence, this is a potassium aryloxide complex devoid of K–O bonds.

The arrangement of the ring centroids of the four bridging rings surrounding potassium is severely distorted tetrahedral with (ring centroid)–metal–(ring centroid) angles in the 96.8 to 127.4° range. The K–C(C<sub>5</sub>H<sub>5</sub>) distances are similar in the two rings attached to potassium and range from 3.01(2)–3.37(2) Å with an average of 3.17(13) Å (K–C(centroid) distances are 2.95 Å and 2.96 Å). In comparison, the average K–C(cyclopentadienyl) distances in  $K[\text{C}_5\text{H}_4(\text{SiMe}_3)]^{15}$  and  $K[\text{C}_5(\text{CH}_2\text{C}_6\text{H}_5)_5]\cdot 3\text{THF}^{16}$  are 3.00(2) and 3.04(4) Å, respectively. In each cyclopentadienyl ring, two adjacent carbons are closest to K with K–C distances less than 3.10(2) Å and the carbon across the ring from these carbon atoms has the longest K–C distance which is 3.30(2) Å or greater. Hence, the rings are oriented with respect to potassium such that the K–(ring centroid)–C angles are in the range 80.8 to 99.8°.

The arene rings are similarly tipped toward the potassium with K–(ring centroid)–C angles in the range 77.8 to 102.2°. The K–C(arene) distances in the two rings are quite different. The C(1)–C(6) ring has K–C(arene) distances from 3.17(2) to 3.54(2) Å with a 3.07 Å K–(ring centroid) distance, while the C(9A)–C(14A) ring has a 3.36(2) to 3.93(2) Å K–C range with a 3.39 Å K–(ring centroid) distance. In both rings, two adjacent carbon atoms have the smallest K–C distances and the longest distances for that ring involve carbon atoms directly across the ring. In comparison, K–C–

(arene) distances in polymeric  $\{K[\text{Nd}(\text{OC}_6\text{H}_3\text{Pr-}2,6)_4]\}_n^{13}$  range from 3.097(10)–3.473(11) Å with a K–(ring centroid) distance of 3.072 Å. In the extended structure of  $\text{KBPh}_4$ , the K–C distances average 3.191(5) Å with a K–(ring centroid) distance of 2.986 Å.<sup>11</sup>

The environment of the neodymium is more conventional and has the distorted tetrahedral arrangement typical for  $[(\text{C}_5\text{R}_5)_2\text{Ln}(\text{ligand})_2]$  complexes.<sup>1,17</sup> The Nd–C(C<sub>5</sub>H<sub>5</sub>) distances fall in a narrow 2.75(5)–2.82(2) Å range (2.79(6) Å average) and the coordination mode is clearly  $\eta^5$ . In comparison, distances of 2.703(7)–2.895(7) Å are found in  $(\text{C}_5\text{H}_4\text{Me})_3\text{Nd}^{18}$  and 2.72(2)–2.85(2) Å in  $(\text{C}_5\text{H}_4\text{Me})_3\text{Nd}(\text{THF})$ .<sup>19</sup> The two 2.206(12) and 2.194(11) Å Nd–O(OAr) distances are similar to the 2.21(2) Å average found in  $K[\text{Nd}(\text{OC}_6\text{H}_3\text{Pr}_2\text{-}2,6)_4]$ .<sup>13</sup> However, the 146.5(10) and 162.8(12)° Nd–O–C angles in **2** are significantly different from each other. A similarly large range of Nd–O–C angles was also found for  $K[\text{Nd}(\text{OC}_6\text{H}_3\text{Pr}_2\text{-}2,6)_4]$ :<sup>13</sup> 132.0(7)–162.1(7)°. The two arene rings in **2** are almost perpendicular to each other with an interplanar angle of 84.6(3)°.

Although complexes of general formula  $[(\text{C}_5\text{R}_5)_2\text{Ln}(\text{OR})_2]^-$  are very reasonable types of yttrium and lanthanide complexes,<sup>20</sup> there are no structurally characterized examples in the literature. The closest examples are the neutral mixed ligand systems such as  $(\text{C}_5\text{Me}_5)_2\text{Sm}(\text{OC}_6\text{HMe}_4\text{-}2,3,5,6)$ ,<sup>21</sup>  $(\text{C}_5\text{H}_5)_2\text{Nd}(\text{OC}_6\text{H}_3\text{Ph}_2\text{-}2,3)$ <sup>22</sup> and  $(\text{C}_5\text{Me}_5)_2\text{Ce}(\text{OC}_6\text{H}_3\text{tBu}_2\text{-}2,6)$ .<sup>23</sup> Hence,  $K[(\text{C}_5\text{H}_5)_2\text{Nd}(\text{OC}_6\text{H}_3\text{Me}_2\text{-}2,6)_2]$  is the first structurally characterized example of a mixed ligand “ate” complex of general formula  $[(\text{C}_5\text{R}_5)_2\text{Ln}(\text{OR})_2]^-$ . More significantly, **2** is the first alkoxide or aryloxide complex containing potassium in which no interaction with the oxygen is found.

**Acknowledgment.** We thank the Division of Chemical Sciences of the Office of Basic Energy Sciences of the Department of Energy for supporting this research.

**Supplementary Material Available:** Tables of crystal data, positional and thermal parameters, and distances and angles and figures giving additional views of **1** and **2** (12 pages). Ordering information is given on any current masthead page.

OM940503B

(17) Evans, W. J.; Foster, S. E. *J. Organomet. Chem.* **1992**, *433*, 79–94.

(18) Burns, J. H.; Baldwin, W. H.; Fink, F. H. *Inorg. Chem.* **1974**, *13*, 1916–1920.

(19) Yuguo, F.; Pinzhe, L.; Zhongsheng, J.; Wenqi, C. *Sci. Sin. Ser. B.* **1984**, *27*, 993–1001.

(20) Evans, W. J.; Sollberger, M. S.; Hanusa, T. P. *J. Am. Chem. Soc.* **1988**, *110*, 1841–1850.

(21) Evans, W. J.; Hanusa, T. P.; Levan, K. R. *Inorg. Chim. Acta* **1985**, *110*, 191–195.

(22) Deacon, G. B.; Nickel, S.; Tiekink, E. R. T. *J. Organomet. Chem.* **1991**, *409*, C1–C4.

(23) Heeres, H. J.; Meetsma, A.; Teuben, J. H. *J. Chem. Soc., Chem. Commun.* **1988**, 962–963.

(15) Jutzi, P.; Leffers, W.; Hampel, B.; Pohl, S.; Saak, W. *Angew. Chem., Int. Ed. Engl.* **1987**, *26*, 583–584.

(16) Lorberth, J.; Shin, S.-H.; Wocadlo, S.; Massa, W. *Angew. Chem., Int. Ed. Engl.* **1989**, *28*, 735–738.

# Influence of Different 4,7-Substituted 1,10-Phenanthroline Ligands on Reactivity and Regio- and Stereocontrol in Tungsten-Catalyzed Allylic Alkylations

Håkan Frisell and Björn Åkermark\*

Department of Organic Chemistry, Royal Institute of Technology, S-100 44 Stockholm, Sweden

Received February 8, 1994<sup>®</sup>

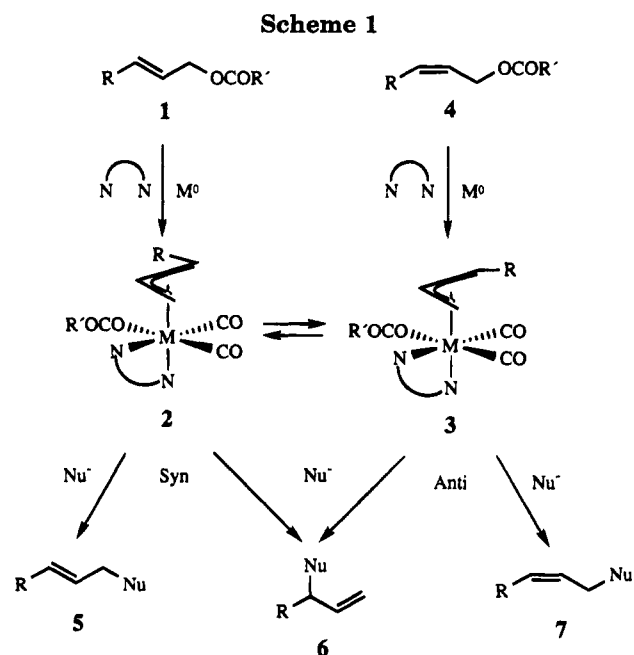
**Summary:** The substitution of allylic carbonate using tetracarbonyl(1,10-phenanthroline)tungsten(0) complexes as catalysts was found to give products with high retention of configuration (>90%) with both (*E*)- and (*Z*)-substrates.

## Introduction

Metal-catalyzed nucleophilic substitution of allylic leaving groups, in principle, offers the possibility to convert allyl alcohols and related compounds into substituted alkenes of specified stereochemistry.<sup>1</sup> For example, a (*Z*)-product **7** could be obtained from an (*E*)-acetate or -carbonate **1** as illustrated in Scheme 1.

Several conditions have to be fulfilled in this specific case. (i) syn–anti isomerization (**2** → **3**) has to be fast relative to nucleophilic addition. (ii) The product between the concentration and the rate of the reaction with the nucleophile has to be greater for the anti isomer. (iii) The nucleophilic attack has to take place preferentially at the least substituted terminus of the intermediate ( $\eta^3$ -allyl) system.

We have recently found that if a palladium catalyst with 1,10-phenanthroline as ligand is used, either a (*Z*)-substrate **4** or an (*E*)-substrate **1** can be converted selectively into an (*E*)-product.<sup>2</sup> In this case, all of the conditions i–iii are evidently fulfilled. During work toward developing a procedure for converting an (*E*)-substrate into a (*Z*)-product, we have earlier shown that in ( $\eta^3$ -allyl)palladium systems, ligands such as 2,9-dimethyl-1,10-phenanthroline (dmphen) are able to induce a preference for the anti configuration **3**.<sup>3</sup> Unfortunately, the continued work has shown that syn–anti isomerization becomes slow with this type of ligand. Furthermore, the regioselectivity is dramatically decreased, and a ca. 1:1 mixture of the two regioisomers **6** and **7** is generally obtained. In order to see if it is possible to overcome these problems, we have started a broad investigation of systems based on other metals and also other ligands. The pioneering studies by Trost and his co-workers using tris(acetonitrile)tungsten(0) tricarbonyl and auxiliary bipyridine and related ligands



suggest a preference for attack of the more substituted terminus of the intermediate  $\eta^3$ -allyl systems.<sup>4</sup> However, we recently observed that, depending on the substitution pattern, 1,10-phenanthroline type ligands induced a wide variation in selectivity in reactions involving ( $\eta^3$ -allyl)palladium systems.<sup>2</sup> We therefore decided to study the reaction of (*Z*)-ethyl hexenyl carbonate **4** ( $R = C_3H_7$ ,  $R' = OEt$ ) with sodium dimethyl methylmalonate using tungsten(0) tetracarbonyl coordinated to a series of 1,10-phenanthroline ligands. Here we would like to report some results, which show that a (*Z*)-substrate **4** may indeed be converted into a (*Z*)-product **7** with high selectivity and with an efficiency that is strongly dependent on the phenanthroline substituents.

## Results and Discussion

Five different catalysts were prepared by refluxing the appropriate phenanthroline with tungsten hexacarbonyl for 20 h at 110 °C in toluene. Tetracarbonyl[4,7-bis(hexanoyloxy)-1,10-phenanthroline]tungsten(0) (**8**), tetracarbonyl-(1,10-phenanthroline)tungsten(0) (**9**), tetracarbonyl(2,9-dimethyl-1,10-phenanthroline)tungsten(0) (**10**), tetracarbonyl(4,7-dimethyl-1,10-phenanthroline)tungsten(0) (**11**), and tetracarbonyl(4,7-dibutoxy-

<sup>®</sup> Abstract published in *Advance ACS Abstracts*, December 1, 1994.

(1) (a) Trost, B. M.; Verhoeven, T. R. In *Comprehensive Organometallic Chemistry*; Wilkinson, G., Stone, F. G. A., Abel, E. W., Eds.; Pergamon: Oxford, 1982; Vol. 8, pp 799–938. (b) Collman, J. P.; Hegedus, L. S.; Norton, J. R.; Finke, R. G. *Principles and Applications of Organotransition Metal Chemistry*; University Science Books: Mill Valley, CA, 1987. (c) Trost, B.; Lautens, M. *Tetrahedron* **1987**, *43*, 4817. (d) Trost, B. M.; Lautens, M. *J. Am. Chem. Soc.* **1982**, *104*, 5543.

(2) Sjögren, M.; Hansson, S.; Åkermark, B.; Vitagliano, A. *Organometallics* **1994**, *13*, 1963.

(3) (a) Hansson, S.; Vitagliano, A.; Åkermark, B. *J. Am. Chem. Soc.* **1990**, *112*, 4587. (b) Sjögren, M.; Hansson, S.; Norrby, P. O.; Cucciolito, M. E.; Vitagliano, A.; Åkermark, B. *Organometallics* **1992**, *11*, 3954.

(4) (a) Trost, B. M.; Hung, M.-H. *J. Am. Chem. Soc.* **1983**, *105*, 7757. (b) Trost, B. M.; Tometzki, G. B.; Hung, M.-H. *J. Am. Chem. Soc.* **1987**, *109*, 2176.

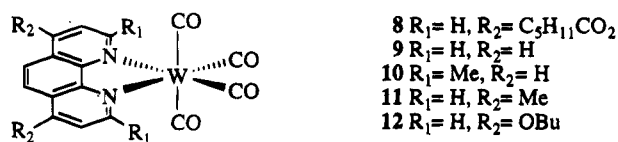


Figure 1.

**Table 1. Product Pattern from Tungsten-Catalyzed Alkylations of (*Z*)-Ethyl 2-Hexen-1-yl Carbonate (Entries 1–8), (*E*)-Ethyl 2-Hexen-1-yl Carbonate (Entries 9–11), and Ethyl 1-Hexen-3-yl Carbonate (Entry 12)**

Entry	Catalyst				% Yield <sup>a</sup>
1	W(CO) <sub>6</sub>	98	1	1	23
2	<b>8</b>	93	6	1	38
3	<b>9</b>	89	2	9	43
4	<b>9</b>	90	1	9	48 <sup>b</sup>
5	<b>10</b>	91	2	7	45
6	<b>10</b>	91	2	7	54 <sup>c</sup>
7	<b>11</b>	88	2	10	67
8	<b>12</b>	92	1	7	100 <sup>d</sup>
9	<b>9</b>	0	91	9	33
10	<b>11</b>	0	84	16	49
11	<b>12</b>	0	80	20	62
12	<b>12</b>	4	73	23	85

The standard reaction conditions are 110°C, 10 mol % of the catalyst and 200 mol % of sodium dimethyl methyl malonate. <sup>a</sup> GC yields after 20 h reaction time, Nu= dimethyl methylmalonate. <sup>b</sup> 20 mol % of 1,10-phenanthroline was added. <sup>c</sup> 20 mol % of 2,9-dimethyl-1,10-phenanthroline was added. <sup>d</sup> Reaction was finished within 60 min.

1,10-phenanthroline)tungsten(0) (**12**) (see Figure 1). These were reacted with (*Z*)-ethyl hexenyl carbonate in toluene at 110 °C with 200 mol % of sodium dimethyl methylmalonate (10 mol % of catalyst). In all cases, high preference was observed for attack at the least substituted terminus of the intermediate  $\eta^3$ -allyl system, leading to ca. 90% selectivity for the desired (*Z*)-product **7** (see entries 1–8, Table 1). A remarkable difference in reactivity among the catalysts was observed. While tungsten hexacarbonyl itself was essentially inactive as catalyst, the phenanthroline catalyst **9** gave ca. 40% and the 4,7-dmphen catalyst **11** a 70% yield of product after 20 h. In bright contrast, the 4,7-dibutoxyphenanthroline catalyst **12** led to complete reaction after 1 h. The reason for this strong influence of the ligands is not clear. A possible explanation is that we are seeing the result of a balance between oxidative addition, which could then lead to the desired product and decomposition of the catalyst. This is supported by the fact that addition of 20% excess ligand (which would be expected to increase the stability of the catalyst) to catalysts **9** and **10** leads to 10–20% increase in yield. The importance of the oxidative addition step is also shown by the fact that allylic acetates fail to react. In order to define the limits for the activity of the catalyst **12**, experiments with only 1% catalyst were performed. After 1 h ca. 30% yield was obtained, but the catalyst degenerates and the yield levels off to become ca. 40% after 20 h. Experiments were also done at lower temperatures and at 80 °C (10 mol % catalyst), the reaction is considerably slower and only ca. 60% yield was obtained after 20 h. However, at this temperature, the catalyst seems stable and there is no leveling off in the yield, which continues to increase on further reaction.

Also the structure of the substrate has a strong influence on the reactivity. While ethyl 1-hexen-3-yl

carbonate was essentially as reactive as the (*Z*)-isomer (entry 12), the (*E*)-isomer was considerably less reactive (entries 9–11). It is interesting to compare the results from the reactions of (*Z*)-ethyl and (*E*)-ethyl hexenyl carbonates and tungsten catalyst with those from (*Z*)- and (*E*)-hexenyl acetates and palladium-dmphen as catalyst. In both cases, the stereochemistry is preserved. With the palladium catalyst, (*E*)-substrate **1** gave exclusively reaction at the less substituted  $\eta^3$ -allyl terminus while (*Z*)-substrate gave a mixture (3/2) of the two products **6** and **7**. By contrast, the tungsten catalyst gave a mixture of (*E*)-product and terminal alkene **6** from the (*E*)-substrate but exclusively the (*Z*)-product **7** from (*Z*)-substrate. Thus the two different catalysts are nicely complementary. A few exploratory experiments were finally performed, using the most active catalyst **12**. With (*Z*)-ethyl hexenyl carbonate, reaction with a  $\beta$ -keto ester enolate, sodium ethyl 2-methylacetoacetate, gave the (*Z*)-product exclusively, but the reaction was fairly slow (ca. 60% yield after 20 h). No reaction was observed with bis(phenylsulfonyl)methyl anion, perhaps due to steric effects. In order to compare the phenanthroline based catalyst **12** with (CH<sub>3</sub>CN<sub>3</sub>)-W(CO)<sub>3</sub>,<sup>4b</sup> (*E*)-cinnamyl ethyl carbonate was reacted with sodium diethyl methylmalonate. While (CH<sub>3</sub>CN<sub>3</sub>)-W(CO)<sub>3</sub> gave exclusive reaction at the more substituted allyl terminus,<sup>4b</sup> the catalyst **12** gave a mixture of products from internal reaction (68%) and (*Z*)-(24%) and (*E*)-(8%) products from reaction at the less substituted allyl terminus. The regiocontrol thus clearly depends on the substrates, but it is clear that simple (*Z*)-substrates can be converted cleanly to (*Z*)-products, using phenanthroline substituted tungsten carbonyl catalysts.

## Experimental Section

**General.** All reactions were performed in oven-dried glassware. Melting points (uncorrected) were determined by using a Büchi SMP-20 melting point apparatus. <sup>1</sup>H and <sup>13</sup>C NMR were recorded on a 400 MHz (Bruker Model AM400) and a 250 MHz (Bruker Model AC250) instrument at 298 K in CDCl<sub>3</sub> (unless otherwise indicated), using CHCl<sub>3</sub> ( $\delta$  7.26 ppm) and CDCl<sub>3</sub> ( $\delta$  77.0 ppm) as internal references for <sup>1</sup>H and <sup>13</sup>C, respectively. The following abbreviations are used in descriptions of NMR multiplicities: s = singlet, d = doublet, t = triplet, q = quartet, m = multiplet, br = broadened and *J* = coupling constant. IR spectra were recorded on a Perkin-Elmer 1725X FTIR instrument. Gas chromatographic determination of yields and product patterns were performed using a Varian Model 3700 spectrometer equipped with a 15 m  $\times$  0.15 mm dimethylpolysiloxane (100%) capillary column and a Varian 4290 integrator. Elemental analyses were performed by Analytische Laboratorien, Gummersbach, Germany. All solvents and reagents were purchased from commercial sources and dried and purified by standard techniques.

**General Procedure for Tungsten-Catalyzed Alkylation.** Toluene (10 mL) was added to a flask containing sodium hydride (48 mg, 2 mmol) under argon. Dimethyl methylmalonate (321 mg, 2.2 mmol) was added with a syringe. After stirring for 45 min at ambient temperature, ethyl hexenyl carbonate (172 mg, 1 mmol) and the internal standard dodecane (70 mg) was added followed by the catalyst (0.1 mmol). The contents of the flask were heated to reflux. The reaction was monitored by GC at regular time intervals (1, 2, 5, and 20 h). Results are presented in Table 1.

**4,7-Dibutoxy-1,10-phenanthroline.**<sup>5</sup> To a mixture of 4,7-dihydroxy-1,10-phenanthroline (0.20 g, 0.94 mmol) in DMF (10 mL) was added NaH (0.67 g, 2.82 mmol) with stirring under argon at room temperature. After 20 min, n-BuBr (0.64 g, 4.67 mmol) was added to the reaction flask and the mixture was stirred at 100 °C for 10 h. The resulting clear, brown solution was cooled down to room temperature. Water (50 mL) was added to obtain a precipitate, which was extracted with CH<sub>2</sub>Cl<sub>2</sub> and dried over MgSO<sub>4</sub>. The pure product (0.25 mg, 80%, mp 131–132 °C) was obtained by chromatography on silica gel (MeOH/CH<sub>2</sub>Cl<sub>2</sub>, 1/20). <sup>1</sup>H NMR (CD<sub>2</sub>Cl<sub>2</sub>, 250 MHz): δ 8.90 (d, *J* = 5.28 Hz, 2H), 8.19 (s, 2H), 6.99 (d, *J* = 5.77 Hz, 2H), 4.25 (t, *J* = 6.36 Hz, 4H), 1.96 (m, 4H), 1.62 (m, 4H), 1.04 (t, *J* = 7.37 Hz, 6H). <sup>13</sup>C (CD<sub>2</sub>Cl<sub>2</sub>, 62.5 MHz) δ 151.3, 119.2, 103.7, 66.7, 31.4, 19.7, 14.0. Anal. Calcd for C<sub>18</sub>H<sub>24</sub>N<sub>2</sub>O<sub>2</sub>: C, 74.0; H, 7.5; N, 8.6. Found: C, 73.5; H, 7.3; N, 8.5.

**Tetracarbonyl[4,7-bis(hexanoyloxy)-1,10-phenanthroline]tungsten(0) (8).** To a mixture of 4,7-dihydroxy-1,10-phenanthroline (0.30 g, 1.41 mmol) in DMF (20 mL) was added NaH (0.10 g, 4.23 mmol) with stirring under argon at room temperature. After 20 min, the solution was cooled down to 0 °C and hexanoyl chloride (0.95 g, 7.05 mmol) was added slowly and was then stirred at room temperature overnight. The reaction product was then filtered off and DMF removed under reduced pressure at 60 °C, giving yellow-brown crystals. Crude yield, 0.50 g (87%). The crystals was used in the following synthesis of **8** without further purification.

Tungsten hexacarbonyl (0.084 g, 0.24 mmol) and 4,7-bis(hexanoyloxy)-1,10-phenanthroline (0.10 g, 0.24 mmol) were dissolved and refluxed in dry toluene (50 mL) overnight under argon atmosphere. The deep red crystals that were formed upon cooling were washed with toluene and dried *in vacuo*. Yield, 0.15 g (89%). <sup>1</sup>H NMR (400 MHz) δ 9.43 (d, *J* = 5.7 Hz, 2 H), 8.07 (s, 2 H), 7.71 (d, *J* = 5.8 Hz, 2 H), 2.82 (t, *J* = 7.5 Hz, 4 H, CH<sub>2</sub>), 1.2 (m, 12 H, CH<sub>2</sub>), 0.98 (t, *J* = 7.6 Hz, 6H, CH<sub>3</sub>). <sup>13</sup>C NMR (100 MHz) δ 222.7 (CO), 204.8 (CO), 170.3, 154.4, 153.8, 147.7, 123.8, 120.7, 116.9, 34.5, 29.7, 24.5, 22.3, 13.9 IR (KBr): 1886 (C=O, broad).

**Tetracarbonyl(1,10-phenanthroline)tungsten(0) (9).**<sup>6</sup> Tungsten hexacarbonyl (1.0 g, 2.80 mmol) and 1,10-phenanthroline (0.50 g, 2.80 mmol) were dissolved and refluxed in dry toluene (50 mL) overnight under argon atmosphere. The deep red crystals that were formed upon cooling were washed with toluene and dried *in vacuo*. Yield, 1.0 g (75%). Mp 190–195 °C dec. <sup>1</sup>H NMR (400 MHz) δ 9.62 (dd, *J*<sub>1</sub> = 5.1 Hz, *J*<sub>2</sub> = 3.76 Hz, 2 H), 8.49 (dd, *J*<sub>1</sub> = 8.1 Hz, *J*<sub>2</sub> = 6.78 Hz, 2 H), 8.00 (s, 2 H), 7.78 (dd, *J*<sub>1</sub> = 8.1 Hz, *J*<sub>2</sub> = 5.1 Hz, 2 H). <sup>13</sup>C NMR (100 MHz) δ 215.6 (CO), 201.2 (CO), 152.9, 147.3, 136.1, 130.4, 127.3, 125.0. IR (KBr): 1997 (C=O), 1846 (C=O, broad). Anal. Calcd for C<sub>16</sub>H<sub>8</sub>WN<sub>2</sub>O<sub>4</sub>: C, 40.36; H, 1.69. Found: C, 40.28; H, 1.77.

(5) Procedure for this ligand synthesis was extracted from: Mäkelä, M. Licentiate thesis, 1992. Department of Organic Chemistry, Royal Institute of Technology, Sweden.

**Tetracarbonyl(2,9-dimethyl-1,10-phenanthroline)tungsten(0) (10).**<sup>6</sup> Tungsten hexacarbonyl (1.0 g, 2.80 mmol) and 2,9-dimethyl-1,10-phenanthroline (0.58 g, 2.80 mmol) were dissolved and refluxed in dry toluene (50 mL) overnight under argon atmosphere. The deep red crystals that were formed upon cooling were washed with toluene and dried *in vacuo*. Yield, 1.20 g (85%). Mp 150–155 °C dec. <sup>1</sup>H NMR (400 MHz) δ 8.26 (d, *J* = 8.2 Hz, 2 H), 7.85 (s, 2 H), 7.71 (d, *J* = 8.3 Hz, 2 H), 3.34 (s, 6 H, CH<sub>3</sub>). <sup>13</sup>C NMR (62 MHz, DMSO-*d*<sub>6</sub>) δ 214.3 (CO), 199.0 (CO), 163.5, 147.0, 138.3, 128.3, 126.6, 126.3 31.0. IR (KBr): 2005 (C=O), 1875 (C=O), 1854 (C=O), 1808 (C=O). Anal. Calcd for C<sub>18</sub>H<sub>12</sub>WN<sub>2</sub>O<sub>4</sub>: C, 42.88; H, 2.40. Found: C, 42.65; H, 2.31.

**Tetracarbonyl(4,7-dimethyl-1,10-phenanthroline)tungsten(0) (11).** Tungsten hexacarbonyl (0.50 g, 1.42 mmol) and 4,7-dimethyl-1,10-phenanthroline (0.45 g, 1.42 mmol) were dissolved and refluxed in dry toluene (50 mL) overnight under argon atmosphere. After cooling, the toluene was removed by distillation under reduced pressure. The residue was then dissolved in CH<sub>2</sub>Cl<sub>2</sub>. Deep red crystals were formed upon slow addition of pentane. The precipitate was filtered off and dried *in vacuo*. Yield, 0.49 g (65%). Mp 205–210 °C dec. <sup>1</sup>H NMR (400 MHz) δ 9.44 (d, *J* = 5.2 Hz, 2 H), 8.15 (s, 2 H), 7.56 (d, *J* = 5.2 Hz, 2 H), 2.91 (s, 6 H, CH<sub>3</sub>). <sup>13</sup>C NMR (62 MHz, DMSO-*d*<sub>6</sub>) δ 219.5, 202.0, 152.6, 147.9, 146.0, 129.7, 126.5, 123.9, 18.7. IR (KBr): 2003 (C=O), 1866 (C=O, broad), 1812 (C=O). Anal. Calcd for C<sub>18</sub>H<sub>12</sub>WN<sub>2</sub>O<sub>4</sub>: C, 42.88; H, 2.40. Found: C, 42.87; H, 2.51.

**Tetracarbonyl(4,7-dibutoxy-1,10-phenanthroline)tungsten(0) (12).** Tungsten hexacarbonyl (0.11 g, 0.31 mmol) and 4,7-dibutoxy-1,10-phenanthroline (0.10 g, 0.31 mmol) were dissolved and refluxed in dry toluene (50 mL) overnight under argon atmosphere. After cooling, the toluene was removed by distillation under reduced pressure. The residue was then dissolved in CH<sub>2</sub>Cl<sub>2</sub>. Deep red crystals were formed upon slow addition of pentane. The precipitate was filtered off and dried *in vacuo*. Yield, 0.17 g (88%). Mp 150–155 °C dec. <sup>1</sup>H NMR (400 MHz) δ 9.29 (d, *J* = 6.1 Hz, 2 H), 8.25 (s, 2 H), 7.06 (d, *J* = 6.1 Hz, 2 H), 4.34 (t, *J* = 6.4 Hz, 4 H, CH<sub>2</sub>), 2.00 (m, 4 H, CH<sub>2</sub>), 1.54 (m, 4 H, CH<sub>2</sub>), 1.06 (t, *J* = 7.4 Hz, 6H, CH<sub>3</sub>). <sup>13</sup>C NMR (100 MHz) δ 215.5 (CO), 202.4 (CO), 162.2, 154.1, 147.9, 122.7, 119.9, 105.4, 69.6, 30.7, 19.3, 13.8 IR. (KBr): 2004 (C=O), 1814 (C=O, broad). Anal. Calcd for C<sub>24</sub>H<sub>24</sub>WN<sub>2</sub>O<sub>6</sub>: C, 46.47; H, 3.90. Found: C, 46.23; H, 3.87.

**Acknowledgment.** We thank TFR (Swedish Research Council for Engineering Sciences) and the foundation "Bengt Lundqvists minne" for financial support. We also thank Dr Joachim Persson and Dr Per-Ola Norrby for valuable comments on this work.

OM9401014

(6) Pardo, M. P.; Cano, M. J. *Organomet. Chem.* **1984**, *260*, 81.

# New Stable Titanocene and Zirconocene Catalyst Precursors for Polysilane Synthesis via Dehydrocoupling of Hydrosilanes

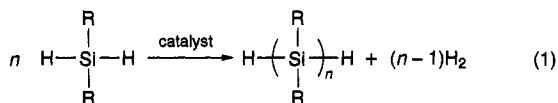
Stéphane Bourg, Robert J. P. Corriu,\* Marcus Enders, and Joël J. E. Moreau\*

CNRS URA 1097-UMR 44, Département de Chimie Organique Fine, Université Montpellier II, Sciences et Techniques du Languedoc, 34095 Montpellier Cedex 05, France

Received April 25, 1994<sup>®</sup>

**Summary:** The titanium and zirconium complexes ( $\eta^5$ -C<sub>5</sub>H<sub>5</sub>)<sub>2</sub>M(OAr)<sub>2</sub> (M = Ti, Zr; Ar = C<sub>6</sub>H<sub>5</sub>, *p*-MeOC<sub>6</sub>H<sub>4</sub>, *p*-MeC<sub>6</sub>H<sub>4</sub>, *p*-ClC<sub>6</sub>H<sub>4</sub>, *p*-CNC<sub>6</sub>H<sub>4</sub>) are shown to be convenient, stable precursors of dehydrocoupling catalysts. Their reactions with a primary silane, at 50 °C or below, generate active catalysts for RSiH<sub>3</sub> dehydrocoupling at 20 °C.

Polysilanes have a number of potential applications owing to their unusual electronic, optical, and chemical properties.<sup>1</sup> These polymers, in most cases, are prepared using the Wurtz coupling of dichlorosilanes by sodium.<sup>1</sup> Alternative polymerization reactions have been developed since they, in principle, could present significant advantages. Among other interesting methods for synthesizing polysilanes, redistribution, electrochemical, disilene polymerization, and cyclosilane ring-opening polymerization reactions have been explored.<sup>2</sup> Another method involves the transition-metal-catalyzed dehydrocoupling of silanes (eq 1).



The development of catalysts for the dehydrocoupling reaction began with the discovery of Harrod and co-workers that ( $\eta^5$ -C<sub>5</sub>H<sub>5</sub>)<sub>2</sub>TiMe<sub>2</sub> and ( $\eta^5$ -C<sub>5</sub>H<sub>5</sub>)<sub>2</sub>ZrMe<sub>2</sub> initiated the polycondensation of primary silanes RSiH<sub>3</sub>.<sup>3</sup> Since then, other transition-metal catalysts have been found, but the group 4 metallocene complexes provide the most active of the dehydrocoupling catalysts.<sup>4–13</sup> The reaction usually produces linear chains containing ca. 10–30 silicon atoms, together with cyclic oligomers.

Despite their sometimes low molecular weight, the MeSiH<sub>3</sub>-derived polysilanes can be converted in high yield to pure SiC.<sup>14</sup> We also have showed that preceramic polysilanes are easily obtained from the reaction of 1,4-disilapentane, in the presence of a titanium catalyst, and lead to high yields of SiC.<sup>15</sup>

We observed recently that ( $\eta^5$ -C<sub>5</sub>H<sub>5</sub>)<sub>2</sub>TiMe<sub>2</sub> and ( $\eta^5$ -C<sub>5</sub>H<sub>5</sub>)<sub>2</sub>TiCl<sub>2</sub>/*n*-BuLi dehydrocoupling catalysts, in the presence of oxygen, can be deactivated to a latent catalytic species.<sup>15</sup> The latter, upon heating, regenerate an active catalyst for the dehydrocoupling reaction. This observation led us to examine the reactions of metallocene complexes containing titanium–oxygen bonds. We wish to report here that ( $\eta^5$ -C<sub>5</sub>H<sub>5</sub>)<sub>2</sub>M(OAr)<sub>2</sub> species (M = Ti, Zr) are stable and tunable precursors of active catalytic species for the dehydrocoupling reaction of silanes.

## Results and Discussion

We first examined the readily prepared diphenoxytitanocene ( $\eta^5$ -C<sub>5</sub>H<sub>5</sub>)<sub>2</sub>Ti(OPh)<sub>2</sub><sup>16</sup> as a catalyst for the polymerization of phenylsilane. No reaction occurred at room temperature between PhSiH<sub>3</sub> and ( $\eta^5$ -C<sub>5</sub>H<sub>5</sub>)<sub>2</sub>Ti(OPh)<sub>2</sub> (0.1 mol %). When it was heated to 50 °C for 15 min, the reaction mixture turned dark blue and hydrogen evolution began. The generated catalytic species was then active at room temperature, and a viscous polymer was formed after 24 h (eq 2). The polymerization rates observed and the products obtained were similar to those using ( $\eta^5$ -C<sub>5</sub>H<sub>5</sub>)<sub>2</sub>TiMe<sub>2</sub><sup>3</sup> and ( $\eta^5$ -C<sub>5</sub>H<sub>5</sub>)<sub>2</sub>TiCl<sub>2</sub>/*n*-BuLi<sup>7</sup> as catalysts. GPC analysis

(7) Corey, J. Y.; Chang, L. S.; Corey, E. R. *Organometallics* 1987, 6, 1595. Chang, L. S.; Corey, J. Y. *Organometallics* 1989, 8, 1885. Corey, J. Y.; Zhu, X. M.; Bedard, T. C.; Lange, L. D. *Organometallics* 1991, 10, 924.

(8) Brown-Wensley, K. A. *Organometallics* 1987, 6, 1590.

(9) Campbell, W. H.; Hilty, J. K.; Yurga, L. *Organometallics* 1989, 8, 2615.

(10) (a) Woo, H. G.; Tilley, T. D. *J. Am. Chem. Soc.* 1989, 111, 1757. (b) Woo, H. G.; Tilley, T. D. *J. Am. Chem. Soc.* 1989, 111, 8043. (c) Woo, H. G.; Walker, J. F.; Tilley, T. D. *J. Am. Chem. Soc.* 1992, 114, 7047 and references therein.

(11) Sakakura, T.; Lantenschlager, M. J.; Nakajima, M.; Tanaka, M. *Chem. Lett.* 1991, 913.

(12) Forsyth, C. M.; Nolan, S. P.; Marks, T. J. *Organometallics* 1991, 10, 2543.

(13) Hengge, E.; Weinberger, M. *J. Organomet. Chem.* 1992, 441, 397.

(14) (a) Zhang, Z. F.; Babonneau, F.; Laine, R. M.; Mu, Y.; Harrod, J. F.; Rahn, J. A. *J. Am. Ceram. Soc.* 1991, 74, 670. (b) Mu, Y.; Laine, R. M.; Harrod, J. F. *Appl. Organomet. Chem.* 1994, 8, 95. (c) Harrod, J. F. In *Inorganic and Organometallic Polymers with Special Properties*; Laine, R. M., Ed.; NATO ASI Series E, Vol. 206; Kluwer Academic: Amsterdam, 1991; p 87.

(15) (a) Corriu, R. J. P.; Enders, M.; Huille, S.; Moreau, J. J. E. *Chem. Mater.* 1994, 6, 15. (b) Corriu, R. J. P.; Enders, M.; Huille, S.; Moreau, J. J. E. Fr. Patent, Dem. 9301648, 1993.

(16) Andra, K. *J. Organomet. Chem.* 1968, 11, 567.

<sup>®</sup> Abstract published in *Advance ACS Abstracts*, December 1, 1994.

(1) For reviews see: (a) West, R. *J. Organomet. Chem.* 1986, 300, 327. (b) Miller, R. D.; Michl, J. *Chem. Rev.* 1989, 89, 1359. (c) Ziegler, C. J. M. *Mol. Cryst. Liq. Cryst.* 1990, 190, 265.

(2) (a) Baney, R. H.; Gaul, J. M.; Hilty, T. K. *Organometallics* 1983, 2, 859. (b) Biran, C.; Bordeau, M.; Pons, P.; Leyer, M. P.; Dunoguès, J. *J. Organomet. Chem.* 1990, 382, C17. (c) Sakamoto, K.; Ohata, K.; Mirata, M.; Nakajima, N.; Sakurai, H. *J. Am. Chem. Soc.* 1989, 111, 7641. (d) Sono, T.; Kashimura, S.; Ishifune, M.; Nishida, R. *J. Chem. Soc., Chem. Commun.* 1990, 1160. (e) Matyjaszewski, K.; Chen, Y. L.; Kim, H. K. *Inorganic and Organometallic Polymers*; Zeldin, M., Wynne, K. J., Alcock, H. R., Eds.; ACS Symposium Series 360; American Chemical Society: Washington, DC, 1988; p 78.

(3) Aitken, C.; Harrod, J. F.; Samuel, E. *J. Organomet. Chem.* 1985, 279, C11. Aitken, C.; Barry, J. P.; Gauvin, F.; Harrod, J. F.; Malek, A.; Rousseau, D. *Organometallics* 1989, 8, 1732 and references therein.

(4) For recent reviews see: (a) Harrod, J. F.; Mu, Y.; Samuel, E. *Polyhedron* 1991, 10, 1239 and references therein. (b) Tilley, T. D. *Acc. Chem. Res.* 1993, 26, 22 and references therein.

(5) (a) Yamamoto, K.; Okinoshima, H.; Kumada, M. *J. Organomet. Chem.* 1970, 23, C7. (b) Ojima, I.; Inaba, S.; Kogure, T.; Nagai, Y. *J. Organomet. Chem.* 1973, 55, C7.

(6) (a) Aitken, C.; Harrod, J. F.; Samuel, E. *Can. J. Chem.* 1986, 64, 1677. (b) Aitken, C.; Harrod, J. F.; Gill, U. S. *Can. J. Chem.* 1987, 65, 1804. (c) Harrod, J. F.; Yun, S. S. *Organometallics* 1987, 6, 1381.





Table 1. Dehydrocoupling of PhSiH<sub>3</sub> (Eq 2)

entry no.	catalyst <sup>a</sup>	induction period	reaction conditions <sup>b</sup>	% of polymer as nonvolatile cyclics <sup>c</sup>	linear polysilane $M_w$ ( $M_w/M_n$ ) <sup>d</sup>
1	( $\eta^5$ -C <sub>5</sub> H <sub>5</sub> ) <sub>2</sub> Ti(OPh) <sub>2</sub>	15 min/50 °C	neat/24 h (20 °C)	25	2400 (1.25)
2	( $\eta^5$ -C <sub>5</sub> H <sub>5</sub> ) <sub>2</sub> Ti(OC <sub>6</sub> H <sub>4</sub> OMe- <i>p</i> ) <sub>2</sub>	2 h/20 °C	neat/48 h (20 °C)	25	3100 (1.55)
3	( $\eta^5$ -C <sub>5</sub> H <sub>5</sub> ) <sub>2</sub> Ti(OC <sub>6</sub> H <sub>4</sub> Cl- <i>p</i> ) <sub>2</sub>	10 min/25 °C	neat/72 h (25 °C)	30	2200 (1.35)
4	( $\eta^5$ -C <sub>5</sub> H <sub>5</sub> ) <sub>2</sub> Ti(OC <sub>6</sub> H <sub>4</sub> CN- <i>p</i> ) <sub>2</sub>	30 min/25 °C	neat/72 h (25 °C)	30	2200 (1.38)
5	( $\eta^5$ -C <sub>5</sub> H <sub>5</sub> ) <sub>2</sub> Ti(OC <sub>6</sub> H <sub>4</sub> Me- <i>p</i> ) <sub>2</sub>	20 min/25 °C	neat/72 h (25 °C)	30	2300 (1.35)
6	( $\eta^5$ -C <sub>5</sub> H <sub>5</sub> ) <sub>2</sub> TiMe <sub>2</sub>	15 min/20 °C	neat/15 h (20 °C)	25	2700 (1.35)
7	( $\eta^5$ -C <sub>5</sub> H <sub>5</sub> ) <sub>2</sub> Zr(OPh) <sub>2</sub>	15 min/50 °C	neat/72 h (20 °C)	10	3200 (1.45)
8 <sup>e</sup>	( $\eta^5$ -C <sub>5</sub> H <sub>5</sub> ) <sub>2</sub> Zr(OPh) <sub>2</sub>	15 min/50 °C	neat/72 h (20 °C)	10	3750 (1.5)

<sup>a</sup> Catalyst concentration: 0.1 mol% throughout. <sup>b</sup> Conversion >95%. <sup>c</sup> Cf. Experimental Section. <sup>d</sup> Determined by GPC, the molecular weight values are relative to polystyrene standards; UV detector. <sup>e</sup> The polymerization was carried out by slow addition of the monomer over a 48 h period.

argon. Solvents were dried using standard techniques. Infrared spectra were recorded on a Perkin-Elmer 1600 FT-IR spectrometer. NMR spectra were obtained with a Bruker AC 250 (<sup>1</sup>H, <sup>13</sup>C) or a Bruker WP 200 SY (<sup>29</sup>Si) (solvent CDCl<sub>3</sub>, TMS as an internal standard).

Gel permeation chromatography of polysilanes was carried out on THF solutions with a Waters Millipore 510. A UV detector, Waters Model 441, and a differential refractometer, Waters Model 410, were used. All molecular weights are reported with respect to polystyrene standards.

The following compounds were prepared according to literature procedures: PhSiH<sub>3</sub>,<sup>23</sup> Ph<sub>2</sub>SiH<sub>2</sub>,<sup>23</sup> ( $\eta^5$ -C<sub>5</sub>H<sub>5</sub>)<sub>2</sub>TiMe<sub>2</sub>,<sup>18</sup> ( $\eta^5$ -C<sub>5</sub>H<sub>5</sub>)<sub>2</sub>Ti(OPh)<sub>2</sub>,<sup>16</sup> ( $\eta^5$ -C<sub>5</sub>H<sub>5</sub>)<sub>2</sub>Ti(OC<sub>6</sub>H<sub>4</sub>Cl-*p*)<sub>2</sub>,<sup>16</sup> ( $\eta^5$ -C<sub>5</sub>H<sub>5</sub>)<sub>2</sub>Ti(OC<sub>6</sub>H<sub>4</sub>Me-*p*)<sub>2</sub>,<sup>16</sup> ( $\eta^5$ -C<sub>5</sub>H<sub>5</sub>)<sub>2</sub>Zr(OPh)<sub>2</sub>.<sup>20</sup>

( $\eta^5$ -C<sub>5</sub>H<sub>5</sub>)<sub>2</sub>Ti(OC<sub>6</sub>H<sub>4</sub>OMe-*p*)<sub>2</sub>.<sup>19</sup> This known complex<sup>19</sup> was obtained according to a slight modification of the reported procedure. To a suspension of NaNH<sub>2</sub> (7.5 mL, 1.6 M in toluene) diluted with toluene (50 mL) was added dichlorotitanocene (1.25 g, 10 mmol). *p*-Methoxyphenol (1.24 g, 10 mmol) in 25 mL of toluene then was added dropwise; the mixture was refluxed for 10 min and then cooled to room temperature. The reaction mixture was filtered and the solvent removed in vacuo. The residue was crystallized from a toluene/pentane mixture to give 1.75 g (70%) of product, mp 87–89 °C. <sup>1</sup>H NMR (CDCl<sub>3</sub>;  $\delta$ , ppm): 6.69 (8H, q); 6.23 (10H, s); 3.77 (6H, s). <sup>13</sup>C NMR (CDCl<sub>3</sub>;  $\delta$ , ppm): 165.2; 152.5; 118.1; 115.8; 114.4; 55.9. Anal. Calcd for C<sub>24</sub>H<sub>24</sub>O<sub>4</sub>Ti: C, 67.92; H, 5.70. Found: C, 67.55; H, 5.99.

( $\eta^5$ -C<sub>5</sub>H<sub>5</sub>)<sub>2</sub>Ti(OC<sub>6</sub>H<sub>4</sub>CN-*p*)<sub>2</sub>. This was prepared by using the above procedure. The residue was crystallized from a toluene/hexane mixture to give 1.15 g (60%) of product, mp 175–176 °C. <sup>1</sup>H NMR (CDCl<sub>3</sub>;  $\delta$ , ppm): 7.53 (4H, d); 6.62 (4H, d); 6.32 (10H, s). <sup>13</sup>C NMR (CDCl<sub>3</sub>;  $\delta$ , ppm): 173.7; 134.4; 120.5; 119.1; 117.3; 101.8. Anal. Calcd for C<sub>24</sub>H<sub>18</sub>O<sub>2</sub>N<sub>2</sub>Ti: C, 69.56; H, 4.35; N, 6.76. Found: C, 69.34; H, 4.66; N, 6.38.

**Reactions of Dihydrosilanes. Diphenylsilanes.** ( $\eta^5$ -C<sub>5</sub>H<sub>5</sub>)<sub>2</sub>Ti(OPh)<sub>2</sub> (7.3 mg, 0.02 mmol) was dissolved in Ph<sub>2</sub>SiH<sub>2</sub> (1.84 g, 10 mmol). The mixture, upon heating at 80 °C, turned dark blue and hydrogen was evolved. After 5 h, the mixture was cooled to room temperature. Crystallization from pentane gave Ph<sub>2</sub>Si(H)Si(H)Ph<sub>2</sub> (0.35 g, 10%), mp 80 °C (lit.<sup>24</sup> mp 78–80 °C).

**Di-*n*-butylsilane.** ( $\eta^5$ -C<sub>5</sub>H<sub>5</sub>)<sub>2</sub>Ti(OPh)<sub>2</sub> (50 mg, 0.14 mmol) and di-*n*-butylsilane (375 mg, 2.6 mmol) were mixed under argon and heated to 110 °C. The solution color change from yellow to dark brown was accompanied by some gas evolution. The mixture was then heated to 130 °C for 30 min and subsequently was allowed to cool to room temperature. The crude reaction mixture was analyzed by GC/MS (temperature range 100–200 °C, 10 °C/min) and revealed *n*-Bu<sub>2</sub>SiH<sub>2</sub> (retention time, 154 s;  $M_r$ , 144; yield, 91%), *n*-Bu<sub>2</sub>Si(OPh)H (retention time, 728 s;  $M_r$ , 236; yield, 2.2%), *n*-Bu<sub>4</sub>Si<sub>2</sub>H<sub>4</sub> (retention time, 834 s;  $M_r$ , 286; yield, 4.4%), and *n*-Bu<sub>2</sub>Si(OPh)<sub>2</sub> (retention time, 1424 s;  $M_r$ , 328; yield, 2.8%).

(23) Benkeser, R. A.; Landesman, H.; Foster, D. *J. Am. Chem. Soc.* **1952**, *74*, 648.

(24) Winkler, H. J. S.; Gilman, H. *J. Org. Chem.* **1961**, *26*, 929.

**Polycondensation of Phenylsilane.** The polymerizations of PhSiH<sub>3</sub> were performed under argon using 0.1 mol % of the titanium or zirconium catalyst without any solvent. The results are given in Table 1. The catalysis by ( $\eta^5$ -C<sub>5</sub>H<sub>5</sub>)<sub>2</sub>Ti(OPh)<sub>2</sub> is described as an example.

**Catalysis by ( $\eta^5$ -C<sub>5</sub>H<sub>5</sub>)<sub>2</sub>Ti(OPh)<sub>2</sub>.** PhSiH<sub>3</sub> (2.16 g, 20 mmol) and ( $\eta^5$ -C<sub>5</sub>H<sub>5</sub>)<sub>2</sub>Ti(OPh)<sub>2</sub> (7.3 mg, 0.2 mmol) were mixed under argon. After dissolution, the solution was slowly heated to 50 °C. After 15 min at 50 °C, the mixture turned dark blue. It was cooled to room temperature and stirred for 24 h. Volatile materials were then removed under vacuum, and the residue was solubilized in toluene and filtered through a Florisil column. The polysilane obtained after removal of the solvent (yield >95%) exhibited characteristics similar to those previously reported.<sup>3</sup> <sup>1</sup>H NMR (CDCl<sub>3</sub>;  $\delta$ , ppm): 4.1–5.2 (m), 6.5–7.5 (m). <sup>29</sup>Si NMR (CDCl<sub>3</sub>;  $\delta$ , ppm): –50 to –65 (m). IR (neat):  $\nu$ (Si–H) 2110 cm<sup>-1</sup>. GPC (on crude polymer, UV detector): 25% cyclics; 75% linear polymer with  $M_w = 2400$ ,  $M_w/M_n = 1.25$ . The proportion of cyclics was determined by GPC and by <sup>1</sup>H NMR by comparing the ratio of resonances above 5 ppm and those below 4.8 ppm.<sup>21</sup> The activation of the catalyst can also be performed at 30 °C. A 4 h induction period was then necessary before the polymerization occurred, leading to the same polysilane.

**Catalysis by ( $\eta^5$ -C<sub>5</sub>H<sub>5</sub>)<sub>2</sub>Ti(OC<sub>6</sub>H<sub>4</sub>OMe-*p*)<sub>2</sub>.** The reaction of PhSiH<sub>3</sub> in the presence of ( $\eta^5$ -C<sub>5</sub>H<sub>5</sub>)<sub>2</sub>Ti(OC<sub>6</sub>H<sub>4</sub>OMe-*p*)<sub>2</sub> was performed as above. When this titanium complex was used, there was a 1–2 h induction period at 20 °C before polycondensation with hydrogen evolution commenced.

**Catalysis by ( $\eta^5$ -C<sub>5</sub>H<sub>5</sub>)<sub>2</sub>Ti(OC<sub>6</sub>H<sub>4</sub>Cl-*p*)<sub>2</sub>, ( $\eta^5$ -C<sub>5</sub>H<sub>5</sub>)<sub>2</sub>Ti(OC<sub>6</sub>H<sub>4</sub>CN-*p*)<sub>2</sub>, and ( $\eta^5$ -C<sub>5</sub>H<sub>5</sub>)<sub>2</sub>Ti(O-C<sub>6</sub>H<sub>4</sub>Me-*p*)<sub>2</sub>.** The reaction of PhSiH<sub>3</sub> in the presence of these titanium catalysts was performed as above. The induction periods at 25 °C were respectively 10, 30, and 20 min, and the polycondensation proceeded as above.

**Catalysis by ( $\eta^5$ -C<sub>5</sub>H<sub>5</sub>)<sub>2</sub>Zr(OPh)<sub>2</sub>.** The reaction was performed as described in the case of the catalysis by ( $\eta^5$ -C<sub>5</sub>H<sub>5</sub>)<sub>2</sub>Ti(OPh)<sub>2</sub>. An induction period of 15 min at 50 °C, after which time the solution turned yellow, was necessary to obtain polycondensation at room temperature.

**Polycondensation of 1,4-Disilapentane.** The reaction was conducted as above using 1,4-disilapentane (10.4 g, 100 mmol) and ( $\eta^5$ -C<sub>5</sub>H<sub>5</sub>)<sub>2</sub>Ti(OPh)<sub>2</sub> (180 mg, 0.5 mmol) as catalyst. After 48 h the reaction was stopped by bubbling air through the liquid until the intense color disappeared. The mixture was diluted with toluene and filtered through a Florisil column. The polysilane was collected after removal of the solvent. GPC (detector: refractive index):  $M_w = 1041$ ,  $M_n/M_w = 1.16$ . <sup>1</sup>H NMR (80 MHz;  $\delta$ , CDCl<sub>3</sub>): 0.0 (t, <sup>3</sup>J(H,H) = 3.5 Hz, 3H); 0.9 (m, 4H), 3.8 (m, 3H). <sup>13</sup>C NMR (62.9 MHz;  $\delta$ , CDCl<sub>3</sub>): 8.3 (CH<sub>3</sub>); 1.4–5.5 (CH<sub>2</sub>); 8.1–9.9 (CH<sub>2</sub>). <sup>29</sup>Si NMR (49.7 MHz;  $\delta$ , CDCl<sub>3</sub>): –65 to –49 (SiH, SiH<sub>2</sub>); –30.2 (t, <sup>2</sup>J(Si–H) = 189 Hz). IR (hexane):  $\nu$  2134 cm<sup>-1</sup> (SiH). Anal. Found: C, 35.11; H, 10.15.

OM940301F

# Direct Conversion of Hydrosilanes to Fluorosilanes with $\text{CuF}_2 \cdot 2\text{H}_2\text{O}/\text{CCl}_4$

Jun-ichi Yoshida,<sup>\*,1</sup> Hidekazu Tsujishima, Kazunori Nakano,<sup>2</sup>  
Toshiyuki Teramoto, Keiji Nishiwaki, and Sachihiko Isoe<sup>\*</sup>

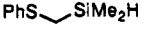
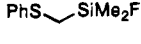
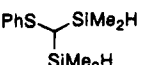
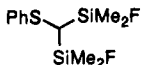
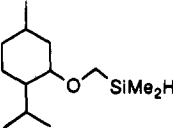
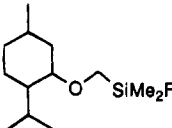
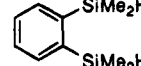
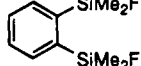
Department of Material Science, Faculty of Science, Osaka City University,  
Sugimoto 3-3-138, Sumiyoshi, Osaka 558, Japan

Received July 14, 1994<sup>®</sup>

**Summary:** The reaction of hydrosilanes with  $\text{Cu}^{\text{II}}\text{F}_2 \cdot 2\text{H}_2\text{O}$  in refluxing  $\text{CCl}_4$  gave the corresponding fluorosilanes in good yields. In THF hydrosilanes were recovered unchanged. X-ray powder analysis of the solid products indicated the formation of  $\text{Cu}^{\text{I}}\text{Cl}$ . These results suggest that both  $\text{CCl}_4$  and  $\text{Cu}^{\text{II}}$  act as oxidants for hydrosilanes.

$\alpha$ -Heteroatom-substituted organosilicon compounds have attracted considerable research interest because of their unique properties in electron-transfer reactions.<sup>3</sup> In an attempt to synthesize sila-functional  $\alpha$ -heteroatom-substituted organosilicon compounds, we needed a convenient method for the conversion of hydrosilanes to the corresponding fluorosilanes. Although there are a great number of methods for the synthesis of chlorosilanes from the corresponding hydrosilanes,<sup>4</sup> only a few methods for the direct conversion of hydrosilanes to fluorosilanes have been found so far. Tang et al. reported monofluorination of  $\text{R}_2\text{SiH}_2$  with  $\text{SbF}_3$ ,<sup>5</sup> but  $\text{SbF}_3$  is highly toxic.<sup>6</sup> Olah and co-workers reported ionic fluorination of  $\text{R}_3\text{SiH}$  using highly reactive  $\text{NOBF}_4$  or  $\text{NO}_2\text{BF}_4$ .<sup>7</sup> Bulkowski et al. employed  $\text{Ph}_3\text{CBF}_4$  to convert  $\text{R}_2\text{SiH}_2$  to  $\text{R}_2\text{SiHF}$ .<sup>8</sup> Finch et al. used  $\text{PF}_5$  to fluorinate  $\text{RSiH}_3$  to give  $\text{RSiH}_2\text{F}$  and  $\text{RSiHF}_2$ .<sup>9</sup> Anderson also reported the conversion of  $\text{Et}_3\text{SiH}$  to  $\text{Et}_3\text{SiF}$  by the action of  $\text{AgF}$ .<sup>10</sup> In this paper we wish to report a new convenient method for the conversion of hydrosilanes to fluorosilanes by the action of  $\text{Cu}^{\text{II}}\text{F}_2 \cdot 2\text{H}_2\text{O}$  in

**Table 1.** Conversion of Hydrosilanes to Fluorosilanes with  $\text{CuF}_2 \cdot 2\text{H}_2\text{O}/\text{CCl}_4$

hydrosilane (mmol)	$\text{CuF}_2 \cdot 2\text{H}_2\text{O}$ (mmol)	product	yield (%)
$\text{Ph}_3\text{SiH}$	(5.03)	$\text{Ph}_3\text{SiF}$	80
	(5.01)		45 <sup>a</sup>
	(5.03)		0 <sup>b</sup>
$\text{Ph}_2\text{SiH}_2$	(5.17)	$\text{Ph}_2\text{SiF}_2$	85
$\text{C}_{10}\text{H}_{21}\text{SiMe}_2\text{H}$	(1.93)	$\text{C}_{10}\text{H}_{21}\text{SiMe}_2\text{F}$	78
	(1.20)		70
	(0.98)		63
	(1.69)		75
	(2.10)		77

<sup>a</sup> The reaction was carried out in refluxing  $\text{ClCH}_2\text{CH}_2\text{Cl}$ . <sup>b</sup> The reaction was carried out in refluxing THF.

$\text{CCl}_4$  under very mild conditions (eq 1).



## Results and Discussion

The fluorination reactions of hydrosilanes with copper(II) fluoride are very simple to perform. In a typical experiment, to a solution of a hydrosilane (5 mmol) in carbon tetrachloride (15 mL) was added copper(II) fluoride dihydrate (15 mmol), and the mixture was heated to reflux overnight. The reaction mixture was filtered through Celite, and the filtrate was distilled to obtain the corresponding fluorosilane. The results obtained for several hydrosilanes are shown in Table 1. The present reaction is effective for arylsilanes, alkylsilanes, and  $\alpha$ -heteroatom-substituted silanes. It is also noteworthy that organosilanes containing two Si-H bonds can be converted into difluorinated compounds by using the present reaction.

It should be pointed out that hydrosilanes are known to be readily converted to the corresponding chlorosilanes by the treatment with metal salts in carbon

<sup>®</sup> Abstract published in *Advance ACS Abstracts*, December 1, 1994.

(1) Present address: Department of Synthetic Chemistry & Biological Chemistry, Faculty of Engineering, Kyoto University, Kyoto 606-01, Japan.

(2) Undergraduate Research Participant, Osaka Institute of Technology.

(3) For example: (a) Yoshida, J.; Maekawa, T.; Murata, T.; Matsunaga, S.; Isoe, S. *J. Am. Chem. Soc.* **1990**, *112*, 1962. (b) Yoshida, J.; Murata, T.; Matsunaga, S.; Maekawa, T.; Shiozawa, S.; Isoe, S. *Rev. Heteroat. Chem.* **1991**, *5*, 193 and references cited therein.

(4) For example: (a) Banovetz, J. P.; Hsiao, Y.-L.; Waymouth, R. M. *J. Am. Chem. Soc.* **1993**, *115*, 2540. (b) Kunai, A.; Kawakami, T.; Toyoda, E.; Ishikawa, M. *Organometallics* **1992**, *11*, 2708. (c) Nagai, Y.; Matsumoto, H.; Yagihara, T.; Morishita, K. *Kogyo Kagaku Zasshi* **1968**, *71*, 1112. (d) Nagai, Y.; Yamazaki, K.; Shiojima, I.; Kobori, N.; Hayashi, M. *J. Organomet. Chem.* **1967**, *9*, 21. (e) Curtice, J.; Gilman, H.; Hammond, G. S. *J. Am. Chem. Soc.* **1957**, *79*, 4754. (f) Baines, I. E.; Eaborn, C. *J. Chem. Soc.* **1956**, 1436. (g) Russel, G. A. *J. Org. Chem.* **1956**, *21*, 1190. (h) Jenkins, J. W.; Post, H. W. *J. Org. Chem.* **1950**, *15*, 556. (i) Whitmore, F. C.; Pietrusza, E. W.; Sommer, L. H. *J. Am. Chem. Soc.* **1947**, *69*, 2108.

(5) Hong, C. M.; Witt, S. D.; Tang, Y. N. *J. Fluorine Chem.* **1983**, *23*, 359.

(6) Damrauer, R.; Simon, R. A. *Organometallics* **1988**, *7*, 1161.

(7) Prakash, G. K. S.; Wang, Q.; Li, X.; Olah, G. A. *New J. Chem.* **1990**, *14*, 791.

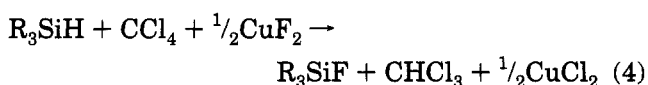
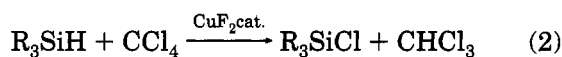
(8) Bulkowski, J. E.; Stacy, R.; Van Dyke, C. H. *J. Organomet. Chem.* **1975**, *87*, 137.

(9) Finch, M. A.; Marcus, L. H.; Smirnov, C.; Van Dyke, C. H.; Viswanathan, N. *Synth. Inorg. Met.-Org. Chem.* **1971**, 103.

(10) Anderson, H. H. *J. Am. Chem. Soc.* **1958**, *80*, 5083.

tetrachloride which acts as both the oxidant and the chloride source. As a matter of fact, hydrosilanes were converted into the corresponding chlorosilanes in refluxing  $\text{CCl}_4$  in the presence of a catalytic amount of  $\text{CuF}_2 \cdot 2\text{H}_2\text{O}$ . The fact that the treatment of hydrosilanes with a stoichiometric amount of copper(II) fluoride in THF gave rise to complete recovery of the starting material also indicates the important role played by carbon tetrachloride. The reaction in 1,2-dichloroethane, which is less effective as a chlorine donor in radical reactions, gave fluorosilanes in lower yields. It is also noteworthy that organotrifluorosilanes are easily converted into organotrifluorosilanes by treatment with copper(II) fluoride.<sup>11</sup>

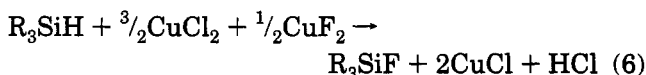
On the basis of these facts, we initially proposed the following mechanism. The first step of the reaction involves copper(II) fluoride catalyzed oxidation of hydrosilanes to chlorosilanes by the action of carbon tetrachloride (eq 2).<sup>4a,c,d</sup> Presumably the reaction proceeds by a radical-chain mechanism.<sup>4d</sup> In the second step, chlorosilanes are converted into fluorosilanes by the halogen-exchange reaction with copper(II) fluoride (eq 3).



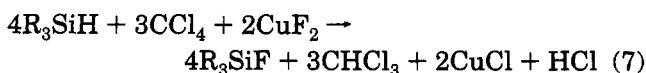
The mechanism of the present reaction, however, was found to be more complicated, because X-ray powder analysis of the solid product indicated the formation of  $\text{CuCl}$  and  $\text{CuOHF}$ . Signals of  $\text{CuCl}_2$  were not detected at all. These results indicate that copper(II) was reduced to copper(I) during the course of the reaction. Kunai and Ishikawa et al. reported that the reaction of hydrosilanes with  $\text{Cu}^{\text{II}}\text{Cl}_2$  in the presence of  $\text{CuI}$  gave the corresponding chlorosilanes and  $\text{Cu}^{\text{I}}\text{Cl}$ .<sup>4b</sup> Therefore, in the case of the present reaction, the initially formed  $\text{Cu}^{\text{II}}\text{Cl}_2$  also seemed to react with hydrosilanes to give  $\text{Cu}^{\text{I}}\text{Cl}$  and chlorosilanes (eq 5).



The combination of eqs 3 and 5 gives eq 6.



By the combination of eqs 4 and 6, we propose the following stoichiometry of the present reaction (eq 7).



The formation of  $\text{CuOHF}$  may be explained in terms of the hydrolysis of  $\text{CuF}_2$  under the reaction conditions.

(11) (a) Tamao, K.; Yoshida, J.; Yamamoto, H.; Kakui, T.; Matsu-moto, H.; Takahashi, M.; Kurita, A.; Murata, M.; Kumada, M. *Organometallics* **1982**, *1*, 355. (b) Shin-Etsu Chemical Industry Co., Ltd. Jpn. Kokai Tokkyo Koho Jp 81,167,693; *Chem. Abstr.* **1980**, *96*, 199870u.

Although the detailed mechanism of the present reaction is not fully understood, as a consequence of mild reaction conditions, the ready availability of  $\text{CuF}_2 \cdot 2\text{H}_2\text{O}$ , and operational simplicity, this method should find extensive use in the chemistry of fluorosilanes.

## Experimental Section

**General Remarks.** Glass-support precoated (Merk silica gel 60 F<sub>254</sub>, 0.25 mm) plates were employed for analytical TLC. Vapor-phase chromatography (VPC) was performed on a Shimadzu gas chromatograph equipped with a 2 m × 3 mm column packed with Silicone OV-1 (2%) on Chromosorb WAW DMCS. Proton NMR spectra were determined on a Hitachi R-90H spectrometer (90 MHz) or a JEOL JNM-GX-400 spectrometer (400 MHz). Carbon NMR spectra were determined on a JEOL JNM-GX-400 spectrometer. Infrared (IR) spectra were determined on a JASCO A-102 diffraction grating spectrophotometer. Mass spectra were obtained on a JEOL JMS-AX500 spectrometer; the ionization potential was 70 eV.

**Materials.**  $\text{CuF}_2 \cdot 2\text{H}_2\text{O}$  was purchased from Nakarai Tesque, Inc., and used as obtained. ((Phenylthio)methyl)dimethylsilane was prepared by deprotonation of thioanisole with BuLi in ether followed by the reaction with chlorodimethylsilane.<sup>12</sup> (Phenylthio)bis(dimethylsilyl)methane was prepared by deprotonation of ((phenylthio)methyl)dimethylsilane with LDA followed by the addition of dimethylchlorosilane.<sup>12</sup> ((Menthyl-oxo)methyl)diphenylsilane was prepared by the transmetalation reaction of ((menthyl-oxo)methyl)tributylstannane with BuLi followed by the treatment with chlorodiphenylsilane.<sup>12</sup> *o*-Bis(dimethylsilyl)benzene was prepared according to the literature method.<sup>13</sup>

**Preparation of Triphenylfluorosilane. Typical Procedure for Fluorination Using  $\text{CuF}_2 \cdot 2\text{H}_2\text{O}$ .** To a stirred mixture of  $\text{CuF}_2 \cdot 2\text{H}_2\text{O}$  (2.052 g, 14.9 mmol) and  $\text{CCl}_4$  (15 mL) was added triphenylsilane (1.309 g, 5.03 mmol) at room temperature. The mixture was refluxed overnight. Solid materials were separated by filtration, and the solvent was removed by evaporation. Recrystallization of the crude product from hexane gave triphenylfluorosilane (1.111 g, 3.99 mmol, 79%): mp 61–63 °C (lit.<sup>7</sup> mp 61–62 °C); VPC  $t_R$  14.4 min (OV-1 2% 2 m 100–240 °C, 10 °C/min); <sup>1</sup>H NMR (90 MHz,  $\text{CDCl}_3$ )  $\delta$  7.26–7.87 (m, 15H); IR 3075 (m), 3020 (w), 2250 (w), 1595 (m), 1430 (s), 1190 (w), 1125 (s), 1000 (w), 890 (s), 840 (m), 695 (s)  $\text{cm}^{-1}$ ; low resolution MS *m/e* 278 (100), 201 (99), 181 (12), 154 (83), 124 (4).

**Diphenyldifluorosilane**<sup>6</sup> (bulb-to-bulb distillation 150–160 °C/20 mmHg): VPC  $t_R$  7.2 min (OV-1 2% 2 m 100–240 °C, 10 °C/min); TLC  $R_f$  0.29 (hexane/ethyl acetate, 99:1); <sup>1</sup>H NMR (90 MHz,  $\text{CDCl}_3$ )  $\delta$  7.14–7.92 (m, 10 H); low-resolution MS *m/e* (%) 220 (100), 199 (19), 154 (66), 143 (23), 77 (28), 51 (4).

**Dodecyldimethylfluorosilane** (bulb-to-bulb distillation 102 °C/19 mmHg): VPC  $t_R$  7.4 min (OV-1 2% 2 m, 100–230 °C/min); TLC  $R_f$  0.85 (hexane); <sup>1</sup>H NMR (90 MHz,  $\text{CDCl}_3$ )  $\delta$  0.22 (d,  $J$  = 7.5 Hz, 6 H), 0.50–1.68 (m, 21 H); IR 2930 (s), 2860 (m), 1460 (w), 1260 (m), 1220 (w), 850 (m), 800 (w), 780–670 (br, m)  $\text{cm}^{-1}$ ; low-resolution MS *m/e* (%) 218 (0.5), 203 (44), 190 (0.1), 175 (0.2), 161 (0.1), 140 (8), 119 (5), 105 (57), 85 (6), 77 (100), 71 (5), 57 (7); high-resolution MS calcd for  $\text{C}_{12}\text{H}_{27}\text{SiF}$  218.1866, found 218.1861. Anal. Calcd for  $\text{C}_{12}\text{H}_{27}\text{SiF}$ : C, 65.99; H, 12.46. Found: C, 66.13; H, 12.38.

**((Menthyl-oxo)methyl)dimethylfluorosilane** (bulb-to-bulb distillation 105–125 °C/30 mmHg): VPC  $t_R$  6.6 min (OV-1 2% 2 m, 100–240 °C, 10 °C/min); <sup>1</sup>H NMR (400 MHz,  $\text{CDCl}_3$ )  $\delta$  0.24 (d,  $J$  = 3.67 Hz, 3H), 0.25 (d,  $J$  = 3.05 Hz, 3H), 0.69–1.00 (m, 12H), 1.13–1.24 (m, 1H), 1.24–1.38 (m, 1H), 1.51–

(12) Yoshida, J.; Tsujishima, H.; Nakano, K.; Isoe, S. *Inorg. Chim. Acta* **1994**, *220*, 129.

(13) Fink, W. *Helv. Chim. Acta* **1974**, *57*, 1010.

1.67 (m, 2H), 2.05–2.21 (m, 2H), 2.82–2.94 (m, 1H), 2.90 (dd,  $J = 5.49$  and  $13.43$  Hz, 1H), 3.45 (dd,  $J = 3.67$  and  $13.43$  Hz, 1H); IR (CDCl<sub>3</sub>) 2960 (s), 2920 (s), 2870 (s), 1451 (w), 1370 (w), 1349 (w), 1260 (s), 1108 (m), 1088 (m), 1073 (m), 852 (s), 810 (m), 708 (br) cm<sup>-1</sup>; low-resolution MS (CI)  $m/e$  (%) 231 (12), 245 (34), 227 (22), 197 (8), 168 (3), 161 (9), 149 (6), 140 (100), 139 (100), 137 (78), 123 (23), 109 (21); high-resolution MS ( $M + H$ ) calcd for C<sub>13</sub>H<sub>28</sub>OSiF 247.1893, found 247.1882. Anal. Calcd for C<sub>13</sub>H<sub>28</sub>OSiF: C, 63.36; H, 11.04. Found: C, 63.07; H, 10.87.

**((Phenylthio)methyl)dimethylfluorosilane** (bulb-to-bulb distillation 120–140 °C/20 mmHg): TLC  $R_f$  0.40 (hexane/ethyl acetate, 39:1); VPC  $t_R$  4.0 min (OV-1 2% 2 m, 100–240 °C, 10 °C/min); <sup>1</sup>H NMR (90 MHz, CDCl<sub>3</sub>)  $\delta$  0.35 (d,  $J = 7.5$  Hz, 6H), 2.35 (d,  $J = 4.5$  Hz, 2H), 7.00–7.50 (m, 5H); IR (neat) 3060 (w), 2960 (m), 2890 (w), 1585 (s), 1485 (s), 1440 (s), 1390 (m), 1255 (s), 1135 (m), 1090 (m), 1070 (w), 1025 (m), 840 (br, s), 735 (s), 685 (s) cm<sup>-1</sup>; low-resolution MS (EI)  $m/e$  (%) 200 (97), 185 (26), 165 (13), 154 (15), 139 (50), 123 (25), 109 (12), 91 (93), 77 (100), 65 (6), 51 (4); high-resolution MS ( $M^+$ ) calcd for C<sub>9</sub>H<sub>13</sub>SiSF 200.0492, found 200.0482. Anal. Calcd for C<sub>9</sub>H<sub>13</sub>SiSF: H, 53.96; F, 6.54. Found: C, 53.97; H, 6.55.

**(Phenylthio)bis(dimethylfluorosilyl)methane** (bulb-to-bulb distillation 123 °C/15 mmHg): VPC  $t_R$  9.2 min (OV-1 2% 2 m, 100–240 °C, 10 °C/min); <sup>1</sup>H NMR (CDCl<sub>3</sub>)  $\delta$  0.27 (d, 5.4 Hz, 6H), 0.38 (d, 5.4 Hz, 6H), 1.82 (t, 4.5 Hz, 1H), 6.93–7.63 (m, 5H); IR (neat) 3100 (w), 3000 (m), 2930 (w), 1595 (s), 1490 (s), 1450 (m), 1410 (w), 1270 (s), 1100 (m), 1035 (m), 1020 (m), 870 (br), 765 (s), 750 (s), 700 (s) cm<sup>-1</sup>; low-resolution MS (EI)  $m/e$  (%) 276 (49), 261 (9), 245 (4), 217 (2), 199 (30), 180 (26), 165 (100), 151 (11), 135 (53), 122 (5), 103 (4), 91 (6), 77 (24),

59 (6); high-resolution MS ( $M^+$ ) calcd for C<sub>11</sub>H<sub>18</sub>SSi<sub>2</sub>F<sub>2</sub> 276.0636, found 276.0648. Anal. Calcd for C<sub>11</sub>H<sub>18</sub>SSi<sub>2</sub>F<sub>2</sub>: C, 47.78; H, 6.56. Found: C, 47.84; H, 6.37.

**o-Bis(dimethylfluorosilyl)benzene** (bulb-to-bulb distillation 120–140 °C/20 mmHg): VPC  $t_R$  5.8 min (OV-1 2%, 100–240 °C, 10 °C/min); <sup>1</sup>H NMR (CDCl<sub>3</sub>)  $\delta$  0.46–0.52 (m, 6H), 7.40–7.46 (m, 2H), 7.64–7.69 (m, 2H); IR (neat) 3120 (w), 3070 (m), 3050 (m), 2960 (s), 2900 (m), 1580 (w), 1560 (w), 1415 (s), 1260 (s), 1125 (s), 1065 (s), 1040 (s), 840 (s, br), 800 (s), 750 (s) cm<sup>-1</sup>; low-resolution MS (EI)  $m/e$  (%) 230 ( $M^+$ , 2), 217 (11), 216 (22), 215 (100), 199 (11), 119 (18), 77 (13); high-resolution MS ( $M^+$ ) calcd for C<sub>10</sub>H<sub>16</sub>Si<sub>2</sub>F<sub>2</sub> 230.0758, found 230.0758. Anal. Calcd for C<sub>10</sub>H<sub>16</sub>Si<sub>2</sub>F<sub>2</sub>: C, 52.13; H, 7.00. Found: 52.15; H, 6.92.

**X-ray Powder Analysis.** After the reaction of triphenylfluorosilane with CuF<sub>2</sub>·2H<sub>2</sub>O in refluxing CCl<sub>4</sub>, solid materials were separated by filtration and dried. X-ray analysis of the solid products with a Rigaku RAD-IA diffractometer (copper) showed signals for CuCl and CuOHF together with those of unchanged CuF<sub>2</sub>·2H<sub>2</sub>O, which were assigned by comparison with the literature data.<sup>14</sup>

**Acknowledgment.** We thank Prof. Nobuyuki Aikawa, Osaka City University, for the use of powder X-ray diffractometer, and valuable discussions. We also thank the Ministry of Education, Science, and Culture of Japan for the Grant-in-Aid for Scientific Research.

OM940561X

(14) Smith, J. V., Ed. *Powder Diffraction File 1967*; American Society for Testing and Materials: York, PA, 1967.

# Preparation of (Aminocarbene)tetracarbonyliron(0) Complexes by the Reaction of Tertiary Amides with $\text{Fe}(\text{CO})_4^{2-}$ and Chlorotrimethylsilane

Dalimil Dvořák<sup>1</sup>

Department of Chemistry, Prague Technical University, 166 28 Prague 6, Czech Republic

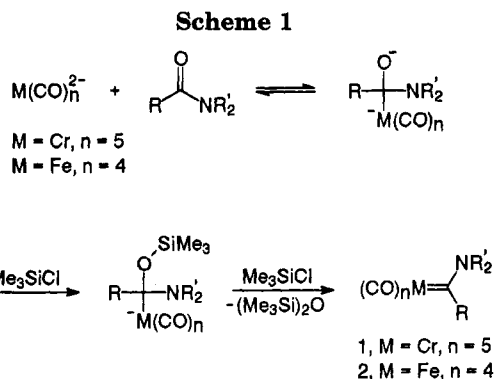
Received July 26, 1994<sup>®</sup>

**Summary:** (Aminocarbene)tetracarbonyliron(0) complexes without hydrogen atoms at the position  $\alpha$  to the carbene atom can easily be prepared by the reaction of formamides or aromatic and heteroaromatic tertiary amides with sodium or potassium tetracarbonylferrate and chlorotrimethylsilane in THF solution.

While the chemistry of chromium aminocarbene complexes has been intensively explored during the last years, resulting in development of many synthetically useful methods,<sup>2</sup> the chemistry of analogous iron aminocarbene complexes remains almost untouched. To the best of our knowledge, there is only one paper dealing with the reactivity of neutral iron aminocarbene complexes.<sup>3</sup> This is apparently due to the relative inaccessibility of these compounds.

Several iron aminocarbene complexes have been prepared to date. The method most used for the preparation of chromium aminocarbene complexes (aminolysis of alkoxy carbene complexes) can, in principle, be used also for the preparation of iron aminocarbene complexes.<sup>4</sup> However, the preparation of the starting iron alkoxy carbene is not as easy as the synthesis of chromium alkoxy carbene complexes.<sup>4a</sup> Furthermore, the exchange reaction with amines has been reported to give satisfactory results only with carbene complexes without hydrogen at the position  $\alpha$  to the carbene atom.<sup>3</sup> Other methods described for the preparation of iron aminocarbene complexes include a photochemical exchange reaction<sup>4c</sup> and the reaction of  $\text{Na}_2\text{Fe}(\text{CO})_4$  with (chloromethylene)dialkylammonium chlorides.<sup>5</sup> However, these methods are either complicated or not general.

A very efficient and relatively general method for preparation of chromium aminocarbene complexes **1**, based on the reaction of  $\text{Na}_2\text{Cr}(\text{CO})_5$  or  $\text{K}_2\text{Cr}(\text{CO})_5$  with amides and chlorotrimethylsilane, was developed by Imwinkelried and Hegedus.<sup>6</sup> This reaction is believed to proceed via nucleophilic addition of  $\text{Cr}(\text{CO})_5^{2-}$  (prepared by reduction of  $\text{Cr}(\text{CO})_6$  with sodium or potassium



naphthalenide) to the carbonyl group of an amide followed by the O-silylation of the adduct and subsequent reaction with an excess of chlorotrimethylsilane and elimination of hexamethyldisiloxane (Scheme 1). The drawback of this procedure—the necessity of separating 2 equiv of naphthalene formed from the sodium naphthalenide from the product by means of chromatography on silica—can be avoided by using  $\text{C}_8\text{K}$  as a reducing agent.<sup>7</sup> A similar concept was used by Hossain, who treated aldehydes with  $\text{FeCp}(\text{CO})_2^-$  and chlorotrimethylsilane to produce unstabilized cationic iron carbene complexes.<sup>8</sup>

$\text{Fe}(\text{CO})_4^{2-}$  is known as a very strong nucleophile. We reasoned that it can react with amides and chlorotrimethylsilane in the same way as  $\text{Cr}(\text{CO})_5^{2-}$ , forming the desired iron aminocarbene complexes. To verify this hypothesis, we chose dimethylformamide, which should give the known product<sup>5</sup> **2a**, for the first experiments. However, the treatment of DMF with the dioxane solvate of  $\text{Na}_2\text{Fe}(\text{CO})_4$  and chlorotrimethylsilane in THF solution gave only traces of the expected [(*N,N*-dimethylamino)methylene]tetracarbonyliron(0) (**2a**). This might be due to the low solubility of the dioxane solvate of  $\text{Na}_2\text{Fe}(\text{CO})_4$  in THF. Therefore, for further experiments, we generated  $\text{Na}_2\text{Fe}(\text{CO})_4$  free of dioxane *in situ* by reduction of iron pentacarbonyl with sodium naphthalenide<sup>9</sup> in THF. With this reagent the desired iron aminocarbene complex **2a** was obtained in high yield. The product **2a** (61%) was separated from the naphthalene byproduct by chromatography on aluminium oxide.<sup>10</sup>

The scope of this method was explored using other substrates with the aim of preparing iron aminocarbene

<sup>®</sup> Abstract published in *Advance ACS Abstracts*, November 15, 1994.

(1) Temporary address: University of Leicester, Department of Chemistry, University Road, Leicester, LE1 7RH, U.K.

(2) For a review, see: Schwindt, M. A.; Miller, J. R.; Hegedus, L. S. *J. Organomet. Chem.* **1991**, *413*, 143.

(3) Semmelhack, M. F.; Park, J. *Organometallics* **1986**, *5*, 2550. For a review of the reactivity of Fischer iron carbene complexes; see: Semmelhack, M. F.; Park, J.; Schnatter, W.; Tamura, R.; Steigerwald, M. *Chem. Scr.* **1987**, *27*, 509.

(4) Preparation of (alkoxycarbene)iron(0) complexes by Fischer procedure: (a) Semmelhack, M. F.; Tamura, R. *J. Am. Chem. Soc.* **1983**, *105*, 4099. (b) Park, J.; Kang, S.; Whang, D.; Kim, K. *Organometallics* **1991**, *10*, 3413. (c) Fischer, E. O.; Beck, H.-J.; Kreiter, C. G.; Lynch, J.; Müller, J.; Winkler, E. *Chem. Ber.* **1972**, *105*, 162. For aminolysis of (alkoxycarbene)iron complexes, see: References 2 and 3c.

(5) Hartshorn, A. J.; Lappert, M. F.; Turner, K. *J. Chem. Soc., Dalton Trans.* **1978**, 348.

(6) Imwinkelried, R.; Hegedus, L. S. *Organometallics* **1988**, *7*, 702.

(7) Schwindt, M. A.; Lejon, T.; Hegedus, L. S. *Organometallics* **1990**, *9*, 2814.

(8) Vargas, R. M.; Theys, R. D.; Hossain, M. M. *J. Am. Chem. Soc.* **1992**, *114*, 777.

(9) Strong, H.; Krusic, P. J.; Filippo, J. S. *Inorg. Synth.* **1986**, *24*, 157.

(10) Aluminium oxide turned out to be the adsorbent of choice, since chromatography on silica gel is accompanied by partial decomposition of the product.

**Table 1. Preparation of (Aminocarbene)tetracarbonyliron(0) Complexes**

entry	complex	R	R'	% yield
1	<b>2a</b>	H	Me	61.7 <sup>a</sup>
2	<b>2b</b>	Ph	Me	63.1 <sup>a</sup> ; 76.0 <sup>b</sup> ; 74.3 <sup>c</sup>
3	<b>2c</b>	4-MeOPh	[(CH <sub>2</sub> ) <sub>2</sub> ] <sub>2</sub> O	48.6 <sup>a</sup>
4	<b>2d</b>	3-ClPh	[(CH <sub>2</sub> ) <sub>2</sub> ] <sub>2</sub> O	39.0 <sup>a</sup>
5	<b>2e</b>	4-BrPh	Me	26.3 <sup>a</sup> ; 54.7 <sup>b</sup>
6	<b>2f</b>	4-CNPh	[(CH <sub>2</sub> ) <sub>2</sub> ] <sub>2</sub> O	29.2 <sup>a</sup>
7	<b>2g</b>	3-pyridyl	Me	28.7 <sup>a</sup>
8	<b>2h</b>	2-furyl	Me	67.0 <sup>a</sup>
9	<b>2i</b>	3-thienyl	Me	65.2 <sup>a</sup>

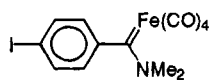
<sup>a</sup> Method A. <sup>b</sup> Method B. <sup>c</sup> Method C.

complexes bearing hydrogen (**2a**), aromatic (**2b–f**), or heteroaromatic (**2g–i**) substituents at the carbene atom. The yield was modest to high (Table 1). However, this method failed in the case of amides bearing  $\alpha$ -hydrogens such as *N,N*-dimethylacetamide or *N*-methylpyrrolidone. Also *N,N*-dimethylamides or cinnamic and pivalic acids failed to give aminocarbene complexes, the latter probably as a result of a steric hindrance.

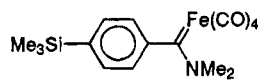
Iron aminocarbene complexes are yellow crystalline solids with IR absorption characteristic for the Fe(CO)<sub>4</sub> moiety. The <sup>1</sup>H NMR spectra of dimethylamino carbenes show characteristic signals of NCH<sub>3</sub> groups at  $\delta$  ~3.10 and 4.00, only slightly influenced by the aromatic substituent. The complexes are infinitely stable at 8 °C under nitrogen<sup>11</sup> and can be handled in air as solids for a limited time without oxidation, but are readily oxidized in solution, especially in the light.

If K<sub>2</sub>Fe(CO)<sub>4</sub> prepared by reduction of Fe(CO)<sub>5</sub> with potassium naphthalene or C<sub>8</sub>K in THF is used instead of Na<sub>2</sub>Fe(CO)<sub>4</sub>, the yields of iron aminocarbene complexes are generally higher (Table 1, entries 2 and 5). In this case, it is crucial to keep the THF solution of K<sub>2</sub>Fe(CO)<sub>4</sub> below –30 °C, otherwise an insoluble THF solvate of K<sub>2</sub>Fe(CO)<sub>4</sub> is formed and the yield of aminocarbene complex drops to zero.

It is known that Cr(CO)<sub>5</sub><sup>2-</sup> does not tolerate aromatic iodo<sup>12</sup> and bromo<sup>13</sup> compounds, presumably because of the electron transfer processes. Fe(CO)<sub>4</sub><sup>2-</sup> behaves differently in this respect: [(4-Bromophenyl)-(N,N-dimethylamino)methylene]tetracarbonyliron(0) was readily formed by the reaction of 4-bromo-*N,N*-dimethylbenzamide with potassium tetracarbonylferrate in 54% yield (Table 1, entry 5). The reaction of 4-iodo-*N,N*-dimethylbenzamide with sodium tetracarbonylferrate appeared to be more complicated. Besides the two singlets at  $\delta$  3.11 and 4.00 characteristic for the carbene dimethylamino group, the <sup>1</sup>H NMR spectrum of the reaction product indicated the presence of two different 4-substituted phenyl groups in 60.5:39.5 ratio and an intensive singlet at  $\delta$  0.27 (a trimethylsilyl group belonging to the compound with less intensive phenyl signals). This spectrum can be interpreted as that of a mixture of two carbene complexes [(4-iodophenyl)-(N,N-dimethylamino)carbene]tetracarbonyliron(0) (**2j**) and [4-(trimethylsilyl)phenyl]-(N,N-dimethylamino)carbene]tetracarbonyliron(0) (**2k**).



**2j**



**2k**

ethylsilyl)phenyl]-(N,N-dimethylamino)carbene]tetracarbonyliron(0) (**2k**). This was confirmed by mass spectrometry showing molecular ions of low intensity for both compounds together with the characteristic<sup>4c</sup> stepwise loss of CO ligands. The silylated product **2k** is likely to be formed by reductive splitting of iodine followed by silylation of the resulting carbanion by Me<sub>3</sub>SiCl.<sup>14</sup>

In conclusion, the reaction of Fe(CO)<sub>4</sub><sup>2-</sup> with tertiary amides without  $\alpha$ -hydrogens provides a useful new route to (aminocarbene)tetracarbonyliron(0) complexes. The chemistry of these compounds is currently under study in our laboratory.

## Experimental Section

**Methods.** Melting points were taken on a Kofler block and are uncorrected. Unless otherwise noted, all <sup>1</sup>H NMR spectral data were recorded in CDCl<sub>3</sub> at 100 MHz and chemical shifts are reported relative to TMS. All IR spectra were recorded as CCl<sub>4</sub> solutions. Elemental analyses were performed by the analytical departments of UOCHB-CSAV and Prague Technical University. The yields are based on starting amides. All experiments were carried out under argon.

**Materials.** Tetrahydrofuran was distilled from benzophenone ketyl under a nitrogen atmosphere just prior to use. Ethyl acetate was distilled over CaH<sub>2</sub>; diethyl ether was dried over sodium metal and distilled. Iron pentacarbonyl, chromium hexacarbonyl, and chlorotrimethylsilane were obtained from Aldrich and used without further purification. Neutral aluminium oxide (Brockman III grade) was obtained from Lachema. Dimethylformamide and dimethylacetamide were obtained from Aldrich; the other amides were prepared from appropriate acid chlorides and dimethylamine or morpholine in ether.

**General Procedure for the Preparation of the Iron Aminocarbene Complexes 2a–i. Method A.** In a 250 mL, round-bottomed flask equipped with a magnetic stirring bar and a septum inlet was placed a solution of iron pentacarbonyl (1.4 mL, 10.5 mmol) in THF (50 mL). The solution was cooled to –78 °C, and the flask was evacuated and filled with argon. This procedure was repeated five times. Then an ~0.8 M stock solution of sodium naphthalene in THF (35 mL, 28 mmol) was added via a double-ended needle over several minutes. The reduction of iron pentacarbonyl proceeds almost immediately with evolution of CO gas. The reaction mixture was then allowed to warm to 0 °C, and the amide (5 mmol) in THF (10 mL) was added through a double-ended needle. The solution was stirred at 0 °C for 10 min and then cooled to –78 °C; chlorotrimethylsilane (2.5 mL, 19.7 mmol) was added via a syringe. The solution was stirred at –78 °C for 0.5 h, then the cooling bath was removed, the mixture was allowed to warm to 0 °C, and neutral alumina (8 g) was added. The solvent was removed under reduced pressure on a rotatory evaporator, and the residue was dried for several hours under high vacuum to remove all the THF. *n*-Hexane (50 mL) was added, and the mixture was stirred vigorously for several minutes under argon atmosphere. The suspension formed was then transferred to the top of a column filled with neutral alumina (150 g). Naphthalene and green Fe<sub>3</sub>(CO)<sub>12</sub> were eluted with hexane, and further elution with hexane–CH<sub>2</sub>Cl<sub>2</sub> (5:1) gave the crude iron carbene complex as a brown-yellow solid. The crude product was dissolved in a small amount of dichloromethane, and the solution was diluted with *n*-hexane and filtered under argon atmosphere. Evaporation of dichloromethane in vacuum at 0 °C and filtration under argon gave the pure iron aminocarbene complex.

(12) Semmelhack, M. F.; Lee, G. R. *Organometallics* 1987, 6, 1839.

(13) Dvořák, D. Unpublished results.

(14) All attempts at separation of **2j** and **2k** by chromatography or crystallization have failed.

(11) The only exception is 2-furyl derivative **2h**, which slowly decomposes even at –18 °C.

**Method B.** To a solution prepared by dissolving potassium (1.20 g, 30 mmol) and naphthalene (4.3 g, 33.5 mmol) in THF (80 mL) in an argon atmosphere was added iron pentacarbonyl (1.4 mL, 10 mmol) at  $-78\text{ }^{\circ}\text{C}$  via a syringe.  $\text{Fe}(\text{CO})_5$  was reduced almost instantaneously, forming a yellow-brown solution of  $\text{K}_2[\text{Fe}(\text{CO})_4]$ . After 15 min at  $-78\text{ }^{\circ}\text{C}$ , the amide (5 mmol) in THF (10 mL) was added. After 0.5 h at  $-78\text{ }^{\circ}\text{C}$ , the temperature was allowed to rise slowly (in  $\sim 0.5$  h) to  $-40\text{ }^{\circ}\text{C}$ , and the mixture was then kept at this temperature for another 0.5 h. The resulting solution was cooled again to  $-78\text{ }^{\circ}\text{C}$ , and chlorotrimethylsilane (2.5 mL, 19.7 mmol) was added. The reaction mixture was stirred at  $-78\text{ }^{\circ}\text{C}$  for 0.5 h and let to warm gradually to  $0\text{ }^{\circ}\text{C}$  over 1 h. Neutral alumina (10 g) was then added, and further workup was identical to that described under (A).

**Method C.** To  $\text{C}_8\text{K}$ ,<sup>7</sup> prepared from graphite (2.5 g, 208 mmol) and potassium (1.06 g, 26 mmol), was added THF (50 mL) under argon. The resulting suspension was cooled to  $-78\text{ }^{\circ}\text{C}$ , and  $\text{Fe}(\text{CO})_5$  (1.4 mL, 10 mmol) was added via a syringe, while CO evolved. The resulting mixture was stirred 0.5 h at  $-78\text{ }^{\circ}\text{C}$ , and then a solution of the amide (8 mmol) in THF (15 mL) was added by syringe. Further procedure was identical to that described for method A, except that only 50 g of alumina was used for chromatography.

**[(*N,N*-Dimethylamino)methylene]tetracarbonyliron(0) (2a).** Procedure A using  $\text{Fe}(\text{CO})_5$  (3.95 g, 20 mmol), a 0.71 M THF solution of sodium naphthalenide (76 mL), dimethylformamide (0.790 g, 10.8 mmol), and chlorotrimethylsilane (4.0 mL, 31.5 mmol) gave 1.99 g (82%) of the crude product. Pure compound was obtained from crystallization as fawn needles: 1.50 g (61.7%), mp  $58\text{--}60\text{ }^{\circ}\text{C}$  (lit.<sup>5</sup> mp  $55\text{--}56\text{ }^{\circ}\text{C}$ ).  $^1\text{H}$  NMR and IR spectra were identical with those in ref 4.

**[(*N,N*-Dimethylamino)phenylmethylene]tetracarbonyliron(0) (2b).** Method A. Crude carbene **2b** (1.03 g, 68.5%) was obtained from *N,N*-dimethylbenzamide (0.745 g, 5 mmol),  $\text{Fe}(\text{CO})_5$  (2.033 g, 10.4 mmol), a 0.71 M THF solution of sodium naphthalenide (42 mL), and chlorotrimethylsilane (2.5 mL, 19.75 mmol). Crystallization gave 0.95 g (63.1%) of yellow crystalline solid: mp  $96\text{--}102\text{ }^{\circ}\text{C}$  (ref.<sup>4c</sup> mp  $106\text{ }^{\circ}\text{C}$ );  $^1\text{H}$  NMR  $\delta$  3.10 (s, 3,  $\text{NCH}_3$ ), 4.00 (s, 3,  $\text{NCH}_3$ ), 6.64–6.80 (m, 2, ArH), 7.00–7.50 (m, 3, ArH); IR  $\nu$  2043 (s), 1972 (s), 1943 (s), 1921 (s)  $\text{cm}^{-1}$  [from ref 3c: IR (*n*-hexane)  $\nu$  2045 (m), 1968 (m), 1955 (m), 1945 (s), 1923 (s)  $\text{cm}^{-1}$ ].

**Method B.** Pure **2b** (0.65 g, 76.0%) was obtained by starting from potassium naphthalenide [K (3.1 g, 77.5 mmol), naphthalene (10.25 g, 80 mmol), and THF (180 mL)],  $\text{Fe}(\text{CO})_5$  (4.2 mL, 30 mmol), *N,N*-dimethylbenzamide (3.03 g, 20.31 mmol), and chlorotrimethylsilane (7.5 mL, 59.1 mmol) in THF (180 mL) after chromatography (250 g  $\text{Al}_2\text{O}_3$ ) and crystallization.

**Method C.** The reaction of  $\text{C}_8\text{K}$  (26.5 mmol),  $\text{Fe}(\text{CO})_5$  (1.4 mL, 10 mmol), *N,N*-dimethylbenzamide (1.2 g, 8.05 mmol), and chlorotrimethylsilane (3 mL, 23.6 mmol) gave 1.80 g (74.3%) of **2b** after chromatography (50 g of  $\text{Al}_2\text{O}_3$ ) and crystallization.

**[(4-Methoxyphenyl)morpholinomethylene]tetracarbonyliron(0) (2c).** The reaction of  $\text{Fe}(\text{CO})_5$  (1.4 mL, 10.3 mmol), a 0.8 M THF solution of sodium naphthalenide (34 mL), *N*-(4-methoxybenzoyl)morpholine (1.12 g, 5 mmol), and chlorotrimethylsilane (2.5 mL, 19.75 mmol) according to method A gave 1.28 g (68.0%) of yellow solid. Crystallization afforded 0.907 g (48.6%) of pure carbene complex **2c**: mp  $121\text{ }^{\circ}\text{C}$  dec;  $^1\text{H}$  NMR  $\delta$  3.59 (s, 4,  $\text{CH}_2$ ), 3.82 (s, 3,  $\text{CH}_3$ ), 3.96–4.10 (m, 2,  $\text{CH}_2$ ), 4.58–4.74 (m, 2,  $\text{CH}_2$ ), 6.68–7.00 (m, 4, ArH); IR  $\nu$  2043 (s), 1972 (s), 1942 (s), 1918 (s)  $\text{cm}^{-1}$ . Anal. Calcd for  $\text{C}_{16}\text{H}_{18}\text{FeNO}_6$ : C, 51.50; H, 4.05; N, 3.75. Found: C, 51.61; H, 4.05; N, 3.87.

**[(3-Chlorophenyl)morpholinomethylene]tetracarbonyliron(0) (2d).** Procedure A was used to produce 1.472 g (77.5%) of carbene **2d** from *N*-(3-chlorobenzoyl)morpholine (1.135 g, 5 mmol),  $\text{Fe}(\text{CO})_5$  (1.4 mL, 10.3 mmol), a 0.8 M THF solution of sodium naphthalenide (34 mL), and chlorotrimethylsilane (2.5 mL, 19.75 mmol) as an oil which solidified after

cooling in refrigerator. Recrystallization gave pure product (0.737 g, 39.0%) as yellow crystals: mp  $89\text{--}93\text{ }^{\circ}\text{C}$ ;  $^1\text{H}$  NMR  $\delta$  3.44–3.74 (m, 4,  $\text{CH}_2$ ), 3.94–4.15 (m, 2,  $\text{CH}_2$ ), 4.58–4.74 (m, 2,  $\text{CH}_2$ ), 6.65–6.89 (m, 2, ArH), 7.10–7.42 (m, 2, ArH); IR  $\nu$  2045 (s), 1976 (s), 1946 (s), 1920 (s)  $\text{cm}^{-1}$ . Anal. Calcd for  $\text{C}_{15}\text{H}_{12}\text{ClFeNO}_5$ : C, 47.72; H, 3.20; Cl, 9.39; N, 3.71. Found: C, 47.94; H, 3.26; Cl, 9.52; N, 3.65.

**(4-Bromophenyl)-*N,N*-dimethylamino)methylene]tetracarbonyliron(0) (2e).** Method A. Reaction of sodium naphthalenide [Na (0.74 g, 32.2 mmol), naphthalene (4.6 g, 35.9 mmol) in THF (100 mL)] with  $\text{Fe}(\text{CO})_5$  (1.4 mL, 10 mmol), 4-bromo-*N,N*-dimethylbenzamide (1.76 g, 7.72 mmol), and chlorotrimethylsilane (2.6 mL, 20.5 mmol) gave 1.53 g (52%) of crude **2e**. Crystallization from ethyl acetate–*n*-heptane mixture afforded 0.771 g (26.3%) of the pure compound: decomposes above  $100\text{ }^{\circ}\text{C}$ ;  $^1\text{H}$  NMR (300 MHz)  $\delta$  3.10 (s, 3,  $\text{NCH}_3$ ), 4.00 (s, 3,  $\text{NCH}_3$ ), 6.73–6.75 (m, 2, ArH), 7.51–7.53 (m, 2, ArH); IR  $\nu$  2045 (s), 1974 (s), 1945 (s), 1922 (s)  $\text{cm}^{-1}$ . Anal. Calcd for  $\text{C}_{13}\text{H}_{10}\text{BrFeNO}_4$ : C, 41.09; H, 2.65; N, 3.69; Br, 21.03. Found: C, 41.35; H, 2.75; N, 3.80; Br, 21.04.

**Method B.** A 2.08 g (54.7%) sample of pure **2e** was obtained from potassium naphthalenide (66 mmol),  $\text{Fe}(\text{CO})_5$  (2.8 mL, 20 mmol), 4-bromo-*N,N*-dimethylaminobenzamide (2.2 g, 10 mmol), and chlorotrimethylsilane (5.2 mL, 41 mmol) in THF (150 mL) upon chromatography (150 g  $\text{Al}_2\text{O}_3$ ) and crystallization.

**[(4-Cyanophenyl)morpholinomethylene]tetracarbonyliron(0) (2f).** The reaction of  $\text{Fe}(\text{CO})_5$  (1.4 mL, 10.3 mmol), a 0.75 M THF solution of sodium naphthalenide (36 mL), *N*-(4-cyanobenzoyl)morpholine (1.10 g, 5.09 mmol), and chlorotrimethylsilane (2.5 mL, 19.7 mmol) according to method A gave 1.08 g (57.8%) of yellow solid. Pure product was obtained by crystallization: 0.548 g (29.2%), mp  $123\text{ }^{\circ}\text{C}$  dec;  $^1\text{H}$  NMR  $\delta$  3.60 (m, 4,  $\text{CH}_2$ ), 4.07 (m, 2,  $\text{CH}_2$ ), 4.67 (m, 2,  $\text{CH}_2$ ), 6.96 (m, 2, ArH), 7.70 (m, 2, ArH); IR  $\nu$  2047 (m), 1979 (m), 1947 (s), 1925 (s)  $\text{cm}^{-1}$ . Anal. Calcd for  $\text{C}_{16}\text{H}_{12}\text{FeN}_2\text{O}_5$ : C, 52.20; H, 3.29; N, 7.61. Found: C, 52.53; H, 3.22; N, 7.54.

**[(*N,N*-Dimethylamino)-3-pyridylmethylene]tetracarbonyliron(0) (2g).** Procedure A using  $\text{Fe}(\text{CO})_5$  (1.4 mL, 10.3 mmol), a 0.8 M THF solution of sodium naphthalenide (34 mL), *N,N*-dimethylnicotinamide (0.850 g, 5.66 mmol), and chlorotrimethylsilane (2.5 mL, 19.7 mmol) gave 0.60 g (35.1%) of crude product as a dark brown oil and 0.490 g (28.7%) of pure yellow crystalline compound after recrystallization: mp  $87\text{ }^{\circ}\text{C}$  dec;  $^1\text{H}$  NMR  $\delta$  3.15 (s, 3,  $\text{NCH}_3$ ), 4.07 (s, 3,  $\text{NCH}_3$ ), 7.13–7.33 (m, 1, Py-H), 7.36–7.60 (m, 1, Py-H), 8.53–8.77 (m, 1, Py-H), 8.87–9.13 (m, 1, Py-H); IR  $\nu$  2045 (s), 1974 (s), 1945 (s), 1923 (s)  $\text{cm}^{-1}$ . Anal. Calcd for  $\text{C}_{12}\text{H}_{10}\text{FeN}_2\text{O}_4$ : C, 47.71; H, 3.34; N, 9.27. Found: C, 47.76; H, 3.41; N, 9.06.

**[(*N,N*-Dimethylamino)-2-furfurylmethylene]tetracarbonyliron(0) (2h).** The reaction of  $\text{Fe}(\text{CO})_5$  (1.40 g, 10.3 mmol), a 0.8 M THF solution of sodium naphthalenide (34 mL), *N,N*-dimethyl-2-furfurylcarboxamide (0.700 g, 5.03 mmol), and chlorotrimethylsilane (2.5 mL, 19.7 mmol) gave, according to method A, 1.18 g (80.56%) of crude product, which afforded after recrystallization 0.981 g (67.0%) of orange crystals: mp  $46\text{--}48.5\text{ }^{\circ}\text{C}$ ;  $^1\text{H}$  NMR  $\delta$  3.23 (s, 3,  $\text{NCH}_3$ ), 3.96 (s, 3,  $\text{NCH}_3$ ), 6.32–6.48 (m, 2, ArH), 7.44 (br s, 1, ArH); IR  $\nu$  2044 (s), 1972 (s), 1945 (s), 1925 (s). Anal. Calcd for  $\text{C}_{11}\text{H}_9\text{FeNO}_5$ : C, 45.40; H, 3.12; N, 4.81. Found: C, 45.09; H, 3.06; N, 4.78.

**[(*N,N*-Dimethylamino)-3-thienylmethylene]tetracarbonyliron(0) (2i).** Method A gave by the reaction of  $\text{Fe}(\text{CO})_5$  (1.40 mL, 10.3 mmol), a 0.8 M THF solution of sodium naphthalenide (36 mL), *N,N*-dimethyl-3-thienylcarboxamide (0.860 g, 5.55 mmol), and chlorotrimethylsilane (3.0 mL, 23.6 mmol), 1.353 g (79.5%) of crude product. Crystallization afforded 1.10 g (64.5%) of yellow solid: mp  $82\text{--}85\text{ }^{\circ}\text{C}$ ;  $^1\text{H}$  NMR  $\delta$  3.16 (s, 3,  $\text{NCH}_3$ ), 3.98 (s, 3,  $\text{NCH}_3$ ), 6.73 (s, 1, ArH), 6.77 (d,  $J = 0.7$  Hz, 1, ArH), 7.24–7.40 (m, 1, ArH); IR  $\nu$  2043 (s), 1972 (s), 1943 (s), 1917 (s). Anal. Calcd for  $\text{C}_{11}\text{H}_9\text{FeNO}_4\text{S}$ : C, 43.02; H, 2.95; N, 4.56; S, 10.44. Found: C, 42.68; H, 2.94; N, 4.73; S, 10.50.



**Reaction of 4-Iodo-*N,N*-dimethylbenzamide with  $\text{Na}_2\text{Fe}(\text{CO})_5$ .** The reaction of sodium naphthalenide [naphthalene (4.5 g, 35.1 mmol), Na (0.70 g, 30.4 mmol) in THF (70 mL)] with  $\text{Fe}(\text{CO})_5$  (1.4 mL, 10.3 mmol), 4-iodophenyl-*N,N*-dimethylbenzamide (1.37 g, 5 mmol), and chlorotrimethylsilane (3 mL, 23.6 mmol) according to method A afforded after chromatography (150 g of  $\text{Al}_2\text{O}_3$ ) and crystallization 0.324 g of a mixture of the [(*N,N*-dimethylamino)-(4-iodophenyl)methylene]tetracarbonyliron(0) (**2j**) and [(*N,N*-dimethylamino)-[(4-trimethylsilyl)phenyl]methylene]tetracarbonyliron(0) (**2k**) in ~60.5:39.5 ratio (based on  $^1\text{H}$  NMR). All attempts to separate **2j** and **2k** by chromatography and crystallization were unsuccessful. For **2j**:  $^1\text{H}$  NMR (300 MHz)  $\delta$  3.11 (s, 3,  $\text{NCH}_3$ ), 4.00 (s, 3,  $\text{NCH}_3$ ), 6.55–6.65 (m, 2, ArH), 7.65–7.78 (m, 2, ArH); MS ( $\text{C}_{13}\text{H}_{10}\text{FeINO}_4$ ) 427 ( $\text{M}^+$ ), 399 ( $\text{M}^+ - \text{CO}$ ),

371 ( $\text{M}^+ - 2\text{CO}$ ), 343 ( $\text{M}^+ - 3\text{CO}$ ). For **2k**:  $^1\text{H}$  NMR (300 MHz)  $\delta$  0.27 (s, 9,  $\text{Si}(\text{CH}_3)_3$ ), 3.11 (s, 3,  $\text{NCH}_3$ ), 4.00 (s, 3,  $\text{NCH}_3$ ), 6.75–6.85 (m, 2, ArH), 7.45–7.55 (m, 2, ArH); MS ( $\text{C}_{16}\text{H}_{19}\text{FeNO}_4\text{Si}$ ) 373 ( $\text{M}^+$ ), 345 ( $\text{M}^+ - \text{CO}$ ), 317 ( $\text{M}^+ - 2\text{CO}$ ), 289 ( $\text{M}^+ - 3\text{CO}$ ), 261 ( $\text{M}^+ - 4\text{CO}$ ). For the mixture of **2j** and **2k**: IR  $\nu$  2044 (s), 1973 (m), 1944 (s), 1920 (s). Elemental analysis of the mixture gave 18.78% I, which corresponds to a 63.15% content of **2j** in the mixture of **2j** and **2k**. This value is in good agreement with that obtained from  $^1\text{H}$  NMR.

**Acknowledgment.** We thank the Prague Technical University and Institute of Organic Chemistry and Biochemistry—AVČR for their support of our program.

OM940596X

## Synthesis and Characterization of a Novel Pentavalent Silane: 1-Methyl-1,1-dihydrido-2,3,4,5-tetraphenyl-1- silacyclopentadiene Silicate, $[\text{Ph}_4\text{C}_4\text{SiMeH}_2\text{-}]\cdot[\text{K}^+]$

Jang-Hwan Hong, and Philip Boudjouk

*Organometallics*, 1995, 14 (1), 574-576 • DOI: 10.1021/om00001a082 • Publication Date (Web): 01 May 2002

Downloaded from <http://pubs.acs.org> on March 9, 2009

### More About This Article

---

The permalink <http://dx.doi.org/10.1021/om00001a082> provides access to:

- Links to articles and content related to this article
- Copyright permission to reproduce figures and/or text from this article



# Synthesis and Characterization of a Novel Pentavalent Silane: 1-Methyl-1,1-dihydrido-2,3,4,5-tetraphenyl-1-silacyclopentadiene Silicate, $[\text{Ph}_4\text{C}_4\text{SiMeH}_2^-][\text{K}^+]$ <sup>1</sup>

Jang-Hwan Hong and Philip Boudjouk\*

Department of Chemistry, North Dakota State University, Fargo, North Dakota 58105

Received July 26, 1994<sup>®</sup>

**Summary:** The reaction of 1-methyl-2,3,4,5-tetraphenyl-1-silacyclopentadiene (**1**) with potassium hydride in THF-*d*<sub>3</sub> gives 1-methyl-1,1-dihydrido-2,3,4,5-tetraphenyl-1-silacyclopentadiene silicate,  $[\text{Ph}_4\text{C}_4\text{SiMeH}_2^-][\text{K}^+]$  (**3**), 1-methyl-5-potassio-2,3,4,5-tetraphenyl-1-silacyclo-2-pentene (**4**), and 1-methyl-5-potassio-2,3,4,5-tetraphenyl-1-silacyclo-3-pentene (**5**). These species are characterized by <sup>1</sup>H, <sup>13</sup>C, and <sup>29</sup>Si NMR. Treatment of the solution of anions with dimethylchlorosilane gives the C-substituted product, 1-methyl-2-(dimethylsilyl)-2,3,4,5-tetraphenyl-1-silacyclo-3-pentene (**2**).

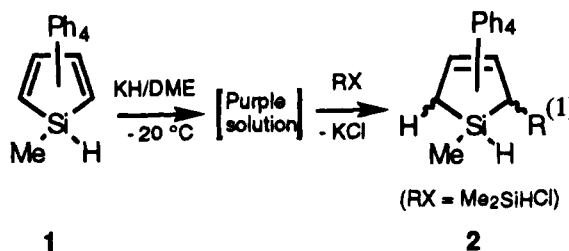
## Introduction

The interest in silacyclopentadienes<sup>2</sup> is largely attributable to their potential for generating aromatic silacyclopentadienide anions<sup>3</sup> and metallocenes featuring silole rings.<sup>4</sup> Recently, they have also been used as precursors to silicon containing dianions.<sup>5</sup> Treatment of hydrosilanes with potassium hydride is a known route to silyl anions<sup>6</sup> and has been used to generate silacyclopentadienide anions. Han and Boudjouk reported that potassium hydride reacts with 1-methyl-2,3,4,5-tetraphenyl-1-silacyclopentadiene (**1**) to give a species thought to be a silacyclopentadienide anion.<sup>7</sup> Corriu et al. later described the reaction of potassium hydride with the less substituted 1-methyl-2,5-diphenyl-1-silacyclopentadiene.<sup>6a</sup> Quenching of the intermediate anion with D<sub>2</sub>O gave quantitative yield of the deuterated product, 1-deutero-1-methyl-2,5-diphenyl-1-silacyclopentadiene.

The unambiguous synthesis of the 1-*tert*-butyl-2,3,4,5-tetraphenyl-1-silacyclopentadienide anion<sup>3a</sup> via reductive cleavage of the Si-Si bond in bis(1-*tert*-butyl-2,3,4,5-tetraphenyl-1-silacyclopentadienyl) and the complete NMR characterization of that anion which indicated substantial  $\pi$ -electron delocalization led us to reinvestigate the reaction of potassium hydride with **1**. Careful analysis of the NMR spectrum of the intermediates and characterization of the major product isolated from treatment of the intermediates with dimethylchlorosilane clearly show that formation of a silacyclopentadienide anion is not an important pathway for the reaction. In this paper we report that the dominant pathway in the reaction of potassium hydride with **1** is simple addition of the hydride anion to the silicon center to give a novel silicate<sup>8</sup> absent of highly electronegative atoms on silicon.

## Results and Discussion

When **1** was stirred with KH in DME at -20 °C, a dark purple solution was produced that gave, after treatment with dimethylchlorosilane, 1-methyl-2-(dimethylsilyl)-2,3,4,5-tetraphenyl-1-silacyclo-3-pentene (**2**) in 71% yield (eq 1).



NMR analysis of **2** led to two noteworthy observations: (1) the dimethylsilyl group exhibits hindered rotation about the bond to the ring carbon, and, (2) only one isomer is produced. Hindered rotation is demonstrated by two methyl doublets of equal intensity with the same coupling constant ( $J = 3.66$  Hz) at 0.21 and 0.33 ppm and a septet of SiH at 4.49 ppm ( $J = 3.66$  Hz). Irradiation at each doublet collapsed the septet to a quartet with no effect on the other doublet. The claim of a single isomer as the product is based on the observation of only two methyl carbon peaks (-4.63 and -4.71 ppm) for the dimethylsilyl group in the <sup>13</sup>C NMR

<sup>®</sup> Abstract published in *Advance ACS Abstracts*, December 1, 1994.

(1) This work has been presented in part: Hong, J.-H.; Boudjouk, P.; Castellino, S. XXVth Organosilicon Symposium, Indianapolis, IN, March 26-27, 1993, Abstract, H-3.

(2) (a) Dubac, J.; Laporterie, A.; Manuel, G. *Chem. Rev.* **1990**, *90*, 215. (b) Colomer, E.; Corriu, R. J. P.; Lheureux, M. *Chem. Rev.* **1990**, *90*, 265.

(3) (a) Hong, J.-H.; Boudjouk, P. *J. Am. Chem. Soc.* **1993**, *115*, 5883. (b) Joo, W.-C.; Hong, J.-H.; Choi, S.-B.; Son, H.-E. *J. Organomet. Chem.* **1990**, *391*, 27. (c) Corriu, R. J. P.; Guérin, C.; Kolani, B. *Bull. Soc. Chim. Fr.* **1985**, 973. (d) Hagen, V.; Rühlmann, K. *Z. Chem.* **1967**, *7*, 462. For silafluorene anions, see: (e) Ishikawa, M.; Tabohashi, T.; Ohashi, H.; Kumada, M.; Iyoda, J. *Organometallics* **1983**, *2*, 351. (f) Gilman, H.; Gorsich, R. D. *J. Am. Chem. Soc.* **1958**, *80*, 3243.

(4) Freeman W. P.; Tilley, T. Don.; Rheingold, A. L. *J. Am. Chem. Soc.* **1994**, *116*, 8428.

(5) (a) Hong, J.-H.; Boudjouk, P.; Castellino, S. XXVth Organosilicon Symposium, Indianapolis, IN, March 26-27, 1993; Abstract, P-50. Hong, J.-H.; Boudjouk, P. *Abstracts of Papers*; 206th National Meeting of the American Chemical Society, Chicago, IL, August 22-27, 1993; American Chemical Society: Washington, D.C.; Abstract, INOR 492. Hong, J.-H.; Boudjouk, P.; Castellino, S. XXVIIth Organosilicon Symposium, Troy, NY, March 18-19, 1994; Abstract, P-23. (b) Hong, J.-H.; Boudjouk, P.; Castellino, S. *Organometallics* **1994**, *13*, 3387.

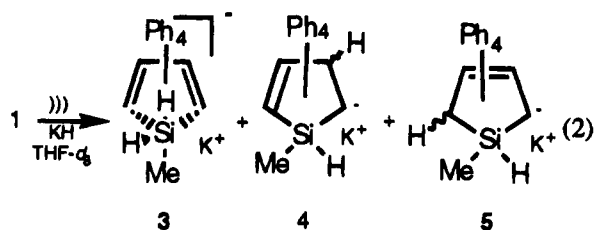
(6) (a) Corriu, R. J. P.; Guérin, C.; Kolani, B. *Bull. Soc. Chim. Fr.* **1985**, 973. (b) Corriu, R. J. P.; Guérin, C. *J. Chem. Soc. Chem. Commun.* **1980**, 168. (c) Gilman, M.; Steudel, W. *Chem. Ind.* **1959**, 1094.

(7) Han, B.-H.; Boudjouk, P. *Chungnam Kwahak Yonguchi* **1984**, *11*, 101. *Chem. Abstr.* **1986**, *105*, 6549u.

(8) (a) Chuit, C.; Corriu, R. J. P.; Reye, C.; Young, J. C. *Chem. Rev.* **1993**, *93*, 1371. (b) Corriu, R. J. P.; Young, J. C. in *The Chemistry of Organic Silicon Compounds*; Patai, S.; Rappoport, Z., Eds.; John Wiley & Sons: New York, 1989; Chapter 20, pp 1241-1288. (c) Tandura, S. N.; Alekseev, N. V.; Voronkov, M. G. *Top. Curr. Chem.* **1986**, *131*, 99-189.

spectrum and only one silicon peak (-15.61 ppm) for that group in the  $^{29}\text{Si}$  spectrum.

NMR studies of the purple solution resulting from sonication of **1** and KH for 2 h in THF- $d_8$  provide evidence for the intermediacy of three novel anions **3**, **4**, and **5** in a ratio of approximately 1:0.8:0.8, respectively.  $^1\text{H}$  NMR shows no significant methyl singlet peaks in the SiCH region which should be present if



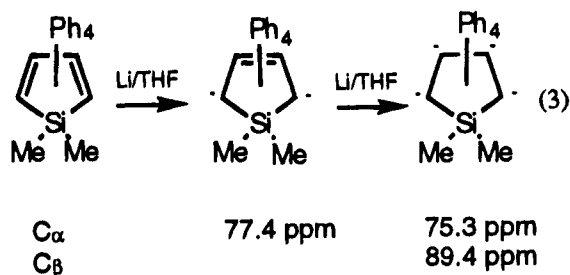
the SiH proton in **1** were removed by the hydride. Instead, the major absorptions attributable to SiCH were a triplet at 0.16 ppm and two smaller doublets at -0.23 and 0.34 ppm. In addition to these SiCH peaks, three SiH absorptions and two *tert*-CH absorptions were observed with phenyl and solvent peaks. The SiH absorptions consisted of a pair of overlapped quartets at 3.79 ppm, a quartet at 4.26 ppm, and a doublet of quartets at 5.19 ppm. The two *tert*-CH absorptions are composed of a singlet at 3.03 ppm and doublet at 3.30 ppm. The three groups of absorptions (SiCH, SiH, and *tert*-CH) are complex but all coupling relationships of SiCH, SiH, and *tert*-CH can be definitively assigned using homo decoupling experiments.

Irradiation at 3.79 ppm (overlapped quartets of SiH) collapsed the triplet of SiCH at 0.16 ppm to a singlet (**3**); irradiation at 4.26 ppm (quartet of SiH) collapsed the doublet of SiCH at 0.34 ppm to a singlet (**4**). Irradiation at 5.19 ppm (doublet of quartets of SiH) collapsed the doublet of SiCH at -0.23 ppm and the doublet of *tert*-CH at 3.30 ppm to singlets, respectively (**5**). Irradiation at 3.30 ppm (doublet of *tert*-CH) collapsed the doublet of quartets of SiH at 5.19 ppm to a quartet (**5**). The positions of the hydrogens on silicon in **3** are distinguishable: overlapped quartets of SiH (**3**) at 3.79 ppm rather than a simple quartet indicates the presence of one axial hydrogen and one equatorial hydrogen on silicon. However, the nearly identical chemical shifts of these hydrogens voided a decoupling experiment: irradiation at 0.16 ppm (the triplet of SiCH) collapsed SiH absorptions to a broad singlet rather than the anticipated pair of separated singlets. As expected,  $^2J$  ( $^1\text{H}$ - $^1\text{H}$ ) coupling was not observed because axial-equatorial coupling constants are typically very small.<sup>9</sup>

The coupled  $^{29}\text{Si}\{^1\text{H}\}$  spectrum resolved the three silicon resonances of the decoupled  $^{29}\text{Si}$  spectrum into a doublet of doublets at -36.30 ppm ( $J_{\text{Si-H}} = 192.5$  and 179.6 Hz) (**3**), a doublet at 7.92 ppm ( $J_{\text{Si-H}} = 177.8$  Hz) (**4**), and a doublet at -3.29 ppm ( $J_{\text{Si-H}} = 168.7$  Hz) (**5**).<sup>10</sup> The Si-H coupling constants in **3** are also very close to

$J(^{29}\text{Si}-^1\text{H}) = 192-225$  Hz in  $[\text{H}_2\text{Si}(\text{OR})^-][\text{K}^+]$ ,<sup>9,11</sup> and are consistent with a trigonal-bipyramidal structure in which one hydrogen and two carbons of the butadiene moiety occupy an equatorial position.

In  $^{13}\text{C}$  NMR, three methyl carbons on silicon are observed at -6.80 ppm for **3**, at -0.70 ppm for **4**, and at -5.02 ppm for **5**; two carbons of *tert*-CH at 45.16 ppm for **4**, 43.22 ppm for **5**; two carbanions of *tert*-C $^-$  at 85.78 ppm for **4** and at 86.20 ppm for **5**. All of these peaks are confirmed by INEPT experiments and are matched to their proton peaks by  $^{13}\text{C}$ - $^1\text{H}$  2D experiments. Both chemical shifts of the two *tert*-C $^-$  are consistent with the observations of O'Brien, in which chemical shifts of the carbanions of 1,1-dimethyl-2,3,4,5-tetraphenyl-1-silacyclopentadiene are observed from 75.3 to 89.4 ppm (eq 3).<sup>12</sup>



The carbanions in **4** and **5** polarize the attached phenyl groups. The chemical shifts of  $\text{C}_p$  and  $\text{C}_m$  in the two phenyl groups are shifted upfield, the chemical shifts of  $\text{C}_p$  are farther upfield than those of  $\text{C}_m$ : 110.75 ppm for  $\text{C}_p$  and 114.93 ppm for  $\text{C}_m$  of the phenyl bonded to *tert*-C $^-$  of **4** and 111.38 ppm for  $\text{C}_p$  and 115.38 ppm for  $\text{C}_m$  of the phenyl bonded to *tert*-C $^-$  of **5**. Similar polarization of phenyl groups has been observed in other silole anions.<sup>3a, 5b</sup> Moreover, all 16 *tert*-C peaks (4 from **3** due to its mirror plane, 6 from **4**, and 6 from **5**) are observed and confirmed by INEPT experiments. Of the possible 26 peaks in the aromatic CH region ( $\text{C}_o$ ,  $\text{C}_m$ , and  $\text{C}_p$ : originally 26 peaks in 123-131 ppm, 6 from **3** due to its mirror plane, 10 from **4**, and 10 from **5**), 18 were observed and could be assigned. Presumably, accidental overlap of some peaks is responsible for the reduced number of peaks.

In  $^1\text{H}$  NMR we observed that the smaller pairs of doublets for **4** and **5** increased with time. Simultaneously, we also observed that **3** diminished to a final ratio of approximately 1:1.4:1.4 for **3**:**4**:**5**, respectively. No evidence that **3** is the source of **4** and/or **5** or that an equilibrium is operating was obtained.

We also determined that the singlet peak attributed to a methyl on silicon in the 1-methyl-2,3,4,5-tetraphenylsilacyclopentadienide anion in an earlier report<sup>7</sup> is actually the methyl peak on polymethylsiloxane which forms when water is present in the reaction mixture. Base cleavage of both Si-C bonds in silole rings has been reported.<sup>13</sup>

## Conclusions

Potassium hydride undergoes an addition reaction with 1-methyl-2,3,4,5-tetraphenyl-1-silacyclopentadiene

(9) Corriu, P.; Guérin, C.; Henner, B.; Wang, Q. *Organometallics* **1991**, *10*, 3574.

(10) For a discussion of the effects on chemical shift of forming a pentacoordinate bond to silicon, see: Williams E. A. In *The Chemistry of Organic Silicon Compounds*; Patai, S.; Rappoport, Z., Eds.; New York, Wiley, 1989; pp 537-540.

(11) Corriu, R. J. P.; Guérin, C.; Henner, B.; Wang, Q. *Organometallics* **1991**, *10*, 2297.

(12) O'Brien, D. H.; Breeden, D. *J. Am. Chem. Soc.* **1981**, *103*, 3237.

(13) (a) Atwell, W. H.; Weyenberg, D. R.; Gilman, H. *J. Org. Chem.* **1976**, *32*, 885. (b) Balasubramanian, R.; Gerge, M. V. *J. Organomet. Chem.* **1975**, *85*, 311. (c) Curtis, M. *J. Am. Chem. Soc.* **1969**, *91*, 6011.

Table 1.  $^1\text{H}$ ,  $^{13}\text{C}$ , and  $^{29}\text{Si}$  Chemical Shifts of **1** and **3**–**5**

		$1^a$	$3^b$	$4^b$	$5^b$
$^1\text{H}$	SiMe	0.57 (d, 3H, $J = 4.15$ )	0.16 (t, 3H, $J = 4.40$ )	0.34 (d, 3H, $J = 3.66$ )	-0.23 (d, 3H, $J = 3.66$ )
	SiH	5.00 (q, 1H, $J = 4.15$ )	3.79 (overlapped q, 2H)	4.26 (q, 1H, $J = 3.66$ )	5.19 (q of d, 1H)
	CH	none	none	3.03 (s, 1H)	3.30 (d, 1H, $J = 4.40$ )
$^{13}\text{C}$	SiMe	-6.94	-6.80	-0.70	-5.02
	CH	none	none	45.16	43.22
	C <sup>-</sup>	none	none	85.78	86.20
	C <sub>p</sub> of C <sup>-</sup>	none	none	110.75	111.38
	C <sub>m</sub> of C <sup>-</sup>	none	none	114.93	115.80
$^{29}\text{Si}$	Si of ring	-11.81	-36.30 (dd, $J_{\text{SiHa}} = 192.5$ , $J_{\text{SiHe}} = 179.6$ )	7.92 (d, $J_{\text{SiH}} = 177.8$ )	-3.28 (d, $J_{\text{SiH}} = 168.7$ )

<sup>a</sup> In  $\text{CDCl}_3$ , reference;  $\text{CDCl}_3 = 7.27$  ppm for  $^1\text{H}$ -NMR,  $\text{CDCl}_3 = 77.00$  ppm for  $^{13}\text{C}$ -NMR, external  $\text{Me}_4\text{Si} = 0.00$  ppm for  $^{29}\text{Si}$ -NMR. <sup>b</sup> In  $\text{THF}-d_8$ , reference;  $\text{THF}-d_8 = 1.73$  ppm for  $^1\text{H}$ -NMR,  $\text{THF}-d_8 = 25.30$  ppm for  $^{13}\text{C}$ -NMR, external  $\text{Me}_4\text{Si} = 0.00$  ppm for  $^{29}\text{Si}$ -NMR.

(1) to form the pentavalent anion, 1-methyl-1,1-dihydrido-2,3,4,5-tetraphenyl-1-silacyclopentadiene silicate,  $[\text{Ph}_4\text{C}_4\text{SiMeH}_2]^-[\text{K}^+]$  (**3**), unique in its composition because of the absence of electronegative atoms on silicon, and two isomeric anions in which the negative charge is on carbon. NMR studies were able to distinguish the axial and equatorial hydrogens in **3**. These results provide strong evidence in support of Corriu's postulation that hypervalent silicon dihydrides are formed in the racemization of 1-NpPhMeSi\*H<sup>14</sup> and of Ishikawa's proposal that silyllithium and organolithium reagents may add to siloles and silafluorenes to give silicates.<sup>15</sup> This study also corrects the earlier report<sup>7</sup> that potassium hydride abstracts a proton from **1**.

### Experimental Section

**General Procedures.** All reactions were performed under an inert nitrogen atmosphere using standard Schlenk techniques. Air-sensitive reagents were transferred in a nitrogen-filled glovebox. THF and DME were distilled from sodium benzophenone ketyl under nitrogen. Hexane was stirred over concentrated  $\text{H}_2\text{SO}_4$  and distilled from  $\text{CaH}_2$ . NMR spectra were recorded on JEOL GSX270 and GSX400 spectrometers. GC-MS and solid sample MS data were obtained on a Hewlett-Packard 5988A GC-MS system equipped with a methyl silicon capillary column. Elemental analyses were done by Desert Analytics (Tucson, AZ).

**1-Methyl-2-(dimethylsilyl)-2,3,4,5-tetraphenyl-1-silacyclo-3-pentene (2).** 1-Methyl-2,3,4,5-tetraphenyl-1-silacyclopentadiene (**1**)<sup>16</sup> (2.50 g, 5.50 mmol) and KH (0.27 g, 6.73 mmol, 1.22 equiv) were placed in a 100 mL flask with 60 mL DME. After stirring at  $-20^\circ\text{C}$  for 40 min, the greenish yellow slurry turned bright red and finally dark purple. Stirring was continued for 8 h at  $-20^\circ\text{C}$ . Filtration of the mixture under nitrogen produced a deep violet solution. This solution was added to an excess of  $\text{Me}_2\text{SiHCl}$  (1.20 mL, 11.0 mmol) in DME at room temperature. Stirring for an additional 3 h produced

a greenish yellow solution. After removing solvent and  $\text{Me}_2\text{SiHCl}$  under reduced pressure, the residual solid was extracted with hexane. Several recrystallizations in hexane gave **2** as colorless crystals (yields: 71% in DME at  $-20^\circ\text{C}$ , 43% in THF  $-20^\circ\text{C}$ , 30% in THF at room temperature), mp, 132–133  $^\circ\text{C}$ ;  $^1\text{H}$  and  $^{13}\text{C}$  NMR patterns of **2** in  $\text{CDCl}_3$  are not different from in benzene- $d_6$ .  $^1\text{H}$ -NMR ( $\text{CDCl}_3$ , ref: solvent = 7.27 ppm), 0.21 (d, 3H,  $\text{SiMe}_2$ ,  $^3J_{\text{Me-H}} = 3.66$  Hz), 0.33 (d, 3H,  $\text{SiMe}_2$ ,  $^3J_{\text{Me-H}} = 3.66$  Hz), 0.60 (d, 3H,  $\text{SiMe}$ ,  $^3J_{\text{Me-H}} = 3.66$  Hz), 3.86 (d, 1H, CH,  $^3J_{\text{H-H}} = 4.40$  Hz), 4.03 (quint, 1H, SiH), 4.49 (sept, 1H, SiH,  $^3J_{\text{Me-H}} = 3.66$  Hz), 6.9–7.8 (brd m, 20 H, Ph).  $^{13}\text{C}$ -NMR ( $\text{CDCl}_3$ , ref: solvent = 77.00 ppm), -4.26 (SiMe), -4.63, -4.71 ( $\text{SiMe}_2$ ), 39.85 (*tert*-CH), 43.33 (CSiMe<sub>2</sub>H), 124.22, 124.28, 125.91, 126.65 (para carbons of four phenyl groups), 127.21, 127.34, 127.90, 128.11, 128.42, 129.01, 130.17, 130.96 (ortho and meta carbons of four phenyl groups), 139.92, 141.48, 142.32, 143.49, 144.81, 146.76 (C<sub>3</sub>, C<sub>4</sub>, and ipso carbons of four phenyl groups).  $^{29}\text{Si}$ -NMR ( $\text{CDCl}_3$ , ref: ext TMS), -15.61 (HSiMe<sub>2</sub>), 28.45 (HSiMe). MS ( $M^+$ , relative abundance)  $m/z$  461 ( $M^+ + 1$ , 5), 460 ( $M^+$ , 13), 400 ( $M^+ - 60$ , 100), 197 (48), 121 (74), 59 (50). Anal. Calcd for  $\text{C}_{34}\text{H}_{32}\text{Si}_2$ : C, 80.81; H, 7.00. Found: C, 81.13; H, 6.94.

**NMR Study of the Reaction of 1-Methyl-2,3,4,5-tetraphenyl-1-silacyclopentadiene (1) with KH.** 1-Methyl-2,3,4,5-tetraphenyl-1-silacyclopentadiene (**1**) (0.141 g, 0.351 mmol) and KH (0.018 g, 0.45 mmol, 1.27 equiv) were placed in a 5-mm NMR tube followed by  $\text{THF}-d_8$  (1.5 mL). Sonication of the NMR tube for 2 h changed the color of the solution from yellow to red and finally to a deep violet. NMR studies were carried out on samples prepared in this fashion.  $^1\text{H}$ ,  $^1\text{H}$ - $^1\text{H}$  homo decoupled,  $^{13}\text{C}$ , INEPT  $^{13}\text{C}$ ,  $^1\text{H}$ - $^{13}\text{C}$  coupled 2D,  $^{29}\text{Si}$ -NMR, and  $^{29}\text{Si}$ -proton coupled NMR data were obtained and are listed in Table 1.  $^{13}\text{C}$  NMR data not included in Table 1: 158.21, 157.44, 150.96, 149.37, 148.88, 148.80, 147.05, 146.99, 146.02, 145.80, 130.51, 128.85, 128.05, 126.95, 111.53, 111.38 (*tert*-C), 131.05, 128.78, 128.51, 128.33, 128.17, 127.75, 127.59, 127.30, 127.25, 126.69, 125.53, 125.16, 124.74, 124.26, 123.07, 122.99, 115.57, 114.75 (aromatic CH).

**Acknowledgment.** Financial support from the Air Force Office of Scientific Research through Grants 91-0197 and F49620-92-J-0431, the National Science Foundation through Grant No. EHR-9108770, and the Korea Science and Engineering Foundation (J.-H.H) is gratefully acknowledged.

OM9405910

(14) Brefort, J. L.; Corriu, R.; Guérin; Henner, B. *J. Organomet. Chem.* **1989**, *370*, 9.

(15) (a) Ishikawa, M.; Tabohashi, T.; Sugisawa, H.; Nishimura, K.; Kumada, M. *J. Organomet. Chem.* **1983**, *250*, 109. (b) Ishikawa, M.; Tabohashi, T.; Ohashi, H.; Kumada, M.; Iyoda, J. *Organometallics* **1983**, *2*, 351. (c) Ishikawa, M.; Nishimura, K.; Sugisawa, H.; Kumada, M. *J. Organomet. Chem.* **1981**, *218*, C21.

(16) Boudjouk, P.; Sooriyakumaran, R.; Han, B.-H. *J. Org. Chem.* **1986**, *51*, 2818.

Tin *N*-*tert*-Butylanilide Compounds

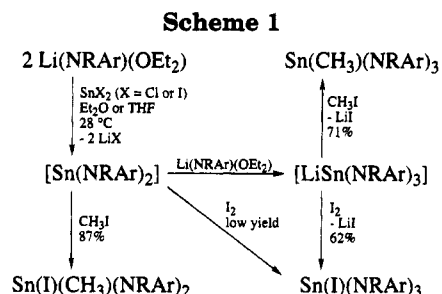
Catalina E. Laplaza, William M. Davis, and Christopher C. Cummins\*

Department of Chemistry, Massachusetts Institute of Technology,  
Cambridge, Massachusetts 02139Received September 1, 1994<sup>®</sup>

**Summary:** Through a combination of salt-elimination and oxidative-addition processes, three new Sn(IV) compounds have been prepared. The derivatives Sn(X)(NRAr)<sub>3</sub> (X = CH<sub>3</sub>, I; R = C(CD<sub>3</sub>)<sub>2</sub>CH<sub>3</sub>; Ar = 3,5-C<sub>6</sub>H<sub>3</sub>-Me<sub>2</sub>) were prepared via an "ate" complex formulated as LiSn(NRAr)<sub>3</sub>, whereas Sn(I)(CH<sub>3</sub>)(NRAr)<sub>2</sub> was obtained by addition of methyl iodide to Sn(NRAr)<sub>2</sub>.

We are currently developing the transition-metal and main-group coordination chemistry of the bulky nitrogen donor ligand NRAr (R = C(CD<sub>3</sub>)<sub>2</sub>CH<sub>3</sub>, Ar = 3,5-C<sub>6</sub>H<sub>3</sub>-Me<sub>2</sub>), an example of an *N*-*tert*-butylanilide ligand. This ligand contains deuterium in the *tert*-butyl group, both to facilitate the ligand synthesis<sup>1</sup> and to provide a spectroscopic handle (<sup>2</sup>H NMR) that is particularly useful for paramagnetic systems,<sup>2</sup> though only diamagnetic compounds are considered in this contribution. Bulky nitrogen donor ligands have played a prominent role in the development of low-valent tin chemistry.<sup>3</sup> Herein we detail the synthesis of HNRAr and give an account of our experiments involving low-valent tin, experiments which resulted in the discovery of synthetic methods for preparing three new compounds containing Sn(IV).

Scheme 1 illustrates chemistry revolving around the Sn(II) entity Sn(NRAr)<sub>2</sub>. Treatment of an ethereal slurry of either stannous chloride or stannous iodide with Li(NRAr)(OEt<sub>2</sub>) (2 equiv) generates orange-red Sn(NRAr)<sub>2</sub>, which is stable in solution. In THF the compound exhibits a single <sup>2</sup>H NMR signal at 1.48 ppm. Sn(NRAr)<sub>2</sub> decomposes upon attempted isolation, giving products we have not yet identified. Oxidative addition of methyl iodide to Sn(NRAr)<sub>2</sub> is rapid and clean, permitting Sn(I)(CH<sub>3</sub>)(NRAr)<sub>2</sub> to be isolated as a pale yellow powder in high yield.<sup>4</sup> Formulation of this product as a monomethyl Sn(IV) compound is indicated,



in part, by the observation of a quartet in the <sup>119</sup>Sn NMR at -188.2 ppm (<sup>2</sup>J<sub>SnH</sub> = 71 Hz).

Oxidation of Sn(NRAr)<sub>2</sub> with iodine is more complicated. The only product we were able to isolate from the reaction of Sn(NRAr)<sub>2</sub> with iodine is Sn(I)(NRAr)<sub>3</sub>, and this was obtained in low yield. This led us to speculate that an "ate" complex, LiSn(NRAr)<sub>3</sub>, is accessible in ethereal, salt-containing solutions of Sn(NRAr)<sub>2</sub>. Furthermore, we thought it should be possible to generate the "ate" complex exclusively, by treating ethereal stannous halide with 3 equiv of Li(NRAr)(OEt<sub>2</sub>).<sup>5</sup> These speculations were substantially borne out, in that Sn(CH<sub>3</sub>)(NRAr)<sub>3</sub> was obtained in good yield by sequential treatment of SnI<sub>2</sub> with 3 equiv of Li(NRAr)(OEt<sub>2</sub>) and excess methyl iodide. This new monomethyl Sn(IV) compound exhibits a quartet in the <sup>119</sup>Sn NMR at -132.2 ppm (<sup>2</sup>J<sub>SnH</sub> = 68 Hz). Sequential treatment of SnCl<sub>2</sub> with Li(NRAr)(OEt<sub>2</sub>) (3 equiv) and the stoichiometric amount of iodine gave Sn(I)(NRAr)<sub>3</sub> efficiently.

X-ray crystallography was used to determine the structure of Sn(CH<sub>3</sub>)(NRAr)<sub>3</sub> and Sn(I)(NRAr)<sub>3</sub> (Figures 1 and 2, Tables 1 and 2).<sup>6</sup> Both evince a coordination geometry that approaches regular tetrahedral. Both compounds have a C<sub>3</sub> axis relating the three *N*-*tert*-butylanilide ligands. The *N*-*tert*-butylanilide ligands themselves are characterized by planar nitrogen atoms, large Sn–N–R angles, and small R–N–Ar angles. Steric interactions appear to dictate the near-perpendicular orientation of the aryl ring relative to the adjacent nitrogen trigonal plane; this orientation minimizes unfavorable interactions involving the aryl ortho hydrogens and precludes overlap between the nitrogen lone pair and the aryl π-system. The nitrogen trigonal plane is tilted with respect to the C<sub>3</sub> axis, by a dihedral angle of 42.9° (C1–Sn–N–C10) in the case of the methyl compound, as compared with 37.0° (I–Sn–N–C9) for the iodide compound. Even so, the bond angles

<sup>®</sup> Abstract published in *Advance ACS Abstracts*, December 1, 1994.

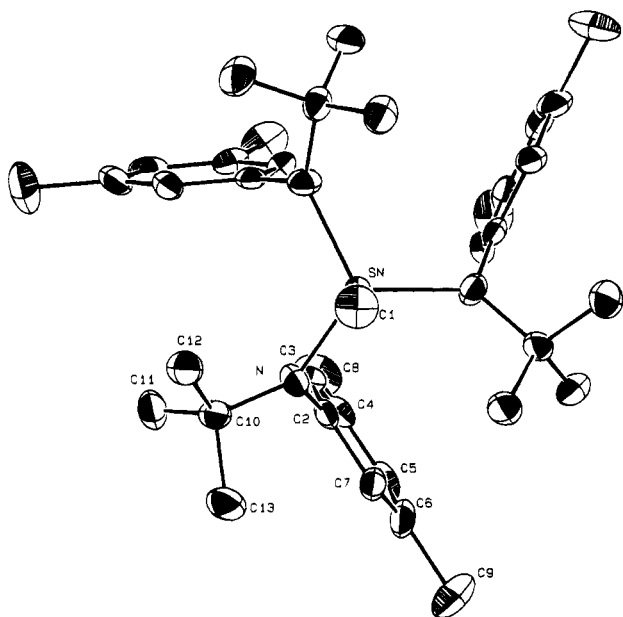
(1) The ligand synthesis involves addition of methylolithium to the imine prepared from acetone-*d*<sub>6</sub> and 3,5-dimethylaniline, followed by aqueous workup. Literature precedent shows that the yield is very low if the imine contains enolizable hydrogens; a 9% yield has been reported for *N*-*tert*-butylaniline by this procedure: Hunter, D. H.; Racoc, J. S.; Rey, A. W.; Ponce, Y. *J. Org. Chem.* **1988**, *53*, 1278. Our yield is much higher due to the substantial primary kinetic isotope effect associated with removal of a deuteron from the *d*<sub>6</sub> imine (see Experimental Section).

(2) The utility of <sup>2</sup>H NMR in studying paramagnetic systems has been addressed both experimentally and theoretically. See: La Mar, G. N.; Horrocks, W. D., Jr.; Holm, R. H. *NMR of Paramagnetic Molecules*; Academic Press: New York, 1973. See also: Johnson, A.; Everett, G. W., Jr. *J. Am. Chem. Soc.* **1972**, *94*, 1419. Also, Sen and co-workers have recently employed the technique in studying the reaction between anionic iron(0) olefin complexes and organic halides: Hill, D. H.; Parvez, M. A.; Sen, A. *J. Am. Chem. Soc.* **1994**, *116*, 2889.

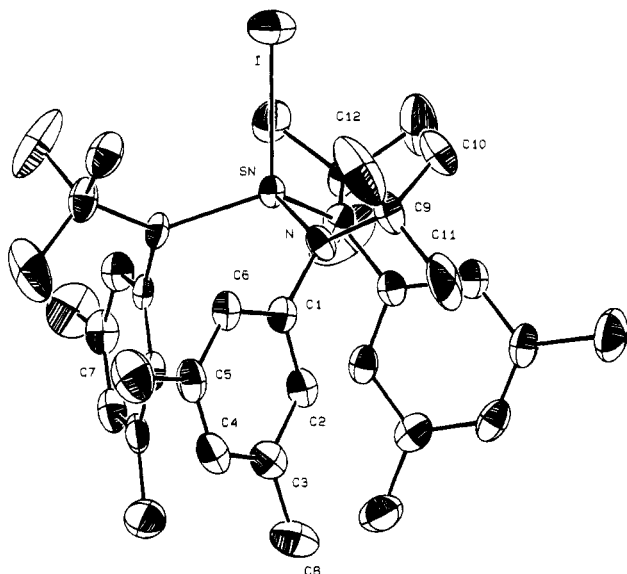
(3) Gynane, M. J. S.; Harris, D. H.; Lappert, M. F.; Power, P. P.; Rivière, P.; Rivière-Baudet, M. *J. Chem. Soc., Dalton Trans.* **1977**, 2004.

(4) For the synthesis of Sn(I)(CH<sub>3</sub>)(N(SiMe<sub>3</sub>)<sub>2</sub>)<sub>2</sub> by treatment of Sn(N(SiMe<sub>3</sub>)<sub>2</sub>)<sub>2</sub> with methyl iodide, see: Lappert, M. F.; Misra, M. C.; Onyschuk, M.; Rowe, R. S.; Power, P. P.; Slade, M. *J. Organomet. Chem.* **1987**, *330*, 31.

(5) Group 14 organometallic anions are sometimes prepared by treatment of a divalent halide with 3 equiv of a Grignard reagent; for the in situ synthesis of Ph<sub>3</sub>PbMgBr see: Seyferth, D.; Son, D. Y.; Shah, S. *Organometallics* **1994**, *13*, 2105. The crystal structure of a tripodal tris(amido)stannate has recently been reported: Hellmann, K. W.; Steinert, P.; Gade, L. H. *Inorg. Chem.* **1994**, *33*, 3859. The latter paper includes several references to other tris(amido)stannates.



**Figure 1.** ORTEP drawing of  $\text{Sn}(\text{CH}_3)(\text{NRAr})_3$  ( $\text{R} = \text{C}(\text{CD}_3)_2\text{CH}_3$ ,  $\text{Ar} = 3,5\text{-C}_6\text{H}_3\text{Me}_2$  (with ellipsoids at the 35% probability level. Selected bond lengths ( $\text{\AA}$ ):  $\text{Sn}-\text{C}(1)$ , 2.151(8);  $\text{Sn}-\text{N}$ , 2.044(4). Selected bond angles (deg):  $\text{C}(1)-\text{Sn}-\text{N}$ , 110.2(1);  $\text{N}-\text{Sn}-\text{N}$ , 108.7(1);  $\text{Sn}-\text{N}-\text{C}(10)$ , 126.2(3);  $\text{Sn}-\text{N}-\text{C}(2)$ , 118.8(2).



**Figure 2.** ORTEP drawing of  $\text{Sn}(\text{I})(\text{NRAr})_3$  ( $\text{R} = \text{C}(\text{CD}_3)_2\text{CH}_3$ ,  $\text{Ar} = 3,5\text{-C}_6\text{H}_3\text{Me}_2$ ) with ellipsoids at the 35% probability level. Selected bond lengths ( $\text{\AA}$ ):  $\text{Sn}-\text{I}$ , 2.752(1);  $\text{Sn}-\text{N}$ , 2.026(5). Selected bond angles (deg):  $\text{I}-\text{Sn}-\text{N}$ , 109.1(1);  $\text{N}-\text{Sn}-\text{N}$ , 109.8(1);  $\text{Sn}-\text{N}-\text{C}(9)$ , 127.5(4);  $\text{Sn}-\text{N}-\text{C}(1)$ , 117.3(3).

about nitrogen are very similar for the two compounds. A slightly shorter  $\text{Sn}-\text{N}$  distance was observed for  $\text{Sn}(\text{I})(\text{NRAr})_3$  as compared with  $\text{Sn}(\text{CH}_3)(\text{NRAr})_3$ , consistent with a more electrophilic tin center in the former.<sup>7</sup> If the solid-state structure of either compound were retained in solution, then two  $^1\text{H}$  NMR signals would be expected for the inequivalent aryl ortho hydrogens. In both cases only one signal is observed at 25  $^\circ\text{C}$ , indicating that rotation about the  $\text{Sn}-\text{N}$  and/or the  $\text{N}-\text{Ar}$  linkage is facile. The  $\text{Sn}(\text{X})(\text{NRAr})_3$  ( $\text{X} = \text{CH}_3, \text{I}$ ) compounds are very similar in structure to  $\text{Ti}(\text{Cl})(\text{NRAr})_3$ .<sup>8</sup>

**Table 1.** Positional Parameters for  $\text{Sn}(\text{CH}_3)(\text{NRAr})_3$

atom	x	y	z
Sn	$2/3$	$1/3$	0.04235(2)
N	0.6679(3)	0.2125(3)	0.0708(1)
C(1)	$2/3$	$1/3$	-0.0441(3)
C(2)	0.6072(3)	0.1612(3)	0.1163(2)
C(3)	0.6403(3)	0.1905(3)	0.1687(2)
C(4)	0.5837(4)	0.1412(3)	0.2129(2)
C(5)	0.4921(4)	0.0612(4)	0.2046(2)
C(6)	0.4564(3)	0.0287(4)	0.1529(2)
C(7)	0.5150(3)	0.0801(3)	0.1091(2)
C(8)	0.6230(4)	0.1712(4)	0.2692(2)
C(9)	0.3554(4)	-0.0607(5)	0.1442(2)
C(10)	0.7286(3)	0.1717(3)	0.0498(2)
C(11)	0.7902(4)	0.1634(4)	0.0938(2)
C(12)	0.7954(4)	0.2378(4)	0.0060(2)
C(13)	0.6619(4)	0.0692(4)	0.0253(2)

**Table 2.** Positional Parameters for  $\text{Sn}(\text{I})(\text{NRAr})_3$

atom	x	y	z
I	$2/3$	$1/3$	-0.06156(3)
Sn	$2/3$	$1/3$	0.04788(3)
N	0.7830(3)	0.3249(4)	0.0743(2)
C(1)	0.8365(4)	0.3859(4)	0.1189(2)
C(2)	0.8067(4)	0.3540(5)	0.1696(3)
C(3)	0.8578(5)	0.4089(6)	0.2145(3)
C(4)	0.9403(5)	0.4978(5)	0.2054(3)
C(5)	0.9723(5)	0.5325(5)	0.1552(3)
C(6)	0.9200(5)	0.4756(5)	0.1114(2)
C(7)	1.0638(7)	0.6285(6)	0.1470(4)
C(8)	0.8255(6)	0.3701(6)	0.2688(3)
C(9)	0.8252(5)	0.2680(5)	0.0507(3)
C(10)	0.7519(6)	0.1881(5)	0.0153(3)
C(11)	0.8509(9)	0.2193(8)	0.0949(4)
C(12)	0.9143(7)	0.3327(7)	0.0176(5)

## Experimental Section

**General Details.** Manipulations were carried out under an atmosphere of dry, oxygen-free nitrogen, in a Vacuum Atmospheres drybox, unless otherwise indicated. THF, ether, pentane, hexane, benzene, and benzene- $d_6$  were distilled from purple sodium benzophenone ketyl. Acetone- $d_6$  was purchased from Isotec and used as received. Iodine was sublimed prior to use.  $\text{CH}_3\text{I}$  was distilled from calcium hydride and stored with 4  $\text{\AA}$  molecular sieves.  $\text{SnI}_2$  (ultra dry, 99.999%) was purchased from Aesar/Johnson Matthey, as was  $\text{SnCl}_2$  (anhydrous, 98%). 3,5-Dimethylaniline was purchased from Aldrich. Molecular sieves (4  $\text{\AA}$ ) were activated by heating to 200  $^\circ\text{C}$  overnight under a vacuum of approximately 0.05 Torr. NMR spectra were obtained on Varian XL-300 instruments.  $^1\text{H}$  and  $^{13}\text{C}$  NMR chemical shifts (ppm) are reported with respect to internal solvent resonances (respectively 7.15 and 128.00 ppm).  $^2\text{H}$  and  $^{119}\text{Sn}$  NMR chemical shifts (ppm) are reported with respect to external  $\text{C}_6\text{D}_6$  and  $\text{SnMe}_4$  (respectively 7.15 and 0 ppm). CHN microanalyses were performed by Oneida Research Services, Inc. Melting points were obtained in sealed glass capillaries and are uncorrected.

**Preparation of Compounds.**  $\text{ArN}=\text{C}(\text{CD}_3)_2$  ( $\text{Ar} = 3,5\text{-C}_6\text{H}_3\text{Me}_2$ ).<sup>9</sup> Freshly distilled 3,5-dimethylaniline (48.24 g, 398.1 mmol) and 4  $\text{\AA}$  molecular sieves (90 g) were added to a flask, which was then fitted with a vacuum adapter. Acetone- $d_6$  (ca. 200 mL, 272 mmol) was then introduced via vacuum transfer. The resulting mixture was stored at 0  $^\circ\text{C}$  under static vacuum for 3.5 days, with occasional stirring each day. The molecular sieves were removed by filtration through a sintered-glass frit, and the filter cake was washed with additional cold acetone- $d_6$ . The excess acetone- $d_6$  was recovered from the filtrate by vacuum transfer, leaving the desired imine as a pale yellow oil (57.43 g, 343.3 mmol). More of the imine (7.17 g, 42.9 mmol) was obtained by immersing the collected sieves in pentane (ca. 100 mL) overnight, followed by filtration and removal of the pentane in vacuo. The total yield of  $\text{ArN}=\text{C}(\text{CD}_3)_2$  was 64.60 g (386.2 mmol, 97%).  $^1\text{H}$  NMR ( $\text{C}_6\text{D}_6$ ): 6.60



(s, 1, para Ar H), 6.44 (s, 2, ortho Ar H), 2.15 (s, 6, Ar CH<sub>3</sub>). <sup>2</sup>H NMR (C<sub>6</sub>H<sub>6</sub>): 1.80 (s, 3, CD<sub>3</sub>), 1.35 (s, 3, CD<sub>3</sub>). <sup>13</sup>C NMR (C<sub>6</sub>D<sub>6</sub>): 166.66 (N=C(CD<sub>3</sub>)<sub>2</sub>), 152.65 (C aryl ipso), 138.41 (C aryl meta), 124.72 (C aryl), 117.51 (C aryl), 27.6 (CD<sub>3</sub>), 21.37 (Ar CH<sub>3</sub>), 19.40 (CD<sub>3</sub>).

**H(NRAr) (R = C(CD<sub>3</sub>)<sub>2</sub>CH<sub>3</sub>, Ar = 3,5-C<sub>6</sub>H<sub>3</sub>Me<sub>2</sub>).** A frozen solution of CH<sub>3</sub>Li (1.4 M in ether, 250 mL, 350 mmol) was allowed to thaw until magnetic stirring became possible, at which point a solution of ArN=C(CD<sub>3</sub>)<sub>2</sub> (23.87 g, 143 mmol) in 40 mL of ether was added dropwise, via pipet, over a few minutes. The reaction mixture was warmed to 28 °C (gas evolution was observed after approximately 25 min), and stirring was continued for 40 h. The reaction mixture was then carefully poured into a 1 L Erlenmeyer flask containing one-third its volume of ice. Petroleum ether (200 mL) was added. After the ice had melted completely, the mixture was transferred to a separatory funnel and the organic layer was separated. The aqueous layer was extracted with additional petroleum ether (2 × 100 mL). The combined organic extracts were flash-filtered through a column of alumina (2 × 20 cm). Additional petroleum ether was used to fully elute the product, giving a final filtrate volume of approximately 900 mL. The solvent was removed in vacuo to provide a yellow oil which proved (according to NMR analysis) to be a mixture of ArN=C(CD<sub>3</sub>)(CD<sub>2</sub>H) and the desired H(NRAr). The oil was stirred with distilled water (225 mL), and concentrated HCl (ca. 25 mL) was added dropwise over 15 min, producing a milky white precipitate. After the mixture was stirred for 4.5 h, aqueous KOH was added via pipet until the white precipitate dissolved, the yellow oil separated, and the pH was >12. Petroleum ether (250 mL) was added, and the mixture was transferred to a separatory funnel. The organic layer was separated, and the aqueous layer was washed with additional petroleum ether (2 × 200 mL). The combined organic extracts were filtered through alumina as before, using additional petroleum ether to fully elute the product, giving a final filtrate volume of 900 mL. Removal of the solvent in vacuo left the desired aniline,

(6) X-ray structure of Sn(I)(NRAr)<sub>3</sub>: a crystal of approximate dimensions 0.28 × 0.28 × 0.28 mm was obtained by slow evaporation of a hexane solution. The crystal was mounted on a glass fiber. Data were collected at 23 °C on an Enraf-Nonius CAD-4 diffractometer with graphite-monochromated Mo Kα radiation. A total of 2176 reflections were collected to a 2θ value of 44.9°, 1905 of which were unique (*R*<sub>int</sub> = 0.032); equivalent reflections were merged. The structure was solved by direct methods. Non-hydrogen atoms were refined anisotropically. The final cycle of least-squares refinement was based on 1329 observed reflections (*I* > 3.00σ(*I*)) and 125 variable parameters and converged (largest parameter shift was 0.01 times its esd) with *R* = 0.042 and *R*<sub>w</sub> = 0.048. A final difference Fourier map showed no chemically significant features. Crystal data are *a* = 15.853(1) Å, *c* = 25.142(2) Å, *V* = 5472(1) Å<sup>3</sup>, space group *R*3̄ (h, No. 148), *Z* = 6, *M*<sub>r</sub> = 792.57 for C<sub>36</sub>H<sub>36</sub>D<sub>18</sub>N<sub>3</sub>ISn, and ρ(calcd) = 1.410 g/cm<sup>3</sup>. Fractional coordinates are given in Table 2. X-ray structure of Sn(CH<sub>3</sub>)(NRAr)<sub>3</sub>: a colorless parallelepiped crystal 0.50 × 0.50 × 0.60 mm was obtained by cooling a pentane solution to -35 °C. The crystal was mounted on a glass fiber under a stream of N<sub>2</sub>. Data were collected at -72 °C on an Enraf-Nonius CAD-4 diffractometer with graphite-monochromated Mo Kα radiation. A total of 910 reflections were collected to a 2θ value of 44.9°, 906 of which were unique (*R*<sub>int</sub> = 0.524); equivalent reflections were merged. The structure was solved by the Patterson method. Non-hydrogen atoms were refined anisotropically. The final cycle of full-matrix least-squares refinement was based on 872 observed reflections (*I* > 3.00σ(*I*)) and 125 variable parameters and converted (largest parameter shift was 0.00 times its esd) with *R* = 0.027 and *R*<sub>w</sub> = 0.039. A final difference Fourier map showed no chemically significant features. Crystal data are *a* = 15.791(1) Å, *c* = 24.885(1) Å, *V* = 5373.9(9) Å<sup>3</sup>, space group *R*3̄ (h, No. 148), *Z* = 6, *M*<sub>r</sub> = 680.70 for C<sub>37</sub>H<sub>39</sub>D<sub>18</sub>N<sub>3</sub>Sn, and ρ(calcd) = 1.228 g/cm<sup>3</sup>. Fractional coordinates are given in Table 1.

(7) The Sn-N distances for Sn(I)(NRAr)<sub>3</sub> and Sn(CH<sub>3</sub>)(NRAr)<sub>3</sub> are both slightly smaller than the 2.056(7) Å distance observed for Sn(Br)(N(SiMe<sub>3</sub>)<sub>2</sub>)<sub>3</sub>.<sup>4</sup>

(8) We recently reported the synthesis and structure of Ti(Cl)(NRAr)<sub>3</sub> in connection with the cleavage of titanium dimethylamides using methyl iodide: Johnson, A. R.; Wanandi, P. W.; Cummins, C. C.; Davis, W. M. *Organometallics* 1994, 13, 2907.

(9) Our imine was prepared according to the procedure given by Eaton and Tong (Eaton, D. R.; Tong, J. P. K. *Inorg. Chem.* 1980, 19, 740) with the substitution of acetone-*d*<sub>6</sub> for acetone.

H(NRAr), as a light yellow oil (13.44 g, 73.31 mmol, 51%). <sup>1</sup>H NMR (C<sub>6</sub>D<sub>6</sub>): 6.43 (s, 1, para Ar H), 6.33 (s, 2, ortho Ar H), 3.06 (s, 1, NH), 2.18 (s, 6, Ar CH<sub>3</sub>), 1.16 (s, 3, C(CD<sub>3</sub>)<sub>2</sub>(CH<sub>3</sub>)). <sup>2</sup>H NMR (C<sub>6</sub>H<sub>6</sub>): 1.02 (s, C(CD<sub>3</sub>)<sub>2</sub>(CH<sub>3</sub>)). <sup>13</sup>C NMR (C<sub>6</sub>H<sub>6</sub>): 147.53 (s, C aryl ipso), 138.19 (q, C aryl meta), 120.62 (d, C aryl), 115.96 (d, C aryl), 50.74 (s, C(CD<sub>3</sub>)<sub>2</sub>CH<sub>3</sub>), 30.08 (q, C(CD<sub>3</sub>)<sub>2</sub>CH<sub>3</sub>), 29.56 (m, C(CD<sub>3</sub>)<sub>2</sub>CH<sub>3</sub>), 21.70 (q, Ar CH<sub>3</sub>). EIMS (low-resolution mode; *M*<sup>+</sup> calcd (found) %): 183.2 (183.2) 37.

**Li(NRAr)(OEt<sub>2</sub>).** A solution of *n*-BuLi (15 mL, 1.6 M in hexanes, 24 mmol) was added via pipet to a solution of H(NRAr) (4.00 g, 21.8 mmol) in hexane at -35 °C. The reaction mixture was warmed to 28 °C, and stirring was continued for 12 h. Removal of the hexane in vacuo left a golden syrup. Addition of ether (10 mL) resulted in the formation of a white, crystalline mass. The solid was broken up and slurried in hexane (ca. 25 mL), and the slurry was chilled to -35 °C for 8 h. The white product was then collected by filtration, washed with cold hexane (10 mL), and dried in vacuo to give Li(NRAr)(OEt<sub>2</sub>) as a white powder (5.20 g, 19.7 mmol, 90%). <sup>1</sup>H NMR (C<sub>6</sub>D<sub>6</sub>): 6.54 (s, 2, ortho Ar H), 6.13 (s, 1, para Ar H), 3.17 (q, 4, OCH<sub>2</sub>CH<sub>3</sub>), 2.30 (s, 6, Ar CH<sub>3</sub>), 1.60 (s, 3, C(CD<sub>3</sub>)<sub>2</sub>CH<sub>3</sub>), 0.95 (t, 6, OCH<sub>2</sub>CH<sub>3</sub>). <sup>2</sup>H NMR (Et<sub>2</sub>O): 2.00 (s, C(CD<sub>3</sub>)<sub>2</sub>CH<sub>3</sub>). <sup>13</sup>C NMR (C<sub>6</sub>D<sub>6</sub>): 159.48 (C aryl ipso), 138.24 (C aryl meta), 116.42 (C aryl), 113.47 (C aryl), 65.34 (OCH<sub>2</sub>-CH<sub>3</sub>), 52.13 (C(CD<sub>3</sub>)<sub>2</sub>CH<sub>3</sub>), 31.72 (C(CD<sub>3</sub>)<sub>2</sub>CH<sub>3</sub>), 31.00 (C(CD<sub>3</sub>)<sub>2</sub>-CH<sub>3</sub>), 22.14 (Ar CH<sub>3</sub>), 14.87 (OCH<sub>2</sub>CH<sub>3</sub>).

**Sn(I)(CH<sub>3</sub>)(NRAr)<sub>2</sub>.** SnI<sub>2</sub> (1.50 g, 4.0 mmol) was added to a solution of Li(NRAr)(OEt<sub>2</sub>) (2.11 g, 8.0 mmol) in 65 mL of THF. The red-orange reaction mixture was stirred for 1 h, and then CH<sub>3</sub>I (1.14 g, 8.0 mmol) was added. In less than 1 min, the color of the reaction mixture changed to pale yellow. The solvent was removed in vacuo. Addition of pentane caused LiI to precipitate, and LiI was removed by filtration. Removal of pentane in vacuo left Sn(I)(CH<sub>3</sub>)(NRAr)<sub>2</sub> (2.18 g, 3.49 mmol, 87.2%) as a pale yellow powder, which was >95% pure by <sup>1</sup>H NMR. The compound can be further purified by recrystallization from pentane with cooling to -35 °C; mp 83–86 °C. <sup>1</sup>H NMR (C<sub>6</sub>D<sub>6</sub>): 6.81 (s, 4, ortho Ar H), 6.71 (s, 2, para Ar H), 2.19 (s, 12, Ar CH<sub>3</sub>), 1.27 (s, 6, C(CD<sub>3</sub>)<sub>2</sub>CH<sub>3</sub>), 0.77 (s, 3, SnCH<sub>3</sub>, <sup>2</sup>*J*<sub>199SnH</sub> = 71.5 Hz, <sup>2</sup>*J*<sub>117SnH</sub> = 68.5 Hz). <sup>2</sup>H NMR (C<sub>6</sub>H<sub>6</sub>): 1.15 (s, C(CD<sub>3</sub>)<sub>2</sub>CH<sub>3</sub>). <sup>13</sup>C NMR (C<sub>6</sub>D<sub>6</sub>): 145.58 (C aryl ipso), 137.46 (C aryl meta), 131.46 (C aryl ortho), 127.27 (C aryl para), 57.35 (C(CD<sub>3</sub>)<sub>2</sub>CH<sub>3</sub>), 32.03 (C(CD<sub>3</sub>)<sub>2</sub>CH<sub>3</sub>), 31 (m, C(CD<sub>3</sub>)<sub>2</sub>CH<sub>3</sub>), 21.43 (Ar CH<sub>3</sub>), 11.83 (SnCH<sub>3</sub>). <sup>119</sup>Sn NMR (C<sub>6</sub>D<sub>6</sub>): -188.15 (q, <sup>2</sup>*J*<sub>SnH</sub> = 71 Hz). Anal. Calcd for C<sub>28</sub>H<sub>27</sub>D<sub>12</sub>IN<sub>2</sub>Sn: C, 48.02; H, 6.29; N, 4.48. Found: C, 47.34; H, 6.20; N, 4.21.

**Sn(I)(NRAr)<sub>3</sub>.** SnCl<sub>2</sub> (264 mg, 1.39 mmol) was added to a solution of Li(NRAr)(OEt<sub>2</sub>) (1.10 g, 4.18 mmol) in 30 mL of Et<sub>2</sub>O. The red-orange reaction mixture was stirred for 2 h, and then it was filtered through a pad of Celite on a sintered-glass frit, thereby removing LiCl. I<sub>2</sub> (353 mg, 1.39 mmol) was then added, causing a rapid color change to orange-yellow. The reaction mixture was stirred for 1 h and then filtered again as before, this time to remove LiI. Et<sub>2</sub>O was removed in vacuo to reveal Sn(I)(NRAr)<sub>3</sub> as an orange-yellow powder. Recrystallization (Et<sub>2</sub>O, -35 °C) provided orange crystals of Sn(I)(NRAr)<sub>3</sub> (0.68 g, 0.86 mmol, 62%); mp 149–151 °C. <sup>1</sup>H NMR (C<sub>6</sub>D<sub>6</sub>): 6.85 (s, 6, ortho Ar H), 6.74 (s, 3, para Ar H), 2.25 (s, 18, Ar CH<sub>3</sub>), 1.36 (s, 9, C(CD<sub>3</sub>)<sub>2</sub>CH<sub>3</sub>). <sup>2</sup>H NMR (C<sub>6</sub>H<sub>6</sub>): 1.23 (s, C(CD<sub>3</sub>)<sub>2</sub>CH<sub>3</sub>). <sup>13</sup>C NMR (C<sub>6</sub>D<sub>6</sub>): 148.40 (s, C aryl ipso), 137.07 (q, C aryl meta), 132.54 (d, C aryl ortho), 127.26 (d, C aryl para), 58.63 (s, C(CD<sub>3</sub>)<sub>2</sub>CH<sub>3</sub>), 32.57 (q, C(CD<sub>3</sub>)<sub>2</sub>CH<sub>3</sub>), 32.03 (m, C(CD<sub>3</sub>)<sub>2</sub>CH<sub>3</sub>), 21.56 (q, Ar CH<sub>3</sub>). <sup>119</sup>Sn NMR (C<sub>6</sub>D<sub>6</sub>): -402.65 (s). Anal. Calcd for C<sub>36</sub>H<sub>36</sub>D<sub>18</sub>IN<sub>3</sub>Sn: C, 54.69; H, 6.87; N, 5.15. Found: C, 54.57; H, 7.05; N, 5.30.

**Sn(CH<sub>3</sub>)(NRAr)<sub>3</sub>.** SnI<sub>2</sub> (566 mg, 1.52 mmol) was added to a solution of Li(NRAr)(OEt<sub>2</sub>) (1.20 g, 4.56 mmol) in 30 mL of THF. The red-orange reaction mixture was stirred for 2 h, and then ICH<sub>3</sub> (900 mg, 6.34 mmol) was added. The color of the reaction mixture changed immediately to a very pale yellow. The reaction mixture was stirred for 1 h prior to the removal of THF in vacuo. The residue was triturated twice

with hexane. Subsequent addition of hexane caused LiI to precipitate, and this was removed by filtration through a pad of Celite on a sintered-glass frit. The hexane was removed in vacuo to give  $\text{Sn}(\text{CH}_3)(\text{NRAr})_3$  as a pale white-yellow powder. Recrystallization (hexane,  $-35\text{ }^\circ\text{C}$ ) provided colorless crystals of  $\text{Sn}(\text{CH}_3)(\text{NRAr})_3$  (0.73 g, 1.1 mmol, 71%); mp  $169\text{--}171\text{ }^\circ\text{C}$ .  $^1\text{H NMR}$  ( $\text{C}_6\text{D}_6$ ): 6.74 (s, 3, para Ar H), 6.48 (s, 6, ortho Ar H), 2.24 (s, 18, Ar CH<sub>3</sub>), 1.20 (s, 9,  $\text{C}(\text{CD}_3)_2\text{CH}_3$ ), 0.75 (s, 3,  $\text{SnCH}_3$ ,  $^2J_{^{119}\text{SnH}} = 69.0\text{ Hz}$ ,  $^2J_{^{117}\text{SnH}} = 66.0\text{ Hz}$ ).  $^2\text{H NMR}$  ( $\text{C}_6\text{H}_6$ ): 1.08 (s,  $\text{C}(\text{CD}_3)_2\text{CH}_3$ ).  $^{13}\text{C NMR}$  ( $\text{C}_6\text{D}_6$ ): 150.08 (C aryl ipso), 136.65 (C aryl meta), 132.69 (C aryl ortho), 126.32 (C aryl para), 56.25 ( $\text{C}(\text{CD}_3)_2\text{CH}_3$ ), 32.34 ( $\text{C}(\text{CD}_3)_2\text{CH}_3$ ), 31.79 (m,  $\text{C}(\text{CD}_3)_2\text{CH}_3$ ), 21.59 (Ar CH<sub>3</sub>), 14.80 ( $\text{SnCH}_3$ ).  $^{119}\text{Sn NMR}$  ( $\text{C}_6\text{D}_6$ ):  $-132.19$  (q,  $^2J_{\text{SnH}} = 67.5\text{ Hz}$ ). Anal. Calcd for  $\text{C}_{37}\text{H}_{39}\text{D}_{18}\text{N}_3\text{Sn}$ : C, 65.29; H, 8.44; N, 6.17. Found: C, 65.59; H, 8.53; N, 6.03.

**Acknowledgment.** We gratefully acknowledge the support of the Massachusetts Institute of Technology Department of Chemistry. C.E.L. also wishes to thank the Undergraduate Research Opportunities Program at MIT for support.

**Supplementary Material Available:** Text giving experimental details and tables of bond lengths and angles, fractional coordinates, and anisotropic thermal parameters for the structures of  $\text{Sn}(\text{CH}_3)(\text{NRAr})_3$  and  $\text{Sn}(\text{I})(\text{NRAr})_3$  (17 pages). Ordering information is given on any current masthead page.

OM940697V